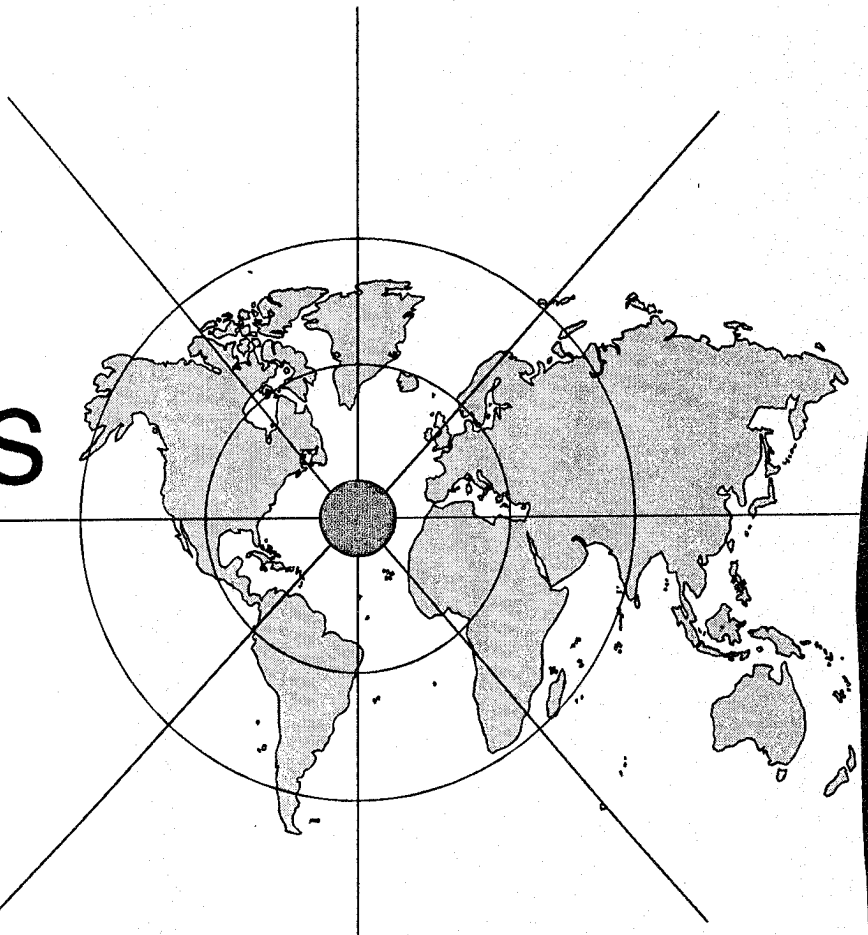
Proceedings of the Forty-Fourth IWCS



Approved for public release
Distribution Unlimited

INTERNATIONAL WIRE AND CABLE SYMPOSIUM

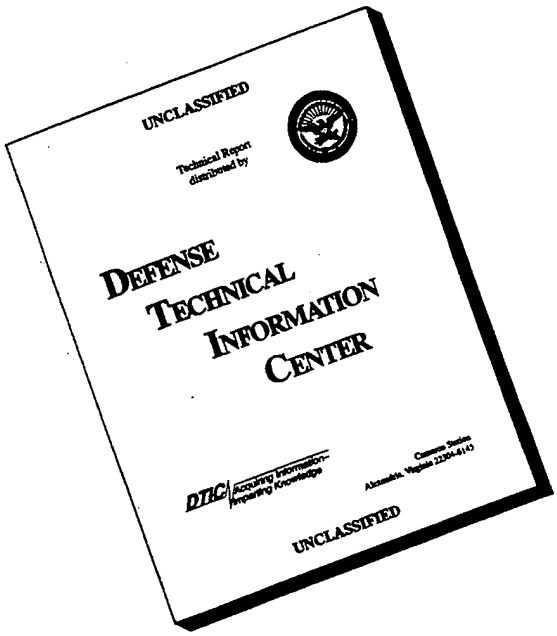
NOVEMBER 13 THRU 16, 1995

19960201 083

Sponsored by
International Wire and Cable Symposium, Inc. (IWCS)
Eatontown, New Jersey

With Participation by
US Army Communications-Electronics Command (CECOM)
Fort Monmouth, New Jersey

DISCLAIMER NOTICE



THIS DOCUMENT IS BEST QUALITY AVAILABLE. THE COPY FURNISHED TO DTIC CONTAINED A SIGNIFICANT NUMBER OF PAGES WHICH DO NOT REPRODUCE LEGIBLY.

PROCEEDINGS OF 44TH INTERNATIONAL WIRE AND CABLE SYMPOSIUM

Sponsored by
International Wire and Cable Symposium, Inc. (IWCS)
Eatontown, New Jersey

With Participation by
US Army Communications-Electronics Command (CECOM)
Fort Monmouth, New Jersey

PHILADELPHIA MARRIOTT HOTEL
PHILADELPHIA, PENNSYLVANIA
NOVEMBER 13, 14, 15 AND 16, 1995

APPROVED FOR PUBLIC RELEASE: DISTRIBUTION UNLIMITED

DTIC QUALITY INSPECTED 1

MISSION

The International Wire and Cable Symposium provides a forum for the exchange of technical information amongst suppliers, manufacturers, and users on technological advancements in materials, processes, and products used for voice, data and video signal transmission systems.

TECHNICAL PAPERS

Tuesday, November 14

9:00 am	SESSION 1	2020 - Visions of Our Communications Future
		Track 1-- Fiber Optic Cables
1:00 pm	SESSION 2	Fiber Optic Cable Design
1:00 pm	SESSION 3	Fiber Optic Connectors
		Track 2 -- Copper Cables
1:00 pm	SESSION 4	LAN Cable/Testing I
		Track 3 -- Materials
1:00 pm	SESSION 5	Fiber Coatings

Wednesday, November 15

		Track 1 -- Fiber Optic Cables
8:00 am	SESSION 6	Submarine Cables
8:00 am	SESSION 7	Fiber Optic Components
		Track 2 -- Copper Cables
8:00 am	SESSION 8	LAN Cable/Testing II
		Track 3 -- Materials
8:00 am	SESSION 9	Hermetically Coated Fiber for Military & Commercial Cable Applications
		Track 1 -- Fiber Optic Cables
2:15 pm	SESSION 10	Polarization Mode Dispersion (PMD)
2:15 pm	SESSION 11	Networks Applications
		Track 2 -- Copper Cables
2:15 pm	SESSION 12	LAN Cable/Testing III
		Track 3 -- Materials
2:15 pm	SESSION 13	Fire Resistance
4:00 pm	SESSION 14	Poster Papers

Thursday, November 16

		Track 1 -- Fiber Optic Cables
8:30 am	SESSION 15	Fiber Ribbons
8:30 am	SESSION 16	Testing & Field Evaluation
		Track 2 -- Copper Cables
8:30 am	SESSION 17	Broadband/Outside Plant
		Track 3 -- Materials
8:30 am	SESSION 18	Fiber Optic Materials
		Track 1 -- Fiber Optic Cables
1:00 pm	SESSION 19	Aerial Cables
		Track 2 -- Copper Cables
1:00 pm	SESSION 20	LAN Media Installers & Manufacturers Roundtable
1:00 pm	SESSION 21	Copper Materials
		Track 3 -- Materials
1:00 pm	SESSION 22	Fiber Coating/Reliability

PAPERS

The papers in this volume were printed directly from unedited reproducible copies prepared by the authors. Responsibility for contents rests upon the authors and not the symposium committee or its members. All rights reserved by the International Wire and Cable Symposium, Inc., 174 Main Street, Eatontown, New Jersey 07724.

PROCEEDINGS/PUBLICATIONS
INTERNATIONAL WIRE AND CABLE SYMPOSIUM (IWCS)

Proceedings - Bound - Available from IWCS

39th IWCS Proceedings - 1990 - $20.00
40th IWCS Proceedings - 1991 - $20.00
43rd IWCS Proceedings - 1994 - $40.00
44th IWCS Proceedings - 1995 - $50.00

Copies of original proceedings not listed above can be reproduced for $75.00 per copy plus shipping.

Publications - Bound - Available from IWCS

Index of IWCS Papers (1983-1990); PUB #1001RP-1991 - $15.00
PIC Insulation Testing Field Experience; PUB #1003RP-1992 - $25.00
Fiber Optic Cables; PUB #1004RP-1992 - $25.00

Extra Copies of the 1995 Proceedings can be obtained for: 1 - $50; 2 - $100; 3 - $150; 4 - $190; 5 - $230; 6 - $270; 7 - $310; 8 - $350; 9 - $390; 10 - $430; 11 and above - $430 plus $30 for each additional copy.

Shipping/Handling:

Proceedings	**Publications**
$ 7.00 per copy USA only	$ 4.00 per copy USA Only
$15.00 per copy Surface Mail (overseas - 4 to 6 weeks)	$ 7.00 per copy Surface Mail (overseas - 4 to 6 weeks)
$35.00 per copy Airmail (Europe)	$15.00 per copy Airmail (Europe and Asia)
$40.00 per copy for (Asia)	

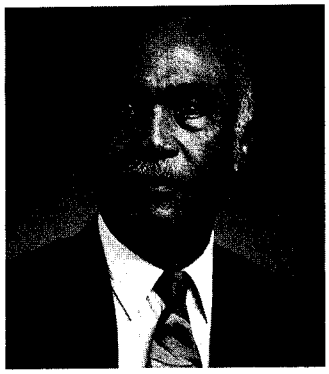
Payment: Make a check or bank draft payable in U.S. Dollars drawn on U.S. Bank only to the INTERNATIONAL WIRE & CABLE SYMPOSIUM, INC. or use your VISA/MC/AMEX by providing number and expiration date and forward request to: International Wire and Cable Symposium, Inc., 174 Main Street, Eatontown, NJ 07724. Telephone inquiries may be directed to Pat Hudak (908) 389-0990. Prices are subject to change.

Photocopies are available for complete sets of papers for 1964 thru 1994. Information on prices and shipping charges should be requested from the:

US Department of Commerce
National Technical Information Service (NTIS)
Springfield, Virginia 22161
Telephone: (703) 487-4650

Include Title, Year and "AD" Number

13th Annual Wire Cable Symposium (1964)	- AD 787164
15th Annual Wire Cable Symposium (1966)	- AD A006601
16th International Wire Cable Symposium (1967)	- AD 787165
17th International Wire Cable Symposium (1968)	- AD 787166
18th International Wire Cable Symposium (1969)	- AD 787167
19th International Wire Cable Symposium Proceedings 1970	- AD 714985
20th International Wire Cable Symposium Proceedings 1971	- AD 733399
21st International Wire Cable Symposium Proceedings 1972	- AD 752908
22nd International Wire Cable Symposium Proceedings 1973	- AD 772914
23rd International Wire Cable Symposium Proceedings 1974	- AD A003251
24th International Wire Cable Symposium Proceedings 1975	- AD A017787
25th International Wire Cable Symposium Proceedings 1976	- AD A032801
26th International Wire Cable Symposium Proceedings 1977	- AD A047609
27th International Wire Cable Symposium Proceedings 1978	- AD A062322
28th International Wire Cable Symposium Proceedings 1979	- AD A081428
29th International Wire Cable Symposium Proceedings 1980	- AD A096308
30th International Wire Cable Symposium Proceedings 1981	- AD A110859
31st International Wire Cable Symposium Proceedings 1982	- AD A125662
32nd International Wire Cable Symposium Proceedings 1983	- AD A136749
33rd International Wire Cable Symposium Proceedings 1984	- AD A152119
34th International Wire Cable Symposium Proceedings 1985	- AD A164384
35th International Wire Cable Symposium Proceedings 1986	- AD A180828
36th International Wire Cable Symposium Proceedings 1987	- AD A189610
37th International Wire Cable Symposium Proceedings 1988	- AD A200903
38th International Wire Cable Symposium Proceedings 1989	- AD A216023
39th International Wire Cable Symposium Proceedings 1990	- AD A233634
40th International Wire Cable Symposium Proceedings 1991	- AD A244038
41st International Wire Cable Symposium Proceedings 1992	- AD A259235
42nd International Wire Cable Symposium Proceedings 1993	- AD A279242
43rd International Wire Cable Symposium Proceedings 1994	- AD A293473
Kwic Index of Technical Papers, International Wire Cable Symposium (1952-1982)	- AD A027588



MESSAGE FROM THE PRESIDENT/DIRECTOR

Welcome to what should be the largest and most exciting International Wire and Cable Symposium (IWCS) since the 1985 symposium in Cherry Hill, New Jersey. The Committee and CECOM, Fort Monmouth are most grateful to all the attendees of the forty-third symposium in Atlanta, GA for making it such a notable success. It is hoped that the return to the east coast will provide the opportunity for many new as well as old attendees to participate in the various technical presentations mixed in with the convivial warmth of meeting old friends and discussing the nostalgia of the early years of symposium activities.

The symposium begins as usual with a plenary session, formerly called the tutorial session, that should be of interest to most attendees, since it covers the expected technical challenges and breakthroughs in communications during the next quarter century. In addition, over 140 other papers are scheduled to be presented on topics of special interest for nearly everyone. This year for the first time a three track program is offered. The third track is dedicated to materials which is in addition to the original tracks on fiber and copper. Another first this year is a session that includes a panel of experts covering the topics of both copper and fiber as experienced by wire/cable installers and manufacturers. This is expected to be an interactive session with participation by the audience. The program also includes the ever popular poster session, suppliers forum and fourteen educational short courses.

On the lighter side, Monday Night Football sponsored by the Alpha Gary Corp. will return, in addition to the usually popular Hospitality Hour on Tuesday and the Awards Luncheon on Wednesday.

Each year the committee bids farewell to several of its hard working and devoted members. This year Brian D. Garrett our present chairman, Dr. Koichi Inada and Dr. Joyce (Chip) Kilmer are leaving the committee. I extend to each, the committee's sincere thanks and appreciation for their cooperation and support.

In addition to the hard working and dedicated committee member, success of the symposium each year is due to the support and participation of its attendees and contributors. The symposium committee salutes and thanks each company for their contribution and each attendees, especially the author's of the more than 140 papers that are included in these proceedings..

The 1996 symposium will be in Reno, Nevada at the Hilton Hotel. It will return to Philadelphia, PA for years 1997 and 1998.

Elmer F. Godwin
President/Director

HIGHLIGHTS OF THE 43RD IWCS

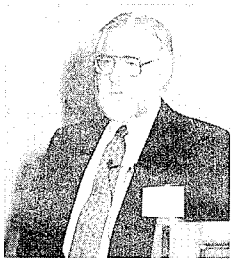
International Wire and Cable Symposium
November 14, 15, 16 and 17, 1994
Atlanta Hilton Hotel, Atlanta, GA

Guest Speakers-Tutorial Session

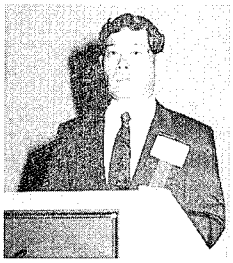
Greetings by



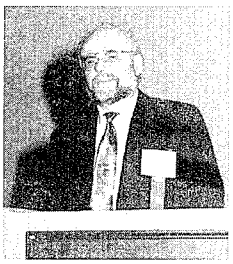
Luncheon Speaker
Durwood Fincher
Atlanta, GA



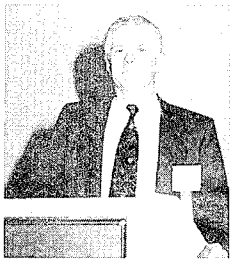
Joseph J. Pucilowski, Jr.
U.S. Army CECOM
Ft. Monmouth, NJ



Yutaka Wakui
NTT Access Network
Systems Labs
Ibaraki, Japan



Eckart Flor
Deutsche Bundespost
Telekon
Darmstadt, Germany



Alex B. Best
Cox Cable
Communications
Atlanta, GA



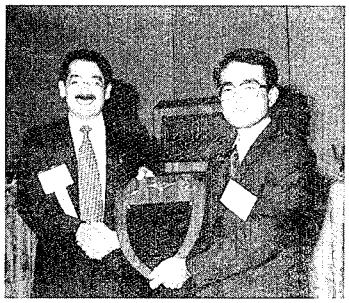
Gerald R. Boyer
Bellcore
Morristown, NJ



Keith Oakley
British Telecom
London, United Kingdom

Award Winners

OUTSTANDING TECHNICAL PAPER



Dr. Yoshinori Namihira
KDD R&D Labs - Saitama, Japan
(Also accepting for Toshio Kawazawa
& Naoki Norimatsu)

OUTSTANDING POSTER PAPER



Willem Griffioen
PTT Research
Leidschendam
The Netherlands

BEST PRESENTATION (Tie)



Dr. Tim Dougherty
AT&T Network
Cable Systems
Phoenix, AZ



Wolfgang Wenski
Kabelmetal
Electro GmbH
Hannover, Germany

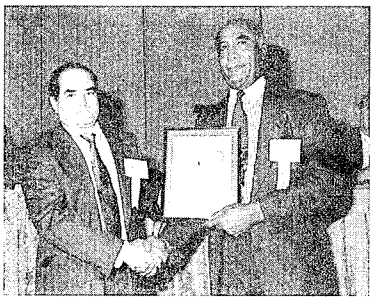
IWCS Retirees



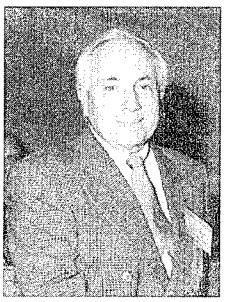
Xavier Mann
AT&T Fitel
Carrollton, GA



Rene Freeman
Union Carbide Co.
Phoenix, AZ



Homero Vela
AT&T ELECON
Telesistemas C.A .- Venezuela



Dieter Nordmann
Kabelmetal - Electro GmbH
Hannover, Germany

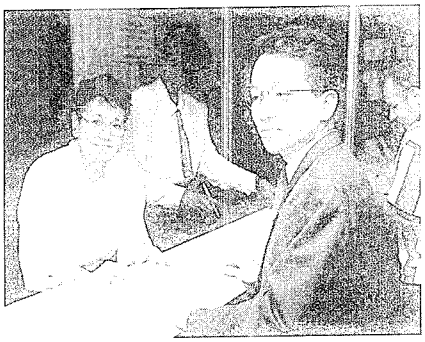
Registration

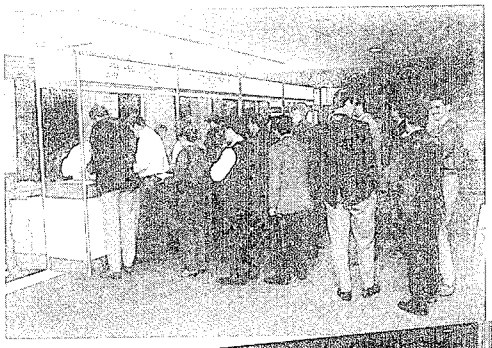


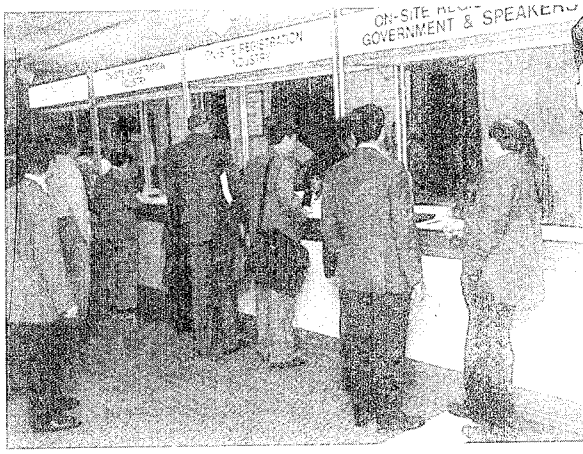




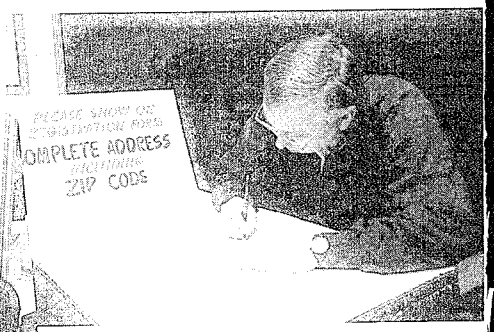


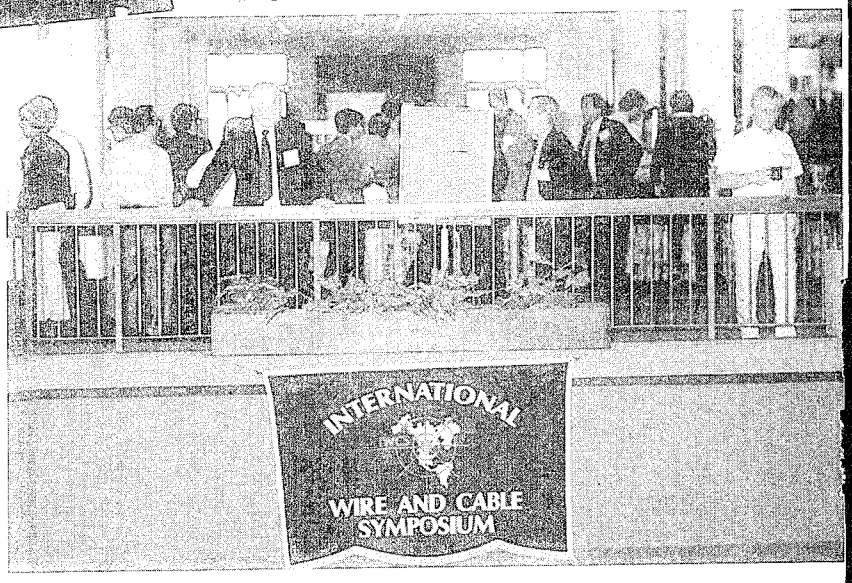






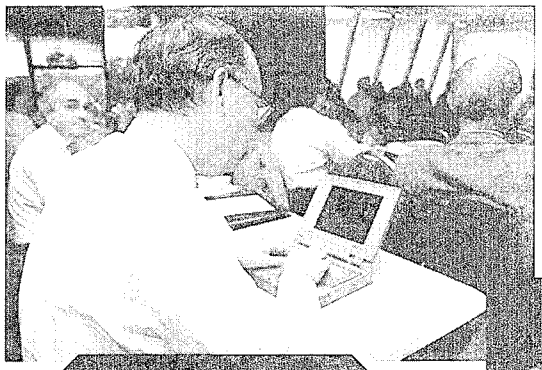


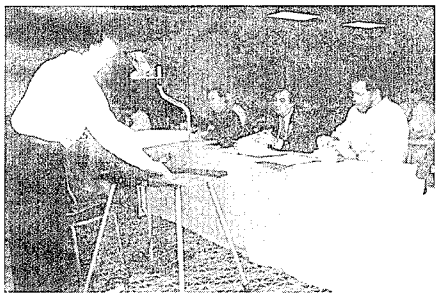


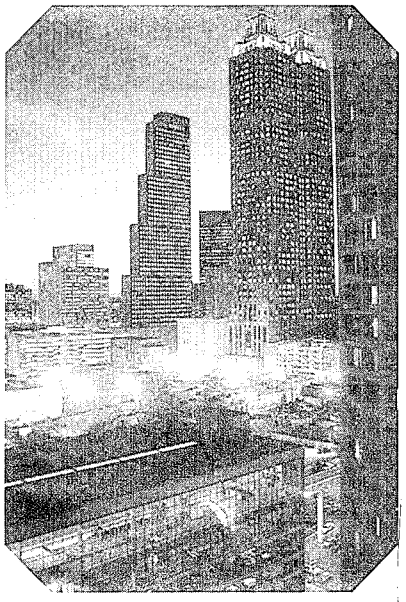




Educational

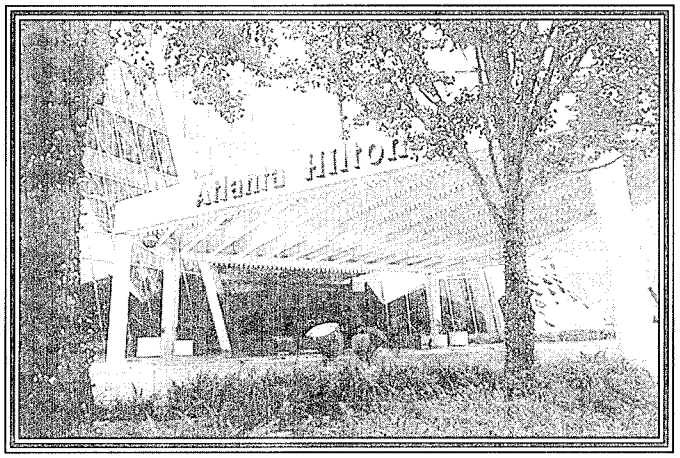


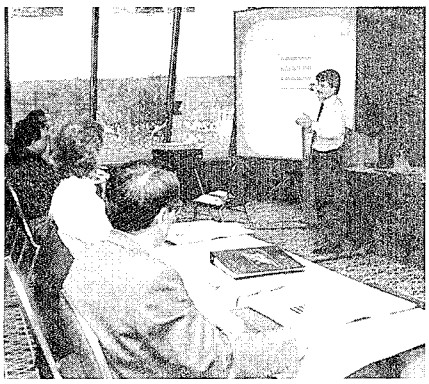




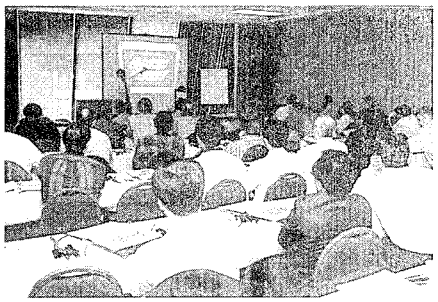


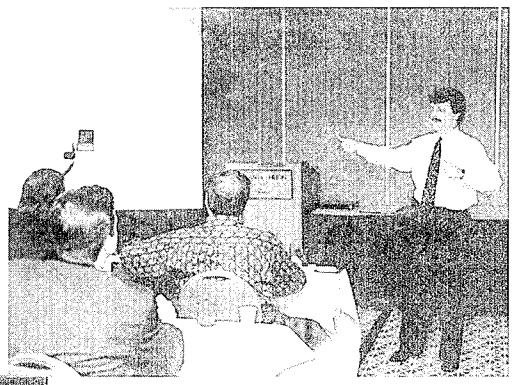




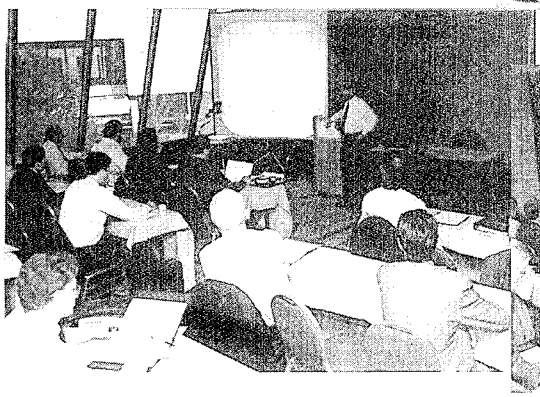


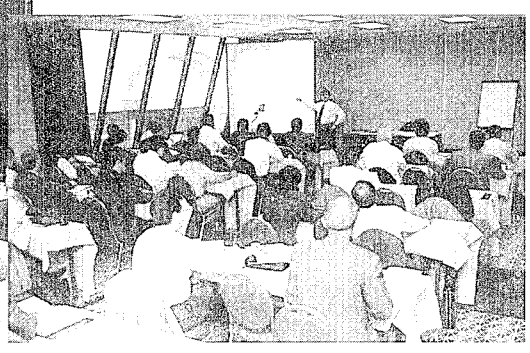


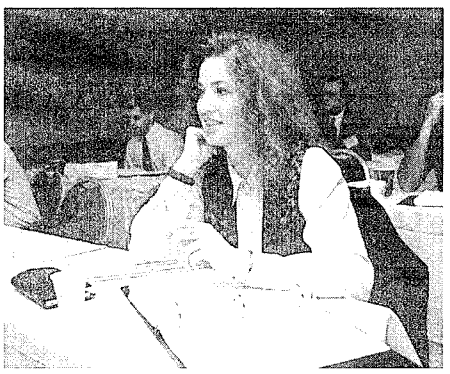




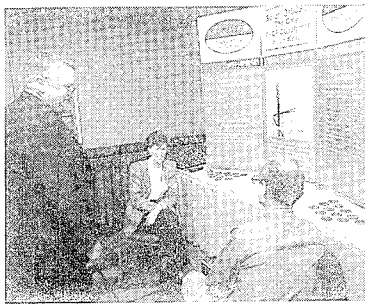




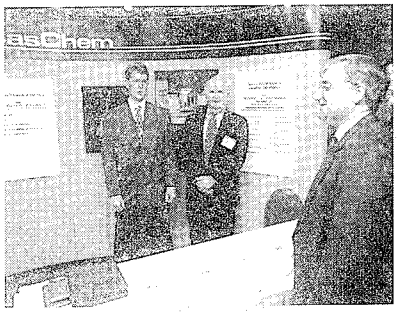




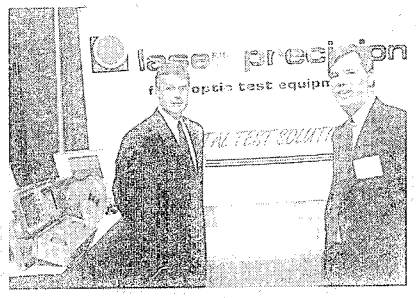




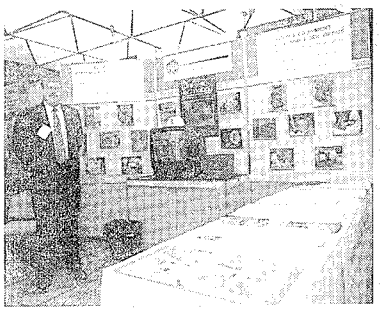

YORK


as-Chem



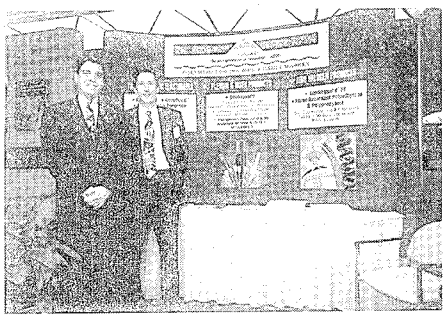

laser precision

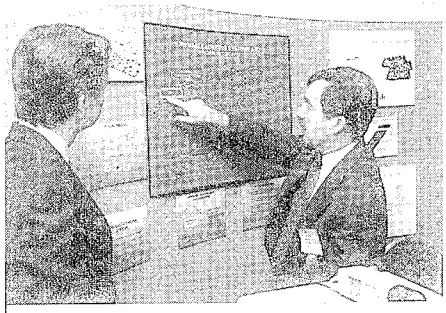




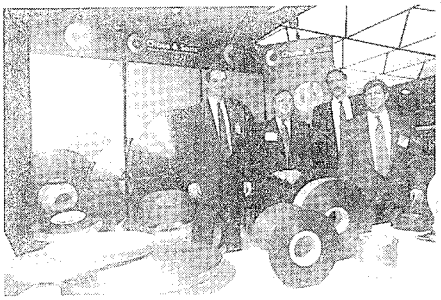



Exhibits

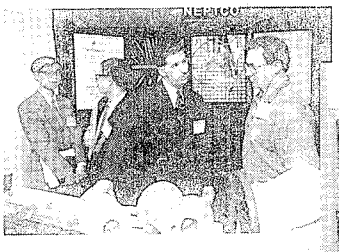




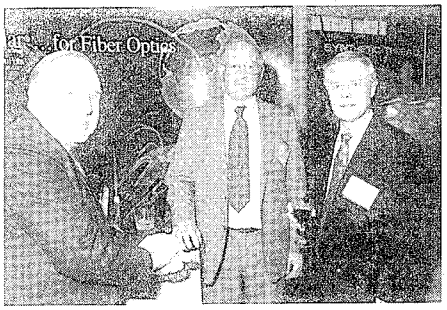

NOKIA-MAILLEFER




WATERGUARD
CABLE PRODUCTS

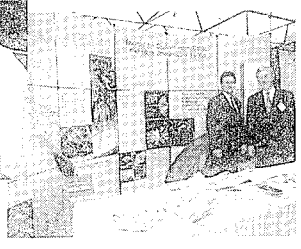


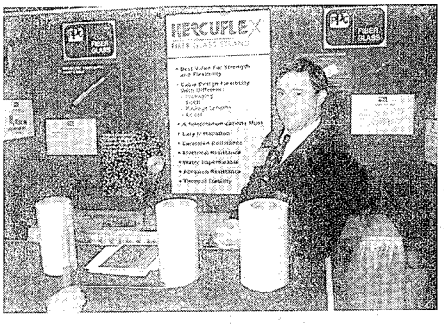

TEXAS
INSTRUMENTS

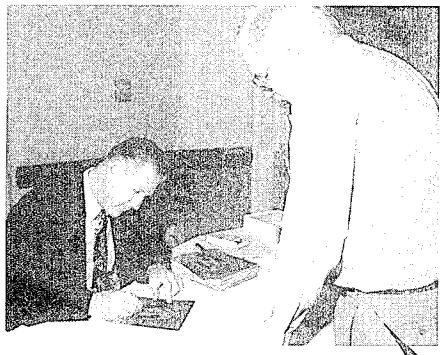

for Fiber Optics








HERCUFLEX



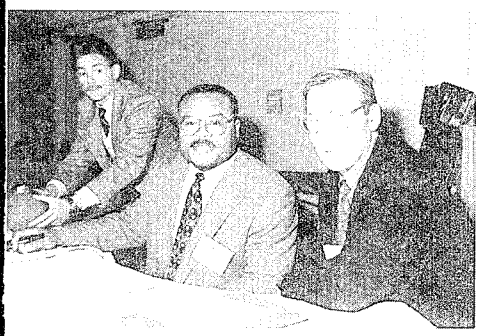
Monday Night Football











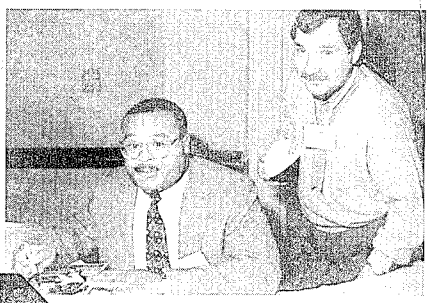


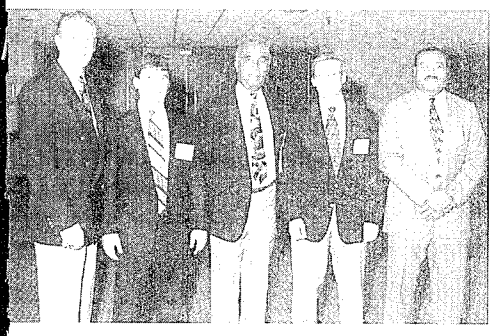






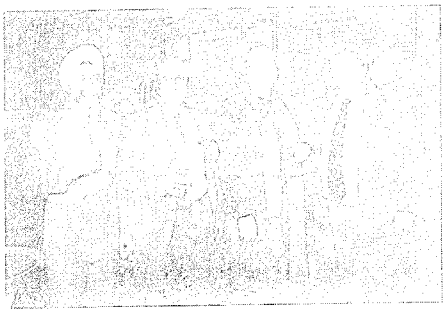


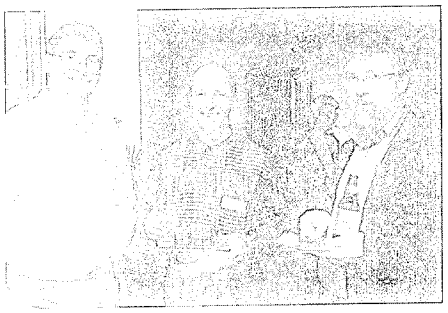






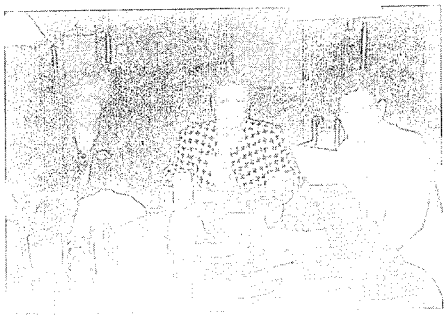


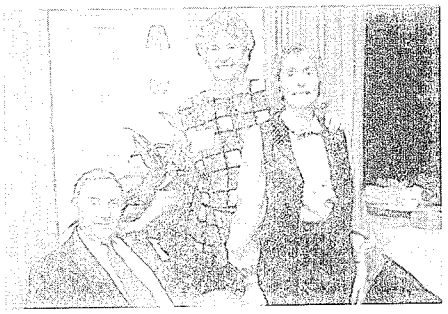


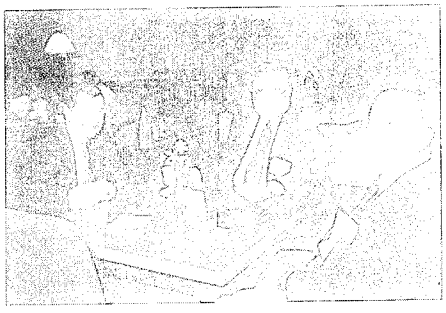






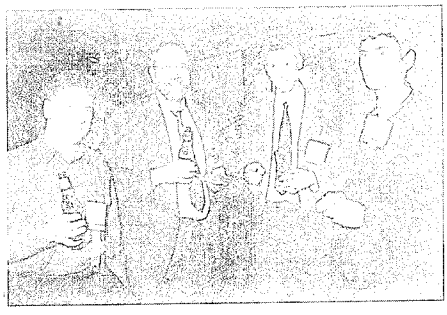


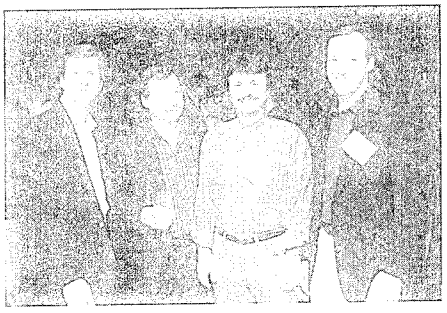


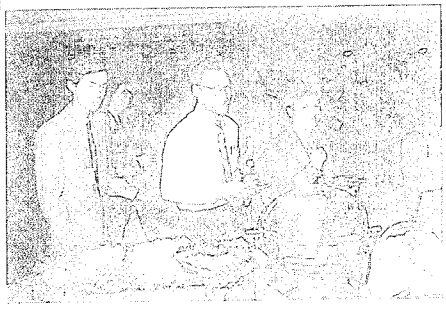


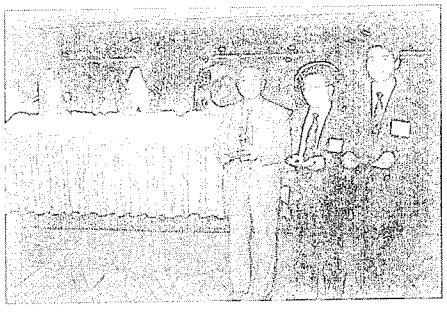

Hospitality

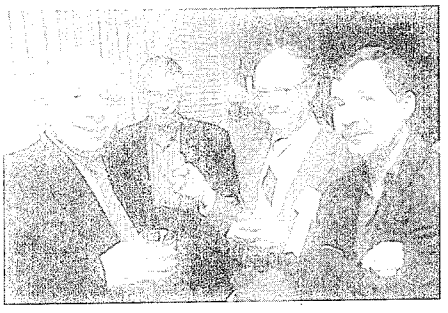


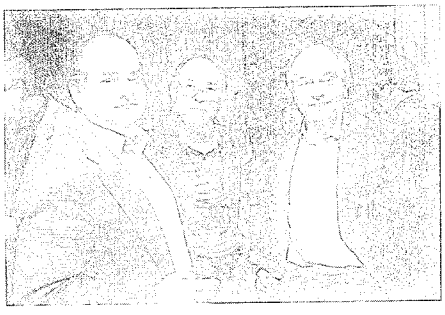




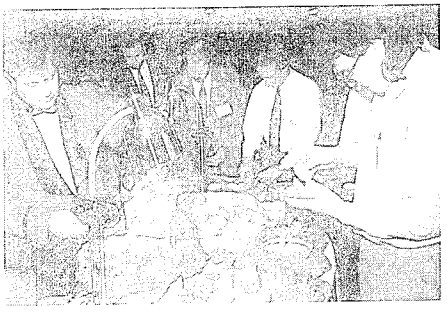






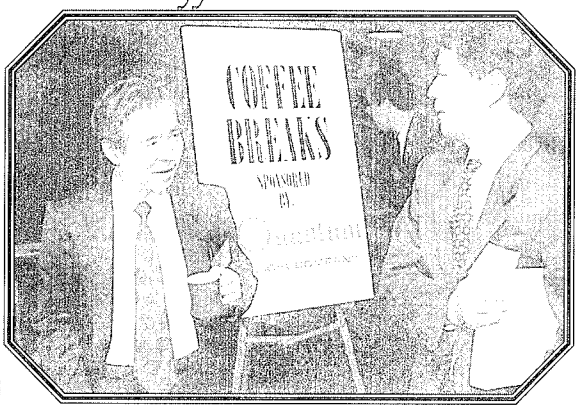




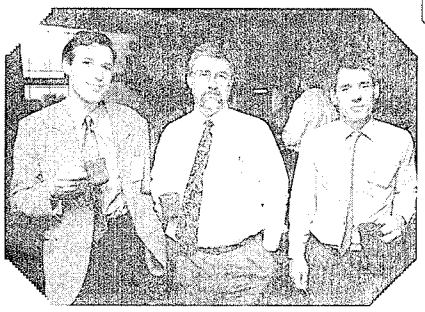


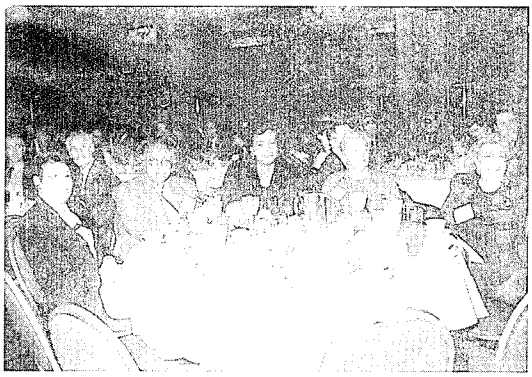
Coffee Breaks

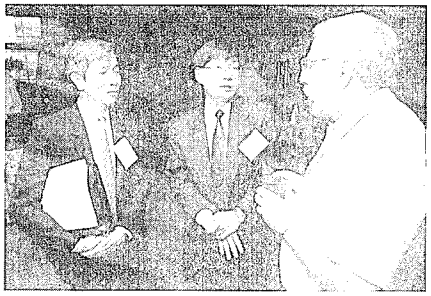


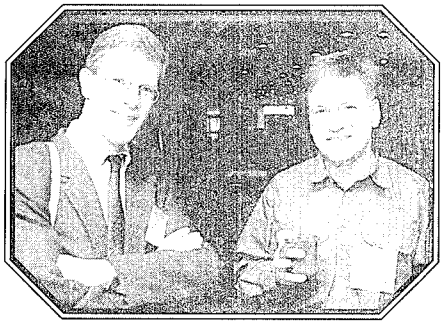


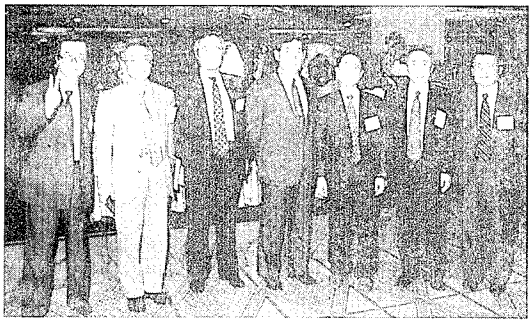


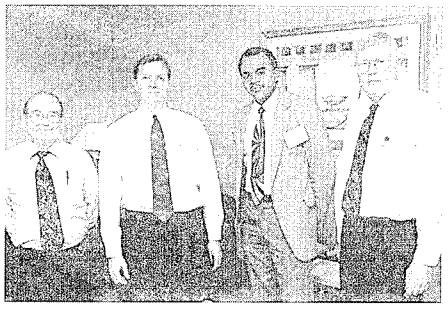


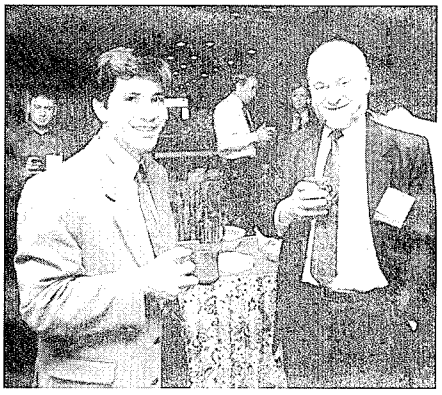


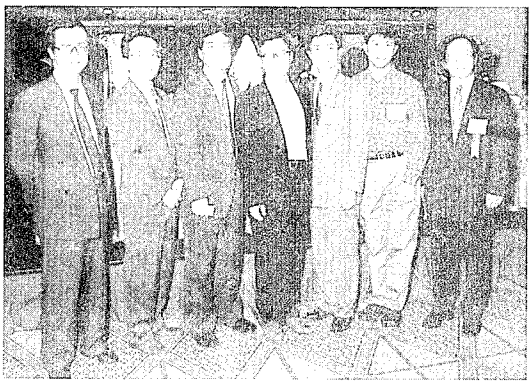




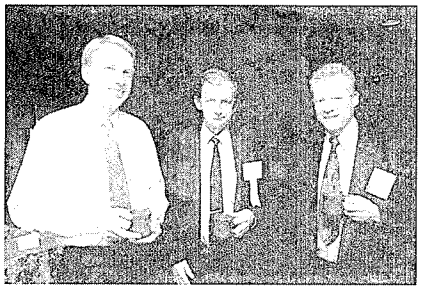




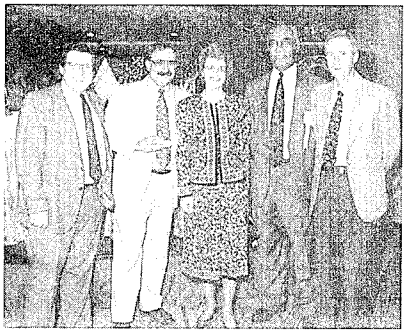


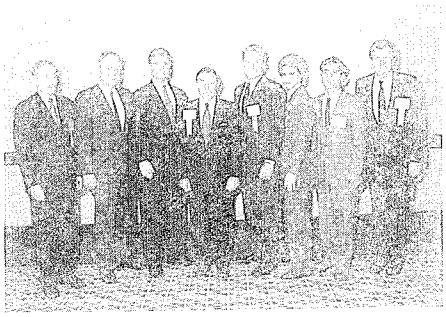
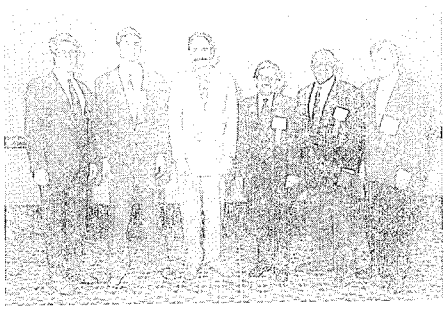
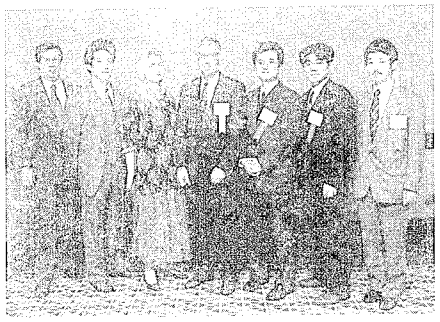
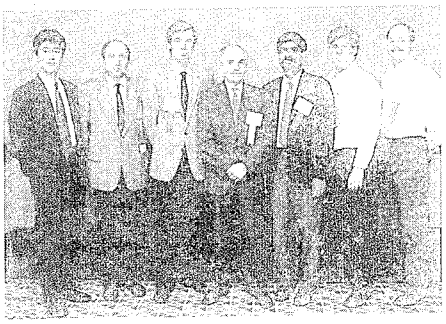
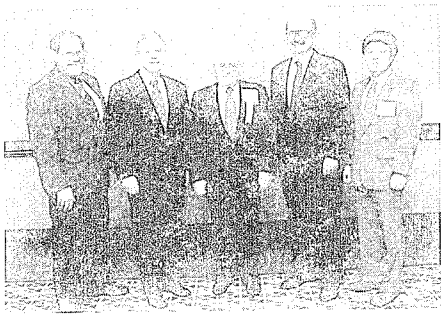
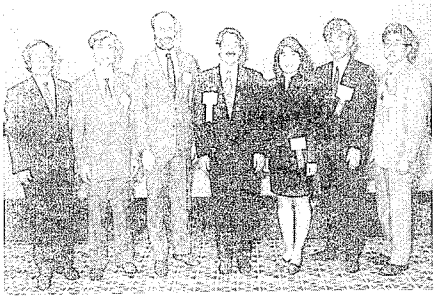
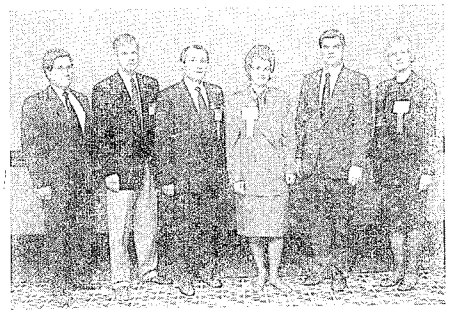
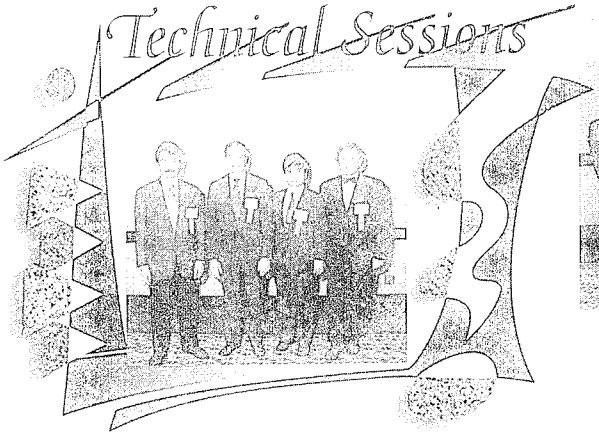
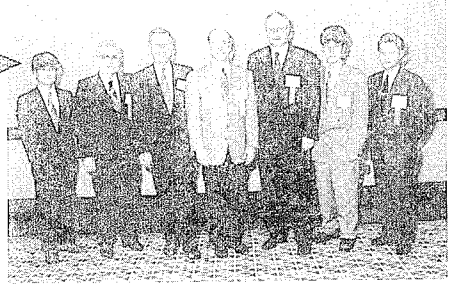


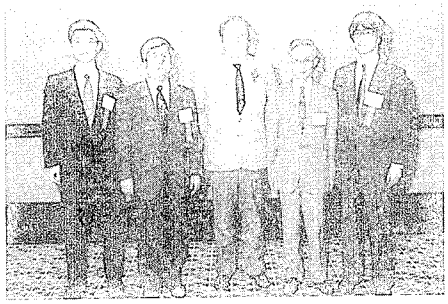
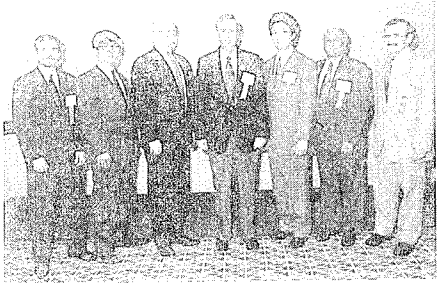
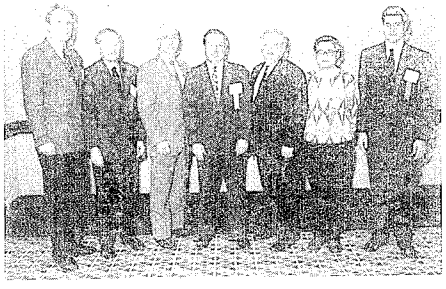
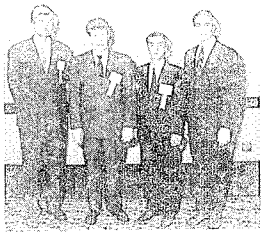
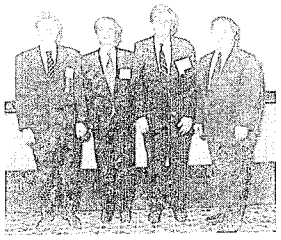


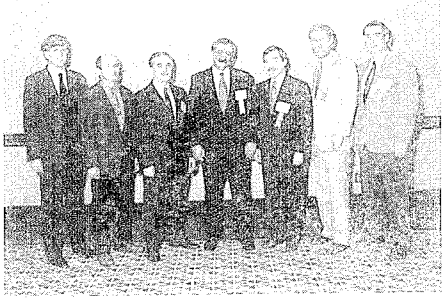
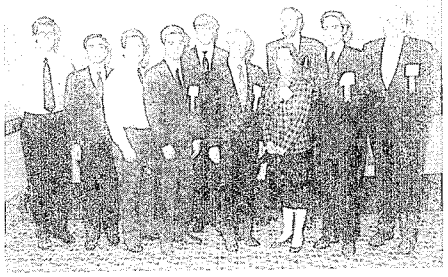
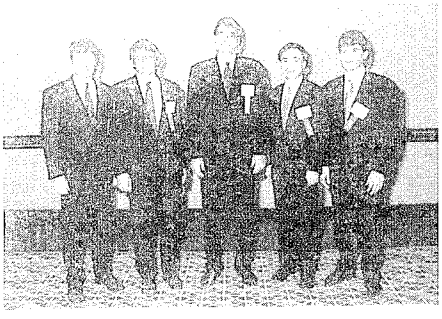


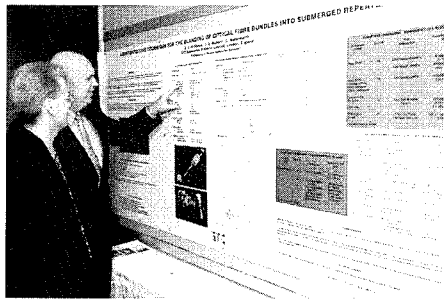


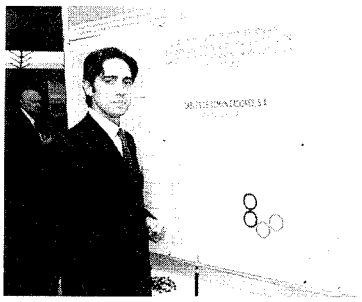


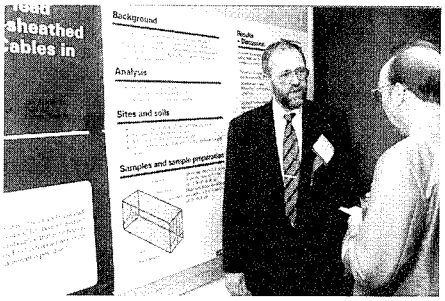








Technical Sessions


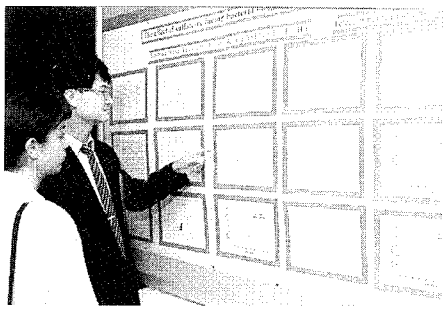






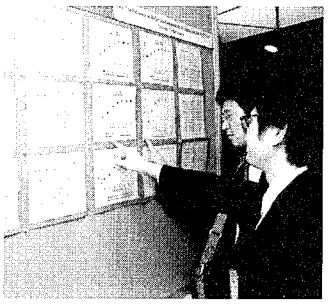




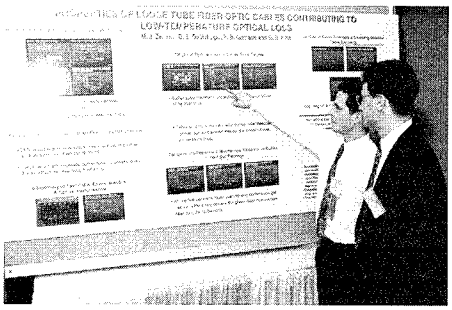


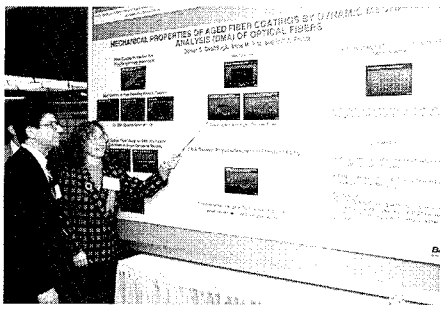


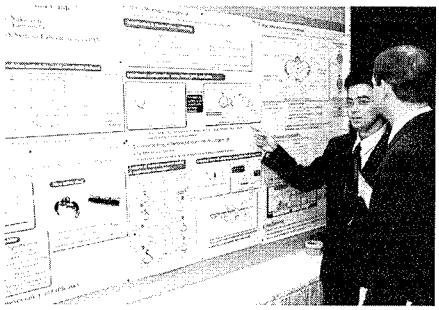
IWCS 1994

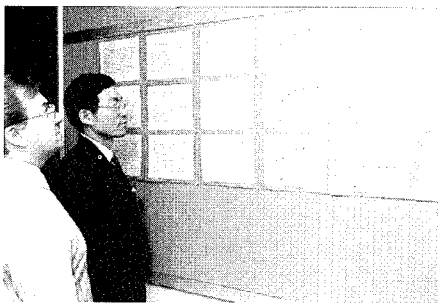


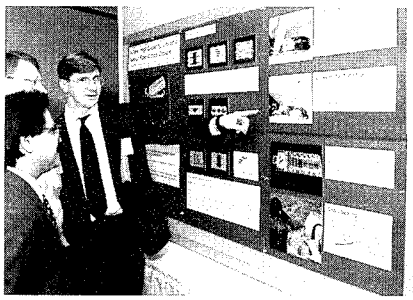
Posters

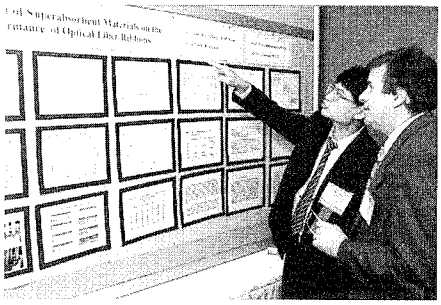


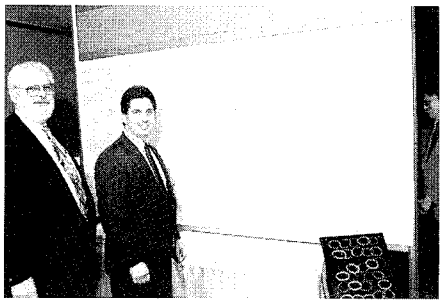


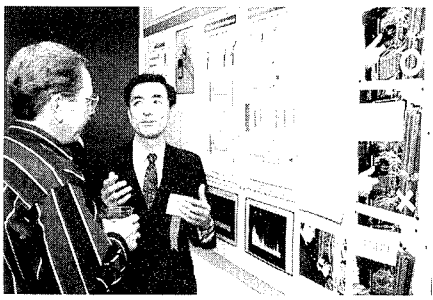


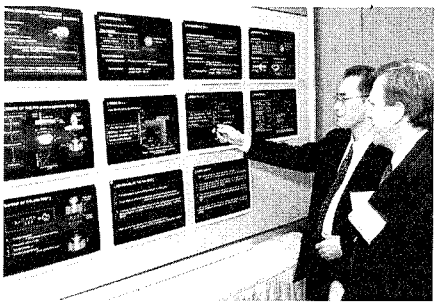


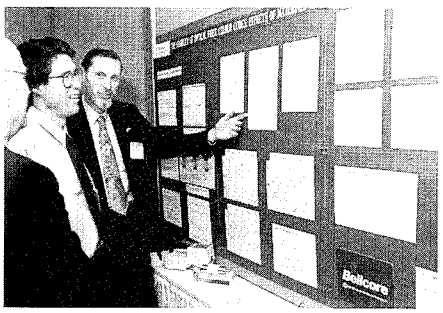


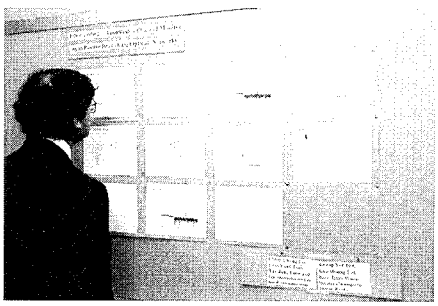


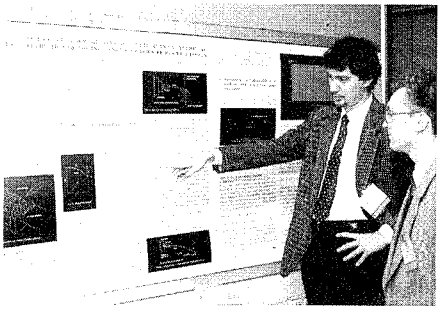












AWARDS

Outstanding Technical Paper

H. Lubars and J. A. Olszewski, General Cable Corp. — "Analysis of Structural Return Loss in CATV Coaxial Cable"

J. P. McCann, R. Sabia and B. Wargotz, Bell Laboratories — "Characterization of Filler and Insulation in Waterproof Cable"

D. E. Setzer and A. S. Windeler, Bell Laboratories — "A Low Capacitance Cable for the T2 Digital Transmission Line"

R. Lyenger, R. McClean and T. McManus, Bell Northern Research — "An Advanced Multi-Unit Coaxial Cable for Toll PCM Systems"

J. B. Howard, Bell Laboratories — "Stabilization Problems with Low Density Polyethylene Insulations"

Dr. H. Margin, Kabelmetal — "High Power Radio Frequency Coaxial Cables, Their Design and Rating"

D. Doty, AMP Inc. — "Mass Wire Insulation Displacing Termination of Flat Cable"

T. S. Choo, Dow Chemical U.S.A. — "Corrosion Studies on Shielding Materials for Underground Telephone Cables"

N. J. Cogelia, Bell Telephone Laboratories and G. K. Lavoie and J. F. Glahn, US Department of Interior — "Rodent Biting Pressure and Chemical Action and Their Effects on Wire and Cable Sheath"

T. K. McManus, Northern Telecom Canada Ltd. and R. Beveridge, Saskatchewan Telecommunications, Canada — "A New Generation of Filled Core Cable"

F. Suzuki, S. Sato, A. Mori and Y. Suzuki; Sumitomo Electric Industries, Ltd., Japan — "Microcoaxial Cables Insulated with Highly Expanded Polyethylene By Chemical Blowing Method"

S. Masaki, Y. Yamazaki and T. Ideguchi, Nippon Telegraph and Telephone Public Corporation, Japan — "New Aluminum Sheath Cable Used for Electromagnetic Shielding"

P. Kish and Y. BeBorgne, Northern Telecom Canada Limited, Montreal, Canada — "General Crosstalk Model for Paired Communication Cables"

C. J. Arroyo, N. J. Cogelia, Bell Laboratories, and B. J. Darsey, Western Electric — "Thermal Behavior of Experimental Plenum Cable Sheaths Determined in a Radiant Heat Chamber"

R. H. Whiteley, Raychem Ltd. — "A Comprehensive Small Scale Smoke Test"

V. A. Fentress, Raychem Corp. and D. V. Nelson, Stanford University — "Fracture Mechanics Evaluation of the Static Fatigue Life of Optical Fibers in Bending"

M. Fujise and Y. Iwamoto, KDD Research & Development Laboratories, Tokyo, Japan — "Self-Core-Alignment Arc-Fusion Splicer Based on a Simple Local Monitoring Method"

James A. Krabec and John W. Kincaid, Jr., Belden Technical Research Center — "Advances in the Optimization of Multi-Layer Shield Design"

Simon D. Dadakarides and Bruce B. Lusignam, Stanford University — "Magnetically Loaded Cables"

Best Presentation

1968 N. Dean, B.I.C.C. – "The Development of Fully Filled Cables for Distribution Network"

1969 J. D. Kirk, Alberta Government Telephones—"Progress and Pitfalls of Rural Buried Cable"

1970 Dr. O. Leuchs, Kable and Metalwerke—"A New Self-Extinguishing Hydrogen Chloride Binding PVC Jacketing Compound for Cables"

1971 S. Nordblad, Telefonaktiebolaget L. M. Ericsson—"Multi-Paired Cable of Nonlayer Design for Low Capacitance Unbalance Telecommunications Network

N. Kojima, Nippon Telegraph and Telephone—"New Type Paired Cable for High Speed PCM Transmission"

1972 S. Kaufman, Bell Laboratories—"Reclamation of Water-Logged Buried PIC Telephone Cable"

1973 R. J. Oakley, Northern Electric Co., Ltd.—"A Study Into Paired Cable Crosstalk"

1974 G. H. Webster, Bell Laboratories—"Material Savings by Design in Exchange and Trunk Telephone Cable"

1975 J. E. Wimsey, United States Air Force—"The Bare Base Electrical Systems"

1976 Michael DeLucia, Naval Ship Research and Development—"Highly Fire-Retardant Navy Shipboard Cable"

1977 William L. Schmacher, AMP Inc.—"Design Considerations for Single Fiber Connector"

1978 Richard C. Mondello, Bell Labs.—"Design and Manufacture of an Experimental Lightguide Cable for Undersea Transmission Systems"

1979 I. Wadehra, IBM Corporation—"Performance of Polyvinyl Chloride Communication Cables in Modified Steiner Tunnel Test"

1980 J. J. Refi, Bell Laboratories—"Mean Power Sum Far-End Crosstalk of PIC Cables as a Function of Average Twist Helix Angle"

1981 G. S. Anderson, Belden Corporation—"Installation of Fiber Optic Cable on 457 Meter Tower"

1982 A. Yoshizawa, The Furukawa Electric Co., Ltd.—"Structure and Characteristics of Cables for Robots"

1983 J. R. Bury, Standard Telecommunication Laboratories, Ltd., Hailow, England—"Development of Flame Retardant, Low Aggressivity Cables"

1984 William E. Dennis, Dow Corning Corporation, Midland, Michigan—"Hydrogen Evolving Tendencies of Cable Fillers and Optical Fiber Coatings"

1985 Stephen Hornung, British Telecom Research Laboratories—"Manufacture and Performance of Fibre Units for Installation by The Viscous Drag of Air"

1986 Dave Fischer, Superior Cable Corp.—"Progress Towards the Development of Lighting Test for Telecommunication Cables"

John C. Chamberlain, Siecor Corp.—"Zero Halogen Fire Retardant Fiber Optic Shipboard Cable"

Outstanding Technical Paper	*Outstanding Poster Paper*	*Best Presentation*
1987 Stephen B. Pierce — Conel Laboratories — "Digital Transmission on Customer Premises Wiring"	William Wood — Bell Communication Research — "Performance Analysis of Optic Fiber Cleavers"	Richard Rossi — General Cable Company — "Cable Sheathing Design and Performance Criteria"
1988 Martin C. Light Jr., James A. Moses, Mark A. Sigmon and Christopher A. Story — Siecor Corp. — "Design and Performance of Telecommunication Cable Optimized for Low Fiber Count"	Dr. R. Raman — Contel Laboratories — "Loss at Dissimilar Fiber Splices"	Janice B. Haber — AT&T Laboratories — "Single-Mode Media and Apparatus for Fiber to the Home"
1989 Michel Plasse, Lise Desroches and Paul-Andre Guilbert — Northern Telecom Canada Limited — "High Performance Twisted-Pair Cable for LAN Systems"	Werner Bernard and Susan C. Grant — Siecor Corporation — "Fiber Optic Drop Cables in the Subscriber Loop"	Michel de Vecchis — Les Cables de Lyon — "Results on a Large Scale Installation of a Fibre Optic Distribution Network"
1990 Trevor N. Bowmer, Russell J. Miner, Irene M. Plitz, Joseph N. D'Amico and Lal M. Hore — Bellcore — "Thermal Stability Tests for Polyolefin Insulations"	Steve Lischynsky, Helmut Lukas, Robin McIntyre and Grant Pacey — Bell-Northern Research Ltd. — "New Technology for a Single Mode Mechanical Splice"	Harold W. Friesen — AT&T Bell Laboratories — "An Improved Characteristic Impedance Measurement Technique"
1991 Shigeru Tomita, Michito Matsumoto, Tetsuro Yabuta and Takuya Uenoya — NTT — "Preliminary Research into Ultra High Density and High Count Optical Fiber Cables"	G. Scott Glaesemann — Corning Inc. — "The Effect of Proof Testing on the Minimum Strength of Optical Fiber"	Sue V. Wolfe — STC Submarine Systems — "Structure and High Voltage DC Behaviour of Submarine Cable Mouldings"
1992 Nathan E. Hardwick III and Kris Kathiresan — AT&T Bell Laboratories and J. G. Hartley — Georiga Institute of Technology — "Analysis of Fiber Optic Cable Design Conditions in Vicinity of Steam Lines — Ruptured and Pristine"	Svend Hopland and Albert Klykken — Norwegian Telecom — "Installation of Submarine Fiberoptic Cables in Rugged Coastal Terrain"	Peter Latoszynski — Telecom Australia — "Development of Co-Extruded Polyethylene/Polyamide 12 Insect Resistant Telecommunications Cable"
1993 Dr. Yoshinori Namihira and Toshio Kawazawa — KDD R&D Laboratories; and Naoki Norimatsu — KDD Company, Limited — "PMD Reduction of Optical Fiber Cables for Transoceanic Optical Amplifier Submarine Cable Systems"	Willem Griffioen — PTT Research — "Mechanical Lifetime of Optical Fibers"	Timothy S. Dougherty — AT&T Network Cable Systems — "The Temperature of Aerial Plant and Its Effect Upon Foam-Skin Insulation Life" and Wolfgang Wenski — Kabelmetal Electro GmbH — "First Large Scale FITL Installation: Experience From Opal '93"
1994 Toshio Kurashima, Kazuo Hogari, Satoshi Matsuhashi, Dr. Tsuneo Horiguchi, Dr. Yahei Koyamada and Yutaka Wakui — NTT Access Network Systems Laboratories; and Hiroshi Hirano — NTT Technical Assistance & Support Center — "Measurement of Distributed Strain in Frozen Cables and Its Potential for Use in Predicting Cable Failure"	Dr. Sverker Forsberg — Swedish University of Agricultural Sciences; and Jan Björkman — Telia AB — "Release of Lead from Lead-Sheathed Telecom Cables in Soil"	Barry J. Keon — Telstra — "The Effects of Optical Fiber Coating and Ink Materials on the Corrosion of the Glass Surface"

GOLD SUSTAINING CONTRIBUTORS

A F A Industries
20 Jewell Street
Garfield, NJ 07026

Akzo Nobel Fibers Inc.
801-F Blacklawn Road
Conyers, GA 30207

Alcatel Cable
30, rue des Chasses
92111 Clichy Cedex
France

AlphaGary Corporation
170 Pioneer Drive
Leominster, MA 01453

Amoco Chemicals
200 E. Randolph Drive
Chicago, IL 60601

Anixter Inc.
4711 Golf Road
Skokie, IL 60048

AT&T Bell Laboratories
2000 Northeast Expressway
Norcross, GA 30071

Breen Color Concentrates, Inc.
11 Kari Drive
Lambertville, NJ 08530

C&S Packaging Group
1300 Commerce Drive
Coraopolis, PA 15108

Cable Systems International
505 N. 51st Avenue
Phoenix, AZ 85043

Chase & Sons
19 Highland Ave.
Randolph, MA 02368

CommScope, Inc.
3642 US 70 East
Claremont, NC 28610-0879

Corning Incorporated
35 West Market Street
MP-RO-02
Corning, NY 14831

DCM Industries, Inc.
2930 Faber Street
Union City, CA 94587

DSM Desotech Inc.
1122 St. Charles Street
Elgin, IL 60120

DuPont Fluoroproducts
Chestnut Run Plaza
Wilmington, DE 19880-0711

E.I. DuPont
PO Box 27001
Richmond, VA 23261

Ericsson Cables AB
Kabelvägen 1
S-824 82 Hudiksvall
Sweden

Facile Holdings Inc.
185 Sixth Avenue
Paterson, NJ 07508

Fujikura Ltd.
1-5-1 Kiba Koto-ku
Tokyo 135, Japan

The Furukawa Electric Co., Ltd.
6, Yawata-Kaigandori
Ichihara, Chiba, 290 Japan

Fusion UV Curing Systems
7600 Standish Place
Rockville, MD 20855-2798

GE Plastics
One Plastics Avenue
Pittsfield, MA 01201

Geca-Tapes
Europalaan 25
5121 DH Rijen
The Netherlands

MM Cables Communication Products
71 Whiteside Road
Clayton, Victoria
Australia

NEPTCO Incorporated
30 Hamlet Street
Pawtucket, RI 02861

Nippon Telegraph and Telephone Corp.
1-7-1, Hanabatake
Tsukuba, Ibaraki, 305
Japan

Nokia-Maillefer, Inc.
1856 Corporate Drive, Suite 135
Norcross, GA 30093

Nortel Cable Group
475 N. Martingale Road
Schaumburg, IL 60173

GOLD SUSTAINING CONTRIBUTORS

Olex Cables
A Division of Pacific Dunlop Ltd.
207 Sunshine Road
Tottenham, 3012
Melbourne, Australia

Optical Fibres
Second Avenue
Deeside Industrial Park
Deeside, Clwyd CH5 2NX
United Kingdom

Owens-Corning
Fiberglas Tower T/12
Toledo, OH 43659

Penreco
4401 Park Ave, PO Drawer C
Dickinson, TX 77539

Photon Kinetics, Inc.
9405 SW Gemini Drive
Beaverton, OR 97008

Pirelli Cable Corporation
700 Industrial Drive
Lexington, SC 29072-3799

Plasma Optical Fibre BV
PO Box 1136
5602 BC, Eindhoven
The Netherlands

PPG Industries, Inc.
One PPG Place, 33W
Pittsburgh, PA 15272

Quantum Chemical Co.
11500 Northlake Drive
Cincinnati, OH 45249

Siecor Corporation (RD)
P.O. Box 489
Hickory, NC 28603

SpecTran Corporation
50 Hall Road
Sturbridge, MA 01566

The Stewart Group Inc.
259 Steelcase Road West
Markham, Ontario
Canada L3R 2P6

Sumitomo Electric U.S.A., Inc.
21221 S. Western Ave., Ste 200
Torrance, CA 90501

Teknor Apex Company
505 Central Avenue
Pawtucket, RI 02861

Telia AB
Network Services
S-123 86 Farsta
Sweden

UBE Industries (America), Inc.
666 Fifth Avenue, 14th Floor
New York, NY 10103-0074

Union Carbide Corporation
39 Old Ridgebury Road, N1-577
Danbury, CT 06817-0001

WaterGuard Cable Products, Inc.
14135 I-10 East
Houston, TX 77015

Weber & Scher Mfg. Co., Inc.
263 Sussex Avenue
Newark, NJ 07107

Witco Corporation
One American Lane
Greenwich, CT 06831

SILVER SUSTAINING CONTRIBUTORS

ACOME
Paris & Mortain, France

Belding Thread Group
Charlotte, NC

CasChem, Inc.
Bayonne, NJ

Daewoo Telecom
Inchon, Korea

Information Gatekeepers, Inc.
Boston, MA

Kroschu-Kabelwerke
Kromberg & Schubert GmbH u. Co.
Rhede, Germany

Mitsubishi Cable Industries, Ltd.
Chiyoda-ku, Tokyo, Japan

Mohawk/CDT
Leominster, MA

Showa Electric Wire & Cable Co., Ltd.
Sagamihara, Kanagawa, Japan

Siemens AG
Muenchen, Germany

TABLE OF CONTENTS

TUESDAY MORNING—9:00 AM–12:00 PM (NOON)
Grand Ballroom, Fifth Floor—Salons E&H

Announcements/Greetings

Elmer F. Godwin, President/Director, IWCS, Inc., Eatontown, NJ

Brian D. Garrett, CommScope, Inc., Claremont, NC, Chairman, IWCS

Barry S. Salis, Deputy Director, Space and Terrestrial Communications, U.S. Army, CECOM, Fort Monmouth, NJ

PLENARY SESSION 1: 2020—VISIONS OF OUR COMMUNICATIONS FUTURE

Chairperson: Dr. Felix P. Kapron, Bellcore, Morristown, NJ

Fiber Optics' Next Quarter Century: Building the Photonic Network—*D. B. Keck*, Corning Inc., Corning, NY 3

The Forty Plus Years of Canadian Cable TV—*J. M. Hood*, Comlink Systems Inc., Oshawa, Ontario, Canada 4

Communications in the Next Quarter Century: The Unexpected Role of the Copper Twisted Pairs!—*G. Dupuy D'Angeac*, Alcatel Cable, Clichy, France 5

Wireless Communications Year 2020—*O. Mäkitalo*, Telia Research AB, Haninge, Sweden 6

Luncheon Speaker—*Ralph Archbold as Ben Franklin*, Philadelphia, PA 7

TUESDAY AFTERNOON—1:00 PM–5:00 PM
Grand Ballroom, Fifth Floor—Salons A/B
TRACK 1—FIBER OPTIC CABLE DESIGN

SESSION 2: FIBER OPTIC CABLE DESIGN I

Chairperson: Dr. Stephen Hornung, Ipswich, UK

Design and Development of a Compact High Fiber Count Ribbon Cable—*W. J. McCallum, M. C. Light, R. S. Wagman*, Siecor Corp., Hickory, NC 8

Buffer Tubes—The Next Generation—*M. Adams, J. Holder*, Alcatel Telecommunications Cable, Claremont, NC; *C. McNutt, O. Tatat*, Alcatel Cable OFCCC, Bezons, France; and *H. Yang*, Alcatel Telecommunications Cable, Claremont, NC 16

Development of Flexible 100-Count Slot-Type Optical Fiber Ribbon Cable—*T. Yasouka, T. Koyama, K. Imamura, M. Fujita, H. Tanaka*, Mitsubishi Cable Industries, Ltd., Itami-City, Japan 22

A Dry Core Loose Tube Cable for Outside Environments—*C. E. Clyburn III, A. G. Bringuier*, Siecor Corp., Hickory, NC 29

Ultra-thin Optical Fiber Ribbon and 108-Fiber Loose Tube Ribbon-Based Cable—*X.-P. Gao, G. X. Shen, B.-S. Yao, Y.-D. Dai*, Shanghai Electrical Cable Research Institute, China 37

Fiber Design for Future High Capacity Digital Transmission—*R. B. Kummer, L. R. Dunn, R. E. Fangmann, A. F. Judy, D. Kalish, D. W. Peckham*, AT&T Bell Laboratories, Norcross, GA; *R. G. Huff, W. A. Reed, A. M. Vengsarkar, K. L. Walker*, AT&T Bell Laboratories, Murray Hill, NJ; *A. R. Chraplyvy, L. Clark, R. Tkach*, AT&T Bell Laboratories, Holmdel, NJ; and *J. J. Thomas*, AT&T Network Technology Development, Bedminster, NJ 42

New Light Weight, Small Diameter Fibre Optic Ribbon Cable for the Norwegian Access Network—*G. Berthelsen, G. Sletten, M. Johansen, K. Skuland*, Alcatel Kabel Norge AS, Oslo, Norway 47

TUESDAY AFTERNOON—1:00 PM–5:00 PM
Grand Ballroom, Fifth Floor—Salons C/D
TRACK 1—FIBER OPTIC CABLES

SESSION 3: FIBER OPTIC CONNECTORS

Chairperson: Dr. Joyce P. Kilmer, Optotec, N.A.A., New York, NY

Direct Fusion Splicing of Optical Connectors: Zero-Length Pigtail Technique for On-Site Installation—*R. Throckmorton, M. Curran*, Siecor Corporation, Hickory, NC; and *K. Hollensett, V. Riech*, RXS Kabelgarnituren GmbH, Hagen, Germany 52

Controlling Reflectance of Optical Connectors—*E. M. Vogel, L. A. Reith, E. Beebe, J. J. Brickel*, Bellcore, Morristown, NJ 58

Automated Assembly and Inspection System for SC Optical Connector—*A. Nagayama, T. Yoshizawa, K. Sasakura, S. Oguchi, T. Saitoh, S. Hosokawa*, NTT Interdisciplinary Laboratories, Tokyo, Japan 63

Testing of Optical Connectors and Splices in High-Stress Service Environments—*L. A. Reith, R. A. Frantz*, Bellcore, Morristown, NJ 71

Study of Lowering Connecting Loss of 16-Fiber Connector—*H. Katsura, T. Ueda, M. Honjo, T. Yamanishi*, Sumitomo Electric Industries, Ltd., Kanagawa, Japan 79

Reference Multifiber Connector—*K. Takizawa, A. Nishimura, T. Arikawa, Y. Kikuchi, H. Yokosuka*, Fujikura Ltd., Chiba, Japan 85

Fiber Optic Feed Through Adapter for Military Applications—*R. J. Patterson, M. F. Petner*, Lockheed Martin Government Electronic Systems, Moorestown, NJ 91

TUESDAY AFTERNOON—1:00 PM–5:00 PM
Grand Ballroom, Fifth Floor—Salons I/J
TRACK 2—COPPER CABLES

SESSION 4: LAN CABLE/TESTING I

Chairperson: Dr. Reiner J. Gerdes, Gerdes Consulting & TransTel Group, Inc., Atlanta, GA

STP-Cables for Data Transmission: 300 MHZ and Beyond—*F. Gaille, J.-C. Ochsner*, Câbleries et Tréfileries de Cossonay S. A., Cossonay, Switzerland 96

The Development of a Multimedia Shielded Twisted Pair Cable—*K. Saito, H. Hondo, K. Negishi, Y. Horie, K. Chiba, Y. Sato*, The Furukawa Electric Co., Ltd., Chiba, Japan 104

Cable Preparation Effects on High Performance Twisted Pair Cable Testing from 100MHz to 350MHz—*R. Alvarez, R. Herrera*, DCM Industries, Inc., Union City, CA 112

An Explanation for Unexpected NEXT Failures on Short UTP Links—*J. R. Sciacero*, Microtest Inc., Phoenix, AZ 119

Modal Decomposition (Non-BALUN) Measurement Technique: Error Analysis and Application to UTP/STP Characterization to 500 MHz—*K. Yanagawa*, Hewlett-Packard Japan Ltd., Hyogo, Japan; and *J. Cross*, Hewlett-Packard Co., Santa Clara, CA 126

Standards Overview and Future Directions for Telecommunications Cabling—*P. Kish*, Northern Telecom, Quebec, Canada 134

TUESDAY AFTERNOON—1:00 PM–5:00 PM
Grand Ballroom, Fifth Floor—Salons K/L
TRACK 3—MATERIALS

SESSION 5: FIBER COATINGS

Chairperson: Michel Rousseau, Alcatel Cable, Clichy Cedex, France

A Viscoelastic Analysis of Thermally Induced Residual Stresses in Dual Coated Optical Fibers—*C. J. Aloisio, Jr., W. W. King, R. C. Moore*, AT&T Bell Laboratories, Norcross, GA 139

Effects of Color Coding on Optical Fiber Performance and Reliability—*R. A. Frantz, E. M. Vogel,* Bellcore, Morristown, NJ; *B. J. Keon,* Telstra, Melbourne, Australia 146

Heat-Resistance Behavior and the Discernibility of the Color of Optical Fibers and Fiber Ribbons—*A. Murata, K. Kobayashi, K. Oohashi, S. Araki, T. Maruoka,* Fujikura Ltd., Chiba, Japan 151

The Characteristics of Polyimide Coated Fiber with UV-Acrylate Overcoating—*Y. Naganuma, A. Mizutani, S. Endo, Y. Kubo, Y. Saito,* Sumitomo Electric Industries, Ltd., Yokohama, Japan 157

Optical Fiber Design for Improved Mechanical Properties—*J. C. Novack, F. Bacon, B. J. Cronk, J. W. Laumer, J. M. Moser, B. A. Rabine,* 3M Co., Maplewood, MN..... 162

TUESDAY EVENING
Grand Ballroom, Fifth Floor—Salons E, F, G & H
Hospitality Hour—6:30 PM–8:00 PM
&
Suppliers Forum—6:30 PM–8:00 PM
Admission by badges issued to all registrants

WEDNESDAY MORNING—8:00 AM–11:45 AM
Grand Ballroom, Fifth Floor—Salons A/B
TRACK 1—FIBER OPTIC CABLES

SESSION 6: SUBMARINE CABLES

Chairperson: Dr. Koichi Inada, Fujikura Ltd., Chiba-ken, Japan

Development of Dispersion Controlled Optical Fiber Submarine Cables and C-OTDR for Long Span Transmission Systems Using In-Line Optical Amplifiers—*T. Numata, S. Goto, Y. Sakuyama,* NTT Network Systems Development Department, Japan; *S. Nishio,* NTT Central Training Institute, Japan; *K. Tanaka, S. Furukawa,* NTT Access Network Systems Laboratories, Japan; and *N. Atobe,* NTT Maintenance Service Planning Department, Japan..... 169

Optical Fiber for Amplified Undersea Systems—*D. L. Philen, R. B. Kummer, D. Kalish, D. Peckham, J. Darsey, R. Heyda, A. Klein, S. Siddiqui, R. Moore, C. Taylor,* AT&T Bell Laboratories, Norcross, GA; *A. Meixner, S. Shapiro, L. Marra, R. Tuminaro,* AT&T Bell Laboratories, Holmdel, NJ; and *D. Applegate,* AT&T Bell Laboratories, Murray Hill, NJ. 176

Optical Performance of Submarine Cables in Optically Amplified High Bit Rate Systems—*J. L. Lang, J. F. Libert,* ASN Calais, Calais, France; *D. I. Curtis, P. Worthington,* ASN Southampton, UK..... 183

On the Reliability of System Integration from Multiple Submarine Telecommunication Suppliers—*L. A. Dissado, J. Bishop, I. Doble,* Alcatel Submarine Networks, Southampton, UK; *S. V. Wolfe,* Alcatel Submarine Networks, Greenwich, London, UK; and *Q. Zhong, W. B. Wargotz, M. M. Sanders,* AT&T Submarine Systems, Inc., Holmdel, NJ..... 192

New High Reliability Design for Submarine Repeaterless Optical System. Qualification Test Results. Installation Background—*J.-F. Libert, Y. Charles,* Alcatel Submarine Network, Calais Cedex, France..... 199

Development of the Optical Cable Unit in Composite Tether Cable for Deep Sea Unmanned Vehicle System (KAIK-OU)—*A. Sano, A. Mogi, O. Koyasu, K. Watanabe, M. Miyamoto,* Fujikura Ltd., Chiba, Japan 205

Investigation of Hydrogen Induced Losses in Installed Fibreoptic Submarine Cable Systems with Submerged Splice Housings—*S. Hopland,* Telenor AS, Telenor Network, Oslo, Norway; *E. Sikora,* BT Laboratories, Ipswich, UK..... 212

WEDNESDAY MORNING—8:00 AM–11:45 AM
Grand Ballroom, Fifth Floor—Salons C/D
TRACK 1—FIBER OPTIC CABLES

SESSION 7: FIBER OPTIC COMPONENTS

Chairperson: Paul M. Kopera, Anixter Inc., Skokie, IL

Splices and Connectors for Bunched Multicore Monomode Fibers—*H. Aoustin, A. M. Blanchard, M. Boitel, J. J. Gueguen, R. Le Marer, T. Mahé, D. Morellec, A. Pécot, G. Perrin,* France Telecom, Lannion, France..... 217

1×7 and 1×8 Monolithic Couplers Manufactured by Indirect Flame Fusion Technique—*S. Pitassi, A. Zucchinali, M. Maglio, V. Spano,* SIRTI S.p.A., Cusano Milanino, Italy..... 224

A 100×100 Optical Fiber Cross-Connect System—*J. Yamaguchi, N. Tamaru, T. Shoji, T. Kanai, Y. Nishida, F. Ohira,* NTT Interdisciplinary Research Laboratories, Tokyo, Japan..... 232

Study of a Compact and Non-Blocking Opto-Mechanical Switch—*Y. Hayashi, H. Furukawa, Y. Nomura, H. Yokosuka,* Fujikura Ltd., Chiba, Japan..... 239

Analysis of Mass Fusion Splice Loss—*T. Sano, T. Watanabe, K. Osaka,* Sumitomo Electric Industries, Ltd., Yokohama, Japan 245

Development of Multi-fiber Backplane Connector—*K. Kanai, H. Yanagase, N. Shimoji,* Furukawa Electric Co., Ltd., Chiba, Japan 250

Filter Embedded Component for Plug Jack Type Connector—*K. Asano, H. Hosoya, H. Yokosuka,* Fujikura Ltd., Chiba, Japan 255

WEDNESDAY MORNING—8:00 AM–11:45 AM
Grand Ballroom, Fifth Floor—Salons I/J
TRACK 2—COPPER CABLES

SESSION 8: LAN CABLE/TESTING II

Chairperson: Hans A. Mayer, Olex Cables (Division of Pacific Dunlop Ltd.), Melbourne, Australia

Relating the Structural Return Loss of Cable Pairs to the Associated Attenuation Deviation and Delay Jitter—*H. W. Friesen,* AT&T Bell Laboratories, Norcross, GA..... 261

Combining Mathematical Modeling with Materials Development to Predict High Speed Telecommunication Cable Properties—The Laplace Model—A Tool for the 21st Century—*B. Burke,* Lightwave Software Corp., Cary, NC; *G. L. Grune,* ABB Corp., Raleigh, NC 269

Achieving Connector Interface Independent Transmission Line Measurements Using Digital Signal Processing Techniques—*T. M. Hayes,* CommScope Inc., Claremont, NC 278

Determining Field Test Instrument Accuracy for Measuring Near End Crosstalk on Twisted Pair Cable—*T. R. Cobb,* Datacom Technologies, Everett, WA 284

Crosstalk Performance of Short Length Data Grade Wires—*J.-H. Walling, M. Bélanger,* NORTEL, Quebec, Canada; and *V. Le Nir,* V.P.S. Enterprises, Canada..... 288

WEDNESDAY MORNING—8:00 AM–11:45 AM
Grand Ballroom, Fifth Floor—Salons K/L
TRACK 3—MATERIALS

SESSION 9: HERMETICALLY COATED FIBERS FOR MILITARY & COMMERCIAL CABLE APPLICATIONS

Chairperson: Dr. Howard Wichansky, CECOM, Fort Monmouth, NJ

Moderator: Dr. Charles R. Kurkjian, Bellcore, NJ

Recent Trends in and New Applications for Carbon-Coated Optical Fibers—*N. Yoshizawa, T. Tanifuji,* NTT Access Network Systems Laboratories, Ibaraki-ken, Japan..... 298

Review of Characteristics and Applications of Commercially Available Carbon-Coated Hermetic Fiber—*K. Moore, A. Dwivedi,* Corning Inc., Corning, NY; *E. Sikora,* BT Laboratories, Ipswich, UK 305

Mechanical Reliability and Hydrogen Diffusion Characteristics of Hermetically Coated Fibres—*J. S. Andreassen, G. M. Sletten,* Alcatel Kabel Norge AS, Oslo, Norway 310

Hermetic Coatings for Optical Glass Fibers—*D. R. Biswas, C. R. Kurkjian, H. H. Yuce,* Bellcore, Morristown, NJ 317

Development of Hermetic, Scratch-Resistant Diamond-Like Carbon Coatings for Silica Optical Fibers—*N. Kumar, S. Amin,* SI Diamond Technology, Inc., Houston, TX; *B. Singh,* David Sarnoff Research Center, Princeton, NJ; *S. DiVita, N. Vallestero,* US Army, Fort Monmouth, NJ; and *R. H. Williams,* Plasmatron Coating Systems, Moorestown, NJ 325

Hermetic and Polymeric Coatings for Military and Commercial Applications—*G. Orcel,* Alcatel Fibres Optiques, Bezons, France; *J. Y. Boniort, J. Y. Barraud,* Alcatel Alsthom Recherche, Marcoussis, France; and *R. J. Overton,* Alcatel Telecommunication Cable, Claremont, NC 330

A Hermetic Carbon/Polyimide Coating Combination for Adverse Environments—*V. A. Cusanello, M. J. Supczak, P. R. Stupak,* SpecTran Corp., Sturbridge, MA; *N. J. Jacobson,* SpecTran Specialty Optics Co., Avon, CT 335

WEDNESDAY AFTERNOON—11:45 AM–2:15 PM
Grand Ballroom, Fifth Floor—Salons G & H
AWARDS LUNCHEON
Admission by badges to all registrants

WEDNESDAY AFTERNOON—2:15 PM–5:00 PM
Grand Ballroom, Fifth Floor—Salons A/B
TRACK 1–FIBER OPTIC CABLES

SESSION 10: POLARIZATION MODE DISPERSION (PMD)

Chairperson: Nils Artlove, Telia AB, Farsta, Sweden

Optimum Dispersion Compensating Fiber: Birefringence and PMD Simulation and Fiber Process Improvement—*J. Ceshnoy, P. Nouchi, J. Y. Boniort, C. Brehm, C. Le Sergent, P. Sansonetti,* Alcatel Alstom Recherche, Marcoussis, France 343

PMD Measurements of Various Twisted Strained and Fully Loose Optical Fibers in the Cable—*D. Boscher, J. C. Bizeul, J. P. Louboutin, C. Mauguen,* France Telecom, Lannion, France 347

Extensive Cabling Effect Analysis and Determination of the PMD Limit—*P. Gaillard, G. Vuillaume,* Alcatel Cable, Bezons, France; *M. Carratt,* Alcatel Fibre Optique, Bezons, France; and *A. Gouronnec,* France Telecom, Lannion, France 353

Characterisation of the Environmental Effects on the Polarization Mode Dispersion (PMD) Measurements on G652 Single Mode Fibers—*A. Gouronnec, R. Goarin, M. Auvray, G. Le Moigne,* France Telecom, Lannion, France... 359

Cable and System PMD Prediction—*D. Gallagher, K. Emig,* Corning Inc., Corning, NY; *M. Ashby, M. Fedoroff,* Siecor Corp., Hickory, NC 366

WEDNESDAY AFTERNOON—2:15 PM–5:00 PM
Grand Ballroom, Fifth Floor—Salons C/D
TRACK 1—FIBER OPTIC CABLES

SESSION 11: NETWORKS & APPLICATIONS

Chairperson: Xavier Mann, AT&T Fitel, Carrollton, GA

A Non-Destructive Optical Talk System Using Fresnel-Reflection Light Signals—*Y. Azuma, H. Izumita, K. Yoshida,* NTT Technical Assistance & Support Center, Tokyo, Japan 372

Development of Multi-Coupler Bi-directional Optical Communication System Employing FM-SCM Video Transmission—*H. Omura, N. Matsuo, T. Kimura,* Furukawa Electric Co., Ltd., Kanagawa, Japan; *Y. Shinoda,* Tokyo Electric Power Co., Kanagawa, Japan 380

Reliability-Centred Approach to the Design and Operation of Plant for the Access Network—*D. A. Brewer, P. G. Hale,* Pirelli Cables Ltd., Gwent, UK 387

A New Application of Air Pulled Cable in Microduct for the Local Loop—*P. Lesueur, D. Lecoq, G. Le Goff, A. Pecot, J. Le Rouzic,* France Telecom, Lannion, France 392

WEDNESDAY AFTERNOON—2:15 PM–5:00 PM
Grand Ballroom, Fifth Floor—Salons I/J
TRACK 2—COPPER CABLES

SESSION 12: LAN CABLE/TESTING III

Chairperson: Leo Chattler, DCM Industries, Inc., Union City, CA

Moderator: Masood Shariff, AT&T Bell Laboratories, Middletown, NJ

Coupling of Electrical Fast Transients from Power Cables to Parallel UTP Cables in Close Proximity—*A. Hashim,* AT&T Bell Laboratories, Whippany, NJ; *M. Makwinski,* The Wiremold Co., West Hartford, CT 397

Link Testing in the Time Domain and Performance Advantages Over Swept Frequency Measurements—*J. S. Bottman, H. Koeman,* Fluke Corp., Everett, WA 404

Research Experiment Demonstrates 622 Mbps Data Transmission Over Commercial Copper Cabling System—*R. C. Pritchard,* AT&T Bell Laboratories, Middletown, NJ 412

A De-Embedding Method for Measuring the Near End Crosstalk of Modular Patch Cords—*A. Hashim,* AT&T Bell Laboratories, Whippany, NJ 416

WEDNESDAY AFTERNOON—2:15 PM–5:00 PM
Grand Ballroom, Fifth Floor—Salons K/L
TRACK 3—MATERIALS

SESSION 13: FIRE RESISTANCE

Chairperson: James R. Leech, Union Carbide Corp., Somerset, NJ

Review of Activities in the International Standardization Organization (ISO) Regarding Toxic Hazards in Fires—*J. C. Norris,* Union Carbide Corp., Export, PA 422

Current State of Fire Corrosivity Testing: Preliminary Electrical Leakage Current Measurements—*L. M. Caudill,* DuPont, Wilmington, DE; *J. T. Chapin,* AT&T Bell Laboratories, Norcross, GA; *R. B. Comizzoli, G. A. Peins, J. D. Sinclair,* AT&T Bell Laboratories, Murray Hill, NJ; and *P. Gandhi,* Underwriters Laboratories, Northbrook, IL 432

Zero-Halogen Flame Retardant Insulation Material for Low Voltage Wire—*Y. Kamei, Y. Inuizawa,* Ube Industries, Ltd., Chiba, Japan; *D. Hashimoto, S. Irie,* Furukawa Electric Co., Ltd., Chiba, Japan 438

WEDNESDAY AFTERNOON—4:00 PM–6:30 PM
Grand Ballroom, Fifth Floor—Salons E&F

SESSION 14: POSTER PAPERS

Chairpersons: Dr. Reiner J. Gerdes, Gerdes Consulting & TransTel Group Inc., Atlanta, GA and Dieter S. Nordmann, Kabelmetal Electro GmbH, Hannover, Germany

Impact of Reflective Components on the Noise Performance of DFB Laser Based AM Video Systems—*K. Y. Chen, T.-J. Sheu, F.-Y. Tsai, C.-Y. Wang, W.-S. Chien, H.-J. Chuang,* Telecommunication Laboratories, Taiwan, Republic of China; *Y. W. Chen,* Chung-Yuang University.... 445

Review on the Excess Length Theory of Fiber Group in the Core Groove—*G. W. Seo, H. S. Han, S. H. Kim,* Daewoo Telecom Co., Ltd., Inchon City, Korea 449

Temperature-Dependent Performance of Buffer Tube Gels in Loose Tube Fiber Optic Cables—*O. S. Gebizlioglu, I. M. Plitz, M. J. Zammit,* Bellcore, Morristown, NJ 457

Development of Single Slotted-Rod Type 1000-Fiber Optical Fiber Cable for Subscriber Loops—*N. Okada, K. Watanabe, K. Kobayashi, A. Sano, M. Miyamoto,* Fujikura, Ltd., Chiba, Japan 463

Development of 1000-Fiber Single Slotted Core Cable—*M. Hara, R. Matsuoka, M. Saito, A. Otake, H. Hondo,* Furukawa Electric Co., Ltd., Chiba, Japan 468

Component Optimization for Slotted Core Cables Using 8-Fiber Ribbons—*R. S. Wagman, G. A. Lochkovic, K. T. White,* Siecor Corp., Hickory, NC 472

A Comparative Study of Polymeric and Fumed Silica Based Optical Cable Fillers—*M. Costello, A. Debska, A. Eckard, W. Thalman,* Witco Corp., Oakland, NJ 479

Mechanical Properties of Optical Fiber Ribbon—*T. Murase, K. Shiraishi, T. Kawano, T. Sakai, M. Ito, T. Shiono,* Showa Electric Wire & Cable Co., Ltd., Kanagawa, Japan 485

New Central Tube Hostile Environment Ribbon Cable Design—*P. E. Neveux, Jr., S. R. Stokes, G. S. Blume,* Sumitomo Electric Lightwave Corp., Research Triangle Park, NC 490

Time of Flight and Optical Skew in Fiber Optic Ribbon Cables Subjected to Thermal Stress—*V. A. Lai, T. Rosenmayer,* W. L. Gore & Assoc., Inc., Austin, TX 497

Micro-analysis for Discoloration of Optical Fibers and Filling Compounds—*J.-C. Lin, S.-H. Chou, C.-M. Hsiao, H.-P. Hsu, Y.-c. Lin, K.-Y. Chen,* Telecommunication Laboratories, Taiwan, Republic of China 502

Effects of Coating Corrosion on the Performance of Optical Fiber—*T.-C. Chang, C.-M. Hsiao, W.-J. Chen, H.-P. Hsu, Y.-c. Lin, K.-Y. Chen,* Telecommunication Labs., Taiwan, Republic of China 507

Development of High Power UV Lamp for Faster Draw Speed of Optical Fiber Manufacturing—*S. Morita, Y. Naito, Z. Komiya, T. Ukachi,* Japan Synthetic Rubber Co., Ltd., Tsukuba, Japan; *T. Naganuma, A. Fujimori,* ORC Manufacturing Co., Ltd., Chofugaoka, Chofu, Japan 513

Reliability Issues Concerning Thermally-Cured Adhesives in Fiber Optic Connectors—*I. M. Plitz, O. S. Gebizlioglu, L. A. Reith, P. B. Grimado,* Bellcore, Morristown, NJ 519

Method for Predicting "On-Fiber" Color Results of UV Curable Inks Using Flat Films—*D. C. Duecker, M. L. Moorman, K. T. Turner,* Borden Packaging and Industrial Products, Cincinnati, OH 528

Development of a New Fiber Cleaning Tool—*T. Kusayanagi, S. Yaguchi, M. Yoshinuma, A. Kubota,* Fujikura Ltd., Chiba-ken, Japan 535

Evaluation of Impact Testing for Simulated Shotgun Damage of Optical Fibre Cable—*I. D. Lang, M. V. Davies,* Pirelli Cables Ltd., Gwent, UK; *N. J. Poole,* University of Glamorgan, Glamorgan, United Kingdom; and *K. J. Cockrill,* BT Laboratories, Suffolk, United Kingdom 540

A New Identification System for Optical Fibers in High Count Buffer Tubes—*H. Haag, G. Hög, M. Hoffart, B. Glessner, K. Nothofer,* Kabel Rheydt Ag, Mönchengladbach, Germany 546

New Fiber Monitoring System Without Fiber Selector—*C.-C. Lee, K.-Y. Chen, F.-Y. Tsai, K.-H. Lai,* Telecommunication Laboratories, Taiwan, Republic of China 554

Development of a Hybrid Loose Tube Cable and Its Field Trial Results—*P. F. Armbruster II, J. Thornton,* AT&T Fitel Co., Carrollton, GA 558

Optical Passive Components: A World Wide Survey and Characterization for FITL Applications—*C. Bastide, O. Stempfel, G. Bourrat, G. Couvrie,* Alcatel Cable, Bezons, France; *M. Gadonna, J. C. Hede,* France Telecom, Lannion, France 563

Communication Cables for Fibre in the Loop—*V. Abadia,* Cables de Comunicaciones, Zaragoza, Spain; *F. Brode, M. Emmerich,* KWO Kabel, Berlin, Germany; *D. G. Dalgoutte, R. Johnson,* BICC Cables Ltd., Warrington, UK; *N. D. Lea-Wilson,* BICC Cables Ltd., Merseyside, UK; and *A. Ragni, F. Zanca,* Ceat Cavi, Torinese, Italy 569

A New Fibre-Optic Cable for Inland Lake Links—*A. Fargahi, H. Etter, H. Zimmermann,* Brugg Telecom AG, Brugg, Switzerland; and *C. Theodossi,* Laser Armor Tech Corp., San Diego, CA 574

Sea Trial of Buried Submarine Cable Detection Using a Parametric Sub-Bottom Profiler—*N. Yoshizawa, T. Tanifuji,* NTT Access Network Systems Laboratories, Ibaraki-ken, Japan 579

Adaptable Moulding Technology for Optical Submarine Cable Joint—*B. Daguet, J. F. Libert,* Alcatel Submarine Network, Calais, France 583

A New Compact 56 Fibre Repair Joint, Remote Pumped Optical Amplifier Housing and Coupling Device for a Low Cost Fibre-Optic Submarine Cable Family—*E. Betten, T. Bjerkeli, I. Vintermyr,* Alcatel Kabel Norge AS, Oslo, Norway 587

Alter Course Cable Behaviour in Water During Laying of Fiberoptic Submarine Cables—*S. Hopland,* Telenor AS, Oslo, Norway 592

Field Experiences of Jelly-Filled Cables for Aerial Trial—*H.-F. Lin, C.-H. Hsieh, C.-C. Pei, Y.-H. Hwang, H.-P. Hsu, Y.-C. Lin, K.-Y. Chen,* Telecommunication Laboratories, Taiwan, Republic of China 599

A Method for Evaluating Cable Resistance to Damage by Pocket Gophers as Adopted by the USDA/APHIS/ADC/DWRC—*G. R. McCann,* U.S. Department of Agriculture, Denver, CO 604

THURSDAY MORNING—8:30 AM–12:00 PM (NOON)
Grand Ballroom, Fifth Floor—Salons A/B
TRACK 1–FIBER OPTIC CABLES

SESSION 15: FIBER RIBBONS

Chairperson: Manuel R. Santana, AT&T Bell Laboratories, Norcross, GA

Coating Design of Thin-Coated Ribbons Using 250µm Coated Fibers—*K. Kobayashi, N. Okada, K. Mitsuhashi, K. Ishida, M. Miyamoto, S. Araki,* Fujikura Ltd., Chiba, Japan..

Investigation on High-Speed Optical Fiber Ribbon Coating and the Characteristics of the Ribbons—*R. Suzuki, H. Sawano, K. Kobayashi, K. Oohashi, S. Araki,* Fujikura Ltd., Chiba, Japan 616

Development of High-Density Optical Fiber Cable Consists of 0.3mm-Thick Fiber Ribbons—*K. Obi, T. Takeda, T. Watanabe, K. Imamura, M. Fujita, H. Tanka,* Mitsubishi Cable Industries, Ltd., Hyogo, Japan 622

Pre-Connectorized 1000-Fiber Single Slotted Core Cable—*H. Iwata, M. Tsutsumi, E. Nakamura, N. Matsumoto, M. Nozawa, S. Hayami, S. Nagasawa, T. Tanifuji,* NTT Access Network Systems Laboratories, Ibaraki, Japan 627

Capability and Control of Ribbon Stripping as Related to Ribbon Material Systems and Stripping Tools—*P. K. Kim, N. W. Sollenberger, K. W. Jackson,* AT&T Bell Laboratories, Norcross, GA 635

THURSDAY MORNING—8:30 AM–12:00 PM (NOON)
Grand Ballroom, Fifth Floor—Salons C/D
TRACK 1–FIBER OPTIC CABLES

SESSION 16: TESTING & FIELD EVALUATION

Chairperson: Dieter S. Nordmann, Kabelmetal Electro GmbH, Hannover, Germany

Optical Fiber Line Test and Management System for Passive Double Star Networks and WDM Transmission Systems—*S. Furukawa, H. Suda, F. Yamamoto, Y. Koyamada, T. Kokubun, I. Takahashi,* NTT Access Network Systems Labs., Ibaraki, Japan 640

Evaluation of Transient Optical Losses When Handling Primary Coated, Secondary Coated and Ribbon Fiber in the Access Network—*D. Daems,* Raychem N.V., Kessel-lo, Belgium 649

Dynamic Range Increase of 1625 nm Monitoring Systems—*E. Cottino, P. G. Peretta,* SIRTI S.p.A., Milano, Italy; *F. Cisternino, E. Riccardi, B. Sordo,* Centro Studi E Laboratori Telecomunicazioni, Torino, Italy 654

Optical Cables Biological Attacks Analysis—*P. J. P. Curado, M. Mendes Filho,* TELEBRÁS, Campinas, Brazil; *A. C. Pereira Netto, J. E. Filho, M. E. Latini,* EMBRATEL, Rio de Janeiro, Brazil 662

Rodent Protected Dielectric Cables: Where is the Solution?—*P. Gaillard,* Alcatel Cable, France; *J. C. Gautun,* Orstom, France; *G. Grolleau,* INRA, France; *J. Rauchs,* Opticable, Belgium; *G. Comezzi,* Alcatel, Cavi, Italy; and *S. Camara,* Alcatel Cable, Iberica, Spain 668

Optical and Mechanical Performances of Different Cable Structures in Frozen Ducts—*M. Agretti, M. Bottanelli,* SIRTI S.p.A., Milan, Italy 675

THURSDAY MORNING—8:30 AM–12:00 PM (NOON)
Grand Ballroom, Fifth Floor—Salons I/J
TRACK 2–COPPER CABLES

SESSION 17: BROADBAND/OUTSIDE PLANT

Chairperson: Brian D. Garrett, CommScope Inc., Claremont, NC

Switched Fiber Twisted Pair (SFTP) Broadband to the Home—*P. Kish, J. Green,* NORTEL, Quebec, Canada; *T. Yeap,* University of Ottawa, Ontario, Canada 682

Study of Stress on Self-Supporting Metallic Cable Under High Mode Galloping Oscillation—*K. Shinmura, Y. Honda, Y. Siba, F. Asiya,* NTT Access Network Systems Labs., Ibaraki, Japan 688

Recent Advancements in Coaxial Cable Design—*H. D. Pixley,* CommScope Inc., Catawba, NC 694

The Sag Behaviour of Aerial Service Wires Using Different Wedge Clamps—*J.-H. Walling,* NORTEL, Quebec, Canada; *J. Druez, J. Bilodeau,* University of Quebec, Chicoutimi, Canada; *C.-T. Nguyen,* Bell Canada, Montreal, Canada 702

New Hybrid Cables for CATV—*C. Schwiering, J. Seidenberg, P. E. Zamzow,* Kabel Rheydt AG, Mönchengladbach, Germany 713

The Deterioration of Transmission Characteristics and Coaxial Cable Longevity—*J. N. D'Amico, T. N. Bowmer, O. G. Chavez, L. M. Hore,* Bellcore, Morristown, NJ 720

THURSDAY MORNING—8:30 AM–12:00 PM (NOON)
Grand Ballroom, Fifth Floor—Salons K/L
TRACK 3–MATERIALS

SESSION 18: FIBER OPTIC MATERIALS

Chairperson: James R. Leech, Union Carbide Corp., Somerset, NJ

A New Hydrolytically Stabilized PBT for Fiber Optic Cable Core Components—*J. M. Finan, M. Jacobson, L. J. Goff,* GE Plastics, Pittsfield, MA 728

New Dimensionally Stable Polymer for Compact and Loose Optical Fiber Buffer Tubes—*M. Hochuli, F. Bühler, D. Jarvis,* EMS-Chemie AG, Domat/Ems, Switzerland; *W. S. Zimmermann,* EMS-American Grilon Inc., Sumter, SC 735

Investigation of the Amount of Extractables or Volatiles Remaining After Ultraviolet Cure of Primary Optical Fiber Coatings—*P. J. Shustack, K. A. Fleisch, M. E. Jones,* Borden Packaging and Industrial Products, Cincinnati, OH 740

Selection of Insulating Materials for Long Distance Optical Submarine Cables—*J.-F. Libert, F. Ruelle, B. Aladenize,* Alcatel Submarine Network, Calais Cedex, France 745

Hydrogen Outgassing of Optical Submarine Cable Materials—*F. Ruelle, J. L. Lang,* Alcatel Submarine Network, Calais Cedex, France 752

Water Getter Flooding Compound for Dielectric Optical Cables—*P. Anelli, C. Bosisio, E. Consonni, A. Ginocchio,* Pirelli Cavi SpA, Milan, Italy 756

THURSDAY AFTERNOON—1:00 PM–5:00 PM
Grand Ballroom, Fifth Floor—Salons A/B
TRACK 1–FIBER OPTIC CABLES

SESSION 19: AERIAL CABLES

Chairperson: Dr. Peter R. Bark, Siecor Corp., Hickory, NC

Development of an All-Dielectric, Self-Supporting Cable for Use in High Voltage Environments—*O. Daneshvar, J. Hill, X. Mann,* AT&T Fitel Co., Carrollton, GA 763

A Novel System for the Installation of All-Dielectric Self-Supporting Optical Cable on High Voltage Overhead Power Lines—*I. V. Nichols, C. A. Platt, S. M. Rowland, A. J. Taha,* BICC Cables Ltd., Helsby, U.K.; *C. N. Carter,* The National Grid Company plc, Leatherhead, U.K. 771

Small Aerial Optic Cable for Multimedia Network—*O. Koyasu, A. Sano, K. Watanabe, A. Mogi, M. Miyamoto,* Fujikura Ltd., Chiba, Japan 778

Design and Reliability Considerations for Long Span, High Voltage, ADSS Cables—*D. A. Keller, O. Tatat, R. Girbig,* Alcatel Cable, Bezons, France; *M. Adams,* Alcatel ATC, Claremont, NC; *R. Böhme,* Kabelrheydt, Mönchengladbach, Germany; and *C. Larsson,* Alcatel IKO Kable, Grimsas, Sweden 786

Mid-span Jointing of Optical Groundwire (OPGW)—*F. Grajewski, W. Stieb,* Alcatel Kabelmetal, Stadthagen, Germany; *H. Haag, G. Hög,* Kabel Rheydt AG, Mönchengladbach, Germany 794

Lightning Strike Resistance of OPGW—*J. P. Bonicel, O. Tatat, G. Couvrie,* Alcatel Cable, Bezons, France; *U. Jansen,* Kabel Rheydt, Mönchengladbach, Germany 800

THURSDAY AFTERNOON—1:00 PM–5:00 PM
Grand Ballroom, Fifth Floor—Salons C/D
TRACK 2–COPPER CABLES

SESSION 20: LAN MEDIA INSTALLERS AND MANUFACTURERS ROUNDTABLE

Chairperson: Irving Kolodny, Consultant, Bellerose Manor, NY

Moderator: Arlyn Powell, Cabling, Installation and Maintenance Magazine, Nashua, NH

Experiences with Cable—*C. Thomasmeyer,* Miller Information Systems, Pittsburgh, PA 807

Experiences with Connectors—*S. Flaherty,* Teledata Systems, Souderton, PA 807

Experiences with Test Equipment—*L. Johnson,* The Light Brigade, Kent, WA 807

Perspectives on Cable—*D. Hess,* Berk-Tek, Inc., New Holland, PA 808

Perspectives on Connectors—*S. Miles,* Mod-Tap, Inc., Harvard, MA 808

Perspective on Test Equipment—*J. Boedekker,* Tektronix, Inc., Beaverton, PA 808

THURSDAY AFTERNOON—1:00 PM–5:00 PM
Grand Ballroom, Fifth Floor—Salons I/J
TRACK 2—COPPER CABLES

SESSION 21: COPPER MATERIALS

Chairperson: Dr. Marek Kapuscinski, Northern Telecom Limited, Quebec, Canada

MFA: A New Perfluoropolymer for Wire & Cable Applications—*G. Vita, M. Pozzoli,* Ausimont S.p.A., Bollate, Italy 809

Development of Irradiated Flexible Flat Cable—*T. Hosokawa, Y. Naruse, K. Tanaka, T. Kuga, Y. Takeda,* Sumitomo Electric Industries, Ltd., Tochigi, Japan 817

Laser Printable Black Cable Jacketing Compounds—*L. Y. Lee, D. E. Roberts, B. L. Vest, K. Tonyali,* Quantum Chemical Co., Cincinnati, OH 823

Using an New Ageing Rate Definition for Thermal Endurance of Cable Materials at Variable Temperatures—*R. A. Widler, R. T. Durham,* Huber & Suhner AG, Pfäffikon, Switzerland 829

Economic & Product Efficiency Relationships With Non-Lead Stabilizers for PVC—*G. R. Bennett, J. A. Caballero,* Synergistics Industries (NJ) Inc., Farmingdale, NJ 835

THURSDAY AFTERNOON—1:00 PM–5:00 PM
Grand Ballroom, Fifth Floor—Salons K/L
TRACK 3—MATERIALS

SESSION 22: FIBER COATING/RELIABILITY

Chairperson: Dr. Raymond E. Jaeger, SpecTran Corp., Sturbridge, MA

Optical Fiber Reliability and Handleability Results from the Biarritz Field Trial—*A. Gouronnec, R. Goarin, G. Le Moigne, J. Martret, M. Baptiste,* France Telecom, Lannion, France 840

Mechanical Behavior of Optical Fibers Removed from a Field-Aged Cable—*J. L. Smith, A. Dwivedi, P. T. Garvey,* Corning Inc., Corning, NY 848

Handleability of Aged Optical Fibers—*W. Griffioen,* KPN Research, Leidschendam, The Netherlands; *T. Volotinen,* Ericsson Cables, Hudiksvall, Sweden; *P. Wilson,* BT Laboratories, Suffolk, United Kingdom; *A. Gouronnec,* France Telecom, Lannion, France; and *T. Svensson,* Telia Research, Haninge, Sweden 857

Investigation on Influence of Coating Materials to Zero Stress Aging of Optical Fiber—*T. Hattori, A. Urano, N. Akasaka, Y. Matsuda,* Sumitomo Electric Industries, Ltd., Yokohama, Japan 865

A New Dual Layer Primary Coating for Optical Fibres with Superior Ageing Behaviour and Improved Cabling Performance—*G. Kuyt, J. W. Leclercq, A. H. E. Breuls,* Plasma Optical Fibre B.V., Eindhoven, The Netherlands 872

OPENING SPEAKERS



BRIAN D. GARRETT
Chairman, IWCS
Vice President & General Manager of
The Network Cable Division
CommScope, Incorporated
Claremont, North Carolina

Mr. Brian D. Garrett was born in 1948 in Cleveland, Ohio. He received his Bachelor of Science degree in Mechanical Engineering from North Carolina State University in 1970 and began working in the materials and process development laboratories of Superior Continental Corporation in that year.

During Mr. Garrett's career he has worked in a variety of assignments including the Engineering Manager of Superior Continental Corporation's apparatus division, Vice President of Engineering for CommScope, Inc. and presently as Vice President and General Manager of CommScope's Network Cable Division. Mr. Garrett has been a past member of ASTM and SCTE as well as an active member of the MCTA engineering committee. He holds a variety of patents in the connector and cable fields and served in the U.S. Marine Corp.

Mr. Garrett is currently located at the Network Cable Division facility of CommScope in Claremont, North Carolina.



BARRY S. SALIS
Deputy Director, Space and Terrestrial Communications
U.S. Army Communications-Electronics Command
Fort Monmouth, New Jersey

Mr. Barry S. Salis has attained the position as Deputy Director of the Space and Terrestrial Communications Directorate after holding increasing positions of responsibility during his twenty-three year Government career.

Providing policy and guidance for the directorate he ensures the resources are allocated for attainment of the multifaceted communications mission of the directorate. He serves on various levels of command level TQM panels, international and joint panels.

Previously he was Chief, Information Security Division, Space and Terrestrial Communications Directorate, USACECOM responsible for all Army RDT&E in the security area which includes: COMSEC, TEMPEST, COMPUSEC, Key Management, Certification and Accreditation, and Network Security. Support to many PEO and PM Offices, various Directorates, and other non-traditional customers is provided routinely by the entire division. The division also supports evaluation and integration of commercial video products with computer and communications systems to meet the Army's Digitization of the Battlefield thrust.

While serving in the Army Signal Corps for three years from October 1971 to October 1974 he worked as an engineer in the COMSEC Division, COMM/ADP Lab, USAECOM at Ft. Monmouth, NJ. Continuing in the same organization as a civilian engineer he worked as Project Leader for the Secure Wire Access Terminal, a VINSON COMSEC ancillary equipment, working it from the development through the production phases. He also was Project Leader for the PARKHILL COMSEC equipment as well as numerous other INFOSEC developments as part of the overall Army tactical system architecture. Assigned to lead an internal task force, he was involved in the initial concepts for usage of modeling and simulation to evaluate combined arms doctrinal changes which today are being implemented.

In 1985 he became Chief of the COMSEC Development Branch, responsible for the embedded COMSEC programs, Key Management, system support to PM Offices to include the Special Operations Forces Offices, and system integration and testing.

Mr. Salis obtained his BSEE degree from Drexel University, Philadelphia, PA in 1971 and his MSEE from Fairleigh Dickinson University, Teaneck, NJ in 1978. He is married to Jan Freeman Salis. They have two children, Rachel and Howard.

Mr. Salis is a member of and on the board of Directors for the Association of the United States Army (AUSA) and the Armed Forces Communications and Electronics Association (AFCEA).

PLENARY SESSION

2020 - VISIONS OF OUR COMMUNICATIONS FUTURE

CHAIRMAN



DR. FELIX P. KAPRON
Bellcore
Morristown, New Jersey

Felix Kapron has been active in fiber optics for over a quarter century. He obtained a B.A.Sc. in Engineering Physics from the University of Toronto, and an M.Sc. and Ph.D. in Physics from the University of Waterloo, all in Canada.

In 1967 Felix began work at Corning Glass Works in Corning, NY, and was a member of the team producing the first low-loss fibers. There he investigated scattering and polarization effects, and predicted zero chromatic dispersion near 1300 nm. In 1972 he joined Bell-Northern Research in Ottawa Ont., and helped start the fiber communications R&D program. He broadened into multimode fiber, cables, active components, long-wavelengths, secure systems, and began early standards work. In 1981 he joined the ITT Electro-Optical Products Division in Roanoke Va., where he was concerned with fiber characterization, reliability, components, and subsystem design, and was involved in international technology transfer between ITT labs.

Since 1987 Dr. Kapron has been at Bellcore in Morristown NJ, at various times responsible for groups dealing with many fiber optic products towards which he contributes to requirements. He is currently Principal Engineer in fiber optics technology.

Felix Kapron has a dozen patents and over a hundred publications, and has served on conference committees for OFC, SPIE, and NIST, currently for the International Wire & Cable Symposium (IWCS) and as a Bellcore co-sponsor of the National Fiber Optic Engineers Conference (NFOEC). He was an Associate Editor of the Journal of Lightwave Technology, is a Topical Editor of Applied Optics, is on the editorial board of the Journal of Optical Communications, and was on an NRC panel for NIST evaluation. He has given numerous courses and tutorials, and has leadership and contributing positions in several domestic and international standards groups such as the Telecommunications Industry Association (TIA), the International Electrotechnical Commission (IEC), and the International Telecommunication Union (ITU). He is a member of the Optical Society of America (OSA), and is nominated for Fellow of the Institute of Electrical and Electronic Engineers (IEEE).

PANELISTS

Dr. Donald Keck, Director of Opto-Electronics Research, Corning Inc., Corning, NY

John Hood, Founding Partner and Vice President, Engineering, Comlink Systems Inc., Ontario, Canada

Gilles Dupuy d'Angeac, Senior Executive Vice-President, Alcatel Cable Group, Clichy Cedex, France

Dr. Östen Mäkitalo, President, Telia Research, Haninge, Sweden

FIBER OPTICS' NEXT QUARTER CENTURY: BUILDING THE PHOTONIC NETWORK

DONALD B. KECK, Ph.D.

Corning Incorporated, Corning, New York

ABSTRACT

In the twenty-five years since the invention of low-loss optical fiber by Corning, fiber has become the transmission medium of choice everywhere except in the "last mile" to the user. However, demands for information -- for example, the recent dramatic growth in use of the Internet for graphics-based or multimedia applications -- continue to increase, so much so that the maximum available transport rate doubles every two years. As a result of this rapid growth, electronic functions in communications transport networks eventually will be replaced by photonic functions to provide higher bandwidth by employing various multiplexing schemes. Much of the current work is concentrated in the area of wavelength division multiplexing (WDM). This latter development in particular will help drive down costs, and optical fiber will extend its reach to the user to accommodate ever increasing bit rates.

These trends present several technical challenges in the areas of fiber-optic lasers, transport, and components. Lasers will need to transmit increasing numbers of wavelengths and generate chirp-free, short pulses at increasingly high bit rates. Long-haul fiber-optic transmission in the high gigabit range gives rise to optical effects that must be taken into account, and work within the industry will continue to study and develop fibers and systems for these applications. Finally, the evolution from all-electronic to all-photonic networks will necessitate improvements in the ability of optical components to split, filter and amplify multiple wavelengths, and eventually will lead to all-optical switching.

In fact, the challenges presented by the evolving all-photonic communications transport network are being met today, and all-optical transport networks are beginning to migrate off the laboratory bench and into real service in small niches. The end-game is becoming clearer: all-optical transport networks with optical fiber extending all the way to the user -- a world filled with light.



Donald B. Keck, Ph.D.
Director, Optics and
Photonics Research
Corning Incorporated
SP-FR-02-9
Corning, NY 14831

Dr. Donald B. Keck is currently the Director of Optics and Photonics Research at Corning Incorporated. He joined Corning in 1968 and did pioneering work on fiber attenuation and dispersion as a member of the team demonstrating first low-loss fibers. He has lectured extensively on optical fibers, has served as editor for the *Journal of Lightwave Technology*, and has been chair or co-chair for several conferences. Dr. Keck's numerous awards include the Technology Achievement Award of the International Society of Optical Engineers, and the Industrial Research IR-100 Award (1982); the Engineering Materials Achievement Award from the American Society of Metals (1983); the John Tyndall Award (1992); and memberships in the National Inventors Hall of Fame and the National Academy of Engineering (1993). Dr. Keck has authored more than 85 papers and publications and holds 25 patents.

THE FORTY PLUS YEARS OF CANADIAN CABLE TV

JOHN M. HOOD

Comlink Systems Inc., Oshawa, Ontario, Canada

ABSTRACT

The Cable Industry in Canada started in 1952 in major urban areas like London, Ontario, Montreal, Quebec, and out west in Vancouver, British Columbia. When it was first developing, cable delivered Canadians improved signal quality and better television service. Forty-three years later, cable passes 95 percent of Canadian homes. Canada is the second most cabled country in the world, with every urban system built and over 2,200 small communities across Canada.

The 90's will see the change of the traditional role as a rebroadcaster of broadcast and specialty programmes to that of a full service provider for all digital services that will allow subscribers to watch or have an alternate access to the digital technologies of the future.

This paper will provide an outline of the technologies and programming used in Canada over the last forty plus years and a brief outline of the future directions expected by cable to survive in 2001.



John M. Hood
Comlink Systems Inc.
1350 Thornton Rd. South
Oshawa, Ontario
Canada L1J 8C4

A founding partner of Comlink Systems in June 1984, John has held the position since then of Vice President, Engineering. In this position, John's responsibilities include satellite system engineering, microwave path engineering, cable TV design and implementation. He was responsible for a number of Telecommunications, Broadcast and Cable projects shown in Comlink's sample of projects completed. John designs and builds very high quality systems with Comlink's suppliers' products, such as Scientific-Atlanta, Hughes Aircraft of Canada, Andrew Antenna, Alpha Technologies, etc.

From 1982 to 1984 John was with Anixter-Microsat as Manager of Applications Engineering. Duties included system design and sales support for Broadcast and Cable products.

From 1967 to 1982, John was with Rogers Cablesystems Engineering in London, Ontario. Duties included technical consulting, field engineering, product evaluations, systems design, proof of performances, system construction projects and special technical evaluations. Major achievements included seven major cable system builds in Canada and the United States.

From 1962 to 1967, John was with London Cable TV Service as Technical Manager and worked in Plant maintenance, construction and headend maintenance. During his employment with London Cable TV, John was privileged to work with Ed Jarmain, a founder, pioneer and operator of one of the first Cable TV systems in Canada. This was a five channel system using electron tube technology that has been rebuilt many times to test and evaluate the many new technologies for the future cable system of tomorrow.

Education: 1961-62 -- H.B. Beal Technical and Commercial High School Advance Electronics; 1968-71 -- Fanshawe College, Industrial Management Certificate Programme (Diploma); 1972-73 -- University of Western Ontario - Engineering.

Professional Affiliations: John is a member of the Society of Cable Television Engineers (SCTE) and the Canadian Cable Television Association (CCTA) Microwave Technical Committee. He is a frequent speaker at conferences and has 12 papers published in the Technical Proceedings of CCTA, NCTA, IEEE and various other technical journals.

COMMUNICATIONS IN THE NEXT QUARTER CENTURY : THE UNEXPECTED ROLE OF THE COPPER TWISTED PAIRS !

Gilles DUPUY D'ANGEAC

ALCATEL CABLE, CLICHY, FRANCE

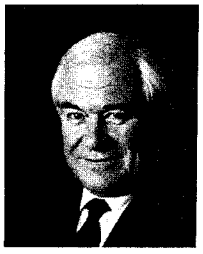
Counting on the well known advantages of optical fibers (bandwidth, attenuation, immunity to electromagnetic interference, dimensions...) as well as on the soaring emergence of broadband transmission systems, most experts dealing with next generation systems have been predicting the switch from copper to fiber in the very near future, even in domains in which up to now copper pairs have been largely implemented : the access network and the Local Area Network (LAN).

In this respect, many papers dating back to 1990 or earlier forecasted the replacement of copper networks by FTTC (Fiber To The Curb) beginning in 1992 and by FTTH (Fiber To The Home) beginning in 1995 in most developed countries. Today, one can notice that, although this trend is undoubtedly confirmed and although a lot of FTTC and FTTH projects are emerging, fiber is not in such a hurry to keep its promises.

In the meantime, copper pairs have been presented as unable to reach the bandwidth performances of fibers and accordingly restricted to narrow band transmissions. However, important progress has been made in the last decade both on the twisted pair cable itself and on the associated transmission encoding techniques which makes twisted pairs a good candidate for high bandwidth distribution systems as well as for current and future LANs.

These unexpected twisted pair technical breakthroughs, at the moment where most telcos are reconsidering their plans of full deployment of fibers by investigating a more economical use of copper pairs to deliver broadband services to their customers, may offer to copper pairs the opportunity to play a key role in the next quarter century. Consequently the full copper solutions and more likely the FTTC designs may benefit from these performance improvements and accordingly the FTTH solutions which were supposed to be under full implementation in 1995 may be somewhat postponed as compared to the early 90's estimates.

To some extent the same situation has occurred in the LAN domain. The recent cost and performance improvements of twisted pairs (category 5 and presumably category 6 cables) could slow down the inescapable progression of the optical fiber.



Gilles DUPUY d'ANGEAC
Senior Executive Vice President
Alcatel Cable Group
30, rue des Chasses
92111 Clichy Cedex
France

Gilles DUPUY d'ANGEAC is graduated from Ecole Centrale (Paris - France). He received his M. S. Degree in Physical Metallurgy from Massachussets Institute of Technology.

He started his career in the Schneider Group and he joined Les Câbles de Lyon (now Alcatel Cable) in 1974.

Since that date, Gilles DUPUY d'ANGEAC has occupied different management positions in the Company.

He is currently Senior Executive Vice President of the Alcatel Cable Group. Among his responsibilities, he is in charge of strategy as well as of technology.

Gilles DUPUY d'ANGEAC is also Vice President of Alcatel NV and President of Alcatel Contracting and of Alcatel USA Corp.

WIRELESS COMMUNICATIONS YEAR 2020

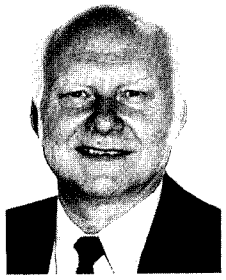
DR. ÖSTEN MÄKITALO

Telia Research AB, Haninge, Sweden

ABSTRACT

Since 1970 there has been a tremendous development in the area of wireless telephony. An obvious question is then, what will be the situation 25 years from now? No matter what we predict it is very likely to be wrong. The technical development is so rapid. For the time being we are introducing the first generation of digital mobile telephones in the world. This first generation is represented by GSM and its North American and Japanese equivalents. We are also talking about PCS and in that context new systems based on CDMA are envisaged. So the second generation of digital systems is not far away.

This development will continue. Telephony will be wireless. Every person can have their own portable telephone. Wireless telephones is probably the only cost-efficient way to provide telephony to the very large number of people in the world who do not have any telephony at the time being. There are large populations having about 1% or lower penetration. In those areas it is very much a question of cost and basic services while in the most densely populated areas in USA, Europe and Japan, availability of spectrum is causing problems. The need of spectrum is linked to the services that the systems will offer. Year 2020 we have to assume that also wideband services are offered wireless. That will require use of higher frequency bands. The radiospectrum extends up to 3000 Ghz. Frequencies higher than 60 Ghz are however because of attenuation not very well suited for communication over greater distances. Wide area coverage is difficult to obtain. There are solutions. Flexible and adaptive use of frequency bands will provide high capacity together with short range over high frequencies in densely populated areas. In areas where the coverage is most important lower frequency bands has to be used. Systems using low elevation orbit polar satellites will also be used. The terminal will have all the necessary intelligence to use the best transmission path in every situation. The systems as such are adaptive. In year 2020 you can go to any place in the world and communicate over your portable phone.



Dr. Östen Mäkitalo
President of Telia Research AB
13680 Haninge
Sweden
Telephone: +46-8-7075200
Fax: +46-8-7075210

Östen Mäkitalo has been with Televerket (Telia since 1993) since he was graduated from the Royal Institute of Technology in Stockholm. From 1977 as head of Radio Laboratory and from 1991 as president of Telia Research, the newly established R&D company of Telia. He has extensive technical and managerial experience in both television transmission and mobile telephony, for which he has won several awards. He has played a key role in the development of a number of commercially successful systems such as NMT (the Nordic Mobile Telephone System), RDS (the Radio Data Service), GSM and HD-Divine (digital HDTV). He has chaired several international working groups. He is holding a number of patents.

LUNCHEON SPEAKER



RALPH ARCHBOLD
as
BEN FRANKLIN
Philadelphia, Pennsylvania

Will the Real Ben Franklin Stand Up

Ralph Archbold is the official "Ben Franklin" for America's Constitutional Bicentennial as designated by *We the People 200.* He has performed for the past five U.S. Presidents and has appeared on *Good Morning America, Today, P.M. Magazine*, over 100 TV interviews and over 200 radio interviews.

He has appeared in *People Magazine, Time, Saturday Evening Post, USA Today cover story, Wall Street Journal, Sunday New York Times* (Front Page), and *Meeting News* plus over 100 national and local news articles.

Mr. Archbold has been acclaimed as the World's Leading Franklin portrayer with over 7000 appearances to his credit.

He has been the official "Franklin" for: The Freedoms Foundation, The University of Pennsylvania, The City of Philadelphia, The State of Pennsylvania, Greenfield Village, The Franklin Institute, The U.S. Constitutional Bicentennial (1987), and The 200 year Franklin Anniversary (1990)

In addition to being a fine actor, he is internationally recognized as an outstanding speaker and is an active member of the National Speakers Association. He is also past president of Philadelphia's National Speakers Association and a member of SAG/AFTRA as well as various civic and business groups.

Ralph was recently awarded the following: *Invest in America Eagle* by Malcolm Forbes, *Constitutional Eagle* by Warren Burger, *Best of Philly Award* by Philadelphia Magazine, and *Constitution Bowl* by Douglas Fairbanks, Jr.

Design and Development of a Compact High Fiber Count Ribbon Cable

William J. McCallum, Martin C. Light, Richard S. Wagman

Siecor Corporation
Research, Development and Engineering
Hickory, NC 28603 USA

ABSTRACT

A new slotted core cable using 12-fiber ribbons has been developed and tested to meet emerging network applications that require high fiber density in a compact cable design. To maintain compatibility with other existing cable and ribbon designs, 250 μm single-mode fibers in standard 12-fiber ribbons are required. To ensure satisfactory fiber attenuation over the operating temperature range, and to meet fiber count, installation, and outer cable diameter requirements, short slot lay lengths are necessary. Super-absorbant polymers (SAPs) are utilized to waterblock the core and increase field splicing productivity. A 360-fiber armored cable has been successfully deployed with standard installation equipment within a 32 mm (1.25 in.) inner duct. This paper addresses design considerations, attenuation performance during environmental and mechanical testing, and installation experience for this new high fiber count ribbon cable.

INTRODUCTION

The demand for high fiber count optical cables continues to increase even as the definition of "high fiber count cable" evolves. In the mid-1980's, 144-fiber cables represented the maximum number of fibers available in a single sheath. Over the next ten years, this upper fiber count limit has increased to hundreds and even thousands of fibers per cable. At the present time, the demarcation point between "standard" and "high fiber count" cables can be placed at 216 fibers.

Two main factors are contributing to the increase in demand for fiber counts more than 216 fibers: new network architectures and limited duct space. Network architectures for SONET rings and emerging broadband networks now being planned in North America rely on deployment of hundreds of fibers. Installation-related economic considerations make placement of a single sheath preferable to multiple sheaths.

Limited duct space in metropolitan areas also makes single-sheath high count cable designs attractive to service providers who are reinforcing optical cable runs between central offices. In many locales, the standard inner diameter of installed innerduct is 32 mm (1.25 in.). In order to successfully place cables in ducts of this size, a cable outer diameter less than 24 mm (0.95 in.) is necessary.

Some requirements for these high fiber count cables, however, are no different from standard cables. A rugged construction is required to withstand the forces encountered during installation using both standard cable pulling and new cable jetting techniques. A ribbon design is preferred to enhance organization of the fibers and provide maximum splicing productivity. To minimize field installation costs, the cable must be easy to prepare and compatible with existing cable closures and mass splicing equipment, which is itself designed around 250 μm optical fibers. Additionally, the cable must have excellent mechanical, environmental, and optical performance over the –40° to +70°C temperature range.

The slotted core cable has several advantages over other high fiber count designs. First, it has excellent packing density for fiber counts above 216 fibers. When compared to a stranded loose-tube design, a 40% or more increase in fiber density can be realized. Second, from a craft handling point-of-view, ribbon stacks are easy to access, simplifying balloon-splicing and mid-span access procedures. The dry core design also greatly increases productivity for cable splicing crews.

A number of previous designs for high fiber count optical ribbon cables have been reported in the literature. Four-fiber and 8-fiber ribbons manufactured with 250 μm fibers are the basic building blocks for some of these designs. Some work with 16–fiber ribbons utilizing standard and reduced-diameter fibers has also been documented. However, particularly in the North American market, the accepted standard is a thinly coated 12-fiber ribbon comprised of 250 μm fibers. To ensure compatibility

with ribbon cables already deployed in North America, high fiber count optical cable designs based on these standard 12-fiber ribbons are required [1], [2], [3].

CABLE DESIGN

A slotted core optical fiber cable, the StarTrac™ ribbon cable, has been developed and tested to meet these requirements. A five-slot core design is used to meet the fiber count, dimensional, and installation demands and to ensure satisfactory performance of the standard 12-fiber single-mode ribbons (see Figure 1).

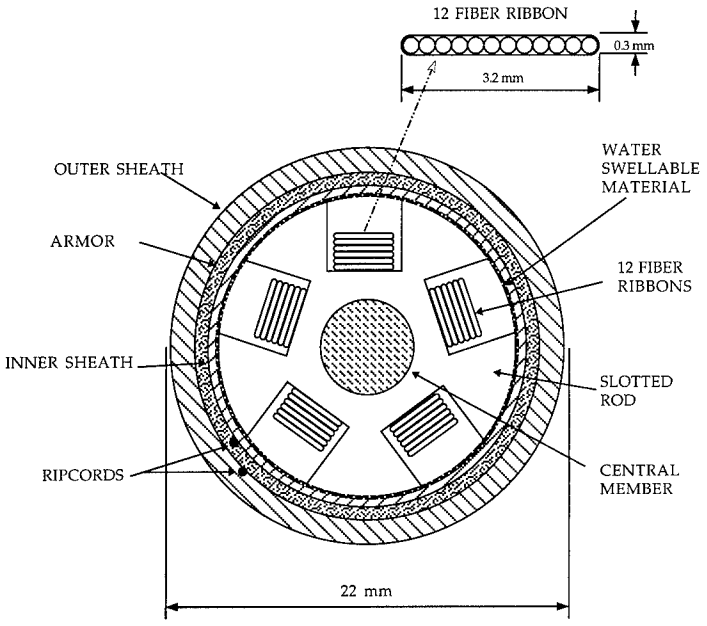


Figure 1: 360-fiber StarTrac™ Armored Cable

Other slotted core cables employed encapsulated ribbons (ribbon wall > 60 μm) to reduce sensitivity to microbending and enhance mechanical protection of the fiber. This design employs a thinner wall of ribbon matrix material over the colored fibers. This thin wall provides less protection to the fiber and increases the sensitivity of the fiber to microbending [4]. Appropriate cable design considerations and manufacturing technologies are utilized to ensure acceptable short-term and long-term fiber performance.

The primary strength member is a flooded stranded steel or solid glass-reinforced plastic (GRP) central element. Polyethylene is extruded over the central element to form a round cross-section with five helical slots to contain the ribbons. A slot depth of 4.3 mm (0.17 in.) was selected to accommodate up to eight 12-fiber ribbons for a total of 480 fibers; however, initial development efforts concentrated on six ribbons per slot for a total of 360 fibers. A non-woven water blocking tape is applied over the core. When exposed to water, the super-absorbant polymers (SAPs) in the non-woven tape form a gel that fills the slots and effectively prevents the ingress of additional water into the cable. This particular design employs a polyethylene inner jacket, corrugated steel armor, and an outer black polyethylene jacket. A non-armored version of this cable design would employ a single protective jacket applied over the wrapped core.

Considerations for the Slotted Rod Design

The slotted core cable design can be viewed as a combination of stranded loose tube and tight buffer cable designs. Since the ribbons are decoupled from the slotted rod, they are free to move during cable shrinkage due to low temperatures. The free space surrounding the ribbons is designed to accommodate the resulting extra relative ribbon length due to cable contraction. This is similar to a stranded loose tube cable design. For tensile loading experienced during cable installations, fiber strain is allowed but is kept low enough to prevent significant strength degradation; the situation is similar to that of a tight buffer cable design.

To place a large number of 12-fiber ribbons in a compact cable, a new slotted rod was developed. By a judicious selection of the slot pitch, the slot depth was kept to a minimum, thereby optimizing the overall core diameter.

Overall, five effects were considered in the choice of pitch for the new slotted rod:

1) bending performance of the cable;
2) length of fiber in the cable;
3) room needed for ribbon rotation during cable bending;
4) room needed for the extra relative ribbon length at low temperatures;
5) fiber strains.

(1) The helical nature of the slot allows the ribbons to move back and forth along the slot to reduce strains during cable bending (reference Figure 2, Straight and Bent Cable). For the entire range of lay lengths tested in this development program, the ribbons were able to move enough to control such bending strains.

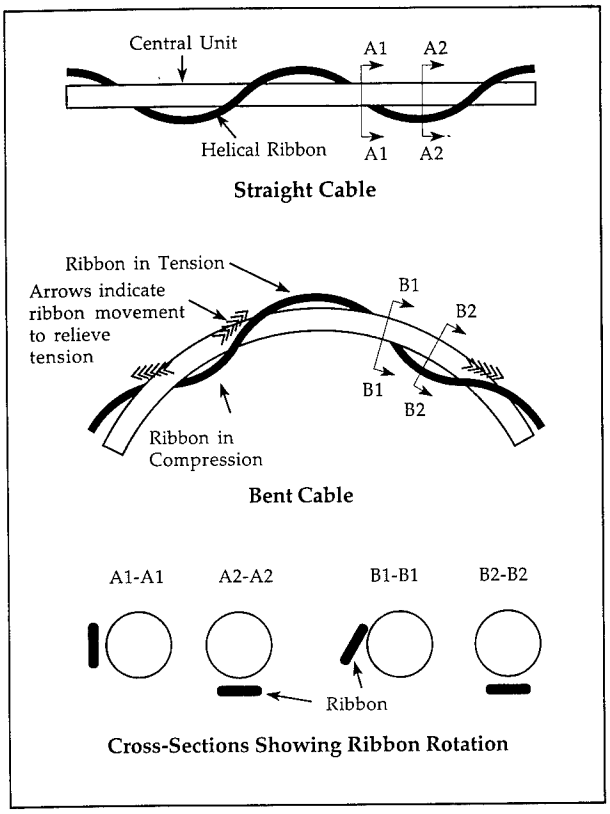


Figure 2: Movement of Helically Stranded Ribbons

(2) Due to the helical nature of the slot, the stranded ribbon length is greater than the cable length. The length of the ribbon relative to the cable length is called the relative helical length and can be calculated by equation (1). The higher relative helical lengths that result from the shorter slot lay lengths yield more ribbon per unit cable length. For the final 360-fiber design, the relative helical length of the ribbons increases 0.3% from the bottom ribbon to top ribbon.

$$\text{Relative Helical Length} = \sqrt{1+(\pi D/P)^2} \qquad (1)$$

where

D is the mean diameter of helical unit,
P is the pitch of helical unit.

(3) During cable bending, the ribbons resist bending sideways by rotating as shown at the bottom of Figure 2. The width and depth of the slot must accommodate this ribbon rotation. There is less ribbon rotation with a shorter slot pitch. The required slot depth is reduced by using a relatively short pitch versus a longer pitch of 450 mm or more. This consideration is especially important with the relatively wide 12-fiber ribbons (in comparison to the 4-fiber and 8-fiber ribbons used in other slotted core ribbon cable designs).

(4) At low temperatures, all cable components shrink. In this slotted core cable design, all the materials except the ribbons are coupled together. Due to the relatively low coefficient of thermal expansion of the glass, the ribbons shrink less than the rest of the cable materials. The ribbons move within the slot to a position that avoids the compression caused by cable shrinkage. At low temperatures, the ribbons increase their radius from the center of the cable, thereby increasing their relative helical length. Equation (1) shows that, as the diameter increases, the helical length increases. Shorter lay lengths require less outward ribbon movement to accommodate cable shrinkage. Therefore, the ribbons require less slot depth when short lay lengths are employed.

(5) There are three types of fiber strain associated with a ribbon in a helical configuration [1]. Each fiber in the ribbon is subjected to both bending and torsional strain due to being in a helix. Over one complete lay length, every fiber in the ribbon experiences nearly one twist. The third type of strain is due to helical length differences. Since the fibers in a ribbon are at different distances from the center of the cable, they have different helical lengths (see Figure 3).

The fibers in a ribbon all start with the same length so their helical length differences result in fiber strain in the edge fibers and fiber compression in the middle fibers. All of these three strains increase with decreasing lay length.

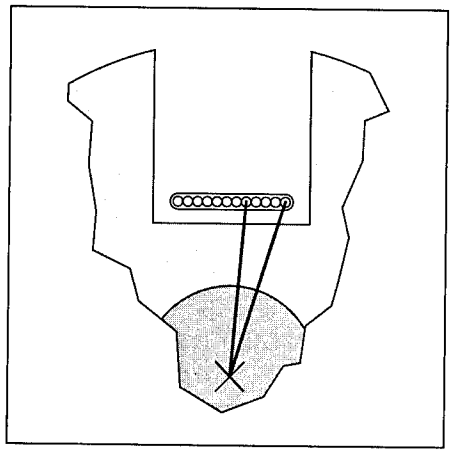


Figure 3: Fiber Distances From Center of Cable

These three strains are combined with any additional tension strains. The maximum effective strain on the outside of the fiber can be calculated by equation (2).

$$\varepsilon_M = 0.5([\varepsilon_{HL}+\varepsilon_B+\varepsilon_\tau]+\sqrt{[\varepsilon_{HL}+\varepsilon_B+\varepsilon_\tau]^2+[(2G/E)\cdot\varepsilon_T]^2}) \quad (2)$$

where

ε_M is the maximum effective strain,

ε_{HL} is the strain due to helical length difference,

ε_B is the strain due to the bending,

ε_τ is the strain due to tension,

G is the shear modulus of the glass,

E is the tensile modulus of the glass,

ε_T is the strain due to torsion.

During the development process, it was found that, at very short lay lengths, attenuation of the middle fibers in the ribbons increases at low temperatures. At those lay lengths, the compression strains from helical length differences are larger than 0.03%. The corresponding strains in the final 360-fiber cable design do not exceed 0.023%.

As previously noted, cables with a shorter lay length require less slot depth. This results in a smaller cable diameter; however, the shorter lay length creates higher strains and the potential of a problem resulting from compression of the center fibers. An optimal lay length was chosen for the final 360-fiber design to balance these considerations. The fiber strain is acceptable in both the unstressed state and during tensile cable loading. No problems were observed at low temperatures as a result of compression of the center fibers and the helical length of the ribbons was acceptable.

CABLE PERFORMANCE

Armored 360-fiber prototype cables were produced and evaluated for optical, mechanical, and environmental performance. EIA/TIA cable test results are summarized in Table 1.

Temperature Cycling

The ribbons essentially form a rectangular cross-section when they are stacked on top of each other. The outer fibers of the ribbon stack are the most susceptible to the effects of bending and side wall pressures exerted as the stack rotates and moves within the slot. The fibers close to the center of a ribbon are susceptible to compression. Edge fibers in the top and bottom ribbons were monitored along with key inner fibers to help characterize cable performance at the temperature extremes (see Figure 4).

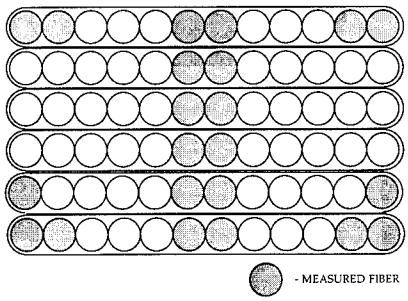


Figure 4: Ribbon Stack Cross Section

Two 120-hour (24 hour transitions, 48 hour soaks) –40°/+70°C cycles were completed. Table 2 shows the mean attenuation changes (relative to the initial attenuation measured at 23°C) and the corresponding standard deviations for a 360–fiber

Test	Results*	Method
Temperature Cycling (-40° to +70°C)	Average change ≤0.05 dB/km	FOTP-3
Cable Aging (+85°C, 168 hrs.)	Average change ≤0.10 dB/km	FOTP-3
High Temperature Bend (+60°C, 4 turns, 450 mm dia. mandrel)	90% of fibers ≤0.05 dB change Remaining 10% ≤0.15 dB change	FOTP-37
Low Temperature Bend (-30°C, 4 turns, 450 mm dia. mandrel)	90% of fibers ≤0.05 dB change Remaining 10% ≤0.15 dB change	FOTP-37
Cyclic Flex (25 cycles)	90% of fibers ≤0.05 dB change Remaining 10% ≤0.15 dB change	FOTP-104
Compression (440 N/cm)	90% of fibers ≤0.05 dB change Remaining 10% ≤0.15 dB change	FOTP-41
Tensile Strength (2700 N)	90% of fibers ≤0.05 dB change Remaining 10% ≤0.15 dB change	FOTP-33
Cable Twist (2 twists in 2 m)	90% of fibers ≤0.05 dB change Remaining 10% ≤0.15 dB change	FOTP-85

*Note: Attenuation measurements at 1550 nm

Table 1: Armored Cable Performance

steel core armored cable. Although the ribbons are free to move within the cable during expansion and contraction due to temperature change, a shift in the mean attenuation at the temperature extremes is apparent. This shift indicates a small degree of coupling between the cable structure and the ribbons. The average attenuation change from initial values was less than 0.05 dB/km, well within expectations.

Temperature (°C)	1310 nm		1550 nm	
	Avg. Change (dB/km)	Std. Deviation (dB/km)	Avg. Change (dB/km)	Std. Deviation (dB/km)
-40	0.00	0.01	0.01	0.02
+70	0.02	0.02	0.02	0.03

n = 110

Table 2: Cable Attenuation Change at Temperature Extremes

Mechanical Testing

Fiber attenuation performance was measured during tensile, compression, twist, and high/low temperature bending tests on the cable. EIA/TIA industry standard test procedures were used for the cable evaluation. Satisfactory results were found in each of these tests.

Water Penetration Protection

Resistance to water penetration in the ribbon slots is achieved through the use of water blocking tape which is applied over the slotted rod (see Figure 1). SAPs in the tape swell and form a gel which fills the free space around the ribbons when water is introduced into the cable. This gel forms a "plug" which blocks movement of additional water into the cable. Unlike filling compounds found in gel-filled cables, SAPs require time to swell and form the water blocking gel. The unique nature of this water blocking design requires special cable testing. An investigation was undertaken to evaluate water penetration resistance and cable performance.

For this test, pressurized water was introduced into the cable through an opening in the sheath. A

25–mm (1–in.) wide section of the outer sheath, armor, and inner sheath were removed from a length of cable. A "T" pipe connection was placed over the opening and 1 meter (3.3 ft.) pressure head of water was continuously applied to the tape-wrapped core for 24 hours. Upon dissection, the SAP had formed a gel to effectively fill the ribbon slots and stop water penetration. The total water penetration was less than 0.2 m (8 in.) in either direction from the point of sheath removal.

Fiber Performance After Exposure to Water

Since water is a component of the water blocking gel, a test was devised to evaluate changes in fiber attenuation after the gel is formed and subjected to temperature extremes. The outer jacket, armor, inner jacket and swellable tape were removed to expose a 50-mm (2-in.) wide section of the slotted rod. A "T" pipe connection was placed over the exposed cable section and water was pressured into the cable (see Figure 5). Six fibers were concatenated and a power meter was used to detect the change in power over the test. Two –30° to +70°C cycles (1 cycle represents 144 hours) were completed. Water was continuously applied throughout the test. [5],[6], [7].

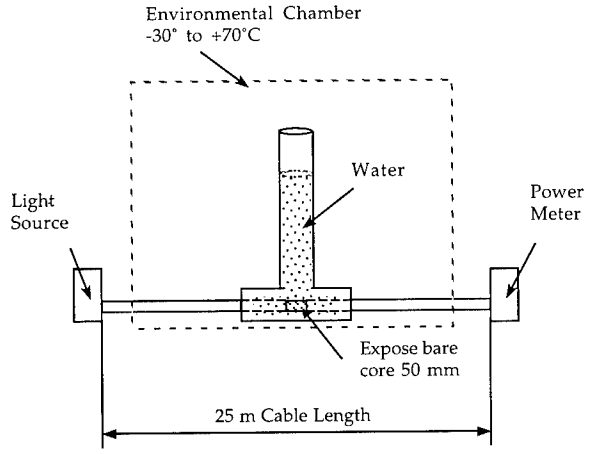


Figure 5: Water Penetration Test During Temperature Cycling

The power change was 0.03 dB (measured at 1550 nm) over the concatenated test fibers. Subsequent cable dissection revealed that gel had formed 2.5 m (8 ft.) in each direction from the "T" connection. The cable itself exhibited no jacket cracking or other damage as a result of the test.

FIELD INSTALLATION

A 360-fiber armored cable was manufactured for field installation. The selected cable route consisted of a concrete conduit in which a 32 mm (1.25 in.) ID polyethylene inner duct had been placed. This connects a central office to a splice location approximately 2.3 km (7,500 ft) away. The route is in a heavily-congested metropolitan area and contains changes in elevation and direction. Mid-span access of the installed cable will be required at a future date.

The cable exhibited the flexibility required for field handling, yet was rigid enough to be installed at speeds up to 30 m/min. (100 ft./min.) using a cable jet machine. The cable was subsequently accessed, spliced, placed into closures, and put into service.

CONCLUSION

A compact high fiber count cable, the StarTrac™ ribbon cable, has been developed to meet emerging network applications. This new cable incorporates 12-fiber ribbons in slots with a short pitch which allows a relatively shallow slot depth.

Test results demonstrate that excellent fiber performance has been achieved during both temperature and mechanical testing. Water penetration protection is achieved through the use of super-absorbant polymers that form a gel when water is present.

Cable has been successfully installed in the field and it exhibited excellent handling during installation. The test results and field experience indicate this cable is suitable for applications that require high fiber counts in a compact design.

ACKNOWLEDGMENTS

The success of this cable development project is the result of significant contributions by many people. Thanks go to Mike Ellwanger, Harriet Cooke, Scott McDowell, Warren McAlpine, Mary Ann Clarke, Kevin White, Andy Jackson, Ron Livingston, and Larry Herman. The authors would also like to thank Ameritech for allowing us to be on-site and to witness the initial installation of this cable design in Chicago, Illinois.

REFERENCES

[1] S. Hatano, Y. Katsuyama, T. Kokubun, and K. Hogari: "Multi-Hundred-Fiber Cable composed of Optical Fiber Ribbons Inserted Tightly Into Slots", *Proceedings of the 35th International Wire and Cable Symposium,* pp. 17 - 23, 1986.

[2] M. Yamanaka, N. Okada, H. Sawano, and M. Miyamoto: "A Study on Reverse Lay Stranding Loose Tube Cable Containing Ribbon Fibers", *Proceedings of the 42nd International Wire and Cable Symposium,* pp. 521 - 526, 1993.

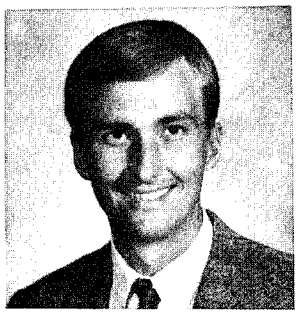
[3] K. W. Jackson, M. R. Santana, and N. W. Sollenberger: "A Modular Ribbon Design for Increased Packing Density of Fiber Optic Cables", *Proceedings of the 42nd International Wire and Cable Symposium,* pp. 20 - 27, 1993.

[4] J. Bonicel, D. Keller, G. Kylen, J. Schulte, G. Paternostro, G. Berthelsen, C. Cortines, and C. Lasne: "An International Development On Ribbon Technology and Evaluation Of Applicability To National Specifications", *Proceedings for the 41st International Wire and Cable Symposium,* pp. 25 - 31, 1992.

[5] A. Bringuier and C. Clyburn, III: "Development of a Loose Tube Cable With Non-Flooded Core For Outdoor Plant Environment", *Proceedings of the National Fiber Optic Engineers Conference,* pp. 376 - 386, 1995.

[6] M. Fukuma, N. Akasaka, and S. Suzuki: "Dry Type Water-Blocking Optical Fiber Tape Cable with Slotted Rod", *Proceedings for the 36th International Wire and Cable Symposium,* pp. 350 - 356, 1987.

[7] T. Uenoya, S. Tomita, and F. Ashiya: "Long-term Reliability of 1000-Fiber Water-blocking Cable", *Journal of Optical Communications,* pp. 86 - 89, 1990.



William J. McCallum, III
Siecor Corporation
PO Box 489
Hickory, NC 28603

William J. McCallum, III received a B.S. degree in Engineering from the University of North Carolina at Charlotte in 1982. Since joining Siecor Corporation in 1982, he has been actively involved with design and development activities for copper and fiber optic telecommunication cables and elevator control cables. He is currently a Supervisor with the Research, Development and Engineering Department. Mr. McCallum has co-authored two previous IWCS papers and has been granted two US patents.



Richard S. Wagman
Siecor Corporation
PO Box 489
Hickory, NC 28603

Richard S. Wagman received a B.S. degree in Engineering Science honors program at Pennsylvania State University in 1978 and a B.S. in Electrical Engineering from Johns Hopkins University in 1984. He worked for seven years as a Product Engineer at Continental Wire and Cable before joining Siecor Corporation in 1985. At Siecor, he has worked with cable, materials, and test design. He is currently a Staff Engineer in the Research, Development and Engineering Department. Mr. Wagman has been granted four US patents and has co-authored three previous IWCS papers.



Martin C. Light, Jr.
Siecor Corporation
PO Box 489
Hickory, NC 28603

Martin C. Light, Jr., received his Bachelor's of Ceramic Engineering degree from the Georgia Institute of Technology in 1985 and his Masters of Business Administration degree from Duke University in 1994. After joining Siecor Corporation in 1985, he was involved with a variety of design, development, and measurements activities for fiber optic telecommunications cable products at the Research, Development and Engineering Department. Currently a Senior Product Specialist in the Telecommunications Marketing Department, Mr. Light has written two previous IWCS papers.

BUFFER TUBES - THE NEXT GENERATION

M. Adams[2], J. Holder[2], C. McNutt[1], O. Tatat[1], H. Yang[2]

[1] Alcatel Cable OFCCC - Bezons FRANCE
[2] Alcatel Telecommunications Cable - Claremont, North Carolina, USA

Abstract

The telecommunications cable industry has an immediate need for reducing optical fiber cable installation times and costs. Operations such as mid-span access, enclosures, and unplanned cable entries are major contributors to these issues. Alcatel has responded to the market place by investigating and targeting cable design improvements in order to meet the customers' needs.

Specifically, the buffer tube's lack of flexibility, desire to kink, and difficulty to enter can present obstacles to the installer during the handling operations of loose tube cables, a commercially popular design.

Alcatel has developed the ABM2 buffer tube to eliminate the aforementioned problems without sacrificing the robust performance of the loose tube cable. The new ABM2 buffer tube has been tested and qualified in a variety of loose tube cable designs and meets or exceeds industry standards. User feedback confirms that the ABM2 buffer tube is easier to use.

Additionally, the ABM2 tube offers significant improvements in heat and humidity environments compared to the current, conventional buffer tubes, polybutylene terephthalate (PBT) and PBT/polycarbonate (PC). This is an important property for cable installations using hardware such as pedestals and enclosures.

Introduction

Fiber optic cable installations continue to increase in order to meet the ever growing demands for more communication availability and capability, nationally and internationally. The progression of a global network of communication transported by fiber optic cables is causing a demand for cables which are easier to install. New fiber in the loop (FITL), fiber to the curb (FTTC), fiber to the home (FTTH) architectures and the need for unplanned entries is driving the demand for quick and easy access to the cable plant [1].

The loose tube cable design is popular and frequently used by many customers worldwide (Figure 1). However, cable installers agree that the buffer tubes currently available for this design can present installation difficulties due to their inflexibility, kinking, and resistance to entering. A synergy of design and materials, combined with process optimization have produced a new buffer tube, ABM2, specifically developed to eliminate these problems without compromising the performance of the cable.

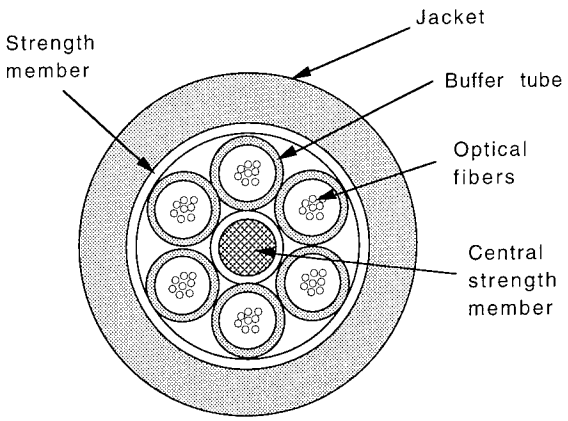


Figure 1

Flexibility

Buffer tube flexibility is a parameter that must be considered during the selection of buffer tubes for fiber optic cables. Conventional buffer tubes tend to offer resistance when being placed into tight arrangements such as splice enclosures. Many times the installer must "wrestle" the tubes into place in order to close the enclosure. This situation may increase the likelihood of fiber stress due to bending, in addition to causing installation delays.

Also, buffer tube materials decrease in flexibility at lower installation and handling temperatures. In some cold weather installations, equipment may be used to preheat the tubes making them more flexible in order to gain access to the fibers without breaking them. Buffer tubes which remain flexible at the lower installation temperatures would then allow the installer to eliminate added handling steps and additional equipment.

The flexibility of the ABM2 buffer tube design was compared to the PBT and PBT/PC designs at -10 °C, 25 °C, and 60 °C using a method which simulates the resistance buffer tubes exert when placed into an enclosure. The temperatures were selected to reflect possible field conditions.

In this method, two coils, 145 mm in diameter, were formed using one continous length of buffer tube. Next the coils were taped together in four locations, 90 ° apart around the circumference of the combined loops. The width of the tape was kept minimal. The coils were then twisted 180 °, forming a "figure eight". The top and bottom of the "eight" were compressed towards each other and placed into a standard compression test unit (Figure 2), with compression plates 50.8 mm apart. The ends were compressed and the force measured until the top and bottom of the "eight" were 6 mm apart. A lower force equates to more flexibility. Compression plate speed was 254 mm/min.

FLEXIBILITY TEST

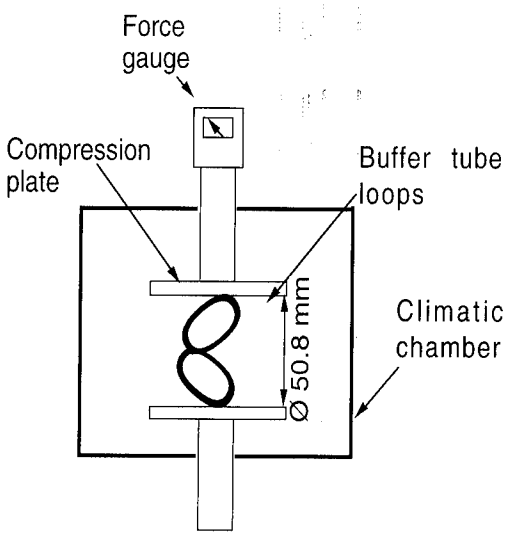


Figure 2

The results demonstrate that the ABM2 buffer tube is much more flexible at typical installation temperatures than PBT or PBT/PC tubes (Figure 3). Furthermore, the ABM2 at -10 °C exhibits the same or better flexibility than either the PBT or PBT/PC at ambient temperatures. This implies that the field installer would not have to preheat the tubes in order to have an acceptable handling flexibility even at sub-ambient temperatures.

Kink

Many times the buffer tubes are bent into tight radii when handled for cable installations. This can present problems when the tubes are bent beyond their minimum acceptable bend radius and kink. If the tube kinks during a mid-span

FLEXIBILITY RESULTS

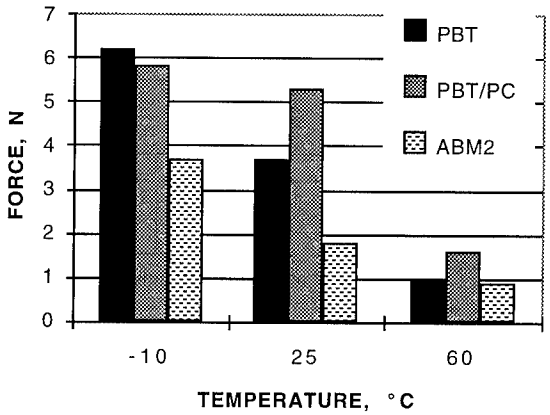


Figure 3

access operation, it must be removed very carefully in order to prevent damage to "live" fibers.

Also, buffer tubes will become much more brittle at lower installation temperatures. This material change will cause the tube's minimum acceptable bend radius to increase, thus further compounding any handling issues. The problem may be minimized by heating the tubes prior to bending.

The ABM2 buffer tubes' kink resistance was compared to the PBT and PBT/PC designs using a modified Kink Performance-Loop Test [2] (the method was modified slightly to eliminate negative values when testing the ABM2 buffer tubes)(Figure 4). A 700 mm tube was marked 225 mm from each end. The tube was then shaped by placing each end of the tube into a ring in order to maintain a loop configuration. The ends of the tube were placed into the tensile test machine clamps and the clamps were adjusted until the two

KINK TEST

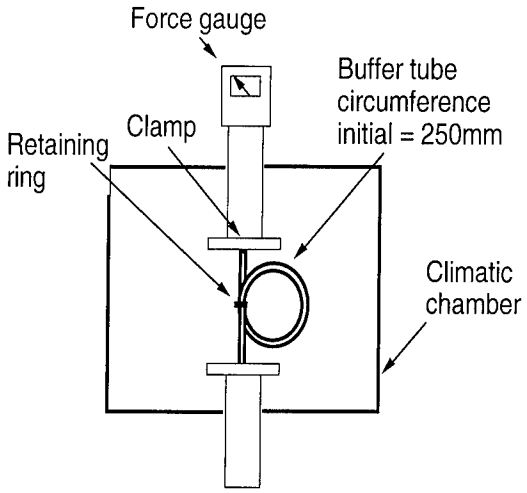


Figure 4

marks coincided. This provided a loop with a starting circumference of 250 mm. Crosshead speed of the test was 254 mm/min and the load versus clamp displacement was recorded. Kink was defined as the first peak load at which point the load then decreases rapidly (visually a kink has occurred). For comparison of buffer tube kink performance, the final circumference is determined using the equation:

Final circumference = starting circumference - crosshead displacement

As in the flexibility test, three different temperatures were evaluated for each tube: -10 °C, 25 °C, and 60 °C. This was to insure a more accurate reflection of actual field installation temperatures and their corresponding tube kink behavior.

As seen, the ABM2 design exhibits a very high resistance to kinking when compared to the PBT and PBT/PC buffer tube designs (Figure 5). Again, as demonstrated in the flexibility results, ABM2's performance at sub-ambient temperatures is better than either the PBT or the PBT/PC tubes at ambient temperatures.

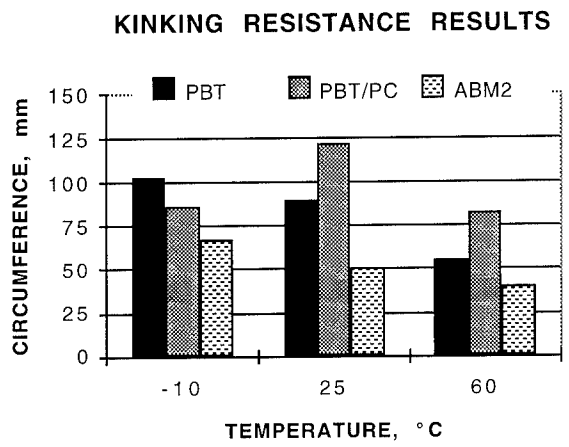


Figure 5

Cutting Resistance

In a successful mid-span access, the buffer tubes must offer minimal resistance when cut or shaved in order to enter the tube and access the fibers. Many variables contribute to the difficulty including access tool design, tube dimensions, the level of operator experience, the material, and the environment. However, proper selection of the material allows the cable manufacturer to have the greatest influence on the ease of entry into the buffer tube.

The cutting resistance of the ABM2 design was compared to the PBT and PBT/PC designs at -10 °C, 25 °C and 60 °C. Cutting resistance is largely influenced by the temperature of the tube and therefore must be examined.

Cutting resistance was evaluated by passing the tube through an Alcatel Easyshaver™ access tool and measuring the amount of force required to enter the tube (Figure 6). The Easyshaver™ opens the buffer tube by shaving off a portion of the tube, allowing the installer access to the optical fibers. The tube speed during the evaluation was approximately eight meters per minute and the length of tube used was between 2 and 3 meters. The force was measured using a portable force gauge.

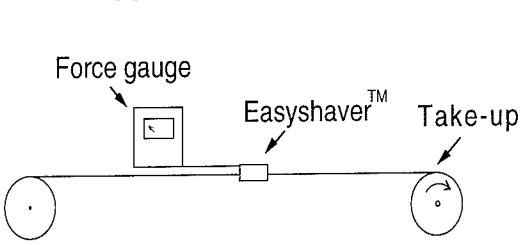


Figure 6

The results indicate that the ABM2 buffer tube requires less shaving force to enter at typical installation temperatures (-10°C to 60°C) than either the PBT or the PBT/PC buffer tubes (Figure 7). The cutting resistance of the ABM2 at sub-ambient temperatures is less than PBT and PBT/PC at room temperature.

Again, actual field experience confirms the improved accessibility of the ABM2 buffer tube design.

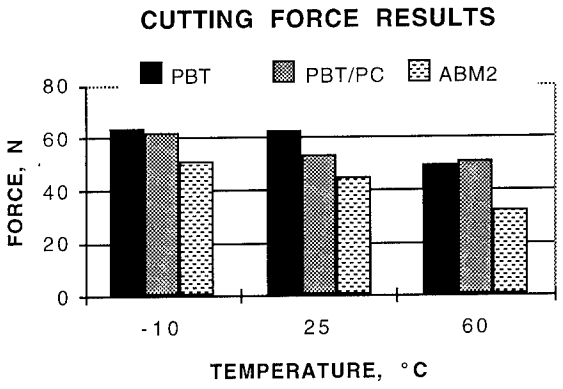


Figure 7

Hydrolytic Stability

PBT and PBT/PC buffer tubes may begin to embrittle when exposed to prolonged heat and humidity environments. The primary reaction causing this degradation is hydrolysis. Industry recognizes that severe tube embrittlement can cause problems in the field, particularly where cables are spliced or

terminated in above-ground pedestal enclosures. In response, new methods of stabilizing, processing and testing conventional buffer tubes are being developed within the industry in order to minimize and predict the degree of hydrolysis occurring over the life of the cable[3,4,5,6].

The ABM2 buffer tubes were aged for 30 days at 85 % RH and 85 °C. Their initial elongation was greater than 300 % and remained unchanged after ageing. Both PBT and PBT/PC buffer tube designs exhibit degradation (lower elongations) during this test. Given the present industrial concerns regarding hydrolytic stability of conventional buffer tubes, plus the time and effort being devoted to further minimizing it, ABM2 buffer tubes offer an excellent alternative.

Cable Installation Simulation

During cable installations into ducts, pulleys are often used to facilitate changes of direction. The pulleys can apply localized pressure on the cable while under the load exerted by the cable pulling device (Figure 8). If the cable design is not sufficiently robust, localized pressure and cable tension during installation may cause fiber breaks.

To duplicate these conditions, a cable installation simulation test, commonly called a "sheave test", was performed on a 216 fiber, loose tube cable (18 buffer tubes) (Figure 9). This test was performed to insure that the fibers were not damaged during actual installations using sheaves and that the cable's optical fiber performance was maintained during and after the installation operation.

The "sheave test" was performed on the cable, using a test length of 250 meters and a 2700 N (607 lbf) load for 120 cycles. The sheave machine moved back and forth over the

DUCT INSTALLATION

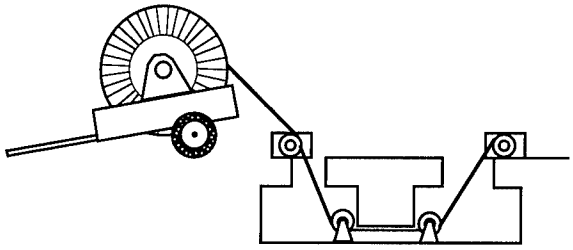


Figure 8

cable at 120 m/min. Sheave diameters were 450 mm. Eighteen fibers in the cable were spliced in series for a total optical fiber length of 4500 meters (14764 ft). The optical fibers were evaluated using an HP 8153A Lightwave Multimeter.

Optical fibers in the cable did not break or exhibit any increase in attenuation upon completion of the evaluation. Typically, the industry requirement for minimum bend radius is approximately 20 times the cable's outside diameter for loaded conditions. This cable was 19 mm in diameter. Therefore, this test was significantly more stringent than the standard minimum bend radius requirement. These "sheave test" results demonstrate that the ABM2 buffer tubes offer very good crush resistance necessary for protecting the optical fibers during actual loose tube cable installations.

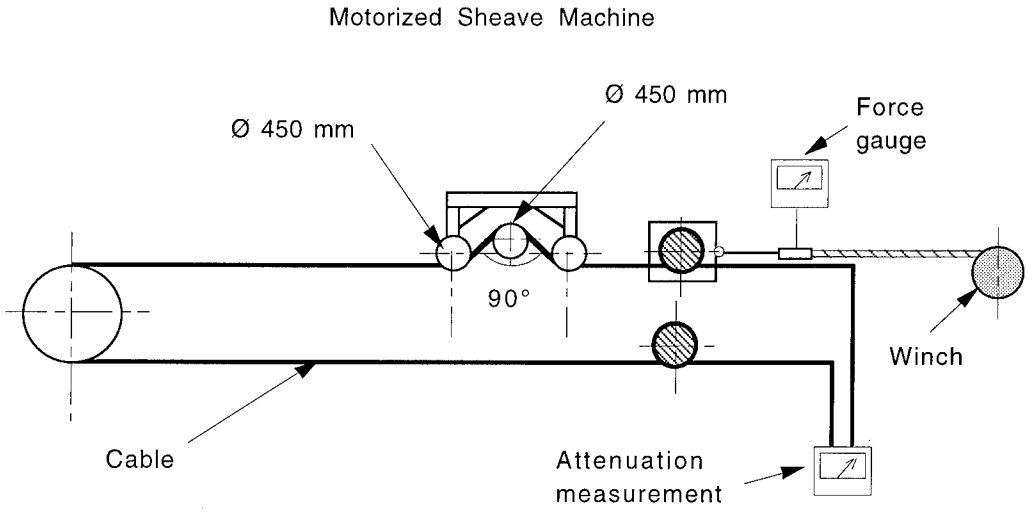


Figure 9

Cable Qualification Testing

Loose tube cables containing the ABM2 buffer tubes meet or exceed industry performance requirements (Figure 10).

CABLE PERFORMANCE RESULTS

TEST METHOD	SPECIFICATION GR-20, Issue 1 (unless noted)	PASS /FAIL*	COMMENTS
Buffer tube cold bend	GTE Sec. 6.3.1	PASS	Maintains high level of flexibility at low temperatures
Color permanence	Sec. 6.6.6	PASS	
Compound flow	Sec. 6.6.3	PASS	
Compression	Sec. 6.5.5	PASS	
Compression ($600\ N.cm^{-1}$)	GTE Sec. 7.4	PASS	
Cyclic flex	Sec. 6.5.8	PASS	
Freeze	Sec. 6.6.5	PASS	
Impact	Sec. 6.5.4	PASS	
Jacket Shrink	Sec. 6.4.4	PASS	
Lightning	Sec. 6.7.1	PASS	Pass 150 kA
Low/high temperature bend	Sec. 6.5.3	PASS	Maintains high level of flexibility at low temperatures
Material compatibility	Sec. 6.3.4	PASS	
Splice enclosure thermal test	Alcatel	PASS	
Temperature cycling and heat ageing	Sec. 6.6.3, Sec. 6.6.4	PASS	Passed cycles to -50°C after heat age
Tensile w/ twist resistance (w/ 720° twist)	Sec. 6.5.6	PASS	
Twist	Sec. 6.5.7	PASS	
Wasp spray exposure	Sec. 6.6.8	PASS	
Water penetration	Sec. 6.6.7	PASS	
Water penetration, aged	Sec. 6.6.7	PASS	

* Includes both armored and non-armored.

Figure 10

Conclusions

Alcatel ABM2 buffer tubes exhibit greater flexibility, less tendency to kink, less resistance to tube entry, and greater hydrolytic stability than the more conventional buffer tubes without sacrificing the cable performance necessary for installation and use. ABM2 tube performance is superior to present buffer tube designs at sub-ambient, ambient and high installation temperatures. These results demonstrate that the ABM2 tube offers significant advantages for installation and handling over present buffer tube designs, particularly for enclosures, mid-span access, and pedestal applications.

References

[1] Beasley W. E., Canady S. T., Karl G., "Choosing the Right Cable for the Right Application", National Fiber Optic Engineers Conference Proceedings, Volume 2, 1995, pp. 491 - 501.

[2] Parris D., Warner B., "Testing of Fiber Optic Cable Core Materials After Accelerated Heat and Humidity Aging", Proceedings of the Thirty - Ninth IWCS, 1990, pp. 237 - 242.

[3] Griswold, G., "Developing Optimal Processing of Hydrolytically Stabilized PBT for Fiber Optic Cable Core Component", Proceedings of the Forty - Second IWCS, 1993, pp. 48 - 55.

[4] Eickholt, J., "Reliability Testing of Fiber Optic Loose Buffer Tubes", Proceedings of the Forty - Second IWCS, 1993, pp. 476 - 478.

[5] Gebizlioglu, O., Plitz, I., "Monitoring Accelerated Aging of Polyester Buffer Tubes in Fiber Optic Cable", Proceedings of the Forty - Second IWCS, 1993, pp. 509 - 515.

[6] Bellcore, "Generic Requirements for Optical Fiber and Fiber Optic Cable, GR - 20 - CORE", Issue 1, September 1994, Section 6.3.4.

Acknowledgements

All the contributions are appreciated and gratefully acknowledged. Many thanks to Jeff Auton, Patrick Bourghelle, Bill Brewer, Gerard Couvrie, Pierre Gaillard, Ray Lovie, Scott Munday, Rachel Roddy and Alcatel Management for their support.

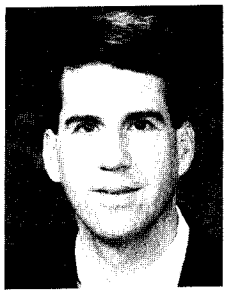
Authors

Michael Adams
Alcatel Telecommunications Cable
Claremont, North Carolina - USA



Michael Adams received his B. S. degree in Mechanical Engineering from the University of Tennessee, Knoxville in 1991. He joined Alcatel the same year and has been engaged in research and development of fiber optic cables.

Jim Holder
Alcatel Telecommunications Cable
Claremont, North Carolina - USA



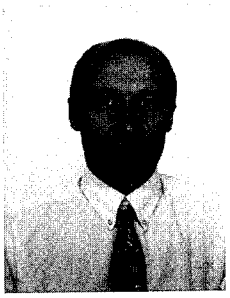
Jim Holder received his B. S. degree in Mechanical Engineering Technology from the University of Dayton in 1983. He worked for 5 years as a Process Engineer at Belden Wire & Cable before joining Alcatel in 1989. At Alcatel, he has worked as a Manufacturing Engineer in both copper and fiber cable plants. He is currently a Cable Development Engineer at Alcatel's Claremont facility.

Christopher McNutt
Alcatel Cable
Optical Fiber Cable Competence Center
Bezons - FRANCE



Christopher McNutt received his B. S. degree in Chemical Engineering from the University of Tennessee, Knoxville in 1985. He is working as a Project Engineer responsible for materials development at the Alcatel Optical Fiber Cable Competence Center.

Olivier Tatat
Alcatel Cable
Optical Fiber Cable Competence Center
Bezons - FRANCE



Olivier Tatat was born in 1959. He received his engineering degree from the Institut des Sciences de l'Ingenieur de Montpellier (ISIM) in 1982. He joined Les Cables de Lyon, now Alcatel Cable, in 1985. Now he is working as Project Engineer, in charge of the development of OPGW, in the Alcatel Optical Fiber Cable Competence Center.

H. Mike Yang
Alcatel Telecommunications Cable
Claremont, North Carolina - USA



Mike Yang is a Materials Scientist in Alcatel's Cable Development Group and is responsible for material related areas for cable products. After working at PPG Industries and W. R. Grace, he joined Alcatel in 1993. Dr. Yang has a B. S. in Industrial Chemistry from National Tsing-hua University in Taiwan, and M. S. and Ph. D. in Chemical Engineering from the University of Maryland at College Park.

DEVELOPMENT OF FLEXIBLE 100-COUNT SLOT-TYPE OPTICAL FIBER RIBBON CABLE

Taro Yasuoka, Teruo Koyama, Kazuo Imamura,
Moriyuki Fujita, Hiroyuki Tanaka

Optical Fiber Cable Engineering Section, Optical Fiber Cable Factory,
Itami works, Telecom. Div., Mitsubishi Cable Industries, LTD.
4-3, Ikejiri, Itami-City, Hyogo-Pref., 664, Japan

Abstract

Recently, an optical fiber cable, especially in measurement and control applications, is required to have multi-count and such properties as to be readily bendable and continuously durable under the working environment where it is continuously bent.

The authors made a prototype of the flexible high-density 100-count slot-type optical fiber ribbon cable, which was evaluated in terms of flexural rigidity and torsion/flexing properties.

The developed cable was constructed to be readily bendable, employing a stranded steel wire with an O.D. of 1.18mm as the tension member at the center, and a cable sheath of the PVC excellently flexible over a wide temperature range.

The cable could have flexibility improved in a great measure.

Introduction

More recently, an optical fiber cable has come to be often employed in controls for instrumentation and large-sized equipment. In a communication application, the fiber cable has been getting oriented for higher and higher density. In such measurement and control applications as referred to above, it is quite natural that the optical fiber cable makes progress toward an increase in both density and number of fibers.

In such applications, moreover, the optical fiber cable is often installed in a relatively small length and by way of a cable feeder or the like, not being secured over a certain fixed section as seen in the optical fiber cable for communications. Under the working environments where the cable is repetitively bent, the optical fiber cable is required to show an excellent level of flexibility.

In the study reported herein, therefore, the cable was constructed into the 4-fiber ribbon slot-type, which was applied to achieve an increase in both density and number of fibers and designed to be made of a material with consideration given to flexibility.

As a measure to represent a level of flexibility, the flexural rigidity was calculated beforehand in the design stages to make the cable, which was in turn evaluated in terms of flexural rigidity and torsion/flexing properties. Thus, it has been verified that the cable is reliable enough for a long period.

Cable Design

The cable was disigned, with consideration given to the following :

- •Increasing both density and number of fibers,
- •Improving flexibility and
- •Achieving long-term reliability against repetitions of bending.

To change an optical fiber cable over to a multi-count type, its construction is conseivable in the following three types:

1. Stranded layer type,
2. Loose tube type and
3. Slot-type with optical fiber ribbon applied.

With attention paid to the cable flexibility, it is naturally important to increase the material flexibility. In addition, a decrease in cable outside diameter would allow the flexibility to increase in a very great measure[1].

If the above-mentioned three types of cabling are compared in number of fibers with an identical cable outside diameter, 3 is found to have the greatest number of fibers. With flexibility taken into consideration, the optical fiber cable of stranded construction reffered to 1 is most advantageous. To increase the number of fibers, however, rigidity increase inevitably since the cable has an outside diameter increase in proportion to the number of fibers. 2, which is of PE tube stranded construction, has a basically structural difficulty to flex. In addition, it has a cable outside diameter also increase in proportion to the number of fibers similarly to 1. Consequently, slot type 3, which allows for the highest fiber density in cable construction, has been employed. To improve the flexibility, the authors have decided to apply a highly flexible material.

The cable had an objective of giving flexibility a general PE-sheathed slot-type optical fiber cable conventionally available.

A general PE-sheathed slot-type optical fiber cable employs a 2.6mm single steel wire as the tension member, with the sheath made of low-density poly-ethylene.

Cable Construction

Fig. 1 shows a construction of the prototype cable. The cable is constructed of twenty 4-fiber ribbons, a tension member, a slotted rod, polyester wrapping tape and a PVC sheath.

To increase both density and number of fibers, a 4-fiber ribbon was employed as optical fiber. Each 4-fiber ribbon is the graded index type fiber which has a core diameter of 50 μm and a cladding diameter of 125 μm. Five 4-fiber ribbons are taken in one slot as identically directed. A total of 100 fibers are emmployed in the cable, with polyester-tape wrapped around the slot-rod.

To improve the flexibility, the cable employed a stranded steal wire tension member to achieve an outside diameter of 1.18 mm. In addition, the cable sheath was made of the PVC material which is highly flexible over a wide temperature range. The cable has an outside diameter of approximately 15 mm while having an estimated mass of 0.16kg/m.

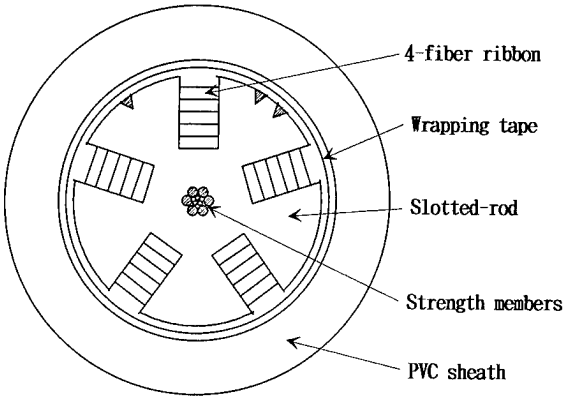


Fig. 1. Cross section of the cable.

Calculating Flexural Rigidity

In the study reported herein, the flexural rigidity was applied as a measure to represent a flexibility level of the cable. The term, flexural rigidity, represents the degree of an object's resistance to bending. It is expressed in a product of Young's modulus E by moment of inertia of area Iz. The smaller the value, the more readily the material will be bendable.

Young's modulus E is a value of the material's properties, which is measured from a rate of unit elongation to unit stress. Fig. 2 shows temperature vs. Young's modulus by component materials of the cable.

Moment of inertia of area Iz represents a geometrical shape of the neutral axis of bending on the section. It is defined by the following expression :

$$I_z = \int y^2 \, dA$$

where, y is distance from the neutral axis, and dA is fine area corresponding to y.

Results of theoretically calculating the flexural rigidity of the cable under the conditions referred to above are shown in Table 1.

Stranded steel wire with an outside diameter of 1.18mm was applied as the tension member while the sheath was made of the PVC material excellently flexible over a wide temperature range. As a result, the cable could be given a flexural rigidity of approximately 1/14 or less of that available in general 100-count slot-type polyethylene-sheathed (at the room temperature). In addition, the flexibility was considered to improve in a great measure at a low temperature.

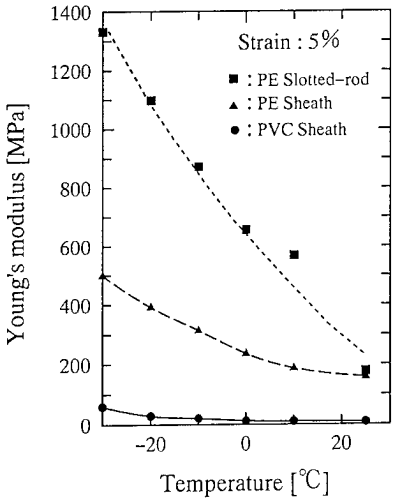


Fig. 2. Relation between temperature and Young's modulus of the cable component materials.

Table 1. Theoretical calculation results of the flexural rigidity of the cables.

	Flexural rigidity(N•m²)
Slot-Type PE Sheathed Optical Cable (25℃)	1.31
Flexible Optical Cable (25℃)	0.09
Flexible Optical Cable (-20℃)	0.41

Cable Performance

The cable was evaluated in terms of flexural rigidity and torsion/flexing properties to make certain that the cable would be reliable enough for a long period.

Bending Test

The bending rigidity was determined by the following two methods :

(1) Horizontal bending method

The cable was banged down, being gasped at both ends. While being secured at one end, the cable was deformed by bending at the other end. Displacement d relative to that load was determined to obtain the flexural rigidity. (Fig. 3)

(2) Cantilever beam method

The cable was secured at one end and had a weight suspended at the other end. Deflection d of the cable relative to that load was determined to obtain the flexural rigidity. (Fig. 4)

Table 2 shows the measurement results.

The horizontal flexing method, which employs a compression testing machine, does not allow for an evaluation at the room temperature. The cantilever beam method, on the other hand, allows for an evaluation at a low temperature.

The cable could have flexibility improved in a great measure, achieving approximately 1/16 of the bending strength in a 100-count slot-type polyethylene sheath optical cable. Even at a low temperature, the cable could have flexibility improved in a great measure.

The flexible cable did not have flexural rigidity fluctuation between calculated and measured values at 25℃ and -20℃.

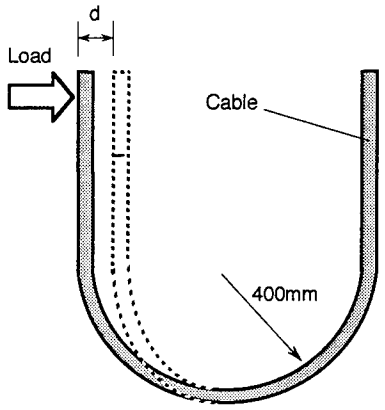


Fig. 3. Horizontal bending method.

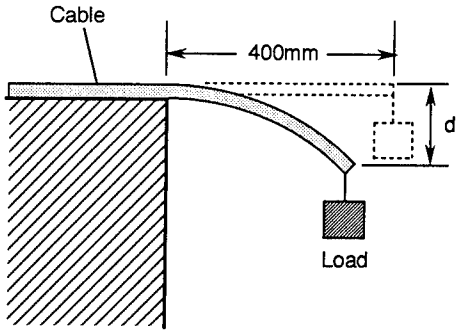


Fig. 4. Cantilever beam method.

Table 2. Measurement results of the flexural rigidity of the cables.

	Flexural rigidity(N•m²)
Slot-Type PE Sheathed Optical Cable (25℃)	2.14
Flexible Optical Cable (25℃)	0.13
Flexible Optical Cable (-20℃)	0.32

Torsion and Flexing Tests

To evaluate the optical transmission and durability characteristics of the cable as repetitively bent, tortion and flexing tests were conducted. Fig. 5 shows the test conditions involved.

For the torsion test, the cable was given 150 thousand twists to +/- 90° at a span of 1m. (Fig. 6.)

For the flexing test, the prototype was mounted on a metal wheel and bent to an angle of 90° . Then, it was flexed 150 thousand cycles over a length of 700 mm, with a tensile load of 150N applied. (Fig. 7.)

As is seen in Fig. 5, to determine a transmission loss fluctuation, the 4-core ribbon was folded back and spliced in series at the cable end to continually determine the transmission loss fluctuations during the torsion and flexing tests.

Fig. 8 shows the measurement results. Transmission loss fluctuations are found relatively stable at a level not specifically detrimental to the practical use. Throughout these tests, moreover, the cable could not be observed damaged to its appearance.

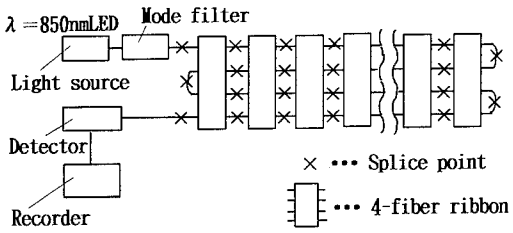


Fig. 5. Measuring system of the torsion and flexion test.

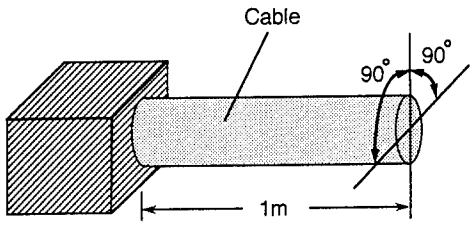


Fig. 6. Torsion test condition.

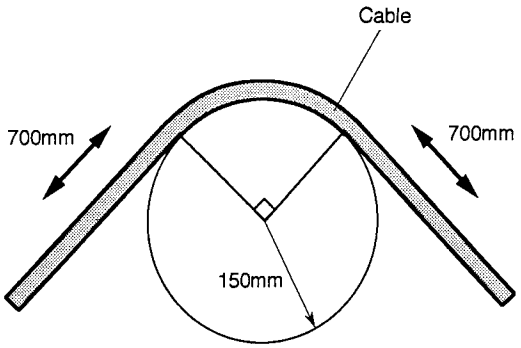


Fig. 7. Flexing test condition.

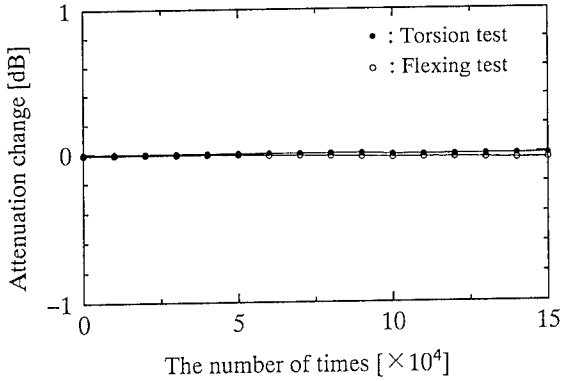


Fig. 8. Results of the Torsion and Flexing test.

Conclusion

In a high-density multi-count optical fiber cable with a 4-fiber ribbon applied, a fine-diameter stranded steel wire was employed as the tension member and a flexible PVC material having a low level of rigidity over a wide temperature range was applied as the sheath. As a result, the cable could have a bending rigidity of approximately 1/16 of that available in a general 100-count slot type polyethylene-sheathed cable (25℃). At alow temperature, moreover, the cable could have flexibility improved in a great measure.

The cable, moreover, had both calculated and measured flexural rigidity values tended to nearly coincide. From this, it may be gathered that any component material could have its flexural rigidity assumed if a Young's modulus and moment of inertia of the material were known.

As a result of continually determining the optical transmission loss fluctuations in the repetitive torsion and flexing tests, transmission power level was stable. This cable was not especially detrimental to the practical use. Throughout these tests, moreover, the cable could not be observed damaged to the appearance, too.

From the evaluation results referred to above, it has been clearly gathered that a high density multi-count slot-type construction is applicable as a flexible optical fiber cable.

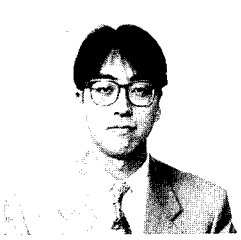
Acknowledgements

The authors would like to thank all who participated in the design, development, construction and testing. Special thanks to Mr. T. Yano, H. Ooizumi, T. Takeda and Y. Yamakawa for useful discussions and their assistance in this program.

Referrences

[1] Hayashi A., Mitsunaga Y. and Koga H., "Optical Fiber Cable Flexibility Design under Plastic Deformation and Its Evaluation", IEICE(B), Vol. J71-B, No6, pp. 725-732, 1988.

[2] Yasuoka T., et al., "Development of Flexible High Density Optical Fiber Ribbon Cable", Proceeding of the 1995 IEICE General Conference, B-1003, Comunication[2], p. 449.



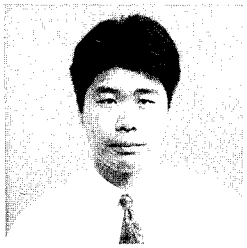
Taro Yasuoka
Mitsubishi Cable
Industries, Ltd.
4-3, Ikejiri, Itami,
Hyogo, 664, Japan

Mr. Yasuoka, staff engineer of Optical Fiber Cable Factory, is engaged in design and development of optical fiber cable. He received his M.S. degree in Geology and Mineralogy from Hiroshima University in 1993.



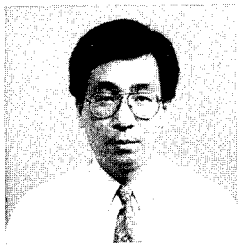
Moriyuki Fujita
Mitsubishi Cable
Industries, Ltd.
4-3, Ikejiri, Itami,
Hyogo, 664, Japan

Mr. Fujita, chief engineer of Optical Fiber Cable Factory, is engaged in design and development of optical fiber cable. He received his B.E. degree in Electrical Engineering from Osaka University in 1973.



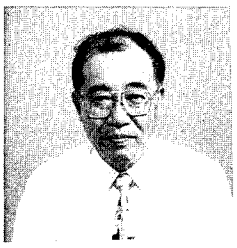
Teruo Koyama
Mitsubishi Cable
Industries, Ltd.
4-3, Ikejiri, Itami,
Hyogo, 664, Japan

Mr. Koyama, staff engineer of Optical Fiber Cable Factory, is engaged in design and development of optical fiber cable. He received his B.E. degree in Electronic Engineering from Osaka Electrocommunication University in 1989.



Kazuo Imamura
Mitsubishi Cable
Industries, Ltd.
4-3, Ikejiri, Itami,
Hyogo, 664, Japan

Mr. Imamura, staff engineer of Optical Fiber Cable Factory, is engaged in design and development of optical fiber cable. He received his M.S. degree in Electrical Engineering from Osaka University in 1983. He is a member of the Institute of Electrical Engineers of Japan.



Hiroyuki Tanaka
Mitsubishi Cable
Industries, Ltd.
4-3, Ikejiri, Itami,
Hyogo, 664, Japan

Mr. Tanaka, manager of Optical Fiber Cable Factory, is engaged in production and development of optical fiber cables. He received his M.S. degree in Electrical Engineering from Osaka University in 1971. He is a member of the Institute of Electronics and Communication Engineers of Japan.

A Dry Core Loose Tube Cable for Outside Environments

Clinton E. Clyburn III, Anne G. Bringuier

Siecor Corporation
Research, Development and Engineering
Hickory, NC 28603 USA

Abstract

This paper presents the development of non-armored (duct) and armored loose tube cable constructions where dry water-swellable materials have replaced flooding compounds outside of the buffer tubes. This results in a craft-friendly product which increases cable handling efficiency while meeting industry performance requirements. Different approaches using dry water blocking components were evaluated. An optimal placement of swellable materials within the cable was selected which reliably limited water migration and which could consistently be manufactured. This approach was then incorporated into duct and armored loose tube designs that were subjected to various mechanical and environmental tests. All cables exceeded industry requirements and displayed good correlation of empirical results to analytical predictions.

Investigation of the the reliability and longevity of water swellable tapes and yarns in the field environment was conducted. The dry swellable materials employed proved to be effective and robust in a variety of ionic and groundwater solutions.

Introduction

The introduction of broadband services employing optical fiber cables has made cable splicing and termination environments more diverse in terms of hardware and procedures. With the increased utilization of Optical Network Units (ONU's) and "breathable" closures, splicing operations are occurring in more unusual locations such as a bucket truck at an aerial ONU location. These changing environments are placing increased demands on the craftsperson in the field and on the products with which they must work. Thus there exists a requirement for an innovative stranded loose tube optical cable which provides field personnel with an easier, craft friendly and efficient method of accessing the cable core.

Loose tube cables typically use a flooding compound around the buffer tubes to block water penetration. Greases can be effective water-block mediums but require tedious cleaning with solvents during cable preparation for termination or splicing in the field.

The main focus for this product was the elimination of the flooding compound outside the buffer tubes while still preventing water penetration, hence the name Mini Bundle® Dry™ cable . Water-swellable materials used in this cable can be quickly removed for cable splicing, decreasing installation time and the need for cleaning chemicals. These advantages are apparent since installation costs are a primary consideration when a cable is being purchased.

Cable constructions utilizing greaseless water-swellable materials have been initially developed for slotted core designs[1,2,3]. In recent years, progress in superabsorbent polymers led to improved quality and performance of water swellable tapes and yarns. The different swellable materials investigated in this study included tape and yarn combinations and superabsorbent coatings attached via different binders on various cable components.

Water Path Considerations

The design of the Mini Bundle Dry cable presented several interesting challenges for both mechanical and ergonomic performance. Our goal was to meet or surpass all characteristics which make stranded loose-tube cables attractive for use. These characteristics include robust protection of the fibers during installation, ease of access and quick identification of buffer tubes.

With the absence of flooding compound, the initial concern was preventing water from flowing down interstitial spaces in the cable. Below the tensile yarns in both duct and armored cables, two main areas of concern were examined for water passage. The first was the area above the central member to the contact point between buffer tubes. The second was the space from the buffer tubes to the inside of the jacket or armor (Figure 1). The total open space in the first region was a function of buffer tube and central member diameter. Since both diameters vary due to different product offerings, a buffer tube outer diameter of 3.0 mm was used in this study to give the largest interstitial space for this product family. The central member diameter was varied from low to high as a function of tube count. The region above the tube layer was influenced by varied thicknesses of dielectric strength members and ripcords. As cable diameter increased, so did the effective area for ingress.

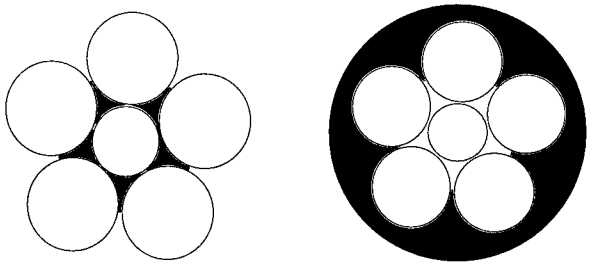


Figure 1: Water passage areas (in black) between central member and buffer tubes (left) and between buffer tubes and jacket or armor (right)

In high-density cables, a third pathway consists of the space between the two layers of buffer tubes (Figure 2). Again, this area was radially maximized by the use of 3.0 mm tubes in both layers and varied in circumference by the number of tubes.

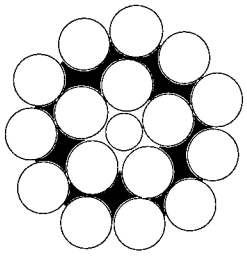


Figure 2: Water passage area (in black) between inner and outer buffer tube rows in dual layer construction

The use of superabsorbent polymers (SAP) for this application was an ideal match. SAPs such as salts of polyacrylic acids have been in use for many years in other industries. They are well characterized and very effective in water absorption. SAPs can be used in different forms and employed with a variety of substrates.

Superabsorbent polymers were analyzed according to swell rate, swell capacity and gel strength. Gel strength of the SAP was selected to be that able to retain blocking ability under expected levels of water pressure in the cable. After a careful study of SAP grades and performance levels, certain materials were selected for further consideration. These included SAPs bound in forms of tensile and non-tensile yarns, binders, tapes and powder. Combinations of these forms and methods of application were investigated in a series of designed experiments to produce a robust, repeatable design which met original goals.[4]

Duct Cable Designs

Alternate Designs

This section describes investigations of different water-blocking approaches aimed at optimizing the non-flooded cable core. Though conducted with duct constructions, this optimized core would also be used as a foundation for armored designs.

Original design criteria for Siecor's Mini Bundle Dry duct cable were covered in a previous article.[4] The outcome of this was a design which employed water swellable yarns placed along the central member and a water swellable tape wrap outside the buffer tubes in a single layer cable (Figure 3). A dual layer design uses a second tape wrap outside the outer buffer tube row (Figure 4). Through statistically designed experiments, this construction proved to be quite robust and repeatable in exceeding industry requirements for water penetration.

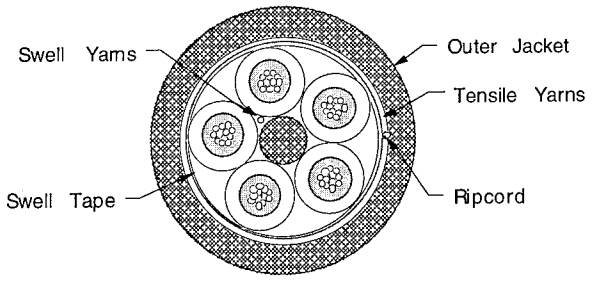


Figure 3: 5 position duct Mini Bundle Dry cable cross-section

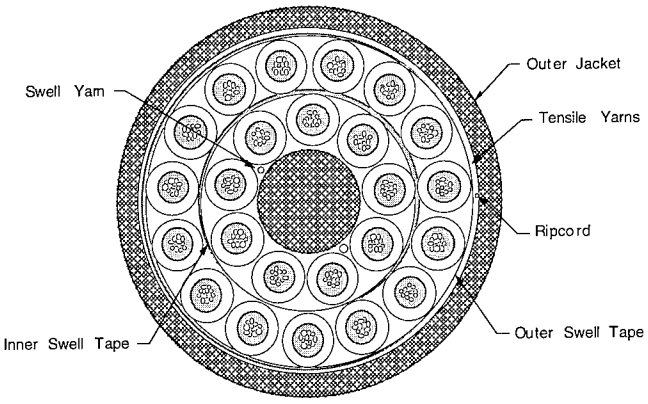


Figure 4: 24 position dual layer duct Mini Bundle Dry cable cross-section

Alternate constructions were developed and examined against the tape-yarns design. In each construction, single layer duct cables were produced consisting of 5 and 16 tubes to examine a low and high level of ingress area. The primary measure of comparison was a water penetration test consisting of the cross-section of a one meter section of cable exposed to a one meter head of tap water. The cable samples were exposed for 24 hours, then removed from testing and dissected. Water ingress was measured along various cable components.

It is worth noting here that all water penetration tests performed in the development of this cable were conducted with instantaneous exposure to the one meter head. Testing has shown that the ingress distance in dry water swell cables decreases by a factor of three as the transition time to full pressure increases from zero to ten minutes.[5] There is a high probability that a cable in field service subjected to water pressure would be exposed gradually to a buildup in water level. The water penetration results reported in this paper represent the most severe application of this test and as such, help to identify relevant variables affecting performance.

The first of these alternate constructions involved the application of SAP directly to cable components. It was required that the powder adhere to the cable and not be allowed to fall freely during cable stripping. Two methods were employed to bind the powder, the first being a prewet system which used an intermediate agent to increase the affinity of the powder to a substrate. The second was the use of a thin film of water-soluble hot melt adhesive. The use of a water-soluble adhesive allowed a greater utilization of SAP swell capacity. Standard adhesives partly encapsulate the swell particles resulting in reduced absorbency.

With both methods, a thin coating of SAP was attached to the central member and to the outside of the cable buffer tube core (the first method is designated in Table 1 as Design 1). A standard commercially-available grade of swell powder identified in the above investigation was used with a particle size range from 1 - 300 μm. Subsequent processing and handling did not cause a loss of powder from the core though the coating could be removed with light wiping action.

The second construction employed a combination of swell yarns and swellable binders (designated in Table 1 as Design 2). As described above, one or more swell yarns were placed along the central member. The buffer tubes were helically stranded over this element and secured with two swellable binders counter-wrapped

to each other. This formed a cell grid pattern over the buffer tube core. Tensile yarn walls were then wrapped over this core and the cable was jacketed as a duct design.

The last alternate core construction used a combination of standard swell yarns and swellable tensile yarns (designated in Table 1 as Design 3). The standard yarns were placed beside the central member under the buffer tubes. Above the stranded buffer tubes, swellable tensile elements were helically wrapped. These elements were comprised of fiberglass yarns impregnated with a swellable matrix. The number of impregnated yarns employed was dictated by the amount needed to give equivalent tensile performance to our standard dry design. Thus, depending on cable size, a varying number of these swell tensile members were needed for a 2700 N rating.

Alternate Designs - Water Penetration Results and Conclusions

Samples of the different core constructions were tested for water penetration in accordance with FOTP-82. A one meter static head pressure was applied at one end of a one meter length of cable for 24 hours. After testing the samples, they were dissected and the length of water ingress was measured along two different sections in the cable: central member and outer core. These responses were identified in order to determine the location and length that the water was able to penetrate along the test sample. Previous work during our original dry design showed that these areas were representative of maximum water penetration in a duct loose tube cable[4]. To identify which designs had the greatest effect on penetration performance, we employed statistical techniques through the application of F-ratio tests. The constructions were evaluated per the following criteria:

1) the mean water penetration distance (X) of 20 samples randomly cut from a 500 m length of cable,
2) the magnitude of the standard deviation (σ) for these samples, and
3) the ease of stripping and installation methods.

In Table 1, water penetration results for the alternate designs have been normalized against the central member distance mean value (center) of the 5 position single layer Mini Bundle Dry cable. For example, if the center water penetration length average of the 5 position Mini Bundle Dry was 88 cm, then the outer core distance mean of 16 position Design 2 cable would be 203 cm (88 cm x 2.31).

5 Position Single Layer Cable

	Mini Bundle Dry		Design 1		Design 2		Design 3	
	Center	Outer Core	Center	Outer Core	Center	Outer Core	Center	Outer Core
X	1.00	1.01	1.62	1.67	1.37	1.45	1.07	1.12
σ	0.05	0.05	0.34	0.37	0.29	0.24	0.15	0.11

16 Position Single Layer Cable

	Mini Bundle Dry		Design 1		Design 2		Design 3	
	Center	Outer Core	Center	Outer Core	Center	Outer Core	Center	Outer Core
X	1.18	1.03	1.52	1.86	1.87	2.31	2.15	2.06
σ	0.13	0.09	0.41	0.59	0.44	0.65	0.33	0.47

Table 1: Normalized Water Penetration Values for Alternate Duct Constructions

Tukey's statistical comparison of means clearly showed a difference between the constructions, with swellable tapes and yarns giving the lowest ingress values.

All designs fared well in stripping exercises to access a 3 m length of buffer tubes. Designs 2 and 3 exhibited potential problems where polyolefin filler rods were used to replace standard buffer tubes in the cable core. If the tensile yarn wall did not provide complete coverage of the core, the extruded outer PE jacket would melt and bond to exposed filler rods making removal of the jacket very difficult. The swell tape wrap over the cable core in the Mini Bundle Dry design protects the tubes and rods from this jacket bonding.

Aged Sample Water Penetration Performance

Five position single layer and 24 position dual layer dry duct cables were subjected to temperature cycling and aging environments described in Table 2. The aging period occurred after two of the four temperature cycles followed by the final two cycles. Twenty samples of one meter length from each cable were then exposed to a one meter head of tap water for 48 hours. Measurements from different ingress areas were compared to unaged results for determining change in water penetration performance.

Statistical ANOVA comparisons did not show a difference between aged and unaged measurements at a 95% confidence level. This supports the idea that the majority of water penetration occurs at the initial exposure to water pressure and that once a gel block has formed, ingress stops.

Unaged 5 and 24 position duct cable samples were subjected to a water penetration test of three weeks with a one meter head. Again, there was no statistical difference between 24 hours ingress values and those measured after 21 days.

Armored Cable Designs

A dry core armored cable was developed as an extension of the Mini Bundle Dry portfolio. It was desired to retain the same core as that designed for the duct version, so concentration was focused on components outside of the tensile yarn wall. Performance levels were expected to be the same or better than Siecor's standard flooded loose tube armored cable.

To take further advantage of the dry cable's weight savings and simplicity, one version eliminated an inner jacket between the tensile yarn wall and the armor wrap (Figure 5). This would allow the swell tape to provide water blockage in areas between the tensile yarns and the armor. The inner jacket elimination provided a decrease in final cable diameter (OD) of 1-2 mm. This equated to a 12% drop in armored cable OD for fiber counts up to 36.

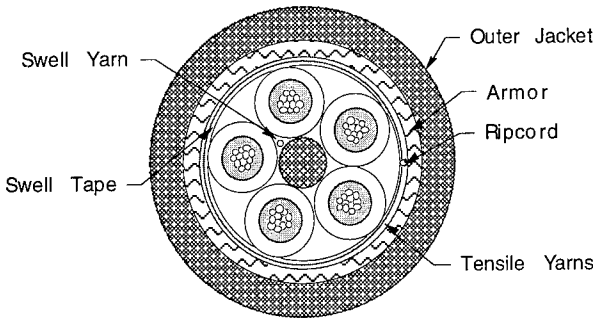


Figure 5: 5 position armored Mini Bundle Dry cable cross-section (no inner jacket)

Another version incorporated the use of an inner jacket between the core and armor (Figure 6). Unfortunately, an additional water path was created in this interface.

To solve this, a water swell tape was wrapped over the inner jacket. Armor tape was then formed over this layer and a final outer jacket was extruded over the cable.

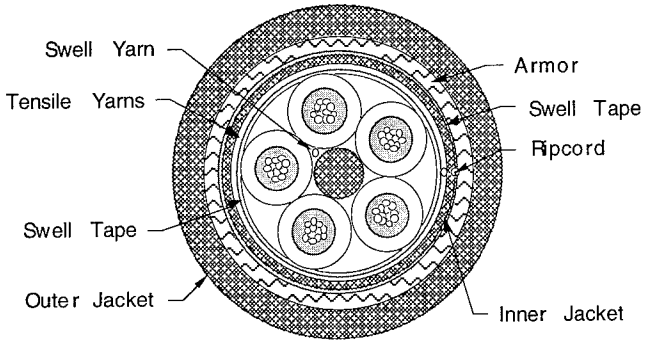


Figure 6: 5 position armored Mini Bundle Dry cable cross-section (with inner jacket)

Cable Performance: Analytical Treatment

The tensile and contraction performance of the armored dry cable can be calculated to predict empirical results. Using equations (1) and (2) published by Horska, one can derive contraction (ε_c) and tensile (ε_T) windows for the loose tube cable core.[6]

$$\varepsilon_c = 1 - \sqrt{1 - \frac{\pi^2}{P_o^2}(D_{BT} - D_{FB})(2D + D_{BT} - D_{FB})} \quad (1)$$

$$\varepsilon_T = \sqrt{1 + \frac{\pi^2}{P_o^2}(D_{BT} - D_{FB})(2D - D_{BT} + D_{FB})} \quad (2)$$

where P_0 = Initial Buffer Tube Pitch
D_{BT} = Buffer Tube Inner Diameter
D_{FB} = Effective Fiber Bundle Diameter
D = Centerline Distance Between Buffer Tube Axes

These equations assume that the fiber bundle is hexagonal close packed to obtain maximum fiber density for this diameter.

Cable shrinkage can be found from the effective coefficient of thermal expansion ($\alpha_{Eff}(T)$) in equation (3).[7]

$$\alpha_{Eff}(T) = \frac{\sum_{i=1}^{n} A_i(T) E_i(T) \alpha_i(T)}{\sum_{i=1} A_i(T) E_i(T)} \quad (3)$$

where T = Temperature
$A_i(T)$ = Initial Buffer Tube Pitch
$E_i(T)$ = Buffer Tube Inner Diameter
$\alpha_i(T)$ = Effective Fiber Bundle Diameter

For this equation, we must assume a composite cable model with full coupling factors between cable components. Dry core cables have a good correlation of this assumption. Gravely and Stokes showed that coupling forces between buffer tubes and central member in dry core loose tube cables were five times higher than flooded cables.[8]

The cold temperature performance can be deduced by comparing the contraction window with the calculated cable shrinkage. The difference between the two equates to a level of micro and/or macrobending of the fibers which results in attenuation change.

A tensile profile of the cable can also be deduced from the composite cable model mentioned above. By assuming contributions from different tensile members in the cable, one can estimate the amount of cable strain at various loads.

From the presence of higher coupling forces, it is surmised that dry core cables will also exhibit improved tensile performance. The increased coupling forces equate to lower slippage between components under tensile loads. In effect, allowances made for construction stretch in stress-strain plots can be reduced. Given equivalent cabled excess fiber lengths (EFLs), higher installation loads are realized before fiber strain is observed in the dry cable.

Cable Performance: Armored Testing Results

Developmental armored cables with and without inner jackets in 6 position single layer and 24 position dual layer constructions were produced and evaluated for optical, mechanical and environmental performance. All cables contained standard single-mode fibers. Tests were chosen to subject the cable to rigors beyond what would be found under typical use. Testing criteria and corresponding results are summarized in Tables 2 and 3. Similar data for dry duct cables was reported in an earlier paper.[4] Attenuation results include a 0.05 dB or 0.05 dB/km allowance for measurement repeatability. Environmental and mechanical performance of the Mini Bundle Dry cable in both duct and armored versions is equivalent to or better than their flooded counterparts.

Test	Results	Method
Temperature Cycling* (-40° to +70°C, 4 cycles)	Average Δ <0.05 dB/km Maximum Δ <0.15 dB/km	FOTP-3
Cable Aging* (85°C, 168 hours)	Average Δ <0.10 dB/km Maximum Δ <0.25 dB/km	FOTP-3
Cable Freezing*	Average Δ <0.10 dB/km Maximum Δ <0.25 dB/km	FOTP-98
Water Penetration	No water leakage (1m/1m: 24 hours-unaged, 1 hour-aged)	FOTP-82
Resistance to Fungus Growth	Grade 0 - 0% growth	ASTM G-21
Filling Compound Flow (80°C)	No compound flow	FOTP-81
Material Compatibility	Buffer tube elongation >10% (45 days in 85°C water)	ASTM D2105

* Note: Attenuation measurements at 1550 nm

Table 2: Environmental test results of armored Mini Bundle Dry cable

Test	Results*	Method
High Temperature Bend (60°C, 4 turns)	90% of fibers <0.05 dB Δ Remaining 10% <0.15 dB Δ	FOTP-37
Low Temperature Bend (-30°C, 4 turns)	90% of fibers <0.05 dB Δ Remaining 10% <0.15 dB Δ	FOTP-37
Impact (25 cycles)	90% of fibers <0.05 dB Δ Remaining 10% <0.15 dB Δ	FOTP-25
Compression (440 N/cm)	90% of fibers <0.05 dB Δ Remaining 10% <0.15 dB Δ	FOTP-41
Tensile Strength (2700 N)	90% of fibers <0.05 dB Δ Remaining 10% <0.15 dB Δ	FOTP-33
Cable Twist (2m - 2 twists)	90% of fibers <0.05 dB Δ Remaining 10% <0.15 dB Δ	FOTP-85
Cyclic Flex (25 cycles)	90% of fibers <0.05 dB Δ Remaining 10% <0.15 dB Δ	FOTP-104

* Note: Attenuation measurements at 1550 nm

Table 3: Mechanical test results of armored Mini Bundle Dry cable

Dry Core Armored Water Penetration Performance

Unaged dry core armored cables with and without inner jackets were extensively tested for water penetration. The test method was the same as that used with the alternate duct constructions. Cables were produced with both armor variants in 6 position single layer and 24 position dual layer configurations. Thirty samples of each cable were randomly cut from a 500 m length. The samples were exposed to water pressure for 24 hours and subsequently dissected. Water ingress was measured along the central member and under the armor in cables without an inner jacket. With inner jacketed cables, the measurements were made between the inner jacket and the armor. Ingress below the inner jacket was not studied since this reflected the same construction as a duct cable.

Table 4 shows comparative results for water penetration testing between the two armored cable types. Results were normalized against the lowest mean distance observed (X = 1.00). All cables were within a one meter industry requirement for water ingress. Those cables with no inner jacket displayed similar numbers to duct versions.

6 Position Armored Cable

	No Inner Jacket		Inner Jacket
	Center	Under Armor	Inner Jacket - Armor Space
X	1.82	1.86	1.00
σ	0.10	0.16	0.29

24 Position Armored Cable

	No Inner Jacket		Inner Jacket
	Center	Under Armor	Inner Jacket - Armor Space
X	1.98	2.19	1.10
σ	0.24	0.19	0.32

Table 4: Mini Bundle Dry armored cable water penetration testing results (cm)

Materials Characterization

Other cable performance aspects were tested. The reliability of swellable materials was investigated in terms of aging and water blocking performance in ionic, acidic and basic solutions.

Aging Performance

Long term reliability of the cable components is of primary importance in the fiber optic industry, where cables are commonly expected to have lifetimes in excess of 20 years while exposed to many possible combinations of temperature and humidity. The water swell tape and yarn selected for this cable were aged at 80°, 100° and 120°C in uncontrolled humidity for 1, 2 and 3 weeks. For the tape samples, swell height was measured in mm. For the yarn samples, swellability was measured in grams of absorbed water per meter of yarn (g/m). Each data point presented in Figures 7 through 10 is the average of 5 measurements. The average standard deviation is 0.5 mm for the tape swell height and 0.15 g/m for the yarn. Performance after aging, monitored in distilled and tap water, is represented in the following graphs:

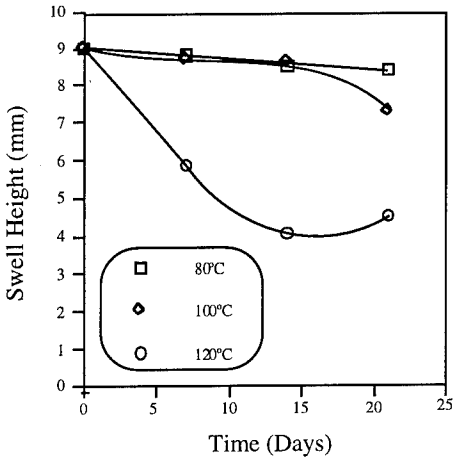


Figure 7: Tape swell height in distilled water as a function of aging time at three temperatures

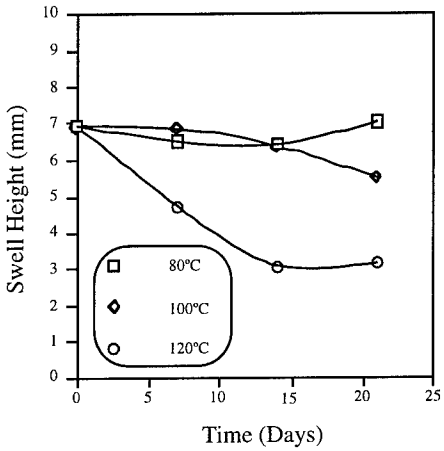


Figure 8: Tape swell height in tap water as a function of aging time at three temperatures

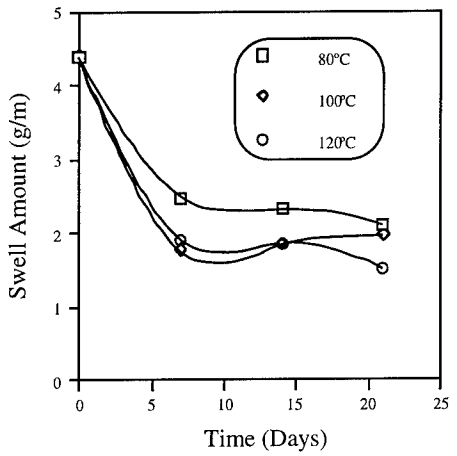


Figure 9: Yarn swell amount in distilled water as a function of aging time at three temperatures

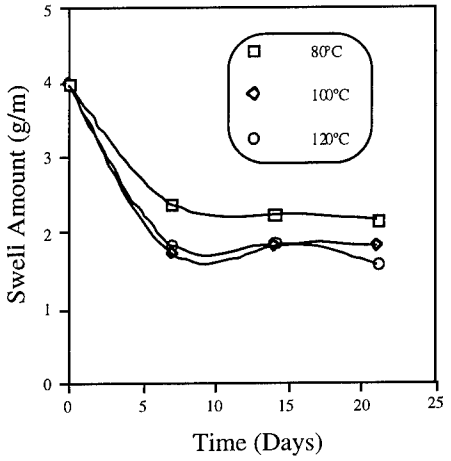


Figure 10: Yarn swell amount in tap water as a function of aging time at three temperatures

From these graphs, the following conclusions were reached:

1. Swell tape:
   - The same trends in aging behavior occur whether distilled or tap water is used.
   - At 80°C, no significant degradation of swell performance is observed.
   - At 100°C, a small decrease in swell performance can be seen after 3 weeks.
   - After 3 weeks at 120°C, the water absorbency is reduced in half, but reaches a plateau.

2. Swell yarn:
   - Again, the same trends in aging behavior occur whether distilled or tap water is used.
   - A significant drop in swell performance is seen after one week at all 3 temperatures.
   - After the initial drop, swell performance levels out.

In summary, the swell tape showed very good aging behavior at 80° and 100°C. The yarn exhibited a quick decrease in swell performance after one week, but its swell performance did not degrade upon subsequent aging.

Additionally, the tape swell rate was monitored because of its direct impact on the cable water penetration performance. A tape which would have a slower rate of swelling may not effectively water block the cable. After aging at 80° and 100°C, the swell rates were equivalent to the one observed at room temperature, where 70% of the swell height was reached within the first minute. However the rates after aging at 120°C were significantly slower.

Ionic Water Effects

FOTP-82 testing for water penetration employs tap water. However, in the field where the cable can be submerged in ground water, ions are present in different concentrations. It is known that ionic solutions can have negative effects on the swellability of SAP. The following testing was conducted to evaluate the effect of the interaction between water swell materials and typical ground waters.

The SAP used in the tape and yarn is a sodium salt based polyacrylic copolymer. Each polymer chain is lined with carboxyl groups (COOH). In water, the carboxyl groups solvate and dissociate into negatively charged carboxylate groups (COO^-).

The repulsion between these negatively charged ions enables absorption of water around the polymer chains and loosening of the polymer coil. Water absorption will decrease with two factors:

(1) the ionic concentration of the water
(2) the molecular crosslinking degree of the polymer.

Water swell performance depends on the ionic density difference and varies in proportion to the osmotic pressure. Hydrogen bonding drives the water absorption mechanism. When the water contains positive ions, these ions position themselves next to the carboxylate ions, thus limiting the swelling and absorbency capacity of the SAP. This explains why distilled deionized water swells the superabsorbent more than tap water which is already slightly ionized. This also explains why swell performance decreases with increasingly ionic water.

Highly crosslinked polymers exhibit lower swell capacity. In the case of a given water swell tape, the crosslinking level is fixed.

In the following study, we investigated the effect of ionic solutions on the swellability of the water swellable tape and yarn selected for the Mini Bundle Dry design. The effect of ionic solutions on the swellability, and thus on the cable water penetration performance, was examined in the case of various monovalent ions (Na^+, K^+) and polyvalent ions (Ca^{2+}, Mg^{2+}, Al^{3+}, Fe^{2+}, Fe^{3+}). Polyvalent ions were expected to have the greatest effect on water absorbency. For example, Ca^{2+} ions will come in contact with twice as many carboxylate ions compared to a monovalent ion like potassium (K^+). Concentrations of these ions vary greatly depending on the geographical location. Typical ground water concentrations were gathered from different reference books on water chemistry.[9,10,11] In particular, cumulative curves displayed in Aquatic Chemistry[11] showed the frequency distribution of ions in ground and surface water. We tested each ion at its 80th percentile concentration, which gave the levels stated in Table 5.

Ion Type	Na	K	Ca	Mg	Al	Fe
Concentration, ppm	100	10	50	50	1	5
Solutions used	NaCl Na_2SO_4	KCl K_2SO_4	$CaCl_2$ $CaCO_3$	$MgCl_2$ $Mg(NO_3)_2$	$AlCl_3$	$FeSO_4$ $Fe(NO_3)_3$

Table 5: Concentration of ions used in study of swell properties

Four compounds were dissolved in very dilute (≤0.1% concentration) acidic solutions: $AlCl_3$, $Fe(NO_3)_3$, $CaCO_3$ and $Mg(NO_3)_2$. These compounds are not soluble in water with a pH = 7. Deionized ultra filtered water was used for the dilutions to insure that no additional ions were introduced. For each ion except aluminum and iron, two solutions were used in order to investigate a possible interaction of the anion (negative ion) on the swellability.

The swell height for the tape and swell amount for the yarn were recorded using the same method as the one previously used in the aging study. Results are displayed in Figure 11. The following conclusions may be reached:

- A very good correlation between the swell performance of yarn and tape may be observed, which confirms that the SAPs chemically react regardless of form.
- It appears that the monovalent ions (Na+, K+) have the same effect on the swellability despite the anion type (Cl^-, SO_4^{2-}).
- With polyvalent cations (Ca^{2+}, Mg^{2+}, Fe^{2+}, Fe^{3+}) however, it appears that the anion type affects the swellability. In the most extreme case, the tape swell height drops from 7.1 to 2.8 mm if we switch from $MgCl_2$ to $Mg(NO_3)_2$.

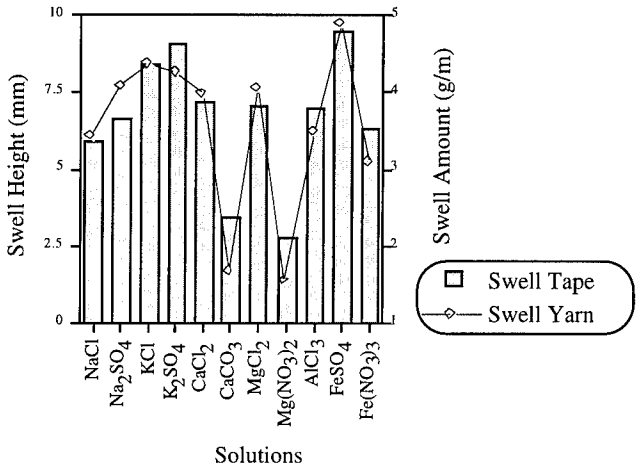


Figure 11: Tape and yarn swellability as a function of ionic solution exposure

In subsequent testing, we subjected the tape to a mixture of $MgCl_2$ and $Fe(NO_3)_2$ to check if the Mg^{2+} cation and NO_3^{-1} anion from different molecules would give the same results as the single solution $Mg(NO_3)_2$. The tape swelled to 2.7 mm. This result is similar to the swell height of 2.75 mm obtained with a solution of $Mg(NO_3)_2$. This leads us to conclude that in the case of polyvalent ions, swellability of SAP may be predicted if we know not only which positive ions but also which negative ions are present in the ground water of interest.

Finally, testing was performed to determine additivity levels of ions found in a typical ground water. To simulate this condition, single solutions using the preset concentrations displayed in Table 5 were mixed together. The substances used were NaCl, KCl, $CaCl_2$, $MgCl_2$, $AlCl_3$ and $FeSO_4$. This swell tape and finished cable samples were subjected to this mixture. If the ion effects were fully additive, the tape swell height should have measured between 0.0 - 1.0 mm. The actual tape swell height was recorded at 4.7 mm. This showed that the mixture of solutions found in a groundwater had less of an effect on swell performance than expected from an additive model. Interactions between ion groups in groundwater and other phenomena serve to alleviate ionic affinity for the swell tape's carboxyl groups. This solution was also used to perform FOTP 82 water penetration testing on duct and armored versions of the cable presented in this paper. All cables passed the one meter requirement.

The last part of the testing was aimed at determining the effect of a basic or acidic water on the tape swellability. In the field, water pH may vary from 4 for acidic water to 10 for basic water. NaOH and HCL solutions were used with respective pH levels of 10 and 4. Tape swell levels are displayed in Table 6.

Solutions	pH	Tape Swell Height Average, mm	σ
Deionized water	7	9.1	0.2
NaOH	10	5.4	0.1
HCl	4	5.5	0.1

Table 6: Tape swell height as a function of water pH

These results demonstrate that the tape performance decreases when the water pH deviates from 7. However, when tested with these acidic or basic waters, all cables passed the one meter requirement.

Conclusions

A dry core loose tube cable without flooding compound outside the buffer tubes has been developed in duct and armored versions. Several alternate methods for dry waterblocking of the cable core were tested and compared to a swellable tape and yarn construction. The tape version showed better performance in water penetration testing and deviations of ingress length than other methods evaluated.

Armored dry cable constructions were designed both with and without inner jackets under the armor. Cables of high and low fiber counts were tested to a variety of industry standard requirements for mechanical and environmental performance. All specifications were met or exceeded.

A study was conducted to characterize the performance of the dry swellable materials after aging and after being subjected to different groundwater solutions. Swell performance was acceptable when aged at temperatures below 100°C. Though some degradation of the swell performance was observed with certain ionic concentrations, the cable's ability to block water ingress within one meter was not compromised.

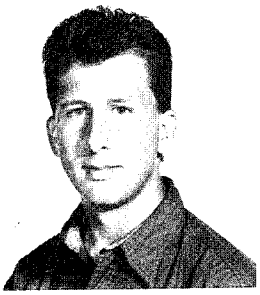
These results, along with excellent performance in all other areas, gives a cable family which is cleaner, craft-friendly and applicable for aerial, duct or buried service.

Acknowledgements

The authors wish to thank everyone involved in the development of Mini Bundle Dry cable. Special thanks go out to Mari Letterman, Larry Barrett and Wesley Nicholson for their hard work in obtaining results for this paper.

References

[1] S. Kukita, T. Nakai, A. Hayashi and H. Koga: "A New Nonmetallic and Waterproof Optical Fiber Cable with Absorbent Polymer Ribbon", Proceedings of the 36th International Wire and Cable Symposium, pp. 357-371, 1987.
[2] M. Fukuma, N. Akasaka, S. Suzuki: "Dry Type Water-Blocking Optical Fiber Tape Cable with Slotted Rod", Proceedings of the 36th International Wire and Cable Symposium, pp. 350-356, 1987.
[3] H. Hiramatsu, N. Ishii and K. Nagai, "Development of Dry-Type Water-Blocking Optical Fiber Cable Using Swelling Material", Proceedings of the 38th International Wire and Cable Symposium, pp. 463-467, 1989.
[4] A. Bringuier and C. Clyburn, III: "Development of a Loose Tube Cable With Non-Flooded Core For Outdoor Plant Environment", Proceedings of the Eleventh Annual National Fiber Optic Engineers Conference, pp. 376 - 386, June 1995.
[5] W. McCallum, Personal Communication.
[6] J. Horska: "Design of Loose Tube Fiber Optic Cable with Adjusted Contraction and Strain Windows", Proceedings of the 43rd International Wire and Cable Symposium, pp. 50 - 58, 1994.
[7] S. Cooper, K. Coupe and B. Zimmerman: "The Effect of Temperature Dependent Materials Properties on Fiber Optic Cable Design", Proceedings of the 35th International Wire and Cable Symposium, pp. 148 - 158, 1986.
[8] R. Gravely III and S. Stokes: "An Improved Loose Tube Cable with Dry Water Blocking Elements", Proceedings of the Eleventh Annual National Fiber Optic Engineers Conference, pp. 367 - 375, June 1995.
[9] J. Hem, "Study and Interpretation of the Chemical Characteristics of Natural Water", Third Edition, U.S. Geological Survey Water-Supply Paper 2254.
[10] F. van der Leeden, F. Troise, D. Todd, "The Water Encyclopedia", Second Edition, Lewis Publishers.
[11] W. Stumm, J. Morgan, "Aquatic Chemistry, An Introduction Emphasizing Chemical Equilibria in Natural Waters", John Wiley & Sons, NY, 1981.



Clinton E. Clyburn III
Siecor Corporation
PO Box 489
Hickory, NC 28603
USA

Clinton E. Clyburn III (Kip) received a B.S. degree in Mechanical Engineering in 1991 and a M.S. in Materials Engineering in 1993 from North Carolina State University. Having earlier service with Raychem Corporation and Alcatel Cable Systems, he joined Siecor Corporation in 1993. He has worked with a variety of design and development projects in cables, materials and testing as well as cable characterization. Mr. Clyburn currently serves as Product Development Engineer in the Research, Development and Engineering Department.



Anne G. Bringuier
Siecor Corporation
PO Box 489
Hickory, NC 28603
USA

Anne G. Bringuier received an Engineering degree in Materials Science and Engineering from the Institut National Des Sciences Appliquees (INSA) in Lyon, France, an "Advanced Studies Diploma (DEA)" in Macromolecular Science from the University of Lyon in 1985 and a M.S. in Polymer Science from Pennsylvania State University in 1987. She worked at Raychem Corporation from 1987 to 1993 in the area of telecommunication closures. In 1993, she joined Siecor Corporation where she has been involved with materials selection and design activities for optical fiber cables. She is currently a Senior Materials Engineer in the Research, Development, and Engineering Department.

ULTRA-THIN OPTICAL FIBER RIBBON AND 108-FIBER LOOSE TUBE RIBBON-BASED CABLE

Gao xiang-ping Shen guo-xun
Yao bo-sheng Dai yu-dong

Shanghai Electrical Cable Research Institute (SECRI), China

ABSTRACT

In this paper, the structures and characteristics of ultra-thin optical fiber ribbon and 108-fiber loose tube ribbon-based cable will be presented. The feasibility of the using normal commercial fiber whose coating is 250 μm in diameter to manufacture the 260 μm height ultra-thin ribbon and cable is demonstrated. The analystical and experimental results of this investigation have indicated that the ribbon and cable can provide good geometrical, optical, physical, and mechanical performances and it is easy to fusion splice. The ultra-thin fiber ribbon was successfully used in a 108-fiber loose tube cable.

1. INTRODUCTION

In recent years, fiber ribbon and ribbon-based cables have been developed widely and rapidly over the world. The outstanding features of ribbon-based cable makes the following facts possible :

.high fibercount while retaining compact and small dimensions;
.easy to identisfication of individual fiber for high fiber count cable;
.convenient and rapidly mass splice and individual fiber breakout and splice;
.small size joint case and closure .

All these features are very important for high fiber-count, high-speed, broadband telecommunication networks with obvious economic benifite.

In China, the development of fiber ribbon and ribbon cable is just started. Some equipments and technology have been imported. SECRI has developed the ultra-thin fiber ribbon and ribbon-based cables by its own's equipments and technology. In this paper, some results will be described.

2. RIBBON STRUCTURE

Optimization of ribbon stucture for performance, reliability and economic is very important. Up to now, there are two kinds of ribbon structure: edge-bonded and encapsulated. In light of manufacture process, it is possible for edge-bonded stucture with one layer ribbon matrix material and it may be difficult for encapsulate structure. Using one layer, it is possible to reduce the thickness of ribbon (by 2/3) and save materials (by 1/3) and simplify the working procedures. Which kind of ribbon is suitable for making cable, shall depend on the structure of cables, but the key factors is also that the ribbon has excellent geometical, optical, physical and mechanical performances. Under the same conditions, choosing of the thinner ribbon is the best way.

There are two ways to reduce the thickness of ribbon: reduce the thinkness of matrix (use the normal primary coating fiber in 250 μm diameter) or reduce the thickness of primary coting (as it being made in Japan, the diameter is 160 μm). The first way is convenient for production, because it does not need special fiber, also, thicker primary coating is useful to prevente ribbon from mechanical damage in the production. consequently, we chooced the first way for our investigate.

The fibers used for manufacturing ribbon are normal commercial fibers including Corning's fiber, Gold-star's fiber and Chinese local fibers

The matrix material was made by SECRI. We think there are two points for matrix:

(1). higher young's modulus insure the mechanical performance of ultra-thin ribbon is necessary, meantime, higher modulus is useful to processes stability and reduce the friction coefficient of ribbon surface, which is very important for tubbing and cabling.

(2). In order to convienently breakout ribbon into individual fiber, the matrix's ingre-

dient must be some difference from fiber's coating or ink.

3. CABLE STRUCTURE

Loose tube stranding structure is that the loose tubes are stranded around a centre reinforce member. Comparing it with other structures, the obvious advantage is that the excess length of fiber in a cable can be controlled by the control of the fiber's excess length in the tube and by the design of the cable st-ructure and lay pitch in the cable. Therefore, they have excellent high-low temperature performance and ability to against tension force.

This structure was choosed for investigation.

The cable structure is shown in FIG. (1). the cable consist of 6-tube in which there are 5-ribbon with 4-fiber, the diameter of cable is less than 17.5mm. In fact, 120-fiber can be involved within it .

Jelly-filled secondary coating tube was made by PBT. The outer diameter is 3.6mm and th-ickness is 0.4 mm for tube .

The lay pitch of cabling is 350 mm, it must be match to the excess length of the ribbon in the tube.

4. RESULTS AND DISCUSIONS

The test results for a batch of ultra-thin fiber ribbon and the 108-fiber cable sample as follows:

The size, attenuation temperature performance, anti-macrobent, machanical performance and splice are shown in table(1), (2), (3), (4), (5), (6), (7).

1). RIBBON PERFORMANCES

All of the ribbons have excellent performance: the geometrical sizes of ribbons are all corre- sponding to IEC .The average height of the ribbons is only 258 μm and the maximum is 268 μm, That is very useful to making the high-count fiber cable, Because of the good machinical and anti-microbent performances for the 250 μm coating diameter fiber, there are not any damage to the fibers in the typping and to the ribbons in the machinical testing.

The average attenuation and maximum attenuation of fibers in the ribbons is 0.36dB/km, 0.39 dB/km at 1310nm wavelength and 0.20dB/km 0.22dB/km at 1550nm wavelength individually.

The average and maximum value of the excess attenuation in the working processes is le-ss than 0.005 dB/km and 0.04 dB/km individua lly, for both at 1310nm and 1550nm wavelength.

In temperature range of the −40∼ +60℃ , the average value and maximum value of attenuations is 0.02dB/km and 0.07dB/km for 1310nm individually, and 0.05 dB/km and 0.10 dB/km for 1550nm individually.

Anti-macrobent performance of the ribbon is also excellent. the excess attenuation of the ribbon wrapied around a mandral in 45 mm diameter can not be obvioused for both at 1310 nm and 1550 nm wavelength.

That is also convienent for the ribbons to fusion splice. All of the ribbons can be splice according to the normal processes by the commercial ribbon splicing machine.

After ten months, the excess loss can not be observered for the ribbon which was immersed in jelly. It is shown in FIG. (2) .

2). CABLE PERFORMANCE

The performance of 108-fiber loose tube cab-le using above ultra-thin ribbon is also exc-ellent . the average value of attenuations is 0.36 dB/km for 1310nm and 0.20 dB/km for 1550 nm. the average and maximum value of the excess attenuation are less than 0.02 dB/km and 0.04 dB/km in both 1310 nm and 1550 nm wavelength in the all of working processes. FIG (3).

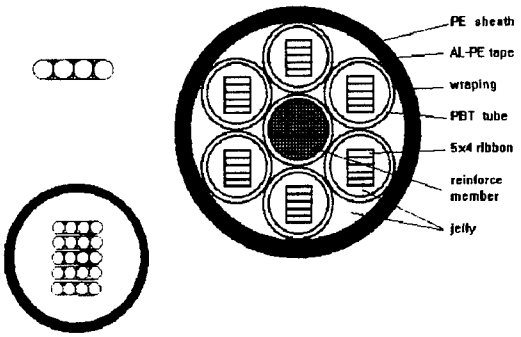
The cable have good temperature, machanical and envirement performances, it can be installated in the duct, tunnel and airal.

3). For the 4-fiber ribbon, in this cable, wether or not the ribbon was twisted in tube, no any obvious difference in fiber's attenuation can be found out. The reasons are that the ultra-thin ribbon's dimensions match the tube's dimensions, and the excess length of ribbon in tube are suitable to the lay pitch of cable, so that the ribbon can move freely and keep located in a minimum stress condition in the tube.

5. CONCLUSION

Using normal commercial fiber in 250 μm diameter to manufacture the ultra-thin ribbon which is less than 260 μm thinkness, it is that not only the ribbon matrix and cable materials can be saved , but also makes the production convienent and cable dimension reduce. The test results indicate that both ribbons and cable has excellent performances for manu-facture, splice and use. That is a good way to manufacture the ultra-thin ribbon and high-count fiber cable.

6. ACKNOWDGEMENT



FIG(j). 108-fiber cable

table (1) structure of 4-fiber ribbon

	width	thickness	fiber alignment		
			orizontal separation		planarity
			djacent	extreme	
	μm	μm	μm	μm	μm
average	1023	256	255	750	<30
maximum	1055	268	269	767	48

table (2) chareactristicsof ribbon

item	condition	result
	on the reel	
transmission loss	wavelength 1310 nm 1550 nm	 ave. 0.36 dB/km max. 0.38 dB/km ave. 0.20 dB/km max.0.22 dB/km
temperature performance	-40~ +60℃ wavelength 1310 nm 1550 nm	excess loss ave. 0.02 dB/km max.0.07 dB/km ave. 0.05 dB/km max. 0.10 dB/km

table (3) machinical prformance of ribbon

item	condition	result
lateral pressure	250 N/50 mm	excess loss <0.0 dB
twist	15 times/1000mm 3N	no break for fiber no breakout for ribbon
friction	3 N Φ6 mm 50 times	no break for fiber no breakout for ribbon

table (4) characteristics of cable

item	condition	result
	on reel	
transmission loss	wavelength 1310 nm 1550 nm	ave. 0.36 dB/km max. 0.38 dB/km ave. 0.20 dB/km max. 0.22 dB/km
temperature performance	-40℃~ +60℃ 1310 nm 1550 nm	excess loss ave. 0.015 dB/km max. 0.05 dB/km ave. 0.025 dB/km max. 0.07 dB/km

table (5) machinical performance of cable

test item	result
tensile 2500 N	increase in loss <0.0 dB
lateral pressure 2500 N	increas in loss <0.0 dB
bending at 350 mm radius	increase in loss <0.0 dB
twist 100 N,10 times + 180° - 180°	 increase in loss <0.0 dB

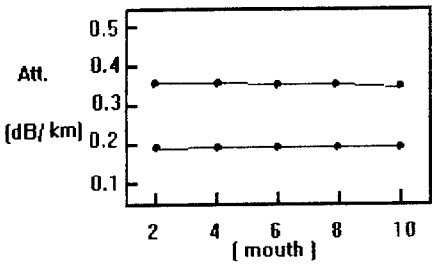


FIG.(2) Attenuation change of Ribbon in Jelly

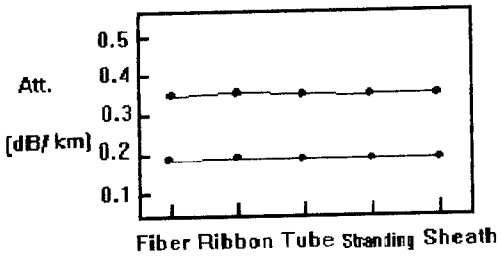


FIG.(3) Attenuation change in Cable Manufacturing Process

table (6) macrobent loss of ribbon

item	condition	result
transmission performance	Φ45 mm 100 turns wavelength 1310 nm	increase in loss < 0.0dB/km
	1550 nm	< 0.0dB/km

table (7) typical splice loss

ribbon NO.	fiber NO.	loss (dB)
SECRI 1-1 4-fiber	red-white	0.01
	yellow-natural	0.04
	natural-yellow	0.05
	white-red	0.03
SECRI-SUMITOMO* 4-FIBER	red-violet	0.05
	red-white	0.01
	natural-red	0.04
	natural-white	0.04
SECRI 5-5 8-FIBER	red-red	0.06
	natural-natural	0.05
	red-red	0.07
	natural-natural	0.04
	red-red	0.05
	natural-natural	0.06
	red-red	0.03
	natural-natural	0.03

* Sumitomo commerical 4-fiber ribbon sample

The authors thank the contributions of Gao huan, Li hui-qin, Feng hai-yun.

7. REFERENCE

1).M.SAITO, S.OKAGAWA," 16 fiber ribbon for ultra-high-density and high-count optical fiber cable".

IWCS 1993, P16-19

2). SHIGERU.TOMITA," ultra high-density optical fiber cable with thin coated fiber and multifiber connectors."

IWCS 1993, P5

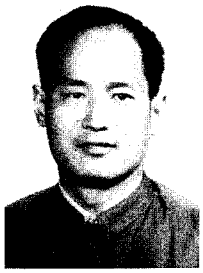
BOGRAPHY



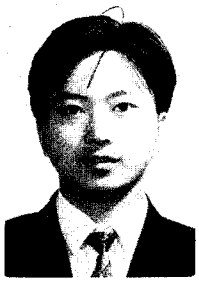
Ms. Gao xiangping
She is a senior engineer, graduated from Xian Jiaotong Univ.in 1966. and joined SECRI in the same time.She used to be engeged in rese-rach on small coaxial cable, optical fiber preform and fiber drawing process,and fiber cable manufacture. She specalizes in fiber ribbon cable and fiber sub scriber cable now.



Mr. Shen guoxun graduated from Haerbin Military Engineering Academy, in 1966.He was employed at the West-north Neauclear Technology Research institute where he worked on optical test and fiber measurement.Since joing SECRI in 1987, he has been involved in all aspect of fiber measurement and in the design of automatical fiber test equipment, as a product development senior engineer. Presently he has been engeged in the research of fiber ribbon.



Mr. Yao bosheng
He is a engineer. He used be engeged in research of optical fiber drawing tower. Since 1994,he has worked on research of ribbon machine and ribbon manufacture process.



Mr. Dai yudong
He was born in 1973. He graduated from Automatic Department of Yanshan University in 1994, and received B.E.degree.he is working on the research of optical fiber ribbon and ribbon cable in SECRI now.

FIBER DESIGN FOR FUTURE HIGH CAPACITY DIGITAL TRANSMISSION

[1] R.B. Kummer, L.R. Dunn, R.E. Fangmann, A.F. Judy, D. Kalish, D.W. Peckham, [2] R.G. Huff, [2] W.A. Reed, A.M. Vengsarkar, K.L. Walker, [3] A. R. Chraplyvy, L. Clark, R. Tkach, [4] J.J. Thomas

[1] AT&T Bell Laboratories, Norcross GA, [2] AT&T Bell Laboratories, Murray Hill NJ,
[3]AT&T Bell Laboratories, Holmdel NJ, [4] AT&T Network Technology Development, Bedminster NJ

Abstract

Erbium Doped Fiber Amplifiers (EDFAs) are dramatically changing the types of fibers needed for digital transmission. With EDFAs, distances are no longer limited by fiber loss, but by dispersion and nonlinear effects. This is driving the development of new fiber designs which minimize both linear and nonlinear distortions in the 1.5 micron EDFA passband. Also needed are special dispersion-compensating fibers to allow optimum use of older fibers at 1.5 microns.

Introduction

The first single-mode transmission systems in the early 1980s operated in the 1310 nm window, and the first single-mode fiber designs were optimized for this window with the nominal zero-dispersion wavelength at 1310 nm. Capacity increases were achieved primarily through Time Division Multiplexing (TDM) with increased bit rates, but 1310 nm systems are still generally limited by fiber loss.

Advances in laser technology in the late 1980s opened the 1550 nm operating window. Thus, the loss limit was pushed out. However, since the initial fiber design, dispersion-unshifted fiber (USF), was optimized for minimum dispersion at 1310 nm, the USF dispersion limit at 1550 nm approaches the loss limit at a transmission rate of about 2 Gb/s, even with a narrow-line DFB laser.

This drove the development of the second-generation fiber design, dispersion-shifted fiber (DSF). Like the first-generation fiber, DSF was designed to minimize chromatic dispersion in the intended operating window, so the DSF zero-dispersion wavelength was shifted to a nominal value of 1550 nm. With DSF, capacity increases could be achieved at 1550 nm through TDM, but transmission distances generally remain limited by fiber loss.

With the development and introduction of the Erbium Doped Fiber Amplifier (EDFA) in the early 1990s, transmission distances are no longer limited by fiber loss, but by dispersion and nonlinear effects. EDFAs operate in the 1550 nm window and when used with DSF, unregenerated distances of thousands of kilometers can be achieved for single-channel transmission, as in transoceanic submarine systems. However, for terrestrial applications, with a few hundred kilometers between terminals, the greatest potential for increasing fiber capacities is with Dense Wavelength Division Multiplexing (DWDM) over the broad range of wavelengths within the EDFA passband. DWDM also provides an optical add/drop capability that promises to revolutionize network architectures. But the ability of DSF to support DWDM is severely limited by nonlinear optical effects such as four-wave mixing. Thus, neither USF nor DSF can take full advantage of EDFA/DWDM systems; and a new non-zero dispersion fiber (NZDF) design has been developed to optimize the performance of these next generation systems.

Optical Nonlinearities and Fiber Characteristics

The development of EDFAs, together with their continually improving output powers, has led to increased power densities in optical fibers. In addition, the lower loss at 1550 nm and the replacement of intermediate regenerators with optical amplifiers allows these powers to interact for longer lengths. This has caused optical nonlinearities to emerge as a major phenomenon that can degrade, and at times enhance, the performance of optical fiber communication systems. The types of degradations are numerous and include: increased noise and fiber loss through stimulated Brillouin scattering (SBS)[1]; distortion of transmitted signals through self and cross-phase modulation (SPM, XPM)[2]; the generation of unwanted frequencies and crosstalk between different wavelengths through four-wave mixing (FWM)[3] or stimulated Raman scattering (SRS); and SRS-induced differential channel loss[4]. Some of these effects can also enhance performance such as the ability to transmit solitons and, at lower powers, to improve standard digital transmission performance by using SPM to narrow pulses.

Thus it has become important to design optical fibers to minimize and control nonlinearities. This is true even though some detrimental effects can be reduced by modifying the light's spectral characteristics. For example, choosing unequal DWDM wavelength spacings can reduce FWM effects. But this places a burdensome restraint on a transmission system designer and the required wavelength control can add substantially to laser cost. So it is always desirable to have a fiber that is inherently optimized for nonlinear distortions and can transmit the widest variety of input signals. There are

various design parameters for accomplishing this. First, all major non-linear interactions are proportional to the fiber's power density which is inversely proportional to its effective area, A_{eff}. For a gaussian mode-field, $A_{eff} \approx \pi w^2$, where w is the radius of the fiber's mode-field. So increasing A_{eff} will decrease most nonlinear effects. However, design limitations preclude changing the A_{eff} by more than a factor of about 2 or 3, and order-of-magnitude improvements cannot be obtained this way.

A more promising fiber parameter to optimize is dispersion. Traditionally, fiber design has always attempted to minimize dispersion since at low power levels, dispersion causes pulse spreading which can limit the maximum bit-rate and transmission distance. But recently it has been appreciated that in the non-linear regime, zero dispersion is not always desirable. The reason is that FWM causes different optical wavelengths to beat together and create new wavelengths. This can substantially degrade a DWDM system if the new wavelengths coincide with transmission wavelengths. The FWM conversion process is maximum when the interacting waves have identical phase propagation constants which only occurs at zero fiber dispersion. That is, three waves with frequency, power and propagation constants (ω_i, P_i, β_i, [i=1,2,3]) will create a fourth wave ($\omega_4 = \omega_1+\omega_2-\omega_3$) with power proportional to:[5]

$$P_4 \approx \frac{P_1 P_2 P_3}{A_{eff}^2}\eta,$$

where the conversion efficiency, η, depends on the difference of propagation constants ($\Delta\beta = \beta_4 + \beta_3 - \beta_1 - \beta_2$) of the four waves:

$$\eta = \left| \frac{\exp(i\Delta\beta L - \alpha L) - 1}{(i\Delta\beta - \alpha)L_{eff}} \right|^2,$$

where α is the attenuation coefficient, L the fiber length and L_{eff} is the effective fiber length ($L_{eff} = (\exp\{-\alpha L\} - 1)/\alpha$). Figure 1 plots η at 1550 nm for equal frequency spacing ($\omega_3 - \omega_2 = \omega_2 - \omega_1 = \Delta\omega \cong c\,\Delta\lambda/\lambda^2$) versus fiber dispersion, D, where $\Delta\beta \cong \left(D + \Delta\lambda \, dD/d\lambda\right) 2\pi c \Delta\lambda^2/\lambda^2$

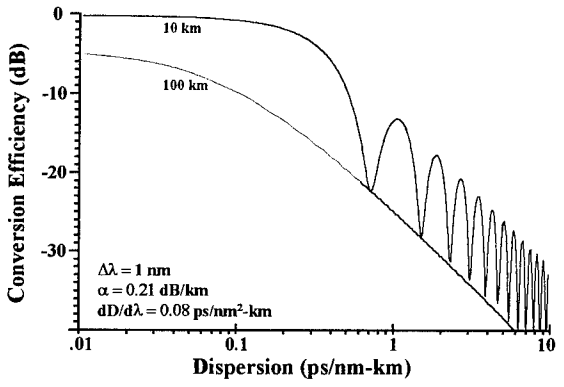


Figure 1

It is seen that increasing the dispersion from .01 to 2 ps/nm-km will decrease the conversion efficiency by over two orders of magnitude. Thus a fiber with a small amount of dispersion will be much more resistant to four-wave mixing than a zero-dispersion fiber and be able to transmit greater powers and more wavelengths in a DWDM transmission system. This is dramatically illustrated in the experimental results shown in Figure 2. The plot in Figure 2(a) shows the severe FWM signals generated when four wavelengths, each with a launch power of 3 dBm, are transmitted through only 25 km of DSF. (The four wavelengths are unevenly spaced so that the mixing products are clearly visible.) Figure 2(b) shows that these FWM signals are completely suppressed even in twice the length (50 km) of NZDF (AT&T's TrueWave™ fiber) with a dispersion of about 2.3 ps/nm-km. Similarly, it has been shown that the effects of XPM are also reduced with non-zero fiber dispersion.[2]

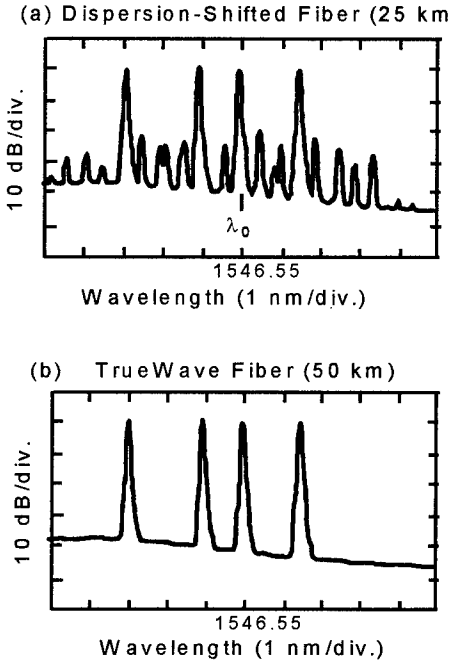


Figure 2

Four-wave mixing can be effectively suppressed with either positive or negative dispersion (i.e. zero dispersion wavelength either below or above, respectively, the operating wavelength). SPM, however, will act to broaden an optical pulse when D is negative and narrow the pulse when D is positive. The choice between the two depends on the anticipated use of the fiber. For terrestrial fiber systems with lengths up to about 1000 km, the pulse narrowing from positive dispersion is generally advantageous because it can improve digital eye patterns thereby lowering the power penalty of a digital transmission system. For much longer, transoceanic system lengths, (~9000 km), negative dispersion may be advantageous because it avoids the possibility of modulation instability.

In either case, the magnitude of dispersion should be kept between 1 and 4 ps/nm-km to avoid FWM and XPM effects, while still restricting the pulse spreading caused by linear chromatic dispersion.

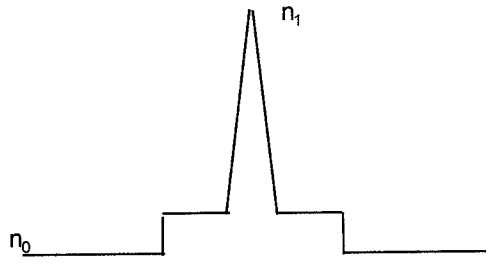
New Fiber Design

The new fiber that is optimized for EDFA/DWDM systems is called non-zero dispersion fiber (NZDF). In addition to obtaining the finite dispersion necessary to mitigate the four-wave mixing effects, several other performance objectives were considered in the design process. First, additional benefits in decreasing the nonlinear effects can be realized by increasing the mode field diameter, and thus the nonlinear effective area. However, the mode field diameter can not be increased arbitrarily without impacting the bending/packaging loss performance of the fiber. Lower fiber attenuation results in longer optimum optical amplifier spacing, when everything else is fixed. Therefore, lower fiber attenuation in the EDFA gain band is desirable. Finally, the long unregenerated transmission lengths require extremely low levels of polarization mode dispersion (PMD). These areas of concern were the focus of efforts to design a fiber that would be optimized for the DWDM systems.

The design objectives of the NZDF design were:

- Provide dispersion at 1550 nm of 1.5 to 4.0 ps/nm-km.
- Increase the nonlinear effective area to greater than 50 μm.
- Maintain bending/packaging performance to at least the level of unshifted fiber designs.
- Maintain low average fiber attenuation at 1550 nm.
- Maintain low sensitivity of transmission properties, such as mode field diameter or zero dispersion wavelength, to manufacturing variations.

The index profile of the fiber that meets these objectives is shown schematically in Figure 3. It consists of a triangular/trapezoidal shaped core, surrounded by a raised-index cladding region or pedestal, which is surrounded by a silica cladding.



Index Profile of AT&T's TrueWave™ Fiber

Figure 3

Also, to achieve the levels of PMD required, a patented, ultra-low PMD process was implemented into the manufacturing processing.[6] Typical production results achieved with this design are shown in Table 1 for AT&T's TrueWave™ fiber.

Table 1
TrueWave™ Fiber Performance
Typical Values at 1550 nm

Attenuation	0.20	dB/km
Chromatic Dispersion	2.3	ps/nm-km
Polarization Mode Dispersion	0.05	ps/√km
Nonlinear Effective Area	55	μm^2
Core/Clad Concentricity Error	0.2	μm

This production performance is maintained through cabling and installation, indicating that the design objective for bending/packaging has been met. And the increase in effective area and excellent core/clad concentricity results in state-of-the-art splice loss performance, for example 0.05 dB/splice with AT&T's rotary mechanical splice.

Dispersion Compensating Fiber

The desire to use the rapidly developing EDFA technology (with amplification in the 1530 - 1560 nm range) to upgrade the large embedded base of USF (with zero dispersion at 1310 nm) has triggered the need for dispersion compensating elements. The compensator, when placed within a USF span, generates zero total span-dispersion by providing negative dispersion that negates the ~17 ps/nm-km dispersion of the typical USF at 1550 nm.

The primary requirements for these compensators are 1) high levels of negative dispersion within the EDFA gain band, 2) low insertion losses, 3) a high threshold level before the onset of deleterious nonlinear effects, and 4) good bending loss performance with packaging diameters less than 6 inches. An additional feature that can significantly increase performance in DWDM systems is for the compensator to have negative dispersion slope. Since USF has positive dispersion slope at 1550 nm, a compensator with negative dispersion slope can provide low total span dispersion over a wide wavelength range.

Practical fiber-based dispersion compensators have been developed that use mainly fundamental-mode, waveguide-induced dispersion to achieve high negative dispersion. Table 2 shows properties of a typical dispersion compensating fiber (DCF). The DCF index profile typically consists of multiple cladding layers surrounding a high delta (greater than 1.5%), small diameter core. Dispersion levels greater than 5 times the USF dispersion have been achieved, while maintaining loss levels around 0.5 dB/km. A figure-of-merit (FOM) for dispersion compensating fiber has been defined in the literature as the ratio of the dispersion in the fiber to the fiber loss. Values for the FOM greater than 150 ps/nm-dB are common.

Table 2
Dispersion Compensating Fiber
Typical Properties

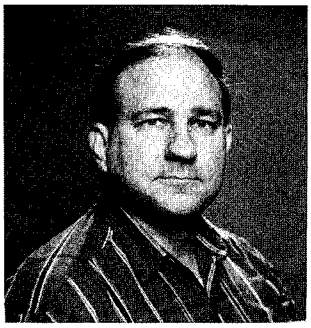
Core Delta	1.8 %
Core Diameter	< 3 μm
1550 nm Dispersion	- 90 ps/nm-km
1550 nm Dispersion Slope	- 0.15 ps/nm^2-km
1550 nm Loss	0.5 dB/km
1550 nm Mode Field Diameter	5.0 μm

Summary

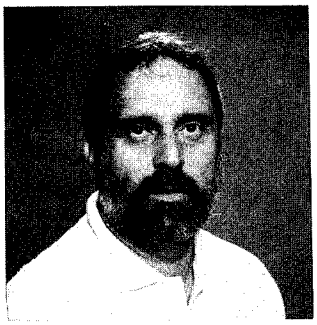
Two new fiber designs have been described. The NZDF is designed to minimize both linear and nonlinear distortions in the 1550 nm EDFA passband and thus it is optimized to take full advantage of EDFA/DWDM systems, which provide the greatest potential for increasing fiber capacity for long distance applications. While NZDF is the clear fiber of choice for new installations, there is a very large embedded base of USF which is optimized for use at 1310 nm. The DCF is designed to allow these older fiber systems to also take advantage of the new EDFA/DWDM technology.

References

[1] X.P. Mao, G.E. Bodeep, R.W. Tkach, A.R. Chraplyvy, T.E. Darcie and R.M. Derosier, *IEEE Photon. Tech. Lett.*, **4**, pp.287-289, (1990).
[2] D. Marcuse, A.R. Chraplyvy, and R.W. Tkach, *J. of Lightwave Tech.*, **12**, 5, pp.885-890, (1994).
[3] K. Inoue, K. Nakanishi, K. Oda, and H. Toba, *J. of Lightwave Tech.*, **12**, 8, pp.1423-1438, (1994).
[4] A.R. Chraplyvy and P.S. Henry, *Electron Lett.*, **19**, pp.641-643, (1983).
[5] N.Shibata, R.P. Braun, R.G. Waarts, IEEE J.Q.E., **QE-23**, 7, pp. 1205-1210, (1987).
[6] A.F. Judy, Proceedings of 43rd IWCS, pp. 658-664, (1994).



R. Brad Kummer is Technical Manager of the Optical Fiber Systems Engineering group at AT&T Bell Laboratories in Norcross, Georgia. He joined Bell Laboratories in 1975, and for the past eighteen years has worked in various areas related to optical fiber development, including exploratory splicing and passive components, fiber measurements, and systems engineering for broadband access and for terrestrial and undersea long haul applications. Dr. Kummer received his BS degree in Physics from Southwestern at Memphis (n.k.a. Rhodes College) in 1970 and a Ph.D. in Physics from the University of Florida in 1975.

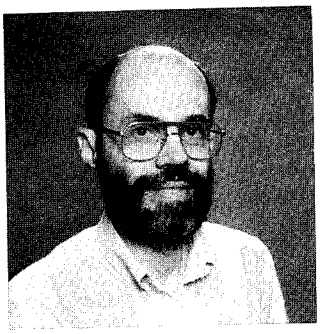


Larry Dunn is currently a Member of Technical Staff in the Fiber Optic Applications Engineering Department of AT&T Network Cable Systems. He joined AT&T Bell Laboratories in 1972 and has worked in various assignments in fiber optic splicing, apparatus, testing, cable and systems engineering. He is a graduate of the State University of New York in Mechanical Engineering. He has been granted three patents in fiber optic cable and apparatus.

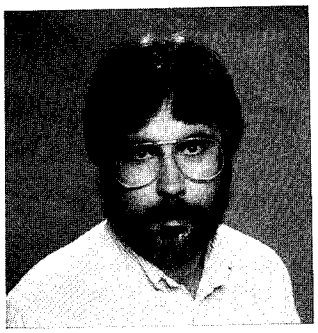


Robert Fangmann is a Member of Technical Staff for Bell Laboratories. He is currently working on Optical Fiber Systems and Applications at Norcross, Georgia. He received a BS in Engineering Physics from Loyola College, Baltimore, and an MS in Engineering Mechanics from the University of Arizona.

David Kalish is Optical Fiber Development and Engineering Director, AT&T Network Cable Systems. He joined AT&T Bell Laboratories in 1971 and, in various assignments, has been involved with fiber design, physical characterization of fibers, development of fiber manufacturing processes and fiber systems engineering. He has S.B., S.M. and Sc.D degrees from M.I.T.



Arthur F. Judy is a Distinguished Member of Technical Staff in the Optical Fiber Systems and Applications Engineering Group. In his 27 years at AT&T Bell Labs, he has worked on the theory, modeling and measurement of optical fibers as well as metallic media. He has a BSEE from the University of Maryland, an MSEE from the University of Michigan, an MS in Physics from Georgia Tech and is currently pursuing a PhD in non-linear optical physics.



David Peckham is a Distinguished Member of Technical Staff with AT&T Bell Laboratories in Norcross, Ga. He received the BS and ME degrees in Electrical Engineering from the University of Florida. Since joining AT&T in 1982 he has worked in the areas of optical fiber characterization, design and manufacture.



William A. Reed is a Distinguished Member of Technical Staff of AT&T Bell Laboratories in the Optical Fiber Research Department. Since joining the Bell Laboratories Materials Science Research Laboratory in 1961, his research has included studies of the Fermi surfaces of metals, transport properties of Type II superconductors, bonding in solids and molecules using gamma ray scattering, the design and characterization of optical waveguides and amplifiers, and the evaluation of new glass compositions for optical waveguide applications. He received a B.A. degree from Oberlin College in 1957 and a PhD degree from Northwestern University in 1962, both in physics. Dr. Reed is a Fellow of the American Physical Society and a member of Sigma Xi and the Optical Society of America.



Ashish M. Vengsarkar received the B. Tech. degree in Electrical Engineering from the Indian Institute of Technology, Bombay, and the M.S. and Ph.D. degrees in Electrical Engineering from Virginia Tech. While pursuing his doctoral degree, he was a Research Associate at the Fiber & Electro-Optics Research Center at Virginia Tech working in the field of fiber optic sensors. In 1991, he joined AT&T Bell Laboratories as a Member of Technical Staff and is presently a Technical Manager for Fiber Gratings and Devices in the Optical Fiber Research Department. He is the Associate Editor (Fibers/Cables) for the Journal of Lightwave Technology and is on the IEEE-LEOS Technical Program Committee for Fiber and Planar Waveguide Technology.



Laurel Clark has a Bachelor of Science Degree in Electrical Engineering from the University of Colorado at Boulder and a Master of Engineering Degree from Cornell University. She is currently a Member of Technical Staff in the Transport Line Planning District of AT&T Network Services Division.

James Thomas is a Technical Manager for Network Technology Development. In his 30 years with AT&T, he has worked on analog and digital radio and lightwave systems. He received a BS in Mathematics from Syracuse University and is currently pursuing an MS degree in Telecommunications Engineering at the University of Colorado.

New light weight, small diameter fibre optic ribbon cable for the Norwegian access network

G.Berthelsen, G. Sletten, M.Johansen, K.Skuland

Alcatel Kabel Norge AS

Abstract

This paper describes the design, properties and advantages of a new light weight fibre optic ribbon cable developed by Alcatel Kabel Norge AS in cooperation with Telenor AS. The cable design is shown in figure 1 below. The cable is designed to be used in access network. The cable is produced and tested according to international standards, and complies with IEC and CECC requirements. Having 24 fibres (6 x 4-fibre ribbons), a cable diameter of 6 mm and a weigth of 30 kg/km, this new light weight cable is 1/2 the diameter and 1/3 the weight of conventional cables with the same ribbon count.

Introduction

As part of a Norwegian Broadband program a national development project, «Fibre Optic ATM-access», was started in 1994. The goal of the project is to develop a broadband subscriber network based on ATM switching and APON access technology with the simplest solution. An important part of this project has been to develop a small diameter and low weight ribbon cable. The considerable reduction of weight and diameter reduces the installation cost between access points, and has lowest initial duct utilization of other designs considered.

Two reasons for introducing ribbon fibres in the cable construction were:

1. The reduced installation cost is due to reduction of splice time, lowering of the transportation cost, light weight and therefor easy handling.

2. The ribbon construction in a tight cable structure improves the fibre protection compared to primary coated fibre, and allows cables with smaller diameter and much lower weight than in a typical loose tube design.

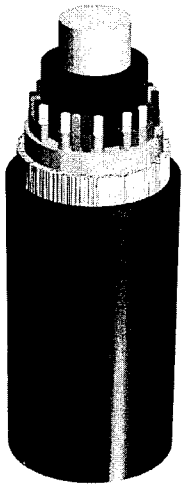


Figure 1.
Light weight 24 fibre small diameter ribbon cable.

The Cable design

The basic idea of the design is to strand the ribbons directly on a coated FRP element. This design is similar to the slotted core design, except for the wall between the slots and the flatness of the bottom of the slot compared to the circular structure of the central element. To compensate for the curvature of the central element, the coating on the FRP serves as a soft bedding between the ribbons and the central strength member to prevent microbending losses. The tensile strength is obtained by the use of aramid yarn in addition to the central strength member. The soft coating of the central strength element and application of aramid yarns between the ribbons and the outer sheath, ensure good mechanical protection against impact and crush.

Dimensions and technical data for a 24 fibre cable:

Diameter :	6 mm
Weight :	30 kg/km
Minimum bending diameter:	110 mm
Maximum allowable tension:	
during installation:	1.5 kN
during operation:	0.5 kN
Temperature range:	
operation:	-40 - +60°C
installation:	-10 - +60°C
storage:	-40 - +70°C

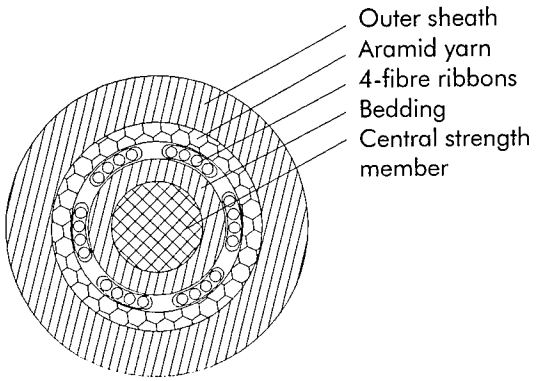


Figure 2.
Cross section of the new light weight, small diameter fibre optic ribbon cable with 24 fibres.

The 24 fibre light weight cable has half the diameter and a third of the weight of comparable cables. The cable is produced in a tandem process allowing stranding and outer sheath extrusion to be performed simultanously.

The design of the cable utilizes standard materials, i.e. polyethylene sheath, aramid yarns, and a FRP-rod as central strength element. The FRP is coated with a thin layer of a soft plastic material. All the cable materials are non-toxic and do not evaporate any harmful gases.

The light weight cable can easily be spliced without breaking all the ribbons for application of midspan access. Standard procedures can be used to remove the outer sheath giving free access to any of the ribbons in the cable.

Both in-line joints and butt joints can be used without the need for special tools.

Design characteristics

The ribbons are stranded directly on a central element. The design principle allows the manufacturer to use both 4-fibre and 8-fibre ribbons in the cable, and makes the cable design flexible and easy to adjust to individual customers. With 8-fibre ribbons the splicing and installation time will be further reduced compared to 4-fibre units.

A multilayer version of the cable is possible. With 3 layers of ribbons, the outer diameter of a 96 fibre cable will be 10 mm and the weight will be 75 kg/km. The cable can be assembled with dry water swellable elements for outdoor and indoor installation. The small diameter and low weight cable is suitable for blown cable installation. The ribbons are embedded in a soft rubberlike material which makes it easy to peal off all the ribbons without the need of any tools. There are no gels to clean out as with loose tube or slotted core cables. Such a cable is shown in figure 3.

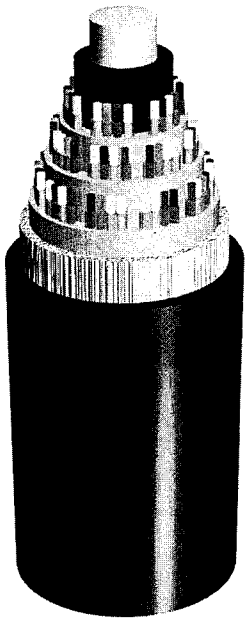


Figure 3.
Light weight multilayer ribbon cable with 96 fibres.

Installation improvements

Conventional slotted core and unitube ribbon cables with the same number of fibres will have an outer diameter of 11 to 13 mm and a weight of 90 to 140 kg/km.

When the weight is reduced to 30 % the length of cable can be increased. 2000 m maximum pull of a 90 kg/km cable relates to 6000 m of this new cable [Ref (2)]. In some cases the cable reduses the need for pulling equipment, allowing faster «hand» installation.

Blowing techniques are often used for fibre optic cable installation. Applying this technique the maximum blowing length is achieved when the friction function equals the air drag function. The friction function is directly proportional to the weight of the cable, and when the cable weight is reduced with a factor 0.3 (from 90 kg/km to 30 kg/km), so is the friction. The air drag function can be shown to be proportional to the radius of the cable [Ref (3)] which is reduced with a factor 0.5. This gives an overall reduction in work required to blow in the cable of approximately 0.6. The result is an increase of the cable length of approximately 40 %.

Accessing the ribbons in this cable for mid-span connections at a later date is facilitated by the initiation of a cut in the jacket and the easy peeling off the layers of aramid over the ribbons.

Critical factors

The improved performance of fibre, fibre coatings, fibre coloring, and matrix materials during the last three years, have enabled a new cable design based on stranding ribbons directly on a central element. The selection of fibres and production parameters for manufacturing the ribbon and the cable, have been optimised to meet the requirements for this type of fiber optic cable. The most important materials and production parameters which have been established are listed below:

- Fibre design
- Tension of each fibre in the ribbon
- Properties of the matrix material
- Diameter of central strength element
- Softness of buffer layer on central strength member
- Lay length of ribbon
- Tension of ribbon
- Tension on the central strength element
- Lay length of the aramid yarns
- Tension of the aramid yarn during stranding
- Properties of filling material
- Distribution of layers
- Radial and lateral shrinking of sheathing material
- Sheath extrusion

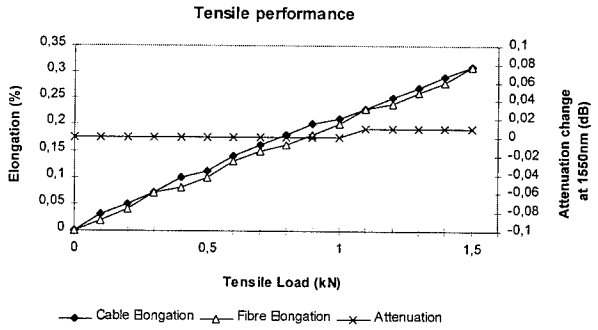
Testing

The cable has been developed to resist harsh environments, and tested according to duct cable specifications. The tests are carried out according to the test procedures issued by IEC, ETSI, ISO and CECC. Exemption are made for bending with 10 turns and stiffness, for which no international tests are issued.

Tensile performance

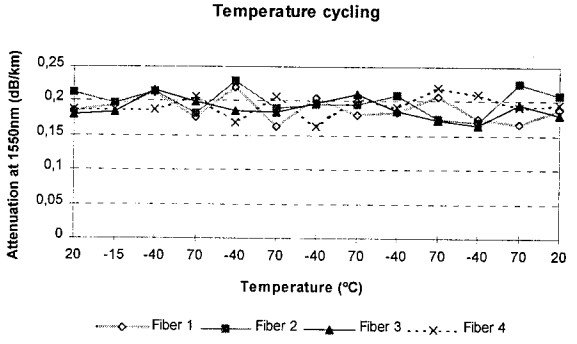
The cable and fibre elongation versus the tensile load is shown in the figure below. The length of cable under test was 144 m and the fibre measurements was made on loops of 4 fibres in each ribbon. The measured fibre elongation is 0.31 % at 1500 N and 0.10% at 500 N.

The fact that there is no fibre excess length in the cable explains the close relation between the fibre and cable elongation.



Temperature cycling

A cable sample was submitted to 7 temperature cycles between +70 °C and -40 °C. The attenuation was measured at both temperatures. The cable passed the test, and the results are given in the figure below. Studies are continuing to reduce the change in attenuation over temperature.



Impact

The cable withstands an impact energy of 15 Nm without any increase in attenuation and with no mechanical damage to the cable elements.

Crush

A load of 1500 N was applied to the cable without any increase in attenuation and with no mechanical damage to the cable elements.

Testing characteristics:

Test	Conditions	Result	Specification/ standard
Tensile perform-ance	100m cable, Load=1500N Fibre strain: 1/3 %	<0,05 dB change in attenuation	CECC EN 187 000, method 501
Bending under tension	Load 1500 N 10 cycles 0.5 m/s	<0.05 dB. No visible damage.	CECC EN 187 000, method XXX, not yet published.
Repeated Bending	Load 100 N 1000 cycles	No visible damage	CECC EN 187 000, method 507
Impact	Anvil dia=50 mm 3 x 15 J	<0.05 dB. No visible damage.	CECC EN 187 000, method 505
Kink	5 cycles L=100 mm	No visible damage.	CECC EN 187 000, method 512
Torsion	L=1 m, Load= 100 N, 5 cycles 1 turn	<0.05 dB No visible damage	CECC EN 187 000, method 508
Bending 10 turns	10 turns, 1 temp. cycling between -40 °C to 70 °C	<0.05 dB No visible damage	No international standard
Cable bend	5 tuns/helix 3 cycles at -15 °C, 20 °C	<0.05 dB. No visible damage or change in attenuation.	CECC EN 187 000, method 513
Crush	Plate/plate load: 1500 N	<0.05 dB. No visible damage.	CECC EN 187 000, method 504
Temp.cycl -ing	7 cycles -40 °C to 70 °C	<0.05 dB increase	IEC 794-1-F1
Water penetrat-ion	3m cable 1 m water	Complying	CECC EN 187 000, method 605B
Drip-test	50 degrees 0.5 m cable	No drip	EIA-Standard 455-81A
Stiffness	0.2 m cable, 500 mm/min	B=0.05 Nm^2	CECC EN187 000, method XXX, not yet published

Stiffness

The cable stiffness is an important parameter when you want to blow the cable through pipes. Stiffness is defined in CECC as the physical force needed to bend the cable.

Blowing is an increasingly popular installation technique. The cable has been blown in the same tubes as traditional slotted core and unitube cables. The performance of the new cable is equal or better than for traditional cables.

The stiffness of the light weight cable is measured to be 0.05 Nm^2 which is fairly flexible compared to 0.50 Nm^2 for ordinary slotted core cables. This is explained by the small diameter of the cable and the reduction of FRP diameter.

However, the FRP diameter to cable diameter ratio is large preventing kinking of the cable during blowing installation.

Conclusion

A new ribbon cable has been developed having a very small diameter and low weight , resulting in the lowest possible installation cost.

A typical cable drum with an outer diameter of 140 cm can accommodate only 4 km of a 13 mm cable compared to 20 km of this cable.

Due to reduced weight the maximum pulling length can be increased to 300 % given equal maximum rated pulling loads.

The cable design has proven its performance according to the tests reported in this presentation. The light weight cable is produced with up to 6 x 4-fibre ribbons. The evaluation and testing of the cable shows that the new light weight ribbon cable is unusually small and robust, and particularily suitable for the access network where splicing, jointing and branching will be main parts of the installation cost. Cable design with armouring for aerial and directly buried applications have been produced and will be tested in order to be able to offer a new generation of fibre optic ribbon cables.

Acknowledgement

The authors would like to thank all who participated in the design, construction, testing and documentation of the cable. We want to thank in particular J.P. Bonicel, D. Keller and J. Påborn, from the Alcatel Cable Optical Fiber Cable Competence Center, who have been of great help in the design and testing of this new light weight cable.

Refrence

(1)
JP. Bonicel, D. Keller, G. Kylen, J. Schulte, G. Paternostro, G. Berthelsen, CG. Cortines, C. Lasne «An international development on ribbon technology and evaluation of applicability to national specifications», Proc. 41st IWCS, p. 29.

(2)
Marks' Standard Handbook for Mechanical Engineers, McGraw-Hill, Inc.. Eighth Edition copyright 1978.

(3)
European Patent Application # 85114013.7. Date of filing 1.11.83, by Michael H. Reeve.

Authors



Gunnar Berthelsen
Alcatel Kabel Norge AS
P.O.Box 130, Økern
N-0509 Oslo, Norway

Gunnar Berthelsen (48) graduated from Heriot Watt University, Edinburgh in 1971, and joined Standard Telefon og Kabelfabrikk (Now Alcatel Kabel Norge AS) the same year. He started work with fibre optics in 1977 and is currently Technical Manager at Alcatel Kabel Norge AS.



Geraldine Sletten
Alcatel Kabel Norge AS
P.O.Box 130, Økern
N-0509 Oslo, Norway

Geraldine Sletten (29) received her B. Eng (Electrical and Electronic Engineering) from Strathclyde University, Glasgow in 1987 and joined STK (now Alcatel Kabel Norge AS), the same year, where she works with research and development into fibre optic cables.



Morten Johansen
Alcatel Kabel Norge AS
P.O.Box 130, Økern
N-0509 Oslo, Norway

Morten Johansen (50) received his degree (Electronics) from Oslo College of Technology in 1973. He has for many years worked with development of silicon chip manufactoring technology, but joined STK (now Alcatel Kabel Norge AS) in 1987. He is currently development manager in Alcatel Kabel Norge AS with responsability for telecommunications cables.



Kåre Skuland
Alcatel Kabel Norge AS
P.O.Box 130, Økern
N-0509 Oslo, Norway

Kaare Skuland (27) received his M.Sc. in Electronics from the Norwegian Institute of Technology in 1992. After finnishing his education he joined Telenor AS and was responsible for specifications and installation procedures concerning splicing of optical fibres and cables. In 1995 he joined Alcatel Kabel Norge AS where he currently is responsible for fibre optic land cables.

DIRECT FUSION SPLICING OF OPTICAL CONNECTORS: ZERO-LENGTH PIGTAIL TECHNIQUE FOR ON-SITE INSTALLATION

Rodney Throckmorton, Martin Curran, *Kai Hollensett, *Volker Riech

Siecor Corporation, Hickory, North Carolina
*RXS Kabelgarnituren GmbH, Hagen Germany

Abstract

A new field installable connector that utilizes a preinstalled fiber stub has been developed using electrical arc fusing instead of a mechanical splicing as a joining method. By using many of the same components that are used in factory installed connectors, performance is similar to that of the factory connector. A micro splicer has also been developed to fuse this connector and maximize craft friendliness during assembly. The mean splice loss achieved with this splicer is 0.09 dB at 1310 nm. Results from thermal cycling show a change in mated pair insertion loss of less than 0.15 dB at both 1310 nm and 1550 nm.

Introduction

As the installation of networks for fiber-in-the-loop, local area, interoffice, campus, and public subscriber increase, the number of connections is also rising. As the desired performance and specifications of cable assemblies improves, field-installable connectors must provide repeatable, reliable, factory-like performance, especially for single-mode applications. Minimal skill level and low overall installation costs are also basic requirements.

As transmission rates also increase with the use of OC-48 (2.488 Kb/s) and faster networks, reflectance performance over temperature is especially important when considering outside plant installations. The polishing process performed in the factory controls the connector end face geometry to insure physical contact, and reflectance performance, is maintained over a wide temperature range.

There are presently three methods to terminate optical cable with a connector. These include:

1. Fusion splicing a factory manufactured "pigtail" connector.
2. Field-installing an "epoxy and polish" or "quick mount" connector which involves part or all of the following: insertion of epoxy, curing (oven or overnight), polishing, and end-face inspection.
3. Field-installing a "quick mount," factory epoxy and polished "stubbed" connector.

This paper compares these three connectorization choices and introduces a new stubbed connector design.

Cable Termination

Factory Connectors

The prevalent method of terminating single-mode fiber optic cable for more than ten years has been fusion splicing of a factory pigtail. This requires a splice tray, storage shelve, and fusion splicer. Since fusion splicers are routinely used for joining cables, the associated cost of this equipment when used for pigtail splicing is minimal. A factory pigtail with one connector, or jumper which is terminated on both ends, provides excellent optical and mechanical performance. With recent improvements in fiber parameters such as core-to-cladding concentricity and circularity, along with assembly processes that include optical ferrule/fiber tuning, insertion loss of a mated pair is now below 0.2 dB. Reflectance of factory connectors is now better than -60 dB due to improved polishing techniques that control fiber extension[1] and apex offset (figure 1.)

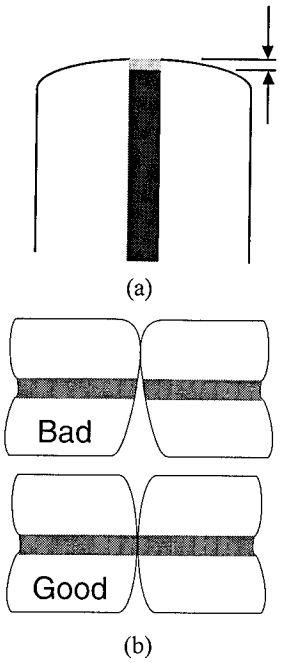


Figure 1 (a) Fiber extension and (b) Apex offset of connector endface geometry

Factory connectors are mechanically robust and pass testing that includes applying tensile forces up to 6.8 kg along the connector/fiber axis and 4.5 kg at 90° to the connector/fiber axis (figure 2.)

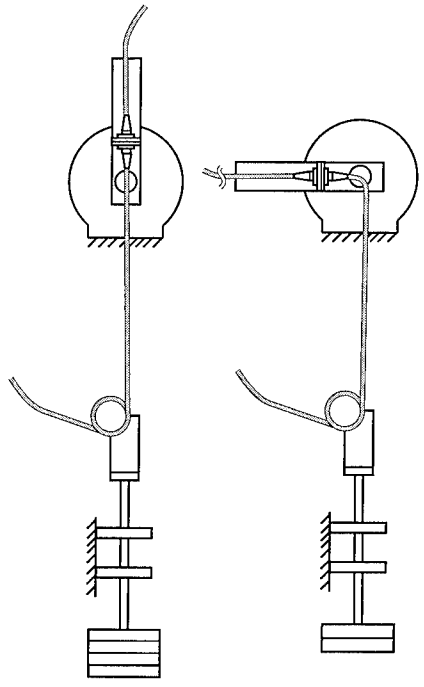


Figure 2 Tensile proof test apparatus

To pass these specifications design improvements in both the boot and retention of the strength member and jacket have been implemented

Field-Installable Connectors

Another common method of termination is to field-install the connector by performing a factory-like assembly process on site. This field installation involves inserting an epoxy into the connector ferrule, inserting a length of bare 125 μm fiber through the ferrule, curing the epoxy, and then polishing the endface to the required specifications. The assembly environment is typically less than optimal for high-volume assembly; small spaces along with poor lighting and dust are often encountered. Curing of either heat or UV curable epoxy may require AC power. Work space and warm-up time are required for the oven used for curing the epoxy. The cure temperature must also be controlled, as most epoxies will not properly hardened without reaching their transition temperature for a required length of time. Work space and set-up time are also required for the materials used in polishing the ferrule. This polish is typically performed by hand and does not control fiber extension or apex offset. The effort required to achieve proper reflectance can lead to longer installation times and higher scrap. Generally, personnel training requirements are higher for these types of connectors, particularly for single-mode installation. Typical insertion loss is around 0.5 dB. Any slack fiber would , again, require storage hardware. Many field-installable applications are multimode fiber where insertion loss and reflectance are not so critical.

Factory Epoxied and Polished "Stubbed" Connectors

Mechanical Spliced, Stubbed Connector An alternative to the epoxy cured field-installable connector is a no-epoxy, no-polish, crimp connector[2,3] which has been in use for more than three years in both single-mode and multimode versions. This connector uses the concept of mechanically splicing a near zero-length pigtail and consists of a short fiber stub epoxied into a ceramic ferrule. The endface is then factory polished to achieve the required reflectance; <-40 dB for Super-PC or <-55 dB for Ultra-PC.

Fiber extension and apex offset are tightly controlled just like a factory-installed connector. This connector uses a precision "V" groove and top flat to align and secure the stub and field fibers (Figure 3.) The splice area contains an index matching material to reduce reflections at the joint. Because the index of refraction of the matching material is temperature dependent, reflectance performance can vary over the standard -40°C to +75°C test range unless two angled cleaves are used. The addition of an angled cleave on the factory-installed stub fiber has increased the temperature range for which it meets Super PC (-40 dB) and Ultra PC (-55 dB) performance.

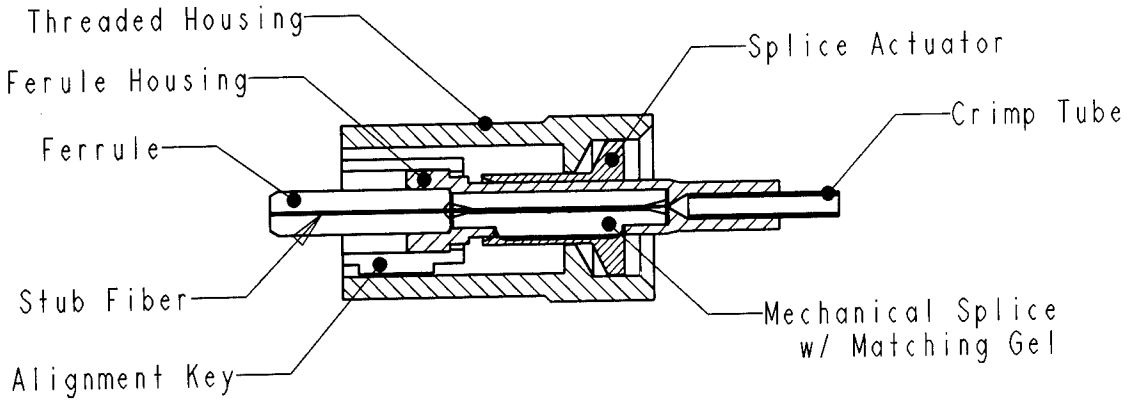


Figure 3 Mechanical spliced stubbed connector

A patented[4] design to control the flow of the index matching material and prevent the occurrence of particle occlusion[5] has also been incorporated into this splice.

Fusion Spliced, Stubbed Connector A new connector has been developed to provide factory installed performance in a field-installable design. This connector design allows fusion splicing within the physical boundaries of the connector, resulting in a near zero-length pigtail. Additionally, no epoxy, polish, or matching material are required for installation.

The absence of index matching gel eliminates any concerns about reflectance performance in the outside plant. The fused connector also has advantages over factory connectors. Cut to length jumpers, which eliminate the need for slack storage and associated hardware, can be quickly and easily produced with near factory connector performance. Repairs can be quickly performed anywhere without sacrificing performance.

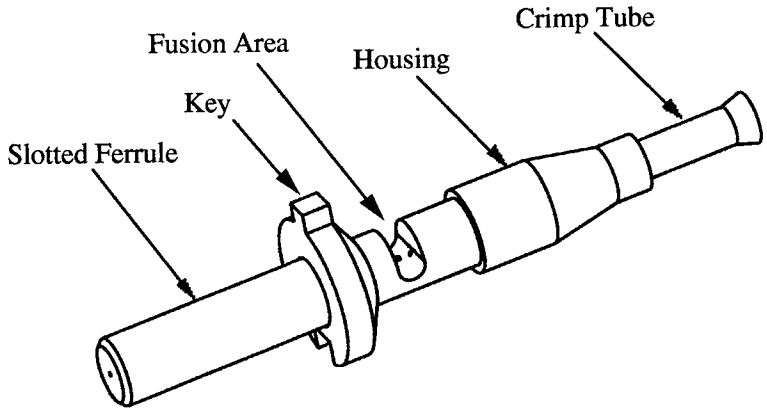


Figure 4 Ferrule assembly for ST™ compatible connector

This connector and the previously described "stubbed connector provide several advantages over other field-installable connectors. The factory polish controls fiber extension in the order of +50 / -50 nm and apex offset of the fiber and spherical dome to < 50 μm. Even if factory polishing process were to be deployed in the field, the inspection equipment to measure and verify these endface specifications would be expensive and impractical.

Connector Design The core component for all versions, SC, FC, and ST™ compatible is the ferrule assembly (Figure 4.) This assembly consists of a short length of fiber precision cleaved at one end and epoxied into a zirconia ceramic ferrule. The ferrule incorporates an extended length and a transverse slot, into which the end of the stub fiber with the precision cleave protrudes. This ferrule assembly also includes a key for aligning eccentricities,and a housing which couples the crimp tube to the ferrule to provide strain relief.

Splicer Design To simplify installation of this connector, a unique fusion splicer has been developed (Figure 5). This splicer provides the ability to fuse within the transverse slot of the ferrule. The splicer incorporates a pivoting arm that positions and orients the connector between the electrodes. 16 different splicing programs can be selected for connector or fiber-to-fiber splicing. Splicing parameters can be easily changed and stored using an optional programming module allowing optimization of splice results for individual fiber types. Insertion and positioning of the bare field fiber has been simplified by a hand-actuated translation stage. A slanted screen provides viewing of the fibers, even in direct sunlight. An integral crimping mechanism performs the 900 μm crimp immediately after splicing to insure a zero stress condition beyond the buffer.

Additionally, standard fiber to fiber splicing can be performed by simply attaching an adapter unit, which takes less than 30 seconds.

Connector Installation Installation of this connector consists of inserting the ferrule assembly into the splicer, stripping, cleaning, and cleaving the field fiber to a predetermined length, and then fusing the fibers together. Fiber alignment is provided by the micro-holes that hold the stub and field fiber. Additionally, surface tension of the molten glass provides self aligning during arcing.

The 900 μm crimp is then performed while the connector remains in the splicer. This prevents coupling of any torsional or tensile forces to the splice joint. The connector is then removed from the splicer and the associated outer hardware, dependent on connector type, is snapped into place.

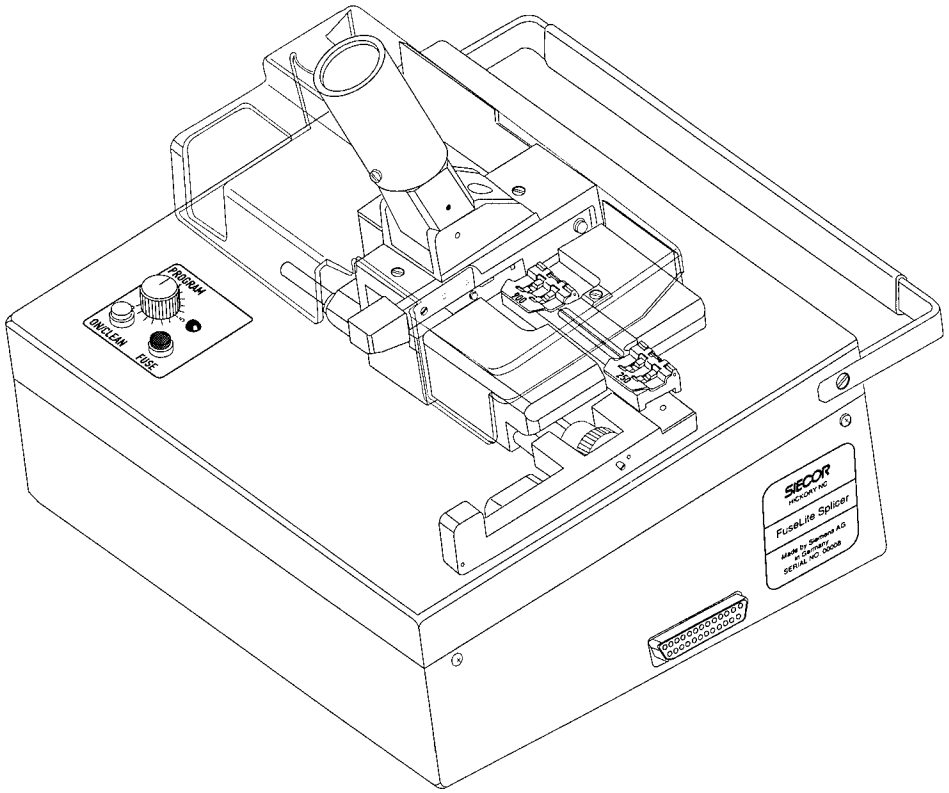


Figure 5 Splicer for field connectorization

If the installation is on single fiber cable, the aramid yarn crimp is performed with a separate hand tool. The jacket is captured with this same crimp. The boot is then slid into place and the connector is ready to use. Typical installation times, whether installing 50 connectors or just one, are only 5 minutes for 250 μm or 900 μm buffered fiber and 7 minutes for single fiber cable.

Test Results Splice loss for 160 assemblies are shown in Figure 6. These measurements were obtained using a 1306 nm laser source and a 25 mm^2 InGaAs detector. The field fiber was first referenced prior to splicing each connector and then the splice loss was measured after splicing by inserting the ferrule into the detector. Values at 1310 nm wavelength show a mean splice loss of 0.09 dB. This loss distribution infers that mated pair losses will be comparable to factory pigtails with their associated fusion splice.

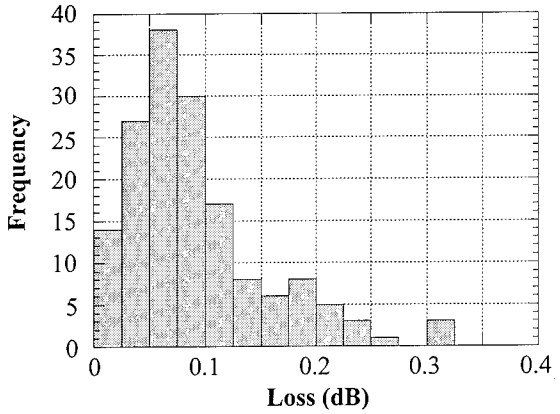


Figure 6 Splice loss histogram at 1310 nm wavelength

Results from thermal cycling per GR-326 show a maximum insertion loss delta of 0.15 dB which occurs at the cold temperature extreme. This loss signature shown in figure 7 of is typical of a factory connector.

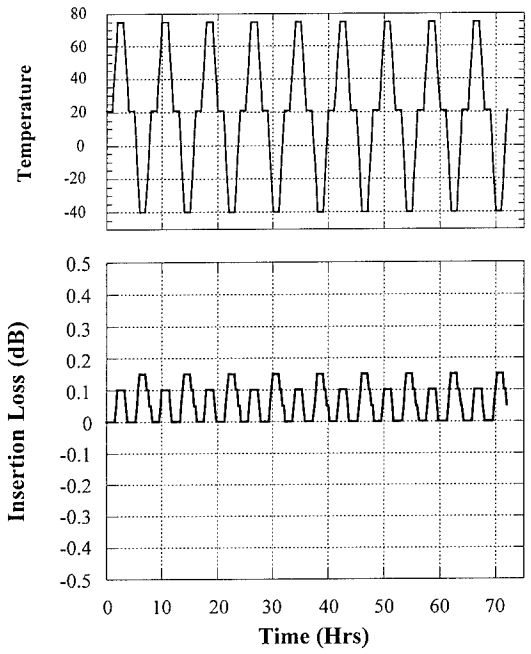


Figure 7 Typical temperature cycling data; only 72 hours shown.

Modal Interference Because modal interference can exist with closely spaced single-mode joints, loss will vary with wavelength. Improved core alignment, along with the selection of a stub fiber for parameters such as cutoff wavelength, mode field diameter, and concentricity error, minimizes the loss variation due to modal interference[6,7]. This variation, which has been characterized both theoretically and empirically for stubbed connectors, is ≤11% as illustrated in Figure 8.

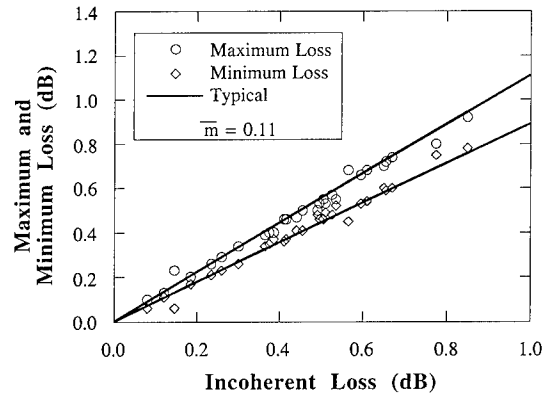


Figure 8 Extreme values of insertions loss versus incoherent loss within the 1310 ± 20 nm operating window for field installable connectors incorporating fiber stubs with a low cutoff wavelength. Discrete points represent measured extreme values, while the solid lines are typical extremes calculated as $(1 \pm m_{avg})$ x (incoherent loss).

Conclusion

With this new fusion spliced, stubbed connector, near factory performance can be achieved with a field-installable single-mode connector. Applications in the outside plant that were previously unacceptable for field-installable connectors can now be terminated quickly and economically with this new connector. Reflectance performance over the full -40°C to +75°C temperature range is achieved by providing a factory polish and a fusion splice,or zero reflectance joint.

References

[1] "Generic Requirements for Single-mode Optical Fiber Connectors," GR-326-CORE, Issue 1, December 1994.

[2] R. Throckmorton, "Single-mode field-installable crimp connector requiring no epoxy or polish," Proc. 8th NFOEC, pp. 361-370, 1992.

[3] M. deJong, "Cleave and crimp fiber optic connector for field installation," *Tech. Dig. Conf. on Optical Fiber Commun.*, paper ThA1, pp. 139-141, 1990.

[4] US Patent SN 8,108,970, "Fiber optic mechanical splice having grooves," R. Throckmorton, M. de Jong, D. Knecht, April, 1995.

[5] G. Kiss and A. Pellegrino, "Erratic loss and reflectance behavior in mechanical splices due to particulate occlusion," Proc. 6th NFOEC, pp. 5.2.1-5.2.12, 1990.

[6] R.A. Throckmorton and D.O. Harris, "Modal interference in field installable single-mode fiber-optic connectors," *Proc. 10th NFOEC*, pp. 399-406, 1994.

[7] R.A. Throckmorton and D.O. Harris, "Azimuthal dependence of modal interference in closely spaced single-mode fiber joints," Photonics Technol. Lett., Volume 6, pp. 1235-1237, 1994.



Rodney Throckmorton was born in Williamsburg, Virginia in 1957. He received his BS in Mechanical Engineering from Virginia Tech in 1980. After working in both design and manufacturing of telephone instruments for Comdial Corporation, he joined Siecor in 1984. As a member of the Hardware and Equipment Technology division, his responsibilities have included development of splice hardware, expert systems for cable configuration, and field-installable connectors. In his present position as Senior Development Engineer he continues to be involved in design and development of single-mode and multimode field-installable connectors. He is a member of ASME and OSA.



Martin Curran received his BBA in Finance from the University of Norte Dame in 1980 and his Masters in Business Administration from the University of Virginia in 1984. He is presently the Marketing Manager for Fiber Optic Joining Points for Siecor Corporation.



Dr. Volker Riech received his Ph.D. from Aachen University, Germany in 1976 and worked as an engineer for Phillips PKI Company developing measurement equipment and fiber optic components. He joined RXS Kabelgarnituren GmbH, a subsidiary of Siemens AG, in 1993 and is presently head of Marketing and Product Management at RXS in Hagen, Germany.



Kai Hollensett studied Economics/Marketing at Dortmund University in Germany and joined RXS Kabelgarnituren GmbH in 1991 after working two years for IBM Corporation developing customer specific applications. He is presently Product Manager for fiber optic hardware products at RXS in Hagen, Germany.

CONTROLLING REFLECTANCE OF OPTICAL CONNECTORS

E. M. Vogel, L. A. Reith, E. Beebe and J. J. Brickel.

Bellcore, Morristown, NJ

ABSTRACT

Over the past several years significant improvements in connector backreflection performance have been achieved by tighter control of the end face parameters and a polishing process that does not significantly change the properties of the contacting fiber surfaces. These improvements have been achieved in response to new technical requirements for optical connectors such as analog AM-VSB video systems that require about -65 dB reflectance.

In addition, the reliability of optical connectors has become an issue because of their increased use in the uncontrolled outside environment. One possible optical connector failure mechanism is an enhanced hydrolysis reaction or corrosion of the damaged glass surface after polishing. Our study suggests the formation of a previously unrecognized *subsurface* damaged layer during the glass polishing. We have developed an etching procedure to further enhance the optical performance of connectors by removing this subsurface damage layer at the fiber endface.

INTRODUCTION

Several techniques are used to reduce fiber-end reflection caused by index discontinuities in the optical path. Low reflectance in straight end-face connectors is achieved by physical contact between the adjacent fiber cores. Over the past several years, changes in the polishing process have produced vast improvements in connector backreflection performance, from about -25 dB in 1984 to below -60 dB by 1993 [1]. These results were achieved by tighter control of the end face parameters (apex offset and fiber undercut), and by a polishing process that does not significantly change the properties of the contacting fiber surfaces.

We have used an environmental scanning electron microscope (ESEM) and an atomic force microscope (AFM) for the physical and chemical endface profile characterization. We also present the results of Fourier Transform Infra-Red (FT-IR) microsampling spectroscopy which was used to characterize polished or cleaved fiber endfaces. It has been recognized that a very high surface stress (compression) can be present during the polishing of glass [2]. We have established that a densified, damaged subsurface layer is responsible for increased reflectance in optical connectors, based on the results of FT-IR microsampling spectroscopy and modeling [3]. Our goals are to understand the polishing process, to establish the etching procedure and to control the etching rate, performance, and reliability of optical connectors.

EXPERIMENT

Connector Assembly: We used an SC Field Connector Tool Kit to terminate fibers with SC connectors. The SC connector is crimped onto the optical fiber, and epoxy adhesive, cured at 100 °C, is used to secure the fiber in the ferrule. After the epoxy cured, we cleaved the end of the fiber and then manually polished the endface of the fiber. We used 15 μm (SiC) down to 0.3 μm (Al_2O_3) lapping films.

For the etching experiment we assembled connectors with protruding fibers to allow for the removal of fiber material during etching.

Etching: We used J. T. Baker Buffered Oxide Etch 6:1 for various times, followed by ultrasonic cleaning in distilled water for 1 min and a final ethanol wash.

Endface Characterization: Different fiber endface inspection techniques were used during this study. We used a surface profile measuring system (Sloan Dektak II) to establish the optimum etching rate using just a ferrule and the fiber, rather than a completely assembled connector. Later we used a Rank-Taylor-Hobson Talysurf profilometer that could accommodate the entire assembled connector. Environmental scanning electron microscopy (ESEM), with an energy dispersive x-ray analyzer for chemical analysis, and atomic force microscopy (AFM) were used to image and analyze the entire endface.

FT-IR Microsampling Spectroscopy: The FT-IR spectra were acquired using a BioRad-Digilab FTS-40 FT-IR with a UMA-300 IR microscope accessory. The samples were mounted on the microscope stage with the fiber axis collinear to that of the IR microscope lens optical path. The fiber tip surface was perpendicular to this path. If the surface was tilted even at a small angle, the IR spectra signal strength would degrade rapidly.

Optical Measurements: We used a Tektronix Fibermaster TFP2 OTDR (Optical Time Domain Reflectometer). A 1 km of a test fiber was connected to each connector under test by a fusion splice and then directly to the OTDR.

RESULTS

The results obtained by ESEM characterization indicated that there are no compositional changes of the glass surface after polishing. Therefore, we employed IR spectroscopy to probe about 5 μm deep into the glass. Figure 1 illustrates the virtually perfect overlap of the traces for two cleaved fibers, demonstrating the excellent reproducibility of this technique. Figure 2 compares a polished fiber in an assembled connector (measured reflectance -48 dB) to that of a cleaved fiber.

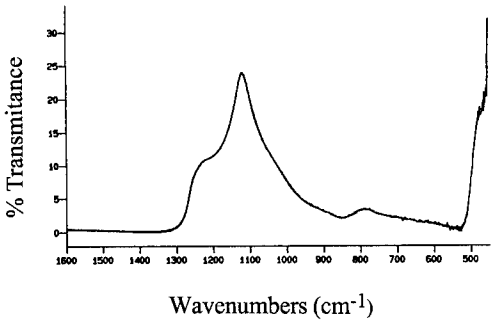


Figure 1. FT-IR spectra of two cleaved fibers.

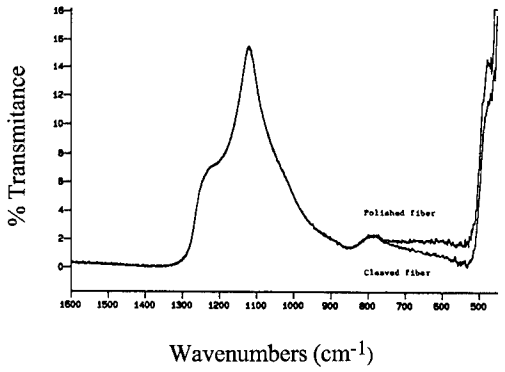


Figure 2. FT-IR spectra of cleaved and polished fiber endfaces.

We probed about 1 μm into the glass fiber endface before and after polishing, looking for the presence of the residual water, polishing agent, or any compositional changes as the result of leaching or stuffing during polishing. We used an energy dispersive x-ray analyzer on ESEM for chemical analysis. All the results indicate no compositional changes of the glass surface. Therefore, a structural change (change in density) occured without the compositional change, as shown in Figure 2 near 800 cm^{-1}.

Table 1 summarizes the results of typical surface profile scans of fibers inside the ferrules, as polished and etched up to 3.5 minutes. The etching rate was 0.02 μm/min.

Table 1

Time (min)	h (μm)	Δ h (μm)
0	0.268	---
1.0	0.248	0.02
1.5	0.235	0.033
3.5	0.206	0.062

Here h is a height of the fiber above the ferrule and Δh is the change in fiber protrusion after an etching interval.

Figure 3 shows the surface profile of a protruding fiber in one of the assembled connectors. This profile, ESEM image in Figure 4 and AFM image in Figure 5 of the etched fiber surface after 3.5 minutes does not show any significant etching pits.

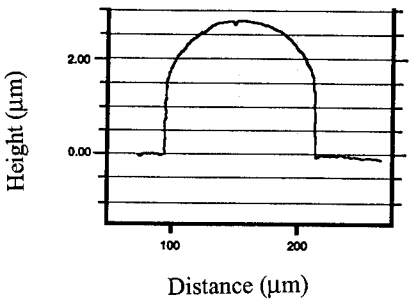


Figure 3. Surface profile of protruding fiber in a connector.



Figure 4. ESEM image of the connector endface after etching.

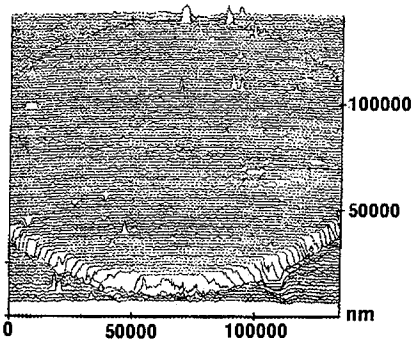


Figure 5. AFM image of the connector endface after etching.

Table 2 presents optical performance (reflectance values) of typical connectors before and after etching as measured by the OTDR. We used an index matching gel (Nyogel OC 431A) to be able to establish the reflectance of the single unmated connector.

Table 2

Endface Conditions	Connector 1	Connector 2
R1	-42 dB	-42 dB
R2	-42 dB	-43 dB
R3	-62 dB	-72 dB

R1 - as is, after polishing
R2 - 2 minutes etch
R3 - additional 6 minutes etch

DISCUSSION

It has been ascertained that a thin layer (about 0.1 μm thick) with increased index of refraction is formed at the polished surface of glass [4] as shown in Figure 6.

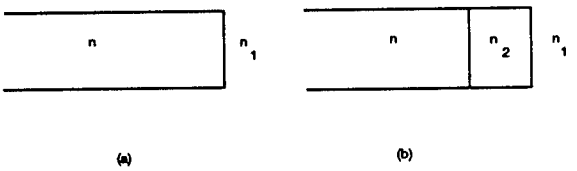


Figure 6. The model of (a) a cleaved and (b) a polished endface with the high index layer.

Here n is a bulk glass refractive index; n_1 is an air refractive index and n_2 is a refractive index of the surface.

A possible explanation for the increase index of refraction of the polished glass surface could be stresses during abrasion, a chemical reaction or an increased density. The results of elemental analysis suggest that there are no compositional changes of the glass surface after polishing. The details of the densification of glasses in the rigid state, at room temperature are still unknown. It has been shown experimentally for fused silica that the index of refraction varies from 1.46 to 1.54 for the densified silica exposed to about 10^7 psi pressure (150 kbars) [5].

In the glass community, the mechano-chemical mechanism of polishing is presently accepted [2]. A recent study that examined the process of glass polishing suggests that there is a transition from brittle to ductile mode grinding for an abrasive size under 1 μm [6] and that a very high surface stress (> 1 kbar) is introduced during polishing. The polishing of glass with very fine abrasives can also result in smearing of the surface layer, i.e., a plastic deformation that covers the permanently disrupted layer.

The subsurface damaged layer can not be examined by techniques such as AFM or SEM that probe surfaces. Therefore we have employed IR spectroscopy to probe about 5 μm deep into the glass. Figure 1 compares two cleaved fibers; the spectra are typical of SiO_2. The 1100 cm^{-1} band arised from Si-O-Si stretching vibrations and the band near 800 cm^{-1} is identified with bond bending modes [7]. The densification in silica could occur by rotating SiO_2 units (changing the bond angle of Si-O-Si) accompanied by a decrease in void volume. A previous infrared study of SiO_2 polymorphs confirmed the existence of 6-coordinated Si with an index of refraction, n = 1.77 [8]. The densities of other polymorphs varied from 2.2 g/cc to 2.9 g/cc with the corresponding indices of refraction varying from 1.46 to 1.6 [9]. This evidence for the existence of compacted silica, combined with the proposed polishing model, helps us to interpret the subsequent spectra. Figure 2 compares a polished fiber in a commercial connector (measured reflectance -48 dB) to that of a cleaved fiber. As in Figure 1, the spectra are nearly identical except for the slight increase in intensity between 800 and 500 cm^{-1}. We consider these results as the first evidence of the presence of densification at the fiber endface due to rotating SiO_2 units and changing the bond angle of Si-O-Si.

We also performed molecular dynamics computer simulations for silica [3], which showed the substantial permanent densification of silica under compression at room temperature without fracture. Our calculations show an unexpected hysteresis (large density change) associated with the change of strain $d\epsilon = -0.04$.

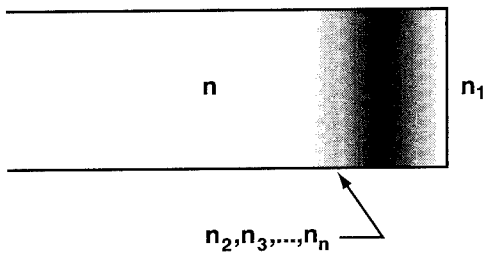


Figure 6. Model of polished endface with a graded refractive index at the surface.

Based on the results of our FT-IR microsampling spectroscopy and modeling, our understanding of the polished fiber endface is that the surface layer is a graded refractive index layer as depicted in Figure 6. We propose that this densified subsurface damage layer is responsible for the increase in reflectance in optical connectors. The precise value of the refractive index and the thickness of the damaged subsurface layer vary with polishing variables such as pressure, chemistry, the size of the abrasive particles, and the fluids used during the polishing.

The stability of the densified glass is of concern because the hydrolysis reaction or corrosion of the glass surface is enhanced due to the increased reactivity of highly deformed bonds in the densified glass. Therefore, it is good practice to remove the surface layer by special polishing or etching, not only because of the undesirable optical properties, but also to achieve long-term physical stability of the glass, thus enhancing the reliability of the mated connector.

The presence of etch pits is a major concern when using a chemical etch to remove the surface layer. Silica glass surface inhomogeneities such as clusters of silanols or of exposed siloxanes can lead to differential dissolution of silica in various chemical environments. Figures 4 and 5 both show only minimal surface etch pits after the etching period required to improve the reflectance values significantly (more than 2 minutes).

Table 2 shows that the etching does improve the reflectance of the individual connector plugs. For ease in tracking the etching process, the connectors used in this experiment were assembled with highly protruding fibers; consequently they were not well suited for proper mating with each other. Therefore we measured the reflectances of these connector plugs using an index matching gel at the fiber endface.

The tighter conditional requirements in Bellcore's Generic Requirements for Optical Fiber Connectors [10] state that connectors intended for use in AM-VSB systems require a reflectance not exceeding -55 dB, with a conditional objective calling for -65 dB.

The measurement accuracy of these very low reflectance values near or below the measurement system reflectance brings to light a potential measurement limitation. The possible reflectance contribution from fusion splices, the limitations that noise imposes on the value of the reflectance, the importance of the backscatter level of different fiber types and the effects of OTDR pulse widths on the measurements have to be considered. Some ambiguity in the value of the backscatter coefficient still exists and as a result, a different reflection modeling method has been proposed that takes into consideration the pulse waveform, the optical fiber and the receiver impulse responses of the OTDR [11]. We have confirmed during our measurements that the system has to be calibrated close to the region of interest for the individual fiber backscatter level.

SUMMARY

Two performance criteria for an optical connector are loss and reflectance. Reflections occur at index discontinuities such as the higher index layer created during the polishing of the connector's endface. We propose that the densified *subsurface* damaged layer is responsible for the increase in reflectance of optical connectors, based on the results of FT-IR microsampling spectroscopy and modeling. The layer is less than 1μm thick and more complex than can be represented by a single surface layer.

The reliability of optical connectors has become an issue because of their increased use in the uncontrolled outside environment. The highly deformed bonds in the densified glass have increased reactivity and as the result the hydrolysis reaction or corrosion of the glass surface is enhanced. Therefore, removal of the densified layer will enhance not only the optical performance but also the physical stability - and hence the long-term reliability of the connector.

We have established that an etching rate of 0.02 μm/min using a buffered HF chemical etch improves the optical performance of connectors with high reflectance. We have shown that the quality of the surface after etching is sufficient not to affect optical performance.

ACKNOWLEDGEMENT

The authors would like to express appreciation to S. W. Martin at Iowa State University, Ames, Iowa for the FT-IR microscopy, and to R. A. Frantz for valuable comments. The experimental assistance of N. B. McLean and C. D. Burpee is very much appreciated.

REFERENCES

1. M. Corke and M. Goduco, "Recent Developments in Single Mode Connector Back Reflection Performance," Proc. 10th Annual NFOEC, June 12-16, San Diego, CA, 389-398, (1994).

2. L. Cook, "Chemical Processes in Glass Polishing," J. Non-Cryst. Solids, 120, 152-171, (1990).

3. E. M. Vogel, M. H. Grabow and S. W. Martin, "Role of Silica Densification in Performance of Optical Connectors," submitted to J. Non-Cryst. Solids (1995).

4. V. Shah, W. C. Young, L. Curtis, "Large Fluctuation in Transmitted Power at Fiber Joints with Polished Endfaces," Proc. Tech. Digest, OFC/IOOC '87, Paper TUF4, (1987).

5. F. M. Ernsberger, "Role of Densification in Deformation of Glasses Under Point Loading", J. of The Am. Cer. Soc., Vol. 51, No. 10, 545-547, (1968).

6. D. Golini and S. D. Jacobs, "Physics of Loose Abrasive Microgriding", App. Optics, Vol. 30, No. 19, 2761-2777 (1991).

7. G. H. Sigel, "Optical Absorption of Glasses", Treatise on Materials Science and Technology, Vol. 12, 5-89, ed. M. Tomozawa and R. H. Doremus, Academic Press, NY (1977).

8. R. J. P. Lyon, "Infra-Red Confirmation of 6-Fold Co-ordination of Silicon in Stishovite", Nature, Vol. 196, 266-267 (1962).

9. C. Fiori and R. A. B. Devine, "Ultraviolet Irradiation Induced Compaction and Photoetching in Amorphous, Thermal SiO_2 ," Mat. Res. Soc. Symp. Proc. Vol. 61, 188-195 (1986).

10. Generic Requirements for Single-Mode Optical Fiber Connectors, Bellcore Generic Requirements, GR-326-CORE, Issue 1, November 1994.

11. P. Blanchard, P-H. Zongo, P. Facq, J. Rochereau, "Very High Optical Return Loss Measurement Using OTDR Technique," NIST Special Publication 792, Technical Digest Symposium on Optical Fiber Measurements, pg. 31-34, Sept. 1990.

Eva M. Vogel is a Member of Technical Staff in Fiber Media and Component Reliability Group at Bellcore, Morristown, NJ. She received her Dipl. Chem. Eng. in Physical Chemistry and PhD degree in Ceramic Engineering from Slovak Technical University, Bratislava, Slovakia. She joined Bellcore in 1984 after working at Bell Telephone Laboratories since 1970. Her research on novel properties of electronic and optical materials is recognized internationally. At Bellcore, she is a subject matter expert for optical component reliability. Her work has resulted in 90 publications and five patents. Dr. Vogel is a Fellow of The American Ceramic Society.

Leslie A. Reith received a BA degree from New York University in 1975, the M.Phil. degree from the City University of New York in 1979, and the Ph.D. degree from The University of Texas at Austin in 1981, all in physics. In 1981 she joined AT&T Bell Laboratories as a Member of Technical Staff and in 1984 she subsequently joined Bellcore. In recent years she has been working on performance and reliability issues related to optical connectors and splices and has been active in national standards activities for fiber optic components.

Edgar D. Beebe is an engineering analyst in the Fiber Media and Component Reliability Group at Bellcore, Morristown, NJ. He joined Bell Laboratories in 1972 where he worked on the development of long wavelength integrated optoelectronic devices. Since coming to Bellcore in 1984 his work has involved the design and fabrication of nanometer scale optoelectronics and more recently optical fiber and component reliability.

Joshua Brickel received a B.Sc. and MS from Columbia University in 1988 and 1990 respectively. He joined Bellcore in 1992 as a Member of Technical Staff. Since joining, Joshua has been active in the area of fiber media and components, specializing in optical fiber connectors. Currently, he authors three Bellcore Generic Requirement documents concerning optical connectors. Additionally, he participates in the TIA/EIA committees which impact optical connectors.

AUTOMATED ASSEMBLY AND INSPECTION SYSTEM FOR SC OPTICAL CONNECTOR

Akira Nagayama, Takashi Yoshizawa, Kunihiko Sasakura, Shigemitu Oguchi, Tadao Saitoh and Shigefumi Hosokawa

NTT Interdisciplinary Laboratories
3-9-11 Midori-cho Musashino-shi Tokyo 180 JAPAN

Abstract

To greatly reduce the assembly and inspection cost of the SC optical fiber connector, we developed a new system that automates all assembly and inspection processes from optical fiber cord cutting to optical performance inspection of the assembled connectors. The system has three subsystems corresponding to the processes for ferrule-fastening to an optical fiber cord, ferrule polishing and polished surface inspection, and connectorizing and optical performance inspection. This system has a building-block configuration based on these subsystems, making it suitable for step-wise automation. The fully-automated system, which consists of all three subsystems and a system control module, can be operated at the tact time of approximately one minute per terminal. Test results of the prototype system employing high-yield-rate, high-performance advanced PC polishing technology and high-speed, high-precision polished surface inspection technology demonstrate the feasibility of an automated assembly and inspection system for SC connectors.

Introduction

The SC type optical fiber connector (SC connector) is being used extensively as an internationally standardized key optical component. However, since assembly and inspection for SC connectors depend on manual handling, the assembly and inspection cost is still very high, making up nearly two-thirds of the total manufacturing cost. Manual handling also causes various quality problems. Therefore, automation of the assembly and inspection of SC connectors is essential.

A few automated assembly systems for SC connectors have been developed [1]-[2]. However, those conventional systems do not realize full automation of the assembly, nor do they deal with automation of inspection.

To reduce the assembly and inspection cost of SC connectors dramatically, we developed a new system which can automate all assembly and inspection processes from optical fiber cord cutting to optical performance inspection. The system is suitable for step-wise automation, and is basically applicable to automation for other optical fiber connectors such as the FC type, ST type and the Plug-in type used mainly in Japan.

This paper explains the system concept and configuration. The new technologies for advanced PC polishing and polished surface inspection adopted in the system are also presented. Furthermore, test results of the prototype system are described.

1. Development Concept

The system (Fig.1) is based on three development concepts. The first is a building-block system configuration, which enables manufacturers to smoothly change manual assembly and inspection lines to fully-automated ones by step-wise introduction of the work modules developed here. Analysis of manual assembly and inspection processes for SC connectors verified that optical fiber connectors were manufactured through three main processes: ferrule-fastening to an optical fiber cord, ferrule polishing and inspection, and connectorizing and optical performance inspection. Therefore, three subsystems corresponding to the three main processes were employed as the basic units for building-block extension. The system is thus

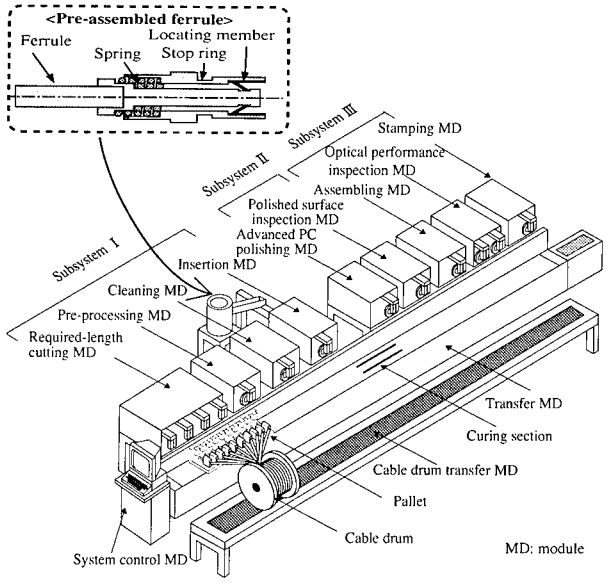


Fig. 1 System outline

composed of nine work modules, a system control module and a transfer module. To apply the system to automation for other optical fiber connectors such as the FC, ST and Plug-in types by making a small change, the handling mechanism in each work module was designed to take hold of the ferrule, which has the same diameter of 2.5mm for all types of connector.

The second development concept is an SC type pre-assembled ferrule suitable for automated assembly [3]. The pre-assembled ferrule is shown in Fig. 1. Since a contrived locating member is adopted, the ferrule, spring and stop ring can be automatically pre-assembled into one component compatible with the conventional SC connector parts specified in the Japanese Industrial Standards. This new component reduces the number of work modules required in the system and simplifies field assembly.

The third concept is the use of new technologies to achieve high-performance, high-reliability, and low cost. Especially, taking account of the importance of reducing return loss in analog signal transmission, an advanced PC polishing and polished surface inspection technologies were thoroughly investigated.

2. System Configuration

2.1 Building-block Configuration

Nine work modules having the same mechanical and electric interfaces form three subsystems. These subsystems can be connected in series, and together with a system control module, make a fully-automated system.

Subsystem I is composed of a required-length cutting module, a pre-processing module, a cleaning module, an insertion module and a related transfer module with an inline curing section (Fig. 1). An optical fiber is glued to a pre-assembled ferrule through several processes in this subsystem. This subsystem dominantly affects the reliability of optical fiber connectors.

Subsystem II consists of an advanced PC polishing module, a polished surface inspection module and a related transfer module. Within this subsystem, a pre-assembled ferrule with an optical fiber cord is polished to the quality of advanced PC and the polished ferrule surface is inspected. This subsystem dominantly affects the performance of optical fiber connectors.

Subsystem III is composed of an assembling module, an optical performance inspection module, a stamping module and a related transfer module. In this subsystem, the connector body and polished pre-assembled ferrule are assembled, its optical performance is tested and the product number is stamped on the optical fiber cord. The quality of the assembled optical fiber connectors is tested in this subsystem.

The related transfer modules corresponding to a subsystem can be connected to each other. The transfer module composed of these related transfer modules synchronously transports pallets. A pallet can hold ten optical fiber cord terminals. The system must also be applicable to assembling SC connectors to an optical fiber cable with many optical fiber cords. From this point of view, a cable drum transfer module with a synchronous transportation function is provided.

2.2 Multi-functional Pallet

The assembly and inspection processes for SC connectors are so complicated that the pallet must have many functions. The main requirements are as follows.

(1) To be capable of holding more than four optical fiber cord terminals, which is necessary for dual-type optical fiber cords and optical fiber cables

(2) To hold an optical fiber cord accurately enough to be handled by a robot in each work module, in spite of its end shape change

(3) To hold connector parts such as crimp ring and boot into which the optical fiber cord must be inserted for connectorization

(4) To provide an inline ferrule heating function for fastening an optical fiber cord by using a thermo-hardening adhesive

Figure 2 depicts the outline of the newly developed pallet. The pallet can hold ten optical fiber cord terminals. Thus, it can be used for both optical fiber cords and optical fiber cables.

As for the holding function of the shape-changing terminal, an optical fiber cord is held by the crimp ring holder in cantilever style at the beginning of assembly. After fastening a pre-assembled ferrule to the optical fiber cord terminal, the ferrule terminal is held in a ferrule holder which has a bore with a tapered entrance (Fig.2). Just after assembling a connector body to the ferrule, the

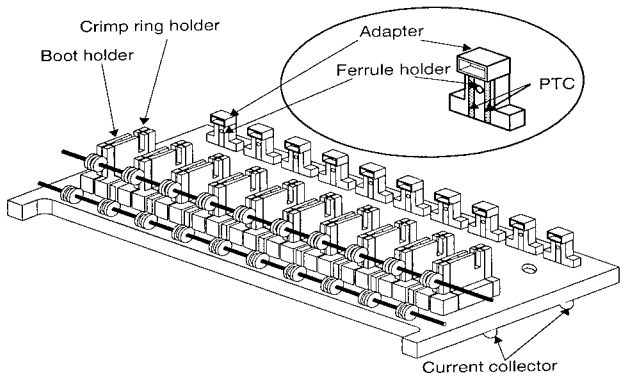


Fig. 2 Pallet outline

adapter on the pallet holds the terminal. To guarantee repeated use, the adapter is made of an abrasion resistant material.

Concerning the connector part holding function, a crimp ring holder and a boot holder are attached to every optical fiber cord position on the pallet. A crimp ring and a boot are set in these holders by a robot of the required-length cutting module.

Regarding the ferrule heating function, each ferrule holder is sandwiched between two positive temperature coefficient thermistor (PTC) elements. The electrical resistance of the PTC element remains low until its critical temperature, while above this temperature it increases suddenly to the extent of an insulator. Thus, the PTC element can be used as a self-regulating heater which is heated to and kept at the critical temperature by simple power control. The pallet has a pair of current collectors at the bottom. The corresponding power supply lines are attached to the curing section of the transfer module, so that the adhesive curing can be completed during pallet transport. The curing temperature can be controlled by changing the critical temperature of the PTC element. The curing time can also be controlled by changing the transport speed or the length of the power supply lines.

2.3 System Control Module with High-availability

Four types of optical fiber connectors (SC, FC, ST and Plug-in) and three kinds of optical fiber cords with different outer diameters (3mm, 2mm, and 0.9mm) are common in Japan. To apply the system to these various connector-cord combinations, each work module has a handling robot whose working range can be changed by varying its operation parameters.

The system control module has three functions. The first function is to transmit the operation parameters to each work module. Operation parameters such as the length of removed PVC sheath and the inspection specifications differ according to the type of optical fiber connector. As for the advanced PC polishing module, the optimal polishing velocity and force in each polishing process may be specific to each manufacturer. Taking such adaptability into consideration, the system is designed to work under flexible operation parameters transmitted through the system control module.

The second function is quality control. To guarantee optical fiber connector quality, the system inspects the surface shape of each polished ferrule and the optical performance of each optical fiber connector. The two inspection modules send their data to the system control module. The data are stored in the system control module along with the production number of the optical fiber connector.

The third function is to serve as a relay base in a remote maintenance system. To realize a quick and adequate response, the remote maintenance system can be constructed by connecting the system control module to a terminal of a distant maintenance center through a public data network. To realize remote maintenance completely, the system control module provides a security administration function for connection to the terminal of the maintenance center, a permission administration function for remote contact with the work module to be maintained, and a file administration function for a diagnostic program.

3. Advanced PC Polishing Technology

3.1 Basic Technology

The newly developed advanced PC (AdPC) polishing technology has the following two main features.

(1) Vertically Mounted Divided Area Polisher

An essential cause of low productivity in the high-performance polishing characteristic of conventional polishing machines is that the polisher must be changed for grinding, coarse polishing and AdPC polishing. This problem also results in an expensive automated polishing machine.

To solve these problems, we developed a divided-area polisher (Fig.3). The polisher is divided into three concentric areas for grinding, coarse polishing, and AdPC polishing. Thus, AdPC polishing can be completed without changing the polisher and by pressing the ferrule against each area of the polisher in order. This polisher can be mounted vertically, another difference from conventional polishing machines. This simplifies the ferrule handling mechanism of the polishing machine, because it is not necessary to change the horizontal ferrule attitude required for transporting the pallet. To be free from scratches on the polished ferrule surface, an inner partition ring is installed to prevent the mixture of polishing agents between coarse and AdPC polishing.

(2) Active Control of Polishing Force

A ferrule end is polished to a spherical contour by being pressed against the polisher made of a tensioned elastic film. Therefore, the accuracy of the radius of curvature for the polished ferrule surface depends on the accuracy of the force with which the ferrule is pressed against the polisher. In conventional handling by a robot, however, some error in this force is inevitable. To solve this problem, we developed an active control for polishing force that maintains a constant contact force between the polisher and the ferrule. This active control is programmable, so the polishing force can be optimized for each polishing process.

3.2 Advanced PC Polishing Module Structure

Figure 3 shows the outline of a prototype of the AdPC polishing module [4]. A robot (not shown in Fig.3) holds a ferrule on the pallet and inserts it into the chuck mechanism of the module. The chuck mechanism, which is fixed to a voice coil motor (VCM) with a linear guide, moves forward to the vertically mounted polisher. To achieve a compact, economical module, the polisher is driven directly by a spindle motor. In addition, the VCM is used as the active pressing element to obtain the optimal polishing force for each polishing process. The two kinds of polishing agents employed in the prototype are supplied by automatic polishing agent suppliers.

Considering both a total polishing time of less than one minute and high polishing performance, various polishing conditions were determined. The required polishing performance involves shape accuracy (Table 1) and a return loss of more than 45dB.

3.3 Polishing Performance

Test results for the prototype show that the process times are 6 seconds for grinding, and 20 seconds each for coarse and AdPC polishing. Including the 24 seconds needed for cleaning off the polishing agents, the total polishing time is 70 seconds. It obviously takes much time to clean off the polishing agents, but a shortened cleaning time results in scars on the ferrule surface, thus increasing in the reflection there. To solve this problem, an improved cleaning method is under investigation.

The vertex eccentricity and the fiber withdrawal from the ferrule measured for the prototype are shown in Fig. 4. The specifications shown in Table1 clearly are satisfied.

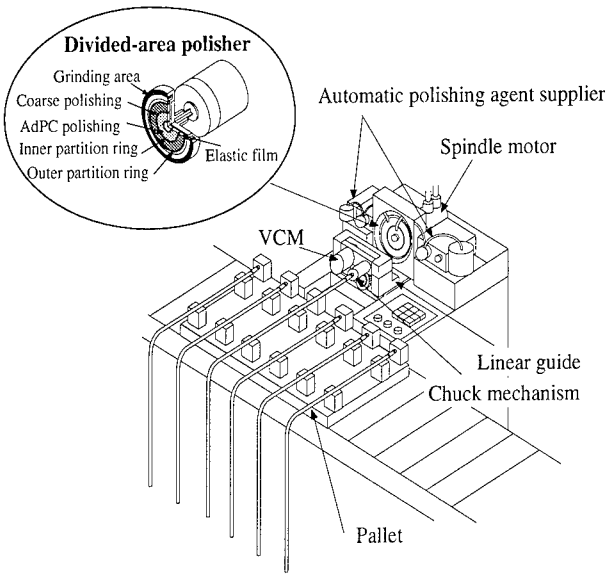


Fig. 3 Outline of AdPC polishing module

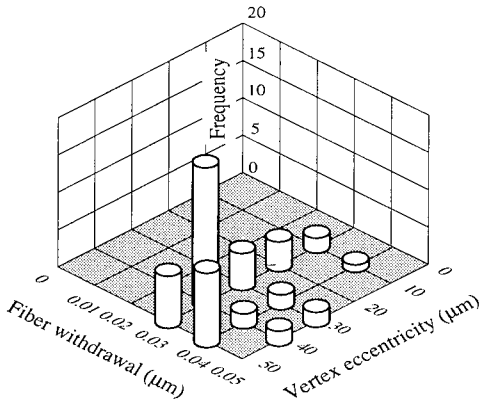


Fig. 4 Polishing characteristics

Table 1 Specifications of Polished Surface Shape

Radius of curvature	10 ~ 25 mm
Vertex eccentricity	less than 50 μm
Fiber withdrawal/protrusion	-0.05 ~ +0.1 μm*

*Minus sign indicates fiber withdrawal; plus sign indicates fiber protrusion

4. Polished Surface Inspection Technology

4.1 Basic Technology

The parameters of a polished ferrule surface, such as vertex eccentricity, radius of curvature and fiber withdrawal, are usually inspected one by one by different inspectors. This is an obstacle to lowering inspection cost and raising productivity. To make a breakthrough in this point, we developed a new inspection method which makes it possible to inspect the multiple parameters simultaneously by using an interference image of a ferrule surface.

The model shown in Figs. 5 explain the principles of this method. A longitudinal section near the end face of the ferrule to be inspected is shown in Fig.5(a); its interference image signal is shown in Fig.5(b). Here, the inspection section must be selected so as to involve the ferrule vertex and the fiber center. To determine the fiber center position, we devised a new method in which the center of the beam emitted from the ferrule under inspection is detected using image processing, when the other ferrule is lighted. The ferrule vertex is obtained by processing an intensity distribution of the interference image.

For rapid image data processing, we normalized the aspect ratio of a charge coupled device (CCD) image area and made a correspondence between the data of the inspection section and a series of interference image signal data in a processor using the Affine transformation technique.

The vertex eccentricity, shown as E in Fig.5(a), is defined as the distance between the fiber center and the vertex or the

highest point on the polished surface. Thus, this parameter can be inspected by simply determining the fiber center coordinates. The radius of curvature, shown as R in Fig.5(a), can be obtained by substituting an interference fringe coordinate X_1 and the next interference fringe coordinate X_2 into eq.(1).

$$R = [X_1^2 + \{ (\lambda/2)^2 - X_1^2 + X_2^2 \} / \lambda^2]^{1/2} \quad (1)$$

λ is the wavelength of the light source

The fiber withdrawal, shown as W in Fig.5(a), is defined as the distance between a fiber end face and a virtual spherical surface fitted to the spherically polished ferrule end face. It is assumed that the ferrule end face is spherical. The distance between the two points in the axial direction can be detected by the phase difference in the interference fringes. Therefore, we employed the fringing scanning method to inspect the fiber withdrawal. In that method, the ferrule under inspection must be moved precisely. A piezo-electric actuator with a positioning resolution of 10nm is used.

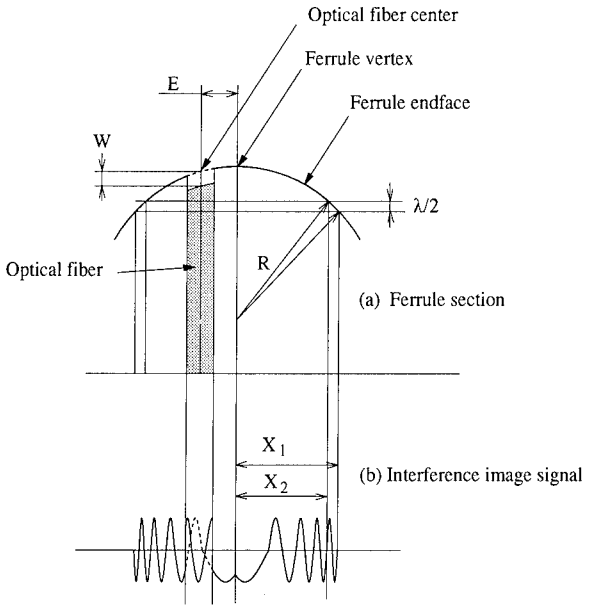


Fig. 5 Model of ferrule section and its interference image signal

4.2 Polished Surface Inspection Module Structure

Figure 6 depicts the outline of a prototype of the polished surface inspection module [5]. A pair of polished ferrules on the pallet are taken into this module by a robot with two hands. The ferrule to be inspected is set into a V groove, and the other ferrule is set in an illuminator. The interference optical system is attached along the V groove. To obtain a high-quality interference image with a low-cost optical system, a two-beam interference technique is employed. Green light produced from white light by an interference filter (wavelength=546 nm) is also used to obtain a high-precision interference image.

The most important point in the module design is to position the center and end face of the ferrule to be inspected at the focal point of the optical system. For high-precision positioning of the ferrule center, the V groove is made of low-friction ceramics. To compensate the ferrule center positioning error, the center of the beam emitted from the ferrule is detected using image processing. Thus, even a small position error of the ferrule center in the V groove does not affect the inspection for the vertex eccentricity. On the other hand, a high-precision positioning of the ferrule end face to the focal point is achieved by compensating the V groove axial position using a piezo-electric actuator.

The image processing speed was much improved to realize the total time of less than one minute for the inspection of the three parameters (vertex eccentricity, radius of curvature and fiber withdrawal). In addition, the prototype provides a Laplacian filtered microscopic image of the ferrule end face. Operators can use this microscopic image to evaluate scars quantitatively.

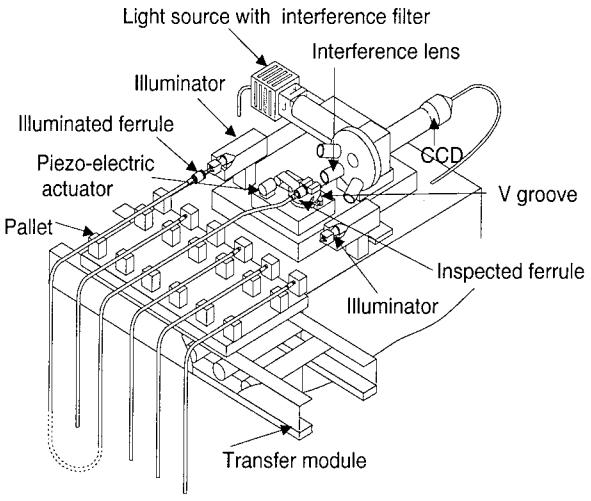


Fig. 6 Outline of polished surface inspection module

The target resolutions in the inspection are less than one-tenth of the polished surface specifications for SC connectors. The specifications of the module are summarized in Table 2.

Table 2 Specifications for Polished Surface Inspection Module

	Inspection range	Resolution
Radius of curvature	5 ~ 30 mm	1 mm or less
Vertex eccentricity	0 ~ 70 μm	5 μm or less
Fiber withdrawal	-0.135 ~ +0.135 μm*	0.01 μm
Inspection time	1 minute or less/terminal	

*Minus sign indicates fiber withdrawal; plus sign indicates fiber protrusion

4.3 Inspection Performance

The repeatability of setting the ferrule at a constant position is important for the polished surface inspection module, because it limits the magnification of the optical system and therefore the inspection resolution. Figure 7 shows a measured example of the repeatability. The position of a sample ferrule center in a X-Y plane orthogonal to the optical axis was measured by detecting the center position of the beam emitted from the sample ferrule, when the other ferrule connected with the sample ferrule is illuminated. The results show that the dispersion of a ferrule center position in the V groove is nearly one pixel. Considering that the permissible dispersion is five pixels, which is determined by the inspection area limitation, the settling repeatability is practically sufficient.

To verify the inspection accuracy, we inspected many sample ferrules which had been polished to the AdPC by using both a conventional inspector (made by ZYGO™) and the prototype. Figures 8 show examples of the comparison. These results show that the radius of curvature and the fiber withdrawal obtained by the developed method correlate well with the results of conventional inspection. The deviation between two inspections is less than 10% for each inspection parameter, confirming that the module has sufficient accuracy for practical use.

Furthermore, the module based on the new method using image processing technique proved that it is possible to inspect multiple parameters of a polished surface in less than one minute.

5. Test Results of the Prototype System

The prototype system, which is a nearly fully-automated system, is shown in Photo 1. The system is composed of eight work modules, a system control module and a transfer module. It is 10m long, 2m wide and 1.5m high.

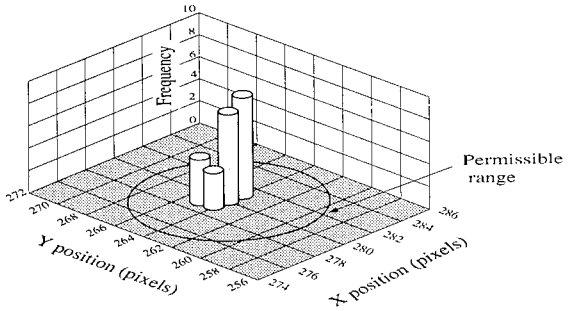
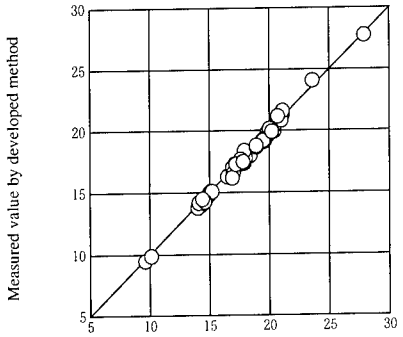
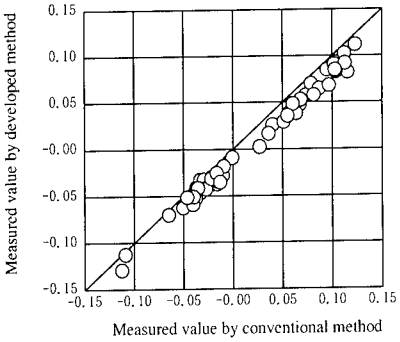


Fig. 7 Setting position distribution



(a) Radius of curvature (μm)



(b) Fiber withdrawal (μm)

Fig. 8 Comparision between conventional method and developed one

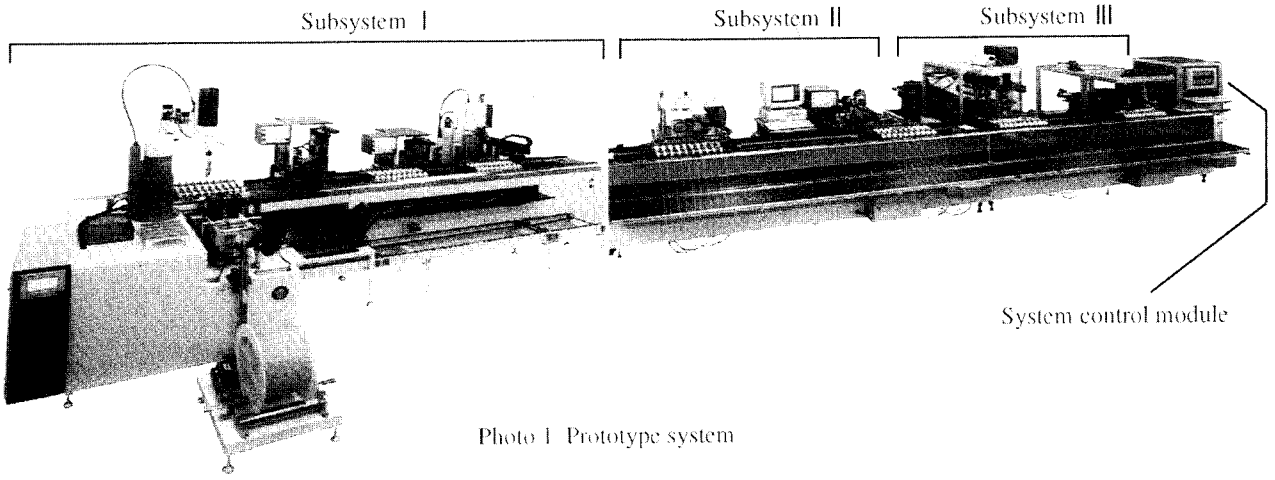


Photo 1 Prototype system

Table 3 shows the test results of the system performance obtained by a series production test of 118 SC connector terminals. The tact time was 75 seconds, which was mainly caused by a long process time, including ferrule cleaning in the AdPC polishing module. The other work modules were completed operation in less than one minute. The total production time for 118 terminals was 9370 seconds including a downtime of 520 seconds. Thus, the operating efficiency is estimated to be 95%. The system was down three times during the production test because of a failure in inserting the ferrule into the pallet, a failure in loading the optical fiber cord into the pallet, and stopping to replace the elastic film of the polisher.

Figure 9 shows the optical performance of SC connectors obtained from the series production test. The average insertion loss is 0.06dB; the average return loss is 47dB. Considering the specifications (insertion loss: less than 0.5dB; return loss: more than 45dB) adopted by optical fiber connector manufacturers in general, only two terminals were out of specification. Therefore, the yield rate is estimated to be 97%. Dust particles or contamination was observed on the ferrule surfaces of the two defective terminals. Those terminals were inspected again after further cleaning, resulting in an improvement of return loss to more than 48dB. This implies that if a higher yield rate is required, the ferrule cleaning function must be enhanced.

These results show that an automated assembly and inspection system for SC connectors that can dramatically reduce the manufacturing cost is feasible.

Table3 Test Results of System Performance

Tact time	75 s/terminal
Operating efficiency	95%
Yield rate	97%

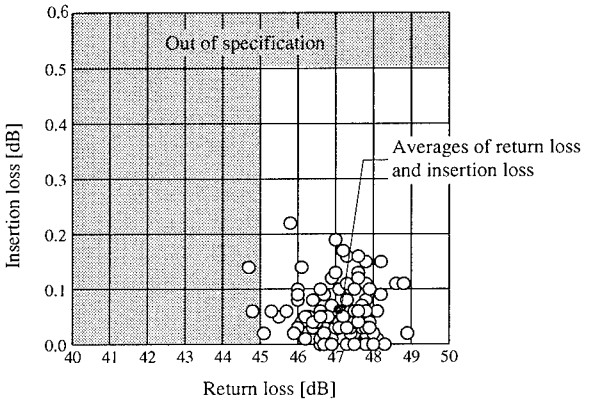


Fig.9 Optical performance of SC connectors manufactured by the prototype system

6. Conclusion

We developed an automated assembly and inspection system for SC connectors based on new concepts and technologies. This system has a building-block configuration suited to step-wise automation in accordance with production scale. It consists of three subsystems and a system control module. To realize a building-block configuration, the mechanical and electrical interfaces between the work modules and the transfer module are unified. With a small change, the system can be applied to other optical fiber connectors such as FC, ST and Plug-in types.

We developed and employed an SC type pre-assembled ferrule that is suitable for automated assembly because it reduces the number of work modules required. This pre-assembled ferrule also simplifies field assembly.

The system employs a new technology for an advanced PC polishing technology featuring a divided-area polisher and active control of polishing force, which enable high-yield, high-performance advanced PC polishing. A polished surface inspection technology featuring interference image processing enables high-speed, high-precision polished surface inspection. The vertex eccentricity, fiber withdrawal and radius of curvature can be inspected with a resolution of less than 10% of the respective specified values.

A tact time of 75 seconds per terminal, a yield rate of 97% and an operating efficiency of 95% were obtained in a production test for SC connectors using the prototype system. These results show that an automated assembly and inspection system for SC connectors is feasible.

Acknowledgments

The authors would like to thank K. Kato, Senior Research Engineer and Supervisor, and R. Nagase and K. Kanayama, Senior Research Engineers of the NTT Opto-electronics Laboratories for their contributions in developing the SC pre-assembled ferrule.

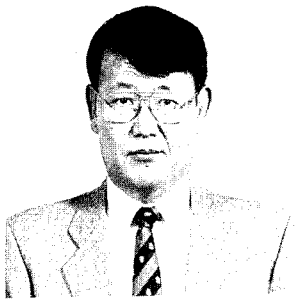
References

[1] J. Schulte, "Automated Mounting of Connectors to Fiber Optic Cables," Proceedings of 40th, International Wire and Cable Symposium, pp.303-308,1991.

[2] M. Tsuda, et al., "Automated Connectorizing Line for Optical Cables," Proceedings of 43th, International Wire and Cable Symposium, pp.781-789,1993.

[3] K. Kanayama et al., "Characteristics of an SC Type Optical Fiber Connector with a Newly Developed Pre-assembled Ferrule," IEEE Photo. Technol. Lett., vol. 7, pp. 520-522, 1995

[4] T. Saitoh et al., "High-speed High-Precision Optical Fiber Connector Polishing by Way of Sharing Polishing Film and Constant Pressure Control," in Autumn National Convention Record (IEICE, Japan, 1993), pp. 4-329
[5] K. Sasakura et al., "The Simultaneous Inspecting Method for the Shape of Polished Ferrule End Face by Using Two-beam Interference," in Autumn National Convention Record (Japan Society for Precision Engineering,1993), pp. 599-600



Akira Nagayama
NTT Interdisciplinary
Laboratories
3-9-11 Midori-cho
Musashino-shi Tokyo 180
JAPAN

Mr. Nagayama received B.E. and M.E. degrees from Osaka City University, Osaka, Japan, in 1967 and 1970. In 1970, he joined Musashino Electrical Communication Laboratory, Tokyo, Japan. He has been engaged in the research and development of servosystems for file memory systems, and automated main distributing frame systems.



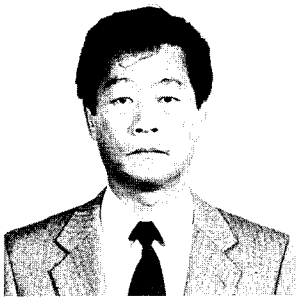
Takashi Yoshizawa
NTT Interdisciplinary
Laboratories
3-9-11 Midori-cho
Musashino-shi Tokyo 180
JAPAN

Mr. Yoshizawa received B.E. and M.E. degrees from Tohoku University, Sendai, Japan, in 1974 and 1976. In 1976, he joined Musashino Electrical Communication Laboratory, Tokyo, Japan. He has been active in the research and development of optical disk devices, and more recently optical fiber connector assembly systems.



Kunihiko Sasakura
NTT Interdisciplinary
Laboratories
3-9-11 Midori-cho
Musashino-shi Tokyo 180
JAPAN

Mr. Sasakura received a B.E. degree from Shizuoka University, Shizuoka, Japan, in 1980. In 1980, he joined Musashino Electrical Communication Laboratory, Tokyo, Japan. He has been active in the research and development of automated main distributing frame systems, and more recently inspection system for optical fiber connectors.



Shigemitu Oguchi
NTT Interdisciplinary
Laboratories
3-9-11 Midori-cho
Musashino-shi Tokyo 180
JAPAN

Mr. Oguchi joined Musashino Electrical Communication Laboratory in 1957 and has been engaged in the research and development of mechanical apparatus for magnetic disks, and mechanical apparatus for automated assembly systems.



Tadao Saitoh
NTT Interdisciplinary
Laboratories
3-9-11 Midori-cho
Musashino-shi Tokyo 180
JAPAN

Mr. Saitoh joined the NTT Musashino Electrical Communication Laboratory in 1959 and has been engaged in the research and development of assembly of optical components and polishers for optical fiber connectors.



Shigefumi Hosokawa
NTT Interdisciplinary
Laboratories
3-9-11 Midori-cho
Musashino-shi Tokyo 180
JAPAN

Dr. Hosokawa received the B.E. degree from Hohsei University, Tokyo, Japan, in 1967 and the Ph.D. degree from Tokyo Institute of Technology, Tokyo, Japan, in 1993. In 1967, he joined the NTT Musashino Electrical Communication Laboratory, Tokyo, Japan. He has been engaged in the research and development of magnetic tapes, mass storage systems, and automated main distributing frame systems.

TESTING OF OPTICAL CONNECTORS AND SPLICES IN HIGH-STRESS SERVICE ENVIRONMENTS

Leslie A. Reith and Rolf A. Frantz
Bellcore, Morristown, NJ 07960

ABSTRACT

Laboratory testing of optical connectors and splices is intended to determine both when and how they will fail under field service conditions. However, typical laboratory tests entail fewer stress factors, applied at significantly higher levels, than are present in the field. In addition, it is impossible to define a single "typical" field environment. Thus, we have established test sites in three very different, high-stress service environments: Louisiana, Maine, and Arizona. Dozens of connectors and splices have been installed in pedestals, aerial closures, and pole-mounted equipment boxes at these sites. After periods up to nearly three years of service, only a few optical performance failures have been observed, although other signs of physical deterioration are present. The failures have been in connectors, and are consistent with poor or intermittent physical contact between the fiber endfaces. Failures in mechanical splices at high humidity, seen in the laboratory, have yet to occur in the field. Monitoring of the components on test continues with the goal of correlating field degradation rates with those measured in laboratory tests.

INTRODUCTION

The installation and use of optical connectors and splices expose fibers to more hazardous environments than are typically encountered inside optical cables. In addition to environmental stresses such as temperature, humidity, and pollutants, the fiber experiences handling stresses as it is segregated, stripped, cleaved, and spliced or mounted in a connector. In the finished splice or connector, the fiber is subject to mechanical stresses—for example, the mating force in a connector or the clamping forces in a splice. Because these stresses act in combination on the fiber, the potential for failure is typically greater at a splice or connector than within a cable.

Laboratory experiments and aging studies typically attempt to identify and accelerate failures by applying one or more of these stresses at elevated levels. High temperatures are often combined with high humidities or with liquid water environments to accelerate the aging of the fiber. Temperature and humidity cycling are used to exercise fiber connections through such effects as differential thermal expansion and contraction of the component materials. However, it is impractical in the laboratory environment to apply simultaneously all of the stresses seen in typical field service. The combined effects of heat, humidity, mechanical stress, stress cycling, dust and dirt, condensation, and contaminants can typically be achieved only in actual service environments.

Bellcore has on an ongoing program to subject optical connectors and splices to three different high-stress service environments: (i) high temperature, temperature cycling, and dust/dirt; (ii) high temperature and humidity, cycling, salt fog, condensation, and pollutants; and (iii) wide-range temperature cycling to very cold temperatures, with moderate humidity. Components under test in these environments include dozens of connectors (representing five major commercial product designs), dozens of mechanical splices (representing five distinct designs), hundreds of fusion splices (made by different splicing technicians on a half-dozen different splicing machines), and a variety of other passive optical components (couplers, WDMs, electro-optic switches, etc.). Our goals are to understand the failure mechanisms of these components under multiple-stress environments, to correlate field failures and degradation rates with those measured in the laboratory, and to develop realistic models of and screening tests for potential failure modes.

We begin with descriptions of the field test sites and enumerations of the components on test. Typical (and atypical) performance data are presented as measured to date. Correlations between the field test data and the results of laboratory experiments are discussed. The capacity for expanded testing and an outline of what future tests are planned are described briefly.

FIELD TEST SITES

Morgan City, LA

This site was constructed in the back yard of the Amelia Central Office (CO) in Morgan City, which is located in the heart of the bayou country of Louisiana. This is an area noted for high temperatures (24-hour averages above 80 °F in the summer) and high humidities (frequently above 85% RH overnight). Trenches and pedestal bases reach the water table only a few inches below ground level. Salt fogs frequently drift in from the Gulf of Mexico. One aftermath of

Copyright © 1995 Bellcore
All rights reserved

the oil boom and bust is a significant amount of industrial pollution in and around the waterways.

The site was built during 1992–93; it includes 21 pedestals of both CAD-12 and CAD-6 sizes, arranged in three rows. Figure 1 gives a plan view of the site. In this figure, the CAD-6 pedestals are in the left-most string, while the center and right-side strings are CAD-12s. The pedestals in the right-most string contain 25W heat-dissipating resistors to simulate the heating caused by fiber-in-the loop electronics. The pedestals are connected to each other and to the CO by buried ducts housing fiber optic cables and shielded copper cabling.[1, 2]

The pedestals provide the test environments for a wide range of optical components:

• 33 connectors, of types FC, SC, ST, and MT. While most of the connectors are mated, some are not, and some of the unmated connector plugs are not covered with protective caps; this provides an opportunity to estimate the extent of contamination experienced by unprotected connectors in service.

• 19 mechanical splices, of four different designs. Each supplier's design takes a unique approach to the alignment and anchoring of the fibers. Most of these splices use an index-matching gel to optimize optical performance. In addition, over 60 fusion splices were made in the process of installing the various components.

• 15 branching components. These include 11 couplers and 2 WDMs which represent designs from ten different manufacturers. Also included are two electro-optic switches.

East Millinocket, ME

This site was constructed in the fall of 1994 on land behind the East Millinocket CO. It was designed to include both aerial and buried plant, and was specifically intended to track the response of optical fibers, cables, and components to bitterly cold temperatures and wide temperature cycles. Overnight low temperatures in northern Maine frequently drop to around -40 °C, due to radiational cooling on clear cold nights. Such nights are frequently followed by clear and sunny days, however, leading to significant solar heating of dark pole-mounted equipment boxes, black aerial cables and splice closures, and even medium-green pedestals. However, snow depths often approach or exceed the height of the pedestals, which then become insulated against the wide temperature swings—up to 55 °C—that can be experienced in the boxes and the aerial plant.[3]

A plan view of this site is shown in Figure 2. As in Morgan City, a buried fiber optic cable and buried innerducts connect the (CAD-12) pedestal and pole locations to each other and to the CO. Because of the concern about snow depth, both pedestals (labeled B1, B2, E1, and E2) and pole-mounted equipment boxes (labeled B3, B4, E3, and E4) were installed on or near the two poles closest to the CO rear wall. In addition, three cables were strung along the five-pole run, with one or more splice closures in each cable, distributed so that at least one closure is installed at each pole location. Because of the concerns about low-temperature-induced cable loss,[4, 5] these cables themselves were selected to be among the items tested at this site. In this paper, however, we are focusing on the connectors and splices under test; these include:

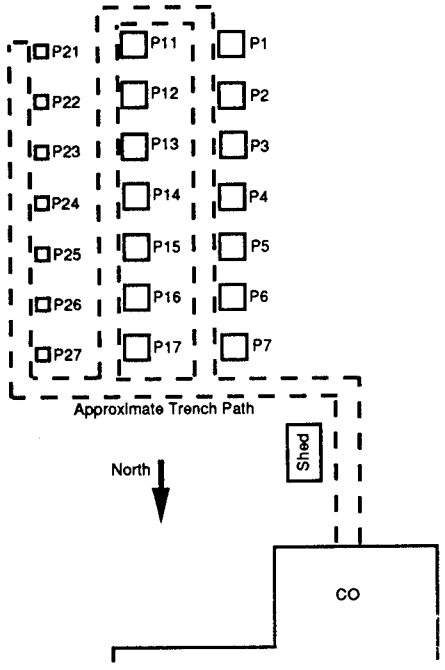


Figure 1. Site Layout in Morgan City, LA

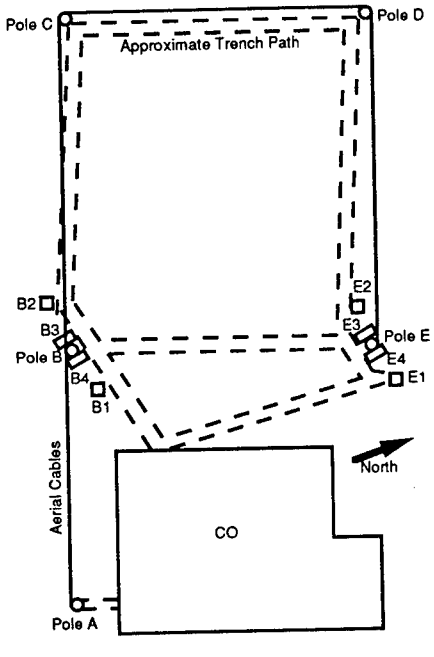


Figure 2. Site Layout in East Millinocket, ME

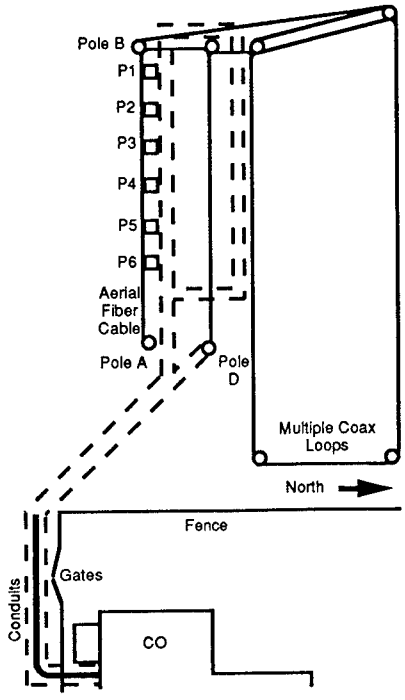


Figure 3. Site Layout in Phoenix, AZ

• 24 connectors, of types FC, SC, and D4. These connectors are all mated and are distributed among the pedestals and pole-mounted equipment boxes. None of the connectors are installed in the aerial closures, since at present it appears highly unlikely that such usage will occur in normal service.

• 31 mechanical splices, of four different designs. These splices are distributed among the pedestals and pole-mounted boxes and among the closures in all three aerial cables at all pole locations. In addition, in the installation of the connectors and branching components, over 100 fusion splices were made by several craft technicians, using different fusion splicing equipment.

• 10 couplers, from two different suppliers. These include both 1 x 8 and 1 x 2 designs.

Phoenix, AZ

This site, located in a field behind the Phoenix Northwest CO, was selected because of the very high summer daytime temperatures (often approaching 120 °F [about 50 °C]). In addition, the intense solar radiation (averaging over 22 million joules/square meter [almost 2000 BTU/ft^2] daily) causes significant solar heating, even in medium-green pedestals; temperatures above 65 °C have been recorded in pedestals at a site in Mesa, adjacent to Phoenix. These high temperatures occur at very low humidities, which offers the opportunity to differentiate between the effects of high temperature and the effects of combined high temperature and humidity as seen at Morgan City. Also, the relatively clear desert skies often allow a significant amount of nighttime radiational cooling, so large daily temperature cycles can occur.

Figure 3 shows a plan view of this site. Note that there are two aerial cable runs, with the upper loop in the figure being a coaxial cable network, where cables and components are being tested in parallel with, but independently from, the optical network. Six CAD-12 pedestals are arranged in an east-west line, spaced to maximize the exposure of each pedestal to solar heating. A four-pole run provides space for installing up to three aerial cables; the initial phase of testing includes one cable, with closures at poles A and D providing mounting locations for splices and connectors. These same types of splices and connectors are installed in the six pedestals; included are:

• 18 connectors, of types FC, SC, and ST. These are installed only in the pedestals. Three connectors of a common type are installed in a pedestal so that unmating and remating in a new configuration can be done at intervals, as would be expected in field service.

• 32 mechanical splices, of four different designs. These are distributed among the pedestals and the aerial closures. In addition, approximately 60 fusion splices have been made as part of the construction process.

DATA COLLECTION

Environmental monitoring

At all of the sites, the monitoring equipment tracks not only ambient temperature and humidity, but also the conditions inside each pedestal, equipment box, and aerial closure to provide a detailed environmental history of each splice and connector on test. Sensors are mounted in each of these locations and connected to computerized monitoring equipment inside the CO.

Because the Morgan City site was also intended to assess any differences in the internal pedestal environment that might arise due to different pedestal orientations and base treatments (gravel, foam sealant, etc.), two temperature/humidity sensors are installed in each pedestal, one near the top and one near the bottom. All components under test lie in the range between these two sensors. The sensors are polled by datalogging equipment inside the CO, and the data are stored in the control computer. In general, data are recorded every few minutes unless the temperature and humidity are unchanged from the previous reading. The data are downloaded to our offices in New Jersey on a weekly basis, and are reduced to hourly averages in order to simplify the daily, weekly, and monthly temperature and humidity plots.

In East Millinocket, the ambient temperature and the temperature at the midpoint of each splice tray (in the pedestals, boxes, and aerial closures) are recorded. Because of the emphasis on cold-weather testing, no localized humidity monitoring was included when the site was built; however, site conditions have suggested that warm-weather humidity data inside the pedestals and boxes may be useful in tracking the component behavior, and this capability is now being designed for addition to the site. The data are again recorded every few minutes and downloaded weekly to our offices; hourly averages have again been found to be sufficiently detailed for all data plots.

Despite the dry conditions in Phoenix, the East Millinocket experience prompted the inclusion of humidity monitors as this site was being constructed. Thus, sensors monitor both the ambient temperature and humidity and the conditions inside each pedestal and aerial closure, as close as possible to the midpoint of the splice trays on which the components are mounted. The site is being completed as this is written, and it is planned that data intervals, downloading, and plotting will be similar to what is done for the other two sites.

Optical monitoring

The optical monitoring system consists of a computer-controlled optical time domain reflectometer (OTDR), one or two optical switches, and an optional source and power meter. The system used in Maine and Louisiana, depicted in Figure 4, uses dual switches connected at opposite ends of

the looped test cables: one to measure loss and reflectance for each component in the forward direction and one to measure in the reverse direction. Measurements in the forward and reverse direction are averaged and stored in data files that are downloaded to our offices from all sites on a weekly basis. The measurement scheme is similar in Louisiana, except that all cable loops are terminated at a single switch, which still allows all connector and splice measurements to be taken in two directions and averaged. Components are concatenated as closely as possible, consistent with the necessary separation to avoid optical "shadowing," so as to maximize the number on test.

In addition, as shown in Figure 4, a source and power meter were included in Maine and Arizona to measure the cumulative loss through each cable loop. The additional measurements were intended to monitor cable loss at low temperatures in Maine, but have proven of sufficient value to be added to the later Arizona site as well.

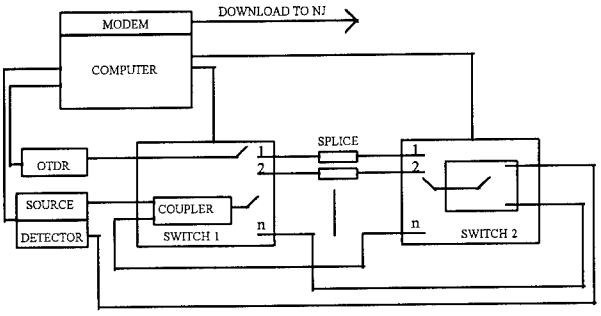


Figure 4. Optical Data Collection Layout

PERFORMANCE DATA

Louisiana temperature/humidity data

Figure 5 shows the maximum and minimum temperatures for a six month period from January through June, 1995 for an unheated pedestal. There are two sensors located in the pedestal, one near the top and one near the bottom. These data are typical for an unheated, medium-green pedestal with a gravel base. The maximum temperatures occur near the top of the pedestal where solar heating has the strongest effect, while the minimum temperatures occur at the bottom of the pedestal.

Figure 6 shows temperature and humidity variations from the top sensor in a heated pedestal during a one week period in June, 1995. The heater is located near the top of the pedestal and, in combination with solar heating, causes the top of the pedestal to be noticeably warmer than the bottom. As temperature increases (decreases) the relative humidity decreases (increases), maintaining an absolute humidity ratio (weight of water to weight of air) of approximately 0.02 to 0.03. Daily temperature swings in the pedestals are typically 20–30 °C. Four connectors, five mechanical splices, and eleven fusion splices are under test in this environment.

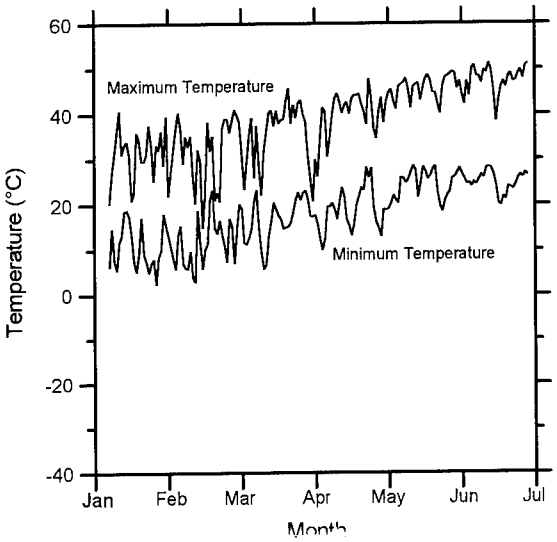


Figure 5. Maximum and Minimum Temperatures

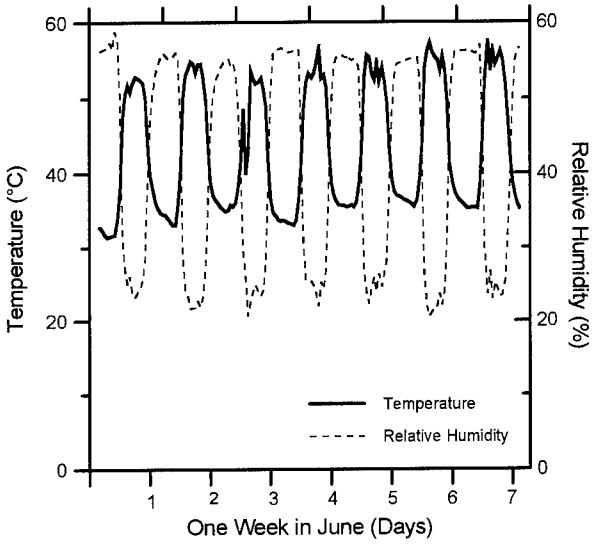


Figure 6. Temperature and Humidity Variations

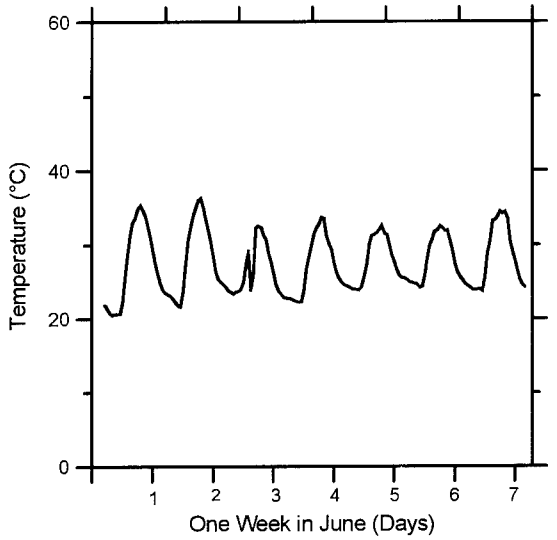


Figure 7. Ambient Temperature

Figure 7 shows the ambient temperature for the same week as shown in Figure 6. The difference in the minimum temperatures illustrates the effect of the heater in holding the temperature above ambient, while the difference in the maximum temperatures shows the effect of both the heater and solar heating.

Louisiana loss/reflectance performance

The optical performance of connectors is typically not strongly dependent on temperature. Figure 8 shows loss and reflectance data for an SC connector over the same time period as shown in Figure 6. Although the loss may show some temperature dependence, the reflectance is quite stable. The refractive index of the glass does not vary, so that as long as the fiber cores maintain good physical contact, the reflectance should remain constant. In the case of a mechanical splice, however, the temperature dependence is stronger. Since the fibers are not making good physical contact, pistoning effects due to temperature fluctuations are likely to be more pronounced. In addition, the refractive index of the matching gel varies with temperature, resulting in a reflectance variation (for perpendicularly-cleaved fiber ends) even if there is no fiber pistoning. This is illustrated in Figure 9, which shows loss and reflectance performance for a typical mechanical splice.

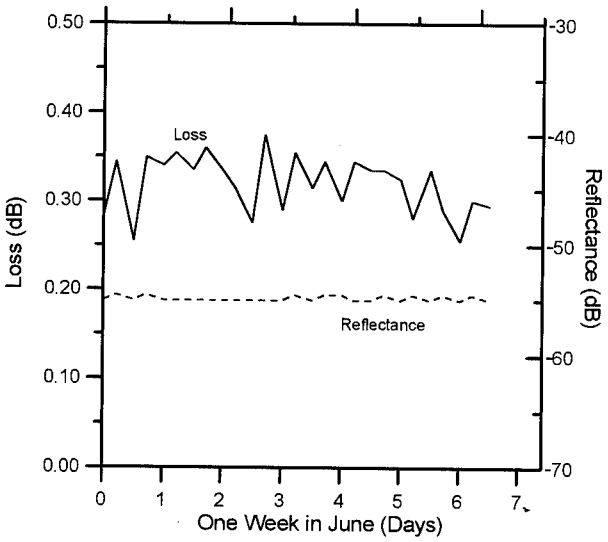


Figure 8. Loss and Reflectance for an SC Connector

After two years on test, there has been no evidence of performance degradation for fusion splices or for mechanical splices. Those splices that utilize a uv-curable adhesive as an index-matching medium had poor reflectance performance from the outset, due to the relatively poor index-matching ability of the adhesive. This made it difficult to track performance variations or degradation over time. We expect that much better reflectance performance would have resulted if the fibers had been cleaved at an angle. The loss performance of uv-curable splices did not show any signs of degradation over the two year period.

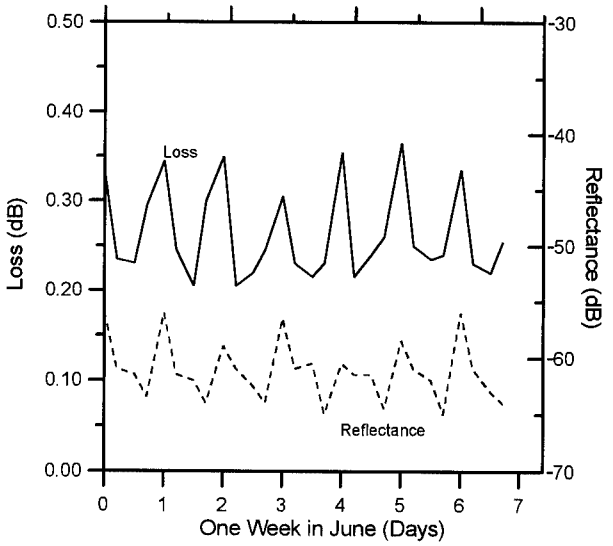


Figure 9. Loss and Reflectance for a Mechanical Splice

One connector has recently experienced reflectance performance degradation, the details of which will be discussed below. All other connectors have had stable performance over time.

Maine temperature data

Figure 10 shows the maximum and minimum temperatures from February through June, 1995 for a typical pedestal. The seasonal variation is quite pronounced compared with Louisiana (Figure 5). The pedestals in Maine are similar to those in Louisiana, so solar loading conditions are expected to be similar. Data shown in this figure come from a single sensor mounted near the components under test at the center of the pedestal; thus, the temperature extremes do not reflect any internal temperature gradients within the pedestal as they do when data from two sensors are plotted as in Figure 5.

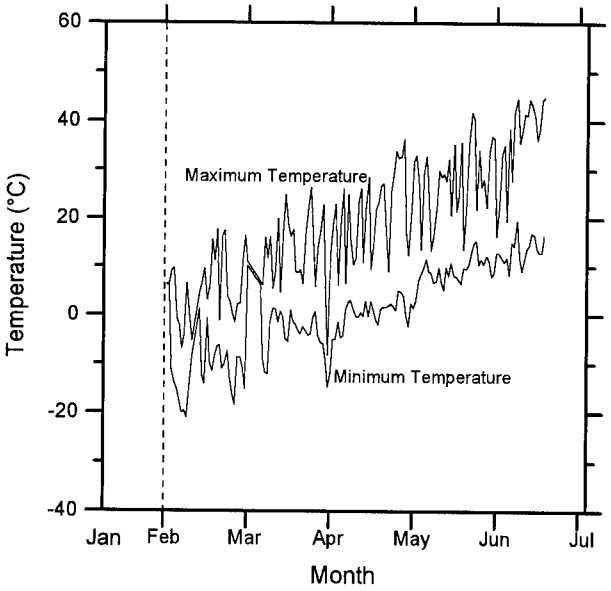


Figure 10. Maximum and Minimum Temperatures

Daily temperature variations are shown in Figure 11 for a typical pedestal, box, and aerial closure, compared with the ambient temperature. The daily variations are somewhat larger than the daily temperature swings in Louisiana, ranging from 25–35 °C inside the pedestals, boxes, or closures. This is due to two factors: daily ambient temperature swings are often larger, and the dark brown boxes and black aerial closures installed in Maine experience increased effects of solar heating.

In general, the aerial closures should experience wider temperature extremes than the ground-mounted pedestals, particularly in the winter months, when the pedestals may be insulated by a covering of snow. This winter, however, had little snowfall. The data collected since February indicate that the maximum difference in temperature between the box, pedestal and aerial closure internal temperatures was 10–12 °C during the winter and ~5 °C during the warmer weather.

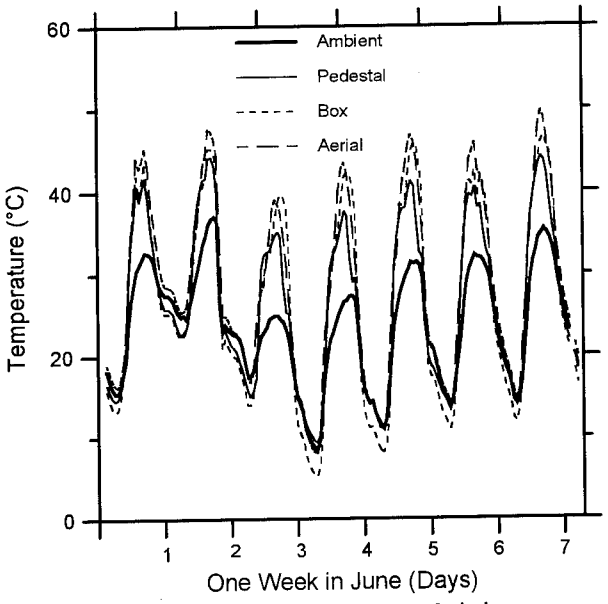


Figure 11. Daily Temperature Variations

Maine loss/reflectance performance

The performance of the fusion and mechanical splices in Maine has so far been similar to what we have seen in Louisiana. There have been no failures or unexpected variations in the performance. There have, however, been some reflectance variations in two of the connectors on test, which will be discussed in more detail in the next section.

Arizona

At the time of preparation of this manuscript, data from the Phoenix test site were not yet available. Earlier studies, however, give us some idea of what type of temperature variations we might expect.[6, 7] The maximum ambient temperature in the summer months is known to go as high as 50 °C. In an unheated medium-green pedestal, such as those installed at the Arizona site, solar loading would raise the temperature to >60 °C. It has been shown that pedestals that are painted white can reduce solar heating.[7] In this case the temperature increase over ambient is expected to be < 5 °C. Despite this fact, medium-green pedestals are still the most common color used. Thus, maximum pedestal temperatures, even without heaters, may be comparable to those in Louisiana.

The aerial plant in Phoenix is expected to be substantially warmer than the pedestals. The data from Maine suggest that the black plastic closures may have ambient temperatures as high as 5–10 °C above those of typical pedestals.

Optical components were placed on test during the last week in July, 1995, and data should be available within the next two to three months.

DISCUSSION

Field failures

One connector at the Louisiana site had an initially high reflectance upon installation. We replaced one of the connector plugs immediately and the reflectance was then acceptable. The connector plug that had been removed was brought back to the laboratory, analyzed, and found to have a recessed fiber. It seemed likely that the large initial reflectance was due to lack of physical contact between the fiber cores. Meanwhile, the connector in the field was found to have a varying reflectance, dependent on the temperature. We believe that the connector plug that was not replaced (which came from the same manufacturing lot) also had a recessed fiber so that only marginal physical contact occurs. This would result in a gap opening up between the fiber cores as the temperature increases, leading to variations in the reflectance. Although the reflectance performance varied with temperature, there was no sign of performance degradation for the first two years. However, the most recent reflectance data show a net degradation. When the component reflectance becomes larger than approximately –35 dB, the OTDR saturates and is no longer able to make accurate measurements. The reflectance gradually degraded during March and April of 1995 and the OTDR measurement has been completely saturated since the beginning of May. Although the increases in the gap size with temperature caused the performance to worsen during the summer months in previous years, the reflectance did not show complete saturation until the summer of 1995.

As noted above, two connectors on test in Maine have also shown evidence of reflectance variation with temperature, indicating marginal physical contact between the fiber cores. Figure 12 shows the reflectance for one of the connectors mounted in box B3 compared to one mounted in pedestal B1. The connector mounted in B1 shows the stable behavior we would expect from a mated connector with good physical contact. The connector mounted in B3 shows varying

reflectance indicative of a varying gap size. As the average temperature has increased with the warmer weather, the average reflectance has also increased, but has not increased above -40 dB. A second connector mounted in box B3 has continued to have relatively stable reflectance throughout the entire period, while the third connector in box B3 has also shown some temperature dependence, which has not worsened with the warmer weather. It is possible that the connectors showing temperature-dependent performance are not completely latched, or that the connector endface geometry is not within proper specifications. Further investigation will be required to determine the cause of the reflectance variations. It is too early to tell whether the performance is degrading over time, or whether the performance will recover when the temperatures become cooler.

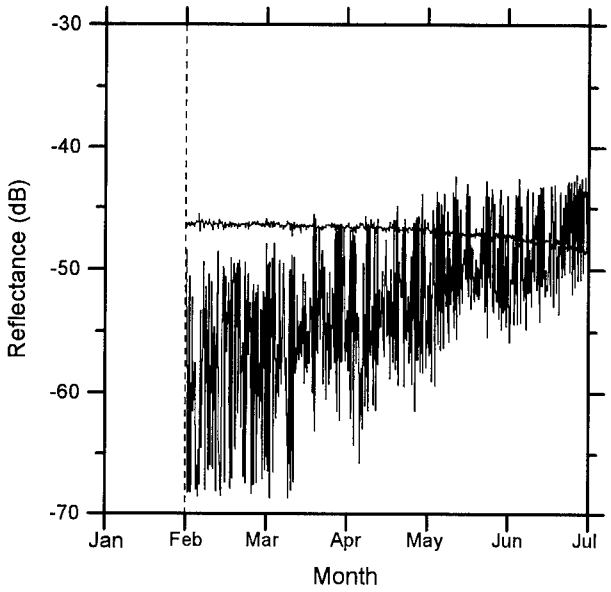


Figure 12. Reflectance Variations for Two Connectors

Laboratory vs. field performance

The performance of splices during temperature cycling in the laboratory and in the field is quite similar. Thus far, we have not seen any unexpected performance variations in the field. Although laboratory experiments show that there exists a potential for field failures due to high humidities, we have not seen any measurable performance degradation in splices exposed to humid field environments. (Some physical degradation—evidence of corrosion and discoloration—has been observed.) Temperature variations in the field, as we have seen in Maine, can be quite large, and the maximum yearly extremes can easily range from -40 to +60 °C. Normal laboratory testing extends over the range -40 to +75 °C. Laboratory testing is accelerated because the cycling is more rapid and because the magnitude of any individual daily temperature cycle in the field is considerably smaller (typically ~30 °C) than the laboratory temperature cycle (115 °C). In terms of humidity exposure, however, the absolute humidity to which the components are exposed in the laboratory is much higher than the components would be expected to see in the field. In the laboratory, the relative humidity is normally held fixed at some high level (typically 85–95 % RH) while the components are either temperature cycled or held at a constant elevated temperature. In the field, the relative humidity varies during the daily temperature cycling so that the maximum absolute humidity is limited, and in addition, the relative humidity is not elevated for prolonged periods of time at elevated temperatures. Certainly, laboratory humidity testing has a larger acceleration factor than laboratory temperature testing compared to actual field conditions. Further laboratory and field investigations are critical to determining the actual acceleration factors.

In terms of connectors, the field performance is again quite similar to the laboratory performance. Optical connectors from the same manufacturer as used in Louisiana have shown similar types of reflectance failures after 30–75 days of high humidity temperature cycling in the laboratory. At this point we do not have sufficient statistics to determine acceleration rates. However, subsequent to placing connectors on test in Louisiana, we have come to a much better understanding of how endface geometry and fiber position within the ferrule determine connector performance. In the future, the endface geometry of all connectors will be characterized before they are placed on test; measurements of changes in the endface geometry may be used to monitor degradation and predict performance failure before it actually occurs.

FUTURE WORK

Expansion capabilities

All three of the test sites have built-in capacity for expansion. A second optical switch is scheduled for installation at the Morgan City site, which will make the optical monitoring system the same as at the later sites. This will provide extra channels which, in combination with the unused fiber capacity in the cables, will enable us to put additional optical components on test. Excess capacity also exists at East Millinocket and in Phoenix, as both optical switch channels and available fiber capacity. At all three sites, additional temperature and humidity monitoring capability exists to accommodate sensors in additional pedestals, aerial closures, pole-mounted boxes, etc. In addition, splices, connectors, and other components on test can be removed for laboratory analysis, either because of a failure or to ascertain the extent of degradation after some years on test.

Future test plans

Because the splices and connectors at Morgan City have been on test for several years, at least some of them will be removed in the near future for laboratory analyses. We also expect to replace one of the aerial cables at East Millinocket,

which will entail replacing a number of mechanical and fusion splices. We have also identified various branching components—couplers/splitters, wavelength division multiplexers, and possibly electro-optic switches and fiber amplifiers—as potential candidates for testing. One goal of future testing is to install components from the same supplier and production lot in all three environments, to develop comparative performance data.

Correlation of laboratory and field results to determine the acceleration factors for high-stress laboratory tests will be facilitated by leaving a number of splices and connectors on test for periods of several years. By removing samples after years of exposure, we should be able to track the rate of change and, by comparison with the changes that occur under laboratory test conditions, develop better predictive capabilities about the service life of splices and connectors in hot, cold, or humid environments. In addition, the simultaneous effects of multiple stresses present in the field can be compared with the effects of fewer but higher-level stresses in the laboratory to ensure that we have identified the failure mechanisms, as well as the failure times, appropriate to field service.

SUMMARY

A total of 75 optical connectors and 82 mechanical splices, plus over 200 fusion splices, are presently under test at sites representing three different high-stress service environments. The optical loss and reflectance performance of all components are measured several times a day, along with detailed temperature and humidity data to record the stress history of each component. There have been relatively few failures to date, which in one respect is a gratifying result, since it would be quite disturbing to see supposedly robust splice and connector designs failing after only a year or two in actual service. The failures that have been seen to date have been in connectors, and the performance changes are consistent with a loss of physical contact between the fiber endfaces. Splice failures in high-humidity environments, observed in the laboratory, have not occurred in the field, although some evidence of physical degradation has been observed. Comparison of the temperature and humidity data from the field with the conditions typically applied during laboratory tests suggests that the acceleration factor for high-humidity testing in the laboratory may be much greater than the acceleration factor for temperature testing. Even as we plan new tests using the existing expansion capacity at each site, we continue to monitor the performance of all splices and connectors on test and will do so for an extended period of time to establish better correlations between laboratory and field testing and to develop better predictive capabilities for the field service life of these components.

ACKNOWLEDGMENTS

The authors would like to thank M. O'Connell, V. Poudyal, and C. Burpee for assisting in various ways, including writing computer programs to download and plot data from the remote sites, and collecting and plotting the data.

REFERENCES

1. P. Briggs, et al., "Establishment of an Environmental Test Facility for Fiber-Optic Components at Morgan City–Amelia, LA," NFOEC '94 Proceedings, volume 2, page 111.

2. L. Reith, et al., "Field Testing of Passive Optical Components in Morgan City, LA," NFOEC '94 Proceedings, volume 4, page 309.

3. R. Frantz, et al., "Construction of a Cold-Weather Environmental Test Facility for Optical Fiber, Cable, and Components," NFOEC '95 Proceedings, page 734.

4. G. Kiss, et al., "Low Temperature Reversible 'Splice Loss' Accompanied by Cable CM Protrusion," NFOEC '94 Proceedings, volume 2, page 411.

5. O. Gebizlioglu, et al., "Investigation of Temperature-Induced Cable Loss," NFOEC '95 Proceedings, page 479.

6. T. Bowmer, R. Miner, and R. Coker, "Field Temperatures in Outside Plant," International Wire & Cable Symposium Proceedings, 1990, page 335.

7. J. D'Amico and T. Bowmer, "Extending the Life of Polyethylene Wire Insulation," International Wire & Cable Symposium Proceedings, 1991, page 476.

Leslie A. Reith received a BA degree from New York University in 1975, the M.Phil. degree from the City University of New York in 1979, and the Ph.D. degree from The University of Texas at Austin in 1981, all in physics. In 1981 she joined AT&T Bell Laboratories as a Member of Technical Staff and in 1984 she subsequently joined Bellcore. In recent years she has been working on performance and reliability issues related to optical connectors and splices and has been active in national standards activities for fiber optic components.

Rolf Frantz is a Distinguished Member of Staff in Bellcore's Fiber Media and Component Reliability program. He received his bachelor's and master's degrees from Cornell University. Upon receiving his Ph.D. from Brown University, he joined AT&T Bell Laboratories, where he worked principally on projects related to the reliability of dielectric and electrical insulating materials. After joining Bellcore at its inception in 1984, he continued to work in that area. Since 1988, he has worked in the field of optical fiber and component reliability, with particular emphasis on fiber coatings, color coding inks, optical adhesives, and materials compatibility issues.

Study of lowering connecting loss of 16-fiber connector

H.Katsura, T.Ueda, M.Honjo, T.Yamanishi

Sumitomo Electric Industries, Ltd.
1,Taya-cho, Sakae-ku, Yokohama, Kanagawa 244 Japan

Abstract

The low loss high count optical connector of 0.2dB random connecting loss is successfully developed. The ferrule offset occurring between two mated ferrules is the dominant factor to guarantee connecting loss as well as fiber core offset in the ferrule. The new master ferrule whose guide pin holes are made of the ceramic sleeves is produced and confirmed to improve measurement accuracy.

1. Introduction

An optical fiber connector used to join high count optical fiber cables with low connecting loss is the important device for the future optical fiber network. NTT reported in 1991's IWCS that the average connecting loss of random pair connection of optical fiber cables in the field should be lower than 0.2dB to realize the future subscriber network[1][2] .

In 1993 we succeeded in producing the 16-fiber connector whose connecting loss with a master ferrule was almost 0.2dB[3].

In this paper we will discuss factors affecting to the random connecting loss and countermeasures to achieve the random 0.2dB connecting loss as well as the new master connector to guarantee measurement accuracy.

2. Structure of 16-fiber connector

The structure of 16-fiber connector is shown in Figure 1. The basic structure is similar to a MT-connector that is the multi-fiber connector for 4 or 8 fiber ribbon. The 16-fiber connector consists of two ferrules with fiber ribbons, two guide pins for precise alignment, and a metallic clamp. The fibers lie with a same interval on the same axis as the two guide pin holes that are the position standards in joining ferrules.

The manufacturing process of the connector is shown in Figure 2. The ferrule is made of an epoxy resin containing silica filler and is made by a transfer molding. And the 16 fiber ribbon is inserted into the ferrule and fixed to the ferrule by a glue. The end face of the ferrule is polished to make an optical surface.

3. Loss mechanism of a multifiber connector

It is well known that there are three main factors which generate connecting loss of a optical fiber. A misalignment of the fiber core is the most important factor among them. A fiber core offset, which is defined as the distance between a actual

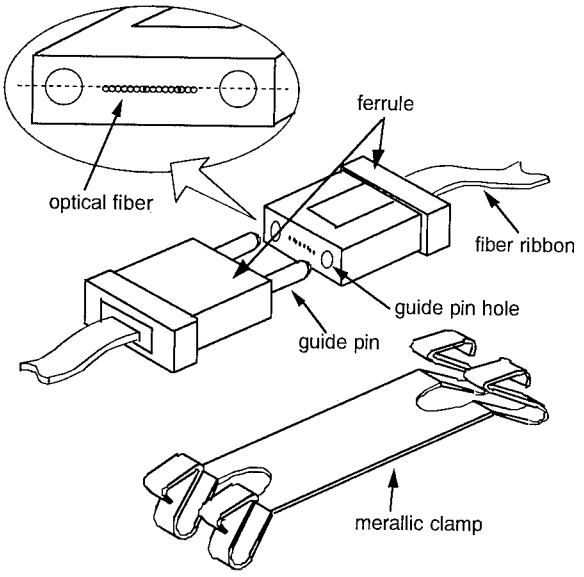


Figure 1. Feature of 16-fiber connector

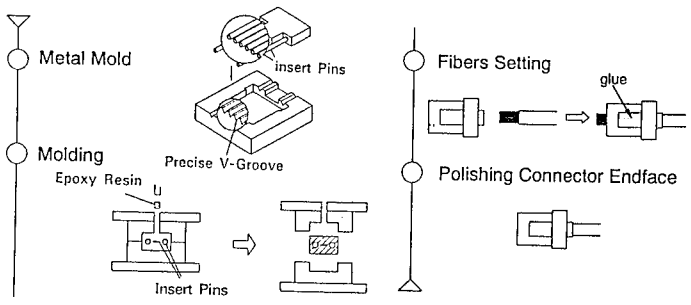


Figure 2. Manufacturing Process of 16-fiber connector

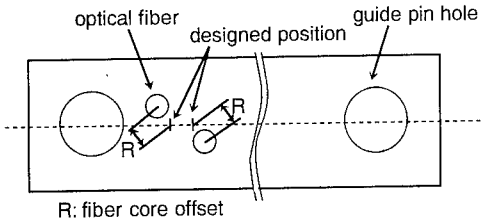


Figure 3. A fiber core offset

position of fiber cores against guide pin holes and a designed position as shown in Figure 3, is the cause of the misalignment at a multifiber connector. We had reported that the 0.2dB of connecting loss with master ferrule for the 16-fiber connector can be achieved by making the fiber core offset lower than 0.9μm. The master ferrule is a standard ferrule for connecting loss whose fiber core offsets of all fibers are lower than 0.5μm. However, the measured connecting loss is not coincident with the estimated loss calculated from the fiber core offsets of two mated ferrules as shown in Figure 4. This result indicate that the other factor besides the fiber core offset should be considered to

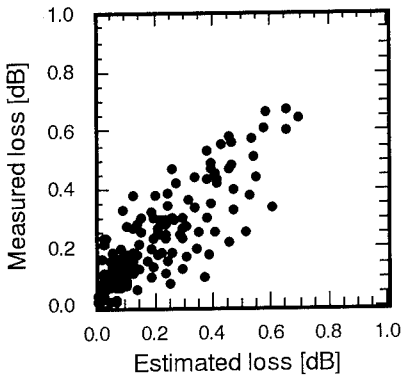


Figure 4. Reration between estimated loss and measured loss

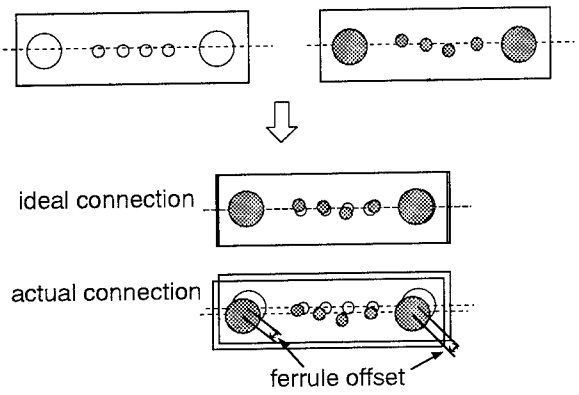


Figure 5. ferrule offset

reduce the connecting loss.

We supposed that the other factor to generate the connecting loss for multifiber connector is the relative displacement of mated ferrules, "ferrule offset", which is described in Figure 5. To prove the hypothesis, we tried to make the ferrule offset to be quantitative value theoretically and experimentally.

After selecting a pair of ferrule, both connecting loss and the ferrule offset of the mated ferrules were measured five times repeatedly. The measurement of ferrule offset was done by tracing the steps of ferrule surfaces utilizing a surface shape contacting measuring equipment as shown in Figure 6.

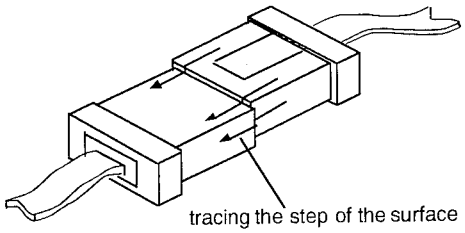


Figure 6. Measurring the steps

The other hand, the relative displacement of the mated ferrules, which best explain the measured loss data, were estimated as follows. As the first step, the fiber core positions against the center of the guide pin holes of each ferrules were measured by the CCD camera measuring system[4]. If the ferrules are joined with no ferrule offset, they are joined with their guide pin hole centers to be equal, and it is possible to calculate the distances of misalignment between each mated fibers from the fiber core position data and to calculate the connecting loss of each mated fibers using the equation

$$loss = \alpha \times \Delta^2, \qquad (1),$$

where Δ is the distance of misalignment of fiber core (in microns), and a is the constant of proportionality, about 0.19. Therefore, when the ferrule offset exists, the connecting loss is calculated by adding the ferrule offset value to the distance of misalignment of fiber calculated above. And the second step, the ferrule offsets which best explain the measured loss were estimated for each mated ferrules by the least square reduction method well known as," hill-climbing searches".

The change of ferrule offset against the first ferrule offset, which is expressed by the relative position change of guide pin hole center, during five times mating are shown in Figure 7. The condensed square marks in Figure 7 mean the

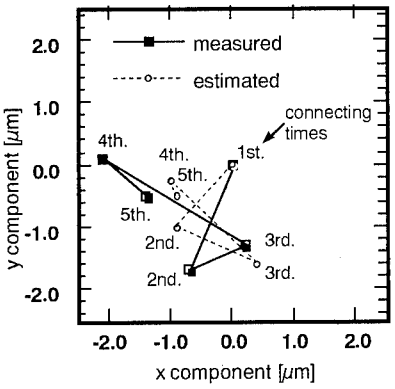


Figure 7(a). Guide pin hole 1

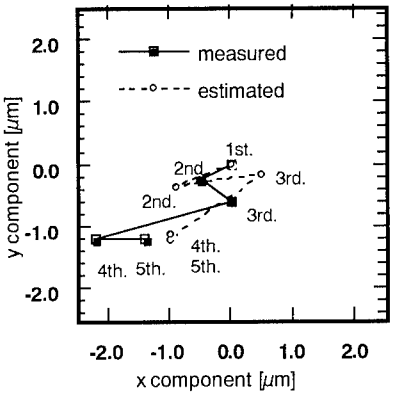


Figure 7(b). Guide pin hole 2

Figure 7. Relative position change during five times reconnecting at the guide pin holes from first connecting state

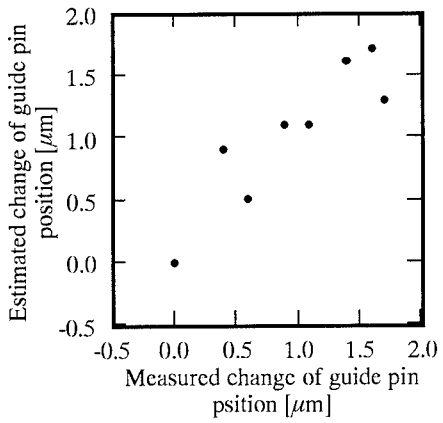


Figure 8. Relation between meatured change of ferrule offset and that of estimated change

actually measured value and the white circled marks mean the estimated value from loss data. The measured value and the estimated value are well corresponded[Figure 8]. So, it indicates that the ferrules are joined with occurring the ferrule offset, and the connector offset is the important factor of connecting loss of multifiber connector.

We thought that the cause of the ferrule offset was the clearance between the guide pin and guide pin hole. So that, to lowering connecting loss of random pair in the field, it is necessary to reduce not only the fiber core offset but also the clearance.

4. Design of low loss connector

Considering the fiber core offset and the ferrule offset as the main factors of the connecting loss, we tried to get the critical value of them by a computer simulation analysis. As shown in Figure 9, the fiber core offset(=R) consists of the ferrule eccentricity error(=Re), the clearance between fiber and fiber hole(=Rc), and the fiber core eccentricity(=Rf), here R=Re+Rf+Rc/2.And we thought the ferrule offset depended on the guide pin clearance and the difference of guide pin hole pitch for each ferrules as shown in Figure 10. The guide pin clearance increases the ferrule offset, but the difference of the guide pin hole pitch decreases the ferrule offset. So, we defined the effective guide pin clearance, Ec, as Equation 2,

$$Ec = \frac{1}{2}\left(Gcm - \Delta Gp\right)$$

Gcm is the minimum value of $Gc_{a1} + Gc_{b1}$ *and* $Gc_{a2} + Gc_{b2}$. (2)

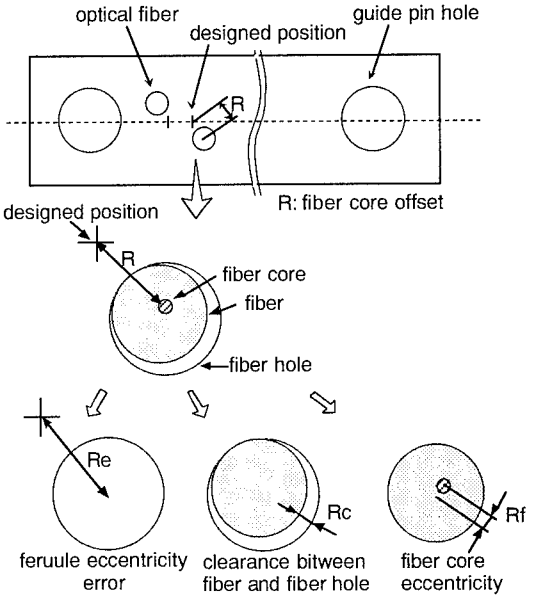


Figure 9. The fiber core offset

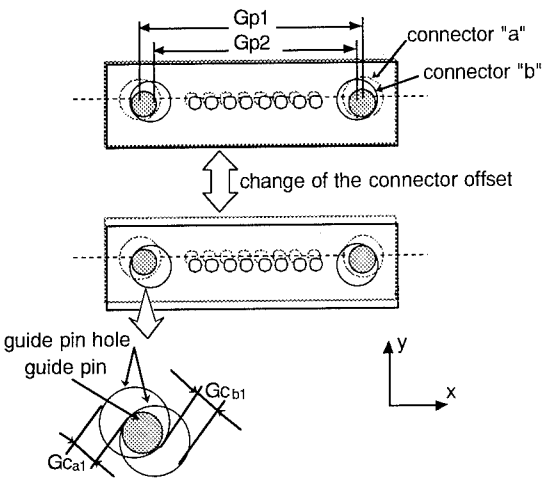


Figure 10. The ferrule offset

,where Gc is the difference between guide pin diameter and guide pin hole diameter, index i means guide pin hole number, index a and b means two mated ferrules, and ΔGp is the difference of guide pin hole pitch. Then, we approximated the ferrule offset as the effective guide pin clearance. Therefore, the connecting loss is approximated as Equation 3 from the fiber core offset, R, and the ferrule offset, Ec, where index k means the fiber number, and index x and y means x component and y component. If Ec is lower than zero, the elastic transform is occurred in the mated ferrules.

$$loss = \alpha \sum_{k=1}^{\infty} \left[\left(R_{xk} + Ec_x \right)^2 + \left(R_{yk} + Ec_y \right)^2 \right], \qquad (3)$$

Assuming Re followed the Rayleigh distribution and Rf, Rc, Gc and Gp followed the normal distribution, random numbers that followed distributions of each variables are made. And the distribution of the total fiber offset and the distribution of the total connecting loss with random pair are calculated by computer simulation, called Montecalro method.

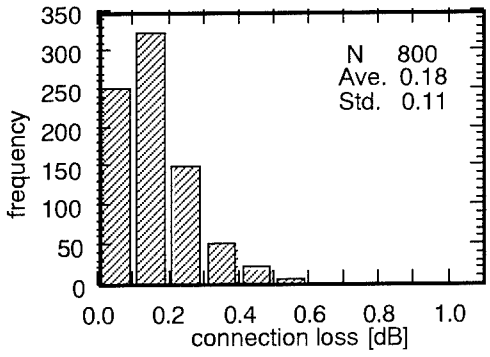


Figure 11. Calculated Distribution of connecting loss of 16-fiber connector

As a result, we found out that both lowering the average of guide pin clearance below 1.0μm and lowering the average of ferrule eccentricity error below 0.4μm made the connecting loss of random pair lower than 0.2dB. The calculated distribution of connecting loss are shown in Figure 11.

Under those rules, we experimentally produced the low connecting loss 16-fiber connector. Adjusting the guide pin clearance is done by controlling molding conditions and changing the diameter of mold guide pin. The ferrule eccentricity error is decreased by making the precise mold and controlling the molding conditions. The average of the guide pin clearance and the ferrule eccentricity error of the 16-fiber connector was 1.0μm and 0.40μm. Figure 12 shows the distribution of the connecting loss of the random pair. The average is 0.19dB. And Figure 13 shows the correlation between the measured connecting loss and the estimated loss calculated from the fiber core offsets, and it shows the good correlation below 0.2dB area.

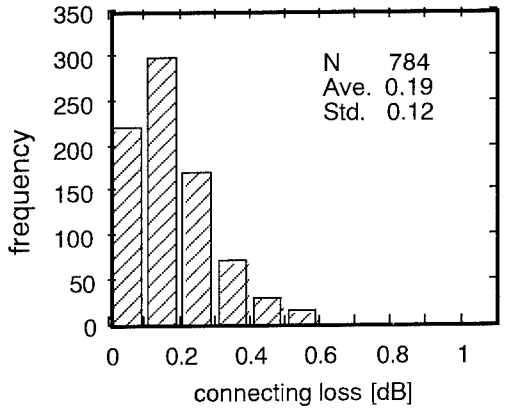


Figure 12 . Distribution of connecting loss of 16-fiber connecor of the random pair

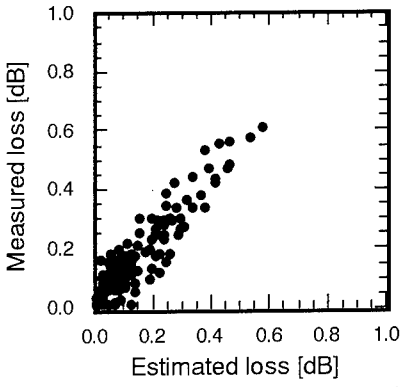


Figure 13. Relation between estimated loss and measured loss

5. Master connector

An examination of connecting loss of an optical fiber connector is made by measuring the connecting loss with a master ferrule. To guarantee the measurement, the master ferrule should have no fiber core offset and no ferrule offset and should have much durability against repeating connecting action. The connecting loss of a 16-fiber connector increases and becomes unstable by repeating connection because of the abrasion of guide pin holes.

We thought to make the guide pin hole out of a ceramic sleeve to improve its durability and to ease controlling the guide pin clearance. And we experimentally produced the 16-fiber connector whose guide pin holes were made out of the ceramic sleeves, zirconium oxide, as shown in Figure 14. The sleeves are inserted in the ferrule by molding. The manufacturing process is same as normal 16-fiber connector. And then, the average of the ferrule eccentricity error and the guide pin hole clearance of produced 16-fiber master connector were both 0.5μm. Figure 15 shows the distribution of the connecting loss of random pair of the 16-fiber master connector. The average was lower than 0.1dB and was enough low for master ferrule. Figure 16 shows the change of the connecting loss during durability test. The change is less than 0.1dB during 10000 times connecting. We confirm the interchangeability between the normal ferrule and the sleeve containing ferrule was good by measuring connecting loss of same ferrule with those two types of ferrules.

Consequently, the usefulness to control the guide pin hole clearance and the improvement of the durability by the new guide pin hole structure was confirmed. And the ferrule whose guide pin holes are made of the ceramic sleeves are promised to be a master ferrule.

6. Conclusions

We found out that the ferrule offset occurring between mated ferrule was important as a factor of connecting loss in addition of a fiber core offset. Decreasing the guide pin hole clearance was effective to reduce the connecting loss. Then we succeed in producing 16-fiber connector which connecting loss with random pair was lower than 0.2dB by both making the guide pin hole clearance lower than 1.0μm and the ferrule eccentricity error lower than 0.4μm. And we produced the 16-fiber connector whose guide pin holes consisted of the ceramic sleeves, and confirm its usefulness for the master ferrule.

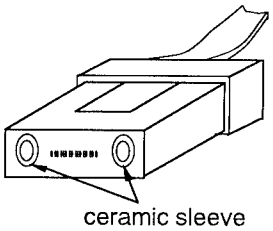


Figure 14. Structure of the master ferrule

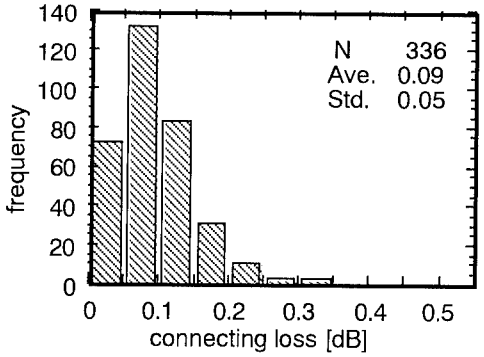


Figure 15. Connecting loss distribution of random pair of the master 16-fiber connector

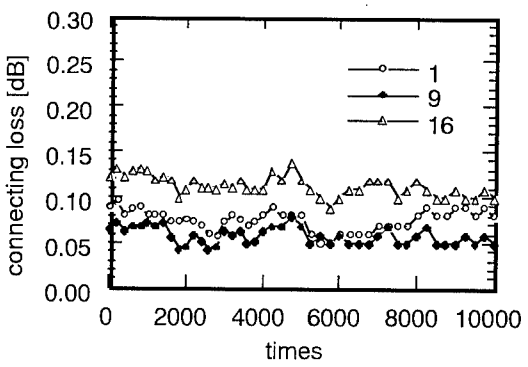


Figure 16. The change of connecting loss of master ferrule during the drability test

References

(1) S.Tomita, M.Matsumoto, S.Nagasawa, T.Tanifuji and T.Uenoya, 'Preliminary Research into High-Count Pre-Connectorized Optical Fiber Cable', 41st IWCS, pp5-12, 1992.

(2) S.Nagasawa, T.Tanifuji, M.Matsumoto and M.Kawase, 'Single-Mode Multifiber Connectors for Future Large Scale Subscriber Networks', 19th ECOC, MoP1.5, pp29-32,1993.

(3) T.Ueda, H.Ishida, I.Tsuchiya, T.Kakii and T.Yamanishi, 'Development of 16-fiber connectors for high-speed low-

loss cable connection', 42nd IWCS, pp244-249, 1993.
(4) M.Shigehara, H.Ishida, H.Katsura and Y.Hattori, 'Investigation on Fiber Core Position Measurement Method for Multi-Fiber Connectors', 2nd OFMC, pp57-60, 1993.



Hiroshi Katsura

Sumitomo Electric Industries, Ltd.

1,Taya-cho, Sakae-ku, Yokohama, 244 Japan

Hiroshi Katsura received a M.E. degree from Tokyo Institute of Technology in 1990. He joined Sumitomo Electric Industries,Ltd. In 1990, and has been engaged in research and development of optical connectors. He is an engineer of Communication R&D Department in Yokohama Research Laboratories.



Makoto Honjo

Sumitomo Electric Industries, Ltd.

1,Taya-cho, Sakae-ku, Yokohama, 244 Japan

Makoto Honjo received a M.E. degree from Osaka University in 1984. He joined Sumitomo Electric Industries,Ltd. In 1984, and has been engaged in research and development of optical fiber, cable and jointing technologies. He is a senior engineer of Communication R&D Department in Yokohama Research Laboratories.



Tomohiko Ueda

Sumitomo Electric Industries, Ltd.

1,Taya-cho, Sakae-ku, Yokohama, 244 Japan

Tomohiko Ueda received a B.E. degree from Tokyo University in 1987. He joined Sumitomo Electric Industries,Ltd. In 1987, and has been engaged in research and development of optical connectors. He is an engineer of Communication R&D Department in Yokohama Research Laboratories.



Toru Yamanishi

Sumitomo Electric Industries, Ltd.

1,Taya-cho, Sakae-ku, Yokohama, 244 Japan

Toru Yamanishi received a B.E. degree from Hokkaido University in 1972. He joined Sumitomo Electric Industries,Ltd. In 1972, and has been engaged in research and development of optical fiber, cable and jointing technologies. He is a chief research associate of Communication R&D Department in Yokohama Research Laboratories.

REFERENCE MULTIFIBER CONNECTOR

Kazuhiro TAKIZAWA, Akito NISHIMURA, Toru ARIKAWA,
Yoshio KIKUCHI and Hiroshi YOKOSUKA

Fujikura Ltd. Opto-Electronics Laboratory
1440, Mutsuzaki, Sakura-shi, Chiba, 285, JAPAN

Abstract

We have developed a highly accurate reference multifiber connector used for the testing of very low loss multifiber connectors. Ceramic sleeves were inserted into the guide pin holes of the MT (Mechanically Transferable) type all-plastic multifiber connector to produce the reference connector. The coefficient of linear expansion of the ceramic sleeves was almost the same as that of the connector material. Thus high accuracy of the reference connector was assured. The ceramic sleeves displayed high durability during repeated use as a reference connector. The mean connection loss of the reference connector was 0.09 dB. After a 10,000 cycles durability test, the maximum change of the connection loss was less than 0.1 dB. The loss change during the temperature cycling test was less than 0.1dB.

1. Introduction

More than one million MT (Mechanically Transferable) multifiber connectors for 4- and 8-fiber optical ribbons have already been installed in optical subscriber loop systems in Japan. In order to enlarge these subscriber systems and construct FTTH (Fiber To The Home) networks for the future, it is necessary to further decrease the connection loss of these multifiber connectors and to achieve high density connection techniques[1-3]. One of the key technologies to accomplish very low loss connectors is highly accurate and reliable reference connectors for inspection. To allow interchangeability, the absolute mating face dimensions of the connector should be determined by a traceable measurement method with an accuracy of less than 0.1 μm. Therefore, we have developed accurate and reliable reference multifiber connectors in which a pair of ceramic sleeves are molded as a guide holes. The dimensions of the connector were the same as that of the MT connectors and the all-plastic 16-fiber connector.

In this paper, we first describe dimensional design and the structure of the developed reference connectors. We then report the results of insertion and return loss tests on reference connectors, as well as durability and performance during temperature cycling. Finally, we verify the correlation between absolute dimensions of the reference connectors and connection losses.

2. Design

Requirements for reference multifiber connector used for inspection are as follows.

1) low connection loss(max.<0.2dB) or slight fiber core location offset (<0.5μm)
2) interchangeability
3) repeatability
4) durability
5) long term reliability

For the first requirement, dimensional design of the reference connector is important. Other requirements are related to the institution and durability of the guide pin holes. Therefore we developed a reference multifiber connector whose guide pin holes consist of ceramic sleeves.

3. Dimensional design and structure

3.1 Dimensional design

Since the low-loss connector requires very high dimensional precision, the reference connector should have even more precise dimensions.

JIS (Japanese Industrial Standard) specify that the connection loss of the MT reference connector should be less than 0.2 dB. In order to satisfy this specification, the transverse offset of fiber cores must be less than 1 μm based on theoretical calculations. The relationship between transverse offset and connection loss is as follows[4].

$$L = -10 \log \{\exp -(d/\omega)^2\} \qquad (1)$$

where L = connection loss (dB)
d = transverse offset
ω = mode field radius

This means that the random transverse offset of one connector plug of a reference connector pair should be less than 0.5 μm. As described in the former section, the average transverse offset deviation is determined by the composition of d_1, d_2 and d_3 which are explained in Fig.1. To keep the transverse offset of a fiber core of a connector pair to less than 0.5 μm, the sum of the maximum of each of the factors (d_1, d_2 and d_3) should be less than 0.5 μm. This, however, is not realistic for manufacturing. Therefore, the relationship between the fiber core offset and each factor is investigated using statistical analysis.

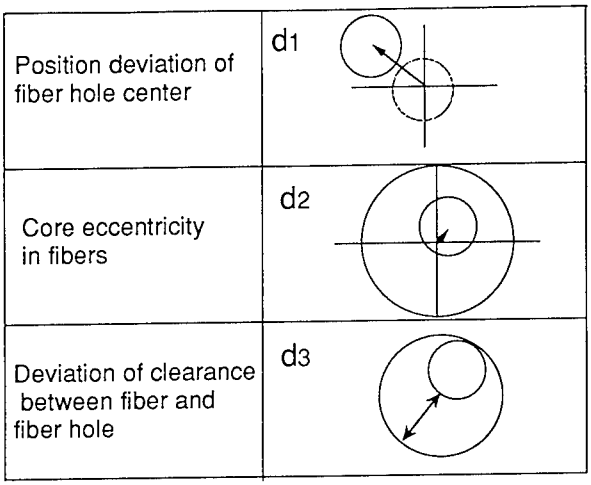


Fig. 1 Transverse offset factors in an MT connector

Assuming that each transverse offset factor has a two-dimensional Gaussian distribution, a probability density function of each factor d_i is expressed by a Rayleigh distribution as follows.

$$f_0(d_i) = d_i/\sigma^2 \cdot \exp(-d_i/(2\sigma^2)) \qquad (2)$$
$$d_i \geqq 0$$

The fiber core offset distribution can be evaluated by calculating the composition of each factor using equation (2). In other words, the probability of the fabrication of reference connectors in which the fiber core offset is less than 0.5 μm can be estimated by determining each factor.

Fig.2 shows the calculated results of the fiber core offset distribution and the probability density when the average of each factor was determined as d_1=0.25 μm, d_2=0.1 μm and d_3=0.25 μm.

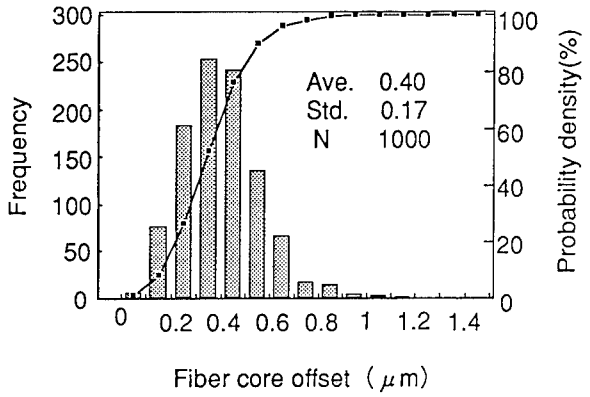


Fig. 2 Calculated results of the fiber core offset

3.2 Structure of reference connector

The structures of a reference connector and a conventional MT connector are shown in Fig.3. The basic structure of reference connector is similar to that of a conventional MT connector.

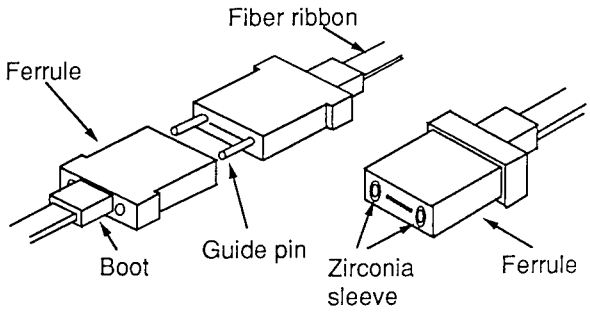


Fig. 3 Structures of MT connector and reference connector

The coefficient of linear expansion of the zirconia sleeves used for this reference connector was almost the same as the molding resin material and had very precise inner diameters and eccentricities so that high accuracy and reliability of the reference

connector were assured. Another advantage of using zirconia sleeves for the reference connector was its high durability. Since the zirconia sleeves were resistant against the deterioration of accuracy by abrasion through repeated use, the newly developed reference connector showed a significant improvement in durability.

4. Performance of reference connector

4.1 Mechanical performance

Fig.4 shows the typical result of the endface flatness of the 8-fiber reference connector. It has the flatness of less than 1 μm. In addition, the angular deviation is less than ±0.1°.

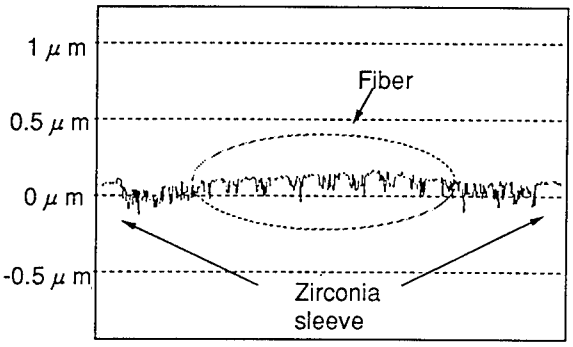
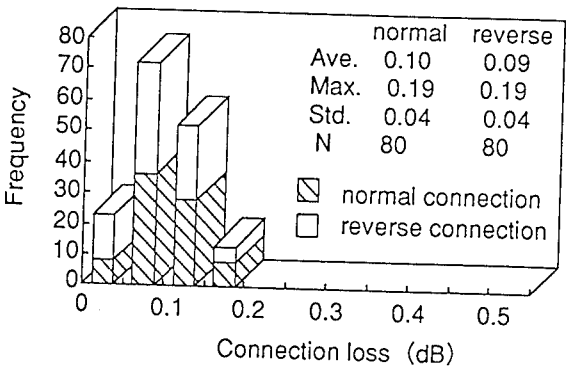


Fig. 4 Endface flatness of the reference connector

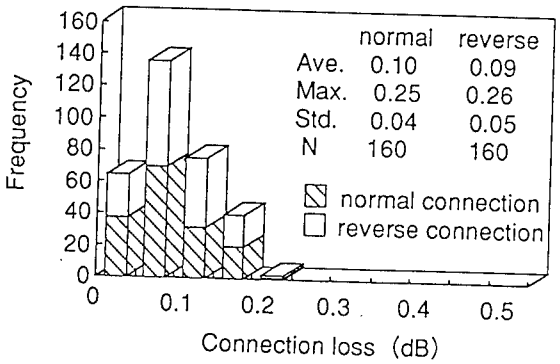
4.2 Insertion loss

The connection losses of the reference connector are shown in Fig.5. The measurements were conducted at a wavelength of 1.31 μm, with the use of index matching materials. The average connection loss of the 8-fiber reference connector was 0.09 dB for normal connection and 0.10 dB for reverse connection. The 16- and single-fiber reference connectors have also been fabricated. Both reference connectors had the same low-loss connection performance as that of the 8-fiber reference connector.

The connection loss of this newly developed 8-fiber reference connector when connected to conventional all-plastic reference connector is shown in Fig.6. Since the average connection loss was less than 0.1 dB for both normal and reverse connections, it is clear that this newly developed reference connector is compatible with conventional reference connectors.



a) 8-fiber reference connector



b) 16-fiber reference connector

Fig. 5 Histogram of connection loss of 8-fiber and 16-fiber reference connector

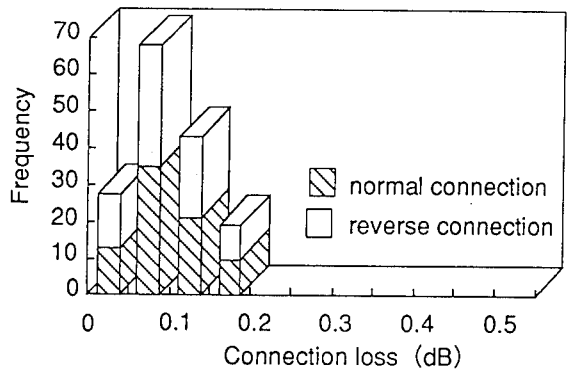


Fig. 6 Histogram of connection loss of nearly developed 8-fiber reference connector with all-plastic reference connector

4.3 Durability

Fig.7 shows the results of the durability test of the 8-fiber reference connector. During a 100 cycle durability test, the change in the connection loss of the 8-fiber reference connector was less than 0.1 dB. Moreover after 10,000 cycles of disconnection and reconnection, the change in the connection loss was less than 0.1 dB and no abrasions or damage were observed on the end-face of the guide-pin holes.

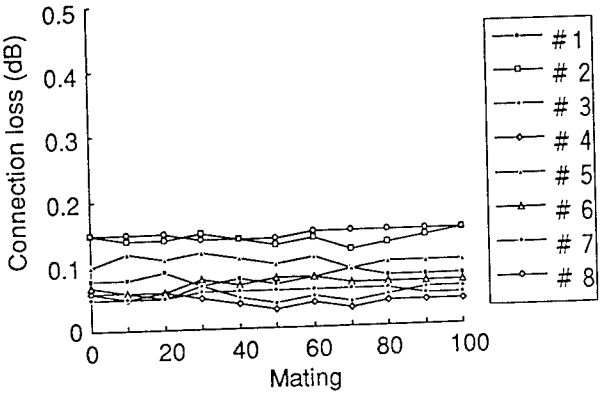


Fig. 7 Durability test results of the 8-fiber reference connector

4.4 Return loss

Fig.8 shows the results of the return loss of the 8-fiber reference connector when measured with the application of index matching materials. The return loss was higher than 40 dB for this reference connector.

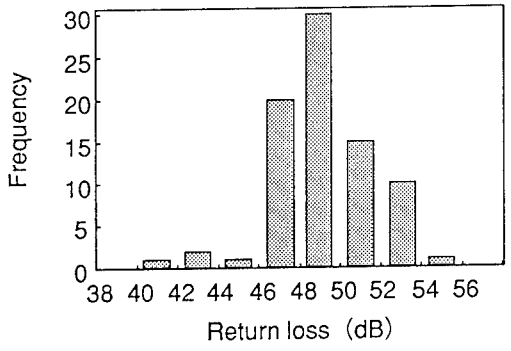


Fig. 8 Histogram of return loss of 16-fiber reference connector

4.5 Temperature cycling

To test environmental performance, the connector pairs were subjected to ten six-hour temperature cycles, where the temperature ranged from -30℃ to 70℃. The insertion loss change during the test is shown in Fig.9. The insertion loss change of these reference connectors was less than 0.1 dB.

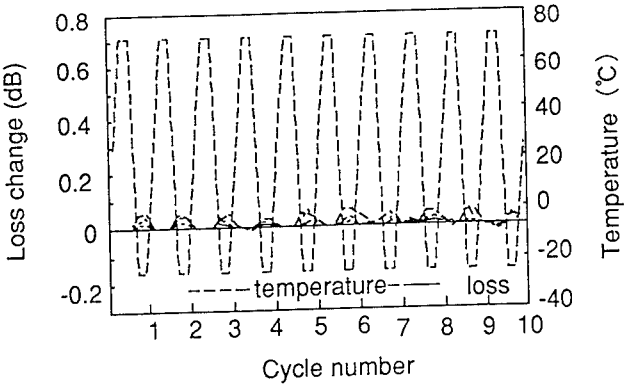


Fig. 9 Temperature cycle test results of 16-fiber reference connector

5. Dimensional analysis

The correlation between the fiber core position and the connection loss was verified using the single-fiber reference connector in which the zirconia sleeveswere inserted as guide pin holes.

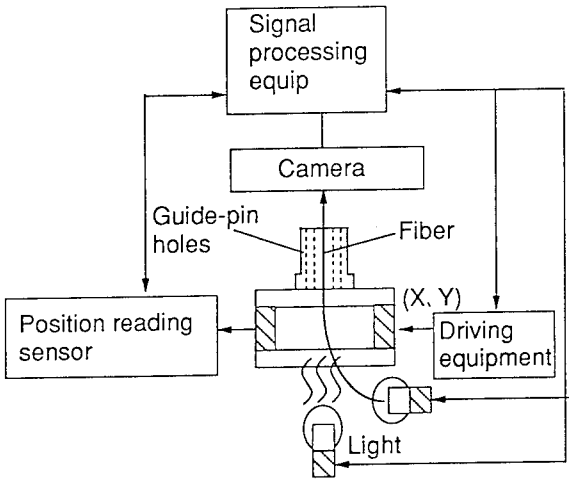


Fig.10 Measuring set-up for fiber core position in multifiber connector

Fig.10 shows the measurement set-up for this analysis. The measurement was conducted by non-contact image processing with a semiconductor image sensor and precision glass scales. The geometric origin was determined by the centers of two guide pin holes.

Fig.11 shows the relationship between the estimated loss from fiber core eccentricity and the measured losses. Since an approximate correlation was confirmed by this investigation, we are now able to verify the absolute position of the fiber core for the newly developed reference connectors.

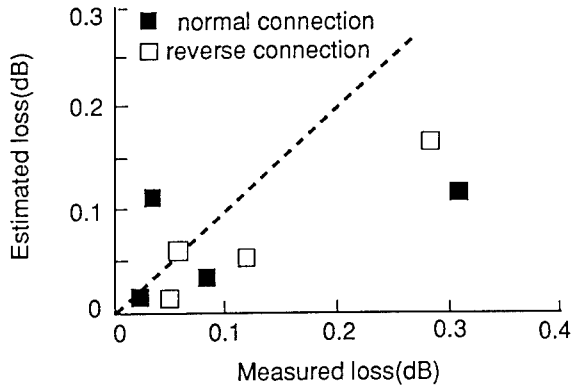


Fig.11 Relationship between estimated loss from fiber core eccentricity error and measured loss

6. Conclusions

We have described a newly developed reference connector for MT type multifiber single-mode connectors. The average connection loss of this reference connector was less than 0.1 dB. After a 10,000 cycles durability test, the maximum change of the insertion loss was less than 0.1 dB. The loss change during the temperature cycling test was also less than 0.1 dB. These results were far superior than these of conventional reference connectors. In addition, we are now able to verify the absolute position of the fiber core for the developed reference connectors.

We are convinced that this newly developed reference connector will contribute towards the construction of large scale fiber optic networks.

References

[1] S. Nagasawa et al.:"Single-Mode Multifiber Connectors for Future Large Scale Subscriber Networks", ECOC'93, MoP1.5, pp.29-32, 1993.

[2] Y. Kikuchi et al.:"HIGH FIBER COUNT OPTICAL CONNECTORS", 42nd IWCS Proceedings, pp.238-243, 1993.

[3] H. Yokosuka:"Recent Progress in Fiber Splicing and Connector Technology", IOOC-95 Technical Digest Vol.1, TuA2-2, pp.20-21, 1995.

[4] D. Marcuse:"Loss analysis of single-mode fiber splices", Bell Syst. Tech.J., Vol.56, pp.703-718, 1977.



Kazuhiro TAKIZAWA

Fujikura Ltd.

1440 Mutsuzaki Sakura,
Chiba, 285, Japan

Kazuhiro Takizawa was born in 1968. He graduated from Yokohama National University with an M.E. degree in 1993. He joined Fujikura Ltd.,and has been engaged in the research and development in the Fiber and Cable Accessory Department of the Opto-Electronics Laboratory.

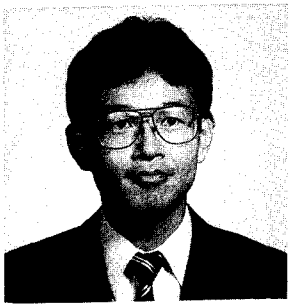


Akito NISHIMURA

Fujikura Ltd.

1440 Mutsuzaki Sakura,
Chiba, 285, Japan

Akito Nishimura was born in 1967. He joined Fujikura Ltd. after his graduation from Ibaraki University with an M.E. degree in 1992. He has been engaged in the research and development of optical fibers, components and accessories.



Toru ARIKAWA

Fujikura Ltd.

1440 Mutsuzaki Sakura,
Chiba, 285, Japan

Toru Arikawa is an assistant manager of Fiber and Cable Accessory Department in Opto-Electronics Laboratory. He received B.E. and M.E. degrees in image science engineering from Chiba University in 1982 and 1984, respectively. He joined Fujikura Ltd. after his graduation, and has been engaged in the research and development of optical fibers, components and accessories.

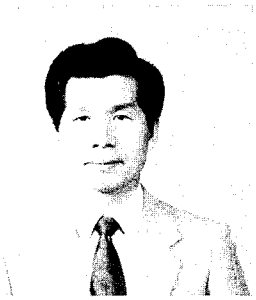


Yoshio KIKUCHI

Fujikura Ltd.

1440 Mutsuzaki Sakura,
Chiba, 285, Japan

Yoshio Kikuchi was born in 1955. He joined Fujikura Ltd. after his graduation from Tohoku University with a M.E. degree in 1980. He has been involved in research and development of optical fibers cables and accessories. He is now a manager in Fiber and Cable Accessory Department of the Opto-Electronics Laboratory and a member of the IEICE of Japan.



Hiroshi YOKOSUKA

Fujikura Ltd.

1440 Mutsuzaki Sakura,
Chiba, 285, Japan

Hiroshi Yokosuka graduated in mechanical engineering from Tokyo Metropolitan Technical Junior College in 1967. He has been engaged in development of telecommunication cables and accessories. He is now a general manager of the Fiber and Cable Accessory Department of the Opto-Electronics Laboratory and a member of IEICE of Japan.

FIBER OPTIC FEED THROUGH ADAPTER FOR MILITARY APPLICATIONS

Richard J. Patterson
Michael F. Petner

Lockheed Martin Government Electronic Systems
199 Borton Landing Road
Moorestown, New Jersey 08057

ABSTRACT

The established requirements for cabling and interconnection of military combat system equipment must not be compromised with the introduction of Commercial-Off-the-Shelf (COTS) hardware. The U. S. Navy and the AEGIS Shipbuilding Program Office have levied stringent requirements upon the installing activities that help mitigate potential interconnection and interface problems. Mission critical systems must maintain multiple and redundant cable paths throughout the ship in order to minimize the effects of casualties and increase system survivability.

The majority of COTS systems being designed and installed aboard ship include many fiber optic interconnections. Several mission critical systems are being designed with COTS components that are housed in ruggedized enclosures. Therefore, mission critical system designers are faced with developing a backplane that must include either costly military heavy duty fiber optic connectors (i.e. MIL-C-28876) or develop a modified design that has to be tested and accepted by the Navy. A fiber optic feed through adapter seemed to be an attractive alternative approach to the use of MIL-C-28876 connectors.

This paper will discuss the development, design, construction, assembly, and test results of three different fiber optic feed through devices. The data obtained from this evaluation will present a low cost alternative design for the penetration of fiber optic cables into equipment enclosures. Navy approval is pending.

INTRODUCTION

Currently, only one type of fiber optic connector has been qualified by the Navy, the MIL-C-28876 connector. The backshell assemblies specified in this specification, capture the outer strength member (aramid yarn) of MIL-C-85045 fiber optic cables. Figure 1 depicts the construction of MIL-C-85045 fiber optic cables approved for shipboard applications.[1] Even though MIL-C-28876 materials are ruggedized to meet the harsh environments found in Naval ships, they are relatively expensive. Use of them with COTS systems does not provide an economical solution that is being promoted throughout the Department of Defense.

In addition to the application of COTS equipment into mission critical systems, more and more COTS based systems are being proposed for shipboard environment applications not considered

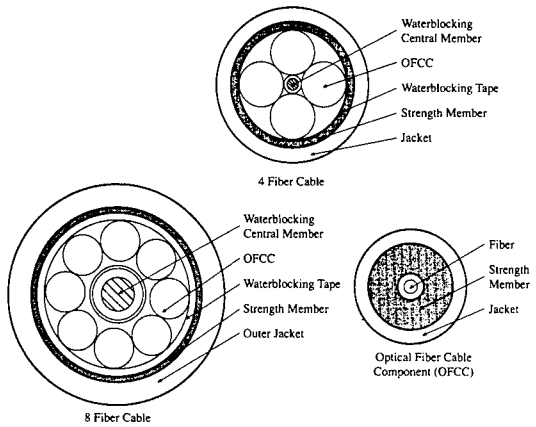


Figure 1. Fiber Optic Cable Construction
(Drawing Courtesy of BICC Brand-Rex Co.)

mission critical. These systems do not utilize military connectors at the equipment interface. Fiber optic cables enter the equipment via nylon stuffing tubes which do not capture the cable's outer strength member for strain relief. The cable is only prevented from moving axially by a rubber bushing being compressed by the force of the backnut.

To ensure the longevity of fiber optic interfaces, especially during periods of shock and vibration, it is essential for fiber optic cables' aramid yarn be used as the primary strength member for terminating. However, there was no device that would allow simplex members of a fiber optic cable to penetrate a cabinet and provide adequate strain relief for the cable. Therefore, the basis was established to develop a low cost, fiber optic equipment feed through device, suitable for use with all systems, including mission critical. Several designs will be introduced which show the capturing technique for the strength members and allow each simplex optical fiber cable component (OFCC) to be installed in the cabinet. Once inside the cabinet, the OFCCs can be terminated with ST connectors, rotary mechanical splices or any other available fiber optic coupling.

The emergent installation of COTS equipment aboard U.S. Naval ships has led to the increased use of fiber optics as the sole interface for implementing Local Area Network (LAN) technology. The Naval Sea Systems Command (NAVSEA) has issued

an edict that contractors must formulate new system designs utilizing COTS based networks.[2]

The initial COTS based system using fiber optics installed on AEGIS hulls was in support of an administrative LAN. Like commercial businesses, the Navy relies on personal computers (PCs) to conduct daily business. These PCs do not perform military functions but they do fulfill word processing, database, spreadsheet, and other office requirements. Since these administrative LANs are not mission critical, COTS equipment along with the optically commercial cable installation practices prevailed except for the use of ruggedized, military fiber optic cable material. Figure 2 depicts a typical commercial hub that is housed in a ruggedized enclosure. As seen in Figure 2, all of the cables are routed into the enclosure and held in place by cable brackets.

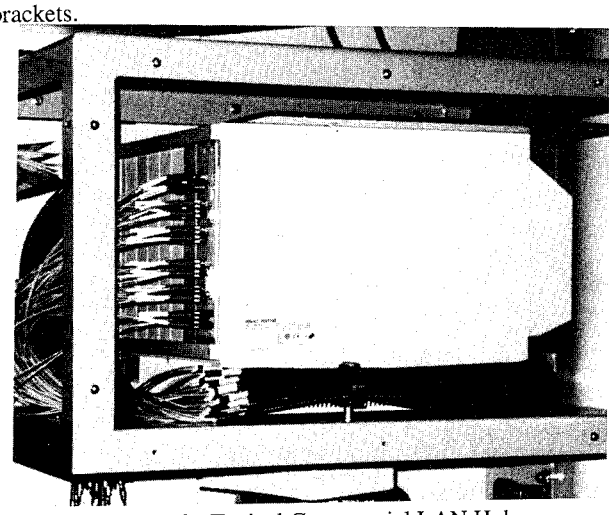


Figure 2. Typical Commercial LAN Hub Shipboard Installation

Figure 3 depicts an enlarged view of fiber optic cables that are routed inside the COTS enclosure shown in Figure 2. Further examination of the fiber optic cables reveals that the aramid yarn strength members are left free flowing. Per U.S. Navy requirements, non-mission critical equipment combinations do not require the strength members to be secured when the cables penetrate the cabinet and are terminated inside.



Figure 3. Enlarged View of Fiber Optic Cables

Regardless of the system classification (i.e. mission critical or non-mission critical), if fiber optic cables are to be terminated at the cabinet or enclosure backplane, then heavy duty MIL-C-28876 multi-terminus connectors must be employed. Nevertheless, COTS equipment is not furnished with MIL-C-28876 connectors. The majority of COTS devices, used for military applications, employ single terminus (ST) connectors or rotary mechanical splices. Therefore, when COTS based mission critical system designs are being developed, designers must make special considerations regarding fiber optic cable terminations:

1. The system loss budget may determine which type of termination is used.
2. The access to the internal terminations of ruggedized consoles or racks which house the COTS systems must be deliberated.

Consoles that are densely populated, therefore not allowing the installing activity to gain entrance to the fiber terminations, will be utilizing MIL-C-28876 multi-terminus connectors and backshell assemblies for fiber optic interconnects. In comparison to MIL-C-83522 ST connectors, MIL-C-28876 assemblies are more expensive and have higher optical loss values but, unlike ST connectors, provide for overall cable strain relief and environmental protection. In an effort to reduce costs, some COTS based systems will be enclosed in ruggedized 19 inch (48 cm) racks. The fiber optic cables are terminated with ST connectors internally located on patch panels that are easily accessed by the installing activity. Current shipboard technology only provides for cable penetration via MIL-S-19622 nylon stuffing tubes. Nylon stuffing tubes provide a secure environmental seal but do not capture the aramid yarn for cable strain relief. However, for mission critical systems, the strength members must be captured and a secure environmental seal is required. Therefore, a fiber optic cable feed through adapter that provides adequate cable strain relief and environmental protection would be ideal.

DISCUSSION

The objective was to develop a low cost shipboard fiber optic feed through device that provides adequate strain relief during high shock events and vibration while offering an environmental moisture resistant seal. The problem is that the only device that enables a fiber optic cable to penetrate equipment is a nylon stuffing tube meeting the requirements of MIL-S-19622. However, MIL-S-19622 contains no provisions for cable pull out or retention. Figure 4 exhibits a cross-section view of the nylon stuffing tube in a straight configuration. As shown in Figure 4, the aramid yarn strength members are not be seized. The restrictive force of the neoprene bushing upon the cable jacket is the only action that holds the cable in place. Consequently, the use of nylon stuffing tubes with mission critical fiber optic cables introduces an unacceptable risk into the cable plant.

The design approach was to utilize currently available RFI/EMI and environmental military bulkhead adapter hardware and make adjustments and improvements where necessary. The concept was to apply the methods by which tinned copper braids, implemented to reduce electromagnetic field effects, are captivated. Two devices were chosen based on their widespread use throughout the military, ease of assembly, and adaptability to fiber optic use. The adapters were altered so that the manner in which the metal braid is held could also be used to grip the ara-

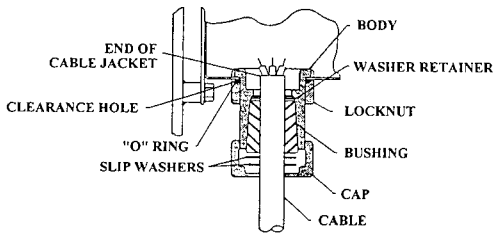


Figure 4. MIL-S-19622/1 Nylon Stuffing Tube

mid yarn. The redesigned fittings were required to meet three basic conditions:

1. The cable pull-out tensile force must be greater than 162 lbs. (720.61 N) with no damage to the cable jacket and optic fiber cable components. There must be no change in optical tranmittance.
2. No epoxies or adhesives may be applied directly to the aramid yarn in an effort to further secure the strength members to the feed through.
3. The aramid yarn must not be damaged, frayed, or cut in any fashion while the cable is under tension or upon completion of the stress event.

Furthermore, the initial military requirements imposed on the original design were not to be infringed upon.

DESIGN NO. 1

Figure 5. exhibits the first of two existing copper cable adapters that were devised to provide a 360° termination, furnish an environmental seal, and allow the cable conductors to continue into an equipment enclosure. The cable overall shield is captured between the RFI conical rings and held in place by compression applied by the body of the fitting as it is torqued in place. The braid is trimmed and is placed as shown in Figure 6. The conical rings are smooth, therefore there is no teeth-like mechanism that grabs the braid.

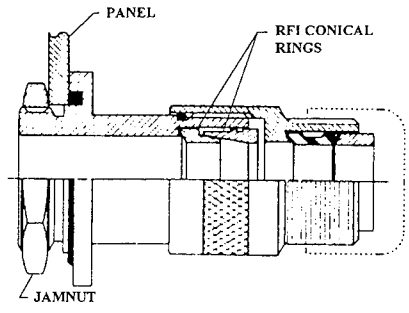


Figure 5. Thru Bulkhead Fitting for Overall Shielded Copper Cables (Drawing Courtesy of Glenair, Inc.)

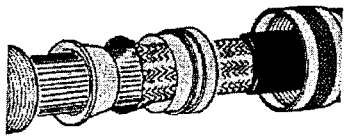


Figure 6. Termination of Cable Overall Shield (Drawing Courtesy of Glenair, Inc.)

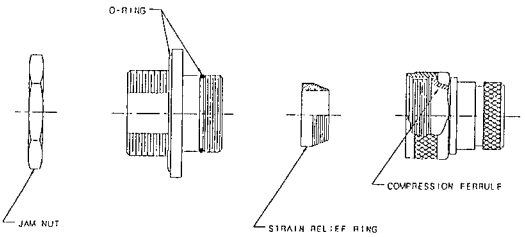


Figure 7. Expanded View of the Fiber Optic Feed Through Adapter Design No. 1 (Drawing Courtesy of Glenair, Inc.)

To transform the copper cable fitting to an optical cable adapter, the conical ring configuration had to be modified. Since the rings were smooth, it was felt that the aramid yarn would not be adequately captured. Therefore several adjustments, as illustrated in Figure 7, were made. The number of conical rings was reduced to one and grooves were embedded into the exterior portion of the remaining ring. Also, any sharp edges were abated. The aramid yarn is fed through the strain relief ring, looped around the ring, laid uniformly and perpendicularly across the grooves of the ring. The body containing the compression ferrule is then torqued down on the main component of the adapter. The grooves are blunted so that the edges do not bisect the yarn. The theory is that the compressive force allows the crevices to grip the strength members and restrain the yarn from moving axially. (Lockheed Martin Government Electronic Systems has submitted a patent application for the design of the fiber optic conical strain relief ring.) To provide for anti-rotation, the threaded end, which penetrates into the cabinet, is shaped in a D-cut configuration. O-rings are required to resist moisture entry into the cabinet via the threaded portions of the main body. Finally, to complete the environmental seal, adhesively lined, heat shrinkable material is applied bonding the fiber optic cable jacket to the compression ferrule segment. The final assembly, which was developed in a joint endeavor between Lockheed Martin Government Electronic Systems Company and Glenair, Inc., is illustrated in Figure 8.

Prototypes, developed by Glenair, Inc., Glendale, CA have undergone initial cable retention tests. These tests are conducted to meet MIL-C-28876 specifications which reference the procedures prescribed in Electronic Industries Association/Telecommunications Industry Association Standard EIA/TIA-455-6B,

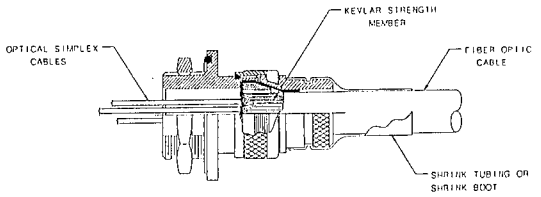


Figure 8. Completed Assembly of the Feed Through Adapter Design No. 1 (Drawing Courtesy of Glenair, Inc.)

Cable Retention Test Procedures for Fiber Optic Cable Interconnecting Devices. Preliminary results have yielded a cable to adapter pullout strength of 277 lbs. (1232.164N) which far exceeds the minimum cable pullout strength of 162 lbs. (720.61 N) required by MIL-C-28876. Also, as required by the specifications, there was no evidence of cable jacket or cable to adapter seal damage. However, the change in optical transmittance has not yet been measured which is required by both the military and commercial specifications.

DESIGN NO. 2

The second design to be introduced is also a variation of another copper cable braided shield termination system. This method uses heat-recoverable rings that shrink down on the spin-coupling adapter upon application of a heat source. This termination system is used with various military circular connectors. Figure 9 presents a straight adapter; notice the ring area where the heat-recoverable ring resides upon completion of the installation.

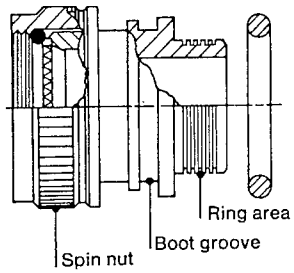


Figure 9. Heat-Recoverable Ring Cable Termination Adapter (Drawing Courtesy of Raychem Corp.)

The cable overall shield is affixed to the adapter body as the ring is heated and recovered upon the braid, therefore providing 360° connection to reduce the effects of electromagnetic interference on the cable inner conductors and to give mechanical protection against shock and vibration. Figure 10 represents a completed termination of the copper braid to the adapter. The ring is fully recovered when the thermochromic paint of the ring changes color as a resistance heater or a heat gun is applied directly to the ring.

Like the transformation that occurred with Design No. 1, minor modifications were made to create a feed through adapter that utilizes heat recoverable rings. The most significant alteration was to replace the spin coupler with a jam nut configuration, since the feed through penetrates into equipment rather than being fastened to the accessory threads of a connector. Like the threaded penetrating end of the first design discussed previously,

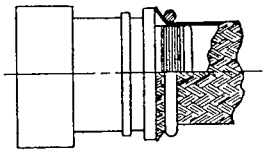


Figure 10. Termination of Cable Overall Shield (Drawing Courtesy of Raychem Corp.)

a D-cut structure was provided for anti-rotation. The ring area basically was not changed. The aramid yarn of the fiber optic cable is captured in the same manner that a copper braid is seized. The strength members are placed perpendicularly to the rings located on the adapter body, the ring is positioned over the aramid yarn at the ring area and shrunk down with a heat source. To resist water intrusion into the equipment via the feed through, an o-ring is placed on the adapter at the point where the adapter interfaces with the panel wall. To complete the assembly, an adhesively lined, heat shrink boot is affixed over the ring area and the aramid yarn, thereby concluding the environmental seal. Figure 11 presents the initial feed through adapter design, developed in a joint venture between Lockheed Martin Government Electronic Systems Company and Raychem Corporation.

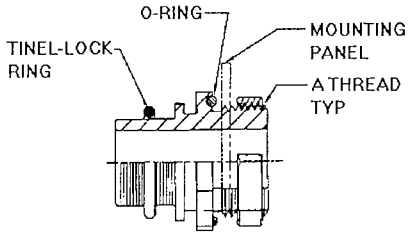


Figure 11. Heat-Recoverable Ring Feed Through Adapter (Drawing Courtesy of Raychem Corp.)

Prototypes, manufactured by Raychem Corp., Menlo Park, CA, have also undergone initial cable retention tests. Testing was conducted during the same period as the tests performed on the first feed through design. Cable retention testing was again performed in accordance with MIL-C-28876. Preliminary results indicate a cable to adapter pullout strength to be 254 lbs. (1129.85.N) which exceeds the MIL-C-28876 requirements of 162 lbs. (720.61 N). There was no evidence of cable jacket or cable to adapter seal damage. However, the change in optical transmittance has not yet been measured.

DESIGN NO. 3

The last design to be discussed has not been entirely developed or tested, but enough information is available for an introduction of this adapter. The third design offers a modification to a backshell that was specifically fabricated to circumferentially seize the strength members of fiber optic cables. This differs from the two designs previously illustrated in this paper that modified devices originally utilized to capture copper overall shielded cables. The key element to this design is the patented method by which the aramid yarn is captured. Specifically, as shown in Figure 12, conical grip rings seize the aramid yarn as the yarn is interlaced through and around the rings. The backnut is torqued

to the adapter body, therefore compressing the rings together and securing the aramid yarn. The o-ring provides the environmental seal which is a distinct method of protection from the use of heat shrinkable material with the previous two designs.

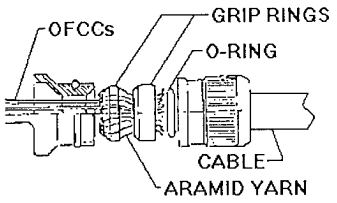


Figure 12. Captivation of Strength Member
(Drawing Courtesy of Litton VEAM)

No test results using this adapter are available at this time. However, the grip method, which is used in MIL-C-28876/27 straight backshells, has undergone extensive qualification testing. Since the fiber optic backshells have successfully passed the requirements specified in MIL-C-28876, then the cable to adapter pull out strength should easily exceed the requirement of 162 lbs. (720.61 N). As with the two other designs, optical transmittance testing should not pose any threats to the acceptance of this adapter and should not damage the cable jacket or cable to adapter seal.

CONCLUSION

The objective of this project was to design and develop a fiber optic feed through adapter that would provide system designers a low cost alternative to the heavy duty MIL-C-28876 multi-terminus fiber optic connector. Commercial-off-the-shelf (COTS) based systems, designed for and installed in naval vessels, utilize single low loss termination devices based upon power budget concerns. That is why the feed through device would lend itself to be more beneficial, since many of the termination designs are enclosed inside equipment. Three feed through designs have been established, two of which have undergone preliminary sets of pull tests and have met or exceeded the cable retention requirements of MIL-C-28876. These low cost feed through adapters allow the optical fiber cable to enter into equipment, provide environmental protection, and supply strain relief during periods of shock and vibration.

ACKNOWLEDGMENT

The authors would like to extend their appreciation to Mr. Greg Noll (Glenair), Mr. Bert Minnella (MTR), Dr. Terry O'Brien (Raychem), Mr. Gary Caporizzo (Raychem), and Mr. William Porzio (VEAM) for their contribution to the success of this endeavor. Also, a special recognition is extended to Mr. Mark Joseph (Lockheed Martin GES) for his influence and advice.

REFERENCES

1. "Shipboard Hardened Fiber Optic Cables Utilizing Thermoset Jackets", Harold J. Russell III, Michael Connaughton, Eli J. Joseph, Larry Rogers, *International Wire and Cable Symposium, 1992.*

2. "Acquisition Reform and Best Product Procurement: An Engineering View", David A. Fisher & Alfred Skolnick, Ph.D., Naval Engineers Journal, November, 1994.

BIOGRAPHIES



Richard Patterson is a Senior Member of the Engineering Staff having joined Lockheed Martin Government Electronic Systems and the AEGIS program in 1988. Combined with his previous position in the Department of Defense, he has eleven years of experience with naval combat systems. His primary responsibilities are as the lead Electrical Engineer for fiber optic and network integration projects. He has received both a ME degree in Engineering Management and a BSE in Electrical Engineering from Widener University in Pennsylvania. He is also an adjunct math instructor with Camden County College in New Jersey.



Michael Petner is a Member of the Engineering Staff who has been employed by Lockheed Martin Government Electronic Systems since November, 1993. He is an Electrical Engineering graduate of Temple University in Philadelphia, PA and has worked on various U.S. Navy programs since 1988. He has provided engineering and project management support to the Gas Turbine Ship Land Based Engineering Site at NAVSSES, contributed analysis and troubleshooting test plans for submarine radars and related systems, and conducted special studies related to EMI reduction aboard AEGIS Class ships. He is currently working in the Standards, Specifications, and Qualification Group conducting special studies and developing new fiber optic components for the U.S. Navy.

STP-CABLES FOR DATA TRANSMISSION : 300 MHZ AND BEYOND

François Gaille and Jean-Claude Ochsner

Câbleries et Tréfileries de Cossonay S.A.
CH-1305 Cossonay, Switzerland

ABSTRACT

This paper describes four families of 100 ohm copper twisted pair cables for data transmission and presents results obtained up to a frequency of 500 MHz.
The first two families, F-UTP and S-UTP cables, consist of unshielded twisted pairs with a common shielding. The electrical characteristics - Z_C, NEXT and ACR parameters - indicate clearly that these cables can operate properly at least up to 155 MHz.
The third family made of S100 QUAD cables, has been measured up to 300 MHz. At this frequency, the cables present an ACR value of about 20 dB indicating that they could operate even at higher frequencies.
The last family, S-STP cables, is formed of shielded twisted pairs with a common shielding. To obtain good electrical performances at 500 MHz or more, the pairs have to be regular, symmetrical and stable. The way to achieve that is to place during the twinning a metallic shielding stabilizing the pairs. Measurements have been made up to 500 MHz. The results - 20 dB of ACR at 500 MHz - show that S-STP cables can transmit signals at frequencies over 500 MHz.

INTRODUCTION

Until a few years ago, telecommunication copper twisted pairs were mostly operating at low frequency. Recently it has been shown that, if correctly designed and produced, twisted pair cables were surprisingly able to transmit signals properly at frequencies up to 100 MHz. Today, even so standards, recommendations or specifications are not defined above this value [1], [2], there is a clear trend and race to produce twisted pair cables operating with good performances at higher frequencies and practically as shown below, a value of 500 MHz has been reached.
A copper twisted pair cable is electrically characterized by three main parameters : its characteristic impedance Z_C, attenuation and near-end crosstalk (NEXT), all three parameters varying with the frequency f. A fourth important parameter is ACR, the attenuation to NEXT ratio, which is an indicator of the real cable performance; practically, ACR (f) = NEXT (f) - ATTENUATION (f). Attenuation and Z_C parameters depend mostly on the geometry of the cable, while NEXT, a more subtle characteristic, is related to structural parameters such as the use or not of an individual shielding of the pairs, the twist pitch ratio of one pair to another and finally the spacing between wire pairs.

These electrical characteristics may be severely affected by problems or irregularities which can arise during production [3]. Twinning - the process of twisting together the two individual conductors forming a pair - is crucial. In order to obtain good performances at very high frequencies (above 100 MHz), a twisted pair has not only to be symmetrically produced, but has also to stay later on geometrically regular. One way to achieve that is to place during its twinning a metallic screen on each individual pair. As a result, the conductors are regularly locked into place to form a perfect helical pair presenting good electrical properties.
In the following sections, four families of data cables are presented with their main electrical characteristics. The last family - the STP's having an individual shielding on each pair - has been measured up to 500 MHz and presents, even at this high frequency, very good electrical performances.

F-UTP CABLES

Foiled - Unshielded Twisted Pairs (sometimes abbreviated FTP) are the most simple and common cables after the UTP's. Two or four pairs of different pitches - a few centimeters long - are stranded together and wrapped with a polypropylene (PP) tape and an aluminium coated foil. The outer sheath could be either made of PVC or halogen free flame retardant material (HFFR). On one side they offer the simplicity of UTP cables and on the other they are noise immune due to the metallic foil.

Figures 1 and 2 show results obtained with a four-pair cable, 100 Ω, AWG 24 (0.51 mm diameter conductor) measured up to 155 MHz, the ATM frequency. Characteristic impedance Z_C of a pair is shown in fig.1; the distribution is centered at 100 ohm and within the ± 15 Ω limits. Figure 2 shows three distributions : NEXT between two pairs, the attenuation of a pair used in the NEXT measurement and finally the ACR parameter versus frequency. Up to 100 MHz, NEXT and ACR are well within the specifications required by present standards or recommendations [1], [2]. At the ATM frequency of 155 MHz, we can still observe an ACR value of more than 10 dB, which indicates that the cable could even perform at a higher frequency.

S-UTP CABLES

Shielded - Unshielded Twisted Pairs (often wrongly abbreviated STP) are up to the metallic foil similar to the F-UTP cables described in the previous section. The foil is then covered by a metallic tinned copper braid and an outer sheath.

Figures 3 and 4, corresponding respectively to figs. 1 and 2, show results obtained also on a four-pair cable, Z_C = 100 Ω, AWG 24. Comments made about the results in the previous section are fully valid and a more than 10 dB ACR value can be also observed at 155 MHz.

S100 QUAD CABLES

This kind of cables is made up of one or more quad(s). Each quad is embedded into a thin PE sheath which is then wrapped with an aluminium coated tape and a metallic braid. Outer sheath could also be PVC or HFFR material. Results obtained on a one-quad cable, 100 Ω, AWG 22 (0.64 mm diameter conductor) are presented in figs. 5 to 7 up to a frequency at 300 MHz. As it can be seen from the plots, the quad presents a good geometrical regularity and stability which are partly due to the PE sheath embedding and blocking the quad conductors. The measured ACR parameter shown in fig. 7, exhibits a 40 dB value at 100 MHz and about 20 dB at 300 MHz, which means that the S100 QUAD cable could operate properly at higher frequencies.

S - STP CABLES

Shielded - Shielded Twisted Pairs are the most elaborate data cables. They are generally composed of two or four pairs having a different pitch. Each pair possesses an individual screen made of a PP tape and an aluminium coated foil. The pairs are then stranded together and the bundle wrapped with a tinned copper braid.

The crucial point here is that in order to obtain an almost perfect geometrical regularity and stability of a pair, the individual metallic shielding is placed during the twinning of the pair and not during a subsequent production step. As a result, the pair conductors are right-a-way locked into a symmetrical position, thus avoiding or minimising asymmetries which could arise in subsequent production steps.

Figures 8 - 10 present results up to a frequency of 500 MHz obtained on a four-pair cable, 100 Ω, AWG 22. All the measurements were made with a network analyzer equipped with wide-band baluns (balanced - unbalanced translators). The geometrical regularity of the pairs is reflected through the flatness of the

characteristic impedance Z_C (see fig. 8) at frequencies well beyond 100 MHz.
As seen on fig. 9, NEXT parameter is also particularly improved by the presence of the individual screen on each pair. Indeed the effect of the metallic screen is double : on one hand to keep the pair symmetrical and on the other, to immune it against external perturbations. Both effects go the same way and improve the NEXT results. For example at 100 MHz, a 80 dB value is obtained, to be compared to about 45 and 55 dB, respectively for the F-UTP and S100 QUAD cables. At 500 MHz, NEXT is still about 60 dB. Finally, the measured ACR parameter shown in fig. 10, presents a value of about 60 dB at 100 MHz and more than 20 dB at 500 MHz. This may suggest that the cable could properly operate even at frequencies beyond 500 MHz.

CONCLUSION

The electrical characteristics and performances of copper twisted pair cables for data transmission are strongly related to the geometrical regularity and stability of the pairs. Consequently, the pairs (or quads) have to be symmetrically produced and have to stay later on geometrically regular.
It has been shown that F-UTP and S-UTP cables, with no individual shielding on each pair, can safely perform (100 m) at least up to 155 MHz, the ATM frequency.
If one wants the cable to operate properly at higher frequencies such as 300 or 500 MHz, the pairs or quads have to be embedded and stabilized. A way to achieve that is to place during its twinning a metallic screen on each individual pair. The resulting S-STP cables present very good electrical performances up to 500 MHz. The results obtained at this particular frequency suggest that this kind of cables could operate properly at frequencies beyond 500 MHz.

REFERENCES

[1] ISO/IEC DIS 11801 : Generic Cabling for Customer Premises Cabling

[2] EIA / TIA - 568 : Commercial Building Telecommmunications Wiring Standard
EIA / TIA - TSB 36 : Additional Cable Specifications for Unshielded Twisted Pair Cables

[3] Paul Z. Vanderlaan, Optimization of High Performance Unshielded Twisted Pair Media, IWCS Proceedings 1994, p.320

François Gaille was graduated in Physics in 1976 from the University of Neuchâtel, Switzerland. He went then to Temple University, Philadelphia, to study and work in High Energy Physics and in 1982 he obtained a Ph. D. in this field. After a few years of pure research, F. Gaille entered at the "Câbleries et Tréfileries de Cossonay S.A." as Chief of the laboratories, which is still his present position. His interests are both in Telecommunication and Power cables.

Jean-Claude Ochsner got in 1987 a diploma of Engineer in Telecommunication from the Engineering School of Geneva, Switzerland. He was then engaged at the "Câbleries et Tréfileries de Cossonay S.A." to develop telecommunication cables. Over the years, Jean-Claude Ochsner specialized in copper cables and today he is responsible for the developments of copper twisted pair cables.

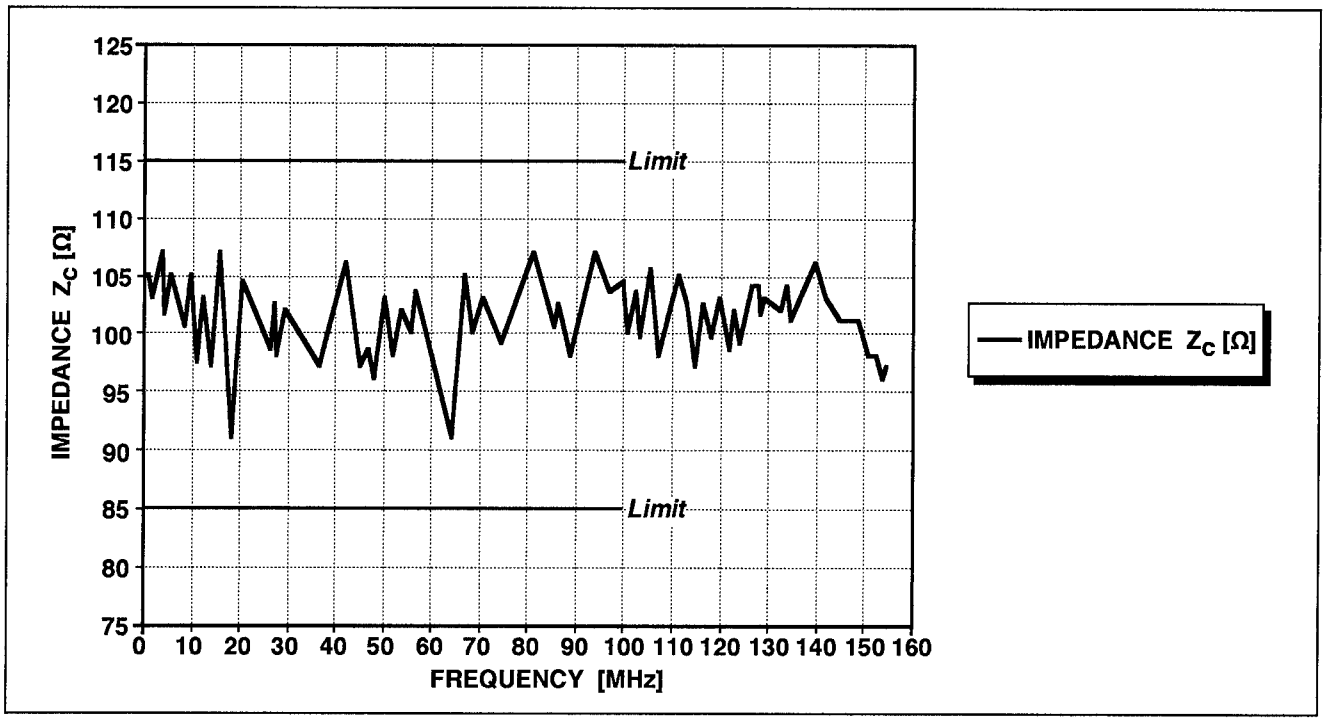


Figure 1. F-UTP 4P AWG24 : Z_C versus frequency of a pair

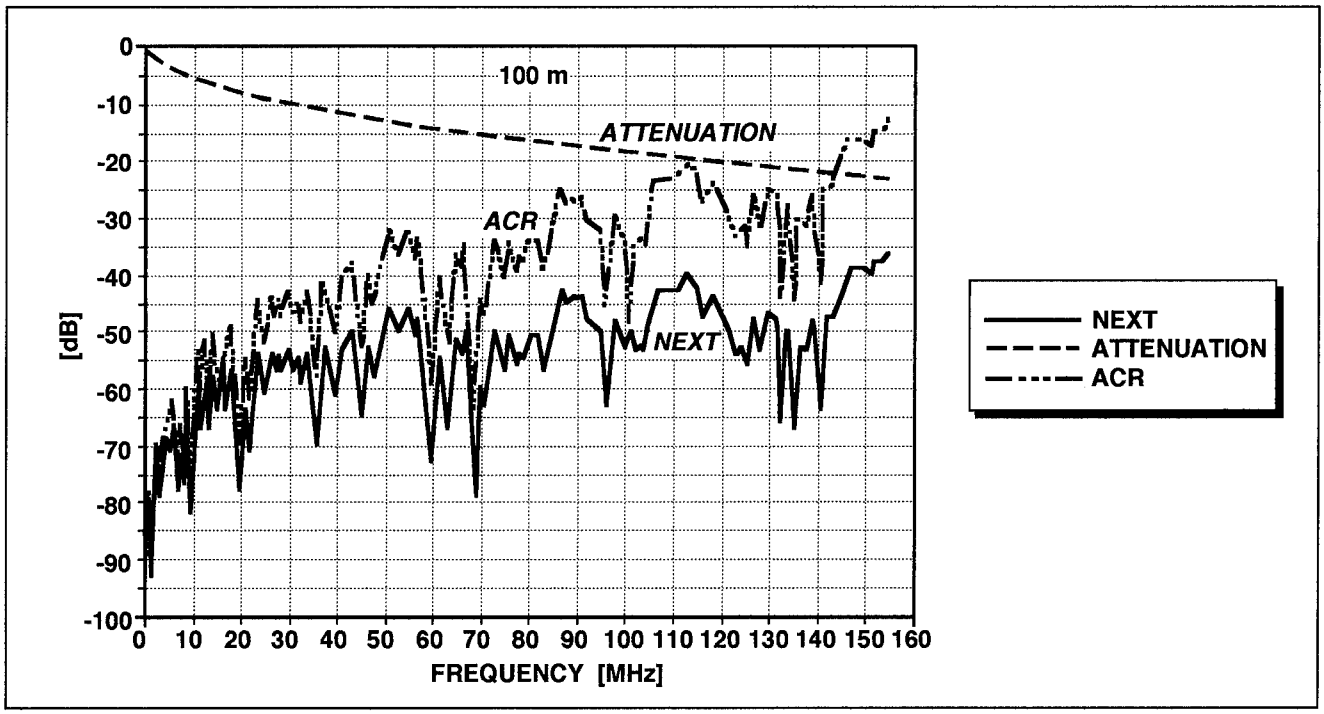


Figure 2. F-UTP 4P AWG24 : NEXT, ATTENUATION and ACR versus frequency

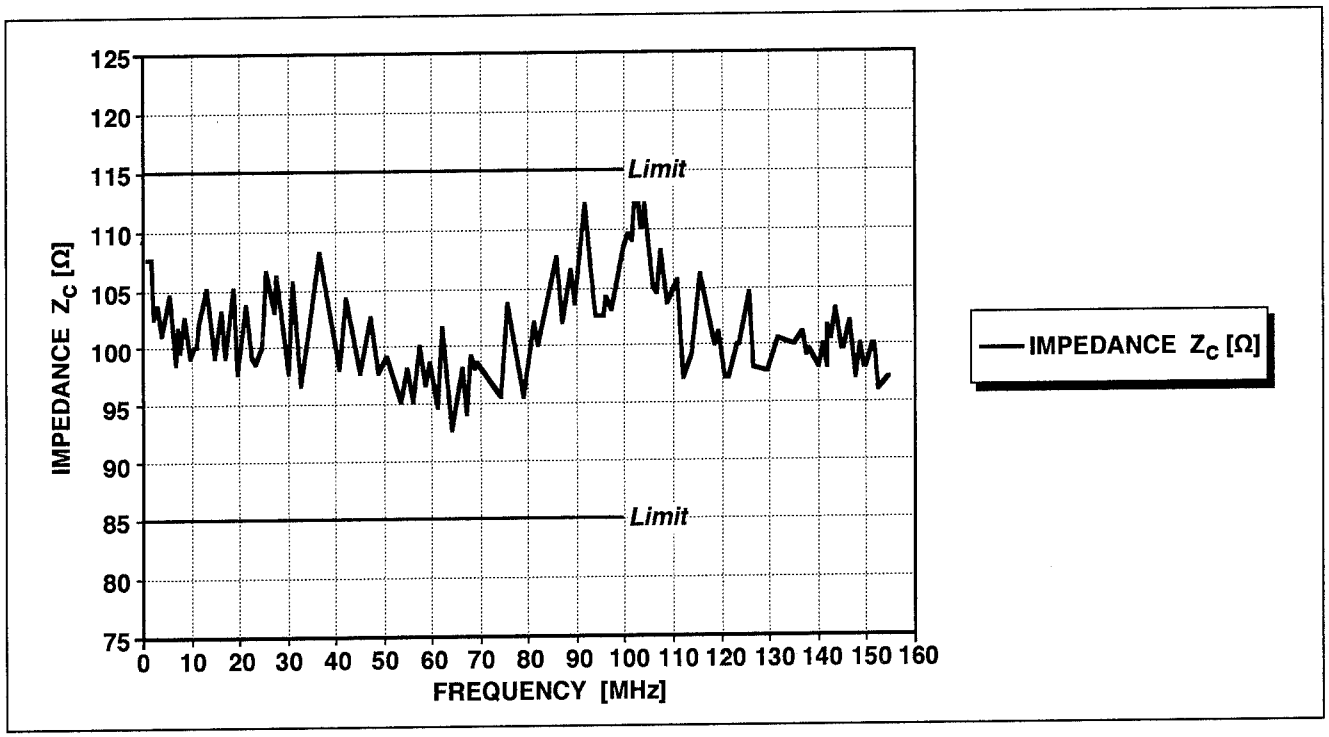


Figure 3. S-UTP 4P AWG24 : Z_C versus frequency of a pair

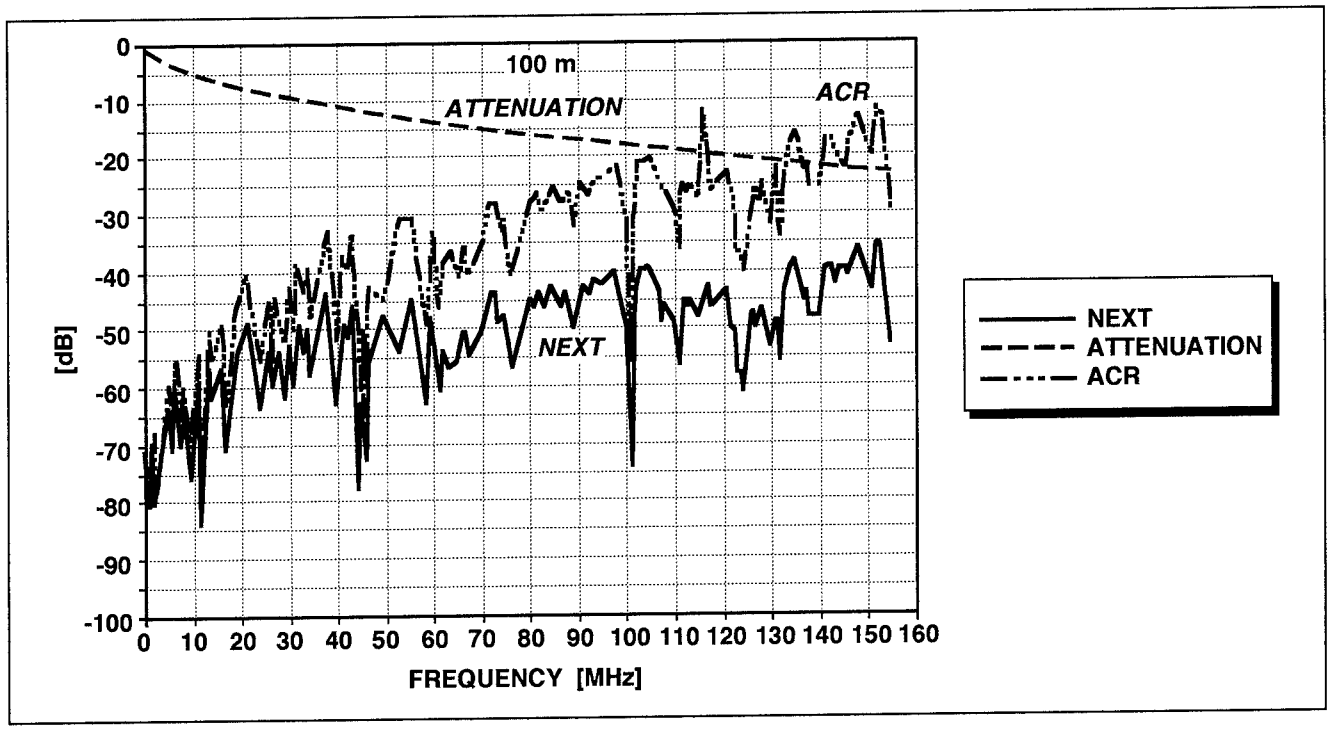


Figure 4. S-UTP 4P AWG24 : NEXT, ATTENUATION and ACR versus frequency

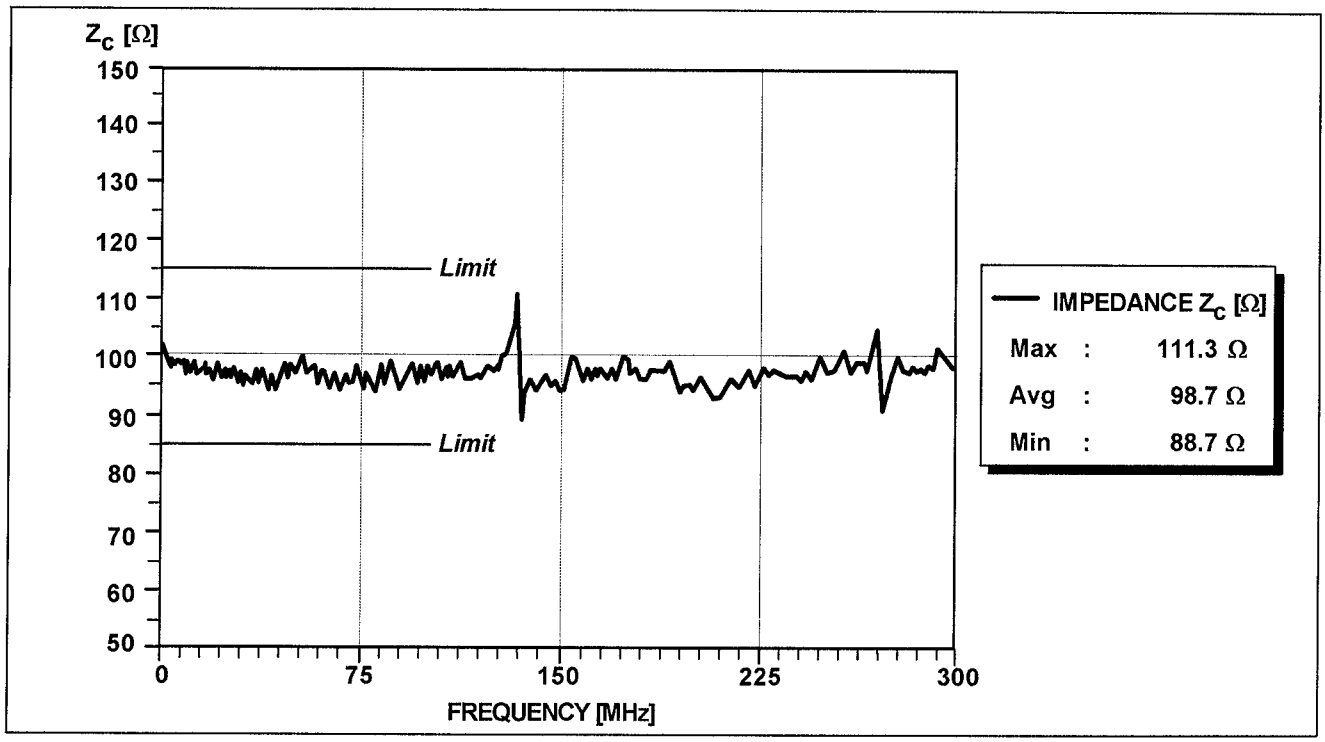


Figure 5. S100 QUAD AWG22 : Z_C versus frequency of a pair

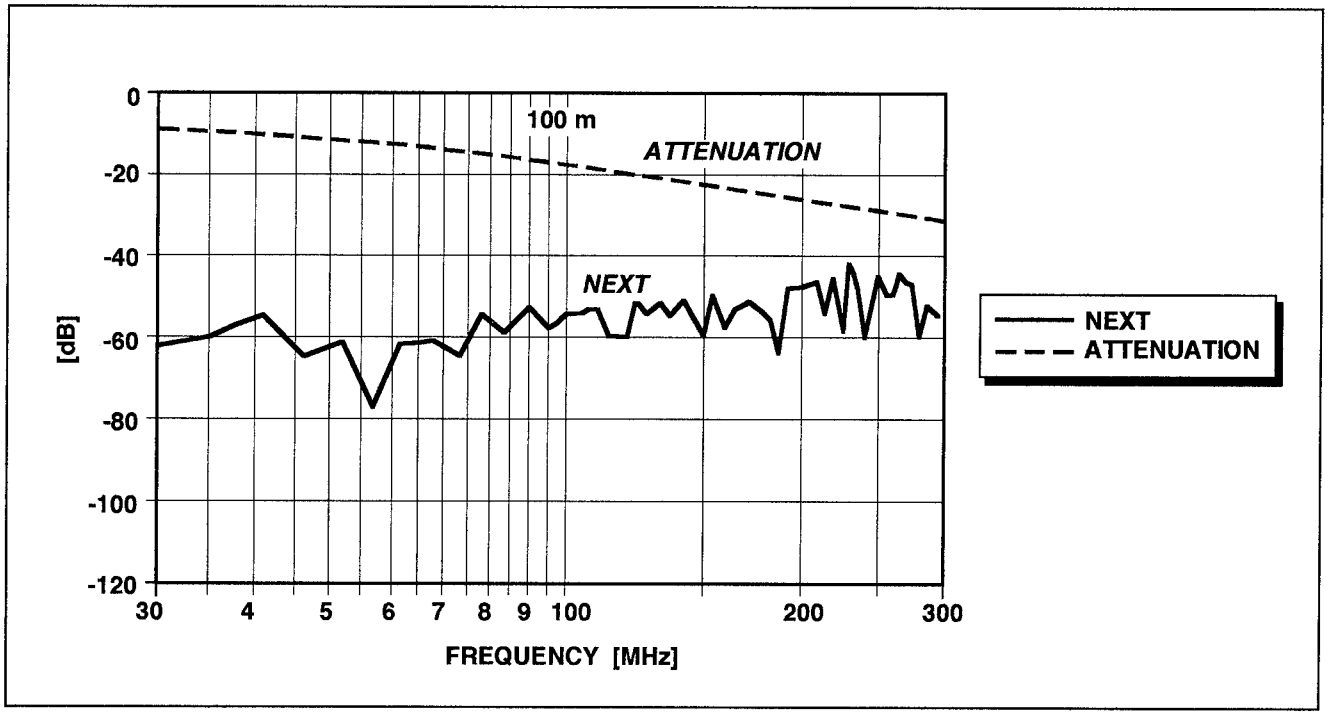


Figure 6. S100 QUAD AWG22 : NEXT and ATTENUATION versus frequency

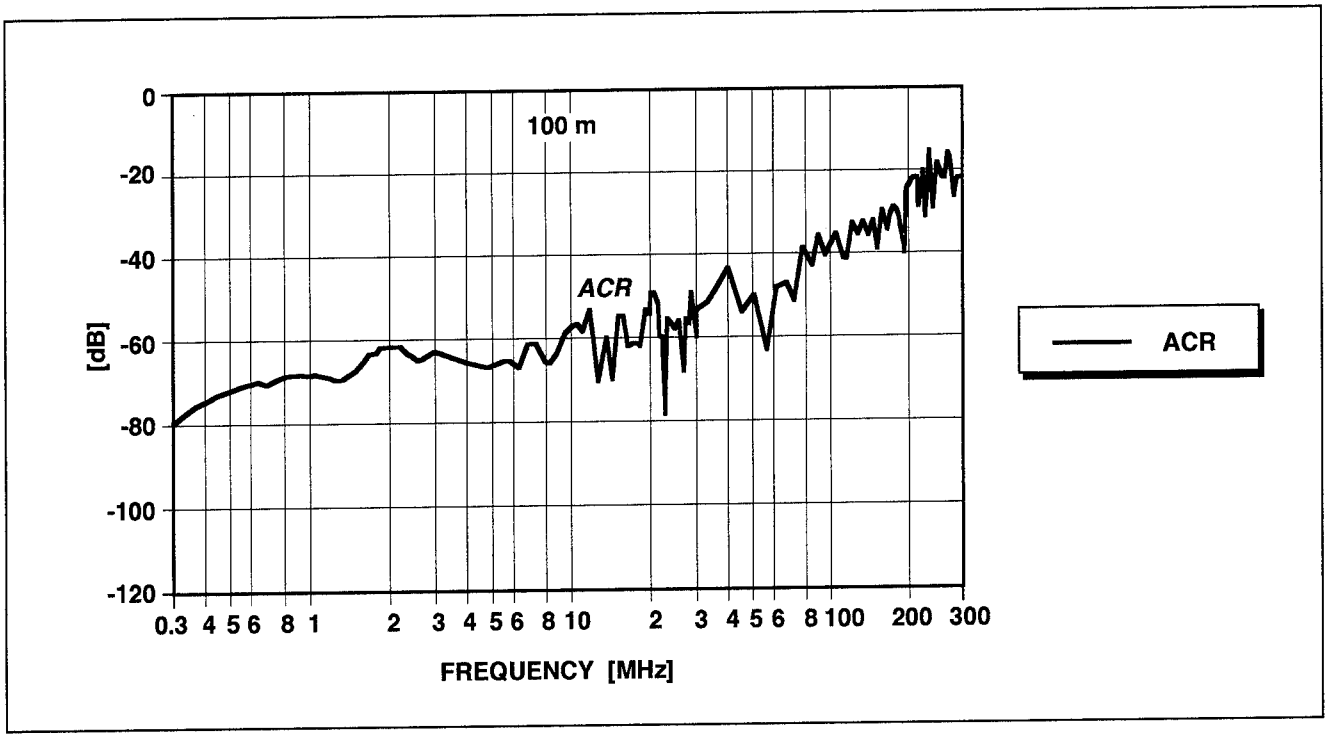


Figure 7. S100 QUAD AWG22 : ACR versus frequency

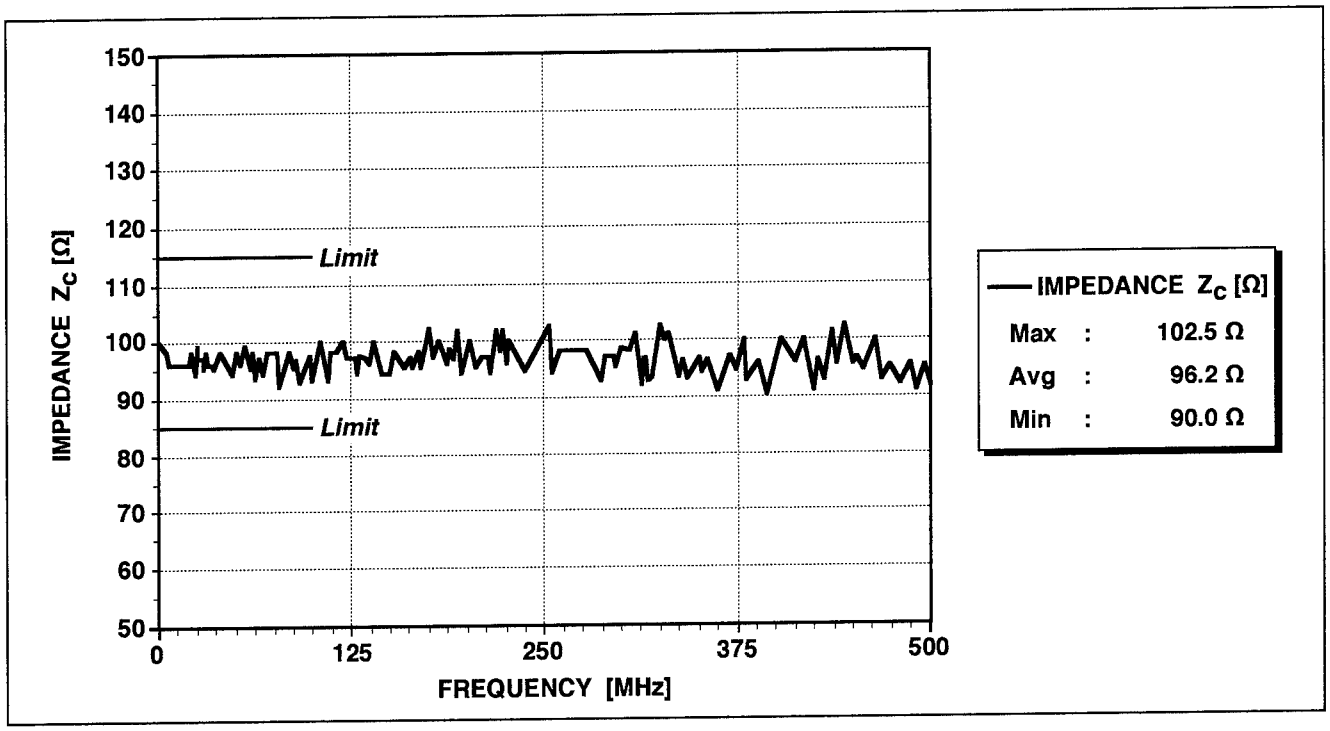


Figure 8. S-STP 4P AWG 22 : Z_C versus frequency of a pair

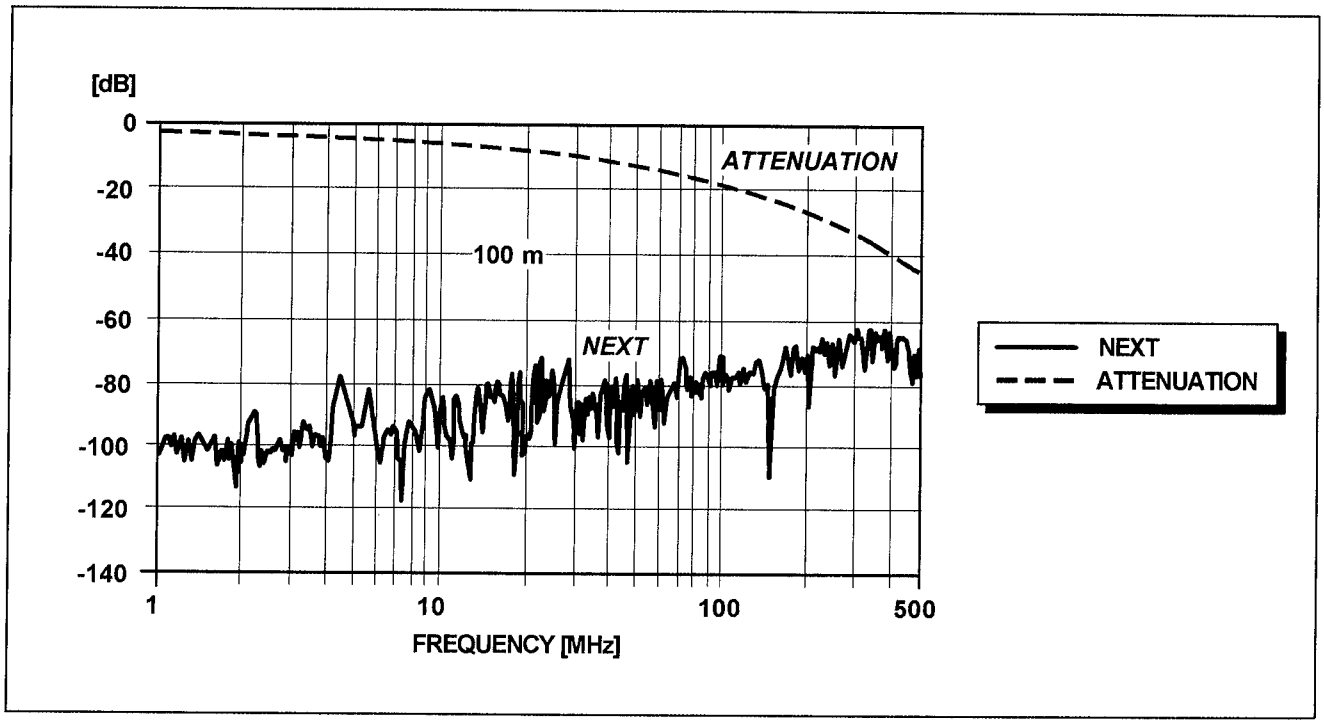


Figure 9. S-STP 4P AWG22 : NEXT and ATTENUATION versus frequency

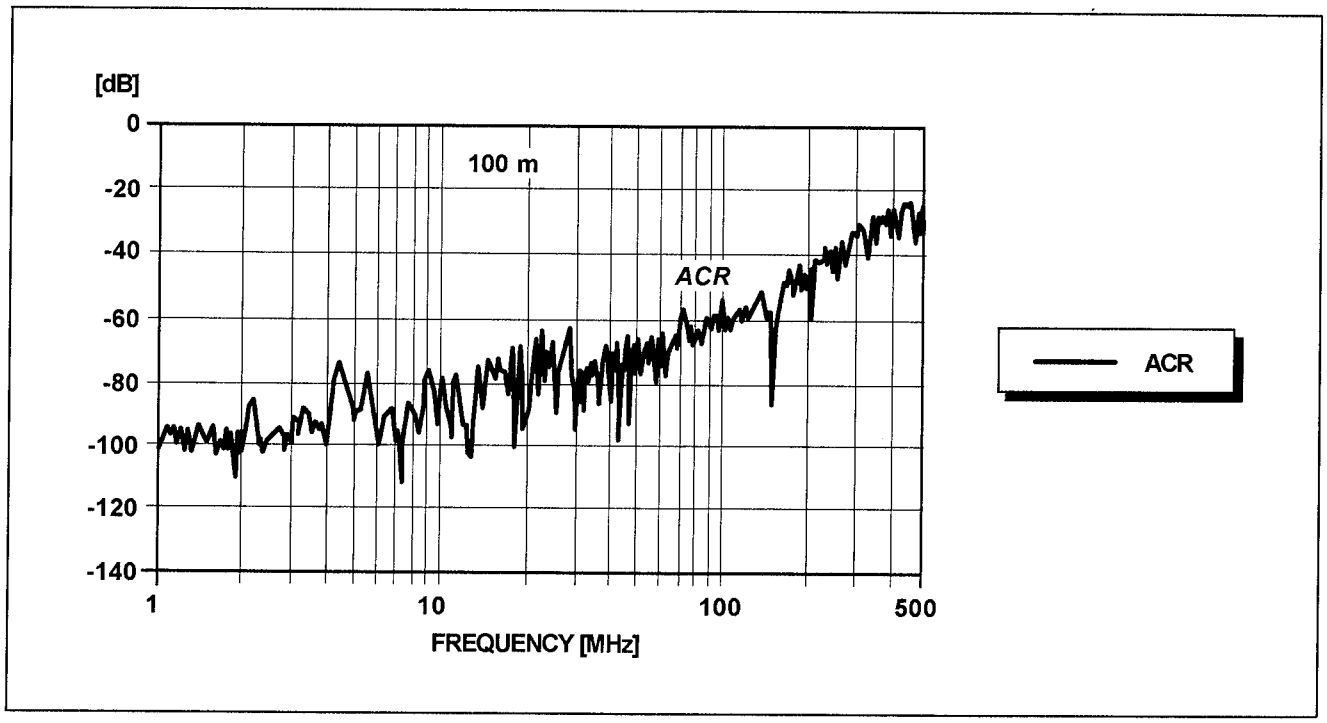


Figure 10. S-STP 4P AWG22 : ACR versus frequency

The Development of a Multimedia Shielded Twisted Pair Cable

Kiyoshi Saito, Hirotoshi Hondo, Kunio Negishi, Yasushi Horie, Kazuo Chiba, Yoshio Sato

The Furukawa Electric Co.,Ltd. Opto-Technology Laboratory,
6 Yawata-Kaigandori, Ichihara, Chiba 290 Japan

Abstract

This paper describes the development of a Multimedia Shielded Twisted Pair Cable which can transmit voice, data and CATV video signals.

The developed cable has following characteristics:

1) The pair for CATV video signal transmission satisfies the maximum attenuation 34dB/100m (at 450MHz), and it is capable of transmitting the CATV video signals up to 450MHz.

2) The pair for voice and data signal transmission satisfies all electrical properties specified by the EIA/TIA-568A Cat.5 UTP cable standard. Further, its attenuation to crosstalk loss ratio (ACR) is 10dB at 200MHz, and it is also applicable to advanced LAN's such as ATM-LAN.

3) The employment of a double shield structure ensures superior shield performance, and it provides the transfer impedance characteristic equivalent to the RG59B coaxial cable.

4) The cable can be terminated with shielded modular connectors.

1. Background

Originating from the announcement of the Information Superhighway information system in the United States, the promotion of Local Area Network (LAN) and the standardization of Asynchronous Transfer Mode (ATM)-LAN have been boosted, and further a demand for video signal transmission has been increased. Consequently, a higher speed and a larger capacity of signal transmission required.

Currently, premise wiring within intelligent buildings, Category 5 Unshielded Twisted Pair (Cat.5 UTP) cable as specified by the EIA/TIA-568A standard is used, but this cable is not suitable for transmitting the video signals such as CATV video signals.

For this reason, a 75 ohm coaxial cable is required for the video signal transmission.

We thought that if the CATV video signals could be transmitted with the Cat.5 UTP cable, it could be used as a multimedia cable capable of transmitting the CATV video signals in addition to the voice and data signals, as well as improved efficiency in premise wiring.

With this in mind, we developed a twisted pair cable that can transmit the CATV video signals in the frequency domain up to 450MHz.

2. Development Goal

The requirements of the cable to transmit both voice and data signals and CATV video signals are as follows;

The detailed cable properties are listed in Table 1.

(1) It can transmit voice and data signals. It satisfies the electrical properties of Cat.5 UTP cable as specified by the EIA/TIA-568A.

(2) It can transmit the CATV video signals in the frequency domain up to 450MHz. The attenuation must be 34dB/100m or less at 450MHz. This value is determined by a difference between the maximum output level of HUB for CATV and the minimum input level of the TV receiver.

(3) It must be shielded for protection from electromagnetic interference (EMI). It must satisfy the EMI standards such as the CISPR standard.

(4) It can be terminated with shielded modular connectors at both ends. The EIA/TIA-568A standard requires the Cat.5 UTP cables to be terminated with modular connectors at the cable ends.

Table 1 Cable Properties Requirements

No.	Item	Requirements	Specifications
①	The cable must satisfy electrical properties of the EIA/TIA-568A Category 5 UTP cable	Characteristic Impedance	100±15Ω (1MHz~100MHz)
		Attenuation	Maximum attenuation 22dB/100m(at100MHz)
		Near End Crosstalk (NEXT)	Minimum 32dB/305m(at100MHz)
②	The cable must transmit CATV video signals up to 450MHz, and provide a shield for protection from EMI	Attenuation	Maximum 34dB/100m(at450MHz)
		Shielding Effectiveness	Double shielded structure with an Al-PET-Al tape wrapping and a braid shield
③	The cable can be terminated with modular connectors (with shield) at the ends of cable	Maximum diameter of Insulation	0.965mm (pairs for voice and data signal transmission)
		Maximum diameter of Shield	6.8mm

3. Cable Design

3.1 Basic construction

The most general cable construction capable of transmitting both voice and data signals and CATV video signals is the Cat.5 4-pair STP cables with the overall shield provided directly outside the twisted pairs as EMI protection. This construction, however, the shield is provided in the vicinity of the twisted pairs, thus causing the attenuation to be increased and the characteristic impedance to be decreased. Accordingly, the following three countermeasures must be taken:

1) Increasing the outside diameter of the insulation

2) Lowering the relative dielectric constant (use of foamed insulation)

3) Increasing the shield diameter.

These countermeasures are taken into the basic structure of cable, which is shown in Figure 1.

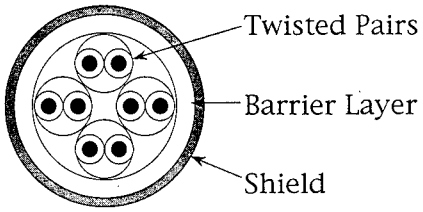


Fig.1 Cable Cross-Section

3.2 Design theory

In designing the cable, we investigated the bibliographies so far pertaining to twisted pair cables. But, we failed to find a twisted pair cable providing electrical properties in the frequency domain as high as 450MHz, nor to find a proper theoretical expression. Thus, we made our own theoretical expression with a way of thinking as follows, and designed the cable.

In a 4-pair cable, as shown in Figure 2-A, the center of each pair is eccentric to the center of shield. This eccentric shield, as shown in Figure 2-B, is replaced with the electrically equivalent shield provided on a pair of the cable, then the characteristic values of a pair of the shielded cable was calculated.

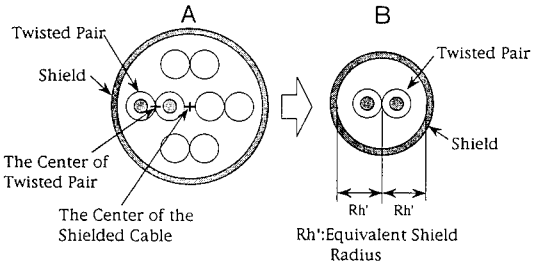


Fig.2 The Basis of the Theoretical Design

3.3 Result of the theoretical design

The conductor, insulation, and the shield diameter are as follows, and the attenuation and characteristic impedance relative to changes of the insulation outside diameter and cell content were theoretically calculated.

1) Conductor: 24AWG (0.511 solid wire) standard conductor of Cat.5 UTP cable

2) Insulation: Low density polyethylene(LDPE) or polypropylene(PP).

3) Shield diameter: The achievement of our analogous products shows that wrapping a tape of low relative dielectric constant several times between the

twisted pair cable core and shield layer is effective in decreasing attenuation and increasing characteristic impedance. We adopted this feature.

3.3.1 Relation of Attenuation (at 450MHz) and Characteristic Impedance (at 1MHz) relative to insulation outside diameter

Figure 3 shows the relation of attenuation and characteristic impedance relative to insulation diameter where the cell content is used as a parameter. The gray zone in the figure shows the range that satisfies both objectives of attenuation below 34dB/100m at 450MHz and characteristic impedance below 115 ohms at 1MHz.

However, there was no range of insulation diameter that satisfies both objectives of attenuation and characteristic impedance at any cell content. Therefore, it is impossible to transmit the CATV video signals and the voice and data signals with a twisted pair cable with the same insulated single conductors.

As a corrective measure, we paid our attention to the fact that in the Cat.5 4-pair UTP cable, 2 of 4 pairs are used for voice and data signals, and remaining 2 pairs are spares. That is, we thought that the attenuation of these 2 pairs should be decreased and they should be assigned as pairs for CATV video signal transmission.

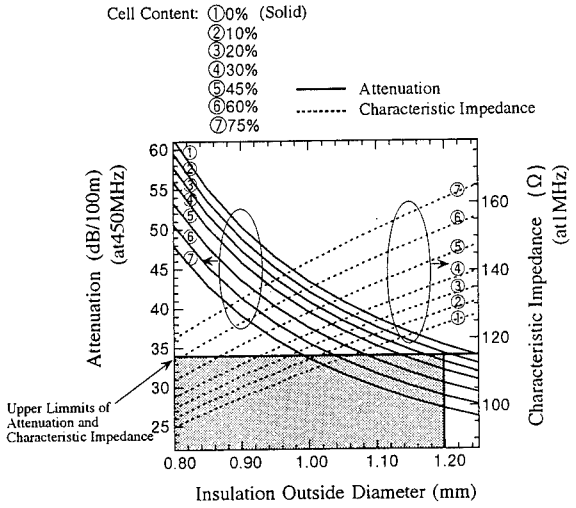


FIg.3 Calculated value of Attenuation and Characteristic Impedance Relative to the Insulation Outside Diameter

3.3.2 Design of a pair cable for CATV video signal transmission

3.3.2.1 Deformation and characteristic variation of foamed insulation

The maximum insulation outside diameter of 1.20mm can be reversely calculated from the maximum outside diameter 6.8mm of shield layer. Even in this case with the maximum insulation diameter, the foamed insulation cell content is over 10% to attain the target attenuation below 34dB/100m, as shown in Figure 3.

With the insulation having such a high cell content, an insulation deformation appears in the twisted pair manufacturing process. If the insulation is deformed, the distance between conductors of a twisted pair becomes smaller, resulting in an increase of attenuation. For this reason, we examined the relationship between cell content and the insulation deformation ratio in the twisted pair process.

The definition of a deformation ratio is shown in Figure 4. We manufactured the twisted pair cables under the following conditions, then evaluated the deformation ratio.

Conductor: 24AWG (0.511 solid wire)
Insulation material: Two kinds of LDPE and PP
Insulation outside dia.: 0.96mm
Twisted pair lay length: 16mm

The result are shown in Figure 5.

The following facts were disclosed:

1) The deformation ratio increases with an increase of the cell content.

2) The deformation ratio of PP is smaller than that of LDPE, showing higher strength.

As a result, we made a decision to adopt the PP as the insulation for the developed cable.

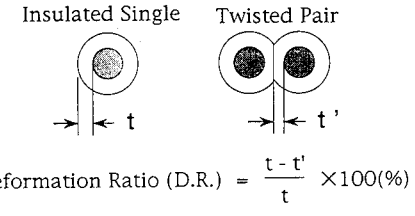


Fig.4 Definition of the Deformation Ratio

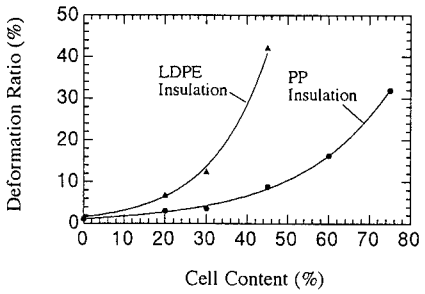


Fig.5 Relationship between Cell Content and Deformation Ratio

3.3.2.2 Theoretical design considering the deformation

The relation of attenuation (at 450MHz) and characteristic Impedance (at 1MHz) relative to cell content, taking the insulation deformation of the twisted pair process into consideration, is shown in Figure 6. The following facts were disclosed:

1) The attenuation decreases with an increase of cell content. But, as the deformation ratio abruptly increases with the increased cell content, the minimum attenuation occurs with a cell content of 55%. On the contrary, it increases when the cell content is over 55%.

2) The range of insulation outside diameter to satisfy attenuation of 34dB/100m is 1.13 to 1.20mm.

As a result, we adopted the following structure for a twisted pair cable for the CATV video signal transmission:

Conductor: 24AWG (0.511 solid wire)
Insulation material: Foamed PP
(cell content 55%)
Insulation outside dia.: 1.16mm nominal
(1.20mm maximum)

The characteristic impedance for this cable will be about 140 ohms (at 1MHz), as estimated from Figure 6.

3.3.3 Design of the twisted pair cable for voice and data signal transmission

The relationship of attenuation (at 100MHz) and characteristic impedance (at 1MHz) relative to the insulation outside diameter is shown in Figure 7. Using solid PP, A 0.95mm insulation outside diameter is expected to satisfy the voice and data signal transmission electrical properties. As a result, we adopted the following structure for a twisted pair cable for the voice and data signal transmission:

Conductor: 24AWG (0.511 solid wire)
Insulation material: Solid PP
Insulation outside dia.: 0.95mm nominal
(0.965mm maximum)

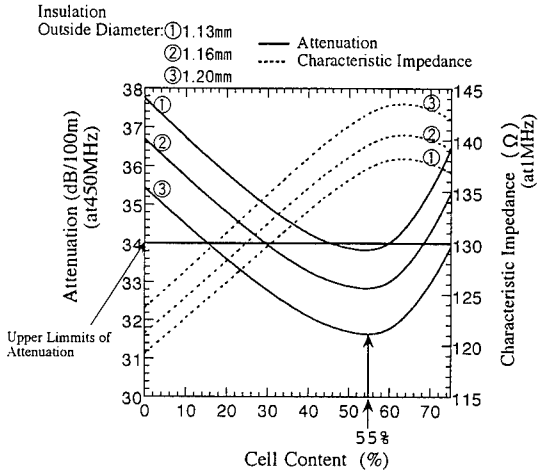


Fig.6 Calculated Value of Attenuation and Characteristic Impedance with Cell Content (Design of the Twisted Pair for CATV Video Signal Transmission)

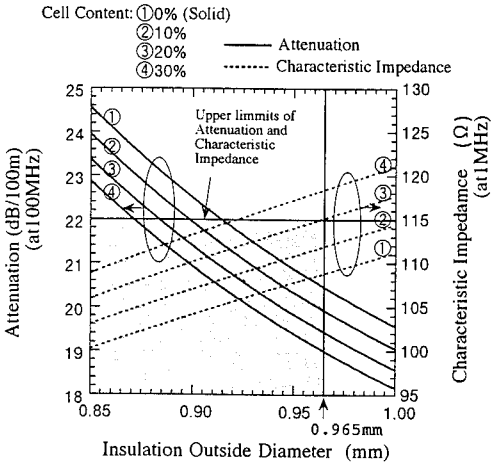


Fig.7 Calculated Value of Attenuation and Characteristic Impedance with Insulation O.D. (Design of the Twisted Pair for Voice and Data Signal Transmission)

4. Trial cable Manufacturing

Through the examination mentioned above, we determined the cable construction, and manufactured a trial cable.

The cross sectional view of the trial cable, and the cable construction are shown in Figure 8, and Table 2 respectively.

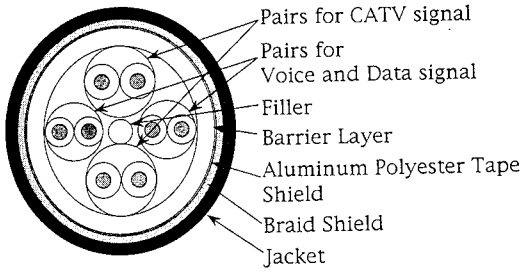


Fig.8 Cross Sectional View of Prototype Cable

Table 2 Trial Cable Construction

Item		Specification	
		Pairs for CATV video signal transmission	Pairs for voice and data signal transmission
Conductor	Material	Bare Copper	
	Size and structure	24AWG,1/0.511	
Insulation	Material	Foamed Polypropylene	Polypropylene
	Cell content (%)	55	Solid
	Mom. Diameter (mm)	1.16	0.95
twisted pairs	Direction	Left-Hand	Left-Hand
Cabling	Direction	Right-Hand	
Barrier layer	Composition and Method	Wrapped two sheets of low relative dielectric constant tape	
Shield	Method	Dual-sided Aluminum faced Polyester tape (AL-PET-AL) and Tin-Plated Copper Braid	
	Diameter (mm)	6.6 (Max. 6.8)	
Jacket	Material	Polyvinyl Chloride	
Overall Nom. Diameter (mm)		7.6	

Table 3 Test Results of Trial Cable

Item	Requirement	Unit	Specification	Result	
				Pairs for voice and data signal transmission	Pairs for CATV video signal transmission
Pairs for voice and data signal transmission	Characteristic Impedance	Ω	100±15 (1~100MHz)	107 (at1MHz) 101 (at100MHz)	(141 (at1MHz)) (134 (at100MHz))
	Attenuation	dB/100 m	22 maximum (at100MHz)	19	(15)
	Near End Crosstalk	dB/305 m	32 minimum (at100MHz)	48	-
Pairs for CATV video signal transmission	Attenuation	dB/100 m	34 maximum (at450MHz)	-	33
	Shielding Effectiveness	-	Transfer Impedance equivalent to RG59B coaxial cable	-	Good
Construction	Insulation O.D.	mm	0.965 maximum (pair for voice and data signal transmission)	0.95	1.16
	Shield O.D.	mm	6.8 maximum	6.5	
	Cable O.D.	mm	7.6 nominal	7.6	

5. Test Result

5.1 Electrical properties test results

The trial cable electrical properties test results for attenuation and near end crosstalk loss in a pair for voice and data signal transmission are shown in Table 3, Figure 9, and Figure 10 respectively.

Further, for the shield characteristics, we made an evaluation of the transfer impedance against IEC Standard 96-1. this result is shown in Figure 11.

Thus, we confirmed that the cable satisfied all development objectives.

5.2 Comparison between the actual measured values and the theoretical design values

The frequency characteristic of attenuation and characteristic impedance respectively for the actual measured values and the theoretical design values in the twisted pair for CATV video signal transmission is shown in Figure 12, and the twisted pair for voice and data signal transmission is shown in Figure 13. The result of the trial cable satisfies the theoretical design values, indicating that our approach is correct.

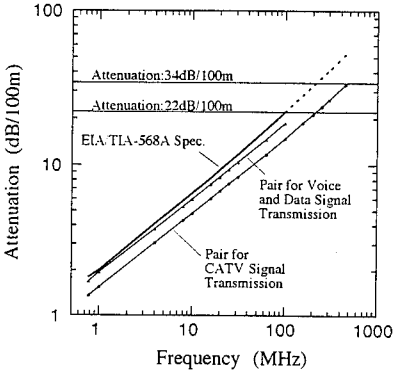


Fig.9 Variation of Attenuation with Frequency of Prototype Cable

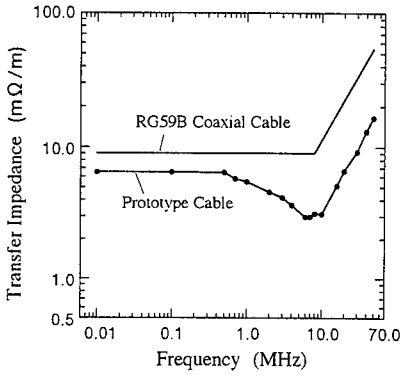


Fig.11 Variation of Transfer Impedance with Frequency of Prototype Cable

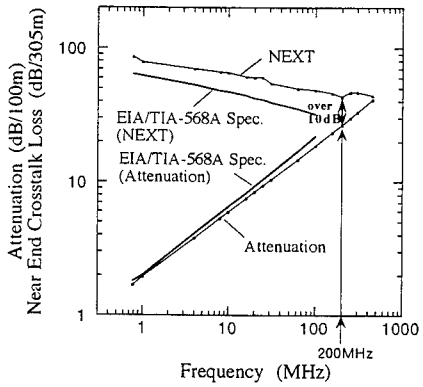


Fig.10 Variation of Attenuation and NEXT with Frequency of Prototype Cable
(Pair for Voice and Data Signal Transmission)

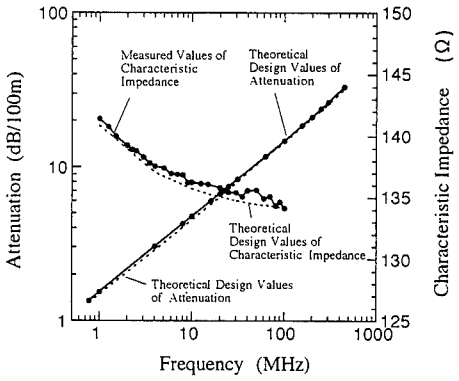


Fig.12 Comparison between Actual Measured Values and Theoretical Designed Values
(Pair for CATV Video Signal Transmission)

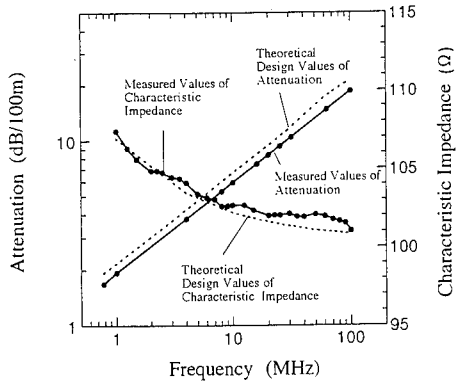


Fig.13 Comparison between Actual Measured Values and Theoretical Designed Values (Pair for Voice and Data Signal Transmission)

5.3 Experiment of CATV video signal transmission

This cable, as shown in Figure 14, is capable of transmitting the CATV video signals using twisted pair cable by connecting a balun (impedance converter transformer) for high frequencies at both ends of the cable with a maximum length 100m. We connected the developed cable to a CATV video signal transmission system as shown in Figure 14, and conducted a CATV video signal transmission experiment. As a result, we confirmed that the cable was capable of transmitting the CATV video signals in the frequency domain up to 450MHz without a failure.

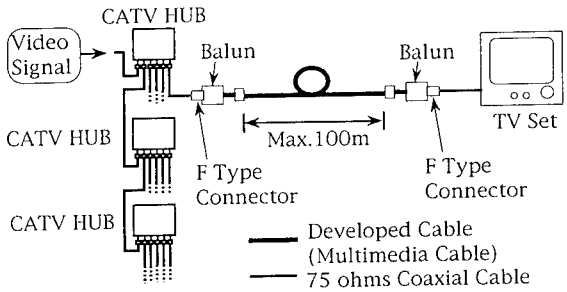


Fig.14 Configuration of CATV Signal Transmission System with Twisted Pair Cable

6. Conclusion

(1) The theoretical electrical properties design values almost met the actual measured values. this indicates that our hypothesis was correct.

That is:

1) A four pair cable with shielding is replaced with a one pair cable with an electrically equivalent shield.

2) The variation of characteristics due to the insulation deformation in the twisted pair manufacturing process is taken into consideration in the design phase.

(2) Due to the insulation deformation in the twisted pair process, there is an upper limit of cell content in every insulation material, where the attenuation becomes the least.

(3) A composite cable consisting of a pair for voice and data signal transmission can be manufactured, which is capable of transmitting both voice and data signals and CATV video signals.

7. Summary

As examined above, we succeeded in making the multimedia twisted pair cable delivering the following characteristics:

1) The pair for CATV video signal transmission satisfies the maximum attenuation 34dB/100m (at 450MHz), and it is capable of transmitting the CATV video signals up to 450MHz.

2) The pair for voice and data signal transmission satisfies all electrical properties specified by the EIA/TIA-568A Cat.5 UTP cable standard. Further, its attenuation to crosstalk loss ratio (ACR) is 10dB at 200MHz, and it is also applicable to advanced LAN such as ATM-LAN.

3) The use of a double shield structure ensures a superior shield performance, and it provides the transfer impedance characteristic equivalent to an RG59B coaxial cable.

4) The shielded modular connectors can be terminated.

8. Acknowledgement

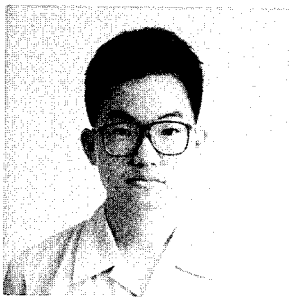
The authors would like to thank the personnel of the Appliance Wire Division, and the Network Integration Division of The Furukawa Electoric for cooperation in manufacturing and evaluating the cable during the development of this cable.

9. References

(1) Natsuo Kobayashi,Tatsuo Saito,"Coaxial Cable and Video Pair Cable", IECE Japan Tech.Rep.,Vol.40 No.4, 1957, pp.325-335

(2) Natsuo Kobayashi, "Miscellanea on Telephone-Cable Transmission-Part7 Resistance and Inductance of a Multi-Paired Cable", FUJIKURA GIHO in Japanese Vol.54, July 1976, pp.71-81

(3) "The Development of Shielded Twisted Pair Cable for Multi-media Applications (Multi-media Cable)", Wire & Cable Focus '94 Seminar Paper 1994 September



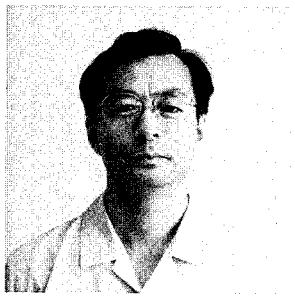
K. Saito
The Furukawa Electric Co.,Ltd.
6, Yawata-Kaigandori,
Ichihara, Chiba 290 Japan

Mr. Kiyoshi Saito graduated from the Chemistry Group of Polytechnic University in 1991 Then he joined The Furukawa Electric Co.,Ltd. and he has been engaged in Production engineering for electronic appliance wire. Now, he is a member of engineer of Metal Cable Section in Opto-Technology Laboratory.



H. Hondo
The Furukawa Electric Co.,Ltd.
6, Yawata-Kaigandori,
Ichihara,Chiba 290 Japan

Mr. Hirotoshi Hondo graduated from Tohoku University in electrical engineering in 1969. He joined The Furukawa Electric Co.,Ltd. and has been engaged in development of telecommunication cables including optical fiber cable, almost during 25 years. During the time period, he was in design engineering department for 6 years and returned to R&D division. Now he belongs to Opto-Technology Laboratory.



K. Negishi
The Furukawa Electric Co.,Ltd.
6, Yawata-Kaigandori,
Ichihara, Chiba 290 Japan

Mr. Kunio Negishi graduated from Sofia University in electrical & electronics engineering in 1972, and joined The Furukawa Electric Co.,Ltd. in the same year. He worked for Engineering Dep. of Appliance Wire Div., during which time, he was engaged in cable design for computers and acoustic equipments. Now, he is a manager of metal cable R&D section of Opto-Technology Laboratory.



Y. Horie
The Furukawa Electric Co.,Ltd.
6, Yawata-Kaigandori,
Ichihara, Chiba 290 Japan

Mr. Yasushi Horie graduated from Nihon University a master of engineering degree majoring in electrical engineering in 1988. Then he joined The Furukawa Electric Co.,Ltd. and has been engaged in production engineering and engineering department of Appliance Wire & Cable Division. He is now a member of Stuff Engineer of Metal Cable Section in Opto-Technology Laboratory.



K. Chiba
The Furukawa Electric Co.,Ltd.
2-6-1, Marunouchi,
Chiyoda-Ku, Tokyo 100 Japan

Mr. Kazuo Chiba received the B.S. and M.S. degrees in materials science from Nagaoka University of Technology, in 1982 and 1984, respectively. In 1984, he joined The Furukawa Electric Co.,Ltd. Since then he has been engaged in design of communication cables. He is currently the Assistant Manager at engineering section of Electronic Appliance Wire & Products Division.



Y. Sato
The Furukawa Electric Co.,Ltd.
5-1-9, Higashi-Yawata,
Hiratsuka, Kanagawa 254 Japan

Mr. Yoshio Sato graduated from Osaka Prefectural University majoring master of science in aeronautical engineering in 1986. Then he joined The Furukawa Electric Co.,Ltd. and has been engaged in development of data communication and cabling system for Local Area Network. He is an assistant manager of Systems Development Department of Network Integration Division.

CABLE PREPARATION EFFECTS ON HIGH PERFORMANCE TWISTED PAIR CABLE TESTING FROM 100MHz TO 350MHz

Ramon Alvarez and Rafael Herrera

DCM Industries, Inc.
Union City, California

ABSTRACT

When testing twisted pairs, as the test frequency increases, the end of the cable nearest to the test equipment becomes more and more important. Essentially, the higher the frequency, the shorter the cable becomes regardless of the cable's actual length. This is true for both Near End Crosstalk (NEXT) and Characteristic Impedance measurements.

The causes for these effects may also produce undesirable accuracy effects when a cable is connected to the test system. Specifically, the intrinsic electro-magnetic cable characteristics are greatly disturbed by the cable jacket removal and corresponding connection to the test system.

Three different 4 pair cables, two unshielded twisted pair cables (UTP) and one shielded twisted pair cable (STP), were evaluated for different lengths of cable jacket removal. The results show that keeping the stripping length to a minimum is necessary for testing at frequencies above 100MHz. In some cases, the intrinsic characteristics of the cable may be acceptably reconstructed by superimposing a polyolefin shrink tubing over the exposed pairs.

INTRODUCTION

As the demand for higher data rate twisted pair cables increases, cable manufacturers have met the challenge by producing cables with higher frequency capabilities. Correspondingly, cable testing requirements have become more stringent and the effects of cable preparation and cable handling during testing have become more critical.

The electro-magnetic configuration located in the first portion of the cable is regarded as the most important consideration for the purposes of testing NEXT and Characteristic Impedance. Some amount of cable jacket must be removed to create access to the pairs under test. Consequently, of paramount interest is the amount of the cable jacket which can be removed without appreciably affecting the characteristics of the cable and thus the accuracy of the measurements. In addition, the effects of cable handling and of the grounding of STP cable must be considered.

MEASUREMENTS AND METHODOLOGY

In order to evaluate the effects of cable jacket removal during cable testing, we chose two 4 pair UTP cables and one 4 pair STP cable: Cable #1 is a traditional UTP; Cable #2 is a UTP with the wires of each pair bonded together to maintain the twist configuration; Cable #3 is a STP with two star quads each with a metallic shield, both quads are then surrounded by a braided shield underneath the cable jacket.

Using a DCM CMS-2XLD Cable Measuring System which includes a network analyzer and a high frequency cable interface, both NEXT and Characteristic Impedance were measured on each cable with a reference minimum jacket removal of 0.1 inches. The amount of jacket was subsequently removed in increments of 0.1 inches up to a total jacket removal length of 1.0 inch. The amount of jacket was then removed in increments of 0.4 inches up to a total jacket removal length of 2.2 inches.

On STP Cable #3, the pairs under test were taken from separate quads (each having its own shield) and the braided shield grounded to the test set up at all times.

The resulting data was first analyzed using Analysis of Variance, in order to determine the existence of measurement changes related to the jacket removal length. If a relationship was determined to exist, the average trend for the measurement changes were shown for five ranges of frequency: 100-150MHz, 150-200MHz, 200-250MHz, 250-300MHz and 300-350MHz.

TEST RESULTS

Characteristic Impedance

UTP Cable #1 showed the most sensitivity to jacket removal length, as shown in Fig. 1. For frequencies up to 300MHz, the cable jacket could be removed up to 1.4 inches before an average change of 3% in the Characteristic Impedance was observed.

UTP Cable #2 showed the best behavior to jacket removal length, as shown in Fig. 2. For frequencies up to 350 MHz, the cable jacket could be removed up to 2.0 inches before an average change of 3% in the Characteristic Impedance was observed.

STP Cable #3, as shown in Fig. 3, showed that the cable jacket could be removed up to 1.8 inches before an average change of 3% in the Characteristic Impedance was observed for frequencies up to 300MHz.

The drastic changes in Characteristic Impedance observed after the jacket removal lengths shown, seemed due to the alteration of the pair's immediate surrounding and not by the influence of external couplings. We noticed the absence of a practical effect when placing an individual shield around each pair under test.

Applying a polyolefin shrink tubing to each pair for isolation reconstruction purposes showed improvements for both UTP Cable #1 and UTP Cable #2. With the shrink tubing applied to the exposed pair, UTP Cable #1 and #2 with a jacket removal length of 2.2 inches presented an average change of less than 2% in the Characteristic Impedance at measurement frequencies up to 350MHz (Fig. 4 and Fig 5). The shrink tubing applied to STP Cable #3 showed a small but insignificant effect (Fig.6).

STP Cable #3 presented a very strong deterioration in Characteristic Impedance when the braided shield was not grounded (Fig. 7).

Near End Crosstalk (NEXT)

UTP Cable #1 and UTP Cable #2 showed no practical correlation to jacket removal lengths for NEXT testing (Fig. 8 and Fig. 9). However, during NEXT testing movement of the pairs between testing may have caused variations in the test results.

NEXT is very sensitive to cable manipulation, and changes due to that effect were observed being on the average of up to 2 dB (Fig. 10). However, NEXT results could individually vary up to 24 dB, especially if they occur at the frequency resonances, only by randomly moving the exposed pairs connected to the test set-up. Consequently, care must be taken when judging the repeatability of a NEXT measurement. A more realistic criteria may be looking at the changes occurring on the envelope (peaks) of the NEXT curve instead.

Based on the observations, a cable under test should be properly clamped or kept unmoved during a test or between consecutive tests.

STP Cable #3 presented the best NEXT characteristic, 70 dB at 100MHz and a non-typical 20 dB/decade slope, as shown in Fig 11. However, Cable #3 also presented an unusual sensitivity to the jacket removal length.

The complete frequency scan of NEXT improved by approximately 6 dB after 0.4 inches of jacket was removed. In fact, NEXT improved by approximately 20 dB at 0.3 inches of jacket removal length, when placing an individual shield on each pair under test. This may suggest a situation where the NEXT for this cable may be determined mainly by the direct NEXT component which occurs solely at the end of the cable. Also, the NEXT was completely deteriorated when the cable braided shield was not grounded.

CONCLUSION

Maintaining the intrinsic Electro-Magnetic characteristics of a cable under test is an important consideration for accurate cable testing. Minimizing the jacket removal length is a major factor for maintaining the accuracy during Near End Crosstalk (NEXT) and Characteristic Impedance tests.

As new processes evolve in the High performance cable manufacturing industry, an evaluation of the measurement conditions may be necessary to detect special connection requirements. This is specially true if the frequency performance continues to increase.

ACKNOWLEDGMENTS

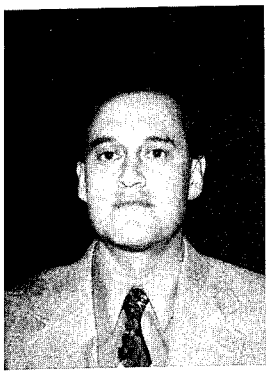
The authors wish to thank Jose Valadez and Jorge Jo for all the work in patiently collecting the data which made possible identifying the importance of the cable preparation and manipulation in testing high performance cables.

REFERENCES

[1] H. Cravis and T.V. Crater, Engineering of T1 Carrier System Repeatered Lines, BSTJ, March 1963, pp 431-486.

[2] N. Holte, A CrossTalk Model for Cross-Stranded Cables, IWCS, 1982, pp 207-220

[3] S. Hinoshita, S. Ishi and K. Ishii, Analysis and Improvement of Crosstalk (NEXT & FEXT) for Multi-unit, Backbone UTP Cable applied up to FDDI/ATM Data Speed, IWCS, 1994, pp 341-350.



Ramon Alvarez
DCM INDUSTRIES
2930 Faber Street
Union City, CA
USA 94587

Ramon Alvarez is currently High Frequency Product Development Manager at DCM INDUSTRIES, INC. He has worked for the past 13 years in the instrumentation development field. He received his Bachelor of Science degree in Electrical Engineering from Universidad de Los Andes in Merida, Venezuela, and has received two Master of Science degrees in Electrical Engineering from the University of California, Berkeley.



Rafael Herrera
DCM INDUSTRIES
2930 Faber Street
Union City, CA
USA 94587

Rafael Herrera is currently the Cable Measuring Systems Marketing Manager at DCM INDUSTRIES, INC. He has worked at DCM for the past 12 years in product support, product development and marketing. He received his Bachelor of Science degree in Electrical Engineering from Pontificia Universidad Javeriana, Bogota, Colombia.

FIGURE 1:

Cable #1, IMPEDANCE Change (%)

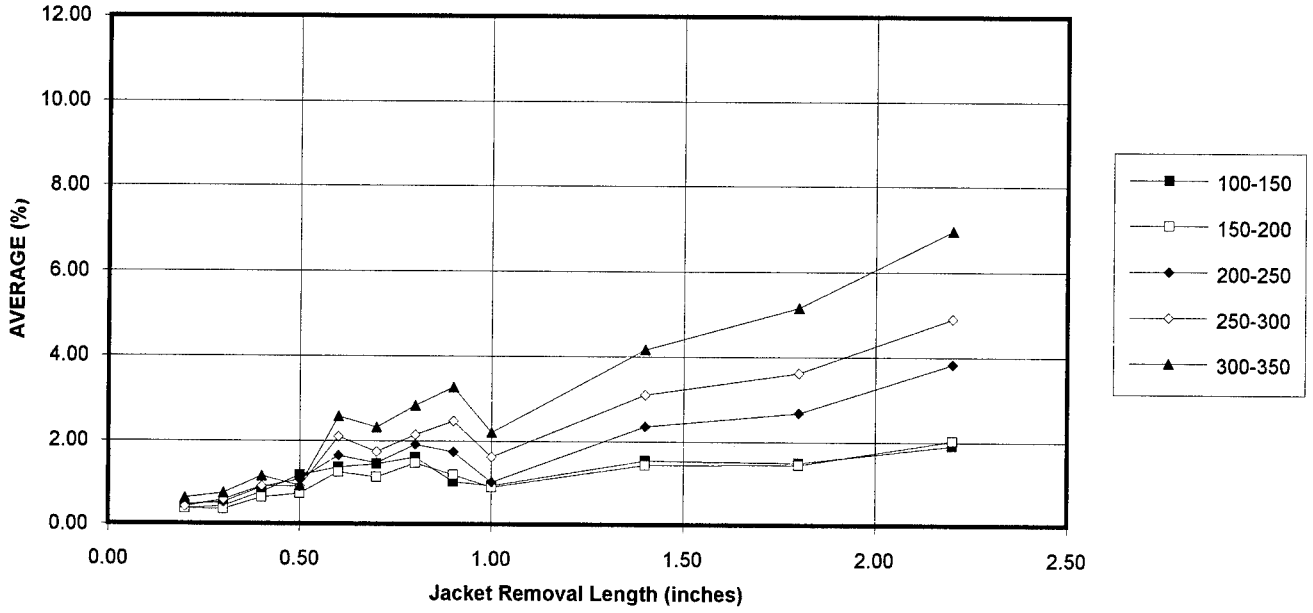


FIGURE 2:

Cable #2, IMPEDANCE Change(%)

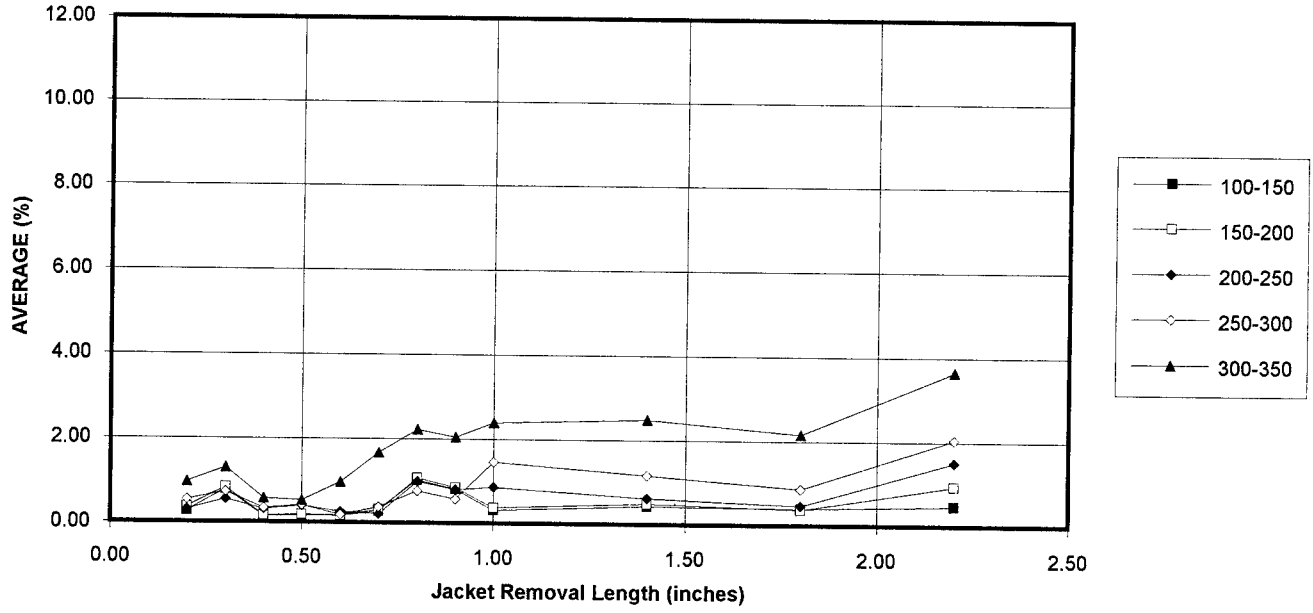


FIGURE 3:

Cable #3, IMPEDANCE Change (%)

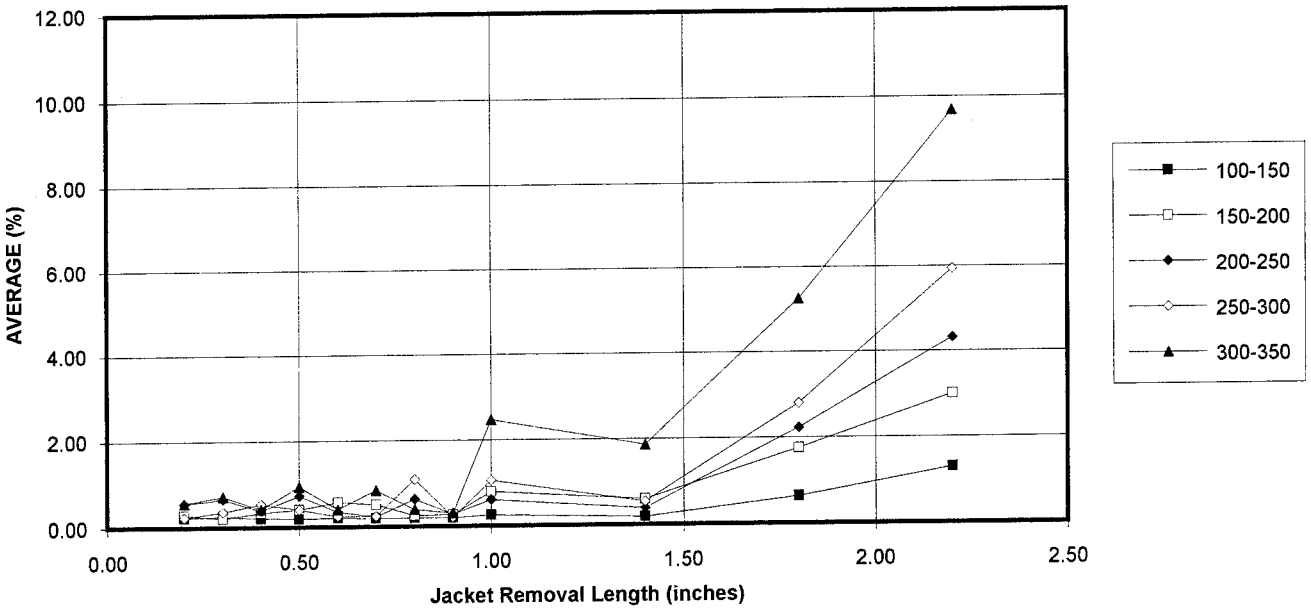


FIGURE 4:

Cable #1 IMPEDANCE
Tubing Effect after 2.2 in of Jacket Removal

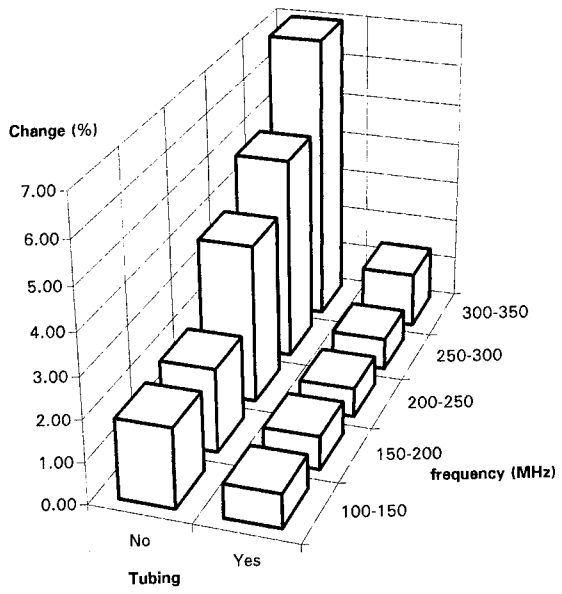


FIGURE 5:

Cable #2 IMPEDANCE
Tubing Effect after 2.2 in of Jacket Removal

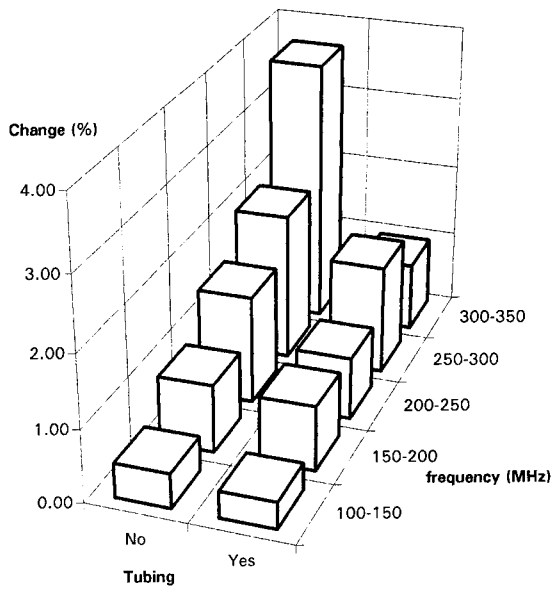


FIGURE 6:

Cable #3 IMPEDANCE
Tubing Effect after 2.2 in of Jacket Removal

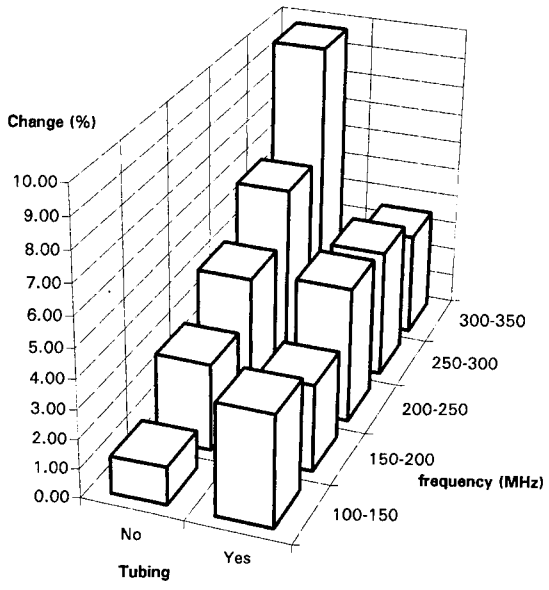


FIGURE 7:

Cable #3 IMPEDANCE
Jacket Removal Length 0.2in

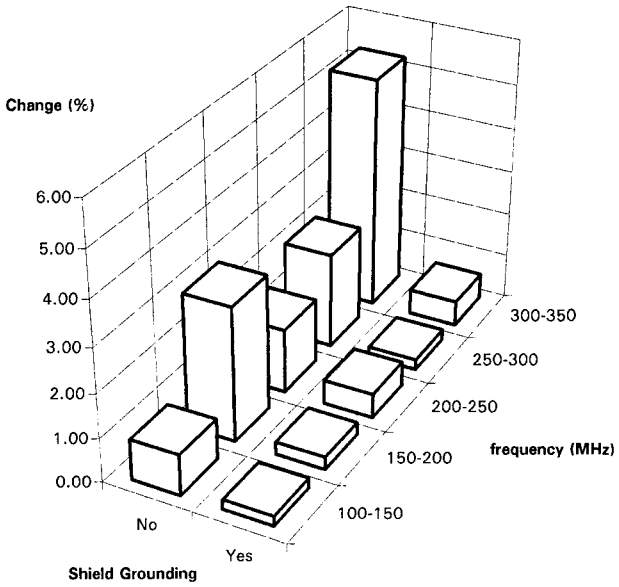


FIGURE 8:

Cable #1, NEXT Change (%)

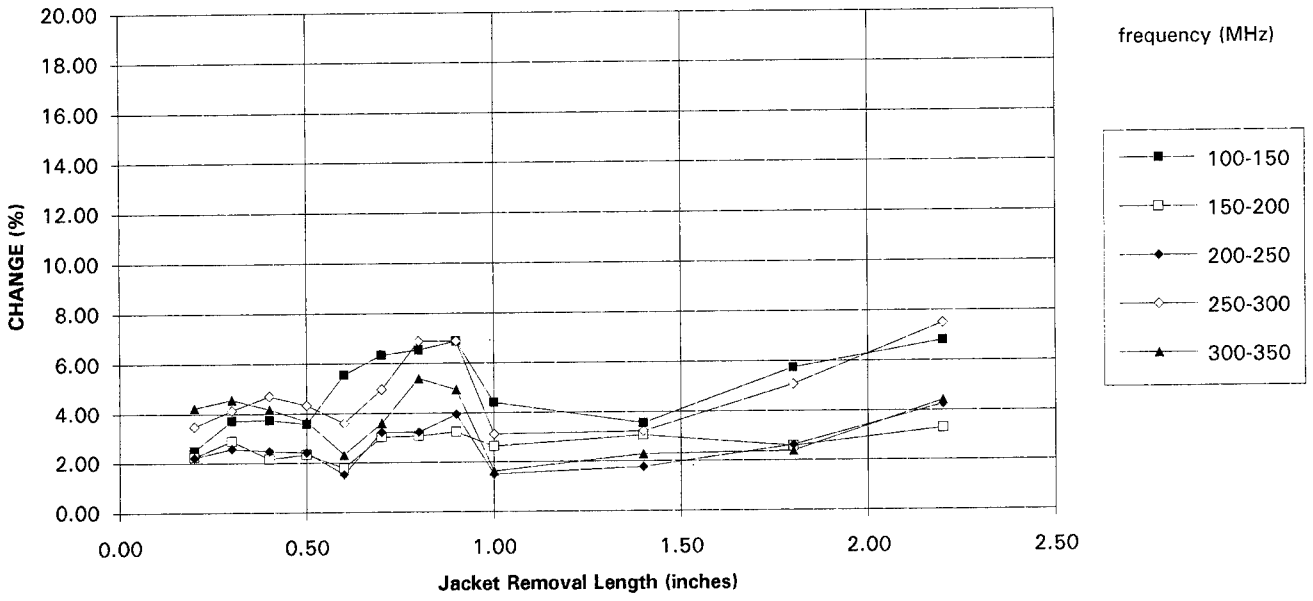


FIGURE 9:

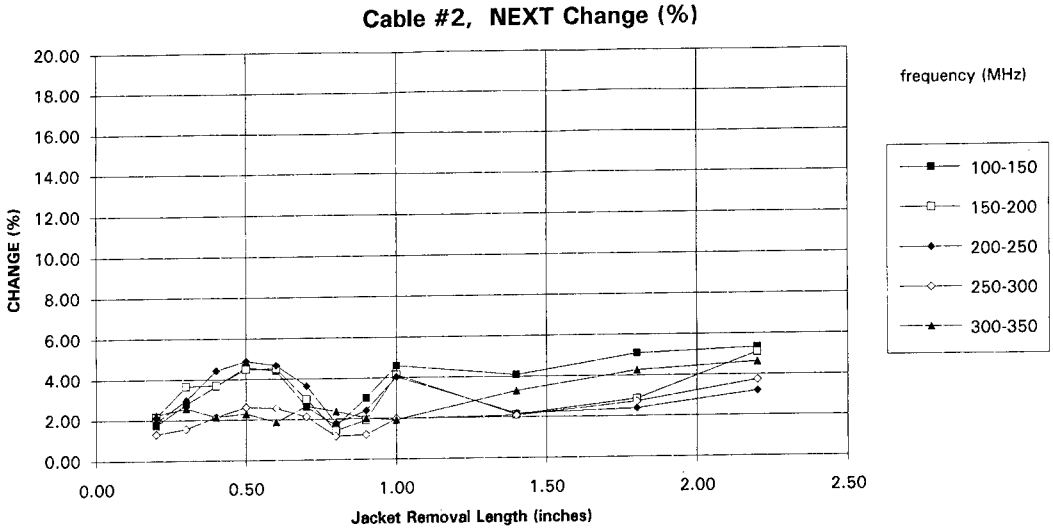


FIGURE 10:

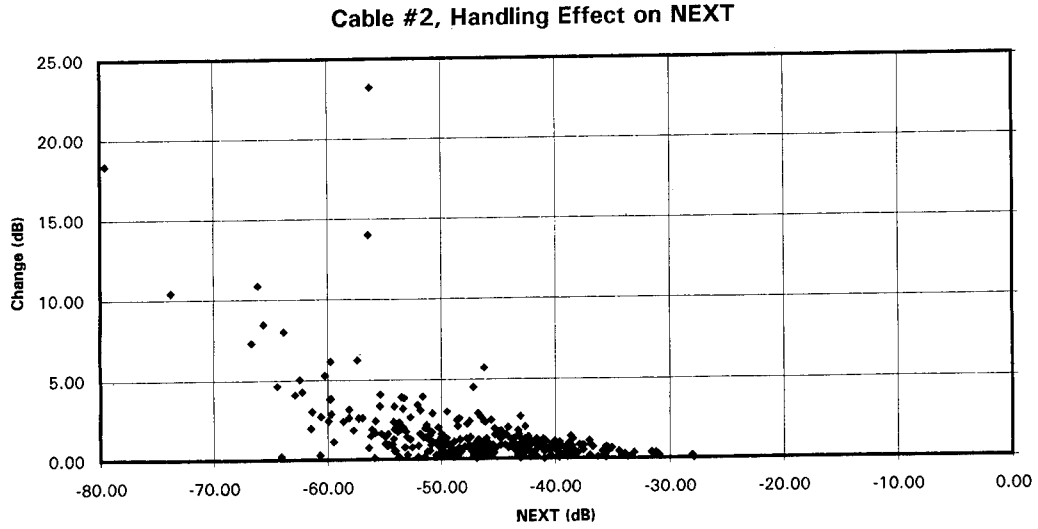
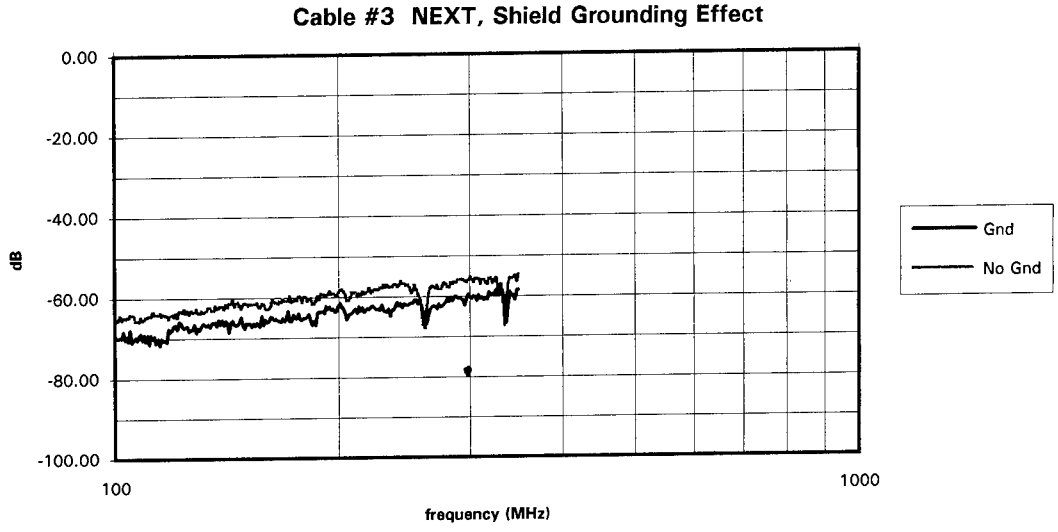


FIGURE 11:



An Explanation for Unexpected NEXT Failures On Short UTP Links

James R. Sciacero
Manager, Hardware Engineering
Microtest Inc., Phoenix, Arizona

ABSTRACT

NEXT on installed category 5 links can be significantly higher than predicted by theoretical models. A major unexpected NEXT source is contributed from common mode (CM) signals. Published link models assume the effects of CM signals are second order and ignore them. These models consider only differential signals as sources of NEXT. Some connectors have high differential to CM conversion characteristics that are sources of CM signals. Thus, the (currently unspecified) connector balance characteristics are very important. Additional connector crosstalk when operating in a real cable impedance environment is also a cause of higher NEXT. This crosstalk results from reflected signals not accounted for by the 100 ohm resistive NEXT qualification test. Both of these effects are magnified on short links. New component qualification tests are needed to guarantee category 5 link performance.

INTRODUCTION

Structured UTP wiring for LANs has enjoyed unprecedented growth in the last three years, with category 5 UTP the most popular choice for new installations. Why has UTP eclipsed its coaxial, STP, and fiber rivals in the horizontal span? It's because it is perceived to be lower cost, easier to install, consistent with the existing wiring infrastructure, more flexible, and able to handle anticipated data rates for the next 5 to 10 years.

As the world's largest manufacturer of LAN cable test equipment, Microtest has been actively involved in copper LAN link testing since 1988. The demand for category 5 UTP testing created a market for test tools prior to the development of standardized category 5 link performance specifications. These tools first appeared in mid 1993. The lack of standards accelerated the creation of a task force under the EIA/TIA TR41.8.1 committee to specify link performance requirements, field test methods, and test equipment accuracy requirements. Microtest has been actively involved with this group since its inception.

MAIN BODY

At Microtest, we have received many calls that links constructed with category 5 components were failing category 5 performance requirements. Once the easy fixes were identified (such as incorrect installation practices and non-category 5 components), a statistically significant number of unexplained failures remained. Connecting hardware and cable vendors felt that since their equipment met category 5 requirements, the problem must be inaccurate test equipment. While we were sure our equipment was operating correctly, we could not account for these unexplained failures.

Eventually, a pattern emerged. These failures were almost always on short links (<25 meters end to end), using modular 8 (RJ-45) connections. Failures often happened with modular 8 connectors from certain vendors and

never happened with products from other connector vendors.

An investigation was conducted to identify the differences in connectors that caused the reported difference in link performance. Connectors from vendors involved in link failures were compared to connectors from vendors with no reports of failures.

Figure 1 shows the crosstalk performance of two popular category 5 modular 8 connectors from different manufacturers on the 54 / 36 pair combination. Note that both products are within the requirements as specified by TIA 568A and seem to have very similar performance.

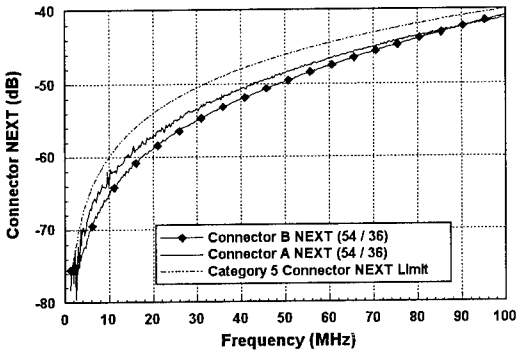


Figure 1: Comparison of Connector NEXT

NEXT performance tests were then conducted on the 54 / 36 pair combination of a 10 meter link using first connector A, then connector B. The same 10 meter segment of UTP cable was used in both test configurations. The test link had one connector at each end which matches the definition of a Basic Link in the new TIA TSB-67 document. Since the connector NEXT test showed similar connector crosstalk performance, it was expected that both link measurements would produce similar results. Figure 2 shows the results of this test. Note that the performance of the link using connector A is well within the link limit, while the NEXT performance with connector B is much worse and even exceeds the link limit. Remember the only difference in this comparison is the connector. This data suggests that there must be some unspecified properties of the connecting hardware that have a significant effect on the overall link NEXT characteristics.

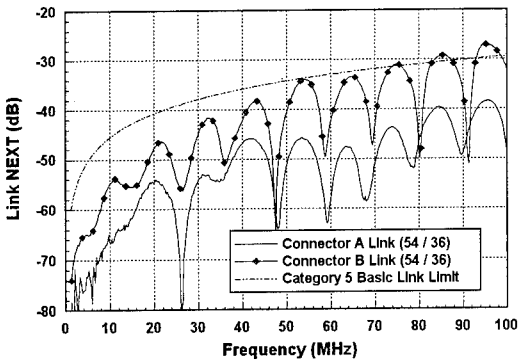


Figure 2: Comparison of Connectors on NEXT in the Same 10 Meter Link

Existing link limit models are based on the assumption that the worst case NEXT will not exceed the in-phase summation of the individual component NEXT characteristics. These models only consider differential NEXT characteristics of link components. Experiments showed that in some cases NEXT on links was significantly higher than predicted by the worst case in-phase prediction of the model. Also, these tests showed that consideration of only differential NEXT characteristics of link components is not adequate to predict the worst case behavior of some connector and cable combinations.

To pursue this investigation a simple 10 meter link was constructed using modular 8 jacks at both ends. The NEXT characteristics of the individual components (cable and connecting hardware) were measured prior to inserting them into the link according to methods outlined in TSB-36 and TSB-40A using an HP4195A Network Analyzer. The NEXT of the 54 / 36 pair combination of the link was measured using

the configuration shown in Figure 3 and compared to the worst case prediction based on the in-phase summation of the individual component NEXT characteristics.

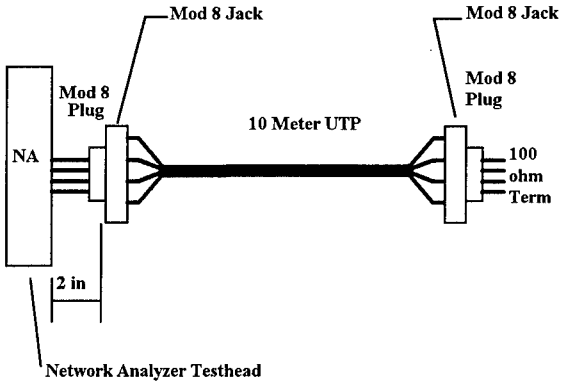


Figure 3: NEXT Measurement of 10 Meter Link Configuration

This comparison of the measured NEXT to the computed in-phase summation of the individual components is shown in Figure 4. The in-phase summation was computed from the NEXT of the near end connector, cable, and far end connector adjusted for round trip attenuation. Figure 4 shows that the measured NEXT for the link with connector B exceeds the worst case prediction by up to 8 dB.

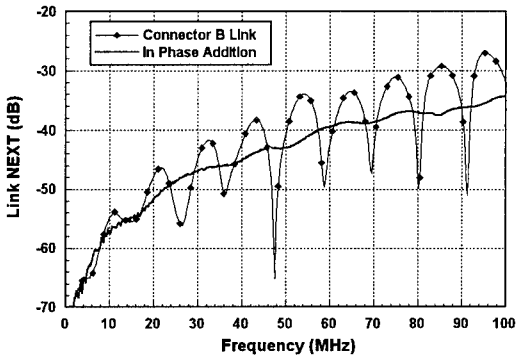


Figure 4: Comparison of Actual NEXT vs. Predicted Worse Case In-Phase Addition

This experiment shows that the existing simple link NEXT model does not adequately account for all transmission parameters when the components are connected in an actual link configuration.

Findings from this investigation revealed that higher than predicted levels of NEXT were attributed to several areas not currently characterized by today's standards. A major source of unexpected NEXT is the contribution from common mode signals. The current model only considers NEXT contributions from differential mode signals. The effects of common mode (or longitudinal mode) signals are assumed to be second order effects and are ignored. This assumption is *not valid* with some samples of connecting hardware. These connectors have a high level of differential to common mode conversion and are a source of common mode signals. This common mode signal is converted to differential NEXT through the common mode to differential conversion properties of the cable. Therefore, the balance characteristic of the connector (which is currently unspecified), is a very important parameter.

The NEXT contribution from common mode signals can be significant. Cables have a common mode to differential conversion function that may be in excess of 20 dB greater than normal differential NEXT conversion. Therefore, small amounts of unexpected common mode signals can generate a significant NEXT component relative to the normal differential NEXT component. NEXT components from common mode signals are not accounted for in the model and can cause the actual NEXT to be much greater than predicted.

Measurements were made on connectors from different manufacturers to determine their relative degree of differential to common mode conversion. In other words, how much common

mode signal is generated as a result of applying a normal balanced differential transmit signal to the connector? It was found that there was a direct correlation between poor performance in the link, and a high degree of differential to common mode conversion in the connector.

The relative differential to common mode conversion of the connectors was measured by injecting a differential signal on a pair under test and observing the amount of common mode signal generated on that pair. All other pairs were terminated in a balanced fashion and carefully spaced the same distance from a common ground reference. The test setup used for this test is shown in Figure 5.

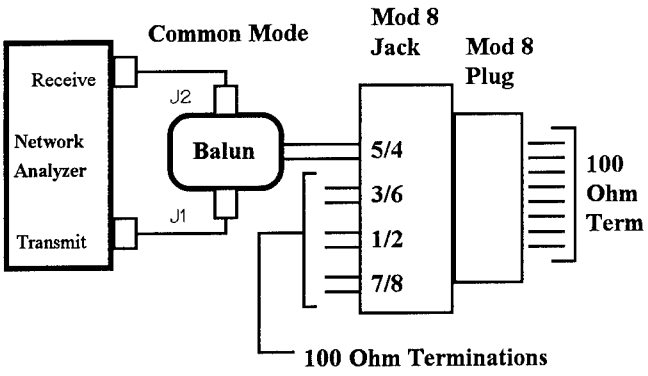


Figure 5: Differential to Common Mode Conversion Test Setup

Figure 6 shows the comparison of the differential to common conversion of connectors A and B when transmitting on the 5/4 pair combination. This data shows that connector B generates a common mode signal component that is 10 dB greater than generated by connector A. The common mode signal is then converted to NEXT in the cable and results in much poorer overall NEXT performance for links built with connector B.

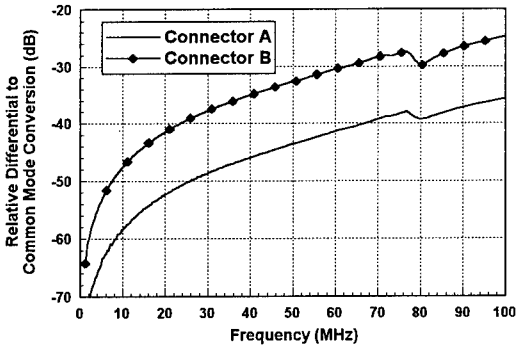


Figure 6: Relative Differential to Common Mode Conversion Due to Transmitting on Pins 5/4

Another potential source of the higher than expected level of NEXT relates to the actual performance of the connecting hardware when connected to a real cable. The performance requirements for modular 8 connections were originally specified in EIA/TIA TSB 40, now updated to be TSB 40A. These TSBs have been recently incorporated into EIA/TIA 568A.

EIA/TIA 568A provides test methods and performance requirements needed to achieve a category 5 rating for connecting hardware. NEXT tests are specified using a 100 ohm resistive load to simulate the cable. An important question is, "Does this test really simulate what happens when the connector is terminated into UTP cabling?"

To explore this, a simple model of NEXT coupling in one pair combination of a modular 8 connector is presented in Figure 7. On the transmit conductor, the signal is composed of two components.

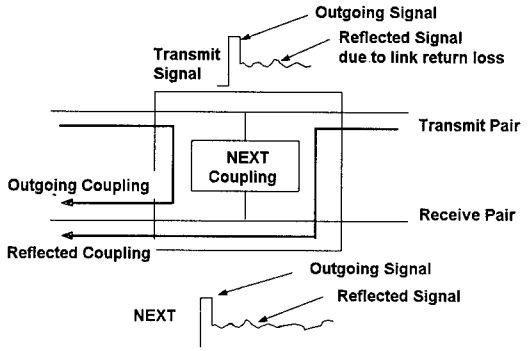


Figure 7: Simplified Connector Crosstalk Model

First, there is the outgoing signal which couples to the receive conductor causing a source of NEXT. A second source of NEXT is caused from reflected energy due to the non-ideal return loss of the link. This reflected NEXT component can be significant, since real links, especially short links, can have return loss characteristics in the order of 10 dB. The over-simplified 100 ohm resistive connector qualification test does not account for this reflected energy NEXT coupling that is present in real links. Therefore, the qualification tests provide an extremely optimistic estimation of the performance of the connector.

A new test environment was needed to determine if the actual NEXT performance of the connector is an issue when operated in a real link. This test environment needed to provide a real cable interface (with its capacitive and inductive elements) and somehow avoid having the cable's NEXT interfere with the measurement of the connector's NEXT.

A "zero-crosstalk" cable test environment was constructed using one pair from each of two separate category 5 UTP cables. All pairs in both cables were terminated at the near and at the far end with 100 ohms . This test configuration allowed the NEXT of the connecting hardware to be measured under real cable loads without the coupling normally associated with the load. The "zero crosstalk" cable was tested on a network analyzer to have less than 80 dB of NEXT at all frequencies below 100 MHz. A diagram of the zero crosstalk test environment is shown in Figure 8.

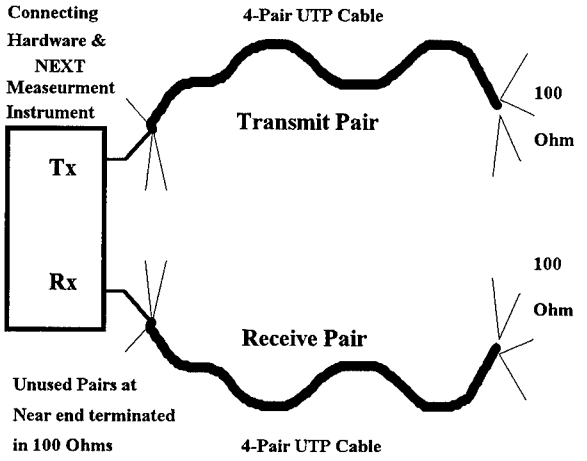


Figure 8: Zero Crosstalk Test Environment

Tests were performed to compare the NEXT of the connecting hardware under real cable and 100 ohm qualification test load conditions. Results from these tests showed that for some connectors, there was a dramatic difference between the NEXT performance with a resistor and the NEXT performance with the "zero crosstalk" cable. An example of the comparison is shown in Figure 9.

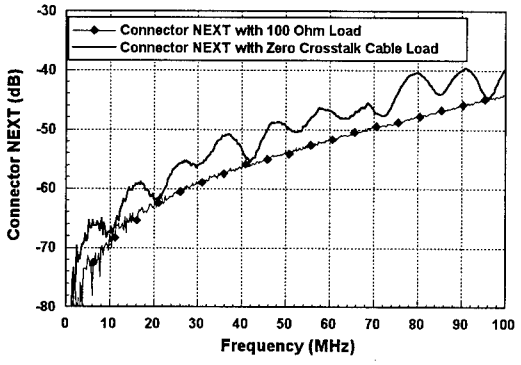


Figure 9: Comparison of Connector NEXT Under Real Cable and Ideal 100 Ohm Load Conditions.

The NEXT measured under a real cable load is up to 8 dB worse than measured with the 100 ohm qualification test. This data proves that connector cancellation is sensitive to load conditions and reflected signal components. The actual NEXT performance of the connector may be significantly worse than assumed in the models used to calculate link limits.

The issue relating to the reflected signal coupling not only has an impact on link performance, but it also affects the performance of interfaces used to test link performance. All the current field test standards require that the test interface have no effect on the instrument measurements. Any NEXT in the test interface is called "Residual NEXT" and is an error term in the measurement.

The coupling associated with the reflected signal component is one of the reasons why modular 8 connectors are an extremely poor choice for link performance test interfaces. There is no cancellation mechanism such as time gating in the time domain or ISO cal in the frequency domain that can remove the deleterious crosstalk effects of the modular 8 connector. The reflected signal component is unknown in time, amplitude and phase and therefore, cannot be canceled.

To explore the effects of the reflected signal component on a test instrument interface, a test was conducted comparing the performance of an extremely low crosstalk connector used in the PentaScanner+ to that of an instrument using a modular 8 jack. A "zero crosstalk" link was constructed to do this test. The "zero crosstalk" link allowed the real "Residual NEXT" of the test instruments to be measured under link load conditions.

The NEXT of the "zero crosstalk" link was first measured with a PentaScanner + through its low crosstalk interface connector. The "Residual NEXT" measured with the PentaScanner+ included both outgoing and reflected signal components since the low crosstalk interface doesn't require any attempts to cancel test interface NEXT. The "Residual NEXT" of the "zero crosstalk" link was then measured with an instrument that attempts to cancel outgoing NEXT coupling through its modular 8 connector. This test allowed a direct measurement of the reflected signal component contribution of "Residual NEXT" since there was little outgoing signal coupling. The results of these tests are shown in Figure 10.

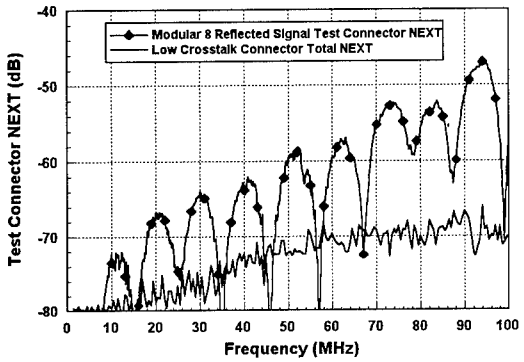


Figure 10: Comparison of "Residual NEXT" Error of Modular 8 and Low Crosstalk Test Interface Connectors

As expected, a low crosstalk connector produces a much lower "Residual NEXT" measurement interface for testing real links. This is because a low crosstalk connector is relatively unaffected by the potential NEXT error introduced by return loss in the link. The comparison in Figure 10 demonstrates that the effect of the reflected signal component on connector NEXT is very real and substantial. For field testers using a modular 8 jack as a primary connection methodology, the "Residual NEXT" caused from the return loss of the link can be a large error source. Under real link conditions this error can account for an *additional* error of up to ±1.0 dB for NEXT measurements near the link limit.

CONCLUSION

When the return loss error and common mode conversion error phenomena are considered together, they explain why in some cases field link test failures occurred where proper installation techniques and category 5 components were used. Simple laboratory testing verified behavior that was not predicted by the model. Other observations from this testing show that some of the effects appear to be magnified in short link configurations. This is especially true of common mode effects described earlier. When links are electrically short, there is little attenuation of common mode signals and their contribution is a very significant contributor to NEXT. Thus, if a user installs a category 5 system with modular 8 connectors that fully meet existing category 5 connector standards, but have other undesirable characteristics, the real NEXT measured may be high enough to fail category 5 link requirements.

In conclusion, current component qualification test methods are not sufficient to guarantee the desired category 5 link performance. The simple model of considering only differential NEXT and return loss parameters does not adequately characterize the components to predict performance in the total link transmission environment. At low frequencies, this simple set of parameters may have been sufficient; however, at the high frequencies associated with category 5 testing, there are many more coupling paths that need consideration. At a minimum, balance must be defined and characterized for modular 8 connectors.

These experiments also showed that choice of interface connectors for link testing is extremely important . Because of the presence of significant return loss characteristics in real links, field testers should avoid the modular 8 connector (or any other relatively high crosstalk connector) in order to achieve accurate measurements.

Further work is required to determine the interaction of the other transmission parameters and their impact on link performance. This work is being pursued by task groups within the standards committees.

Author



Jim Sciacero
Manager, Hardware Engineering
Microtest Inc.
4747 N. 22nd Street
Phoenix, Az 85016

Jim Sciacero is Manager of Hardware Engineering at Microtest Inc. He holds an MSEE degree from the University of Southern California. Jim is a voting member of EIA/TIA TR41.8.1 and is an active member in the Link Performance Task group which developed TSB-67.

MODAL DECOMPOSITION (NON-BALUN) MEASUREMENT TECHNIQUE: ERROR ANALYSIS AND APPLICATION TO UTP/STP CHARACTERIZATION TO 500 MHz

Koichi Yanagawa
Hewlett-Packard Japan Ltd.
1-3-2 Murotani, Nishi-Ku, Kobe-Shi, Hyogo, 651-22 Japan

Jon Cross
Hewlett-Packard Company
5301 Stevens Creek Blvd., Santa Clara, CA. 95052, U.S.A.

Abstract

A BALUN transformer is often used to measure balanced parameters of twisted pair cable. However, at high frequencies, these transformers may cause measurement errors and calibration is not traceable for the balanced condition. This paper provides a method by which balanced parameters are calculated from unbalanced data measured by a conventional vector network analyzer with a S-parameter test set, eliminating the need for BALUN transformers. Error analysis and measurement results are shown. In addition, specific measurements, such as longitudinal conversion loss (LCL) are discussed.

Introduction

In the communication industry, twisted pair cables have been widely used for transmission lines because of their cost advantage and simplicity. Recently, they are used not only for telephone systems but also for high speed digital signal transmission for local area networks (LAN). Today, data rates as high as 155 megabits/second are being transmitted and received as balanced (differential) signals over high-quality twisted pair data cable. The need for measuring the balanced (and unbalanced) characteristics of such twisted pair cables over higher and wider frequency ranges is increasing.

Usually, a vector network analyzer is used for transmission characteristics measurements at higher frequencies. Network analyzers typically offer 50 ohm unbalanced test signal inputs and outputs. To use a network analyzer for twisted pair cable measurements, an balanced/unbalanced conversion transformer (BALUN) is needed between the twisted pair cable and the unbalanced measurement instrument. As the frequency range BALUN transformers are limited, a number of transformers are needed for wide band measurements. At the high frequencies, measurement becomes difficult because of the lack of availability of transformers. As a result, the calibration of BALUN characteristics and the traceability of calibration standards of the balanced system at high frequency are not established. On the other hand, the subject of multiconductor transmission lines has been studied in the past, and the technique of modal decomposition to diagonalize the matrix product for solving transmission-line equations is well known.

Basic Theory

The modal decomposition theory in the measurement of a twisted pair cable is summarized as follows: [1],[2]

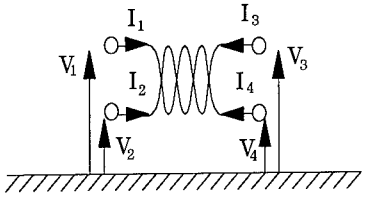


Figure 1: Voltage and current of a twisted pair on or surrounded by a ground plane.

$$\begin{bmatrix} V_1 \\ V_2 \\ V_3 \\ V_4 \end{bmatrix} = \begin{bmatrix} Z_{11} & Z_{12} & Z_{13} & Z_{14} \\ Z_{21} & Z_{22} & Z_{23} & Z_{24} \\ Z_{31} & Z_{32} & Z_{33} & Z_{34} \\ Z_{41} & Z_{42} & Z_{43} & Z_{44} \end{bmatrix} \begin{bmatrix} I_1 \\ I_2 \\ I_3 \\ I_4 \end{bmatrix} \quad (1)$$

Once an impedance matrix **Z** is known, which was measured referred to ground, the modal domain impedance matrix is calculated by using the conversion matrices **P** and **Q**.

$$\mathbf{Z}^m = \mathbf{P}_e^{-1}\mathbf{Z}\mathbf{Q}_e \quad (2)$$

where,
$$\mathbf{P}_e^{-1} = \begin{bmatrix} \mathbf{P}^{-1} & \mathbf{0} \\ \mathbf{0} & \mathbf{P}^{-1} \end{bmatrix}, \quad \mathbf{Q}_e = \begin{bmatrix} \mathbf{Q} & \mathbf{0} \\ \mathbf{0} & \mathbf{Q} \end{bmatrix} \quad (3)$$

In the case of a perfect one-pair cable, the size of the conversion matrices become 4×4 with these values;

$$\mathbf{P} = \begin{bmatrix} \frac{1}{2} & 1 \\ -\frac{1}{2} & 1 \end{bmatrix}, \quad \mathbf{Q} = \begin{bmatrix} 1 & \frac{1}{2} \\ -1 & \frac{1}{2} \end{bmatrix} \quad (4)$$

These conversion matrices operate as transformers, in other words, we can replace BALUN transformers with these conversion matrices. These operations are sometimes referred to as mathematical BALUNs.

$$\begin{bmatrix} V_1 \\ V_2 \\ V_3 \\ V_4 \end{bmatrix} = \mathbf{P}_e \begin{bmatrix} V_{b1} \\ V_{u1} \\ V_{b2} \\ V_{u2} \end{bmatrix}, \quad \begin{bmatrix} I_1 \\ I_2 \\ I_3 \\ I_4 \end{bmatrix} = \mathbf{Q}_e \begin{bmatrix} I_{b1} \\ I_{u1} \\ I_{b2} \\ I_{u2} \end{bmatrix} \quad (5)$$

By substituting equation (5) in equation (1), we get equation (6).

$$\begin{bmatrix} V_{b1} \\ V_{u1} \\ V_{b2} \\ V_{u2} \end{bmatrix} = \begin{bmatrix} Z^m_{11} & Z^m_{12} & Z^m_{13} & Z^m_{14} \\ Z^m_{21} & Z^m_{22} & Z^m_{23} & Z^m_{24} \\ Z^m_{31} & Z^m_{32} & Z^m_{33} & Z^m_{34} \\ Z^m_{41} & Z^m_{42} & Z^m_{43} & Z^m_{44} \end{bmatrix} \begin{bmatrix} I_{b1} \\ I_{u1} \\ I_{b2} \\ I_{u2} \end{bmatrix} \tag{6}$$

These matrices are equivalent to a set of ideal hybrid transformers connected at each end of a cable pair.

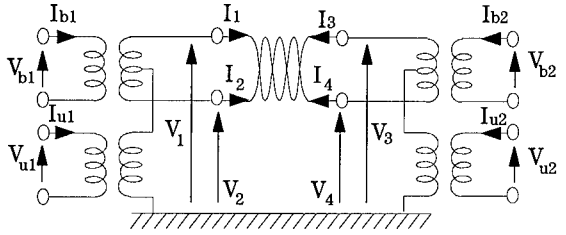


Figure 2: Voltage and current conversion by two hybrid transformers.

Due to the configuration of most vector network analyzers, it's preferable to measure S-parameters rather than Z-parameters. Generally, the relationship between an impedance matrix and a S-parameter matrix of a 2n-port circuits can be represented by the following equations.

$$\mathbf{Z} = \mathbf{R}^{\frac{1}{2}}[\mathbf{E}+\mathbf{S}][\mathbf{E}-\mathbf{S}]^{-1}\mathbf{R}^{\frac{1}{2}} \tag{7}$$

where $\mathbf{E}$ is a $2n \times 2n$ unit matrix and $\mathbf{R}^{\frac{1}{2}}$ represent a diagonal matrix with these values:

$$\mathbf{R}^{\frac{1}{2}} = \begin{bmatrix} \sqrt{r_1} & 0 & \cdots & 0 \\ 0 & \sqrt{r_2} & 0 & \vdots \\ \vdots & 0 & \ddots & 0 \\ 0 & \cdots & 0 & \sqrt{r_{2n}} \end{bmatrix} \tag{8}$$

In most applications, all the measurement ports of a network analyzer have the same impedance, typically 50 ohms; that is, $r_1 = r_2 = \cdots = r_{2n} = 50$.

Furthermore most of the cable parameters of interest are represented in the form of S-parameters in the modal domain.

This can be done by converting the modal domain Z-parameters into S-parameters using the following equation:

$$\mathbf{S}^m = \mathbf{R}_m^{-\frac{1}{2}}[\mathbf{Z}^m - \mathbf{R}_m][\mathbf{Z}^m + \mathbf{R}_m]^{-1}\mathbf{R}_m^{\frac{1}{2}} \tag{9}$$

where $\mathbf{R}_m$ is a matrix of termination resisters in the modal domain, and typically set to 100 ohms for the balanced mode and set to 25 ohms for the unbalanced mode.

$$\mathbf{R}_m^{\frac{1}{2}} = \begin{bmatrix} \sqrt{r_{m1}} & 0 & \cdots & 0 \\ 0 & \sqrt{r_{m2}} & 0 & \vdots \\ \vdots & 0 & \ddots & 0 \\ 0 & \cdots & 0 & \sqrt{r_{m2n}} \end{bmatrix} \tag{10}$$

Thus we can convert the S-parameters measured by a conventional unbalanced network analyzer into

S-parameters in the modal domain, which contain both balanced and unbalanced mode S-parameters.

$$\begin{bmatrix} S_{11} & S_{12} & S_{13} & S_{14} \\ S_{21} & S_{22} & S_{23} & S_{24} \\ S_{31} & S_{32} & S_{33} & S_{34} \\ S_{41} & S_{42} & S_{43} & S_{44} \end{bmatrix} \Rightarrow \begin{bmatrix} S^{11}_{bb} & S^{11}_{bu} & S^{12}_{bb} & S^{12}_{bu} \\ S^{11}_{ub} & S^{11}_{uu} & S^{12}_{bu} & S^{12}_{uu} \\ S^{21}_{bb} & S^{21}_{bu} & S^{22}_{bb} & S^{22}_{bu} \\ S^{21}_{bu} & S^{21}_{uu} & S^{22}_{ub} & S^{22}_{uu} \end{bmatrix} \tag{11}$$

The suffix bb means it is the S-parameter from the balance mode to the balanced mode, and the suffix bu means the S-parameter from the unbalanced mode to the balanced mode. Similarly, the prefix 21 mean the transmission from the port 1 to the port 2. For example, S^{11}_{bu} is a ratio of the reflected power of the balanced mode at port-1 to the unbalanced mode incident power at port-1 , and S^{21}_{bb} represent the ratio of the transmitted power of the balanced mode output to port-2 to the balanced mode input power at port-1.

Transmission of a Hybrid Transformer

Consider the transmission between the balanced port and the unbalanced port of a hybrid transformer . This is essential in the consideration of mode conversion (or isolation) of these two ports.

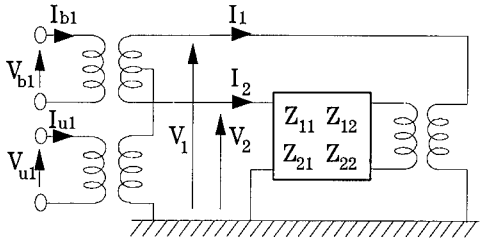


Figure 3: Impedance conversion by a hybrid transformer.

Obviously the transmission depends on the device under test (DUT) which is connected to the DUT port of the hybrid transformer. Let the impedance matrix of DUT, Z be:

$$Z = \begin{bmatrix} Z_{11} & Z_{12} \\ Z_{21} & Z_{22} \end{bmatrix} \tag{12}$$

By using the voltage and the current relationship of a hybrid transformer, we get the impedance matrix between the two ports, that is the balanced port and the unbalanced port.

$$\begin{bmatrix} V_b \\ V_u \end{bmatrix} = \begin{bmatrix} Z_{bb} & Z_{ub} \\ Z_{bu} & Z_{uu} \end{bmatrix} \begin{bmatrix} I_b \\ I_u \end{bmatrix} \tag{13}$$

$$= \begin{bmatrix} Z_{11}+Z_{22}-Z_{21}-Z_{12} & (Z_{22}-Z_{11}+Z_{21}-Z_{12})/2 \\ (Z_{22}-Z_{11}-Z_{21}+Z_{12})/2 & (Z_{11}+Z_{22}+Z_{21}+Z_{12})/4 \end{bmatrix} \times \begin{bmatrix} I_b \\ I_u \end{bmatrix} \tag{14}$$

Applying the equation (9) to the equation (13) with using $\mathbf{R}_m^{\frac{1}{2}}$ in the form of $\begin{bmatrix} \sqrt{r_b} & 0 \\ 0 & \sqrt{r_u} \end{bmatrix}$, we get

$$S_{bb} = \frac{(Z_{bb}-r_b)(Z_{uu}+r_u)-Z_{bu}Z_{ub}}{(Z_{bb}+r_b)(Z_{uu}+ru)-Z_{bu}Z_{ub}} \quad (15)$$

$$S_{bu} = \frac{2\sqrt{r_b r_u}\, Z_{bu}}{(Z_{bb}+r_b)(Z_{uu}+ru)-Z_{bu}Z_{ub}} \quad (16)$$

$$S_{ub} = \frac{2\sqrt{r_b r_u}\, Z_{ub}}{(Z_{bb}+r_b)(Z_{uu}+ru)-Z_{bu}Z_{ub}} \quad (17)$$

$$S_{uu} = \frac{(Z_{bb}+r_b)(Z_{uu}-r_u)-Z_{bu}Z_{ub}}{(Z_{bb}+r_b)(Z_{uu}+ru)-Z_{bu}Z_{ub}} \quad (18)$$

When the impedance matrix of DUT is given by a resistive T-network as shown by the following figure,

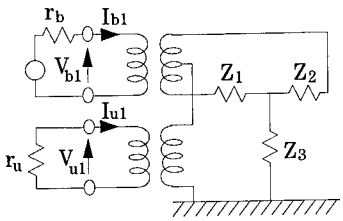
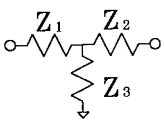


Figure 4: Impedance conversion of a T-circuit.



$$Z_{11} = Z_1 + Z_3$$
$$Z_{12} = Z_{21} = Z_3 \quad (19)$$
$$Z_{22} = Z_2 + Z_3$$

Figure 5: Z-parameters of a T-circuit.

then, the balanced mode and the unbalanced mode elements of the impedance matrix $\mathbf{S}^m$ in the modal domain are expressed by

$$Z_{bb} = Z_1 + Z_2 \quad (20)$$

$$Z_{bu} = Z_{ub} = (Z_2 - Z_1)/2 \quad (21)$$

$$Z_{uu} = Z_3 + (Z_1 + Z_2)/4. \quad (22)$$

In this case, each element of the $\mathbf{S}^m$ matrix in the modal domain becomes

$$\Delta \cdot S_{bb} = Z_1 Z_2 + (r_u - r_b/4)(Z_1 + Z_2) - r_u r_b + (Z_1 + Z_2 - r_b)Z_3 \quad (23)$$

$$\Delta \cdot S_{bu} = S_{ub} = \sqrt{r_b r_u}\,(Z_2 - Z_1) \quad (24)$$

$$\Delta \cdot S_{uu} = Z_1 Z_2 + (r_b/4 - r_u)(Z_1 + Z_2) - r_u r_b + (Z_1 + Z_2 + r_b)Z_3 \quad (25)$$

$$\Delta = Z_1 Z_2 + (r_b/4 + r_u)(Z_1 + Z_2) + r_u r_b + (Z_1 + Z_2 + r_b)Z_3 \quad (26)$$

The condition in which the reflection of the balanced port becomes zero is $r_u = r_b/4$, $Z_1 + Z_2 = r_b$, $Z_1 Z_2 = r_b^2/4$. As $S_{bu} = r_b(Z_2 - Z_1)/2/\Delta$ and $\Delta = r_b^2 + 2r_b Z_3$ in this condition, S_{bu} can be greatly influenced by the magnitude of Z_3. In other words, the transmission from the balanced port to the unbalanced port of a hybrid transformer depends on the impedance of the device connected to the output of the hybrid. This can be significant at such high frequency where the common mode impedance of a twisted pair cable becomes low.

Terminated Connection of a Hybrid Transformer

By choosing Z_1, Z_2, Z_3, r_b, and r_u as $r_u = r_b/4$, $Z_1 = Z_2 = r_b/2$, $Z_3 = 0$, we can get

$$\begin{bmatrix} Z_{bb} & Z_{ub} \\ Z_{bu} & Z_{uu} \end{bmatrix} = \begin{bmatrix} 0 & 0 \\ 0 & 0 \end{bmatrix} \quad (27)$$

In this case, the two ports are isolated with the balanced port terminated by r_b and with the unbalanced port terminated by r_u. This shows how to make the isolation calibration of a hybrid transformer for LCL measurements.

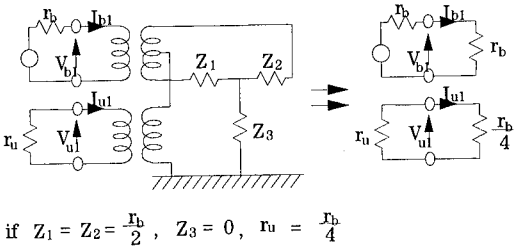


Figure 6: Terminated isolation connection.

Through Connection of a Hybrid Transformer

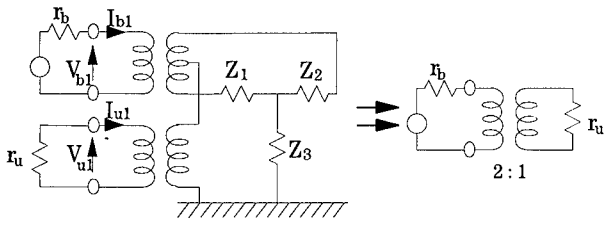
If we set Z_1, Z_2, and Z_3 as $Z_1 = Z_3 = 0$ and $Z_2 = \infty$ we get

$$\begin{bmatrix} Z_{bb} & Z_{ub} \\ Z_{bu} & Z_{uu} \end{bmatrix} = \begin{bmatrix} 0 & 1 \\ 1 & 0 \end{bmatrix} \quad (28)$$

Similarly, by setting Z_1, Z_2, and Z_3 as $Z_2 = Z_3 = 0$ and $Z_1 = \infty$, we get

$$\begin{bmatrix} Z_{bb} & Z_{ub} \\ Z_{bu} & Z_{uu} \end{bmatrix} = \begin{bmatrix} 0 & -1 \\ -1 & 0 \end{bmatrix} \quad (29)$$

This means that the balanced port and the unbalanced port is through connected. (Note that we can make a through connection between two ports, each of which has a termination impedance of r_b and r_u, respectively, by connecting a $\sqrt{r_b} : \sqrt{r_u}$ ideal transformer.) This shows how to make through calibration of a hybrid transformer for LCL measurement.



if $Z_1 = Z_3 = 0$, $Z_2 = \infty$, $r_u = \frac{r_b}{4}$

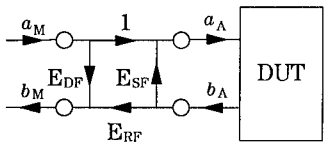
Figure 7 :Through connection of a hybrid transformer.

Error Analysis[3]

Generally speaking, many network parameters are expressed as relative values. For example, the return loss is a ratio of the reflected power to the input power. The measured power which is input to and reflected from the DUT are slightly different from the actual values. They are typically represented by linear combinations like

$$\left.\begin{aligned} a_M &= E_{11}a_A + E_{12}b_A \\ b_M &= E_{21}a_A + E_{22}b_A \end{aligned}\right\} \qquad (30)$$

The four unknown factors, normally appear in linear equations, can be reduced to three by taking ratios.



$$S_{11M} = \frac{b_M}{a_M} = E_{DF} + \frac{E_{RF} \bullet S_{11A}}{1 - E_{SF} \bullet S_{11A}}$$

$$S_{11A} = \frac{b_A}{a_A}$$

Figure 8: Error model of a reflection measurement.

$$S_{11M} = \frac{b_M}{a_M} = \frac{E_{21}}{E_{11}} + \frac{\left(\frac{E_{22}}{E_{11}} - \frac{E_{12}E_{21}}{E_{11}E_{11}}\right)\frac{b_A}{a_A}}{1 + \frac{E_{12}}{E11}\frac{b_A}{a_A}}$$

$$= E_{DF} + \frac{E_{RF}S_{11A}}{1 - E_{SF}S_{11A}} \qquad (31)$$

A normal 2-port measurement consists of a forward and reverse measurement. In the reverse measurement, because the signal source switching from port-1 to port -2 will cause a change to the network constants, another 6 sets of error factors are assumed.

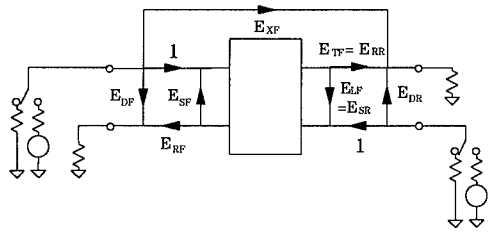


Figure 9: Error model of a transmission measurement.

If the receiver input impedance in the forward measurement is perfectly equal to the source output impedance in the reverse measurement, the load match E_{LF} in the forward measurement should be equal to the source match E_{SR} in the reverse measurement. Similarly, the transmission tracking E_{TR} in the reverse measurement becomes equal to the reflection tracking E_{RF} in the forward measurement. Thus, the error factor which relates the balanced port with the unbalanced port is the isolation E_{XF}. The isolation E_{XR} in the reverse measurement should be equal to the E_{XF} if the system is assumed to be linear. In this case, the forward transmission measured is represented by the following equation.

$$S_{21M} = E_{XF} + \frac{E_{TF}S_{21A}}{(1+E_{SF}S_{11A})(1+E_{LF}S_{22A}) - E_{SF}E_{LF}S_{21A}S_{12A}} \qquad (32)$$

By setting $S_{11A} = 0, S_{22A} = 0$ and $S_{21A} = 0$, we can measure the isolation coefficient E_{XF} between the unbalanced port and the balanced port of the hybrid transformer.

Errors of Modal Decomposition

Measurement parameters for balanced mode characterization are: return loss (RL), insertion loss (IL), near-end crosstalk (NEXT) far-end crosstalk (FEXT) and characteristic impedance (Zc). Because NEXT is an insertion loss from the driven port of a pair to the near-end port of another pair, and FEXT is an insertion loss from the driven port to the far-end of another pair, the errors for both parameters are treated as the error for the insertion loss. Thus the number of errors is decreased to three, the return loss, the insertion loss and the characteristic impedance.

A measurement error is represented by a linear sum of lower level errors assuming that the lower level errors are small enough. The system performance data of a network analyzer is calculated using lower level errors[4]. It consists of a reflection uncertainty and a transmission uncertainty. Theoretically, the errors (or uncertainties, or measurement accuracy) of the modal decomposition method should be calculated using these data.

First, we tried to express each terms of Sm by the terms of S. But it was very difficult and time consuming work , and the results were pages of equations which did not provide a useful perspective. Another way to resolve this problem is the approximation. We derived the series approximation equation which is given in the appendix, but it is still hard to get a perspective from the approximation due to the unclear convergence conditions. The third method was to apply our knowledge of the single transmission mode, like for unbalanced coaxial cable, to the balanced transmission mode assuming mutual independence between the balanced mode and the unbalanced mode.

This means that the equation (31) and (32) can be applied to the balanced mode.

Return Loss Measurement Error

We can use the equation (31) to express the error of return loss measurements. Because the specification of E_{SF} is -20 dB and the maximum magnitude of S_{11A} is 1, the denominator of the second term of the equation (31) is 1 +/- 0.1 and we can approximate the denominator is equal to 1 allowing 10% error for E_{RF}. Thus we get:

$$S_{11M} \cong E_{DF} + E_{RF} S_{11A}. \qquad (33)$$

We evaluated the magnitude of each error term E_{DF} or E_{RF}, we measured those values with the temperature variation at 23+/-5 degree C. Figure 10 shows the estimated worst case value of E_{DF} based on data measured from the three test sets. Similarly, Figure 11 shows the estimated worst case of E_{RF}.

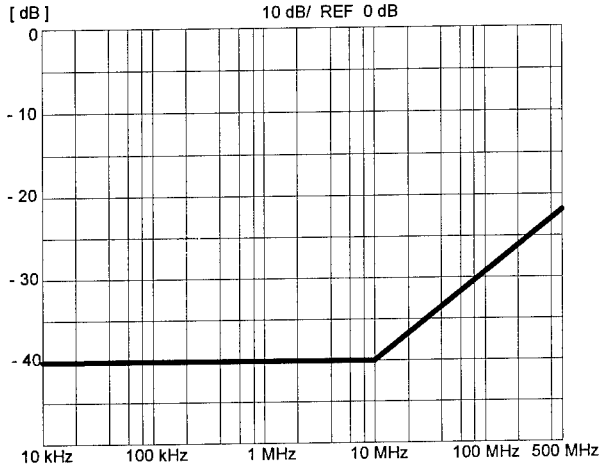


Figure 10: EDF; Residual response of return loss measurement. (Basically caused by the temperature change of the instrument and measurement cables.)

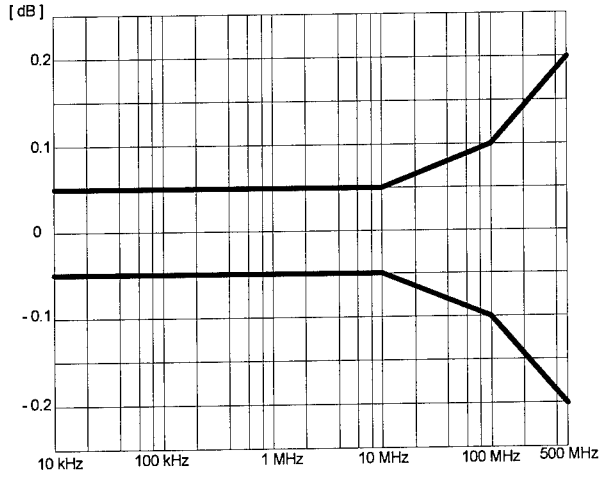


Figure 11: ERF and ETF; Proportional error for reflection and transmission measurements.

Insertion Loss Measurement Error

The equation (32) shows that the measured transmission is a function of both transmission and reflection characteristics of the DUT. By assuming E_{SF} and E_{LF} are small enough, we get a simplified equation of

$$S_{21M} = E_{XF} + E_{TF} S_{21A}. \qquad (34)$$

The errors in the measurement of one of the two modes, that is, the balanced mode will now be discussed.

Insertion loss error is divided into three parts; linearity, stability, and noise. When the signal level is high enough, the stability and the linearity are the main portions of the error. In this method, the final results are calculated after all the S-parameters are measured. In the default setting, the resolution band width (RBW) is set to 200Hz and it takes 5.5 minutes to measure all the S-parameters. The characteristics drift of the network analyzer, measurement cables, test set and the cable under test (CUT) causes errors at the final result. In addition, any changes in the external environment with relation to grounding or interfering signals can also cause errors. If we will ignore the change of the CUT and the external changes around the CUT, the main portion of the error is the stability of the network analyzer. The stability of the network analyzer was measured as a characteristics change of the balanced mode insertion loss due to the temperature change of 23 ± 5 degree C after calibration.

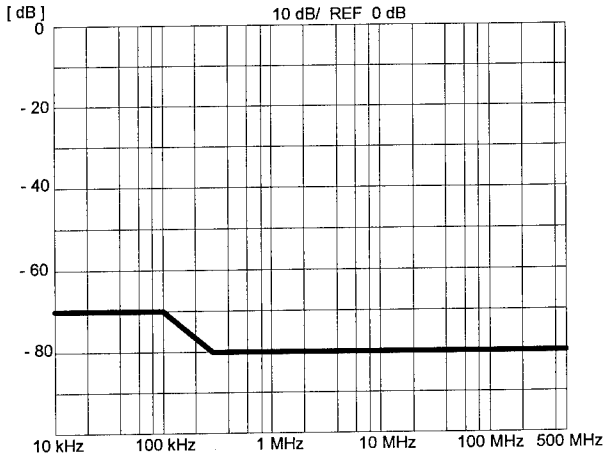


Figure 12: EXF; Residual error for transmission measurement of the modal decomposition system.

Combining these two data gives the typical error data for an insertion measurement as shown in Figure 13.

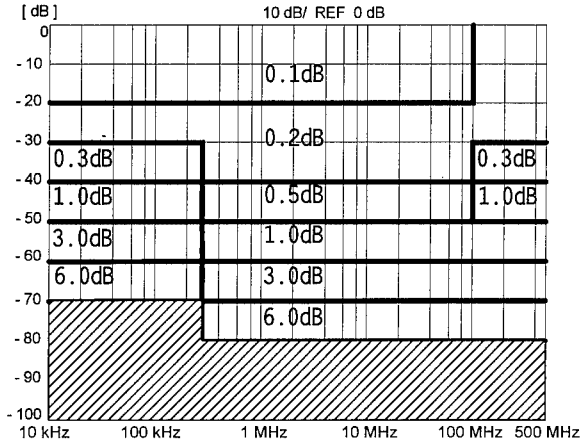


Figure 13: Total error for transmission measurements.

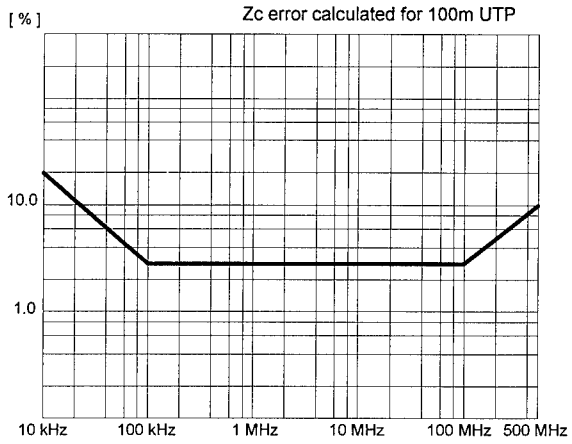


Figure 14: Zc error calculated for 100m UTP cable.

Zc Measurement Error

The characteristic impedance Z_c expressed by the scattering parameters is given below:

$$Z_c = \sqrt{\frac{Z_{11}}{Y_{11}}} = Z_0 \times$$

$$\sqrt{\frac{\{(1+S_{11})(1+S_{22})-S_{12}S_{21}\}\{(1+S_{11})(1-S_{22})+S_{12}S_{21}\}}{\{(1-S_{11})(1-S_{22})-S_{12}S_{21}\}\{(1-S_{11})(1+S_{22})+S_{12}S_{21}\}}} \qquad (35)$$

When the characteristics of the CUT is linear, that is, they are independent of the signal level and time, the S-matrix becomes symmetrical and $S_{12} = S_{21}$. By assuming further that the cable is symmetrical and therefore, $S_{11} = S_{22}$, the equation for Z_c reduces to

$$Z_c \cong Z_0 \times \sqrt{\frac{(1+S_{11})^2-S_{21}^2}{(1-S_{11})^2-S_{21}^2}} \qquad (36)$$

By substituting S_{11} and S_{21} with $S_{11} + \Delta_1$ and $S_{21} + \Delta_2$ respectively, Z_c can be approximated by

$$Z_c \cong Z_0 \times \sqrt{\frac{(1+S_{11})^2-S_{21}^2}{(1-S_{11})^2-S_{21}^2}} \times \sqrt{\frac{1+E_1}{1+E_2}} \qquad (37)$$

$$E_1 \cong \frac{2\Delta_1(1+S_{11})-2\Delta_2 S_{21}^2}{(1+S_{11})^2-S_{21}^2}, \quad E_2 \cong \frac{-2\Delta_1(1-S_{11})-2\Delta_2 S_{21}^2}{(1-S_{11})^2-S_{21}^2}$$

$$E = \frac{1}{2}E_1 - \frac{1}{2}E_2 \cong \frac{2\Delta_1\left(1-S_{11}^2-S_{21}^2\right)+4\Delta_2 S_{11}S_{21}^2}{\left(1+S_{11}^2-S_{21}^2+2S_{11}\right)\left(1+S_{11}^2-S_{21}^2-2S_{11}\right)} \qquad (38)$$

The total error of the Zc measurement can be calculated by substituting the error Δ_1 given by Figure 10 and the error Δ_2 given by Figure 11. As a result we get Figure 14.

LCL Measurements

Consider the non-diagonal cross terms. S_{ss}^{ij} $(i = 1.2; a = b, u)$ means the reflection coefficient at the i-port in the balanced or the unbalanced mode depending on the notation a = b(alanced) or a = u(nbalanced). $S_{kl}^{ij}(i,j = 1,2;\ k,l = b,u)$ means the transmission from the j-port of the l-mode to the i-port of the k-mode. The longitudinal conversion loss (LCL) is defined as follows[3]:

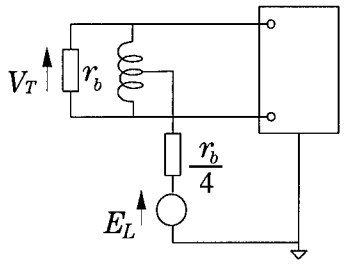
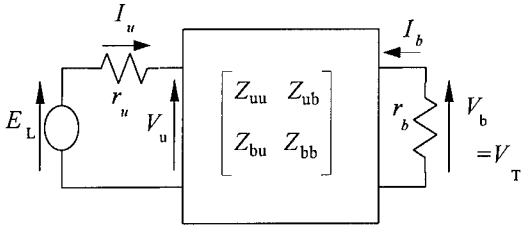


Figure 15: CCITT definition of LCL measurement.

In the recommendation G.117 of CCITT, four measurement parameters are defined. Consider the longitudinal conversion ratio k.



Consider the circuit as a two-port network.

Figure 16: Equivalent model to calculate LCL.

$$V_u = Z_{uu}I_u + Z_{ub}I_b$$

$$V_b = Z_{bu}I_u + Z_{bb}I_b$$

$$V_T = V_b = -r_bI_b,\ V_u = E_L - r_uI_u$$

$$k = \frac{E_L}{V_T} = \frac{(Z_{bb}+r_b)(Z_{uu}+r_u)-Z_{bu}Z_{ub}}{r_bZ_{bu}}$$

When $r_u = r_b/4$, from the equation (16), we get

$$S_{bu} = \frac{r_bZ_{bu}}{(Z_{bb}+r_b)(Z_{uu}+ru)-Z_{bu}Z_{ub}} \quad .$$

Thus, LCL $(= 20\log\left(\frac{E_L}{V_T}\right))$ is equal to $20\log(S_{bu})$ (except the sign) when the CCITT condition $r_u = \frac{r_b}{4}$ is satisfied and expressed in dB.

Measured Data

The basic performance issues when using a hybrid transformer in the measurement of the longitudinal conversion loss are the insertion loss and the isolation between the unbalanced port and the balanced port. Figure 7 shows how to make a through connections for the measurement of insertion loss. Figure 17 shows the equivalent insertion loss of the mathematical balun according to the modal decomposition method. Note that this data shows the characteristics after calibration, so the actual signal level decreases to about -10 dB at high frequencies.

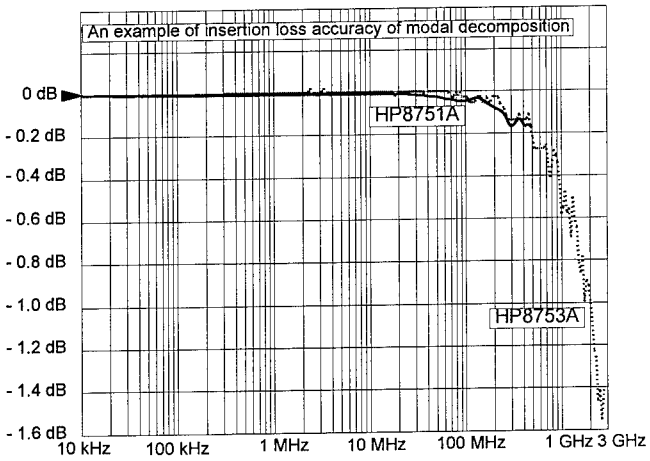


Figure 17:Insersion loss of mathematical hybrid transformer.

The isolation, or in other words, the common mode rejection ratio (CMRR), can be measured by terminating the measurement port of a hybrid transformer with two $\frac{r_b}{2}$ ohm resistors connected to the ground as shown in the Figure 6. The measured data is shown in Figure 18.

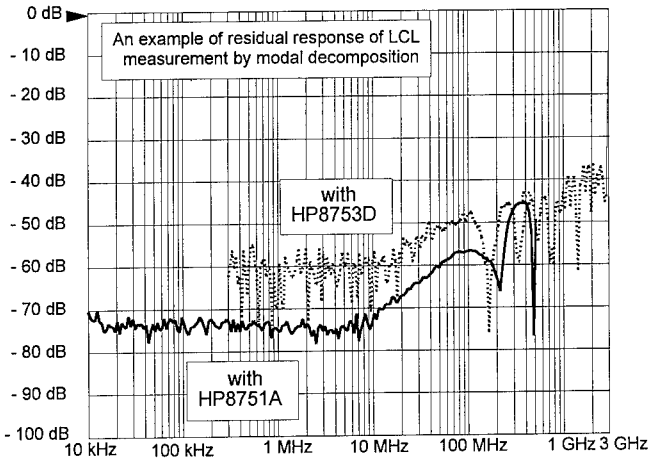


Figure 18: Common mode rejection ratio of the mathematical hybrid transformer.

Figure 18 shows that the degradation of CMRR of the mathematical balun is moderate over 100 MHz. At the frequency lower than 10 MHz, the CMRR is limited by the system noise, the main portion of which is due to the resolution of the analog-to-digital (A/D) converter used in the network analyzer. The performance of this mathematical balun depends on the stability of the measurement system, including the measurement instruments, measurement cables and the environment of the system.

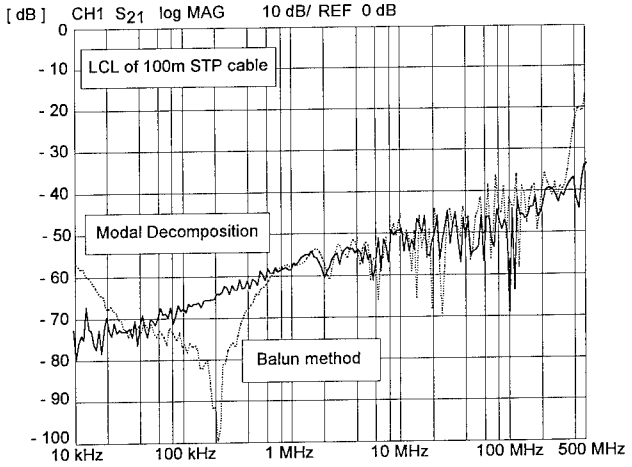


Figure 19: LCL data measured by balun and modal decomposition.

The data in Figure 19, measured by physical balun and by mathematical balun (modal decomposition theory), shows good agreement between both methods.

Finally, the dependency of isolation between the unbalanced port and balanced port of a hybrid transformer on the impedance to the ground was measured. As shown by the equation (24), the isolation depends greatly on the common mode impedance of the device connected to the DUT port. As seen from Figure 20, the isolation data differs depending on the termination impedance of the unbalanced mode.

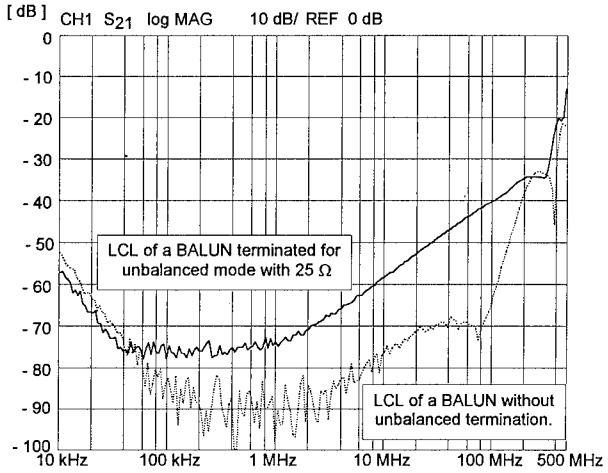


Figure 20: Common mode termination effect on CMRR.

Conclusions

The error of the modal decomposition method was analyzed based on the error model which is popular for S-parameter measurements. Although the errors practically depend on the performance and stability of the network analyzer and measurement cables including the environmental stability, it was shown that the system has good performance for the measurement of twisted pair cable parameters.

The versatility of this method was shown by proving that LCL is included in the non-diagonal components. It was shown that LCL depends directly on the common mode impedance of the DUT, and specifying it is important to get compatible data between different test systems and environments. Common mode termination with one fourth of the differential mode impedance is recommended.

The CMRR of physical BALUN at the frequency lower than 100 MHz goes down to -60 dB to -70 dB without common mode termination, but it becomes worse above 1 MHz when the common mode is terminated, raising to - 40 dB at 100 MHz.

The CMRR of the modal decomposition method is almost -55 dB flat to 10 MHz when an HP 8753D analyzer was used. (Levels of about -72 dB were obtained with an HP 8751A analyzer). The HP 8753D data increases to around -48 dB at 100 MHz and to around -40 dB at 1 GHz.

Appendix

$\mathbf{S}^m$ in terms of $\mathbf{S}$

Because the calculation of the expression $\mathbf{S}^m$ in terms of $\mathbf{S}$ is not easy, we derived the approximated series equation.

$$\mathbf{S}^m = \mathbf{R}_m^{-\frac{1}{2}}[\mathbf{Z}^m - \mathbf{R}_m][\mathbf{Z}^m + \mathbf{R}_m]^{-1}\mathbf{R}_m^{\frac{1}{2}} \tag{9}$$

By substituting $\mathbf{R}_m^{-1/2}\mathbf{P}_e^{-1}\mathbf{R}^{1/2}$ with V, we get

$$\mathbf{S}^m = [\mathbf{T} + \mathbf{US}][\mathbf{U} + \mathbf{TS}]^{-1} \tag{a-1}$$

$$\text{where } \mathbf{V} = \mathbf{R}_m^{-\frac{1}{2}}\mathbf{P}_e^{-1}\mathbf{R}^{\frac{1}{2}},\ (\mathbf{V}^t)^{-1} = \mathbf{R}_m^{\frac{1}{2}}\mathbf{Q}_e^{-1}\mathbf{R}^{-\frac{1}{2}} \tag{a-2}$$

$$\mathbf{T} = \mathbf{V} - (\mathbf{V}^t)^{-1},\ \mathbf{U} = \mathbf{V} + (\mathbf{V}^t)^{-1} \tag{a-3}$$

From equation (a-1), we get

$$\mathbf{S}^m[\mathbf{U} + \mathbf{TS}] = [\mathbf{T} + \mathbf{US}] \tag{a-4}$$

$$\text{Thus, } \mathbf{S}^m = \mathbf{TU}^{-1} + \mathbf{USU}^{-1} - \mathbf{S}^m\mathbf{TSU}^{-1} \tag{a-5}$$

From equation (a-5), we get the first order approximation 1Sm of Sm as

$${}^1\mathbf{S}^m \cong \mathbf{TU}^{-1} + \mathbf{USU}^{-1}. \tag{a-6}$$

Substituting (a-6) into the right term of (a-5), we get the second order approximation. By iterating this procedure, we get the series expression of Sm in terms of S as follows.

$$\mathbf{S}^m = (\mathbf{TU}^{-1} + \mathbf{USU}^{-1})\left\{\mathbf{E} + \sum_{n=1}^{\infty}(-\mathbf{TSU}^{-1})^n\right\} \tag{a-7}$$

Equipment Used

Network analyzer:	HP8751A, HP8753D
8-port test set:	HP4380A
BALUN:	NH0322BF
PC for modal decomposition calculations:	HP Vectra XU 5/90C

Acknowledgements

The authors thank Atsushi Ishihara for the development of the software used here.

References

[1] Ken Yamanaka, Koichi Yanagawa, "A Balanced Parameter Measurement using S-parameters," Technical Conference Report EMCJ92-2, May, 1992 (in Japanese)

[2] K. Yanagawa, K. Yamanaka, T. Furukawa, A. Ishihara, " A Measurement of Balanced Transmission Lines Using S-Parameters," IEEE, Instrumentation and Measurement Technology Conference '94, vol. 2, pp. 866-869

[3] Hewlett-Packad Company, HP8753C Operating Manual, Appendix to Chapter 5, pp. 5.53-5.64

[4] Hewlett-Packad Company, HP8753C Operating Manual, System Performance section of General Information, pp. 25-52

[5] CCITT Recommendation G.117



Koichi Yanagawa received his B.E. degree in Electrical Engineering from Tohoku University in March 1971 and M.E. degree in Electronics from Kyoto University in March 1974. After joining Yokogawa-Hewlett-Packard, he has been working for the development of component test equipment as a design engineer and a project manager.

Jon Cross received his B.S. degree in Electrical Engineering from Purdue University in 1965. He then joined Hewlett-Packard Company as a design engineer. During his career at Hewlett-Packard, he has held positions in R&D and marketing. Currently he is a product manager for the Kobe Instrument Division.

STANDARDS OVERVIEW AND FUTURE DIRECTIONS FOR TELECOMMUNICATIONS CABLING

by

Paul Kish
NORTEL

Abstract

The TIA/EIA 568-A Telecommunications Cabling Standard specifies the minimum requirements of a structured cabling system for voice and data. This paper will provide an overview of the US, Canadian and International Standards for telecommunications cabling and their inter-relationship. The standardization process is also described as it applies to TIA and CSA committees. Today, over 70 members actively participate in TIA TR 41.8.1 working group activities to develop standards for high performance cables and components. TIA TR 41.8.1 also provides input to the international standards bodies involved in telecommunications cabling through the US TAG (Technical Advisory Group). This paper will summarize the status of some of the new projects currently under study by the TIA TR 41.8.1 working group.

Introduction

The publication of the first edition of ANSI/EIA/TIA 568 Commercial Building Telecommunications Cabling Standard in July 1991 was a major achievement of global significance. The need for the Standard was identified following deregulation of the telecommunications industry in the US. The standard was developed with broad participation from the telecommunications industry. EIA/TIA 568 covers the requirements for the "Contents" of a structured cabling system for voice and data. A companion standard EIA/TIA 569 covers the requirements for the "Container" (Pathways and Spaces) that will accommodate the cabling system. These standards and subsequent bulletins published by TIA formed the basic input for an international standard under development by ISO/IEC JTC 1/SC25/WG3. The international standard ISO/IEC 11801 "Generic Cabling for Customer Premises" is expected to be published by the time of this symposium.

ANSI/EIA/TIA 568 standard is a living document. Since the standard was published in July 1991, the TR 41.8.1 working group has remained active. The group has spearheaded many new developments in the industry. For example, cabling systems that are being installed today need to support more sophisticated applications at ever increasing data rates. This has led to the development of high performance twisted-pair copper cables and connecting hardware and the increased deployment of optical fiber cabling for system interconnection.

TIA has published supplementary bulletins, namely TSB-36, TSB-40 and TSB 40A which cover additional requirements for Categories 3, 4 & 5 Unshielded Twisted Pair (UTP) cables and connection hardware. The higher categories correspond to the so-called "data grade" twisted pair cabling. The transmission performance of Category 5 cabling is specified up to 100 MHz. The technical content of these bulletins has been incorporated into the current revision of TIA/EIA 568-A Standard. This document is in the final stage of approval at the American National Standards Institute (ANSI) and is also expected to be published by the time of this symposium.

TIA Organizational Structure

Within TIA there are various Committees responsible for developing Standards reporting to the Telecommunications Standards Subcommittee (TSSC).

TR 41, an Engineering Committee in the User Premises Division of TIA, is the principal committee responsible for developing and maintaining voluntary standards for telecommunications terminal equipment, telecommunications systems, private telecommunications networks and auxiliary equipment and devices. This Committee is broken down into various Subcommittees of which TR 41.8 Subcommittee has prime responsibility for Commercial and Residential Building Distribution Systems. This Subcommittee is further subdivided into Working Groups of which TR 41.8.1 is responsible for developing the TIA 568 / 568-A Commercial Building Telecommunications Cabling Standard.

Process of Approval

A Standard issued by TIA must be processed through various stages to ensure acceptance by Industry and Users. First, the need for a Standard must be documented. When recognized as needed and approved by the Engineering Committee responsible for that subject, it is referred to the appropriate Subcommittee for action. A Working Group is then formed with technical experts from the industry including users, manufacturers and government agencies. The Standard is formulated and

developed by this Working Group following a consensus principle. The draft Standard is sent out for letter ballot to all interested members of TIA. At this stage many comments and suggested changes are received. The Working Group then meets to resolve any comments and negative ballots. If substantial changes are made it must be sent out for reballot. When all negative ballots have been addressed and resolved, the proposed Standard is forwarded to ANSI for their balloting and approval before it can be published.

Overview on TIA Standard 568-A Commercial Building Telecommunications Cabling Standard

TIA Standard 568-A starts with Section **1. Introduction**, Section **2. Scope** and Section **3. Definitions**. This is done to establish clearly the area of applicability. The main body of the standard covers the following topics:

4. Horizontal Cabling

- specifies requirements for horizontal cabling distances, recognized cables, choosing media, installation practices, and grounding considerations.
  - ⇒ Note: "media" is the type of cable or wire.

5. Backbone Cabling

- specifies requirements for backbone cabling topology, recognized cables, and choosing media.
  - ⇒ The fundamental topology is a hierarchical star. Accommodation is made for non-star configurations as well as cabling directly between telecommunications closets.
- specifies the backbone cabling distances for both intra- and inter-building distances.
- specifies requirements for the main and intermediate cross connections, the cabling to related telecommunications equipment, and the link performance of the backbone cabling.
- specifies some cabling installation practices and considerations for grounding.

6. Work Area

- specifies requirements for cabling in the work area.
  - ⇒ Note: work area components extending from the outlet/connector to the work area equipment are outside the scope of this Standard.

7. Telecommunications Closets

- specifies requirements for the cabling and related cabling practices at the telecommunications closet.
  - ⇒ covers cross connections and interconnections.

8. Equipment Rooms

- specifies requirements for the cabling and related cabling practices at the equipment room.

9. Entrance Facilities

- specifies requirements for cabling at the entrance facility as well as entrance facility connections.
  - ⇒ covers the design and functions dealing with the network demarcation point, necessary electrical protection, bonding and grounding.

10. 100 Ω Unshielded Twisted-Pair (UTP) Cabling Systems

- specifies mechanical and transmission requirements and performance markings for horizontal UTP cable.
  - ⇒ mechanical requirements cover insulated conductors, pair assembly, color codes, cable diameter, the breaking strength and bending radius.
  - ⇒ transmission requirements cover dc resistance and unbalance, mutual capacitance and unbalance, characteristic impedance, structural return loss, attenuation, NEXT loss, propagation delay and measurement precautions.
- specifies requirements for backbone UTP cabling under the same headings as those for horizontal. In addition,
  - ⇒ covers mechanical requirements for core assembly, core wrap, core shield and jacket.
  - ⇒ covers transmission requirements for dielectric strength, and core shield resistance.
- specifies mechanical and transmission requirements and performance marking for UTP connecting hardware.
  - ⇒ mechanical requirements cover environment compatibility, mounting, mechanical termination density, design and reliability.
  - ⇒ transmission requirements cover attenuation, NEXT loss, return loss and dc resistance.
- specifies requirements for UTP patch cords and cross-connect jumpers.
- specifies UTP installation practices.
  - ⇒ covers connector termination practices, cabling practices and multiple connections.

11. 150 Ω Shielded Twisted-Pair (STP-A) Cabling Systems

- specifies mechanical and transmission requirements and performance marking for horizontal 150 Ω STP-A cable.
  - ⇒ mechanical requirements for STP-A cable cover the insulated conductor, pair assembly, color codes, core wrap, core shield, braided shield, jacket and jacket slitting, cable diameter, breaking strength, low temperature bending radius and additional durability requirements.
  - ⇒ transmission requirements for STP-A cable cover the dc resistance and unbalance, capacitance unbalance, balanced and common mode attenuation, characteristic impedance, NEXT loss, dielectric strength and propagation delay.
- specifies requirements for backbone STP-A cable.
- specifies requirements for connecting hardware for STP-A cable.
  - ⇒ transmission requirements cover attenuation, NEXT loss, shielding effectiveness, connector return loss and marking.
  - ⇒ mechanical requirements cover the outlet/connector that is used with 150 Ω STP-A cable, installation and reliability.
- Specifies requirements for 150 Ω STP-A patch cable.
  - ⇒ mechanical requirements cover insulated conductor, jacket slitting cord, cable diameter and additional mechanical durability requirements for tensile strength and number of flexes.
  - ⇒ transmission requirements cover dc resistance, balanced mode attenuation, characteristic impedance and NEXT loss.
- specifies 150 Ω STP-A cabling practices.

12. Optical Fiber Cabling Systems

The last large body of the Standard deals with horizontal 62.5/125 μm optical fiber cable, backbone optical fiber cable, connecting hardware, optical fiber patch cords, optical fiber splices and cabling practices.

- specifies physical and transmission requirements and marking for horizontal 62.5/125 μm optical fiber cables.
- specifies physical and transmission requirements for 62.5/125 μm and single mode backbone optical cables.
- specifies requirements for connecting hardware for optical fiber cables.
  - ⇒ covers the physical design, identification of 62.5/125 μm and single-mode fiber, keying, labeling and the pull strength.
  - ⇒ covers attenuation, return loss and durability.
- specifies requirements for patch panels and patch cords
  - ⇒ covers environmental compatibility, mounting, mechanical termination density, design and the installation.
  - ⇒ covers the optical fiber connector and its configuration.
- specifies requirements for optical fiber splices and cabling practices.
  - ⇒ covers polarization and passive system testing.

13. Hybrid and Undercarpet Cables

- specifies hybrid cable requirements and additional requirements for the application and installation of undercarpet cables.

There are three normative and seven informative Annexes in the TIA 568-A Standard. Normative means that it is an integral part of the Standard placed in a separate location for convenience. Informative means that the Annex gives additional information and does not contain requirements.

Annex A Reliability Testing of Connecting Hardware Used for 100 Ω UTP Cabling

- specifies requirements for contact resistance measurements, insulation resistance, durability, vibration, stress relaxation, thermal shock, humidity temperature cycle and other testing.

Annex B Transmission Testing of Connecting Hardware Used for 100 Ω UTP Cabling

- specifies requirements for test set-up and apparatus, test method, measurement precautions, termination procedure and set-up verification for modular jack and plug testing, and NEXT measurement procedures .

Annex C Transmission Testing of Connecting Hardware Used for 150 Ω STP-A Cables

- specifies requirements and test methods for NEXT, attenuation, return loss, and shielding effectiveness for STP-A connecting hardware.

Annex D to J are informative in nature and cover the following subjects:

Annex D "Shared sheath guidelines for multi-pair UTP cables"
Annex E "Unshielded twisted pair (UP) channel performance"
Annex F "Migration paths for optical fiber connections"
Annex G "Other cable specifications"
Annex H "Optical fiber link performance testing"
Annex I "Bandwidth considerations"
Annex J "Bibliography"

Overview of TSB's

A "Telecommunications Systems Bulletin" is issued by TIA as an interim document to provide information, but it is not considered a Standard. Rather, it is a temporary way of getting information out for consideration by the interested public at large. The intention is that ultimately this information will become part of a new Standard and at that time the TSB will be withdrawn.

TIA have issued some TSB's relative to the subject of telecommunications cabling:

TSB-36 Additional Cable Specifications for Unshielded Twisted Pair Cables
TSB-40 Additional Transmission Specifications for Unshielded Twisted-Pair Connecting Hardware (This was replaced by TSB-40A).
TSB-40A Additional Transmission Specifications for Unshielded Twisted-Pair Connecting Hardware

Since the pertinent information in TSB 36, and TSB 40A has now been included in TIA Standard 568-A, these TSB's will be withdrawn once TIA Standard 568-A is issued. The TIA Standard 568-A is currently going through the ANSI accreditation procedure and should be published by Nov/95.

CSA Standard T529

The Canadian Standards Association issues National Standards applicable in Canada. In this case they have attempted to use the same TIA Standard making only those changes necessary to meet minor differences in practice and code requirements and other regulations that are unique to Canada. The objective is to work towards having a Standard that is essentially common to North America.

In the case of TIA Standard 568-A the most important changes or amendments apply to clarification of intent as it applies to the Canadian Electrical Code, Part I, and the reference to other applicable Canadian Standards.

The Telecommunications Cabling Standard for Commercial Buildings in Canada will be identified as CSA T529-1995.

Structure of CSA Committees

In Canada the CSA Committees develop Standards following the consensus principle to meet the requirements of Industry, Government and Users. CSA does not write the Standards, they merely administer the development of them by Committees following the consensus principle.

The main Committee in this case is the Steering Committee on Telecommunications (SCOT). It has formed various Technical Committees including the Technical Committee on Telecommunications Facilities in Buildings. This committee is comprised of members in a balanced matrix operating under strict guidelines and has the responsibility for various Subcommittees. The Subcommittee on Telecommunications Wiring Systems has the prime responsibility for the development of this Standard.

Process of Approval

CSA follows a similar process to TIA to ensure acceptance of a Standard by Industry and Users.

The need for a Standard is documented and submitted to the Steering Committee responsible for that subject. When it is recognized as needed and approved by the steering committee, it is referred to the appropriate Technical Committee for action to form a Subcommittee. A Chairman is named and then together with the CSA Administrator they form a Subcommittee with interested representatives of industry, government and users. The Standard is formulated and developed by this Subcommittee following the consensus principle.

Once the draft standard is approved by subcommittee members, it is sent to the CSA Editors for pre-approval editing to ensure that the CSA guidelines have been followed, as regards format, layout, English etc. The draft standard is sent out for letter ballot to the supervising Technical Committee members and balloted by the Steering Committee but only for due process. The Subcommittee and/or Technical Committee then meet to address any comments and resolve negative ballots as necessary. When all negative ballots have been addressed and resolved it is sent to the CSA Editors before the Standard can be published.

CSA Standards are not mandated by CSA but they are voluntarily accepted by users. In some cases, concerning safety, CSA standards are mandated by government authorities.

International Standards

At the national level, the development of standards and the ability to reach consensus is an involved process, requiring much discussion because of differing viewpoints from manufacturers and users. At the international level, the process is even more involved. It can be more difficult to reach a common base because of different practices in different countries. Consequently, the international standard must recognize more options and cover a broader range of requirements.

The applicable International Standard for Customer Premises Cabling is IS 11801. This standard was developed by the ISO/IEC JTC 1 SC25 WG3 Working Group. It is more broadly based than TIA 568-A standard but is essentially compatible regarding the performance requirements for the cables and connecting hardware. This standard makes reference to IEC 1156 for "Multicore and symmetrical pair/quad cables for digital communications" which was developed by IEC SC 46C committee.

The following points highlight the main differences between the IS 11801 and the TIA 568-A Standard.

IS 11801 requirements:

- a channel (Class A, B, C or D) is specified in terms of the end-to-end transmission performance independent of the components used to comprise a channel. For example, it may be possible to meet Class D performance using Category 3 components for short distances.
- worse case NEXT performance can be traded off for lower Attenuation.
- 120 Ohm cables may be used as an alternative to 100 Ohm cables.
- cables using star quads may be used interchangeably with cables using twisted pairs.
- multipair/quad cables may be used in the horizontal (i.e. when the optional transition point is used as a breakout point).
- a minimum of two pairs can be used for each 8-pin modular connector. **Note:** Certain data applications currently under development require the use of four pairs.
- cable sharing is allowed making it possible to serve two telecommunication outlet/connectors with one 4-pair or one 2-quad cable.
- metric conductor sizes are specified (e.g. 0.5 mm conductor compared to 0.51 mm for 24 AWG).
- higher attenuation values are specified for patch cords (50% increase vs. 20% increase) thus allowing the use of a finer conductor.

The use of shielded cables is more prevalent in Europe than in North America. Currently, there are differing opinions regarding the need for and value of shielding, the type of shielding (foil/braid) that is required and the earthing, bonding and grounding practices that are required. These items have not been standardized and are still a subject of further study.

What's coming next?

The TIA TR 41.8.1 working group has completed the work leading up to the publication of TIA 568-A revised Standard. Telecommunications System Bulletin (TSB-67) will soon be published which covers requirements for testing of installed cabling using field test instruments. TSB-67 has been in preparation for over 18 months and is urgently anticipated by the user community. In addition, two other TSB's are currently under development, one dealing with "Open Office Cabling" guidelines and the other dealing with "Centralized Optical Fiber" Cabling guidelines.

The following topics are currently under study by TIA TR 41.8.1 working group. The results of this work will be published in a future revision of the standard or as a TSB.

- 100 Ω Screened Twisted Pair cabling
- Test methods and test requirements for patch cord assemblies
- Short link resonance phenomena
- Cable and connector balance measurements
- Effect of common-mode terminations
- Power Sum Far End Crosstalk of multipair cables
- Harmonization (ASTM vs. IEC test procedures)

In summary, the National and International Cabling Standards fulfill an essential purpose for the telecommunications industry. These standards establish a minimum level of performance for the cabling system and components. They are widely recognized in the industry and are used as the basis for cabling procurement specifications and referenced by application standards. Standardization ensures that the same cabling will serve a wide range of applications. The cabling standards are continually evolving to meet the needs of the industry.

Biography

Paul Kish received an M.A.Sc. degree in Electrical Engineering from the University of Waterloo in 1972. He has over 20 years experience with BNR and Northern Telecom in the design and development of telecommunications cables. He is currently Senior Manager, PLM for the Cable Group of NORTEL. Mr. Kish has been an active member of TIA for the last seven years. He initiated the work leading up to the publication of TSB-36 on enhanced UTP cable specifications. He serves as the current chairman of TR 41.8.1 working group responsible for the Telecommunications Cabling Standard for Commercial Buildings.

A VISCOELASTIC ANALYSIS OF THERMALLY INDUCED RESIDUAL STRESSES IN DUAL COATED OPTICAL FIBERS

C. J. Aloisio, Jr. W. W. King R. C. Moore

AT&T Bell Laboratories

ABSTRACT

The analysis of thermoviscoelastic effects in the performance of optical fibers and package configurations, such as ribbons,[1] must incorporate both the time and temperature dependence of the component polymer properties. In the case of dual coated fibers, both the primary and secondary coatings are applied to the glass fiber at temperatures above their respective glass transition temperatures. As the coated fiber cools to below the secondary coating glass transition temperature, the primary coating is placed in a stress state that is almost hydrostatic.

In the present paper the magnitude of the primary-glass interface viscoelastic tensile stresses are presented and include the contribution due to the compliance of the secondary coating neglected in earlier work.[2] The results for (1) a quasi-elastic approximation with a step change in temperature, (2) a quasi-elastic approximation with time varying temperature, and (3) an exact viscoelastic analysis are compared.

Introduction

The stress distribution in the coatings on optical fibers may impact the fiber performance in requirement tests, such as pullout, as well as in coloring, rewinding, cabling, and handling in the field. The response of the primary and primary-glass interface to mechanical perturbations applied at the free surface of the secondary coating can be affected by temperature and the rate of loading. The mismatch between the coefficients of thermal expansion in the vicinity of room temperature is a major driver of the stresses at the primary-glass interface. Efforts have been made to estimate the magnitude of such stress,[2,3] but have neglected the compliance of the secondary coating and the viscoelastic response of both coatings. The purpose of this paper is to calculate the tensile stress at the primary-glass interface including the compliance and the viscoelastic response of the secondary coating. In addition, the consequences of changes in the secondary coating glass transition temperature, temperature dependence, or shape of the relaxation modulus curve on the primary-glass interface stresses are presented. For these calculations data for two UV cured secondary coatings - one Coating S, exhibiting a more rapid decrease in relaxation modulus than the second, Coating B -- are used ("S" is chosen to indicate a "sharp" drop off in modulus; "B" indicates a "broad" dropoff). Photos from microscope videos of mechanically perturbed coating showing the propagation of damage demonstrate the presence of radial tensile stresses at the primary-glass interface.

The primary coatings of many fiber suppliers ranges from 30 μm (0.00118") to 40 μm (0.00156") thick, depending upon fiber design philosophy. The high modulus secondary and the even higher modulus silica glass fiber effectively constrain the low modulus primary. This configuration has been studied extensively because of the unusual failure mode exhibited by soft rubbers, like the primary, under these constraints.[4] Under the near-hydrostatic tension (negative pressure referred to in Ref.(4)) induced by the geometry, the soft rubber exhibits spherical voids opening at the center of poker-chip shaped samples, eventually forming cracks and propagating through the sample as the tensile stress increases. The failure stress, 5/6 of the rubbery tensile modulus, is independent of the strength and extensibility of the material; this has been verified experimentally and analytically.[5] for similar materials. According to References (4) and (5), a diameter to thickness ratio of greater than 3-4 was sufficient to produce near-hydrostatic tension in the center of the sample.

In our case of a rubbery primary coating, far from fiber ends[a] the coating is constrained against longitudinal displacement (and strain) such that if the secondary exerts a stress (either tensile or compressive) the stress state will be almost hydrostatic. Since the days of single coated fiber it has been generally accepted that the coating exerts a compressive stress on the fiber. When the coating system was changed to a high modulus secondary over a low modulus primary, primarily for improved microbending loss performance, a difference in thermal expansion coefficients between the two layers was unavoidably introduced. In the next section we will determine the magnitude and sign of the stresses developed at the primary/silica glass interface.

[a] According to the principle of Saint-Venant, "far" is defined as several times the cross sectional dimension; in the case of the 40 micron primary, 100 to 150 microns from the free end would be sufficient.

Residual Thermal Stress

When the coated fiber exits the UV ovens the temperature of both the primary and secondary is normally above the glass transition temperature of the secondary coating. When the secondary glass transition temperature is reached, the secondary mechanical properties transform from a rubbery type material to that of a rigid plastic. Between this temperature and room temperature the thermal expansion coefficient of the primary is approximately three times that of the secondary.[6] The short time modulus of the secondary is in the 100,000 psi range while the primary is in the 200 psi range during this part of the cooling process. Depending on the geometry of the coatings and fiber, either compressive or tensile stresses may develop at the primary/silica glass interface; in either case the constrained, plane-strain state of the nearly incompressible primary coating sandwiched between two high modulus materials insures that the stress state will be very nearly hydrostatic[5] (triaxial with equal components).

The moduli of viscoelastic materials, such as the primary and secondary coatings, are both time and temperature dependent.[b] The relaxation moduli for secondary Coating B and a primary Coating P are shown in Figure 1 for various temperatures. Initially, we will treat the thermal stress elastically and use a quasi-elastic approximation to account for the time dependence; in the next section we will account for the time varying temperature in this approximation, using a temperature reduced time parameter. In a subsequent section, the exact solution is obtained from the solution of the convolution integral form of the viscoelastic constitutive equation. It will be shown that the first approximation yields an upper bound to the exact solution and the second approximation yields a lower bound.

Because of the rapid relaxation of the primary modulus the analysis assumes the primary to have the long time, rubbery value of 150 psi[c] subscripts 1 and 2 refer to the primary and secondary, respectively. The Poisson's ratios were set to 1/2 for the primary and 1/3 for the secondary. The small magnitude of the ratio of the primary modulus to the secondary modulus permitted further simplification. The resulting equation follows (details are presented in the Appendix) and was used to calculate the thermal stresses at the primary/silica glass interface as a function of coating geometry and time for a temperature drop, ΔT.

$$\sigma_1 = \alpha_1 \Delta T \left[\frac{3}{2}(1-\gamma_1^2) - \frac{4\alpha_2}{3\alpha_1} \right] \frac{(3E_2(1-\gamma_2^2))}{4\left(1+\frac{\gamma_2^2}{3}\right)} - (1-\gamma_1^2) E_1 \alpha_1 \Delta T$$

Equation 1

[b] See Ref. 6, in particular Chapter 1 and 2 provide an informative overview.

[c] 6.9×10^4 dynes/cm^2 equals 1 psi or 6.9×10^3 Pa.

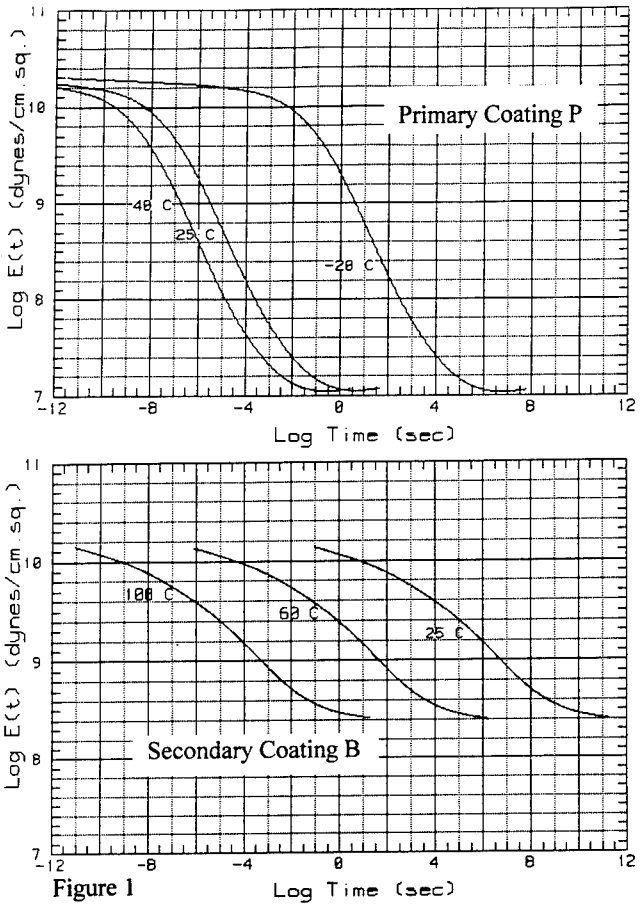


Figure 1

In equation 1, α is the thermal expansion coefficient; the primary value was taken as 10^{-3} °C^{-1} and the ratio of secondary to primary was 1/3 (see Ref. 6, p. 281). γ_1 is the ratio of the silica glass diameter to that of the primary coating and γ_2 is the ratio of the primary coating diameter to that of the secondary coating. The only time dependent modulus to appear in the final expression for the tensile/compressive stress at the primary/silica glass interface is E_2, the tensile modulus for the secondary coating.

Quasi-Elastic Approximation

Figure 2 shows the thermal stress as a function of the primary coating diameter for an initial, short time, secondary modulus of 145,000 psi and for a one day modulus of 36,000 psi; the secondary coating diameter is held constant at 250 microns. Using the short-time and one-day values allows an estimate of the consequences of secondary relaxation on the induced thermal radial stress at the primary/glass interface. The maximum value for an equal volume of primary and secondary coating design is initially greater than 500 psi, changing to less than 200 psi in one day. In Figure 3 the thermal stress is shown for the case of an oversized secondary (290 microns). If the increase in secondary coating diameter is not accompanied by an increase in primary coating diameter, the equal volume of primary and secondary design (at 250 μm secondary OD) would exhibit an increase in radial tensile stress of 300 psi to 800 psi.

Some may find it surprising that there is a tensile interfacial stress when the primary coating is relatively thick. That this is plausible can be envisioned in the following way: imagine the primary and secondary coatings to be disconnected and let the radius defining the interface between the two coatings be very much greater than the radius of the glass fiber. Then for all practical purposes the primary will be a solid uniform cylinder which can contract freely (no stress) with a drop in temperature. The outer circumference would experience a certain contraction. The inner circumference of the (disconnected) secondary coating would, with the same drop in temperature, experience a lesser contraction, since that coating has the smaller coefficient of thermal expansion. Now, because the coating layers are in fact joined, in the composite there must be, for this extreme of geometry, radial tension at the interface between the two coating layers. And because there is basically hydrostatic stress in the primary, tension at the primary/secondary interface will be accompanied by tension at the glass/primary interface. Using a similar analysis Bouten et. al.[2] estimated the temperature at which the radial stress in the primary changes from compressive (at high temperatures) to tensile (at low temperatures). Note in Figure 2 that for a primary thickness of 10 microns or less the radial stesses are compressive.

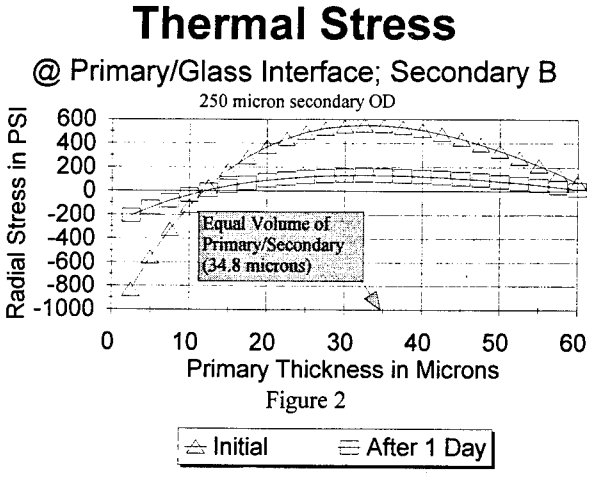


Figure 2

We do not have a reliable measure of the adhesive tensile stress working to keep the primary on the glass, but some judge that they are significantly lower than the previous results. Why then do we not observe even more primary/glass interface failure if the tensile stresses are several hundred psi? Also, if the hydrostatic tension were as high as the previous analysis indicates, we would expect rupture of the primary coating during cooling. In the next section we will extend Equation 1 to account for time and temperature viscoelastic effects which greatly reduces the calculated tensile stress levels, using a quasi-elastic/temperature reduced time approximation..

Quasi-Elastic/Temperature Reduced Time

We can see in Figure 1 that the secondary modulus exhibits a time scale change of 5 decades from 60°C to 25°C; for example at the higher temperature the modulus reaches log E=9.2 in 10 seconds (log seconds=1), at the lower temperature it takes 11.6 days (log seconds=6) or 11.6 days to reach the same modulus value. Through the introduction of a temperature reduced time variable we can account for the thermoviscoelastic effects with the following modifications of Equation 1.

$$\sigma_1(t) = K\Delta T(t)E_2(\xi) - (1-\gamma_1^2)E_1\sigma_1\Delta T$$

$$where, K = \left(\left[\frac{9\alpha_1}{8}(1-\gamma_1^2) - (\alpha_2)\right]\frac{(1-\gamma_2^2}{\left(1+\frac{\gamma_2^2}{3}\right)}\right)$$

Equation 2

The argument, $\xi = t/a_T$ of the secondary modulus is called the temperature reduced time; the temperature enters in through the function $a_T(T)$ which describes the way in which curves, such as the relaxation moduli in Figure 1, shift along the time axis with changes in temperature. Since the temperature drop occurs rapidly between the UV ovens and the draw take-ups, we will assume a linear change in temperature and cooling times of 1 and 0.5 seconds (dependent on fiber draw line speeds and cooling distances.) Also, data for log a_T indicate that a linear approximation over the temperature range being considered is reasonable.

In order to facilitate the stress calculation a modified power law form for the relaxation modulus was determined.

$$E(t) = E_e + \frac{(E_e - E_g)}{\left(1+\left(\frac{t}{a_T\tau}\right)^m\right)^n}$$

Equation 3

The Modified Power Law (MPL) is a convenient equation that reproduces a variety of the features of the relaxation modulus. The parameters E_g and E_e are readily picked off the data for the relaxation modulus. The parameter τ locates the curve on the time axis without changing the shape. The parameters ***m*** and ***n*** modify the shape of the curve; for example, the sharpness of the drop off in modulus with increasing time.

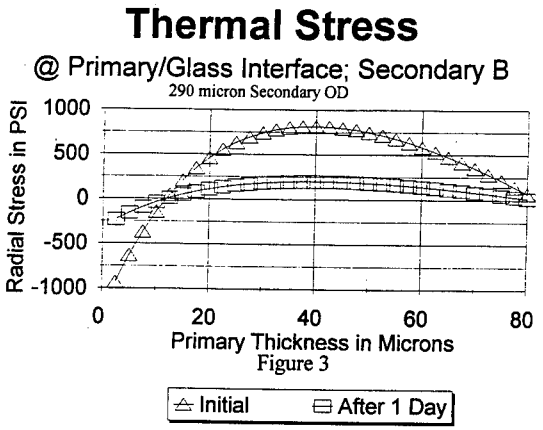


Figure 3

For coating B, the values of the glassy modulus, E_g, and the rubbery or equilibrium modulus, E_e, were estimated from the relaxation curve of Figure 1 as $10^{10.2}$ and $10^{8.4}$, respectively. The time constant, τ, was selected to locate the function correctly on the time axis for 25°C; for use at other constant temperatures, the appropriate value for a_T is used (the value is 1 at the reference temperature; 25°C in this case). After several iterations a satisfactory fit was obtained using the following constant values,

τ=0.04 seconds
m=0.3
n=1.0

The entire curve is displayed in Figure 4 in order to show all of the essential features, such as the glassy modulus and the rubbery or equilibrium modulus. The modulus calculated using Equation 3 is compared to the 25°C Secondary B modulus curve in Figure 5.1 and for Secondary S in Figure 5.2. The two MPL representations are compared in Figure 5.3. Coating B (for broad) exhibits a more gradual (i.e., slower relaxation) than Coating S (for sharp).

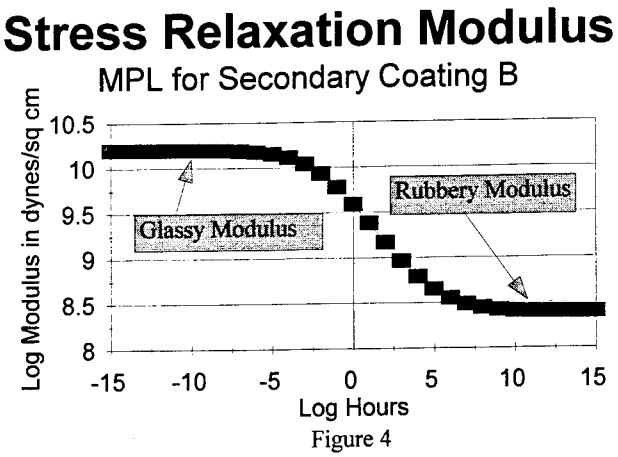


Figure 4

We are now ready to calculate an approximate time dependent stress developed at the primary/silica glass interface during cooling. Using the following values

silica glass OD=125 microns
primary OD=181 microns
secondary OD=250 microns

for the geometry, the tensile stresses as a function of time during cooling were calculated and are shown in Figure 6 for a 1 second and a 0.5 second cooling time. For the 1 second cooling time the tensile stress reaches 161 psi; for the 0.5 second cooling time a stress of 189 psi is developed, significantly lower than the 500 psi calculated using the quasi-elastic approximation. In both cases, after one day the stress level is reduced to 100 psi.

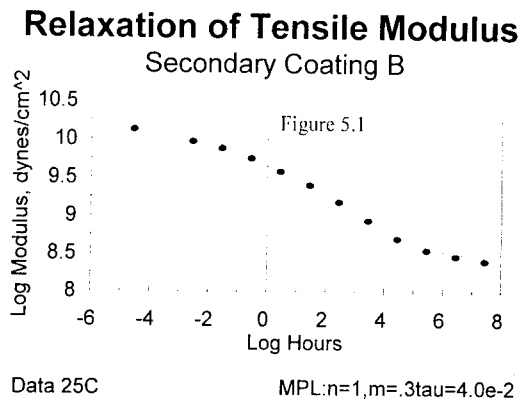


Figure 5.1

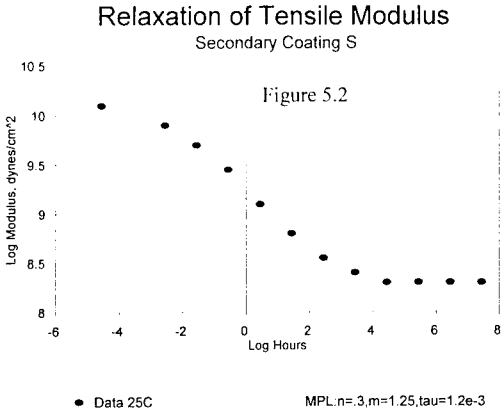


Figure 5.2

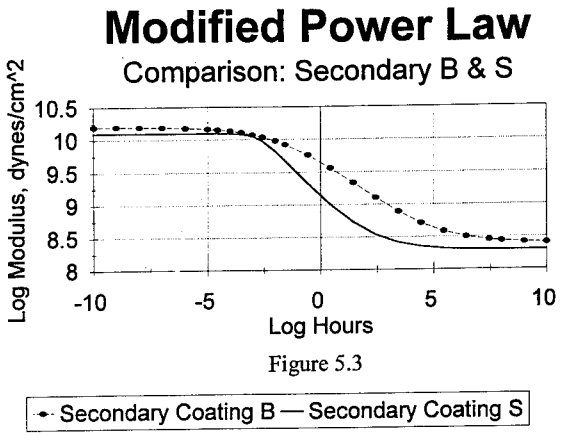


Figure 5.3

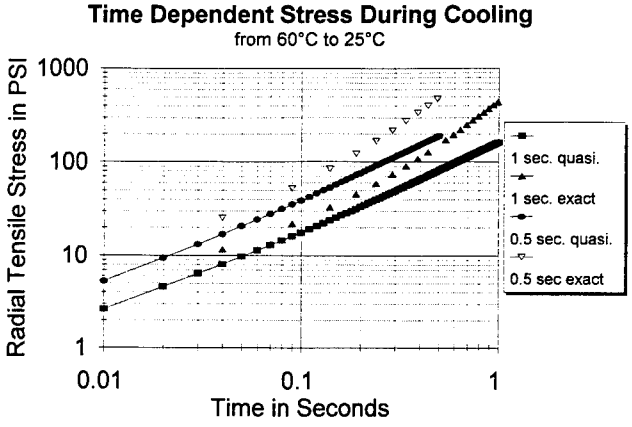


Figure 6

Exact Viscoelastic Analysis

Using the MPL properties shown in Figure 5 for the Coatings B and S the stresses were calculated using the following convolution equation (see Ref. 6, p. 7).

$$\sigma(t_f) = K \int_o^{t_f} \left(E_e + \frac{(E_e - E_g)}{\left(1 + \left(\frac{1}{\tau}\int_t^{t_f} \frac{1}{a_T(e)}\,de\right)^m\right)^n} \right) \frac{d\Delta T(t)}{dt} dt$$

Equation 4

The constant **K** contains coating geometry and non time dependent material parameters from the earlier equations (1) or (2). The entire relaxation curve and the material's temperature dependence are scanned by equation (4) in the calculation of stress. Table A is a tabulation of all of the MPL factors along with the temperature dependence factor over the 25 to 60°C temperature range. In addition the maximum achieved stresses are plotted in Figure 7.

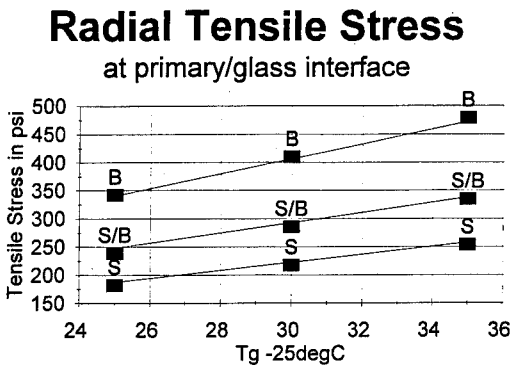


Figure 7

Table A
Modified Power Law Parameters
Delta T(Tg-25) and Radial Tensile Stress

deg C Tg-25	n	m	hours tau	dec/degC	dsc logEg	dsc logEe	psi stress	Coating Parameters
35	1	0.3	0.04	0.14	10.2	8.4	479	B
30	1	0.3	0.04	0.14	10.2	8.4	410	B
25	1	0.3	0.04	0.14	10.2	8.4	342	B
35	0.3	1.25	0.0012	0.2	10.1	8.3	254	S
30	0.3	1.25	0.0012	0.2	10.1	8.3	218	S
25	0.3	1.25	0.0012	0.2	10.1	8.3	182	S
35	0.3	1.25	0.0012	0.014	10.1	8.3	335	S/B
30	0.3	1.25	0.0012	0.14	10.1	8.3	286	S/B
25	0.3	1.25	0.0012	0.14	10.1	8.3	239	S/B

The two secondaries have distinctly different shaped relaxation modulus curves at 25°C; this is readily seen in Figure 5.3 where the MPL for the two materials are compared. The two materials also have different temperature dependent factors; 0.20 decades/°C for Secondary Coatings and 0.14 decades/°C for Secondary Coating B. The effect of this factor is demonstrated by the data marked **S/B** in Figure 7 and Table A; the MPL factors for these entries are for Coating S and the temperature dependence is 0.14 decades/°C for Coating B.

Summary and Experimental Observations

We have calculated the thermally induced radial stresses at the primary/glass interface using two quasi-elastic approximations (one with a step increase in temperature and one with a time varying temperature) and an exact viscoelastic analysis. As shown in Figure 6 and Table B, the quasi-elastic solution, with a step increase in temperature, provides an upper bound estimate while

Table B
Maximum Radial Tensile Stress
at
Glass/Primary Interface
Radial Tensile Stress in PSI

	Exact	Quasi-Elastic	Quasi-Elastic
Type of Cooling		with time varying temperature	step increase in temperature
0.5 sec	471	163	
1 sec	438	141	
10 sec	329		
100 sec	229		
step/initial modulus			551
step/1 day modulus			135

the quasi-elastic with time varying temperature provides a lower bound estimate. The approximation using the step temperature increase permitted an analysis of the effect of primary or secondary thickness variations on the radial tensile stress (Figures 2 and 3).

It is clear from these results that increasing the secondary Tg or broadening the relaxation response increases the radial tensile stresses at the primary/glass interface. One would need to design a coating system with a primary thickness of 10 microns or less to have compressive stresses at the primary/glass interface; an unrealistic design for microbend loss resistance.

When an optical fiber is subjected to a mechanical perturbation, the bond between the primary and glass surfaces may be broken. This damaged interface would be expected to grow, similar to a "crack", in the presence of radial tensile stresses. This is, in fact, observed. Induced separations at the primary/glass interface continue to grow for as long as 5 minutes after initiation. Once the interface separation occurs, the analyses presented here no longer apply since the primary coating is not constrained in the vicinity of the separation. The accompanying modification of the boundary conditions at the "crack" tip contributes to the eventual stopping of the separation growth.

In addition to the observations of interface damage growth after mechanical perturbation, we have observed spontaneous primary/glass interface separation, within hours after draw, in experiments with secondary coatings having glass transition temperatures around 100°C. It is clear from our analysis and experimental observations that the secondary coating relaxation modulus shape, the glass transition temperature, and temperature dependence can impact the magnitude of the maximum radial tensile stress (Figure 7).

Acknowledgments

We thank Larry Sweatt for programming the exact viscoelastic solution and Carl Taylor and Jerry Anderson for helpful discussion and encouragement. Prof. Richard Schapery, of the University of Texas, is also acknowledged for his valuable inputs. Also, we want to recognize Brenda Odom for her patience and expertise in preparing this manuscript.

[1] Brockway, G. S. and Santana, M. R.: Analysis of Thermally Induced Loss in Fiber-Optic Ribbons, The Bell System Technical Journal, April, 1983, Vol. 62, No. 4, Part 1, pp. 993-1018.

[2] Bouten, P. C. P.; Broer, D. J. ; Jochem, C. M. G.; Meeuwsen, T. P. M.: Optical Fiber Coatings: High Modulus Coatings for Fibers with a Low Microbending Sensitivity, Polymer Engineering and Science, mid-September, 1989, Vol. 29, No. 17, pp. 1172-1176.

[3] Reddy, S. S.; Overton, B. J.; Watson, S. M.: Design Parameters of Coatings for Low Temperature Applications of Optical Fibers, Proceedings of National Fiber Optic Engineers Conference, June 18-22, 1995, Boston, MA pp. 260-270.

[4] Gent, A. N.; Lindley, P. B.: Internal rupture of bonded rubber cylinders in tension, Proceedings of Royal Society A, Vol. 249, pp. 195-205, 1959.

[5] Lindsey, G. H.; Schapery, R. A.; Williams, M. L.; Zak, A. R.: The Triaxial Tension Failure of Viscoelastic Materials, Aerospace Research Laboratories Office of Aerospace Research United States Air Force, ARL 63-152, September, 1963.

[6] Ferry, J. D. , Viscoelastic Properties of Polymers, John Wiley & Sons, 1980.

[7] Popov, E.P. Engineering Mechanics of Solids, Prentis-Hall, 1990.

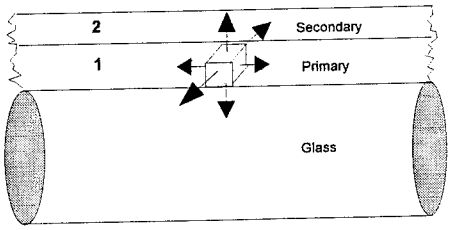
Appendix

Thermoelastic Stress Analysis

In this analysis each of the coating layers is treated as a uniform elastic cylinder, constrained to plane-strain deformation because of attachment to the relatively rigid glass fiber (as shown in Figure 1a) and subjected to the temperature drop ΔT. Geometric and material parameters are defined as follows:

r = radial coordinate
a = radius of glass fiber
b = outer radius of primary coating
c = outer radius of secondary coating
E_1= Young's modulus of primary coating
E_2= Young's modulus of secondary coating
ν_1= Poisson's ratio of primary
ν_2= Poisson's ratio of secondary
α_1= thermal expansion coefficient of primary
α_2= thermal expansion coefficient of secondary
σ_1= radial tensile stress at glass-primary interface
σ_2= radial tensile stress at primary-secondary interface
γ_1= a/b
γ_2= b/c

Triaxial tensile stress throughout primary due to the constraint of the high modulus glass and secondary coating. As the primary and secondary cool down after exiting the UV lamps their respective thermal expansion coefficients are approximately equal down to 60 degrees C.



From 60 degrees C to 25 degrees C (delta of 35 degrees) the primary has about 3 times the thermal expansion coefficient of the secondary. Constrained by the secondary and the glass stresses develop in the primary that are tensile for the fiber coating dimensions.

Figure 1a

The basic analytical results, from which a solution of our problem follows, are given in standard texts[7] on the mechanics of solids. We find that for the primary coating the circumferential strain is given by:

at r=a;

$$\varepsilon_1 = -(1+\nu_1)\alpha_1\Delta T - \frac{(1+\nu_1)}{E_1}\frac{[1+(1-2\nu_1)\gamma_1^2]\sigma_1}{(1-\gamma_1^2)} + \frac{2(1-\nu_1^2)\sigma_2}{E_1(1-\gamma_1^2)}$$

and at r=b;

$$\varepsilon_1 = -(1-\nu_1)\alpha_1\Delta T - \frac{2(1-\nu_1^2)\gamma_1^2\sigma_1}{E_1(1-\gamma_1^2)} + \frac{(1+\nu_1)(1+\gamma_1^2-2\nu_1)}{E_1(1-\gamma_1^2)}$$

In the secondary at r=b the circumferential strain, ε_2, is given by

$$\varepsilon_2 = -(1+\nu_2)\alpha_2\Delta T - \frac{(1+\nu_2)}{E_2}\frac{[1+(1-2\nu_2)\gamma_2^2]\sigma_2}{(1-\gamma_2^2)}$$

Assuming the glass to be relatively rigid, the radial displacement and hence circumferential strain in the primary at r=a must vanish, so that

$$0 = -(1+\nu_1)\alpha_1\Delta T - \frac{(1+\nu_1)}{E_1}\frac{[1+(1-2\nu_1)\gamma_1^2]\sigma_1}{(1-\gamma_1^2)} + \frac{2(1-\nu_1^2)\sigma_2}{E_1(1-\gamma_1^2)}$$

Equation 1a

Contact between the primary and secondary at r=b requires that the circumferential strains in the two layers be equal there. Thus

$$-(1+\nu_1)\alpha_1\Delta T - \frac{2(1-\nu_1^2)\gamma_1^2\sigma_1}{E_1(1-\gamma_1^2)} + \frac{(1+\nu_1)(1+\gamma_1^2-2\nu_1)}{E_1(1-\gamma_1^2)} = -(1+\nu_2)\alpha_2\Delta T - \frac{(1+\nu_2)[1+(1-2\nu_2)\gamma_2^2]\sigma_2}{E_2(1-\gamma_2^2)}$$

Equation 2a

Solving (1a) and (2a) simultaneously for σ_1 we obtain

$$\frac{4\left(1+\frac{\gamma_2^2}{3}\right)\sigma_1}{3E_2(1-\gamma_2^2)} = -\frac{4}{3}\alpha_2\Delta T + \frac{3}{2}\alpha_1\Delta T - \frac{3}{2}\gamma_1^2\alpha_1\Delta T - \frac{4E_1\left(1+\frac{\gamma_2^2}{3}\right)(1-\gamma_1^2)\alpha_1\Delta T}{3E_2(1-\gamma_2^2)}$$

where we have set ν_1=1/2 and ν_2=1/3, which are typical. Rearranging yields the Equation (1) in the body of this memo.

$$\sigma_1 = \alpha_1\Delta T\left[\frac{3}{2}(1-\gamma_1^2) - \frac{4\alpha_2}{3\alpha_1}\right]\frac{3E_2(1-\gamma_2^2)}{4\left(1+\frac{\gamma_2^2}{3}\right)} - (1-\gamma_1^2)E_1\alpha_1\Delta T$$

Equation 3a

The last term in Equation (3a), over the range of parameters important for fiber coating, represents the compressive stress contribution of the primary coating. The magnitude, shown in Figure 2a, is not significant. This component of the stress is not time dependent since the primary mechanical behavior is out on the rubbery plateau of the relaxation curve. At long times it becomes a more significant portion of the stress because of the time dependence of the secondary coating, though the stress remains tensile.

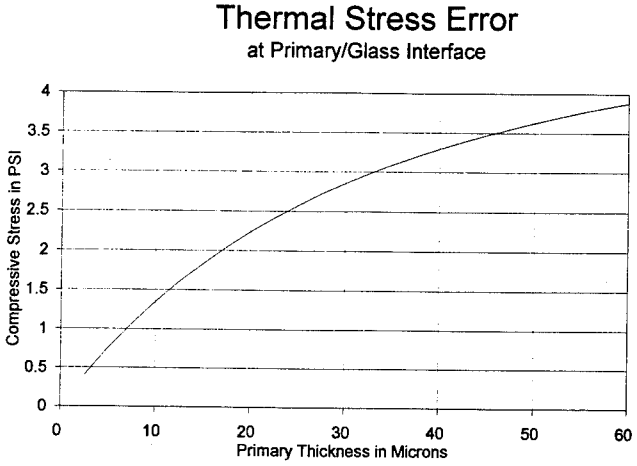
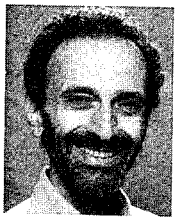


Figure 2a

Dr. C. J. Aloisio, Jr.
AT&T Bell Laboratories
2000 Northeast Expressway
Norcross, GA 30071



Charles Aloisio began his career with Bell Laboratories in 1952. After two years in the Murray Hill Drafting Department and two years in the U.S. Marine Corps, he joined the Chemical Research Department. For the majority of his career, he has been involved in the study of the rheology of polymeric materials. He worked in the Materials Group with Bell Labs in Indianapolis from 1967 to 1972, while obtaining his MS and Ph.D. from Purdue University.

Charles joined the Atlanta Bell Labs in January, 1972, as a Member of the Technical Staff in the Materials Chemistry Group working on the characterization of polypropylene and polyethylene for cable sheathing and DEPIC insulation. He became the supervisor of the Polymer Characterization Group in 1973 initiating the use of rheology and viscoelastic analysis in a variety of copper and fiber optic applications.

In 1986, he became the supervisor of the Glass Technology Group. Since January 1992, he has been a Distinguished Member of the Technical Staff in the Material Technology Group, applying rheology and viscoelasticity to fiber optic coating technology.

EFFECTS OF COLOR CODING ON OPTICAL FIBER PERFORMANCE AND RELIABILITY

Rolf A. Frantz*, Eva M. Vogel*, and Barry J. Keon†

*Bellcore, Morristown, NJ; †Telstra, Melbourne, Australia

ABSTRACT

Optical fibers are color coded for ease of identification in service. However, the application of color coding inks raises a number of performance-related issues. Some colors can be so similar as to result in mismatching of fibers at splice points. Fibers discolored by aging can be difficult to identify during repair work. Interactions of the ink with the coating, ribbon matrix material, or buffer tube gel can be detrimental to the performance of the materials involved. LID compatibility of the ink is necessary to facilitate the use of various fiber measurement tools. The addition of the thin ink layer can have a greater than anticipated effect on the microbending sensitivity of the fiber and on its aging and strength retention characteristics. This paper discusses each of these issues and cites specific examples of the behaviors involved.

INTRODUCTION

Color coding inks for optical fibers have typically been viewed solely as a means of identifying the fibers within an optical cable. A thin ink layer is applied over the dual-layer polymeric fiber coating. By controlling the color of this ink to be one of a specified set of colors, the fiber should be uniquely identifiable within a cluster of fibers within a buffer tube or fiber ribbon in a cable. However, color-coding a fiber can affect its performance and long-term reliability in a variety of ways. Among the issues involved are: color repeatability (lot-to-lot and supplier-to-supplier); color stability during aging; compatibility of the ink with other cable materials, notably buffer tube gels; compatibility of the inked fiber with LID devices; changes in the fiber's microbending sensitivity; and effects of the ink layer on fiber aging characteristics, particularly fiber strength.

- Color repeatability between suppliers is poorer than the lot-to-lot repeatability from a single supplier. Problems can arise in identifying fibers or in matching them by color, particularly when splicing cables from different suppliers.
- Color changes during aging can cause fiber identification problems when splicing older cables, or when revisiting splice closures for rearrangements or maintenance.
- Incompatibilities between color coding inks and surrounding cable materials, particularly buffer tube gels, can cause the ink to change color or to delaminate from the coating, so that it easily flakes off during handling.
- Ideally, fiber inks should pass signals at transmission wavelengths with minimal attenuation. However, non-uniformities in the ink layer can cause large fluctuations in the signal strength registered by LID and clip-on devices.
- Finally, the ink layer acts as a thin supplementary coating layer. As such, it can impact the sensitivity of the fiber to microbending stresses. The ink layer can also act as an additional barrier to environmental penetration, particularly by humidity or liquid water. In so doing, it can delay the onset of surface roughening on the glass and of the reduction in fiber strength that typically accompanies aging in moist environments.

In this paper, we discuss each of these various effects and cite specific examples of each problem.

COLOR MATCHING

Fiber identification and matching by color are prerequisites for accurate splicing during service installation, maintenance, or restoration. The colors on fibers in different cables vary for a number of reasons. Each manufacturer typically specifies a set of colors—within the tolerances of EIA/TIA-359-A and TIA/EIA-598-A[1]—that are visually distinct; individual colors can and do vary among manufacturers. Cable manufacturers purchase their inks from different suppliers; colors may vary slightly depending upon the recommendations and capabilities of each ink supplier. Inks may be solvent-based or uv-curable, introducing differences in the processing and ink layer thickness. Even within a single manufacturer's product line, the color may vary from cable to cable because of variability in the ink and factors that affect the inking process: the wettability of the coating by the ink; settling of the ink pigment in the applicator; the speed and extent of the ink curing; and abrasion as the colored fiber is spooled, unspooled, and cabled.

Table 1 shows the variations in the non-neutral colors for fibers from three suppliers, while Table 2 shows the variations in color for different lots from one supplier. The data in both tables were collected over the past two years using the stacked-fiber samples and colorimetric measurement techniques we have described previously.[2] The Munsell coordinates for some colors are quite different, particularly among different manufacturers and in both tables, some colors lie outside the tolerance ranges.

Table 1. Variations in colors from several suppliers

COLOR	SUPPLIER 1	SUPPLIER 2	SUPPLIER 3
Red	0.2R 4.5/11.9	2.8R 4.2/12.5	3.3R 3.6/9.7
Orange	9.2R 5.8/13.9	10.0R 5.4/14.5	1.2YR 5.1/10.2
Brown	2.4YR 4.4/4.5	3.2YR 3.3/3.3	0.9YR 2.5/2.8
Yellow	4.8Y 8.2/12.1	2.0Y 7.0/11.9	3.7Y 7.2/10.0
Green	4.2G 4.7/6.6	4.6G 4.8/9.5	8.2G 3.5/6.3
Blue	3.4PB 3.9/10.0	4.1PB 2.7/7.5	8.3B 3.4/8.0
Violet	4.6P 5.3/7.5	2.5P 3.5/4.6	0.4RP 4.0/6.3
Rose	2.3R 6.5/7.7	2.7YR 6.3/9.2	7.4R 7.0/6.0
Aqua	8.5B 6.5/7.6	2.0B 6.5/6.9	7.3BG 6.3/5.4

Copyright © 1995 Bellcore. All rights reserved.

Table 2. Variations in colors from a single manufacturer

COLOR	SAMPLE 1	SAMPLE 2	SAMPLE 3
Red	3.1R 4.2/11.8	3.3R 4.3/12.5	3.1R 4.1/11.5
Orange	0.8YR 5.6/13.3	1.0YR 5.9/14.1	0.8YR 6.0/14.2
Brown	3.3YR 3.3/3.3	2.8YR 3.5/3.9	3.7YR 3.3/3.1
Yellow	3.9Y 8.1/12.5	3.5Y 8.0/12.2	3.6Y 7.9/12.4
Green	1.1G 4.5/9.0	0.9G 4.8/9.7	1.1G 4.5/8.6
Blue	3.6PB 3.4/10.6	3.6PB 3.3/10.5	1.5PB 3.4/9.5
Violet	3.7P 3.7/4.6	3.0P 3.6/4.7	4.3P 3.6/4.8
Rose	5.6R 6.7/7.6	6.0R 6.4/9.0	4.8R 6.3/9.1
Aqua	10.0BG 5.6/7.0	9.8BG 5.6/6.7	9.9BG 5.7/7.0

However, even within the tolerances, it is possible to have colors that are subject to mismatching. Figure 1 shows the tolerance regions in color space for Red and Orange. Because of the wide range of Hues allowed, the most orange shade of Red (5.5R) is actually closer to the red limit for Orange (10R) than it is to the opposite Hue limit for Red (10RP). Confusions of color such as this are particularly possible if the fiber colors have changed due to aging, and can cause delays when technicians are forced to spend significant time properly identifying fibers in closures or matching fibers in lengths of different cables.

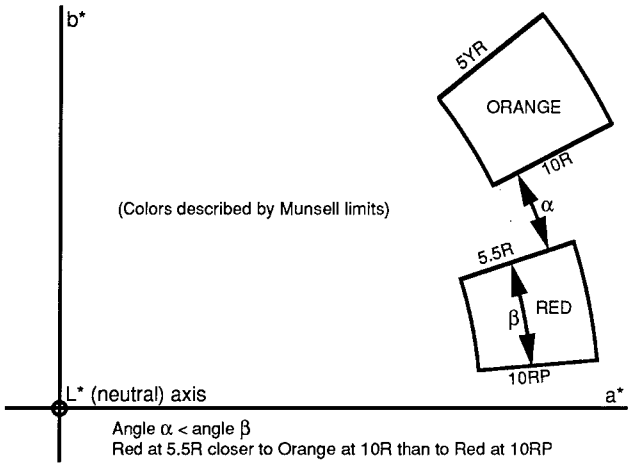


Figure 1. Sample color tolerances that allow fiber mismatching

STABILITY DURING AGING

Fibers must be readily identifiable by color when the inks are first applied and also after years of field service. Aging of the fibers may take place inside a cable or in a splice closure, pedestal, or similar enclosure. In a cable, the fiber is surrounded by a buffer tube gel or ribbon matrix material; the stability of the color will depend upon the interactions (or lack thereof) between these various materials. In a pedestal or closure, the fiber is exposed to the external ambient, at least to some extent; humidity, liquid water, airborne contaminants, and materials introduced when handling the fiber (cleaning compounds, skin oils, etc.) are part of the aging environment. The fiber colors must be sufficiently stable that each color is readily recognizable and matchable to an unaged color so that new service installation, rearrangement, or service restoration can be done quickly and accurately.

Previous studies have examined the effects of aging on the color stability of inked fibers.[2–4] Not surprisingly, the extent of discoloration is affected by the ink, the coating, the environment (gel, air, humidity, etc.), and the aging temperature. Table 3 shows the effects of aging on a sample fiber. The color changes (ΔE, the distance between the aged and unaged colors in three-dimensional L*a*b* color space) are larger for the fibers aged in gel than for those aged in air, and larger yet for fibers aged inside buffer tubes. This suggests that an interaction between the gel and the ink is contributing to the discoloration; when the gel is exposed to the air, rather than being protected inside the buffer tube, an alternate reaction (e.g., evaporation and/or oxidation of gel constituents) reduces the interaction between the gel and the ink. The uninked fiber also experiences a measurable color change, which contributes to the changes seen on the inked fibers. Finally, light colors (Yellow, White) show much greater color changes than dark colors (Brown, Slate, Black). Unfortunately, human perception is also more sensitive to color changes in light colors than in dark ones.

Table 3. Color changes (ΔE) after aging 14 days at 85 °C in different environments

COLOR	AGED IN AIR	AGED IN GEL	AGED IN TUBE
Uninked	7.2	3.0	8.5
Red	5.7	10.4	23.6
Orange	8.2	17.7	30.7
Brown	8.3	24.6	16.9
Yellow	26.0	35.1	48.4
Green	13.9	23.0	41.4
Blue	8.2	11.6	24.9
Violet	8.2	12.7	23.9
White	22.9	26.1	38.2
Slate	2.3	5.1	9.1
Black	4.4	6.1	2.8

Figure 2 (from [4], edited) shows just how troublesome the effects of aging can be. Three fibers whose colors were distinctly different initially became virtually non-identifiable after aging for one month in air at 85 °C. All three samples turned brown, and all were close enough to each other and to the actual Brown fiber that sample lengths could not be separately identified when intermixed. A technician opening a splice closure or pedestal to install, rearrange, or restore service would require a means other than color to identify these fibers with sufficient confidence to work with them.

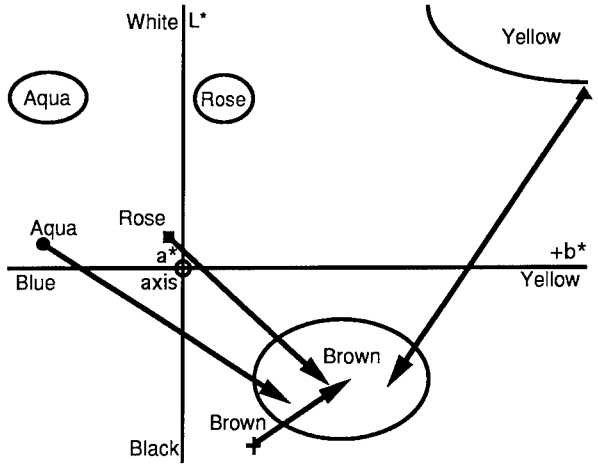


Figure 2. Color changes causing difficulty in fiber identification

MATERIALS COMPATIBILITY

Color coding inks should be compatible with the materials with which they come in contact, particularly the fiber coating and the ribbon matrix material or buffer tube gel. Compatibility with the coating means that the ink should thoroughly wet the surface, should adhere well when cured, and should not cause any chemical or physical changes in the coating that affect the fiber's optical or mechanical performance. Compatibility with a matrix material means that the ink should not dissolve in the uncured material, should remain on the fiber rather than with the matrix when the fibers in the ribbon are separated, and should not affect the material's performance. Finally, compatibility with a buffer tube gel means that the ink should not dissolve in the gel, nor absorb elements of the gel in such a way that either the ink or the gel is adversely affected. Because each of these interactions can be thermally stimulated, short-term aging at elevated temperatures will typically reveal any compatibility problems that might exist.

If such a screening test is not performed, the incompatibility may appear after a period of field service. One particular instance involved the migration of low molecular weight oils from a buffer tube gel, which penetrated the ink layer and caused it to delaminate from the coating. Handling the fiber and wiping off the gel caused the ink to flake and peel. Figure 3 shows two such fibers that were gently wiped. The dark stripe on the upper edge of the top fiber is where the ink was almost completely removed during the wiping; the bottom fiber shows the nearly complete removal of the ink during subsequent handling. When a technician opened the cable in the field, separated the fibers, and wiped off the gel, almost all of the ink came off on his hands and the wiping cloth.[5] It was necessary to separate the individual fibers at the end of the tube (using extreme care so as not remove the small amount of ink remaining), identify each fiber and trace it to its end, and splice it while reasonably confident of its identity. Time-consuming though this procedure was, fiber identification will be even more difficult if the closure must be re-entered and the spliced fibers identified for rearrangement or maintenance.

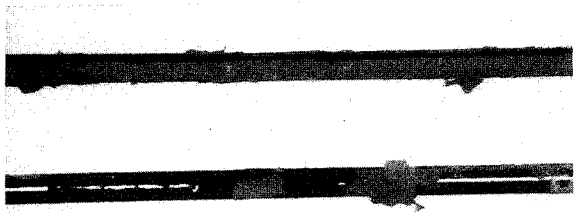


Figure 3. Ink peeling and flaking due to wiping and handling

INK TRANSMISSIVITY

The proper operation of fiber identifiers, light injection and detection (LID) systems, and clip-on devices depends upon their ability to detect transmission-wavelength light passing through the coating and ink. If the ink layer is highly opaque, either because of its pigment density or its thickness, only minimal light will reach the detector. If the ink layer is not uniform, signals injected or detected at different locations can have very different strengths, resulting in erratic performance and results that are difficult to interpret.

Development of a standard technique for assessing "LID compatibility" has been hindered by the differences among fiber-contacting devices. Measurements that depend upon the characteristics of a "standard" device often have little relevance to the fiber performance with a different device. Workers at BICC Cables have proposed measuring the light radiated from a fiber loop inside an integrating sphere,[6] thus avoiding the dependence upon a specific fiber-contacting device. However, the *average* transmittance so determined can be difficult to correlate with actual fiber/LID performance if the ink layer is nonuniform and contact with the fiber occurs at locations with very different opacities. Table 4 rank orders the opacities of inked fibers from one supplier as measured by different techniques.[7] The colors are listed in the first column in the rank ordering obtained through integrating sphere measurements; the second and third columns present averaged results from a LID system and a clip-on device, respectively. Although there is some agreement that Black, Brown, and Slate are relatively opaque, behavior such as that of the Red fiber (ranked third, twelfth, and ninth) preclude any general conclusions. Both the LID and clip-on data are highly variable, and the rank-ordering can be significantly affected by averaging more or fewer measurements.

Table 4. Opacity rankings for a sample set of inked fibers[7]

COLOR	LID	CLIP-ON
Black	2	1
Brown	1	3
Red	12	9
Slate	3	2
Yellow	11	11
Violet	7	10
Green	9	5
Blue	5	7
Orange	8	12
Rose	6	4
Aqua	10	8
White	4	6

Nonuniform inking caused problems for technicians using a LID system to estimate splice losses in the field. Their unacceptably large percentage of high-loss splices was attributed to problems of fiber geometry.[8] However, OTDR measurements in the laboratory showed that the "high loss" splices had low losses typical of "good" fusion splices. We examined the fibers under a microscope and found that the ink was both opaque and non-uniform; irregular uninked stripes and patches were clearly visible, as shown in Figure 4. Because of the opaque ink, the fiber colors were readily discernible; however, in the LID measurement system, loss estimates differed greatly, depending upon whether fiber contact was made at inked or uninked locations. Table 5 summarizes the results of measurements on these fibers (A) and on fibers from three other suppliers (B–D). The latter inks were less opaque, and the LID measurement technique worked quite well. Note that fiber A would not have created a problem if the ink had been uniform, since all splices would have shown high estimated losses, and the measurements, rather than the fiber, would have been suspected from the beginning.

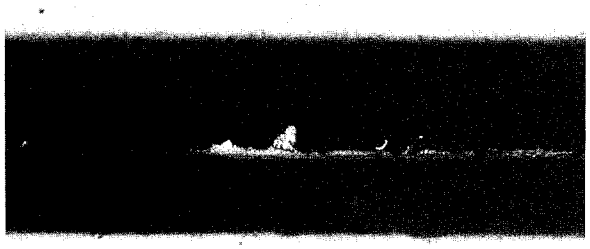


Figure 4. Nonuniform application of an opaque ink

Table 5. Splice loss results for fibers inked by four suppliers

SUPPLIER	NUMBER OF SPLICES MEASURED	NUMBER OF ERRONEOUS HIGH-LOSS READINGS
A	59	20
B	55	1
C	60	3
D	50	6

INKS AS COATINGS

Because the ink layer, while thin, adds to the coating at its outside diameter, it might be expected to provide additional stiffness against microbending. However, published work from Northern Telecom shows that inking increases the sensitivity of fibers to microbending.[9] The measurements were made by winding the fibers on glass drums in a basket weave pattern; OTDR readings were taken as the sample was cooled to -40 °C, at which temperature the stiffened coating provides only minimal elastic cushioning of the fiber against the bending introduced at the winding crossover points. As shown in Table 6, adding a uniform layer of uv-cured ink increased the microbending loss by 40–50%, while a layer of thermally-cured ink increased the loss by a factor of three. Possible causes for this behavior could include: an increased stiffening of the coating due to the ink curing process (heating or uv radiation); compression of the coating due to circumferential shrinkage in the ink during curing; or nonuniform stresses in the ink and coating due to interactions and adhesion at the interface. Of particular interest is the additional increase in the loss of nearly 80% that occurred when the ink layer was applied nonuniformly; this provides additional evidence of the importance of assuring that the ink layer uniformly wets and adheres to the coating surface.

Table 6. Microbending loss, in dB/km, at 1550 nm, -40 °C, for fibers with different inking conditions[9]

CONDITION	FIBER 1	FIBER 2
UNINKED	0.59	0.26
UV INK, UNIFORM	0.93	0.36
UV INK, NONUNIFORM	1.65	—
THERMAL INK, UNIFORM	1.8	—

We have previously reported on the effects of the ink layer on the mechanical behavior of fibers, particularly after aging.[10, 11] Among the variables included in our investigations have been: ink type (uv or thermal curing); ink color; fiber/coating (several commercial products); aging environment (water, humidity); aging time and temperature; and post-aging conditioning. For fibers in which the uninked samples experienced significant changes during aging, both thermally cured and uv cured inks enhanced the stability of the coating strip force and the retention of fiber strength (in two-point bending) during aging.[10] For another set of fibers which nominally differed only in the color of the uv ink, the extent to which the tensile strength was retained during aging was apparently dependent upon the color of the ink.[11] Table 7a presents normalized median tensile strength data for the latter fiber, colored with three different inks, in both 85 °C/85% relative humidity and 85 °C deionized water aging environments. Table 7b presents similar data for the two-point bending strength of three commercial fibers all colored with the same inks. (Direct comparisons should not be drawn between the two sets of strength measurements because of the differences in the test methods.) Our gas chromatography/mass spectroscopy analyses suggest that volatile compounds such as uv photoinitiators, thermally-evaporated solvents, and stabilizers can be extracted during water aging and that the extent of such extraction can affect the ability of the environment—especially liquid water and water vapor—to penetrate to the glass surface. Thermally cured and uv cured inks obviously contain significantly different extractables, both in types and in quantities. Even within one ink family, differences in pigment content and in the amounts and types of additives required to suspend and disperse the pigment particles can result in significant differences in extractables, as can the extent of cure of the ink on the fiber. These variations help to explain the differences in behavior between the uninked, uv inked, and thermal inked samples, as well as among the three samples inked with different uv colors, in Table 7. None of these results should be taken to imply that either uv or thermally cured inks are inherently superior. Both types of ink can offer additional protection against environmental penetration, but the specifics of each ink application (formulation, uniformity, cure, and environment) will strongly affect the extent of this protection, as well as what other, possibly counteracting, effects (e.g., reactive chemical constituents) may be present.

Table 7. Fraction of initial strength retained by sample fibers after seven days of aging

FIBER IDENTIFICATION	85 °C/85% RH	85 °C DI Water
a: Fiber A — Tension		
Green UV Ink	0.95	0.70
Blue UV Ink	0.85	0.86
Red UV Ink	0.81	0.73
b: Fibers X, Y, Z — Two-point Bending		
X, Uninked	1.04	0.61
X, Thermal Ink	1.09	1.02
X, UV ink	1.06	0.96
Y, Uninked	0.90	0.95
Y, Thermal Ink	0.93	1.01
Y, UV Ink	0.85	0.96
Z, Uninked	1.09	1.16
Z, Thermal Ink	1.09	1.14
Z, UV Ink	1.06	1.10

SUMMARY

The perception of color coding inks for optical fibers as thin layers added for ease of fiber identification does not take into account the many ways in which the ink affects fiber performance. Even in their basic function as a means of identification, inks raise performance issues with regard to how readily they can be identified—especially after discoloration due to aging—and be matched with other inked fibers during service installation, maintenance, and restoration. Interactions with the surrounding environment raise additional issues, such as the potential delamination of the ink due to the action of oils in the buffer tube gel, or the adhesion of the ink to the fiber, rather than to the matrix material in a ribbon. The transmissivity and uniformity of the ink layer have significant effects on the performance of fiber-contacting equipment such as LIDs and fiber identifiers; the worst situation may not be that this equipment does not work, but that it works only intermittently, giving false or misleading information about the condition of the fiber or splice. Nonuniformity of the ink layer, which gives rise to this intermittent LID performance, also can add significantly to the microbending sensitivity of the fiber; the magnitude of the effects can be surprisingly large, considering the limited thickness of the ink layer. Finally, the ink layer can delay the onset of strength degradation during fiber aging, acting as an additional barrier to the penetration of the environment (particularly water) to the glass surface. On the other hand, the ink may contain chemical species that enhance the surface roughening of the glass once they do reach the surface. Careful selection and thorough testing are required before an ink is applied to fibers for cables in field service environments.

ACKNOWLEDGMENTS

The measurements reported in this paper were made by many people over the past several years; we particularly thank Ed Beebe and Joel Mann for collecting the most recent data. The permission of the Director, Telstra Research Laboratories, to publish and present this paper is also acknowledged.

REFERENCES

1. TIA and EIA documents are available from Global Engineering Documents, 15 Inverness Way East, Englewood, CO 80112.

2. B.J. Keon and R.A.Frantz, "The Stability of Optical Fiber Color Codes: Effects of Material Choices and Service Environments," Proceedings of the 43rd International Wire and Cable Symposium, p.522, 1994.

3. J.R. Petisce, M.D. Kinard, S. Siddiqui, and C. Taylor, "Effect of Environmental Aging on Optical Fiber Color Codings," Proceedings of the 42nd International Wire and Cable Symposium, p.552, 1993.

4. R.A. Frantz and I.M. Plitz, "The Effects of Aging on the Discernibility of the Color Identification of Optical Fibers," Proceedings of the 42nd International Wire and Cable Symposium, p.850, 1993.

5. Private communication from fiber splicer.

6. N.R. Haigh, P. Crahay, R. Grigsby, and S. McCabe, "Direct Measurement of the Transmittance of Coating Layers on Optical Fibers," Proceedings of OFC '92, paper WK9, p. 151, 1992.

7. R. Frantz and J. Berardinelli, "Transmissivity of Optical Fiber Inks and Coatings," Proceedings of the 10th National Fiber Optic Engineers Conference, volume 2, page 155, 1994.

8. Private communication from splicing supervisor.

9. Z. Pasturczyk and C. Saravanos, "Microbend Loss of Colored Optical Fibers Measured over Extended Temperature Range," Proceedings of the 42nd International Wire and Cable Symposium, p.527, 1993.

10. R.A. Frantz, B.J. Keon, E.M. Vogel, T.N. Bowmer, and H.H. Yuce, "The Effects of Optical Fiber Coating and Ink Materials on the Corrosion of the Glass Surface," Proceedings of the 43rd International Wire and Cable Symposium, p.742, 1994.

11. E.M. Vogel, B.J. Keon, C.R. Kurkjian, R.A. Frantz, and H.H. Yuce, "Mechanical Properties of Color Coded Fiber," Proceedings of the 11th National Fiber Optic Engineers Conference, volume 2, page 237, 1995.

Rolf A. Frantz is a Distinguished Member of Staff in Bellcore's Fiber Media and Components Reliability group. He received his bachelor's and master's degrees from Cornell University and his Ph.D. from Brown University. He joined AT&T Bell Laboratories, where he worked principally on the reliability of electrical insulation materials, an area in which he continued to work after coming to Bellcore in 1984. Since 1988, he has worked in the field of optical fiber and component reliability, with emphasis on fiber coatings, color coding inks, adhesives, and materials compatibility. An active participant in national standards work, he chairs the TIA Task Group on optical cable color coding standards.

Eva M. Vogel is a Member of Technical Staff in the Fiber Media and Components Reliability group at Bellcore. She received her Dipl. Chem. Engr. in Physical Chemistry and her Ph.D. in Ceramic Engineering from the Slovak Technical University in Bratislava, Slovakia. She joined Bellcore in 1984 after having worked at AT&T Bell Laboratories since 1970. Her research on novel properties of electronic and optical materials is internationally recognized, and she is one of Bellcore's subject mater experts on optical component reliability. Dr. Vogel is a Fellow of the American Ceramic Society.

Barry J. Keon is a Senior Materials Engineer in the Telecommunications Science and Technology Branch of the Telstra Research Laboratories in Melbourne, Australia. He holds a B.Sc. degree from Monash University, a post-graduate Diploma of Polymer Chemistry from the Chisholm Institute of Technology, and an M.Eng.Sci. from Monash University. He has worked in the telecommunications industry since 1991, with responsibilities in the areas of optical fiber reliability and cable materials performance. In 1994 and 1995, he was a Visiting Researched in the Fiber Media and Components Reliability group at Bellcore, working on reliability issues affecting optical fibers and cables.

Heat-Resistance Behavior and the Discernibility of the Color of Optical Fibers and Fiber Ribbons

Akira Murata, Kazunaga Kobayashi, Keiji Oohashi,
Shinji Araki, and Toshikuni Maruoka

Fujikura Ltd., Opto-Electronics Laboratory
1440, Mutuzaki, Sakura-shi, Chiba, 285 Japan

Abstract

We investigated that the heat resistance behavior of UV-curable urethane acrylate resin widely used as optical fiber coatings. Low Young's modulus primary coatings showed lower heat resistance than high Young's modulus secondary coatings. We examined some relationship between the molecular structure of the soft coatings and their heat-resistance behavior. Optical loss of the fibers coated with these primary coatings were stable and fiber strength did not change after three month aging at 120℃. Yellowing of ribbon coatings made it difficult to discern the fiber ribbons. After two weeks aging at 120℃, blue and green ribbons were the most difficult to distinguish. We calculated the discernibility life span of fiber ribbons based on yellowing values of the ribbon coatings aged at five levels ranging.

1. Background

The recent rapid growth of optical access networks and the high-performance requirements of telecommunication systems has meant that optical fiber cables will be increasingly used for aerials. Since such cables must endure harsh service conditions, such as storage in place where temperature reaches up to 60℃, it is particularly important that the optical fibers are highly heat- and weather- resistant.

UV curable urethane acrylate resin is most widely used as a protective coating for silica-based optical fibers. The resin degrades, losing mechanical properties and yellowing, as a result of by heat aging and/or exposure to UV light. It is likely that decrease of mechanical properties of the resin causes optical-loss and lessens fibers' strength. It is also possible that yellowing makes it difficult to discern between fiber ribbons. To design fibers that will be highly reliable outside of the laboratory, it is important to understand not only the degradation behavior of urethane acrylate resin, but also the degradation mechanism and the relationship between this degradation mechanism and the molecular structure.

We have studied the heat-degradation behavior of the UV-curable urethane acrylate resins used in fiber coatings. In this work, we first investigated the relationship between heat-degradation behavior and molecular structure, focusing on the change in mechanical properties and color. Next, we researched the optical-loss characteristics and mechanical strength of these coated fibers after heat aging. Finally, we examined the color discernibility of fiber ribbons, and estimated how long these colors would be discernible under ordinary service conditions.

2. Experiments

2.1 UV Curable Urethane Acrylate Resin

We employed four types (A, B, C, and D) of UV-curable primary coatings with different oligomer structure and one hard coating (E), as shown in Table 1. UV-curable urethane acrylate resin is composed of di-isocyanates, di-ols, hydroxy-acrylate, an initiator, and some additives. In this experiment, we examined the molecular structure of di-isocyanates and di-ols. Isocyanate groups in oligomers A and B bond to electron-attracting groups (aromatic isocyanate : TDI). In contrast, isocyanates groups in oligomers C and D bond to electron-donating groups (alicyclic groups : IPDI). The di-ol components of the oligomer have different structure as shown in Table 1. The crosslinking density of A ~ D are comparable. Similar antioxidants are used for A ~ D.

Table 1 Detailes of Employed UV Coatings

Coating	S/H	isocianate	poly-ol
A	soft	Aromatic (electron atracting, TDI)	PTMG
B	soft	Aromatic (electron atracting, TDI)	PPG
C	soft	Alicyclic (electron donating, IPDI)	PTMG/PPG
D	soft	Alicyclic (electron donating, IPDI)	PEG
E	hard	Aromatic (electron atracting, TDI)	PTMG/PPG

The coatings were applied to a plate glass and cured by being passed under a UV lamp. The cure dose was 300mJ/cm^2; after curing, the film thickness of the coatings was 0.2mm for the tensile test and 0.07mm for color observation. The cured films were aged in a convection oven for three months. After aging, the mechanical properties of the films (Young's modulus defined by 2.5% modulus and elongation at breakage) were measured by the tensile method. Yellowing rate was measured with a spectroscopic colorimeter . Transparency film was put on white paper, and reflection was measured. Yellowing was calculated from the difference in the yellowing rate before and after aging.

2.2 Fibers and Fiber Ribbons

We prepared SM fibers coated with four types of primary coatings (A~D) and one secondary coating (E). The fibers were aged in a convection oven at 90 and 120℃; ribbon fibers were aged at 5 levels ranging from 60 to 120℃. After aging for a certain period, OTDR was used to measure the optical transmission loss, and fiber strength was measured at a strain rate of 10%/min with 300mm span. Number of the sanple are 20. After three months of aging, changes in the optical transmission loss of the fibers undergoing a heat cycle (-40 ~ 90℃) were monitored. Color change and the color discernibility of the fiber ribbons were judged visually.

3. Results and Discussion

3.1 Heat-resistance behavior of two types of UV-curable resins

Two types of coatings are used for ordinary optical fibers. Soft coatings (primary coatings) have from 0.1 to 1kg/mm^2 Young's modulus, and are used as buffer layer. Hard coatings (secondary coatings and ribbon coatings) have from 10 to 100kg/mm^2 Young's modulus, and are used as protective layers. Figure 1 shows the changes in elongation retention and yellowing of these two types of coatings after they were aged at 120℃. The elongation of soft coatings decreases substantially over time, but that of hard coatings does not change appreciably. Yellowing of soft coatings increases more than that of hard coatings, but not very significantly. Since hard coatings have a high crosslinking density compared with soft coatings, heat aging does not affect polymers' bonds and change their crosslinking. So, mechanical properties of hard coatings do not change drastically. However, it is suspected that yellowing does not depend on crosslinking density, the yellowing of hard coatings is same as that of soft coatings. Thus, the relationship between the heat-resistance behavior and oligomeric molecular structure is best seen in soft coatings with a low crosslinking density. We therefore use primary coatings to examine heat resistance behavior and molecular structure.

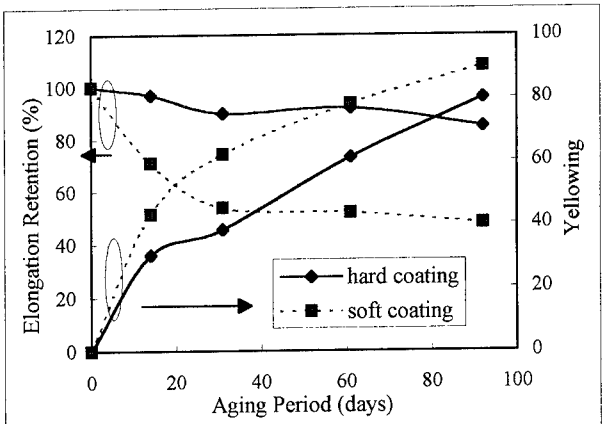


Figure 1. Mechanical Properties and Yellowing of UV Coatings after Aging at 120℃

3.2 Relationship between the molecular structure and the heat-resistance behavior of UV-curable resins

We investigated the mechanical properties and yellowing of four primary coatings with different molecular structure, aged at 90℃. Figure 2 shows the changes in elongation retention aged at 90℃ for three months. The elongation changes for A and C are imperceptible. After aging for three months, the elongation retention for coatings B and D decrease to 50% and 70%, respectively. Young's modulus

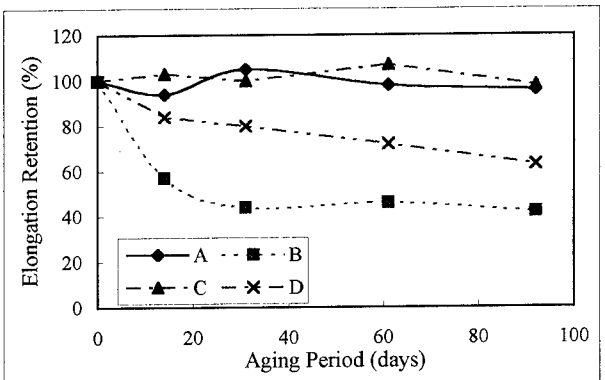


Figure 2. Elongation Retention after Aging 90℃.

changes similarly with elongation. Coating B has the lowest mechanical heat-resistance. Since the isocyanate species of A and C are different, we suspect that the decreased mechanical properties is not related to the isocyanate species. It has been suggested that the branches in poly-ols' main chains break easily and that poly-ols with more branches have lower heat tolerance. We believe that the poly-ol structure of the coatings governs the degradation of their mechanical properties. The degree of yellowing, in contrast, depended on the isocyanate species from which urethane bonding is composed. Figure 3 shows the change in yellowing of four coatings aged at 90℃ for three months. The rate of yellowing for A and B is very large compared with that for C and D. The reason for this drastic color change is as follows: A's and B's urethane bonding, synthesized from aromatic isocyanates and di-ols, can be more easily decomposed by heat than that of C and D. This decomposition forms highly conjugated double bonds that cause yellowing. Thus, coatings with aromatic isocyanate groups yellow easily. Figure 4 shows the relationship between the coatings' elongation retention and yellowing after they were aged at 90℃. Coating A retains its elongation although A's yellowing increases considerably. In contrast, D's yellowing does not increase, but it has a relatively low rate of elongation retention. From the above results, we conclude that there is no clear relationship between yellowing and the retention of mechanical properties when the coatings are aged , as shown in Figure 4. The coatings with high rate of yellowing might still retain their mechanical properties well.

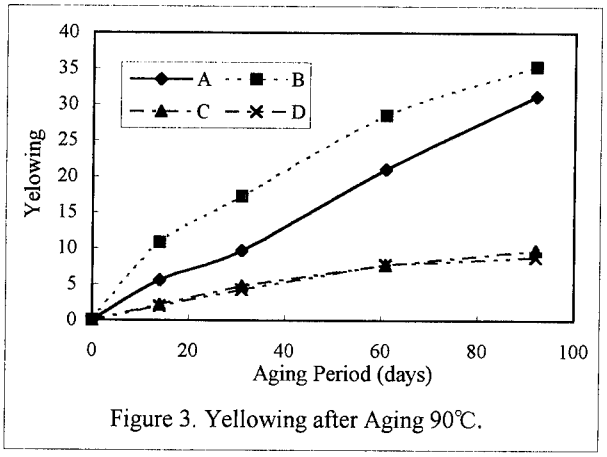


Figure 3. Yellowing after Aging 90℃.

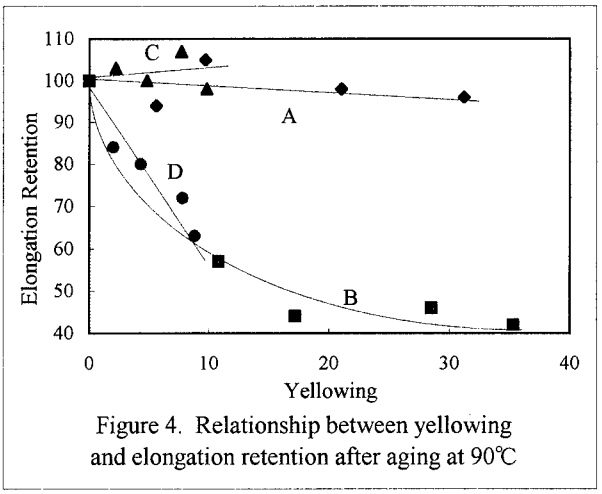


Figure 4. Relationship between yellowing and elongation retention after aging at 90℃

3.3 Characteristics of silica fibers after aging

We measured the tensile strength of silica fibers coated with the primary coating A and the secondary coating E, aged at 90℃ and 120℃. Medium break strength (F50) and constant m values in weibrll plot with time are shown in Figure 5. The F50 and m value did not change. Even if the coatings are degraded by heat aging, the silica fibers maintain their original strength.

The optical transmission loss for SM fibers coated with the primary coatings A ~ D and the secondary coating E are shown in Table 2. There was no change in the loss of the loose coil fibers aged for three months. Figure 6 shows the optical loss of these SM fibers measured during heat cycled test (-40 ~ 90℃), after aged at 90℃ for three months. The coatings degrade, but the loss of SM fibers remains stable, since Young's modulus does not increase and/or primary coatings do not disappear after aging.

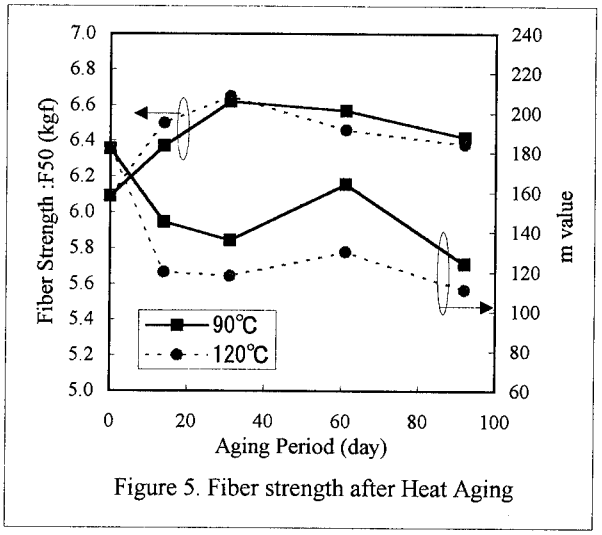


Figure 5. Fiber strength after Heat Aging

Table 2 Optical Loss at 1.55 μ m of SM Fibers Coated with four primary coatings

		Optical Loss (dB/km)			
Temp.		2weeks	1month	2months	3months
90℃	A	0.20	0.21	0.20	0.19
	B	0.20	0.20	0.21	0.20
	C	0.19	0.20	0.20	0.19
	D	0.20	0.20	0.19	0.20
120℃	A	0.20	0.19	0.21	0.20
	B	0.20	0.19	0.20	0.19
	C	0.20	0.20	0.19	0.20
	D	0.19	0.20	0.20	0.21

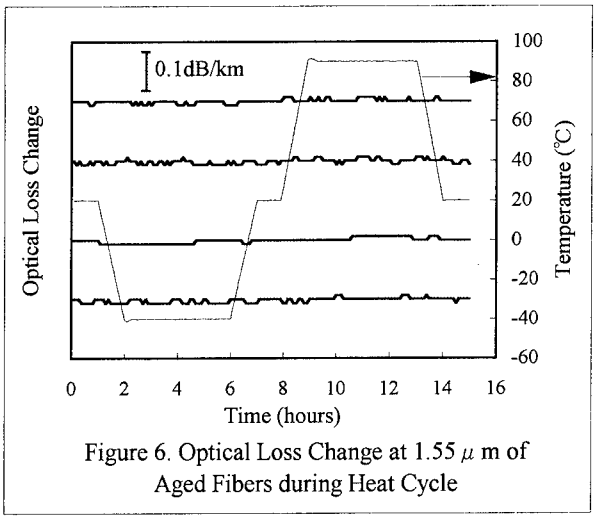


Figure 6. Optical Loss Change at 1.55 μ m of Aged Fibers during Heat Cycle

3.4 Reliability of discernibility between fiber ribbons

After one month of aging at 120℃, there is no change in fibers' mechanical strength and optical loss. However, the coatings' color change may make it difficult to discern of colored fiber ribbons. We examined whether it would be possible to discern the colors of colored fiber ribbons that were subject to deterioration over time. Colored four-fiber ribbons ({blue, yellow, green, red, purple}, white, white, pink) were aged at 120℃. Ribbons' thickness are 0.4mm and diameter of colored fibers are 0.26mm. First, we examined the color combinations and aging time at which the color of the ribbons became difficult to discern. We found that blue and green ribbons became hard to discern after two weeks aging. At this time, we could only discern the blue and green color coded fibers by peeling away the ribbon coatings. The difficulty in discernibility seemed mainly to be caused by the yellowing of ribbon coatings. We confirmed this by measuring the color change of the laminated sheets. The laminated sheets are composed of ribbon coatings, color coatings, secondary coatings and primary coatings on a glass plate layered to nearly the same thickness as the fiber ribbons' actual coating thickness. After aging at 120℃, we measured the yellowing of the laminated sheets with and without ribbon coatings. The yellowing change for blue is shown in Figure 7. The yellowing of the laminated sheet with ribbon coatings is greater than that of the laminated sheet without ribbon coatings. This indicates that the main factor for difficulty with blue and green fibers is overlapping yellowing ribbon coatings and blue coded fiber. When yellowing ribbon coatings overlaps blue coded fiber, blue appears green due to adsorption of spectra around 400 ~ 500nm. Ribbon coatings' yellowing most visually influences of blue coded

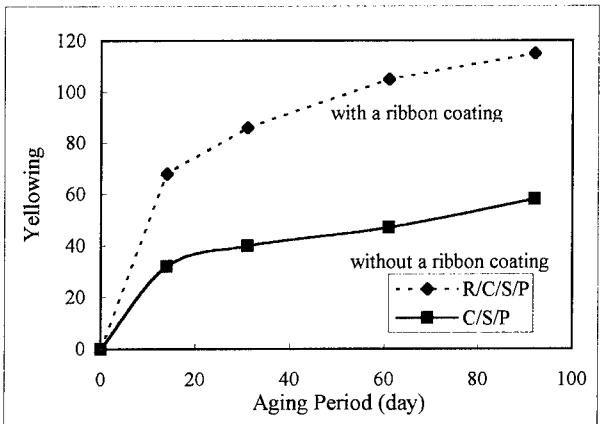


Figure 7. Yelowing of Laminated Sheets with and without a Ribbon Coating

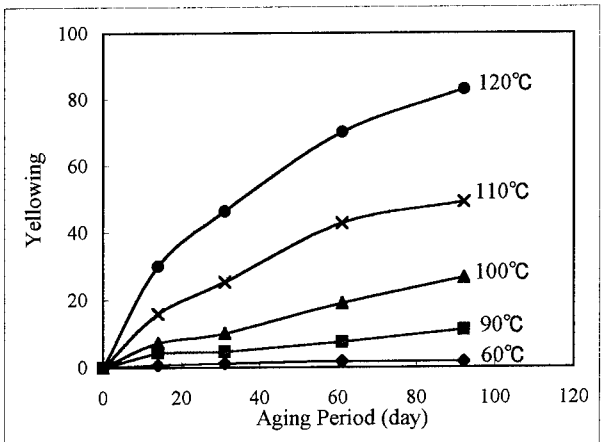


Figure 8.. Yellowing of Ribbon Coatings.

fiber, since blue is complementary to that of yellow. In contrast, the yellowing of primary coatings whose yellowing is larger than that of ribbon coatings does not affect discernibility, because of masking effect of color coatings.

From the above results, we consider that it is possible to judge the discernibility of fiber ribbons by measuring the yellowing of ribbon coatings. Figure 8 shows the yellowing of ribbon coatings after aging at 60 ~ 120℃. The rate of yellowing increases over time and is large at high temperatures. To estimate the life span of discernibility, it is necessary to define the maximum amount of yellowing that we can have and still discern blue and green. From the result of aging test using actual fiber ribbons of the previously mentioned, we took the yellowing value 30 of the ribbon coating after two weeks of aging at 120℃ as a threshold for differentiation between fiber ribbons. Thus the time it takes for yellowing to reach 30 is the discernibility life span. We calculated the life span for fiber ribbons at each temperature based on Figure 8. To determine the life span for fiber ribbons at 90 and 100℃, we assumed that the yellowing increases initially. By drawing an Arrhenius plot of testing temperature and life span, we calculated the life span under ordinary conditions. The Arrhenius plot in Figure 9 shows that the measured points are in a straight line; yellowing is caused by a certain thermal activation reaction. Activation energy is 28kcal/mol. We determined that the life span of color discernibility and differentiation between fiber ribbons is more than 20 years at 60℃ and more than 280 years at 40℃.

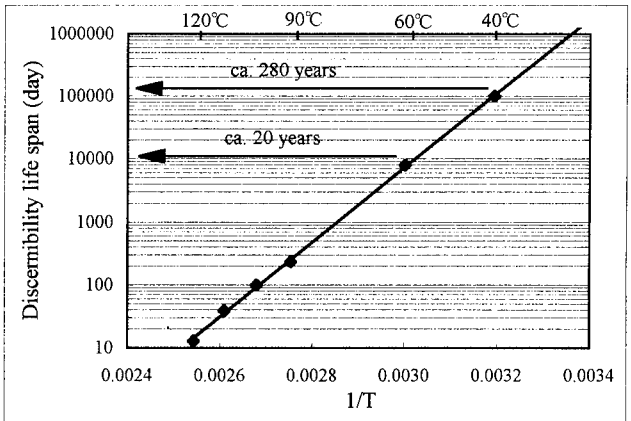
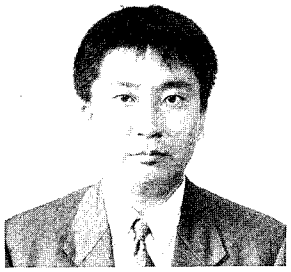


Figure 9. Arrhenius plot of Discernibility Life Span of Ribbon Fibers

4. Conclusions

The thermal degradation of the mechanical properties of UV-cured primary coatings is primarily governed by the poly-ol structures in the oligomer, while changes in their color are affected by the isocyanate species from which urethane bonding is composed. There is no certain relationship between these two characteristics of heat resistance.

Yellowing of the ribbon coatings is the main cause of probrems with differentiation between the fiber ribbons after heat aging. After aging, blue and green ribbons are the most difficult to distinguish. We suspect that the colors of these fiber ribbons will be discernible after more than 20 years at 60℃.

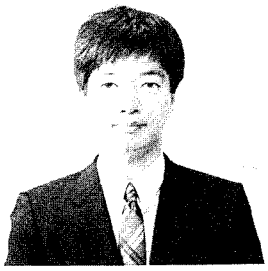


Akira Murata

Opto-Electronics
Laboratory
Fujikura LTD.

1440, Mutuzaki, Sakura-shi, Chiba, 285, Japan

Akira Murata was born in 1963. He joined Fujikura LTD. in 1992 after receiving his ph. D. degree in environmental since from Chiba University. He has been engaged in research and development of optical fibers He is now an engineer in the Telecommunication Cable Material section and a member of the IEICE of Japan.

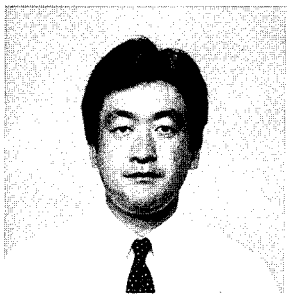


Kazunaga Kobayashi

Opto-Electronics
Laboratory
Fujikura LTD.

1440, Mutuzaki, Sakura-shi, Chiba, 285, Japan

Kazunaga Kobayashi was born in 1961. He joined Fujikura LTD. in 1985 after graduating from Gunma University with a M.E. degree of chemistry. He has been engaged in research and development of optical fibers and optical fiber coatings.. He is now an engineer in the Telecommunication Cable Material section and a member of the IEICE of Japan.

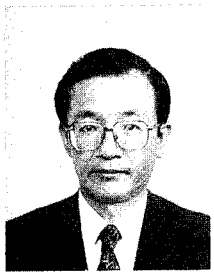


Keiji Oohashi

Opto-Electronics
Laboratory
Fujikura LTD.

1440, Mutuzaki, Sakura-shi, Chiba, 285, Japan

Keiji Oohashi was born in 1956. He graduated from the Tokyo Institute of Technology in 1980 with a B.E. degree of chemistry. After eight years of work as an engineer in materials for motor vehicles, he joined Fujikura LTD. in 1988. He has been engaged in research and development of optical fibers and optical fiber coatings. He is now assistant chief of the Telecommunication Cable Material section and a member of the IEICE of Japan.

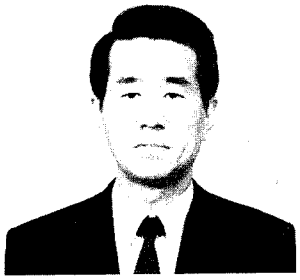


Shinji Araki

Opto-Electronics Laboratory
Fujikura LTD.

1440, Mutuzaki, Sakura-shi, Chiba, 285, Japan

Shinji Araki was born in 1950. He joined Fujikura LTD. in 1974 after graduating from Tokyo Metropolitan University with a B.E. degree of chemistry. He has been engaged in research and development of optical fibers and optical fiber coatings. He is now a chief in the Telecommunication Cable Material section and a member of the IEICE of Japan.



Toshikuni Maruoka

Opto-Electronics Laboratory
Fujikura LTD.

1440, Mutuzaki, Sakura-shi, Chiba, 285, Japan

Toshikuni Maruoka was born in 1943. He joined Fujikura LTD. in 1967 after graduating from Tokyo University with a B.E. degree. He has been engaged in design, research, and development of transmission cables. He is now the manager of Opto-electronics Laboratory and a member of the IEICE of Japan.

The characteristics of polyimide coated fiber with UV-acrylate overcoating

Yasuhiro Naganuma, Akihiko Mizutani, Shigeki Endo, Yuji Kubo and Yasunori Saito

Sumitomo Electric Industries , LTD

1 Taya-cho , Sakae-ku, Yokohama, Japan

Abstract

Polyimide coated fiber is used in harsh environment because of the excellent heat resistance and low expansion coefficient of the polyimide resin. The polyimide coated fiber with silicone and nylon overcoating had been reported [1]. Recently 250 or 400 μ m UV coated fiber has been widely used as an industry standard, consequently new structure with overcoating UV resin on polyimide is required. Therefore we had developed the manufacturing technology of UV overcoating on polyimide coating. The optical and mechanical characteristics of UV overcoated polyimide fiber are comparable to the conventional polyimide coated fiber.

Introduction

The polyimide coated fiber is used in harsh environments or in special area such as the temperature sensor [2] because of the excellent heat resistance performance and low expansion coefficient of the polyimide resin. For instance, polyimide coated fibers are applied to the feed through portion of the repeater in submarine cables, where the fiber and the housing are sealed with the metal alloy [3][4]. In this application, the heat resistance performance is required on every a few centimeters along several meters of fiber. Since the polyimide coating is so thin, careful handling is required to protect the resin from the mechanical damages. Therefore the silicone and nylon overcoating was developed. Recently 250 or 400 μ m UV coated fiber has been widely used. Moreover for the higher fiber count system, the thinner diameter coating system is also required. Therefore we developed the manufacturing technology of the UV-acrylate overcoating on polyimide coating. This paper describes the characteristics of newly developed polyimide coated fiber with UV overcoating, the optical and mechanical properties of developed fiber are comparable to usual UV fibers and the conventional polyimide coated fiber with silicone and nylon.

Coating structure

The coating structure of developed polyimide coated fiber with UV overcoating is shown in Fig.1, together with the conventional silicone and nylon overcoated fiber. The polyimide resin was coated on the glass fiber with the diameter of 140 μ m. The UV overcoating with soft and hard resin is applied on the polyimide layer. The diameters of the overcoating are 250 μ m and 400 μ m respectively. These diameters are quarter and two third size of conventional polyimide coated fiber , and the same as usual commercial UV coated fiber. In this paper, we used the 1.3 μ m single mode fiber, but this coating system is also applicable on the dispersion shifted fiber or the polarization-maintaining optical fiber.

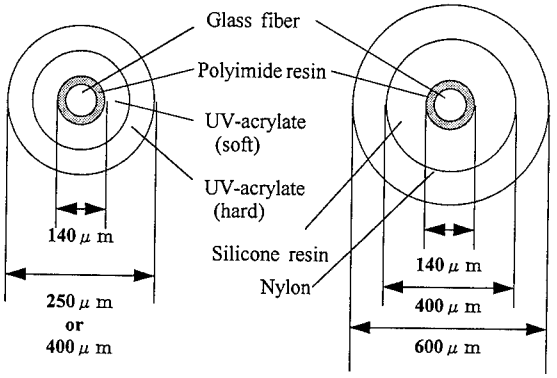


Fig.1 . Structure of polyimide coated fiber with UV and silicone / nylon overcoatings.

Optical characteristics

The attenuation of the manufactured UV overcoated polyimide fiber is 0.36dB/km and 0.23 dB/km at 1.30 and 1.55 μ m respectively. The temperature dependence of the attenuation of the two types UV overcoated polyimide fiber is shown in Fig.2 . The attenuation changes are less than 0.05dB/km at 1.55 μ m in the temperature range from 0℃ to 45℃.

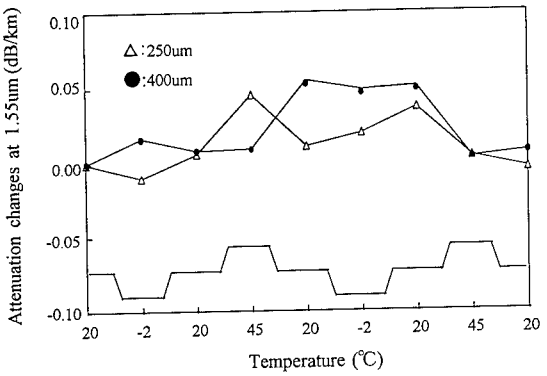


Fig. 2. Temperature dependence of the attenuation of UV overcoated polyimide fiber

Moreover heat cycling test was also conducted. The attenuation variation during 100 times heat cycling from -10℃ to +60℃ is less than 0.03 dB / km at 1.55 μ m as shown in Fig.3.

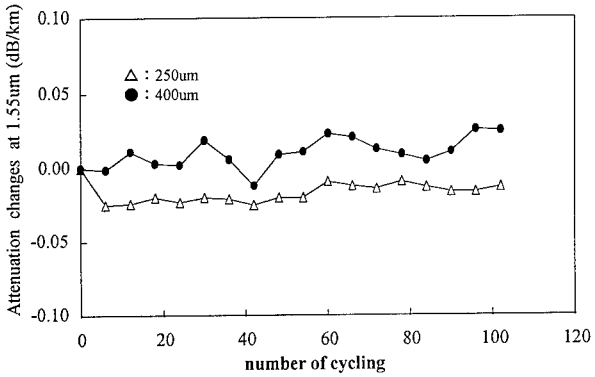


Fig.3. The attenuation changes of polyimide coated fiber with two types of UV overcoating in heat cycling test.

To evaluate the bending and pressure performance , we conducted mandrel winding test and the plate pressure test . In the plate pressure test , 20 kg weight was applied on the 10 cm length of the fiber. The induced attenuation at 1.55 μ m is 0.05 dB /m for 50 mm bending and 0.1 dB under 2kg/cm pressure.

These characteristics are comparable to the usual UV fiber and the conventional polyimide coated fiber with silicone and nylon overcoating.

Mechanical characteristics

Fiber Strength

Tensile strength testing was conducted with 20m gauge length and 1 m / min tensile speed in air at room temperature. Fig.4 shows the tensile strength of manufactured 250 and 400 μ m UV overcoated polyimide fiber. The Weibull distribution of tensile strength is linear and steep. The average strength of each fiber is 5.4Gpa.

250 μ m UV overcoated polyimide fiber was used to evaluate the strength behavior during agings. We chose 60 ℃ 95% Rh and 85 ℃ dry condition as aging environments. Samples were aged for a predetermined period up to 120 days. Fig.5 shows the strength of aged UV overcoated polyimide fiber. The fiber strength of aged UV overcoated fiber is stable under the high humidity condition.

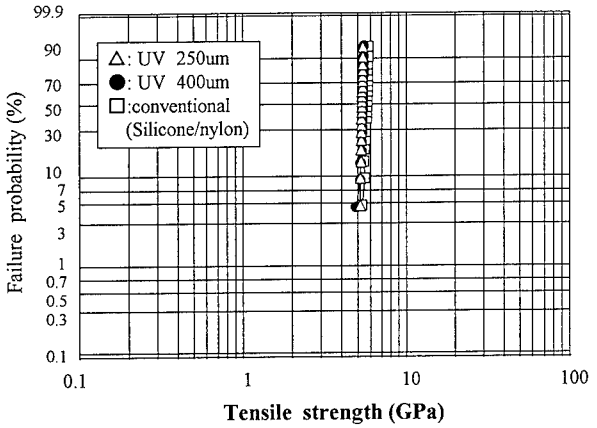


Fig.4. Tensile strength of UV overcoated and conventional polyimide fiber

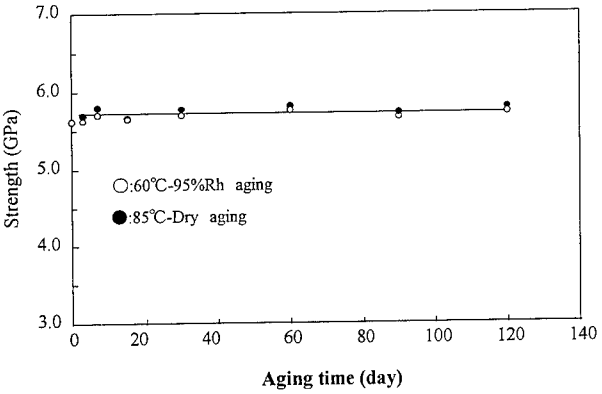


Fig.5. Fiber strength of aged 250 um UV overcoated polyimide fiber

The stress corrosion factor was examined by means of static and dynamic fatigue tests. In the static test, a constant tensile stress was applied to the fiber by winding on mandrels and the test environment was at room temperature in air. The static fatigue plots of the two types of the UV overcoated polyimide fiber are shown in Fig.6 .

Dynamic fatigue test were conducted at 300mm gauge length and 10mm / min to 300 mm / min loading rate under 25℃and 50%Rh in air. The dynamic fatigue plots of the two types UV overcoated polyimide fiber are shown in Fig.7.

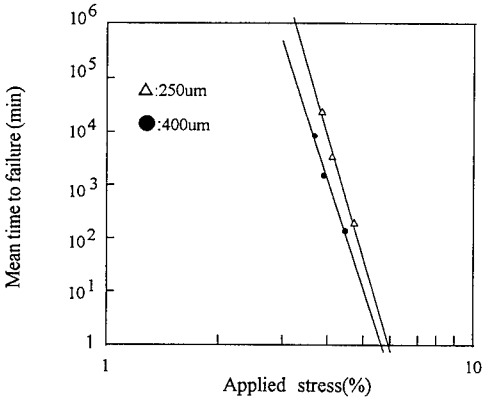


Fig.6. Static fatigue plots of UV overcoated polyimide fiber

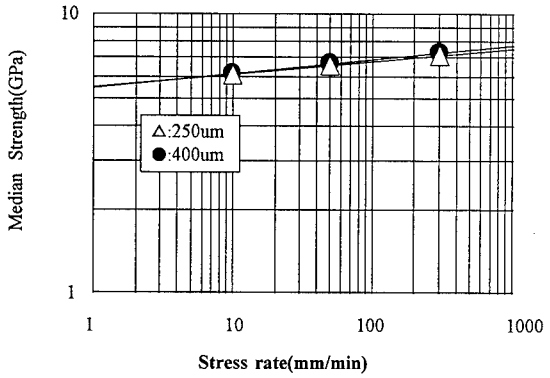


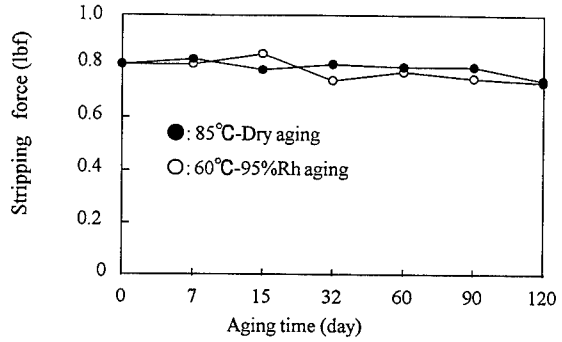
Fig.7. Dynamic fatigue plots of UV overcoated polyimide fiber

It is estimated that the stress corrosion factor of the manufactured UV overcoated polyimide fiber is about 20 to 23.

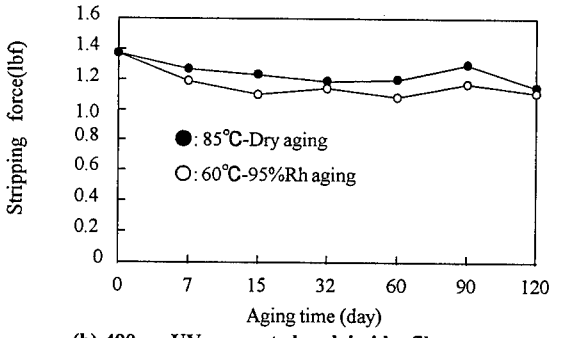
These characteristics are comparable to the usual UV fiber and the conventional polyimide coated fiber.

Stripping force

We investigated the stripping force behavior during aging. We chose 60℃ 95%Rh and 85℃ dry condition as aging conditions. Samples were aged for a predetermined period up to 120 days. The stripping force of aged UV overcoated polyimide fiber is shown in Fig.8. The variations of stripping force under these aging conditions were less than about 20%.



(a) 250um UV overcoated polyimide fiber



(b) 400um UVovercoated polyimide fiber

Fig. 8. Stripping force of aged UV overcoated polyimide fiber

Conclusion

We developed the manufacturing technology of the UV overcoated polyimide fiber. The optical and mechanical properties of UV overcoated polyimide fiber are summarized in Table 1. We found there was no performance degradation for usual UV fibers and conventional polyimide coated fibers.

Table 1. Optical and Mechanical properties of polyimide coated fiber with UV overcoating.

Properties	Type of fiber		
	Polyimide coated fiber		usual UV fiber
	UV overcoated	conventional	
Attenuation (dB/km) 1.30 μ m	0.36	0.36	0.35
1.55 μ m	0.23	0.23	0.20
Temperature dependence of attenuation at 1.55 μ m (dB/km)	<0.05	<0.04	<0.02
Attenuation changes in heat cycling test at 1.55 μ m (dB/km)	<0.03	<0.05	<0.03
Bending (dB/m at φ 50mm diameter)	<0.05	<0.05	<0.05
Plate pressure (dB at 2kg/cm)	<0.1	<0.1	<0.1
Strength(GPa)	5.4	5.5	5.3
Stress corrosion factor	20～23	20～23	20～23

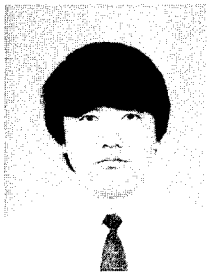
References

1)T. Ono et al., IEICE Transactions on Communications .,pp.115, Oct. 1984.

2) T.Fujii et al., IECE Transactions on Communications., pp.125, Oct. 1991.

3)Y. Iwamoto and H. Fukinuki, , J. of Lightwave Technology ., vol. LT.-3, No.5, pp.1005-1016,Oct. 1985.

4) Y. Noguchi, I. Marugome, N. Norimatsu, Y. Yamazaki, H. Yamamoto., IWCS Proceedings., pp.620-627,1991.

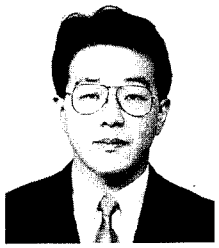


Yasuhiro Naganuma

Sumitomo Electric
Industries, LTD.

1, Taya-cho, Sakae-ku,
Yokohama, 244, Japan

Yasuhiro Naganuma received a M.S. degree from Tokai University in 1990. He joined Sumitomo Electric Industries, LTD. in 1990 and has been engaged Analytical Characterization Center in R&D Group. He is an engineer of the fiber optics production engineering section.

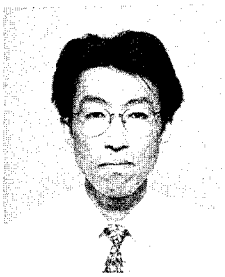


Yuji Kubo

Sumitomo Electric
Industries, LTD.

1, Taya-cho, Sakae-ku,
Yokohama, 244, Japan

Yuji Kubo was received the M.S. degree from Hokkaido University in 1987. He joined Sumitomo Electric Industries, LTD. in 1987. and has been engaged in research and development of optical fibers in Fiber Optics Division. He is a member of Institute of Electronics, Information and Communication Engineers of Japan



Akihiko Mizutani

Sumitomo Electric
Industries, LTD.

1, Taya-cho, Sakae-ku,
Yokohama, 244, Japan

Akihiko Mizutani received a M.S. degree from Nagoya University in 1985 and joined Sumitomo Electric Industries, LTD. He has been engaged in development of manufacturing optical fiber. He is a senior engineer of the fiber optics production engineering section .

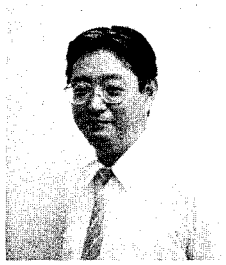


Yasunori Saito

Sumitomo Electric
Industries, LTD.

1, Taya-cho, Sakae-ku,
Yokohama, 244, Japan

Yasunori Saito received his B.S. degree in Electrical Communication Engineering from Tohoku University in 1969. He then joined Sumitomo Electric Industries, LTD. and has been engaged in research and development of optical fiber cable. Mr. Saito is a manager of Fiber Engineering Department , Fiber Optics Division. He is a member of Institute of Electronics and Communication Engineers of Japan.



Shigeki Endo

Sumitomo Electric
Industries, LTD.

1, Taya-cho, Sakae-ku,
Yokohama, 244, Japan

Shigeki Endo received the B.S. degree for Electrical Engineering from Waseda University in 1976. He joined Sumitomo Electric Industries, LTD. and worked on the production engineering of 9.5 and 4.4 coaxial cable. Thereafter he has been engaged in the development of manufacturing optical fiber. He is a plant manager of fiber optics division.

OPTICAL FIBER DESIGN FOR IMPROVED MECHANICAL PROPERTIES

James C. Novack, Fredrick Bacon, Bryon J. Cronk, James W. Laumer, Julie M. Moser and Bruce A. Rabine

3M Company, 3M Center, Maplewood, MN 55144

Abstract

Fiber to the home (FTTH) and fiber to the desk (FTTD) provide excellent opportunities for increasing the deployment of optical fiber. Associated with these types of deployment is an increased density of termination sites. With the need for overall long term reliability in fiber optic systems many question have been raised about the reliability of the termination sites in the fiber system.

This article reports the results of a new fiber design which prevents damage to the glass fiber surface during the preparation of a fiber end for termination. This design leads to an overall increase in the mechanical reliability of the fiber at the termination site based on fiber strength analyses conducted in our laboratory.

Introduction

The processes of stripping and cleaning optical fiber in preparation for fiber termination imparts damage, via physical contact, to the surface of the glass fiber. The type of damage inflicted on the fiber surface has been documented as have the effects of that damage on the reliability of the fiber system [1,2,3]. Though the sources of damage have been identified, little has been done to provide a means by which to protect the fiber from the processes which cause the damage. This, combined with a lack of complete understanding of the degradation of strength of bare silica fiber results in a continued concern about the reliability of termination sites and system lifetime calculations.

A new fiber design has been identified which protects the glass surface of the optical fiber with a polymeric coating that is designed to remain intact through the stripping, cleaning, and termination processes. This design relies on a combination of the material properties of the coating and process controls to provide a fiber which is protected from the mechanical detriment of the fiber end preparation processes while maintaining the required properties of the particular fiber type. The term GGP has been designated as a generic descriptor of this fiber design with specific reference to the glass/glass/polymer construction and will be used in that context in this paper.

Fiber Design

The original design was directed towards a fiber for use in a data communication application and therefore was structured around a 62.5 μm graded index core. The construction depicted in Figure 1 shows the 62.5μm core (1) surrounded by a reduced diameter (100μm) glass clad (2). This is done such that a permanent polymeric coating (3) can be applied to an industry standard diameter of 125μm thereby being compatible with existing connector ferrule hole dimensions. This coating acts as a physical barrier which protects the glass fiber surface from contact damage during the stripping and cleaning processes of fiber end preparation in very much the same way that coatings in general protect the glass fiber. Additionally, by proper selection of material properties, the coating allows installed fiber optic connectors to perform as they would on an all-glass fiber construction.

The subsequent coatings are selected to provide the usual benefit of the inner and outer primary buffer coatings typical of a conventional fiber design (i.e. the secondary coating (4) is selected to be a lower modulus coating which acts to minimize effects of microbending and the tertiary coating (5) is a higher modulus material that provides abrasion resistance). Additionally, this fiber can be subsequently jacketed and cabled with the numerous materials that are currently used in the industry.

Process

Regardless of the material being coated, the process used to coat a 100μm fiber to 125μm diameter must be very exacting in that the ferrules used in commercially available connectors do not allow for much variation in diameter. Coating diameters in excess of the standard 125μm dimension create problems with insertion of the fiber into the ferrule. Coating at diameters much less than the 125μm will create a problem of core misalignment and associated signal loss. This would be most noticeable in smaller core fibers.

The coating process used in the production of this fiber allows for very close tolerances in the dimension of the

polymeric clad. Figure 2 shows a histogram of the primary coating diameter from a typical draw of the described fiber design. It can be seen that the coating diameter can easily be controlled to tolerances necessary to achieve compatibility with connector ferrule hole dimensions.

Material

The material for the polymeric clad is selected for a number of properties related to general process considerations in the manufacture of the fiber and properties specific to termination performance as the connector is fastened to the fiber via this polymeric layer. A partial list of desired characteristics of the material may include:

- provides a smooth continuous coating
- curable with ultraviolet radiation
- be mode stripping
- have surface properties that allow subsequent coating materials to be readily removed while providing good adhesion with standard connector adhesives
- have mechanical properties which provide stable connector performance over desired temperature ranges.
- can be cleaved

While much effort is put into the proper materials selection to optimize the necessary properties, the aspect of the coating being addressed in this work is the ability of the material/design combination to protect the glass surface from mechanical detriment during fiber end preparation.

Testing

The method used to investigate the contention that the polymeric coating protected the fiber during the stripping and cleaving processes was a dynamic strength analysis. The testing was performed on GGP fiber and a commercially available 62.5/125μm multi-mode fiber in 2-point bend and axial load configurations.

Test specimens were prepared for the 2-point bend analysis by stripping 1 cm of the buffer coatings from the central portion of a 10 cm length of fiber using a 203μm fiber optic stripper. The section of stripped fiber was then cleaned with two wipes of a lint-free material which was wet with 2-propanol (HPLC grade, 99.8% minimum). The samples were allowed to sit for ~1 minute in the ambient laboratory environment (74°F, 58% R.H.) to allow any residual alcohol to evaporate. During this time no additional physical contact was made with the stripped portion of the specimen.

The strength of the samples were then measured using a 2-point bend apparatus. The faceplate separation at loading was 15 mm to insure that the sample could be loaded without contacting the stripped portion of the specimen thereby avoiding abrasions during loading. The samples were then subjected to a constant strain rate of 9%/minute to failure which was detected acoustically. The unstripped specimens provide a baseline of fiber performance for each of the fiber types.

Test specimens were prepared for the axial loading samples by mounting the fiber on the test bed at a gauge length of 1 meter and then stripping a 2 cm section at the midpoint using a 203μm fiber optic stripper. The stripped section was cleaned with two wipes of a lint-free material which was wet with 2-propanol (HPLC grade, 99.8% minimum). To allow any residual solvent to evaporate the specimens were allowed to sit for ~1 minute in the ambient laboratory environment (74°F, 58% R.H.) making sure that no additional physical contact was made with the stripped portion of the specimen. The fibers were then strained to failure at a strain rate of 9%/minute with the stress at failure being reported. The unstripped specimens provide a baseline of fiber performance for each of the fiber types.

Results & Discussion

The results, which follow a Weibull distribution, are shown in Figures 3-6. Figures 3 and 4 show the results for the 2-point bend testing. In the Weibull plot shown in Figure 3 it is easily seen that the GGP fiber suffers no degradation in strength as a result of the stripping and cleaning processes. The Weibull plot shown in Figure 4 clearly shows a significant reduction in strength of the commercial 62.5/125μm multi-mode fiber when subjected to the stripping and cleaning processes.

Dynamic fatigue in axial load was conducted to verify that the decrease in strength of the commercial fiber was due to the stripping and cleaning processes rather than the physical contact that the bare fiber makes with the faceplates of the 2-point bend apparatus. Figures 5 and 6 show the results of the dynamic fatigue testing in axial loading. In this testing mode the stripped portion of the fiber is freely suspended therefore the only contact with the bare fiber is that which occurs during the stripping and cleaning processes. Since the axial loading test show a result similar to that seen in 2-point bend, it is reasonable to assume that the reduction in strength seen in 2-point bend is not a result of faceplate contact.

Note that the dynamic fatigue testing in axial tension does reveal a broader strength distribution in the GGP fiber than in the commercially available fiber and that there is a small change (≤400 MPa) in strength subsequent to the stripping and cleaning processes. This change is not evident in the results from 2-point bend testing.

Conclusions

Our tests confirm reports that commercial optical fiber is significantly weakened by conventional stripping and cleaning methods. When the GGP fiber design is subjected to the same testing only a minimal degradation in the strength of the fiber is observed indicating that the permanent polymeric layer indeed protects the glass surface from the mechanical detriment of the stripping and cleaning processes. As the amount of damage imparted to the glass surface during stripping has an effect on the reliability of the termination it can be seen that the GGP fiber design offers the potential for terminations of increased reliability. Furthermore, as the fiber is not stripped to expose a bare fiber surface, the uncertainties associated with the strength degradation of bare fiber are not an issue.

Acknowledgments

The authors would like to acknowledge the contributions of Justin Black for his contributions in the collection of dynamic 2-point bend data.

References

1. Extrinsic Fiber Damage And Its Effect On The Reliability Of Optical Fiber Connectors And Splices, W.R. Wagner, SPIE Vol. 1580 Fiber Optic Components and Reliability (1991).

2. Failure Analysis Of Fiber Optic Connectors, W.R. Wagner, Advances in Ceramics, Vol. 22 (1988).

3. Friend or Foe?, T.Wei and F.S. Leong, Telephony, June 12, 1989.

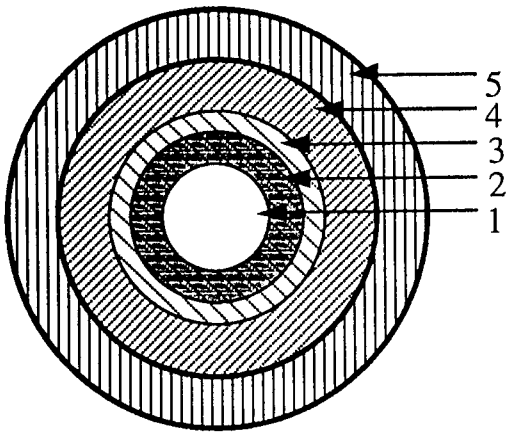


Figure 1 Cross section of fiber construction.

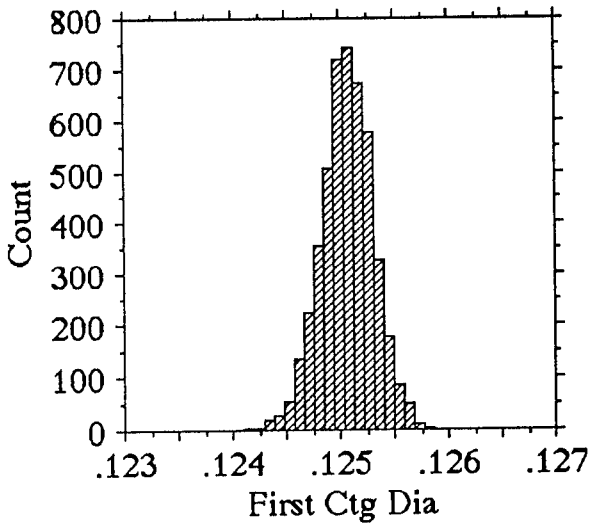


Figure 2 Process histogram of primary coating diameter.

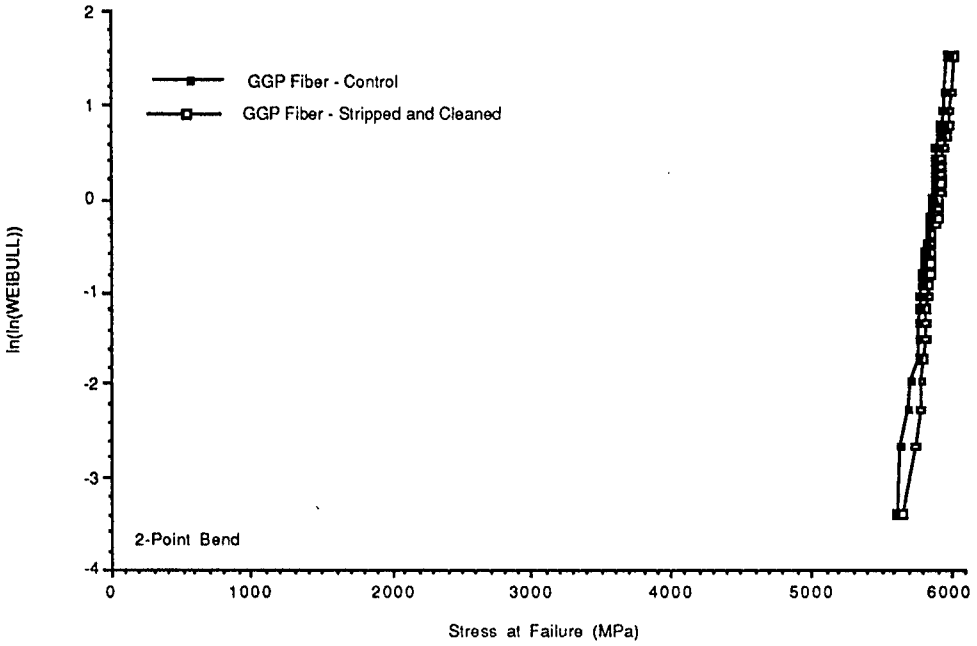


Figure 3 Weibull plots of the GGP fiber in 2-point bend.

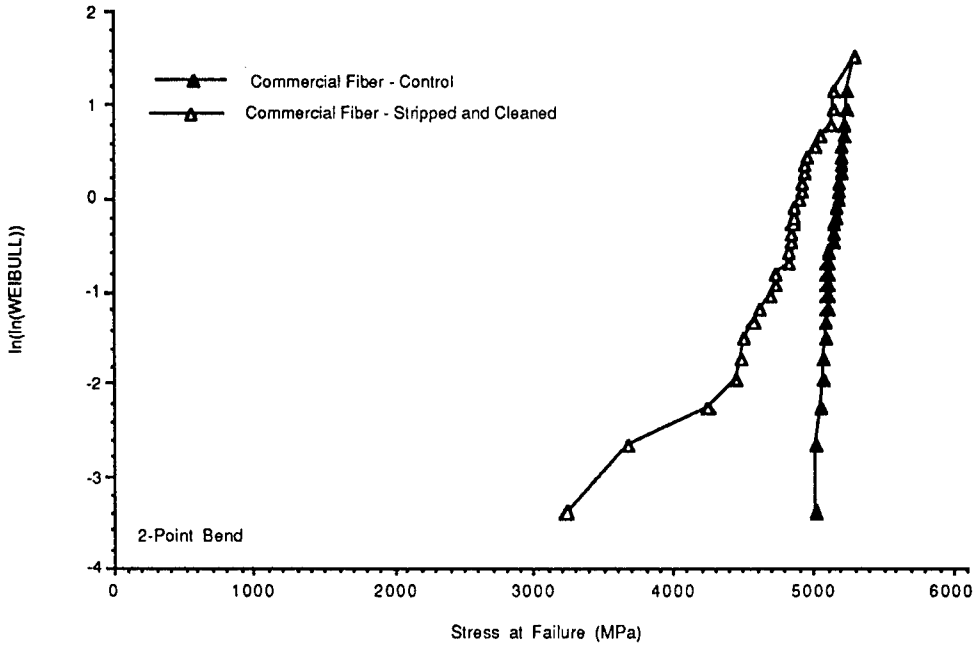


Figure 4 Weibull plots of the commercial fiber in 2-point bend.

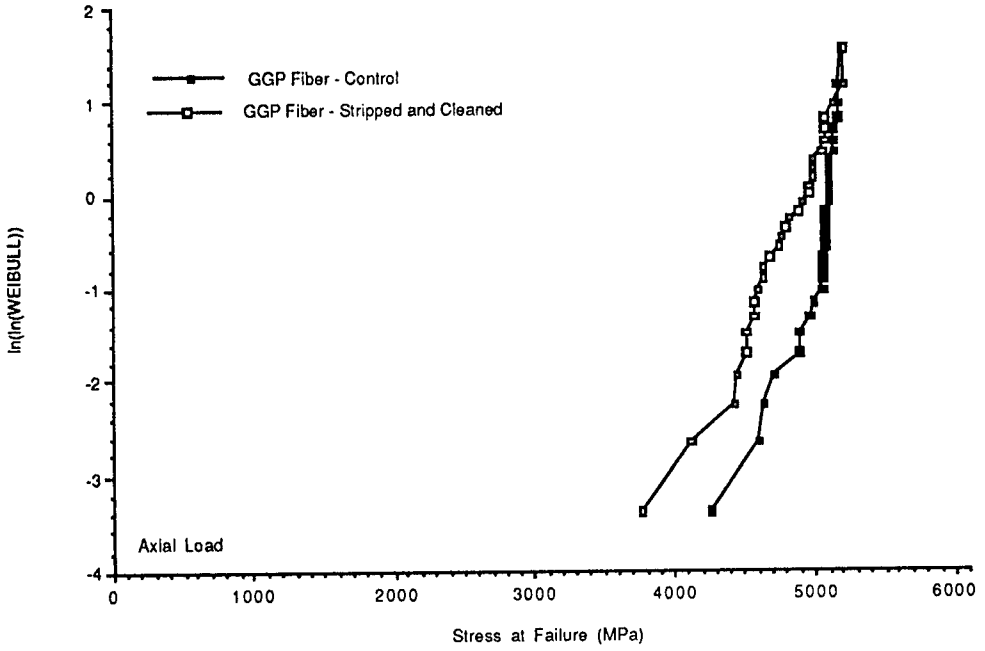


Figure 5 Weibull plots of GGP fiber in axial load.

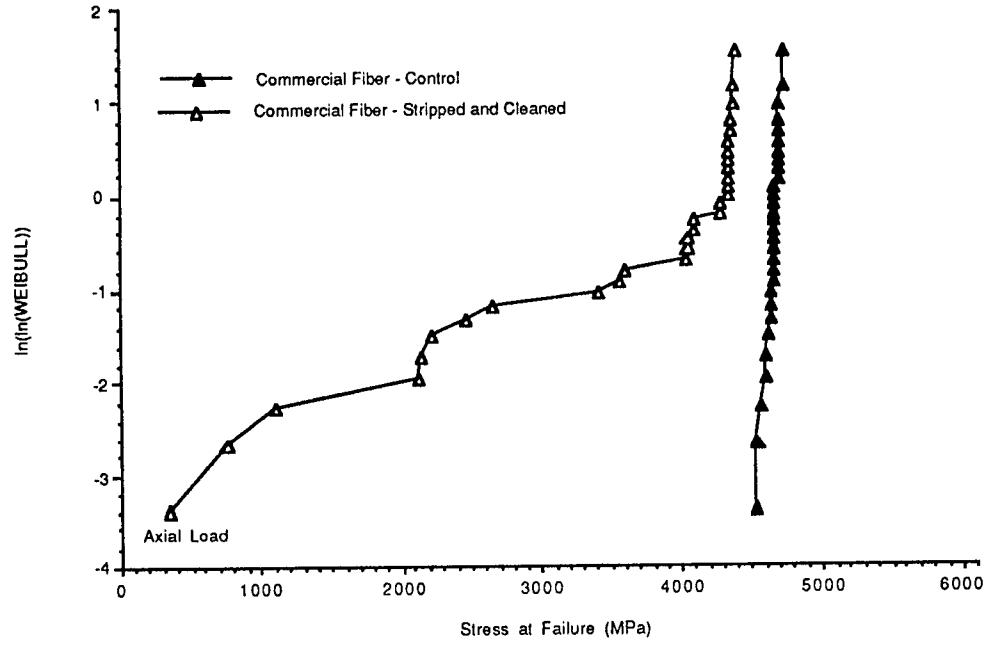
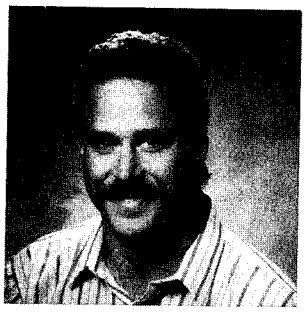


Figure 6 Weibull plots of commercial fiber in axial load.



James C. Novack
3M Company
Maplewood MN 55144
USA

Jim Novack received a Bachelors of Science Degree in Chemistry from the University of Minnesota and is near completion of a Masters of Materials Science at the University of Virginia. Jim joined 3M Company in 1977 and is currently a Senior Research Chemist in the 3M Fiber Optics Laboratory. His research and development interests include fiber reliability, coating materials development for specialty fibers, fiber optic connector adhesives, and index matching materials.



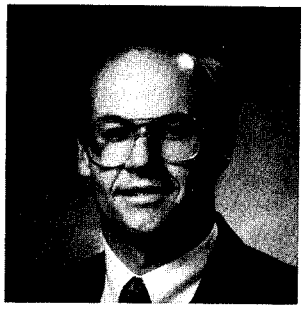
Fredrick Bacon
3M Company
Maplewood MN 55144
USA

Fred Bacon received a Bachelors of Science Degree in Chemistry from Morehouse College and a Ph.D. in Physical Chemistry from the University of California at Berkeley. Fred joined 3M Company in 1982 and is currently a Research Specialist in the 3M Fiber Optics Laboratory. His research is devoted to fatigue strength analysis and specialty coating development for optical fibers.



Bryon J. Cronk
3M Company
Maplewood MN 55144
USA

Bryon Cronk is a Research Specialist in the 3M Fiber Optics Laboratory with over twenty years experience in fiber optics and related technologies. Bryon has made significant contributions in the areas of novel fiber processes and components and is named as an inventor on five patents on the topic of fiber optics.



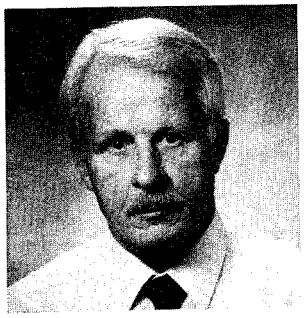
James W. Laumer
3M Company
Maplewood MN 55144
USA

Jim Laumer received a Bachelor of Science Degree in Chemical Engineering from Michigan Technological University. Jim joined 3M Company in 1977 and is currently a Research Specialist in the 3M Fiber Optics Laboratory. His research and development interests include fiber draw and coating process development, and plastic optical fiber product and process development.



Julie M. Moser
3M Company
Maplewood MN 55144
USA

Julie Moser works part time as a Technical Aide in the 3M Fiber Optics Laboratory while pursuing a degree in Chemical Engineering at the University of Minnesota. Julie's activities include fiber drawing, optical measurements, and mechanical and strength analyses.



Bruce A. Rabine
3M Company
Maplewood MN 55144
USA

Bruce Rabine joined 3M in 1966 and has been a key member of numerous new product development teams. Bruce is currently a Senior Technologist in the 3M Fiber Optics Laboratory. Bruce maintains a state of the art R&D draw facility and his current interests/activities include fiber draw operations, draw and coating process R&D, equipment calibration and equipment evaluation.

DEVELOPMENT OF DISPERSION CONTROLLED OPTICAL FIBER SUBMARINE CABLES AND C-OTDR FOR LONG SPAN TRANSMISSION SYSTEMS USING IN-LINE OPTICAL AMPLIFIERS

Tetsuhiro Numata*, Shuichi Nishio**, Shinji Goto*, Kuniaki Tanaka***,
Yuki Sakuyama*, Naoyuki Atobe****, and Shinichi Furukawa***

* NTT Network Systems Development Department
** NTT Central Training Institute
*** NTT Access Network Systems Laboratories
**** NTT Maintenance Service Planning Department

Abstract

Optical fiber submarine transmission systems using an erbium-doped fiber amplifiers as submarine repeaters demand optical properties different cable specifications namely,properties are chromatic dispersion and polarization mode dispersion. The higher the bit rate, and the longer the transmission distance, the more severe is the demand for these modes. We clarify the requirement for an optical fiber cable that can transmit for 1000 km using an ultra-high-speed 10 Gbit/s signal , and introduce a new optical fiber submarine cable having this property.

In a optical amplifier repeater, unlike a conventional repeaters the optical signal is not converted to an electrical signal. Thus, a optical time domain reflectometer measurement is possible by adding a loopback pass transmitting backscattering to every repeater. But, the long distance and low signal level necessitate high receiver sensitivity. So, we developed and introduced a coherent optical time domain reflectometer.

1. Introduction

To make the optical fiber cable networks spanning Japan's many islands, NTT has deployed an optical fiber submarine transmission system to the straits between the islands. As transmission systems for a submarine cable, there are the repeaterless transmission system, which is used in the same way as a land system, and the repeater transmission system, which attempts to expand the transmission distance by interposing submarine repeaters on the way. The conventional submarine repeater in the repeater transmission system was the regenerating type, so we planned the development and introduction of a system that is an applied optical amplifier repeater (we call this the FSA system). Application of an optical amplifier offers the follow advantages:

(1) The repeater is made more economical by simplification.
(2) The FSA system is able to pack twice as many fibers into the conventional box size.
(3) A change of transmission speed is possible merely by exchange of the transmission device at both ends.

But application of an optical amplifier causes two problems. One is that the requirement for chromatic dispersion and polarization mode dispersion becomes severe because the regenerating transmission interval becomes long. The other is that, because the optical injection power to the optical fiber is high, signal degradation by the non-linear effect of optical fiber is produced near the injection. We will first describe the results of our search for a method for solving these problems.

In the system that uses the conventional regenerating-type repeater, optical time domain reflectometer (OTDR) measurement was impossible because the optical signal pulse could not be transmitted through the repeater. Hence, we measured the fault location by means of minute electric current examinations. But there was a problem: the measurement error was big. OTDR measurement became possible by applying an optical amplifier in the repeater. We controlled the output optical signal intensity from an optical amplifier for optical signal to the most suitable level. This output intensity is lower than the output intensity from the usual OTDR. So, the sensitivity of the OTDR receiver device had to be raised higher than that of the usual OTDR so that this system could measure an interval of 100 km.

Next, we will describe the results of our examination of the coherent optical time domain reflectometer (C-OTDR), which applies a coherent detection technique to raise receiver sensitivity .

We also consider the loss of adding a loopback pass in the repeater to transmit backscattering produced in the optical fiber.

2. Optical fiber submarine cable for FSA system

The structure of the optical fiber submarine cable applied in the FSA system is equivalent to the structure of the 12-fiber unit type optical fiber submarine cable that NTT has used in previous applications. This is because conventional cable structure has satisfactory mechanical and electrical properties for the FSA system cable. The following is a description of the optical requirements of the optical fiber used in the optical fiber submarine cable and its implementation in the FSA system.

2.1 Optical loss The submarine repeater was developed so that the submarine transmission interval would be a maximum of 100 km, which is equal to the interval of the regenerating system. As a result, there was no change from the conventional optical loss design of this cable because we determined that the optical loss of the conventional optical fiber submarine cable could be applied in the FSA system. Fig. 1 shows a histogram of cable loss applied to a transmission to Kagoshima from Naha.

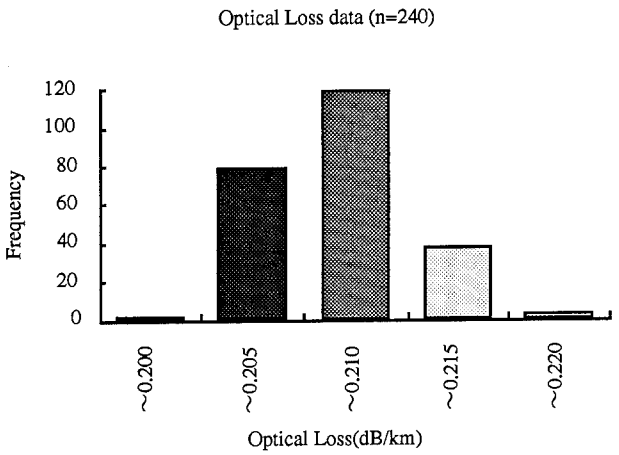


Fig. 1 Histogram of cable loss

2.2 Chromatic dispersion

Different from a conventional cable, the optical fiber submarine cable applied in the FSA system requires chromatic dispersion. Because the optical injection power to the optical fiber becomes high by an application of an optical amplifier near the injection edge, there is a risk of optical signal degradation from the non-linear effect of the optical fiber. Therefore, it is necessary to apply normal-dispersion optical fiber in the signal wavelength while optical intensity is decremented fully.

In a conventional regenerating transmission interval of around several hundred km,we have investigated influences such as stimulated Raman scattering and stimulated Brillouin scattering as the non-linear effect within the optical fiber. These phenomena become a problem in optical signal levels of more than around several tens of mW. However, the influence of the phase change of the optical signal due to the optical Kerr effect appears even in an optical electricity level of several mW when the transmission distance gets longer, into the 1000 km level, as in the FSA system.

In the FSA system, because the optical signal and the amplified spontaneous emission (ASE) from an optical amplifier are transmitted together inside the fiber, the phase change from the optical Kerr effect is divided by the intensity of the optical signal itself and by the optical signal, interacting with the ASE. These are respectively called self-phase modulation and four-wave mixing.

Self-phase modulation causes frequency chirping corresponding to the optical intensity change in the optical signal. Moreover, it brings an expanse of the optical signal spectrum. The signal wave shape degrades due to this expanse and chromatic dispersion of this optical signal spectrum. In particular, the transmission wave shape does a complex change for transmission distance in the abnormality dispersion domain. Therefore, the wave shape degradation cannot be treated as a power penalty. Accordingly, normal dispersion fiber needs to be applied in the domain in which this interacting wave shape degradation is big (the domain in which optical intensity is big).

Phase shaking by the four-wave mixing modulation phase of the optical signal causes an extension of the optical signal spectrum. Hence, it becomes easy to receive the influence of chromatic dispersion. By contrast, the influence by four-wave mixing appears at 0 value of chromatic dispersion, and the bigger the dispersion, the smaller the influence.

Generally, wave shape degradation by these non-linear effects is dependent on three factors: the maximum transmission electricity, the regenerating transmission interval, and the optical amplifier transmission interval. In the FSA system, the maximum transmission electricity is +6 dBm, the maximum regenerating transmission interval is 1000 km, and the maximum optical amplifier transmission interval is 100 km. Our goal was to reduce the power penalty to less than 1 dB by wave shape degradation. We deterimined experimentally that application of normal dispersion is good to the distance at which optical electricity in the fiber become to 0 dB, from the end. Accordingly, we supposed the fiber loss to be 0.2 dB/km, and decided to apply normal dispersion fiber to a span 30 km from the output edge of the optical amplifier, as shown Fig. 2. Fig. 3 shows the chromatic dispersion data.

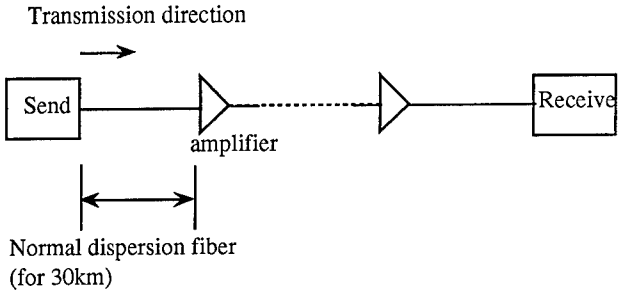


Fig. 2 Application of normal dispersion fiber

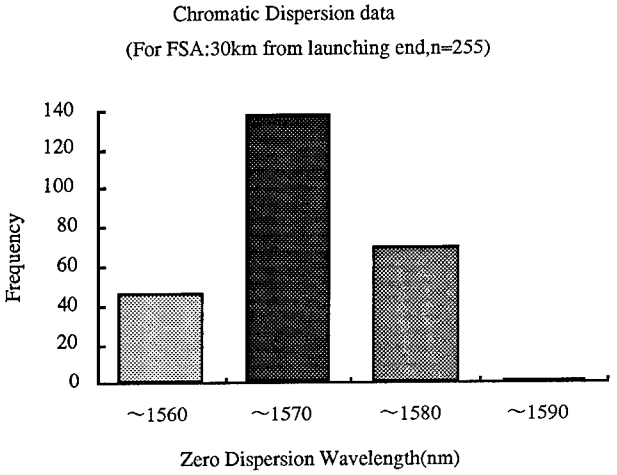


Fig. 3 Histogram of chromatic dispersion

The conventional cable is designed with chromatic dispersion on the premise that the regenerating transmission interval is around 100 km. But, because the FSA system's regenerating transmission interval is 1000 km, it must consider a chromatic dispersion design of full length. As mentioned

above, we decided to apply normal dispersion fiber to a span 30 km from the output edge of the optical amplifier. But in this situation, the degradation by chromatic dispersion became too big, because the regenerating transmission interval was long. So, an accumulation dispersion value of the full length of the cable was brought to roughly 0 (Zero dispersion wavelength is almost equivalent to signal wavelength 1.552μm).by controlling the dispersion in the section beyond this 30 km span to the reception point, as shown Fig. 4 . Fig. 5 shows the chromatic diperson data.

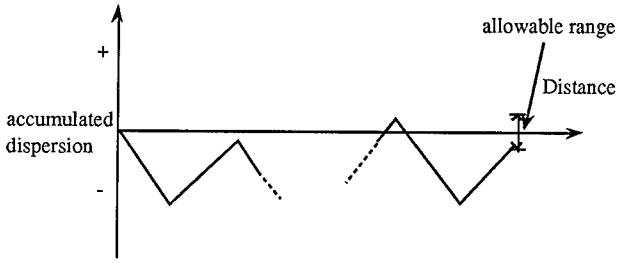


Fig. 4 Controlling the dispersion

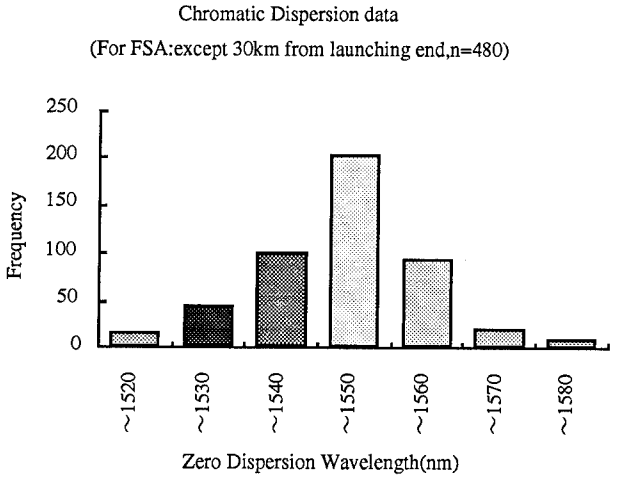


Fig. 5 Histogram of chromatic diperson

2.3 Polarization mode dispersion

In conventional optical fiber cable, a standard for polarization mode dispersion value has not yet been established. The reason is that the regenerating transmission interval is short, and the transmission speed is at the several-hundred-Mbit/s level, and it is thus necessary to consider the influence on the transmission characteristic by polarization mode dispersion. But in the FSA system, because the regenerating transmission interval is long (from several hundred to 1000 km) and the transmission speed is very high (10 Gbit/s), the influence of the warp of the wave shape by polarization mode dispersion is a subject of concern. Hence, we measured the polarization mode dispersion of the present optical fiber submarine cable. We examined the necessity of standardization by comparing the demand level in the FSA system and this result. In the FSA system, with a regenerating transmission interval of 1000 km, the polarization mode dispersion requirements for an optical fiber cable at a transmission speed of 10 Gbit/s are 0.35 ps/$\sqrt{}$km (full length average), 0.16 ps/$\sqrt{}$km (maximum), and a maximum of full length average (power penalty 0.5 dB). Fig. 6 shows the polarization mode dispersion measurement results for the optical submarine cable.

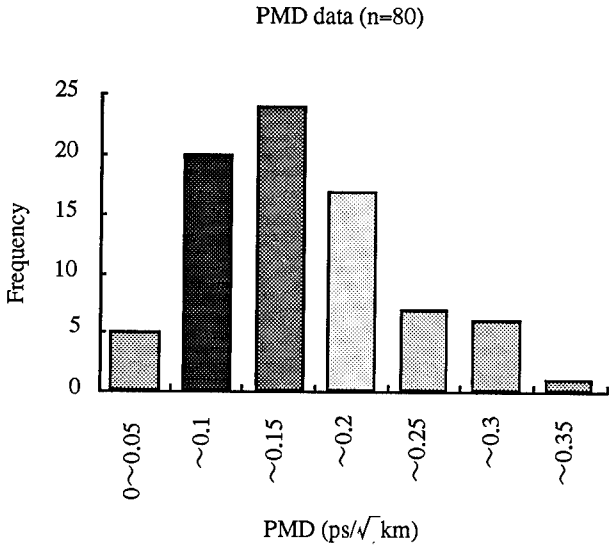


Fig. 6 Histogram of polarization mode dispersion

As a result, the average was 0.14 ps/$\sqrt{}$km, and the maximum value was less than 0.35 ps/$\sqrt{}$ km. And, we determined that it satisfied even the present situation's requirement. Therefore, we determined that we did not need to make a different standard of polarization mode dispersion regarding optical fiber submarine cable for the FSA system.

3. C-OTDR

3.1 Requirement for C-OTDR

For monitoring of the FSA system, we examined the configuration of OTDR and its dynamic range.

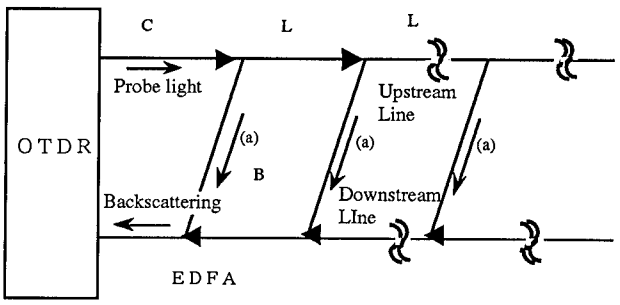


Fig. 7 Configuration of an FSA system using OTDR

Fig. 7 shows the configuration of an FSA system that uses an OTDR for monitoring. A probe light from the OTDR is injected into the upstream line. Because the backscattering produced in the upstream line cannot be transmitted on a reverse course by the isolator in each repeater, a loopback pass is added to transmit through the downstream line with each repeater. To be specific, an optical coupler is used for return in the upstream and the downstream line. Moreover, backscattering does not pass the erbium-doped fiber amplifier (EDFA) to the downstream line, but loops back via course (a) of Fig. 7. After the backscattering turned down by the downstream line goes by way of each repeater of the downstream line, it is detected by the OTDR detector. When the optical pulse using the usual OTDR is injected as an output light from the OTDR in the optical repeater of the optical transmission line, its power jumps suddenly to a level of several hundred μW of the input light, from a level of no optical signal in the optical amplifier operated by the APC (automatic power control). This is called optical surge. As a result, there is a risk of damage of the receiver devices for the APC. Output optical signal intensity must be as fixed as possible so that optical surge does not occur when the OTDR is applied in the optical transmission line. And, the OTDR receiver device detects both backscattering and amplified spontaneous emission (ASE) output simultaneously from the downstream line repeater. Therefore, a configuration of the OTDR that considers the SN ratio by ASE (a signal and the ratio of noise) is needed. If in the FSA system the EDFA compensates for line loss between each transmission optical line section, the dynamic range of aim (SWDR) is represented by equation (1).

$$SWDR=L+(B+C)/2 \quad (1)$$

Here, L represents the line loss of each transmission optical line. B represents the loss in the loopback pass. C represents downstream line loss.

In the FSA system, the output optical intensity from an optical amplifier is controlled at +6 dB to restrain the non-linear effect. The output optical intensity is much smaller than the output optical intensity from the usual OTDR(+15 dBm). For getting high dynamic range from the low output power in OTDR, coherent detection system can be considered. So, it is appropriate to change configuration slightly to monitor the FSA system.

3.2. Configuration of the C-OTDR

Fig. 8 shows the configuration of the C-OTDR for monitoring of the FSA system. The output light from the distributed-feedback-laser (DFB-LD) with linewidth narrowed by splicing a 1 km length of optical fiber is diverged to local light for coherent detection and probe light for monitoring the optical line by coupler 1. The output light wavelength is 1.552 μm. The probe light is done in a pulse by AO-SW1 working with the pulse mode, and it shifts in optical frequency simultaneously with the plus side. The AO-SW2 frequency is synchronized with that of the AO-SW1, and it shifts the optical frequency to the minus side when the pulsed probe light setup passes the AO-SW2. And, CW light having another wavelength, 1.554 μm , is inserted between pulses from the 0-dimension optical terminal of the AO-SW2 so that the output light level from the OTDR is fixed. The polarization control device reduces change in the OTDR wave shape due to polarization of probe light. And, after passing this control part, the probe light is amplified by the EDFA , and it is injected into the upstream line through coupler 2. The backscattering from the line is led through coupler 2 to coupler 3 , and is mixed with the local optical signal by coupler 3 to produce signal light. After the beat signal is received in the detector, the beat signal undergoes AD conversion, and signal processing. The drive frequency of the AO-SW1 is set at +120 MHz, the drive frequency of the AO-SW2 is set at -120 MHz, and the beat signal was produced at 20 MHz. The backscattering by CW light at 1.554 μm, which was inserted into the output light from the OTDR to render a fixed constant, cannot be received, so the influence on the OTDR is small. On the other hand, as for the ASE from the EDFA transmitting from downstream line, the beat signal noise resulting from the ASE and local signal is produced when power becomes big. For this reason, the dynamic range of the OTDR becomes degraded.

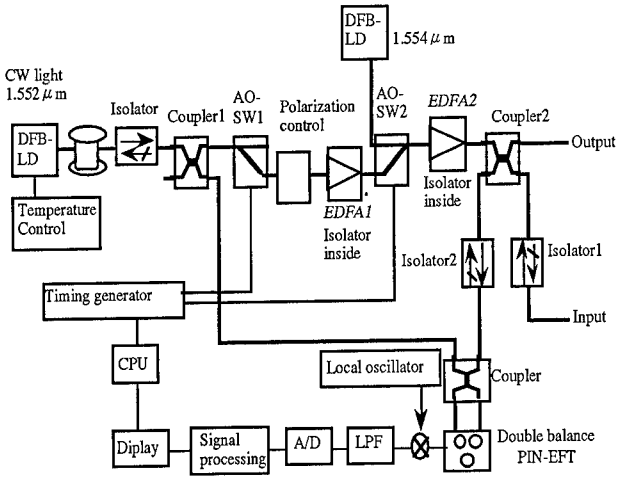


Fig. 8 Configuration of the C-OTDR

3.3 Property examination

The repeater connection of the FSA system was completed from Okinawa to Kagoshima in February, 1995. We evaluated a feature of the C-OTDR, which was the measurement device for fault location identification into the FSA system. Fig. 9 shows the measurement system (measurement system 1) that assumes a case of two fibers fault in the optical cable . Fig. 10 shows the measurement (measurement system 2) for a case that assumes only one fiber fault in the optical cable.

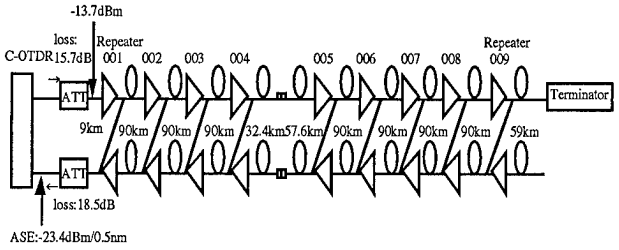


Fig. 9 Measurement system 1

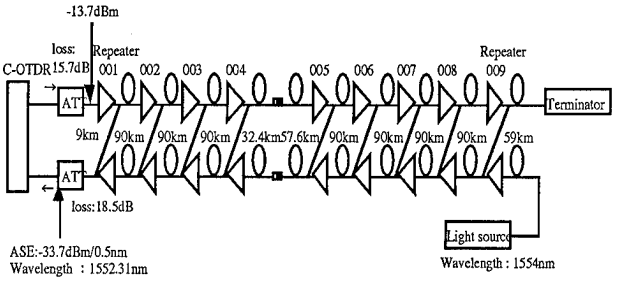


Fig. 10 Measurement system 2

The resolution ability of the failure point measurement is 1 km when the pulse width of the injection light of the C-OTDR is 10 μs. We were able to measure approximately 61 km between each transmission section when averaging was done 2^{16} times in this pulse width. Fig. 11 shows the measurement result. This result shows that a distance of 45 km can be sufficient for measuring optical fiber submarine cable in both directions. The distance is the measurement distance that is necessary to include the whole line.

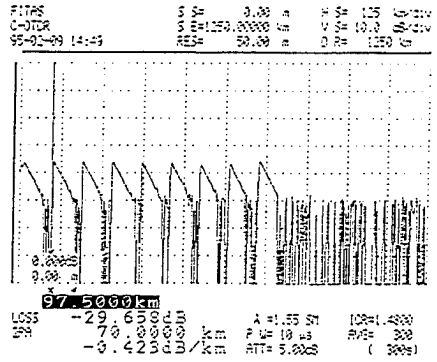


Fig.11 Measurement result by measurement system 1

Fig. 12 shows the result measured with a pulse width of 10 μs using measurement system 2. By this measurement, because light is injected in repeater 009, the ASE level falls 10 dB compared with measurement system 1. Therefore, we were able to identify the measurement of all sections with this pulse width . And, the connector insertion part is located in the fifth section. Therefore, we investigated to determine the connection insertion point. We were able to identify a reflection of about 0.4 dB, and were able to identify the distance of the point by an error of less than 1 km as shown in Fig.13.

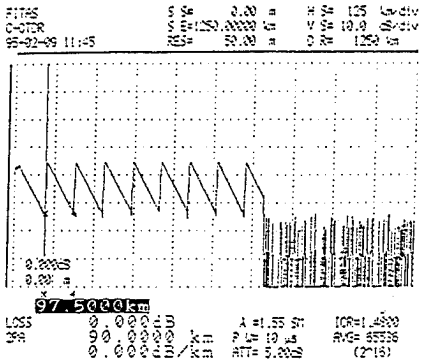


Fig.12 Measurement result by measurement system 2

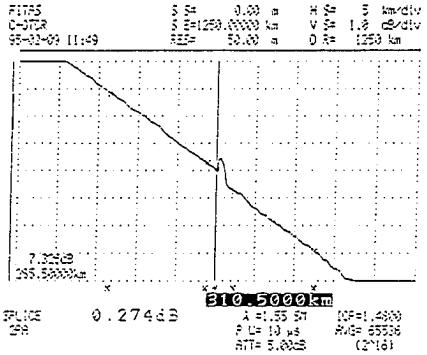


Fig.13 Measurement result (connection insertion point)

4. Conclusions

We examined chromatic dispersion and polarization mode dispersion for the development and introduction of an FSA system with a 1000 km transmission applied in-line optical amplifier.

As a result, by controlling chromatic dispersion of the cable longitudinally, we achieved on accumulation dispersion value of full length cable of roughly 0. This meets with the requirement of the FSA system. And, we examined the requirement for a coherent OTDR which applied a coherent detection system to measure the FSA system, evaluated a property with a real transmission line, and identified that measurement in all sections was possible.

5. Acknowledgements

The authors thank N. Isikawa, Y.Sato, N.Nakao and M.Kuroiwa for their discussions. The authors gratefully thank S.Sugiura for encouragement.

6. References

(1) N.Suzuki, T.Ozeki "Simultaneous Compensation of Laser Chrip, Kerr Effect, and Dispersion in 10-Gb/s Long-Haul Transmission Systems", Jounal of Lightwave Technology, Vol 11. No.9, pp 1486-1494,1993

(2)T.Imai, M.Murakami and A.Naka "Oprimum Parameter Guidelines for 10Gbit/s, Multi-Megametre Transmission Systems Considering The Nonlinear Effect", Electronics Letters, Vol 29,No.16,1993

(3) S.Furukawa, H.Izumita, I,Sankawa and Y.koyamada "High dynamio range, low fading noise coherent OTDR using erbium fiber amplifier and LD temperature changing techniques",Proc, ECOC'91/IOOC'91, Mo.C1-3,pp,81-84,Paris,1991

(4) Y.Koyamada, H.Nakamoto and N.ohta "High Performance Coherent OTDR Enhanced with Erbium Fiber Amplifiers",J.Opt.Cmmun.,Vol.13,No.4,pp.127-133,1992



Tetsuhiro Numata

NTT Network Systems Development
Chiba, Japan

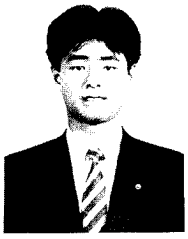
Tetsuhiro Numata received B.E. and M.E.degree in 1990 from Tohoku University.He is a Engineer, Acces Networks Project Group in Network Systems Development of NTT. He joined NTT in 1990.



Shyuichi Nishio

NTT Central Training Institute
Tokyo, Japan

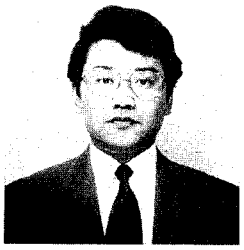
Shyuichi Nishio received B.E. degree in 1989 in Electrical Engineering from Sophia University,Tokyo,Japan.In 1989,he joined Nippon Telegraph and Telephone Coopporation(NTT) Network Systems Development Center and had been engaged in the development of optical fiber cable systems. He was transferred to NTT Central Training Institute in 1995.



Shinji Goto

NTT Network Systems Development
Chiba, Japan

Shinji Goto is a Engineer, Access Networks Project Group in Network Systems Development Department of NTT. He received his B.S. degree from Yamagata University in 1989. He joined NTT in 1989.



Kuniaki Tanaka

NTT Access Network
Systems Laboratories
Ibaraki, Japan

Kuniaki Tanaka received B.S.degree from the Koch University and M.S.degree from Kyushu University.He joined NTT in 1988.Since 1992,He has been worked in development of optical fiber measuring and testing technologies.



Yuki Sakuyama

NTT Network Systems
Development
Chiba, Japan

Yuki Sakuyama received B.E. in 1981 in electrical engineering from Tohoku University. After joining the Engineering Bureau, Nippon Telegram Telephone Public Corporation, in 1981, he worked on research and development of communication cables and splicing technologies. He is a Senior Engineer in the Access Networks Project Group in NTT Network Systems Development Department, and is currently engaged in the development of optical fiber cable .

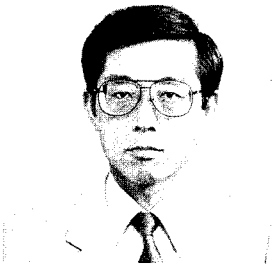


Naoyuki Atobe

NTT Maintenance Service
Panning
Department
Tokyo, Japan

Naoyuki Atobe received the B.E. degree in electrical engineering from Kyushu University in 1979. After joining the Engineering Bureau, Nippon Telegram Telephone Public Corporation, in 1979, he worked on Presearch and development of communication cables and splicing technologies. He had worked on planning and investment of telecommunication plants at Hokuriku regional head quarter in 1986. He was a Senior Manager, superviser in the Access Networks Project Group in NTT Network Systems Development Department, and had been engaged in development of testing system for fiber optics network systems, optical fiber cable, and fiber termination systems. He was transferred to NTT Maintenance Service Panning Department in 1995.

Mr. Atobe is a member of the institute of electronics, information and communication engineers of Japan.



Shin-ichi Furukawa

NTT Access Network
Systems Laboratories
Ibaraki, Japan

Shin-ichi Furukawa received B.E. and Dr. Eng. degrees in electrical engineering from kyushu University in 1974 and 1987,respectively. He joined the Ibaraki Electrical Communication Laboratory, NTT, Ibaraki, Japan, in 1974, where he engaged in the research and development of submarine cables and joints, and optical fiber measurement techniques. Since 1989, he has been engaged in the research and development of optical fiber measurement and surveillance systems. From this March, he is currently engaged in the research and development of optical fiber cables. He is presently a Senior Research Engineer, Supervisor of NTT Access Network Systems Laboratories. Dr.Furukawa is a member of the IEEE and IEICE of Japan.

OPTICAL FIBER FOR AMPLIFIED UNDERSEA SYSTEMS

Dan L. Philen, Raymond B. Kummer, Dave Kalish, David Peckham, Joel Darsey, Robert Heyda,
Alan Klein, Shahab Siddiqui, Robert Moore, Carl Taylor
AT&T Bell Laboratories
2000 Northeast Expressway
Norcross, Georgia 30071

Art Meixner, Seymour Shapiro, Lou Marra, Ray Tuminaro
AT&T Bell Laboratories
101 Crawfords Corner Rd.
Holmdel, New Jersey 07733

David Applegate
AT&T Bell Laboratories
600 Mountain Avenue
Murray Hill, New Jersey 07974

ABSTRACT

A dispersion shifted fiber with zero dispersion wavelength optimized for 1561.5 nm has been developed for matching the 1558 nm optical amplifier cascaded gain peak using both MCVD and VAD technologies. Long amplifier systems require a very narrow distribution of zero dispersion wavelength, achieving a mean of 1561.5 with a sigma of 0.6 nm. To minimize non-linear effects from the high power amplifiers, the effective area of the fiber is increased to greater than 50 μm^2. PMD is required to be very low, and a special process for producing low PMD results in a mean of 0.07 and a sigma of 0.03 ps/$\sqrt{}$ km. These parameters are stable through cable processing. Constituent fibers are selected using a proprietary selection algorithm that matches the constituent fiber across a matched set of spliced fibers. The fiber is colored with a solvent free material, that also allows for high strength splicing after coloring. The dispersion between colored fibers is also managed to reduce the color-to-color variation possible in long system lengths.

INTRODUCTION

The rapid advance in undersea communications systems brings with it new demands on the transmission medium; specifically the optical fiber and its associated cable. System capabilities that were envisioned a few years ago are now a practical reality. For instance a 2,000 km optically amplified system was placed into service in 1994 that operates at 2.5 Gbit/sec. In 1995, systems were installed that operate at 5.0 Gbit/sec. and span distances of 9,000 km, and even higher bit rate systems are being considered for future systems.[1]

This technology advance places additional demands on the optical fiber and its configuration into the final system. This paper describes the various technical considerations required to manufacture an optical fiber undersea cable system using optical amplifiers rather than electrical repeaters.

DISPERSION SHIFTED FIBER CHARACTERISTICS

AT&T systems that use optical amplifiers rather than electrical repeaters are known as SL-2000 for Submarine Lightguide 2000, and represent the current generation in undersea optical fiber systems. The first generation dispersion shifted fibers (DSF) were optimized for operation at 1550 nm and have several weaknesses regarding their use in amplified transoceanic undersea systems. First, the mean zero dispersion wavelength (lambda zero) does not coincide with the 1558 nm gain peak that develops in long cascaded amplifier links. In addition, with the effective area less than 50 square-microns and the high power levels of the erbium-doped optical amplifiers, unacceptable levels of system degradation occur as the result of the onset of nonlinear optical effects due to the high power density. Furthermore, the long unregenerated transmission lengths require extremely low levels of polarization mode dispersion. These areas of concern were the focus of efforts to design a dispersion shifted fiber that would be optimized for the these ultralong distance systems.

The design objectives of the new dispersion shifted fiber intended for optically amplified transoceanic undersea systems were:

1. Decrease the nonlinear effect by increasing the effective area to greater than 50 μm.

2. Move the mean zero dispersion wavelength to be slightly higher than 1558 nm.

3. Maintain bending/packaging performance to at least the level of unshifted fiber designs.

4. Decrease the average fiber attenuation at 1550 nm.

5. Decrease the sensitivity of transmission properties, such as mode field radius or zero dispersion wavelength to manufacturing variations, compared to that of existing designs.

The index profile of the fiber that meets these objectives consists of a triangular/trapezoidal shaped core, surrounded by a raised-index cladding region or pedestal, which is surrounded by a silica cladding. Fibers meeting these objectives have been manufactured using both MCVD and VAD processes. To achieve the low levels of PMD required, a patented ultra-low PMD process was implemented into the manufacturing operation. Typical results achieved with this design are shown below in Table 1.

TABLE 1

Mode Field Diameter	8.4 μm
Avg. Attenuation at 1550 nm	0.201 dB/km
Effective Area	> 50 μm^2
Avg. Lambda Zero	1561 nm
Avg. PMD	0.07 ps/√km

FIBER SELECTION FOR SPLICING LONG LENGTHS

In order to assemble long lengths of fiber with a very tight zero dispersion wavelength (lambda zero) distribution, shorter lengths of constituent fibers are spliced together to make the longer lengths. The spliced lengths vary depending on the particular application, but in general vary between 45 and 90 kilometers, with the typical length being about 71 kilometers.

The constituent fibers have a lambda zero distribution that has a mean of about 1561 nm and a standard deviation of about 8 nm. This would normally give a distribution that is ± 25 nm, however in practice, the distribution is truncated at ± 20 nm.

Fibers are selected from an inventory pool to be spliced together such that the lambda zero of the final spliced length is near 1561.5 nm ± 1.5 nm at room temperature. The wavelength of 1561 is chosen so that when the cable is placed on the sea floor, the final lambda zero for the system will be correct taking into account the decrease in temperature at the ocean bottom. The parameter of interest is actually the group velocity dispersion, in ps/nm-km, but since the dispersion slope has a narrow distribution, the zero dispersion wavelength (lambda zero) is usually specified for spliced fiber assembly.

If constituent fibers were randomly chosen from the inventory pool, it would be possible to achieve the average of the inventory distribution over some large number of fibers. However, this would lead to dispersion variation over wide ranges within the same cable section. It is obvious that some form of dispersion management in assemblying the concatenated fiber lengths is necessary right from the start of any system.

Concatenating Fibers

The simplest dispersion management for concatenating constituent fibers would be to require that the average lambda zero for any spliced length be within the target value, such as 1561.5 nm ± 1.5 nm. This would give spliced fibers of length of 71 km whose spliced lambda zero values could range from 1560.0 nm to 1563.0 nm This is accomplished by taking a fiber with a low lambda zero (less than 1561.5 nm) and splicing it to another fiber with high lambda zero (higher than 1561.5 nm) to achieve a spliced fiber whose average of the constituents is exactly 1561.5 nm.

In practice, there are usually three constituents to make up the spliced length, and there could be as many as five depending on the loss requirements of the system and the constituent fibers. Thus, the "cut-length" (the length where the constituent fiber is intentionally broken during fiber drawing) is carefully chosen to minimize the number of splices and constituent fibers, while maximizing the ability to use the available inventory to achieve the desired lambda zero target. Because some shorter lengths always occur during fiber drawing the selection of fibers from the inventory pool needs to consider how to best utilize these shorter lengths.

This simplest scheme for concatenating constituent fibers into spliced lengths involves splicing random fibers together so that the final average lambda zero is 1561.5 nm. This will produce the final required lambda zero, and will give individual fibers having a total length of 71 km each, but each spliced length would have different constituent fiber properties from every other length.

Set Assembly

The next level in building a concatenated fiber length is to consider the idea of a "Set" of fibers where each fiber in the set would be matched to every other fiber in the set along some system parameter. Since undersea cables usually use a small number of fibers in each cable section the idea of a set becomes the number of fibers actually in a cable section at any one point. Most cables today use 4 or 6 fibers in the core section[2], and some are as high as 18 to 24 in higher fiber count cables[3]. Thus, a "Set" is a group of 4 or 6 fibers that are matched together for a particular parameter. The simplest case would be for a set of 4 fibers having matched loss i.e. all spliced fibers less than 0.205 dB/km, for each and every one of the four fibers.

When considering the effects of dispersion, the considerations about set matching become much more complex. A set of four fibers all having their individual spliced lambda zero values in the range of 1561.5 ± 1.5 nm would constitute a set of matched lambda zero fibers. This type of set would be matched on both lambda zero and attenuation, because one must meet the system loss budget as well as the dispersion requirements.

Matching Sets of Fibers

Yet a third level of dispersion management involves considering what happens when a cable section is cut. For efficiency in the cable manufacturing operation, as long a length as is possible is desirable. However, the section lengths between amplifiers rarely corresponds to the manufactured length. Cutting and reassembly of the cable sections is typically required.

In the above matched dispersion set, all of the constituents may be different lengths and different lambda zero providing that the final spliced length lambda zero is within the target range. In this case, cutting the cable at any point will give cable sections that may vary widely in their dispersion properties.

To minimize this effect, each constituent fiber within a set is matched to each other constituent fiber at the same point in the

set. Because of fiber-to-fiber variation some tolerances are allowed in the selection process. A set might be configured as follows in order to match each constituent fiber: Consider that for a 4 fiber set, each spliced length has 3 constituent fibers. Each fiber at position #1 in the spliced length for each of the 4 fibers must match each of the other three fibers to within ± 4 nm for lambda zero. Likewise, the second and third fibers also match each other to within ± 4 nm. In order to accomplish this, the lengths of the constituent fibers must also match to within ± 2.5 km. The final set will have four fibers each of whose lambda zero will be 1561.5 ± 1.5 nm, and if the set (final cable) is cut at any point in the spliced fiber, the cut sections will have the same dispersion properties, although each of these will not meet the 1561.5 nm target. Because both cable sections are eventually used in the same system, the system dispersion incorporates these lengths, and averages out to 1561.5 nm.

This process becomes more complicated as the number of constituent fibers increases. Figure 1 shows the lambda zero distribution for an undersea system that uses such a dispersion matching system.

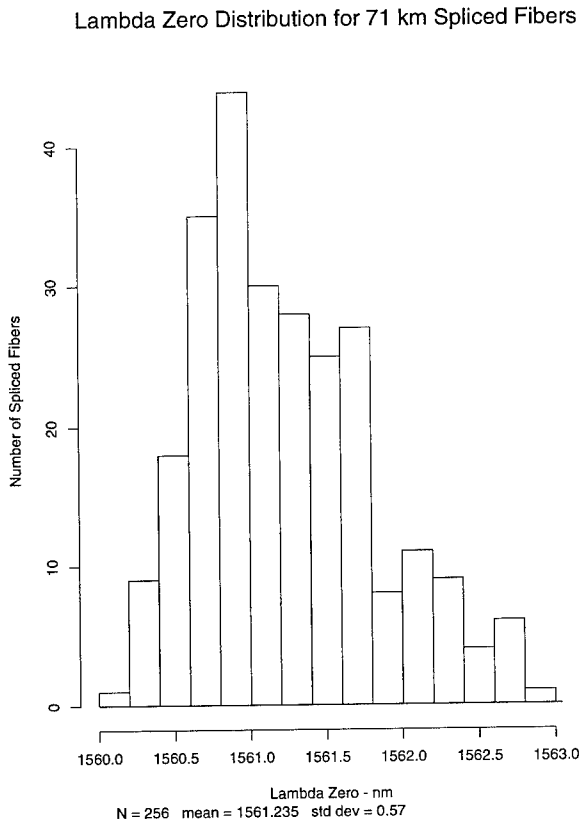


Figure 1. Lambda Zero Distribution of matched sets for an undersea cable system.

Color-to-Color Variation

For fiber identification purposes, each fiber is given a distinct color coding. The usual colors are red, brown, blue, yellow, orange, and green. Even though the fiber sets are now matched, there is a tolerance range of ± 1.5 nm within the matching boundary, and each spliced fiber in the set is colored a different color. In the system assembly, all of the fibers of the same color are spliced to each other throughout the system. Thus, it possible to get differences in total dispersion over the different color paths. Even though all of the spliced fibers in a system average 1561.5 nm ± 1.5 nm, if all of the low lambda zero fibers are colored red and all of the high ones are colored blue, there will be a sizable accumulated dispersion between the red and blue colors over the interval of 500 to 800 km (distance between compensators) when dispersion compensation occurs.

To minimize this effect, active monitoring of the average lambda zero of the colored fibers is performed as a system is being spliced in the fiber factory. Should a bias develop between any two colors, corrective measures can be undertaken to change the order of the coloring such that subsequent colored fibers correct for the accumulated bias of the previous ones. Figure 2 shows such a color-to-color dispersion running average.

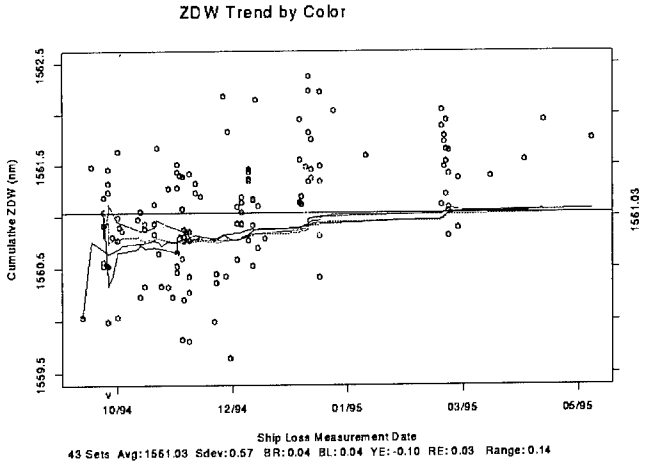


Figure 2. Average lambda zero by color of spliced fiber monitored as a project is completed.

High Strength Fiber Splicing

The splicing of constituent fibers is necessary to attain the stringent requirements on the final dispersion properties of the spliced length. The splice, however, must not be allowed to cause any strength degradation to the total fiber length. The use of a "splinted" splice to add strength reinforcement is not permitted because the splice must go through the fiber coloring operation. The splice also gets processed into the Unit Fiber Structure (UFS) of the cable core; thus, high strength splices are required. Typically the fiber is proof tested to 200 kpsi (1.38 GPa) and the splices are required to be at least that level. In practice, the splices are manufactured to a higher level around 230 kpsi (1.58 GPa), to insure that no splice proof test level is lower than 200 kpsi (1.38 GPa) after subsequent operations.

The splice loss can add significantly to the total loss of the spliced lengths. Each splice of 0.1 dB adds 0.0015 dB/km to the final loss of a 71 km length, and a 0.15 dB splice adds 0.002 dB/km. Thus low loss high strength splices are required for today's low loss systems.

Figure 3 shows the distribution of splice loss for a typical undersea system.

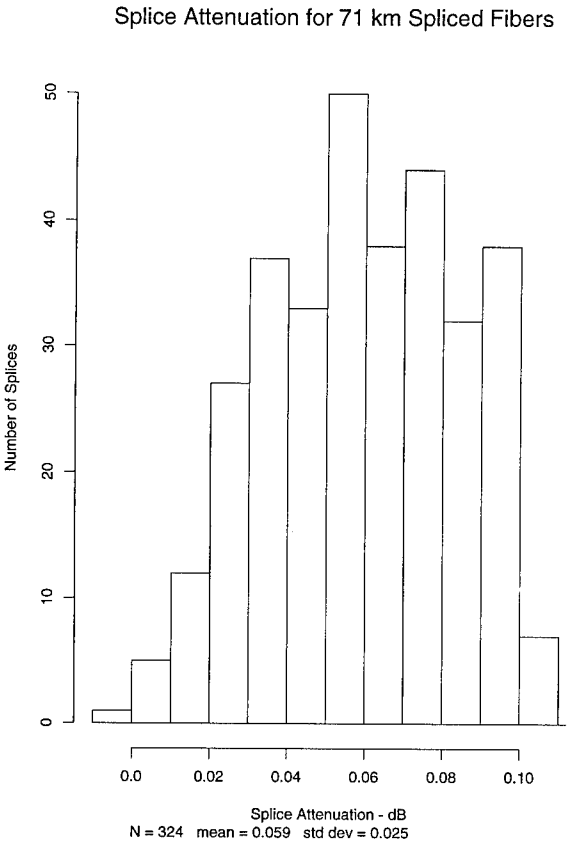


Figure 3. Attenuation of high strength arc fusion splices.

The splices shown in this figure were made using a commercial arc fusion splicing machine with each splice passing a minimum of 230 kpsi (1.58 GPa).

Once a fiber is spliced, the area of the splice must be re-coated with urethane acrylate coating material similar to the fiber coating. In order to use fiber coloring materials that incorporate a fixed die applicator, the reconstituted coating material must meet maximum and minimum diameter requirements similar to the original fiber. The splice re-coat tolerances need not be as stringent as for the bulk of the fiber length, provided that some maximum tolerance for the die clearance is not exceeded.

Fiber Color Code

In order to provide fiber identification in the cable for subsequent splicing and connectorization, each fiber in the cable must have a color code that allows it to be distinguished from other fibers in the cable. Several commercial suppliers of pigmented color material are available. These pigmented materials are generally mixed with a material similar to the fiber coating itself, and processed using a fixed die applicator.

As outlined above, fibers are spliced into long lengths and then colored. Should a fiber break occur during or after coloring, it is necessary to repair the fiber by re-splicing it. These commercial materials generally have the drawback that they contain certain ingredients that are suspected of causing strength degradation when making high strength splices after the fiber has been colored.

For high strength splices, a proprietary ink formulation has been used in the past, but it also contains a material for decreasing the viscosity for ease of processing. Recently, a formulation of this material has been developed that removes the viscosity modifying material and allows the ink to be processed using the fixed die technology. Since this ink does not contain these suspect ingredients, high strength splicing is possible both in the fiber factory and in the cable factory.

This ink formulation provides high adhesion of the color material to the optical fiber coating, high strength splicing capability, and high speed application using solvent free materials.

POLARIZATION MODE DISPERSION

The management of chromatic dispersion as outlined previously, is essential for long distance undersea systems. However, that accumulated dispersion must be compensated every few hundred kilometers. The dispersion that occurs because of the difference in propagation velocity between orthogonal fiber modes (Polarization Mode Dispersion) can not be compensated, but accumulates over the fiber path of the system.

In order to minimize the effect of PMD, a patented fiber processing technology is used to produce low PMD fiber. The PMD of this fiber is also stable with respect to the cabling operation, showing negligible increase through the final cable operation.[4]

Figure 4 shows the PMD of the constituent fibers used to concatenate into spliced set lengths.

Figure 5 shows the PMD of the final spliced length for the fibers prior to shipping to the cable factory.

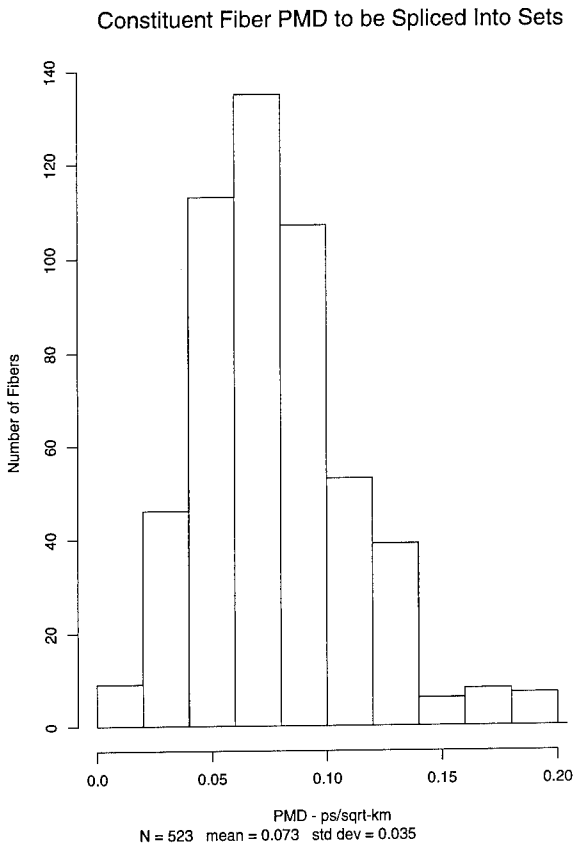


Figure 4. PMD of constituent fiber to be spliced into sets.

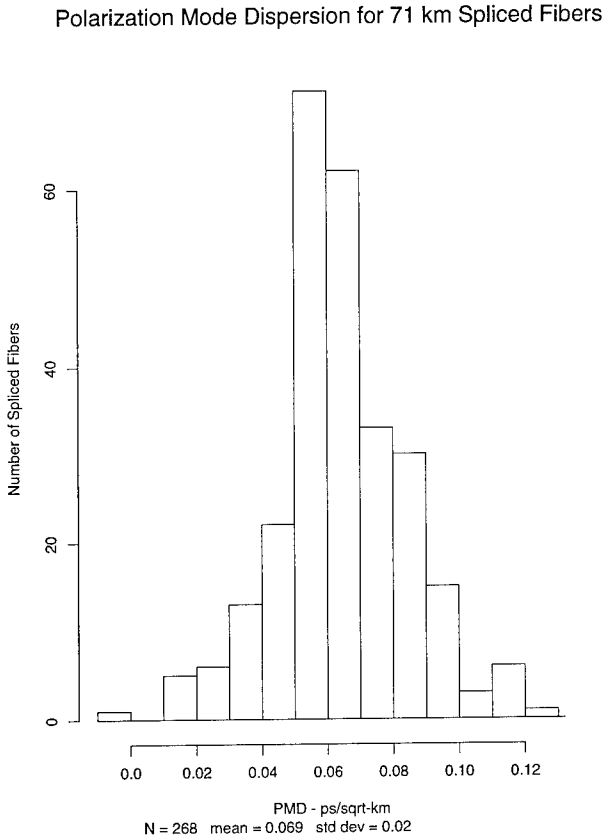


Figure 5. PMD of spliced 71 km lengths in matched sets.

The PMD after the final cable extrusion process has a mean of 0.08 ps/√km which is similar to the fiber after splicing, and shows that there is no appreciable increase in the PMD with the cabling operation. This level of PMD is about one-half the system requirement of 0.15 ps/√km, average

CABLING PROCESS

Fiber

As described before, a constituent fiber is a drawn, coated, and proof tested unspliced fiber. A unit fiber is a 71 km fiber which typically contains three to five constituent fibers which are spliced together. For SL-2000 applications, unit fibers are color coated to provide unique identification over the length of the system. An SL-2000 fiber set consists of up to eight such uniquely colored unit fibers.

When a fiber set arrives at the cable factory, each unit fiber is remeasured for loss, zero dispersion wavelength, and slope to insure agreement with fiber factory measururements. These unit fibers are then stranded into a elastomeric material which forms the Unit Fiber Structure (UFS). Strict dimensional control is applied to all component elements and processing variables of the UFS manufacture. Fibers are color-coated to extremely tight tolerances (± 5 μm) to ensure proper cabling into the UFS. The UFS itself is manufactured by first extruding a thin layer of elastomer over a copper-clad kingwire. The dimensions of both the kingwire and the first-layer extrudate are controlled to within tenths of mm. In addition the temperature of the first layer extrudate is precisely controlled to achieve a dimensionally stable, yet suitable compliant material, unto which the fibers are embedded. This latter operation is accomplished at a "closing die" whose surfaces are maintained very smooth, and whose dimensional tolerances are critically controlled. The final UFS operation is the co-extrusion of a second layer of elastomer along with a layer of nylon to further protect the fibers. The result of this UFS manufacture is a precise, robust intermediate product, in which the fibers are captured in a relaxed, low loss state for subsequent cabling operations.

Figure 6 shows the arrangement of the fibers, kingwire, and hytrel in the unit fiber structure for a six fiber unit.

Nominally, this 71 km UFS will be used to fabricate a 71 km SL-2000 cable. In actual production, the cabling process introduces some variation in the range of extruded cable lengths; the finished cable lengths are called "subsections". The average cable subsection length is typically in the range of 40 kilometers. These cable subsections are optically characterized at 10°C, for loss,

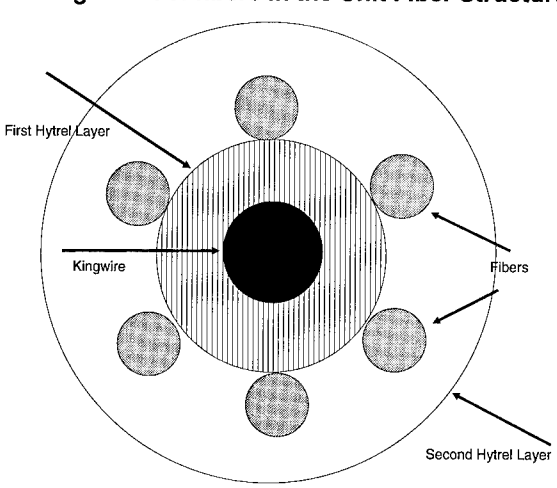


Figure 6. Arrangement of kingwire, optical fibers, and hytrel in a unit fiber structure for a 6 fiber cable.

chromatic dispersion, and PMD, and are then placed into inventory. Typical performance of cabled SL-2000 fibers to date is shown in Table 2.

TABLE 2

Finished Cable Loss	0.205 dB/km (typ.)
Added Cabling Loss (change from fiber to finished cable	0.003 dB/km (avg.) 0.003 dB/km (std.dev.)
PMD (UFS)	0.12 ps/√km
PMD (finished cable)	0.08 ps/√km

CABLES

Cables are designed to isolate the fibers, insulate the electrical conductor from the ocean environment, and provide a range of levels of mechanical protection from known and unexpected hazards. The cable design and manufacture must reliably maintain the optical performance of the fibers at minimum cost. The SL-2000 undersea lightwave cable consists of four major sub units that are built in a modular process to provide flexibility in cable manufacture . The four sub units are [5]:

1. The Unit Fiber Structure (UFS), as described previously.

2. The Composite power conductor, which consists of steel strength wires and water blocking material surrounded by a continuously welded copper sheath.

3. Polyethylene insulation that is extruded over the power conductor.

4. Armour protection that can be added on top of the polyethylene layer as needed depending on the depth and terrain of the cable route.

SYSTEM CABLE REQUIREMENTS

Prior to the assembly of a system cable, the system optical requirements are used to determine cable assembly requirements. These requirements include:

System Cable Length

Determined by the location of terminals, bottom terrain (depth profile), and required cable slack of the proposed cable route.

Optical Amplifier Loss Budget

The high level requirements which specify the minimum and maximum section loss between amplifiers, as well as the average section loss for the entire system cable.

Dispersion Map

These requirements include the allowed minimum and maximum accumulated dispersion, in ps/nm at all points along the cable, and may also include a nominal value for the dispersion depth, in ps/nm for every compensating interval. (A compensating interval is defined as a segment of a cable, for which the accumulated dispersion goes from a nominal value of zero ps/nm, to a required dispersion depth, and returns to zero ps/nm, using dispersion compensating cable.) A typical dispersion map is shown in Figure 7.

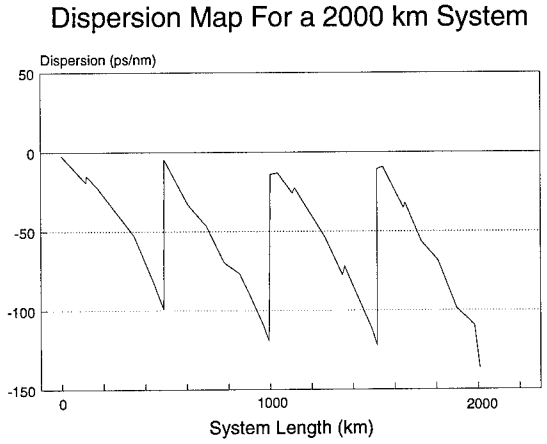


Figure 7. Typical dispersion map of a fiber path in a 2000 km optically amplified system.

Cable Operating Temperature

The undersea temperature profile must be known, in order to design the system cable dispersion map. The fiber zero dispersion wavelength has a temperature sensitivity of + 0.028 nm/^{O}C.

CABLE ASSEMBLY REQUIREMENTS:

The above requirements are then used to derive the cable assembly requirements. These include;

1. Nominal Section Length (Distance between optical amplifiers): The nominal section length is derived from the required average section loss, and average expected cabled fiber attenuation. Actual cable section lengths are adjusted to reflect measured cable loss at the transmitter wavelength.

2. Nominal Dispersion Map: Once the nominal section length has been determined, one may determine the dispersion map targets using the system requirements outlined above.

3. Dispersion Interval: For a generic terminal-to-terminal cable segment, an interval will be (the cable length, plus the amount of fiber in the receiving terminal)/N, where N is an integer which will produce a dispersion map which meets the requirements for accumulated dispersion and dispersion depth at the cable operating temperature.

CABLE ASSEMBLY

Cable assembly is accomplished in the following manner: Cell Selection: To reduce cable assembly complexity, the total cable segment is broken into a series of subsegments, or cells. Typically a cell will amount to roughly one half of a dispersion interval. Requirements for a cell include a loss and dispersion filter. A dispersion filter sets requirements for the total accumulated dispersion of a cell. Constituent cable subsections are selected from the total cable subsection inventory. The measured dispersion, in ps/nm of each subsection selected is summed over the cell. A loss filter is employed to insure that the loss section is within the specified window, and that the average section loss is also on target. When the loss and dispersion filter requirements are met, the cable factory joins all subsections for that cell. Additional cells are fabricated, and all cells are placed in a sequence within the cable installation ship, consistent with the overall cable assembly plan.

SUMMARY

Design and manufacturing considerations for producing optical fibers and cables for optically amplified systems have been presented. The high data rates being installed today, and proposed for the future, demand that, in addition to low attenuation, fibers must meet strict chromatic dispersion and PMD requirements. Constituent fibers must be matched and concatenated into matched fiber sets, and colored with materials that allow high strength splicing. Finished cables must also be assembled into loss and dispersion cells to meet the overall cable assembly plan consistent with the final system requirements.

REFERENCES

1. J. M. Sipress, "Undersea Communications Technology", AT&T Technical Journal, vol. 74, no. 5, Jan/Feb 1995.

2. R. E. Frantz, et al,"The Design and Manufacture of Fiber and Cable for Undersea Optical Amplifier Systems", Proceedings IWCS, 1993.

3. W. R. Wright, et al, "Design and Development of High Fiber Count Repeaterless Submarine Cable", Proceedings IWCS, 1994.

4. A. F. Judy, "Improved PMD Stability in Optical Fibers and Cables", Proceedings IWCS, 1994.

5. R. L. Mortenson, et al, "Undersea Amplified Repeatered Technology, Products, and Challenges", AT&T Technical Journal, Feb. 1995.



Dan L. Philen is a Distinguished Member of Technical Staff in the Systems Engineering Group at AT&T Bell Laboratories. He joined AT&T Bell Laboratories in 1979 and is responsible for the technical requirements and specifications for optical fibers used in undersea applications. He received a B.S. degree in chemistry from Auburn University, and a Ph.D. degree in physical chemistry from Texas A&M University, and was a Robert A. Welch Postdoctoral Fellow in electrical engineering at Rice University. He is the author of numerous publications on measurements of optical fiber properties and holds patents in fiber measurements and cable design. He is a member of The American Chemical Society, The Optical Society of America, Sigma Xi - The Research Society of North America, Sigma Pi Sigma - Physics Honorary, and Phi Lambda Upsilon - Chemistry Honorary.

OPTICAL PERFORMANCE OF SUBMARINE CABLES IN OPTICALLY AMPLIFIED HIGH BIT RATE SYSTEMS

J.L. Lang ASN Calais D.I. Curtis ASN Southampton
J.F. Libert ASN Calais P. Worthington ASN Southampton

SUMMARY

Several long haul high bit rate optically amplified systems have now been installed or are under construction. The systems place more stringent requirements on the optical performance of the cable, particularly in respect of dispersion characteristics. The chromatic dispersion must be closely controlled and equalised to maintain the zero dispersion wavelength close to the operating wavelength. The polarisation mode dispersion must also be maintained at a low figure to avoid degradation of system margins.

Alcatel Submarine Networks (ASN) has supplied two types of cable for the long haul systems which have required significant development and qualification work to meet the stringent optical targets. A common approach to solution of the low PMD requirement was adopted for the two cables. Results of the optical performance of installed optically amplified systems are presented.

1. INTRODUCTION

Over the past 10 years ASN has supplied optical cable systems for long haul (repeatered) and short haul unrepeatered systems. Repeatered systems which were regenerated and retimed at each repeater (typically 100 km spacing) did not require particularly low or closely matched dispersion of the fibre paths. For 560 Mbit/sec systems, standard (non-DS) fibre could be used. For a 2.5 Gbit/sec repeatered system DS fibre was used, but no selection or matching of fibre dispersion was needed during cabling.
Optically amplified long haul systems operating at high bit rates (5 Gbit/sec) however require close control of both chromatic dispersion and polarisation dispersion. Chromatic dispersion of installed cable on the sea bed must be accurately predicted from factory measurements so that compensation cable can be inserted to maintain the overall dispersion close to zero.

In the case of polarisation mode dispersion, compensation is not possible as the effect is randomly varying with time and temperature. The mean value of the PMD increases with the square root of the length of the system so that for long haul systems it must be controlled by ensuring all cable has low and stable PMD. System margins or BER may be degraded when the instantaneous value of PMD exceeds a certain level. Because of the statistical distribution of PMD with time, the mean value must be specified at a level which avoids the extreme values of the distribution exceeding a critical level.

2. CABLE DESIGNS

The deep water cable designs used for long haul amplified systems are shown in Figs. 1a and 1b. Figure 1a shows the ASN 21.5 cable using a loose structure (slotted core) fibre package. Figure 1b shows the ASN NL LW cable using a tightly buffered fibre package. The cable characteristics are summarised in Table 1. The cables were developed from the same basic designs used for deep water optical repeatered systems. The modifications that were made were to the fibres and optical package in the centre of the cable to improve the optical transmission characteristics.

	Cable Type		
	Dn	NL	Units
O/D	21.5	26.2	mm
weight in air	0.79	1.28	kg m^{-1}
weight in water	0.42	0.73	kg m^{-1}
UTS	100	160	kN

Table 1 - Deep water Cable characteristics

3. REQUIREMENTS

The exact requirements for the optical transmission characteristics vary with system length, bit rate, etc. Typical requirements for the first generation long haul systems operating at 5 Gbits/sec are:-

- Average λ_0 of system approximately 2.85 nm higher than the operating wavelength (typically 1558.65 nm). Equalisation added to keep dispersion within limits of 0 and -150 psec/nm on all fibre paths.
- Mean polarisation mode dispersion less than 0.15 psec/$km^{\frac{1}{2}}$ (equivalent to about 10 psec on a 5000 km link).
- Low and stable attenuation (<0.21 dB/km) with negligible ageing characteristics.

4. CONTROL OF PMD

Tests had been carried out on 2 short haul systems using DS fibre installed in 1988 and 1991 (Figs. 2a and 2b). These showed typical mean PMD figures of 0.5-0.6 psec/$km^{\frac{1}{2}}$ and clearly did not meet the requirements for long haul systems. The measurements also show the statistical nature of PMD with the distribution of instantaneous values in time closely fitting a Maxwell distribution. Investigation into the cause of the relatively high PMD of the early systems was made difficult because of the inter-dependency of PMD on both birefringence and coupling. The fibre birefringence is determined mainly by the asymmetry of the core

geometry or asymmetry of the refractive index profile due to stress.
Without coupling between modes, the dispersion increases linearly with length. However, coupling between the polarisation modes causes the accumulation to be proportional to square root of length for long lengths:-

$$\langle \tau \rangle = \tau_B (L.Lc)^{\frac{1}{2}}$$

where:- $\langle \tau \rangle$ = Mean PMD in psec
τ_B = Birefringence (psec/km)
L = Length
Lc = Coupling length

Coupling can be introduced by external stress to the fibre from (for example) bending or twisting the fibre. As a result, the PMD of fibre when measured under tension on a small shipping bobbin is usually low (~0.1 psec/$km^{\frac{1}{2}}$) independent of the true "intrinsic" PMD of the fibre which would be observed without external coupling mechanisms. It should therefore be possible to reduce the PMD in cable by introducing the same type of external coupling to the fibre in the cable as it experiences on the shipping bobbin. Figure 3 shows such reduction in PMD in a slotted core structure where the pitch of the helical groove which guide the fibres has been systematically reduced with a corresponding reduction in cabled fibre PMD. However the method could not reduce the mean PMD to the level required for high bit rate systems.
Similar trials were carried out with the tight buffered cable by introducing an S-Z lay in the fibres. Although some reduction in PMD was observed, the method could not reliably reduce the PMD of all fibres. It was suspected that this was because of the wide range of 'intrinsic' PMD of fibre which could not be measured on fibre supplied on shipping bobbins.

4.1 PMD Measurement methods
Two methods were devised for measuring intrinsic PMD of fibre in conditions where there was little or no external stress acting on the fibre.

4.1.1 Fibre laid out straight method
In this method fibre was laid out straight (250 m length in 2 x 125 m legs) with a turn-round loop at the far end of about ½ metre diameter. Fibre was maintained under slight tension (25 g) to keep it straight. The configuration is shown schematically in figure 4. PMD was measured using the Jones Matrix method (tuneable laser plus polarimeter) in the wavelength range 1480 - 1560 nm. The resolution of the method is better than 0.005 psec or <0.01 psec/km for a 250 metre length.

Coupling between the 2 legs could be changed by turning the end loop. By making measurements with 0, ½T, 1T, clockwise and anti-clockwise in the end loop, a statistical distribution of PMD was obtained from which a mean value could be determined.

Tests showed that fibres had a very wide range of intrinsic PMD (0.03 to > 1 psec/$km^{\frac{1}{2}}$).

The test also confirmed that fibre made with a spinning process (in which the fibre is twisted during pulling) consistently has very low intrinsic PMD (0.025 psec/$km^{\frac{1}{2}}$).

Fibres that were not made with a spinning process could have very high intrinsic PMD (>1 psec/$km^{\frac{1}{2}}$).
A cut back test on such a fibre showed that the high PMD was due to a very long coupling length (> 200 m) rather than high basic birefringence (see Fig. 5).
The measured results of PMD vs. length shown in Fig. 5 fit well to the theoretical model given by Suzuki (Ref. 1) for PMD as a function of coupling length:-

$$\langle \tau \rangle = \tau_B (L.L_c)^{\frac{1}{2}} \left[1 - \frac{Lc}{2.L} \left\{ 1 - \exp\left(-\frac{2L}{Lc} \right) \right\} \right]^{\frac{1}{2}}$$

Where:- L = Fibre length
Lc = Coupling length
τ_B = Linear birefringence (psec/km)

This fibre had linear birefringence of approximately 2.5 psec/km and a coupling length of 280 m.

Applying a small amount of twist to a fibre with high "intrinsic" PMD caused a dramatic reduction in PMD (Fig. 6).

The effect of twisting a fibre that had been manufactured with the spinning process is also shown in Fig. 6. Here there is no improvement to the initial (very low) PMD. At high levels of twist the PMD starts to rise, presumably from circular birefringence introduced by the twist put in during the test.

The method of laying out straight of 250 m samples has proved to be a reliable method for correlating intrinsic fibre PMD and performance in cable (see table 2).

	PMD /ps $km^{-1/2}$		
Fibre Type	**on shipping bobbin**	**laid out straight**	**in cable**
UNSPUN	~0.1	0.03 → >1	0.03 → >1
SPUN	~0.1	0.025	0.05*

Table 2 - Summary of Intrinsic and cabled PMD results.

* mean value of production cable for long haul systems to date

4.1.2 Tension free winding onto spool
This method of measuring intrinsic fibre PMD consists of winding fibre tension free onto a spool. Results with unspun fibre wound onto a 400mm diameter spool at zero tension showed an increase in PMD at zero tension compared to shipping bobbin results (figure 7a).
With spun fibre the opposite effect was seen (figure 7b). Winding from a shipping bobbin onto the 400 mm bobbin at zero tension reduced the PMD from typically 0.1 ps $km^{-\frac{1}{2}}$ to 0.05 ps $km^{-\frac{1}{2}}$.

For unspun fibres with intrinsic PMD of less than about 0.2 ps $km^{-\frac{1}{2}}$, it was found that there was good correlation between the PMD of cabled fibre (loose structure) and the results obtained from the zero tension winding measurement.

For unspun fibres with intrinsic PMD greater than about 0.25 ps $km^{-\frac{1}{2}}$ the method becomes less reliable because the bending induced mode coupling (due to the winding) is sufficient to significantly reduce the PMD in the fibre wound onto the bobbin. Figure 8 illustrates this.

The table in figure 9b illustrates the effect of twist on unspun fibres. The PMD of the fibres was measured on the bobbin wound under zero tension conditions prior to and after twisting. The results show that the PMD of unspun fibre may be significantly reduced by putting even a small amount of twist into the fibre. e.g. in the experiment 1 turn per m twist reduced the PMD from 0.2 ps $km^{-\frac{1}{2}}$ to 0.09 ps $km^{-\frac{1}{2}}$ and 1 turn in 10m reduced the PMD from 0.3 ps $km^{-\frac{1}{2}}$ down to 0.14 ps $km^{-\frac{1}{2}}$.

4.2 Reduction of PMD in cables

4.2.1 Reduction of PMD in ASN tight buffered design

The results with twisted fibre suggested that one approach to making low PMD cable would be to package the fibres and then twist the package during cabling. Trials with this showed that twisting was effective in initially reducing the PMD of the fibres in the package. Figure 9a shows the corresponding reduction in PMD for tight buffered package.

However, it was found that subsequent processing in which the fibre package is subjected to thermal cycling could cause a significant increase in final PMD. This was because of the stresses that were produced in the elastomer when subjected to thermal cycling.

The original material used in NL cable had a tensile modulus of 50 MPa at ambient temperature and the modulus had a high temperature coefficient. Fig. 10 shows an example of the effect on PMD of temperature cycling this type of package. PMD falls rapidly with temperature (the initial high PMD is a combination of intrinsic fibre PMD plus additional stress from the elastomer). After cooling, the PMD increases as the stress in the elastomer increases. The rise in PMD on cooling follows a similar curve to the estimated stress in the elastomer caused by thermal contraction.

This thermal contraction puts both radial and tangential stress on the fibres.

Some tests were carried out to measure the sensitivity of fibres to effects of unidirectional radial stress by crushing fibre between flat plates.

Fig. 11a shows the change of diameter of 4 types of fibre coating when subjected to this lateral loading.
Fig. 11b shows the corresponding change in PMD of the fibres. It can be seen that the fibre coating has a very significant effect on the sensitivity.

Dual coating with a high modulus outer coating and low modulus inner coating (Type C) shows improved performance.

Increasing the coating diameter (400 µm, Type D) is also very effective in reducing the sensitivity of fibre to lateral stress.

An alternative approach of reducing the stress on the fibres by using a lower modulus elastomer was also investigated.

A material with a lower modulus and also a much lower temperature coefficient of modulus compared to the original material was selected.

This approach produced a fibre package with low PMD when used with fibre with low intrinsic PMD (spun fibre) and also low sensitivity to temperature. Fibres with normal size coatings (250 µm) could be used.

4.4.2 Reduction of PMD in ASN loose structure cable

As mentioned previously, it is possible to introduce coupling in fibre by bending and/or twisting the fibre. This can appreciably reduce the PMD of the fibre.

Bending

The ASN loose structure cable uses a slotted core as the fibre package. Fibres are guided in helical slots hence are bent to a certain degree. The amount of curvature in the fibre is dependant on the pitch of the slot. Four prototype cables were manufactured using slotted cores with 4 different pitches, the fibres used in the cables all had the same level of PMD before cabling. The PMD of the cabled fibres were compared with their PMD levels on shipping spools. The best results were obtained with core with the smallest pitch (prototype 1). In the cable with the longest pitch, the PMD of the cabled fibre was 9 times higher than the PMD on the shipping spool (see fig. 3).

Twist

For this experiment 6 fibres were used, chosen to have the same level of PMD (when wound under zero tension onto a 400 mm bobbin) $\cong$ 0.24 ps.$km^{-\frac{1}{2}}$. Four of the fibres were then twisted on the spool prior to cabling, two of them with 1 turn per metre and two of them with 0.5 turns per metre.
After manufacture the cabled results were compared with those obtained under tension free conditions (Fig. 9b). The two fibres which were not twisted prior to cabling showed an increase in PMD (0.24 ps $km^{-\frac{1}{2}} \rightarrow$ 0.33 ps $km^{-\frac{1}{2}}$).
The two fibres which had 1 turn per metre showed a significant reduction in PMD after cabling (0.24 ps $km^{-\frac{1}{2}} \rightarrow$ 0.07 ps $km^{-\frac{1}{2}}$).

Spun fibre

Figure 12 shows the results of a thermal cycling test on loose structure cable using spun and unspun fibre. It is interesting to note that there is no fluctuation of PMD during the test with spun fibre, which have very low levels of intrinsic PMD, whilst on the other hand unspun fibres in the cable showed a high sensitivity to temperature fluctuating between 0.2 ps $km^{-\frac{1}{2}}$ and 0.7 ps $km^{-\frac{1}{2}}$ over the temperature range -20°C to +65 °C.

This allowed a common approach for the two ASN deep water cable designs.

i.e. To use fibre with low intrinsic PMD (spun fibre) with standard coatings and to cable them in a low stress environment with negligible stress change over the operating temperature range. In the case of the slotted core design only minor modifications were required to the fibre package to achieve the required stable low stress condition. For the tight buffered elastomeric package using the low modulus elastomer, extensive processing trials were carried out to optimise conditions to give stable and predictable performance.

Results of qualification tests on the cables are given in section 6.

5. CONTROL OF CHROMATIC DISPERSION

If in a long amplified system the zero dispersion wavelength λ_0 of the majority of fibre is at or below the operating wavelength of the system, the signal will suffer from non linear distortion. These non linearities arise from a number of sources including Four Wave Mixing (FWM) and self Phase Modulation (SPM) (ref. 2). To largely avoid non linear effects fibre λ_0 is chosen to be between 1-3 nm above the system operating wavelength. The effect of this is to produce a slow build up of negative chromatic dispersion along the length of the system. Chromatic dispersion does not by itself cause distortion of the signal, only a phase delay between the different components. Compensation does, however need to be carried out before the leading and trailing edges of adjacent pulses interfere with one another. In practice this means the introduction of short lengths (usually less than 10 km) of Non Dispersion Shifted Fibre (NDSF) about every 600 km along the length of the system producing the characteristic 'saw tooth dispersion map' (fig. 16) adopted in the first generation of amplified systems.

6. QUALIFICATION TEST RESULTS

The ASN optical cables had been extensively used for long haul repeatered systems. Some additional qualification testing was carried out with the modified designs to ensure the stability of the optical characteristics.

Fig. 12 shows the variation of PMD vs. temperature in the range -20°C to +60°C for the two ASN cable structures. There is no significant trend of PMD vs. temperature in either case when using spun fibre.

Fig. 13 shows PMD vs. hydrostatic pressure for the two cables. Again there is no significant change in PMD with pressure. (This is not surprising in view of the fact that the fibres are protected from the effects of hydrostatic stress by the cable structure in both cases.)

Fig. 14 shows the results of an accelerated ageing test for stress in the ASN tight structure cable. There is a small trend of decreasing PMD with time, which may be expected as a result of long term stress relaxation in the elastomer.

The temperature coefficient of chromatic dispersion of the fibre in cable was also measured. Fig. 15 shows the results of dispersion vs. temperature for the two ASN cable structures as well as earlier results obtained for DS fibre only.
Tests on DS fibre only had given the following coefficients for λ_0:-

Temperature:	0.030 nm/°C
Elongation:	1.7 nm per %

In the ASN tight structured package, the fibre is subject to a tensile elongation of about 11 ppm/°C due to expansion of the steel strength member of the cable. Hence the overall temperature coefficient of λ_0 should be:-

$(0.030 + 1.7 \cdot 11 \times 10^{-6} \times 100) \cong 0.032$ nm/°C

The fibres in the ASN loose structure contain a certain amount of slack and therefore do not experience any strain due to thermal expansion of the cable. Hence the temperature coefficient for λ_0 for the ASN loose structure cable will be 0.030 nm/°C.

These values are in good agreement with figure 15.

This figure is important in order to correct factory measurements made at ambient temperature to sea bed temperatures and allow the correct length of compensation cable to be determined. Results of factory and system measurements after installation are given in section 7.

Figure 16 shows the result of a tensile test performed on 1 km of loose structure fibre package. This long length test was performed in order to improve the accuracy of the measurement of PMD and chromatic dispersion as a function of elongation. Furthermore, it gives more reliable information on the behaviour of fibre inside cable.

Fibres are looped to increase the length under test, and package tension is increased to give elongations of up to 0.7%.

In total 6 km of dispersion shifted fibre were under test, monitored in PMD and chromatic dispersion.
The results show that there was no significant change in PMD when the fibre package was subject to elongation. With chromatic dispersion however it is interesting to note that there is no significant change in λ_0 with elongation until cancellation of fibre slack occurs at around 0.5 % elongation.

7. SYSTEM RESULTS

The PMD of four long haul systems with the ASN loose and tightly buffered construction have been measured. the results reflect the changes made in the cable design to reduce the PMD.

Systems A & C were manufactured with fibres that were not spun during pulling. For system A a high modulus matrix material was used to encapsulate the fibres. The conventional loose slotted core was used for system C.

Systems B & D on the other hand operates at a higher bit rate than Systems A and C. With an installed mean PMD requirement of 0.15 ps $km^{-½}$ it was necessary to adopt the modified tight buffered design with spun fibres for system B. For system D it was necessary to incorporate spun fibres into the conventional slotted core design.

Table 3 summarises the PMD measurements made on the four systems. All measurements were made using either the Jones Matrix Eigenanalysis method or the interferometric method. The results for System B and D show a marked improvement in PMD performance over designs A and C. The installed mean PMD of System A is about 6 times higher than that of B and, in addition, System B did not show the increment that System A did after installation. This later effect is attributed to the temperature reduction between factory and ocean, something that was predicted quite accurately from earlier tests with the tight structured cable.

The installed mean PMD of system D is about 3 times lower than that of C. This is mainly due to the use of spun fibre with low intrinsic PMD in conjunction with the loose structure which does not induce stress on the fibre.

SYSTEM	PMD / ps $km^{-½}$			
	cable only	system in factory	system installed	System requirement
A	0.26	0.27	0.44	0.45
B	0.05	0.065	0.07	0.15
C	0.35	0.35	0.33	0.75
D	0.04			0.15

Table 3 - Factory and installed PMD Results

Fibres were selected for Chromatic Dispersion on the basis of those used in the previous sections. The intention was to keep the overall chromatic dispersion of all of the fibres close together at the end of each amplifier span. This helps to simplify the task of selecting fibre for, and length of the equalisation sections. With one or two exceptions this was achieved and the result (corrected to seabed temperature) is shown in figure 17. After the system was installed the end to end Chromatic Dispersion was measured, the results (Table 4) are in excellent agreement with those predicted from figure 17.

Loop	Predicted from factory measurements	Measured after installation
Red + Green	-121 ps nm^{-1}	-116 ps nm^{-1}
Brown + Blue	-115 ps nm^{-1}	-103 ps nm^{-1}

Table 4 - Factory and Installed Chromatic Dispersion Measurements

8. CONCLUSIONS

ASN has conducted a major investigation to understand the phenomena that have an effect on PMD evolution. To this effect a large number of tests were performed with unspun and spun fibres in cable and as bare fibre.

In parallel of that, modifications of cable structure were experienced.

Finally, the optimised solutions were adopted for manufacturing of optically amplified systems which require very low PMD (<0.15 ps $km^{-½}$) and very constant chromatic dispersion.
The results of the qualification tests and data from manufactured and installed systems show that the ASN cables, using loose and tight structure for fibre package have met the optical requirements for first generation long haul optically amplified systems.

REFERENCES

(1) Suzuki et al. Electronics Letters 1983

(2) Russell et al. IWCS Proceedings 1993.

AUTHORS

J.F. LIBERT
Alcatel Submarine Network
536 Quai de la Loire
62225 Calais Cedex
FRANCE.

Jean-Francois LIBERT recieved his engineering degree from 'Hautes Etudes Industrielles' of Lille (FRANCE). He joined Alcatel in 1984. He is now Technical Manager for Optical Submarine Cable in Calais.

J.L. LANG
Alcatel Submarine Network
536 Quai de la Loire
62225 Calais Cedex
FRANCE.

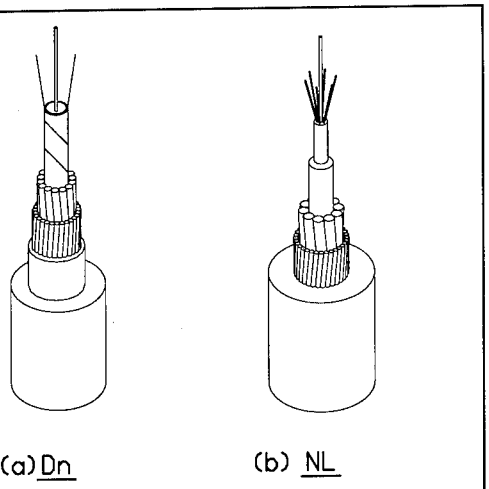
Jean Luc LANG recieved his degree from 'Institut Universitaire de Technologie' of ORSAY (FRANCE). He joined Alcatel in 1975. He is now involved in optical transmision in the technical directorate in Calais.

Peter Worthington
STC Submarine Systems Ltd,
West Bay Road,
Southampton
ENGLAND

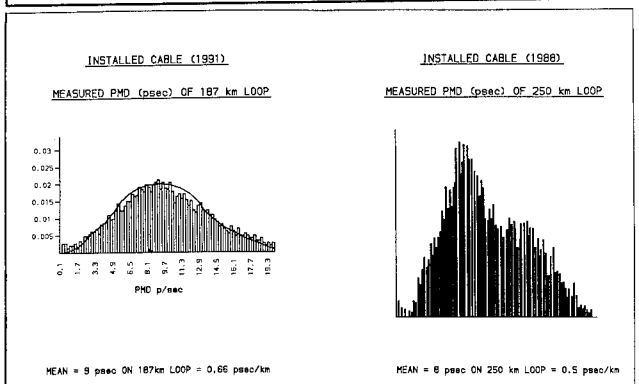
Peter Worthington is a development engineer with STC Submarine Systems which he joined in 1974. He recieved a BSc in Electronics and Electrical Engineering from the University of Birmingham in 1971. Since 1977 he has been involved in the development of optical cables for submarine systems.

David Curtis
STC Submarine Systems Ltd,
West Bay Road,
Southampton
ENGLAND

David Curtis graduated from the University of East Anglia, Norwich in 1980 with a BSc in mathematics. He worked as a development engineer in the coaxial cable industry before joining STC Submarine Systems in 1987, where he has been involved in cable design and deployment issues.



ASN DEEP WATER CABLES USED FOR FIRST GENERATION OPTICALLY AMPLIFIED SYSTEMS | FIG.1



MEASUREMENTS ON INSTALLED SYSTEMS | FIG.2

PMD behaviour of DS unspun fiber in ASN Loose Cable Structure

Effect of the Structure

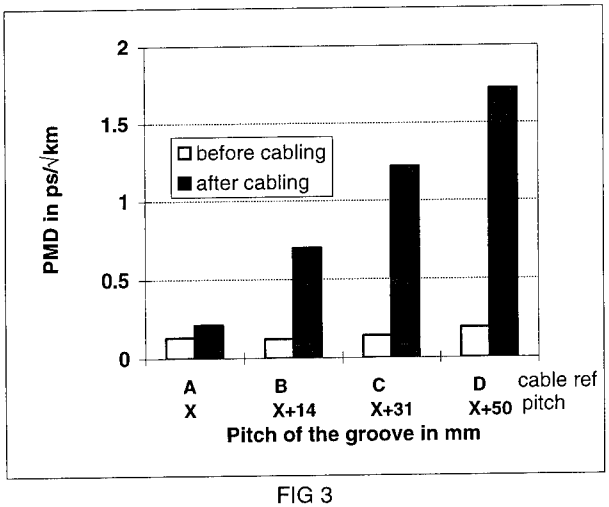
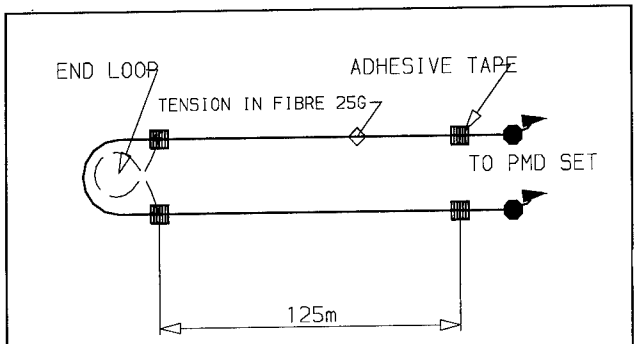
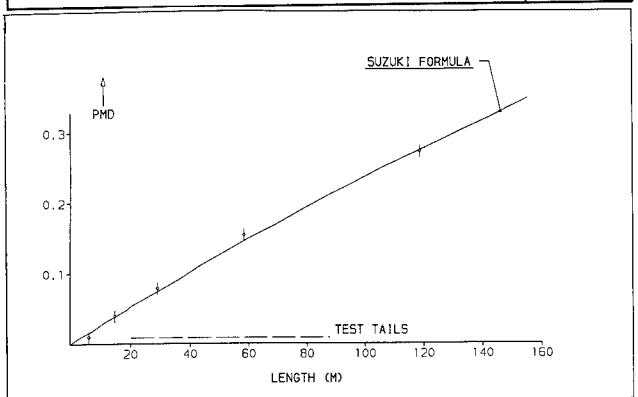


FIG 3

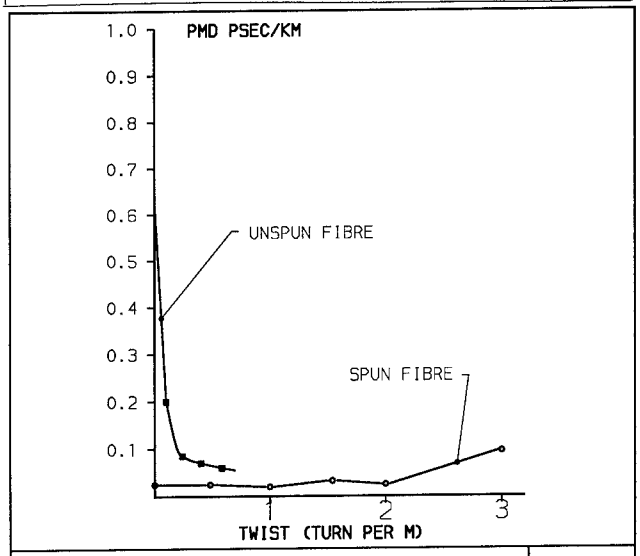


MEASURE WITH 0, 0.5, 1, 1.5, 2 TURNS CLOCKWISE AND ANTI-CLOCKWISE IN THE END LOOP (~ 10 SCANS)

"INTRINSIC" PMD MEASUREMENT ON 250m OF FIBRE | FIG.4



PMD vs LENGTH OF FIBRE WITH HIGH INTRINSIC PMD | FIG.5



EFFECT OF TWIST ON INTRINSIC PMD OF FIBRE | FIG.6

⊗ Short Pitch of helix can induce mode coupling

PMD evolution with winding conditions
Unspun DS fibers

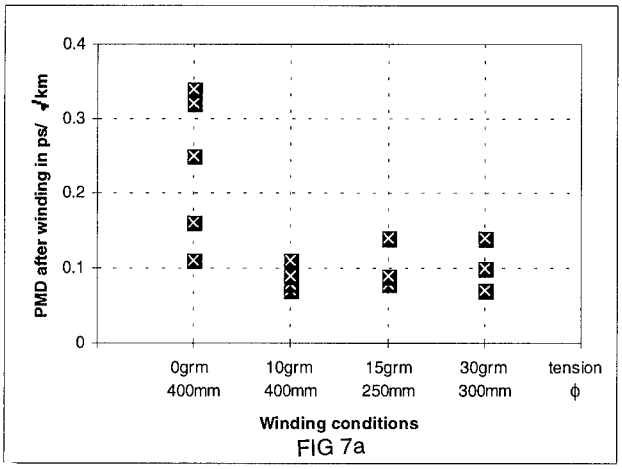


FIG 7a

With Unspun DS fiber, we observed that the PMD decreases when winding tension increases from 0grm to 30grm , the winding diameter being within the range 250mm - 400mm

PMD for Unspun DS fiber in ASN Loose Cable Structure

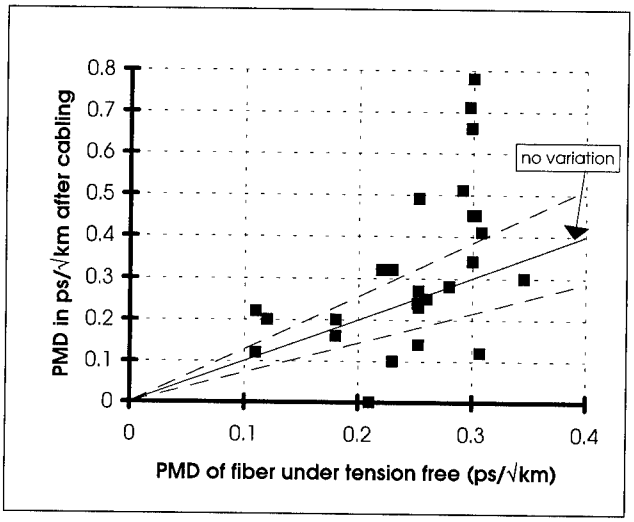


FIG 8

⊕ Low intrinsec PMD FIBER GIVES Low PMD after cabling in ASN Loose Structure Cable

⊕ Good prediction on PMD after cabling, for fibers having intrinsec PMD< 0.25ps/√km.

PMD evolution with winding conditions
Spun DS fibers

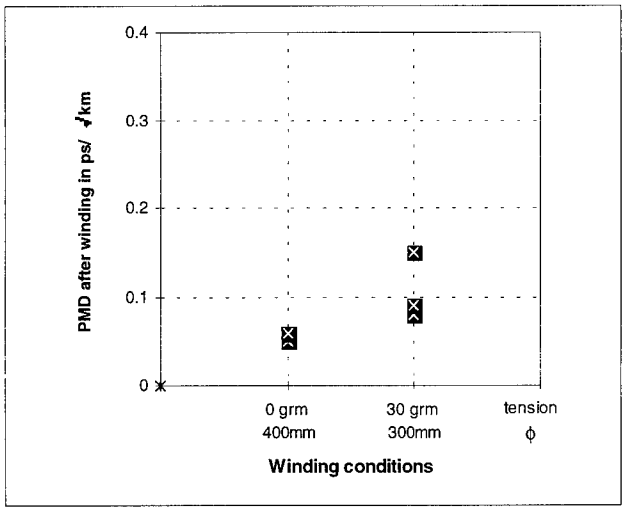
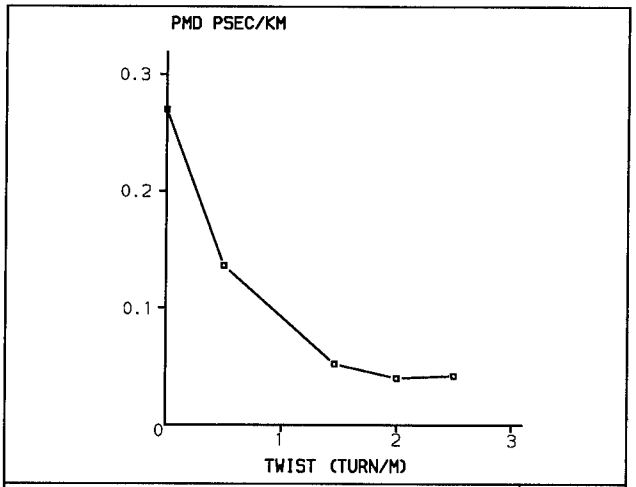


FIG 7b

With Spun DS fiber, we observed that the PMD increases when winding on spool decreases (Ø400mm to Ø300mm) with tension increasing from 0 to 30 grm.



EFFECT OF TWIST ON PMD OF FIBRE IN HIGH MODULUS ELASTOMER

FIG 9a

Effect of twist on Unspun DS fiber and Unspun DS fiber in ASN loose cable structure.

⊗ Effect of twist on fiber

PMD (ps/√km) on unspun DS fiber under tension free on 400mm spool ϕ		
Before twist	After twist	number of twist
0.2	0.09	1 twist/meter
0.3	0.14	1 twist/10 meters

Table 9b

⊗Effect of twist on fiber in ASN loose Cable Structure

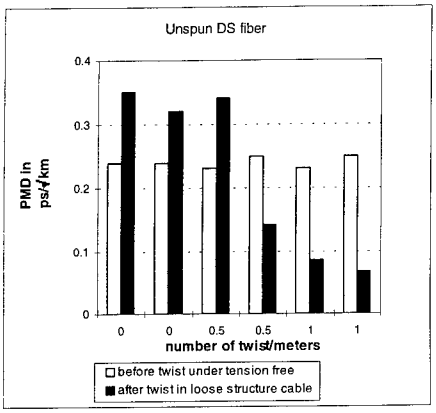
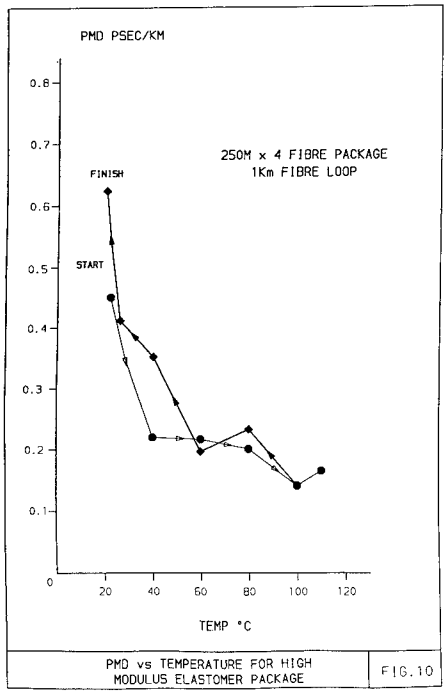


FIG 9b



Thermal Test on ASN Cable Structures
Behavious of spun DS Low PMD fiber and Unspun DS High pmd fiber

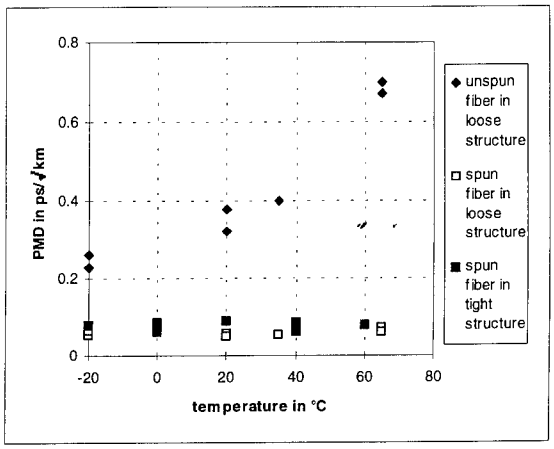


FIG 12

- Spun DS low PMD fiber is no sensitive to T°, in Loose and tight Cable Structures.
- Unspun DS High PMD fiber is very sensitive to T° : PMD decreases when T° decreases.

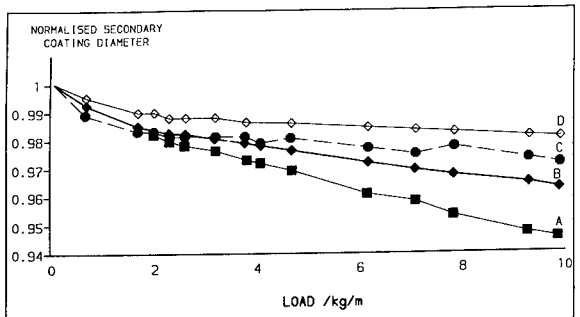


FIG.11a SECONDARY COATING DIAMETER vs LATERAL LOAD

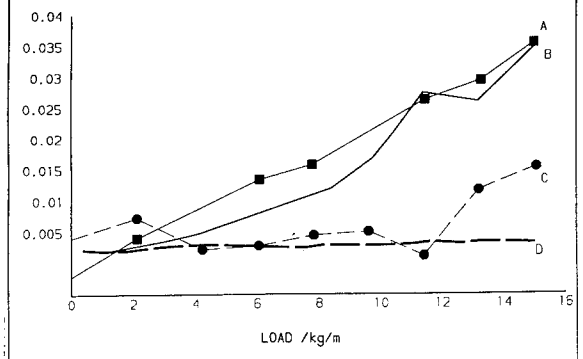


FIG.11b PMD vs LATERAL PRESSURE

PMD vs External Pressure
for ASN Tight Structure NL LW
and for ASN Loose cable Structure 21.5LW

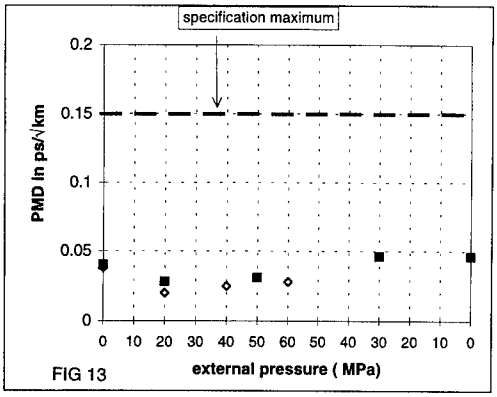


FIG 13

◊ ASN LW Tight Cable Structure
1 km cable 4 fibers looped tested at 10°C.

■ ASN LW Loose Cable Structure
1 km cable 12 DS fibers looped tested at 20°C.

λo vs Temperature on DS fiber
in ASN Loose and Tight Cable Structure

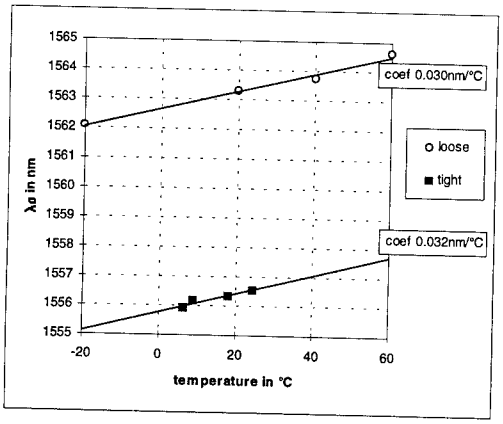
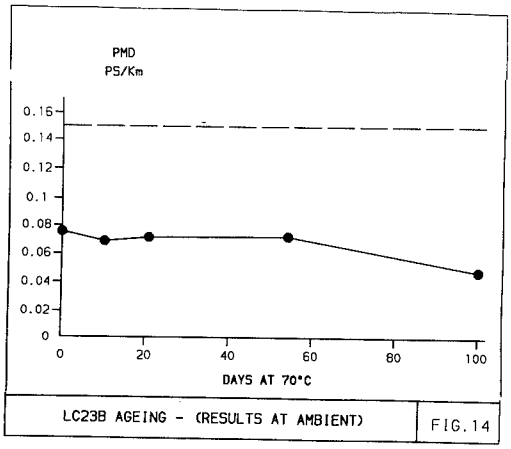
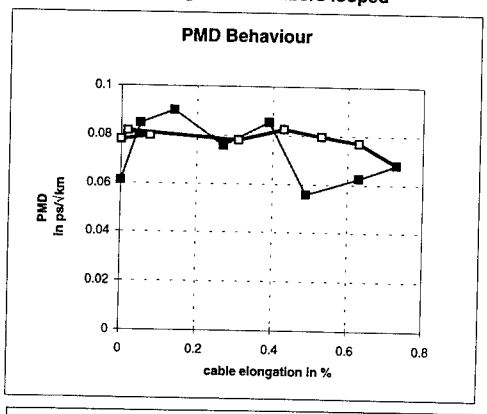


FIG 15



LC23B AGEING - (RESULTS AT AMBIENT) FIG.14

Long Length Elongation Test on DS Spun fiber
in ASN Loose Cable Structure
Cable length 1km 6 fibers looped



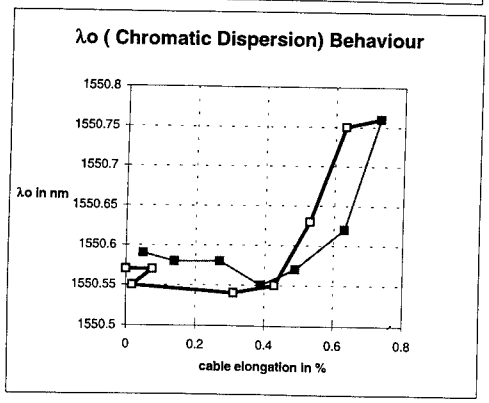
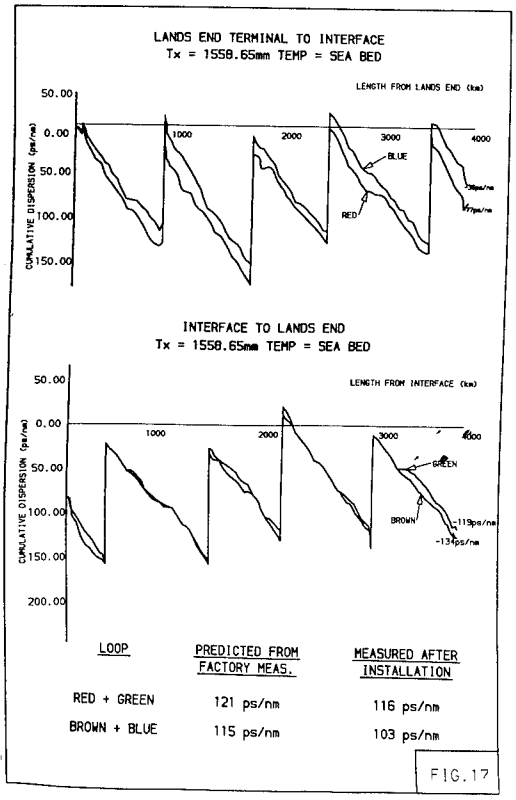


FIG 16



LOOP	PREDICTED FROM FACTORY MEAS.	MEASURED AFTER INSTALLATION
RED + GREEN	121 ps/nm	116 ps/nm
BROWN + BLUE	115 ps/nm	103 ps/nm

FIG.17

ON THE RELIABILITY OF SYSTEM INTEGRATION FROM MULTIPLE SUBMARINE TELECOMMUNICATION SUPPLIERS

L. A. Dissado[(1)], J. Bishop[(1)], I. Doble[(1)], S. V. Wolfe[(2)], Q. Zhong[(3)], W. B. Wargotz[(3)], M. M. Sanders[(3)]

(1) Alcatel Submarine Networks, Southampton, UK;
(2) Alcatel Submarine Networks, Greenwich, London, UK;
(3) AT&T Submarine Systems, Inc., Holmdel, NJ, USA

ABSTRACT

A joint program has been carried through to investigate the high-voltage reliability of submarine telecommunication cables, which are integrated through joints overmolded with polyethylene. A statistical analysis of test data in conjunction with over decades of manufacturing and service experience has provided a "*modus operandi*" for the quantitative determination of the minimum reliability of systems. This methodology comprises a high-voltage quality assurance (QA) sampling test, together with a high-voltage proof-test and an x-ray inspection of the overmolded joint to reveal material/processing imperfections and eliminate moldings with severely hazardous defects. With such, it is expected that different suppliers will allow a standard to be established for the future assembly of submarine telecommunication systems from multiple sources with the various components rated by their estimated reliability. This approach relies on a quantitative reliability factor instead of subjective pass criteria, and therefore, will ensure that long-term reliability of submarine telecommunication systems can be achieved through a substantial margin of safety.

INTRODUCTION

With the globalization of submarine telecommunication business, systems can be manufactured by multiple suppliers. This leads to an increasing need to develop common standards worldwide, which will facilitate the potential integration of a range of designs within a system, including factors such as the supply of spare cable.

If the development of common standards is interpreted as the development of common test procedures, then the valuable experience gained by major suppliers over many years of cable service and development may be lost when testing procedures are changed.

The aim of a test procedure for submarine cables is to produce results which can confirm or verify a high reliability over 25 years of service life. If the reliability is quantified, then it is possible to set a common standard based on this, thereby enabling flexibility in the testing routes which can be used to quantify and then verify the common reliability standard.

Traditionally, in many fields of engineering, there has been a tendency for a degree of overdesign, to a large extent obviating the need for precise reliability calculations. The need for standardization therefore gives manufacturers the opportunity to gain a better insight into the quantification of the product reliability, whilst at the same time retaining some flexibility and independence in terms of specific test regimes. In this way, reliance on potentially poorly defined pass tests will be eliminated in favor of quantitative reliability.

This paper uses the example of high-voltage reliability to demonstrate how a common reliability standard could be achieved between two different suppliers, which can be verified using two different testing processes.

METHODOLOGY FOR QUANTIFICATION OF HIGH VOLTAGE RELIABILITY IN CABLE SYSTEMS

For most transoceanic systems, optical amplifiers or repeaters are typically deployed along the cable at about 45~100 km spacing. Amplifier or repeater termination to the cable employs a polyethylene injection molding technique to complete the continuity of the high-voltage insulation[1]. This technique, which is also used when cable sections are joined together, introduces amalgamations between the undisturbed cable insulation and the polyethylene injectate which effectively act as discontinuities in the insulation system. Extensive work on laboratory samples[1] has shown that the region of amalgamation is potentially a weak site in the system, and hence the moldings contribute most to the risk of electrical failure of the complete system.

Moldings are therefore the controlling components governing the high-voltage reliability of a cable system, such that quantification of high-voltage reliability of moldings will dictate the high-voltage reliability of the system. It is clear, therefore, that although tests on raw material can be useful, system reliability cannot be quantified without testing full-scale joint assemblies. This will enable factors such as the system geometry and design, conductor-insulation interface, raw material and processing effects to be taken into account.

The lifetime of polymeric insulation in a field is generally accepted to obey an inverse power law[2,3]:

$$t \propto E^{-n} \quad (1)$$

where t is the time to failure at a given field E, and n is the life exponent. In order to understand and use this relationship, it is necessary to consider values of t and/or E of statistical significance, and it is widely accepted[4,5] that experimental data of this type provide a good fit to the Weibull function. The Weibull function can be expressed in two ways, dependent upon the testing conditions employed to generate the data. For a ramp test, where the voltage is increased until failure occurs:

$$P_s = \exp\left[-\left(\frac{E}{E_c}\right)^b\right] \quad (2)$$

where:

P_s is the cumulative survival probability

E is the electrical breakdown strength

b is the Weibull ramp exponent

E_c is the characteristic breakdown field, defined as the field E for which $P_s = \frac{1}{e} \approx 0.368$, and the probability of failure, $P_f = 1-\left(\frac{1}{e}\right) \approx 0.632$

For a life test, where the field (voltage) is maintained at a constant level until failure occurs at time t, the Weibull survival probability P_s is given by:

$$P_s(V) = \exp\left[-\left(\frac{t}{t_c(V)}\right)^a\right] \quad (3)$$

where $t_c(V)$ is the characteristic time to failure at voltage V and a is the Weibull time exponent.

In order to quantify the reliability of a molding at service voltage V_o, it is necessary to determine the life exponent, n, and the Weibull time exponent, a. The life exponent n can be obtained by constructing a life plot (log E vs. log t) from ramp data and at least two sets of life tests at different voltages. In constructing the plot, the characteristic ramp field, E_c, is located at the line E_c/R, where R is the ramp rate dE/dt. This procedure overestimates the time to breakdown at the characteristic field E_c, since it includes all the preceding ramp-up time in the value. This means that the failure at E_c is too far along the log time axis, so that the gradient $\left(-\frac{1}{n}\right)$ is too steep and hence the life exponent is underestimated. The procedure therefore gives a worst case prediction of low-field lifetimes. It is adopted here because the conventional technique, verifiable in AC fields[4], has been shown not to apply in DC fields[4,6]. In this latter conventional approach, the cumulative effect of the ramp (or other prestressing) is described through the joint probability of surviving $[P_s(E)]$ for a sequence of time increments, dt, i.e.,

$$1-P_f(E)=P_s(E)=\exp\{-D\int_o^t t^{a-1}E^{na}dt\} \quad (4)$$

where D is a system constant with dimension of [time]$^{-a}$ [field]$^{-na}$ which may be size-dependent. When the field E is independent of time, integration of equation (4) gives $P_s(E)=\exp[-(t/t_c)^a]$ with $t_c=(a/D)^{1/a}E^{-n}$, whereas linear ramp conditions, i.e., $E=tR$, give

$$P_s(E)=\exp\{-DE^{a+na}/[(a+na)R^a]\} \quad (5)$$

Equation (5) predicts a dependence of the characteristic field ($E_c=[bR^a/D]^{1/b}$, $b=a+na$) upon ramp rate R that is not observed experimentally in DC fields[4,6,7]. Thus ramp data alone cannot be used to make DC life predictions[4,6], and the cumulative stressing of the ramp cannot be represented by equation (5).

In normal service conditions, molded joints generally experience a constant voltage. Therefore equation (3) can be used in conjunction with the relationship shown in equation (1) which can be expressed as:

$$t_c\, V^n = \text{constant} \quad (6)$$

to obtain t_c at the operating voltage, V_o. The probability, P_s, of a molding surviving 25 years can then be estimated. This figure defines the electrical reliability of the moldings, and the number of molding failures in a system under any given set of conditions can therefore be obtained by multiplying the failure probability $P_f(V)$,

$$P_f(V) = 1 - P_s(V) \quad (7)$$

by the number of moldings in the system. The value of V_o can be set at the maximum operating voltage for the system. This, of course, overestimates the voltage experienced by most of the joint moldings in the system, and the reliability will in practice be higher than that predicted.

RELIABILITY ESTIMATES ON JOINT MOLDINGS-- EXPERIMENTAL DATA AND RESULTS

The two types of joint moldings, used in this investigation and designated Group A and Group B, have a number of different features with respect to internal geometry, conductor-insulation interface, raw material and processing methods, and might therefore be expected to display somewhat different electrical characteristics.

Three sets of joint moldings were tested from each group--one set was ramped to failure at a ramp rate of 60 kV min^{-1}, the second set was subjected to a life test at 100 kV and the third set was subjected to a 30 kV life test. Additional life data was also available for group B samples at 70 kV.

Figures 1 and 2 show Weibull plots of the ramp test data for group A and B moldings, respectively. In addition, ramp test data for 10m sections of development cable with the same

nominal insulation thickness as joint moldings is shown in Figure 1 for group A, as a comparison.

It is interesting to note that both sets of data in Figure 1, cable and moldings, have very similar Weibull ramp exponents, $b \approx 3.0$ for cable and $b \approx 3.4$ for moldings. However, the characteristic breakdown voltage for cable is considerably higher than for molded joints (V_c for cable ~ 330 kV compared with V_c for molded joints ~ 240 kV). This is to be expected since the electrical strength of the joint moldings is dominated by the electrically weaker material in the amalgamation zone.

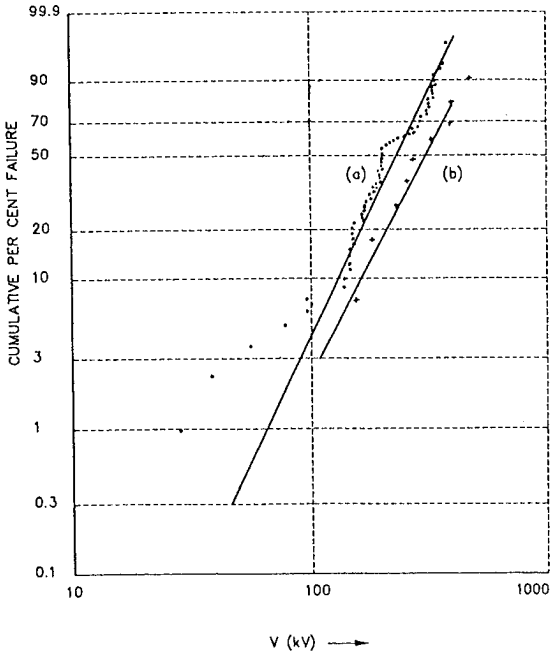


Fig. 1 Weibull plot of ramp test data (60 kV min^{-1}) for (a) full set of Group A moldings, and (b) cable sections.

In Figure 2 for Group B, as expected, a difference in behavior has been observed. The ramp exponent, b, for molded joints is approximately 2.5, whilst the characteristic voltage is higher at around 350 kV. The ramp data for both groups of moldings is summarized in Table 1.

Parameter	Group A	Group B
Weibull Ramp Exponent, b	3.4	2.5
Characteristic Breakdown Voltage, V_c (kV)	240	350

Table 1. Ramp Data for Group A and Group B Moldings

Figures 3 and 4 show Weibull plots of life tests at 100 kV for groups A and B, respectively. Group A (Figure 3) gives a value of the time exponent, a, of approximately 0.5, well below unity. The physical significance of a is in the measure of the time-

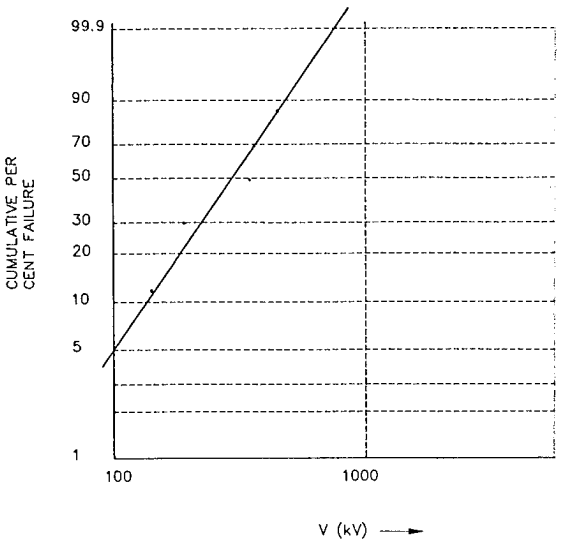


Fig. 2 Weibull plot of ramp test data (60 kV min^{-1}) for Group B moldings.

dependence of processes which age to failure at a constant applied field or voltage. It is interesting to note that thin sections of molded material from Group A also give a similar, low value of, a, (~ 0.26), therefore indicating that physical processes of aging is derived from the processed bulk materials rather than anything relating to the joint geometry.

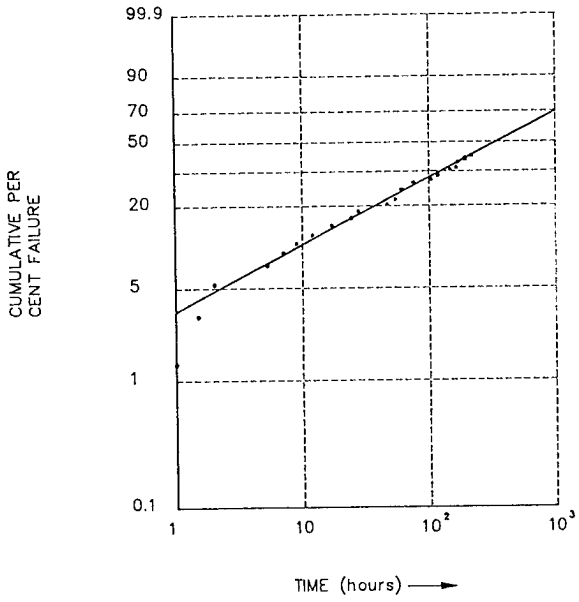


Fig. 3 Weibull plot of life test on Group A moldings at 100 kV, censored at 9 days.

The time exponent, a, for Group B moldings, (Figure 4) is substantially higher, approximately 1.45~1.8, which implies a difference in the nature of the statistical processes occurring.

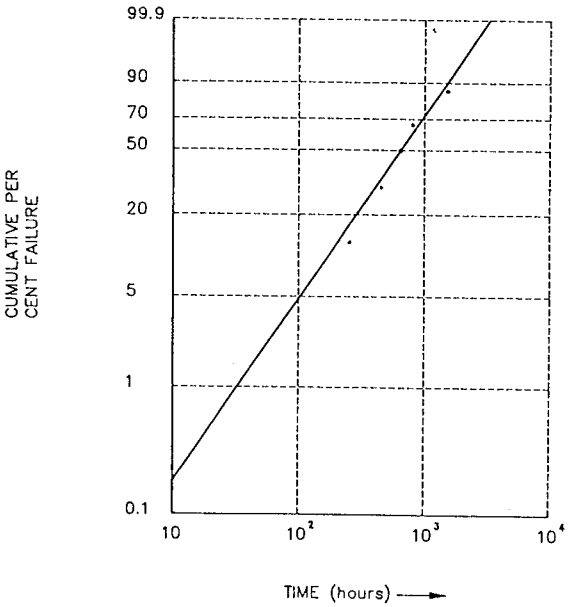


Fig. 4 Weibull plot of life test on Group B moldings at 100 kV.

Figures 5 and 6 show the full life plots for Groups A and B moldings, respectively. At 100 kV and 70 kV, not all samples failed, and the characteristic time plotted in Figures 5 and 6 is that estimated from a censored data plot (see Figures 3 and 4). No samples failed at 30 kV, and the time plotted pertains to that when the test was terminated. This point is shown by an arrow indicating that the characteristic time lies to the right along the time axis.

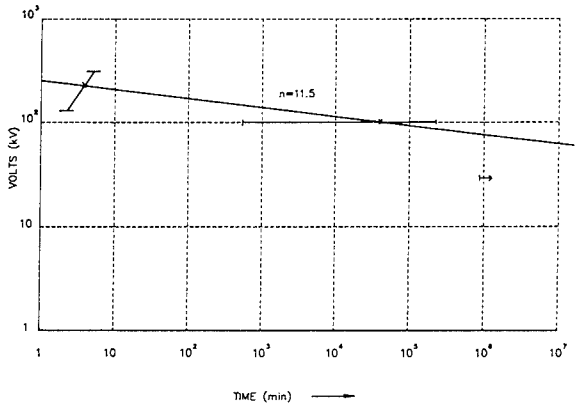


Fig. 5 Life plot of Group A moldings.

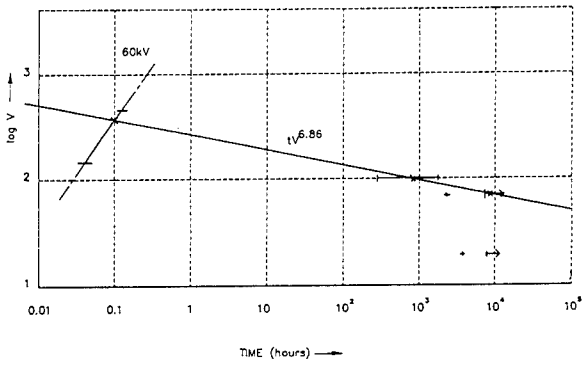


Fig. 6 Life plot of Group B moldings.

The values of n thus obtained for Group A and Group B moldings are approximately 11.5 and 6.9, respectively. The difference in these values reflects the difference in the aging process which has also been observed in the statistical time exponent, a.

In order to estimate the probability of survival, P_s , it is necessary to obtain not only values of a, n, and t_c, but also some indication of the confidence limits of the values. During the experimental testing schedule, it was possible to test a higher number of samples in Group A than in Group B, such that confidence in the estimated parameters will be higher from Group A than Group B.

Table 2 shows a summary of values of a, n, and t_c (for 100 kV life tests) for both groups of moldings. Values of a and t_c are shown as a range for Group B samples, taking into account of the smaller sample size. To consider the difference in confidence limits, calculations of P_s have been carried out for nominal values of the Weibull time exponent, a, for both Group A and Group B, and also for the minimum likely value of a for the Group B samples. The service life is assumed to be 25 years, and the operating voltage V_o is assumed to be 10 kV. Values for P_s (nominal) and P_s (minimum) are also shown in Table 2.

Parameter	Group A	Group B
Weibull Time Exponent, a	0.5	1.45~1.8
Characteristic Time, t_c (at 100 kV) (hr)	695	750~850
Life Exponent, n	11.5	6.9
P_s (10 kV), nominal	0.99997	0.9999995
P_s (10 kV), minimum	0.99997	0.99994

Table 2. Summary of Experimentally Determined Data for Group A and Group B Moldings

The values of P_s (minimum) are very similar for both Group A

and Group B moldings, despite the large differences in the experimentally determined breakdown parameters, and the nature of the physical processes occurring in the two groups of moldings. Even taking the minimum values for the survival probability, P_s, it is assumed that a typical submarine telecommunication system has ~300 molded components, then this level of reliability indicates a safety margin of around two orders of magnitude. This level of high-voltage reliability therefore gives some indication of what could reasonably be set as a standard figure--it is achievable and also gives a good safety margin in the product.

MAINTAINING RELIABILITY IN MANUFACTURING--QUALITY ASSURANCE REQUIREMENTS

As in any manufacturing process, a routine quality assurance measure is required in addition to an initial determination of reliability, in order to guarantee that manufacturing quality is maintained. An effective procedure is to combine inspection tests, factory tests and a high-voltage QA sampling test. Severe stress-enhancing defects (typically those which would fail a ramp test below 30 kV) can currently be eliminated by optical and x-ray inspection techniques, combined with a proof test, such as 1 minute at 30 kV, with the possibility of other techniques becoming available in the future[8]. This can be routinely employed as 100% inspection/testing. This type of routine testing therefore eliminates the possibility of "infant mortalities" in systems typically operating at around 10 kV.

This inspection and testing will not, however, eliminate moldings which could fail at longer times, such as those which would fail between 30 kV and 100 kV on a ramp test, and hence constitute a potential risk to the system. Such moldings can be expected to fail not only when ramped to 100 kV but also when aged for a suitable period at a lower voltage. For these reasons a high-voltage QA test is applied to a regular sampling. The rationale behind the regular sampling test is that "high-risk" moldings contain stress-enhancing defects which reduce the quality of manufacture below the level normally achievable (i.e., the standard distribution which has been shown to give an acceptable service reliability with substantial safety margins). This type of manufacture would only occur when manufacturing conditions drift out of specification; otherwise, moldings in the standard distribution are produced. A regular sampling test therefore serves to monitor the production quality and as a mechanism to verify the molding conditions.

The QA test must be designed to verify that the molding standards achievable in development are retained during manufacture. This can be achieved by two means. Either the values of a and n are verified each time a qualification or quality test is carried out, or the assumption can be made that the values of a and n originally estimated do not change. Either approach is acceptable, providing that, for the second case, there is sufficient molding and service experience to justify the assumption. For example, this would be fully valid for the case of a manufacturer or manufacturing process which has shown a decade's worth of stability and field performance.

Enabling both philosophies to be used yields a wide range of possible test regimes which can verify the molding standards. If we take an example of the first type of test, sample moldings are ramped to 100 kV in order to reveal failures lying outside the standard distribution. The test is then continued for a given dwell time at 100 kV, survival to indicate a pass. The length of the dwell time is fixed to demonstrate that the moldings passing the test lie in the standard distribution and retain its characteristics in terms of the exponents, a and n, and might typically be set at 48 hours, to demonstrate the quality of moldings such as those in Group A. In an example of the second type of test, sample moldings would require a typical pass time of 21 hours at 70 kV, assuming that the life exponent has remained at n=6.9. In either case, the selection of the test regime can vary depending upon the design, optimization of manufacturing and development experience; yet, the quantified reliability is comparably high.

CONCLUSIONS

A method has been described by which a common high-voltage reliability standard could be achieved for different products made by different manufacturers. To establish or quantify the product reliability, an initial development program is required. However, it is possible thereafter to ensure that the quantified reliability is maintained by simple proof-testing and batch testing techniques derived from the reliability data, and these can vary from manufacturers to manufacturers. Examples have been given of typical achievable probabilities of survival, and typical quality assurance testing regimes which guarantee that the survival probabilities are routinely maintained.

Acknowledgment

The authors would like to acknowledge their colleagues, S. R. Barnes, R. C. Nilsson, and S. O'Bow-Hove of Alcatel Submarine Networks, and R. F. Gleason and S. Shapiro of AT&T Submarine Systems for their support and comments.

REFERENCES

1. J. Bishop, I. Doble, H. K. Chan, L. A. Dissado, S. V. Wolfe, and A. E. Davies, "Structure and High Voltage D.C. Behavior of Submarine Cable Moldings", Proc. 40th IWCS (St. Louis), 1991, 634-642.

2. G. C. Montanari and L. Simoni, "Aging Phenomenology and Modeling", IEEE Trans. EI-28, 1993, 755-776.

3. M. Cacciari and G. C. Montanari, "Probabilistic Models for Life Prediction of Insulating Materials", J. Phys. D. Appl. Phys. 23, 1990, 1592-1598.

4. L. A. Dissado and J. C. Fothergill, "Electrical Degradation and Breakdown in Polymers", ed. G. C. Stevens, IEE Materials and Devices Series 9 (P. Peregrinus, London, 1992).

5. G. C. Stone and R. G. Van Heeswijk, "Parameter Estimation for the Weibull Distribution", IEEE Trans EI-12, 1977, 253-261.

6. F. Colla, "Life Test on IC Capacitors", IEE DMMA Conf. Pub. 239, 1984, 253-261.

7. K. Kitagawa, G. Sawa, and M. Ieda, "Electrical Breakdown of Solution Grown Polyethylene Films Without Spherulites", Jap. J. Appl, Phys., 1981, 87-94.

8. N. Hozumi, H, Suzuki, T. Okamoto, K. Watanabe, and A. Watanabe, "Space Charge Measurement in XLPE Cable Insulation under High Field", Proc. ISE8, Sept, 1994, 916-921.



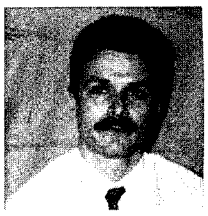
L. A. Dissado
Alcatel Submarine Networks
Southampton, UK

Len Dissado gained his Ph.D. from University College, London University in 1966, and was awarded a Research Fellowship at the Australian National University (ANU). After a period with the Atomic Energy Authority at Harwell, and a further period at ANU, he joined the Dielectrics Group at Chelsea College (which later amalgamated with King's College), London University, in 1977. He has been working as a consultant with STC (now part of Alcatel) since 1980, specializing in the area of dielectrics and DC insulation. He has recently become Reader in Engineering at Leicester University.



J. Bishop
Alcatel Submarine Networks
Southampton, UK

Jim Bishop was born in London, England in 1965. He obtained a B.Sc. in Chemistry with Polymer Since in 1989. After spending a year researching fire retardant polymers, he joined STC in 1990 (STC became a part of Alcatel in 1994), where he has worked on high-voltage reliability, jointing, and contract engineering.



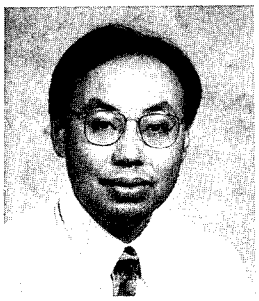
I. Doble
Alcatel Submarine Networks
Southampton, UK

Ian Doble joined STC Submarine Systems (now part of Alcatel) in 1987, after receiving a B.Sc. in Physics from Southampton University in 1982. In addition to maintaining close links with the University, he has been responsible for many aspects of cable and joint development. In 1994, he became Technical Manager for Southampton, and has since assumed responsibilities across the whole of Alcatel Submarine Networks, Cable.



S. V. Wolfe
Alcatel Submarine Networks
Greenwich, London, UK

Sue Wolfe joined STC (now part of Alcatel) in 1970, working on cable materials and cable development. She gained her B.Sc. in Materials Science from Thames Polytechnic in 1976, and her Ph.D. in Materials Engineering from Queen Mary College, University of London in 1982. After a period as Head of Department in the London School of Polymer Technology, University of North London, she returned to STC in 1984, working on optical fiber cables. She is now Manager, Materials and Support Division, Alcatel Submarine Networks, Cable.



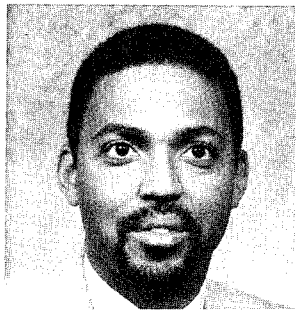
Q. Zhong
AT&T Submarine Systems
Holmdel, NJ, USA

Qian Zhong is a Member of Technical Staff at the Undersea Cable Development and Implementation Department of AT&T Bell Laboratories, Submarine Systems, Inc., in Holmdel, NJ. He is responsible for various aspects of materials development in submarine lightwave cables. He joined the company in 1992, and has a B.S. degree from Shanghai Jiao Tong University and a Ph.D. degree from the University of Pennsylvania, both in Materials Science and Engineering.



W. B. Wargotz
AT&T Submarine Systems
Holmdel, NJ, USA

Bernard Wargotz's work experience includes supervising and conducting research and development in the chemistry industry on new polymers. He has contributed, as manager and member of technical staff, toward the design, material investigations and process development both in communication and power wire and cable, as well as interconnection/electronic assembly technology. His Bachelor and Master of Science Degrees were received from the University of Michigan and his Ph.D. from the University of Rochester. Before his retirement, he was a Distinguished Member of Technical Staff at AT&T Bell Laboratories and concerned with design, materials and processes related to the development of undersea fiber optic cable systems. He is the recipient of 11 patents and authored over thirty publications. Since his retirement, he has been a visiting scientist at the National Oceanic and Atmospheric Administration, National Marine Fisheries Service Center at Sandy Hook, NJ.



M. M. Sanders
AT&T Submarine Systems
Holmdel, NJ, USA

Michael Sanders is a technical manager in the Undersea Cable Products Realization Group in AT&T Submarine Systems, Inc. in Holmdel, NJ. His group is responsible for the technology transfer of submarine lightwave cable product design and manufacturing processes to the cable and repeater factory, and shipboard operations. He joined the company in 1979 and has a B.S.M.E. degree from the Illinois Institute of Technology and an M.S.M.E. degree from the Massachusetts Institute of Technology.

NEW HIGH RELIABILITY DESIGN FOR SUBMARINE REPEATERLESS OPTICAL SYSTEM. QUALIFICATION TEST RESULTS. INSTALLATION BACKGROUND

Jean-François LIBERT - Yves CHARLES

ALCATEL SUBMARINE NETWORK
536 Quai de la Loire - BP 849 - 62225 CALAIS CEDEX - FRANCE

ABSTRACT

ASN has developped a new high reliability cable design specifically devoted to unrepeatered coastal and medium depth systems (5 000 m).

The design has emphasized high fibre count and integrated the background acquired by ASN in the S 560 and GIGA 5 systems.

A presentation of the design and its advantages will be done. The fully qualification and the already huge background of installation will be presented.

INTRODUCTION

The 14 mm cable family, designed for a 25 years period life time, covers armoured and deep sea cables which can be laid and recovered from respectively 2 000 m and 5 000 m depth.

I - CABLE DESCRIPTION

1 - Key points of the structure

Fibers and fiber unit structure

The fiber unit structure is based on the use of a stainless steel tube. This tube is designed to provide a loose structure which is very friendly and powerful with regard to optical performances.

The material and process answer to the following fonctionalities :

- very low elongation under load,
- good hydrogen barrier close to the fibres,
- high crush and impact performances,
- high fiber count (≤ 24 fibres).

Fibers are laid straight inside the cable core.

In addition to that, a small fiber slack allows the use of low proof test level and prevents any fiber stress even when the cable is bended.

Inside the tube, a jelly acts as a buffer around the fibers and as a barrier against water ingress and moisture.

Composite Conductor

The steel wires and the vault construction provide a very high strength member to the cable (the ultimate tensile strength garanteed for the LW cable is greater than 60 kN). This vault provides also a good hydrostatic pressure behaviour. It can sustend 1 000 bars pressure.

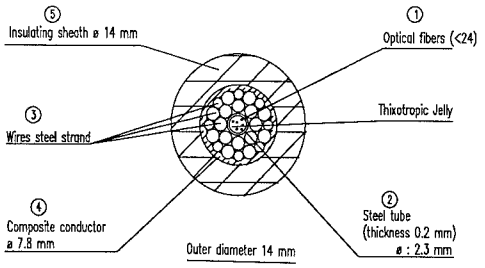
A welded copper tube is formed, welded and reduced around the vault in order to get a very compact composite conductor.

This composite conductor provides a double H_2 barrier thanks to the use of a welded stainless steel tube and to this welded copper tube.

Polyethylene sheath

The use of high density polyethylene sheath gives very good abrasion performances and increases the cable density by reduction of the requested PE thickness.

All that is integrated in the following LW cable design.

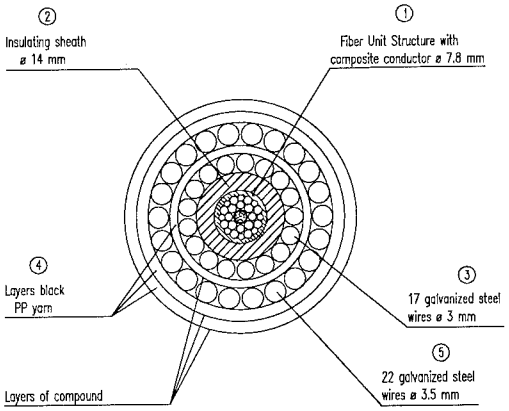


2 - Armoured cables

Three types of armouring are proposed to protect the deep sea cable against rocks, trawlers damage and fish bite. Armoured cables and LW cable have been designed to allow the recovery of any cable type from its maximum depth by any adjacent other cable.

Double armour (DA)

The protection is provided by two layers of preformed galvanised steel wires. The armoured cable is suitable for shallow water down to 500 m.

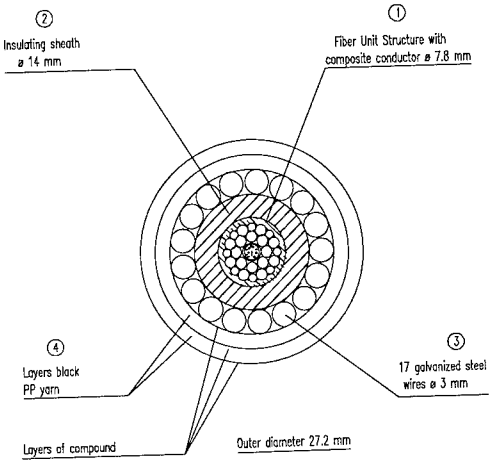


Single armour (SA)

Protection of the cable is provided by one layer of galvanised steel wire. The single armour design is suitable for sea depth down to 2 000 m.

Laying and recovery from such a depth are achieved thanks to the wires preformation which prevents any residual torque and twist normally induced during the armouring process.

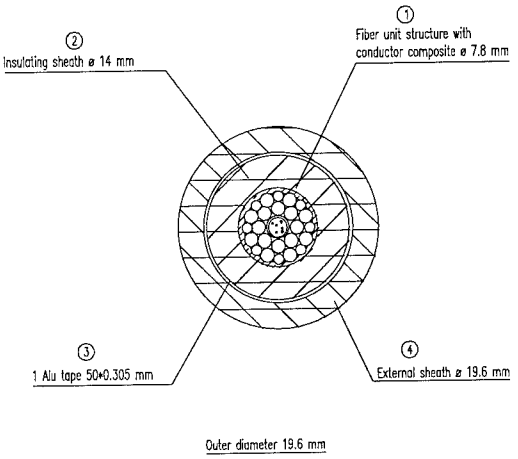
The optimisation of the armoured designs provides good flexibility and handling performances.



Screened cable (LWP)

Protection of the cable is provided by an aluminium tape overlaid by an outer high density polyethylene sheath.

The LWP cable protects the deep sea cable against abrasion and fishbite down to 5 000 m water depth.



Hereafter are presented the main performances of the 14 mm cable family.

		LW	LWP	SA	DA
CHARACTERISTICS	UNIT	VALUES	VALUES	VALUES	VALUES
C C electric resistance at 10°	Ω/km	< 1.6	< 1.6	< 1.6	< 1.6
Water ingress ; 15 days 500 bars	m	< 1 000	< 1 000	< 1 000	< 1 000
Insulation sheath thickness	mm	3	3	3	3
Aluminium resistance at 10°	Ω/km	-	< 1.8	-	-
Protection Sheath thickness	mm	-	2,5	-	-
Armour steel wires first lay	Nb x mm	-	-	17 x 3	17 x 3
Armour steel wires sec lay	Nb x mm	-	-	-	22 x 3.5
OUTER CABLE DIAMETER	**mm**	**14**	**19.6**	**27.2**	**36.8**
Cable weight into the air	kN/km	4.4	6.2	16	34.7
Cable weight into the water	kN/km	2.8	3.1	10	24
UTS	kN	60	60	186	264
Modulus	km	21	19	18	11
NPTS	kN	12	12	58	50
NOTS	kN	24	24	117	147
NTTS	kN	42	42	156	196
Maximum use depth	m	5 000	4 500	2 000	500

II - QUALIFICATION

An extensive test programme (130 tests), designed to explore all the extreme in-service conditions has been performed. The tests include factory based tests and sea trial.

1 - Factory based tests

Most of the following tests have been successfully achieved on each cable type and follow the IEC 794.

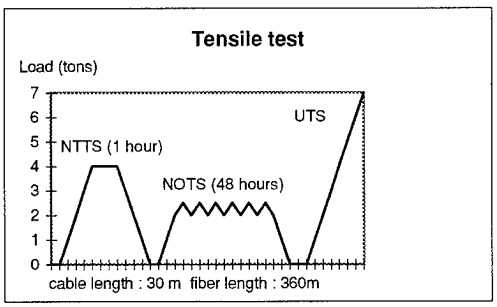
TESTS	SAMPLES	REQUIREMENTS / RESULTS
Cumulated NOTS, NTTS, UTS under fixed gyration (0.4 turn / m)	- LW cable - LW cable with jointing box - SA cable - DA cable	**AFTER NOTS / NTTS** - No residual attenuation(< 0,002 dB). - No significant residual elongation. **AFTER UTS** . Breaking load > UTS. . Fibre and cable break and same location (~ 1 m). . Cable expertise compliant . Joint box expertise compliant.
Cumulated NTTS, UTS under free gyration	- LW cable - SA cable - DA cable	Same requirements as above.
Long length tensile test under NTTS elongation	LW cable	No residual attenuation (< 0,02 dB)
Sheave test	- LW cable with jointing box - SA cable with jointing box - DA cable with jointing box	No residual attenuation (< 0,02 dB). Cable expertise compliant. Joint box expertise compliant.
Thermal test 0° C /, 35° C - 20° C / 65° C	- LW cable - SA cable - DA cable	No significant evolution between 0° and 35° (< 0.002 dB / km). Optical reversibility after test (-20° C / 65° C).
Ageing test	LW cable with jointing box	No significant evolution for 1 240 nm pic. No evolution between 1 530 and 1 570 nm.
Water ingress 15 days - 500 bars	LW cable	Penetration less than 330 m.
Hydrostatic pressure 500 bars	LW cable	Optical attenuation < 0.02 dB during test. No fiber stress.
Bending / Crush / Impact 15 alternative bends on 1 m radius. Impact : LW - 2 kg weight released from height of 1.5 m. SA -DA : 1 ton pannel pulled at 4 knots. Crush : 2 LW cable samples crossed and load at 30 DaN for 1 month.	- LW cable - SA cable - DA cable	Cable expertise compliant.
Joint box expertise	-	. X-ray examination conform . Pressure test 1 000 bars - 24 h * 45 kV - DC for 1 mn conform, * examinantion of PE amalgamation conform, * DC resistance < 0.2 Ω, * visual internal inspection conform, * breaking load of cable, anchoring (LW base) > 50 kN.
Cable expertise	-	. Visual assessment . Pressure test 500 bars - 24 h * 45 kV - DC for 1 mn compliant, * cable ovality < 100 µm.

In order to have a good idea of the originality and severity of these factory based tests, four of them are detailed hereafter.

Tensile Test

The originality of the test is based on the cumulation of strength, and in final, verification of integrity of fonctionality of the cable.

This test has been carried out successfully on Deep sea cable and on Armoured cables (LW, SA, DA).



A 12 fibre sample of 30 meters is subjected to forced paying out at 0.4 rev / m, and then is submitted for 1 hour to a static load equivalent to NTTS with elongation and optical measurements. No residual optical attenuation has to be seen after NTTS test.

The same sample is then submitted to dynamic fatigue for a duration of 48 hours equivalent to NOTS (28800 cycles of 6 seconds period to simulate sea waves). After this test, no residual attenuation has to be seen. The elongation during NOTS is measured.

The residual elongation after the NTTS and the NOTS test must not be significant and have no effect on the 25 period life of the cable. That means that the elongation after test must be less than elongation at NPTS. Finally, the same sample is submitted to UTS test. The cable break must not appear before designed UTS. The cable and fibre breaks must be located in the same area. The fiber break must not appear before the cable break.

At the end of the test, the cable expertise must satisfy :

- hydrostatic pressure for 24 hours under 500 bars,
- dielectric strength greater than 45kV for 1 mn,
- vault ovalisation lower than 100 µm.

Sheave test

This test has been carried out successfully on Deep sea cable and on Armoured cables with jointing boxes (LW, SA, DA).

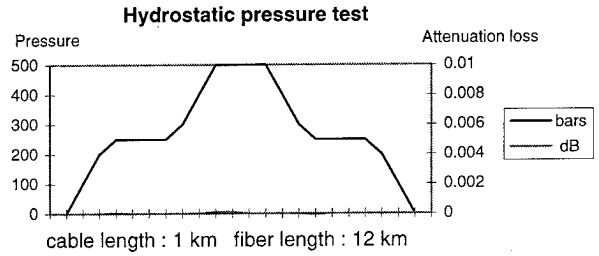
A 12 fibres cable sample of 100 m long is submitted to 15 go and back around a 3 metres diameter sheave. The angle is fixed to 135°. Fibers are optically monitored and after test no residual attenuation must be seen.

After completion of this test, the jointing box expertise must satisfy :

- X ray on PE overmoulding,
- dielectric strength greater than 45 kV / 1 mn,
- ohmic resistance lower than 0.2 Ω on joint
- pressure test 1 000 bars for 24 hours,
- anchoring performance greater than 90 % of cable UTS,
- no degradation of amalgamation zone,
- no visual damage.

Hydrostatic pressure test

This test has been successfully performed on a deep sea cable. A 12 fibre cable sample of 1 000 m long is inserted in a longitudinal pressure vessel. Fiber attenuation and fiber stress are recorded under different pressure up to 500 bars.



No optical attenuation and no fiber stress must be revealed before, during and after test.

Long length tensile test

This test has been successfully performed on optical module. The purpose of the test is to check satisfactory optical performance of the fibers when the cable is subjected to longitudinal mechanical stresses. The length of fiber monitored is long enough to get a great accuracy on optical measurement.

An optical module of approximatively 700 meters, incorporating 12 fibers is subjected to tensile loading up to 90 DaN, equivalent to 0.6 % elongation.

The 12 fibers (i.e 8.4 km) are monitored for attenuation at 1.5 µm and for stress.

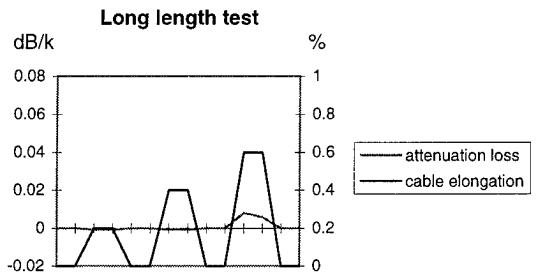
Elongation of the optical module is measured during the test.

Requirement :

The fiber shall not break during the tensile test. After return to nil load, there shall be non remanent attenuation.

The obtained results were :

- no increase of attenuation before and after the fiber slack resorbtion,
- there was a very slight evolution of attenuation above slack resorbtion,
- the evolution was reversible on return to 0 DaN.



Sea trial

The cable design was finally qualified in a sea trial performed in the Atlantic sea.

The purpose of the trial was to validate the cable repair in real operation and to evaluate the behaviour of each cable type during different life period of the cable (laying, recovery, standby).

Cable samples

37 km manufactured spared in 10 km of armoured cable and 27 km of deep sea cable, containing 12 fibers.

Weather conditions

Wind : 5 -7 Beaufort.
Waves : 4 - 5 m height.

The sea trial was carried out under severe conditions as it could be frequently encountered in Bay of Biscay at this period of the year (January -February).

Results

The 14 mm cable family emphasised good behaviour during laying, hanging and recovery.

The deep sea cable and the jointing box proved that they can recover the armoured cable from 2 000 meters water depth under severe weather condition.

The armoured cables were laid and recovered from their maximum specified depths (500 meters and 2 000 meters),

The quality of the cable transition and the armour wire preformation process proved their efficiency.

The cable proved its good handling performances and was laid and recovered both by LCE engine and by motorised capstan.

FIBRE TYPE	AT FACTORY	BEFORE LAYING	1RST LAY BY STERN	2ND LAY BY BOW	RECOVERY
NDS TYPE A	0.186	0.186	0.185	0.184	0.186
NDS TYPE B	0.222	0.222	0.221	0.223	0.224
NDS TYPE C	0.228	0.229	0.229	0.229	0.229

From the optical point of view results were also significantly good since during any stage of the sea trial (loading, laying and recovery from both LCE and motorised capstan) they do not have significant evolution.

III - INSTALLATION BACKGROUND

The 14 mm cable family has been already laid in various world areas. This design optimizes all the improvment done on the S 560 and GIGA 5 systems of ASN. It has exhibited good behaviour all along the 2 000 km already manufactured and installed.

Hereafter 4 links already laid are presented.

- KINYRAS,
- ECFS,
- CC5,
- BASS-STRAIT.

KINYRAS

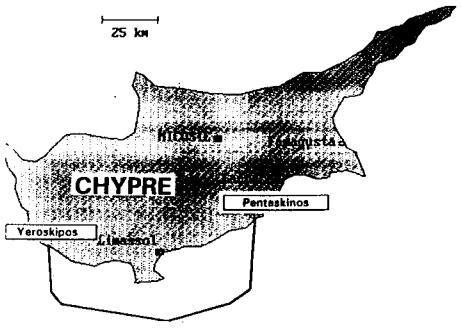
KINYRAS is a domestic link in Cyprus. 150 km length between Pentaskinos and Yeroskipos.

. Fiber count : 12.

. Cable attenuation loss : 0.18 dB/km.

. Laying speed :

LW cable	: 5.5 knots,
SA and DA cables	: 3 knots.



In only 36 hours, two shore ends and the laying operation were carried out in spite of the fact that the survey gave locally some great bottom slope (25° up to 30°).

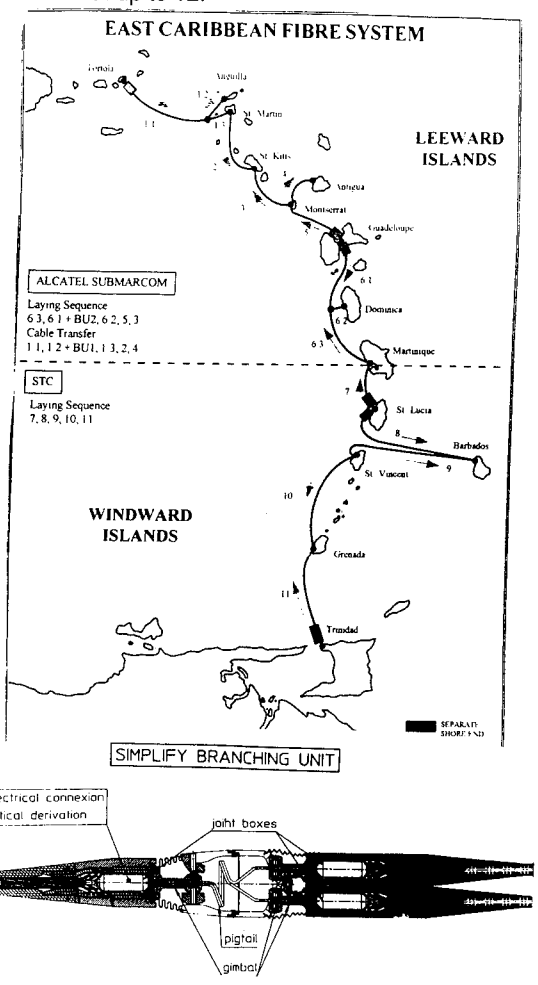
The straight line diagram contains :

- 14 km double armour (DA),
- 46 km single armour (DA),
- 90 km deep sea cable (LW).

The Deep sea cable was laid down to 2 400 m and the armoured cable down to 1 300 m.

Eastern Caraibbean Fiber System (ECFS)

ECFS is a festoon which links islands in the Caribbean Sea : fiber count : up to 12.



For this link 1011 km were manufactured :

- 133 km land cable,
- 128 km double armoured cable (DA),

- 291 km single armoured cable (SA),
- 459 km screen cable (LWP).

The SLD of this festoon required 25 transitions :

- 10 transitions LWP-SA,
- 25 transitions SA-DA.

During this link two simplified Branching Unit developped and qualified by ASN were laid.

MAIN LAND - CORSICA 5 - (CC5)

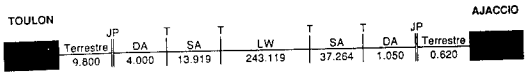
CC5 is a point to point link of 300 km long between Toulon and Ajaccio (France).

. Fiber count : 12.
. Cable attenuation loss : 0.18 dB / km.

The straight line diagram is presented hereafter :

Maximum depth : 2 700 m

Maximum speed :
* LW cable : 5.5 knots,
* SA, DA cable : > 3 knots.



TYPE DE CABLE	QUANTITES (km)
Terrestre	10.420
DA	5.050
SA	51.183
LW	243.119
TOTAL	309.772

BASS STRAIT

The BASS STRAIT system length is 244 km long from Sandy point, Australia to Boat Harbour, in Tasmania. The entire length was armoured and ploughed.

The installed cable attenuation including splices and joints was 0.179 db / km.

During phoughing the cable was easy to handle. The phoughed depth was 1 meter. The phoughing average speed was 1.5 knots :

The good performances of the armoured designs of the 14 mm cable family was well confirmed by this laying.

On shore ends, some articulated pipe specifically designed for this cable were used to increase the abrasion performances.

- CONCLUSION -

A new cable design has been developped and qualified for unrepeatered medium depth system down to 5000 meters depth.

It is based on the use of a longitudinally welded stainless steel tube which gives a lot of advantages with regard to fiber protection and fiber count. (up to 24).

In addition to that, the rest of the design get the benefit of S560/5 GIGA bits cable design.

A huge program of factory based tests, enabled to explore the capability of this new cable design and its reliability for 25 years life time is proven.

Untill now, more than 2000 km of cable have been manufactured.

During installations and sea trial, maximum deployment depths for any cable type have been achieved, ploughing performances have been well proven, passive branching units have been installed and articulated pipes for extra protection were successfully used.

Acknowledgments

The authors wish to thank the TCC staff for their contribution to this paper

Authors

Jean-François LIBERT received his engineering degree from «Hautes Etudes Industrielles» of Lille (FRANCE). He joined Alcatel in 1984. He is now Technical Manager for Optical Submarine Cable in Calais.

Yves CHARLES was born in 1967 He is graduated from « Ecole Universitaire Des Ingenieurs de Lille».(FRANCE). He joined Alcatel in 1993 where he is now in charge of cable design qualification and tests programs inside the Submarine technical department.

Development of the Optical Cable Unit in Composite Tether Cable for Deep Sea Unmanned Vehicle System (KAIKOU)

Akira Sano,Akio Mogi,Osamu Koyasu,Koichiro Watanabe and Matsuhiro Miyamoto

FUJIKURA Ltd.Opto-electronics Laboratory

1.ABSTRACT

The optical fiber cable unit for the KAIKOU system was required to have some specific properties. As its diameter had to made as small as possible (within permissible limits), it was necessary to obtain such properties as flexibility, tensile strength, water tightness and water pressure resistance.
As a result of out investigations including those under high water pressure, we developed a high performance cable unit for the KAIKOU system. The system succeeded in transmitting information on the deepest seabed in the world on March 24, 1995.

2.INTRODUCTION

In Japan, scientific and technical interest in deep sea bed has been increasing for the survey of oceanic resources. The Japan Marine Science and Technology Center (JAMSTEC) has been developing many kinds of seabed survey systems for that purpose.
Shinkai 6500, a manned deep submergence vehicle capable of diving to deep seabeds, was developed to obtain seabed information.
The KAIKOU system, a new unmanned deep submergence vehicle capable of diving to a depth of about 11,000 m (the deepest seabed), was developed to survey the seabed where it is too dangerous for manned deep submergence vehicles to operate.

For the success of the KAIKOU system, we had develop a high performance optical fiber cable unit that can resist to high water pressures.

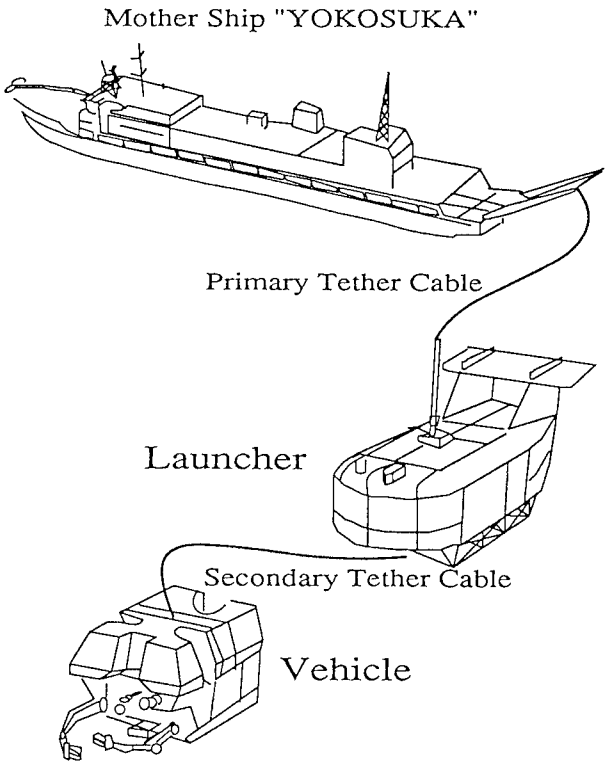
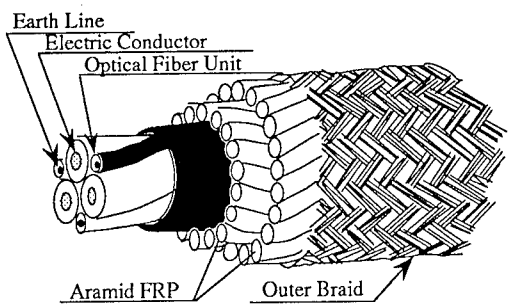


Fig.1 "KAIKOU" System

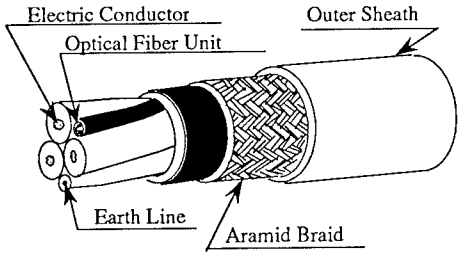
3.BRIEF DESCRIPTION OF KAIKOU SYSTEM

Fig. 1 shows the composition of the KAIKOU system. The system consists of a control station,

mother ship "Yokosuka," launcher as relay station, and unmanned vehicle, The primary tether cable connects the mother ship and launcher and the secondary tether cable the launcher and vehicle. The primary tether cable has to sustain the total gravity of the launcher, secondary tether cable and vehicle in the water.



Primary Tether Cable Structure



Secondary Tether Cable Structure

Fig.2 Primary and Secondary cable Structures

Main specifications of the primary cable are as follows:

Cable Diameter : 44mm (1.7inch)
Cable Length : 12,000m (40,000ft)
Break Strength : more than 40tons
Voltage : AC 3000V,3 ϕ ,60Hz
Optical Fiber Unit
Fiber type : single mode
Fiber number : 4
MFD : 10 μ m

The secondary tether cable has to sustain only the gravity of the vehicle in the water. Compared with the primary tether cable, the secondary tether cable requires greater flexibility and lighter weight for manipulation of the vehicle. Main specifications of the secondary cable are as follows:

Cable Diameter : 28mm (1.1inch)
Cable Length : 250m (820ft)
Break Strength : 3tons
Voltage : AC 3000V,3 ϕ ,60Hz
Optical Fiber Unit
Fiber type : GI
Fiber number : 3
MFD : 50 μ m

Fig.2 shows the structure of the primary and secondary tether cables. The primary tether cable has many stranded aramid FRP rods for sustaining the heavy gravity, while the secondary tether cable has an aramid braid. The secondary cable is made lightweight by allowing the primary cable to share most of the total gravity in the water.

In this report, we will describe the development of an optical fiber unit of the secondary tether cable exposed to the highest water pressure in the world.

4.EXPERIMENT

The most difficult problem was resistance to high water pressure. We had to develop a high performance optical fiber cable unit that can resist to high water pressures. After careful consideration, we designed three types of structure for the optical fiber unit of the secondary tether cable.

4.1Structure

Fig. 3 shows the structures of the experimental optical fiber units of the secondary tether cable. For the secondary cable which throughout its length goes down to the deepest seabed in the world, it is desirable that its structure be capable of minimizing the fiber strain by water pressure. Therefore, we adopted a four-groove slotted rod, single-fiber structure as the basic unit design and investigated for comparison three fiber units different in the groove

filling method which exerts the greatest effect on water pressure resistance. The actual secondary cable is a composite with power cable, so the water pressure applied to it is relieved to some degree. In terms of reliability , however, the fiber unit itself is also required to have a property enough to withstand the conditions of the deepest part in the world. The A unit is of a perfect mobile type in which the grooves are filled with air. In this structure, the grooves take their own share of water pressure resistance.

The B unit is of a type in which the grooves are filled with semi-fluid material to enable the fiber to move to some degree. In this structure, water pressure is shared by the entire unit, but on the other hand high water pressure is applied to the fiber itself.

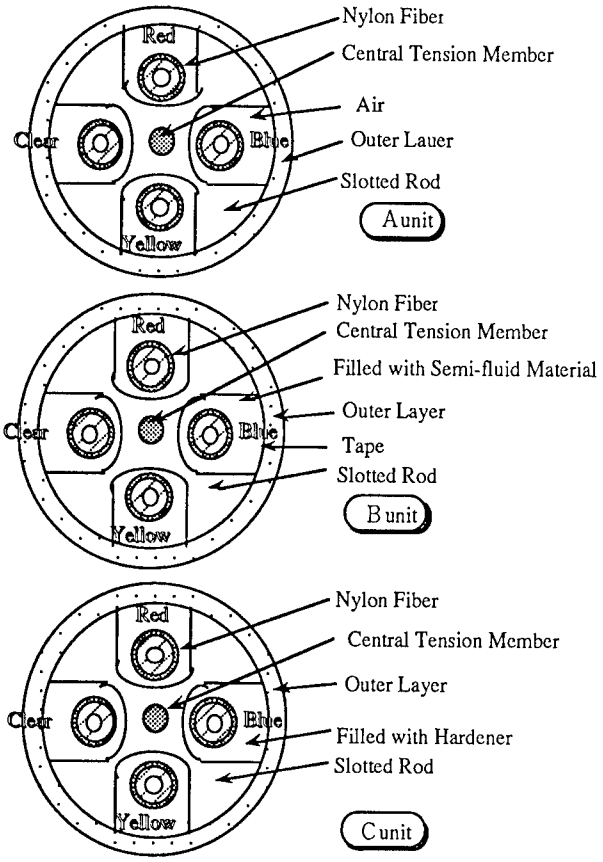


Fig. 3 Cross section structures of test units

The C unit is of the so-called tight type in which the fiber is fully fixed in the groove. In this structure, water pressure is shared by the entire unit as is the case with the B unit. The secondary cable itself is required to be small-size and lightweight, and the unit stranded in it is placed in a vacant space in the power cable. Therefore, the outside diameter of the unit is limited to about 4.0 mm.

4.2 In-process Variation in Transmission Loss

Fig.4 shows the in-process variation in transmission loss. Variations in transmission loss produced in each stage of the cabling process and those caused by changes in environmental temperature were measured by the OTDR method at a wavelength of 1.31 μ m. There were no clear differences due to the difference in the groove filling method, and variations in transmission loss were within measurement error.

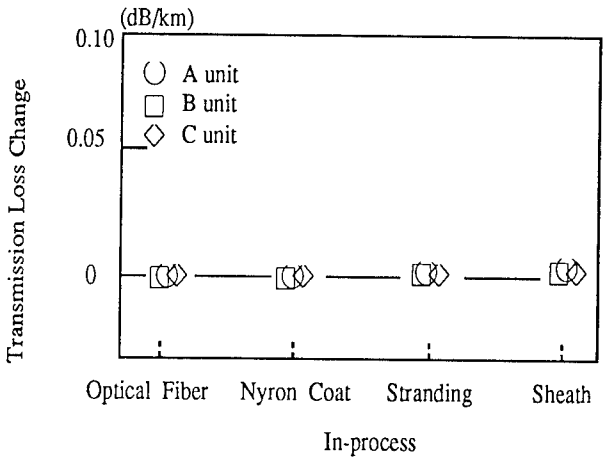


Fig.4 In-process Variation in Transmission Loss

The fibers used in the experiment were the same for the A, B and C units, i.e., they were cut from a length of fiber. Table 1 shows the fiber parameters.

Table-1 Fiber Parameters

Kind	GI Fiber
Fiber Diameter	125 μ m
MFD	50 μ m
Optical Fiber Diameter	0.4mm
PA coating Diameter	0.6mm

4.3 Thermal Properties

Fig5 shows the thermal properties of the optical fiber unit. Four heat cycles from -20℃ to +60℃ were performed with good result: variations in transmission loss were less than $\pm$0.02 dB/km in each of the A, B and C units. During the test, the filler was seen leaking out slightly at the end portion of the B unit, but the degree of leakage did not affect measurements. In general, the environmental temperature of cables laid on the seabed is very stable, but the KAIKOU system is required to be also stable against the short-term temperature variation due to submergence and withdrawal from the water.

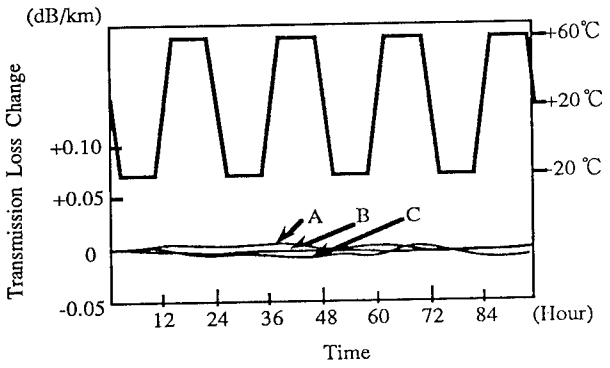


Fig. 5 Temperature Dependence of Transmission Loss

4.4 Water Pressure Resistance

4.4.1 Variation in transmission loss

Fig. 6 shows the water pressure dependence of transmission loss. In the A unit with no filler in the grooves of the slotted rod, degradation in transmission loss performance begins when the water pressure exceeds 100 kg/cm^2 . The loss begins to increase suddenly at about 400 kg/cm^2 or higher and continues to increase until the fiber breaks at 600 kg/cm^2 .

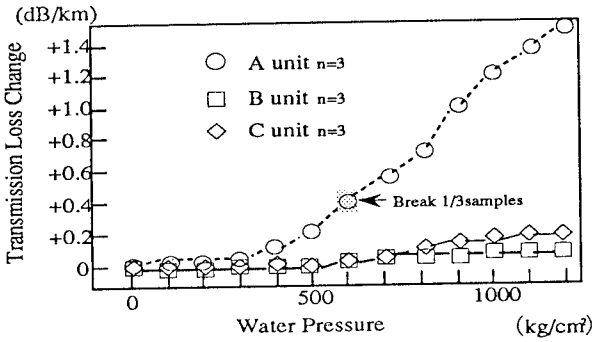


Fig.6 Relation Between Water Pressure and Transmission Loss Change

After pressure testing , we observed test samples and found that the outer sheath had fallen in the groove, causing a side pressure to be applied to the fiber and thus leading to its break.

Concerning the B block, the test results were generally good, but the end portion was difficult to fix in this experiment as well as before.

That is, the problem of handling sill remains unsolved. The C unit showed no such degradation in transmission loss performance as was observed in the A unit but tended to increase in loss a little more than B unit. Deformation of the unit under high water pressure was expected to some extent from simulation by the finite element method.

It was, however, necessary to investigate what amount of strain is applied to the fibers of the actual unit. Reducing the amount of fiber strain to permissible limits permits to obtain stable pressure resistance and high reliability.

Considering the amount of longitudinal strain applied to the fiber, the A and B units, in which the fiber can move freely, are advantageous.

However, the A unit cannot sustain the structure

under water pressure and the B unit is not easy to handle. Therefore, We tried to reduce fiber strain on the basis the C unit having the strongest structure, and started out to develop a unit having stable pressure resistance.

4.4.2Water pressure dependence of fiber strain

In this experiment, fiber strain measurements were made using the BOTDA method which makes use of Brillouin scattering.

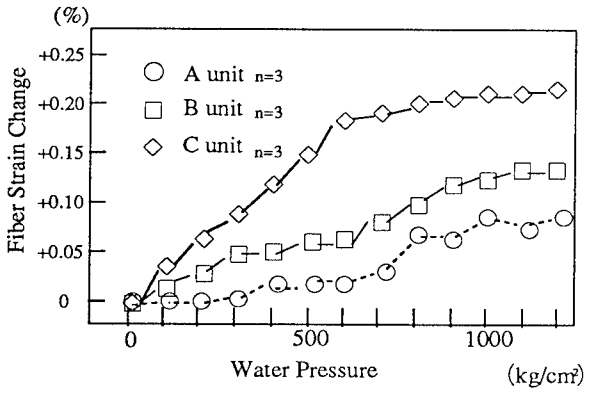


Fig.7 Relation Between Water Pressure and Fiber Strain Change

Fig.7 shows the water pressure dependence of fiber strain for each unit. In the A unit, the transmission loss performance degraded remarkably, making it impossible to take measurements. The longitudinal strain applied to the fiber by water pressure is compressive in any unit, so size reduction is confirmed. The difference in the amount of strain between the B and C units is due to the difference in structure between them. That is, in the B unit the fiber moves in the slotted rod groove, allowing to relieve strain, while in the C unit the deformation of the unit components appears directly as strain. The factors contributing to producing strain are roughly divided into two. One is the mechanism in which the pitch diameter of the fiber is decreased by water pressure, resulting in producing compressive strain in the longitudinal direction. The other is the mechanism in e\which fiber strain results directly from size reduction in longitudinal direction of the unit. The fiber strain by the former mechanism can be improved by presetting the fiber pitch diameter at the smallest possible value to provide a longer pitch. Making the pitch longer results in increasing the amount of strain in the latter mechanism, so it is necessary to acquire balance. In addition, this improvement method was not so suitable because the twist pitch of the fiber should preferably be shorter for flexibility. To relieve fiber strain by the latter method, it is necessary to increase the rigidity of the central tension member. It was important to increase the rigidity as much as possible under the restriction that the outside diameter should be less than 4.0 mm.

5.CONCLUSION

Making a challenge to the deepest part in the world, the KAIKOU system successfully reached the target point on March 24, 1995. The newly developed optical fiber unit reported in this paper was only a part of the system and an elemental technique that supported this project. Particularly with the secondary tether cable exposed throughout its length to high water pressures over 1,000 atm, it was difficult to ensure stable transmission. We made three types of trial units and evaluated them minutely for in-process transmission loss, thermal and mechanical properties, and so on. As a result, a unit improved in water pressure resistance, the most important property for the system, obtained. The unit exhibits stable performance with transmission loss variation less than 0.2 dB/km under a water pressure of 1,200atm. The optical unit is, of course, a part of the secondary cable, so similar efforts and

devices must have been used for the other parts of the cable. And accumulation of such exertions led to the great success of the system.

6.REFERENCE

[1] H.OKADA etal "OUTLINE OF 1000m CLASS REMOTELY OPERATED VEHICLE UNDER DEVELOPMENT"ROV'91,(1991)

[2] Y.IWAI etal "KEY TECHNOLOGIES OF 1000m CLASS ROV SYSTEM UNDER CONSTRUCTION" ROV'92,(1992)

[3] SHINOZAKI etal "THE MATERIAL OF A TENSION MEMBER USED FOR DEVELOPING MARINE CABLE" TECHNO OCEAN'92 (1992)

[4] MOGI etal "DEVELOPMENT OF OPTICAL CABLE FOR 1000m CLASS ROVS"IEIEC SPRING(1993)

[5] T.HORIGUCHI etal "TENSILE STRAIN DEPENDENCE OF BRILLOUIN FREQUENCY SHIFT IN SILICA OPTICAL FIBERS" IEEE PHOTON.TECHNOL.LETT.,vol.1,pp.107-108,(1989)

[6] T.HORIGUCHI etal "BOTDA-NONDESTRUCTIVE MEASUREMENT OF SINGLE-MODE OPTICAL FIBER ATTENUATION CHARACTERISTICS USING BRILLOUIN INTERACTION: THEORY",J.LIGHTWAVE TECHNOL.,vol.7,pp.1170-1176 (1989)

[7] M.TATEDA etal "FIRST MEASUREMENT OF STRAIN DISTRIBUTION ALONG FIELD-INSTALLED OPTICAL FIBERS USING BRILLOUIN SPECTROSCOPY",J.LIGHTWAVE TECHNOL.,vol.8,pp.1269-1272 (1990)

7.AUTHOR



Akira Sano
Opto-Electronics Laboratory
Fujikura Ltd.
1440 Mutsuzaki
Sakura-shi,Chiba-ken
285 Japan

Akira Sano was born in 1960.He joined Fujikura Ltd.after his graduation from Kyoto University with a B.E. in1983 and has been engaged in research and development of cable materials.He is an engineer of the Telecommunication Cable Section and a member of IEICE of Japan.



Kohichirou Watanabe
Opto-Electronics Laboratory
Fujikura Ltd.
1440 Mutsuzaki
Sakura-shi,Chiba-ken
285 Japan

K.Watanabe was born in 1959. He recieved a B.E. degree in electrical engineering from Tohoku University in 1982. Since joining Fujikura Ltd. in 1988, he has worked on the development of optical fiber cable section and a member of the IEICE of Japan.



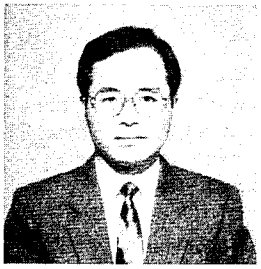
Osamu Koyasu
Opto-Electronics Laboratory
Fujikura Ltd.
1440 Mutsuzaki
Sakura-shi,Chiba-ken
285 Japan

Osamu Koyasu was born in 1953. He joined Fujikura Ltd. from Kisarazu Technical College in 1973. And He has been engaged in research and development of transmission cable. He is now engineer in the Telecommunication Cable Section and a member of the IEICE of Japan.



Akio Mogi
Opto-Electronics
Laboratory
Fujikura Ltd.
1440 Mutsuzaki
Sakura-shi,Chiba-ken
285 Japan

Akio Mogi was born in 1946.He joined Fujikura Ltd.after his graduation from Haneda institute High School in1967 and has been engaged in research and development of the metallic cables and optical cables.He is now the manager of the telecommunication line deoartment and a member of IEICE of Japan.



Matsuhiro Miyamoto
Opto-Electronics
Laboratory
Fujikura Ltd.
1440 Mutsuzaki
Sakura-shi,Chiba-ken
285 Japan

Matsuhiro Miyamoto was born in 1953.He received the M.S. degree from the Tokyo Institute of Technology in 1978.He joined Fujikura Ltd.and has been engaged in research and development of optical fibers and cables .He is now the manager of the Telecommunication Cable Section and a member of IEICE of Japan.

INVESTIGATION OF HYDROGEN INDUCED LOSSES IN INSTALLED FIBREOPTIC SUBMARINE CABLE SYSTEMS WITH SUBMERGED SPLICE HOUSINGS

Svend Hopland and Edmund Sikora*.

Telenor AS, Telenor Network, Oslo, NORWAY.

BT Laboratories, Martlesham Heath, Ipswich, UK*.

ABSTRACT

Telenor and BT have used a hydrogen sensitive OTDR-module to investigate the hydrogen induced losses in a number of cable systems with different cable and splice housing designs, that have been installed at different times. The data has revealed a number of important features. Hydrogen induced loss is present at joints on all systems. The magnitude of the hydrogen induced loss varies greatly between different joints in the same system. The losses due to hydrogen in joints increases with time. In one system the average loss associated with each joint was found to be approximately 0.026 dB/joint/year at 1550 nm, and is expected to continue to increase with the same rate. In another system one single joint have shown an increase rate of approximately 0.002 dB/year at 1550 nm. Hydrogen induced loss was also found in one system at positions other than at joints. Since the twenty-five years lifetime margins for hydrogen induced losses in long unrepeatered systems are small, these results give rise for some concern.

1. INTRODUCTION

In a fibreoptic submarine cable construction, the fibres are usually hermetically sealed in order to protect the fibres against hydrogen ingress resulting from corrosion of the cable armouring. However, in cable splice housings, which are frequently used in submarine cable systems, the hermetic seal is broken *, and small lengths of fibre are left unprotected against hydrogen ingress which may result from corrosion of the splice housing/armour wires. Furthermore, if hydrogen does migrate into the joint cavity, it may also diffuse along the cable, and the length of fibre affected by hydrogen induced loss will thus increase with time.

Hydrogen induced loss increase in submarine cable joints due to splice housing corrosion has recently been identified as a possible optical loss mechanism [1]. However, no field measurements were reported. Thus, the question of magnitude and time dependence of the hydrogen induced loss at submerged cable splices in real installed cable systems, remained open.

Many submarine cable manufacturers use joint housings as an integrated part of their cable systems. Cable joints are used to splice together cable sections of different types of cable armouring and/or to splice together cable section lengths to make it one single submarine cable length. In addition, any repair after installation of the system, will increase the number of submerged cable joints.

The general trend in system design is to reduce optical loss margins. New long unrepeatered systems may therefore have only small margins allocated to ageing and hydrogen induced loss over their expected lifetimes. Any unexpected optical loss may therefore be critical. In order to determine whether the present optical loss budgets allocated for hydrogen induced loss are sufficient, it is important to obtain data on hydrogen induced losses in installed systems.

Telenor has earlier investigated the magnitude and distribution of hydrogen induced losses in domestic installed systems by using a hydrogen sensitive OTDR-module at 1241 nm [2]. Using this technique, we have collected field measurement results in order to evaluate the magnitude and the time dependence of hydrogen induced losses in submerged splice housings and along cables with hermetically sealed fibres. In this work, Telenor and BT have investigated 3 different cable systems with 3 different cable splice housing designs and 2 different hermetic tube cable designs, installed at different times.

* The only exception from this are cables with hermetically coated fibres.

2. ANALYSING METHOD

2.1 General

We have used a four-wavelength OTDR at 1306 nm, 1550 nm, 1567 nm and the hydrogen sensitive wavelength 1241 nm. The best way to reveal the presence of hydrogen is to compare the OTDR curves at 1306 nm and 1241 nm. Since the hydrogen induced losses have a narrow attenuation peak at 1244 nm, the loss curve at 1241 nm will be strongly affected by hydrogen. In comparison, the influence of hydrogen on fibre loss at 1306 nm will be much less and even smaller than at the wavelengths 1550 nm and 1567 nm.

Furthermore, it is well known that other loss effects such as microbends, macrobends and splices, are of approximately equal size both at 1241 nm and 1306 nm. Therefore, any presence of hydrogen will cause the 1241 nm loss curve to differ significantly in form from the corresponding 1306 nm curve, thus indicating the presence of hydrogen. To determine whether hydrogen is present it is sufficient to examine one fibre in a cable. Observations of a number of cables has shown that the hydrogen induced loss of fibres within and close to a joint is not always the same. The reason for this is unclear. Therefore, to get an accurate estimate of the loss due to hydrogen, we have examined all the fibres and used average values in the calculations.

From numerous measurements at many different levels of hydrogen, we have established the relationship between the hydrogen induced losses at the different OTDR wavelengths [3]. These relations have turned out to be:

$$1) \quad \Delta\alpha_{1306} = 0.027 \times \Delta\alpha_{1241}$$

$$2) \quad \Delta\alpha_{1550} = 0.061 \times \Delta\alpha_{1241}$$

$$3) \quad \Delta\alpha_{1567} = 0.090 \times \Delta\alpha_{1241}$$

, where:

$\Delta\alpha_{1241}$, $\Delta\alpha_{1306}$, $\Delta\alpha_{1550}$ and $\Delta\alpha_{1567}$ are the hydrogen induced losses at the wavelengths 1241 nm, 1306 nm, 1550 nm and 1567 nm, respectively. When $\Delta\alpha_{1241}$ is known, the other losses can be estimated using Equations 1), 2) and 3).

2.2 Submerged splices.

In submerged cable splices, possible hydrogen will be present in very short fibre lengths and will therefore be masked by the fibre splice loss.

Normally, without any hydrogen present, the one-way splice loss at 1241 nm is nearly equal or slightly higher than the one-way splice loss at 1306 nm. For each cable system, we have provided typical one-way splice losses at 1241 nm and 1306 nm without any hydrogen present by measuring the splices on land, and a typical one-way splice loss difference has been established.

If hydrogen is present at joints, the "splice" loss at 1241 nm will be significantly higher than the "splice" loss at 1306 nm, compared to the above normal situation. In the first approximation, the 1241 nm loss increase can be calculated as the average splice loss difference. By using Equation 1) in Section 2.1, an approximate 1306 nm loss increase can be calculated. An improved estimate of the 1241 nm loss increase is then obtained by adding the approximate 1306 nm loss increase, and subtracting the typical small one-way splice loss difference value. Examples of such calculations are shown later in detail in Section 3.1.1.

A more straightforward way to calculate the hydrogen induced losses, applicable when no 1241 nm data are available, is to examine the difference between measured splice loss and splice loss data when the system was manufactured/installed.

3. MEASUREMENTS RESULTS

3.1 Cable system A, joint design A.

Cable A is a submarine cable system with a copper C-tube and joint design A. The insertion loss of the system has been measured, using a cutback technique on two fibres spliced together, at intervals of ≈ nine months since installation approximately six years ago. The results are shown in Figure 1. The measurements carried out at 1550 nm suggest that the insertion loss starts to increase after ≈ 6 months and continues to increase at a linear rate of ≈ 0.0033 dB/km/year.

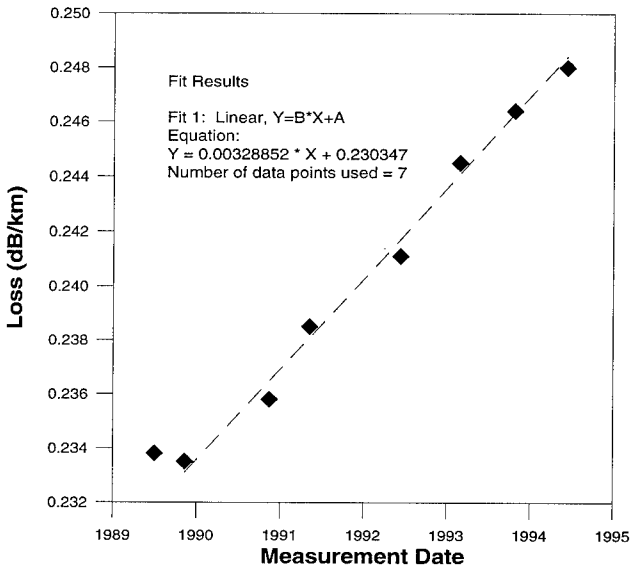


Figure 1: Increase in loss at 1550 nm of fibres (d,e) in cable system A.

In late 1994 we used the hydrogen sensitive OTDR to examine the first 40 km from each end terminal in order to determine whether the loss was evenly distributed and to reveal possible hydrogen induced losses. Five fibres were available for measurements. In Figure 2 are shown OTDR-traces for one fibre at 1241 nm and 1306 nm taken from one terminal.

By carefully studying the traces, a substantial number of regions with hydrogen ingress were found, including all the submerged splices as well as some portions of cable. Similarly, a number of regions affected by hydrogen ingress was also apparent on the OTDR traces taken from the other terminal.

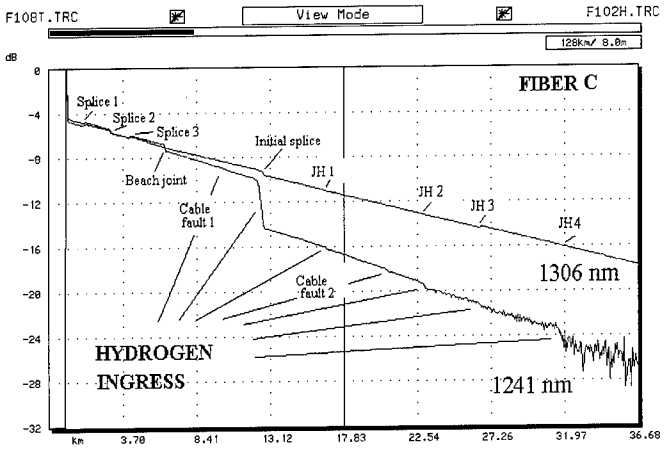


Figure 2: OTDR-curves taken from one terminal in cable system A.

3.1.1 Estimation of hydrogen induced losses.

The magnitude of the hydrogen induced loss at the submerged cable splices have been estimated. We first measured typical one-way splice losses at 1241 nm and 1306 nm without any hydrogen present. The relevant data was obtained from the cable system by calculating the splice loss for the splices on land. The results are shown in Table 1.

Land splice ID	Fibre no.	Splice loss 1241 nm (dB):	Splice loss 1306 nm (dB):	Difference 1241 nm-1306 nm (dB):	Average difference (dB)
Splice 1	a	-0.028	-0.017	- 0.011	0.019
	b	0.168	0.139	+ 0.029	
	c	- 0.153	- 0.180	+ 0.027	
	d	0.073	0.065	+ 0.008	
	e	0.267	0.227	+ 0.040	
Splice 2	a	0.207	0.217	- 0.010	- 0.003
	b	0.017	0.025	- 0.008	
	c	0.259	0.269	- 0.010	
	d	0.229	0.216	+ 0.013	
	e	0.059	0.059	+ 0.000	
Splice 3	a	0.029	0.019	+ 0.010	0.011
	b	- 0.031	- 0.035	+ 0.004	
	c	- 0.173	- 0.185	+ 0.012	
	d	0.153	0.132	+ 0.022	
	e	- 0.027	- 0.033	+ 0.006	
Beach joint	a	0.491	0.477	+ 0.014	0.013
	b	0.405	0.385	+ 0.020	
	c	0.292	0.282	+ 0.010	
	d	0.205	0.208	- 0.003	
	e	0.503	0.479	+ 0.024	

Table 1: One-way splice losses and differences for land splices in system A.

We note from Table 1 that the one-way splice loss at 1241 nm is nearly equal or slightly higher than the one-way splice loss at 1306 nm. On average, the splice loss for the 20 fibre splices are 0.010 dB higher at 1241 nm than at 1306 nm. We have thus assumed that a splice loss difference of 0.010 dB is typical for the fibres in system A, provided that average is taken over several fibres.

We then measured and tabulated the hydrogen induced losses for the sea portion of the cable system. A selection of results obtained from the measurements from one terminal, are shown in Table 2. We note that splice loss differences are higher than normal, and it is evident that there is hydrogen ingress in the submerged joints.

Sub-merged splice/ cable	Fibre no.	"Splice" loss 1241 nm (dB):	"Splice" loss 1306 nm (dB):	Diff. 1241 nm -1306 nm (dB):	Approx. 1241 nm loss incr. (dB):	Approx. 1306 nm loss incr. (dB):	Corrected 1241 nm loss incr. (dB):
JH 1	a	0.127	0.026	0.101	0.095	0.095 x 0.027 = 0.002	0.095 + 0.002 - 0.010 = 0.087
	b	0.138	0.032	0.106			
	c	0.126	0.036	0.090			
	d	0.091	0.010	0.081			
	e	0.128	0.031	0.097			
JH 4	a	1.055	0.265	0.790	0.928	0.928 x 0.027 = 0.025	0.928 + 0.025 - 0.010 = 0.943
	b	1.079	0.295	0.784			
	c	0.586	0.039	0.547			
	d	2.042	0.457	1.591			
	e	Noise	Noise	Noise			
Initial splice + 400m	a	3.436	0.002	3.434	3.496	3.496 x 0.027 = 0.094	3.496 + 0.094 - 0.010 = 3.580
	b	3.503	0.013	3.490			
	c	3.867	0.375	3.492			
	d	3.626	0.115	3.511			
	e	3.374	- 0.177	3.551			
Cable fault 2	a	0.107	N.A.	N.A.	N.A.	N.A.	0.096
	b	0.076					
	c	0.123					
	d	0.076					
	e	0.099					

Table 2: Calculations of hydrogen induced losses at 1241 nm for some features in system A.

For each splice housing, the approximate 1241 nm loss increase has been calculated as the average splice loss difference. Then, by using Equation 1) in Section 2.1, an approximate 1306 nm loss increase can be calculated. Finally, a better estimate of the 1241 nm loss increase is obtained by adding the approximate 1306 nm loss increase, and subtracting the found value of 0.010 dB.

For the pure cable faults, if the fibre length affected by hydrogen ingress is short, the 1241 nm loss increase was calculated simply as the average value of measured "splice" losses. This is the case for cable fault 2, which is included in Table 2.

Finally, we have used Equations 1), 2) and 3) in Section 2.1 to quantify all the hydrogen induced losses seen from both terminals at all the OTDR wavelengths. A summary of the results are shown in Table 3.

In the middle part of the system, where no 1241 nm data were available, hydrogen induced losses at joints (data not included here) were estimated using the splice loss data at 1550 nm and comparing them with splice loss data measured in the factory when the system was made. However, not all joints in the system was reached with the OTDR, and the total hydrogen induced loss estimated for system A was therefore probably underestimated.

Submerged splice/cable	Estimated average $\Delta\alpha_{1241}$ (dB):	Estimated average $\Delta\alpha_{1306}$ (dB):	Estimated average $\Delta\alpha_{1550}$ (dB):	Estimated average $\Delta\alpha_{1567}$ (dB):
JH 1	0.087	0.002	0.005	0.008
JH 2	0.285	0.008	0.017	0.026
JH 3	0.477	0.013	0.029	0.043
JH 4	0.943	0.025	0.058	0.085
JH 5	1.027	0.027	0.063	0.092
Initial spl.+ 400 m	3.580	0.097	0.218	0.322
Cable fault 1	0.067	0.002	0.004	0.006
Cable fault 2	0.096	0.003	0.006	0.009
JH 6	0.966	0.026	0.059	0.087
JH 7	0.061	0.002	0.004	0.006
JH 8	2.599	0.070	0.159	0.234
Final spl. + 100 m	1.522	0.041	0.093	0.137
Cable fault 3	0.416	0.011	0.025	0.037
Cable fault 4	0.233	0.006	0.014	0.021

Table 3: Estimated hydrogen induced losses of a number of features on cable system A.

3.1.2 Discussion

We have identified and quantified hydrogen induced losses at all visible splice housings in the sea, a number of which are reported in Table 3. The magnitude of the hydrogen induced losses varied significantly from one cable joint to another. There are a number of factors which may account for this difference. The local corrosion conditions may vary at the different joint locations giving rise to different levels of hydrogen. The hydrogen may also diffuse along the inside of the copper C-tube at different rates depending on the local diffusion constant. As indicated in Table 1, the diffusion of hydrogen along the cable was most clearly seen at the Initial Splice and Final Splice close to the end points of the cable where the OTDR could be used at its highest spatial resolution.

Hydrogen ingress has also been identified at points other than cable joints. A possible cause is incomplete welding of the C-tube at these positions.

The total hydrogen induced loss at 1550 nm for system A was estimated, using the OTDR-measurements, to be approximately 80 % of the cutback measurement at 1550 nm. The correlation between the OTDR and cutback measurements is reasonable given that not all of the cable joints could be viewed with the OTDR.

The latest cutback measurements indicate the loss will probably continue to increase at ≈ 0.0033 dB/km/year. As the majority of the loss occurred at the joints, the rate of increase of loss would better be described as ≈ 0.026 dB/joint/year.

3.2 Cable system B, joint design B.

Cable system B is a submarine cable with lead tube and joint design B. We measured approximately 40 km of the system from one terminal approximately 2 years after installation of the system with the four wavelength OTDR. In this system, two fibres were available for measurements.

3.2.1 Induced losses

We carefully analysed all visible joints and cable for hydrogen induced losses by the same method as outlined in Section 3.1.1. The results are summarised in Table 4.

Submerged splice	Estimated average $\Delta\alpha_{1241}$ (dB):	Estimated average $\Delta\alpha_{1306}$ (dB):	Estimated average $\Delta\alpha_{1550}$ (dB):	Estimated average $\Delta\alpha_{1567}$ (dB):
JH 1	Zero	Zero	Zero	Zero
JH 2	0.040	0.001	0.002	0.003
JH 3	Zero	Zero	Zero	Zero
JH 4	Zero	Zero	Zero	Zero
JH 5	0.040	0.001	0.002	0.003

Table 4: Estimated hydrogen induced losses for features in cable system B.

There are no signs of any hydrogen induced losses along the cable itself. The hydrogen induced losses in 3 of 5 measured submerged splices, are virtually zero. In 2 joints, a small hydrogen induced loss can be observed.

3.3 Cable system C; joint design C.

In Telenor's domestic submarine cable network, submerged cable splices are generally not used, except for repairs. A specially designed repair splice (joint design C) has been developed. Up to now, repairs splices have been applied only 3 times since 1989. We have measured two of Telenor's repair splices deployed in 1989 and 1992, respectively, several times after their deployment. 4 fibres were available for measurements at each joint.

3.3.1 Induced losses.

The cables contained no hermetic seal, and we have therefore analysed only the joints for hydrogen induced losses. The results are summarised in Table 5.

Submerged splice	Estimated average $\Delta\alpha_{1241}$ (dB):	Estimated average $\Delta\alpha_{1306}$ (dB):	Estimated average $\Delta\alpha_{1550}$ (dB):	Estimated average $\Delta\alpha_{1567}$ (dB):
R. Spl. 1 -91	0.087	0.002	0.005	0.008
-93	0.119	0.003	0.006	0.009
-94	0.139	0.004	0.009	0.013
R. Spl. 2 -93	0.038	0.001	0.002	0.003
-94	0.052	0.002	0.003	0.005

Table 5: Estimated hydrogen induced losses for Telenor's repair splices.

We have found that the hydrogen ingress in both repair splices has increased with time. In our case, the hydrogen induced losses in Repair Splice 1 have increased more than 50 % during 3 years.

A time plot for hydrogen induced loss at 1550 nm for Repair Splice 1 is shown in Figure 3.

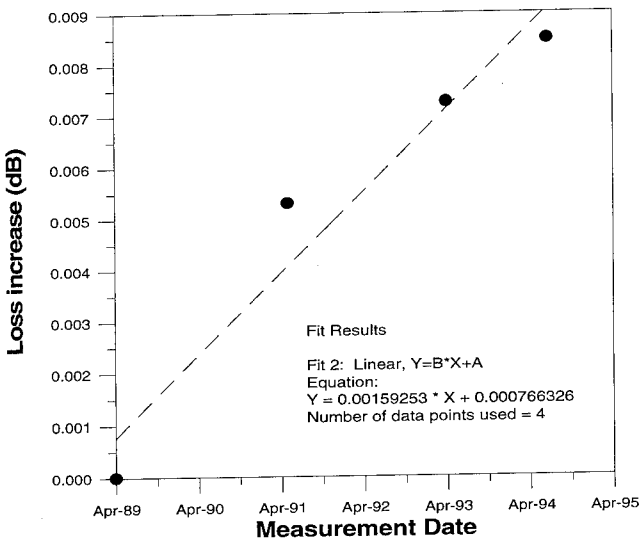


Figure 3: Hydrogen induced loss increase at 1550 nm for Repair Splice 1.

The loss at 1550 nm of Repair Splice 1 is found to increase at an approximate linear rate of 0.002 dB/year, which is considerably lower than the average increase rate estimated for the splices in system A. However, if the rate of increase remains constant, the magnitude of the hydrogen induced loss in Repair Splice 1 is comparable to the observed hydrogen induced losses in some of the joints in cable system A, after deployment for a similar time.

4. CONCLUSIONS

We have investigated the hydrogen induced losses in 3 different cable systems with 3 different submerged splice housing designs, installed at different times.

From the data we have collected a number of interesting features can be observed:

- There are indications of hydrogen induced loss associated with joints on all systems examined.
- The losses due to hydrogen can start to increase after a relatively short period after deployment of the cable.
- The magnitude of the hydrogen induced losses can vary greatly between different joints in the same system.
- The losses due to hydrogen in joints increases with time. In one system the average loss associated with each joint was found to be approximately 0.026 dB/joint/year at 1550 nm. In another system one single joint have shown an increase rate of approximately 0.002 dB/year at 1550 nm.
- The hydrogen permeating into the joint cavity can diffuse along the cable.
- A small amount of hydrogen was found to diffuse into cable A at positions other than at joints. This is probably due to manufacturing faults rather than damage to the cable on or after deployment. An increase with time is expected also for these losses.
- As the tendency is to reduce system margins for hydrogen induced losses the above results give rise for some concern.

5. ACKNOWLEDGEMENT

The authors would like to thank Knut Langeland and Idar Gangsø of Telenor AS and John Lyle, Mark Scopes, Kevin Linsell and Andy Cook of BT Laboratories, for carefully collecting the field data.

6. REFERENCES

[1] B.R. Ridd, C.J. Brown and G. McGurk: "Hydrogen Generation and Diffusion at Submarine Cable Joints: An Experimental Investigation": International Wire & Cable Symposium, Atlanta, Georgia. USA, 14-17 Nov. 1994.

[2] S. Hopland: "Measurements of low hydrogen levels in installed open fibreoptic submarine cables" Proceedings International Wire & Cable Symposium 1991, St. Louis, Missouri, pp. 742-749.

[3] S. Hopland: "Relation between hydrogen induced losses at different wave-lengths for Telenor's four-wavelength hydrogen sensitive OTDR." Telenor internal communication 1995.



Svend Hopland

Telenor AS
Telenor Network
P.Box. 6701, St.Olavs Plass
Oslo, NORWAY.

Svend Hopland graduated from the Norwegian Institute of Technology in 1985 with a PhD. on optical fibres. In 1986 he joined Norwegian Telecom (now Telenor), where he is presently a senior engineer on fiberoptic cables.

Edmund Sikora

BT Laboratories
Martlesham Heath
IP5 7RE
Ipswich, UNITED KINGDOM.

Ed Sikora joined BT Laboratories in 1989. He is at present working in the Fibre System Unit examining a number of aspects related to fibre transmission.

SPLICES AND CONNECTORS for BUNCHED MULTICORE MONOMODE FIBERS

H. Aoustin, A. M. Blanchard, M. Boitel, J. J. Gueguen, R. Le Marer, T. Mahé, D. Morellec, A. Pécot, G. Perrin

FRANCE TELECOM CNET/FCI/CAI, Lannion, FRANCE.

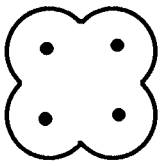
ABSTRACT

To achieve a full star optical network, which remains the most evolutive solution, answers have to be found to reduce the price and the volume of passive components.

A new kind of optical fiber has been developped by the CNET : the Bunched Multicore Monomode Fiber (1)(2)(4). This fiber includes many cores in the size of a classical unimodal fiber (125 µm). This new technique decreases drastically the cost per cabled monomode guide and leads to very thin cables (basically, cable capacity multiplied by the number of cores).

This paper describes the work done for connecting a BMMF to another BMMF or to classical fibers. It is focused on 4-core BMMF.

Cross section of a 4-core fiber :



CONNECTORS

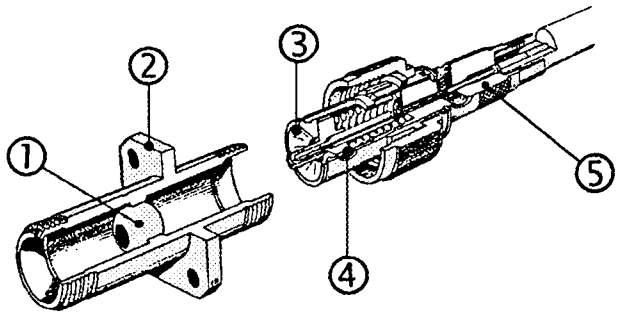
As the fiber is inscribded in a 125 µm circle, it is possible to use classical components to connect it. Connectors which allow a rotation but maintain the alignement already exist as they have been designed for polarisation maintaining fibers.

The first connector we used was a VFO MP (trade mark of RADIALL). This connector is based on the VFO Optaball principle : a coupling system with a sphere in the receptacle and a cone in the plug, a dynamic centering of the core and an optical continuity realised by index matching gel. The external part of the connector is maintained but the middle part can rotate.

The VFO MP plug is made basically of three mobile parts :

- ④, containing the fiber, which can translate relativly to ③ (X and Y axis)
- ⑤, containing ③, which can rotate relativly to the plug main part (Z axis)

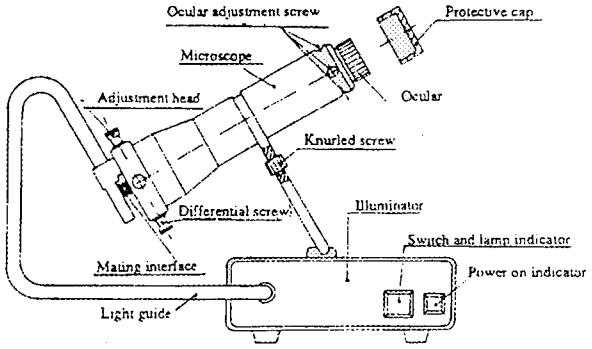
the VFO MP



Connectorisation process : the fiber is sticked in the plug, which is then set in a microscope. Four micrometric screws are used to align the cores in a reticule by moving part 4 relatively to part 3. Part 4 is then glued to part 3. By turning 5, the cores can be orientated to match the reticle, then ⑤ is sticked to the main body of the plug.

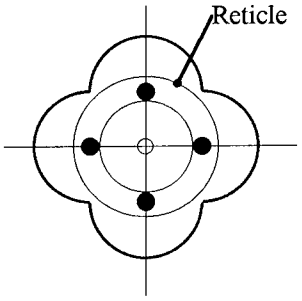
The performances depend on the fiber geometry but are basically those of the classical VFO MP and lead to an average insertion loss of 0,5 dB.

the microscope



This microscope has been designed for on-site installation and is still in use at FT for mounting monomode connectors.

View in the microscope :



We experienced ST type connector too. We used the receptacle and the plug whithout its indexation. As the four cores are not centered in the fiber, physical contact is not possible therefore we used flat polishing and index matching gel.

SPLICES

Cleavage

In all the following splicing methods, the first operation is to cleave the fiber. The cleavage has to be straight (90°) for fusion splice, but an angle is often prefered for mechanical splices (decreasing of the return loss).

Most of the cleaving tools are based on the following principle :

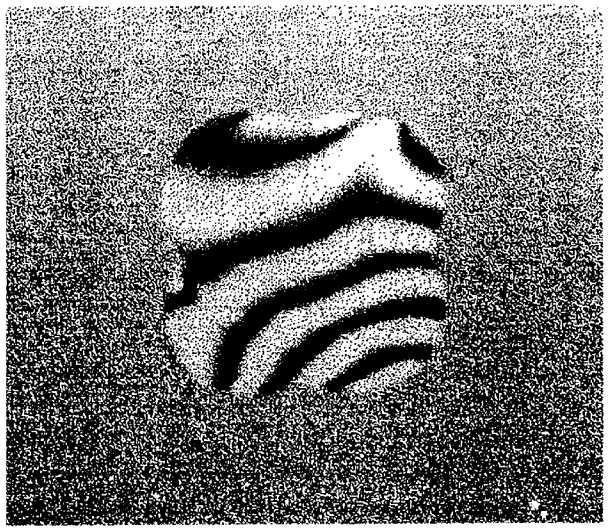
- scoring of the fiber

- application of appropriate stresses (tension, flexion and torsion if angle-cleavage)

The fiber tends to cleave along a direction perpendicular to stresses, but as the BMMF is not circular, cleavage is not easily predictable. The stress calculation is possible, but there are concentration stresses areas and heterogeneities may interfer (4 cores, 4 optical cladding).

The trials we made shows that cleaving BMMF is possible with tools not very different from the usual ones. A good combination between flexion and tension leads to a flat and straight surface.

Interferogram of a cleaved face :



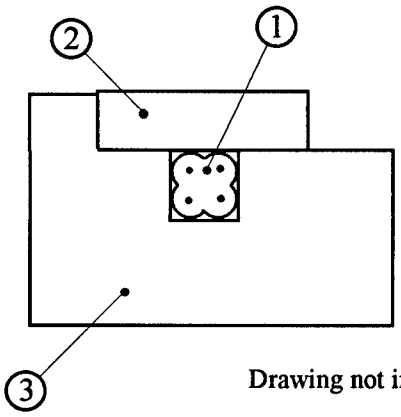
The number and shape of the fringes show that the surface is flat and that the angle is smaller than 1°.

Mechanical splice

In an elastomeric groove

This splice has been developped on the basis of a technique made for usual unimodal fibers. This method

has been used for years to splice unimodal fiber on France Telecom networks (ATI device).



Drawing not in scale

① is the multicore fiber
② is a glass slide
③ is a moulded elastomer, the groove is a little smaller than the fiber.

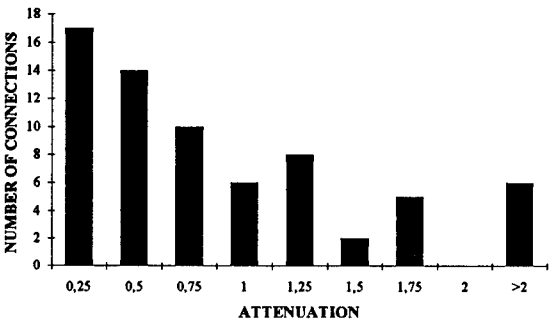
The groove is filled with UV-curing glue, ② is set on ③. The two fibers are cleaved and inserted in the groove, the splice is then insulated.

③ is removed and a mechanical protection is added.

As the fiber section is basically a square and the fiber is bigger than the groove, the two fibers are self orientated and centered.

The glue and the fiber cores indexes are close : it has a matching effect and decreases the insertion loss.

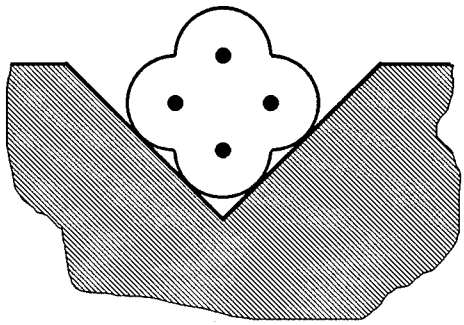
Performances of the splice :



With usual fibers, the average insertion loss of this splice is smaller than 0.15 dB. The same attenuation is not to expect because a fiber orientation is needed and the fiber geometry is more complex, but with more accurate groove and with fibers of better precision, there must be only a light difference (average insertion loss of BMMF splice close to the average insertion loss of the usual fiber).

In vee grooves

A 90° vee groove can be used to connect the BMMF. The groove must be sharper than those used for conventionnal splices and the angle very accurate (+ 1° means 1 μm of misalignment for the upper core).



For conventionnal fiber, we know Vee grooves made by plastic moulding, metal stamping, glass...

Apropriate grooves can be made by all these means. For our trials, we made it by grinding. The fibers were maintained by mechanical ways, but there are many solutions (glue, thermoretractable...).

Our splices had an average value of 0,5 dB.

Fusion splice

The fusion is the favourite splicing method for unicore fiber. It gives very low insertion and return losses, and as it rebuilds the silice guide, there is no doubt that is long term reliable.

The usual splicing proceeding is :

① straight cleavage of the fiber
② core alignment (static or dynamic)

③ spark-cleaning of the fiber
④ fusion spark and penetration
⑤ mechanical protection

The splicing of our multicore fiber add two difficulties :

- alignement of four cores instead of one

- circularisation of the fiber during fusion

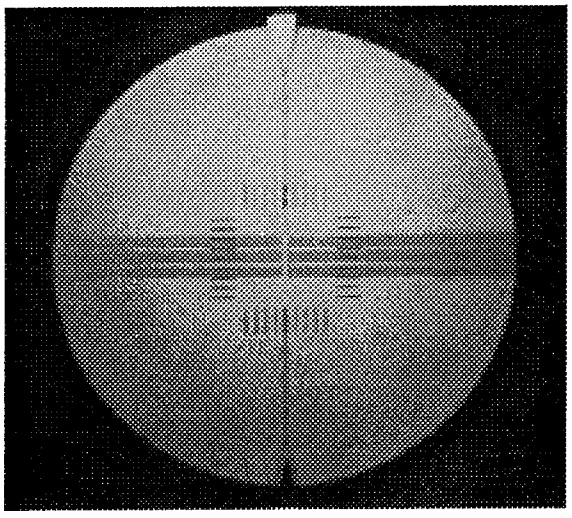
There are many ways to overcome the first difficulty. For example, it is possible to make an orientation in vee-grooves and to use micro-motors to optimise the transmitted light.

Even if the fiber is not circular, fusion without deformation is possible, it needs only a good combination between spark power, time and penetration.

The two next pictures show the multicore fibers before and after fusion, on the splicer screen. The two clear lines are the light reflected by the upper side of the fiber (there are not the cores).

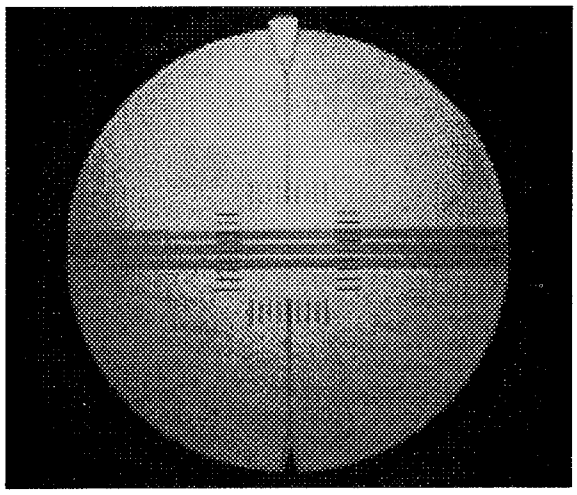
The first picture shows the cleaved fiber before the cleaning spark.

Splicer screen before fusion

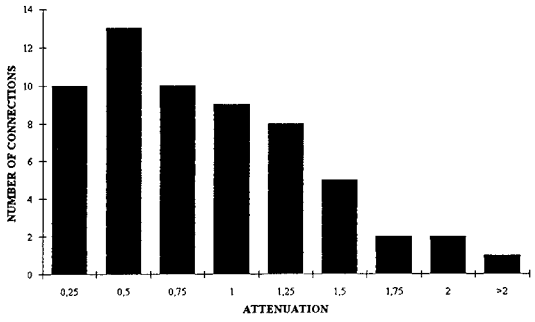


The second photographs shows the splice, the fusion is complete, the return loss is low and the tensile strenght is good.

Splicer screen after fusion



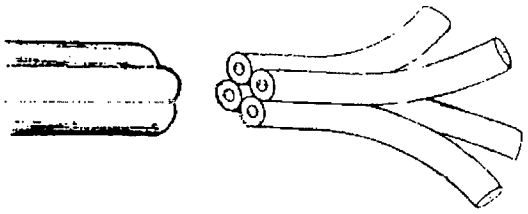
Fusion splice insertion loss



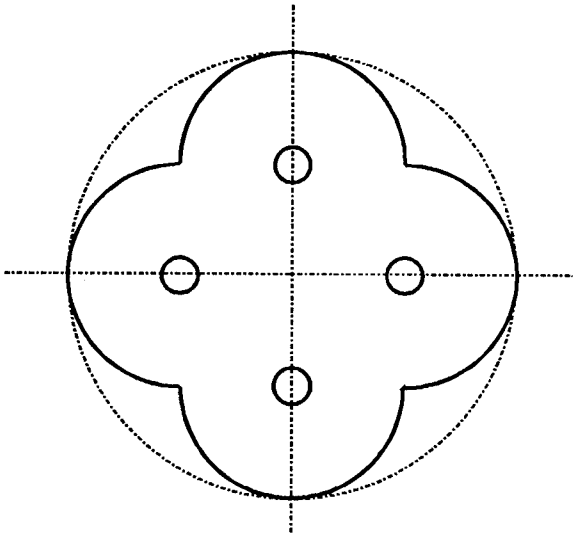
The diagram shows results obtained with different parameters, various time, penetration and spark power, because measurements were made during the elaboration of the process. With an optimisation of all these conditions, the insertion loss should decrease drastically.

FAN-OUT

The fan-out allows the connexion of a BMMF onto four unicore fibers. It can be used at each end of the fiber (connexion of four customer on one BMMF, connexion of four lasers...).

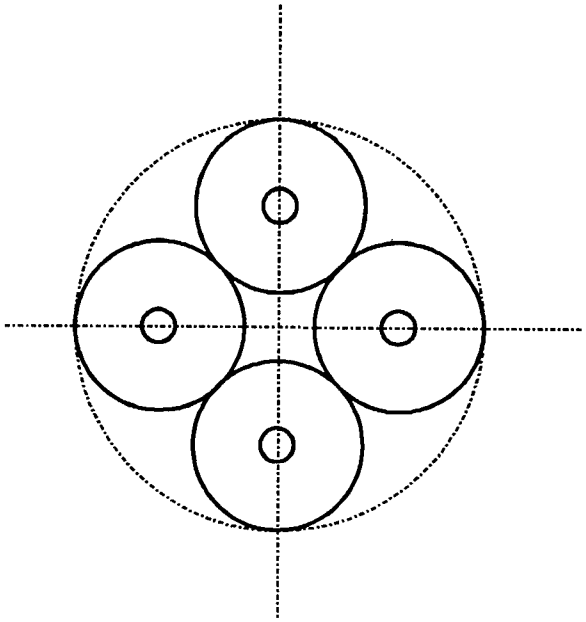


Cross section of a BMMF



In the BMMF, the four cores are at the corners of a 44.2 μm square. The diameters of 4 classical fibers are reduced at one end to 44.2 μm by chemical attack (fluorhydric acid), then these fibers are connected to the 4-core fiber.

Cross section of the 4 fibers (reduced ends)



Two methods to connect the 44.2 μm fibers to the BMMF are licensed (CNET) :

- the first one is to stick then together and to connect it to the BMMF by using a VFO MP

- the second is to assemble them in a special ferule of 106.7 μm and to connect it to a usual ceramic ferule containing the BMMF.

The connection loss depends on :

- the geometrical quality of the assembled fibers, for a sample of 14 fan-outs, the average distance between neighbouring cores is 43,9 (σ = 0,7) and 62,2 for opposite cores (σ=0,9)

- the quality of the connection itself

Connected to a BMMF of perfect geometry (cores on a 44.2 μm square) it leads to an average insertion loss better than 1 dB at 1.3 μm.

PRE-DEMONSTRATOR

A model of a distribution network using 4-core fibers has been installed at the CNET Lannion. It is composed of real cables, joints, fan-outs, connectors and splices and then could have been installed on-site.

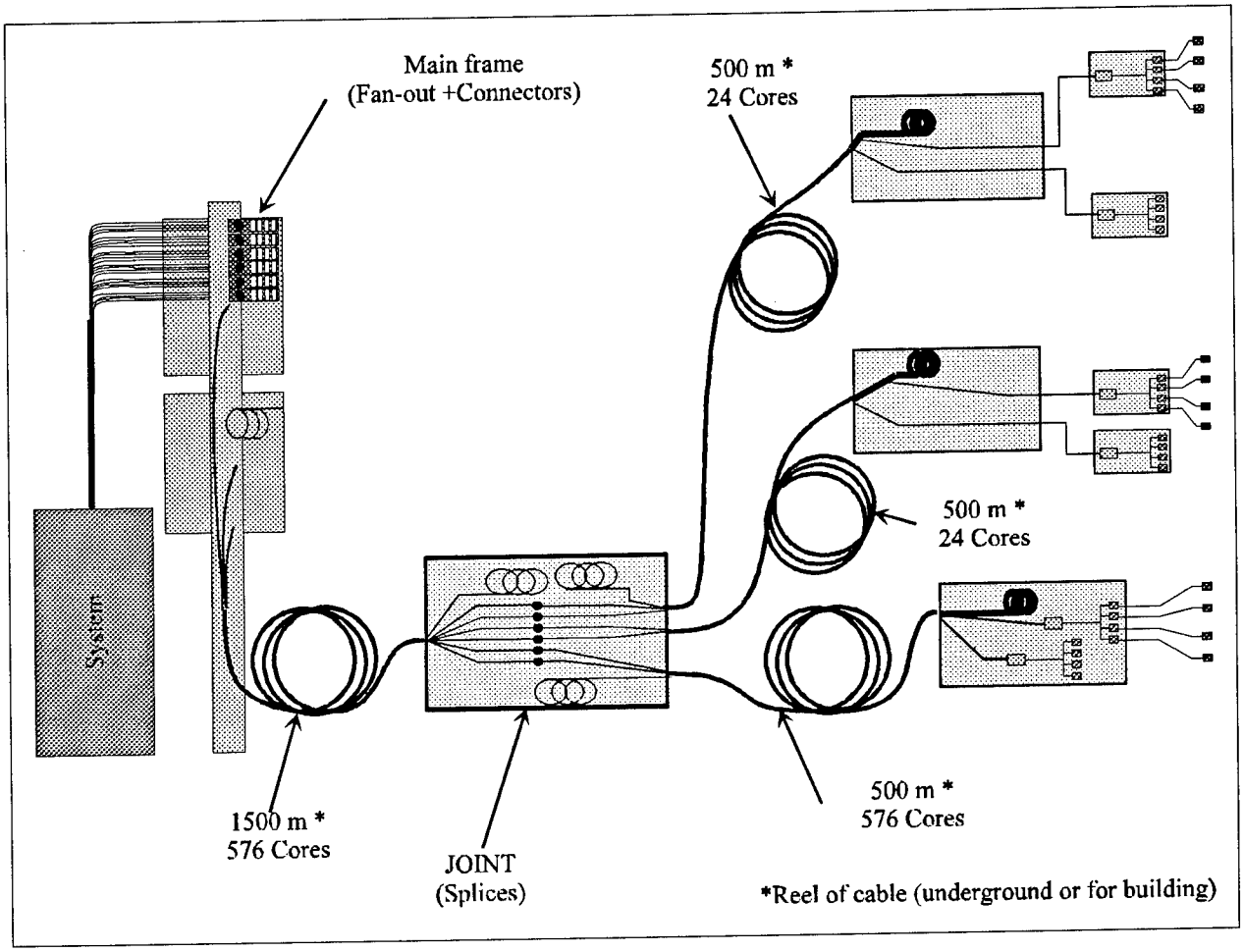
The drawing below is not in scale, it only shows the different elements of the model. Most of the parts are those used nowadays on FT network or only lightly modified. Everything is designed for the cables capacities but only 6 fibers (24 cores) are connected from the central to the customer.

The different elements are, from the left to the right :

- the central with electrooptics (system) and the distributing frame containing fan-outs and connectors

- a cable joint containing splices

- the customer end, with one fiber per customer (4 cores) or only one core.



CONCLUSION

We have presented the different kind of connexion needed to link the customer to the central office (connectors, fan-outs, splices).

Performances (insertion loss...) are still low but will be ameliorated, by progress in the connection technology itself and by amelioration of the fiber geometry.

Anyway the model we have made (pre-demonstrator) shows that building a distribution network using BMMF is already possible.

The main conclusion is that connecting BMMF is possible and as the technology is not very different from the usual one, the connexion price and volume of a unimodal lightguide will be basically divided by the number of cores in the fiber.

REFERENCES

(1) G. Le Noane et al. "Bunched multicore monomode fibers (BMMF) : A new key for the furure FTTH networks", EFOC & N 94 p 31 to 36.

(2) G. Le Noane et al. "Ultra high density cables using a new concept of bunched multicore monomode fibers : a key for the future FTTH networks" IWCS p 203 to 210

(3) R. Le Marer, G. Perrin "Composant d'éclatement pour fibres multicoeurs monomodes - L'éclateur, un composant clé", OPTO 95

(4) G. Le Noane et al. "La fibre multicoeur : un élément décisif pour le réseau FTTH"

(5) R. Le Marer, G. Perrin "Fan-out Component for Bunched Multicore Monomode Fibers : "Fan Out" a Key Component", EFOC&N 95.

(6) "Fibres Multicoeurs Monomodes" in OPTOELECTRONIQUE n°81 Mars-Avril 1995.



Hervé AOUSTIN

FRANCE TELECOM
CNET/LAB/FCI/CAI
3, Av. Pierre MARZIN
Technopole Anticipa
22307 LANNION
FRANCE

Hervé AOUSTIN received his engineering degree from the Ecole Nationale des Arts et Metiers in 1990. He joined the CNET in 1992 and works on optical Fiber connections since then.

"1X7 AND 1X8 MONOLITHIC COUPLERS MANUFACTURED BY INDIRECT FLAME FUSION TECHNIQUE"

Stefano Pitassi, Alberto Zucchinali, Maurizio Maglio, Vittorio Spano

SIRTI S.p.A. - Direzione Cavi e Tecnologie Ottiche
Via Manzoni 44, 20095 Cusano Milanino (MI) - ITALY

Abstract

The growing interest in broadband applications (e.g. CATV) involves optical components having high-level characteristics and performances. In this paper a new methodology to obtain 1x7 and 1x8 monolithic fused couplers will be described; the problems related to the use of biconic-tapered technology will be analyzed.

This paper will provide an overview of the main theoretical aspects related to the fabrication of 1x7 and 1x8 monolithic fusion couplers as well as the experimental results over a wide population of components. A comparison between the two configurations will be given, in order to achieve a wideband component, able to work in both optical windows.

Finally a packaging technique, developed to solve environmental problems and to obtain field reliable and compact couplers will be described.

1. INTRODUCTION

The wide diffusion in the worldwide market of the interest related to telecommunication highways and, in particular, to multimedia applications involving video, audio and data has brought a renewed effort to answer the problem of splitting a signal into different pathways. Couplers are divided in two main categories: fusion (all-fiber) and integrated devices. The use of ion exchange on silica or silica on silicon allows the production of a number of components characterized by a good repeatability but low cost just for high numbers.

The tree structure, used for integrated devices but also for many commercial fused couplers, is not an optimum solution for a compact size package. A monolithic splitter with a unique coupling zone can offer good performances considering insertion loss and return loss, moreover giving a size-effective, low-cost and all-fiber device. The new technique described allows the production of wavelength-flattened couplers, to be placed in networks working in the 2nd and/or 3rd optical windows, using a configuration in which a number of fibers surround a central one, having two resulting configurations, with 7 and 8 output ports respectively. The second solution has greater technical problems that forced us to develop a different geometry as it will be explained in the following.

2. A NEW METHOD OF FABRICATION

To obtain a regular coupling, it is fundamental that all fibers stay reciprocally in contact, at least for all the coupling zone length. Two methods exist to reach the desired geometry.

Up to now, monolithic splitters have been obtained by the use of a Vycor capillary fused and stretched together with the fibers during the heating process. One of the requests to be satisfied to obtain a wavelength-independent performance is the control of the difference between the propagation constant of the central fiber compared with the outer fibers. This process can be hardly controlled because of the deformation of the capillary and the ring fibers.

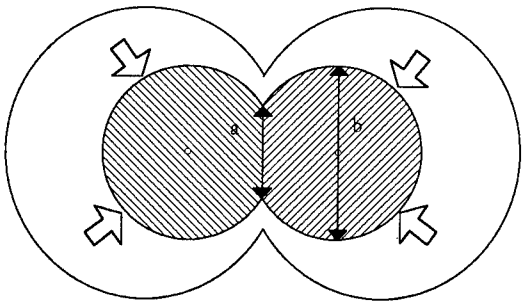
The new technique we have developed is based on the use of a tube with non-collapsing walls which avoids the direct contact between the flame and the twisted fibers; this allows a uniform and distributed heating which, together with an accurate control of the mechanical, thermal and dimensional parameters of the process, gives the possibility of obtaining good results.

The control of the temperature is obtained by a regulation of the burning gas flow. A light pulling of the fibers during the fusion causes a reciprocal compenetration and a subsequent reduction of the transversal section of the coupler.

The design of the fabrication procedure and its impact on the performances needed a separate study of four different items:

- fibers twist;
- fibers pulling;
- fused fibers configuration;
- difference between the propagation coefficients.

It is important to define the differences between the theoretical and the experimental approach. Theory says that coupling coefficients between external fibers should be constant. Another assumption is that these coefficients do not change while coupling length is increasing. Mostly this second assumption differs deeply from the real situation in which the coupling zone becomes longer and longer and the distance between the centers of the fibers reduces more and more in a non-symmetrical way. This forces to define an optimum pulling speed; the central zone of the twisted fibers gets longer and tapered, giving a limit to the degree of fusion W (figure 1) and consequently to the compenetration of the claddings. An excessively high speed implies that optical power coming from the central fiber hardly couples with outer fibers; on the other side, a low speed brings to possible deformations of the structure, giving worse uniformity.



Degree of fusion W = a /b

Figure 1

The choice of the twist rate depends on the strength of the fibers and on the maximum macrobending loss introduced by the twist itself. The length of the twisted zone has to ensure the parallelism and the physical contact among the fibers and consequently it has to be much greater than the length of the fused zone.

Another request to be satisfied is a time-constant tapering of the fused region, able to maintain a constant ratio among the fibers. To achieve this aim, a balance between two items is needed:

- the reduction of the pulling speed of the fibers in order to prevent them from different tensile loads;
- the minimization of the fusion process time so that fibers do not risk unwanted deformations.

Another fundamental parameter to consider is the nominal value tolerance of the twisted fibers starting diameter: it is important that all the fibers refer to the same reel or stock to avoid a bad uniformity.

As it concerns the twist, our method implies a difference between the length of the external fibers and the central one; that results in a mismatching between the propagation constants. To obtain the length L_{tw} and the equivalent radius of curvature R_{eq} the following equations can be used:

$$L_{tw} = (4\,\pi^2\,r^2 + p^2)^{1/2}$$
$$R_{eq} = r + p^2/(4\,\pi^2\,r)$$

where r is the radius of the cylinder and p the stranding pitch. The lateral fibers are about 0.3 % longer, while the radius of curvature is about 18 mm (0.7 in), causing a stress on the fibers and therefore a need for a short processing interval between twist and fusion. On the other side, the helicoidal arrangement implies lower per cent elongation with respect to the central fiber.

The parameters that have an influence on the tapered zone are the following:

- the shape of the transverse section of the fused region;
- the longitudinal profile of the fused region;
- the separation between the cores (the degree of fusion) of the fibers.

It is well known how the combined effect of fusion and pulling causes a tapered zone with an increasing section from the center of the coupler (figure 2).

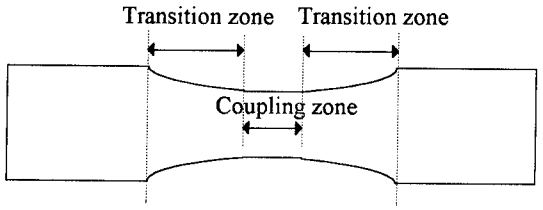


Figure 2

It is possible to notice a central part with a constant diameter (coupling zone) and two symmetrical zone apart from it with a variable diameter (transition zone). To minimize the loss of the guided modes (excess loss) it is necessary that the profile of the transition zone be sufficiently smooth to be considered adiabatic [1].

Another cause of excess loss is an uncontrolled deformation of the fused region because of an insufficient pulling of the fibers; the thermal gradient caused by the longitudinal and transversal distribution of temperature modifies the degree of fusion among the claddings and the coefficient of coupling between the fibers.

To avoid undesired stress, it is important to start pulling just when the fibers have the right degree of softening and to stop just when the flame is turned off. In our case, the use of intermediate walls recommends to move them away from the fused zone to prevent from thermal drifts.

With our method the fine adjusting of the different parameters of the process is obtained by monitoring in real time the performance of each fiber at the two wavelengths of interest on an automated bench.

3. THEORETICAL ASPECTS

The coupling mechanism that takes place in a wavelength flattened 1xN coupler can be understood by considering a central fiber (figures 3 and 4) surrounded by a ring of N identical fibers in an infinite cladding medium.

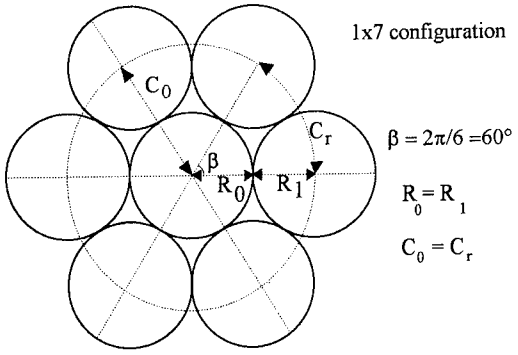


Figure 3

If we assume an illumination through the central waveguide and an equal and regular spacing of the ring cores, only two coupling constants (C_0 and C_r in figures 3 and 4) can be taken into consideration. Due to the circular symmetry of the problem, the analytical solution [2] represents the beating of two normal modes with different phase velocities, and that looks like an exchange of power between the central and the ring waveguide.

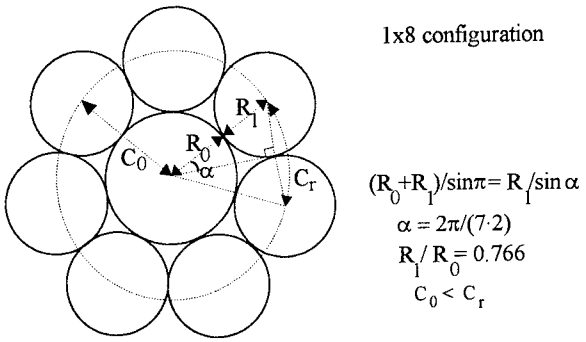


Figure 4

If we consider a simple two-core structure, under the assumption of weakly guiding fields, the coupling constant C_{rs} can be calculated by separating the total field into the sum of the fields of the cores in isolation (perturbation theory). This is not always true, in particular when the fibers compenetration, during the fusion process, is so high that the weakly guiding fiber hypothesis is not valid any more. From now on we suppose a core separation great enough to apply the perturbation assumption, so that the familiar step-fiber approximation [3] can be used:

$$C_{rs} = \frac{(2\Delta)^{0.5} U^2}{\rho V^3} \cdot \frac{K_0(W d_{rs}/\rho)}{K_1^2(W)} \qquad (1)$$

where ρ is the fiber radius and d is the center-to-center separation. The core and cladding parameters are for one fiber in isolation while K_n are the modified Bessel function. The task for a coupler manufacturer is to evaluate the coupling coefficient C_0 and C_r (figures 3 and 4) in 1xN structure, in order to calculate the total fraction F of power coupled out of the central fiber:

$$F = N \frac{C_0^2}{C_0^2 + \left(C_r + \frac{\beta_r - \beta_0}{2}\right)^2} \qquad (2)$$

Formula (2) shows that the coupled power fraction depends on the number N of fibers, the difference in the propagation constants and the relative degree of fusion

between them. An accurate calculation requires a detailed and complete knowledge of the internal structure and taper geometry which could be rather complicated. Therefore the main purpose of the theoretical model is to describe in qualitative terms the overall coupling trends for these kind of components.

To obtain a wavelength flattened coupler the power amount in each fiber must be the same at both 1310 nm and 1550 nm, and this condition can be achieved by varying the coupling constants and/or the propagation constants of the central fiber and the ring fibers [4]. In other words the maximum optical power in each of the surrounding fibers is higher than the related minimum of the power remaining in the central one, so that the two wavelength-flattened points (points A and B in figure 5) get closer.

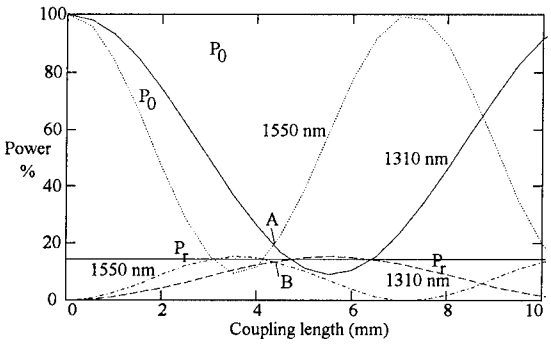


Figure 5

As the structures fuse together, the outer fibers collapse partly on the central one generating a cladding compenetration between adjacent fibers. This interaction changes not only the core separation but also the degree of fusion, and therefore affects the coupling mechanism.

Another phenomenon which influences the split ratio is related to our specific fabrication process, where the pulling action, performed along the axis of the helicoidal structure of the twist, causes a different elongation of the surrounding fibers with respect to the central one and a variation of their radii. The result consists in a mismatch between propagation constants ($\beta_r > \beta_0$) that reduces the transferred power F (equation (2)) and can be controlled by a proper choice of the twisting parameters and the initial diameter of the fibers.

Two-mode problem

Due to the illumination of the central core only and the arrangement of surrounding fibers, coupling is reduced to a two-mode problem where the power carried by the central fiber P_0 and by each fiber in the ring P_r have an oscillating behavior [1].

The analytical results can be applied either for 1x7 or for 1x8 fusion couplers, taking into account the different array geometries. In a seven core array arrangement the constants C_0 and C_r are equal and the maximum coupled power coincides with the uniform power split between the seven fibers (14.3%). The curves of figure 5 represent the coupling characteristics of this component calculated at two wavelengths 1.31 and 1.55 μm, using equation (1) with ρ = 1.8 μm, n_{core} =1.467 and $n_{cladding}$ = 1.457. The distance between adjacent cores is supposed to be about 15 μm, as a consequence of the starting diameter of the fibers and the fusion process which ideally should not change the geometrical ratio between core and cladding diameters. Unfortunately this can be hardly guaranteed during the process because of the temperature distribution and the asymmetry of pulling strength (among fibers).

An unbalance between fusion temperature and pulling speed can be expressed mathematically with the variation of the ratio d/ρ where d is the core-to-core separation and ρ is the core radius. Assuming a sufficient degree of fusion, which implies a normalized fused width W (figure 1) of about 0.4÷0.5, a d/ρ decrease reduces the theoretical coupling length, improving the uniformity of the component at 1310 nm and 1550 nm (i.e. the two curves in the figure 5 get closer each other).

For the particular configuration of 1x8 fusion couplers with a central fiber surrounded by a ring of seven fibers, the previous analytical model leads to different results.

The cores separation in the ring guides (about 13 μm) is lower than the external-to-central separation (about 15 μm) and therefore the coupling coefficients are not equal any more but show a difference that increases as wavelength decreases (figure 6).

Even if no propagation constant mismatch ($\beta_0 = \beta_r$) takes place during the process, the amount of power remaining on the central fiber is higher than the power split in each surrounding fiber so that a satisfactory uniformity can not be achieved in these conditions.

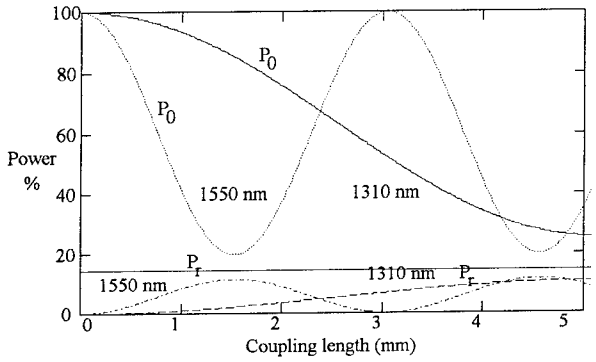


Figure 6

By a suitable choice of the fusion parameters (such as prefusion, temperature and pulling speed) it is also possible to increase the difference between C_0 and C_r which causes the same effect as the phase mismatch in 1x7 couplers; in this way the uniformity of the component is lower than 2 dB, but only at 1550 nm (figure 7). A second drawback regards the actual excess loss obtainable; our experimental results confirmed that its average value exceeds 2 dB due to an excessive waveguide distortion, while maximum insertion loss is never below 14 dB.

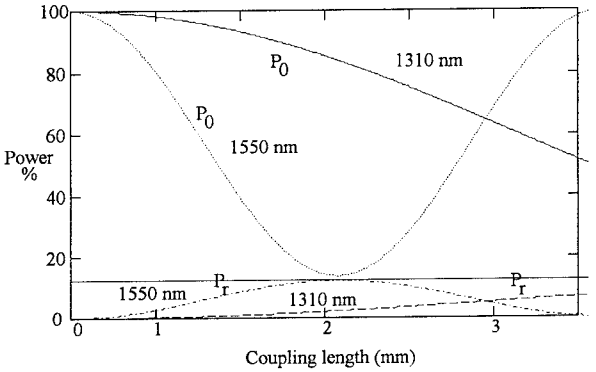


Figure 7

An alternative approach to get through the previous problem consists in changing the starting diameter of the fibers; that results in higher coupling coefficients and shorter coupling length (figure 8).

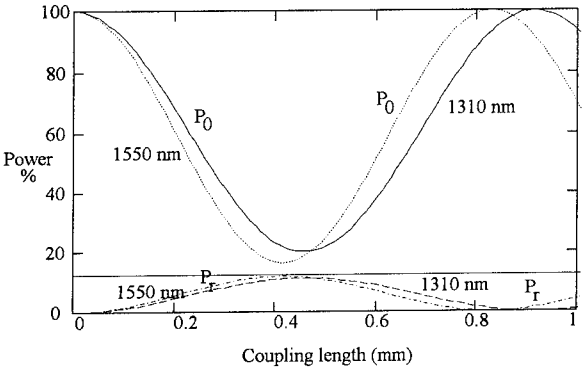


Figure 8

Three-mode problem

Due to the different diameters of the fibers, the configuration of 1x8 couplers comprising a central fiber surrounded by a symmetrical heptagonal array does not meet the requirements of low excess loss and high uniformity. Therefore we studied and experienced an alternative geometry where all the fibers have the same diameter and are placed in two concentric rings (figure 9); one is in the center, six in the first ring and one in the second.

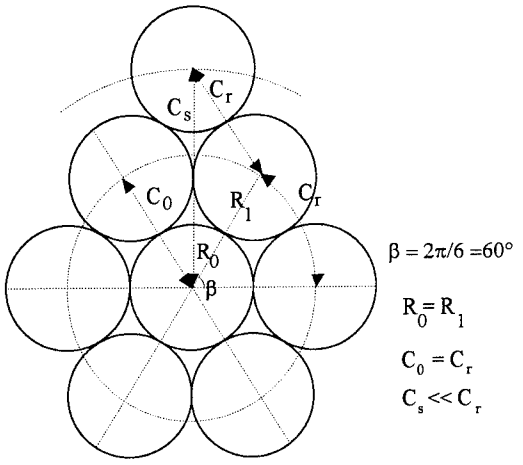


Figure 9

The modal field of this structure can be constructed by normal mode analysis. Under the approximation of weak guidance theory we can use a linear superposition of the

fundamental modes of N fibers to represent the normal mode field (sometimes referred to as supermode) of the whole cross-section of the coupler.

After much algebra we obtain the following set of equations [5]:

$$\sum_j C_{ij} \cdot a_j = (\beta - \bar{\beta}) \cdot a_i \qquad (4)$$

where a_i means the individual modal field, C_{ij} the coupling coefficients and $\bar{\beta}$ the propagation constant of the fiber. The geometrical features of the structure suggest that there is only one coupling constant involved (in figure 9 C_s can be neglected), while the eigensystem can be reduced from order 8 to order 5 by setting $a_2=a_3$, $a_4=a_5$ and $a_6=a_7$. Each eigenvector represents a mode of the structure, and a linear combination of the four eigenvectors gives the field and the power at position z, under the assumption that for $z = 0$ (launch condition) only the central fiber is illuminated. The analytical problem must be solved numerically and the resulting power swapping between the cores is similar to that calculated for 1x13 coupler (figure 10 [5]), which has a more regular structure. The coupling coefficient has the same value calculated for 1x7 couplers so that a similar uniformity at 1310 nm and 1550 nm is expected. One way to improve the power split in area A (figure 10) could be to change the coupling constant between the outer fiber and the inner ring fibers.

On the basis of the previous considerations, it is clear that 1x8 coupler (with all equal fibers) is only a near equal-splitting device, as is evident looking at the area A in figure 10, but can guarantee a better wavelength dependency with respect to the former configuration where the ring fibers have smaller diameters.

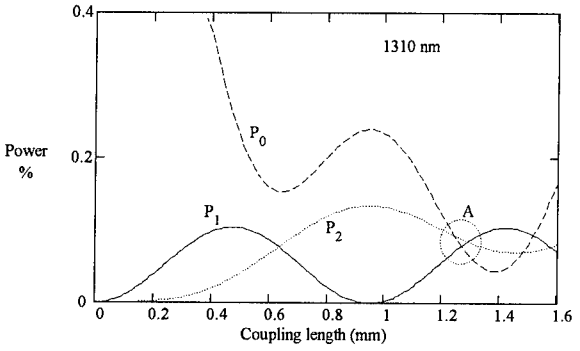


Figure 10

4. PACKAGING

One of the main requests to solve is that the optical parameters of the device remain constant and independent from temperature, humidity and vibrations. Therefore it is important to choose materials with a thermal coefficient similar to silica to prevent the coupler from stress caused by different dilatations. Moreover, the package should be compact, robust and possibly with a low cost.

In our method we do not move the coupler from the bench in order to fix it to a glass substrate with a curing resin without damages or breaks to the fragile fused zone. A second phase consists in positioning and collapsing a heat shrinkable tube along the glass substrate, followed by index matching the ports on one side of the device. The final procedure consists in the insertion of the coupler into a steel tube with a length of 7 cm (2.75 in) and an external diameter of 4.5 mm (0.18 in) (figure 11). An assembly with two rubber boots completes the packaging.

Temperature cycle tests (-40°C +70°C) revealed that our couplers exhibited variations of the insertion loss lower than 0.2 dB.

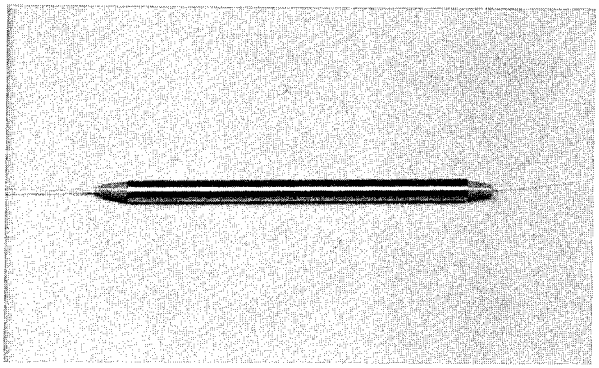


Figure 11

5. RESULTS

A first group of 125 1x7 couplers has been produced optimizing the procedure to obtain better insertion loss and better uniformity at 1310 nm and 1550 nm. Figures 12 and 13 show that in the last 15 samples the maximum insertion loss has always been less than 10.5 dB and in the 80% of the cases less than 10 dB; the uniformity has always been under 3 dB and in more than 60% of the samples less than 2 dB. Excess loss was under 0.3 dB, showing how our

process was adiabatic enough to prevent the fibers from deformations.

As it concerns 1x8 couplers, we achieved the best performances by adopting the configuration with all fibers with the same diameter, as explained previously.

Figures 14 and 15 show that in the last 15 samples the maximum insertion loss has always been less than 15 dB and in the 67% of the cases less than 14 dB; the uniformity has always been under 7.5 dB and in 67% of the samples less than 6 dB. Excess loss was under 0.7 dB. In one case (sample n.3 in figure 14) a maximum insertion loss lower than 12 dB (most commercially available integrated 1x8 couplers have 11.5 -12 dB max insertion loss) with an excess loss of 0.5 dB was obtained; that demonstrates the feasibility of this device, even if the repeatability of the process cannot be considered satisfactory yet.

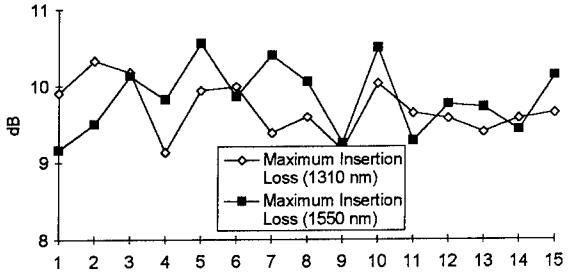


Figure 12 - 1x7 couplers maximum insertion loss

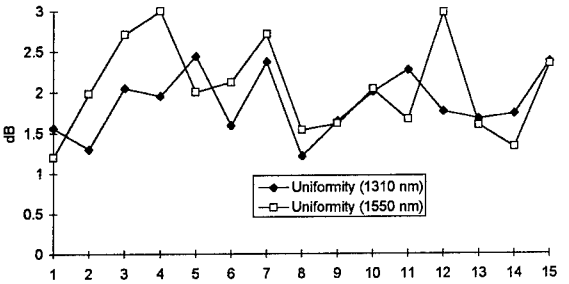


Figure 13 - 1x7 couplers uniformity

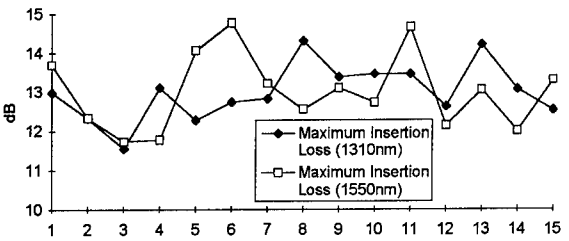


Figure 14 - 1x8 couplers maximum insertion loss

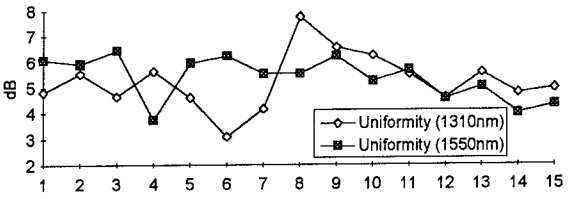


Figure 15 - 1x8 couplers uniformity

6. CONCLUSIONS

We have described a new method for fabricating wavelength-flattened 1x7 monolithic couplers with good repeatability and optical performances. Our experimental results confirm the potential of this method also for 1x8 devices, where the intrinsic geometry of the structure makes more difficult to assure a satisfactory splitting ratio. Unfortunately, theory is not sufficient to control the whole process, due to the high number of parameters interacting each other. This implies a fine-tuning of the procedure which however has still given encouraging results in order to obtain compact, cheap and reliable devices for the optical networks.

REFERENCES

[1] W.J.Stewart, J.D. Love: "Design limitation on tapers and couplers in single-mode fibres" - IOOC-ECOC, 1992

[2] D.B. Mortimore, J.W. Arkwright: "Theory and fabrication of wavelength-flattened 1xN single-mode couplers", Appl. Opt., pp. 1814-1818, 1990

[3] A.W. Snyder, J.D. Love: "Optical waveguide theory", Chapman & Hall, 1983

[4] D.B. Mortimore, J.W. Arkwright: "Monolithic wavelength-flattened 1x7 single-mode fused fibers couplers: theory, fabrication and analysis", Appl. Opt. pp. 650-659, 1991

[5] F. Ladouceur, J.D. Love: "Multiport single-mode fibre splitters", Opt. and Quantum El. pp. 453-465, 1990

Authors

Stefano Pitassi was born in Udine, Italy, in 1965. He received the doctor degree in Opto-Electronics Engineering from "Politecnico di Milano" in 1990. At the beginning of 1991 he joined R&D Dept. of Sirti, where he

has been engaged in passive optical components (connectors, fusion splices and biconical fusion couplers) as a Senior Engineer. He also studies the reliability of components and connecting techniques related to optical fibers. He had some papers in national and international conferences.

Alberto Zucchinali was born in Milan in 1962. He received his degree in Electronics Engineering from "Politecnico di Miliano"; he has been working for 4 years in Sirti in Cables and Optical Components Dept. He is involved as a Senior Engineer in optical components (attenuators, filters, couplers and gratings) research and development activity, from the study of theoretical problems up to device characterization. He is involved in national and international standard committees (ISO/IEC JTC1 SC25 WG3). He had some papers published in national and international conferences.

Maurizio Maglio was born in 1961. Since 1985 he has been working as an Engineer in R&D Dept in Sirti. After a long experience on passive optical components, since 1989 he has been engaged on the optimization process of multi-mode and single-mode fusion couplers.

Vittorio Spano was born in Lagonegro (Italy) in 1967. Since 1989 he has been working as an Engineer in R&D Dept in Sirti. He has been engaged in the development of passive optical components. Since 1994 he has been working on monolithic fusion couplers.

A 100x100 OPTICAL FIBER CROSS-CONNECT SYSTEM

Joji YAMAGUCHI, Naoyuki TAMARU, Tetsufumi SHOJI,
Tsuneo KANAI, Yasuhide NISHIDA and Fumikazu OHIRA

NTT Interdisciplinary Research Laboratories
3-9-11 Midori-cho, Musashino-shi, Tokyo 180, Japan
Phone: +81-422-59-2608 Fax: +81-422-59-4622

ABSTRACT

We developed an optical fiber cross-connect system that automatically makes any connections among 100 pairs of optical fibers. This cross-connect system uses optical fibers, micro-optical connectors, and a robot hand, thereby allowing the system to be compact, and to provide stable, self-holding, low-loss connections. The average connection loss for 100 connections is 0.19 dB, and cross-connect time is 55 seconds. This system can be used to construct flexible optical networks; for example, inter-module connection systems for intelligent buildings.

1. INTRODUCTION

The recent transition to optical access networks has made optical inter-module connections increasingly important.[1] Optical cross-connect systems are necessary to supply efficient access networks and to construct flexible optical distributing systems, such as inter-module connection systems in intelligent buildings. Optical cross-connect systems for such applications require the following characteristics:

- low-loss optical connections,
- self-holding connections (connections are stable even when power supply fails),
- low dependency on optical wavelength, and
- small size.

A mechanical cross-connect system, which uses optical fibers and optical connectors, is one system that meets these requirements.[2] This system has the advantages of low-loss connections and low dependency on wavelength.

This paper describes a prototype mechanical cross-connect system with a robot hand that holds an optical connector to connect and disconnect fibers. The system can automatically make any connections among 100 pairs of optical fibers. The system configuration and experimental results are described.

2. SYSTEM CONCEPT

2.1 BASIC CONFIGURATION

The basic configuration of the system is shown in Fig. 1. The main parts of this system are a robot hand, a connection board, an arrangement board, a roll-up mechanism, and 100 pairs of single-mode optical fibers and optical connectors.

A connector consists of a plug and an adaptor. Each of 100 fibers has a plug at one end and the other end is connected to an external interface port through the arrangement board which has 100 through-holes in a horizontal line. 100 adaptors are arranged on the connection board. Another 100 fibers whose ends are attached to the adaptors are also connected to the external interface ports. The arrangement board and the connection board are positioned in parallel.

The hand can grip and carry a plug from the arrangement board to the connection board, and connect or disconnect it with any adaptor. Two reference positions are provided on the connection board to be used for correction of adaptor positional

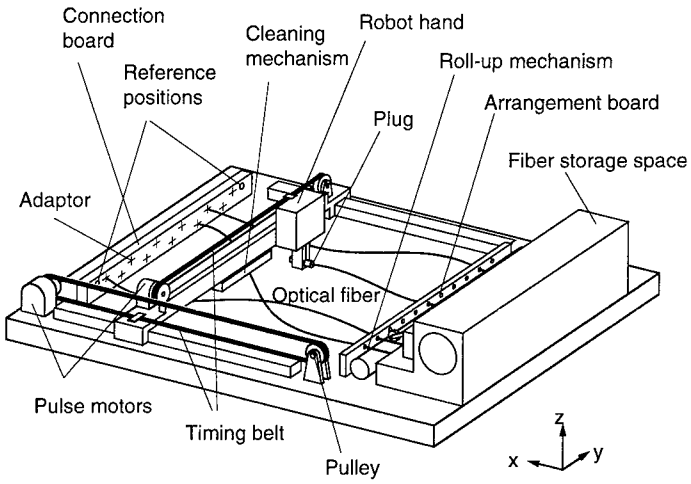


Fig. 1 Basic configuration

errors (see 3.2.2). This compensation achieves precise alignment of plugs and adaptors. A roll-up mechanism is provides behind the arrangement board to roll up and store optical fibers. The mechanical parts and the control circuits are linked to a computer.

The system has the following characteristics.

- The cross-connect procedure described later achieves reliable operation without fiber entanglement.
- The micro-optical connectors used in this system achieve low-loss, self-holding connections. They provide a dense configuration of adaptors that results in a small system.
- Remote operation is possible using a computer.

2.2. CROSS-CONNECT OPERATION PROCEDURE

During operation, the robot hand pulls on a fiber and draws it across to the connection board. Therefore, there is a risk that the fiber will be entangled and finally broken. To avoid this, the system uses the following procedure, for example, to cross-connect plugs Pi and Pj when Pi is connected to adaptor Ai and Pj is connected to Aj in the initial state. Figure 2 also shows the procedure.

(1) The robot hand grips Pi and disconnects it from Ai. Then the hand releases Pi.

(2) The roll-up mechanism rolls up the optical fiber attached to Pi until Pi is on the arrangement board. This process avoids entanglement with other fibers.

(3) Pj is disconnected and arranged on the arrangement board in the same way.

(4) The hand moves to the arrangement board and grips Pi. It carries this plug to the connection board and connects it to Aj

(5) The hand connects Pj to Ai in the same way.

This procedure prevents fibers from entangling even if the operation is repeated many times.

In steps 2 and 3 of the above procedure, dust can get on the plug while the fiber is rolled up. This may worsen the connection loss. The system is therefore equipped with a cleaning mechanism. In steps 4 and 5, the plug is cleaned while the plug is being transferred. This process achieves low connection loss.

The system connects all plugs to the adaptors even if there are plugs that do not need to be connected. Thus all the plugs and adaptors are protected from dust contamination.

3. PROTOTYPE SYSTEM

A photograph of the prototype system is shown in Fig. 3. The size of the mechanical part is 685x495x200 mm^3. This section describes the structure and functions of the main components of the prototype system.

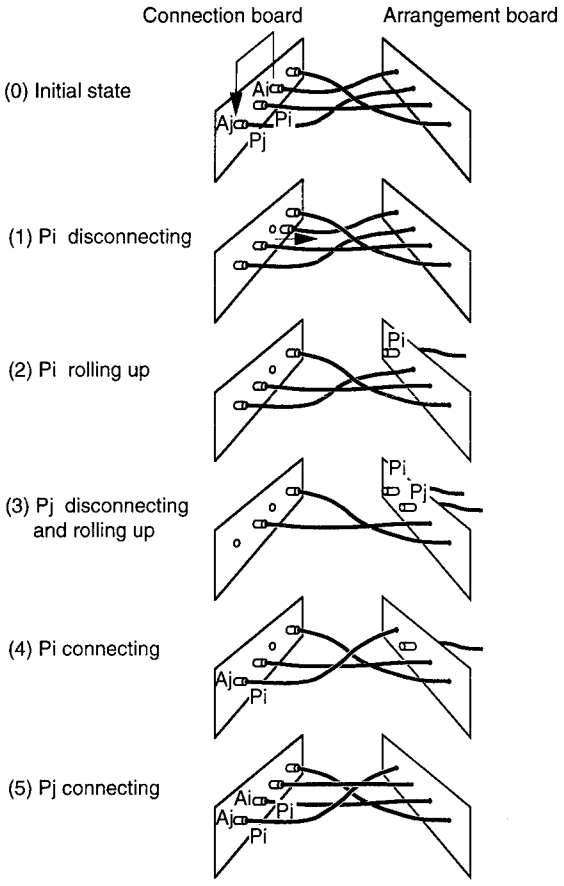


Fig. 2 Cross-connect operation procedure

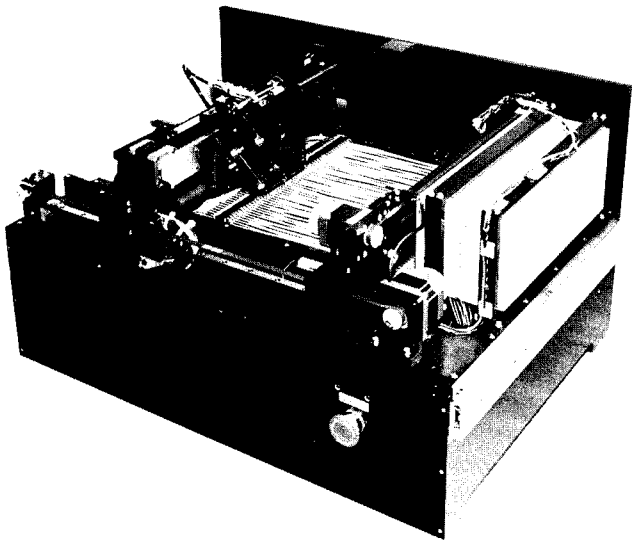


Fig. 3 Prototype system

3.1 Micro-optical connector [3]

A micro-optical connector has a split alignment sleeve and two ferrules with a diameter of 1.25 mm. So high-density, low-loss connections can be achieved. Figure 4 shows the structure of the connectors. The adaptor has a split alignment sleeve and a ferrule. The adaptor also has a pair of leaf springs that holds the plug by spring force. The plug has a ferrule. The step part on the plug expands the space between the two springs and releases the force when the plug is disconnected.

The arrangement of adaptors on the arrangement board is shown in Fig. 5. 100 adaptors (A00-A99) are arranged in two lines and the adaptors in one line are shifted by a half pitch from those in the other line. High density is achieved and the robot hand can approach any of the adaptors from the +z direction. Figure 6 is a histogram of the measured connection loss for 100 connections. The average connection loss is 0.19 dB.

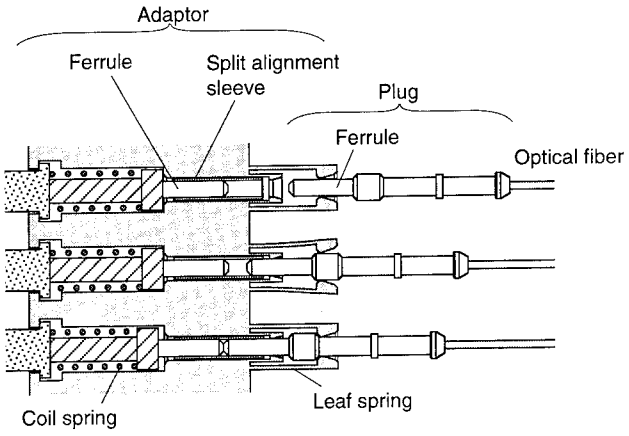


Fig. 4 Micro-optical connector

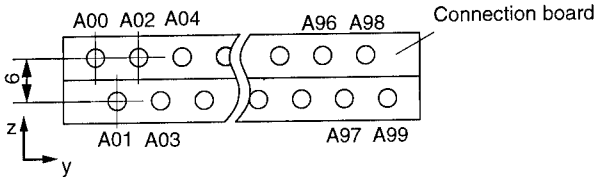


Fig. 5 Adaptor arrangement

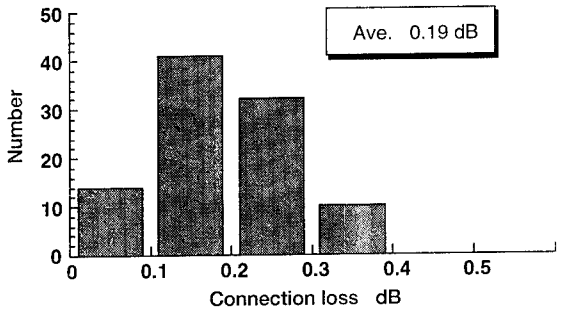


Fig. 6 Histogram of connection loss

3.2 Robot hand

3.2.1 Drive system The hand can move in the x and y directions as shown in Fig. 1. It is driven by a pulse motor through pulleys and a timing belt in each direction. The drive system for the y direction is attached to the carriage for the x direction. Positioning resolution of the hand is determined by the step angle of the motor and the pulley diameter. The resolution is 10 μm in each direction.

When the hand connects a plug to the adaptor, the axes of the plug and the adaptor must be precisely aligned. Therefore, the positioning in the y direction is very important. Figure 7 shows the positioning repeatability in the y direction when the hand moves from A00 to A99. The deviations from the average position of 50 positionings are shown. The standard deviation of the result is approximately 1.0 μm.

3.2.2 Offset compensation [4] In order to align the axis of the plug with the axis of the adaptor by hand positioning, it is necessary to determine the adaptor position in the coordinates of the hand drive system. The adaptor positions are different from

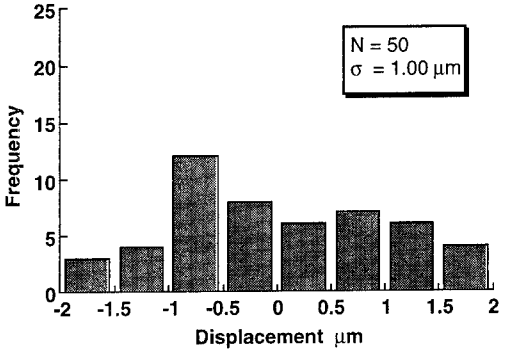


Fig. 7 Positioning repeatability

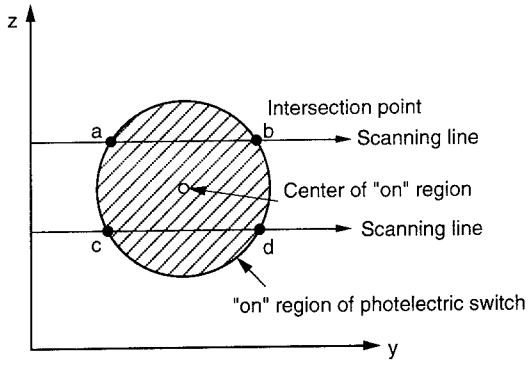


Fig. 8 Offset compensation

the designed positions because of assembly errors, machining error, thermal deformation of mechanical parts and so on. These differences in adaptor positions (offsets) are compensated by an offset compensation method that assumes the following.

- Machining errors and assembly errors in the pitch of the adaptors are negligible and the adaptor positional errors are mostly caused by assembly error and thermal deformation of the connection board.
- The connection board is uniformly deformed by thermal change.

With these assumptions, the adaptor positions can be calculated from any two points on the connection board. A reflective type photoelectric switch is attached at each end of the connection board to provide reference positions on the board. Figure 8 shows the method of measuring these two positions. The photoelectric switch outputs "on" if there is a reflective object in front or nearly in front of the switch. The positions at which the object cause the switch output to become "on" is represented by the circle shown in Fig. 8 which is perpendicular to the switch axis. This area is called the "on" region. When the hand grips a plug, which is the reflective object, and scans the y-z plane, intersections of the "on" region, points a, b, c and d are measured. The center of the "on" region is then calculated from these intersection points. This operation is done for both switches to measure the reference positions on the connecting board. The adaptor position is then calculated relative to these two reference positions. This method achieves precise alignment and reliable connection.

3.2.3 Finger part Figure 9 shows the configuration of the finger. The gripping force is produced by leaf springs deformed by a cam. The designed gripping force is 46.2 N. The finger incorporates a sliding table in the z direction to align with the adaptors on either upper or lower lines (see Fig. 5).

The hand positioning repeatability is good and the offset compensation achieves precise alignment of plug and adaptor axes as already explained. However, there are adaptor pitch errors that are neglected in the offset compensation method. Therefore, there is a possible alignment error in the connecting operation, which could cause damage to the adaptor and plug. To avoid such damage, the finger has a compliance mechanism.

Figure 10 shows the structure of the compliance mechanism. It consists of parallel leaf springs for the y and z directions. So the mechanism has translational compliance in both directions. Experimental compliance values are approximately 4.2 μm/N in the y direction and 8.8 μm/N in the z direction. Designed values are 6.7 μm/N and 6.1 μm/N respectively. Differences between the experimental and designed values are mainly caused by machining error of the hinges.

The total compliance of the plug griped by the hand consists of the compliance values of the finger, the compliance mechanism, the timing belt and so on. The experimental compliance of the plug is 28.2 μm/N in the y direction and 28.5 μm/N in the z direction. If there is 100 μm alignment error, the force between the plug and the adaptor is only 3.5 N. The compliance mechanism lowers the force and decreases the possibility of damage. In practice, connection was achieved without any connector damage even when 100 μm alignment error was produced intentionally.

3.3 Roll-up mechanism

Figure 11 shows the configuration of the roll-up mechanism. A fiber is rolled up by an idler pulley pressing on a drive roller behind the arrangement board. The idler pulley can be positioned at any fiber, so it can be rolled up.

To prevent rolled-up fibers from becoming entangled with

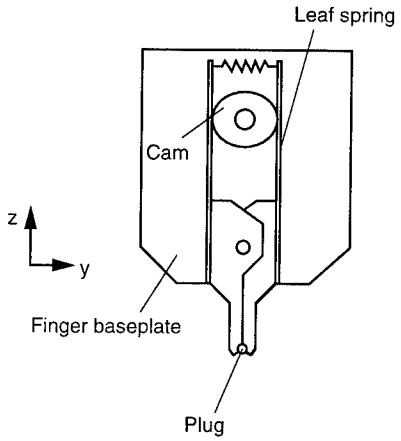


Fig. 9 Structure of the finger

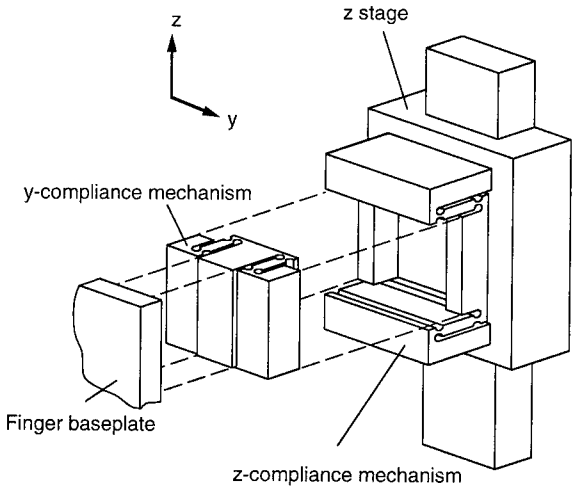


Fig. 10 Compliance mechanism

other fibers, each of the 100 fibers has its own separate storage space. Figure 12 shows a stored fiber. Five turns of fiber are stored in the shape of a vortex in the space. The depth of the space is 1.0 mm which is slightly larger than the fiber diameter of 0.9 mm. This depth achieves smooth storage and prevents the fiber from being caught and stopped in the space.

Maximum fiber length needed for connection to any adaptor is 370 mm, for example, when the plug P00 is connected to adaptor A99. The space can store 570 mm length of fiber which is longer than the required fiber length.

3.4 Cleaning mechanism

Figure 13 shows the cleaning mechanism. It is installed at the center of the hand guiderail (see Fig. 1). The plug is carried in front of the cleaning mechanism by the hand, then the cleaning tape is pushed to the plug end and it cleans by horizontal movement

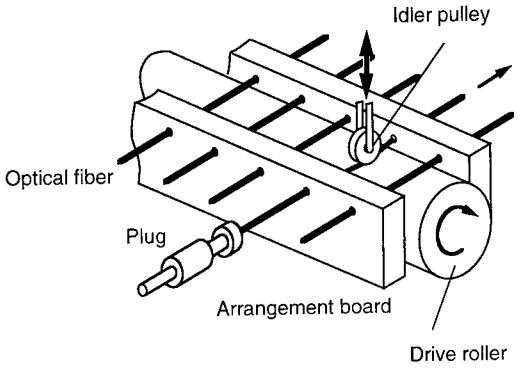


Fig. 11 Roll-up mechanism

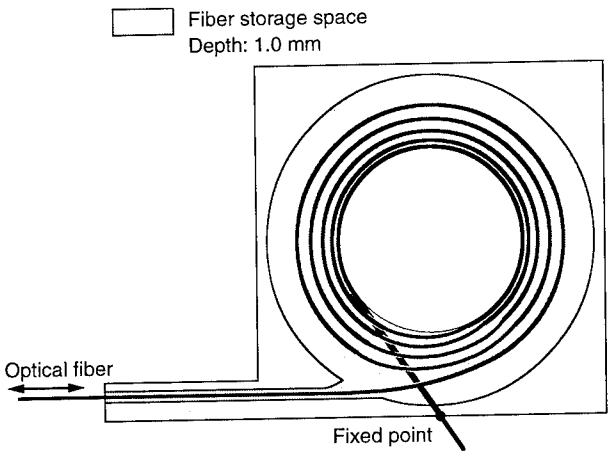


Fig. 12 Fiber storage space

4. EXPERIMENTAL RESULTS

Plug P50 which was connected to Adaptor A30 was disconnected then connected to adaptor A80. Figure 14 shows the change in connection loss at each connection. The solid line shows the loss of P50 and A30, and the dotted line shows the loss of P50 and A80. Low-loss connections were achieved at both connections. It took approximately 55 sec to do this operation.

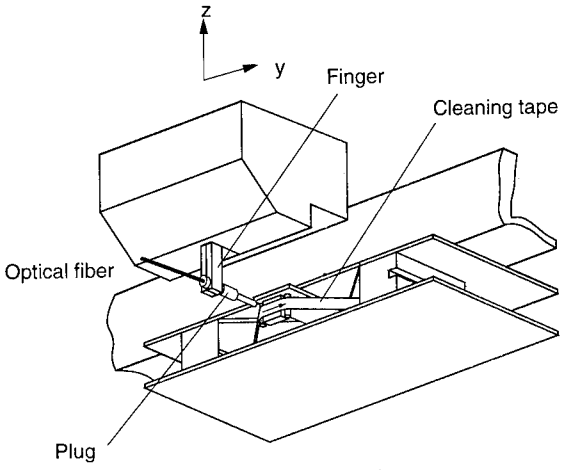


Fig. 13 Cleaning mechanism

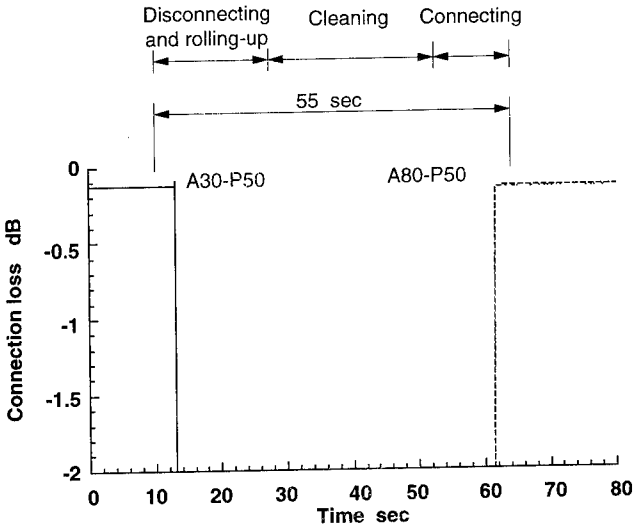


Fig. 14 Cross-connect operation

5. SUMMARY

A cross-connect system was developed that can automatically make any connections among 100 pairs of optical fibers. The system makes low-loss, self-holding connections, and is remotely operated by computer. Highly reliable connection is achieved by using offset compensation and a cleaning mechanism. The average connection loss was 0.19 dB and the cross-connect operation time was 55 sec.

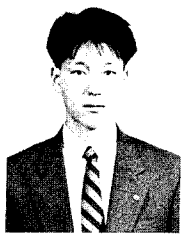
REFERENCES

(1) Tetsuya MIKI: "Fiber-Optic Access Networks and Services", NTT Rev., Vol. 6, No. 3, pp. 17-25 (1994)

(2) Toshiaki KATAGIRI, Yahei KOYAMADA, Masao TACHIKURA and Yutaka KATSUYAMA: "Nonblocking 100x100 optomechanical matrix switch for subscriber networks", International Wire & Cable Symposium Proceedings, pp. 285-290 (1991)

(3) Yasuhide NISHIDA, Fumikazu OHIRA, Tsuneo KANAI, Naoyuki TAMARU, Tetsufumi SHOJI, Joji YAMAGUCHI and Hirofumi KIMURA: "Main distributing frame using a fiber-handling method in optical access networks", OFC '95 Technical Digest, Vol. 8, TuK6, pp. 57-58 (1995)

(4) Naoyuki TAMARU, Joji YAMAGUCHI, Yasuhide NISHIDA and Fumikazu OHIRA: "Offset compensation method using photoelectric switches for positioning control system", Preprints of the 37th Japan Joint Automatic Control Conference, Osaka, pp. 225-228 (1994)



Joji YAMAGUCHI

NTT Interdisciplinary Research Laboratories
3-9-11 Midori-cho, Musashino-shi, Tokyo
180, Japan

Dr. Yamaguchi was born in São Paulo, Brazil, in 1965. He received B.E., M.E. and Dr. degrees in mechanical engineering, all from Tokyo Institute of Technology, Tokyo, Japan, in 1988, 1990 and 1993, respectively. He joined NTT Interdisciplinary Research Labs., Tokyo, Japan, where he is engaged in research on optical cross-connect systems. Dr. Yamaguchi is a member of the Japan Society of Mechanical Engineers, and the Japan Society for Precision Engineering.



Naoyuki TAMARU

NTT Interdisciplinary Research Laboratories
3-9-11 Midori-cho, Musashino-shi, Tokyo
180, Japan

Naoyuki Tamaru was born in Tokyo, Japan, in 1947. He received the B.E., M.E. and Dr. degrees in electrical engineering from Waseda University, Tokyo, Japan, in 1970, 1972, and 1992 respectively. Since joining NTT in 1972, he has been engaged in research on the tracking control for mass memory systems and for optical disk drives. He started researching optical switching equipment for optical communications in March 1992. He is a member of the Society of Instrument and Control Engineers, Japan, and the Institute of Electronics, Information and Communication Engineers of Japan.



Tetsufumi SHOJI

NTT Interdisciplinary Research Laboratories
3-9-11 Midori-cho, Musashino-shi, Tokyo
180, Japan

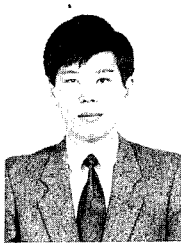
Tetsufumi Shoji was born in Tokushima, Japan, in 1965. He received the B.E. and M.E. degrees in mechanical engineering from Keio University, Tokyo, Japan, in 1989 and 1991 respectively. Since joining NTT in 1991, he has been engaged in research on the optical measurement technology. He started researching optical switching equipment for optical communications in March 1992. He is a member of the Japan Society of Mechanical Engineers, the Japan Society for Precision Engineering, and the Institute of Electronics, Information and Communication Engineers of Japan.



Tsuneo KANAI

NTT Interdisciplinary Research Laboratories
3-9-11 Midori-cho, Musashino-shi, Tokyo
180, Japan

Tsuneo Kanai received the B.E. and M.E. degrees in mechanical engineering from Kyoto University in 1969 and 1971, and a doctor's degree in engineering from Tokyo Institute of Technology in 1993. He joined NTT Electrical Communication Laboratories in 1971 and since then he has been engaged in research and development on connectors for electronic switching and transmission systems, on pin-board-matrix switches for automated main distributing frame systems. He is now a Senior Research Engineer and Supervisor at NTT Interdisciplinary Research Laboratories. Dr. Kanai is a member of the Institute of Electronics, Information and Communication Engineers of Japan.



Yasuhide NISHIDA

NTT Interdisciplinary Research Laboratories
3-9-11 Midori-cho, Musashino-shi, Tokyo
180, Japan

Yasuhide Nishida was born in 1954. He received the B.E. and M.E. degrees in mechanical engineering from Tohoku University, Sendai, Japan in 1976 and 1978, respectively. He joined NTT Electrical Communication Laboratories in 1978 and since then he has been engaged in research and development on mass storage systems and telecommunication mechatronics systems. He is now a Senior Research engineer, Supervisor at Interdisciplinary Research Laboratories. Mr. Nishida is a member of The Japan Society of Mechanical Engineers and The Japan Society of Applied physics and Optical Society of America.



Fumikazu OHIRA

NTT Interdisciplinary Research Laboratories
3-9-11 Midori-cho, Musashino-shi, Tokyo
180, Japan

Fumikazu Ohira was born in Kagawa, Japan, on November 19, 1949. He received the B.E., M.E. and Ph.D. degrees in precision engineering from Osaka University, Osaka, Japan, in 1973, 1975 and 1989, respectively. In 1975 he joined the Nippon Telegraph and Telephone Public Corporation, Tokyo, where he has been engaged in research and development of precision machining and packaging technology of electronic and optical components or modules. Dr. Ohira is a member of the Institute of Electronics, Information and Communication Engineers of Japan, and the Japan Society for Precision Engineering.

STUDY OF A COMPACT AND NON-BLOCKING OPTO-MECHANICAL SWITCH

Y. Hayashi, H. Furukawa, Y. Nomura, H. Yokosuka

Opto-Electronics Laboratory, Fujikura Ltd.
1440 Mutsuzaki, Sakura-shi, Chiba, 285 Japan

ABSTRACT

A compact and non-blocking opto-mechanical switch has been developed for optical fiber networks. It consists of 100 inputs and a corresponding number of outputs whereby any input can be freely connected to any of the outputs. The switch is composed of a pair of robot hands and fiber terminated ferrules having a diameter of 0.6 mm. 100 such ferrules are arranged linearly. The fibers are prevented from entangling during the switching process. The switch size is $300mm^{W} \times 130mm^{D} \times 250mm^{H}$. The switch had a mean insertion loss of 1.3 dB for standard single-mode fibers. The average switching time was 4.8 min.

1. INTRODUCTION

The use of optical fibers in subscriber networks has increased tremendously these past few years. It has become necessary to find efficient ways of installing and maintaining these networks. In particular, efforts at reducing the workload of network reconfiguration require automatic switching capability. To meet this requirement, various non-blocking opto-mechanical switches have been developed previously [1]-[7]. A non-blocking opto-mechanical switch with a 100x100 matrix size has been developed [1]-[4]. In this switch, any input can be randomly connected to any of the 100 outputs. In subscriber networks, it is important that switches have a large matrix in a compact size. A switch consisting of a simple square array with 100 inputs and 100 outputs needs 10,000 (100^2) crosspoints. In this paper, a compact 100x100 switch which reduces the number of crosspoints to 100 and uses thin zirconia ferrules is described.

2. Design of the switch

2.1 Principle of switching

Fig. 1 shows the basic configuration of the non-blocking 100x100 matrix switch with 100 crosspoints. The switch is composed of a pair of robot hands, a housing comprising of 100 adapters which are arranged linearly, 100 fiber terminated ferrules which are connected to the adapters, and a corresponding number of fiber terminated ferrules which are fixed to the opposite side of the adapters. There are excess vacant adapters for the temporary placement of a disconnected ferrule during switching. The robot hands are located on both sides of the adapter array. Switching is accomplished automatically by changing connections at the adapter array. A ferrule to be reconnected at a different adapter is transported by the robot hands. The switching procedure is shown in Fig. 2. Changing the connection between a ferrule a and b in Fig. 2 is described by the following.

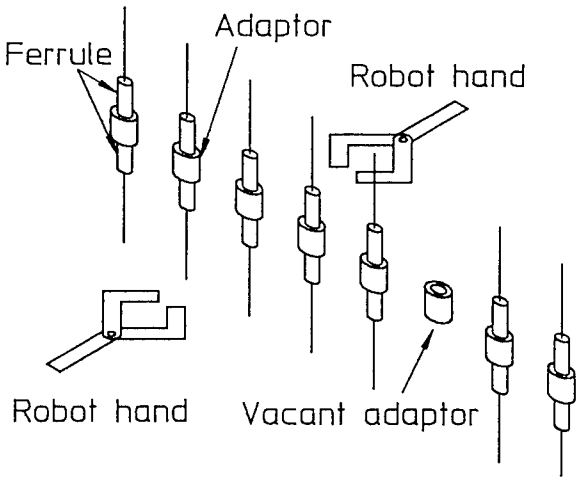


Figure 1 Switch configuration

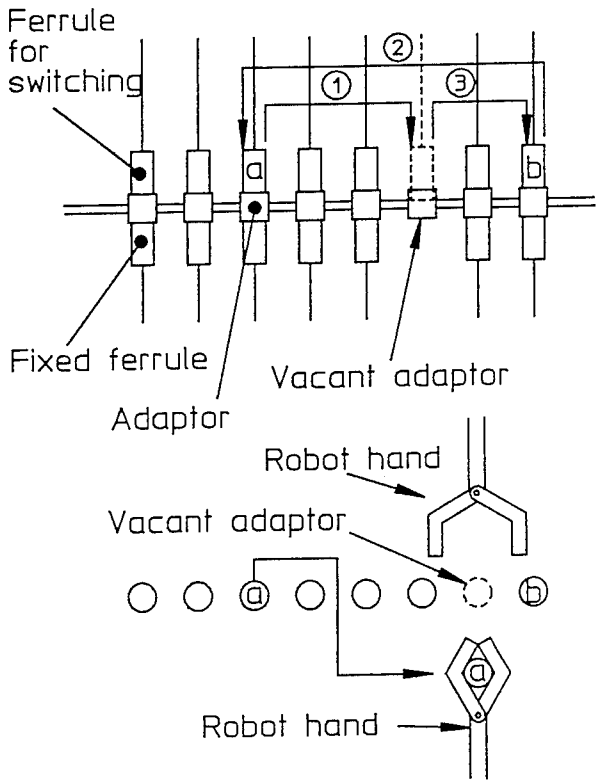


Figure 2 Switching procedure

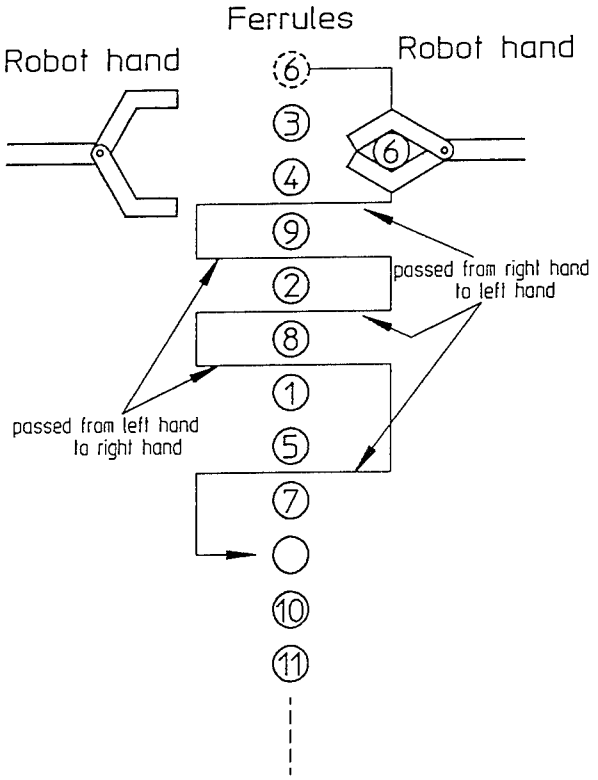


Figure 3 Transport procedure

(1) The robot hand disconnects ferrule **a** from the adapter and connects it to a vacant adapter.
(2) The robot hand disconnects ferrule **b** and connects it to the adapter in which ferrule **a** was located.
(3) Ferrule **a** is transported to the adapter in which ferrule **b** was located.

Thus changing the connection between ferrules **a** and **b** is accomplished.

If the switching is done randomly, the fibers become entangled. The fibers are prevented from entangling during the connection process by adhering to the following transport procedure. Each of the ferrules are numbered at the beginning. The number of the ferrule to be transported is compared to the ferrule number which is to be passed by it. When the transported ferrule number is bigger than the passed ferrule, the robot hand on one side moves the transported ferrule. When the transported ferrule number is smaller than the passed ferrule, the robot hand on the opposite side moves the transported ferrule. Fig. 3 shows an example where the robot hands transport ferrule 6 to a vacant adapter located between ferrule 7 and ferrule 10. In this case, as switching has been already carried out several times, the arrangement of ferrules is not in numerical order. Ferrule 6 transported by the robot hand on the right has passed ferrule 3 and is about to pass ferrule 4. Since the following ferrule number is 9 (which is bigger than 6), the transported ferrule is handed from the robot hand on the right to that on the left. Thereafter, the ferrule as transported by the robot hand on the left passes ferrule 9. The next ferrule number is 2, therefore the transported ferrule is handed to the robot hand on the right and passes ferrule 2. When switching is carried out following the above mentioned procedure, the fibers are prevented from entangling. The intention is to maintain the initial non-tangled condition of the ferrules. By following the rules stated above, as a ferrule is moved up or down along the array, it follows a fixed path that in

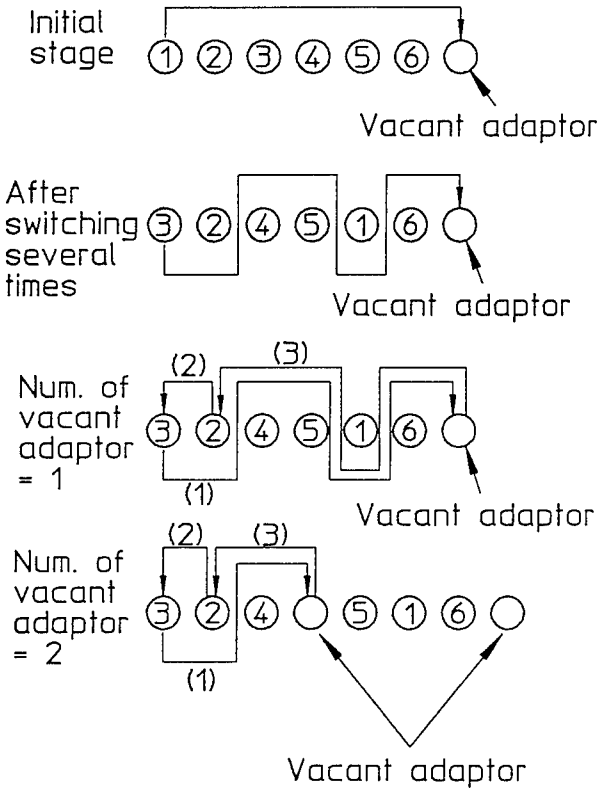


Figure 4 Pass times between robot hands

fact retraces its own movement.

The arrangement of ferrules becomes random compared with the initial numbering after a number of switching operations. (See Fig. 4) When the arrangement of ferrules is random, the number of times the ferrule is switched between the robot hands increases. Consequently, the switching time increases. By increasing the number of excess vacant adapters, the transfer length of a ferrule can be shortened and the number of passing times between the robot hands can be decreased. Therefore, switching time is also decreased. However, the switch size becomes bigger as the adapter array is extended in the longitudinal direction. For determining the optimum number of excess vacant adapters, we simulated passing times between robot hands during switching of ferrules by varying the number of excess vacant adapters. The simulation was

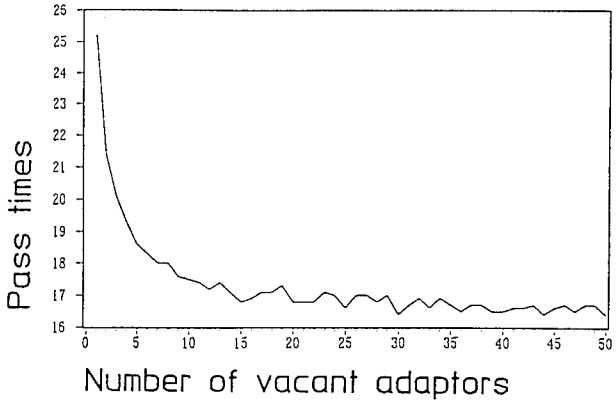


Figure 5 Determination of optimum number of vacant adaptors

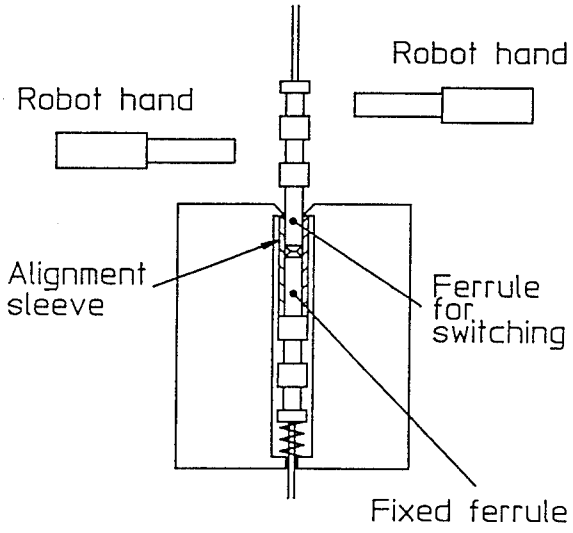


Figure 6 Structure of connection mechanism

carried out as follows.

There are 100 connectors. Excess vacant adapters are located at equal spacing within the adapter array. The arrangement of ferrules and the combination of ferrule numbers for switching is determined at random. The experiment was carried out 10,000 times for each number of excess vacant adapters. The results are shown in Fig. 5. The average value of passing times reduces rapidly when the number of excess adapters is increased from 1 to 5. Thereafter the reduction is small. Therefore, we decided that the optimum number of excess adapters is 5.

2.2 Developed switch

Fig.6 shows the structure of the connection mechanism. We manufactured zirconia ceramic ferrules with a diameter of 0.6 mm and alignment sleeves with a diameter of 0.7 mm in order to make the switch compact. The pitch of the ferrules is 2 mm. A ferrule is held by an alignment sleeve. Through this alignment sleeve, precise connection is achieved. The hole of the adapters has a taper. The ferrules also have a taper. These tapers help to connect the ferrule and the adapter even if the robot hand has a positioning error of 0.3 mm. Standard 10/125 μ m single mode fiber was used in this switch. The switch size is $300mm^{W} \times 130mm^{D} \times 250mm^{H}$.

3. Performance

3.1 Insertion loss

This switch has one fusion splice point and three connections at the input and two ferrule connection pairs for switching. Therefore, the insertion loss of this switch is the sum of these three connections and a fusion splice. Fig. 7 shows the insertion loss measurement setup. A MT connector is used for the input connector. A 1.3 μ m wavelength LED light source was used. The histogram of insertion losses for 50 measurements is shown in fig.8. The average insertion loss was 1.3 dB. The maximum insertion loss was 1.93 dB. The minimum insertion loss was 0.51 dB. The average insertion loss of the MT connectors was about 0.3 dB. The insertion loss of a ferrule connection pair is estimated to be about 0.5 dB.

The loss fluctuation of five repeated switchings for five randomly selected ferrules was less than 0.1 dB.

3.2 Return loss

The return loss measurement setup is shown in Fig. 9. The measured return loss varied with ferrule combinations from 29.7 dB to 47.5 dB at a 1.3 μ m wavelength. The average return loss was 34.4 dB. This variation is mainly due to the polishing technique for a thin zirconia ceramic ferrule. Further investigations are required to refine this.

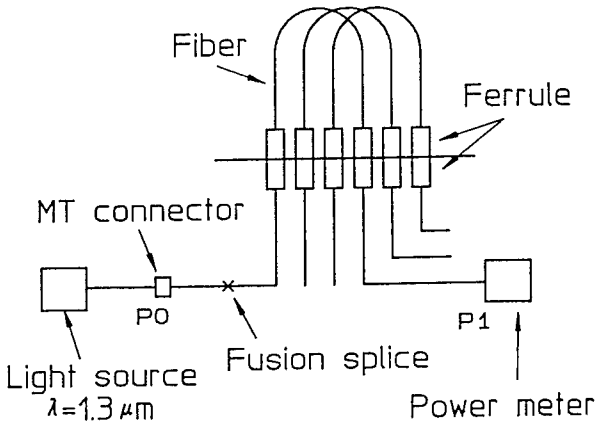


Figure 7 Loss measurement setup

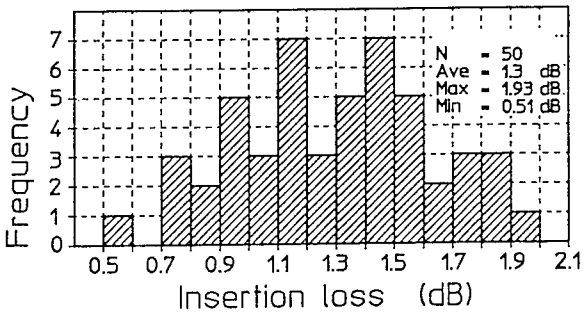


Figure 8 Insertion loss

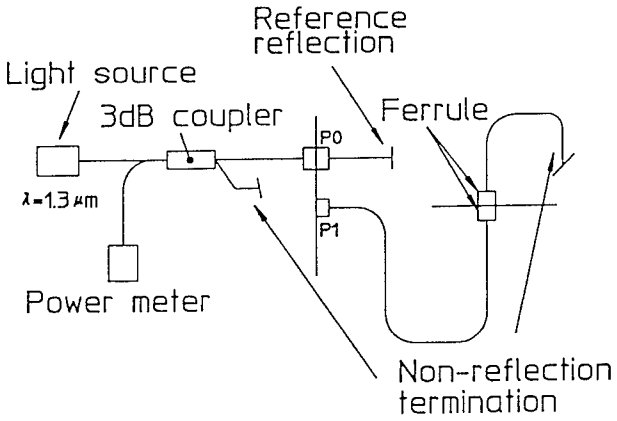


Figure 9 Return loss measurement setup

3.3 Switching time

The switching time is dependent on the arrangement of ferrules and the ferrule combinations required for switching. The switching time was measured with the robot hand starting from the origin, finishing the switching and returning to the origin. The average switching time for 50 randomly selected ferrules was 4.8 minutes.

4. Conclusions

A compact and non-blocking opto-mechanical switch has been developed. An average insertion loss of 1.3 dB was obtained. The switch size was $300mm^{W} \times 130mm^{D} \times 250mm^{H}$.

REFERENCES

[1] T. Katagiri and M. Tachikura, "Cassette-type non-blocking 100x100 optomechanical matrix switch", IEICE Trans. Commun., vol. E75-B, No.12, pp.1373-1375, 1992.

[2] T. Katagiri, Y. Koyamada, M. Tachikura, and Y. Katsuyama, "Non-blocking 100x100 optomechanical matrix switch for subscriber networks", 40th IWCS, pp.285-290, 1991.

[3] M. Tachikura, T. Katagiri, and H. Kobayashi, "Compact and perfectly-free fiber-crossconnect switch with 100 fiber ports", 6th International Workshop on Optical Access Networks, paper:S3.7, 1994.

[4] Y. Hayashi, H. Naidu, Y. Nomura, and H. Yokosuka, "Development of a Non-Blocking Opto-Mechanical Switch", 42nd IWCS, pp.265-269, 1993.

[5] M. Tachikura, T. Katagiri, and H. Kobayashi, "Strictly non-blocking 512x512 optical fiber matrix switch based on three-stage Clos network", IEEE Photon. Tech. Lett., vol. 6, No. 6, pp.764-766,1994.

[6] T. Katagiri, M. Tachikura, and H. Kobayashi, "A construction method for non-blocking, large matrix-size optomechanical switch", IEICE Trans. Commun., vol. E76-B, No. 11, pp.1470-1473, 1993.

[7] M. Tachikura, T. Katagiri, and H. Kobayashi, "Matrix enlargement in connector-type optical switching apparatus by a novel technique which eliminates fiber tangling", IEICE Trans. Commun., vol. J76-B-I, No. 12, pp.989-997, 1993. (in Japanese)



Yukio Hayashi

Opto-Electronics Lab.
Fujikura Ltd.
1440 Mutsuzaki,
Sakura-shi, Chiba,
Japan

Yukio Hayashi was born in 1963. He received the M.E. degree in mechanical engineering from Chiba University in 1988. He joined Fujikura and has been engaged in the research and development of the telecommunication cables and accessories. He is a member of the Institute of Electronics, Information and Communication Engineers of Japan.



Hiroshi Furukawa

Opto-Electronics Lab.
Fujikura Ltd.
1440 Mutsuzaki,
Sakura-shi, Chiba,
Japan

Hiroshi Furukawa was born in 1959. He received the B.E. degree in mechanical engineering from Chiba University in 1984. He joined Fujikura and has been engaged in the research and development of the telecommunication cables and accessories



Yoshikazu Nomura

Opto-Electronics Lab.
Fujikura Ltd.
1440 Mutsuzaki,
Sakura-shi, Chiba,
Japan

Yoshikazu Nomura was born in 1951. He graduated in mechanical engineering from Shinshu University. He has been engaged in the research and development of the telecommunication cables and accessories. He is presently a manager in the Fiber and Cable Accessory Department.



Hiroshi Yokosuka

Opto-Electronics Lab.
Fujikura Ltd.
1440 Mutsuzaki,
Sakura-shi, Chiba,
Japan

Hiroshi Yokosuka graduated in mechanical engineering from Tokyo Metropolitan Technical Junior College in 1967. He has been engaged in the research and development of the telecommunication cables and accessories. He is presently a general manager of the Fiber and Cable Accessory Department. Mr. Yokosuka is a member of the Institute of Electronics, Information, and Communication Engineers (IEICE) of Japan and the Japan Society of Mechanical Engineers, respectively.

Analysis of Mass Fusion Splice Loss

Tomomi Sano, Tsutomu Watanabe, Keiji Osaka

YOKOHAMA RESEARCH LABORATORIES
SUMITOMO ELECTRIC INDUSTRIES, LTD
1, Taya-cho, Sakae-ku, Yokohama, 244 JAPAN

Abstract

Using numerical simulation and experimental analysis, the relationship between splice loss and core deformation for mass fusion splice was analyzed. Core deformation was classified into two types, one is named α type whose core was bent to the opposite direction at the splice point and other one is β type whose core was bent to the same direction. The α type results from a core axis misalignment and β type results from cleave angle of optical fiber end face. A model of core deformation was made from experimental data and analyzed using finite difference beam propagation simulation. These relationships were successfully formulated.

1.Introduction

Fusion splice of optical fiber has a high reliability , a low splice loss and is an important technique for optical fiber network deployment.

A splice loss mainly depends on misalignment of optical fiber core axis. For single fiber splice, core alignment system has been widely used which mechanically manipulates V grooves in 2 directions. By this system we successfully obtained low loss splice of that less than 0.1dB in average [1]. In this case a low-loss splice is easily obtained even if the core eccentricity is large. Splice loss can be easily estimated with direct core monitoring system.

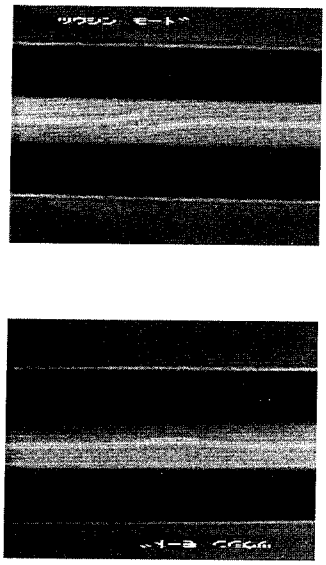
For mass fusion splice that does not adopt a mechanically active alignment system, a large misalignment due to geometrical difference of the fibers and a small dust on V groove is inevitable. In order to decrease this misalignment , a longer arc duration, a higher discharge power and a longer stuffing stroke are adopted in mass fusion splice[2]. This splice condition difference makes the occurrence of core deformation higher. Furthermore, direct core monitoring is practically impossible in case of mass fusion splice due to the small magnification in optical system in order to get a wider view field. These facts make the loss estimation problem in mass fusion splice more complicated.

In this paper we describe splice loss analysis for mass fusion splice and new estimation method.

2.Analysis of mass fusion splice loss

Mass fusion splice loss depends on many parameters such as arc duration, power and so on. Among them, we consider the dependence of splice loss on core deformation at splice point.

The relationship between core deformation at splice point and splice loss for mass fusion splice was actually



(2) β type core deformation

Fig.1 Photographs of splice point for mass fusion splice

measured using single mode four fiber ribbon at 1.3 μm. These data were classified into two groups, one is named α type whose core was bent to the opposite direction at the splice point (Fig.1(a)) and other one is β type whose core was bent to the same direction (Fig.1(b)). Fig.2 shows the dependence of splice loss on core deformation at splice point. Splice loss in α type are lower than those in β type at the same core deformation radius and both α and β type splice loss decrease while core deformation radius R increase.

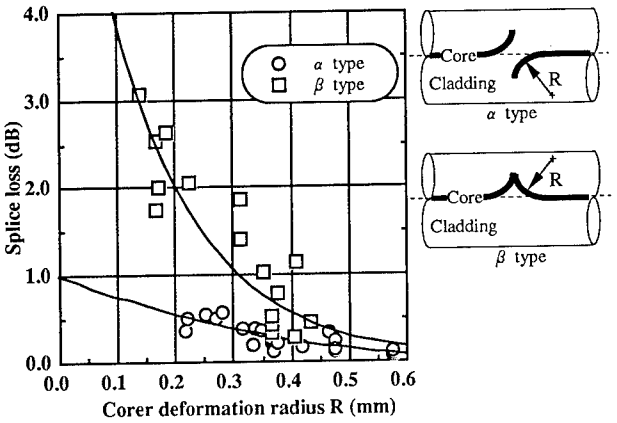


Fig.2 Dependence of splice loss on core deformation radius

3. *Observation of Core deformation at splice point*

A real-time observation of the core deformation process was observed by direct core monitoring technique during arc fusion. The set-up is shown in Fig.3. Fig.4 shows fusion splicing process in case that fibers have a both large axial misalignment and a large cleave angle at the end faces.

When axial misalignment occurred before fusion splice as is shown in Fig.4 (a), misalignment still remained after splicing. And core deformation was proceeded until optical fiber contour became flat with self-alignment effect between the right and the left hand side fibers. From this process, core was bent to the opposite direction each other at the splice point that is α type core deformation. The dependence of core deformation radius on axial misalignment before fusion splice is shown in Fig.5. A core deformation radius decreases while axial misalignment increases.

The core deformation process for angled end face of optical fiber was shown in Fig.4 (b) and (c). In case of (b) that direction of end face angle in the right hand side is identical to that in the left hand side, a core deformation was not occurred. However for case (c), a core is deformed with self-alignment effect. This core deformation type is named β type. Fig.6 shows the relationship between cleave angle and core deformation radius at splice point. When the cleave angle become lager than 6 degrees, a core deformation radius became rapidly smaller.

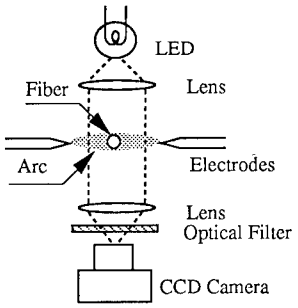


Fig.3 Schematic view of direct monitor system during arc duration

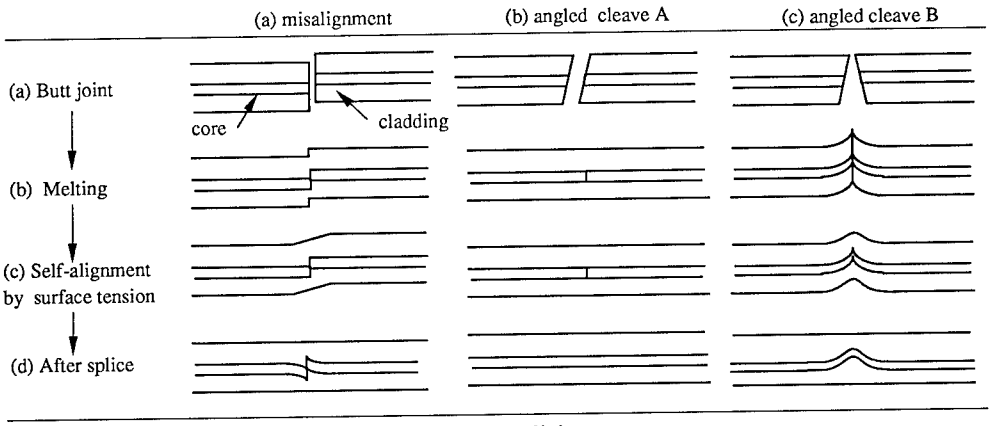


Fig.4 Fusion splicing process

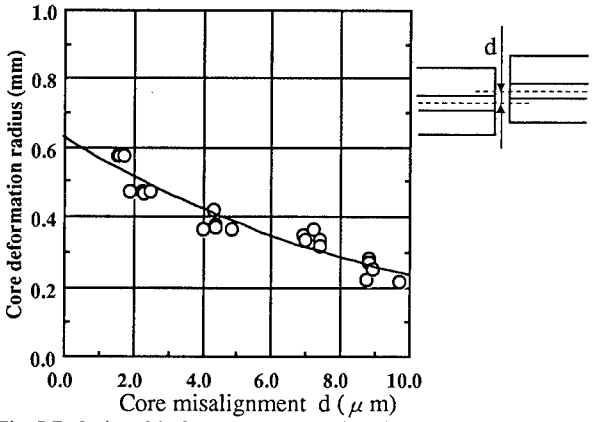


Fig.5 Relationship between core axis misalignment before splice and core deformation radius

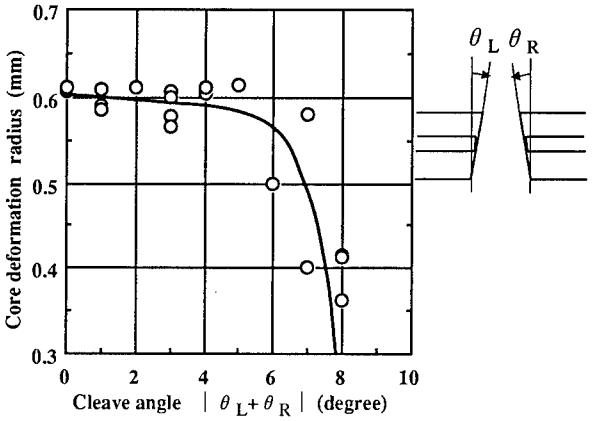


Fig. 6 Relationship between cleave angle and core deformation radius

4.Simulation of splice loss with core deformation

When core deformation occurred, it is too difficult to apply Marcuse`s equation[3] for splice loss estimation. In this section we explain a finite difference beam propagation simulation (FD-BPM)[4] that can estimate a splice loss with core deformation at splice point. Then actual splice loss was compared with the calculated splice loss using FD-BPM.

4.1 FD-BPM simulation

Fig.7 shows a model for this simulation. Z axis shows a propagation direction of optical beam. X and Y axes are defined as the directions perpendicular to Z axis,respectively. Helmholtz equation for 3 dimension was given by

$$\frac{\partial^2 \varepsilon}{\partial x^2} + \frac{\partial^2 \varepsilon}{\partial y^2} + \frac{\partial^2 \varepsilon}{\partial z^2} + k_0^2 n^2 \varepsilon = 0 \qquad (1)$$

where $\varepsilon(x,y,z)e^{j\omega t}$ is electric field, k_0 $(=2\pi/\lambda)$ is the wave vector in the vacuum and n(x,y,z) is the reference refractive index.

Then electric field ε is written as

$$\varepsilon(x,y,z) = E(x,y,z)e^{-jk_0 n_0 z} \qquad (2)$$

where n_0 is refractive index of cladding.

By substituting equation (1) into equation (2), equation (3) is obtained.

$$\frac{\partial^2 E}{\partial x^2} + \frac{\partial^2 E}{\partial y^2} + \frac{\partial^2 E}{\partial z^2} - 2jk_0 n_0 \frac{\partial E}{\partial z} + k_0^2(n^2 - n_0^2)E = 0 \qquad (3)$$

If electric field changes smoothly as following ,

$$\left|\frac{\partial^2 E}{\partial z^2}\right| << k_0 n_0 \left|\frac{\partial E}{\partial z}\right| \qquad (4)$$

then we obtain equation (5) that is basic equation for FD-BPM.

$$2jk_0 n_0 \frac{\partial E}{\partial z} = \frac{\partial^2 E}{\partial x^2} + \frac{\partial^2 E}{\partial y^2} + k_0^2(n^2 - n_0^2)E \qquad (5)$$

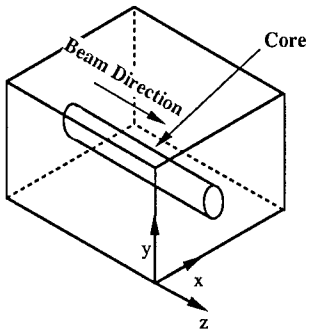
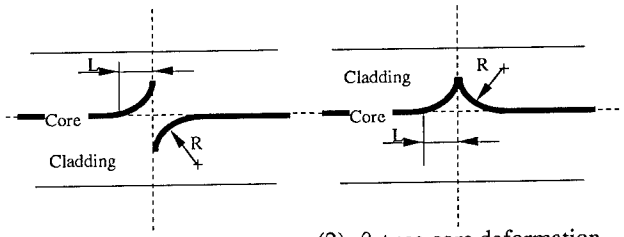


Fig.7 Model of FD-BPM simulation

4.2 Simulation result

Fig.8 shows a core deformation model that (a) is α type and (b) is β type. In this model parameters are defined as follows : R denotes a core deformation radius. L denotes a distance between the splice point and the core deformation starting point.



(1) α type core deformation (2) β type core deformation

Fig.8 Model of core deformation

Fig.9 shows a relationship between splice loss and core axis misalignment before splice. In this figure, the solid curve was obtained by Marcuse`s equation and the dotted curve was calculated from FD-BPM. When core misalignment becomes larger than 6.1 μ m, a good agreement between experimental data and FD-BPM simulation result is obtained.

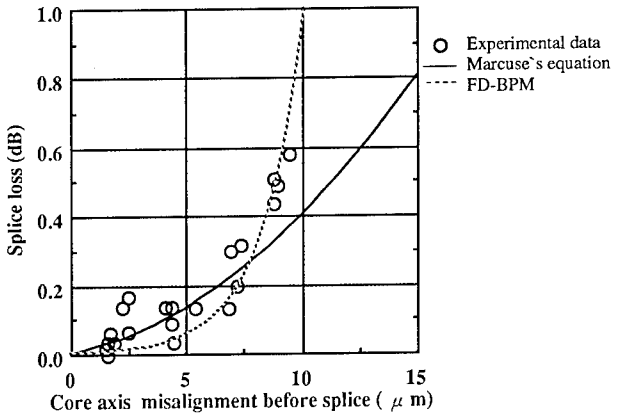


Fig 9 Relationship between splice loss and core axis misaligemet before splice

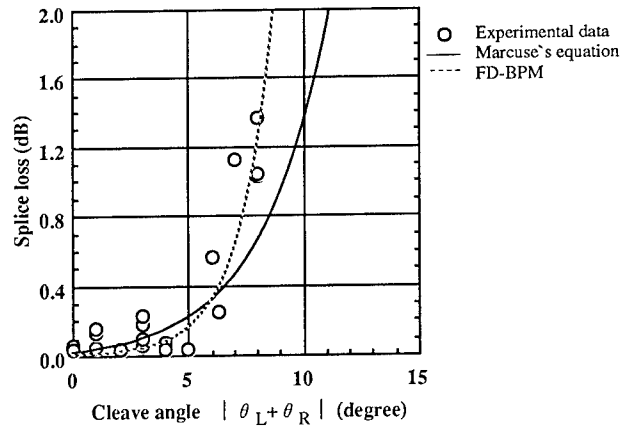


Fig .10 Relationship between splice loss and cleave angle before splice

Fig.10 shows a relationship between splice loss and cleave angle before splice. When cleave angle become bigger than 6.0 degrees, a good agreement between experimental data and FD-BPM simulation result is obtained. We consider that there is a limit in an ability of Marcuse`s equation when core deformation occurred at the splice point.

5. New estimation method for splice loss

We can estimate core deformation from axial misalignment and cleaved angle of optical fiber end face before splice, both of which can be measured by image processing technique in conventional mass fusion splicer. Then splice loss is estimated using FD-BPM simulation.

Fig.11 shows the relationship between actual splice loss and estimated splice loss using our new estimation method. The estimation is kept within $\pm$ 0.05dB error for both α and β type .

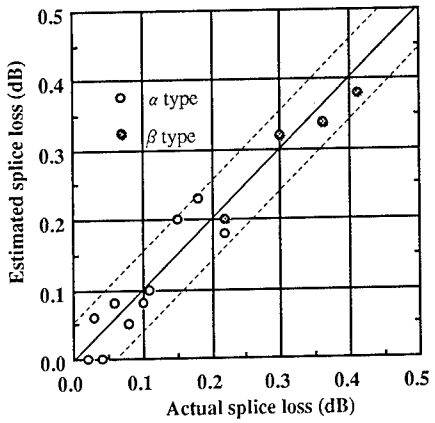


Fig.11 Accuracy of estimated splice loss

6.Conclusion

The main cause of mass fusion splice loss was clarified by the core deformation at splice point. The mechanism for core deformation occurrence was also clarified.

From these results, the mass fusion splice loss was classified into two types, α and β. By FD-BPM simulation, we showed the limit in the ability of Marcuse`s equation. We also established the new estimation technique for the splice loss with a big core deformation. The estimation accuracy by the technique was kept within $\pm$ 0.05dB.

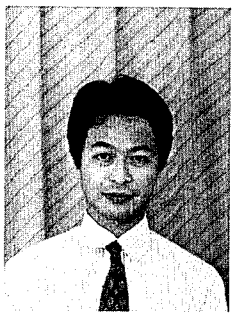
Reference

(1) N.Hakamata et al .,"Development of Compact Fusion Splicer with Direct Core Monitoring System SUMIOFCAS T-34" Sumitomo Electric Technical Review,Nov.27,Jan.1988, pp37-41

(2) K.Osaka et al .,"Mass Fusion Splicing Technique for single-Mode Optical Fiber Ribbon for Subscriber Networks" Sumitomo Electric Technical Review,Nov.29,Jan. 1990, pp85-91

(3) D.Marcuse,"Loss Analysis of Single-Mode Fiber Splices", B.,S.,T.,J.,56,No.5(May-June 1977)

(4) Y.Chang and N.Dagli,"Analysis of Z-invariant and Z-variant semiconductor rib waveguides by explicit finite difference beam propagation method with nonuniform mesh configuration",IEEE J.Quantum Electronics, vol.27, no.10, pp2296-2305, Oct.1991.



Tsutomu Watanabe
Sumitomo Electric Industries,Ltd.
1,Taya-cho,Sakae-ku,
Yokohama,Japan

Tsutomu Watanabe was born in 1964 and received his B.S.degree in mechanical engineering from Tokyo University in 1987. He joined Sumitomo Electric Industries the same year and has been engaged in research and development of fusion splicing technologies for optical fiber. He is a member of Mechanical Engineers and the Institute of Electronics, Information and Communication Engineering of Japan.



Tomomi Sano
Sumitomo Electric Industries, Ltd.
1,Taya-cho,Sakae-ku ,
Yokohama,Japan

Tomomi Sano was born in 1965 and received his M.S.degree in electric engineering from Tokai University in 1990. He joined Sumitomo Electric Industries the same year and has been engaged in research and development of fusion splicing technologies for optical fiber. He is a member of Japan Applied Physics.



Keiji Osaka
Sumitomo Electric Industries.Ltd.
1,Taya-cho,Sakae-ku,
Yokohama,Japan

Keiji Osaka was born in 1955 and received his M.S.degree in precision mechanical engineering from Kyoto University in 1981. He joined Sumitomo Electric Industries the same year and has been engaged in research and development of fusion splicing and mechanical switching technologies for optical fiber. He is now a chief research associate of Optomechatronics Systems R&D Dept.Yokohama Research Laboratories and a member of Electronics,Information and Communication Engineering of Japan.

Development of Multi-fiber Backplane Connector

Ken Kanai,Hiroyuki Yanagase,Naoko Shimoji

THE FURUKAWA ELECTRIC CO.,LTD.

6,Yawata-kaigandori,Ichihara,Chiba 290 Japan

Abstract

Multi-fiber Push-On type connector (MPO connector) has been used at where connections are repeated many times, for example, at the terminals of equipment.

This type of connector has an oblique endface, so it is able to eliminate Fresnel reflection without index matching materials. It has also achieved low insertion loss due to physical contact between fibers.

Applying the connector described above, backplane type connector has been developed which can connect backplane and printed board with self-retentive mechanism.

Backplane connector has almost the same insertion loss of MPO connector and has high return loss of over 50dB. That connector keeps good characteristic during 5000 times reconnection test, and no damage is observed on the surfaces of the fibers after the test.

1. Introduction

In the near future, very high-count cables will be introduced into the subscriber cable systems. The connection point is expected to increase, so high-count optical fiber connectors play an important roll in the cable networks[1].

At the connection point, refractive index matching materials are usually supplied on the endface of connectors to eliminate Fresnel reflection. There are a lot of connection points and it takes a long time to supply index matching gel. So it is proposed to develop a connector which doesn't need gel.

On this point of view, MPO connector has been developed to make connection easy at where connections are repeated many times, for example, at the terminals of equipment. This type of connectors has an oblique endface, so it is able to eliminate Fresnel reflection without index matching materials. It has also achieved low insertion loss due to physical contact between fibers.

And recently, the technology of arraying light-emitting devices has been improved, so it is necessary to develop a connector which connect the device and fiber ribbon.

For the purpose described above, multi-fiber backplane connector has been developed applying MPO connector. This type of connector can make connection easily by push-pull coupling mechanism.

This paper presents the structure and the characteristics of multi-fiber backplane connector.

2. Structure of backplane connector

2.1. Structure

Figure 1 shows the structure of MPO connector which has been already used. This type of connector consists of an adaptor and two connector plugs. The endface of this connector is polished at an angle of 8 degrees to eliminate Frenel reflection without index matching materials. And it has also achieved low loss connection by direct contact between fibers.

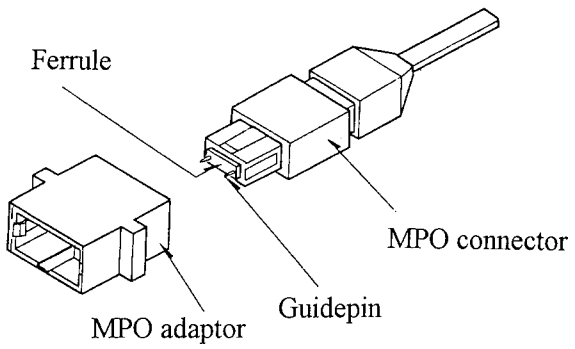


Figure 1 Structure of MPO connector

Figure 2 shows the structure of backplane connector. This type of connector consists of backplane housing, printed board housing, and connector plugs which are inserted within both housings. These plugs are the same ones as those of MPO connector. And backplane housing and printed board housing are used instead of adaptor for MPO connector, and which have push-pull coupling mechanism. The structure of both housings were designed based on almost the same concept of Miniature Unit-coupling (MU) backplane connector which had been already developed[2]. Furthermore, these housings can connect 12-fiber ribbon which has 0.25 mm in distance between fibers in the same space of the backplane housing which connect 2 MU connectors.

Backplane housing consists of an inner housing and an outer housing. As the printed board is inserted into the backplane, the inner housing of backplane is coupled with the printed board housing, then the inner housing comes to free from the outer housing. So the pressing force onto the backplane can be canceled. This is called self-retentive mechanism and it overcomes the problem of lack of strength of backplane.

These housings also have floating mechanism which can absorb horizontal, vertical and axial misalignments.

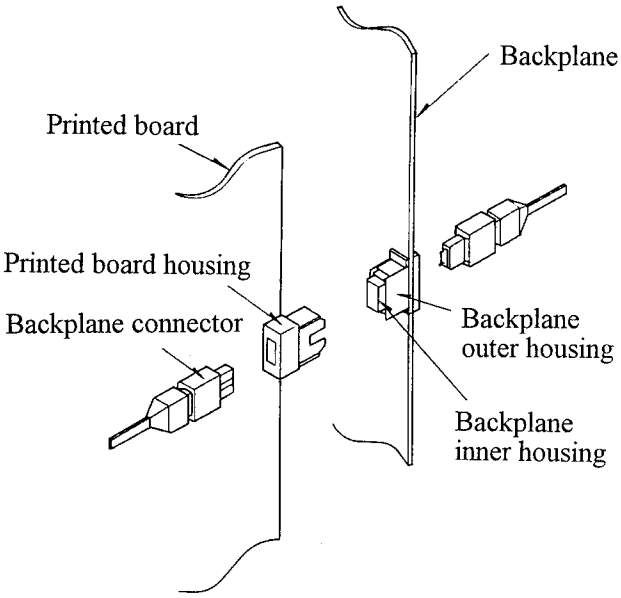


Figure 2 Structure of backplane connector

2.2. Sequence of mating

Figure 3 shows the sequence of mating of backplane connector. As the printed board is inserted into the backplane, the housings are aligned and the floating mechanism comes into operation to absorb horizontal and vertical misalignment of housings. After that the plugs are aligned and ferrules are mated. At this point optical connection is completed and this gives rise to pressing force to the backplane. The printed board is inserted into the backplane furthermore, the main latch of the printed board housing is locked and inner latch is released. Then the self-retentive mechanism comes into operation and the inner housing comes to free from the outer housing. So the pressing force onto the backplane is canceled with optical connection completed.

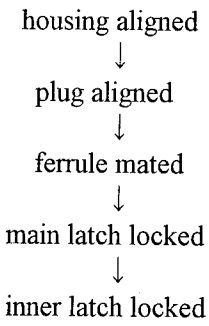


Figure 3 Connecting sequence of backplane connector

3. Characteristics

3.1. Insertion loss

The design of the housing of backplane and printed board is very important as well as the precision in size of ferrule. So it is necessary to verify that housings are designed accurately.

The method is as follows.

At first, insertion loss was measured with MPO adaptor. And next, connectors which have rather high insertion loss were selected, and assembled into the backplane housings. Then insertion loss was measured again. The reason for this sequence is that the change in insertion loss can be observed remarkably as the connectors are assembled into the backplane housings.

Figure 4 shows the insertion loss measured with MPO adaptor. Every plug has 12 fibers. The number of fibers measured was 168 (14 connections). The insertion loss was 0.346 dB in average.

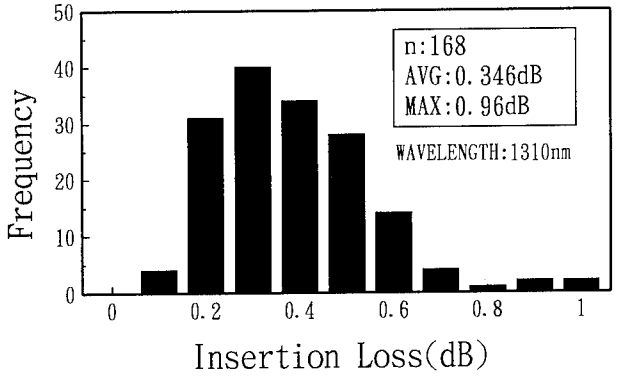


Figure 4 Insertion loss measured with MPO adaptor

Figure 5 shows the insertion loss measured with the backplane housing. The number of fibers measured is as same as with MPO adaptor. The insertion loss was 0.406 dB in average and there were no remarkable difference between the insertion losses measured with MPO adaptor and backplane housing.

The results descried above verified accuracy in design of the housings.

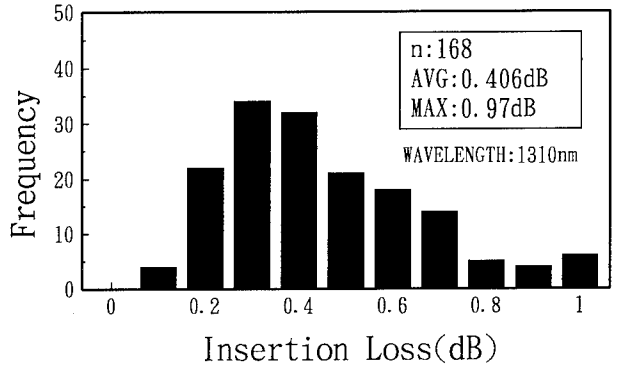


Figure 5 Insertion loss measured with backplane housing

3.2. Return loss

Backplane connector has an oblique endface, so Fresnel reflection can be avoided without index matching materials. It is necessary to verify that backplane connector has high return loss as well as MPO connector.

Figure 6 shows the return loss of backplane connector. It has 58.46 dB in average.

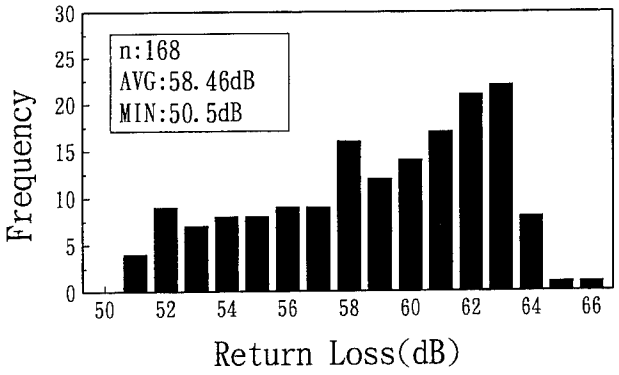


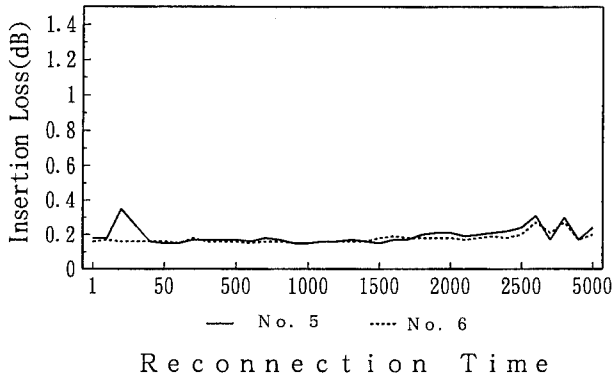
Figure 6 Return loss of backplane connector

3.3. Reconnection test

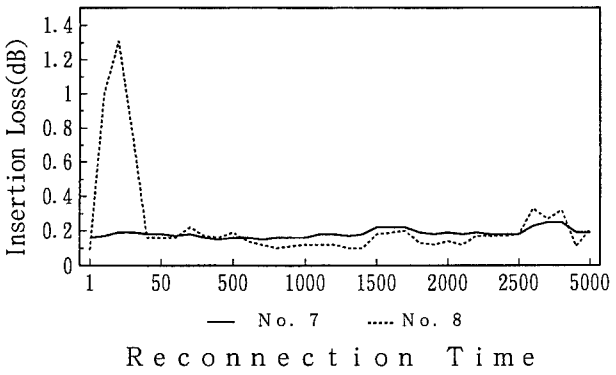
Backplane connector is used at where connection is repeated many times. So it is necessary to verify that the backplane connector is durable for reconnection.

Figure 7 shows the change of insertion loss during the reconnection test. No. 5, 6, 7 and 8 fibers were measured and the number of reconnection times was 5000.

It can be observed that remarkable increase in insertion loss at No. 5 and No. 8 fibers at 20 and 30 reconnection times in figures 7(a) and (b), respectively. But after the endface of the connectors were cleaned up, then it came back to the first level. So it seems that the increase of insertion loss was due to the dust on the endface of the connectors. At another 2 fibers, there were no remarkable increase in spite of rather high losses at the first level. And no damage could be observed at the surfaces of fibers. The stability of backplane connector during the reconnection test was verified.



(a) No.5 and No.6 fibers



(b) No.7 and No.8 fibers

Figure 7 Change of insertion loss during the reconnection test

4. Conclusion

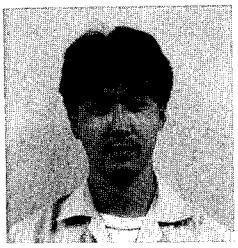
Applying MPO connector, high-count backplane connector has been developed which has the self-retentive mechanism.

Backplane connector has almost the same insertion loss of MPO connector. And that connector has high return loss of over 50 dB. That connector also keeps good characteristic during 5000 times reconnection test, and no damage is observed on the surfaces of the fibers after the test.

5. References

(1)S.Nagasawa, T.Tanifuji, M.Matsumoto, M.Kawase, "Single-Mode Multifiber Connectors for Future Large Scale Subscriber Networks, "ECOC'93, pp29-32, 1993

(2)S.Iwano, R.Nagase, K.Kanayama, E.Sugita, K.Yasuda and Y.Ando, "Compact and Self-Retentive Multi-Ferrule Optical Backpanel Connector, "J.Lightwave Technol., vol.10, no.10, pp1356-1362, 1992

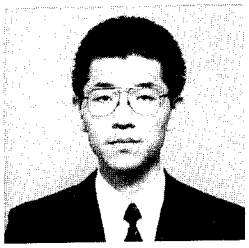


Ken Kanai

The Furukawa Electric Co. , Ltd.

6, Yawata-kaigandori, Ichihara, Chiba, 290, Japan

Ken Kanai was born in Niigata, Japan, in 1967.
He received the M.E. degree in materials science engineering from Keio University, Kanagawa, Japan, 1992.
He joined The Furukawa Electric Co., Ltd., in 1992. Since then he has been engaged in development of optical fiber connectors.

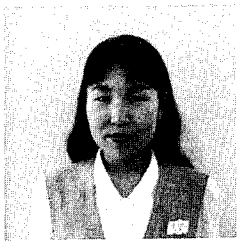


Hiroyuki Yanagase

The Furukawa Electric Co., Ltd.

5-1-9, Higashi-yahata, Hiratsuka, Kanagawa, 254, Japan

Hiroyuki Yanagase was born in Niigata, Japan, in 1966.
He received the M.E. degree in electrical engineering from Niigata University, Niigata, Japan, 1991.
He joined The Furukawa Electric Co., Ltd., in 1991. Since then he has been engaged in development of optical components.



Naoko Shimoji

The Furukawa Electric Co., Ltd.

6, Yawata-kaigandori, Ichihara, Chiba, 290, Japan

Naoko Shimoji was born in Tokyo, Japan, in 1968.
She received the M.S. degree in physics engineering from Chuo University, Tokyo, Japan, 1993.
She joined The Furukawa Electric Co., Ltd., in 1993. Since then she has been engaged in development of optical fiber connectors.

Filter Embedded Component for Plug Jack Type Connector

K. Asano, H. Hosoya, H. Yokosuka

Opto-Electronics Laboratory, Fujikura Ltd.
1440 Mutsuzaki, Sakura, Chiba, 285 Japan

ABSTRACT

Filter components have an important function in remote fiber test systems used in the maintenance of optical fiber networks. In the past, various filter components have been developed.

This time we developed a filter embedded plug jack type connector and confirmed its reliability for use in outdoor environments.

A connector housing similar to that of optical attenuators was used for the filter embedded plug jack connector. The optical filter chip was embedded in the ferrule of the connector. A slit was machined in the ferrule using a mirror finish grinding technique. The average insertion loss was 0.7 dB at pass wavelength and greater than 50 dB at block wavelength. The average return loss was greater than 50 dB. We investigated methods of protecting the embedded filter to ensure reliability in outdoor environments. To confirm its environmental reliability, we subjected the filter component to various environmental tests. Excellent results were obtained.

INTRODUCTION

Filter components have an important function in remote fiber test systems used in the maintenance of optical fiber networks.[1) 2)] In the past we developed various filter components such as filter embedded fiber ribbon, filter embedded connector, etc.[3) 4) 5)] These filter components have been put to practical use in remote fiber test systems. Presently, there is a rapid introduction of optical fibers in subscriber networks. Many proposals on various transmission configurations have been made. Filter components need to be suitably designed so as to fit various networks and systems. Desired characteristics for such devices include small size, environmental durability and easy removal / addition among others.

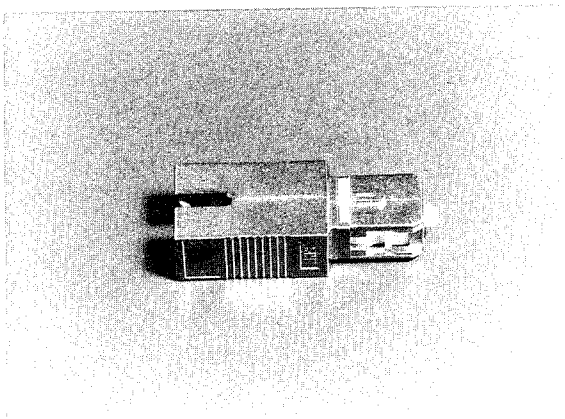
We have developed a filter component that is implemented in a plug jack type housing that hitherto has been mainly used in optical attenuators. Up to now, in incorporating optical devices within this type of connector, the optical device has been inserted between two ferrules. This method has a weakness in that there is a need to align the optical axis, and consequently, insertion loss is high due to fiber axis offset. To overcome this, we have examined a mirror finish grinding technique for fibers contained inside a ferrule, and managed to machine a thin slit (about 40 μm width) on the ferrule and embed a filter into the slit. We also investigated methods of protecting the embedded filter for use in outdoor environments. The results of environmental tests of the filter components confirmed its reliability for use in outdoor environments.

CONSTRUCTION

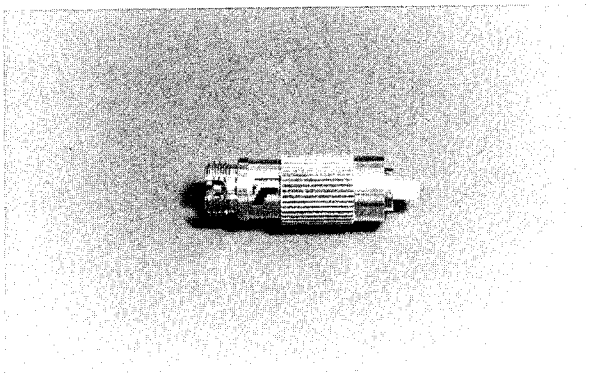
The external views of the filter embedded plug jack SC and FC connectors are shown in Fig. 1. Both consist of a plug on one side and an adapter on the other. It has been designed so as to enable easy removal / addition according to system or service requirements. This construction has been widely used in optical attenuators.

Fig. 2 shown the structure of the ferrule we used. A single ferrule was used with both end faces polished to a Super PC finish. The optical filter chip was embedded at the center

of the ferrule. To fix the filter, we used epoxy optical adhesive that maintains a high bonding strength against moisture. The assembly was enclosed within a metal case and then sealed with resin to ensure mechanical and environmental stability.



a) SC connector type



b) FC connector type

Fig. 1 External view of the Filter Embedded Plug Jack Connectors

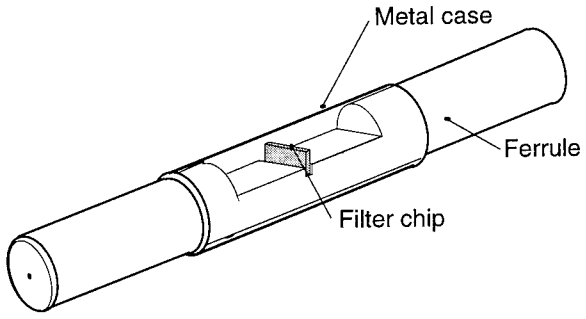


Fig. 2 Structure of the ferrule

MACHINING OF FILTER PART

The section where the filter was embedded is located at approximately the center of the zirconia ferrule as shown in Fig. 2. To achieve a low insertion loss, the filter chip was embedded in a slit that was machined using a micro lapping machine, to be approximately 40 μm wide on the fiber. This is the same as ordinary filter components.

Micro lapping consists of grinding and polishing simultaneously using a fast revolving blade while supplying a grinding fluid containing abrasive materials continuously[6]. This results in an end face with a mirror surface and free from damage. Thus far, the micro lapping machining technique has been applied to machine 2 layers of similar materials (at the same time). For example, in the case of a filter embedded optical fiber ribbon, the fiber was placed on a glass V-groove substrate and then machined. However in the case of a filter embedded ferrule, it is necessary to machine dissimilar materials i.e. glass and zirconia in the same machining operation. Therefore, we investigated the mirror finish grinding technique as applied to different materials using the micro lapping machine. In our experiments to determine the optimum speed of the slitting blade, we varied the work speed of the slitting blade and the slit width. The insertion loss was measured as it gives an indication of the surface roughness inside the slit. The slit width between the surfaces was measured by a microscope. In the case of the loss measurement, matching oil was applied prior to measurement of the insertion loss. The slitting blade used was a thin metal-bonded diamond wheel and the polishing fluid consisted of silica powder in grinding fluid. The work speed was varied from 1 mm / min to 8 mm / min while other parameters of the slitting process were kept constant. This experiment investigated the relationship between the work speed and surface roughness. Fig. 3 shows the relationship between the work speed and the slit width and loss. From the point of view of the slit width, at a work speed of 5 mm / min, the unbalance of the slit width was at a minimum and the insertion loss obtained approaches the theoretical value. On the other hand when the work speed is increased to 8 mm / min, the loss will be

significantly greater than the theoretical value due to surface roughness. Fig. 4 shows a photograph of a fiber end face as seen through a microscope. Based on the above results, we made prototypes of the filter embedded component plug jack type connector at a work speed of 5 mm / min.

The slitting angle of fiber was maintained at 8 degrees with respect to the fiber axis to remove any reflected light (return loss).

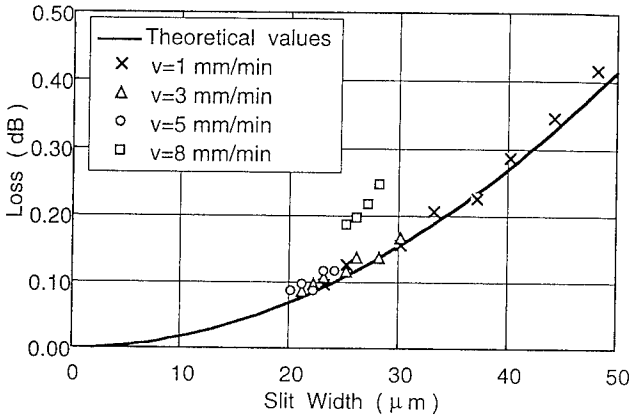


Fig. 3 Relationship Between Loss and Slit Width Filled with Matching Oil

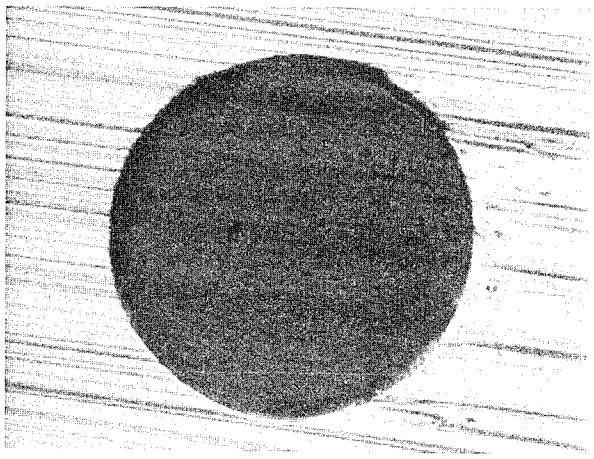


Fig. 4 Mirror Finish of Fiber End Face

Fig. 5 outline's the various steps involved the filter in embedding process.

(1) Optical fiber is inserted into the zirconia ferrule and fixed by adhesive. The ferrule end faces are then polished.
(2) A slit is formed in the center of the ferrule using micro lapping machining.
(3) A filter chip with a thickness of about 20 μm is inserted into the slit and bonded with optical adhesive.
(4) The assembly is enclosed within a metal case, and sealed with resin (including inside the case).

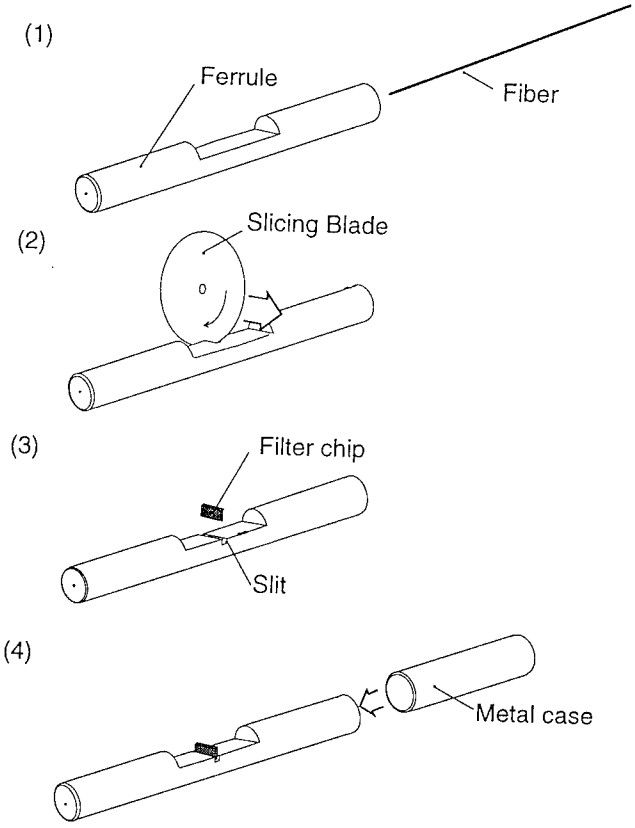


Fig. 5 Filter Embedding Process

OPTICAL CHARACTERISTICS

The filter we used was a Short Wavelength Pass Filter (SWPF) which means that a light signal of wavelength 1.31 μm can

pass through the filter chip while a wavelength of 1.55 μm is blocked.

Fig. 6 shows the insertion loss histogram of the prototype at a wavelength of 1.31 μm and 1.55 μm. At the pass wavelength, the average loss of the prototype was about 0.7 dB. These results include the loss of the filter part and two connection losses. The filter part loss includes the loss of the filter chip and the longitudinal offset loss of the slit. Calculations[7] indicate that the longitudinal offset loss is about 0.25 dB for a slit width of 40 μm. The average loss of the filter chip is about 0.1 dB. The average insertion loss at the blocking wavelength is 55 dB which is almost the same as that of the filter chip.

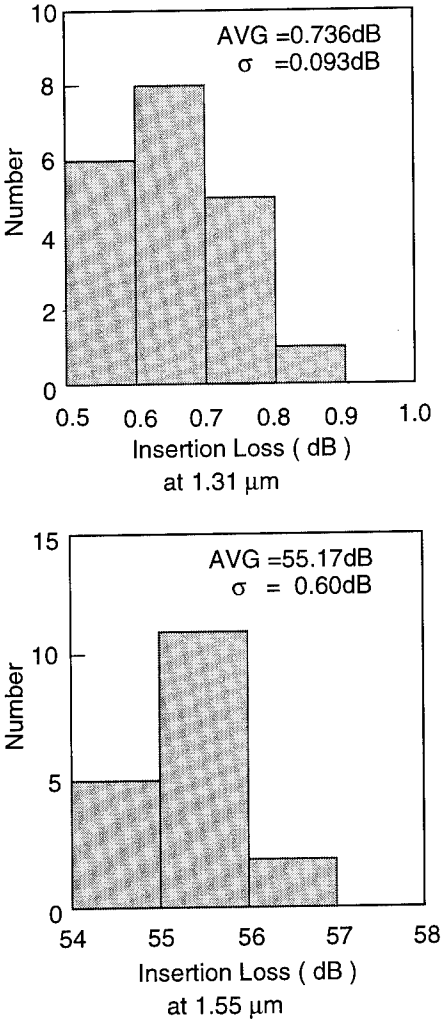


Fig. 6 Insertion Loss Histogram

Fig. 7 shows an example of the loss-spectrum of the filter embedded component for the plug jack connector.

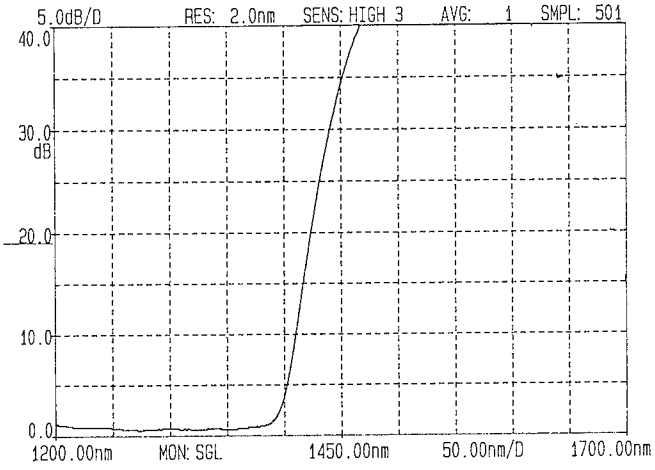


Fig. 7 Insertion Loss-Spectrum

The histogram of the return loss is shown in Fig. 8. These results include the return loss of the filter part as well as two connections. The average return loss of the prototype is about 50 dB, which is a typical result of Super PC polishing. The return loss of the filter part is extremely high and exceeds the measurement range of ordinary measurement equipment. This is because the slit was formed at an 8 degree angle to the fiber axis in order to reduce any reflection around the filter part. If the fiber end face inside of the slit is not mirror finished, the return loss deteriorates. Fig. 9 shows the result of the return loss of each part (connector and filter) measured using optical coherence domain reflectometry based on the Michelson interferometer. This result shows that the fiber end face inside the slit was mirror finished, as the return loss of the filter part is greater than 70 dB.

Table 1 summarizes the optical characteristics.

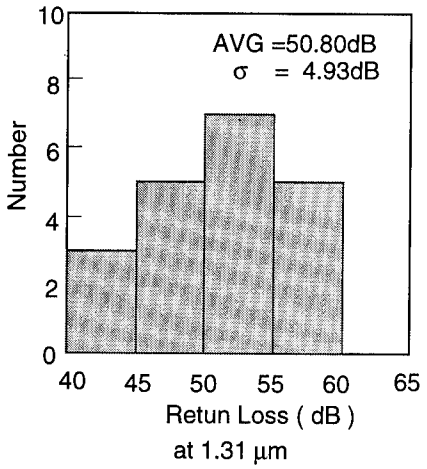


Fig. 8 Return Loss Histogram

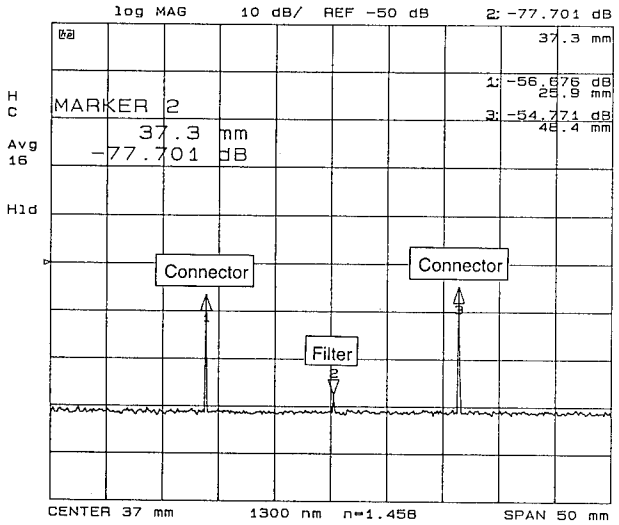


Fig. 9 Return Loss of Individual Parts

Table 1 Results of Optical Characteristics

Items	Wave length	Results (average)
Insertion Loss	1.31 mm	0.74 dB
	1.55 mm	55.2 dB
Return Loss	1.31 mm	50.8 dB
	1.55 mm	48.3 dB
Polarization Dependent Loss	1.31 mm	0.05 dB

RELIABILITY

Environmental reliability tests were carried out taking into account use in outdoor environments. Table 2 shows the results of the environmental reliability tests. The filter embedded components have given us satisfactory results in terms of environmental resistance and long term reliability. In the future we plan to investigate the following areas :

1. Thermal aging
2. Low temperature storage test
3. Thermal shock test
4. Temperature-Humidity cycling test
5. Salt spray test etc.

Table 2 Results of Environmental Reliability Tests

Items	Test Conditions	Results (Residual Loss)
High temperature storage test	75℃, RH 90%, 5000 hours	Less than 0.1dB
Temperature cycling test	-40~+75℃, 1℃/min, 1000 cycles	Less than 0.1dB
Water immersion test	43℃, 340 hours	Less than 0.1dB

Table 3 shows the results of mechanical reliability tests. Excellent results were obtained.

Table 3 Results of Mechanical Reliability Tests

Items	Test Conditions	Results (Residual Loss)
Vibration test	1.5mm, 10~55 Hz, 3 directions	Less than 0.1dB
Impact test	50G, 11 ms	Less than 0.1dB

CONCLUSIONS

We developed a compact and easy addition / removal filter component, using a plug jack type connector. A high precision micro lapping technique was used to machine a slit in a ferrule into which a filter chip was inserted and fixed with epoxy optical adhesive.

We investigated methods of protecting the embedded filter, as a result of which we managed to realize high reliability when used in both outdoor and indoor environments.

Hereafter we plan to develop other optical components with various embedded filter chips as well as other optical devices, in addition to optical device embedded adapter etc.

REFERENCES

1) H. Takasugi, N. Tomita, T. Uenoya & Y. Yokoo ; IWCS, pp. 623-629, 1990.
2) N. Tomita, K. Sato & I. Nakamura ; NTT REVIEW, vol. 3, No. 1, pp. 97-104, 1991.
3) H. Hosoya, K. Asano, M. Ohsawa & H. Yokosuka ; IWCS, pp. 440-444,1991.
4) H. Hosoya, K. Asano, M. Akiyama & H. Yokosuka ; IWCS, pp. 250-254, 1993.
5) H. Hosoya, K. Asano, M. Akiyama & H. Yokosuka ; FUJIKURA TECH. REVIEW, No. 23, pp. 5-9, 1994.
6) S. Matsui, J. Watanabe, T. Saitoh & J. Noda ; ECOC, pp. 517-520, 1990.
7) D. Marcuse ; Bell Syst. Tech. J., vol. 56, No. 5, pp. 703-718, 1977.



Kenichiro Asano

Opt-Electronics Laboratory
Fujikura Ltd.

1440, Mutsuzaki, Sakura, Chiba, 285, Japan

Kenichiro Asano was born in 1966. He graduated in opto-electronics engineering from Tokyo Kougakuin College of Technology. He joined Fujikura Ltd. in 1989 and has been engaged in the research and development of telecommunication cables and accessories. He is a member of the Institute of Electronics, Information and Communication Engineers of Japan.

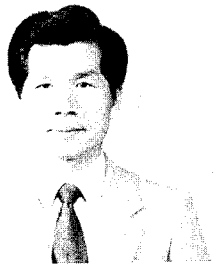


Hideyuki Hosoya

Opt-Electronics Laboratory
Fujikura Ltd.

1440, Mutsuzaki, Sakura, Chiba, 285, Japan

Hideyuki Hosoya was born in 1959. He received the M.Sc. degree in Physics from Yamagata University in 1983. He joined Fujikura Ltd. in 1983 and has been engaged in the research and development of telecommunication cables and accessories. He is a member of the Institute of Electronics, Information and Communication Engineers of Japan.



Hiroshi Yokosuka

Opt-Electronics Laboratory
Fujikura Ltd.

1440, Mutsuzaki, Sakura, Chiba, 285, Japan

Hiroshi Yokosuka graduated in mechanical engineering from Tokyo Metropolitan Technical Junior College in 1967. He has been engaged in the research and development of telecommunication cables and accessories. He is presently a general manager of the Fiber and Cable Accessory Department. Mr. Yokosuka is a member of the Institute of Electronics, Information and Communication Engineers of Japan and the Japan Society of Mechanical Engineers, respectively.

RELATING THE STRUCTURAL RETURN LOSS OF CABLE PAIRS TO THE ASSOCIATED ATTENUATION DEVIATION AND DELAY JITTER

H. W. Friesen

AT&T Bell Laboratories
Norcross, Georgia 30071

Abstract

Structural Return Loss (SRL) is a common way of specifying the amount of roughness a cable pair can exhibit. Structural roughness also results in loss roughness and delay jitter at the receive end. In this work numerical calculations are used to relate both the transmit end reflected signal and the roughness at the receive end to the roughness function of distance. Simulation results establish the relationship between the signals appearing at the two ends both qualitatively and quantitatively. Calculated results and actual cable roughness data demonstrate agreement. RMS roughness function amplitudes greater than about 1.5 Ohms result in failing the Category 5 SRL specification. This SRL specification implies loss roughness noise that is secondary to near end crosstalk by about 10 dB. Delay jitter for the same amount of roughness runs only about 0.02 ns RMS for 100 m lengths. Loss roughness and delay jitter increase at a rate only slightly greater than the square root of length for random roughness. This is a lower rate than the first power of length rate associated with periodic structural variation. Loss roughness increases with the first power of frequency.

I. Introduction

The present day Category 5 LAN cable structural return loss (SRL) specification has been in place for several years. This standard consists of a fixed 23 dB portion out to 20 MHz followed by a sloping portion out to 100 MHz with a -10 dB/decade slope. The basis of the Category 5 cable SRL specification and also that of Categories 3 and 4 is extensive calculations performed when the standard was established. Those calculations are reviewed here along with the relationships between the reflected signal roughness and that of the attenuation and delay.

The calculations under review here, demonstrate the relationship between the structure in the reflected signal and amplitude and phase roughness appearing in the receive end signal. Roughness in the reflected signal is of interest in that it is readily measured[1]. Roughness in the received signal is what is really important. The amplitude roughness can be translated into a noise component and related to other noise signals such as the near end crosstalk (NEXT). Phase or delay roughness (jitter) is of consequence in the situation where timing recovery may be impaired.

The approach in this paper is to first consider an example set of actual cable data. Calculated results, where rough cable performance is modeled, are considered next. These calculations are based on numerical modeling of the transmission line in a way that allows random roughness to be simulated. A differential element line, where elements can readily be varied, is used to represent the transmission line. Finally, a summary set of relationships are presented. These allow the user to relate a given amount of reflected roughness to the transmitted roughness and relate both to the common roughness function amplitude. A sample set of calculations is discussed.

Prior work discussed the theoretical basis for structural return loss decreasing and consequently degrading with frequency[2]. It was found that SRL relates to the roughness function, W(x), as near end crosstalk relates to the coupling unbalance function (referred to as U(x)). Near end crosstalk exhibits a -15 dB/decade slope when the coupling between the pairs is random with distance. For near end crosstalk, random coupling results when different twist lengths are used to break up the phasing in the coupling for otherwise strongly coupled adjacent pairs.

Periodic structural variation is generally not present in well designed cable made with well controlled processes. Random structural roughness with distance is what remains when any tendency towards periodic variation in the manufacturing process is identified and brought under control. The amount of the random component of roughness is further subject to the control of such variables as insulation uniformity and wire centering.

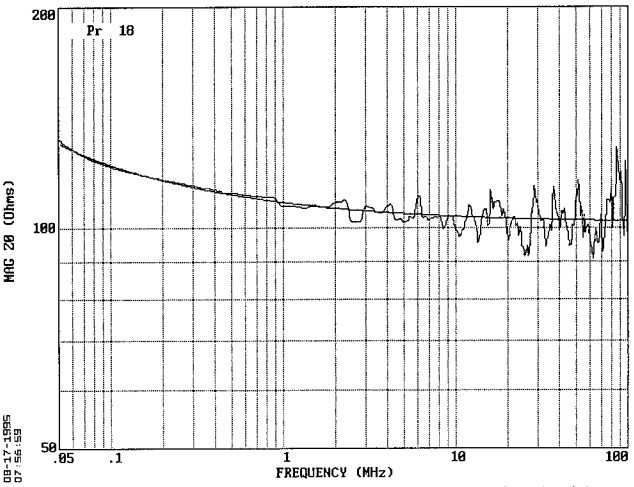


Fig. 1 Input Impedance Scan Least Squares Fitted with Characteristic Impedance Like Function

II. A Review of Cable Data for Structural Return Loss and Transmission Data Exhibiting Roughness

This section reviews both reflected signal data and received signal data with regard to roughness. Figure 1 shows a typical square route of open and short impedance trace, $Z_{OS} = \sqrt{Z_{OC} Z_{SC}}$, plotted versus frequency. This trace, which exhibits structural roughness, is fitted with an impedance-like function consisting of at least a constant and a $1/f^{1/2}$ component. It is apparent that the roughness of the impedance trace, increases with frequency for this situation where roughness is considered random. Furthermore, this example pair is one that passes the SRL requirement with a margin of less than one dB.

$$SRL = -20 \log \left| \frac{Z_{OS} - Z_0}{Z_{OS} + Z_0} \right| \qquad (1)$$

The structural return loss is calculated from the Z_{OS} trace and the fitted impedance which is termed the characteristic impedance of the pair, Z_0. Equation 1 shows that SRL is related to the difference of the impedances divided by the sum on a logarithmic (dB) basis. The impedances are complex values consisting of magnitude and angle or the real and quadrature components. The quadrature component of Z_0 is small at frequencies above 1 MHz. A parameter that will be used as a measure of reflected signal roughness throughout this work is S_{11}. It is defined as the difference over the sum expression inside the vertical lines in Equation 1. Clearly as impedance deviations from the fitted value increase both SRL and S_{11} worsen.

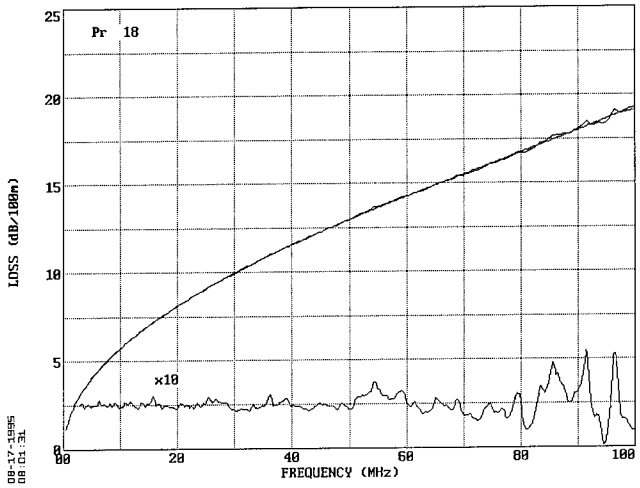


Fig. 2 Attenuation Trace Showing Roughness due to Structural Variation

Related to the impedance roughness is the attenuation roughness and delay jitter. Figure 2 shows the corresponding measured attenuation trace for the pair for which an impedance trace was exhibited in Figure 1. The attenuation trace has been fitted with an attenuation-like function of frequency. The roughness in the attenuation trace is obtained by computing the difference between the measured attenuation and the fitted function. The difference, expanded by a factor of 10, is plotted at the bottom of the graticule at the first major division level. The fluctuations exhibit mostly randomness with there being a gradual increase of amplitude with frequency.

Peaks in the attenuation trace in Figure 2 cannot necessarily be associated with the impedance extremes in Figure 1. This is due to the roughness being random. If the roughness were periodic there would be a definite coincidence of the poor SRL frequencies and the attenuation roughness peaks. There is, however, a strong statistical type of relationship between the amount of structural roughness appearing at the transmit end and the through-the-cable roughness as will be seen later.

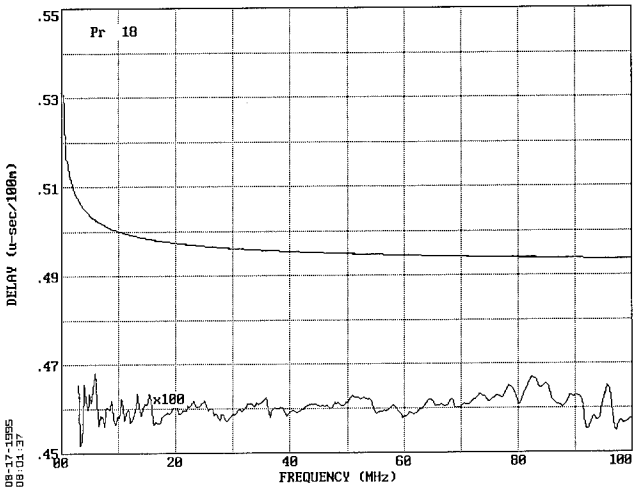


Fig. 3 Delay Trace Showing Roughness due to Structural Variation

Figure 3 shows the delay for the same example considered earlier. Again function fitting was used to obtain a smooth reference delay trace. Here the actual and fitted traces coincide so well that no difference is visible. The trace which is plotted up one graticule division from the bottom shows the difference multiplied by a factor of 100.

Structural content observed in the expanded delay trace does coincide with that observed in the attenuation trace. The delay difference trace is a first derivative version of the loss difference trace. Where one is at a maximum or minimum the other crosses the axis. Loss deviation can be related to phase on a nepers and radians basis. For instance, in Figure 2 at 96 MHz the loss has a peak to peak amplitude swing of 0.5 dB or 0.058 nepers. The delay at that frequency has a 1 x 10^{-4} μs transition. This is equivalent to a phase change of 0.059 radians which agrees well with the 0.058 neper loss transition.

III. Modeling the Impedance and Transmission Roughness

3.1 Numerical Method for Evaluation of Structural Effects

The relationship between a given amount of roughness (variation in the W(x) function) and the effects on SRL, loss roughness and delay jitter can be approached analytically for periodic roughness. Random roughness is not as amenable to an analytic approach but can be handled numerically. The methods used here are similar to

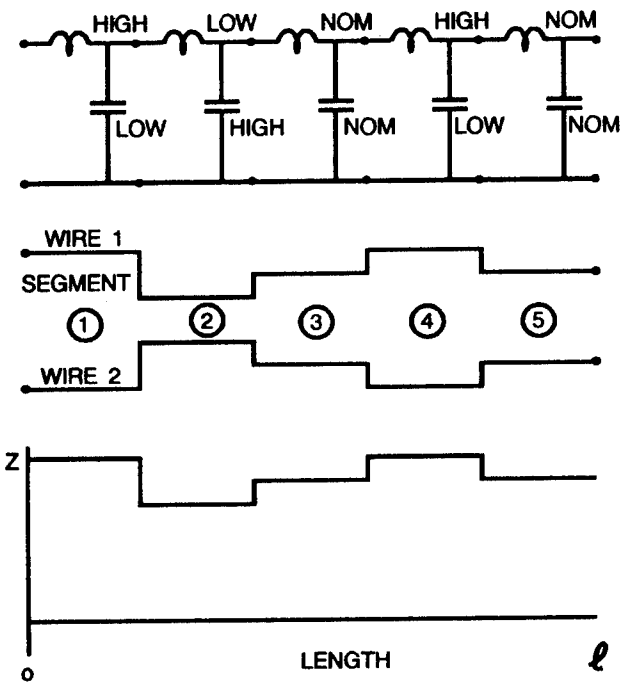


Fig. 4 Structural Variation Associated with Wire Separation Variation

those discussed in a previous paper[2]. The cable pair is viewed as consisting of many segments, each of which differs from the nominal structure by some small amount. The equations for voltage and current changes across the segment are evaluated in sequence for each segment resulting in a solution for the whole line. The segments are permitted to vary in a random manner. Solutions pertaining to many different random sequences are evaluated to allow modeling of the performance as a function of the magnitude of the roughness, variation with length, etc.

Figure 4 indicates how the line segments might vary. One segment might have high inductance and low capacitance (high impedance and a positive value for W(x)) as a result of added wire separation. The next segment might represent the opposite from the first with the result being low impedance (a negative value for W(x). Another segment might have fairly nominal wire separation and electrical values.

A line segment in Figure 4 can be represented by the T circuit

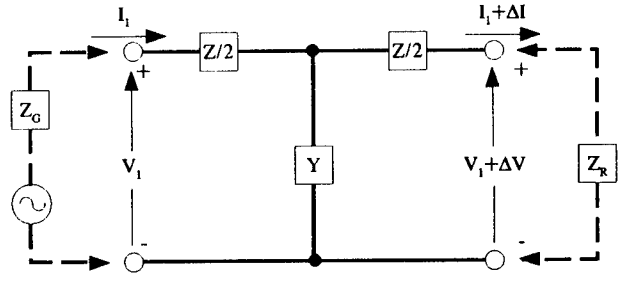


Fig. 5 Short Segment of Line Represented by T Circuit

appearing in Figure 5 where the series **Z** effect consists of the R and ωL and the shunt **Y** effect consists of G and ωC. If the input is defined as consisting of voltage $\mathbf{V}_1$ and current $\mathbf{I}_1$ then the output differs from the input by the incremental changes in voltage $\Delta\mathbf{V}$ and current $\Delta\mathbf{I}$ which are defined by a set of difference equations (Equations 2 and 3). The effect of many segments can be totaled up readily by means of a computer program. Both the input impedance and the transfer function, (loss and phase) can be obtained for the line consisting of many randomly varying segments.

$$\Delta V = \frac{YZ}{2}V_1 - \left(Z + \frac{YZ^2}{4}\right)I_1 \qquad (2)$$

$$\Delta I = \frac{YZ}{2}I_1 - YV_1 \qquad (3)$$

While the difference equations are the actual basis for the calculations, Equation 4 lends some insight to what happens when a line is rough. This equation relates the reflected signal S_{11} to the roughness function W(x) of distance along the cable pair in a manner similar to the way frequency is related to time by the Fourier transform[3]. S_{11} can be thought of as indicating the frequency spectrum (somewhat weighted) of the roughness function. The localized element of roughness, W(x), contributes to the overall reflected signal appearing at the sending end of the pair as modified by the propagation effect ($e^{-2\gamma x}$) to the location x and back. Effects of all points along the pair are summed at the transmitting end. The nearby portion of the pair contributes heavily at all frequencies while the distant end contributes little at high frequencies if attenuation is substantial. The integral effect is multiplied by the ratio of the propagation constant γ to characteristic impedance which supplies frequency dependence.

$$S_{11}(\omega) = \frac{\gamma(\omega)}{Z_0(\omega)}\int_0^l W(x)\,e^{-2\gamma(\omega)x}\,dx \qquad (4)$$

There is good reason for SRL and NEXT having similar behaviour versus frequency. The equations are similar in form. The main difference is that in the crosstalk equation there is a coupling function of distance instead of a roughness function of distance. The transfer function can be evaluated by the relatively complicated double integration formula, Equation 5. This expression is more difficult to interpret than Equation 4 but some effects can be deduced. Since the roughness function appears twice, as (W(x)

$$S_{21} = e^{-\gamma(\omega)l}\left[1 - \frac{\gamma(\omega)^2}{Z_0(\omega)^2}\int_0^l W(x)\,e^{2\gamma(\omega)x}\int_x^l W(y)\,e^{-2\gamma(\omega)y}\,dy\,dx\right] \qquad (5)$$

and W(y)) in this formula, there is the likely prospect that results represented by this equation will exhibit W^2 dependence. The negative sign inside the square brackets indicates that the roughness effect subtracts from the smooth cable signal strength.

3.2 Numerical Results for Sending End Structural Effects

The starting point for the numerical calculations is the roughness function W(x). An example of one is shown in Figure 6. This

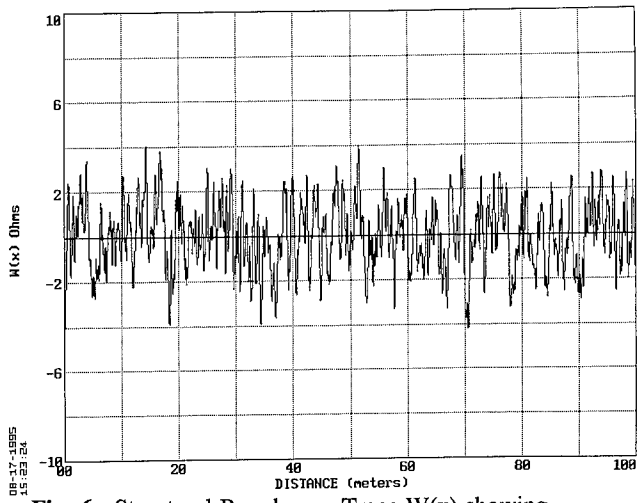


Fig. 6 Structural Roughness Trace W(x) showing Impedance Deviations

roughness function was obtained from a random number generator. A sequence of six hundred different element values were used to represent 100 meters of cable. This one has a peak to peak variation of about 6 Ohms and an RMS of 1.5 Ohms.

Earlier work using this numerical approach indicated that SRL traces exhibited slope values centered around -15 dB/decade, just like NEXT. From measurements it has been found that SRL slope values in the vicinity of -10 dB/decade are more common. To more closely simulate actual cable behavior the roughness functions obtained from a random number generator were filtered digitally to reduce high end frequency content by about 5 db relative to content a decade lower.

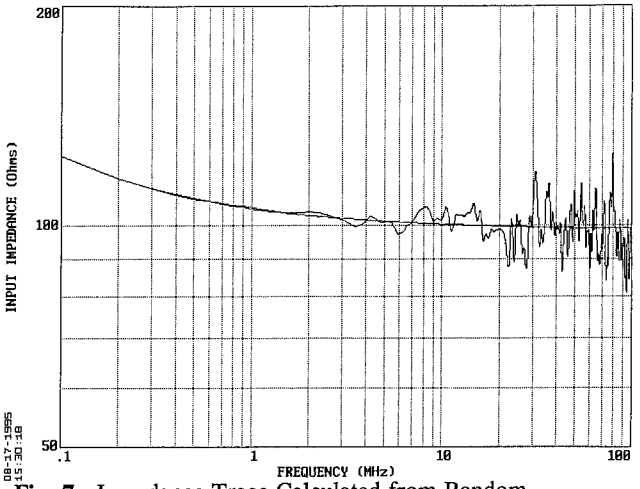


Fig. 7 Impedance Trace Calculated from Random Structural Sequence

Figure 7 shows a 1000 point Z_{OS} trace resulting from the numerical procedure. It is the result of a sequence of many segments varying randomly about the nominal. This trace having features similar to those found in the example of actual data such as was considered earlier in Figure 1 is important. The trace does resemble the one found in Figure 1 in that it is smooth at the low frequency end where roundtrip distance is a fraction of a wavelength and becomes progressively rougher with frequency. It appears to have about the same degree of flaring or worsening with frequency. A smooth characteristic impedance trace has been drawn through the rough impedance trace. In this procedure function fitting is not required since the smooth impedance trace is readily calculated from the assumed primary transmission parameters (the R, L, G and C). The pair assumed here is one with a 100 Ohm nominal impedance of the 24 gauge variety with zero dissipation factor (no dielectric loss).

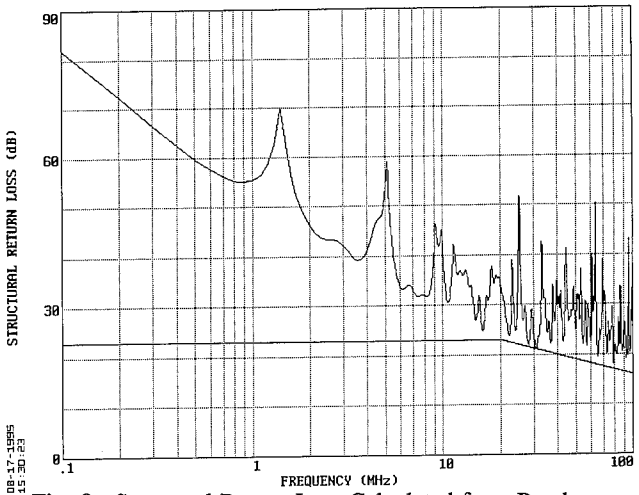


Fig. 8 Structural Return Loss Calculated from Random Structural Sequence

Results for the SRL which are shown in Figure 8 follow readily from Equation 1. This trace is for the calculated input impedance results obtained from the difference equations. It shows a definite decrease with frequency. The decrease is about 10 dB over the upper decade of frequency extending from 10 to 100 MHz.

3.3 Numerical Results for Receive End Structural Effects

Figure 9 is a key illustration in that it compares the noise resulting from receive signal roughness to the Category 5 NEXT specification. In the lower half of the graticule appear several calculated loss traces. The crosstalk specification line appears in the middle and the noise resulting from roughness towards the top. The loss traces are similar to the ones considered in Figure 2 except that these are calculated. There are two loss traces ending at about 20 dB at 100 MHz for the 100 m span. These traces nearly coincide. The difference between these two traces, expanded 10x, shows near the bottom of the graticule. This difference trace is readily calculated since the smooth pair values are available from the assumed primary constants.

The difference between the rough and smooth traces is the additional loss due to roughness. This difference trace appears to consist of two parts, the first a monotonically increasing component and the second a varying component. Only the variation in loss is of real concern provided that the total loss is not excessive (greater than the applicable standard permits). At the high end of the frequency scale the peak excess loss is about 0.3 dB which is

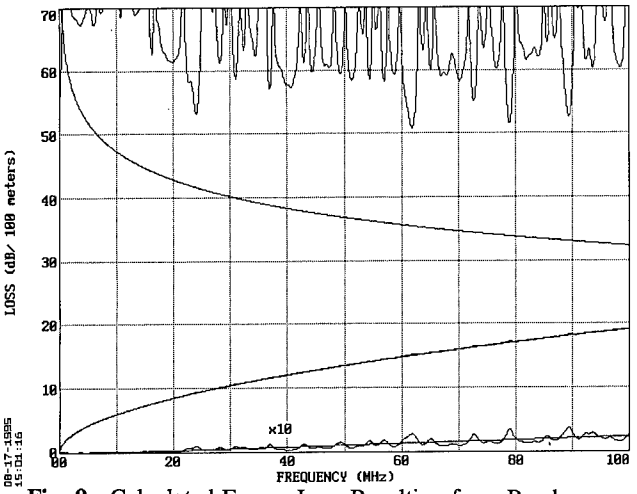


Fig. 9 Calculated Excess Loss Resulting from Random Structural Sequence

small compared to a frequently used 1 dB benchmark value.

The trace at the top of the graticule is the actual noise voltage amplitude resulting from the excess loss variation. This trace is computed by taking the difference between the added loss variation and the line fitted to it and converting it to an isolated noise amplitude trace. This can be seen by considering the 79 MHz peak which deviates from the fit line by 0.2 dB. The smooth cable loss at this frequency is about 17 dB and the effect of adding the excess loss brings the total loss to 17.2 dB. Converting both loss values to amplitudes, taking the ratio of the two, and converting back to the dB scale results in the 51 dB peak noise value at 79 MHz. This point is about 18 dB above the NEXT specification line at this frequency. This is for a roughness function where SRL is at the limit as observed in Figure 8. Two other points in this noise trace are a bit closer to the crosstalk specification line with the nearest point coming within about 12 dB. This example demonstrates how the noise due to excess loss is at least 10 dB weaker compared to that permitted for Category 5 NEXT.

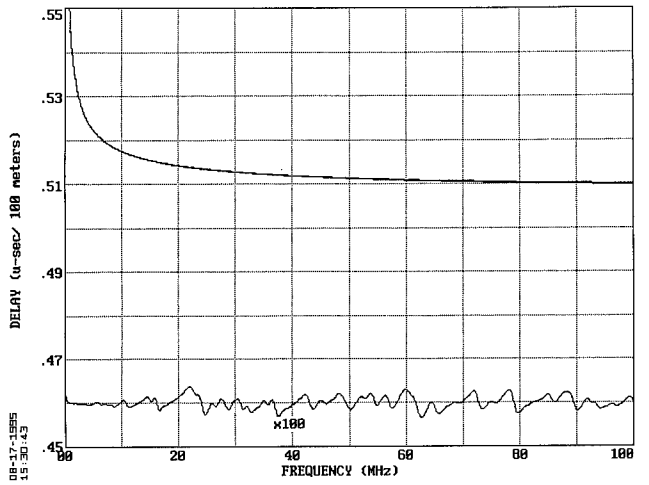


Fig. 10 Delay Roughness calculated from the Random Sequence

Figure 10 shows the delay roughness resulting from the same roughness function. As mentioned earlier, attenuation and delay noise are closely related. When a noise vector has the same or opposite phase as the desired signal the amplitude is affected. When the noise vector is at quadrature the delay is affected. Here there are actually two delay curves, one including the roughness and the other a smooth cable representation, which nearly coincide. The roughness is not visible with the slightly expanded delay scale where the vertical scale is about 4% of nominal delay per division. Centered one division up from the bottom of the graticule is the varying component of delay expanded by a factor of 100. This trace was obtained by function fitting the computed delay trace to establish a reference.

The delay roughness trace appearing in Figure 10 has roughness that corresponds to the loss roughness where one is the derivative of the other as was the case with the traces obtained from actual cable. Where the loss roughness peaks, the delay roughness trace crosses the axis. The RMS delay roughness for this example is about 0.02 ns for the 100 meter length.

IV. Results Obtained from a Set of 50 Roughness Sequences

Calculations were made for a set of 50 random roughness sequences extending from those that are of minimal RMS amplitude to ones that typically result in failing to meet the Category 5 SRL performance requirements. The independent variable in these calculations was the RMS roughness of the W(x) function. Calculations were performed with W_{RMS} values of the roughness functions extending up from 0.04 Ohms to 2.0 Ohms with the step interval being 0.04 Ohms.

The dependent responses that were computed for each roughness function amplitude (W_{RMS}) setting were the reflection coefficient (S_{RMS}), the loss roughness (L_{RMS}) and delay roughness (D_{RMS}). Maximum values were also used to quantify the responses resulting from the individual random sequences. The summary values for these responses were calculated to represent only a portion of the 0 to 100 MHz frequency range representative of the upper end of the copper FDDI system. Knowledge of how the parameters scale with frequency and length allow extension to other ranges. The frequency range represented by the RMS values extends from 32 MHz to 64 Mhz. By keeping the frequency range down to an octave, problems with RMS results being heavily influenced by the upper end of the range, as in the case of loss, are minimized.

The first scatter plot, Figure 11, to be considered plots the S_{RMS} and S_{MAX} values from the 50 runs against W_{RMS}. The plot shows that the reflection coefficient amplitude does indeed increase linearly with roughness amplitude with only a minimum of scatter. Straight line fits yield coefficients relating S_{RMS} (unitless) and S_{MAX} to W_{RMS} in Ohms whose values are 0.037 and 0.080. This set of calculated S_{RMS} values correlates with W_{RMS} with an R^2 of 0.926. So if the roughness W_{RMS} is known the reflection coefficient can readily be predicted.

The reason for presenting both RMS and MAX values is that later in Section V a peak factor will be needed. The ratio of the MAX

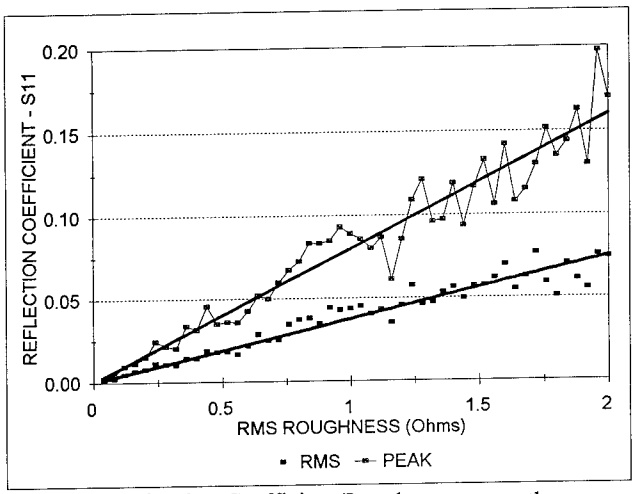


Fig. 11 Reflection Coefficient Roughness versus the RMS Roughness of W(x)

and RMS coefficients does not result in a peak factor but is a step in that direction. Here the ratio of the two coefficients is 0.08/0.037 = 2.16. A slightly larger value of 2.5 (8 dB) will be used later in Section V.

Figure 12 shows how loss roughness relates to the roughness function. Recall that these values are relative to a function fitted to loss versus frequency plots such as were exhibited in Figures 2 and 9. When the roughness component of the loss is plotted against the mean square of the W function (square of the RMS roughness) a straight line trend is exhibited. This is not surprising since W(x) appears twice in the equation for S_{21} (Equation 5) examined earlier.

Both MAX loss and RMS loss points are shown in Figure 12. These two sets of points and the corresponding fitted lines show that there is MAX/RMS ratio of 0.0682/0.0204 = 3.34 of the coefficients for loss. The PEAK values for loss run quite a bit higher, about 5 times as high as RMS. A PEAK/RMS ratio of 5 (14 dB) is used in the calculations in Section 5.2.

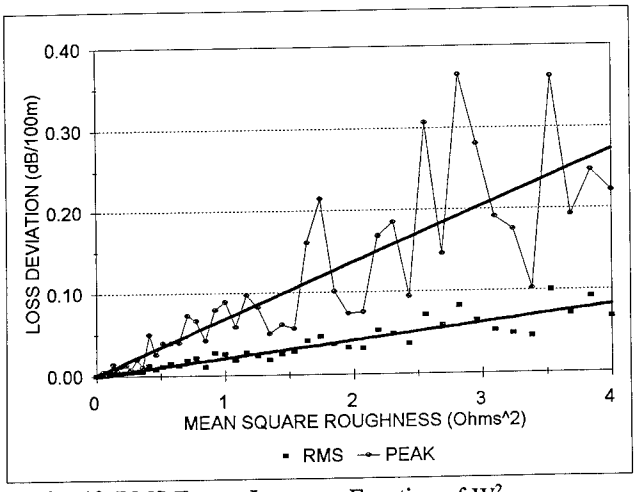


Fig. 12 RMS Excess Loss as a Function of W^2_{RMS}

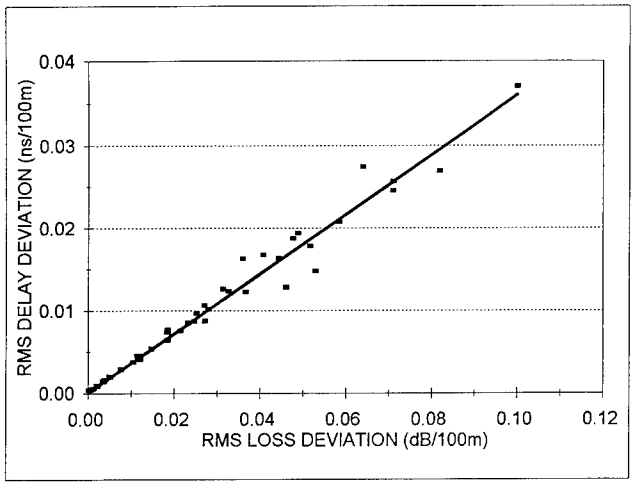


Fig. 13 RMS Delay Deviation versus Loss RMS

Delay roughness, D_{RMS} relates to W_{RMS} in a way similar to that of loss RMS, on a W^2 basis. The MAX/RMS ratio obtained from the corresponding fit coefficients was 0.0206/0.0074 =2.8 and PEAK/RMS ratio about 4. These ratios run somewhat less than the ones obtained for loss.

Figure 13 is included to show how well delay and loss RMS values correlate. A correlation coefficient of 0.979 was obtained for this relationship. This is not surprising since the size of transistions in one can be calculated from the other for individual features as was demonstrated with Figures 2 and 3 in Section II.

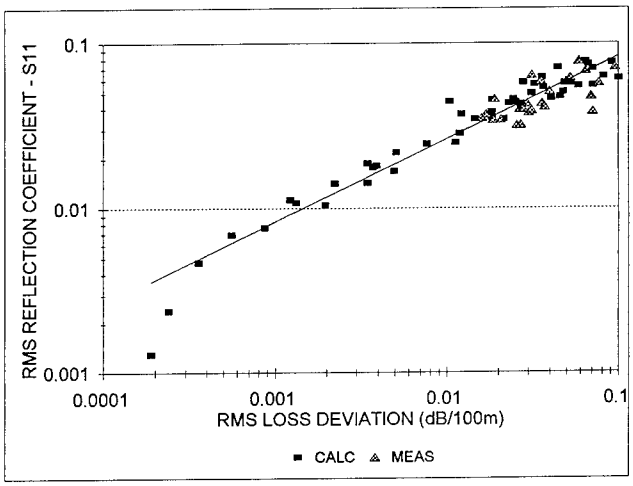


Fig. 14 Reflection Coefficient RMS versus the Loss RMS

Plotting the reflection coefficient RMS against the loss RMS is of considerable interest. This relationship is key in relating how much reflected signal can be tolerated when the real concern is roughness in the received signal. Since the received signal varies with the square of the roughness function amplitude and the reflected signal as the first power it is useful to use log-log scaling. Figure 14 demonstrates that the slope is indeed 0.5 as anticipated. The points span approximately 1.5 decades vertically for three

decades horizontally.

Figure 14 also shows points calculated from the cable reflection coefficient and loss measurements. The RMS values for the cable measurements were calculated in a manner similar to that for the simulation runs. These points were obtained from a 25 pair Category 4 cable. They appear at the high end of the calculated distribution with some points running close to the Category 5 SRL specification. Most of the points fall within or close to the calculated distribution with four points falling somewhat below. These points generally support the slope of one-half exhibited by the simulation points. Points from smoother cable are more difficult to obtain because the demands on the necessary function fitting become greater.

Length dependence of transmission roughness is reviewed next. The situation where roughness varies randomly with length is thought to be different from the one where roughness is periodic. Periodic effects build rapidly with length. A line with a periodicity acts like a bandstop filter. More length with the same periodicity sharpens the tuning effect. The result is an excess loss buildup where peak excess loss builds with the first power of length. Random roughness builds at a lower rate. It is conceivable that the rate, like that for far end crosstalk with random coupling, is more like the square root of length.

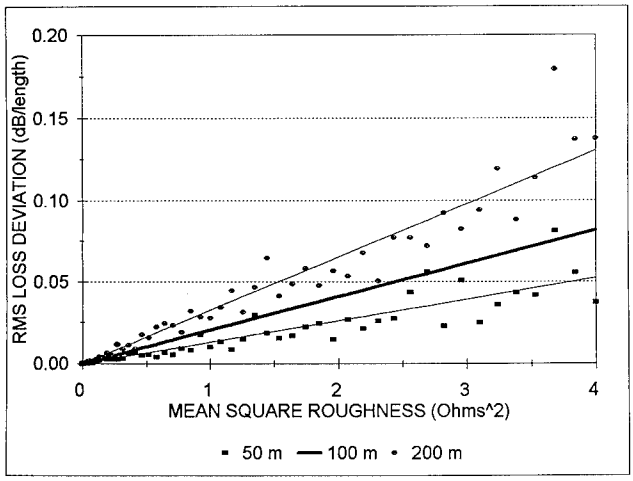


Fig. 15 Excess Loss for Various Lengths

Figure 15 plots calculated L_{RMS} values for 50 m, 100 m, and 200 m lengths against W^2_{RMS}. Calculated points are shown for the 50 m and 200 m lengths. Including the 100 m points in this plot would make it too busy. These values were presented in Figure 12. The three fitted lines appears to be log spaced. The fit coefficients are 0.0131, 0.0204 and 0.0326 dB/Ohm^2. These coefficients ratio as 1.58 with length doubling which is $2^{0.66}$ The rate appears to be closer to the square root of length rate than first power of length but is somewhat higher than square root. The coefficient for 200 m is about 2.49 times as large as the one for 50 m instead of only 2 times as large. Results affirming this rate of scaling were obtained for delay as well. A plot of those results was reviewed and found very similar in appearance to the one for loss.

V. Summary of Calculated Results

5.1 Summary Table of Modeling Results

The calculations and plots reviewed in Sections III and IV form the basis for relating the various response parameters to W_{RMS} and in some cases to each other. These relationships can be used to set a standard for the situation where the preferred measurement parameter (such as SRL) is different from an important performance parameter (such as jitter).

Table I summarizes the various relationships, the coefficients, and the associated correlation (R^2) values based on the 32 to 64 MHz frequency range. The relationships are of the form Y = Coef • X where Y is the dependent response, Coef is the coefficient and X is the independent variable. The units for the variables are roughness W in Ohms, excess loss L in dB/100 m, and delay jitter D in ns/100 m with S_{11} parameter values being unitless.

Table I: Table of Calculated Coefficients and R^2 Values Based on 32 to 64 MHz Frequency Range

Y	Coef	X	R^2	Figure #
S_{RMS}	0.0374	W_{RMS}	0.926	11
S_{MAX}	0.0799	W_{RMS}	0.929	11
L_{RMS}	0.0204	W^2_{RMS}	0.878	12
L_{MAX}	0.0682	W^2_{RMS}	0.721	12
D_{RMS}	0.359	L_{RMS}	0.979	13
D_{RMS}	0.00739	W_{RMS}	0.886	NA
D_{MAX}	0.0206	W_{RMS}	0.849	NA
S_{RMS}	0.2786	$L^{0.5}_{RMS}$	NA	14

Consider now the first row in Table I which relates S_{RMS} to W_{RMS}. It indicates that a 2 Ohm W_{RMS} value results in an S_{RMS} value of 0.0748 (22.5 dB SRL value). The resultant S_{MAX} value according to the second row is 0.16. The correlation coefficient for row one is high at 0.926. The data points used to calculate these values appear in Figure 11. The S_{RMS} versus L_{RMS} coefficient in row 8 is actually calculated from the first and third row values.

5.2 Example Calculation of Specification Values

The coefficients in Table I are the basis for determining specification values for SRL, excess loss and delay jitter. Most of the coefficients relate back to the W_{RMS} value. The coefficients for L_{RMS} versus W^2_{RMS} and S_{RMS} versus W_{RMS} are used in this section to start with a given amount of loss roughness and arrive at an SRL specification. Table II steps through the calculations needed, step by step from top to bottom. Two designs, Category 4 and Category 5 are examined. This table can obviously be applied in the reverse direction to go from SRL to excess loss or jitter.

Table II starts with the design frequency values where 16 MHz is considered to be applicable for 16 Mbit token ring and 48 MHz to copper FDDI. The starting assumption is that the roughness noise

Table II: Calculation of SRL Limits Starting with an RMS Excess Loss Effect 24 dB Below NEXT

Parameter	Category 4	Category 5
Design Frequency	16 MHz	48 MHz
NEXT with 10 + 14 dB Offset	62.3 dB	61.1 dB
Permitted Noise Voltage Relative to 1 V_{RMS}	0.772 mV	0.881 mV
Loss at Design Frequency	15.74 dB @ 200 m	13.63 dB @ 100 m
Received Signal Voltage Minus Noise	0.1624 V	0.2072 V
Loss of Signal minus Noise	15.78 dB	13.67 dB
RMS Excess Loss	0.041dB	0.056 dB
W^2 Coef of Loss Adjusted for Frequency and Length	0.009621	0.02041
W_{RMS}	2.07 Ω	1.34 Ω
W_{RMS} Coef of S11 Adjusted for Frequency	0.02162	0.03745
S_{11} @ Design Frequency	0.0447	0.0503
SRL with 8 DB Peak Factor	21.0 dB	18.0 dB
SRL Spec. Value	19.0 dB	19.2 dB

be secondary to NEXT generated noise running at the specification limit. For the Category 5 example this results in a 48 MHz noise level of 61.1 dB or 0.881 mV relative to a 1 V reference with a 10 dB margin and 14 dB peak factor included. Pair loss at this frequency and length is 13.63 dB. Subtracting the noise voltage from the received voltage yields 0.2072 V or 13.67 dB. The excess loss of 0.056 dB is the difference between the loss values with and without noise. Using the W^2 coefficient of loss roughness of 0.0204 from Table I, yields a W_{RMS} value of 1.34 Ohms. The W_{RMS} coefficient of S_{11}, also a value appearing in Table I, results in a design frequency S_{11} value of 0.0503 or 18.0 dB when an 8 dB RMS to Peak factor is used. The resultant SRL value is 1.2 dB more permissive than the specification value of 19.2 dB. The sensitivity of the SRL value to the starting excess noise level is about 1 dB lower SRL for two dB more loss noise.

The Category 4 example follows in a similar manner with the result being good agreement with the existing standard. The main difference in the calculations is that both the design frequency and the length are different from the values of 48 MHz and 100 m for which Table I values are applicable. The coefficient for loss roughness is larger in accordance with the square root of length ratio and smaller in proportion to frequency. The coefficient for S_{RMS} is smaller in accordance with the square root of frequency.

VI. Conclusion

The main focus has been to relate the various structural effects to a common source, the roughness function W(x). Doing this makes it possible in turn to relate the reflected signal roughness to the transmitted signal roughness. The degree to which the received signal is affected is of primary importance.

The numerical results were used to relate the SRL specification to the excess loss and delay jitter. Calculations performed to arrive at SRL specifications in place in the LAN cable industry today, demonstrated that the peak noise due to excess loss is smaller than that due to NEXT by about 10 dB. This result indicates that improving the crosstalk performance needs to have priority over improving the SRL in the event that better performance is desired. Improving only the SRL will not result in substantial performance improvement.

The modeling of rough performance demonstrated that excess loss variation and delay jitter increase at a rate slightly greater than the square root of length when the roughness function is random with position down the length of the pair. This differs from periodic structural effects where the buildup is with the first power of length. It means that roughness effects do not build much faster with length than far end crosstalk.

References

1. ASTM D 4566-94, Standard Test Methods for Electrical Performance Properties of Insulations and Jackets for Telecommunications Wire and Cable

2. Friesen, H. W., "An Evaluation of Measurement Techniques for Determining Copper Cable Structural Effects", 40th International Wire & Cable Symposium Proceedings, 1991, pp 93-104

3. Bolinder, F., "Fourier Transforms in the Theory of Inhomogeneous Transmission Lines", Transactions of the Royal Institute of Technology, Stockholm, Sweden, No. 48, 1951.



HAROLD W. FRIESEN
AT&T Bell Laboratories
Norcross, GA 30071

Harold W. Friesen is a Distinguished Member of Technical Staff at AT&T Bell Laboratories. He received a BSEE degree from the University of Colorado in 1963 and a MEE degree from New York University in 1965. Hal has been involved in cable design, the development of fabrication methods and cable measurement techniques. He holds seven patents in this area. He is a member of the IEEE. This is his fifth IWCS paper with a 1990 paper winning the "best presentation" award.

Combining Mathematical Modeling with Materials Development to Predict High Speed Telecommunication Cable Properties - The Laplace Model - A Tool for the 21st Century

Brian Burke
Lightwave Software Corporation
104 Laurie Lane
Cary, North Carolina 27513

Guerry L. Grune
ABB Corporation
Transmission Technology Institute
1021 Main Campus Drive
Raleigh, North Carolina 27606

Abstract

The need to establish a modeling technique which will allow the cable designer the necessary tools to shorten the development time required to establish the tradeoffs between electrical, mechanical and flammability properties of the various materials available has been a long term goal of many in the industry.
Ultimately it should be possible to design high speed transmission cables with such modeling tools prior to determining which parameters wield the greatest influence on final overall product performance. The Laplace model described in detail in this paper is an initial attempt toward reaching this goal.

I. Introduction

For wire and cable developers/designers there is a constant need to address three fundamental criteria specific to governing the final transmission properties of their products. These include;

1. Mechanical properties (i.e. tensile strength, flex modulus, etc.)
2. Electrical transmission characteristics (i.e. dielectric constant, dissipation factor, dielectric breakdown strength, etc) and
3. Flammability, smoke and toxicity characteristics (i.e. NEC, IEC and U.L. standards)

The various electrical insulating materials available to the designer must include determination of the key parameters necessary to accomplish the initial goals associated with cable fabrication. High speed transmission requires the use of relatively low (for thermoplastics) loss properties combined with high mechanical/physical strength and flame/smoke resistance.

In today's office environment, the building will have a network of vertical and horizontal shafts and designated plenum areas which act as a medium for flame propagation from floor to floor and department to department. As the computerization of this environment accelerates, a wide range of twisted pair, coaxial, power and fiber optic cables are installed for a myriad of uses from computer terminals to telephones, from lighting to alarm systems. [1] As more and more cables are installed (and older ones are left in ceilings and walls), the associated potential fire hazard requires increased scrutiny.

Unfortunately, the historical development of materials and processes for reducing flame spread, smoke generation and toxic potency properties of conventional extruded thermoplastics has not included the concurrent need for "low loss" transmission characteristics. This trend has been

reversing, however, since the 1975 NEC adoption of the U.L. 910 plenum test for flame propagation and smoke generation. As standards evolve, the issue of not only smoke generation, but also the toxic and corrosive nature of the smoke has become a primary focus.

II. Motivation

The need therefore existed to try to determine how to develop a synergistic relationship between the various physical, electrical and flammability requirements by the use of computer modeling and simulation. The time required to manufacture and test a cable for electrical and flammability acceptance can be substantially reduced with the Laplace tool. The current cycle time required from the actual design to final product is usually a minimum of several weeks. The motivation for this work was to develop a program which would allow for manipulation of design and electrical material properties, and allow the user to indicate the direction in which the final cable transmission characteristics would proceed.

The Laplace CAE tool developed is capable of handling any arbitrary shaped geometry without restriction to the number and type of conductors. It is also possible to include varying dielectric properties based on the thermoplastic characteristics. This model has evolved from a software package specifically designed for high speed analog system simulation for connectors, cables and interconnect media design. The "Helmholtz" electromagnetic transmission CAE tool is comprised of an electromagnetic field solver and a transmission line modeling tool.

Key features of the enhanced "Laplace" version includes;

- transmission line analysis of any graphically selected cross-section
- frequency dependent analysis of eddy current losses which includes proximity and skin effects with results inserted into a full resistance matrix
- frequency dependent analysis of dielectric losses based on a selected loss tangent
- flexible cross-section determination of unit matricies for R,L,C and G as well as impedance, admittances,and propagation modes
- use of a combination of boundary and finite element electromagnetic field solvers to address the lossy conductor and dielectrics in open space
- solution of the Helmholtz and Laplace equations for a selected frequency range
- analysis of the characteristic impedance with options for various loading conditions
- automatic generation of optimized SPICE models for lossless or lossy, multiconductor transmission lines for a selected frequency range

The wire and cable industry development and design work for the 21st century will no longer be able to afford the time and costs associated with producing actual cables that are subsequently tested electrically and then burned in some standard test scenario. The Laplace Model allows one the ability to acquire quickly and with lower cost: Impedance, Attenuation, Cross-Talk, Skew, Propagation Delay, and Rise-Time Degradation.

III. Development of the Laplace Model

Transmission Line Problems

High speed logic families bring data transmission frequencies into the GigaHertz range creating sub-nanosecond pulse risetimes which require high quality, well designed transmission lines for high speed data transfer. To successfully transfer data without severe pulse distortion, signal paths which are longer than approximately one eighth the wavelength propagating down the line are classified as transmission lines and should be designed as such. Poorly designed systems suffer problems like crosstalk, ringing, reflections, impedance mismatches, and severe attenuation which all contribute to pulse degradation and large error margins in logic circuits.

Computer speeds are influenced by digital pulse risetimes. Improperly designed transmission line systems will increase pulse risetimes which results

in decreased computer speed. A single pulse is comprised of many pulse harmonics of different frequencies. The higher frequency components give a square pulse with sharp edges which give a square rise-time. To transmit a pulse with negligible distortion, its first ten harmonics should be passed which requires the system to have a large bandwidth. If the bandwidth of the system is too narrow, usually due to design flaws, high frequency components will be lost resulting in severe pulse distortion at the receiving end.

Interconnect media can contain numerous, densely packed, transmission lines which cause crosstalk. Crosstalk is the undesired transmission of a signal to adjacent quiet lines. Low crosstalk levels are negligible but high levels will cause false triggering and overloading in logic circuits. Crosstalk is measured by taking the ratio of the amplitude of a quiet line to that of an adjacent driven line. Crosstalk can be reduced in interconnects by proper design considerations and by application techniques such as signal-ground pin configurations.

Impedance of a conductor is defined as the opposition to current flow. The impedance of various components in any system should be matched for proper system operation. Optimally, the system impedance should be large to keep power requirements to a minimum but the system may still be susceptible to large amounts of noise. Systems typically use characteristic impedance between 30 and 150 ohms depending on the applications. Characteristic impedance is defined in terms of the inductance and capacitance per unit length or SQRT(L/C). For proper system operation, all interconnects, loads and source impedances should be matched for maximum power transfer and proper system operation.

Reflections are caused by impedance mismatches between interconnections. Any changes in characteristic impedance would cause reflections in the system causing significant pulse degradation, and noise generation. Maintaining a constant characteristic impedance throughout the system is a major design criteria.

In general, faster signals and longer lines require more elaborate models to accurately represent transmission line effects. Systems running above 50 MHz will require accurate models to represent the transmission line effects in high speed interconnects.

Electromagnetic Field & Circuit Analysis

The nature of electromagnetic fields in the presence of conducting materials can be described in two distinct ways. The first is often referred to as the electromagnetic field approach. The second is the lumped approach which leads to an equivalent circuit description and circuit analysis.

The field approach is based on the solution of Maxwell's equations in their original form, or - more frequently in their reduced form. The reduced form accounts for position and symmetry of analyzed objects and their material properties. The reduction process is often based on the introduction of a set of new variables known as potentials.

This leads to second order partial differential equations of the following types:

Laplace: for static electric and magnetic fields without sources (excited by boundary conditions),
Poisson: for static fields with sources,
Helmholtz : for linear quasi-stationary fields - solved for a specific frequency,
Heat transfer: for lossy time dependent fields, and
Wave : for time dependent fields.

The field approach is the most comprehensive method of solving electromagnetic problems. However, it is also the most time consuming and complex approach, which cannot be applied to the majority of practical problems that include complex geometries and hundreds of active and passive components. Structuring the problem into a set of subregions (circuit components) and evaluating interactions between them (circuit analysis) is often considered to be the only option for practical applications. In the Computer Aided Engineering (CAE) modeling tool, the electromagnetic field

analysis is applied to the much simpler task of constructing equivalent circuit models.
The equivalent circuit approach makes use of certain regularities of geometrical structures and the direction of energy transmission. The analyzed region is considered as a composite structure, with subregions of principle types described as transmission lines and circuit components (L,R,C,G). The transmission line regions -in the frequency range of interest for designers of high performance digital circuits - can be characterized by a set of TEM (transverse electromagnetic modes). The justification for such a simple procedure lies in the fact that it is the dominant mode that determines the energy transmission and the interaction characteristics of the system. In most applications the presence of the longitudinal modes (TE and TM), which result from conductor and dielectric loss and non-uniformity of the structure, can be neglected. These higher level modes are rapidly damped out in the transmission region. Therefore, the discontinuity may be regarded as a lumped circuit device, with the frequency characteristics representing its effect on the propagation of the dominant mode. Such a representation may be schematically described in the form of an equivalent circuit.

Modeling Considerations

CAE modeling tools offer a unique feature of constructing optimal circuit representations for multi-conductor transmission lines. To accurately model interconnecting media, the electrical length of the conductor(s) and wavelength must be considered. There are several techniques for developing an accurate model. A simple method is to determine the propagation delay through the interconnect. If this delay is greater than approximately 10% of the signal risetime, then a distributed transmission line model must be used. For example, with a 1 ns risetime, interconnects with a propagation delay less than 100ps, can be modeled by lumped elements. If the propagation delay through the interconnect is greater than 100ps, then distributed elements must be used. This rule can also be applied when determining the number of subsections to be used in a distributed model. It is important to choose enough subsections so the delay through any subsection is less than 10% of the signal risetime. Increasing the number of subsections improves the accuracy of the model at the expense of larger memory requirements.

Another consideration when developing an interconnect model is whether loss effects should be included (lossy) or ignored (lossless). Losses come in the form of conductor resistance and conductance. Conductor losses are modeled by a small series resistance, and dielectric losses are represented by a small conductance to ground. In the case where cables are concerned it is generally true that losses need to be considered for proper attenuation results. This is due to the long lengths of the cable, and therefore the significant contribution toward attenuation from resistance. To model an interconnect the current distribution in the conductors must be calculated. Current distribution in a conductor could be calculated from a simplified form of Maxwell's equations known as the Helmholtz equation.

There is a range of frequencies for which the Helmholtz solution is required. For low frequencies, the DC approximation of current distribution (uniform throughout the conductor cross section) is fairly accurate. The situation is similar for very high frequencies where the surface currents screen the interior of the conductors. Both cases can be determined (in two dimensions) by the Laplace equation which is used by static field solvers.This phenomenon is illustrated in Figure 1.

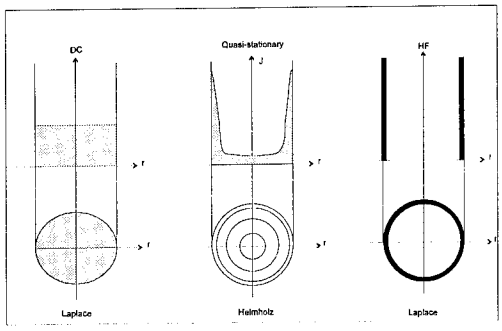


Figure 1: Schematic Indicating the Range of Frequencies for Which the Helmholtz Solution is Required

The transition between the low (DC) and high-frequency (HF) range can be described as the quasi-stationary region. This region is characterized by a non-uniform current distribution. To estimate the frequency range of the quasi-stationary region one must calculate the skin depth for different frequencies as shown in Table 1.

Table 1

Skin Depth for Aluminum Conductors as a Function of Frequency

f	1 MHz	20 MHz	100 MHz	1 GHz	10 GHz	100 GHz
Skin depth (μm)	81.47	25.76	8.147	2.576	0.815	0.258

One can draw conclusions about the need for a detailed analysis of the current distribution of interconnects by comparing wire cross-sectional dimensions and skin depth. If the skin depth is in the range of the conductor cross-sectional dimensions then the current is distributed in a non-uniform way (quasi-stationary solution in Figure 1) and a solution of the Helmholtz equation is required for calculating equivalent circuit components.

To address practical problems, the Laplace method provides the user with a field analysis module that solves the complex Helmholtz equation for lossy conductors and lossy dielectrics. It is assumed that all signals propagate as quasi-TEM waves.

Inductance is strongly dependent on frequency when the skin depth is within the conductor cross-sectional dimensions. A region of significant changes in the value of inductance is located in the Helmholtz region and is based on a comparison between skin depth and the conductor's cross-sectional dimensions. The area below the Helmholtz region (below f_{MIN} skin) is qualified as the DC region, and the area above the Helmholtz region (above f_{max} skin) is qualified as the high frequency (HF) region.

It is quite clear that most MCM designs and some VLSI and packaging applications require a detailed analysis of the current distribution based on the Helmholtz equation. Using a DC model for some of the VLSI applications may result in satisfactory results whereas most of the PCB and cable applications can be considered HF applications which are based on the surface distribution of currents.

Benchmarking the Model

In order to evaluate the validity of the model we must first establish a benchmark to compare theoretical versus calculated results. For this purpose we will use a Two-Wire Open Loop problem as is shown below in Figure 2.

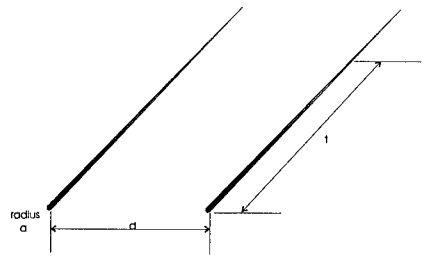


Figure 2: Two Wire Loop Diagram

In order to obtain L and C, neglecting the effects of frequency (frequency will be considered for resistance),for this model the following equations are used, Shaum's Outline Series on Electromagentics.

For the general case where d>>a, the inductance can be found in a relatively simple manner and is easily shown to be:

$$L = \frac{\mu_0}{\pi}\cosh^{-1}\bullet\frac{d}{a}\ \frac{henries}{meter} \quad (1)$$

From the reciprocity theorem the capacitance is given by:

$$C = \frac{\varepsilon\mu_0}{L}\ \frac{farads}{meter} \quad (2)$$

The characteristic impedance is seen to be:

$$Z0 = \frac{1}{\pi}\bullet\frac{\mu_0}{\varepsilon}\bullet\ln[\frac{d}{a}] = \sqrt{\frac{L}{C}}\ ohms \quad (3)$$

Where:

$$\mu_0 = 4\bullet\pi\bullet 10^{-7}, \varepsilon = 8.848\bullet 10^{-12} \quad (4)$$

The results for Capacitance, Inductance, and Impedance for the Two-Wire Loop are presented in Table 2 below where the "Calculated" value is from equations (1)-(4) above, and the Laplace CAE tool results are marked as "Model":

Table 2
Calculated and Modeling Results for the Two-Wire Loop

Electrical Property	Calculated Value	Model Value
Capacitance (farads/meter)	12×10^{-12}	11.5×10^{-12}
Inductance (henries/meter)	$.921 \times 10^{-6}$	$.952 \times 10^{-6}$
Characteristic Impedence (ohms)	277	287

The comparison of the results for this model in comparison with the calculated values are considered acceptable, since equation (1) assumes the current is at the surface of the conductor but is actually shifted inward due to frequency. This phenomena is taken into account by the CAE tool.

In order to obtain attenuation results for cable problem resistance as a function of frequency is necessary, therefore skin depth must first be calculated. The solution for skin depth for the two wire loop can be derived in the following way:

The conductivity of the wire material was chosen to be copper and is:

$$\sigma = 5.814\bullet 10^{7}\ S/m \quad (5)$$

The wires are placed in free space with relative permeability:

$$\mu_0 = 4\bullet\pi\bullet 10^{-7}\ H/m \quad (6)$$

and separated by the distance:

$$D = 100\bullet 0.001\bullet 2.54\bullet 0.01\ m\ \ (i.e.\ 100\ mil)$$
$$D = 2.43\bullet 10^{-3} \quad (7)$$

The cross section of the wire is circular, with the radius:

$$r = 10\bullet 0.001\bullet 2.54\bullet 0.01\ m\ (i.e.100\ mil)$$
$$r = 2.54\bullet 10\text{-}4\ m \quad (8)$$

Values of resistance are required for the following frequencies *f:*

i. DC Case - find R0
ii. 1MHz, 10MHz, 100MHz, 1GHz, 10GHz - find R

The resistance values for a single wire are marked 'half'; those without this mark are for the double-wire loop. The skin effect is taken into account, but not the proximity effect. The following calculates the resistance from the skin depth d:

$$\delta(f) = \sqrt{\frac{2}{\omega(f)\bullet\mu\bullet\sigma}},\ S(f) = 2\bullet\pi\bullet r\bullet\delta(f) \quad (9)$$

$$Rskinhalf(f) = \frac{1}{\sigma\bullet S(f)},\ Rskin(f) = 2\bullet Rskinhalf(f) \quad (10)$$

In the following we use:

$$\omega(f) = 2\bullet\pi\bullet f \quad (11)$$

A numerical analysis of these cases were performed using the Laplace Method.

The numerical results are compared against the analytical values in Table 3. The analytical values obtained from Kelvin functions ber(),bei(),ber1,bei1 were found [2]. The relationships between different Bessel and Kelvin functions used were obtained from, Abramowitz, et. al.[3] as well as the use of asymptotic formula (approximations valid for x>=8). These values are denoted "Exact". The analytical results calculated by use of the skin-depth are labeled "Skin". The values acquired from numerical methods within the Laplace Model are

depicted as 'Model', where the circular structures were broken into ten equal segments. The geometry was augmented so that after subdivision into elements these objects have circumferences equal to those of the original circles.

Table 3
Resistance (Ohms/meter) of the Two-Wire Loop
(Rounded to 5 significant digits)

f	Exact	Skin	Model
1 MHz	0.37316	0.32656	0.37034
10 MHz	01.0327	1.0327	1.0769
100 MHz	3.2656	3.2656	3.3086
1 GHz	10.327	10.327	10.369
10 GHz	32.656	32.656	32.684

Modeling Process

The Laplace CAE tool can handle any arbitrarily shaped geometry, enabling it to solve complex geometric structures such as cable and connector problems. Once the model geometry has been described (within any CAD tool which is capable of exporting DXF or IGES files), materials and material properties can be applied by selecting them from a material table (this table can be easily extended through user input). This is where the modeling process significantly reduces cost and time by allowing the user to arbitrarily change materials and ascertain the relative differences in the interconnect and compare with allowable thresholds, before a prototype is created. The modeling process is comprised of 3 main steps:

1. Geometry:
Creation of model drawing files within "off-the-shelf" CAD tools capable of exporting DXF or IGES files.

2. Importing DXF Files into the Laplace tool:
When the 2.5 Dimensional geometries (2-D cross sections with a constant depth, such as used for a cable) are complete, the DXF files are imported into the Laplace tool, all material properties and signal - ground configurations are then defined. Once this is accomplished, an EM analysis can be performed for the various cable sections. The outcome of this analysis provides an EM report which includes L,RC,G, Time Delay, Eigenvalues, and Characteristic Impedance. In addition, a Lossy Modal SPICE configuration which can further be evaluated is included. (the Laplace CAE tool has an interface to SPICE specifically designed for the cable and connector industry).

3. Building a system SPICE model:
Once the SPICE model has been created, the system elements (such as sources, grounds, probes, terminating resistors) are placed on the circuit for further analysis. The types of analysis performed are Time Domain Reflectometry (TDR,impedance scan), cross-talk (near and far end), propagation delay, rise time degradation, and attenuation.

Effects of Materials

In addition to size and location of conductors (signals and grounds), materials play a significant role in the performance of the interconnect. Two material variations are performed on the above model shown in Figure 2, to reveal the impact of material properties on a Two-Wire Loop (this could be twin-ax or a twisted pair). It is assumed (although not a restriction) that the wires are completely surrounded by dielectric (it is possible to have circular insulating materials around the circumference of the conductors, and enclosures, such as a jacket, around the entire model). The materials for each case are as follows:

Case 1 Solid Fluorinated Ethylene-Propylene Copolymer (FEP);2.1 dielectric constant and loss tangent of .0005

Case 2: Solid Flame Retarded Polyethylene (PE) of 2.7 dielectric constant and loss tangent of.006

The Boundary Element Method (BEM) is used for analysis of the field equations. For this structure a 1 x 1 matrix including LRCGZ is obtained. SPICE uses capacitors to represent both capacitance to ground and coupling capacitance. An inductor is used to model self inductance. To model mutual inductance, SPICE references two inductors and defines a coupling coefficient, k, between the two inductors. The coupling coefficient is a ratio of the mutual inductance between conductors to the square

root of the product of the two conductors ' self inductance. For the cable models due to their relativley long length, a modal model is used. This model is comprised of controled sources derived from the eignevalues to establish the coupling between the lines. In addition, a timel delay is placed in the circuit which accounts for the actual signal propagation through the cable.

For the two-wire loop, general equations can be derived for behavior estimation. The equations are as follows:

$$\Gamma^2 = (R + j\omega l) j\omega C = jR\omega C - \omega^2 LC \quad (12)$$

where Γ is the propagation constant

$$\Gamma = \omega\sqrt{LC}\sqrt[4]{1+x^2}\, e^{j\,arctg\frac{R}{\omega L}} \quad (13)$$

where $X = \frac{R}{\omega L}$

which reduces to:

$$\mathrm{Re}(\Gamma) = \omega\sqrt{LC}\sqrt[4]{1+x^2}\left[\cos\frac{arctg\ \frac{R}{\omega L}}{2}\right] \quad (14)$$

Conclusion: As $\varepsilon\uparrow$, $\mathrm{Re}(\Gamma)\uparrow$, $\therefore\ \alpha\uparrow$

Table 4 below indicates the final results obtained for the two-wire loop system using the insulation materials for case 1 and case 2 described above.

Table 4
Laplace CAE Results for the Two-Wire Loop Model for Case1 and Case 2

	Inductance L(H/m)	Resistance R(Ω/m)	Capacitance C(F/m)	Impedance $Z_o\Omega$	Time Delay T_d(m/s)	Attenuation α(dB/ 100m)
$\varepsilon_{r2.1}$	1.0037e-6	3.26	23.3e-12	207.64	4.83e-9	1.06
$\varepsilon_{r2.7}$	1.0037e-6	3.26	29.9e-12	183.12	5.48e-9	1.15

As shown in Table 4 above, and as is often the case for high speed transmission lines, the attenuation increases as the dielectric constant and dissipation factor increases. Further efforts with various wire and cable designs are continuing.

IV. System Evaluation

The techniques used to create these SPICE subcircuits can be expanded to form accurate and detailed interconnect models. Printed circuit board (PCB) traces and other passive circuit components can be included in a total system simulation for the highest degree of accuracy. Thus, system level analyses are no longer restricted to driver and receiver circuitry as it becomes apparent that interconnect components and board traces can have a significant impact on the total signal integrity of high speed systems.

Early in the design stage when system engineers develop specifications and evaluate the performance of components and devices, they commonly refer to technical data sheets. As more electronic manufacturers provide SPICE models of their products, and with the application of CAE tools earlier in the design cycle, a manufacturer's "virtual" product may be evaluated on the computer before the actual product ever qualified. Use of these tools can facilitate quick and accurate comparisons of competitive products or aid in the selection of the most appropriate part within a given product line. The term computer-aided prototyping (CAP) is now being used to describe this integration of CAE evaluation tools early in the design cycle.

This trend will continue as more manufacturers provide SPICE subcircuits in conjunction with mechanical drawings and as more companies develop advanced CAE capabilities. Almost all time domain solvers have the ability to interface to SPICE or are capable of including SPICE subcircuits into the final circuit design. This trend is facilitated by the emergence of SPICE as a "de facto" standard analysis technique used among electrical engineers. Low cost SPICE simulation packages running on standard PC's are currently available with powerful simulation capabilities. These packages allow smaller companies to perform detailed system evaluations without major hardware/software purchases.

V Conclusions

The use of CAE tools for delivery of reliable products to market in the shortest amount of time is a trend that is certain to continue. Increasing design complexity and faster clock speeds will demand accurate modeling of every element of a system design including interconnection components.

Interconnection manufacturers should be prepared to provide SPICE models in conjunction with mechanical drawings for all high speed components. The use of such SPICE models has helped a number of computer and telecommunications companies better predict the operation system designs.

The Laplace model serves as a primer on how to integrate mechanical and electrical property tradeoffs during high speed transmission cable design. Future work should include addressing the flammability and smoke characteristics so that full scale prototype flame testing of the finished product can also be minimized.

VI. References

1. Grune, G.L., "Wire and Cable Material Selection Criteria for the 90's," International Wire and Cable Symposium Proceedings, pp. 634-640, 1990.

2. Sikora, A. "Terio Pola Elektomanetcycznego", PWN, (1979), p. 145.

3. Abramowitz and Stegun, "Handbook of Mathematical Formulas", Dover, New York, NY. (1974), p. 385.

Brian Burke graduated from Florida Institute of Technology (Melbourne, Fl) in 1986 with a B.S.E.E. Beginning in 1987, he began working with Amp Corp.developing CAE tools for the connector industry for thermal optical analysis. In addition he supported off the shelf EM and CAE tools. In 1988 he established Compusol, Inc., specifically for consulting in the area of CAD CAM CAE developement. From 1989 - 1991, received grants from Ben Franklin partnership of PA to develop fiber optic simulation tools for the fiber cable industry. In 1991 established Light Wave Software Corp. continuing software development for fiber optics. In 1992, he began partnershipping with OptEM Engr., Inc.for development of the Helmholtz Cable and Connector EM/Transmission Line CAE tool. This work continues through the present.

Guerry L. Grune obtained his B.S.M.E. from Duke University, 1978 (graduation with distinction) with a double major (A.B.) in Chemistry the same year. After working for Fiber Industries Incorporated, a subsidiary of Celanese and ICI of Great Britain, from 1978-1980 in the heavy denier polyester filament and liquid crystal high modulus organic fiber group, her returned to graduate school at the University of Massachussetts. There he obtained his M.S.ChE. (1982), from the Departments of Chemical Engineering and Polymer Science and Engineering working for Professor Robert W. Lenz in the area of thermotropic liquid crystal polyesters. Upon finishing his M.S. degree requirements, in May 1982, he joined IBM in the Research Triangle Park, NC. His major responsibilities there included development of the token ring local area network cabling system , fiber optic cables and connectors, and corrosive gas testing of metallurgical components within the IBM-RTP Materials Laboratory. Completion of the doctorate in Chemical Engineering from North Carolina State University under the direction of Professor Vivian T. Stannett, involving the use of modified allyl amino polyphosphazenes by radiation for possible microlithographic resist applications occurred in 1992. Currently he is working for the Transmission Technology Institute of ABB Corporation on the North Carolina State University Centennial Campus within the area of materials and process development,corrosion control, and computer simulation for various power transmission and distribution technologies.

ACHIEVING CONNECTOR INTERFACE INDEPENDENT TRANSMISSION LINE MEASUREMENTS USING DIGITAL SIGNAL PROCESSING TECHNIQUES

Trent M Hayes
CommScope Inc.
3642 US Highway 70 East
Claremont, NC 28610

Abstract: Today, the advanced CATV, Telco, and LAN markets are requiring field tests of the cables they purchase and install. Due to the nature of field testing conditions, it is often not possible or practical to duplicate the conditions of laboratory tests. Consequently, it can be difficult to correlate field and laboratory measurements. The main difference between the two conditions is the cable termination quality, the cable remains unchanged. This paper will develop a method of time domain filtering and filter loss compensation that will yield measurements that are independent of the connector interface and closely correlate to laboratory measurements.

Introduction: The techniques developed in this paper are equally valid for all measurements sensitive to the connector interface (e.g., NEXT, FEXT, SRL, etc.), however structural return loss (SRL) will be used for the purpose of development and verification. The traditional method of SRL measurements involves a variable impedance bridge and a vector network analyzer. This method is described in the Society for Cable Television Engineers Subcommittee Standards for cable impedance and structural return loss (IPS 406 and 407). Using this method, the bridge is adjusted to minimize the reflection across the entire bandwidth.

$$\text{Eq 1:} \quad \frac{\partial[(\overline{\rho}, Z_0)]}{\partial(Z_0)} = 0$$

Partial Derivative Condition for Minimum Reflection (Optimum Match)[3]

When this minimum is achieved the variable bridge optimally matches the characteristic impedance (both real and reactive components) of the cable to that of the test equipment. This bridge adjustment requires a level of operator competence and introduces a source of measurement variability. Other difficulties arise such as the bridges ability to compensate uniformly across the entire bandwidth. The following graph shows a bridge's capacity to adjust 4 ohms from a 75Ω calibration standard over a 1 - 1000MHz bandwidth.

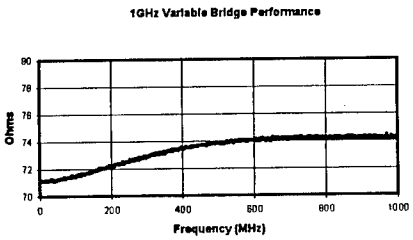


Figure 1: 1GHz Variable Bridge Performance

The bridge's ability to "tune" is relatively good up to 200MHz, however, beyond this point adjusting both real and reactive terms have little effect on the match.
One method of eliminating these limitations is through Fourier analysis.

Theory: In a linear time invariant system; time and frequency domains are related by the Fourier transform pair.

$$\text{Eq 2:} \quad F[x(t)] = X(j\Omega) \equiv \int_{-\infty}^{+\infty} x(t) e^{-j\Omega t} dt$$

$$\text{Eq 3:} \quad F^{-1}[X(j\Omega)] = x(t) = \frac{1}{2\pi} \int_{-\infty}^{+\infty} X(j\Omega) e^{-j\Omega t} d\Omega$$

Fourier Transform Pair

In the application of measuring SRL, the continuous frequency domain is approximated

by sampling a finite spectrum with a finite number of points. A discrete sequence now represents the frequency response. Discrete time and frequency domains are related through the Discrete Fourier Transform Pair (DFT and IDFT).

$$\text{Eq 4:} \quad DFT[x(n)] = X(k) = \sum_{n=0}^{N-1} x(n) e^{-jk\omega_0 n}$$

$$0 \le k \le N-1 \quad \text{where } \omega_0 = \frac{2\pi}{N}$$

$$\text{Eq 5:} \quad IDFT[X(k)] = x(n)$$

$$= \frac{1}{N} \sum_{k=0}^{N-1} X(k) e^{-jk\omega_0 n} \quad 0 \le n \le N-1$$

Discrete Fourier Transform Pair

Figure 2 illustrates the Fourier transform pair for a band limited impulse response signal.

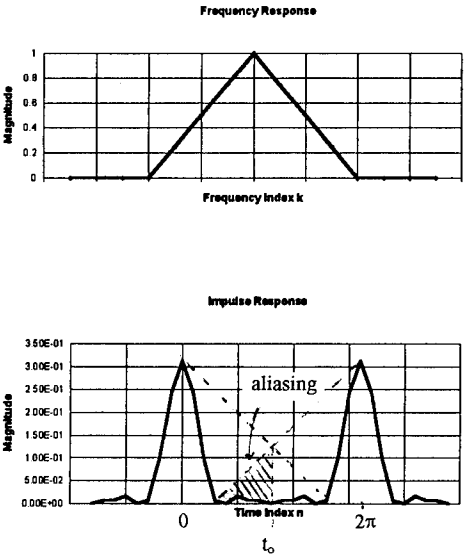


Figure 2: Frequency and Impulse Responses

Notice the inverse DFT (IDFT) is periodic with 2π. If the translated versions of x(n) overlap, the condition of aliasing occurs. In order to prevent aliasing, it is necessary to sample in the frequency domain at a rate equal to or grater than the Nyquist sampling rate. It can be seen from the above figure that this condition will be satisfied if the following inequality is met.

$$\text{Eq 6:} \quad \frac{1}{F} > 2t_o$$

Nyquist Sampling Rate

In this application, normally this condition is easily satisfied because sampling rate in frequency to capture high Q peaks is beyond the Nyquist rate. Additionally, cable loss works in favor of limiting the impulse response duration. Limiting cable length to t_0 will also satisfy the Nyquist criterion (this may become important in low loss cable measurements and is analogous to prefiltering in classical DSP applications). Given that the Nyquist sampling theorem is satisfied, it is possible to transform the sampled SRL frequency response to the time domain (impulse response).

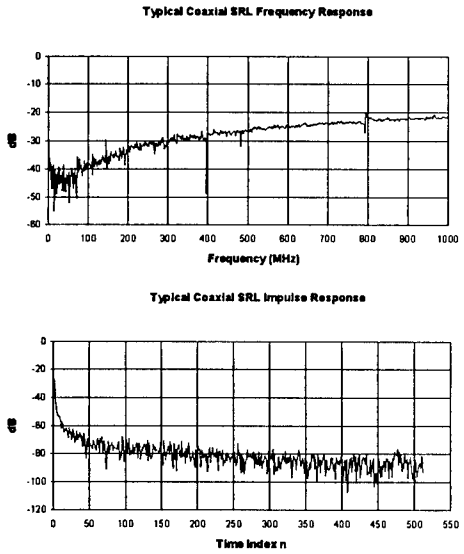


Figure 3: Frequency and Impulse Responses of Typical Coaxial SRL

While the first graph represents the frequency response of SRL measured on a typical 75Ω coax, the second graph shows its impulse response and can be interpreted as SRL versus distance. The following equation relates time to distance of SRL peaks.

$$\text{Eq 7:} \quad distance(m) = \frac{n \cdot c \cdot v_p}{N \cdot F}$$

where n = sample index

N = sequence length

F = sample period (Hz)

$c = 3 \times 10^8 \text{ m/s}$

v_p = cable velocity

Relationship between Time and Distance

The decimation in frequency FFT was used to compute the IDFT while the decimation in time FFT was utilized for the DFT computation. These algorithms provide the most straight forward computation but restrict the sequence length to be a power of 2, $N=2^{\nu}$. If necessary, other techniques can be used to allow for arbitrary sequence length.

Application: The following graph shows the SRL frequency response of a 75Ω mini-coaxial cable measured under both matched and mismatched conditions.

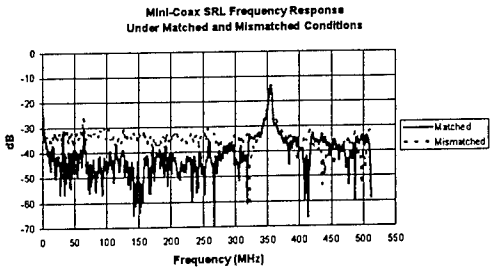


Figure 4: 75Ω Mini-Coax Frequency Responses

The measurements include 1022 sample points from 1 to 511.5 MHz at a spacing of 500kHz. *SRL values at .5 and 0 MHz are extrapolated from the average performance between 2 and 10 MHz.* The average SRL level difference is approximately 8dB and can be attributed to a 4Ω mismatch (magnitude of real and reactive components). A severe discontinuity was placed in the cable periodically every 0.33m resulting in a major SRL spike at approximately 360MHz (typical of severe defects caused in the manufacturing process). The reflection coefficient at this frequency is an order of magnitude greater than reflection resulting from the mismatch. Because of the relative magnitude of this reflection, the SRL value at 360 MHz is essentially unchanged for both the matched and mismatched conditions. This illustrates a special case where the measured value of SRL at 360MHz is largely independent of the connector interface. Simply correcting values based upon the initial mismatch would incorrectly compensate this peak by 8dB.

Time domain analysis lends itself as a correction technique due to the nature of the information. Connector interface information is embedded in the cable performance frequency response but it can be distinguished in the time domain. Shown below are the IDFT sequences (impulse responses) of the previously shown SRL data.

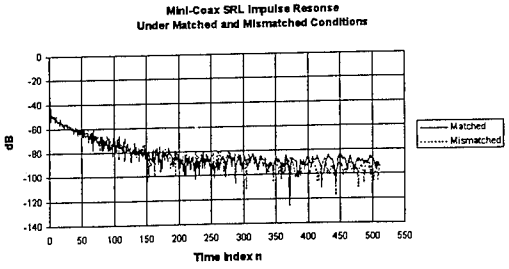


Figure 5: 75Ω Mini-Coax Impulse Responses

Notice the traces are virtually identical with the exception of sample at time index n=0. This sample represents the reflection at the connector interface. The obvious question at this point would seem why not adjust the first value of the impulse response to magnitude that accounts for loss but not connector reflection. The answer lies in the frequency response of such a correction. An example of this will be investigated later.

Its necessary to remove the portion of the impulse response resulting from the connector interface while leaving the remaining data unaffected. Several approaches from the signal processing filtering arena are well suited for this task. This application deviates from traditional applications in that samples are taken in the frequency domain and filtering is applied in the time domain.

Eq 8: $y(n) = x(n) \cdot h(n)$

Output as a Function of Input and Filter Impulse Responses

x(n) is the SRL impulse response, h(n) is the filter response, and y(n) is the desired SRL response independent of connector interface.

However, it must be recognized that multiplication of two sequences in one domain is convolution in the other domain.

Eq 9: $Y(k) = X(k) * H(k)$

$$\equiv \sum_{n=-\infty}^{+\infty} X(n)H(k-n)$$

Convolution Sum

Y(k) = X(k)*H(k) where X(k) is the measured SRL frequency response, H(k) is the filter Frequency response, and Y(k) is the desired cable frequency response independent of connector interface.

The challenge lies in designing a filter response h(n) that optimally removes the connector interface, leaves the cable response intact, and does not distort the frequency response. The following figure illustrates an ideal filter.

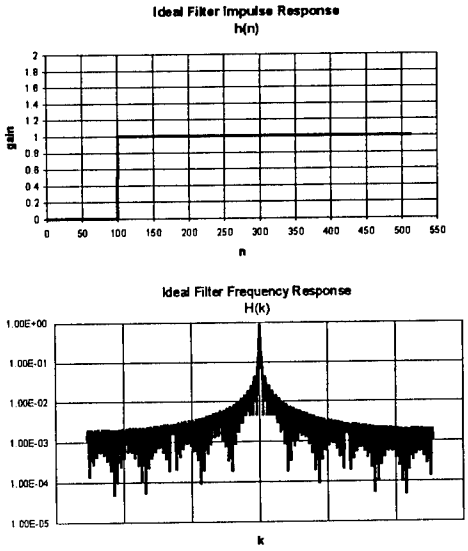


Figure 6: Impulse and Frequency Responses of an Ideal Filter

Notice that the ideal filter has an infinite frequency response with non-decaying side lobes. Because multiplying the impulse response of the filter with x(n) is convolution in frequency, Y(k) is a smeared version of X(k). Consequently, much of the information about the cable's SRL frequency response has been corrupted. The previous case of adjusting the n=0 sample of x(n) is analogous to implementing an ideal filter. The following graph shows the result Y(k).

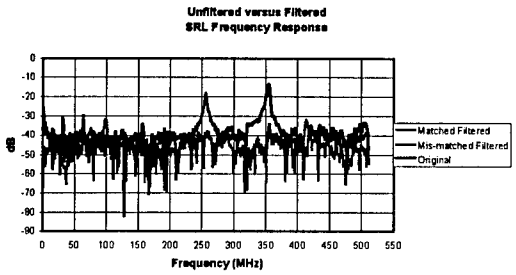
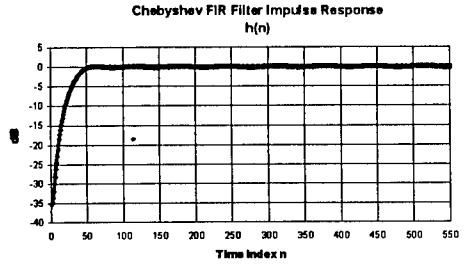


Figure 7: Frequency Responses X(k) and Y(k) with Rectangular Filter

Several filter techniques should be considered. First of all a filter of the type FIR (finite impulse response) should be used due to the advantage of linear phase. Gating implements FIR filtering by multiplying a window function. Several window types exist (rectangular, Bartlett, Hanning, Hamming, Blackman, and Kaiser) and their time and frequency responses are well known. Each window type has advantages and disadvantages in approximating and ideal filter while maintaining control of sidelobes. Advances have been made in algorithms implementing digital FIR filters based upon classical analog filter types such as Butterworth, Chebyshev, and elliptic. While many of these filter realizations could provide satisfactory results, this paper focus on the Chebyshev filter due to its advantages of transition band slope.

The compromise in filter design is bandwidth and dynamic range. The higher the filter order, the steeper the transition band. The equates to closer approximation the ideal filter. The advantage is less sequence energy in the desired band is removed; however, its frequency response has more terms resulting in reduction of bandwidth. After several iterations, a 31st order filter exhibited a reasonable compromise. The following table enumerates the filters frequency response.



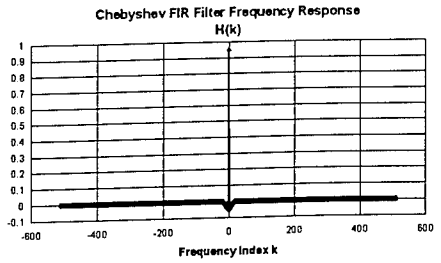


Figure 8: Impulse and Frequency Responses of 31st (M=31) Order Chebyshev FIR Filter

H(1)	$-1.256e^{-2}$	H(31)
H(2)	$-9.218e^{-3}$	H(30)
H(3)	$-1.226e^{-2}$	H(29)
H(4)	$-1.568e^{-2}$	H(28)
H(5)	$-1.941e^{-2}$	H(27)
H(6)	$-2.337e^{-2}$	H(26)
H(7)	$-2.747e^{-2}$	H(25)
H(8)	$-3.159e^{-2}$	H(24)
H(9)	$-3.561e^{-2}$	H(23)
H(10)	$-3.944e^{-2}$	H(22)
H(11)	$-4.292e^{-2}$	H(21)
H(12)	$-4.595e^{-2}$	H(20)
H(13)	$-4.841e^{-2}$	H(19)
H(14)	$-5.024e^{-2}$	H(18)
H(15)	$-5.136e^{-2}$	H(17)
H(16)	$+9.483e^{-1}$	H(16)

Table 1: Filter Frequency Response Coefficients

After the filter is designed, it can be implemented as a linear constant coefficient difference equation in the frequency domain. Because the filter is of type FIR with linear phase, its frequency is symmetric about its midpoint. This eases computation in the frequency domain to M/2 multiplies and M-1 adds per frequency sample. It is not necessary to take forward and reverse Fourier transform to implement this filter.

$$H(k)\cdot X(k)+H(k-1)\cdot [X(k-1)+X(k+1)]+\ldots$$

Eq10: $$Y(k)=\sum_{n=0}^{N}+H(k-N)\cdot[X(+\frac{N}{2})+X(-\frac{N}{2})]$$

Difference Equation Realization of FIR Filter

The following graph results from applying this filter to the matched and mismatched SRL frequency response data.

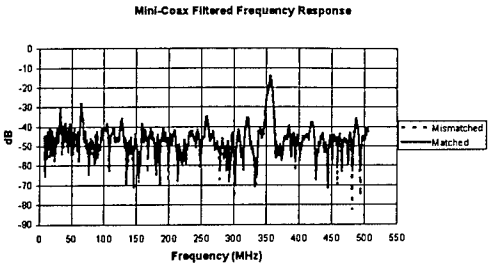


Figure 9: 75Ω Mini-Coax Filtered Frequency Responses {Y(k)}

Notice the two traces are virtually identical (the degree of similarity will be evaluated shortly). The results show SRL performance of cable independent of the connector interface. Since the filter has finite transition slope some energy was removed from the frequency response. It will be necessary to determine the magnitude of this reduction and apply it back into the response. This is analogous to raising the noise floor of the measurement hence the decrease in dynamic range.
Using Parseval's Energy theorem, sequence energies can be computed to determine the value of energy inadvertently removed from the frequency response.

Eq 11: $$E=\sum_{n=-\infty}^{+\infty}x(n)\cdot x^{*}(n)=\frac{1}{2\pi}\sum_{k=-\infty}^{+\infty}|X(k)|^{2}$$

unitless

Parseval's Theorem

The following table shows the sequence energy of X(k) and Y(k) under both matched and mismatched measurement conditions.

	Original X(k)	Filtered Y(k)
Matched	0.506	0.177
Mismatched	0.800	0.175

Table 2: Sequence Energy

The sequence energies of Y(k) differed by 0.5% while X(k) differed by 22.5%. The magnitudes of Y(k) differed from the matched version of X(k) by a factor of 1.432. A scalar multiplier

(gain) can be applied to x(n) or y(n) to account for the level difference in X(k) and Y(k).

Eq 12: $$\sum_{n=+1}^{+N} x(n) \cdot x^*(n) = G \sum_{n=\alpha}^{+N} x(n) \cdot x^*(n)$$

α = filter 3dB break point

G = gain

Finally, figure 10 illustrates the scaled version Y(k) for both matched and mismatch versions of X(k). SRL results Y(k) with the relative magnitude of the X(k) under matched conditions is achieved.

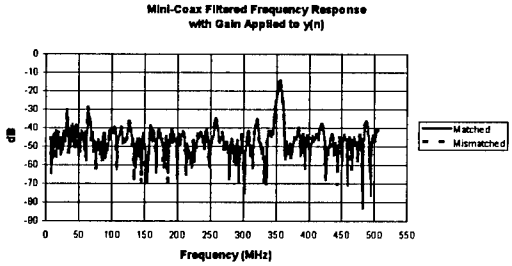


Figure 10: 75Ω Mini-Coax Filtered Frequency Responses {Y(k)}with Gain applied to y(n)

Conclusions: A technique for achieving connector interface independent transmission line measurements was developed utilizing DSP techniques. Careful consideration was given to satisfy the Nyquist sampling theorem. A digital filter was designed to give optimum rejection of connector interface data in the time domain while leaving as much cable information as possible. Further, through Parsevall's energy relationships; it was possible to adjust relative signal level at the cost of dynamic range. Finally, the filter was applied to the gain adjusted cable frequency response as a linear constant coefficient difference equation. The end result was SRL traces from both matched and mismatched interface conditions that were identical to within 0.5% of each other and maintained the same relative SRL values as the original trace under matched conditions. Using these techniques, repeatability and correlation of connector sensitive measurements between lab and field environments are possible.

References:

1. *Fundamentals of Digital Signal Processing*, Lonnie C. Ludeman, copyright 1986 by John Wiley & Sons, Inc.

2. *Discrete-Time Signal Processing*, Alan V. Oppenheim • Ronald W. Schafer, copyright 1989 by Prentice-Hall, Inc.

3. "Cable Impedance and Structural Return Loss Measurement Methodologies", Joe Rowell, Joel Dunsmore, and Les Brabetz, Hewlett Packard Company, Sata Rosa, California.



Trent M. Hayes

Product Engineering
CommScope, Inc.
General Instrument
Claremont, NC 28610

Trent Hayes received his BEE from the Georgia Institute of Technology and his MSEE from Clemson University. He joined CommScope, Inc. in 1991 and has worked primarily in new product development and ATE design.

DETERMINING FIELD TEST INSTRUMENT ACCURACY FOR MEASURING NEAR END CROSSTALK ON TWISTED PAIR CABLE

Terry R. Cobb

Datacom Technologies
Everett, WA.

Abstract

In the last few years the requirements of testing installed cabling for conformance to standards has grown significantly. As the performance of copper twisted pair cabling and applications increased so did the need for more accurate measurements in the field. One of the more important and difficult measurements is that of Near End Crosstalk, NEXT. To determine the accuracy for measuring NEXT requires identifying potential error sources in the instrument and how they combine with the cable under test. To analyze this, a model was developed for the measurement. The model includes such terms as residual crosstalk, balance, and the mode coupling between the pairs of a cable. The result is an error model that provides a first order approximation for NEXT measurements and a method of standardizing on field test instrument parameters.

Introduction

Structured wiring was introduced into the market for Local Area Networks with the publication of TIA/EIA 568. The standard defines a wiring scheme with a fixed performance, allowing applications to be added later. With a guaranteed cabling and the production of higher speed copper twisted pair cabling, users began to require at installation the cabling be tested in the field for conformance to these specifications. In some applications the margin of performance over the cabling is only a few dB. This required a measurement accuracy to within one or two dB. To study the problem a group within TIA was formed and eventually published a Technical Systems Bulletin, TSB, on Field Testing.

The TSB deals with twisted four pair cable and includes tests to verify that the installation conforms to the specifications in the standard. The most difficult of the field tests is that of measuring NEXT, Near End Crosstalk. NEXT is determined by injecting a signal on one pair of a multi-pair cable and measuring the coupling ratio of the signal on another pair, Figure 1. Since most applications are full duplex, sending and receiving at the same time, this coupling of the sending signal to receive signal accounts for most of the disturbance or noise to the received signal and requires an accurate measurement.

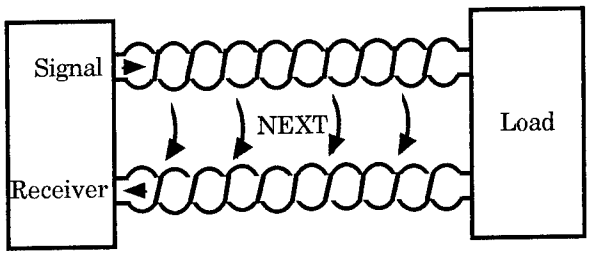


Figure 1: NEXT Measurement

Measurement Accuracy

To calculate an instrument's accuracy the potential error sources in the instrument must be identified. These errors are ultimately determined by the instrument parameters and how they combine with the cabling under test. To calculate the error between the actual value of NEXT and what is measured, a model was developed for the measurement. Once the instrument parameters are determined along with the parameters of the cable, then the model predicts the error. Limiting the error or fixing the accuracy of a field measurement requires limiting the instrument parameters for a set of cabling parameters. This also provides a traceability to the measurement when the instrument parameters are measured with standard references, traceable to NIST.

Cable Model

Modeling the measurement requires defining the cabling under test. Figure 2 is a flow diagram for differential mode NEXT. In the model a balanced signal is injected into the source pair. Some of this signal will be coupled, S21, to a receive pair. In addition part of the signal is reflected back from the cabling, S11, to the signal source. The balanced coupled received signal is the actual NEXT. For an imperfect receiver match, some of the signal is reflected and either absorbed by the cabling, reflected by the cable, S22, or couple in the reverse direction to the signal source, S12. The actual value of NEXT is S21, and the measured value is V2/V1.

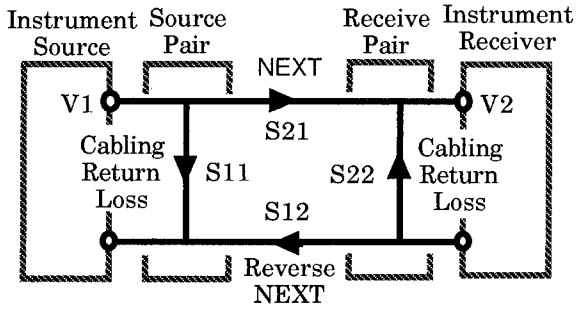


Figure 2: Differential Mode NEXT Cable Model

The cable model in Figure 2 depicts single mode coupling: differential to differential. In reality the signal along the cable consists of a differential mode and common mode component,often referred to as metallic and longitudinal. Perfect balance is impractical in either the instrument or cabling. Some common mode will be present in the instrument signal output or generated by the cabling. Coupling between any two pairs is then one of four possible combinations of the two modes on each pair. Tests on the mode couplings indicate they can be significant (Figure 7). Although common mode or even differential mode could be generated by a cable pair this analysis will deal only with instrument and pair to pair mode generation, considered the dominant source in the model.

Instrument Model

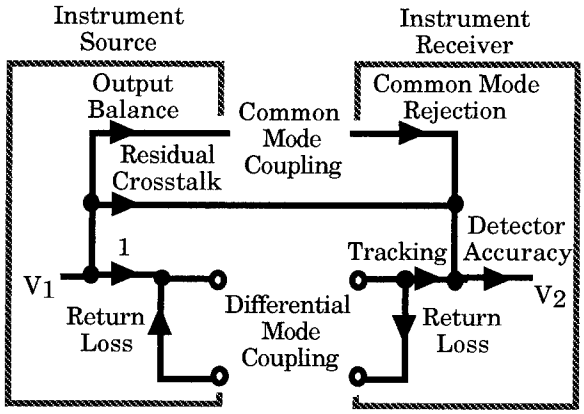


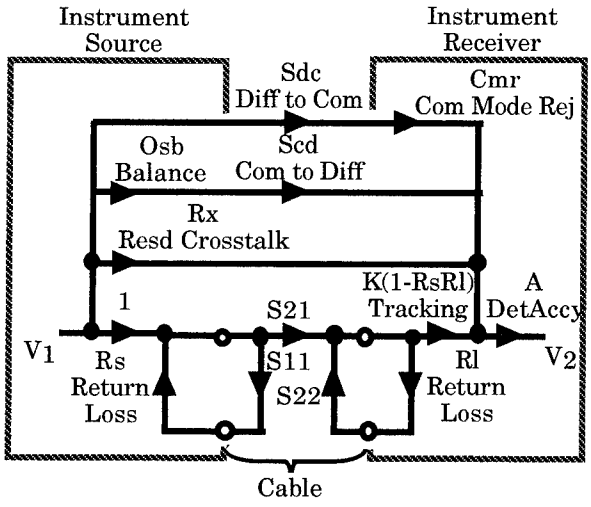
Figure 3: Instrument Error Sources

The instrument's error characteristics can be defined in a similar model, Figure 3. In the model any returned signal from the instrument contributes to the error by adding to the source or the measured received signal. Tracking, included in Figure 3, determines how accurate the received signal is calibrated or is tracking the source. In most systems noise will alter the final reading. In measuring NEXT, a measurement conducted at a near end, some of the source will be coupled to the receiver as residual crosstalk. Additional noise is usually an order of magnitude below the residual crosstalk and is not included in the model. Also not accounted for are the effects of any far end residual crosstalk; as the dominant contributors are at the near end. Measuring the final signal at the receiver uses a detector. Detector errors include such terms as front end compression, non-linearity, spurs, drift, resolution, and others. Together all of these are lumped into a detector accuracy.

Common mode signals on a cable can effect the results. The model includes an output balance term to account for unbalances in the instrument that produce a common mode signal. In addition the receiver includes a common mode rejection term that accounts for the effect that a common mode signal would have on the received differential signal. These terms will be combined with the cable mode coupling terms.

Error Model

Before inserting the cable model in the instrument model several simplification's are possible. First any reverse NEXT is an order of magnitude below that reflected by the cable and can be ignored. This eliminates the return path in the cable model, S12. If the mode coupling is common to common, its contribution to an error would include the generation of the common mode signal by the instrument source and the rejection at the receiver. When taken together the result is small compared to the other mode coupling errors. The common to common mode coupling term consequently is not included in the model. To determine the measured value of NEXT the cable and instrument model are combined as shown in Figure 4.



Measured NEXT =
A x {Rx + (OsbScd) + (SdcCmr)
+ K x S21 x [(1 - RsRl) / (1 - RsS11)(1 - RlS22)]} (1)

Actual NEXT = S21 (2)

Figure 4: NEXT Measurement Error Model

The effects of return loss on the common mode terms is not included. Their contribution complicates the model and is considered of second order for longer cable lengths or connector spacing. With this assumption the mode coupling terms are combined in Figure 4 with the instrument mode conversion parameters and summed with residual crosstalk, as additional error signals. The intent of the error model was to define a reasonable first order approximation to the accuracy and include parameters that could easily be measured.

Results

Tests were conducted in the laboratory on the effects of the instrument parameters predicted by the model by measuring NEXT on a cable. Illustrated in Figure 5 is an error due to residual crosstalk, created by including crosstalk at the near end in the measurement setup. By unbalancing the signal source, an error is created with the common to differential mode coupling, Figure 6. The mode coupling terms in the model were also determined by laboratory measurements on the cabling. Figure 7 is a comparison of the common to differential mode and differential to differential mode coupling (NEXT).

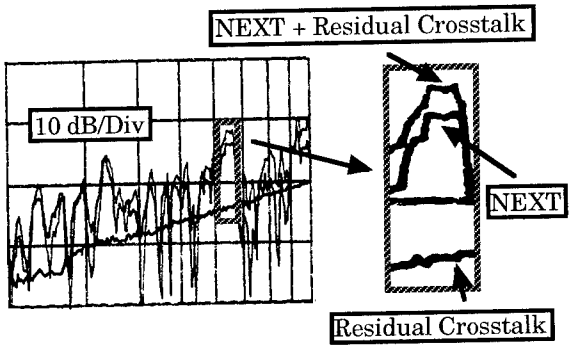


Figure 5: Measurement Error Due to Residual Crosstalk

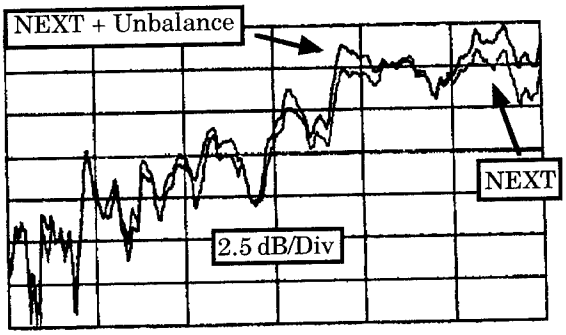


Figure 6: Measurement Error Due to an Unbalanced Signal Source

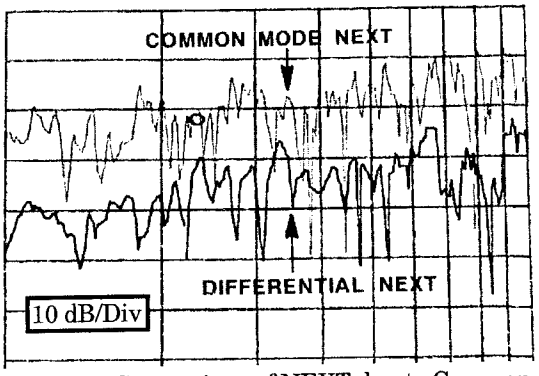


Figure 7: Comparison of NEXT due to Common and Differential Mode

With the error model, the measured value of NEXT V2/V1, Figure 4 (1), can be calculated and compared to the actual value (2). In the TSB, parameters for instruments are specified and then with an approximation of the model the error is determined for the instrument. A comparison of a Network Analyzer (assumed close to actual) to an instrument whose parameters meet those specified in the TSB, Figure 8, indicate that the error is well within the 1.6 dB predicted by the approximation in the TSB. Other experiments indicate that the model is a reasonable representation of the field test instrument accuracy in measuring near end crosstalk on twisted pair cables.

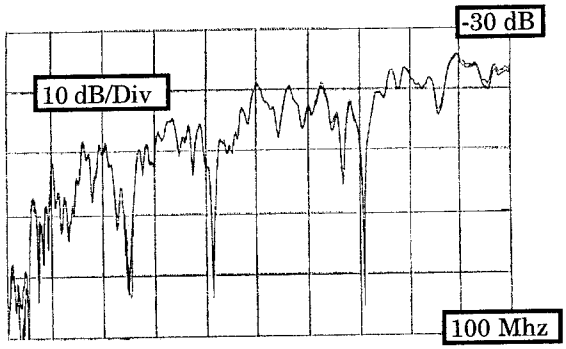


Figure 8: Instrument Comparison to a Network Analyzer

The analysis of the parameters was near the level of the requirements defined for category 5 cabling. It is expected that the results are different at other levels. The model is limited to first order terms, and an order of magnitude improvement in the parameters from those defined in the TSB, should require consideration of additional contributors. Network Analyzer comparison on the same cable indicate an uncertainty of 1 dB for any NEXT measurement, and should be considered a minimum for the error.

Conclusion

A field test instrument's accuracy can be predicted as illustrated by the modeling of the instrument error sources and how they combine with the characteristics of the cable under test. Standardizing on instrument parameters then determines the accuracy for the result and provides a consistency to the measurement. Standards in the future that define specifications for installed cabling should always consider their measurement to insure correct field testing.

Acknowledgment

The author would like to thank Douglas Kent Rytting of the HP Network Measurement Division, for providing a copy of his paper on "Improved RF Hardware and Calibration Methods for Network Analyzers". Also the members of TIA/EIA TR41.8.1 for their support and contribution to the error model.



Terry R. Cobb
Datacom Technologies
Everett, WA.

Terry R. Cobb is the President of Datacom Technologies, a manufacturer of Field Test Equipment for Data and Telecommunications Systems. He developed the model for the instrument parameters and accuracy defined in Annex A of the TSB. He taught a class on cable testing at the University of Texas at Arlington where he received a Bachelors and Masters degree in Electrical Engineering.

Crosstalk Performance of Short Length Data Grade Wires

J.- H. Walling * , M. Bélanger * and V. Le Nir **

* NORTEL ** V.P.S.Enterprises

Abstract

NEXT and FEXT measurements are performed on two wires, specially made, having large differences in propagation constants while meeting the requirements for Category 5. Large differences in propagation constant ought to have an impact on crosstalk. However, we obtain for both types of wire, terminated for differential mode, crosstalk matrices which are comparable in their asymmetry.

We also terminate all pairs with respect to their common mode suppression. We confirm that NEXT matrices are symmetric for nearly all types of baluns and termination modes. FEXT matrices show substantial deviations, due to the indirect crosstalk coupling over tertiary circuits amplified by continuous signal reflections in the idle pairs. We show this using different terminations of the idle pairs.

Hence, the differences of the absolute values of the propagation constants are not responsible for the crosstalk matrix asymmetry. The asymmetries are therefore only caused by the performance of the baluns with respect to their common mode rejection and longitudinal balance.

It is necessary to use common mode termination, since some of the baluns, we use for cable testing, are not sufficiently accurate for the purpose of our experiments. We are able to achieve very consistent results using North Hills BF-0322 baluns, although the scatter of the data suggests a lack of signal balance.

In order to obtain a true characterization with respect to NEXT and FEXT for short cables (shorter than 100 m), our recommendation is that the full crosstalk matrix should be measured with common mode terminations. For this purpose the use of high performance baluns is imperative.

Introduction

An understanding of crosstalk concepts is gaining renewed importance. In this context the following areas are subject to special attention :

- Crosstalk performance of tapered cable structures for bi-directional data traffic. By tapered cable structures we understand real installations in the backbone or loop, using higher pair count cables which branch out over smaller pair count cables to the individual connection of a station or customer premises having only two or four pairs total.
- Crosstalk of data grade cable links, especially for short link length and at high frequencies.
- Crosstalk performance of multiple pair data grade cables under the combined impact of NEXT and FEXT.

Note: Here and in the following we will understand FEXT as the Input-to-Output FEXT only. The equal level far end crosstalk will be designated as such, i.e. EL-FEXT.

Tapered cable structures are required for the deployment of FSTP (Switched Fiber Twisted Pair) broadband systems, as proposed by NORTEL and reported upon concurrently by P. Kish et al. [1] Tapered structures have a tapered trunk and branches. The branches result from the splicing of drop or service wires from the feeder or backbone cable to individual stations or customers.

Similar structures are also obtained if hybrid cables of the same category are deployed as break-out cables. Such cables are covered in TIA/EIA 568A. Included in such structures is the branching out of two or four pairs from a backbone or horizontal distribution cable. In this case the drop is only exposed to station specific self crosstalk, and is exposed to effective powersum crosstalk by the remaining pairs in the tree part of the structure.

The subject of the present paper deals with crosstalk in short lengths of wires and cables. These results are part of a study of crosstalk performance in tapered structures.

Crosstalk in short wires or cables is not well understood and the problem in links is, furthermore, amplified by the connectors used for patchcords. For the objective of standardization it is important to evaluate the impact of the length/frequency dependency of the entire link. This is an actual undertaking of the TR 41.8.1 Standards Committee of TIA/EIA. A model for plug-ended patchcords has been recently proposed. [2] Here we will focus only on the wire aspect of this issue, i.e. the behaviour of the data grade

wires, cables or the patchcord-wire, under the condition that the wire is relatively short, with a length anywhere from 1.5 m to 100 m.

The shorter the link length of a cable, the more the systematic crosstalk becomes predominant. Patch cords are generally terminated in such a way that they are end reversible, i.e. the entire patch cord may be used in either direction. The crosstalk performance requirements must be met for both cases. Performance requirements are actually based upon two pair data protocols, but four pair protocols are increasingly being deployed, either to increase the available bandwidth of installed systems or to substantially increase the bit rate of future systems.

Multiple pair protocols have either two transmit and receive pairs or use switching of the data traffic direction in two or four pairs according to data traffic requirement. In these cases, patchcord requirements must cover both NEXT and FEXT, and eventually powersum limits. In addition, the requirements must be met from both ends, i.e for INEXT, ONEXT, IFEXT and OFEXT.

For multiple pair data grade cables the importance of specification requirements for combined NEXT and FEXT has been demonstrated. [3];[4] The impact of the combined powersum of NEXT and FEXT upon an individual pair, i.e. the effective powersum, was proposed as well. [3]

The standards covering multiple pair data grade cables are actually under revision by IEC - WG 46C and by TIA/EIA. TIA/EIA recently mandated NEMA to handle the wire and cable performance requirement issues for high performance wires and cables.

Two new work item proposals, dealing with FEXT performance requirements, are at present in the IEC-WG46C for discussion. Their main difference is the specific FEXT definition which is proposed for specification purposes, i.e. Input-to-Output FEXT versus EL-FEXT. Though EL-FEXT in itself represents the attenuation to crosstalk ratio ACR_{FEXT} for far end crosstalk, it seems to be more advisable to use the Input-to-Output FEXT, as it impacts directly upon the effective powersum crosstalk. One of the main arguments for the use of Input-to-Output FEXT is that it can be directly measured. The proponents of EL-FEXT support their choice by the utilization of average crosstalk values and respective standard deviations. However, the statistical crosstalk model is useful primarily for high pair count telephone cables with relatively long twistlays. For these cables the longitudinal irregularity of the twistlays and the displacements of individual pairs from their intended design location yields a relatively high proportion of unsystematic crosstalk. [5] Hence, this model is correct only if the crosstalk power has a perfectly normal distribution (log-normal Gaussian distribution) [6]. This is not necessarily the case for low paircount wires and cables, for cables with short twist lays and for short wires or cables having short twistlays. It is better to use the convolution of the double helix or the 'twist frequency' than the twistlay itself. EL-FEXT values would have to be calculated from the measured Input-to-Output FEXT and attenuation and is therefore subject to higher error levels.

FEXT is more pertinent from a performance requirement point of view, as it allows the direct computation of effective powersums with the complementary NEXT, i.e. we obtain powersums which are generated in a disturbed pair exposed to its neighbouring disturbers. EL-FEXT does not allow the combined impact of FEXT and NEXT to be evaluated on any disturbed pair, though this is really the final objective of any subject specification requirement.

In all cases crosstalk performance will have to be assessed for the pair combinations and for both cable ends. Hence, the present paper will focus on crosstalk data for different wire lengths, with crosstalk being measured from both ends and for all the pair combinations. To limit the amount of data, we only used four pair wires.

Rationale

It is well known that the pair to pair near end crosstalk matrix is symmetric provided the propagation constant of the pairs involved is considered to be equal. We have then :

$$NEXT_{i,j} = NEXT_{j,i} \quad \ldots\ldots\ldots\ldots\ldots\ldots \quad (1)$$

If the propagation constants are substantially different, this equation does not necessary hold any more. [6];[7]. The difference may be amplified by the manner in which the adjacent pairs, which cause indirect crosstalk coupling, are terminated.

Uniformly manufactured wires, i.e. wires with a high degree of uniformity of the twist and strand convolution, are subject predominantly to systematic crosstalk, and an end change will not substantially change the near end crosstalk, i.e. the following equations should hold :

$$INEXT_{i,j} = INEXT_{j,i} \quad \ldots\ldots\ldots\ldots\ldots\ldots \quad (2)$$

$$ONEXT_{i,j} = ONEXT_{j,i} \quad \ldots\ldots\ldots\ldots\ldots\ldots \quad (3)$$

For far end crosstalk we have similar equations, i.e.:

$$IFEXT_{i,j} = OFEXT_{j,i} \quad \ldots\ldots\ldots\ldots\ldots\ldots \quad (4)$$

$$OFEXT_{i,j} = IFEXT_{j,i} \quad \ldots\ldots\ldots\ldots\ldots\ldots \quad (5)$$

Real data grade wires and cables show some deviations from the equations (2) to (5). The amount of asymmetry of the crosstalk matrices gives an indication of :

- the impact of differences of the propagation constant in different pairs. This effect increases with length of the cable.
- the uniformity of the cable, primarily with respect to the regularity of the twist frequency.
- the impact of indirect crosstalk coupling over tertiary circuits. This effect is amplified with decreasing length of cable.
- the performance of the baluns used for testing the cable.

Depending upon the results we will be able to decide whether the specification requirements for data grade cables should be expanded to cover the measurements of all pair combinations, i.e. including the reversal of the pairs under test, or if the specification requirement should cover the performance of the baluns used for the test as well.

If we assume a high degree of systematic crosstalk for wires, we may expect the equations (2) and (3) to hold very closely. This is primarily due to the indirect crosstalk coupling paths and the mode of termination of the adjacent pairs.

For FEXT measurements the conditions of equations (4) and (5) may not hold up any more. We therefore expect slightly deviating results for the corresponding measurements, depending on the termination of the idle pairs, i.e. those which are not under immediate test. These pairs may be shorted, left open or may be terminated to their real part of the characteristic impedance either in a straight differential fashion, or in such a way that the common mode propagation is suppressed.

Though the coupling functions can be derived directly from full matrix measurements, it is not in the scope of this paper to do so. The coupling functions can be obtained using Fourier series developments. Preliminary steps towards this goal are indicated in [7]. These results must be expanded for impedance matching terminations of adjacent pairs and the complex crosstalk values must be used. Additionally, the strongly helicoidal electromagnetic fields, which result from the relative tight twistlays, may have to be taken more accurately into account, as is indicated in references [8] to [15].

Here we will focus on the following questions: Can we continue to assume the symmetry of the NEXT and FEXT matrices, or should we consider measuring the full matrix, i.e. all possible wire combinations ? Alternatively, do we have to consider the performance of the baluns used for the testing of wires and cables ?

Description of Wires Investigated

We made extensive tests on two different types of wire. These wires are designed for the trials with certain purposes in mind. We use two specific twist frequency patterns. One of the wires is characterized having twist frequencies as postulated for good crosstalk performance [7]; [8]; [16]; [17]. Similar twist frequencies are commonly used for data grade wires. The second wire contains two pairs with very narrowly spaced twist frequencies and two pairs with widely spaced twist frequencies. The crosstalk influence functions are shown in Table I for each pair combination and are calculated as shown by Oakley et al. [18], although expanded to cover both differences and sums :

$$CIF = \log\left(\frac{1}{t_i} \pm \frac{1}{t_j}\right) = \log(C_i \pm C_j) \quad \ldots\ldots\ldots (6)$$

Here t_i and t_j are the twistlays of the considered pair combination whereas C_i and C_j are the corresponding convolutions or twist frequencies.

Incidentally, Holte utilizes similar coupling terms, but does not use the Neperian logarithm. [8]

Wire #	1		2	
Pair Combination	CIF			
	Pos.	Neg.	Pos.	Neg.
1 = 2	0.567	0.388	0.421	0.476
1 = 3	0.602	-1.097	0.231	-0.207
1 = 4	0.557	-0.320	0.700	-0.570
2 = 3	0.558	0.308	0.463	-0.454
2 = 4	0.507	-1.044	0.750	0.375
3 = 4	0.547	0.398	0.722	0.435

Table I

To give an idea of the differences in twist frequencies over unit length of the wire, we indicate the resulting relative propagation velocities in Fig. 1 and 2 for all the four pairs of the wires # 1 and 2 respectively.

Two extremes of twist frequency spacing are selected for these wire designs because:

- they can occur in reality in multiple pair data grade cables between the pairs with the largest differences in twist frequencies.
- their relatively large deviations of propagation velocity should have an impact upon crosstalk behaviour, which is one of the objectives pursued in our investigation.
- they have an impact on the attenuation, since the helix loss of a pair is directly proportional to the twist frequency.
- they yield the maximum variation of the absolute value of the propagation constant without using specially

designed delay or continuously loaded lines.

Hence, we try to obtain the largest differences in propagation constant, while not sacrificing the Category 5 requirements. Therefore, the signal delay for the wire # 2 is relatively large, exceeding the values which are normally accepted for an individual station connection.

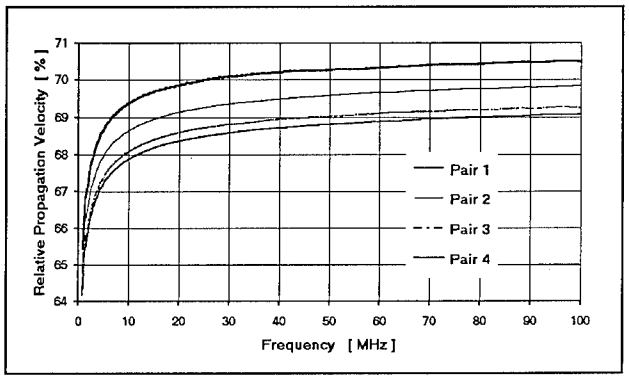


Figure 1 : Relative propagation velocity of wire # 1

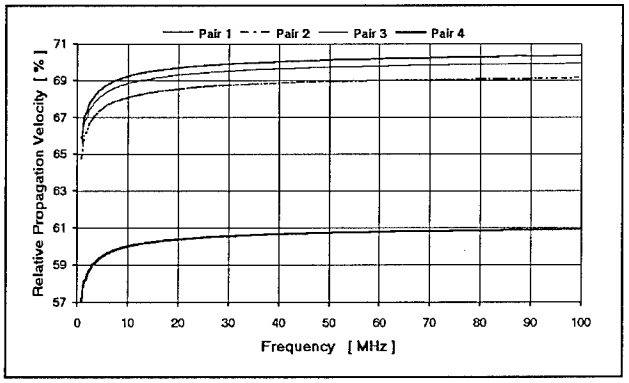


Figure 2 : Relative propagation velocity of wire # 2

Methodology and Measurements

We build a matrix switch for the measurements which allows the automatic measurement of the entire crosstalk matrices from both ends in the same fan-out. The schematic of the corresponding crosstalk denomination is shown in Fig. 3.

We use the same baluns which are normally used for cable testing equipment for the matrix switch. The driving software for the switch as well as for the network analyzer is developed in conjunction with VPS Enterprises. We measure 1601 linearly incremented frequency points. Though the amount of data is large, we feel that the interpolation curves of the traces obtained justify this choice.

In addition to crosstalk values, we also record the attenuation, the phase angle of the propagation constant and the impedance. The impedance is recorded only as a control measure for a wire length of 100 m for the wires, primarily with respect to the pair having the extremely short twistlay. The results fall in a range of 100±6 Ohms. The SRL values obtained are better than 30 dB over the entire frequency range, i.e. up to 100 MHz. These results are, however, of no importance in the context of this work and will not be elaborated further.

We always start with a wire length of 100 m. In those cases where the wire length is stepwise reduced, we cut the length down gradually to 1.5 m, starting from the outside end.

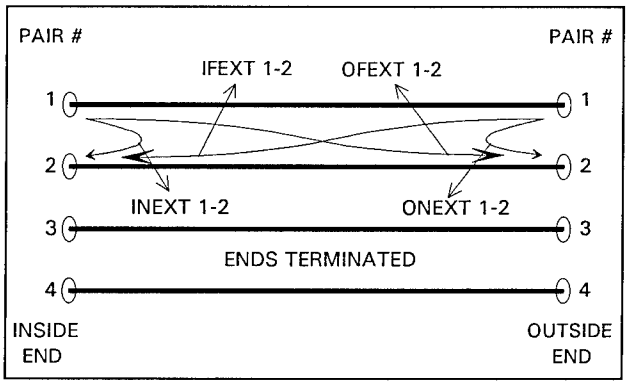


Figure 3 : Schematics of NEXT and FEXT coupling an the inside and outside end of a line. The termination of tertiary circuits is not indicated.

In order to assess the impact of adjacent idle pairs, which are the cause of indirect crosstalk coupling over tertiary circuits, the idle pairs are terminated differently, i.e. they are shorted, left open or terminated in their real part of the characteristic impedance. In the last case we use two different termination modes, i.e. we use either a straight differential measurement or we try to suppress common mode propagation. This is shown schematically in Fig. 4.

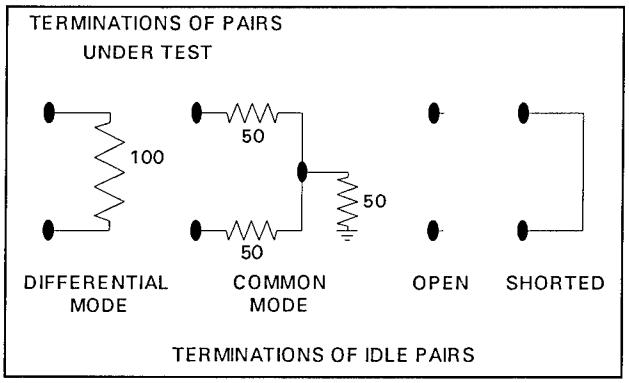


Figure 4 : Terminations used for idle adjacent pairs.

All the measurements are carried out over a frequency range of 0.772 to 100 MHz with linear frequency division, as already mentioned.

Results

The amount of results gathered is massive and we will only discuss some representative results. We first report the measurements with differential terminations of all the pairs. Fig. 5 shows the NEXT for 100 m of wire #1. The result clearly indicates that the NEXT matrix seems to be symmetric. Fig. 6 proves that the FEXT matrix obtained is clearly asymmetric. At a length of 10 m the asymmetry of the matrix reaches 3 dB. (see Fig. 7) Shortening the length of the wire increases the asymmetry of the FEXT

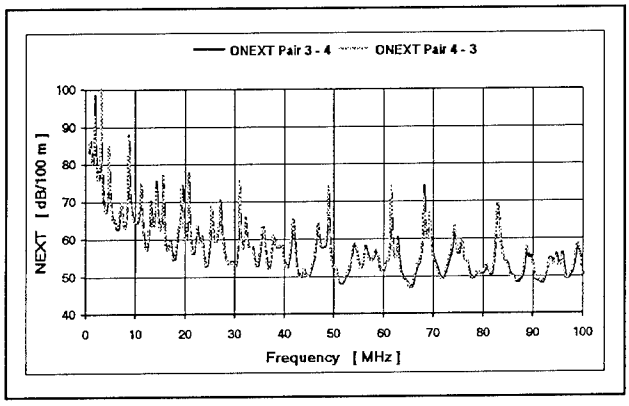


Figure 5 : ONEXT for 100 m of wire #1 between the pairs 3-4 and 4-3 with differential mode termination of all pairs

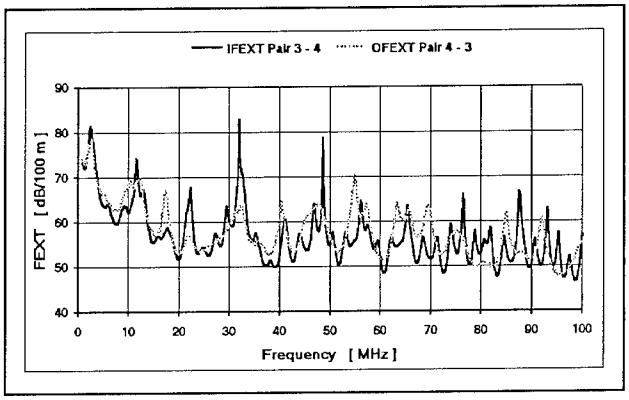


Figure 6 : IFEXT/OFEXT for 100 m of wire #1 between the pairs 3-4 and 4-3 with differential mode termination of all pairs

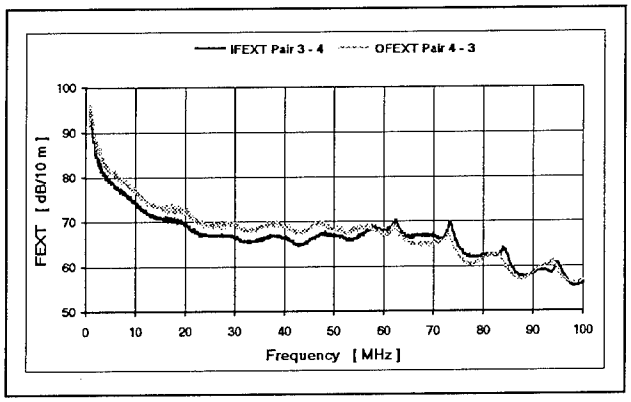


Figure 7 : IFEXT/OFEXT for 10 m of wire #2 between the pairs 3-4 and 4-3 with differential mode termination of all pairs

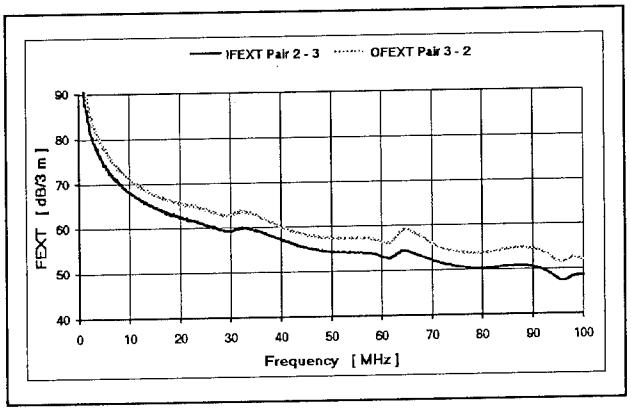


Figure 8 : IFEXT/OFEXT for 3 m of wire #2 between the pairs 2-3 and 3-2 with differential mode termination of all pairs

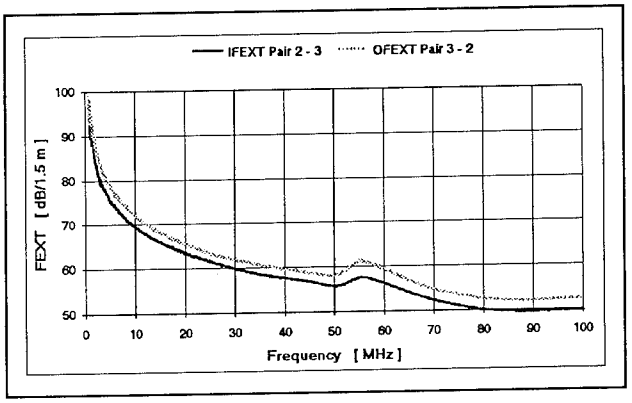


Figure 9 : IFEXT/OFEXT for 1.5 m of wire #2 between the pairs 2-3 and 3-2 with differential mode termination of all pairs

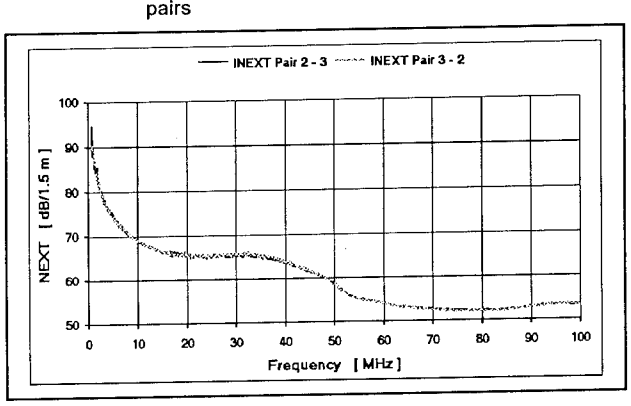


Figure 10 : INEXT for 1.5 m of wire #2 between the pairs 2-3 and 3-2 with differential mode termination of all pairs

matrix as shown in Fig. 8 and Fig. 9. The NEXT matrix measured with differential mode termination of all pairs seems however to yield a complete symmetry down to a length of 1.5 m, as shown in Fig. 10.

The measurements with differential mode termination do not yield symmetric results for the FEXT matrix. For wire # 1 the common mode termination of all pairs is compared against the differential mode termination. Incidentally, the differential mode termination is generally used in commercially available equipment which normally does not allow for common mode terminations.

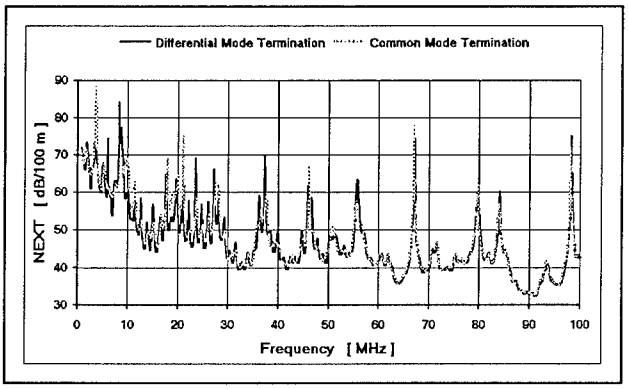


Figure 11 : INEXT for 100 m of wire #1 between the pairs 1-3 with differential and common mode termination of all pairs

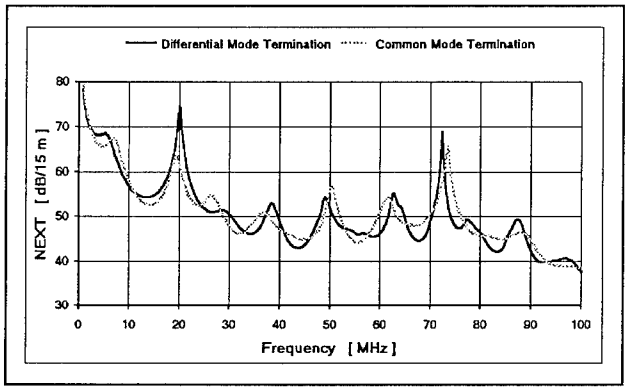


Figure 12 : INEXT for 15 m of wire #1 between the pairs 1-2 with differential and common mode termination of all pairs

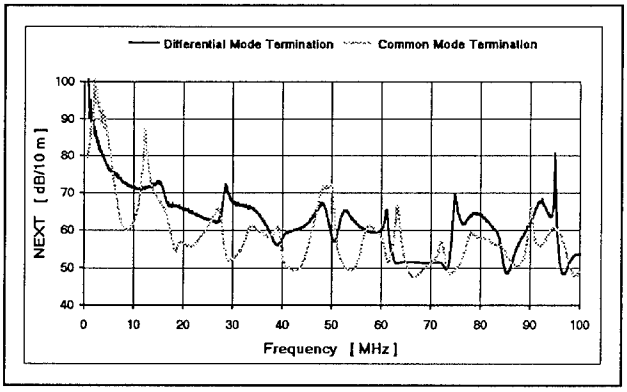


Figure 13 : INEXT for 10 m of wire #1 between the pairs 1-4 with differential and common mode termination of all pairs

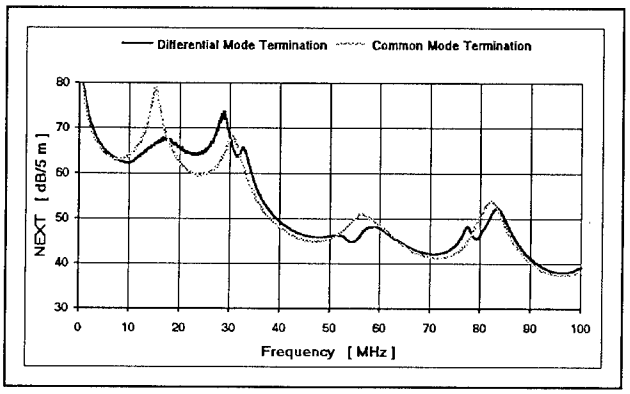


Figure 14 : INEXT for 5 m of wire #1 between the pairs 2-4 with differential and common mode termination of all pairs

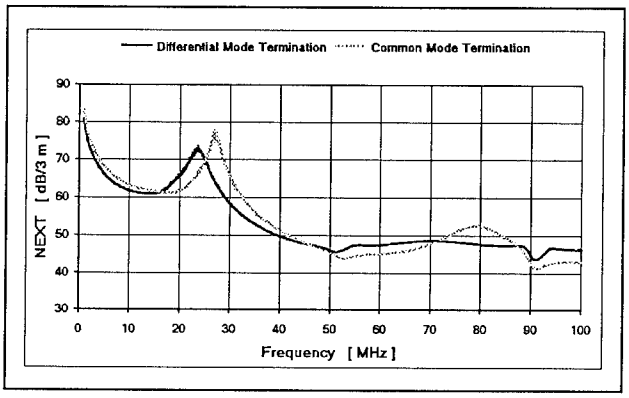


Figure 15 : INEXT for 3 m of wire #1 between the pairs 2-4 with differential and common mode termination of all pairs

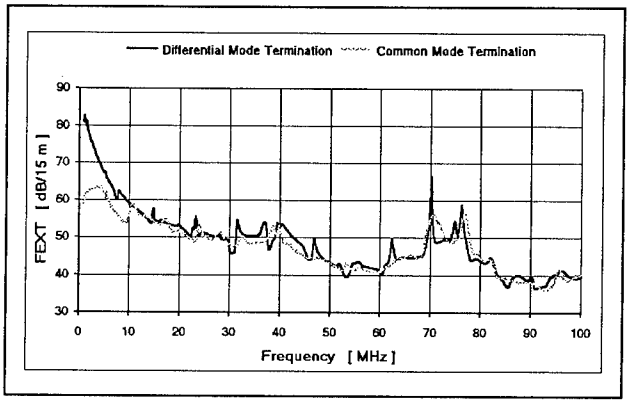


Figure 16 : IFEXT for 15 m of wire #1 between pairs 2-4 with differential and common mode termination of all pairs

The results of NEXT are indicated for different lengths of wire #1 in Fig. 11 to Fig. 15. Equivalent results for FEXT are given in Fig. 16 and 17 for two different lengths of wire.

Common mode termination of all pairs also yields symmetric NEXT matrices over the entire frequency range for 100 m of wire #2, as indicated in Fig. 18. Only some NEXT combinations at a length of 100 m show minor deviations as depicted in Fig. 19. Comparable results are obtained for the FEXT, as may be seen in Fig. 20. Both traces show some ripple, due to the indirect crosstalk

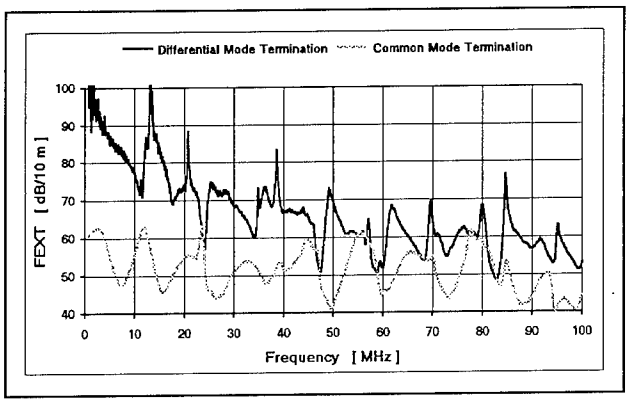


Figure 17 : IFEXT for 10 m of wire #1 between the pairs 1-4 with differential and common mode termination of all pairs

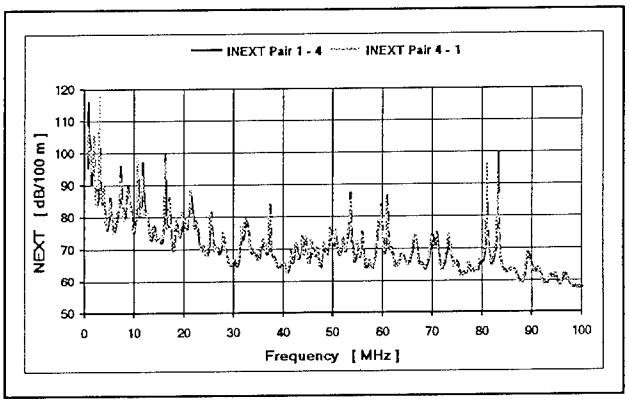


Figure 18 : INEXT for 100 m of wire #2 between the pairs 1-4 and 4-1 with common mode termination of all pairs

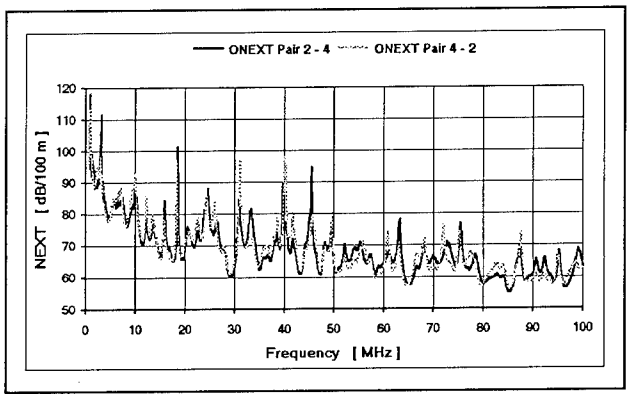


Figure 19 : ONEXT for 100 m of wire #2 between the pairs 2-4 and 4-2 with common mode termination of all pairs

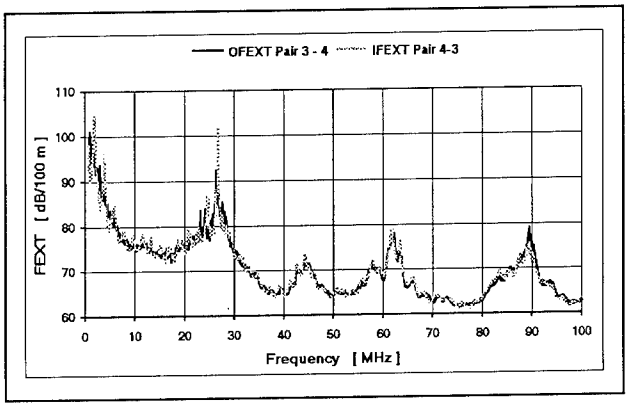


Figure 20 : IFEXT/OFEXT for 100 m of wire #2 between the pairs 3-4 and 4-3 with common mode termination on all pairs

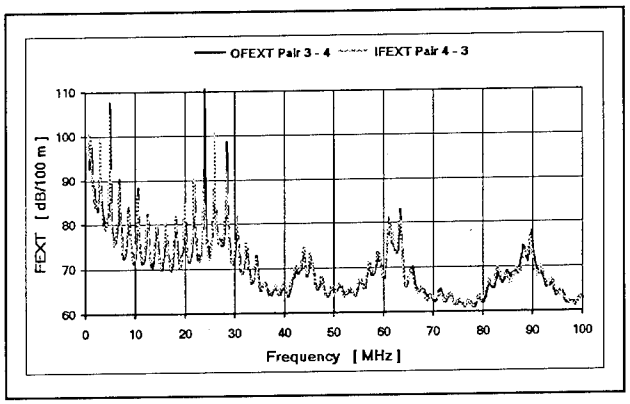


Figure 21 : IFEXT/OFEXT for 100 m of wire #2 between the pairs 3-4 and 4-3 with common mode termination and open idle pairs

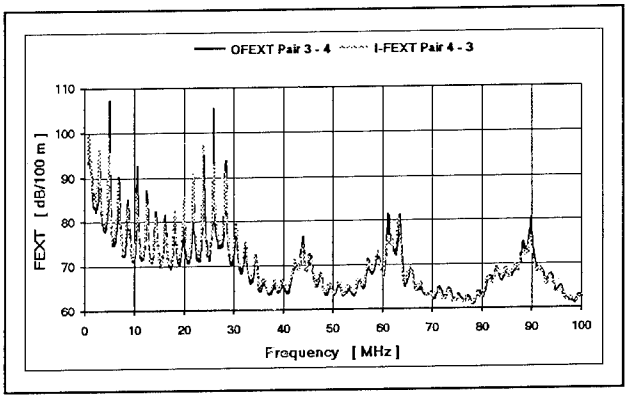


Figure 22 : IFEXT/OFEXT for 100 m of wire #2 between the pairs 3-4 and 4-3 with common mode termination and shorted idle pairs

coupling over the tertiary circuits, but are otherwise equivalent. The lower envelope of the curves is nearly identical, though shorted or open idle pairs show slightly lower crosstalk minima. The ripple is amplified substantially if the idle pairs are either left open or are shorted as is shown in Fig. 21 and Fig. 22. The same effect occurs also at a length of 5 m. This is shown in Fig. 23 to Fig. 25, although the ripple is much less pronounced over frequency, since it depends on length and frequency as previously mentioned.

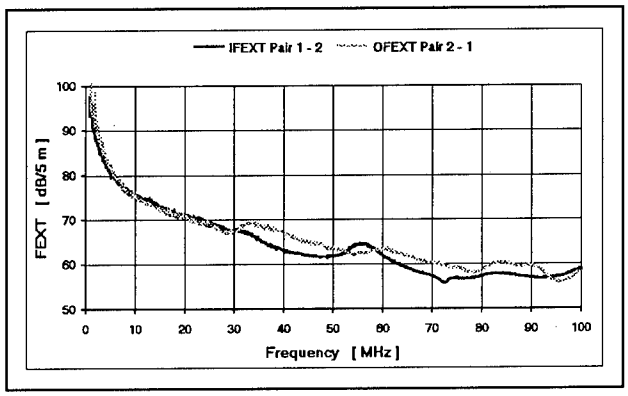


Figure 23 : IFEXT/OFEXT for 5 m of wire #2 between the pairs 1-2 and 2-1 with common mode termination on all pairs

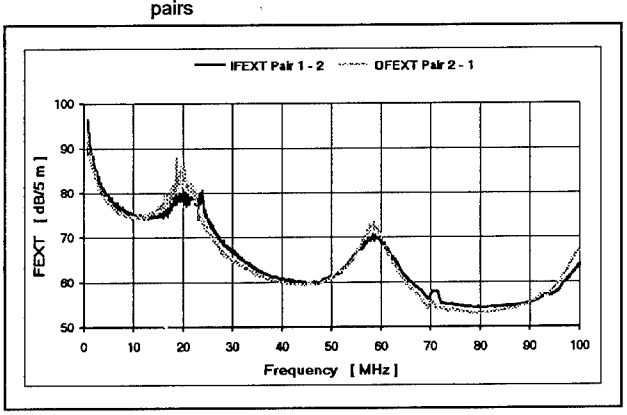


Figure 24 : IFEXT/OFEXT for 5 m of wire #2 between the pairs 1-2 and 2-1 with common mode termination and idle pairs open

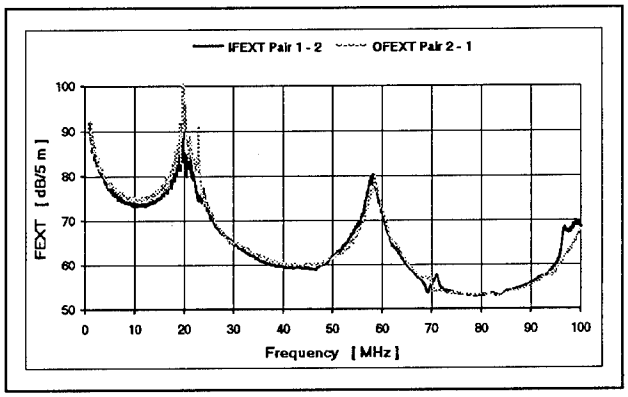


Figure 25 : IFEXT/OFEXT for 5 m of wire #2 between the pairs 1-2 and 2-1 with common mode termination and idle pairs open

In Fig. 26 we have the NEXT for a length of 1.5 m of the

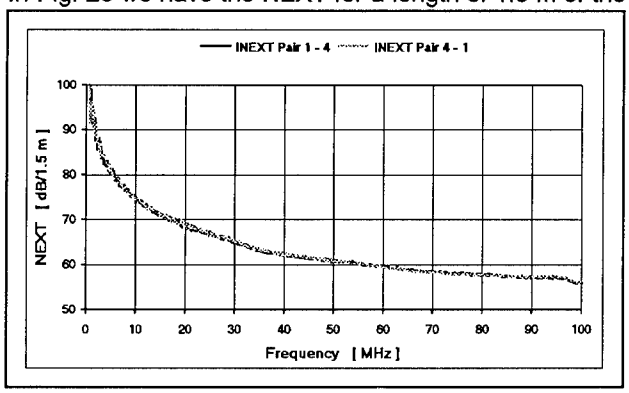


Figure 26 : INEXT for 1.5 m of wire #2 between the pairs 1-4 and 4-1 with common mode termination on all pairs

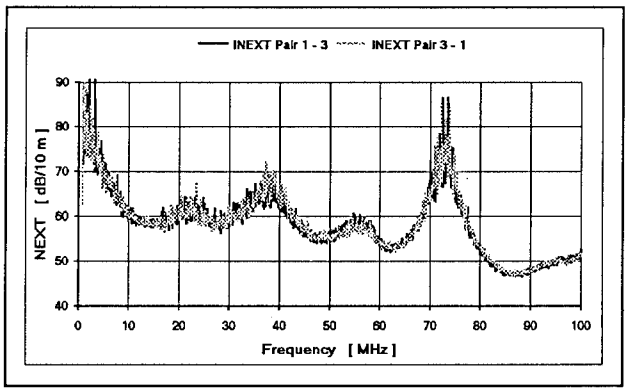


Figure 27 : INEXT for 10 m of wire #2 between the pairs 1-3 and 3-1 with common mode termination on all pairs, measured with North Hills BF-0322 baluns

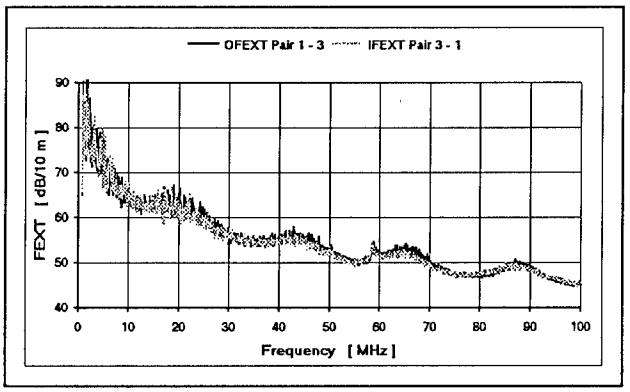


Figure 28 : OFEXT/IFEXT for 10 m of wire #2 between the pairs 1-3 and 3-1 with common mode termination on all pairs, measured with North Hills BF-0322 baluns

wire #2. It shows a near perfect symmetry for the NEXT matrices down to a very low length. Generally, we find for common mode termination that the NEXT measurements for all pair combinations hold the equality according to equations (2) and (3).

Finally Fig. 27 and 28 show the results obtained using baluns with high longitudinal balance and common mode rejection. These results are consistent with our expectations, though the scatter of the data, which shows a decrease of the difference of upper and lower envelope over frequency from approximately 3 dB to less than 1 dB, suggests a lack of signal balance of the baluns.

Discussion of Results

Our results indicate that the difference in propagation constant within one wire has only a minor impact on the observed asymmetries of the crosstalk matrices. This is also supported by the results from the short length of wire, where the effect of different propagation constants would be substantially less.

Indirect crosstalk coupling over tertiary circuits has a minor impact on these crosstalk matrix asymmetries. This is corroborated by the fact that the lower crosstalk envelope is affected by the termination mode of the idle pairs. It should be mentioned that the differences which were observed are the result of combined common and differential mode propagation in the idle pairs, both for shorted or open idle pairs (see Fig. 20 to Fig. 22). This is simply due to the fact that both termination modes do not provide for any suppression of common mode propagation. Therefore, we have additional indirect crosstalk coupling from the disturbing pair over differential to common crosstalk coupling into the idle pairs and over common to differential crosstalk coupling from the idle pairs into the disturbed pairs. The result is that the absolute value of the crosstalk for open or shorted idle pairs is lower than the one obtained if the idle pairs are common mode terminated. This demonstrates that the observed deviations of the FEXT matrices are caused by indirect crosstalk coupling if the pairs are not common mode terminated. If the all pairs are common mode terminated however, then the asymmetry of the FEXT matrices has to be attributed to the performance of the baluns.

Tests with baluns, having a high longitudinal balance and a good common mode rejection ratio, indicate that the results obtained on full crosstalk matrix measurements yield, for all practical purposes, symmetric matrices for the lengths of wires or cables considered here. However, it should be mentioned that these measurements are based upon full common mode suppression at both ends of all pairs and could be improved using baluns with matched high signal balance.

Summary and Conclusions

The selection of high performance baluns is of prime importance for full crosstalk characterization and testing of short lengths of wire or cable.

For commercial cable testing equipment, baluns with high longitudinal balance are not yet industry standard. It is highly desirable to standardize on the cable testing baluns. In this context it is noteworthy to mention that in TIA TSB 67 output signal balance and common mode rejection are defined and proposed as a standard for baluns for short link testing. This is especially important with respect to the correct assessment of FEXT, and should be taken into account in the standardization process of the FEXT performance requirements of data grade cables.

We have conclusively demonstrated that it is necessary to measure all crosstalk modes, i.e. differential to differential, differential to common, common to differential and finally common to common crosstalk coupling, if the objective is to obtain a true crosstalk characterization.

The construction of a matrix switch using high performance baluns will result in substantial gains in testing time over the modal decomposition method, primarily with respect to four pair or multiple pair testing with adequate frequency interval spacing. The results obtained will then be equivalent to those achieved with the modal decomposition method proposed by Yanagawa et al [19]; [20].

References

[1] P. Kish et al : Switched Fiber Twisted Pair Broadband to the Home.
44th IWCS 1995

[2] P. Kish : NEXT Model for Plug-ended Patch Cords.
Proposal to the members of the TIA/EIA TR 41.8.1 Committee.
June 12, 1995

[3] J.-H. Walling et al: Performance Evaluation of Multiple Pair Category 5 Backbone Cable for High Speed Data Services.
43rd IWCS 1994, p. 328-430

[4] S. Hinoshita et al: Analysis and Improvement of Crosstalk (NEXT & FEXT) for Multi-unit, Backbone UTP cable applied to FDDI/ATM Data Speed.
43rd IWCS 1994, p. 341-350

[5] M. Yotsuya et al : An Approach to Crosstalk Coupling Reduction of Pair Type Cable.
23rd IWCS 1974, p. 182-193

[6] E.W. Riley et al : Understanding Transmission. Crosstalk between Cable Pairs.
abc TeleTraining, Inc Vol 7(1988), Chapter 7 p. 20-27

[7] W. Klein : Die Theorie des Nebensprechens auf Leitungen.
Springer Verlag, Berlin / Göttingen / Heidelberg 1955

[8] N. Holte : A Statistical Model for Calculation of Crosstalk in a Balanced Pair Cable.
25th IWCS 1977, p.25-31

[9] A.Y. Alksne : Magnetic Fields Near Twisted Wires.
IEEE - Transactions Space Electr. & Telemetry, Volume SET-

10(1964),12 p.154-158
[10] S. Shenfeld : Magnetic Fields of Twisted Wire Pairs.
IEEE - Transactions Electromagnetic Compatibility Volume EMC -11(1969), 4 p. 164-169
[11] L.P. Dikmarova et al : The Electromagnetic Field of Two-Wire Line with Pair and Quad Twist.
Scripta Publishing Co.
Telecomm. & Radio Engineering (1984), p. 64-69
[12] Y.V. Balovlenkov et al : Calculation of the Components of the Electromagnetic Field of a Helical Line with Arbitrary Periodic Structure.
Scripta Publishing Co.
Telecomm. & Radio Engineering (1983), p. 28-31
[13] H.H. Adelaar : The Steady-State Magnetic Field of a Twisted Pair.
IEEE - International Convention Record, Part 5, 1964. Session on Wire and Data Communication, March 23-26, 1964, New York, p. 130-145
[14] J.R. Moser et al : Predicting the magnetic Fields from a Twisted-Pair Cable.
IEEE - Trans. Electromagnetic Compatibility Vol.EMC-10(1968), 3 p. 324-329
[15] V. Belevitch et al : Cross-Talk in Twisted Multiwire Cables.
Philips J. Res. 35(1980),1 p. 14-58
[16] D.P. Dalzell : A New Contribution to the Rational Design of Telephone Cables.
Electrical Communication VIII(1930),3 p. 173-178
[17] H. Schiller : Über Nebensprechstörungen in Fernsprechkabeln.
Elektrische Nachrichten-Technik 8(1931),3 p. 114-121 and 9(1932),3 p. 81-91
[18] R.J. Oakley et al : A Study into Paired Cable Crosstalk.
22nd IWCS (1973) p.136-149
[19] K. Yanagawa et al : A measurement of Balanced Transmission Lines Using S-parameters.
[20] R. Conte : A Tutorial on Modal Scattering in Multiconductor Transmission Lines
AT&T Bell Laboratories, July 1995

Appendix

Abbreviations

We use the following abbreviations :

C	-	Twist Frequency or Convolution
i; j	-	Indices of the pair combination for the crosstalk measurement
t_i	-	Twistlay of pair i
t_j	-	Twistlay of pair j

Equipment used

1	Compaq Deskpro 486 S/16M
1	Impedance Switch Test Unit HP-3235 (a dual 32x32 matrix switch)
1	Network Analyser HP-8753 D
1	DCM Testset with Fanning Fixture (used for low frequency measurements only)
1	HP Cable Testset HP Z-2010 equipped with North Hills baluns type NH, having no centre tap on the balanced side
2	The Siemon Company RD-TRAN-100 Four-Pair, 100-ohm Transmission Test Fixture
8	North Hills baluns NH13734
1	Matrix switch of own design
2	North Hills baluns 0322BF

Software used

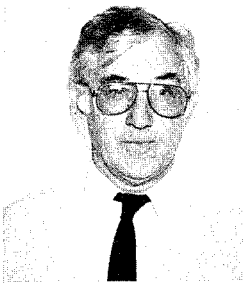
Designer 3.0
Jandel Scientific PeakFit 3.0M
Jandel Scientific TableCurve 2D
Microsoft Access 2.0
Microsoft Excel 4.0 and 5.0
Microsoft Visual Basic 3.0
VPS Cabmeas
Wolfram Research MathLink
Mathematica 2.22
WordPerfect 5.0 and 6.0



Jörg-Hein (Jo) Walling received his diploma in Mechanical Engineering in 1966 at the Technical University of Berlin. In 1974 he obtained a Doctor's degree (Dr.-Ing.) at the same University. In 1974 he joined Northern Telecom in the Research and Development department. Since 1976 he has been a senior engineer at the NORTEL Lachine Cable Plant, responsible for the design of Outside Plant and Data Grade Wires and Cables.



Martin Bélanger received his B.E. in Electrical Engineering from Université de Sherbrooke. He joined Northern Telecom Canada Limited Technology Cable Group in 1992 where he was initially responsible for cable design and electrical test methods. He is at present responsible for the manufacturing aspects of data grade cables, for quality assurance, for the development of new test and manufacturing facilities.



Victor LeNir received a B.Sc in Physics from Manchester University, England in 1960 and a M.Sc. in Computer Science from London University in 1968. He was employed at the Northern Telecom Cable Division in Lachine, Quebec in the Research & Development Group from 1963 to 1991. Since then he is with V.P.S. Enterprises working on the development of specific software packages, especially with regard to data grade wires and cables.

Recent Trends in and New Applications for Carbon-Coated Optical Fibers

Nobuyuki YOSHIZAWA and Tadatoshi TANIFUJI

NTT Access Network Systems Laboratories
Tokai-Mura, Naka-Gun, Ibaraki-ken, 319-11, Japan

ABSTRACT

The total length of carbon-coated fibers (CCF) used in NTT submarine cables will reach about 34000 km by the end of 1995. The contribution of CCF has been invaluable in the construction of a highly reliable submarine optical network. This applies not only to submarine cable as CCF has the potential to be applied to many other technical fields. This paper describes the practical application of CCF to submarine cables and examines recent investigation results by NTT. CCFs were tested in hot artificial sea water over a 6 month period and these tests proved their ultra-high reliability.

This paper also introduces recent studies and new applications in many technical fields by referring to the technical reports of various researchers. A local carbon coating method using a CO2 laser, and a continuous method to coat the CCF with metal are also introduced. Recent investigations into the relationship between carbon structure and fiber strength are also reported. As examples of new applications, indoor and towing cables are described. Application to optical couplers and optical amplifiers and application of metal-coated CCFs to laser diodes are also introduced.

(1) PRACTICAL APPLICATION

In 1993, NTT developed a 100-fiber submarine cable. Figure 1 shows a cross section of the non-armored cable, which can be laid up to a depth of 3000 meters. This is the first transmission cable in service to use carbon-coated optical fiber (CCF). It uses CCFs in a 4-fiber ribbon arrangement.

NTT has a long history with both submarine optical fiber cables and CCFs. NTT has been investigating submarine optical fiber cables since 1979 and it developed a deep-sea submarine cable, which can be laid up to a depth of 8000 meters, in 1985. In this cable, we adopted a conventional fiber with a 2% proof level. During this period, hermetic optical fiber was proposed at OFC[1] [2] and NTT began basic research. As a result of these studies, NTT developed a high-reliable high-strength CCF[3] in 1991. In comparison to conventional fibers, CCF has no apparent faults from the technical point of view and its fiber proof level is able to reduced to less than 1%. Because of this, NTT adopted CCF for its 100-fiber submarine cable. One hundred-fiber cables were used in the short-span routes of non-repeatered systems. The cables were directly connected to high-fiber-count land-cables.

Figure 2 shows the trends in total number of submarine optical fiber cable routes. The black bars represent 100-fiber cables. During the early stages of development, low-fiber-count submarine cables were introduced into trunk networks. The fiber count gradually increased with time firstly from 6 to 12 and then to 48. After 1994, 100-fiber cables were introduced into nearly all new routes so that they could be connected to the high-fiber count land optical cable networks which had been extended all over Japan. Figure 3 shows the

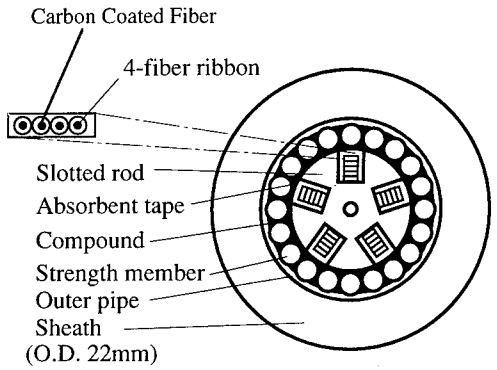


Fig.1 Cross section of 100-fiber submarine cable using carbon-coated optical fiber.

total fiber length of submarine cables laid by NTT. The hatched bars represent conventional fibers, while the black bars are CCFs. After 1994, CCF became dominant and the length of cable laid has been increasing annually. The total length for CCF will be 34000 km by the end of 1995, which represents about 40% of the total fiber length.

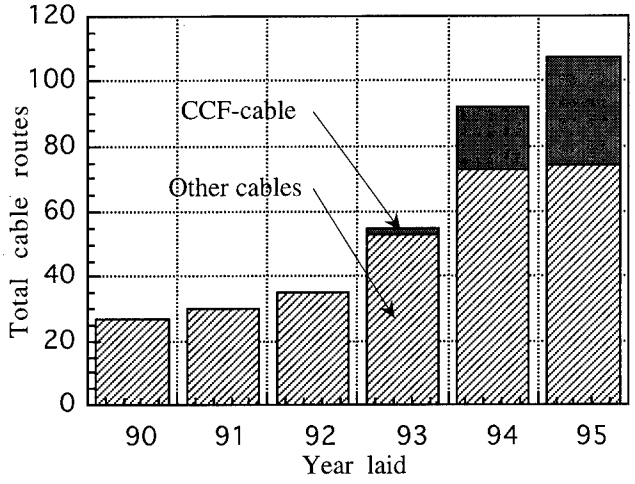


Fig.2 Total number of NTT's submarine optical fiber cable routes.

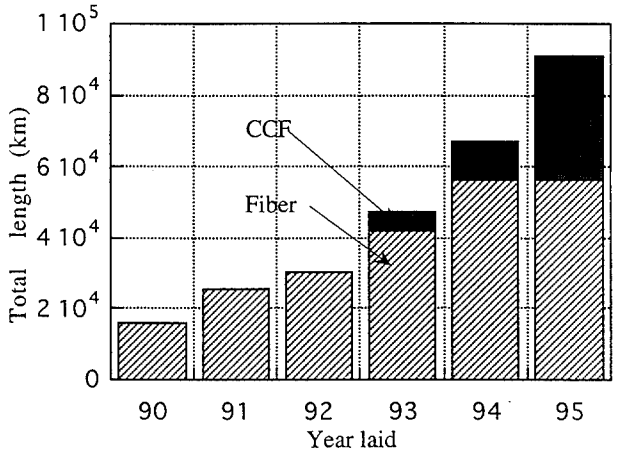


Fig.3 Total fiber length of submarine cables.

(2) RECENT INVESTIGATIONS

CCF has thus been responsible for achieving a highly reliable submarine optical network. The dynamic fatigue parameter n of CCF is more than 100, and optical losses were as small as those for conventional fibers. Many kinds of accelerated fatigue tests have established the ultra-high reliability of CCF. In 100-fiber submarine cables, CCFs are free of moisture, because the water solvent tape around the slotted rod draws humidity from the cable. Please see Fig.1 again. It also seals against water penetration in case the cable is damaged on the sea bed. Recent test results have shown a new possibility of using CCFs in other wet conditions.

Figures 4 to 7 show the test results after immersing CCFs in artificial sea water at a temperature of 80°C for 6 months. The fiber coating resins were also maintained under the same conditions. Figure 4 shows the dependence of optical loss on wavelength after hot water immersion. The fiber length was 6000 m. The characteristics completely coincides with those at the start of the trial. After this, the fiber was suspended in a chamber which was filled with Hydrogen to 1 atm. These conditions were maintained at 80°C for 20 hours. No increase in loss at 1.24μm were observed. The test results indicate that the hermetic properties of the carbon-layer were retained even under these stringent conditions. Figure 5 shows dynamic fatigue test

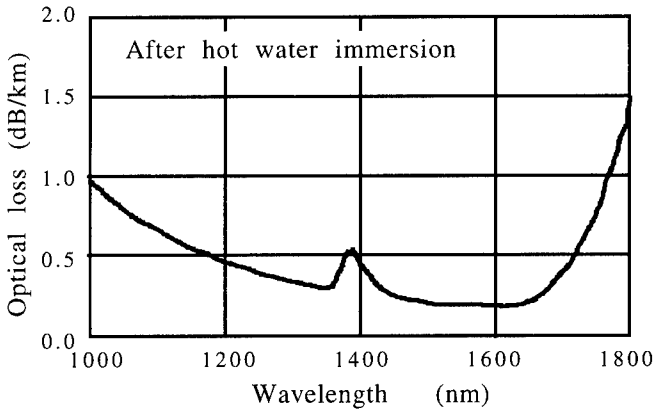


Fig.4 Wavelength vs. optical loss for CCF after 6 months of hot water immersion.

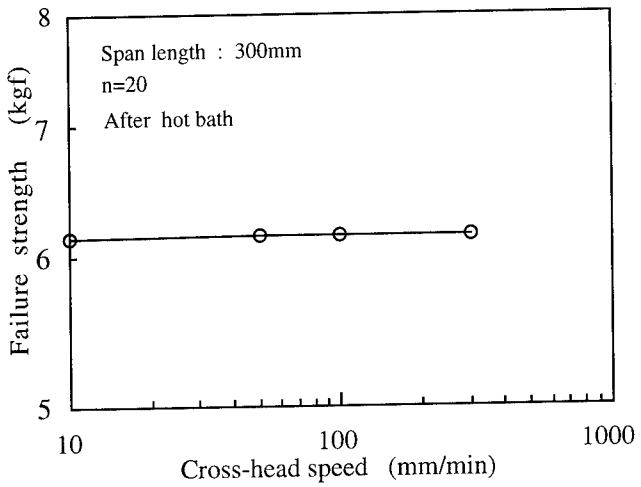


Fig.5 Dynamic fatigue test results for CCF after 6 months of hot water immersion.

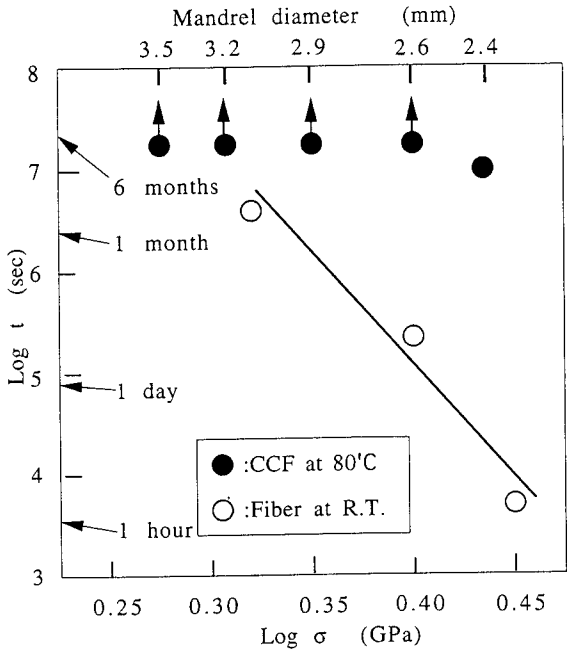


Fig.6 Static fatigue test results. One meter long fibers were coiled around a mandrel and suspended in baths.

results after hot water immersion. The tensile breakage load of 30 cm long specimens was measured at 4 stages of cross-head speed. The breakage load of the CCFs was about 6.2 kgf and dynamic fatigue factor n was more than 200. Degradation in mechanical strength due to the hot water treatment was not observed.

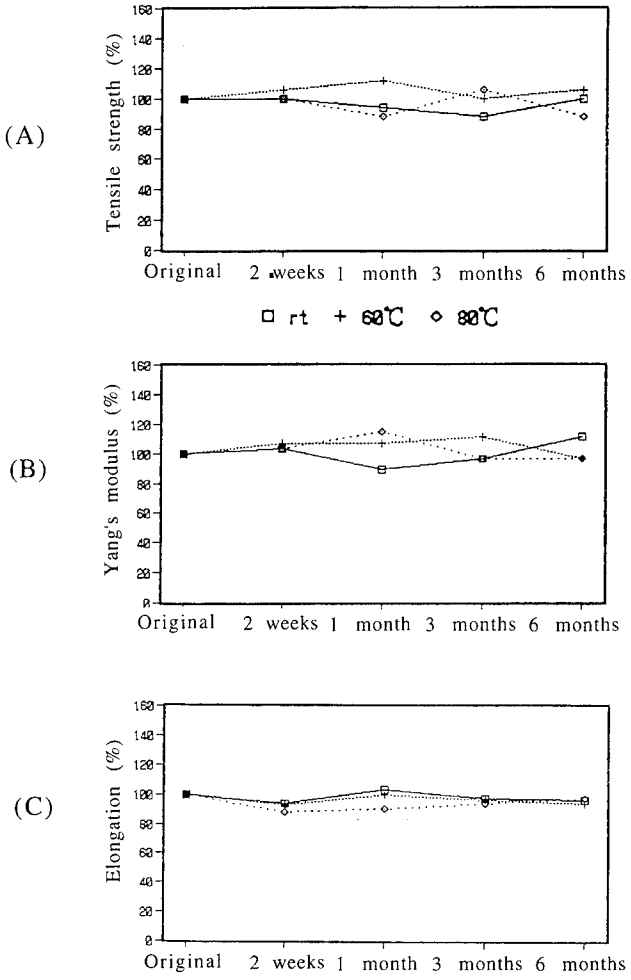


Fig.7 Hot water immersion results for buffer material of optical fiber.

Figure 6 shows static fatigue test results during hot water immersion. One meter long specimens were completely coiled around a thin mandrel and immersed in a hot bath. The time required for fibers to break was measured. Mandrel diameters were 2.4mm, 2.6mm, 2.9mm, 3.2mm and 3.5mm. The calculated bending strain of the fiber surface was from 6.7 % to 9.5%. The black dots indicate CCFs which were immersed in hot water at 80°C , while the circles indicate conventional fibers which had been immersed in water at room temperature. The number of specimens is 20 for both conditions. The arrows in the figure indicate that no CCF specimens failed for 6 month when the mandrel diameter was more than 2.6mm. By comparison, conventional 2.6mm diameter

fiber broke within a few days at room temperature. Figure 7 (A)(B)(C) shows the characteristics of ultra-violet curable resins which experienced the same hot bath treatment over 6 months. The resins are used as the buffer layer coating CCFs. Figure 7(A) shows tensile strength. Figure 7(B) shows Young's modules. Figure 7(C) shows tensile elongation. The perpendicular scale in each figure is normalized by values prior to the hot water immersion. Test results were almost constant over the 6 months. These test results indicate that CCFs can be used even under wet conditions for indefinite periods of time. Optical cable structures can also be simplified for limited purposes.

The practical application of CCFs in submarine cables has accelerated improvements of related technologies. We will report on recent findings by respected researchers in associated fields. A non contact testing method for the carbon layer has been established[4], and a local carbon coating method using a CO2 laser has also been developed[5]. Figure 8 shows a schematic view of the local carbon coating equipment. During this process, a high-strength spliced fiber is placed in a reaction chamber. The chamber is then charged with hydrocarbon gas, and a CO2 laser beam is introduced into the chamber through a zinc selenide window. The laser beam converges on the surface of the bare fiber and heats up the region near the spliced bare fiber. Carbon film is deposited onto the region through thermal chemical vapor deposition. The reaction chamber then traverses at an appropriate speed to coat carbon film for a length of about 7 mm along the spliced portion. This method is useful for the local carbon-coating of optical devices.

A method to coat the CCF with metal has been established. The metal layers can be coated by an electroplating technique[6]. Figure 9 illustrates the process. Three to twenty μm thick metal is deposited onto a CCF, by using the graphite layer as the cathode. The anode is suspended in a bath surrounding the fiber. Optical loss after metal coating is reportedly 1 to 4 dB/km at 1.55μm wavelength[6]. The metal layer is advantageous not only in terms of ' improving fiber strength, but also in providing a surface for soldering.

The relationship between the structure of the carbon layer and such fiber characteristics as strength and hydrogen resistance have been investigated[7]. Although those relationships are very important from the practical and academic points of view, they have not been reported enough because of their proprietary value. It is claimed that the orientation of graphite structure affects these characteristics. It is claimed that if the micro graphite structure is random, the hermetic properties are low and failure is high. If the structure is stable, the hermetic properties are high and failure is low.

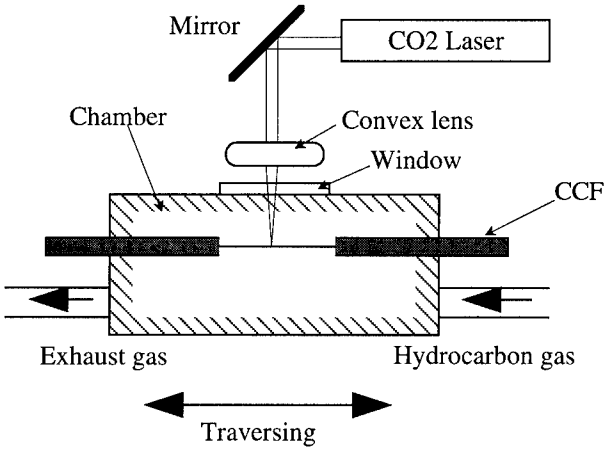


Fig. 8 Schematic view of local carbon coating equipment.

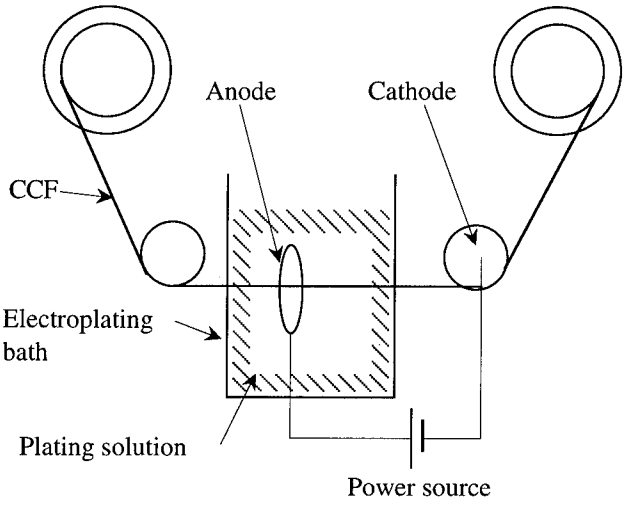


Fig.9 Schematic view of metal coating equipment for CCF.

(3) NEW APPLICATIONS

CCF is a promising material for use in the fields where high mechanical reliability is required. It is also attractive because it is able to be coated with metal and consequently soldered.

3-1: Application to indoor optical cables

Indoor optical cables and drop cables are essential in bringing "fiber to the home" ; it is important that these have a small bending radius. Figure 10 shows a typical view of a fiber cable laid around the molding of a window. A kind of corner guide was used to moderate fiber curvature. The curvature obtained was 30mm in radius. There were two reasons for this. One was to prevent curvature loss increase which depends on both fiber parameters and optical wavelengths. The other was to prevent any degradation of fiber reliability. The bending test results in Fig.6 indicate that CCF should be a promising candidate for applications where extreme bending strains are encountered.

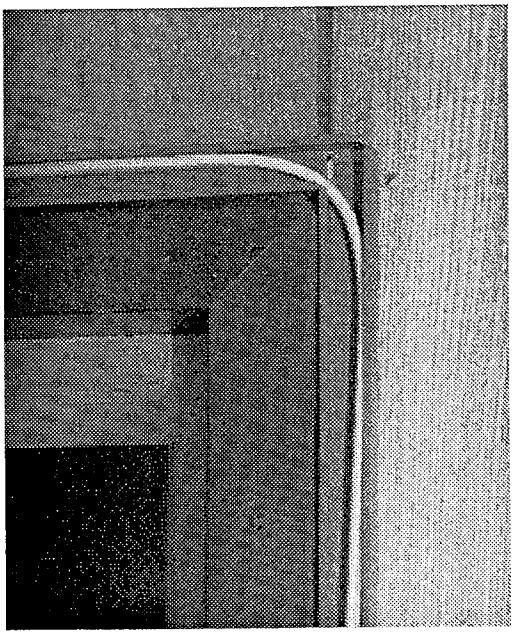


Fig.10 Typical view of fiber cable laid around the molding of a window.

3-2: Applications to tow cables

Optical fibers have been widely used in long length signal cables and control cables. Figure 11 shows a tow cable which suspends an ocean equipment. A variety of ocean equipment have been developed to investigate the deep sea bottom. When towing an ocean equipment, large amount of tension are applied to the cable. Figure 11 shows the calculated relationship between cable strain and sea depth when towing an ocean equipment with a weight of 1 to 10 tons in water. The fiber strain in the cable reaches 0.8% at a depth of 6000 m when equipment weight is 5 tons. Strain can not be reduced by increasing the amount of steel wire because the weight of the cable itself increases accordingly. CCF is suitable for these extreme application.

3-3: Applications to optical couplers

An important consideration is to decrease the size of optical components. Optical couplers are important passive devices in constructing optical networks. They are made by coiling fusion-spliced fibers on both sides of the coupler and encasing these coils in a housing. There are 7 couplers and 6 sleeves containing fusion-spliced points in the housing of a 1x8

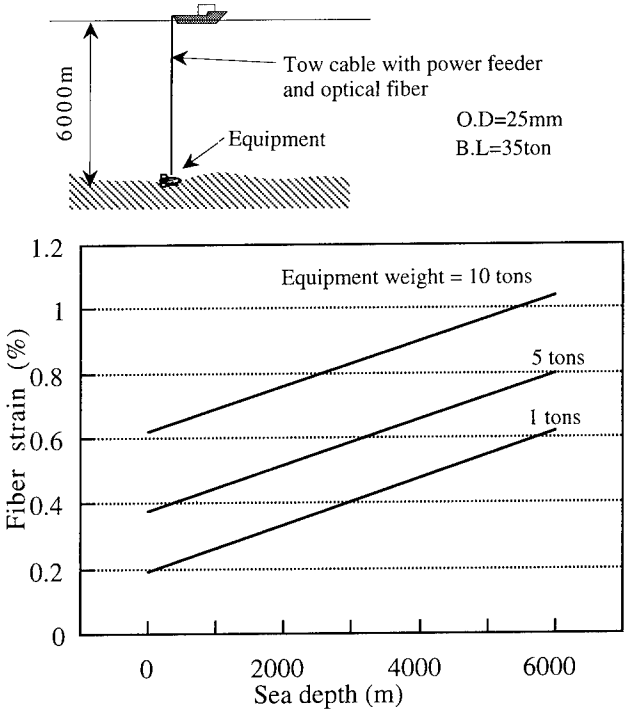


Fig.11 Calculated fiber strain for tow cable at various sea depths.

coupler[8]. The coiling diameter affects the size of the housing. For conventional couplers using normal 1 % proof tested fiber, the coil diameter is 60 mm. Such a diameter is necessary to maintain the long term mechanical reliability of the fiber. However, the coil diameter of a CCF is 30 mm, which was established to prevent bending loss at a wavelength of 1.3μm. Through the use of CCFs, a 1x8 couples that was 62mm wide, 90mm long and 8.5mm thick was able to be produced. Volume decreased by above 60% when compared with conventional ones.

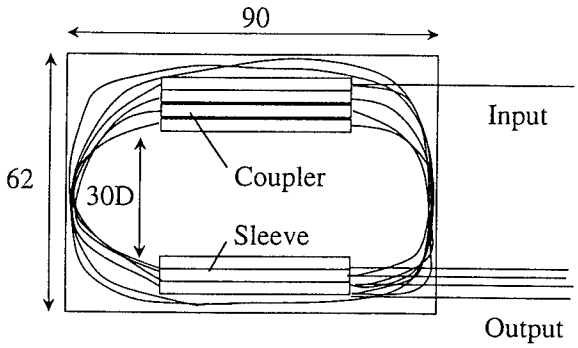


Fig. 12 Schematic view of 1x8 coupler.

3-4 Applications to optical amplifiers

Erbium-doped fiber amplifiers (EDFAs) have been used as boosters, repeaters, and pre-amplifiers in various system experiments, such as intensity-modulation-direct-detection (IM-DD), coherent transmission, CATV, and soliton transmission. Long EDFs must be coiled in the fabrication of compact EDFA modules. There are two important requirements for the optical fibers used in compact and efficient EDF coils. The first is small bending loss and the second is high mechanical reliability. CCFs have permitted the production of compact coils[9]. A 200 meter long carbon-coated EDF was coiled around a spool. The coil had a 15 mm inner diameter, a 32mm outer diameter, and a height of 20mm.

3-5: Application to laser package

CCF also shows promise from the viewpoint of hermetic sealing. The carbon layer can easily be coated with Ni or Au[9], and such a metallic coat is useful in allowing fiber to be fixed to the package by soldering. This method has also been used to fix fiber to laser diodes. A compact and reliable connecting method for fibers with diodes has also been investigated[10]. Figure 13 shows the schematic view of a laser diode housing. The metal coated CCF is able to be soldered and is useful in allowing fiber to be fixed to the waferboad. Also, it is useful in hermetic sealing on the window of the metal housing.

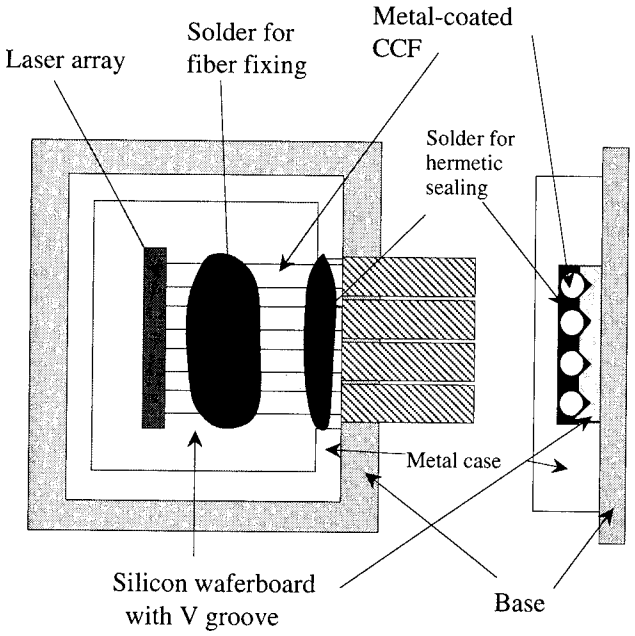


Fig. 13 Schematic view of laser diode housing. Metal coated CCFs are fixed by soldering .

CONCLUSION

A 6 month test of CCF in artificial sea water confirmed its ultra-high reliability. CCF is being increasingly applied in many fields and it is expanding the utility of optical fibers.

ACKNOWLEDGMENTS

The authors want to express their thanks to Dr. T. Yabuta and Dr. Y. Koyamada for coordinating this work to make presentation.

REFERENCES

[1] R. Hiskes, C. A. Schantz et al., "High performance hermetic optical fibers," Post Deadline Paper W16 , OFC, 1984

[2] K. J. Beales, D. M. Cooper, W. J. Duncan and J. D. Rush, " Practical barrier to Hydrogen diffusion into optical fibers", OFC, 1984

[3]N. Yoshizawa, H. Tada and Y. Katsuyama," Strength improvement and fusion splicing for carbon-coated optical fiber", IEEE, J. Lightwave Technol., Vol. 9, No.4, pp. 417-421, (1991).

[4]T. Shimomichi, K. Oohashi, S. Araki and T. Maruoka, " In-Line Methods of Assuring the Characteristics of Hermetically Carbon-Coated Optical Fibers", IWCS, pp. 651 to 656, (1994)

[5] K. Oohashi, T. Shimomichi, S. Araki and N. Sato, " High-Strength Spliced Optical Fiber Manufactured Using a Localized Carbon Coating Technique With A CO2 Laser," IWCS, pp.111-118 (1992)

[6] T. Nozawa, D. Tanaka, A. Wada, R. Yamauchi, "Novel Metal-Coated Solderable Optical Fiber", in Technical Digest, Optical Fiber Communication, Paper ThF3 (1992)

[7] M. Koguchi, K. Hirabayashi and K. Kokura, "Microstructure of Carbon Layers Deposited on Optical Fibers and Hydrogen Diffusion in the Layers," J. Ceramic Society of Japan. Int. Edition, Vol. 101, No.3, pp. 293-296 (1993)

[8] S. Yodo, A. Hasemi, T. Sato and M. Shimizu," Development of 1x8 Optical Star Coupler using Carbon-Coated Fiber", Technical Report of IEICE (in Japanese),

[9] A. Wada, D. Tanaka, T. sakai, T. Nozawa, K. Aikawa and R. Yamauchi," Highly Er-Doped Almino-Silicate Optical Fiber Synthesized by High Temperature Plasma and its application to compact EDF coils," Optical Amplifiers and their Applications, Technical Digest Services, Vol. 17, Paper 222/FD6-1, (1992)

[10] T. Kato, F. Yuuki, K. Tanaka, T. Habu, Y. Akiyama, T. Shimura, A. Takai, K. Mizuishi, T. Teraoka and Y. Motegi, " A New Assembly Architecture for Multichannel Single Mode-Fiber-Pigtail LD/PD Modules," IEEE Trans. Comp., Hybrids, Manuf. Technol., Vol. 16, No.1, pp. 89-94 (1993)



Nobuyuki YOSHIZAWA

NTT Access
Network Systems
Laboratories
Tokai, Ibaraki,
319-11, JAPAN

Nobuyuki Yoshizawa is an executive research engineer. He was born in 1954 and received the B.S., M.S., and Ph.D. degrees in mechanical engineering from Waseda University in 1977, 1979, and 1986, respectively. He joined NTT in 1979, and since then he has been engaged in research on submarine optical fiber cables. His major work was the design of shallow-sea submarine optical fiber cable, deep-sea submarine optical fiber cable, 48-fiber submarine cable and 100-fiber submarine cable. He also investigated a UV-coated optical fiber and a carbon-coated optical fiber. Dr. Yoshizawa is a senior member of the IEEE.



Tadatoshi TANIFUJI

NTT Access
Network Systems
Laboratories
Tokai, Ibaraki,
319-11,JAPAN

Tadatoshi Tanifuji is the leader of the optical cable and connecting research group. He was born in 1949. He received the B.S., M.S., and Ph.D. degrees in electronics engineering from Hokkaido University in 1972, 1974, and 1983, respectively. He joined NTT in 1974. Since 1991 he has been engaged in research on high-density and pre-connectorized optical fiber cable. Dr. Tanifuji is a member of the IEEE.

REVIEW OF CHARACTERISTICS AND APPLICATIONS OF COMMERCIALLY AVAILABLE CARBON-COATED HERMETIC FIBER

Karen Moore, Corning Incorporated
Anurag Dwivedi, Corning Incorporated
Ed Sikora, BT Laboratories

Abstract

This paper will review the characteristics of carbon-coated hermetic fiber, and report on their performance in hydrogen and stress environments. Existing manufacturing techniques that demonstrate the ability of fiber manufacturers to consistently deliver a reliable product will be discussed. Data will be presented to show fiber performance after 21 days exposure to 11 atm. hydrogen at 85 °C. The results of several years of dynamic fatigue testing will show that carbon-coated hermetic fiber may offer an advantage in high stress environments. In addition to the development work and data regarding optical and mechanical reliability of carbon-coated hermetic fiber, this paper will also discuss some of the development work done for product commercialization. A review will be provided on how customers' manufacturing and field handling concerns have been addressed. Specifically, these concerns include the effect the carbon layer has on fiber stripping, splicing, and strength. Lastly, this paper will present a perspective on the future deployment of carbon-coated hermetic fiber.

Introduction

The presence of hydrogen, or polar molecules such as water when in a stress environment, can degrade the optical and mechanical performance of silica optical fiber. Hydrogen ingress may increase attenuation in the standard optical transmission band, whereas the presence of water vapor may cause weakening of the silica fiber through subcritical crack growth in a high stress environment. Fiber deployed where these conditions exist may require additional protection for the glass surface. One solution is the use of carbon-coated hermetic fiber where the layer of amorphous carbon deposited on the surface of the glass provides a barrier between the silica fiber and hydrogen or water.

The trend towards high capacity systems have had the effect of reducing system margins allowed for aging. Thus, significant effort in the cable design process continues to be spent in minimizing the effect of hydrogen due to corrosion of the metal components of the cable and the degradation of the polymers within the cable. Carbon-coated hermetic fibers give the system/cable designer greater flexibility in reducing cable costs while maintaining the required reliability.

Carbon-coated hermetic fiber is being used in both military and commercial submarine cables. The U.S. Navy selected this type of fiber in 1992 for its submarine cables that link undersea acoustic sensors in their Fixed Distributed System (FDS.) Several thousand kilometers of carbon-coated hermetic fiber have been deployed in this application. Commercial submarine cable manufacturers have also deployed tens of thousands of kilometers in several applications worldwide since 1992 as an alternative to expensive cable designs which incorporate copper tubing as the hermetic barrier. Hermetic fiber cables are deployed in countries such as France, Greece, Korea, and New Zealand as well as in fiber-optic links between Iran and United Arab Emirates, and between Norway and Denmark. More than 35,000 km of carbon-coated hermetic fiber are in use today.

The information presented in this paper will show that carbon-coated hermetic fiber is a mature technology and has demonstrated its ability to perform in adverse environments. The deployment of hermetic fiber is not limited by supply or performance, but by the ability of cable designers to realize a cost/performance advantage when incorporating new cable designs using hermetic fiber. As new cost effective cable designs are developed that take advantage of the benefits of carbon-coated hermetic fiber, its usage is likely to increase.

Description of Carbon-Coated Hermetic Fiber

Hermetic fiber is manufactured by depositing a thin layer, typically 200 to 700 Angstroms (20 to 70 nm), of amorphous carbon which bonds directly to the glass surface prior to the application of an acrylate polymer coating (Figure 1). Based on electron diffraction studies, this carbon layer consists of a microstructure of disordered graphitic platelets or ribbons. Such a structure creates a barrier against the diffusion of hydrogen or water molecules[1-2]. An evolution model of the carbon layer is shown schematically in figures 2a to 2f. Due to the random orientation of the platelets/ribbons, the carbon layer must be of a minimum thickness to prevent the occurrence of microvoids which, if large enough, would provide paths for diffusion of hydrogen or water molecules. Correlations have been established for Corning hermetic fiber between the carbon layer thickness and performance measures such as hydrogen induced attenuation and effective dynamic fatigue.[3] These correlations indicate that for very thin coatings, the microvoids are too big to prevent the migration of hydrogen. These migration paths can be obstructed by increasing the carbon layer thickness. For a given microstructure, or carbon deposition process, there is a minimum threshold carbon layer thickness to prevent hydrogen molecules, as well as the larger water molecules, from permeating through the carbon layer and reaching the glass surface. This minimum layer thickness depends on factors of the deposition process such as time, temperature, and concentration of carbon.

Ensuring Hermetic Fiber Product Performance

Manufacturing processes exist for hermetic fiber that ensure the entire fiber length has a uniform carbon layer thickness greater than the minimum required to block hydrogen and water from reaching the glass surface. On-line manufacturing techniques control the carbon layer deposition and verify layer thickness and uniformity. As previously reported at IWCS[3], a number of techniques have been used to demonstrate and verify the ability of Corning's

manufacturing process to deposit and maintain exceptional layer thickness control. On-line techniques include optical detection of thickness and radial thickness differences of the carbon layer, and a non-contact electrical detection technique to determine the total carbon layer thickness. Other off-line tests were used during process development which include an electrical contact device for measuring total carbon deposited and Scanning Tunneling Microscopy (STM) for measuring surface roughness. Figure 3 shows the correlation map of hydrogen induced attenuation and fatigue resistance vs. the on-line measured resistivity of the carbon coating.[3] These tests show that significant attention is given to ensure the consistent performance of hermetic fiber.

Verification Data for Hermetic Fiber Performance

The maturity of carbon-coating technology has lead to the steady use of carbon-coated hermetic fiber in harsh environment applications. Available test data verifies that manufacturing control systems have been put in place that ensure the effectiveness of the carbon layer to inhibit hydrogen and water ingress. A selection of hydrogen and dynamic fatigue test data is discussed below.

Hydrogen Resistance

One manufacturer of carbon-coated hermetic fiber reported that 500 samples taken from more than two years of manufacturing, have not shown any increase in attenuation, within experimental error, at 1240 nm (the first harmonic wavelength of the fundamental hydrogen vibration) after 21 days exposure to 11 atm. hydrogen at 85^{o}C.[3] This result corresponds to an immeasurable attenuation change in dB/km at 1550 nm for 25 years of normal submarine use. Hermetic fiber with this performance characteristic can be deployed in environments where hydrogen is likely to exist in cables without resorting to the use of a copper tube or other means of providing a hermetic barrier.

Dynamic Fatigue

The mechanical reliability of optical fiber depends on the inherent strength of the fiber, the fiber's processing and handling history, including cabling, and subsequent deployment. The strength of the fiber is not uniform along the entire length. Microscopic surface flaws introduced during the manufacturing process are distributed along the length of the fiber. Given an appropriate cable design that minimizes the stress on the fiber, the fiber performance remains unaffected by these microscopic flaws. However, these flaws grow slowly under stress (subcritical crack growth) until a time at which the flaw growth is sufficient to cause failure and the fiber breaks. It has been reported that it is the reaction between water and the strained silica bonds that leads to subcritical crack growth.[4-5] In the absence of water molecules, subcritical crack growth cannot occur.

Subcritical crack growth is commonly referred to as fatigue. A fiber with an effective hermetic layer would therefore be expected to perform well in tests modeling fatigue behavior. Figure 4 shows a typical dynamic fatigue plot of a hermetic fiber using FOTP-76. For silica fibers, the typical dynamic fatigue susceptibility constant is 20 which is several orders of magnitude lower than that for hermetic fiber with dynamic fatigue susceptibility constants greater than 200. Figure 5 is a compilation of dynamic fatigue values for Corning hermetic fiber with each data point representing a valid dynamic fatigue test.

Field Handling of Carbon-Coated Hermetic Fiber

Carbon-coated hermetic fiber is optimized for use in certain severe applications and as a result, even though the optical properties of the fiber remain the same as compared to its non-hermetic counterparts, some of the mechanical properties of the hermetic fiber differ from those of silica fiber. Some of these differences are discussed below.

Fiber Stripping and Splicing

Stripping and splicing tools and procedures need to be optimized for handling hermetic fiber. It is important not to nick the carbon layer when stripping hermetic fiber as this may cause crack propagation and lead to fiber breakage. This can be minimized by using heated strippers, or using mechanical strippers with a larger hole size. Carbon-coated hermetic fiber can be easily spliced using a profile or clad alignment splicer. Special settings may be required when using a LID (Light Injection/Detection) fusion splicer in order to detect sufficient light through the black carbon layer of hermetic fiber . To maintain optimum splice performance, it is also important to clean the electrodes of the fusion splicer frequently, since carbon is deposited on the electrodes during the splice operation.

Many users of hermetic fiber require continuous lengths from 42 to 82 kilometers long. To deliver these lengths, shorter lengths of fiber may need to be spliced together. During the splicing process, carbon is burned off from a small region of fiber in the vicinity of the splice. Techniques have been developed to reconstitute the hermetic layer over the splice region.[6-7] Hermetically reconstituted splices are proof tested to the same level as the constituent fiber lengths and are tested to verify the integrity of the carbon layer of the reconstituted area.

Fiber Strength

The intrinsic strength, or high strength region of carbon-coated hermetic fiber, is believed to be controlled by the fracture of the carbon layer,[8] whereas the intrinsic strength of standard fibers is governed by the fracture of silica. The carbon layer has the effect of reducing the intrinsic strength region of hermetic fiber from 650 kpsi, which is typical for silica fibers, to 450 kpsi. However the strength region of interest for long term reliability of long length applications is not the intrinsic strength region, but the low strength region where flaws may exist near the proof stress level. Glaesemann has recently suggested that the strength distribution of hermetic and silica fiber are nearly the same for the lower strength region.[9] Figure 6 compares the predicted inert strength distribution of silica fiber to the measured strength distribution of hermetic fiber

Given a particular microstructure for the carbon layer, thicker layers generally result in lower intrinsic strength,[10] but provide greater protection against hydrogen and water diffusion. The thickness of the carbon layer of hermetic fiber can be varied to optimize the fiber for strength or hermeticity. Some fibers, optimized for hermeticity, have a typical carbon-coating thickness of 500 Angstroms (50 nm.) These fibers have a slightly lower intrinsic strength when compared to fibers with thinner carbon layers or non-carbon coated fibers. This thickness should provide adequate protection from hydrogen and water diffusion, whereas a thinner carbon layer , though higher in intrinsic strength, could potentially allow hydrogen or water diffusion over time. Data previously presented has shown that the attenuation due to hydrogen begins to increase as the carbon layer thickness is reduced below 250 Angstroms (25 nm.)[3] Slightly lower intrinsic strength of the hermetic fiber is not a limiting factor, since fiber handling and installed stresses are usually significantly lower than the intrinsic strength.

In addition to the virtual elimination of flaws in the low strength region in a typical carbon-coated hermetic fiber, the high dynamic fatigue constant allows cable designers to increase the allowable stress placed on the fiber. As previously presented by Glaesemann et al.[5], the allowable long term stress for long lengths of fiber in a given application depends on the fatigue constant of the fiber. Based on Glaesemann's conclusions, silica fibers with a typical fatigue constant of 20 should see no more than 20% to 30% of the

proof stress level, but carbon-coated hermetic fiber can see as high as 80% of the proof stress level. This performance advantage for hermetic fiber gives greater deployment flexibility or an enhanced safety margin for users of hermetic fiber.

Future Deployment

Since substantial data exists to suggest that hermetic fiber is a robust product that may offer several performance advantages over non-hermetic fiber in harsh environments, one might ask why this product has not been deployed in every harsh environment application. The answer lies in understanding the selection criteria used by cable manufacturers and the implications of major cable design changes.

Undersea cable manufacturers operate in an environment of continuous improvement. Cable designs and production processes are re-examined frequently to improve the product and reduce material and production costs. The need to re-examine cable designs, materials and production processes may occur because of a change in the cost of incoming material, or the need to improve the cabled characteristics of the fiber regarding resistance to stress or hydrogen. For example, Polarization Mode Dispersion (PMD) has caused manufacturers to review and modify their designs to minimize the effect of PMD. Another example is hydrogen. Significant work continues to be carried out to minimize hydrogen evolution and its associated loss in fibers as can be seen by the number of papers presented at IWCS over the years. This is driven by the trend to reduce the loss margins attributed to aging and hydrogen in, for example, unrepeated submarine systems.

For undersea communication system cables, a major element of their design and production is meeting the technical specifications and the cost and the reduction of cost of the cable. Fiber costs are a significant part of the total cable cost. For a typical long haul, high bit rate system the fiber cost for an eight fiber package is ~ 40% of the material costs of a lightweight cable. In the finished cable the fiber cost will be ~ 26% of the total cost. For a single armored cable the fiber cost will be ~ 13% of the total cost of the cable. Although these figures are approximate, they show that the fiber costs are not considered insignificant.

A further cost occurs when cable manufacturers make a large change to their designs. Substantial testing and verification must be done to ensure that the fiber can be processed successfully and, more importantly, requalification of the design to prove that it can meet the end user specifications. If, for example, a new cable design incorporating hermetic fiber were to be used instead of standard fiber, some of the important factors of the manufacture and performance of the new cable that would need to be examined would be:

- Hermetic integrity along the fiber and over time
- Splicing, the need for reconstitution and proof testing
- Fiber handling and initial strength
- The fiber proof stress requirements for different systems
- Color coding or identification techniques

This process adds considerably to the development costs. Changes to current cable designs and/or the production processes by major undersea cable manufacturers are therefore not considered lightly. While hermetic fiber gives a number of advantages, including the potential for new lower cost cable designs, its higher cost is an issue. However, given large enough volumes, the cost of hermetic fiber may be reduced to more closely approach non-hermetic submarine fiber.

Although one can assume that hermetic fibers are primarily of interest to undersea cable manufacturers, hermetic fiber will also allow manufacturers of terrestrial cables to enter the undersea market for nonrepeated links in, for example, coastal festoon systems, or buried cable applications in low lying coastal areas.. Also, as more fiber is being used in the junction and access networks, the fatigue properties of hermetic fiber will become more useful where cables/fibers are deployed in higher strain environments such as drop cables or in fiber enclosures where the fiber curvature is high, and steam ducts where the presence of water vapor makes fatigue a concern. But again, their use will largely depend on cost and system requirements.

The quality control of hermetic fiber production has been successfully addressed, as described above, giving cable manufacturers additional flexibility in designing cables for new markets and uses or potentially reducing the cost of present cable designs for existing markets.

The main conclusions of this paper are:

- The deposition and testing of carbon coatings on optical fiber is a mature technology.
- More than 35,000 km of hermetic fiber have been deployed in undersea systems.
- Current hermetic fiber manufacturing has been optimized to minimize the hydrogen and water vapor diffusion through the coating.
- Consistency of the product has been demonstrated through a combination of on-line monitoring and off-line measurements of hydrogen diffusion and dynamic fatigue resistance.
- Special procedures have been developed to strip and splice hermetic fiber.
- Hermetic fiber can give cable designers a competitive edge but the cost needed to design new cables or modify existing designs must be considered.

References

1. T. Akiyama, Y. Kawada, H. Hiramatsu, and K. Hirabayashi, "Long-term Reliability of a Carbon Coated Optical Fiber Cable", pp 155-160 in proceedings of the 40th International Wire and Cable Symposium, St. Louis, Mo., 1991.
2. E. S. R. Sikora, J. V. Wright, S. J. Pycock, and M. J. Yates, "Examination of the Strength and Characteristics, Hydrogen Permeation and Electrical Resistivity of the Carbon Coating of a Number of 'Hermetic' Optical Fibers," pp 20-26 in the proceedings of the Ninth Annual European Fiber Optic Communication and Local Area Network Conference, 1991.
3. M. R. Tuzzolo, A. E. Allegretto, and E. H. Urruti, "Hermetic Product Performance: Ensuring the Uniformity of the Carbon Layer," pp 381-384 in the proceedings of the 42nd International Wire and Cable Symposium, St. Louis, Mo., 1993.
4. T. A. Michalske and S. W. Freiman, "A Molecular Interpretation of Stress Corrosion In Silica," Nature 295(2), 511-512 (1982).
5. G. S. Glaesemann and S. T. Gulati, "Design Methodology for the Mechanical Reliability of Optical Fiber," Optical Engineering 30(6), 709-715 (1991).
6. C. A. Schantz, U. S. Patent #4,727,237, 1988.
7. M. G. Estep and G. S. Glaesemann, "The Effect of Carbon Overcoating on the Mechanical Behavior of Large Flaws," in Optical Materials Reliability and Testing: Benign and Adverse Environments 1992, Roger A. Greenwell, Philip K. Paul, Editors, Proc. SPIE 1791, 18-24 (1993).
8. M. M. Bubnov, E. M. Dianov, A. M. Prokhorov, S. L. Semjonov, A. G. Shchebunyaev, and C. R. Kurkjian, "High-strength Carbon-coated Optical Fiber," Sov. Lightwave Commun. 2, 245-250 (1992).
9. G. S. Glaesemann, "High Speed Testing of Optical Fibers," in proceedings of SPIE's Photonics East '95 Symposium, Philadelphia, PA, 1995.

10. N. Yoshizawa, and Y. Katsuyama, "High Strength Carbon Coated Optical Fiber," Electronic Letters, 12 Oct., 1989, Vol. 25, No. 21, pp 1429-31.

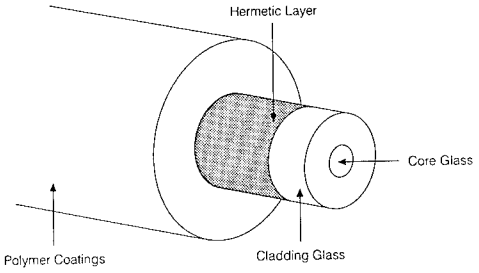


Figure 1: Schematic of Carbon-Coated Hermetic Fiber

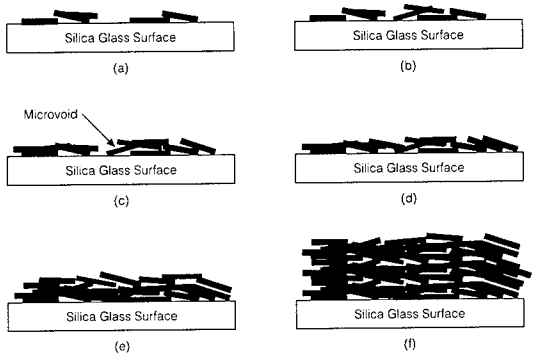


Figure 2. Schematic Representation of the Evolution of Pyrolytically Deposited Carbon Layer

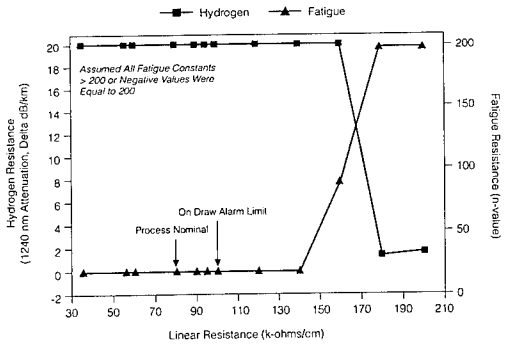


Figure 3. Correlation of Hydrogen and Fatigue Resistance vs Linear Resistance for Corning Hermetic Fibers

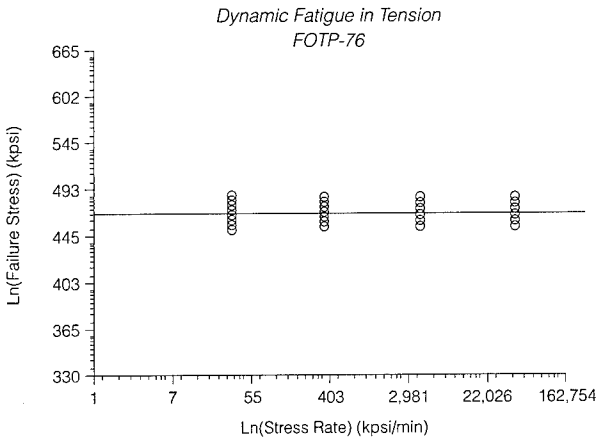


Figure 4. Typical Dynamic Fatigue Plot of Corning Hermetic Fiber

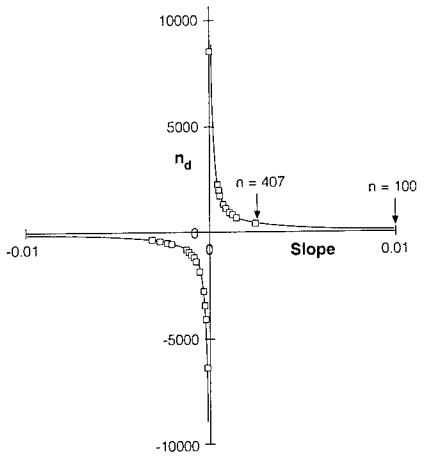


Figure 5. Compilation of All Valid (SEE<0.0017) nd Data Collected Using FOTP-76 at Corning's Center for Fiber-Optic Testing Between 1991 and 1993

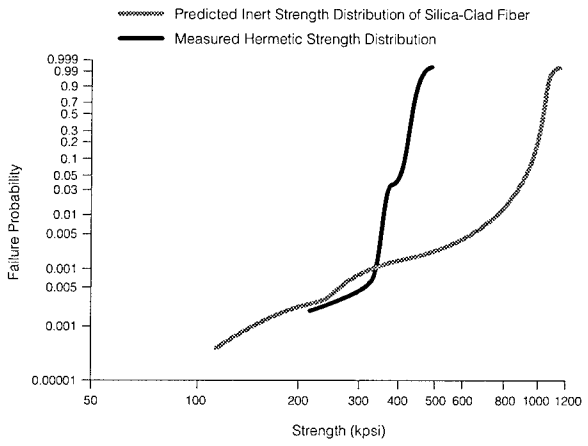


Figure 6. Comparing Measured Hermetic Fiber Strength Distribution to Predicted Silica Fiber Inert Strength Distribution

Biographies



Karen Moore received a BS degree in Systems Engineering from the U. S. Naval Academy in 1986 and served six years as a military officer in the US Navy prior to joining Corning in 1992. She has worked as a Senior Applications and Sales Engineer for Corning's Industrial/Government Fiber & Components Group.



Anurag Dwivedi is a Senior Engineer at the Center for Fiber-Optic Testing (CFT), Corning Incorporated, Corning NY. Currently he is responsible for leading the ribbon and strip force testing team at CFT. He joined Corning in 1992 as a Senior Product Engineer. From 1991-1992 he was employed by Alfred University, Alfred, NY as a post-doctoral research associate.

Anurag received a Ph.D. in ceramics in 1991 and M.S. in ceramic Engineering in 1988 from Alfred University and a B.S. in ceramic engineering in 1986 from the Institute of Technology, Benaras Hindu University, Varanasi, India.

Ed Sokira joined BT Laboratories in 1989. He is at present working in the Fiber Systems Unit examining a number of aspects relating to fiber transmission.

MECHANICAL RELIABILITY AND HYDROGEN DIFFUSION CHARACTERISTICS OF HERMETICALLY COATED FIBRES

Jon S. Andreassen, Geraldine Moe Sletten

Alcatel Kabel Norge AS
P.O. Box 130 Økern, N-0509 Oslo, NORWAY

ABSTRACT

Carbon coated fibres have been used by Alcatel Kabel Norge AS for more than 5 years. The carbon coatings have proven their efficiency with respect to isolating the silica glass surface against the environment. This ensures resistance against degradation of mechanical properties, as well as reduction of hydrogen reaching the fibre core.

The performance of the evaluated carbon coated fibres, shows variation with respect to hydrogen diffusion and inert strength, and there seems to be a trade off between the two properties. The fatigue resistance is in general high for the carbon coated fibres.

The performance difference of the carbon coated fibres indicates that the harshness of the environment together with the cost efficiency of the cable design should determine the choice of fibre for the particular application.

1. INTRODUCTION

Throughout the last decade, the performance of hermetically coated fibres with respect to fatigue resistance and hydrogen induced losses have been reported in the literature [1,2,3,4,5,6,7,8]. As the word «hermetic» indicates, the coating provides a protection of the silica glass fibre, making the fibre less susceptible for environmental exposures. Thus, the beneficial properties are related to long term reliability with special focus on high fatigue resistance and low diffusion rates for hydrogen molecules and consequently small induced losses. The older work was mainly focused on metal coated fibres, whereas carbon coated fibres has taken more attention since late 80's.

Hermetic carbon coated fibres have been used by Alcatel Kabel Norge for more than 5 years. In 1991, the first commercial submarine cable containing carbon coated fibres was installed[5] between the North and South Islands of New Zealand. Since then, more than 30.000 km of hermetically coated fibre has been used for submarine cable applications by Alcatel Kabel Norge. The cable for which hermetically coated fibres have been used has no metallic barrier against hydrogen or moisture, and the main reason for using such fibres is the diffusion barrier properties of the carbon layer. For submarine cables, different mechanisms such as corrosion of steel wire armouring and sulphate reducing bacteria[9] generates hydrogen. Measurements on installed fibre optic submarine cables with polyethylene outer sheath and two layers of steel wire armouring, but no shielding or other moisture barriers have shown levels of hydrogen corresponding to partial pressures of approximately 0.1 atm.[10]. For long length repeaterless communication links, even the small extra losses induced by hydrogen in «open» submarine cable constructions is of importance to avoid considering total system power budgets.

2. HERMETICALLY COATED FIBRES

The most common types of fibre coatings available on the market today are either metallic[1,2,8] or made by a thin layer of pyrolytic carbon[3,4,5,6,7,8]. For both types of fibres, the increased reliability ensured by the sealing of the glass makes them an attractive choice for applications featuring harsh environments. The isolation of the silica glass surface from the environment provides low fatigue rates, and the diffusion rate of hydrogen is delayed significantly. In fact, a proper coating can delay the permeation of hydrogen to the fibre core beyond the specified fibre lifetime.

For the metal coatings, materials as aluminium, tin or even gold are used. These fibres are however, very expensive compared to standard telecommunication fibres, as well as they in general suffer from microbending induced excess losses which are strongly dependant on temperature and thermal history. This makes such fibres probably more interesting in systems where initial loss is of less importance, and where the fibre volumes are small or moderate, as found in fibre based sensor systems where extremely harsh environments are considered. Thus, for long distance repeaterless communication, where fibre loss

can be a limiting factor and the volumes are large, the carbon coated fibres are most interesting. The work covered in this paper is solely on carbon coated fibres.

Several fibre manufacturers do supply or have supplied carbon coated fibres. Typically, the hermetic layer is a thin, 300 to 500 Å, layer of amorphous graphite. This coating is applied directly onto the silica glass fibre in the drawing process. As will be shown later, the properties of the carbon layers varies significantly between different suppliers. This variation is due to differences in material morphology, which again is depending on the fibre drawing and carbon deposition reactor conditions. Due to this, different primary polymer coatings may restrict the optimisation of the carbon coating as these may require special drawing conditions for application.

3. HYDROGEN DIFFUSION

Considering the diffusion of hydrogen, the hermetic layer significantly delays this process[3,4,11,12]. The loss caused by interstitial hydrogen molecules is proportional to the concentration of dissolved hydrogen in the fibre core. Thus, one can actually measure the diffusion rate through the coating by studying the obtained loss spectra. Here one should of course be careful to isolate the effects solely caused by molecular hydrogen.

After an initial period needed for establishing a concentration gradient across the carbon layer the diffusion into the silica glass fibre can be expressed by [11,12] :

$$\frac{C_{H_2}(t)}{C_{equilibrium}} = \left(1 - e^{-\left(\frac{t-\tau_i}{\tau_f}\right)} \right) \qquad \text{Eq. 1}$$

where $C_{H2}(t)$ and $C_{equilibrium}$ are the time dependent hydrogen concentration in the fibre at time t and the equilibrium concentration (t=∞), respectively. The time coefficients τ_i and τ_f are given by :

$$\tau_i = \frac{\delta^2}{6 D_c} = \tau_{i,o}\, e^{\frac{E_{ia}}{RT}} \qquad \text{Eq. 2}$$

$$\tau_f = \frac{r\,\delta}{2 D_c}\,\frac{K_s}{K_c} = \tau_{f,0}\, e^{\frac{E_{f,a}}{RT}} \qquad \text{Eq. 3}$$

where δ is the thickness of the carbon layer, D_C is the diffusion constant of hydrogen, Ks and Kc is the solubility of hydrogen in silica glass and carbon, respectively. In eq.1 it is assumed that reactions of hydrogen with defect sites in the silica material has no significant effect on the concentration of dissolved hydrogen molecules in the fibre.

One sees from eq. 1 through 3 that for characterisation of the diffusion properties, one has to determine the two time coefficients in general. That is, one has to measure them at different temperatures, and extract the corresponding activation energies (E_{ia},E_{fa}) and constant terms (τ_{i0},τ_{f0}).

When carrying out such measurements, the loss growth will after some initial lag time, reach a constant rate given by the time coefficient τ_f. The initial lag time, τ_0 is then found by extrapolating the curve back to zero loss increase. By plotting the logarithm of the time coefficients vs. the inverse temperature, the activation energies can be found.

The problem with performing measurements like this is of course that for good hermetic barriers, there is a need of either plenty of time or facilities for high temperature and high pressure testing. For the studies performed by Alcatel Kabel Norge, pressure chambers designed for a hydrogen pressure of 150 atm. at temperatures up to 185°C has been used.

For a comparison of different hermetically coated fibres in connection to the first submarine cable to be installed[5], testing was performed at 85°C and 20 atm. H_2. In fig.1 below, the relative hydrogen concentration ($C(t)/C_{equilibrium}$ in eq. 1) is plotted vs. time.

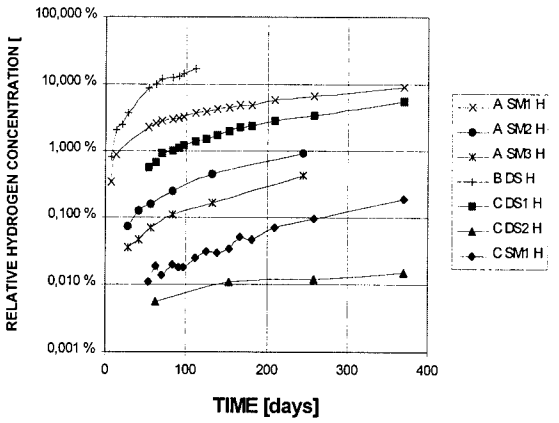


Figure 1 Hydrogen concentration build up in hermetically coated fibres in 20 atm. H2 at 85°C.

The fibre samples shown in fig.1 originates from 3 different fibre manufacturers, "A","B" and "C", and one clearly sees the difference between fibres, not only from different producers, but also between fibres from the same supplier. For comparison, a non hermetic fibre would have reached its equilibrium within less than one day at the same temperature.

With reference to eq. 1 through 3, the estimated time coefficients are for the fibres in fig.1 are as shown in table 1 below. In table 1, the question marks indicates that the estimated curve fit returns with a negative τ_i, which again indicates the uncertainty in the determination of the time coefficients. For closer studies, several samples of the same type of fibre should be measured at different temperatures, to obtain an improved basis for parameter estimation.

Fibre	τ_i [days]	τ_f [days]
A SM1 H	?	3650
A SM2 H	19	55400
A SM3 H	13.5	25800
B DS H	1,5	650
C DS1 H	60	200000
C DS2 H	20.5	6600
C SM H	?	3600000

Table 1 Time coefficients for hydrogen diffusion at 85°C

For a more detailed investigation, fibres from one of the above vendors was more detailed investigated, by performing similar tests at a set of different temperatures on three different samples of the same product. Results from 150 atm. H_2 test at 130°C and 150°C are shown in fig. 2.

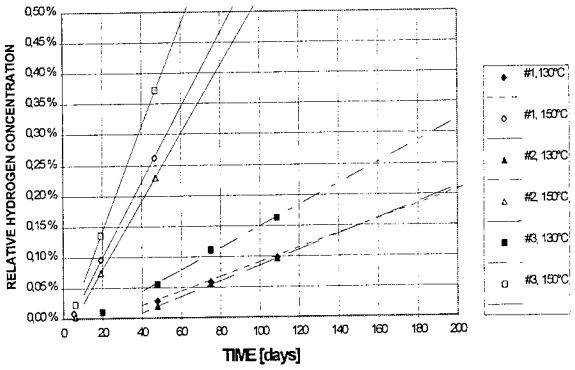


Figure 2 Hydrogen concentration vs. time for three different samples of fibre from the same manufacturer. Results from 1991/92 (130°C and 150°C, 150atm H_2).

In fig.3, the lines corresponding to the estimated curve fit according to eq.1. are shown for a period of approx. 25 years.

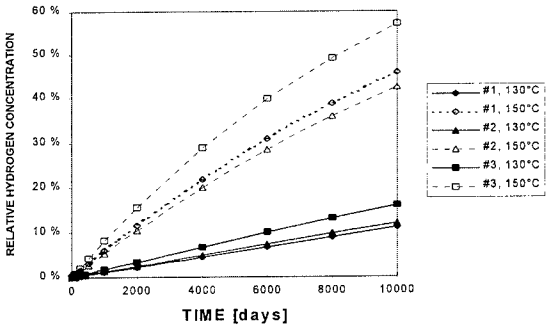


Figure 3 Estimated long term hydrogen concentration increase in hermetically coated fibres tested in 1991/92

From the results shown in fig.2, the characteristics of the diffusion properties was found as given in table 2. There is a

	τ_i		τ_f	
Fibre	$\tau_{i,0}$ [s]	E_{ia} [J/mole]	$\tau_{f,0}$ [s]	E_{fa} [J/mole]
#1	$1.27 \cdot 10^{-10}$	124700	$4.05 \cdot 10^{-6}$	117750
#2	$1.35 \cdot 10^{-10}$	125900	$2.13 \cdot 10^{-4}$	104170
#3	$8.46 \cdot 10^{-9}$	109300	$1.40 \cdot 10^{-5}$	112250
Mean	$2.91 \cdot 10^{-9}$	119970	$7.70 \cdot 10^{-5}$	111390

Table 2 Hydrogen diffusion characteristics

wide spread in the estimated parameters given in table 2, due to that the testing of all fibres were carried out at two different temperatures only. A control measurement on one fibre at 180°C, however, confirmed that the mean values are representative. In fig.4, the individually estimated time coefficients are plotted against temperature, together with their best fit curves.

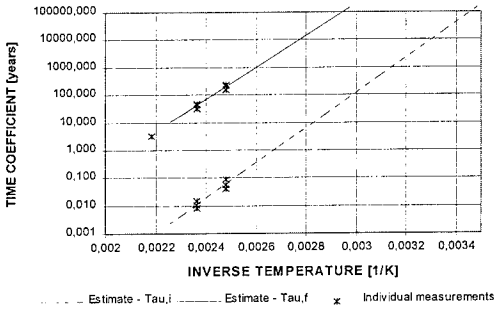


Figure 4 Time coefficients for diffusion through carbon layer.

One sees from fig.4 that for temperatures below 60°C, the initial lag time is more than 100 years !

The results given in figures 1 through 4 are all originating from 1991/92. More recently, some new (experimental) fibres from the same fibre manufacturer have been evaluated under the same conditions together with fibres

from a fourth fibre manufacturer. Some of these results are given in fig. 5.

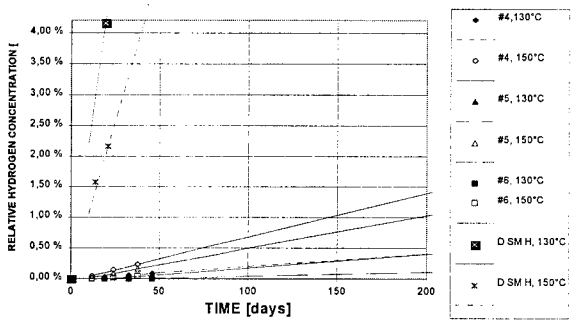


Figure 5 Hydrogen concentration vs. time for three different samples of fibre from the same manufacturer. Results from 1995 (130°C and 150°C, 150atm H_2).

It should be noted that for fibre denoted "D SM H", the lengths tested at the two temperatures were not from the same preform, so that the otherwise surprising observation of a faster diffusion at 130°C than at 150°C probably reflects variation in manufacturing process. Noteworthy is the performance of the fibre denoted #6, which showed extremely low diffusion rate at 150°C , and has not suffered from any loss growth at 130°C after nearly 50 days treatment (test is still ongoing). The estimated long term behaviour is shown in fig.6.

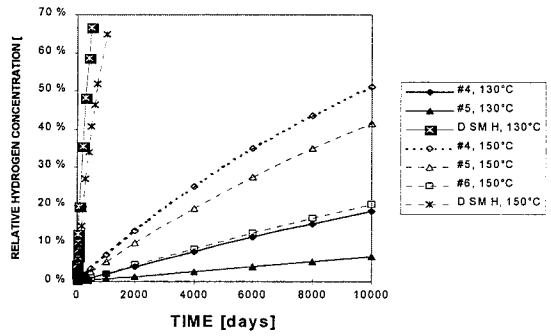


Figure 6 Estimated long term hydrogen concentration increase in hermetically coated fibres tested in 1995.

The time coefficients corresponding to the fibres in fig.5 and 6 are given in table 3.

Fibre	130°C		150°C	
	τ_i [days]	τ_f [days]	τ_i [days]	τ_f [days]
#4	2.2	49000	4.8	14000
#5	31	147000	8.1	18600
#6	?	?	20.5	44100
D SM H	≈0	455	≈0	960

Table 3 Time coefficient for hydrogen diffusion (1995 data).

It is definitely hard to establish one general picture on the long term performance with respect to hydrogen. One reasonable approach is to look at the hydrogen concentration vs. time coefficient as shown in fig.7 for 1, 10 and 30 years. From this, one can define requirements to the carbon layer according to the environment such as expected hydrogen level, temperature and the system margin of the application. As a conservative approximation, the initial time lag is assumed to be negligible in the calculations shown in fig.7.

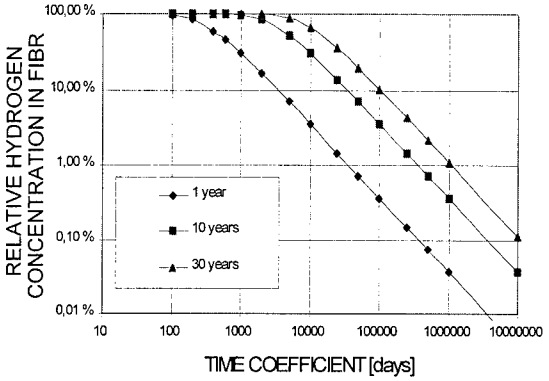


Figure 7 Hydrogen concentration in fibre relative equilibrium concentration after 1, 10 and 30 years vs. τ_f

4. MECHANICAL PROPERTIES

The fatigue of optical fibres can be expressed by the power law approximation[13], considering the subcritical crack growth regime. For this model, the stress corrosion factor, n, gives the fatigue rate for a stressed fibre. For carbon coated fibres, this n value is indeed high, requiring huge populations for experimental determination with reasonable statistical uncertainty. High n values ranging from 35 to infinity have been indicated[3,4,5,6], based on dynamic fatigue measurements. It has however been proposed that the mechanical properties of the fibre are closely connected to the carbon layer itself[14,15], and that the fatigue parameter is limited to the one of the carbon coating itself. This implies that the n value will not exceed 150[14]. For calculations, however, the practical importance using n=150 or higher is small.

In fig.8 below, the measured breaking strength at different strain rates are shown for some of the fibres which diffusion

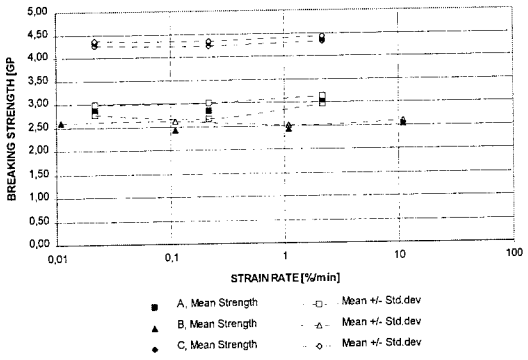


Figure 8 Breaking strength vs.fibre strain rate

rates at 85°C were presented in fig.1. It is evident that the breaking strength is nearly independent of the strain rate, indicating a high n value. The inert strength, however ,is varying between fibres[5]. From the results, it can seem like the n-value of fibre C is somewhat higher than the others, however, the statistical uncertainty is too large to make any conclusion on this. However, the higher strength on this fibre may in general indicate "better mechanical properties" in terms of a higher slope for the strength distribution.

Apart from the fatigue, much work has been focusing on phenomenons acting in addition to fatigue, such as stress free ageing[16,17,18]. Studies on fibres aged in water have shown increased surface roughness corresponding to weakening of the fibre which can not be explained by the power law model. In fig.9 below the measured strength is plotted against ageing period in deionised water at 70°C for non-hermetic and hermetic fibre. The hermetically coated fibre is of same type as in fig.2. For the non hermetic fibre, a clear decrease in strength is observed after 3 months. However, after 4 months, the strength seems to increase. Strengthening induced by ageing due to blunting of existing flaws has previously been reported[19] , but assuming that the fibres initially was pristine, the reason for the observed

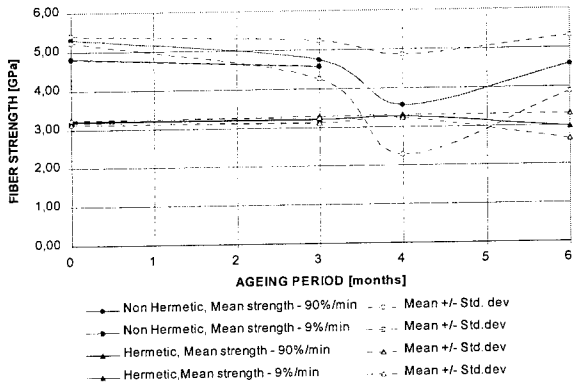


Figure 9 Breaking strength of fibres aged in deionised water at 70°C

increase in strength is unclear, since the ageing is expected to result in etched pits which should have been blunt already[16,18]. The zero stress ageing has been connected to the dissolution of silica glass which certainly is depending on the environment. Temperature, pH and humidity[16,17] are some factors of importance. Due to this the type of coating and its ability to resist its surroundings and protect the glass surface is a critical factor. As expected, for the carbon coated fibre, there was no effect of the ageing, indicating the protection of the silica glass surface by the carbon coating, avoiding water attack. This corresponds to previously published work[18]. The somewhat wider spread in strength after 6 months is due to statistical uncertainty. In fact, all measured samples are within the high strength region for this type of fibre shown in fig.10, for 9.5m gauge lengths.
In fig.10, also the strength distribution for carbon coated fibres aged in cable without any metallic moisture barrier (70°C water, 4 months) is shown [20].

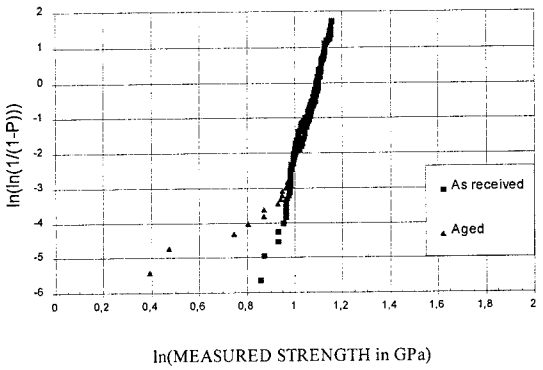


Figure 10 Tensile srength distribution, 9.5m gauge lengths, hermetically coated fibres.Aged population : 232 specimens aged 4 months in cable in water at 70°C. As received : 280 specimens [20]

From fig.10, one sees a slight deviation between the strength distributions of the as received and the aged populations. Due to the considerable amount of manual handling of relatively long bare fibre lengths (removing 15 m lengths of fibres from cable), the weak spots were most likely caused by damage of the coating due to handling, such as accidentally stepping on the fibre. The possible effect of this was investigated by strength measurements on mechanically abraded carbon coated fibres. . Typically, the mechanical abrasion caused either immediate breakage of the fibre or no weakening at all, however strength distributions including a few weakened samples as for the aged fibre, were reconstructed, where the tensile strength reduction of the weakest spots was found to correspond to dynamic fatigue for non hermetic fibres [20] .Thus, it is less likely that any weakening was introduced by the ageing. The only possibility of weakening due to ageing would have been discontinuity in the hermetic sealing possibly introduced by mechanical exposures or due to cracking of

carbon at extrinsic surface flaws in the glass[6]. A discontinuity in the carbon layer will naturally lead to non hermetic behaviour at that particular spot. However, it has been shown that the carbon ensures a hermetic protection also at large surface flaws[15,21], provided a sufficient thickness of the carbon layer[15]. For an adequate coating thickness, the risk of damaging the coating by tensile loading of the fibre without breakage of the fibre is very low[15].

Considering fatigue to be the main mechanism for limiting the mechanical reliability of carbon coated fibres, the extrinsic part of the strength distribution, thus remains to restrict the allowed service load on the fibre. Here, the high fatigue resistance results in an effective truncation of the post screen test strength by the negligible fatigue during unloading.

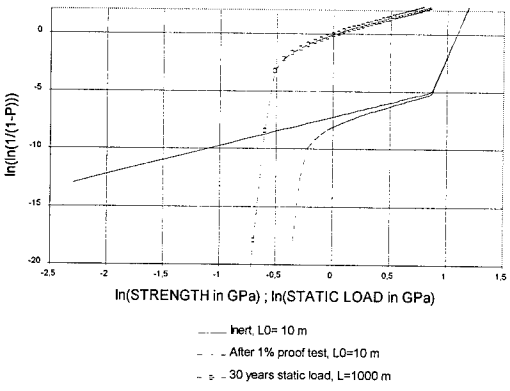


Figure 11 Weibull plots for inert and post-screening strength distributions and 30 years static load.

In fig.11, a hypothetic extrinsic strength distribution with a slope of m_e=2.5 is added to the measured distribution on as received fibres shown in fig.9. The effect of proof test is calculated according to[13,22] :

$$P(\sigma_f) = 1 - e^{-\frac{L}{L_0}\left[\left(\frac{\sigma_f}{\sigma_0}\right)^{n_p-2}+\left(\frac{\sigma_i^*}{\sigma_0}\right)^{n_p-2}-\left(\frac{\sigma_{f,\min}}{\sigma_0}\right)^{n_p-2}\right]^{\frac{m}{n_p-2}}} e^{-\frac{L}{L_0}\left(\frac{\sigma_i^*}{\sigma_0}\right)^m} \quad \text{Eq. 4}$$

where

$$\sigma_f^{n-2} = B^{-1}\sigma_a^{n_a} t_a$$

$$\sigma_{f,\min}^{n-2} = \sigma_p^{n_p-2} - \frac{\sigma_p^{n_p+1}}{B(n_p+1)\sigma'_{pu}}$$

$$\sigma'_{pu} = \frac{\sigma_p}{t_{pu}} \quad \text{Eq. 5}$$

$$\sigma_i^{*n-2} = B^{-1}\sigma_p^{n_p} t_{p,eq} + \sigma_{f,\min}^{n_p-2}$$

$$t_{p,eq} = t_{ph} + \frac{t_{pl}+t_{pu}}{n_p+1}$$

A n value of 100 has been assumed for both service and proof test environment. $\sigma_{f,min}$ and σ^*_i are the minimum strength after screening and the minimum inert strength surviving the screen test, respectively. One sees from fig.11 that 70% of the proof test level is to considered as a safe region for static loads of a carbon coated fibre.

5. DISCUSSION

It is clear that the hermetically coated fibre exhibit properties regarding mechanical behaviour and resistance against hydrogen diffusion which makes them applicable for more harsh environments than the standard coated fibre. The performance, however, varies strongly between different fibre types. This suggests careful selection of fibre, based on the specific need and application.

From the test results in 1991[5], there seems to be a trend that the better the mechanical performance, the poorer the diffusion barrier. The mechanical properties of carbon coated fibres have been suggested to be determined by the carbon layer itself[14,15] which again depends on morphology, that is the orientation and quality of the crystallites of the coating material[6]. The diffusion properties can be expressed in terms of time coefficients (eq.2 and 3), where one should have proportionality to thickness and square thickness of the coating for τ_f and τ_i , respectively. This dependency, however, does not solely explain the performance difference of the hermetic coatings. It probably would have done this, provided otherwise equal material structures, but as for the mechanical performance it is the material structure that seems to determine the diffusion characteristics. Thus, there should be no law by nature stating that one has to live with a trade off between strength and diffusion properties.
It is believed that the end users of hermetically coated fibres only to a small degree have specified the performance of hermetically coated fibres in detail, and that the products supplied well have satisfied the customer needs, which for most applications probably have been focused on strength and fatigue.

There seems to be quite a potential for further development on carbon coatings to meet even more severe environments than experienced for standard land and submarine cables.
The carbon coating has proven that it protects the fibre from the environment, which otherwise has to be provided by a proper cable design. The cable manufacturers alternatives include metallic moisture and hydrogen barriers, hydrogen absorbing filling compounds, sufficient fibre strain relief, etc.. The cost connected to the different alternatives will finally decide the preferable method of ensuring a reliable product.

6. CONCLUSION

Carbon coatings when processed properly, improves strongly the resistance to possible environmental threats against fibre reliability. This resistance features low hydrogen diffusion into the fibre and low fatigue rates.

Typically, the fatigue resistance has been found to be very high for the products evaluated by Alcatel Kabel Norge. The variation in mechanical properties between fibres from different suppliers concerns the inert strength, which in general is lower than for non hermetic fibres. The hydrogen barrier properties are strongly variable between the products, although all coatings perform as nearly hermetic at low temperatures.

From the results obtained on different available products, there seems to be a to be a general trend that there is a trade off between strength and H_2 diffusion barrier properties. This makes the choice of fibre type, first the choice between hermetic or non hermetic and next possibly between the available hermetic products, clearly connected to both the cable design and the environmental harshness. Eventually, the choice will be dictated with respect to cost efficiency of the total cable design.

7. ACKNOWLEDGEMENTS

The authors would like to thank Audun Hordvik, Optoplan.

8. REFERENCES

[1] D.A. Pinnow, et.al., "Reductions in static fatigue of silica fibers by hermetic jacketing", Appl. Phys Lett. 34(1), January 1979.

[2] J.A. Wysocki , "Static fatigue of silica in hermetic environments", J. Am. Ceram. Society, Vol 66, No3, March 1983.

[3] K.E. Lu, et.al.,, "Recent developments in hermetically coated optical fiber", J. of Lightw. Techn., Vol6, No2, February 1988.

[4] K.E. Lu, et.al; "Mechanical and hydrogen characteristics of hermetically coated optical fibre "; Optical and Quantum Electronics 22 (1990) pp. 227-237.

[5] G. Berthelsen et.al., "The worlds first commercial submarine cable with hermetic fibres", Proc. 40th. Int. Wire & Cable Symp. (1991), pp 628-632.

[6] E.S.R. Sikora, et.al; "Examination of the strength characteristics, hydrogen permeation and electrical resistivity of the carbon coating of a number of 'hermetic' optical fibres"; Proc. 40th. Int. Wire & Cable Symp. (1991), pp 663-672

[7] H.H. Yuce, J.P. Varachi Jr, " Mechanical behaviour of hermetically coated optical fiber", "; Proc. 40th. Int. Wire & Cable Symp. (1991), pp 686-692.

[8] A.Abramov, et.al; "Prospects in application of hermetically coated fibers in submarine optical cables"; Proc. 2nd Int. Conf. on Optical Fiber Submarine Telecomm. Syst. (SUBOPTIC '93), 1993, pp. 315-319.

[9] K. Schick, et.al; "Hydrogen Sources for Signal Attenuation in Optica Fibers"; Optical Eng., Vol.30, No6, June 1991.

[10] S. Hopland; "Measurements of Low Hydrogan Levels in Installed Open Fiberoptic Submarine Cables"; Proc. IWCS , Nov. 1991, St. Louis, pp 742.

[11] P.J. Lemaire; "Hydrogen permeation in optical fibres with carbon coatings"; Electron. Letters Vol 24, No21 1988, pp.1323-1324.

[12] P.J. Lemaire; "Reliability of optical fiber exposed to hydrogen: prediction of long-term loss increases"; Opt. Eng., June 1991, Vol. 30 No. 6, pp. 780.

[13] E.R. Fuller, et.al ; "Proof testing of ceramics, Part 2 Theory"; J. Mat. Science 15 (1980) pp. 2282-2295.

[14] M.M. Bubnov, et.al; "Maximum value of strength and fatigue parameter n for hermetically coated optical fibers"; Proc. 41st. Int. Wire & Cable Symp. (1992), pp 629-635

[15] S.L. Semjonov, et.al.; "Mechanical behaviour of low- and high-strength carbon-coated fibres"; Proc. SPIE Vol. 2290, Fiber Optic Materials and Components, pp.74 (1994)

[16] M.J. Matthewson, C.R. Kurkjian;"Environmental effects on the static fatigue of silica optical fiber"; J. Am. Ceram. Soc., 71(3) pp.177-183

[17] C.R. Kurkjian; "Strength and fatigue of silica optical fibers"; J. Lightw. Techn., Vol 7, No 9, September 1989.

[18] W. Griffioen; "Ageing of optical fibres in water"; Proc. 41st. Int. Wire & Cable Symp. (1992), pp 622-628

[19] G.S. Glaesemann; "The mechanical behaviour of large flaws in optical fiber and their role in reliability predictions"; "; Proc. 41st. Int. Wire & Cable Symp. (1992), pp 698-704.

[20] J.S. Andreassen; "Experimental study on reliability and stress free ageing efects on hermetically coated fibres"; Proc. SPIE Vol. 2290, Fiber Optic Materials and Components, pp.229 (1994)

[21] M.G. Estep, G.S. Glaesemann; "The effect of carbon overcoating on the mechanical behaviour of large flaws"; Proc. SPIE Vol 1791 pp.18-24, (1992)

[22] Y. Mitsunaga, et.al; "Failure prediction for long length optical fibre based on proof testing"; J. Appl. Phys. 53(7), July 1982.



Jon S. Andreassen
Alcatel Kabel Norge AS
P.O. Box 130, Økern
N-0509 Oslo, Norway.

Jon Steinar Andreassen graduated from the University of Trondheim, Norwegian Institute of Technology (Physical Electronics) in 1985, and joined STK (now Alcatel Kabel Norge) in 1986, where he works with research and development of fiber optic cables.



Geraldine M. Sletten
Alcatel Kabel Norge AS
P.O. Box 130, Økern
N-0509 Oslo, Norway

Geraldine Sletten received her B. Eng (Electrical and Electronic Engineering) from Strathclyde University, Glasgow in 1987 and joined STK (now Alcatel Kabel Norge) the same year, where she works with research and development of fiber optic cables.

HERMETIC COATINGS FOR OPTICAL GLASS FIBERS

D. R. Biswas, C. R. Kurkjian and H. H. Yuce

Bellcore, 445 South Street, Morristown, NJ 07960

ABSTRACT

Polymeric coatings are not impervious to moisture, and as a result the strength of polymer-coated optical fibers degrades under stress over a period of time due to fatigue. Exposure to harsh environments, such as moisture, high stresses, and hydrogen, can adversely affect the reliability and attenuation of optical fibers. Considerable work has been done in the field of hermetic coatings for optical glass fibers. In this paper, we will review the status of different hermetic coatings - both metal and inorganic on glass optical fibers, the techniques used to apply them, and their performance in different environments. In addition, we will endeavor to evaluate the practical problems associated with such coatings, the reasons for their lack of acceptance, and the possibilities of their future use.

INTRODUCTION

When standard telecommunication fibers from field trials have been tested for strength degradation and fatigue after some time in service, conflicting results have been reported. In the case of the field trial in Biarritz, France, when the fibers were tested after ten years of field aging,[1] a strength reduction of ~40% and a reduction of the dynamic fatigue parameter from a typical n-value of 20 to a value of 15 was observed. In another report,[2] when a fiber-optic cable which was in service for eight years in a duct that was routinely flooded and always had standing water was tested for strength and fatigue, there was no degradation in either strength or fatigue. In the case of hermetically coated optical fibers, another report[3] showed that when three cables containing a large volume of carbon coated hermetic and standard non-hermetic coated fibers were installed in duct and aerial routes and later tested for strength and fatigue, the hermetically coated fibers showed much higher fatigue resistance ($n > 200$) than the standard fibers ($n = 20$).

Copyright © 1995 Bellcore. All rights reserved.

Despite their apparently superior aging and fatigue resistance, no large scale use of hermetically coated optical fibers has been reported in this country. This might be somewhat surprising, since hermetic coatings can compensate for some of the shortcomings of polymeric coatings. The viscoelastic character of polymer coatings is important in their ability to protect fibers from mechanical damage and at the same time isolate them from added optical losses due to microbending. However, their permeability to water gives rise to strength degradation through aging and fatigue.

An ideal hermetic coating should be simple and easy to apply at high draw speeds, should not contribute any additional optical loss, and should provide protection and isolation from liquid water or water vapor, and hydrogen. If the coating performs this latter function satisfactorily, it would be expected that the fiber's initial, short-term strength at room temperature would be the same as that measured at room temperature in vacuum: 12 to 14 GPa.[4]. In addition, the fiber's n-value would be the theoretically expected maximum, $n = \sim 150$ (see the discussion of Bogatyrjov et al[4a]). Two presently available hermetic coatings have been successfully applied in-line to lightguide fibers: melt-applied metallic coatings and reactor-applied inorganic coatings. Since neither of these types is viscoelastic, they each suffer from deficiencies when compared to organic polymers and also to the ideal coating described above. For some applications, however, they have important advantages which may outweigh these disadvantages. It is our purpose here to describe these coatings and their properties and to discuss their present applications as well as to indicate where improvements in their properties could be made which would enhance their usefulness.

METAL COATINGS

The advantages of using metal coatings which are applied from the melt are: (i) hermetic sealing of the glass fiber surface from moisture and the resultant high fatigue parameter (n), (ii) higher strength, (iii) possible higher temperature resistance than organic polymer coatings, and (iv) solderability.

In 1967 Arridge and Heywood[5] demonstrated the application of an aluminum coating onto a silica fiber using a freeze coating process. More recently, others[6,7] have used a similar process for applying a variety of different metal coatings. Wysocki et al.[6a] claimed that metals with a melting point near the softening point of glass can be used for coatings, and that a dual metal coating (with the primary metal being non-reactive to silica) can also be used for coating glass fiber.

A typical melt coating process for optical fiber is shown in Figure 1. In this set-up, a silica fiber passes through a pool of a molten metal or alloy which freezes onto the fiber surface. The exact mechanism which controls the application of a metal coating from the melt is not well understood. It appears that freezing may take place either within or upon exiting the coating cup, or by a combination of the two, depending on the metal being applied, as well as on the details of the coating process[8,9]. Approximately 20-micron thick coatings are typically applied.

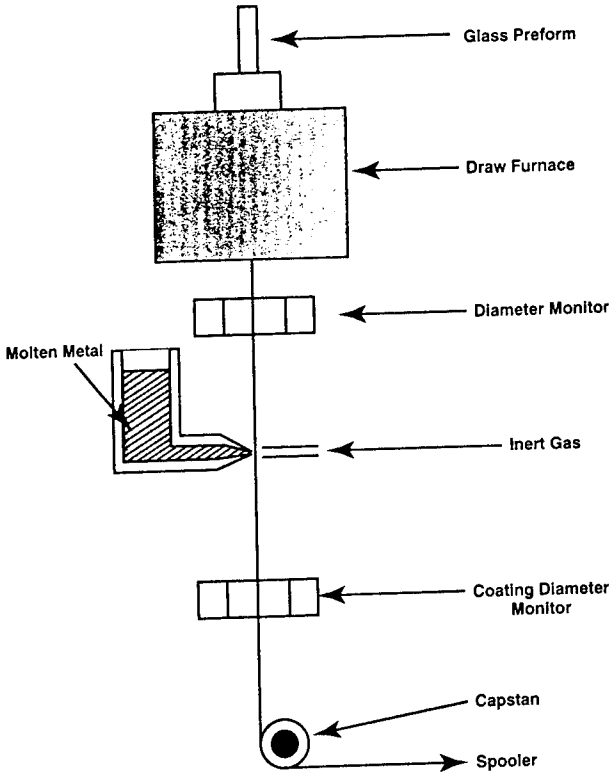


Figure 1. A typical metal coating set-up.

Other methods used for coating fibers with metal are sputtering[10], ion plasma deposition [11], vapor deposition [12] and dip coating in metallo-organic liquids [13]. In the case of the vapor deposition of nickel[12], the resultant coating was apparently not hermetic, since the measured value of n was ~20 and the strength was essentially the same as for the polymer coated fiber. However, the hermeticity of the coating cannot be determined simply by the measurement of n. The amount of water already on the fiber surface, as well as the sensitivity of the hermeticity to stress are both factors in determining the value of n. To date it has not been shown that any but melt-applied metallic coatings are hermetic. A novel metal coated solderable fiber has been produced by plating copper and nickel on top of a conductive carbon coated optical fiber[14]. Since the carbon coated fiber itself is hermetic, the composite fiber is presumably also hermetic.

Although the basic metal coating deposition process (melt and freeze) is similar for different coatings, the strength of the fibers varies as evidenced by the data in Figure 2. The original aluminum coated fiber[5] had a low and variable strength ($\sigma \sim 4.5$ GPa) when compared to normal uncoated fibers. Somewhat higher strengths ($\sigma = \sim 5.5$-6.5 GPa) and apparent hermeticity were reported by Pinnow et al[6a]. Recently, substantially higher strengths have been reported [7].

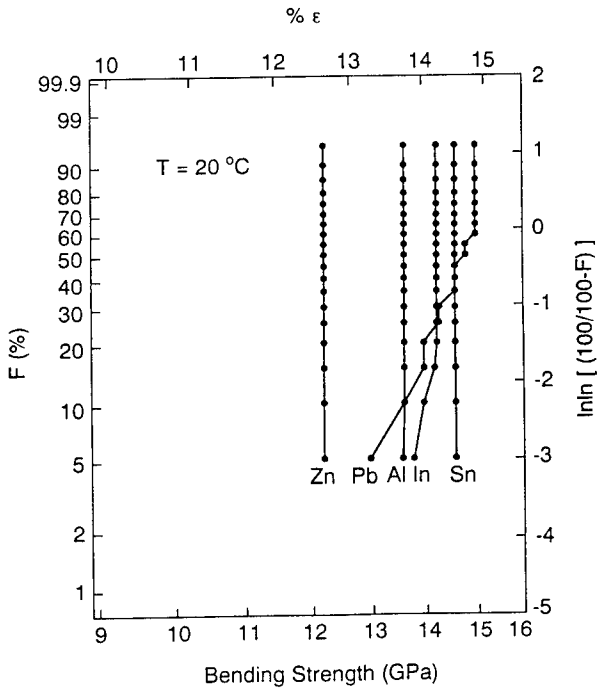


Figure 2. Bending strength of different metal coated fibers [7].

It was originally thought that the reduction in strength of aluminum coated fiber was due to the interaction of the Al with the silica surface. Measurements of the strength of the fiber[6a] with the aluminum coating removed gave a value only one-half that of an ordinary bare silica fiber[15]. Clearly the fiber surface was somehow damaged by the application of the Al or by the process itself. Inada, et al.[16] showed that the activation energy for the kinetics of the reaction of silica and aluminum agrees with that observed in the reduction of strength in these fibers at elevated temperatures. Subsequently Bogatyrjov et al confirmed these results in detail for lightguide fibers [17].

In 1988 Bogatyrjov et al[7] were able to produce very high strength fibers with a variety of metal coatings, apparently by the proper control of the details of the drawing process. These results are shown in Figure 2. In this and subsequent work by the Moscow group, the results from two-point bending studies are given in terms of failure stress. While the modulus of silica is known to be a function of strain of the form $E = E_0 (1 + 3\varepsilon)$, the validity of this expression has only been measured to a strain of ~5%. Indeed, it is expected that at a strain of ~10%, it fails to hold. The original data of these Russian workers is presented as published, though this discussion must be borne in mind.

These high strengths in Figure 2 indicate that the coating is indeed hermetic. The reason for the variation in strengths with the different metals is not clear. Differences in the extent of reaction with the silica surface, possible differences in the silica surface itself, differences in the failure strain possible with different metals, or differences in the modulus of the coating may all play a part. Bogatyrjov et al.[18] have shown that by developing single crystals of tin (Figure 3a) properly oriented along the fiber axis rather than a random array of tin polycrystals in the coating, higher and more consistent strengths are obtained. In the case of aluminum, the microstructure of a polycrystalline aluminum coated fiber with a somewhat lower strength of 10 GPa is shown in Figure 3b. Tin has four independent slip systems, and as Taylor [19] has shown, at least five different slip systems are necessary for unlimited change in the crystal grain shape. Thus, crystal alignment is necessary. In addition, by varying the water content of the environment during the melt coating process, variations in strength as well as the fatigue parameter are observed[20].

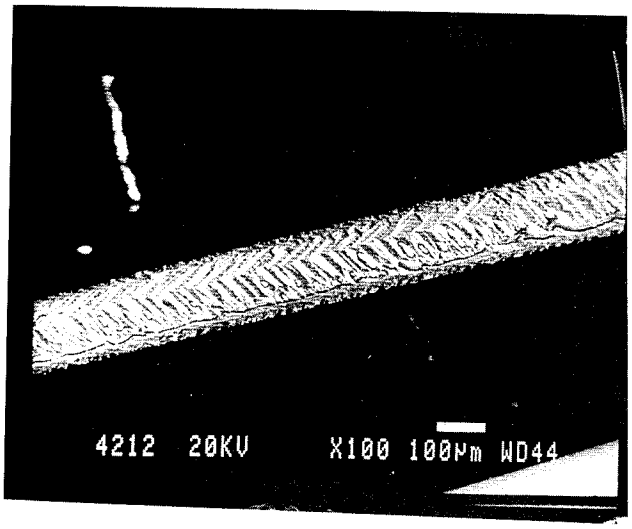


Figure 3a. Microstructure of a tin coated fiber after selective etching [18].

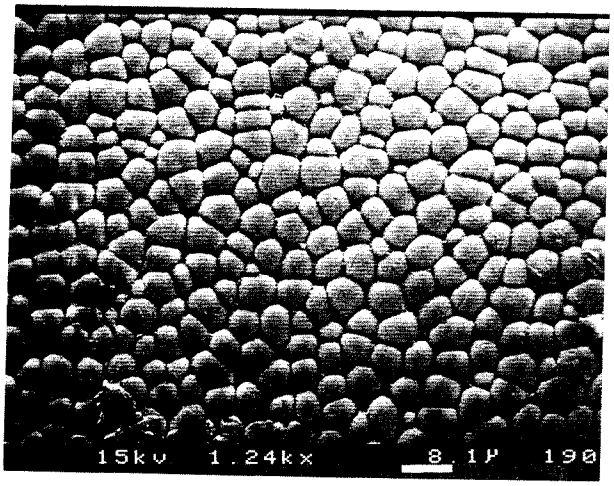


Figure 3b. Microstructure of an aluminum coated fiber surface with polycrystalline grain structure.

It was suggested above that since high temperature coatings are desirable in some applications, and since polymer coatings have a rather limited temperature capability[21], the use of metal coatings might provide a means of increasing this temperature limit. The strength of aluminum coated fiber degrades rapidly above 400°C and, as discussed earlier, it appears that this degradation is the result of the Al + SiO_2 reaction. When used at 250°C or below, however, aluminum coated fibers can have a lifetime of more than 10 years when subjected to 1 GPa stress [22]. For an even higher temperature resistant coating as well as for ease of soldering, copper, gold or silver coatings may be considered. Presumably because of the difficulty of coating at the required temperatures (~1075°C) and the possible reaction of copper with the silica surface, two-point bend strengths of only ~9 GPa [23] (corrected), combined with a rather broad strength distribution, are found. It is expected that these strengths can be improved, however. Gold and silver coated fibers are available commercially and should be useful for high temperature applications, but details of their strengths are not available. Copper coated fibers are easy to solder[24] and seem to be promising for a variety of applications such as pigtails.

In the absence of copper coated fiber, aluminum coated fiber has been investigated for pigtail applications. While such fibers can be soldered, the process is rather difficult to control. Because of this, Simpkins et al. [25] have recently reported the successful soldering of aluminum coated fibers which have been coated with a thin layer of electroless nickel at room temperature. The soldering of the Ni/Al coated fiber is rather straightforward, with average tensile pull-out forces ~6 lb_f. Also in this work, some interesting data on the tensile and bend strengths of aluminum coated fiber are reported. In the original work of Bogatyrjov et al.[7], it was shown that there was a major difference between the two-point bend and tensile strengths of metal coated fibers. Part of this is undoubtedly the result of the improper use of the formula for the modulus correction at high strains. In addition, it is difficult to make tensile tests on these fibers, which fail at tensile loads as high as thirty or forty pounds. Simpkins et al. however, found that for their aluminum coated fiber, a bend strength of 8.5 GPa (uncorrected) could be shifted to the value of tensile strength which they measured (4.4 GPa.) using Weibull statistics. This takes into account the gauge length difference in the two cases and assumes similar flaw distributions in the bending and tensile samples. More work needs to be done to verify this since in their case an unusually wide strength distribution was found in bending (m ~15).

As can be seen from the above, the high strength, hermeticity, high use temperature and solderability which were suggested as advantages for melt-applied metal coated fibers can usually be realized. However, all metal coated fibers show added optical losses due to microbending caused by the plastic flow of metals when stressed.

INORGANIC AND CARBON COATINGS

The main advantages of using an inorganic coating such as SiON or carbon on optical fibers are: ease of application, high deposition speed, and hermetic sealing of the glass fiber from moisture (thus obtaining high fatigue resistance) and from hydrogen atmospheres.

Carbon coatings were successfully applied as early as 1967 by Cooper [26] but no detailed study of hermeticity was carried out. In 1978 the possible use of an inorganic coating of SiON was suggested by AuCoin et al.[27] and later deposited on optical fiber by Hiskes et al.[28] This particular coating and other coatings of different oxides and carbides were developed, but were not extensively used. Later, as carbon coatings were further developed by a number of laboratories[29-34] and showed significant promise, carbon became the prime hermetic coating for optical glass fibers. The application process and mechanical behavior of these carbon coatings as described by different workers are very similar. The coating process (as shown in Figure 4) consists of feeding a hydrocarbon precursor gas into a reactor placed beneath the draw furnace. The retained heat of the hot fiber exiting from the bottom of the furnace is sufficient to crack the hydrocarbon and to deposit a carbon coating onto the fiber surface. A 500-Angstrom thick carbon coating can be deposited at draw speeds at least as high as 5 m/s. Because of the thinness and lack of abrasion resistance of these coatings, they are protected from mechanical damage by the application of a standard polymeric coating over the carbon coating. The quality and uniformity of the carbon coating can be monitored in-line during the deposition process[35,36]. The carbon coatings are either amorphous or microcrystalline [37-39] in structure.

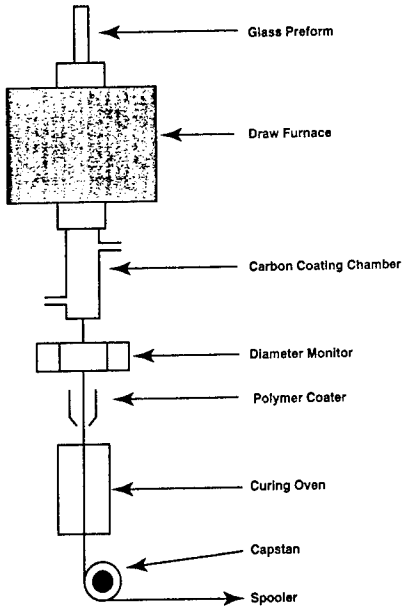


Figure 4. A typical carbon coating set-up.

Carbon coated fibers generally are weaker than polymer or metal coated fibers. The carbon coating is brittle and has a higher coefficient of thermal expansion, and thus applies a residual tensile stress. In addition, the failure strain for the carbon coating is apparently not as high as for silica. The coating therefore fails before the fiber, either damaging the fiber or allowing it to come into contact with the ambient and thus to fail by fatigue. An additional possibility is that, as in the case of metal coating applications, the surface of the silica may have been damaged during the reactor treatment, either due to the deposition or to some other feature of the process itself.

Carbon coated fibers usually fail at ~4.5 GPa or at a strain of ~5%. The failure strain of a bare silica fiber under inert conditions is significantly higher (18%). Thus, absolutely, and also in comparison to metal coated fibers, carbon coated fibers would appear to show properties which are far below their potential.

Although the deposition processes used by all workers appear to be similar, variations in precursors, the use of additional chlorine, the reactor temperature, etc. would appear to have an effect on the properties of the final coated fiber.

In general, carbon coatings appear to be either amorphous or microcrystalline. However, French workers[37] have observed spherical SiC inclusions in their films and these could seriously affect their strength. The surface roughness of the carbon is also seen to show substantial variation. In fact, one of the puzzles is that both increased and decreased roughness are claimed to produce higher strengths. It would appear that some factor other than the carbon surface roughness is actually controlling the strength in these cases.

The available hydrogen radical concentration in the chemical vapor deposition (CVD) reaction for forming the carbon coating[32,34] has also been shown to influence the strength and fatigue as well as the H_2 permeability. The addition of chlorine during the deposition of carbon coatings on fibers apparently increases the carbon coating's ultimate elongation. The strength of the coated fiber increased to 6.0 GPa. This increase was noticeable when the chlorine content was maintained at 30 (arbitrary units), but the strength decreased at higher chlorine levels (Figure 5). Possible explanations for the increase in strength of carbon coated fibers with an increase in chlorine content are the reduction in hydrogen radicals along with a modification in the carbon structure, as well as a possible reduction in the residual stresses in the carbon coating.

As mentioned earlier, the carbon coating thickness is only 500-Angstroms. This is less than the possible flaw or defect size of 0.1-1 micron at the proof-test level of 0.3-1.5 GPa. Now, the question is whether the carbon coating can seal such defects.

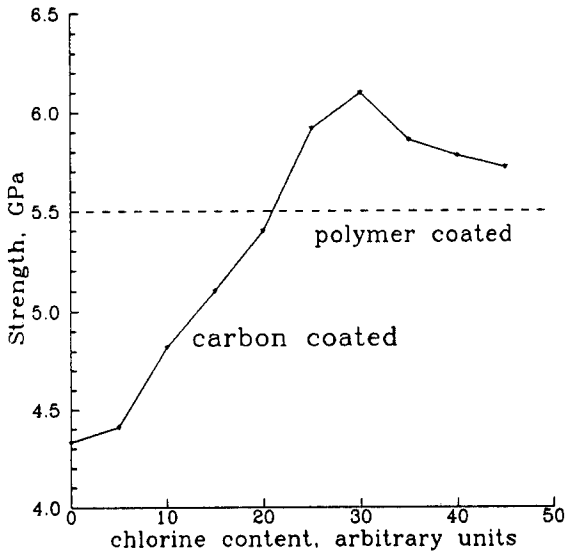


Figure 5. Bend strength of carbon coated fibers as a function of chlorine content in the precursors [34].

A recent study of the strength and fatigue of carbon coated fibers with large mechanically-induced cracks has indicated that the carbon coating might have the potential to cover or heal large surface flaws on glass fibers and to increase the strength of abraded fiber[40]. In another experiment[34], large flaws were generated by drawing fibers from a silica rod coated with <1 μm zirconia particles. The fiber was then coated with carbon. The strength of the carbon coated fiber with the melted-in zirconia particles increased as the carbon coating thickness increased that was more than twice that of similar polymer coated fibers. The carbon coated fibers were also hermetic if the coating thickness was sufficient. Thus, if the carbon coating can seal the defects, the fibers can be hermetic.

The aging of carbon coated fibers in hot water appears to have little effect on either their strength or fatigue resistance[41], as shown in Figure 6.

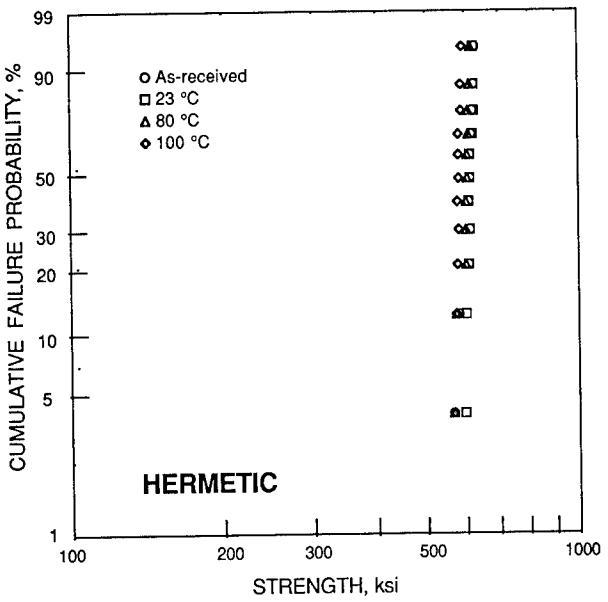


Figure 6. Bend strengths of carbon coated fibers in water at different temperatures [41]

The carbon coating itself does not contribute any added optical losses in normal or in hydrogen-containing atmospheres. Carbon coated fibers were tested extensively [42-44] in hydrogen atmospheres at different temperatures, and in all cases, the carbon coating resisted hydrogen diffusion into the glass. Thus, although the strength of carbon coated fibers is substantially less than that of metal coated fibers, carbon coated fibers have enjoyed more practical success.

The capability of fusion splicing carbon coated fibers has been developed recently [3,45]. The mass fusion splice losses of hermetic coated fibers were found to be identical to those of standard polymer coated fibers. The restoration of the carbon coating on fusion splices of carbon coated fibers (and ribbon fibers) has also been demonstrated [46-48] by using a carbon-dioxide laser as a heat source. A maximum strength of 4 GPa and an n-value of 85 have been achieved for recoated splices[47]. Although in the production of normal quality splices it has been found that it is neither necessary nor desirable to remove the carbon coatings before splicing, for very high strength splicing it is necessary to remove the coating. Since there are no known satisfactory chemical solvents for the carbon, it is normally oxidized, i.e., burned off. Neither the details of the kinetics nor the resultant bare fiber strength are known. It is clear that the carbon can be easily removed by a rather modest thermal treatment in air or oxygen. While this simplifies the carbon removal, it obviously reduces the promise of these coatings for high temperature use.

In view of the lack of promise for high temperature use of either the carbon coating or the metal coatings generally available, it has been suggested that a dual coating might be successful. The idea was that the carbon would be applied first in order to eliminate the silica-aluminum reaction. The aluminum would then be applied in order to protect the carbon from oxidation. While this dual coating system was not really a success for high temperature use, it was, however, demonstrated that a 1 GPa strength can be maintained after an exposure at 400°C for 25 years[49].

A substantial amount of development effort has gone into carbon coatings, and a reasonable compromise can be achieved between strength and fatigue. Thus it would appear that, because they contribute no added loss, carbon coated hermetic fibers may have a better chance of success for long-haul applications provided issues related to the color coding and field splicing of dark colored carbon coated fibers are solved.

SUMMARY

Metal coatings on glass optical fibers can be hermetic and lead to an extremely high strength fiber. The bend strength of monocrystalline tin coated fibers is as high as 14 GPa. Metal coated fibers can survive relatively high temperatures (350°C for aluminum coated fibers), but all metal coated fibers show additional optical losses due to microbending. No information is available regarding the splicing and reconstitution of metal coated fibers.

Carbon coating, on the other hand, is relatively easy to apply and is hermetic (with a very high fatigue resistance, and also resistance to hydrogen permeation), but the fibers are not as strong as the metal coated fibers (~ 6 GPa). An important advantage is that the carbon coating does not contribute any additional optical loss. Carbon coated fibers can also be used for reliable pigtails. Field splicing and reconstitution of the carbon coating on splices are feasible, but the color coding, practical field splicing and recoating, and costs are the major hurdles for the widespread use of such fibers. Still, carbon coated optical fibers appear to have a much better chance than metal coated fibers for performing as reliable hermetic coated fibers for long-haul applications in harsh environments provided future development effort is devoted to addressing the above shortcomings.

REFERENCES

1. A. Gouronnec, R. Goarin, G. LeMoigne and M. Baptiste, Proc. SPIE, 2290, 191 (1994).
2. D. Taylor, TIA FO-6.6.8 Meeting, April 6, Arlington, VA (1995).
3. Y. Katsuyama, N. Yoshizawa and T. Yashiro, J. Lightwave Tech., 9, 1041 (1991).
4. W. Griffioen, G. Segers and E. van Loenen, Proc. IWCS, 368 (1990).
4a. V. Bogatyrjov, et al., Opt. Eng., 30, 690 (1990).
5. R. Arridge and D. Heywood, Brit. J.Appl. Phys., 18, 447 (1967).
6. D. Pinnow, G. Robertson and J. Wysocki, Appl. Phys. Lett., 34, 17 (1979).
6a. J. Wysocki, G. Blair and M. Vince, US Patent 4,418,984 (1983).
7. V. Bogatyrjov, M. Bubnov, E. Dianov, A. Prokhorov, S. Rumyantsev and S. Semjonov, Sov. Tech. Phys. Lett., 14, 343 (1988).
8. P. Simpkins, Mater. Sci. and Eng., B23, L5 (1994).
9. A. Biriukov, V. Bogatyrjov, E. Dianov and A. Khitun, Sov. Lightwave Comm., 3, 235 (1993).
10. P. Hale, J. Almeida and J. Sheppard, Adv. in Ceramics, 2, 115 (1981).
11. M.Stein, S. Aisenburg and J. Stevens, ibid., 124 (1981).
12. D. Biswas and S. Raychaudhuri, Tech. Digest OFC/OFS, 124 (1985).
13. J. Williams, P. Garmon, D. Biswas and D. Nath, US Patent 4,485,122 (1984).
14. T. Nozawa, D. Tanaka, A. Wada and R. Yamauchi, Tech. Digest OFC, 217 (1992).
15. C.R. Kurkjian and C.R. Kurkjian, Jr., unpublished results, 1987.
16. K. Inada and T. Shiota, Proc. SPIE, 99 (1985).
17. V. Bogatyrjov, et al., J. Tech. Phys., (in Russian) 18 , 1991.
18. V. Bogatyrjov, E. Dianov and S. Rumyantsev, Tech. Digest OFC, 219 (1992).
19. G. Taylor, J. Inst.Met., 62, 307 (1938).
20. M. Bubnov, E. Dianov and S. Semjonov, Mat. Res. Sys., 244, 97 (1992).
21. D. Biswas, Proc. IWCS, 634 (1989).
22. S. Tanaka, K. Inada, O. Fukuda, R. Yamauchi and T. Shiota, Fujikura Tech. Rev., 15 (1986).
23.V. Bogatyrjov, E. Dianov, S. Rumyantsev and A. Sysoliatin, Tech Digest OFC/IOOC,78 (1993).
24. C.Kurkjian and P. Simpkins,unpublished results, 1994.
25. P. Simpkins, C. Kurkjian and C. Schroeder, Elec. Lett., 31, 747 (1995).
26. G. Cooper, J.Mater. Sci., 2, 206 (1967).
27. T. AuCoin, S. DiVita and M. Wade, US Patent 4,118,211 (1978).
28. R. Hiskes, Tech. Digest OFC, 74 (1979).
29. R. Huff, F. DiMarcello and A. Hart, Tech. Digest OFC, (1988).
30. N. Yoshizawa and Y. Katsuyama, Elec. Lett., 25, 1429 (1989).
31. K. Lu, Tech. Digest OFC, 174 (1990).
32. K. Oohasi, T. Shimomichi, S. Araki and N. Satoh, Proc. ECOC, 33 (1991).
33. D. Biswas, Solid State Optical Materials, 28, 551 (1992).
34. S. Semjonov, M. Bubnov, E. Dianov, C. Kurkjian and A. Breuls, Proc. SPIE, 2290, 74 (1994).
35. M. Tuzzolo, A. Allegretto and E. Urruti, Proc. IWCS, 381 (1993).
36. T. Shimomichi, K. Oohashi, S. Araki and T. Maruoka, Proc. IWCS, 651 (1994).
37. J. Boniort, C. Brehm, J. Rousseau, J. Saugrain, G. Roussy and J. Ayache, Proc. ECOC, 37 (1991).
38. E. Sikora, J. Wright, S. Pycock and M. Yates, Proc. IWCS, 663 (1991).
39. M. Nakamura, A. Urano, H. Aikawa, H. Ishikawa and T. Danzuka, Proc. IWCS, 43, 644 (1994).
40. M. Estep and G. Glaeseman, Pro. SPIE, 1791, 18 (1992).
41. D. Biswas, C. Burpee and H. Yuce, Proc. SPIE , 1791 (1992).
42. K. Lu, G. Glaesemann and G. Kar, Pro. IWCS, 87 (1987).
43. G. Berthelsen, J. Andreassen, T. Birkeland, G. Lang and K. Nyaaas, ibid., 628 (1991).
44. T. Akiyama, Y. Kawada, H. Hiramatsu and K. Hirabayashi, ibid., 155 (1991).
45. T. Wtanabe, K. Osaka, T. Yanagi, Y. Ishiguro and Y. Asano, ibid., 294 (1990).

46. D. Innis and J. Krause, Tech. digest, OFC (1991).

47. K. Oohashi, T. Shimomichi, S. Araki and N. Sato, Proc. IWCS, 111 (1992).

48. I. Fijita, M. Hamada, H. Aikawa, K. Nagayama and Y. Asano, ibid., 119 (1992).

49. M. Bubnov, S. Semjonov, A. Shchebunyaev and C. Kurkjian, Tech. Digest OFC/IOOC, 77 (1993).



Dipak R. Biswas received his M.S. and Ph.D. degree in Materials Science and Engineering from the University of California, Berkeley in 1974 and 1976 respectively. He started working on optical fiber coating development at ITT-EOPD since 1981. After working for Alcatel Cable Systems, SpecTran and Fiberguide, he joined Bellcore in Morristown, N.J. in 1994. He is currently working on the strength and reliability of optical fibers with different coatings.



Charles R. Kurkjian received his B.S. degree in Ceramics from Rutgers University in 1952 and his Sc.D. in Ceramics from M.I.T. in 1955. After post-doctoral positions at M.I.T. and the University of Sheffield in England, he spent 35 years at A.T.&T. Bell Labs in Murray Hill, N.J. During this time he did research and development on glass and glass fibers. In September of 1994 he retired from Bell Labs and joined Bellcore in Morristown, N.J. where he continues his work on the strength and reliability of lightguide fibers.



Hakan H. Yuce is Chief Scientist and Director of Transport Technology at Bellcore, Morristown, N.J. His group is responsible for fundamental work in the areas of fiber/coax media and component reliability. His group is also responds to clients' immediate needs related to consultation on reliability and field problems. He received his B.Sc. Degree in Mechanical engineering from Technical University of Istanbul, his M.S. Degree in Mechanical engineering from M.I.T. and his Ph.D. Degree in Mechanical Engineering and Materials Science from Stanford University.

Dr. Yuce plays an active role in the establishment of U.S. and international standards regarding optical fiber and component test procedures to assure reliability. He has published over 100 technical papers, contributed to three books, and presented hundreds of talks and educational courses. He is the recipient of the 1980 NATO Fellowship, the 1986 ASTM Engineering Foundation Fellowship and the 1992 Telephony's Ray Blain Outside Plant Achievement award.

DEVELOPMENT OF HERMETIC, SCRATCH-RESISTANT DIAMOND-LIKE CARBON COATINGS FOR SILICA OPTICAL FIBERS

Nalin Kumar[1], Bawa Singh[2], Sam DiVita[3], Neil Vallestero[3], Samiul Amin[1,2], R.H. Williams[4]

[1]SI Diamond Technology, Inc., Houston, Texas; [2]David Sarnoff Research Center, Princeton, New Jersey
[3]US Army, Fort Monmouth, New Jersey; and [4]Plasmatron Coating Systems, Moorestown, New Jersey

ABTRACT

Diamond-like Carbon (DLC) films have numerous potential applications, particularly in optics and as abrasion and chemical resistant coatings. Amorphous DLC films have been produced by rf plasma deposition from hydrocarbon gas such as butane. The DLC films being developed are intended to provide improved reliability and performance, and maintain the design and dimensional characteristics of the optical fibers against abrasion, chemical erosion and environmental degradation. DLC coatings are typically inert, moisture and H_2 impermeable and are applied at near room temperatures. SEM data for coated fibers, electron diffraction for flat substrates show the films to be smooth, uniformly adherent coatings. The films have excellent optical transperancy in the 0.8 to 1.6μm wavelength used in fiber optics and have a refractive index around 2.0.

INTRODUCTION

Despite tremendous advances in fiber optic technology, one of the limiting characteristics of the present generation optical fibers is the lack of long-term stability and performance reliability. These limitations are due mainly to mechanical and chemical damage of the fiber surface by abrasion and the corrosive effects of adverse environments. The mechanical damage can be caused by scratches or surface abrasion in the cable environment and during handling. The chemically induced degradation arises from moisture and chemical attack of the fiber surface. Three major coatings for optical fibers are commonly used in industry. These coatings are polymeric, metallic, and inorganic; but no single coating can fulfill all of the mechanical, optical, and environmental requirements [1].

DLC films possess a range of properties that make them ideal for use as protective coatings for optical fibers. The films are of high hardness, higher thermal conductivity, scratch resistance, inertness to most materials, gases, organic solvents and chemicals, stability up to 400°C in reactive or inert atmospheres, high electrical insulation, transperancy from visible through the far infrared wavelength and hermiticity to moisture, H_2 and acids.

PRIOR APPROACHES TO PRODUCE IMPROVED FIBERS

The long-term reliability and enhancement of the performance of optical glass fibers can be improved by protecting the fibers against mechanical abrasion, microbending losses, scratches, radiation damage, fatigue, chemical and corrosive environment, moisture attack and hydrogen permeation. These goals can be realized either by developing a new class of silica glasses which corrode/degrade slowly in the harsh environmental conditions, or by modifying the cladding of the standard silica glass fiber or by developing the fiber glass coatings. Fiber coatings provide a more promising and flexible approach to achieving fiber reliability. These coatings, however, have to meet stringent requirements as discussed below.

Fiber Coatings : Needs and Requirements

It is desirable that the ideal applied coatings meet the following requirements :

- Coating must be thick enough and compliant to neutralize the effects of stress concentrating flaws on the fiber.
- Must produce stiff fiber coating composite to minimize conformity to contacting the surfaces.
- Provide superior dimensional and structural characteristics.
- High deposition rate with uniformity and concentricity.
- Low moisture sensitivity, chemical resitant and abrasion resistant.
- Refractive index higher than that of cladding glass at the highest service temperature to achieve cladding mode stripping.
- Long term durability in severe environment with widely varying conditions.
- Inert to vapors or liquid that may penetrate the optical fiber.
- Coating should offer low micro bend losses.

In addition, the most important requirement is that the coating is able to maintain design characteristics of the fiber over the entire projected life and during continuous contact with cable filling compounds/gels.

LIMITATIONS OF EXISTING FIBER COATINGS

There are three types of coatings which have been developed as optical fiber coatings. These are (i) polymer, (ii) metallic,

and (iii) inorganic and amorphous carbon coatings. each of these coatings provide substantial improvement over uncoated fiber.

(i) Polymer Coatings

Optical fibers are generally coated with ultraviolet (UV) cured coatings. Typical strength of UV cured acrylate coated 125 μm diameter fiber is around 750 kpsi (5.17 GPa). These fibers exhibit lower strength when they are subjected to a long term stress (such as wound fiber on a FOG-M bobbin), particularly in a moist environment. The applied stress induces a slow crack growth of pre-existing flaws to a critical level before failure. The crack growth accelerates in presence of moisture/water until failure. This phenomena is called fatigue. The static fatigue parameter (n-value) of UV -acrylate coated optical glass fiber is around 22-24. In contrast polymide coated optical fiber has an n-value of 32 [2]. Normally, a dual layer coating, which is more popular among manufacturers due to high reliability predictions, is applied to the fiber and acts for both protection and microbending. However, it has been observed that even a double layer polymer coating is unable to protect the fiber completely from harsh conditions.

(ii) Metal Coatings

Studies of various aspects of silica fibers coated with metals have been investigated. Coatings of a variety of materials, such as Sn, In, Zn, Pb, and Al have been reported to influence the strength of the fibers. Development of metal coatings of 10-20 μm thickness demonstrates superior bend stresses and tensile strength and improved survival in humid atmosphere as compared to polymer[3]. However, being relatively hard, metal coated fibers tend to exhibit excess losses due to microbending. In addition, metal coated fibers are sensitive to electromagnetic interference.

(iii) Inorganic and Amorphous Coatings

A significant improvement in fatigue resistance has been achieved by applying inorganic and amorphous coatings on glass fibers [4-8]. Several coatings such as TiC, SiC, amorphous carbon showed very high n-value (near or greater than 100). In general, these coatings are applied by very high temperature CVD process. Even though the n-value of these coated fibers are high, the strength of the coated optical fiber is usually low (in the range of 400 to 600 kpsi).

It is quite explicit that a hermetic coating of a non-metal is desirable to improve both the mechanical and environmental durability of optical fibers and thus improve the long term reliability of the optical fibers.

EXPERIMENTAL SET-UP

DLC films have been successfully synthesized by using a variety of plasma and ion beam based processes [9-14]. The properties of films produced by these different methods can vary quite considerably[14]. We have modified a cylindrical magnetron sputter source into a high-intensity plasma chemical vapor deposition (CVD) reactor developed by Kumar[15]. This reactor configuration has the advantages of being able to deposit DLC films with high uniformity and concentricity, and at high deposition rates onto long lengths of fiber. We were able to deposit hard, durable, and chemically inert DLC films on commercial silica fibers using butane.

The modified PECVD deposition source used for DLC film deposition is shown in Figure 1. This source concept is very suitable for scaling-up for high-rate coating of optical fibers in an in-line draw tower configuration. The fiber is held in the geometric center of the reactor by the fiber transport system. Deposition occurs from the dissociation of butane gas in the rf plasma and subsequent condensation of the film forming DLC on the substrate. Plasma is generated applying rf (13.56 MHz) excitation using a capacitively coupled "L" type impedance matching network.

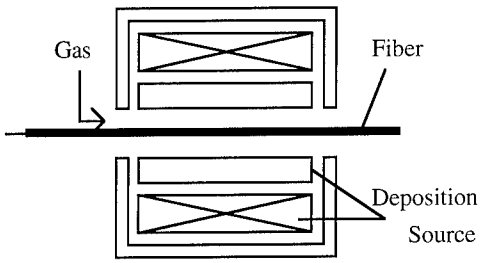


Figure 1. Cylindrical PECVD reactor module used for depositing DLC layers on optical fibers.

EXPERIMENTAL RESULTS

DLC layers were synthesized using butane as the gaseous precursor. Film properties routinely measured included :

- depositon rate,
- coating composition,
- microstructure,
- surface morphology,
- optical and mechanical properties.

These properties were measured as a function of the deposition process parameters, such as incident rf power, gas pressure, substrate bias, and gas flow.

Deposition rate

The variation of deposition rate of DLC films on silica fibers vs. applied rf power is shown in Figure 2. As shown in Figure 2, the deposition rate increases almost linearly with applied power. The rf power supply is capable of supplying a maximum power of 1.0 KW. No saturation of the increase in deposition rate with increasing power was observed upto 1KW. The deposition rate is also highly dependent on flow rate and pressure. Typically highest deposition rates (>5μ m/min) are obtained when flow rates exceed 50sccm and the pressure is >100 millitorr.

Refractive Index

The refractive index is a good indicator of the film density and hardness as well as other "diamond-like" properties. Films with refractive index below 1.8 generally tend to be soft, more transparent and more polymer-like. Films with refractive index greater than 1.8 are harder, less transparent and have properties that resemble diamond. Refractive index of the deposited films was measured using a dual wavelength Gertner ellipsometer and the measurements were done using HeNe laser with a wavelength of 6320Å. Figures 3 and 4 show the dependence of refractive index with rf applied power and substrate bias power respectively.

Optical Transmittance

A Beckman UV/VIS/NIR spectrophotometer was used to measure the optical transmittance of DLC films. Figure 5 shows the transparency of the DLC layers on silicon substrates from 1.0 to 2.5μm. It is seen from this data that the films are completely transparent in this wavelength (i.e. the near infrared) region. The increase in transmittance of the silicon sample indicates that the films are able to act as anti-reflection coatings due to their refractive index between 2.0 and 2.2.

Visible appearance of DLC layers

The deposited DLC layers can have different colors depending on process conditions. The films can vary from transparent which have a very high degree of transparency to black coatings that are virtually opaque to visible light. The clear films are relatively soft and the darker films tend to be hard.

Substrate rf bias and gas pressure have an effect on the hardness and transparency of the films. At low substrate bias and low gas pressures the deposited films are clear and fairly soft. As the bias and pressure are increased, film hardness increases dramatically and the films become increasingly less transparent. It has been observed that at high pressure film deposition rate increases considerably.

SEM Characterizations on Flat Substrates

Figure 6 shows scanning electron microscope (SEM) micrographs of DLC films on silicon wafers. The films have an extremely smooth surface and they display no grain structure. The usual columnar structure observed for most thin films is generally absent. Surface scans using commercial profilometers such as Dek Tak also confirm the very smooth surface of these layers.

Etchability of DLC layers

DLC films were found to be stable against most common laboratory solvents including all commonly available acids. However, DLC films can be easily patterned or completely removed by plasma etching when oxidizing gases such as O_2 or N_2O are employed. Figure 7 is a micrograph showing etched DLC lines on silicon wafers. The etch rates are high, typically 1μm/min in standard parallel RIE etch tools.

Scratch Resistance

The hardness of the DLC films was assessed using a custom scratch tester that is based on Mohs scale. Depending on the deposition conditions, films with hardness exceeding SiC can be obtained at high coating rates.

Hermiticity Evaluation

Thin film metals, such as aluminum and silver, approximately 5mm in diameter were deposited on glass slides. The whole slide was then coated with DLC approximately 3,000Å thick. The coated slide was then immersed in a mixture of hydrochloric and nitric acid for 15 minutes. No degradation or etching of the metal dots was observed indicating that the DLC films were dense and pore-free and impervious to acid.

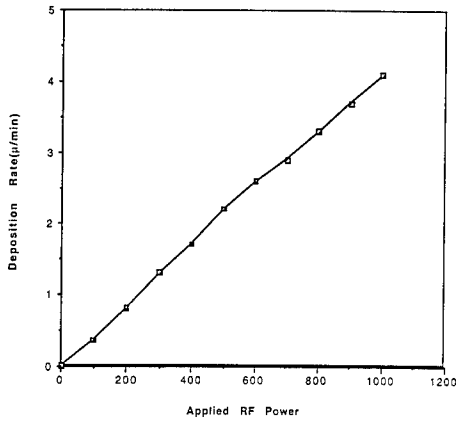


Figure 2. Variation of deposition rate of DLC films on silica fiber (100 μm diameter) vs. applied rf power
(Gas : Butane, Pressure : 10 millitorr, Flow rate : 30sccm)

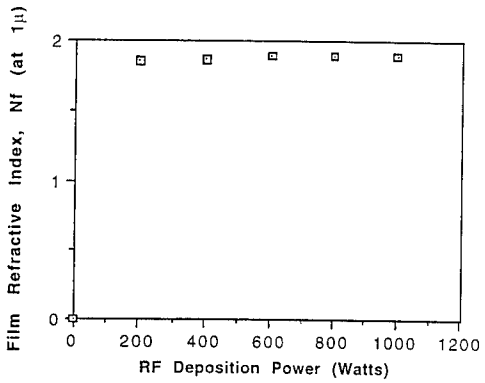


Figure 3. Variation of refractive index with rf power
(Substrate : flat quartz slides, film thickness : 1.0 μm
Gas : Butane, Pressure : 10 millitorr, Flow rate : 30sccm)

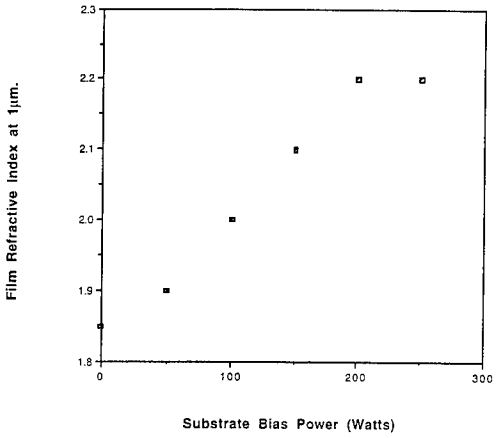


Figure 4. Variation of refractive index with substrate bias power.
(Substrate : flat quartz slides, film thickness : 1.0 μm
Gas : Butane, Pressure : 10 millitorr, Flow rate : 30sccm)

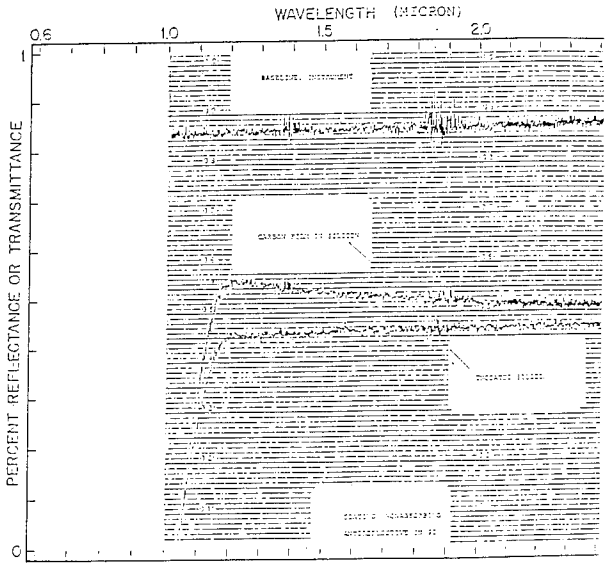


Figure 5. Optical transmittance of DLC films on Silicon.

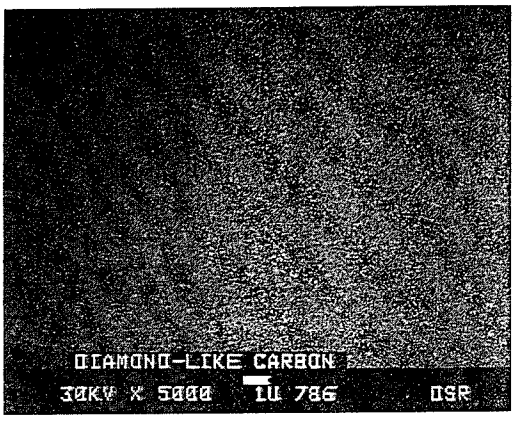


Figure 6. SEM of DLC films on Silicon wafer.

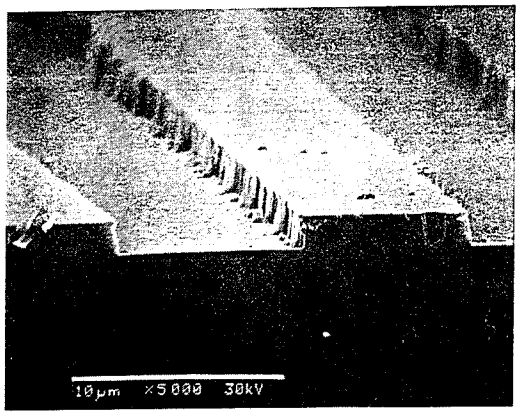
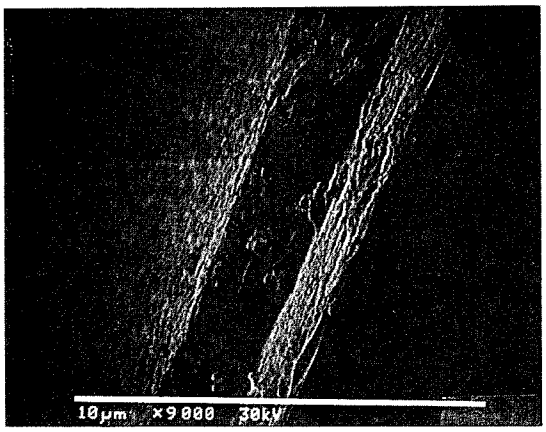


Figure 7. SEM of plasma-etched DLC films on Silicon wafer.



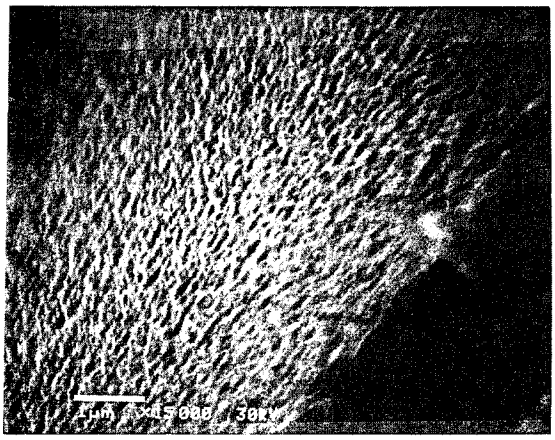


Figure 8. Silica fibers - with no pre-coating, DLC layer thickness : 2µm.
(Deposition conditions : rf power 100 Watts, Gas : Butane, Pressure : 25 millitorr, Flow rate : 30sccm, Time : 5min.)

Fiber Coating Results

SEM of DLC coatings on uncoated CeramOptec single mode optical fibers are shown in Figure 8. The DLC films on uncoated silica fibers are very smooth and the films have excellent adherence. Furthermore, the coatings do not appear to degrade the fiber strength. It is possible to bend DLC coated fibers into circles of 0.25" diameter or smaller. The adhesion of DLC films to uncoated fibers is so good that it is very difficult to peel or chip sections of the coating for SEM examination. As seen in these micrographs, there is very little chipping or lift-off of the DLC film from the fiber surface. Figure 8 shows a typical DLC film applied at 100 Watts of rf power. As can be seen, the film has very dense, pore-free structure and is uniformly applied to the fiber. A slight granular surface morphology is seen at magnifications greater than 15,000.

SUMMARY

DLC films possess a range of properties that make them near ideal for use as protective coatings for optical fibers. DLC films, if they can be successfully applied, can provide a hard, hermetic, non-toxic, chemically resistant, inert coating for optical fibers that is smooth and has a low coffecient of friction, the required optical properties and can be applied at near room temperatures. Moreover, DLC coatings on optical fibers will eliminate the organic plastic coatings used in FOG Missiles, thus reducing the weight and thickness of the coatings.

ACKNOWLEDGEMENT

This work has been sponsored by the U.S. Army, Communication and Electronics Command, Fort Monmouth under contract DAA07-93-CB001. The authors are thankful to Ramazan Soydan and Bogdan Brycki for their assistance in the experimental work at David Sarnoff Research Center.

REFERENCES

1. D. Biswas, Optical Engg, 31(7), 1400 (1992).
2. D. Biswas, Optical Engg, 30(6), 772 (1991).
3. V. Bogatyrjov etal., Sov. Tech. Phys. Lett., 14 (5), 343 (1988).
4. S. Divita etal., US Patent 4,110,211 (1970).
5. P. Schultz and S. Raychoudhary, US Patent 4,735,932 (1988).
6. D. Biswas and S. Raychoudhary, US Patent 4,592,932 (1988).
7. R. Huff etal., Tech Digest OFC, TUG2 (1988).
8. K.Lu, ibid., THH4, 174 (1990). SPIE 842 (1987).
9. B. Singh etal., App. Phys. Lett. 57(22), 1990.
10. B. Singh David Sarnoff Research Center, Unpublished Work.
11. B. Singh etal., Appl. Phys. Lett. 52, 451 (1988).
12. B. Singh etal., Proc. SPIE Symp. on Microelectronic Materials, 877 (70) (1988).
13. B. Singh etal., Sarnoff Technical Report No. PRRL-88-TR-022.
14. Diamond and Diamond-Like Films, Proc. Electrochem. Soc. 89(12), (1989), Ed. J.P. Disukes.
15. N. Kumar, US Patent.

Dr. Nalin Kumar is Director of advanced Technology at SI Diamond Technology, Inc., Houston, Texas. He holds an M.Sc and Ph.D. in electrical Engineering from Drexel University, Philadelphia, PA.

Dr. Bawa Singh is currently Head of Advanced Materials and Applications Group at David Sarnoff Research Center. He holds a B.Sc. degree in Physics and Ph.D. in Plasma Physics from the University of Aston in Birmingham, England.

Neil John Vallestero received his BE in Electrical Engineering from Stevens Institute of Technology in 1991. He is currently pursuing his Masters degree in EE at Stevens with a concentration on lightwave/microwave communication. Since 1991, Neil has been with the US Army CECOM in the Photonics Group in Space and Terrestrial Communication Directorate. His current area of research is in optical heterodyning.

Samiul Amin received his M.S. degree in Electrical Engineering from New Jersey Institute of Technology (NJIT) in 1993. He is currently enrolled in the Ph.D. program at NJIT and working on developing DLC as a coating material for optical fibers.

Mr. Robert H. Williams is currently General Manager of Plasmatron Coating Systems, Inc. a division of SIDT.

HERMETIC AND POLYMERIC COATINGS FOR MILITARY AND COMMERCIAL APPLICATIONS

G. Orcel, J.Y. Boniort*, J.Y. Barraud*, and R.J. Overton +

Alcatel Fibres Optiques, Bezons, France
*Alcatel Alsthom Recherche, Marcoussis, France
+Alcatel Telecommunication Cable, Claremont, NC

ABSTRACT

Optical fibers with a hermetic coating are very attractive for applications in harsh environment due to their resistance to corrosion and hydrogen permeation. Alcatel has been active in the field of carbon coated fibers for many years. This paper reviews the main results obtained by the different laboratories.
For specific applications where hydrogen resistance is not a strong requirement, it might be more interesting to develop a polymeric coating with a high n value. The second part of this paper reviews the work on fluorination of UV-curable urethane acrylate polymers. Fibers drawn with this polymer as a secondary layer have a static fatigue parameter greater than 50.
Finally, preliminary results on thin coatings (200 µm outside diameter) are presented. They indicate that comparable properties to the ones of 250 µm OD fibers should be attainable.

INTRODUCTION

More and more applications are available to optical fibers provided that they can meet the technical challenges which are inherent to them. Optical fiber networks are expanding with for example the fiber-in-the-loop (FITL) concept. Bringing the optical signal to businesses and homes is an attractive idea. Military applications are also developing with the use of fibers for guided vehicles and for adverse environment. All these applications require the fiber to survive in increasingly harsher environments in terms of water aggression and bending, with long lifetime (20 years or more).
Another aspect is that fibers must be as small as possible, either to fit in existing conduits for FITL, or to optimize space utilization for military applications.
There are several approaches which can be followed to address these issues. The first approach, which has been extensively used and studied over the past few years, is the hermetic coating. The most successful process is the heterogeneous pyrolysis of hydrocarbon gas on the fiber surface. Coatings with a fatigue parameter « n » well in excess of 100 are easily obtained. In this paper, the main parameters which govern the coating characteristics will be briefly reviewed. The impact of the process on the fiber output of the plant will be evaluated.

When the resistance to hydrogen is not a strong requirement for the product, it might be interesting to consider another approach. Most optical fibers which are available on the market have a dual polymeric coating of the urethane acrylate family. The static fatigue parameter « ns » measured for these coatings is typically 20. The newest Alcatel's primary coating[1] was designed taking into account the glass polymer interface and « ns » values greater than 30 were obtained. This coating can also be applied in smaller thicknesses (about 200 µm OD) and still provides a significant protection to the fiber. It is possible to further increase the « ns » value of the coating by introducing fluorine in the formulation of the secondary coating, and « ns » values in excess of 50 were obtained. The latest work on the fluorination of the resin will be presented.

HERMETIC COATING

Manufacturing Process.

Over the past few years, pyrolytic carbon coating has been extensively studied in the field of hermetic coating and is the most efficient material in terms of fatigue resistance. It is deposited on the silica fiber by on-line pyrolysis of hydrocarbon gases such as acetylene, ethylene, butadiene, methane, propane or benzene. The optimum pyrolysis temperature is related to the bond energy of the hydrocarbon molecule. Consequently, the structure and the quality of the carbon coating depends on the fiber temperature in the reactor, which is in turn determined by the draw speed.
Another important parameter in terms of factor « n » is the coating thickness. It is necessary to deposit a layer with a thickness above a threshold value to effectively protect the fiber.
For the industrial process, it is important to monitor the coating properties on-line. It has been demonstrated that the electrical resistance provides a good indication of the coating property. Alcatel developed a measuring device based on microwave absorption.[2] The introduction of a dielectric wire into a helical microwave cavity reduces the power output of the cell. This power drop is directly correlated to the mean electrical resistance of the carbon coated fiber. Figure 1 illustrates the variation of the electrical resistance and the factor « n » as a function of the drawing speed, with the reactor at a fixed position. At low speed, the electrical resistance is high because the carbon layer is thin (less than 10 nm). This is not enough to provide hermeticity and the n

parameter is low. At median speed (270 m/min to 360 m/min) the carbon thickness is about 30 nm, and the n parameter is greater than 500. At higher speed, the fiber temperature increases and the carbon coating becomes polycrystalline as shown by electron diffraction (figure 2) and « n » decreases rapidly.

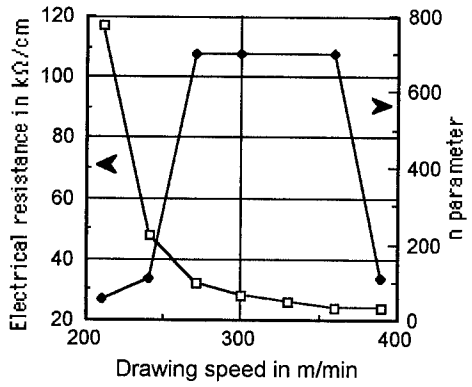


Figure 1. Influence of the draw speed on the electrical resistance and n parameter of a carbon coated fiber.

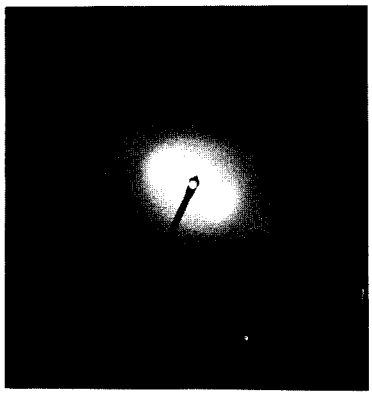


Figure 2. Electron diffraction picture of a polycrystalline carbon layer.

Fiber Strength.

The other fundamental parameter which determines the lifetime of the fiber is the mechanical strength. It is well known that the hermetic coating reduces the mean strength of the fiber. However, it is important to note that if the manufacturing process is well under control then there should not be additional low stress breaks, as illustrated on the following Weibull plot (figure 3).

The influence of the process parameters on fiber strength is illustrated in figure 4. As the thickness of the hermetic coating increases, the fiber strength decreases. Finally, there is a sharp decrease of the strength, which is due to crystallization of the carbon coating. Although this data cannot be translated into coating roughness, which is the main parameter which affects fiber strength,[3] it is possible to identify the operating set points from such a diagram. Also, deposition of soot on the coating must be avoided, because it decreases fiber strength.

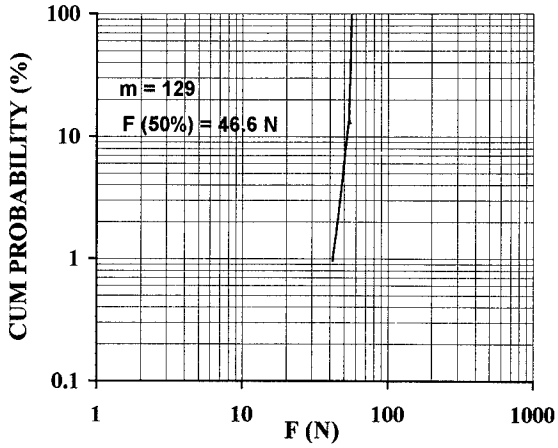


Figure 3. Weibull distribution plot of a hermetic carbon coated fiber.

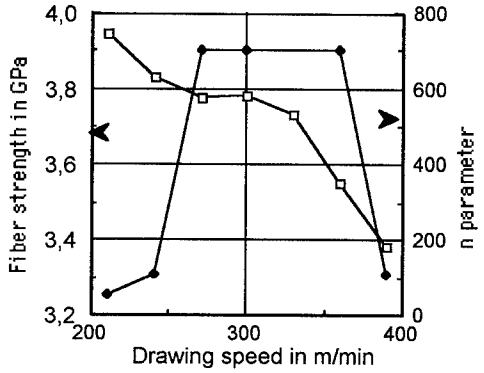


Figure 4. Influence of the draw speed on the mean strength and n parameter of a carbon coated fiber.

Fiber Characterization.

From the curves presented in figures 1 and 4, it can be seen that it is possible to manufacture fibers with a hermetic coating with an « n » value about 500 and with a mean strength which is about 80% of the value for the fiber without hermetic coating. Fibers prepared with a coating with such an « n » value did not present any attenuation increase at 1224 nm after 21 day exposure to 11 atmospheres of hydrogen at 85°C. For specific applications, it is necessary to submit the fiber to more exotic test, such as weathering under vibration. The sensitivity to vibration of the hermetic coating is determined by two types of tests : 1) vibration of a coiled fiber during 8 hours between 5 and 500 Hz with an acceleration of 5 times the gravity; and 2) vibration at resonance (about 140 Hz) of fibers loaded under 1.5 N. After these tests no modification of fiber strength and n parameter has been observed.[4]

POLYMERIC COATING

For most terrestrial applications, it is not necessary that the fiber presents an improved resistance to hydrogen. It is possible to guarantee the same lifetime (t) using a fiber with a lower « ns » value and by proof testing it at a higher level. As a first approximation, the proof test level (σ_p) to ensure a 20 year lifetime can be deduced from the following equation as a function of the applied stress in operation (σ_a).

$$\sigma_p = (A\ \sigma_a^{n})^{1/(n-2)} \qquad (1)$$

where A = t/B, B being the crack strength preservation parameter (known as B-value and taken = 0.1 GPa^2.ms). The results are presented in figure 5. It can be seen that for an applied stress in operation of 0.5 GPa, a factor « ns » greater than 33 will ensure a 20 year lifetime at a fiber prooftested under 1 GPa. It is then interesting to develop a polymeric coating with a high « n », which will ensure a significant protection against water corrosion, and which can be drawn at the same speed as for the existing process. This can be achieved by introducing fluorine into the formulation of the secondary polymeric layer.

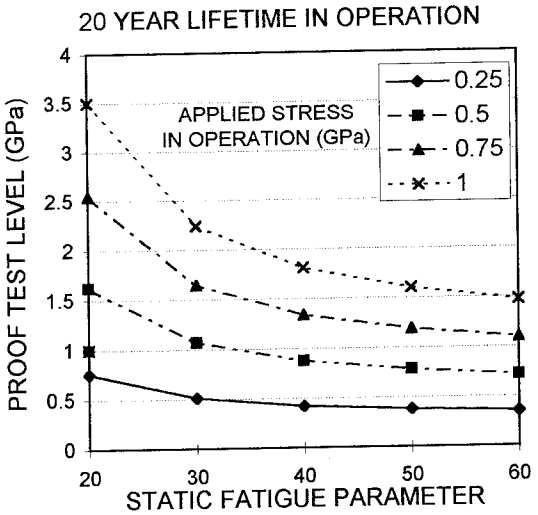


Figure 5. Influence of the factor n on the prooftest level for ensuring a 20 year lifetime under various applied stress.

Composition of the Resin.

UV-curable acrylates and especially urethane acrylates are widely used as optical fiber coatings. They combine good rheological properties for high-speed low-tension extrusion, high curing rates and extended pot lives. Both primary and secondary resins have similar compositions:
- a urethane acrylate oligomer,
- one or two monomers having one or several acrylate functions and acting as reactive diluents,
- a photoinitiator.

Oligomers and reactive diluents copolymerize under UV light to give a cross-linked network which is the final coating. The coating properties are affected by the length of the diol chain. When the chain length increases, the crosslink density and the volume fraction of polar urethane groups decrease. As a result, the glass transition temperature (Tg) and the Young modulus (E) decrease.[5] Functionality and length of the acrylate diluents modify also the whole range of mechanical and chemical properties of the final material. They must be optimized to provide the coating the desired characteristics.

Improvement of the Watertightness.

Water permeability of the polymeric coating is an important concern since it is strongly correlated to the static fatigue parameter. In moist environment the organic coating preserves fiber strength by hindering water diffusion.[6] However, this protection is not good enough with the classically used material.
Previous studies have shown that the incorporation of fluorine atoms in polymers decreases strongly water permeability.[7] Two different approaches for the fluorination of the resin are presented in this work. They are first the addition of fluorinated reactive diluents; and second the incorporation of fluorinated chains in the oligomer.

Fluorinated reactive diluents: First, commercially available fluorinated reactive diluents were tested. Only a few percents of diluent could be incorporated in a classical secondary resin because of poor miscibility. Consequently, it was decided to design reactive diluents having a polar function compatible with the polar urethane links of the resin oligomer. The molecules which present the maximum miscibility with the resin are of the type

$$R_1SR_2O\overset{\overset{O}{\|}}{C}CH{=}CH_2$$

with $R_1 = C_mF_{2m+1}C_nH_{2n}$ and $R_2 = C_pH_{2p}$.

Films of the different new formulations were prepared and tested for the water vapor permeability (by measuring the weight loss at 20 °C and 50% R.H. of a permeability cup covered with a 10 cm^2, 50 µm thick film). The permeability values, P, measured for these films are very similar to the one obtained for a film made with the neat resin. This is probably due to the fact that the polar functions which are necessary for the compatibility with the resin cancel the hydrophobic effect of the fluorine. In order to avoid these antagonist effects, a direct fluorination of the oligomer was explored.

Fluorinated urethane acrylate: The oligomer is the reaction product of a diol, a diisocyanate and an hydroxy alkyl acrylate. The easiest way to incorporate a fluorinated chain in such an oligomer is to fluorinate the diol. Fluorine can be introduced in the backbone or in a side chain.

The fluorinated oligomers thus produced are then mixed with one or two reactive diluents to reach the desired viscosity (about 6 Pa.s at 20°C). The permeativity values are 0.020 g.cm/m^2.24h.mm Hg for fluorination of the main chain, and between 0.008 and 0.020 g.cm/m^2.24h.mm Hg for fluorination of the side chain. The best formulation in terms of permeability and mechanical properties was tested on fiber and the results compared with two Alcatel coating systems, AFC1 and AFC3. The results are presented in table 2. It can be seen that the best combination is with the primary of the AFC3 system and with the fluorinated secondary, which gives a static fatigue parameter of 51. From equation 1, it can be deduced that such a fiber proof tested at 1 GPa will survive 20 years under 0.64 GPa of applied stress in operation. This is much more than what is usually requested by the users.
It is worth noting that although the surface of the coated fiber is hydrophobic due to the presence of fluorine atoms, it can be processed without problem through an inking line. The fibers are undergoing extensive testing at the present time.

ALCATEL coating system	secondary coating permeability (a)	static fatigue n-value
AFC 1	0.045	n = 22
AFC 3	0.035	n = 30
primary AFC3/ fluorinated sec.	0.011	n = 51

a: in g.cm/m^2.24h.mm Hg

Table 1. Permeability and static fatigue parameter values for various Alcatel coating systems.

Future Direction.

Thinner coatings (200 to 210 µm outside diameter) are being more and more considered.[8] They find application in higher count cables, they can fit the small conduits which are found in the existing networks in many cities, and they also allow a more efficient use of space in military vehicles. The challenge is to develop a coating system which can provide the same level of protection. Several coating systems are under testing in different laboratories within Alcatel. Preliminary results indicate that it is possible to achieve a significant level of protection with a 200 µm outside diameter coating. Figure 6 presents the Weibull distribution plots for a 250 and a 200 µm outside diameter fibers. Although a slight decrease in median strength can be observed (about 1.5%), there is no additional breaks under proof testing. These fibers are more sensitive to lateral stress induced by micro bending than the 250 µm outside diameter fibers, but this can be easily compensated for by slightly modifying the refractive index profile. The aging behavior of these fibers is being studied at the present time.

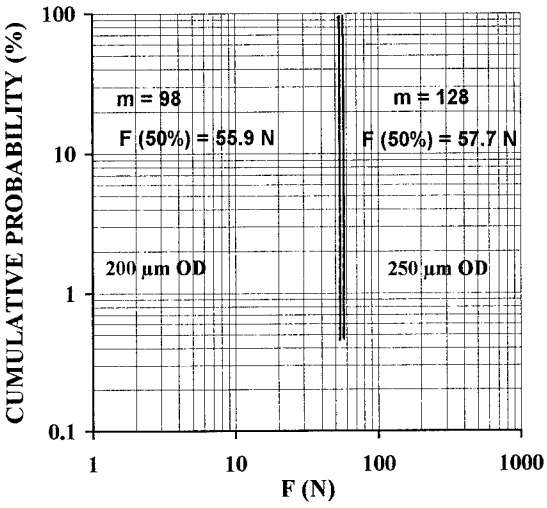


Figure 6. Weibull distribution plot for a 250 and a 200 µm outside diameter fibers.

CONCLUSION

Fibers with hermetic coatings are the prime candidate for applications in harsh environments especially when a good resistance to hydrogen permeation is needed. Over the years, Alcatel developed specific equipment (such as a carbon thickness measuring device) to produce carbon coated fibers with competitive properties. Fatigue resistance parameters in excess of 500 were produced with a mean strength of about 80% of the strength of the un-coated fiber.
However, for most specific applications, it might be more interesting to develop a polymeric coating with a high n value, and which is more compatible with the non-hermetic manufacturing process. This was achieved by fluorinating the side chains of UV-curable urethane acrylate formulation.
Static fatigue parameter in excess of 50 were obtained. This coating is also compatible with actual inking processes.
These progresses in polymeric coating technology are significant enough to predict that smaller outside diameter fibers with comparable properties to the actual fibers will be soon achievable.

ACKNOWLEDGMENTS

The authors gratefully acknowledge the financial support of FRANCE TELECOM, contract number 91-35-145.
The contributions of S. Gervat from Alcatel Alsthom Recherche is greatly appreciated.

REFERENCES

1. R.J. Overton, C. Lasne, H.M. Michaud, R.G. Sommer, « Designing an Optical Fiber Dual Coating System for Loose Tube and Ribbon Cable Long Line and Local Loop Applications », IWCS, p 701, 1993.

2. J-Y Boniort, C. Brehm, J.C. Rousseau, J.M. Saugrain, G. Roussy, J. Ayache, « New Characterisation Techniques for Hermetic Carbon Coated Fibers », ECOC 91, MoB1-4, p 37.

3. N Yoshizawa et al., « High Strength Carbon Coated Fibre », Elec. Let. 12th oct 1989, Vol 25, N° 21.

4. M. Carratt, « L'Etude et Développement de Fibres Monomodes à Revêtement Hermétique », report CNET number 91-35-145, 1993.

5. D.J. Broer, G.N. Mol, « Fast Curing Primary Buffer Coatings for High Strength Optical Fibers », J. Lightwave Technol., vol. LT-4, p 938, 1986.

6. D.M. Szum, C.P. Chawla, T.E. Bishop, K.P. Murray, J.M. Zimmerman, « Water Sensitivity and its Relationship to Stability in Optical Fiber Coating », IWCS, p 703, 1990.

7. J.F. Imbalzano, D.N. Washburn, P.M. Mehta, « Minimized Failure in Fluoropolymers », Chemical Engineering 98, p 105, 1991.

8. K. Oishi, W. Katsurashima, T. Kakuta, Y. Matsuda, S. Tanaka, « Coating Design of Thin Coated Fiber for Ultra-High-Count Optical Fiber Cable », IWCS, p 687, 1993.

BIOGRAPHIES



Gérard Orcel received his MS and Ph.D. degrees from the University of Florida in the field of Materials Science and Engineering in 1985 and 1987 respectively. He held positions at GelTech and Spectran before joining the R&D group of Alcatel Fibres Optiques in 1992 as Project Manager. Since then, he has been involved in preform design, CVD and draw technology and coating development.



Jean-Yves Boniort was born in 1942. He received an Engineering degree from Ecole Nationale Supérieure de Céramique Industrielle de Sèvres in 1967. He joined Alcatel Alsthom Recherche in 1970. He is presently is in charge of the drawing process and development of new coating technics within the Fibers and Photonics Systems group.

Jean-Yves Barraud was born in 1941. After a Ph.D. in crystallography he joined Alcatel Alsthom Recherche in 1970, where he held several positions in the field of analytical chemistry and polymer science. He is now Manager of the « Laboratoire Diagnostic Intervention Service », which is devoted to the characterization of materials used by the different Alcatel units in the fields of electrochemistry, energy, and telecommunication. He also leads a group involved in research on polymers for industrial applications.

Bob J. Overton is a Senior Principal Scientist in the Fiber Development Group at Alcatel Telecommunications Cable. He received a B.S. in Chemistry from Mercer University and a M.S. in Polymers from the Georgia Institute of Technology. After 14 years with AT&T Bell Laboratories working in fiber optic coatings and cable materials, he joined Alcatel in 1991. At the present time he is responsible for the development of coatings and fiber strength improvement.

A HERMETIC CARBON/POLYIMIDE COATING COMBINATION FOR ADVERSE ENVIRONMENTS

V.A. Cusanello, N.J. Jacobson*, M.J. Supczak, and P.R. Stupak

SpecTran Corporation 50 Hall Road Sturbridge, MA 01566

*SpecTran Specialty Optics Company 150 Fisher Drive Avon, CT 06001-1260

Abstract

Optical fibers made for operation in adverse environments including high temperature (>100C), aggressive chemicals, environmental hydrogen, and where space constraints require small bending radii, require specialized coatings. One such coating consists of an amorphous carbon layer overcoated with a thin polyimide layer. This paper examines the strength characteristics of hermetic carbon/polyimide coated fibers subject to water aging and aging at elevated temperatures. This coating combination effectively blocks strength degradation due to water induced stress corrosion at the fiber surface. The strength reduction due to high temperature aging was found to follow an Arrhenius type time-temperature dependence. A microscopic examination of temperature aged fibers provided insight into the coating damage accumulation process.

Introduction

The primary function of an optical fiber coating is to preserve the fiber strength by protecting the glass surface from both mechanical damage and the external environment. For most data and telecommunication applications, the protection provided by coatings based on acrylate polymers is sufficient to assure mechanical integrity of the system. However, for adverse environments such as high temperature (>100°C), aggressive chemicals, environmental hydrogen, and where space limitations require small bend radii, more specialized coatings are required. Metal coated fibers providing hermetic coatings were first proposed and demonstrated by Pinnow and co-workers[1,2]. Several non-metallic coatings have also been shown to provide hermeticity[3-5]. However, most such coatings are complex to apply and induce high losses. Thin amorphous carbon coatings are easy to apply and provide good hermetic protection[3,4,6-11].

We report here on the strength characteristics of a composite coating consisting of a thin (<1um) amorphous carbon layer overcoated with 5 to 15um polyimide polymer coating in comparison with fiber coated only with polyimide. The amorphous carbon is continuously deposited during the fiber draw process and is the product of a gas phase CVD reaction. The polyimide coatings use a special applicator and are thermally cured. The carbon coating provides hermeticity, and thus lowers the time dependent strength degradation resulting in a high fatigue exponent. The thin polyimide coating provides the full benefit of mechanical protection while maintaining a small fiber diameter, an important feature for small bend radii and constrained space application. Furthermore, the polyimide coating allows connectorization directly over the coating which eliminates the reduction in reliability inherent to the coating stripping process.

The short length unaged strength of the hermetic coated fiber was less than the polyimide coated fiber. However, the dynamic fatigue exponent and zero-stress aging performance for the hermetic fiber were superior to the polyimide coated fiber. The post-temperature aging strength of the hermetic and polyimide coated fibers was found to follow an Arrhenius type time-temperature dependence. Microscopic examination of the temperature aged fibers showed that localized pitting formed in the polyimide surface coincident with the degradation in strength of the polyimide coated fiber. However, the carbon hermetic/polyimide coated fiber lost strength prior to the pit formation, suggesting a second strength degradation mechanism for this coating material combination.

Sample Fiber Preparation

Two coating variations were considered in this study. The first fiber sample was coated only with a polyimide layer, while the second was coated with an amorphous carbon layer followed by a polyimide layer. The carbon thickness was estimated from electrical resistance measurements[12] to be 34nm thick. The polyimide coating was 15um thick for both fiber samples. The two coating types were applied to 125um clad diameter graded index multimode fiber drawn from the same preform. The fibers were exposed to a 25°C and 50% humidity environment for a minimum of 48 hours prior to testing in the same environment.

Strength Testing

The short length fiber strength of both fibers was measured from 0.5m gauge length tensile specimens tested using a rotating capstan unit operating at a reference strain rate of 4%/min. Fifteen specimens of each coating variation were tested.

The Weibull strength distributions for the coated fibers are shown in Figure 1. The polyimide coated fiber exhibited higher strength, but a similar Weibull modulus compared to the hermetic coating. The strength reduction associated with the presence of a hermetic carbon coating has been noted frequently in the technical literature[3,6,7,13,14]. However, the mechanism for the strength reduction has not been clearly established. Some workers suggest that particle impact during the deposition process[15] or thermal residual stress in the carbon layer results in defect formation in the silica surface[16]. An alternate view claims that the low strain to failure of the carbon layer (5.5%) allows the external environment to reach the silica and activate the stress corrosion reaction in existing surface defects[9,14]. Other workers concluded that a combination of carbon coating smoothness and thickness resulted in higher strength carbon hermetic fibers[6,11,13].

Dynamic Fatigue

Dynamic fatigue tests were performed to determine the susceptibility of the fibers to time dependent stress corrosion as quantified by the dynamic fatigue exponent. The 0.5m gauge length tensile specimens were tested on a rotating capstan apparatus operating at 0.025%, 0.25%, 2.5%, 4%, and 25%/min strain rates. The dynamic fatigue exponent was calculated from the slope of the bi-logarithmic plot of fracture stress versus strain rate. Fifteen specimens of each coated fiber were tested.

Although the polyimide coated fiber possessed a higher unaged fiber strength, the carbon hermetic coated fiber exhibited superior dynamic fatigue performance with n>100 compared to n=23 for polyimide (Figure 2).

Zero Stress Aging: 85C Water Soak

The effectiveness of the sample coatings in preventing strength reduction under near zero stress conditions was determined by measuring the fiber strength as a function of immersion time in 85°C water. Loose coils of the fiber were totally immersed in water while the ends of each coil were isolated from direct water contact. Strength testing was conducted immediately after the fiber was removed from the water after aging for 1, 4, 7, and 10 days. Fibers were fractured as 0.5m gage length tensile specimens using the rotary capstan unit operating at 4%/min strain rate. Ten fibers were tested for both of the fiber samples.

The experimental results in Figure 3 illustrate that the advantage of the greater unaged strength of the polyimide coated fiber relative to the hermetic fiber is lost after less than four days in the harsh environment. Notice that the carbon hermetic fiber retained the unaged strength throughout the ten day aging period.

High Temperature Aging Strength

The relationship between fiber strength as a function of exposure time and temperature at elevated temperatures was investigated for both coating types. The test consisted of preparing approximately fifteen fiber specimens, 80mm in length, and placing the fibers into a silica tube (10mm inner diameter). One tube of fibers was prepared for each exposure time at a given temperature. Thirteen exposure times were selected over the period between six minutes to 100 hours. The thirteen tubes of fibers prepared for each of the coating types were placed within a preheated resistance furnace operating in an air environment. The tubes were withdrawn from the furnace at the prescribed time intervals and the fiber strengths evaluated using the two-point bend method after a 24 hour equilibration in a 25°C and 50% humidity environment. Five aging temperatures were investigated, including, 300, 350, 375, 415, and 500°C. The fibers contained in each tube were allowed to remain in physical contact, since tests showed that little inter-fiber adhesion occurred even at long aging times.

Figure 4 shows the resulting mean strength as a function of exposure time and temperature for the coated fiber samples. For both cases, the fiber strength decreased with both increasing exposure time and temperature. A comparison between the different coatings shows that the polyimide coated fiber retained its strength at higher temperatures and for longer times compared to the hermetic fiber. The strength of the carbon hermetic fiber decreased to a minimum value of 2.4GPa for the temperatures investigated. Severely aged carbon hermetic coated fibers exhibited an apparent strength increase after the minimum mean strength was reached, whereas the polyimide fiber mean strength continued downward after degradation initiated. Both the apparent strength increase of the hermetic and strength loss of the polyimide fibers were accompanied by an increase in strength variability as seen in Figure 5, where the deviation of the strength is plotted as a function of aging time for each fiber type. The strength distributions for the severely aged hermetic coated fibers were bi-modal (Figure 6). For the hermetic fiber, one strength population was located near the low strength minimum observed in Figure 4b (i.e. 2.4GPa) and the other distribution was located above the unaged carbon hermetic fiber strength, such that the strength attained, but did not exceed the strength of the unaged polyimide (i.e. 7GPa) (Figure 6). The polyimide coated fiber strength distribution consisted of some fibers showing nearly the unaged strength and a low strength distribution indicative of damage to the fiber.

The mechanism of strength degradation for both coated fiber types is not currently known. However, useful insight into the degradation process was obtained through microscopic examination of the aged fibers.

The polyimide coated fiber outer surface was initially smooth prior to aging with no inhomogenieties apparent on the surface. Increased aging time at elevated temperature resulted in a change in the polyimide coating color from yellow to brown in localized regions around the fiber circumference and along the fiber length. Closer examination showed that the darkened areas contained circular shaped roughened regions followed by the formation of circular pits in the coating after further aging (Figure 7a,b). Energy dispersive X-ray (EDS) elemental analysis of the pit interior revealed a strong presence of silica and no carbon, indicating that the polyimide coating had been removed. The diameter of the circular pit regions increased with continued aging (Figure 7c). Ultimately the polyimide coating was completely removed for the most severely aged fibers.

The formation and growth of the circular pits in the coating corresponded to the decrease in the mean strength of the polyimide fiber. Figure 8 shows the polyimide coated fiber mean strength data at 415°C as a function of time (Figure 4a) with the position of the micrographs of Figure 7 noted. A plausible mechanism for the observed strength degradation, therefore, is mechanical damage to the silica surface caused during sample handling and occuring with a greater probability as more polyimide material is lost from the surface.

A microscopic examination was also conducted for carbon hermetic coated fibers aged at 415°C to allow direct comparison to the aged polyimide samples. The polyimide/carbon hermetic coated fiber outer surface was also initially smooth prior to aging with no inhomogenieties apparent on the surface. The polyimide outer layer followed the same pitting type degradation process as the fiber coated only with polyimide. The pits were first observed after 5 hours of aging and increased in diameter with increasing aging time (Figure 9). EDS elemental analysis showed that the carbon layer was present at the bottom surface of the circular pits, but was not present for severely aged fibers which had lost the majority of the polyimide coating. However, the mean strength of the aged hermetic fiber began to degrade sooner than the polyimide coated fibers aged at comparable times and temperatures (Figures 4a,b), suggesting that a different strength controlling mechanism was operative. Further observation revealed that fibers aged as little as 19 minutes at 415°C were occasionally found with portions of the polyimide layer absent. The polyimide appears to have detached from the fiber during testing and was observed as separated pieces of full thickness (Figure 10). The loss of sections of polyimide was never observed for the polyimide coated fiber. EDS elemental analysis verified the presence of the carbon layer at the regions where the polyimide had detached. The detachment of polyimide from the fiber coincided with the onset of the strength degradation in the hermetic coated fiber and suggests a reduction in the polyimide to carbon adhesion. Severely aged fibers which possessed a bi-modal strength distribution (Figure 6), exhibited regions where both the polyimide and carbon layers were removed.

Following the analysis of Bubnov and co-workers[14] for aging of a dual hermetic carbon/tin coating, the mean strength curves in Figure 4 were shifted horizontally along the time axis to form a master curve according to the Arrhenius relationship (Equation 1) (Figure 11),

$$\ln\left(\frac{t_1}{t_2}\right) = \frac{Ea}{R}\left[\frac{1}{T_1} - \frac{1}{T_2}\right] \qquad (1)$$

Where t_1 is the time required for the fiber strength to decrease to a given value at the aging temperature T_1 and t_2 is the calculated time for the strength to degrade to the same chosen value after aging at temperature T_2. The activation energy is given by Ea and is calculated from the slope of a plot of the time shift factor versus the inverse of the absolute temperature, and R is the gas constant. The mean strength data for both the polyimide and hermetic coated fibers were shifted to a reference temperature of 300°C for comparison. The data for both fiber coatings superimposed well and a plot of the time shift factor versus the inverse absolute temperature produced substantially linear curves, indicating that the strength degradation mechanisms in both cases can be described by a thermally activated process over the temperature range explored (Figure 12).

The use of the master curve and Equation 1 suggests that the influence of adverse service environment on both polyimide and hermetic coated fiber strength can be quantitatively predicted. However, it is important to note that the data presented in Figures 4 and 11 pertain to short fiber segments and not necessarily to long fiber lengths that do not suffer from possible fiber end effects. The effect of elevated temperature aging on long fiber lengths is in process.

Conclusions

The strength of short lengths of polyimide and hermetic carbon/polyimide coated fibers was investigated as a function of carbon layer thickness, strain rate, zero-stress aging, and elevated temperature aging. The short length unaged strength of the hermetic coated fibers was less than the polyimide coated fiber. However, the dynamic fatigue exponent and zero-stress aging performance for both hermetic fiber types was superior to the polyimide coated fiber. The post-temperature aging strength of the hermetic and polyimide coated fibers was found to follow an Arrhenius type time-temperature behavior. Microscopic examination of the temperature aged fibers showed that localized pitting formed in the polyimide surface coincident with the degradation in strength of the polyimide coated fiber. However, the carbon hermetic/polyimide coated fiber lost strength prior to the pit formation, suggesting a second strength degradation mechanism for this coating material combination.

Acknowledgment

The authors gratefully acknowledge both the assistance of Carey Williams in performing the fracture testing and microscopy and SpecTran for the permission to publish the results of this study.

References

1. D.A. Pinnow, G..D. Robertson, Jr., J..A. Wysocki, Appl. Phys. Lett. 34(1979)17.
2. D.A. Pinnow, J..A. Wysocki, and G.D. Robertson, IECE E61(1978)171.
3. K.E. Lu, "Hermetic Coatings," OFC, 1990, p. 174.
4. R. Chaudhuri and P.C. Schultz, SPIE Vol. 717, 1986, p. 27.
5. M. Stein, Proc. of Conference of Laser and Electro-optics, (1982).
6. N. Yoshizawa and Y. Katsuyama, Electronics Letters, 25(1989)1429.
7. M. Koguchi, Y. Matsuda, K. Kokura, M. Mishimoto, and K. Hirabayashi, OFC, 1990, p. 176.
8. F.V. Dimarcello, R.G. Huff, A.C. Hart, K.L. Walker, R.M. Atkins, D.H. Smithgall, D.R. Edmonston, H.C. Chandan, and K.H. Chang, OFC, 1990, p. 175.
9. V.A. Bogatyrjov, M.M. Bubnov, E.M. Dianov, S.D. Rumyantzev, and S.L. Semjonov, Optical Engineering, 30(1991)690.
10. T. Zushi, S. Nakahara, T. Takeda, T. Kaide, and H. Tanaka, IWCS, 1992, p. 273.
11. Y. Katsuyama, N. Yoshizawa, and T. Yashiro, J. of Lightwave Technology 9(1991)1041.
12. Y. Ishida, Y. Kohmura, S. Arai, NIST Special Publication 839, 1992, p.67.
13. N. Yoshizawa, Y. Miyajima, and Y. Katsuyama, J. of Lightwave Technology, 9(1991)417.
14. M.M. Bubnov, E.M. Dianov, and S.L. Semjonov," IWCS, 1992, p. 629.
15. R.G. Huff and F.V. Dimarcello, Proc. SPIE 867, 40(1987).
16. K.E. Lu, G.S. Glaesemann, and M.T. Lee, Opt. Quant. Electron., 22(1990)227.

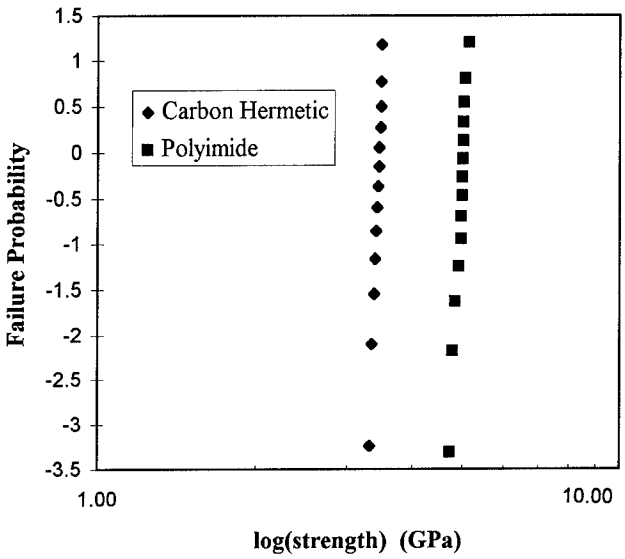


Figure 1: Weibull strength distribution for the polyimide and carbon hermetic/polyimide coated fibers. The test were conducted in uniaxial tension using a 0.5m gauge length.

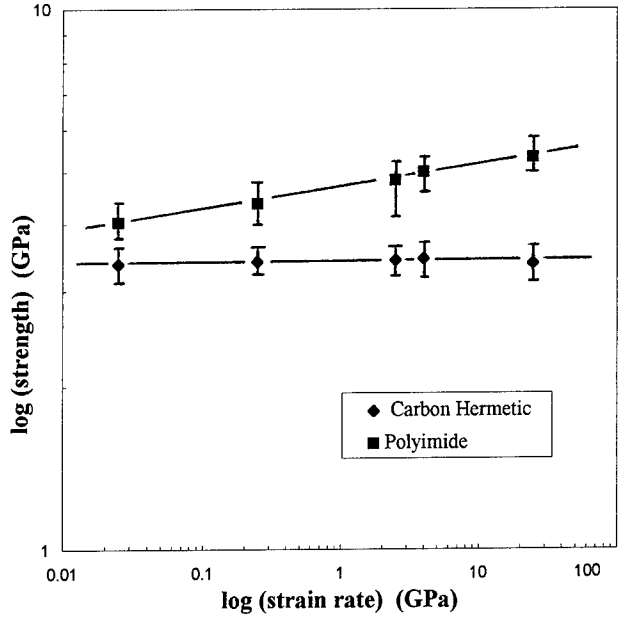


Figure 2: Dynamic fatigue test results for the polyimide and carbon hermetic/polyimide fibers. The error bars represent the strength at 15 and 85% failure probability.

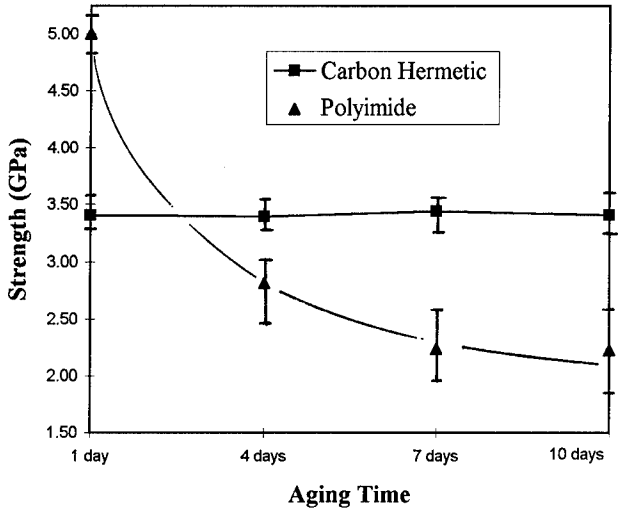


Figure 3: Zero stress aging test results for the polyimide and carbon hermetic/polyimide fibers. The error bars represent the strength at 15 and 85% failure probability.

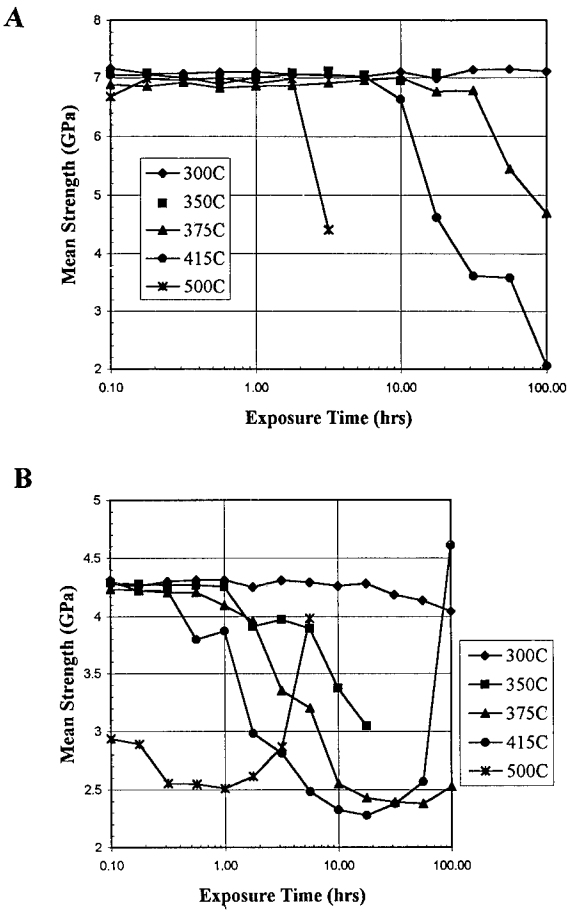


Figure 4: Mean fiber bending strength as a function of aging time and temperature for the A) polyimide coated and B) carbon hermetic/polyimide coated fibers.

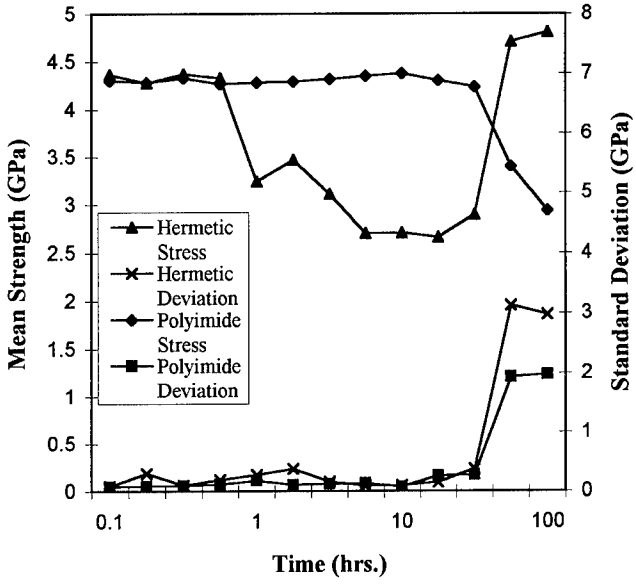


Figure 5: Mean fiber bending strength and strength standard deviation as a function of aging time at 375C for polyimide and carbon hermetic/polyimide fibers.

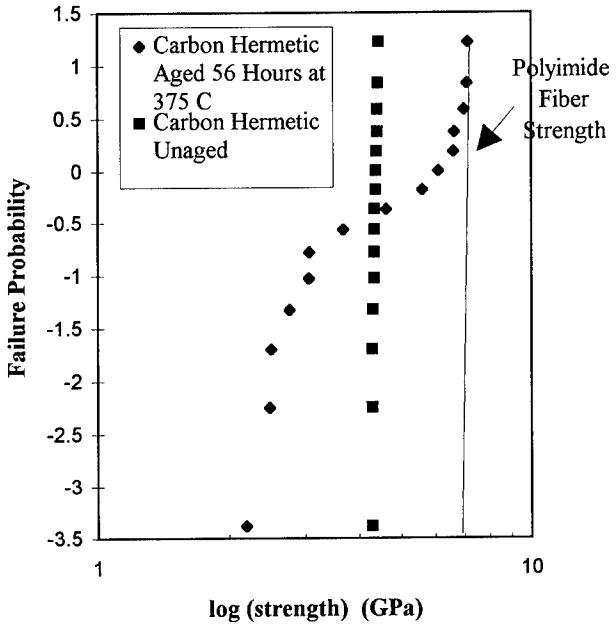
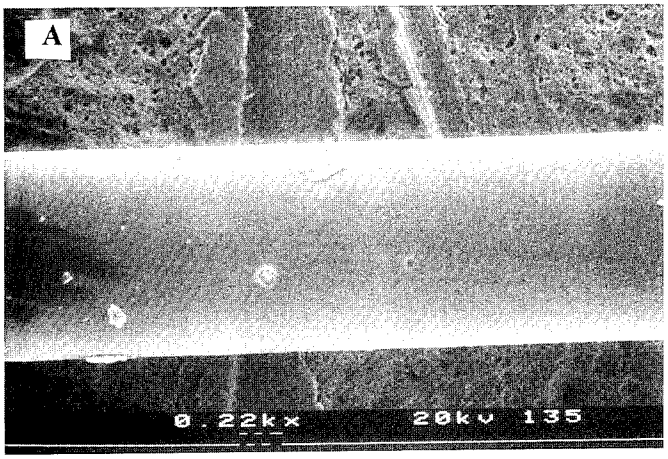
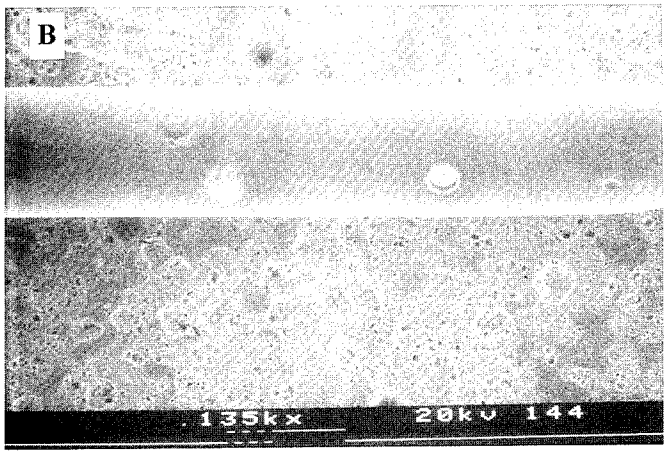


Figure 6: Weibull strength distribution of unaged and severely aged carbon hermetic/polyimide fibers. Note the high strength distribution of the aged fibers equals the unaged strength of the polyimide coated fibers.





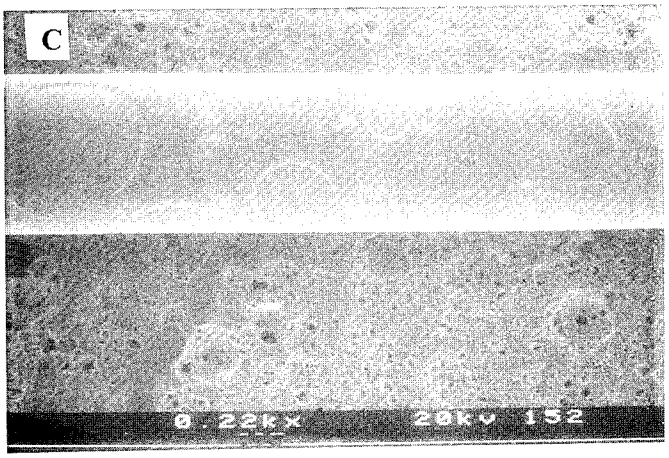


Figure 7: Scanning electron micrograph (SEM) micrographs of polyimide coated fiber after aging at 415C for A) 5hrs 37min., B) 17hrs. 45min., and C) 100hrs. Note the increasing pit diameters as a function of increasing aging time.

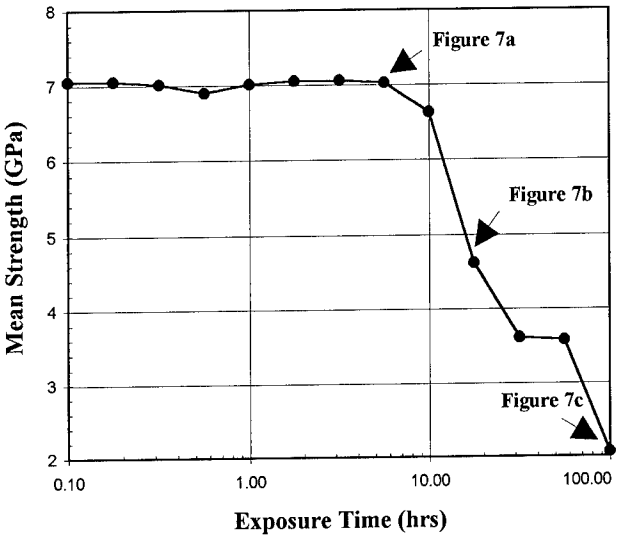
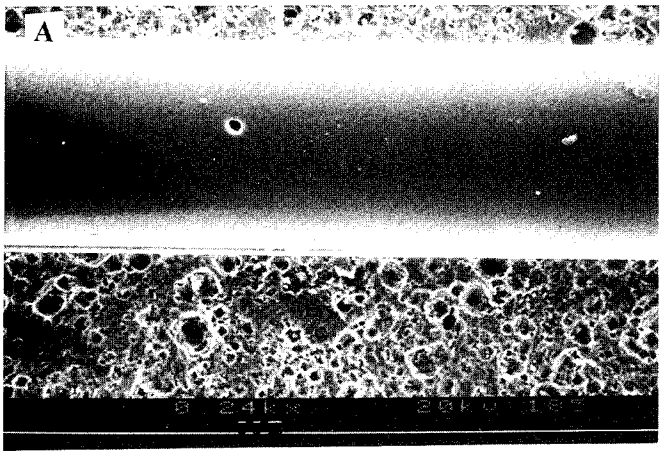


Figure 8: Mean bending strength of polyimide coated fibers (Figure 4a) aged at 415C, with the time position of the micrographs in Figure 7 denoted.



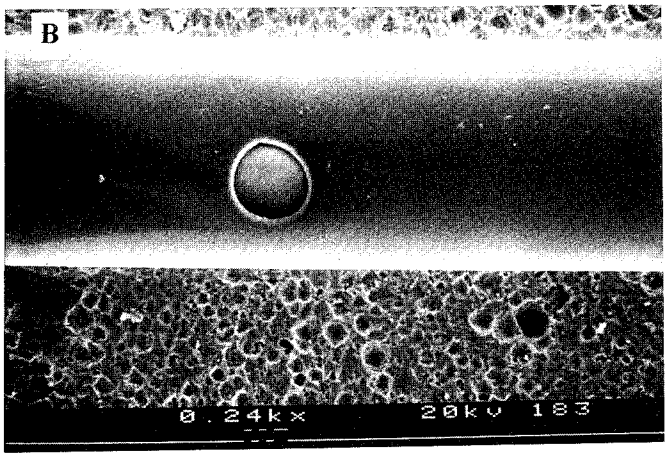


Figure 9: SEM micrographs of carbon hermetic/polyimide coated fiber after aging at 415C for A) 5hrs 37min., B) 56hrs.

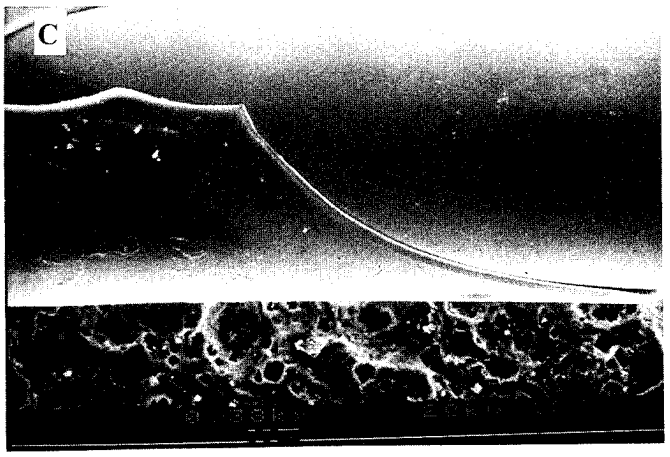


Figure 9 - Continued: SEM micrographs of carbon hermetic/polyimide coated fiber after aging at 415C for C) 100hrs. Note the increasing pit diameters as a function of increasing aging time.

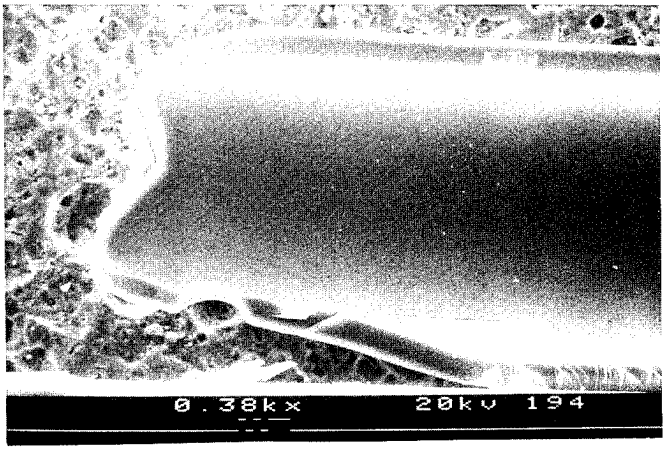
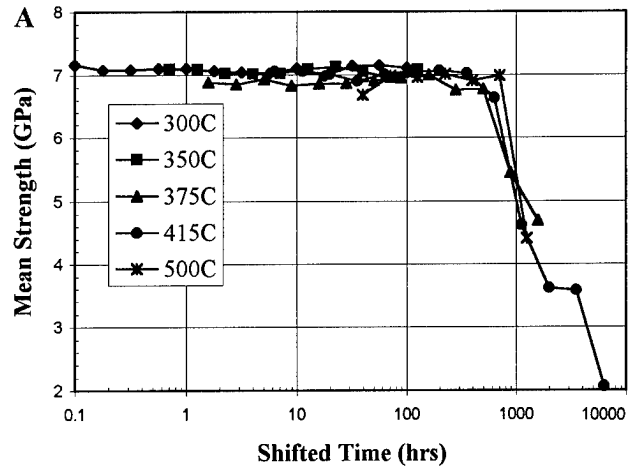


Figure 10: SEM micrograph of a section of polyimide coating that debonded after fracture testing from a carbon hermetic/polyimide coated fiber aged at 415C for 20 minutes.



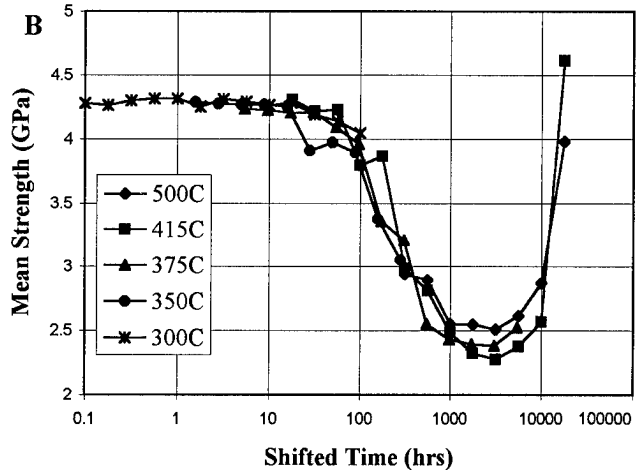


Figure 11: Master curves of mean fiber bending strength as a function of aging time and shifted to 300C reference temperature for the A) polyimide and B) carbon hermetic/polyimide coated fibers.

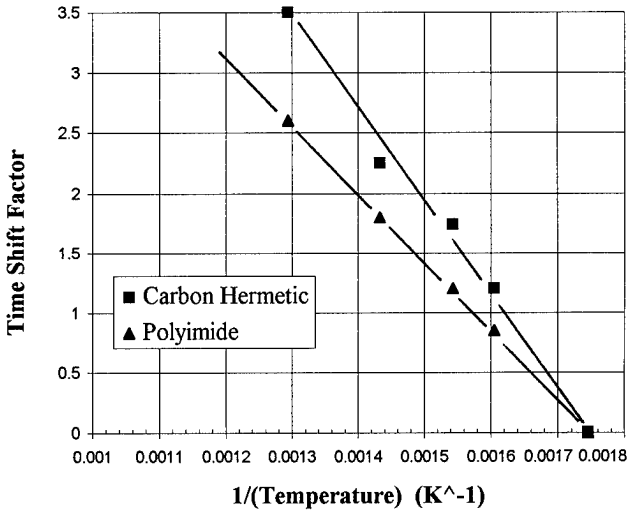
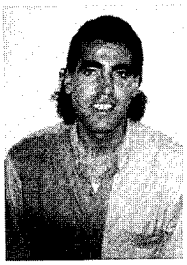


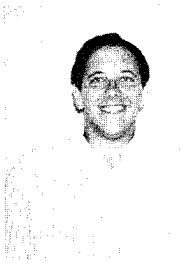
Figure 12: Arrhenius type plot of the time shift factors used to construct the strength aging master curves in Figure 11.



Victor Cusanello is a Draw Process/Project Engineer at SpecTran Corporation. He has worked at SpecTran for 13 years holding positions in preform and draw development and was responsible for the development of the hermetic/ polyimide draw process. Prior to joining SpecTran Victor was employed by Valtec Corporation for three years where he held various positions in preform manufacturing and draw development.



Michael J. Supczak is a Process Engineer, joining SpecTran Corporation in the summer of 1995. He graduated in 1994 with a Bachelor of Science degree in Mechanical and Aerospace Engineering from Cornell University. He subsequently followed his undergraduate degree with a Master of Science degree in Engineering Mechanics and Astronautics from the University of Wisconsin-Madison in 1995. At SpecTran, Michael is focused on manufacturing process improvements. He has also worked extensively on the fatigue, fracture and reliability of optical fibers. He is a member of the American Society of Mechanical Engineers.



Nick Jacobson received his B.S. degree in chemical engineering in 1982 and is completing a Masters in Business Administration degree, both from Worcester Polytechnic Institute. Nick is currently a Senior Product Line Engineer with SpecTran Specialty Optics Company and has over ten years of fiber optics and electro-optics experience at Galileo Electro-optics Corporation, SpecTran Corporation and SpecTran Specialty Optics Company. Nick's primary experience has been in the drawing of optical fiber, fiber optic coatings and the development of optical fiber metallized pigtails. Nick was previously a EIA/TIA optical fiber coating and reliability working group member for two years and is presently a member of the American Institute of Chemical Engineers, The International Society for Optical Engineers and the American Electroplaters and Surface Finishers Society.



Peter R. Stupak is a Fiber Draw Scientist at SpecTran Corporation. He received a Ph.D. in Mechanical Engineering from the University of Massachusetts in 1992. After graduation he held a one-year postdoctoral position at the University of Naples, in Naples, Italy, studying the mechanical properties of glass fiber reinforced polymers. Since he joined the SpecTran R&D Department in 1993, he has conducted research on the influence of the fiber draw process on fiber optical and mechanical properties.

OPTIMUM DISPERSION COMPENSATING FIBER : BIREFRINGENCE AND PMD SIMULATION AND FIBER PROCESS IMPROVEMENT

José CHESNOY, Pascale NOUCHI, Jean Yves BONIORT, Claude BREHM,
Christian LE SERGENT, Pierre SANSONETTI.

ALCATEL ALSTHOM RECHERCHE
Route de Nozay, 91460 Marcoussis, France

ABSTRACT

We show polarization mode dispersion (PMD) can be very high in dispersion compensating fibers (DCF).
However fibers with high figure-of-merit (FOM) up to 230 ps/nm/dB and polarisation mode dispersion (PMD) lower than 0.1 ps/√km have been made, by improving MCVD preform process and fiber drawing to reduce fiber loss and polarization mode dispersion.

INTRODUCTION

The availability of erbium doped fiber amplifiers in the 1.53 - 1.56 µm range and the lack of such amplifiers in the 1.31 µm window has impelled system designers to upgrade earlier 1.31 µm systems to 1.55 µm. Already laid conventional single-mode fibers have zero dispersion wavelength near 1.31µm and a positive dispersion close to 17 ps/nm/km at 1.55 µm. Therefore maximum achievable bit-rate distance is limited and dispersion compensating elements are needed. Adjusting chromatic dispersion to specific values is also needed for various system applications [1].
Dispersion compensating fibers (DCF) can be added quite easily with the 1.55 µm optical amplifiers, if extra loss and PMD are not too high and the ratio of chromatic dispersion to fiber loss, or figure-of-merit (FOM), far over 100 ps/nm/dB.

DCFs have already been presented by American and Japanese laboratories [2,3]. Their index profile were either step-like, W or triple clad and few data have been shown about PMD.
There we present results on low PMD dispersion compensating fibers.

In what follows, we first present theoretical investigation of short-length PMD or linear PMD (in units of ps/km) : we find that whatever the index profile is, PMD_{lin} is more than one order of magnitude higher than that of standard or dispersion-shifted fibers.
In the second part, we present our triple-clad design together with experimental results showing low PMD (as low as 0.07 ps/√km) and FOM around 200 ps/nm/km.

THEORETICAL INVESTIGATION OF FORM BIREFRINGENCE AND LINEAR PMD.

It is well known PMD arises from a difference in group velocity between two orthogonal principal polarization states *x* and *y*.
In short fibers, linear PMD (ps/km) is simply given by :

$$PMD_{lin} = \frac{d(\Delta\beta)}{d\omega} = -\frac{\lambda^2}{2\pi c}\frac{d(\Delta\beta)}{d\lambda} \quad , \qquad (1)$$

where birefringence $\Delta\beta$ is the difference in the propagation constants of the two orthogonally polarized principal states ($\Delta\beta = \beta_x - \beta_y$).
In a single mode fiber, this difference is caused by a combination of core ellipticity (form birefringence) and an associated thermal stress anisotropy (stress birefringence).

In long fibers ($L >> L_c$), PMD(ps/√km) and linear PMD(ps/km) are related through coupling length L_c :

$$PMD = PMD_{lin} * \sqrt{L_c}.$$

Theoretical contribution of core ellipticity to linear PMD has been shown to be very high in such high dispersion waveguide structure.

Using a perturbation theory by R.A. Sammut [4], we computed form birefringence $\Delta\beta_{form}$ and linear PMD for any profile as :

$$\Delta\beta_{form} = \frac{e^2(2\Delta)^{3/2}}{a}\Delta B(V) \qquad (2)$$

$$PMD_{lin} = \frac{4e^2(\Delta n)^2 d(\Delta B)}{c\, n_2 \quad dV} \qquad (3)$$

Where e is the ellipticity ($e^2 = 1 - a^2/b^2$), a the core radius and b the major axis, Δ is the relative index difference between the core and the cladding, $\Delta = (n_1^2 - n_2^2)/2n_1^2$), $\Delta\beta(V)$ is the normalised birefringence.

Figure 1 represents computed linear PMD for three index profiles commonly used for DCFs : step, W and triple clad. Profile parameters were chosen to yield chromatic dispersion of - 100 ps/nm/km with the lowest possible value for Δn (maximum of normalized waveguide dispersion), i.e. Δn = 20, 30 and 40. 10^{-3} for triple clad, W and step profile respectively. This operating point corresponds also to the maximum of linear PMD curve of figure 1.
PMD_{lin} is more than one order of magnitude higher than that of standard or dispersion-shifted fiber.

PREFORM AND FIBER FABRICATION

Triple clad index profile was chosen for fabrication due to a lower germanium doped central core part.

MCVD preform process has been improved for fluorine doped inner cladding deposition with SiF_4 and more accurate index profile and geometry control (figure 2) .

With high germanium content preforms, fiber drawing conditions are more critical to minimize drawing induced defects and low drawing temperature is better for lower fiber losses [5].

Fiber drawing conditions, like temperature gradient, protective gas flow, drawing speed and tension, have been explored to reduce fiber loss, while keeping residual stress to an adequate level for fiber end cleaving and connecting process.
Fiber loss is lower with higher drawing tension or lower furnace temperature, drawing speed has little influence (figure 3) .
Maximum FOM is up to 230 ps/nm/dB at 1.55 µm with loss as low as 0.5 dB/km and chromatic dispersion as high as - 117 ps/nm/km. (figure 4).
Mode field diameter is 2Wo = 6.2 µm,
with λc = 1.18 µm,
i. e. MAC number is ($2Wo/\lambda c$) = 5.3
This ensures a good compromise between high bending resistance [2] and low non-linear effects.

We could measure PMD_{lin} on short lengths of those fibers: computed form PMD_{lin} is close to measured values (Figure 5) showing how important contribution of form is. We believe the combination of high Δn and high "normalized waveguide PMD" explains high measured PMD values in DCFs.

Knowing how critical the preform core ovality is, we introduced special care in MCVD process as silica tube selection, appropriate alignment of tube burner lathe and modified collapse condition. Then the PMD of these fibers is between 0.5 and 1 ps/$\sqrt{}$km.

Furthermore by introducing mode coupling effects into fiber, very low PMD fibers, (< 0.1 ps/$\sqrt{}$km), have been obtained (figure 6).

CONCLUSION

We have shown that form PMD can be very high in DCFs.
However by improving MCVD preform process and fiber drawing triple clad fibers with high figure-of-merit (FOM) up to 230 ps/nm/dB and low PMD have been made.

ACKNOWLEDGMENT :

This work was partly supported by France Telecom.

REFERENCES

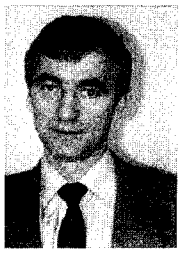
[1] S.S Sian et al, PD26, K. Olla et al, PD 22, M. Suzuki et al, PD 20 - OFC'95 San Diego

[2] A. M. Vengsarkar et al, - Symp. Opt. Fiber Meas. Rech. dig. Boulder)1994) pp 175-179.

[3] M. Onishi et al, - ECOC 94 Firenze Tech. dig. pp 681-684

[4] R.A. Sammut et al, - I.E.E. Proc., vol 3, pp. 173-187 (1981)

(5) C. Brehm et al, - Fiber and Integrated Optics vol. 7, (1988), pp 333-341.



José CHESNOY

ALCATEL ALSTHOM RECHERCHE

Route de Nozay

91460 Marcoussis FRANCE

José Chesnoy was born in 1954.
He is an "ancien élève" of the Ecole Polytechnique. and Docteur d'Etat (Orsay University 1981).
He was initially involved in research activities in the CNRS, after which he joined Alcatel Alsthom Recherche in 1989.
Dr Chesnoy is at present the manager of the Fiber and Photonic Systems Unit (UFP) a research department involved in new optical fibers and systems studies.

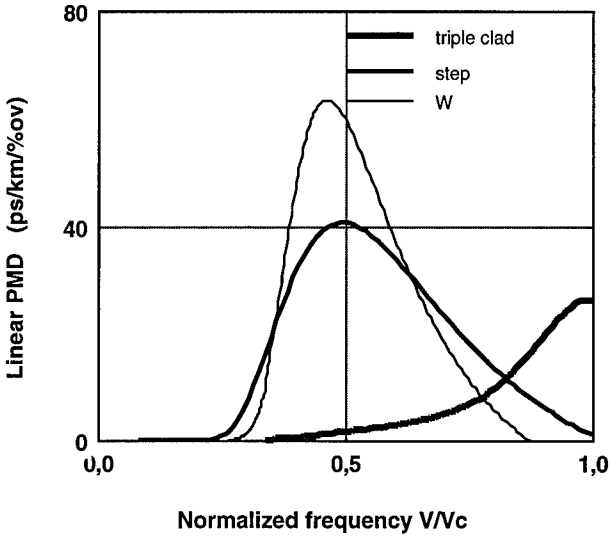


Figure 1 : Computed linear PMD per percent of core ovality versus ratio of normalized frequency V over cut-off frequency Vc.

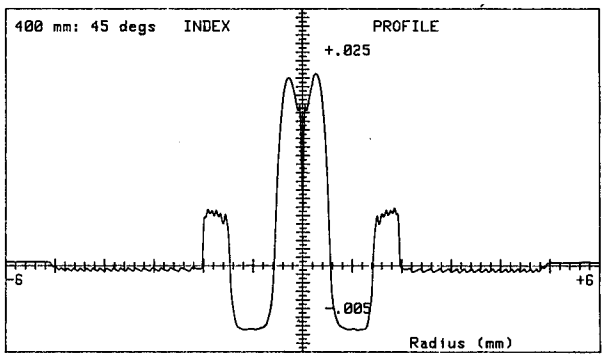


Figure 2 : Typical preform index profile for "optimum" dispersion compensating fiber

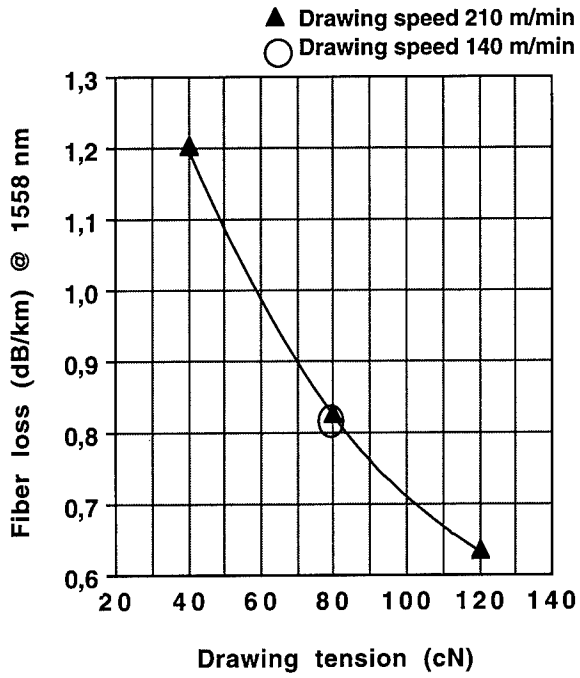


Figure 3 : Fiber loss versus drawing tension on bare fiber (same preform)

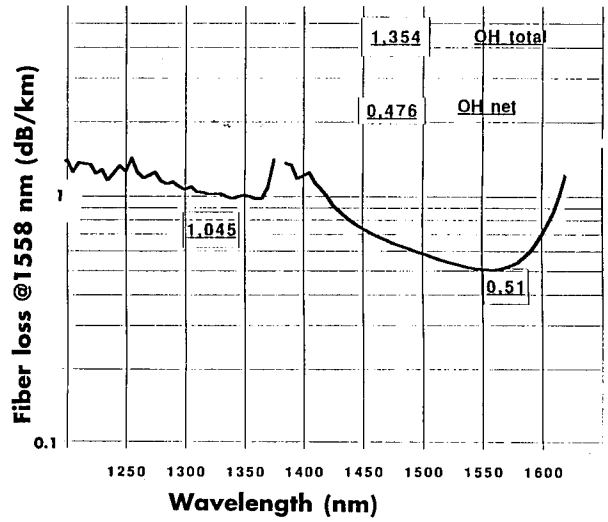


Figure 4 : Spectral loss of dispersion compensating fiber : length 25 km
C = - 117 ps/nm/km, FOM = 230 ps/nm/dB
MFD = 6.2 µm, λc = 1.18 µm, MAC = 5.3

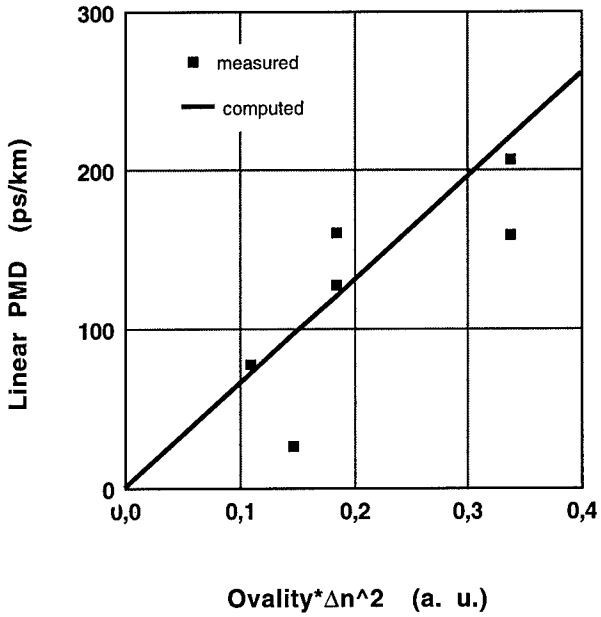


Figure 5 : Measured linear PMD versus core ovality*Δn^2. Computed values correspond to equation (3).

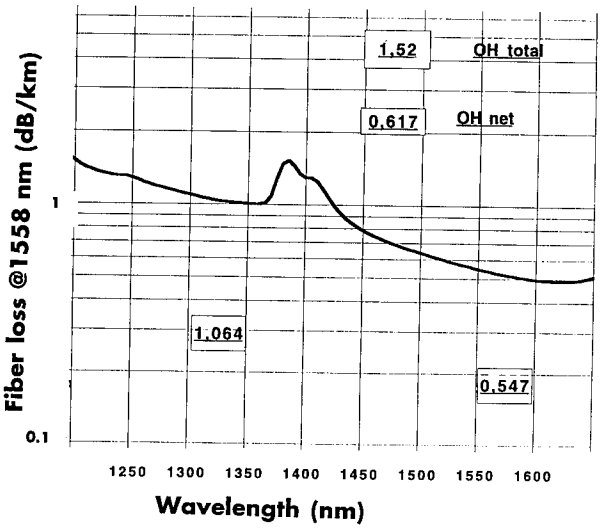


Figure 6 : Spectral loss of dispersion compensating fiber : length 18 km,
C = - 95 ps/nm/km slope = - 0,27 ps/nm^2/km
PMD = 0.07 ps/√km
MFD = 5.64 µm, λc = 1.25 µm, MAC = 4.5

PMD MEASUREMENTS OF VARIOUS TWISTED STRAINED AND FULLY LOOSE OPTICAL FIBERS IN THE CABLE

D Boscher , JC Bizeul , JP Louboutin , C Mauguen

FRANCE TELECOM-CNET/LANNION B/FCI/FCM 22300 LANNION FRANCE

ABSTRACT

PMD level of the fiber is very dependant of the fiber packaging. A cabling machine has been specially adapted for provide in a same cable , fibers with twists or strains or with a fully loose cabling.

Three experiments with twisted, strained and loose fibers, with thermal behaviour give the PMD variation in these conditions. Concatenation laws have been also investigated and analysis of all these results let us a large understanding of cabling phenomena which could allow to define the specifications levels versus the different steps of the cable manufacture.

1) INTRODUCTION

The PMD phenomena have been studied for the submarine applications, where the doped fibre amplification can give very long distance of link without regeneration. Now the very high bit rate and espacially the analog MABLR transmission ,require a maximum level of PMD for the installed link. As we have not, today,CCITT specifications and as the PMD measurements are very critical, we need a perfect understanding of phenomena ,like the variation law versus length , and the PMD values versus packaging. About that, many theoretical approaches defining geometrical and stress birefringence have shawn basic phenomena , but the final value of PMP with random perturbations is very dependant of mode coupling length which is strongly ,itself, dependant of the fiber packaging. Several papers (1) (2) have studied some aspects, and the goal of this presentation is to complete these studies with other aspects, and to know, if it is possible, to fix fiber specifications on manufacture drums ,to guarantee a maximum level of PMD for the cabled and installed link.

For that, it is necessary to characterize the fiber in each step of manufacturing process and to measure PMD variation with, only, one parameter fluctuation.

2) MEASUREMENT SET UP

Two kinds of measurement can be used ,which are wavelength scanning and interferometric method, and we have selected the first one, using laboratory set up with wavelength peak analysis for a first experiment, and a commercial set up, including a FFT fonction, for our two others experiments.

Nevertheless ,at the time of an very large, in the field ,characterization for fiber PMD, we established,with other laboratories the agreement between WS and interferometric values. These results will be now published in other papers, but the final correspondence in ps is given fig.1.

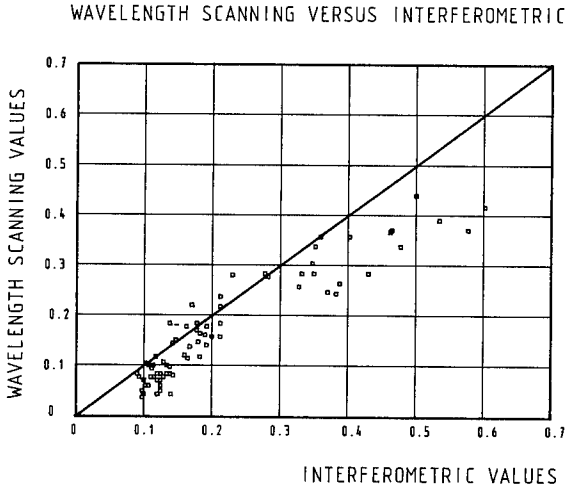


Fig 1

We can define three PMD categories :

D<0,15ps / √km interferometric is pessimistic

0,15ps / √km < D <0,3ps / √km both methods are equivalent

D>0,3ps / √km interferometric is again pessimistic

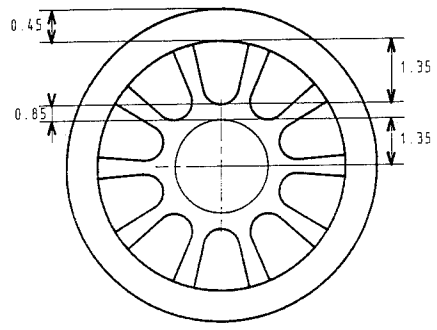
All measurements have been carried out on 60cm drums with minimum strain.

For our other experiments, measurements have been made firstly on these large drums, and after cabling with 50cm diameter small reel (A,C) or medium reel (∅ 1,20m C) and in thermal room with 2m diameter free strain reel.

3) CABLING EXPERIMENTS

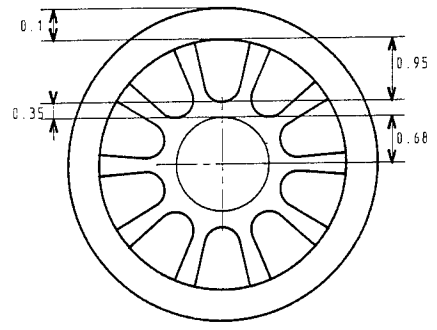
We must to change stress states of the fiber, but it essential to control them and the helical ve groove structure, several years ago described (3) ,guarantees, with laying technics developed for this rod, a perfect knowledge of stress parameters in the cable. Two kinds of rod have been used ,where geometrical characterics are given fig 2

EXPERIMENT B



helical pitch
130 mm
thermal coefficient
$1,38.10^{-5}$ / °C

EXPERIMENT A and C



helical pitch
210 mm
thermal coefficient
$1,7.10^{-5}$ / °C

FIG2

Deep of groove and helical pitch determine the minimum excess length of the fiber and the constant radius of curvature induced by helix. With the thermal expansion coefficient we can calculate the thermal range of fully loose fiber.

	Excess length	Radius curvatere	T° range
A, C	10–3	750mm	58°C
B	8,8 10–3	150mm	~600°C

4) TWISTED FIBERS,EXPERIMENT A

For this experiment we use 5 fibers with high core ovality (>6%) and 5 Kms length. It is well know that this parameter influences the fiber PMD, but the induced stress due to this ovality is surely more penalyzing ,and the PMD level gaps between 0,25ps/$\sqrt{km}$ and 8,1ps/$\sqrt{km}$ show it well. These five fibers have been cut in two sections where one of them will be fullyloose cabled (untwisting on the cabling machine with one rotation by helix pitch) and the other will be cabled with fixed drum on the machine.

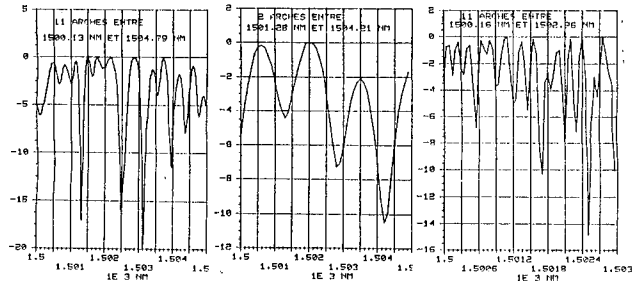
Fibers 0, 2, 4, 6, 8, are fully free and fibers 1, 3, 5, 7, 9, are twisted with about five turns/m. The following table give the results.

Fibre 5000 m before cabling	ps/$\sqrt{km}$	Fibre 2450 m after cabling	ps/$\sqrt{km}$
A	8.1	**0**	3.3
		1	20.3
B	.25	**2**	.72
		3	.97
C	.6	**4**	.55
		5	.2
D	3.9	**6**	10.4
		7	14.5
E	.35	**8**	.3
		9	6

Table

FIBER A 0&1

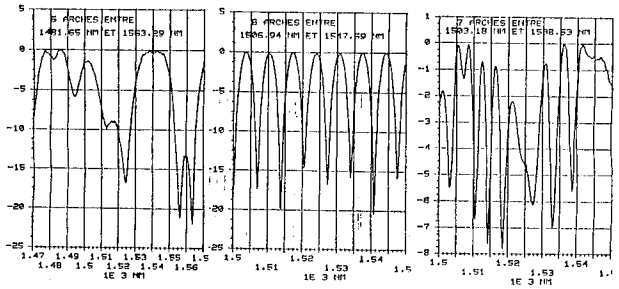
Before Cabling | Loose | Twisted



$\tau = 8,12$ ps/ km $^{1/2}$ 3,3 20,3

FIBER B 2&3

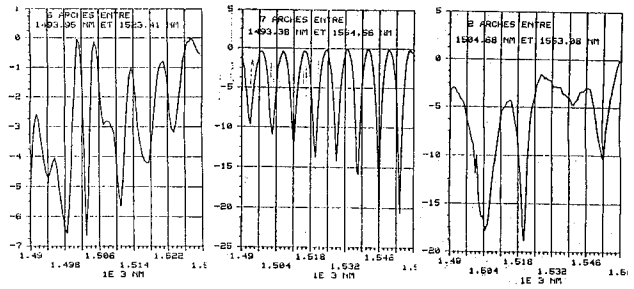
Before Cabling | Loose | Twisted



$\tau = 0,21$ ps/ km $^{1/2}$ 0.72 0.97

FIBER C 4&5

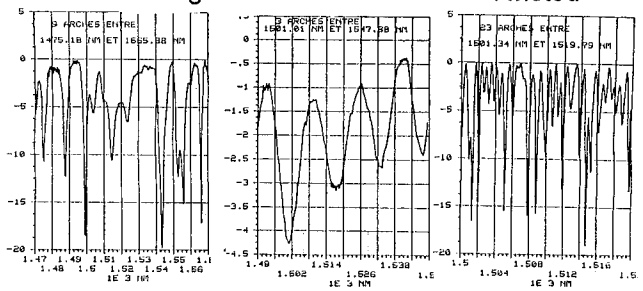
Before Cabling | Loose | Twisted



$\tau = 0,57$ ps/ km $^{1/2}$ 0.56 0.45

FIBER E 8&9

Before Cabling | Loose | Twisted



$\tau = 0,34$ ps/ km $^{1/2}$ 5.9

Fig 3

We notice,in the table, that these fibers with high ovality have non identical behaviour and that, the simple-minded interpretation of PMD values is very difficult. It appears more interesting to analyze the wavelength spectrums given fig 3.

For all fibers ,we can remark that, even on free strain drum, there is mode coupling ,which disappears on all fibers fully loose cabled, showing quasi perfect sinusoidal spectrums. Nominal PMD values have trends to increase.

In opposition to that, the spectrums of twisted cabled fibers are very disturbed with PMD levels which are decreasing for C fiber, and strongly increasing for A,B and E fibers. We can, therefore ,say that,the predicting of PMD in cable for such fibers with high ovality is almost impossible, without much more elaborate investigations about mechanical stress and optogeometrical parameters.

5) STRESS FIBER CABLING, EXPERIMENT B

In order to agree concatenation classical laws with $\sqrt{\ }$ kms variation, we have selected a 25km length fiber with ordinary 0,1ps/$\sqrt{km}$ PMD. We cut this fiber in 10 sections,where,we measured ,at each time, PMD values of fully fiber and the cut section. Fig 4 shows the results, where we notice that,the variation is rather a square law than a square root law. This is due to a decreasing of PMD value along the 25 Kms of fiber explicated by a variation of residual stress during the drawing process.

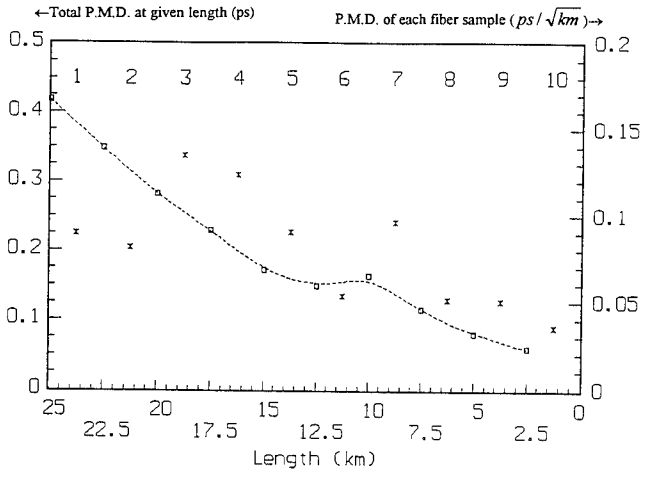


Fig 4

Consequently, we can not surely determine the PMD value of a fiber section by a square root calculation of a high length fiber PMD.

Fiber sections are marked off 1 to 10 with a decreasing trend of PMD. The five first sections were fullyloose cabled, and the five others, cabled in bottom of groove with small strain.

PMD histograms are given fig 5 before cabling ,then on 1,20m reel and finally on ∅2m in heating room at 20 C.

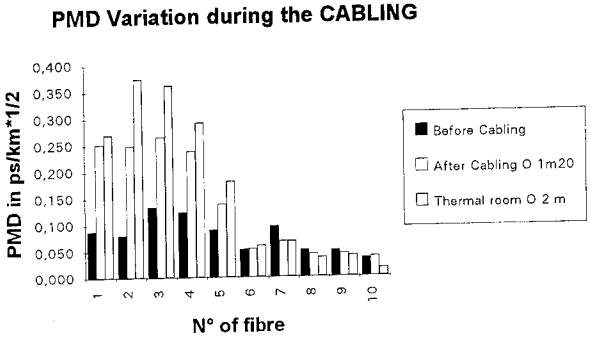


Fig 5

We can see that the fully loose PMD levels are increasing in 1,5 to 2,5 ratio after cabling, and these values are again more high when the cable is on a 2m reel (ratio 3,5 for the fiber n 2).

In the other hand, small tensile strain fibers show roughly the same PMD values.

This cable has been then tested in thermal cycles, between -40 C and +70 C, with 10 C steps of measurement. The PMD values and insertion losses at 1.55 μ wavelength are given in fig 6.

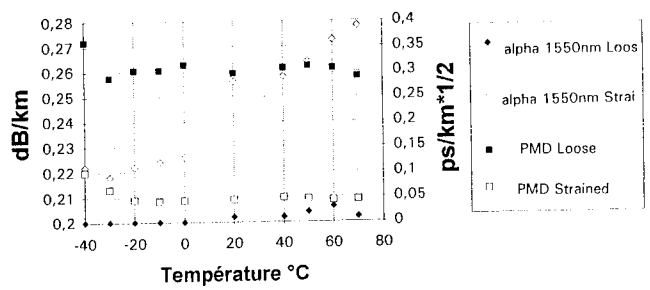


Fig 6

The five first fibers (1 to 5) had a more high intrinsic PMD and are fully loose cabled (0,3ps/√km) and the five other fibers (6 to 10) are in tensile strength (0,05ps/√km).

We notice that the fully loose fibers have an attenuation at 1,55μ and a PMD level roughly stable on the full range, when small tensible strength fibers show an increase of attenuation between -20 C and +70 C whereas the PMD level is constant, and we can see that ,between -20 C and +40 C, fibers have trends to go back free, with a stable attenuation and a PMD value which is increased of 0,05ps/√km to 0,1ps/km.

Restoration of initial fiber

We have then, restored the initial fiber with rotation optimized connector and by fused splice . The rotating optimization gave not perceptible variations and the classical laws giving $\tau=\sqrt{\Sigma\tau_i^2}$ have been applied to compare with experiment in fig 7.

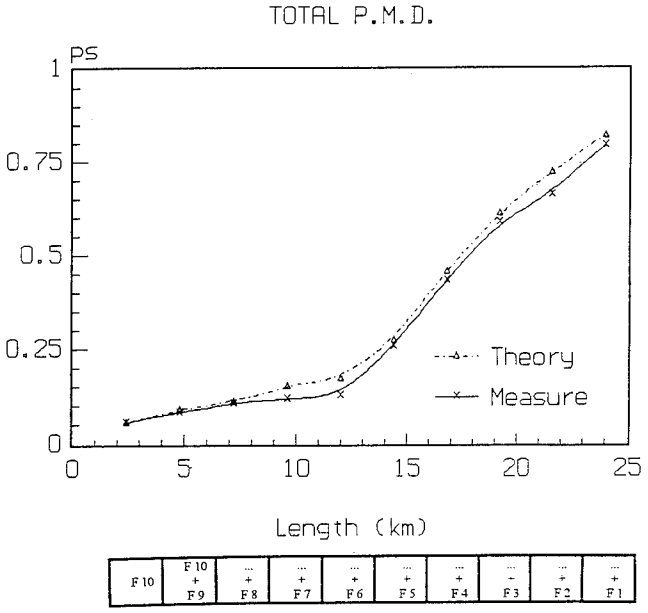


Fig 7

We have a good agreement between theoretical approach and experimental measurements of total dispersion for the restored fiber at each step. Between 0 and 12.5km we have tensile strength fibers and 12.5km - 25km fully loose fibers . We remark the clear slope variation between both cabling types. The conclusion of this test is ,therefore, that a good cabling of the fiber increase the PMD level in

comparison with the drum level,even with zero strain, whereas a bad cabling conceal these phenomena.

6) INFLUENCE OF MANUFACTURING PROCESS OF THE FIBER ON PMD VARIATION DURING CABLING STEPS

Process of preform manufacture or coating material are different for some providers and we have investigated four kinds of manufacturer and one spun fiber. Each fiber has been cut in two parts and one section was fully loose cabled and the other without excess length in the cable. We must notice that this cabling has been carried out with a small cylindrical ve groove ,and a high helical pitch, giving a high helix curvature. Results are given fig 8.

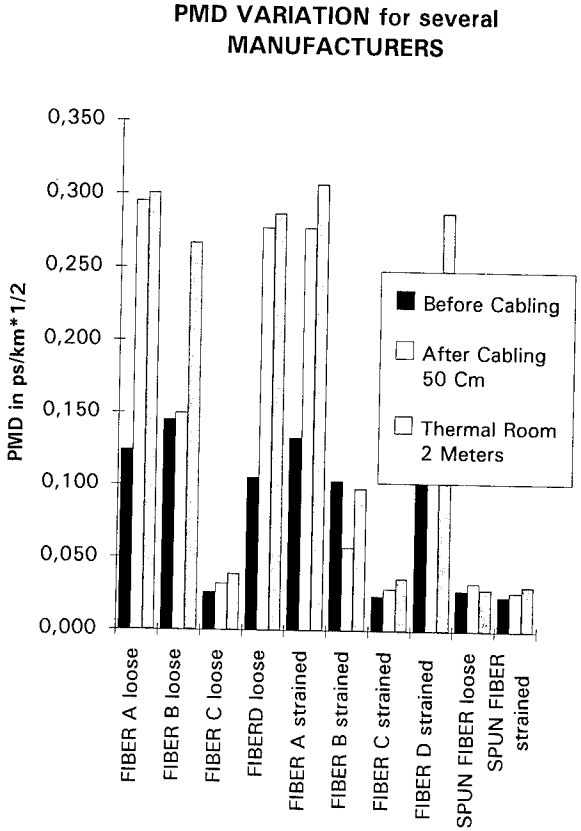


Fig 8

We can remark an increasing of PMD during the cabling, even for the C manufacturer which had an ultra low initial level,except for the spun fiber. In the other hand we can see that fiber B is sensible with small tensile strain ,whereas A, B, and D fiber seem no affected.

It is abvious that the coating material used ,is very critical , such as the high helix curvature of the rod.

This cable was tested thermically between -40 C and +70 C and fig 9 shows the difference of behaviour.

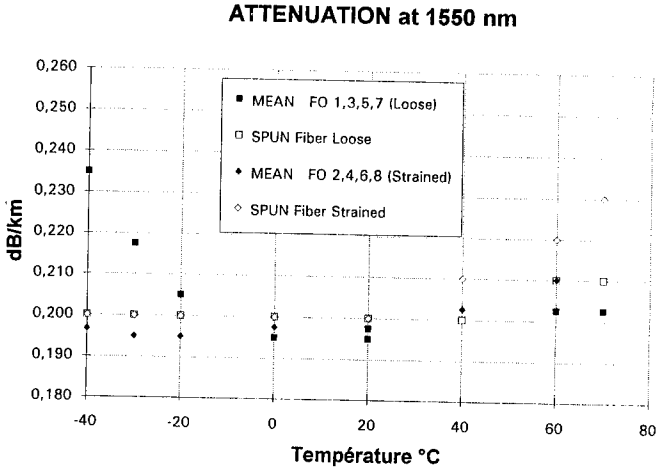


Fig 9

In the same time, PMD measurements have been carried out each 10 C step, giving PMD variation. Fig 10 shows that the fiber C which means insensitive to the cabling process PMD level was not affected during the cabling process , neither thermical cyclings.

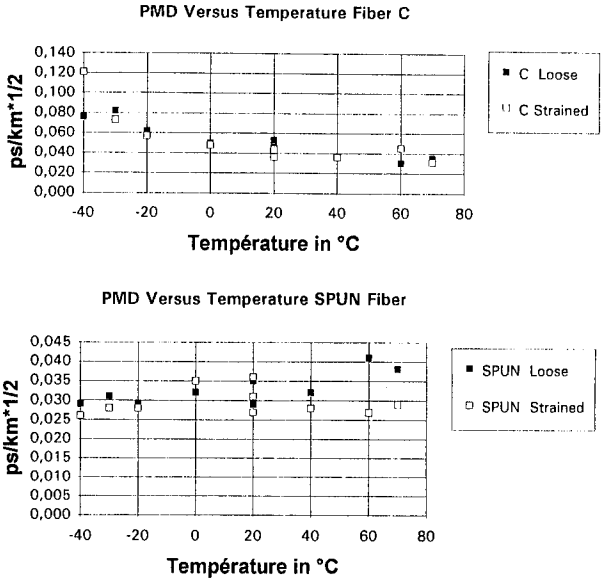


Fig 10

CONCLUSIONS

With these three experiments carried out in order to determine fiber specifications required to guarantee the maximal total PMD of the installed link, we can advance some outlines :

- It's very dangerous to determine the PMD of cut fibers in small length by a square root calculation of the high length fiber PMD.
- In many cases the fully loose fiber PMD is greater than the PMD on the drum even with zero strain, (1 to 3 ratio) except for the spun fibers where the PMD level is very stable, in all packaging states.
- This ratio is not constant from a manufacturer to another and the coating effect affect strongly these phenomena.
- For the high core ellipticity fibers, the twist of the fiber in the cable can improve or make worse the PMD values.
- Generally the bad cabling process, with twist or small tensile strain of fiber, perceptibly, improves final values of PMD.
- Concatenation law $\tau=\sqrt{\Sigma\tau_i^2}$ is in good agreement for the calculation of installed link.

REFERENCES

(1) AF JUDY Improved PMD stability in optical fibers and cables IWCS 94

(2) T SEKITO Bending induced PMD with random mode coupling IWCS 94

(3) D BOSCHER Ultra low loss optical fiber cable design ECOC 81



Daniel BOSCHER

FRANCE TELECOM
CNET/LAB FCI/FCM
BP 40 22300 LANNION
FRANCE

Daniel BOSCHER born in 1951 receveid his engineering degree from the Ecole Nationale Supérieure des Arts et Métiers and joined CNET in 1973.

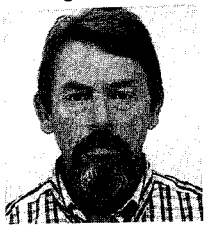
Working on circular waveguide until 1979 ,he then joined the optical fibers and cables department.Since 1993 he is manager of the "Fibers ,Cables and Measurement" Department.



Jean Claude BIZEUL

FRANCE TELECOM
CNET/LAB/FCI/FCM
BP40 22300 LANNION
FRANCE

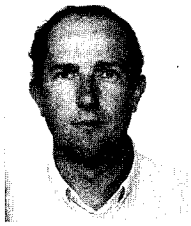
Jean Claude BIZEUL was born in 1948 .In 1973 he joined the CNET.He was engaged in research on fabrication and characterization of optical fibers .Since 1988 he is involved in optical fiber and cable measurement goup with special interests on transmission and geometrical single mode features.



Christian MAUGUEN

FRANCE TELECOM
CNET/LAB/FCI/FCM
BP40 22300 LANNION
FRANCE

Christian MAUGUEN was born in 1940.In 1971 he joined CNET and is responsible of optical measurements in the laboratory.



Jean Pierre LOUBOUTIN

FANCE TELECOM
CNET/LAB/FCI/FCM
BP40 22300 LANNION
FRANCE

Jean Pierre LOUBOUTIN was born in 1954 .Doctor in solid physics ,he joined CNET in 1982 .He is now Head of Group "Cables in Distribution"

EXTENSIVE CABLING EFFECT ANALYSIS AND DETERMINATION OF THE PMD LIMIT

P. GAILLARD [1], M. CARRATT [2], A. GOURONNEC [3], G. VUILLAUME [1]

[1] ALCATEL CABLE-OFCCC, FRANCE ; [2] ALCATEL FIBRE OPTIQUE - OFCC - FRANCE [3] FRANCE TELECOM - CNET, LANNION, FRANCE

ABSTRACT

This paper presents some investigations conducted in order to estimate the cabling influence on the polarisation mode dispersion (PMD) of various optical fibers :

- Statistical analysis of the PMD evolution from the bare fiber to the cabled fiber by comparing individual results of the fiber measured under zero tension and the corresponding value in a loose structure cable ;
- evaluation of the intrinsic PMD of some selected fibers by laying them loosely coiled in large diameter tanks or on a large diameter drum ;
- estimation of one of the possible cabling effects, arising when applying a torsion on the fiber (either helical or SZ twisting of the fibers during the cabling process) ;
- verification of the PMD homogeneity along the fiber on several long length (25 km) of fiber, splitted into 2.5 km individual lengths and then cabled and measured in PMD , and concatenation effect estimation.

From all these results the preliminary conclusion is that some fibers present a significant sensitivity in PMD during the cabling process and in relation with the initial value on bare fiber. The state of the art of high performance PMD fibers is finally described in term of evolution versus different winding conditions and packaging. Demonstration of very low and stable PMD values, leading to a 0.5 ps/√km limit on cable, suitable with all kinds of application and use, is made.

INTRODUCTION

The polarisation mode dispersion (PMD) effect on transmission systems has been already extensively studied regarding its impact either on analog (e.g. for video transmission) or high bit rate digital systems (e.g. 2.5 or 10 Gbit/s systems), and it has been found that this parameter is of a great importance as it can degrade significantly the transmission if it reaches too high values. In addition, the PMD random aspect and the fact that its origin can be either intrinsic to the fiber (e.g. core ovality) or extrinsic (i.e. due to external causes, for example the uncabled fiber packaging conditions during the measurement or stresses resulting from the cabling process) makes it difficult to be measured accurately and can lead to a significant change of the PMD value after cabling. This latter phenomenon can be due to either a wrong estimation of the bare fiber PMD (inhomogeneity along the fiber, problems related to the fiber packaging during the measurement...) or a strain, induced by the cabling process or the cable structure, generating birefringence and thus PMD.

In order to clarify these points and to be able to predict the cabled fiber PMD from the uncabled value as provided or guaranteed by the fiber manufacturer, we have performed a series of investigations which are presented and the obtained results are commented.

MEASUREMENT METHOD

Among the various possible measurement methods for PMD measurement (interferometric, fixed analyser and polarimetric methods) we have chosen the interferometric method, performed with a commercially available test set, due to its easiness of use. The principle of the measure is given in figure 1. The measurement wavelength is 1550 nm.

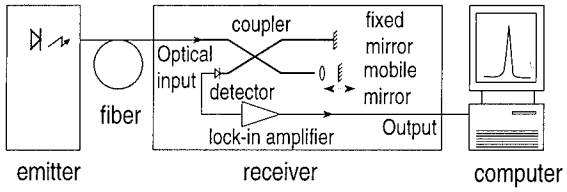


figure 1 : interferometric measurement principle

CURRENT PRODUCTION PMD CABLING EVOLUTION ANALYSIS

In order to estimate statistically what is the evolution of the PMD from the bare fiber to the cabled fiber, an analysis has been performed on a significantly large quantity of fiber, by comparing individual results obtained when measuring the uncabled fiber under very low tension and the corresponding value in a standard, loose tube structure cable.

The obtained results, presented under the form of an histogram of the PMD change between the uncabled fiber value and the cabled fiber value is given in figure 2. It can be seen

on these results that the population of the deltas is centered around a value which is slightly negative, but that the population distribution shows a tail on the positive values, with a maximum at + 0.97 ps/√km ; statistical data are summarized in table 1.

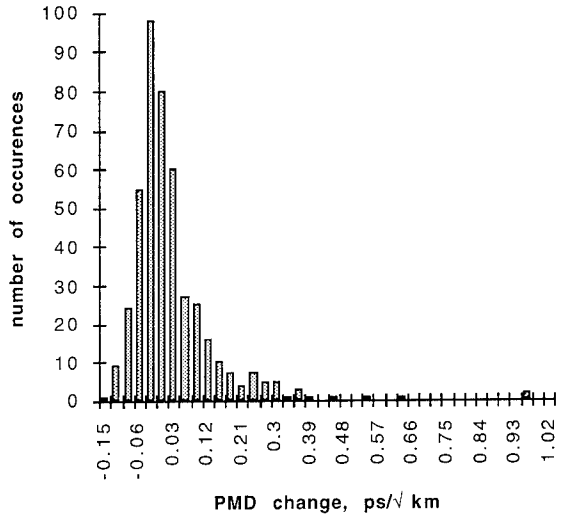


Figure 2 : PMD evolution when cabling

item	(ps/√km)
sample size	443
average	0.026
standard deviation	0.117
minimum	-0.139
maximum	0.967

Table 1 : PMD evolution when cabling (data)

It has also been noted in this analysis that the PMD change from the bare fiber to the cabled fiber was in relation with the fiber initial PMD value : big changes occur preferentially on fibers having a high initial PMD ; this result is in accordance with previously reported data (1).

In addition to this statistical analysis different types of fibers have been cabled in a standard loose tube structure ; the corresponding results are given in table 2 (average value, standard deviation and maximum value over the six fibers of each tube).

FIBERS INTRINSIC PMD EVALUATION

The intrinsic PMD of some selected fibers has been also evaluated by laying them loosely coiled in large diameter tanks (Ø 2800 mm) in a similar way than the experiment described in (2) with the exception that the fiber coating has been kept intact and that the coiling diameter was much larger ; obtained results are given in table 3. The fibers attenuation has been verified at 1550 nm after laying in order to check that this operation did not induce a measurable strain. The fibers were selected according to their high «initial» PMD value (PMD measured under a very low tension on Ø 630 mm drums). The results show that under these conditions of laying, there is a significant increase in PMD compared to the initial value on these selected high PMD fibers, probably due to the mode coupling created by the spooling diameter and the packaging conditions (microbendings).

tube	fiber type		zero tension Ø 400 mm	coiled Ø 1200 mm	delta
1	MCVD,	ave.	0.175	0.194	0.018
	matched	s	0.108	0.135	0.046
	clad	max.	0.342	0.385	0.078
2	MCVD,	ave.	0.093	0.084	-0.045
	matched	s	0.015	0.015	0.016
	clad	max.	0.106	0.076	-0.025
3	MCVD,	ave.	0.084	0.055	-0.029
	matched	s	0.026	0.018	0.039
	clad	max.	0.125	0.089	0.021
4	MCVD,	ave.	0.034	0.036	0.002
	depressed	s	0.005	0.004	0.005
	clad	max.	0.04	0.041	0.008
5	VAD,	ave.	0.081	0.036	-0.045
	matched	s	0.003	0.004	0.003
	clad	max.	0.087	0.041	-0.039
6	OVD,	ave.	0.102	0.16	0.059
	matched	s	0.016	0.053	0.062
	clad	max.	0.127	0.227	0.140

Table 2 : various fibers PMD evolution vs. cabling (ps/√km)

ref.	zero tension Ø 630 mm	loosely coiled Ø 2800 mm
1	0.87	1.718
2	0.84	2.46
3	096	3.336
4	0.91	2.665
5	0.99	4.621

Table 3 : PMD evolution, fibers loosely coiled on a large diameter tank (1300 nm, ps/√km)

In addition to this test fibers from different origins have been loosely coiled around a large diameter (Ø 2000 mm) drum, in the same purpose ; the tested fibers and the obtained results are given in table 4. In this case there is no important evolution of the PMD, probably due to the fact that initial PMD is low.

EFFECT OF FIBER TORSION WHEN CABLING

Actual loose structures of optical cables are designed so as to avoid microbending on the fibers, and to limit macrobending to the one due to fibres stranding ; however one added strain due to cabling arises when applying a torsion on the fiber (either helical or SZ twisting of the fibers during the cabling process). This effect has been investigated on a loose tube structure, by helically twisting selected single or bundled fibers, here again the fibers being selected according to their high «initial» PMD value (PMD measured under zero tension on Ø 630 mm drums). Obtained results are given in table 5,

ref.	fiber type	zero tension Ø 400 mm	coiled Ø 1200 mm	delta
1	OVD matched clad	0.100	0.032	- 0.068
2	OVD matched clad	0.08	0.091	+0.011
3	MCVD depressed clad	0.033	0.032	- 0.001
4	MCVD depressed clad	0.033	0.037	+ 0.004
5	MCVD matched clad	0.092	0.034	- 0.058
6	MCVD matched clad	0.089	0.036	- 0.053
7	VAD matched clad	0.087	0.037	- 0.050
8	VAD matched clad	0.08	0.035	- 0.045

Table 4 : PMD evolution, fibers loosely coiled on a large diameter drum (ps/√km)

where references 1, 2 and 3 correspond to 6 bundled fibers (the given value corresponding to the average over the 6 fibers), and references 4 to 7 to single fibers. The corresponding curve of PMD vs. torsion for single fibers is given in figure 3 ; for the bundled fibers the cumulative effects of torsion and bending do not allow to separate the effect of torsion itself, and it seems that this «stranding bending» limits the PMD increase on these selected fibers when cabling.

ref.	torsion (t/m)	bare fiber value	loose tube value	delta
1	1	0.63	0.70	+ 0.07
2	2	0.58	0.55	- 0.03
3	5	0.60	0.41	- 0.19
4	0.5	0.53	1.83	+ 1.30
5	1	0.53	1.02	+ 0.49
6	2	0.53	0.47	- 0.06
7	5	0.53	0.36	- 0.17

Table 5 : PMD vs. torsion data (ps/√km)

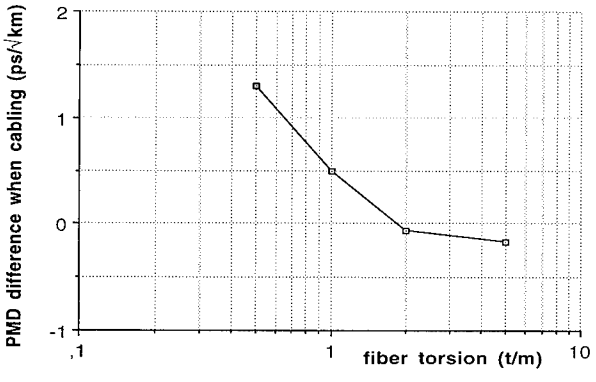


Figure 3 : PMD vs. torsion curve

The results on the single fibre confirm the influence of the torsion on the PMD, which decreases when the amount of torsion increases ; in addition it is confirmed that initially high PMD values can lead to a significant increase during the cabling process, probably due to the complete relaxation of the fiber in loose conditions compared to its packaging during the initial measurement. The obtained curve of PMD vs torsion is similar to previously reported results (3).

The «SZ» stranding has been also investigated, but the fibers being loosely laid into the tubes the obtained results were not significant as it is not possible to be sure that the stranding and its induced combination of bending and torsion is preserved in the completed cable.

PMD HOMOGENEITY ALONG THE FIBER AND CONCATENATION EFFECT

An other aspect to be taken into consideration for the cable manufacturing is the PMD homogeneity along the fiber This point has been verified on six long length (25 km) of fiber, splitted into 2.5 km individual lengths and then cabled (standard loose tube structure) and measured in PMD ; in addition, two of these 2.5 km lengths sets have been spliced together so as to restore the original length, and the concatenation effect derived from the obtained results. The obtained results are given in tables 6.1 to 6.6 and the graphs giving the comparison of calculated and measured PMD in the restoration experiment for fibers 1 and 6 are given in figures 4.1 and 4.2. The conclusions drawn from these results are that some discrepancies can occur for some fibers when considering their homogeneity, and that the concatenation results are in good agreement with predicted values.

25 km initial value	2.5 km bare fiber value	2.5 km cabled fiber value	delta bare/ cabled
0.115	0.21	0.295	0.085
	0.263	0.147	-0.116
	0.201	0.352	0.151
	0.139	0.166	0.027
	0.152	0.275	0.123
	0.194	0.155	-0.039
	0.332	0.200	- 0.132
	0.475	-	-
	0.353	0.876	0.523
	0.257	-	-

Table 6.1 : PMD homogeneity, fibre 1 (ps/√km)

25 km initial value	2.5 km bare fiber value	2.5 km cabled fiber value	delta bare/ cabled
0.057	0.131	0.109	-0.022
	0.145	0.154	0.009
	0.192	0.31	0.118
	0.189	0.109	-0.08
	0.13	0.109	-0.021
	0.125	0.09	-0.035
	0.098	0.097	-0.001
	0.151	0.135	-0.016
	0.101	0.096	-0.005
	0.111	0.09	-0.021

Table 6.2 : PMD homogeneity, fibre 2 (ps/√km)

25 km initial value	2.5 km bare fiber value	2.5 km cabled fiber value	delta bare/ cabled
0.105	-		
	0.158	0.22	0.062
	0.104	0.155	0.051
	0.111	0.116	0.005
	0.108	0.09	-0.018
	0.122	0.122	0
	0.156	0.166	0.01
	0.178	0.147	-0.031
	0.15	0.102	-0.048
	0.112	0.109	-0.003

Table 6.3 : PMD homogeneity, fibre 3 (ps/√km)

25 km initial value	2.5 km bare fiber value	2.5 km cabled fiber value	delta bare/ cabled
0.151	0.184	0.154	-0.03
	0.156	0.135	-0.021
	0.372	0.366	-0.006
	0.275	0.224	-0.051
	0.278	0.205	-0.073
	0.262	0.282	0.02
	0.146	0.32	0.174
	0.173	0.4	0.227
	0.245	0.224	-0.021
	0.182	0.192	0.01

Table 6.4 : PMD homogeneity, fibre 4 (ps/√km)

25 km initial value	2.5 km bare fiber value	2.5 km cabled fiber value	delta bare/ cabled
0.063	0.141	0.096	-0.045
	0.098	0.096	-0.002
	0.1	0.103	0.003
	0.13	0.135	0.005
	0.109	0.09	-0.019
	0.128	0.103	-0.025
	0.129	0.103	-0.026
	0.141	0.103	-0.038
	0.118	0.096	-0.022
	0.133	0.096	-0.037

Table 6.5 : PMD homogeneity, fibre 5 (ps/√km)

25 km initial value	2.5 km bare fiber value	2.5 km cabled fiber value	delta bare/ cabled
0.14	0.214	0.161	-0.053
	0.382	0.199	-0.183
	0.233	0.462	0.229
	0.465	0.302	-0.163
	0.577	0.257	-0.32
	0.348	0.269	-0.079
	0.385	-	-
	0.43	0.263	-0.167
	0.35	0.25	-0.1
	0.217	0.193	-0.024

Table 6.6 : PMD homogeneity, fibre 6 (ps/√km)

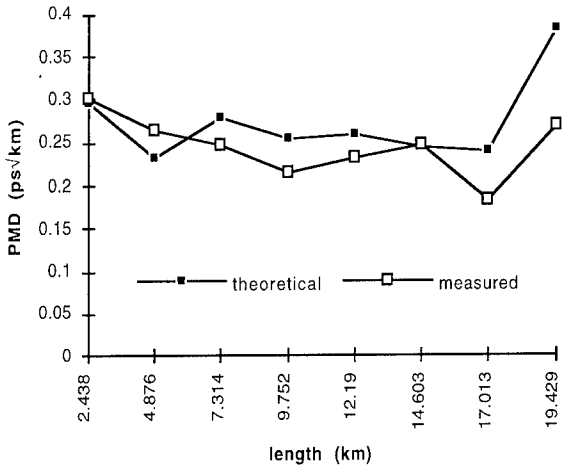


Figure 4.1 : PMD concatenation, fibre 1

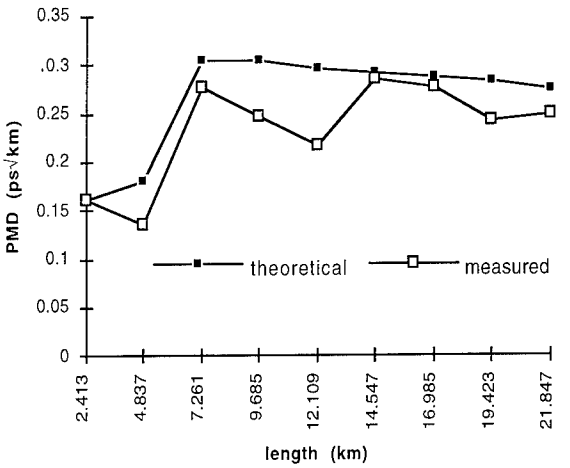


Figure 4.2 : PMD concatenation, fibre 6

DISCUSSION

From all these results the preliminary conclusion is that some fibers can present a significant sensitivity in PMD during the cabling process, in relation with the initial value on the bare fiber, and that a long fiber may not be homogeneous throughout its length. This leads to the conclusion that it is not possible to predict at 100% the PMD of the cabled fiber from its initial value, due to a small part of the fiber population for which it is difficult to estimate the intrinsic PMD.

A solution to solve this problem could be to apply a torsion during the cabling process in order to create mode coupling ; however, we consider that such a solution to reduce the PMD is not recommendable, as it presents some disadvantages, such as it leads to the application of a permanent strain on the fiber and therefore presents some risks of reduction of the fiber lifetime.

As a consequence, the best solution is to have a fiber with very low intrinsic PMD and insensitive to bending and microbending, regarding PMD. For this purpose, a high performance PMD fiber is obtained with a tight management process, in term of geometry improvement and internal stress decrease.

The very low intrinsic value and insensitive extrinsic effect lead to a constant PMD with respect to the packaging. No change have been found, lower than few hundreds, between a loosely coiled or winding from zero tension to 15 and 50 grammes.

The following histograms (figures 5.1 and 5.2) present the initial PMD repartition and the variation after cabling in a loose tube structure.

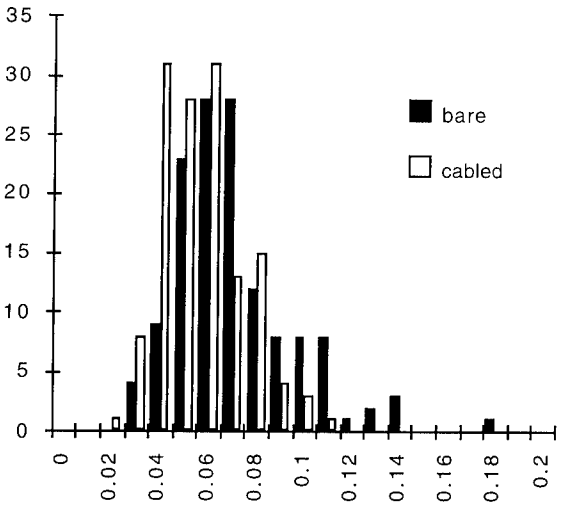


Figure 5.1 : PMD distribution, before and after cabling (high performance PMD fibers, ps/√km)

The initial PMD is 0.070 ps/√km in average, standard deviation 0.026, 0.18 maximum and 0.03 minimum. The final PMD values after cabling are 0.058 ps/√km in average, standard deviation 0.018, and 0.11/0.03 for max. and min. This experiment demonstrates the efficiency of the so-called high performance PMD fiber applied in the process.

CONCLUSION

We have conducted various investigations in order to estimate the cabling influence on the polarisation mode dispersion (PMD) of various optical fibers ; from the obtained results it has been concluded that some fibers presenting a significant sensitivity in PMD during the cabling process, it is not possible to predict at 100% the PMD of the cabled fiber from its initial value.
As a consequence it is necessary not only to have a fiber which has a very low intrinsic PMD but primarily which is insensitive (regarding PMD) to bending and microbending.
Demonstration of very low and stable PMD values, leading to a 0.5 ps/√km limit on cable, suitable with all kinds of application and use, has been demonstrated.

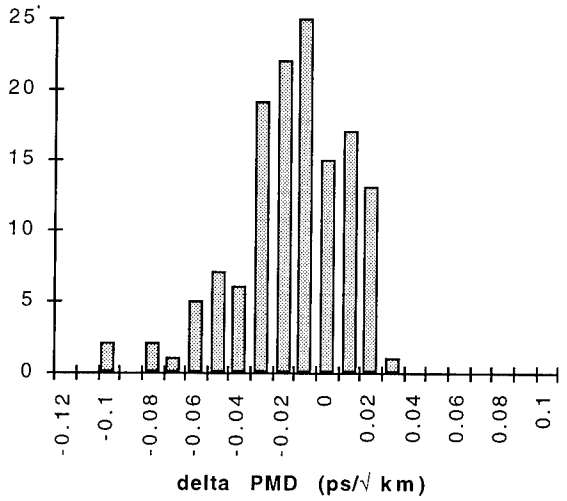


Figure 5.2 : PMD evolution when cabling (high performance PMD fibers, ps/√km)

ACKNOWLEDGMENTS

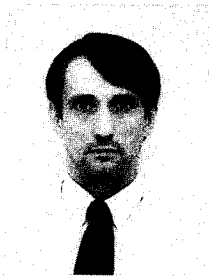
The authors would like to acknowledge their colleagues from CNET Lannion, Alcatel Cable and Alcatel Fibres Optiques for their assistance and the valuable and fruitful discussions.

REFERENCES

(1) Extrinsic stress effects on polarisation mode dispersion in optical fiber cables, S. Grindstaff and al., IWCS 1993
(2) Bending induced PMD with random mode coupling, T. Sekito and al., IWCS 1994
(3) Improved PMD stability in optical fibers and cables, A. F. Judy, IWCS 1994

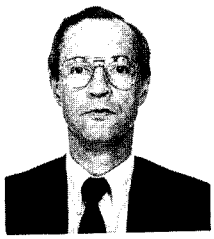
AUTHORS

Pierre GAILLARD
ALCATEL CABLE, STT/OFCCC
35 rue J. Jaurès BP 20 95871
Bezons cedex, FRANCE



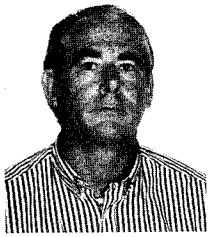
P. GAILLARD was born in 1956. He received his engineer degree from the Ecole Catholique des Arts et Métiers (ECAM) in 1980. He joined Alcatel Cable in 1983, where he is now working as project engineer in the Optical Fiber Cable Competence Center.

Michel CARRATT
ALCATEL FIBRES OPTIQUES, OFCC
35 rue J. Jaurès BP 20 95871 Bezons cedex, FRANCE



M. CARRATT was born in 1949. He received his engineer degree from Institut National des Sciences Appliquées (INSA) of Lyon. He worked from 1974 to 1978 on the development of circular waveguides for Les Câbles de Lyon, and then joined the CLTO in 1978 where he was in responsible for research and development. In 1990 he joined Alcatel Fibres Optiques, where he is now deputy general manager at the head of research and development programs.

Alain GOURONNEC
FRANCE TELECOM - CNET
22301 Lannion, FRANCE



A. GOURONNEC was born in 1946. He received his engineer degree from the Conservatoire National des Arts et Métiers (CNAM) in 1978. He joined the CNET in 1971, where he was in charge of the pulling and multipulling of optical fibers studies. In 1986 he started to work on the development and specification of telecommunication cables ; since 1993 he is in charge of the evaluation and the qualification of optical fibers for France Telecom needs. He is also in charge of the optical fiber reliability studies in CNET.

Gérard VUILLAUME
ALCATEL CABLE, STT/OFCCC
35 rue J. Jaurès BP 20 95871 Bezons cedex, FRANCE



G. VUILLAUME was born in 1942. He joined Les Câbles de Lyon in 1966, where he was working on the development of circular waveguides ; he moved in 1976 to the optical fiber activity and optical test set development. He is now in charge of optical fibers and optical cables characterisation in the Optical Fiber Cable Competence Center of Alcatel Cable.

CHARACTERISATION OF THE ENVIRONMENTAL EFFECTS ON THE POLARIZATION MODE DISPERSION (PMD) MEASUREMENTS ON G 652 SINGLE MODE FIBERS

Alain GOURONNEC, R. GOARIN, M. AUVRAY, G. LE MOIGNE
France Telecom-CNET
Technopole Anticipa
2, avenue Pierre Marzin
22307 LANNION, France

ABSTRACT.

In a single mode optical fiber two series of dispersive effects are observed: The chromatic dispersion and the polarization mode dispersion (PMD). The polarization mode dispersion generates a limitation in high speed digital transmission and also in high quality analog systems. The PMD is induced in an optical fiber principally by core birefringence and index core axis variations. The stresses induced in the fiber depend on fiber packaging and manufacture inducing random index variations along the fiber. After a comparison of measurement methods we have tested the fibers under different environments. We have tested on specific fibers the PMD core ovality dependance and we have measured the PMD evolution regarding different kinds of packaging conditions. The concatenation effects are treated. We have tested the PMD dependance of the fibers according to bending, axial strength and coating effects.

Keywords : Optical Fiber, Optical Cable, Polarization mode dispersion, Reliability.

INTRODUCTION.

In a single mode optical fiber, along the axis the structural caracteristics could have assymetrical variations such as core non circularity, core index fluctuation, glass birefringence principally induced by mechanical constrains. These imperfections generate on the transmitted light signal a second type of dispersion, called the Polarization Mode Dispersion (PMD).

In high bits rates transmission PMD causes the optical pulse to spread in the time domain. This could affect the performance of the digital system. The effect is related to the differential group delay time $\Delta\tau$ (DGD) between the two orthogonal polarized states of polarization (PSP) of the transmitted wavelength. With analog system the combination of the PMD in the fiber, the frequency chirp in the transmitter and polarization dependent loss of the receiver could generate high level of the composite second-order distorsion of the transmitted signal.

The paper presents the investigations on the G 652 optical fibers and cables used in the FRANCE TELECOM network.

I: PRINCIPAL CARACTERISTICS OF PMD ON FIBERS AND CABLES.

We have seen that PMD depends on the quality of the fiber core. Core non circularity is the main parameter inducing the polarization mode dispersion [1]. This non circularity gives a fiber core stress state inducing a birefringence state sensitivity of the fiber. Through the photoelastic effect, external mechanical or thermal constrains can

change this stress state. The optical fiber transmission thus depends on the fluctuation of these environmental parameters, inducing random variations to the differential group delay (DGD).

In components or short length of optical fibers, the differential group delay is the difference in the propagation time for the two orthogonal polarisation modes, it is scaled in pico-seconds (ps). In long length of optical fibers a high degree of coupling energy between each polarization mode is observed and the polarisation mode dispersion is expressed as the expected value of the differential group delay $<\Delta\tau>$. PMD is expressed in terms of this $<\Delta\tau>$ divided by the square root of the fiber length ($ps/\sqrt{km}$).

II: THE MEASUREMENT METHODS.

Different methods for the measurement of the polarization mode dispersion of an optical fiber or cable can be used. These methods are described by many authors [2] to [6]. From CNET we have made PMD investigations in order to define the best way for field measurements. Figures 1 and 2 show the results obtained on a specific 36 fibers loose tube cable, using fibers with different selected levels of PMD. Figure 3 is a measurement comparison at the two windows (1310 & 1550 nm) using the interferometric technique[7]. After this first PMD evaluation we have decided to use the interferometric technique for our field measurements.

III. THE FIBERS PMD EVALUATION.

III.1: The packaging effects on PMD.

We have seen above that the environmental conditions influence hardly the measurement results. So we have compared the PMD for fibers on shipping spools to the values obtained on the same fibers rolled up on large diameter drums under differents winding tensions (15 gr and "0" gr). The results are given in table I. We have also made some concatenation tests. Firstly we have used long length fibers on large diameter drums -(multi layers). After PMD measurement we have winded these fibers with one layer per drum. We have measured the PMD under this environment. Then we have cut the fibers in two parts and have done the new measurements. The results are given in figure 4. We can see a good correlation between theory and measurement when the initial fiber PMD value is low. For these fibers measurements the principal result is that the more initial PMD we have, the greater are the fluctuations of the PMD results.

In a same approach we have tested different cables [8] in the lab and on the field. Long length fibers have been choosen and PMD tested, cut in cable length ($\cong$ 2.4 km) and PMD measured on large drums firstly and after cabling secondly. The results are given in figure 5a. In figure 5b we have results obtained from field measurements [9]. When PMD is low, the cabled fibers and the layed down cables didn't present any PMD over values. So from our experience, PMD values less or equal to 0.2 $ps/\sqrt{km}$ on the fiber is a limit to secure low PMD on field cabled fibers and cables.

III.2:Fiber behaviour influence on PMD.

We have done some investigations on the effects of mechanical and chemical fiber behaviour on PMD. We have used our axial tension test equipment able to receive long length samples as shown on figure 6. We have strengthed from 0 to 0.5 % elongation in ambient air and in water fibers of 540 meters long. The results are given in figure 7. We see that axial strength has no influence on the fiber PMD for elongation less than 0.3 % until the stresses bending effect becomes higher than those of the axial tension when the initial PMD is relatively high (fibers A, B). Put in water with the same equipment under the same elongations, measured after 72 hours we

observe a decrease in the PMD values. The coating swelling stresses the fiber inducing mode coupling in the fiber. After drying the initial values were found. When the initial PMD is low we can see the stability of the values obtained (fiber C, D). We have seen that bending effect is a critical parameter for PMD. So we have made bending and micro bending tests. The first results are given in table II. We can observe that bending is more critical than micro bending for PMD.

All these tests show that the 0.2 ps/√km as a maximum PMD value for the fiber gives the same PMD values under conditions of harsh environment and for cabled fibers.

III.3:The PMD specification.

After those experimental evaluations on the PMD effects on the single mode G 652 optical fibers we have defined a maximum fiber PMD value of 0.2 ps/√km in our France Telecom-CNET specification. Our results show that this level gives a very low probability for having PMD values of cabled fibers higher than 0.5 ps/√km which is compatible with the actual and also with the next generation of high bits rates systems. So our final goal, for terrestrial fibers is only to have a statistical measurement on the optical fibers and to have no more measurements on the cables.

IV: CONCLUSION.

Like on fibers, the same results are observed on cabled fibers when the initial PMD is low: the cabling process did'nt degrade the PMD.

When the initial PMD is high, the results are not stable and great fluctuations are observed. We have seen that PMD is a critical parameter when the initial PMD value on the optical fiber is high.

Our investigations and field measurements show that specifying PMD values lower than 0.2 ps/√km on fibers is the best way to pratically solve the problems induced by the Polarization Mode Dispersion effects on cabled optical fibers for transmission networks.

V: ACKNOWLEDGMENT.

The authors would like to thank all the colleagues who have performed the PMD measurements in the laboratory and in the field. Particular thanks to M. BIZEUL for his collaboration. Thanks also to M. D. RIVIERE from the Components Failure Analysis Laboratory for the MEB measurements. All they have permitted by their collaboration to find an optimised solution to the PMD effects. All thanks also to our qualified fibers and cabling manufacturers for their helpfull actions. The authors also would like to thank M. G. DESERT for his help with results presentation.

VI: REFERENCES.

[1]-A. MABROUKI et al. *Analysis and Measurement of Polarization Mode Dispersion of single mode Optical Fibers.* Journal of Lightwave Technol. 1995 (sumitted) - France Telecom-CNET/LAB.

[2]-C.D. POOLE *Measurement of polarisation-mode dispersion in single mode fibers with random mode coupling.* Optics Letters, Vol 10. N° 10, may 15, 1989.

[3]-N. GISIN, J.P. VON DER WEID, J.P. PELLAUX. *Polarisation Mode Dispersion of short and long single mode fibers.* Journal of ligthwave technology, Vol 9. N° 7, july 1991.

[4]-N. GISIN et al. *Definition of Polarization Mode Dispersion and first results of the COST 241 Round -Robin measurements.* January 22, 1995.

[5]-P.HERNDAY. *Polarization Mode Dispersion measurement by the JONES MATRIX EIGENANALYSIS and WAVELENGTH-SCANNING METHODS.* HP technical data, january 5, 1995.

[6]-N. GISIN, R. PASSY, J.C. BISHOFF, B. PERNY. *Experimental investigation of the statistical properties of Polarization Mode Dispersion in single mode fibers.* IEEE Photonics Technology Letters, Vol5, N° 7, july 1993.

[7]-N. GISIN. *Polarization mode dispersion measurements with white light interferometry:principles, comparison with other methods and results.* 2nd OPTICAL FIBRE MEASUREMENT CONFERENCE; september 21-22,1993/p 165-170.

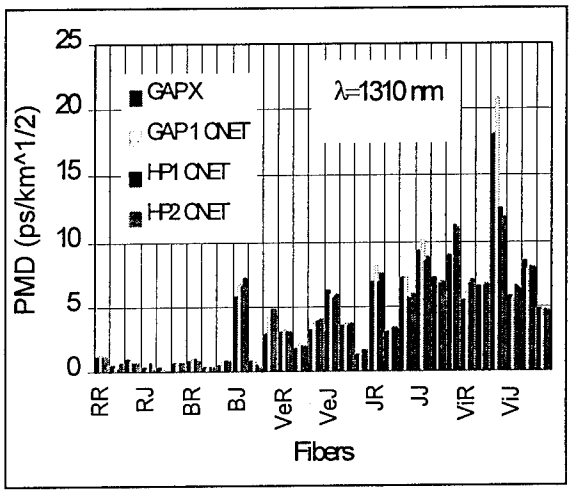


Fig.1 PMD measurement comparison

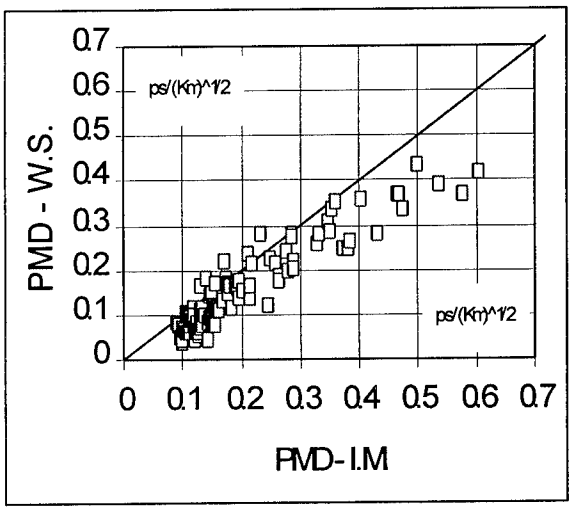


Fig.2 Comparison WS and IM

[8]-P. GAILLARD, M. CARRAT, A. GOURONNEC. *Extensive cabling effect analysis and determination of the PMD limit.* Proc. 95's IWCS, nov 1995.

[9]-A. JARLOT, J. LESPINASSE. *Technical Report from SILEC & France Telecom/SCTT study*, July 1995.

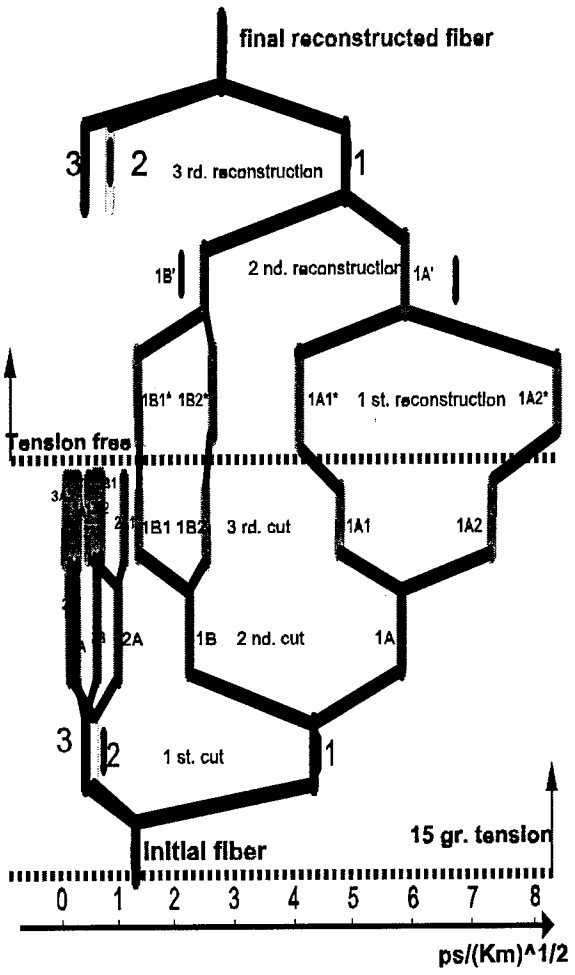


Fig.4 Concatenation test on a single mode fiber (fiber B, 1550 nm, IM)

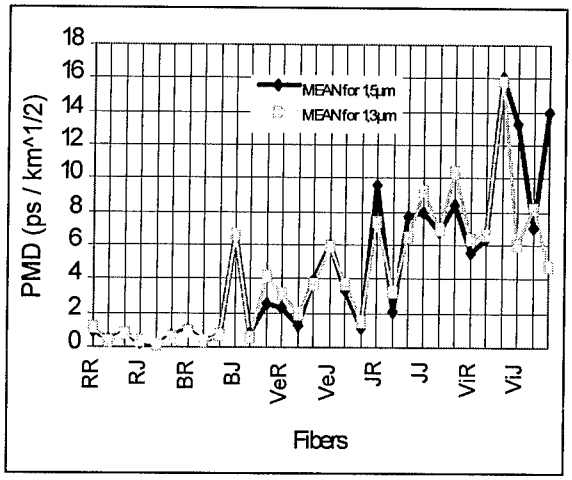


Fig.3 Interferometric measurement comparison at 1310 and 1550 nm

	Diameter		
	d=15 cm (15 gr)	D>=60cm ("0" gr)	η=D/d
Low Level PMD (ps/Km^1/2)	0.088	0.059	0.67
	0.106	0.04	0.38
	0.13	0.131	1.01
High Level PMD (ps/Km^1/2)	0.87	1.49	1.71
	0.91	2.31	2.54
	0.99	4.08	4.12

Table I Packaging effects on PMD

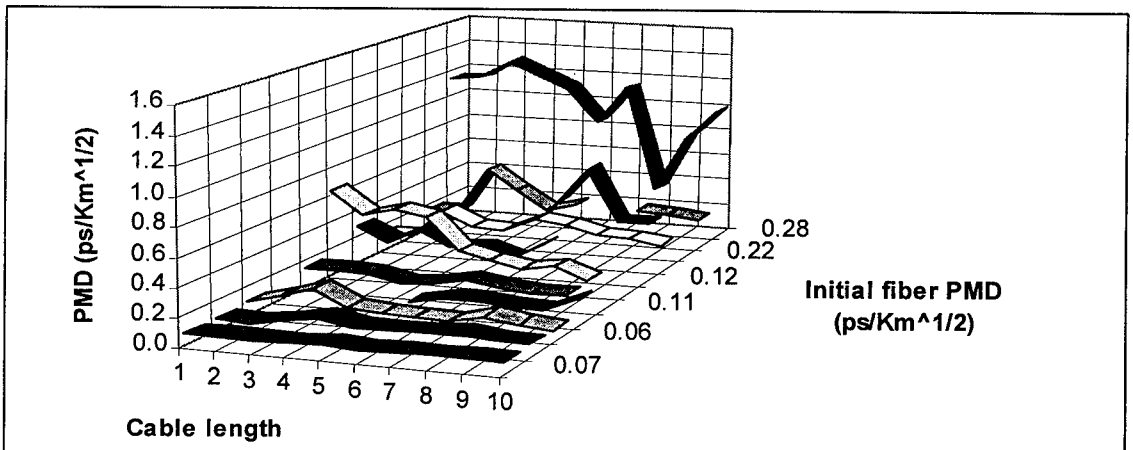


Fig.5a Cabling effects on PMD

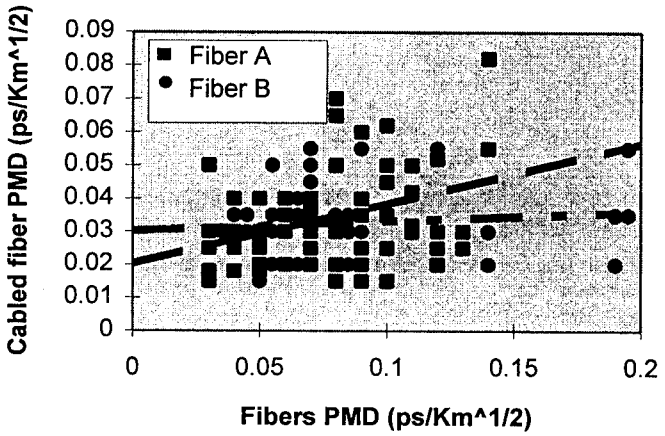


Fig. 5b Field measurement comparison

Fig. 5 PMD cabling effects



Fig.6 Axial tension test equipment

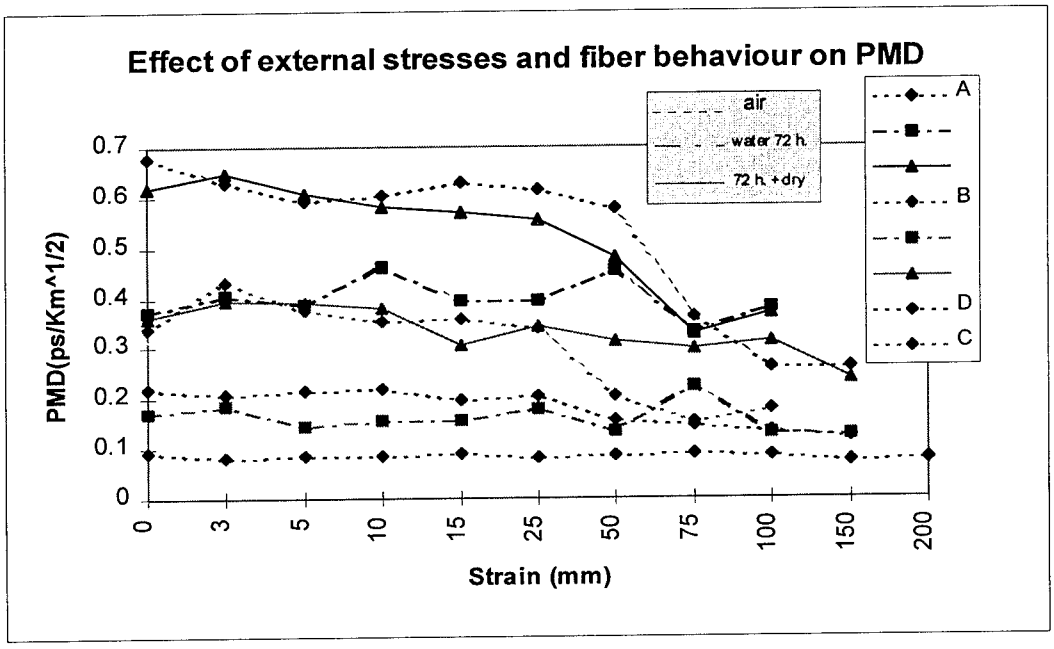
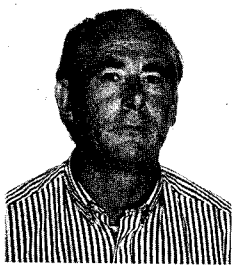


Fig.7 Effects of axial elongation and behaviour conditions on PMD

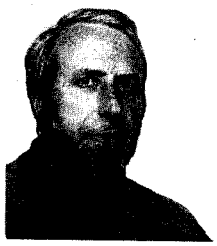
	Bending						micro bending				
	ϕ = 20				ϕ = 15	ϕ = 10	M=0 gr	M=500 gr	M=1500 gr	M=2500 gr	M=3500 gr
	1	2	5	10	5	5					
Fiber A (ps/Km^1/2)	0.626	0.626	0.57	0.47	0.48	0.58	0.78	0.802	0.846	0.844	Failure
Fiber B (ps/Km^1/2)	0.217	0.175	0.193	0.189	0.183		0.267	0.261	0.253	0.264	0.267

Table II Bending and micro bending effects on PMD

Authors BIOGRAPHIES



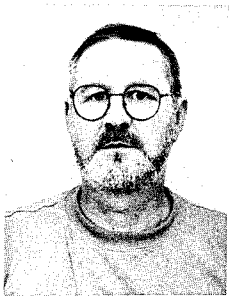
Alain GOURONNEC was born in 1946. He received his engineer degree from the CONSERVATOIRE NATIONAL DES ARTS ET METIERS in 1978. He joined the CNET in 1971 where he was in charge of the pulling and multipulling of optical fibers studies. In 1986 he started to work on development and specification of telecommunication cables; since 1993 he has been in charge of evaluation and qualification of optical fibers for France Telecom needs; he is also in charge of the optical fiber reliability studies in CNET.



Roland GOARIN was born in 1942. He received his doctorate in electronics in 1968 and joins the CNET during the same year. He is an international expert for components reliability. He is now the head of the "Components and Devices for Optronics" department.



Monique AUVRAY is a technician in electronics. She is "DPCT" graduated from the "Conservatoire des Arts et Métiers". She is in charge of transmission measurements in the CNET Laboratory for Evaluation and Qualification of Optical Fibers.



Gerard LE MOIGNE was born in 1943. As a technician in electronics he joined the CNET in1965. Since 1984 he has been in charge of the mechanical reliability test for the CNET Laboratory for Evaluation and Qualification of Optical Fibers.

Cable and System PMD Prediction

Dan Gallagher and Keith Emig
Corning Incorporated
MP-RO-02
Corning, NY 14831
Phone: 607-974-4939
Fax: 607-974-7522

Marvin Ashby and Mike Fedoroff
Siecor Corporation
P.O. Box 489
Hickory, NC 28603-0489
Phone: 704-327-5957
Fax: 704-327-5533

Abstract

The authors have performed PMD experimentation which demonstrates that cabled optical fiber and installed plant performance can be predicted by characterization of the source optical fiber distribution. Experimentation includes cabling effects, cable deployment, concatenation and temperature dependence. Quadrature average is presented as a practical metric for comparison of distributions.

Introduction

Polarization Mode Dispersion (PMD) has quickly become an important consideration in both analog, cable TV and digital (long-haul) applications which utilize single-mode optical fiber in the network. This paper describes experimentation conducted to understand and quantify the effects of cabling and concatenation on the PMD performance of single-mode optical fiber cables.

The experiments described below involve testing of matched clad, single-mode fiber in stranded loose tube cable designs used in the cable TV and telephony industry. These results do not necessarily reflect the performance of other fiber or cable designs. Either the Jones Matrix Eigenanalysis (JME) technique or the wavelength scan method with Fourier data analysis referenced to the JME equipment [1] was used to collect the PMD data.

PMD Contributors

PMD performance has two contributors: birefringence and mode coupling. Birefringence is the relative delay between the two polarization states of the fundamental mode. This delay is from differences in the refractive indices in the two orthogonal planes caused by asymmetry in the dopant concentration or stress non-uniformities. Mode coupling [2] refers to the exchange of optical energy between modes as they propagate. Increased birefringence leads to more dispersion while mode coupling reduces the dispersion. Both of these factors can have intrinsic or extrinsic sources.

Intrinsic (defined here as within the optical fiber) birefringence is driven by asymmetries within the fiber profile, either form or stress induced. Intrinsic mode coupling is caused by coupling sites (such as minute axial variations in the dopant profile) within the glass itself.

Extrinsic birefringence is primarily caused by lateral loading of the waveguide in the cable. Extrinsic mode coupling can be induced by bends, twists and fiber-to-fiber contact in the cable structure.

Developing a Metric for Comparing Distributions

Selection of a metric is fundamental to any effort to compare the impact of different distributions of PMD. A proven metric enables one to quantitatively compare one fiber distribution with another or a given fiber distribution before and after cabling.

Addition in quadrature has been suggested as a theoretical predictor for concatenated PMD performance [3]. If confirmed, it would be a good metric to predict the performance of cabled and concatenated system lengths created from a fiber distribution. In other words, to predict the performance of links created from a distribution, calculate the normalized quadrature average of that distribution. For shorter length systems, some type of Monte Carlo analysis might be needed, but for longer lengths the quadrature average yields the expected link performance from a distribution.

For τ representing the non-normalized individual fiber delays in psec and L the length in km, the normalized PMD is:

$$PMD_i = \tau_i/\sqrt{L_i}$$

And the normalized, quadrature average PMD of a distribution of fibers, the metric we will use throughout this paper, is:

$$PMD_{QA} = \sqrt{(\Sigma \tau_i^2 / \Sigma L_i)}$$

To test the ability of this metric to predict concatenated performance, we spliced the fibers from three 30 fiber cables in a combination of lengths ranging from three to 90 km. Figure 1 shows both the measured delay and the delay predicted by the quadrature addition of the constituent fiber delays. Although there is some variability about the unity line, this calculation appears to predict concatenated performance within the limits of the Maxwellian variability [4] of any PMD measurement.

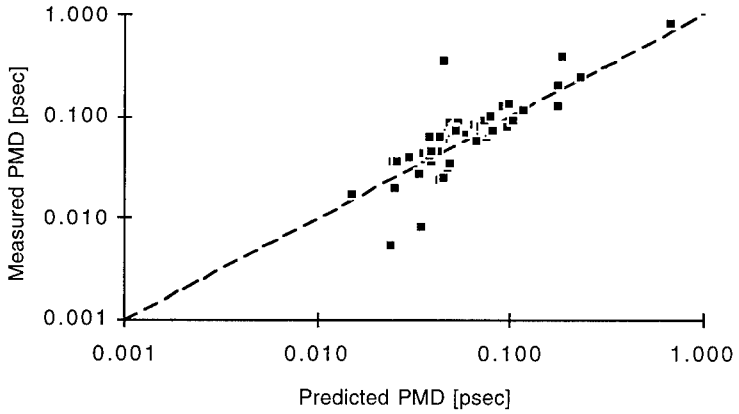


Figure 1: Comparison of predicted and measured PMD for concatenated lengths

Cabling Effect on Fiber PMD

It is important to be able to predict the effect of cabling on fiber PMD. Due to the inherent Maxwellian variability of any single measurement, the prediction of cabling effects on individual fibers will be limited in accuracy. However, by looking at even small populations such as those presented here, these effects can be quantified using the quadrature average PMD.

Cable Design

The optical fiber cable acts as a protective package for the optical fiber, providing a buffer from the mechanical and environmental stresses presented by the environment in which it is deployed. If not properly designed and manufactured, this protective package can induce stress on the fiber during manufacturing and deployment.

The cable design used in these experiments was the reverse oscillation stranded loose tube construction, widely deployed in such outdoor cable applications as telephony, cable TV and premises communications systems. The basic building block of the cable is a protective polymer buffer tube housing the optical fibers. This buffer tube is extruded over a maximum of 12 fibers and serves to protect the individual fibers from external forces exerted on the cable. This is accomplished by placing a controlled excess length of fiber in the tube and through critical selection of the tube material. The buffer tube also provides isolation of the fiber from any lateral loading, thereby minimizing induced birefringence.

Figure 2 below shows the results of 60 non-dispersion shifted fibers before and after cabling. The variability about the unity line is not

unexpected, given the Maxwellian variability of PMD.

The quadrature average for this cabled population was 25 percent lower than before cabling; the median showed a similar reduction. A larger data set has also shown significant reduction in both quadrature average and median.

Note that the fiber values were generated while the fibers were deployed on large, catenary-wound drums. Errors in comparison between fiber and cable often occur when the fiber performance from a shipping spool is compared to that in the finished cable. The random occurrence of fiber-to-fiber contact associated with commercial fiber shipping packages serves to induce a high level of extrinsic mode coupling, resulting, in some cases, in an artificially low measured PMD. Comparisons from fiber on a controlled wind measurement spool to that in the finished cable serve to yield a more practical predictor of the true cabling influence.

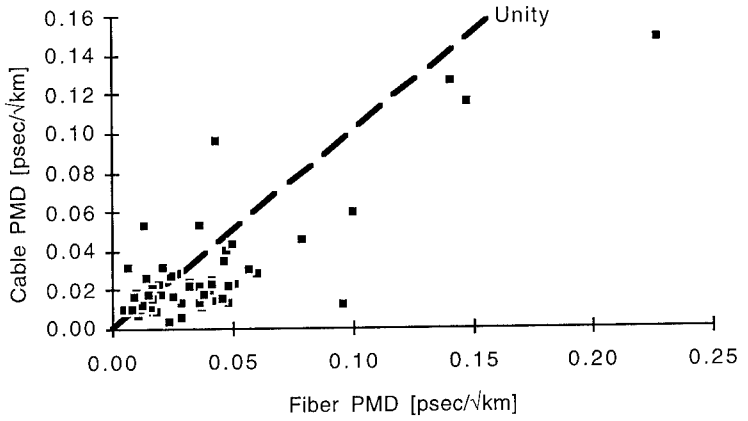


Figure 2: Comparison of PMD before and after cabling.

Field Deployment

The ability to assess and accurately predict the distribution of cabled PMD performance in a spooled condition was then followed by work to understand the cabled fiber performance in a deployed condition. A Siecor LiteTube® cable was placed on the ground with a random distribution of bends and twists, similar to that which is routinely experienced in outside plant environments. Figure 3 shows deployed PMD values compared to the initial measurements of the cable on the reel.

The results of the deployment study indicate that there is little effect on the PMD distribution as the cable deployment is changed. Comparison of the quadrature averages of these two conditions leads us to conclude that the measurements on the cable spool are representative of the deployed performance. Other testing of deployed cable has yielded supporting results.

Verification of Concatenation Work

While in this deployed state, fibers from this cable were concatenated and re-measured to confirm that addition in quadrature predicted installed cable performance. Results from that experimentation are shown in Figure 4. As can be seen, the quadrature average results in a practical, if slightly conservative, prediction of deployed, concatenated performance. The splice frequency in this concatenated link was higher than would be expected in a typical outside plant installation. Mode coupling contributions from splicing may have reduced the measured performance [5].

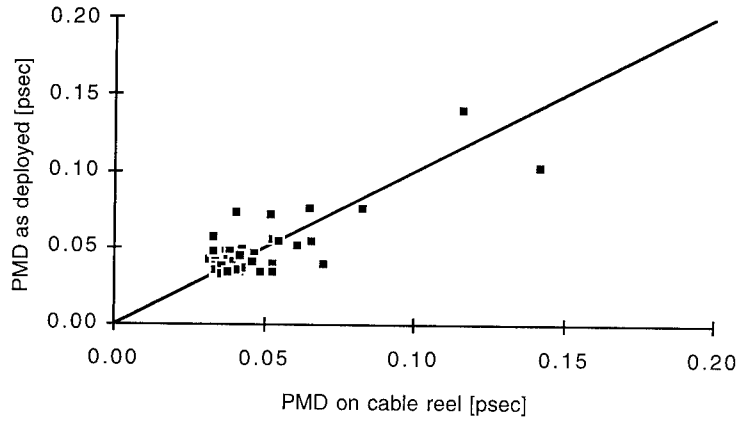


Figure 3: Comparison of PMD performance on cable reel and deployed

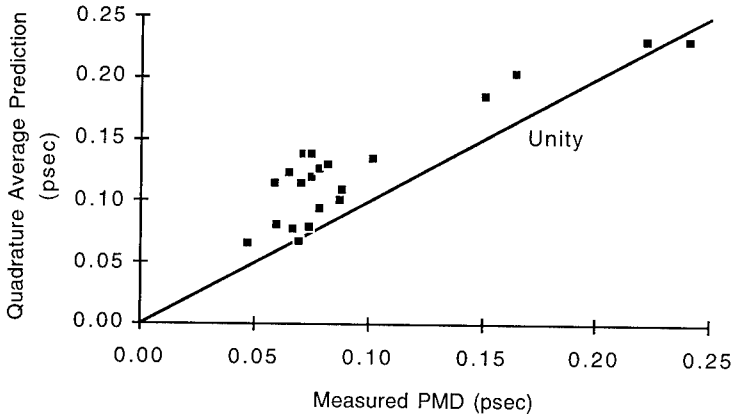


Figure 4: Comparison of measured and predicted PMD performance of deployed, concatenated cable

Temperature Dependence

Another aspect of the installed plant PMD performance that must be understood is the contribution of temperature variations and aging. A single-mode cable was subjected to environmental extremes of -40°C and + 70°C and aged at a temperature of +85°C for a period of 120 hours. Characterization of the PMD performance for each fiber was conducted prior to testing as well as at the temperature extremes and after the aging period.

By looking at the change in the quadrature average for the group of fibers tested, uncertainty due to the variability of PMD is reduced. As shown in Figure 5, only small changes were detected in the quadrature averages. We conclude that temperature changes can induce variability within the Maxwellian distribution of a concatenated link but a shift in the distribution would not be expected. The magnitude of the changes shown should not be of concern for installed systems.

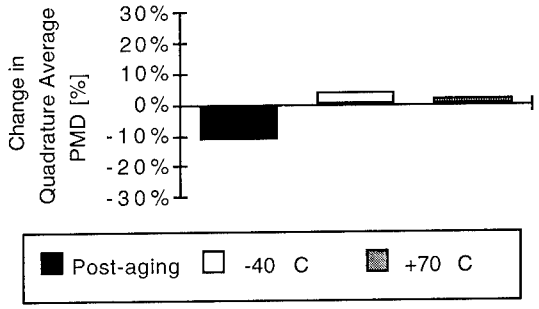


Figure 5: Temperature dependence of PMD

Prediction of Digital System Performance

System PMD limitations for digital transmission can be calculated for a given length and bit rate.

Since regeneration will remove the signal degradation caused by PMD, we are only concerned with the length between regeneration sites regardless of the use of optical amplifiers. We estimate that for most digital system designs, the pulse broadening from PMD should be limited to 25 percent of the bit period. Furthermore, given the Maxwellian variability of PMD, that bit period "budget" must be further reduced by a safety factor calculated to protect against some low probability excursion. We calculate that a factor of 4.2 protects against 10e-9 probability excursions in the Maxwellian distribution. Using these inputs, Figure 6 shows the maximum PMD allowed for a given system length (between regeneration sites) and bit rate.

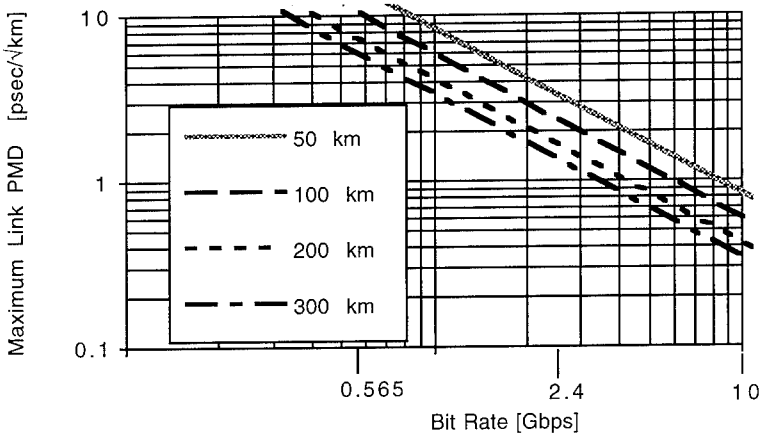


Figure 6: Maximum PMD as a function of bit rate and distance between regeneration

Other Fiber Types

The authors have initiated similar studies on another fiber design, Corning®'s SMF-LS™ fiber. These studies indicate that the fiber distribution, having a quadrature average well below 0.1 psec/√km, did not degrade during cabling or deployment. Using the system model described above, the resulting cabled performance ensures that PMD will not limit 10 Gbps transmission at lengths in the thousands of kilometers.

Summary

In conclusion, experimentation has been performed which demonstrates that, for the fiber and cable designs tested, cabled PMD performance can be predicted using measured fiber PMD distributions. Additionally, it has been demonstrated that the PMD of concatenated fiber lengths can be well predicted using the quadrature average as a metric.

Acknowledgments

The authors would like to recognize Gene Brarens, Ralph Westwig, Jerry Racki, Jim Warder, Bing Fung and Joyce Fidler for their extensive efforts in acquiring supporting data and numerous other individuals for review and comment on the work.

References

1. D.Q. Chowdhury and D.A. Nolan, "Quantitative Comparison Between the Jones Matrix Eigenanalysis & Wavelength Scan Method for Polarization Mode Dispersion Measurement: A Simulation Study", NIST Special Publication 864, 1994.

2. D.A. Nolan and D.Q. Chowdhury, "Mode Coupling Model for the Jones Matrix Eigenanalysis Method", NIST Special Publication 864, 1994.

3. A. Galtarossa, et al., "Polarization Mode Dispersion in Long Single-Mode Fiber Links: A Review", Fiber and Integrated Optics, Volume 13, pp. 215-229.

4. F. Curti, et al., "Statistical Treatment of the Evolution of the Principal States of Polarization in Single-Mode Fibers", Journal of Lightwave Technology, Vol. 8, No. 8, Aug. 1990.

5. Y. Suetsugu, et al., "Effects of Random Mode Coupling on Polarization Mode Dispersion and Power Penalty in Single-Mode Fiber Systems", Optical Fiber Technology 1, pp. 81-86, 1994.

Biography

Marvin Ashby is currently the Manager of Applications Engineering at Siecor Corporation and is responsible for worldwide technical support for optical fiber cable, connectors, connectorized assemblies, and hardware. Prior to Applications Engineering he worked in Process Engineering, Quality Control, and Product Evaluation. He currently is active in the development of national standards for the optical fiber industry through the Telecommunications Industry Association and the Insulated Cable Engineers Association. He is a graduate of Purdue University with a B.S. in Electrical Engineering.



A Non-destructive Optical Talk System using Fresnel-Reflection Light Signals

Yuji Azuma, Hisashi Izumita, and Koji Yoshida

NTT Technical Assistance & Support Center
Midori-cho, Musashino-shi, Tokyo, 180 Japan

***Abstract*:**

A previously proposed non-destructive optical talk system with local amplitude modulation and local light detection can be used at any point along an optical fiber without cutting and splicing the fiber. It is used for the maintenance of trunk communication lines. However, since this system needs a light source at each end of the optical fiber, it cannot be applied to subscriber networks. A non-destructive optical talk system with only one light source has thus been newly developed. This system uses masking detection of Fresnel-reflection light signals at the open-end face of the fiber or at an optical filter.

1. Introduction

The capacity of subscriber optical fiber networks[1] is being increased by using high-density, high-count optical fiber cables[2]. This requires an effective operational system[3] for testing and maintaining the optical fiber cables. During cable installation and maintenance, it is often necessary for the workers in the end office and at outside points to talk via the optical fiber. This is usually done by cutting the optical fiber in order to be able to send and detect a signal light. However, this requires fusing the optical pigtail cords with optical connectors, which takes a long time and reduces operational efficiency. It would be better if talking could be done from any point without cutting the fiber.

We previously proposed a local amplitude modulator[4] that enables transmitting a light signal without damaging the optical fiber. It is based on the property that fiber bending loss is proportional to the change in the bending radius of a U-bent optical fiber.

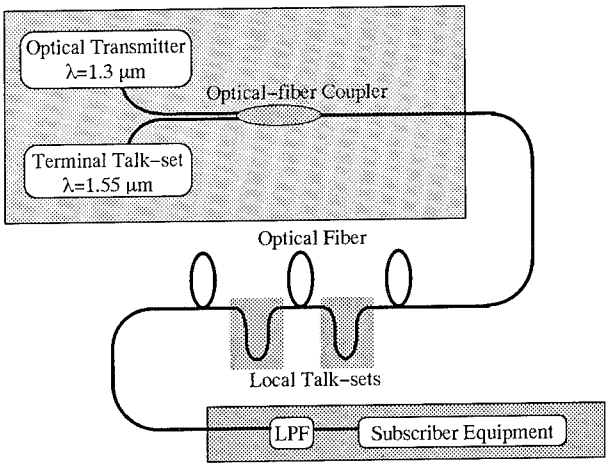


Fig. 1 Configuration of proposed talk system on subscriber network.

A system using the proposed amplitude modulator enables conversation between workers at outside points and at both ends of an optical transmission line. However, this system needs a light source at each end of the optical fiber, which means that it cannot be applied to subscriber networks in which one of the optical-fiber ends is terminated at subscriber equipment. We thus propose a new non-destructive optical talk system with a light source at only the input end of the optical fiber. This paper describes our theoretical and experimental studies on this talk system.

2. Principle

2-1 System Configuration

The configuration of the proposed talk system at a subscriber network with an optical fiber is shown in Fig. 1. It uses a 1.3-μm single-mode optical fiber;

the propagated light wavelength for commercial use and maintenance use is 1.3 μm and 1.55 μm, respectively. The optical fiber is terminated at the user's end by an optical pigtail cord with an optical low-pass filter (LPF). This LPF transmits the 1.3-μm-wavelength light for commercial use and reflects the 1.55-μm-wavelength light for the maintenance use. The reflected light barely transmits through the LPF. This LPF is used to separate the user's transmission equipment from the outside line when a problem is being located with an optical time domain reflectometer (OTDR).

This talk system is composed of a terminal talk-set and several local talk-sets. The terminal talk-set is placed at the end office and connected to the optical fiber. The local talk-sets can be placed at any points along the optical fiber; they are mounted by bending the optical fiber into a U-shape without cutting it. A local talk-set can easily be connected with an optical ribbon fiber and secured with a clip. Communication between the terminal talk-set and a local talk-set is done using Fresnel-reflection light signals at the optical LPF.

The flow of a signal sent from the terminal talk-set is as follows. The terminal talk-set sends an optical fiber a pulsed light signal through an optical fiber coupler. A local talk-set detects the propagated light signal by using a local detection technique. The light is modulated by a voice-band signal at the terminal talk-set and demodulated to a voice-band signal at the local talk-set. At the same time, the propagated light through the local talk-set is modulated by the worker's voice by using local amplitude modulation. This modulated light is reflected at the optical LPF at the fiber end, returned to the terminal talk-set, detected by the terminal talk-set, and demodulated to a voice-band signal. It is thereby possible for workers at the terminal talk-set and at a local talk-set to talk via the optical fiber.

The flow of signals between local talk-sets is as follows. Light modulated at local talk-set A is detected and demodulated at local talk-set B. The light modulated at local talk-set B is reflected at the optical LPF and returned to local talk-set A through local talk-set B. However, local talk-set A cannot directly detect the returned light by using local detection, because the coupling loss of local detection is large. Therefore, the returned light is detected at the terminal talk-set, which amplifies it and returns it to the optical fiber. Local talk-set A then detects the light radiated from the bending region and demodulates the signal propagated from local talk-set B through the repeater function of the terminal talk-set. At least theoretically, local talk-sets can talk to each other.

2-2 Detection Method using Advanced Sensitivity

The output light from the terminal talk-set is placed into the optical fiber through a coupler. However, some of the incident light are returned back to the photodetector of the terminal talk-set through the coupler due to the optical power of the Rayleigh backscattering in the optical fiber and the Fresnel reflection that occurs at some type of connectors with the exception of the fiber end. These multiple values decrease the detection sensitivity of the photodetector.

We therfore set pulse period T of the light source to be longer than the time it takes to send and detect the pulse at the terminal talk-set through reflection at the LPF. This enables the light signal modulated at the local talk-sets to be separated from the optical power of the Rayleigh backscattering in the optical fiber and the Fresnel reflection at other connectors. Assuming that the fiber length is L and the velocity of the light in the fiber is v_g, this pulse period condition is given by

$$T > 2L / v_g . \qquad (1)$$

In addition, we set pulse width τ to be less than pulse period T in order to decrease the noise level of the Rayleigh backscattering power. Rayleigh scatter capture level R_R is given by[5]

$$R_R=\alpha_R S\,(1-\exp(-\alpha v_g \tau))/2\alpha, \qquad (2)$$

where α_R is the power attenuation coefficient due to Rayleigh scattering, α is the optical-fiber loss factor, and S is the recature ratio of the Rayleigh power scattered back into the fiber.

For example, when 1.55-μm-wavelength light pulsed at τ =1 μs is transmitted into a 1.3-μm-

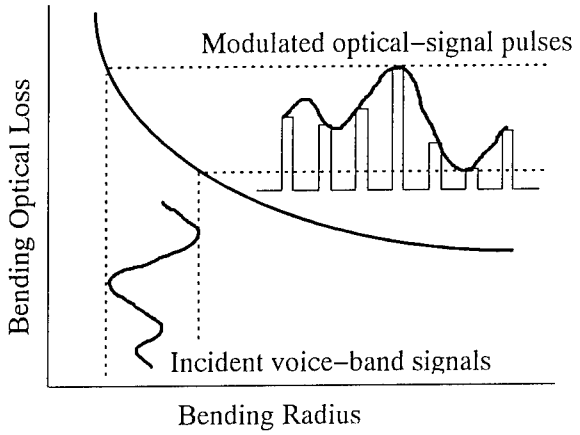


Fig. 2 Modulation principle.

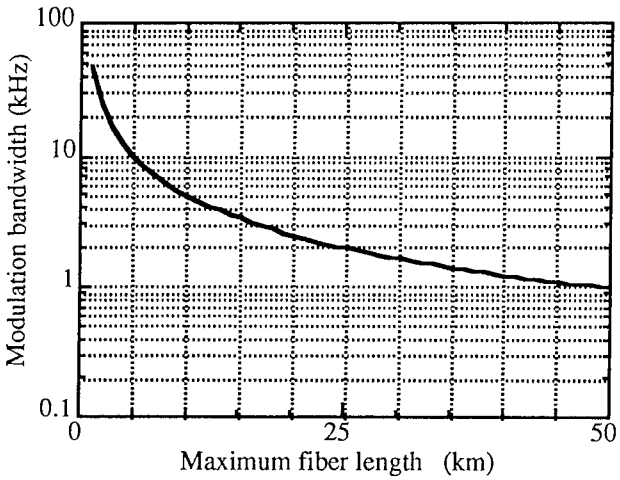


Fig. 3 Calculated maximum fiber length as a function of modulation bandwidth.

wavelength single-mode optical fiber, Rayleigh scatter capture level R_R is -53 dB ($\alpha_R=3.59\times10^{-5}m^{-1}$, $\alpha=4.83\times10^{-1}m^{-1}$, and $S=1.33\times10^{-3}$). This is 20 dB lower than the Rayleigh scatter capture level for a continuous-wave. Pulsed light clearly decreases the Rayleigh backscattering noise.

2-3 Modulation Bandwidth of Local Talk-set

The relation between the optical-fiber bending loss and the bending radius is shown in Fig. 2. The optical power propagating in the fiber depends on the bending radius; its variation tracks with the variation of the bending radius. By using this characteristic, the vibration of the diaphragm (audio speaker) used to input the voice-band signal can be used to modulate the propagating pulsed light.

Since the propagating light is pulsed, the signal modulated at a local talk-set is sampled by the terminal talk-set at pulse period T. Therefore, modulation bandwidth f of the local talk-set is defined by

$$f < 1/2T. \quad (3)$$

2-4 Maximum Fiber Length

From the two condition of Eqs. 1 and 3, pulse period T is given by

$$2L/v_g < T < 1/2f. \quad (4)$$

Therefore, maximum fiber length L is given by

$$L < v_g/4f. \quad (5)$$

Figure 3 shows maximum fiber length L as a function of modulation bandwidth f as calculated using Eq. 5. The length is in inverse proportion to the modulation bandwidth. For example, when modulation bandwidth f is 2 kHz, applied fiber length L is less than 25 km.

3. Experimental Results

3-1 Verification of Basic Operations

The experimental setup we used to verify the basic operations is shown in Fig. 4. The FP-LD light source is driven by pulses with a 1.55-μm-wavelength; the pulse width and peak optical power are 1 μs and 0 dBm, respectively. The pulsed light signal is sent to a 1.3-μm single-mode optical fiber through an optical-fiber coupler at a pulse period of 250 μs. The fiber length is 25 km. The local talk-set is placed 20 km from the terminal talk-set. The propagating light is amplitude modulated by an 800-Hz sine-waveform at the local talk-set, which is connected to a signal generator. The modulated light

reflects at the open end of the optical fiber and returns to the terminal talk–set, where it is detected by the PIN photodiode and demodulated.

Figure 5 shows the waveform detected by the PIN photodiode of the terminal talk–set. The pulse period is 250 μs; the waveform and frequency of the envelope is a sine–wave and 800 Hz, respectively.

Figure 6 shows the spectrum of the light signal detected by the PIN photodiode of the terminal talk–set. The detected signal shows that the notable frequency is 800 Hz with an *SNR* of 26 dB. The second harmonic frequency of 1600 Hz is generated due to the nonlinearity of the bending loss characterictics of optical fiber. When the detected signal is input into an audio speaker through an electrical low–pass filter (LPF) of 2 kHz, an 800–Hz tone can clearly be heard from an audio speaker.

We experimentally verified that the light modulated at a local talk–set is reflected at the open end of the optical fiber and that the reflected light signal is detected at the terminal talk–set and demodulated to a voice–band tone. We thus achieved communication between the terminal talk–set and the local talk–sets.

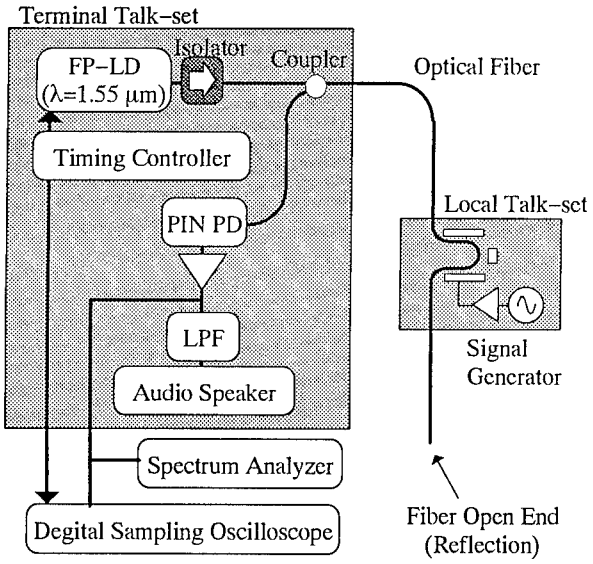


Fig. 4 Experimental setup to verify basic operations.

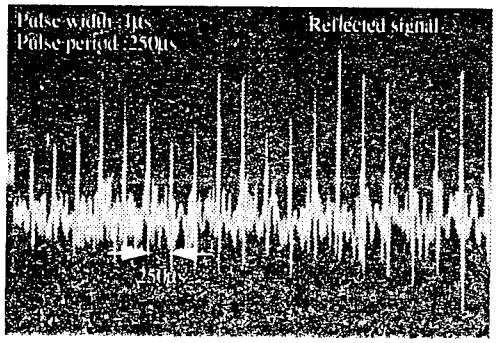


Fig. 5 Waveform of returned light signal.

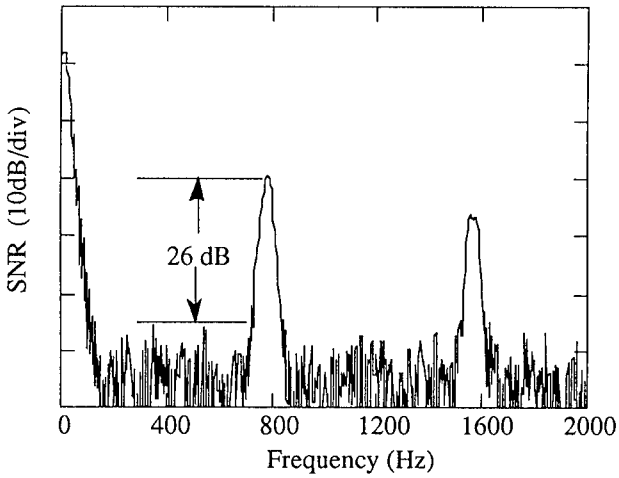


Fig. 6 Spectrum of reflected light signals.

3–2 Light Signal Sampling Method

Figure 7 shows the experimental setup we used to verify the sampling method of the light signal modulated at a local talk–set. In a terminal talk–set, there is a gate circuit and a timing controller. The gate circuit is opened for 10 μs, delayed $2L/v_g$ from the clock signal of the timing controller to eliminate the backscatterd light noise. The clock signal is synchronized with the pulse period of the light source. The eliminated backscattered light noise consists of Rayleigh backscattering light in the optical fiber and Fresnel reflection light at the connectors.

We experimentally investigated the sampling method assuming that there are several optical connectors in the line located immediately after a fiber coupler and before the local talk–set. The local talk–set is located 20 km from the terminal talk–set, as shown in Fig. 7.

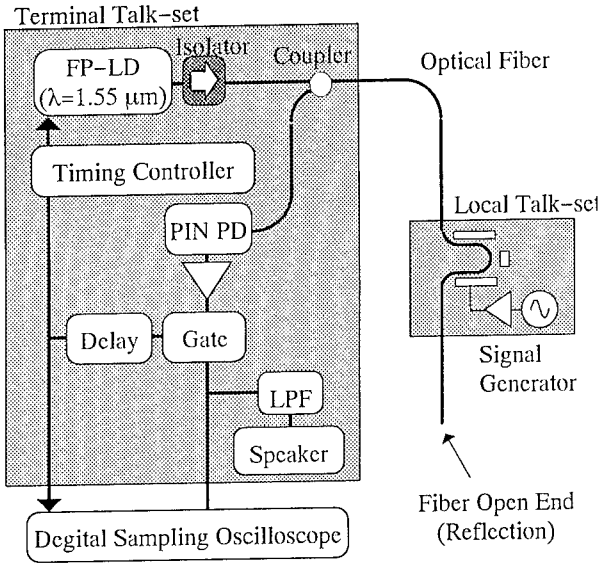


Fig. 7 Experimental setup to verify sampling method.

Figure 8 shows the waveforms detected through a fiber coupler by the PIN photodiode. Figure 8 (a) shows the output waveform before the gate circuit. The large optical power of the Rayleigh backscattering and Fresnel reflection is detected as noise. Figure 8 (b) shows the output waveform after the gate circuit. The detected signal is masked for the time region of the Rayleigh backscattering and Fresnel reflection; the Fresnel reflection light is sampled only at the fiber end. The envelope frequency of the sampling pulses was 800 Hz. The envelope is a signal modulated at the local talk-set. In the measured waveform, there was still some Fresnel reflection at the connector after an optical coupler; however, we think that it is possible to remove it completely by improving the isolation of the gate circuit. Figure 8 (c) shows the clock signal synchronized with the light source signal.

We verified that the light signal modulated at a local talk-set and reflected at the fiber end can be sampled at the terminal talk-set by using a masking technique based on Eq. 1.

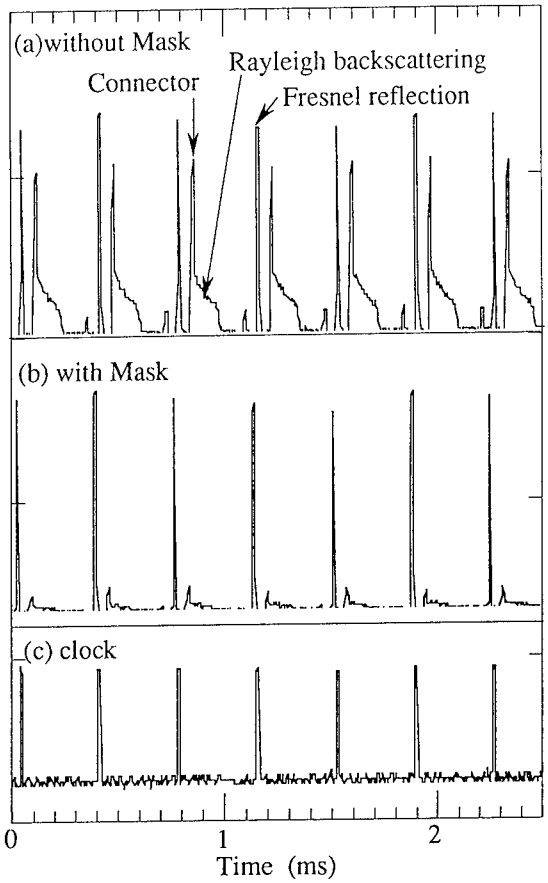


Fig. 8 Waveforms of returned light signals.

3-3 Modulation Bandwidth

The propagation bandwidth of the talk system is limited by the modulation bandwidth of the local talk-set. Modulation bandwidth f is in inverse proportion to optical fiber length L (Eq. 5). We experimentally investigated the propagation bandwidth.

Using the experimental setup shown in Fig. 4, we measured the signal-to-noise ratio (SNR) with a spectrum analyzer in the band from 400 Hz to 2 kHz. The modulation index of the input signal was 3% at a frequency of 800 Hz. Optical fiber length L was 25 km.

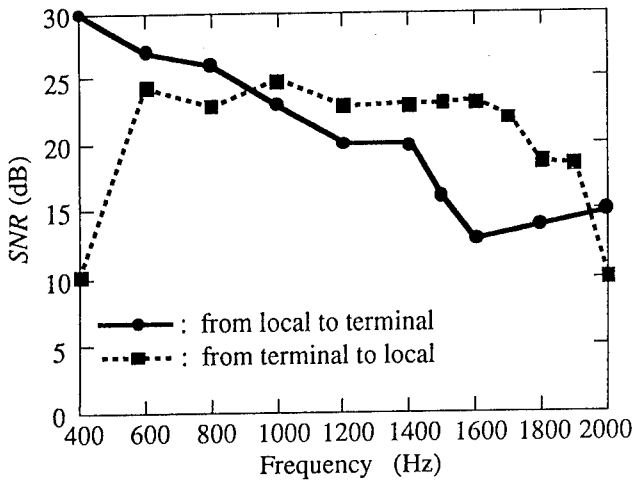


Fig. 9 Frequency characteristics of terminal talk–set and local talk–set.

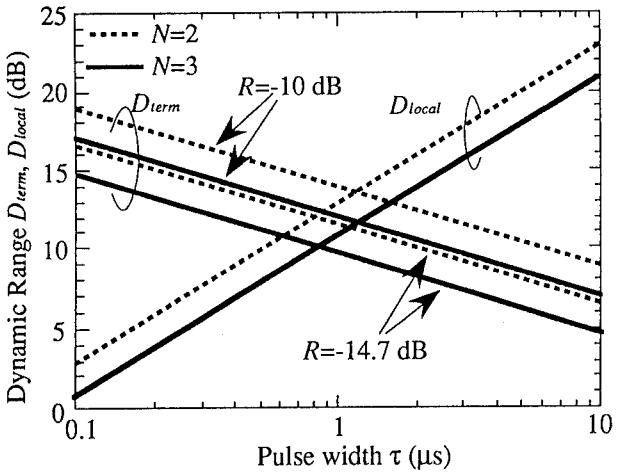


Fig. 10 Calculated dynamic ranges D_{term} and D_{local}.

Figure 9 shows the measured results. The *SNR* from a local talk–set to a terminal talk–set gradually decreased as the frequency increased. The 6–dB normalized *SNR* at 800 Hz was from 400 to 1400Hz. This is the gain characteristic of the electromagnetic transducer of the diaphragm. For the *SNR* from a terminal talk–set to a local talk–set, the 6–dB normalized bandwidth was from about 500 to 1900 Hz. This satisfies the modulation bandwidth limit of Eq. 3. This bandwidth is sufficient for normal conversation between a terminal talk–set and a local talk–set.

4. Dynamic Range of Talk System

This talk system consists of one terminal talk–set and several local talk–sets. The number of local talk–sets is assumed to be N. Reflectivity R of the fiber end is −10.0 dB when the fiber is terminated by an optical LPF for maintenance work and −14.7 dB when the fiber is open ended for installation work, respectively.

The effective minimum detectable optical power ($P_{min,term}$) of the terminal talk–set is given by

$$P_{min.term}=\mathrm{Max}(P_{term}, P_0+R_R-2\alpha_c+SNR_m), \quad (6)$$

where P_0 is the peak power of the pulsed light source, α_c is the coupler insertion loss, SNR_m is the demodulation margin, R_R is the Rayleigh scatter capture level, and P_{term} is the minimum detectable optical power with SNR_m=20 dB at 1 kHz. Therefore, dynamic range D_{term} from a local talk–set to a terminal talk–set is given by

$$D_{term}=(P_0-2\alpha_c+R_R-P_{min,term}-2N\alpha_{local})/2\ . \quad (7)$$

The local talk–set has an InGaAs photodiode with a diameter of 3 mm. The detectable optical power with an *SNR* of 20 dB at 1 kHz is assumed to be P_{local}. The fiber bending radius of the local talk–set is approximately 10 mm, so fiber–bending optical loss α_{local} is less than 2 dB. Coupling loss η between the optical power propagating through the bending region and the optical power detected at the photodetector is approximately 23 dB. The average optical power of the pulsed light signal decreases by the ratio of the pulse width and the pulse period. Therefore, dynamic range D_{local} from a terminal talk–set to a local talk–set is given by

$$D_{local}=P_0+10\log(\tau/T)-\alpha_c-(N-1)\alpha_{local}-P_{local}-\eta. \quad (8)$$

Figure 10 shows calculated dynamic ranges D_{term} and D_{local} as a function of pulse width τ. Parameter N is the number of local talk–sets. For talk from a local talk–set to a terminal talk–set, when pulse width τ is larger, dynamic range D_{term} decreases. For talk from a terminal talk–set to a local talk–set, dynamic range

D_{local} increases. In these calculations we assumed P_0=10 dBm, α_c=3 dB, α_{local}=2 dB, SNR_m=7 dB, P_{term}=−55 dBm, η=23 dB, and T=250 μm.

On the subscriber line, the optical line loss cofficient and the splice loss of a connector is assumed to be 0.36 dB/km and 1 dB, respectively. When the line length is 25 km and the number of connectors is one, the required dynamic range is more than 10 dB. For N=3, the pulse width τ that produces dynamic ranges D_{term} and D_{local} greater than 10 dB is approximately 1 μs. We verified that workers can communicate between a terminal talk−set and three local talk−sets over an optical fiber.

5. Conclusion

We have proposed and demonstrated a non−destructive optical talk system using a Fresnel reflection light signal. This talk system uses only one light source, yet enables bi−directional conversation between a terminal talk−set and several local talk−sets over a 25−km single−mode optical fiber. This system is a suitable communication tool for the maintenance of subscriber networks.

Acknowledgements

We are grateful to Mr. Yasutaka Imori, Mr. Shigeru Kawakami, and Dr. Nobuo Kuwaki for their helpful suggestions and encouragement, and to Mr. Mitsunori Hasebe and Mr. Toshihide Koma for their insightful discussions.

References

[1] T. Miki, "Fiber−optic access networks and services", NTT Review, Vol. 6, No. 3, pp. 17−25, 1994.

[2] K. Hogari, K. Takagi, and F. Ashiya, "Nonmetallic 1000−fiber cable", J. Lightwave Technol., Vol. 10, No. 2, pp. 130−134, 1992.

[3] H. Takasugi, N. Tomita, T. Uenoya, I. Nakamura, and Y. Yokoo, "Design and evaluation of automatic optical operation support system", 39th IWCS, pp. 623−629, 1990.

[4] Y. Azuma, Y. Shibata, S. Tamura, and N. Kuwaki, "Non−destructive optical fiber amplitude modulation for optical talk system", 41st IWCS, pp. 97−103, 1992.

[5] E. Brinkmeyer, "Backscattering in single−mode fibers", Electron. Lett., Vol. 16, No. 9, pp. 329−330, 1980.



Yuji Azuma

NTT Technical Assistance & Support Center
Midori-cho, Musashino-shi, Tokyo, 180 Japan

Yuji Azuma received the B.S. degree in electrical engineering from Doshisha University, Kyoto, Japan, in 1984, and then jointed NTT Laboratories. He was engaged in research on characteristics of high-density optical fiber cable, and fiber nonlinearity. Since 1989, he was engaged in research of evaluation for optical device reliability, and optical fiber transmission characteristics, at Technical Assistance & Support Center. He is now a senior engineer of the Fiber Optics Group.

He is a member of the Institute of Electronics, Information and Communication Engineers of Japan.

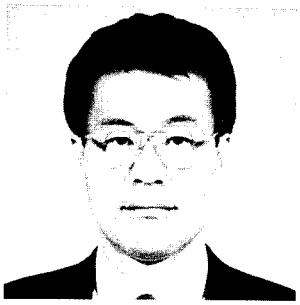


Hisashi Izumita

NTT Technical Assistance & Support Center
Midori-cho, Musashino-shi, Tokyo, 180 Japan

Hisashi Izumita received B.S.and M.S. degrees in Physics from Waseda University, Tokyo, Japan, in 1987 and 1989, respectively. He joined NTT Transmission Systems Laboratories in 1989. He has been engaged in research on coherent ligthwave technology for optical fiber distributed sensing and the development of non-destructive optical talk system. He is presently a Research Engineer of NTT Access Networks Systems Laboratories.

Mr. Izumita is a member of the Institute of Electronics, Information and Communication Engineers(IEICE) of Japan, Japan Society of Applied Physics and an associate member of IEEE.



Koji Yoshida

NTT Technical Assistance & Support Center
Midori-cho, Musashino-shi, Tokyo, 180 Japan

Koji Yoshida received the B.S. degree in electrical engineering from Osaka University, Osaka, Japan, in 1973, and then jointed NTT Laboratories. He was engaged in research on characteristics of optical fiber cable. Since 1985, he was engaged in research of evaluation for optical fiber transmission characteristics, at Technical Assistance & Support Center. He is now a supervisor of the Fiber Optics Group.

He is a member of the Institute of Electronics, Information and Communication Engineers of Japan.

Development of Multi-Coupler Bi-directional Optical Communication System Employing FM-SCM Video Transmission

Hideyuki OMURA, Nozomu MATSUO, Toshinori KIMURA
FURUKAWA ELECTRIC CO.,LTD. Information & Electronics Laboratories,
5-1-9, Higashiyawata Hiratsuka, Kanagawa, 254, JAPAN
Telephone:81-463-24-8446 Facsimile:81-463-24-8491

Yukihisa SHINODA
TOKYO ELECTRIC POWER COMPANY Computer & Communications R&D Center,
4-1, Egasaki-cho Tsurumi-ku Yokohama, Kanagawa, 230, JAPAN
Telephone:81-45-585-8853 Facsimile:81-45-585-8872

Abstract

We have developed a novel bi-directional system employing SCM technique for FM-video transmission. This system is attractive for several reasons. The transmission line of the system consists of conventional optical couplers and optical fibers only. Other active and usually expensive components, such as optical repeaters, (E/O-O/E) or optical amplifiers, are not used in this system. Each signal from the terminals can be received at a center individually and simultaneously with only one photo-detector. Therefore a trouble at any terminal dose not interfere the signal from other terminals. Thus highly reliable and cost effective system can be constructed.

In this paper we present not only the features of the novel multi-coupler system, but also describe the consideration on optical beat interference on the system for FM-SCM video transmission. As the result, the 110km transmission experiment was successfully carried out on an 8 optical coupler system.

1.Introduction

Recently, the optical fiber network has made great progress rapidly. Especially in video distribution systems, such as CATV, taking advantage of the wide bandwidth of optical fiber have been already in practical use[1]-[3], where the subcarrier multiplexing technique (SCM) is widely used to multiplex many channels of video signals on an optical carrier. Additionally, recent progress of optical fiber amplifiers has realized a long haul transmission of such downstream signals. On the other hand, upstream transmission system, where all terminals (subscribers) have their own optical signal transmitters, should be studied and developed for the future bi-directional transmission network applications such as interactive television systems, video monitoring systems, and video on demand systems.

Passive optical networks (PON's) have great potential for the realization of highly reliable and cost effectiveness. Without any active components in the network, construction costs of the transmission line is reduced. Furthermore, passive components like optical fibers and optical couplers have a great advantage of reliability rather than that of active components.

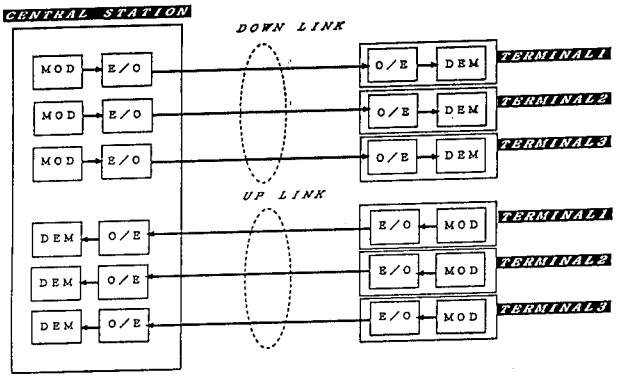
In upward link of PON, where each user uses different RF subcarrier from each other to transmit information, the optical signals from different users can be identified at the receiver set in a central station using SCM technique. But in such a system a problem happens when the optical signals from two or more users get too close to each other in wavelength. The beating of these two lasers causes increase of noise at the detector. This problem is known as optical beat interference (OBI) [4]-[6].

In this paper, we propose and demonstrate a new bi-directional all passive system employing SCM technique for FM-video transmission based on the detailed analysis on the OBI. By using conventional optical coupler to combine the optical signals from each terminal, a cost effective and reliable video transmission system has been realized. And we have applied this system to video monitoring systems to keep watching high-voltage electric power cable, railway, highway, etc. We also show an example of application for video monitoring system to supervise a high-voltage electric power transmission system.

2.Features of the multi-coupler system

2.1 Architecture comparison of PON Systems

Fig.1. (a) to (c) show a typical configurations of bi-directional video transmission system on PON network.



MOD:modulator E/O:electrical/optical converter
DEM:demodulator O/E:optical/electrical converter

Fig.1 (a) Point to point system configuration

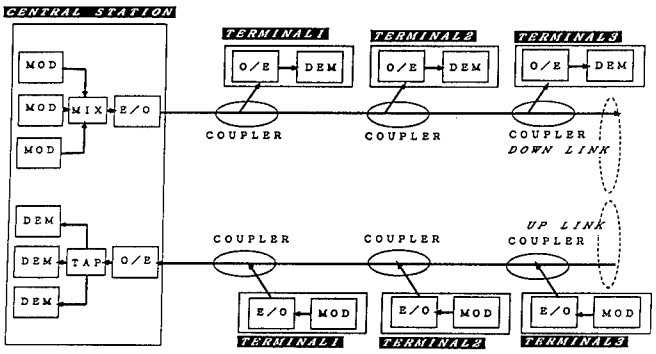


Fig.1 (b) Multi-coupler system configuration

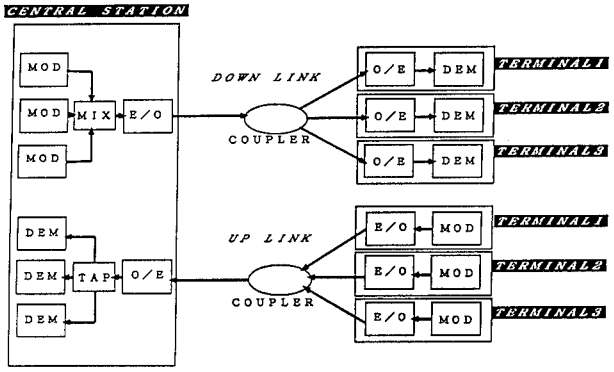


Fig.1 (c) Tree system configuration

2.1.1 Point to Point configuration

In a point to point transmission route between a terminal and a central station, large volume of data can be transmitted at high speed rate, and independent transmission can be realized for each terminal.

On the other hand, as the disadvantage of this configuration, the system requires as many optical fiber lines, receivers and transmitters as terminals, resulting in more expensive system than the multi-coupler system described below. Additionally, in the case of many terminals, many optical fibers must be gathered at a central station and the maintenance of such a system becomes very difficult.

2.1.2 Multi-coupler configuration

To construct reliable and cost effective system, we propose a new architecture, multi-coupler system.

In this system, the optical signals are multiplexed or demultiplexed for each terminal by optical couplers, which are located along the only one transmission line.

In a conventional optical repeater (E/O-O/E) system, the trouble at any optical repeater may disturb the transmission of all signals from other terminals. In Fig.2, a example of optical repeater system configuration is shown. If the terminal 1 has any trouble, the information cannot be reached to central station from terminal 2 and terminal 3. In a multi-coupler system, on the other hand, high reliability will be realized because each signal from each terminal can reach the central station individually. Even if a terminal has any trouble, it does not interfere other terminals.

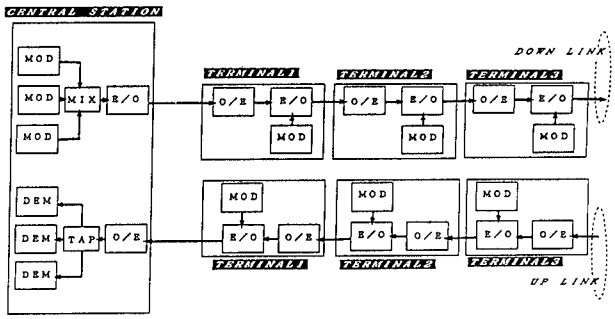


Fig.2 Optical repeater system configuration

2.1.3 Tree configuration

Tree system is one of the multi-coupler system.

The terminals are divided into some blocks and wiring is centralized for each block. The passive double star system is one of the typical tree system. This type is particularly effective when the central station is located at the center point of transmission area and the terminals are distributed uniformly.

2.2 Detailed design of the multi-coupler system

Fig.3 shows a schematic diagram of multi-coupler system.

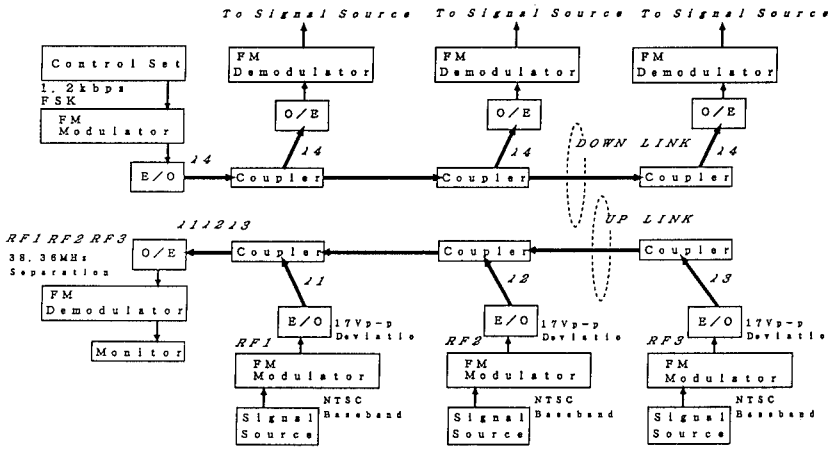


Fig.3 Detailed design of the multi-coupler system

In upward link, the video signals from terminals are frequency-modulated with FM modulator, and the laser-diodes are directly modulated by the output of FM modulators to construct a FM Sub-Carrier Multiplexing (FM-SCM) system. We used the same frequency allocation and FM modulation format as those used in Satellite Broadcasting in Japan. Sub-carriers are allocated around 1 GHz with channel separation of 38.36MHz. Because of FM improvement of Satellite Broadcasting format, Carrier-to-Noise Ratio (CNR) required for the optical links is relatively small. CNR of 14 dB is required in order to transmit a broadcast satellite FM signal below the interference detection. By choosing the subcarrier frequency allotted to each terminal, we can easily receive the signals from each terminal separately at a central station.

The optical signals from each terminal are combined by conventional optical couplers with transmission line. All optical signals are transmitted to the central station along the transmission line, and received simultaneously by single photo-detector.

In downward link, the optical signal from the central station is distributed to each terminal by the conventional couplers. The optical signal from the central station is usually used as control signals to the terminals. Moreover, it can be used for video signal or some kind of data signal as well.

3. Transmission quality

3.1 Optical beat interference

In a conventional system, noise usually consists of Relative Intensity Noise (RIN) of lasers, shot noise from photo-detectors, and thermal noise from electrical amplifiers.

Additionally, in upward link of our system, when the lasers for each terminals become too close to each other in wavelength, the beating of these lasers generates noise at photo-diode at a frequency corresponding to the optical wavelength difference. If this noise overlaps a frequency band of the subcarriers, CNR is degraded.

Due to the square law nature of the photodetection process, the generated photocurrent contains beat signal as the cross-mixing terms at the different frequencies corresponding to each pair of optical fields. This phenomenon is expressed as follows:

$$E^2=2E_0^2\sin^2(\omega_0 t)+2E_1^2\sin^2(\omega_1 t) +4E_0E_1\cos(\theta)\sin(\omega_0 t)\sin(\omega_1 t) \quad (1)$$

where: E_0 and E_1 are the field intensities of the two optical signals and θ is the angle formed by the polarization planes. The third term expresses the optical beat. It can be expanded into following equation (2).

Third term :

$$2E_0E_1\cos(\theta)\{-\cos(\omega_0 t+\omega_1 t)+\cos(\omega_0 t-\omega_1 t)\} \quad (2)$$

In this equation, the sum component of optical frequency rises at much higher frequency than the sub-carriers. But the differential component can be very close to sub-carriers. In Fig.4, measured optical beat frequency can be shown as a function of wavelength difference between two lasers. This differential component deteriorates the CNR quality.

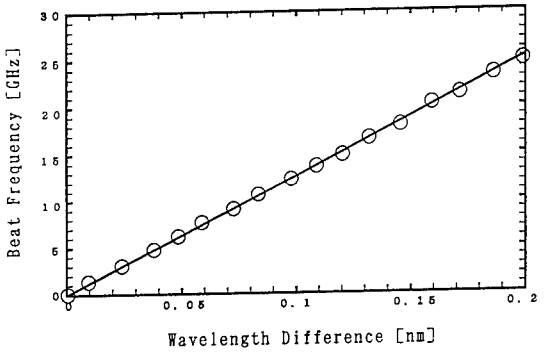


Fig.4 Optical beat frequency versus wavelength difference

3.2 Investigation of improvement in CNR quality

When some lasers set on the terminals have the same wavelength, the same polarization, no chirping, and very narrow linewidth, then CNR will be worst because of the optical beat interference. But there are some effects that make CNR better in practical systems.

3.2.1 Chirping effect

Firstly, we made sure experimentally that the beat interference noise can be reduced due to the optical power spread by the chirping effect.

When a laser-diode is modulated by RF signal, the frequency chirping will be generated by the refractive index of the laser diode change according to the input RF signal level. Thus the optical frequency will be modulated simultaneously with the output intensity modulation. By this phenomenon, the beat noise power will be spread out over some frequency range, and amplitude of each frequency will come to bessel function.

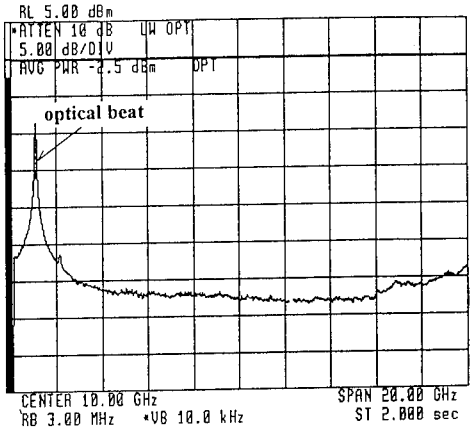


Fig.5 (a) Optical beat spectrum for Unmodulated optical signal

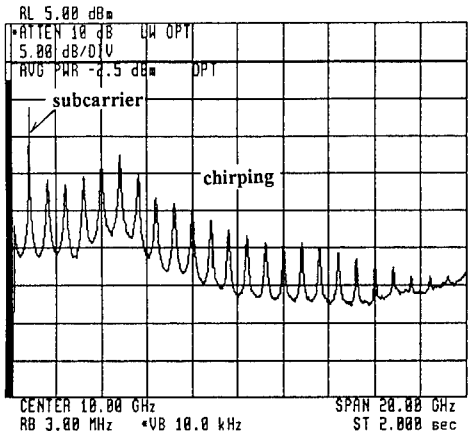


Fig.5 (b) Optical spectrum for modulated optical signal

When the frequency difference between two laser-diodes is about 0.01 nm and both lasers have the same polarization, the unmodulated beat spectrum like Fig.5 (a) is observed. And Fig.5 (b) shows the modulated beat spectrum at the same polarization condition as Fig.5 (a), where optical modulation index m is 1. It is obvious that beat peak level is reduced by spreading a optical power spectrum.

3.2.3 Polarization effect

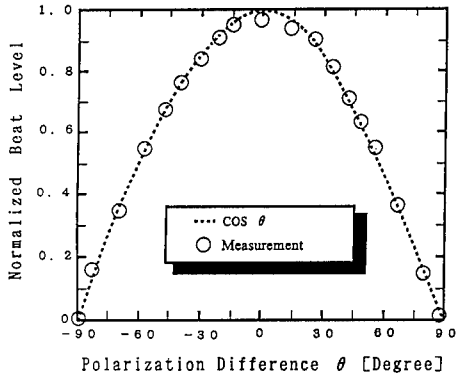


Fig.6 Optical beat level versus polarization difference between tow lasers

Secondly, we confirmed experimentally that the beat interference noise is not so high because of the random polarization of the optical carriers.

It can be seen from equation (2) that the optical beat level depends on the polarization of two optical signals.

For simplicity, when we assume the liner polarization, optical beat level is varied as Fig.6 according to the polarization condition θ . In usual case, the polarization condition between lasers are not consistent exactly. So it is considerable that the beat level cannot be the worst value.

Fig.7 shows the measured value of CNR dependence on the number of optical beat, in the case where the polarization among optical signals were not controlled. It is made clear that CNR become under 14 dB when three or more beats generate on the subcarrier frequency band.

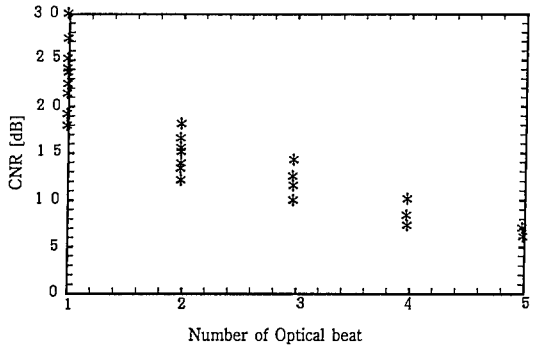


Fig.7 CNR versus number of optical beat, in the case where the polarization of optical signals are random

3.2.3 Random wavelength distribution effect

Thirdly, we made quantitative analysis of the beat interference noise generated on subcarrier frequency band by the simulation considering the random distribution for optical wavelengths of practical lasers.

Although some laser-diodes are used in a system, it is extremely rare for the output wavelength of them to coincide. Therefore, the number of beat was derived by numerical simulation assuming a wavelength distribution.

Fig.8 shows the results of simulation for the relation between number of optical signals and probability of beat generation.

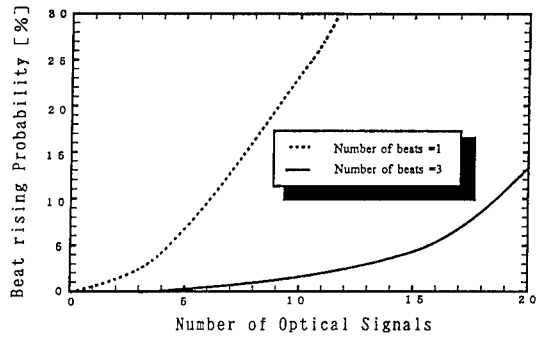


Fig.8 Result of simulation for the relation between number of optical signals and probability of beat generation. 3 σ is assumed to be 20 nm

It is assumed that the OBI will affect to the frequency band of subcarriers (about 1 GHz) only when two optical signals come closer than 0.1 nm. It is also assumed that the wavelength distribution has gaussian probability density function with standard deviation of σ . We calculated how many optical signals can be picked up without making more than three beat noises in subcarrier band. When 3 σ is 20 nm, which is the typical distribution of wavelength for actual laser-

diodes, it is shown in Fig.8 that we can combine as many as19 optical signals if we permit 10% probability of beat generation.

4. Transmission experiments

Based on the above fundamental consideration, the 110km transmission experiment was carried out with the system which consists of 8 terminals, 8 couplers, and one optical amplifier as shown in Fig.9.

The signal sources launched a NTSC baseband signal to FM modulators. FM modulators converted a baseband signal into a RF signal and launched it to DFB-lasers, and then DFB-lasers were modulated with optical modulation depth of 100%. In this condition, the spectrum was spread by chirping most widely without signal clipping of the laser. The 8 modulated optical signals were combined into a SM-fiber with conventional couplers,and they were received at a photo diode simultaneously. CNRs and RIN were measured with signal analyzer set on the end of photo-diode and video signals were observed with a monitor. The received optical power from each laser were adjusted to the same level at photo-detector with optical attenuater. We did not intentionally control the wavelengths and the polarization of the optical carriers.

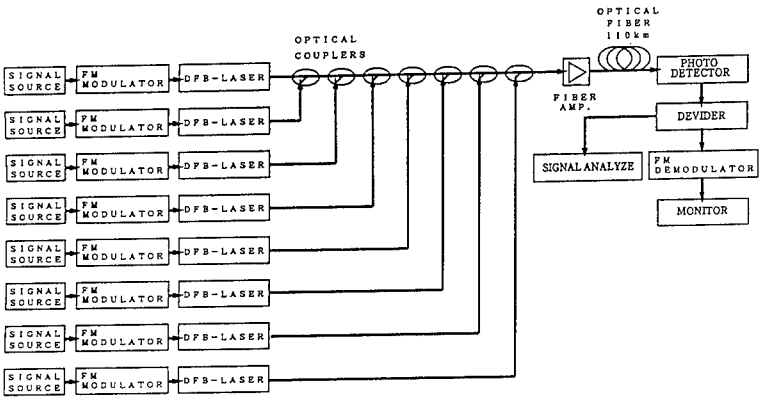


Fig.9 Experimental scheme to confirm transmission quality of 8 channel system

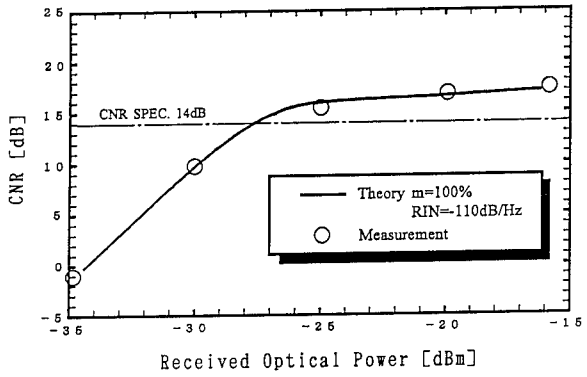


Fig.10 C/N characteristic versus received optical power

In this experiment, RIN caused by OBI was about -110dB/Hz. Fig.10 shows the CNR measured as a function of received optical power per channel. The open circles indicate the measured level with varying received power of a optical signal. They are found in good agreement with theoretical analysis, the solid line. We were able to obtain a desirable CNR over 14 dB with the minimum received optical power below -25 dBm. And we confirmed that the video signals were transmitted very clearly.

5. Application to video monitoring system

TOKYO ELECTRIC POWER COMPANY (TEPCO) decided to equip the power transmission line with an video transmission system to monitor operating conditions of power transmission line on real time. The purpose is to improve maintenance efficiently and assure the reliability of electrical power supply.

We applied our multi-coupler system to video transmission system to supervise a power transmission system. Fig.11 shows the system architecture. There are three monitoring sites at each of which one camera is mounted approximately 60m above the ground level.They are connected to the central equipment at center station with optical ground wire (OPGW) consisting of SM-fiber.

The system handles bi-directional system. On upward stream, the video signals from each terminal are transmitted. The control signal for monitoring cameras is transmitted on downward stream. In this system, the lasers set into E/O are modulated by FM video signal with modulation index of 40%. The polarization conditions are not controlled. The wavelength difference among the lasers is 16nm at maximum. Such wavelength difference are held constant with temperature control around the lasers.

Main specifications of this monitoring system are shown in Table.1. Actually we realized very good CNR of 29dB.

6. Conclusion

We investigated the improvement of CNR on upward link of multi-coupler system theoretically and experimentally. As the results, it was demonstrated that the successful video transmission was achieved for the 8 terminal system with the total length of 110km. We believe that this multi-coupler system is useful for the bi-directional networks such as interactive TV system and remote video monitoring system because of its simple configuration and high reliability. We have already installed several systems with this configuration for the video monitoring on electric power cables in Japan.

Table.1 Main specification of the monitoring system

Item		Up-link	Down-link
Modulator	Method	FM modulation (audio & video)	FM modulation (audio)
	Propagation frequency	Broadcast or communication satellite allocation	80MHz
	Transmission signal	Audio,video :1 channel each per set	Audio :1 channel per set
Demodulator	Method	FM modulation	
	Propagation frequency	Audio subcarrier signal :6.5MHz	80MHz
E/O converter	Light source	1300nm band distributed-feedback laser diode	
	optical output level	6dBm(tipical)	
	optical connector	NTT Type FC	
O/E converter	Photo-detector	1300nm band APD	
	Min. detection level	≧ −30dBm	
	Optical connector	NTT Type FC	
Optical coupler	Branching ratio	10 : 1	

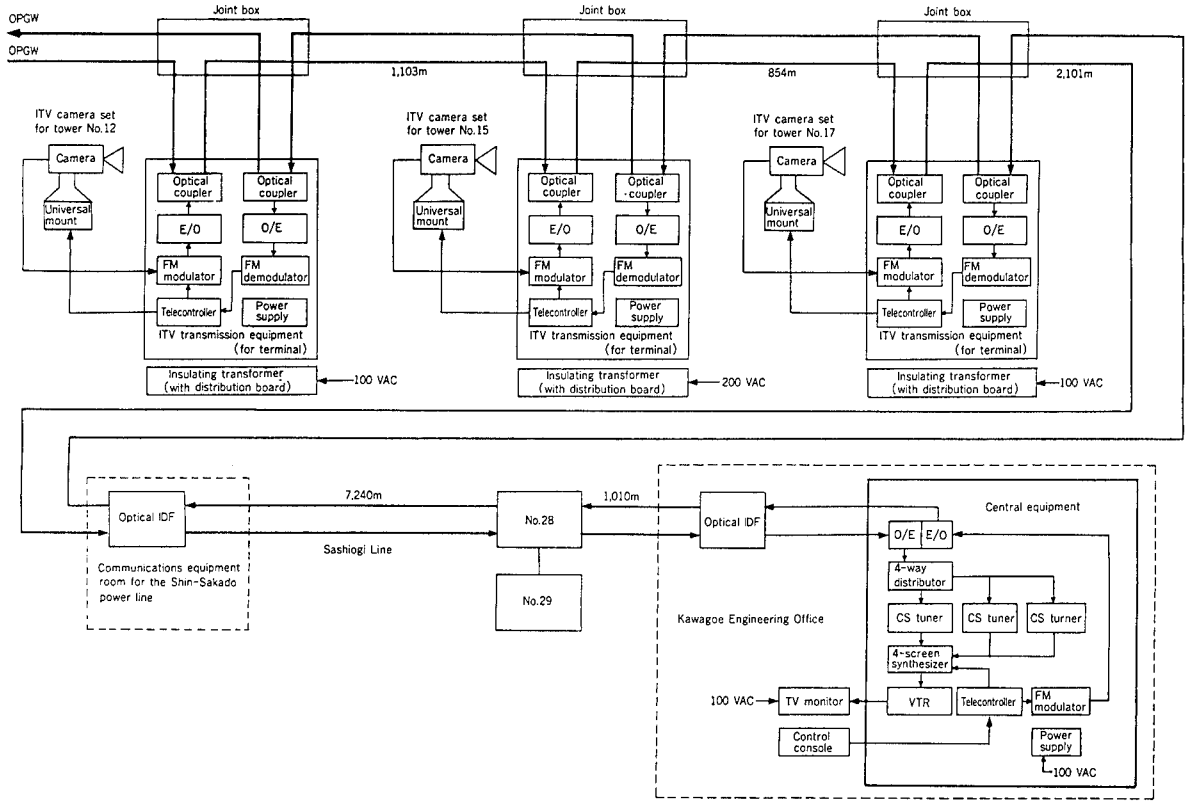


Fig.11 Architecture of the monitoring system for power cable line employing multi-coupler system

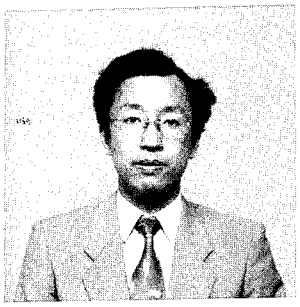
Reference
[1]DARK et.al:'Lightwave System Using Microwave Subcarrier Multiplexing', Electron.Lett.,vol22,pp.774-775,1986
[2]DARCIE.T.E:'Subcarrier Multiplexing for Multiple-Access Lightwave Networks', J.Lightwave Technol.,LT-5,pp1103-1110,1987
[3]OLSHANSKY.R:'RF Multiplexing Techniques Applied to Video Distribution in Local Networks', ECOC'87 Technical Digest,pp.122-125,1987
[4]DESEM.C:'Optical Interference in Lightwave Subcarrier Multiplexing Systems Employing Multiple Optical Carriers',Electron.Lett.,vol24,pp.50-51,1988
[5]DESEM.C:'Measurement of Optical Interference Due to Multiple Optical Carriers in Subcarrier Multiplexing',IEEE PTL.,vol.3,pp387-389,1991
[6]Wood.T.H et.al:'Operation of Passive Optical Network with Subcarrier Multiplexing in the Presence of Optical Beat Interference', J.LightwaveThecnol.,vol.11,pp1632-1640,1993



Hideyuki Omura

Furukawa Electric Co.LTD
5-1-9, Higashiyawata
Hiratsuka, Kanagawa, 254,
JAPAN

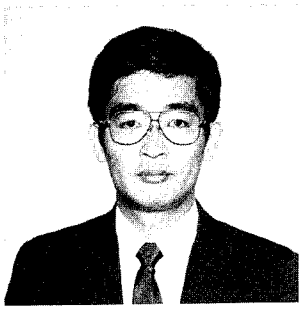
Hideyuki Omura received the Master Degree in electrical engineering from Tokai University, Kanagawa, Japan in 1987. He joined Furukawa Electric CO., LTD in 1987 and he has been involved in the development of bi-directional CATV for 4 years. At present he is working in Video transmission system and equipment research section of Information & Electronics Laboratory. Mr. Omura is a member of the institute of Electrical Engineers of Japan



Toshinori Kimura

Furukawa Electric Co.LTD
5-1-9, Higashiyawata
Hiratsuka, Kanagawa, 254,
JAPAN

Toshinori Kimura received the Master Degree in electrical engineering form Muroran Institute of Technology, Hokkaido, Japan in 1990. He joined Furukawa Electric CO., LTD in 1990 and at present he is working on Information & Electronics Laboratory. Mr. Kimura is a member of the institute of Electronics, Information and Communication Engineers of Japan.



Nozomu Matsuo

Furukawa Electric Co.LTD
5-1-9, Higashiyawata
Hiratsuka, Kanagawa, 254,
JAPAN

Nozomu Matsuo received the Master Degree in electrical engineering from Hokkaido University, Hokkaido, Japan in 1984. He joined Furukawa Electric CO., LTD in1984. Since then he has engaged in the development of laser-diode for optical communication. At present he is working on Information & Electronics Laboratory and he is a chief researcher of the optical video transmission. Mr. Matsuo is a member of the Japan Society of Applied Physics.



Yukihisa Shinoda

Tokyo Electric Power Company
4-1, Egasaki-cho Tsurumi-ku
Yokohama, Kanagawa, 230,
JAPAN

Yukihisa Shinoda received the Master Degree in electrical engineering from Chiba University, Chiba, Japan in 1987. He joined Tokyo Electric Power Company in 1987. He has been engaged in developmental research on optical transmission system. At present he is working in Computer & Communications R&D Center.

RELIABILITY-CENTRED APPROACH TO THE DESIGN AND OPERATION OF PLANT FOR THE ACCESS NETWORK

David A. Brewer, Peter G. Hale

Pirelli Cables Limited, Wednesbury Street, Newport, Gwent, NP9 0WS, UK

ABSTRACT

Optical fibre and other passive components are being deployed world-wide for the provision of high capacity, reliable networks. This paper describes a reliability-centred design philosophy adopted for optical fibre plant and system configurations intended for the access network.

A computational technique for the assessment of component and end-to-end reliability is shown, including the generation of Mean Time Between Failure (MTBF) and Availability statistics. The network sensitivity to the failure rate distribution of key components is considered.

Network optimisation to meet local topological, climatic and operational requirements is discussed in terms of component selection and configuration options, with examples.

INTRODUCTION

Fibre in the access network (fibre in the loop) is now being deployed in increasing quantities. Although trials are in progress, an increasingly large number of installations are full time traffic carrying and are being designed for operation over a long period. It is essential that such installations are reliable over their anticipated lifetime (decades) and a considerable amount of research has been undertaken by network operators and their suppliers to understand the operation of both point-to-point links and Passive Optical Networks (PONs) which utilise fibre branching devices. Work has been conducted both at the component level[1,2] and the network level[3,4], the network effort resulting in FIT rate specifications for components.

There is no doubt that fibre is a long term solution for providing bandwidth to the customer. As well as offering high bandwidth, optical fibre in the access network must offer *flexibility, upgradability and reconfigurability* matching or exceeding copper infrastructures (addressed by attention to plant design[5,6,7]) and *reliability* with a similar proviso.

In response to the requirements for such plant, Pirelli Cables has introduced a modular system which provides a complete end-to-end solution between the exchange/office and customer premises (OLTE and ONU). OAsys™[8] plant is designed to fulfill the requirements addressed in this paper.

RELIABILITY WITHIN A PASSIVE OPTICAL NETWORK

The definition of what constitutes a reliable network depends upon the perspective. A single customer is only concerned with the availability of the spectrum of services which have been subscribed to. The fact that a neighbouring installation may be experiencing disruption is generally inconsequential.

The network operator has additional concerns, primarily aimed at making the provision of network services into a viable business. The network operator is concerned with keeping all customers up and running. The selection of an effective operation and maintenance (O&M) strategy is core to this, and is heavily dependent upon network topology, the number of maintenance engineers in the field, labour rates, spares provision, etc. As will be shown, the needs of the customer and the network operator may diverge.

A supplier of network plant must understand both of these perspectives, gearing design and manufacturing facilities to servicing the network operator. A process of continuous improvement is fundamental to optimising plant design and responding to changing network operator requirements. For example, a design review procedure has been implemented for OAsys™ plant which incorporates a feed-back loop from the Installation Training function.

Modelling reliability may be readily broken down into component and system related issues.

COMPONENT RELIABILITY

A network comprises a large number of diverse components, each having an associated reliability which contributes to the overall system reliability. The most commonly used indication of equipment reliability is the Mean Time Between Failures (MTBF) parameter, which is defined thus:

$$\text{MTBF, } \theta = \int_0^\infty R(t)\,dt \qquad (1)$$

where R(t) is the reliability of the component as a function of time. For repairable systems, the MTBF may be combined with the Mean Time To Restore (MTTR) giving rise to Availability, A, according to (2).

$$A = \frac{MTBF}{MTBF + MTTR} \quad (2)$$

As an example, a system availability of 99.9% means that service will be interrupted, on average, for 8.76 hours per year.

At this stage it is necessary to emphasise that the MTTR incorporates more than the actual repair function. The restore activity may be divided into a number of constituents:

- realisation (determining that a fault condition has occurred);
- reaction (organising spares, mobilise repair crews, arrival on site);
- repair;
- test (commission new equipment);
- return to service;
- record failure (nature of failure, list affected components etc.).

Repair time estimates, and the subsequent MTTR assessments must be made under service conditions. The time necessary to replace plant in a clean, warm laboratory offering unrestricted access to both equipment and tools generally bears little relation to field conditions, and could potentially lead to optimistic predictions of restore times.

At a practical modelling level, the Hazard Rate (effectively the instantaneous failure rate) of each component also proves to be useful. The Hazard Rate, z(t), represents the conditional probability of failure in a time interval t to t+δt, and may be defined as follows:

$$z(t) = \frac{f(t)}{R(t)} \quad (3)$$

where f(t) is the failure probability density function (PDF). Analysis of the variation of component Hazard Rates with time determines the implications of prolonged operation on network Quality of Service (QoS) levels.

A cautionary note should be introduced at this point. A number of mathematical means exist to determine the Hazard rate for a particular component or network. Depending on the exact form of the probability distribution function involved, some iterative methods do not converge. Where possible, more than one method should be followed to check the resulting prediction. As an example, Equation 3 may be written in the following forms:

$$z(t) = \frac{f(t)}{R(t)} = \frac{f(t)}{\int_t^\infty f(t)\,dt} \quad (4a)$$

$$z(t) = \frac{f(t)}{R(t)} = -\frac{d}{dt} \ln \{R(t)\} \quad (4b)$$

The integral contained within Equation 4a may be solved numerically be any of the common iterative methods (secant, Newton-Raphson etc.) whilst the numerical solution of the derivative in Equation 4b may be found using Ridder's method.

Key Components - Passive Optical Splitters

Passive optical splitters provide branching points at specific locations within the network and give a fibre-lean network. Fused biconic tapers (FBTs) and planar devices have been widely used for this purpose, typically located in exchanges which offer comparatively benign operating environments. Different philosophies have now been proposed (for example the OPAL project in Germany and deployment of OTIAN® in the United Kingdom) which require such devices to operate in an external plant environment, either underground in jointing chambers or within street-side cabinets.

External plant experiences greater ranges of temperature and humidity than would normally be found in an exchange. To understand the short-term effects of such variation, condensation tests such as those proposed by IEC 68-2-38 may be followed. Long-term accelerated ageing tests have been conducted and reported by a number of organisations [1,2]. Such tests characterise individual device designs by monitoring optical performance over time under continuous exposure to various combinations of temperature and humidity. An activation energy may then be derived for both temperature and relative humidity allowing lifetime predictions under any given service condition. As an example, when considering the effects of temperature changes, the Arrhenius relationship is adopted:

$$R = R_0 \exp\left(\frac{-E_A}{k.T}\right) \quad (5)$$

where R is the failure rate, R_0 is a constant, E_A is the thermal activation energy, k is Boltzmann's constant and T is the absolute temperature. The sensitivity of failure rate to temperature change can then be derived, as shown in Figure 1.

The joint chamber is a very different operating environment to a street-side cabinet. Although the chamber may become flooded for considerable periods, the temperature remains relatively stable. In contrast, the street-side cabinet will experience greater temperature fluctuations due to solar radiation, etc. The Joule heating effect of any electrically powered equipment also in the jointing chamber or street cabinet should also be considered. Poor ventilation and the materials typically used in cabinet construction will slow heat dissipation, consequently the internal temperature can remain high for some considerable time after removal of any heat source.

Each scenario presents its own individual set of problems for the plant design engineer. Where available, information gathered from representative sites under actual service conditions should be used to define realistic working limits for

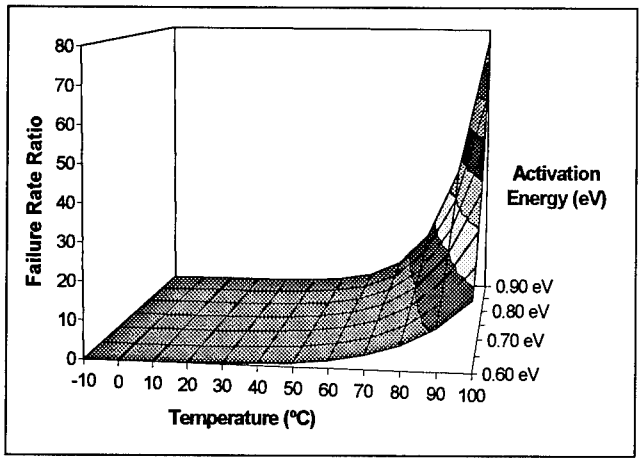


Figure 1 : Variation of Failure Rate Ratio With Thermal Activation Energy

plant. It is entirely possible that due to a combination of failure rate and intended service condition, specific components may be precluded from a particular installation.

Consider a ring-based network which utilises 2x4 splitters at primary node points, and 2x8 splitters at secondary nodes. The ring is assumed to use cable containing 96 optical fibres. Using the network modelling techniques described later, sensitivity analyses of the contribution made by the splitters to both the customer (or path) reliability and the total network reliability may be conducted under various operating scenarios. The results a specific study are included as Table 1.

Combined Splitter Failure Rate (FITs)	% Contribution Made By Splitters At Primary (P) and Secondary (S) Nodes				
		% Utilisation of Overall Network			
	Path	50% P 50% S	100% P 50% S	50% P 100% S	100% P 100% S
1050	26%	22%	22%	19%	19%
10500	78%	74%	74%	70%	70%

Table 1 : Sensitivity Analyses To Splitter Failure Rate

SYSTEM RELIABILITY

System reliability depends on the topology adopted. Typically, ring or spine based configurations are used, as shown schematically in Figure 2.

Analysis of system reliability can be accomplished using a Reliability Block Diagram (RBD) approach. Each component is assigned a specific reliability, derived from experimental data where possible, from which an instantaneous hazard rate may be calculated. The RBD analysis can readily accommodate redundant configurations, where standby systems are put in place to protect key areas of the network.

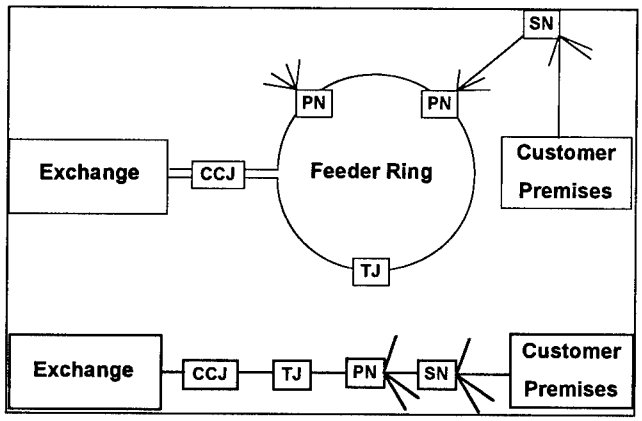


Figure 2 : Ring Topology (top) and Spine Topology (bottom)

Typically, an electronic network fault sensing system (ENFSS) is used which is responsible for redirecting telecommunications traffic from the main to the standby path under fault conditions. The reliability of the ENFSS equipment, considered only in terms of sensing faults and correctly reacting to them, may be included as a non-unity value. Following this approach, the reliability of a main and standby system which utilises switched redundancy (refer to Figure 3) may be described thus:

$$R_{system}(t) = 1 - \left[\left(1 - R_1(t) \,.\, R_{ENFSS}(t)\right) . \left(1 - R_2(t)\right)\right] \qquad (6)$$

where $R_{system}(t)$ is the reliability of the system, $R_1(t)$ is the reliability of the component on the main system, $R_{ENFSS}(t)$ is the reliability of the ENFSS with respect to fault sensing and subsequent transfer of communications traffic to the standby route, and $R_2(t)$ is the reliability of the component on the standby system. Note that a time dependency is implicit in all reliability calculations.

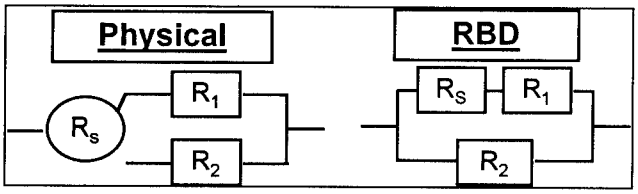


Figure 3 : Reliability Block Diagram (RBD) Diagram Showing Switched Active Redundancy

Other analytical techniques exist for describing networks, an example of which is Markov transitions. Whichever method is adopted, flexibility is vital. Examples of factors which influence network reliability are:

- Network operating procedures - will the network be switched between the two potential transmission paths only under fault conditions, or will this occur more regularly? The reliability of both pathways must be considered.
- For ring topologies, the cable lengths between the exchange and a primary node may be different, depending on the

direction travelled around the feeder ring. The associated intrinsic cable failure rate (i.e. those failures which are attributable only to degradation mechanisms of the optical fibres or cable itself) may then vary.

- The cable dig-up rate may vary depending on location.

Common Cause Failures (CCF)

Common cause failures are the result of an event(s) which, because of dependencies, causes a coincidence of failure states of two or more separate channels of a redundant system. Common cause failures may be equipment related, or may be attributable to human error. Considerable time and effort must be committed to designing and implementing comprehensive training programmes for manufacturing, installation and maintenance personnel to minimise such errors. The benefits of training programmes, when correctly incorporated into the design review procedure are two-fold:

- human errors, at all stages of implementation, are minimised for existing plant;
- potential areas of improvement of design, documentation or working practices can be highlighted and incorporated into future revisions.

A checklist is used to assess the risk of encountering CCFs at each stage of the network. A common cause failure rate may then be derived, and the implications on system reliability investigated. It is a sobering thought that, without due care at the plant design stage, common cause failure rates can be comparable to the failure rate contribution of the rest of the redundant section or even the entire network.

An example of the sensitivity analyses which can be performed is shown in Figure 4. A particular network configuration was subjected to varying CCF rates and ENFSS reliabilities. The effect of these changes on the failure rate of the redundant section are shown, in this case normalised to typical predicted values of CCF and ENFSS applicable to OAsys™ plant.

Sensitivity Analyses Based on Topology

The spine topology generally utilises less equipment than a ring network for a comparable catchment area. The fact that less plant is employed reduces the total network failure rate. A lower total failure rate results in a reduced maintenance burden, eases stores provisioning and reduces labour overheads as fewer maintenance engineers are needed. A comparison between spine and ring topologies for total network reliability is given in Figure 5.

However, from a customer stand-point service can be disrupted by a single incident such as a cable dig-up between the cable chamber joint (CCJ) and the primary node (PN). The provision of a standby path as part of the ring topology means that such a single dig-up incident would not cause the same disruption.

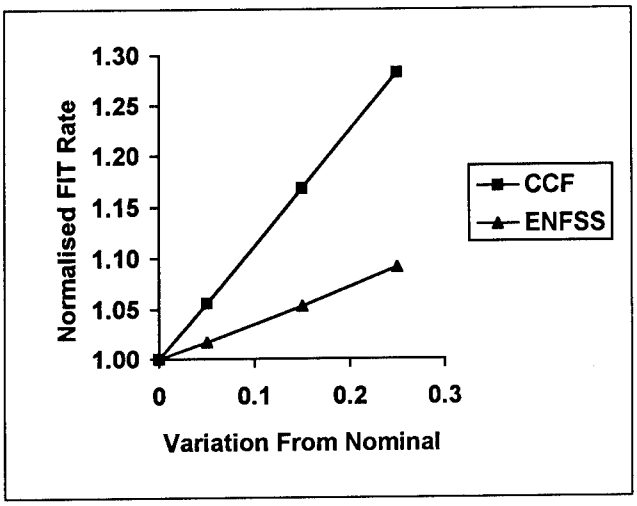


Figure 4 : Redundant Section Sensitivity to CCF and ENFSS Reliability

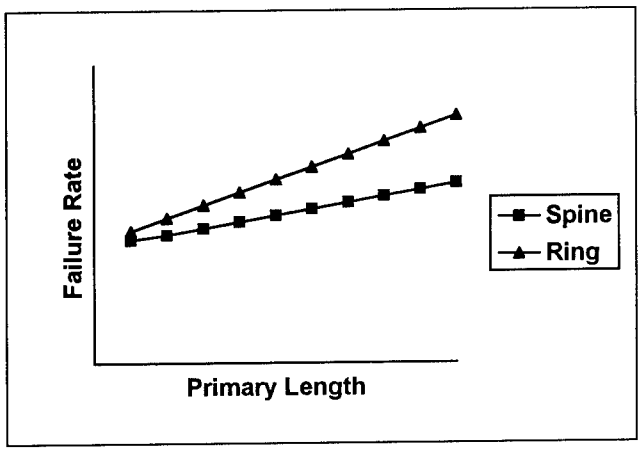


Figure 5 : Total Network Reliability

Figure 6 shows a comparison between the individual customer site reliability of ring-based and spine-based topologies.

Furthermore, the ring topology allows greater flexibility and control over preventative maintenance and repair. Should a fault occur, a risk assessment can be made of a further failure affecting the standby path. This can then be used to decide whether to defer the repair activity until it may be scheduled into an optimised maintenance programme.

CONCLUSION

Fibre in the access network is now being deployed in increasing quantity, not only on a trial basis but also commercially. Reliability assessments of components and potential network configurations are core to optimising network deployment and subsequent operating and maintenance strategies. Suppliers of

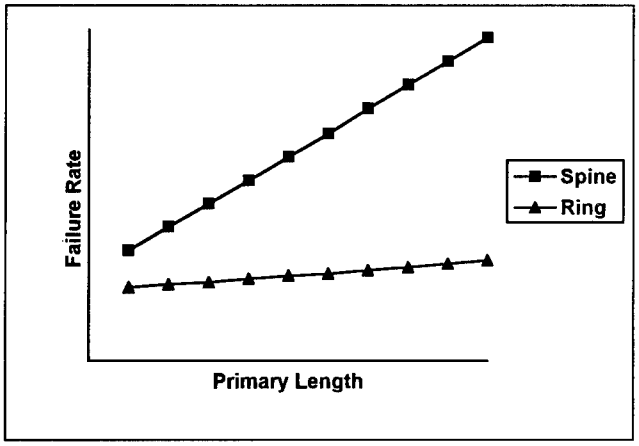


Figure 6 : Individual Customer Site Reliability

network plant must accommodate the sometimes competing needs of customers and network operators, with the intention of providing turn-key system capability.

Sensitivity analyses of key parameters such as components, common cause failure and network topology are tools which should be used not only when planning networks but also prior to implementing any plant design improvements.

ACKNOWLEDGMENTS

The authors wish to acknowledge the work of the access network team at Pirelli Cables, UK, that has made this paper possible.

REFERENCES

[1] Gadonna, M., Redstall, M., Gundersen, S.; **Reliability Evaluation for PON Power Splitters**, Proc. SPIE, July 1994, pp 170-184.

[2] Gadonna, M., Draycott, T., Gundersen, S.; **Results of Accelerated Lifetests on Passive Optical Splitters**, Proc. EFOC & N (Technology and Infrastructure), 1995, pp 65-69.

[3] Gardan, D., Haagh, L., Larson, L., Margarito, R., Redstall, M., Socard, A., Steffensen, H., Stroetzel, J.; **Availability Analysis of the Fibre Optic Local Loop**, Proc. EFOC & N (Communication Systems and Optical Access Networks), 1994, pp 28-32.

[4] Brewer, D., Hale, P., Peacock, J., Walling, R.; **Modular Optical Plant for the Access Network: Operational Aspects**, Proc. EFOC & N (Technology and Infrastructure), 1995, pp 164-167.

[5] Hornung, S., Frost, P., Kerry, J., Warren, J., **Flexible Architecture and Plant for Optical Access Networks**, Proc. IWCS, 1992, pp 53-58.

[6] Hale, P., Brewer, D., Peacock, J., Bell, P., **Modular Optical Plant for the Access Network: A Practical Solution**, Proc. EFOC & N (Technology and Infrastructure), 1995, pp 158-161.

[7] International Telecommunication Union Draft Recommendation L.17 (L.imp), 1995.

[8] OAsys is a trademark of Pirelli Cables Ltd.

BIOGRAPHIES



David A. Brewer

Pirelli Cables Limited,
Communication Cables,
Wednesbury Street,
Newport,
Gwent NP9 0WS
United Kingdom

Dave joined Pirelli in 1988 after graduating from University College, Cardiff, with a B.Sc. in Physics. Working in the cable design section, he was responsible for the design and development of aerial communication cables until 1994, when he moved to the access plant development team. Dave is now responsible for component and system reliability analyses for the OAsys™ plant within Pirelli Cables Limited.



Peter G. Hale

Pirelli Cables Limited,
Communication Cables,
Wednesbury Street,
Newport,
Gwent NP9 0WS
United Kingdom

Peter Hale gained an M. A. in Engineering Science and Economics from the University of Oxford, from which he also holds a D. Phil. for work on the metal coating of optical fibres. He is a member of the Institution of Electrical Engineers and is a Chartered Engineer. Peter made the move to manufacturing at Pirelli after nine years at Standard Telecommunication Laboratories (now BNRE) researching into optical cables, sensors and local area networks, and is now responsible for advanced fibre applications, with particular reference to optical technology in the local loop.

A NEW APPLICATION OF AIR PULLED CABLE IN MICRODUCT FOR THE LOCAL LOOP

Philippe LESUEUR, Daniel LECOQ, Gerard LE GOFF, Alain PECOT, Jean LE ROUZIC

FRANCE TELECOM CNET/FCI/CAI, Lannion, FRANCE

Abstract

An installation technique in microduct using air and an airtight piston is described. Average lengths in the drop part of the french network or in business building are less than 100m. It is possible to install a cable with a diameter of 2mm in a microduct with an inner diameter of 6mm, on a distance of 90m with 8 right angled curves. The test have been conducted with no lubricated ducts and we consider that longer distances with more right angled can be installed.

Introduction

Optical cables bave been first installed in the trunk part of FRANCE TELECOM network. These lightweight and small diameter cables make new installation techniques developped. Length of 2400m are regularly installed by blowing the cable with air and a piston. We are now working on adapting this method in the local network. Our equipment is shown in fig. 1. Microducts 6/8mm are used to install a 2mm diameter cable containing two or four optical fibers. The pushing and the pulling forces are respectively applied in the blowing head by two rubber wheels and a piston connected with the cable by a crimping cylinder.

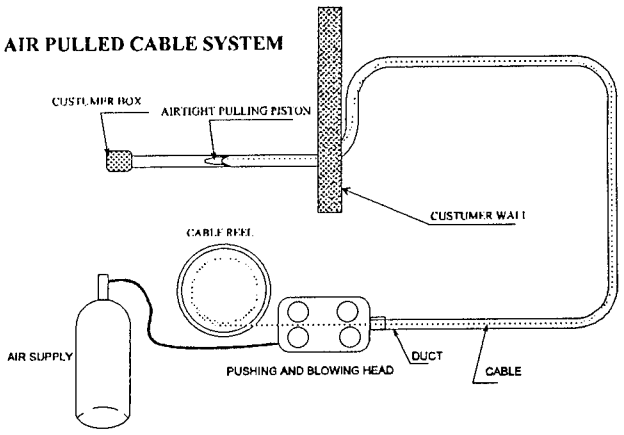


fig.1 Blowing system equipment

Installation Lengths Objectives

We have defined the need in term of length installation in three categories:

Business buildings: In France an inquiry shows that, in 98% of case, offices are setted from a technical room at a distance less than 80m.

Residential drop length: In Paris and suburbs, ten percent of drop cables are longer than 50m.

Buildings drop length: an inquiry on hundreds buildings in Paris shows that the medium installation length is 39m.

In these three cases small diameter ducts could be installed to feed customer houses or offices in buildings.

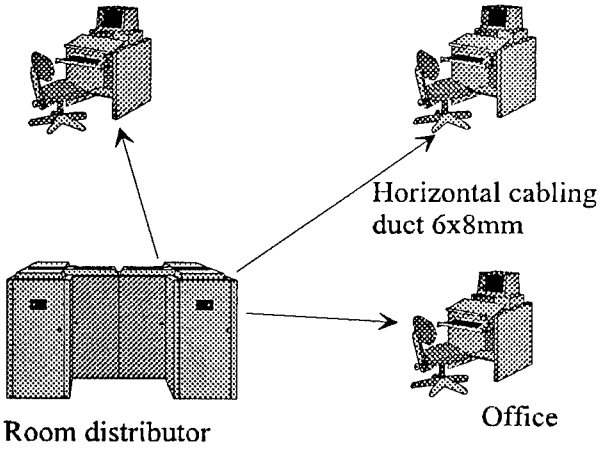


fig.2 Business buildings

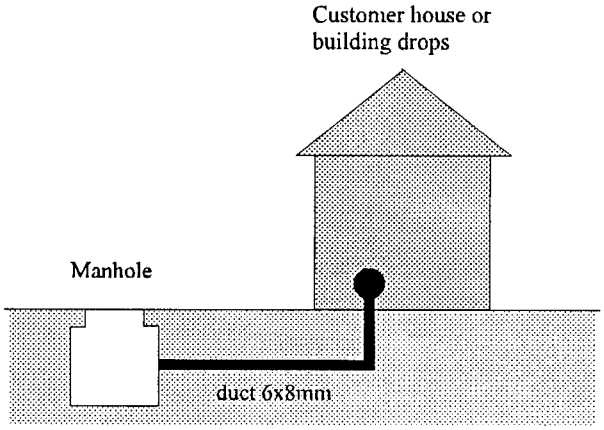


fig. 3 Residential and buildings drops

Theorical analysis of forces involved

Description of the test circuit:

The test circuit is 90m long with eight right angled bends.

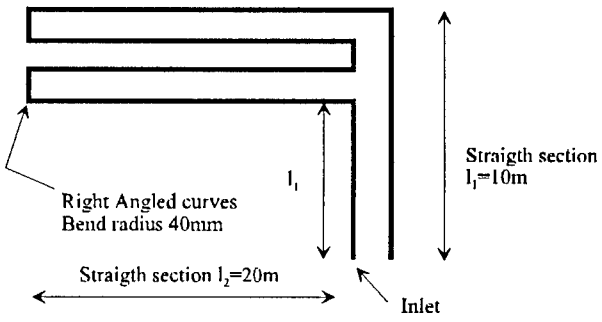


fig.4 test circuit

Friction forces:

refering to Buller's equations ([1]), in curved sections the force necessary to pull a cable is:

$$T_s = T_e e^{f\theta} \quad (1)$$

Where f is the friction coefficient, T_e the force at the inlet and θ the bending angle. For straigth sections the force is given by:

$$T_s = T_e + fwl \quad (2)$$

where w is the weigth of the cable per unit of length and l the length of the section. Refering to (1) and (2) the total friction force on the test circuit is:

$$F_{tot} = fwl_2\left(\frac{e^{8f\theta}-1}{e^{2f\theta}-1}\right)e^{f\theta} + fwl_1 + \left(T_e + fwl_1\right)e^{8f\theta} \quad (3)$$

where T_e is tail force at the inlet of the circuit. We recorded the tail force (tension in the cable) during an installation on the test circuit:

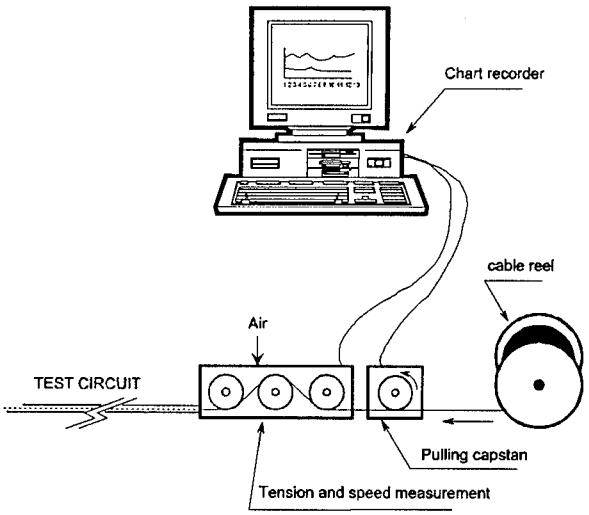


fig.5 Experimental setup to measure the tail force

The installation speed is controlled at 0,1m/s by the capstan. The absolute air pressure is 2,5 bars. The cable diameter is 2mm and the duct internal diameter is 6mm. Materials are respectively cellular polyethylen and HDPE.

Experimental record is:

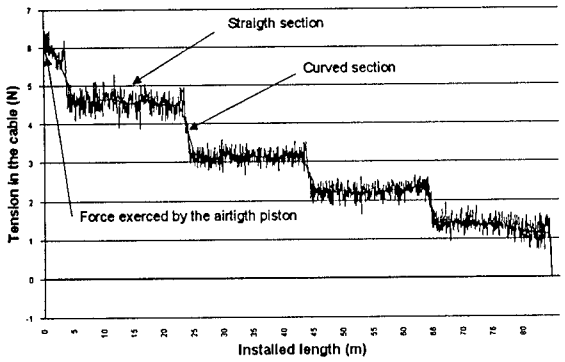


fig.6 Measurement of the tail force T_e at the inlet of the circuit

We observed first the force exerced by the airtigth piston on the cable equal to 6,04N on the section 0-1m. The tail force is then decreasing in each curved sections and is relatively regular in straigth section. We have compared the force exerced by the piston to the theorical friction force (3) using, in each straigth sections, the tail force T_e given in fig.6. We have first experimentally dertermined the friction coefficient at 0,11 ([2]). The results are:

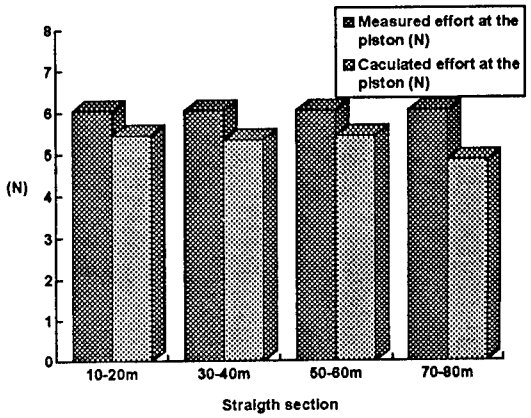


fig.7 Comparison between calculus and measured efforts at the head of the cable (piston)

Remark: Calculated friction coefficient f for best values of the calculated effort at the piston is 0,13.

This is a good estimate of the friction forces during installation. We get high values of T_e for the need of the experimentation and calculus. Normally there is no such tail force at the inlet of the duct because of the adding of a pushing force in the blowing head. With (3) and T_e=0N, total friction force is calculated to be equal to 1,06N on the test circuit. As the piston pulling effort is 6,04N this allows to lay greater lengths of cable than the test circuit. Theorically (with f=0,13), we can lay a cable on a 28 right angled bends route (one bend per meter). 20 bends were achieved in our labs. With such a friction coefficient, 2300m in straight section could be laid. This had not been tested in our labs.

We plan to test new duct flame retardant materials and smaller diameter ducts in the future.

Pushing force:

In the field, we add a pushing force by two rubber wheels in the blowing head. Because of the buckles of the cable an extra friction force per unit of length appears, given by the formula ([3]):

$$F_{push} = f \frac{D_d - D_c}{\pi^2 EI} F^2$$

Where EI is the stiffness of the cable , F the pushing force and D_d and D_c respectively the diameters of the duct and the cable. We experimentally measured the pushing force of a cellular polyethylen cable in a HDPE duct on the test circuit.

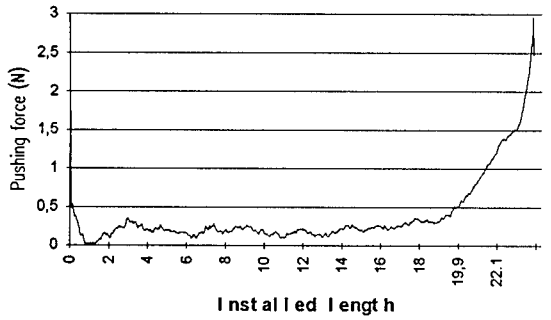


fig.8 measurement of the pushing force on the test circuit

The cable stop before the second rigth bend angle on the test circuit (see fig.4). We observe a very quick increasing of the extra friction force at 20m wich is predicted by GRIFFOEN theory ([3]). The installation length reached by pushing can be added to the pulling installation length. So regarding to the last paragraph, a cellular polyethylen cable wich diameter is 2mm can be easily installed in a HDPE duct (internal diameter 6mm) on a 90m long route with 8 right angled bends. Longer distances can be achieved with the technique of air pulled cable.

Installation equipment

These technique does not require a great volume of air because of the presence of the airtight piston. The whole equipment is light and can be easily carry by one man. This equipment is composed of a blowing head, a battery (12V) to supply the pushing motor, pistons and pliers to crimp them with a cylinder on the cable and a compressed air bottle.

Conclusion

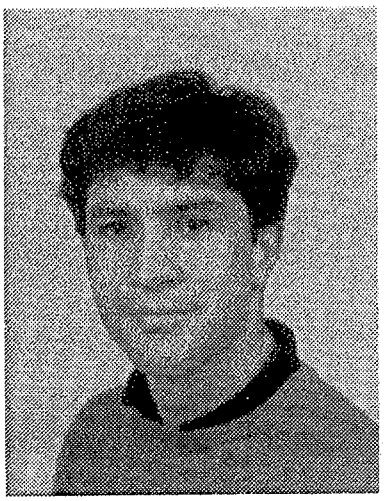
It is possible to blow a polyethylen cellular sheated cable (diameter 2mm) in a HDPE duct (internal diameter 6mm) on a distance of 90m with 8 right angled bends. Greater distances can be achieved with air pulled cable technique. This performance allows to lay cable in the applications considered in France Telecom plant and to industrialize equipments for the deployment of air pulled cable technique.

References

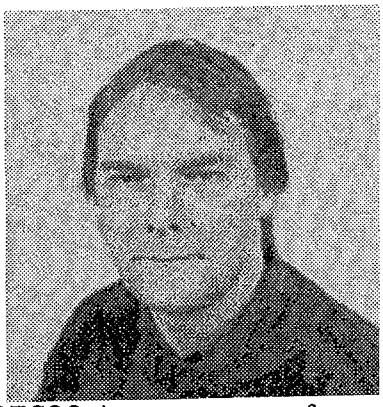
[1] F.H. BULLER "Pulling tension during cable installation in ducts or pipes" General Electric review Aug. 1949

[2] Howard M. KEMP "Procedure for the experimental determination of friction coefficient between a cable and a duct" IWCS1987 page 557

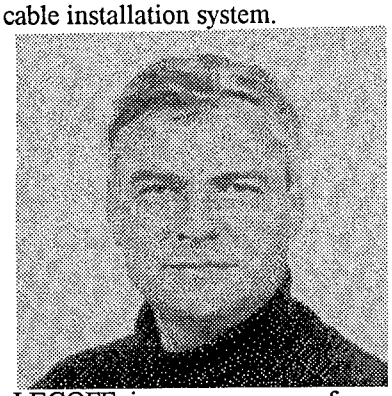
[3] W. GRIFFOEN "The installation of conventionnal fiber-optic cables in conduit using the viscous flow of air" Journal of lightwave tech. vol7 n°2 feb1989



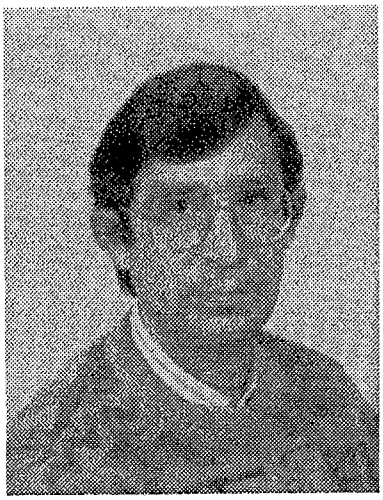
Philippe LESUEUR is a member of connecting and laying cable departement in France Telecom Research Center. He graduated from the Ecole Nationale Superieure des Arts et Metiers in 1990. He is presently engaged in development of optical cable installation system.



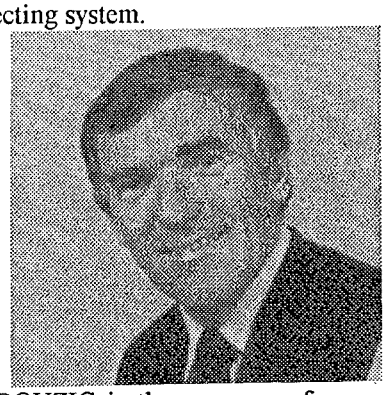
Daniel LECOQ is an engeneer of connecting and laying cable departement in France Telecom Research Center. He is presently engaged in development of optical cable installation system.



Gerard LEGOFF is an engeneer of connecting and laying cable departement in France Telecom Research Center. He is presently engaged in development of optical cable installation system.



Alain PECOT is a member of connecting and laying cable departement in France Telecom Research Center. He graduated from the Institut National des Sciences Appliquées in 1979. He is presently responsible of development of optical cable installation and connecting system.



Jean LE ROUZIC is the manager of connecting and laying cable departement in France Telecom Research Center.

COUPLING OF ELECTRICAL FAST TRANSIENTS FROM POWER CABLES TO PARALLEL UTP CABLES IN CLOSE PROXIMITY

Amid Hashim
AT&T Bell Laboratories
Whippany, New Jersey*

Mark Makwinski
The Wiremold Company
West Hartford, Connecticut

Abstract

It is not uncommon in today's commercial buildings for power and UTP data lines to be run parallel and in close proximity, for considerable distances, as is the case when they are run around room perimeters, in the adjacent channels of a raceway, to enable the delivery of power and data to work station locations. In such an implementation, and when the power conductors are subjected to the type of transients produced by the arcing associated with the closing or opening of air contactors (successive re-ignitions and clearings), termed electrical fast transients, inevitably a portion of these transients capacitively and inductively couples across from the power line to the UTP pairs. In this paper a simplified model is used to derive a frequency domain formulation of this coupling effect. In addition, experimental data for various test configurations representing different real life installations is presented.

Introduction

Power lines inside buildings are frequently subjected to disturbances from some of the loads they serve. This occurs when air contactors, that are used to switch capacitive and inductive loads, arc as they near or depart from each, as explained by Martzloff et al [1]. The disturbance generated by this phenomenon consists of a series of pulses each having a slow rise time and a fast decay that behave in a similar manner to the fast rise time slow decay electrical fast transient (EFT) pulses specified in the IEC-801 document [2]. This standardized waveform consists of bursts each containing a sequence of pulses. Each pulse is characterized by a 5 ns rise time and 50 ns duration at half maximum. This waveform is shown in figure 1.

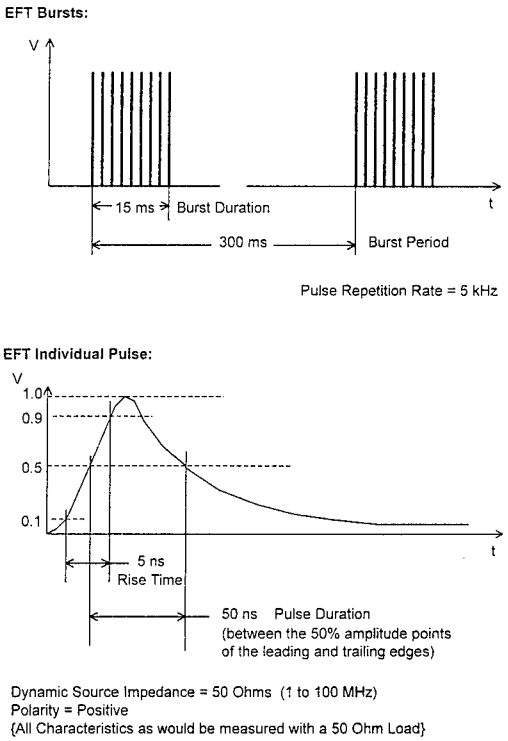


Figure 1: The IEC 801-4 EFT Waveform

The need to deliver power, voice and data circuits to each workstation in the office environments of today has made it convenient to co-route the power, voice and data lines. In one prevalent implementation, raceways that skirt the perimeters of floors and rooms are used to provide an integrated wire management system for all cables. In such an application the power, voice and data lines are run in adjoining parallel raceway channels over significant distances. Electrical fast transients

*Note: The work supporting this paper was performed by Amid Hashim while he was an employee of the Wiremold Company

existing on the power lines transfer over by capacitive and inductive coupling from the power lines to the voice and data lines in the adjoining channels. Particularly sensitive to the coupled EFT disturbances are the data lines that typically carry information signals of 100 MHz spectral bandwidth.

Coupling Model

The model consists of a power conductor and a data conductor that are parallel to each other and are equidistant from a ground plane over which they are suspended, as shown in figure 2.

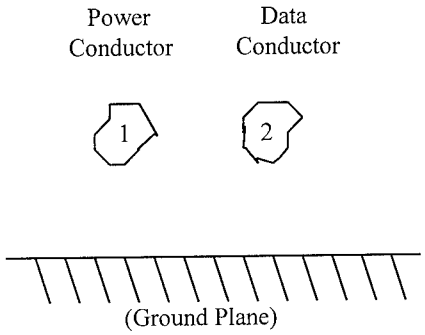


Figure 2: The Model Consisting of Parallel Power and Data Conductors over a Ground Plane

This model attempts to simulate disturbances appearing on line and neutral in common mode, here treated as one conductor termed the power conductor. It is assumed that the main coupling mechanism is common mode resulting in common mode voltages appearing on the data pair which is consequently represented in this model by one conductor. The appearance of differential voltages on the data line is assumed to take place as a result of conversion of the common mode signals to differential mode signals due the degree of unbalance of the data pair and not due to differential coupling. This conversion of common mode to differential mode signals is not treated in the following analysis, although differential voltage data is presented as part of the experimental results section that follows.

Data has shown that because of their high frequency contents the EFT transients attenuate within a very short distance as they propagate down the line, and become non-existent after approximately after 12 ft (3.7 m). The model deals with runs greatly exceeding 20 ft (6 m), which means that signals reflected from the far end are considered negligible at the near end and are therefore not considered in this model.

It is also assumed that coupling takes place from the power to the data conductors only and that no coupling takes place from the data to the power conductors.

The voltage and current at a point x along the power conductor can be represented by a forward traveling wave (the first term) and a backward traveling wave (the second term) as follows:

$$V_p(x) = \frac{V_{pin}}{2}(e^{-\Gamma_p x} + e^{\Gamma_p x})$$

$$I_p(x) = \frac{V_{pin}}{2Z_{11}}(e^{-\Gamma_p x} - e^{\Gamma_p x})$$

where,

$V_p(x)$ is the voltage at point x

$I_p(x)$ is the current at point x

V_{pin} is the EFT voltage applied to the near end of the power conductor

Z_{11} is the characteristic impedance of the power conductor, and

Γ_p is the power conductor propagation constant and is given by,

$$\Gamma_p = \sqrt{(R_{11} + j\omega L_{11})(G_{11} + j\omega C_{11})}$$

Assuming $G_{11} = 0$ and Using an approach similar to that presented by Martzloff et al [1], the expression for Γ_p can be simplified by expanding it into a Taylor series in R_{11} and retaining the first two terms,

$$\Gamma_p = j\omega\sqrt{L_{11}C_{11}} + \frac{R_{11}}{2}\sqrt{\frac{C_{11}}{L_{11}}}$$

This can be written more conventionally as,

$$\Gamma_p = \frac{R_{11}}{2}\sqrt{\frac{C_{11}}{L_{11}}} + j\omega\sqrt{L_{11}C_{11}}$$

Considering the coupling current that occurs at point x over the region Δx and travels back to the near end provides,

$$I_d(x) = \frac{j\omega V_{pin}}{4}(e^{-\Gamma_p x})(C_{21} + \frac{L_{12}}{Z_{11}Z_{22}})\Delta x$$

where Z_{11} and Z_{22} are the characteristic impedances associated with the power and data conductors respectively.

Since the near end coupled voltage is the product of Z_{22} and the summation over the length, ℓ, of all the currents coupled along the conductors for all values of x, each modified by the data conductor propagation characteristics as it travels back to back to the near end, the voltage coupling ratio can be expressed as;

$$\frac{V_{nd}}{V_{pin}} = \frac{j\omega}{8}(Z_{22}C_{21} + \frac{L_{12}}{Z_{11}})\int_0^{\ell}(e^{-(\Gamma p+\Gamma d)x}dx$$

where, using the same procedure used for the power conductor propagation constant,

$$\Gamma_d = \frac{R_{22}}{2}\sqrt{\frac{C_{22}}{L_{22}}} + j\omega\sqrt{L_{22}C_{22}}$$

$$Z_{11} = \sqrt{\frac{L_{11}}{C_{11}}}$$

$$Z_{22} = \sqrt{\frac{L_{22}}{C_{22}}}$$

Evaluating the integral and substituting for Z_{11} and Z_{22},

$$\frac{V_{nd}}{V_{pin}} = \frac{j\omega}{8}(C_{21}\sqrt{\frac{L_{22}}{C_{22}}} + L_{12}\sqrt{\frac{C_{11}}{L_{11}}})(\frac{1-e^{-(\Gamma p+\Gamma d)\ell}}{\Gamma_p + \Gamma_d})$$

Substituting for Γ_p and Γ_d and deriving the magnitude we obtain the expressions at the bottom of the page.

$$\left|\frac{V_{nd}}{V_{pin}}\right| = \frac{\omega}{8}(C_{21}\sqrt{\frac{L_{22}}{C_{22}}} + L_{12}\sqrt{\frac{C_{11}}{L_{11}}})\sqrt{\frac{1-\{e^{-(R_{11}\sqrt{C_{11}/L_{11}}+R_{22}\sqrt{C_{22}/L_{22}})\ell}\}\{\cos\omega(\sqrt{C_{11}L_{11}}+\sqrt{C_{22}L_{22}})\}+e^{-2(R_{11}\sqrt{C_{11}/L_{11}}+R_{22}\sqrt{C_{22}/L_{22}})\ell}}{(R_{11}\sqrt{C_{11}/L_{11}}+R_{22}\sqrt{C_{22}/L_{22}})^2+\{\omega(\sqrt{C_{11}L_{11}}+\sqrt{C_{22}L_{22}})\}^2}}$$

For longer lengths the above expression can be approximated by:

$$\left|\frac{V_{nd}}{V_{pin}}\right| = \frac{1}{8}(C_{21}\sqrt{\frac{L_{22}}{C_{22}}} + L_{12}\sqrt{\frac{C_{11}}{L_{11}}})\sqrt{\frac{\omega^2}{(R_{11}\sqrt{C_{11}/L_{11}}+R_{22}\sqrt{C_{22}/L_{22}})^2+\{\omega(\sqrt{C_{11}L_{11}}+\sqrt{C_{22}L_{22}})\}^2}}$$

From these final expressions a number of insights into the effects of the various parameters can be obtained:

1. The magnitude of the voltage induced on the data cable is linearly dependent on the magnitude of the EFT disturbance voltage injected on the power cable.

2. The effect of housing the conductors in a metal raceway is to increase C_{22} (smaller distance to ground plane) and to decrease L_{22} (smaller loop subtended by conductor 2 and ground plane), without much affecting C_{11} and L_{11} which are determined by the more closely coupled power conductor. Consequently, the coupling ratio when the conductors are housed in metal raceways is less than when they are housed in plastic raceways or suspended in air.

3. The introduction of a grounded metal divider between the two conductors reduces C_{21} thus reducing the coupling ratio.

4. For low frequencies the magnitude of the coupling voltage increases linearly with frequency until ω approaches a value of :

$$\omega = \frac{R_{11}\sqrt{C_{11}/L_{11}} + R_{22}\sqrt{C_{22}/L_{22}}}{\sqrt{C_{11}L_{11}} + \sqrt{C_{22}L_{22}}}$$

For higher frequencies the coupling ratio asymptotically approaches:

$$\frac{(C_{21}\sqrt{L_{11}L_{22}} + L_{12}\sqrt{C_{11}C_{22}})}{8(C_{22}\sqrt{L_{11}L_{22}} + L_{11}\sqrt{C_{11}C_{22}})}$$

Experimental Results

The Test Background and Set-up:

The idealized model of a power & data cable environment utilized to develop the forgoing relationships can provide useful insight into the problem being studied only if the model can be determined to be at least adequately representative of a "real world" environment. To examine the assumption of the model's validity, its predictions are compared to the measured performance of a test bed which had previously been constructed to investigate the problem. The test bed, whose development and performance has been previously described in detail, ref. [3], is outlined briefly below.

Testing was conducted using typical constructions of 100m of both non-metallic (plastic) and metallic (steel) multichannel raceways. Figure 3 schematically depicts the basic test setup. An EFT (electrical fast transient)

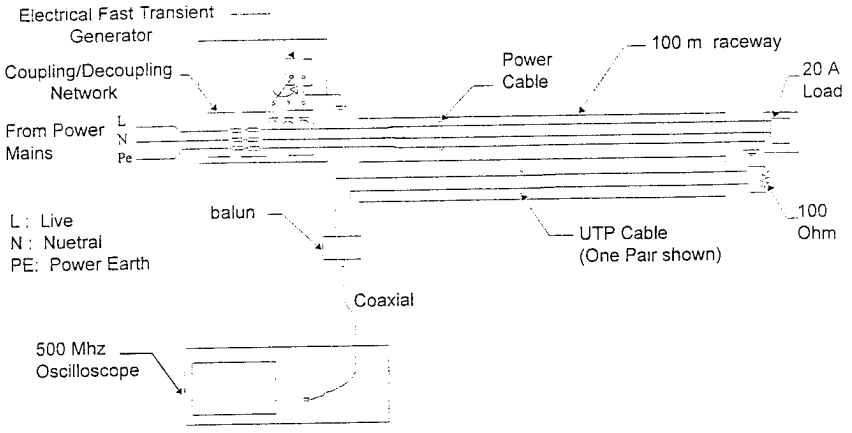
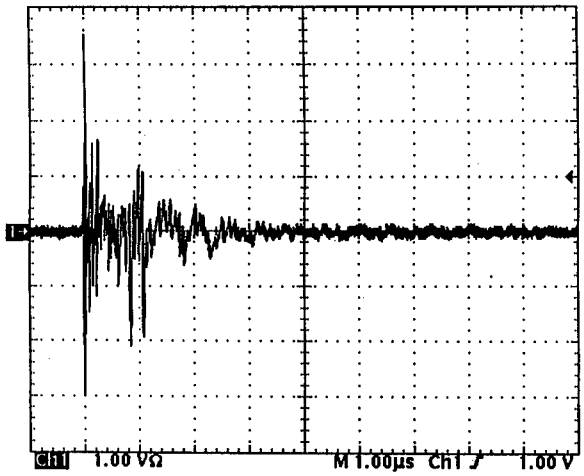


Figure 3: Experimental Test Set-up Schematic

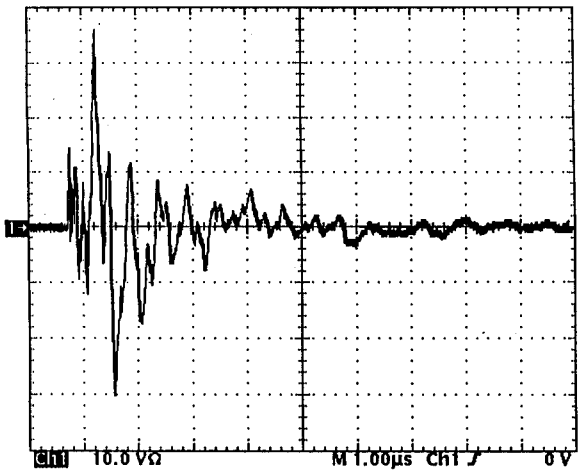
generator was used as a controlled means to introduce the waveform of figure 1 onto the power lines. The peak-to-peak voltage level of the resultant voltage coupled onto the data lines was then measured through a wideband high balance balun using a 500Mhz digitizing oscilloscope.

Test Results - Metal vs. Plastic (Common Mode):

The lower coupling ratio predicted in the mathematical analysis for metal raceways as compared to plastic raceways is supported by the plots shown in figure 4. (Note that the vertical, or voltage, scale for the second plot is ten times that of the first plot.)



Metal Raceway: 6.54 v peak-to-peak



Plastic Raceway: 66.2 v peak-to-peak

Figure 4: Common Mode Coupled Voltage for a 1kv injected EFT (Metal vs. Plastic Raceways)

EFT level:

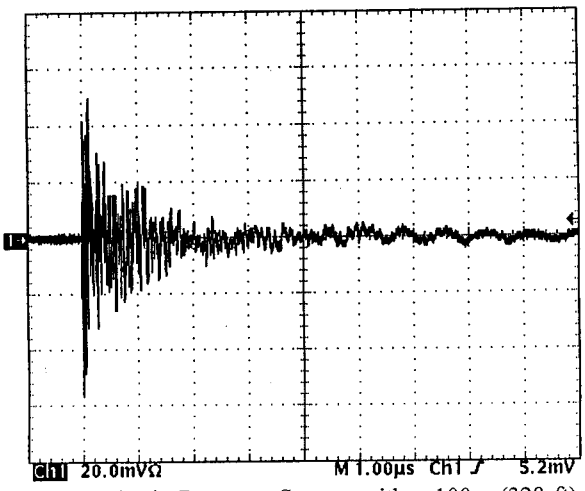
Table 1 supports the prediction of the analytical model about the linear dependence of the coupled voltage magnitude on the injected EFT voltage magnitude. As can be seen in the table, the resultant differential voltages observed are proportional to the levels of injected voltages used, throughout the range of voltages involved in the experimental investigations.

Vpin (volts)	Vnd (volts)
250	17.6
500	35.0
750	54.6
1000	71.6
1250	87.6
1500	107.2
1750	124.8
2000	148.0

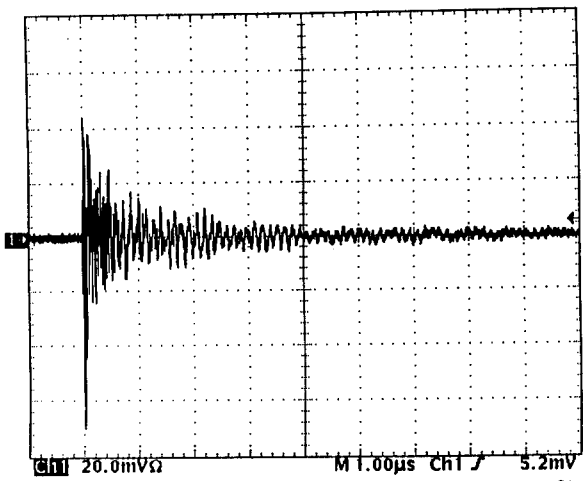
Table 1: Tested Differential Mode Coupled Voltage Linearity with Injected EFT Voltage (peak-to-peak measurements for a metal raceway system)

Coupling Length:

Figure 5 supports the assumption that coupling length ceases to be a factor beyond approximately 12 ft (3.7m). The first plot shows a peak-to-peak coupled voltage level of 108.0 mv measured on a 100m test installation. The second plot illustrates the comparable coupled voltage of 113.2 mv for a 2.5m test installation. Numerous similar tests have demonstrated that once the test length (i.e. the distance over which the power and data cables are held in close parallel proximity to each other) exceeds this approximate threshold, additional length has a negligible effect on the level of voltage coupling observed.



Plastic Raceway System with a 100m (328 ft)
Coupling Length: 108.0 mv peak-to-peak



Plastic Raceway System with a 2.5m (8.2 ft)
Coupling Length: 113.2 mv peak-to-peak

Figure 5: Comparative Differential Mode Coupled Voltages for different coupling lengths

Conclusions

Testing of representative raceway installations supports the validity of the simplified analytical model developed for investigating the case of UTP data cables run in close proximity to power cables. The model therefor can be used as a basis for predicting the effect of system changes (e.g. cable routing, shielding options, required levels of noise robustness, etc.) on the overall level of system performance. Further correlative studies between actual results and model predictions should help to refine the model. Additionally, it is recommended that this simplified model be enhanced, (or a more general model be developed), to address more complex cabling environment issues such as the possible interactions between multiple nearby power and data circuits.

References

[1] Martzloff, F.D., and Leedy, T.F., "Electrical Fast-Transient Tests: Applications and Limitations," IEEE Transactions on Industry Applications, Vol. 26, No. 1, January/February 1990.

[2] International Electrotechnical Commission International Standard: Electromagnetic Compatibility for Industrial-Process Measurement and Control Equipment, Part 4: Electrical Fast Transient/Burst Requirements.

[3] Hashim, A., and Makwinski, M., "The Coupling of Electrical Fast Transients from Power Lines to Data Lines in Close Proximity", presented at Power Quality '94, September 17-22, 1994, Dallas/Ft. Worth, Texas.



Amid Hashim
AT& T
Bell Laboratories
Whippany, NJ

Amid Hashim is currently a member of the Technical Staff at AT&T Bell Laboratories. During the past four years of his professional experience, he worked on telecommunications premise distribution systems. He received his B.S. degree in Electrical Engineering from the University of Illinois and his M.S. degree in Electrical Engineering from Case Western Reserve University.



Mark Makwinski
The Wiremold Company
West Hartford, CT

Mark Makwinski is currently a Chief Project Engineer with the Wiremold Company where he is working on the integration of communications into wire management systems. He received his B.S. degree in Mechanical Engineering from Cornell University and his M.E. degree in Mechanical Engineering from Rensselaer Polytechnic Institute.

LINK TESTING IN THE TIME DOMAIN AND PERFORMANCE ADVANTAGES OVER SWEPT FREQUENCY MEASUREMENTS

J.S. Bottman, H. Koeman

Fluke Corporation, Everett, WA, USA

ABSTRACT

Time Domain Response Measurement methods for twisted pair cable transmission characteristics offer significant advantages over traditional swept frequency methods. These advantages include: substantial increase in measurement speed, greatly enhanced diagnostic capability and state-of-the-art accuracy, even when user patch cords are used to connect the link to equipment.

The time samples are used to calculate the equivalent frequency response using digital signal processing and Fast Fourier Transforms. The DSP methods include estimating the unwanted Near End Crosstalk (NEXT) contributions from the local and remote instrument connectors and excluding this response from the NEXT performance of the link that is reported.

The basic measurement and practical performance results concepts are described.

INTRODUCTION

Swept frequency methods are commonly used to specify performance of components and links for data communication [1-3]. They are also commonly used in specific applications as well as field test equipment.

The pulse response approach to LAN cable testing results in a unified, uniquely capable measurement system. Time domain measurements include Time Domain Reflectometry, Time Domain Crosstalk, and cable impedance estimation. The frequency domain parameters of attenuation and NEXT are obtained by Fourier analysis of the steady state pulse response, and are exactly equivalent to results obtained through the traditional swept frequency approach. The pulse based approach simultaneously applies a large number of harmonically related test frequencies to the cable under test, and analyzes the resulting pulse response with the Fast Fourier Transform algorithm to find the amplitude and phase of each harmonic. By comparing these results with calibration data obtained under a known reference condition, transfer functions are calculated. This approach is inherently faster and more efficient than sequential application and measurement of the large number of test frequencies required for adequate cable verification.

Both phase and amplitude information are available through pulse based analysis. This makes measurement of complex impedance, and thus return loss, possible. Return loss cannot be measured with a scalar swept frequency test system.

In the formal definition of a link the connection to the equipment at both ends of the interconnect cabling is excluded, although physically those end connections are part of the patch cord [1]. The reason is

that the electrical performance of data communication equipment is tested at the cable side of the plug mating with the instrument jack and there should be no double accounting for the transmission performance by connections. International standards [4] define the link slightly different: they exclude also the cordage of the patch cord at both ends, but include the plug making connection to the fixed wiring.

This presents serious problems for test equipment designers, who have to perform a measurement through an instrument jack/mating plug, but somehow have to suppress measurement errors resulting from this component. This is a very serious problem during the measurement of Near End Crosstalk (NEXT), the most important parameter affecting high frequency transmission. NEXT is also the parameter most affected by workmanship errors, so it is important to test NEXT in the field.

Connecting hardware is a point source of NEXT, and practically cause serious limitations of link performance. NEXT contributions in cable are distributed in nature and tend to be far less harmful. Figure 1 shows a typical time domain response as displayed on a tester that illustrates this.

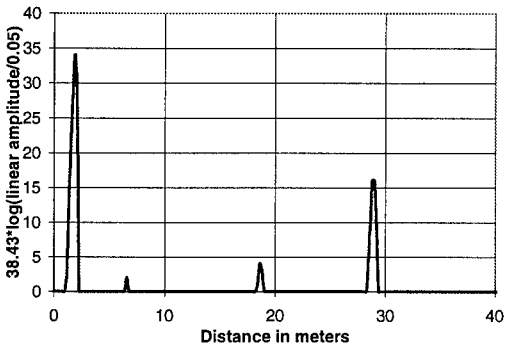


Figure 1: Typical time domain response of a link showing NEXT contributions from cable and connecting hardware.

The link committee of the Telecommunications Industries Association (TIA) recognized that tighter requirements were appropriate for the horizontal cabling portion of a link and defined a "basic link" configuration [2]. The equipment cord, delivered with the field tester is used in this configuration. The solution to overcoming the impact of the instrument connector by several manufacturers of field test equipment has been to use a low NEXT connector with a special equipment cord with a mating plug at one end and a standard modular plug at the other end. This overcomes the measurement error by NEXT introduced at the connection to the field tester and its remote unit. This solution is suitable for the basic link configuration (see figure 2), which is intended to represent the fixed horizontal wiring portion of the link.

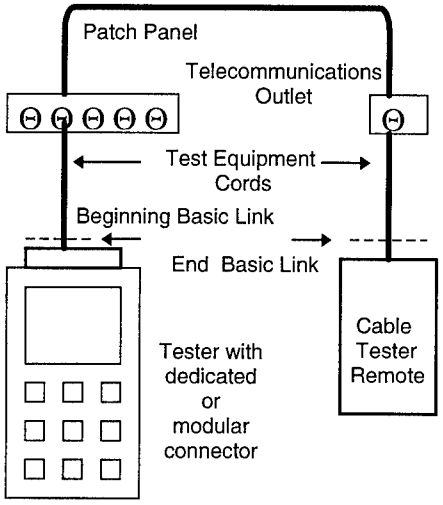


Figure 2: Basic Link configuration per TSB-67

This solution is not available for the channel configuration (see figure 3), where provisions for mating with a modular plug are needed. The channel is intended to represent the end-to-end connection including the user patch cords. In this case the end-plug, which is typically of the modular variety, must be accommodated by the tester.

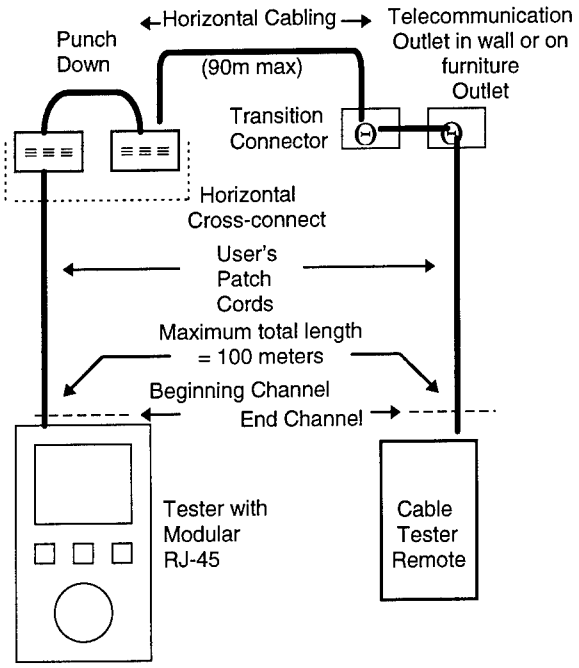


Figure 3 Definition of "channel" type link.

The time domain measurement approach provides means to selectively eliminate portions of the time response associated with the local and remote connector. Principles of operation and practical performance aspects for the NEXT measurement of a link equipped with modular end connectors are described.

PULSE RESPONSE MEASUREMENT SYSTEM

A pulse response digitizer generates a data record for the cable under test that provides input for subsequent signal processing. Sample rate and record length are determined by requirements of the test modes. For example, frequency measurement to 100MHz requires a sample rate of at least 200Ms/s, and must be much higher to allow for practical anti-alias filtering. Thus 500Ms/s was chosen as the fastest sample rate. Data record length is determined by NEXT frequency spacing. A 4096 point record length was chosen to meet the 150kHz requirement in TSB-67. The internal frequency step size is 0.122MHz. Values at 100kHz increments are obtained by linear interpolation. The NEXT and TDR functions require a number of pulse widths to cover the dynamic range with sufficient signal-to-noise ratio. Table 1 summarizes the capabilities of the digitizer.

Parameter	Values
Sample Rate	62.5, 125, 250, 500 Ms/s
Record Length	4.096 to 16.384 μs
Pulse width	5, 16, 64, 240 ns

Table 1: Digitizer capabilities

Sequential sampling is used to obtain effective high sample rates with a much lower real time sampling rate of 3.91Ms/s. A data record is built over a large number of excitation pulses by measuring only a subset of the total record with each pulse, and storing the result in the appropriate indexed locations in acquisition memory. Averaging reduces the noise floor and is achieved by summing A/D output data into acquisition memory on the fly. For example, each data point in a NEXT record is the sum of 128 A/D converter readings.

Computer modeling of the measurement system revealed two major sources of transfer function error: amplitude error, such as A/D quantization and non-linearity, and sample time errors. The A/D converter has 10 bits of resolution. Variable DC offset injection over a 7 bit range is used during data record acquisition in order to smooth the quantization curve, thereby increasing linearity and resolution. This technique provides adequate amplitude accuracy. Sample time uniformity is of critical importance for accurate transfer function measurement, and timing circuits were optimized for adequate uniformity.

NEXT MEASUREMENT

Category 5 LAN cabling is tested for NEXT over a 1-100MHz frequency range. The pass/fail test limit is approximately the following function of frequency:

$NEXT_{limit} = 27 - 15 * \log(f / 100)$

where f is the frequency in MHz. Thus a measurement system with constant signal power and noise floor will have 30dB worse signal-to-noise ratio at 1MHz than at 100MHz when measuring near the limit.

Signal power is increased at lower frequencies during the NEXT measurement by using three pulse widths, corresponding to three frequency bands as shown in table 2.

Freq. Range	Pulse Width	1st Null Power Spectrum.
1-10MHz	64ns	15.6MHz
1-40MHz	16ns	62.5MHz
40-100MHz	5ns	200MHz

Table 2: Pulse width selection

This technique results in a signal power spectrum that maintains approximately uniform signal-to-noise ratio when measuring close to the test limit. A NEXT noise floor of about 100dB is achieved in the 1-10MHz range, providing about 40dB of margin at the 60dB test limit at 1MHz. Note that the measurement accuracy is most critical in the region close to the pass/fail test limit.

NEAR END CONNECTOR COMPENSATION

The link definition requires exclusion of crosstalk from the test instrument. Most often the modular connector is used. Unfortunately, its physical design results in a high, unpredictable crosstalk (e.g., 40dB typical at 100MHz). Fortunately, the pulse response based measurement approach allows exclusion of most of the NEXT from the instrument connector.

The technique essentially constructs an estimate of the the near end connector pulse response from the measured pulse response. The measured response includes crosstalk from the near end connector as well as the link under test.

An example of the 5ns response of the near end connector (nec) NEXT and the total link NEXT response is shown in figure 4. During calibration the beginning of the connector response is identified. During the measurement of the link, the near end connector pulse response is obtained from the 10ns time interval that follows the defined start of the connector response. Other adjustments are made for the long term response contribution from the connector. The connector estimate is then effectively subtracted from the uncompensated NEXT that is calculated.

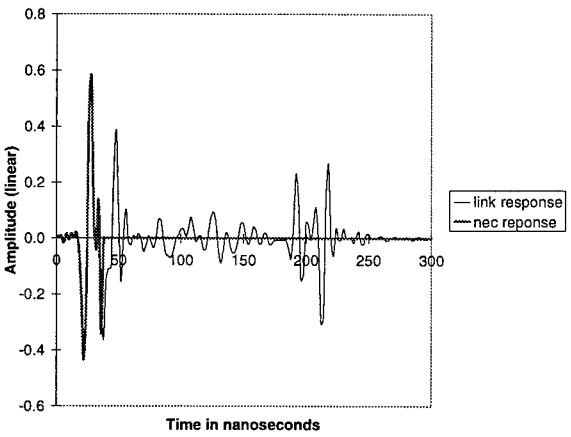


Figure 4: 5ns Response of near end connector and 15m basic link.

Patents related to the measurement principles, which were described in this article have been applied for.

MEASUREMENT PERFORMANCE

The performance of a time domain measurement based field tester is illustrated with key performance parameters related to the measurement of NEXT. It includes consideration of sources of error from excluded cable NEXT, and variations in local connector NEXT performance by modular connector.

Overall measurement performance relative to network analyzer measurements are shown as well.

Residual NEXT performance

The immediate benefit is rejection of the NEXT of the local connector. When terminated by just 100Ω, the residual NEXT improves from approx. 40dB to approx. 70dB at 100MHz. However, reflections and coupling inside the instrument jack/mating plug reduces this to approx. 60dB. See figure 5 for a typical result measured per TSB-67 guidelines.

As expected, the worst performance occurs with the 3,6-4,5 pair combination.

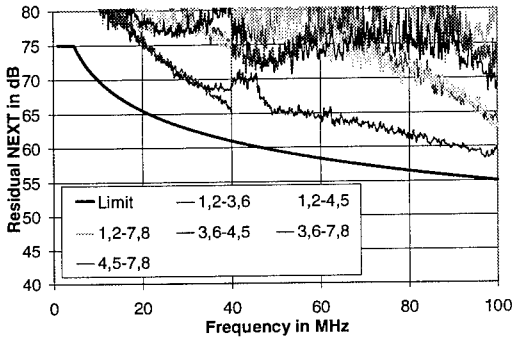


Figure 5: Residual NEXT of modular connector measured with DSP techniques.

Transition of sensitivity

While suppression of unwanted connector NEXT is achieved, some portion of NEXT from cable near the local instrument connector is lost as well. Figure 6 shows the sensitivity as a function of distance from the local connector for the NEXT at 100MHz.

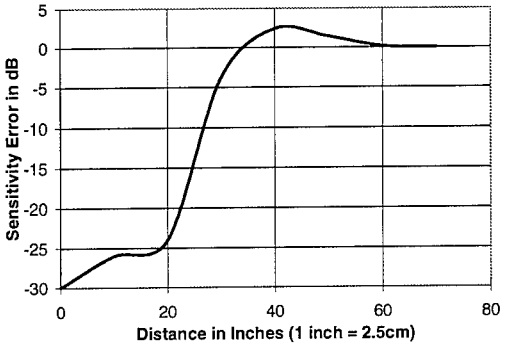


Figure 6: Sensitivity as a function of distance from the local connector at 100MHz

Note that the rejection of the connector NEXT is approximately 30dB. The sensitivity turns on rapidly between 50cm (20") and 75cm (30") from the equipment connector and is slightly overly sensitive at 1m (40")..

Measurement Error Considerations

The error in the NEXT of the link is lack of NEXT from a portion of jacketed cable. This amount can be measured and calculated. For a short segment of cable, the result is

$$NEXT_{dB,length} = 10 * \log(K_N * f^2 * length)$$

where the length is expressed in meters and frequency f is in MHz. Constant K_N for nominally performing category 5 cable is $6*10^{-9}$. At 100MHz, the result is:

$$NEXT_{dB,1m} = -42.2dB$$

Since the NEXT in a cable is distributed in nature, the error caused at a nominally performing channel is given by:

$$E_{dB,1m} = -10 * \log(1 - K_N * f^2 * 10^{\frac{NEXT_{dB,nom}}{10}})$$

In this equation, $NEXT_{dB,nom}$ represents the nominal signal level, e.g., the test limit for a category 5 channel. At 100MHz the error is 0.13dB for a 1m long cable and insignificant relative to the overall 1.5dB accuracy objective.

Instead, the potential error contribution from a local connector NEXT is fixed in phase relative to the point of measurement and therefore can easily add worst case with the NEXT of the link to be measured. For a nominally performing category 5 connection, the error is 1.8dB @ 100MHz at the test limit for a channel.

In-situ measurement of local connector NEXT

Since the time record includes the response of the local connector, it is possible to determine the frequency domain equivalent of the amount that is excluded from the computation of the NEXT for the defined link. An example of the frequency response on a logarithmic frequency scale is shown in figure 7.

Note that the slope closely resembles 20dB/decade, as predicted for NEXT from connecting hardware; cable "slopes" at 15dB/decade. This result confirms that short segments of cable contribute very little error. Also note the dynamic range at low frequencies. In order to avoid passing any seriously damaged patch cord, if not already detected during other tests, the time domain tester can issue warnings, if expected NEXT for the compensated amount is outside normal levels.

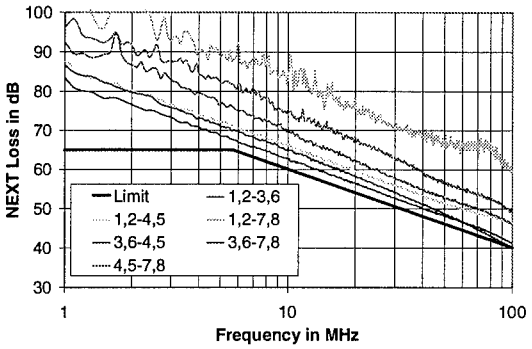


Figure 7: Local connector compensation amount as a function of frequency.

Not every plug inserted into a category 5 compliant modular jack results in a connection that complies with the category 5 requirements [1]. The explanation might be that the qualification procedure in [1] selects first a test plug and then verifies performance of the plug/jack combination. Instead, the jack of a field tester is always fixed and plugs of user patch cords vary.

Comparisons with network analyzer measurements

Reference [3] contains in Annex B information on how to properly make measurements so that results from field testers and network analyzers are directly comparable.

Sample results of comparison are reported on the very same basic link by several independent and very qualified parties, using laboratory equipment. All parties used 0322BF North Hills baluns, but different network analyzers. Along with these results, the response of a time domain measurement field tester is plotted. The links that were tested tended to have less favorable balance properties, and represent potentially worst

case quality links. The 3,6-4,5 pair combination examined as generally representing a worst case situation.

One will note that in some cases very good correlation exists between the independently obtained network analyzer results. It will be found that the agreement with the response of a field tester is as good. See figure 8. The fat line is the time domain tester; the thin lines represent the results of laboratory equipment. For some links, the level of agreement is superb.

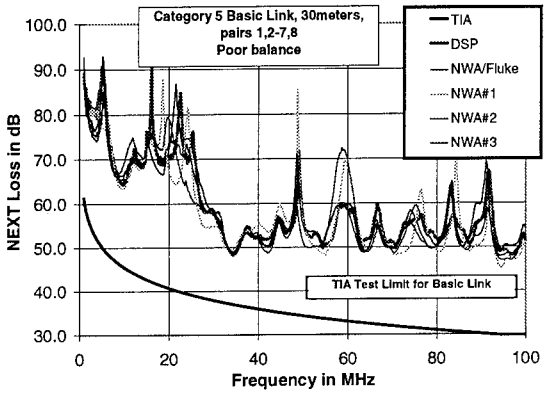


Figure 8: Comparison network analyzer responses vs. time domain tester, better correlation.

In other cases relatively poor correlation exists between independently obtained network analyzer results. In those cases, the agreement with the response of a field tester is not as good as well. See figure 9.

One may conclude that secondary link parameters affect the measurement accuracy. The current draft of [3] contains the initial error model and it has been agreed that it is satisfactory for an initial step. It will be subject of future research and will likely be enhanced in future issues of [3].

It is found also that in any case, the agreement between worst case NEXT margins is well within the measurement errors of the field tester and network

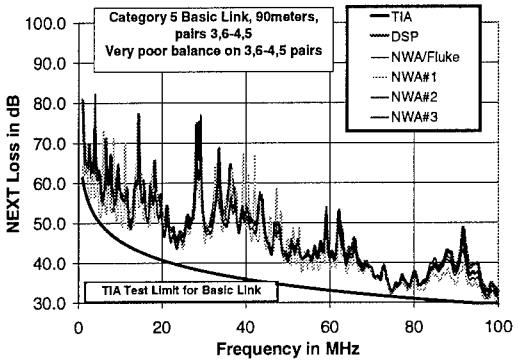


Figure 9: Comparison network analyzer responses vs. time domain tester, worse correlation.

analyzer. Table 3 shows typical results for three links. The first column contains information on the link. Good (longitudinal) balance is 40dB or better, Average balance is 30-35dB, Poor balance is <30dB. The Network Analyzer Result column (NWA) shows the worst case NEXT margin as

Link	Pairs	NWA (dB)	Delta #1 (dB)	Delta #2 (dB)	Tol. (dB)
Cat 5	1,2-3,6	3.9	+0.2	+0.4	2.5
30m	1,2-4,5	7.3	-0.8	-0.9	2.7
Ave	1,2-7,8	11.0	+1.4	+1.3	3.3
bal.	3,6-4,5	2.1	+0.1	-0.2	2.4
	3,6-7,8	9.2	+0.3	+0.1	3.0
	4,5-7,8	7.7	0.0	+0.1	2.8
Cat 5	1,2-3,6	14.8	-0.2	-0.3	4.2
60m	1,2-4,5	8.7	+0.6	+0.5	2.9
Good	1,2-7,8	12.4	+1.5	+1.0	3.7
bal.	3,6-4,5	7.7	+1.7	+1.5	2.8
	3,6-7,8	11.1	-0.9	-0.8	3.3
	4,5-7,8	7.7	+0.3	+0.2	2.8
Cat 5	1,2-3,6	3.1	-0.3	-0.2	2.5
90m	1,2-4,5	2.4	-0.4	-0.3	2.4
Poor	1,2-7,8	1.4	+0.9	+1.1	2.3
bal.	3,6-4,5	1.3	+0.2	+0.2	2.3
	3,6-7,8	5.2	+0.2	+0.3	2.6
	4,5-7,8	3.4	0.0	+0.1	2.5

Table 3: Comparisons of worst case margins by two time domain testers against network analyzer results.

measured by the network analyzer. The deviation of the worst case margin by two time domain testers is shown in the columns marked Delta #1 and Delta #2. The tolerance column (Tol) is the allowed difference computed guidelines of Annex B of [3].

Note that the observed differences are always less than approx. 60% of the tolerance that is allowed, even under relatively unfavorable conditions. Furthermore that the two different testers tend to be very consistent in their results. This is confirmed by the frequency plots which are virtually on top of each other.

CONCLUSIONS

The time domain measurement method has been shown to provide accurate NEXT measurements, even when modular connectors are used, since it includes the ability to electronically "cut off" unwanted responses. Integrated circuits that incorporate fast Fourier transform functions have made it practical to design a hand held instrument.

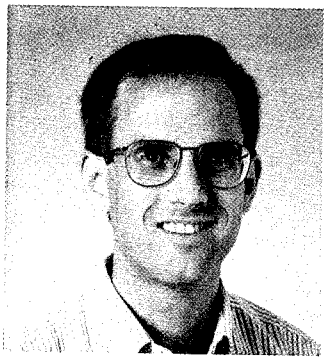
Also, the deviations from "ideal" network analyzer based test results are no worse than the variations observed between results obtained from different network analyzer based setups.

In addition to achieving the highest level of measurement accuracy, it can be shown that the time domain based tester meets the required performance for random noise, residual NEXT, output signal balance, common mode rejection, dynamic accuracy and return loss for Accuracy Level II performance for both a basic link and channel configuration. The results of these tests are not discussed in this paper.

Furthermore, the speed of the measurement is very high. Time domain responses provide excellent means to diagnose and locate transmission problems on the link.

REFERENCES

1. TIA standard TIA/EIA-568-A
2. ASTM standard ASTM D-4566-1994
3. TIA Telecommunications Service Bulletin (TSB) - 67.
4. ISO/IEC standard ISO/IEC IS-11801
5. IEC standard IEC 1156-1994



Jeff Bottman is a Senior Staff Engineer with Fluke. He has worked on a time domain cable tester since its inception. He designed the high speed measurement system and also specified the digital signal processing algorithms. Jeff holds a MSEE degree from Stanford University.



Henriecus Koeman has a PhD degree from the University of Nymegen (The Netherlands) and is a Principal Engineer with Fluke. He is the Fluke representative to the TIA link committee.

RESEARCH EXPERIMENT DEMONSTRATES 622 Mbps DATA TRANSMISSION OVER COMMERCIAL COPPER CABLING SYSTEM

Robert C. Pritchard
AT&T Bell Laboratories
Middletown, NJ 07748

ABSTRACT

The market for commercial premises distribution systems is evolving rapidly. As data systems reach ever higher bandwidth requirements, concerns have been raised about the capabilities of Unshielded Twisted Pair (UTP) copper cabling systems. An experimental data link demonstrating high-speed data transmission over a commercially available UTP copper cabling system has been designed and built at AT&T Bell Laboratories. Using all four pairs in the cable, the research prototype transports digital data at a rate of 622 Mbps, far beyond the capability of currently existing LANs. The cabling system is made up of off-the-shelf Category 5 components, including 100m of cable, cross connect hardware, modular outlets, and jumper cords. The application supplying the digital data stream is studio-quality RGB video equipment. The proprietary data link hardware transports this digital video using the 64-point Carrierless AM/PM (64-CAP) encoding technique.

INTRODUCTION

The requirements placed on cabling systems for commercial premises have changed a great deal in recent years. After being stable for roughly a century (since the invention of the analog telephone), data systems are rapidly evolving to faster data transfer rates, starting with the comparatively recent appearance digital telephone and the local area network (LAN). Users have come to realize that the electronic distribution of data deserves as much attention as its collection and processing. In fact, in many cases companies find it easier to evolve and update their data processing equipment than the distribution infrastructure in their buildings. A customer doesn't want to be in the position of having a distribution system that can't support her/his needs.

To address these concerns, Bell Labs has focused a great deal of effort on discovering and exploring the fundamental theories of electronic and optical data transmission, to better understand and exploit their application to commercial data transmission.

This paper describes a demonstration system that is one example of that exploration. Currently widespread commercial data transmission systems (LANs) operate at 10 or 16 Mbps. Next generation LAN offerings are beginning to gain market acceptance, touting data rates of 25, 51, or 100 Mbps. Beyond that, attention is focused on channels to and from ATM switches or channels, at 155 Mbps. By contrast, the point-to-point data connection in this demonstration is operating over a 24 AWG unshielded twisted pair (UTP) cabling system at 622 Mbps, achieved by combining four 155 Mbps channels in a single 4-pair cable. Simple arithmetic shows that this connection is sufficient to carry (roughly) 23,000 pages of text per second.

Two Bell Laboratories organizations have collaborated to design and build the demonstration system, one expert in data transmission and encoding techniques, the other in cabling system technology and performance. The cabling system connecting the endpoints consists of standard off-the-shelf Category 5 products. This demonstration shows the ability of the well-engineered and complete commercial cabling system to transport a very high bit-rate data stream — far beyond the capability of currently existing LANs.

The remainder of the paper describes the components of the system and system operation, including a brief discussion of the encoding scheme. The paper does not describe cable performance in any detail. The references contain more thorough treatments of these complex topics for interested readers.

SYSTEM DESCRIPTION

The very first problem we faced when conceiving this demonstration system was finding a source of data which was capable of supplying roughly a half-Gigabit per second of data in a user-friendly format. After weighing a number of alternatives, we selected digitized high-quality RGB (red/green/blue) video as the application to supply the digital data stream to our transport electronics. This kind of video, sometimes called studio-quality video, is higher quality than the typical NTSC/PAL video you would see on most televisions. It is referred to as "component video" (as opposed to "composite video") by the video industry, and is used by television stations and production studios to record shows and distribute signals for broadcast.

The major components used in the demo are schematically represented in Figure 1. A few interconnections (such as AC power) have been omitted for clarity. The boxes labeled Transmitter and Receiver contain the proprietary electronics we designed and built for this system; all other components are commercially available items.

In our experimental system, we have a commercial-grade RGB video camera capturing a full-motion high-resolution image. The codec labeled ADC converts the analog video signal from the camera to a digital video data stream in an industry standard protocol[1,2] called D1. This digital data stream is provided to our proprietary hardware, which arranges the bits and adds some control overhead to facilitate transmission, applies the

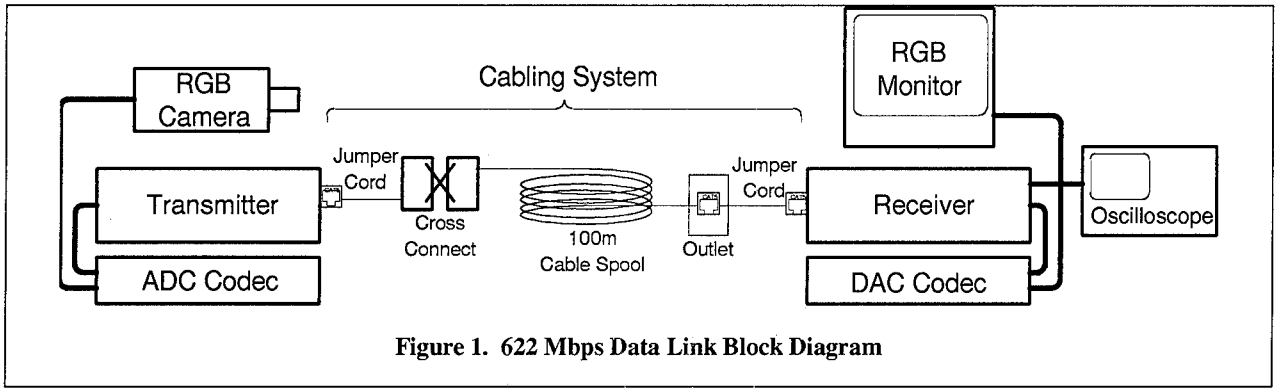


Figure 1. 622 Mbps Data Link Block Diagram

64-point Carrierless AM/PM (64-CAP) encoding technique, and then drives the signal onto the UTP cabling system.

The receiver hardware decodes the incoming CAP signal and recreates the same digital data stream we started with. This data stream is sent to the DAC codec for conversion back into an analog RGB video signal which is displayed on the monitor. Special purpose hardware within the receiver allows the received CAP signal constellation (described below) to be displayed on an oscilloscope.

The cabling system is intended to be a realistic representation of the horizontal subsystem of a premises distribution system[3,4]. All components used are high-performance Category 5 items from our product line, currently available off-the-shelf. Using low quality or lower performance cabling components will definitely affect the system performance (i.e. the error rate will increase).

Our transmitter and receiver each have a standard modular jack at the rear of their cabinets. The transmitter end is treated as the "hub" electronics in the equipment closet. One end of a jumper cord is plugged into the jack on the rear of the transmitter. The other end of this cord (without a plug) is punched down onto the IDC terminals of the cross connect field. A 100m length of our 4-pair Category 5 cable is punched down on another field, and the two terminations are connected by a patch cord. The cable is coiled and placed either in a WE-TOTE box or left visible on the table. The other end of the cable is punched down onto a modular jack mounted in a wall outlet. A jumper cord then connects to the modular jack on the back of the receiver, completing the link. We deliberately took no special care in selecting or assembling the components, but rather used factory stock and followed our standard installation procedures.

64-CAP ENCODING

The complexities of CAP encoding are well beyond the scope of this paper. However, a short discussion of some general coding concepts assists in understanding the operation of the demo system. Readers interested in pursuing the topic in depth are recommended to the excellent references cited[5,6].

One of the simplest encoding schemes is the non-return-to-zero (NRZ) line code. This scheme uses a pair of voltage levels to represent the two possible states of a single bit of digital information. For example, the transmitter might send a high voltage level to represent a 0 bit, and low level to represent a 1 bit. The receiver samples the incoming signal near the center of each bit time, and decides whether the signal is high or low for a 0 or 1 bit. Each *symbol* sent over the wire carries one *bit* of information.

A straightforward extension to this simple encoding scheme is to use several amplitude levels. For example, a four-level system might send symbols at ± 1 and ± 3, so that each symbol represents two bits. This is a powerful step because it reduces the bandwidth necessary to carry a designated bit rate, improving the *bandwidth efficiency*. With two bits per symbol, the frequency can be half that required by a system using one bit per symbol, and so the bandwidth efficiency is doubled.

Next, consider extending the encoding scheme by sending multiple symbols simultaneously. Of course, this is only useful if the symbols are *orthogonal*, meaning the symbols don't interfere with each other and can be recognized and distinguished at the receiver. Sending multiple orthogonal symbols is called multi-dimensional encoding. In a system with two orthogonal symbol sets, the set of possible received data values can be represented as a two-dimensional matrix. This matrix is called a *constellation*. Each point in the constellation represents a pair of orthogonal symbols, called a complex symbol. To continue our example from the preceding paragraph, with four possible values per symbol, we would have a 4×4 matrix with 16 possible values.

CAP encoding is an example of such a 2-dimensional scheme, using sophisticated digital signal processing techniques to send two orthogonal symbols simultaneously. The transmitter partitions the incoming data, and uses the bits to select a pair of orthogonal waveforms, then combines and sends them. At the receiver, there are two filters, each of which will recognize one symbol and ignore the other. The 64-CAP scheme used in our system uses a set of 8 symbols in each dimension, for a total of 8×8 or 64 points, as illustrated in Figure 2. Thus, each complex symbol transmitted over the link conveys one of those 64 or 2^6 points, and represents 6 bits of data.

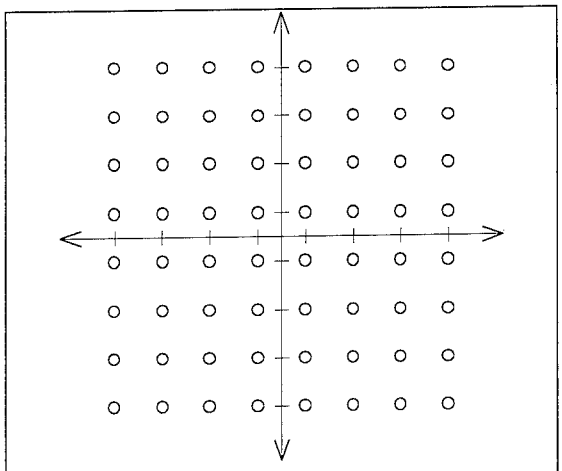


Figure 2. 64-point Constellation

In our demonstration system, the received constellation is graphically displayed on an oscilloscope connected to the receiver, showing the actual received data points. Intuitively, one can see that the receiver must make a decision on each received complex symbol, determining which of the 64 points was received.

In order for the receiver to distinguish this many constellation points, the receiver includes adaptive equalization, and the data is scrambled. The adaptive equalization makes continual adjustments to make sure that all receiver parameters are at optimum values. For example, the electronic components in the transmitter and receiver will all perform slightly differently depending on the ambient temperature, and the adaptive equalization will adjust the receiver to compensate for this phenomenon. The data are scrambled to ensure that all 64 dots in the constellation are populated. If this were not the case, the adaptive algorithm would have difficulty making these adjustments. In other words, the scrambling makes sure that the adaptive equalization algorithm is adjusting the receiver based on a complete picture of all values, and not some subset of values.

FOUR-PAIR OPERATION

We are using all four pairs in the UTP cable to achieve the high bit rate of 622 Mbps. To accomplish this, we must partition the data stream into four "channels" at the transmitter, and then recombine the channels into a single data stream at the receiver.

Partly because the link bandwidth is so high, the method selected to perform this partitioning and recombining was chosen not for efficiency but rather for circuit design simplicity. The incoming digital video data is arriving at the board through an 8-bit wide parallel connection. This data stream is widened to 16 bits at half the rate. This 16-bit data stream is then sliced into four 4-bit channels, and then two control bits are concatenated to form a 6-bit word. These 6-bit words are supplied to the CAP transmitters, which encode the 6-bit word as one of the 64 complex symbols discussed above, and then the symbol is sent.

In addition to the control bits sent with every data word, there are also dedicated channel alignment words added to the data stream and sent periodically in every channel. These data are multiplexed into the data stream at fixed intervals, and encoded and sent by the CAP transmitters just as is the video data.

At the receiver, the received complex symbol is decoded by the CAP receiver, and the 6-bit word is sent on to the combiner circuitry. The channel alignment information is used to align the four channels into a single data stream during initialization, and is also continually checked during normal operation. Once the channels are properly aligned, the control information is stripped from the data stream, and the valid video data emerges as the half-speed 16-bit wide data stream. This is then rearranged and sped up, then sent off the board as the same 8-bit wide data stream with which we started.

Even though the data is driven by the transmitter at the same time onto all four pairs of the UTP cable, there will be some variation from pair to pair in propagation time through the cabling system. This difference is due to variation in parameters like twist rate, absolute length, and the adaptive equalization algorithm in the CAP receivers. As a result of these variations, the receiver includes a small flexible store between the CAP receivers and the combiner circuitry. This flexible store is adjusted during an initialization phase to compensate for any pair-to-pair differences, and guarantee that a coherent data stream is reconstructed from the four separate received streams.

The channel-to-channel alignment of this data stream is continually monitored during system operation. If the cable is disconnected, or part of the link electronics fails, the system will detect the failure and begin the initialization alignment procedure.

The D1 digital video data emerges from the ADC codec at a nominal rate of 8 bits at 27 MHz, or 216 Mbps. As described above, two control bits are added to every four data bits, adding 50% overhead onto this rate, plus some slight additional overhead for the channel alignment information. In all, the data with overhead accounts for roughly half of the available 622 Mbps capacity. The remaining capacity is filled by idle characters, generated at the transmitter and stripped at the receiver. An auxiliary channel is included in the system design, with a maximum capacity of 155.52 Mbps actual data rate plus overhead, but this port is not used in the current system setup.

Currently, some types of data errors can be detected by the receiver, but the system has no provision for error correction or retransmission. This kind of function is typically provided by a high-level protocol, such as those used by a LAN or ATM link, and not by the physical link layer, and so was not included in the system design. The error rate of the complete 622 Mbps link has not been characterized. However, individual CAP transmitter/receiver pairs operating at 155.52 Mbps have been measured at 10^{-10} error rate over 100m of cable.

CONCLUSION

The experimental system described in this paper has been used to demonstrate the high-performance capability of present-day commercial cabling systems. The system transports an encoded digital data stream at 622 Mbps over a realistic horizontal cabling link. The cabling link incorporates all necessary components, including outlets, cross connect hardware, jumper cords, and 100m of 4-pair cable. The cabling system components are all commercially available, although the transmission electronics portion of the system is strictly a research prototype containing experimental hardware.

ACKNOWLEDGEMENTS

Along with the author, the demonstration system described in this paper was designed and built by G. D. Fowler, J. A. Grandle, Jr., and R. Hartung. N. C. Stathum has provided ongoing lab and field support for the system.

REFERENCES

[1] CCIR Recommendation 656, "Interfaces for Digital Component Video Signals in 525-Line and 625-Line Television Systems", 1986.

[2] CCIR Recommendation 601-1, "Encoding Parameters of Digital Television for Studios", 1986.

[3] "AT&T SYSTIMAX® Structured Cabling Systems", Document Number 4062B, AT&T Network Systems, 1992.

[4] "SP-2840A, Commercial Building Telecommunications Cabling Standard", Proposed TIA/EIA-568-A standard, July 13, 1994.

[5] G. H. Im, D. D. Harman, G. Huang, A. V. Mandzik, M.-H. Nguyen, J. J. Werner, "51.84 Mb/s 16-CAP ATM LAN Standard", IEEE Journal on Selected Areas in Communications, Vol. 13, No. 4, May 1995.

[6] G. H. Im, J. J. Werner, "Bandwidth-Efficient Digital Transmission up to 155 Mb/s over Unshielded Twisted Pair Wiring", ICC'93 Geneva.



R. C. Pritchard received the B.S. degree in Engineering and Applied Science from Yale University in 1977, and the M.S. degree in Electrical Engineering from Cornell University in 1981. From 1977 to 1979 he was a staff member at M.I.T. Lincoln Laboratory in Lexington, MA. He joined AT&T Bell Laboratories in 1981, and became a Distinguished Member of Technical Staff in 1989. He was initially involved with development of the Definity™ family of PBXs, and later participated in photonic switching research. Since 1988, he has been a member of the SYSTIMAX® Structured Cabling System Department. His work at Bell Labs has encompassed circuit design, firmware design, software design, project management, field support, systems design, systems engineering, EMC testing, and applied research. He is an IEEE member.

A DE-EMBEDDING METHOD FOR MEASURING THE NEAR END CROSSTALK OF MODULAR PATCH CORDS

Amid Hashim

AT&T Bell Laboratories, Whippany, New Jersey*

1. Abstract

This paper outlines a method for non-destructively measuring the near end crosstalk (NEXT) of unmated patch cords. Prior to this method it was only possible to measure this parameter destructively. Any non-destructive method that existed could not extract the unmated patch cord NEXT values from the test fixtures. The proposed method is based on storing reference data pertaining to the test fixtures and using this data to mathematically eliminate the effects of these fixtures on the measurement, thus enabling the extraction of the unmated standalone patch cord NEXT. In the following, a presentation is made of the mathematical basis for the de-embedding method. Test results obtained using the de-embedding method are compared with results obtained using a destructive method. In addition data is presented correlating the NEXT of the unmated patch cord to the TOC (Terminated Open Circuit) NEXT values of its plug terminations.

2. Introduction

This paper focuses on measuring NEXT of modular patch cords that are made from 100 Ω twisted pair cables specified in TIA-568-A [1] and modular plugs compliant with IEC 603-7 [2]. The NEXT performance of such cords is very much affected by the way in which the plugs are terminated to the cable when they are assembled. TOC NEXT, which is described in TSB-40A [3], is a measure of the quality of the terminations on a test plug assembly. While measuring TOC on a test plug assembly is possible by attaching the raw conductors to 100 Ω terminated baluns, such a measurement would be impossible on an assembled patch cord, since the raw conductors are inaccessible. Apart from the de-embedding method, all non-destructive tests contain inextricable portions of NEXT pertaining to the test head and terminating test jacks. The de-embedding method extracts the unwanted NEXT values associated with these jacks from the measurement, thus yielding the NEXT of the patch by itself. To achieve this a set of test fixtures, described in this paper , are constructed. NEXT values for these fixtures are measured and stored for subsequent use in deriving the NEXT to be vectorially subtracted from patch cord measurements.

3. Analyzing the Patch Cord

As shown in figure 1 the mated patch cord consists of a near end jack , the patch cord and the far end jack .

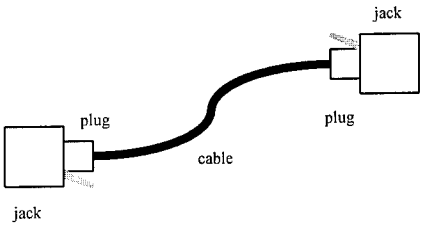


Figure 1: A mated Patch Cord

The NEXT loss of a mated patch cord, $\overline{N}_m$,can be expressed as follows:

$$\overline{N}_m = \overline{N}_{nj} + \overline{N}_{np} + \overline{N}_c + (\overline{N}_{fp\Delta} + \overline{N}_{fj\Delta})10^{-2\alpha/20} \qquad (1)$$

where,

*Note: The work supporting this paper was performed by Amid Hashim while he was an employee of the Wiremold Company

$\overline{N}_{nj}$ is NEXT loss vector for the near end jack

$\overline{N}_{np}$ is NEXT loss vector for the near end plug of the patch cord

$\overline{N}_c$ is NEXT loss vector for the patch cord cable

$\overline{N}_{fp\Delta}$ is NEXT loss vector for the far end plug delayed by the round trip patch cord group delay

$\overline{N}_{fj\Delta}$ is NEXT loss vector for the far end jack delayed by the round trip patch cord group

α is the attenuation of the patch cord cable in dB

NEXT loss of the patch cord alone (without the mating jacks), $\overline{N}$, can be expressed as follows:

$$\overline{N} = \overline{N}_{np} + \overline{N}_c + (\overline{N}_{fp\Delta})10^{-2\alpha/20} \quad (2)$$

Combining equations (1) & (2),

$$\overline{N} = \overline{N}_m - \overline{N}_{nj} - (\overline{N}_{fj\Delta})10^{-2\alpha/20} \quad (3)$$

which can be written as,

$$\overline{N} = \overline{N}_m - \overline{N}_{nj} - \overline{N}_{fj\Delta} + (1-10^{-2\alpha/20})\overline{N}_{fj\Delta}$$

To determine the unmated patch cord NEXT, $\overline{N}$, we need therefore to measure NEXT for the mated patch cord, $\overline{N}_m$ and the near end jack, $\overline{N}_{nj}$, delayed NEXT for the far end jack, and the attenuation of the patch cord cable.

The term $(1-10^{-2\alpha/20})\overline{N}_{fj\Delta}$, which represents the attenuating effect of the patch cord cable on the far end jack only, has an insignificant effect on $\overline{N}$ and is ignored. This results in simplifying the test method in that the attenuation of the patch cord cable does not need to be measured. In the proposed test method therefore, we use the following simplified expression shown below for $\overline{N}$

$$\overline{N} = \overline{N}_m - \overline{N}_{nj} - \overline{N}_{fj\Delta}$$

4. The Test Method:

4.1 Fixtures

First the following fixtures need to be constructed:

4.1.1 (a) The Near End Termination Plug:

The near end terminating plug, illustrated in figure 2, consists of a modular plug with each pair terminated with a 100 Ω resistor. The resistors are located at the cable entrance of the plug and are connected to its mating contacts via insulated 24 AWG wires. The insulated wires are kept parallel within the body of the plug.

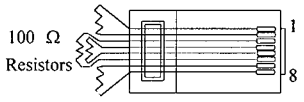


Figure 2: The Near End Terminating Plug

4.1.2 (b) The Near End Plug Reference:

The Near End Plug Reference, illustrated in figure 3, is identical with the terminating plug described in item b above with the exception that 50 mm (2.0 in) UTP test leads are connected to its mating contacts, as shown in figure 8.

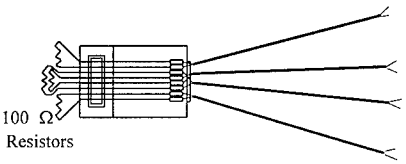


Figure 3: The Near End Reference Plug

4.1.3 (c) The Far End Test Plug:

The far end test plug, illustrated in figure 4, consists of 50 mm (2.0 in) UTP test leads attached to a modular plug. The test leads enter the body of the plug from the cable entrance.

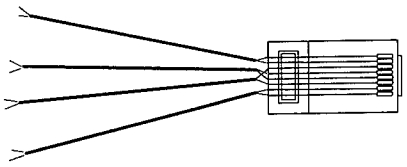


Figure 4: The Far End Test Plug

4.1.4 (d) The Far End terminating Jack:

The far end terminating jack consists of a category 3, printed-circuit mountable jack with 100 Ω resistors connected to its terminals , as shown in figure 5.

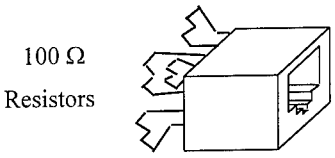


Figure 5: The Far End Terminating Jack

4.1.5 (e) The Far End Plug Reference:

The Far End Plug Reference is identical with the far end test plug with the exception that 100 Ω terminating resistors are connected to its mating contacts, as shown in figure 6.

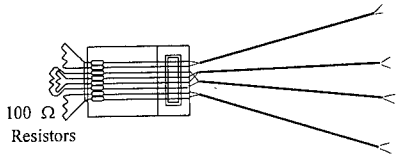


Figure 6: The Far End Plug Reference

4.1.6 (f) The Far End Through Jack:

The Far End Through Jack consists of a category 3 jack with its terminals interconnected in a through configuration, as shown in figure 7.

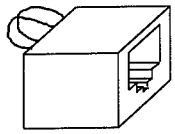


Figure 7: The Far End Through Jack

4.2 The Test Procedure

4.2.1 The Test Set-up:

The test set up uses a vector network analyzer with a group delay measuring capability. As shown in figure 8 all pairs are terminated at the near end with common mode terminations and at the far end with differential mode terminations. As is common in all balanced NEXT measurements the network analyzer accesses the device under test, whether it is a reference fixture or a device under test, through wideband precision baluns.

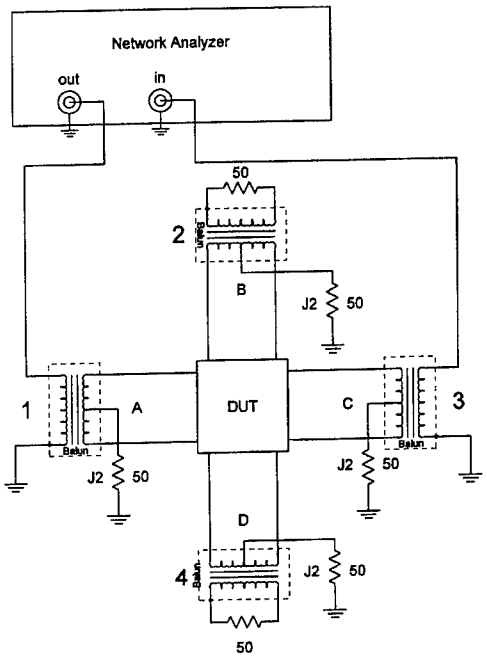


Figure 8: Test Configuration

4.2.2 Instrument Calibration

To eliminate the effects of the test leads the network analyzer is first calibrated for reflection, transmission and isolation using the calibration standards shown in figure 9.

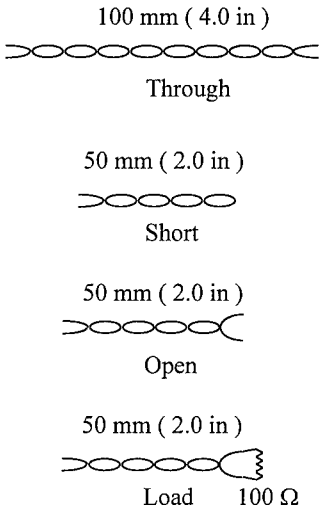


Figure 9: UTP Calibration Standards

4.2.3 Near End Measurements

STEP 1: The real and imaginary components of the crosstalk of the reference near end plug are measured. Let these be Re_{NRP} and Im_{NRP}.

STEP 2: The real and imaginary components of the crosstalk of the near end test jack mated with the near end terminating plug are measured. Let these be Re_{NRPJ} and Im_{NRPJ}.

4.3.1 Mated Patch Cord Test

The real and imaginary components of the crosstalk of the patch cord under test mated at its near end with the near end test jack and its far end with the far end terminating jack are measured. Let these be Re_{MC} and Im_{MC}.

4.3.2 Far End Measurements

STEP 1: (Patch Cord Electrical Length Compensation): An electrical length measurement is performed on the patch under test, mated at its near end with the near end test jack and at its far end with the far end through jack. The network analyzer is then set to subtract an electrical delay equal to the electrical delay noted above. This setting is maintained for the remainder of the far end measurements.

STEP 2: The real and imaginary components of the crosstalk of the reference far end plug are then measured . Let these be $Re_{FRP\Delta}$ and $Im_{FRP\Delta}$.

STEP 3: Measure the real and imaginary components of the crosstalk of the far end test plug mated with the far end terminating jack. Let these be $Re_{FRPJ\Delta}$ and $Im_{FRPJ\Delta}$.

4.4 Computing Unmated Patch Cord NEXT

The NEXT components of the unmated patch cord, X and Y can be obtained from the following equations:

$$X = Re_{MC} - (Re_{NRPJ} - Re_{NRP}) - (Re_{FRPJ\Delta} - Re_{FRP\Delta})$$

$$Y = Im_{MC} - (Im_{NRPJ} - Im_{NRP}) - (Im_{FRPJ\Delta} - Im_{FRP\Delta})$$

To obtain the logarithmic magnitude of the NEXT loss of the unmated patch , in dB's, the following formula can be used:

$$N = -20 \log \sqrt{X^2 + Y^2}$$

4.3 Interpreting the NEXT vs. Frequency Plots

In order to obtain a worst case reading of NEXT at any frequency in the range and for the purpose of pass/fail determination, NEXT is read using the 20 dB/decade intercept criterion. This is achieved by sliding down a 20 dB/decade straight line onto the NEXT vs. frequency curve, to the offset level at which it intercepts any point on the curve. This line is the used for NEXT vs. frequency determination.

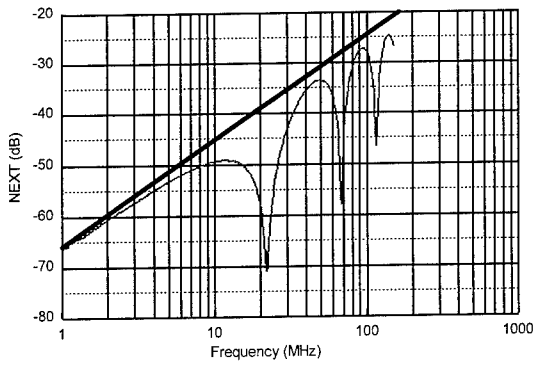


Figure 10: The 20 dB/decade Intercept

5. Experimental Results

An experiment was performed to determine the relationship between patch cord NEXT, measured using the method described in this paper and plug TOC values for different length cords. A constructed patch cord was assembled using a 7 ft (2.1m). category 5 UTP cable terminated with an IC socket at each end. Plug assemblies covering a range of TOC values were then inserted into the IC sockets at the ends (see figure 11). Figure 12 is a plot of the average of the two TOC plugs vs. the patch cord NEXT.

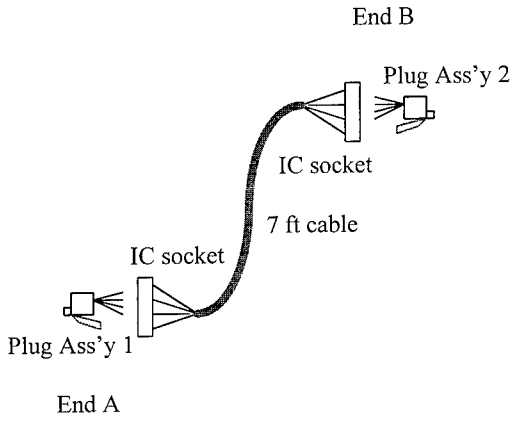


Figure 11: The Constructed Patch Cord

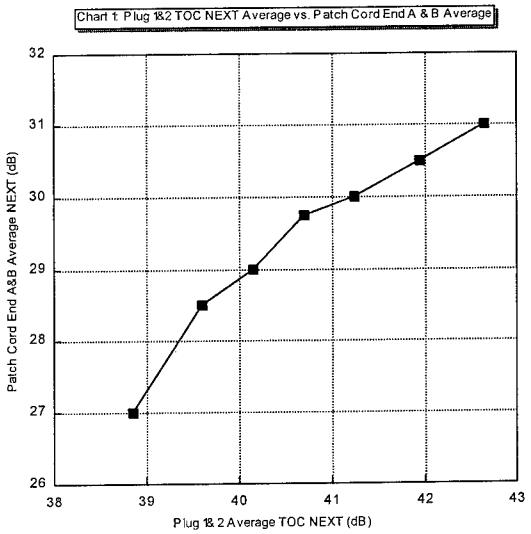


Figure 12: Patch Cord End vs. TOC average NEXT

6. Conclusions:

1. A non-destructive method for measuring NEXT of a patch cord independently from the test fixtures is proposed.

2. For a constructed patch cord, patch cord NEXT increased with increasing plug TOC values. A similar trend is expected with a pre-assembled patch cord.

3. A pass/fail limit can be selected based on the relationship between patch cord NEXT and TOC NEXT although no such selection is made in this paper.

References

[1] Electronic Industries Association/ Telecommunications Industries Association Commercial Building Telecommunications Wiring Standard

[2] International Electrotechnical Commission International Standard: Connectors for frequencies below 3 Mhz for use with printed boards - Part 7: Detail specification for connectors, 8-way, including fixed and free connectors with common mating features.

[3] Electronic Industries Association/ Telecommunications Industries Association Telecommunications Systems Bulletin: Additional Transmission Specifications for Unshielded Twisted-Pair Connecting Hardware



Amid Hashim
AT& T Bell Laboratories
67 Whippany Road
Room 1s-301
Whippany, NJ 07981-0903

Amid Hashim is currently a member of the Technical Staff at AT&T Bell Laboratories. During the past four years of his professional experience, he worked on telecommunications premise distribution systems. He received his B.S. degree in Electrical Engineering from the University of Illinois and his M.S. degree in Electrical Engineering from Case Western Reserve University.

REVIEW OF ACTIVITIES IN THE INTERNATIONAL STANDARDIZATION ORGANIZATION (ISO) REGARDING TOXIC HAZARDS IN FIRES

James C. Norris, Ph.D.
Toxicologist

Union Carbide Corporation
Bushy Run Research Center
Export, PA

Abstract

Reasons for the wire and cable industry to be concerned about toxic hazard development in the International Standardization Organization (ISO) are explained. Several examples are cited illustrating the scientific, public and political pressures surrounding this issue and the wire and cable industry. The documents developed by ISO Technical Committee 92 Subcommittee 3 are reviewed and the principles therein discussed. Future standards are also described.

Introduction

The wire and cable industry has many reasons to be concerned about the toxic hazards of the combustion gases from their products. This sensitivity is due not only to the hazards posed to humans and property, but also to the public and political pressures that have resulted in legislation affecting the industry. The latter reason has manifested itself in several different ways. Two of the most obvious in the US are legislation for the state of New York and New York City. These have their similarities and differences regarding what was enacted. Both require LC_{50} values generated by the University of Pittsburgh Toxicity Test Method. In New York State the toxic potency value must only be filed, and it can be part of a classification system to reduce the number of products tested. Wire insulation was among the products required by New York State to file LC_{50} values during the first year of implementation. New York City, however, has a pass/fail criterion for the LC_{50} values submitted. Transit systems have required the application of advanced products of non-halogen or zero halogen cables to reduce fire hazard. In fact, New York City became interested in the above mentioned legislation in part from transit fires involving cables.

This emphasis in cables is also present in Europe. The Channel Tunnel connecting the Britain and Europe had a safety theme requiring zero halogen low smoke cables [Nicholls and Roberts, 1992]. In another IWCS presentation [Barker and Ness, 1993], it was reported that the transit authorities reviewed and tightened cable specifications after the Kings Cross transit fire. Other applications have also been reviewed for changes in cable construction. For example, the UK Ministry of Defence (Navy) reviewed all cable specifications after the loss of the H.M.S. Sheffield in the Falklands conflict [Barker and Ness, 1993].

This presentation will focus on the activities of one International Standardization Organization subcommittee and it's efforts to understand toxic hazards and develop standards regarding toxic hazards of building products.

International Standardization Organization and Toxic Hazard

Within the International Standardization Organization (ISO), the responsibility of Technical Committee 92 (TC 92) are defined by its title "Fire Tests on Building Materials and Structures." Four subcommittees exist under the auspices of TC 92: Subcommittee 1 - Reaction to Fire; Subcommittee 2 - Fire Endurance; Subcommittee 3 - Toxic Hazards in Fire; and Subcommittee 4 - Fire Safety Engineering. Subcommittee 3 will be the subject of this presentation.

The Working Groups, convenors, and the US designated experts are listed below.

Working Group	Title	Convenor	US Designated Expert
1	Fire Model	Dr. Jim Norris	Dr. Gordon Hartzell
2	Analytical Methods	Mr. Peter Fardell	Dr. Art Grand
3	Biological Assay	Work Completed	
4	Guidance Document	Dr. Don Christian	Dr. John Punderson
5	Bio-Analytical Approaches	Dr. Gordon Hartzell	Dr. Barbara Levin

The first publication from this subcommittee was a series of six technical reports designed to described the state of the art for 1989. These technical reports are referred to as TR 9122 Parts 1-6 and entitled, "Toxicity Testing of Fire Effluents,". Each working group contributed one technical report pertaining to its particular area of responsibility. The sixth technical report was an overview. The titles of these technical reports are noted below.

Part	Title
1	General
2	Guidelines for Biological Assays to Determine the Acute Inhalation Toxicity of Fire Effluents (Basic Principles, Criteria and Methodology)
3	Methods for the Analysis of Gases and Vapours in Fire Effluents
4	The Fire Model (Furnaces and Combustion Apparatus Used in Small-Scale Testing)
5	Prediction of Toxic Effects of Fire Effluents
6	Guidance for Regulators and Specifiers on the Assessment of Toxic Hazard in Fires in Buildings and Transport

Part 1 - General

No consensus was reached as to a particular combustion toxicity test methodology. However, this part provides an overview of the topic.

The threat to life in fires is a consequence of toxic hazards associated with fire. The inability of fire victims to escape can be attributed to three major factors: (1) smoke or obscuration of vision, (2) heat, and (3) toxic factors such as narcosis and irritancy.

Trends in fire statistics

From 1955 to 1971 in the United Kingdom, the number of fatal and nonfatal casualties significantly increased for those overcome by toxic gas or smoke. Two hypotheses were proposed to explain this increase. First, the composition of fire products has changed so that the fire effluents are more toxic. Second, the rate of fire growth is much more rapid and thus the rate of evolution of products is much greater. However, additional mitigating factors could be that fire loads have increased in the typical residential housing and that the reporting of fire statistics may have changed.

Fire scenarios and victim incapacitation

In the United Kingdom and the United States fire statistics indicate that the majority of fire deaths occur in residential housing. However, a difference exists between the two countries in that a large percentage of the deaths in the United Kingdom occur in the near proximity of the fire's origin, whereas in the United States the deaths seem to occur outside the room of the fire's origin.

These deaths may arise from inhalation of combustion products generated from non-flaming and/or flaming conditions. Each fire would have different times for the non-flaming and flaming conditions yielding different combustion products. These differences would influence the time that the occupants have to escape before being incapacitated.

Classification of fires

Characterization of fire atmospheres is dependent on the type of material, temperature, and ventilation conditions. Factors that are necessary for defining fire atmospheres are carbon dioxide (CO_2), carbon monoxide (CO), and oxygen (O_2) concentrations. The concentrations of additional specific toxic gases, such as hydrogen cyanide and hydrogen chloride, and the types and concentrations of "unburnt" organic products should be measured. Other contributing factors to the hazard in fire atmospheres are rate of production of smoke, total amount of smoke produced, temperature of the fire effluent, and the radiation from the effluent.

The classification of fires are listed as being smoldering (self-sustained), nonflaming (oxidative) decomposition, nonflaming (pyrolytic) decomposition, fully developed flaming (low ventilation), and fully developing flaming (well ventilation). These are defined by some of the above mentioned parameters such as CO_2/CO ratios, O_2 concentrations, irradiance, and the temperatures. The table below correlates the fire parameters with the fire classifications or stages.

Fire Stage	Oxygen[1] (%)	CO_2/CO Ratio[2]	Temperature[1] (C)	Irradiance[3] (kW/m^2)
1 Decomposition				
a) Smoldering (self-sustained)	21	N/A	< 100	N/A
b) Non-flaming (oxidative)	5 to 21	N/A	< 500	< 25
c) Non-flaming (pyrolytic)	< 5	N/A	< 1000	N/A
2. Developing Fire (flaming)	10 to 15	100 to 200	400 to 600	20 to 40
3. Fully developed (flaming)				
a) Relatively low ventilation	1 to 5	< 10	600 to 900	40 to 70
b) Relatively high ventilation	5 to 10	< 100	600 to 1200	50 to 150
[1] General environmental condition (average) within compartment.				
[2] Mean value in fire plume near to fire.				
[3] Incident irradiance on to sample (average).				
N/A - not available				

Test Methods

Several combustion toxicity test methods or fire models are cursorily reviewed representing different countries, such as DIN 53 436 (Germany), FAA (USA), National Bureau of Standards Cup Furnace (USA), Radiant Furnace (USA), University of Pittsburgh (USA), Japanese Government Building Regulation (Japan), and University of San Francisco (USA).

Limitations exist for all of these fire models. The major limitation is the result of the complex nature of a fire making it impossible for a small-scale test method to simulate all of the fire stages. Other limitations would be the specimen size, real time monitoring of weight loss, and/or simulating vitiated combustion. However, each fire model should be able to generate at least one fire stage.

Analytical Methods as Alternative to Animal Testing

The role of small-scale testing is confirming the toxicity of the generated combustion products. Two mechanisms are used to accomplish this task, analytical techniques and animal exposure. The analytical methodology is sufficient for the known toxicants typically present in a fire atmosphere. However, if there are other toxicants present that are not included in the analytical procedures, then the animal exposures provide evidence of their existence. Chemical analysis alone cannot completely analyze the fire atmosphere. (However, in recent years some countries feel that sufficient information has been obtained

such that they are willing to rely only on chemical analysis. This may be due in part to the fact that a strong movement exists against the use of animals in testing.)

Mitigation of Toxic Hazard

Control of toxicity, rate of fire growth, and the generation of toxic species will greatly influence the ability to mitigate the toxic hazard for potential fire victims. Their escape times will depend on control methods such as smoke extraction and management, sprinklers and compartmentalization. Prime considerations for reducing the toxicity of the fire environment may be ignitability and overall flammability. Toxicity should not be confused with toxic hazard and information derived from a toxicity test (based on a simple fire model may be very limited in application to hazard.

Part 2 - Guidelines for Biological Assays to Determine the Acute Inhalation Toxicity of Fire Effluents (Basis Principle, Criteria, and Methodology)

Nature of Toxic Effects

Most toxicity evaluations are intended to predict the consequences of human exposure. Two categories for toxic effects have been defined as narcotic and irritants. Fire victims' blood have been found with compromising carboxyhemoglobin and hydrogen cyanide concentrations. Both these toxicants depress the central nervous system resulting to incapacitation leading to death. These effects are referred to as "narcotic." Another important category of fire gases is the "irritants," such as hydrogen chloride. The effects are coughing, choking, and eye irritancy (reduced visual acuity).

Relevance of Animal Data to Human

A major concern is the applicable of animal data to humans. Narcotic and irritant toxicants have the same mechanisms of action for inducing their toxicity effect in both animals and humans. The acute effects of many chemicals are the same in animals and humans. However, some physiological differences do exist, such as the ratio of respiratory minute volume to body weight is greater in animals than in humans. Another difference is the pattern of breathing air into the body. The rodent is an obligate nose breather as opposed to the humans who breathe through the nose or the mouth. During times of stress, heavy workload, or the presence of irritants, humans become totally mouth breathers, and this is an important difference in regard to water soluble toxicants such as hydrogen chloride. The rodent breathes those toxicants through the nose which acts as a scrubber to remove them from the air prior to reaching the lungs. Thus, the biological damage to the lung could be reduced or abated because of the toxicants' removal from the air prior to reaching the lungs.

A reasonable correlation does exists between animals and humans. Consequently, the justification for the comparison is acceptable for general toxicology as well as combustion toxicology.

Thermal Decomposition Methods and Exposure Methods

Two exposure methods, dynamic or static, are utilized by the existing fire models. For the dynamic exposure systems, the combustion products are generated and then passed by the animals and analytical measurement devices using a flow through system. For the static exposure system, the combustion products are generated in a defined volume of air and maintained in the chamber for animal exposure

and analytical measurements for the length of the exposure period. Several criteria for the fire model are repeatability and reproducibility should be established, heat stress and oxygen depletion should be avoided, and concentration-response or time-response relationships should be determinable. For the animals, two exposure techniques have been used, whole body and head-nose only. The head-nose mode is the predominant technique used in the fire models.

Observations

Animals should be observed during exposure, immediately after exposure and daily for at least a 14-day post-exposure period. Observations of the breathing behavior, motor activity, changes in the mucous membranes (such as tearing and salivation), and effects on the central nervous system (such as tremors and convulsions) should be recorded. Time of death and body weights for each animal should also be noted. A post mortem examination should be performed and should include an assessment of the major abdominal and thoracic organs. Organ weights should be collected for the lungs, liver and kidneys. Histopathological evaluations should be performed depending on the results of the animals' response.

Part 3 - Methods for the Analysis of Gases and Vapors in Fire Effluents

The purpose of this part is to provide analytical techniques for the analysis of gases present in fire effluents. It includes the analytical methods for 9 gases commonly found in fire effluents along with references. The gases are carbon monoxide, carbon dioxide, oxygen, hydrogen cyanide, hydrogen chloride, hydrogen bromide, hydrogen fluoride, oxides of nitrogen, and acrolein. As part of the discussion, sampling techniques, calibrations, interferences, limitations, and reproducibility are also examined. Several other gases of potential interest are briefly reviewed including, nitrogen, sulfur dioxide, carbonyl sulfide, ammonia, isocyanates, nitriles organophosphorous compounds, styrene, aldehydes, polynuclear hydrocarbons, antimony and arsenic compounds, total hydrocarbons, and solid particulates.

A new task for the Working Group # 2, the responsible working group for Part 3, is to write a document entitled, "Toxic Species In Blood," including carboxyhemoglobin and cyanide. This is one of the important biomarkers in fire victims for the cause of death. The author will be the chairperson of the task group to formulate the initial document for presentation to Working Group #2.

Part 4 - The Fire Model (Furnace and Combustion Apparatus Used in Small-Scale Testing)

Selection of a fire model

The fire model functions as a surrogate to a real fire, and no consensus has been obtained that one fire model is superior to any other. Its ability to serve in this capacity is arguable. But with the proper use of the fire model as defined by its accuracy and limitations, a knowledgeable user should be able to obtain useful data. Additionally, it must be understood that no fire model simulates all fire stages, and the toxic potency from a fire model is related to the conditions under which that fire model generates its fire effluents. The selection of the fire model must result from an understanding of the characteristics of the real fire to be simulated. Considerations should be given to the previously mentioned parameters, CO_2/CO ratio, temperature, heat flux, and

ventilation by comparing the conditions of the real fire to the capabilities and limitations of the fire models.

Fire models

Detailed information of the equipment and procedure are reviewed for the National Bureau of Standards Cup Furnace, the University of Pittsburgh Furnace, the DIN 53 436 Tube Furnace, the Radiant Furnace, the Cone Calorimeter, Japanese Building Research Institute Cone Furnace, Research Institute for Polymers and Textiles Cone Furnace and the Japanese Ministry of Construction Model. Two models are not recommended, the Ohio State University (OSU) Rate of Heat Release Apparatus and the NES 713. The OSU Rate of Heat Release Apparatus can be related to fire stages but is not able to accommodate animal exposures. Whereas, the NES 713 does not satisfy the relevant criteria and is not recommended by the UK national standards body.

Part 5 - Prediction of Toxic Effects of Fire Effluents

Bioanalytical methodologies applicable to a toxicological assessment of fire effluent atmospheres are reviewed. Available mathematical models are included in the review. Also, the minimization of animals through the application of the these models is considered. An additional objective is the ability to estimate the time to untenable conditions during a fire.

Two types of data are needed for these calculations. First, the exposure dose for the major toxic gases generated during fires or the mass loss of the combusted materials. Second, the exposure dose for each toxicant to produce incapacitation and/or lethality. Exposure dose is one of the basic concepts for these predictions and is the sum of the products of the fire gas concentrations multiplied by the times of exposure. Some values that have been employed are 900 $g \cdot m^{-3} \cdot min$ used by the US National Standards and Technology Hazard Model I and 500 $g \cdot m^{-3} \cdot min$ used by the British Standards Institution. Using these numbers avoids the use of individual toxic potency (LCt_{50}) values which are not always known.

Mass loss methodology is another approach for the predictions. It requires only the rate of mass loss of the materials in the fire and the LCt_{50} values of the materials burned. Differentiation of the mass losses and toxic potency values during non-flaming and flaming has to be made. The major advantage is their simplicity of application to either small or large fires.

Fractional effective dose (FED) models, based on the assumption of additivity between the individual fire gas toxicants, are introduced. This is the most powerful method for predicting rat lethality, particularly since the fire gas effluents concentrations change with time. Human incapacitation model is also introduced. The FED equations involved in this model are derived primarily from human and primate experimental data. It uses rodent sensory irritation and lethality data only for the assessment of irritancy. A certain degree of incapacitation from sensory irritation is produced from a mass loss concentration of 1.0 $g \cdot m^{-3}$; and serious post-exposure lung inflammation results from an accumulated exposure dose of 300 $g \cdot m^{-3} \cdot min$.

In conclusion, it is useful to combine the results of more than one model. The guidance of an expert professional skilled in the various techniques should be used in the selection and appropriate use of these predictive models.

Part 6 - Guidance for Regulators and Specifiers on the Assessment of Toxic Hazard in Fires in Buildings and Transport

It is recognized in many countries that life threat hazard from fires is a concern and, thus, several small-scale tests were developed for regulatory purposes. It is also recognized that these tests have limitations as listed below:

1. The rates of fire growth and toxic product generation are not provided.
2. The decomposition conditions used in these tests are reliable to actual fires.
3. Toxicity data based on only chemical analytical data can never be comprehensive in assessing toxicity.
4. The LC_{50} value is too simplistic for sublethal effects that may prevent escape from fire.
5. The end-use configuration of the materials or in conjunction with other materials cannot be utilized.
6. The environmental aspects of fires which may influence escape and overall hazard are not addressed.
7. Representing the effects on humans from animal data must be correlated with humans and disallowing any differences may introduce errors.

Life threat depends on more than just the toxic potency and should encompass the toxic hazard. For toxic hazard to be predictable, the time/concentration profiles of the important toxic products in the fire and the time/concentration/toxicity relationships of these products in humans have to be known.

For the regulator, toxic hazard has yet to be fully addressed. Voluntary codes of practice could provide the necessary regulations. However, in the absence of these voluntary codes of practice, the regulatory system chosen should have several features:

1. The case must be arguable and defensible.
2. The quantification and qualification of the identified hazards must have a scientific and valid basis.
3. The regulation must be expressed with precision and clarity.
4. Practical and relatively simple methods (i.e., rapid and inexpensive) for enforcement should be employed.

The regulator is dependent upon experts to identify problems for which regulation is necessary and to provide the most practical tests on which to base the implementation of the regulations.

With an understanding of these limitations and requirements, a procedure of logical steps to assess a particular fire scenario is described. This begins with defining the circumstances in terms of the type and number of occupants and activities, the provision for warnings and escape procedures, and the building contents and their location with reference to the local environment. Experience and historical data should be reviewed to identify loss patterns and life threats. Recommendation for a three-tier assessment, i.e. "likely to occur," "unlikely to occur," and "very unlikely to occur," is suggested. Also, selection of the different fire scenarios should be made and this will influence the toxic hazard analysis. The fire growth curves, the volume into which the composition products will be flowing, the yields of the different toxic products, and the

exposure dose and toxic potency values of the various toxicants must be defined. With these decisions having been delineated, the time to incapacitation and lethality can be calculated. However, an assessment will require the incorporation of the effects of heat exposure and visual obscuration by smoke.

International Standard 13344: Standard for the Determination of the Lethal Toxic Potency of Fire Effluents

This standard does not specify any particular fire model. However, a fire model can be employed that demonstrates relevance to one or more fire stages as identified in ISO TR 9122 "Toxicity Testing of Fire Effluents, Part 4: The Fire Model." Collection of only analytical data is an acceptable option to not using animals. It incorporates the concept of FED's for the determination of the toxicity potency values. An FED equation is also presented which includes an irritancy factor.

Conclusion

Much work over at least two decades has gone into the development of the principles described herein for ISO TR 9122 Parts 1-6 and the International Standard 13344. Work continues in the development of new standards, such as draft International Standard 13571 entitled, "Fire Hazard Analysis - Life Threat Components of Fire." This standard is to provide input data for fire safety engineering standards being developed in ISO Technical Committee 92 Subcommittee 4. Also, combustion toxicity is currently being considered in International Electrotechnical Commission TC 89 for which a standard is undergoing development.

References

Barker, J. R. and Ness, E. M. (1993). Low Fire Hazard Cable - The European Experience. International Wire and Cable Symposium Proceedings. p. 757-764.

Nicholls, A. W. and Roberts, D. G. (1992). Development of Low Smoke and Fume Cables and Joints for the Channel Tunnel. Transfil Europe. October. p.30-35.

ISO TR 9122 "Toxicity Testing of Fire Effluents, Part 1: General

ISO TR 9122 "Toxicity Testing of Fire Effluents, Part 2: Guidelines for Biological Assays to Determine the Acute Inhalation Toxicity of Fire Effluents (Basic Principles, Criteria and Methodology)

ISO TR 9122 "Toxicity Testing of Fire Effluents, Part 3: Methods for the Analysis of Gases and Vapours in Fire Effluents

ISO TR 9122 "Toxicity Testing of Fire Effluents, Part 4: The Fire Model (Furnaces and Combustion Apparatus Used in Small-Scale Testing)

ISO TR 9122 "Toxicity Testing of Fire Effluents, Part 5: Prediction of Toxic Effects of Fire Effluents

ISO TR 9122 "Toxicity Testing of Fire Effluents, Part 6: Guidance for Regulators and Specifiers on the Assessment of Toxic Hazard in Fires in Buildings and Transport

Acknowledgements

The author wishes to acknowledge the assistance of Dr. W. D. Claus in the preparation of this paper and to thank Union Carbide Corporation for permission to present this paper.

James C. Norris

Dr. Norris has bachelor's and master's degrees in chemistry and a doctorate in pharmacology and toxicology. He has been working in the area of combustion toxicology since graduate school. He was employed by the Weyerhaeuser Company as the toxicologist at its Fire Technology Laboratory. Later, he worked at Union Carbide Corporation's Bushy Run Research Center as a toxicologist in the inhalation department. He is active in the American Society of Testing and Materials as a subcommittee chairperson, in the National Fire Protection Association as a member on the Fire Test Committee and Life to Safety Fundamentals Committee, and in the International Standardization Organization as a designated expert and an acting convenor. Currently, he is employed by the Oak Ridge National Laboratory performing human health risk analysis.

CURRENT STATE OF FIRE CORROSIVITY TESTING: PRELIMINARY ELECTRICAL LEAKAGE CURRENT MEASUREMENTS

L. M. Caudill, DuPont, Wilmington, DE
J. T. Chapin, AT&T Bell Laboratories, Norcross, GA
R. B. Comizzoli, AT&T Bell Laboratories, Murray Hill, NJ
P. Gandhi, Underwriters Laboratories, Northbrook, IL
G. A. Peins, AT&T Bell Laboratories, Murray Hill, NJ
J. D. Sinclair, AT&T Bell Laboratories, Murray Hill, NJ

Abstract

In this paper, the various test methods currently available for evaluating the corrosivity of combustion products are reviewed, the limitations of the various classes of methods are discussed, and a new approach for smoke corrosivity testing is considered. The goal of combustion testing is to stimulate the development of materials with low flame spread, low smoke density, and low corrosivity of combustion products. No single product known to the authors can stand with the best in all three categories. A basic premise of this discussion is that criteria for flame spread and smoke density should be met before it is even appropriate to undertake a corrosivity test. Products should only be considered satisfactory if they meet all minimum performance criteria at each phase of testing. Arguments supporting this premise and a suggested test methodology are presented following the review and critique of corrosivity test methods.

Introduction

Development of test methods for evaluating the corrosivity of combustion products is a topic of vigorous discussion standards organizations world wide[1-6]. These initiatives are driven by the cost to telecommunications service providers and insurance companies of fires at large telecommunications facilities. The outcome of the standards development process could have a substantial economic effect on many players in this industry. It is essential that the standards coming out of these discussions be based on appropriate technical data and sound judgment.

A key issue with respect to evaluation of smoke corrosivity is the design of facilities and test substrates for evaluating smoke corrosivity. The common practice today is to measure the acidity of the corrosive gases (pH, conductivity) or to expose metal coupons, typically copper, to the combustion products that are collected in or pass through a standardized chamber. Metal loss is monitored through resistivity changes or weight loss. The degree of metal thickness reduction is a gauge of whether equipment or structural materials can be restored or are damaged beyond repair. Based on the authors' experience[7-12], this method does not get at the key telecommunications equipment reliability issues following a fire. The greatest threats to service restoration for such electronic equipment are electrical leakage, arcing, and electrolytic corrosion caused by the deposition of hygroscopic, ionic contaminants on insulating surfaces. Following a discussion of existing/draft methods for corrosivity testing, an alternative test methodology that has been used by AT&T for many years for evaluating these failure mechanisms is suggested[9]. This method accounts for all of the components of smoke that may bear on equipment reliability, not just corrosive gases.

Existing/Draft Methods For Corrosivity Testing

Throughout the world there are a number of test methods to assess the corrosivity of smoke from the combustion of plastics and cables. These methods are frequently cited in cabling specification documents. A list of smoke corrosivity methods is found in Table 1.

Table 1. Smoke Corrosivity Test Methods[13]

Method	Standard	Measure	Country
1. Halogen Gas	IEC 754-1	pH	International
2. Halogen Gas	BS 602 Part 1	pH	UK
3. Acid Gas	JCS C No. 53/397	pH	Japan
4. Acid Gas	CSA 22-2 No. 0.3M	pH	Canada
5. Halogen Gas	SAA AS 1660.5.3	pH	Australia
6. Acid Gas/Conductivity	IEC 754-2	pH/cond.	International
7. Acid Gas/Conductivity	BS 602 Part 2	pH/cond.	UK
8. Acid Gas/Conductivity	DIN 57472 Part 813	pH/cond.	Germany
9. Static Corrosivity	ISO 11907-2	metal loss	International
10. Dynamic Corrosivity	ISO 11907-3 draft	metal loss	International
11. Cone Corrosimeter	ASTM D5485	metal loss	US
12. Radiant Apparatus	ASTM E5.21 draft	metal loss	US

There are two major types of corrosivity test methods; those based on acid gas generation and those based on metal loss. The acid gas methods are an indirect measure of one characteristic of smoke corrosivity - acidic components (gas and solid), while the metal loss methods measure only one degradation mechanism associated with corrosive smoke: metal loss associated with corrosion. Prevoiusly, in the development of the ASTM standards (Methods 11 and 12 in Table 1), consideration was given to electrical leakage and contact resistance. However, the methods did not include these phenomena as there was insufficient information on their measurement techniques.

There are several variables in the methods found in Table 1 that can influence smoke corrosivity; they are: a) combustion conditions, b) air flow conditions, and c) design of the test target exposure chamber. The combustion conditions are listed in Table 2; the chamber and combustion atmosphere conditions are listed in Table 3.

Table 2. Combustion Conditions for Smoke Corrosivity Methods

Method	Condition
1. **Stationary Heat Sources**:	
A. Isothermal:	
* SAA AS 1660.5.3	800°C for 10 minutes
* IEC 754-2	935°C for 30 minutes
* ASTM D5485	Various heat fluxes, typically 50 kW/m^2 with 70% combustible mass loss of sample
* ASTM E5.21.70 draft	Various heat fluxes, typically 50 kW/m^2 for 15 minutes
* ISO 11907-2	800°C for 2.5 minutes
B. Ramped:	
* IEC 754-1	23-800°C for 40 min. ramp/20 min. isothermal
2. **Traveling Heat Sources:**	
* ISO 11907-3 draft	600°C for 20 minutes
* CSA C22.2	800°C for six, 5 min. steps, 10 min. isothermal

Table 3. Test Apparatus Chamber and Atmosphere Conditions

Method	Chamber	Atmosphere
1. Static		
* ISO 11907-2	20 liter at 50°C	Air at 40-60% RH
* ASTM E5.21.70	200 liter	Air at 60% RH
2. Dynamic		
* ASTM D5485	11 liter	Air at 50% RH

The heating conditions and combustion atmosphere of the test methods determine the nature of the smoke generated from the test material. Two questions can then be posed: 1) do any of the heating conditions represented by the test methods resemble an actual fire, and 2) will the determination of "corrosivity" by any of the methods accurately predict the performance of electronic equipment exposed to smoke from the combustion of the telecommunications cables?

AT&T Experience With Fire Related Equipment Failures

From the authors experience with damage associated with fires in telecommunications equipment[7-12], metal loss associated with smoke generation and deposition is not the most important damage mechanism. Acid gases are important, but ionic contaminants associated with fillers, flame retardants, colorants, processing aids and/or impurities in the polymers, or by-products of the polymerization reactions, can also be important. The most common cause of equipment malfunction following exposure to smoke is not loss in thickness of metals or metal circuitry from direct deposition of corrosive gases but rather electrical shorts and arcing that cause cross-talk and malfunctioning components[9]. The low insulation resistance associated with smoke-related contamination leads to metal migration (dendrites), electrolytically corroded conductor lines (quite distinct from the direct corrosion caused by deposition of corrosive smoke on conductors), and other electrochemical degradation processes[7,8]. The full array of contaminants from the smoke includes the halide gases, but also includes other ionic contaminants, organic gases, and, in some cases, graphitic carbon. High humidity exacerbates the effects of ionic contaminants[7,8]. Graphitic carbon is conductive at all humidity levels. While specific data on the effects of smoke on equipment performance are proprietary, data showing the effects of these kinds of contaminants on electrical leakage are shown in Figure 1[11]. The Figure shows that ionic contamination from several different sources produces electrical leakage on an AT&T standard interdigitated test pattern that exhibits a pronounced exponential dependence on humidity. It is this exponential dependence that necessitates tight control of humidity if the functionality of smoke damaged equipment is to be restored. One curve in the Figure, for soot deposited on equipment exposed to the oil fires following the Gulf War, shows that graphitic carbon can also cause failures. In this case, even short term restoration of service requires cleaning the equipment.

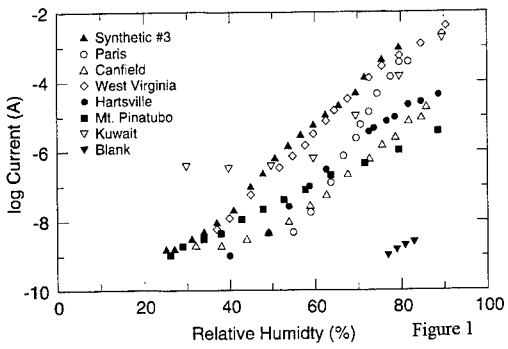
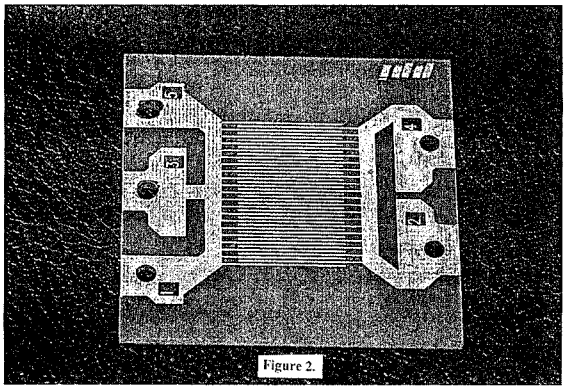


Figure 1

Smoke can travel hundreds of feet before some of the components deposit on equipment surfaces. During this aging process, the smoke composition and particle size distribution change dramatically. Combustion gases react with each other to form new gases or particles, react with components of existing particles, or condense adding to liquid aerosol mass. At the same time particles coalesce to form larger particles with changing hydrodynamic properties. Deposition to surfaces is driven by a combination of convective diffusion and inertial impaction, as well as thermophoretic, gravitational, and electrostatic forces. As smoke moves through a building it continues to cool leading to further condensation. In view of this complexity, it seems unlikely that collection on a single test substrate at one point in the combustion process will give a representative view of the potential for equipment damage from a cable fire. Clearly, sampling needs to be undertaken at multiple sampling points that simulate the range of aging characteristics of smoke in a fire situation.

New Smoke Corrosivity Investigations

Considering the data shown in Figure 1 and our experience with smoke damaged electronic equipment, a more appropriate test of smoke corrosivity is to expose interdigitated test structures to the smoke and measure leakage current as a function of humidity. Measured current/humidity curves are then compared to threshold curves for various damage levels. The threshold levels depend on the geometry of the circuitry on the test substrate. A test pattern in common use that fits the minimum requirements for corrosivity testing is the AT&T test pattern which is illustrated in Figure 2[14]. An alternative is the ASTM IPC B25 pattern, which has also been adopted by Bellcore for some of its electrical leakage test specifications[15]. A new pattern could also be developed that would enable leakage current and metal resistivity to be measured simultaneously. Whatever test substrate is used, it is important that the experiment be designed so the precision of the data can be assessed and confidence limits can be specified in comparing different materials and different test positions within the same test. This can be accomplished by using multiple test patterns on the same substrate or multiple test substrates at equivalent sampling points.


Figure 2.

Perhaps the most difficult issue to resolve in evaluating smoke corrosivity is how much material should be combusted during the exposure of test substrates. Some polymeric materials with high flame spread (e.g., non-flame retarded polyolefins) may show low corrosivity in a standard test chamber and the amount of corrosive material produced per unit mass of polymer may be less than that found for low flame spread materials (e.g., flame retardant polyolefins). None of the current or proposed small scale corrosivity methods allow for flame spread. In many of the methods listed in Table 1, the limited amount of material in the test apparatus is completely combusted in a relatively short time of a much longer exposure period (combustion conditions found in Table 2). In an actual fire situation, high flame spread material would likely take

much longer to exhaust. Thus the effective exposure time in the small scale test apparatus may be low. Other materials with low flame spread may be consumed to only a small amount no matter how large the starting mass. It may be inappropriate to use some of the existing small scale tests as a source of smoke for a corrosivity test. For an accurate comparison a sufficient mass of material should be used to ensure that some remains uncombusted at the end of the test. In this way, the effective exposure periods would be equal. However, for materials with high flame spread, such a test is probably not practical.

Experimental Details

The tests were conducted using a combustion tube furnace (modifying the IEC 754-2 test protocol), and the Cone Corrosimeter (modifying the ASTM D5485 test protocol). The test apparatus, samples, corrosion targets, and test procedure are described below.

Combustion Tube Furnace

The combustion tube furnace consists of furnace, silica tube, combustion boat, air supply system, and a mixing chamber for the combustion products. The tube furnace has an inside diameter of 60.3 mm and a heating zone of 300 mm. The test temperature was controlled by an electronic temperature controller. The silica tube is 1600 mm long, 47.5 mm inside diameter and a wall thickness of 2.75 mm. The silica tube is placed in the tube furnace such that it extends 400 mm from the rear end of the furnace. The rear end of the silica tube is ground and was fitted with a glass adapter connected to an air supply from a dry compressed air cylinder. A porcelain combustion boat, 97 mm in length, is used to hold the test sample during the test.

The mixing chamber is made from polymethyl methacrylate (PMMA), with dimensions of 310 x 310 x 340 mm. A stainless steel plate is attached to the inner side of part of the chamber connected to the silica tube. The purpose of the plate is to protect the PMMA surface from flames emanating from the silica tube. The top of the mixing chamber serves as a blowout panel to release excessive pressure. The chamber has a 6.3 mm opening at the bottom of one of the sides to permit exhaust of combustion products to a smoke abatement system. The mixing chamber is placed 385 mm away from the end of the tube furnace, such that 55 mm of the silica tube protrudes inside the chamber.

A schematic of the test apparatus is shown in Figure 3.

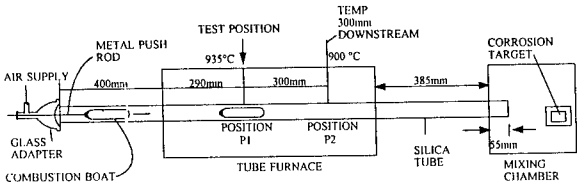
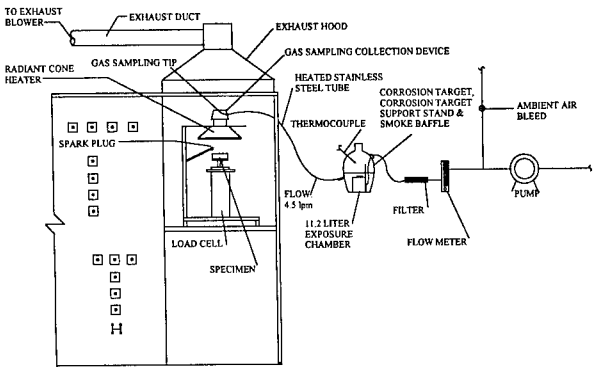


Figure 3
SCHEMATIC OF MODIFIED IEC 754-2 TEST APPARATUS

Cone Corrosimeter

The cone corrosimeter consists of a load cell, a radiant cone shaped electric heater, an electric spark to ignite the thermal decomposition products, an exhaust system, and a gas sampling system to transport a portion of the combustion products to a chamber. The details of the apparatus are provided in ASTM D5485[9]. A schematic of the apparatus is shown in Figure 4.



CONE CORROSIMETER Figure 4

Test Samples

Test samples were obtained commercially. Six were used in this investigation. In the combustion tube furnace experiments the IEC 754-2 test specifies a sample weight of 1,000 ± 5 mg. The ASTM D5485 Cone Corrosimeter method calls for sample plaques dimensions to be 100 mm x 100 mm x 6 mm thick. The samples are described in Table 2.

Table 2 - Smoke Corrosivity Test Samples

Sample Identification	General Composition
A	Halogenated, flame retardant polyolefin
B	Commercial PVC formulation
C	Nonhalogenated, flame retardant polyolefin
D	Nonflame retardant polyolefin
E	Halogenated, highly flame retarded polyolefin
F	Commercial fluorinated polymer
G	Nonhalogenated, flame retarded polyolefin

The samples were conditioned for at least 16 hours at a temperature of 23 ± 2 °C, and relative humidity of 50 ± 5 %.

Corrosion Target

The corrosion target consists of an interdigitated circuit with a spacing between the digits of 12.5 mm. A schematic of the circuit is shown in Figure 2. Prior to testing, the target was cleaned in an ultrasonic bath with 75% isopropyl alcohol, followed by rinsing in de-ionized water for 30 seconds, and drying with compressed nitrogen.

The surface resistance can be calculated approximately as:

$$R(\text{surface}) = 2000\ V/I\ \text{Ohms/square}$$

where V = applied voltage in volts and I = measured current in amps. The samples were placed in the controlled RH chamber. A voltage of 5, 50 or 200V was applied. For each voltage, the RH was increased from 30 to 90% and currents were recorded at RH intervals of 5%. Four samples were run as a group.

Test Procedure - Combustion Tube Furnace

For each test, the following test procedure was used. Test temperatures of 935 °C at test position "P1" and 900 °C at position "P2" were established in the tube furnace. One corrosion target was placed at the bottom and at one of the ends of the mixing chamber as shown in Figure 3. The test samples were weighed to an accuracy of 1 mg and evenly distributed on the bottom of the combustion boat. The test samples with the combustion boat were also weighed. The combustion boat with the test sample were placed inside the rear end

of the tube prior to test initiation. The end was closed with the adapter, and an air flow rate of 0.45 liters per minute was established through the silica tube. The combustion boat was then moved, using a push rod, to the test position "P1", as shown in Figure 3. The combustion products were allowed to react with the corrosion target for 1 hour. At the end of one hour, the target was removed and leakage current characteristics were determined. The combustion boat with residue was weighed and the sample weight loss was determined. One test was performed for each test sample.

Test Procedure - Cone Corrosimeter

The procedure used was in accordance with the method described in ASTM D5485. The radiant cone heater was set to provide a heat flux of 75 kW/m^2. The test was conducted in two phases. In the first phase, the weight loss characteristics of the test sample were first determined by conducting two tests without the gas sampling system activated. The weight loss data was used to calculate the 70% of the combustible mass. In the second phase, the test was conducted with the gas sampling system activated and corrosion target positioned in the exposure chamber. The gas sampling was continued until the test sample had lost 70% of its combustible mass as determined by the previous tests. The exposure chamber was then sealed until one hour had elapsed from the beginning of the test. Subsequently, the target was then removed from the chamber and the leakage characteristics were measured. One corrosion test (with gas sampling activated) was performed for each test sample.

RESULTS AND DISCUSSION

Weight Loss Measurements

The sample weight loss results for the tube furnace and the cone calorimeter are presented in Table 5.

Table 5 - Tube Furnace and Cone Corrosimeter Weight Loss Data

Sample Identification	Tube Furnace	Cone Corrosimeter
	% Weight Loss	% Total Weight Loss
A	98	68
B	94	62
C	55	42
D	99	47
E	98	62
F	99	89

Leakage Current Data

The leakage current data for the tube furnace at 5, 50 and 200 volts are found in Figures 5, 6 and 7. The leakage current data for the cone corrosimeter at 5, 50 and 200 volts are found in Figures 8, 9, and 10.

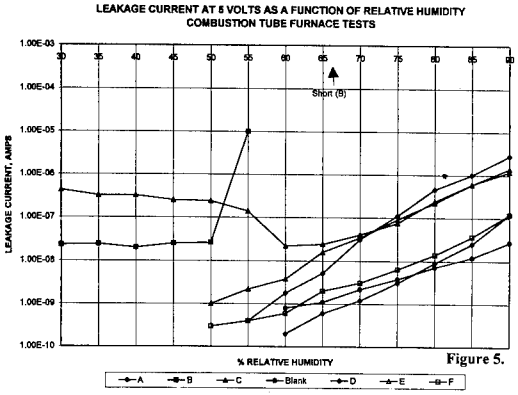


Figure 5.

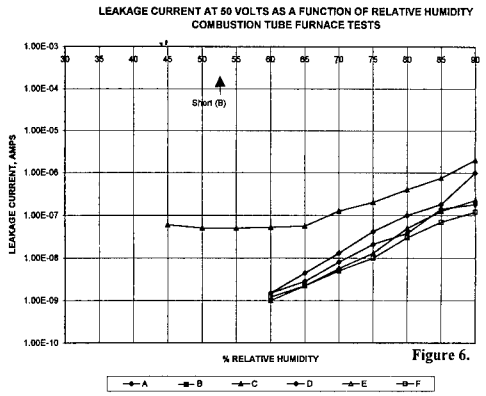


Figure 6.

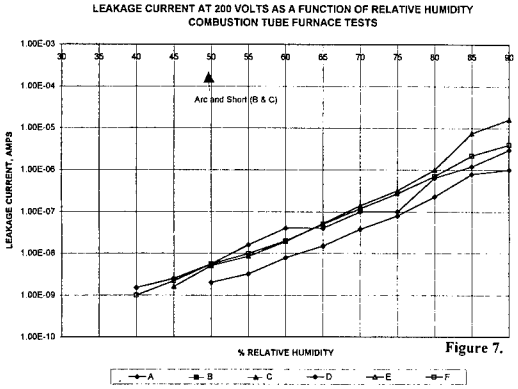


Figure 7.

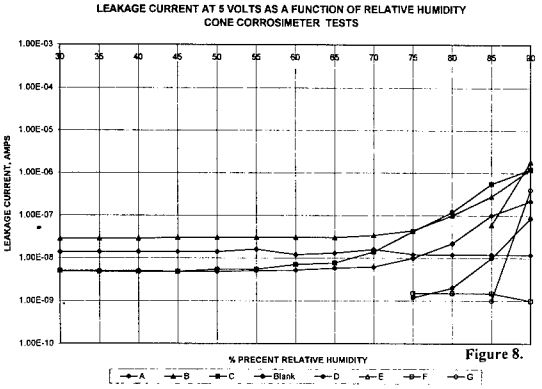


Figure 8.

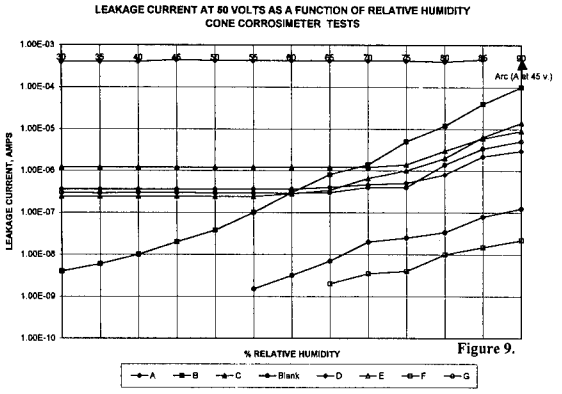


Figure 9.

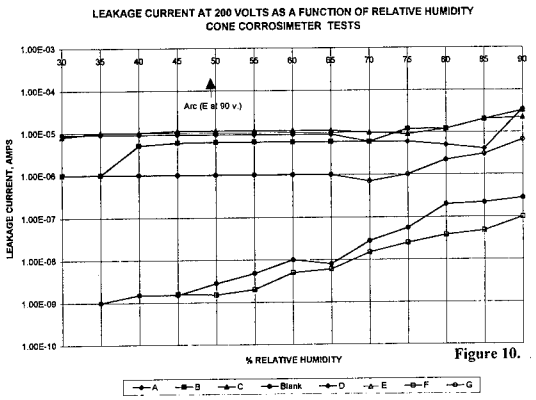


Figure 10.

The leakage current measured on a test pattern will depend not only on the type and quantity of deposited species, but also on the RH, temperature, applied voltage, and the history of the sample including the duration of the RH exposure and voltage application. In light of these factors, the present experiment is a first step demonstration of RH-dependent surface currents after deposition of combusted polymer formulations. Until the effects of RH, time, and voltage are more clearly resolved by the data, a detailed comparison of the polymer formulations may be premature. However, some general observations can be made.

Below about 50% RH, the currents in Figures 5, 6 and 7 are measurable but small, except for Samples B and C. Sample B has significant leakage current, even at 30% RH. At 55% RH Sample B shorted out. Inspection revealed little corrosion, no "growths" of corrosion product, and an apparent smoke "dendrite" bridging two lines. Sample C exhibited unusually large currents at low RH. The current decreased as the RH increased, which is most likely a time effect rather than an RH effect. The current is decaying with time, rather than decreasing because the RH is higher. The current decay is probably related to polarization effects or to formation of corrosion product.

A comparison of current levels at high RH for the three voltages (for the tube furnace and the cone data) shows that only Sample F has a consistently low current, (for data in Figures 5, 6, 8, 9 and 10) indicating it is the most benign, at least for these test conditions. Sample B has a consistently large current, suggesting it may have the most serious smoke effects.

Some of the data shows an approximate exponential dependence of current on RH above about 50% RH. This behavior is typical for surface currents on a wide variety of insulators[12]. In other cases, for example samples A and C at 50V for the Cone Corrosimeter (Figure 9), the current is constant over a wide range of RH. This is attributed to the formation of conducting regions between the metal lines. These regions are conducting independent of RH. In some cases microscopic examination revealed bridging structures of presumably conducting smoke. In other cases, charred regions of circuit board material or conducting corrosion product bridges were observed.

Conducting bridges of corrosion product or of smoke particles can usually be disrupted by the passage of sufficient current. Following the disruption, the resistance of the sample increases and lower currents are measured even at higher voltages. The testing sequence at different voltages is clearly an important variable. For example, Sample A had a larger current at 5V than at 50V for the tube furnace exposure (Figures 5 and 6).

Future Work

This study provides information for understanding the smoke corrosivity behavior of cable jacket and insulation materials. We are anticipating continuing this investigation to refine the test protocol and correlate to large scale testing. Some areas of future work include: 1) comparison of data to metal loss behavior, 2) comparison of data to pH and conductivity data, 3) expanded materials list for testing, 4) conduct SEM/EDAX analysis of test patterns, 5) analysis of smoke particulate, 6) small and large scale product testing.

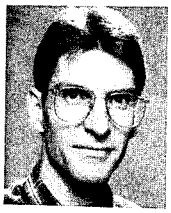
References

1. Briggs, Peter J., "Smoke Generation - Developments in International Test Methods and Use of Data for Selection of Materials and Products", *Fire Safety Journal*, V20, 1993, pp. 341-351.
2. Fazzari, A.M. Stratta, J. J., and Panzer, L.M. "Plastic Building Products with Reduced Combustion Emissions", *Technical Proceedings 43rd Annual Conference, Composites Institute*, 1988, pp. 8A.1-8A.4.
3. Cider, L, "Cleaning and Reliability of Smoke Contaminated Electronics", *Fire Technology*, Third Quarter 1993, pp. 226-245.
4. IEC Technical Committee 89, Working Group 8 is responsible for the development of international standards pertaining to smoke corrosivity and safety issues.
5. Bottin, M.F., "Acidity and Corrosivity Measurements of Fire Effluent", *International Wire and Cable Symposium Proceedings*, 1990, pp. 205-213.
6. Rogers, C.E., Bennett Jr., J.G. and Kessel, S.L., "Corrosivity Test Methods for Polymeric Materials, Part 5. A Comparison of Four Test Methods", *Journal of Fire Sciences*, Vol. 12, No. 2, March/April 1994, pp. 196-233.
7. Sinclair, J.D., "Corrosion of Electronics", *Journal of the Electrochemical Society* March 1988, pp. 89C-95C.
8. Comizzoli, R.B., Frankenthal, R.P., Milner, P.C. and Sinclair, J.D., "Corrosion of Electronic Materials and Devices", *Science* Vol. 234, 1986, pp. 340-345.
9. Frankenthal, R.P., Siconolfi, D.J., and Sinclair, J.D., "Accelerated Life Testing of Electronic Devices by Atmospheric Particles: Why and How", *Journal of the Electrochemical Society*, Vol. 140, N0. 11, November 1993, pp. 3129-3134.
10. ASTM D5485 - Fire Test Response Standard For Determining The Corrosive Effect Of Combustion Products From Electrical Insulations Or Coverings Using The Cone Corrosimeter ASTM, 1916 Race Road, Philadelphia, PA.
11. Comizzoli, R.B., Frankenthal, R.P., Lobnig, R.E., Peins, G.A., Psota-Kelty, L.A., Siconolfi, D.J., and Sinclair, J.D., "Corrosion of Electronic Materials and Devices by Submicron Atmospheric Particles", *Interface*, Fall 1993.
12. Comizzoli, R.B., "Materials Developments in Microelectronic Packaging Conference Proceedings", Montreal, August 1991, ASM International, pp. 311-316.
13. A list of acronyms used in this paper are found in Attachment 1.
14. This test pattern can be obtained from Precision Prototypes, Inc., Garfield, NJ.
15. This test pattern can be obtained from Electronic Controls Design, Inc., Mulino, OR.

Attachment 1.

Acronym List

ASTM - American Society of Testing and Materials
BS - British Standard
CSA - Canadian Standards Association
DIN - Deutsches Insititut fur Normung
IEC - International Electrotechnical Commission
IPC - (comb pattern)
ISO - International Standards Organization
JCS - Japanese Cable Standard
NIBS - National Institute of Building Sciences
SAA - Standards Association of Australia
UK - United Kingdom



J. Thomas Chapin is a Member of Technical Staff in the Chemistry, Environment and Safety Group at AT&T Bell Laboratories in Norcross, Georgia. He is responsible for fire technology research and materials development for copper and fiber optic building cables. He joined AT&T Bell Laboratories in 1980 after working at the Upjohn Company for three years. He received his B.S. in Chemistry and Ph.D. in Polymer Science from the Institute of Materials Science at the University of Connecticut. Since 1980 he as worked in in the ares of outside plant materials failure phenomena, optical fiber coating development and fiber optic cable development. He has been awarded 11 patents and has 15 publications.

ZERO-HALOGEN FLAME RETARDANT INSULATION MATERIAL FOR LOW VOLTAGE WIRE

*Yasuhiro Kamei, *Yoshihiro Inuizawa
**Dai Hashimoto, **Shinichi Irie

*UBE Industries, LTD. Chiba. Japan.
**FURUKAWA ELECTRIC Co., LTD. Chiba. Japan.

ABSTRACT

A non-crosslinked, halogen-free and flame retardant insulation material has been developed for low voltage wires. This new material has satisfactory mechanical properties, heat and abrasion resistances, and flame retardancy comparable to poly vinyl chloride (PVC) insulation materials for low voltage wires.

This material is a thermoplastic compound that is environmentally friendly without causing pollution problems. Furthermore, the processability of this material is excellent and existing extrusion line for PVC insulation materials can be used as is.

The various properties of the new material also meet the application requirements of electrical equipment and communication cables.

INTRODUCTION

Until now PVC insulation materials have been widely used for wire insulation. Although PVC has better mechanical and flame retardancy characteristics, it is a difficult material to properly dispose of. (1)

On the other hand it is technically and economically difficult to recycle the low-voltage wires with a smaller diameter, in particular from automobiles and electrical equipment, simply by the mechanical separation of conductors and insulation materials.

Therefore these types of wires are disposed of presently by usually incineration or land-filled. However with incineration, hydrogen chloride gases are emitted into the atmosphere unless a suitable process of neutralization is installed. With land filling, there is a release of heavy metal stabilizers.(2,3)

In this situation, flame retardant, halogen-free and pollution-free new materials for insulation have long been sought for. Unfortunately, zero-halogen type flame retarding insulation materials reported up until now have not been acceptable for thinner insulation wires with respect to mechanical strength, and heat and abrasion resistance properties.(4,5)

In this paper, we will describe the newly developed halogen-free insulation material with flame retardancy being applicable to high quality low voltage automotive wires. This material includes a non-combustible inorganic filler component as conventional zero-halogen type compounds do.

We have, however, attained a great improvement in the mechanical properties for the new material. Furthermore, we have achieved high speed processing at an existing extrusion line ,even when used the material has a large amount of an inorganic filler.

DEVELOPMENT

Conventional zero-halogen type flame retarding compounds (NHFRs) have polyethylene copolymers (EVA, EEA, and so on) as base polymers. This is because there is less deterioration of mechanical properties for the polyethylene copolymers with high contents of non-combustible inorganic fillers.

However the conventional NHFRs have limitations in mechanical strength and heat-resistance based on the intrinsic natural state of the base polymers. Crosslinking is one of the ways to overcome this limitation. However, crosslinking makes recycling unfavorable and results in higher cost.(6,7)

In this view we decided to develop a new non-crosslinked NHFR which has better mechanical and heat-resistant properties. At first, we screened various polymers and fillers and found a superior polymer alloy system including a well examined inorganic filler.

The newly developed NHFR was designated F-88 .

The low-voltage wires for automobile covered by F-88 (0.35mm insulation thickness) possess the same or better mechanical and heat-resistant properties as PVC insulation materials. In addition, the F-88 coated automotive wire exhibited a self extinguishing nature at a horizontal position in a flame test.

MECHANICAL PROPERTIES

Tables 1 and 2 show mechanical properties of F88, a PVC insulation material (PVC-IM), and a conventional NHFR.

The PVC-IM used in this study for a comparison purpose is one called AVSS a high intensity type among the automobile wire insulation materials. The conventional NHFR being commonly used in Japan comprises ethylene copolymers as base polymers.

The tensile strength of F88 are 20Mpa for a sheet specimen, and 25Mpa for a wire insulation specimen. These values are twice as high as those for the conventional NHFR. It can be said F-88 is one of the NHFRs which exhibits heat resistance against a high extension force. The excellent tensile strength and elongation shown in Tables 1 and 2 arise from superior mechanical properties of base polymers in addition to powder properties of the inorganic filler used.

The inorganic filler used for F-88 is magnesium hydroxide, which SEM picture and physical properties are shown in photograph 1 and table 3 respectively. It was found that the magnesium hydroxide used exists as hexagonal crystals without forming aggregates of secondary particles. Photograph 2 is the cross-section of an automotive wire with F-88 insulation. The planner crystals of magnesium hydroxide are dispersed homogeneously in the insulation matrix and line up to a machine direction.

It is considered that, by the homogeneous dispersion and orientation of the magnesium hydroxide having high aspect ratios, excellent mechanical properties are achieved in the wire insulation.

Table-1
Mechanical properties (sheet specimen)

properties	F-88	PVC-IM	conv.NHFR
tensile strength (MPa)	21	29	12
elongation (%)	650	320	650
hardness (shore D)	59	56	52

Table-2
Mechanical properties
(wire insulation specimen)

properties	F-88	PVC-IM
tensile strength (MPa)	25.7	25.8
elongation (%)	680	220

Table-3
Physical properties of filler

properties	typical values
crystallite size (μ m)	0.8
average secondary particle size (μ m)	0.8
specific surface area (BET),(m2/g)	5.5
temperature of commencing dehydration (℃)	340
amount of heat absorbed (cal/g)	312

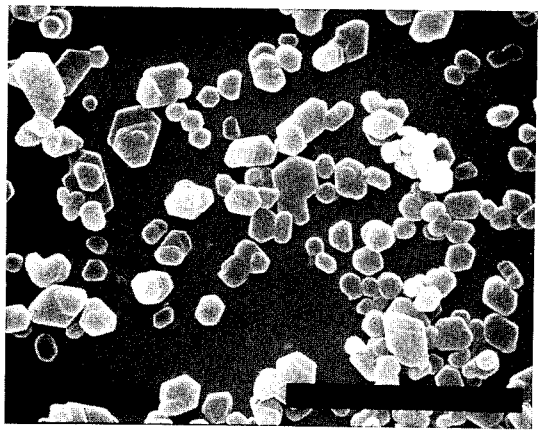


Photo-1
SEM picture of magnesium hydroxide 2 μ m

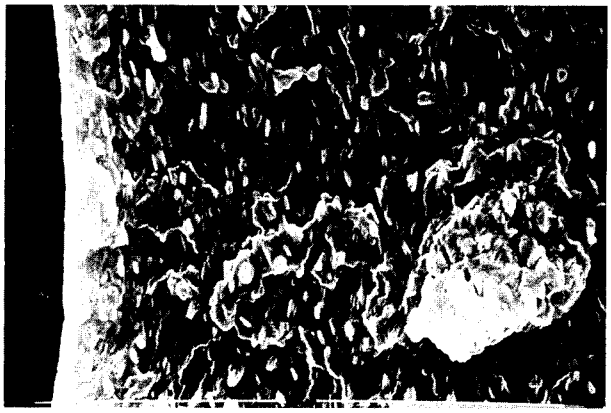


Photo-2
The cross-section of a automotive wire with F-88 insulation.

4 μ m

THERMAL AGING

Table 4 shows the tension test results of the insulation wires from F-88 and PVC-IM after various heat agings. F-88 maintained sufficient tensile strength and elongation after a heat aging at a high temperature (130℃) for 336 hours.

Photo-3 shows the result of a "pig tail test" for the F-88 insulated wire.Even after 1000 hours exposure of the F-88 insulated wire at 120℃, no cracks were observed on the surface and a better heat-resistant property was confirmed.

Table-4

Thermal aging
(wire insulation specimen)

Mechanical properties

test condition	F-88	PVC-IM
after 7days at 110℃		
tensile strength retention (%)	96	105
elongation retention (%)	90	100
after 7days at 130℃		
tensile strength retention (%)	94	124
elongation retention (%)	82	14
after 14days at 130℃		
tensile strength retention (%)	93	---
elongation retention (%)	76	---

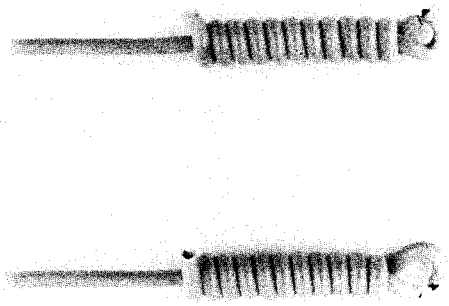


Photo-3
The result of "pig-tail " test for the F-88 insulated automotive wire.
(after 1000hours at120℃)

HIGH TEMPERATURE PERFORMANCE

The test results of high temperature deformation and vicat softening temperature are presented in table 5.

The deformation test consists of the measurement of the change of a sheet thickness before loading the pressure of 9.8N on it and after the loading for 30 minutes at 120 ℃. The size of the sheet is 15x30x2mm(t), and it is placed on an iron half cylinder of 10mm diameter and 35mm length.

F-88 can be applied to wires used at a high temperature due to its high vicat softening temperature and slight deformation at 120 ℃ as compared to the conventional NHFR.

Table-5
High temperature performance

properties	F-88	PVC-IM	conv.NHFR
heat deformation (%) penetration at 120℃	7.5	12	60<
vicat softening temp. (℃)	100	85	73

ELECTRICAL PROPERTIES

The electrical properties of F-88 and the PVC-IM are shown in table 6.

F-88 has a better volume resistivity and breakdown voltage than those of the PVC-IM. Dielectric constants and dissipation factors being important specifications required for communication cables are still higher compared to polyethylene. We consider that the dielectric constants and the dissipation factors of F-88 are possibly improved to ca. 2.8 (1Mhz),and ca. 0.001 (1Mhz) respectively.

Table-6
Electrical properties

properties	F-88	PVC-IM
dielectric constant (1MHz)	3	3.16
dissipation factor (1MHz)	0.004	0.057
volume resistivity (ohm cm $x10^{15}$)	18	0.3
breakdown voltage (kV/mm)	25	22

COMBUSTION PROPERTIES

The results of a flame test, a smoke test, and acid gas evolution for F-88 and the PVC-IM are shown in table 7.

Flame test ---- In the iron test box, the sides and the sectional area of which were provided, covers about 600mm(H)x 310mm(W)x 360(D), a wire specimen of about 360mm length was held horizontally.

A Bunsen burner with a 10mm diameter was used to conduct the test. The length of the oxidizing flame was adjusted to about 35mm. And the tip of the reducing flame was applied to center the specimen from the underside until it started to burn within 30seconds. Then, the self-extinguishing time was measured after removing the flame.

Both,F-88 and PVC-IM are self-extinguishing, and the oxygen indexes for both materials are nearly the same.

Smoke test ---- Smoke tests were performed in a NBS smoke chamber using 0.5mm thickness sheets.

The smoke density of F-88 is much lower than that of the PVC-IM in either a flaming or non-flaming mode.

Acid gas generation --- An acidity of gas generated in combustion was measured by the IEC-754-2 test.

The gas generated was introduced into distilled water for 30minutes and then the pH value of the water was recorded.

As a result, the generation of acid gas from F-88 is much less than the PVC-IM.

A cable using F-88 insulation will generate very little acid gas and black smoke in a fire. This will reduce the harm to a human body and the damage to electrical equipment to the minimum level.

Table-7
Combustion properties

properties	F-88	PVC-IM
oxygen index	26.5	26.5
flame test (horizontal burning)	S.E *1	S.E
smoke density (NBS chamber)		
Ds max. (flaming)	50	180
Ds max. (non-flaming)	108	200
acid gas generation (pH) IEC 754-2	5	2

*1) self extinguish

PROCESSABILITIES

Rheological property ---- The rheological properties of F-88, the PVC-IM, and the conventional NHFR are shown figure-1. Viscosity data were obtained against different shear rates at 200℃ using a capillary rheometer.

F-88 having the suitable combination base polymers and the non-combustible filler, exhibits a lower melt viscosity at each shear rate in comparison with that of the conventional NHFR. The processability of F-88 is quite satisfactory and is equivalent to the PVC-IM.

Extrusion property ---- The dimension of the extruded wire for automobile and the conditions of extruding are shown in table 8 and 9 respectively. The machine used for this test is used daily in the production of PVC insulated automotive wires. The test processing was performed at extrusion speeds of 300 m/min. and 500 m/min.

The surface of the insulated wire extruded at these high speeds was extremely smooth as seen in photograph 4.

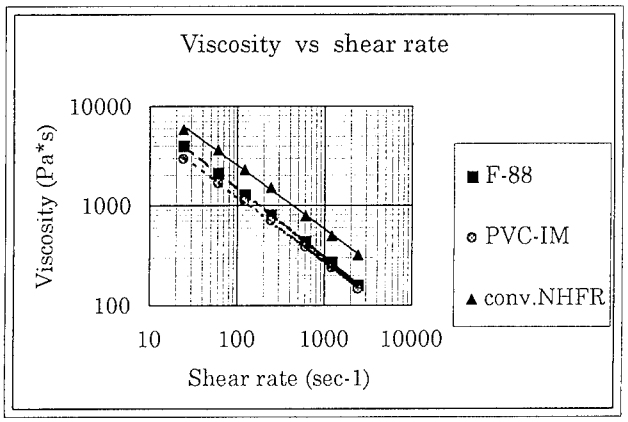


Figure-1
Viscosity data were obtained at 200 ℃ using a capillary rheometer.

Table-8
Dimension of F-88 insulated automotive wire

conductor		insulation	overall
no.stands/ mm size	outside diameter	thickness	diameter
7 / 0.32	0.96mm	0.35mm	1.66mm

Table-9
Extruder conditions

extruder type : single screw , ϕ =50mm, L/D=26

temperature profile

cylinder	zone 1:	170℃
cylinder	zone 2:	190℃
cylinder	zone 3:	200℃
head	:	220℃

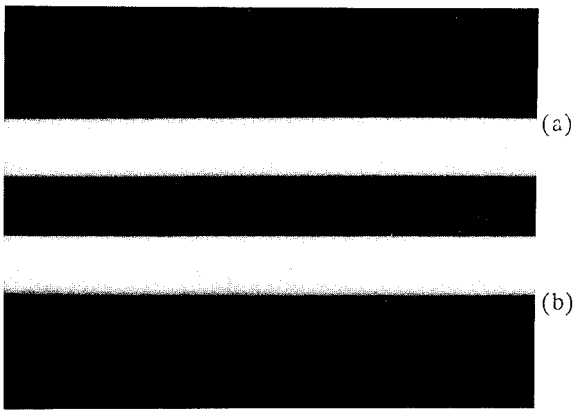


Photo-4
Surface appearance versus extrusion rate
(a) 300m/min. (b) 500m/min.

WIRE PROPERTIES

The property of the F-88 insulated automotive wire are summarized in table 10.

It is clear that the insulated wire using F-88 easily meets the requirements for automotive wire specifications.

Table-10
properties of F-88 insulated automotive wire

item	condition	performance required	result (F-88 insulated wire)
dielectric test	dip it in 5% NaCl solution for 5hours	withstands a voltage of 1KV for 1min.	pass
tensile strength of insulation	tensile speed: 50mm/min	15MPa or more	25.7MPa
elongation of insulation	tensile speed: 50mm/min	125% or more	680%
oil absorption test	dip it in oil mixed the equivalent amount of lubricating oil and kerosene for for 20 hours	after bending it across a 75mm diameter mandrel,withstands a voltage of 1KV for 1 minute	pass (with no crack)
hot bend test	heat it at 120℃ for 120 hours.	after bending it across a 115mm diameter mandrel,withstands a voltage of 1KV for 1 minute.	pass (with no crack)
cold bend test	cool it down at -40℃ for 3hours.	after bending it across a 75mm diameter mandrel,withstands a voltage of 1KV for 1 minute.	pass (with no crack)
flame test	holding it horizontally,apply flame to it	self extinguishes within 15 seconds.	pass
heat shrinkage	heat it at 150℃ for 15 minutes.	shrinkage rate should be 4% or less.	0.40%
abrasion test	blade method(ISO 6722 /1) tip end of blade : piano wire with a diameter of 0.25mm weight : 8.8N	abrasion resistance value should be equal to that of the pvc automotive wire.	equal

CONCLUSION

F-88 is an excellent insulation material which has better mechanical and heat-resistant properties when compared to conventional NHFR. In addition, it has the same processability as PVC insulation materials.

Therefore, currently used extrusion lines are available for F-88 without any special modification.

Since F-88 has no heavy metal and halogen, we are able to minimize the environmental influence when disposing it. Most importantly, loss of life and economical damages can be reduced greatly in case of a fire.

REFERENCE

(1)H.Nisikawa,et.al, Emission of organic compounds by combustion of waste plastics involving vinyl chloride polymer, Chemosper, vol. 25, pp. 1953-1960 (1992)

(2)M.M.Nir, J.Miltz, and A.Ram, Update on plastics and the environment , Plastics Engineering, March, pp. 75-93, (1993)

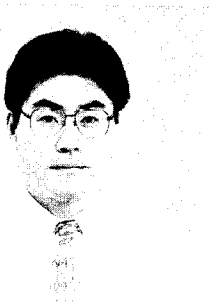
(3)F.Tamaddon, and W.Hogland, Review of cadmium in plastics waste in Sweden , Waste Management & Research, pp. 287-295, (1993)

(4)C.A.Glew, Halogen versus non-halogen materials for telecommunication wire & cable , Wire Technology International, vol. XXII, July, pp. 64-67, (1994)

(5)M.Taylor, P.Richardoson, J. Preston, and J.Taylor, Second generation thermoplastics, zero-halogen, low-smoke, fire-retardant, insulation compound , 39th IWCS, pp. 673-681, (1990)

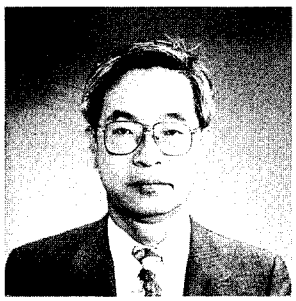
(6)J.Kosin, New non-halogenated flame retardants in ethylene-vinyl acetate , ANTEC, pp. 1404-1407, (1988)

(7)L.H.Gross, New low-voltage insulation systems , WIRE INDUSTRY, August, pp. 609-612, (1990)



Yasuhiro Kamei
UBE INDUSSTRIES, LTD.
8-1, Goi-Minamikaigan, Ichihara, Chiba ,290, JAPAN

Yasuhiro Kamei received the B.S degree in chemical engineering from Science University of Tokyo in 1985.
He joined The UBE Industries LTD. in 1985.
He is now a member of Chiba Technical Section Polyolefin Group of Research & Technical Dept.



Yoshihiro Inuizawa
UBE INDUSTRIES, LTD.
2-3-11, Higashi-Shinagawa, Shinagawa-ku, Tokyo, 140 Japan

Yoshihiro Inuizawa received the B.S degree in chemical engineering from Kyushu University in 1967.
He joined The UBE Industries LTD. in 1967.
He is now a leader of Super Polyethylene Marketing Group of Polyolefin & Synthetic Rubber Division.



Dai Hashimoto
FURUKAWA ELECTRIC Co.,LTD.
6, Yawata-Kaigandori, Ichihara, Chiba, 290 JAPAN

Dai Hashimoto received the B.S degree in chemical engineering from University of Tsukuba in 1989.
He joined The Furukawa Electric Co.,Ltd.in 1989 and he was developing fluoroplastics insulated electronic wire.
Since 1993, He has been developing a flame-retarding jacketed materials for electronic wire and optical fiber.



Shinichi Irie
FURUKAWA ELECTRIC Co.,LTD.
6, Yawata-Kaigandori, Ichihara, Chiba, 290 JAPAN

Shinichi Irie received master degree in chemical engineering from Waseda University in 1972.
He joined The Furukawa Electric Co.,Ltd.in 1972, and worked on the development of material for power cable, telecommunication cable and fiber optical cable.
From 1988 to 1991, he was staying in Atlanta, Georgia as a senior engineer of Furukawa America, and did market research of power cable and dicing tape for semiconductor.
He is currently manager in the Opto-Technology Laboratory of Furukawa Electric responsible for developing material for fiber optical cable and electro appliance wire.
Mr. Irie is a member of Chemical Society of Japan, and The Society of high polymer Science, Japan.

Impact of Reflective Components On The Noise Performance of DFB Laser Based AM Video Systems

*K.Y. Chen, Tien-Jey Sheu, Fwu-Yuan Tsai, *Y.W. Chen*
Chih-Yih Wang, and Wei-Shyan Chien ,Hsiu-Jung Chuang,

Telecommunication Laboratories *Chung-Yuang University**
D.G.T. MOTC,Taiwan, **R.O.C***China.*

Abstract:
This paper presents our study of the noise performance of AM-VSB systems, including CNR, CSO, and CTB, and discusses the influence of the optical reflectance of fiber components by varying the optical return loss of fiber connectors. The system performance was measured at five channel frequencies between 55.25 MHz to 445.25 MHz (channel 2 - channel 61) using two directly modulated DFB lasers operating at 1.3 um and 1.55 um.
The test results indicate that the AM system performance using the 1.55 um DFB laser is less sensitive to the change in the optical return loss of connectors. Therefore, the outside plant specification of optical reflectance for 1.55 um DFB based AM systems could be less restrictive than that for 1.3 um system to meet the same CNR requirement.

1.Introduction

AM-VSB CATV systems are being developed for deployment in Taiwan. Some CATV program providers intend to use telecommunications fiber cables in the subscriber loop to transmit the video signals.
Among many video transport systems investigated, the AM-VSB multichannel system is being considered for CATV programs in Taiwan. It is therefore important to consider if the existing outside plant can support such services. One of the considerations is the impact of the optical reflectance of passive components, including connectors and splices, on the noise performance of the AM systems.[1-5]
In a video system where multiple channels are transmitted, and nonlinerarity results in the production of distortion products. As the nonlinerarities can generally by represented as second- and third- order terms in an expansion, the distortion products are due to the beating of combinations of two and three channels, respectively. The sum of the distortion products, due to the beating of any two channels, is defined as composite second order (CSO) and the sum of those due three tones as composite triple beat (CTB).[7]

In this study, we investigated the AM-VSB system performance using DFB lasers operating at two different wavelengths. This study allows us to specify the return loss of optical components used in the subscriber loop for transmitting AM CATV signals.

2. Theoretical

It is reported [1]that every system has some theoretical calculate CNR which is a function of the double Rayleigh backscattering of the fiber. and the laser spectral width and the modulation depth. The equation of cavity CNR is expressed as[4]

$$CNR_{cav} = 10\log\left[\frac{\sqrt{2\pi}\,m^2}{16\sqrt{\ln 2}}\frac{B_{fwhm}}{B_n R_{eq}}e^{2f^2\frac{\ln 2}{B_{fwhm}^2}}\right] \qquad (1)$$

where B_{fwhm} is the full width of half maximum of the laser spectrum under modulation. **B**n is the noise bandwidth (4 MHz).and ***m*** is the modulation index of the laser .f is the measured frequency. **R**eq is the equivalent reflectance of fiber Rayleigh backscattering

$$R_{eq} = \frac{S\alpha_s}{4\alpha}R_i\left[\left(1-e^{-2\alpha l}\right)+\left(1-e^{-2\alpha l}\right)\right] \qquad (2)$$

where l is the fiber length. α is the total attenuation of the fiber α s is the fiber Rayleigh scattering coefficient = 0.076/km.S is the fraction of scattered light captured and guided by the fiber back to the source.The CNR of the system can then be given as:

$$CNR_{sys} = -10\log\left[10^{-\frac{CNR_{base}}{10}}+10^{-\frac{CNR_{cav}}{10}}\right] \qquad (3)$$

where **CNRsys** is the CNR of the system. **CNRbase** is the baseline CNR of the system.

The composite triple beats is computer simulation by expression

$$p = \sum_{\pm}\left\lfloor 6\sum_{q1=1}\sum_{q2=q1+1}\sum_{q3=q2+1}B(q1,\pm q2,\pm q3)+ 3\sum_{q1=1}\sum_{q2=q+1}\left[B(q1,\pm q2,\pm q2)+B(q2,\pm q1,\pm q1)\right]+\sum_{q=1}B(q,\pm q,\pm q)\right.$$

3.Experimental Results

3.1 Test Setup

Diagrams of the experimental setup to evaluate the noise and distortion characteristics of the AM system are shown in Fig.1. Two wavelength(1311 nm and 1555 nm) of commercially available CATV lightwave video transmitters were used.The 1311 nm laser transmitter has an optical power of 8.2 dBm with side mode suppresion ratio (SBSR)44.8 dBc and low relative-intensity-noise. The 1555 nm laser transmitter has an optical power of 8.3 dBm with side mode suppresion ratio (SBSR)50.2 dBc and low relative-intensity-noise. The source consisted of a DFB laser driven by a multi-channel CATV generate which is set up with 61 channels from 55.25 MHz to 445.25 MHz. Angle FC/APC connectors or fusion splices with an optical reflection less then -60 dB are applied for the measurement. The link consisted of a test optical connector with different reflection loss from -55 dB to -20dB. We also used a variable backreflector(VBR).The optical signal was sent through 4.4 km of conventional single-mode fiber (SMF),and was detected at an optical power level of 0 dBm at the receiver. RF signal generator is used Matrix SX-16. Distortion analyzer is Matrix R-75. The CNR,the composite second-order (CSO) distortion, and the composite triple-beat (CTB) distortion are measured under 61 channel modulation according to the NTSC frequency plan.[]

3.2 Test Result &Discussion

The measured CNR degraded after transmission through the SMF, which is caused by transmission effects such as double Rayleigh backscattering and chromatic dispersion from the fiber. Fig. 2 shows the measured CNR as a function of the optical connector reflection loss for both two different wavelength (1311 nm and 1555 nm) of DFB laser transmitters,measuing at 55.25 MHz (CH 2) with same modulation index 4 %,and the optical connector position is near the receiver end (Rx).The test results indicate that the 1550 nm wavelength DM-DFB laser transmitter performance has about higher CNR of 5 dB than the 1310 nm wavelength DM-DFB laser transmitter. The reason is that the fiber loss at the wavelength 1310 nm is higher than at the wavelength 1550 nm. The use of 1550 nm DFB lasers allows the CATV system designer to take advantage of the optical fiber's better sttenuation and CNR performance at 1550 nm.

Fig. 3 and 4 show the measured CSO and CTB distortions, which were corrected for the receiver noise,as a function of the optical reflection for the DM-DFB laser transmitter with different channel frequencies. This results can explained below, In a multichannel AM system, the number of CSO terms increase linearly as the number of channels (N) increases. Fig. (5) shows the CSO for a 60-channel system,where the terms fa-fb are clearly seen to be dominate at the lower end of the multichannel spectrum while, at the upper edge , it is the terms of the type fa+fb that dominate. Most cable systems use carrier frequencies which are offset 1.25 MHz from the harmonics of the 6 MHz channel spacing. Thus the fa+fb and fa-fb fall in a narrowband on either side of the carrier frequency. This results may explain Fig. (3) channel 2 near the left side which have higher number of terms means CSO value more lower compare with channel 20 and channel 29.because from Fig. (5)consider terms fa-fb, the number of terms channel 2 >channel 20>channel29.Channel 44 (343.25 Mhz) have less number of terms, show the lowest CSO figure in Fig.3 .

The number of terms and their type that make up the CTB are shown in Fig. (6). It is clear that the terms of the type fa+fb-fc contribute the most to the CTB ,since the terms fa+fb-fc fall on the carrier frequencies, while fa+fb+fc and fa-fb-fc fall 2.5 Mhz above and below the norminal carrier frequency positions,In this system with 40 channels ,the terms that contribute the most to the CTB are those of the form fa+fb-fc. The maximum value of the CTB occurs at the center of the channel group.This may explained the reason why in Fig. 4 with which channel 29 have more number of terms by computer simulated shown in Fig.6 measured the lowest figure of CTB. The measured position of optical connector near transmitter end (Tx) and Receiver end (Rx) are show in the Fig. 7(a) and 7(b). It shows that using 1550 nm laser transmitter locate both in Tx end or Rx end , the CSO are independent with optical reflection. But using 1310 nm laser transmitter the CSO may degrade about 14 dB. Since our laser is to use 1550 nm DFB's which incorporate an RF predistortion circuit.This adjustable circuit predistorts the analog signals, so that the CSO products are minimized at constant link length. Fig. 8 shows CTB as a function of connector reflection loss under 61 channel modulation. however, CTB is degraded by 1 dB after reflection loss is change from -50 dB to -30 dB.It shows that only 1550 nm laser located near the transmitter end may effect the CTB. The measured frequency range was 55.25 MHz to 445.25 MHz,and the fiber total length was 4.4 Km.

4.Conclusion

By varying the reflectance of the connectors, we compared the noise performance (CNR, CSO, etc.) of the AM system at 1310 nm and 1550 nm. We observed that the CNR is less affected by the reflectance at 1550 nm, indicating that the reflectance specification of connectors at 1550 nm could be less restrictive than that at 1310 nm.

This study allows us to specify the return loss of optical components used in the subscriber loop for transmitting AM CATV signals.

Acknowledgments

The author would like to thank Dr.Winston I. Way for his encouragement and with his fruitful teaching HFC Communication Syetems in NCTU.

Reference

[1] K.Y. Chen,T.J. Sheu,etc.“ The influence of reflective components in lightwave AM-VSB CATV systems performance”International Wire and Cable Synposium Proceedings 1994 Atlanta,p484-487.

[2]W.I. Way,C.L. Lin,etc.“Multiple-Reflection-Induced Intensity Noise Studies in a Lightwave System for Multichannel AM-VSB Television Signal Distribution”,IEEE Photonics Technology Letters 2, 360 (1990)

[3]S.Ovadia,L.Eskildsen,C. Lin,“BER degradation due to optical reflections in multichannel AM/16-QAM video lightwave transmission systems”,*Conference on Optical Fiber Communication*,1995 Technical Digest p.62

[4] Darcie, T.E.and G.E. Bodeep."Fiber reflection-Induced Impairments in Lightwave AM-VSB CATV Systems." *Journal of Lightwave Technology*.Vol.9,No.8,1991,pp 991-995

[5] Judy,A.f."Reflections and Fiber Video System."*Proceedings Southcon*/91.1991,pp 181-188.

[6] A.F.Judy,"Intensity noise from fiber Rayleigh backscatter and mechanical splices,"in ECOC'89,1989,PP 486-489.

[7] M.J. Labiche,"Noise due to reflective components in fiber optic AM-VSB CATV systems" NFOEC Conference Proceedings 1993 pp290- 299.

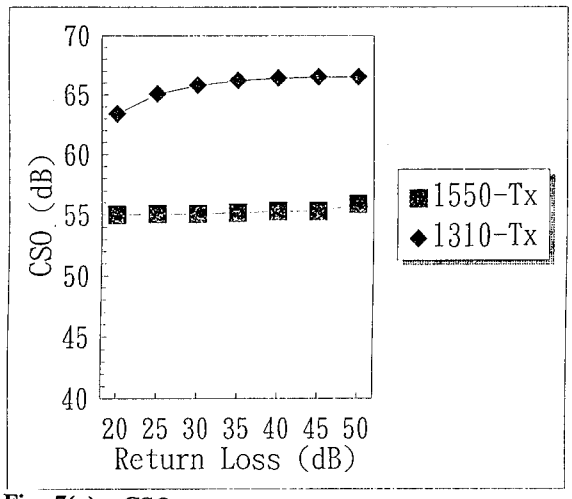


Fig. 7(a) CSO versus reflection levels for an 1310 nm transmitter and a 1550 nm DFB laser transmitter.The optical reflection position near transmitter end (Tx).the measuing frequency is at 55.25 MHz.

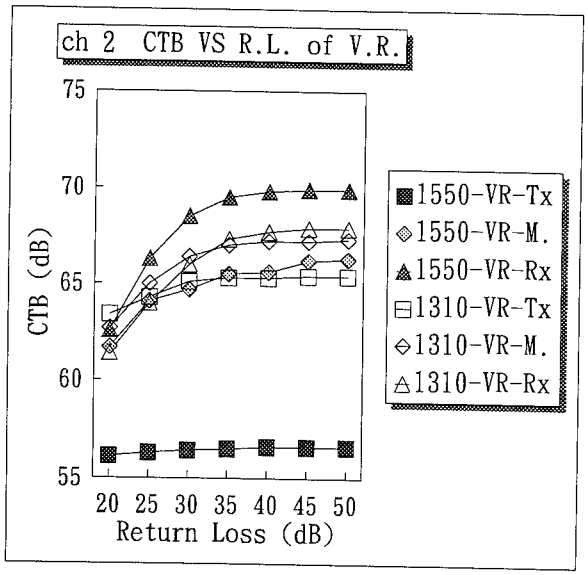


Fig. 8 The measured CTB distortions(relative to the carrier) as a function of optical reflection for the DM-DFB laser transmitter.the measured frequency is at 55.25 MHz.

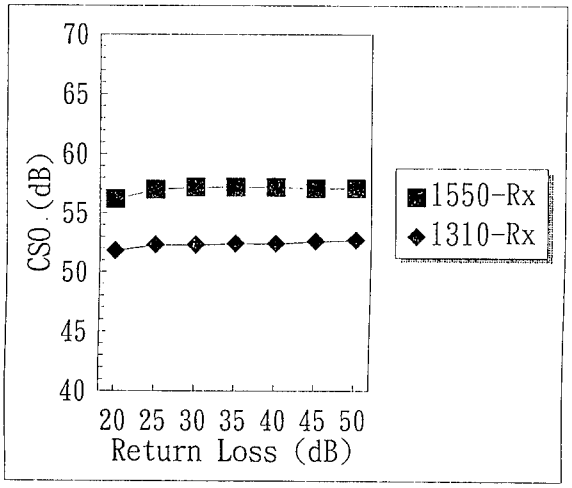


Fig. 7(b) CSO versus reflection levels for an 1310 nm transmitter and a 1550 nm DFB laser transmitter.The optical reflection position near Recriver end (Rx).the measuing frequency is at 55.25 MHz.

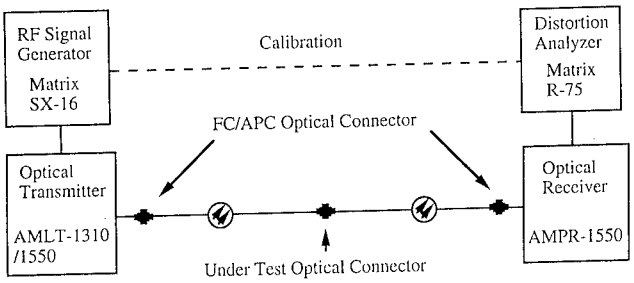


Fig.1 Schematic diagram of the lightwave AM-VSB CATV system's parameter test configurations.

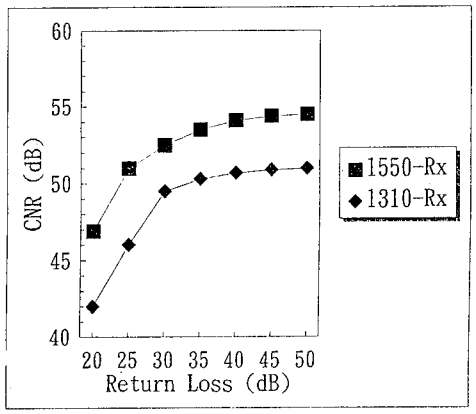


Fig. 2 CNR versus reflection levels for an 1310 nm transmitter and a 1550 nm DFB laser transmitter with same MOI.the measuing frequency is at 55.25 Mhz.

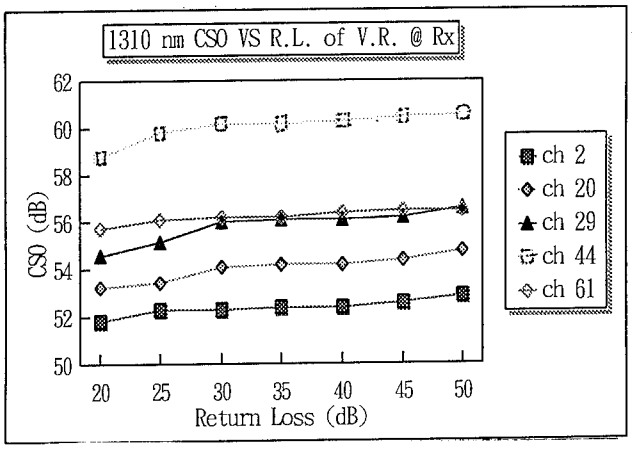


Fig. 3 CSO versus connector reflection on different channel frequency 55.25, 157.25, 253.25, 343.25 ,445.25 MHz.

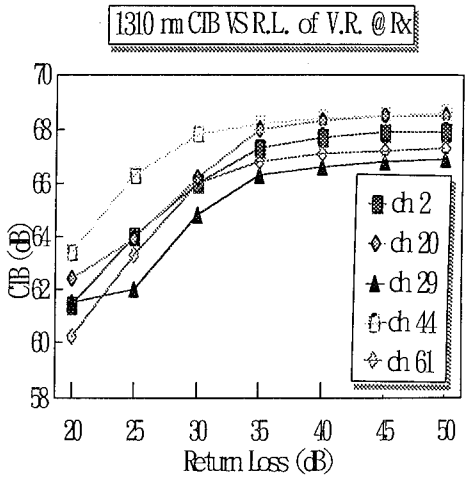


Fig. 4 CTB versus connector reflection on different channel frequency 55.25, 157.25, 253.25, 343.25 ,445.25 MHz.

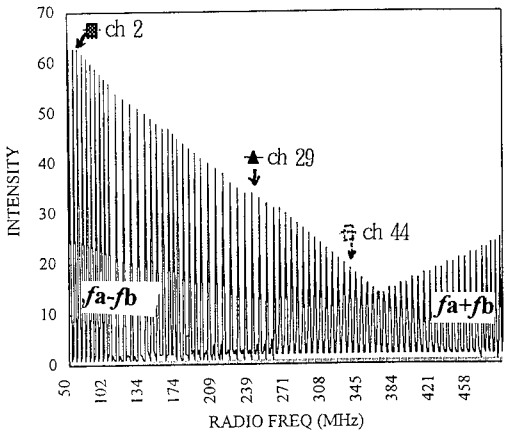


Fig.5 Number of terms of the type *fa+fb*,*fa-fb* conribute to CSO versus the channel number for a 60-channel system.

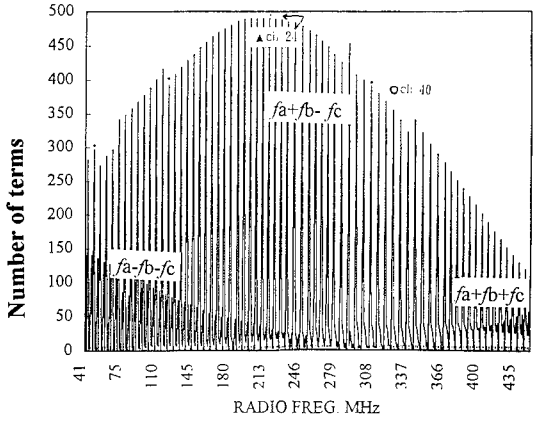


Fig.6 Number of terms of the type *fa+fb-fc*, conribute to CTB versus the channel number for a multi-channel system.

REVIEW ON THE EXCESS LENGTH THEORY OF FIBER GROUP IN THE CORE GROOVE

G.W.SEO H.S.HAN S.H.KIM

FIBER OPTIC R&D CENTER, DAEWOO TELECOM CO.,LTD.,
531-1,GAJWA-DONG,SEO-GU,INCHON CITY,KOREA

ABSTRACT

The study on High-density cable has been under way actively all over the world and most of its structure has a dense shape. Because it is natural that fibers in cable like this become more sensitive to the cabling process than that in general cable, it is very important to forecast the average excess length of fibers in the core groove correctly in order to design optimum cable. Therefore, we re-examined the general excess theory and made a few new equations based on our new conception. The average excess length calculated by them was nearer to the actual one as the groove size and the pitch of the slot core were larger than before.

1. INTRODUCTION

In general, the compact structure has been used for the high density cable and in case of the cable like this, the dimension and pitch of the slot core have an important effect on the average excess length of fibers in the core groove. Also, because the average excess length exercise its influence over the optical property and the life time of the cable under the mechanical and environmental stress to be given to a cable before and after installation, we think that it is necessary to design the cable with much thought of the average excess length of fibers in the core groove correctly to minimize those effects. Although we have used the slot core with helical and S/Z stranding for improving the mechanical and environmental property, the study on how fibers move in the core groove has not almost been proceeded. Therefore, for designing the more stable cable, we studied their movements and induced a few new excess length equations based on our new conception. We used [the sine curve] and [Straight line + Inscribed circle] one as the theoretical approximation method. Also, we practiced verification on each theory and for supporting the confidence of those new equations, we measured the actual average excess length of fibers in the groove and compared them with the theoretical one calculated by those new equations. As a result of the test, we think that those new equations can be used for forecasting the Max./Min. excess length of fibers in the core groove correctly.

2. THE ANALYSIS ON THE MAX./MIN. PATH OF FIBERS IN THE CORE GROOVE

1) Helical type

In case of the helical groove, the path lengths of fibers depend on the stacked radius only, the distance from the center of the slot core to the center of stacked fiber group in the groove. That is, the length passing on the point that the stacked radius is the smallest or the largest is the minimum or the maximum. Therefore, in Fig.1,3, the path length of the point (1) or (2) becomes the largest and the path length to go along the point (3) becomes the shortest. Here, we can mistake the maximum path as path (a) in Fig.1 but if you see Fig.3, you can understand easily that the length passing on the point (1) or (2) is the largest because they rotate with a radius larger than path (a).[Fibers can't go along path (c) actually due to W/B tape or binding yarn.]

2) S/Z type

In case of the S/Z groove, the maximum path length within unit pitch is path (b) and the minimum path is formed when fibers go along the path (b'). If we draw the upper tip lines of the core groove with helical and S/Z stranding more minutely in order to check which path is larger as shown in Fig.2, we can find out that the helical groove has a straight line generally and the S/Z core groove has a sine curve around the center of the slot core. Therefore, fibers in the S/Z groove will naturally form a sine curve in the groove.

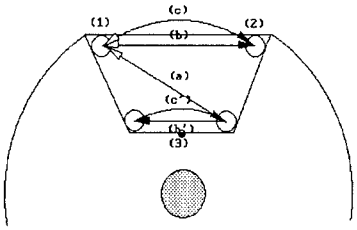


Fig.1 The expectation paths of fibers in the core groove to be seen on the cross section

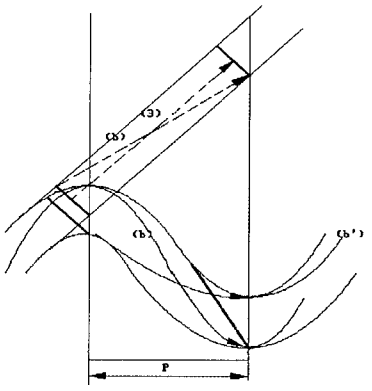


Fig.2 The Max./Min. path of fibers in the helical groove and the S/Z groove.

Also, when the two groove types are compared with each other, while fibers in the helical groove nearly form a straight line because a sine curve is not proper to be formed inside the groove, fibers in the S/Z groove can move along the longer path than them in helical groove within unit pitch. Consequently, the maximum and the minimum length that fibers move in the S/Z groove are longer and shorter than in the helical groove as shown in Fig.2. That is, that the S/Z groove gives more effect to the average excess length of fibers than the helical groove. In addition, the S/Z groove has the merits that the cabling machine is small in size comparatively and it is easy to extract them from the grooves for connecting fibers together. So, we conclude that it is more desirable to study S/Z groove preferentially. The expectation paths of fibers in a S/Z groove is shown in Fig.3.(Twist angle is below 360°)

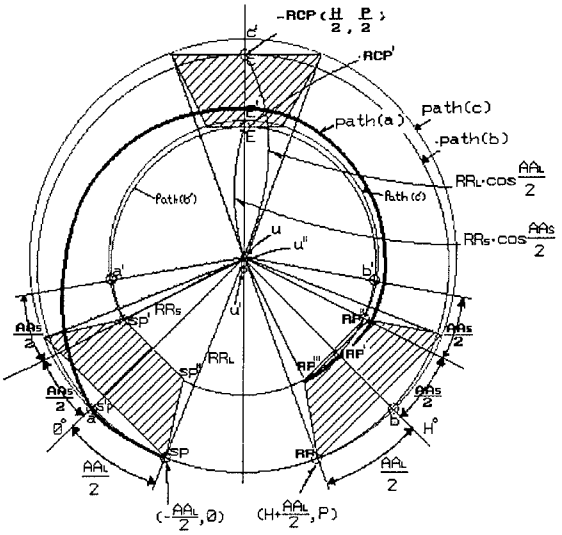


Fig.3 The expectation paths of fibers in a S/Z groove within 1 pitch.

3. The definition and verification of a angle formed when tip lines change their direction at a twist angle.

The helical part(Straight line) and reverse part of a S/Z groove need to define clearly so as to calculate the path lengths of fibers in the core groove. Therefore, we assumed them like the following and the verification is practiced on the definition.

Assumption	When upper tip lines of a core groove move helically from 0 pitch to the reverse point P/2 and from the point to another point P without a curve, the curve around the reverse point divides the line connecting two tip lines at P/2 into two equal parts as shown in Fig.4.

Herein, the angle I_1 shown in Fig.4 is expressed like the below formula.

$$I_1 = Tan^{-1}[\frac{2}{P}\frac{\pi}{180}R_L(\frac{H}{2}+\frac{A_L}{2})]$$

Where, I_1:The angle between the helical direction of the groove and the center of the core

P :The distance from one reverse point to next
R_L:The distance from the center of the core to upper tip lines
H :The twist angle within 1 pitch
A_L:The angle between the center of the core and upper tip lines

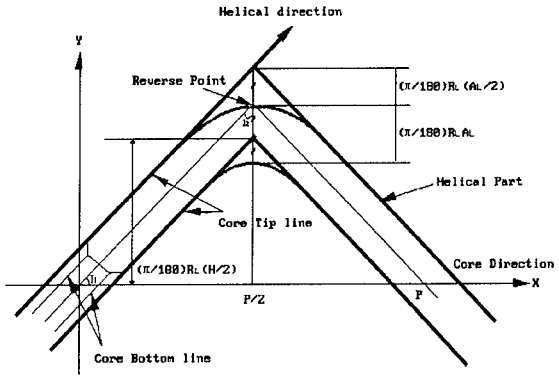


Fig.4 Analysis on the helical & reverse parts when upper tip lines of the core groove is unfolded on a plane.

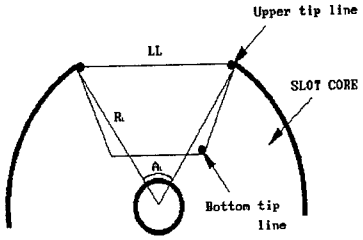


Fig.5 The diagram showing the angle A_L

But we have to check surely whether there are any faults in the above assumption. Therefore, we compared both theoretical and the actual measurement value.
Its procedure is as follows.

Verification on the above assumption

- Dimension of the core groove used for verification

  . Upper width : 4.00 mm
  . Bottom width : 0.95 mm
  . Groove height : 1.85 mm
  . H : 320°
  . P : 400 mm

① The theoretical value

The result calculated by theoretical equations is as follows.

  . A_L : 46.4°
  . I_1 : 4.6°
  . I_2 : 85.4°

Here, the theoretical value of I_2 is 85.4°.(Namely, $2I_2$ = 170.8°)

② The actual value(The measured value)

For measuring the actual angle, we painted black ink on the upper tip lines and left their traces on a white sheet to measure I_2. The result is that the curve around the reverse point to be traced on it almost divided the line connecting upper tip lines at the point P/2 into two equal parts, as well as actual values of $2I_2$ to be measured were as follows.

No	1	2	3	4	5	6
Values(°)	171	171.3	171.1	171	170.5	170.7

- Average(x) = 170.9
- The standard deviation(Sx) = 0.3

Therefore, 170.9 ± 0.3(170.6 ~ 171.2)

The result of comparison of the theoretical and actual values shows that they are almost the same as each other and the difference between them is below 0.06%. Therefore, it is convinced that there is no problem in our assumption and this assumption will be used for calculating the average excess length of fibers in a core groove without any doubt.

4. Analysis on the expectation paths of fibers in a core groove

On the preceding page, we assumed that upper lines of a core groove formed a curve around the reverse point to calculate the expectation path lengths of fibers and ascertained that there was no problem in the assumption through verification. Then, from now on, let's study the expectation paths that fibers may pass in a core groove actually.

1) 4 positions that fibers may be placed on in the core groove to form the max./min. path length.

In general, as the slot core is wrapped by water blocking tape to protect water permeation from outside after the fibers were inserted in the groove, their paths must be considered only to the point just below them when fibers move in the core groove. Then, after locating fibers on 4 positions that they may pass in the groove as shown in Fig.6, let's define some parameters for calculating each path length. Those parameters can be expressed as follows.

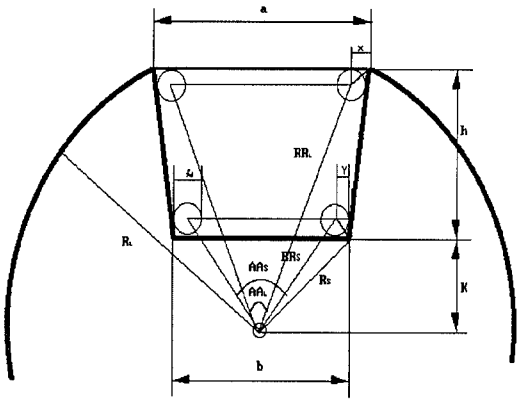


Fig.6 Four positions of fibers in a core groove

$$AA_L = 2Tan^{-1}\left[\frac{\frac{a}{2}-X}{K+h-\frac{1}{2}f_d}\right]$$

$$RR_L = \left[\left(\frac{a}{2}-X\right)^2+\left(K+h-\frac{1}{2}f_d\right)^2\right]^{\frac{1}{2}}$$

$$AA_S = 2Tan^{-1}\left(\frac{\frac{b}{2}-Y}{K+\frac{f_d}{2}}\right)$$

$$RR_S = \left[\left(\frac{b}{2}-Y\right)^2+\left(K+\frac{f_d}{2}\right)^2\right]^{\frac{1}{2}}$$

2) The max./min. path of fibers in the core groove.

As previously expressed in Fig.1,2,3, Path (b) is generally longer than path (a) except for special cases, but needs to check which path is longer between two paths as they depend on the structure of the slot core. Therefore, parameters for calculating each path length are induced as follows by Fig.3 and 7.

① The induced equation showing path (a)[=G_2]

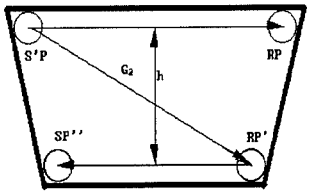


Fig.7 The diagram showing Path (a), G_2, on the cross section of the slot core

$$G_2 = \left[\left(\frac{\pi H}{360}\,\frac{D_L+D_S}{2}\right)^2+h^2\right]^{\frac{1}{2}}$$

$$= \left[\left(\frac{\pi H}{360}\,(RR_L+RR_S)\right)^2+h^2\right]^{\frac{1}{2}}$$

② The induced equation showing path (b)[=G_1]

On the other hand, fibers can't actually pass Path (c) due to the binding yarn or the water blocking tape, but provided that it is possible, path (c) is one passing from the point SP to the point RP with a radius RR_L and path (b) is one that the radius decreases from SP to RCP having minimum radius[$RR_L\cos(AA_L/2)$] and increases from RCP to RP again. Now, let's induce a general equation for showing path (b) by making good use of parameters of path (c). First, if we draw only path (b),(c) on the plane, they are the same as Fig.8.

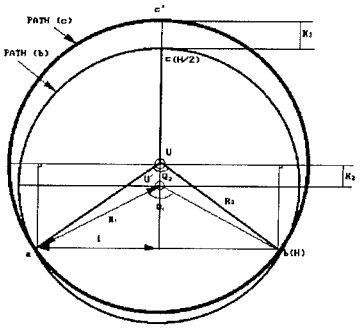


Fig.8 A detailed diagram of path (b),(c)

If we regard an arc $\overset{\frown}{acb}$ passing three points a,c,b as a part of the circle with the new center U' and the radius R_1, we can induce new factors(R_1,U',Q_1) of path (b) by making use of factors(R_2,U,Q_2) of path (c) that are already known. The result is as follows.

$$i = R_1 Sin(\frac{Q_1}{2}) = R_2 Sin(\frac{Q_2}{2})$$
$$R_2 - R_1 = K_3 - K_2$$

$$K_2 = R_2 Cos(\frac{Q_2}{2}) - R_1 Cos(\frac{Q_1}{2})$$
$$K_3 = R_2[1 - Cos(\frac{AA_L}{2})]$$

R_1 : The radius of the circle that path (b) makes
R_2 : The radius of the circle that path (c) makes
K_3 : The distance between radii of circles that path (b),(c) make at P/2
K_2 : The distance between centers of circles that path (b),(c) make at P/2

We, consequently, can induce the general equation for calculating the length of path (b) from the above equation as follows.

$$F(Q_1) = i\ Cos(Q_1/2) + j\ Sin(Q_1/2)$$

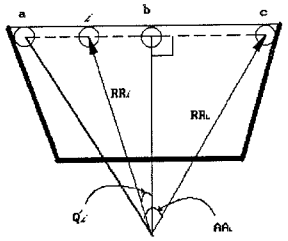
Where, i,j is constant. {$j = K_3 - R_2[1+Cos(Q_2/2)]$}

We can calculate G_1, which is the length of path (b), by using Q_1 and R_1 values from the above equation. That is, G_1 means the total length when path (b) move helically with the radius R_1 and the twisted angle ($360°-Q_1$).

$$G_1 = \frac{\pi}{180}(360 - Q_1)R_1$$

On the other hand, because G_1 is based on the assumption that the arc $\overset{\frown}{acb}$ has the radius R_1 and the new center U', we must ascertain through verification whether the assumption has any problem or not. With reference to this, we verified, accordingly to procedure as follows, the difference of the results was below ±1%. And we concluded that path (b) almost formed a circle because the difference between the lengths was very small when compared to the total length. But we must keep an eye on which fibers don't necessarily move along the ideal paths, G_1,G_2 and they will be used only as references to estimate the max./min. length of fibers in the core groove.

Verification on the assumption that path (b) form a circle



- the principle

When a arc is divided into infinite parts, a line connecting two points is almost the same as a straight line.

- The verification procedure

① When the core groove is proceeded toward the same direction as that of the center of the slot core, induce a general equation calculating the distance(RR) between the center of the slot core and any point on $\overline{abc}$.
② After dividing the angle AA_L into infinite parts, calculate each RR_i
③ Calculate the total length connecting the every points on $\overset{\frown}{abc}$ to be formed by each RR_i and the twisted angle(H).
④ Compare the total length with G_1.

5. Models for calculating the max./min. length of fibers in the core groove.

Up to now, we made a few equations by assumptions and verifications as a preparatory stage to apply to calculation of the max./min. length of fibers in the core groove. Now, let's induce the more complete equations to calculate the max./min. lengths by making good use of those equations. For those inductions, we suggest a [Straight line+Inscribed circle] model to be presented below, In addition, during our study, we found that another model by a sine curve can be used for calculating those path lengths. Those models will be shown in detail below.

1) The method by the sine curve

As previously stated, fiber group in the S/Z groove naturally draw a sine curve because the S/Z groove forms a sine curve itself, which is the function of the twisted angle(H) and the pitch(P) around the center of the slot core unlike the helical groove as shown in Fig.9. Here, the amplitude(F) is proportioned to the twisted angle(H) of the core groove and the radius(R) from the center of the slot core to some point.
The following is the general equation of the sine curve.

$$Y = \frac{\pi R}{360} H\ Sin\frac{\pi}{P} X$$

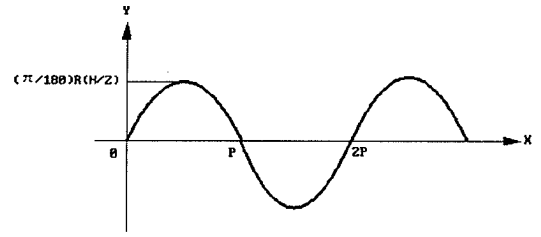


Fig.9 The shape of the S/Z groove around the center of the slot core

If the shape is drawn more minutely with being focused on upper tip lines, it can be presented as Fig.10.

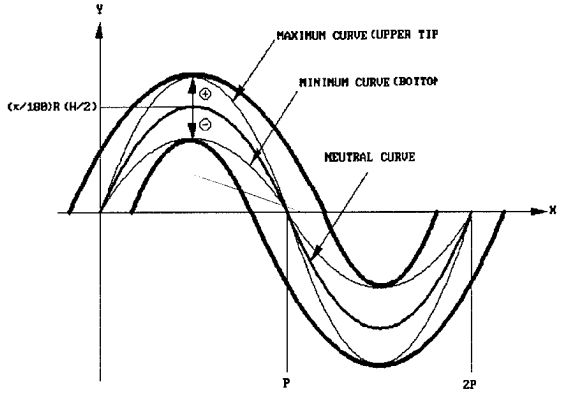


Fig.10 The shape of upper tip lines of the S/Z groove

If the angle(AA_L or AA_S)) that the center of the slot core forms with upper or bottom lines is considered, Y can be presented again as follows.

$$Y = \frac{1}{2}\,\frac{\pi D}{360}\,(H \pm A)\,Sin\,\frac{\pi}{P}X$$

Where, (+) : *Max.*
(−) : *Min.*

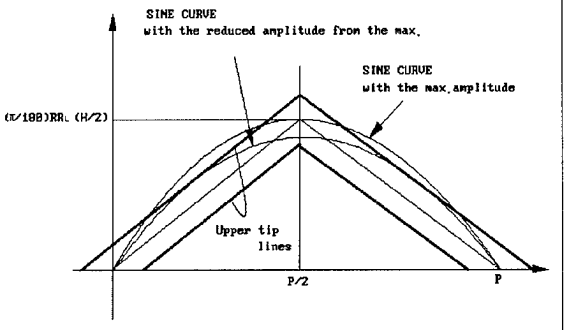
Thus, the total length of the sine curve is the same as the result of a integral equation(S_P) from 0 to the unit Pitch.

$$S_P = \int_0^P \sqrt{1+(\frac{dy}{dx})^2}\,dx$$

$$Where,\ \frac{dy}{dx} = \frac{\pi^2 D}{360P}(H \pm A)\,Cos\,\frac{\pi}{P}X$$

We can calculate the max./min. length of sine curves from the above equation. However, we must ascertain whether those sine curves exist within upper or bottom lines. That is, because we don't know whether those sine curves can form inside the groove, it needs to be ascertained through verification. In view of the results verified, if the sine curve goes off the groove, we should find the new equation surely by subtracting or adding the proper value(angle) from or to (H±A)

Verification procedure for ascertaining whether sine curves exist in the core groove.



① Y(Max.) = $(\pi/180)RR_L(H/2 + AA_L/2)Sin(\pi/P)X$
Y(Upper tip line) = $(\pi/180P)RR_L(H+AA_L)X + (\pi/180)RR_L(AA_L/2)$

First, get X value(s) by making the two equations equal. [The same procedure is applied to Y(Min.)]

--> If there are solutions more than two in X, the sine curve overpasses the gap between two tip lines. Also, if there is only one solution, we can see that the sine curve touches internally on a tip line or a bottom line. That is, if X has solution less than one, we can see that the sine curve moves within them. We found that there were always two solutions in X from the above equations. Thus, we modified those equations as follows.

② Y(Max.) = $(\pi/180)RR_L[H/2 + (AA_L-I_L)/2]Sin(\pi/P)X$
Y(Min.) = $(\pi/180)RR_L[H/2 - (AA_S-I_S)/2]Sin(\pi/P)X$

Second, get I value that there exists only one solution in X.

--> The truth that the sine curve may or may not be within upper or bottom lines depends on I. Consequently, We could get Y(Max.) because I_L was smaller than AA_L, but could not get Y(Min.) because I_S was larger than AA_S.

2) The method by [Straight line + Inscribed circle]

We learned that fibers in the S/Z groove might pass along a sine curve as we have said above. Also, we could get the maximum sine curve but couldn't get the minimum sine curve by the sine curve method. Now, we want to suggest an another model as shown in Fig.11,12, [Straight line+Inscribed circle] one which is better than the sine curve model. About this, we already defined the curve part on the preceding page and the truth on the definition was confirmed by verification.
The [Straight line + Inscribed circle] model is like the below.

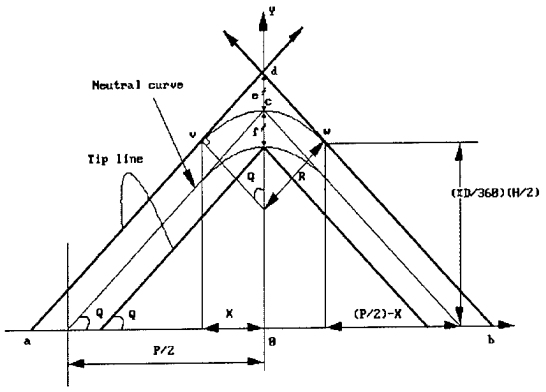


Fig.11 The [Straight line + Inscribed circle] model

Where, R: The radius of the circle that touch internally on straight lines($\overline{ad}$, $\overline{bd}$) and pass the point(c)
Q: The angle that the twisted direction of the groove forms with that of the center of the slot core
e, f: A half of the distance between upper tip lines
X: A half of the straight line when is drawn paralleled with the direction of the center of the slot core from the start point(v) to the end point(w)

As previously assumed and measured, the curve part around the reverse point passes on the cross point(c) and touches internally on two straight lines($\overline{ad}$, $\overline{bd}$), $\widehat{vcw}$ is expressed as follows.

$$\widehat{vcw} = \frac{\pi}{180} RQ \times 2$$

Also, R and Q are as follows.

$$e = f = \frac{\pi D}{360} \frac{A}{2}$$

$$(R+f)CosQ = R$$

$$TanQ = \frac{\pi D(H+A)}{360P}$$

$$\therefore,\ R = \frac{f\ CosQ}{1-CosQ}$$

$$Q = Tan^{-1} \frac{\pi D(H+A)}{360P}$$

Consequently, the max./min. path of fibers in the groove is expressed as the sum of the straight line and the curve part. They are like the equations below.

① The minimum path length(S_P) of fibers in the core groove

$$S_P = 2[\sqrt{(\frac{P}{2} - X_S)^2 + [\frac{\pi R_1}{360}(360 - Q_1)]^2} + \frac{\pi}{180}(SR)Qs]$$

Where, P : Pitch(400mm)
H : Twist angle(320°)
D_S: $2RR_S$
Q_S: $Tan^{-1}[\pi D_S(H+AA_S)]/360P$
SR: $(f_S\ CosQ_S)/(1-CosQ_S)$
f_S: $(\pi Ds/360)(AAs/2)$
AAs: The angle that the center of the slot core forms with two inner bottom lines at the radius RRs(=Ds/2)
Xs: (SR) SinQs
R_1, Q_1: Refer to Fig.8 (R_2=RRs, Q_2=360-H+2AAs)

② The maximum path length of fibers in the core groove

Two paths, which are much the same as (a),(b) paths in Fig.3 are drawn in Fig.12 and we can't see which is the longer one only on the drawing because their path lengths depend on the slot core profile. Thus, in order to judge that, we should calculate all two values and compare the two with each. In general, if G_1 is larger than G_2, path (b) will be the maximum one and if G_1 is smaller than G_2, path (a) will be the maximum one. In case that we draw paths (a),(b) three-dimensionally, their path lengths are expressed again in the equations below.

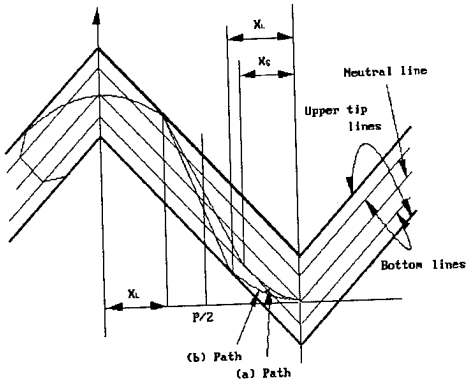


Fig.12 The diagram showing two maximum paths

i) The length of path (a)[G_2']

$$G_2' = \sqrt{h^2 + [\frac{\pi H}{360}(RR_L + RR_S)]^2 + [P - (X_L + Xs)]^2} + \frac{\pi}{180}[(LR)(Q_L) + (SR)Qs]$$

ii) The length of path (b)[G_1']

$$G_1' = \sqrt{[\frac{2\pi R_1}{360}(360 - Q_1)]^2 + (P - 2X_L)^2} + \frac{2\pi}{180}(LR)(Q_L)$$

Where, D_L : $2RR_L$
Q_L : $Tan^{-1}[\pi D_L(H+AA_L)]/360P$
LR : $f_L CosQ_L/(1-CosQ_L)$
f_L : $(\pi D_L/360)(AA_L/2)$
X_L : $(LR)SinQ_L$
P : Pitch(400mm)

H : Twist angle(320°)
R_1, Q_1 : Refer to Fig.8($R_2=RR_L, Q_2=360°-H$)

Till now, we induced and verified some equations that can theoretically calculate the max./min. path length of a fiber group in the core groove by using the Sine curve and [Straight line+Inscribed circle] models. We also summarized both the results of the induced equations and the general equation to be applied to the helical groove all over the world to understand easily. That is as follows.

Items	methods	in. /Max.	Formula	Result (mm, %)
S/Z	1 By the sine curve	Min.	There is in no existance.	
		Max.	$\int_0^P \sqrt{1+[(\frac{\pi^2 R_1}{360P})\frac{(360-Q_1)}{2} Cos\frac{\pi}{P}X]^2}\, dx$	401.0634 (0.2671)
	2 By [Straight line + Inscribed circle]	Min.	$[\sqrt{(\frac{P}{2}-X_S)^2+[\frac{\pi R_1}{360}(360-Q_1)]^2} + \frac{\pi}{180}(SR)Q_S] \times 2$	400.3152 (0.0788)
		Max. (a)	$\sqrt{h^2+[\frac{\pi H}{360}(RR_L+RR_S)]^2+[P-(X_L+X_S)]^2} + \frac{\pi}{180}[(LR)(Q_L)+(SR)Q_S]$	400.7755 (0.1839)
		Max. (b)	$\sqrt{[\frac{2\pi R_1}{360}(360-Q_1)]^2+(P-2X_L)^2} + \frac{2\pi}{180}(LR)(Q_L)$	401.1893 (0.2973)
Helical	3 By the general equation used over world	Min.	$\sqrt{P^2+(\frac{\pi D_S}{360}H)^2}$	400.3392 (0.0848)
		Max.	$\sqrt{P^2+(\frac{\pi D_L}{360}H)^2}$	400.9103 (0.2277)

6. Test

In view of the result that we studied two models to calculate the possible max./min. path of fibers in the core groove so far, between the two models, because the method by the sine curve is troublesome, we should always re-adjust its amplitude properly after construing whether the sine curve is bounded in the core groove, the method is difficult to use for calculating their path lengths. Therefore, we concluded that the method by the [Straight+Curve] is practically the better one and of course, this was used for comparing with the actual values below. Also, if those that are inserted in the core groove have any volume regardless of fibers or ribbons, the above model can be used for calculating their excess lengths in the groove. But in order to make our test simple, we inserted multi-fiber in the core groove and tested them.

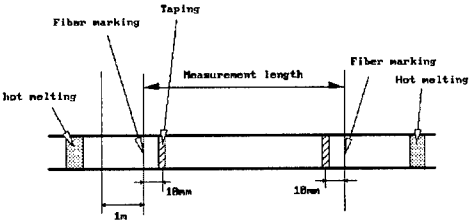
1) Measurement details

① The preparation of the sample (The total 500m x 4 kinds of pitch)

- Measurement length : 50m
- Sample No. : 10 Ea/Pitch
- The dimension(6 grooves type) of the slot core
  . R_L : 5.05mm
  . The upper width : 4.00mm
  . The bottom width : 0.95mm
  . Height : 1.85mm
- Pitch : 400, 300, 250, 200mm
- Twist angle : 320°

② Measurement method

- The preparation and measurement of the sample
  . Fix fibers to the core groove with hot melting after deciding the length of the sample as shown below.(To prevent fibers from moving in the core groove)
  . Mark on its proper point and cut it after straightening the fixed sample out on a floor and fixing its two ends to the floor.
  . Measure their lengths after extracting fibers from the core groove.



2) Test results and analyses

The slot core		Test results			Ave. excess length (Theoretical)
Outer Dia. (mm)		Pitch (mm)	Excess length(%)	Theoretical comparition ratio(%)	
φ 10.1	First	400	0.13	72	0.19
		300	0.23	67	0.34
		250	0.31	63	0.49
		200	0.39	58	0.67
	Second	400	0.18	95	0.19

As a result of the first test, the actual excess length is comparatively smaller than the theoretical one, and the gap became more and more widen in proportion as the slot core pitch become smaller and smaller. We were in a great confusion for a time because of the result of the first test but realized soon that is because the tension control in inserting fibers into the core groove was not proper and the inserting die rotated rapidly when compared to the line speed of the slot core. So, after inserting only 10 ea fibers in the groove with the pitch 400mm carefully during the second test, we measured their excess lengths with the same method as before. Consequently, the actual average excess length(about 0.18%) was almost the same as the theoretical one(0.188%). Therefore, we conclude that there will no problem though the theoretical equation is used for calculating a excess length in the future.

7. Conclusion

Up to now, we reviewed the methods making an estimate of the excess lengths of fibers in the S/Z and Helical groove which have been used for improving its mechanical/environmental properties on designing a cable. For which, we used a S/Z stranded slot core because the the maximum and minimum length of fibers moving in the groove are longer and shorter than that in the helical groove. If we want to make the optimum cable with no attenuation from any outside circumstance, we have to design to make fiber group in the limited groove have more space.

Anyhow, we made a few assumptions and verifications in process of inducing the new excess length equations based on our new conception and finally, we induced two models, which are the sine curve and [Straight line+Inscribed circle] model. However, between the two models, because the method by the sine curve has a troublesome that we should always re-adjust its amplitude properly after construing whether the sine curve is bounded in the core groove. Therefore, the method is difficult to be applied as that for calculating those path lengths. Now, we concluded that the method by the [Straight+Curve] is practically the better one and of course, Also, in order to confirm whether the theoretical excess length by the method and the actual one coincide, we measured over the first/second and as a result of those tests, there was a difference between the two at the first, but the two almost coincided at the second. Also, there was a gap between the excess length by the [Straight line+Inscribed circle] and by the current method(Helical method). And the maximum and minimum of the former were larger and smaller than of the latter as previously expected. In addition, the actual excess length approached to the theoretical one as the diameter and pitch of the slot core were larger and larger.

Finally, we conclude that it is desirable to apply our new model to its design for improving the properties of a cable.

REFERENCE

1) P.A.McGettigan, Technical report(Report No.TR-4140 -81-02), NT cable division
2) T.S.Swiecickt, Unit cable structure for optical communication system, NT cable LTD.



G.W.Seo
DAEWOO TELECOM. Co.,Ltd.
531-1,Gajwa-Dong,Seo-Gu,
Inchon-City,Korea

He joined Daewoo Telecom.LTD.after graduating from Pusan University with M.S. degree in the inorganic material engineering in 1993 and, since then, has been engaged in R&D center of the optical fiber cable. He is now the assistance manager and is working as the cable designer.



H.S.Han
DAEWOO TELECOM. Co.,Ltd.
531-1,Gajwa-Dong,Seo-Gu,
Inchon-City,Korea

He received bachelor's degree in the inorganic material engineering at Yonsei University in 1984. He joined DAEWOO TELECOM. LTD. as the cable manufacturing engineer, where he has been involved in developing and designing the optical cable. He is currently the assistance manager and working on development of multi-fiber cable.



S.H.Kim
DAEWOO TELECOM. Co.,Ltd.
531-1,Gajwa-Dong,Seo-Gu,
Inchon-City,Korea

He is a member of CCITT(Study group 6) and in charge of development of multi-fiber cable. He obtained bachelor's degree in the precision mechanical engineering from Hanyang University and joined DAEWOO TELECOM. LTD.in 1982. Since then, he has been engaged in R&D of the optical fiber cable. He is now the manager of the R&D center.

TEMPERATURE-DEPENDENT PERFORMANCE OF BUFFER TUBE GELS IN LOOSE TUBE FIBER OPTIC CABLES

Osman S. Gebizlioglu, Irene M. Plitz, and Michael J. Zammit
Bellcore
445 South St.
Morristown, New Jersey 07960

ABSTRACT

In loose tube fiber optic cables, buffer tubes are filled with hydrocarbon-based gels to protect the optical fibers against water entry. These gels must be chemically and thermomechanically stable. They must show no drip at 80 °C and no appreciable contribution to cable transmission loss at -40 °C. The buffer tube gels consist of a low-molecular weight polymer blended with fumed silica. The large variations in the polymer molecular weight and in the surface chemical structure of the fumed silica cause these gels to exhibit a broad range in two key mechanical properties: storage modulus and dynamic viscosity. The buffer tube gels examined in this study exhibit strongly temperature-dependent moduli and dynamic viscosities over the -40 °C to 25 °C range. Our results suggest that buffer tube gels may be formulated to reduce the temperature dependence of their mechanical properties, thus simultaneously achieving high-temperature drip resistance and minimal contribution to low-temperature transmission loss in loose tube fiber optic cables.

I. INTRODUCTION

In loose tube fiber optic cables, hydrocarbon-based gels are used to fill buffer tubes to protect the optical fibers against water. While these gels fill the voids within a cable, they also serve to isolate the optical fibers from contact with the buffer tube inner surfaces during installation, maintenance operations, and service at low temperatures. A key performance requirement is that they maintain their room-temperature mechanical properties over a broad temperature range. They must retain their room-temperature viscosity at service temperatures that may rise to 80 °C or drop to -40 °C.

A critically important issue of buffer tube gel performance is its fluidity at high and low temperatures. At high temperatures, a buffer tube gel tends to drip out of buffer tubes within splice closures. Requirements R6-54 and CR6-55 in the Bellcore generic requirement for optical fiber and cable (GR-20-CORE)[1] address the drip performance at 65 °C and 80 °C, respectively. At these temperatures, buffer tube gels are required to exhibit no flow out of a fiber optic cable. At low temperatures, on the other hand, the gels are potential contributors to service-affecting transmission loss[2,3] in loose tube fiber optic cables deployed in aerial applications. Hence, buffer tube gel design involves finding a trade-off between two conflicting performance requirements: 1) low viscosity to minimize the risk of cable transmission loss at low temperatures, and 2) high viscosity to maximize drip resistance at high temperatures. The relationship of these requirements to gel material properties has attracted considerable attention.[4-7] In earlier work[4-6] on fiber optic cable filling compounds, the cone penetration method and oven drip tests were used to correlate compound material properties to the cable drip performance. In more recent work,[7] however, gel rheological properties such as storage modulus (as a measure of stiffness) and dynamic viscosity (as a measure of fluidity) were measured to correlate gel material properties with cable drip (or low-temperature transmission loss) performance. In this report, we examine the temperature dependence of these two mechanical properties and explore the sensitivity of this temperature dependence to the gel composition and matrix molecular weight. The overall objective of our work on the buffer tube gels is to develop gel formulation strategies to achieve the high-temperature drip resistance while minimizing the risk of low-temperature transmission loss in loose tube fiber optic cables. Our work in progress is aimed at correlating the temperature-dependent gel mechanical properties to the cable drip/low-temperature performance.

II. EXPERIMENTAL METHODS

II.1 Buffer Tube Gel Components and Composition

Three of the four gel samples that we discuss in this paper were from cables provided by three manufacturers. We designate them as samples 1, 2, and 3. Sample 4 was

copyright @ 1995 Bellcore All rights reserved

recovered from a cable that exhibited service-affecting transmission loss at low temperature. We used FTIR (Fourier Transform Infrared) spectroscopy and DSC (Differential Scanning Calorimetry) to identify the gel components, TGA (Thermogravimetric Analysis) to determine the inorganic filler content of these gels, and GPC (Gel Permeation Chromatography) to analyze the gel matrix molecular weight (MW) and its distribution (MWD).

II.2 Gel Mechanical Properties

Buffer tube gels exhibit viscoelastic behavior over the typical outside plant temperature range. Depending on the temperature and time scale of measurement, they behave in a solidlike and/or liquidlike manner. The most commonly used technique for the mechanical analysis of gels is dynamic mechanical analysis (DMA). For buffer tube gels, this technique can be applied in the simple shear (deformation) mode where a gel sample confined between two parallel plates is subjected to a cyclic sliding motion of one of the plates while the other plate is kept stationary. For a selected cyclic shear strain at constant frequency, the shear stress is monitored over the temperature range of interest. A portion of the measured shear stress is in phase with the applied strain, while the remainder is out of phase. The in-phase component represents the elastic (solid-like) response; it is characterized by the storage modulus, G'. The out-of-phase component gives the viscous (liquid-like) response by which a portion of the initial mechanical energy input is dissipated; this component is characterized by the loss modulus, G". For gels, we prefer to represent the viscous response by the dynamic viscosity, η'; this quantity is equal to the loss modulus (G") divided by the measurement frequency ω. The storage modulus is expressed in Pascals (Pa = Newtons per square meter in SI units). The dynamic viscosity is expressed in Pascal-seconds (Pa-sec.).

We used a Rheometric Scientific DMTA (Dynamic Mechanical Thermal Analyzer) to measure the gel mechanical properties over the temperature range from -40 °C to 80 °C. In the DMTA, parallel plates that hold the gel sample are called shear clamps; the stationary plate is called the fixed clamp, and the moving plate is called the drive clamp. The stationary shear clamps (7-mm disks) were positioned horizontally with a gap of 0.5 mm from the drive clamp. For all DMTA measurements on the gels, the average dynamic shear strain was less than 1%, and the frequency was 1 Hz.

II.3 Drip Tests of Fiber Optic Cables

The fiber optic cables that provided gel samples 1,2, and 3 were tested for drip in accordance with the fiber optic test procedure, FOTP-81,[8] *Compound flow (drip) test for fiber optic cable.*

III. RESULTS and DISCUSSION

III.1 Components and Composition of Buffer Tube Gels

The two major components of the four buffer tube gel samples were poly(isobutylene) and fumed silica. Poly(isobutylene) melts over a broad temperature range from -5 °C to 128 °C[9], and its glass-to-rubber transition temperature is about -70°C. For these samples, the gel matrix consists of poly(isobutylene) with a broad molecular weight distribution. Fumed silica consists of aggregates of nanometer-sized (colloidal) silica particles and is used to modify the viscosity of the matrix oils. TGA showed that the fumed silica content varied from 4% to 9% by weight. Table 1 presents a summary of the gel analysis results. In Table 2, we show number-average molecular weight (M_n), weight-average molecular weight (M_w), and polydispersity index (PDI, the ratio of M_w to M_n) that indicates the breadth of the molecular weight distribution. These tables show the variations in the fiber optic buffer tube gel formulations. Table 1 indicates that the fumed silica content may vary by a factor of 2. Table 2 reveals that the average molecular weights and molecular weight distributions may cover a very broad range; moreover, the MWD is tri-modal for sample 3, indicating that the gel matrix material consists of three distinct fractions of PIB molecular sizes.

Table 1. Buffer Tube Gel Components

	Sample 1	Sample 2	Sample 3	Sample 4
Matrix Material	PIB Poly(Isobutylene)	PIB	PIB	PIB
Fumed Silica % by weight	9	8	4	4

Table 2. Gel MW and MWD

	Sample 1	Sample 2	Sample 3	Sample 4
M_w	1280	350	8980 1240 187	315
M_n	1050	320	8960 1040 186	280
PDI	1.22	1.10	1.003 1.19 1.003	1.12

III.2 Temperature Dependence of Storage Modulus and Dynamic Viscosity

Figures 1 and 2 present a storage modulus - temperature profile and a dynamic viscosity - temperature profile, respectively, for gel sample 4. Each profile shows one complete thermal cycle from -40 °C through 80 °C back to -40 °C; the upper segment shows a heating (at 2 °C per minute) profile from -40 °C to 80 °C while the lower segment corresponds to cooling at the same rate from 80 °C to -40 °C. These segments appear indistinguishable over the temperature range from about 0 °C to 80 °C. From 0 °C down to -40 °C, however, the cooling segment runs below the heating segment, suggesting some thermally-induced breakdown in the gel structure during the heating segment. Samples 1 through 3 showed similar trends in their modulus/viscosity profiles to those shown in Figures 1 and 2.

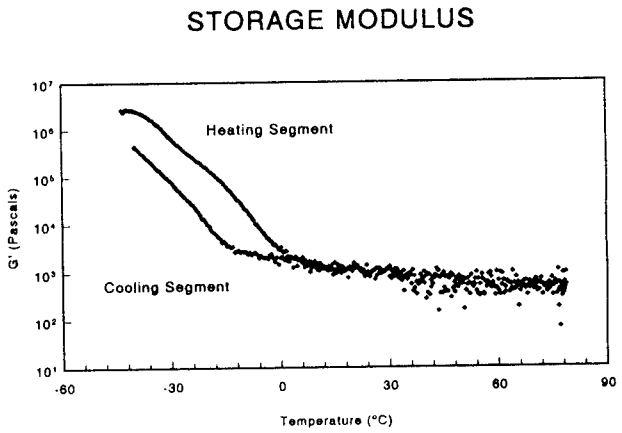


Figure 1. Modulus profile for gel 4

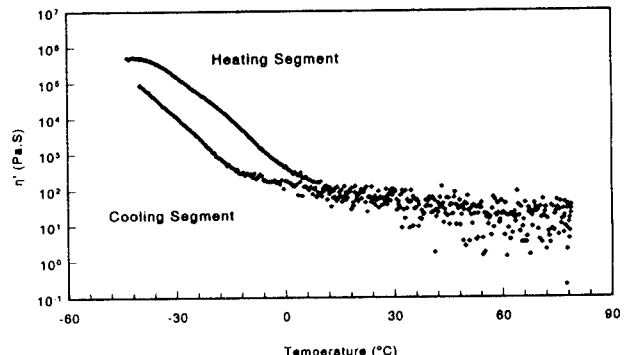


Figure 2. Viscosity profile for gel 4

In Figures 3 and 4, we compare point values of the moduli and dynamic viscosities, respectively, at -40 °C, 25 °C and 80 °C for the gel samples of Table 1.

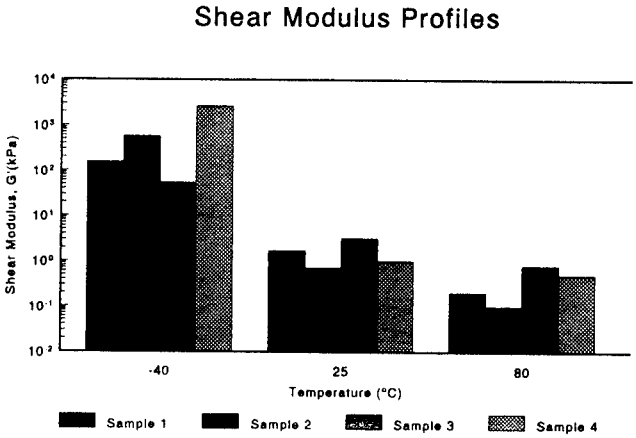


Figure 3. Moduli at selected temperatures for all gel samples

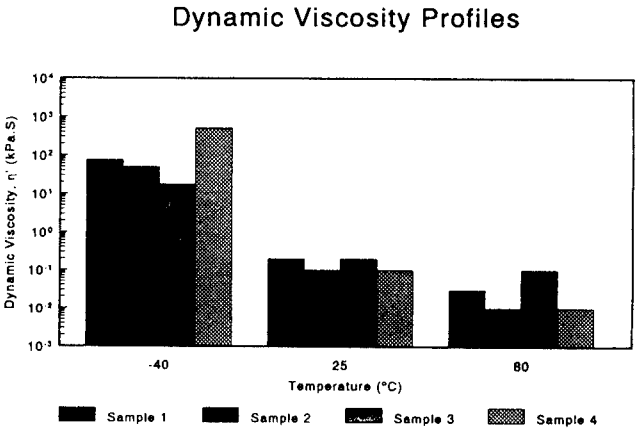


Figure 4. Dynamic viscosity at selected temperatures

In these bar graphs, we note that each sample exhibits a unique temperature dependence for storage modulus and dynamic viscosity. For instance, gel sample 4 shows the highest storage modulus and dynamic viscosity of the four gel samples at -40 °C. At 25 °C and 80 °C, however, the highest moduli are those of gel sample 3; at 25 °C, the dynamic viscosities of samples 1 and 3 are the highest, while the 80 °C dynamic viscosity is the highest for gel sample 3. These trends suggest that the temperature dependence of the gel mechanical properties varies with the gel composition and structure. The magnitude of the -40 °C modulus of gel sample 4 in Table 2 is comparable to the shear modulus of a cross-linked rubber at 25 °C. The shear moduli of rubbers at room temperature fall in the range from 30×10^5 to 300×10^5 Pa.[10] This comparison points out that these gels become progressively rubber-elastic within the buffer tubes as the temperature drops to -40 °C. The most important consequence of this rubberlike behavior is the large volumetric thermal strain associated with a

rubberlike coefficient of volume expansion. For the matrix material, poly(isobutylene), the coefficient of volumetric thermal expansion over the 25 °C to -40 °C range is 6.0×10^{-4} /°K.[11] When cooled from 25 °C to -40 °C, the matrix material would undergo a 4% compressive volumetric strain. However, the thermal expansion coefficient of the gel may differ significantly from that of the matrix material alone due to the composition and chemistry of the fumed silica, the hydrocarbon-based additives used in the matrix material, and the molecular weight distribution of the matrix material itself.

Poly(isobutylene) exhibits a shear modulus of 10^6 Pa over the temperature range from 25 °C down to 0 °C.[11] Below this temperature, its shear modulus rises sharply through its rubber-to-glass transition (at about -70 °C) to about 10^9 Pa. The shear moduli of Figure 3 fall both above and below the shear modulus of poly(isobutylene) through the 25°C to 0 °C range, suggesting that variations in the (molecular weight) characteristics of the matrix material, and in the additives and fillers, can result in buffer tube gels with a broad range of mechanical properties. In particulate-filled and fiber-filled polymer composites, inorganic fillers (with a higher modulus than the matrix material's modulus) result in a substantial increase in the composite modulus.[12] This effect is known as reinforcement, and its magnitude is proportional to the volume fraction of the filler material in the composite. If the gel samples of this investigation were of similar matrix/filler characteristics, the gel sample 1 would exhibit the largest modulus at a given temperature since it has the largest fumed silica weight fraction (0.09). This observation further confirms that the gel samples differ in the fumed silica and matrix material characteristics.

III.3 Drip Performance and its Relationship to the Gel Modulus/Viscosity

The drip tests performed on the fiber optic cables that provided gel samples 1, 2, and 3 indicated no appreciable drip at 80 °C, yet these samples exhibited a ten-fold change in their 80 °C dynamic viscosity and an eight-fold change in their 80 °C modulus values. However, we should not interpret these preliminary results as indicating the absence of any correlation between the drip test and the gel mechanical properties. If we represent the flow of a buffer tube gel by a relatively simple fluid model such as the Bingham model, we can then describe the gel drip from a fiber optic cable suspended vertically in an oven by the following expression[13]:

$$Q=\frac{\pi \rho g}{8\mu_0} R^4\left[1-\frac{4}{3}\left(\frac{\tau_0}{\tau_R}\right)+\frac{1}{3}\left(\frac{\tau_0}{\tau_R}\right)^4\right]$$

where

Q = the volumetric flow rate of a buffer tube gel under the gravitational force $\left[\frac{m^3}{s}\right]$

ρ = gel density, $\left[\frac{Kg}{m^3}\right]$

g = local gravitational acceleration, $\left[\frac{m}{s^2}\right]$

μ_0 = flow rate-independent gel viscosity, $\left[\frac{K_g}{m-s}\right]$

R = buffer tube inner diameter, $[m]$

τ_0= shear yield stress of a buffer tube gel, [Pa]

τ_R = shear yield stress at the buffer tube wall, [Pa].

For a Bingham fluid, shear stress at the tube wall must exceed the yield stress τ_0 for fluid flow to occur. The two material parameters that determine whether or not a gel will flow are the viscosity μ_0 and the shear yield stress τ_0; for a Bingham fluid, the shear yield stress τ_0, by itself, may determine the outcome of a drip test since τ_0 must exceed the product $(\rho gR)/2$ for flow to occur. The tube inner diameter also affects the flow rate, which is proportional to the fourth power of the effective tube diameter. However, fiber optic cables have varying buffer tube diameters, fiber counts, and fiber excess lengths; therefore, the effective tube diameter may vary significantly from one cable to another. Hence, the Bingham model does not adequately represent the complexities of relating the gel flow rate to the material properties. Thus, we will defer a detailed analysis of the drip test results until we develop a statistically significant set of drip test data for well characterized buffer tube gels.

To understand the dynamic viscosity values shown in Figure 4, we first note that the absolute viscosity of water at 25 °C is 0.9×10^{-3} Pa-sec. Thus, the 25 °C gel dynamic viscosities of Figure 4 are ten thousand to one hundred thousand times larger than that of water. At 80 °C, the highest dynamic viscosity (sample 3) is ten times larger than the lowest viscosity (samples 2 and 4). At 25 °C, the lowest value gel viscosity (samples 2 and 4) differs from its its highest value (samples 1 and 3) by a factor of two, while the -40 °C viscosity values can differ by a factor of about thirty. In Figures 5 and 6, we examine the temperature dependence of the gel modulus and dynamic viscosity, respectively, normalized to their 80 °C values.

The normalized moduli and viscosities of Figures 5 and 6, respectively, clearly indicate the much larger gel-to-gel variability of the low-temperature (-40 °C) mechanical properties than at 25 °C and 80 °C. This variability combined with the large increases observed in the gel modulus and viscosity at low temperatures point to a potential reliability risk in the low-temperature performance of the buffer tube gels.

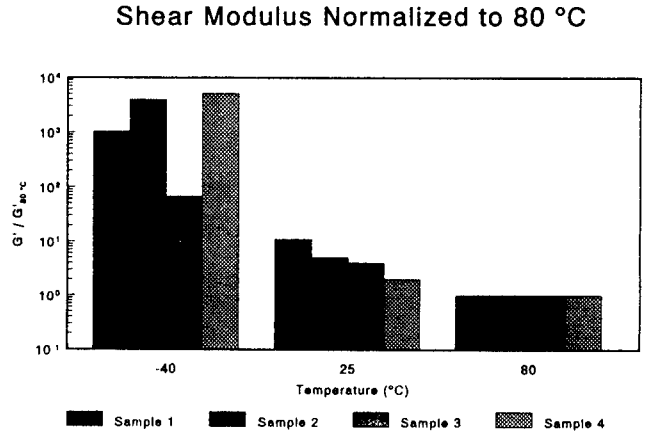


Figure 5. Moduli normalized to the 80 °C values

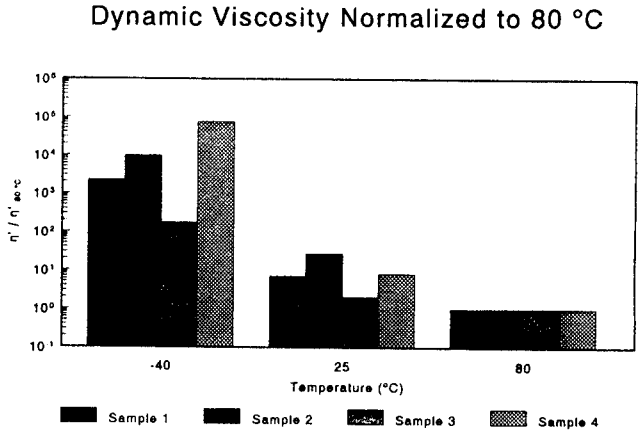


Figure 6. Dynamic viscosities normalized to the 80 °C values

III.4 Gel Molecular Weight and Molecular Weight Distribution

Referring back to Table 2 and Figure 4, we note that the dynamic viscosities at 80 °C correlate in accordance with their M_w and M_n. Thus, sample 3 with the highest average molecular weights exhibits the highest dynamic viscosity. At 25 °C, however, the sample dynamic viscosities are closer together. In addition, the dynamic viscosity of sample 3 at 25 °C does not increase appreciably over its 80 °C viscosity. At -40 °C, however, the ordering in the dynamic viscosity values changes dramatically. At this temperature, sample 3 with its tri-modal MWD shows the lowest dynamic viscosity while sample 4 with its lowest average molecular weight and uni-modal distribution exhibits the highest η' value. The modulus-temperature trends of Figure 3 show an even more complex set of relationships between the gel MW's and the storage moduli. Remarkably, however, sample 3 with its tri-modal MWD, covering a broad MW range from 186 to 8960, exhibits the smallest temperature dependence of both storage modulus and dynamic viscosity. Consequences of this weak dependence on the cable drip performance at 80 °C and low-temperature transmission loss performance at -40 °C are unknown at this time. Nevertheless, this preliminary evaluation suggests that the temperature dependence of the gel mechanical properties can be reduced by a judicious choice of gel components and compositions. A definitive study of the role that the buffer tube gel properties play in the low-temperature cable performance should involve a standared cable structure filled with buffer tube gels that exhibit systematic variations in their moduli and viscosities.

IV. SUMMARY

We examined buffer tube gels from a set of loose tube fiber optic cables. All four gels consisted of poly(isobutylene) and fumed silica (4 - 9 % by weight). The poly(isobutylene) (PIB) molecular weight distributions were uni-modal for samples 1, 2, and 4, but tri-modal for sample 3. While the molecular weight distributions (MWD's) were narrow (as indicated by polydispersity indices (PDI's) that are close to 1), the average molecular weights covered a broad range from 187 to 8960. In general, the storage moduli and dynamic viscosities showed a strong temperature dependence, especially over the range from -40 °C to 25 °C. The gel sample with the smallest temperature dependence was sample 3, which had a tri-modal MWD covering a range from 186 to 8960. The results to date show promise that the buffer tube gel mechanical properties may be tailored to provide both high-temperature drip resistance and low-temperature fluidity for minimizing transmission loss.

ACKNOWLEDGMENTS

We thank Prof. S. Khan, North Carolina State University, Raleigh, North Carolina, for many fruitful discussions and suggestions. We also acknowledge the invaluable assistance of R. Kanen in sampling the buffer tube gels from commercial fiber optic cables.

REFERENCES

1. GR-20-CORE, "*Generic Requirements for Optical Fiber and Fiber Optic Cable,*" Bellcore, Issue 1, September 1994.

2. G.D. Kiss, M.J. Zammit, O.S. Gebizlioglu, and P.B. Grimado, NFOEC Proceedings ,pp 411-427 (1994).

3. M.J. Zammit, O.S. Gebizlioglu, P.B. Grimado, and G.D. Kiss, IWCS Proceedings, Vol. 43, pp 538-544 (1994).

4. A.C. Levy and R. Sabia, IWCS Proceedings, Vol. 31, pp 313-319
(1982).

5. G.J. Hughes, IWCS Proceedings, Vol. 36, pp 148-154 (1987).

6. T.Hattori, N. Akasaka, M. Fukuma, S. Masuda, and S. Suzuki, IWCS Proceedings, Vol. 37, pp 12-15 (1988).

7. G. Morland, D. Rees, and G. White, IWCS Proceedings, Vol.40, pp 469-475 (1991).

8. EIA/TIA-455-81A, FOTP-81, *Compound Flow (Drip) Test for Filled Fiber Optic Cables.*

9. L.E. Nielsen and R.F. Landel, "Mechanical Properties of Polymers and Composites", Marcel Dekker, New York, p521 (1993).

10. M.F. Ashby and D.R.H. Jones, "Engineering Materials," Pergamon, Oxford, p31 (1982).

11 . N.G. McCrum, C.P. Buckley and C.B. Bucknall, "Principles of Polymer Engineering"
Oxford Univ. Press, Oxford, p49 (1991).

12. F.R. Eirich, "Science and Technology of Rubber", Academic Press, New York, p352 (1978).

13. R.B. Bird, W.E.Stewart, and E.N. Lightfoot, "Transport Phenomena," John Wiley & Sons, Inc., New York, p50 (1960).



Osman Gebizlioglu holds BS and MS degrees in chemical engineering from the Middle East Technical University, Ankara, Turkey. After receiving his PhD. in the Polymer Materials Program at Princeton University, he was a Monsanto Postdoctoral Fellow in the Mechanical Engineering Department of MIT where he investigated the physics of toughening glassy polymers. Since he joined Bellcore in 1987, he has focussed his research on polymers used in optical fiber cables and components



Irene Plitz received her BS in Chemistry and immediately joined Bell Labs where she worked on outside plant materials, primarily wire and cable applications. She joined Bellcore in 1984 and focused her work principally on the chemical and structural analyses of polymers. Early this year, she transferred to the Fiber Media and Component Reliability Group where her work will concentrate on assuring reliable optical fiber cable and components.



Michael Zammit holds BS and MS degrees in Mechanical Engineering. His responsibilities include the development of generic requirements, test procedures, and technical analyses for fiber optic splice closures, Optical Network Unit (ONU) enclusures, and innerduct.

Development of single slotted-rod type 1000-fiber optical fiber cable for subscriber loops

Naoki Okada, Kohichiro Watanabe, Kazunaga Kobayashi, Akira Sano, Matsuhiro Miyamoto

Fujikura, Ltd. Telecommunication Cable Section Opt-electronics Laboratory
1440 Mutuzaki, Sakura, Chiba, 285, Japan

Abstract

The single slotted rod type optical 1000-fiber cable with small diameter has been developed successfully. Ten thin coated 8-fiber ribbons which are 0.3mm in thickness are inserted into a slot. This cable structure has high fiber-packing density and small diameter, therefore some pieces of cables can be installed in a underground duct using sub-pipes. The trial cable has been manufactured actually and tested that cable performance. As a result, it is confirmed that the single slotted rod type optical 1000-fiber cable has good transmission characteristics and mechanical properties.

1. Introduction

The full optical fiber loop will be constructed for the high speed digital transmission networks in the future. In urban area, the telecommunication cables are installed in the under ground ducts in Japan[1,2]. In order to construct the new networks economically, the constructed ducts should be used efficiently, therefore the optical fibers should be packed in the ducts at high density. We are aiming to install some pieces of cables in a duct using sub-pipes. Therefore, the high fiber-packing density and thin optical fiber cables are demanded.

We have attempted to design the new cable with high fiber packing-density and small diameter. The most important target is to reduce the diameter of the 1000-fiber cable and the 600-fiber cable. The ordinary 1000-fiber cable is 40mm in diameter, and the ordinary 600-fiber cable is 30mm[3,4,5]. In case of installing some pieces of cables, the diameter must be reduced down to about 30mm or 24mm in diameter[6]. Moreover, the small diameter cables can be installed in long distance, so the jointing points will be reduced when the networks are constructed.

The water blocking and flame retardant characteristics are also required. The water blocking property is obtained with water absorbent tape, and the flame retardant property is achieved by non-halogen flame retardant poly-ethylene sheath.

2. Cable design

In order to get the high-density and small diameter cable, we have designed fiber ribbon structure and cable structure. The cable design criteria are shown in Table 1.

Table 1. Cable design criteria

Fiber count in a cable	1000	600
Dia. of cable	30 mm	24 mm
Compatibility with ordinary cables	8-fiber ribbon (Divisible into 4-fiber ribbons)	

2-1. Ribbon structure

We tried to develop the thin coated 8-fiber ribbon. Considering compatibility with ordinary 4-fiber and 8-fiber ribbon, the 250micron coated fibers are used. The thickness of the ribbon is reduced from 0.4mm to 0.3mm as shown in Fig.1. This newly developed 8-fiber ribbon can be divided into two 4-fiber ribbons easily in order to splice with 4-fiber ribbon.

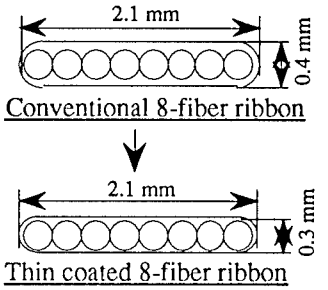


Fig.1 Thin coated 8-fiber ribbon structure

2-2. Cable structure

The following three types of cable structures are designed and compared each other.

One is the multi slotted-rod structure. This structure is adapted ordinary 1000-fiber cables in Japan as shown in Fig.2. Five slotted-rod units are stranded around the central strength member. The cable diameter can be reduced down to 37mm using thin coated 8-fiber ribbon, but this cable diameter is too large to install the cable in a sub-pipe.

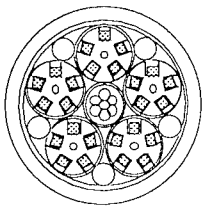


Fig.2 Multi slotted rods type 1000-fiber cable

Second is the U-groove stranded structure. This structure has been investigated to design the ultra high count and ultra high density optical fiber cables as shown in Fig.3[7,8,9]. The U-grooves are stranded around the central strength member. This structure is suitable for the high count fiber cable, because the U-grooves can be stranded at multi layers.

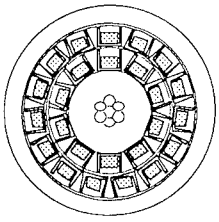


Fig.3 U-groove type 4000-fiber cable

Third is the single slotted-rod structure. This structure has been used for ordinary 100 and 300-fiber cables in Japan as shown in Fig.4. These single slotted-rod type structures have been optimized for low count optical fiber cables.

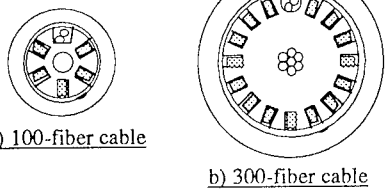


Fig.4 100 and 300-fiber single slotted rod type cable

In order to select the cable structure, U-groove stranded structure or single slotted-rod structure, we have designed the 1000-fiber cable changing ribbon count in a slot. The results are shown in Fig.5. The cable diameter of the 2-layers U-grooves stranded structure is smaller than other cable structures in the range of low ribbon count in a slot. However, in the range of high ribbon count in a slot, the single slotted-rod structure is best. We adopted the single slotted-rod structure, considering the identification of the ribbons, manufacturing process, etc.. Ten thin coated 8-fiber ribbons are stacked in a slot as shown in Fig.6.

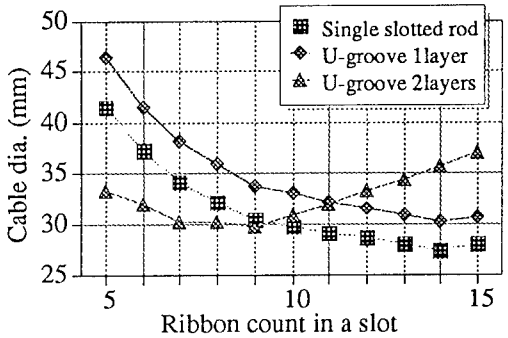


Fig.5 Relationship between cable diameter and ribbon count in a slot

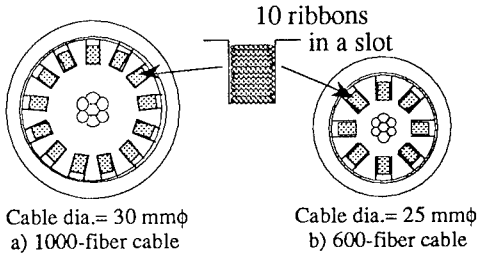


Fig.6 Single slotted-rod type 1000-fiber and 600-fiber cable

3. Cable characteristics

The prototype cables were manufactured actually, and these cable performance was researched. We manufactured 4 kinds cables as shown in Table 2. Transmission characteristics, mechanical characteristics, water blocking characteristics, and flame retardant characteristics were investigated.

Table 2 Prototype cables

Cable	Wrapping	Sheath
1000SM-WB	Water absorbent tape	Polyethylene sheath
1000SM-WB-FR	Water absorbent tape	Non-galogen FR sheath
600SM-WB	Water absorbent tape	Polyethylene sheath
600SM-WB-FR	Water absorbent tape	Non-galogen FR sheath

3-1. Transmission characteristics

The histogram of loss after sheathing is shown in Fig.7. Moreover, temperature characteristics is shown in Fig.8. These results are obtained from the prototype 1000-fiber cable. It is confirmed that the single slotted-rod 1000-fiber cable shows good transmission characteristics.

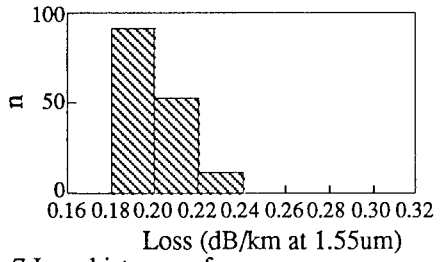


Fig.7 Loss histgram of the single slotted-rod 1000-fiber cable

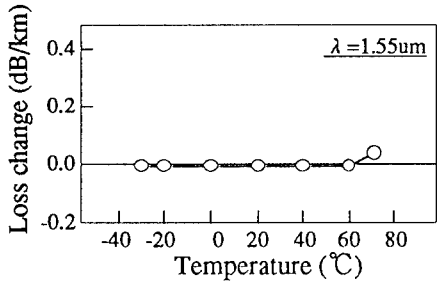


Fig.8 Temperature characteristics of the single slotted-rod 1000-fiber cable

3-2. Mechanical characteristics

The results of several mechanical tests are listed in Table 3. As results, the mechanical characteristics are enough to use the actual field.

Table 3 Mechanical test results

	Test conditions	Results
Bending	400 mmϕ ±90° bending	No change in loss
Lateral pressure	30 N/100 mm	No change in loss
Tensile	1000 kgf	Less than 0.02 dB/100m
Squeezing	800 kgf/600 mmR-roller	Less than 0.02 dB/100m

3-3. Water blocking characteristics

These prototype cables have water blocking performance by using water blocking tapes for wrapping. Test setup is shown in Fig.9. As a result, water leak at the cables end was not observed 240 hours after water injection. Newly designed cables have excellent water blocking capacity as well as the ordinary 1000-fiber cable structure.

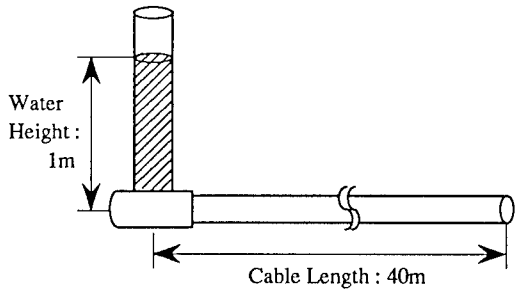
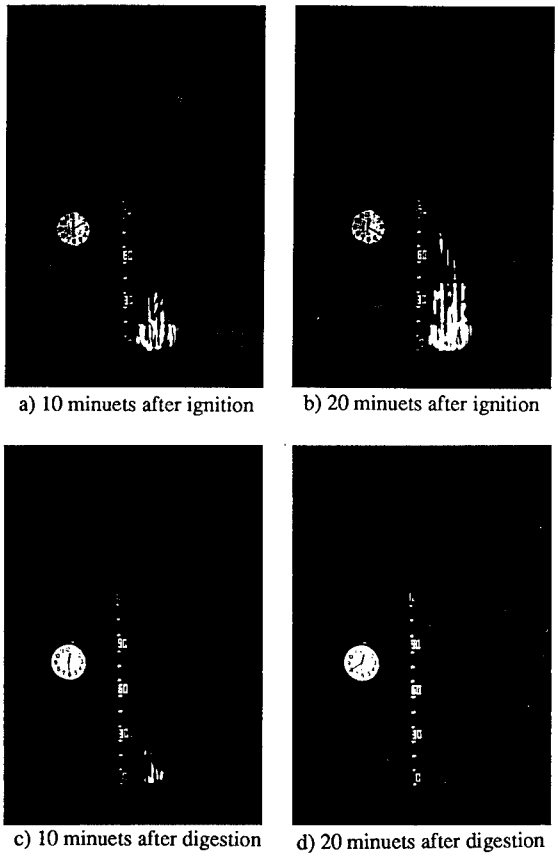


Fig.9 Water blocking test set up

3-4. Flame retardant characteristics

The flame retardant characteristics of the prototype FR(Flame Retardant) cables was executed in accordance with "JIS C 3521", "Flame Test Method for Flame Retardant Sheath of Telecommunication Cables". One of the test views are shown in Fig.10. As a result, fire could not continue and extend within 1.4m length. Good flame retardant characteristics are confirmed.



a) 10 minuets after ignition b) 20 minuets after ignition

c) 10 minuets after digestion d) 20 minuets after digestion

Fig.10 Flame retardant test view of newly developed 1000-fiber cable

4. Conclusion

The newly developed single slotted-rod 1000-fiber cable makes the diameter of the cable reduced about 25%, and fiber-packing density increased about 80% compared with ordinary multi slotted rods type 1000-fiber cable. And the excellent cable performances, including water blocking and flame retardant characteristics, are achieved. From the late 1995, these newly developed cables will be used actual field in Japan.

References

[1] T. Uenoya, "The Optical Fiber Loop 21 Plan" , OEC, 1990

[2] T. Miki, "Introduction Plan for Optical Network of the B-ISDN", ECOC'90, 1990

[3] S. Hatano et al., "Multi-hundred-fiber Cable Composed of Optical Fiber Ribbons Inserted Tightly into Slots", 35th IWCS, 1986

[4] H. Sawano et al., "One-thousand-fiber Optical cable Composed of Eight Fiber Ribbons", 38th IWCS, 1989

[5] Y. Kikuchi et al., "Characteristics of One-thousand-fiber Water Proof Cable", 39th IWCS,1990

[6] H. Iwata et al., "Design and Performance of Pre-connectorized High-density Optical Fiber Cable", TECHNICAL REPORT OF IEICE, OCS95-15, 1995

[7] T. Tomita et al., "Preliminary Research into Ultra High Density and High Count Optical Fiber Cables", 40th IWCS, 1991

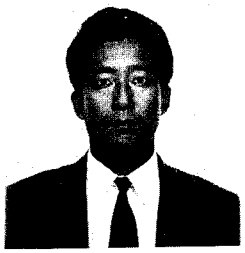
[8] T. Tomita et al., "Ultra High-Density Optical Fiber Cable with Thin Coated Fibers and Multi-Fiber Connectors", 42th IWCS, 1993

[9] N. Okada et al., "Ultra High-Density Optical Fiber Cable with Thin Coated Multi-Fiber Ribbons for Subscriber Networks", 43th IWCS, 1994

Naoki Okada

Opto-Electronics
Laboratory
Fujikura Ltd.

1440, Mutsuzaki,
Sakura-shi, Chiba,
285, Japan

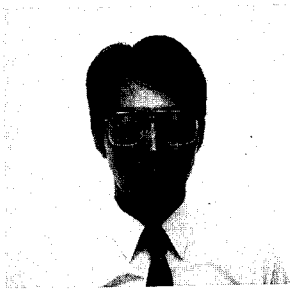


Naoki Okada was born in 1964. He joined Fujikura Ltd. after his graduation from Chiba University with a B.E. degree in 1986 and has been engaged in research and development of optical fiber cables. He is now an engineer in the Telecommunication Cable Section and a member of the IEICE of Japan.

Kohichiro Watanabe

Opto-Electronics
Laboratory
Fujikura Ltd.

1440, Mutsuzaki,
Sakura-shi, Chiba,
285, Japan

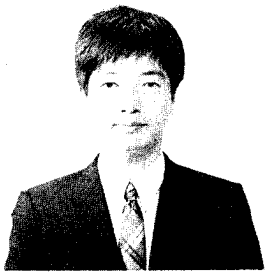


Kohichiro Watanabe was born in 1959. He received a B.E. degree in electrical engineering from Tohoku University in 1982. Since joining Fujikura, Ltd. in 1988, he has worked on the development of optical fiber cables. He is currently employed in the Telecommunications Cable Section of the Opto-electronics laboratory.

Kazunaga Kobayashi

Opto-Electronics
Laboratory
Fujikura Ltd.

1440, Mutsuzaki,
Sakura-shi, Chiba,
285, Lapan

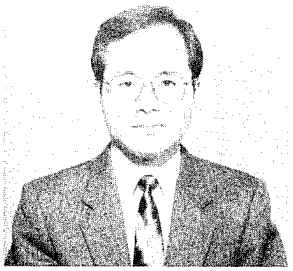


Kazunaga Kobayashi was born in 1961. He joined Fujikura Ltd. after his graduation from Gunma University with a M.E. degree in 1985 and has been engaged in research and development of optical fibers. He is now an engineer in the Telecommunication Cable Material Section and a member of the IEICE of Japan.

Matsuhiro Miyamoto

Opto-Electronics
Laboratory
Fujikura Ltd.

1440, Mutsuzaki,
Sakura-shi, Chiba,
285, Japan



Matsuhiro Miyamoto was born in 1953. He graduated from Nagoya Institute of Technology with a B.E. degree of electrical engineering. He joined Fujikura Ltd. after his graduation from Tokyo Institute of Technology with a M.S. degree in 1978 and has been engaged in research and development of optical fiber and optical fiber cables. He is now a manager of the optical fiber cable section.

Akira Sano

Opto-Electronics
Laboratory
Fujikura Ltd.

1440, Mutsuzaki,
Sakura-shi, Chiba,
285, Japan



Akira Sano was born in 1960. He joined Fujikura Ltd. after his graduation from Kyoto University with a B.E. in 1983 and has been engaged in research and development of cable materials. He is an engineer of the Telecommunication Cable Section and a member of IEICE of Japan.

Development of 1000-fiber Single Slotted Core Cable

M.Hara, R.Matsuoka, M.Saito, A.Otake and H.Hondo
The Furukawa Electric Co., Ltd.
6, Yawata Kaigandori, Ichihara, Chiba, 290, Japan

Abstract

With the object of realizing higher-density and smaller-diameter optical fiber cables, a 1000-fiber single slotted core cable was developed by stacked ten thin coated 8-fiber ribbons in one slot. Thin coated 8-fiber ribbons were manufactured experimentally at two levels of materials, ordinary Young's modulus and high Young's modulus, but no notable differences were observed, and favorable properties were obtained in both types. Varying the cable twisting pitch from 500 to 1000 mm resulted in a problem in bending characteristic at 1000 mm pitch, but no problems were noted at smaller pitches, and satisfactory cable characteristics were obtained.

1. Introduction

For construction of optical fiber networks for subscriber systems, attempts have been made to achieve higher density and smaller diameter in optical fiber cables. [1)]

To reduce the diameter, it has been proposed to decrease the thickness of ribbon fiber and increase the number of ribbons of one slot, or combine multiple slotted rods into a single slotted rod, and optical fiber cable with new structures are being developed according to these method.

However, it is considered that the practice of increasing the number of ribbons and decreasing the radius of curvature by single slotted rod structure increase the lateral pressure on the ribbon and adversely affects the cable characteristics. The radius of curvature of ribbon depends on a large extent on the cable twisting pitch.

Accordingly, after fabricating trial cables by varying the cable twisting pitch, we investigated the relation between the cable characteristic and the twisting pitch in order to ascertain the optimum pitch, and successfully obtained favorable cable characteristics, as reported in the following.

2. Cable structure

Fig. 1 shows the structure of the cable we have developed. In consideration of compatibility with the existing cables, the ribbon is composed by eight conventional 0.25 mm fibers, and the ribbon thickness is reduced from the conventional 0.4 mm to 0.3 mm. These ribbons are assembled in 13-slots of single slotted rod by stacked ten layers in one slot, and the maximum number of fiber is 1040.

Table 1 shows a comparison with a conventional 1000-fiber cable. As compared with the conventional cable, the outside diameter is smaller by 10 mm, and the fiber density is 1.75 times higher.

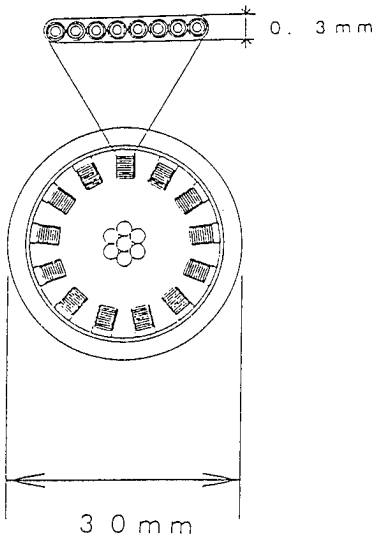


Fig. 1 Cable Structure

Table 1 Comparison with Cable Structure

	trial cable	conventional cable
fiber diameter	0.25mm	0.25mm
ribbon thickness	0.3mm	0.4mm
number of ribbon	10/slot	5/slot
cable diameter	30mm	40mm
fiber density	1.4fiber/mm2	0.8fiber/mm2

3. 8-fiber ribbon

In the ribbon, the ribbon coating thickness is reduced from the conventional 0.4 mm to 0.3 mm. When the coating thickness of the ribbon is decreased, there appears to be a risk of deterioration of lateral pressure characteristic. Accordingly, transmission loss in the free coil state and lateral pressure characteristic were evaluated. The lateral pressure characteristic was evaluated in a drum winding test. In this test, the ribbon is wound around a drum under tension and the loss increase at wavelength 1.55 um is measured. [2)]

Evaluated samples are shown in Table 2. The Young's modulus of ribbon coating was prepared at ordinary level and high level, and a conventional 0.4 mm thick 8-fiber ribbon was tested as reference. Transmission loss in the free coil state is also shown in Table 2. It can be seen that there is no problem in transmission loss in the free coil state.

Results of the drum winding test are given in Fig. 2. As can be seen from the diagram, the lateral pressure characteristic deteriorates as the ribbon thickness is reduced. It can also be seen that the Young's modulus of the ribbon material is almost unrelated to the performance. It seems that the effect of the ribbon material is small because the ribbon coating thickness is very small.

Table 2 Samples of Ribbon

No.	ribbon thickness (mm)	Young's modulus (arb. unit)	transmission loss, 1.55um (dB/km)
1	0.3	1	0.19
2	0.3	1.3	0.19
3	0.4	1	0.19

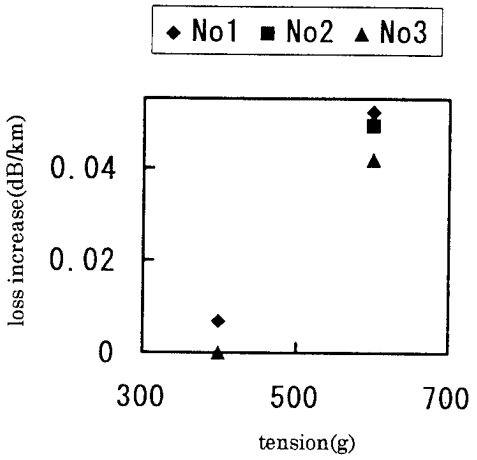


Fig. 2 Result of Drum Winding Test

4. Slot pitch

In this cable structure, since the ribbons are stacked with ten layers in one slot, when a lateral pressure acts on the ribbons, it is considered that the lateral pressure acting on the ribbon in the lowest layer is greater than in the conventional five layer stacked structure.

Moreover, in this structure, because of single rod design, the slotted rod diameter is larger and the radius of curvature of the ribbon is smaller. Accordingly, when a tensile force acts on the ribbons, the force of pressing the ribbons on to the slotted rod is also considered to be greater.

The radius of curvature of the ribbon varies with the slot pitch: the broader the pitch, the greater the radius of curvature. It is hence considered important to study the relation between the slot pitch and cable characteristic.

Fig. 3 shows the radius of curvature when the pitch is varied in this cable structure, in comparison with the radius of curvature in the conventional structure. In this cable structure, the radius of curvature is quite small, and is about one-third at the same pitch. For the radius of curvature to be the same as in the conventional structure, it is known that the pitch must be about 1000 mm.

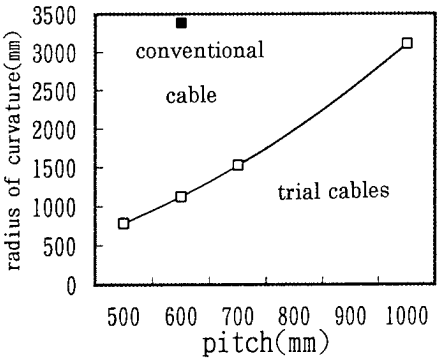


Fig. 3 Relation between Pitch and Radius of curvature

5. Trial fabrication of cable

On the basis of the above studies, trial cables were fabricated by varying the slot pitch at four levels, from the conventional 500 mm to 1000 mm that is roughly equal to the radius of curvature. The cables were then evaluated.

5.1 Transmission loss

Fig. 4 shows the transmission loss at 1.55 um of fibers at both ends in the lowest layer ribbons. An acceptable transmission loss was obtained at all levels. At pitch 500 mm, however, it was noted that the transmission loss showed a slight tendency to increase.

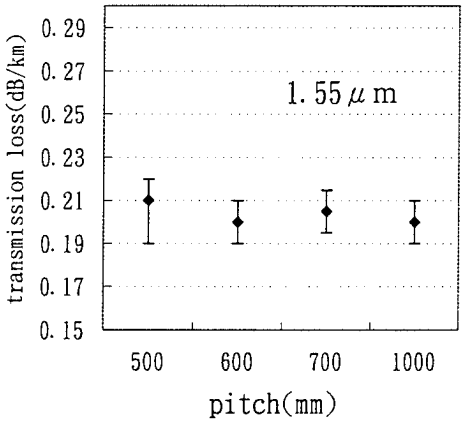


Fig. 4 Relation between Pitch and Transmission Loss

5.2 Bending characteristic

When the pitch is varied, this is thought to have an effect on the bending characteristic of the cable. Fig. 5 shows loss fluctuations at 1.55 um when the cable is bent at a radius of 200 mm. From pitch of 500 mm to 700 mm, no loss fluctuations were observed, but at 1000 mm, a loss increase of about 0.4 dB was detected.

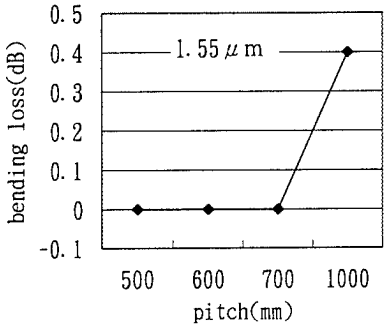


Fig. 5 Relation between Pitch and Bending Loss

5.3 Other mechanical characteristics

With regard to temperature characteristic, crushing characteristic, and tensile characteristic, no problems occurred at any level, as shown in Table 3.

Table 3 Mechanical Characteristics

item	condition	result (at1.55um)
temperature characteristic	-30~60℃	<0.01dB/km
crushing characteristic	2000N/100mm	no loss increase
tensile characteristic	8000N	no loss increase

6. Conclusion

The relation between slot pitch and characteristic was studied in a 1000-fiber single slotted rod cable using thin coated 8-fiber ribbons. It was determined from the study that the pitch from 500 mm to 700 mm was the optimum pitch from the viewpoints of both transmission characteristic and mechanical characteristics, and problem-free, satisfactory cable characteristics have been demonstrated.

References

1) H. Iwata, M. Matsumoto, Y. Ishino, S. Tomita, S. Nagasawa and T. Tanifuji, "Field Test Results for Pre-connectorized Cable with 16-fiber Ribbons", 43rd IWCS, 1994.

2) M. Saito and S. Okagawa, "16-fiber Ribbon for Ultra-high-density and High-count Optical Fiber Cable", 42nd IWCS, 1993.

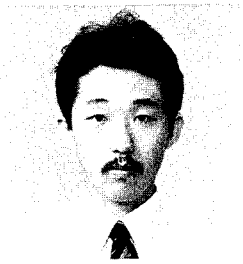


Masami HARA

The Furukawa Electric Co., Ltd.

6, Yawata Kaigandori, Ichihara, Chiba, 290, Japan

Mr. Hara received his M.E. degree in Physics from Osaka University in 1987. He joined The Furukawa Electric Co., Ltd. and has been engaged in research and development of optical fiber cable. He is now a research engineer of optical fiber transmission research department, opto-technology laboratory.



Ryuichi MATSUOKA

The Furukawa Electric Co., Ltd.

6, Yawata Kaigandori, Ichihara, Chiba, 290, Japan

Mr. Matsuoka received his M.E. degree in electronics from Osaka University in 1991. He joined The Furukawa Electric Co., Ltd. and has been engaged in research and development of optical fiber cable. He is now a research engineer of optical fiber transmission research department, opto-technology laboratory.



Minoru SAITO

The Furukawa Electric Co., Ltd.

6, Yawata Kaigandori, Ichihara, Chiba, 290, Japan

Mr. Saito received his M.E. degree in chemistry from Kyushu University in 1992. He joined The Furukawa Electric Co., Ltd. and has been engaged in research and development of optical fiber cable. He is now a research engineer of optical fiber transmission research department, opto-technology laboratory.



Akihiro OTAKE

The Furukawa Electric Co., Ltd.

6, Yawata Kaigandori, Ichihara, Chiba, 290, Japan

Mr. Otake graduated from Tohoku University in 1974. He joined The Furukawa Electric Co., Ltd. and has been engaged in research and development of optical fiber cable and those accessories. He is now the chief of optical fiber transmission research department, opto-technology laboratory.



Hirotoshi HONDO

The Furukawa Electric Co., Ltd.

6, Yawata Kaigandori, Ichihara, Chiba, 290, Japan

Mr. Hondo graduated from Tohoku University in electrical engineering in 1969. He joined The Furukawa Electric Co., Ltd. and has been engaged in development of telecommunication cables including optical fiber cable, almost during 25 years. During the time period, he was in design engineering department for 6 years and returned to R&D division. Now he belongs to opto-technology laboratory.

Component Optimization for Slotted Core Cables Using 8-Fiber Ribbons

R. S. Wagman, G. A. Lochkovic, K. T. White

Siecor Corporation
489 Siecor Park, Hickory, North Carolina 28603

Abstract

A development program was initiated to reduce the diameter of 600 and 1000 fiber slotted core ribbon cable designs. The development focused on three key areas: the ribbons, the slotted rod and the jacketing process. The development objectives were (1) to develop a thin, 8-fiber ribbon, separable into two 4-fiber ribbons, (2) to develop a slotted rod of optimized diameter with the capacity to hold ten 8-fiber ribbons in each slot, and (3) to apply a cable jacket that is tight enough to minimize water penetration without interfering with the ribbons.

A newly developed 8-fiber ribbon design with a dual-layer coating was found to enhance the ribbon separation characteristics. The thin outer ribbon coating has a lower Young's modulus than the inner ribbon coating. For the slotted rod design, experiments were used to establish an optimum slot depth for the stack of 10 ribbons. No significant differences were found between the two experimental slot widths. Jacket experimentation was used to set the process limits for polymer melt temperature, line speed and jacket tooling. These parameters interactively affect slot intrusion and core extraction.

A 1000-fiber cable prototype was made accordingly. This new cable compares favorably to existing slotted core ribbon cables in a standard battery of tests.

1.0 Introduction

Nippon Telegraph and Telephone (NTT) is deploying a fiber optic subscriber network that requires high fiber count cables to utilize their underground facilities economically [1] [2]. This has led to the development of new 600 and 1000 fiber slotted core cables which have greatly reduced diameters.

The new 600 and 1000 fiber cables attain their compact size compared to previous cables through the use of (a) a single slotted rod as opposed to multiple slotted rods, (b) 10 ribbons per slot as opposed to 5, (c) 320 μm thick ribbons as opposed to 400 μm thick ribbons, and (d) 8-fiber ribbons separable into 4-fiber ribbons as opposed to individual 4-fiber ribbons. (The previous 1000 fiber cable did use thick, separable, 8-fiber ribbons [3], but the previous 600 fiber cable used 4-fiber ribbons). Figure 1 compares the relative sizes of the new designs versus the previous designs.

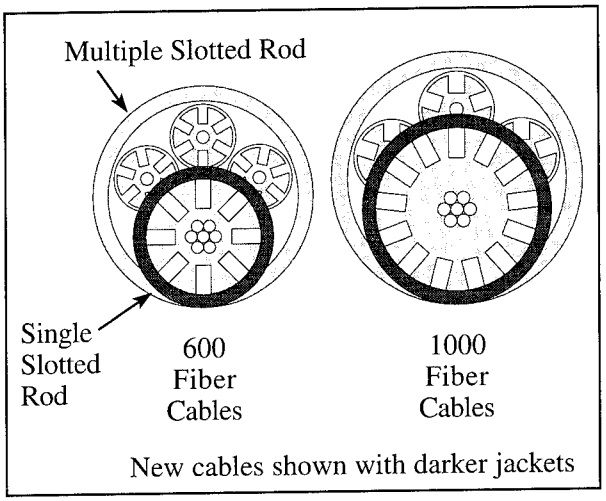


Figure 1. Cross-Sections of the New Cable Designs

These new cables presented three key development challenges: (1) to develop a thin, 8-fiber ribbon, separable into two 4-fiber ribbons, (2) to develop a slotted rod of optimized diameter with the capacity to hold ten 8-fiber ribbons in each slot, and (3) to apply a cable jacket that is tight enough to minimize water penetration without interfering with the ribbons.

2.0 8-Fiber Ribbon

Previous 8-fiber ribbons were 400 μm thick and separable into two 4-fiber ribbons [3]. The goal of the ribbon development was to maintain acceptable separation properties and attenuation properties in the cable while reducing the thickness of the ribbon to 320 μm. The development process consisted of three stages.

The first stage in the development was to investigate alternate ribbon geometries. Generic examples are shown in Figure 2. Short lengths of these geometries were manufactured and evaluated for general properties. Based on this investigation, the dual-layer geometry was chosen for further development. A dual-layer

ribbon is made by applying an inner ribbon coating over the fibers to form two 4-fiber units, and then applying an outer ribbon coating over the 4-fiber units to form the 8-fiber ribbon.

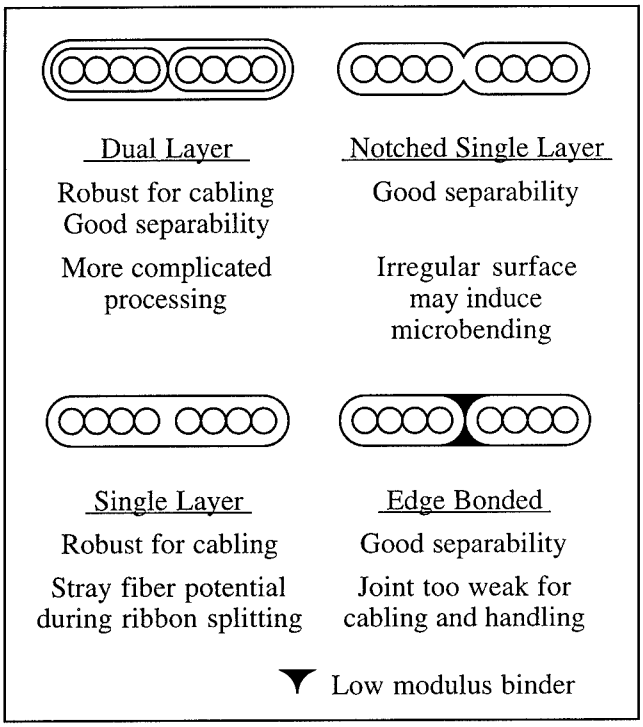


Figure 2. Ribbon Geometries with Comments

In the second stage of development, the focus was on two tests. The first test measured fiber attenuation while separating the ribbon into its 4-fiber units using a tool. In addition, the appearance and the integrity of the 4-fiber units were characterized. The second test measured the attenuation of the ribbon wound under tension on a reel [4]. This test is used to predict attenuation properties in cable.

In this second stage of development, the optimum materials for the dual-layer ribbon were determined. Materials of various Young's moduli were used for the fiber outer primary coating, the inner ribbon coating and the outer ribbon coating. Preliminary testing showed that ribbons with materials of the same modulus did not separate well. The results of the second stage trials using various combinations of different moduli are shown in Table 1. Each attenuation change in the table is the maximum average attenuation increase observed for each of the various ribbons.

Ribbons #1, 2 and 5 in Table 1 had a low modulus inner ribbon coating. During the separation testing, the 4-fiber units did not maintain structural integrity which resulted in stray fibers. These ribbons did show good winding under tension results. Ribbons #5, 6 and 7 had a high modulus fiber outer primary coating. These ribbons had either high attenuations in the winding under tension test or in the separation test. Consequently, a lower modulus fiber outer primary coating, a higher modulus inner ribbon coating and a lower modulus outer ribbon coating were chosen.

In the third stage of the ribbon development, emphasis was placed on improving the appearance of the 4-fiber units. The outer ribbon coating did not always separate in the middle of the 8-fiber ribbon. The 4-fiber units had stringers of extra outer ribbon coating (See Figure 3).

Two improvements were made to minimize stringers. (1) Reduction in the thickness of the ribbon's outer coating resulted in a split closer to the center of the ribbon which decreased stringer length. (2) Processing additives used to enhance the coating's flow characteristics were removed from the inner ribbon coating. These additives caused inconsistent adhesion between the ribbon coatings, and their removal minimized

Parameter		#1	#2	#3	#4	#5	#6	#7
Young's Modulus of the Coatings (MPa)	Fiber Outer Primary	Med	Med	Med	Med	High	High	High
	Inner Ribbon	Low	Low	Med	High	Low	Med	High
	Outer Ribbbon	Med	High	Low	Low	Med	Low	Low
Winding Under Tension Test: Attenuation Increase (dB) @ 1550		0.02	0.00	0.02	0.03	0.01	0.03	0.07
Separation Test: Attenuation Increase (dB) @ 1550	Upon Closing Tool	0.04	0.03	0.12	0.04	0.22	0.01	0.32
	During	0.06	0.01	0.01	0.00	0.11	0.10	0.01
	After	0.00	0.01	0.00	0.01	0.01	0.00	0.00
Stray Fiber During Separation		Yes	Yes	No	No	Yes	No	No

Table 1. Second Stage Ribbon Parameters and Test Results

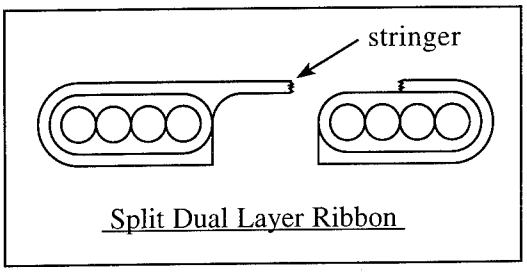


Figure 3. Example of a Stringer

stringers with no significant impact on the processing. Running over 1,000 kilometers of ribbon with these modifications has demonstrated both the robustness of the ribbon and the efficiency of its production.

This final design for the 8-fiber ribbon is a dual-layer ribbon that uses materials similar to ribbon #3 in Table 1. The attenuation change during the separation test is lower, however, for the final design than for ribbon #3. In addition, the length of the stringer was reduced by more than 75%. This final design compares favorably to the previous 400 μm thick ribbons which had separation attenuation changes less than 0.5 dB [3].

3.0 Slotted Rod

The design of the slotted rod has the greatest impact on low temperature attenuation performance. There are three key variables that affect this performance. They are slot width, depth and pitch. The slotted rod, shown in Figure 4, is manufactured by profile extrusion over a central strength element.

A designed experiment was conducted to determine the optimum slot dimensions and pitch needed to contain stacks of ten 8-fiber ribbons. A U-Groove cable [5] was used to perform the experiment. U-Grooves can be stranded around a central element to form a cable that functions similarly to a slotted core cable. The advantage of a U-Groove cable during experimentation is that the pitch can be easily changed. For each experimental cable, two U-Grooves contained ribbon stacks.

Prior experience with 4- and 16-fiber ribbon cables provided guidelines for choosing the ranges for slot depth, width and pitch. High and low values were chosen for each of the variables.

The average attenuation of the top corner fibers of each ribbon stack at -30°C was the response variable for the experiment. These fibers are most likely to have increases in attenuation at -30°C if there is insufficient room in the slot to accommodate the ribbons

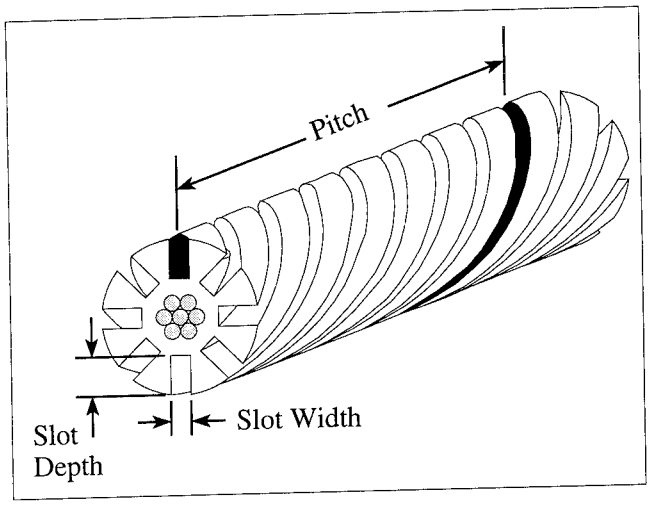


Figure 4. Diagram of Slotted Rod Showing the Key Variables

when the cable shrinks longitudinally. To ensure good comparisons, all of the optical fibers had 1550 nm attenuations between 0.19 and 0.20 dB/km before processing, and all of the cables were processed identically.

The results of the experiment are shown in Table 2. For an attenuation difference of 0.22 dB/km between the average for the top corner fibers in any two slots, the difference is statistically significant at a 98% level of confidence (t-Ratio). In step A of the experiment, five cables were made. All of the cables with the smallest depth had unacceptably high top corner fiber attenuations. The slot width was not a significant factor. Results showed that the 375 mm pitch resulted in better attenuation performance than the 450 mm pitch. The two cables with the largest slot depth had acceptable top corner fiber attenuations. Again, slot width was not a significant factor.

In step B of the experiment, the slot depth was investigated while keeping the slot width and pitch constant. Both of the slot depths resulted in low attenuations. When these cables were also tested at high temperatures, the average 1550 nm attenuation of the bottom corner fibers was 0.23 dB/km Historically, these are the most vulnerable fibers at high temperature because the ribbons move down to the bottom of the slot as the cable length increases with increasing temperature.

A slot depth that is slightly less than the larger depth in step B was selected to allow for processing tolerances, and to make the cable design robust.

Cable Group	Variables			-30°C Attenuation at 1550nm (dB/km)			
	Relative Slot Depth (mm)	Relative Slot Width (mm)	Relative Lay Length	Top Corner Fibers		Other Fibers	
				Slot #1	Slot #2	Slot #1	Slot #2
A	0.0	0.0	0.83	0.42	0.42	0.22	0.23
	0.0	0.3	0.83	0.50	0.28	0.22	0.22
	0.0	0.3	1.00	0.77	0.92	0.23	0.22
	1.0	0.0	1.00	0.26	0.26	0.21	0.22
	1.0	0.3	1.00	0.25	0.29	0.23	0.21
B	0.4	0.0	1.00	0.27	0.27	0.21	0.20
	0.7	0.0	1.00	0.21	0.23	0.20	0.20

Table 2. Cable Results for the Slotted Rod Experiment

4.0 Jacket

The jacketing process is especially important for the new slotted core cables because 8-fiber ribbons require wider slots than 4-fiber ribbons. Increasing slot width will increase slot intrusion given the same jacket application method. A water-blocking tape and a polyethylene jacket are applied over the slotted rod to form the top of the slot. If the jacket is applied too tightly, the tape and jacket will intrude into the slot. This will reduce the effective slot depth and cause low temperature attenuation problems (see Figure 5). Conversely, a loose jacket may lead to water penetration failures as well as installation problems.

As shown in Figure 5, slot intrusion is defined as the thickness of the jacket at the middle of the slot (Tmax) minus the thickness of the jacket over the slotted rod (Tmin). The jacket deformation pushes the water-blocking tape into the slot. So in effect, the tape position determines the effective slot depth. True intrusion is difficult to assess because the tape is compressible.

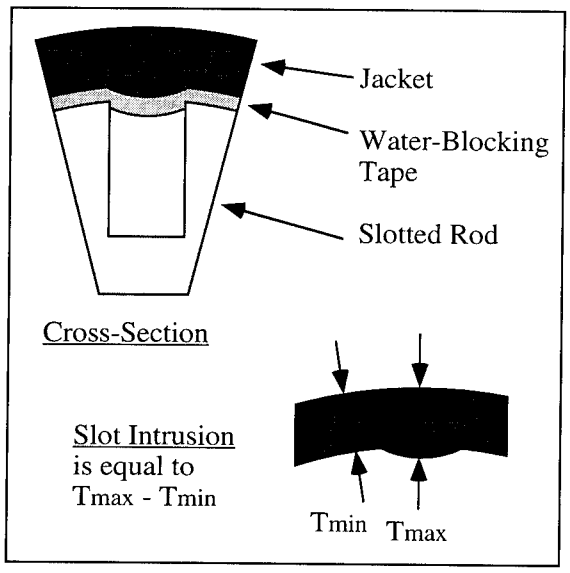


Figure 5. Section of Slotted Rod Cable Showing Jacket and Water-Blocking Tape Intruding into the Slot

The force required to extract the core longitudinally from the jacket is also measured. A loosely applied jacket will have a low extraction force. Core extraction is the peak force required to slide 40 cm of jacket off the cable core.

Four critical jacket parameters were identified for experimentation.

Polymer Melt Temperature can affect slot intrusion and core extraction. A higher melt temperature lowers the viscosity which may cause higher slot intrusion due to increased flow rate.

Line Speed can have several effects. Increased line speeds require additional extruder output which leads to increased shear rates and higher polymer melt temperatures. Line speed can also affect the cooling of the jacket by changing the cable's residence time in the cooling trough.

Cable Core Cooling was investigated for its effect on slot intrusion. The cable core was passed through a container of dry ice before entering the crosshead.

	Net Effect of an Increase in		
	Melt Temperature by +20°C	Line Speed by +10 mpm	Draw Down and Draw Ratio Increase
Slot Intrusion (mm)	+0.19	+0.05	+0.23
Core Extraction (N)	+43	+140	+220
Shrinkback (%)	Not Available	+0.2	0.0

Table 3. Effects of Process Parameters on Jacket Properties

Jacketing Extrusion Tooling is chosen to provide the desired draw down ratio and draw ratio balance. These ratios affect how the jacket is applied to the core by determining the velocity gradient with which the polymer exits the extruder. Typically, a specific polymer will have a recommended range for these variables which can be used as a starting point in experimentation. Early in the development process, semi-pressure tooling was replaced with landed tips and dies to reduce jacketing process variability. Also, a fixed center crosshead eliminated any adjustment of the tip and die.

Jacket shrinkback was also measured. It was necessary to verify that the variable ranges did not have a negative impact. The experimental results are shown in Table 3. No data is provided for cable core cooling because the jacket was so loose.

Slot intrusion is minimized by decreasing the melt temperature, decreasing the line speed and using optimized jacket tooling. However, these parameters affect slot intrusion and core extraction interactively so that fine tuning of the process is required. The experiments were used to set the jacketing process parameters for a consistent and optimized product.

5.0 Cable

A 1000 fiber cable prototype was made using the thin, separable, 8-fiber ribbons, the optimized slotted rod and the optimized cable jacket. A diagram of the 1000 fiber cable design is shown in Figure 6. The actual experimental cable, however, had only 3 slots filled. Standard testing [5] was conducted as shown in Table 4. The cable, as manufactured, had attenuations close to initial fiber values. The attenuation changes observed during all mechanical testing were within the range of measurement repeatability. At high temperatures, there was a 0.01 dB/km increase in the average 1550 nm attenuation. The water penetration tests (T-Tests) were conducted with a one meter head of artificial sea water, and the water was applied to a 2.5 cm section of the cable length where the jacket was removed. The T-Test was conducted with the water-blocking tape in place. In the modified T-Test, the tape was removed. The test results for this new cable compare favorably to those of existing slotted core ribbon cables. In addition, 600 fiber cable prototypes have shown similar results.

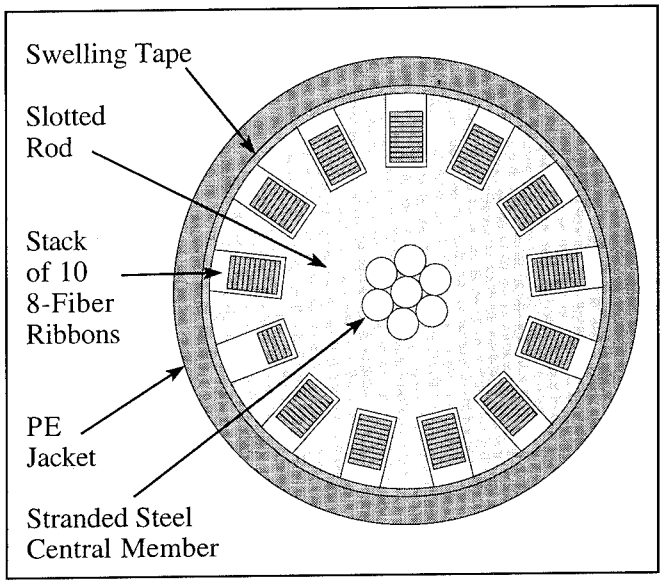


Figure 6. 1000 Fiber Cable Diagram

Description of Test		Result	
Attenuation on the reel at 1310 nm (dB/km)	except corners (n=228)	0.34	Average
	corner fibers (n=12)	0.34	
Attenuation on the reel at 1550 nm (dB/km)	except corners (n=228)	0.19	Average
	corner fibers (n=12)	0.20	
Bend (dB/90°)	200 mm Radius	<0.02	Increase in Loss @ 1550 nm for Every Fiber
Lateral Load (dB/100mm)	3000 N	<0.02	
Elongation (dB/19.5m)	0.15%	<0.02	
	0.25%	<0.02	
Squeezing (dB/0.95m)	0.20% Elongation, 600 mm Radius	<0.03	
Attenuation at Temperature Extremes (dB/km)	at -30°C	0.00	Average Increase in Loss @ 1550 nm
	at 60°C	0.01	
Water Penetration (m)	T-Test	0.08	Maximum Length of Penetration (24 Hours)
	Modified T-Test	9.32	

Table 4. 1000 Fiber Cable Test Results

6.0 Conclusions

A new family of slotted core ribbon cables has been developed that utilizes a single slotted rod with 10, separable, thin, 8-fiber ribbons in each slot. In the development, three key challenges were addressed.

- A thin, separable, 8-fiber ribbon was developed that has enhanced separation characteristics and that performs well in the cable. The ribbon has a dual-layer coating where the outer coating is relatively thin and has a lower modulus than the inner coating.
- Slotted rods were developed to provide low temperature performance. A designed experiment was used to establish a slot depth for the stack of 10 ribbons. No significant differences were found between the two experimental slot widths.
- A cable jacketing process was developed to provide an optimum jacket. Experiments were used to set the process limits for polymer melt temperature, line speed and jacket tooling.

A 1000-fiber cable prototype was made accordingly. This new cable compares favorably to existing slotted core ribbon cables in a standard battery of tests.

Acknowledgements

The authors thank the many people who contributed to this development program. Special thanks go to Mary Ann Clarke, Derwin Nelson, Chris Eoll, John Keesee, Ronnie Livingston and Jeff Dellinger.

References

[1] Y. Wakui, The Fiber-Optic Subscriber Network in Japan, *IEEE Communications Magazine*, pp. 56-63, February 1994.

[2] H. Ishihara, Plans for an Optical Access Network, *NTT Review*, pp. 11-18, Vol. 6 No. 4, July 1994.

[3] H. Sawano, Y. Kikuchi, Y. Kobayashi, N. Okada, M. Misono, H. Suzuki, N. Sato, One-Thousand-Fiber Optical Cable Composed of Eight Fiber Ribbons, Proceedings of the 38th International Wire and Cable Symposium, pp. 240-245, 1989.

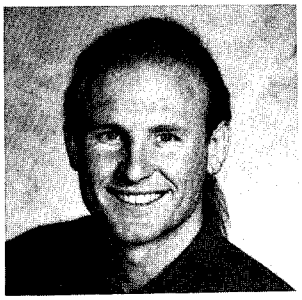
[4] J. Keesee, G. Lochkovic, D. Smith, R. Toler, A Comprehensive Approach to Ribbon Design with a Focus on Materials, Proceedings of the 43rd International Wire and Cable Symposium, pp. 430-439, 1994.

[5] R. Wagman, P. Bark, H. Cooke, C. Eoll, R. Livingston, G. Lochkovic, W. McAlpine, F. Sears, S. Sodhi, Design Concepts for a 4000-fiber Cable with Thinly Coated Fibers, Proceedings of the 43rd International Wire and Cable Symposium, pp. 12-21, 1994.

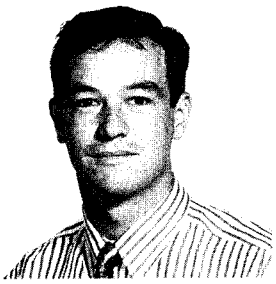
Authors



Richard S. Wagman was born in Dallastown, PA in 1956. He received his B.S. degree in the Engineering Science honors program at Pennsylvania State University in 1978, and his B.S. in Electrical Engineering from Johns Hopkins University in 1984. In 1985 he joined Siecor where he has worked with cable, materials and test design. He is currently employed as a Staff Engineer in the Research, Development and Engineering Department.



Gregory A. Lochkovic was born in Evansville, IN in 1962. He received a B.S.M.E. in 1985 from Purdue University and a M.S. in Manufacturing Systems from Clarkson University in 1993. He has worked on various fiber optic cable product and process development projects since graduation in 1985, and has been with Siecor Corporation since 1991. His responsibilities include development of UV-curable and related products. He is currently Supervisor for UV Development in the Research, Development and Engineering Department.



Kevin T. White was born in Boston, MA in 1969. He received a B.S. and M.S. in Plastics Engineering from the University of Massachusetts Lowell. Since starting at Siecor Corporation in 1994, his work has focused primarily on jacketing development for high fiber count slotted core cables. He is currently a Process Development Engineer in the Research, Development, and Engineering Department.

A COMPARATIVE STUDY OF POLYMERIC AND FUMED SILICA BASED OPTICAL CABLE FILLERS

M. Costello, A. Debska, A. Eckard, W. Thalman

Witco Corporation, Petroleum Specialties Group, Oakland Technical Center, 100 Bauer Drive, Oakland, NJ 07436

Abstract

A comparative study of the differences between fumed silica and various polymeric cable filler combinations was completed. The cone penetration, volatility, oil separation, and rheology appear to be significantly different for the two classes of compounds. Within the class of polymeric cable filling compounds there are two types, which we will call Type A and Type B. The Type A polymeric cable fillers possess superior physical and rheological properties to the Type B blends. It appears the tendency of Type A polymers to form a non-networked three dimensional lattice in oil reduces the viscosity and amount of oil bleed. The Type A polymers can serve the dual purpose of gelling agent and anti-bleed agent.

Introduction

Optical fiber cables have made great inroads into the communication cable market. Since the fiber optic element is fragile the fibers are placed in a bundle, which is then inserted into a protective buffer tube. Although the presence of water is not detrimental to its performance, moisture may eventually damage optical fibers,[1] and passage of the water along the cable interior to the connection points, terminals, or associated equipment, may cause problems and should be prevented. When a cable is buried, it may be immersed in water and plastic insulation alone is not enough to protect against the effects of water, if at any point along the length there is mechanical damage. Water which enters through perforations in the sheath can travel a considerable distance along an unfilled cable via capillary action. Current industry standards address this problem with various water blocking provisions.

Waterblocking (also referred to as flooding or filling) compounds have been used to fill cable cores and coat portions of the cable sheath to prevent the movement of water longitudinally along the cable. The filled cable design was developed to overcome the short-comings of plastic insulated cables.[2] In the filled cable the interstitial spaces are filled and the sheaths are flooded with hydrophobic compounds. In some designs, the fiber optic elements can not be allowed to remain loose in the buffer tube, since mechanical shock or bending could damage the fiber. Accordingly the filling compound also acts as a cushion, to protect the fibers. Typical compositions are thixotropic in nature and cause maintenance problems during splicing in the field. These cable fillers are typically semi-solid or semi-liquid substances comprising a gelling agent in a liquid carrier. Frequently used gelling agents are: fatty acid soaps, clays, silicas, waxes, rubber copolymers, and petrolatums. The industry is currently moving toward polymeric gelling agents and hydrogenated copolymers of styrene and rubber are preferable to the polyisoprene copolymers (SIS) since they are more compatible with hydrocarbon fluids, do not degrade at high blend temperatures, and are not tacky in compositions of interest to cable filling applications.

Over the years the properties of a good cable filling material have been enumerated several times and an amalgamation of typically desirable properties are as follows:

1. The filler must perform well over the range of temperatures from -40°C to 76°C.
2. The filler must be free of syneresis (oil bleed) over the same temperature range.
3. The filler must yield and recover under strains experienced when the cable is made or handled
4. The filler must be thermally and oxidatively stable.
5. The filler must not be effected by water, and prevent its incursion.
6. The filler must be compatible with the sheath and buffer tube materials.

Additionally, the compound must be economical, safe, and compatible with existing filling equipment. These remaining criteria are

obvious and need not be included with the physical criteria of the filler. In this study we will investigate the properties in statements 1, 2, and 3 through the use of the standard test methods for fillers gelled with polymer, silica, and combinations of the two.

Procedures

Preparation of Blends

The hydrocarbon carriers chosen were a low pour napthenic white mineral oil, a 4 cSt PAO and a 5 cSt PAO. Typical properties are listed in Table 1. In terms of volatility and low temperature flexibility, these hydrocarbons were the best match for comparison of cable filler properties.

The blends of the silica and polymer based cable fillers were prepared in the lab and heated to 130°C with mixing for 2-4 hours to insure proper dissolution of the gelling agent in the carrier oil. These samples were then cooled and centrifuged at moderate speed to remove any entrapped air in the samples. Blends 1 to 9 were made with differing combinations of the Type A polymers, since Type B polymers do not form soft

Table 1

Property	Mineral Oil	4 cSt PAO	5 cSt PAO
Viscosity 40°C, cSt	37.5	16.9	23.9
Viscosity 100°C, cSt	5.4	3.9	5.1
Viscosity Index	53.9	123	145
Pour Point, °C	-37	-73	-48
Flash Point, °C	190	219	238
Color, Saybolt	+30	+30	+30

gels, blends 10 to 13 were made with a combination of Type A and Type B polymer. Blends 14 to 18 contain different amounts of hydrophobic and hydrophilic fumed silica for comparison with the block copolymer blends. Blends 19 to 26 contain poly-α-olefins for comparison with mineral oil carriers.

For non-Newtonian fluids, of which our blends are of the type which are pseudo-plastic and thixotropic, the viscosity changes as the shear rate is varied. Thus, the viscometer model, spindle type, and rotational speed all have an impact on the on the measured viscosity value. The rheological properties of the gels were studied with a Brookfield Model RVF Viscometer with a #7 spindle at 22°C and 55% humidity according to ASTM D1824 (which recommends 23±1°C and 50±5% humidity). Each sample sheared for two minutes at four different rotations (2, 4, 10, and 20 rpm, which corresponds to shear rates of 0.1, 0.05, 0.02, and 0.01 sec^{-1}, respectively). In order to evaluate the handling characteristics of the samples the apparent viscosities were measured and the following criteria were calculated: shear thinning index, degree of thixotropy, and thixotropy index. These criteria which are defined below, were calculated as recommended by ASTM 2196 with one modification. The apparent viscosities measured in consideration for the shear thinning index evaluation were made at 2 and 10 rpm, whereas the method specifies typical combinations of speeds as 2 and 20 rpm.

As defined by ASTM D2196 the shear thinning index is the ratio between the viscosity at 2 rpm to the viscosity at 10 rpm. The degree of thixotropy is a ratio of the viscosity at 2 rpm, taken with increasing speed to that with decreasing speed. The thixotropy index is the ratio of the viscosity at 2 rpm taken after a rest period of 30 minutes to that before the rest period.

The volatility tests were conducted at 150°C and 80°C and aged for 24 and 48 hours, respectively. The volatilities were measured by comparing the weight loss of the filling compound before and after the aging. The oil separation test was conducted according to FED 791 at 80°C for 48 hours. The cone penetration values were determined by ASTM D937, with a 150g weight.

Results and Discussion

Appearance

In evaluating the appearance of the filling compound it is important to observe the homogeneity and consistency of the material. The cable fillers tested typically ranged in appearance from clear (C) to slightly hazy (SH) to hazy (H). Blends made with Polymer Type A and B appear clear, while silica based formulations appear hazy (See Table 2 and 3). The advantage of a clear appearance is the ability to visually identify impurities or air bubbles in the filler.

Oil Separation

Oil separation is a property of a gelled material which describes the tendency to bleed oil during the lifetime of the cable. Oil separation (or syneresis) is controlled by assuring the complete dispersion of an adequate amount of

colloidal thickener or other gelling agent. There are several types of oil separation tests and the techniques to measure the separation are varied. Some of the current procedures involve the use of high speed centrifugation[3], modified paper bleed tests[4], or grease tests with mesh cones.[5]

Due to fabrication difficulties, filling of short lengths of cable for drip testing is usually not feasible, therefore, the results of modified oil separation tests have been previously correlated to the loose tube cable drip test (REA PE-90).[6] Our test method utilizes the cone bleed test (FED 791) for lubricating grease. We would expect, in a like manner, that these tests will be correlated with cable drip performance.

Oil separation results reveal that the Type A polymers which bleed 0.1% oil are superior to both Type B (Blend 10 to 13) and fumed silica formulations (Blend 14 to 18) which bleed between 3.6 and 98% oil. In fact, after several months of storage, the Type A polymers show no signs of oil bleed, even with repeated centrifugation.

Volatility

Ideally, a gel with a low volatility would be desirable for a filling compound. The volatility of the cable filling compound can limit both the filling temperature[7] and the compatibility of the filler with the buffer tube and jacket. The volatility of the filler depends almost entirely on the choice of the liquid carrier used. Fillers which contain synthetic carriers like poly-α-olefins or polybutenes are lower in volatility, but are very expensive when compared to mineral oil based products.[8]

The 80°C volatility of the Type A, Type B, and fumed silica formulations are indistinguishable (see Table 2 and 3). Since the values are the same, the oil separation at 80°C for the Type A polymers can be attributed solely to the volatility of the oil at this temperature and not to the syneresis of the gel. It does not appear there is any differentiation in the products until a high temperature volatility test is performed at 150°C for 24 hours. Under these conditions it appears that the silica based fillers may be less volatile than the polymer based blends (16.9-18.5% weight loss vs. 19.8-23.4% weight loss). Surprisingly, the 150°C volatility shows no correlation with the 80°C volatility values (r^2 = 0.01) and demonstrates that extreme test conditions such as these may reveal differences in volatilities of blends, but may not correlate with observed behavior in filling operations, which are conducted at 80°C or less.

Cone Penetrations

It is important that the cable filler possess good flexibility at low temperatures. A well formulated cable filler not only should not drip at elevated temperatures, but remains flexible at temperatures down to -40°C. The cone penetration value of a filling compound is an easy and quick way to estimate the low temperature flexibility. It has also been reported that cone penetrations above 200 dmm at -40°C are required to minimize attenuation loss in the optical fiber.[9] Recent formulations of fillers have also incorporated poly-α-olefins into the formulation to improve the low temperature flexability.[10]

Although mineral oil carrier blends (Blend

Table 2

Blend	1	2	3	4	5	6	7	8	9	10	11	12	13
Mineral Oil	X	X	X	X	X	X	X	X	X	X	X	X	X
Polymer Type A	X	X	X	X	X	X	X	X	X	X	X	X	
Polymer Type B										X	X	X	X
Appearance	C	C	C	C	C	C	C	C	C	H	H	H	C
Cone Pen. (dmm) -60°C	98	93	91	81	136	143	116	98	80	126	104	83	60
-40°C	207	202	193	181	-	249	223	199	177	184	220	147	74
-20°C	290	272	257	248	-	-	306	261	188	237	227	162	93
0°C	352	333	323	304	-	-	362	326	296	271	242	202	117
+21°C	366	340	344	337	-	-	-	364	337	295	282	229	156
Oil Separation, 80°C, 48h,%	0.2	0.2	0.2	0.1	97.8	97.3	88.6	22.8	0.2	76.1	84.6	94.3	98.7
Volatility, 80°C, 48h., %	0.2	0.2	0.1	0.1	0.1	0.2	0.2	0.2	0.2	0.1	0.1	0.0	0.1
Volatility, 150°C, 24h., %	22.2	23.4	23.1	22.5	22.6	23.4	20.3	20.2	19.8	18.2	17.6	18.5	16.9
Viscosity (cps X 1000)	170	205	295	420	20	40	105	270	640	-	-	-	-
Shear Thinning Index	2.3	2.5	2.5	2.6	1.8	2.0	2.1	2.3	2.3	-	-	-	-
Degree of Thixotropy	1.0	1.0	1.0	1.0	1.0	1.0	1.0	1.0	0.9	-	-	-	-
Thixotropy Index	1.0	1.0	1.0	1.0	1.0	1.0	1.1	1.0	1.0	-	-	-	-

1 to 18) exhibit poor -60°C cone penetrations, blends of the Type A polymers and fumed silica exhibit penetrations above 200 dmm at -40°C, while blends of the Type B polymers are considerably less flexible at all temperatures. The cone penetrations at -60°C appear to be below the low temperature phase transition for these gels, and, therefore, yield very low penetrations.

Rheology

The viscosity of a filling material is important with respect to processing and handling. Most desired is a low viscosity material which facilitates low temperature pumpability. This requirement is usually antagonistic with oil separation, where typically a reduction in the oil separation is accompanied by an increase in the viscosity and yield stress.[11] Since cables are filled as units or cores, the viscosity-temperature profile of the filling compound is limited by the thermal properties of the insulation.

When low stress is applied to a grease-like material the material acts substantially like a solid. If the stress is above a critical value, then the material flows and the viscosity decreases. Such materials are commonly called thixotropic, and the decrease in viscosity is usually reversible since the three dimensional lattice of particles which form the structure can be easily reformed following the release of the critical stress. Upon shearing a filling compound it is important that the gel reforms upon removal of the shear. These tendencies to recover from an applied shear are measured by the degree of thixotropy and the thixotropy index. A degree of thixotropy and thixotropy index of 1.0 indicates excellent recovery of properties. The decrease in viscosity with applied shear can be measured by the shear thinning index, and is indicative of pumpability of the filler. A low shear thinning index indicates that the product will not change substantially under conditions of handling, which lessens the danger of oil separation.

Many of the samples produced were visco-elastic and these methods were insufficient to measure the thixotropy of these materials. Samples of the Type B polymer and the high viscosity fumed silica formulation (Blends 10 to 13 and 17) were of this class and some of their rheological measurements were excluded.

The Type A polymers possess both a degree of thixotropy and a thixotropy index of 1.0, which indicates excellent recovery under our conditions. The shear thinning index of the Type A polymers increases as the amount of polymer is increased (Blends 1 to 4 and 5 to 9). The fumed silica based blends (14 to 19) possess a higher shear thinning index than the polymer formulations which would facilitate better pumpability, but their large degree of thixotropy and thixotropy index indicates an irreversible recovery at ambient conditions. We are currently investigating Blend 15 which seems to possess anomalous rheological properties when compared to other fumed silica based formulations.

Poly-α-olefins

As mentioned above the low temperature flexibility and the volatility of the gel depend almost completely on the carrier oil used in the

Table 3

Blend	14	15	16	17	18	19	20	21	22	23	24	25	26
Mineral oil	X	X	X	X	X	X		X		X		X	
4 cSt PAO						X	X			X	X		
5 cSt PAO								X	X			X	X
Polymer Type A						X	X	X	X				
Fumed Silica	X	X	X	X	X					X	X	X	X
Appearance	H	H	H	H	H	SH	SH	SH	SH	SH	C	SH	C
Cone Pen. (dmm) -60°C	130	135	132	78	76	199	253	206	77	189	204	92	66
-40°C	260	185	265	211	184	281	299	266	297	262	230	215	285
-20°C	-	251	-	297	227	319	333	320	333	285	251	255	320
0°C	-	286	-	332	259	332	349	342	336	310	290	274	280
+21°C	-	-	-	362	312	355	359	355	357	370	271	316	383
Oil Separation 80°C, 48h., %	11.9	3.6	8.2	10.0	4.8	0.3	0.0	1.0	0.1	8.3	5.3	6.9	9.9
Volatility 80°C, 48h., %	0.3	0.7	0.2	0.6	0.4	0.3	0.1	1.1	0.2	0.2	0.2	0.3	0.2
Volatility 150°C, 24h., %	17.7	24.2	18.1	23.2	22.8	12.3	1.9	10.0	0.4	12.8	5.6	9.8	2.4
Viscosity (cps X 1000)	145	263	271	276	-	125	200	140	200	165	220	148	88
Shear Thinning Index	4.0	2.6	4.2	4.2	-	3.3	3.4	3.5	3.3	1.8	2.5	2.5	2.6
Degree of Thixotropy	1.1	2.4	1.3	1.5	-	1.0	1.0	1.1	1.0	-	-	-	-
Thixotropy Index	0.9	0.9	0.6	0.8	-	1.0	1.0	1.0	1.0	0.9	1.3	0.8	0.8

gel. Poly-α-olefins (PAO) are known for their excellent volatility and low temperature phase transition which aides in their low temperature flexibility. Blends of mineral oil, PAO, and combinations of the two are compared in Table 3. Again it can be observed that blends of polymer Type A separate less oil than blends of fumed silica, regardless of whether PAO is present (Blends 19 to 22 vs. 23 to 26). It can also be observed that the 80°C volatility of gels of PAO are no better than the straight mineral oil blends, and in fact the blends which contain both PAO and mineral oil actually faired worse (Blend 20. 21, 24, and 25). As was previously observed the 150°C volatility was greatly affected by the use of PAO as a carrier and the PAO blends were considerably less volatile than the mineral oil and combination mineral oil and PAO blends. Although an interesting academic results this may well not prove to be useful in fully formulating a cable filler.

The low temperature cone penetration (flexibility) of the polymer Type A blends with PAO was improved over mineral oil blends, but a combination of mineral oil and PAO (which is considerably less expensive) faired no worse than strictly PAO alone (Blend 18 and 20 vs. 19 and 21). The shear recovery of the polymer Type A and fumed silica blends were the same as for straight mineral oil blends, with the polymer possessing superior recovery to the fumed silica blend. In fact, due to their visco-elastic nature, the degree of thixotropy for the fumed silica blends could not be accurately measured by our method.

Conclusions

The preceding work has demonstrated the need to define physical parameters for successful performance testing of a cable filling compound. It appears cone penetration, oil separation, and viscosity are three important physical properties which can define a filling compound, and further work in this area will concentrate on correlating these properties with field testing.

Future work will concentrate on investigating the sheath and buffer tube compatibility, oxidative stability, and water penetration of polymer and fumed silica cable fillers. This will subsequently lead to a correlation with performance testing results and better understanding of cable filler properties.

Acknowledgments

The authors would like to thank the Polymer Additives Group and Petroleum Specialties Group for instrumental and financial support.

References

1. Davis, K. M.; Tomozawa, M., Journal of Non-Crystalline Solids, 185, 203-220, **1995**.

2. Mitchell, D. M.; Sabia, R., 29th International Wire And Cable Symposium, 15, **1980**.

3. U.S. Patent #5,187,763 and references cited therein.

4. U.S. Patent #5,358,664.

5. American Society for Testing and Materials, " Standard Test Method for Oil Separation from Lubricating Grease During Storage", ASTM D1742-83, **1983**.

6. Light, M. C., 37th International Wire And Cable Symposium, 459, **1988**.

7. U.S. Patent #4,870,117.

8. U.S. Patent #5,050,959.

9. Hattori, T.; Akasaka, N.; Fukuma, M.; Masuda, S.; Suzuki, S., 37th International Wire And Cable Symposium, 12, **1988**.

10. U.S. Patent #5,276,757 and references cited therein.

11. U.S. Patent #5,285,513.



Dr. Michael T. Costello has received his B.S. degree in Chemistry from Virginia Polytechnic Institute and his Ph.D. degree in Inorganic (Organometallic) Chemistry at Purdue University in West Lafayette, IN. Dr. Costello has been involved in the pilot development of hydrogenation and sulfonation technologies and is currently developing improved cable fillers for the fiber optic market. He is employed as a Research Chemist for the Petroleum Specialties Group of Witco Corporation at their research center in Oakland, NJ.



Dr. Anna Debska-Chwaja has received Masters degrees in Chemical Engineering and Petroleum Technology and a Ph.D. degree in Petroleum Engineering. She was trained and worked in Poland, Romania, Italy, and France. She is a member of the ACS and STLE and is currently employed by the Petroleum Specialties Group of Witco Corporation as a Research Scientist specializing in solid hydrocarbons, lubricants, cable fillers and tribology. Dr. Debska is the author of over 30 publications and 5 patents.



Dr. Alan D. Eckard has received his B.S. degree from Rensselaer Polytechnic Institute and his Ph.D. in physical chemistry from the University of Liverpool, England. After research fellowships at Keele University (UK) and the University of Toronto, Dr. Eckard has been involved in the development and application of industrial lubricants, coatings and surface treatment chemicals with several international manufacturers of these products for the over 20 years. He is currently Director of Research and Development for the Petroleum Specialties Group of Witco Corporation at their research center in Oakland NJ.



Mr. William J. Thalman has received his Masters degree in Chemistry from Montclair State College and is nearing completion of his Ph.D. degree in Physical Chemistry at Rutgers University. Mr. Thalman has been involved in the pilot development of hydrogenation and sulfonation technologies and is currently investigating methods to improve cable filler performance. He is employed as a Research Chemist for the Petroleum Specialties group of Witco Corporation at their research center in Oakland, NJ.

MECHANICAL PROPERTIES OF OPTICAL FIBER RIBBON

T. Murase, K. Shiraishi, T. Kawano, T. Sakai, M. Ito, and T. Shiono

Showa Electric Wire & Cable Co., Ltd.
4-1-1, Minami-Hashimoto, Sagamihara, Kanagawa 229, Japan

1. Abstract

Using the finite element method, a stress analysis was performed varying the Young's modulus and ribbon thickness of the ultraviolet-cured optical fiber coating material (ribbon coating material) of optical fiber ribbon, assuming it is subjected to lateral-pressure outside force. It was found that the stress of the glass fiber declines with higher Young's modulus and with greater thickness. Also, an evaluation with long-length of ribbon instead of short-length which is used in the conventional method yielded good agreement between calculated values and experimental values. This series of new evaluation methods is valuable for the design of ribbon coating materials and ribbon manufacturing dimensions.

2. Introduction

When lateral pressure or bending is applied to the optical fiber ribbon inside an optical cable, its transmission loss increases. In recent years, extensive research is being done for the type of cable that accommodates spacers, and "structures that allow extra length" in order to meet the stringer requirement for the optical cable to withstand against lateral pressure and bending. From another angle, many attempts have been made to improve the mechanical properties by changing the Young's modulus of the coating material that makes up the optical fiber ribbon. In this paper, we have made an analysis of the stress imparted to the fiber using the finite element method (FEM) when an outside force (lateral pressure) is applied to a four-fiber ribbon. The mechanical properties of four-fiber ribbon were measured experimentally using a method different from conventional methods. We found good agreement between the experimental results and the results the stress analysis.

3. Stress analysis by the finite element method (FEM)

When lateral pressure is applied to a four-fiber ribbon, the layer of coating that protects the fiber reduces the stress that propagates to the fiber. This propagated stress must be reduced to a minimum, because it causes an increase in the transmission loss of the fiber. Fig.1 shows stress analysis model used in FEM to calculate the stress that propagates to the fiber when a concentrated load is applied to a four-fiber ribbon from outside. An analysis was carried out by applying constraint to the outer diameter and coating of the fiber, primary, secondary, and color (Table 1), and varying the ribbon thickness(t) as a structure parameter and the Young's modulus of the ribbon coating (E_t) as a material parameter. The load condition was applied to the top of the boundary of ribbon.

3-1 Effect of the ribbon thickness

When the material parameter (Young's modulus of the ribbon material) is held constant and the ribbon thickness is varied

Fig.2 shows the change in the normalized stress (σ/W) when the stress (σ) that is propagated to the surface of the fiber is divided by the applied lateral pressure load (W). It is clear that

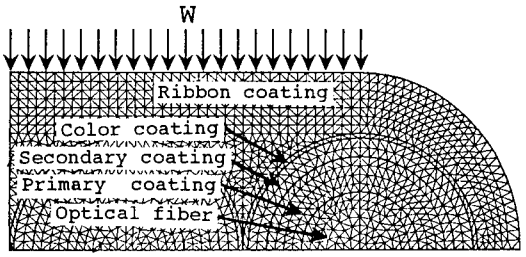


Fig.1 Stress analysis model of 4-fiber ribbon by finite element method

Table 1 Typical parameters used in the FEM

	fiber	Primary	Secondary	Color	Ribbon
Diameter (mm)	0.125	0.200	0.240	0.250	t
Young's Modulus (MPa)	72000	1.0	500	400	E_t
Poison ratio	0.16	0.45	0.45	0.35	0.45

increasing the thickness of the ribbon reduces the stress propagated to the fiber surface, and that the normalized stress is highly dependent on the ribbon thickness.

3-2 Effect of the Young's modulus of the ribbon layer

Figure 3 shows the change in the normalized stress (σ/W) as a function of the Young's modulus of the ribbon when the ribbon size (structural parameter) is at 1.1 mm x 0.38 mm and the Young's modulus of the ribbon material is varied.

It can be said that as the Young's modulus of the ribbon material grows larger, the stress propagated to the fiber surface decreases. It is clear that the stress is highly dependent on the Young's modulus of the ribbon, but above a certain Young's modulus the propagated stress remains nearly constant.

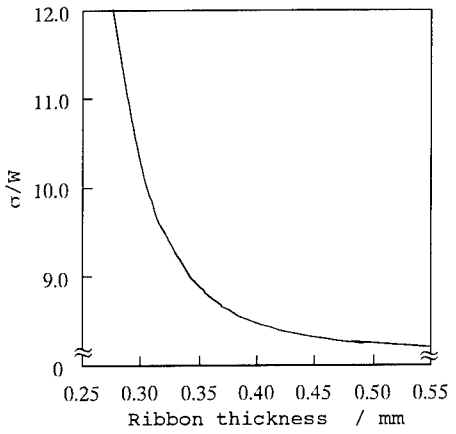


Fig.2 Relationshiop between ribbon thickness of ribbon coating and σ/W

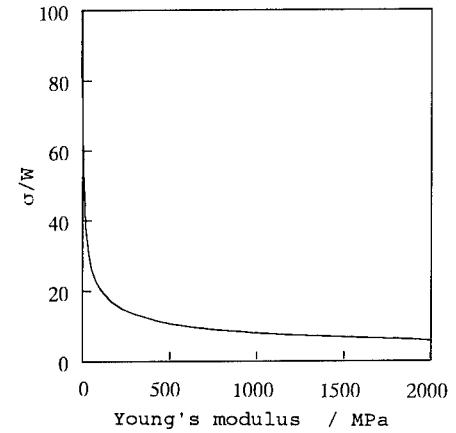


Fig.3 Relationshiop between young's modulus of ribbon coating and σ/W

4. Experiments

The flat plate lateral pressure method has long been used for evaluating the lateral pressure properties. In this method, an approximately 2m sample is sandwiched between flat plates covered with sandpaper, a load is applied to the upper plate, and the loss increase is measured. In this method, only about 500mm of lateral pressure is applied which makes difficult to observe noticeable changes in loss. Therefore, the increase of the load or the use of rough sandpaper is necessary. But it results in breaking of the coating resin and yields large fluctuations in the measured value. Therefore we studied new methods for evaluating lateral pressure properties bending properties.

4-1 Lateral pressure properties

(Lateral pressure among the ribbon thickness direction)

The schematic diagram to evaluate the lateral pressure on a four-fiber ribbon from the direction of its thicknesses shown in Fig.4. The fiber ribbon was sandwiched between two plate which had sandpaper on their inner surface. The microbend loss was measured as a function of load such that the fiber ribbon should not overlap and come under any tension (the lateral pressure was applied to the 2.7 m length of the fiber ribbon). Fig.5(a) shows the loss increase as function of lateral pressure per kg for a different ribbon thickness 0.3mm and 0.38mm at a constant Young's modulus of the ribbon coating. It was found that as the lateral pressure load increases, the effect of the ribbon thickness on loss increase becomes more apparent and thus the loss increase in the fiber is reduced. Fig.5(b) shows the loss increase as a function of lateral pressure per kg for a different Young's modulus of the ribbon coating (such as typical Young's modulus E_{st} and 1.6 and 1.9 times of the typical Young's modulus) at a constant ribbon thickness 0.30mm. It showed that as the lateral pressure load increases, the variation of loss increase becomes more apparent among the different Young's modulus of the ribbon material. Therefore higher Young's modulus can reduce the loss increase of the fiber.

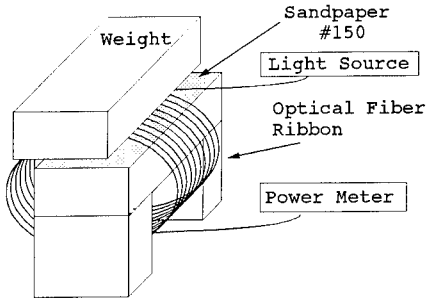


Fig.4 Schematic diagram of loss increase measurement due to lateral pressure

4-2 Lateral pressure properties

(Lateral pressure among the ribbon width direction)

The experimental set up to measure the loss increase as a function of lateral pressure along the direction of the ribbon width is shown in Fig.6. First four-fiber ribbon was aligned (sample length 34 m). A load of 3 kg was applied to two pipes 2.5 mm in diameter. Then the change in the loss increase was measured as shown Fig.7. In this case, the loss increase of fiber closed to the pipe was measured as a function of side thickness of ribbon while varying the ribbon thickness and Young's modulus of the ribbon material. When the Young's modulus was held constant, changing the thickness of the ribbon produced no observable change in the loss increase. This indicates that the thickness of the ribbon is independent of the lateral pressure from the ribbon width direction. On the other hand, with regard to the effect of the Young's modulus of the ribbon material, this indicates that increasing the Young's modulus can reduce the loss increase in the fiber (also, the propagation of stress to the fiber on the inner side is very small for lateral pressure from the direction of the ribbon's width).

4-3 Bending properties

A study was conducted concerning the relationship between the loss increase and bending for the following case (1)the inner-side fiber of the four-fiber ribbon, (2)the individual strands of fiber after peeling off the ribbon layer of the four-fiber ribbon. The schematic diagrams of loss measurement under bending condition of four-fiber ribbon are shown in Fig.8(a) and (b). Initially, the four-fiber ribbon was wound onto a rod of constant outside diameter without putting it under tension, and it was

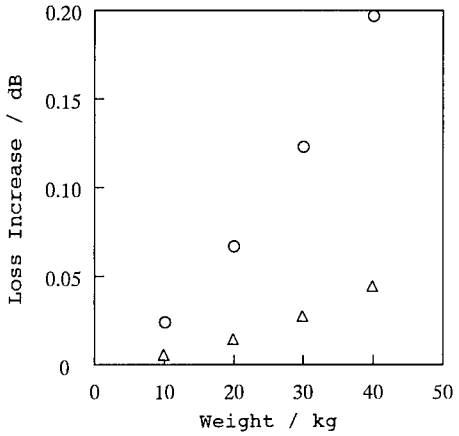


Fig.5(a) Relationship between lateral pressure and loss increse of 4-fiber ribbon

○ : ribbon thickness (0.30mm)
△ : " (0.38mm)

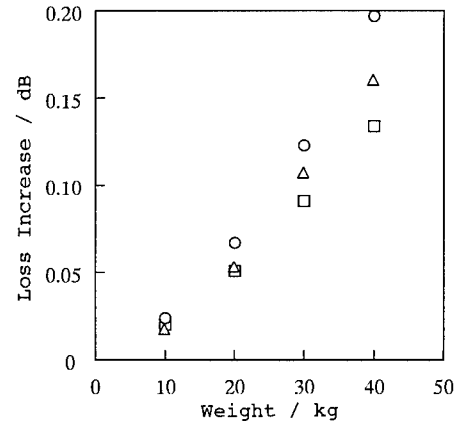


Fig.5(b) Relationship between lateral pressure and loss increase of 4-fiber ribbon

○ : Young's modulus of ribbon coating (Est)
△ : " (1.6Est)
□ : " (1.9Est)

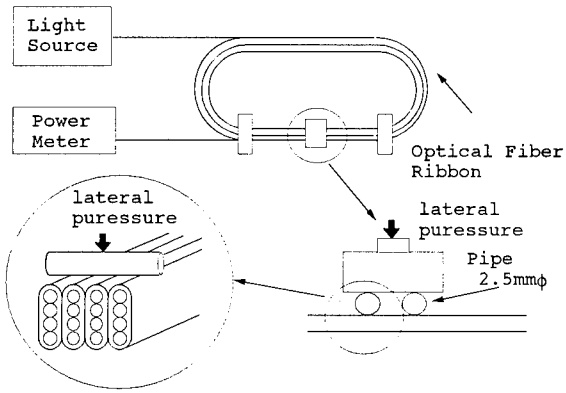


Fig.6 Schematic diagram of loss increase measurement due to lateral pressure

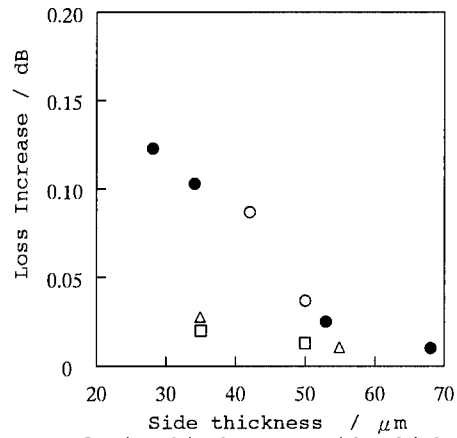


Fig.7 Relationship between side thickness and loss increase

● : ribbon thickness 0.38mm, Young's modulus Est
○ : " 0.30mm, " Est
△ : " 0.30mm, " 1.6 Est
□ : " 0.30mm, " 1.9 Est

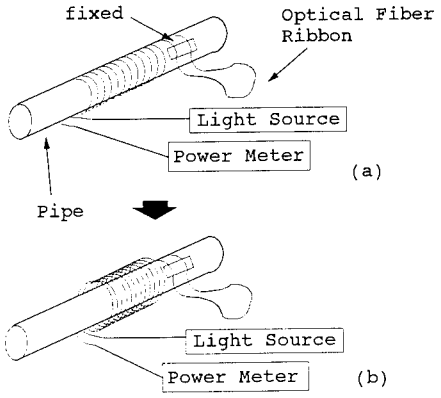


Fig.8 Schematic diagram of loss increase measurement due to wind

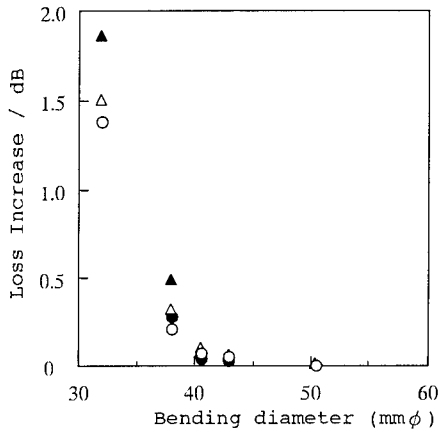


Fig.9 Relationship between bending diameter and loss increase of 4-fiber ribbon and fiber

○ : 4-fiber ribbon(ribbon thickness 0.30mm)
● : fiber in 4-fiber ribbon (")
△ : 4-fiber ribbon(ribbon thickness 0.38mm)
▲ : fiber in 4-fiber ribbon (")

left standing for 30 minutes as shown in Fig.8(a). Then, as in Figure 8(b), the four-fiber ribbon was loosened and released, and its recovery value was taken as its loss increase. The loss increase as a function of bending diameter was measured for case (1) and (2) as shown in Fig.9. It was found that there was a steep loss increase at a bending radius of 40 mm or less. Also, no difference was found in the measured values of loss increase between the cases (1) and (2), indicating no significant effect of the ribbon thickness or ribbon layer.

5. Discussion

We discuss the relationship between the results of the stress analysis by FEM and of experiments with respect to the lateral pressure properties of four-fiber ribbon. Fig.10 shows the loss increase and the stress in the fiber ribbon as a function of ribbon thickness. The stress is the result of multiplication of the normalize stress (σ/W) and the applied load (W) in the

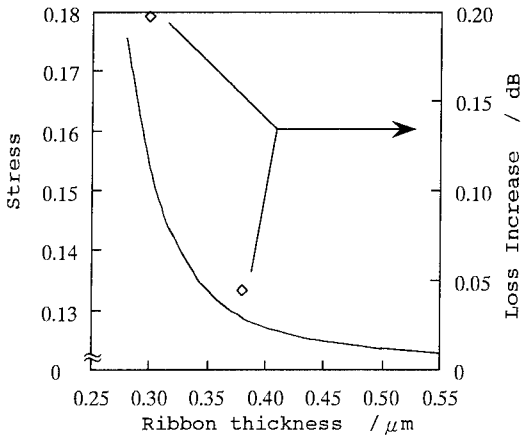


Fig.10 Relatioship between ribbon thickness, stress, and loss increase
—: Stress : Loss increase

lateral pressure test (Fig.4). In Fig.10, the stress analysis calculated values by FEM and the experimentally measured values showed the same trend, and therefore we concluded that the measurement method was valid. Hence, the evaluation method studied here may be useful for determining the material and structure of the ribbon.

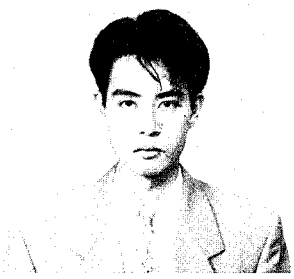
6. Conclusion

A stress analysis of the lateral pressure properties of four-fiber ribbon was made using the finite element method. The results of the stress analysis agreed closely with mechanical property evaluation tests of four-fiber ribbon and optical fiber strands, and were useful as an indication for determining the material and structure of ribbon.

The lateral pressure testing method studied here was a testing method for lateral pressure only it was assumed that any other outside forces were absent (such as bending). Similarly, in case of bending test the active force was only due to bending. That is, these method are effective from the viewpoint of designing the ribbon material and structural dimensions for the respective mechanical properties.

7. References

1) Mochizuki et al.: " Structure Design of Optical Fiber Cable," Rev. Electr. Commun. Lab., 27, 2451(1978)
2) Ishihara et al.: " Determination of Optimum Structure in Coated Optical Fiber and Unit," Trans. IECE J-63-B, 71(1980)
3) Timoshenko: "Strength of Materials, Elementary Theory and Problems" Tokyotosho (1957)
4) Higashimachi: "Finite Element Method Know-how" Morikitasyuppan (1993)



Tomotaka Murase
Showa Electric Wire & Cable Co.,Ltd., 4-1-1, Minamihashimoto, Sagamihara, Japan

T.Murase received his B.E.degree from Kanagawa University in 1993. He joined Showa Electric Wire & Cable Co,. Ltd. in 1993. He is an engineer working with the Material Research Division of Telecommunication R&D Dept.



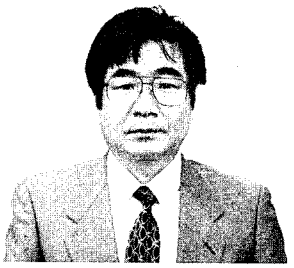
Tomonori Sakai
Showa Electric Wire & Cable Co.,Ltd., 4-1-1, Minamihashimoto, Sagamihara, Japan

T.Sakai received his B.E.degree from Nagasaki University in 1984. He joined Showa Electric Wire & Cable Co,. Ltd. in 1987. He is an engineer working with the Material Research Division of Telecommunication R&D Dept.



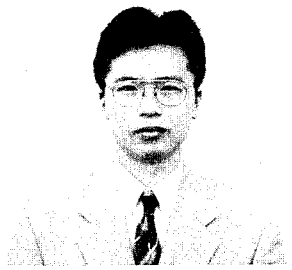
Keiko Shiraishi
Showa Electric Wire & Cable Co.,Ltd., 4-1-1, Minamihashimoto, Sagamihara, Japan

K.Shiraishi received her B.E.degree from Tokai University in 1993. She joined Showa Electric Wire & Cable Co,. Ltd. in 1993. She is an engineer working with the Material Research Division of Telecommunication R&D Dept.



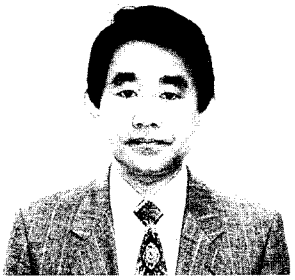
Mitsuo Ito
Showa Electric Wire & Cable Co.,Ltd., 4-1-1, Minamihashimoto, Sagamihara, Japan

M.Ito passed from Yokohama Syouko Highschool in 1962. He joined Showa Electric Wire & Cable Co,. Ltd. in 1962. He is an engineer working with the Material Research Division of Telecommunication R&D Dept.



Taketo Kawano
Showa Electric Wire & Cable Co.,Ltd., 4-1-1, Minamihashimoto, Sagamihara, Japan

T.Kawano received his M.S.degree from Science University of Tokyo in 1994. He is joined Showa Electric Wire & Cable Co,. Ltd. in 1994. He is an engineer working with the Material Research Division of Telecommunication R&D Dept.



Takeo Shiono
Showa Electric Wire & Cable Co.,Ltd., 4-1-1,Minamihashimoto, Sagamihara, Japan

T.Shiono received his Ph.D.degree in Chemical Engineering from the University of Tokyo in 1979 and works in the development of telecommunication cable's materials. He is the manager of the Material Research Division of Telecommunication R&D Dept.

NEW CENTRAL TUBE HOSTILE ENVIRONMENT RIBBON CABLE DESIGN

Paul E. Neveux, Jr., Stephen R. Stokes, Grant S. Blume

Sumitomo Electric Lightwave Corp.
78 Alexander Drive, Research Triangle Park, NC 27709

ABSTRACT

A hostile environment central tube ribbon cable has been designed with exceptional resistance to thermal and hydrolytic degradation while improving the cable flexibility and ease of entry when compared to existing commercially available constructions. The central tube, inner and outer jacket materials are shown to be oxidation, hydrolysis and oil resistant as well as craft person friendly. The cable core, composed of glass reinforced strength elements and a heat and moisture resistant inner sheath, is easily entered with ripcords placed alongside the strength elements. The cable core is hermetically sealed with a seam welded corrugated copper sheath. Testing of the cable was performed in a custom designed hostile environment autoclave. Test results met or exceeded all Bellcore's mechanical and environmental requirements for steam resistant optical cable.

INTRODUCTION

Leaky steam pipes in large cities are a well-documented problem for telecommunication companies throughout the United States. In major U.S. cities, stranded and central loose tube optical cables have been, and are being installed in underground ducts adjacent to steam pipes. In some cases, steam pipes have been in service for over 100 years and are now producing leaks.[1] Catastrophic failure can occur in conventional cables when they are subjected to high temperature and humidity generated by the faulty pipes as shown in Figure 1.

Standard stranded and central loose tube designs which meet Bellcore's GR-20-CORE[2] requirements are not sufficient to protect the optical fibers from high temperature steam. Steam related failures of loose tube fiber optic cable have been reported as early as 10 months after installation. The vulnerability of cables arises from a combination of the cable design and the materials used: the sheath material, typically polyethylene, can melt away and the tube material, typically condensation polymers (nylon, polyesters, polycarbonates), can become brittle and crumble. Even standard armored and aluminum lap tape constructions are insufficient since moisture passes easily through the overlap. While current steam cable designs have much improved resistance to high temperatures and moisture, drawbacks still remain.

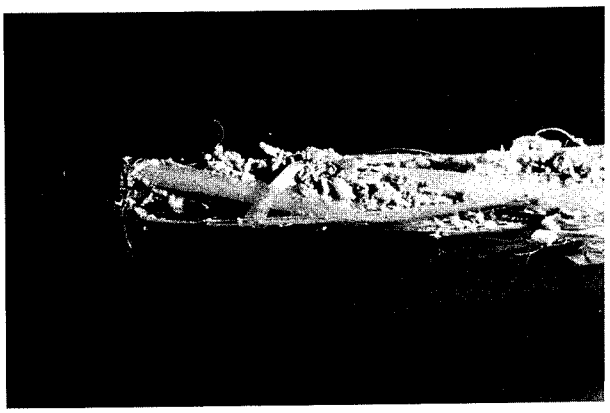


Figure 1.

The comment heard most often from the field is that the available central ribbon tube hostile environment cable designs are too rigid for installation: the cable does not readily conform to sheaves or bends and turns in the ducts. In response to customers' requests, a cable has been designed which improves the ease of installation. Using a combination of properly applied anti-buckling and tensile strength elements, flexible inner jacketing material, and kink resistant central tube material, a new hostile environment cable was designed to be easy to handle yet remain mechanically and environmentally robust. These properties were confirmed by subjecting the cable to mechanical and accelerated aging tests in excess of what is required by Bellcore's TR-NWT-001322.[3]

In order to to confirm the cable's reliability in a saturated steam environment, a hostile environment autoclave was designed and manufactured. The autoclave is capable of testing up to three one-meter sections of cable while maintaining a saturated steam pressure of at least 70 psia and 150°C. Its design and construction features are discussed.

CABLE DESIGN AND CONSTRUCTION

The cable structure, shown in Figure 2, includes a jelly filled central tube containing optical fiber ribbons. Use of optical fiber ribbons allows for higher fiber densities than loose fiber and quicker connectivity via mass fusion splicing. Table 1 shows the material properties necessary for hostile environment cables. Because of the 130°C aging requirements of TR-1322, both the central tube and inner sheath materials are high temperature fluoropolymers which have improved performance and reliability over standard loose tube materials as well as previous materials investigated for steam cable use.[4] As discussed below, these characteristics result in excellent retention of physical properties after 130°C steam exposure, allowing the tube and inner sheath to remain craftsperson friendly throughout the life of the cable. As a tube material, the fluoropolymer provides excellent kink resistance and notch-break properties, allowing easy entry. As an inner sheath material, it provides excellent resistance to the catalytic oxidation of the hermetic copper armor.

Table 1. Material Properties Necessary for Steam Cables

Material	Oil Resistance	Moisture Resistance	Oxidation Resistance	Relative Stiffness	Melting Point
Fluoro-polymer	Excellent	Excellent	Excellent	Moderate	160°C
Polyether sulfone	Excellent	Excellent	Excellent	Very High	T_g= 232°C
Polyolefin	Poor	Excellent	Poor	Moderate	121°C
Polyester	Excellent	Poor	Good	High	221°C
Nylon	Good	Fair	Poor	Moderate	178°C

Tensile strength and anti-buckling members are stranded in two counter-helically applied layers about the central tube. The anti-buckling elements are composed of flat, glass reinforced plastic (GRP) tapes. Both layers are applied with a pitch and tension which are optimized for efficient utilization of tensile strength, -40°C cold temperature performance, and exceptional cable flexibility when compared to similar cable structures. Water blocking of the cable core is ensured through the use of water swellable components around the core elements and a thixotropic gel filling compound for the central tube. Two ripcords of a contrasting color are stranded with the strength elements to facilitate removal of the inner sheath. The inner sheath is applied over the core without imbedding the strength elements, maintaining overall cable flexibility and allowing for easy removal during entry. Additionally, the inner sheath material is translucent so that the contrasting color ripcords can easily be seen through the sheath.

A seam welded corrugated armor of high purity copper is applied over the cable core to provide a hermetic barrier to steam. The corrugation pitch, depth, and profile were optimized to provide improved mechanical strength and overall cable flexibility. Water blocking between the core and the armor is ensured with the use of water swellable tape. A high strength ripcord is located longitudinally beneath the copper to facilitate its removal.

For the jacket material, a special grade of high temperature fluoropolymer, having properties similar to the tube and inner sheath materials, is applied over the copper armor. The outer jacket is easily removed using standard sheath entry tools.

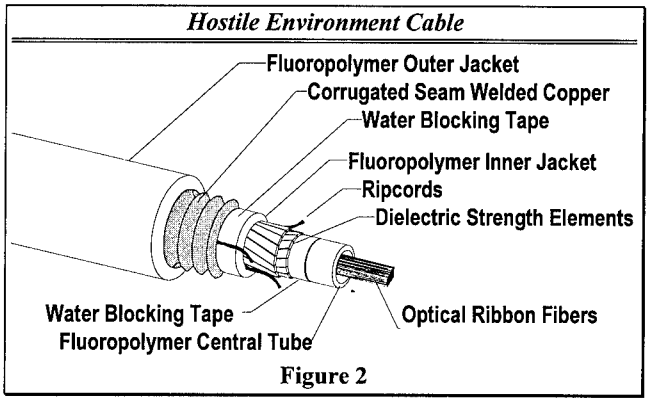


Figure 2

EXPERIMENTAL

Material Performance Testing

Tensile bars of the tube, inner sheath and jacket materials were aged in a "pressure cooker" at 130°C saturated steam. The inner sheath material was also tested for oxidation resistance at 130°C by making a "sandwich" of copper and inner sheath material on the outside separated by water blocking tape. Mechanical testing was performed on an Instron Tensilometer. All percent elongation results were calculated using the tensile bar gauge length and the change in crosshead position.

Optical fiber tensile strength was performed per FOTP-28B[5] using a 500 mm gauge length. Testing was done at 23°C ± 2°C and 50% ± 5% RH. Commercially available tube jelly was used for the optical fiber immersion aging.

Cable Performance Testing

Cable performance testing was performed per Bellcore TR-NWT-0001322 and references included therein, unless noted otherwise in the results. Optical fiber attenuation changes in cable during mechanical testing were measured using an automated discrete light source and power meter arrangement. Attenuation changes during temperature cycle and aging were measured using a spectral attenuation measurement system. For the steam aging testing, as specified in TR-1322, a 50 meter was used with the fibers concatenated by fusion splicing into 12 fiber loops. The attenuation measurement systems conform to general requirements for measurement repeatability of less than or equal to ± 0.05 dB.

The central tube kink test was performed as specified in IEC 794-1-E10.[6]

Autoclave Construction and Operation

In order to conduct the steam permeability test, a steam autoclave, shown below in Figure 3, was custom designed and manufactured. Constructed entirely of stainless steel, it consists a test chamber, where the cable sample(s) are held in place, and a water reservoir. The temperature is monitored by a thermocouple located at the midpoint of the sample chamber. A pressure tight seal is maintained around the cable samples at the entry ports to prevent excess moisture loss. Level sensors and valves allow for automatic water filling. The entire unit is insulated to ensure a stable, uniform interior temperature. For safety, a pressure relief valve is included.

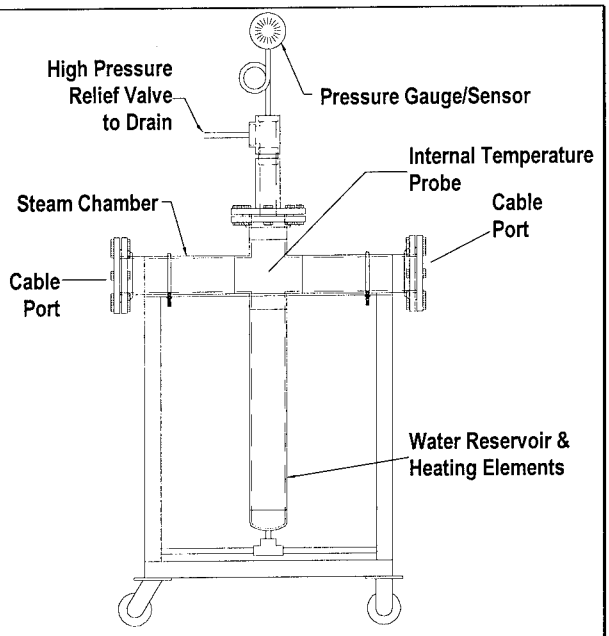


Figure 3. Steam Autoclave

The autoclave operates by heating the water until the temperature of the steam saturated air adjacent to the test sample(s) is reached. The pressure generated is simply the water vapor pressure at that temperature. To insure that the correct steam pressure is being generated, a combination pressure gauge and sensor is located at the top of the autoclave. Both the temperature and the pressure electrical output signals are connected to a chart recorder which is operated during the entire experiment. Operating in this manner, the autoclave can run very consistently for well over the required aging period. The autoclave has been certified to 70 psia steam pressure at a temperature of 150°C. In the present case, the cable samples were aged at 39.2 ± 2.4 psia at 130°C ± 2°C for 60 days.

MATERIAL RELIABILITY TEST RESULTS

Buffer Tube Material

Selection of the central tube material is critical because it provides the most immediate layer of protection for the optical fibers. Previous studies have shown that typical poly(butylterephthalate) (PBT) loose tubes can show significant degradation after exposure to high temperature and humidity for only seven (7) days.[7] Therefore, the high temperature fluoropolymer used in this tube was tested for degradation of mechanical properties after exposure to 130°C saturated steam (shown in Figure 4.) and 130°C filling compound (shown in Figure 5.).

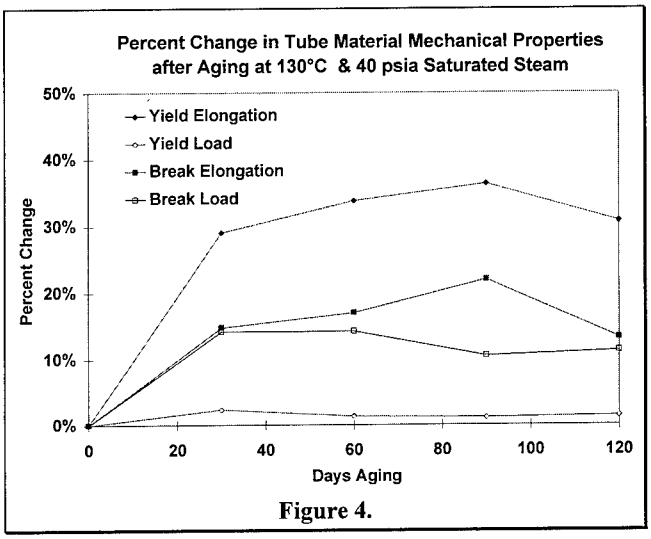


Figure 4.

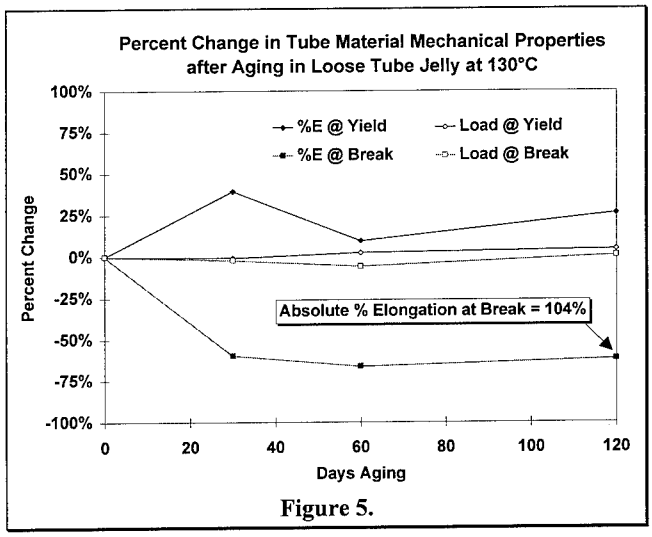


Figure 5.

The aging results of the tube material in the saturated steam environment indicate an initial reduction in the modulus as shown by the increases in percent elongation at yield,

however, little change occurs afterward. The material essentially becomes more elastic with aging as opposed to becoming more brittle, as is typical of PBT.

After 130°C aging in loose tube filling compound, the tube material percent elongation at break drops by approximately 60% immediately after aging 30 days but remains at that value for up to 120 days indicating that the change is initial and not sustained. The absolute percent elongation after 120 days is approximately 104%, far exceeding the minimum 10% elongation required after 60 days aging.

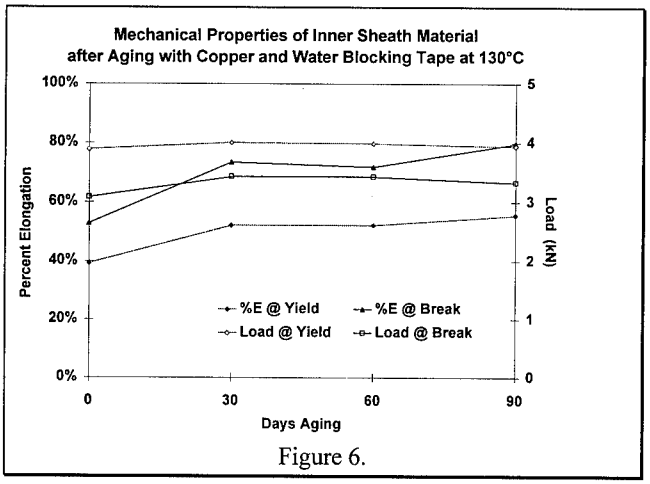


Figure 6.

Inner Sheath Material

Selection of inner sheath material was extremely important to ensure that future mid-span entry of the cable would be possible, even after the cable had been exposed to extreme environments. Previously available hostile environment cables contained a polyester inner sheath which is very stiff and difficult to handle when new. Additionally, polyester materials degrade rapidly when exposed to high temperature and humidity associated with a failure of the hermetic barrier. The high temperature fluoropolymer used in this inner sheath exhibited similar performance characteristics to the tube material described in the preceding section. In addition, the inner sheath material was tested for resistance to oxidation by copper (see Experimental section above). As can be seen in Figure 6, the copper, which typically acts as an oxidizing catalyst for materials such as polyethylene and nylon-12, does not affect the inner sheath material significantly.

Outer Jacket Material: As shown below in Figure 7, 120 days of steam aging has virtually no effect on the jacket material yield or break properties.

Optical Fiber Tensile Strength: In order to insure that the fiber reliability was being compromised, a fiber was aged in tube filling compound at 130°C for 60 days. As shown below in Figure 8, the median tensile strength of the fiber actually increased slightly over the unaged control samples, indicating that the jelly had no effect on the reliability of the fiber after aging at 130°C for 60 days.

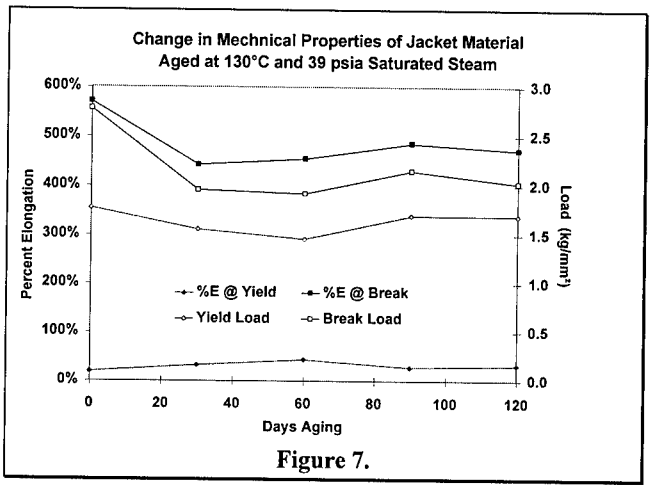


Figure 7.

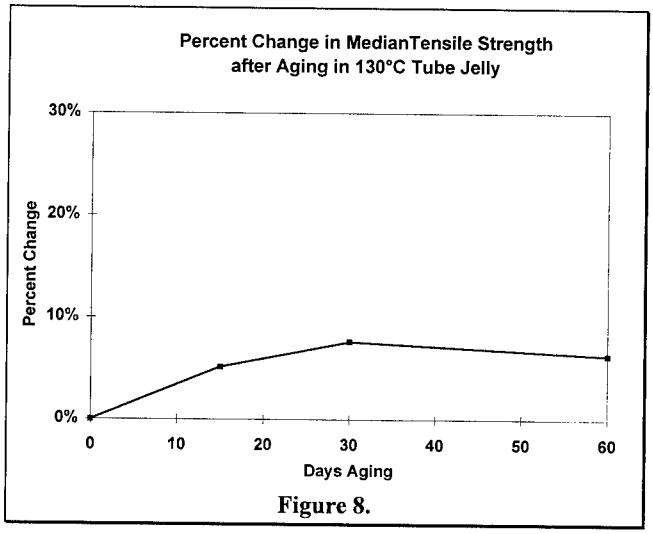


Figure 8.

CABLE PERFORMANCE TESTING

The cable was tested in accordance with the requirements of Bellcore TR-NWT-001322. The Bellcore requirements were considered to be the absolute minimum performance standards. And, as mentioned above, major design goals were set to increase cable flexibility and cable entry ease with an ultimate goal to reduce installation time. Some of the test results which highlight these improvements are discussed below. A summary of all test results is shown in the following tables.

Cable Material Test Requirements

Cable Material Compatibility: Both optical fibers and ribbons were subjected to immersion in the tube filling compound at 130°C: no delamination or splitting was observed. As mentioned in the above section, the tube jelly had no effect on the tube material, even after 120 days of aging

at 130°C and the copper had no effect on either the inner or outer sheath.

Jacket Abrasion Resistance: This test was performed in accordance with Bellcore TR-1322, Section 5.4.1, which specifies a minimum of 1000 passes with an abrading surface. After over 10,000 passes there was no significant loss of sheath thickness or wear, indicating an extremely durable sheath.

Corrosion Resistance: The copper sheath exhibited only cosmetic discoloration after aging at 130°C saturated steam in the autoclave. In addition, there was no evidence of copper oxide, indicative of corrosion of the copper.

Table 2. Cable Test Results for Material Requirements

TR-1322 TESTS	TR-1322, Issue 1, Conditions/Requirements	RESULTS
Compound Flow Section 5.3.3	• 80°C, 4/5 No Flow.	• 5/5 No Flow
Cable Core Materials Compatibility Section 5.3.4	• 130°C, 60 days, No splits or delamination in ribbon/fiber, • Tube % Elong. ≥ 10% @ 60 d	• No splits or delam. • Tube % Elong. ≥ 100 % at 120 days
Jacket Thermal Stability Section 5.4.2	• $T_O \geq 140°C$ • $T_P \geq 160°C$	T_O =156°C, T_P =170°C
Jacket Abrasion Resistance Section 5.4.1	• 1,000 × 4 lb force, 8/10 no Cu exposed	• 10 / 10 pass, 10,000 cycles
Corrosion Resistance Section 5.4.7	• No cracks, pits, perforations. • Pits ≤ 5 μm	• No pits, cracks, perforations.

Environmental Requirements

Moisture in Cable Core: Due to the hermetic seal of the copper armor, it is very important that the cable core not contain any residual moisture after manufacturing. Previously available hostile environment cables used a polyester based inner sheath and tube material which retains moisture, leaving open the possibility of hydrolytic degradation of the polyester and acrylate fiber coating. In addition to hydrolytic resistance, the fluoropolymers used in the inner sheath and central tube are hydrophobic and do not contribute moisture to the cable, thus preventing damage to the fiber coating. The cable was tested in accordance with TR-001322, Section 5.3.5, which requires that the core contain less than 2.6 mg of moisture per cm of length per cm of cable outer diameter. Less than 1.8 mg/cm/cm was detected.

Sheath Permeability to Steam: Using the specially designed steam autoclave described above, this test was performed in accordance with Bellcore TR-1322, Section 5.4.6, which specifies a maximum of 0.1 mg per hour per linear foot per inch cable outer diameter of moisture may penetrate the cable armor when the cable is exposed to saturated steam at 39.2 ± 2.4 psia and 130°C ± 2°C for 7 days. After 14 days, twice the required time period, there was no measurable moisture permeation.

Temperature Cycling : This test was performed in accordance with Bellcore TR-1322, Section 5.6.3 with the exception that low temperature measurements were conducted at -40°C instead of the specified -20°C. Even when tested at these much more severe cold temperatures, the average attenuation change for all tested fibers was only 0.003 dB at a test wavelength of 1550 nm compared to an allowable average of 0.10 dB. Therefore, this cable can comfortably be used in any outside plant application with a temperature range for operation extending down to -40°C.

Table 3. Cable Environmental Test Results

TR-1322 TEST	TR-1322, Issue 1, Conditions/Requirements	RESULTS
Moisture in Cable Core Section 5.3.5	• 2.6 mg/cm/cm	• 1.8 mg/cm/cm
Sheath Permeability Section 5.4.6	• 130.5°C and 39.7 psia max. of 0.1 mg/hr/ft/in	• 0.0 mg/hr/ft/in
Temperature Cycling Section 5.6.3	• 50 m sample; -20°C / 24 hours to +130°C / 60 days • Avg. $\Delta\alpha_{1.55} \leq 0.10$ dB over all fibers tested • Maximum $\Delta\alpha_{1.55} \leq 0.20$ dB for any individual fiber	**For 12 fiber loop: @130°C, 60 day:** • Ave. $\Delta\alpha_{1.55}$= 0.005 dB • Max. $\Delta\alpha_{1.55}$= 0.06 dB **@-40°C Temp. Cycle:** • Ave. $\Delta\alpha_{1.55}$= 0.003 dB • Max. $\Delta\alpha_{1.55}$ = 0.04
Water Penetration Section 5.6.5	EIA/TIA-455-82A • 1m sample, 1m head, 24 hours, under copper only; No water leak from open end.	No leak after 24 hours.

Mechanical Test Results

Central Tube Kink Test: A tube kink test per IEC 794-1-E10 was performed to determine the minimum diameter which the tube could be coiled without kinking. The maximum diameter that the central tube kinked was 8".

Cable Twist : This test was performed in accordance with Bellcore TR-1322, Section 5.5.7, which specifies a maximum test length of 3 meters. The results of this test showed no measurable fiber attenuation change or observable damage to the armor or any other component of the cable, even when tested as a 1 meter sample length. Therefore, the results of this test easily exceeded the Bellcore requirements when tested at conditions that are 3 times as severe as Bellcore specifications.

Cable Cyclic Flex : This test was performed in accordance with Bellcore TR-1322, Section 5.5.8 which specifies a minimum of 5 flex cycles. The cable was tested for 25 cycles before testing was discontinued. Even after exceeding the required number of cycles by 5 times the specification, there was no observable damage to any cable components and no measurable change in fiber attenuation.

Table 4. Mechanical Test Results

TEST	CONDITIONS/REQUIREMENTS	RESULTS
Tube Kink Test IEC 794-1-E10	Loop until kink	~ 8"
Low & High Temperature Bend TR-1322 Section 5.5.3	• 18" diam. × 4 wraps; @ -20 C to 60 C; 4 hrs. soak times • $\Delta\alpha_{90}$; $\Delta\alpha_{10}$ • Armor cracks ≤ 5mm @ 5X magnification	Max. $\Delta\alpha_{1.55}$ = 0.02 dB No cracks in armor or jacket
Impact Resistance TR-1322 Section 5.5.4	• EIA/TIA-455-25A • 25 Cycles • $\Delta\alpha_{90}$; $\Delta\alpha_{10}$ • No outer jacket damage	Max. $\Delta\alpha_{1.55}$ = 0.0 dB No cracks in armor or jacket
Compressive Strength TR-1322 Section 5.5.5	• 4.4 kN/10cm, 10 min. under load; (O) 8.0 kN/10 cm, 5 min. after load • $\Delta\alpha_{90}$; $\Delta\alpha_{10}$ • No outer jacket damage	Max. $\Delta\alpha_{1.55}$ = 0.02 dB No cracks in armor or jacket
Tensile Strength TR-1322 Section 5.5.6	• Minimum 600 lbf / 1 hr. hold • 200 lbf residual load • 360° twist / < 3 m under 600 lbf minimum load • $\Delta\alpha_{90}$; $\Delta\alpha_{10}$ • No outer jacket cracking or splitting • (O) Fiber strain ≤ 66% of proof test strain; residual fiber strain ≤ 0.05% load removed	Max. $\Delta\alpha_{1.55}$ = 0.04 dB No cracks in armor or jacket Max. Fiber Strain ε_f < 33% of proof test strain
Cable Twist TR-1322 Section 5.5.7	• Length ≤ 3m ± 180° • $\Delta\alpha_{90}$; $\Delta\alpha_{10}$ • No outer jacket cracking or splitting	Maximum $\Delta\alpha_{1.55}$ = 0.0 dB and no cracks in armor or jacket for 1 meter sample length
Cable Cyclic Flexing TR-1322 Section 5.5.8	• Mandrel diam. 18 inch • 5 cycles @ 30cycles/min • $\Delta\alpha_{90}$; $\Delta\alpha_{10}$ • Armor cracks ≤ 5mm @ 5X • (O) No visible cracks in armor	Maximum $\Delta\alpha_{1.55}$ = 0.0 dB and no cracks in armor or jacket after 25-cycles

$\Delta\alpha_{90} = \Delta\alpha_{1.55} \leq 0.05$ dB for 90% of fibers; $\Delta\alpha_{10} = \Delta\alpha_{1.55} \leq 0.1$ dB for 10% of fibers

Cable Entry and Handling

One of the significant drawbacks of previous commercially available hostile environment cables was its difficult handling characteristics, both in installation and entry. Previous designs have utilized a polyester inner sheath with imbedded strength elements resulting in a cable which is extremely stiff and difficult to cut for entry. With the translucent fluoropolymer as the inner sheath and the non-embedded strength elements, several advantages were realized.

Since the inner sheath material was resistant to degradation from the steam environment, it was easily entered at mid span even after steam aging, unlike a polyester sheath which may have been severely degraded under the same conditions. The material retained its flexibility, even after aging, thus maintaining its craftsperson friendliness. Being translucent, the contrasting colored ripcords were easily seen through the jacket, allowing quicker cable entry. And with the tensile strength and anti-buckling elements not imbedded within the inner sheath, the elements were easier to strip away for splice preparation.

As shown in the test results, the pitch, depth, and profile of the corrugated copper armor ensured both an armored shield resistant to both compression and impact while maintaining with maximum flexibility as reflected in the cyclic flex results. Placement of a high strength ripcord beneath the copper facilitated its removal and reduced end preparation time. This feature was not available on previous designs. The effect of these improvements are evident when comparing cable end preparation times for various armored cable designs. In fact, this hostile environment cable is quite comparable to a standard, armored, ribbon cable[8] in end preparation time as shown in Table 5. Preliminary field results indicate up to a 30% reduction in end entry time compared to previous commercial designs of hostile environment cables.

Table 5. 144 Fiber Armored Cable End Preparation Times (min.)

Preparation Step	Cable Type		
	Loose Tube[8]	Standard Ribbon[8]	Hostile Environment
Jacket Removal / Ground Armor	13	12	14
Clean Tubes	20	N/A	N/A
Clean Ribbons	N/A	9	9
Clean Fibers	42	12	12
Unit Splitter / Tubing	N/A	N/A	N/A
Ribbonized Fiber	78	N/A	N/A
Total (min)	153	33	35

CONCLUSION

A new central tube, hostile environment, ribbon cable has been designed which offers many improvements over previous commercially available hostile environment cables. Through careful selection and testing of oxidation, hydrolysis and oil resistant materials, the cable design is capable of withstanding harsh environmental conditions without significant degradation of material or optical properties. The cable structure was also designed to provide improved flexibility and ease of handling over previous designs. With the addition of a ripcord beneath the copper armor and inner sheath ripcords that are easily locatable, the sheath removal time is comparable to a standard armored ribbon cable. The geometry of the copper corrugations and the stranding of the strength elements also contribute to a cable with dramatically improved flexibility. Finally, this cable design does not require any special tooling for the craftsperson.

All material compatibility, material aging, cable environmental, and cable mechanical tests meet or exceed Bellcore TR-1322 requirements. The temperature stability of

this cable extends to -40°C, increasing its usefulness in outside plant applications.

In order to simulate a high pressure steam environment a specially designed autoclave was manufactured. The autoclave allowed multiple samples to be aged in a saturated steam environment of up to 150°C and 70 psia. Conditions within the autoclave were constantly monitored and automatically adjusted to ensure stability throughout the entire testing period.

ACKNOWLEDGMENTS

The authors would like to thank members of Lightwave Laboratory, the Materials Laboratories, Ted Wilkins, Jeff Andrews, Jeff Truckner and Brad Hogg for their help and support.

REFERENCES

[1] Madalli, P.S.V.; presentation to "Telecommunications Wire and Cable Standard Technical Advisory Committee," New Orleans, May 1990.

[2] GR-20-CORE, "Generic Requirements for Optical Fiber and Optical Fiber Cable," Issue 1, Bellcore, September, 1990.

[3] TR-NWT-001322, "Generic Requirements for Steam Resistant Optical Cable," Issue 1, Bellcore, 1994.

[4] Vyas, M.K.R.; Buckland, E.L.; Neveux Jr., Paul; "Design and Development of Steam Resistant Fiber Optic Cable," Proceedings of the Fortieth International Wire and Cable Syomposium, pp 55-65, 1991.

[5] EIA/TIA-455-28B (FOTP-28), "Method for Measuring Dynamic Tensile Strength of Optical Fiber," October, 1991.

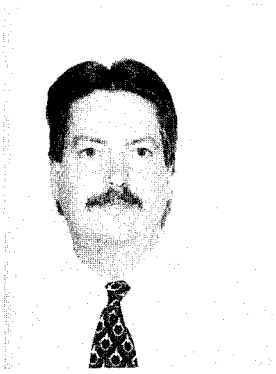
[6] IEC 794-1-E10 (Tube Kink Test), "Generic Specifications: Optical Fiber Cables."

[7] Neveux Jr., Paul E.; Buckland, Eric L.; "Cable Polymer Reliability Testing," Proceedings of the Fortieth International Cable And Wire Symposium, pp 341-347, 1991.

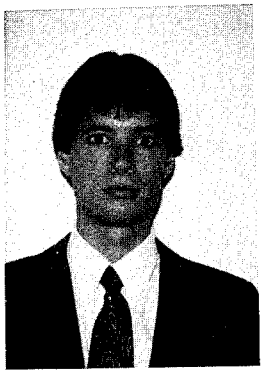
[8] Beasley, William; Canady, Shannon T.; Karl, Greg; "Choosing the Right Cable for the Right Application," Proceedings of the National Fiber Optics Engineering Conference, pp 491 - 501, 1995.



Paul E. Neveux, Jr. obtained his double B.S. in Chemistry and Biology in 1979 from Antioch College, Yellow Springs, Ohio. After completing his Doctorate in Inorganic Photochemistry at the University of North Carolina in Chapel Hill, he held a post-doctoral fellowship investigating conducting liquid crystal polymers at Duke University in Durham, North Carolina. In 1986, he joined Sumitomo Electric Lightwave Corp. and currently supervises the Materials Testing & Reliability Laboratory. Dr. Neveux is an active member in the Telecommunications Industries Association and the American Chemical Society.



Stephen R. Stokes obtained a B.S. degree in Electrical Engineering from Virginia Polytechnic Institute and State University in 1988. He was employed by ITT Electro Optical Products Division and, subsequently, Alcatel Cable Systems from 1980 to 1990 in the development of fiber optic measurement systems. From 1990 to 1991 he was employed by Galileo Electro-Optics Corporation as a Design Engineer in the development of light guide and imagescope products. He has been engaged in the research and development of fiber optic cables since joining Sumitomo Electric Lightwave Corp. in 1991. He is currently Manager of Product Design Engineering.



Grant S. Blume obtained his B.S. degree in Mechanical Engineering in 1989 from The Pennsylvania State University and his Masters degree in Mechanical Engineering from North Carolina State University in 1995. He worked as a Mechanical Engineer / Enforcement Agent for the U.S. Environmental Protection Agency from 1989 to 1991 investigating violations of the Clean Air Act. Since joining Sumitomo Electric Lightwave Corp. in 1992 as a Product Design Engineer he has been engaged in the research and development of optical fiber cables. He is currently the supervisor of the Research and Development Optics Laboratory.

TIME OF FLIGHT AND OPTICAL SKEW IN FIBER OPTIC RIBBON CABLES SUBJECTED TO THERMAL STRESS

Vu Anh Lai and Tom Rosenmayer

W.L. Gore & Associates, Inc., Austin, Texas

Abstract - Fiber-to-fiber time-of-flight differential (skew) is an important factor in high bandwidth parallel fiber optic data transmission applications. Fiber optic cables can undergo substantial changes in temperature in service. Temperature swings may affect skew in ribbon cables because of non-uniformity in coefficients of thermal expansion (CTE)-induced stress across the cross-section of the cable. A method is developed whereby the skew of fiber optic ribbon cables can be measured at various temperatures. Results indicate relatively low skew at all temperatures in the particular sample s tested. This indicates that proper design, materials selection, and manufacturing techniques were used.

Introduction

The purpose of fiber optic ribbon cables is data communication. Channel capacity defines the amount of data that may be communicated within a certain period of time. Channel capacity is determined by signal-to-noise ratio, bit error rate, and bandwidth.

The common dominant consideration for long distance, single-mode applications is signal-to-noise ratio. Hence, traditional testing methodologies and specifications for determining the effect of mechanical stresses on fiber optic cables focus on measuring signal-to-noise ratio (attenuation) vs. applied mechanical load. One type of such load results from thermal cycling of the cable. For high speed (approaching 1Gbit/s), short length (< 1km) multi-mode fiber ribbon applications, bandwidth is a critical consideration to channel capacity.

In addition, it is anticipated that multichannel arrays for parallel optical data transmission will be commercially available in the near future. This consideration increases the importance of determining skew (fiber to fiber propagation delay differential) in fiber optic ribbon cables.

It is possible that skew may vary with temperature. This is because of non-uniform mechanical stresses within the cable. The mechanical stresses are a result of differing CTE in the various materials used in the construction of the cable (ie., core, cladding, coating, buffer, strength member, jacket). The stresses may be non-uniform because the ribbon cable (Figure 2) is not radially symmetric. The fibers near the outer edge of the ribbon are surrounded by substantially different (in volume % as well as in geometrical configuration) material set from those fibers near the center of the construction.

Optical Time of flight Test Setup

Figure 1 shows an Opto-Electronic Optical Time Domain Reflectometer (OTDR). This setup was used to conduct all measurements in this report. This OTDR system is designed to detect Fresnel reflection rather than the Rayleigh backscattering used by conventional OTDR systems. Sub-millimeter resolution is routinely achieved with this system [1]. An interchangeable laser source of 680, 850, or 1550 nanometer wavelength can be used. However, all data collected in this report were obtained using a 860 nanometer laser.

This system consists of three main components. These are the laser source, photon counter, and optical coupler. The test setup works very similarly to a radar system. First, the laser source injects a very fast light pulse into one end of the fiber optic cable under test via the optical coupler. This light pulse travels along the test fiber until it reaches the opposite end of the fiber under test. Because of the mismatch in index of refraction between glass fiber and air, some of the light energy reflects and travels in the reverse direction. The reflected light will travel back towards the pulse origin and reach the photon counter with help from the coupler. With minor corrections for all the test leads, the amount of time the light pulse took to travel down and back the fiber optic cable is accurately measured. The one direction time-of-flight (TOF) and skew was calculated using the equations below:

$$T_f = T_2 - T_1 \quad \text{ns} \quad (1)$$

$$\text{Skew} = (T_{fmax} - T_{fmin})/L \quad \text{ns/m} \quad (2)$$

Where T_1 and T_2 are the time in ns at the beginning and ending of each fiber, respectively. T_f is the TOF in ns, T_{fmax} and T_{fmin} are the longest and shortest TOF per cable under test. L is the length of the cable under test, in meters.

Test Sample

The tested sample was a Skew matched Optical Ribbon Fiber. This cable consisted of twelve 62.5/125/250 micron graded multi-mode fibers held together in a flat configuration with 250 micron pitch. Figure 2 shows a cross section of this cable [2]. The overall length of the test cable is 135.52 meters. The length of cable was loosely wrapped around a paper spool with a diameter of 12 inches.

Test Procedure

The test sample was placed into a thermal chamber that is capable of maintaining constant temperatures at -55°C, 25°C, and 100°C. These temperatures were selected to represent a typical indoor temperature environment. No effort was made to control humidity during this procedure. The initial condition was established after a standard warm up time for all equipment had elapsed and the sample under test had reached a static condition at room temperature for at least 12 hours. Throughout this experiment, all measurements were taken after the thermal chamber had reached the desired temperature with a soak time of two hours. An average of 512 readings were taken for each T_1 and T_2 measurement. T_1 and T_2 are the signal delays at the beginning and the ending of the fiber under test, respectively. In addition, the average of five T_1 and T_2 pairs was used to calculate the TOF for each fiber under test.

As described by the above procedure, the TOF of each fiber within the cable under test was measured and recorded at the preset temperature conditions. The temperature sequence was 25°C, -55°C, 25°C, 100°C, and 25°C. From these measurements, the skew for the cable under test was calculated using equations 1 and 2 at each of the temperature condition.

Results & Discussion

To our knowledge, the lowest skew reported up until now is 1.25 ps/meter/12-fibers. In this report, a skew of less than 1 ps/meter/12 fibers at various temperature conditions was obtain in a new generation of skew matched optical cable. Table 1 shows the TOF results for each fiber at different temperature conditions. Figure 3 is a graphical representation of the data from Table 1. The effect of temperature can be seen by noting that TOF becomes shorter at low temperatures and longer at high temperatures. Two interesting phenomena were observed. First, the test cable appeared to have a good recovery characteristic when extreme temperature conditions were removed. Second, even though the absolute TOF varied with temperature, the overall skew seemed to be stable. This stability is shown in Table 3 and Figure 4.

Using the skew data in Table 2, the average skew over the temperature range tested was 0.69 ps/meter with a standard deviation of 0.0547 ps/meter. The best skew previously reported was 1.25 ps/meter/12-fibers [1] which is larger than the 0.77 ps/meter/12-fiber finding that is reported herein.

Conclusion

As parallel laser arrays become more commercialized in the near future, the market for short run fiber optic interconnects will greatly increase. Parallel computers and telecommunication cross switch systems will demand high quality, ruggedized, low optical signal skew fiber optic interconnect systems. As is demonstrated here, a ribbon fiber optic cable system that has a stable optical signal skew of less than 1 ps/meter/12-fibers over the temperature range of -50 C and 100 C is possible.

References

1 Opto-Electronics Inc. 'Reference Manual, 'Milimeter Resolution OTDR System', 1991, p 1-1

2 W. L. Gore & Associates, Inc.,'FLEX-LITE® High Reliability Fiber Optic Interconnects', Gore Fiber Optic Products Catalog, pp 8-9

3 S. Siala, A.P. Kanjamala, R.N. Nottenburg and A.F.J. Levi, 'Low skew multimode ribbon fibres for parallel optical communication', Electronics Letters Online No: 19941190, % July 1994.

Authors' biographies

Vu Anh Lai is a product manager at the Electronics Product Division of WL Gore & Associates, Manor, TX, where he has worked for 10 years. Warren received a BSEE from the Lamar University, Beaumont, TX. In his spare time, he enjoys camping, hiking, and computers.

Tom Rosenmayer is the product development leader at the Industrial Electronics Business Group of WL Gore & Associates, Austin, TX, where he has worked for three years. Rosenmayer holds a BS in metallurgical engineering form the University of Missouri, Rolla, MO, and MS and a PhD in materials science from Rise University, Houston. He enjoys golf and computers.

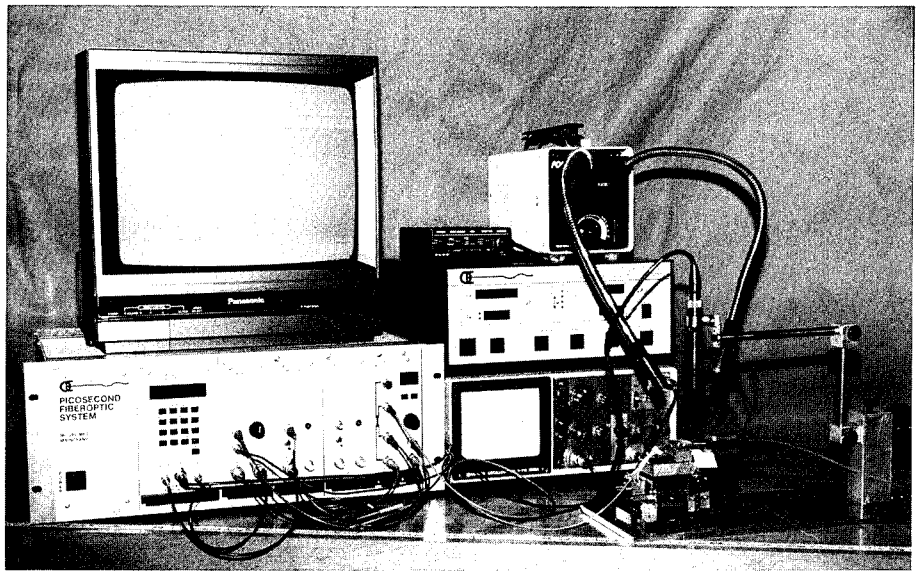


Figure 1. Optical Time Domain Reflectometer test setup

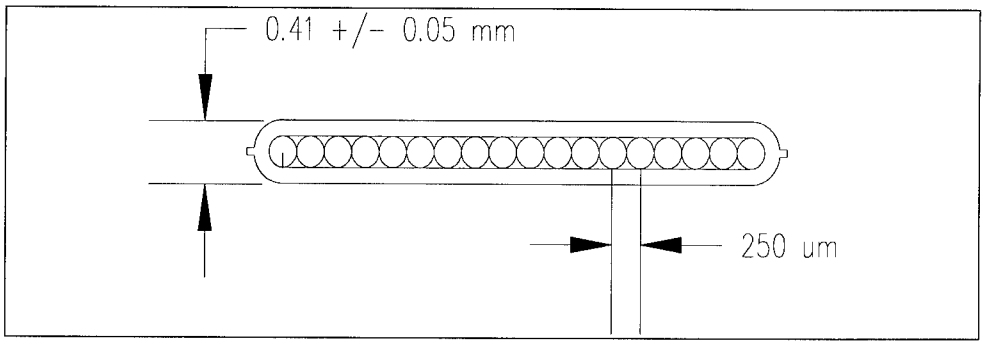


Figure 2. Cross section of Test Sample

Raw Data:

	Time of Flight (ns/test length)				
Fiber Number	**25 C**	**-50 C**	**25 C**	**100 C**	**25 C**
1	1356.70	1355.47	1356.74	1357.56	1356.64
2	1356.74	1355.49	1356.74	1357.59	1356.67
3	1356.72	1355.44	1356.69	1357.54	1356.62
4	1356.76	1355.52	1356.82	1357.63	1356.71
5	1356.77	1355.48	1356.79	1357.59	1356.68
6	1356.65	1355.46	1356.66	1357.50	1356.61
7	1356.62	1355.41	1356.68	1357.46	1356.53
8	1356.80	1355.56	1356.67	1357.64	1356.70
9	1356.74	1355.54	1356.80	1357.59	1356.67
10	1356.63	1355.46	1356.68	1357.48	1356.56
11	1356.63	1355.42	1356.67	1357.47	1356.54
12	1356.59	1355.39	1356.64	1357.45	1356.52
SKEW(ns/Length)	0.21	0.17	0.18	0.19	0.19

Table 1. Time of Flight at different temperatures (ns/test length)

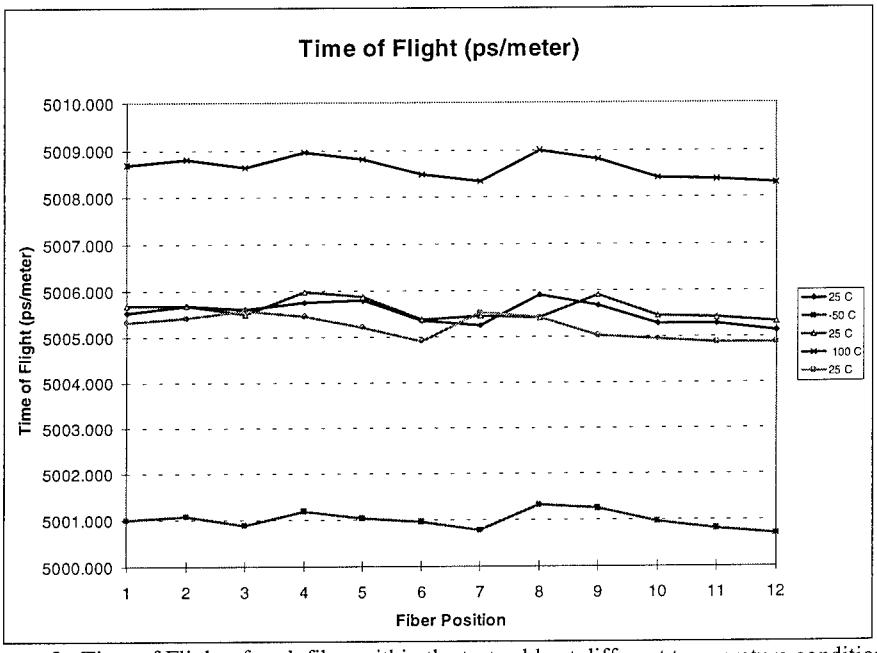


Figure 3. Time of Flight of each fiber within the test cable at different temperature conditions

	Time of Flight (ps/meter)				
Fiber Number	25 C	-50 C	25 C	100 C	25 C
1	5005.534	5000.996	5005.682	5008.707	5005.313
2	5005.682	5001.070	5005.682	5008.818	5005.424
3	5005.608	5000.885	5005.497	5008.633	5005.571
4	5005.756	5001.181	5005.977	5008.965	5005.460
5	5005.793	5001.033	5005.866	5008.818	5005.202
6	5005.350	5000.959	5005.387	5008.486	5004.907
7	5005.239	5000.775	5005.460	5008.338	5005.534
8	5005.903	5001.328	5005.424	5009.002	5005.424
9	5005.682	5001.254	5005.903	5008.818	5005.018
10	5005.276	5000.959	5005.460	5008.412	5004.944
11	5005.276	5000.812	5005.424	5008.375	5004.870
12	5005.128	5000.701	5005.313	5008.301	5004.870
Skew (ps/meter)	0.77	0.63	0.66	0.70	0.70

Table 2. Time of Flight at different temperatures (ns/meter)

Temperature (°C)	Skew (ps/meter)
25	0.77
-55	0.63
25	0.66
100	0.70
25	0.70

Table 3. Signal skew as a function of temperature conditions

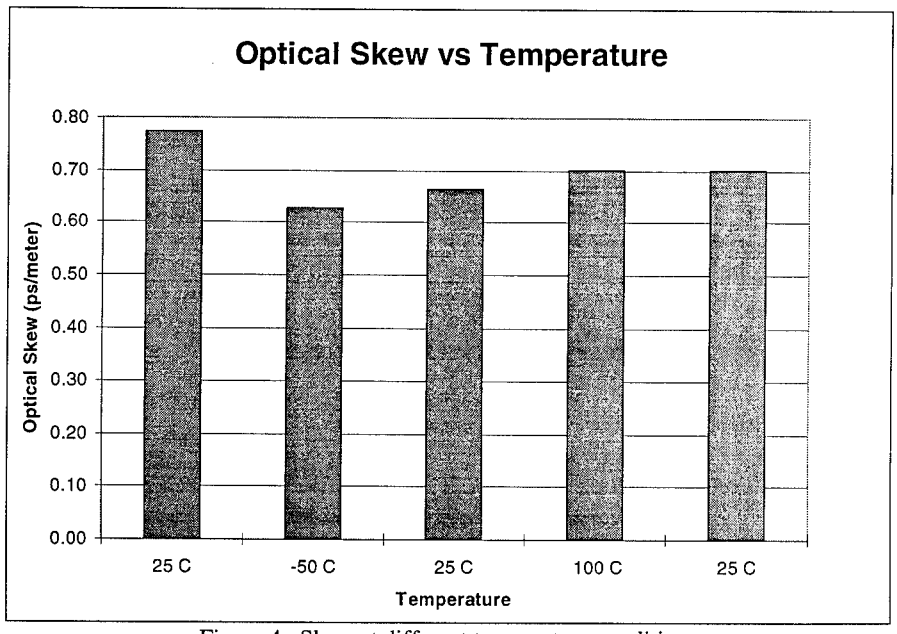


Figure 4. Skew at different temperature conditions

Micro-analysis for Discoloration of Optical Fibers and Filling Compounds

J.-C. Lin, S.-H. Chou, C.-M. Hsiao, H.-P. Hsu, Y.-c. Lin, K.-Y. Chen

OSP, Telecommunication Laboratories, DGT, MOTC
12, Lane 551, Min-Tsu Rd., Sec. 3, Yang-Mei, Taoyuan 326, Taiwan, R.O.C.

ABSTRACT

Micro spectro colorimeter, which is available to measure an extremely small area, has been used to study the colors of the optical fibers in this work. The colored fibers, having six different colors, obtained from three manufacturers have been used to examine the initial colors and the color changes under various aging environments. The color changes of filling compounds are also examined by a large area measurement method. The $L^*a^*b^*$ notation is used to quantitatively describe the colors and the color changes. The color change parameters including L^*, a^*, b^*, and E^*_{ab} are used to discuss the discoloration phenomena. Good color discernibility should state the meaning of good specification for each color and good distinction one another for all colors within a group. The discernibility of fiber colors is adversely influenced by aging. The amount of color change depends on time, temperature, and the service environment around the fibers.

INTRODUCTION

The optical fiber applied in telecommunication and data transmission is usually coated with polymeric materials immediately after drawing to preserve its strength and optical properties. In order to identify polymer-coated optical fibers which are grouped together in a tube, visually distinct color inks are applied to the surface of polymer-coated optical fibers.[1-4] A coloring layer should be bonded strongly to the surface of the secondary coating to remain the color identification of optical fibers. However, it can also form a separate layer which may not adhere well to the secondary coating.

It is well known that the color discernibility of fibers is adversely influenced by aging, because the coloring layer and/or the secondary coating may undergo color changes.[1-4] Exposed to the service environments with time, coating materials have been observed to exhibit color changes. [1] An opaque coloring layer may mask the color change of secondary coating. Although the coloring layer can present as a protective layer to inhibit the discoloration of secondary coating, the coloring layer itself may occur color changes due to the binder resin.[2] The color stability of coloring layer relates to the characteristics of the inks, the characteristics of the secondary coating, and the interactions with the environment to which the fiber is exposed.[3] However, changes in the fiber colors must be acceptable over the service life of the cable.

The specific characteristics of the inks in the colored fiber involve the thickness, the opacity, and the uniformity of the coloring layer, which are normally affected by the manufacturing processes. The inks may be solvent-based and thermally cured, or cured by exposure to ultraviolet (uv) light.[3] Usually, the coloring layer cured by the latter method can provide a more uniform surface. Regardless of the inking technology used, the color must ensure well-defined identification of each fiber by its own unique color throughout the service life of the cable.

Color is a sensation and has three essential properties, lightness, hue, and chroma.[2-4] The color specification may be performed through using Visual Reference Standards or through the use of color measuring instruments, spectrophotometers or colorimeters.[5] Visual Reference Standards describe a color by Munsell notation which is used internationally as a basis of color specifications. However, this method executed by comparing with standard color reference chips is a person-dependent method. On the other hand, the color description can be quantitatively performed by using a color measuring instrument.

The principal problem to measure the color of optical fiber is attributed to the small size of the fiber which is inherent to the optical fibers. For providing a large viewing area to measure the color, the fibers have to be laid parallel and touching in a square holder by hand.[6] It however is a time-consuming work. If micro spectro colorimeter to measure a small area is used, a short piece of individual fiber is sufficient to examine the fiber colors. Compared with the diameter of the optical fiber (250 μ m), the measurement area by micro-analysis method (4 μm in diameter) is very small. In addition, because the thickness of the coloring layer for the optical fibers is normally about 4 to 5 μm, so thin thickness that a uniform surface is not easy to obtain. The sampled location therefore dominates the micro-analysis results. However, the main disadvantage of micro-analysis method is that the data seem more sample-specific due to the measurement area and the uniformity of the coloring layer.

Optical fibers in cables are identified using standard color codes specified by ANSI/EIA-359-A[5] and ANSI/EIA/TIA-598.[7] Colors are specified by centroid and tolerance ranges. If two or more fibers in a unit or a tube cannot be uniquely identified by their colors and distinguished one another, the bad color identification can trouble craft persons for matching the fibers during field splicing. The initial colors of fibers from different manufacturers must be clearly identifiable as to color and lot-to-lot variations in color should be controlled within the tolerance range. Fiber colors change during the service life of the cable, but they must remain distinct and identifiable. Minimal color changes after the cable aging test assure that changes occur slowly enough to permit unique identification of the colors after years in service.

Micro spectro colorimeter is used to measure the color data quantitatively in this work. The objective of this work is to examine the variability of the initial colors of fibers and to study the effects of aging on colored fibers and filling compounds. The color difference between the fibers before and after aged should be minimized to keep the color identifiable and each aged color must be followed to its initial color.

EXPERIMENTAL

Three commercially-available optical fibers, identified as fibers AF, AM and AE, were chosen as the samples in this work. Six different colored fibers (blue, yellow, green, red, violet and white) were provided from

each manufacturer. Fibers supplied from AM and AE were colored with uv-cured inks, whereas fibers from AF were with solvent-based inks.

The colored fibers were aged in various environments to study the effects of temperature, gel, humidity, and time on the color stability. The fibers from AF and AM were aged at 50°C, 70°C, and 100°C in the ovens, and at the same temperatures submerged in filling compounds supplied from their original manufacturers. The former provided the thermo-oxidative environment, while the latter condition was used to study gel effect. The filling compounds were also individually aged at 50°C, 70°C, and 100°C in the ovens. The fibers from AE had different original situation, which the fibers were enclosed in a buffer tube and already immersed in filling compounds. The gel effect therefore was investigated when the fibers in the buffer tube were aged at room temperature (RT), 50°C, and 70°C in the ovens. In addition, the tubes soaked in water were aged at the same temperatures to study the effect of water penetration on the fiber colors.

Micro spectro analytical system including an Olympus BH2-MJLT microscope and an Otsuka MCPD-1000 Spectro Multi Channel Photo Detector was used for micro-area color measurement. The D_{65} standard source was used as the light source. The measurement diameter was 4 μm. The colorimeter equipped with a Y-shaped optical fiber to connect the microscope and the photo detector. The optical fiber directed the light at a 0° angle to the fiber surface and guided it at the same angle back to the photo detector which monitored the emitted light by a photodiode array. The detection wavelength range was 380-780 nm. Color and color difference data were calculated via the colorimeter software using a data processing unit. Black background was chosen during the measurement. The sampling time was 7 sec for fibers. The color data were stated as the average of values at 10 measurement locations to eliminate sample specific problem. On the other hand, the large-area measurement could be used to examine the color of fibers and filling compounds. MCPD-1000 using an accessory, MC-955, made it available to measure a large-area sample. The light source was the same as micro-area method used. Compared with micro-analysis method, there are some typcial difference as follows. The 0°/45° illumination and receiving geometry was used. The measurement area was 5 mm in diameter and the sampling time was 1 sec. The holder shapes of fibers and filling compounds are different, but the holders are made of Teflon plates. The holder for filling compounds is a round hollow with 20 mm in diameter and about 1 mm in depth, while the holder for placing the fibers is a square hollow with 20 mm in each side and 1 mm in depth.

Although the color notations have been introduced somewhere else,[2-4] it should be noted here again. Definition of the color in $L^*a^*b^*$ space is used in this study. It uses an xyz coordinate system to describe a color. Values of L^* state the lightness, while a^* and b^* define the x and y axes, respectively. Values of a^* and b^* depict hue and chroma. Compared with Munsell notation, the main advantages of the $L^*a^*b^*$ color space are the clear specification of colors and the simplicity of the calculation. The values of a^* and b^* indicate clear physical meaning. For example, high positive value of b^* means that the sample color has high yellow component and high negative value of a^* denotes that the sample color has high green component. ΔE^*_{ab} is used to describe the distinction between $color_1$ (L^*_1, a^*_1, b^*_1) and $color_2$ (L^*_2, a^*_2, b^*_2), which is expressed as the following, the linear distance between these two points.

$$\Delta E^*_{ab} = ((\Delta L^*)^2 + (\Delta a^*)^2 + (\Delta b^*)^2)^{1/2}.$$

Low ΔE^*_{ab} value indicates a color difference between $color_1$ and $color_2$ which cannot be distinguished by the naked eye, while high ΔE^*_{ab} value indicates clear distinction from each other.

RESULTS AND DISCUSSION

The initial color data of fibers from three manufacturers measured by micro-analysis method are summarized in Table 1. The color data listed in this Table include L^*, a^*, and b^*. It clearly shows that the color named the same from different manufacturers can be visually different and have significantly different color data. However, the initial colors behave visually clear and bright, and can be easy to distinguish one from the others within a group.

The colors from AM have lower values of a^* and/or b^* than those from the others, especially green and blue. Based upon the definition of $L^*a^*b^*$ notation, negative a^* value indicates the degree of green, whereas negative b^* value indicates the degree of blue. For the fibers supplied from AM, blue ones having small a^* value (-5.80) denote low blue component in the coloring layer, whereas green ones having small a^* value (-3.48) denote low green component. Furthermore, the blue and green fibers supplied from AM inspected by eye seem translucent. This observation is in agreement with the shown color data. The result may be attributed to the low concentration of the pigment and the low opacity of the coloring layer.

Figure 1 shows color data for five initial colors (except white) graphically through an a^*-b^* diagram, which provides more detailed information about the colors. The points marked the same symbol exhibit that they are from the same manufacturer. Each ellipse involves three points with different symbols represented from three manufacturers as shown in Figure 1. The point near to the zero point means that it approaches to an achromatic color. Among five colors, except yellow, compared with the data of the fibers from AF and AE, the points from AM are much near to the zero point. The data show that the colored fibers from AM are close to achromatic color.

Another important information shown in Figure 1 is to describe the color difference between two colors. The distance between two points can be used to identify how good the color distinction for the color pair is. The longer distance, the better color distinction. The fibers from AF and AE exhibit better color distinction than those from AM. Minimal ΔE^*_{ab} value of the fibers from AM is only about 9. Again, this value is between green and blue. Although they are distinguishable at the beginning, it however is not a good initial existing state. The requirements for having good color discernibility in a group should include good color specification for each color and good color discernibility one another for all colors in the group.

For understanding the difference between micro-area (4 μm in diameter) and large-area (5 mm in diameter) measurements, few large viewing area samples were also examined. To obtain a large viewing area, the short fiber pieces were placed in a square holder as described in experimental section. Double layers of fibers were needed and must be orthogonal to each other. Except the measurement area, the essential difference between two methods is illuminating/viewing geometry which may influence the measured color data. However, the preliminary results of blue and green fibers measured by both methods are shown in Table 2, except higher values of L^* obtained by micro-area method, the values of a^* and b^* obtained by these two methods seem quite similar. Higher L^* values obtained by micro-area method are possible due to the uniformity of the small local area. Although optical fibers may not provide a wholly uniform surface, small measurement area is supposed to be a uniform surface. On the other hand, the large area by placed the fibers provides an uneven surface, which may scatter the light and decreases the measured lightness. Different measurement methods and/or even different analytical instruments however may result in different color data. The result therefore suggests that obtained from the same measurement method and the same instrument, the color data then are comparable.

The color changes of fibers from AF aged under six different environments for 30 weeks are shown in Figure 2. Roughly to inspect the data, all colors remain stable below 70°C. Red color seems inert to the aging environments. Though the red fibers are immersed in filling compounds at 100°C, the color change is still undetectable by eye. The result suggests that the red color is thermally stable and the color difference measured by ΔE^*_{ab} below 4 is within experimental error. Some colors have higher ΔE^*_{ab} values at 100°C than at low temperatures. Temperature therefore is an important factor to affect the color stability.

On the other hand, the data exhibit that the filling compounds left on the fibers provide a more severe environment. If the fibers are immersed in filling compounds at 100°C, the color changes exhibit significantly high, especially blue up to 18. The blue color change from (52.01, -5.74, -38.65) to (52.54, -12.71, -22.41) clearly shows that the large color change is from Δa^* and Δb^*, but not from ΔL^*. The aged blue has less blue (lower negative b^*) and more green (higher negative a^*) components. It means that the aged color is far from blue and approaches to green. Although the aged blue color approaches to green, the color difference between aged green and aged blue is still high to 37. However, all aged colors from AF experienced the most harsh environment are still distinct identification one another.

The color changes of fibers from AM under the same aging environments as AF experienced are shown in Figure 3. Though the red color seems thermally stable under thermo-oxidation, all colors however are sensitive to the aging environments. Regardless of the aging environments experienced, temperature effect is still the main factor to influence the color. There is only slight effect at 50°C and 70°C; nevertheless, it is clear that 100°C is an unacceptable temperature to the samples supplied from AM.

It is well known that the colors are perceived as darker and duller after aging in harsh environments. Higher ΔE^*_{ab} value denotes large deviation from the original color. However, ΔE^*_{ab} cannot clearly depict the direction of color change. If L^*, a^*, and b^* are separately discussed, then the discoloration direction becomes clear. Low L^* value indicates that the color becomes darker. High a^* value implies a yellowing process. In addition, extremely low values of both a^* and b^* indicate that the color is near to an achromatic color.

Figure 4 involving an a^*-b^* diagram and a L^* diagram presents more detailed description about the colors at 100°C. Three different symbols in the a^*-b^* diagram represent the color data including the initial colors and the aged colors experienced in two different aging environments, under thermal-oxidation and immersed in filling compounds. There are several features displayed in this Figure. Except white, all other aged colors shift the initial colors to achromatic range. The L^* values of the colors except white decrease slightly under thermo-oxidation, on the contrast, the L^* values decrease greater in amount when the fibers are submerged in filling compounds. White fibers experienced different environments provide interesting results that the ΔE^*_{ab} values are similar and, however, different discoloration phenomena are displayed in Figure 4. Under thermal-oxidation environment, ΔL^* is 6, furthermore, the b^* value increases from 0.6 to 10.8 and the a^* value (Δa^* is 0.6) is almost invariable. It is significantly a yellowing phenomenon. By contrast, when the white fibers are immersed in filling compounds, ΔL^* is 15, while Δa^* is 1.3 and Δb^* is 5.6. The fibers by this reason become darker and however are not a meaningful yellowing process.

The color differences for aged color pairs are also shown in Figure 4. Under thermal-oxidation, the b^* value of blue color shifts to a positive value, indicating that there is completely no blue contribution to the coloring layer. Another feature has to be noted that the color difference between aged blue and aged green is only 4.13, which means completely hard to distinguish each other. However, the fact is that there is originally no good color discernibility between blue and green. All fibers immersed in filling compounds behave darker having low lightness values. There are five color pairs having the color differences below 7. The most unacceptable color pairs involve blue-green and green-violet which are only 3.1 and 4.5, respectively. The aging study therefore suggests that the colored fibers supplied from AM do not have good color discernibility over the service life of the cable.

The fibers from AE had different original situation, the study therefore was different from the others. Except gel effect, the effect of water penetration was also studied. The color changes of fibers from AE under different aging environments for 34 weeks are shown in Figure 5. Enclosed in a buffer tube, the fibers are already submerged in filling compounds. Except white, the color changes of the other colors below 4 are within experimental error. The colors therefore remain stable up to 70°C. When the buffer tube is soaked in water at 70°C, all colors have extremely high ΔE^*_{ab} values which exhibit large color changes during aging. The result ensures that the effect of water penetration on color change is significant. It means that water penetrates to the tube, reacts with the filling compounds, and significantly influences the colored fiber.

Figure 6 includes a^*-b^* diagram and L^* diagram. Three different symbols represent the color data of three different conditions. There is a clear feature shown in the a^*-b^* diagram. When the colored fibers is enclosed in the buffer tube even at 70°C, compared with the initial colors, the a^* and b^* values are almost stationary. On the contrast, when the tube is soaked in water, the colors approach to achromatic range significantly. However, the high ΔE^*_{ab} value of white is attributed to dominantly the color darker during aging. Among six colors, the ΔE^*_{ab} value of violet color is extremely high up to 18 as shown in Figure 5. The reason is also clearly shown in Figure 6, which an exceptional data appears in L^* diagram. Although the violet color approaches to achromatic area, the L^* value of this color increases after aging, which is an unusual result. To inspect the aged violet fiber, it approaches to an achromatic color but becomes brighter than the initial fibers. The results conclude again that the discoloration phenomena cannot be wholly described by the ΔE^*_{ab} values, but can be completely discussed by ΔL^*, Δa^*, and Δb^*.

As mentioned previously, fibers from AF were colored with thermally cured inks, while fibers from AM and AE were colored with uv-cured inks. It was generally noted that the uv-inked layer had good thermal stability attributed to the uniformity of the uv-inked layer. However, based upon the experimental results, the colored fibers from AF exhibited better color stability and better color discernibility than those from AM and AE. It therefore suggested that the color stability during aging was not completely affected by the inking technology used, but by the manufacturing processes controlled.

The color changes of filling compounds from AF and AM aged under thermal-oxidation over 40 weeks at 100°C are shown in Figure 7. At initial condition, both are milky color and transparent. Up to 40 weeks, the color change of filling compounds from AF is only 8.6. To inspect the color data detailedly, it is a slightly yellowing process. On the other hand, filling compounds from AM show a significantly different phenomena. At first 7 weeks, it proceeds a yellowing process. However, after 7 weeks, the lightness value drops fast, while the a^* and b^* values increase rapidly. The color therefore approaches to dark brown. Furthermore, based upon the thermogravimetic results,[8] the discoloration of the filling compounds was correlated with the chemical changes. At high temperature, volatilization of low molecular weight compounds is the dominant process for the filling compounds from AF, while for the filling compounds from AM, thermal degradation of high molecular weight compounds is dominating. Different phenomena therefore are attributed to different chemical reaction occurred.

SUMMARY

Micro-analysis method is one of the methods to measure the color of the optical fiber. It suggests that it can be used as an alternative method, which provides the color data very fast. $L^*a^*b^*$ notation can be clearly describe the color and the color difference. Good color discernibility should include good color specification for each color and good color distinction one another for all colors in the group. The discernibility of fiber colors is adversely affected by aging. The amount of discoloration depends upon time, temperature and the service environment around the fibers. To interpret the discoloration phenomena, the color parameters including ΔL^*, Δa^*, and Δb^* are necessary. For most colors, aging in the gel environment caused greater color changes than aging in thermal-oxidative environment.

REFERENCES

1. T. Bishop, C. Chawla, D. Szum, and E. Poklacki, *Proc. 41st IWCS*, 442, 1992.

2. R.A. Frantz and I.M. Plitz, *Proc. 42nd IWCS*, 850, 1993.

3. B.J. Keon and R.A. Frantz, *Proc. 43rd IWCS*, 522, 1994.

4. J.R. Petisce, M.D. Kinard, S. Siddiqui, and C. Taylor, *Proc. 42nd IWCS*, 552, 1993.

5. ANSI/EIA-359-A-1984, Electronic Industries Association, Washington, DC 20006.

6. TR-NWT-000020, Bell Communications Research, Technical Reference, Issue 5, 5-8, 1992.

7. ANSI/EIA/TIA-598-1992, Electronic Industries Association, Washington, DC 20006.

8. Unpublished results.



J.-C. Lin received his M.S. degree in polymer science in 1983 from Tsing Hua University and then directly joined TL. He is presently a research scientist and a member of Outside Plant Laboratory in TL.

S.-H. Chou received a Ph.D. degree in Physical Chemistry from University of Delaware in 1990. She worked as a Postdoctoral Fellow in Academia Sinica after graduation and joined OSP, TL in 1994. Her interests have concentrated on the reliability of polymer materials used in the telecommunication applications.

C.-M. Hsiao received her M.S. degree in Chemical Engineering from Tsing Hua University. She joined TL in 1981 and presently worked as a research scientist and a member of Outside Plant Laboratory in TL.



H.-P. Hsu is currently a project manager of the material group of Loop and Outside Plane Laboratory, Telecommunication Labs.. He received his Ph.D. degree in Chemistry in 1983 and has engaged in industrial materials research since then.

Y.-c. Lin received his B.S. degree in Chemistry in Taiwan and his Ph.D. degree in Photochemistry from Georgetown University. After working as a Postdoctoral Fellow in the Institute of Materials Science at the University of Connecticut, he joined Telecommunication Laboratories in 1989 and presently is a project leader of O.S.P. material and construction.

K.-Y. Chen was born in 1953 and received his Ph.D. degree in Electro-Optics from National Central University in 1990. He has been engaged in research and development of optical fabrication and communication technologies since 1977. He is currently the director of outside plant technology laboratory of Telecommunication Labs.

TABLE 1 Initial colors data (L^*,a^*,b^*) of fibers from three manufacturers

color	AF	AM	AE
Blue	52.01, -5.74, -38.65	47.10, -1.31, -5.80	52.55, -7.31, -22.15
Yellow	59.41, -1.40, 22.83	70.89, -3.46, 34.36	55.73, -3.54, 27.18
Green	67.57, -31.84, 13.03	48.02, -3.48, 3.11	47.28, -12.37, 11.41
Red	42.27, 27.19, 0.40	48.65, 13.40, 4.38	38.88, 11.05, 3.16
Violet	47.56, 11.03, -11.73	51.75, 8.58, -7.72	53.92, 12.43, -17.02
White	60.28, 0.94, -2.16	76.72, 0.04, 0.58	76.16, -0.40, -0.05

TABLE 2 Color data (L^*,a^*,b^*) of blue and green fibers measured by micro-area and large-area methods

	blue	green
micro-area	46.45, 1.45, -36.70	60.45, -31.54, 13.24
large-area	36.77, 6.60, -37.66	47.66, -35.19, 13.72

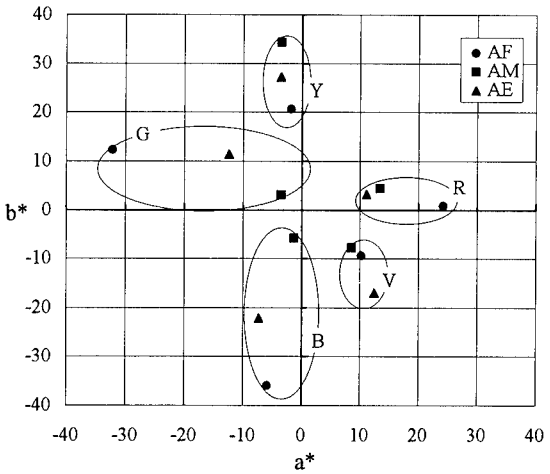


FIGURE 1 Color data for five initial colors (blue-B, yellow-Y, green-G, red-R, violet-V) graphically through a*-b* diagram, the points marked the same symbol from the same manufacturer.

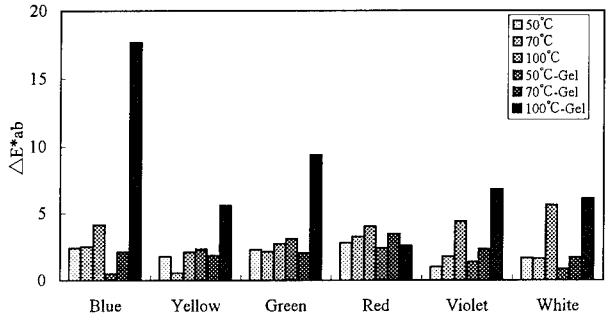


FIGURE 2 Color changes △E*ab for colored fibers from AF during six different environments.

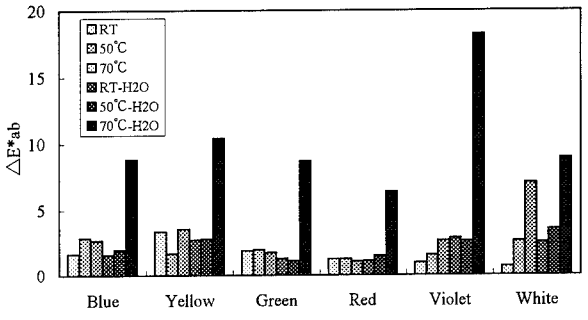


FIGURE 5 Color changes △E*ab for colored fibers from AE during six different environments.

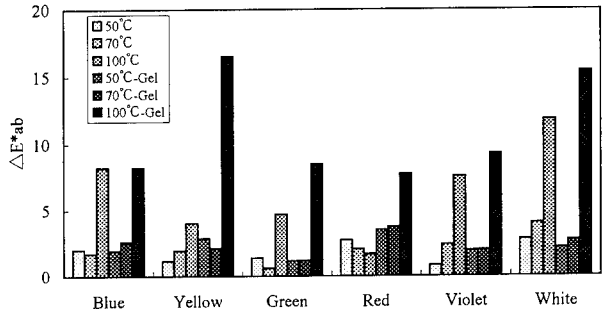


FIGURE 3 Color changes △E*ab for colored fibers from AM during six different environments.

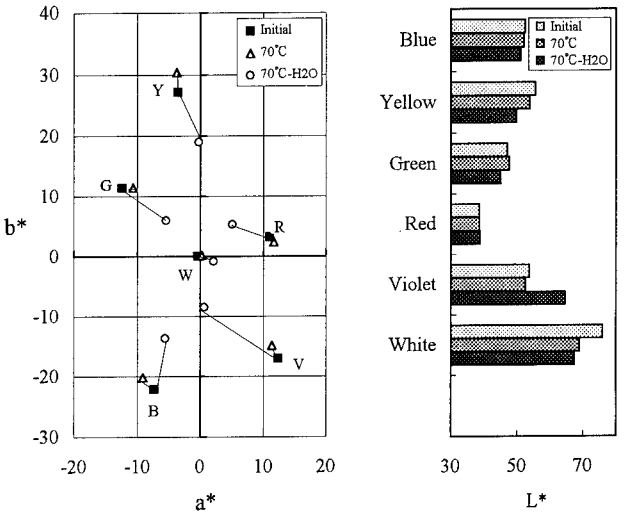


FIGURE 6 a*-b* diagram and L* diagram for colored fibers from AE aged at 70°C soaked in water or not.

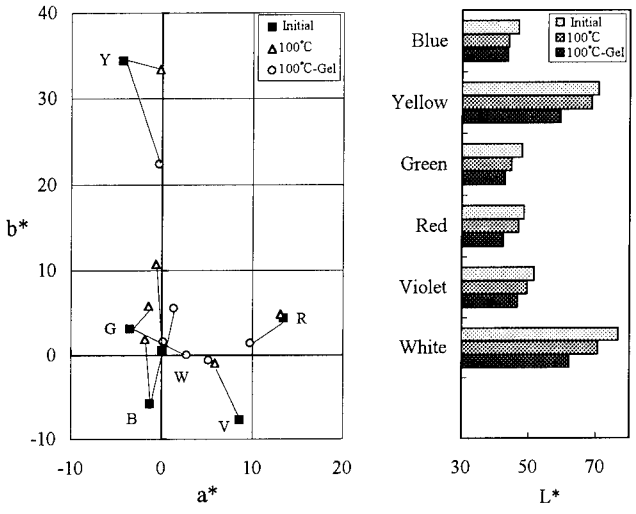


FIGURE 4 a*-b* diagram (white-W) and L* diagram for colored fibers from AM aged at 100°C with and without filling compounds.

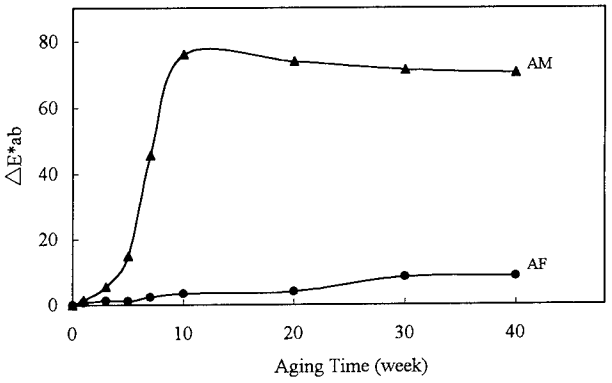


FIGURE 7 Color changes △E*ab for filling compounds from AF and AM at 100°C over 40 weeks.

Effects of Coating Corrosion on the Performance of Optical Fiber

Ting-Chung Chang, Chieh-Mei Hsiao, Whei-Jen Chen, Hsi-Pai Hsu, Y-c Lin, Kuang-Yi Chen

OSP, Telecommunication Labs, DGT, MOTC
12,Lane 551, Min-Tsu Rd., Sec. 3, Yang-Mei, Taoyuan 326,Taiwan,R.O.C.

Abstract

Two types of optical fibers designated as fiber-A and fiber-B are aged in aqueous solutions at different pH values, 3.5% NaCl solution and superabsorbent material saturated solution at ambient temperature. Tensile strength measurements indicated that the strength of fiber-A dropped by 7% of initial strength while fiber-B dropped by 15% after 7 days aging. No apparent additional drop was observed for aging up to 210 days. For aging in solutions with different pH values, fiber-A showed no dependence of the drop of tensile strength on pH values while fiber-B showed an increase of drop when the pH values increased. However, in low pH condition, the tensile strength measurements showed a large discrepancy since the acidic condition had caused a random corrosion on protective coating as observed by SEM.

When aged in 3.5% NaCl solution and superabsorbent material saturated solutions, both fibers show continuing drops of tensile strengths and strip forces as a result of the charge accelerating corrosion occurs between the coating and glasses.

Introduction

As a trend of replacing copper wire with optical fiber, optical communication has essentially taken most of the load in numerous telecommunications and data transmission applications. This has prompted intensive researches on the materials used for optical fibers cable plant as result of the concern of fiber reliability, especially in harsh environments. It has been recognized that optical fiber is extremely susceptible to water or moisture that can cause the deterioration of fiber strength and the increase of transmission loss(1,2,3). To prevent the moisture from attacking the fiber surface or physical damage and scratches on fiber surface that result flaws, UV-cured polyurethane acrylates are widely coated on the fiber surface as a protective barrier. In addition, optical cables are designed as waterproofing by incorporating waterproofing jellies and water-blocking tapes (superabsorbent materials) into the cable structures. Although this may provide certain degrees of protection, doubts on the fibers whether to persist their performance when encountering hash environments such as high humidity and sea water floods still undermine our confidence to apply optical fibers in such areas without special cautions. This work is intended to understand the environmental effects such as in water solutions and soaked superabsorbent material solutions on the long term reliability of optical fiber.

Experimental

Samples

Samples of fiber designated as fiber-A and fiber-B are commercial available. Both fibers are single mode fiber (125 μm)coated with dual coating in a diameter of ca. 250 μm.

Aging

Fiber-A and fiber-B were cut to numbers of samples at a length of ca. 2000 m that were loosely wounded as circles (diameter = 300 mm) and placed in containers with the ends of fibers outside the container. The samples were aged in different pH value solutions, distilled water and 3.5% sodium chloride solution. Samples of fibers were removed from aging at period of time and the change of tensile strength and strip forces were measured.

Tensile strength

Minimum of 25 specimens for each sample was measured in a Universal testing machine using a gage length of 500 mm and a strain rate of 20 mm/min in a laboratory ambient environments of 23℃ and relative humidity of 60%.

Strip force

Minimum of 10 specimens for each sample was measured in a customized stripping tensile testing machine mounted with a

commercial stripping tool(0.18/0.30). The gage length is 100 mm and stripping length is 30 mm with a stripping rate of 500mm/min. Strip force collected through out the stripping process with a data acquisition rate of 20 Hz.

Coating morphology observation

The aged fiber samples were cleaned to remove dirt particles that might have collected on aging environments and adhered to a metal tape. The cleaned fibers are then coated with a gold-palladium coating (40-100 A. thickness). The fiber coating surface is then examined under a scanning electron microscope.

Result and discussion

Change of tensile strength

The tensile strength changes of both fibers aged in aqueous solutions with different pH values are shown in fig.1 and fig.2. All the figures also show the maximum and minimum point of measured specimens for each sample. For fiber-A no systematic relationship between the loss of tensile strength and aging pH condition can be seen. It looks as the loss of tensile strength of fiber-A aged in acidic or alkaline conditions are similar to aged in distilled water. The protective coating of fiber-A is still well performed even in harsh conditions (such as in pH=2 or pH=11). However, for fiber-B, the degree of loss tensile strength is pH depended. As show in fig.1.a an erratic change (shown as larger standard deviations) of strength that sometimes dropped to half of the prior-to-aging tensile strength is obtained. The erratic changes become smaller when the pH value increase and a progressive loss of strength are clearly seen in pH=11 for prolonged aging. This indicates that the coating of fiber-B apparently is chemically reacted especially in acidic condition and alkaline condition and the reactive sites that may induce the cracks of fiber glass have developed upon aging. The coating that usually made of urethane acrylates is much easily hydrolyzed in strong acidic and alkaline conditions and alkaline condition is even stronger than acidic conditions. As a result, alkaline aging will produce much more reactive sites that may also contain hydroxy anion attacking the glass surface to give the progressive loss of strength for prolonged aging. Furthermore, the effect of alkaline aging shows stronger corrosion on the fiber tensile strength is more evident as shown in fig.2. For fiber-A, no apparent change on the strength shift was observed. For fiber-B, a shift to lower strength can be clearly seen as the pH increases. Fig. 3 shows the change of tensile strength of fiber-A and fiber-B aged in a superabsorbent solution. The strength of Fiber-A dropped sharply at the initial aging stage and became steady after 28 days of aging. Yet the strength of Fiber-B keep dropping as the aging goes. Since the superabsorbent solution has a bulky pH value near 7, it is expected that fiber strength deterioration in superabsorbent solution is similar in distilled water. Nevertheless, as seen in fig.3 and fig.1c, the tensile strength drop in superabsorbent solution is more serious than in distilled water. This phenomenon can be explained by the surface charge effect reported by D. I. Inniss, D. L. Brownlow, and C. R. Kurkjian (4). The structure of superabsorbent materials is polyacrylic, chemically the major functional groups are carboxylates. In water, sodium ions of -COONa dissociate to increase the ionic density and absorb water through hydrogen bonding(5,6), This result will increase the surface charge surrounding the glass fiber and accelerate the fatigue rate and strength deterioration. Fig. 4 shows the tensile strength change of both fibers in a 3.5% sodium chloride solution. A dramatic drop of both fiber's tensile strengths on the first 14 days of aging is observed and is more serious than that of aging in distilled water. This result can also be explained by the surface charge that exists in the glass fiber surface. In fact, any ion that can increase the surface charge can accelerate the fatigue rate(4).

Strip force

Coating strip force measurements were carried out after each fiber sample removal from various aging conditions and were equilibrium with test environment as described above for a minimum of 48 hours. The strip force is an index of coating protecting ability and directly reflects the handling ability. Figure 5 shows the average strip force change of both fibers after aging. Upon aging in acidic or alkaline solutions, Fiber-A shows a slight drop of strip force. On the other hand, Fiber-B shows a quickly drop of strip force and is only 1/2 of its initial value when aged in alkaline solution. Since the strip force depends on the adhesion between the glass and coating and the inherent properties of coating, and any factor that changes above may have effect on strip force. The strip force result indicates that Fiber-B's coatings were easily corroded in aging condition, as a result of lower strip force. It is worth noting that for both fibers, the pH=9 solution was more severe than other aging conditions.

Coating morphology observation

Figure 6 is the coating surface pictures obtained from a scanning electron microscope. Fiber-A's coating had no apparent corrosion under the aging conditions while fiber-B's coating had been critically corroded by aging conditions. This can explain why erratic results of strength measurements were obtained for Fiber-B. The corrosive coating has virtually no protection on the fiber, and an extreme low value of measurement will result on the test machine.

However, the broken coating is not equally distributed on an aged fiber. When the specimens adopted from the fiber contain no broken coating, a stronger strength will be obtained in contrast.

Conclusion

The mechanical performance of optical fiber aged under harsh environments is depend on the protective ability of its fiber coating. From our study, when coating is corroded in aging conditions, the tensile strength, strip force will drop erratically. However, proper coating formulation is available to preserve the fiber coating from corrosion upon aging. Usually, acidic aging results erratic corrosion on fiber coatings and give randomly drops of tensile strength for fibers. In alkaline aging condition, more severe corrosion on fiber can occur due to the induce of more reactive site on fiber coating. In addition, aging in 3.5% sodium chloride solution and superabsorbent solution were more serious than in distilled water due to the charge effect that acerbates the corrosion. Results of strip force measurements echo the results of tensile strength measurement and the mechanical properties of optical fiber are determinate by the resisting ability of coating to environmental, especially in the environments with higher or localized ionic environments is considered harsher.

Reference

1. M.J. Matthewson, C.R. Kurkjian, J. Am. Ceram. Soc., pp. 177-83 (1989)
2. T.T. Wang, H.M. Zupko, J. Mater. Sci., pp. 2241-48 (1978)
3. V.A. Bogatyrjov, M.M. Bubnov, A.N. Guryanov, G.G. Devyatykh, Electron. Lett., pp1013-14(1986)
4. D. Inniss, D.L. Brownlow, C.R. Kurkjian, J. Am. Ceram. Soc. , pp. 364-68 (1992)
5. F.L. Buchholz, CHEMTECH SEPTEMBER pp. 38-43 (1994)
6. C.J. Arroyo, J.J. Sheu, W.J. Paucke, 40th IWCS, pp 326-31 (1991)

Authors



Ting-Chung Chang received his M.S. degree in Applied Chemistry in 1984 from Tsing Hua University and then directly joined T.L.. He is now a research scientist and a member of outside plant laboratory in T.L..



Whei-Jen Chen received her M.S. degree in Applied Chemistry in 1991 from Tsing Hua University and then directly joined T.L.. She is now a research scientist and a member of outside plant laboratory in T.L..

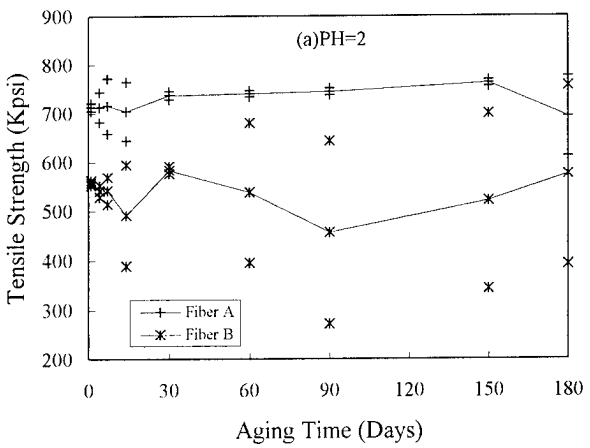


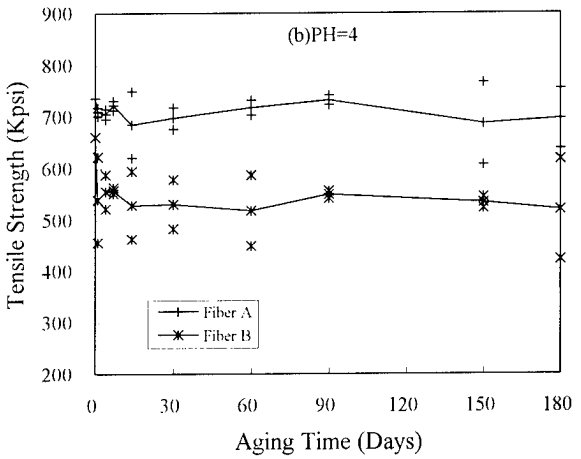
Hsi-Pai Hsu is currently a project manager of the material group of Loop and Outside Plant Laboratory, Telecommunication Labs. . He received his Ph.D. degree in Chemistry in 1983 and has engaged in industrial materials research since then.

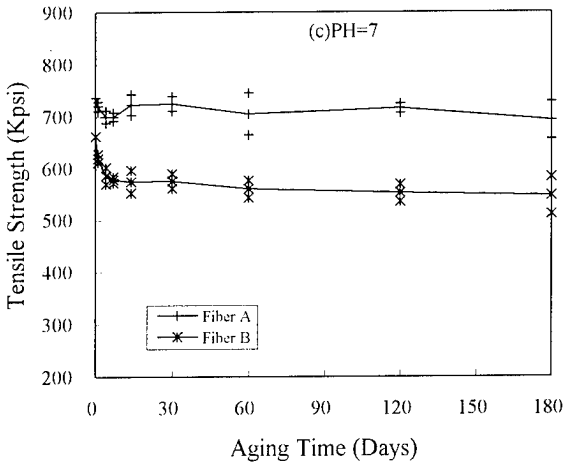
Chieh-Mei Hsiao received her M.S. degree in Chemical Engineering from Tsing Hua University. She joined T.L. in 1981 and presently worked as a research scientist and a member of outside plant laboratory in T.L..

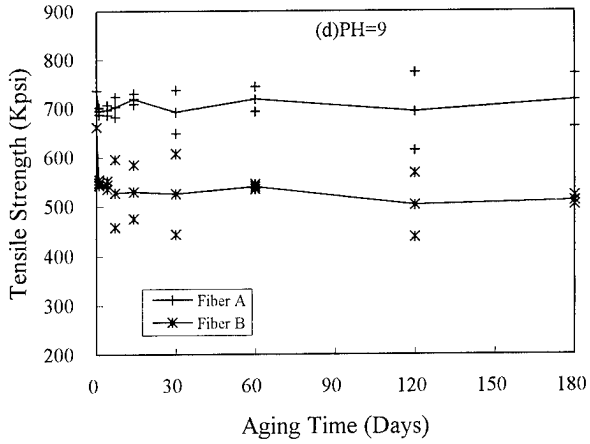
Yih-Chyuan Lin received his B.S. degree in chemistry in Taiwan and his Ph.D. degree in Photochemistry from Georgetown University. After working as a postdoctoral Fellow in the Institute of Materials Science at the University of Connecticut, he joined Telecommunication Laboratories in 1989 and presently is a project leader of O.S.P. material and construction.

Kuang-Yi Chen was born in 1953 and received his Ph.D. degree in Electro-optics from National Central University in 1990. He has been engaged in research and development of optical fabrication and communication technologies since 1977. He is currently the director of outside plant technology laboratory of Telecommunication Labs.









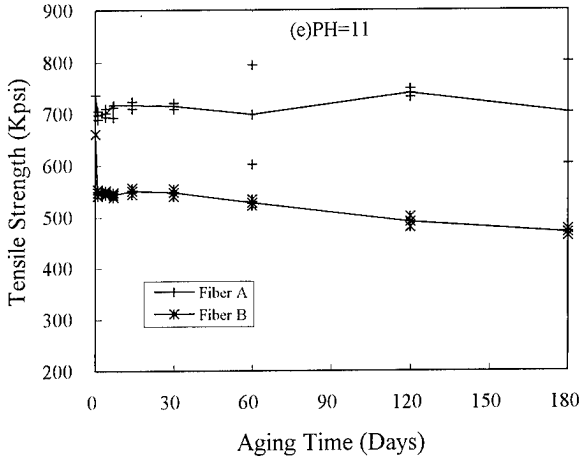


Fig.1 The tensile strength change of fiber aged in aqueous solution (a)pH=2 (b)pH=4 (c)pH=7 (d)pH=9 (e)pH=11

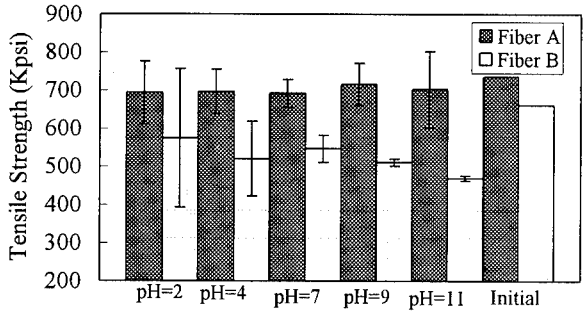


Fig.2 The effect of pH value on the tensile strength after 180 days aging

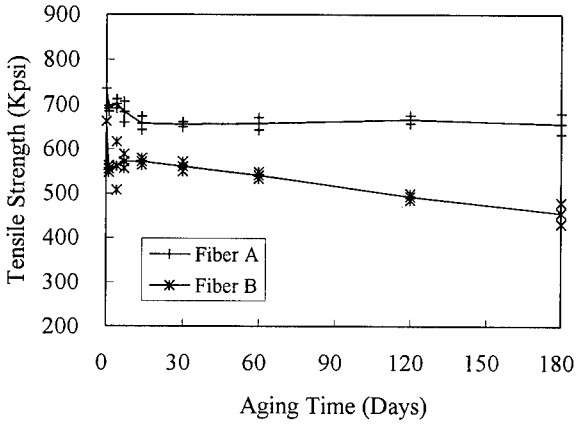


Fig.3 Tensile strength change of fiber aged in superabsorbent solution

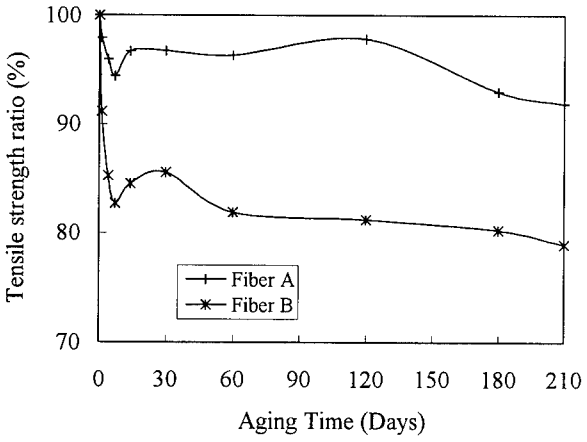
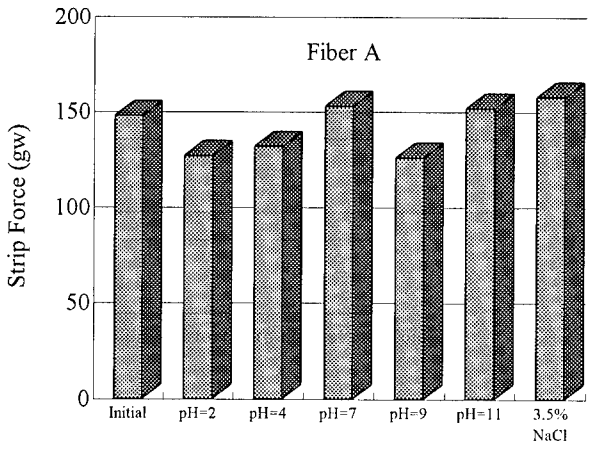


Fig.4 Tensile strength change of fiber aged in 3.5% sodium chloride solution



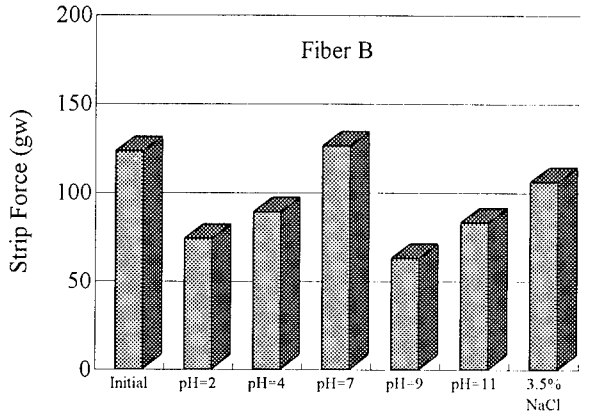


Fig.5 The strip force change of fiber after 60 days aging in different pH solution

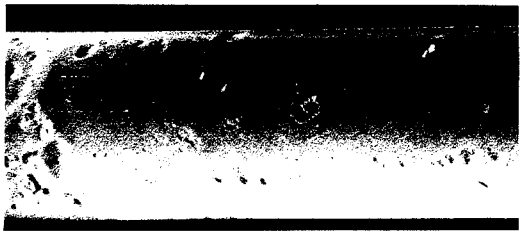
(a)Fiber A in acidic solution(pH=2)



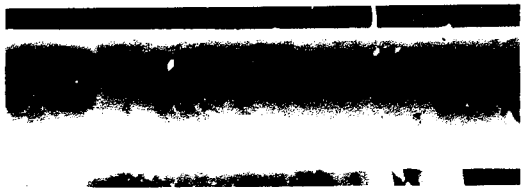
(b)Fiber A in acidic solution(pH=4)



(c)Fiber A in acidic solution(pH=9)



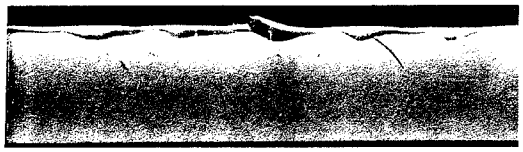
(d)Fiber A in acidic solution(pH=11)



(e)Fiber B in acidic solution(pH=2)



(f)Fiber B in acidic solution(pH=4)



(g)Fiber B in acidic solution(pH=9)



(h)Fiber B in acidic solution(pH=11)



Fig.6 SEM pictures of fiber aged in aqueous solution

DEVELOPMENT OF HIGH POWER UV LAMP FOR FASTER DRAW SPEED OF OPTICAL FIBER MANUFACTURING

Shigeji Morita, Yuji Naito, Zen Komiya, Takao Naganuma,¶ Akiyoshi Fujimori,¶
and Takashi Ukachi

Tsukuba Research Laboratory, Japan Synthetic Rubber Co., Ltd.
25 Miyukigaoka, Tsukuba, 305 Japan
¶ ORC manufacturing Co., Ltd. 3-34-1 Chofugaoka Chofu, 182 Japan

ABSTRACT

Recent high demand for optical fiber is promoting acceleration of a draw speed of optical fiber. In order to achieve high draw speed, a high power UV lamp (12 kW input) was manufactured and its curing performance was evaluated. Cure behavior was evaluated by Young's modulus and gel fraction of cured coatings. It was found that a cure rate was proportional to the square root of UV lamp intensity in good accordance with a theoretical expectation. Curing behavior of UV curable coatings at high UV intensity was also estimated by using a real-time infrared spectroscopy (RT-IR). The RT-IR experiments revealed that the increase of UV intensity decreases induction period and cure rate drastically. It was estimated that the induction period would be short enough when the coatings were irradiated by the high power UV lamp.

INTRODUCTION

Optical fiber telecommunication networks have developed both in quality and quantity. Recent so-called "Information Super Highway" project and rapid economical growth in Asian countries have accelerated installation of optical fiber cables. Under such circumstances, it is necessary not only to build additional draw towers but to increase the draw speed to meet the high demand.

The increase of draw speed would result in various changes in the curing condition for UV coatings. For example, it was demonstrated that the temperature at which the UV coatings were cured was strongly affected by the draw speed.[1] The high draw speed requires UV coatings which are curable in a very short period of time. For instance, if the glass fiber is drawn at 1200 m/min, a coated fiber would run through a UV lamp house of 50 cm long in 25 msec. Shorter irradiation period leads smaller UV dose to the coating and to solve this problem. First one is to install additional UV lamps to the draw tower. However, it is difficult to increase a height of draw tower due to the limited space. The second choice is to employ high power UV lamps to obtain enough UV dose to cure coatings.

In this study, we evaluated a newly developed high power UV lamp of 12 kW input, which is more than twice of energy comparing to conventional UV lamps. We thus investigated the relationship between curing behavior of UV coatings and UV intensity using a real-time infrared spectroscopy (RT-IR). The RT-IR has been demonstrated to be very powerful method to investigate the curing kinetics of UV curable materials in millisecond order.[2]

EXPERIMENTS

Material

A urethane acrylate based secondary coating J-1 was employed for this study. Liquid and cured film properties of J-1 are listed in Table 1.

Table 1. Characteristics of UV Coating J-1.

Liquid	
Viscosity (@ 25°C, cps)	6500
Density (@ 25 °C, g/ml)	1.10
Cured film [1)]	
Young's modulus (kg/mm^2)	75
Tensile strength (kg/mm^2)	4.0
Tensile elongation (%)	60

1) Cured at 1 J/cm^2 under air. Film thickness is 200 μm.

UV Lamps

Characteristics of UV lamps employed here are summarized in Table 2. A high power of UV lamp Q-1 was achieved by applying high electric power to the UV lamp tube of the same length of P-2. The lamp house of Q-1 is bigger than that of P-2 because of a stronger cooling system which allows stable UV emission and assures long life. The power supply of Q-1 is electronically controlled and delivers rectangle-wave electric power resulting constant UV light emission. UV lamps, P-1 and P-2 use sine-curved current which gives waved UV light emission at 100 Hz when the power source is driven by alternate current of 50 Hz.

Table 2. Characteristics of UV Lamps.

	P-1	P-2	Q-1
Input (kW)	3.5	6	12
Diameter (mm)	18.5	24.2	24.3
Length (cm)	25	50	50
Shape of input power	Sine curve	Sine curve	Rectangle
UV light emission	Waved	Waved	Constant

Drawing Experiments

Drawing experiments were carried out using metallic wire of 125 μm in diameter instead of optical fiber glass. Configuration of the drawing experiments is depicted in Figure 1. The urethane acrylate coating J-1 was coated on the wire with a thickness of 63 μm. The draw speed was varied from 200 to 1200 m/min. The extent of cure was evaluated by measuring Young's modulus and gel fraction of the cured coating. The coating was removed from the metallic wire to give a tubular specimen. The specimen was clamped in a tensile testing machine with a gauge length of 25 mm and extended at a rate 1 mm/min. The area of cross section of the specimen for calculation of Young's modulus was measured by observing the cross sectional area using microscope after cutting the specimen. Gel fraction was measured by the following method. The sample was extracted by refluxing methylethylketone (MEK) for 12 hours and the resultant sample was dried under vacuum. The amount of extracts was measured by weight change. Gel fraction was calculated from the amount of unextracts in the sample.

RT-IR Experiments

Coating J-1 was drawn on a KBr disc to 25 μm thickness. The sample was placed in the RT-IR chamber under nitrogen atmosphere and irradiated with a high pressure mercury lamp. The intensity of UV light was controlled from 25 to 75 mW/cm^2 by changing the distance. Details of the RT-IR apparatus are reported elsewhere.[2, 3] Consumption of acrylic double bond corresponding to the degree of cure was followed by monitoring the decrease of absorption at 812 cm^{-1} at the sampling time of 2 msec.

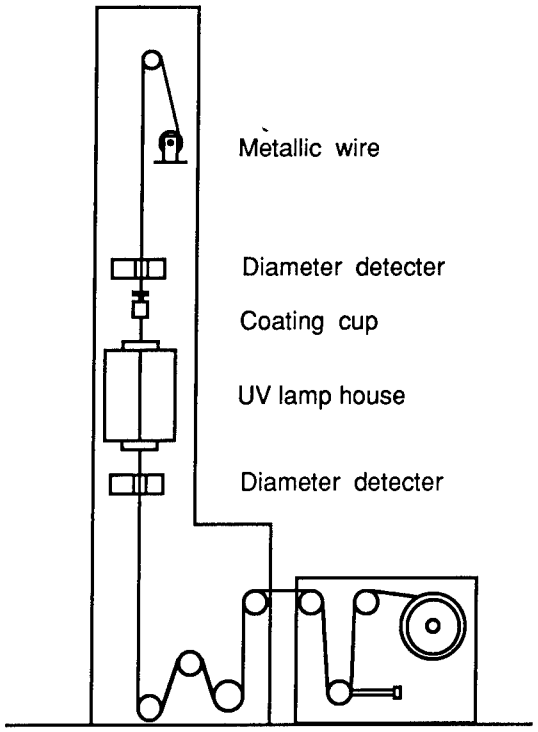


Figure 1. Configuration of Draw Tower.

RESULTS AND DISCUSSION

Performance of High Power UV Lamp

Young's moduli and gel fractions of coatings were plotted against the draw speed in Figures 2 and 3. The increase in draw speed leads steady decline in both Young's modulus and gel fraction. It is obvious that a single P-1 lamp of 3.5 kW input does not have sufficient ability to cure coatings at the draw speed more than 200 m/min. The difference between P-2 and Q-1 is not clear from Figures 2 and 3. In order to compare the performance of these lamps, normalized values of Young's moduli and gel fractions based on the values obtained at the draw speed 200 m/min are plotted in Figures 4 and 5. Again, it is clear that the high power lamp Q-1 gives better performance at high draw speed.

Relationship between UV light intensity and polymerization rate is well established for photo-initiated radical polymerization reaction in dilute solution.[4] Overall polymerization rate, Rp, is proportional to the square root of UV light intensity I_0 as shown in the equation (1), where k_p is a rate for polymerization, k_t is a rate for termination reaction, A is a constant defined by the photoinitiator employed, [C] and [M] are concentrations of photoinitiator and monomer.

$$R_p = k_p \left(\frac{A[C]}{k_t}\right)^{0.5} [M] [I_0]^{0.5} \qquad (1)$$

Since the UV intensity of Q-1 is twice of that of P-2, the polymerization rate is expected to be about 1.4 times (square root of two) larger. The decline in Young's modulus and gel fraction were approximated to linear relation by the least square method as shown in Figures 4 and 5. The slope of each line is considered to represent the polymerization rate. Comparison of the slopes indicates that Q-1 shows 1.3 times higher polymerization rate in Young's modulus and 1.5 times in gel fraction. These values are in good accordance with what was expected from the consideration of the polymerization kinetics described above.

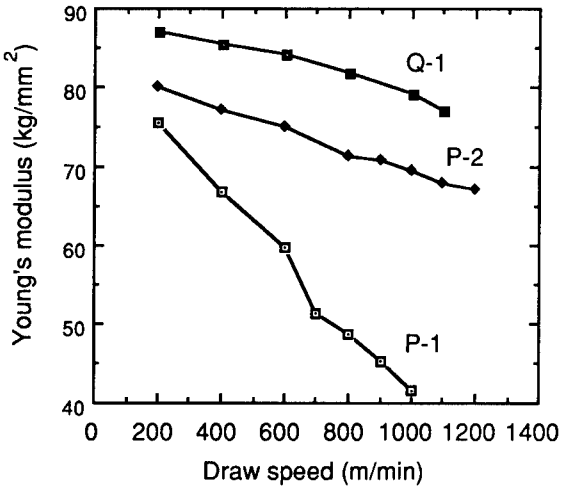


Figure 2. Changes in Young's Modulus as a Function of Draw Speed.

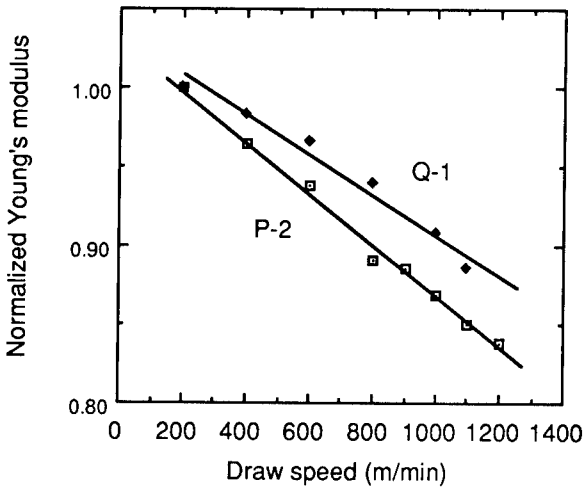


Figure 4. Normalized Young's Modulus as a Function of Draw Speed.

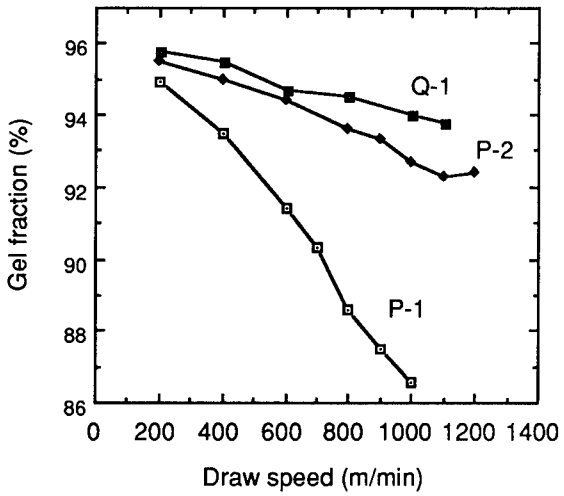


Figure 3. Changes in Gel Fraction as a Function of Daw Speed.

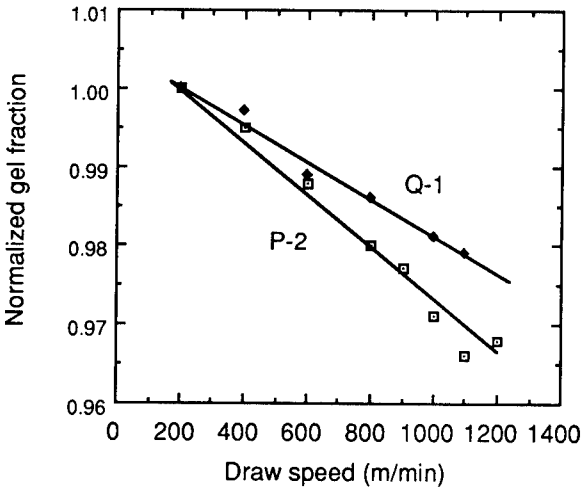


Figure 5. Normalized Gel Fractions as a Function of Draw Speed.

It should be noted that the performance of P-1 was far poorer than that expected from P-2. Since the lamp length of P-1 is a half of the others, the difference in the UV intensity and/or the amount of irradiated heat might cause the discrepancy.

The new UV lamp Q-1 uses an electronically controlled power source which generates rectangle-wave current to the lamp so that the lamp emits UV light without flickering. On the other hand, P-1 and P-2 radiate flickering UV light at 100 Hz due to the sine-curved alternating current of 50 Hz. If the draw speed is high enough to allow the coating run through the lamp house less than 10 msec, it could produce unevenly cured coating layer in the direction of optical fiber axis. In our case, the draw speed was as high as 1200 m/min. At this draw speed, the coated fiber runs through the 50 cm long lamp in 25 msec. This duration corresponds to that the UV light flickers twice. Thus, the coating receives the same amount of UV dose. If the draw speed exceeds 3000 m/min, when the lamp length is 50 cm, the flickering of the light could result in the unevenly cured coating layer. Using a microscopic ATR FT-IR[5], we examined the cure degree of the coating cured at 1200 m/min by the P-2 lamp. There were no fluctuations in cure degree as expected.

Effect of UV intensity on the curing behavior

Using the RT-IR instrument, we investigated effects of UV intensity on an induction period and a polymerization rate of urethane acrylate coating J-1. A typical RT-IR chart is shown in Figure 6. When the coating is irradiated, there is time when the consumption of acrylic double bond does not start yet, which is called an induction period. During the induction period, photoinitiator is producing radicals, but those radicals are believed to be consumed by polymerization inhibitors and oxygen dissolved in the liquid coating and do not initiate the polymerization. Assuming the amount of the inhibitors and oxygen in the coating is constant, the induction period would be inversely proportional to the UV intensity. In other words, UV dose applied to the coating during induction period remains constant at various amount of UV intensity. The results summarized in Table 3 indicate that the amount of UV dose applied during the induction period was somewhat fluctuated but in the same order. The average UV dose for the induction period is estimated to be 5.4 J/cm^2. Intensity of the UV lamps for optical fiber drawing is much higher than that of UV lamp used for the RT-IR measurement. The exact amount of the UV intensity must be estimated because of the lack of an

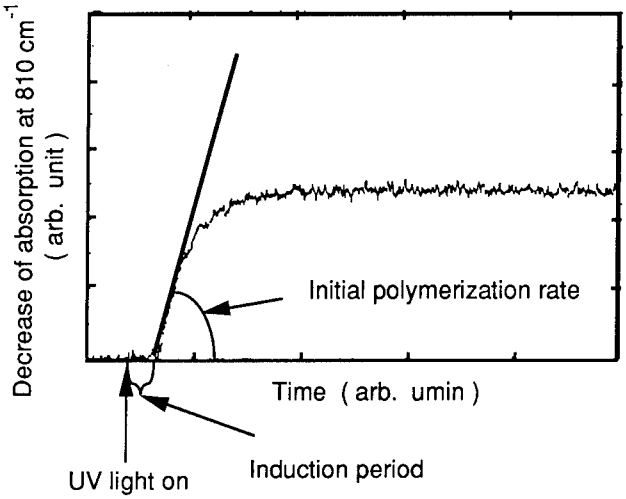


Figure 6. A Typical RT-IR Chart for H-1.

appropriate method to measure the UV intensity at the focal point of the UV lamp. Assuming that a radiation efficiency of UV lamp is 50 % and an efficiency of a reflector to focus onto the fiber is 75 %, the estimated intensity of P-1 (3.5 kW) would be about 9.0 W/cm^2. The induction period irradiated at 9.0 W/cm^2 is calculated to be 0.6 msec from the average UV dose, 5.4 mJ/cm^2, which is necessary for the induction. In the same manner, the induction periods irradiated with P-2 and Q-1 are estimated to be 0.9 or 0.5 msec respectively. At draw speed of 2000 m/min, optical fiber travels about 3 cm in one millisecond which is much shorter than the length of UV lamps (25 or 50 cm). It is therefore concluded that the induction period would not be a significant obstacle to achieve the high speed drawing.

The dependence of an initial polymerization rate on the UV intensity was also examined by the RT-IR method. The results are listed in Table 4. As described in the previous

Table 3. Change in Induction Period at Various UV Intensities.

UV intensity (mW/cm^2)	Induction period (msec)	UV dose (mJ/cm^2)
25	172	4.3
50	138	6.9
75	67	5.0

Table 4. Change in Initial Polymerization Rate at Various UV Intensities.

UV intensity (mW/cm^2)	Initial polymerization rate (sec^{-1})
25	1.20
50	1.44
75	2.64

section, polymerization rates are proportional to the square root of the UV intensity. The plots of polymerization rates against square root of the UV intensity exhibit a fair linear relationship as shown in Figure 7. As the UV intensities of P-1, P-2, and Q-1 are estimated to be 9.0, 5.9, and 12 W/cm^2 respectively, the initial polymerization rates would be 35, 28, and 40 sec^{-1} respectively. It is difficult to define the time required for full cure of the coating, we use half life periods for a rough estimation using the initial polymerization rates. Half life periods for P-1, P-2, and Q-1 are in the range of 17 to 25 msec which correspond to 57 to 83 cm of traveling distance at 2000 m/min of draw speed. The fact that the distances are longer than the length of the lamp indicates that coatings with fast cure rates should be applied for the high draw speed production. In other words, the employed urethane acrylate coating J-1 has sufficient cure rate if it is applied at less than 2000 m/min of draw speed.

CONCLUSION

We developed a new high power UV lamp of 12 kW input power and examined the curing ability at high draw speed using a draw tower. The tensile modulus and gel fraction of cured coating revealed that the high power UV lamp cured the coating well at fast draw speed up to 1200 m/min. The RT-IR study of the curing behavior indicated that the increase in UV intensity decreases both the induction periods and the polymerization rates. It was estimated that the induction period would be negligibly short at high UV intensity. However, the enhancement of cure rate of coating would be necessary to obtain the high draw speed production.

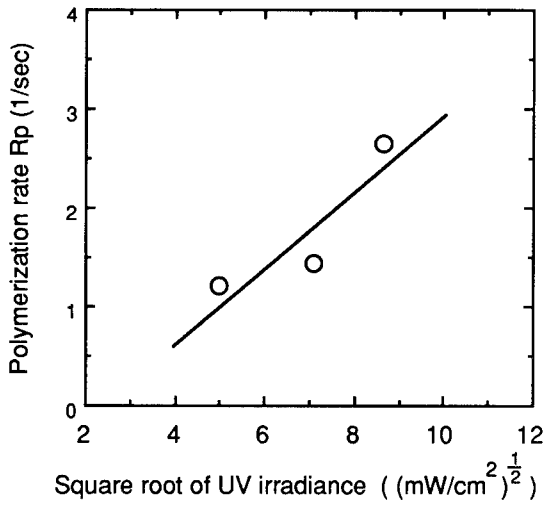


Figure 7. Changes in Initial Polymerization Rate as Afunction of Square Root of Intensity.

REFERENCES

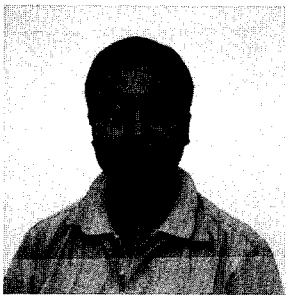
[1] T. Ukachi, A. Aoyama, Y. Naito, K. Igarashi, Proceedings **41**st IWCS, 261 (1992).

[2] N. Saito, Y. Hashiguchi, Y. Takasugi, Proceedings of RadTech Asia **93**, 221 (1993).

[3] H. Takase, Y. Hashiguchi, Y. Takasugi, N. Saito, T. Ukachi, Proceedings **43**rd IWCS, 72 (1994).

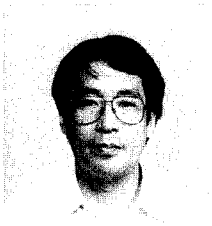
[4] Kh. S. Bagdasaryan, Zhur. Fiz. Khim, **18,** 294 (1944); ibid., **21,** 25 (1947); ibid., **22,** 1181 (1948); ibid., **28,** 498 (1954).

[5] JASCO MFT-2000 was employed for this measurement. JASCO MFT-2000 enables us to measure the surface of the coated fiber by using focused IR beam in 4x4 μm^2.



Shigeji Morita
Tsukuba Research Laboratory,
Japan Synthetic Rubber Co., Ltd.
25 Miyukigaoka, Tsukuba, 305
Japan

Shigeji Morita received his M. E. degree in Science and Engineering from Osaka University, Osaka, Japan and joined Japan Synthetic Rubber Co., Ltd. in 1992. He has been engaged in research and development of radiation curable materials for optical fiber coatings.



Takao Naganuma
ORC manufacturing Co., Ltd.
3-34-1 Chofugaoka Chofu, 182
Japan

Takao Naganuma received his B. E. degree in Electronics and Communication Engineering from Musashino Institute of Technology in 1978 and joined ORC Manufacturing Co., Ltd. He is now a manager of Lamp division.



Yuji Naito
Tsukuba Research Laboratory,
Japan Synthetic Rubber Co., Ltd.
25 Miyukigaoka, Tsukuba, 305
Japan

Yuji Naito graduated in Chemical Engineering Course of Sagamidai Technical High School in 1971 and joined Japan Synthetic Rubber Co., Ltd. He has been engaged in development of draw process of optical fibers. He is now a chief engineer of Radiation Curable Material Development division.



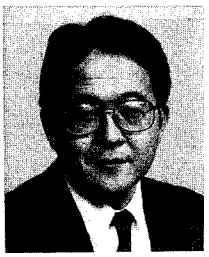
Akiyoshi Fujimori
ORC manufacturing Co., Ltd.
3-34-1 Chofugaoka Chofu, 182
Japan

Akiyoshi Fujimori received his B. E. degree in Communication Engineering from Tokai University and joined ORC Manufacturing Co., Ltd. He is currently a general manager of Lamp division.



Zen Komiya
Tsukuba Research Laboratory,
Japan Synthetic Rubber Co., Ltd.
25 Miyukigaoka, Tsukuba, 305
Japan

Zen Komiya received his Ph. D. in Organic Chemistry from Hokkaido University in 1984 and joined Japan Synthetic Rubber Co., Ltd. He was engaged in research on development of new transparent plastics and currently has been engaged in research and development on radiation curable materials.



Takashi Ukachi
Tsukuba Research Laboratory,
Japan Synthetic Rubber Co., Ltd.
25 Miyukigaoka, Tsukuba, 305
Japan

Takashi Ukachi received his B. E. degree in Biophysics and Bioengineering from Osaka University and Ph. D. in Material Science from Kyushu University. He started his professional carrier at Japan Synthetic Rubber Co., Ltd. in 1976 and has been engaged in research and development of radiation curable materials.

RELIABILITY ISSUES CONCERNING THERMALLY-CURED ADHESIVES IN FIBER OPTIC CONNECTORS

I.M. Plitz, O.S. Gebizlioglu, L.A. Reith, P.B. Grimado
Bellcore
445 South Street
Morristown, NJ 07960-6438

ABSTRACT

Fiber optic connectors are likely to be exposed to high temperature/humidity conditions. To determine this reliability risk, we focused on the effects of high temperature and humidity on commonly used connector adhesives. DMA and DSC measurements on bulk epoxy samples exposed to high humidity/temperature aging revealed that some epoxies were more susceptible to thermomechanical deterioration after heat and high humidity exposure. We also confirmed that the epoxy dimensional instability that contributes to fiber motion can be minimized by selecting an adhesive with a T_g that is much higher than the maximum temperature in the service environment. A theoretical model of fiber motion in physical contact (PC) fiber optic connectors was developed. Experimental fiber motion data compared well with the model predictions and demonstrated that large fiber withdrawal is expected when the connector epoxy T_g is low. The rationale for developing a performance test procedure based on absolute fiber motion for Bellcore's optical fiber connector generic requirements was established from this understanding of epoxy thermomechanical properties.

INTRODUCTION

Fiber optic connectors must maintain alignment and physical contact at the fiber cores to achieve low reflectance. For deployment flexibility in outside plant applications, these connectors may be installed in adverse environments of high relative humidity and temperature where they are expected to perform with high reliability and low maintenance. Therefore, it is essential that we assess connector reliability based on an adequate understanding of the performance characteristics of the materials that comprise these connectors. In this report, we focus on the thermomechanical characteristics of the epoxy-based adhesives that are used to hold the fibers aligned and in physical contact within the connector.

Adhesive materials commonly used in fiber optic connectors consist of two main components, namely, a resin (or a prepolymer mixture) and a hardener (or a catalyst). A selected adhesive formulation must have a low viscosity to easily fill the connector body and cure rapidly at temperatures ≤ 120 °C to avoid degradation of fiber coatings and other materials. During the thermal cure process, the liquid epoxy compound is transformed into a rigid three dimensional (cross-linked) network. The cross-link density increases rapidly as the cure temperature is raised.[1] The epoxy compound must be exposed to a high enough temperature over a specific time to ensure maximum cross-linking but not introduce thermooxidative degradation. Thus, the selection of the correct cure temperature and time for a given connector epoxy is one of the most important steps in the manufacturing of high-quality and reliable fiber optic connectors.

Cure temperature and time determine the extents of two principal transformations that may occur during cure. These are gelation and vitrification. The gelation process takes place with the development and extension of three-dimensional branch structures throughout the entire sample, whereas vitrification refers to the solidification process that occurs when the glass transition temperature (T_g) of the growing molecular network reaches the cure temperature. These two principal processes control the rheological (flow)

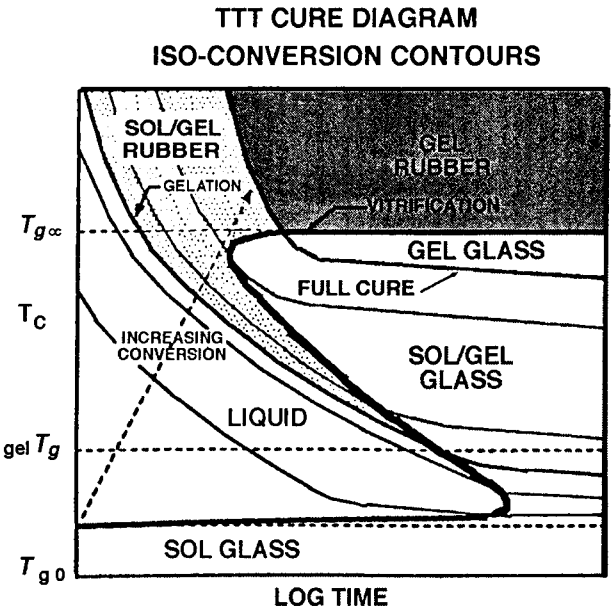


Figure 1.

Copyright @ 1995 Bellcore All rights reserved

properties, cure reaction rate, dimensional stability of the final cured product, and other properties. Therefore, the selection of an optimum time/temperature cure path becomes critically important.

We will now illustrate how one can select the correct cure path from a generalized TTT (Time-Temperature-Transformation) isothermal cure diagram shown in Figure 1, adapted to thermally-curing (thermosetting) polymers.[2-4] In this TTT diagram, cure temperature T_c is plotted against cure time (on a logarithmic scale). During cure to full conversion, the T_g increases from T_{g0} for the uncured mixture to $T_{g\infty}$ for the fully cured adhesive. Following the dashed arrow from the T_{g0} corner, a liquid epoxy compound crosses the gelation line into the sol/gel rubber region where the rate of the initially steep T_g increase drops. In this region, one sees iso-T_g (constant T_g) contours, some of which cross the vitrification line into the sol/gel glass region. For T_c values lower than $T_{g\infty}$, the curing process is diffusion-controlled, and results in a limiting value of the adhesive T_g. When T_g reaches T_c, the curing mixture crosses the bold s-shaped vitrification line. For rapid curing, one should avoid diffusion control and move the system into a regime where reaction kinetics control the overall cure rate. This can be accomplished by heating the system more rapidly than the upper limiting heating rate. For maximum material density and minimum internal stress, curing must occur in the glass transition region below T_g. The final T_c must be lower than $T_{g\infty}$ so that the system temperature remains below T_g throughout the curing operation. Thermally-cured fiber optic connector adhesives must attain their maximum density to assure their long-term dimensional stability.

In an earlier report,[5] we showed that ultraviolet (UV)-curable adhesives used in optical devices pose a significant reliability risk if deployed in the outside plant environment because they have relatively large thermal expansion coefficients and creep compliance. In order to assess the impact of thermally-curable adhesive performance on the reliability of fiber optic connectors, we began a parallel study to determine the effects of high temperature and high humidity on connectors and bulk adhesives. Initial results indicated some epoxy degradation that might have contributed to fiber movement within the connector and poor intermateability.[6] Some connectors exhibited high reflectance during high-humidity aging. Generally, we observed that fiber optic connectors assembled with low-T_g adhesives fail when exposed to a combination of heat and high humidity.[7]

In this report, we present our results on the effects of aging on connectors and selected bulk adhesive samples. We first discuss the effects of 65 °C/95% RH (Relative Humidity) aging on the bulk thermomechanical properties of the connector adhesives. We then analyze fiber movement in physical contact (PC) connectors theoretically and experimentally. We identify key adhesive characteristics that control fiber withdrawal in PC connectors. The results reported here confirm our earlier findings that laid the groundwork for the development of generic product requirements and the performance test procedure in the appropriate Bellcore requirements.

ANALYSIS OF BULK ADHESIVE PROPERTIES

High-Humidity Aging of Connector Adhesives

We used DSC (Differential Scanning Calorimetry) and DMA (Dynamic Mechanical Analysis) to determine the effects of aging on adhesive thermomechanical properties such as the T_g, the extent/enthalpy of residual cure, and the storage modulus/loss tangent (Tan δ)-temperature profiles. In the aging tests, adhesive samples (20 mm × 10 mm × 0.1 mm), cured in accordance with each manufacturer's recommendations, were exposed to 65 °C and 95% RH for a maximum of 12 weeks. Table 1 presents the T_g and Tan δ data as measured at 1 Hz by DMA, and the cure state determined by DSC, for five adhesives commonly used in PC connectors. In this table, T_g indicates the temperature about which a sample softens and turns rubbery (glass-to-rubber transition) as the sample temperature is raised, while the loss tangent gives the magnitude of this transition.
The glass transition temperature is very sensitive to curing-induced and aging-induced changes in the material structure. As illustrated earlier on the TTT diagram of Figure 1, the sample T_g undergoes an initially sharp increase through the liquid region. Although the rate of T_g increase drops once the gelation line is crossed, the sample T_g continues to increase to the T_g of the final "fully-cured" product. If an under-cured sample continues to cure during the aging process, its T_g will rise while its Tan δ will drop; if the sample takes up moisture that does not bind to the adhesive structure, its T_g will decrease while its loss tangent increases. If, however, both curing and moisture take-up occur simultaneously without any sample degradation, the T_g and the loss tangent may increase or decrease together.

We note that the Tg values for samples I through III are below their (recommended) cure temperatures; the curing reaction takes place in the rubbery (softened) state, and the overall cure rate is controlled by the kinetics of the curing reaction. High Tan δ values and residual DSC cure peaks, however, point out that these Tg values may not correspond to their fully cured state. The Tg values for samples IV and V, on the other hand, are higher than the recommended cure temperatures. In this case, curing occurs in the glassy state, and the overall cure rate is diffusion-controlled. Relatively low Tan δ values for these samples indicate that they are in

Table 1

Thermomechanical Properties Before Aging @ 65 °C / 95 % RH

Sample	T_g (°C)	Tan δ	DSC Cure State
I 1.5 Hrs @ 120 °C	83	1.98	Residual Cure @ 171 °C, 6 cal/gm
II 20 Min. @ 90 °C	84	0.84	No Residual Cure
III 2 Hrs @ 120 °C	105	1.10	Residual Cure @ 175 °C, 4 cal/gm
IV 10 Min. @ 100 °C	128	0.65	Residual Cure @ 148 °C, 4 cal/gm
V 15 Min. @ 100 °C	146	0.58	Residual Cure @ 105 °C, 10 cal/gm

the vicinity of their full cure condition. One may be tempted to raise the cure temperatures to bring these samples closer to their fully-cured condition. However, degradation reactions at higher temperatures may prevent some samples from attaining their full cure state.

Table 2

Thermomechanical Properties After 30-Day Aging @ 65 °C / 95 % RH

Sample	T_g (°C)	Tan δ	Volume Change (%)
I	75 No Residual Cure	1.14	1.2
II	108 No Residual Cure	0.57	0.5
III	103 No Residual Cure	0.82	3.8
IV	117 No Residual Cure	0.65	1.2
V	118 No Residual Cure	0.44	1.5

Table 2 shows that 30-day aging at 65 °C/95% RH eliminates the residual cure shown by the unaged samples, while Table 3 indicates that no additional aging takes place beyond 30 days. Lower loss peak values for some 30-day aged samples with the absence of residual cure peaks may suggest that further curing accompanies 30-day aging. However, the reduced T_g values and the volume increases shown in the last column of Table 2 indicate that swelling occurs in all samples. Tables 2 and 3 clearly show that these epoxy adhesives are susceptible to aging-induced dimensional instability. However, dimensional instabilities in adhesives are also related to the viscoelastic nature and glass transition temperatures of these materials. In an earlier publication,[6] we indicated that dimensional instabilities that contribute to fiber pushback can be minimized by selecting an adhesive with a T_g that is much higher than the maximum temperature that may be encountered in the telecommunications service environment. In the following paragraphs, we show the results of fiber motion measurements in some fiber-ferrule assemblies and compare them to calculated results from an analytical fiber withdrawal model that uses dynamic modulus-temperature profiles directly measured on five connector adhesives.

Table 3

Thermomechanical Properties After 3-Month Aging @ 65 °C / 95 % RH

Sample	T_g (°C)	Tan δ	Volume Change (%)
I	74	1.43	1.2
II	109	0.65	1.5
III	103	0.82	3.5 - 4.0
IV	139	0.67	1.3
V	118	0.44	1.5 - 2.0

Fiber Withdrawal at Elevated Temperature

In PC connectors, the adhesive is required to provide a rigid mechanical linkage between the connector ferrule and fiber as schematically shown in Figure 2. However, the rigidity of this linkage is temperature-dependent since the adhesive modulus decreases with temperature for two entirely different reasons:

1) Due to thermal expansion, the intermolecular distance increases with a consequent decrease in the intermolecular forces. The modulus decreases in accordance with the following relationship[8]

$$-\frac{1}{E}\frac{dE}{dT} \approx 10.5\,\alpha_c \qquad (1)$$

where α_c is the volumetric thermal expansivity.

2) The second reason for the decrease in modulus with temperature is relaxation. An increase in temperature accelerates the relaxation processes, thereby reducing the modulus at a constant frequency. The steepest decrease in modulus occurs through the glass transition region as shown by the modulus-temperature profiles of adhesive samples I through V in Figures 3a through 3e, respectively. These profiles show a two to four orders-of-magnitude drop in the

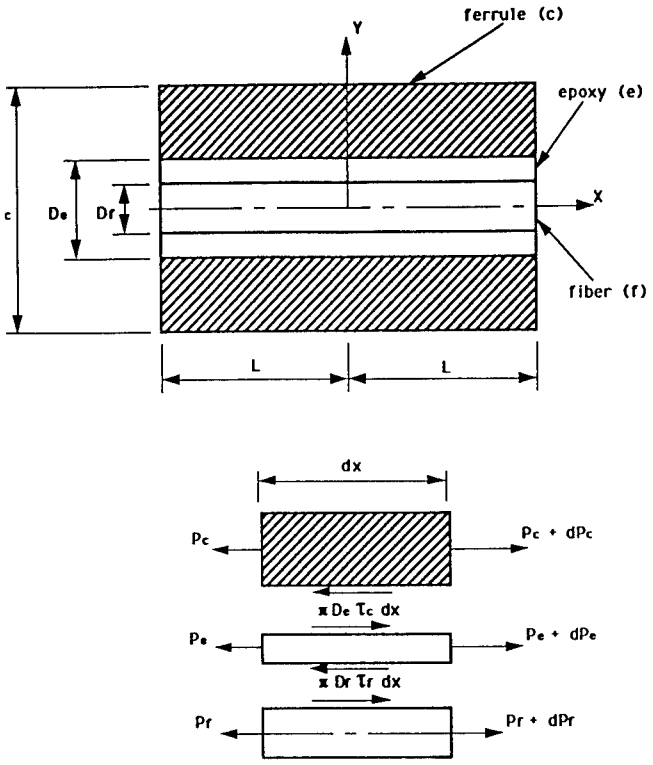


Figure 2.
A Schematic Representation of the Forces on a PC Connector Axial Cross-Section

modulus through the glass transition region, and the inflection points in these profiles correspond to the glass transition temperatures measured by DMA at 1 Hz. As shown in Table 4, the ferrule material, zirconia, and fiber material, silica, exhibit much higher moduli, and these are temperature-independent. Thus, within the composite structure of a PC connector, the fiber is expected to move axially as the temperature rises since the connector adhesive thermal expansivity is very large compared to those of the ferrule and fiber materials as shown in Table 4.

Table 4

Thermophysical Properties of the Connector Materials

Material	Coeff. of Thermal Exp. ($°C^{-1}$)	Modulus of Elasticity (GPa)
Fiber, Silica	5.5×10^{-7}	73
Ferrule, Zirconia	10^{-8} - 10^{-7}	150
Adhesive	$(0.5 - 1.7) \times 10^{-4}$	0.001 - 2

Figure 3a. Modulus Profile for Sample I

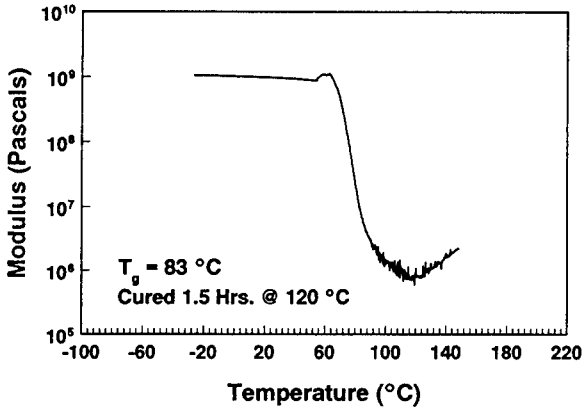


Figure 3b. Modulus Profile for Sample II

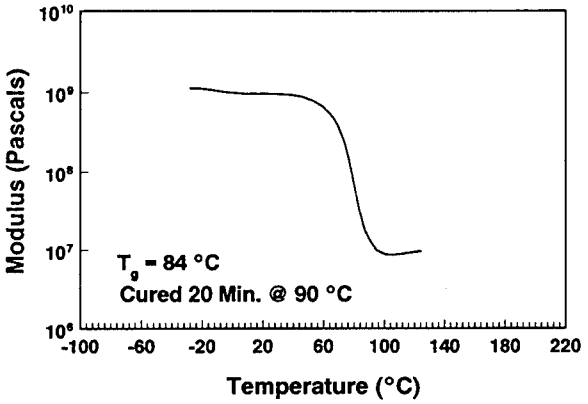


Figure 3c. Mod. Profile for Sample III

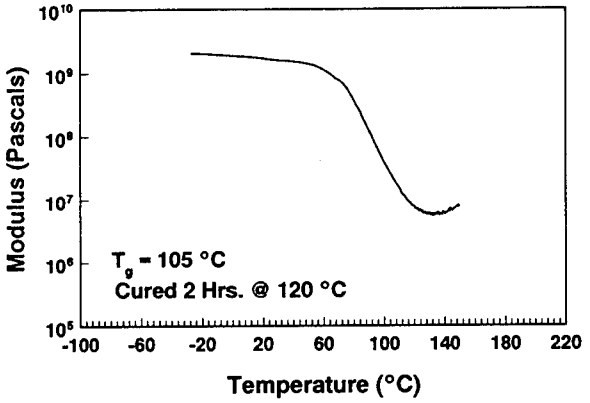


Figure 3d. Mod. Profile for Sample IV

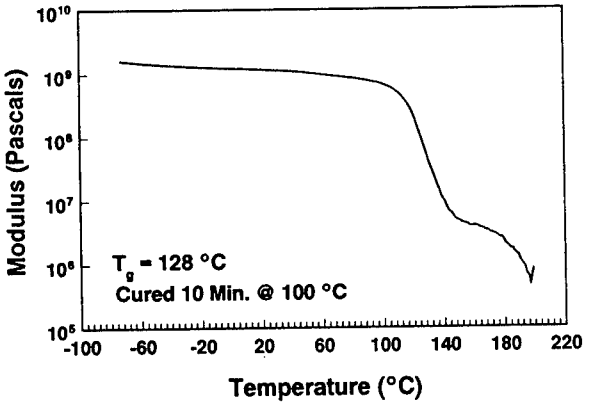
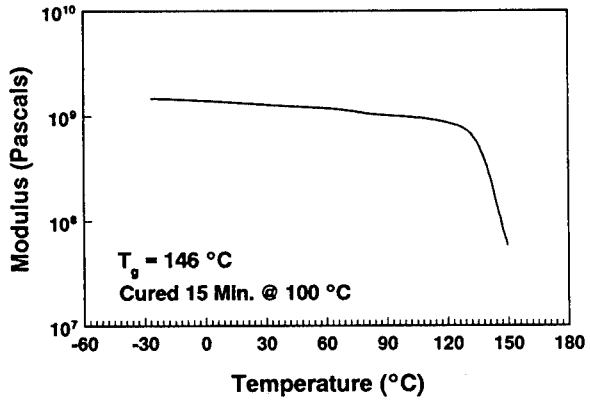


Figure 3e. Mod. Profile for Sample V



Considering the mechanical equilibrium of the ferrule-fiber assembly shown in Figure 2, we developed an analytical model of fiber motion in a PC connector subjected to a temperature change. The derivation of this model is presented in the Appendix. In Figure 4, we show the model results and measured fiber motion for an unaged connector assembled using adhesive IV. For fiber motion measurements, we used a contact profilometer with an accuracy of 0.02 μm; data squares with error bars show mean values of the measured fiber withdrawal. These results compare well with the fiber motion calculated from the analytical model. The tolerances on the diameter of the optical fiber and the ferrule opening suggests that the thickness of the epoxy can vary form 0.5 micron to 1.0 micron. Figure 4 gives the calculated results for the two limiting adhesive thicknesses of 0.5 μm and 1.0 μm; the experimental data show a good correlation with this model at the 1.0 μm limiting thickness. This figure also demonstrates that fiber motion increases with temperature. Figure 5 shows a plot of the calculated fiber motion versus the glass transition temperature, confirming the experimentally observed trend of increased fiber motion with adhesives of lower T_g's.

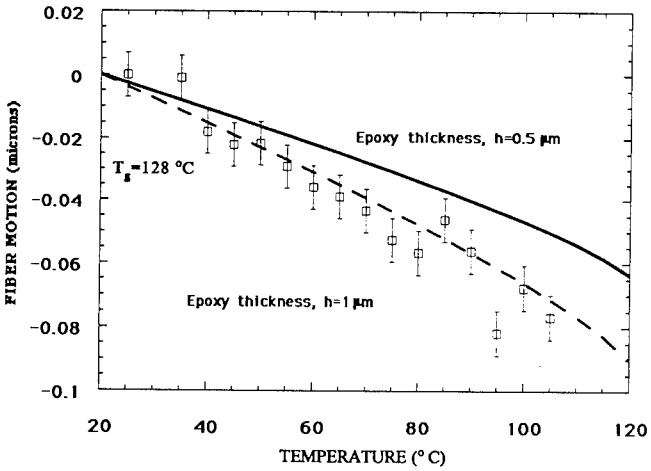


Figure 4 - Measured (data points) and Predicted by the Model (curves) Fiber Motions in a PC Connector Using Epoxy IV

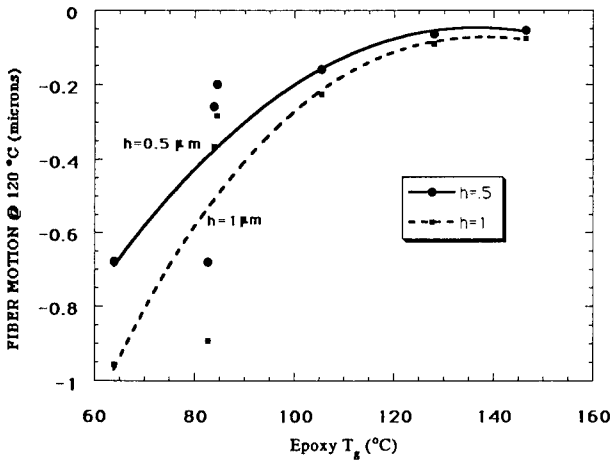
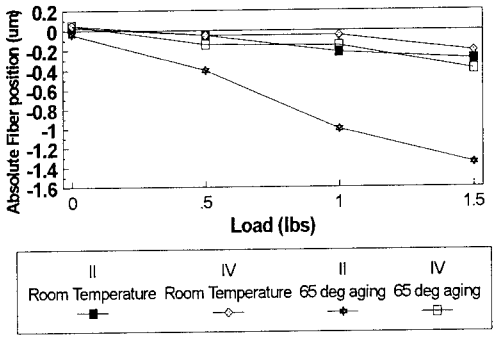


Figure 5
Predicted Fiber Motion as a Function of Epoxy T_g

Our previously published data on connectors and ferrules showed that significant fiber motion or pushback occurred at room temperature when the loading force applied directly to the fiber was increased to greater than one pound.[9] This motion significantly increased in connectors exposed at 65 °C (see Figure 6). The ability of the epoxy to withstand the loading force is shown for commercially available connectors from two different manufacturers. The connectors were assembled using epoxies II and IV from Table 1. The Tg for epoxy II is 30 °C lower than that measured for epoxy IV. Even under room temperature

loadings, fibers in the connector with the lower Tg showed larger motion. When fibers become recessed more than approximately 0.1 μm, physical contact of the fiber cores may be lost and large reflectances can result.[10]

Figure 6
Fiber Movement in Two Commercial Connectors



We also showed that the change in fiber position for samples aged at 65 °C in hand-assembled ferrules correlated to the epoxy T_g.[7] Table 5 shows the comparison of bulk epoxy T_g with the fiber position (with respect to the ferrule) after aging in hand-assembled ferrules using these epoxies. Again, the experimental data compares well with the model predictions as well as the epoxy data, emphasizing the significance of the epoxy glass transition temperature as an indicator of the magnitude of fiber withdrawal at elevated temperatures. Some of these ferrules were subjected to additional aging at 65 °C /95% RH that resulted in further fiber motion.

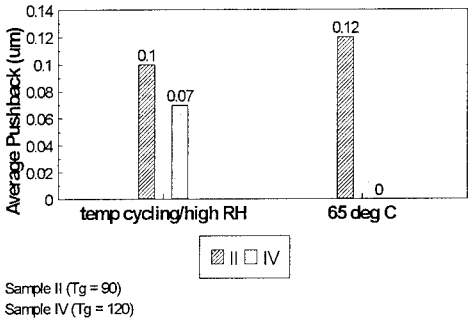
TABLE 5

Comparison of Final Fiber Position and Epoxy T_g

Sample	Fiber Position (μm)	T_g (°C)
I	-0.07	83
II	-0.07	84
III	-0.03	105
IV	+0.01	120
V	+0.03	146

Figure 7 shows the average pushback from two sets of commercially available connectors after exposure to high humidity and temperature cycling or to 65 °C with uncontrolled humidity. These epoxy T_g's were determined from DSC measurements of the epoxy recovered from unaged connectors. As expected, the set IV connectors (high T_g epoxy) had much better performance at 65 °C than set II. However, the addition of humidity and temperature cycling degraded the epoxy performance, which led to significant pushback. The set II connectors do not appear to degrade significantly during exposure to the high humidity. However, the data are inconclusive because these connectors had fibers that were initially more recessed than any of the other connectors in this test. This means that the initial load carried by the fibers (epoxy stress) was less than for the set II connectors aged at 65 °C. From Tables 2 and 3, we have shown that the epoxies all showed volume changes caused by the absorption of humidity. Although not conclusively established yet, the results to date indicate that increasing humidity or temperature cycling will adversely affect connector reliability.

Figure 7
Average Pushback after Aging for Two Commercial Connectors



DMA analysis of bulk epoxy samples already pointed out that dimensional changes can be minimized by selecting adhesives with glass transition temperatures higher than the anticipated service temperature of the connector. Physical measurements on hand-assembled ferrules and connectors corroborated this finding. The theoretical model (see the appendix) served to further confirm this result.

Our work on the thermomechanical properties of bulk epoxy adhesives in conjunction with experimental and theoretical analyses originally led to a materials requirement in Bellcore's GR-326-CORE.[11] However, this work has now led to the development of a performance test procedure. This document currently requires a 30 mm radiussed indentor test which allows limited fiber motion after 24 hours at 85 °C. The fiber must not move out of the specified envelope required for the ferrule end face geometry during the test time.

CONCLUSION

DMA and DSC measurements on bulk epoxy samples exposed to high humidity/temperature aging revealed that some epoxies were more susceptible to thermomechanical deterioration after heat and high humidity exposure. These measurements also confirmed that epoxy dimensional instability, which contributes to fiber motion in connectors, can be minimized by selecting an adhesive with a T_g that is much higher than the maximum anticipated service temperature.

A theoretical model of fiber motion in PC fiber optic connectors was developed. This model used temperature-dependent epoxy moduli that were measured by DMA on bulk adhesive samples. Experimental fiber motion data compared well with the model predictions. These analyses demonstrated that the epoxy T_g characterizes the magnitude of fiber withdrawal at elevated temperatures. That is, a large fiber withdrawal is expected when the connector epoxy T_g is low. The rationale for developing a performance test procedure for GR-326 based on absolute fiber motion is based on this understanding of epoxy thermomechanical properties.

REFERENCES

1. A.F. Lewis, "Epoxy Resin Adhesives", in **Epoxy Resin, Chemistry and Technology**, Marcel Dekker, inc., NY (1973).

2. J.B. Enns and J.K. Gillham, **J. Appl. Polym. Sci.**, 28, 2567 (1983).

3. J.K. Gillham, **Polym. Eng. Sci.**, 26(20), 1429 (1986).

4. S.L. Simon and J.K. Gillham, **J. Appl. Polym. Sci.**, 53, 709 (1994).

5. I.M. Plitz, O.S. Gebizlioglu and M.P. Dugan, **Proc. SPIE**, (1994).

6. L.A. Reith, R.A. Frantz, P.B. Grimado, I.M. Plitz, O.S. Gebizlioglu, and D.A. Dolinoy, **IWCS Proceedings**, 43, 790 (1994).

7. L.A. Reith, et. al., **Proceedings of 11th Annual NFOEC**, (1995).

8. L.C.E. Struik, "Internal Stresses, Dimensional Instabilities and Molecular Orientations in Plastics," John Wiley & Sons, Inc., New York, p 47 (1990).

9. L.A. Reith, R.A. Frantz, I.M. Plitz, W.W. Wood, **IWCS Proceedings,** 42, 256 (1993).

10. R. Ziebol, H. Roberts, B. Daniel, **Proceedings of 8th Annual NFOEC,** 11, 241 (1993).

11. Generic Requirements for Single-Mode Optical Fiber Connectors, Bellcore, GR-326-CORE, Issue 1 (1994).



Irene Plitz received her BS in Chemistry and immediately joined Bell Labs where she worked on outside plant materials, primarily wire and cable applications. She joined Bellcore in 1984 and focused her work principally on the chemical and structural analyses of polymers. Early this year, she transferred to the Fiber Media and Component Reliability Group where her work will concentrate on assuring reliable optical fiber cable and components.



Osman Gebizlioglu holds BS and MS degrees in chemical engineering from the Middle East Technical University, Ankara, Turkey. After receiving his PhD. in the Polymer Materials Program at Princeton University, he was a Monsanto Postdoctoral Fellow in the Mechanical Engineering Department of MIT where he investigated the physics of toughening glassy polymers. Since he joined Bellcore in 1987, he has focussed his research on polymers used in optical fiber cables and components.

Leslie Reith received a BA degree from New York University in 1975, the M.Phil. degree from the City University of New York in 1979, and the Ph.D. degree from the University of Texas at Austin in 1981, all in physics. In 1981, she joined AT&T Bell laboratories as a Member of Technical Staff and in 1984, she subsequently joined Bellcore. In recent years, she has been working on performance and reliability issues related to optical connectors and splices and has been active in national standards activities for fiber optical components.

Philip B. Grimado received the BS degree in civil engineering from the City University of New York and the MS and PhD degrees in applied mechanics from Columbia University, New York, in 1962 and 1968, respectively. He joined Bell Laboratories in 1968 where his responsibilities included vulnerability studies of antiballistic missile systems, fire protection studies involving fire-risk analyses, heat transfer calculations, development of standard fire testing methods for telephone company equipment and development of algorithms for optimum control of building environmental equipment. Since 1983, he has been with Bellcore, engaged in outside plant activities concerned with fiber optic cable placement, damage assessment and stress analysis studies.

APPENDIX

In the schematic diagram of a fiber optic connector cross-section shown in Figure 1, we consider the mechanical equilibrium of axial and shear forces on three major connector components, namely, the ferrule, the fiber and the adhesive. This equilibrium is expressed by the following equations:

$$P_c(x) + P_e(x) + P_f(x) = 0 \qquad (2)$$

$$\frac{dP_c}{dx} = \pi D_c \tau_c, \quad \frac{dP_e}{dx} = \pi(D_f \tau_f - D_e \tau_e), \quad \frac{dP_f}{dx} = -\pi D_f \tau_f \qquad (3)$$

P_c, P_e, and P_f are the axial forces acting on the ferrule, the epoxy adhesive and the fiber, respectively. τ_c designates the shear stress on the ferrule-adhesive interface while τ_f refers to the shear stress acting on the fiber-adhesive boundary. D_c, D_e, and D_f refer to the diameters of the connector ferrule, epoxy adhesive, and the glass fiber, respectively. The stresses on the connector components originate from the differential thermal expansion of these components. Assuming linear elastic deformation, we write the following expression for the strain on each component:

$$\frac{du_c}{dx} = \alpha_c T + \frac{P_c}{K_c}, \quad \frac{du_e}{dx} = \alpha_e T + \frac{P_e}{K_e}, \quad \frac{du_f}{dx} = \alpha_f T + \frac{P_f}{Kf} \qquad (4)$$

In these expressions, u is the displacement, α is the coefficient of linear thermal expansion, K is a measure of component stiffness defined as the product of the cross-sectional area and the modulus of elasticity (Young's modulus), and T is the temperature change from the ambient conditions. Again, the subscripts c, e, and f distinguish the variables and the material properties associated with the ferrule, the epoxy adhesive and the fiber, respectively. By substitutions and algebraic manipulations of Equations 2 through 4, a fourth-order linear differential equation is obtained. The solution of the differential equation produces the following expression for the fiber motion (withdrawal) at the tip of the ferrule, x=L:

$$m_c - m_f)_{x=L} = \left[K_f(b^2 - a^2)G\right]^{-1} \left\{ \begin{array}{l} -a(Db^2 + d)\left[-\left(\frac{D_f}{D_e} + \frac{D_f K_e}{D_e K_f} + 1\right) + \frac{a^2 D_f K_e}{G D_e K_f}\right] \\ +b\left(Da^2 + d\right)\left[-\left(\frac{D_f}{D_e} + \frac{D_f K_e}{D_e K_f} + 1\right) + \frac{b^2 D_f K_e}{G D_e K_f}\right] \end{array} \right\}, aL, bL)) \qquad (5)$$

The terms α, β, δ, Δ, and Γ are defined in terms of the geometrical and material parameters of the connector components by the following relationships:

$$\alpha = \sqrt{\frac{\Gamma}{2}}\left\{1 + \frac{K_f}{K_c} + 2\frac{K_f}{K_e} + \left[\left(1 - \frac{K_f}{K_c}\right)^2 + 4\left(\frac{K_f}{K_e}\right)^2\right]^{0.5}\right\}^{0.5}$$

$$\beta = \sqrt{\frac{\Gamma}{2}}\left\{1 + \frac{K_f}{K_c} + 2\frac{K_f}{K_e} - \left[\left(1 - \frac{K_f}{K_c}\right)^2 + 4\left(\frac{K_f}{K_e}\right)^2\right]^{0.5}\right\}^{0.5}$$

$$\delta = -\Gamma K_f(\alpha_e - \alpha_f)T$$

$$\Delta = \frac{K_f^2}{K_e} \frac{\left[(\alpha_c - \alpha_f) + \frac{K_e}{K_f}(\alpha_e - \alpha_f)\right]}{\left[\frac{K_f}{K_c} + \frac{K_f}{K_e} + \frac{K_f^2}{K_c K_e}\right]} T$$

$$\Gamma = \frac{2\pi G D_f}{h K_f}$$

where h is the thickness of the adhesive layer, and G is the adhesive shear modulus.

Eq. 5 describes the fiber motion relative to the ferrule for connector components with temperature-independent material characteristics. We use this equation to calculate the instantaneous incremental change in fiber position at any given temperature. As the modulus-temperature profiles of

Figure 3a-3e show, adhesive moduli are strongly temperature-dependent. For total fiber withdrawal over a wide temperature range, we need to use the temperature-dependent modulus for the epoxy adhesive and integrate Eq. 5 over the temperature range of interest:

$$\left(u_c - u_f\right)_{x=L} = \int_0^T (eq.5)dT$$

where the appropriate data from Figure 3 are used to determine the values in eq. 5. $(u_c - u_f)$ is the total motion of the fiber endface and is plotted in Figure 4.

METHOD FOR PREDICTING "ON-FIBER" COLOR RESULTS OF UV CURABLE INKS USING FLAT FILMS

David C. Duecker, M. Linda Moorman, Kelvin T. Turner

Borden Packaging and Industrial Products
Cincinnati, Ohio

ABSTRACT

A procedure for color analysis of UV curable fiber optic inks has been developed. Thin uniform ink films were coated onto clear plastic substrate and cured. The color of these films was evaluated using a color spectrophotometer. The correlation between film and fiber results was good.

INTRODUCTION

Color is only one characteristic of optical fiber. Though it will not determine whether an optical fiber will perform according to its designed function, color is important in the day-to-day use of the technology. As with most wire and cable applications, color identification is necessary in assembling the optical cable and later during its use in the field.

The perception and interpretation of color is highly subjective and can vary greatly from one individual to another. A person's color perception can be affected by ambient lighting, eye fatigue, color blindness, and other physiological factors. The interpretation of color will depend upon the observer's color references which can lead to different expressions of color. An alternative to these limitations is to determine a common frame of reference and a mutually agreed upon way of communicating color. A standard method for the measurement of color will provide for consistent analysis and interpretation.

The optical fiber industry has recognized the need for controlled color identification. As a result, the industry has standardized to the color specification defined in EIA-359-A. This specification defines the desired colors along with acceptable limits for each. The standard is defined in Munsell color space though it can be translated into other color measurement systems.

The Munsell system of color originated in the early 1900's as a way to visually order color. The Munsell system is based on three numerical values which define a specific color. These values are known as Hue, Chroma, and Value and are assigned in equal intervals of visual perception. Figure 1 shows the three dimensional color space as defined by the Munsell color system.

Color analysis equipment now common in the optical fiber industry, are more useful for color interpretation than the Munsell color system. The newer color systems utilize mathematical interpretation of instrumental measurements rather than the physical determinations on which the Munsell system is based. The most common of the mathematical systems is the CIE - - Commission Internationale de l'Eclairage (translated as the International Commission on Illumination, the body responsible for international recommendations for photometry and colorimetry).

When color is expressed in CIELAB, L* defines lightness, a* denotes the red/green value, and b* the yellow/blue value. As shown in Figure 2, the color scales of CIELAB are based on the opponent-colors theory of color vision that states: a color cannot be both green and red at the same time, nor blue and yellow at the same time. In this way, each set of L*a*b* values will refer to a unique point in three dimensional color space. An important characteristic of the instrumental measurement is the ability to quantify the differences between colors. Another feature is the ability to define the value of color as it relates to specific light sources and a "standard observer's" point of reference. These are important distinctions since changes in light source or observer's point of reference can impact the interpretation of color. For the purpose of this paper all measurements were made using CIELAB with "C" illuminant (approximately equivalent to overcast daylight) and 2 degree observer.

In addressing the issue of color as it relates to the manufacture of optical fiber there are additional

obstacles to overcome beyond those inherent in the expression of color. Processing parameters such as line speed and ink deposition tolerances will impact on the ultimate color perceived.

Optical fiber manufacturers desire to have inks which will consistently result in acceptable color when applied to fiber. An obstacle confronting the ink manufacturer is his inability to color fiber. In order to evaluate color during the ink development, a method must be created which will adequately predict the color as it will appear on a finished spool. This may seem a trivial matter but it certainly is not.

Several manufacturers of optical fiber have chosen to do their color evaluation on full spools of colored fiber. In this way they can determine whether an acceptable color has been achieved. This means of measurement causes the color to be the accumulation of many separate layers of ink. Also, because the number of individual layers of fibers is large, the bulk effect essentially removes the possibility that another layer of fiber will change the measured color.

Any technique for measuring the color in the laboratory must satisfy several criteria.

1. The color measurement must be reproducible.
2. The characterization must correlate with results measured on fiber.
3. The evaluation must be quick and inexpensive.
4. The method must be acceptable to customers who color fibers.

EXPERIMENTAL

The process of developing a proofing method for optical fiber involved many variables. For instance, a reasonable substitute for the substrate had to be identified since it is impractical to color fiber for routine QC purposes. Furthermore, a means of depositing a uniform and reproducible ink film was required. A method for measuring color on film and fiber had to be chosen. A controllable process to cure the ink was included in the method.

The method chosen must provide color results that correlate to those obtained on fiber. The method development process was iterative.

The choice of substrate began with consideration of the uncolored optical fiber. The optical fiber was essentially clear and did not contribute significantly to the appearance of the color. An attempt to prepare proofs at the expected film thickness of ink on the fiber was not practical. Also it was noted that color on a spool of fiber is the cumulative effect of many layers.

A substrate which reasonably approximates the conditions of the uncoated fiber was transparency film used in photocopiers. This film was readily available, is not prohibitively expensive, and is essentially optically clear. It also was sufficiently rigid, non-porous, and flat to allow a consistent proof to be prepared. The drawback to using this film was that the proof would not be totally opaque so a backing of Leneta 3NT-4 ink test paper was used when measuring all proofs.

Methods of applying ink to substrate were also considered. These were evaluated for film uniformity, reproducibility and correlation to fiber. The best of these application methods was chosen for this study. Films were prepared using a 0.5 mil Bird film application.

The films prepared required controlled handling in order to insure adequate cure. A Conrad Hanovia UV curing unit was used to cure the proofs. The unit was equipped with a medium pressure mercury vapor lamp with an output of 200 watts/inch. A belt speed of 24 ft/min was used. The proofs were exposed three times (twice from the front and once from behind) to the radiation source since they were relatively thick.

The color measurements were made on films and fiber using an X-rite® 968 spectrophotometer. The color measurements were done as noted earlier using C illuminant and 2 degree observer.

RESULTS AND DISCUSSION

Figures 3 - 5 are plots of L*, a* and b* for film versus fiber. The fitted lines, obtained using least - squares, are also shown. The film and fiber results correlate well. Some deviation from each of the fitted lines was observed. These deviations could be due to uncertainty in the L*, a* and b* values or perhaps they result from trends in the data. L*, a* and b* values for various batches of fiber prepared from the same lot of ink were compared. The uncertainties in L*, a* and b* values were too small to account for all of the deviations found. Additional ink films were prepared and L*, a* and b* values measured. The uncertainties in the L*, a* and b* values from film to film is also too small to explain the results . Therefore, the deviations observed indicate that trends exist. The trends can be readily evaluated if the inks are placed systematically into groups. Black, slate and white which have a* and b* values of approximately zero, comprise one group. For this group of inks, L* is the primary parameter of change. Aqua, rose and brown differ from the six remaining inks since they have significant levels of white or contain black. To make the trends apparent Δ L*, Δ a* and Δ b* were plotted against the fiber L*, a* and b*, values respectively. The Δ values were calculated using the following equations:

$$\Delta L^* = L^*(\text{fiber}) - L^*(\text{film})$$

$$\Delta a^* = a^*(\text{fiber}) - a^*(\text{film})$$

$$\Delta b^* = b^*(\text{fiber}) - b^*(\text{film})$$

The Δ L* values for black, slate and white inks are plotted as a function of L* in Figure 6. The horizontal line on the plot corresponds to a Δ L* of zero. Notice that Δ L* decreases when moving from the black to the white ink. The Δ L* for the black ink is a positive number. This means that black ink appears to be slightly darker on film than on fiber. The Δ L* for white ink is a negative number. The white ink, therefore, appears to be slightly lighter on film than on fiber. For the slate ink, Δ L* is about zero. The lightness/darkness of the slate ink is the same whether on film and fiber.

Next it is convenient to consider the colored inks shown in Figures 7 and 8 and consider the results collectively. Figure 7 shows the relative values of Δ a* for each of six inks. The horizontal line in the plot corresponds to a Δ a* of zero.

The trend may not at first be obvious. However, remember that the value of a* is directly related to the perceived degree of redness/greenness of an ink. Note that the inks close in color to red (i.e. violet, red and orange) have lower Δ a* values, and that inks close to green (i.e. yellow, green and blue) have larger Δ a* values.

Figure 8 is a similar plot, but of the relative values of Δ b* for each of the six inks. The horizontal line corresponds to a Δ b* of zero. Recall that b* is directly related to the degree of yellowness/blueness of an ink. It is seen that the inks close to yellow (i.e orange, yellow and green) have negative b* values while those close to blue (i.e. blue and violet) have positive b* values. Combining the results of the two figures with the equation for calculating chroma,

$$C = (a^{*2} + b^{*2})^{1/2}$$

it can be seen that the chroma value for inks printed on film is slightly higher than those printed on fiber.

In Figure 9, Δ L* for the six colored inks is plotted versus L*. The trend is similar to that seen in Figure

6 for the black, slate and white inks. Dark inks appear slightly darker on films than on fiber; light inks appear slightly lighter.

Next consider the rose and aqua inks. They are essentially slightly tinted "whites inks" so that, in terms of Δ L*, they behave like white. With respect to a* and b* they behave more like red and blue, respectively.

The hue for brown is very similar to that of orange. However, it contains black pigment and thus has a smaller L* value. There is little difference between L*, a* and b* for brown ink on film and fiber. The behavior of the brown ink with respect to L* is similar to that of slate.

The high chroma values for the group of six inks along with the L* values of black and white suggest that the ink films in this study are slightly too thick. However, because of difficulties associated with using thinner ink films and because the method described already gives good color correlation to fiber, the thicker films of this study are preferred. If desired the results could be refined by subtracting Δ L*, Δ a* and Δ b* from the film data.

CONCLUSION

The reproducibility achieved between testing done in the development laboratory and in the manufacturing laboratory has been good. This method of preparing ink proofs allows interpretation of lot-to-lot color variation in the laboratory. It can also be used by optical fiber manufacturers as a way to predict fiber results as a part of their quality control procedures. The ink proofing method as described is able to meet requirements for an acceptable evaluation technique.

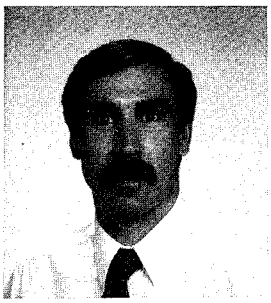
REFERENCES

A Guide to Understanding Color, X-rite Inc., Grandville, MI.

A Guide to Understanding Color Tolerancing, X-rite Inc., Grandville, MI

Munsell Color Charts for Color Coding - EIA-359-A,
Macbeth Division of Kollmorgen Instruments Corporation, Newburg, NY.

Nassau, Kurt, The Physics and Chemistry of Color - The Fifteen Causes of Color, Wiley - Interscience Publication.



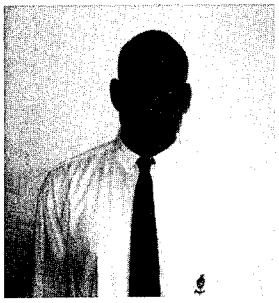
Dave C. Duecker
Borden Inc.

Dave Duecker obtained his B.S. in Chemistry from Indiana Wesleyan University in 1975. He earned a PhD. from the University of Cincinnati in 1988. He has been employed at Borden, Inc. since 1988, where he developed coatings for ribbons. He also has developed UV curable fiber optic inks.



M. Linda Moorman
Borden, Inc.

M. Linda Moorman is a Chemist in the Coatings/Graphics group of the Packaging and Industrial Products division of Borden, Inc. in Cincinnati, OH. She received her undergraduate engineering degree and a graduate degree in business from the University of Dayton. She works for Borden developing radiation curable or waterborne printing inks for a variety of industrial applications. She has worked for Borden for more than two years. Before that, she worked for 5 years for another supplier of inks to the wire and cable industry.



Kelvin T. Turner
Borden, Inc.

Kelvin T. Turner is a Laboratory Technician in the Specialty Coatings Division of Borden Packaging and Industrial Products in Cincinnati, OH. He holds an Associates degree from Cincinnati State and Technical College. He has worked in the Chemical Industry as a Laboratory Technician in the Beverage, Foods, and Oils Division of the Winton Hill Branch of Procter and Gamble. His current responsibilities are working with Ultraviolet Fiber Optic coatings and inks.

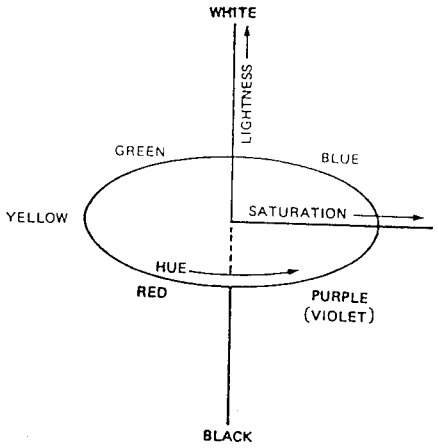


Figure 1

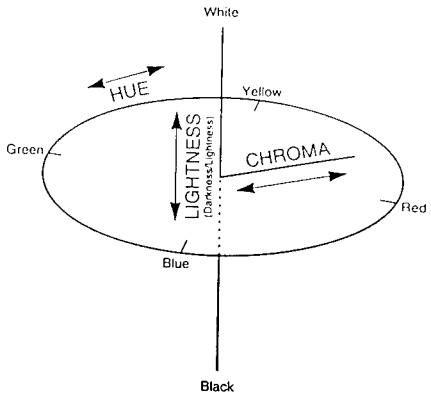


Figure 2

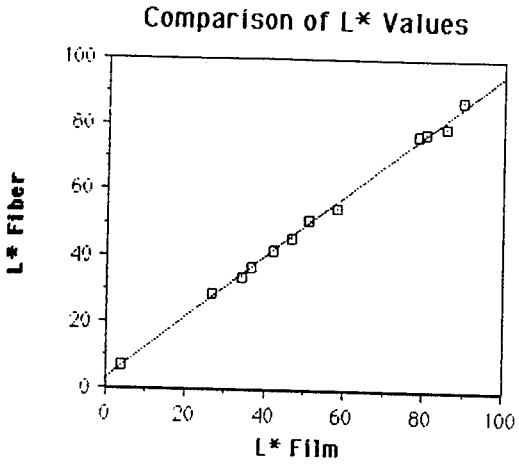


Figure 3

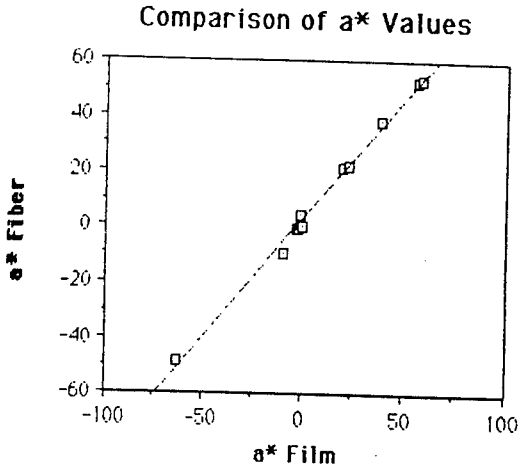


Figure 4

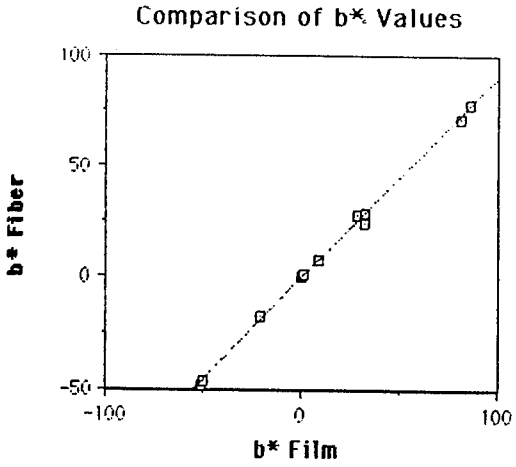


Figure 5

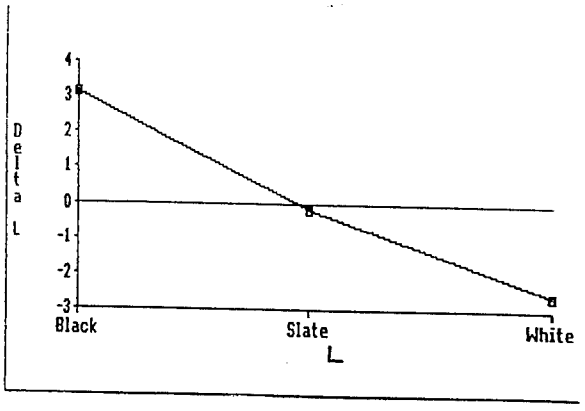


Figure 6

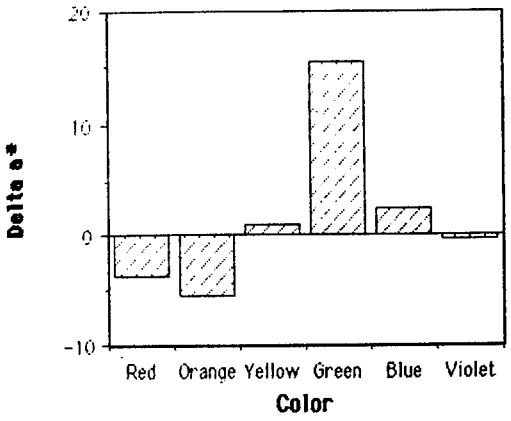


Figure 7

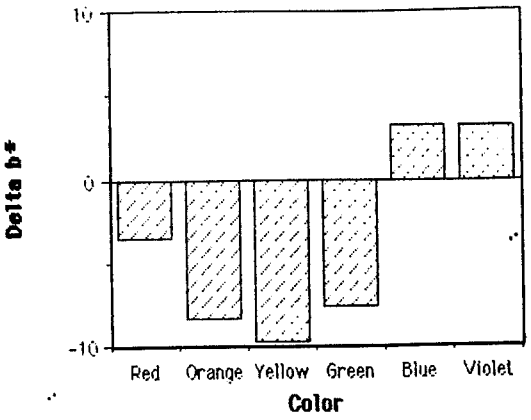


Figure 8

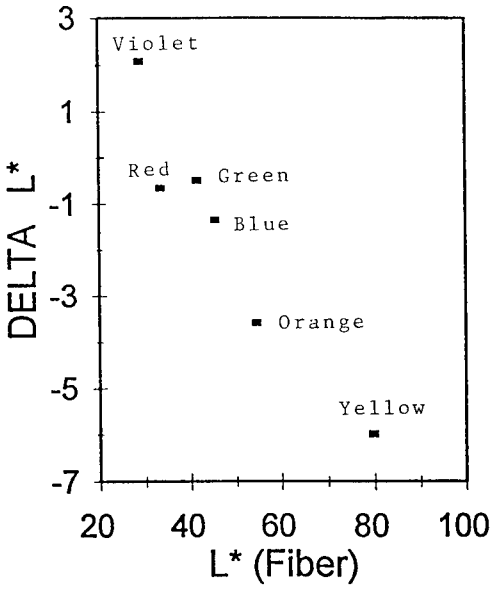


Figure 9

Development of a New Fiber Cleaning Tool

T.Kusayanagi S.Yaguchi M.Yoshinuma A.Kubota

Precision Instruments R&D Dept. Fujikura Ltd.
1440, Mutsuzaki, Sakura-shi, Chiba-ken, 285, JAPAN

ABSTRACT

There are three methods of joining optical fibers; arc fusion splicing, mechanical splicing, and fiber connectors. In particular, fiber cleanliness affects the splice quality (splice loss and fiber strength) in the case of arc fusion splicing and mechanical splicing. Also in the field, in order to clean the fibers, operators are pinching and wiping fibers by hand, and hence, splicing quality is not stable. We have developed a convenient new tool for fiber cleaning. This tool will facilitate better splice quality and it is operator skill independent. This tool is compact, light weight, and does not require any power source. Therefore this tool is very suitable for use both in the field, and in the laboratory.

1. INTRODUCTION

Work installing and interconnecting fiber cables has been increasing, as demand of optical fiber shows an increase of more than 10% per year in recent years. Reliable, good quality interconnections are essential to these fiber deployments, and this is dependent on cleanliness. Of the three means of joining optical fibers, only fiber connectors are typically factory pre-installed where conditions and cleanliness are controllable during fiber cleaning operations. Of course, the ends of the fiber connector must be clean when the connectors are mated together as the fiber cable is deployed.

In the case of fiber interconnections using fusion splicing or mechanical splicing methods, the fiber coating and/or jacket is removed in the field. Hence, both fusion and mechanical splice quality is dependent upon the fiber cleaning process which follows coating removal.

In the field, operators are pinching and wiping fibers with a cloth or a tissue soaked with alcohol in order to clean coating debris, dust, and dirt from the fibers. The number of wiping passes and the method and compression applied to the fiber all vary, depending upon the operator's skill and habits. Hence splice quality is not stable.

In order to correct these problems, we have developed a convenient new fiber cleaning tool. The advantages of this tool are that it is possible to achieve better and more uniform fiber cleaning, which will facilitate better splice quality, and furthermore, the tool operation is repeatable and independent of operator cleaning technique.

2. SPECIFICATION AND FEATURES

2.1. Specifications

Cleaning tool size and weight:
148mm(W)×50mm(D)×115mm(H), 400g.
This cleaning tool does not require any power source.
The cleaning tool is shown in Fig. 1.

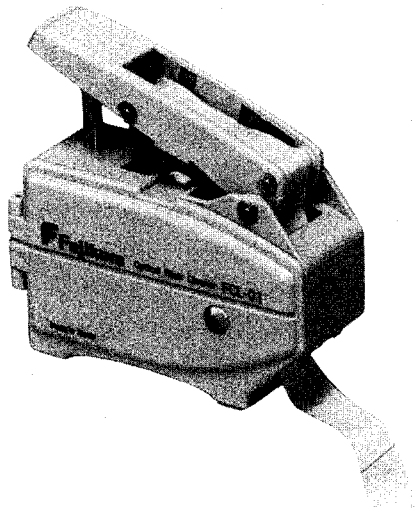


Fig. 1 Appearance of the new cleaning tool.

2.2. Features

The cleaning tool has the following features:

(1) Fibers are wiped clean by a special material tape.
(2) The new cleaning tool contains the cleaning tape reel.
(3) Fibers are inserted into the space between the tool body and the lever, and the lever is closed. The fiber is thereby compressed by the cleaning tape on both sides.
(4) There are two sponges soaked with alcohol at the fiber cleaning position. Alcohol soaks the cleaning tape also.
(5) When the fibers are pulled from the cleaning tool with the lever closed, the fibers are wiped by the cleaning tape and cleaned.
(6) Because the stroke of the lever is limited by a mechanical stop, fiber compression is consistent and stable.
(7) When the lever is released, the cleaning tape reel is uncoiled by an internal mechanical device, providing a new portion of tape to the fiber cleaning position. Hence, the tool is always ready to clean a fiber.

3. PERFORMANCE

First, inadequate cleaning of the fiber causes high splice loss. When the coating is stripped from the fiber, there is still a great deal of coating debris, dust, etc. on the fiber surface. Without adequate cleaning, foreign material will be left on the fiber surface and will prevent proper fiber alignment, leading to substandard and unstable splice loss results.

On the other hand, cleaning more than needed causes low fiber strength. Other problems are that some operators may not only wipe the fiber too many times, but also with too much compression or bending stress, also resulting in reduced fiber strength.

We have performed a comparison between splice quality when the fibers were cleaned by hand (the former/conventional method), and when cleaned by use of the new cleaning tool. The results prove the utility of the new cleaning tool.

3.1.1. Fiber Offset and Splice Loss

Generally speaking, there are several factors for good splicing quality as follows: (1) cleave angle, (2) fiber axial offset, (3) fusion arc discharge conditions. In particular, mass fusion splicers and the new generation compact fusion splicers utilize a fixed V-groove system to provide for fiber alignment. Therefore, fiber pre-splice axial offset will arise from dust or contamination remaining on the fiber surface due to inadequate cleaning. This pre-splice misalignment causes deformation of the fiber cores during the fusion arc, as the fibers tend to self align due to surface tension of the molten glass, resulting in a splice loss increase. (In the case of mechanical splicing, contamination on the fibers will also lead to axial offset of the fibers, and increase splice loss.)

In the experiments conducted, we have performed a comparison between the cleaning results with conventional fiber cleaning methods (cleaning by hand) and the new cleaning tool, gathering pre-splice fiber offset and splice loss data. These tests were performed with various fibers.

The condition of this experiment is as noted below:

(1) In the case of the former method, 10 cleaning passes were generally performed.
(2) In the case of using the new cleaning tool, 5 cleaning passes were performed.

The fiber utilized in this experiment is as noted below:

(1)SM (single-mode) single fiber (Fujikura).
(2)SM 4-fiber ribbon (Fujikura).
(3)SM 12-fiber ribbon (AT&T).

3.1.2. Result and Discussion

Fiber axial offsets and splice losses when splicing SM single fibers (Fujikura) are shown in Fig. 2 and Fig. 3. Fiber axial offsets and splice losses when splicing SM 4-fiber ribbon (Fujikura) are shown in Fig. 4 and Fig. 5. Fiber axial offsets and splice losses when splicing SM 12-fiber ribbon (AT&T) are shown in Fig. 6 and Fig. 7.

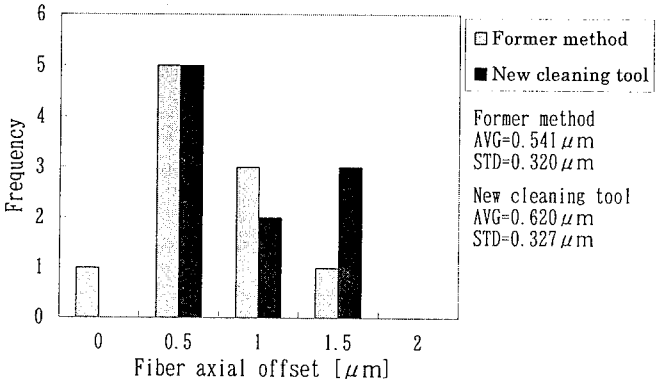


Fig.2 Fiber axial offset for SM single fiber

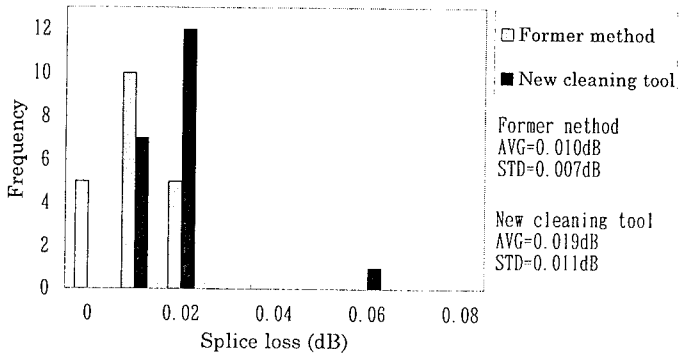


Fig.5 Splice loss for SM 4-fiber ribbon

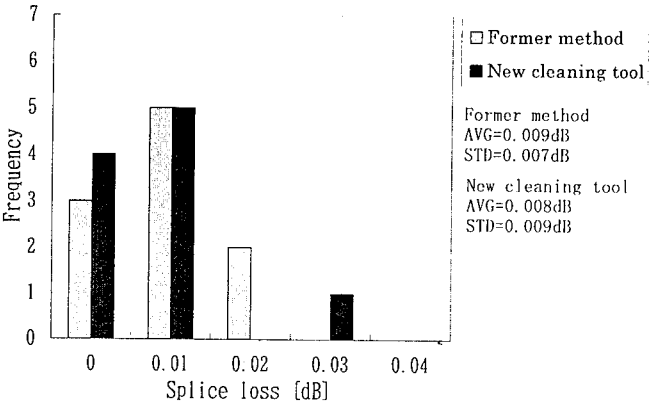


Fig.3 Splice loss for SM single fiber

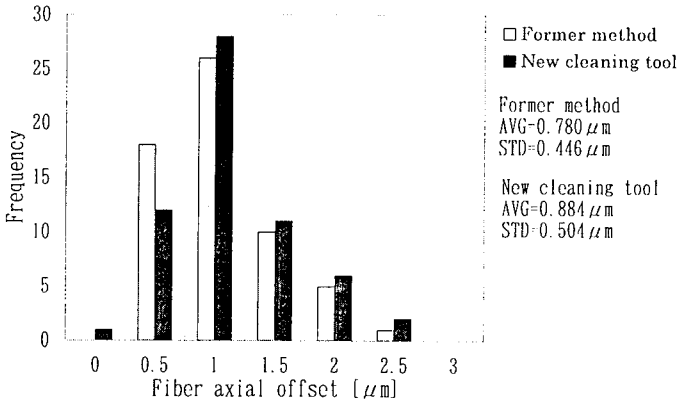


Fig.6 Fiber axial offset for SM 12-fiber ribbon

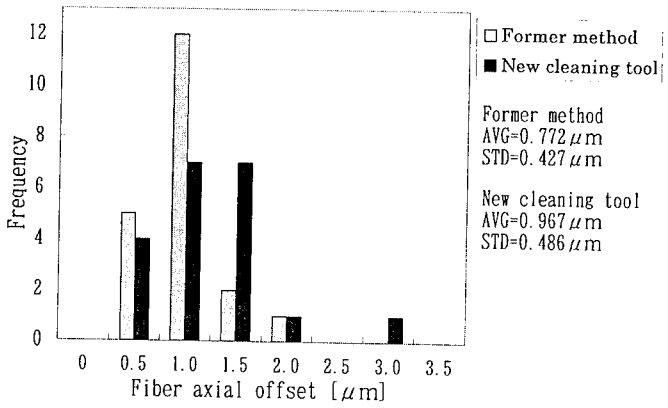


Fig.4 Fiber axial offset for SM 4-fiber ribbon

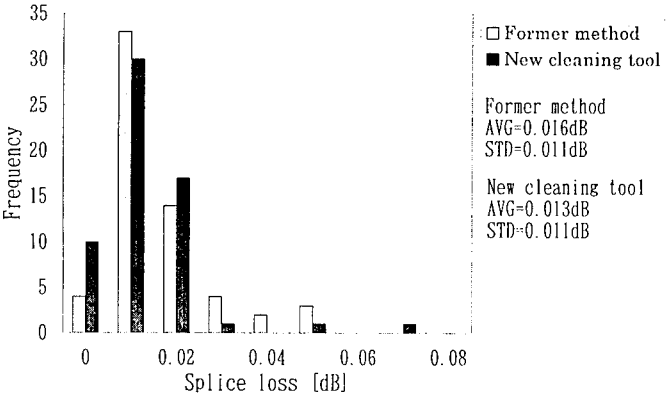


Fig.7 Splice loss for SM 12-fiber ribbon

The results demonstrate that the averages of the fiber axial offset and the splice loss achieved using the new cleaning tool are essentially equal to the case of the former cleaning method (despite using fewer cleaning passes). While there is some slight deviation in the above data obtained with the new cleaning tool, it is with allowable limits, demonstrating that the new cleaning tool yields very consistent and reliable results even with fewer cleaning passes.

3.2.1. Fiber Strength

There are several factors for the decline of fiber strength during splicing operations; (1) During fusion splicing, a chemical reaction between the silica glass and burning debris on the fiber surface occurs during the heating, (2) Scratches on the surface of the fiber are caused by wiping and cleaning the fiber, (3) Scratches on the surface of the fiber are caused by loading the fiber into the splicer V-grooves (or into the mechanical splice). In particular, considering fiber cleaning, wiping more than needed causes low fiber strength. Other fiber cleaning practices which may lead to reduced fiber strength are : (a) too much compression applied to the fibers during cleaning (which can also lead to an increased tensile stress on the fibers as they are pulled through the compressed cleaning tissue) (b) bending stress (c) the use of previously used cleaning tissues, already contaminated with fiber coating debris. All of these cleaning issues relate to the specific habits of the individual operator.

We have performed a comparison between the spliced fiber strength obtained after cleaning the fibers using the former (conventional) fiber cleaning method, and the new cleaning tool. This spliced fiber strength data was collected using various fibers.

The condition of this experiment is as noted below:

(1) In the case of the former method, the cleaning passes were generally performed.

(2)In the case of using the new cleaning tool, 5 cleaning passes were performed.

The used fiber of this experiment is as noted below:

(1)SM (single-mode) single fiber (Fujikura).

(2)SM 4-fiber ribbon (Fujikura).

(3)SM 12-fiber ribbon (AT&T).

3.2.2. Result and Discussion

Fiber strength results when splicing SM single fibers (Fujikura) are shown in Fig. 8. Fiber strength results when splicing SM 4-fiber ribbon (Fujikura) are shown in Fig. 9. Fiber strength results when splicing SM 12-fiber ribbon (AT&T) are shown in Fig. 10.

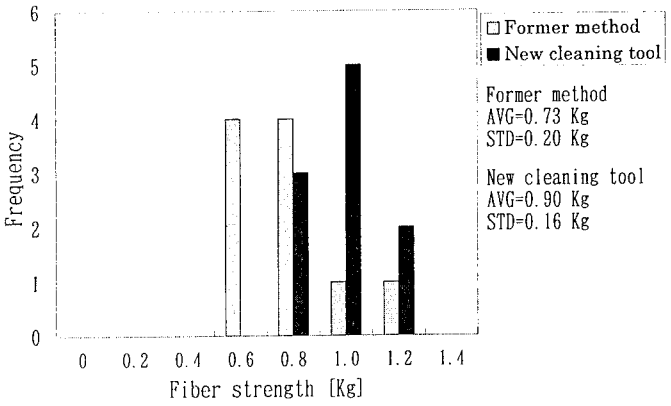


Fig.8 Fiber strength for SM single fiber

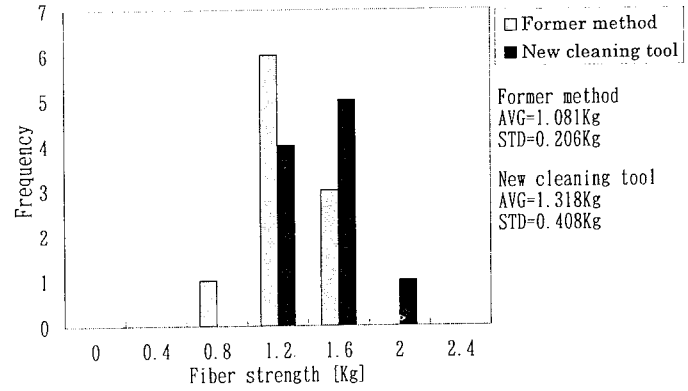


Fig.9 Fiber strength for SM 4-fiber ribbon

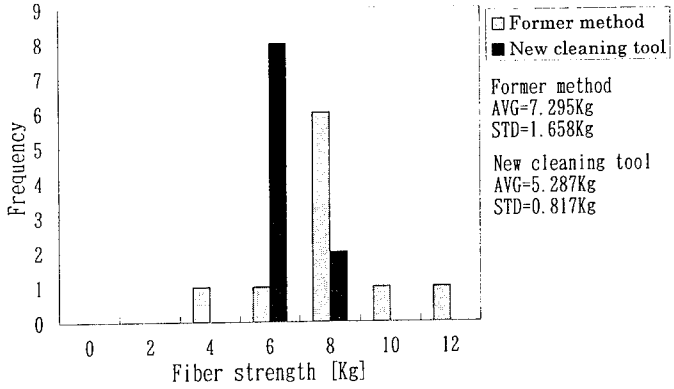


Fig.10 Fiber strength for SM 12-fiber ribbon

We have also confirmed that the average spliced fiber strength obtained when the fibers are cleaned by the new cleaning tool is essentially equal to the average result obtained by use of the former (conventional cleaning by hand) method. However, the deviation of splice strength by using the new cleaning tool is generally smaller than the former method. Therefore, consistent fiber strength can be achieved irrespective of the operator's level of skill, habits, or cleaning techniques when the new cleaning tool is utilized, and weaker splices are more readily avoided.

4. CONCLUSION

Both splice loss and fiber strength are very consistent in the case of cleaning fiber using this new fiber cleaning tool. Because this new cleaning method is not dependent upon the skill or techniques of the operator, this new cleaning method is more reliable than conventional hand cleaning of the fibers, and will result in more consistent results in the field. The new cleaning tool is suitable for use in the field, as well as in the laboratory.

REFERENCE

T.Wei, H.H.Yuce, C.H.Hasz and P.L.Key
"DEGRADATION OF FIBER STRENGTH DURING COATING STRIPPING",
International Wire & Cable Symposium Proceedings, p199-204, 1989



Tadahiro Kusayanagi

Precision Instruments
R&D Dept.
Fujikura Ltd.

1440, Mutsuzaki,
Sakura-shi,
Chiba-ken, 285,
JAPAN

Tadahiro Kusayanagi was born in 1961. He received the B.E. degree in mechanical engineering from Tokyo Denki University in 1985.

He joined Fujikura Ltd. in 1991 and has been engaged in the research and development of an optical fiber splicers and related products.



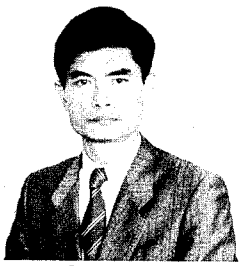
Shonosuke Yaguchi

Precision Instruments
R&D Dept.
Fujikura Ltd.

1440, Mutsuzaki,
Sakura-shi,
Chiba-ken, 285,
JAPAN

Shonosuke Yaguchi was born in 1955. He graduated in mechanical engineering from Keio University in 1979.

He joined Fujikura Ltd. in 1979 and has been engaged in the Plant Engineering Section for 12 years and currently is a manager of the Precision Instruments R&D department.



Mikio Yoshinuma

Precision Instruments
R&D Dept.
Fujikura Ltd.

1440, Mutsuzaki,
Sakura-shi,
Chiba-ken, 285,
JAPAN

Mikio Yoshinuma was born in 1947. He graduated in mechanical engineering from Chiba University in 1971.

After graduation, he joined Fujikura Ltd. and has been engaged in research and development on mechanical equipment and tools for communication wires, cables, and parts. He is now a general manager of the Precision Instrument R&D Department, including responsibility for fusion splicer R&D.



Akinobu Kubota

Inter'l Telecom. Engr'g
Dept.Fujikura Ltd.

1-5-1, Kiba, Koto-ku,
Tokyo, 135, JAPAN

Akinobu Kubota was born in 1949. He graduated in Electronics from Tokyo Institute of Technology in 1972.

He joined Fujikura Ltd. in 1972. He had been involved in Telecom R&D Department for 3 years and has been in Telecom Engineering Dept. since 1975. He is currently general manager of International Telecommunications Engineering Department.

Evaluation of Impact Testing for Simulated Shotgun Damage of Optical Fibre Cable.

Lang* I.D., Davies† M.V., Poole+ N.J., Cockrill§ K.J..

Pirelli Cables Ltd UK*†, University of Glamorgan*+, BT Laboratories§.

Abstract

This paper investigates the characteristics and variables of shotgun testing as applied to communication cables, and has led to the development of a new impact test method. The method allows a quick evaluation of shotgun resistance of cables and materials. A combined mass and shotgun pellet are given a specific amount of potential energy by fixing them at a given height. On release the stored potential energy provides an impact energy that allows the pellet to penetrate through the layers of the cable. Field variables such as shot distribution, gun variance, strike angle, and cable orientations are eliminated by the impact test method.

Good correlation was found between the impact test and shotgun testing for the worst case shotgun damage of individual pellets.

The impact test was also found to be a reproducible, safe and cost-effective method that has allowed quick, accurate modelling of cable shotgun protection.

Introduction

Customers of the cable industry may specify shotgun testing to evaluate a cable's resistance to shotgun damage, the aforementioned requirement having arisen from practical experiences of cable damage caused by stray shot. Current proposed tests[1] can produce results varying both within or between test houses. This is caused by variations between guns, cartridges, and the accuracy of the person firing the shot. Also, this method is time consuming and expensive as full production samples are required for field tests. This has led to the development of a simple method to simulate shotgun damage quickly, consistently, and fairly.

The impact method, which is based on impact testing, was developed by investigating field variables including shot characteristics. Only conditions which produced the highest damage during shotgun testing have been modelled by the impact. Plaques of cable sheathing materials were then used to compare the impact test method with field shooting. This became a useful means to assess materials and the test equipment performance. Cable testing then confirmed the assumptions made during plaque testing. The impact method has been found to be a safe and controlled test to assess materials and designs.

Field Variables

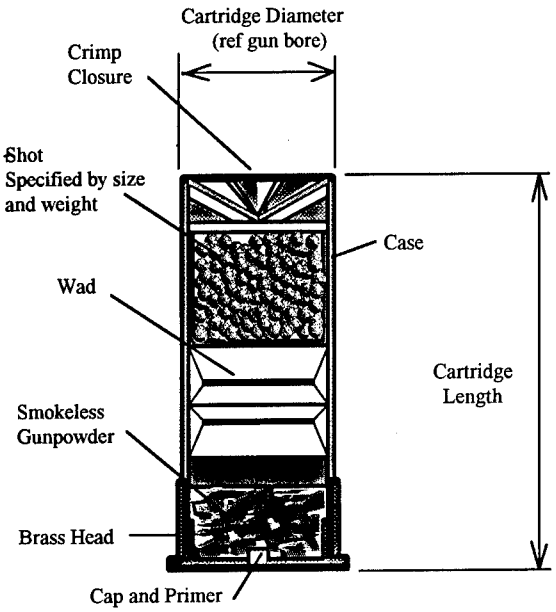


Figure 1 Section of Shotgun Cartridge.

Cartridge length and diameter. The shotgun's cartridge size is limited by the gun's barrel inside diameter (the bore), and chamber length. Unless otherwise stated, this paper considers British 12 bore shotguns.

Shot size. The shot size used depends on the prey being shot. Table 1 outlines the range of shot sizes, the larger shot size having smaller diameter pellets. Throughout this paper all further references will be made to the English sizes. The common range of shot size used varies from seven, used for small light targets (for example pigeons) to shot size four, which might be used for larger birds (for example duck).

Shot weight. The cartridge shot load is specified as a weight. This can vary from 9 g for a .410 bore gun, to 46 g for a 12 bore magnum cartridge.

Shot material. The shot material used for field and impact tests was lead, alternatives include copper, alloys, steel, and polymers.

Wad and case. Cartridges made from the common combination of plastic wad and plastic case were used for field tests. Biodegradable composites are an alternative choice.

Gun choke. The discharged pellets form a 'cloud', with each pellet having a different speed and direction. As the cloud travels away from the gun the pellets' speeds reduce and the 'cloud' diameter increases. An insert into the end of the gun barrel, called the *choke*, controls this spread. This varies from *skeet* which gives maximum spread, to full *choke* which gives the tightest pattern. For fast moving, close range targets, *skeet* might be used to maximise the spread and increase the chances of hitting the target. At long ranges full *choke* would be used so that an adequate number of pellets would strike the target

Barrel length. Field tests where carried out with 28 inch barrel gun. British law[2] requires shotguns to have a minimum barrel length of 24 inches.

Cartridge design. The cartridges range from low recoil to high velocity. The variations exist to cope with the range of targets, the gun limits, and the preference and experience of the user. Standard cartridges were used for field testing.

Shot size						Nominal Shot Diameter		Lead weight
English	American Swedish	French	Belgian Dutch	Italian	Spanish	mm	inch	grams
LG	-	-	-	-	-	9.1	0.36	5.000
SG	00 Buck	-	9G	11/0	-	8.4	0.33	3.333
Spec.SG	1 Buck	C2	12G	9/0	-	7.6	0.30	2.500
SSG	3 Buck	C3	-	-	-	6.8	0.27	1.818
AAA	4 Buck	5/10	-	-	-	5.2	0.20	0.800
BB	Air rifle	1	00	00	1	4.1	0.16	0.400
1	2	3	-	1 OR 2	3	3.6	0.14	0.278
3	4	4	-	3	4	3.3	0.13	0.200
4	5	5	-	4	5	3.1	0.12	0.167
5	6	6	5	5	6	2.8	0.11	0.128
6	-	-	6	6	-	2.6	0.10	0.105
7	7.5	7	7	7.5	7	2.4	0.095	0.083
7.5	8	7.5	7.5	8	7.5	2.3	0.090	0.071
8	-	8	8	-	8	2.2	0.085	0.063
9	9	9	9	9.5	9	2.0	0.080	0.048

Table 1 Shot Size and Pellet Weight[2,3]

The Principle of the Impact Test

The impact test method is based on providing a single pellet, supported by a drop weight, the same energy as a pellet when shot. As a fired pellet may have a barrel velocity over 375 ms^{-1}, the drop weight is used to achieve the equivalent energy at a lower impact velocity. This lower impact velocity has a maximum value limited by gravitational acceleration and the practical limits of drop heights.

Using Newtonian mathematics the average pellet kinetic energy at the point of impact may be calculated and an equivalent potential energy defined. The calculations are based on cartridge information which considers the pellet's flight resistance forces (see table 2).

Shot Size	Range [m]			
	20	25	30	35
BB	284	269	254	238
3	272	253	236	219
4	269	249	231	214
5	265	244	224	205
6	261	239	219	199
7	257	234	212	191
9	247	220	196	171

Table 2 Striking Speed [ms^{-1}] Compared with Shot Size[2] (Based on 12 Bore Standard Game Cartridge, 325 ms^{-1})

Calculations are completed for selected target ranges using the drop height as the variable. The drop weight masses were initially selected to provide convenient drop heights within the limits of a typical room. The results for shot sizes 4 and 7 can be seen in table 3, for example, to simulate the firing of a shot size 4 pellet at a range of 20 m, the 418 g drop weight is used from a drop height of 1470 mm.

Shot Size (English)	Drop Weight (grams)	Range				
		10 m	15 m	20 m	25 m	30 m
4	418	2000	1710	1470	1260	1078
7	233	1690	1438	1200	1000	860

Table 3 Impact Simulation Test Variables. Drop Height [mm] for Specific Shot Size and Range

Test Equipment

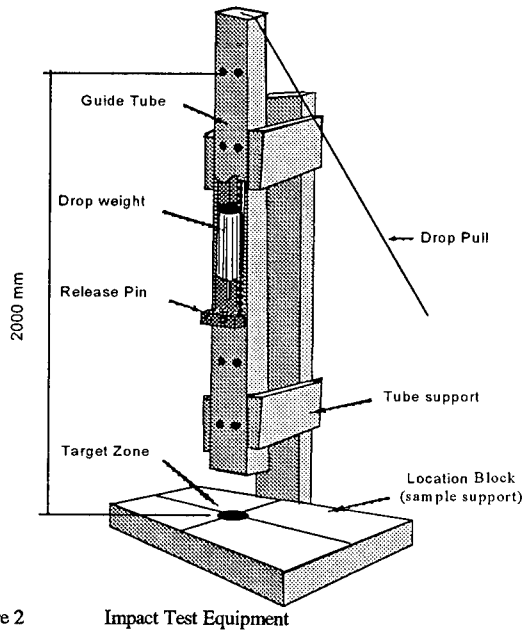


Figure 2 Impact Test Equipment

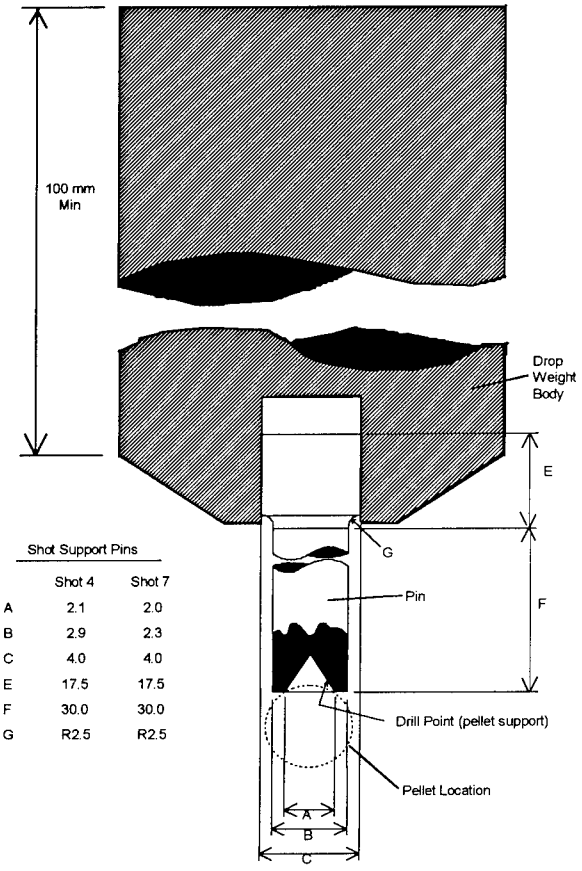
The impact test equipment consists of a drop weight, a guiding drop tube, and a location block (see figure 2). The drop weight is designed to impact a supported shotgun pellet into, and in some cases through, the test sample. The test sample is placed on the location block, over the target zone hole. The drop weight is fitted with a pellet of the appropriate size and material. The pellet is held to the drop weight pin with 'Blu-Tack' or other similar material.

The guide tube is made from 25.4 mm square section tubing which provides four line contacts with the cylindrical drop weight. The geometrical difference between the guide tube and drop weight allows room where tube flaws and release pin holes will not influence the drop weight fall.

The Drop Weight

The drop weights have been designed so that a minimum of 100 mm is guided by the tube. This length was a compromise to provide a controlled drop while not adversely increasing the frictional drag. Mild steel was chosen to achieve the required weight within the proposed dimensions.

Clamped to the weight's leading nose is the 'shot support pin' (figure 3). This holds a pellet so that it is supported without slipping from the tip, while not constrained so that the resulting deformation is governed by the impacting surface profile.



Shot Support Pins

	Shot 4	Shot 7
A	2.1	2.0
B	2.9	2.3
C	4.0	4.0
E	17.5	17.5
F	30.0	30.0
G	R2.5	R2.5

Figure 3 Shot Support Pin

The Target

The target zone and test piece support will affect both transient attenuation changes and material testing results. The support consists of a wooden block with a hole directly below the impact location. The hole protects the shot support pin from impacting with the block. When cables are tested they are held flat and taut with the addition of toggle clamps. The restrained cable simulates field tests where cables show little movement when shot. Cable freedom would lead to optical performance errors induced by the cable slapping against the support block when impacted by the drop weight. For material testing, plaques are placed flat over the hole. If a fair comparison is to be made between test houses, then the hole shape and size must be defined to allow equal sample support. It is recommended that this hole is 15 mm in diameter.

Experimental Results of Plaque Testing

To obtain results for materials and composite structures, plaques can be tested for shotgun damage resistance. Plaque testing allows modelling of cables prior to costly cable manufacture. Samples which have been tested but not pierced are quantified by measuring the deformation, as shown in figure 4.

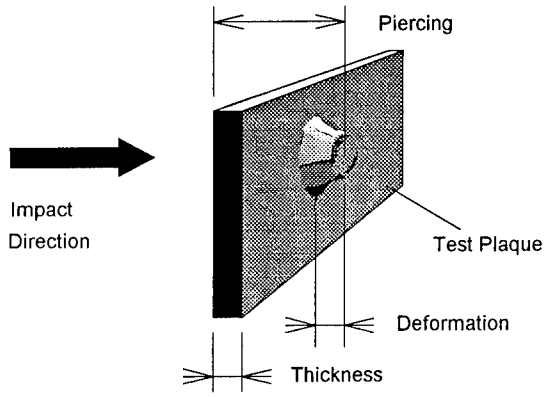


Figure 4 Test Plaque Deformation

The testing of plaques built up to simulate cable layer has been a powerful tool in the prediction of shotgun protection for cables. Testing allows a quick assessment of a broad range of materials from corrugated steel to tight woven aramid yarn. Plaque testing was also used to investigate correlation between test houses and variation between impact and field tests.

Test House Comparison

Two test sets were independently constructed at BT Laboratories, Martlesham and Pirelli Cables, Newport. Comparison tests were made with plaques of various thickness and cable sheathing materials. The materials tested were a range of polyethylenes from low to high density, of thicknesses between 2.2 and 6.0 mm, and shot sizes four and seven were impacted into samples from varying heights.

The results showed that the difference between the sets for the measured deformation as a percentage of the plaque thickness was less than 8%. For example a loaded medium density polyethylene of 4.4 mm thickness showed deformations of 0.63 mm on the first fixture and 0.50 mm on the second fixture when impact tested to simulate firing with shot size 7 from 15 m. This is considered acceptable since field testing produced variations greater than 20%.

Field Comparisons

The difference between field and impact testing was investigated using plaques. The materials tested were a range of polyethylenes from low to high density, of thicknesses between 1.3 mm and 4.9 mm, and shot from ranges between 5 m and 30 m.

The worst field pellet strike for each test was compared with the equivalent impact test result. Field deformation values were found to be within 7% of impact results, for example, a medium density polyethylene of 2.4 mm thickness showed deformations of 0.40 mm when shot and 0.54 mm impacted test to simulate shot size 7 from 30 m. This again was considered an acceptable value.

Pellet deformation differed between field and simulated tests. Field fired shot tended to become penned into the material, the pellet flattening under the broken surfaces whereas impact test shot tends to absorb the energy through shear. The difference was more noticeable with dense homogenous material where the pellet was retarded abruptly. The differences in deformation did not affect the total damage correlation between field and impact tests.

Cable testing

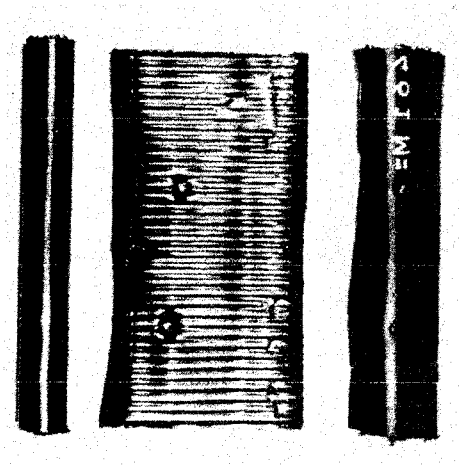
Both physical damage and optical performance may be monitored using the impact test method. For optical performance the fibres from one element of a short cable sample are spliced together and connected to a light source and detector. This sample is then impacted above the active element using the lay length to predict the element position.

Cables may also be tested under loading conditions, for example the maximum working tension, by combining the impact equipment with tensile testing.

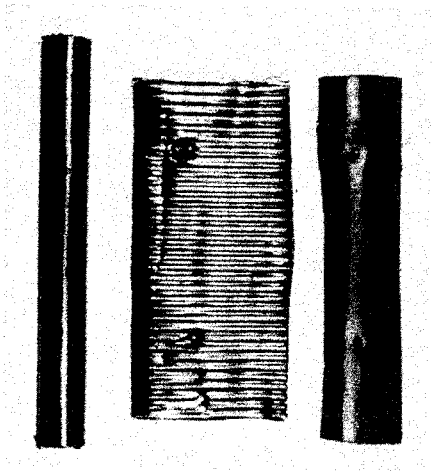
Field cable testing was compared with impact simulated damage, being of multiple loose tube construction with sheaths consisting of:

- Corrugated steel polymer laminate tape, double sheathed
- Aluminium polymer laminate tape, single sheathed
- Stranded aramid yarn, single sheathed
- Stranded aramid yarn, double sheathed
- Stranded glass yarn, double sheathed

It was found that the worst pellet strike hitting the cable normal to the surface was accurately simulated by impact tests. From the cables tested the shot penetration and fibre tube damage was indistinguishable. Figure 6 shows one cable which has been field and impact tested.



Simulated Impact, Shot 7, 25 m



Field Tests, Shot 7, 25 m

Figure 6 Comparison Between Field and Impact Testing

The resulting damage did vary for a glancing shot. As the impact testing is primary mass controlled, the pellet is driven in the same direction as the drop weight. Impact testing will therefore represent the worst case normal strike.

Equipment and Field Variations

Besides the comparative tests, two trials were made to investigate impact and field variations, the first investigation dealt with drop weight drag, the second was field shot density.

Impact speed will be reduced by drag losses acting on the drop weight. The concern was investigated by timing the drop weight fall through known distances. The effect of drag on the drop time was under 2% for the 418 g and 233 g weights. This is equivalent to a 4 ms^{-1} change in the pellet velocity, and is considered insignificant compared with field variations.

Shot density will vary considerable depending on the gun, choke, range, and ammunition. At ranges over 15 m the charge spreads so that each strike may be considered a separate event. For a 5 m, full choke, direct hit, the pellets' damages start to merge causing multiple strikes in one place. The problems caused by shot distribution and aim are illustrated in figure 7. Assuming that the damage is caused by stray shot at the outer limits of the spread, the density along a cable would be low and random. This pattern would change completely if the cable was directly struck. Therefore field results are random in nature, but dependant upon the accuracy of shooting.

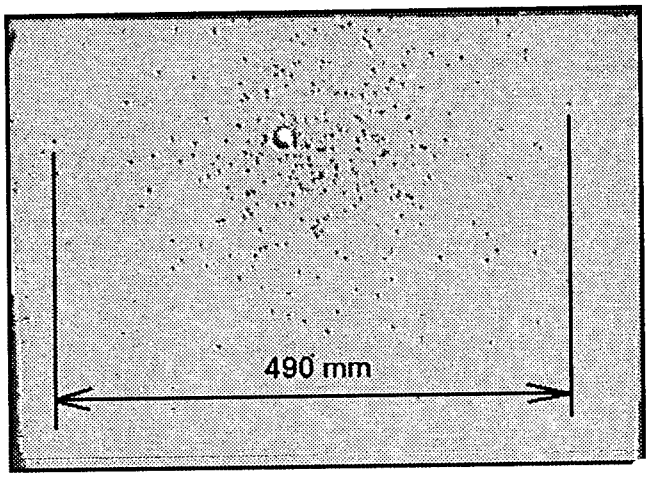


Figure 7 Pellet distribution of shot size 7, from 15m, with $^1/_2$ Choke (The centre hole is produced by the wad and not pellets)

Proposed Test Specification and Reporting

To ensure fair and repeatable testing the following variables should be defined in any impact test specification.

- Shot size
- Drop weight
- Drop height
- Shot material
- Cable length
- Optical circuit
- Light source wavelength
- Test temperature

Criteria such as the limit of mechanical damage requires definition on a case-by-case basis. Figure 8 shows a report sheet that allows quick visual analysis of the results. In this example the cable failed between 15 m and 20 m when the fibre tube was damaged and there was a significant attenuation increase.

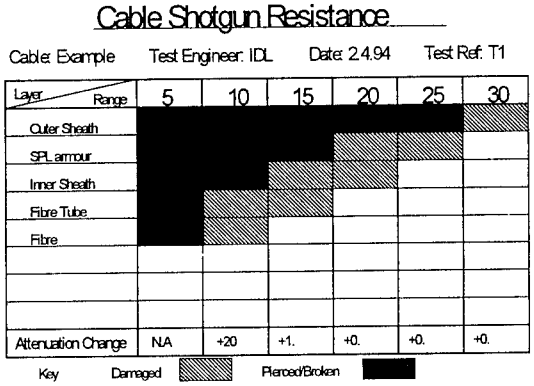


Figure (8) Typical Results

Conclusions

A new test method to simulate shotgun damage using impact testing has been developed. A measurement of the test damage generated by an equivalent impact energy to that of shotgun pellets correlates well with the worst damage produced from a single projectile strike.

The method eliminates the poor reproducibility of field shotgun testing and provides reproducible testing, both within and between test houses. The impact test is a safe and cost-effective alternative to field testing and is a useful product development tool to assess material selection and construction before cable manufacture.

The test method allows fibre monitoring combined with cable tensile loading to simulate the effects of shotgun damage at high loads.

Acknowledgements

The authors would like to thank the many people who positively supported and aided the investigation. In particular the marksmanship of Ray Studd (BT Laboratories), the enthusiasm of Nigel Fishlock (Pirelli) and the help of Dr Ron Seho (Pirelli). In addition a special acknowledgement is made to Dr David Rees (University of Glamorgan) who is responsible for the related Teaching Company Programme that has made this project possible.

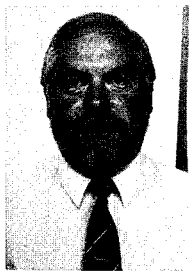
References

1. Method IEC 794-1-XXX Shot-gun Damage, SC 86A (secretariat) 233

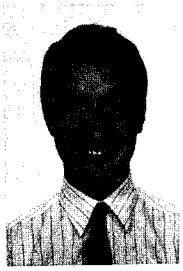
2. Trade Literature, Eley Hawk LTD, Witton, Birmingham, UK

3. Trade Literature, Hull Cartridge LTD, Hull,.UK

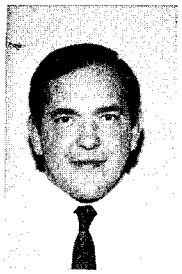
Authors



KEITH COCKRILL joined British Telecom (Then the GPO) in 1967 working as a Representative at Contractors works on Submarine and Land cables and as a maintenance engineer on complex test equipment. In 1975 he transferred to British Telecom Research Laboratories to enable him to use his expertise on a wide range of submarine system related projects. His 25 years of work in this area has gained him an international reputation for universal solutions to world-wide moulding problems. With the transfer of Submarine cable work out of BT in 1994 he transferred to his current position supplying technical and reliability support on Optical fibre and cables to BT and the cable industry.



MARTIN DAVIES gained an honours degree in Statistics at the University of Bath. He is Chief Engineer with the Communication Cables division of Pirelli Cables UK, and has represented the company on a number of standardisation bodies including BSI, ETSI and IEC.



Dr N.J.POOLE is a principle lecturer and responsible for research co-ordination in the Department of Electronics and Information Technology at the University of Glamorgan. He is a chartered physicist and has research interests in mathematical modelling, quality assurance, and reliability.



IAN LANG gained a degree from Loughborough University and is currently studying for a masters degree at the University of Glamorgan through the Teaching Company Programme while working with Pirelli Cables Newport. He is an associate member of the Institute of Mechanical Engineers and has previously worked in the automotive industry.

A New Identification System for Optical Fibers in High Count Buffer Tubes

H. Haag, G. Hög, M. Hoffart, B. Glessner, K. Nothofer

KABEL RHEYDT AG, 41048 Mönchengladbach, Germany

Summary.

Up to now, in most optical fiber cable applications a 12-color identification scheme using either solvent- or UV-inking has been adequate for the identification of individual fibers. For higher fiber counts per tube, *e.g.,* in order to reduce the number of steel tubes in Optical Ground Wire (OPGW) constructions, more than 12 individual fiber colors would be necessary to achieve unduplicated identification. Therefore, a new identification system has been developed in which up to 48 fibers can be uniquely identified within one tube. Different colors and ring marks are utilized. This obviates the need to use a tandem identification system in high fiber count tubes such as, for example, colored binders around 12-fiber bundles as a means of distinguishing fibers of the same color.

Introduction.

Until recently the maximum fiber count in one tube in most loose tube optical fiber cables has been twelve. For reasons of cost reduction today's trend is to increase the fiber count to greater than twelve per tube, This applies especially to OPGW with stainless steel tube and to single-tube cable constructions. This paper describes a new 48-fiber color-coding process, its coloring technology and the related behavior of the single mode fiber. Test results describing the temperature and mechanical behavior of two representative loose tube cable construction types are described.

A highly important part of this paper deals with the description of an OPGW with 96 single mode fibers, using 2 stainless steel tubes, each containing 48 fibers.

A New 48-Color- Code Identification System.

A coloring process for optical fibers which allows unique identification of individual fibers in high counts has been developed. This process is an extension of the conventional 13-color scheme (12 pigmented colors and neutral) to a 48-color system. The premise of the new process is to superimpose single-ring and double-ring markings on the 13 basic colors. Today, two different fixed-length marking intervals and one ring color are used to yield a 48-color process. Higher count solutions are possible with different fixed-length intervals and the use of more than one ring color. Additionally, triple or quadruple rings are possible. The technology developed results in a color-coding that is easily distinguishable, permanently fast and having no discernible effect on the attenuation of the fiber "as manufactured" or in use in the cable. Both aerial and buried cable designs have been evaluated as reported below.

Color Coding.

The 48-fiber color identification system which has been implemented is shown in Fig. 1. Basically, this coding system is composed of five elements:

- Without ring marks
- Single rings 25 mm apart ("Standard 25")
- Single rings 50 mm apart ("Standard 50")
- Double rings 25 mm apart ("Tandem 25")
- Double rings 50 mm apart ("Tandem 50")

The identifying details of the process are shown in Figure 2. The rings (single or double) are black. These black rings are combined with various fiber colors to create 48 clearly distinguishable identifications. The standard 13-color process is the starting point for the extended color-coding system.

As black rings are not clearly visible against gray, brown, violet and (naturally) black background, ring markings are not used with these colors.

Color Codes for up to 48 Fiber Counts

Color	Color without ring	Color with one ring Type 50	Color with one ring Type 25	Color with double ring Type 50	Color with double ring Type 25
red	1	13	22	31	40
green	2	14	23	32	41
blue	3	15	24	33	42
yellow	4	16	25	34	43
white	5	17	26	35	44
grey	6				
brown	7				
violett	8				
aqua	9	18	27	36	45
black	10				
orange	11	19	28	37	46
pink	12	20	29	38	47
uncolored		21	30	39	48

= not used

number = color code

Fig. 1 48-fiber color coding system

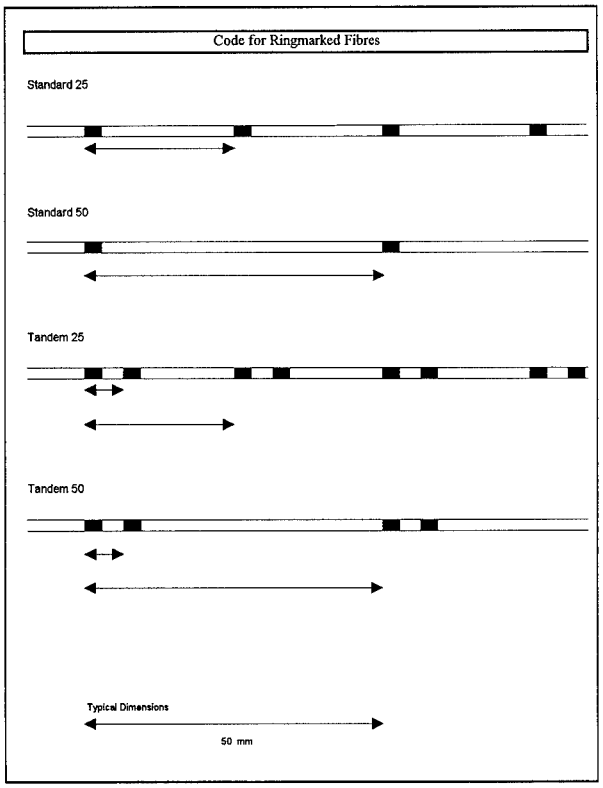


Fig. 2 Ring-marking codes

Ring Marking and Coloring Process.

The manufacture of the ring-marked colored fiber is done in two steps:

- Application of the single or double rings
- Inking of the ring-marked fiber

(Fibers that are not ring-marked go through only one inking step.)

The ring marking is performed using a spray technology in which ring width, spacing between the two rings within a double ring, and the interval between ring markings (single or double) are precisely controlled.

The thickness of the ring coating is between 0.5 and 0.8 µm. The inking is, in all cases, controlled to within 4 ± 1 µm.

Ring-marked colored fibers are of the same high quality as unmarked colored fibers. No optical, mechanical or geometrical differences between the two types are discernible. Both finished fiber products have the same surface properties and chemical surface inertness[1].

Fiber Test Results.

Three criteria must be met for ring-marked colored fibers to be acceptable for cable use:

- the ring-marked colored fiber must be as compatible with all cable elements, such as filling compounds, *etc.,* as colored fiber that is not ring-marked;
- the ability of fibers to move against each other when in close proximity in limited space (for example, in a high fiber count loose tube) must not be not impeded;
- the same behavior with regard to temperature cycling as for standard colored fibers must be guaranteed.

Solid-colored fibers without ring-marking and inked by the same process as reported here have been used in cables for several years with excellent performance. As stated in the previous section there is no discernible difference in the surface characteristics of the ring-marked colored fiber from the colored fiber without ring-mark. Thus,

with respect to the first two criteria above, there exists no immediate concern. With respect to temperature cycling, the changes in optical losses between -60 °C and +85 °C are shown in Figures 3 to 5
for unringed, single-ring and double-ring fiber, respectively. The attenuation changes are negligible. This good performance is confirmed in the complete cable , as reported further down. Ring-marked colored fiber as manufactured in our plant has, in addition, been evaluated with Light Injection Detection (LID) testing in the course of fiber splicing, tensile testing, macro- and micro-bending testing and so on. No negative influence of the ring marking has been observed[1].

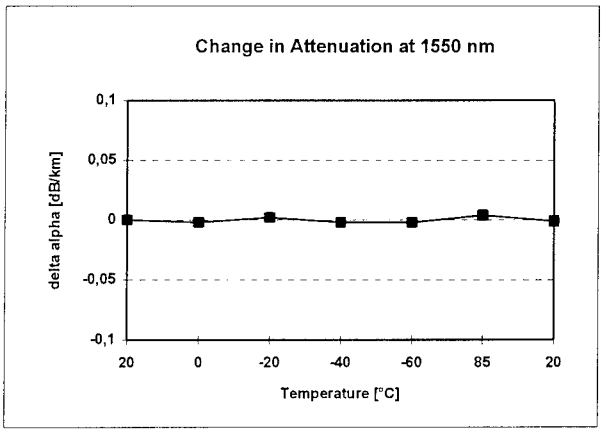


Fig. 3 Temperature cycling test on fibers without ring-marks

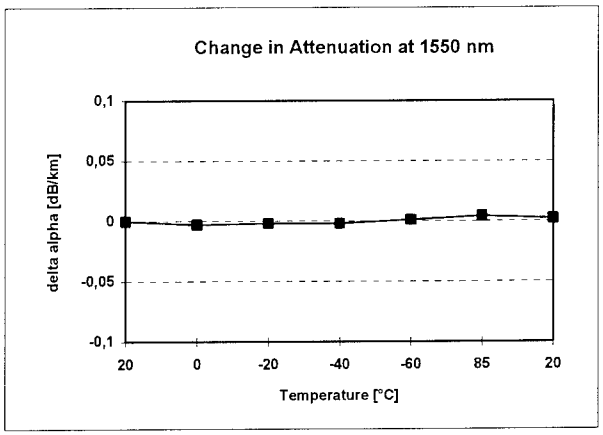


Fig. 4 Temperature cycling test on fibers with standard 50 mm ring-marks (ST 50)

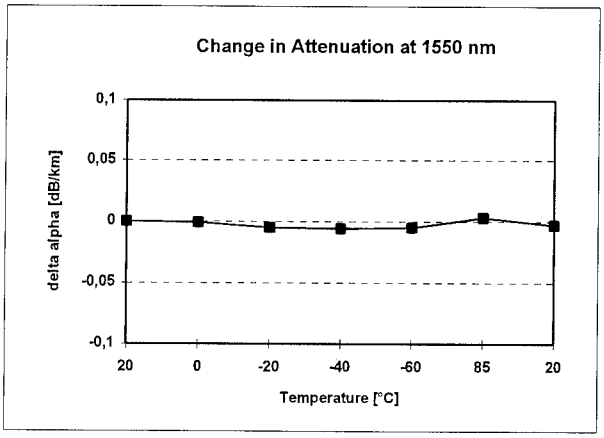


Fig. 5 Temperature cycle test on fibers with tandem 50 mm ring-marks 50mm (T 50)

Cable Applications for the new Color-Coding System.

The use of a color code for up to 48 fibers allows for very small tube dimensions. This is because no binders are necessary to distinguish one fiber bundle from another. Binders, which have been in use in some high fiber count loose tubes to separate fibers into groups of twelve, require extra space in the tube. Therefore the tube diameter is increased with the use of binders. The new color identification process in realizing very high fiber counts in comparatively low diameter tubes results in lower weight and lower diameter cables.

Cable Construction.

Optical Ground Wire (OPGW).

The relatively recent OPGW design which uses fibers in stainless steel tubes is one of the most rapidly growing types of cable construction[2,3,4,5]. Power utilities all over the world are expanding their telecommunication networks. OPGWs must have similar mechanical and electrical properties as the standard ground wire which they replace. This means that the allowed cable diameters are small. Maximizing the fiber count in the OPGW optimizes the capacity of the line.

Therefore, the aim is to get the highest possible fiber count per allowed cable diameter. As a result, the highest number of fibers in the smallest possible steel tubes is specified. The new color identification process reported here accomplishes this. A specially-designed and manufactured 96-fiber OPGW with two stainless steel tubes, each containing 48 fibers identified with the new color codes, is described. This cable design is illustrated in Figures 6 and 7.

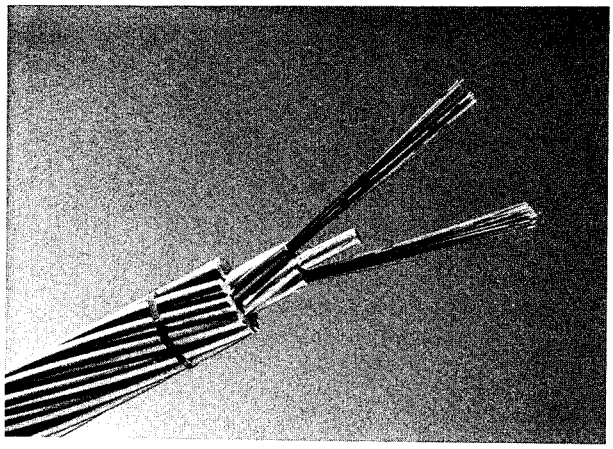


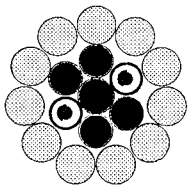
Fig. 7 Optical Ground Wire

Unitube Cable Construction.

For optical fiber cables with a central loose tube design the new color coding system provides equally the opportunity to implement very small tube dimensions for cables with up to 48 fibers. Cable designs utilizing a standard PE-jacket (metal-free design) with an overall diameter of less than 10 mm are easily realizable. Figure 8 displays the design of an outdoor 12 mm rodent- protected cable possessing considerable crush- and impact resistance. It consists of a PE-jacketed, laminated, corrugated steel strip with two embedded steel wire strength elements in the jacket design. This cable has a maximum allowable pulling strength of 2,700N and a maximum permanent allowable load of 600N.

96 - Fiber Optical Ground Wire

Type: **ASLH-D(S)bb 2x48E9/125 (Ay/Aw 138/50-14,7)**



Cable Design:

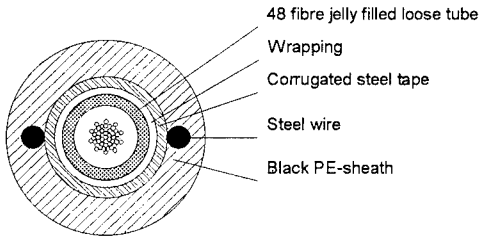
Center	3,75mm Aw-Wire
1. Layer	4 x 3,5mm Aw-Wire 2 Steel Tubes 3,0/3,4mm with 48 Fibers each
2.Layer	11 x 4,0mm Ay-Wire

Technical Data:

Diameter	: 18,1	mm
Weight	: 777	kg/km
Supporting Cross-Section	: 187,8	mm²
Ultimate Tensile Strength	: 104,7	kN
Young's Module	: 84,7	kN/mm²
Thermal Elongation Coefficient	: 18,0	10^{-6}/K
DC-Resistance	: 0,218	/km
Nominal Short Time Current	: 14,7	kA

Fig. 6 Optical ground wire with 96 fibers

Outdoor Cable with 48 Fibers



Cable diameter	12 mm
Cable weight, approx.	150 kg/km
Bending radius, min.	20 x D
Max. pulling load	2700 N
Crush resistance	3000 N/100 mm
Operating temperature range	- 40°C up to + 70°C

Fig. 8 48-fiber unitube cable for duct or direct-burial application

Cable Properties and Tests.

The fact that the attenuation of the fibers in a cable using this new process is not affected by the color-coding is of primary interest. It makes no difference whether the fibers are colored without rings, whether they are single-ringed with 25 mm or 50 mm spacing (ST25 and ST50), or double-ringed with 25 mm or 50 mm spacing (T25 and T50). None of these variations has any effect on the fiber attenuation in the cable. Figures 9 through 16 illustrate the statistical attenuation data for the different color codes through the cable manufacturing production steps as well as the results of temperature cycling of both the aerial (OPGW design, Fig. 6) and the buried (unitube, Figure 8 design) cables. The attenuation measurements show excellent results; they are totally independent of the type of individual color coding with the new color identification process.

Test Results: OPGW Design (Fig. 6).

After stranding the attenuation values were very close to those of the unmarked fibers. There is no discernible difference in attenuation between ring-marked fibers and colored fibers without ring marks (Figs. 9 and 10). The finished OPGW cable underwent a temperature cycling test of two cycles from -40 °C to +80 °C (Fig. 11). The average attenuation changes over this temperature range for both ring-marked fibers and colored fiber without ring marks were less than 0.008 dB/km. This shows that there is no effect on the attenuation due to ring-marking (Fig. 12).

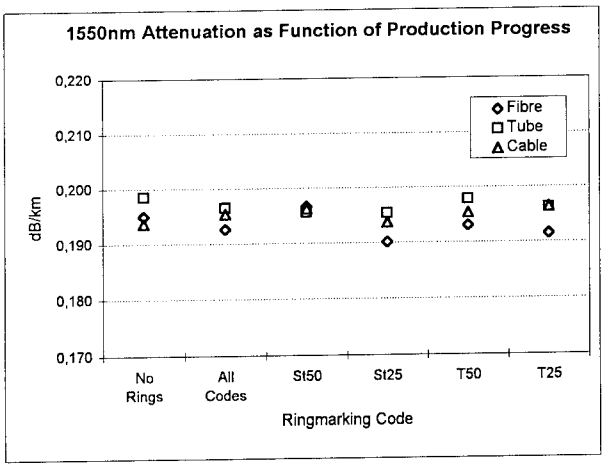


Fig. 9 OPGW with 2 x 48 Fibers, attenuation as a function of production status and color coding

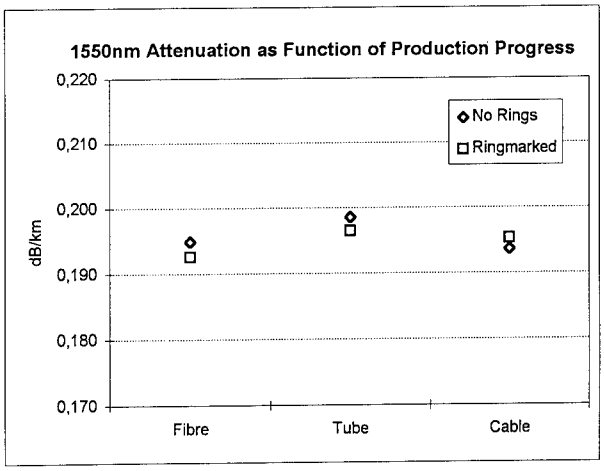


Fig. 10 OPGW, attenuation as a function of production status

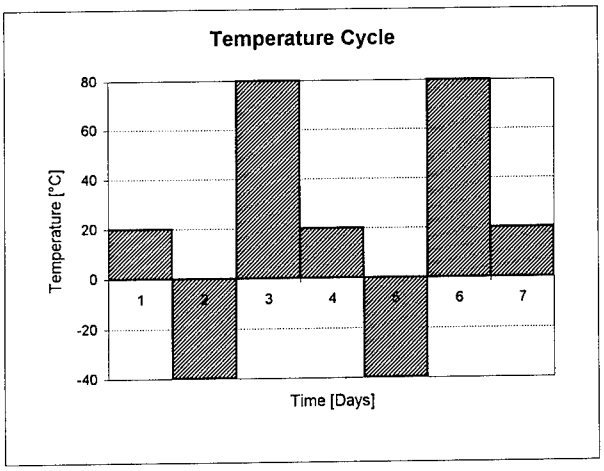


Fig. 11 OPGW: temperature cycling plan

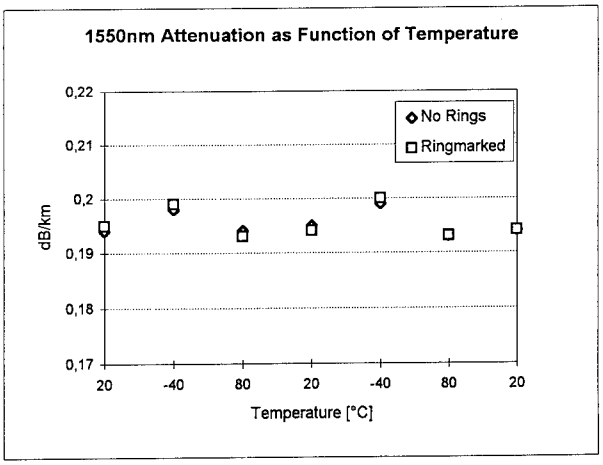


Fig. 12 OPGW: attenuation as a function of temperature

Test Results: Unitube Cable Design (Fig. 8).

The behavior of the unitube buried cable design was comparable to that of the OPGW. The attenuation decrease at lower temperatures is due to the slight variation in excess length of each of the 48 fibers in the tube (up to 0.05 % absolute difference). This length difference leads to micro-bending losses resulting from radial forces between the fibers. When the cable shrinks at lower temperature, the fibers are given more freedom of radial movement with decreasing fiber-to-fiber forces. Therefore, there is reduced microbending and thus less attenuation. The attenuation behavior of the ring-marked fibers when compared to that of fibers without ring marks, as is the case for the aerial cable (OPGW), is equally good with no measurable difference within the range of bi-directional OTDR accuracy. Figure 17 shows, in addition, the result of a tensile test which was performed on the unitube cable. The cable was tested up to the maximum pulling force of 2,700 N specified in the cable design, which corresponds to 0.2 % elongation. For the measurement of fiber strain and attenuation six ring-marked fibers were spliced together to give a total measurement length of 600 meters. The test result is excellent. This test result is no different than that of low fiber count, central loose tube constructions with fibers that are not ring-marked.

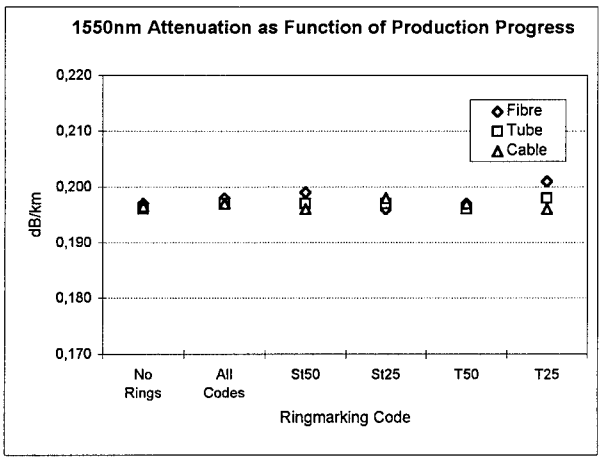


Fig. 13 48-fiber unitube cable: attenuation as a function of production status and color-coding

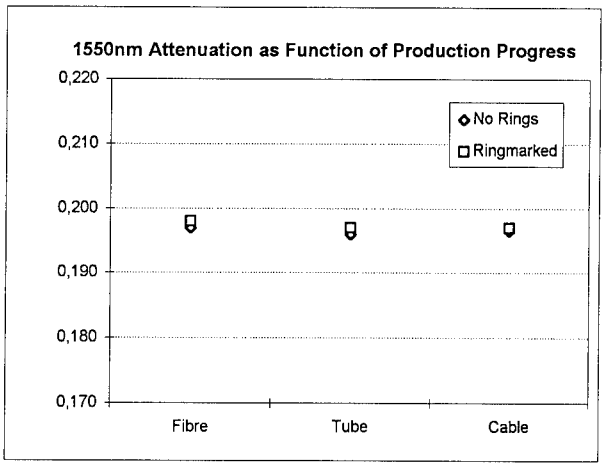


Fig. 14 Unitube Cable: attenuation as a function of production status

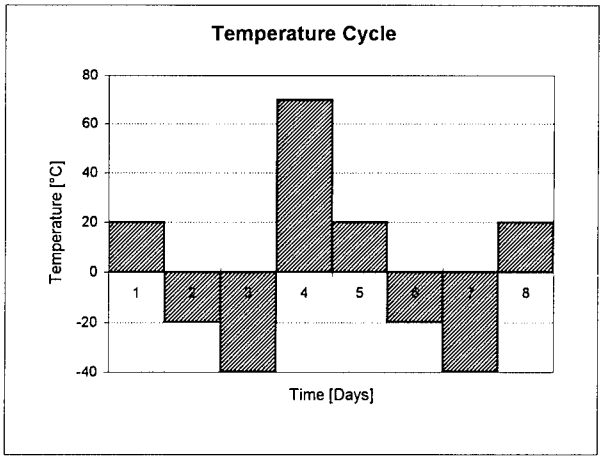


Fig. 15 Unitube cable: temperature cycling plan

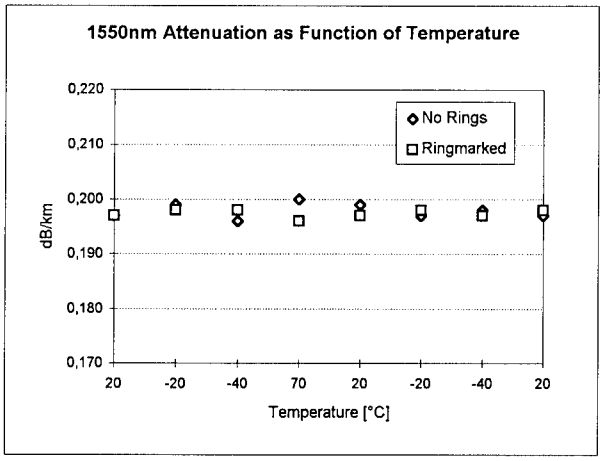


Fig. 16 Unitube Cable: temperature cycling test

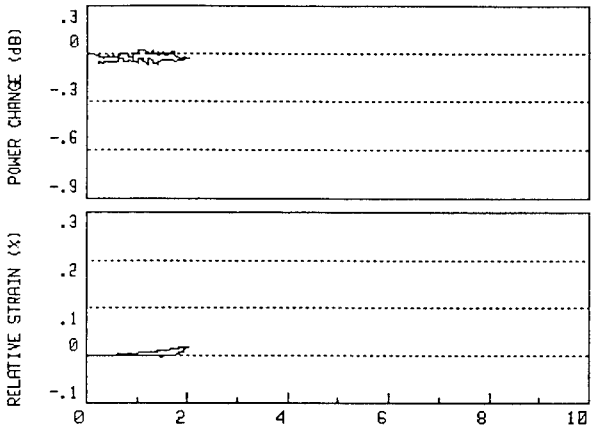


Fig. 17 48-fiber unitube Cable, fiber strain and cable strain at maximum pulling force

Summary.

The new fiber color-coding process reported here uniquely identifies up to 48 fibers in one loose tube without any need for additional identification binders or tapes. This leads to high fiber counts in comparatively low diameter tubes and lower diameter, lower weight cables. The manufacture of high fiber count buffer tubes with the new style color-coded fibers is as easy as that for low fiber count tubes with no special equipment needed to separate fibers into groupings. The attenuation characteristics of both steel tube OPGW (aerial cable) and unitube loose tube (buried cable) have been shown to be excellent for standard production cable, including temperature cycling. They are independent of the type of color coding used in both cable designs. There is no noticeable difference in attenuation between colored fibers without ring marks, single-ring-marked colored (25 or 50 mm spacing), or double-ring-marked colored (25 or 50 mm spacing) fibers. For cable designs which require large fiber counts in limited available space, such as for submarine cables and OPGWs, the new color coding system is an excellent solution for optimum space utilization. The 48-color coding process can be expanded to a higher count scheme if so desired in the future.

References.

1. G. Hög, H.G. Haag, *"Der Einsatz von Luftkabeln für die Telekommunikation im Spiegel der Zeit"*, Proc. ITG FA 6.7, Kommunikationsanlagen, Dec. 1994.

2. H.G. Haag, G. Hög, U. Jansen, J. Schulte, P.E. Zamzow, *"Optical Ground Wire and All Dielectric Self-Supporting Cable - A Technical Comparison"*, Proc. 43rd IWCS (1994) 380.

3. H.G. Haag, G. Hög, M. Hoffart, R.G. Sommer, J. Wienskowski, P.E. Zamzow, *"Self Supporting Optical Fiber Aerial Cable Construction and Related Fiber Parameters for the Transmission at λ = 1550 nm"*, Proc. 40th IWCS (1991) 206.

4. J.P.Bonicel, C.G. Cortines, J.C. Delomel, G. Hög, S. Pouilly, O. Tatat, P.E. Zamzow, *"Optical Ground Wire - A Worlwide Technical Survey and Comparison"*, Proc. 42nd IWCS (1993) 42.

5. R.G. Sommer, J. Rosenkranz, R.J. Overton, P. Dupont, *"Fiber Coating Strip Force Testing: Meaningfully Predictive?"*, Proc. EFOC & N '95 (1995), 241

Authors

Helmut G. Haag
KABEL RHEYDT AG
41048 Mönchengladbach
Germany



Helmut G. Haag (46) is Director of the Sales Division for Telecommunications. After reaching his Dipl.-Physiker-degree from the University of Stuttgart he joined KABELRHEYDT in 1975 for the development of coaxial cables. Later he has also been responsible for the development of optical cables. From 1980 to 1983 he built up the production plant for these cables. From 1984 to 1989 he has been responsible for the technical sales department. In 1990 he took over his present position.

Georg Hög
KABEL RHEYDT AG
41048 Mönchengladbach
Germany



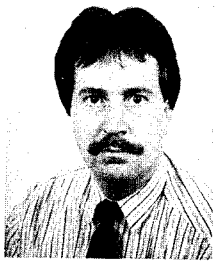
Georg Hög was born in 1950. After studying electronics at the Technische Hochschule Aachen he joined KABELRHEYDT as a development engineer for copper cables in 1977. In 1980 he became responsible for the development of symmetrical telecommunication cables. In this position he also was active in the standardization for copper cables for the German Telekom. In 1985 he became the head of the development for optical fiber cables. From 1987 to 1988 he was the head of the technical department of BETEFA (special cables for telecommunications). Since 1989 he returned to KABELRHEYDT where he was responsible for the development and construction department for optical fiber cables. Since 1995 he is responsible for the technical sales department of telecommunication cables. He is also responsible for the standardization of optical fiber cables for the DBP Telekom and he is a member in the standardization committees of VDE ETSI and IEC for optical fiber cables.

Bertram Glessner
KABELRHEYDT AG
41048 Mönchengladbach
Germany



Bertram Glessner was born in 1948. He received his Dipl.-Physiker degree from the University of Saarbrücken and joined the Optical Fiber Group of AEG KABEL (now KABELRHEYDT) in 1979. Since then he was responsible in various positions in the development and production of optical fibers. In 1990 he became head of the Administration Department of the Fiber Product Group. In 1995 he was promoted to Deputy General Manager of the group.

Klaus Nothofer
Kabel Rheydt AG
41048 Mönchengladbach
Germany



Klaus Nothofer was born in 1956. He obtained his Dipl.-Ing. degree from the Fachhochschule Düsseldorf and joined AEG KABEL (now KABELRHEYDT) in 1981 as development engineer for optical fiber cables. From 1984 he was responsible for the optical fiber cable manufacturing technology. In 1993 he became leader of the Optical Fiber Cable Design Group. He was appointed Manager of Optical Fiber Cable Development and Design in 1994.

Michael Hoffart
KABELRHEYDT AG
41048 Mönchengladbach
Germany



Michael Hoffart (39) is General Manager of the Optical Fibre and Optical Cable Plant. He received his Dipl.-Ing. degree from the Bergische University, Wuppertal in 1983. He joined KABELRHEYDT on graduation and has been engaged in the fields of optical measurement techniques and telecommunication cables.

NEW FIBER MONITORING SYSTEM WITHOUT FIBER SELECTOR

Chien-Chung Lee, Kuang-Yi Chen,
Feu-Yuan Tsai, Kuo-Hsiang Lai

Telecommunication lab.,Directorate General of Telecommunications,
Ministry of transportation and communication,Taiwan,Republic of China.

Abstract

We design a new fiber monitoring system(FMS) that can overcome the drawbacks caused by fiber selector in conventional FMS.This new FMS does not need to switch the optical path, so it can provide zero switching time and has no limitation for monitoring times. The new FMS experimental system in our lab. is able to monitor 32 fibers at one time, and has less than 0.5 second per line monitoring time and 0.2 dB loss detection sensitivity.

1. Introduction

Fiber monitoring system(FMS) is an operating system that supports the maintenance of optical fiber line. FMS monitors active optical line by using different wavelength light with transmission system. Conventional FMS, as shown in Fig. 1, consists of measurement module、fiber selector module and optical wavelength division multiplexing module. By controlling fiber selector module, conventional FMS is able to switch the monitoring light path to the wanted optical fiber line. However, the finite switching lifetime of fiber selector limits FMS monitoring times, and the several ten milliseconds switching time causes conventional FMS to have a slow monitoring speed. Therefore, conventional FMS is unable to take the real-time and all-time fiber monitoring task.

In this paper, we propose a new FMS design that can overcome the above drawbacks, and we present its measurement principle and the experiment results.

2. System Design

This new FMS, as shown in Fig. 2, consists of optical branch module、WDM module、fiber monitoring module and fiber fault locating module. The function of every module is described as follows:

Optical branch module

Optical branch module provides point-to-multipoint optical path, which allows monitoring light to inject into several ten optical fiber lines at the same time. Its schematic diagram is shown in Fig. 3. The 1x32 splitter provides point-to-multipoint optical path and allows FMS to monitor 32 fiber lines at the same time. When we want to locate the fiber fault, we terminate other normal fiber lines by controlling the variable benders. The WDM module in optical branch module allows the different wavelength monitoring light to inject into fiber system.

Fiber monitoring module

Fiber monitoring module is able to monitor several ten fiber lines at the same time. It uses short optical pulse to probe fiber lines, and measure the fiber line loss by reflection signal. Because every fiber line has different time delay reflective signal, fiber monitoring module can measure the losses of all fiber lines by detecting their reflective signals.

Fiber fault locating module

When fiber fault happens, this FMS will terminate the other normal fiber lines by controlling the optical branch module and start fiber fault locating module to find the fiber fault location. Fiber fault locating module probes the fiber lines by using long optical pulse. It detects backscattering signal and locates the fiber fault.

WDM module

The far-end WDM module stops the monitoring light into the transmission system. It also generates different time delay reflective signal for different fiber line. Therefore the new FMS can identify fiber line and measure each fiber line loss.

3. Measurement principle

The fiber monitoring and fault locating flow chart is shown in Fig. 4. The considerations for measurement are described as follows:

(a) fiber line loss monitoring

We measure the fiber line loss by using optical time domain reflectometry method. We use different time delay reflective pulses to mark the individual fiber lines. The far-end reflective pulse height variation represents the loss variation of the fiber line. When the reflective pulse reduces

its pulse height or even disappears, we know that the fiber line loss is increased or the fiber line is broken. Line loss(L_{system}) can be shown as follows:

$$L_{system} = DR_{4\%} - H_p - 0.5 \times (R - 14), \quad (1)$$

where H_p=pulse height,
R=far-end return loss,
$DR_{4\%}$=4%Fresnel reflection dynamic range.
$DR_{4\%}$ can be calculated as following formula.

$$DR_{4\%} = DR_B + 0.5 \times (14 - BL), \quad (2)$$

where DR_B=backscattering dynamic range,
BL=backscattering level.

If we detect out 1 dB pulse height variation, the fiber line loss also has 1dB variation. Therefore, we can monitor each fiber line loss. When measurement dynamic range is not enough, we can adjust return loss R and do not need to increase pulse width for larger $DR_{4\%}$.

(b) Fiber fault location

We use fiber backscattering signal to detect the fiber fault position. If the fiber fault happens in the fiber line, the loss shown on backscattering signal trace will be less than the true loss. The measured loss(L_{OTDR}) in N branching fiber line can be shown as the function of true loss(L_{true}) as follows:

$$L_{OTDR} = -10\log\left(\frac{N-1}{N} + \frac{1}{N} \bullet 10^{Ltrue/10}\right), \quad (3)$$

If 1XN branching splitter has unequal splitting ratio, L_{OTDR} will change measured loss to L_{OTDR} +d L_{OTDR} and d L_{OTDR} can be shown as following formula.

$$dL_{OTDR} = \frac{10}{\ln 10} \bullet 10^{-L_{OTDR}/10} \bullet \frac{(1 - 10^{-L_{true}/10})}{N^2} \bullet dN, \quad (4)$$

where dN=ratio difference,

$dN=(10^{dU/10}-1) \cdot N$,

dU=uniformity in dB.

If the fiber line has 1dB loss, there is only 0.11dB loss shown on backscattering signal trace for 8 branching lines. If the uniformity dU is 1.5dB,then d L_{OTDR} is about 0.04dB.

(c) Loss measurement error

When we use reflective pulse to detect fiber line loss, the measurement errors come from the pulse height linearity and receiver noise. Normally, the pulse height linearity is less than ±0.05dB/dB. If we intend to detect 10 dB loss variation, the linearity error will be less than 0.5 dB.

The pulse height linearity noise(Np) can be shown as the function of signal-to-noise-ratio(SNR) as follows:

$$N_p = 5\log(10^{-SNR/5} + 1) \quad (5)$$

For 10dB pulse height, the pulse height noise is about 0.02dB. If the fiber line loss increases 1dB, the possible maximum total detection error is about 0.07dB. Therefore, we can detect fiber line loss variation precisely by proper pulse height value.

4. Experimental results

We set up the new experimental FMS with a 32-optical branch module in our lab..It uses 1550nm wavelength light as the monitoring light. The experimental results are as follows:

(1) Dynamic range

The dynamic range measurement set up is shown as Fig. 5. The 1550nm dynamic range of this experimental FMSs can reach 14dB for real-time detection and 18dB for 50s average detection by 1.95dB far-end return loss setting.

(2) Reflective pulse height linearity

The pulse height linearity for this new FMS is shown in Fig. 6. When the reflective pulse is too high, the receiver of FMS will be saturated and distort the linearity. So we have to controll far-end return loss carefully. The pulse height linearity of this new FMS is better than 0.05dB/dB.

(3) Loss detection sensitivity.

We control far-end return loss and average times to keep SNR larger than 5dB for this new FMS. The result is shown in Fig. 7. The fiber line loss monitoring deviation is less than 0.07dB. So we can easily detect out 0.2 dB line loss variation and the loss detection sensitivity is better than 0.2dB. The loss deviation becomes large when pulse height is small. Therefore the high detection sensitivity will cause the effective dynamic range decreasing. The monitoring speed for real time loss monitoring depends on program execution. This new FMS in our lab. can reach 0.5 second per line.

(4) Fiber fault location

The fiber fault loss will be less than true loss when branching lines are larger than 1. We use 1550nm optical light to detect 1300nm transmission fiber system. 1550nm optical source is more bending sensitive than 1300nm optical source. So we still can detect fiber fault when using large branching lines. When detection fiber line number is increased, the fiber fault loss will become small as we describe in Eq.(4). For 0.13dB fiber loss by 1310nm,we detect 1.56dB by 1550nm, 0.41dB for 3 lines and 0.70dB for 2 lines. Therefore when locating the fiber fault, we terminate the other normal fiber lines by controlling variable benders to increase small fault loss locating ability. In our experimental FMS, it is easy to locate 0.1dB 1310nm fiber fault.

5. Conclusion

This proposed FMS,which does not need to switch the optical path, can monitor optical fiber line very fast and provide all-time fiber monitoring. This experimental system is able to monitor 32 fiber at one time, and has less than 0.5 second per line monitoring time and 0.2 dB loss detection sensitivity. It is very suitable and useful for fiber monitoring task.

Reference

1. Ray savich and Marvin D.Ashby,"Testing and troubleshooting the passive branching plant",Lightwave, Oct.1993.
2. Ofred scheu,"Testing fiber in the loop ",Lightwave,Oct.1993.
3. Chien-Chung Lee and Kuang-Yi Chen,"Optical Fiber Monitoring Systems for Passive Optical Networks",IWCS 1994,pp494-498.

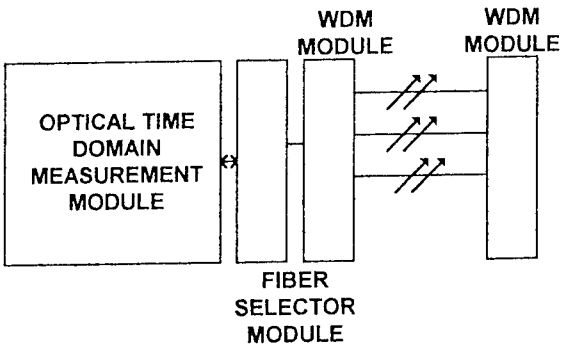


Fig. 1 The schematic diagram of the conventional fiber monitoring system

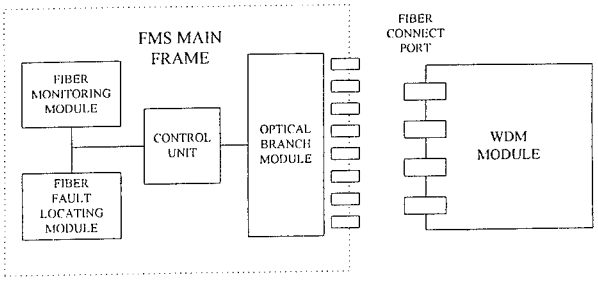


Fig. 2 The schematic diagram of the new fiber monitoring system

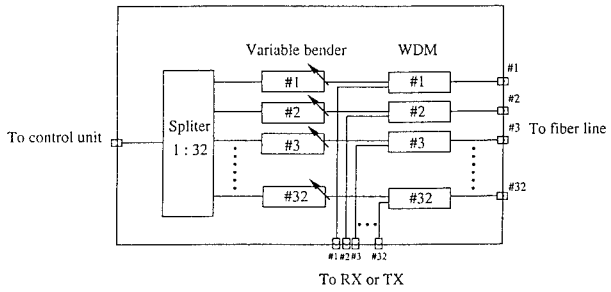


Fig. 3 The schematic diagram of optical branch module

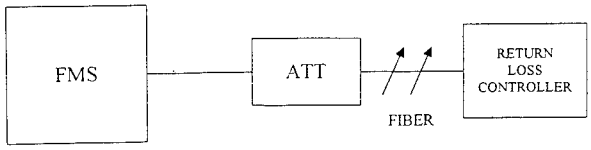


Fig. 5 The set up of the dynamic range measurement

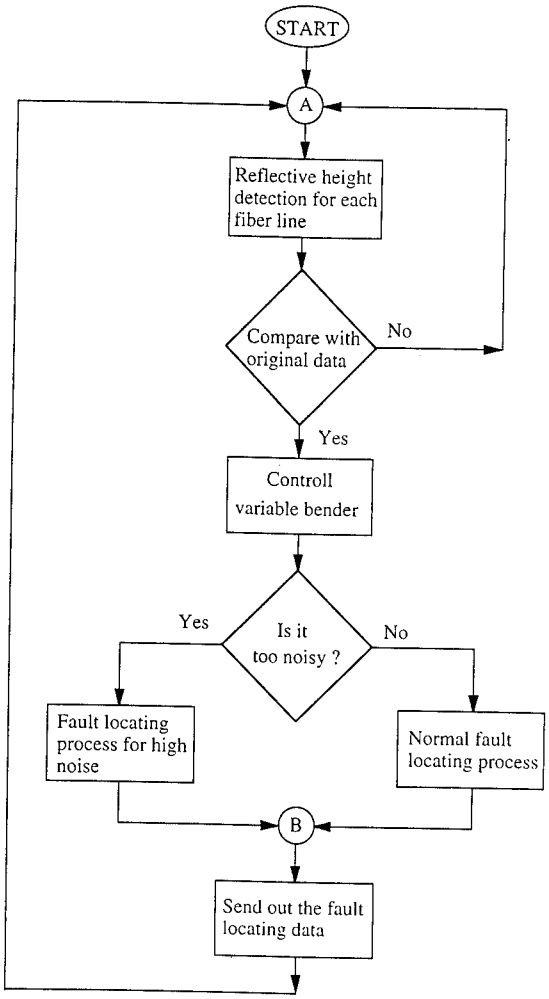


Fig. 4 The fiber monitoring and fault locating flow chart

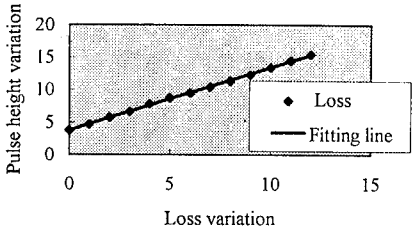


Fig. 6 The pulse height linearity of the experimental FMS

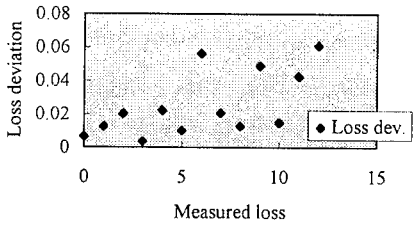


Fig. 7 The monitoring loss deviation for this experimental FMS

DEVELOPMENT OF A HYBRID LOOSE TUBE CABLE AND ITS FIELD TRIAL RESULTS

Paul F. Armbruster II, James Thornton

AT&T Fitel Company, Carrollton, Georgia

Abstract

A hybrid loose tube cable that contains both single mode fibers and copper conductors was developed which replaced the need for a separate power cable and communications cable. Environmental and mechanical testing was conducted in accordance with REA PE-90 and the appropriate Fiber Optic Test Procedures (FOTP) for this cable and it met or exceeded all of the requirements. During the development and field trial, a number of issues were resolved. These included accommodating copper conductor and fiber splices and the effect of the conductors on cable performance.

Introduction

As more optical subscriber systems are being deployed in rural areas, a hybrid loose tube optical fiber cable has become desirable. The hybrid loose tube cable that was developed for the rural subscriber application contained #16 AWG copper conductors that had the capability to power the transmission system. By combining both the optical fibers and the power conductors into one cable, the need to rely on the local power could be eliminated. The hybrid loose tube cable provided better protection for the power circuits than two separate cables. The corrugated steel armor was applied around the cable core improving the mechanical parameters and the overall protection of the copper conductors. This paper presents the design, performance, application, installation and field trial of a hybrid loose tube cable designed for rural applications.

Design Application

The existing rural exchange designs are quickly becoming obsolete. Greater bandwidth and higher data speed transmissions are necessary to support current and future customer equipment. The existing analog station carrier with its deteriorating air core cable plant will not support future services such as Asymmetrical Digital Subscriber Line (ADSL), High Bit Rate Digital Subscriber (HDSL), or Integrated Service Digital Network (ISDN). These (and other) higher bandwidth technologies will be more widely deployed in the future.

New designs, utilizing optical fiber technology have been the solution to these issues in the subscriber loop and the Rural Fiber Network. The introduction of electronic equipment capable of serving rural subscribers with optical fiber facilities has been developed by several manufacturers in the past few years. The designs utilize wideband capabilities of fiber optic systems and existing copper distribution concepts. These systems use a basic 24 channel Digital Loop Carrier (DLC), some with multiplexing capabilities to serve up to 192 subscribers. The DLC equipment has a fiber interface toward the central office and a copper interface toward the subscriber. The various systems employ fiber transport ranging from a single fiber for short systems, to multiple fibers for longer systems. The systems may be either protected or non-protected depending on local requirements.

One of the problems that needed to be addressed was one of providing reliable power to the Digital Loop Carrier (DLC) distribution sites, while maintaining the level of dependable service that is expected in the traditional copper loop. The Remote Terminal sites require a considerable amount of power, so commercial AC power with battery backup and emergency generator receptacle is necessary. The Serving Area Interfaces (SIA), however, require relatively low power consumption (as little as 40 Watts), and could be powered from the Remote Terminal. (See fig. 1).

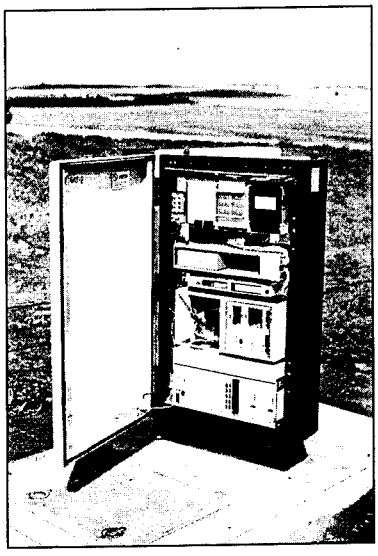


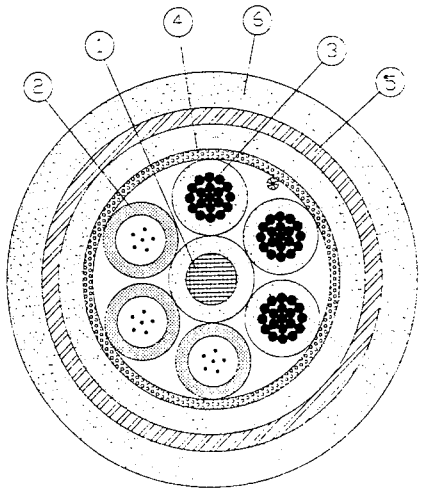
Figure 1 - Serving Area Interface

There were two options to providing this reliable network power to the SIA's. The traditional method was to place two cables, one copper and one optical fiber. The second, to develop a hybrid cable, that contains both optical fiber and copper conductors, under one sheath. Studies by Finley Engineering Company Inc.,[1] showed that the cost (labor and materials) and environmental impact (on minimizing of farm land damage) favor the innovative hybrid cable approach. Projected savings based on the hybrid cable were nearly $200,000 on the field trial alone.[2]

The REA, the Engineering firm, and the end users, jointly decided that a hybrid cable be designed for a field trial, that would provide optical fiber and remote power to SIA sites on a new rural fiber distribution system in the midwest. The particular installation utilized the AT&T SLC Series 5 and SLC 2000 transmission systems.

Cable Design

The hybrid cable design was developed to meet the need for network power for cable electronics. Currently, electronics need either local power provided by a customer (via the electric utility) or network power provided by the telephone company's cable network. Our cable design is a loose tube design that includes optical fibers and metallic conductor(s). The hybrid cable design replaces one or more of the buffer tube positions with an insulated conductor(s). Because the metallic element is similar to a buffer tube in size, the hybrid cable's size and performance is the same as cables that do not contain copper conductors. The copper conductors do add to the cable weight compared to buffer tubes and/or filler rods.



1 : Dielectric Central Member
2 : Buffer Tubes Fiber
3 : Insulated Conductor
4 : Aramid Yarn
5 : Steel Armor
6 : Polyethylene Jacket

Figure 2 - Core Cross-section

The core construction of the hybrid cable design consists of buffer tubes, metallic insulated conductors, binder thread, and a dielectric central member that is upjacketed with polyethylene. Reverse oscillating lay (ROL) stranding is used to strand the buffer tubes and metallic conductor(s) to the jacketed central member. The buffer tubes and cable core are fully filled with gel to prevent water ingress and migration. The core is wrapped with several ends of Aramid yarn for good pulling grip and tensile performance. An inner jacket of polyethylene is applied to protect the core. Corrugated steel armor is formed over the inner jacket and a jacket of polyethylene is applied to form an outer sheath.

The hybrid cable offers lower cost, easier installation and improved reliability. This is because this design will eliminate the need to bury a separate power cable (to be buried with the fiber cable) to provide network power. The steel armor will also provide excellent rodent protection which many power cables do not.

Cable Performance

In order to qualify the Hybrid cable design, a trial cable was manufactured for the purpose of testing. The trial cable was a double jacket, dielectric central member, 8 position cable with 2 buffer tubes with 6 optical fibers each, and 6 x 16 gauge copper conductors. The trial cable was also constructed with Aramid yarn and steel corrugated tape. The trial cable was subjected to the environmental, material and mechanical qualification tests per REA PE-90[3] and related FOTP tests. In general, the trial cable performed well during mechanical and environmental tests with no evidence of mechanical weakness or attenuation increase. The cable meets or exceeds all REA PE-90 and related FOTP specifications.

Mechanical Testing

The trial cable passed all related FOTP and REA PE-90 specifications for mechanical testing. The cable tensile test result is noteworthy due to its high performance. The cable specification for tensile test is 600 lbs with no fiber strain. The hybrid cable performed better than this and went to 1400 lbs with no fiber strain. This is attributed to the added tensile strength afforded to this design by the metallic insulated conductors. The following is a summary of the mechanical test results:

Test Performed	Performance	Test Procedure
Cable Bend	-20 C for 24 hrs., 202mm mandrel, 1 = 1274 m	REA PE-90
Jacket Adhesion	avg. force 21.59 N/mm of circumference	FOTP-84
Low/High Temp.	-30 C to +60 C 0.01 dB change	FOTP-37
Impact Resistance	25 impacts, 9 kg mass -0.04 dB change	REA PE-90
Compressive Strength	440 N/cm after release of load, no residual loss	FOTP-41
Cable Twist	10 cycles, 1.7 m, -0.01 dB change, no damage	FOTP-85
Cyclic Flex	100 cycles, 300 mm, -0.01 dB change	FOTP-104
Cable Tensile Test	0.00% fiber strain @ 1400 lbs.	FOTP-33

Table 1 - Mechanical Test Results

Environmental Testing

The trial cable passed all related FOTP and REA PE-90 specifications for environmental testing. The following is a summary of the environmental test results:

Test Performed	Performance	Test Procedure
Temp. Cycling	Temp. -40 +70 @ 1550 nm Max: 0.02 0.02 dB/Km Avg: 0.01 0.01	FOTP-3
Cable Aging (7 days, 85°C)	Temp. -40 +70 @ 1550 nm Max: 0.03 0.02 dB/Km Avg: 0.01 0.01	Bellcore GR-20, Issue 1
Water Penetration	1 meter/1 hour, avg pen 5cm 1 meter/24 hours, avg pen 3cm	FOTP-82
Compound Flow	3/3 showed no drip @ 80°C	REA PE-90
ESC	10/10 showed no evidence of cracking after 7 days @ 50°C	REA PE-90
Melt Flow	0.71 g/10 min, 8.5% increase from incoming material	REA PE-90
Jacket Shrinkage	Avg. shrinkage 0.3% after 4 hours at 115°C	REA PE-90

Table 2 - Environmental Test Results

Field Trial Installation

The installation of the trial hybrid cable was a direct buried one. A cable plow train was used to place the cable directly into the ground. In some areas, the soil was pre-ripped with a tractor using a ripper blade to aid the cable plow by opening the soil in front of it. (See fig. 3).

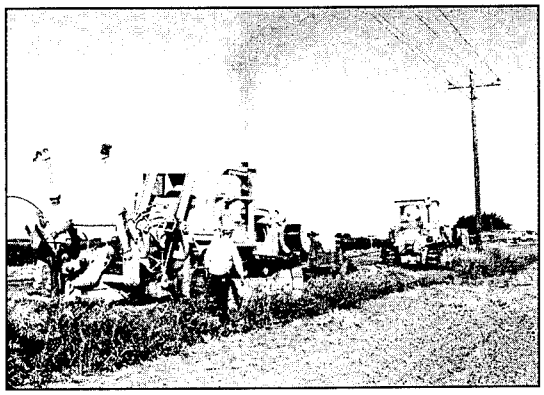


Figure 3 - Cable Plow Train

Although the copper conductors slightly increased the weight of the cable, the diameter was not affected, and cable handling was identical to standard optical fiber cable. The installation crew indicated that during the entire trial (over 100 Km) installation was normal with no problems encountered. "Figure eighting" the cable onto the ground, (before pulling through an obstacle), went smoothly. (See fig. 4).



Figure 4 - Making A "Figure 8"

Cable Splicing

Splice Closures

Standard "off the shelf" splice closures for optical fiber splicing are available that provide ample space for splicing

and storage of both copper and fiber. The splice closure chosen for the field trial was a six and a half inch diameter stainless steel closure, that is split longitudinally in half. Cables enter through one endcap, and a series of fastening nuts provide the environmental sealing once the splicing is complete. Typically used to store multiple optical fiber splices in a stacked tray configuration, the closure provides enough area to accommodate the copper conductors.

Optical Fiber Splicing

Cable end preparation for splicing was accomplished by accessing the ripcord under the armor, and pulling to the desired length. Once the jackets were removed, the flooding compound was cleaned from the conductors and buffer tubes with an approved cable cleaner. Standard shield bond connectors (supplied with the splice closure) were attached to the sheath armor, and the cables were fastened into the closure. The buffer tubes were removed and attached to the splice trays. Copper conductors were easily routed out of the way for splicing later.

Optical fiber can be mechanically spliced or arc fused together. Both of these methods are well established. The method of optical fiber splicing chosen for the trial cables was arc fusion. Both Profile Alignment System (PAS) and Local Injection and Detection (LID) Fusion Splicers were used to obtain high quality fusion splices. Optical fiber splice losses averaged well below the Engineers specification of .20dB average per fiber. Heatshrink splice protectors were placed over the optical fiber spliced and placed into the fusion splice tray.

Copper Conductor Splicing

Most of the copper splices were a direct one to one butt splice. A crimpable connector with a heat shrinkable protective insulator was chosen as the most effective means to splice the conductors. Copper conductors were stripped and placed into the splice and crimped together using a recommended crimping tool. Using the crimping tool, the craft applies the correct amount of force each time, to ensure consistent results. After the crimp is made, a heatgun is used on the splice which activates the encapsulating epoxy. (See fig.'s 5 and 6).

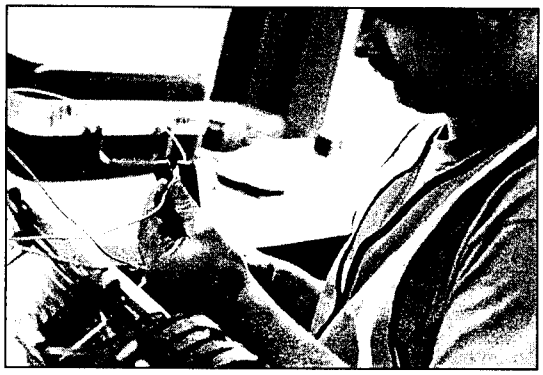


Figure 5 - Crimping The Copper Splice



Figure 6 - Activating The Epoxy Heatshrink

Where more than two copper conductors were to be spliced, the twist and solder technique was used. Heat shrink protection was applied to the splice to ensure insulation from moisture. Conductors were resistance tested before and after splicing, to ensure their integrity. Copper splices were conveniently stored on the inside endcap, secured with a fastening tape that is provided with the splice trays. (See fig. 7).

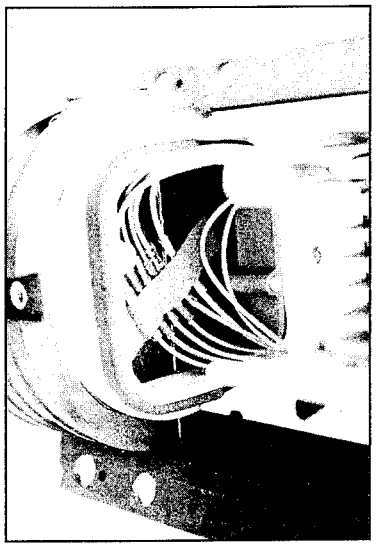


Figure 7 - Copper Splices

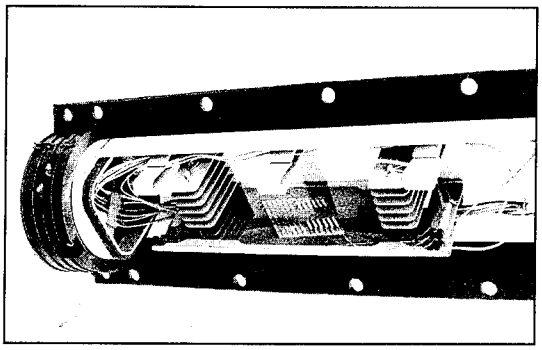


Figure 8 - All Splicing Is Complete

Conclusion

A hybrid cable design has been developed that meets REA PE-90 specifications and FOTP procedures. The design met or exceeded all performance requirements of REA PE 90.

Acknowledgment

The authors gratefully acknowledge Finley Engineering for their important contributions to this product development and paper. Roger Toedter is acknowledged for his efforts in beginning this project.

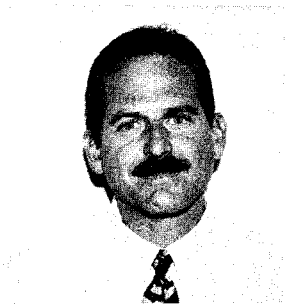
References

1. Finley Engineering Company, Inc., "Composite Cable and Design Reports" May 1993.

2. Ibid. "Rural Fiber Network Design Considerations." April 1993.

3. REA PE 90 (1986), etc.

Biographies



Paul F. Armbruster II
AT&T Fitel Company
Carrollton, Georgia

Paul F. Armbruster II is Senior Field Service Engineer with AT&T Fitel. He is responsible for product support and field service in the CATV, independent telephone company and competitive access provider markets. Mr. Arbruster has more than ten years experience with the installation, splicing and testing of optical fiber cable systems and is a member of the Society of Cable Telecommunications Engineers.



James Thornton
AT&T Fitel Company
Carrollton, Georgia

James Thornton is a Design Engineer in The R&D Department at AT&T Fitel in Carrollton, Georgia. Since joining the company this year, he has been responsible for the development of Fiber Optic Cable. He has a Bachelor degree in Mechanical Engineering from the Georgia Institute of Technology.

OPTICAL PASSIVE COMPONENTS : A WORLD WIDE SURVEY AND CHARACTERIZATION FOR FITL APPLICATIONS

C. BASTIDE[1], O. STEMPFEL[1], G. BOURRAT[1], G. COUVRIE[1], M. GADONNA[2], J. C. HEDE[2]

[1] ALCATEL CABLE-OFCCC, FRANCE
[2]FRANCE TELECOM - CNET, LANNION, FRANCE

Abstract

The deployment of optical access networks requires the availability of optical passive components as connectors, couplers... For these applications, there is particular requirements in term of optical characteristics, environment and reliability performances. This paper presents the preliminary results of an evaluation of some optical passive components. This work includes couplers, wavelength multiplexers (WDM) and angled connectors.
In this paper, the optical measurements and the preliminary results on environmental tests are given. The first conclusion shows that the choice of the technology will depend on the requirements, for example, the isolation level for WDMs. Also the results show for the same technology, the performances are different according to the manufacturing process.

1. Introduction

Fiber Into The Loop (FITL) systems are expected to be widely deployed in many countries to deliver existing telecommunication services as well as video services to residential and small business customers. Deployment of the fiber in the local loop will require passive optical components with particular characteristics for optical performances, environment, reliability and cost. The key components include inter-connecting devices, splitters and WDMs. Interconnecting devices as connectors and splices must have low insertion loss (IL) and often a high return loss (RL) is required ; they must be easy to install and to use. The splitters allow sharing of expensive hardware. WDMs increase the transmission capacity.
The life time of the systems is expected to be between 20 to 25 years. Various environmental conditions could be encountered, sometimes very hard with a high humidity level. The components used must prove to be of good quality and reliability and to meet the targets. In order to demonstrate the long term capability of the devices to perform their function, they must pass a comprehensive reliability test program which attempts to duplicate the stresses the components would experience over a 20-year operating life. The reliability tests take a long time and are costly. A selection of tests, measurements and technical analyses will allow an evaluation of the technologies and the designs. The aim of this paper is to present the preliminary results of the evaluation of some components of each type : angled connectors, splitters and WDMs. This paper includes :

- an overview of the optical passive component technologies,
- the optical performances and tests required versus international standards,
- the measurements and test results,
- the main conclusions from the results.

2. Splitters and WDMs

2.1. Technologies of couplers and WDMs

They are classified into three major types : bulk, fused-fiber and waveguide.

2.1.1. Bulk type

This technology is attractive for multimode fiber components. The positioning of the micro-optical elements are much more critical for single mode fiber and the detrimental effects of lens aberrations are significant.

Advantages :
- good directivity and isolation
- easy to make WDM/WDDM (grating, prism, filter, thin film,..)

Drawbacks :
- high insertion loss
- big volume
- pigtailing
- vibration behaviour
- alignment

2.1.2. Fused-fiber type

Fusion has proved to be the simplest, most versatile and efficient technology allowing the industrial implementation. Fibers are heated by a flame or by an electric discharge and are simultaneously pulled : fibers are fused together. In the tapered part, the distance between cores in fibers becomes close and non negligible coupling takes place between the cores ; this coupling produces the directional coupler.

Advantages :
- low insertion loss
- low return loss
- good thermal stability

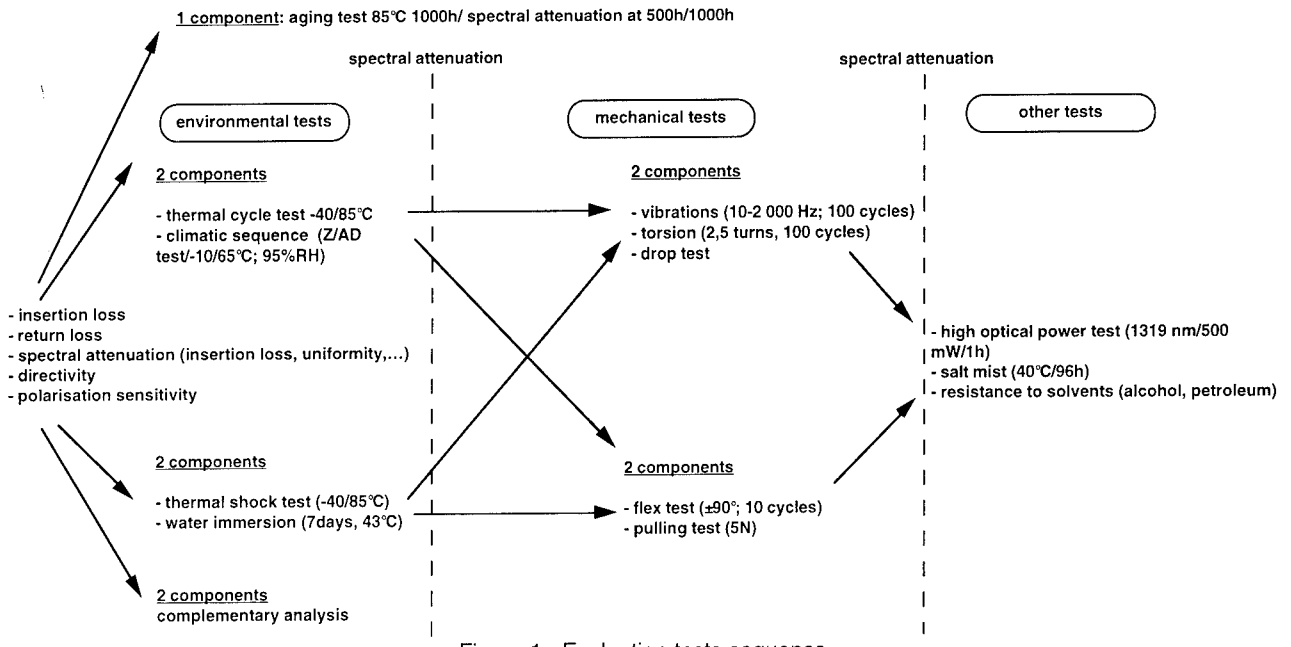


Figure 1 : Evaluation tests sequence

Drawbacks : - non achromaticity,
- difficulties for high splitting ratio (monolithic components only up to 7 ports today),
- uniformity for high splitting ratio (specially for monolithic components),
- low directivity (for WDDM).

2.1.3. Integrated optics

Passive components based on integrated optics (IO) available today are made with two main manufacturing processes. The first one consists in making waveguides by ionic diffusion in glass. The second one is based on the formation of waveguides of silicon or silica substrate by several processes, such as flame hydrolysis deposition (FHD) or chemical vapor deposition (CVD). The fiber pigtailing design and process is very important for the performances and the reliability of integrated optics components.

Advantages : - achromaticity
- reproductibility
- high splitting ratio (up to 32)
- easy to industrialize
- small size for high splitting ratio

Drawbacks : - difficult pigtailing
- thermal behaviour
- insertion loss

2.2. Test program

The splitters tested are 1X16 or 2X16, wavelength independent couplers (1260 nm - 1600 nm). The components were from 11 suppliers, 3 for integrated optics technology and 8 based on fused biconical taper design.
The WDMs are 1310 nm/1550 nm multiplexers. Two technologies have been selected : fused biconical taper (FBT) and filter based design with bulk optics or integrated optics. In order not to disclose the names of the manufacturers, they are identified as A, B, C, ...K.

The test sequence (figure 1) is divided into 4 parts :

- optical characteristic measurements,
- environmental tests,
- mechanical tests,
- aging test.

2.3. Evaluation results on splitters

Couplers A, B and C are integrated optic couplers ; the others are FBT couplers.

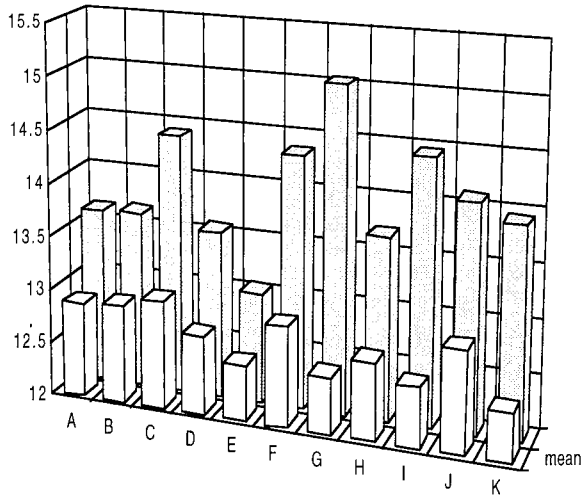


Figure 2 : splitters insertion loss (dB for the different suppliers, mean and maximum values)

2.3.1. Insertion loss

Insertion loss (IL) is measured versus wavelength (spectral attenuation) or at 2 wavelengths with laser diodes at 1310 nm and 1550 nm. Figure 2 represents insertion loss (mean and max. values) at 1310 nm. We can see that the mean of IL is nearly identical to all of the designs and is around 12.7 dB at 1310 nm and 12.9 dB at 1550 nm.

The high maximum value for design G is due to one component. For all other designs, the maximum IL is lower than 14.5 dB.

2.3.2. Wavelength dependence

Wavelength dependence is calculated from spectral attenuation measurements : U= ILmax. - ILmin. Figure 3 represents the wavelength dependence in the range 1270 nm - 1350 nm.

The device H has shown very high uniformity in the two windows.

All IO designs have shown a uniformity near or lower than 1.5 dB.

Uniformity for some FBT couplers was lower than 2 dB in the second window and lower than 2.5 dB in the third window (1450 nm - 1600 nm).

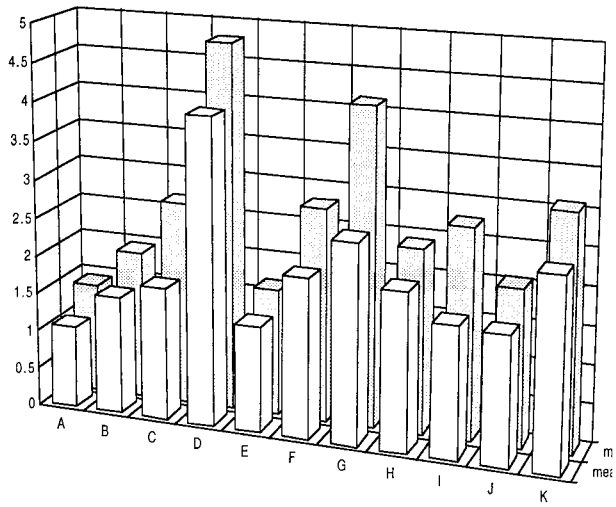


Figure 3 : splitters wavelength dependance (dB for the different suppliers, mean and maximum values)

2.3.3. Return loss

Return loss is measured at 1310 nm and 1550 nm by the coupler method (optical continuous wavelength reflectometry, OCWR). Results are similar at both wavelengths. For both wavelengths, RL is higher than 60 dB, except for 2 splitters A and D (>55 dB).

2.3.4. Polarisation sensitivity

IL changes are measured versus states of polarization using fiber loops. For devices from suppliers A, B, D, E and G, the polarization sensitivity has been found to be lower than 0.1 dB at 1310 nm; for A, B, E, and G, it is still lower than 0,15 dB at 1550 nm. In other cases, these values have been found higher than 0,2 dB with some values around 0,5 dB.

2.3.5. Aging test

One component of each supplier is placed into dry heat at 85°C. IL is not controlled during the test. Spectral attenuation is performed before the test, at 500 hours, 1,000 hours and 5,000 hours.

The devices from manufacturer G have shown IL increase of 0.2 dB, from B of 0.5 dB and from H of 2.6 dB. No degradation has been observed for the other designs.

2.3.6. Climatic tests

Sequence "thermal shock; water immersion"

Thermal shocks are performed using a thermal chamber with two temperature zones ; the transition time between -40 and 85°C was fixed at 5 seconds. The number of cycles is five. The dwell time was one hour. Two components from each design have been tested. Optical power fluctuations of each output port were controlled at 1310 nm or 1550 nm. IL changes observed were between 0 and 0.1 dB (improvement) for positive temperature and between -0.1 and -0.5 dB (degradation) for negative temperature; after the test, IL returned to their initial values.

Then, components were plunged into a bath filled with water at 43°C during 7 days, according to Bellcore TA-NWT-1221. IL was not controlled during the test.

At the end of the sequence, a spectral attenuation is performed again. No mechanical and optical degradation has been observed, only rust on the screws of the boxes.

Sequence "thermal cycling and climatic sequence"

Two components have been tested, between -40°C and 85°C with non controlled relative humidity (RH), according to IEC 68-2-14:Nb. The dwell time was 2 hours ; the transition time between two steps was one hour. IL has been measured every 15 minutes, at both wavelengths. Then, climatic sequence was performed according to IEC 68-2-38: Z/AD, between 65°C and -10°C with controlled RH.

At the end of the sequence, a spectral attenuation was performed again.

Only the A, C, E and F couplers passed the tests without degradation. Others couplers have shown either an increase of IL or some broken ports.

2.3.7. Mechanical tests

Tests are running; results are not available yet.

2.4. Results of WDMs evaluation

WDMs I, J and K are filter WDMs. The others are FBT technology WDMs. Measurement conditions and measurement equipment are the same as for the couplers.

2.4.1. Insertion loss

Figure 4 represents insertion loss (mean and max values) at 1310 nm. The mean of IL is lower than 0.2 dB for all FBT designs. For filter based WDMs, IL are near 1 dB, the design I has shown good performances of IL.

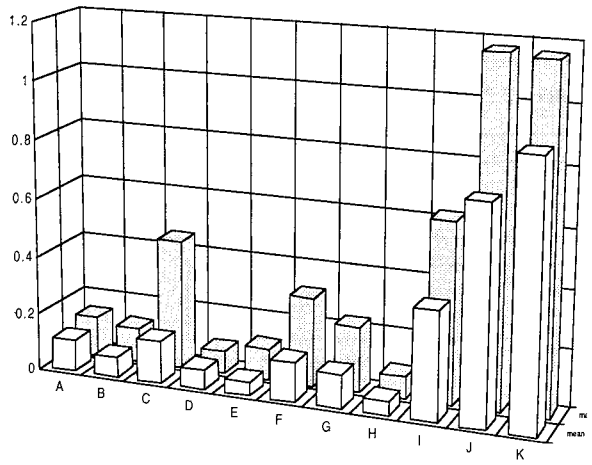


Figure 4 : WDM insertion loss (dB for the different suppliers, mean and maximum values)

2.4.2. Isolation

Isolation is measured at both wavelengths 1.3 and 1.55 µm; this parameter could be also calculated from spectral attenuation ; but for filter technology, the dynamic of the measurement equipment is not large enough.
Isolation depends strongly on wavelength ; generally, the maximum value is centered at 1310 nm and 1550 nm.
WDMs based on FBT technology have shown isolation values between 20 to 25 dB at both wavelengths. For filter based devices, the typical value was higher than 50 dB, only isolation for devices J at 1550 nm was observed at 45 dB.

2.4.3. Return loss

The two technologies have shown different performances in RL. FBT devices have shown values exceeding 60 dB. For filter designs, RL were around 50 dB.

2.4.4. Polarisation sensitivity of IL

All the devices have shown polarization sensitivity of IL less than 0.13 dB for both wavelengths. It could be observed that this sensitivity is often lower at 1310 nm than at 1550 nm, particularly for FBT based designs.

2.4.5. Aging test

One component from each supplier is placed into dry heat at 85°C. IL was not controlled during the test. Spectral attenuation is performed before the test, at 500 hours, 1,000 hours and 4,000 hours. No degradation has been observed except for the WDM J for which the 1550 nm port was found broken after 4 000 hours (IL has increased from 500 hours).

2.4.6. Environmental tests

Sequence "thermal shock; water immersion"

One mechanical failure has been observed after water immersion test ; fibers of one WDM D were no longer attached to the package.
Degradations have been observed after the tests sequence : WDM I and K shown IL increase higher than 0.2 dB.

This test has shown that filter based designs are more sensitive to temperature change than FBT based WDMs. The IL change observed for filter designs was of several tenths of a dB and for FBT less than 0.1 dB.

Sequence "thermal cycling and climatic sequence"

Some designs have shown IL increase : 0.5 dB for the 1300 nm port of one WDM G, 0.6 dB for both ports (1310 and 1550 nm) of one WDM I, 1.5 dB for both ports (1310 and 1550 nm) of one WDM J.

2.4.7. Mechanical and miscellaneous tests

Tests are running; results are not available yet.

3. Single fiber connectors

3.1. Connectors technologies

For FITL applications, optical connectors with a low IL, high RL and a low sensitivity to environment are required. Two main designs are used for fiber alignment in optical connectors :

- cylindrical ferule / sleeve alignment. The material used is ceramic in order to obtain the precision required and the stability. Generally, in this design, fibers are in contact. The performances depend on fiber offset, surface finish quality and fiber undercut or protrusion.

- cone to sphere alignment. Fibers are not in contact ; an index matching, gel or a thin film, inserted in the adaptor allow a low IL.

Several methods exist to reduce RL : convex polishing and physical contact, index matching, angle polish. For some applications (analog transmission), RLs higher than 60 dB are required. This is obtained by angle polish with physical contact (APC) or with index matching (EC).

3.2. Test program

In this work, we decided to consider only push-pull connectors with high RL. The test includes :

- SC/APC from 8 suppliers
- EC from 1 supplier
- E 2000 from 1 supplier

For each type, 8 patchcords have been tested. The evaluation test sequence is presented in figure 5. The mechanical and aging test are still in progress.

3.3. Evaluation results on connectors

3.3.1. Angle of the ferule

We have measured the connector ferule angle ; all the tested SC/APC and E 2000 connector ferules have a 8° angle, except the supplier A (9°).
The angle of the EC connector is 12°.

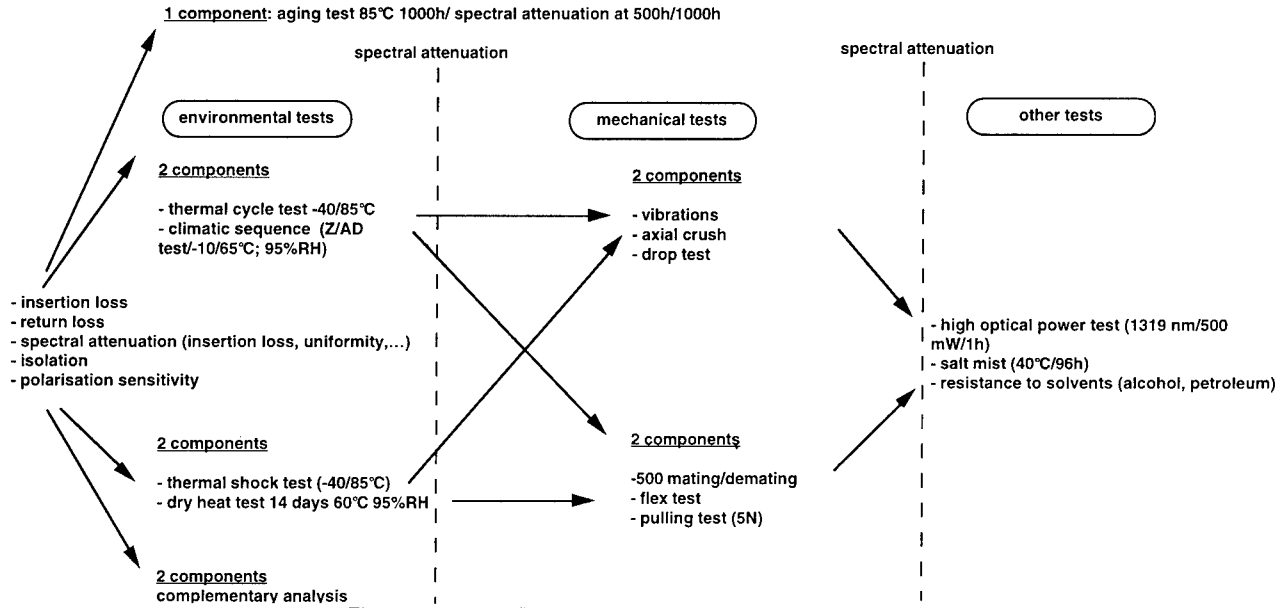


Figure 5 : single fiber connectors evaluation test sequence

3.3.2. Insertion loss

IL has been measured at two wavelengths with 2 laser diodes at 1310 and 1550 nm, according to the IEC 874-1 method 7 and also in spectral attenuation.
IL was found around 0.25 dB for B, C, E, G and H suppliers. For A, D and F SC/APC designs, IL was found around 0.45 dB with some values up to 1 dB.
Spectral attenuation for some APC designs have shown oscillations versus wavelength with amplitude up to 0.2 dB. It is supposed that these variations are due to index discontinuities at the fiber interface.

3.3.3. Insertion loss with intermating

We have measured IL with mixed SC/APC plugs, for example a plug A with all the others. IL are good (0.25 dB) if none of the plugs are from manufaturers A, D or F. Otherwise, the mean value of IL was measured around 0.45 dB with some values up to 1.2 dB.

3.3.4. Return loss

RL of a complete connection has been measured according to the OCWR method. For all the tested connectors, RL was found better than 55 dB, with a mean value at around 60 dB.

3.5. Aging test

One connection of each supplier have been placed into 85°C dry heat with non controlled relative humidity. Spectral attenuation has been performed before the test, after 21 days and 42 days : no optical degradation has been observed after 42 days. Test is still running.

4. Conclusion

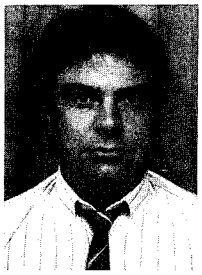
This evaluation, which is not finished, has allowed us to compare several technologies for each kind of passive components.

The choice of the technology and the choice of the supplier for FITL applications, depend upon requirements (splitting ratio, wavelength dependence, insertion loss, return loss, isolation, reliability, volume...).
For high splitting ratio couplers (> 8), integrated optics couplers seem to be the best choice.
The main criteria for selecting 1.3/1.55 µm WDMs are isolation and insertion loss. For applications needing isolation more than 30-40 dB, filter technology WDMs are more suitable. For applications needing low insertion loss and an isolation around 20 dB, FBT WDMs seem to be the best choice.
In term of quality, few couplers have passed the tests with success. The test sequence thermal cycling followed with climatic sequence, is very stringent and shows the importance of the packaging.
For connectors, it appears that the different designs tested, SC/APC, EC and E 2000 are able to meet the performance targets for FITL applications. The manufacturer must prove that he controls very well all of the manufacturing processes in order to assure a good quality of connectors. The choice depends if the connectors are made at the manufacturing site or in the field. Their reliability tests will be also important for the selection.

Tests are still in progress and more complete results will be reported later.

Authors

Christian BASTIDE
35 rue Jean Jaures-95871 Bezons, FRANCE



C BASTIDE was born in 1957. He received his engineer degree from Institut National Polytechnique de Grenoble (INPG) in 1982. He joined Compagnie Lyonnaise de Transmissions Optiques (CLTO) now ALCATEL FIBRES OPTIQUES where he was in charge of fiber measurements. In 1988, he joined ALCATEL CIT where he worked on CATV applications. Now, he is in the ALCATEL OPTICAL FIBER CABLE COMPETENCE CENTER where he is in charge of the Metrology team.

Olivier STEMPFEL
35 rue Jean Jaures-95871 Bezons, FRANCE



O STEMPFEL was born in 1969. He received the Diplome Universitaire Technologique (DUT) in 1990 and a certificate in opto-electronics domain. In 1992, he joined the ALCATEL OPTICAL FIBER CABLE COMPETENCE CENTER where he is in charge of optical passive component characterization.

Gérard COUVRIE
35 rue Jean Jaures-95871 Bezons, FRANCE



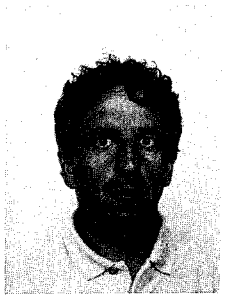
G COUVRIE was born in 1949. He received his General Certificate of Education in 1968. After two years in Mathematics and Physics, he joined Les Câbles de Lyon Outside Plant Operations Department. He is now working on the development of OPGWs and testing some optical connectors in the OPTICAL FIBER CABLE COMPETENCE CENTER of ALCATEL CABLE.

Gilles BOURRAT
35 rue Jean Jaures-95871 Bezons, FRANCE



G BOURRAT was born in 1954. He received his General Certificate of Education in 1974 and joined Les Câbles de Lyon Outside Plant Operations Department. He is now working on optical passive components in the OPTICAL FIBER CABLE COMPETENCE CENTER of ALCATEL CABLE.

Michel GADONNA
France Télécom - CNET
22301 LANNION FRANCE



M. GADONNA graduated from Ecole Supérieure d'Électricité in 1977 in the field of micro-electronics. He joined France Télécom/CNET in Paris in 1980 and was involved in development of test and measurement equipments on copper subscriber lines. Since 1986 he has the responsibility of quality and reliability assessment studies on optical passive components at CNET Lannion.

Jean Claude HÉDÉ
France Télécom - CNET
22301 LANNION FRANCE



JC. HÉDÉ was born in 1938. After secondary studies he followed technical formation in French Telecommunications Institute of Paris. He joined France Télécom/CNET in Paris in 1962 where he was in charge of cable quality control for Telecom. He joined CNET Lannion in 1966, where he was first in charge of new electrical contact technologies, connectors and interconnection designs for telecom applications. He is since 1980 active in the development of optical passive components quality control and reliability.

COMMUNICATION CABLES FOR FIBRE IN THE LOOP

V Abadia[**], F Brode[*], M Emmerich[*], D G Dalgoutte[+], R Johnson[+], N D Lea-Wilson[†], A Ragni[++], F Zanca[++]

[+]BICC Cables Ltd, Helsby Technology Centre, Helsby, Warrington, WA6 0DJ, UK
[†]BICC Cables Ltd, Whiston, Merseyside, L35 1RZ, UK
[**]Cables de Comunicaciones, Poligono Ind. Malpica, Calle D, num 83, 50016 Zaragoza, Spain
[++]Ceat Cavi, 10036 Settimo Torinese, Italy, Via Brescia 16
[*]KWO Kabel, Friedrichshagener Straße 29-36, D-12555 Berlin, Germany

Abstract

Optical cables are penetrating deeply into the local loop using different competing network strategies including single star, double star and ring structures. Despite this diversity of architectures, common themes are emerging when it comes to cable designs for the access network. Similar cable designs can be employed in very different network topologies. Expenditures for the access network amount to some 50% of total network expenditures. Accordingly the efficiency and economics of the cable plant are of the utmost importance. It is vital to create the most favourable cable design as a compromise between costs, installation behaviour, reliability and future network evolution. In this paper we describe different solutions adopted across Europe for the implementation of Fibre in the Loop (FITL) distribution networks. Existing and new optical cable designs for different levels of the access network are outlined, with the different constructions being compared from the network point of view.

Introduction

Cost reductions in recent years for optical transmission systems and cables have steadily shifted the strategies of Public Telecommunication Operators (PTO's) in favour of optical transmission techniques. Based on the increased bandwith demands of many customers and dramatic cost reductions of optical transmission equipment, the introduction of single-mode optical fibre cables into the local network has become increasingly cost-effective. Strategies for FITL deployments in Europe include OPAL in Germany (Deutsche Telekom), OTIAN® networks in the UK (British Telecom), FOTON in Spain (Telefónica) and Telecom Italia's optical ribbon cable system. Deregulation and privatization are acting as powerful catalysts in the ongoing process of access network evolution and change.

PTO's have very different starting points for their network planning. Operators with mature copper networks can deliver enhanced customer services by Passive Optical Network (PON) or point-to-point fibre network overlays, or by transmission technique improvements such as HDSL and ADSL. PTO's with less well developed networks are using optical cables extensively to help achieve rapid build rates and accelerated network coverage over wide geographical areas. An example of this latter approach is cable television operators in the UK, with most franchises deploying fibre to nodes passing 500 homes, and some seeing deeper fibre penetration to the 80 home point.

PTO's require access network infrastructures which provide a continuously stable platform for service delivery, with some stipulating simultaneous support for both PON and point-to-point fibre connectivity [1-4].

Optical Cables for Fibre In The Loop

In general the Local Loop network is based on three or four cable types. Figure 1 gives an example of a generic Local Loop network, which can be divided into the following areas:

- main or feeder cables
- distribution cables
- drop cables
- indoor cables.

Indoor cable constructions are not addressed in detail in this paper.

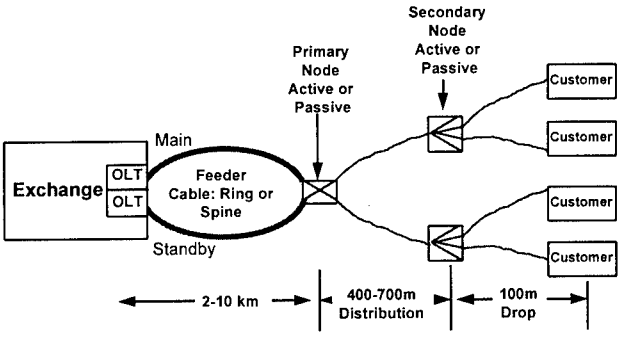


Figure 1: Typical Local Network

Nodes with internal components as different as passive optical splitters and SDH add-drop multiplexers, may nevertheless require similar input and output cable sizes.

Main or Feeder Cables

The constructions of the main cables which connect the exchange and primary node are strongly influenced by the network architecture adopted. For ring and double star structured local networks, optical cables with up to 200 fibres are commonly employed. A significant advantage of the ring topology is its higher system reliability against cable cut-through.

Frequently, an essential design feature requested is the ability to perform simple mid-span access, that is, to easily intercept selected cable elements in such a way that they are the only cable elements spliced, with all other cable elements passing unbroken through the joint. This in turn implies that cable elements should have good breakout characteristics from the cable structure and be rugged enough to provide good fibre handling inside joint closures. Usually, stranded cable structures are laid up using S-Z (alternating lay) stranding to assist in achieving easy mid-span access. Figure 2 shows a typical optical cable used in the main or feeder portion of the access network.

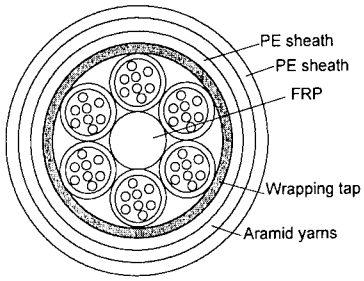


Figure 2: Optical Cable based on loose-tubed fibres

Cable structures having a single stranded layer of loose-tubes (8 to 12 fibres per tube) are amongst the most common designs found in the feeder part of the access network. Fibre counts range from 48 up to 160 fibres. Sometimes however, a PTO requires more fibres than can be accommodated in a single layer loose-tube structure. In this case, a double layer structure with up to 264 fibres is often deployed, as in Figure 3. The nominal diameter of this cable is 22mm. Many of the fibres in such higher fibre count cables are used for point-to-point (PTP) links to business customers.

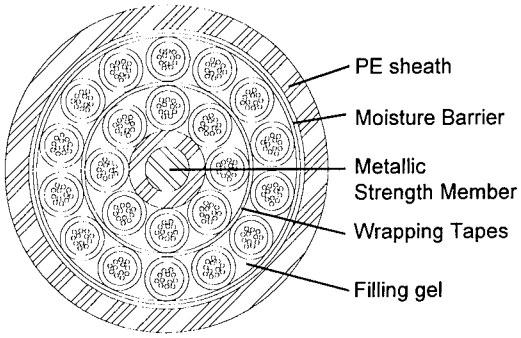


Figure 3: Double stranded layer loose-tube cable

In order to develop a cost effective network, it is essential that time spent on installation is minimized. Splicing of fibres is one of the most costly items in the installation of fibre optic cables. In long distance trunk networks the average length between splices is approximately 2-3 km, whilst in distribution networks this length is reduced to a few hundred meters, due to the neccesity of branching and distributing fibres to all customers in the feeding area. This leads to a notable increase in splicing costs for FITL networks. The only significant drawback of the cable structure shown in Figure 3 is the cost of splicing. Some PTO's may be prepared to pay the extra cost in time and money of single-fibre splicing. Alternatively, fibres in tubes can be 'ribbonized' on site by a sprayed on lacquer and splicing can then proceed using ribbon fusion splicers. But this approach, despite yielding significant time savings over single-fibre splicing, is slower than true ribbon splicing. Also, it introduces the possibility of errors such as mis-placed fibres in creating the ribbon. This is not surprising since craft personnel will have to perform the ribbonizing process in non-ideal conditions (eg freezing cold, dark winter days etc). For these reasons, the ribbonizing technique usually gives way to true ribbon cable solutions.

A typical ribbon cable using a slotted core design is shown in Figure 4. This five-slot design uses 4-fibre ribbons with five ribbons in each slot to achieve a 100 fibre cable in a conveniently small package (diameter less than 20mm). Large quantities of this type of cable have been successfully deployed in Europe, for example in Italy. The design delivers good splicing efficiency and high fibre cross-sectional densities, essential for full utilisation of congested ducts.

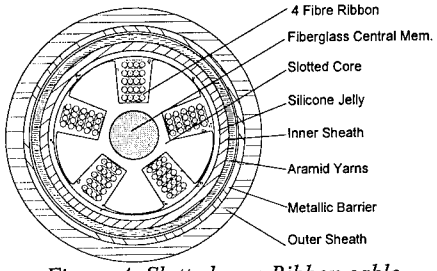


Figure 4: Slotted core Ribbon cable

Higher fibre counts, up to 500 fibres are achieved by stranding the basic 100 fibre units, as in Figure 5.

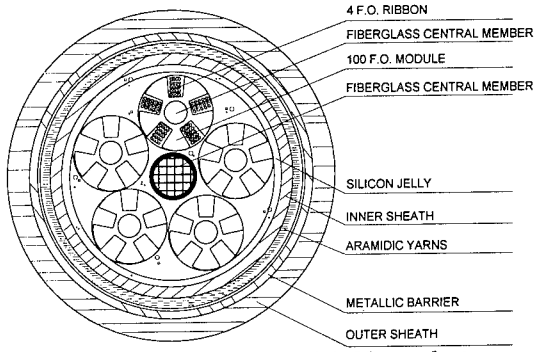


Figure 5: High Fibre count Optical Cable employing stranded ribbon in slotted core units

Some PTO's however, require cable elements to have a greater degree of ruggedness and better break out behaviour at joints than the bare fibre ribbons of slotted core cables as in Figures 4 and 5. They prefer a cable construction which uses ribbons packaged in tubes. Figure 6 shows a 96 fibre version with a nominal diameter of 17mm [5].

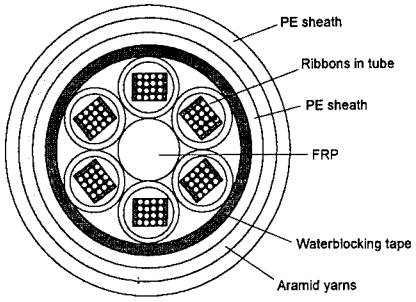


Figure 6: Ribbon in Tube Optical Cable

This cable combines the advantages of the good break out and cable element handling behaviour of tubes, with the low splicing costs of ribbons.

Table 1 provides a qualitative comparison of the advantages of the different feeder cable constructions.

Cable Type	Prod. costs	Install costs	Splice costs	Break out	Range of applic'n	Relia bility
Fibres in tubes	+	++	+	++	Up to 250 fibres	++
Fibre ribbons in tubes	+	++	++	++	Up to several hundred fibres	++
Ribbon in slotted cores	++	+	++	-	Up to several hundred fibres	+

Key: - negative, + good, ++ very good

Table 1 Feeder cable constructions compared

Distribution Cables

Distribution cables fan out from primary node positions and are usually based on central tube construction, containing fibres or ribbons. They are characterized by:

- Short installed lengths
- Low tensile forces
- Normally only up to 12 fibres
- Low production costs
- Good connectivity with main cables (eg cable elements matched)
- Suitable for cable blowing technology.

Sometimes, in addition to tensile requirements the cable must be stiff enough to be pushed up a small plastic duct without jamming or buckling. Figure 7 shows a typical 4 fibre cable designed for the distribution network.

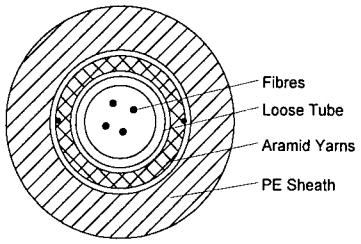


Figure 7: Optical Distribution Cable (4 fibre)

Figure 8 shows an 8 fibre distribution cable commonly used in the UK by cable companies to bring fibre to neighbourhood nodes (usually passing 500 homes, but with some operators bringing such cables as far as the 80 home point). The nominal cable diameter is 9.9mm

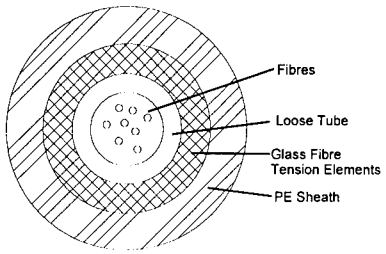


Figure 8: Optical Distribution Cable (8 fibre)

Cables as in Figure 8 but with twelve rather than eight fibres are also in common use bringing fibre to neighbourhood nodes. Usually only three of the fibres are lit, two for telephony and one for broadcast TV. The remaining dark fibres are ready for use if increasing upstream bandwidth demands require a greater dedicated bandwidth per node. The neighbourhood node will then be sub-divided, for example a 500-home area is likely to split into four 125-home areas.

Drop Cables

Many, if not the majority of drop cables in FITL networks are expected to be copper cables for some time to come, either copper pairs for Fibre to the curb (FTTC), or coaxial drops for Hybrid Fibre Coax (HFC) networks. However, Fibre to the Building (FTTB) is also a vital strategy for many PTO's, both for business customers, and for domestic customers living in apartment blocks. The low-cost distribution cables shown in Figures 7 and 8 above can also be used as drop cables. In addition, cables as shown in Figure 9 can be employed.

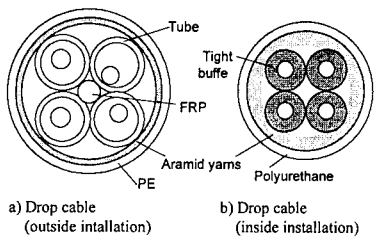


Figure 9: Examples of Optical Drop Cables

Blown Fibre Cables

An important technique useful in both distribution and drop networks is the blown-fibre concept[6] which is now seeing volume deployment in the UK by BT. This technology employs small diameter tubes or microduct, typically 5mm in diameter, to act as a conduit for the fibre.

Bundles of 2, 4 or 7 tubes which have been over-sheathed are pulled into ducts using conventional installation techniques. As the name suggests, optical fibres, which are produced in 4 fibre units, are installed into the tubes using the viscous flow of air. The benefit of this approach is that the relatively inexpensive tubes can be installed into the network and jointed using simple tools and materials at an early stage, to be equipped with blown fibre when service is requested on a 'just in time' basis. Blown fibre units can be installed over hundreds of metres quite easily given the correct blowing equipment.

The total installed cost of a 'completed' blown fibre cable (tubes equipped with blown fibre units) is about the same as the total installed cost of a conventional distribution cable. The difference is that the blown fibre approach helps to minimize stranded investment in outside plant fibre, that is, installed fibre which will never earn revenue because it is in the wrong place, eg due to planning errors or uncertainties. Errors such as these are likely to increase as competition in the local loop intensifies.

Installation and Costs

In view of the massive expenditure required in the local network, achieving the most economical implementation is very important. A typical analysis of plant and labour costs modelled for an OTIAN® FTTB network and giving the breakdown of expenditure per site is shown in Figure 10 [7,8].

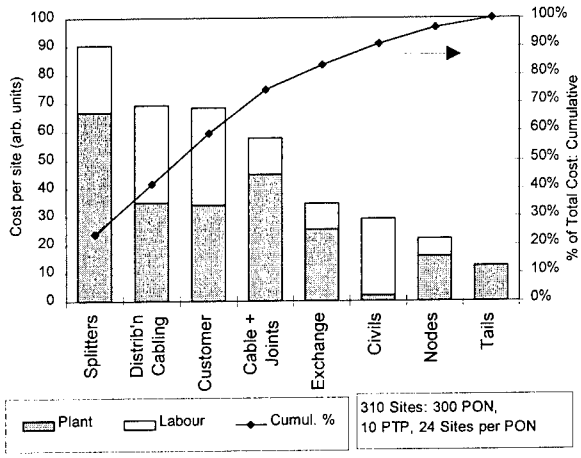


Figure 10: Installed first Costs per Site

It can be seen that distribution cabling, in this case blown fibre and tubing, is the second largest cost item after optical splitters, due to the significant labour component involved. In order to develop a cost effective network, it is essential that time spent on installation is minimized. As can be seen in Figure 10, this is particularly important not only in areas such as distribution cabling but also the customer plant items.

The 'Cable + Joints' category represents the cost to install cable in the feeder network. It is not uncommon to find problems with tortuous duct routes in the access network. As a result, cable installation rates are often slower than those achieved for the long distance network. Other primary cost areas include Civils, which includes the cost for new civil works, Nodes, which is the cost for underground nodes excluding splitters and Tails, which is the cost for connectorised leads.

System Reliability

It is recognised that system availability depends not only on the reliability of the network components but on other factors including maintenance and time to repair and that ultimately these factors will determine the whole life costs of a network. System design and product selection is therefore of key importance in addressing the required level of availability. As a result, much work has gone into developing accurate and realistic values for the reliability of network elements in order to predict overall system reliability. Major accelerated ageing programmes for key components such as optical splitters have been established to provide the necessary data. Table 2 summarizes the component failure rate and time to repair information used to develop system reliability models for OTIAN® networks.

Component	Failure rate (FITs)	MTBF (yrs)	MTTR (hrs)
Cable - Main or Feeder	1000	114/km	21
Cable - Distribution or Drop	2330	49/km	21
Splices - Field	30	3803	21
Splices - Internal	3	38026	21
Connectors	30	3803	21
Splitter - 2x16	950	120	21

Key: FIT - failure in 10^9 hours
MTBF - Mean Time Between Failures
MTTR - Mean Time To Repair

Table 2: Failure rates of passive components

Conclusions

Despite the plethora of competing approaches to FITL network construction at the system and architectural level, the number of different optical cable designs required is modest. Main or feeder cable structures are commonly fibre in loose-tube and ribbon in slotted core designs, with ribbon in tube structures an attractive alternative. Distribution and drop cables are usually low cost central tube designs, with blown fibre solutions a complementary approach. Ongoing modelling of passive networks helps to clarify the main cost and reliability issues still to be addressed.

Acknowledgments

The authors would like to thank Dave Seddon, Don White and Steve Davies for useful discussions on cable designs, and Iain Cook for his input on system reliability aspects.

Abbreviations:

PTP: Point-to-Point
OLT: Optical Line Terminal
HDSL: High bit-rate Digital Suscriber Line
ADSL: Asymmetric Digital Subscriber Line
OTIAN® is a registered trade mark of British Telecommunications plc.

References:

1. 'Flexible architecture and plant for optical access networks', Hornung S et al, Proc. 41st IWCS, Nov 16-19, 1992, pp.53-58.

2. 'OTIAN™ - An Infrastructure System for Networks in the Future', Frost P & Peacock J, Proc. 1st Communication Networks Symposium, 11-12 July 1994, Centre for Communication Networks Research, Manchester, UK, pp 97-100.

3. 'OTIAN™ - An Outside Plant System for the Access Network', Dalgoutte D G, Hewins A R, Hornung S, Peacock J, Proc. 12th EFOC&N, June 1994, pp37-40.

4. 'Implementation of connecting customers into the Public Switched Telephone Network (PSTN) via optical fibres', ITU-T Recommendation L.17, June 1995.

5. 'Study, manufacture and test on a S-Z stranded loose tube optical fibre ribbon cable with no pretwisting and no filling compound.', Baguer L, Proc. 43rd IWCS, 14-17 Nov 1994, pp.499-508.

6. 'Blown fibre experience in the Local Loop', Howard M, Proc. ISSLS 88, 11-16 Sept 1988, pp.197-201.

7. 'Installation Cost Issues in External Plant Deployment', Dalgoutte D G & Lea-Wilson N D, Proc. 13th EFOC&N, June 1995, pp 146-149.

8. 'Key Factors Governing Cost Effective Deployment of Passive Optical Network Infrastructures', Lea-Wilson N D, Proc. 2nd Communication Networks Symposium, 10-11 July 1995, Centre for Communication Networks Research, Manchester, UK, pp 102-105.

A NEW FIBRE-OPTIC CABLE FOR INLAND LAKE LINKS

Amir Fargahi*, Hanspeter Etter*, Chambos Theodossi** and Hubert Zimmermann*

* BRUGG TELECOM AG, CH-5200 BRUGG, SWITZERLAND
** LASER ARMOR TECH CORP., SAN DIEGO, CA 92121, USA

Abstract

Due to the rapid expansion of the digital data highways, new innovative cable constructions are needed to fully exploit the potential economic advantages of deploying fibre-optic cables in inland lakes, rivers and canals. In order to satisfy these needs in a cost-effective way, Brugg Telecom AG has developed and successfully installed a new generation of fibre-optic cables for underwater installation.

The cable is specifically optimised for small diameter, high strength and high crush resistance. The tests have shown that the newly developed rope can withstand very high lateral loads of up to 1000 N/mm.

Introduction

Optical fibres are the media of choice for voice and data transmission. With the expansion of the fibre-optic network, it has become clear that the deployment of fibre-optic cables in inland lakes, rivers and canals is a very cost-effective method to build parts of the fibre-optic network. The use of underwater installation for fibre-optic cables has many advantages compared to duct, direct burial and aerial installation on land, the most significant ones are:

- a very significant reduction of installation time and cost;
- problems with deployment in rugged terrain or in densely populated regions can be avoided;
- less problems to negotiate the rights of way;
- a shorter cable route is used.

To fully exploit the potential advantages of underwater installations, it was necessary to develop a new cable generation.

The new cables comply fully with the requirements of this kind of installation and provide a very value-effective and environmental-friendly option for a fast and economical expansion of the fibre-optic network.

In addition to developing the fibre-optic cables, we have also set up the capability to engineer, furnish and install turn key systems.

Design goals

The optical fibres have to be protected from excessive tensile, bending and compressive forces as well as from effect of moisture and hydrogen gas to guarantee a system life time of more than 30 years. Therefore the fibre elongation at the rated tensile force has to be minimised, the fibres have to be protected with a hydrogen barrier and the materials inside the hermetic sealing has to be carefully chosen in order to minimise the release of hydrogen gas.

Property	Design goal
Fibre count	30/60/90
Diameter	minimal
Weight	minimal
Density	> 3 kg/dm^3
Tensile Force	>3 weight per km
Fibre elongation	< 0.25 %
Crush resistance	> 400 N/mm
Hydrogen barrier	required
Hydrogen partial pressure after 30 years	< 10 mBar

Table 1: Design goals for the new cable generation.

Because in most cases the cable will be laid in depths of less than 200 m, there is a risk of cable damage due to anchors, rocks and ground movement. In this case a cable with higher density than the surrounding material of the lake bed is favourable, since it will provide a self bury effect, resulting in an additional protection of the cable. Therefore a cable with a density higher than 3 kg/dm^3 and a crush resistance of more than 400 N/mm is required.

For this kind of applications, long continuous lengths are necessary. To minimise transport and deployment costs a small diameter cable is advantageous.

Design

The construction uses jelly filled stainless steel tubes, which contain the optical fibres. The tube provides a hydrogen diffusion barrier and an excellent protection against hydrostatic pressure. The tubes are stranded together with zinc-coated high strength steel wires, in a way that the fibres are protected against stress and lateral pressure. The space between the stranding elements is filled with a compound to achieve water tightness in longitudinal and radial direction and to avoid corrosion. The cable core is coated with a polyethylene sheath (Figure 1).

Property	Type I	Type II	Type III	Type IV
Max. Fibre count	12	36	72	96
Diameter (mm)	11	17	20	22
Cross section (mm^2)	100	230	330	400
Weight in air (kg/km)	300	770	1200	1500
Weight in water (kg/km)	200	540	870	1100
Density (kg/dm^3)	3.0	3.4	3.6	3.8
Long term tensile strength (kN)	18	56	91	120
Min. breaking load (kN)	40	120	200	260
Min. crush resistance (N/mm)	400	600	800	1000
Min. bending radius (m)	0.15	0.22	0.26	0.30

Table 2: Properties of the new generation underwater cable.

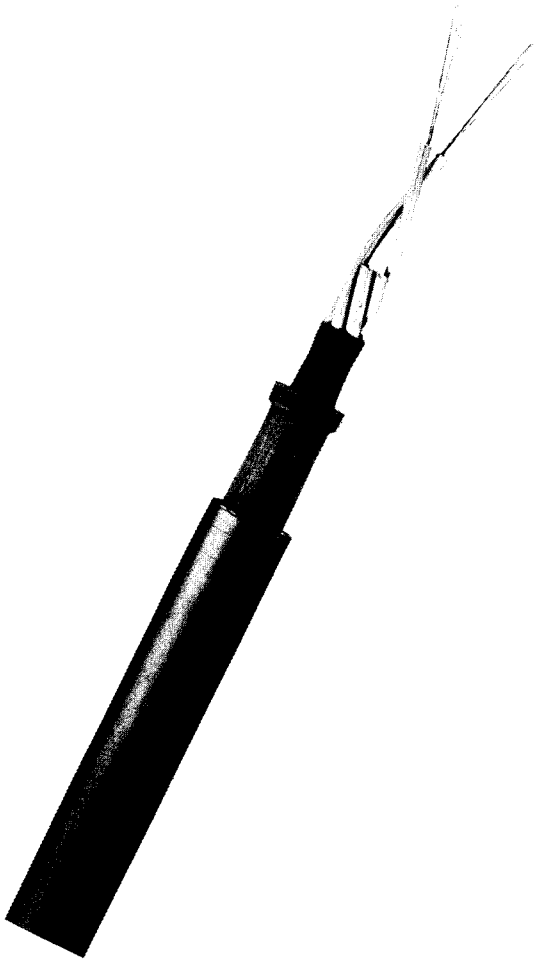


Figure 1: The new developed fibre-optic underwater cable.

The tube itself is made from a stainless steel strip which is formed into a tube through a precision forming mill. Optical fibres and thixotropic filling compound are introduced into the tube, which is then welded longitudinally with a CO_2-laser beam. This welded stainless steel tube provides the hydrogen barrier.

The cable construction can accommodate up to 96 standard single-mode or dispersion shifted single-mode fibres with the same fibre specifications as in standard outdoor cables. The optical specifications are according to Swiss PTT Telecom [1], IEC 793, ITU-T G652 and ITU-T G653 requirements.

Design Validation

In order to validate the new cable design we compare it to the standard cable used for lake links up to now (Figure 2).

The design installed so far uses a standard outdoor cable with stranded polymer loose tubes (1 in Figure 2). A corrugated welded copper tube (2 in Figure 2) provides the necessary barrier against humidity and hydrogen gas. To protect the copper from corrosion the tube is coated with a filling compound and a polyethylene sheath (3 in Figure 2). To achieve the required tensile strength a double layer of steel flat wire armouring (4 in Figure 2) is added, which in turn is covered with a polyethylene sheath (5 in Figure 2).

Property	Earlier design	New design Type III	Improve-ment (%)
Max. Fibre count	50	72	44
Diameter (mm)	35	20	43
Cross-Section (mm^2)	962	330	66
Weight (kg/km)	2430	1200	51
Density (kg/dm^3)	2.5	3.6	42
Long term tensile strength (kN)	15	91	500
Bending radius (m)	0.9	0.26	71

Table 3: Comparison of the two designs for the underwater cable with optical fibres.

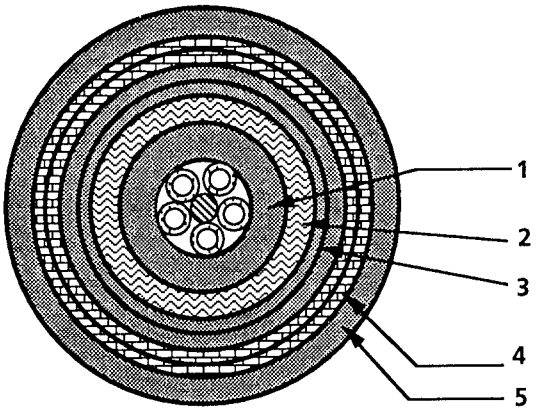


Figure 2: Earlier design of the underwater cables used for lake links.

Comparing diameter, weight, density and material consumption it is obvious that the new design is a real quantum step concerning customer benefit, system cost and economical use of materials (Table 3).

Mechanical and Environmental Performance

Prototype cables have been produced and tested to evaluate the optical, mechanical and environmental properties. Some results obtained on different ropes with different diameter are summarised below.

Properties of the tube

Some of the properties of the tubes have already been published (Ref. 2).

In addition we carefully studied the effect of hydrogen gas on the attenuation properties of the optical fibre inside the hermetic closed stainless steel tube to guarantee a system life time of more than 30 years. In order to accelerate the ageing process of the jelly and the fibre coating, the tubes was heated up to different temperatures for 24 hours and the spectral attenuation of the fibres was measured after cooling down the tube to 20 °C. The results obtained at 1550 nm are shown in Figure 3.

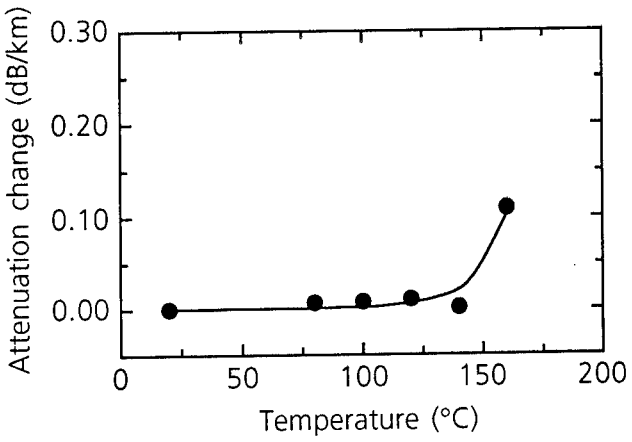


Figure 3: Average attenuation increase of single-mode fibres at 1550 nm due to hydrogen generation as a function of heat treatment.

The properties of different filling compounds has been evaluated to find a jelly causing low H_2-partial pressure at high temperatures and providing good low temperature attenuation properties of the embedded fibres. The evaluated jelly can fulfil both requirements (Figure 3 and 4).

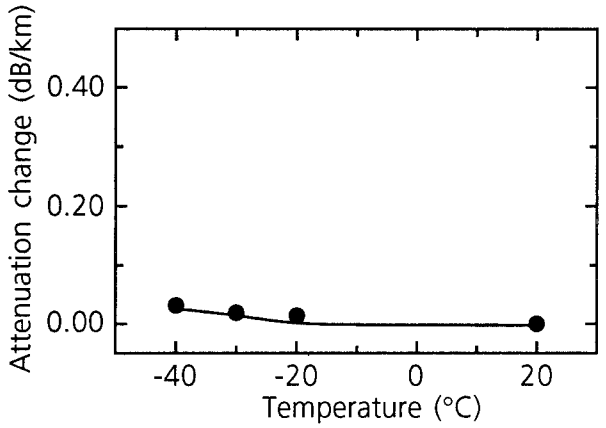


Figure 4: Attenuation increase at low temperature measured on single-mode fibres in the bare tube at 1550 nm.

Tensile Performance of the cable

The rope is designed to have an elongation window of about 1%, implying that no fibre elongation will occur at rope elongation's below 1%. The obtained data from tensile performance test provide a maximum rope elongation of about 0.6% at 150 kN well above the maximum rated tensile force of 120 kN (Figure 5). Up to the maximum rated tensile force no fibre elongation was observable, confirming that the fibres are embedded in the cable without any stress even at maximum rated tensile load.

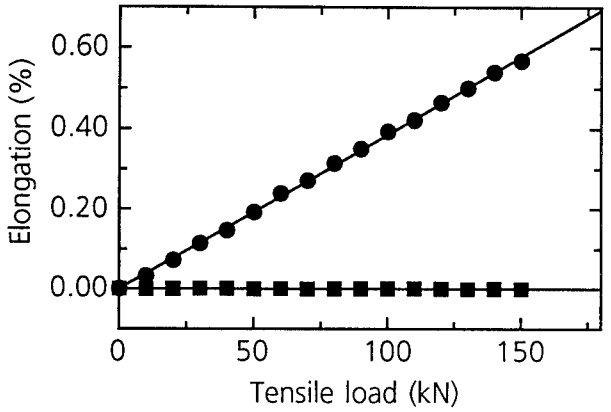


Figure 5: Rope (●) and fibre elongation (■) as a function of load, for the 22 mm diameter cable.

Crush resistance

A crush test was executed in accordance with IEC 794-1-E3. The experiment didn't show any significant attenuation change under crush load of up to 1000 N/ mm (Figure 6).

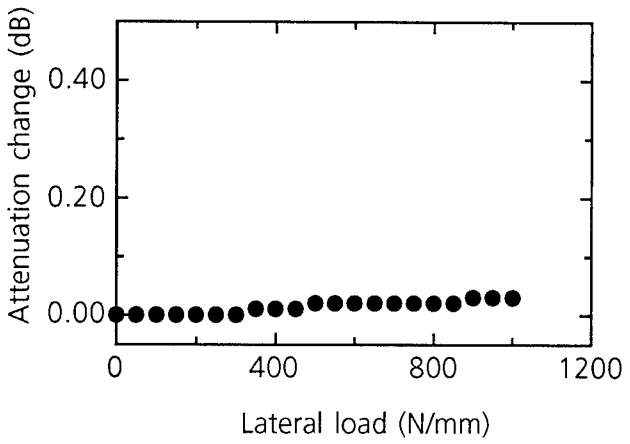


Figure 6: Attenuation change as a function of lateral load for a standard single-mode fibre in a 20 mm diameter cable measured at 1550 nm.

Installation

We have successfully deployed several cables in inland lakes. Due to the low weight per meter and the small diameter of the cable, it was possible to deploy the cable directly from a small, specially equipped vessel. The navigation of the vessel is achieved with a global positioning system (GPS), to ensure a precise positioning of the cable. In this way all of the already installed cables were deployed in less than one day without any serious problem. Divers have controlled the introduction of the cable in the tubes leading to the junction boxes at the landing points as well as other critical points.

Extensive measurements of the optical performance in the factory and after deployment have shown full conformance with the specifications for all deployed cables.

The experience with these installations fully confirmed the results obtained from the tests conducted prior to the first deployment and proved that the cable can fulfil the requirements under practical conditions.

Conclusion

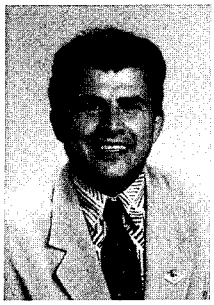
Brugg Telecom AG has successfully developed, manufactured and installed a new generation of fibre-optic cables for underwater installation. This newly developed product shows from a technical point of view a significant improvement compared to the standard cable used up to now. From the economical point of view, it increases substantially the already highly cost-effective method of deploying fibre-optic cables in inland lakes, rivers and canals.

The practical experience has shown that the new cable generation proves to be the ideal product for a fast and economical expansion of the underwater fibre-optic network.

References

[1] Detail Specification for Standard Single-Mode Optical Fibre.
Swiss Telecom PTT, PTT 840.05.01, July 1994.

[2] A. Fargahi, C. Zehnder, A. Banfi, D. Schoepke, C. Theodossi, H. Hagmann, W. Nägele and H. Zimmermann
Design and test of a new metallic fibre-optic cable for aerial cable ways.
International Wire & Cable Symposium Proceedings, p. 182-188, 1993.



Amir Fargahi
BRUGG TELECOM AG
CH-5200 Brugg,
Switzerland

Amir Fargahi graduated from Swiss Federal Institute of Technology, Zurich, with a Dipl.-Ing.-degree in Material Science. He joined Brugg Telecom AG in 1991 and has been engaged in the field of telecommunication cable development.



Chambos Theodossi
LASER ARMOR TECH CORP.
SAN DIEGO, CA 92121,
USA

Chambos Theodossi is Director of Business Development at Laser Armor Tech Corporation. He received his degree in Electrical Engineering from Faraday House College, London, England in 1958 and he has been involved in the field of telecommunications ever since.



Hanspeter Etter
BRUGG TELECOM AG
CH-5200 Brugg,
Switzerland

Hanspeter Etter was born in 1966. After receiving his Electrical Engineering degree from HTL Burgdorf, Switzerland, he joined development department of Brugg Telecom AG in 1993. He is responsible for product development projects.



Hubert Zimmermann
BRUGG TELECOM AG
CH-5200 Brugg,
Switzerland

Dr. Hubert Zimmermann - product development manager - joined Brugg Telecom AG in 1991. He received his degree in Applied Physics as well as his PhD. in Solid State Physics from University of Zurich, Switzerland.

Sea trial of buried submarine cable detection using a parametric sub-bottom profiler.

Nobuyuki YOSHIZAWA and Tadatoshi TANIFUJI
NTT Access Network Systems Laboratories
Tokai-Mura, Naka-Gun, Ibaraki-ken, 319-11, Japan

ABSTRACT

A remote sensing method for submarine optical fiber cables buried under the sea bed is proposed. The method uses acoustic waves to find the cable and can directly measure its depth under the sea bed. A prototype sub-bottom profiler using a parametric ultrasonic transducer is developed. The transducer can produce a narrow wave of between 10 to 30kHz in spite of its small diameter. A cable buried one meter under the sea bed was detected successfully for the first time in an experimental sea trial.

INTRODUCTION

NTT has already laid about six thousand kilometers of submarine optical fiber cable. This is still increasing because of its superiority in both transmission quality and cost performance. The transmission capacity of the submarine optical fiber cable system has also been improved and the transmission speed is increasing towards several decade Gb/s. In addition, wavelength division multiplexing is an attractive method to increase this capacity. The transmission capacity of a coaxial cable for the CS-36M system was about 2700 voice channels. The capacity of the optical system at 100 Gb/s of 10 wave mixing can be more than 10 million channels through a pair of optical fibers; that is, about five thousand times that of the coaxial system. A satellite system was used as backup for the coaxial submarine system. However, it is impossible for the optical system to use the satellite because of the difference in transmission capacity.

Submarine systems require high reliability because any repairs typically take several weeks. As a result, it is very important to prevent malfunctions in the submarine optical fiber cable system. Submarine cable can avoid external attacks only by burying it beneath the sea bed. It is very important to maintain a necessary buried depth because the condition of the sea bottom changes over time as a result of the flow of the sea current. However, it has not been possible to verify the cable depth because of the lack of reliable sensing methods. It is therefore very important to develop a sensing method which can directly and accurately measure the buried depth.

SENSING PRINCIPLE

A lot of sonar systems have been developed for sensing in the sea. However, none of them can detect a buried submarine cable. Figure 1 shows the relationship between frequency and wavelength in water. The wavelength determines the distance resolution of the system. The frequency of the conventional sub-bottom profiler is less than a few kHz and the wavelength is longer than several meters. The attenuation of acoustic waves in sea soil is dependent on the first power of frequency[1]. Therefore, a low frequency is required in order to propagate deeply under the sea bed. However, the distance resolution decreases in proportion to the reduction in frequency. Submarine cable is normally buried less than 2m under the sea bed and the required distance resolution is about 10cm. The dotted line in Fig.1

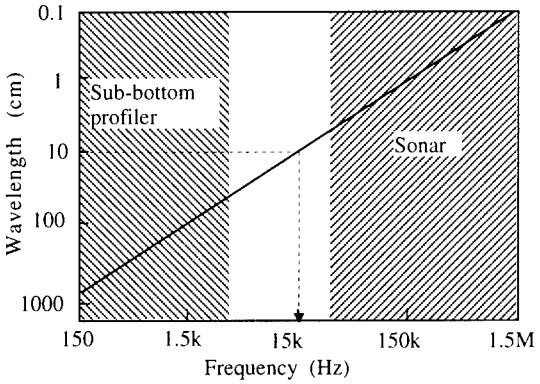


Fig.1 Relationship between frequency and wavelength in water.

shows that a wavelength of 10cm can be attained when the frequency is 15kHz if the wave can propagate down to the sea bed. The frequency must be experimentally clarified because the attenuation of acoustic waves depends on the quality of sea sediment. This is the first technical problem.

Submarine cable diameter is about 5 to 10cm. Directional resolution is also important to identify a cable. A transducer diameter which can produce a beam width of 10cm at a distance of 3m was calculated. Figure 2 shows the relationship between the transducer diameter and the frequency. The diameter would be more than 2m at 20kHz, which is too large for an economical and compact sensing system. This is the second technical problem.

A practical method must be found to satisfy these two requirements at the same time. Parametric technology is attractive in constructing a compact system with a frequecy tunable narrow beam. Figure 3 shows a schematic view of a parametric transducer. It has long been known that when traveling in the same direction, two plane waves of differing frequencies generate two new waves, one of which has a frequency equal to the sum of the primary two frequencies and the other a frequency equal to the frequency difference[2]. Those second waves are generated from the interaction of the two waves according to the non-linear effect of the sea water. The frequency difference component is useful because the beam is as narrow as that of the primary wave. Figure 2 shows that the transducer diameter can be smaller than 0.5m if the primary frequency is higher than 100kHz. The frequency difference component is also useful because the frequency can be tuned by changing the primary frequency around the resonance frequency. Replacement of the transducer is not necessary to change the frequency. However, the second wave power is low. This is a disadvantage of parametric technology.

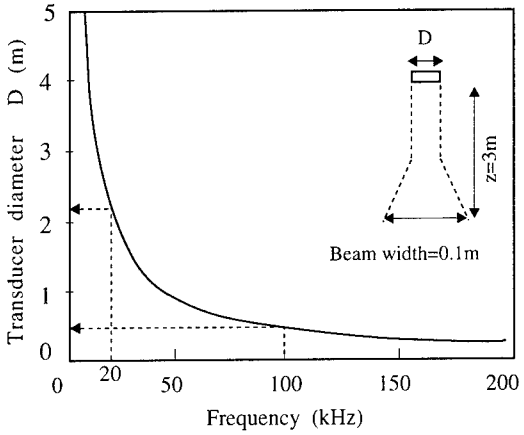


Fig.2 Diameter and frequency for a narrow beam transducer

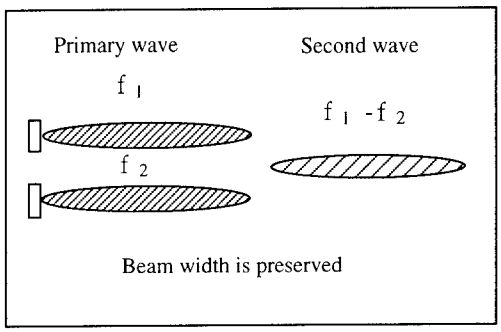


Fig.3 Principle of parametric transducer

PROTOTYPE SYSTEM

A prototype sub-bottom profiler using a parametric transducer has been developed in order to detect a buried submarine cable. The parametric system uses the frequency difference component for sensing. The advantages of the system include superior directivity and an ability to tune frequency. Figure 4 shows the external view of the parametric transducer and a receiver. The transducer is 48cm in diameter

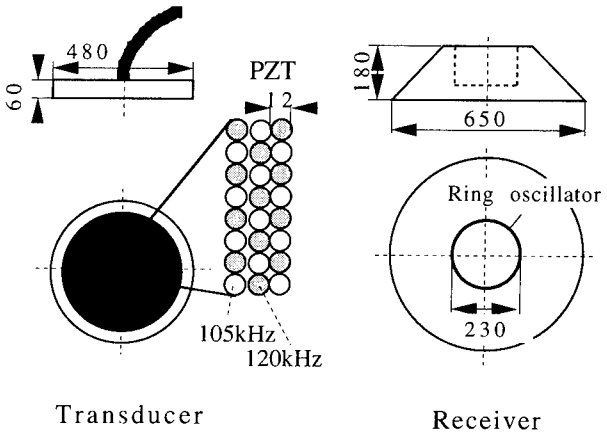


Figure 4 Prototype system

and 6cm in height. The transducer is composed of two sets of PZT elements of 250 pieces each. The primary wave frequencies are 105kHz and 120kHz. The output power of the primary wave is 220dBrelμPa. The receiver is 65cm in diameter and 18cm in height. Figure 5 shows the beam pattern of the second wave at 10kHz, and the beam width is about 3 degrees. The second wave frequency can change from 10 kHz to 30 kHz. The system can select frequency in order to adjust to the quality of the sea soil.

SEA TRIAL RESULTS

A sea trial was performed offshore of Yamaguchi prefecture. A submarine optical fiber cable route of 13km was constructed there in 1994. The cable was armored, about 4cm in diameter, and was buried to a depth of about 1m. This cable was selected as the detection target. The maximum sea depth was about 30m. Before the detection, sea-bed soil samples were taken at several points along the cable route. The soil was mud or sandy mud. Figure 6 shows the experimental set-up. A prototype transducer and a receiver were attached to the side of a ship and the ship was anchored over the buried cable. The ship's position was controlled above the cable because the cable position had been measured precisely during the burial process by a high accuracy radio positioning system. The positioning was accurate to within 1m. The received second wave power of 10 kHz is shown in Figure 7. The vertical axis shows the distance and the perpendicular axis shows the time. The sea depth is about 26m. As is indicated, when the ship position was above the cable, a strong cable reflection was detected one meter beneath

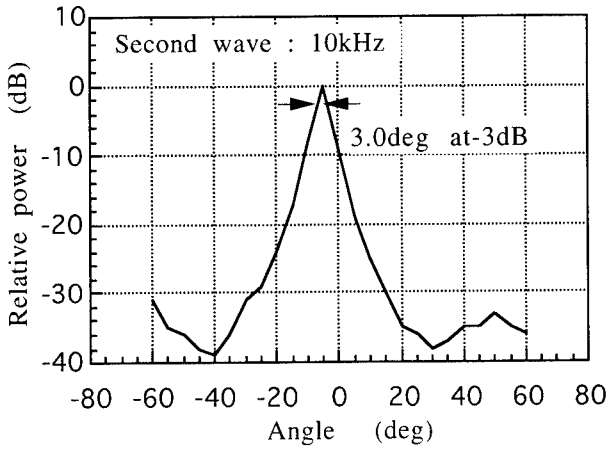


Figure 5 Beam pattern of second wave.

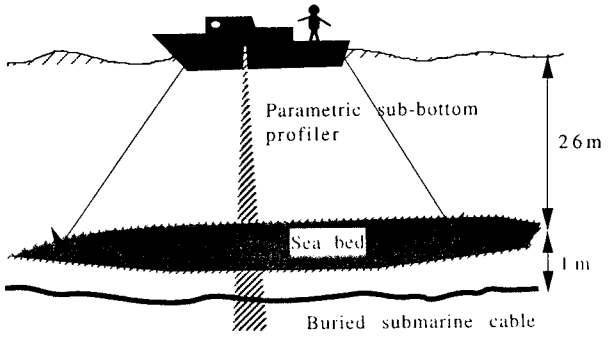


Figure 6 Sea trial setup

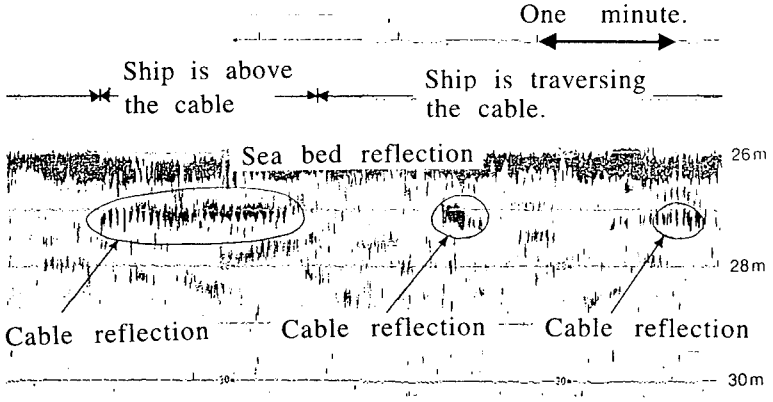


Fig. 7 Sea trial results.

the sea bed. When the ship traversed the cable, the strong reflection changed according to the ship position. The surface sedimentary layers were observed at the same time.

The feasibility trial demonstrated that a compact system which can "observe" and trace a buried cable can be constructed. Figure 8 shows the image of a practical sensing system. The compact system will be useful in assuring the reliability of the submarine cable because it can detect critical points on the cable route where the buried depth is reduced as a result of the flow of the sea current.

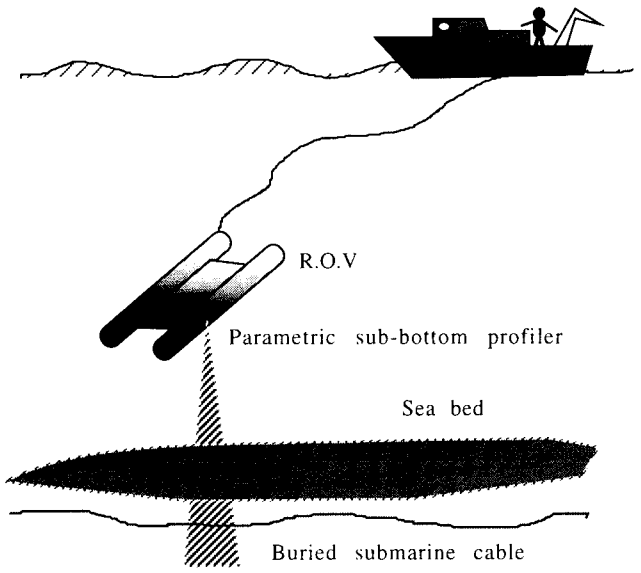


Figure 8 System image for buried cable survey

CONCLUSION

A remote sensing method for buried submarine cable using parametric acoustic technology was proposed. A feasibility sea trial was performed and a submarine cable 1 meter under the sea bed was detected acoustically for the first time.

ACKNOWLEDGMENTS

We would like to express thanks to Dr. T. Yabuta and Dr. Y. Koyamada for their encouragement during this work.

REFERENCES

[1] Edwin L. Hamilton," Compressional-wave attenuation in marine sediments ", Geophysiscs, Vol. 37, No. 4, pp. 620-646, 1972

[2] Peter J. Westervelt," Parametric acoustic array ", J. of acoustic society of America, Vol. 35, No. 4, pp. 535-537,1963



Nobuyuki YOSHIZAWA

NTT Access
Network Systems
Laboratories
Tokai, Ibaraki,
319-11, JAPAN

Nobuyuki Yoshizawa is an executive research engineer. He was born in 1954 and received the B.S., M.S., and Ph.D. degrees in mechanical engineering from Waseda University in 1977, 1979, and 1986, respectively. He joined NTT in 1979, and since then he has been engaged in research on submarine optical fiber cables. His major work was the design of shallow-sea submarine optical fiber cable, deep-sea submarine optical fiber cable, 48-fiber submarine cable and 100-fiber submarine cable. He also investigated a UV-coated optical fiber and a carbon-coated optical fiber. Dr. Yoshizawa is a senior member of the IEEE.



Tadatoshi TANIFUJI

NTT Access
Network Systems
Laboratories
Tokai, Ibaraki,
319-11,JAPAN

Tadatoshi Tanifuji is the leader of the optical cable and connecting research group. He was born in 1949. He received the B.S., M.S., and Ph.D. degrees in electronics engineering from Hokkaido University in 1972, 1974, and 1983, respectively. He joined NTT in 1974. Since 1991 he has been engaged in research on high-density and pre-connectorized optical fiber cable. Dr. Tanifuji is a member of the IEEE.

ADAPTABLE MOULDING TECHNOLOGY FOR OPTICAL SUBMARINE CABLE JOINT

B. DAGUET - J.F LIBERT

ALCATEL SUBMARINE NETWORK - CALAIS FRANCE

ABSTRACT

This document deals with optical submarine cable jointing operations and more specially moulding taking place during manufacturing, laying or maintenance operations.

Optical submarine cables are usually insulated with an outer sheath of polyethylen. When a cable joint is required, the water sealing is usually provided by a polyethylen overmoulding when high dielectric insulation performances are requested (case of repeatered systems).

This paper describes and compares the different existing technologies for polyethylen (PE) overmoulding to a «fast moulding» technique that is now in use in Alcatel Submarine Network (ASN).

I - INTRODUCTION

Due to cable evolution, the concept of upgradability and adaptability becomes a key issue regarding jointing operations. It's obvious that mechanical differences between cables can be overcame and adapted in any joint design with quite small modifications. Moreover, equipment investments are rather low if any change is required. However the problem concerning insulation differences between cable types, is much difficult to be solved :

- an important range of polyethylens (PE) is now adapted for the submarine cable use. Properties of these PE can be really different according to family types (for instance : linear low density and high density),

- moulding qualification programms are always heavy to complete because of the complexity of the process and the reliability that must be achieved,

- moulding equipment investments are usually expensive specially when several moulds are needed to fit different sizes of cable for instance.

The jointing activity must take into account that the cable ranges available on the market are now increasing a lot. This is critical specially for maintenance that must be available during the cable life time (usually 25 years).

II - CABLE STATUS AND FUTURE DEVELOPMENTS

Two main families are existing today :

- long distance optical submarine cables for repeatered systems,

- cables for unreapetered systems.

The main difference between these two types is the insulating sheath (without taking into account mechanical aspects).

Unrepeatered cables are usually insulated with a thin HDPE (High Density Polyethylen) layer (1,5 mm to 3 mm). Cables for repeatered systems generally use the LLDPE (Linear Low Density Polyethylen) or the LDPE (Low Density Polyethylen).

In this last case the thickness of polyethylen is higher in order to get a high dielectric strength and compensate a lower abrasion resistance. The thickness of such layer is typically between 5 and 6 mm.

The next table shows a short comparison between both PE.

	LLDPE	HDPE
Typical abrasion resistance (Volume of PE lost - Taber abrasimeter - mm3)	120	70
Melting temperature (degree Celsius)	120 to 130	About 170

Some studies and ageing tests made in ASN[1] demonstrate than HDPE can also be used for long distance repeatered systems, since they are providing very good abrasion resistance and dielectric insulation with better ageing properties.

III - JOINTING STATUS

In the field of cable jointing activity, some differences also exist depending on the system type (unrepeatered system or long distance repeatered system).

Unrepeatered systems

For unrepeatered systems, there is no or a small voltage requirement for fault location or electroding (typical voltage is about 500 V). Different solutions are available to provide insulation and sealing at the area of the joint :

- conventional moulding techniques,
- heatshrinks,
- metal sealing with internal insulation of the conductor.

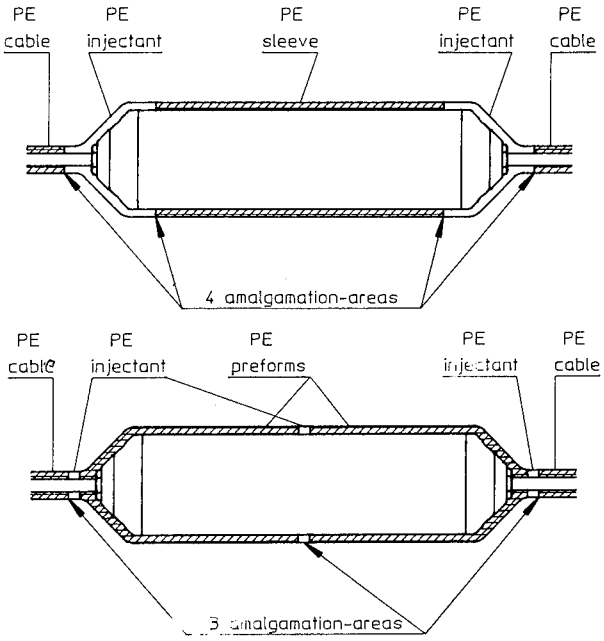
Repeatered systems

For repeatered systems using high voltage supply (maximum 10 KV), PE overmoulding is the only solution that has been used since the beginning of Submarine optical fiber cables. The purpose is to obtain the same dielectrical and mechanical properties than the PE cable layer by itself.

The usual technique is to use a PE pre-manufactured sleeve as shown in the following drawing. The moulding by itself consists in filling the gap between the sleeve and the cable with PE injectant.

An alternative solution is to use 2 PE preforms instead of the sleeve in order to limit the volume of PE injectant (so the risk of contamination).

This technique is shown in the following picture.



It's easy to understand that there is no major problem when using the same type (LLDPE or LDPE) for cable, sleeve or preforms and injectant. The melting of the cable and sleeve ends is done by thermal conduction from the mould, which is heated to above 200 °C, for about 20 mn.

However the problem is much more difficult to solve with HDPE cable due to melting temperature that is 40° C higher than LLDPE.

IV - FAST MOULDING TECHNOLOGY

1) Status on fast moulding technology

This new ASN technology for joint moulding is based on intrusion and injection of PE injectant (PE granules) inside a mould cavity at high pressure and high filling speed rate.

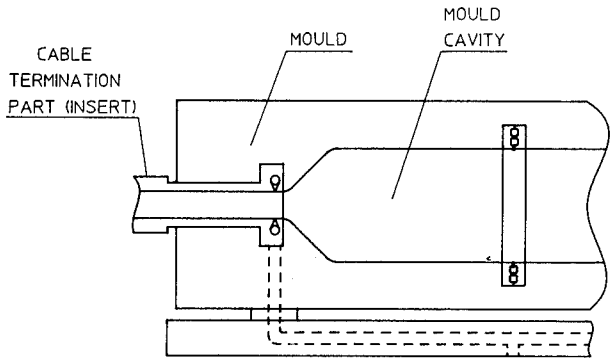
There is no need to use PE sleeve or preform. In addition to that, the heating of the PE cable ends is very local and is provided by pulsing hot air for 5 mn.

Only the useful volume of cable end PE, close to the interface (for the amalgamation) is heated. This gives many advantages :

- the mould is only heated at 110° C, that means that fibers and joint components are not submitted to high temperatures (even when cable is insulated with HDPE),

- all types of cable PE can be moulded without changing the mould temperature regime (LDPE, LLDPE, HDPE).

In addition to usual advantages of this technique (time saving, completion of moulding in 20 minutes, from installation of the joint to opening of the mould), reliability with only 2 amalgamation areas), another important aspect is the flexibility regarding all types of cables as shown in the following drawing.



Considering that, the joint shape is identical for all types of cables ; only the cable termination part need to be adapted to each diameters. The mould remains on the machine and is identical for all types of cables providing :

- minimal mould investment,
- minimal mould handling,
- the same moulding parameters.

2) Results on mouldings

a) Qualification

Today, this technique is qualified with 2 types of cable :

- the ASN 14 mm cable for repeaterless systems

This cable is insulated with a 3 mm layer of black HDPE. Up to now, 5 systems have been built using that «Fast Moulding» technique :

* Kyniras,
* Mainland Corsica 5 (CC5),
* ECFS (East Caraibean Feston System),
* Sumatra Java Bali,
* Bass-Strait.

The datas about the moulding are as follow :

. PE cable end : HDPE 1 or LDPE 5,

. PE injectant : LLDPE 2.

. Moulding sucess rate : 100 %.

. Moulding qualification regime : 45 kV - DC for 5 mn.

- the ASN 21.5 mm cable for repeatered systems

The cable is insulated with a 5.5 mm layer of LLDPE, LLDPE2 or LLDPE3.

Up to now, two systems have been built with that «Fast Moulding» technique. The datas about the moulding areas follow :

. Moulding sucessfull rate : 98 %.

. Moulding qualification regime : 150 kV - DC for 36 mn (contractual).

. PE cable end : LLDPE2 or LLDPE3 or LDPE5.

. PE cable injectant : LLDPE2.

In addition to the contractual qualification regime, extra high voltage tests have been performed to proove the reliability of the moulding. The voltage was increased to find the higher limit resistance. It

was not possible to reach the breakdown voltage for most of the samples (for instance in the following table ; No failure at 400 kV means that during the test, moisture content in air did not enable to reach more than 400 kV. It was not possible to get breakdown voltage).

Results are presented in the following table :

* short term test (1 h) :

Joint number	PE Injectant type	PE cable ends type		150 kV / 1 h	200 kV / 1 h	250 kV / 1 h	Higher limit
1	LLDPE 2	LLDPE 3	LLDPE 3	Pass	-	-	No failure at 400 kV
2	LLDPE 2	LLDPE 3	LLDPE 3	Pass	-	-	No failure at 300 kV
3	LLDPE 2	LLDPE 3	LLDPE 3	Pass	-	-	No failure at 400 kV
4	LLDPE 2	LLDPE 3	LLDPE 3	-	Pass	-	No failure at 300 kV
5	LLDPE 2	LLDPE 3	LLDPE 3	-	Pass	-	No failure at 300 kV
6	LLDPE 2	LLDPE 3	LLDPE 3	-	Pass	-	Failure at 220 kV
7	LLDPE 2	LLDPE 3	LLDPE 3	-	-	Pass	No failure at 350 kV
8	LLDPE 2	LLDPE 3	LLDPE 3	-	-	Pass	No failure at 400 kV
9	LLDPE 2	LLDPE 3	LLDPE 3	-	-	Pass	No failure at 400 kV

* medium term test (9 days) :

Joint number	PE Injectant type	PE cable ends type		150 kV / 36 mn	100 kV / 9 days	Higher limit
10	LLDPE 2	LLDPE 2	LLDPE 2	Pass	Pass	No failure at 425 kV
11	LLDPE 2	LLDPE 2	LLDPE 2	Pass	Pass	No failure at 425 kV
12	LLDPE 2	LLDPE 2	LLDPE 2	Pass	Pass	Failure at 354 kV
13	LLDPE 2	LLDPE 2	LDPE 4	Pass	Pass	No failure at 425 kV

Table shows that results are always much better than the contractual specification which is 150 kV - DC for 36 mn.

b) Evaluation of wide range of PE combination

Until now, 7 different combinations have been successfully tested at 150 kV - DC for 36 mn using the same moulding temperature regime.

PE INJECTANT	PE CABLE ENDS TYPE	
LLDPE 2	HDPE 1	HDPE 1
LLDPE 2	HDPE 1	LDPE 5
LLDPE 2	LLDPE 2	LLDPE 2
LLDPE 2	LLDPE 2	LLDPE 3
LLDPE 2	LLDPE 3	LLDPE 3
LLDPE 2	LLDPE 2	LDPE 4
LLDPE 2	LLDPE 3	LDPE 5

PE characteristics :

	DENSITY	GRADE
HDPE 1	0.955	10.5 - Condition 7
LLDPE 2	0.934	4 - Condition 4
LLDPE 3	0.923	0.65 - Condition 4
LDPE 4	0.932	
LDPE 5	0.92	0.14 - Condition 4

CONCLUSION

All the kinds of cable tested up to now have been moulded using the same mould and the same parameters (moulding temperature regime). Taking into account development of new cable types probably using HDPE with a thickness of about 5 mn, the flexibility of that technique gives a major advantage for manufacturing purposes and maintenance issues. All the moulding parameters can be also used to mould termination joint (Extremity Box for coupling of cable to repeater).

This flexibility combined with the intrinsec quality of the fast moulding :

- moulding time : 20 mn,
- remoulding : yes,
- raw material : only PE granules (no need of PE shots, preforms or sleeves),
- available and tested on cable ship for laying and maintenance,

gives many advantages to that technique.

A wide range of combination, using wide range of PE type (density : 0.92 to 0.955, grade 4 condition 4 up to grade 10.5 condition 7) were successfully tested under 150 kV - DC for 36 minutes.

Such a flexible moulding technique can be a major advantage if cable optimization is required in the future (PE layer thickness with regard to abrasion resistance, supply voltage, lifetime requirement).

REFERENCES

[1] Selection of insulating materials for long distance optical submarine cables (44th IWCS).
Authors : F. RUELLE ; JF. LIBERT, B. ALADENIZE

Authors

Jean-François LIBERT received his engineering degree from «Hautes Etudes Industrielles» of Lille (FRANCE). He joined Alcatel in 1984. He is now Technical Manager for Optical Submarine Cable in Calais.

Bruno DAGUET was born in 1968. He received a degree in plastic material engineering from the institut of Alençon (France). He joined Alcatel in 1991 where he is in charge of cable jointing technologies and development.

A NEW COMPACT 56 FIBRE REPAIR JOINT, REMOTE PUMPED OPTICAL AMPLIFIER HOUSING AND COUPLING DEVICE FOR A LOW COST FIBRE-OPTIC SUBMARINE CABLE FAMILY.

Einar Betten, Terje Bjerkeli, Inge Vintermyr

Alcatel Kabel Norge AS

ABSTRACT

As part of the new generation of fibre-optic submarine cables, Alcatel Submarine Networks has developed a low cost cable family for unrepeatered cable links.[1]

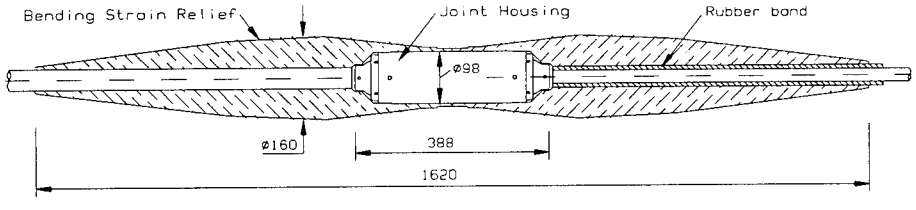
A 56 fibre splice capacity repair joint has been developed. The same armoured housing is also used for a remote pumped optical amplifier unit, as joint housing for a passive submarine branching unit and a loop-box/earth electrode for cable end deployment during shore end and branching unit laying. The joint housing and armour terminations are dimensioned for the strongest cable in the family, and can unaffected sustain 360 kN tension for more than one hour. The joint tolerates more than 200 kN tension while passing around a 3 m diameter capstan, and is pressure resistant down to 3000 m water depth.

This new joint is assembled with simple handtools, and has a hermetically sealed fibre housing, achieved by metal seals.

INTRODUCTION

To complete the new low cost steel tube cable family from Alcatel Submarine Networks, a cable accessories line was required. The "10mm" cable family (named after the diameter over its inner polyethylene sheath) is tailored for the continental shelf national and unrepeatered international connections and festooning networks. Key words are low cost, high fibre counts, large variety in armour designs and light installation equipment. Primary accessory need was for a simple repair joint. Secondly, demand for increasing unrepeatered transmission span lengths introduced the remotely pumped optical amplifier. These amplifiers are due to their nature convenient to install submerged, and thus requires a submersible housing. Thirdly, festooning of unrepeatered cables has led to the requirement of passive branching units in the submerged plant. Finally, a need for a loop box / earth electrode exists associated with cable end deployment during shore end and branching unit laying. To reduce number of contingency kits required by the cable operator, and keep volume of training of installation personnel at a minimum, a versatile concept based on a common armoured joint housing were designed.

The common armoured housing was given the same outer dimensions as the Alcatel Submarine Networks' moulded deep sea joint for repeated cables, i.e. 98 mm diameter, and less than 400 mm length.



Joint Housing with Bending Strain Relieves

FIGURE 1

DESIGN

Materials

The joint housing is made of a seawater corrosion resistant stainless steel. The chosen high alloy steel does not require any corrosion protective coating, and has a substantially higher strength than standard stainless steel.

The inherent strength of the material used allows the cylindrical outer tube of the joint to double as both tensile strength element, and pressure housing. Thus it has been possible to keep dimensions at a minimum, and the armoured joint has a rigid length approximately half of that commonly used in the business today.
The joint does not involve polyethylene moulding or bonding techniques, and is therefore quick to assemble and requires a minimum of special tooling. A 24 fibre armoured joint can be assembled in less than 12 hrs by two jointers.

Bending strain relieves

The joint housing including the armour terminations are designed as a compact cylinder, tapered in each end over the armour termination. Bending Strain Relieves (BSRs) are used to avoid excessive bending and subsequent rupture of the armour wires at the entry of the armour termination. Again the outer dimensions of the joint housing allows utilisation of proven techniques from the experience of repeatered cables. The basic design and outer shape of the BSRs from the repeatered cable deep sea joint is used. The centre hole through the BSR is enlarged to fit the largest diameter cable in the family, the Heavy Armoured cable. To allow a single set of BSRs to be used for the whole range of cables, rubber bands (3 - 4 mm thick, 30 mm wide) are used to build up the diameter of the smaller cables. The rubber band material is chosen with consideration given to the similarities in hardness with the BSR material itself. This prevents the cable to cut through the filler material when the joint is exposed to tension around a capstan or laying wheel. The width of the band allows it to be wrapped onto the cable serving in a matter of minutes.

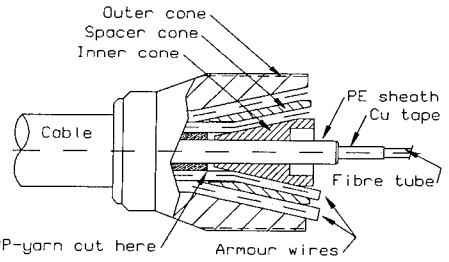
The external shape of the BSRs are functional through their small diameter, maximum 160 mm, and gently tapered design. This has proven to be well suited for cable ship operation and equipment like ploughs etc. The fact that the maximum diameter of the BSR is located over the cable a distance outside of the armour termination, ensures that the cable is exposed to tension rather than bending at the entrance of the armour termination when the joint passes around a capstan or laying wheel.

To prevent the BSRs to be pulled away from the joint housing during passage through linear cable engines, a metal insert is moulded into the BSRs. This metal insert is threaded on the inside to secure the BSRs onto external threads on the joint housing. The threads also acts as a water blocking zone, and prevents circulation of water over the better part of surface area over the joint. By this only a small area at the tapered ends of the joint housing is effectively exposed to seawater, and does not increase the corrosion of the armour wires.

Armour termination

The cable armour is locked in the armour termination by the well proven technique of threaded cones as used in the Articulated Joint[2] since 1988. Termination units for single and double armoured cables are available with a set of interchangeable armour-locking- and spacer cones. It has been demonstrated that the armour termination can sustain more than 90% of the cable tensile strength. This is achieved both through specific testing of the armoured joint and by the fact that all tensile testing of the cable itself has been executed with the same type of armour terminations. Each cone is individually pushed in by a portable handoperated hydraulic tool, ensuring repeatability of the process through the amount of hydraulic pressure applied. The same hydraulic tool is also used for jointing of repeatered cables from Alcatel Submarine Networks, and thus allows standardisation in the tooling of cable operators.

Assembly of the armour termination is the first step in the process of completing the joint. A length of less than 20 cm of the armour lay-up is handled during the assembly. Consequently the armour wires close to the joint preserves their original lay-angle, no time-consuming armour wire lay-back or outer serving reconstitution is necessary.



Armour termination (HA shown)

FIGURE 2

Joint housing

The joint is designed with a cylindrical body. At each end of this body the armour terminations are screwed into a bulkhead flange, through which the cable core enters the splice compartment. The sealing and mechanical securing of the cable core is provided in the bulkhead and will be described later in the next chapter. Inside the joint housing, a bracket between the two bulkheads absorbs the forces by the external water pressure onto the bulkheads. The bracket also provides storage of fibre overlength and means for fastening of storage trays for fibre working tails and fibre splices. Equipped with fibre/splice storage trays on both sides of the bracket, the joint can accommodate 56 fibre splices.

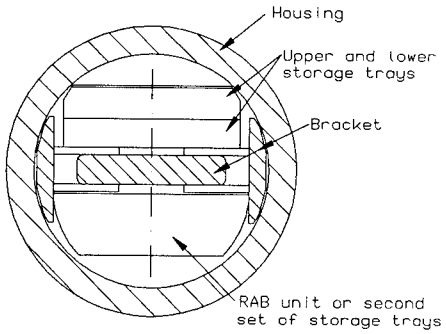


FIGURE 3

Joint housing hermetic seals

In the cable core, the hermeticity is preserved by a steel tube around the fibres. The cable core consists of this tube, with an optional cu-sheath for electrical purposes, built up to a diameter of 10 mm by a polyethylene sheath. The sealing system of the joint housing is contained in the bulkhead between the armour termination and the joint housing chamber. A ceramic gland preserves the electrical insulation through the bulkhead. In this insulating gland an elastomeric seal ensures the electrical integrity of the polyethylene sheath. This partly pressure compensated seal system (patent pending) will not be degraded by the limited yield of the polyethylene sheath, as experienced with standard elastomer (O-ring) seals. The seal will sustain the pressure at 3000 m water depth. Being an elastomeric seal, it is however not a hermetic seal. The purpose of this first seal system is to preserve the electrical properties of the polyethylene sheath.

The hermeticity of the steel tube of the cable is preserved by a second metallic compression seal. After the first elastomeric seal the polyethylene sheath of the cable core is removed. Inside the ceramic gland a metal tube is located. In this tube a connection to the optional cu-conductor is achieved by a spring system. Only the steel tube is guided into the joint housing. A metal compression seal ensures the hermeticity between the steel tube of the bulkhead gland, and the steel tube of the submarine cable. The compression fitting is of the same type as found in high pressure hydraulic systems. To avoid the steel tube of the cable to collapse under the pressure from the compression fitting, a supporting insert is fitted. This insert has a gently curved inner profile, ensuring that the fibres does not chafe against any sharp edges resulting from the cutting of the steel tube. Thus any meticulous and hazardous polishing of the inside edge of the tube end is avoided. Tests have proved that with this termination the steel tube can be pulled to an elongation of more than 6 %, i.e. ten times that of the allowed cable elongation at Nominal Transient Tensile Strength (NTTS) without being pulled out. The tube will ultimately break outside of the compression fitting.

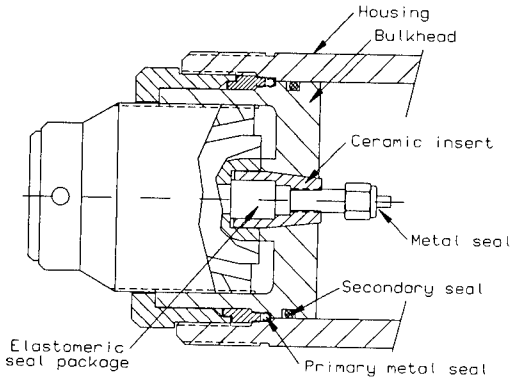


FIGURE 4

To complete the hermetic closure a metal seal is utilised between the bulkhead and the outer tube of the joint. The seal is of a C-ring type. The energising of the seal is carried out during assembly of the joint, as the seal with a simple tool is pushed in over a conical section on the bulkhead circumference into its highly polished seat. Increasing waterpressure inside the "C" will only improve the sealing forces. The metal C-ring seal requires tight mechanical tolerances of the associated parts. Behind the metal seal a secondary elastomeric seal is positioned. The primary function of this O-ring is however centralising of the bulkhead inside the outer tube, and protection of the seal surfaces inside the outer tube as this is fitted over the bulkhead.

Fibre and splice storage

Inside the joint housing an initial storage space for fibre excess length is provided directly on the central bracket. On top of (optionally also beneath) the central bracket a standard set of coiling trays are used. The lower tray has a pattern that allows coiling of the working length required for splicing. To allow for 6 repeated splices, an initial working length of 800 mm is used. The assembly procedure provides instructions for how the fibre should be cut back for repeated splicing, and the lower tray has a system of tracks that allows defined coiling paths for the different lengths that may remain. In the upper tray(s) the splices in their standard heatshrink protective sleeves are stored. The tray has two layers with slots for 14 splices in each. The splice sleeves are secured with foam rubber sheet in-between plates that are locked with screws. The coiling paths in both trays ensures that a minimum bending diameter of 50 mm is maintained.

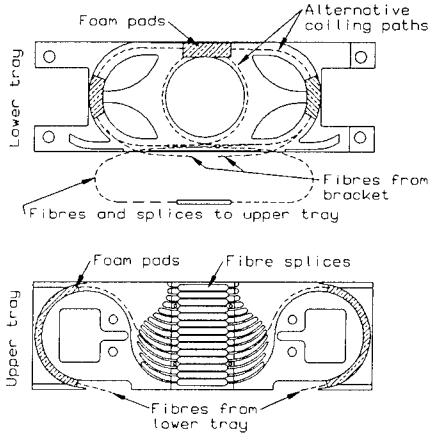


FIGURE 5

Electrical continuity and insulation

The electrical conductor path is led inside the joint through the ceramic gland in the bulkhead by the metal entry tube. An insulated jumper lead is connected to the nut of the metal compression fitting at the end of the entry tube. Insulation of the entry tube is provided by a polymer sleeve with a feed through hole for the jumper lead and obviously also for the fibres. The end of the polymer sleeve is gently curved on the inside, to provide suitable curvature for the fibres that may be led to the upper or lower side of the central bracket.

Inside the joint housing all spark distances are greater than 20 mm allowing for 10 kVDC test voltage.

The electrical jumper lead is jointed with a standard insulated crimp sleeve and again covered by an insulating heat shrink tube.

Remotely pumped optical amplifiers

With the joint equipped with one set of fibre/splice storage trays, the other half of the joint compartment can house a unit with remotely pumped optical amplifiers. A Remote Optical Amplifier Box (RAB) unit containing 6 lengths of Erbium doped fibres, each with an optical isolator can be fitted into the joint housing. As the external shape of the repair joint is unchanged, no special precautions are required in the handling of the amplifier joint on the cable ship. As the present RAB contains 6 Erbium fibres, it is suitable for amplification of a 12 fibre cable. However, with the large splice storage capacity still available in the joint housing (28 on one side) a scheme with two amplifier joints in series will facilitate remote optical amplification for a 24 fibre cable.

Branching unit

Alcatel Submarine Networks has qualified a passive branching unit. Due to the similar external shape of the new joint and the previous moulded joints for these repeatered cables, the new joint fits in the simplified branching unit. As the new joint contains both armour terminations and sealing devices, it relies on the branching unit only for the gimbal hinges and mechanical coupling between the different arms of the branching unit.

Cable end loop-box, earth electrode

If required the new joint can be used as an cable-end loop-box and/or earth electrode during shore end laying or in conjunction with installation of a branching unit. The only difference in this application is that one bulkhead will be exchanged with a pulling eye and/or earth electrode.

Assembly and tooling

The assembly of the joint can be completed by two jointers in less than 12 hrs for an armoured 24 fibre cable. In addition to standard jointers handtools, and equipment for fibre fusion splicing, a set of simple special tools is required. First the hydraulic press tool, which provides a compressive force of up to 200 kN. The hydraulic tool-kit is contained in two boxes 600x400x330 mm weighing less than 40kg in total. The remaining of the special tools consists of a set of purpose designed jigs and spanners, all contained in a box 800x400x330 mm weighing less than 20 kg.

TESTING

Test programme

The repair joint has been developed so as to be able to sustain any anticipated strain during installation and recovery of a submarine fibreoptic cable. A qualification programme was defined from the cable characteristics, industry standards and through discussions with leading cable operators. Completed joints have been tested with respect to ;

Straight Tensile Test: (360 kN maximum tensile load, 1 hr)
The Straight Tensile test was carried out with a load of 90% of the Nominal Transient Tensile Strength rating of the strongest cable in the family (NTTS = 400 kN). To simulate realistic operation, the joint under test and ~75 m of cable under tension to one side of the joint were straight during the test, while the cable under tension on the other side of the joint (also ~75 m) was passed 180 degrees around a 3 m diameter wheel. This simulates the laying wheel of a cable ship after the joint has been passed over the laying wheel with full load on the cable. The long cable length used in the test assures the possibility for separation of end effects related to pulling heads from effects related to the function of the joint itself.

Sheave Passage Tensile Test: (200 kN maximum tensile load, 5x2x180° cycles, around 3m diameter sheave)
Again a total length of 150 m of cable with the joint in the middle were under tension during the test. This length allows the individual fibres and splices to be identified during the test. The test represents a worst case situation as the cable and joint is passed 180 degrees around the wheel. It is otherwise often only used an angle of 135 degrees to simulate a lay angle of 45 degrees.

Temperature cycling (+20°C,-10°C,+35°C,5 cycles, 8hrs.)
Temperature storage (+20°C,-30°C,+60°C, 24 hrs.) :
Both temperature tests were executed on a joint that first had been through the tensile tests. The joint and 70 m of cable each side was reeled onto a drum and placed in the temperature chamber. No effects were observed during the test.

Repeated Bending (Bend Fatigue): (±45° bending, 1m sheave diameter, 100 cycles)
During the repeated bending the joint is kept with a moderate tension, enough to ensure proper function of the BSR. The joint is suspended so that the pivot point is at the maximum diameter of the BSR as it would be over a laying wheel. The repeated bending is executed by a airdriven pendulum ensuring rapid cyclic rate.

Hydrostatic pressure : (300 bar for 24 hrs.)
The joint with ~50 m of cable each side were placed in a pressure tube. Again due to the long cable length under pressure it is possible to isolate effects due to feedthroughs into the pressure chamber from the actual sample under pressure. Pressure is increased in a rate simulating normal laying speed. The sealing arrangements has also been subjected to long term pressurisation (28 days at 300 bar) on component basis to evaluate whether any long term effects could be detected. No long term deterioration were detected, hence the standard pressurisation period of 24 hrs was maintained.

Electrical tests were carried out after the hydrostatic pressure test period, before the hydrostatic pressure were released.

All the tests were carried out with satisfactory results. Neither additional loss nor mechanical degradation were detected in the joint during any of the tests.

The tests demonstrate that the repair joint can be handled as an integral part of the cable, and that more than 90 % of the cable NTTS is preserved in the joint.

REFERENCES

1 G.Berthelsen, I.Vintermyr "New low weight/small diameter optical fibre submarine cable for unrepeatered system" IWCS 1994, p 249 - 255.

3 M.Johansen, E.Betten "Design of an articulated repair joint for a light weight,open fibre optic submarine cable", IWCS 1991, p 531 - 534



Einar Betten

Alcatel Kabel Norge AS
Telecom Cables Division
P.O. Box 130 Økern
N-0509 Oslo, NORWAY

Einar Betten (34) received his M.Sc. in Electrical Machines from the Norwegian Institute of Technology in 1984. He then joined Alcatel and worked with termination, jointing and installation of composite control cables for subsea oilwells in the North Sea. In 1988 he joined the Telecom Cables division, technical department for fibre optics, and has since then worked with development of fibre optic submarine cable accessories, jointing and installation. He has also been cable responsible during marine installations, and project manager for fibre optic submarine cable deliveries.



Terje Bjerkeli

SINTEF
Measurement Technology
P.O.Box 124 Blindern
0314 OSLO, NORWAY

Terje Bjerkeli (58) graduated from Oslo Technical Institute as a Mechanical engineer in 1963 and was employed at SINTEF, Society of Industrial and Technical Research. He has worked in more departments with design and development of a broad range of equipment for various applications and industries. In recent years as a Senior Engineer at the Measurement Technology department he has mainly worked with development of subsea equipment, including electrical and fibre optical oil well instrumentation, high pressure testing equipment, and Subsea Joints for fibre optical cable.

ALTER COURSE CABLE BEHAVIOUR IN WATER DURING LAYING OF FIBEROPTIC SUBMARINE CABLES

Svend Hopland

Telenor AS, Telenor Network, Oslo, NORWAY

ABSTRACT

We have investigated the detailed geometry of fiberoptic submarine cables during laying in alter course regions by studying the shape of towed cable lengths by a transponder technique. We have shown that the towed cable lengths behave individually and attain characteristic geometries through the alter course regions. The alter course region has been found be asymmetric. At the alter course point, the distance between the ship and the horizontal projection of the far end transponder increases approximately linearly with increasing course change as well as increasing sea depth. Actual values of parameters characterising the alter course region have been found for course changes up to 90 degrees and sea depths of up to 650 meters. Found parameter values are valid when a well defined alter course procedure is followed, and can be used for precise cable laying when the cable is laid with zero bottom tension in the alter course region.

1. INTRODUCTION

The installation of light fibreoptic submarine cables in rugged undersea topography has proven to be a difficult task. Telenor AS has during the last years developed an automatic laying concept which is based on selection of optimal cable routes from high quality topography maps provided by a multibeam echosounder route survey [1]. The exact amount of cable payout during laying to accurately fit the bottom topography, is precalculated and fed into the laying computer which automatically pays out cable as the laying ship moves along the cable route's surface line.

Along the uneven Norwegian coastline there are several factors preventing the individual cable routes to be one single straight line between the landing points. Burial of submarine cables into the seabed are costly and therefore generally avoided. Instead we have to round-route the local trawling fields, which also enhances the importance of knowing the exact position of the cable on the sea bed. In addition, when selecting an optimal route through the rugged terrain, the cable route may often change its course. As a result, the final cable route will typically consist of several straight lines; each line connected to the neighbouring line with a suitable curvature.

During laying, the cable ship will typically have to alter course several times. The magnitude of the course changes varies typically between 10 and up to 90 degrees and the sea depth at the alter course points varies typically from 100 meters up to 700 meters. Each time a suitable surface compensation has to be made in order to place the cable in correct position on the sea bed.

We have earlier investigated the cable behaviour when the cable ship moves along straight lines. Here we found that the cable positions in water were generally very close to the vertical plane through the ship's surface line [2]. However, in the alter course regions, the cable positions may differ significantly from the ship 's surface line. Up to now, no experimental investigations in a practical scale have been reported showing the detailed behaviour of cables in water in alter course regions. In this work, we have used a towing technique to reveal the actual shape of practical cable lengths in water near alter course points.

2. CABLE CHARACTERISTICS

We have investigated lengths of single armour (SA) cable and double armour (DA) cable. The cable weights in water are 1.1 kg/m, and the outer diameters are 25.1 mm and 23.2 mm for the SA cable and the DA cable, respectively. The cables have outer sheaths consisting of HDPE with a smooth outer surface. The hydrodynamic constants for the cables have been determined in a separate steady state towing experiment. The key parameters are shown in Table 1.

Cable type	Weight in water (kg/m)	Outer diameter (mm)	Outer sheath	Hydrodynamic constant (degree-knots)
SA	1.1	25.1	HDPE	68.8
DA	1.1	23.2	HDPE	68-72

Table 1: Cable parameters of the investigated cables.

3. EXPERIMENTAL METHOD

When cables are laid with zero bottom tension, the normal drag force acting on the cable will determine the actual shape of the cable in water. The tangential water resistance is negligible for our cable types at normal laying speeds, and the cable geometry in water during laying will be equivalent to the geometry of a corresponding towed cable length in water [3]. We can therefore investigate cable behaviour in water during cable laying by studying the behaviour of towed cable lengths.

3.1 Equipment

The towing was performed in Norwegian fjords at suitable sea depths. Several small size and low weight cylindrical hydroacoustic transponders were attached to the cables.

The towed cable lengths were typically 200-1000 meters in order to investigate cable lengths which were of the same length as in a practical laying situation. The cable length interval between two neighbouring transponders was typically 75-100 meters, and up to eight transponders were used simultaneously on the cable. The far end transponder was attached 25 meters from the cable end in order to avoid end effects. Since transponder sizes and weights are small, we may assume that the transponders have marginal effect on the towed cable geometries.

On board the ship, a hydroacoustic transducer unit collected continuously data from the submerged transponders and the position of each transponder relative to the ship was accordingly calculated with high accuracy. During towing, the transponder positions are continuously monitored in 3 dimensions, and the actual shape of the towed cable lengths in water have been calculated. The chosen transponder spacing gave a satisfactory resolution of the towed cable geometry.

The towing ship used differential GPS navigation equipment, which monitored accurately the ship' s position, velocity and course. Also cable tension was recorded in order to observe possible variations in tension during towing.

3.2 Course change procedure.

It is of great importance that the procedure for course change is well defined, simple and easy to perform, and reproducible from time to time. We have chosen a method which fulfils these requirements.

The towing took place along straight lines with intermediate course changes of varying magnitude of up to 90 degrees in both directions. In the alter course region, the ship followed the two intersecting lines as closely as possible. The ship speed was kept constant in the typical laying speed range of 1.5-2.0 knots. Due to the requirement to maintain a constant laying speed through the alter course region, the actual surface line of the ship will show a small radius of curvature in the close vicinity of the alter course point. During the towing tests and during actual cable laying, we have experienced that course changes with a ship's radius of curvature of typically 50-100 m, can be routinely performed.

4. RESULTS

4.1 General

An alter course region where the projected lines of the transponders on the surface deviates from the ship's surface line, defines the area of interest.

The instant cable geometry in the alter course region is described by a horizontal and a vertical projection. The horizontal projection shows the projected positions on the surface of all transponders as well as the position of the ship. The vertical projection shows the corresponding layback of each transponder projected on the vertical plane in the direction of the ship's gyro, as well as the depth.

By calculating cable geometries at regular intervals during the alter course period, and plotting the results into the horizontal and the vertical projections, a clear picture of the behaviour of the cable in water through the entire alter course region, can be obtained.

We have found that the horizontal projections of cable geometries through the alter course region can be described by a few key parameters. A schematic drawing of a typical horizontal projection is shown in Figure 1, where the key parameters describing the cable behaviour, are shown.

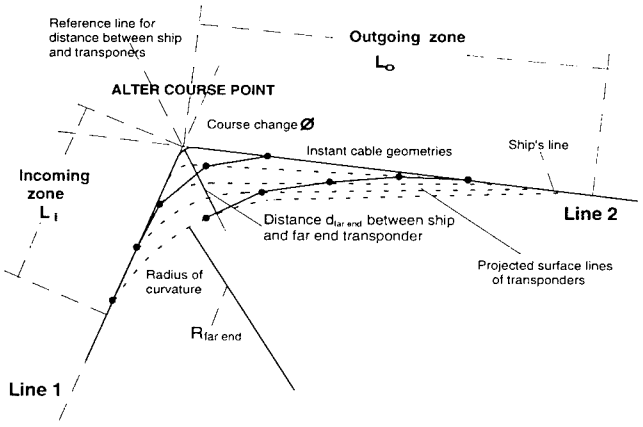


Figure 1: Horizontal projection of cable with 4 transponders: key parameters.

The total length of the alter course region is $L = L_i + L_o$, where L_i is the length on the incoming side of the alter course point and L_o is the length on the outgoing side.

At the incoming side and tangential to the ship's incoming line (LINE 1), each transponder line can be characterised by a radius of curvature R, which increases when the transponder depth increases.

At the outgoing side, the transponder lines are nearly straight lines which slowly approach the ship's outgoing line (LINE 2).

Finally, an important parameter is the distance $d_{far\ end}$ between the ship's line and perpendicular to the far end projected transponder line, which is at its maximum at the alter course point.

4.2 Experimental results

Initially, a cable length of approximately 420 m of DA cable, containing 4 transponders, was deployed. At the speed of 1.5-2.0 knots, the far end transponder was travelling at a sea depth of 225-275 m. The cable length was then reduced to 220 m and 2 tranponders were removed. In this case, the far end transponder was travelling at a sea depth of 120-140 m.

Secondly, a cable length of approximately 1000 m of SA cable, containing 8 transponders, was deployed. When towing at normal laying speed, the far end transponder was travelling at a depth of 550-650 m.

In Figure 2 is shown the actual horizontal projected geometries through the alter course region of the DA cable with 4 transponders, when the ship have performed a course change of 71 degrees. In Figure 3 is shown the corresponding vertical projection.

From Figure 2 we find that the distance $d_{far\ end}$ between the ship and the projection of the far end transponder at the alter course point, is approximately 80 m when performing a course change of 71 degrees at a sea depth of 250 m. The corresponding value of $R_{far\ end}$ is approximately 250 m, and the total length of the alter course region L is approximately 950 m.

From Figure 2 and Figure 3 we can observe some features which were common for all deployed cable lengths. These are:

- The alter course region is asymmetric with a length of the outgoing zone L_o which is considerably greater than the length of the incoming zone L_i. A typical ratio have been $L_o/L_i = 3$, which have been nearly constant for all deployed cable lengths and nearly independent of the magnitude of the course change. However, L_o and L_i have increased when the deployed cable length have increased, as shown later in Figure 8.

- The transponders closer to the ship follow markedly different lines, while the deeper part of the cable, represented by the transponders closer to the end of the cable follow nearly the same trajectories. This effect is also evident from Figures 4-6, shown later in Section 4.2.

- In the alter course region, the depth of the far end transponder and the other transponders as well, increases temporarily by a small amount. This could also be registered on the cable tension, which increased correspondingly. One reason for this was that the speed of the ship tended to decrease in a short period in the close vicinity of the alter course point. Also, the fact that the cable experience on average a lower speed than the ship through the alter course region, will cause a similar effect, which will increase when the magnitude of the course change increases.

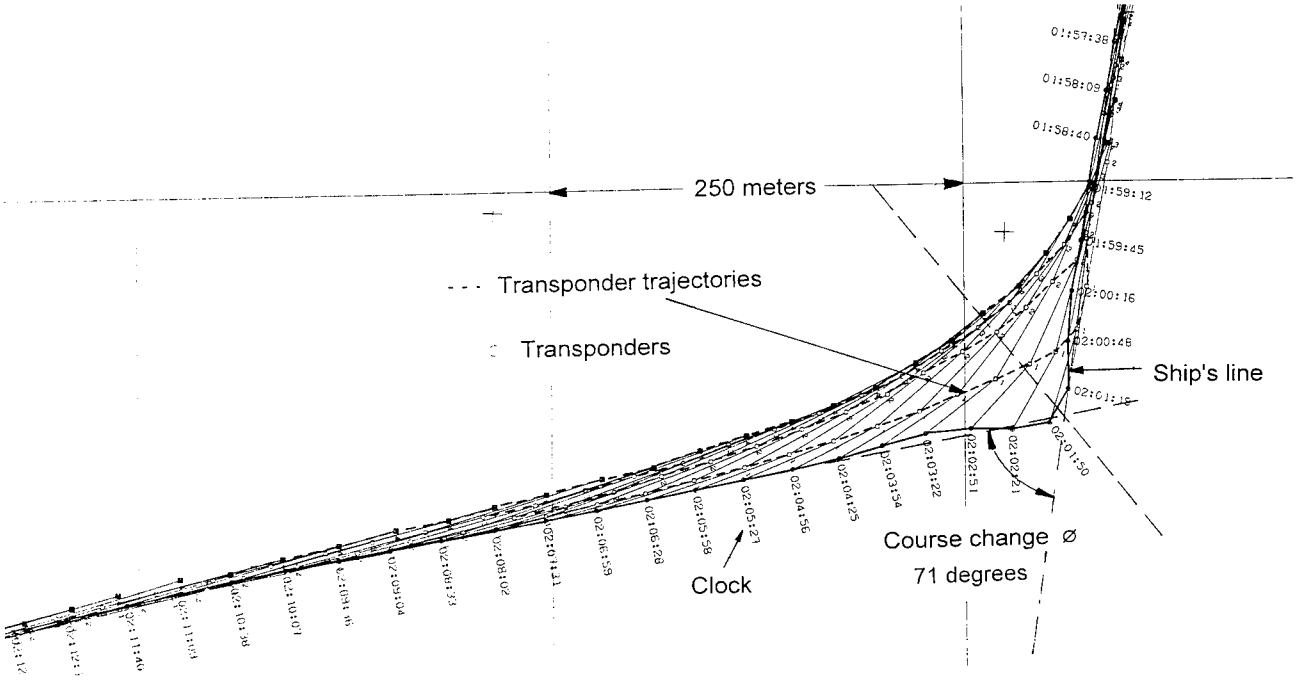


Figure 2: Horizontal projection of geometries for DA cable with 4 transponders.

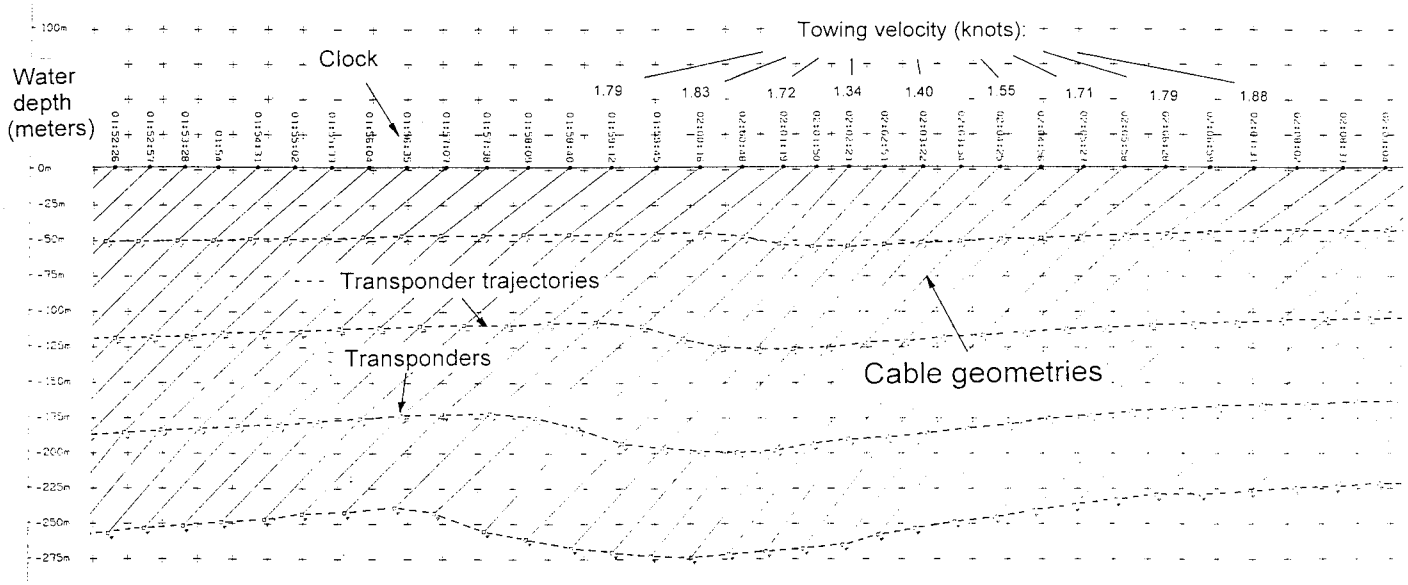


Figure 3: Vertical projection of geometries for DA cable with 4 transponders.

Using the horizontal plots for each deployed cable length, we have measured the distance between the ship and the projected transponder lines with reference to a line drawn through the alter course point and perpendicular to the projected line of the far end transponder. In Figure 4-6 are shown the distances between ship and transponders at the reference line as a function of the magnitude of the course change, for the different deployed cable lengths. Included in the figures are also the corresponding radius' of curvature for the far end transponders.

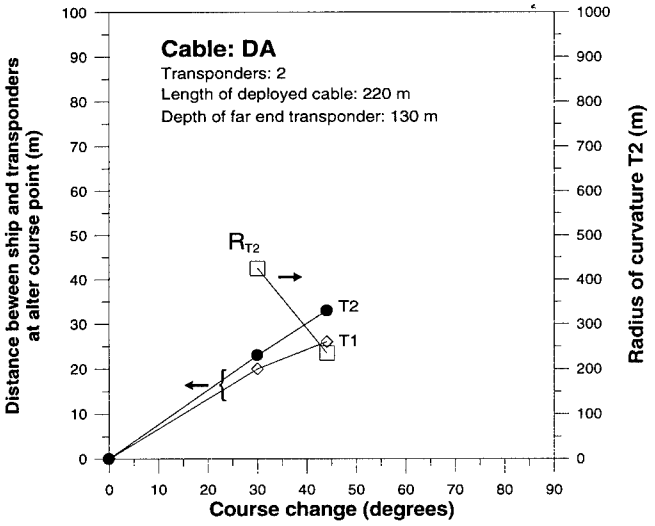


Figure 4: Horizontal distance between ship and transponders at alter course point/ Radius of curvature for far end transponder: DA cable with 2 transponders.

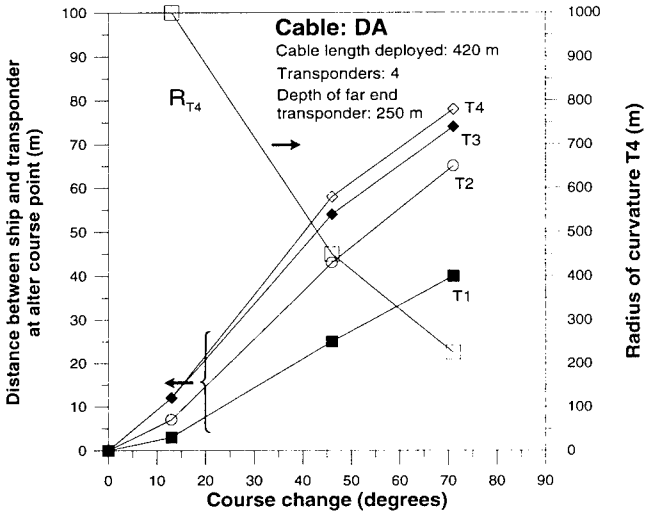


Figure 5: Horizontal distances between ship and transponders at alter course point/ Radius of curvature for far end transponder: DA cable with 4 transponders.

We observe from Figures 4-6 that the horizontal distance between the ship and the far end transponder as well as the intermediate transponders increases nearly linearly with the magnitude of the course change in the range of course changes that we have examined.

Furthermore, the results in Figure 4-6 clearly show that each deployed cable length has its own individual geometry behaviour and the far end transponder will thus represent the deployed cable length as a whole. We note as a consequence that it is not possible to predict the geometry of the towed 220 m DA cable length from the results of the deployed 420 m DA cable.

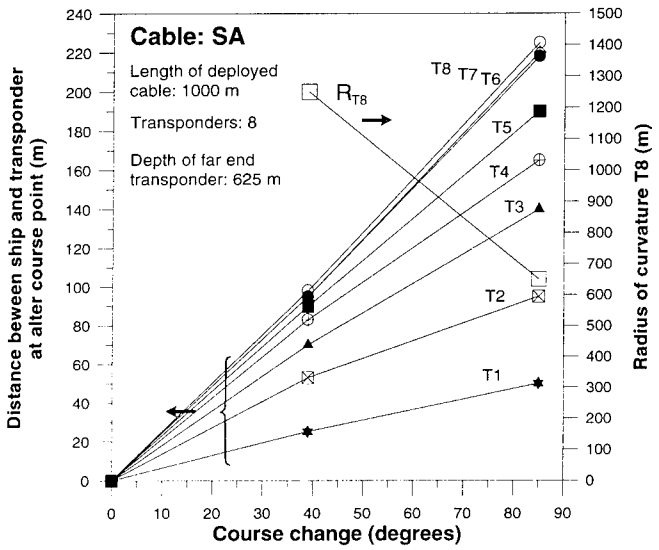


Figure 6: Horizontal distances between ship and transponders at alter course point/ Radius of curvature for far end transponder: SA cable with 8 transponders.

Since the weights, outer diameters and hydrodynamic constants for the SA and DA cable are essentially identical, the results in Figures 4-6 can be compared directly. Using both DA and SA results, we have plotted the horizontal distance between the ship and the far end transponder, $d_{far\ end}$, versus sea depth at constant course change angle. We have also included corresponding calculated values of radius of curvature for the far end transponder. The results are shown in Figure 7. We observe that $d_{far\ end}$ increases approximately linearly with increasing sea depth.

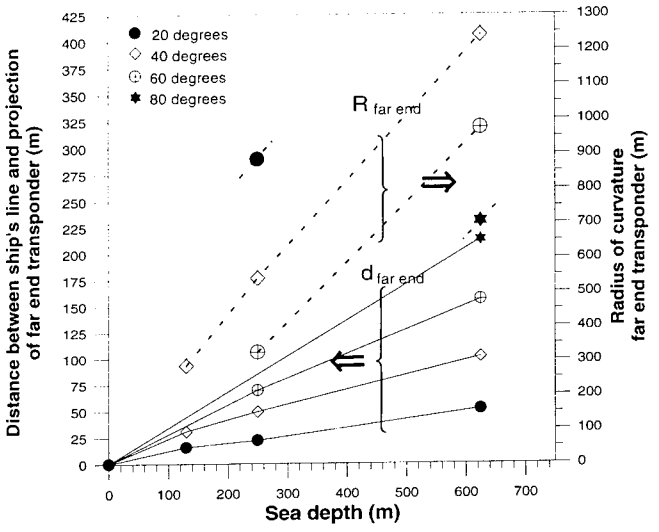


Figure 7: Horizontal distance between ship and far end transponder at alter course point/Radius of curvature far end transponder versus sea depth at constant course change.

Furthermore, we have measured the length of the incoming zone and outgoing zone as well as the ratio L_o/L_i . There is little variation of L_o and L_i when the magnitude of the course change varies for the same deployed cable length. However, L_o and L_i increases when the deployed cable length increases, as shown in Figure 8. We note that L_o and L_i increases almost linearly with increasing sea depth, while the ratio L_o/L_i remains nearly constant at 2.5-3.0.

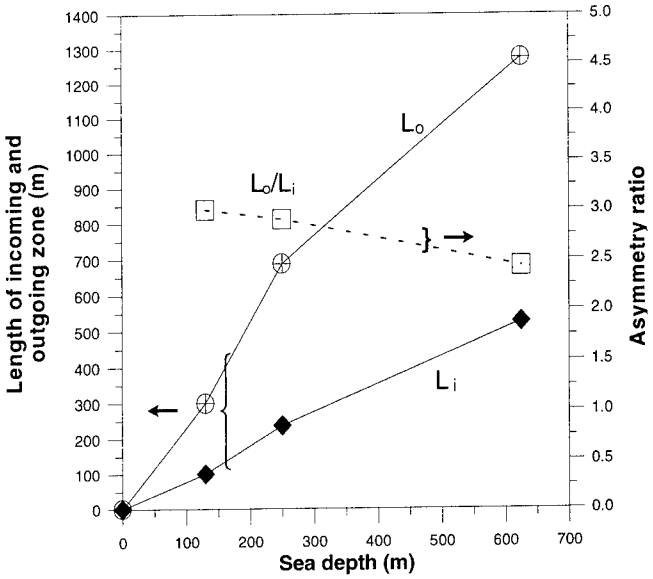


Figure 8: Length of incoming and outgoing zone/asymmetry ratio versus sea depth.

5. INSPECTION OF LAID CABLE

In an early phase of the development of our cable laying concept, an ROV-inspection was performed on a small number of laid cables including a few alter course regions. During laying of these cables, cable payout was manually controlled and attention was not strongly focused on the detailed alter course procedure and laying with zero bottom tension through the alter course region. However, in one occation a SA cable was laid under conditions comparable with the towing experiments. The results of the ROV-inspection of the SA cable are shown in Figure 9.

We note that the horizontal distance between the cable ship and the cable position on the sea bed is approximately 110-120 m for a course change of 58 degrees at a sea depth of 450 m. The results from the towing experiments indicate a value of approximately 120 m (Fig. 7), which is in good agreement. Due to varying sea depth through the alter course region, it is not possible to directly compare the values of the other parameters.

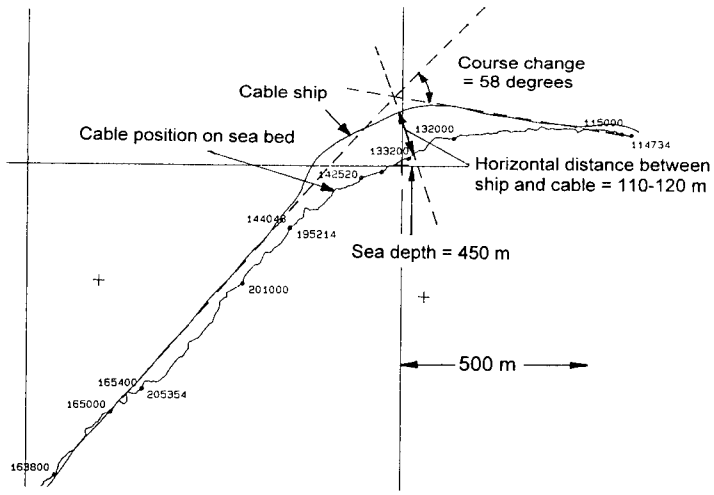


Figure 9: ROV-inspection of laid SA cable.

6. DISCUSSION

The results of the towing experiments are valuable for cable laying in alter course regions. By basically steering the cable ship accurately along the straight lines, the results give guidance for estimating the actual position of the cable on the sea bottom. Vice versa, the straight lines can be chosen to give a desired position of the cable on the sea bottom.

The results are obviously only valid under the conditions that the cable is laid with zero bottom tension, and that the defined alter course procedure has been followed. Laying with bottom tension will result in greater distance between the laying ship and the projection of the actual cable position on the sea bed than indicated in Section 4.2.

During the towing experiments, we have seen indications that if the ship has followed a large surface radius of curvature when changing course, the distance between the towing ship and the projection of the far end transponder has been less than indicated in Section 4.2. If the towing ship in the alter course region has made an outdrop in opposite direction of the course change, the distance between the towing ship and the projection of the far end transponder has been greater than indicated in Section 4.2.

Our full range of fibreoptic submarine cables have different types of armouring and the cable weights in water and outer diameters are varying between 0.6-1.8 kg/m and 22-31 mm, respectively. All cables have outer sheaths consisting of HDPE with a smooth outer surface.

The resistance against lateral movement in water increases as the square of the lateral velocity and proportionally with cable diameter [3]. In an alter course situation, the average lateral velocity experienced by the cable is determined by the towing speed and magnitude of the course change, and should be independent of cable type. Cables with 10-20 % higher or smaller diameter than the cables investigated here, "resists" somewhat more or less against lateral movements, and the displacement of such cables from the ships line could be expected to be less or greater than indicated in this investigation. However, the towing situation is very complex, and one should await further experiments to draw any conclusion. Nevertheless, significant differences are not likely to occur.

We have improved our laying concept in alter course regions by selecting the distance between the cable ship's surface line and the projection of the desired position of the cable on the sea bed according to the results of the towing experiments. Also, the cable payout in the alter course region has been calculated according to the towing results and used during laying, in order to lay the cable with zero bottom tension through the alter course region as well as to obtain the correct position of the cable on the sea bed.

7. CONCLUSION

We have investigated the detailed behaviour of fiberoptic submarine cables in water in alter course regions by towing practical cable lengths at depths frequently encountered in our coastal waters.

The results of the towing experiments have shown that towed cable lengths behave individually in water and attain characteristic geometries through the alter course region. The far end transponder will in fact represent the deployed cable length as a whole, and the intermediate transponders will only give information about the geometry of the deployed cable length, and cannot be used to predict the behaviour of other towed cable lengths.

We have found that the alter course region is asymmetric, with a length of the outgoing zone L_o of typically 3 times the length of the incoming zone L_i. The distance between the ship and the projection of the far end transponder, $d_{far\ end}$, increases approximately linearly with increasing course change ϕ as well as increasing sea depth. For a fiberoptic cable with weight in water of 1,1 kg/m and an outer diameter of 23.2 mm, $d_{far\ end}$ is approximately 80 m when performing a course change of 71 degrees at a sea depth of 250 m. The corresponding value of $R_{far\ end}$ is approximately 250 m, and the total length of the alter course region L is approximately 950 m.

Good agreement is found between towing results and actual found positions of an SA cable on the sea bed in an alter course region.

The values of the parameters $d_{far\ end}$, $R_{far\ end}$, L_i and L_o are not expected to be significantly different for cables with slightly higher or lower outer diameters.

With respect to cable laying, the results are valuable for estimating cable position on the sea bed in alter course regions. It should be noted, however, that the found parameter values are valid only when the defined alter course procedure is

followed, and when the cable is laid with zero bottom tension in the alter course region.

We have used these results in our cable laying concept to estimate the correct surface compensation and cable payout in alter course regions in order to obtain the correct position of the cable on the sea bed.

8. ACKNOWLEDGEMENT

The author wishes to thank Emil Marhaug and his crew at Telenor AS, for supplying mechanical equipment and invaluable assistance with the deployment of the cables during the fjord trials. Also great thanks to Kjell Martin Dukefoss and Dag Viken at Geoteam A/S, for supplying ship and navigation equipment, and assisting with processing and plotting the data.

9. REFERENCES

[1] Svend Hopland and Albert Klykken: "Installation of submarine fiberoptic cables in rugged coastal terrain". Proceedings IWCS 1992, Reno Nevada, pp. 492-496.

[2] Svend Hopland: "Investigation of cable behaviour in water during laying of fiberoptic submarine cables". Proceedings IWCS1993, St. Lois Missouri, pp.734-739.

[3] E. E. Zajac: "Dynamics and Kinematics of the Laying and Recovery of Submarine Cable". Bell System Technical Journal, September 1957, pp.1129-1207.



Svend Hopland

Telenor AS
Telenor Network
P.Box. 6701, St.Olavs Plass
Oslo, NORWAY.

Svend Hopland graduated from the Norwegian Institute of Technology in 1985 with a PhD. on optical fibres. In 1986 he joined Norwegian Telecom (now Telenor AS), where he is presently a senior engineer on fiberoptic cables.

Field experiences of jelly-filled cables for aerial trial

Hui-Fen Lin, Chi-Hsiang Hsieh, Chih-Chiang Pei, Yih-Horng Hwang, Hsi-Pai Hsu, Y.-C. Lin, Kuang-Yi Chen

OSP, Telecommunication Laboratories, DGT, MOTC
12, Lane 551, Min-Tsu Rd., Sec. 3, Yang-Mei, Taoyuan 326, Taiwan, R.O.C.

Abstract

A jelly-filled copper cable is testing to evaluate its feasibility and reliability of aerial deployment. Its characteristics were measured in laboratory for its water (humidity) resistance and high temperature aging effects. Further field trials were also conducted in a test field for three years and rural mountain areas for one year. Results have shown no apparent degradation on the insulation (e.g. no cracks or mechanical properties drops). The evidences prove the improved jelly-filled cable is suitable for aerial deployment and is superior to air-core cable in humidity resistance, specially, in the mountain areas where the cables are suffered by foggy humidity and animal destruction.

Introduction

Traditionally, aerial deployment cables in rural mountain areas are neither gas-pressurized nor jelly-filled. In Taiwan, the mountain areas usually are foggy and under high humidity all the year around. Telecommunication cables in such areas have long been suffered by insulation problems arising from broken sheath mostly caused by animal destruction. Therefore, jelly-filling as a humidity-barrier is taken for serious consideration since it is economical, easy deploying, and, most importantly, is compatible with existing system and equipment. However, Taiwan is located in the semitropical weather zone. Temperatures recorded in aerial outside plants can be as high as 70°C[1], and the possibilities of jelly flowing and leaking, or interaction with insulation resulting to insulation cracks, oxidative induction time (OIT) drops are the first thing to be solved if such cables are intended for aerial deployments. By adapting improved jelly compounds and insulation materials for aerial cable, we have finished several laboratory tests[2,3] for water-resistance and high temperature aging from original jelly filled cable. Furthermore, laboratory field trial for three years[4] and mountain field trial also have been conducted to evaluate its feasibility and reliability under actual weather conditions and environmental destruction. After 12 months mountain field trial, the results and experiences of general jelly-filled cable are collected and reported here.

Experimental

Test cables, trial sites and deploy time

Two jelly-filled cables, one 50 pair 0.65mm conductor diameter and the other 30 pair 0.65mm conductor diameter, were deployed at mountain areas in central Taiwan on the end of July 1994. The original air-core cable in this route remained in service and served as a control.

Cable capacitance test

Cable capacitance was measured by cable capacitance tester DCM (Model:MINI-C6B) with 1 KHz frequency.

Cracks of insulation, mechanical properties and OIT test

Two sets of insulation samples, straight and twist, were placed in RA boxes for field aging. Straight samples are used for monitoring mechanical properties changes(e.g. break load and elongation) and twist samples for checking OIT and crack of insulation. Twist samples were prepared by twisting both end of a 15 cm insulation together for 10 times. Both straight and twist samples contain 10 pieces of colored insulations (blue, yellow, green, red, purple, brown, black and 3 pieces of white) in a set. Each RA box has 6 sets of samples that allow six tests.

(1) Insulations crack

The cracks of insulation was judged by visual examination directly from the skin of insulation.

(2) Mechanical properties test

Break loads and elongation of insulation was test by Instron(model 1122). Gauge length and pull speed were set as 30 mm and 200 ± 20mm per minute at ambient temperature.

(3) Insulations OIT test

The OIT values were obtained from three samples (white, brown and black) of twist insulation. OIT test was following the method of ASTM D4565-86[5]. 5 mg sample was placed in an aluminum pan that was then moved into the chamber of Differential Scanning Calorimeter (Perkin Elmer, DSC-2C). The initial temperature was set at 100 ℃. After purging nitrogen for 5 minutes, the temperature was quickly increased to 200 ℃ in a rate of 40 ℃ /min. The temperature was hold for 2 minutes and then the oxygen was introduced into the chamber to replace the nitrogen in a flow rate of 50 ml/min . The OIT values were measured from the start of oxygen inlet to the time when exothermic decomposition occurred. Each sample was tested 3 times and the average value was reported.

Results and Discussion

Fig. 1 shows the map of cable deployment. Thick line represents the 50 pair cable and thin line corresponds to 30 pair cable. Pole number were labeled to indicate where the cable ended.

The changes of cable capacitance in the period of 12 months deployment are shown in Table 1. The cable was installed on the end of July 1994 and the initial test of capacitance was done two weeks after the installation on the beginning of August 1994. Pair 11 to 16 and pair 23,24 were used as temperature sensor's wires, and therefore were not monitored. Pair 3 to 8 and pair 17 to 20 show very low capacitance values in the first 2.5 months beginning. This was corrected when a knife, a scar on the cable was found near the pole #70R12. And broken conductors were reconnected. Apparently, the damage was caused shortly after the deployment. The unusual capacitances shown on pair 4 and 5 at the 12th month were caused by customers' phonesets, and the obvious loss values of pair 41 and 42 at the 12th month were caused by disconnected wire. There are other irregulars, for example the pair 26 displayed unusual high values and the pair 9's value dropped from 54 to 25 after two month deployment. Since this route was designed to be free access, T-taps complicate the testing situation and we were still working on to resolve those problems.

During the field trial, we do not see any dropping jelly until the 12th month. The RMS test[6] relates that the higher temperature results the lower viscosity of jelly. According to our current specification, the temperature for drip test is 60±1 ℃. It is clear from this field trial that the temperature for drip test for aerial jelly-filled cable has to be increased.

With visual examination, we could not find any crack on the surface of insulation samples. Table 2 shows the changes of their mechanical properties. The result indicated that there are no significant difference throughout the trial.

The OIT value of insulation is an important indicator for insulation aging. Table 3 shows the insulation OIT values. We find that the OIT values are decreasing and those samples in the RA box of lower elevation have the largest change. This result is reasonable, since the higher temperature causes the aging fasten.

The customers' fault complain record were also collected as a reference to the status of the trial cable , since the field trial jelly-filled cable is the final part of the whole cable plant at the same time. During the deployment, 5 customers' lines were moved from original air-core cable to the trial cable. Table 4 shows the customers' fault complain record of both original and trial cables. We can see the user of new cable is increased at the expense of original cable. In jelly-filled trial cable, there are 14 fault complains after the deployment of jelly-filled cable in a period of 12 months. However, the first 8 complains were due to the knife damage mentioned above. Among the rest 6 complains, one was due to a fault from trunk cable and one other was caused by customer's phoneset. Thus, only 4 complains were probably due to faults of the trial cable in a period of 8 months. This result is much better compared with those of the original air-core cable in the period of July 1993 to June 1994.

Conclusion

After 12 months trial of jelly-filled cable for aerial deployment, we found no apparent degradation on the insulation (e.g. no crack or mechanical properties drops) but that jelly drop test temperature has to be increased to well above 60 ℃. In addition, the record of customer fault complains showed significant improvement of reducing users' fault complains by using the jelly-filled cable.

Reference

1. S.I. Wang, H.F.Lin, D.M.Fann, *Telecommunication Labs. internal report* 80-LL-083, 1991
2. D.M.Fann, H.F.Lin, H.Y.Shih, *ANTEC* 1989, p.1178.
3. S.I. Wang, H.F. Lin, C.H. Hsieh, D.M. Fann, *Telecommunication Labs. internal report* 82-LL-055, 1993
4. H.F. Lin, S.I. Wang, C.H. Hsieh, D.M. Fann, *Telecommunication Labs. internal report* 82-LL-074, 1993
5. ASTM D4565-86, "Standard test method for physical and environmental performance properties of insulations and jackets for telecommunications wire and cable".
6. D.M. Fann, H.Y.Shih, H.F. Lin, T.F. Chan, H.M. Chang, *Telecommunication Labs. internal report* 78-LL-043, 1993

Authors



Hui-Fen Lin received her B.S. degree in Chemistry from Chung-Yuan University and joined T.L. in 1981. She is now a associate research engineer and a member of outside plant laboratory in T.L..



Chi-Hsiang Hsieh received his M.S. degree in chemical engineering in 1991 from National Taiwan Institute of Technology and then directly joined T.L.. He is now an assistant research engineer and a member of outside plant laboratory in T.L..



Chih-Chiang Pei received his M.S. degree in chemical engineering in 1993 from National Taiwan Institute of Technology and then directly joined T.L.. He is now an assistant research engineer and a member of outside plant laboratory in T.L..



Yih-Horng Hwang received his M.S. degree in Fiber and Polymer Engineering in 1992 from National Taiwan Institute of Technology and then directly joined T.L.. She is now an assistant research engineer and a member of outside plant laboratory in T.L..



Hsi-Pai Hsu is currently a project manager of the material group of Loop and Outside Plant Laboratory, Telecommunication Labs. . He received his Ph.D. degree in Chemistry in 1983 and has engaged in industrial materials research since then.

Yih-Chyuan Lin received his B.S. degree in chemistry in Taiwan and his Ph.D. degree in Photochemistry from Georgetown University. After working as a postdoctoral Fellow in the Institute of Materials Science at the University of Connecticut, he joined Telecommunication Laboratories in 1989 and presently is a project leader of O.S.P. material and construction.

Kuang-Yi Chen was born in 1953 and received his Ph.D. degree in Electro-optics from National Central University in 1990. He has been engaged in research and development of optical fabrication and communication technologies since 1977. He is currently the director of outside plant technology laboratory of Telecommunication Labs.

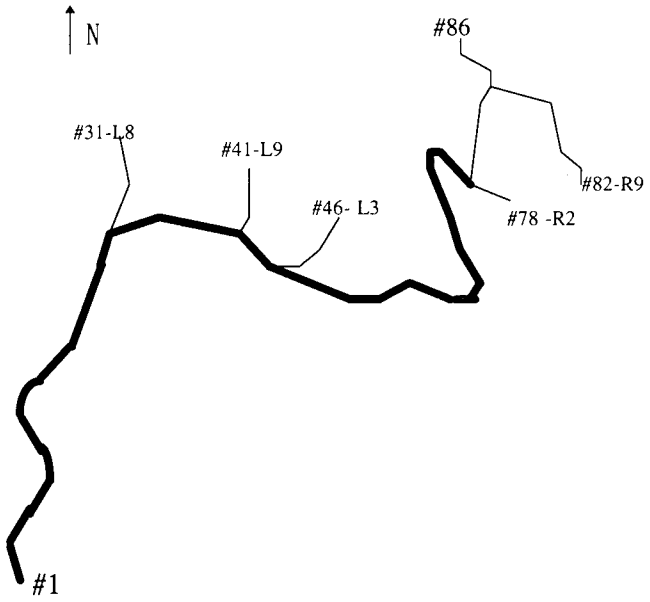


Fig. 1 The map of cable deployment

Table 1. Changes of cable capacitance (unit: nf/km)

No. of pair	initial	1 Month	2.5 Months	4 Months	6 Months	8 Months	12 Months
1	51.36	51.58	51.69	51.49	51.24	51.27	51.76
2	53.85	53.85	49.86	49.68	50.07	50.11	53.62
3	3.91	3.82	3.52	51.18	51.70	51.72	51.13
4	7.13	7.13	7.13	52.89	52.99	52.76	271.04
5	6.92	6.92	7.01	54.00	54.25	54.32	28.79
6	7.01	7.13	7.01	54.59	54.71	54.8	62.44
7	11.2	11.02	11.37	54.37	54.66	54.66	54.75
8	11.47	11.47	11.40	54.71	56.09	56.09	55.43
9	53.85	53.85	25.29	26.09	26.07	24.28	27.83
10	55.20	55.20	55.48	55.48	55.79	55.93	54.75
17	7.13	7.06	7.05	54.95	55.09	55.18	54.52
18	7.10	7.08	7.05	54.91	55.18	55.18	54.75
19	7.01	7.01	7.03	54.30	54.52	54.55	53.85
20	11.61	11.31	11.21	54.89	55.09	55.09	54.75
21	60.02	60.02	62.80	62.82	63.11	63.16	62.49
22	62.93	62.9	63.14	65.44	65.08	66.18	65.40
25	64.28	64.50	64.61	64.64	64.88	64.97	64.28
26	111.98	111.98	112.99	86.45	85.11	86.67	78.61
27	64.28	64.28	64.32	64.37	64.70	64.73	28.44
28	64.73	64.73	64.88	64.82	65.98	66.00	64.50
29	63.83	64.05	61.43	62.19	62.35	62.26	60.47
30	80.40	80.18	82.02	80.09	79.73	81.75	100.11
31	43.99	43.99	44.08	44.08	44.36	44.38	42.68
32	43.99	44.18	44.23	44.16	44.45	44.51	44.73
33	44.18	44.36	44.36	44.34	44.55	44.60	44.18
34	44.55	44.55	44.62	44.60	44.83	44.90	44.36
35	44.55	44.55	44.62	44.64	44.85	44.92	44.36
36	45.11	45.10	45.24	45.24	45.41	45.52	45.11
37	45.11	45.30	45.22	45.20	45.44	45.52	45.11
38	37.47	37.65	37.60	37.60	37.89	37.89	37.47
39	44.73	44.73	38.58	44.81	45.67	45.09	44.55
40	45.11	45.30	38.60	38.40	38.45	38.12	38.68
41	40.82	40.26	40.19	39.89	39.93	39.74	5.41
42	44.55	44.73	44.70	44.66	44.86	44.94	5.41
43	42.87	42.68	43.00	42.44	43.17	43.04	42.31
44	9.69	9.71	9.63	44.68	44.94	45.01	40.26
45	44.73	44.73	44.77	44.75	45.00	45.11	44.55
46	44.73	44.73	44.81	44.77	45.00	45.13	45.55
47	44.73	44.92	44.96	44.99	45.24	45.29	44.73
48	45.11	45.30	45.33	45.33	45.57	45.63	45.11
49	45.11	45.30	45.14	45.20	45.39	45.52	45.11
50	45.48	45.67	45.59	45.59	45.83	45.93	45.29

Table 2. Changes of break loads and elongation of insulation

Time	Break load(kg)			Elongation(%)		
	#15	#63	#78-1	#15	#63	#78-1
0	0.89 ± 0.11			607 ± 26.8		
3M	0.89 ± 0.11	0.88 ± 0.11	0.91 ± 0.13	599.6 ± 35.5	599.6 ± 27.5	612.7 ± 27.8
6M	0.87 ± 0.12	0.93 ± 0.12	0.89 ± 0.09	590.6 ± 36.1	600.4 ± 26.9	597.2 ± 22.8
12M	0.77 ± 0.13	0.86 ± 0.12	0.85 ± 0.12	599.5 ± 27.5	600.6 ± 33.6	600.9 ± 28.2

Table 3. Changes of OIT value of insulation

Time	#15	#63	#78-1
0	45.5 ± 5.9		
3M	50.4 ± 6.9	46.7 ± 6.2	51.9 ± 7.1
6M	40.2 ± 7.4	46.5 ± 5.0	48.6 ± 5.5
12M	35.4 ± 1.1	43.6 ± 5.7	45.5 ± 1.1

Table 4. Fault complains of both new and old copper cable

Date	Original air-core cable				Jelly-filled trial cable			
	Customer lines	No. of fault complains	Total	fault complains /(user x month)	Customer lines	No. of fault complains	Total	fault complains /(user x month)
7-12 '93	19	19	19	0.17				
1-6 '94	19	23	23	0.20				
7 '94	21	2	32	0.01			9	
8 '94	16	11		0.69	5	6		1.20
9 '94	16	13		0.81	5	0		0
10 '94	14	1		0.07	7	2		0.29
11 '94	14	2		0.14	7	0		0
12 '94	13	3		0.23	8	1		0.13
1 '95	10	0	2	0	11	0	5	0
2 '95	8	0		0	13	0		0
3 '95	7	1		0.14	14	2		0.14
4 '95	6	1		0.17	15	0		0
5 '95	6	0		0	15	1		0.07
6 '95	5	0		0	16	2		0.13

A METHOD FOR EVALUATING CABLE RESISTANCE TO DAMAGE BY POCKET GOPHERS AS ADOPTED BY THE USDA/APHIS/ADC/DWRC

Geraldine R. McCann
Biological Science Technician (Wildlife)

U.S. Department of Agriculture/Denver Wildlife Research Center
Denver, Colorado

ABSTRACT

Pocket gopher damage to underground cables causes significant economic losses to the communications and power industries. The Denver Wildlife Research Center (DWRC) has confidentially collaborated with these industries for many years in the development of cables and duct resistant to pocket gopher damage. The laboratory testing developed by DWRC has provided a valuable challenge for many industry engineers and has stimulated the research and development of rodent proof communications and power cables.

INTRODUCTION

Initial cable evaluations were conducted at the Denver Wildlife Research Center (DWRC) by J.R. Tigner. Procedures have been modified and improved by several researchers, including N.J. Cogelia, R.A. Connolly, R.E. Landstrom, and G.K. LaVoie. Effective laboratory analysis of the potential for pocket gopher damage to cables provides the initial data for field evaluations. The pocket gopher (family Geomyidae) is a medium-sized fossorial (burrowing) rodent having a powerfully built upper body, large, strong claws on the forefeet[1], and rapid incisor growth which facilitates digging or chiseling. To keep the incisor length in check, the pocket gopher routinely finds materials to gnaw, and buried cable is a likely item [2,3,4].

The plains pocket gopher (Geomys bursarius) was selected for the cable evaluation because it is widely distributed in the U.S. on the Great Plains (generally occurring from the Rocky Mountains to the Mississippi valley and from northern Minnesota to the gulf coast of Texas). It is larger and more capable of damaging cable than most Thomomys species, and it has been identified as a major cause of damage to communication and power cables.

METHODS

Cable preparation: An evaluation involves 10 cable replicates, each approximately 100-152 mm long. An individual sample is attached (using 18-gauge steel wire) horizontally across an opening of 51 x 50 mm in a stainless steel panel (18 cm square). When the cable is positioned on the panel, the gaps between the panel and the cable must be large enough for the gopher to get its incisors on the cable without interference from the panel. The pocket gopher must have non-restrictive access across the majority of the top and bottom edges of the cable. Cables are attached securely enough to prevent shifting or rolling. Each panel is numbered to coincide with the pocket gopher's number, and inserted widthwise into the cage.

Many types of cable have an overlapping armor shield with an unsoldered horizontal seam; this is recognized as a potential weakness in the cable. To enter this variable into the evaluation, it is necessary to position the cable with the outer edge facing in (towards the animal) and downward. This enables the gopher's bottom incisors to grip the metal lap, thus providing the most potential for damage. When cables are being evaluated for a chemical repellent treatment, it is important that the cable manufacturer's specifications be reviewed for handling precautions. A Material Safety Data Sheet (MSDS) is filed to document any hazards.

Pre-evaluation: A section of 13 mm Overall Diameter (OD) cable similar to those routinely examined is given to a pocket gopher on a prepared panel. Observations are recorded for 7 days; if the animal demonstrates an inclination to gnaw on the cable, it is placed into the laboratory population. Each pocket gopher is maintained in the population as long as its biting performance is appropriate (as determined by subsequent evaluations). Age and sex are not performance criteria.

7-day evaluation: Prior research has indicated that 7 days of laboratory exposure to pocket gopher activity is a very rigorous evaluation for the cable; field vulnerability is usually not this extreme[4]. Ten pocket gophers are randomly selected from the laboratory population and each animal is given a prepared cable sample. A cable evaluation form for the group of cables is assigned a unique identifier indicating the year and an ascension number (88-01, 88-02, etc.). All foodstuffs remain in the

partitioned section with the pocket gopher to eliminate any inducement to gnaw on the cable solely to obtain food. Daily, the cables are visually inspected and a damage index is recorded for each sample as follows:

0 = no damage; the outer jacket shows no evidence of pocket gopher activity.

1 = outer jacket scratched; pocket gopher activity is limited to surface marking to a depth not including penetration of the protective outer jacket by the incisors and/or claws.

2 = outer jacket penetrated; this denotes piercing of the jacket into sublayer material that can be a protective armor or spacer substance. When armor is present, this damage index does not include penetration of the armor. Where the sublayer within the jacket is used primarily as a filler or to secure the conductors, this damage index includes penetration or damage to this material but does not include activity directly upon the conductors.

3 = armor penetrated; the specifically designed protective layer between the jacket and the conductors is pierced without damage to the conductors.

4 = conductors damaged; the transmitting wire or filaments are affected to the extent that they evidence contact by the pocket gopher (scratched, bent, or severed).

5 = cable severed; the cable is cut in at least one location denoting a complete loss of continuity in the conductors.

If a cable is found to be completely severed before the conclusion of the 7-day period, it is removed at that time. All remaining cables are removed from the cages after 7 days. Two researchers independently inspect the cables and then compare final damage assessments. If an index value discrepancy exists between the individual assessments, the cable is reviewed until a consensus is reached. Then, a mean of the damage index values for the group of ten cables is calculated.

Extended evaluation: The 7-day evaluation can be extended to 3 or 6 weeks. The cable is inspected daily and assigned a damage index value on the 7th day, the 21st day, and the 42nd day. Progressive damage after the 7th day is noted on an "as it occurs" basis. This lengthy observation is particularly useful for comparing slight variations between the composition or design of two cables. Extended exposure may reveal subtle differences.

DISCUSSION

Denver Wildlife Research Center studies using this method of cable evaluation have benefited the communications and power industries. The new fiber-optic cables will need to be subjected to the same scrutiny as their metallic predecessors.

A wide variety of materials such as polyethylene, polypropylene, polyurethane, coal tar, vinyl chloride, and glass reinforced epoxy have been evaluated for the outer jacket of cables[3,4]. Jackets have been combined with rodenticides and chemical repellents but significant reduction of pocket gopher damage has not been achieved[5]. The ability of the pocket gopher to gnaw on cables without ingesting cable material makes the animal virtually immune to chemicals in treated cables[2,3]. A soil treatment of tert-butylsulfenyl dimethyldithiocarbamate diluted in kerosene also has been evaluated[6,7,8]. Although the results of that study were positive, soil preparation may not be a viable option in light of potential soil contamination, hazards to humans, questionable effectiveness because of leaching, and a poor cost:benefit ratio[3,4,5]. Stainless steel has been found to be the most effective armor against pocket gopher penetration, but the electrical resistance of this metal has increased the vulnerability to lightning damage[3]. Materials of carbon steel, copper, brass, or phosphor bronze, and combinations of metal laminate and various wire wrappings also have proven to be highly protective armors. Glass epoxy materials for protecting fiber-optic cables are showing promise for pocket gopher resistance. Research has shown that the diameter of the cable influences the degree and the rate of damage; cables larger than 53 mm OD do not sustain significant damage[3,4]. Based on an industry standard, a cable type is considered rodent resistant if "at least 80 percent of the test specimens are not penetrated through the armor"[9].

Individual animal behavior, in relation to a cable sample, varies continually during an evaluation period. Although all pocket gophers in the laboratory population are "pre-evaluated" to insure an inclination to gnaw on cable, an animal may occasionally display brief behavioral periods of total disregard for a cable or periods of undeterred aggression.

In conclusion, this procedure has proven to be an effective laboratory method for determining the potential of pocket gopher damage to cables. Most cables showing significant damage in the laboratory also have been damaged in the field. However, the absence of damage in the laboratory is no assurance that damage will not occur in the field. Laboratory evaluations are valuable because they are the basis for eliminating those cable types that show a high degree of vulnerability to pocket gopher damage[5].

ACKNOWLEDGEMENTS

I would like to say "Thank you" to Carol Schafer for helping me prepare the manuscript and the poster paper and Paul Hegdal for his interest in continuing the cable research.

REFERENCES

1. Hall, E.R., The Mammals of North America, Vol. I, 2nd Ed., 1981.

2. Colorado State University Experiment Station, Pocket Gopher In Colorado, Bulletin 508-S, April 1960.

3. Connolly, R.A. and N.J. Cogelia, "The Gopher and Buried Cable," The Bell Laboratories Record, Vol. 48, No. 4 (April 1970), pp. 98-103.

4. Connolly, R.A. and R.E. Landstrom, "Gopher Damage to Buried Cable Materials," Materials Research and Standards, MTRSA, Vol. 9, No. 12, December 1969, pp. 13-16.

5. Howard, Walter E., "Tests of Pocket Gophers Gnawing Electric Cables," Journal of Wildlife Management, Vol. 17, No. 3, July 1953, pp. 296-300.

6. Mailen, T.H. and R.E. Stansbury, "Protection of Geophysical Communication and Power Transmission Cable Against Rodent Species Attack by R-55 Rodent Repellent Treatment," Fifteenth Annual Wire and Cable Symposium, Atlantic City, NJ, 7-9 December, 1966.

7. Anthony, Jr., C., and J.R. Tigner, "Rodent Repellent Cable Coating Development, " Sixteenth International Wire and Cable Symposium, Fort Mammouth, NJ, November 30, 1967.

8. Tigner, J.R., "Chemical Protection Methods Progress," Electronic Packaging and Protection, April 1968.

9. Cogelia, N.J., G.K. LaVoie, and J.F. Glahn, "Rodent Biting Pressure and Chewing Action and Their Effects on Wire and Cable Sheath," Twenty-fifth International Wire and Cable Symposium, Cherry Hills, N.J., Nov. 1976, pp. 117-124.



Geraldine R. McCann
Biological Science Technician (Wildlife)

USDA/APHIS/ADC/DWRC
Building 16, Denver Federal Center
Denver, CO 80225-0266
(303)236-7816
FAX (303)236-7863

Geraldine McCann is a Biological Science Technician (Wildlife) at the USDA/APHIS/Denver Wildlife Research Center in Denver, Colorado. She is a graduate of the University of Wisconsin-Stevens Point and has been with the Center for the past 7 years. Geraldine has worked with various rodent species in her career, specifically pocket gophers doing toxicity testing and testing telecommunications cable for various cable companies across the United States and abroad. She was the main technician on this project.

Coating design of thin-coated ribbons using 250 μm coated fibers

K. Kobayashi, N. Okada, K. Mitsuhashi, K.Ishida,
M. Miyamoto, and S. Araki

Fujikura, Ltd. Telecommunication Cable Section Opto-electronics Laboratory
1440 Mutuzaki, Sakura, Chiba, 285, Japan

Abstract

We investigated thin-coated fiber ribbons using 250 μm coated fibers.

First, we calculated the relationship between the fiber coating structures and the microbending characteristics of thin-coated ribbons. It has been clarified that the Young's modulus of the primary coating is the dominant parameter for microbending loss.

We then tested low-Young's-modulus primary coatings of various chemical compositions. A low-Young's-modulus primary coating with excellent physical properties can be made using the optimized chemical composition.

Finally, we fabricated prototype thin-coated divisible 8-fiber ribbon that for application to a slotted-core cable with high fiber density and a high fiber count. Thin-coated ribbons with the same optical transmission characteristics and mechanical characteristics as conventional fiber ribbons can be made using 250 μm coated fibers with the low-Young's-modulus primary coating.

1. Introduction

Higher fiber density and higher fiber count cables are needed to construct subscriber networks. Reducing optical fibers' coating diameter and the fiber ribbons' size seems to be the most effective method for realizing small-diameter cables with high fiber density [1] [2].

However, reducing the coating diameter can degrade mechanical durability. Coated fibers should be proof tested to ensure glass fiber reliability. During the test, the thin-coated fiber tended to fail more frequently than conventional fibers. Therefore, the protective strength of the coating seemed to be an essential factor in determining the fiber failure rate during proof test.

1-1 Mechanical durability of thin-coated fibers

Recently, we investigated the mechanical durability of coated fibers by a special fiber strength test [3]. Coated fibers with outer diameters varying from 180 μm to 250 μm were tested using a tensile machine with the capstan covered with sandpaper, as shown in figure 1.

Figure 2 shows the relationship between the F50 value of the failure strength and the coating diameter of the coated fibers. The strength degrades as the coating diameter decreases and also as the particle size of the sandpaper increases.

Figure 3 shows the results when using sandpaper with a particle size of 50 μm and changing coating structure, such as primary diameter, secondary diameter, and the secondary Young's modulus, of thin-coated fiber.

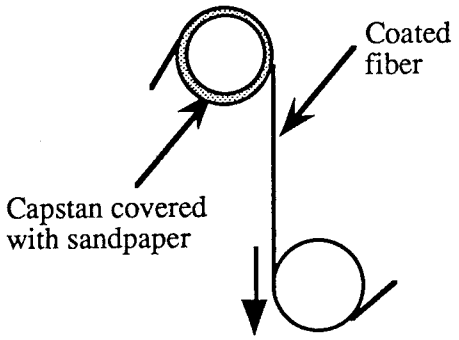


Fig. 1 Arrangement for evaluating the mechanical durability of coated fiber.

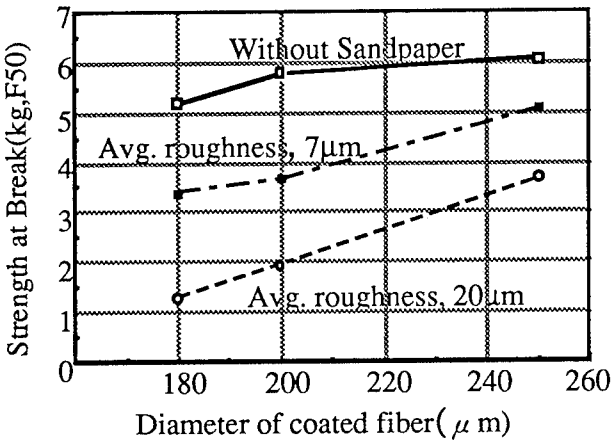


Fig. 2 Relationship between the measured fiber strength and the secondary diameter

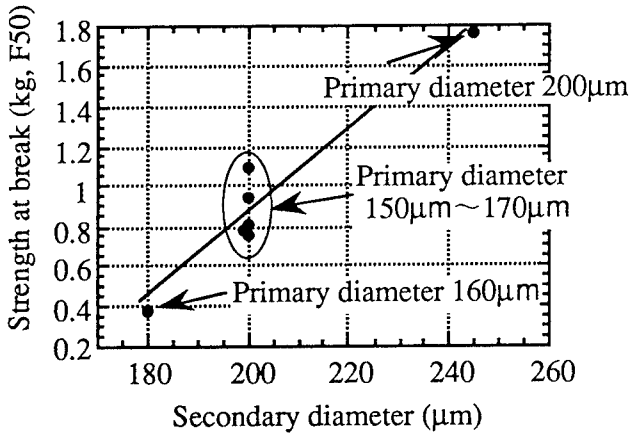


Fig.3 Relationship between the measured fiber strength and the secondary diameter

$$F_{50} = \frac{C}{X+1} \qquad (1)$$

Formula 1 shows the appropriate equation. C is the original failure strength. Index X contains factors of the secondary thickness (Ts), the primary thickness (Tp), and the secondary Young's modulus (Ys), respectively. We then searched for the best fit between the test result and Formula 1.

Consequently, we obtained an approximate relationship between the F50 value and the value of X for the tensile test conditions (Formula 2).

$$X = 1.57 \times 10^4 \times (Ts)^{-1.54} \times (Tp)^{-0.81} \times (Ys)^{-0.18} \qquad (2)$$

The Formula 2 shows that the secondary diameter is the dominant parameter.

Therefore, we concluded that the thicker secondary coating is desirable for sufficient mechanical durability.

1-2 Thin-coated ribbons with 250 μm conventional coated fiber

An alternative technique for realizing high fiber density cable is using high fiber count and a reduced thickness ribbons such as 8-fiber, 12-fiber, or 16-fiber with 250 μm conventional fiber [4].

However, in the case of a tight-structure cable, such as a slotted-core cable, reducing the ribbon thickness may degrade of the microbending characteristics against lateral forces. Using glass fiber with a low MAC value or optimized coating material can improve microbending loss.

Here, we investigated relationship between the coating structure of thin-coated fiber ribbons and microbending characteristics.

2. Microbending characteristics of thin-coated ribbons

In a previous study, we found that the microbending loss of coated fiber can be expressed as a function of the coatings' mechanical parameter, Cmech, as shown in Formula 3. [2] [5]

$$\alpha_{\text{microbending loss}} \sim C_{\text{mech}} \frac{f_0 \sigma}{H_f^2}$$

$$C_{\text{mech}} = \frac{k_s^2}{D_o^{0.375} H_o^{0.625}} \qquad (3)$$

In this study, we used the mechanical parameter, Cmech, to investigated the relationship between the microbending loss of 0.3 mm thin-coated ribbon with 250 μm coated fiber and the coating structure (the Young's modulus of the primary coating, the Young's modulus of the secondary coating, and the primary diameter).

To determine the coating's mechanical parameter, the Ks and the D0 were calculated using the Finite Element Method shown in Figure 4, and the H0 was calculated from Formula 4.

The calculation results are shown in Figure 5. It is apparent that a lower Young's modulus of the primary coating, a higher Young's modulus of the secondary coating, a thicker primary coating diameter, and a higher Young's modulus of ribbon coating are all factors that lower microbending loss.

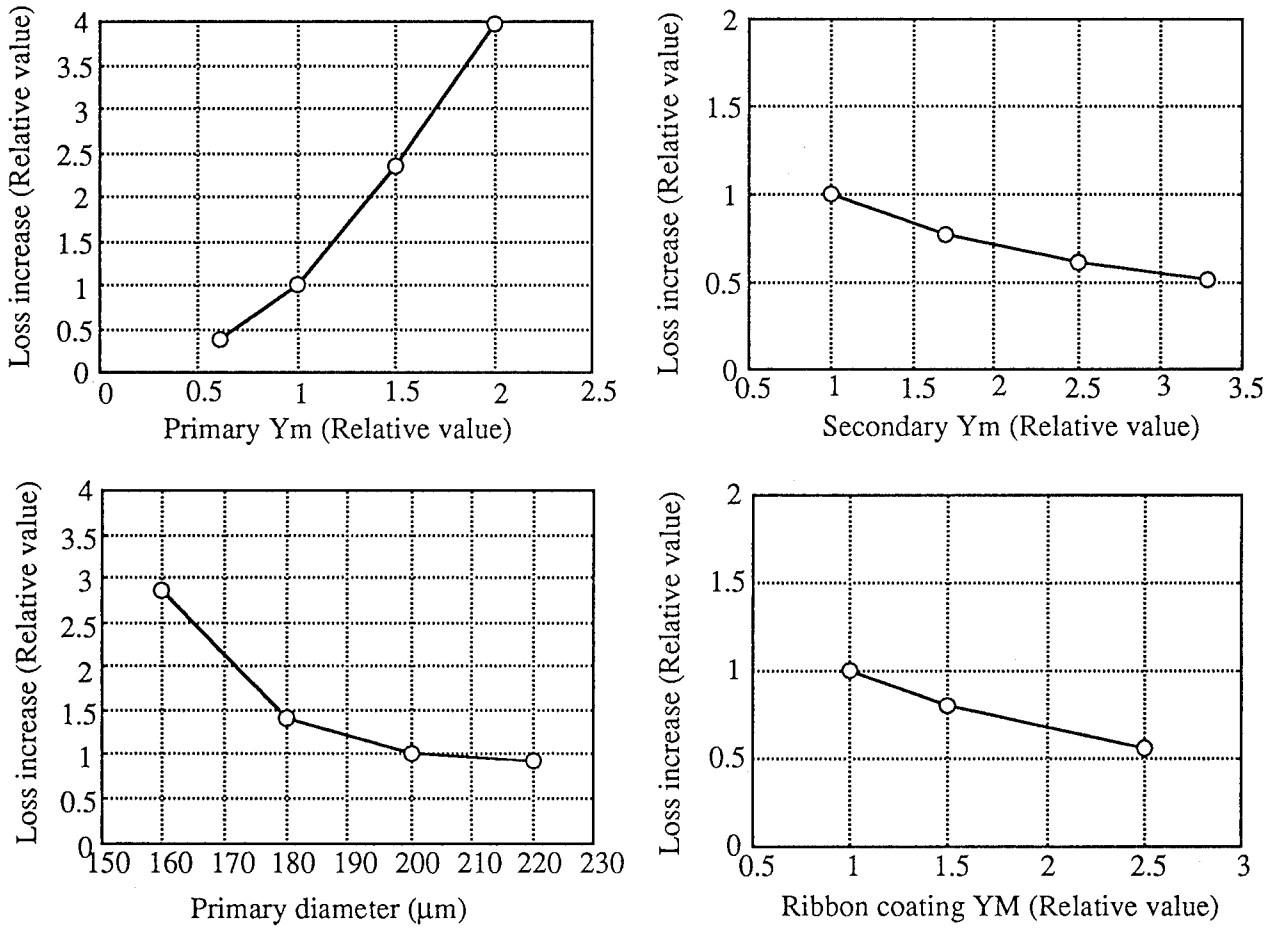


Fig. 5 Relationship between the theoretical microbending loss and the coating structure of 0.3 mm thin-coated ribbons

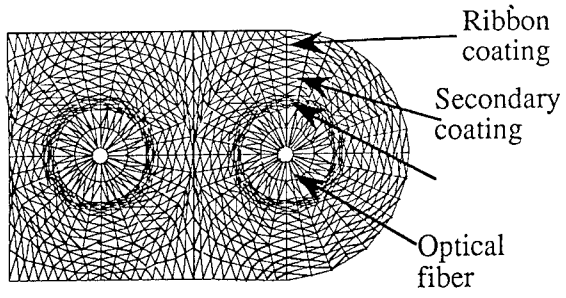


Fig. 4 Fiber ribbon model for FEM analysis

$$H_0 = \sum_{n=1}^{\#\ layers} \frac{\pi}{4} E_n (r_n^4 - r_{n-1}^4) \qquad (4)$$

This analysis also clearly shows that the Young's modulus of the primary coating is the dominant parameter for the microbending characteristics of the thin-coated ribbon. The thin-coated ribbon with a 60% lower Young's modulus primary coating is subject to approximately one-third as much microbending loss as is the thin-coated ribbon with a conventional primary coating.

We can conclude from this analysis that low-Young's-modulus primary coating can be used to design 0.3 mm thin-coated ribbon that has the same microbending loss as conventional fiber ribbon.

3. A composition design of low-Young's-modulus UV-curable resin

We then investigated low-Young's-modulus primary coating. An oligomer with a high molecular weight was introduced into the composition to lower the Young's modulus of the resin.

However, composition involving a high-molecular-weight oligomer tends to have a high resin viscosity and be inferior to resin in long-term reliability. Therefore, selecting resin is particularly important and requires careful consideration.

We prepared three kinds of low-Young's-modulus UV-curable resins with a Young's modulus approximately 60% that of our conventional primary resin. Their compositions include various monomers and stabilizers.

We then examined the curing rate and reliability of Young's modulus of these resins.

Figure 6 shows how the Young's modulus of the resins depends on UV dose. The low-Young's-modulus resins of the Tno.2 and 3 have the same curing rate as conventional resin.

Figure 7 shows the changes in Young's modulus when aged at 80°C. The low-Young's-modulus resin of the Tno.1 and 2 has the same reliability as

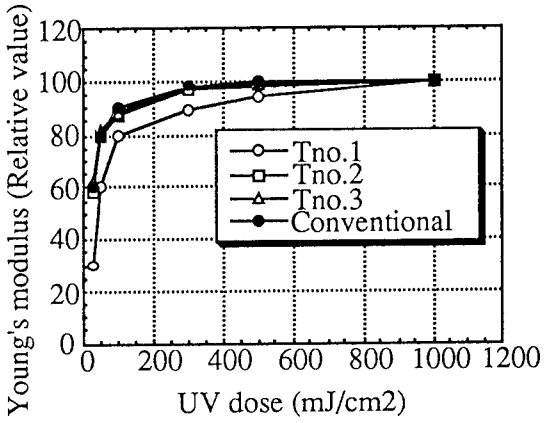


Fig. 6 Young's modulus of the resins' dependence on UV dose

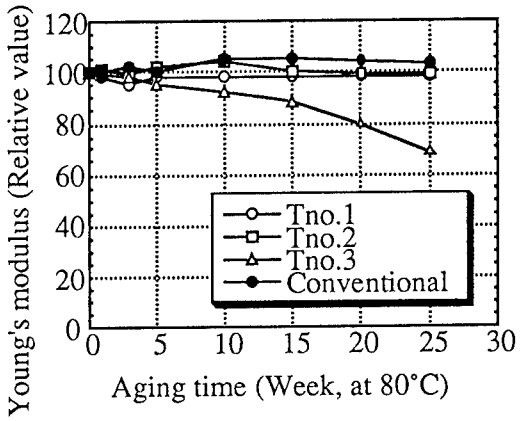


Fig. 7 Changes in Young's modulus during aging at 80°C

conventional resin.

These results show that a low-Young's-modulus resin with excellent physical properties can be made using the optimized composition.

However, the low-Young's-modulus primary coating still has a few problems that must be solved. We have been researching improvements.

4. Experimental results for microbending characteristics of prototype thin coated ribbons

To estimate the microbending characteristics, we used the drum winding test as shown in Figure 8. The microbending loss of the tested ribbons was determined by winding each ribbon on the drum under constant backtension. Then, the optical loss of the fiber and the loss of the fiber in a loose coil was measured. The microbending loss is the difference in loss between the fiber wound on the drum and the loosely coiled fiber (formula 5).

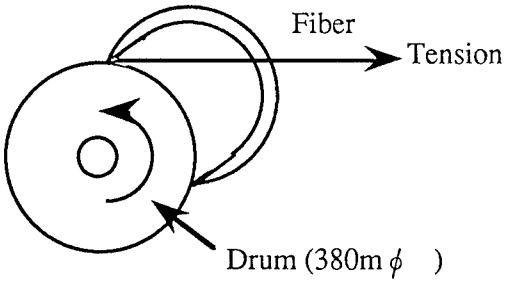


Fig. 8 Illustration of the drum winding test

$$\alpha_{microbend}(dB/km) = \alpha_{drum}(dB/km) - \alpha_{free}(dB/km) \quad (5)$$

We fabricated 4-fiber ribbons to compare their microbending performance: a thin-coated ribbon with low-Young's-modulus primary of the Tno.2, a thin-coated ribbon with conventional primary, a 0.4 mm thick conventional ribbon.

Figure 9 shows the measured microbending loss of these ribbons. The thin-coated ribbon with the low-Young's-modulus primary has approximately the same microbending performance as does the 0.4 mm thickness conventional ribbon.

Therefore, Proper primary material can be used to make a thin-coated ribbon with the same microbending characteristics as the conventional ribbon .

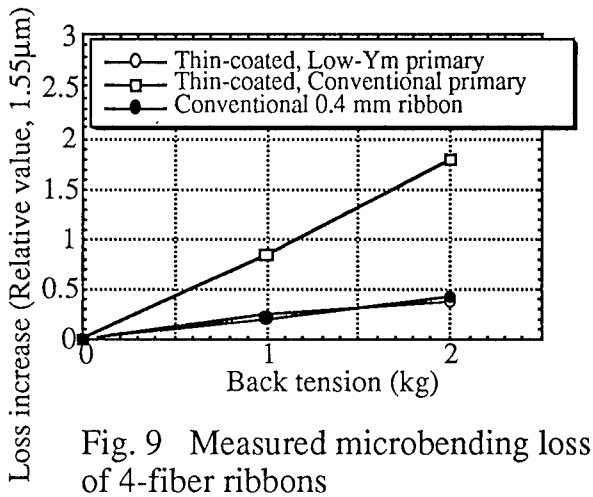


Fig. 9 Measured microbending loss of 4-fiber ribbons

5. Thin-coated divisible 8-fiber ribbon

The structure of thin-coated fiber ribbon for future high density slotted-core cable will be thin-coated 8-fiber or 16-fiber ribbon that can be easily divisible into 4-fiber ribbons for splicing to other 4-fiber ribbons.

We investigated 0.3 mm thin-coated divisible 8-fiber ribbons using 250 μm coated fibers with the optimized low-Young's-modulus primary coating. A cross section of the ribbon is shown in Figure 10. The ribbon should be easily divisible into two 4-fiber ribbons without break in the fiber and ribbon coatings. Again, the ribbon should not break or deform during processes such as ribbon rewinding and cable installation.

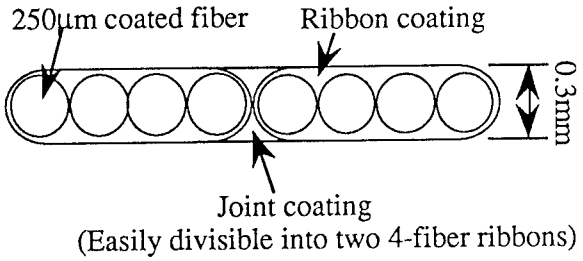


Fig. 10 Structure of the thin-coated 8-fiber ribbon

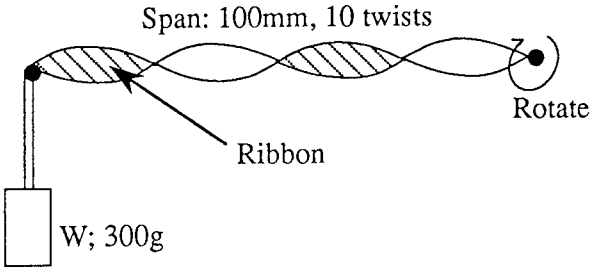


Fig. 11 Illustration of the twisting test

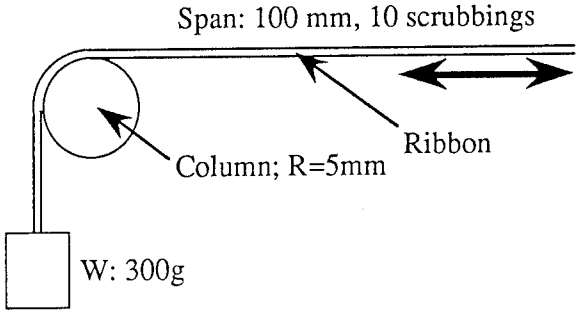


Fig. 12 Illustration of the scrubbing test

However, reduced ribbon thickness degrade mechanical durability and divisibility, because the thinner the ribbon coating, the more breakable and more transformable the ribbon becomes.

Therefore, we then investigated the divisibility and mechanical durability of the ribbon coating and joint materials.

5-1 Mechanical durability and divisibility of the thin-coated ribbons

We fabricated a prototype thin-coated divisible 8-fiber ribbon using proper ribbon and joint materials. To estimate the mechanical durability of the thin-coated ribbon, we performed twisting and scrubbing tests. Figure 11 and Figure 12 show the test conditions and Table 1 contains the test results. The twisting and the scrubbing tests did not damage either the thin-coated ribbon or the 0.4 mm conventional divisible 8-fiber ribbon.

We then used a ribbon-dividing-tool to examine the divisibility of the thin-coated ribbon. The ribbon coating did not break and the division was completed in all 50 trials.

Therefore, the thin-coated divisible 8-fiber ribbon with proper ribbon material and joint material has the same excellent mechanical durability and divisibility as does the conventional ribbon.

Table 1 Mechanical durability of the ribbons

	Twisting	Scrubbing
Thin-coated ribbon	No damage	No damage
Conventional ribbon	No damage	No damage

5-2 Transmission characteristics of the thin-coated ribbons

To investigate transmission characteristics, we performed a temperature cycling test and a long-term reliability test. Figure 13 shows the loss changes during a temperature cycle ranging from -40 to +60°C. The loss changes for all fiber in the ribbon are less than 0.02 dB/km.

Figure 14 shows the loss changes during aging at 80°C and 60°C/95%RH. Almost no loss increases were observed in either test.

This investigation confirmed that the prototype 8-fiber ribbon has excellent loss performance.

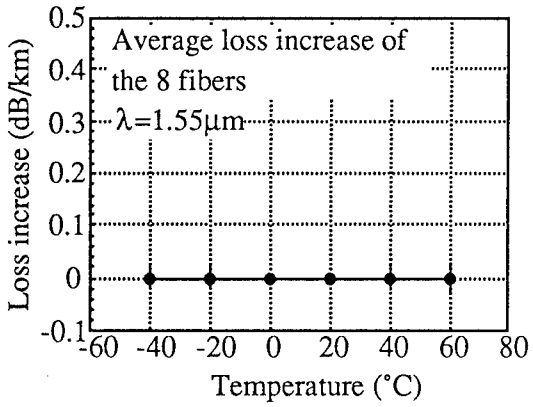


Fig. 13 Loss stability at high and low temperatures

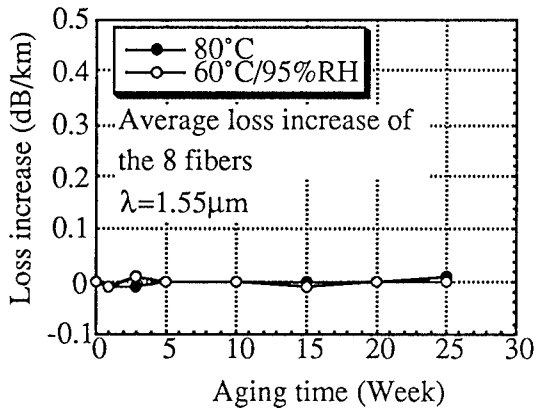


Fig. 14 Loss changes during aging at 80°C and 60°C/95%RH

5-3 Other general mechanical properties of the thin-coated ribbons

To investigate the mechanical properties of the thin-coated ribbons, we performed lateral pressure and fiber-stripping tests.

Figure 15 illustrates the lateral pressure test. The loss increases at 100 kg were scarcely observed, as shown in Figure 16.

We then used a conventional fiber-stripping-tool to perform the fiber-stripping test. The fiber did not break and the coating material did not remain on the fiber during all 50 trials.

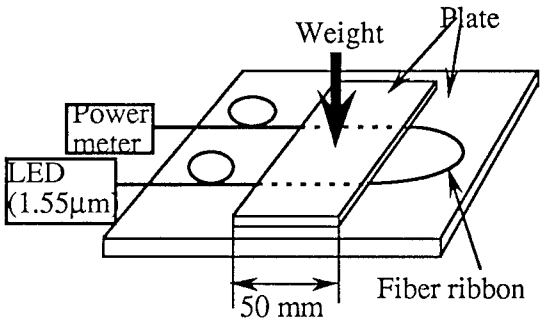


Fig. 15 Illustration of the metal plate test

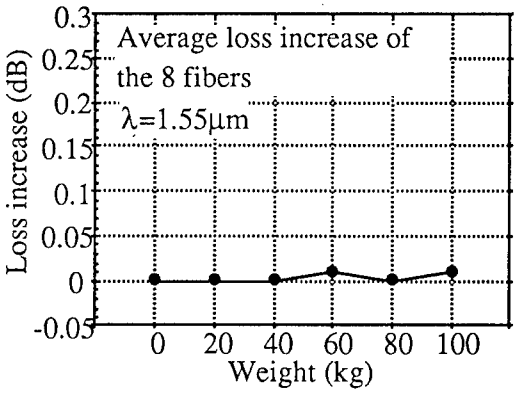


Fig. 16 Metal plate lateral pressure test

6. Conclusion

This study clarified that a thin-coated ribbon with the same microbending characteristics as a conventional ribbon can be designed using a low-Young's-modulus primary coating.

The optimized chemical composition can be used to make a low-Young's-modulus primary coating with excellent physical properties.

The prototype divisible 8-fiber ribbon has excellent mechanical and transmission properties, as well as excellent divisibility.

References

[1] S. Tomita et al, "Preliminary research into ultra high density and high count optical fiber cables," IWCS Symposium Proceedings, 1991, pp.8-15.

[2] K. Kobayashi et al, " Study of Microbending Loss in Thin Coated Fibers and Fiber Ribbons," IWCS Symposium Proceedings, 1993, pp. 386-393.

[3] K. Kobayashi et al, "Microbending characteristics and mechanical strength of thin coated fibers," OFC '94, 1994 Technical Digest Series, Vol. 4, paper ThA4.

[4] H. Iwata et al, "Characteristics of a 1000-fiber single slotted rod optical cable," IEICE General Conference, March 1995, B-999.

[5] J. Baldauf et al, "Relationship of mechanical characteristics of dual coated single mode optical fibers and microbending loss," IEICE Trans. Commun., vol. E76-B, no. 4, April 1993, pp. 352-357.



Naoki Okada

Opto-Electronics Laboratory
Fujikura LTD.

1440 Mutsuzaki,
Sakura-shi, Chiba-ken
285 Japan

Mr. Okada was born in 1964. He joined Fujikura LTD. after his graduation from Chiba University with a B.E. Degree in 1986 and has been engaged in research and development of optical fiber cables. He is now an engineer in the Telecommunication Cable Section and a member of the IEICE of Japan.

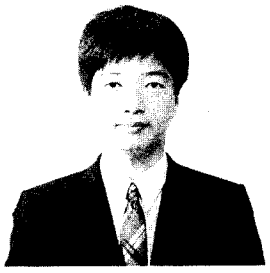


Keiko Mitsuhashi

Opto-Electronics Laboratory
Fujikura LTD.

1440 Mutsuzaki,
Sakura-shi, Chiba-ken
285 Japan

Ms. Mitsuhashi graduated from Chiba University with a B.E. Degree in 1986. After six years of work as an engineer for functional organic materials, she joined Fujikura Ltd. and has been engaged in research and development of optical fibers. She is now an engineer in the Telecommunication Cable Section and a member of the IEICE of Japan.



Kazunaga Kobayashi

Opto-Electronics Laboratory
Fujikura LTD.

1440 Mutsuzaki,
Sakura-shi, Chiba-ken
285 Japan

Mr. Kobayashi was born in 1961. He joined Fujikura LTD. after his graduation from Gunma University with a M.E. Degree in 1985 and has been engaged in research and development of optical fibers. He is now an engineer in the Telecommunication Cable Section and a member of the IEICE of Japan.

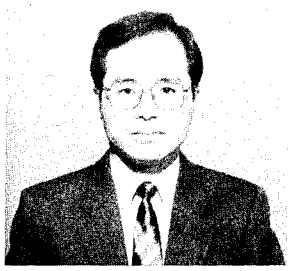


Katsuyoshi Ishida

Opto-Electronics Laboratory
Fujikura LTD.

1440 Mutsuzaki,
Sakura-shi, Chiba-ken
285 Japan

Mr. Ishida was born in 1967. He joined Fujikura LTD. after his graduation from Gunma University with a B.E. Degree in 1991 and has been engaged in research and development of optical fibers. He is now an engineer in theTelecommunication Cable Section and a member of the IEICE of Japan.



Matsuhiro Miyamoto

Opto-Electronics
Laboratory
Fujikura LTD.

1440 Mutsuzaki,
Sakura-shi, Chiba-ken
285 Japan

Mr. Miyamoto was born in 1953. He joined Fujikura LTD. after his graduation from Tokyo Institute of Technology with a M.S. Degree in 1978 and has been engaged in design and research of optical cables. He is now a section chief of the Telecommunication Cable Section and a member of the IEICE of Japan.



Shinji Araki

Opto-Electronics
Laboratory
Fujikura LTD.

1440 Mutsuzaki,
Sakura-shi, Chiba-ken
285 Japan

Mr. Araki was born in 1950. He joined Fujikura LTD. after his graduation from Tokyo Metropolitan University with a B.E. Degree in 1974 and has been engaged in design and research of optical fibers. He is now a section chief of the Telecommunication Cable Section and a member of the IEICE of Japan.

Investigation on high-speed optical fiber ribbon coating and the characteristics of the ribbons

R.SUZUKI, H.SAWANO, K.KOBAYASHI, K.OOHASHI and S.ARAKI

Fujikura Ltd.,Opto-electronics Laboratory,
1440 Mutsuzaki, Sakura, Chiba, 285, JAPAN

ABSTRACT

We attempted to make four-fiber ribbon coated with UV-curable resin at a rate of more than 600 m/min without any surface distortion in the resin by optimizing the fluid viscosity and coating die shape. While the material properties of the cured resin showed slight changes in accordance with changes to the coating speed, transmission loss and polarization mode dispersion (PMD) after ribbonization did not.

1. Introduction

Optical fibers have become an indispensable part of communication networks[1]. However, the rapid growth in optical fiber networks has caused the price of fibers to fall drastically. This has meant that fiber and cable manufacturers have had to establish high-speed deposition, drawing, and cabling technologies. Furthermore, the demand is for cheap ribbons that are usually used in subscriber networks. One key technology that can achieve low-cost ribbon is high-speed ribbonization. In high-speed ribbonization, two key factors - shear stress during coating and the amount of energy that cures the UV-curable resin - affect the manufacturing speed and ribbon properties. A high shear stress causes surface distortion of the resin, as well as orientation and /or cutting of the molecule. Sometimes, this orientation and /or cutting of the molecule causes transmission loss and unstable chromatic dispersion due to the irreversible change in the mechanical and thermal properties of the coating material. Also, insufficient curing energy can cause degradation in the reliability of the coating material and/or the transmission characteristics.

2. Manufacturing condition

2-1. Sizing factors

Ribbon sizing is governed by fluid dynamics, and as a result, the following factors affect ribbon sizing:

1) Coating speed
2) Die shape
3) Viscosity of the resin

From a structural viewpoint, the coating speed depends on the degree of surface distortion of the coating resin. In a region of critical shear stress, the surface of the coated resin will distort due to the nonlinearity in the relationship between the shear rate and shear stress[2].

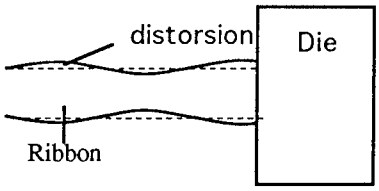


Fig. 1 Sketch of surface distortion

Assuming that the flow rate is Newtonian, the length of the parallel part of the die (L) must satisfy the following condition.

$$L \geqq \Delta P \cdot H / \{2\eta \ (\gamma - V/H)\}$$

Where, η is the viscosity of the fluid, γ is the critical shear rate which correspond to the critical shear stress, H is the separation of the parallel part, and ΔP is the pressure difference at the inlet and outlet of the parallel

part of the die. However, since ΔP for a used die will depend upon the coating speed and Pin (the pressure at the inlet of parallel part of the die), the actual flow will not appear Newtonian in the high-speed region. To date, L has been determined experimentally.

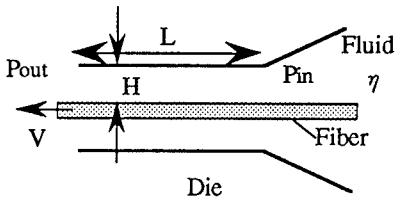


Fig. 2 Coating Parameters

Table 1 Experimental results for a stable surface.

		L (mm)					
		0.2	0.5	1.0	1.5	2.0	2.5
Shear rate (/S)	10^4	NG	NG	OK	OK	OK	OK
	10^5	NG	NG	OK	OK	OK	OK
	$5x10^5$	NG	NG	NG	OK	OK	OK

2-2. Curing conditions

The following factors governs UV curing:

1) Geometrical layout of the UV-curing lamp and the object to be cured.
2) Spectra of the UV-curing lamp and the amount of energy,
3) Reactivity of the photo initiator and matrix resin.

Of these factors, curing energy is the fundamental parameter.

The minimum energy that is needed for curing was determined by Young's modulus and from the residual reactivity of the cured resin. Young's modulus for cured resin is the most important of its kind and directly indicates the mechanical property because it is generally included in the analysis of lateral force. Residual reactivity is a direct indicator that reflects the conversion ratio of the resin. The residual reactivity after ribbonization was measured by photo differential calorimetry (PDC). Table 2 lists the measuring conditions used.

Table 2. Conditions of PDC measurement

Item	Unit	
Sample mass	mg	1.5
Initial temp.	℃	45
UV dose	mW/cm^2	10
Curing time	sec.	10
Atmosphere		Nitrogen gas

Figure 3 shows the relationship between Young's modulus and residual reactivity. Here, residual reactivity is defined as the ratio between the exothermic energy of cured resin during recuring and that of uncured resin during complete curing. As the coating speed or the residual reactivity increased, Young's modulus of cured resin became decreased.

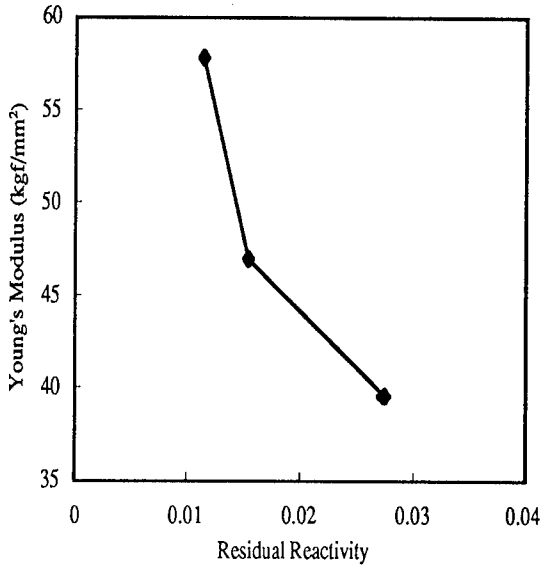


Fig. 3 Relationship between Young's modulus and residual reactivity

3.Characteristics of cured resin

3-1. Investigated material properties

The mechanical and thermal properties of cured resin that we investigated were dynamic elastic modulus, deformation, and glass transition temperature. Dynamic elastic modulus and deformation were measured as the function of temperature.

Figure 4 shows the relationship between thermal deformation and the coating speed. As the speed of ribbonization increased, the glass transition

Table 3. Measuring conditions for thermal deformation and dynamic elastic modulus.

Item		Unit	
Thermal deformation	Method		TMA
	Sample length	mm	10
	Area	mm^2	0.1 - 0.15
	Weight	gf	1
	Temperature elevating speed	℃/min	3
	Atmosphere		Nitrogen gas
Dynamic elastic modulus	Method		DMS
	Sample length	mm	10
	Area	mm^2	0.35
	Frequency	Hz	1
	Amplitude	μm	5
	Weight	gf	10
	Temperature elevating speed	℃/min	5
	Atmosphere		Nitrogen gas

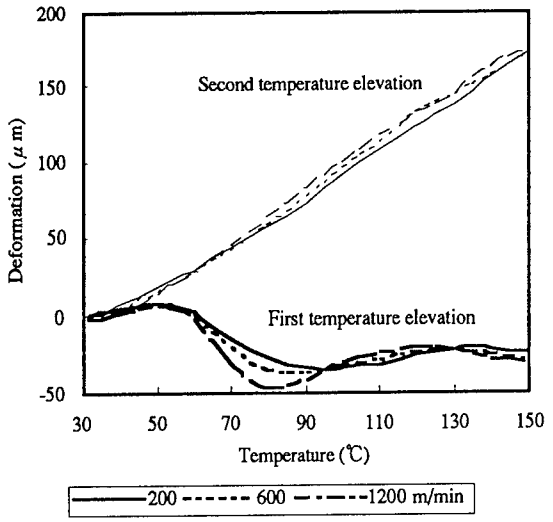


Fig. 4 Relationship between thermal deformation and coating speed

temperature decreased. It seems that the orientation effect was observed as the negative linear expansion coefficient in the elevating temperature process for each sample. However, this negative linear expansion coefficient was not observed after the history of the temperature, which was higher than glass transition temperature. It seems that orientation of the molecule occurs at a shear rate of more than 10^4/s, and was slightly dependent on the shear rate.

The results of dynamic elastic modulus investigation (see Fig. 5) show that dynamic elastic modulus does not depend strongly on the shear rate. As the coating speed increased, the glass transition temperature dropped.

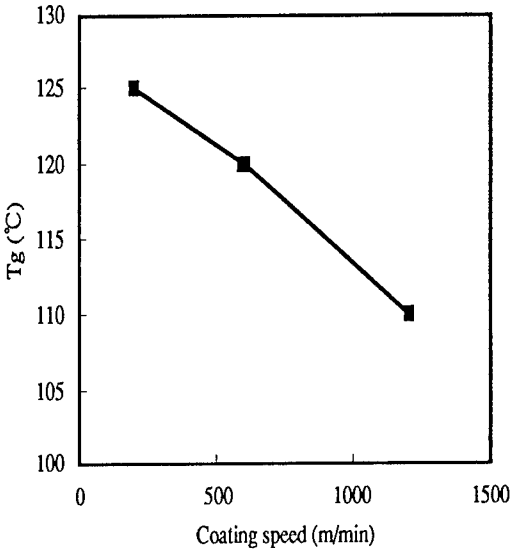


Fig. 5 Relationship between the glass transition temperature and coating speed.

4. Transmission characteristics of the ribbon

4-1. Investigated ribbon

The investigated optical fiber was a single-mode fiber for 1.3 μm transmission. We examined a ribbon coating matrix whose Young's modulus was between 20 and 120 kgf/mm^2 to research the anisotropic stress on the optical fiber.

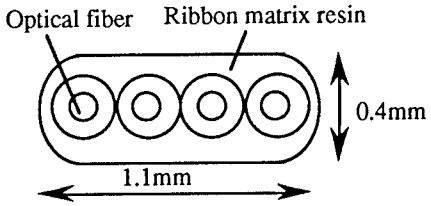


Fig. 6 Sketch of the investigated ribbon

Table 4 Parameters of the investigated ribbon

Item		Unit	
Optical fiber	Diameter	μm	125
	MFD	μm	9.5
	λ cf	μm	1.26
Primary coating	Diameter	μm	200
	Young's modulus	kgf/mm^2	0.1
Secondary coating	Diameter	μm	250
	Young's modulus	kgf/mm^2	75
Ribbon	Dimension	mm	1.1 x 0.4
	Young's modulus	kgf/mm^2	20 - 120

We investigated transmission loss and PMD as fundamental transmission characteristics. PMD is an important consideration for long-distance telecommunication such as a submarine cable installed in the ocean[3-5]. The fibers used in the investigated ribbons were the same for each ribbon and located at the outer edge of the ribbon.

The measuring conditions of transmission loss and PMD were as follows:

1) Ribbon: Free coil with a diameter of 30 cm
Length: 1,000 m,
2) Loss: OTDR, 1.55 μm,
3) PMD: Frequency sweeping method.

We paid special attention to the layout of the investigated ribbon to ensure that there were no small bends in it.

4-2. Results of the investigation

The investigated parameters were Young's modulus dependence and temperature dependence at low temperatures.

Figure 6 shows the relationship between optical loss, PMD, and Young's modulus after ribbonization. The loss changes after ribbonization were less than 0.01 dB/km at 1.55 μm. However, as shown in Fig. 8, a slight increase in loss was observed at a low temperature (-40℃) for ribbons coated with large Young's modulus resin. On the other hand, PMD after ribbonization depended upon Young's modulus. The larger the Young's modulus of the coated resin, the greater the PMD. At a low temperature, PMD decreased (see Fig. 8). Given the transmission losses and changes in PMD, it seems likely that the stress in and on the fibers after ribbonization is anisotropic, and that this anisotropic stress degraded the PMD. On the other hand, at a low temperature, microbending of the fiber occurred due to the compressive force exerted by the coating resin. This microbending causes two kinds of mode coupling: random mode coupling between orthogonal polarized modes, and mode coupling between the propagation modes and radiation modes.

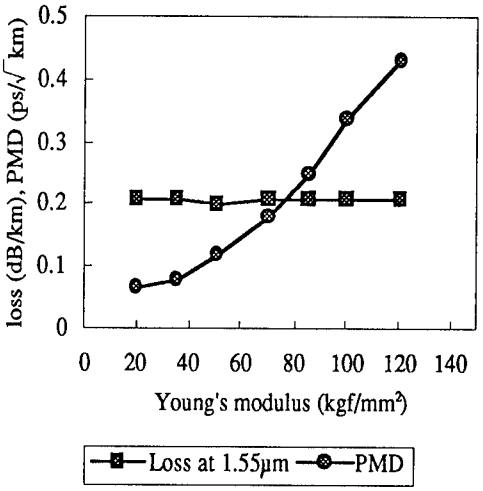


Fig. 6 Relationship between loss, PMD and Young's modulus of the cured resin.

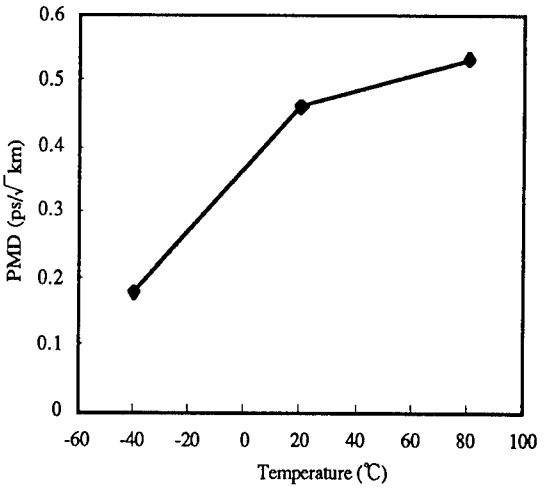


Fig. 7 Temperature dependence of PMD.

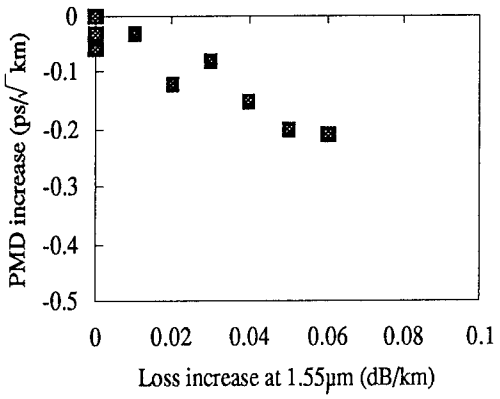


Fig.8 Relationship between PMD change and Loss change due to the temperature change from 20 to -40℃.

5. Conclusion

We attempted to make four-fiber ribbons coated with UV-curable resin at a rate of more than 600 m/min using several kinds of coating resins whose Young's modulus was between 20 and 120 kgf/mm^2. The investigated shear rate was between 10^4 and $5x10^5$.

We could make four-fiber ribbons without any surface distortion of the resin by optimizing the fluid viscosity and coating die shape at a coating speed of more than 600m/min. The investigated properties of the cured resins were the linear expansion coefficient, dynamic elastic modulus, and glass transition temperature. The linear expansion coefficient of each cured resin was negative between 50℃ and 70℃. This phenomenon depended to a small extent upon the shear rate. From the results of the dynamic elastic modulus, it seems that no cutting of the molecule was occurred. The transmission loss did not increase after ribbonization at room temperature, although a slight increase in loss was observed at -40℃ for hard resin. The PMD after ribbonization depended upon the elastic modulus. At -40℃, the PMD tended to decrease in contrast to the slight increase in loss.

Acknowledgements

We would like to thank the many people who supported our investigation. Special thanks go to Mr. Maruoka for his encouragement.

References

[1] S. Tomita, M. Matsumoto, S. Nagasawa and T. Tanifuji, "Ultra High-Density Optical Fiber Cable with Thin Coated fibers and Multi-Fiber Connectors", IWCS Proceedings, P5, 1993

[2] N. Wagatsuma, T. Kimura, Y. Shuto and S. Yamakawa,"Optical Fiber Coating Speed Prediction from Flow Properties of Coating Materials", Electronics Letters, Vol.18, No.17, 1982.

[3] J. Sakai and T. Kimura, "Birefringence and Polarization Characteristics of Single-Mode Optical Fibers under Elastic Deformations", IEEE Journal of Quantum Electronics, Vol. QE-17,No.6, 1981

[4] Y. Namihira and J. Maeda, "Polarization mode dispersion measurements in optical fibers", Proceedings of SOFM, Invited paper, Boulder, USA, Sep. 1992.

[5] A. F. Judy, "Improved PMD Stability in Optical Fibers and Cables", IWCS Proceedings, P658, 1994



Ryoji Suzuki

Opto-Electronics Laboratory
Fujikura LTD.
1440 Mutsuzaki,
Sakura, Chiba
285 Japan

Mr. Suzuki was born in 1961. He graduated from Tokyo Institute of Technology with a M.E. Degree in 1987. He joined Fujikura Ltd. and has been engaged in research of optical fiber and cables. He is now an engineer of the Telecommunication Cable Section.



Hiroyuki Sawano

Opto-Electronics
Laboratory
Fujikura LTD.
1440 Mutsuzaki,
Sakura, Chiba,
285 Japan

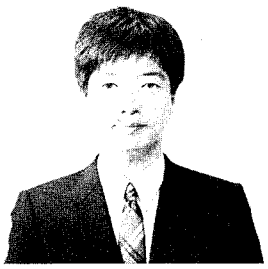
Mr. Sawano was born in 1955. He joined Fujikura LTD. after his graduation from Hokkaido University with a M.S. Degree in 1984 and has been engaged in research and development of optical cables. He is now an assistant chief in the Telecommunication Cable Section and a member of the IEICE of Japan.



Keiji Oohashi

Opto-Electronics
Laboratory
Fujikura LTD.
1440 Mutsuzaki,
Sakura, Chiba
285 Japan

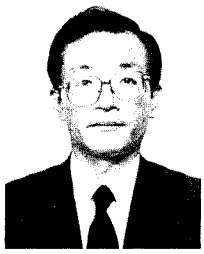
Mr. Oohashi was born in 1956 and graduated from Tokyo Institute of Technology with a B.E. Degree in 1980. After eight years of work as an engineer in materials for motor vehicles, he joined Fujikura Ltd. and has been engaged in design and research of optical cables. He is now an assistant chief of the Telecommunication Cable Section and a member of the IEICE of Japan.



Kazunaga Kobayashi

Opto-Electronics
Laboratory
Fujikura LTD.
1440 Mutsuzaki,
Sakura, Chiba,
285 Japan

Mr. Kobayashi was born in 1961. He joined Fujikura LTD. after his graduation from Gunma University with a M.E. Degree in 1985 and has been engaged in research and development of optical fibers. He is now an engineer in the Telecommunication Cable Section and a member of the IEICE of Japan.



Shinji Araki

Opto-Electronics
Laboratory
Fujikura LTD.
1440 Mutsuzaki,
Sakura, Chiba
285 Japan

Mr. Araki was born in 1950. He joined Fujikura LTD. after his graduation from Tokyo Metropolitan University with a B.E. Degree in 1974 and has been engaged in design and research of optical fibers. He is now a section chief of the Telecommunication Cable Section and a member of the IEICE of Japan.

DEVELOPMENT OF HIGH-DENSITY OPTICAL FIBER CABLE CONSISTS OF 0.3mm - THICK FIBER RIBBONS

Kazuya Obi Tetsuya Takeda Tamishige Watanabe Kazuo Imamura
Moriyuki Fujita Hiroyuki Tanka

MITSUBISHI CABLE INDUSTRIES, LTD
4-3, Ikejiri, Itami-city, Hyogo-Prefecture, 664, Japan

Abstract

We have developed a cable of higher density than cables currently in practical use and enabled highly efficient mass production.

First, we tested 4-fiber and 8-fiber ribbons whose thickness were reduced from 0.4 mm to 0.3mm. Two kinds of ribbon were made of each resin. Young's modulus of a resin is about 2 times that of another (conventional) resin. Initial loss and loss-temperature characteristic of both thin ribbons were found to be equivalent to those of the conventional ribbons and free of problem.

Next, we have designed a cable of 0.3mm-thick 4-fiber ribbons and succeeded in making a 420-count cable with the same outer diameter as the conventional 300-count cable. The initial loss of this cable is 0.21dB/km at 1.55μm. Loss change in cabling process is less than 0.03dB/km.

Introduction

Optical fiber cables widely used in Japan have a tight structure consist of about 0.4mm-thick fiber ribbons. Up to 300-count cables have the single-slotted rod cable structure consist of 4-fiber ribbons, 300 to 600-count cables have the multi-slotted -rod cable structure cosist of 4-fiber ribbons, and 600 to 1000-count cables have the multi-slotted-rod cable structure consist of 8-fiber ribbons. We designed and developed the cable with view to achieving a higher density while enabling mass production. It is 420-count cable that have the single-slotted-rod cable structure consist of 0.3mm-thick 4-fiber ribbons.

Characteristics of 0.3mm-thick Fiber Ribbon

Construction of Fiber Ribbon

The coated optical fibers applied were ϕ 0.25mm coated single-mode type fibers similarly to the conventional product. The ribbon, however, was thined to the thickness of 0.3mm as compared with 0.4mm conventional ribbon . Fig.1 depicts a comparison of construction between thinned and conventional ribbons.

Two kinds of ribbons were made of resin Types A or B respectively. Resin B has a Young's modulus of about twice that of A.

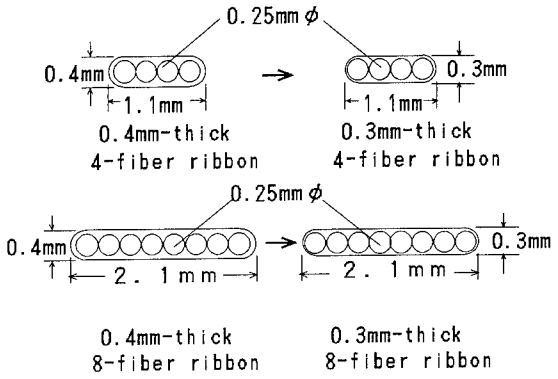


Fig.1 Optical Fiber Ribbon Construction

Transmission Loss Characteristic

Table 1 shows the transmission losses by ribbon. Every ribbon made of either Resin A or B showed a favorable initial loss.

From -30℃ to 70℃, moreover, the loss-temperature characteristic was determined. And any loss temperature fluctuations were found to be within 0.015dB/km(λ=1.55μm).

Table.1 Initial loss of 0.3mm Thick Ribbon

	Loss at 1.3μm	Loss at 1.55μm
4-fiber ribbon (A)	0.34	0.20
4-fiber ribbon (B)	0.34	0.21
8-fiber ribbon (A)	0.33	0.19
8-fiber ribbon (B)	0.33	0.19

Splice Characteristics

Splicing 4-fiber Ribbons Different in Thickness As referred to above, the 0.3mm thick ribbon showed favorable characteristics. As compared with the conventional 0.4mm thick ribbon, the 0.3mm thick one allows us to except of higher cable density

than usual. A matter of concern in this case is the case where the existing 0.4mm thick ribbon cable must be spliced with the 0.3mm thick ribbon cable to be newly laid. With such splicing case assumed, the 4-fiber ribbon was tested to determine a splicing loss and a loss-temperature characteristic at the fusion splice. Fig. 3 is a histogram of the initial splice loss.

A sample with ten splices, moreover, was evaluated for a loss-temperature characteristic at -30℃～70℃. As a result, the loss fluctuation was found to be within 0.03dB.

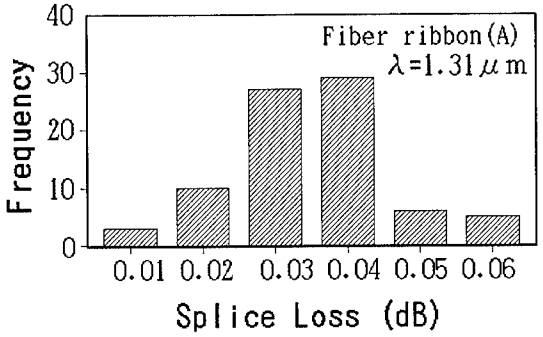


Fig. 2 Splice Loss between 0.3mm and 0.4mm Thick 4-fiber ribbons

Splicing 8-fiber Ribbon with Two 4-fiber ribbons Although it is described later, the 8-fiber ribbon is advantageous for high density if the single slotted rod type cable 400 or more fibers. If the cable has less than 400 fibers, the 4-fiber ribbon is advantageous. We assumed the case where a 4-fiber ribbon cable is spliced with an 8-fiber ribbon cable, and tested such splices. The 8-fiber ribbon was placed on the holder to one side of the multi-fiber fusion splicer for an 8-fiber. And two 4-fiber ribbons were placed in parallel on the holder to the opposite side. Thus blanket-fusion splicing test was conducted. Fig. 3 is a conceptual illustration of the fusion splice.

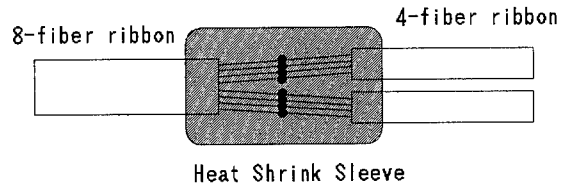


Fig. 3 Blanket Splicing 8-fiber Ribbon with Two 4-fiber Ribbons

The test was conducted in each of the following combinations:

1) 0.3mm thick 8-fiber ribbon vs. 0.4mm thick 4-fiber ribbon
2) 0.3mm thick 8-fiber ribbon vs. 0.3mm thick 4-fiber ribbon

Fig. 4 is a histogram of splice loss of combination 1), and fig. 5 is one of combination 2).

Samples with ten splices, moreover, were evaluated for a loss-temperature characteristic at -30℃～70℃. As a result, the loss fluctuations of each combinations were found to be within 0.03dB.

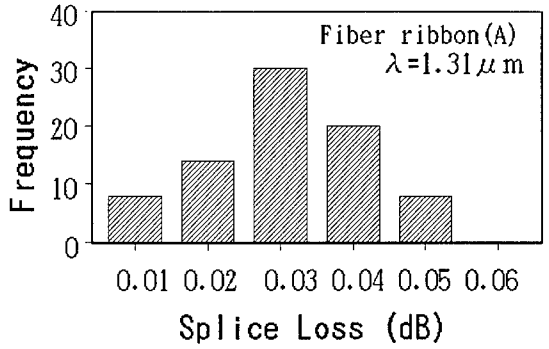


Fig. 4 Blanket Splice Loss between 0.3mm Thick 8-Fiber Ribbon and 0.4mm Thick 4-Fiber Ribbons

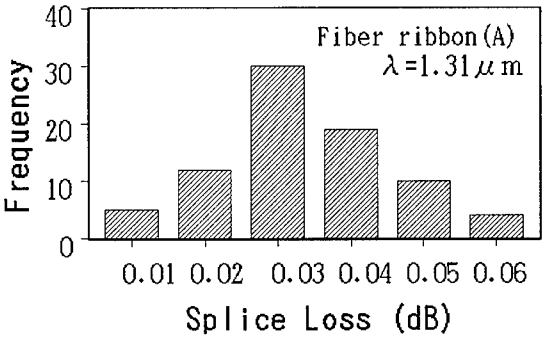


Fig. 5 Blanket Splice Loss between 0.3mm Thick 8-Fiber Ribbon and 0.3mm Thick 4-Fiber Ribbons

Optical Fiber Cable with 0.3mm Thick Ribbon

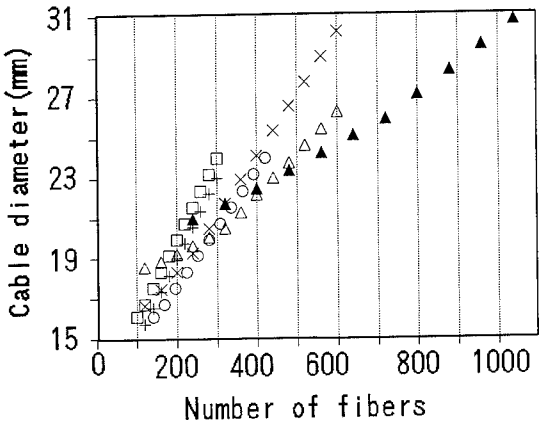
High Density Oriented Design

To determine which is more advantageous for a higher density in the single slotted rod type case, 4-fiber or 8-fiber ribbon, we calculated diameters of cables.

Fig. 6 shows the outside diameters of those cables which were manufactured in the following six patterns where:

1) Five 0.4mm thick 4-fiber ribbons are packed in one slot.
2) Five 0.3mm thick 4-fiber ribbons are packed in one slot.
3) Seven 0.3mm thick 4-fber ribbons are packed in one slot.
4) Ten 0.3mm thick 4-fiber ribbons are packed in one slot.

5) Five 0.3mm thick 8-fiber ribbons are packed in one slot.
6) Ten 0.3mm thick 8-fiber ribbons are packed in one slot.



□Conventional +Thin 4-fiber ribbon*5
○Thin 4-fiber ribbon*7 △ Thin 4-fiber ribbon*10
×Thin 8-fiber ribbon*5 ▲ Thin 8-fiber ribbon*10

Fig. 6 Number of Fibers and Cable Outside Diameter

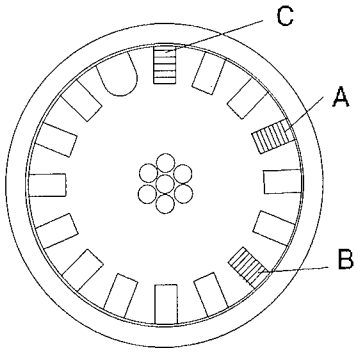
From the figure above, it may be gathered that:

- Even if the 0.3mm thick 4-fiber ribbon is applied, the outside diameter can be reduced by about 1mm as compared with the conventional product with five ribbons packed in one slot.
- If a cable having up to 280 fibers is constructed to have seven 0.3mm thick 4-fiber ribbons packed in one slot, the smallest outside diameter can be achieved.
- If a cable having from 320 to 400 fibers is constructed to have ten 0.3mm thick 4-fiber ribbons packed in one slot, the smallest outside diameter can be achieved.
- A cable having more than 400 fiber is advantageous if ten 0.3mm thick 8-fiber ribbons are packed in one slot.

Making a prototype of 420 fiber Cable

Cable Construction The cable which is able to have 420 fibers was made on a prototype basis to determine the characteristic of the cable constructed to have seven 0.3mm thick 4-fiber ribbons packed in one slot.

The slotted rod which had been put into practical use for a 300-fiber type optical cable was used directly to pack seven 0.3 mm thick ribbons in the slot in which five 0.4mm thick ribbons had been packed conventionally. As a result, 420 fibers could be mounted in the cable which has the same outside diameter (approx. 25mm) as of the conventional 300-fiber cable. On a slot by slot basis, ribbons made of different resin were dropped in, while the five conventional 0.4mm thick ribbons were also inserted in one slot for comparison. Fig. 7 is a sectional view of the prototype cable.



Diameter: about φ25mm
A: Thin ribbon (A), 7pcs.
B: Thin ribbon (B), 7pcs.
C: Conventional ribbon, 5pcs.

Fig. 7 Construction of Prototype Cable

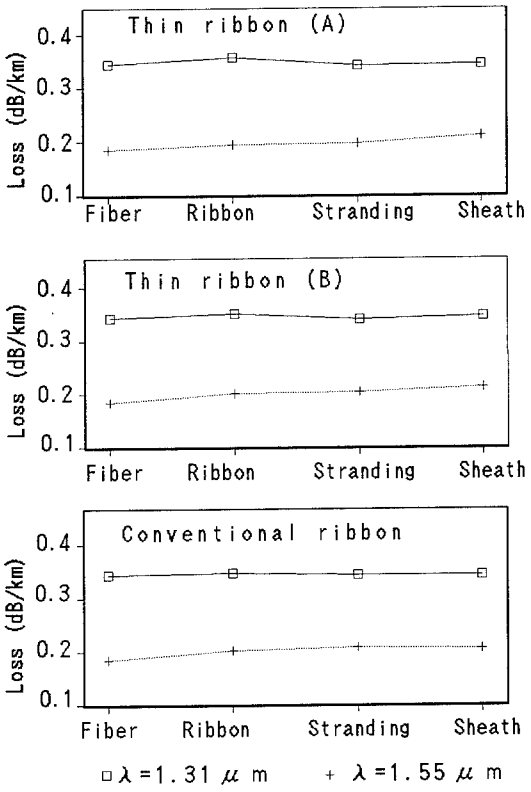


Fig. 8 Inter-Process Loss Fluctuation

Inter-process Loss Fluctuation Fig. 8 shows the fluctuations of each ribbon's inter-proces loss. In either case, the loss fluctuation fell within 0.03dB/km(λ =1.55 μ m), which is an absolutely acceptable value.

Loss-Temperature characteristic With a heat cycle of -30℃ to 70℃ applied, a loss -temperature characteristic was determined. In either case, a fluctuation fell within 0.05dB/km. Thus, the test resulted acceptably. No characteristic could be observed changed while employing ribbons different in both thickness and resin.

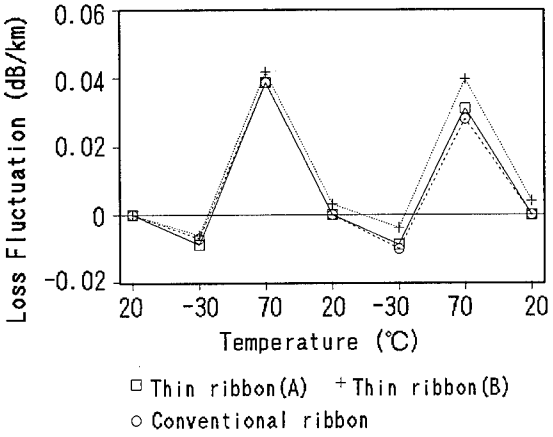


Fig. 9 Loss-Temperature characteristic, 420-fiber type Cable

Mechanical Properties

Concerning those slots only in which ribbon resin A was applied, a mechanical test was conducted as summarized in table 2. A measuring wavelength of 1.55 μ m applied.

In either case, the test showed the properties equivalent to those those with the conventional type 300-fiber cable.

Table. 2 Mechanical Properties, 420 fiber Type Cable

Test Items	Results
Bending (at 150mmR)	increase in loss <0.1dB
Lateral pressure (1960N/100mm)	increase in loss <0.1dB
Tensile (2940N)	increase in loss <0.1dB
Squeezing (1960N 300mmR)	increase in loss <0.1dB

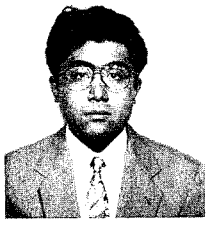
Conclusion

We have designed and developed 4-and 8-fiber ribbons(0.3mm thick)thinner than the conventional fiber ribbon(0.4mm thick). Initial loss and temperature loss characteristics of thin ribbons were found to be favorable and equivalent to those of the conventional ribbon. Thin fiber ribbon could be spliced problem-freely with the conventional ribbon.

Using the thin 4-fiber ribbon, we have also developed the 420-count slot-type optical fiber cable with a tight structure. This cable has the same outer diameter as the 300-count cable made of the convention al fiber ribbon and has good loss characte ristic of 0.21dB/km at 1.55 μ m. This structure will reduce cable costs.

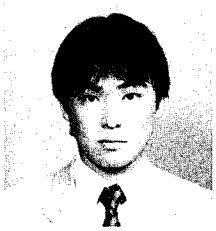
Reference

- M. Kawase, T. Fuchigami, M. Matsumoto, S. Nagasawa, S. Tomita, and S. Takashima "Subscriber Single-Mode Optical Fiber Ribbon Cable Technology Suitable for Midspan Access", J. of Lightwave Technology, Vol. 7, NO. 11, November, 1989
- S. Tomita, M. Matsumoto, S. Nagasawa, and T. Tanifuji "Ultra High-Density Optical Fiber Cable with Thin Coated Fibers and Multi-Fiber Connestors" 42th IWCS, pp5-14, 1993



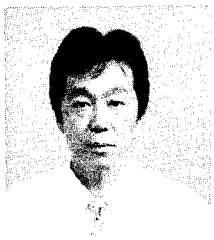
Kazuya Obi
MITSUBISHI CABLE INDUSTRIES, LTD.
4-3, Ikejiri, Itami, Hyogo Pref., 664, Japan

Mr. Obi, Engineer of Optical Fiber Cable Factory, is engaged in design and development of optical fiber cables. He received his B.S. degree in Communication Engineering from Tohoku University in 1986.



Tetsuya Takeda
MITSUBISHI CABLE INDUSTRIES, LTD.
4-3, Ikejiri, Itami, Hyogo Pref., 664, Japan

Mr. Takeda, Engineer of Optical Fiber Cable Factory, is engaged in production and development of optical fiber cables. He received his B.S. degree in Electrical Engineering from Osaka Institue of Technology in 1989.



Tamishige Watanabe
MITSUBISHI CABLE
INDUSTRIES, LTD.
4-3, Ikejiri, Itami,
Hyogo Pref.,
664, Japan

Mr. Watanabe, Staff Engineer of Optical Fiber Cable Factory, is engaged in production and development of optical fiber cables. He received his M.S. degree in Electrical Engineering from Kinki University in 1985. He is member of Institue Electrical Engineers of japan.



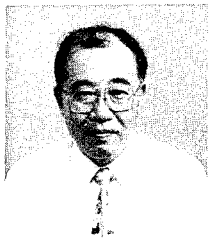
Kazuo Imamura
MITSUBISHI CABLE
INDUSTRIES, LTD.
4-3, Ikejiri, Itami,
Hyogo Pref.,
664, Japan

Mr. Imamura, Staff Engineer of Optical Fiber Cable Factory, is engaged in design and development of optical fiber cables. He received his M.S. degree in Electrical Engineering from Osaka University in 1983. He is member of Institue Electrical Engineers of japan.



Moriyuki Fujita
MITSUBISHI CABLE
INDUSTRIES, LTD.
4-3, Ikejiri, Itami,
Hyogo Pref.,
664, Japan

Mr. Fujita, chief Engineer of Optical Fiber Cable Factory, is engaged in design and development of optical fiber cables. He received his B.S. degree in Electrical Engineering from Osaka University in 1973 .He is member of Institue Electrical Engineers of japan.



Hiroyuki Tanaka
MITSUBISHI CABLE
INDUSTRIES, LTD.
4-3, Ikejiri, Itami,
Hyogo Pref.,
664, Japan

Mr. Tanaka, manager of Engineer of Optical Fiber Cable Factory, is engaged in production and development of optical fiber cables. He received his M.S. degree in Electrical Engineering from Osaka University in 1971 .He is member of Institue Electrical Engineers of japan.

Pre-connectorized 1000-fiber Single Slotted Core Cable

Hideyuki IWATA, Mikio TSUTSUMI, Ei-ichi NAKAMURA,Noriyoshi MATSUMOTO,
Masaru NOZAWA,Shigekazu HAYAMI, Shinji NAGASAWA and Tadatoshi TANIFUJI

NTT Access Network Systems Laboratories
Tokai, Naka, Ibaraki, 319-11 JAPAN

Abstract

We studied component optimization for pre-connectorized slotted core cables by reducing 8-fiber ribbon thickness, by stacking 10 ribbons in each slot and by using low insertion loss 4 and 8-fiber connectors. As a result, the diameter of 1000-fiber cable has been reduced from 40 to 30 mm. Also the 1000-fiber cable joining time was reduced from 10 to 4.5 hours by using 5 stacks of 4 mechanically transferable (MT) connectors and a newly developed joint box. The performance of the pre-connectorized cable examined in the field was satisfactory.

1. Introduction

NTT plans to construct Fiber-To-The-Home (FTTH) networks to support the multi media services required by future access networks. Optical fiber cables will be needed to construct these networks economically. By reducing the cable diameter and weight, it will be possible to install longer lengths of cable and use conduits more effectively.[1] Also low loss multifiber connectors reduce the joining time.[2],[3] It is expected that these results will lead to reductions in installation and joining costs.

We describe the design and performance of 1000-fiber single slotted core cable with a reduced diameter , low loss 4 and 8-MT connectors, a pulling head and a joint box which reduces the joining time.

Finally, we present field test results for pre-connectorized 1000-fiber cable.

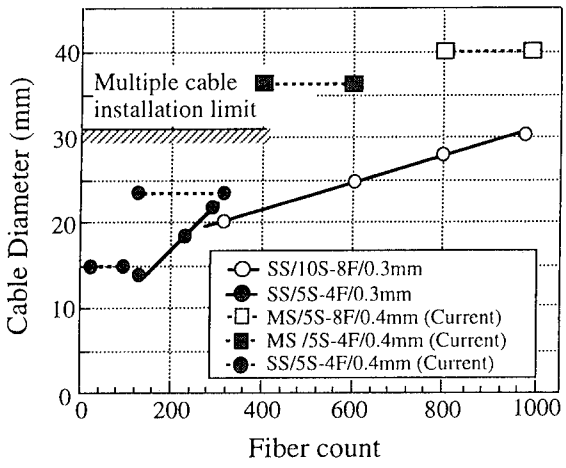
2. Design of high density optical cable

2.1 Cable structure design

Figure 1 shows the cable diameter for two different cable structures with 4 and 8-fiber ribbon. The dotted lines show the relationship between fiber count and cable diameter for current optical cable family. For a fiber count below 300, cables consist of single slotted rod with 5 stacks of 4-fiber ribbons in each slot. For a cable containing more than 400 fibers, a multi slotted rod structure is used taking ease of manufacture into consideration. 4-fiber ribbon is used for cable containing up to 600 fibers and 8-fiber ribbon is used for 800 to 1000 fiber cables to reduce the outer diameter. 8-fiber ribbon can be easily separated into two 4-fiber ribbons. The solid line with filled circles shows the same relationship for single slotted core cables with 5 stacks of 4-fiber ribbons in each slot. The solid line with open circles shows the same relationship for single slotted core cable with 10 stacks of 8-fiber ribbons. In this design, the thinner ribbons are effective both in reducing the outer diameter and for facilitating slotted rod manufacture.

From the figure, it can be seen that for a fiber count of more than 400, the single slotted core optical cable with reduced thickness 8-fiber ribbon achieves the highest fiber density in our cable family. The single slotted core 1000 fiber cable enables subduct installation after the cable has been installed in a conduit, as shown in Fig.1.

Cross sectional views of the current and newly designed 1000-fiber cables are shown in Fig.2. The cable diameter has been reduced from 40 to 30 mm and the fiber density is about 1.8 times greater than the density in the currently used cable.



SS & MS:Single and multi slotted core cable.
5S-8F:5 stacks of 8-fiber ribbons in a slot.
0.3 mm & 0.4 mm:Fiber ribbon thickness.

Figure 1 Relationship between fiber count and cable diameter

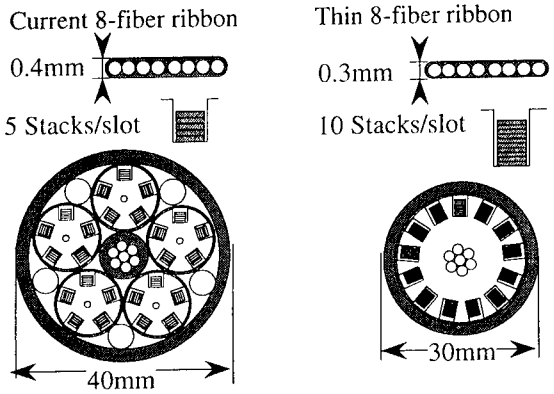


Figure 2 Cross sectional view of currently used and newly designed 1000-fiber cables

2.2 Thin fiber ribbon design

The fiber ribbon structure was designed from the view point of its the adaptability both for fusion splicing with current fiber ribbon and optical loss increase during ribbon handling at joint boxes.

(1)Compatibility with current splicing tools

We examined the compatibility of thin 8-fiber ribbon with currently used splicing tools.

(1-1) Separator

Optical losses were measured while separating thin 8-fiber ribbons into 4-fiber ribbons using the current separator. The loss increase was less than 1dB.

(1-2) Stripper and holder

Figure 3 shows the relationship between stripability and ribbon thickness for when using the current stripper and holder. Current holders fail to remove the UV curable coating from a ribbon with a thickness of less than 0.32 mm. By sticking 0.1 mm thick tape on the bottom groove of the holder, the stripability was good for a ribbon with a thickness of 0.30 mm.

(1-3) Fusion splicing machine and cutter

The average splicing loss between the current and thin 8-fiber ribbons was below 0.1 dB. Thin fiber ribbon can be cut well using existing cutters.

From the above results , it is concluded that thin ribbons with a thickness more than 300 μm are compatible with the existing splicing tool and there are no problems as regards low loss splicing between currently used and thin ribbons.

(2) Handling characteristics

For such operations as cable repositioning and network reconfiguration, the fiber ribbons are handled at cable joining boxes. There is the danger of a loss increase during handling because of the reduced fiber ribbon thickness. Therefore we measured the optical loss change during handling, which is shown in Fig.4.

The fiber ribbon handling procedure we used had four stages, a sheet was removed from an enclosure, the slack fiber ribbons and MT connectors were taken out of the sheet, put back into the sheet, and the sheet re-accommodated. In this experiment we used two types of thinly coated 8-fiber ribbon separated into 4-fiber ribbons. One type was coated with conventional material and the other with hard material. Their characteristics were the same as currently used 8-fiber ribbon.

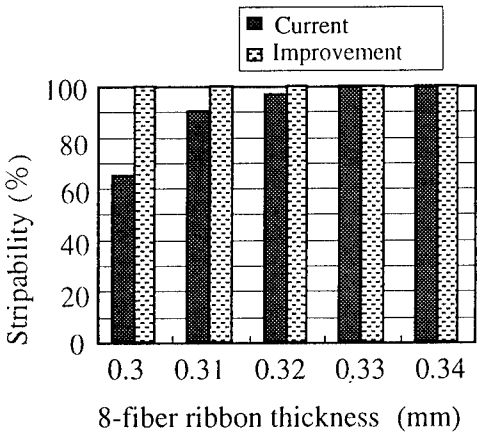
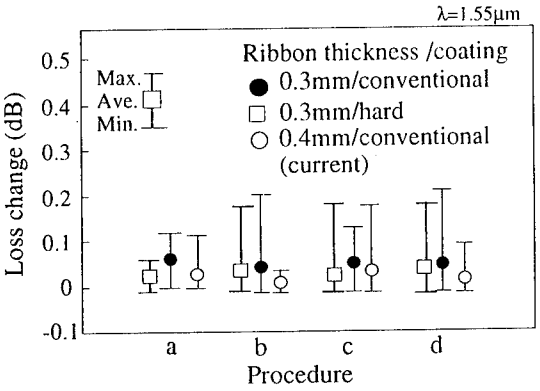


Figure 3 Relationship between stripability and ribbon thickness



a:Sheet is removed **b**:Ribbon is removed from sheet
c:Ribbon is replaced in sheet **d**: Sheet is re-accommodated

Figure 4 Optical loss change during handling

2.3 Strain design of fibers in 1000-fiber single slotted core cable

Optical fiber strains due to the cabling process are classified into three types, elongation strain, bending strain, and twisting strain. The relationship between the total strain and the stranding pitch is shown in Fig.5.[1] If the total strain is required to be below 0.05%, the stranding pitch must be longer than 500 mm. However the bending characteristics must be considered when the stranding pitch is increased as shown in Fig.5. Therefore, the stranding pitch must be between 500 and 1000 mm.

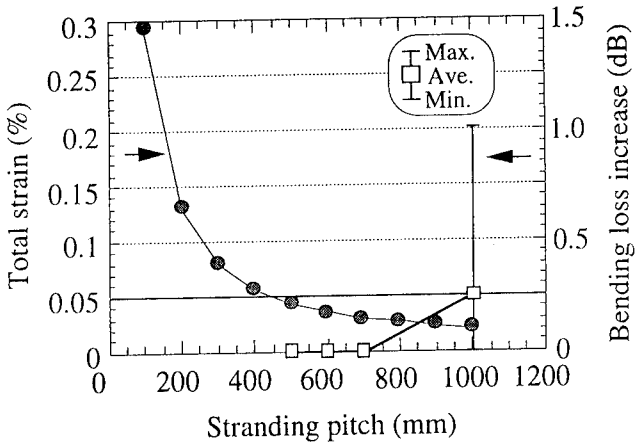


Figure 5 Relationship between total strain and stranding pitch

2.4 1000-fiber cable performance

(1) Cable performance

In our trial cable, three kinds of 8 fiber ribbon with different combinations of secondary fiber coating and ribbon coating material were inserted into three slots to confirm the effect of the coating material. The three combinations were conventional-conventional, conventional-hard and hard-conventional ultraviolet curable resins. The attenuation and mechanical performance with the different coating materials were found to be similar. The optical loss changes were measured for temperatures between -30 and 60℃ on a reel 1600mm in diameter. The optical loss changes of the bottom corner fibers in a slot increased by 0.04 dB/km at 60℃, but there were no loss changes when the cable was off the reel.

The mechanical and water-blocking performance is shown in Table 1. These levels of performance are almost the same as those of current 1000-fiber water blocking cable.

Table 1 Trial cable performance

Test item		Result
Attenuation at 1550nm	on the reel	0.20dB/km (Ave.) 0.22dB/km (Ave.) (bottom corner fiber)
	off the reel	0.20dB/km (Ave.)
Temperature cycle at1550nm: -30(-20)*~+60℃	on the reel	0.04dB/km increase:60℃ (bottom corner fibers)
	*off the reel	No loss increase
Bending: 200mmR		No loss increase
Lateral Force: 40N/mm		No loss increase
Tension: 8000N		No loss increase
Squeezing: 8000N,600mR		No loss increase
Penetration Length :After 10 days		0.5m

(2) Strain distribution of fiber in the cable.

The strain distribution of fibers in the cable was measured by Brillouin Optical-Fiber Time Domain Analysis (BOTDA) using identical strain free fibers as references. The fiber strain in the prototype cable is shown in Fig.6. The strain was measured for the edge and center fibers in the top, center and bottom fiber ribbons. This fiber strain due to cabling was below 0.05%. The fiber strains on and after applying a pulling force of 8000N were also measured. The remaining fiber strain after a pulling force of 8000N was below 0.01%. These strain characteristics are sufficient to assure long term reliability. The temperature induced strain was about 0.002%/℃.

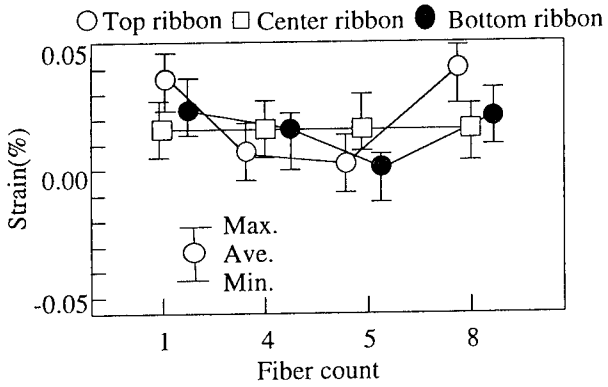


Figure 6 Fiber strain in this cable structure

3. Low loss multi-fiber connector.

3.1 Connector structure

Multifiber connectors are a more appropriate method for rapidly joining high count optical cables than fusion splicing in terms of high speed cable joining and cable network rearrangement. But the connection loss of current MT connectors for 4 and 8 fiber ribbons is as high as 0.35 dB. We have adopted a target loss value of below 0.2dB, which is the average value of current MT connector loss plus fusion splicing loss. To achieve this target, we must consider the causes of fiber offset in the MT connector. These are the clearance between a pin and a hole, fiber-hole positional deviation, fiber-hole clearance, and fiber core eccentricity. Figure 7 shows the relationship between connection loss and fiber positional deviation. To obtain an average connection loss of below 0.2dB, the fiber-hole positional deviation and the clearance between a pin and a hole must be below 0.4μm. These dimensional deviations can be improved by using a high precision plastic molding technique.

3.2 Connector performance

Based on the above design parameters, a precisely molded 8-MT connector was constructed. An average connection loss of below 0.2dB was attained as shown in Fig. 8 .

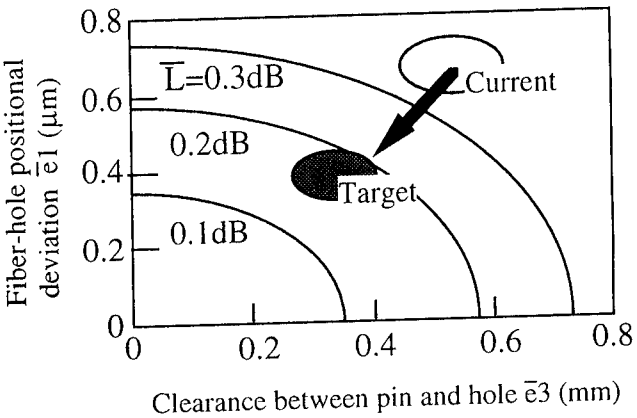


Figure 7 Relationship connection loss and fiber positional deviation

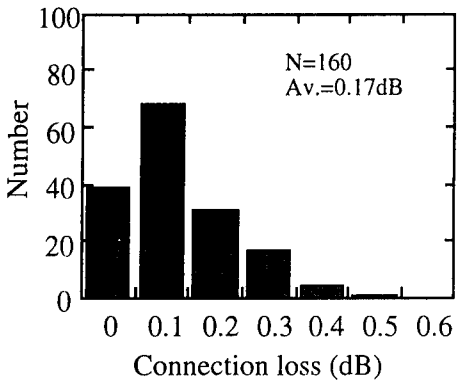


Figure 8 Connection loss of precisely molded 8-MT connector

4.1000-fiber pre-connectorized pulling head and joint box

4.1 Pulling head structure

There are certain requirements for the compact pulling head. The outer diameter and length must be less than 60mm and 1200mm, respectively, to allow the use of current installation tools. The pulling force must be 8000N, the same as the pulling force for cable. With 1000-fiber cable, 250 4-MT plugs must be packed in a pulling head. A schematic view of a pre-connectorized pulling head is shown in Fig.9. A flexible metallic tube is attached to the cable sheath and strength member to maintain mechanical strength. 4-MT plugs and 4-fiber ribbons are stacked every fiber pieces and are stored in the tube by turning them back on themselves. Thus the pulling head can accommodate and protect 250 4-MT plugs .

4.2 Pulling head performance

The pulling head and connectors were undamaged by the same squeezing test used for the cable. The pulling head remained in 1m of water for 24 hours without water penetration.

4.3 Joint box structure

There are certain requirements for the joint box.

With pre-connectorized 1000-fiber cable, 250 4-MT connectors must be packed in an enclosure compatible with those currently used in NTT. The joining time must be shorter than 6 hours or one working day.

A schematic view of our developed joint box for accommodating 250 4-MT connectors is shown in Fig.10. Five excess 4-fiber ribbons are stored by turning them back on themselves in the current enclosure. Five 4-MT connectors are held in a case and the case is then stored in a tray. Before cable joining, five 4-MT plugs are stacked in a shell as shown in Fig.11. By using a pin applicator, five pins are inserted together into pin holes with one operation. The five stacked plugs are coupled together. To enable individual access, the shell is removed after coupling and a pair of mated plugs is held with a clamp spring.

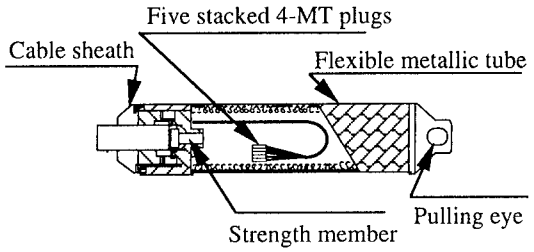


Figure 9 Pulling head structure

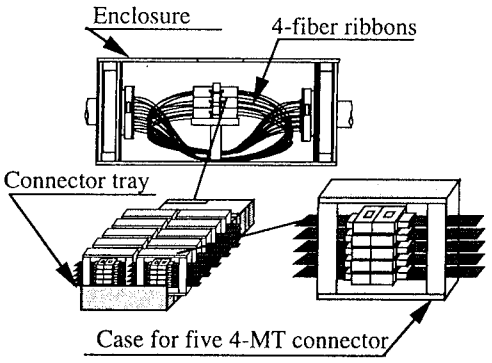


Figure 10 Joint box structure

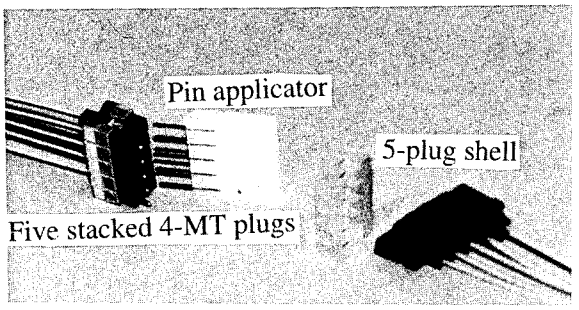


Figure 11 Five stacked 4-MT plugs

4.4 Joint box performance

Figure 12 compares the joining time for 1000-fiber cable using the current method and our new method. The procedure is divided into four stages, removing the pulling head, positioning the enclosure, joining the cable and sealing the enclosure. The total joining time is 4.5 hours for 1000 fiber cable using the developed technology and this is about half the time required for the conventional joining procedure.

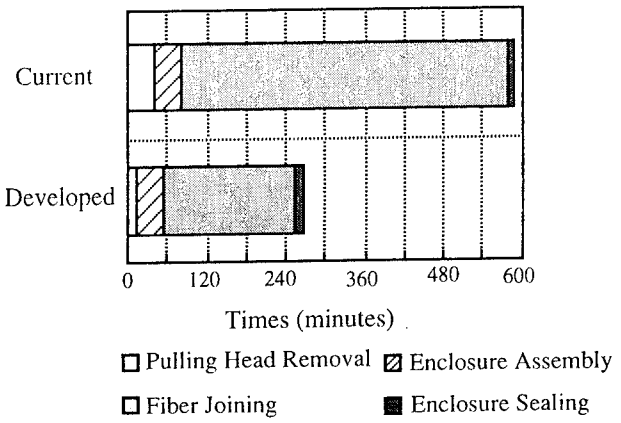


Figure 12 Joining time for 1000-fiber cable

5. Field test

5.1 Outline

We trial manufactured 1000-fiber pre-connectorized cables and evaluated their performance in the field.

Figure 13 shows a schematic view of the underground facilities used in field tests at Tsukuba R&D Center. The total conduit length is about 1.4 km, one pre-connectorized cable 577 m long and another 805 m long were installed by an optical cable pulling machine with a pulling force of 800 kgf. In this trial cable, 240 fibers (60 4-MT connector plugs) were inserted in the cable and 190 4-MT dummy connector plugs were added at the cable ends.

5.2 Results

The optical loss of the cable was measured before and after installation, and after removal from the conduit. In all cases, the optical cables were joined in a similar way when installed in the conduits. The optical loss in each cable and the joining loss were measured by OTDR at wavelengths of 1.31 and 1.55 μm.

The optical loss change both at 1.31 and 1.55 μm was within measurement accuracy.

The joining loss change for 4-MT connectors was also measured after installation and removal from the conduit. The average connection loss was 0.2 dB at 1.31 μm. The average connection loss change was within the repeatability margin for connection loss.

The strain distribution was measured by BOTDA before and after installation and after removal from the conduit. The measurement wavelength was 1.55 μm and fibers both at the side and in the center of ribbons were measured. The remaining fiber strain after a pulling force of 800 kgf was below 0.01%.

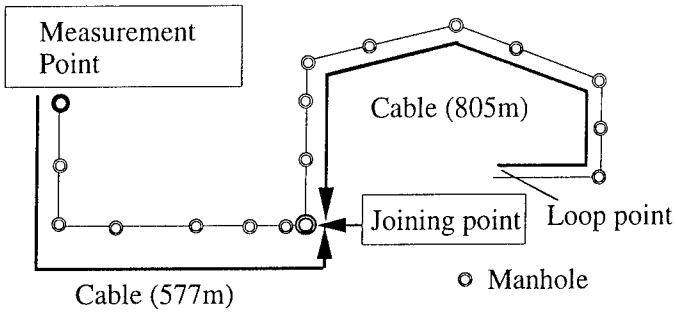


Figure 13 Field test arrangement

6. Conclusion

The 1000-fiber pre-connectorized optical cable with optimized components can be used to increase installation length from 1 to 2 km and the maximum fiber count in a conduit for multiple installation from 600 to 1600.

The connection loss of the 4 and 8-MT connectors is reduced from 0.35 to 0.2 dB on average.

The cable joining time was greatly reduced by using 5 stacks of 4-MT connectors and newly developed enclosures.

In field tests, this cable is sufficiently stable with present installation methods.

The 1000-fiber pre-connectorized single slotted core cable is promising with regard to upgrading the access network towards FTTH.

Acknowledgments

The authors are grateful to K.Ishihara,Y.Koyamada, T.Yabuta and T.Kurashima for their helpful suggestions and comments.

References

[1] S. Tomita, M. Matsumoto, T. Yabuta and T. Uenoya

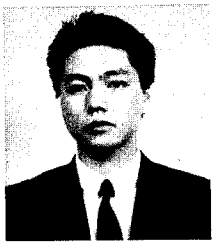
"Preliminary Research into Ultra High Density and High Count Optical Fiber Cables",Proc. of 40th IWCS, pp.8-15, 1991.
[2] T. Haibara, S. Tomita, M. Matsumoto and T. Yabuta "High-Speed Low-Loss Connection Techniques for High Count Pre-Connectorized Cables", Proc. of 40th IWCS, pp.296-302, 1991.
[3] S.Nagasawa, T. Tanifuji, M. Matsumoto, K.Kawase "Single-Mode Multi-fiber Connectors for Future Large Scale Subscriber Networks",Proc. of 19th ECOC, pp29-32,1993.



Hideyuki IWATA

NTT
Access Network
Systems Laboratories
Tokai, Ibaraki,
319-11, JAPAN

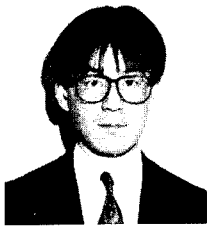
Hideyuki Iwata is enginner. He was born in 1965 and received B.E. and M.E. degrees in electronic engineering from Yamagata University in 1989 and 1991, respectively.
He joined NTT in 1991. Since 1993 he has been engaged in research on high-density and pre-connectorized optical fiber cable.
Mr. Iwata is a member of IEICE of Japan.



Mikio TSUTSUMI

NTT
Access Network
Systems Laboratories
Tokai, Ibaraki,
319-11, JAPAN

Mikio Tsutsumi is enginner. He was born in 1963 and graduated from Kumaishi High School in 1981.
He joined NTT in 1981. Since 1993 he has been engaged in research on optical cable ends and enclousures.



Ei-ichi NAKAMURA

NTT
Utsunomiya
Branch Office
Utsunomiya, Tochigi,
329, JAPAN

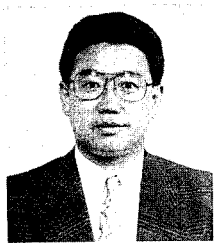
Ei-ichi Nakamura is engineer. He was born in 1968 and graduated from Kuroiso High School in 1986.
He joined NTT in 1986. Since 1992 he has been engaged in research on high-density and pre-connectorized optical fiber cable.



Noriyoshi MATUMOTO

NTT
Access Network
Systems Laboratories
Tokai, Ibaraki,
319-11, JAPAN

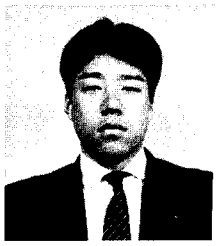
Noriyoshi Matsumoto is engineer.
He was born in 1965 and received a B.E. degree from Osaka Industrial University in 1988.
He joined NTT in 1988. Since 1993 he has been engaged in research on multifiber connectors.



Masaru NOZAWA

NTT
Access Network
Systems Laboratories
Tokai, Ibaraki,
319-11, JAPAN

Masaru Nozawa is a research engineer.
He was born in 1956 and graduated from Aomori Technical High School in 1974.
He joined NTT in 1974. Since 1994 he has been engaged in research on high-density and pre-connectorized optical fiber cable



Shigekazu HAYAMI

NTT
Access Network
Systems Laboratories
Tokai, Ibaraki,
319-11, JAPAN

Shigekazu Hayami is a research engineer. He was born in 1965 and received a B.E. degree from Yamanashi University in 1988.

He joined NTT in 1988. Since 1993 he has been engaged in research on aerial optical fiber cable.



Tadatoshi TANIFUJI

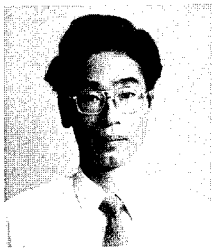
NTT
Access Network
Systems Laboratories
Tokai, Ibaraki,
319-11, JAPAN

Tadatoshi Tanifuji is the leader of the high count optical fiber cable research group.

He was born in 1949. He received B.E. , M.E. , and Ph.D . degrees in electronic engineering from Hokkaido University in 1972, 1974, and 1983, respectively.

He joined NTT in 1974. Since 1991 he has been engaged in research on high-density optical fiber cable and jointing technologies.

Dr. Tanifuji is a member of IEEE.



Shinji NAGASAWA

NTT
Access Network
Systems Laboratories
Tokai, Ibaraki,
319-11, JAPAN

Shinji Nagasawa is an executive research engineer. He was born in 1950 and received B.E. and M.E. degrees in electrical engineering from Chiba University in 1974 and 1976, respectively.

He joined NTT in 1976. Since 1990 he has been engaged in research on multifiber connectors.

Mr. Nagasawa is a member of IEEE.

CAPABILITY AND CONTROL OF RIBBON STRIPPING AS RELATED TO RIBBON MATERIAL SYSTEMS AND STRIPPING TOOLS

P.K. Kim, N.W. Sollenberger, K.W.Jackson

AT&T Bell Laboratories

Norcross, GA

Abstract

Mass fusion splicing with fiber ribbon cable can significantly reduce the splicing cost for broadband access networks in the subscriber loop. The high productivity of mass fusion splicing has spawned a host of suppliers of ribbon cable, ribbon stripping tools and mass fusion splicing machines. To achieve and maintain the high productivity of mass splicing operations in the field, it is important that the ribbons strip well over a range of field conditions. The capability of the ribbon stripping process, as measured by yield, depends upon ribbon geometry, all the material components and interfaces that exist in the ribbon, as well as the design, the temperature, and blade separation settings of the stripping tool. Because factory made ribbons involve precisely controlled conditions, the stability or state of control of the stripping process is only weakly influenced by the ribbon parameters but is more strongly influenced by consistency of the strip tool operating parameters. In this paper, we examine the ribbon stripping process with respect to both capability and control. We clarify the relation between strip yield and other important performance characteristics. We also examine practical guidelines that can be used to assess the stability or degree of control of the stripping process.

1. Introduction

Design of ribbon structures that have suitable stripping characteristics and still maintain high long term reliability requires an understanding of the interactions among the various material systems and subprocesses involved [1-5]. The statistical concepts of capability and control are relevant to the laboratory experiments that generate design data as well as to ribbon stripping and mass fusion splicing in the field [6]. Whereas capability relates to the yield of the stripping process, control relates to the time dependence or stability of the yield. Strip yield or capability is meaningful only when there exists no time dependence for the yield. Thus, experiments that aim to investigate strip yield must be designed and conducted such that process stability is assured. Sources of instability include temperature drift, blade movement and misalignment, and debris buildup at the blades of the tool. Attention to both capability and control permits a more accurate assessment of the design robustness of different material systems and of different stripping tools and their operating parameters. As mentioned earlier, for factory made ribbons, precise control of the manufacturing process results in stringent dimensional and quality specifications so that the stability of the stripping process is virtually independent of the ribbon itself. For field ribbonized fibers, it is more difficult to control the ribbon geometry and quality specifications and both the ribbonizing method and operator technique can influence stability and yield.

For a stable process with geometrically uniform ribbons, the critical parameters that affect ribbon strip yield include the bulk and interfacial properties of the primary and secondary coating, the coloring ink and the ribbon matrix [1-4]. Specific properties and parameters of interest include the following:

- Modulus/Time/Temperature Function for Primary/ Secondary Coatings
- Adhesion of Primary Coating to Glass Fiber
- Adhesion of Ink to Secondary Coating
- Adhesion of Matrix to Ink
- Modulus/Time/Temperature Function for Matrix
- UV Dose/Cure Response of Coatings, Inks and Matrix
- Thickness of Matrix
- Thermal/Moisture Aging Characteristics of Adhesion and Moduli

Other issues of concern involve the relation among the foregoing properties and parameters along with other important functional characteristics of ribbons such as placing/handling robustness and the retention of easy fiber and subribbon breakout after thermal or moisture aging. Lastly, it is important to keep in mind that, in addition to good ribbon strippability, the ribbon material system must maintain sufficient adhesion at all the interfaces to resist delamination induced by handling or environmental exposure [7,8].

2. Experimental

2.1 Ribbons

Both factory and field made ribbons were evaluated in this work. Edge bonded ribbons comprising 12 color coded fibers were factory made with various coloring inks while keeping the coating and matrix materials the same.. The 12-fiber field made ribbons (FMR) were made using a commercially available ribbonizer tool (Fiber Arranger Tool). Table 1 lists the characteristics of the ribbons tested.

Table 1. Test Ribbons

Ribbon #	Coating	Ink	Matrix
1	A	D	K
2	A	E	K
3	A	F	K
4	A	G	K
5	A	H	K
6	A	I	K
7(FMR)	A	I	L

2.2 Ribbon Stripping

We used three commercial ribbon stripping tools designed to remove the coatings, color code and matrix from the end of the fiber ribbon. Two of the tools are currently available. The detail description of these two tools, the temperature measurement methods, the ribbon stripping procedure and the ribbon stripping test conditions are described in reference 1. The third tool used is an older model tool no longer available. The temperature settings used for each tool during the test program are listed in Table 2.

Table 2. Tool Temperatures for Strip Yield Robustness Tests.

Stripping Tool	Test Temperatures
A	155°C
B	75°C, 105°C, & 135°C
C	75°C, 105°C, & 135°C

To achieve high productivity of mass splicing operations in the field, it is important that the ribbon strip well over a range of field and tool conditions. When stripping ribbons, it is desirable to achieve, in order of importance, the following results:

- No broken fibers
- Matrix, color inks and coatings composite removed as a single piece
- No tenacious residue remaining on fibers (can be removed with one alcohol wipe)
- No debris or particles on or around tool blade

For a given stripping tool, the ability to cleanly strip a 12 fiber ribbon can be measured by its characteristic strip yield profile over the temperature range shown in Table 2. For a given ribbon type, tool and temperature, the stripping yield is the percent of strips in a sample of size, N, for which the matrix, ink and coatings composite is integrally removed without breaking a fiber and no tenacious residues remain on the fibers. Because field conditions and tool temperatures can be highly variable, it is useful to define a more comprehensive and robust metric of ribbon stripping yield. One such metric is provided by the strip yield when averaged over all tools for a specified temperature range. For the purposes of this study, the ***average strip yield*** is defined as the overall, sample size weighted average of the ribbon strip yields for the three tools when used at the respective temperatures of 75, 105, 135, and 155°C Thus, defined, the ***average strip yield,*** provides a quantitative measure of the stripping robustness of a given ribbon design (as determined by coatings, inks, and matrix materials and their geometry). The ***average strip yield*** is subsequently referred to as the ribbon robustness strip yield **(RRSY).**

A less stringent definition of strip yield is useful to assess the degree of stability or control of the ribbon stripping process as related to the ribbon and tool design, as well as the diligence exercised in cleaning the blades of the stripping tool after each strip. During the stripping process, coating, ink, or matrix can build up around the blades in the form of debris or particles. Such debris , if it remains on the tool, greatly increases the risk of fiber breaks in subsequent strips. Moreover, the risk of fiber breaks increases with improper cleaning. The less stringent measure of average yield relaxes the requirement that the coatings, ink and matrix composite be removed in a single piece as specified by the **RRSY** measure. The less stringent measure of yield allows for varying degrees of diligence in cleaning of the tool blades and clearly demonstrates the importance of cleanly stripping the coatings/ribbon materials from the glass fiber as a single piece. Figures 1a and 1b, respectively demonstrate the criteria for the **RRSY** and the less stringent definitions of strip yield.

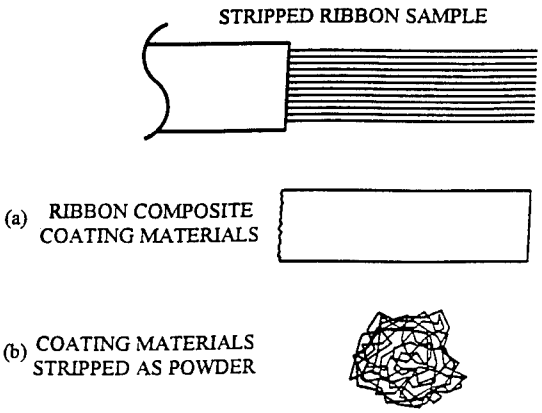


Figure 1. Stripped Ribbon Sample and Ribbon Composite Coating Materials (a) stripped in one piece, (b) stripped as powder

3. Results

The effect of primary and secondary coatings, on ribbon strippability has been studied extensively for a given color and matrix system [1-4]. For a given ink and matrix system, the **RRSY** increases as the fiber pull-out force decreases (Figure 2: Type 1). However, for a given coating system, it is possible to vary the ribbon strip yield by changing the ink and/or the ribbon matrix materials (Figure 2: Types 2 & 3). Also, a condition of instability in the ribbon stripping process

can be generated by debris buildup at the blades of the tool when the ribbon does not strip in one piece. In this section we present results for the effect of ink system on strip yield and the effect of debris buildup on the strip yield stability. This work extends our laboratory's efforts to identify and control factors which affect performance and reliability of ribbon structures.

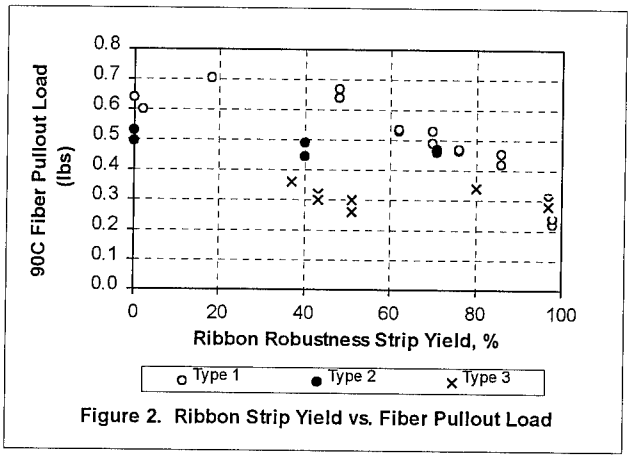


Figure 2. Ribbon Strip Yield vs. Fiber Pullout Load

3.1 Ribbon Robustness Strip Yield (RRSY)

The **RRSY** results for the test ribbons listed in Table 1 are presented in Table 3. Ribbons #3, #4, and #6 performed very well for all tools

Table 3. Ribbon Robustness Strip Yield Results for the Test Ribbons.

Ribbon #	Tool A	Tool B			Tool C			RRSY
	155°C	75°C	105°C	135°C	75°C	105°C	135°C	
1	0	0	0	0	40	0	20	**9**
2	20	0	80	0	0	0	0	**14**
3	100	100	100	100	100	100	80	**97**
4	100	100	100	100	100	100	100	**100**
5	100	100	100	0	100	20	0	**60**
6	100	100	100	100	100	100	100	**100**
7	100	40	100	80	0	0	0	**46**

over the entire temperature range with a **RRSY** of 97 to 100. In contrast, ribbons #1 and #2, which have an **RRYS** of 14 or less performed poorly for all tools at almost all temperatures. Ribbon #5 performed well at the lower temperatures for Tools B and C, but the ribbon composite coating crumbled at higher temperatures. It is noted that the ribbons were heated for ten seconds before stripping with Tools B and C, while for Tool A it was only one second. This may account for why Ribbon #5 stripped well on Tool A at 155°C, but stripped poorly on Tools B and C at 135°C.

3.2 Effect of Matrix to Ink Adhesion on RRSY

The effects on **RRSY** of the adhesion of the matrix to the inked fiber were measured on four ribbons made with the same primary and secondary fiber coatings and matrix but with different inks. The glass transition temperature of the matrix as measured by the peak in tanδ in the DMA (Dynamic Mechanical Analysis) is about 30°C. Ribbons with different levels of adhesion of matrix to inked fiber were prepared by coloring the fiber with different inks. These results are summarized in the Figure 3. The adhesion of matrix to inked fibers can be characterized by both a solvent swell and peel test. The relative adhesion parameter is a measure of the matrix to inked fiber adhesion, and is the ratio of the measured 90° peel force of the ribbon and the percent solvent swell of the ribbon.

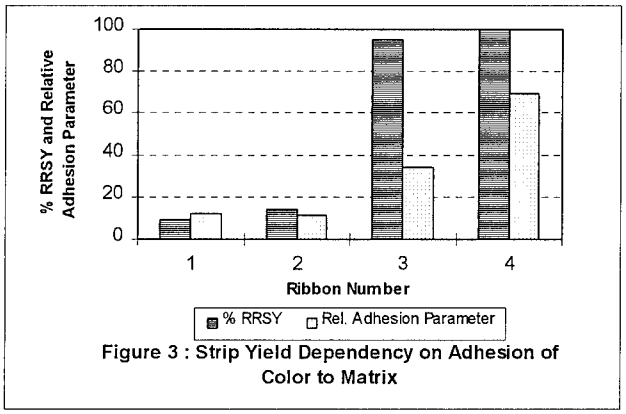


Figure 3 : Strip Yield Dependency on Adhesion of Color to Matrix

If the adhesion between the ink and the matrix becomes too low, as in Ribbons #1 and #2, the matrix tends to separate from the fiber at the beginning of the ribbon stripping process and starts to disintegrate before the fiber fully separates from its coating. Because the ribbon is firmly held in between two plates, the disintegrating matrix forces fibers to separate and spread laterally in front of the blade. The coatings of individual fibers are then stripped off as a loose residue which causes more build-up of debris which in turn forces the fibers to spread away from the stripping front even more. As the adhesion level increases, the coating/ink/matrix composite remains together as one unit throughout the stripping process, as demonstrated by Ribbons #3 and #4. In general, the higher the adhesion between the matrix and the ink the higher the **RRYS** for a given material system.

The adhesion of the matrix to the inked fibers also has significant influence on other important functional characteristics of ribbons such as placing/handling robustness, long term environmental resistance to delamination and ability to access individual fibers and subribbons before and after environmental aging [8]. As the matrix to colored fiber adhesion increases, it becomes more difficult to access individual fibers without either damaging the coatings or causing transient

bending-induced attenuation increase. On the other hand, if the adhesion level is too low, then there is a risk of delamination at the interface between the matrix and the inked fiber during handling or environmental aging. It is important to evaluate any changes in this adhesion after aging. For instance, when one of the ink/matrix combination ribbon was aged according to the Bellcore material compatibility test procedure, the matrix was difficult to remove to access individual fibers compared to an unaged ribbon. This type of aging condition is typical in aerial closures, pedestals and steam applications. Possible causes for this difficulty in removing the matrix after aging are either increase in adhesion between colored fiber and matrix caused either by the migration of some mobile release agents (or weak boundary layer) away from this interface or by some chemical interactions between ink and matrix during aging. We are continuing our efforts to better understand this change in adhesion during aging.

3.3 Control/Stability of Stripping Process

The **RRYS** is useful for evaluating ribbon composite materials. First, it characterizes the effect of tool temperature and heating-up time on the stripping performance of a given ribbon. This is important because, even though a tool's operating temperature is preset at the manufacturer, temperature drift and changes may occur in the field. Also, the requirement for the composite material to come off in one piece is important.

When it comes to the actual mass splicing of ribbon, it is important for just the coating to be completely removed without any broken fibers, and for any residue left on the fiber to be removed with an alcohol wipe. So, why is it desirable for the composite coating ink and matrix to come off in one piece? If the coating disintegrates and builds up at the stripping tool blades then the fibers are bent during stripping which increases the risk of a broken fiber. Also, according to the stripping tool manufacturers, the most frequent cause for an unsuccessful strip is the build up of coating materials on or behind the tool blades. When the ribbon coating composite crumbles and disintegrates during stripping, debris build-up at the blades is greatly increased.

We designed and conducted a test to compare the stripping performance of ribbons which did and did not disintegrate during stripping. For this study, only the optimum tool temperature was used, that is Tool A was set at 155°C and Tool B was set at 105°C (these temperatures correspond to the recommended setting by the tool's manufacturer). The strip yield was calculated as the percent of successful strips for the given number of attempts without cleaning off the tool (with the exception of removing the composite coating material if it came off in one piece). The results are presented in Figure 4 for 1, 5, 10, and 25 strip attempts without cleaning the tool. For reference the overall **RRSY** is presented at the right hand side of the Figure 4. Except for the field made ribbons, all of the ribbons stripped successfully on the first attempt.

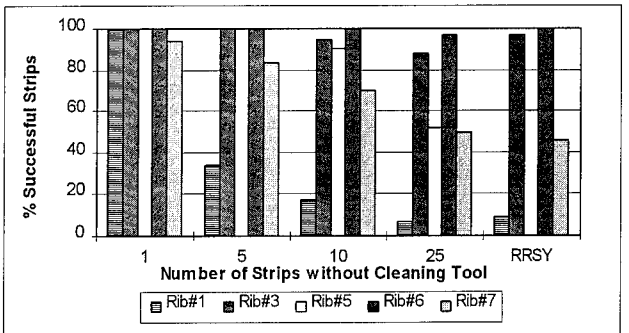


Figure 4. Strip Yield Dependence on Tool cleaning

Fibers sometimes broke on the first attempt to strip the field made ribbon primarily because of an irregular ribbon geometry. After five attempts without cleaning the tools, the strip yield for Ribbon #1 dropped below 40 percent and continued to drop below 20 percent after ten attempts. The **RRSY** for Ribbon #1 was 9 percent. The strip yield of ribbon #5, which had a **RRSY** of 60 percent, stays at 100 percent even after five attempts without cleaning the tool. It drops only to 90 percent after ten attempts and finally falls to about 50 percent after twenty five attempts without cleaning the tool. Ribbons #3 and #6, which had **RRSY** values of 97 and 100 respectively, performed excellently with Ribbon #6 having a strip yield of 97 percent even after 25 attempts without cleaning the tool.

Other factors involving "wear and tear" of the stripping tool can also affect stripping performance. As part of our ribbon program, whenever new ribbon composite coating materials are evaluated for ribbon stripping, a control ribbon is tested along with the ribbons to be evaluated. The control ribbon is a well-characterized production ribbon having a **RRSY** of 95 to 100 percent. The control ribbon is used to detect and correct for any change in the performance of the stripping tools themselves.

Figure 5 shows the results of stripping a control ribbon with two different ribbon stripping tools over a period of about a year and a half. At the beginning, Tool B was relatively new, while Tool C was an older tool which had been used extensively in previous tests. These results demonstrate that Tool B performed consistently at 100 percent yield throughout this time period, with the exception of one time at 95 percent. On the other hand, Tool C had intermittent drops in yield of below 75 percent. When the yield dropped below 95 percent, the tool was inspected and readjusted for optimum performance. The most recurring problem with Tool C was that the space between the blades changed over time. Sometimes only one side of one blade moved causing the cutting edges to be skewed with respect to each other. When this happened, either the coating would not be completely removed from one side of the ribbon (because the blades were too far apart) or fibers would break on one side (because the blades were too close together). Other problems we

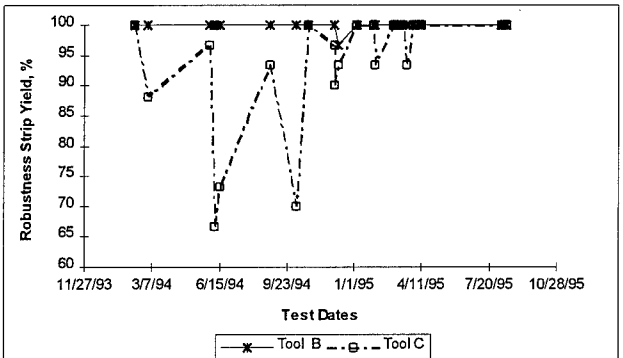


Figure 4. Robustness Strip Yield with Tool Aging for Different Stripping Tools

encountered included the heating surface becoming loose, movement of the pads behind the blades, or blade wear.

4. Summary and Conclusions

This work focused on evaluating the ribbon stripping process with respect to both capability and control. We measured the effects of the coating system, fiber inks, matrix and adhesion at both glass/coating and ink/matrix interfaces on stripping capability as measured by an overall temperature/tool averaged strip yield. We demonstrated that a balance in physical and adhesion properties of each layer of materials in the ribbon is required for robust stripping performance and presented results for ribbon material systems that provide a high strip yield. We also examined practical ways to assess the stability or degree of control of the stripping process as determined by the ribbon and tool design.

Acknowledgments

The authors thank Ken Kroupa and Joel Darsey for coloring and ribboning, Heng Ly and Ray DeFabritis for test measurements. We acknowledge the contributions of Charles Aloisio and Shahab Siddiqui, and support of Carl Taylor and Manuel Santana.

References

1. Jackson, K.W., Parker, T.L., Petisce, J.R., Sollenberger, N.W., Taylor, C.R., *Proceedings of the 42nd International Wire and Cable Symposium*, U.S. Army Communications and Electronics, Fort Monmounth, N.J., 1993, pp. 28-35.

2. Jackson, K.W., Moore, R.C., Petisce, J.R., Sollenberger, N.W., Taylor, C.R., Turnipseed, J.M., Proc. 10th NFOEC, June 12-16, 1994, pp. 93-100.

3. Keesee, J.R., Lochkovic, G.A., Smith D. and Toler, J.R., *Proceedings of the 43rd International Wire and Cable Symposium*, U.S. Army Communications and Electronics, Fort Monmounth, N.J., 1994, pp. 430-439.

4. Bonicel, J.P., Keller, D., Kylen, G., Schulte, J., Paternostro, G., Cortines, C.G. and Lasne, C., *Proceedings of the 41st International Wire and Cable Symposium*, U.S. Army Communications and Electronics, Fort Monmounth, N.J., 1992, pp. 25-31.

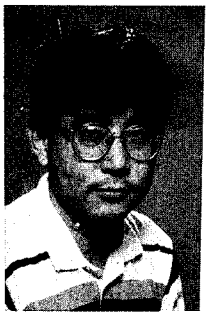
5. Greco F. and Ragni, A., *Wire Journal International,* v.25 (12), 1992, pp. 63-72.

6. Moen, R.D., Nolan, T.W., and Provost, L.P., Improving Quality Through Planned Experimentation, McGraw-Hill, 1991, pp. 420-426.

7. Abel, A. and van Eekelen, J., *Proceedings of EFOC & N '93 the Eleventh Annual Conference*, July 1993, pp. 298-302.

8. Cocchini, F., Cuomo, D., Ferri, G. and Pudia, A., *Proceedings of the 43rd International Wire and Cable Symposium*, U.S. Army Communications and Electronics, Fort Monmounth, N.J., 1994, pp. 66-71.

Biography



Peter K. Kim is a Member of Technical Staff in the Materials Engineering Department at AT&T Bell Laboratories in Norcross Georgia. After receiving a BS in Chemical Engineering from MIT, he received a Ph.D. in Polymer Science and Engineering from the University of Massachusetts at Amherst in 1986. He worked at the Aerojet Propulsion Company and the Dow Chemical Company before joining AT&T in 1994. His present responsibility include development of materials for optical fiber, ribbon and cable.

Neil W. Sollenberger is a Member of Technical Staff in the Outside Plant Fiber Optic Cable Group at AT&T Bell Laboratories in Norcross, GA. He is responsible for various aspects in the development of fiber optic ribbons and cables. Prior to his current assignment, he has worked in areas of both copper and fiber optic closures and terminals, as well as cabinets for loop electronics. He joined AT&T Bell Laboratories in 1978. He has B.S. degree in Agricultural Engineering from University of Georgia, and he has a M.S. degree in Mechanical Engineering from the Georgia Institute of Technology.

Kenneth W. Jackson is a Distinguished Member of Technical Staff in the Outside Plant Fiber Optic Cable Group at AT&T Bell Laboratories, Norcross, GA. He joined the Western Electric Company in 1970 having received a B.S.M.E. from Auburn University. He joined AT&T Bell Laboratories in 1981 having received a M.S.M.E. and Ph.D. from the Georgia Institute of Technology. Since 1981, he has worked in the areas of Optical Fiber Fabrication, Fiber Optic Connectors, Materials Design, and Fiber Optic Ribbon and Cable Design and Development.

OPTICAL FIBER LINE TEST AND MANAGEMENT SYSTEM FOR PASSIVE DOUBLE STAR NETWORKS AND WDM TRANSMISSION SYSTEMS

Shin-ichi FURUKAWA, Hiroyuki SUDA, Fumihiko YAMAMOTO,
Yahei KOYAMADA, Toshinao KOKUBUN and Ikuya TAKAHASHI

NTT Access Network Systems Laboratories
Tokai-mura, Naka-gun, Ibaraki-ken, 319-11 JAPAN

ABSTRACT

We have constructed for the first time an optical fiber line remote test and management (OFTM) system for passive double star (PDS) networks and wavelength division multiplexing (WDM) transmission systems operating at wavelengths of 1.31 and 1.55 μm. A fault isolation technique, using a high spatial resolution OTDR operating at 1.65 μm and optical filters which reflect the OTDR light, has been developed for the in-service testing of a practical PDS network with eight-branch splitters. A UNIX system work station and an object-oriented database (OODB) are used to control and manage the system. We have applied a prototype OFTM system in an experiment on new multimedia info-communication services in Japan, and confirmed its usefulness.

1. INTRODUCTION

Optical subscriber systems using PDS networks and WDM transmission techniques at wavelengths of 1.31/1.55 μm have been actively investigated in order to provide customers with economical services [1-2]. OFTM systems are needed in order to reduce the testing time required for installed fiber cables and to perform preventative fiber network maintenance. Furthermore, they must effectively manage numerous outside optical facilities of various types.

NTT has already developed the Automatic Optical Fiber Operation Support System (AURORA) for test and management in single star subscriber networks [3-4]. With a view to constructing a new OFTM system for PDS/WDM systems, we have already investigated such areas as a 1.65 μm fiber measurement technique [5-8], a fault isolation technique [9], and an outside plant management database [10]. A monitoring system has been developed which uses the 1.6 μm wavelength band for the preventive maintenance of the optical fiber cable plants [11].

We have now constructed a practical prototype OFTM system for a PDS/WDM system and applied it to a multimedia experiment. It is the New Generation Communication Network Pilot Model Project which has provided about 300 subscribers with integrated telecommunications and broadcasting services in the Kansai-Science-City in Japan since July 8, 1994.

This paper outlines the OFTM system, its key technologies and results of the multimedia experiment.

2. OFTM SYSTEM FUNCTIONS AND CONFIGURATION

2.1 OFTM System Functions

Table 1 shows the system functions of the OFTM for PDS/WDM systems, which are almost the same as those of AURORA [4].

There are two main functions: testing and management. With regard to testing, first, fiber loss tests and OTDR tests are performed remotely at communication wavelengths at the request of a field worker when outside work such as cable installation, service orders, repair, or cable transfer has been carried out. Second, fault isolation and location and periodic surveillance tests can be undertaken without any interruption of multimedia services.

Table 1 System functions of OFTM for PDS/WDM

	Function	Contents
1	Remote loss test and OTDR test	Remote test light injection into a fiber under test and remote OTDR measurement after cable installation or repair and during service order or cable transfer work.
2	Fault isolation and location	Remote isolation of a fault between an optical fiber line and an ONU and remote fault location in an optical line.
3	Periodic surveillance test	Preventive maintenance by periodic OTDR tests.
4	Fiber identification	Remote identification light injection into an object fiber.
5	Optical facility information management	Registration and reference of outside optical facility information such as fibers, fiber connections, splitters, users and tested data.
6	Information provision	Providing information about fiber assignment to users, cable routes, outside facilities, etc. with intelligent graphical user interface (GUI).

2.2 OFTM System Configuration

Figure 1 shows an outline of the PDS networks and WDM systems that we must test and manage and a configuration of the OFTM system designed for them.

Optical splitters are located outside or inside a telephone office as shown in Fig. 1. When they are located in or near the customer's premises, fiber testing and facility management for the PDS networks become much difficult because of their splitting characteristics. Therefore, we have mainly investigated PDS networks where the splitters are located outside the telephone office.

Signal lights transmitted at wavelengths of 1.31 and 1.56 μm propagate in an optical fiber for telecommunication services and video distribution services. They are mixed or divided with WDM couplers located both in customer premises and in the telephone office. An optical network unit for narrowband digital system (N-ONU) and an ONU for video distribution system (V-ONU) are installed in customer premises. An optical subscriber unit for narrowband digital system (N-OSU) and an OSU for video distribution system (V-OSU) are installed in the telephone office. Here we show them as a subscriber line terminal (SLT) in Fig. 1.

A measurement wavelength of 1.65 μm was selected for in-service testing since 1.31 and 1.56 μm are used for the WDM transmission system and fiber bending loss occurs easily in the 1.6 μm wavelength band. We used short wavelength pass filters (SWPF), which allow the signal light to pass and cut off the test light. They are arranged in front of the ONU and in the optical branch module. Their cut off wavelength, however, was different from that of conventional SWPFs [3-4]. We carefully designed the return loss in the components of the OFTM system because it is a more important factor in analog video distribution services than in conventional services.

Optical couplers were installed in the optical branch module and two types of fiber selectors using MT-type and SC-type mechanisms were installed in an FTM and a TEM in order to inject the test light into the fiber under test [3-4]. The SC-type fiber selector in the TEM was slightly changed as regards the input ports of the test equipment because their number was increased for the PDS/WDM system.

A 1.65 μm optical pulse from the OTDR is launched into all the branched fibers via fiber selectors, a coupler and a splitter. The pulses reflected by the SWPFs are superimposed in one OTDR trace since they are mixed by the splitter. Therefore, an OTDR with high spatial resolution (H-OTDR) has been developed and installed in the TEM to isolate each reflected pulse. An optical power meter has been modified, which can measure a transmission signal light power individually when two signal lights enter it simultaneously.

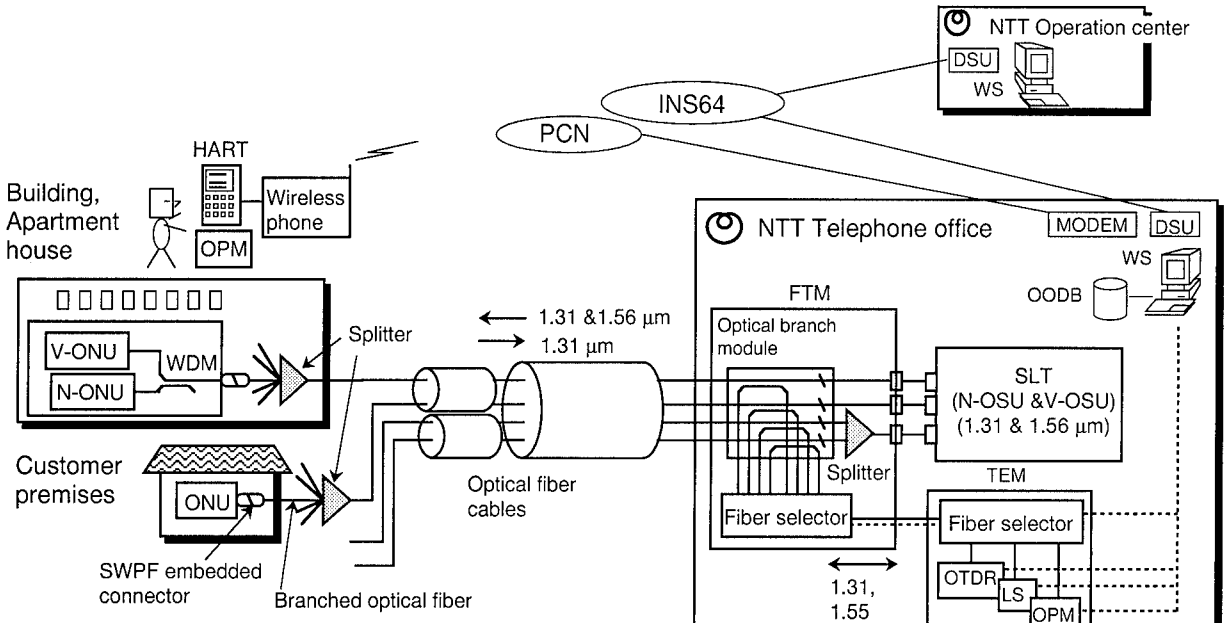


Fig. 1 Outline of PDS/WDM systems and configuration of optical fiber line test and management (OFTM) system

A UNIX system work station (WS) was used to control the fiber selectors and test equipment and manage an object-oriented database. A wireless phone was used to transfer some measurement data from customer premises to the WS. Features of the OFTM system for PDS/WDM are summarized in Table 2.

3. OPTICAL FIBER LINE TEST TECHNIQUES

3.1 Tested Item, Equipment and Measurement Wavelength

Table 3 summarizes the tested items, the equipment installed in the OFTM system and the test wavelengths used for PDS/WDM systems.

It is important to measure the reflected pulse peak level and the distance from the telephone office to each SWPF installed in front of the ONU just after finishing each stage of service order work. This is because the reflected pulse is the only way to identify the customer on the H-OTDR trace.

3.2 1.65 μm SWPF Embedded in SC-Connector

A short wavelength pass filter (SWPF), which allows 1.31 and 1.56 μm wavelengths to pass and which cuts off the 1.65 μm wavelength, was embedded in a fiber with an angle of inclination to the fiber axis in an SC-connector in the conventional way. Figure 2 shows the relationship between the transmittance and wavelength of the SWPF. The filter was made by depositing multilayers of TiO_2 and SiO_2 on a polyimide film substrate [12]. The thickness of the SWPF was about 30 μm. There was a slight hump in the transmittance characteristics at a wavelength of 1.575 μm, however, the optical loss between 1.3 and 1.565 μm was less than 0.2 dB. The optical loss at 1.65 μm was more than 30 dB.

The return loss from an SWPF embedded in an SC-connector is very important, since an analog video distribution system operating at 1.56 μm is very sensitive to reflections from the devices and the dynamic range for fault isolation depends on its return loss at 1.65 μm. We measured the return loss of trial SC-connectors in which the SWPF was embedded in the fiber with various angles of inclination. Figure 3 shows the measured relationship between the return losses at 1.31, 1.56 and 1.65 μm and the filter angle.

As is clear from the diagram, the larger the filter angle became, the bigger the return losses became. The angle dependence of the return loss at 1.31 μm became smaller than those at other wavelengths because the measured data included the reflected optical power from the connection between the trial SC-connector and a reference SC-connector. The filter angle must be about 3.5 degrees to achieve a return loss of more than 35 dB at 1.56 μm. It was also clear that a return loss of about 20 dB could be obtained at a wavelength of 1.65 μm.

Table 2 Features of OFTM system for PDS/WDM

	Item	Feature
1	Test wavelength	1.31 and 1.55 μm (for installation, etc.) 1.65 μm (for maintenance)
2	Filter cut off wavelength	1.65 μm
3	Return loss	more than 35 dB
4	Fault isolation	High spatial resolution OTDR
5	Controller	UNIX system work station
6	Database	OODB

Table 3 Tested items, equipment and wavelength

Work	Item	Equipment	Wavelength (μm)
Installation, Repair, Cable transfer	Line loss	LS, OPM	1.31, 1.55
	Connection loss	OTDR	1.31, 1.55
	Fiber identification	LS, Identifier	1.65
Service order	Optical power	OPM	1.31, 1.55
	Reflected pulse	H-OTDR	1.65
Maintenance	Fault isolation	H-OTDR	1.65
	Fault location	OTDR	1.65
	Periodic surveillance	OTDR, H-OTDR	1.65

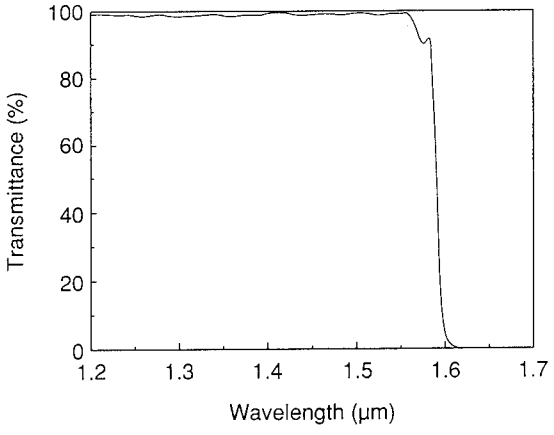


Fig. 2 Relationship between transmittance and wavelength in the SWPF

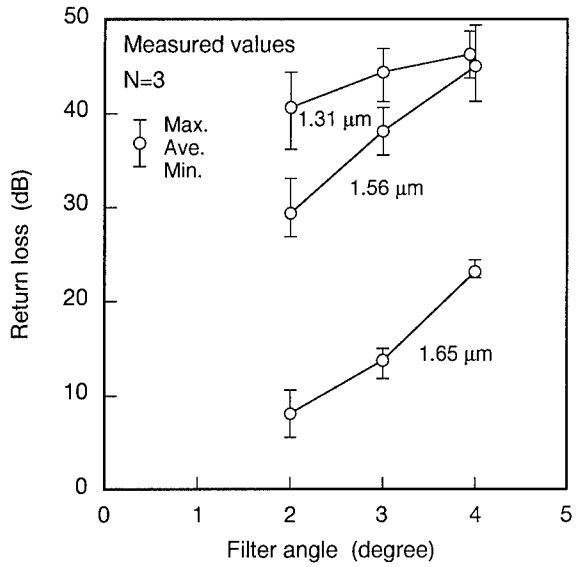


Fig. 3 Measured relationship between return loss and filter angle with the trial SC-connector including the SWPF.

3.3 High Spatial Resolution OTDR

We have designed a high spatial resolution OTDR (H-OTDR). Our targets were a dynamic range of more than 35 dB for fault isolation and a spatial resolution of less than 1 m when the reflected pulse from the filter is -20 dB at that point [9].

Table 4 shows the characteristics of our prototype H-OTDR. The light source was a high power DFB laser operating at a wavelength of 1.654 μm. The output peak power from the H-OTDR into the fiber was 11 dBm with a 10 ns pulse width. We achieved a 1 ns pulse width, however, the difficulty of constructing a broadband and high dynamic range APD receiver and the high target for the dynamic range made it impossible to use the 1 ns pulse. A sampling resolution of 6.5 cm was achieved using an equivalent sampling method for OTDR signal processing in the analog to digital transformation. When the return loss of the filter was about 20 dB, the single-way dynamic range (SWDR) of the H-OTDR itself was 33 dB with 2 to 16 integrations. Here, the SWDR means the difference between the reflected pulse peak or backscattered signal level and the noise peak level on the OTDR display. The SWDR for the backscattered light from the fiber was 5 dB with the same pulse width and integrations.

We experimentally confirmed using an 8-branch splitter that all the reflected pulses from the filters could be distinguished when the distance from the splitter to each filter varied by more than 2 m [9].

3.4 Test Light Injection

The optical branch module was composed of optical couplers, filters, attenuators and an accommodation box, slightly modified from a previously reported module [3-4] in order to inject the test light into the fiber under test.

Table 4 Characteristics of prototype H-OTDR

	Item	Characteristics
1	Wavelength	1.654 μm
2	Output power	11 dBm
3	Pulse width	10 ns
4	Receiver bandwidth	100 MHz
5	Sampling resolution	6.5 cm
6	Single-way dynamic range (with 10 ns pulse width and 2^{16} integrations)	33 dB (for -20 dB reflected pulse)
		5 dB (for backscattered signal)

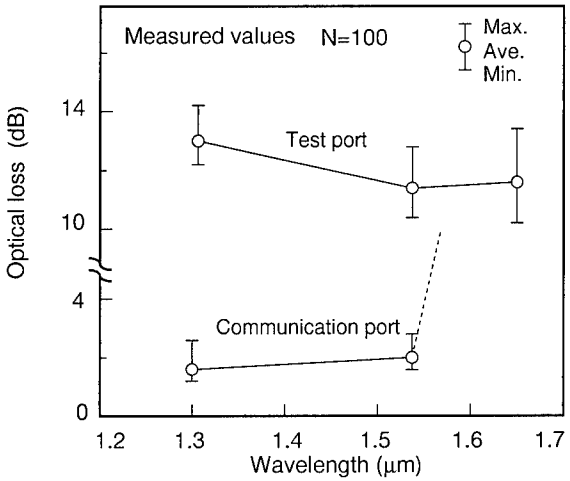


Fig. 4 Measured optical losses of the prototype optical branch module.

A coupler was used with a splitting ratio of about 8 to 2 between the communication and test ports, since the ratio of the coupler was almost flat in the 1.25 to 1.65 μm wavelength band [3]. The filter was the same SWPF described in 3.2. An attenuator with a loss of about 3.5 dB was inserted between the test port of the coupler and the MT-type fiber selector in order to increase the return loss due to the reflection at the surface of the MT-connector in the fiber selector.

Figure 4 shows the optical losses of the prototype optical branch module. The loss in the communication port at 1.65 μm was more than 40 dB using the SWPF.

3.5 Effect of Nonlinearity in 1.65 μm Test

A strong communication light at 1.55 μm, such as the light generated by an erbium-doped fiber amplifier for video distribution services, affects in-service OTDR testing at 1.65 μm due to stimulated Raman scattering [13]. A strong test pulse at 1.65 μm from the OTDR similarly affects services in the 1.5 μm wavelength band [14].

The level of the backward propagating optical power generated by the stimulated Raman scattering of a 1.55 μm communication light is about -54 dB at a wavelength of 1.65 μm [13]. So, the optical power at the near end of the test fiber due to the stimulated Raman scattering can be assumed to be -44 dBm when a 10 dBm communication light is launched into the fiber under test. We performed an experiment to determine the effect of nonlinearity. A continuous light of -40 or -30 dBm at 1.65 μm was injected into the H-OTDR from the far end of a 10 km long test fiber and an OTDR test with 1 μs wide pulse was carried out with an output pulse power of 11 dBm. There was no change in the OTDR backscattering trace except for a slight increase in the noise level.

This experiment showed that the influence of a 1.55 μm strong communication light on an in-service OTDR test at 1.65 μm is negligible except for a slight decrease in dynamic range.

We also carried out an in-service OTDR experiment using an amplitude modulated vestigial-sideband (AM-VSB) video signal distribution system operating at 1.55 μm. We also used a high power OTDR operating at 1.65 μm, an SWPF which cuts off the 1.65 μm light and a coupler to mix the test pulse into the video distribution system. The video distribution system included a transmitter, a receiver, a video source, a TV monitor and a standard fiber. The OTDR, which incorporated a Raman fiber amplifier [15], was used to generate a high power pulse.

White spots were periodically observed in the picture on the TV monitor when OTDR pulses of about 20 dBm were injected into the fiber. This is because communication signal depletion occurs repeatedly with the strong 1.65 μm pulse [14]. However, there was no change in the picture with 7 dBm pulse injection. So, we confirmed that the H-OTDR test on the OFTM system had no influence on the 1.56 μm video service because the launched pulse power into the test fiber was less than -2 dBm due to connection losses. Here, the connection losses are those of the optical branch module, fiber selectors, fiber connections with MT-connectors and SC-connectors and the communication light cut off filter which is installed in front of the equipment when necessary.

3.6 Test System Performance

(1) System Dynamic Range

System dynamic range (SDR), which means a fiber loss measurable using the test system, can be derived by subtracting the connection losses from the dynamic range of each piece of equipment.

The SDR for fault isolation using the H-OTDR was about 20 dB after subtracting the 13 dB connection loss from its 33 dB SWDR. The SDR for the loss test was 32.5 dB at 1.31 and 1.55 μm wavelengths, respectively, since both LED output lights modulated at 270 Hz were about -31 dBm, the detectable minimum power level of the optical power meter was about -80 dBm within 0.2 dB accuracy and the connection loss was about 15.5 dB.

(2) Standard Uncertainty of Loss Test

The fiber line loss was calculated using the optical power value P1 measured manually in the field with a portable power meter, the value P0 measured automatically with the power meter installed in the TEM and fiber connection losses between the coupler in the optical branch module and the power meter in the TEM. We used the average loss values of the fiber connections for the calculation, so the standard uncertainty for the loss test was assumed to be as large as 0.6 dB. The value will become small if all the connection losses in the fiber selectors are stored in the database and each connection loss is applied to the calculation of each fiber under test.

4. OPTICAL CABLE NETWORK MANAGEMENT

We have applied an object-oriented database (OODB) to manipulate optical cable networks and tested data [10].

Figure 5 shows part of the object model of the optical cable facilities in subscriber loops, the modeling and notation of which is based on Object Modeling Technique (OMT) [16]. Since the cable facilities in optical subscriber loops have numerous and various data, we separated them into several layers such as the fiber layer, the cable layer and the outside facility layer to clarify the inclusive relationships among entities. In the database schema, individual fibers are connected to one another through a fiber connection class, which can manipulate a many-to-many connective relationship such as a branched connection. Dynamic modeling and functional modeling were also applied to design the task applications for PDS systems using optical couplers.

The OODB allows the arbitrary long data collection of objects such as image data, for example the spread figure of a manhole and facility photograph, as shown in Fig. 5, which provide precise maintenance information.

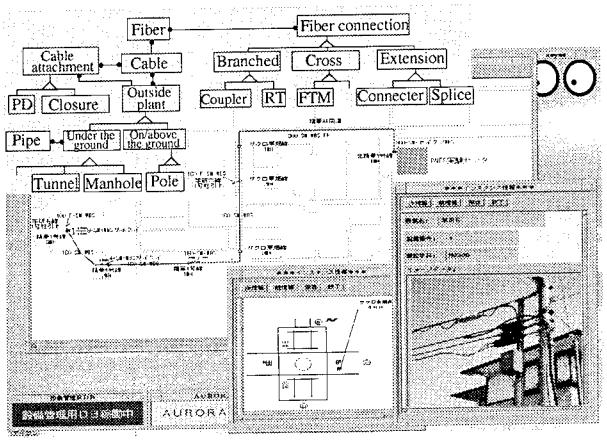


Fig. 5 Object model and GUI of the optical cable network database.

5. EXPERIMENT ON NEW MULTIMEDIA INFO-COMMUNICATION

5.1 Outline of Experiment

Figure 6 shows the location of Kansai-Science-City in Japan and an outline of the optical cable network configuration where several kinds of multimedia services using FTTH have been provided since July 8, 1994. The trial services are telephone, video phone and video conferencing using the N-ONU and video-on-demand (VOD), CATV and HDTV using the V-ONU [17]. The transmission system used in the experiment is the WDM described in 2.2. The number of the customers participating in the experiment is about 300 in both areas A and B.

Feeder cables were installed in ducts and the maximum length was about 1.7 km. Aerial distribution cables were used in areas A and B. Their total length was 3.8 km. When dropping fiber to customers, several kinds of optical drop wires and optical indoor wires were used.

2x8 optical splitters were installed in three places; namely in aerial closures installed near residential premises, in cabinets installed in apartment houses and in an FTM in the experiment center. The prototype OFTM system was also installed in the center.

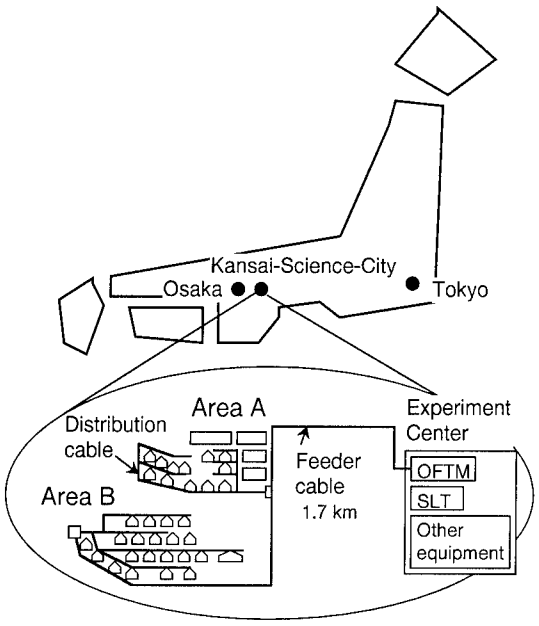


Fig. 6 Location and optical cable network configuration of the experiment in Kansai-Science-City.

5.2 Test Results of PDS Network in the Experiment

(1) Optical line loss

Figure 7 shows the losses of optical lines tested at 1.31 and 1.55 μm using the OFTM system during service order work. In addition to fiber losses and connection losses, the line loss includes the splitting loss of a 2x8 splitter, the coupler loss in the optical branch module and the SWPF losses in the SC-connector and the optical branch module.

The losses at 1.31 μm were similar to those at 1.55 μm. This was because the loss of the splitter occupied close to two thirds of the whole line loss and its wavelength dependence was very small.

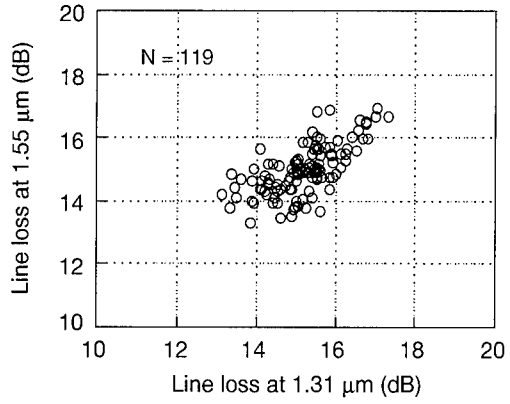


Fig. 7 Experimental optical line losses of the PDS network at 1.31 and 1.55 μm including a 2x8 splitter.

(2) Reflected pulse waveforms from the SWPFs

Figure 8 shows an example of the H-OTDR trace for an optical line with eight SWPFs and a 2x8 splitter installed in a four-storied apartment house. The apartment house was about 1.1 km from the experiment center, so Fig. 8 is an enlarged H-OTDR trace obtained near the SWPFs. A reflected pulse peak corresponding to the SWPF installed in each customer premises was clearly observed. The pulse peaks were gathered to two groups of four peaks. This indicates customers living from the first to the fourth floor on either side of the apartment house with an intra-office cable between the two sides. It is clear from the H-OTDR trace that we could distinguish individual customers when the fiber length difference was more than 2 m.

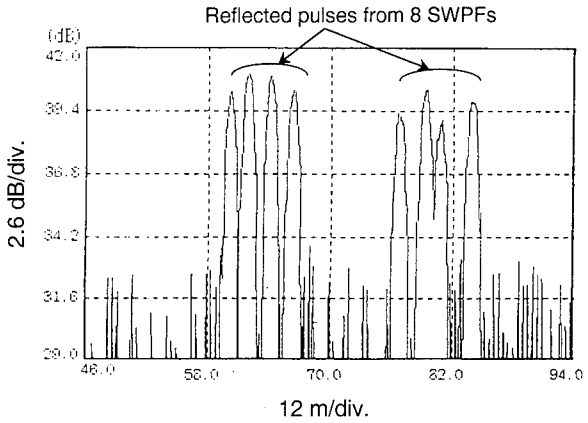


Fig. 8 High spatial resolution OTDR trace of a PDS network with eight SWPFs and a 2x8 splitter.

(3) Fault isolation test

When the service is interrupted and the cause is outside the telephone office, a fault isolation procedure is carried out using the OFTM system. The first step is to input a customer's name or an optical line number into the OFTM system via the key board of the WS or the touch panel keys of the HART. Then, the system automatically executes a self check test, the selection of the fiber to be tested, an H-OTDR test under the measurement conditions stored in the OODB, a comparison of the tested trace with the one stored just after the service order work and then presents the fault isolation result.

Figure 9 shows the overlapping H-OTDR traces which are the result of a fault isolation test when an in-service optical drop wire was accidentally cut by a construction machine. There was no splitter in the optical fiber line between the customer and the FTM. So, we can observe one pulse waveform on the H-OTDR trace. The pulse indicated with a solid line shows the waveform reflected from the fault and the dotted line shows the waveform reflected from an SWPF embedded in an SC-connector, which was stored in the OODB just after the service order work was completed. The two pulses should coincide unless a fault has occurred. The OFTM system showed us, by analyzing two traces, that the fault occurred in the optical drop wire providing services to the customer.

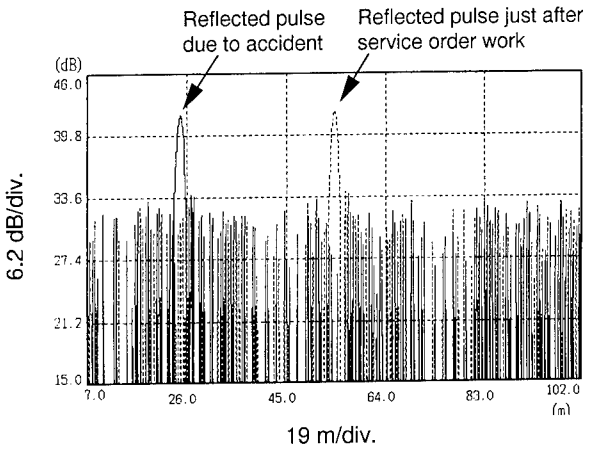


Fig. 9 H-OTDR traces from a fault isolation test when an optical drop wire was accidentally cut.

6. CONCLUSION

We have constructed for the first time an optical fiber line remote test and management (OFTM) system for passive double star (PDS) networks and wavelength division multiplexing (WDM) transmission systems operating at wavelengths of 1.31 and 1.55 μm. It incorporates an OTDR and a light source operating at 1.65 μm for preventive maintenance in the WDM transmission system and in-service testing of a PDS network with splitters.

A fault isolation technique, using a high spatial resolution OTDR operating at 1.65 μm and optical filters which reflect the OTDR light, has been developed. A UNIX system work station and an object-oriented database (OODB) were used to control and manage the system.

We have applied the prototype OFTM system in an experiment on new multimedia info-communication services in Kansai-Science-City and confirmed its usefulness.

ACKNOWLEDGEMENT

The authors thank Dr. M. Tateda, Dr. T. Yabuta, Dr. K. Ishihara and Mr. Y. Wakui for their continuous encouragement. The authors also thank Dr. T. Horiguchi, Mr. T. Sato and Mr. N. Kanda for useful discussions and help in experiments.

REFERENCES

[1] K. Okada et al., "Passive double star system features", 3rd IEEE Workshop on Local Optical Networks Proceedings, pp.5.1.1-5.1.10, Tokyo, Sept. 1991

[2] H. Lemberg et al., "A generalized summary of presently available passive optical networks", 3rd IEEE Workshop on Local Optical Networks Proceedings, pp.2.3.1-2.3.8, Tokyo, Sept. 1991

[3] H. Takasugi et al., "Design and evaluation of automatic optical fiber operation support system" 39th IWCS Proceedings, pp.623-629, 1990

[4] N. Tomita et al., "Design and performance of a novel automatic fiber line testing system with OTDR for optical subscriber loops", IEEE J. Lightwave Technol., Vol. 12, No. 5, pp.717-726, May 1994

[5] K. Koyamada et al., "Basic concepts of optic subscriber loop operation systems", IEEE ICC Proceedings, pp.1540-1544, 1990

[6] I. Sankawa et al., "Fiber measurement techniques for passive double star networks", 3rd IEEE Workshop on Local Optical Networks Proceedings, pp.4.2.1-4.2.10, Tokyo, Sept. 1991

[7] I. Sankawa et al., "Optical fiber line surveillance system for preventive maintenance based on fiber strain and loss monitoring", 40th IWCS Proceedings, pp.81-87, 1991

[8] S. Furukawa et al. "1.65-μm optical surveillance and test system for subscriber lines and ultralong-span trunk lines", OFC'94 Technical Digest, pp.156-157, Feb. 1994

[9] F. Yamamoto et al., "Fault isolation technique using high resolution 1.6μm-band OTDR for passive double star networks", 6th International Workshop on Optical Access Networks proceedings, pp. 6.2.1-6.2.7, Kyoto, Oct. 1994

[10] T. Kokubun et al., "A common optical cable network database system using object-oriented design", IEEE ICC Proceedings, pp. 1087-1093, May 1994

[11] E. Cottino et al., "1625 nm monitoring system design for the preventive maintenance of fiber optical plants", 42th IWCS Proceedings, pp.799-804, 1993

[12] T. Oguchi et al., "Dielectric multilayered interference filters deposited on polyimide films", Electron. Lett., Vol. 27, No. 9, pp. 706-707, 1991

[13] S. Goto et al., "Remote optical-fiber testing system for unrepeatered long-span optical-fiber trunk lines", 43th IWCS Proceedings, pp. 608-613, 1994

[14] T. Sato et al., "Cross talk due to in-service monitoring at

1.6 μm -band", 1993 Spring Natl. Conv. Rec. IEICE, B-923, 1993 (in Japanese)
[15] T. Sato et al., "A 1.6 μm band OTDR using a synchronous Raman fiber amplifier", IEEE Photonics Technol. Lett., pp. 923-924, 1992
[16] J. Rumbaugh et al., "Object-oriented modeling and design", Prentice-Hall, Inc. 1991
[17] K. Iida, "New multimedia info-communication services towards the FTTH", O plus E, No. 170, pp. 65-68, Jan. 1994 (in Japanese)



Shin-ichi FURUKAWA
NTT Access Network
Systems Laboratories
Tokai-mura, Naka-gun
Ibaraki-ken, 319-11
Japan

Shin-ichi Furukawa was born in Kagoshima, Japan, on January 3, 1952. He received B.E. and Dr. Eng. degrees in electrical engineering from Kyushu University in 1974 and 1987, respectively. He joined the NTT Ibaraki Electrical Communication Laboratory in 1974, where he engaged in the research and development of submarine cables and joints, and optical fiber measurement techniques. Since 1989, he has been engaged in the research and development of optical fiber measurement and surveillance systems. Since March 1995, he has been engaged in the research and development of optical fiber cables. He is presently a Senior Research Engineer, Supervisor of NTT Access Network Systems Laboratories. Dr. Furukawa is a member of the IEEE and IEICE of Japan.



Fumihiko YAMAMOTO
NTT Access Network
Systems Laboratories
Tokai-mura, Naka-gun
Ibaraki-ken, 319-11
Japan

Fumihiko Yamamoto was born in Yamaguchi, Japan, on January 25, 1966. He received the B.E. and M.E. degrees, in mechanical engineering from Kyushu University, Fukuoka, Japan in 1989 and 1991, respectively. In 1991, he joined NTT Transmission Systems Laboratories, Ibaraki, Japan where he has been engaged in research on measurement techniques for passive double star networks. He is now a member of NTT Access Network Systems Laboratories, Ibaraki, Japan. Mr. Yamamoto is a member of the IEICE of Japan.



Hiroyuki SUDA
NTT Access Network
Systems Laboratories
Tokai-mura, Naka-gun
Ibaraki-ken, 319-11
Japan

Hiroyuki Suda was born in Kanagawa, Japan, on May 9,1953. He received B.E., M.E. and Dr. Eng. degrees from Keio University, in 1976, 1978 and 1992, respectively. He joined the NTT Electrical Communications Laboratories in 1978. He worked on optical fiber fabrication by the Vapor-phase Axial Deposition process and assembly technology for silica planar lightwave circuits. Since 1993, he has worked in the field of testing and management systems for outside facilities. He is presently a Senior Research Engineer, Supervisor of NTT Access Network Systems Laboratories. Dr. Suda is a member of the IEEE and the IEICE of Japan.



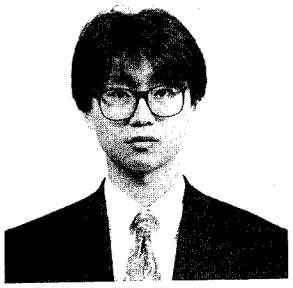
Yahei KOYAMADA
NTT Access Network
Systems Laboratories
Tokai-mura, Naka-gun
Ibaraki-ken, 319-11
Japan

Yahei Koyamada was born in Mie, Japan, on September 15, 1947. He received B.E., M.E. and Dr. Eng. degrees, all in electrical engineering from Osaka University, in 1970, 1972 and 1978, respectively. He joined the NTT Electrical Communications Laboratories in 1972. From 1972 to 1977, he was engaged in research on surface acoustic wave devices. Since 1978 he has been engaged in development research on optical fiber cables and related measurement techniques. He is now Executive Manager of the Optical Transmission Line Systems Laboratory, NTT Access Network Systems Laboratories, Ibaraki, Japan. Dr. Koyamada is a member of the IEEE and the IEICE of Japan.



Toshinao KOKUBUN
NTT Access Network
Systems Laboratories
Tokai-mura, Naka-gun
Ibaraki-ken, 319-11
Japan

Toshinao Kokubun was born in Fukushima, Japan, on November 7, 1957. He received the B.E. and M.E. degrees in electrical engineering from Ibaraki University in 1980 and 1982, respectively and a Ph.D. degree from Osaka University, Japan, in 1992. He joined NTT in 1982. He has been engaged in research and developmental work on the design and characterization of optical-fiber cables for subscriber loops and high-speed optical transmission systems. He is presently engaged in research on optical cable network operation systems. He is now a Senior Research Engineer of NTT Access Network Systems Laboratories. Dr. Kokubun is a member of the IEICE of Japan and Information Processing Society of Japan.



Ikuya TAKAHASHI
NTT Access Network
Systems Laboratories
Tokai-mura, Naka-gun
Ibaraki-ken, 319-11
Japan

Ikuya Takahashi was born in Akita, Japan, on April 25, 1966. He received B.E. and M.E. degrees from Hokkaido University, Japan, in 1990 and 1992, respectively. He joined NTT in 1992. He has been engaged in research and developmental work on the object-oriented database system and information modeling for the subscriber cable network. He is a member of the IEICE of Japan and Information Processing Society of Japan.

EVALUATION OF TRANSIENT OPTICAL LOSSES WHEN HANDLING PRIMARY COATED , SECONDARY COATED AND RIBBON FIBER IN THE ACCESS NETWORK.

Daniel Daems

Raychem N.V.
Diestsesteenweg 692, 3010 Kessel-lo, Belgium

ABSTRACT

Compared to the optical trunk and junction network, more fiber handling and craft activities are expected in the optical fiber access network. These activities can cause transient optical attenuation losses, which could lead to an increase in transmission errors (= bit errors). The majority of optical fibers used in telecommunications applications are coated with a 250 µm protective coating. It might be expected that buffered fibers, like secondary coated or ribbonized fibers, would be preferred in this part of the network because they look more rugged to the craft personnel. Several papers and articles (examples given in [1] and [2]) mention better protection against fiber handling, but no further evaluation is done on the optical performance during fiber manipulation. This paper will quantify and compare the transient loss sensitivity of different types of commercially available fibers that are in use in some European fiber access networks.

INTRODUCTION

During investigation of their optical networks, BT engineers noticed an increase in bit errors [3] during activities of a working party on the network. This even occurred in systems with optical margins far above (15 dB at 1550 nm) the nominal 10^{-9} bit error rate operating point. The cause of these bit errors was the transient attenuation losses, due to (uncontrolled) fiber movements. The probability of causing a number of sharp bends in live fibers during handling is high. It is known that when standard single mode fiber is bent beyond a critical bend radius (~ 15 mm) optical attenuation occurs.

The relationship between system performance and transient optical attenuation is complex. The occurrence of a transient loss will not necessarily result in bit errors, but the probability of having bit errors will certainly increase. Several parameters need to be considered:

- System characteristics (bit rate, system margin)
- Receiver characteristics (gain, noise, line code)
- Static characteristics (loss, reflections, wavelength)
- Dynamic characteristics (transient losses)

There are several ways to overcome the effects of this transient loss problem. These include the redesign of optical receiver circuits, transmission codes, use of bend insensitive fiber or total controlled fiber management. Some of these solutions would result in either a significant cost increase or would be impractical to implement. An interesting solution would be one that reduces the amount of transient attenuation losses. This can be achieved by specifying a new type of optical network infrastructure (e.g. a single circuit approach with total control of fiber routing) or by selecting a fiber type with good handling performance. In order to quantify the handling sensitivity of the different fiber types a test programme was setup.

EXPERIMENTS

A number of experiments were carried out to simulate working party operations, e.g. installing or re-arranging fibers in organizer trays. The optical power (at 1550 nm) was continuously monitored while the organizer tray underwent typical handling operations. The selected organizer tray was originally designed for trunk and junction networks, but is also used in access networks. Up to 12 fiber splices can be stored in this tray and it has been designed in such a way that the bend radii of the stored fibers is always above 30 mm.

Types of Fiber

The fibers used in the experiment are currently used in several fiber optic access networks in Europe. A selection was made of the following single mode fiber types found in commercially available fiber optic cables:

Type	Description
A	Primary coated fiber (250µm)
B	Secondary coated fiber (900 µm)
C	Semi-tight coated fiber (900 µm)
D	Ribbon fiber I (4 fibers)
E	Ribbon fiber II (4 fibers)

Fiber A is a primary coated single mode fiber with an outer diameter of 250 µm. Fiber B is a primary coated single mode fiber of 250 µm with an additional buffer coating (tight buffered 900 µm). Polyamide-10 was used

as buffer material. Fiber C is a loose buffered construction. It contains a primary coated fiber of 250 µm inside a loose buffer tube of 900 µm. The buffer tube material was a soft poly(1,4-butylene terephthalate) material. Fiber types D and E are both 4 fiber ribbons used by different PTT's in Europe.

The static bend sensitivity of the selected fibers was checked first. This was realized by inserting a fiber loop in a tube with inner diameter 20 mm (Figure 1). 100 optical loss measurements (at 1550 nm) were taken for each fiber type.

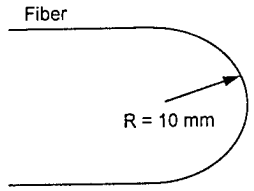


Figure 1: Fiber bend sensitivity test

Fiber Type	Average loss (in dB)
A	0.6
B	1.4
C	1.7
D	0.5
E	0.9

It appeared that most fiber types had about the same sensitivity to macrobends (measured at 1550 nm), except fiber types B and C which were more bend sensitive.

Experimental Procedure

The following handling operations were carried out on fiber stored in the conventional multi fiber organizer tray:

1. Re-accessing fiber stored above and underneath the active fiber: a non-active or "dark" fiber was taken out the organizer tray, spliced and restored in the organizer tray.
2. Re-positioning the active fiber: the "live" fiber was taken out the organizer tray and restored in another splice location.

An active fiber is defined as a fiber carrying an optical signal. The optical power was monitored continuously in one active fiber loop that was spliced and stored in the organizer tray. The other non-active fibers were stored above and underneath the active fiber. In total 56 operations were carried out by 7 installers for each fiber type.

Test Set-up

To determine the effects of fiber handling on an active circuit, experiments have been conducted using the system depicted in Figure 2.

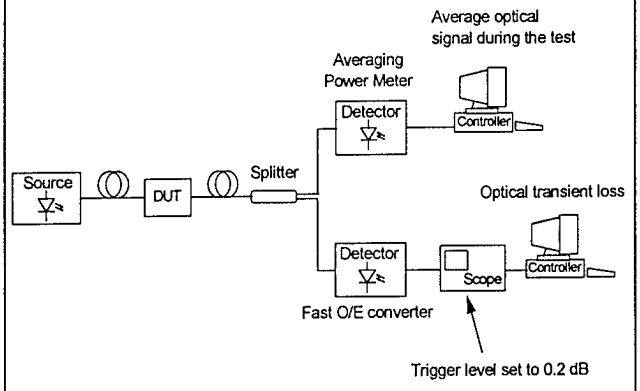


Figure 2: Experimental set-up.

The trigger level of the oscilloscope was set to 0.2 dB

RESULTS

Re-accessing a Non-active Fiber

Re-accessing a non active fiber stored together with an active fiber resulted in transient attenuation losses. By manipulating the non-active fibers uncontrolled bends with small radii were introduced in the active circuit. Figure 3 shows a typical transient loss in an active ribbonized fiber when another ribbon was manipulated:

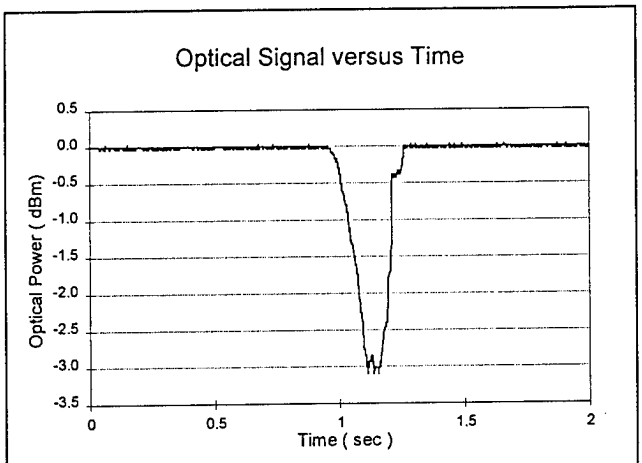


Figure 3: Optical transient loss.

A comparison between the average number of transients per operation (= non-active or "dark" fiber was taken out the organizer tray, spliced and restored in the organizer tray) and the average transient peak loss for each fiber type is shown in Figure 4. An overview of the maximum recorded loss for each fiber type is given in Figure 5.

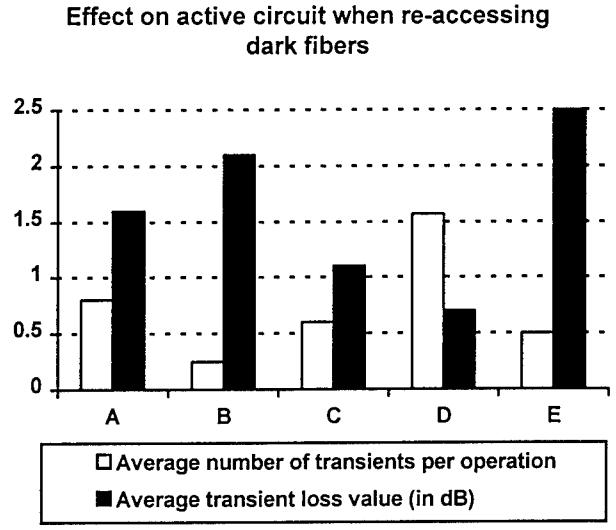


Figure 4: Comparison between occurrence of transients and average loss for each fiber type.

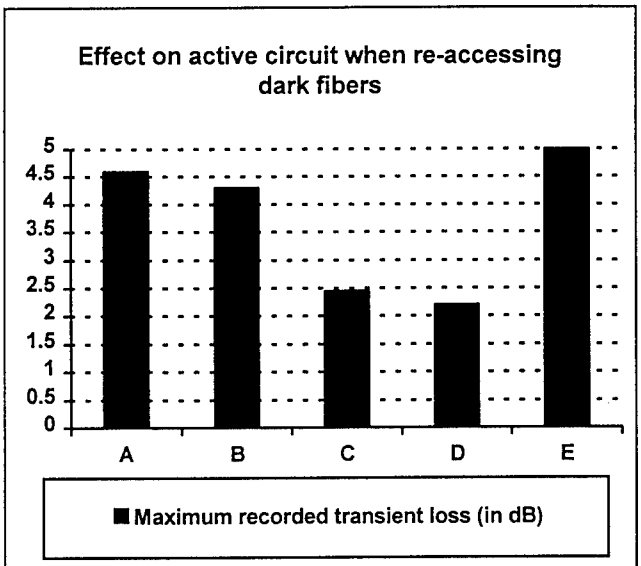


Figure 5: Comparison between highest transient for each fiber type.

Re-accessing an Active Fiber

The re-positioning an active fiber led to a high level of transients in this fiber. A comparison between the average number of transients per operation (= the "live" fiber was taken out the organizer tray and restored in another splice location) and the average transient peak loss for each fiber type are shown in Figure 6. An overview of the maximum recorded loss for each fiber type is given in Figure 7.

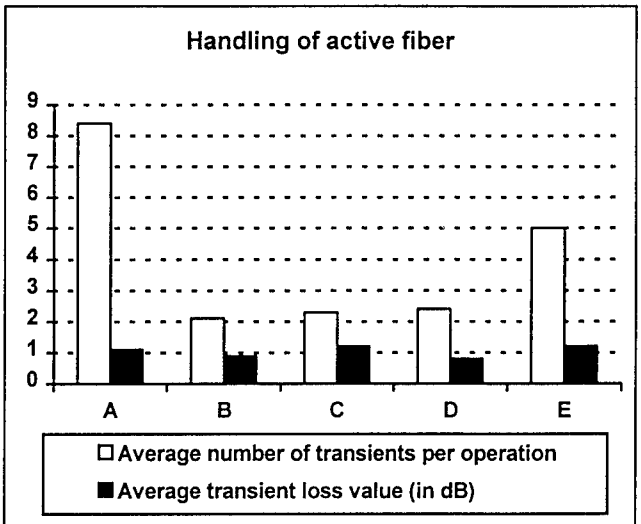


Figure 6: Comparison between occurrence of transients and average loss for each fiber type.

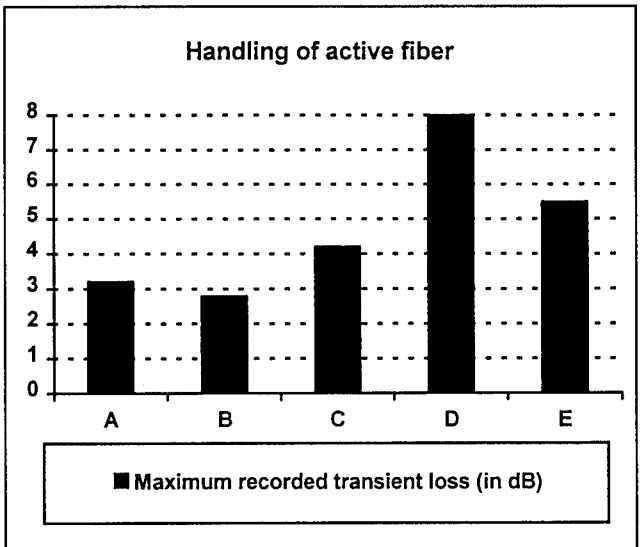


Figure 7: Comparison between highest transient for each fiber type.

CONCLUSIONS

Testing carried out on several fiber types showed that there is a high probability of having optical transient losses when fibers are manipulated in a conventional multi fiber organizer tray. This must be considered as an important issue as more and more fiber handling activities are expected in the optical access network. None of the tested fiber types seem to give excellent results in a multi fiber organizer system. The only way to minimize the number of transient losses on active fibers when other fibers are re-accessed, is to use a single fiber or single circuit approach. These were also the recommendations made by BT. They proposed a new type of optical network known as the OTIAN® (see note) infrastructure [4]. Invited by BT, Raychem has designed and developed a Fiber Infrastructure System Technology (FIST™) to meet all the fiber access network requirements. This was achieved by storing each optical circuit (a send and receive fiber) in a separate organizer tray (Figure 8). In this case it is possible to work on one circuit without disturbing the services in other circuits.

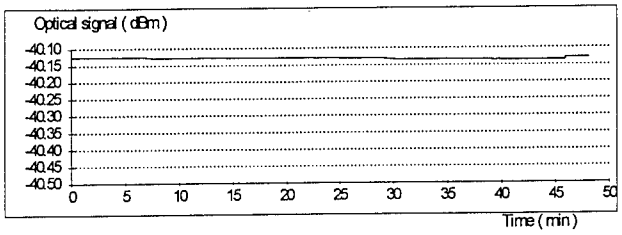


Figure 8: FIST single circuit fiber organizer trays

The evaluation of this system showed a real improvement on the reduction of transient losses [4]. In order to prove the increased optical performance of this system a comparative test was conducted. The FIST™ product (organizer A) and the conventional multi fiber organizer B were tested. The optical power in a primary coated fiber was monitored at 1550 nm while the other fibers (or circuits) in the organizer trays underwent typical handling operations. The outcome of this test is given in Figure 9. Organizer B had multiple loss events while organizer A showed none. Using such a single circuit organizer system will not only guarantee optimal services to the subscribers, but it will also make the network independent of future transmission equipment (= future proof).

Effect on active circuit when re-accessing other fibers.

Organizer A (FIST System)



Organizer B (Multi fiber organizer)

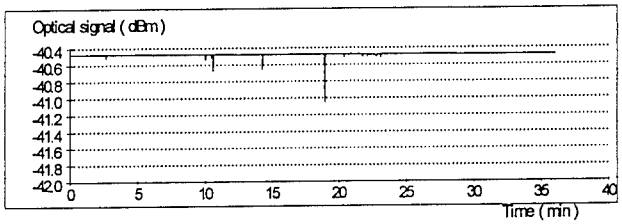
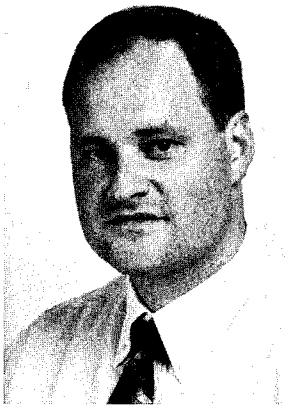


Figure 9: Optical power level versus time for organizer systems A and B.

References

1. J.J. Farro, R.A. Frantz, J.P. Kilmer, C.J. Wieczorek, H.H. Yuce: "Long term reliability of 900 µm buffered fibers", International Wire & Cable Symposium Proceedings 1991, p693.
2. R.G. Lindsay, S.D.Robbins, S.C. Mettler, C.F. Cottingham, K.W. Jackson: "Ribbon cable and mass-fusion splicing technologies accrue extended benefits", Lightwave, p40, June 1995
3. J. Peacock: "Measurements of optical transient attenuation losses and their effect on deployed optical systems in the BT Network", Electronics Letters September 1994.
4. J. Franckx, J. Peacock: "A new generation of products for the access network infrastructure", EFOC&N '95

Note: OTIAN® is a registered trademark of British Telecommunications plc.



Daems Daniel
Raychem N.V.
Diestsesteenweg 692
B-3010 - Kessel-lo
Belgium

Daniel Daems is a Department Manager of the Fiber Optics Development Group in the Telecom Division of Raychem. He received his M.S. degree in Electromechanical Engineering at the Polytechnic Institute of the Free University of Brussels (VUB) in 1982. Since joining Raychem in 1988 he has been involved in the development of fiber organizer systems.

DYNAMIC RANGE INCREASE OF 1625 nm MONITORING SYSTEMS

E. Cottino, P. G. Peretta
SIRTI S.p.A. - Direzione Cavi e Tecnologie Ottiche
Via Manzoni, 44 - Cusano Milanino - Milano (Italy)

F. Cisternino, E. Riccardi, B. Sordo
CSELT - Centro Studi E Laboratori Telecomunicazioni
Via G. Reiss Romoli, 274 - Torino (Italy)

ABSTRACT

Optical time domain reflectometers (OTDR) operating in the 1.6-1.65 μm region are currently utilised for in line monitoring of the fibre optics plants. Great effort are devoted to improve the capability (dynamic range) of such instrument in order to monitoring long fibre links. To increase the dynamic range of the OTDR, optical fibre amplifiers (by means of Raman effect or Er doped fibres) are under developement, with output pulses reaching peak power level up to 1W.

The aim of this paper is to describe a system that has proved to be able to increase the dynamic range of a commercial OTDR by more than 6.5 dB; this corresponds to a ≈30 km improvement in the monitoring capability, without introducing resolution penalties.

1. INTRODUCTION

Monitoring systems of installed fiber optics plants are becoming widely used by Telecom operators [1]; the key measuring instrument in these apparatuses is an Optical time domain reflectometer (OTDR) operating at a wavelength far from those used in the transmission systems. In practice the spectral region of 1.6-1.65 μm [2] has been chosen for OTDR measurements, because it allows an easy (low cost components) and good separation (no crosstalk penalties) among the transmission and the monitoring channels; on the other hand, in this wavelength region the measured attenuation coefficient is very close to the value experienced by the transmission systems near 1.55 μm [3].

The present generation of the OTDR instruments allows a somewhat limited measurement dynamics in the range of 80-120 km of monitored fiber, the precise value depending on the chosen resolution. However, due to the growing length of the unrepeatered optical links, more dynamics would be desirable from these measurements. A possible choice in upgrading the OTDR instruments consists in boosting the power of the launched pulses, so overcoming the limitation imposed by the available laser sources. Optical fiber amplifiers have been considered to this end, both with Er doped [4] and Raman type [5] fibres. In any case, improving the receiver side of the OTDR would be welcome and is compatible with the work done on the pulse source.

In the present work we have chosen to build a Raman amplifier, in order to boost the pulses available from a commercial OTDR, because this form of optical amplification seems to be more flexible with respect to the instrument wavelength (as far as we know, no result has been published on Er amplification above 1600 nm). Moreover this solution allows to use general purpose optical components, as opposed to the specialized custom fiber used for Er amplification [4].

With our Raman amplifier it has been possible to increase the dynamic range of a commercial OTDR by more than 6.5 dB; this corresponds to a ≈ 30 km improvement in the monitoring capability, without introducing resolution penalties.

2. DESCRIPTION OF THE INSTRUMENT

The instrument we have built is composed of a commercial OTDR apparatus, working around 1625 nm, and a Raman fiber optical amplifier working in pulsed mode.

The commercial OTDR provides a pulse train with selectable time width and distance range; we have chosen to work with 0.5-1 μs pulses, which allow a good compromise between dynamic range and resolution. The maximum power of the launched pulses is about 25 mW (measured at the output connector, after the Acousto-Optic switch); with these pulses, 1 μs wide, about 18 dB dynamic range is available, which corresponds to ≈ 85 km of conventional SM fiber.

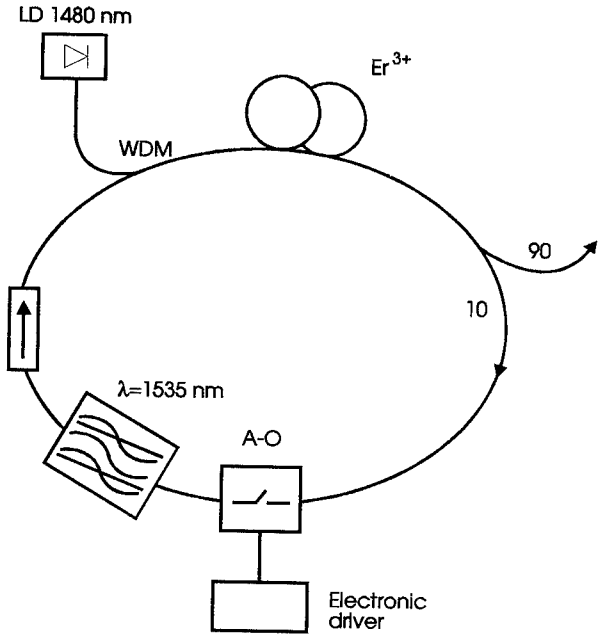


Fig. 1: Scheme of the Q-Switched Er fiber laser.

The optical amplifier is made up of a Raman shifting fiber and a pulsed Er doped fiber laser, operating at 1535 nm, which acts as a pump for the non linear amplification effect. More than 2 W optical pulses from the Er laser allow more than 23 dB small signal gain at 1625 nm; on the other side, high signal input (25 mW pulses from the commercial OTDR) causes full depletion of the pump and produces, after due filtering, about 800 mW output pulses at 1625 nm.

2.1. RAMAN AMPLIFIER

The pulsed operation of the Er doped fiber laser is obtained by Q-Switching an active fiber ring cavity (Fig. 1); an Acousto-Optic device, synchronous with the OTDR pulse train (< 1 kHz repetition rate), modulates the gain of the fiber cavity and provides a short time window for the growth of the giant pulse (2 ≈ 2.5 W peak power, ≈ 1.5 μs FWHM; see Fig. 2). The Er doped fiber, 30 m long, is CW pumped by a laser diode emitting approximately 30 mW at 1480 nm; stronger pumping of the active fiber is possible, but higher power pulses could damage the commercial optical components utilized inside the cavity. The output coupler has been chosen with a splitting ratio of 10-90, which allows a high efficiency power extraction without reducing the lasing level; moreover, with this choice, a safer region is created inside the cavity, where the power level is compatible with the optical components (< 300 mW peak power).

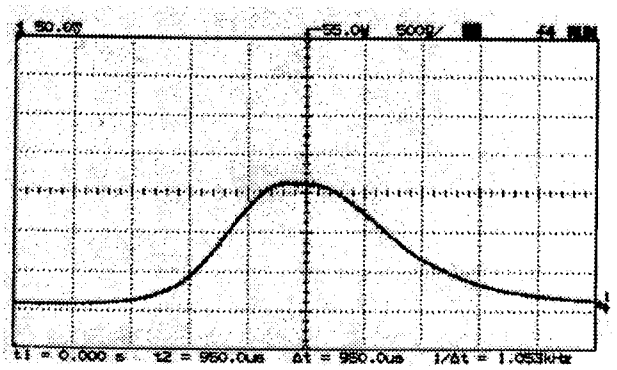


Fig. 2: 2 W at 1535 nm output pulse from the Q-S Er laser.

In this region, between the output coupler and the active fiber, are placed the A-O modulator, an optical isolator and a narrow-band tunable filter that forces the lasing wavelength to the optimum value. In this context the best wavelength turns out to be around 1535 nm, which is a compromise between maximum Raman gain for the signal to be amplified at 1625 nm and good lasing within the Er bandwidth.

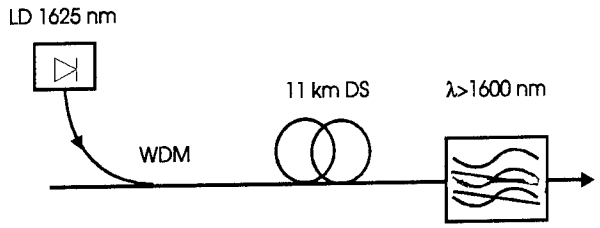


Fig. 3: Scheme of the fiber Raman amplifier.

Fig. 3 shows the scheme of the Raman section of the device. By means of a WDM coupler, the high power pulses from the Er Q-S laser are mixed synchronously with the pulses to be amplified into the Raman fiber. This stimulated non linear process converts pump power toward infrared wavelengths, with an efficiency that is maximum at approximately 100 nm shift. This Raman gain profile can be easily appreciated from the spectrum of the amplified spontaneous emission (Raman noise) which is the output of the amplifier when there is no signal at the input (Fig. 4). From this measurement it also turns out that the whole region from 1620 to 1650 nm can be easily amplified.

The Raman fiber is a commercial one, dispersion shifted, 11 km long; the choice of a DS fiber is due to the small core diameter, which permits higher power density and consequently stronger Raman effect. Other fibers (conventional SM and DCF fibers) have been tested, but the efficiency was lower or the loss higher. Finally, at the end of the Raman fiber, a spectral filter cuts out the remaining power at the pump wavelength and delivers pure 1625 nm amplified pulses.

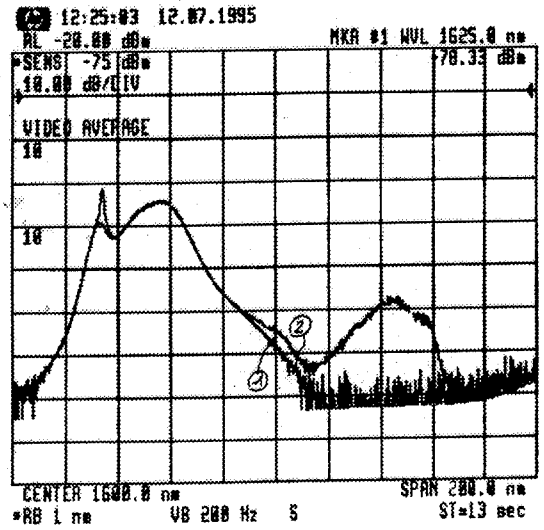


Fig. 4: ASE spectrum from the fiber Raman amplifier.

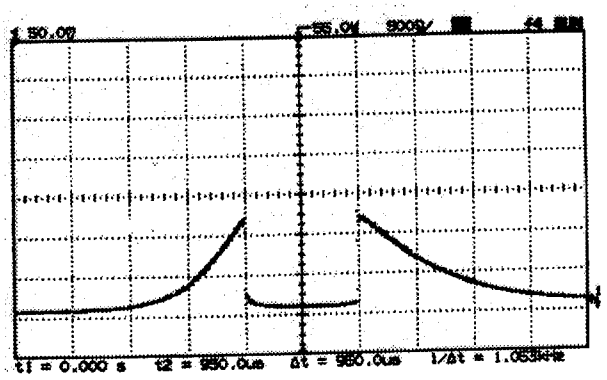


Fig. 5: Pump pulse depletion for 1μs, 25 mW input signal.

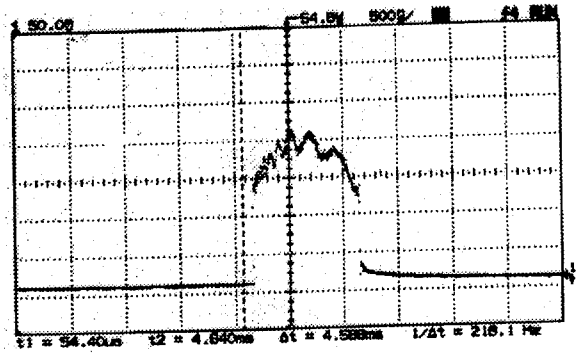


Fig. 6: 1 μs, 800 mW at 1625 nm amplified output pulse.

The small signal gain of this amplifier has been measured to be more than 23 dB; of course, with 25 mW input pulses from the commercial OTDR, a deep saturation of the pump pulse is reached, as can be seen from Fig. 5. In Fig. 6 is reproduced the output amplified pulse at 1625 nm, which is more than 800 mW peak power; this value, as compared to the pump pulse power, can be understood by considering that the overall loss of the Raman section (WDM, fiber and filter) is about 4.5 dB. Similar results are also obtained with 0.5 μs input pulses. An interesting measurement is reported in Fig. 7, where the input spectrum of the pulses to be amplified (the lower trace) is compared to the optical spectrum at the output of the Raman amplifier (before the final filter; so the peaks to the left are due to the Er laser): the Raman amplification of the signal is clearly seen and is of the order of 20 dB.

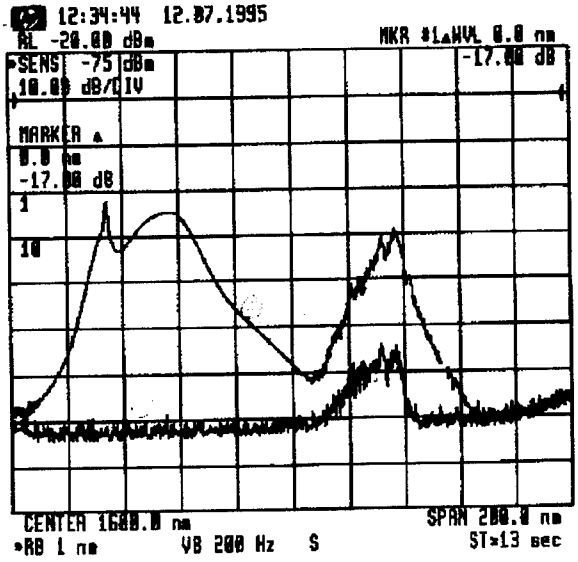


Fig.7: Spectrum of OTDR input signal against the spectrum of the amplified signal after the Raman fiber.

2.2. OTDR AND RAMAN AMPLFIER

In order to interface the Raman amplifier to the commercial OTDR instrument, three different system configurations have been tested. The simpler one (Fig. 8) consists in directly interposing the Raman amplifier between the OTDR output and the fiber under test; the main advantage of this configuration would be its simplicity, because no operation would be required inside the instrument at the optical level.

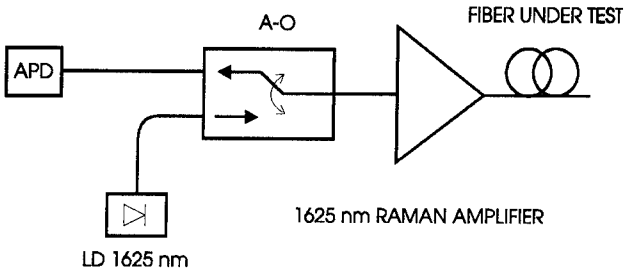


Fig.8: First set-up of the amplified OTDR: direct connection.

However, in this case the optical amplifier is crossed in the backward direction by the backscattered signal, and this introduces an unnecessary penalty of approximately 5 dB on the received signal. Moreover a dramatic drawback of this scheme is that the CW ASE noise, emitted from the Er laser after the output of the giant pulse, is partly converted by linear Raman backward scattering (inside the amplifying fiber) to the 1.65 μm band and severely interferes with the zero level calculation of the OTDR instrument. In practice, highly curved backscattering traces are seen on the instrument, which eliminates any advantage produced by the amplification process.

A second configuration (Fig. 9) consists in amplifying directly the pulses inside the OTDR, by-passing the A-O switch of the instrument; the amplified pulses are then coupled to the fiber under test through a 3 dB coupler and the backscattered signal is sent to the OTDR receiver via the masking function of the A-O switch. In this case, one obtain the maximum isolation of the OTDR receiver from the CW

noise produced inside the Raman amplifier, but again at the expense of the received signal, due to the presence of the 3 dB coupler.

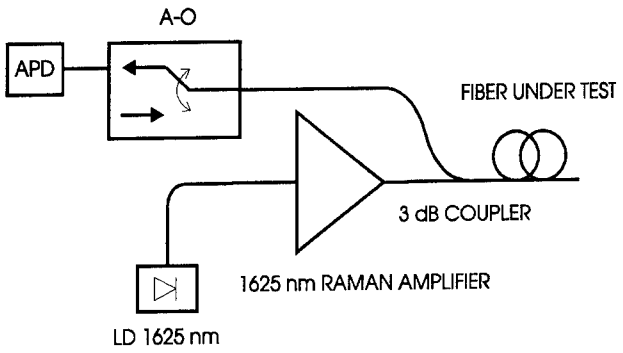


Fig. 9 - Second set-up of the amplified OTDR: A-O bypass.

Finally we have chosen a third configuration (Fig. 10), which consists in amplifying directly the OTDR pulses and using the instrument A-O switch as the coupler to the fiber under test; this has been possible because this A-O device is able to tolerate up to 1 W optical power. In this case no additional 3 dB coupler is needed; the only unavoidable penalty is due to the attenuation introduced by the first crossing of the A-O switch (about 2 dB).

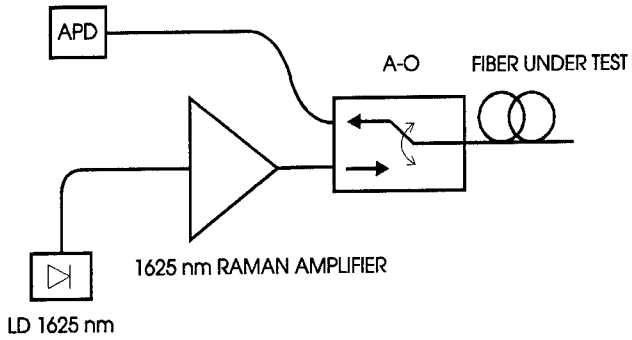


Fig.10: Final set-up of the amplified OTDR: source booster.

This effect reduces the available pulses at 1625 nm to about 500 mW peak power.

3. PERFORMANCES OF THE INSTRUMENT

The input power level increase obtained in the chosen configuration is 13 dB with respect to the original instrument, which amounts to a 6.5 dB increase in the dynamic range of the measurement. In terms of the monitored fiber length, this corresponds to an improvement of approximately 30 km (the exact value depending on the fiber attenuation), which can be added to the 85 km span already explored with the commercial instrument. In Fig. 11 is reported (in logarithmic scale) a measurement made with the commercial instrument, with 1 μs time resolution and 2^{17} averages (the chosen distance range being 160 km).

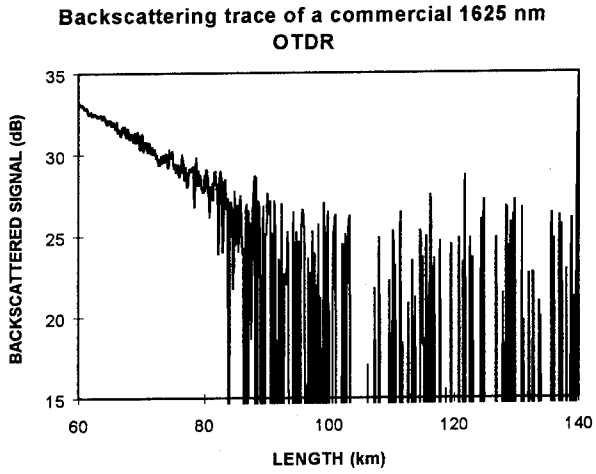


Fig. 11: OTDR trace (1 μs pulses - 2^{17} averages) using the commercial instrument.

By comparison, in Fig. 12 is reported the backscattering trace recorded with the amplified OTDR instrument, by preserving the same measurement conditions; it appears clearly the increase obtained in the dynamic range.

A compact version of the fiber Raman amplifier, inserted in a 19" rack and ready for use in a telephone exchange, is in an advanced development stage; together with

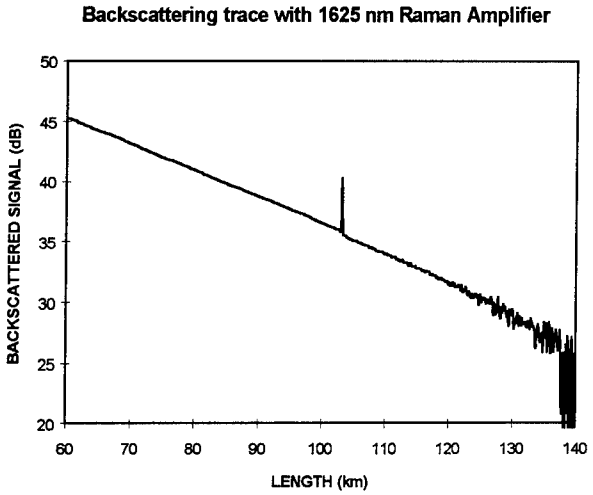


Fig. 12: OTDR trace (1 μs pulses - 2^{17} averages) using the upgraded instrument (with Raman amplifier, set-up of Fig. 10).

the commercial OTDR instrument, it will constitute an upgraded monitoring system which will be tested in the Italian optical network.

4. IMPACT ON THE TRANSMISSION LINE

The question of the possible perturbations that a monitoring system, operating at 1625 nm, can produce on the installed optical traffic has already been investigated, with the answer that no penalty has to be expected, as far as the present generation of OTDR instruments is concerned [3]. However, the use of such intense pulses, as those obtained after our Raman amplifier (but in fact independently on the way they are generated), poses again the question, within this new context. The point is now that non-linear effects can mix the propagation at 1.55 μm (transmission system) with that in the 1.6 μm region (monitoring system).

By performing a transmission experiment at 1540 nm (622 Mbit/s on 40 km DS fiber), while simultaneously propagating in the fiber high power pulses at 1620 nm (for OTDR measurement), we observed the presence, on the data stream, of a train of micro-attenuations, synchronous with the monitor pulses [6]. This is due to a non-linear effect, again of the Raman type, which is produced in the transmission fiber and which depletes the transmission wavelength in favour of the co-propagating intense monitor pulse. With 200 mW monitor pulses, the observed depth on the average transmitted signal was approximately 4 dB (Fig. 13).

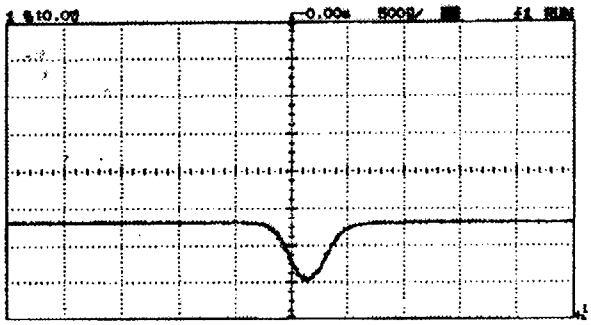


Fig. 13 - Dip in the transmitted average signal.

Of course, the impact of this train of micro-attenuations on the transmission system can be very severe (presumably depending on the receiver design). In our experiment we observed a dramatic BER increase for 200 mW monitor pulses and still a considerable penalty (to 10^{-7} level, starting from an error-free system) with 60 mW pulses (Fig 14).

However we found also an effective remedy to this drawback: in fact, if the system is monitored from the receiver end, the 1.6 μm pulses counter-propagate with respect to the data stream and the degradation is completely eliminated (the non-linear effect is reduced by orders of magnitude, due to the low duty-cycle of the monitoring system). This result has been confirmed by direct measurement on the BER value (Fig.14).

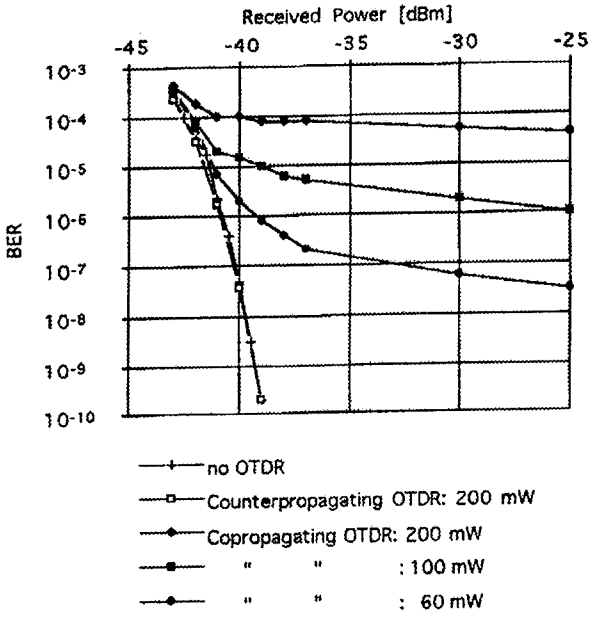


Fig. 14: BER at 622 Mbit/s, due to Raman scattering.

5. CONCLUSIONS

Stimulated Raman amplification has been demonstred to be a good way to generate very high pulses (≈ 1 W, 1μs). The interface of the optical amplifier with a commercial OTDR is quite easy: some configuration has been tested and the more performed permits a dynamic increase of 6.5 dB, wich corresponds a ≈30 km in terms of the monitored fiber length.

Many pulses can be used (0.1, 0.5 and 1 μs) with the same dinamic gain. Figures 15 and 16 show, respectively, a OTDR trace (0.1 μs pulses-2^{17} averages) using the commercial instrument and a OTDR trace (same conditions) using the upgraded instrument (with Raman amplifier, set-up of Fig. 10). The dynamics limits are clear in fig.15 where the backscattering trace is very distant from a straight line.

The possible perturbations that a monitoring system, with such intense pulses operating at 1625 nm, can produce on the installed optical traffic has already been investigated. With 200 mW monitor pulses, the observed depth on the average transmitted signal was approximately 4 dB; the impact of this train of micro-attenuations on the transmission system can be very severe. If the system is monitored from the receiver end, the 1.6 μm pulses counter-propagate with respect to the data stream and the degradation is completely eliminated. This result has been confirmed by direct measurement on the BER value (Fig.14).

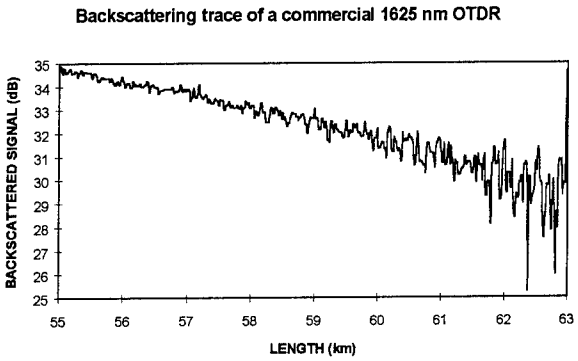


Fig. 15 - OTDR trace (0.1 μs pulses - 2^{17} averages) using the commercial instrument

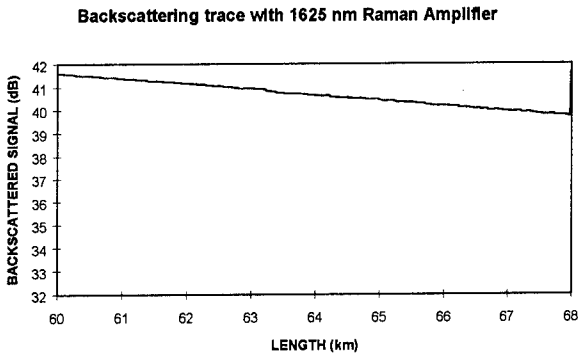


Fig. 16 - OTDR trace (0.1 μs pulses - 2^{17} averages) using the upgraded instrument (with Raman amplifier, set-up of Fig. 10).

REFERENCES

[1] M.Artiglia, E.Cottino, Proceedings of Symposium on Optical Fiber Measurements, Boulder (1994)

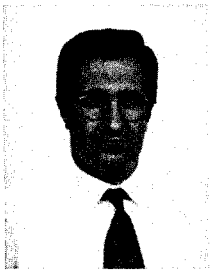
[2] More specifically, the 1600-1640 nm spectral region is a good candidate to become a reference standard for these systems (ETSI stc-TM1).

[3] E.Cottino et al, Proceedings of IWCS '93, pp.799-804 (1993)

[4] S.Seikai et al., Electronics Letters, Vol.30, pp.1225-1226 (1994).

[5] T.Sato et al., IEEE Photonics Technology Letters, Vol.4, pp.923-924 (1992)

[6] F.Cisternino et al., Proceedings of OFC, pp.181-183 (1995)



Edoardo Cottino

Sirti S.p.A.

Direzione Ricerca e Sviluppo

Milano, Italia

Edoardo Cottino was born in Turin, Italy, in 1957. He received his degree of electronic engineering from Politecnico di Torino in 1982. He joined in AET Telecomunicazioni from 1983 to 1995 in the fiber optic laboratories, this year he moved in SIRTI where currently holds the position of manager, Cables and Opltical Technologies R&D Division.

Dr. Cottino is a member of SPIE and his present responsibilities include ITU-T and ETSI activities.

OPTICAL CABLES BIOLOGICAL ATTACKS ANALYSIS

* Paulo J. P. Curado, * Manuel Mendes Filho
** Antonio C. Pereira Netto, ** João Elias Filho, ** Marcilio E. Latini

* TELEBRÁS - Research and Development Center - Campinas - SP
** EMBRATEL - Optical Systems Division - Rio de Janeiro - RJ
BRAZIL

ABSTRACT

In the last four years, the need to link Brazil's main cities using optical fiber cables stimulated the use of direct buried cables, even because Brazil has a huge territorial area.

Relates considering biological attacks around the world[1] leaded Research and Development Center (CPqD) of Telebrás - Brazilian telecommunications holding company - and Embratel - Long distance operating company - to join and develop studies to certify the requirements and protections foreseen for the cables used in these links.

Cables used in these long distance routes were submitted to an evaluation based on brazilian fungi, ants and termites specimens, due to know the damages kinds and consequences.

This paper will present the test methodology and results obtained in tests performed in local labs. The results indicate that used protections are efficient against insects attacks, the materials are fungi resistant and the cables are suitable to use. Also, we are able to perform these test in other cables.

INTRODUCTION

The long length optical systems implementation in Brazil increased very quickly in the last four years with EMBRATEL linking the main cities of the country. It was planned to install 10.000 km of optical cables.

During these systems planning step, technical and economics studies indicated that direct buried cable was the most suitable solution for use in some routes and there was a need to develop this kind of cable. Other types of routes used in long distance system are in duct cables and optical ground wire cable (OPGW).

Table 1 shows the direct buried routes planned to install in the 93-97 period. Two cables are planned to install in each route, one of them is point-to-point and the other serving intermediate cities.

Table 1 - Routes of direct buried cables (93-97)

Route	Length (km)
São Paulo - Belo Horizonte	600
Rio de Janeiro - Belo Horizonte	450
Natal - Fortaleza	550
São Mateus - Porto Seguro	380
Belo Horizonte - Brasilia - Goiania	1000
São Paulo - Curitiba	700

This routes are very long and will link some of the main cities of Brazil, as we can see in the map of figure 1.

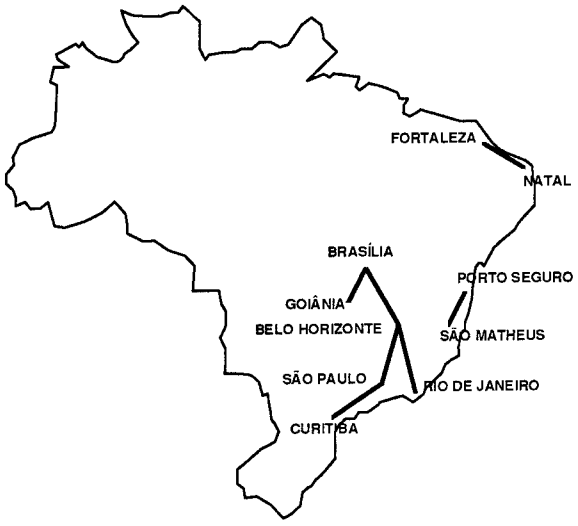


Figure 1 - Direct buried routes

A direct buried cable to use in these links was developed, adapted for the national's conditions. An all dieletric cable was adopted because of the high lightning protection installation costs. It is also very difficult to access the route for maintenance procedures. Studies for this cable considered

biological attacks. There are few informations about fungi actions over cables in the world[1], but the environment in Brazil is suposed to stimulate fungi growth due to high humidity levels.

On the other hand, insects like termites and ants are very commom in the regions of country where this cable will be installed. Operating companies have experiences with damages caused by these insects in buried cables, although they don't have a large amount of direct buried cables installed. These attacks are also related in other countries [2].

For these reasons, Embratel and Telebrás Research and Development Center (CPqD) joined to study biological attacks against optical cables with the following objectives :

- Direct buried optical cable evaluation for these routes;

- Test procedures stablishment for insects and fungi attacks evaluation.

This work will present the studies evolution, with the considerations to define test procedures and the cables tests results.

DIRECT BURIED OPTICAL CABLES

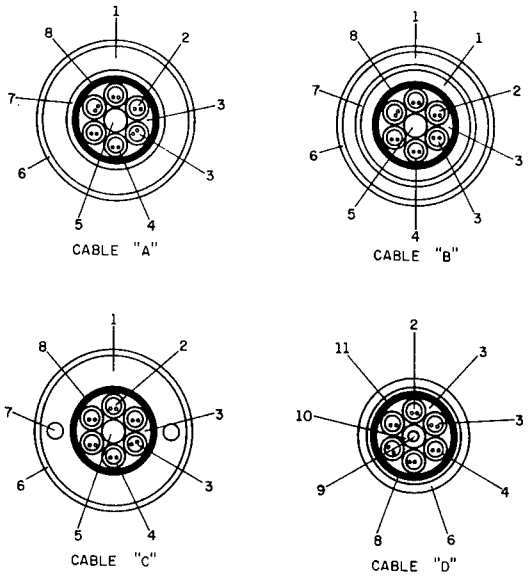
For Embratel long distance links showed in figure 1, a direct buried optical cables with loose technology was developed, with 36 singlemode optical fibers, six fibers per tube, jelly filling compound, dieletric strength member (usually aramid fiber) and with a 4 mm polyethilene outer jacket. Other material can be used like non oven tapes, polyester tapes and ripcords.

Telebrás specifications do not require a specific design for optical cable but ask for some design features able to become its functionality easier to the operators. It's main worry is cable's performance. This way the manufacturers can choose a most proper design.

Protection against insects atacks was first recommended by Telebrás based on an ITU-T recommendation and Australian Telecom studies[1,2], and it was used by all brazilian cables suppliers. This protection is a thin nylon outer jacket with 0.3 or 0.4 mm of thickness with a smooth surface without imperfections.

Our study, used samples of four different cables types. One of them was an optical cable for use in duct, with LAP sheath and metallic sthength member for control purposes and the others were direct buried optical cables developed by differentes suppliers.

For identification purposes the cables are identified by letters and in Figure 2 is shown the cables design.



1- outer jacket
2- fiber optics
3- jelly filling compound
4- plastic tub (PBT)
5- central member (GRP)
6- poliamide jacket
7 - strength member (aramid fiber)
8 - polyester tape
9 - strength member (steel)
10 - strength member coating
11 - LAP

Figure 2- Optical cables evaluated

FUNGI ATTACKS EVALUATION

Fungi attacks against polymers occur in two different ways :

- Fungi grows over polymer but the resin does not serve as a carbon source, only over other components such as colorants, stabilizers, plasticizers and lubricants caused by its nonuniform dispersion.

- material attacks from excreted metabolic products.

Damages can be described as attack, discoloration, change in weight, dimensions and physical, mechanical or electrical properties.

These listed damages in cables sheaths can expose the cable's core to moisture and many environmental agents that can early age and affect optical or mechanical characteristics of optical fibers. It happens in the cable route, manholes and places where cable is exposed to moisture and air.

The evaluation of optical cables and its components was based on the ASTM G-21 test procedure[3], "Determining resistance of Synthetic polymer material to fungi".

In this test, fungi cultures are prepared in sufficient nutrient-salts agar that is inoculated by spraying over polymer's surface.

Polymers materials are exposed to fungi action during, at least, 21 days. After this period, samples are visual examined for fungi's growth and verified if there are damages over the polymer after washed. If there are damages like surface attacks, discoloration or other visual effects, it will be verified material's physical changes that can affect its performance.

Fungi used in this test are recommended in ASTM procedure and usually found in Brazil. The cultures used are show in table 2.

Table 2 - Fungi cultures used in test

Cientific name	ATCC* number
Aspergillus Niger	9642
Penicillium funiculosum	9644
Chaetominum globosum	6205
Gliocladium virens	9645
Auerobasidium pullulans	9348

* American Type Culture Collection

The fungi growth was measured in 0 to 4 scale recommended in ASTM G 21 that is showed in table 3.

Table 3 - Fungi evaluation scale

Observed growth of specimens	Rating
None	0
Traces (less than 10 %)	1
Ligth (10 to 30%)	2
Medium (30 to 60%)	3
Heavy (60 to complete coverage)	4

All cables showed in figure 2 and materials used in their construction were evaluated with the procedures described before but with 28 days exposure period. The results found in cable's test are summarized in Table 4.

Table 4 - Cable's test results

Cable	outer material	rating	Observation after wash
A	poliamide 12	3	no damages
B	poliamide 11	1	no damages
C	poliamide 12	2	no damages
D	polyethyline	3	no damages

Actually, fungi grew in all cables samples, but after washed they were removed with no visible damages or attacks evidence. Due to these results physical properties verification were not necessary.

As can be seen, fungi's growth rating is different among the samples but no any presented visible damages due to specimens attacks. Cable "D" is the most sensitive sample, cable "B" the less and althougth "A" and "C" are the same material they have different behavior. It shows that fungi growth depends on the material and also manufacturing process.

After fungi removal, there were no visible damages and all samples are suitable to use.

Supplementary tests were performed with cables materials and components usually used in its construction, like plastic tubes, dieletric strength members, outer jacket, polyester tapes and non oven tapes. Also samples of different jelly filled compounds were tested. Type "A" is a jelly usually used in optical cables and type "B" is one out of specification product (oil separation test).

Results found in these tests are presented in table 5.

Table 5 - Summary of materials test

Compon.	Material	Rating	Observation after washed
Tube	PBT	1	Fungi removed/no damage
Jelly "A"	-	0	not applicable
Jelly "B"	-	2	not applicable
Str. Men	Aramide	2	Fungi removed/no damage
Tape	poliester	1	Fungi removed
Tape	no oven	2	not applicable
Jacket	HDPE	2	Fungi removed/no damage

Results indicate that almost all materials behave very good except jelly type "B" that presented a high rate of fungi growth when compared with jelly type "A".

In materials that allowed washing after test, no visibles damages were observed. For non oven tapes a future detailed study is recommended, because this material can be submitted to fungi action and the results are not conclusive.

INSECTS ATTACKS EVALUATION

Cables damages caused by termites and ants have been related for many decades in many contries of the world. These attacks occur mainly over direct buried cables and in some cases chews the cables sheath. Reasons for these attacks aren't clear.

In Brazil, operating companies don't have a large buried plant, but even so there are insects attacks. It indicates that problems will probabily happen with the planned network if no action to protect the cable would be taken.

Besides that, places where the cables will be installed have a large potential of different insect specimens, and it is very common to find concentrations of mounds as showed in photograph 1.



Photograph 1 - Termites mounds in Brazil's central region

Termites and ants attacks over cables does not occur because it is a food source, but because the cable is in their way when they are seaching for food source behind the cable. Some ants can cause degradation due to formic acid liberation.

Insects graw and chew cable sheath exposing fibers and components around to environmental actions (humidity, gases, soil) .

Agressive specimens used to perform an actual evaluation were searched even in thecnical papers [1,2] and in field investigations. Also there was low artificial nests avaiability in Brazil. The chosen specimens were:

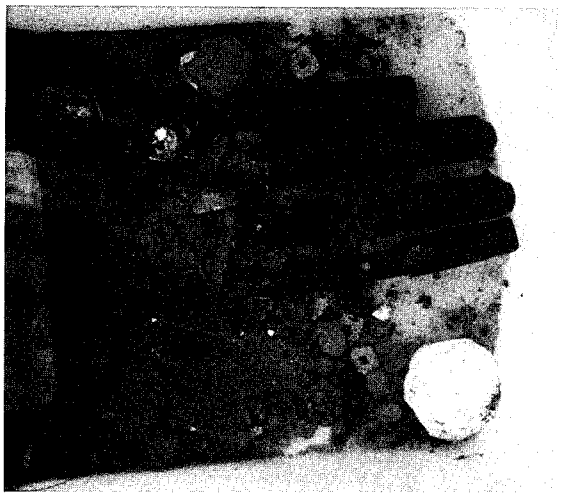
Termites :
- Cornitermes cumulans
- Coptotermes spp

Ants :
- Pheidole spp
- Irydomyrmex humilis

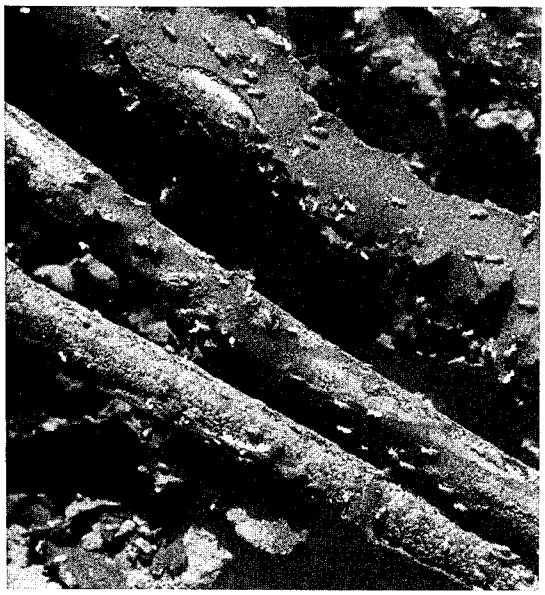
Coptotermes spp nest was found in Morrinhos, a city in the state of Goias, after attacking and damaging installed metallic cables. Pheidole spp was field colected and tests were performed in laboratory conditions.

Four groups of 50 cm optical cables samples were prepared, one group per tested specimens. In each group the four cables types showed in figure 1 (Cables A,B,C and D) were tested with five samples each. 80 samples were prepared at all.

It was observed that both ants specimens involved the whole samples. After cleaning no attacks evidence (pitchs or material removing) was observed. Photographs 2 and 3 show samples in testing.



Photograph 2 - Sample during ant lab test

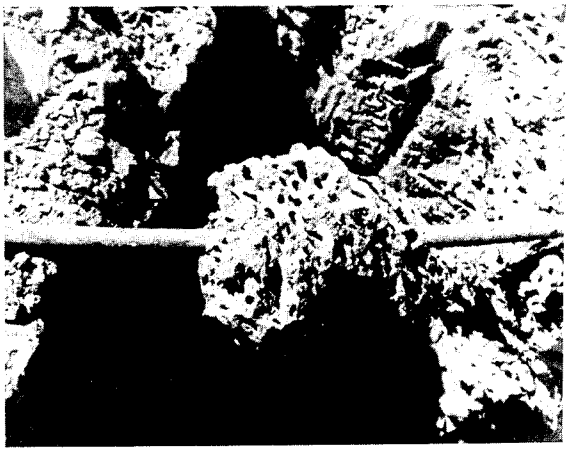


Photograph 3 - Sample during ant field test

For termites tests, cables were introduced in mounds and indentified by numbers. Samples were involved in paper to certify insects presence.

Samples verifications were performed after 3 months and after 1 year exposure. No damage occured in the samples.

Photograph 4 shows samples after removed of in termites nests.



Photograph 4 - Sample removed from termite test (Coptotermes spp)

Termites nests involved all samples and the paper used to detect insects presence was destroyed but was no material removing in the cable sample. Was detected that termites tried to chew cables sheath.

An analysis performed in the old installed metallic cable attacked by termites in Morrinhos, indicated that the damages were done by the soldiers, that are responsible by nest's defense. As optical cables were not damaged, two reasons may be considered: optical cables are actually resistant or attacks in metallic cables occured due to eletrical excitement (current or frequency). A study of transmission effects on insects attacks intensity would be an interesting continuation. The test method was considered suitable because there were attack against other cables in the same place and tried attacks over cables sheath were observed.

Anyway optical cables used in tests performed very good against termites.

CONCLUSIONS

This paper presented a study for biological attacks evaluation against direct buried optical cables used in long distance routes.

The fungi attack was evaluated using an ASTM standard and all cables tested showed fungi growth but after washing samples, all fungi were removed and there was no damage in cable samples. Materials from cables also presented fungi growth over them. Some of them could not be evaluate only by visual examination, like non oven tapes and jelly filled compounds. In these cases we recommend a future study to evaluate physical properties.

Insect attacks were evaluated in laboratory and field tests. Results indicate that optical cables tested are resistant against termites attacks, because no damages were presented in cables installed besides a destroyed metallic cable and there was traces of tried attacks. Results with insects tests indicates that these attacks can occur due to electrical excitement in metallic cables. This possibility will be studied in future work.

In ants test there were no visible damages in lab or field evaluation. These results indicates that these types of cables are resistant or are not attacked by ants. Ant's specimens used in test are very commom in Brazil.

All results presented in this work indicate that tested cable are suitable to use in buried routes, and test methodologies are efficient to test other cables.

ACKNOWLEDGMENTS

The authors would like to thanks to Mr Derval S. Rosa and Mr Júlio Cezar R. Martorano for their helpful discussion and suggestions to the work described in this paper.

REFERENCES

[1] ITU-T, "Outside Plant thechnology for Public Networks" Geneve 1992.

[2] Ruddell, H.J., "Development of an Insect Resitant Telecommunication Cable for the Australian Environment" ; Telecommunication Journal of Australia, vol 35, n 2, 1985.

[3] ASTM G 21 - "Determining Resistance of Synthetic polymeric Material to Fungi", Standard Pratice, 1988.



Paulo José Pereira Curado
Telebras - R&D Center (CPqD)
Campinas - SP - Brazil

Paulo José Pereira Curado was born in 1962. He graduated in mechanical engineering from Campinas State University (UNICAMP) in 1985 and in this year he joined Telebras Research and Development Center at Outside Plant Department. He has been engaged in research and development of optical fiber cables for trunk lines. Presently is working with Optical Subscriber Networks in Outside Plant area.



Manuel Mendes Filho
Telebras - R&D Center (CPqD)
Campinas - SP - Brazil

Manuel Mendes Filho was born in 1945. He graduated in Biological Science from Campinas Catholic University (PUCC) in 1981 and Chemical Technician in 1970. He joined Telebras Research and Development Center in 1979 and has been working in Outside Plant Department with new materials and degradation of polymers.



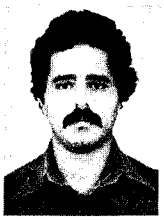
Antonio Costa Pereira Netto
Optical Systems Division
Embratel
Rio de Janeiro - RJ - Brazil

Antonio Costa Pereira Netto was born in 1950. He received his B.S. degree and M.S. degree in Telecommunication Engeneering from Rio de Janeiro Catholic University (PUC) in 1972 an 1981 respectly. He received his Ph.D. degree from Gama Filho University in 1983. Presently is Optical System Division manager of Embratel.



João Elias Filho
Optical Systems Division
Embratel
Rio de Janeiro - RJ - Brazil

João Elias Filho was born in 1948. He is Telecommunication Technician from National Technical School of Rio de Janeiro. Since 1990 is staff member of Optical System Division of Embratel.



Marcilio Estevão Lattini
Optical Systems Division
Embratel
Rio de Janeiro - RJ - Brazil

Marcilio Estevão Lattini was born in 1954. He received his B.S.C. degree in Telecommunication Engeneering from General Roberto Lisboa University in 1982. Since 1992 is staff member of Optical System Division of Embratel.

RODENT PROTECTED DIELECTRIC CABLES : WHERE IS THE SOLUTION ?

P. GAILLARD[1], JC. GAUTUN[2], G. GROLLEAU[3],
J. RAUCHS[4], G. COMEZZI[5], S. CAMARA[6]

1 : ALCATEL CABLE, FRANCE ; 2 : ORSTOM, FRANCE ;
3 : INRA, FRANCE ; 4 OPTICABLE, BELGIUM ;
5 : ALCATEL CAVI, ITALY ; 6 : ALCATEL CABLE IBERICA, SPAIN

ABSTRACT

Direct buried cables used in the telecommunication networks are preferably protected with a metallic armouring. However, this metallic protection presents several disadvantages, such as its sensitivity to electromagnetic perturbations and safety aspects ; therefore there is a substantial advantage to use dielectric cables in these applications, but it is necessary to check the resistance vs. rodents of these designs. This paper describes a series of tests conducted in this objective.

The different test methods used are detailed and discussed, together with the acceptance criteria applicable to the tested samples :

- test #1 : simple exposure to rodents
- test #2 and #3 : exposure as obstacles to rodents

Various cable protections have been submitted to these different tests ; these protections are described, and tests results presented and discussed. Some added environmental and mechanical tests results are presented to demonstrate the good adaptation of these structures to a direct burial laying.

As a result of this study, the conclusion includes recommendations for dielectric cable protection versus rodents.

1. BACKGROUND

Dielectric optical cables are widely used in the telecommunication networks, mainly in ducts; direct buried cables are preferably protected with a metallic armouring. However, this metallic protection presents several disadvantages, such as its sensitivity to electromagnetic perturbations with all the safety aspects related to induced tensions or currents (security of the maintenance staff...) ; therefore there is a substantial advantage to use dielectric cables in these applications. These cables have to present an equivalent or similar degree of protection compared to metallic cables, specifically regarding rodents attacks.

Dielectric optical fibers cables present among other points a main advantage versus metallic cables : they avoid to have to realize earthings, and they solve radically electromagnetic and lightning cable susceptibility. As a drawback, some of them are mechanically less protected, particularly against rodents for direct buried cables.

To better estimate this aspect, the present work has been performed in order to test a wide range of cable protections against rodents, and to derive from the obtained results a solution which ensures a suitable protection taking into account the following criteria :

- dielectric cable structure
- design fitted for direct buried applications
- to include a rodents protection (actually ensured by steel tape(s) or steel wires)
- to match or exceed existing 'metallic' cable specification requirements
- cost analysis compared with the metallic solution.

There is about 2,000 rodent species throughout the world. These rodents are very diversified :

- according to their size (weight from several grams for the harvest rat to several tens of kg for a south american rodent) ;
- according to their habits : diurnal, nocturnal, arboreal, combined, terrestrial, subterranean, aquatic ;
- according to their affinity for mankind (anthropophile rodents), its cultivation and its food stock, its confining to wildest areas ;
- according to their herbivorous, granivorous, omnivorous or insectivorous nutrition.

On the other hand all rodents have the capacity to gnaw, thanks to strong and often sharp, continuously growing incisor teeth moved by a specialized and extremely strong muscle fascicle. This capacity to gnaw frequently turns into a vital need, so as to wear out their continuously growing incisor teeth. In these circumstances, it is not surprizing that construction constituents, industrial products or cables be submitted to rodents attacks.

The main rodents harmful to cables are either commensal rodents living in man-built subterranean ducts and sewers,

such as *Rattus norvegicus* and *Rattus rattus*, or field arboreal rodents such as Squirrels for damages caused to aerial cables, or underground rodents *(Geomys* or american Pocket Gopher) which try to cut cables when encountering them during their subterranean burrowing or moving.

It is clear that it is not possible to give here a complete list of harmful rodents, and that in new sites one can find and must expect to encounter problems caused by rodent species not yet involved in such damages.

2. EXPERIMENT #1

2.1. Tested cable protections

The different cable protections tested in this first experiment (11 in total) are summarized in table 1 ; examples of some typical cable cross sections is given in figure 1. All cables have a double sheath protection except cables #A & B ; cables #B (dielectric, non protected) and #J (metallic protection) were used as reference.

cable #	protection design	outer dia.
A	impregnated glass yarns, 226000 dTex, HdPe sheath	13.4
B	aramid yarns, HdPe sheath	12.7
C	GRP rods Ø2.5 mm (n=18), HdPe sheath	21.5
D	impregnated glass yarns, 131000 dTex, HdPe sheath	17.5
E	polyamid inner sheath (0.7 mm thick), aramid yarns, HdPe sheath	14.5
F	glass yarns, 432000 dTex, HdPe sheath	17.5
G	glass yarns, 288000 dTex, LdPe sheath	17.5
H	glass yarns, 120000 dTex, HdPe sheath	17.5
I	corrugated steel tape, 0.25 mm thick, HdPe sheath & polyamid outer sheath (0.2 mm)	18.2
J	corrugated steel tape, 0.15 mm thick, HdPe sheath	16.5
K	9 GRP rectangular rods, HdPe sheath	15.5

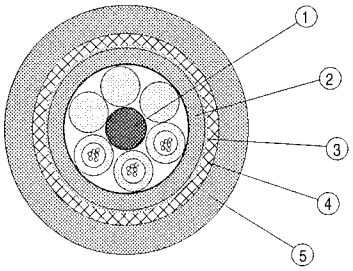
Table 1 : experiment #1, cables protection

2.2. Test method

The test procedure for the experiment #1 was as follows :

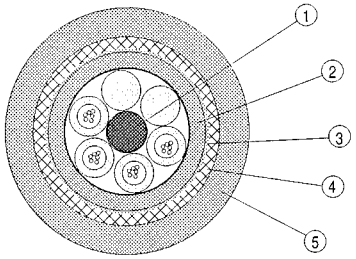
- test #1 : simple exposure to rodents (simulation of a 'normal' situation where rodents attacks correspond to a 'play' activity or to the need they have to wear their teeth); *Rattus norvegicus*, wild and laboratory (domestic) species. The cable samples to be tested are introduced into the cages (eight different cages per type of rat, three series of tests) together with a non protected dielectric cable sample and a steel tape armoured cable sample (reference), for a three weeks exposure. Rats are fed normally.

cable # E



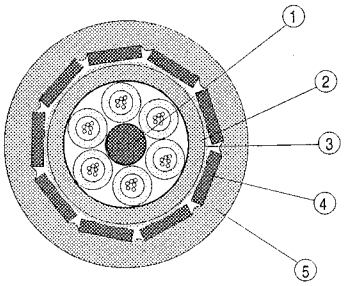
1 : cable core
2 : polyamid inner sheath, 0.7 mm thick
3 : swellable tape
4 : aramid yarns reinforcement
5 : HdPe outer sheath, 2 mm thick
Outer diameter : 14.5 mm

cable # F



1 : cable core
2 : LLdPe inner sheath, 1.5 mm thick
3 : hot melt flooding
4 : glass yarns 1200 Tex
5 : HdPe outer sheath, 2 mm thick
Outer diameter : 17.5 mm

cable #K



1 : cable core
2 : LLdPe inner sheath, 1.5 mm thick
3 : swellable tape
4 : flat FRP helically applied armouring
5 : HdPe outer sheath, 2 mm thick
Outer diameter : 15.5 mm

Figure 1 : experiment #1, examples of cables cross section

3. EXPERIMENT #2

3.1. Tested cable protections

15 different cable protections have been tested in this second experiment, performed in order to confirm and complete the previous one ; they are summarized in table 4. All cables have a double sheath protection except cables #5, 9, 10, 11 and 12 ; cables 4, 5 and 7 (labelled with an *) contain as a rodent protection a polyamid outer sheath. Cables #14 (dielectric, non protected) and #13 (metallic protection) were used as reference.

cable #	protection design	outer dia.
1	43,200 Tex glass rovings reinforcement, HdPe outer sheath	17.5
2	10 GRP rectangular rods, HdPe sheath	16.5
3	Polyamid inner sheath, 1.5 mm thick, aramid yarns reinforcement, HdPe outer sheath	14.5
4	aramid yarns reinforcement, polyamid 2.1 mm thick outer sheath	13.5
5	aramid yarns reinforcement, thick HdPe outer sheath, polyamid 0.5 mm thick oversheath	18.5
6	aramid yarns reinforcement, two glass tapes S and Z helically applied, MdPe outer sheath	13.3
7	corrugated 0.15 mm thick steel tape longitudinally applied, LdPe outer sheath, polyamid 0.6 mm thick oversheath	17.5
8	LdPe inner sheath, two steel tapes 0.1 mm thick helically applied, LdPe outer sheath	17
9	43,200 Tex glass rovings reinforcement, LdPe outer sheath	11.6
10	57,600 Tex swellable glass rovings reinforcement, HdPe outer sheath	12
11	45,600 Tex swellable glass rovings reinforcement, HdPe outer sheath	17.2
12	86,400 Tex flooded glass rovings reinforcement, HdPe outer sheath	16.3
13	corrugated 0.15 mm thick steel tape longitudinally applied, HdPe outer sheath	16.5
14	aramid yarns reinforcement, HdPe outer sheath	12.5
15	18 round GRP armouring, helically applied, HdPe outer sheath	21.5

Table 4 : experiment #2, cables protection

3.2. Test method

For this experiment the procedure was as follows :

- test #3 : identical to test #2 of experiment #1, except for the rodents (Gophers and *Rattus norvegicus*, wild and domestic) and the number of experiments (ten tests with Gophers, three tests with *Rattus norvegicus*).

- test #4 : according to BellCore GR20 specification ; *Rattus norvegicus*, wild and laboratory (domestic) species and Pocket Gophers. The cable sample to be tested is located across an opening between two cages (ten samples), for a seven days exposure. Rats are fed normally.

The estimation of the damages caused by the rodents is identical with the one used for experiment #1.

3.3. Results

The results are given in following tables 5.1 to 5.6. The numbers correspond to the number of samples found under the corresponding category ; a cable presenting a damage of 3 or more is considered as non satisfactory, except cables 4, 5 and 7 for which a damage of 2 or more is considered as non satisfactory, the tested protection being an outer polyamid sheath.

cable	0	1	2	3	4	5	mean	max
1	1		1		1		2	4
2	1	1	1				1	2
3		2	1				1.3	2
4*		2			1		2	4
5*	1				2		2.7	4
6	1		1		1		2	4
7*		2	1				1.3	2
8	1	1	1				1	2
9		1		1	1		2.7	4
10		3					1	1
11	1	1		1			1.3	3
12		1			2		3	4
13	1		2				1.3	2
14	1	1	1				1	2
15	1	2					0.7	1

Table 5.1, wild rats, test #3

cable	0	1	2	3	4	5	mean	max
1			2	1			2.3	3
2		1	2				1.7	2
3		1		1		1	3	5
4*		1			1	1	3.3	5
5*		1			1	1	3.3	5
6			1			2	4	5
7*		1	2				1.7	2
8			3				2	2
9				1		2	4.3	5
10			2			1	3	5
11		1	2				1.7	2
12			1		2		3.3	4
13		1	2				1.7	2
14					1	2	4.7	5
15		1	2				1.7	2

Table 5.2, domestic rats, test #3

- test #2 : exposure as obstacles to rodents (simulation of a specific situation where rodents attacks are caused by a vital need); *Rattus norvegicus*, wild and laboratory (domestic) species. The cable sample to be tested is located across an opening between two cages, rats being on one side of the opening and rats food being on the other side in the cages (five different cages per type of rat, three series of tests), for a two days exposure. Rats are not fed.

The estimation of the damages caused by the rodents has been set as follows :

0 : no damage
1 : the outer jacket is scratched, but not penetrated
2 : the outer jacket is penetrated, the protection layer is not penetrated
3 : the protection layer is penetrated, the fibers are not damaged
4 : the fibers are damaged
5 : the cable is severed (cut into two parts)

Illustration of damage index 2 (cable K) and 4 (cable H) are given in figure 2.1 and 2.2.

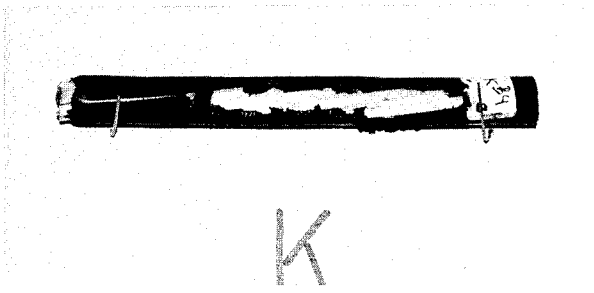


Figure 2.1, example of index damage 2

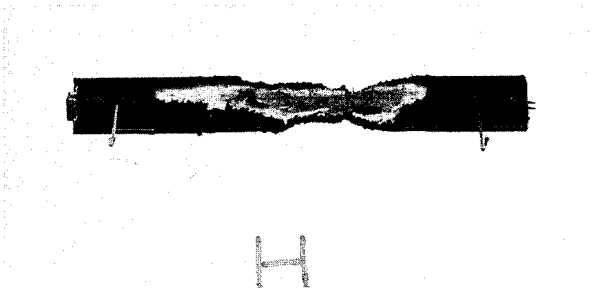


Figure 2.2, example of index damage 4

2.3. Results

The results are given in following tables 2.1, 2.2, 3.1, and 3.2. The numbers correspond to the number of samples found under the corresponding category ; a cable presenting a damage of 3 or more is considered as non satisfactory, except cable I for which a damage of 2 or more is considered as non satisfactory, the tested protection being an outer polyamid sheath.

cable	0	1	2	3	4	5	mean	max
A	1	1		1			1.3	3
B	4	4	4	8	4		2.2	4
C			3				2	2
D	1	1		1			1.3	3
E				1	2		3.7	4
F			3				2	2
G	1			1		1	2.7	5
H		2		1			1.7	3
I	1		2				1.3	2
J	6	4	14				1.3	2
K								

Table 2.1 : domestic rats, test #1

cable	0	1	2	3	4	5	mean	max
A	2		1				0.7	2
B	10	10	2		1		0.8	4
C		3					1	1
D	2		1				0.7	2
E		1	1				1.5	2
F		2	1				1.3	2
G	1	1	1				1	2
H	1	2					0.7	1
I	2	1					0.3	1
J	6	13	4				0.9	2
K								

Table 2.2 : wild rats, test #1

cable	0	1	2	3	4	5	mean	max
A					5		4	4
B					5		4	4
C			5				2	2
D				1	4		3.8	4
E					5		4	4
F			1		4		3.6	4
G					4	1	4.2	5
H					4	1	4.2	5
I			5				2	2
J			5				2	2
K			4		1		2.4	4

Table 3.1 : domestic rats, test #2

cable	0	1	2	3	4	5	mean	max
A				1	4		3.8	4
B	1				3		3	4
C			5				2	2
D					4	1	4.2	5
E					5		4	4
F				3	2		3.4	4
G		1			3	1	3.6	5
H			1		7		3.8	4
I			5				2	2
J			5				2	2
K			4	1			2.2	3

Table 3.2 : wild rats, test #2

cable	0	1	2	3	4	5	mean	max
1		2	1	1	5	1	3.2	5
2		8	2				1.2	2
3		3		6	1		2.5	4
4*		9	1				1.1	2
5*		5	2		3		2.1	4
6		3	1		2	4	3.3	5
7*		4	6				1.6	2
8		1	9				1.9	2
9					2	8	4.8	5
10		1		1		8	4.4	5
11		3	1		4		2.6	4
12		1		1	7	1	3.7	5
13		3	7				1.7	2
14		1	1	1	7		3.4	4
15	1	3	6				1.6	2

Table 5.3, Pocket Gophers, test #3

cable	0	1	2	3	4	5	mean	max
1		2			8		3.4	4
2		3	6	1			1.8	3
3		3		2	5		2.9	4
4*		3			7		3.1	4
5*								
6								
7*		2	8				1.8	2
8		1	9				1.9	2
9		1			2	7	4.4	5
10								
11								
12								
13								
14								
15								

Table 5.4, wild rats, test #4

cable	0	1	2	3	4	5	mean	max
1	1	6	3				1.2	2
2		8	2				1.2	2
3		7		3			1.6	3
4*		10					1	1
5*								
6	1	5	3	1			1.4	3
7*		7	3				1.3	2
8		5	5				1.5	2
9		3	3			4	2.9	5
10	1	4	5				1.4	2
11								
12								
13								
14								
15								

Table 5.5, domestic rats, test #4

cable	0	1	2	3	4	5	mean	max
1		3			5	2	3.3	5
2		3	5		2		2.1	4
3		4		3	3		2.5	4
4*	1	3	1	2	3		2.3	4
5*	1	7			2		1.5	4
6		3			2	5	3.6	5
7*		7	3				1.3	2
8		5	5				1.5	2
9		2	1		1	6	3.8	5
10		4			1	5	3.3	5
11	2	1		1	3	3	3.1	5
12	1	3			3	3	3	5
13		3	7				1.7	2
14		3	1		5	1	3	5
15		4	6				1.6	2

Table 5.6, Pocket Gophers, test #4

4. DISCUSSION

Regarding these results the following point can be noted :

- as shown in table 6, the test #1 is the less stringent as it can be expected ; the tests #2 & 3 and #4 are comparable, with a slight advantage (in terms of severity) for the tests #2 & 3
- as shown in table 7, the most destructive rodent is the Pocket Gopher, closely followed by the domestic *Rattus norvegicus*. However such a comparison has to be balanced with the number of rodents introduced into the cages (several for the domestic species, only one for the wild ones)
- approximately 37% of the rodents attacks did not penetrate the cable outer sheath. These unsuccessful attacks allow to evaluate the degree of efficiency for cables having an outer Pa sheath as protection (samples I, 4, 5 and 7), but do not permit to estimate other protections efficiency
- only the metallic (samples J, 8, and 13) and ruggedized GRP armouring protections (samples C and 15) have passed all the tests ; a lighter GRP armor

test # (all species, all samples)	nr of tests	mean results		max. results
		mean	max	mean
1	20	1.4	3.7	2.5
2 & 3	67	2.7	4.8	3.4
4	31	2.3	4.4	3.3

Table 6 : tests severity comparison

rodent (all tests, all samples)	nr of tests	mean results		max. results
		mean	max	mean
wild Rattus n.	43	2.1	4.4	2.9
dom. Rattus n.	45	2.2	4.7	3.2
Pocket Gopher	30	2.6	4.8	3.7

Table 7 : rodents comparison

(samples K and 2) showed good results and failed in only approx. 10% of the tests, which is in compliance with BellCore GR 20 requirements

- polyamid (preferably outer) sheath protection and glass roving armoured (preferably with a sufficient amount of glass to ensure a complete covering of the core) cables present an acceptable level of protection for standard situations (exposition test #1), but fail (cable core penetrated) in approximately 50% of the other tests which is comparable to an unprotected cable. Best results are obtained on samples #10 (glass protection, 44%) and #4 (Pa sheath, 37%).

These considerations are illustrated in figure 3 and in table 8.

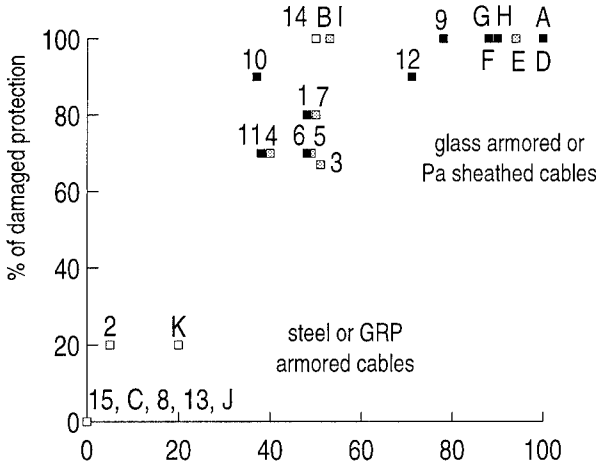


Figure 3 : tests results summary

sample #	protection	number of tests	failures	
			prot.	core
A	glass yarns	16	11	9
B	none	56	21	13
C	GRP rods	16	0	0
D	glass yarns	16	11	9
E	Pa inner sheath	15	13	12
F	glass yarns	16	9	5
G	glass yarns	16	11	10
H	glass yarns	18	13	12
I	Pa outer sheath	16	7	-
J	steel tape	57	0	0
K	GRP rods (light)	10	2	1
1	glass yarns	46	24	14
2	GRP rods (light)	46	3	0
3	Pa inner sheath	46	25	7
4	Pa outer sheath	46	17	10
5	Pa outer sheath	26	11	9
6	glass tapes	36	17	16
7	Pa outer sheath	46	23	-
8	steel tapes	46	0	0
9	glass yarns	46	35	34
10	glass yarns	36	16	15
11	glass yarns	24	12	10
12	glass yarns	26	19	18
13	steel tape	26	0	0
14	none	26	17	16
15	GRP rods	26	0	0

Table 8 : tests results summary

These results also show that the main point to be considered in addition to the expected rodents when designing a dielectric rodent protected cable is the estimation of the risk incurred according to the cable laying conditions (possible rodents obstruction due to the cable) :

- low risk : glass yarns or tape reinforcement or polyamid outer sheath
- medium risk : light GRP armouring
- high risk : strong GRP armouring

From the economical point of view, the glass roving protection is the cheapest solution, comparable to a steel tape armored cable ; next come the Pa sheathed cables, the GRP armoring representing by far the most expensive choice.

5. MECHANICAL TESTING

In addition to these tests cables E, F and K have been submitted to mechanical and environmental tests in order to evaluate their ability to be used for direct burial application.

The tests realized and obtained results are given in table 9 ; they show a good behaviour compared to the actual direct buried cables, with a tensile performance better than 270 daN, a minimum crush resistance of 45 daN/cm (without loss increase when subjected to the load) and an impact resistance of 10 N.m minimum. The thermal range has been checked between -40°C and +70°C (before and after ageing at 85°C for 7 days) with a loss increase of less than 0.1 dB/km. Test methods are in compliance with IEC 794-1 international standard ; the attenuation changes were monitored at 1550 nm. The aging mechanical test has been performed in order to evaluate the aging in water of a glass roving protection. A duct pulling and a direct burying (using a ploughing machine) tests have also been performed on cable K under real conditions, without any measurable loss increase or mechanical damage.

test	severity	result
tensile	270 daN	$\Delta\alpha \leq 0.1$ dB
crush	45 and 80 daN/cm	$\Delta\alpha \leq 0.1$ dB under 45 daN/cm no residual loss after 80 daN/cm
impact	10 N. m and 100 N.m	$\Delta\alpha \leq 0.1$ dB at 10 N.m no residual loss after 100 N.m
thermal	-40°C/+70°C 2 cycles	$\Delta\alpha \leq 0.1$ dB
aging (optical)	85°C, 168 h + thermal test	$\Delta\alpha \leq 0.1$ dB
aging (mechanical)	85°C, 15 days (in water)	no change in modulus (cable F)
water tightness	168 h	no leakage

Table 9 : mechanical and environmental testing

6. CONCLUSION

Two series of fully dielectric cable protection have been tested regarding their behaviour vs rodents.

Obtained results show that for simulations conducted in a laboratory rodent attacks strongly depend on the way the test is conducted ; it is concluded that in real conditions for current situations a glass yarns or polyamid outer sheath protection might represent a sufficient solution, but that a true dielectric rodent resistant protection can be achieved only with an FRP armouring.

Other mechanical and environmental tests showed that the proposed cable designs are well suited for a direct buried use.

ACKNOWLEDGEMENTS

The authors would like to thank France Telecom CNET for the duct and direct burying tests, and Genesis Laboratories Inc., CO, for rodents tests.

AUTHORS

Pierre GAILLARD
ALCATEL CABLE, STT/OFCCC
35 rue J. Jaurès BP 20 95871 Bezons cedex, FRANCE



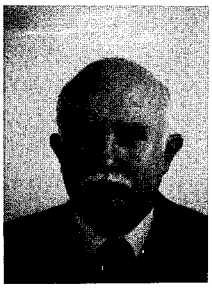
P. GAILLARD was born in 1956. He received his engineer degree from the Ecole Catholique des Arts et Métiers (ECAM) in 1980. He joined Alcatel Cable in 1983, where he is now working as project engineer in the Optical Fiber Cable Competence Center.

Jean Claude GAUTUN
ORSTOM, département MAA/UR 33
213 rue La Fayette 75480 Paris cedex 10, FRANCE



JC. GAUTUN was born in 1941. He received his Docteur es Sciences degree from Paris 6 University. He is now working as Directeur de Recherche at the ORSTOM, where he is a specialist of ecology and of the fight against harmful rodents, particularly from African tropical countries.

Gérard GROLLEAU
INRA, département Phytopharmacie et Écotoxicologie, unité Phytopharmacie et Médiateurs chimiques
route de Saint Cyr, 78026 Versailles cedex, FRANCE



G. GROLLEAU was born in 1935. He received his engineer degree from ENSH at Versailles ; he is now working as research engineer at the Institut National de la Recherche Agronomique (INRA), where he is in charge of the Eco-etho-toxicologie Group and a specialist of the fight against commensal and field rodents in France, as well as of the effects of fertilizers, herbicides...on the animal wildlife.

Gerardo COMEZZI
ALCATEL CAVI
via del Crocifisso, Latina, ITALY



G. COMEZZI was born in 1958. He was graduated as Electrical Engineering Doctor at Rome University. He joined SIP (Telecom Italia in 1985, attending a TCL master (1985 - 1986). He joined Alcatel Cavi in 1989, working in OF cables design & development. Now he is Technical responsible for the Optical Cable Product Line in Latina plant.

Jean RAUCHS
OPTICABLE SA
Frameries, BELGIUM

Jean RAUCHS was born in 1965. He obtained his Dip. Ing. Degree in mechanics from the Faculté Polytechnique de Mons, Belgium, in 1989.
He joined Opticable in August 1989 in the R&D department. He became in 1991 responsible for the Engineering department.

Susana CAMARA
ALCATEL CABLE IBERICA
Santander, SPAIN



S. CAMARA received her Master Degree in Chemistry from Oviedo University in 1983. She joined Alcatel Cable Iberica in 1987, where she was in charge of material development for telecommunication cables. She is actually reponsible of the Product Engineering for copper and optical fibre cable in Alcatel Cable Iberica.

OPTICAL AND MECHANICAL PERFORMANCES OF DIFFERENT CABLE STRUCTURES IN FROZEN DUCTS

Marco Agretti, Mauro Bottanelli

SIRTI S.p.A. - Via Pirelli 20, 20124 Milan - ITALY

ABSTRACT

This paper describes the results of experimental freezing tests carried out on eight different cable structures. The cables have been tested in steel and plastic tubes filled with cyclically frozen water, according to standardized and non standardized test procedures. The aim of the work was to evaluate the optical and mechanical behaviour and reliability of different optical cable types for terrestrial installation and to develop the most realistic test procedure to do that. The experimental results seem to point out that the choice between metal free cables and metal sheath ones, loose tube cables and slotted core ones, have to be carefully considered for installation in ducts, according to cable and duct diameters, ground morphology and environmental temperature variations.

1. INTRODUCTION

Nowadays, the optical fiber cable world market offers a huge number of different products to meet every kind of requirements for installation in very different applications and geographical and climatic conditions: submarine, aerial or terrestrial cables; loose or tight, metal free or armored cables; single fiber or fiber ribbon cables; low cost limited life cables or more expensive long life ones.

However, in spite of this wide availability of typologies, the proper choice of a cable is not always a simple matter, and could depend on different and contrasting requirements. So, for instance, a metal sheath cable can offer a suitable solution against rodents, but under particularly severe climatic conditions (frozen water in the cable duct) could show mechanical irreversible failures; on the contrary, in the same situation, a metal free cable can show reversible mechanical strain though being unprotected against rodents.

In general, the reliability of optical cables for installation in ducts under severe climatic conditions is a very important and difficult property to measure. Little differences in the cable structure, in the duct material and geometry, in the ground morphology and in the thermal exposure can give rise to even opposite cable optical and mechanical behaviours. For these reasons, laboratory tests on optical cables are essential to get at least some fundamental criteria to avoid future (and often very expensive) problems in the field.

This paper collects the results of different tests carried out on eight optical cable structures during a two years period, originally under the pressure of an immediate need, and only recently with a more organized approach. For this reasons, it could be observed that it is difficult to get comparisons among the eight different cable structures, because they have been generally tested by means of different set-ups and procedures. However, the aim of this study was not only to test and compare different cable structures, but also to develop the most realistic procedure to do that. As we will see in the following, the best test procedure, that is the procedure giving us the possibility of best comparing the different cable structures, is, in our case, the less realistic one in comparison with field installations.

2. CABLE STRUCTURES UNDER TEST

The experimental freezing tests have been carried out on eight different cable structures. Schematic cross-sections of the cables are reported in figure 1, according to the following classification:

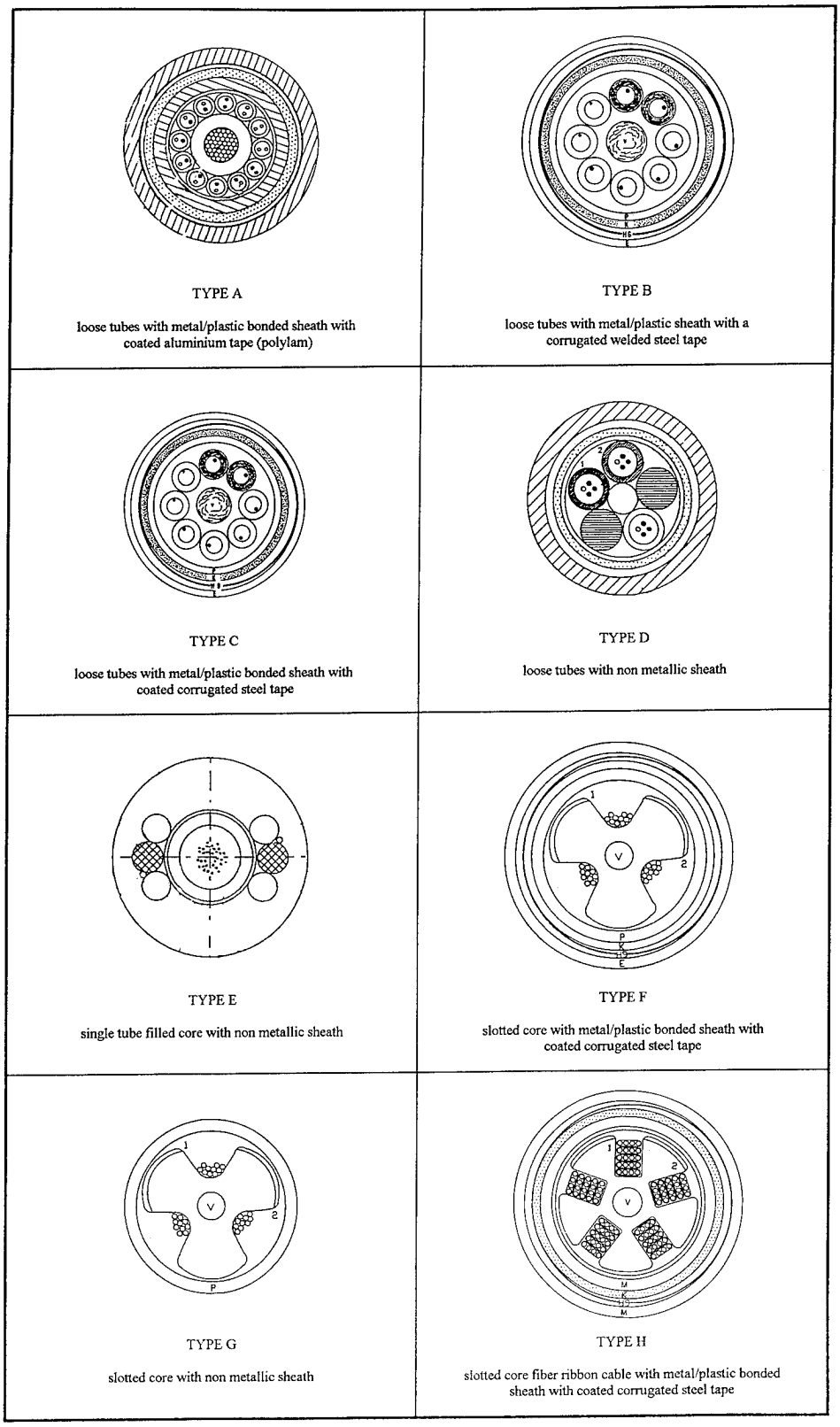


Fig. 1 - The eight optical cable structures under test

loose tube cables:

- loose tubes with metal/plastic bonded sheath with coated aluminium tape (polylam) (type a);
- loose tubes with metal/plastic sheath with a corrugated welded steel tape (type b);
- loose tubes with metal/plastic bonded sheath with coated corrugated steel tape (type c);
- loose tubes with non metallic sheath (type d);
- single tube filled core with non metallic sheath (type e);

slotted core cables:

- slotted core with metal/plastic bonded sheath with coated corrugated steel tape (type f);
- slotted core with non metallic sheath (type g);
- slotted core fiber ribbon cable with metal/plastic bonded sheath with coated corrugated steel tape (type h).

Apart from the previous subdivision, we emphasize the fact that cable types d, e and g are metal free ones, while cable types a, b, c, f and h have a metal sheath of different thickness and composition: these differences fundamentally influence the optical and mechanical behaviour of cables under freezing tests, as we will show in the following.

3. TEST SET-UPS AND PROCEDURES

The eight different cable structures have been tested in steel and plastic tubes filled with cyclically frozen water.

a) Steel tube set-up and procedure (figure 2 and 3)

A limited length of the cable under test is inserted into a 2 meters long steel tube; the ends of the tube are capped with flanges and the cable portion inside the tube is sealed into it by means of thermo-shrinkable sheaths. The tube is filled with water and placed in a freezing chamber; the cable optical fibers are monitored by means of an automatic OTDR-optical switch-computer system; they are typically looped together to reduce the number of monitored channels (to have high monitoring rate). The

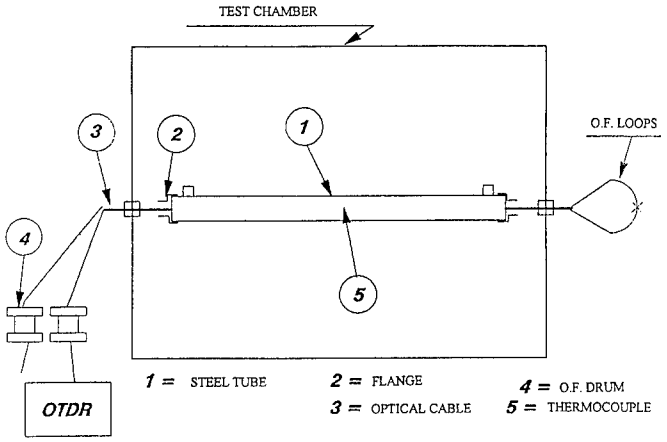


Fig. 2 - Set-up for the steel tube test

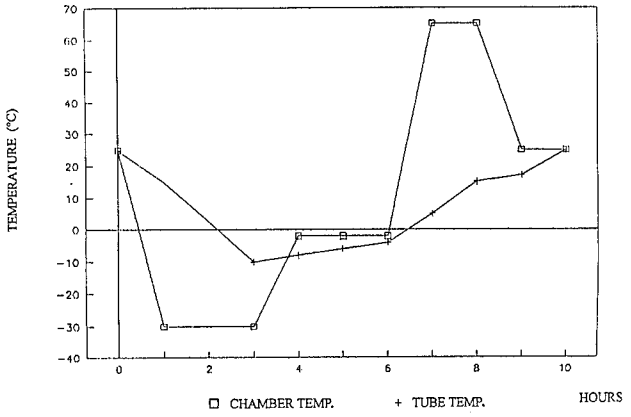


Fig. 3 - Thermal cycle for the steel tube test

test thermal cycle of the freezing chamber is reported in figure 3 together with the thermal behaviour of the tube outside surface temperature, which is monitored by means of a thermocouple. This kind of test (EIA/TIA-455-98A, method B) should reproduce the situation of cables in ducts with completely frozen ground, where the crush force caused by ice can not be compensated by duct expansion and it entirely acts on the cable. After a first and destructive attempt on the cable type a, with a 45 millimetres inner diameter steel tube and only 5 meters of global cable length, we decided to use a 35 mm inside diameter steel tube and at least 25 meters of cable length to avoid fast migration of water-blocking material towards the cable ends and no realistic test situations.

b) Plastic tube set-up and procedure (figure 4 and 5)

About 11 meters of cable length is inserted into a 34 mm inner diameter plastic tube with free ends, filled with water. The cable optical fibers are monitored by means of the same set-up previously described. The cable is the subjected to 25 thermal cycles of the type reported in figure 5. The main differences between this kind of test and the previous one are:

- the plastic tube expansion can partially compensate the ice expansion;
- the thermal cycle is less severe. (A more severe test cycle with a -25 °C lower temperature was considered at the beginning of this study; see for instance in table 2 the results on a and f cable structures).

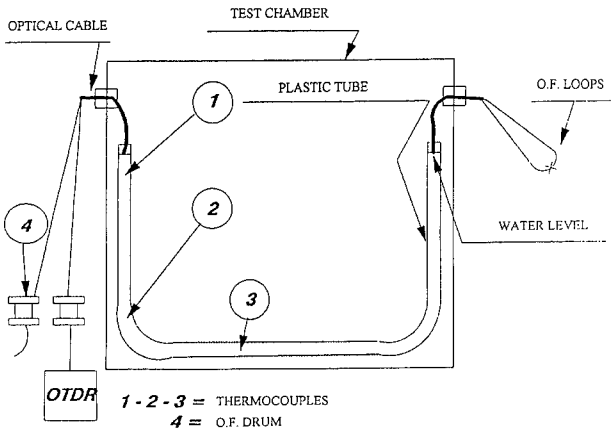


Fig. 4 - Set-up for the plastic tube test

In conclusion, this kind of test procedure seems to be more realistic than the previous one, but it gives also poor information on the mechanical behaviours of the different cable types.

A detailed comparison between this two different test procedures and the actual situation in the field, both for duct installations in the ground and in the open air, can be found in table 1.

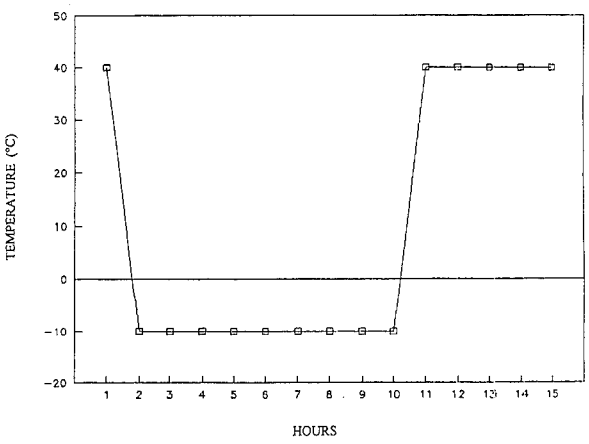


Fig. 5 - Thermal cycle for the plastic tube test

TEST PROCEDURE	DUCT IN THE GROUND	DUCT IN THE OPEN AIR
STEEL TUBE TEST		
• the tube can not expand	W	WW
• the tube ends are capped	WW	W
• the thermal cycle is very severe	WW	W
• only one thermal cycle	B	B
PLASTIC TUBE TEST		
• the tube can expand	B	N
• the thermal cycle is severe	W	N
• more than one thermal cycle	N	N

B = better condition than that in the field

N = normal condition in the field

W = worse condition than that in the field

WW = very worse condition than that in the field

Tab. 1 - Comparison between the two freezing test procedures and the actual situation in the field

TEST PROCEDURE / CABLE TYPE	OPTICAL SET-UP FOR MONITORING	45 mm inner Ø STEEL TUBE EIA/TIA 455-98A, method B Tchamber = -30 ÷ +65 °C 5 m cable length	35 mm inner Ø STEEL TUBE EIA/TIA 455-98A, method B Tchamber = -30 ÷ +65 °C 25 m cable length	PLASTIC TUBE Tchamber = -25 ÷ +40 °C 25 m cable length 11 m tube length	PLASTIC TUBE Tchamber = -10 ÷ +40 °C 25 m cable length 11 m tube length
TYPE A loose tubes with metal/plastic bonded sheath with coated aluminium tape (polylam) (24 O.F. - 17 mm Ø)	1 optical loop on 24 O.F.	out of OTDR dynamic range at the first freezing cycle water-blocking compound migration towards the cable ends cable diameter reduction of about 0.75 mm tube and fiber squashing	0.06 dB attenuation at the first freezing cycle out of OTDR dynamic range at the second freezing cycle after water filling up tube and fiber squashing	out of OTDR dynamic range at the fourth freezing cycle fibers permanently squashed after the fifth cycle about 0.5 l of water filling up after every cycle tube cutting and squashing external sheath broken	to be performed
TYPE B loose tubes with metal/plastic sheath with a corrugated welded steel tape (8 O.F. - 21 mm Ø)	1 optical loop on 8 O.F.	no longer performed test	permanently out of OTDR dynamic range at the third freezing cycle (no attenuation variations before) insignificant wather filling up between cycles up to 4 mm irregular diameter reduction of the metal sheath metal sheath slipping of about 5 cm out of the cable ends tube and fiber squashing	no longer performed test	25 cycles without attenuation variations, filling up and significant cable modifications
TYPE C loose tubes with metal/plastic bonded sheath with coated corrugated steel tape (8 O.F. - 13.5 mm Ø)	1 optical loop on 8 O.F.	no longer performed test	fiber broken at the first freezing cycle up to 2 mm irregular reduction of the metal sheath tube and fiber squashing	no longer performed test	25 cycles without attenuation variations, filling up and significant cable modifications
TYPE D loose tubes with non metallic sheath (12 O.F. - 14.2 mm Ø)	3 optical loops 4 O.F. in each loop one loop for each loose tube	no longer performed test	3 fibers broken in a tube after the first freezing cycle (about 4 dB attenuation on the other two optical loops) filling compound migration towards one end of this tube tube and fiber squashing	no longer performed test	to be performed

Tab. 2/a - Freezing test results on a, b, c and d cable structures

TEST PROCEDURE / CABLE TYPE	OPTICAL SET-UP FOR MONITORING	45 mm inner Ø STEEL TUBE EIA/TIA 455-98A, method B Tchamber = -30 ÷ +65 °C 5 m cable length	35 mm inner Ø STEEL TUBE EIA/TIA 455-98A, method B Tchamber = -30 ÷ +65 °C 25 m cable length	PLASTIC TUBE Tchamber = -25 ÷ +40 °C 25 m cable length 11 m tube length	PLASTIC TUBE Tchamber = -10 ÷ +40 °C 25 m cable length 11 m tube length
TYPE E single tube filled core with non metallic sheath (24 O.F. - 12.8 mm Ø)	1 optical loop on 24 O.F.	no longer performed test	out of OTDR dynamic range at every freezing cycle but coming back to the initial conditions at the thaw up to 2 mm irregular diameter reduction of the sheath large quantity migration of water-blocking compound towards the cable ends during the first cycle	no longer performed test	25 cycles without attenuation variations, filling up and significant cable modifications
TYPE F slotted core with metal/plastic bonded sheath with coated corrugated steel tape (30 O.F. - 17 mm Ø)	1 optical loop on 30 O.F.	no longer performed test	out of OTDR dynamic range at the first freezing cycle but coming back to the initial conditions at the thaw irregular squashing of the metal sheath squashing of the polypropylene ribbons towards the slots water-blocking compound migration towards the cable ends	no attenuation variations after 4 freezing cycles in spite of 0.2 l water filling up between cycles	25 cycles without attenuation variations, filling up and significant cable modifications
TYPE G slotted core with non metallic sheath (30 O.F. - 10 mm Ø)	3 optical loops 5 O.F. in each loop one loop for each slot of the core	no longer performed test	about 8 dB attenuation on each loop, but coming back to the initial conditions at the thaw sudden attenuation variations during freezing	no longer performed test	to be performed
TYPE H slotted core fiber ribbon cable with metal/plastic bonded sheath with coated corrugated steel tape (100 O.F. - 20 mm Ø)	4 optical loops: a - most external ribbons of every slot b - most internal ribbons of every slot c - 3 middle ribbons of a slot d- 3 middle ribbons of another slot	no longer performed test	no attenuation variations at the first freezing cycle second cycle: a: 1.5 dB; b: 0.3 dB; c: 1.0 dB; d: 0.0 dB. third cycle: a: 2.0 dB; b: 0.4 dB; c: 1.5 dB; d: 0.0 dB. note that on d we monitor the second fiber of the ribbons; the first one on all the other loops irregular squashing of the metal sheath 0.13 l water filling up between cycles	no longer performed test	to be performed

Tab. 2/b - Freezing test results on e, f, g and h cable structures

4. EXPERIMENTAL RESULTS AND DISCUSSION

Table 2 summarizes the results of our freezing tests on the different eight cable structures. Some of the tests are still to be performed, but it is already possible to draw same important conclusions:

- Only the cable type e seems to be able to pass the EIA/TIA steel tube test without any substantial functional modifications, in the sense that its optical fibers attenuation cyclically increases during the freezing, coming back to the initial conditions at the thaw. Note that this kind of cable is completely metal free, and that the optical fibers are contained in a single large and straight plastic tube along the cable axis. All the other cable structure seems to suffer an immediate or a cycle-by-cycle degradation up to fiber breaking.

- Fibers in loose tube cables with little loose tube diameters are generally less protected than in slotted core cables. During the EIA/TIA steel tube test, the fiber loose tubes generally collapse due to the ice expansion, squashing the fibers in a permanent way. However, the loose tube cable structure is more elastic than the slotted core one, and it seems to be possible to prevent fiber damage by means of a proper distribution of empty space in the cable.

- Fibers in metal sheath cables are initially more protected than in metal free ones. However, cycle-by-cycle the metal sheath suffers a plastic deformation if, as in the EIA/TIA steel tube test, the force of the ice expansion is stronger than the metal sheet endurance. So, due to the water filling up, the water quantity in the duct increases up to a complete cable damage during the following cycles.

- All the eight cable structures passed the plastic tube freezing test at -10°C without any particular trouble; this is a good result, especially considering that this kind of test is probably very similar to the actual situation in the field.

- Finally we have to stress the fact that the differences among the cables outer diameters have obviously to be carefully considered when comparing the experimental test results: a big outer diameter reduces the water quantity (that is the test severity) in the test tube with respect to a little one.

5. CONCLUSIONS

We have reported the experimental results of freezing tests carried out on eight different cable structures according to different tests procedures. These results point out that the choice between metal free cables and metal sheath ones, loose tube cables and slotted core ones, have to be carefully considered for installation in ducts, according to cable and duct diameters, ground morphology and environmental temperature variations.



Mauro Bottanelli

Cables and Optical Technologies - R&D Division
SIRTI S.p.A.
Via Manzoni 44 - 20095 Cusano Milanino (MI) - ITALY

Mauro Bottanelli was born in 1963. He received the Dr. Ing. degree in Nuclear Engineering from Politecnico of Milan. After a two years activity in the field of industrial automation, he joined SIRTI in 1990 as research engineer in the field of optical fiber cables and optical components measurement techniques. He is a member of the ITU-T 4/15 National Working Group on fibers, cables and optical components.

Switched Fiber Twisted Pair (SFTP) Broadband to the Home

Paul Kish & Jon Green,
NORTEL

Tet Yeap,
University of Ottawa

Abstract

This paper covers the distribution of broadband services to the home over a Switched Fiber Twisted Pair (SFTP) copper network. A new broadband PIC cable and drop wire was developed that provides the capability of up to 52 Mb/s data transmission between the Node and the subscriber for a distance of 1 kilometer. A broadband loop including cable, connection and protection hardware has been tested. The test results indicate a six fold increase in available bandwidth compared to existing outside plant cabling. It is concluded that high performance twisted pair copper provides a practical and economical means for the delivery of digital broadband services in the foreseeable future. This architecture will permit mapping of the broadband network onto the existing network with minimum disruption to the planning, installation, management and maintenance of the outside plant.

Introduction

We are entering an exciting new era in telecommunications that will offer business and residential subscribers unprecedented access to new broadband services. Today one can only see a glimpse of the emerging market for broadband services in the field of education, work at home, advertising, information retrieval, home entertainment, etc. Market drivers such as user friendly graphical interfaces and voice activated systems are attracting many new users and are stimulating demand for new services in a growing multibillion dollar industry.

New broadband service offerings are being made possible through rapid advances in digital technology. The technological factors that are shaping the future include:

1. The digitisation of all kinds of information, e.g. voice, text , image and video
2. The tremendous increase in digital signal processing and computing power
3. The availability of high capacity, fast and efficient memory storage devices
4. New developments in digital encoding and digital compression techniques
5. The rapid growth of world-wide information networks (Internet)
6. International Standard protocols for access and transfer of information
7. The deployment of ATM technology for assembling and routing information
8. Increased bandwidth availability for cable transmission using
   - Optical fibre in the backbone
   - Enhanced twisted-pair **Copper** for distribution

In spite of the wrong perception that copper is not suited for broadband, twisted-pair copper cabling is the media of choice for high speed LAN and data applications in buildings. The local exchange carriers, after looking at different alternatives (Fiber to the Home, Fiber to the Curb, Hybrid Fiber Coax,..) are arriving to the same conclusion for the outside plant. The use of twisted pair copper distribution cables makes sense both technically and economically as a practical vehicle to deliver broadband to the home. This paper will present the rationale for choosing copper, not as an interim stopgap technology, but to fulfil the requirements for the delivery of broadband services looking forward for the next 20 years.

In 1989, the Cable Group of Northern Telecom presented an award winning technical paper at this symposium which demonstrated the capability of 16 Mb/s data transmission over a new design 100 Ohm UTP cabling. Shortly thereafter, the industry quickly adopted the new technology and standardised on enhanced 100 Ohm UTP cabling as the preferred media for LAN and data applications in commercial buildings. Today, transmission of 100 Mb/s (TP PMD) and 155 Mb/s (ATM) is commonplace in the industry with 622 Mb/s being experimented with in the lab. As a natural extension of this technology, the same principles were applied to the design and manufacture of high performance multipair PIC distribution cables.

The results presented in this paper which, in a sense, is an analogy to the in building evolution, will demonstrate the technical capability of 52 Mb/s (STS-1) data transmission for a distance of 1 km or alternatively, 26 Mb/s for a distance of 1.5 km over twisted pair copper cabling.

SFTP Architecture

The reach objective is based on the maximum distance between the Distribution Serving Area (DSA) and the furthest subscriber. With few exceptions, nearly all subscribers are located within 1.5 km of the DSA and more than 95% are located within 1 km of the DSA. The most attractive economic model would be to locate the remote electronics (Node) at the Distribution Serving Area interface which is also called the Jumper Wire Interface (JWI), i.e. at the junction between the feeder and the distribution cables. A DSA typically serves between 400 to 600 subscribers. Fig. 1 illustrates the concept of Switched Fibre Twisted Pair (SFTP) broadband distribution to the home. This architecture will permit the mapping of the broadband network onto the existing network with a minimum disturbance to the outside plant, right of way, network management, planning, maintenance, etc.

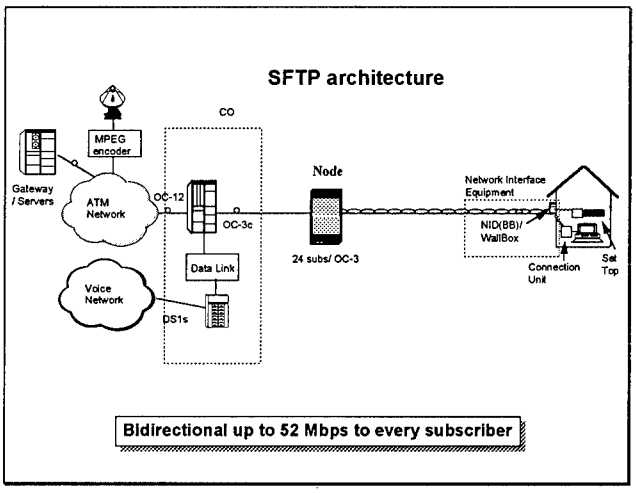


Figure 1

The Switched Fiber Twisted Pair architecture uses optical fiber (OC-3 or OC-12) as the transmission media between the central office equipment and the Node. The broadcast channels at the head end are digitally encoded using MPEG-2 and delivered over the ATM network along with the digital video interactive, text and image information residing on high power gateway/servers. Voice service can be maintained over the existing subscriber loop plant or, optionally, provided over the ATM network through a data link in the central office. The Node contains the common equipment for ATM bandwidth management and plug-in line cards that interface with the broadband loop. Initially, an OC-3 link from the central office can serve 24 subscribers providing an average data throughput of 6.5 Mb/s per subscriber. Depending on traffic density and traffic patterns, this can be upgraded later to an average of 26 Mb/s by providing an OC-12 link. The maximum data throughput is only limited by transmission characteristics of the broadband loop between the node and the subscriber.

The broadband loop interface can be over one or two twisted copper pairs. Use of two twisted pairs, one for each direction of transmission, provides the greatest flexibility for symmetrical, bi-directional transmission using all of the available bandwidth and relatively simple electronics. Alternatively, a single pair can be used for asymmetrical transmission such that most of the available bandwidth is allocated for downstream transmission and only a small portion for upstream transmission. The latter scheme would require a relatively more complex electronic interface.

An **important** consideration in the design of the electronic interface is to provide a scaleable technology such that the data rate can be adjusted (sub multiple of the STS-1 rate) depending on the quality of the transmission channel. This would allow the possibility to utilise existing copper at a lower data rate for basic broadband service while providing an upgrade path to full bi-directional 52 Mb/s transmission by installing a new broadband cable and drop wire. The new broadband loop can provide up to 10 times the bandwidth of existing outside plant copper for less than 10% of the total cost for providing broadband service to each subscriber (mostly electronics). Given the fact that there are many projects today for new build and for rehabilitation of existing outside plant, the Telco should seriously consider putting in best cable and OP hardware that will be able to deliver the 26 or 52 Mb/s data rates that will be required in the near future.

Fig. 2 illustrates different options for providing voice telephony and broadband service as an overlay to an existing installation.

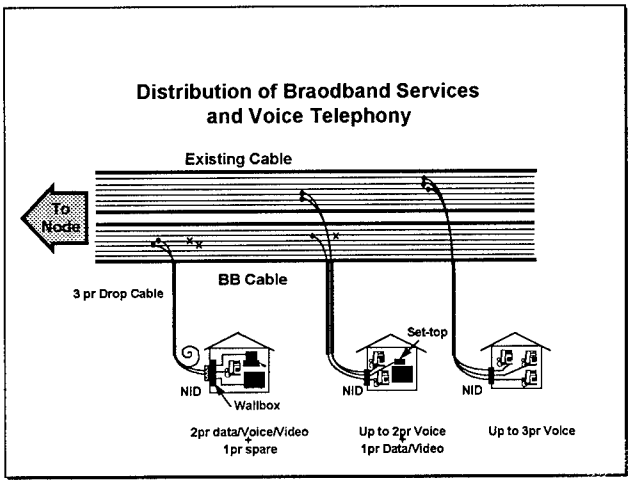


Figure 2

As one option, a home terminal (wallbox) is installed at the residence. The home terminal is linked by two high performance twisted pairs that are dedicated to each residence. The home terminal receives, decodes and processes the ATM signal and provides suitable interfaces for all the services required including voice telephony, ISDN, LAN and broadband video.

Note: The inside wiring is not included as part of the overall channel from the Node to the Wallbox. It can be reused without modification for distribution in the home.

As another option, voice service is provided over existing outside plant cable and drop wire. Interactive broadband video service is provided over a single broadband pair which terminates at the NID and extends to the settop box through the inside wiring. The interactive broadband signal may be combined with the CATV broadcast signal through a passive coupler and fed over an existing 75 Ohm coaxial cable inside the home. The settop box provides all the decoding and control functionality.

The last option represents a subscriber that is not interested in broadband services and is adequately served with three telephone lines over the existing outside plant network.

Channel Performance

The channel is comprised of many elements and includes all the cables, splices, jumpers, connecting hardware and protection devices that are linked together to form a twisted pair circuit between the node and the home terminal. For existing outside plant, it may also include bridge taps where one pair can have multiple appearances at different locations. All these elements can have a significant affect on the transmission performance and the available bandwidth of the channel. The most critical transmission parameter is the **signal-to-noise ratio** at the input to the receiver. Fig. 3 illustrates the sources of **internal** noise due to crosstalk coupling between pairs in the same cable or in close proximity to each other such as connection points.

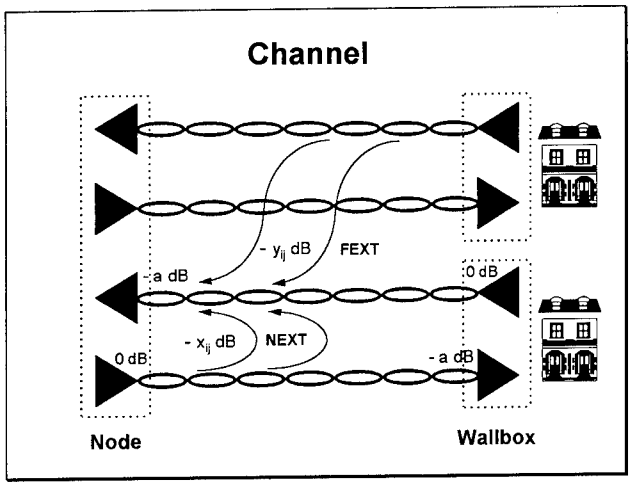


Figure 3

Noise due to Near End Crosstalk (NEXT) coupling between pairs in opposite direction of transmission is usually the dominant form of interference. NEXT is controlling whenever a high level transmit signal (0 dB) is located in close proximity to a low level receive signal (-a dB). Far End Crosstalk (FEXT) coupling between pairs in the same direction of transmission can be equally strong or stronger. However, the noise due to FEXT is attenuated by the time it reaches the far end of the cable and its affect on the receive signal is very much diminished.

There can be many **external** noise sources such as power line interference that can have a significant effect on performance. The effects of external noise are being investigated at different sites and is part of the ongoing work activity

Cable Design

The physical construction of broadband PIC cables is similar to conventional outside plant PIC cables. The cable is comprised of tightly twisted balanced pairs that are assembled into binder groups of 25-pairs and formed into a compact core. The core is fully filled with an EPW (or EPR) compound and enclosed in a bonded Alpeth (or ASP) sheath. The cable dimensions are slightly larger than conventional cables of the same gauge and pair count. Apart from some minor considerations for splicing and terminating pairs, standard practices can be followed for cable installation and maintenance.

Broadband cable is designed to provide at least a 20 dB improvement in signal-to-crosstalk noise ratio compared to conventional outside plant cable designs. Broadband PIC cable also provides a much more controlled impedance compared to standard PIC cables. The Structural Return Loss (SRL) is greater than 30 dB at frequencies up to 10 MHz.

Test Configuration

The performance of broadband PIC cable and broadband drop wire was evaluated by simulating an actual field installation from the jumper wire interface to the protector block at the subscribers premises. The broadband cable connections, patchcords and terminating cables were modified to conform to data cabling installation guidelines. In all other respects, the installation was done in accordance with standard practices by experienced installers. As a benchmark, the same test set-up was duplicated for a standard 26 AWG and a standard 22 AWG loop. The test set-up is illustrated in Fig. 4.

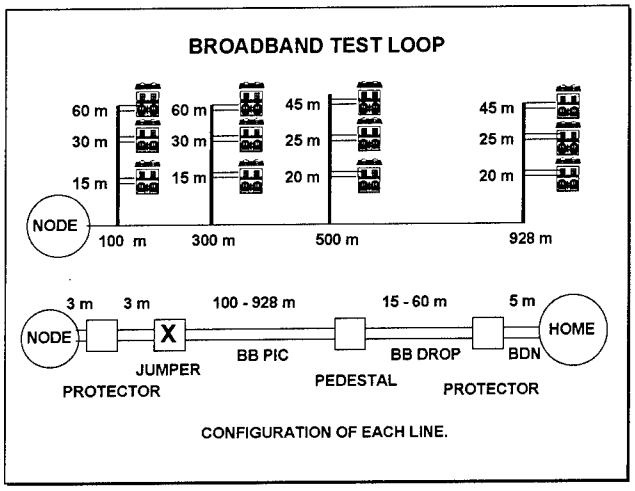


Figure 4

Comprehensive transmission measurements were performed using a network analyser over the frequency range from 300 kHz to 30 MHz from both ends as follows:

- for short and for long loops (100 m to 1 km)
- for short and for long drops (15 m to 60 m)
- for different protectors (solid-state, carbon and gas tube)
- with and without bridge taps
- with different x-connect/termination hardware i.e. binding post, quick clip, ...

Test Results

The Insertion Loss was measured for all pairs. In addition, all pair-combinations of NEXT and FEXT were measured within a 25-pair cable and the power sum calculated. The results for the worst pair power sum NEXT are presented in Fig. 5 and for the worst pair power sum FEXT are presented in Fig. 6. These results apply for a loop length of 1 km with no bridge taps using carbon or gas tube protectors.

The signal-to-crosstalk noise margin (SCR) can be easily observed from Fig. 5 and 6. as the difference in dB between the upper NEXT or FEXT curves and the lower Insertion Loss curves. The frequency at which the two curves intersect is the theoretical upper bound for useful transmission. It is the point at which the crosstalk noise is equal to the signal level at the receiver. The available bandwidth occurs at some frequency less than the upper bound. The required SCR can vary from 6 dB to 26 dB depending on the line encoding scheme and the error rate criteria. The available bandwidth for a 1 km 22 AWG broadband loop is in the range of 8 to 10 MHz compared to a bandwidth of 1.3 to 1.7 MHz for 26 AWG standard loop, i.e. a sixfold increase in bandwidth.

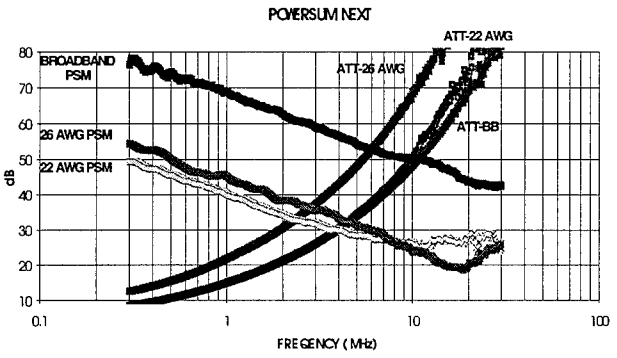


Figure 5

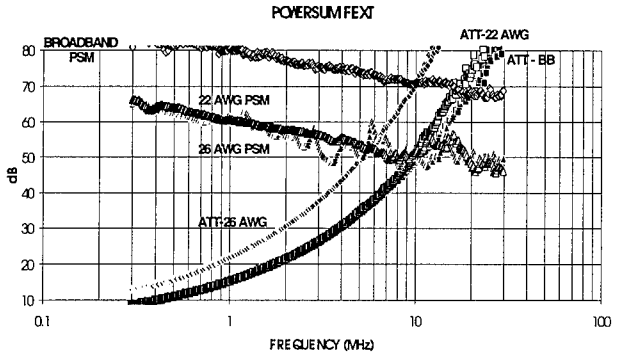


Figure 6

MHz vs. Mb/s

The practical information carrying capacity of a channel is a function of the available bandwidth in MHz, the type of encoding/decoding scheme and the design sophistication of the transceiver electronics. The data modem is a good example to illustrate the efficiency of data transmission. Today, modems are available that can transmit 28,800 bits/s of information in an available voice frequency bandwidth of 4 kHz. This corresponds to a coding efficiency of approximately 7 bits/Hz. Fig. 7 shows the coding efficiency of some of the encoding schemes that are being considered for broadband digital transmission over twisted pair copper. DMT is the most efficient and sophisticated encoding scheme. It packs 12 bits/Hz and was developed for the Asymmetric Digital Subscriber Line (ADSL) which provides up to 6 Mb/s data rate over existing copper. Fig. 7 also shows the required bandwidth for MPEG-2 digital video and the number of MPEG-2 video channels that can be accommodated for an available bandwidth of 10 MHz.

Encoding Matrix

Studio Quality MPEG-2 Video Signal

Line Code	bits/Hz	BW (MHz)	# ch/10 MHz
NRZ	2	3	3
CAP-16	4	1.5	6
64QAM	6	1	10
CAP-64	6	1	10
DMT	12	0.5	20

Figure 7

Observations

A lot of data was generated to characterise the transmission performance of a broadband channel and a standard channel under different conditions. We will only report on some of the more significant observations. For more information, please contact the author.

It was observed that bridge taps contribute to large amplitude variations of the receive signal and are to be avoided for a broadband channel.

There are indications that drop wires with parallel conductors can have a detrimental effect on performance.

The results indicate that the type of protection device can be a significant source of signal impairment at high frequencies. These devices can cause large fluctuations in the measured impedance characteristics of a channel. In particular, protection devices with heat coils showed the greatest impairment.

The results indicated that certain modifications to the packaging of protection hardware or the configuration of terminating cables and connectors can have a beneficial effect on transmission performance at high frequencies.

Simulation Results

The data carrying capacity of the proposed broadband cable was estimated using a simulation software implementing a QAM (Quadrature Amplitude Modulation) transmission system. QAM is used in the simulation because it is a bandwidth-efficient modulation technique that allows two message signals to be transmitted in the same frequency band without mutual interference.

The baseband continuous-time channel model used in the simulation is presented in figure 8. An adaptive LMS equalizer is positioned at the front end of the QAM receiver to combat the distortions such as intersymbol interference caused by the dispersive effects of unshielded twisted pair (UTP) cable, as depicted in figure 8. The QAM modulated carrier a(t) is transmitted through a dispersive channel whose transfer function is modelled by

$$H(s)=\frac{b_0}{a_3 s^3 + a_2 s^2 + a_1 s + a_0}$$

where the coefficients are functions of 4 primary constants (series inductance, series resistance, shunt capacitance and shunt conductance) derived directly from a T-equivalent circuit of a twisted pair. The UTP channel output y(t) is corrupted by noise n(t) due to NEXT and FEXT interference. The received signal is

$$x(t) = y(t) + n(t)$$

whose two components are uncorrelated with each other. The signal x(t) is applied to an adaptive LMS equalizer which is designed to generate an estimate $\hat{a}(t)$ of the original QAM signal a(t) at the transmission end. The estimated signal $\hat{a}(t)$ is then sent to a QAM receiver to recover the transmitted symbol.

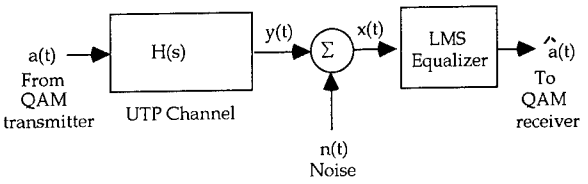


Figure 8. Baseband continuous-time data transmission model

For a one kilometer broadband loop, the available bandwidth is approximately 10 MHz. Therefore, a 16-QAM transceiver was simulated using a carrier frequency of f_c = 10 MHz. Fig. 9 and 10 present the simulated signal constellations for data transmission over 1 km of the broadband cable at bit-rates of 20 and 30 Mb/s. The simulation results for 16-QAM show that at 40 Mb/s, the probability of an error, i.e., the probability of a signal point being moved by noise into an adjacent decision region, is not feasible to support very low BER (bit-error-rate) required in a broadband service. However, the signal constellations in figures 9 and 10 show that the probability of an error is low when the bit rate is between 20 and 30 Mb/s. An error would occur if a sampled data point would move outside the decision threshold region for each cluster. Even though 25.94 Mb/s of broadband service over 1 km of the proposed cable with low BER can be supported using 16-QAM encoding, more efficient line codes may be required to achieve higher bit-rate broadband service (for example 51.84 Mb/s).

We note that these simulations were performed by assuming that the NEXT and FEXT interferences are negligible, and there is no phase jitter with perfect timing recovery. Distortion in the data signal is strictly due to the dispersive effect in the UTP channel. Further work is needed to study the effects when NEXT, FEXT and phase jitters are included in the simulation. Also, the effects of a different equalizer design need to be studied to further optimise performance.

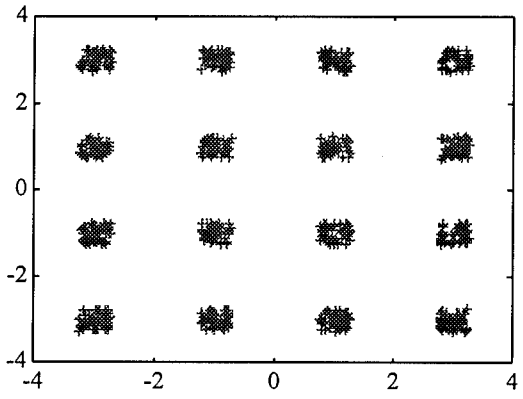


Figure 9. Signal constellations for data transmission over 1 km of broadband cable at 20 Mb/s

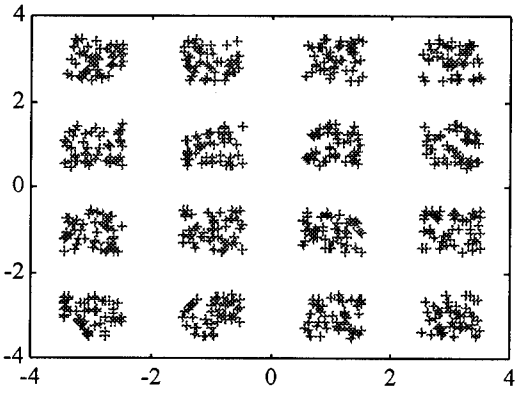


Figure 10. Signal constellations for data transmission over 1 km of broadband cable at 30 Mb/s

Summary and Conclusions

Switched Fiber Twisted Pair (SFTP) architecture effectively addresses interactive broadband requirements by providing high speed switched digital access to information gateways and video service providers.

The key points are as follows:

SFTP infrastructure is supported by optical fiber cable in the backbone and twisted-pair copper for distribution. The Node is located at the Distribution Serving Area (DSA) and contains the common equipment for ATM bandwidth management and plug-in line cards that interface with the twisted-pair copper cabling. The line cards can provide a scaleable data rate from 6.5 Mb/s up to 52 Mb/s depending the quality of the transmission channel.

SFTP supports an evolutionary approach for broadband provisioning. For broadband overlay, existing copper can be used initially to provide basic broadband service at a lower data rate. The cable facilities can be upgraded later as the need for higher bandwidth unfolds in the market. For new build, it makes sense to install the best outside plant copper cable that can deliver the 26 Mb/s or 52 Mb/s data rates that will be required in the near future.

A new broadband PIC cable and drop wire was developed which provides a dramatic improvement in transmission performance. Measurements performed under worst case conditions indicate a minimum 20 dB improvement in the signal-to-crosstalk noise ratio. As a result, there is a six fold increase in available bandwidth compared to standard outside plant cabling.

Biography

Paul Kish received his B.A.Sc. and M.A.Sc. degree in electrical engineering from the University of Waterloo, Ontario in 1971 and 1972 respectively. He is currently a senior manager, PLM for IBDN at NORTEL. His experience with Northern Telecom includes telecommunications cable design, development and product management. Paul is also actively involved in industry standards and committees. He is the current chairman of the TIA TR 41.8.1 working group responsible for the Telecommunications Cabling Standard for Commercial Buildings.

Jon Green graduated from McGill University in 1981 with a B.E. in Electrical Engineering. Jon has worked for NORTEL for the past 14 years, initially in the Research and Development Group in the Lachine, Quebec Plant and currently in the Technology Group in the Kingston, Ontario Plant where he is senior design engineer responsible for the in-building cabling portfolio and electrical test methods.

Tet Yeap received the B.A.Sc. degree in electrical engineering from Queen's University in 1982, and the M.A. Sc. and Ph. D. degrees in electrical engineering from the University of Toronto, in 1984 and 1991, respectively. He is currently an assistant professor in the Department of Electrical Engineering, University of Ottawa. His research interest include transceiver design for high speed digital subscriber loop, design of optical indoor wireless system, optical communications, multi-media, dynamics and control, neural networks, parallel computer architectures and VLSI.

"STUDY OF STRESS ON SELF-SUPPORTING METALLIC CABLE UNDER HIGH MODE GALLOPING OSCILLATION"

Koji Shinmura, Yuji Honda, Yosiki Siba, Fumihiro Asiya

NTT Access Network Systems Laboratories

Abstract

This paper discusses the characteristics of self-supporting metallic cable under galloping oscillation with higher mode, especially the stress on the cable, and proposes countermeasures against the stress.

We observed the high mode galloping oscillation and the damage of cables due to the oscillation in the field test.To estimate the influence of high mode galloping oscillation, we measured the strain on the cables in high mode and compared them with that in low mode.

It is shown that high mode galloping oscillation gives stress to the cable about 2 times more than low mode. The cause and the mechanism of the damage can also be explained based upon the strain measurement results.

For countermeasure, a stress decreasing method by fixing with a cord and application of the cable with stainless steel tape are discussed. It is shown both countermeasures have the effect of preventing cables from the damage.

1. Introduction

Self-supporting metallic cables become so familiar because they cope with material and manpower reduction in construction and improve workability and security, through eliminating cable hanger ring installation onto strand wires for round cables.

Self-supporting cables have a defect that galloping oscillation can easily be made because of its shape, aerodynamically non symmetric cross section. This can cause material fatigue in the cable.

The twisting method has been applied to suppress the galloping oscillation. The critical wind speed, which causes galloping oscillation, can be made higher by twisting, because it diffuses wind force coefficients by changing shape of the cable along the axis.*2)

In addition to the twisting method, the Cable suspension method has been developed (Fig. 1, *1).

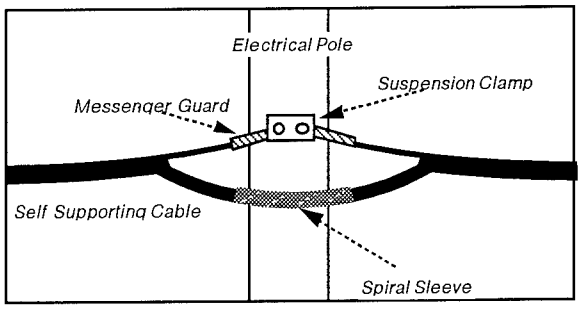


Fig.1 Cable Suspension Method of Self Supporting Cable

After those countermeasures were proved to be effective in the field, the self-supporting cables have been applied to strong wind areas. On the other hand, it is also reported that not only 2nd mode galloping oscillation but also high mode galloping oscillation can cause in these areas. We also have observed 5th to 7th mode galloping oscillation in the field, as shown in Fig. 2.

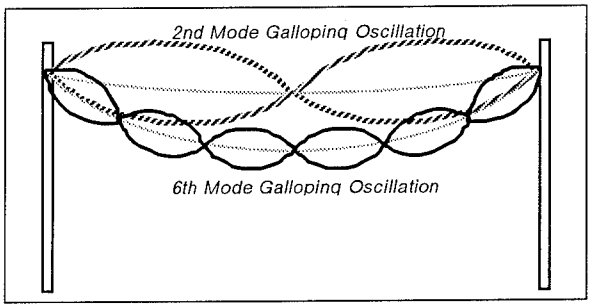


Fig.2 Galloping Oscillation with Low and High Mode

In this paper, we discuss the stress on the self-supporting cable in high mode galloping oscillation. The high mode galloping oscillation is shown to give stress to the cable about 2 times larger than that in 2nd

mode. It is shown that this large stress causes a crack of an aluminum tape in strong wind areas.

Based on the result, this paper proposes a stress decreasing method where the cable and the messenger wire are bound with a cord at the edge of the messenger guard. This method can be proved, in the laboratory test, to decrease maximum stress on the cable.

It is also proposed that a stainless steel tape is used in place of an aluminum tape because the elastic limit stress of stainless steel is 3 times larger than that of aluminum.

2. Stress Under High Mode Galloping Oscillation

We estimate conducted both laboratory and field tests. In laboratory tests we analyzed characteristics of strains on cables. We conducted field tests to observe the condition of galloping oscillation in the field and to estimate the effect of the stress decreasing method.

2-1. Laboratory Test

2-1-1. Test Conditions and Samples

We simulated galloping oscillation using the experimental equipment as shown in Fig. 3, where we can gallop cables in 2nd mode of 36m wavelength and 6th mode of 12m wavelength.

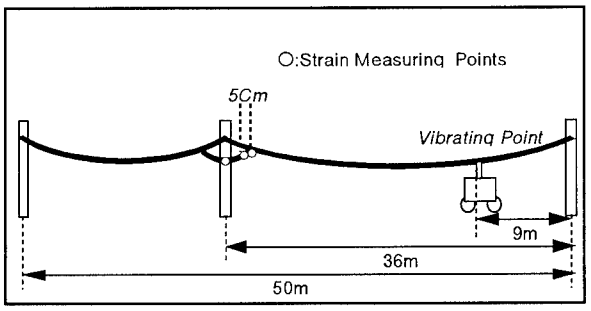


Fig.3 Experimental Equipment

We measured the strain of cable under various amplitudes of oscillations. The strains were measured at the points in a separated part, the ripped end, 5cm far from the end and the middle of the separated part. (Fig.3) We measured the maximum strain of cables laid with the cable suspension method and countermeasures.

We measured strains on the self-supporting cables shown in Table 1. Cables with an aluminum tape and with a stainless steel tape were tested so that a relationship between material and the damage due to galloping oscillation could be discussed.

Table 1

	Cable with Aluminum Tape in Jacket	Cable with Stainless Steel Tape in Jacket
Cable Diameter (mm)	11.0	16.0
Cable Weight (kg/m)	0.27	0.45
Thickness of Tape(mm)	0.20	0.12

2-1-2. Cable laying Conditions

Cables were laid with a standard dip in NTT and a smaller dip to estimate dip-dependence of stress.

From some experimental results, it is known that the maximum stress at the edge of separated part can be moved to the other point and be decreased when the cable and the messenger wire are fixed between the suspension clamp and the ripped point.

Considering the reduction of the maximum stress in the separated part, we measured strains in two cases ; (1)Cables were fixed onto a pole by the cable suspension method, and (2) a new method proposed in Fig. 4.

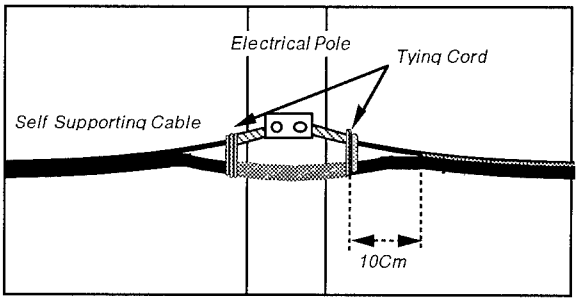


Fig.4 Stress Decreasing Method

The cable and the messenger wire are bound with a tying cord at the edge of the messenger wire. The proposed method is called the stress decreasing

method hereafter.

2-2. Field Test

Field test was conducted in Hokkaido, where is well known as strong wind area in Japan. Tested cables were laid in two routes as shown in Fig. 5.

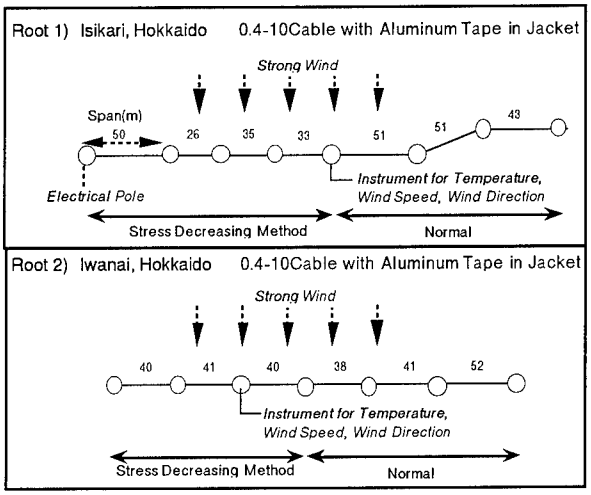


Fig.5 Field Tests in Hokkaido

A cable with aluminum tape were laid with the cable suspension method for 8 months. Another cables with aluminum tape were laid with the cable suspension method and the stress decreasing method for 4 months.

We observed the galloping oscillation phenomenon and the amplitude of the oscillation in winter. In April, we investigated the appearance of cables at the separated part.

3. Experimental Results

3-1. Laboratory Test

3-1-1. The strain in the separated part

Strains on cable with aluminum tape in a small dip are shown in Fig. 6. The standard dip is 0.31m to a span of 36m. We adopt the dip of 0.23m as the smaller dip.

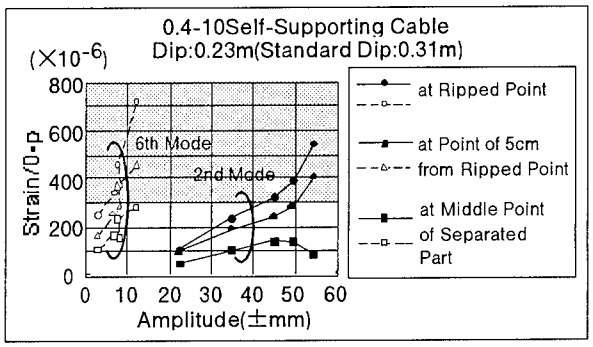


Fig.6 Cable strain on Points in the separated part with Smaller Dip

In Fig. 6, it is shown that strain are decreasing along the cable to the middle of the separated part, and the strain at the ripped point is over 300×10^{-6}, the elastic limit strain of aluminum, in larger amplitude of 2nd and 6th mode.

It is also shown galloping oscillation in 6th mode with small amplitude makes larger strain than in 2nd mode.

3-1-2. Cable with Stainless Tape in Jacket

To avoid breaking of an aluminum tape within the cable jacket, it is necessary to use another metal which has large elastic limit strain. Thus, we examine a cable with stainless steel tape in its jacket.

Maximum strain of cables with aluminum tape and with stainless steel tape in 2nd mode and 6th mode are shown in Figs. 7-1 and 7-2.

-2nd Mode

Strain of cable with stainless steel is as same as that of cable with aluminum tape in standard dip. In smaller dip of 0.23-0.25m, strain of cable with aluminum tape rises up over 300×10^{-6} as amplitude becomes larger than 30mm(0-p) . The strain of cable with stainless steel tape can not reach to 1500×10^{-6}, which is the elastic limit strain of stainless.

-6th Mode

Strain of cable with stainless steel tape are less than the elastic limit strain of stainless steel in both dips.

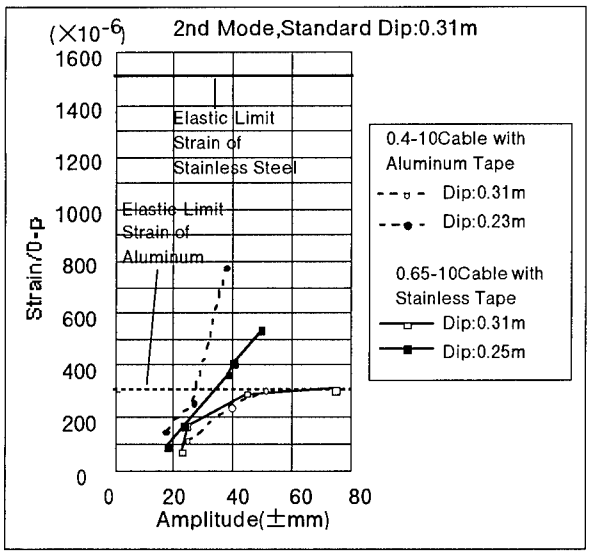


Fig.7-1 Strain at Ripped Point of Both Cable with Stainless Tape and Cable with Aluminum Tape (2nd Mode)

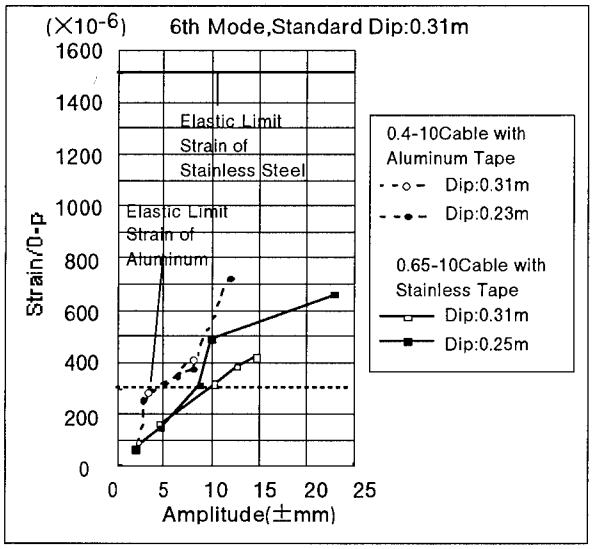


Fig.7-2 Strain at Ripped Point of Both Cable with Stainless Tape and Cable with Aluminum Tape (6th Mode)

3-1-3. Strain and Dips

Relationships between strain and dip are also shown in Figs. 7-1 and 7-2.

In 2nd mode oscillation, strain increases in smaller dip. In 6th mode, strain in smaller dip is almost same as that in standard dip.

3-1-4. Stress Decreasing Method

The strain of cables with the cable suspension method (normal method in Fig. 8-1) and the stress decreasing method (tying cord method in Fig. 8-1) are shown in Figs. 8-1 and 8-2.

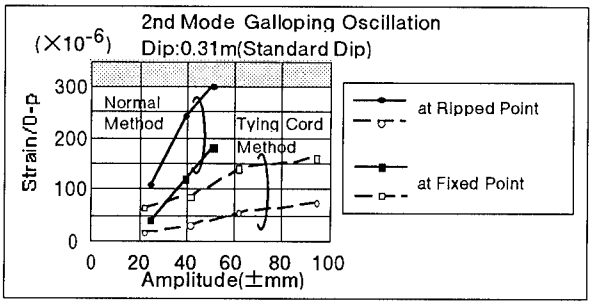


Fig.8-1 Strain on Cable with "Stress Decreasing Method"(2nd Mode)

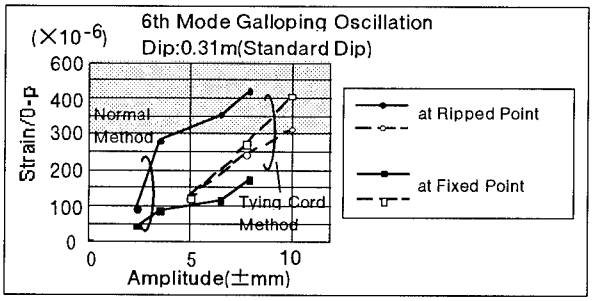


Fig.8-2 Strain on Cable with "Stress Decreasing Method"(6th Mode)

In the normal method, strains are measured at the ripped point and the point of 10cm apart from the ripped point.

In the normal method, strain at the ripped point is larger than that at the point of 10cm in both 2nd and 6th mode.

In the stress decreasing method, strain at the ripped point is smaller than that at the fixed point in both 2nd and 6th mode. Strain at the fixed point in the tying cord method is smaller than that at the ripped point in the normal method. Thus, maximum strain can be decreased by using a tying cord in both 2nd and 6th mode.

Strains at the ripped point and fixed point decrease to less than 300×10^{-6} in 2nd mode. In 6th mode, strain at the fixed point is smaller than 300×10^{-6} in the region of amplitude under 8mm(0-p) .

3-2. Field Test Results

We observed high mode (5th to 7th) galloping oscillations in every cable laid in field test routes. Amplitude of galloping in high mode were 10mm(0-p) .

A cable laid for 8 months suffered the damage. Jacket and aluminum tape are cut in ring at the ripped point. Cables laid with the cable suspension method also suffered the damage. Cracks were observed in aluminum tape at the ripped point of an electric pole. However, cables laid with the stress decreasing method did not suffer any damage.

4. Discussion

4-1. Cable Damage due to High Mode Galloping Oscillation

From the field test results, high mode galloping oscillation can be observed in strong wind areas. High mode galloping oscillations have amplitudes of 10mm(0-p). At the amplitude of 10mm(0-p) in 6th mode, by the laboratory test, strain of the cable with aluminum tape laid with the cable suspension method is shown to be larger than the elastic limit strain of aluminum at the ripped point.

Thus, high mode galloping oscillation, at first, causes a crack of aluminum tape at the ripped point, where the maximum strain over the elastic limit strain is measured in the laboratory test. Then the crack of aluminum tape impairs the cable jacket and the jacket is cut.

4-2. Stainless Steel Tape

From the laboratory test results, strains of the cable with a stainless steel tape laid with the cable suspension method are less than the elastic limit strain of stainless steel, which suggests that the cable with a stainless steel tape will not suffer the damage.

4-3. The stress decreasing method

We proposed the stress decreasing method in Fig. 4. The strain of the cable laid with the method is shown by the laboratory test to be less than the elastic limit strain of aluminum in 6th mode galloping oscillation of amplitude under 8mm(0-p). Therefore, even if the high mode galloping oscillation with amplitude under 8mm(0-p) occurs, a cable with an aluminum tape will be prevented from the damage when the cable is laid using the stress decreasing method.

In the field tests, the cables laid with the method did not show any cracks in both cable jacket and aluminum tapes at the ripped points. The proposed method can be effective to some extent.

5. Conclusion

The high mode galloping oscillation can be observed in the field. Some cables with an aluminum tape have suffered the damages.

We clarify the characteristics of strain on self-supporting cable both in low mode and high mode by the laboratory test. Maximum strain in high mode is larger than that in low mode. This result suggests that galloping oscillation in high mode can give more critical influence than that in low mode.

From the field and laboratory tests, the cause and the mechanism of the cable damage due to high mode galloping oscillation can be explained.

For countermeasures against the damage, we propose cable with stainless steel tape instead of aluminum tape. It is experimentally shown that strain of cable with stainless steel tape is less than 1500×10^{-6} in both 2nd and 6th mode, which suggests those cables will not suffer damage due to high mode galloping oscillation.

We also propose the stress decreasing method using a tying cord which is a easy and cost effective method. In the field tests, the method can be prevent the cable from the damage to some extent.

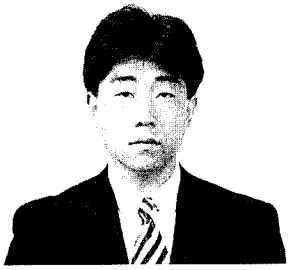
6. Acknowledgements

The authors wish to gratefully acknowledge the cooperation of engineers at Sapporo and Otaru Branches and Hokkaido Technical Center, NTT Hokkaido Telecommunications Service Region.

References

*1) M. Iwazaki, K. Katagiri, A. Sekiguchi, S. masaki "Theoretical Analysis and Reductional Countermeasure of Dancing Phenomena on Self-Supporting Cable" Proc. of 29th I.W.C.S. p.432-437(1980)

*2) T. Kawanabe, S. Matsuhasi, I. Fujibayasi "Aerodynamic Force of Aerial Cables" Proc. of 40th I.W.C.S. p.172-177(1991)



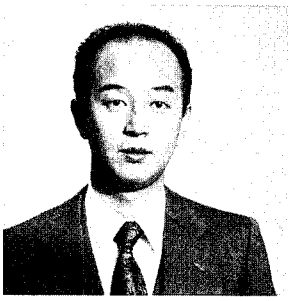
Koji Shinmura
NTT Access Network Systems Laboratories
1-7-1 Hanabatake, Tsukuba-city, Ibaraki, 305 Japan

Koji Shinmura received his B.E. and M.E. degrees in electrical engineering from Osaka University in 1990 and 1992. He joined NTT in 1992. He is engaged in the development of copper cables at NTT Access Network Systems Laboratories, Japan.



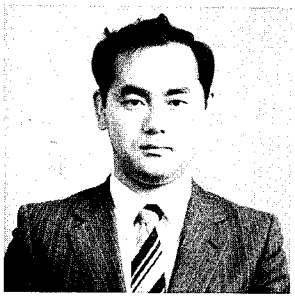
Yuzo Honda
NTT Access Network Systems Laboratories
1-7-1 Hanabatake, Tsukuba-city, Ibaraki, 305 Japan

Yuzo Honda is an Engineer at NTT Access Network Systems Laboratories.
He received his B.E. degree in economics from Hokkai Gakuen University in 1975. He joined NTT in 1969. He is engaged in the development of copper cables.



Yoshiki Siba
NTT Access Network Systems Laboratories
1-7-1 Hanabatake, Tsukuba-city, Ibaraki, 305 Japan

Yoshiki Siba is Senior Engineer at NTT Access Network Systems Laboratories.
He received his B.E. and M.E. degrees in electrical engineering from Electric Communication University in 1981 and 1983. He joined NTT in 1981. He is engaged in the development of copper cables at NTT Access Network Systems Laboratories, Japan.



Fumihiro Asiya
NTT Access Network Systems Laboratories
1-7-1 Hanabatake, Tsukuba-city, Ibaraki, 305 Japan

Yoshiki Siba is Senior Research Engineer at NTT Access Network Systems Laboratories.
He received his B.E. and M.E. degrees in electrical engineering from Waseda University in 1971 and 1973, respectively. Since joining Electrical Communication Laboratories of NTT in 1973, he has been engaged in research and development of submarine coaxial cables, optical fiber cables, optical connectors and copper wires.

RECENT ADVANCEMENTS IN COAXIAL CABLE DESIGN

Henry D. Pixley

CommScope Inc., General Instrument
Catawba, NC 28609

ABSTRACT

Hybrid Fiber/Coax (HFC) architectures are being deployed as a low cost, broadband solution for the delivery of video, voice and data services to and from the home. In order to increase the reliability/survivability and powering performance of the coaxial cable network, new advancements have been made in the design and development of coaxial cable transmission lines.

This paper presents the design and performance of smooth wall copper coaxial cables with significantly enhanced electrical, mechanical and corrosion performance. In addition to affording a superior connector/cable system, this design also exhibits lower cost, weight and attenuation as well as improved Structural Return Loss (SRL) or Voltage Standing Wave Ratio (VSWR) and phase stability compared to conventional corrugated coaxial cables.

INTRODUCTION

Today's telecommunications systems are quickly evolving into full service networks with the deployment of HFC architectures. These networks, due to their providing life-line services, such as telephony, will demand system reliability/survivability and powering performance.

In the HFC architecture, fiber is used as the backbone for the two-way delivery of signal to and from the central office or headend to the serving node, where the optical to electrical conversion takes place. Coaxial cable is then used for the two-way delivery of signal along with the transmission of power from the serving node to the Customer Interface Unit (CIU) located on the side of the home.

It is because of this high level of required reliability that many of the networks are being designed to provide network powering to the home. In order to increase network powering reliability, however, centralized powering schemes are being deployed as opposed to distributed powering schemes. In other words, one centralized power supply will service a single node, where one node typically serves 500 homes with four distribution coaxial cables leaving a node, one distribution coaxial cable per quadrature (see Figure 1).

Powering schemes being considered, and in some networks deployed, include 90V/60Hz, 90V/1Hz and minus 90V/DC. Maximum current levels placed on the coaxial cable are limited by the current passing capability of network components and are around 12 Amperes. The power is inserted onto the inner and outer conductors of the coaxial cable and delivered to the network load which includes both coaxial cable components and CIU's located on the side of the home.

It is both the centralization of power supplies and the fact that the network be required to provide power to the home that have introduced new powering requirements for coaxial cables. These network requirements have increased the distance, therefore, resistance between source and load as well as the currents found on the coaxial cable. This increase in both resistance and currents results in an increase in the IR voltage drop between source and load, therefore, limiting the reach of voltage out into the network. The increase in currents also creates great concern regarding corrosion and, therefore, reliability/survivability within the coaxial cable network.

It is these powering and reliability/survivability issues that have initiated the design and development of new coaxial cables. This paper presents the design and performance of smooth wall copper coaxial cables with significantly enhanced electrical, mechanical and corrosion performance.

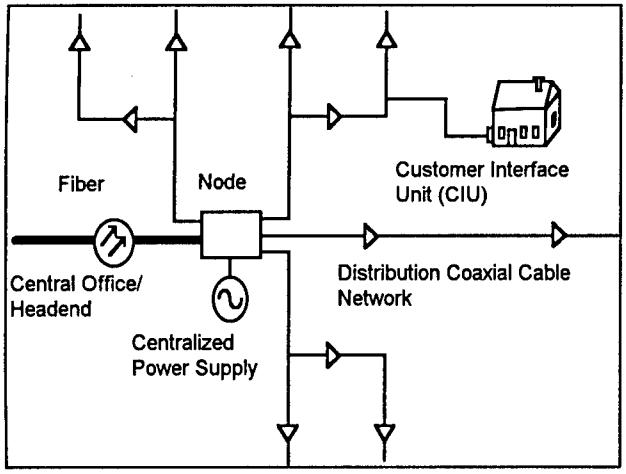


FIGURE 1.
Hybrid Fiber/Coax (HFC) Architecture

DESIGN CONSIDERATIONS

The design of a coaxial cable is ultimately governed by its application and the environment in which it is used in. This section reviews design considerations pertaining to coaxial cables used within the HFC architecture.

Reliability/Survivability Improvements

The reliability/survivability of the coaxial cable network is primarily a corrosion issue, within the buried plant. Corrosion protection has become of increasing concern for the HFC network, due to the fact that the coaxial cable network will be seeing greater levels of current than have been traditionally found within broadband type plants; and the fact that these networks, due to their providing life-line services, will demand system reliability/survivability.

The two basic forms of corrosion found within the buried plant include both galvanic corrosion which occurs between dissimilar metals at the connector and cable interface and between the outer conductor of the coaxial cable and ground soil, in the event that the outer conductor becomes exposed. These mechanisms of corrosion occur due to the presence of an electrolyte and become accelerated with increasing levels of current found on the coaxial cable.

In order to provide enhanced corrosion protection of the coaxial cable, copper alloy is used as a continuous non-overlapping outer conductor material as opposed to aluminum alloy, which has been traditionally used within the CATV industry. The word continuous is used to indicate that the outer conductor is both mechanically and electrically continuous about its length and circumference. This design provides superior performance, both environmentally and electrically by preventing moisture from entering the cable as well as providing superior RF shielding performance.

Copper alloy used as an outer conductor significantly reduces the effects of galvanic corrosion which might take place between dissimilar metals found at the connector and cable interface and between the outer conductor and ground soil. The connector and cable system will, therefore, consist of galvanically friendly materials such as the connector being brass or nickel/tin plated brass in contact with the copper coaxial cable. A Medium Density Polyethylene (MDPE) jacket is then used to protect the coaxial cable's outer conductor during and after installation. Corrosion inhibitors can also be used between the outer conductor and jacket and are optional to provide added protection.

It is the use of copper alloy as an outer conductor material which provides significantly enhanced corrosion protection compared to aluminum coaxial cables. This enhanced corrosion protection, in turn, provides increased reliability/survivability of the coaxial cable network.

Powering Transmission Improvements

The powering transmission performance of the coaxial cable network is primarily a dc loop resistance issue. Both the centralization of power supplies and the fact that the network be required to provide power to the home, have increased powering requirements for coaxial cables. These network requirements have increased the distance and, therefore, resistance between source and load as well as currents found on the coaxial cable. This increase in both resistance and currents results in an increase in the IR voltage drop between source and load, therefore, limiting the reach of voltage out into the network.

When using the coaxial cable for the transmission of power, a low dc loop resistance between source and load is required, in order to reduce voltage drops, therefore, increasing the reach of voltage further out into the network. The dc loop resistance circuit between the source and load is largely dependent on the dc loop resistance of the coaxial cable which is

the sum of the inner and outer conductor dc resistances, expressed in Ohms/1000ft at 68 °F.

In order to cost effectively design a coaxial cable with minimum dc loop resistance, several factors must be considered. First, the RF attenuation and characteristic impedance of the coaxial cable are usually already set for a given size coaxial cable and application. For the present application the characteristic impedance is 75 Ohms and the outer conductor material is of continuous copper alloy to provide enhanced corrosion protection along with superior RF shielding performance. For the purpose of this demonstration the coaxial cable will be 1/2" in size.

The next major design parameter is the selection of the dielectric medium to be used to separate the inner and outer conductors coaxially. The selection can usually be narrowed down to foamed polyethylene, air dielectric (bamboo style, helical construction or longitudinal tubes) and solid polyethylene. Solid polyethylene increases attenuation and cost for large size coaxial cables. The helical and longitudinal air dielelectrics do not prevent water penetration while the bamboo style does not provide uniform compressive stiffness along the length of the coaxial cable, therefore, reducing mechanical performance. Foamed polyethylene appears to be the optimum choice, due to its combination of good electrical and mechanical performance along with its prevention of moisture migration, processibility and low cost.

It, therefore, makes sense to use a low loss, low density closed cell foamed polyethylene dielectric. Low densities of around 0.2 g/cc are standard with today's technology. Low densities result in low dielectric constant and high velocity of propagation, allowing the designer to use a larger size center conductor, in order to maintain impedance. This results in lower attenuation and dc loop resistance. The attenuation is reduced two fold, first by reducing the amount of lossy dielectric material within a given volume and second, the cross sectional area of the center conductor RF current path is increased. Low RF attenuation allows the network designer to maximize the distance between amplifiers and minimize network costs. The center conductor dc resistance is also reduced, due to increasing the center conductor's cross sectional area. Being able to add material to the center conductor has significant advantages. First, for standard aluminum 75 Ohm coaxial cables, the center conductor contributes approximately 70% of the total dc loop resistance. Second, adding material to the outer conductor adversely affects the cable's mechanical handling performance without enhancing its RF electricals, such as attenuation. For these reasons the present coaxial cable design will utilize the low loss, low density closed cell foamed polyethylene dielectric.

The cable designer, when selecting center conductor material, usually has the choice of either copper clad aluminum (10% Cu by volume) or solid copper, where there is a trade off between resistivity and cost (see Table 1).

Material	Resistivity, Ohm-Meters at 68° F
CuAl (10% Cu by Volume)	2.68×10^{-8}
Solid Copper	1.72×10^{-8}

TABLE 1. - Material Resistivity

When deciding whether to use CuAl or solid copper for the center conductor, it should be noted that the change in center conductor resistance, due to a change in the material's resistivity is inversely proportional to the center conductor's cross sectional area. This can be seen from equation 1.

$$\Delta R = \frac{\Delta\rho \cdot l}{a} \qquad \text{(Eq. 1)}$$

where,

R is the resistance, Ohms/1000m
ρ is the resistivity, Ohm-meters
a is the cross sectional area, sq. m.
l is the length, meters

Therefore, due to the 1/2" size 75 Ohm coaxial cable having a center conductor of small cross sectional area and because dc loop resistance is such an issue, the present coaxial cable design will utilize a solid copper center conductor.

It is also interesting to note that an optimum relationship exists between the inner and outer conductor cross sectional areas of the coaxial cable design, in order to obtain the lowest possible dc loop resistance for a given amount of material. This can be seen from Equation 2.

$$DCLR = \frac{\rho_{ic} \cdot l}{a_{ic}} + \frac{\rho_{oc} \cdot l}{a_{oc}} \qquad \text{(Eq. 2)}$$

Where,

DCLR is the dc loop resistance, Ohms/1000m
ρ_{ic} is the resistivity of the inner conductor, Ohm-m
ρ_{oc} is the resistivity of the outer conductor, Ohm-m
a_{ic} and a_{oc} are the cross sectional areas of the inner and outer conductors respectively, sq. m.
l is the length of the coaxial cable, meters

For the present coaxial cable design, because both the inner and outer conductors are of the same material ($\rho_{ic} = \rho_{oc}$), equation 2 reduces to:

$$DCLR = \left(\frac{a_{ic} + a_{oc}}{a_{ic} \cdot a_{oc}}\right) \cdot (\rho_{ic} \cdot l) \qquad \text{(Eq. 3)}$$

From looking at equation 3, it can be seen that, in order to optimize the coaxial cable design to obtain the lowest possible dc loop resistance for a given amount of material, the inner and outer conductor cross sectional areas should approach equalness ($a_{ic} = a_{oc}$). Figure 2 shows the increase in DCLR vs difference in inner and outer conductor cross sectional areas.

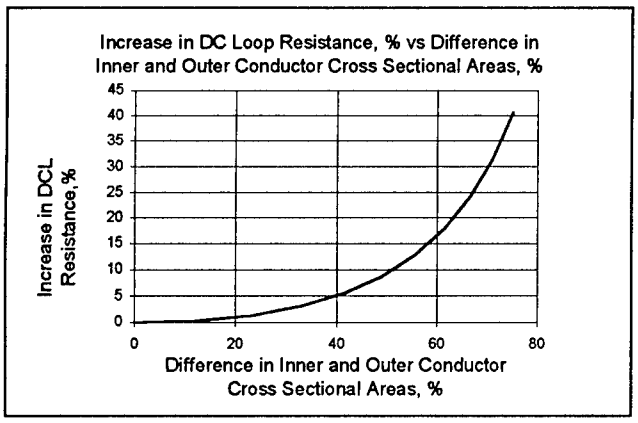


FIGURE 2.
Increase in DCLR vs Difference in Inner and Outer Conductor Cross Sectional Areas

Although it is not always possible to fully meet this design criteria, it is however important that the other coaxial cable design parameters help aid in approaching this optimization in design. For example, it will be seen later in this paper that the design parameters necessary for achieving enhanced mechanical bending performance and reduced coaxial cable cost also aid in allowing the inner and outer conductors to approach equal cross sectional area.

Finally, a discussion regarding the coaxial cable's characteristic impedance and its affect on dc loop resistance and cost is felt to be both interesting and important. Besides the selection of materials, the coaxial cable's impedance plays a significant role in determining the coaxial cable's dc loop resistance and cost.

In the beginning of this section, the coaxial cable's impedance was set at 75 Ohms, due to its application. However, the coaxial cable's application determines its electrical performance which in turn should determine the impedance (system) of the coaxial cable design. 75 Ohms has traditionally been used to support CATV type applications due to its low attenuation performance. 50 Ohms, on the other hand, has been used for applications such as cellular and broadcast, due to its high RF powering capability at the expense of attenuation. Changing from 75 to 50 Ohms allows the center conductor cross sectional area to be increased considerably, therefore, reducing the overall dc loop resistance of the coaxial cable. Figure 3 shows the change in attenuation and dc loop resistance with a change in the cable's characteristic impedance for the 1/2" copper coaxial cable using a CuAl center conductor.

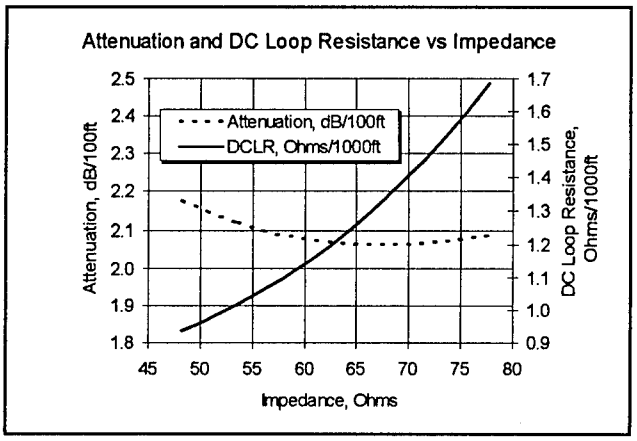


FIGURE 3.
Change in Attenuation (at 1 GHz) and DC Loop Resistance vs Change in Characteristic Impedance
Coaxial Cable Size: 1/2"
Center Conductor: CuAl

From Figure 3, the attenuation is seen to increase less than 4%, while the dc loop resistance is seen to decrease 40%, due to a change in impedance from 75 Ohms to 50 Ohms. The 50 Ohm design using CuAl as a center conductor achieves lower dc loop resistance and lower cost compared to the 75 Ohm

design using solid copper as a center conductor material. This is because the dc resistance/$ value is lower for CuAl than it is for solid copper. It should be noted, however, that the solid copper design provides enhanced corrosion protection of the center conductor at the connector and cable interface. This is due to concerns regarding the center conductor seizure mechanism of the connector biting through the copper surface and exposing the aluminum.

RF Electrical and Mechanical Improvements

The important RF electrical parameters for coaxial cables of this application are of course attenuation and Structural Return Loss (SRL) along with RF shielding performance. The RF shielding performance, however, has already been optimized, due to the selection of a continuous copper alloy outer conductor. The SRL requirement for coaxial cables of today's HFC network is greater than 30 dB (5 - 1000 MHz). The mechanical parameters include minimum bend radius and flexibility, in order to aid in the handling and installation of the coaxial cable along with sidewall compressive strength and pulling tension to endure the rigors of installation. The objective, therefore, consisted of the design and development of a copper coaxial cable which would exhibit electrical and mechanical properties similar to those of aluminum coaxial cables already found within the broadband industry.

Traditionally, within the coaxial cable industry, improvements in bending performance of coaxial cables utilizing continuous outer conductor materials, such as copper alloy, have been achieved by corrugating the outer conductor. While some improvement in the bending performance can be achieved by corrugating the outer conductor, the improvement in performance marginally justifies the expense. Corrugating the outer conductor adversely affects the cable's electrical performance, such as attenuation, SRL and dc loop resistance, while increasing the cost and weight of the coaxial cable. The optimum RF electrical design of a coaxial cable, in fact, consists of both inner and outer conductors being continuous smooth wall surfaces of homogeneous high conductivity material.

Therefore, in order to design the coaxial cable for optimum electrical performance, i.e., without the use of corrugations, such that it would exhibit electrical and mechanical properties similar to those of aluminum coaxial cables already found within the broadband industry, the following design concepts were utilized:

The copper outer conductor is of "O" temper (soft) and its wall thickness considerably reduced in relation to its diameter, in order to reduce its stiffness and force necessary to plastically deform. The low loss, low density foamed polyethylene dielectric core, on the other hand, is of considerably high core stiffness (compression), in order to increase the core to shield stiffness ratio. In doing this, in combination with drawing down the smooth wall tube over the dielectric core and bonding all elements, i.e., center conductor, dielectric core, outer conductor and jacket allows the coaxial cable to behave as a single composite monolithic structure, providing a synergistic effect which significantly improves its mechanical performance. The results are a smooth wall copper coaxial cable with significantly enhanced bending characteristics compared to those of prior smooth wall copper coaxial cable designs.

This concept is based on the recognition that greatly enhanced bending characteristics are achieved by reducing the stiffness of the tubular sheath in relation to the stiffness of the core, such that the core serves a much greater role in contributing to the cable's physical properties. In order to accomplish this, however, it is required that the dielectric core compressive strength be increased without adversely affecting its electrical performance. Figure 4 shows a plot of minimum bend radius vs core to shield stiffness ratio for smooth wall aluminum coaxial cables.

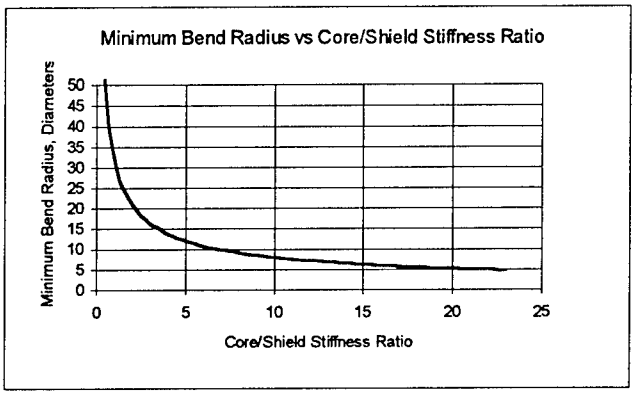


FIGURE 4.
Minimum Bend Radius vs Core to Shield Stiffness Ratio For Smooth Wall Aluminum Coaxial Cables

Figure 4 was obtained from empirical data taken from smooth wall aluminum coaxial cables within the industry. It can be seen that significantly enhanced bending performance can be achieved for core to

shield stiffness ratios greater than five (5) and that the bending performance improves with increasing core to shield stiffness ratios.

Mechanical Tests

Stiffness: The core and shield stiffness ratio is determined by independently evaluating the compressive stiffness of the core (inner conductor and dielectric) and the outer conductor as would be observed from its side. A sample of core and outer conductor of one inch in length are placed within a compressive load chamber and compressed to 12% of their original diameter. The ratio of stiffness is then expressed as the ratio of the measured loads at the 12% deflection point.

Minimum Bend Radius (MBR): The minimum bend radius is measured by bending the coaxial cable over the smallest mandrel of uniform radius such that there are no signs of outer conductor deformation or waviness.

RESULTS AND DISCUSSION

In utilizing these design concepts the smooth wall copper coaxial cables are capable of achieving similar electrical and mechanical performance, along with significantly enhanced corrosion performance compared to standard aluminum coaxial cables within the industry. The smooth wall copper coaxial cables also achieve significantly enhanced electrical performance compared to copper corrugated coaxial cables within the industry. Table 2 shows a performance comparison among 1/2" coaxial cable designs.

Electrical vs Mechanical Performance

There exists a trade-off between electrical and mechanical performance for smooth wall and corrugated coaxial cable designs. While corrugating the outer conductor provides some improvement in flexibility, it also adversely affects the cable's electrical performance such as attenuation, SRL, dc loop resistance and phase stability. Corrugated coaxial cables are typically limited to 20 dB SRL (1.2 VSWR), while smooth wall coaxial cables can achieve greater than 30 dB SRL (1.06 VSWR) from 5 to 1000 MHz. Figure 5 shows a typical SRL measurement for a smooth wall copper coaxial cable.

The choice between smooth wall and corrugated coaxial cable designs is, therefore, governed by the coaxial cable's application. For example, for applications such as HFC networks where electrical and mechanical performance similar to that of standard aluminum coaxial cables are required, the smooth wall copper coaxial cable becomes transparent, due to its having similar electrical and mechanical performance to that of standard aluminum coaxial cables within the industry.

Coaxial Cable Size	1/2" Coaxial Cable			
Coaxial Cable Impedance	75 Ohm		50 Ohm	
Coaxial Cable Design	Standard Aluminum	Copper (Smooth Wall)	Copper (Smooth Wall)	Copper (Corrugated)
Material Specification				
Inner Conductor	CuAl*	Solid Copper	CuAl*	CuAl*
Dielectric	Foamed PE	Foamed PE	Foamed PE	Foamed PE
Outer Conductor	Aluminum (Smooth Wall)	Copper (Smooth Wall)	Copper (Smooth Wall)	Copper (Corrugated)
Physical Specification				
Inner Conductor OD, in.	0.137	0.124	0.201	0.189
Dielectric OD, in.	0.563	0.523	0.523	0.485
Outer Conductor OD, in.	0.625	0.540	0.540	0.47 min./ 0.55 max.
Electrical Specification				
Impedance, Ohms	75	75	50	50
Attenuation at 1 GHz, dB/100ft	2.1	2.1	2.25	2.34
DC Loop Resistance, Ohms/kft	1.10	1.26	1.00	1.03
SRL, dB (Min. from 5 - 1000 MHz)	30 (1.06 VSWR)	30 (1.06 VSWR)	30 (1.06 VSWR)	20 (1.2 VSWR)
Mechanical Specification				
MBR, in.	5	5	5	5
Bending Moment, ft-lbs.	12	9	9	3
Pulling Tension, lbs.	475	600	500	325

* 10% Cu by Volume

TABLE 2. - Performance Comparison Among 1/2" Coaxial Cable Designs

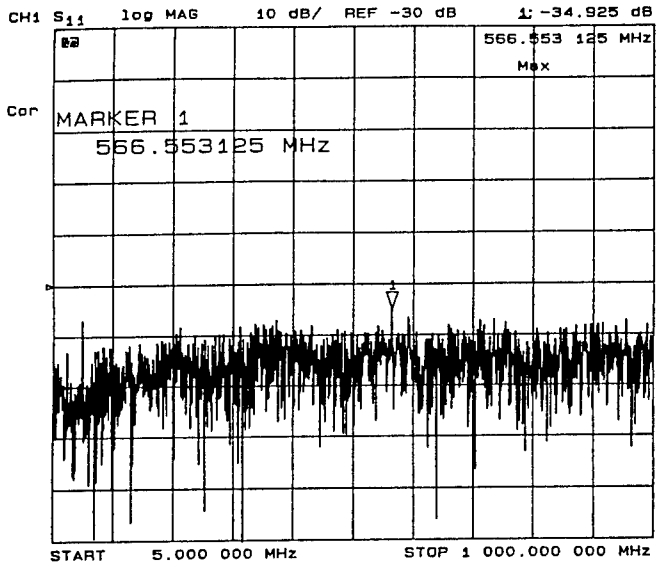


FIGURE 5.
Structural Return Loss (SRL) Measurement of 1/2" Smooth Wall Copper Coaxial Cable

Corrugated coaxial cables, on the other hand, have valid applications, such as for jumper cables, where the flexibility is required and the SRL, attenuation and cost can be tolerated, due to the short lengths.

In fact, in applications requiring long aerial runs where copper corrugated coaxial cables are traditionally used, the reduced flexibility and internal ruggedness of the smooth wall copper coaxial cable design reduces the sag and number of clamps necessary for install, while significantly improving the electrical performance of the network and reducing cost.

Connector and Cable System

The connector and cable system is an integral part of the coaxial cable network and has a significant affect on both electrical and reliability/survivability performance. Figure 6 shows a typical connector and cable system for a smooth wall coaxial cable.

Connector and cable systems of smooth wall coaxial cables have significantly enhanced performance characteristics compared to those of corrugated coaxial cables. Table 3 shows a performance comparison of connector and cable systems for both smooth wall and corrugated coaxial cables.

	Smooth Wall	Corrugated
Installation Performance		
Installation Tools	(1) Coring Tool	Multiple Hand Tools
Installation Time, minutes	2 to 5	5 to 30
Craftsman Variance	Minimum	Maximum
User Friendly	Yes	No
Mechanical Performance		
Seizes Inner Conductor	Yes	No
Seizes Outer Conductor	Yes	Yes
Seizes Jacket	Yes	No
Pull-Off Force, lbs. (Data for 1/2" coaxial cables)	600	250
Electrical Performance		
Return Loss, dB (VSWR) (Data for 5 to 1000 MHz)	40 (1.02)	30 (1.06)
Attenuation, dB max.	0.2	0.2

TABLE 3.
Performance Comparison of Connector and Cable Systems for 1/2" Smooth Wall and Corrugated Coaxial Cables

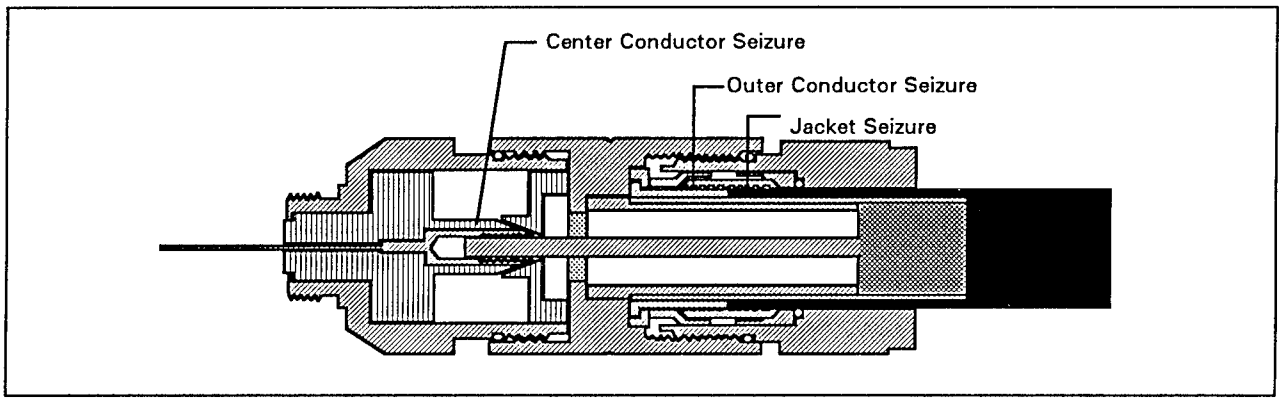


FIGURE 6. - Typical Connector and Cable System for a Smooth Wall Coaxial Cable

The connector and cable system of the smooth wall coaxial cable design is seen to have twice the mechanical pull-off force compared to that of corrugated coaxial cables, due to the connector mechanically seizing all components, i.e., inner conductor, outer conductor and jacket.

FIELD TRIALS

At the time of this writing, the 1/2" and 3/4" smooth wall copper coaxial cables are undergoing a full scale field trial consisting of 2,000 homes.

SUMMARY AND CONCLUSIONS

This paper has presented the most recent advancements in the design and performance of smooth wall copper coaxial cables. The primary conclusions of this work are:

1. Coaxial cables of the present design provide significantly enhanced bending performance compared to that of prior smooth wall copper coaxial cable designs.

2. Coaxial cables of the present design provide significantly enhanced corrosion protection compared to standard aluminum coaxial cables within the industry.

3. Coaxial cables of the present design achieve similar electrical and mechanical performance to that of standard aluminum coaxial cables.

4. Coaxial cables of the present design provide significantly enhanced electrical performance compared to that of copper corrugated coaxial cables within the industry, while reducing cost and weight.

ACKNOWLEDGMENTS

The author would like to extend his sincere appreciation to Mr. Bruce Carlson, Director of R&D, for his support and direction during the writing of this paper. The author also wishes to thank several of his colleagues at CommScope Inc. for the development and manufacture support. Special thanks to Mr. Alan Moe, Senior Research Engineer, Scott Adams, Extrusion Process Engineer and Harold Edwards, Process Development Technician.

Finally, the author is grateful to the management of CommScope Inc. for granting the permission to communicate this paper and supporting its publication.

REFERENCES

[1] "Powering Issues Of Coaxial Cable In HFC Networks", 1995 NFOEC, Bruce Carlson

[2] "Coaxial Cable Having Enhanced Handling And Bending Characteristics" US Patent 4,472,595, Fox et al.

[3] "Powering Study Of Broadband Coaxial Cable Distribution Plants", 1994 IWCS, Henry D. Pixley



Henry D. Pixley
Product Development Engineer
CommScope Inc.
General Instrument Corporation
6519 CommScope Rd.
Catawba, NC 28609

Henry graduated from SUNY New Paltz, NY with a Bachelor of Science in Electrical Engineering in 1991 and joined Cablewave Systems, Div. of Radio Frequency Systems, CT. There he designed and developed a line of radiating coaxial cables for the North American market.

He joined CommScope Inc. in the beginning of 1994 and is responsible for the design and development of new coaxial cable transmission lines for the telecommunications Industry. He is also a member of the Society of Cable Television Engineers (SCTE).

The Sag Behaviour of Aerial Service Wires Using Different Wedge Clamps

J.- H. Walling[1], J. Druez[2], C.-T. Nguyen[3] and J. Bilodeau[2]

[1] Nortel (Northern Telecom Canada Ltd.)
[2] University of Quebec at Chicoutimi
[3] Bell Canada

Abstract

The performance of wedge clamps for glass fiber reenforced aerial service wires has been evaluated with respect to their contribution to the sagging of aerial wire spans. It has been demonstrated that the clamps contribute substantially to the sagging of the wires, and that some design changes of the clamps are required. This seems to be especially important if the wires are used for road crossings, in order to avoid damage by trucks. Small design changes of the clamps will effectively reduce the impact of the clamps upon the sag.

The elasticity of the wires themselves also contribute to a sag increase. We found, however, that these sag increases are small compared to copper clad steel reenforced wires. Our results indicate that thermally induced sag increases cannot be neglected. Thermally induced sag increases may be reduced by using reenforcing material with lower linear expansion coefficients.

Our data suggests, furthermore, that it is advantageous to use bail eyelets to prevent the deformation of the bail over the drive hook or the "bull's-horn", and thus to decrease the effective length increase on the span, and, therefore, also the sag.

Introduction

The installation practices for aerial service wires require the use of wedge clamps. Wedge clamps serve to suspend the service wire from the pole line to the customer premises or occasionally between poles on road crossings.

Initially wedge clamps were made from copper alloys. Later on, the clamp material was changed to aluminum alloys and to stainless steel. More recently plastic clamps have also been introduced.

Originally the wedge clamps were designed for single pair self supporting copper clad steel reenforced aerial service wires. The design of these wires was based upon a common insulation layer, which was covered by a textile braid. An outer jacket was provided for the mechanical long term protection of the wire. These service wires have poor electrical transmission characteristics rendering high speed data transmission difficult and restrict link length.

Over time the jacket, the braid and the insulation were replaced by a single layer of material used as insulation and jacket simultaneously.

Modern aerial service wires for single dwellings have two copper pairs. This is necessary to cope with an increasing dual service line demand combined with higher transmission performance requirements. These wires have a glass fibre reenforcement. The development and introduction of such wires has been initiated originally in Germany by "Lynen Werke". Later on, similar designs appeared also in North America. To date, this design concept has been generally accepted and deployed globally.

Though wedge clamps may vary slightly in their design, their working principle is identical. The clamps use a wedge, which progressively tightens the wire under increasing load. The tightening of the clamps is coupled with a displacement of the wire and the wedge with respect to the suspension point. Therefore, the progressive tightening yields a length contribution to the wire on the span.

Rationale

Two pair wires were designed to match the existing hardware, hence, the same wedge clamps that were developed for single pair aerial service wires. However, the suitability of these clamps for the new glass fibre reenforced wires has not yet been assessed. It is interesting, in this context, to remind that a corresponding Bellcore specification covers only wedge clamps for single pair aerial service wires [1]. These requirements are not extended to clamps for two pair wires.

It is therefore the objective of this paper to investigate the behaviour of wedge clamps in conjunction with glass fibre reenforced aerial service wires. To this purpose

wedge clamps from different suppliers have been investigated.

The scope of the present paper is the evaluation of the clamp performances upon the sagging behaviour of conventional service spans only. The significance of the results for non-standard applications is not covered.

As a baseline comparison of the clamps influence upon the sag of different spans we assume an inelastic wire. We then focus upon the additional sagging due to the slightly higher elasticity of glass fibre versus copper clad steel reenforced aerial service wires.

We will see that the frequently expressed impression of higher sags of glass fibre reenforced aerial service wires versus those with a copper clad steel reenforcement is primarily a result of the clamps and their relatively poor performance in conjunction with glass fibre reenforced service wires.

Finally we try to derive some conclusions for an improved wedge clamp design which is better suited for the modern service wires.

Description of Wedge Clamps and Wires Investigated

We selected six clamp types from four different suppliers. In Table I are listed some design characteristics of the clamps investigated.

Clamp Type	Material			
	Shell	Shim	Wedge	Bail
A	Aluminum	Aluminum	Aluminum	Stainless Steel
B	Stainless Steel	Stainless Steel	Stainless Steel	Stainless Steel
C	Aluminum	Aluminum	Aluminum	Stainless Steel
D	Stainless Steel	Stainless Steel	Stainless Steel	Stainless Steel
E	Stainless Steel	Stainless Steel	Stainless Steel	Stainless Steel
F	Stainless Steel	Plastic	Stainless Steel	Stainless Steel

Table I : Description of clamp types investigated

Methodology and Measurements

To quantify the performance of the clamps, we used a tensile testing machine. The clamp wire combination were attached to the cross heads with drive hooks. Drive hooks are used in outside plant installations to suspend the span. They were used here, to obtain the real life deformation of the bails while they form under tension around the drive hook. Thus we obtained the impact of the bail geometry upon the sagging characteristics. However, a separation of the crimp yielding between bail and wedge and the bail wire deformation itself could not be obtained in our measurements. Detailed results are compiled in two detail reports. [2];[3]

Small metal angles were glued to the wedge and the shell of the clamps. The displacement of these angles was measured with linear displacement transducers relative to the suspension point (see Fig. 1), while at the same time recording the load on the clamp/wire combination. The data were collected with an acquisition system. The speed of the crosshead of the tensile tester was set to 0.2 inch/min (5.08 mm/min). The trials were carried out at room temperature.

The analysis of very old spans with copper alloy clamps, recently replaced, yielded the condition of the wires with a shape stabilizing braid inside the jacket. The wires showed hardly any deformation. Therefore, the clamps did not contribute to the sag increase through excessive displacement of the shell over the shim. Analysis of different glass fiber reenforced aerial service wires showed a much larger deformation of the wires in the clamp area as shown in Fig. 2 (flattening of the wire in the clamp). These conditions were the same as those obtained after static load tests at slightly raised temperatures over several days.

After a static load test at elevated temperature, the wire fills out the entire space between the shell and the shim, i.e. the clamp deformation will be at its maximum. This represents closest the equilibrium condition of a suspended wire span, after several years under cycling temperature and load conditions.

Hence this long term effect can be simulated using a static load test. The static load tests were carried out with a load of 365 lbf at 35 °C for 5 days.

The wires were tested in the tensile tester using a precision extensometer in order to assess the elastic properties of the wires upon the sag of a span. This tensile testing has been made, starting with a pre-load of 200 N at a cross head speed of 0.2 inch/min (5.08 mm/min) under load cycling conditions. This permits the measurement of the cable elasticity upon loading and also the residual elongation upon unloading.

Fig. 3 shows the stress-strain curve of this wire. Upon cyclic loading and unloading, glass fiber reenforced service wires show in their load deformation curve an hysteresis, yielding a residual elongation. The residual elongation is generally temperature and time dependent, and is subject to a recovery through relaxation.

We checked the sensitivity of the cross section of the wire upon the performance of the individual clamps. We used three different types of service wires with increasing cross section. However, our results indicate only minor differences of the relative movements of shell, shim and bail for different clamp-wire combinations when measured during a tensile test.

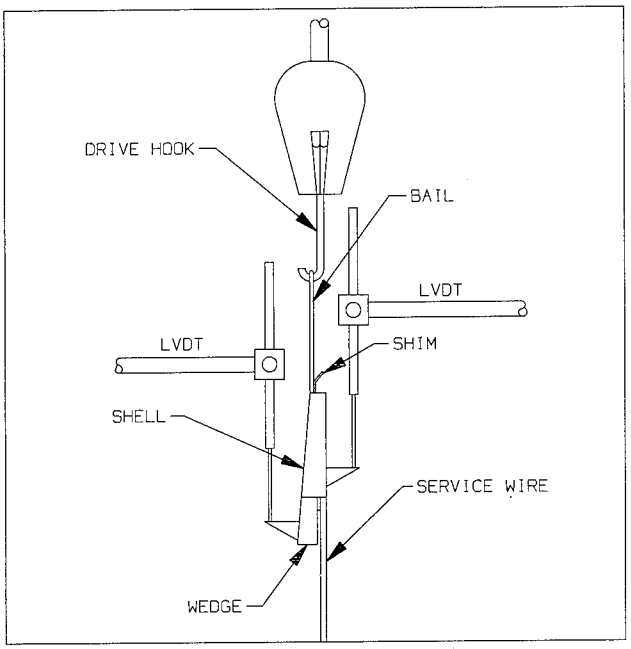


Figure 1 : Schematic test set-up

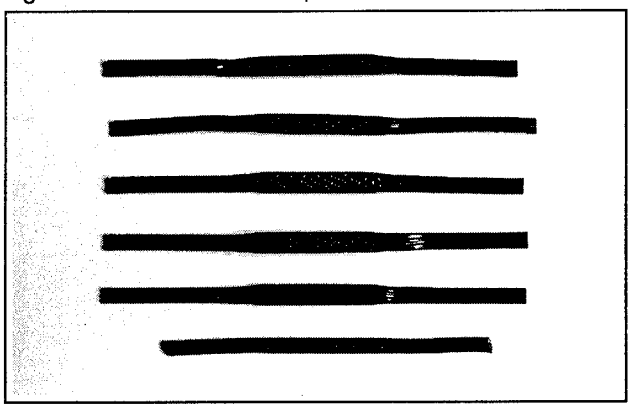


Figure 2 : Wires taken out of clamps. Top five samples are two pair aerial service wires bottom sample is a copper clad steel wire

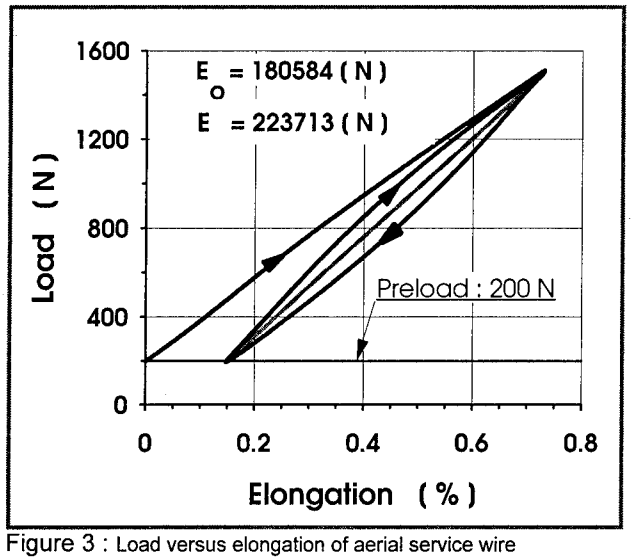


Figure 3 : Load versus elongation of aerial service wire

Hence we only report on the results of one of these wires in conjunction with the clamps. The wire selected for the tests was an aerial service wire NT-2ADW ICEA-Type I, produced by NORTEL. This wire was fully evaluated with respect to the mechanical data required. The same conclusions would be expected for similar aerial service wire products. All the data presented was obtained using a few clamps, probably from one production lot. The conclusions drawn assume there to be negligible lot to lot variations. The conclusions presented are intended to guide the user of clamps to the selection of optimum designs for the glass fiber reenforced two pair aerial service wires. There is no intention to "rank" manufacturers, or to comment on the reliability of these clamps for conventional one pair copper clad steel drop wires.

The same test specimen which we used to evaluate the clamp in the tensile tester were subsequently exposed to a static load test to simulate the long term behaviour of the clamp-wire combinations.

For this purpose the tensile test samples which were loaded only to 1513 N (340 lbf), were consecutively subjected to a static load test at 1624 N (365 lbf) for five days at 35 °C. The clamps were measured before and after the static load test, and the observed deformations were added to those measured during the tensile test. We refer here and in the following only to the displacement of both clamps, assuming two clamps per span.

For the string-up condition we can define an initial wire modulus (E_o) and a hysteresis modulus (E), which in fact, is derived from the average values of the unloading and reloading curve. It should be noted that deviating from the common definition we use the wire moduli not cross section specific (see also in the Appendix). We use for the calculations the hysteresis modulus. In Fig. 3 both elastic wire moduli are indicated. For comparison purposes the elastic modulus of a copper clad steel reenforced aerial service wire is given here to be approximately $E \approx 320{,}000$ [N] (71,694 lbf) [4]

Incidentally, the sagging of a service wire as a function of both moduli and the loading history, is quite complex and leads to solutions in terms of incomplete elliptical integrals. An analysis of this problem would be very interesting.

Results

The results obtained are generally reported for both clamps, i.e. the displacements for both clamps are added and are given as a function of the load. For these data we used Jandel Scientifics Table Curve 2D curve fitting software. This has been done for interpolation and extrapolation purposes. The load corresponds to the load at the suspension point. Thus the results represent directly the values obtained for a real span. In Fig. 4 to Fig. 6 are shown for three clamp

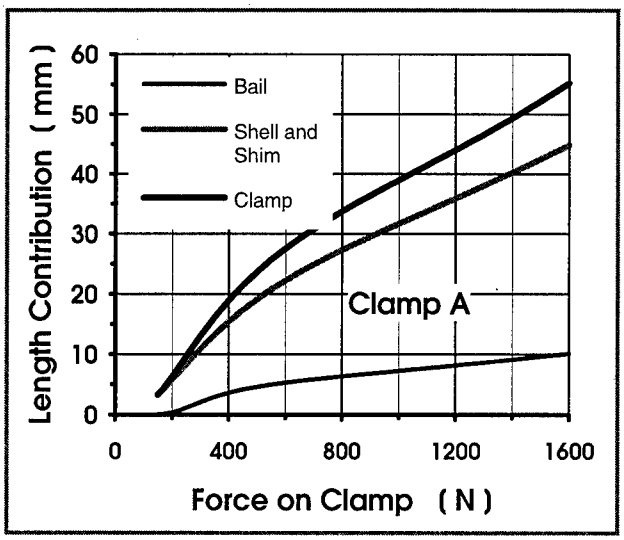


Figure 4 : Length contribution of clamp A

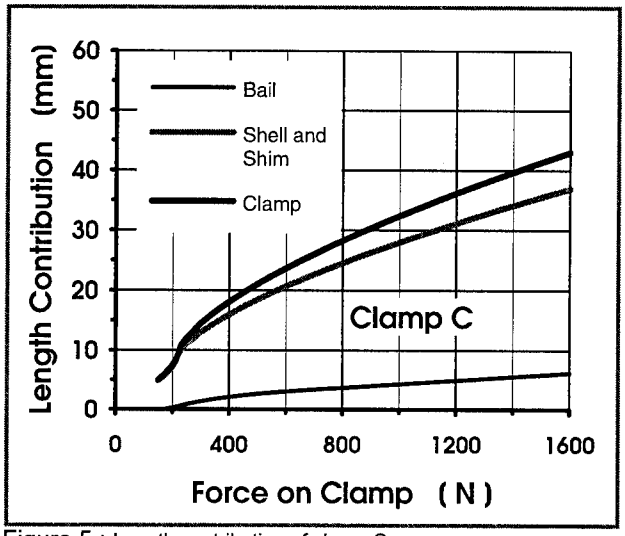


Figure 5 : Length contribution of clamp C

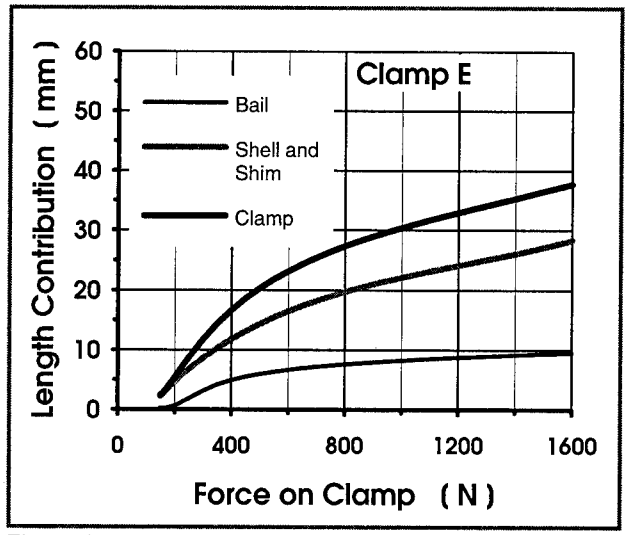


Figure 6 : Length contribution of clamp E

types the results for the displacements and deformations, as measured in the tensile tester.

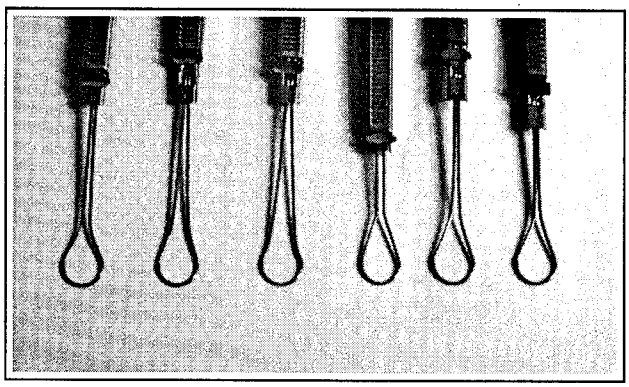


Figure 7 : Shape of bails from clamp A to F (left to right)

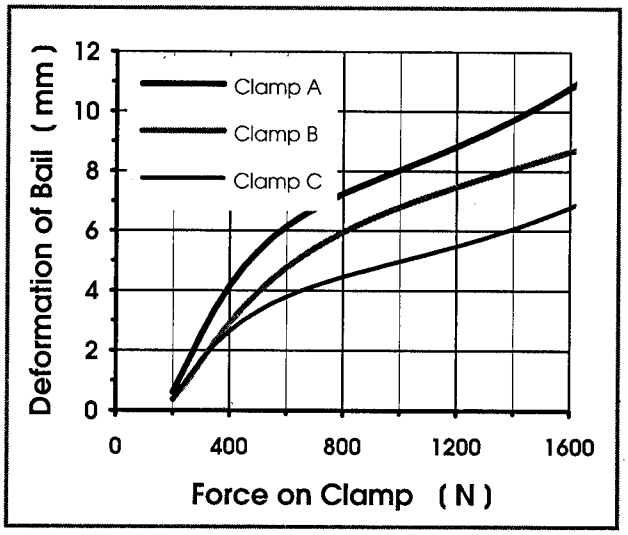


Figure 8 : Deformation of bail versus force applied to clamp

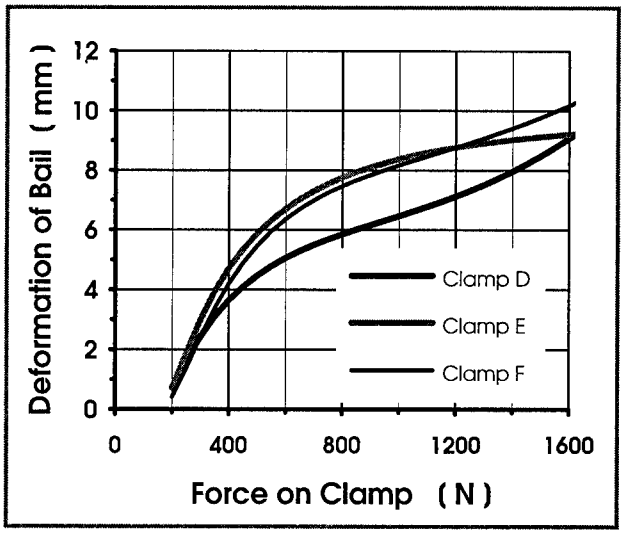


Figure 9 : Deformation of bail versus force applied to clamp

The original form and the shape after utilization of the bails is shown in Fig. 7 for the different types of clamps. Fig. 8

and Fig. 9 show for the same types of clamps the deformation of the bails alone.

Fig. 10 to Fig. 12 show the added total deformations for the clamp types investigated which contribute directly to the length increase of the unstretched wire on the span.

Fig. 13 to Fig. 15 show the sags obtained for an inelastic wire on three different span length. Additionally the sags of the same spans were calculated under the assumption that the length of the wire on the span increased by the contribution due to the clamps. This is equivalent to a change in load on the span, which yields a displacement of the clamps, as the wire itself was assumed to be inelastic.

For the same clamp types the sag increases for the different span lengths were calculated and are shown in Fig. 16 to 18. These increases are computed from differences of the sags of the inelastic wire including the length increase due to the clamps and the sag of the inelastic wire on the entire span. This yields the impact of the clamps upon the applied load at the string-up points. For the calculations we use the sag equations for equal height at the suspension points given in the Appendix. These formulæ are more elegant than the first derivations of the "elastic catenary" [5]. We use the tension at the suspension points, which yields the maximum elongation of the wire on the span. In order to obtain the behaviour of an inelastic wire we assume that $E \Rightarrow \infty$. We obtain then the well known catenary.

Fig. 19 gives the results for a span of 30 m pole to pole distance for an inelastic and for an elastic wire using the clamp type E. It also indicates the sag for different temperature differentials. We use ± 75 °C a maximum temperature differential between the installation temperature range (- 15 °C to + 35 °C) and the extreme operating temperature range (-40 °C to +60 °C). The linear thermal expansion coefficient is $7.2 \cdot 10^{-5}$ [m/m·°C] for the glass fiber reenforced aerial service wire. It is dominated by the linear expansion coefficient of type of glass used for the reenforcement rovings (E-glass).

Fig. 20 to Fig. 22 indicate the sag increases for three different types of clamps for the same pole to pole distance of 30 m. Additional to the sag increase of an inelastic wire as reference, the sag of the elastic wire with its variations over temperature has been indicated.

Finally in Fig. 23 we have the sag for clamp type E under the same conditions as previously mentioned, however, for a copper clad steel reenforced wire with a wire elasticity of $E \approx 320{,}000$ [N] and a linear expansion coefficient of $1.11 \cdot 10^{-5}$ [m/m·°C]. In this case, it is assumed, that the deformation of the clamp is comparable to the one obtained with the glass fiber reenforced wires. This assumption is justified, as the one pair copper clad steel wire does not show any more a shape stabilizing braid between the insulation and the jacket, which prevents

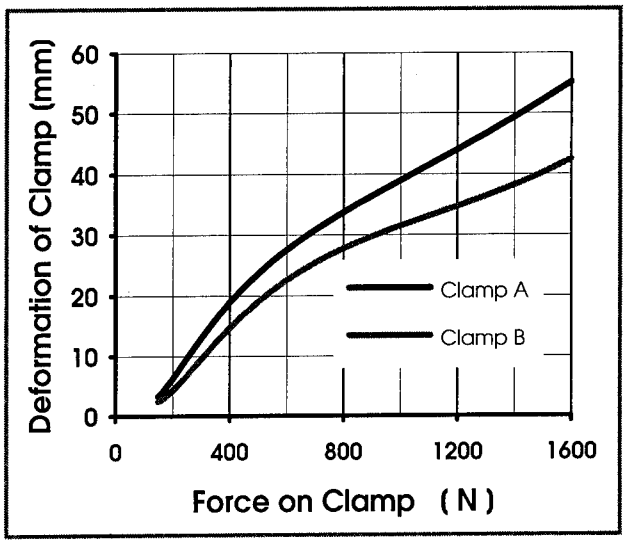


Figure 10 : Entire length contribution of clamp versus load

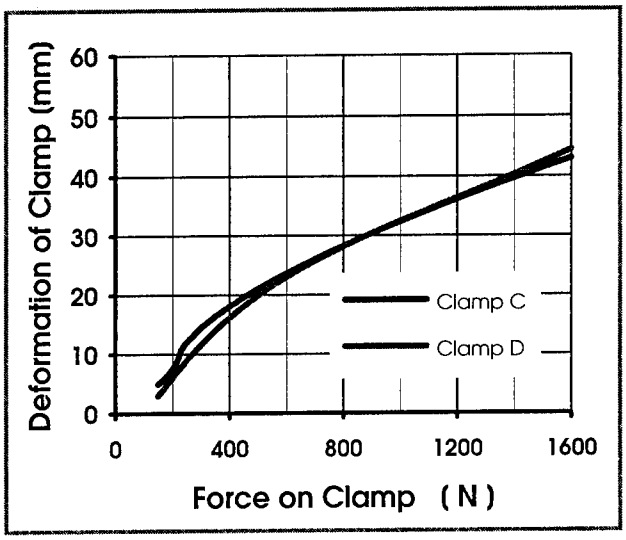


Figure 11 : Entire length contribution of clamp versus load

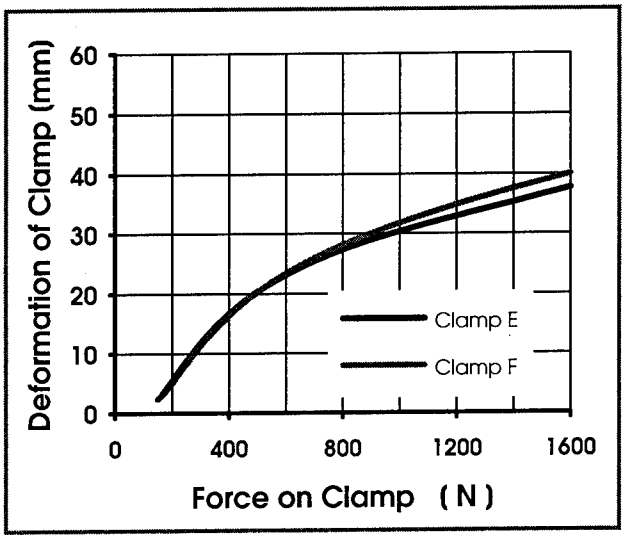


Figure 12 : Entire length contribution of clamp versus load

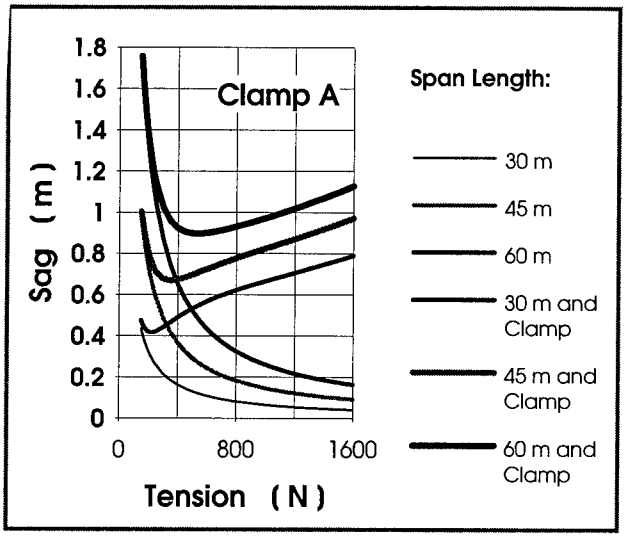


Figure 13 : Sag versus tension at suspension point for clamp A

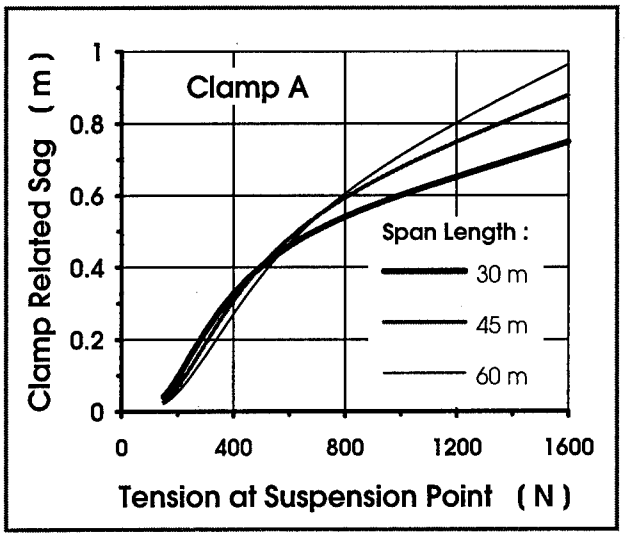


Figure 16 : Sag increase caused by the clamp A

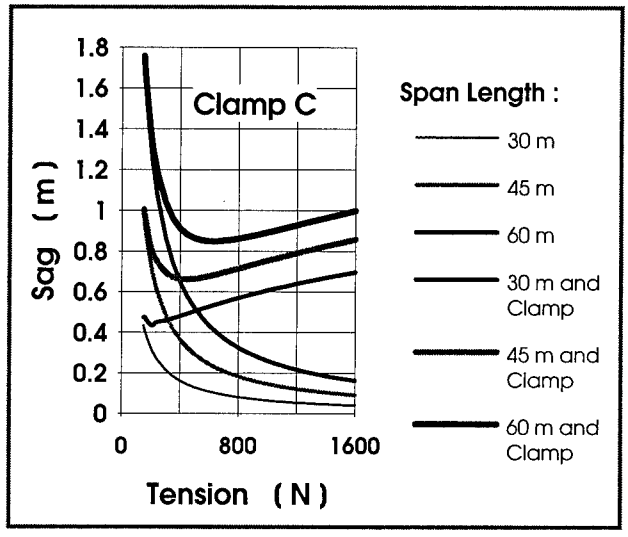


Figure 14 : Sag versus tension at suspension point for clamp C

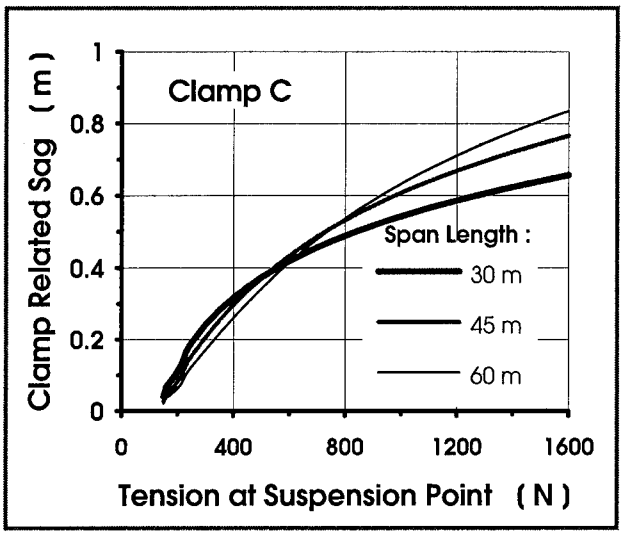


Figure 17 : Sag increase caused by the clamp C

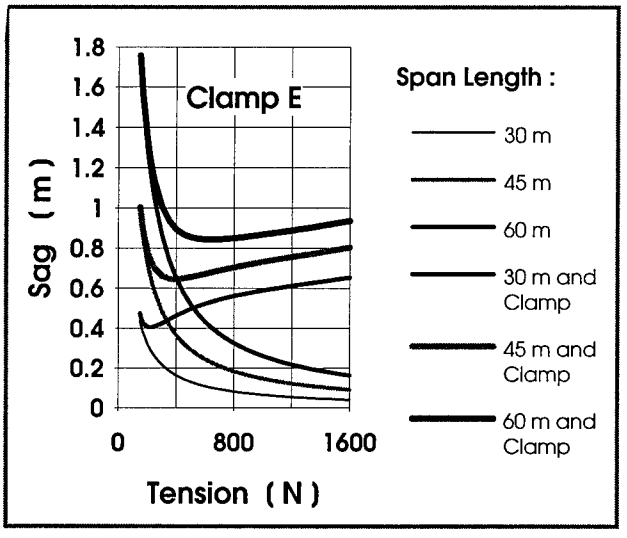


Figure 15 : Sag versus tension at suspension point for clamp E

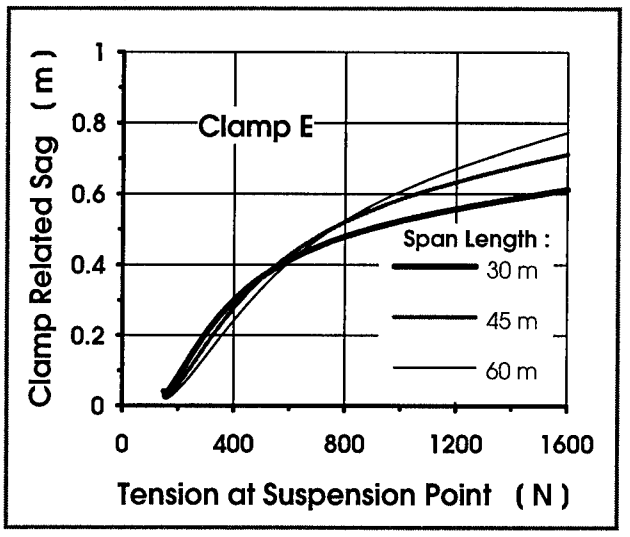


Figure 18 : Sag increase caused by the clamp E

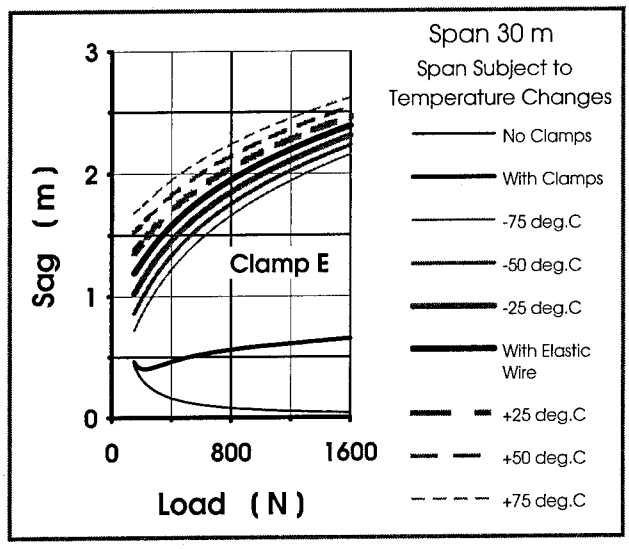


Figure 19 : Sag versus load subject to temperature changes

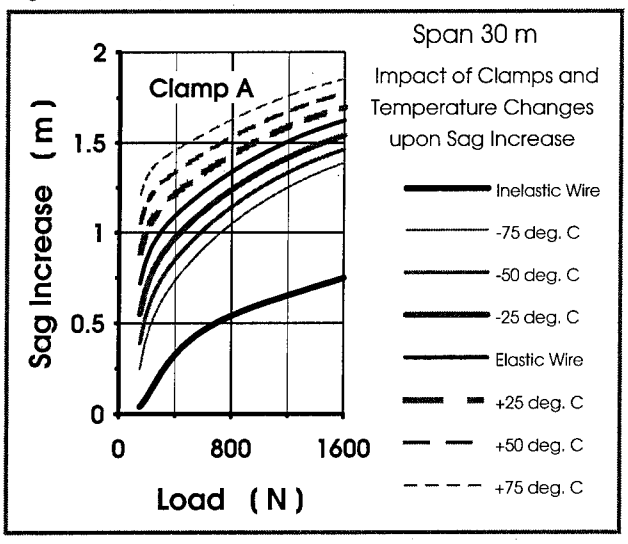


Figure 20 : Sag increase of clamp A after temperature changes

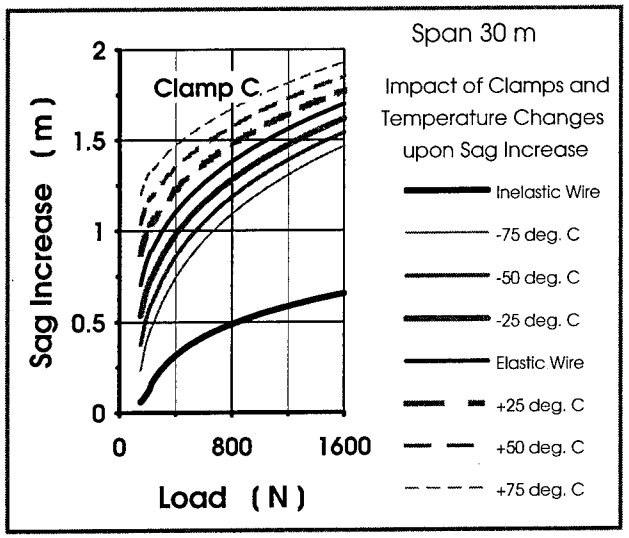


Figure 21 : Sag increase of clamp C after temperature changes

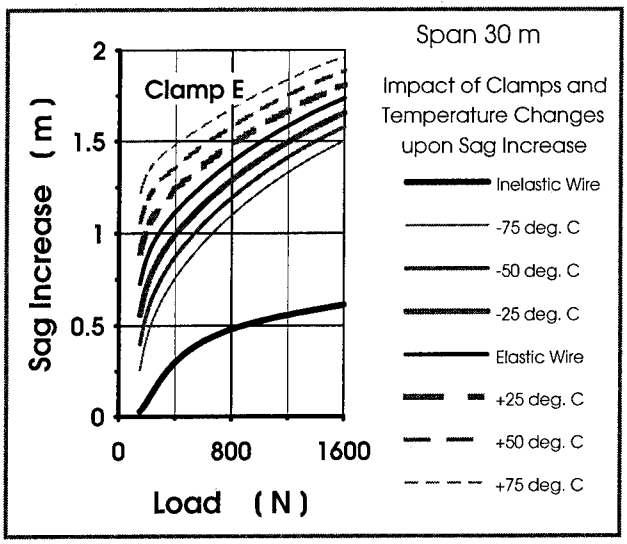


Figure 22 : Sag increase of clamp E after temperature changes

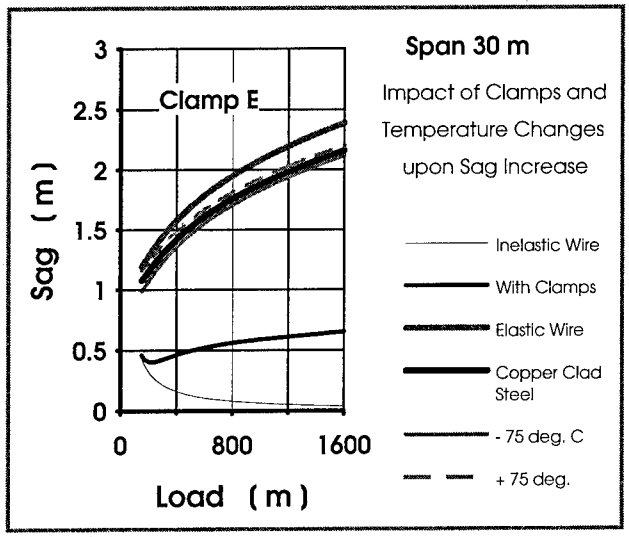


Figure 23 : Sag of different aerial service wires

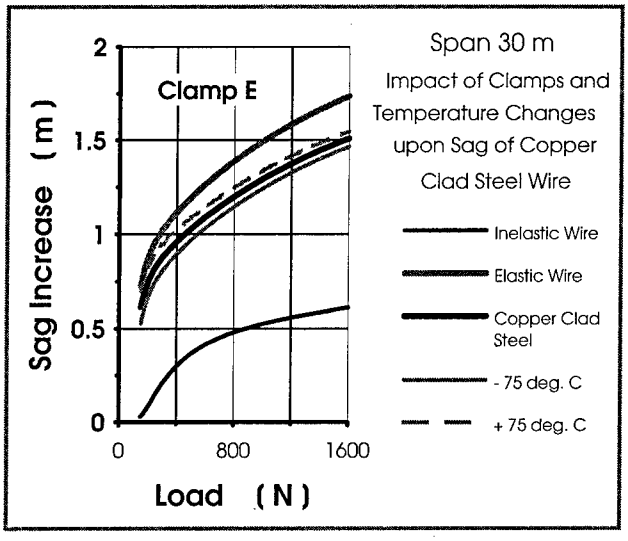


Figure 24 : Sag increase versus load for the wires in Fig. 23

major clamp displacements by flattening of the wire inside the clamp. Fig. 24 shows the sag increase relative to an inelastic span without any clamps.

Discussion of Results

The clamp type C shows the least bail deformation (see Fig. 4 to 6 and Fig. 8 and 9). This indicates that bails with a shape resembling the deformed bail are the best performing with respect to deformation. The deformation of the bail depends upon the original shape of the bail at string-up (see Fig. 7). The contribution of the bails to the sagging can, therefore, be reduced through proper shaping of the bails at point of manufacture or, more awkwardly, at installation time.

Another method to reduce the bail deformation effectively is to use bail-eyelets (see Fig. 25). Bail eyelets help to reduce sag, corrosion and friction induced wear in wind prone areas. Incidentally, the use of bail-eyelets was formerly recommended in the installation practices of the Bell System and they were commonly used, but, unfortunately over time, they gradually disappeared and it seems that, today, they are very difficult to find.

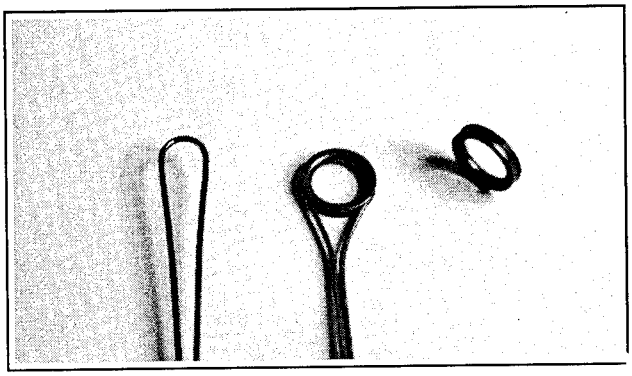


Figure 25 : Deformed bail and bail eyelet to prevent deformation

The results of the entire clamp deformation (Fig. 10 to 12) show, that the clamp type E has the best performance, though clamp type C and D perform nearly as well. However, it should be mentioned that the clamp type D failed in several cases, as the wire slipped through the clamp, i.e. this clamp does not show sufficient gripping to allow for the self-tightening of the clamp. This may have to do with the bottom profile of the shell or with the profiling of the shim.

Fig. 5 and 6 show the ratio of the bail deformation and the slip of the shell over the wedge. From these diagrams, it is obvious that the performance of the clamp type E could be substantially improved by reducing the contribution of the bails, and that the clamp type C is subject to a relatively high slip of the shell over the shim.

If the theoretical sag curves for elastic wires are calculated at string-up without any clamps, and with the same elongation at the suspension point, then the sag curves are deviating only very little from the inelastic case. In fact, the sag-load curves are nearly identical, also for relatively low cable elasticities. We therefore omit to show these results in the Fig. 13 to 15, and we use an inelastic wire to evaluate the pure impact of the clamps upon the sag for different pole to pole distances. With increasing load and raising pole to pole distances the sag increases. The increasing load on the wire over its length is identical to an increase of tension. The increase in sag due to the clamps is in accordance with expectation high at short pole to pole distances (see also Fig. 16 to 18). However at high loads the sag increase on long spans is more pronounced than on shorter spans. This is somewhat surprising and only explainable out of the minimum of the sag tension curves, illustrating that the minimum clearly shifts to higher tensions with increasing span length.

The elasticity of the wire becomes important if the contribution of the clamps is taken into account. This is demonstrated in Fig. 19 for the clamp type E. If we take additionally the thermal expansion coefficient into account, then we get for different temperature differentials with respect to the string-up temperature the curves shown as well in Fig. 19. It is clear from this diagram that the impact of the cable elasticity has, in conjunction with the clamps a substantial influence upon the sagging under equal tension at suspension point. However, it is also obvious that the temperature influence is predominant at the lower end of the sag tension curve (see Fig. 19 to 22 for different clamp types).

It could be argued now, that it is recommendable to increase the elasticity and therewith the strength of the wire. However, if we assume a copper clad steel reenforced wire in comparison to a glass fiber reenforced wire, then we have in Fig. 23, for the same clamp type E, only a very marginal improvement of the sag (see also Fig. 24). Considering the thermal expansion of copper clad steel wires on the other side we can conclude that a reduction of the thermal expansion coefficient yields a major reduction of the sag over the temperature range considered.

Summary and Conclusions

We performed extensive measurements of the mechanical performance of clamps in conjunction with a glass fiber reenforced aerial service wire and made a detailed analysis of the results obtained. We then applied the obtained results into the calculation of the sag of service wire spans of different pole to pole distance and under different load conditions. We stress that the load conditions were always related to the tension at the suspension point, and not as usually communicated as a constant horizontal force which is a function of variable length specific load. However, the length specific loads can be easily computed, using load

and the slope of the wire at the suspension point.

Our results indicate that

- the tightening of the clamps has a major impact upon the sag of an aerial service wire, if the wire is compressed and flattened in the clamp.
- the deformation of the bails of the clamps shows also a not negligible impact upon the sag.
- clamps should be improved with respect to their bail shape, to reduce excessive deformation. In Fig. 25 on the left side is shown a deformed bail, whereas Fig. 7 shows the bails of the clamps type A to F from left to right. The comparison shows that clamp type C has the most suitable formed bail.
- it is recommended to return to the old practice to use bail eyelets to avoid the impact of the bail deformation upon the sag.
- the angle of the wedge and shell can be improved to allow a faster compression of the wire in the clamp, yielding a lower contribution of the effective wire length on the span.
- the elasticity and thus the load carrying capacity of glass fiber reenforced aerial service wires is sufficient to limit excessive sagging under extreme loads.
- the thermally induced variations of the sag under same load conditions are high if compared to those of copper clad steel reenforced aerial service wires.
- it would be advantageous to use reenforcement members with a reduced thermal expansion.

Acknowledgements

The authors would like to express their thanks to :

- Mr. J.-G. Després from Bell Canada for his permission to utilize the results compiled in two Bell Canada sponsored research reports.
- Mr. K. Kress from Cincinnati Bell Telephone for his help in obtaining very old spans with copper clad steel reenforced wires and copper alloy clamps for analysis.
- Mr. J. Ellard from Newfoundland Telephone for his indications on bails eyelets, and for providing a sample of such.

References

[1] Bell Communications Research
Technical Reference TR-TSY-000267
Issue 1, July 1986
Drop Wire Clamp for Single Pair Aerial Service Wire

[2] J. Druez and J. Bilodeau : Étude sur le Comportement des Fils de Service Aériens et de leurs Systèmes de Fixation en Fonction des Conditions Climatiques.
Part I : Comportement des Systèmes de Fixation
Research Report for Bell Canada ERIGS-94-10-01
University of Quebec at Chicoutimi, January 1995

[3] J. Druez and J. Bilodeau : Étude sur le Comportement des Fils de Service Aériens et de leurs Systèmes de Fixation en Fonction des Conditions Climatiques.
Part II : Effet des Conditions Climatiques
Research Report for Bell Canada ERIGS-94-10-01
University of Quebec at Chicoutimi, May 1995

[4] J.-H. Walling : The mechanical characteristics of glass fiber versus copper clad steel reenforced wires.
Northern Telecom Technical Memorandum 1989

[5] F. Skrobanek : Gleichgewichtsform eines elastisch dehnbaren Fadens (elastische Kettenlinie)
Zeitschr. f. Angew. Mathematik und Mechanik 2 (1922),p. 472-474

Appendix

Sag Calculation

The linear elasticity in the classical sense is described essentially by three constants, the elasticity modulus, the modulus of transverse elasticity and finally Poisson's ratio. These constants are interrelated and cannot be determined in a straight forward fashion for composites. The shear stresses in between the components of differing elasticities yield three dimensional stress strain conditions which are very difficult to assess.

It is for all practical purpose impossible to derive for glass-fibre reenforced aerial service wires an elasticity modulus based upon the elastic moduli of its components. Hence, we use the entire cable elasticity (longitudinal stiffness), and consequently instead of integrated cross-sectional stresses only the entire applied load on the wire over the elongation.

We use the following abbreviations :

a	-	Abbreviation
b	-	Abbreviation
c	-	Abbreviation
E	-	Elastic modulus of entire wire
f	-	Sag
F_o	-	Horizontal force
l	-	Horizontal distance between suspension points
L_o	-	Unstretched wire length on span
L_w	-	Unstretched wire length including length increase due to clamps
p_1	-	Slope of tangent to clamp free span at suspension point

p_w	-	Slope of tangent to span at suspension point
ΔT	-	Temperature differential between the actual and string-up temperature
α	-	Thermal expansion coefficient
δ	-	Length increase due to one clamp
ε_{max}	-	Maximum elongation at suspension point
μ	-	Length specific weight of wire, including other length specific loads

For the following formulas :

$$F_o = \frac{E}{\sqrt{1 + p_1^2}} \cdot (\varepsilon_{max} - \alpha \cdot \Delta T) \qquad (1)$$

$$a = \frac{l \cdot \mu}{2 \cdot E}$$
$$b = \varepsilon_{max} - \alpha \cdot \Delta T \qquad (2)$$
$$c = 1 + \alpha \cdot \Delta T$$

Transcendental equation solved iteratively to obtain the slope at suspension point of clamp free span:

$$\frac{a}{b} \cdot \sqrt{1 + p_1^2} - b \cdot \frac{p_1}{\sqrt{1 + p_1^2}} - c \cdot \operatorname{arcsinh} p_1 = 0 \qquad (3)$$

$$f = \frac{F_o}{\mu} \cdot \left[\frac{F_o}{2 \cdot E} \cdot p_1^2 + (1 + \alpha \cdot \Delta T) \cdot (\sqrt{1 + p_1^2} - 1) \right] \qquad (4)$$

$$L_o = \frac{2 \cdot F_o}{\mu} \cdot p_1 \qquad (5)$$

$$L_w = L_o + 2 \cdot \delta \qquad (6)$$

$$F_w = \frac{\mu_w \cdot L_w}{2 \cdot p_{1w}} \qquad (7)$$

$$a = \frac{\mu_w \cdot L_w}{2 \cdot E}$$
$$b = \frac{l}{L_w} \qquad (8)$$
$$c = 1 + \alpha \cdot \Delta T$$

The following transcendental equation has to be solved iteratively to obtain the slope at suspension point of the span including the length contribution of the clamps:

$$a - b \cdot p_{1w} + c \cdot \operatorname{arcsinh} p_{1w} = 0 \qquad (9)$$

$$f = \frac{L_w}{2} \cdot \left[\frac{\mu_w \cdot L_w}{4 \cdot E} + (1 + \alpha \cdot \Delta T) \cdot \frac{(\sqrt{1 + p_{1w}^2} - 1)}{p_{1w}} \right] \qquad (10)$$

Software Used

WordPerfect 5.0 and 6.0
Microsoft Excel 4.0 and 5.0
Wolfram Research MathLink
Wolfram Research Mathematica 2.22
Jandel Scientific TableCurve 2D
Designer 3.0
Microsoft PowerPoint 3.0

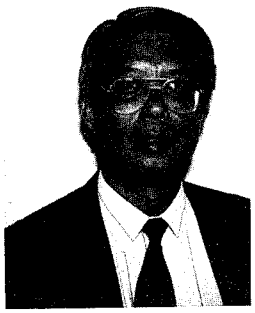


Jörg-Hein (Jo) Walling received his diploma in Mechanical Engineering in 1966 at the Technical University of Berlin. In 1974 he obtained a Doctor's degree (Dr.-Ing.) at the same University. In 1974 he joined Northern Telecom in the Research and Development department. Since 1976 he is senior engineer at the Lachine Cable Plant, responsible for the design of Outside Plant and Data Grade Wires and Cables.

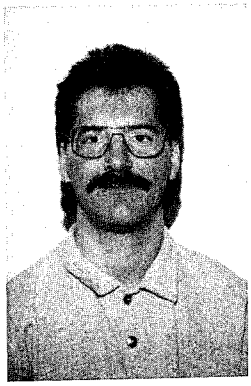


Jacques Druez received his diploma in Mechanical Engineering in 1968 at the National Institute of Applied Sciences (INSA), Lyon, France. In 1969 he obtained a M.Sc.A. degree in Mechanical Engineering from the University of Sherbrooke, and in 1983 a Ph.D degree from École Polytechnique, Montréal. Since 1969 he is Professor of Engineering at the University of Québec at Chicoutimi, Canada. Since 1973, his research involves atmospheric icing on cables and structures, using both laboratory and nature icing test site facilities. In 1991 he founded a Research team on the Engineering of Atmospheric Icing on Structures (ERIGS) at the University of Québec at Chicoutimi.

Chi-Than Nguyen received his B.A.Sc degree in Electrical Engineering in 1971 from École Polytechnique, Montréal.



He has over 22 years of experience in the phone industry working for Bell Canada, Bell Northern Research, Bell Canada International and Stentor. He was involved in many different aspects of telephony, including Outside Plant, Transmission, Consultant and O.P. Technology Development. He is currently with Bell Canada as a Staff Manager in the Outside Technology Research group, responsible for the copper and coaxial cable standards. Mr. Nguyen represents Bell Canada at various cable standard committees of IEC, IEEE and the Telecommunication Wire and Cable Standard Technical Advisory Committee of ICEA where he has served for the last two years, as Vice-Chairperson and Chairperson consecutively. He is also a member of the Order of Professional Engineers of Québec, the Canadian Council of Professional Engineers, the CSA, the ASTM and the SCTE.



Julien Bilodeau received a Baccalaureate in Engineering in 1992 from the University of Québec at Chicoutimi. He is currently completing a M.Sc.A. degree in engineering at the same university. As a research assistant he is involved in the determination of the mechanical behaviour of atmospheric ice.

NEW HYBRID CABLES FOR CATV

C. Schwiering, J. Seidenberg, P. E. Zamzow

KABEL RHEYDT AG, Mönchengladbach, Germany

Abstract

For the further development of the CATV hybrid fiber coax (HFC) network, customers require hybrid fiber/coaxial cables.

This paper deals with a new hybrid cable construction for trunk and distribution applications. The cable is based on an aluminum coaxial cable design whose popularity increased in recent years. The electrical, optical and mechanical characteristics of the hybrid cable will be presented. We shall show that the optical fibers which are located in the center conductor to optimize the cable geometry, have no effect on the high-frequency characteristics of the coaxial element and that they are sufficiently protected to maintain the integrity of their performance.

Solutions for special accessories (connector, splice and closure) which are necessary for the installation and operation of the system and for hybrid drop cable construction will be proposed.

Introduction

In recent years the CATV networks changed from coaxial cable plants to hybrid networks. In the hybrid fiber coax (HFC) network architecture optical fiber cables are used for feeder applications from the head-end to the node near the subscriber. For the distribution from the node to the subscriber coaxial cables are installed. Fiber to the home (FTTH) solutions that provide a fiber for each subscriber often go unrealized because of the present high cost of the electronics.

The first step in developing a new network structure which offers increased flexibility for future applications was recently taken. Cable plant architectures with hybrid cables for the distribution and drop area are under consideration. They provide an electrical and optical path for optional use.

This paper describes the new hybrid cable construction for CATV application which consists of a coaxial and of a fiber optic transmission element. As aluminum coaxial cables became more and more popular in recent years the coaxial part of the hybrid cable is based on this aluminum design. The optical fibers are standard single-mode fibers. The design of trunk and distribution (T&D) cables will be discussed in detail. A cable construction for hybrid drop cables will be briefly presented.

Accessories, such as cable splices, connectors and closures that are necessary for the installation of this new cable generation, are included in this paper.

Trunk and Distribution Cable

Cable Construction.

The integration of optical fibers in leaky coaxial cables, which have much larger dimensions than CATV cables, has been described at IWCS 1994 /1/. For our investigations the hybrid cable is based on an aluminum coaxial cable type that is very often used in conventional coaxial cable plants. The center conductor had to be modified to allow the integration of the optical fibers. Since the diameter of this center conductor is one of the smallest that is commonly used for trunk and distribution CATV cables, the presented hybrid cable design can easily be applied to other coaxial cable types. Figure 1 shows the construction of the hybrid cable and Figure 2 a cable sample.

Optical Fibers and Loose Tube. The design and properties of the single-mode optical fibers used for the hybrid cable correspond to CCITT Rec. G652 /2/.

Four optical fibers are located in a central plastic loose tube as it is commonly used in optical fiber cables. The tube is filled with a thixotropic jelly which protects the fibers. During the production process a fiber excess length in the tube of typically 2 ‰ can be achieved.

Center Conductor. Normally a copper-clad aluminum center conductor is used for aluminum coaxial cables. It contains 10 % copper by volume (corresponding to 0.08 mm wall thickness for this type). It meets the ASTM B 566 Standard /3/.

For the hybrid cable the copper-clad conductor is replaced by a welded copper tube which contains the loose tube with the optical fibers. The copper tube has an outer diameter of 3.15 mm and a wall thickness of 0.25 mm.

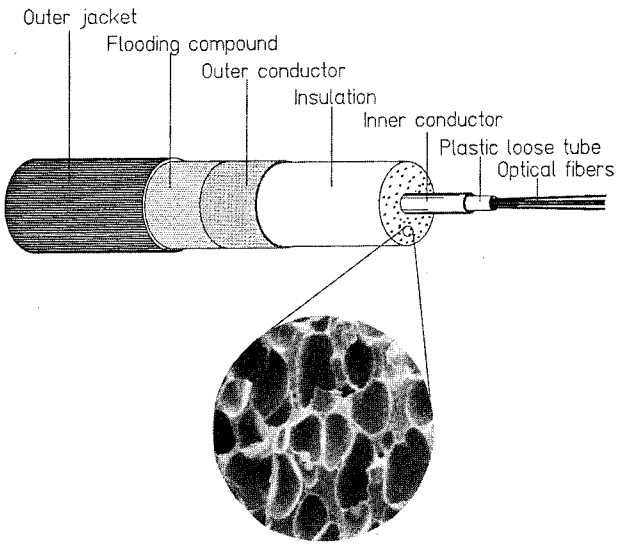


Figure 1: Hybrid cable construction

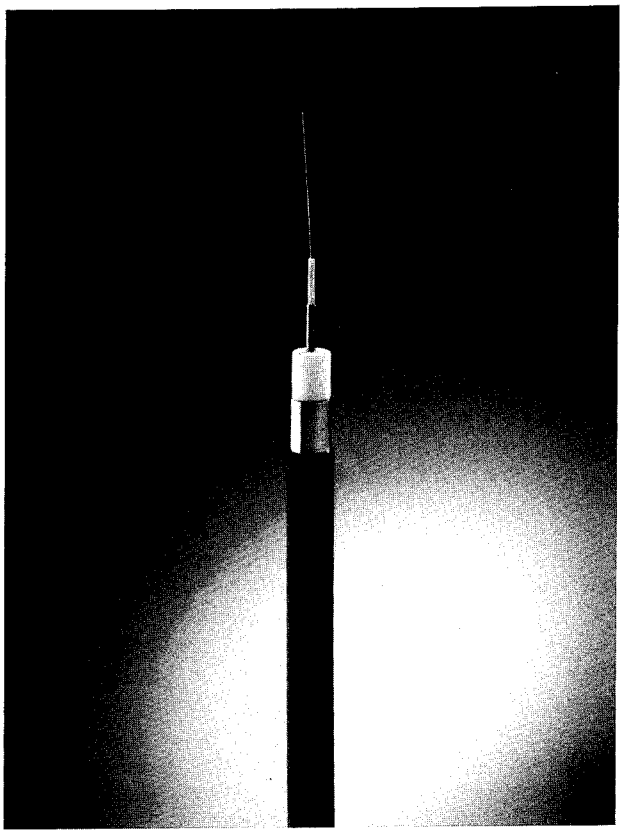


Figure 2: Hybrid cable sample

Insulation. The insulation consists of physically foamed polyethylene (PE) of about 80 % blowing degree which forms a closed cell structure (Fig. 1).

To achieve excellent electrical characteristics small cells and homogenous distribution as well as good concentricity and ovality are required. A special low-loss insulation material must be used for low electrical attenuation.

The foamed PE combines the mechanical advantages of homogeneous insulation with the properties of bamboo insulation (less weight and attenuation).

Outer Conductor. The outer conductor is made out of a welded aluminum tube with a 0.35 mm wall thickness. The welded construction ensures the high screening attenuation of the cable which is greater than 110 dB. The cable therefore meets the requirements of the prEN 50117-4 Standard /4/ which prescribes 85 dB for trunk and distribution cables.

Jacket. A flooding compound between the outer conductor and the jacket provides additional protection against corrosion. The standard material for the outer protective jacket is medium density PE according to ASTM D 1248 Type II /5/.

Table 1 summarizes the main constructional characteristics of the hybrid cable.

Center conductor with a plastic loose tube and four optical fibers		
Wall thickness of the center conductor	mm	0.25
Outer diameter of the center conductor	mm	3.15
Diameter of the gas-injection insulation	mm	13.0
Wall thickness of the outer conductor	mm	0.35
Outer diameter of the outer conductor	mm	13.7
Outer diameter of the cable	mm	15.5
Cable weight (appr.)	kg/km	136

Table 1: Constructional characteristics of the hybrid cable

Electrical Characteristics.

Due to the construction of the hybrid cable as described above the electrical high-frequency characteristics do not differ from those of the corresponding aluminum coaxial cable.

Attenuation. One characteristic that influences the attenuation of a coaxial cable is the material and construction of the center conductor. Due to the well-known "skin effect" caused by electro-magnetic forces, the penetration of the current into the conductor decreases with increasing frequency.

To evaluate the contribution to the attenuation by the center conductor, the field penetration depth δ must be calculated:

$$\delta = \sqrt{1/(\pi f \sigma \mu)}$$

with f - frequency
σ - conductivity
μ - permeability

For copper and assuming a minimum frequency of 5 MHz, δ = 0.03 mm. This is much less than the wall thickness of the welded copper tube of the hybrid cable.

Figure 3 illustrates the measured attenuation of the coaxial element of the hybrid cable for different temperatures.

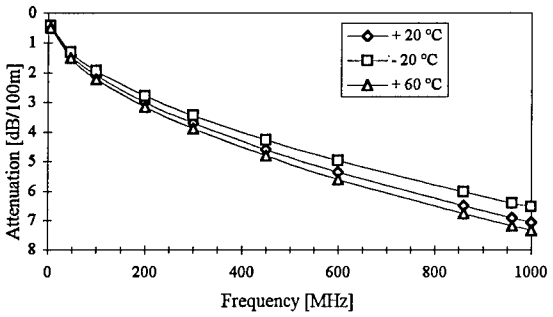


Figure 3: Electrical attenuation at - 20 °C, + 20 °C and + 60 °C

DC Resistance of the Center Conductor. Due to the design of the center conductor the DC resistance differs from the one of a copper-clad aluminum center conductor, which is normally used in a conventional aluminum coaxial cable.

According to ASTM B 566 /3/ a copper-clad conductor with 10 % copper by volume and a diameter of 3.15 mm has a DC resistance of 3.52 ohms/km.

The welded copper tube of the hybrid has a higher DC resistance. This difference must be considered in the design of the power supply.

Return Loss. The return loss of a coaxial cable is a characteristic value of the quality of the production process. The curves measured from both ends of the cable are given in Figure 4.

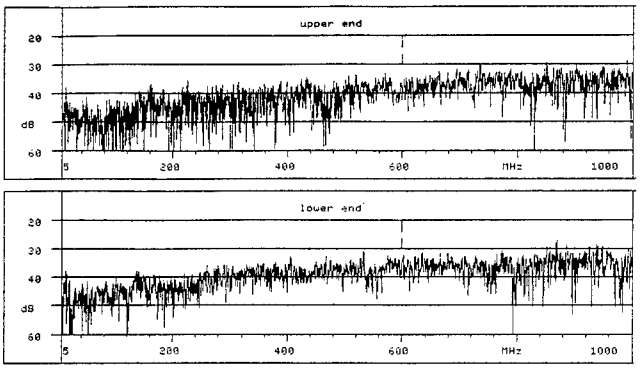


Figure 4: Return loss

Regularity of Impedance. The regularity of the characteristic impedance also characterizes the production quality and gives information of local defects. The curves measured from both ends of a cable (length = 502 m) are given in Figure 5. The regularity of impedance is better than 50 dB.

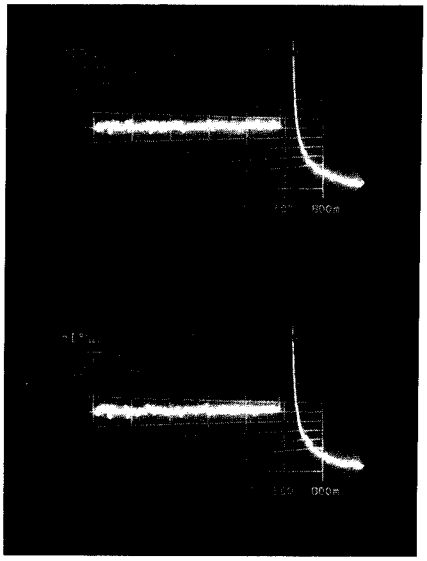


Figure 5: Regularity of impedance

The electrical characteristics of the hybrid cable are summarized in Table 2.

	Value	Test method according to prEN 50117-1 /6/
Center conductor resistance	8.4 ohms/km	11-1
Outer conductor resistance	1.9 ohms/km	11-1
Insulation resistance	> 10 Gohms*km	11-2
Dielectric strength	2 kV AC / 1 min	11-3
Characteristic impedance (40ns-impuls)	75.2 ohms	11-5-2
Regularity of impedance (40ns-impuls)	> 50 dB	11-9-1
Capacitance	51 pF/m	

Table 2: Electrical characteristics

Mechanical Characteristics.

Several tests were performed to determine the ability of the hybrid T&D cable to withstand mechanical stress and meet environmental requirements.

Torsion. A torsion test according to IEC 794-1-E7 was carried out. A cable sample of 2 m was tested. A weight of 10 kg was applied. After two cycles of ± 180 ° the increase of the optical attenuation was less than 0.05 dB at 1550 nm. The center and outer conductor did not show any cracks or breaks and the weld was not damaged.

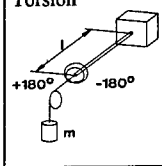
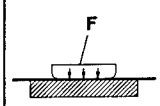
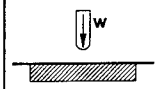
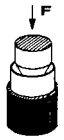
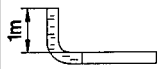
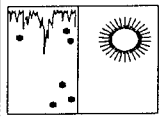
	Test method	Results
Torsion 	IEC 794-1-E7 weight: m = 10 kg length: l = 2 m	no cracks or breaks in the center and outer conductor, no damage of the weld, increase in optical attenuation $\Delta\alpha_{opt}$ < 0.05 dB at 1550 nm
Crush 	IEC 794-1-E3 prEN 50117-1 10-4 and 11.9.1 force: F = 8,000 N	no cracks or breaks in the center and outer conductor, no damage of the weld, increase in optical attenuation: $\Delta\alpha_{opt}$ < 0.05 dB at 1550 nm, regularity of impedance: r > 50 dB
Impact 	IEC 794-1-E4, radius: r = 5 mm energie: W = 8.8Nm	increase in optical attenuation: $\Delta\alpha_{opt}$ < 0.05 dB at 1550 nm
Cone 	internal test	destruction of the outer conductor but not of the weld
Waterblocking 	DIN VDE 0472 part 811	longitudinal watertight between insulation and outer jacket
Temperature Cycle 	IEC 794-1-F1	see Figures 3 and 6

Table 3: Mechanical and environmental characteristics

Crush Test. Crush tests are described in IEC 794-1-E3 for optical fiber cables and in prEN 50117-1 10-4 for coaxial cables. Testing the coaxial element of the cable results in a force f = 8000 N that can be applied (regularity of impedance: r > 50 dB, 10 ns impulse). The increase in optical attenuation at that force was less than 0.05 dB at 1550 nm. No cracks or breaks in the center and outer conductor could be found. The weld was not damaged.

Impact Test. An impact test according to IEC 794-1-E4 was performed to show that the optical fibers are very well protected in the center conductor of hybrid cable. The cable was exposed to an energie of 8.8 Nm. The increase in optical attenuation was $\Delta\alpha_{opt}$ < 0.05 dB at 1550 nm.

Cone Test. A test with a metal cone was performed to determine the quality of the weld. For this test the insulation and the outer jacket were removed. A cone was driven into the outer conductor until it broke. The test has shown that the weld was perfect: the outer conductor tore but not the weld.

Temperature Cycle. The cable was tested by temperature cycling (+ 20 °C, - 20 °C and + 60 °C). The electrical attenuation and optical attenuation at 1310 nm and 1550 nm were measured. The results are shown in Figure 3 (electrical) and Figure 6 (optical).

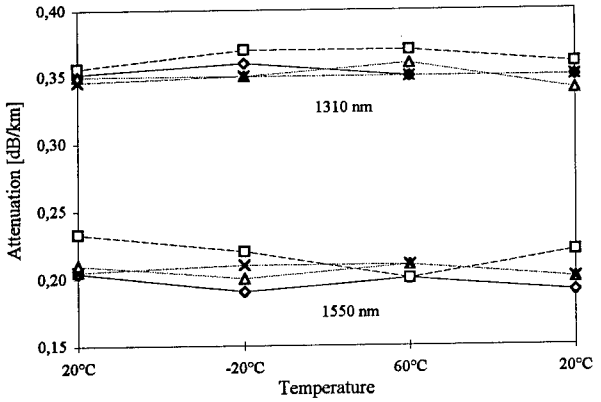


Figure 6: Optical attenuation during temperature cycle

The mechanical and environmental characteristics of the hybrid cable are summarized in table 3.

Drop Cable

One suitable design for hybrid fiber/coaxial drop cables is the figure-8 siamese construction. The coaxial and fiber optic parts of the cable are connected by a web. They can easily be separated, e.g. for the installation of connectors. Therefore, no special accessories are required for these hybrid drop cables. On the other hand, this is no optimum cable geometry. Figure 7 shows a sample of a siamese hybrid cable.

Accessories

Connector.

For the connection of the hybrid T&D cable with other components special connectors must be used. An outlet for the optical fibers and the loose tube must be provided as illustrated in Figure 8. Figure 9 shows a model of an assembled connector.

Since a plastic tube is used instead of a metallic tube, no short-circuit can arise. The minimum bending radius for the optical fibers is maintained inside the connector. The connector must absorb the pulling forces and has to be moisturetight for the operation in an environment that is not protected against humidity.

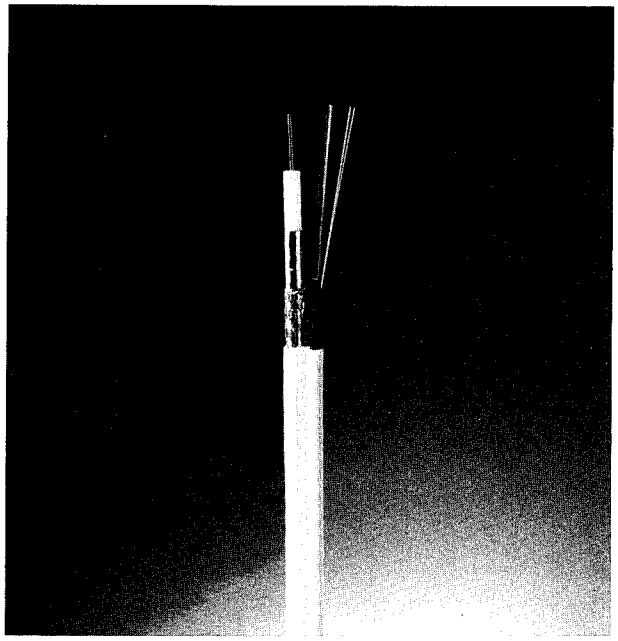


Figure 7: Sample of a siamese drop cable

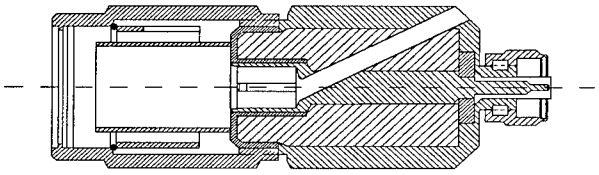


Figure 8: Sketch of a hybrid connector

Splice and Closure

The splicing of two hybrid cables means that the coaxial element as well as the optical fibers must be connected. For ease of installation and increased flexibility the fibers are spliced outside the coaxial splice.

Coaxial Splice. The coaxial splice for the hybrid cable ensures the electrical connection between both cables. It provides two outlets, one for the loose tube of each cable. For the installation of the coaxial splice several meters of the plastic tubes of each cable must be exposed at the cable end and fed through the outlets. The preparation and installation of the coaxial elements are executed in the conventional way. Due to the use of the PEX-O-FO closure described below the coaxial splice need not be watertight nor bear any tensile stress.

Hybrid Cable Closure. The fiber splices are secured in conventional splice cassettes in the closure. The PEX-O-FO is a general purpose closure which can be used for the hybrid system. A heat-shrinkable sleeve seals the whole joint independent of the number or diameter of the cables. The PEX-O-FO allows for easy re-opening and simple re-sealing of the joint.

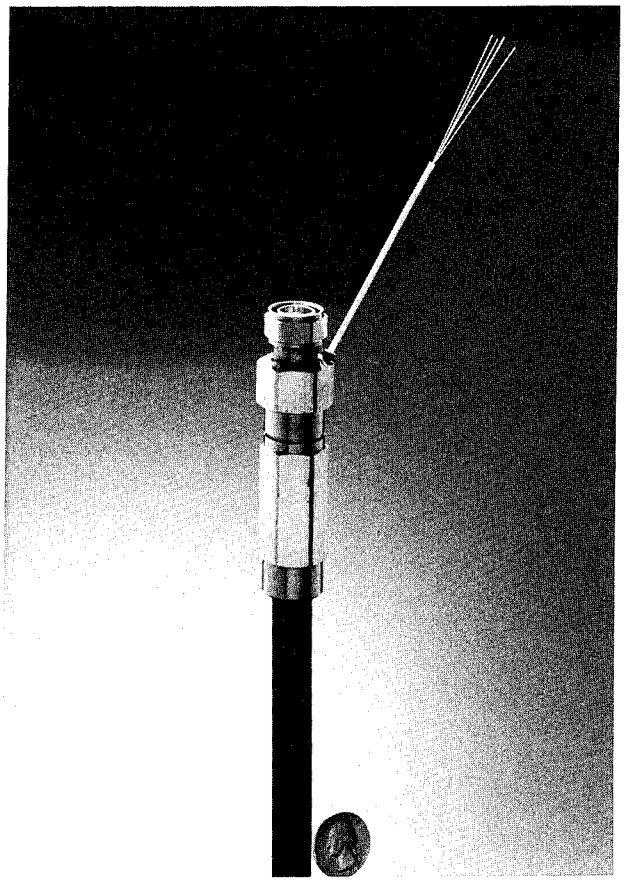


Figure 9: Hybrid connector sample

The concept described does not only allow to join two hybrid fiber/coaxial cables but it also provides, for example, a possibility to connect the fiber(s) of a hybrid cable with the fiber(s) of other fiber optic cables as illustrated in Figures 10 and 11. It therefore provides a high degree of flexibility using the components that are available now. A more compact solution for the splicing of two hybrid cables is under investigation. This can e.g. be achieved by using fiber ribbons.

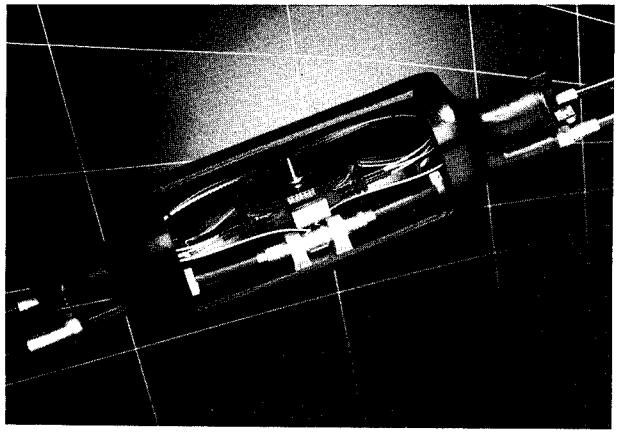


Figure 10: Photograph of a closure with an installed splice

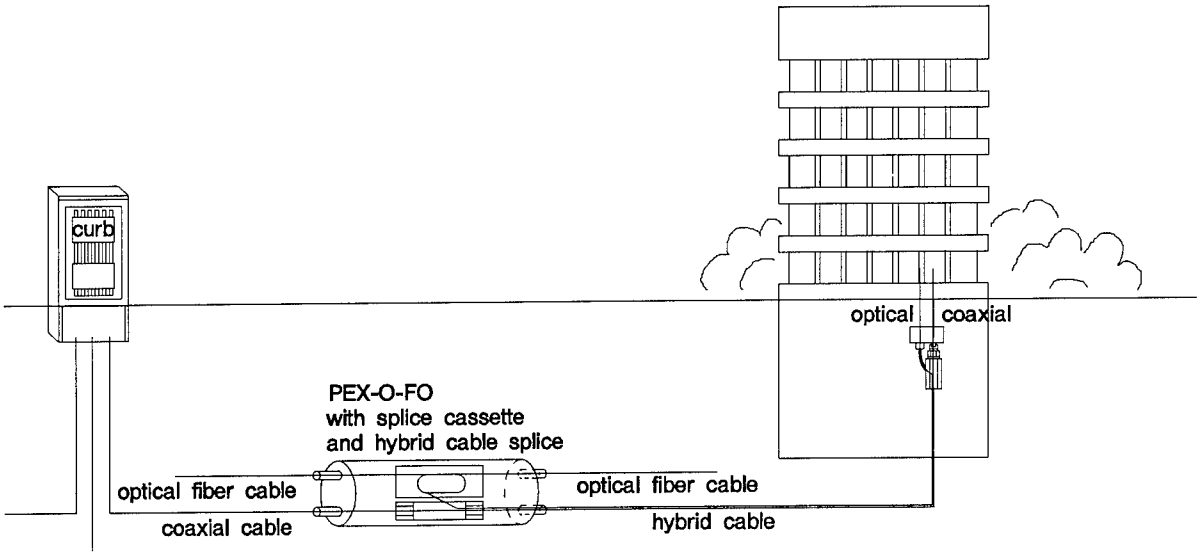


Figure 11: Use of hybrid cable accessories (example)

Conclusions

A new hybrid fiber/coaxial cable for trunk and distribution applications has been introduced. The optical fibers are well protected in the center conductor. The cable construction is based on a widely used aluminium coaxial cable and characterized by a smallest possible diameter and cable weight. These features, as well as its circular cross-section and the characteristics described in this paper contribute to render the transportation, installation and operating properties of the cable very attractive.

Accessories necessary for the installation and operation of the hybrid cable have been presented as well as a solution for hybrid drop cables.

Later installation of optical fibers in the center conductor of a coaxial cable consisting of an empty, welded copper tube, is presently under investigation.

Acknowledgements

The authors gratefully acknowledge the cooperation of Messrs. H. Hofheimer and D. R. Stein of Cable Consultants Corp., Larchmont NY in reviewing this paper and of Dr. Ziemek of ALCATEL kabelmetal, Hannover.

References

1. "Optimized VARIO Leaky Feeders for 900 and 1800 MHz Frequency with Optical Fibers Integrated in the Inner Conductor for Use in Mobile Radio Communication Systems in Tunnels and Buildings", G. Brambilla, H. G. Haag, K. Schulze-Buxloh, A. Weiss, Proceedings IWCS 1994, pp. 710 - 714

2.) "Characteristics of a single-mode optical fiber cable" CCITT Rec. G652 , 1988

3.) "Standard Specification for Copper-Clad Aluminum Wire", ASTM B 566

4.) "Coaxial cables used in cabled distribution networks Part 4: Sectional specification for distribution and trunk cables" prEN 50117-4

5.) "Standard Specification for Polyethylene Plastics Molding and Extrusion Materials", ASTM D 1248

6.) "Coaxial cables used in cabled distribution networks Part 1: Generic specification" prEN 50117-1



Peter E. Zamzow
KABEL RHEYDT AG
Mönchengladbach, Germany

Peter E. Zamzow (55) is director of the Telecommunication Division. He finished his postgraduate studies in telecommunications in Munich and Graz as Dipl.-Ing. He joined AEG KABEL in 1970. He has been engaged in development and production of telecommunications cables. In 1980 he became head of the fiber optic division at AEG KABEL and in 1982 he was nominated as a senior engineer. From 1992 on he was plant manager of the new Optical Fiber Cable Plant Rheydt. Since July 1994 he is director, manager of the product group CATV, product line telecommunication, sector Germany.

Jürgen Seidenberg
KABEL RHEYDT AG
Mönchengladbach, Germany

Jürgen Seidenberg (38) received his degree and his Ph.D. in high-frequency engineering from the Technische Hochschule Aachen and joint AEG KABEL in 1989. Presently he is head of the department for optical CATV systems.



Carsten Schwiering
KABEL RHEYDT AG
Mönchengladbach, Germany

Carsten Schwiering (32) finished his studies at the University Hannover in 1991 with a degree in high-frequency engineering (Dipl.-Ing.). In the same year he joined kabelmetal electro where he was engaged in the engineering of telecommunications cables. In 1994 he joined KABEL RHEYDT where he is now responsible for the engineering of CATV cables.

The Deterioration of Transmission Characteristics and Coaxial Cable Longevity

Joseph N. D'Amico, Trevor N. Bowmer, Orlando G. Chavez and Lal M. Hore

Bellcore
Morristown, New Jersey 07962
USA

ABSTRACT

Historical data show that the long term electrical and physical reliability of CATV type coaxial drop cables is a matter of serious concern. Service providers are worried about the longevity of coaxial drop cables in new hybrid fiber-coax networks since their projected useful lives have remained largely uncertain. Moreover, we have lacked data on their possible high frequency (500-1000 MHz) transmission deterioration with aging.

We aged coaxial drop cables at temperatures of 60, 70, 80, 90 and 100 °C for over 170 days. We measured the cables' transmission characteristics and correlated their deterioration with the depletion of stabilizer in the dielectric as determined by its decrease in oxidative induction time (OIT). With the loss of stabilizer, the cables' attenuation increase; a change that is most pronounced at the higher frequencies (e.g., at 1 GHz.). We have supplemented the attenuation measurements with structural return loss and characteristic impedance measurements. These studies have enabled us to correlate stabilizer depletion with cable RF transmission loss, and also, through an Arrhenius projection, to present a method for predicting useful cable life.

INTRODUCTION

Coaxial cables have long been used in telecommunications. Early investigations by Bell Laboratories in the 1930s[1] demonstrated their ability to transmit information at high frequencies. Indeed, the telephone companies used coaxial cables to interconnect their Central Offices before the advent of optical fiber cables. Coaxial cables also have been used for decades by the CATV industry for the broadband transmission of video.

Copyright © Bellcore All rights reserved

In a previous paper, we reported that some CATV industry sources stated that installed CATV coaxial drop cables had an average useful life of only three years[2]. While we can often attribute a drop cable's premature failure to the use of low quality connectors, improper installation, and/or a low quality cable, we have remained unable to predict the useful life of a properly manufactured and installed coaxial drop cable. Such information has become critically important with the convergence of the telecommunications and the CATV industries and the expansion of broadband networks.

In this paper, we examine the changes that occur in a coaxial drop cable as it ages. We correlate those changes and propose a method for projecting useful drop cable life.

TEST METHODS

We accelerated the deterioration of coaxial drop cables by aging them at 60, 70, 80, 90 and 100 °C in forced air ovens. Before aging and then periodically, we examined the relative oxidative stability of the cables' dielectric by measuring its oxidative induction time. We also measured the cables' signal attenuation, their structural return loss (SRL) and characteristic impedance.

Since the number of test samples could easily become unmanageably large, we limited our investigation to two Series 7 coaxial drop cables: a non-messengered aerial cable and a cable designed for direct burial. The cables were cut into individual 500 ft. coils to form the aging and reference electrical test specimens. These samples were terminated with weatherproof series 7 "F" connectors having an integral center conductor . (The connectors contained a heat resistant silicone gel to resist moisture ingress.) A second series of coils of 100 ft. length were prepared for aging in the same ovens as the 500 ft. electrical test specimens. The samples were periodically removed from the ovens. The electrical test samples were measured and an approximately 3 ft. length was removed from the 100 ft. coils for stabilizer analysis. They were dissected and the dielectrics were analyzed for residual stability by differential thermal analysis. The aging ovens were continually monitored by a temperature data logger[3].

We measured the cables' electrical characteristics from 5 MHz to 1 GHz with a vector network analyzer equipped with an "S" parameter test set[4]. We also measured an unaged reference cable to determine the intrinsic error in the measurement method. We then plotted the length of time elapsed for a ten percent deterioration of cable attenuation versus the different aging temperatures to present a method for projecting the useful longevity of a real-world cable.

The residual thermal stability was determined by measuring the oxidative induction time of the cables' dielectric with a differential scanning calorimeter (DSC)[5]. The tests were conducted according to ASTM D 4565, Section 17, at 180 °C in oxygen as specified in GR 1398-CORE, Bellcore's generic requirements document for coaxial drop cables.

EXPERIMENTAL

Samples

We tested two coaxial drop cables representing the two most widely used drop cable designs:

A. A series 7 non-messengered aerial drop cable with a standard shield. This cable consists of a 16 gauge copper-clad steel center conductor, a foamed polyethylene dielectric, an inner shield of an aluminum-polypropylene-aluminum laminated tape overlapped and bonded to the dielectric, an outer shield consisting of 34 AWG aluminum braid wire providing 60% coverage, and a flame retardant black PVC (polyvinyl chloride) jacket extruded overall.
B. A series 7 coaxial drop cable designed for direct burial. This cable is similar in construction to that of the aerial cable. It, however, contains a flooding compound between its shields and its sheath, an extruded black polyethylene jacket.

Both these cables were manufactured with a stabilizer system designed to meet Bellcore's drop cable dielectric oxidative thermal stability requirements. They were supplied as single lengths (>4000 ft.) on oversized reels to ensure the uniformity of the test specimens.

Testing

We measured the cable attenuation, structural return loss (SRL) and characteristic impedance at frequencies of 5 MHz to 1 GHz. We employed time delay to allow for the electrical length of the cable. When making SRL and characteristic impedance measurements, the effects of test leads and connectors were removed by the time domain inverse Fast Fourier Transform (FFT) gating function of the network vector analyzer.

The residual oxidative stability of the cable dielectric was characterized by measuring its oxidative induction time (OIT) at 180 °C in oxygen. Samples were prepared as cylindrical cross-sectional disks to average the stabilizer in the various components of the dielectric. At least an inch of insulation was removed and discarded before cutting the specimen disk. (Prior analysis had shown that end effect oxidation did not penetrate more than 0.25 to 0.5 inches into the cable.) The test was conducted according to ASTM D 4565, Section 17 (Revised 1994) and Bellcore GR-1398-CORE. Since we were interested in determining when the stabilizer content would approach zero (or some plateau) as the cable aged and in correlating that time with the deterioration of the cable's transmission characteristics, we drew the baseline intercept from the dielectric's first appreciable oxidation exotherm rather than as described in the specification. (See Figure 1.) The indicated OIT determinations are therefore lower then they would be if we were performing this test for quality assurance purposes.

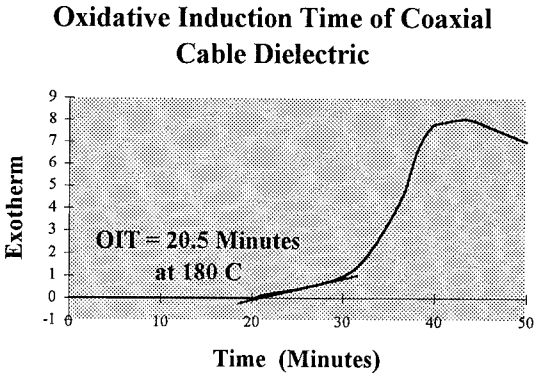


FIGURE 1

Lastly, we used a ten percent increase in cable attenuation in developing our method for projecting cable lifetimes by an Arrhenius projection to service temperatures. The attenuation, for example, of a 600 ft. long Series 7 drop cable is approximately 30 dB at 1 GHz. A 3 dB increase in loss would halve the strength of the transmitted signal. The attenuation of a lower series cable would obviously be greater.

RESULTS AND DISCUSSIONS

Electrical Measurements

In Table 1 we present attenuation measurements taken on Sample "A", the coaxial aerial drop cable, at selected frequencies from 5 MHz to 1 GHz. Prior to aging, the cable's attenuation over this frequency range was 0.41 dB to 4.9 dB per hundred feet at 20° C. These results follow from the well known fact that the attenuation of a coaxial cable increases both with its length and according to the square root of the transmitted frequency[6]. Figure 2 shows

the attenuation curve of a 500 ft. unaged Series 7 drop cable. On a 500 ft. length of test cable, a 5% increase in attenuation at 5 MHz would be only 0.1 dB. Such a change is difficult to measure accurately and reproducibly. At 1 GHz, that same percent change would be over 1.2 dB. It is reasonable, therefore, that upon aging, we should first see a noticeable increase in a cable's attenuation at the highest frequency at which it is tested. As the cables aged at elevated temperatures, their attenuation, indeed, began to increase. Table 2 shows that the attenuation of Sample "A", aged at 100 °C, averaged over the test frequencies given in Table 1, increased 5.6% in 46 days, 8.6% in 80 days and 23% in 151 days. As the aging time of the cable increased, the stabilizer in the cable's dielectric was consumed and it began to degrade (as shown by the reduction in OIT in Figure 3). As the degradation progressed, the cable's attenuation increased ever more rapidly. While there is some evidence that the percent deterioration in a cable's transmission ability increases with increasing frequency, the data are not yet conclusive.

	Attenuation (dB)				
Cable aged at 90 C					
5 Mhz.	0.4	0.4	0.4	0.4	0.4
55 Mhz.	1.2	1.2	1.2	1.2	1.2
300 MHz.	2.6	2.6	2.6	2.7	2.8
433 MHz.	3.1	3.2	3.2	3.3	3.4
754 MHz.	4.2	4.2	4.3	4.5	4.5
1000 MHz.	4.9	4.9	4.9	5.2	5.3
Cable aged at 100 C					
5 Mhz.	0.4	0.4	0.4	0.4	0.4
55 Mhz.	1.2	1.2	1.3	1.4	1.4
300 MHz.	2.6	2.7	2.8	3.3	3.4
433 MHz.	3.1	3.3	3.4	4.0	4.1
754 MHz.	4.2	4.4	4.6	5.4	5.6
1000 MHz.	4.9	5.2	5.4	6.3	6.6
	0	**46**	**80**	**151**	**171**
	Cables Oven Aged (Days)				

The Accelerated Aging Of Series 7 Aerial Drop Cable Sample "A"

Signal Attenuation (dB) Per 100 Feet At 20 C

TABLE 1

Returning to Table 2, let us look at the attenuation of this same cable when it is aged at 90° C. After 46 days there is no significant deterioration in the cable's transmission ability. (Later we will see that OIT measurements show that the dielectric's stabilization system was still intact at that time.) After aging for 80 days, and when tested at the same

Coaxial Drop Cable - Attenuation vs. Frequency

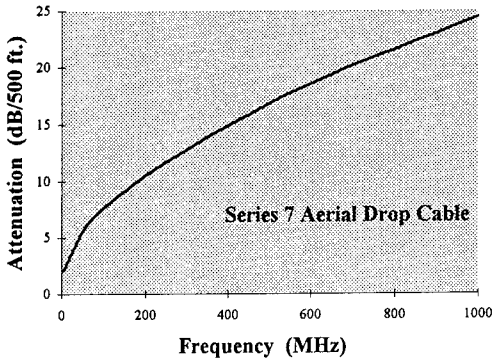


FIGURE 2

frequencies as in the previous example, the attenuation of this cable has increased 1.5%, and after 151 days, 5.9%. At the time of this writing (171 days of accelerated aging), there have been noticeable changes in cable attenuation at these higher aging temperatures, but there has been little change at the lower aging temperatures.

Aging Temp. (C)	%			
80	0.0	0.5	2.3	3.4
90	1.2	1.5	4.9	5.9
100	5.6	8.6	19.2	23.3
	46	**80**	**122**	**151**
	Days Aged			

Series 7 Aerial Drop Cable Sample "A" Percent Increase In Attenuation Upon Aging*

*Average increase in attenuation from 5 to 1000 MHz at frequencies indicated in Table 1

TABLE 2

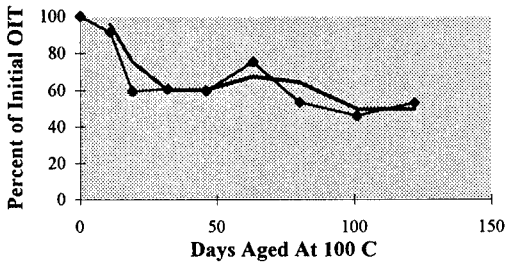
Structural return loss and characteristic impedance measurements before and after aging at 90 °C are illustrated in Figures 4 and 5. There we can see the deterioration that has occurred in those electrical transmission characteristics after 171 days of accelerated aging.

Stabilizer Measurements

A coaxial cable's long term transmission depends on the continued integrity of the dielectric separating its center conductor from its shield. Each cable has a (foamed) material-specific dielectric constant and a very low dissipation factor. Today, almost all coaxial drop cables use a gas injected foamed polyethylene dielectric. It is usually extruded over a center conductor that has been coated with a polymeric adhesive. To ensure its longevity, the foamed polyethylene is stabilized to resist thermally-induced oxidation. A practical way to measure the degree of stabilization is to measure its oxidative induction time (OIT). This test provides an indication of the stabilizer's effectiveness by measuring the length of time that oxidation of the polymer is inhibited at an elevated temperature (e.g., 180 °C). It has long been used by the telephone industry to measure the oxidative stability of polyolefin insulated conductors (PIC cables). There it has been related to real-world cable longevity[7]. The OIT test requirement for coaxial drop cable as given in the Bellcore generic requirements[8, 9] is less than that for polyolefin insulated conductors since the coaxial drop cable dielectric is partially protected from oxidation by its shielding tape.

In Table 3 we present OIT test results on the coaxial aerial drop cable (Sample "A"). If we correlate the onset of increasing cable attenuation (Tables 1 and 2) with the OIT measurements, we find that noticeable increases in attenuation occurred when the OIT retention time was 55 to 65% of its original value. The OIT values plateau at that level, one which is specific to this cable. We also found a large variation in our test results. Through infrared analysis and high performance liquid chromatography (HPLC), we found that the stabilizer system contained additional antioxidants along with those traditionally used in PIC telephone cable. It appears from OIT testing that the stabilizer in sample "A" is consumed in a stepwise fashion. Cable transmission deterioration appears to have begun when stabilizer depletion reached a plateau, a phenomenon which indicates that the dielectric's deterioration may have begun upon the consumption of a major component of the stabilizer system.

Stabilizer Retention In Coaxial Aerial Drop Cable Upon Oven Aging*



*As indicated by the oxidative induction time measured on samples aged at 100 C and shown as a percent of .the OIT of unaged samples.

FIGURE 3

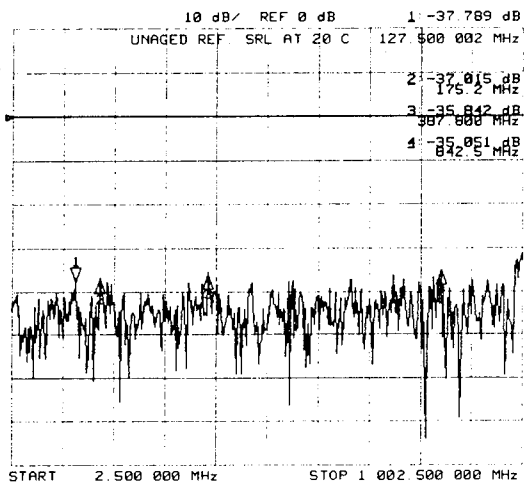
	OIT (Min.)	% of Orig.	OIT (Min.)	% of Orig.	OIT (Min.)	% of Orig.	OIT (Min.)	% of Orig.	OIT (Min.)	% of Orig.
Cable aged at 90 C	24.6	100	24.6	100	21.8	89	14.9	60	15.0	61
Cable aged at 100 C	24.6	100	14.7	60	18.5	75	13.2	54	11.3	46
	0		**46**		**63**		**80**		**101**	
	Days Aged									

Series 7 Aerial Drop Cable Dielectric
Sample "A"

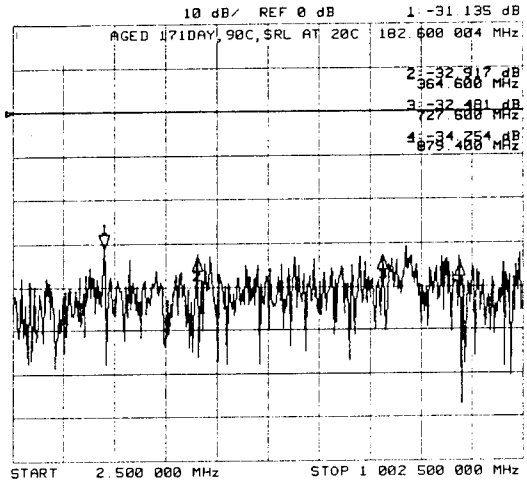
Oxidative Induction Time (Minutes)
And
Percent OIT Retention After Oven Aging

TABLE 3

Structural Return Loss (SRL) In dB Of Coaxial Aerial Drop Cable
Before and After Oven Aging



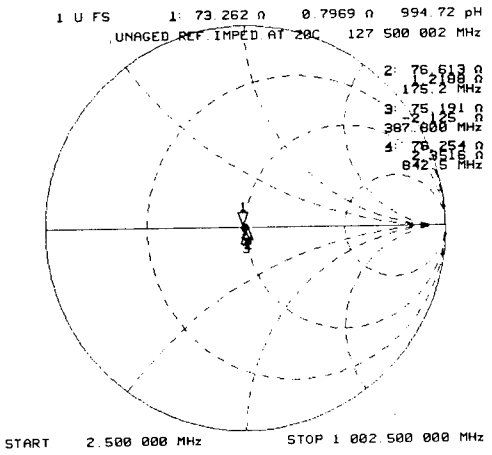
Before Aging



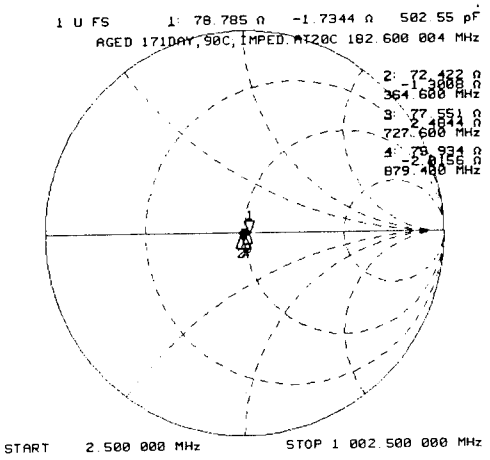
After Aging

FIGURE 4

Characteristic Impedance In Ohms Of Coaxial Aerial Drop Cable
Before and After Oven Aging



Before Aging



After Aging

"Smith Charts" showing calculated characteristic impedance of series 7 aerial drop cables. Reactance values in the upper half of the Smith chart circles are positive (inductive) reactance while those in the lower half of the circles are negative (capacitive) reactance.The indicated data points are those marked in Figure 4.

FIGURE 5

The distribution in OIT measurements is more difficult to interpret. Repeated measurements taken on adjacent sections of the same cable specimen usually agreed within ± 2 minutes. At times, however, the measurement variations were considerably greater; for example, the OIT values of four adjacent samples taken from cable "A" aged 80 days at 90 °C were 21.1, 11.8, 6.4, and 20.1 minutes respectively. With increased sampling, the data average approached the "expected" value. We have attributed this wide data distribution to a non-uniform dispersion of the stabilizer. We have seen this effect in many coaxial cables from several manufacturers and it is likely the result of non-uniform stabilizer dispersion at the extruder line.

Cable Lifetime Projection

Figure 6 shows the percent increase in coaxial cable attenuation that occurred as the cables were aged at the four selected aging temperatures. This Figure also shows the cable's attenuation as smooth curves derived by polynomial regression which are then projected into the future. We have selected data points representing 5.0, 7.5, and 10.0 percent increases in attenuation upon cable aging and derived the extrapolations shown in Table 4. By plotting the time (on a logarithmic scale) required for a selected percent change in signal attenuation to occur in aged cables as a function of the reciprocal of the (absolute) aging temperature [Log_{10} T(time) vs. $°K^{-1}$(temp.)], we can make an Arrhenius projection to the expected useful lifetime of a coaxial drop cable. We consider the effective service temperature of outdoor coaxial drop cable will be 35 to 40 °C[10]. Its actual service temperature will depend on where in the country the

Cables	Days Cable Aged		
Aged At 100 C	44	60	78
Aged At 90 C	133	*176	*215
Aged At 80 C	*220		
	5%	7.50%	10%
	Percent Increase In Attenuation		

*Extrapolated Data

Series 7 Aerial Drop Cable
Sample "A"
Increase In Attenuation Upon
Accelerated Aging

TABLE 4

cable is deployed and on whether it is placed aerially or buried. As of this writing we do not yet have data at the lower accelerated aging test temperatures for the selected 10 percent increase in cable attenuation. We cannot, therefore, accurately project the expected useful cable

The Attenuation of Coaxial Aerial Drop Cable Upon Oven Aging

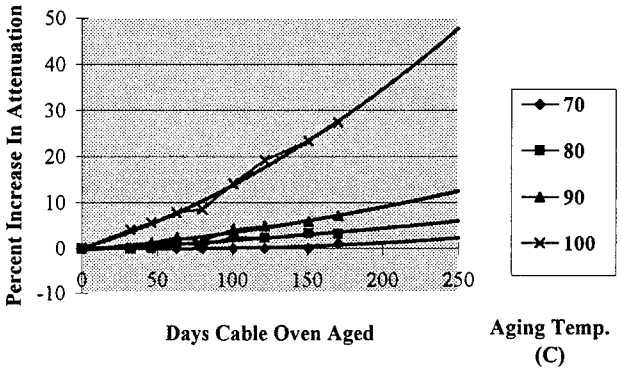


FIGURE 6

lifetime. Data at three to four temperatures are required. Earlier work on PIC cable also indicates that the Arrhenius projection from the higher to lower test temperatures may not be linear.

	Attenuation (dB)			
Cable aged at 90 C				
5 Mhz.	0.4	0.4	0.4	0.5
55 Mhz.	1.2	1.2	1.2	1.3
300 MHz.	2.6	2.7	2.7	2.7
433 MHz.	3.2	3.2	3.2	3.2
754 MHz.	4.3	4.3	4.3	4.3
1000 MHz.	5.0	5.0	5.0	5.0
Cable aged at 100 C				
5 Mhz.	0.4	0.4	0.5	0.5
55 Mhz.	1.2	1.3	1.2	1.3
300 MHz.	2.6	2.7	2.7	2.9
433 MHz.	3.2	3.3	3.3	3.6
754 MHz.	4.3	4.4	4.4	4.8
1000 MHz.	5.0	5.0	5.1	5.6
	0	81	122	175
	Cables Oven Aged (Days)			

The Accelerated Aging
Of Series 7 Buried Drop Cable
Sample "B"

Signal Attenuation (dB) Per 100 Feet
At 20 C

TABLE 5

	OIT (Min.)	% of Orig.	OIT (Min.)	% of Orig.	OIT (Min.)	% of Orig.	OIT (Min.)	% of Orig.	OIT (Min.)	% of Orig.
Cable aged at 90 C	28.5	100	25.5	89	18.1	63	14.6	51	15.0	53
Cable aged at 100 C	28.5	100	13.4	47	8.5	30	7.3	26	5.4	19
	0		25		39		53		81	
	Days Aged									

Series 7 Buried Drop Cable Dielectric
Sample "B"

Oxidative Induction Time (Minutes)
And
Percent OIT Retention After Oven Aging

TABLE 6

We have consciously resisted making cable lifetime projections until we have more data. Nonetheless, projections based on a five percent increase in cable attenuation on cables that have been aged at high temperature suggest that the cable dielectric stabilization requirement presented in Bellcore's GR-1398-CORE may be adequate to ensure a 20+ year cable dielectric lifetime. This conclusion is tentative and needs to be verified by our continued testing. The reader is cautioned that not all cables having the same OIT test result will have the same longevity. To have equal longevity, they must also contain the same stabilization package equally dispersed. OIT test results must be correlated with long term aging and field test data.

Sample "B"

In Tables 5 and 6 we present similar data for Sample "B", the buried coaxial drop cable. This cable is aging somewhat more slowly than Sample "A". Its oxidative induction times are approaching zero as the cable ages.

CONCLUSION

History has shown that coaxial drop cables are often the weak link in a CATV distribution plant. Within the past two to three years, telecommunications companies have recognized that coaxial drop cable may be the most cost effective medium for delivering broadband services (telephony, video, data) the final step, from "curb" to home. There is no inherent material or technical reason that a coaxial drop cable cannot be made reliable and long lasting. Coaxial cable manufacturers have responded to the industry's concerns and, along with other improvements, have reformulated the stabilization system for the coaxial drop cable dielectric. We have evaluated two such (reformulated) cables in this report.

From our analysis we conclude:

1. Coaxial drop cable transmission degradation in the form of increased signal attenuation begins upon the depletion of at least one major component of the cable's dielectric stabilization system. The loss of stabilizer can be tracked by oxidative induction time analysis on aging cable samples.
2. The attenuation of a coaxial cable increases rapidly once degradation of the dielectric begins. While aging degrades cable transmission at all frequencies, its effects are more serious at high frequencies. For example, a ten percent increase in attenuation at one GHz could result in as much as a 2.5 dB signal loss on a long (500 ft., Series 7) drop cable, reducing to almost half the signal delivered to the customer. That same percent loss at five or fifty MHz would be small and would not noticeably affect signal reception.
3. Lastly, we present a method for extrapolating accelerated cable aging data to real-world cable-use temperatures. We suggest that the slope of the Arrhenius projection to service temperatures, once established, can be judiciously used to project the lifetime of cables with different levels of stabilization so long as the dielectric remains a foamed polyethylene blend.

REFERENCES

[1] L. Espenschied and M. E. Strieby, "Systems For Wideband Transmission Over Coaxial Lines", Bell System Technical Journal, 13, 654 (1934)

[2] P. L. Key et al., "Reliability of Coaxial Cable Drops In The CATV Industry", National Fiber Optics Engineers Conference, Technical Paper, 3, 103 (1994)

[3] Model 50 Datalogger, mfd. by Electronic Controls Design, Inc., Milwaukie, OR

[4] Models HP 8753C with external "S" Parameter Test Set and HP 8753D with integral "S" Parameter Test Set, mfd. by Hewlett-Packard Corp., Englewood, CO

[5] Model 2100 Differential Scanning Calorimeter (DSC), mfd. by TA Instruments, Inc., New Castle, DE

[6] Cable Television, 2nd. Edition, W. Grant, Society of Cable Telecommunications Engineers, Exton, PA

[7] T. N. Bowmer et al., "Thermal Stability Tests For Polyolefin Insulations", Proceedings of the 39th. International Wire and Cable Symposium, 316 (1990)

[8] Bellcore GR-1398-CORE, "Generic Requirements For Coaxial Drop Cable", Issue 1, 7/1994, 4.2.3, Bell Communications Research, Inc., Morristown, NJ

[9] TR-NWT-000421, "Generic Requirements For Metallic Telecommunications Cables - Thermal Oxidative Stability Requirements For Cables With Polyolefin Insulated Conductors", Issue 3, 9/1991, Revision 1, 12/1992, 2.1.1, Bell Communications Research, Inc., Morristown, NJ

[10] T. N. Bowmer, "Cracking of Foam-Skin Insulation In Pedestals", Proceedings of the 37th. International Wire and Cable Symposium, 475 (1988); Referenced therein.



Joe D'Amico is a member of the Plastics and Metals Technology Group at Bellcore. He has worked on engineering and materials issues affecting all types of telecommunications and power cables in his career. He first worked with communications cable at the Western Electric Company before joining the General Cable Company. There as a senior research physicist, he investigated the structure and composition of all types of telecommunications wire, cable and optical fiber as well as electrical power cables. Since 1985 Joe has worked for Bellcore, initially as a quality assurance engineer and since 1989 as a researcher in the Applied Research and the Network Integrity Organizations. Joe is a graduate of Seton Hall University. He received his MS degree from Fairleigh Dickinson University.



Lal Hore is responsible for the preparation of Bellcore's Generic Requirements for Outside Plant Cables and the development of high speed transmission requirements for coaxial cable and other wire products. After receiving a M.Sc. Tech. degree in Applied Physics from the University of Calcutta and a Dr. Tech. degree from the Technical University of Budapest in Electrical Engineering, he joined Bell Northern Research in 1970 to design and develop communications cables. In 1972, Lal moved to General Cable Company where he worked as a manager in the Communications Cable Section and next as a Staff Project Manager in the Applications Engineering Section until 1987 when he joined Bellcore.

Dr. Hore has authored numerous technical papers on dielectric materials and telecommunications wire and cable and holds a number of patents on telecommunications cables.

Trevor Bowmer is a member of the Plastics and Metals Technology Group at Bellcore. He received his Ph.D. in chemistry from the University of Queensland, Australia, where he studied radiation chemistry of polymers. Joining Bell Laboratories in 1980, he investigated radiation cured systems and lithographic materials. In 1984, he came to his present position where his research on network integrity problems has centered on the degradation mechanisms and characterization of polymeric materials used in telecommunications applications.

A NEW HYDROLYTICALLY STABILIZED PBT FOR FIBER OPTIC CABLE CORE COMPONENTS

James M. Finan *Product Development Chemist*
Misha Jacobson *Process Development Engineer*
Leslie J. Goff *Product Line Design Leader*

GE Plastics
1 Plastics Avenue
Pittsfield, MA 01201

ABSTRACT

A new Polybutylene Terephthalate has been developed for use in the buffer tube component of optical cables. This material has been designed to drive processing productivity and performance. Improvements made in this LOW VISCOSITY HR PBT formulation over its predecessor, a HIGH VISCOSITY HR PBT, have yielded a robust material capable of excellent performance at speeds well beyond current industry standards. A combination of GE stabilization technology and proprietary resin technology, has yielded lower viscosity and improved stress relaxation while maintaining hydrolysis resistance beyond the Bellcore GR-20-Core, Issue 1, specification.

INTRODUCTION

Polybutylene Terephthalate (PBT) is an engineering thermoplastic that provides many attractive mechanical and physical properties. It is a semi-crystalline polymer with good chemical resistance, good flow, and very fast crystallization under typical processing conditions. PBT melts at approximately 225°C and has a glass transition temperature (T_g) ranging from 40-60 °C [1,2]. It has found widespread use in the buffer tube component of loose tube fiber optic cables. However, because PBT is a condensation polymer and therefore susceptible to hydrolysis under certain conditions, the hydrolytic performance of buffer tube material has been a key concern in the fiber optic market. Bellcore's document, GR-20-Core, Issue 1, addresses field performance by proposing methods for predicting buffer/core tube degradation.

In 1993 GE Plastics introduced a hydrolysis resistant PBT (HIGH VISCOSITY HR PBT) for use in loose tube fiber optic cable constructions. This material was based on a proprietary stabilization technology which provided very good hydrolysis resistance, as well as enhanced product capability after processing and during the life of the cable.

Since the introduction of HIGH VISCOSITY HR PBT, material requirements in the fiber optic market have changed. The performance changes are reflected in Bellcore's document GR-20-Core, Issue 1. The processing requirements are a result of market trends which point toward reducing manufacturing costs while increasing productivity. These trends are complicated by the increasing competitive pressures from a global marketplace that has seen tremendous growth in the past 18 months. As part of its Multi-Generation Product Planning, GE Plastics has developed LOW VISCOSITY HR PBT to address these shifting market needs.

Productivity and reduced costs in the manufacture of buffer tubes have been achieved by driving higher extrusion line speeds to produce more cable on existing equipment. The next generation, a low viscosity Hydrolysis Resistant PBT resin, has been designed with the specific objective of optimizing processability while maintaining material performance. Modifications in the rheological and thermal properties coupled with GE proprietary stabilization technology, have resulted in the generation of a robust PBT capable of adapting to the wide variety of equipment and screw designs used by buffer tube manufacturers.

CHEMISTRY

As part of the polyester family, PBT is subject to hydrolysis. The hydrolysis of polyesters has been widely studied and well documented [3]. A variety of factors such as molecular weight, end groups, residual polymerization catalyst and additives, such as glass, mineral fillers and flame retardants, can affect the hydrolytic stability of polyesters.

Of particular concern in the fiber optic market is hydrolysis under conditions of high humidity. This reaction can be either acid- or base-catalyzed and results in chain scission, which, with sufficient loss in molecular weight, can lead to loss of mechanical properties. The mechanism for acid hydrolysis is represented by the equilibrium equation in Figure 1.

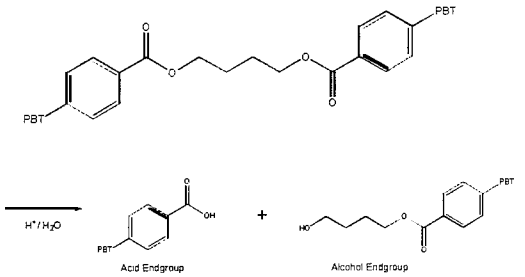


Figure 1. Acid hydrolysis.

Hydrolysis of PBT, by this mechanism, is dependent on the Carboxylic Acid End Group (CEG) concentration present in the material. There are several sources for carboxylic acid end group formation in polyester resins: residual end groups resulting from the polymerization process; acid end groups formed by thermal degradation during melt processing; and acid end groups as a consequence of chain scission during the hydrolysis reaction.

Understanding and controlling these reactions is critical in stabilizing PBT. In general, lower CEG concentration equates with better resistance to hydrolytic degradation. GE Plastics' proprietary stabilization technology is based on modification of the resin during manufacturing, thereby reducing the concentration of carboxylic acid end groups. This technology also offers control of the CEG formation during processing and hydrolysis. HIGH VISCOSITY HR PBT and LOW VISCOSITY HR PBT have been shown to maintain low carboxyl end group concentrations for long periods of time under harsh testing conditions. Earlier work has shown that these materials are 2-3 times better than standard PBT resins under these test conditions [4,5].

Evaluation of relative hydrolysis resistance under two sets of testing conditions is shown in Figures 2 and 3. The graph in Figure 2 plots the generation of acid end groups under accelerated test conditions of 120°C and 100% relative humidity as a function of time.

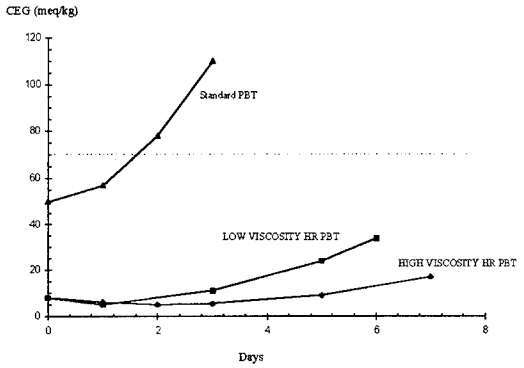


Figure 2. Hydrolytic Stability Testing - Accelerated Testing Conditions (120C/100%RH)

The initial decrease in the CEG levels for HIGH VISCOSITY HR PBT and LOW VISCOSITY HR PBT demonstrates the effectiveness of GE Plastics' Stabilization Technology in controlling acid end group generation. This is in contrast to the results for standard PBT, which exhibits an increase in CEG immediately upon processing, and again at aging. This same behavior will be true of any unmodified PBT, irrespective of initial CEG content.

Measurement of CEG provides a chemical understanding of material performance under hydrolytic aging conditions. Material performance will begin to deteriorate at CEG levels over 70 meq/kg. The results of tensile testing under conditions similar to Bellcore's GR-20-Core, Issue 1, specification are plotted in Figure 3. The data shows that the LOW VISCOSITY HR PBT formulation retains over 70% of the hydrolysis resistance of HIGH VISCOSITY HR PBT and clearly surpasses the Bellcore GR-20-Core requirement of 10% elongation after 45 days.

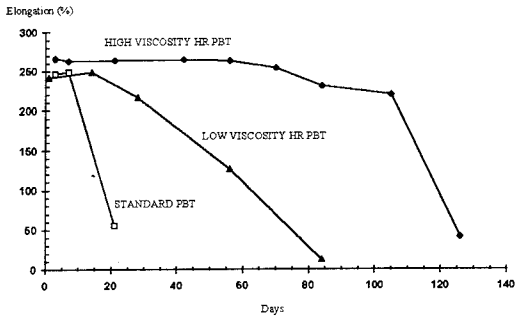


Figure 3. Hydrolytic Stability Testing - Conditions: 85C/94% RH

MATERIAL CHARACTERIZATION

GE Plastics' main goal in the development of LOW VISCOSITY HR PBT was to improve processability and performance at high line speeds through improved rheological properties. Implicit in the development of this new, lower viscosity product, was a need to maintain the mechanical properties of the parent resin, HIGH VISCOSITY HR PBT. As shown in Table 1, tensile properties, which are key in fiber optic tubes, are maintained. In addition, LOW VISCOSITY HR PBT retains the flexural properties of the higher molecular weight HIGH VISCOSITY HR PBT.

Table 1
Material Properties of LOW VISCOSITY HR PBT and HIGH VISCOSITY HR PBT

	LOW VISCOSITY HR PBT	HIGH VISCOSITY HR PBT
Melt Viscosity (poise)	4,000	13,000
Tensile Strength (psi)	8100	8100
Tensile Elongation (%)	300	280
Flexural Modulus (psi)	325,000	340,000
Flexural Strength (psi)	12,000	12,000

Rheological measurements on this new product are shown in Figures 4 and 5. The rate sweep in Figure 4 highlights the viscosity difference between HIGH VISCOSITY HR PBT and LOW VISCOSITY HR PBT. Included for comparison is the curve for STANDARD

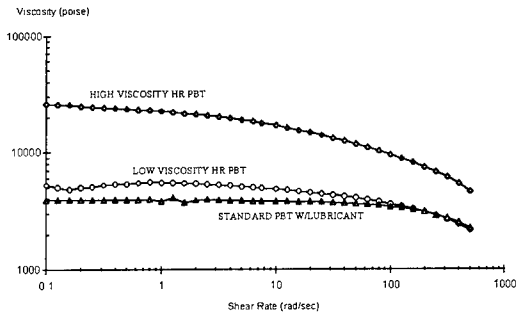


Figure 4. Rate Sweep at 250C.

PBT with an equivalent viscosity to the LOW VISCOSITY HR PBT. The behavior of LOW VISCOSITY HR PBT exhibits some shear thinning, which is a key to the improved processability of this new material.

Figure 5 shows the changes in viscosity on extended heating. The increase in viscosity observed for the LOW VISCOSITY HR PBT provides processing advantages which will be discussed in the following section.

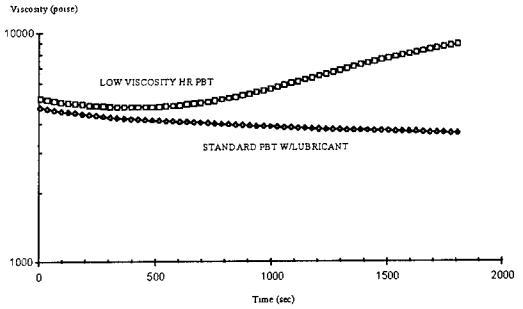


Figure 5. Time sweep at 250C.

PROCESSING STUDIES

A key criterion in the evaluation of a new material is the size of the processing window. With an overall goal of developing the most thorough assessment of the processability of LOW VISCOSITY HR PBT, data was gathered from industry trials, as well as process development laboratory lines at GE Plastics' Polymer Process

Development Center, Davis-Standard and Nokia-Maillefer.

Equipment Studies

A first look at the processability of LOW VISCOSITY HR PBT involved an assessment of its ability to be processed on equipment of varying design, size and configuration.

Output rates are sensitive to both pressure and screw rate. That is, the pumping action changes with increasing shear. Figures 6 and 7 consider output from two perspectives. Figure 6 compares output rates per revolution for LOW VISCOSITY HR PBT as a function of different extruder sizes, as well as different design screws.

Examination of the output-per-revolution ratio can demonstrate the range over which a material will exhibit stable processing. The data indicates that LOW VISCOSITY HR PBT is capable of maintaining a stable, linear output rate, independent of screw design and extruder size, over a wide RPM range.

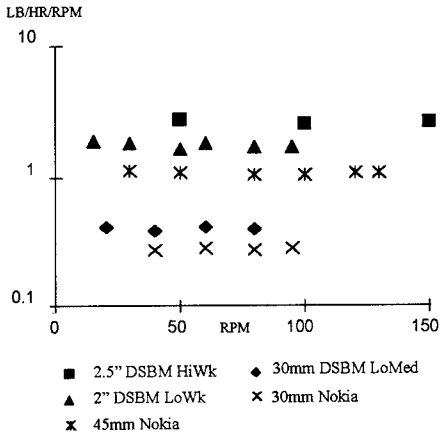


Figure 6. Pumping efficiency.

Figure 7 shows the variation in pumping efficiency for several different screw designs. The data demonstrates that a linear relationship between speed and output can be maintained throughout a wide operating range for each screw.

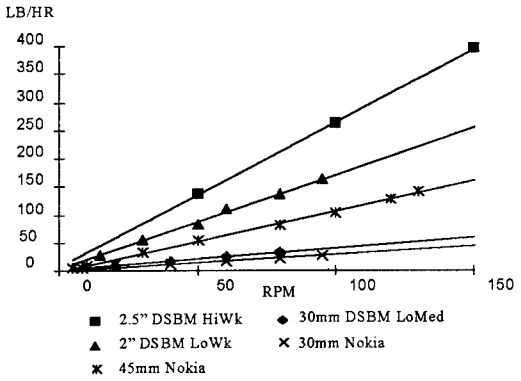


Figure 7. Pumping efficiencies of various size and design screws for LOW VISCOSITY HR PBT.

Thermal Stability

The optimum temperature profile is different for each combination of screw design and extruder. The thermal stability of LOW VISCOSITY HR PBT plays a key role during melt processing and gives the resin the ability to process linearly, independently of screw design, even in regions of temperature induced shear, where other polyesters might fail due to degradation or melt fracture.

Thermal performance experiments were designed for LOW VISCOSITY HR PBT [6]. Long-term thermal stability trials were performed on a Davis-Standard, 2.5", 24:1 extruder fitted with a valved test head to simulate tubing die flow restriction. Feed and head pressure were monitored at constant RPM, over a two hour period. A total variation of 1.3% in head pressure indicated a linear, stable output as indicated by Figure 8.

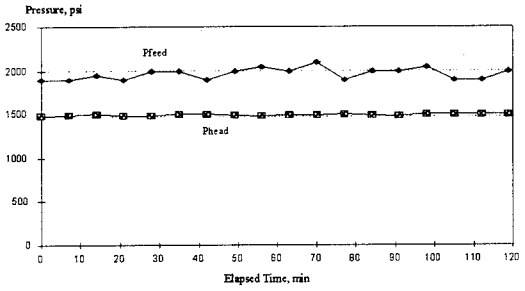


Figure 8. Long term stability check.

Another check of thermal stability involved a study to determine the effects of lower barrel zone settings on melt temperature at a constant RPM setting. Beginning with 520°F (feed), 510°F, 500°F and 490°F barrel temperature sets, the profile was iteratively reduced in 20°F increments to 460°F (feed), 450°F, 440°F, 430°F. The graph in Figure 9 plots pressure and melt temperature variation as a function of the four different temperature profiles trialed (referenced by the barrel 4 temperature setting on the abcissa).

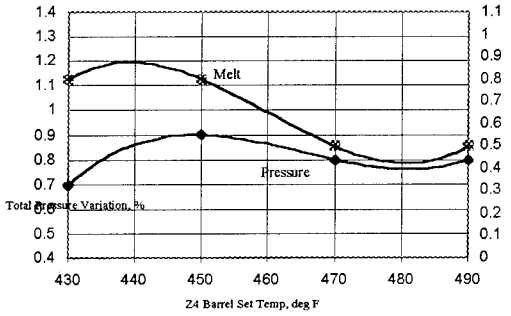


Figure 9. Pressure and Melt Temperature variation as a function of temperature profile.

The data indicates that LOW VISCOSITY HR PBT melt temperature variations did not exceed 0.9%. The plot shows that melt temperature and pressure variations track one another with the exception of the 460°F/450°F/440°F/430°F profile. This profile consists of barrel sets that are lower or within the onset of melt temperature range for LOW VISCOSITY HR PBT (T_m approximately 432°F). Melt homogeneity is not expected at these conditions.

In addition to the pressure and melt temperature variations, output and melt temperature were studied as a function of the same four barrel temperature profiles. Figure 10 represents a plot of that data. It was observed that melt homogeneity was maintained within 1 °F. The decrease in output rate seen at the second profile trialed is explained by the rheological behavior of LOW VISCOSITY HR PBT as shown in Figure 5. The competing mechanisms of increase in viscosity with time and decrease

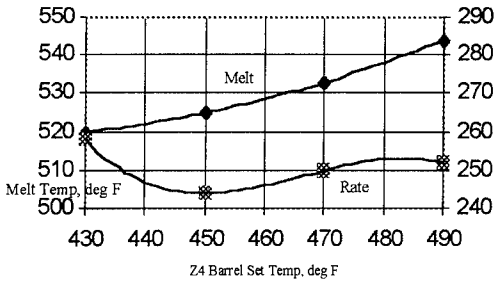


Figure 10. Melt temperature and rate as a function of temperature profile.

in viscosity due mechanical and shear heat in the extruder are dominated by the former at this temperature. The CEG reduction that takes place during extrusion is manifested rheologically by an increase in molecular weight at this temperature. CEG reduction results in chain extension and thereby, an observed "dip" in output.

Line Speed/Dimensional Stability

Having established the processing stability of LOW VISCOSITY HR PBT, experiments were undertaken to understand the correlation of the output studies to tube dimensional stability and post extrusion shrinkage characteristics.

Data for this study was generated on two different manufacturers' extrusion lines. The first is a 2", 24:1 Davis-Standard extrusion line with a standard tubing die and a DSBM low work screw. The second is a Nokia-Maillefer 45mm, 24:1 extrusion line with a standard design PBT barrier screw and tube die.

Line speeds up to 300 mpm were validated on 2.5 mm OD, filled, and variously stranded tubes. Ovality and OD measurements taken on both machines at line speeds ranging from 50 to 300 mpm were averaged and are shown in Table 2.

Table 2
Average Total Ranges for OD and Ovality.
2.5 mm OD tubes, filled and variously stranded.

	DAVIS STD	NOKIA MAILLEFER
OD AVERAGE RANGE	0.02 mm	0.02 mm
OVALITY AVERAGE RANGE	0.01 mm	0.01 mm

A second series of experiments was designed to benchmark LOW VISCOSITY HR PBT versus:

- ◊ HIGH VISCOSITY HR PBT - the parent resin;
- ◊ STANDARD PBT - a standard, non-hydrolysis resistant PBT;

and

- ◊ STANDARD PBT WITH LUBRICANT - a standard PBT formulation with a viscosity equivalent to that of LOW VISCOSITY HR PBT.

This experiment established that LOW VISCOSITY HR PBT processes within and beyond the stable range of the parent HIGH VISCOSITY HR PBT (maximum stable output achieved with the HIGH VISCOSITY HR PBT was 200 mpm). The high line speed capability of the LOW VISCOSITY HR PBT is attributable to formulation improvements over HIGH VISCOSITY HR PBT which allow the LOW VISCOSITY HR PBT to offer improved flow, with retention of melt viscosity, and relatively unchanged mechanical properties.

As Figure 11 shows, the experiment also established that the enhanced processability of LOW VISCOSITY HR PBT is not due solely to viscosity since the STANDARD PBT WITH LUBRICANT performed poorly from a tube dimensional stability standpoint.

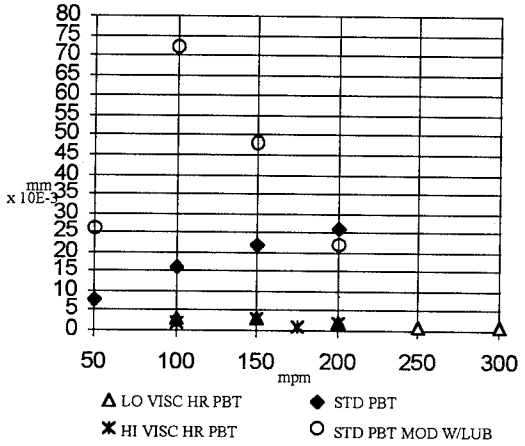


Figure 11. Total Variation in Outer Diameter as a Function of Line Speed.

CONCLUSION

Optimal processing for LOW VISCOSITY HR PBT has been established on a wide cross-section of industry and laboratory equipment, demonstrating stable, repeatable output which is independent of screw design and size over a wide rpm range.

Market trends which point toward reducing manufacturing costs while increasing productivity and quality can be met by LOW VISCOSITY HR PBT. With tube dimensional stability and post extrusion shrinkage which has been validated at line speeds up to 300 meters per minute, LOW VISCOSITY HR PBT is poised to meet these current as well as evolving needs of the fiber optic industry.

REFERENCES

1. Halser, R.S., Joshi, M., Misra, A., J.Appl. Poly Sci, Vol. 39, 1251-1264, 1990

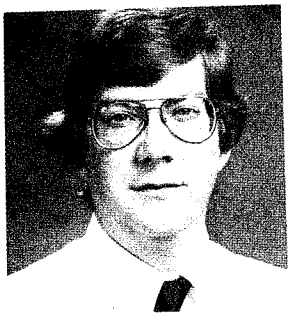
2. Brandurp, P., Immergut, E.H., Polymer Handbook, John Wiley & Sons, N.Y., 1975

3. Borman, W.F.H., Polym. Eng. Sci, 22, 883, 1982

4. Gallucci, R.R., Hamilton, D.G., Plastics Engineering, Nov. 94, pp 52-54

5. Griswold, G.N., International Wire and Cable Symposium, Nov. 1993

6. Thompson, J.R., Davis-Standard Development Report 1892, Oct. 94



James M. Finan is a VALOX® Product Development Chemist with GE Plastics, Mt. Vernon, Indiana. He holds a Bachelor of Science degree in Chemistry from Michigan State University and Masters and Ph.D. degrees in Chemistry from Harvard University.



Misha Jacobson is a Process Development Engineer with GE Plastics in Pittsfield, MA. She is a Bachelor of Science with Honors graduate of Rensselaer Polytechnic Institute with a degree in Mechanical Engineering.



Before his recent transition to Electronics Industry Management for GE Plastics, Pittsfield, MA, Leslie J. Goff was a VALOX® Product Line Design Leader with G.E. Plastics, Mt. Vernon, Indiana. He holds a Bachelor of Science degree in Biochemistry from Mississippi State University and a Ph.D. in Polymer Science from the University of Southern Mississippi.

NEW DIMENSIONALLY STABLE POLYMER FOR COMPACT AND LOOSE OPTICAL FIBER BUFFER TUBES

Martin Hochuli, Dr. Friedrich Bühler, David Jarvis
EMS-CHEMIE AG, CH-7013 Domat/Ems, Switzerland
Werner S. Zimmermann, EMS-AMERICAN Grilon Inc., Sumter, SC, 29151, USA

ABSTRACT

A new buffer tube material for compact and loose buffering of optical fibers has been developed and tested. Improvements in the polymer were made in the following areas: coefficient of thermal expansion, post shrinkage at room and elevated temperatures and heat deflection temperature. These advantages allow for the design of compact buffer tubes for installation cables, as well as cost-effective cables with central loose tube design, that exhibit excellent attenuation properties over a wide temperature range.

INTRODUCTION

The thermal expansion coefficient of optical fibres is different from that of the buffer tube materials. To achieve a length compensation free of tension, the optical fiber always has a certain overlength in the buffer tube.
Common buffering materials such as polybutylene terephthalate (PBT), the most widely used material for standard cables, or polyamide 12 (PA12) have a relatively high coefficient of thermal expansion and due to their semi-cristalline structure, a high post shrinkage at elevated temperatures. The use of such materials is limited for use in very thin buffer tubes, e.g. compact tubes in installation cables or loose tubes in high performance cables, e.g. aerial cables. A material with a lower coefficient of thermal expansion and a minimal post shrinkage is required.

It is known that mineral filled polymers, compared to unfilled, have an improved dimensional stability and increased heat distortion temperatures. However, mineral filled polymers, besides being difficult to extrude, are generally too hard and too brittle for optical fiber buffer tubes. Therefore the purpose of this projekt was to develop a new polymer which should have increased dimensional stability without compromising toughness and extrudability.

NEW DIMENSIONALLY STABLE POLYMER BASED ON POLYAMIDE 12

Based on PA 12 a new polymer which meets the above mentioned requirements has been developed. This modified material has a clearly reduced coefficient of thermal expansion and reduced post shrinkage at elevated temperatures. These facts combined with the reduced water absorption, result in a very high dimensional stability over a wide range of temperatures. Compared to an unmodified PA12 grade, the heat distortion temperature has been improved to 100°C (212°F) and the tensile E-modulus has been increased to 2000 N/mm^2. While maintaining its superb hydrolysis resistance properties, this modified polymer also retains its excellent resistance to chemicals common in cable applications.

General Properties

Table 1 shows the general properties of the new dimensional stable PA12 (PA12 DS) in comparision to a standard PBT, a modified PBT (PBT/PC-Blend) with improved dimensional stability, a standard PA12 and an amorphous PA (ISO 1874/1 PA12/MACMI, MT, 12-020) the common material for the inner layer of o.f. dual loose tubes.

Property	Norm	Unit	new PA12DS	PA12	amorphous PA	PBT	PBT/PC-Blend
Density	ISO1183	g/cm³	1.05	1.01	1.06	1.31	1.28
Tensile E-modulus	ISO 527	N/mm²	2000	1100	2200	2500	2400
Tensile strength at yield	ISO 527	N/mm²	55	45	75	55	60
Elongation at yield	ISO 527	%	6	15	8	5	6
Tensile strength at break	ISO 527	N/mm²	52	50	60	40	-
Elongation at break	ISO 527	%	>50	>50	>50	>50	>50
Notched impact strength at							
23°C	ISO180/1A	kJ/m²	8	8	8	5	6
- 30 °C	ISO180/1A	kJ/m²	5	6	4	4	5
Heat distortion temperature							
HDT/A 1.8N/mm²	ISO 75	°C	100	50	135	50	-
HDT/B 0.45 N/mm²	ISO 75	°C	150	130	145	130	-
Coefficient of thermal expansion 23 - 80°C	DIN 53752	10^{-4}/K	0.65	1.3	0.8	1.3	0.8

Table 1: General properties of the new dimensional stable PA12 (PA12 DS) in comparison to other o.f. bufffer tube materials [1]

Resistsance against hydrolysis and chemicals

The resistance against hydrolysis was tested on tubes ⌀ 1.8/2.8 mm stored at 85°C in water (Fig. 1). The test was concluded after 80 days, because no change in properties were found.
The chemical resistance was tested on tensile test bars with 3.2x10mm cross section stored in aceton and methanol at 23°C and in a glycol/ water mixture 50:50 at 110°C. This test was running over 1000 h (Fig. 2).
Compared to PBT-based polymers due to its structure PA12 generally has an excellent hydrolysis resistance and can be used also in warm and humid regions. Also due to the high chemical resistance, buffer tubes made in PA12 based materials are preffered for cables where it can not be guaranteed that the buffer tube will never be exposed to humidity, e.g. installation cables or so called "mid-span" cables.

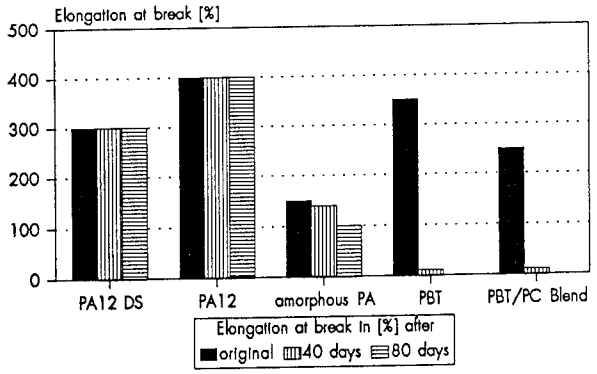


Fig. 1 Hydrolysis resistance of PA12 DS in comparison to other o.f. buffer tube materials

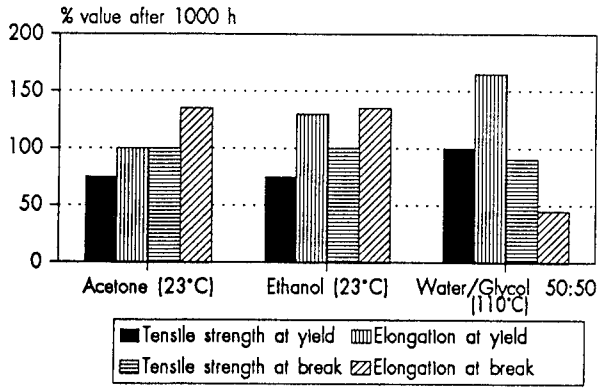


Fig. 2 Resistance of PA12 DS against acetone, methanol and water/glycol 50:50

Compability with filling compounds

The compatibility to filling compounds was tested on tubes ø 1.8/2.8 mm stored at 85°C in following three filling compound types:

a) Mineral oil based
b) Synthetic aliphatic hydrocarbon based
c) Silicon based

This test, too, was closed after 80 days, because no changes in properties were found.

Dimensional stability

To achieve minimal attenuation values over a wide temperature range, a material with the lowest coefficient of thermal expansion and minimal post shrinkage after extrusion is required.

The new PA12 DS has a clearly reduced coefficient of thermal expansion and reduced post shrinkage at room and elevated temperatures compared to PBT or standard polyamide 12.

The dimensional stability was measured on tubes ø 2.8x1.8 mm. The tubes were cut immediately after extrusion to a length of 10 m. After 1 and after 8 days stored at room climate (23°C/50% r.h.) and after 1 day stored in an oven at 80°C, the change of length was measured (Fig 3).

The coefficient of thermal expansion was measured on test bars according DIN 53752 between 23°C to 80°C (Fig. 4).

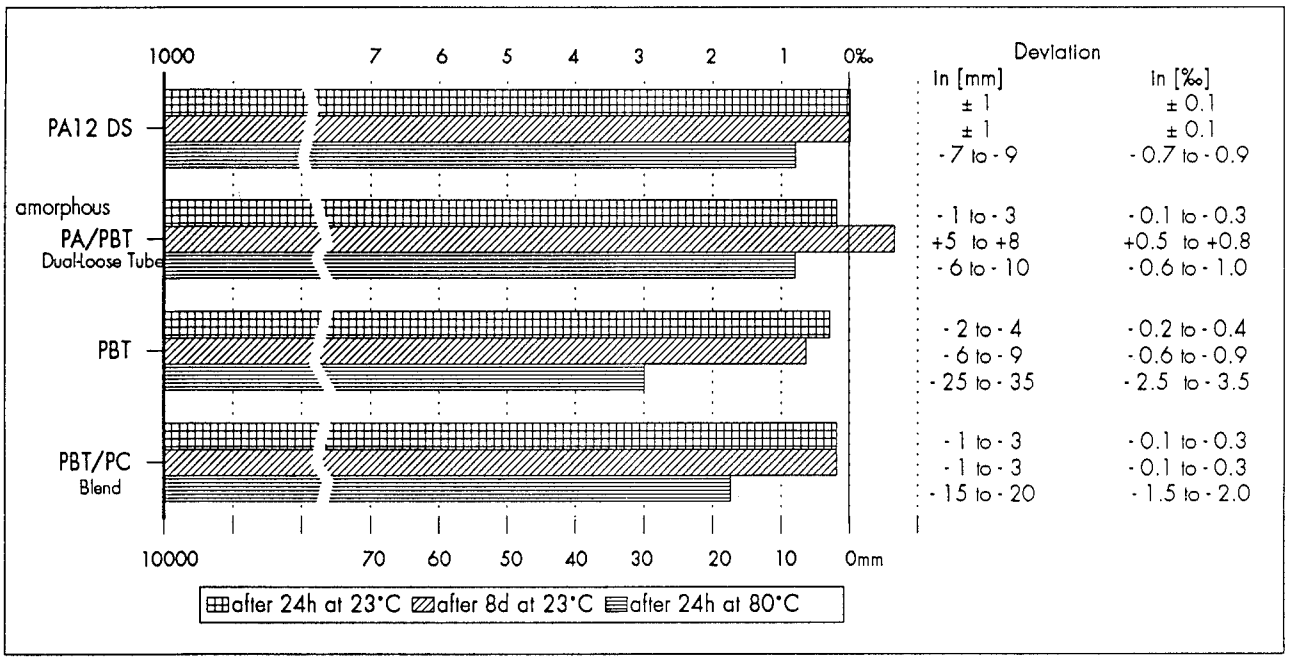


Fig. 3 Change of length of a 10 m long buffer tube ø 2.8x1.8 mm after storage at room climate (23°C/50% r.h.) and in an oven at 80°C of PA12 DS in comparison to other o.f. buffer tube materials [2]

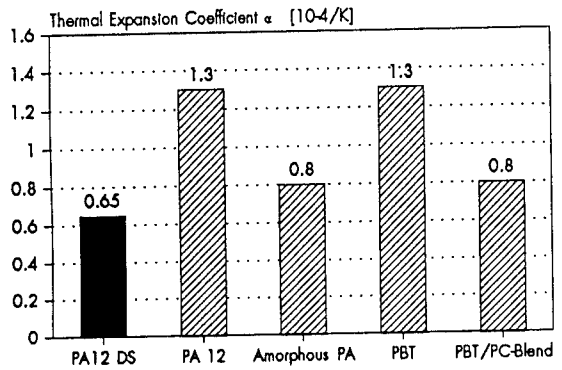
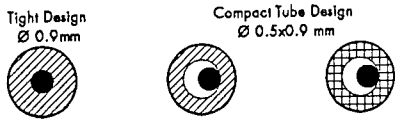


Fig. 4 Coefficient of thermal expansion between 23°C and 80°C of PA12 DS in comparison to other o.f. buffer tube materials

APPLICATION EXAMPLES

a) Installation cable: compact buffer tube design

The compact tube ø 0.5x0.9 of an installation cable was made in a modified PBT-grade. The maximum operating temperature of the specific cable was 50°C (132°F). The same cable with a compact buffer tube made in the new PA12 DS reached a maximum operating temperature of 70°C (158°F). In addition the resistance against chemicals and hydrolysis was also improved. In the end similar property results as with a polyamide 12 tight buffering but without strippability problems (Fig. 5).



Material	PA12	PBT/PC-Blend	PA12 DS
Temperature range			
operating	-5 to 70°C	-5 to 50°C	-5 to 70°C
storage	-25 to 85°C	-25 to 50°C	-25 to 85°C
Chemical resistance	very good	limited	very good
Strippability	difficult	problemfree	problemfree
Processing	difficult	easy	easy

Fig. 5 Comparison of tight and compact tube designs

c) Development of a cost effective central loose tube cable

Central loose tube cables are cost effective in production and installation. To reach good attenuation properties over a wide temperature range is more difficult, due to the special design where the loose tube is not fix stranded around a strength member element. A high dimensional stable material is requested.
The use of the new PA12 DS allows the engineering of a simply designed cable with excellent storage and operating temperature range (Fig. 6).

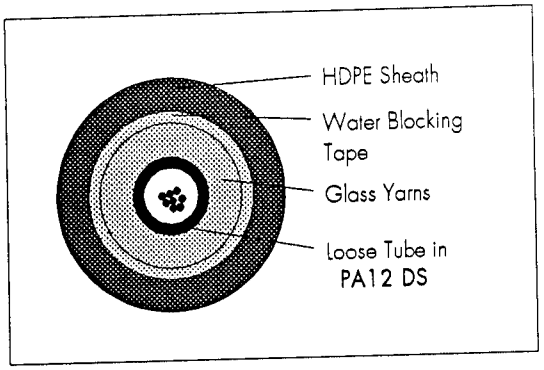


Fig. 6 Central loose tube cable with PA12 DS loose tube and excellent storage and operating temperature range

CONCLUSION

The new PA12 DS has when compared to common o.f. buffer tube materials advantages in dimensional stability and chemical resistance. This allows the engineering of cables with improved usage temperature or permits new cost effective designs.

REFERENCES

[1] CAMPUS, Version 2.4, Polymer Data Base, CFWG, Frankfurt am Main, 1993

[2] Ems-Chemie AG, Internal Test Report

AUTHORS



Martin Hochuli (CH) was born in 1966. He received his engineering degree from HTL Brugg-Windisch (CH) in 1990. He joined Ems-Chemie AG, Domat/Ems Switzerland, in 1992 where he was in charge of Technical Customer Service for Extrusion Application.
Since 1994 Martin Hochuli is the head of the Application Development Group for the Cable and Electrical Market Segment.



David Jarvis (GB), born in 1955, started with the EMS group in 1976. Has held various positions in field Sales, Product Management, Market Management both in UK and in Switzerland. In 1990 moved from EMS headquarters Switzerland to Stafford, England as Managing Director of EMS- Grilon (UK) LTD..
In 1991 returned to Switzerland as Product Manager Technical Thermoplastics. Since August 1995 worldwide Marketing Manager for the Cable and Electrical Market Segment.
Currently studying for MBA.



Dr. Friedrich Bühler (D) was born in 1954. In 1986 he received is PH.D degree in macromolecular chemistry from the Albert Ludwigs University of Freiburg (D). He joined Ems-Chemie AG, Domat/Ems Switzerland 1986, where he was in charge of adhesives development. 1989 he led the development and technical application of biodegrable materials.
Since 1995 Dr. Friedrich Bühler is responsible for the development of polyamide 12 materials for electrical, cable and automotive applications.



Werner S. Zimmermann (CH) was born in 1965. He received his engineering degree from HTL Brugg-Windisch (CH) in 1989. He joined Ems-Chemie AG, Domat/Ems Switzerland, in 1989 where he was in charge of Technical Service for Polymers in Electrical and Cable Industry. After further Marketing Education he was responsible Product Manager for Nylons and PBT-resins for Electrical and Cable applications. Now he is responsible for the North American Market as Product/Market Manager Electrical/Cable for the company Ems-American Grilon Inc. in Sumter (SC).

INVESTIGATION OF THE AMOUNT OF EXTRACTABLES OR VOLATILES REMAINING AFTER ULTRAVIOLET CURE OF PRIMARY OPTICAL FIBER COATINGS

Paul J. Shustack, Kelli A. Fleisch, Mardelle E. Jones

Borden Packaging and Industrial Products
Cincinnati, Ohio

ABSTRACT

In this study, various model primary optical fiber coating formulations were evaluated in order to determine the amount of chemically unbound material that remains in the coating after ultraviolet cure. Experimental primary optical fiber coating formulations were cured under ultraviolet light. The cured films were then subjected to both solvent extraction and thermogravimetric analysis. The results of this study indicate that even though ultraviolet curable coatings are generally considered 100% solids, they still contain a certain amount of chemically unbound material after cure. The unbound material appears as an extractable in the solvent extraction study and/or a volatile in thermogravimetric analysis. The source of these extractables and/or volatiles was hypothesized. The hypotheses were tested by developing and testing experimental formulations were specifically designed to theoretically minimize the amount of extractables and/or volatile material that remained after UV curing. Coating formulations, that had a lower amount of extractables and/or volatiles, were further evaluated to determine the effect that the formulational modification had on the other physical properties of the coating. Subsequent formulational modifications were made in order to attempt to achieve an optimum balance of all physical properties. Mechanistic ideas have been proposed to possibly explain the experimental results. Possible ramifications of the presence of extractables and/or volatile material have been considered. Primary optical fiber coating formulations with lower extractables/volatiles were developed which had an optimum balance of physical properties.

INTRODUCTION

Ultraviolet curable materials are often referred to as 100% solids. However, these materials can still contain a significant amount of chemically unbound material after the ultraviolet cure (1,2). This unbound material can be extractable with solvent or water or it can be volatile under certain conditions. The presence of an extractable or volatile component in optical fiber products can be problematic. These potential problems may manifest themselves at any point throughout the lifetime of the optical fiber.

Chemically unbound materials may become volatilized in the presence of the high heat encountered in the ultraviolet curing chamber on the fiber draw tower. This can create a smoke inside the center tube which can decrease the transmission of the ultraviolet light necessary for curing. The volatilization of material in the curing chamber can also contribute to the fogging of the center tube itself.

If there are chemically unbound materials present in the cured fiber materials, it means that there is potential for migration of this uncured material to other areas of the optical fiber structure during the lifetime of the fiber. For example, suppose the primary coating contains unbound material that may migrate or exude over time. The unbound material may migrate to the glass-coating interface. This may affect the coating adhesion characteristics. If the unbound material moves in the other direction, it may enter the secondary coating and potentially plasticize or soften it. This can also affect fiber performance.

Chemically unbound materials present in the secondary coating may migrate inward into the primary coating affecting its properties or migrate outward and affect the adhesion of ink to the secondary coating. Similarly, if unbound materials are present in the inks or matrix material, they can potentially move about and cause ribbon integrity problems, fiber breakout problems, etc. If the unbound materials are volatile, an odor problem during storage can also occur.

Another potentially detrimental aspect of the presence of chemically unbound material is what happens to the physical properties of the coating after this material is removed. The coating may undergo shrinkage or embrittlement, both of which may induce stress on the fiber and result in microbending and signal attenuation. It is very likely that optical fiber products will be exposed to agents that can volatilize or extract chemically unbound material at some point during their lifetime. These agents can be heat, water, solvent, filling compounds, etc. Therefore, formulations which minimize the amount of this material present after ultraviolet cure are desirable.

Potential sources of chemically unbound material in a cured ultraviolet curable coating, ink, adhesive or matrix material are varied. Since most fiber optic formulations are urethane acrylate based, they may contain trace levels of unreacted polyol or non-acrylated urethane. Also, since most formulations are acrylate based, they may contain trace levels of

unacrylated alcohol, residual water or solvent. These materials can be by-products of the esterification reaction when the acrylate monomers are manufactured.

Other sources of unbound material could be shelf stabilizers either present in the acrylate raw materials or added to finished formulations. Other non-chemically bonding materials can be present in formulations like antioxidants, surface tension modifiers, release agents, COF modifiers etc. Any impurity or material present in the finished formulation that does not contain a chemically reactable group could potentially be extractable or volatile.

Chemically unbound material may result from incomplete photocure reaction. An incomplete reaction could result in unreacted monomer, oligomer, or other material that may be extractable or volatile. Also, it is possible for the raw materials to polymerize but to polymerize to a low molecular weight. The low molecular weight polymer may be extractable with solvent. Another source of chemically unbound material could be unreacted photoinitiator. It is known that a significant amount of the photoinitiator present in an ultraviolet curable formulation does not chemically react into the polymer network during cure. There is also a potential for other photoproducts resulting from the photochemical reaction (3). These materials may also be extractable.

Finally, an equilibrium amount of water will be present in all coatings exposed to the atmosphere. This water will appear as a volatile in a volatile experiment.

All of these potential sources for volatiles or extractables were considered in this study. Attempts were made to formulate to minimize these sources. Ramifications of these formulational changes were considered. Reformulation was done in order to achieve an optimum balance of properties.

EXPERIMENTAL

Urethane acrylate based model primary coating formulations were prepared. These formulations were drawn down on glass using a 3½" wide 6 mil Bird applicator. The coatings were cured in air under a Conrad Hanovia 200W/in medium pressure mercury vapor lamp at 0.7J/cm^2. For the extraction studies the cured coatings were removed from the glass and placed into a preweighed 33mm x 80mm Whatman single thickness cellulose extraction thimble. Each thimble was filled with approximately five 3½" x 5" x 6 mil drawdowns. The thimbles were conditioned at 23 ± 2°C and 50 ± 5% RH for at least 40 hours and then weighed. The thimbles were then extracted in a Soxhlet extractor for approximately 16 hours using 180mL of EM Science OmniSolv grade methyl ethyl ketone (MEK). After extraction, the thimbles were allowed to dry to a constant weight at 23 ± 2°C and 50 ± 5% RH.

For the volatiles analysis, the samples were cured on glass as above , after removal from the glass the free films were conditioned at 23 ± 2°C and 50 ± 5% RH for at least 16 hours. TGA analysis was done using Perkin Elmer TGS-2 thermogravimetric analyzer. This analysis was done under nitrogen at a flow rate of 50 cc/min. The TGA heat program was isothermal at 25°C for one minute, then heat at 35°C/min to 200°C, then held isothermal at 200°C for 40 min.

All modulus data was determined according to ASTM method D882 using an Instron Model 1122 Tensile Tester. A rough estimate of cure speed was done by measuring the modulus of a drawdown cured at 0.2J/cm^2 and another drawdown of the same material cured at 0.7J/cm^2 . A ratio of the modulus at 0.2J/cm^2 to 0.7J/cm^2 converted to a percentage is referred to as the cure ratio. For most conventional ultraviolet curable optical fiber coatings, a dose of 0.7J/cm^2 will result in a fully cured coating.

RESULTS AND DISCUSSION

Twenty three urethane acrylate based experimental primary coating formulations were prepared. These formulations were evaluated for modulus, cure speed, volatiles and extractables. The results of this initial screening appear in Table 1. The data has been normalized to formulation number 1 which is representative of a typical primary fiber optic coating formulation. Using the MEK extractables and TGA volatiles techniques described and used in this study, commercial primary coatings from multiple sources yield approximately 10-15% extractables and 3-8% volatiles. The volatile results normally are significantly lower than the extractables. It is hypothesized that this result is due to the chemically unbound material being of sufficient molecular weight or low enough volatility so that it does not volatize at 200°C but it can be solubilized and extracted by the hot refluxing MEK. Another factor contributing to this result could be that the MEK tends to swell the primary coating polymer. It is possible that chemically unbound material is trapped enough in the polymer network so that it does not appreciably volatilize in the TGA volatiles test but when the polymer network swells in the solvent the material becomes extractable.

From the initial screening, seven coating formulations exhibit a lower amount of MEK extractables. Three of the seven (Formulas 16, 17, 21) have an unacceptably high modulus. In general, the results indicate that higher modulus coatings tend to have lower extractables. This can be expected because higher modulus coatings tend to have higher acrylate functionality, higher crosslink density and lower swelling in solvent. Formula 9 had an unacceptably slow cure speed. Formula 11 was very unstable and it gelled on the lab bench in about one week. Formulations 20 and 23 had viscosities much too high for fiber application. The results on these seven formulations were taken under consideration and the products reformulated so as to address the problems mentioned.

The results on the reformulated products appear in Table 2. Formulation 24 exhibited no improvement in the percent extractables. Formulations 25, 27, and 28 were only a modest improvement. However, formulations 26 and 29 show a distinct improvement. These formulations were further considered and evaluated. From this evaluation, optimized coating formulations 30 and 31 were developed. The results on these optimized formulations appear in Table 3.

The results on formulations 30 and 31 indicate that the amount of extractables can be lowered by 52 and 54% respectively over a typical primary optical fiber coating. For both formulations, the volatiles were lowered by 74%.

The formulations were also evaluated after being cured under nitrogen. In this case the extractables are lowered by 62% on both formulations. The lower amount of extractables when cured under nitrogen can be expected because oxygen is known to inhibit free radical polymerization at the surface. This inhibition can result in uncured monomer, low molecular weight polymer, peroxide type photoproducts or polymerization by-products being formed. These materials would be expected to be extractable after cure. Since almost all fiber towers are engineered to cure the primary coating either under nitrogen or under a secondary coating, the results after cure under nitrogen merit consideration.

Further experimentation was conducted on formulation 30. This experimentation included most of the testing that any commercial primary coating formulation must undergo. This testing included long term accelerated aging, adhesion, low temperature modulus, viscosity, shelf life stability, refractive index and solvent swelling. All of the results on this testing proved favorable.

CONCLUSIONS

It is a requirement that coatings for optical fibers maintain their physical properties over an extended time frame. In order to do this, it is desirable that

the coatings contain a minimal amount of chemically unbound material after ultraviolet cure. Chemically unbound material has the potential, under certain conditions, to migrate and alter the initial physical properties of the coating system. This can result in potential transmission problems of the optical fiber.

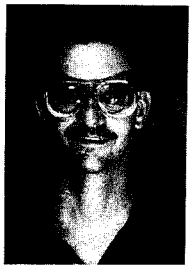
Although ultraviolet curable coatings are considered to be 100% solids, this study indicated that these coatings do contain an amount of chemically unbound material after cure. The techniques of solvent extraction and thermogravimetric analysis were used to evaluate experimental primary optical fiber coating formulations. The evaluation served to identify the cause of the extractables and/or volatiles. This allowed for the development of formulations with a significantly reduced amount of chemically unbound material and still achieve an optimum balance of the necessary physical properties of a primary optical fiber coating.

REFERENCES

(1) W. Baeumer, M. Koehler, J. Ohngemach, "Copolymerizble Photoinitiators", Proc. of Radcure 1986 pp 4-43 to 4-55 (1986).

(2) G. Li Bassi, L. Cadona, F. Broggi, "Advance in Low-Odor Coatings: A new class of Polymeric Nonyellowing Photoinitiators", Proc. of Radcure Europe 1987, pp 3-15 to 3-36 (1987).

(3) P. K. T. Oldring ed., K.K. Dietliker, "Chemistry and Technology of UV and EB Formulation for Coatings, Inks, and Paints", Vol. 3, SITA Technology Ltd. London, UK (1991).



Paul Shustack
Borden, Inc.

Paul Shustack received a BS in Chemistry from Bloomsburg State College in Bloomsburg, PA. He received a M. S. degree in chemistry from Indiana University of Pennsylvania in Indiana, PA. He joined Borden in 1985 as a member of the UV/EB curable products group. He has served in the position of Senior Scientist and currently is UV Development Lab Manager for Borden.



Mardelle Jones
Borden, Inc.

Mardelle Jones received a BS in chemistry from Miami University in Oxford, OH. She worked as an analytical chemist for 6 years at Borden.



Kelli Fleisch
Borden, Inc.

Kelli Fleisch received an A.S. degree in industrial laboratory technology from University of Cincinnati. She joined Borden in 1986 as a member of the UV/EB curable products group. she is currently working on her B.S. in chemistry from University of Cincinnati.

Table 1 Data for Experimental Primary Coating Formulations

Formula Number	Normalized Modulus at 0.7J/cm²	Normalized Modulus at 0.2J/cm²	Care RATIO (%)	Normalized Trial 1 MEK Extractables	Normalized Trial 2 MEK Extractables	Normalized Avg. MEK Extractables	Normalized TGA Volatiles
1	1.00	0.73	73.0	1.00	1.00	1.00	1.00
2	1.04	0.86	82.7	0.96	0.99	0.98	1.01
3	0.90	0.75	83.3	1.06	1.06	1.06	0.98
4	1.08	0.95	88.0	1.10	1.10	1.10	1.05
5	1.05	0.83	79.0	1.02	0.99	1.03	0.99
6	1.01	0.79	78.2	0.99	0.95	0.97	1.00
7	1.03	0.82	79.6	1.00	1.03	1.02	1.01
8	0.84	0.45	53.6	1.06	1.07	1.06	0.56
9	0.96	0.45	46.9	0.71	0.73	0.72	0.25
10	1.07	0.87	81.3	1.02	1.02	1.02	1.00
11	1.06	0.96	90.6	0.91	0.95	0.93	0.99
12	1.07	0.95	88.8	1.13	1.15	1.14	1.03
13	1.19	1.12	94.1	1.09	1.10	1.10	0.91
14	1.07	0.92	86.0	1.21	1.22	1.22	0.99
15	1.05	0.88	83.8	0.94	0.94	0.94	1.00
16	2.25	2.11	93.8	0.78	0.78	0.78	1.00
17	4.62	4.07	88.1	0.61	0.61	0.61	0.94
18	1.37	1.27	92.7	1.00	1.01	1.00	0.85
19	1.46	1.41	96.6	1.13	1.15	1.14	0.74
20	1.46	1.43	97.3	0.92	0.93	0.92	0.69
21	2.12	1.86	87.7	0.58	0.60	0.59	0.65
22	1.55	1.33	85.8	0.99	1.03	1.01	0.79
23	1.37	1.19	86.9	0.60	0.62	0.61	0.53

Table 2 Data for Reformulated Experimental Primary Coating Formulations

Formula Number	Normalized Modulus at 0.7J/cm²	Normalized Modulus at 0.2J/cm²	Care RATIO (%)	Normalized Trial 1 MEK Extractables	Normalized Trial 2 MEK Extractables	Normalized Avg. MEK Extractables	Normalized TGA Volatiles
24	1.35	1.26	93.3	0.98	1.00	0.99	0.96
25	1.71	1.50	87.7	0.90	0.90	0.90	0.95
26	1.25	1.07	85.6	0.81	0.72	0.76	0.91
27	1.38	1.29	93.5	0.92	0.90	0.91	0.92
28	1.39	1.17	84.2	0.90	0.91	0.90	0.91
29	1.58	1.45	91.8	0.64	0.62	0.63	0.33

Table 3 Data for Optimized Experimental Primary Coating Evaluations

Formula Number	Normalized Modulus at 0.7J/cm²	Normalized Modulus at 0.2J/cm²	Care RATIO (%)	Normalized Trial 1 MEK Extractables	Normalized Trial 2 MEK Extractables	Normalized Avg. MEK Extractables	Normalized TGA Volatiles
30	1.30	1.14	87.1	0.48	0.48	0.48	0.26
31	1.35	1.25	92.6	0.43	0.49	0.46	0.26

SELECTION OF INSULATING MATERIALS FOR LONG DISTANCE OPTICAL SUBMARINE CABLES

Jean-François LIBERT - Franck RUELLE - B. ALADENIZE

ALCATEL SUBMARINE NETWORK
536 Quai de la Loire - BP 849 - 62225 CALAIS CEDEX - FRANCE

ABSTRACT

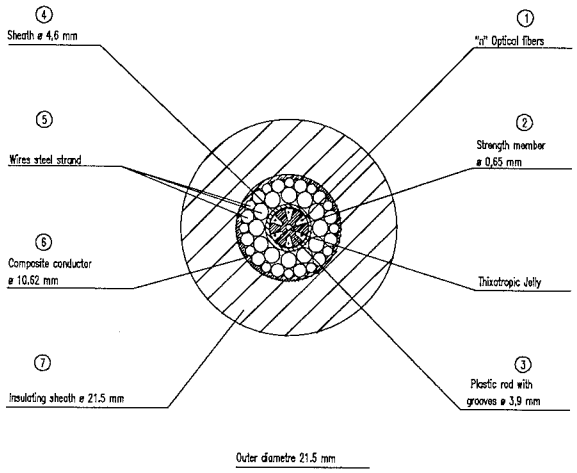
In long distance optical submarine systems, cable is exposed to an agressive environment. In high depths, the insulating material which ensures the reliability of the system in term of dielectric strength, is not mechanically protected.

This insulating material has to sustain electrical, mechanical and chemical stresses during 25 years. Furthermore, the amount of material has to be optmized in order to reach a minimal cable size.

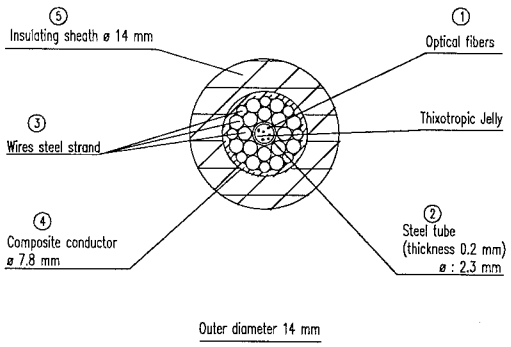
In this article, we describe the way we have selected an alternative insulating material and we specially present test methods used to address the risk assessment of submarine cable design in real environment.

INTRODUCTION

Alcatel Submarine Network has been manufacturing optical submarine cables for several years. One of the current design is based upon a slotted core enclosed in a vault which is insulated thanks to linear low density polyethylene (see figure 1). The outer diameter of the cable reaches 21.5 mm.



In 1990, it was decided to develop a new kind of cable in order to optimize cable dimensions. So a loose tube cable structure has been considered. First, a 14 mm outer diameter cable has been developed and qualified . The design philosophy has been kept since the loose tube is enclosed inside a vault (see figure 2).



This cable is devoted to unrepeatered systems down to 5 000 m depth and is jacketed with black high density polyethylene since electrical requirements are low.

Since the mechanical properties of such a High Density Polyethylene (HDPE) appeared to be better than those of current Linear Low Density Polyethylene (LLDPE), it seemed to be worth evaluating the potential use of a HDPE for power feeded repeatered systems purposes.

This paper describes the way followed in order to select the optimized insulating material.

INSULATING MATERIAL REQUIREMENTS FOR REPEATERED SYSTEMS

The insulating material has to sustain the required voltage for 25 years in an aggressive submarine environment.

The life conditions of the cable (including manufacturing, laying and operating) lead to the main following qualitative requirements (non exhaustive list) :

- good abrasion resistance (better than LLDPE one),
- good ESCR (environmental stress cracking resistance),
- low water intake,
- good dielectric behaviour when ageing,
- standard material.

Several materials from different sources have been selected. The choosen insulating materials were then evaluated. The following tests have been performed :

- mechanical characteristics,
- abrasion resistance,
- ESCR,
- water intake,
- dielectric performance (before and after ageing).

MATERIAL SELECTION

The following materials were found conforming to our requirements. The table 1 summarizes the main characteristics given by the suppliers :

	HDPE1	HDPE2	HDPE3	HDPE4	HDPE5	HDPE6
Resistivity (Ω.cm)	-	10^{16}	10^{16}	-	-	-
Dielectric strength (kV / mn)	-	20	22	-	-	-
Density	0.945	0.939	0.947	0.951	0.961	0.946
MFR (melt flow ratio)	0.05	0.25	0.7	0.5	0.4	0.75
Breaking strength (MPa)	30	20	20	20	15	22
A % at break	1 100	600	500	700	700	700
ESCR (h)	> 400	> 1 000	> 484	> 1 000	> 1 000	-

Table 1 : Selected materials characteristics

As abrasion resistance is known to be related to density, all preselected insulating materials were HDPE.

On the other hand, for cost effectiveness reasons, polymer alloys, copolymers and compounds have been rejected.

TEST RESULTS

Mechanical characteristics

Stripping resistance of polymers (abrasion against rocks for example) can be well related to the $\sigma_r \cdot \varepsilon_r$ product where :

σ_r : Breaking strength,
ε_r : Breaking elongation [1].

This relationship is only valid for rigid polymers (semi-crystalline or amorphous polymers below their glass transition temperature).

It is also known that the ESCR is related to the elongation of the polymer at the yield point (upper point).

The results are given in the table 2 :

MATERIAL	YIELD ELONGATION (%)	BREAKING STRENGTH (Mpa)	BREAKING ELONGATION (%)	σ_r X ε_r
HDPE1	20	35	900	31 500
HDPE2	10	34	830	28 220
HDPE3	10	13	420	5 460
HDPE4	12	31	503	15 593
HDPE5	11	34	501	17 034
LDPE	10	30	800	24 000
LLDPE1	15	20	650	13 000
LLDPE2	12	20	700	14 000

Table 2 : Mechanical properties

All the materials have been tested following the ISO R527 standard.

HDPE3 exhibits the lowest theoritical stripping resistance.

Abrasion resistance

All the materials have been abraded thanks to a «Taber» abrasimeter.

The test method conforms to the ASTMD 1044 standard : a calibrated abrasive disc is pressed against the sample and is rotating at a given speed and during a given duration.

The results are given in the following table 3 :

MATERIAL	ABRASION LOSSES (mm^3)	DENSITY
HDPE1	77	0.945
HDPE2	79	0.939
HDPE3	86	0.947
HDPE4	84.5	0.951
HDPE5	90.6	0.961
LDPE	100	0.932
LLDPE1	113	0.923
LLDPE2	110	0.934

Table 3 : Abrasion resistance

We notice relationship between abrasion resistance and PE type i.e HDPE exhibited better performances than LLDPE and LDPE.

ESCR

All the materials have been tested following the NFC 32-031 standard : samples are immersed in water containing 10 % of Antarox at 50° C during 48 hours.

All the materials passed this test except HDPE3. This behaviour is certainly related to its molecular weight distribution and is well related to mechanical performances.

At this stage, we were able to do a classification of the different kind of tested polymers.

The different parameters are collected in the table 4 and are marked.

	PEHD1	PEHD2	PEHD3	PEHD4	PEHD5	LDPE	LLDPE1	LLDPE2
Abrasion resistance	++	++	+	+	+	-	-	-
Mechanical properties	++	+	-	+	+	+	-	-
ESCR	+	+	-	+	+	+	+	+

Table 4 : Classification of polymers

PEHD1 was found to be the optimized insulating material. Later on in this paper it will be called HDPE.

Electrical tests

As LDPE, LLDPE1, LLDPE2 were well known materials we have compared them to the preselected HDPE.

The insulating material has to sustain the specified voltage for 25 years in a submarine environment. In term of electrical performance, we have to choose the material showing the lowest breakdown probability under these conditions.

The breakdown probability of the insulating material at the end of the life time of the cable depends mainly on three parameters :

- initial breakdown probability of the polymer under the specified electrical stress,
- electrical ageing of the polymer,
- ageing in sea water.

Dielectric behaviour before ageing

The dielectric strength of an insulating material is a highly stochastic characteristic and can only be described by a probability function [2]. The most commonly accepted functions are the Weibull ones [3-4]. The two parameter Weibull function

$$p(E) = 1 - \exp. \{-(E/Eo)^{\beta}\}$$

considers that at each electrical field E > 0, the breakdown probability takes a non-zero value p.

The three parameters Weibull function

$$p(E) = 1 - \exp. \{-(E/Es) / Eo)^{\beta}\}$$

considers that below the electrical field Es, the breakdown probability is zero and increases above that field Es.

The aim of this part is to compare p(E) for different polyethylenes before ageing.

The experiments are conducted with 0.3 mm thick samples submitted to a 2 kV / s DC ramp voltage till breakdown. 20 samples are used for each test in order to perform a statistical analysis. Figure 3 shows the results obtained with five polyethylenes represented in a 2 parameters Weibull plot. A three parameter distribution gives a slightly better estimation for LLDPE1 : for this polymer, the correlation coefficient grows from 0.97 to 0.996 when the threshold field increases from 0 to 210 kV / mm.

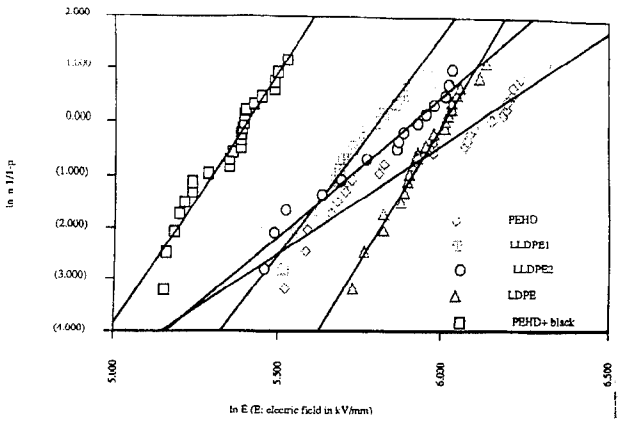


Fig 3:field dependent probability of breakdown

HDPE loaded with 2.5 % carbon black exhibits a lower dielectric strength than the other polymers. For this reason, it will be disregarded for the further tests.

The parameters of the Weibull distribution for the polymers are given on table 5 :

POLYMER	BREAKDOWN MEAN VALUE (kV / mm)	β
HPDE NATURAL	438	10
LLDPE1	330	19
LLDPE2	364	12
LDPE	402	24
HDPE BLACK	220	9.65

Table 5 : Weibull parameters for non aged polymers

This tests give us an evaluation of the intrinsic electrical behaviour of the materials. Effects of ageing have now to be investigated.

Electrical ageing

To evaluate the electrical ageing behaviour of the polymers, we apply a constant DC field of 100 kV / mm to the samples and we measure their life time.

The breakdown time at constant field is also of stochastic nature and known to follow a Weibull law. Figure 4 shows the time until breakdown for LLDPE1 in a three parameter Weibull plot. The threshold time is 480 h.

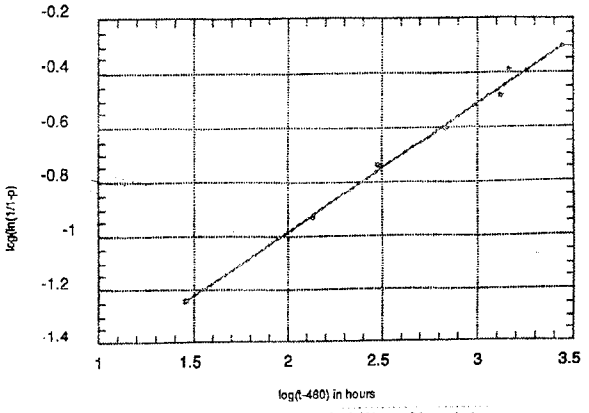


Fig 4: time dependent probability of breakdown

In most experiments (that is the case for HDPE natural, LLDPE2, LDPE, but not for the LLDPE1), the ageing time was limited to 2 000 hours and this duration was not sufficient to lead to a significant proportion of breakdown. In this case, we measured the dielectric breakdown probability after ageing and compared it to the value measured before ageing.

As a rule, the electrical ageing causes a decrease of the mean breakdown field and an increase of the scattering of the results (see for example figure 5 concerning the effect of ageing on LDPE). However, for HDPE, the electrical ageing has no significant effect on dielectric strength (figure 6).

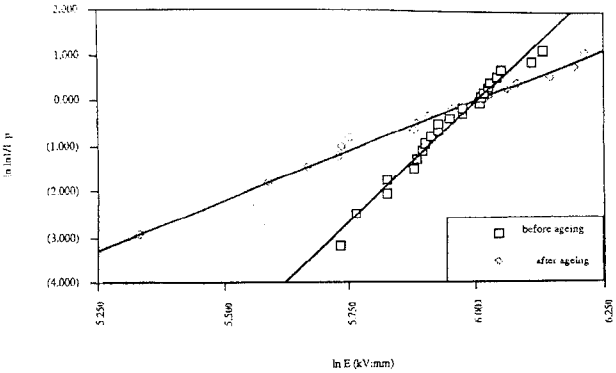


Fig 5: effect of electrical ageing on LDPE

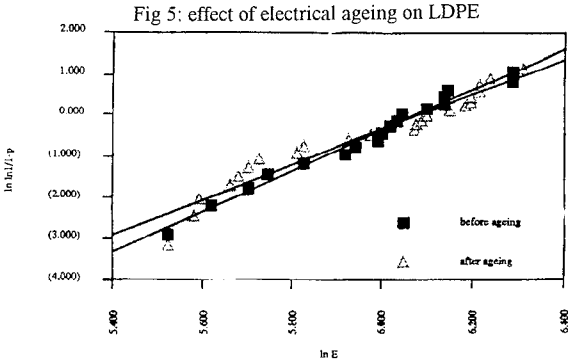


Fig 6: effect of electrical ageing on HDPE

The validity of Weibull laws both for the electrical field and the time under electrical stress leads to a relation following a power law form between the applied field E and the life time t under this stress :

$$E.t^n = cte.$$

Thus, the extrapolated life time under any stress requires the knowledge of the exponent «n» of the power law. This exponent is computed by analysing two sets of life time obtained at different fields, for example before and after ageing. The said life time is the time needed to reach a specified level of breakdown probability. The values of «n» are given in table 2 for the polymers tested.

POLYMER	n
HDPE	(*)
LLDPE1	15
LLDPE2	25
LDPE	15

Table 6 : «n» values

(*) For the natural HDPE «n» can not be given since there is no effect of ageing. However, «n» is much better than 25.

Ageing in sea water

In high depths, the insulating material is in direct contact with sea water. With time, sea water will diffuse into the material and affect its electrical performances.

We previously determined that pressure has no significant effect on water intake. All the following measurement are made under atmospheric pressure. We measured water intake as a function of time on 0.3 mm thick samples submitted to sea water on both faces. Results are given on figure 7.

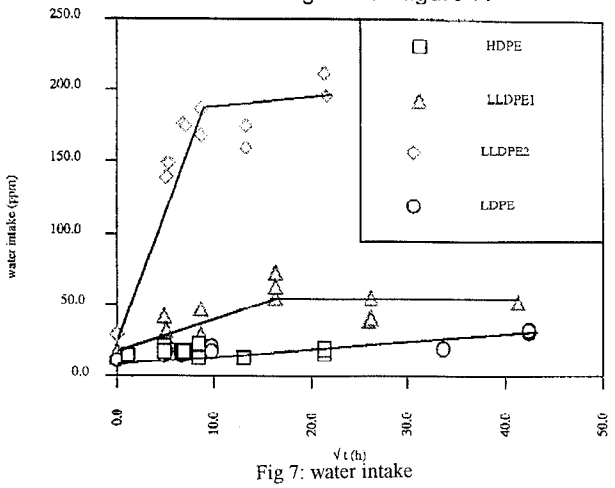


Fig 7: water intake

Water intake linearly increases with the square root of the immersion time (fitting of a Fickean law) till a saturation value. According to the Fick law, the water intake follow the function :

$$Wi = \frac{k \times t}{l^2}$$

were Wi : water intake
k : coefficient
t : ellapsed time
l : thickness of sample

Thus, the water intake after 25 years of a 3 mm thick sample is equivalent to the water intake of a sample of 0.3 mm thick after 3 months immersion.

Electrical breakdown tests were performed on 0.3 mm thickness samples after 3 months immersion in sea water. Figure 8 shows that the deleterious effect of this ageing is directly connected to the water intake in the polymer : natural HDPE which shows a very low water intake is not strongly affected by ageing in sea water whereas this ageing has a deleterious effect on LLDPE2.

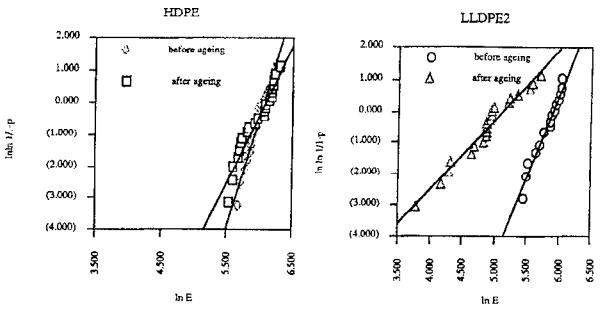


Fig 8: effect of sea water ageing
on dielectric breakdown probability

Evaluation of long term dielectric breakdown probability

In order to estimate the breakdown probability after 25 years in a submarine environment, we have to combine the results from initial breakdown test, the effect of electric ageing and the effect of sea water intake on dielectric strength. Moreover, all the tests are made on thin plates (0.3 mm) and the insulating layer of long distance optical submarine cables are several mm thick (say 3 mm) ; thus we have to take into account the thickness effects.

As a basic hypothesis, we considered that electrical ageing and sea water ageing were independent. The validity of this hypothesis is perhaps not relevant, however we used it as a first assumption. It allows to apply the electric ageing law derived from results obtained before and after electrical ageing (power law : $E.t^n$ = cte) to the statistics of dielectric breakdown obtained after ageing in sea water, and then to extrapolate an evaluation of the breakdown probability of a material submitted to electrical and sea water ageing.

The electrical field E at which breakdown of a polyethylene sample occurs is linked to thickness L by a power law $E.L^{\alpha}$ = cte, where α = 0.5 is currently admitted and theorically predicted from a thermal breakdown process [5]. Thanks to these assumptions, we can estimate the breakdown probability of 3 mm thick samples of different polyethylenes after 25 years in a sea water environment as a function of the applied voltage (figure 9).

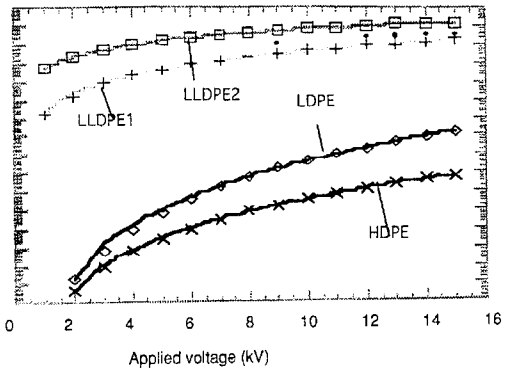


Fig 9: comparisson of estimated reliability of moulded samples

We are now able to quote the general performances of the different polymers (see tables 6-7) :

	Density	Abrasion (mm^3)	Yield elongation (%)	Breaking strength (MPa)	Breaking elongation (%)	σ_r X ε_r
HDPE	0.945	77	20	35	900	31 500
LDPE	0.932	100	10	30	800	24 000
LLDPE1	0.923	113	15	20	650	13 000
LLDPE2	0.934	110	12	20	700	14 000

Table 6 : General physical properties

	Mean value before ageing (Kv / mn)	β before ageing	Mean value after electrical ageing (Kv / mn)	β after electrical ageing	Mean value after sea water ageing	β after sea water ageing
HDPE	438	10	435	5	426	7
LDPE	402	24	399	4.4	379	9.7
LLDPE1	330	19	-	-	282	2.54
LLDPE2	364	12	229	2.9	167	2.25

Table 7 : Electrical performances

CONCLUSION

The thickness of insulating material is an important issue because of the total amount, involved in the cable.

In this paper we described a systematic way in order to choose an optimised material. We demonstrated the advantages we can take when using HDPE.

The selected material exhibits better mechanical performances and higher electrical reliability than LDPE and LLDPE currently used as insulating materials for long haul submarine systems.

This study proved that the use of High Density Polyethylene on long haul repeatered optical systems can be considered. It requires cables able to sustend higher temperature during cable insulation process.

REFERENCES

[1] J.K. Lancaster Abrasive wear of polymers wear 14 (1969)

[2] L.A. Dissado, J.C Fothergill - «Electrical Degradation and Breakdown in Polymers» Peter Peregrinus Ed (1992)

[3] A. Bradwell «Electrical Insulation» Peter Peregrinus Ed (1984)

[4] W. Weibull «Fatigue testing and Analysis of Results (1961)

[5] R. Coelho, B. Aladenize - «Les diélectriques» Hermes Ed (1993)

Authors

J.F LIBERT
Alcatel Submarine Network
536 Quai de la Loire
62225 Calais Cedex

Jean-François LIBERT received his engineering degree from «Hautes Etudes Industrielles» of Lille (FRANCE). He joined Alcatel in 1984. He is now Technical Manager for Optical Submarine Cable in Calais.

F. RUELLE
Alcatel Submarine Network
536 Quai de la Loire
62225 Calais Cedex

Franck RUELLE was born in 1965. He is graduated in chemistry from the «Ecole Nationale Supérieure de Chimie de Clermont-Ferrand». He joined Alcatel in 1991 where he is in charge of cable materials development.

B. ALADENIZE
Alcatel Alsthom Recherche
Route de Nozay
91460 Marcoussis - France

Bernard ALADENIZE is graduated from «Conservation National des Arts et Métiers» in polymers engineering. He joined Alcatel Alsthom Recherche in 1974 where he is now in charge of research on materials for Telecommunication and power cables.

HYDROGEN OUTGASSING OF OPTICAL SUBMARINE CABLE MATERIALS

Franck RUELLE - Jean-Luc LANG

ALCATEL SUBMARINE NETWORK
536 Quai de la Loire - BP 849 - 62225 CALAIS CEDEX - FRANCE

ABSTRACT

Long haul optical submarine systems are designed for a 25 years lifetime. Ageing of materials used in cables has to be taken into account.

This paper describes a reliable technique for evaluation of materials ageing, in the domain of hydrogen generation. This technique gives good accuracy of measurement.

Several materials have been tested with this technique. It enabled to select materials in term of low hydrogen generation.

Optical fiber cable prototype, manufactured with selected materials was submitted to accelerated ageing. During this ageing test, measurements of hydrogen peak at 1 240 nm were performed and they confirmed the low level of hydrogen generated by raw materials.

1) INTRODUCTION

One of the most critical ageing effect in optical submarine cables is the hydrogen diffusion into optical fibers that can cause signal attenuation in long haul optical systems because of chemical reactions that involve -OH formation with doping agents.

There are several sources of hydrogen in optical cables, but in this paper we describe the work that has been done to establish the amount of hydrogen outgassed by polymers degradation after a 25 years lifetime.

More precisely, we propose and describe a reliable procedure in order to perform accelerated ageing tests. Furthermore, we discuss the advantages that this method exhibits when compared to the former one.

2) SOURCES OF HYDROGEN

Major sources of hydrogen in optical cables are polymers degradation, metallic outgassing and galvanic corrosion.

In this paper, we only take into account the first phenomenom. In this case, it is difficult to have a complete understanding of all the reactions leading to hydrogen outgassing as the structures of polymers used in submarine cables are complex.

Nevertheless, it is commonly admitted that oxydation and hydrolysis produce hydrogen. This is confirmed by the changes in color of some of the tested organic materials : yellowing is often observed. Such discoloration is typical of oxydation products (conjugated systems exhibiting delocalized electrons).

3) DESCRIPTION OF THE TECHNIQUE

Principle

Since polymers degradation phenomena leading to hydrogen outgassing are known to be thermally activated, the common way to practice is to heat the said polymers in sealed cells at higher temperatures than service ones in order to accelerate hydrogen generation. Then the hydrogen that has been produced is measured.

We assume that the degradation phenomena follow an Arrhenius law and the linear representations of hydrogen generation as a function of reciprocal absolute temperature are used for extrapolating assessments to actual conditions of service (3° C over 25 years).

Procedure

Since measured concentrations of hydrogen are very low, it is necessary to take care of possible leakages of the cells but also of possible disturbances due to the cell materials outgassing by themselves (mainly sealing materials).

Usually the sealed cell used is a 20 cm^3 glass tube (SVL pyrex tube) sealed with PTFE septum inserted inside bakelite plug.

With this new technique, a new type of sealed cell is used. This is a full glass cell (see figure 1) which offers a 13.5 cm^3 volume.

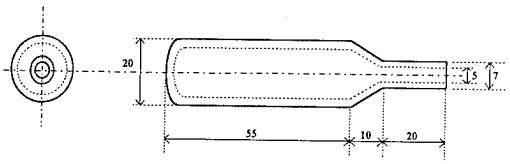


Fig 1: glass cell

The tested material is introduced in the cell which is then sealed thanks to a torch which fuses the glass of the cell neck. The whole is then heated at the required temperature for 18 hours (arbitrary duration).

After natural cooling at room temperature during 24 hours, the cell containing the thermally accelerated aged material is introduced inside an hydrogen proof metallic container. This one is then sealed thanks to a plug with PTFE (polyethylen fluoroethylene) septum.

The volume of the container is 40 cm^3 (see figure 2).

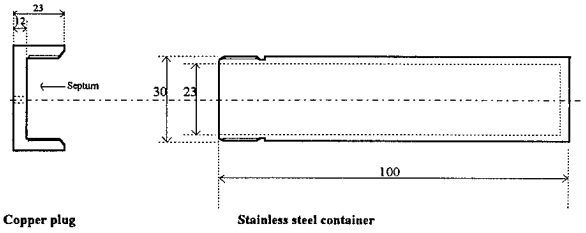


Fig 2: metallic container

The whole is then bumped in order to break the glass cell inside the metallic container.

Hydrogen generation is then monitored by withdrawing 500 µl via a gas syringe from the headspace of the sample in the metallic container. The gas is then injected into a gas chromatograph equiped with a thermal conductivity detector. The analysis are performed under the following conditions :

- column :
  * ∅ : (1/8)"
  * L : 4.5 m
  * Packed with 60 - 80 meshs silicagel
- carrier gas : Argon N 60
- flow rate : 10 ml / min
- temperatures :
  * oven : 35° C
  * injection port : 60° C
  * thermal conductivity detector : 60° C

4) EVALUATION OF THE METHOD

Reliability

The following trials have been performed in order to evaluate the reliability of the procedure :

- 10 empty glass cells are sealed and hydrogen is immediately monitored at room temperature. No evidence of hydrogen was found.

CELL N°	HYDROGEN CONTENT (ppm)
1 to 6	0
7-8	2
9-10	4

Table 1 : Influence of cell sealing

It means that there is no hydrogen introduction in the empty cell due to the combustion of the torch gases during sealing.

- 10 glass cells containing PVC are sealed and hydrogen is immediately monitored at room temperature. No evidence of hydrogen was found :

CELL N°	HYDROGEN CONTENT (ppm)
1 to 7	0
7 to 10	3

Table 2 : Influence of cell sealing on tested material

That means that the procedure followed in order to seal the glass cell doesn't have any influence on the hydrogen outgassing of the tested raw material.

- 5 empty glass cells are sealed and then heated at 150° C for 18 hours. After cooling, hydrogen is then monitored. No evidence of hydrogen traces was found. On the other hand, same experiments were performed with the former kind of cell (20 cm^3 glass tube made of SVL pyrex, sealed with PTFE septum inserted inside Bakelite plug). Traces of hydrogen were found as shown below in table 3 :

CELL N°	HYDROGEN CONTENT (ppm)
1	77
2	110
3	109
4	174
5	94
6	145

Table 3 : Hydrogen generation of former sealed cell

This hydrogen outgassed from organic materials of the sealing device may have an influence on measurements when low amounts of hydrogen are measured.

- 5 glass cells containing a styrene - ethylene - butylene - styrene + polypropylene compound are heated at 120° C during 18 hours. After cooling at room temperature, hydrogen has been monitored after 50, 100, 200, 300, 700 hours.

The five values recorded were consistant. It means that there is no leakage of hydrogen from the fusionned sealed glass cells (see figure 3).

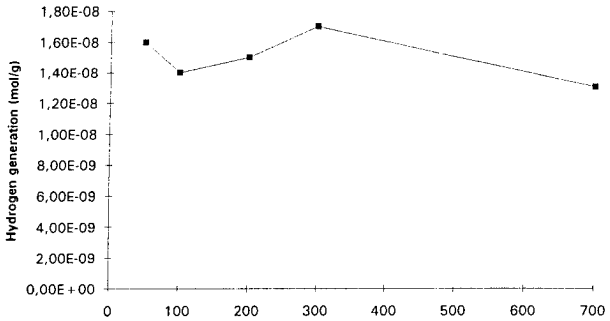


Fig 3: evaluation of long term leakages

5) RESULTS ON AGEING OF CABLE MATERIALS

Several organic materials have been evaluated in order to establish their behaviour when ageing.

It has been assumed that metallic components will release a very little amount of hydrogen at service temperature since it is generally tightly trapped in sites such as grain boundaries or dislocations.

We now describe as an example the tests performed on a PVC compound used to manufacture a slotted core in which optical fibers will be inserted further in the cable manufacturing process.

An average of 8 grams of raw material pellets are introduced in the glass cells. The different samples are heated at 110° C, 120° C and 150° C for 18 hours. Results are given in table 4 :

T°	AMOUNT OF HYDROGEN (mol / g)
110° C	$2.5\ 10^{-8}$
120° C	$4.62\ 10^{-8}$
150° C	$2.18\ 10^{-7}$

Table 4 : Hydrogen generation of PVC compound

By extrapolating these figures thanks to an Arrhenius law (see figure 4), the total amount of hydrogen generated by this material after 25 years at 3° C can be calculated. It has been found equal to $1.4\ 10^{-7}$ mol / gram that is equivalent to $1.38\ 10^{-3}$ mol per km of cable in the considered cable structure.

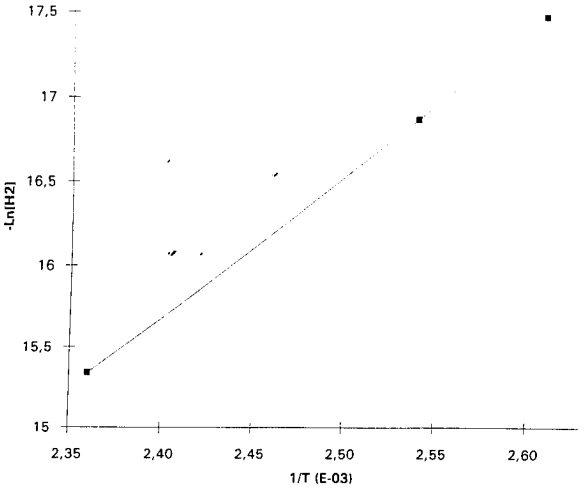


Fig 4: Arrhenius plot of PVC compound

The analysed mechanism is thermally activated and can be described by an Arrhenius law between 110° C and 150° C. In this example, the activation energy is 17.1 k Cal / mol.

6) SELECTION OF MATERIALS

This method allows us to be more confident in the raw materials evaluation in term of hydrogen outgassing. We are now able to make a hard selection of material for submarine optical cable purposes.

As an example, several optical filling compounds have been evaluated thanks to this method.

Results are summarized in the table 5 :

	110° C mol / g	115° C mol / g	120° C mol / g	130° C mol / g	140° C mol / g	150° C mol / g
Jelly A	-	-	$8\ 10^{-10}$	$9\ 10^{-10}$	$2\ 10^{-9}$	-
Jelly B	0	-	0	-	-	0
Jelly C	$3\ 10^{-10}$	-	$1\ 10^{-9}$	$2\ 10^{-9}$	$2\ 10^{-9}$	-
Jelly D	$8\ 10^{-10}$	$7\ 10^{-9}$	$5\ 10^{-9}$	-	-	-

Table 5 : Hydrogen generated by 4 different jellies

All these filling compounds are silicone based jellies and are standard references purchased from different sources.

We notice several kinds of behaviours that are not yet explained since the actual structure of these compounds are not well known by Alcatel Submarine Network.

Since jelly B gives the best results, it was selected as filling material for Submarine cable.

This kind of evaluation has been performed as well on other organic components such as PVC compounds and two parts cured polyurethannes. Then a selection of materials was made in order to improve the ageing behaviour of submarine cables.

7) VERIFICATION ON CABLE PROTOTYPE

A light weight cable prototype (see figure 5) has been manufactured with the raw materials showing the lowest hydrogen outgassing.

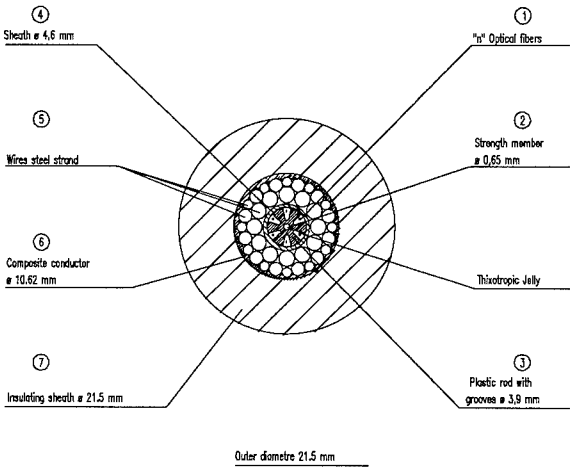


Figure 5

The 4 km length deep sea cable has been heated in a temperature controlled chamber for 1 500 hours at 80° C in order to simulate a 25 years ageing at 3° C if a 12 k Cal / mol energy is assumed.

The attenuation performance between 1 190 nm and 1 600 nm wavelength of four different kind of fibers has been monitored. Thanks to fiber loop, 12 km of each type of fiber were under test.

Fiber A : non dispersion shifted fiber.

Fibers B, C, D : dispersion shifted fibers from different sources.

We focused on the 1 240 nm area by measuring the hydrogen peak height at this wavelength.

Values are given by :

$$\Delta\,\alpha\,(H_2) = \alpha_{1\,240} - \alpha_{1\,265} - \frac{(\alpha_{1\,215} - \alpha_{1\,265})}{2}$$

where α_{xxxx} = loss at the xxxx wavelength in dB / km.

Before heating, cable ends are prepared in order to prevent any hydrogen leakages (copper plugs).

Results are given in figure 6.

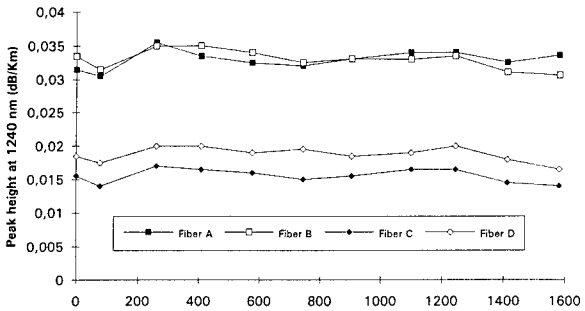


Fig 6: evolution of hydrogen peak at 1240 nm

Losses evolution is within the accuracy of measurement whatever the fiber type is.

No measurable effect of hydrogen was noticed (maximum evolution of 0.002 dB / km on 1 240 nm hydrogen peak).

CONCLUSION

A new technique, for evaluation of hydrogen outgassing of raw materials used in optical submarine cable has been experienced. This showed good reliability and accuracy.

Selection of materials was made thanks to this new technique. This selection was validated through an ageing test on optical cable prototype, using the selected materials.

Authors

Franck RUELLE was born in 1965. He is graduated in chemistry from the «Ecole Nationale Supérieure de Chimie de Clermont-Ferrand». He joined Alcatel in 1991 where he is in charge of cable materials development.

Jean-Luc LANG received his degree from «Institut Universitaire de Technologie» of ORSAY (FRANCE). He joined Alcatel in 1975. He is now involved in optical transmission in the technical directorate in Calais.

WATER GETTER FLOODING COMPOUND FOR DIELECTRIC OPTICAL CABLES

P. Anelli, C. Bosisio, E. Consonni, A. Ginocchio

Pirelli Cavi SpA - Milano, Italia

ABSTRACT

The market demand for fully dielectric optical cables both for the subscriber loop and for the trunk network is rapidly growing. In order to guarantee high transmission reliability in all environments such cables must incorporate a truly effective non metallic moisture barrier.
Some theoretical considerations for evaluating the effect of permeability and absorption capacity of the cable materials on the water vapor partial pressure inside the cable versus time are described. A new flooding compound with a high water absorption capacity and effective in delaying the development of saturation condition around the fibers for cables immersed in water is presented. Laboratory tests carried out on this new flooding compound and a real scale test performed on cables manufactured with and without this material are described. The results obtained demonstrate that this new flooding compound is very effective in reducing the water vapor partial pressure inside the cable structure and in preventing contact between fibers and liquid water.

INTRODUCTION

The use of dielectric cables is growing due to the introduction of optical fibers in the subscriber loop. In fact the challenge for successful penetration of optical fibers into the local distribution network is dependent on the development of new cables that must be small, flexible, light and cost effective. On the other hand, some Telecom operators ask for dielectric cables to be installed in regions characterized by high lightning risk. The development of these cables requires a high transmission reliability also when installed in particularly wet environments, without using any kind of metallic moisture barrier.
Work has been undertaken to provide:
- a coating system more resistant to water soak [1];
- new cable materials effective in reducing the water vapor partial pressure around the cabled fibers.

In the present paper only the investigations related to the new flooding compound with a high water absorption capacity are described. In fact, some theoretical considerations for evaluating the water vapor partial pressure inside the cable vs. time show that an high water absorption capacity inside the cable can delay the development of saturated environment around the fibers for cables immersed in water.
Laboratory tests have been carried out on this new flooding compound in order to measure its absorption capacity and its effectiveness in delaying the diffusion of water vapor.
Three different single jacket cables have been manufactured using conventional flooding compounds both alone and with commercially available water absorbing tapes and the new water flooding compound alone to realize a full-scale test. Each cable was manufactured using different types of fibers, some having a coating very sensitive to water swelling. Attenuation measurements and fiber visual inspections have been carried out systematically during the water aging.

THEORETICAL CONSIDERATIONS

Water is supposed to be generally present at any moment in a dielectric cable, both in small internal spaces (not completely jelly filled) as a gaseous phase and in the polymeric components as dissolved molecules. In equilibrium the water content is proportional to the vapor pressure (perfect gas law in empty spaces and Henry's law for dissolution in solids). The driving force for the diffusion of water into the cable is the difference of water vapor partial pressure between the external environment and the interior of the cable. The water vapor diffusion rate through polymeric sheaths is proportional to the gradient of partial pressure (Fick's law) and the proportionality factor which increases with temperature is called permeation rate. Also the water absorption is influenced by the temperature and in general it decreases with temperature. In this case the proportionality factor is named solubility.
Let's consider a cable with one sheath as representing the most general case of dielectric construction. The sheath is characterized by the permeation rate Q (water quantity diffused through the sheath per unit time, unit cable length and unit of pressure difference across the thickness) and the internal region is characterized by the absorption coefficient K (water quantity that can be

absorbed in every form in that region per unit cable length and unit vapor pressure).

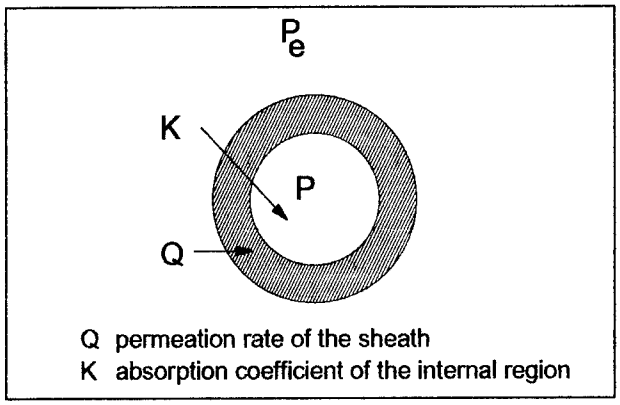


Fig. 1 - Cable model for numerical simulations

Indicating with P_e the external vapor pressure and with P the internal vapor pressure, we have the following differential equation:

$$Q (P_e - P) = d (K P) / dt$$

The solution is given by:

$$P = (P_e - P(0)) (1 - \exp (-Q t / K)) + P(0)$$

and has the following physical interpretation: the factor of time in the exponent is the ratio of the permeation rate to the absorption coefficient. It has the dimension of the inverse of time and therefore its reciprocal, the time constant, is the time for the system to reach 1 - 1/e = 63.2 % of the differential between the external vapor pressure and the initial vapor pressure in the cable.
Let us consider two different cable structures. The cable 1 contains a commercial flooding compound and its absorption capacity is mainly due to the presence of aramid yarns. The cable 2 contains the new flooding compound, that from now on we will call "water getter compound", with a typical absorbing capacity value. The global physical constant are reported in Table 1.

Cable	Absorbing Capacity (mole H_20 / km / bar)	Permeation Rate (mole H_20 / km / year /bar)
1	540	550
2	18847	550

Table 1 - Global physical constants for numerical simulations

The global absorption coefficients are deduced from the specific solubilities, multiplying them by the quantity of each material present in the unit cable length and adding these contributions. The permeation rate is related to the material and geometry of the sheath.

The numerical simulation is performed assuming 5 different situations summarized in the following Table 2.

	Simulation				
	1	2	3	4	5
Cable	1	1	2	2	2
Environmental Temperature	25	25	25	25	25
External humidity	100%	100%	100%	100%	100%
Initial inner humidity	50%	0%	50%	20%	0%

Table 2 - Conditions for numerical simulations

All the simulations are calculated assuming saturation conditions for the external vapor pressure (R.H. 100%) and a temperature of 25°C. These conditions represent rather severe situations for the ingress of water in the cable, because the slowing down of the permeation rate for temperatures less than 25°C is not taken into account.
The simulation 1 is typical for a cable without any particular absorption capacity while the simulation 2 cannot be considered realistic because it needs a manufacturing environment completely dry and it is reported only for comparison. The simulation 3, 4 and 5 consider different initial R.H. in the cable.
Using the new flooding compound, an initial R.H. of 50% in cable type 2 (simulation 3) is not realistic because the presence of the water getter compound reduces quickly the humidity inside the cable. Initial R.H. values between 0 and 20% are in this case more realistic (see simulations 4 and 5).
Figure 2 reports these simulations. It can be seen that in the case of the cable 2 , the saturation condition at 25°C (water vapor pressure of 24 mmHg) is reached definitely after 20 years, while in the cable 1 the same condition is reached before 5 years.

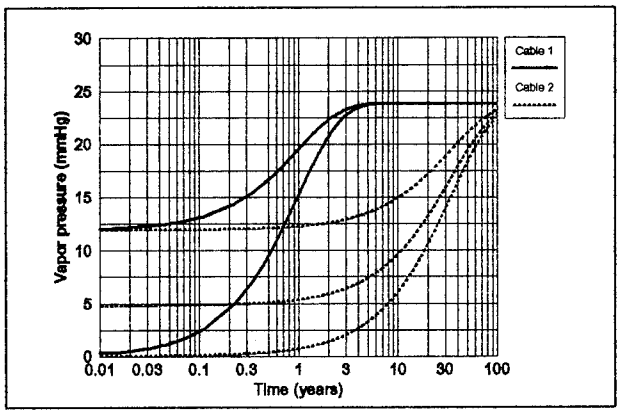


Fig. 2 - Numerical simulations (vapor partial pressure vs. time inside the cable)

Some experiments and field experience indicate that optical fibers can withstand high R.H. values in cables (typically above 90 %) without problems, while R.H. in excess of this range can promote delaminations and associated problems. In terms of water vapor pressure at 25 °C this means that the safe limit is about 21 mmHg. The cable 2 is below this limit for all the service life (20 years).

QUALIFICATION OF THE NEW FLOODING COMPOUND: LABORATORY TESTS.

Absorption capacity from the vapor phase.

To evaluate the absorption capacity of the compound, 5 mm thick layers were prepared on Petri dishes in a dry atmosphere. The dishes were then exposed to high R.H. (slightly low than 100 % to avoid droplet condensation on the compound and consequent unrestrained absorption and swelling) at various temperatures. Therefore, periodic weighting of the dishes have been made in order to evaluate the absorption capacity. Figure 3 shows the test results carried out at three different temperatures (5 , 25, 60 °C) and at 90 % R.H..

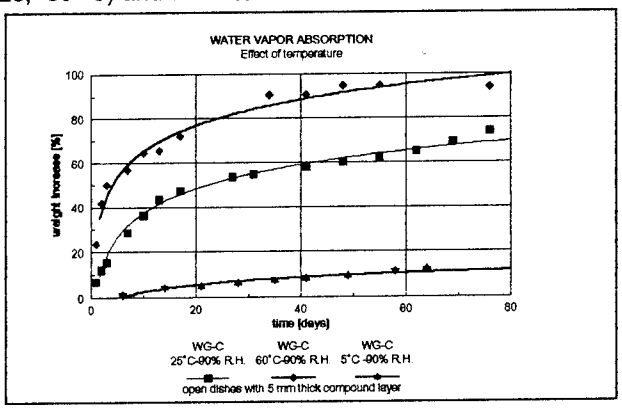


Fig. 3 - New flooding compound: water vapor absorption

In the range 25 to 60 °C the saturated absorption capacity of the new flooding compound is of the order of 70 to 90 % (corresponding to solubilities of 1200 to 250 mole/Kg/bar).
A special test has been developed in order to evaluate the stability of the water absorbed by the compound. Two 15 mm thick layers of compound were conditioned in vapor saturated containers both at 60°C for about 50 days and at 25°C for more than 80 days and, then, were dried at 0% R.H. at 60 °C.
Measurements of weight change have been carried out, initially day by day. The results are reported in figure 4. It can be seen how in the first days of drying the water getter compound releases only a minimum amount of the absorbed water. For instance, considering short term effects, in 1 day at 60 °C and 0% R.H. only 8 - 9 % of the previously absorbed water is released.

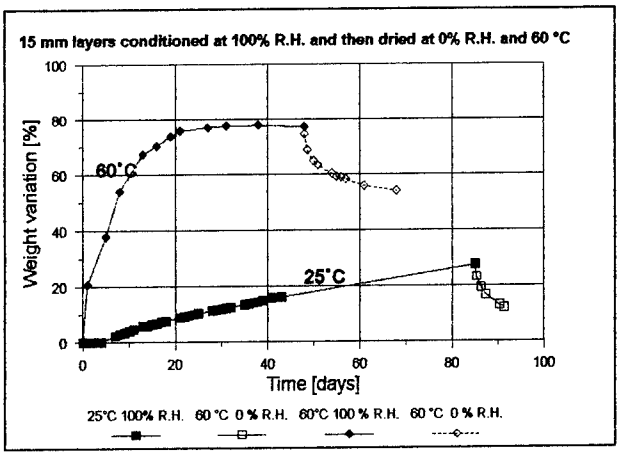


Fig. 4 - New flooding compound: water retention capability

Diffusion of water vapor.

To evaluate the kinetics of vapor diffusion through a compound layer, a special measurement technique has been implemented from standard ASTM E96 test (see figure 5). A compound layer (3 mm thick and 12.6 cm^2 in surface) is enclosed between two polyurethane films 0.5 mm thick that have a very high permeability to water vapor and a metallic flange. The ensemble is clamped with an o-ring seal and bolts to a small metallic container (about 30 cm^2 internal volume) that encloses a relative humidity sensor (Panametrics Hybrid cap 99I capacitive transducer, sensitivity about 2 mV/%R.H.).

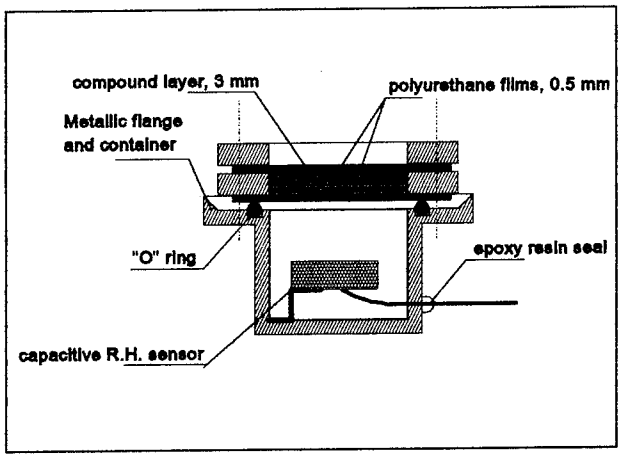


Fig. 5 - Equipment for vapor diffusion measurement

The device with the compound layer is assembled in a glove box under continuos dry air flow so that initial R.H. values in the order of 10-20 % are easily obtained. The device is then placed in a container where 85% R.H. at room temperature is maintained by a proper water-glycerine mixture, and the sensor output continuously monitored.

The time constant of the R.H. transient can be taken as a relative measure of the permeability of the compound to water vapor, provided that the same geometry is employed for all materials and that the delay offered by the PUR films be negligible in comparison to that of the compound layer.
The materials considered and the results obtained are summarized in the Table 3.

	Materials	time constant
1	two 0.5 mm thick PUR layers with empty space in between	10 hours
2	one 0.5 mm thick MDPE layer	2500 hours
3	3 mm thick water getter compound between 2 PUR layers	10000 hours
4	3 mm thick conventional compound between 2 PUR layers	2500 hours
5	5 layer stratum of commercial water absorbent tapes between 2 PUR layers	10 - 20 hours

Table 3 - Water vapor diffusion: materials and results

The time constant is the time for the system to reach 1-1/e = 63 % of the differential between the external vapor pressure and the initial vapor pressure in the container.
It must be outlined that the new water getter compound (item 3) presents a time constant not only higher than that of a conventional compound, but also higher than that of the combination in cable between a conventional compound and a commercial water absorbent tape (item 4 + item 5).

Capability of avoiding delamination in OF.

Cable models have been used to test directly the effective protection given to OF by a layer of flooding compound. The cable models are fabricated starting form a standard 6 PBT tubes optical core, containing particular optical fibers very sensitive to water swelling. A piece 250 mm long of the core is cut, cleaned from the external compound and both ends of the tubes sealed with epoxy X60 resin. The core is then smeared with a weighed quantity of the compound to be evaluated, inserted into a pre cut piece of PUR or MDPE sheath that is finally closed with two thermoretractable caps. The cable models contain between 40 and 60 g/m of compound. Figure 6 shows a simplified drawing of the cable model used.

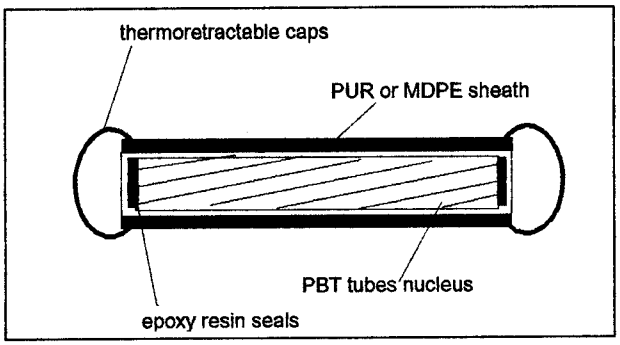


Fig. 6 - Cable model used to test the protection given to optical fibers by the flooding compound

Cable models are then directly soaked in 60 °C water and periodically weighed to measure the amount of water absorbed by the compound. In addition some were dismantled for OF examination.
A first set of cable models was aimed to verify the difference between conventional flooding compound and water getter flooding compound. The results are shown in Table 4.

Elapsed time [hours]	Sheath material	Compound	H_2O absorbed	Optical fiber delamination
48	PUR	Water getter	19%	NO
48	PUR	Conventional	≅ 0%	YES
720	PUR	Water getter	54%	NO
720	PUR	Conventional	≅ 0%	YES
2880	MDPE	Water getter	1.1%	NO
2880	MDPE	Conventional	≅ 0%	YES

Table 4 - Tests on cable models: results

From the microscopic analysis of the fibers, the protective effect of the water absorbent compound with respect to the traditional one is apparent. It is worth noting that the results on models with PUR sheath show that the water absorbent compound is effective also when close to the saturated absorption value.
A second set of cable models has been used to show the degree of stability of the water absorbed by the compound. Six cable samples with PUR sheath where kept in water for 720 hours at 60 °C. Two samples were then dismantled to be sure that no delamination was present on the fibers. The remaining four samples were immediately sealed in glass vials at atmospheric pressure in order to keep all the absorbed water in. The vials were then submitted to daily thermal cycles between 25 °C (8 hours) and 60 °C (16 hours). Four samples were dismantled after 30 cycles with no sign of delaminations. The test corresponds to extremely hard conditions due to the presence of both high temperature and humidity and confirms the findings of figure 4. The results are summarized in the following Table 5.

Elapsed time [hours]	Compound	H_2O absorbed	Temperature	Optical fiber delamination
720	Water getter	54%	60 °C	NO
720+720	Water getter	–	60°C + 30 cycles (25 - 60 °C)	NO

Table 5 - Stability of the water absorbed by the new flooding compound: results

QUALIFICATION OF THE NEW FLOODING COMPOUND: TESTS ON CABLES.

In order to evaluate the water getter compound behavior in a real scale test, a set of cables has been manufactured using this new material and, for comparison, also standard "materials". The cables were coiled and immersed in water, the attenuation monitored every week during the first 3 months, every 15 days during the 4th and 5th month and later every month. The cables have been under test for 2 years. After 2 years, all fibers have been checked using a microscope to detect possible coating delaminations.
The cable structure is shown in figure 7, while the Table 6 summarizes the materials used in each sample.

	Cable 1	Cable 2	Cable 3
Central member	GRP	GRP	GRP
Loose tubes	PBT	PBT	PBT
Filling compound	Conventional	Conventional	Conventional
Flooding compound	Conventional	Conventional	Water getter
Wrapping	Conventional	Water absorbent tapes	Conventional
Outer sheath	MDPE	MDPE	MDPE

Table 6 - Full scale test: cable model materials

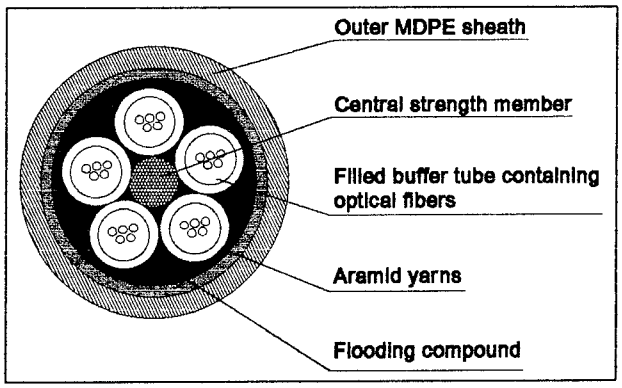


Fig. 7 - Full scale test: cable cross section

The buffer tubes contain different type of fibers, indicated as type A, B. Fiber A has a coating very sensitive to water swelling, while fiber B has been developed by Pirelli in order to achieve enhanced performance in wet environments [1]. Every fiber is colored with a standard transparent UV ink. In each cable two tubes contain 12 fibers type A, other three tubes contain 18 fibers type B. Figures 8, 9 and 10 show the attenuation versus time for all the fibers contained in the cable 1, 2 and 3. It can be seen that no significant attenuation increase has been recorded in two years under test.

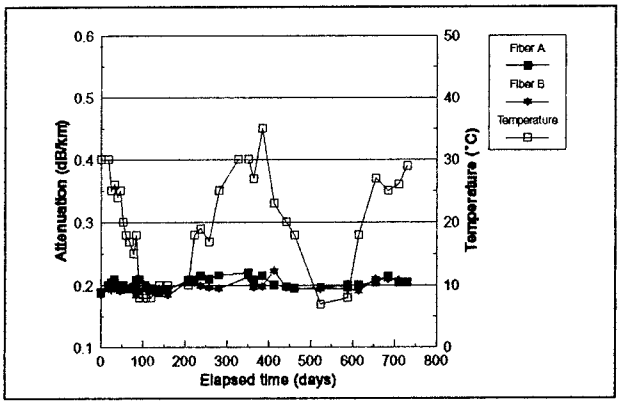


Fig. 8 - Water soak test: cable 1

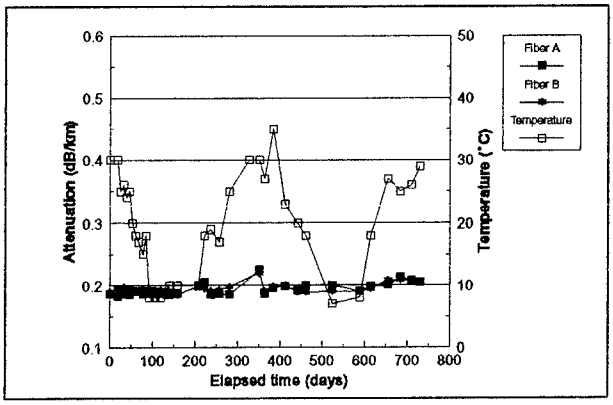


Fig. 9 - Water soak test: cable 2

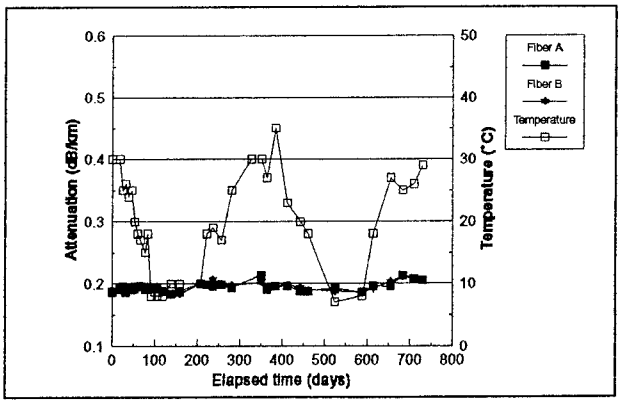


Fig. 10 - Water soak test: cable 3

Table 7 summarizes the results of the visual inspections carried out on the fibers after two years of immersion in water.

	Cable 1	Cable 2	Cable 3
Fiber A	YES	YES	NO
Fiber B	NO	NO	NO

Table 7 - Delaminations after 2 years of immersion in water

The results related to delamination detection show that only the cable manufactured with the new water getter flooding compound shows no delamination at all.
As a complementary test, measurements of pull-out force on fiber samples taken from the cables after 2 years of immersion in water have been carried out. The measurements are performed on 10 mm of fiber embedded in resin with a gauge length of 100 mm and a crosshead speed of 10 mm/min (figure 11).

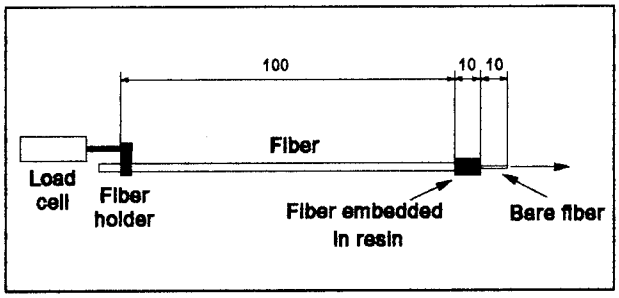


Fig 11 - Test apparatus for the pull-out force measurement

This test verifies the adhesion between glass and coating. Table 8 summarizes the results obtained.

	Cable 1	Cable 2	Cable 3
Fiber A	739.6	1528	2203
Fiber B	739	875	880

Table 8 - Pull out force (g / 10 mm) after 2 years of immersion in water

It can be seen that the highest values of the pull-out force were measured generally in the cable 3. In particular it must be outlined that a correlation between pull-out force and delaminations is evident for the fibers type A.

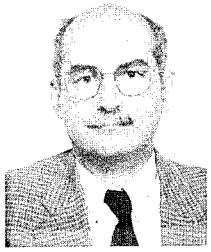
CONCLUSIONS

A novel water absorbent flooding compound, specially devoted to fiber optical cables, has been developed . Testing both in laboratory and in full size prototype cables show that the new compound presents effective protection capacity against water for the fiber coatings. Theoretical evaluations of relative humidity inside the cable vs. time show that cables employing the new water getter compound are much better protected than conventional ones.
In conclusion the new water getter compound seems to be very effective in:
- reducing the water vapor partial pressure inside the cable structure
- preventing contact between fibers and liquid water
- as a consequence, assuring a longer lifetime of the cable.

Water soak tests are still in progress in order to confirm the present results after a longer aging time.

REFERENCES

1) A.Ginocchio, A.Portinari, E.Consonni, G.Roba, F.Nanni, "A new coating system for fibers with enhanced resistance to environmental conditions" 1994, IWCS p.96-104
2) H.Sawano, Y.Sato, M.Miyamoto, "The reliability of water proof optical cable with a plastic sheath and water swellable materials" 1991, IWCS p.333-340



P. Anelli

Pirelli Cavi SpA
Milano, Italy

P. Anelli was born in 1942 in Cremona, Italy. He received his degree in physics from the University of Parma in 1966 and joined Pirelli, where he has been involved in metallurgy, electrochemistry and polymer physics at the Central Cable Research Laboratory. At present he is responsible for the chemical laboratory.



C. Bosisio

Pirelli Cavi SpA
Milano, Italy

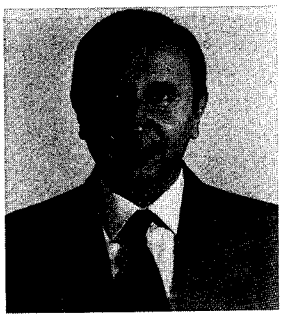
C. Bosisio was born in 1942 in Milano, Italy. He received his diploma as chemist from the technical school "Istituto Esperia" of Bergamo in 1961. In the same year he joined Pirelli, were he has been involved in the study and application of new materials at the Central cable Research Laboratory. At present he is responsible for the development of new chemical materials.



E. Consonni

Pirelli Cavi SpA
Milano, Italy

E. Consonni was born in Seregno (Mi) in 1964. He graduated in Aeronautical Engineering from Politecnico di Milano in 1991 and joined Pirelli in 1991, where he has been engaged in research and development of telecommunication Cables, dealing mostly with environmental tests on optical fibres/cables and manufacturing technology.



A. Ginocchio

Pirelli Cavi SpA
Milano, Italy

A. Ginocchio was born in Milano in 1947. He graduated in Electrical Engineering from Politecnico di Milano in 1972 and joined Pirelli in 1974, where he was engaged in the research and development on submarine cables. Since 1987 he has been responsible for the technological development of optical fiber cables.

DEVELOPMENT OF AN ALL-DIELECTRIC, SELF-SUPPORTING CABLE FOR USE IN HIGH VOLTAGE ENVIRONMENTS

Omid Daneshvar, Joseph Hill, Xavier Mann

AT&T Fitel Company, Carrollton, Georgia

Abstract

An all-dielectric, self-supporting (ADSS) aerial cable was developed which is resistant to tracking damage. A new, specially designed sheath material was developed for this purpose. Critical demands for this sheath were good mechanical and environmental characteristics, resistance to electrical tracking damage, and easy processability. Tracking damage resistance of the material was performed using both a Japanese Industrial Standard (JIS) method and dip track method, and good results were found. A tracking test was performed on a finished cable in a salt fog chamber with electrodes directly attached to the cable. Salt fog was created to simulate the contamination that the cable might see during its lifetime. The cable was tested in electrical fields up to 30 kV/m, and excellent performance was found. The cable was also evaluated for the attachment hardware's gripping performance to this new jacketing material at elevated temperature and during galloping vibration. In addition, an ADSS cable produced with this new jacket material met the flame retardancy requirements of UL 1581.

Introduction

Power utilities often have established right-of-ways and existing support structures in their systems that can easily accommodate a communication or data transmission network. In the past, high amounts of electromagnetic interference (EMI) prevented traditional networks from being used. Because optical cables are resistant to EMI, utilities are able to create networks using their existing plant. All-Dielectric, self-supporting (ADSS) fiber optic cables are commonly used for above ground installations such as these.[1,2,3]

In the past, electric utilities installed fiber optic cable for their internal use. In this case, an electric utility could satisfy its fiber needs with a low fiber count cable containing as few as six fibers. Recently many US electric utilities are providing new services along their right of ways, acting as (or with) interexchange carriers or alternate access providers. Fiber counts greater than 100 fibers are often needed to provide these new services.

Three major types of fiber optic cables are installed along utilities' high voltage power transmission and distribution lines. These include a cable directly wrapped around the ground wire, optical ground wire (OPGW) and ADSS cable.

The cable wrapped around an existing ground wire has the advantages of low cost installation and no clearance issues. However, this design is limited to only the lowest fiber counts and requires a power interruption during installation.[4]

OPGW has been widely used in utility networks. It provides optical fibers for communications while acting as the ground (or shield) wire of the powering network. OPGW is considered cost effective when installing new or replacing existing ground wire. Installation methods are well understood and there is substantial field experience with this product. However, OPGW is limited to relatively low fiber counts (typically 72 fibers or less), has the highest installation cost of the three cable designs and requires power interruption during installation.[5]

ADSS cables have also been widely used in electric utility networks. Like OPGW, ADSS cable installation methods are well understood and there is a significant amount of field experience with this product. ADSS cable designs offer the highest fiber counts (144 fibers or more), can be installed less expensively than OPGW and require minimal interruption in power transmission during installation. ADSS cables must meet clearance requirements and perform properly in a high electric field environment.

Two major challenges exist when utilizing ADSS cables on utility structures. One complication is the distance between structures, which sometimes can be more than 1000 meters. This requires the cable to have high strength. This can be compounded by clearance limitations which restrict the allowable cable sag therefore further necessitating additional cable strength. This challenges the cable manufacturers to design very high strength cables without the use of metallic strength members, so that the cable's dielectric nature is maintained.

The second difficulty relates to the environment in which the cable is placed on utility structures. The structures usually carry high voltage distribution conductors, which produce a high electrical field environment. The potential created on the cable by capacitive coupling of the cable to earth and transmission lines induces a current on the optical cable. When the cable is wet, the surface current in the presence of dry and wet spots can cause surface tracking and flashover in the dry band region.[6] If the outer jacket of the cable is not designed properly, the heat created by this phenomenon will eventually erode the sheath. Cable manufacturers can often calculate the midspan voltage on the cable by using commercially available software and recommend a cable installation location on the towers to minimize the induced electrical field on the conductor; however, due to the voltage of the conductors, clearance requirements, tower architecture, and tower loading, a sufficiently low electrical field location may not be available. No tracking problem has been reported for cables strung on lines with the system voltage levels of 150 kV or less with calculated space potential levels on the cable of 10 kV or less.[8,9] However, most sheath damages have been seen on spans where the calculated induced potential is 20 kV or more.[8] Our objective was to have a jacket material that can pass the tracking requirements at 25 kV, and its mechanical performance to be similar to standard polyethylene to withstand the rigor of aerial cable installation and operation using standard hardware.

Sheath Selection

Because dry-band arcing is a cable surface phenomenon, the critical cable design difference from standard cables is the sheath material. Standard polyethylene sheathing materials are eroded by tracking and are therefore inappropriate for high-voltage environments. The primary criteria used in designing a sheath material were its tracking resistance, mechanical properties, environmental properties, and processability.

Tracking Resistance

The tracking resistance of various materials can be evaluated by many methods. The first test we used was Japanese Industrial Standard C 3005. In the test, a 4 kV potential is applied over a 100 mm section of cable. The test sample is sprayed with a conductive test water solution while the voltage is applied. The test solution is composed of 1 L of water, 2 g of sodium chloride, and 1 ml of nylphenyl polyoxyethlene glycoether, having a conductivity of approximately 3000 $\mu\Omega$/cm. This is continued until observable damage occurs to the sheath or 101 spray applications are completed. A diagram of the test is shown in Figure 1 below.

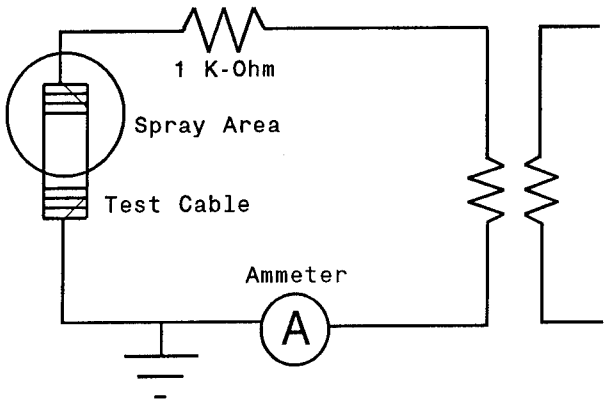


Figure 1 - JIS C 3005 Test Setup

We tested standard polyethylene and the new sheath material using this standard to determine the relative performance improvement. Four tests were completed using standard polyethylene, and the average number of spray applications before failure was 21. Two tests were conducted with the improved material and were carried beyond the minimum requirement to try to determine a failure point. The number of cycles before the test was discontinued was 248 for the first test and 148 for the second test. In neither case was there any signs of sheath damage.

After exhibiting good performance using the JIS method, a second measure of relative performance was conducted. The second method employed is known as Dip Track Testing. In this method, four cable samples are attached to a test wheel using fiberglass supports to give the cable better rigidity. The inside cable end was grounded while the outer end was wrapped with copper tape to provide a conductive electrode contact surface. The wheels four positions represent 0°, 90°, 180°, and 270° from horizon. The wheel rotates counterclockwise (0° → 270° → 180° → 90°) at fifteen second intervals. The cycle beings at 180°, where the cable sample is submerged in a test solution, containing water plus a 1.4 ± 0.06 g/l salt content. The 90° position allows the cable to "drip dry" for 15 seconds. The partial drying creates dry bands that can intensify the tracking action. At 0°, a voltage potential is applied through the cable for 15 seconds. The last position allows cable cool down before being resubmerged in the salt water solution. The test lasts for 10,000 complete cycles (40,000 step revolutions) or until damage is sever enough to cause a short circuit. A test setup drawing is shown in Figure 2, and setup photograph shown in Figure 3.

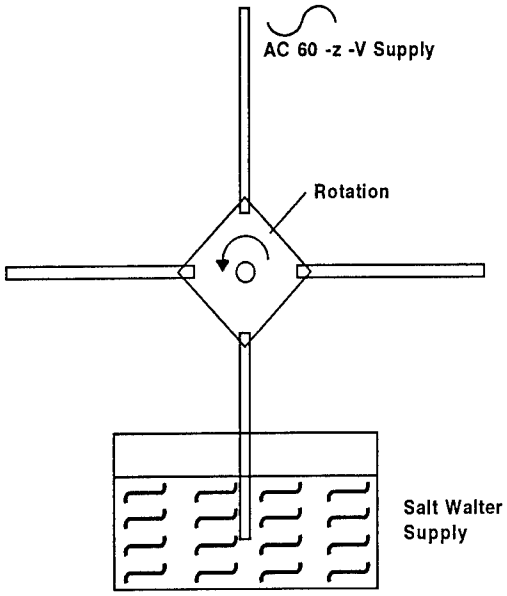


Figure 2 - Dip Track Test Setup

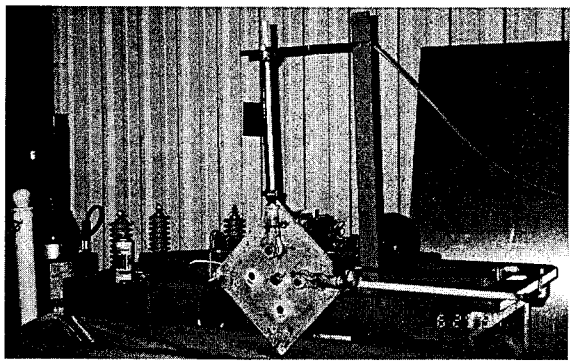


Figure 3 - Dip Track Testing

We performed two test iterations using different voltage levels. The cable was tested at voltage levels of 25 kV/m and 40 kV/m, and showed marked improvements in performance over cables jacketed with standard polyethylene.

Mechanical Performance

All-dielectric, self-supporting optical cables require a tough outer sheath to stand up to the rigors of installation and service. Tracking resistant materials typically give up some of the mechanical performance of standard sheathing materials. It is imperative that the sheathing material chosen possess sufficient mechanical strength to meet the installation and service requirements.

The tracking resistant material chosen has the material properties shown in Table 1 below:

Property	Value	Unit	Method
Tensile Strength	13.8	Mpa	ASTM D638
Elongation	160	%	ASTM D638
Hardness	88	Shore A	ASTM D2240
Abrasion	1.4	%	ASTM D1044
ESCR	>30	days	ASTM D1693
Sunlight Resistance	>720	hours	UL 1582
Track Resistance	>240	hours	ASTM D2132

Table 1 - Material Properties

The tensile properties of this material are slightly less than that of standard polyethylene jacketing materials, but greater than that of other tracking resistant compounds on the market. The hardness and abrasion resistance are sufficient to eliminate damage due to cable pulling and dead end installation. Finally, the chemical resistance makes this material appropriate for direct buried use when transitioning from the aerial plant to a utility substation.

Environmental Properties

A sheathing material for an all-dielectric, self-supporting cable must be able to withstand both sunlight and temperature extremities associated with outdoor service. The sheathing material was tested in accordance with the UL 1581 for sunlight resistance. In this test, material samples are attached to a rotating drum. The samples are exposed to continuous radiation, and water is sprayed on the samples for 3 minutes on and 17 minutes off to complete a cycle. The samples were tested continuously for 720 hours, and the tensile strength and ultimate elongation ratios exceeded 0.80.

Testing to ensure good performance in temperature extremities was conducted on a qualification cable, and results are presented in a later section.

Processability

One important property of the material is its processability. Other commercially available tracking resistant materials offer cable manufacturers the disadvantages of shelf life, component mixing, extrusion inconsistency and moisture crosslinking.

Some compounds on the market have a short shelf life, in some cases as little as 6 months from date of manufacture. This can cause problems for a cable manufacturer because of the inconsistency of demand for cables requiring tracking resistance. The material used for this cable has no expiration date.

A second disadvantage of other tracking resistant compounds is that they contain two components. This requires either the compound to be mixed before being placed in the hopper or to have an auger mixer attached to the extruder. This requires additional difficulty to the manufacturer, and is avoided by using our new material.

The extrusion consistency of this material is excellent. Earlier generation materials can be difficult to extrude which can be compounded if the material has any moisture. The new material offers processability using standard extrusion equipment with the ease of extruding standard polyethylene. A final disadvantage of other tracking resistant materials is their requirement to be crosslinked. The materials require moisture crosslinking, which necessitates the use of environmental chambers or the construction of hot water pits. Insufficient crosslinking affects both the tracking resistance and mechanical performance of the material. The material for our cable does not require any crosslinking to maintain its tracking resistant nature.

Cable Design

The ADSS cable uses the loose tube construction for its cable core. Individual fibers are placed within buffer tubes that are stranded around a dielectric central member. Reverse oscillating lay (ROL) stranding is used to improve mid-span accessibility. Up to 12 buffer tubes, each containing up to 12 fibers, can be used to allow a maximum of 144 fibers in this design. The buffer tubes and cable core are fully filled to prevent water ingress and migration. The core is protected by an inner polyethylene sheath.

Tensile Strength

ADSS cables require considerable tensile strength to resist damage during installation and to support its weight under storm loading. Because induced electrical fields sufficient to require a tracking resistant sheath are often found on transmission structures, the span distance is much greater than traditional ADSS installations might see. The aramid yarn content is tailored to the specific application. Yarn is applied counter-helically to prevent cable rotation during tensile loading. sufficient yarn can be applied to the cable to have spans of 1000 meters with a minimum amount of cable sag. Finally, the tracking resistant material is extruded over aramid yarn.

To guarantee a long life time, the cables are designed such that the axial fiber strain is zero during the life of the cable. The cable design also considers the National Electric Safety Code Rule 250B, which defines different storm loading conditions for various geographic regions of the United States.

Cable Performance

Because of the high tensile strength requirement of this cable, it is imperative that the cable operate as a unit. The outer sheath of the cable must have good adhesion to the cable core to effectively couple the load to the cable. The cable's performance were verified by performing the following tests:

- Ultimate Tensile Test
- Elevated Temperature Test
- Galloping Test
- Flame Retardant Test
- Cable's Mechanical and Environmental Test
- Tracking Resistant Test

Ultimate Tensile Test

For this test, a 30 m sample of tracking resistant ADSS cable with a diameter of 17.0 mm was terminated with dead ends. The sample then loaded to 3358 kg (7400 lbs.), the maximum rated load of the cable. The cable was maintained at this load for 1 hour. At the completion of the 1 hour, the sample dead end grips were removed, and jacket was closely observed for any signs of jacket damage. No damage was noticed. The cable then tensioned to destruction. The aramid fiber strength members broke in the middle of the cable away from the dead-ends, and there was no slippage of the dead-ends.

Elevated Temperature Test

An 8 meter sample of the cable was used for this test. Cable was terminated at each end with dead-ends. One end of cable was placed in a solar simulated box, and the other end was kept at room temperature. Tension was increased to the maximum installed load of 2632 kg (5800 lbs.), and temperature in the box was raised to 60 °C. This condition was maintained for 3 days. At the completion of the test, the dead-ends were removed for verifying the mechanical integrity of the jacket. No jacket damage was noticed at either dead-ends.

Galloping Vibration Test

Galloping can cause severe wear on cable hardware and jacket. This test is conducted in accordance with Institute of Electrical and Electronics Engineers (IEEE) P1222 (draft) to prove the adequacy of the cable and hardware at withstanding large amplitude vibrations. The test setup is shown in Figure 4.

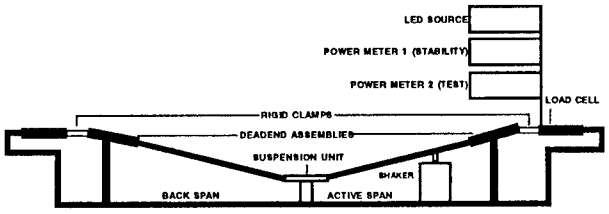


Figure 4 - Galloping Test Setup

During this test, the cable is tensioned to 500 kg (1100 lbs.) A shaker is placed on the cable to cause galloping vibration. For this test, a peak-to-peak amplitude of 24 inches (610 mm) was observed for a 110 foot (34 m) span at a frequency of 5.92 Hz. The vibration and tension were maintained for 100,000 cycles. At the end of the test there was no wear under either the dead-ends or the suspension clamp.

Flame Retardant Test

A concern for ADSS cable installations is flammability. It has been reported that overhead communication cables have contributed to fire spreading.[7] Because of the cross-country routes that transmission lines often take, the biggest concern is forest fires.

The tracking resistant ADSS cable we designed contains a non-halogen, flame retardant additive in the sheath material. The additive allows the cable to pass UL 1581 tests of horizontal burn, VW-1 and vertical tray flame test.

Mechanical and Environmental Test

Qualification cables were manufactured for performance characterization. The cables were tested for mechanical and environmental performance per EIA/TIA test standards. Table 2 shows the performance of the test cables.

Test	Results	Method
Compound flow	Pass at 80°C	FOTP 81
Water penetration	1 m/1 hour	FOTP 82
Jacket yield strength	11.16 Mpa	FOTP 89
Jacket elongation	154%	FOTP 89
Jacket shrinkage	1.3%	FOTP86
Cable tensile strength	0.00 dB at rated load	FOTP 33
Impact resistance	0.01 dB at 50 impacts	FOTP 25
Compressive strength	0.03 dB at 250 N/cm	FOTP 41
Cable twist	0.01 dB, d=1.7 m	FOTP 85
Cable flex	0.01 dB at 50 cycles	FOTP 104
Low/high bend	0.01 dB, -30°/60°C	FOTP 37
Cable freezing	0.01 dB	FOTP 98
Temperature cycling	0.02 dB/km max	FOTP 3
Cable aging	0.04 dB/km max	FOTP 3

Table 2 - Cable Performance

Tracking Resistant Test

The completed cable was tested for tracking resistance per IEEE P1222 (draft). In this test, the cable is subjected to continuous salt fog while being energized with ac voltage. Two sections of cable were installed through a chamber with the ability to produce a salt fog. Figure 5 shows the top view of the chamber looking down into it.

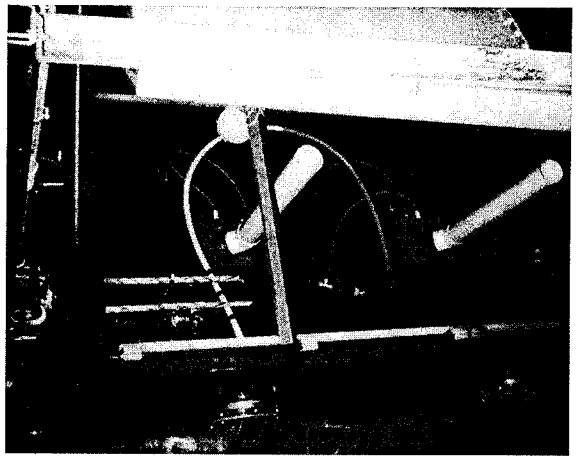


Figure 5 - Salt Fog Chamber (Top View)

Deadends were installed to the cables, and the cables were tensioned to 817 kg (1800 lbs.) using calibrated springs. This tension represents the value existing for 90% of the service life of the cable. A photograph of the tension setup is shown in Figure 6 below:

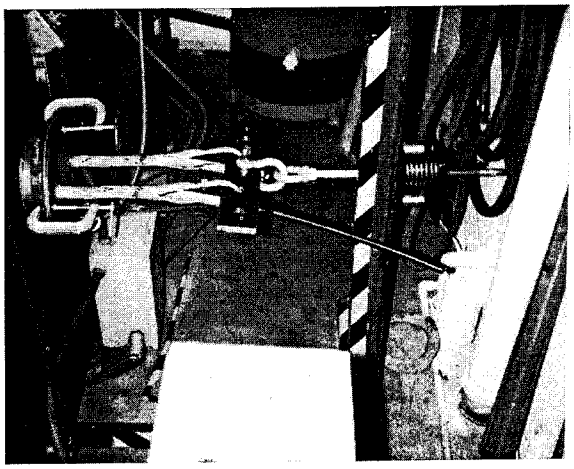


Figure 6 - Tension Application

The cable attachment hardware was grounded, and electrodes were attached to the midspan of the cable. Wire braids were used to obtain complete coverage of the circumference of the cable. See Figure 7 below for attachment details.

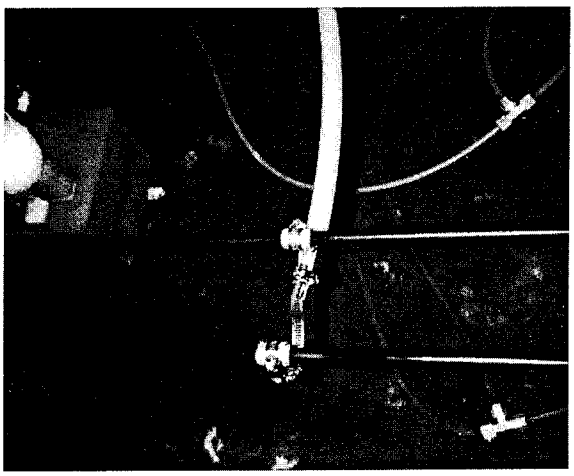


Figure 7 - Electrode Attachment

The top of the chamber was covered, and a salt fog was produced inside. A high voltage potential was placed on the cable using a Hipotronics high voltage supply, as shown in Figure 8 below.

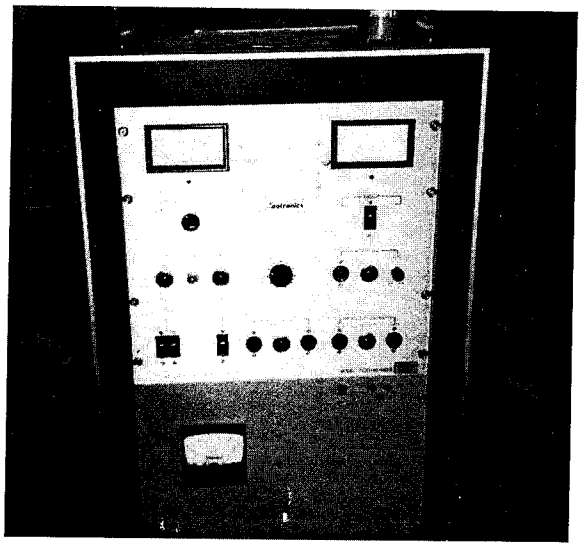


Figure 8 - High Voltage Supply

The test was conducted for 1000 hours. The testing was briefly suspended for weekly observations to verify the jacket surface was not affected. At the end of the 1000 test, the cable was removed for a more detailed observation. The first test was completed using a test voltage of 25 kV/m (16.6 kV). At the end of the test, only a slight surface damage could be observed. See Figure 9 below for more detail.

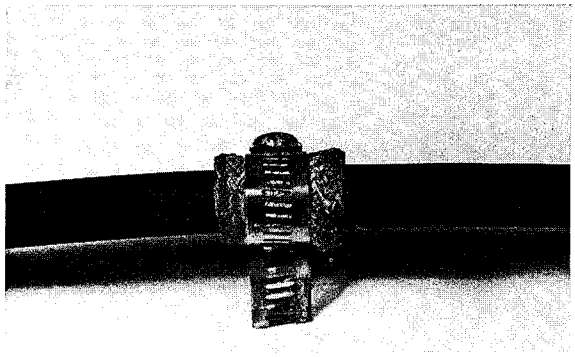


Figure 9 - Completed Cable Sample

The cable was dissected to verify that the aramid yarn strength member was not damaged below the sheath surface. Figure 10 below shows that no damage was evident to the aramid yarn.

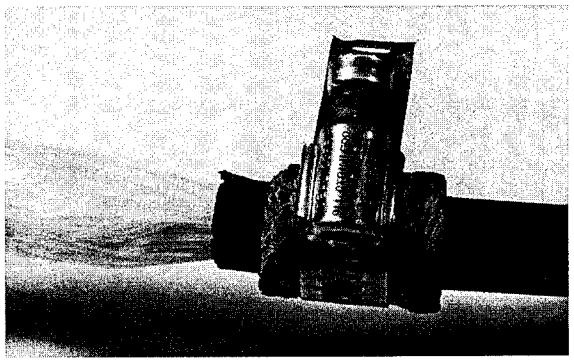


Figure 10 - Dissected Test Cable

After successfully completing the test at 25 kV/m, additional samples were tested at 38 kV/m (25 kV). No damage occurred to the cable.

Conclusion

An all-dielectric, self-supporting cable which is resistant to tracking damage associated with high voltage environments. The cable met all industry standards for mechanical and environmental performance, and in addition, met tracking and flame resistance test standards. The cable can be used with standard cable hardware and in standard environments.

References

1. Grooten, *et al*, "Practical Experience with Metal-Free Self-Supporting Aerial Optical Fiber Cable in High Voltage Networks", 36th International Wire and Cable Symposium, 1987.

2. Oestreich, U. "Fiber Optical Aerial Cable", Fiber and Integrated Optics, Volume 4, Number 1, 1982.

3. Hayasaka, E., *et al*, "Non-metallic Optical Cable with Optical Fiber Catenary for Long Span Aerial Applications", 32nd International Wire and Cable Symposium, 1983.

4. Yoshida, *et al*, "Winding of Optical Fiber Cable onto Existing Ground Wire", 35th International Wire and Cable Symposium, 1986.

5. Rowland, *et al*, "The Development of a Metal Free, Self Supporting Optical Cable for use on Long Span High Voltage Overhead Power Lines," 36th International Wire and Cable Symposium, 1987.

6. Carter, C. "Dry Band Electrical Activity on Optical Cables Separately Strung on Overhead Power Lines", 37th International Wire and Cable Symposium, 1988.

7. Nakano, *et al*, "A New Non-Halogenated Flame Retardant Compound and Its Jacketed Telecommunications Cables", 34th International Wire and Cable Symposium, 1985.

8. Carter, C., *et al.* "Mathematical model of dry-band arcing on self-supporting, all-dielectric, optical cables strung on overhead power lines", IEE PROCEEDINGS-C, Vol. 139, No. 3, MAY 1992.

9. Rowland, S., *et al.* "Electrical ageing and testing of dielectric self-supporting cables for overhead power lines", IEE PROCEEDINGS-A, Vol. 140, No. 5, SEPTEMBER 1993.

Biographies



Omid Daneshvar
AT&T Fitel Company
Carrollton, Georgia

Omid Daneshvar is the Research and Development Manager at AT&T Fitel Company. He holds B. Sc. and M. Sc. degrees in Electrical Engineering from Georgia Institute of Technology. He joined AT&T Fitel in 1985 and has since had responsibilities in the development of fiber optic cables and measurement systems. Mr. Daneshvar is a member of the Optical Society of America (OSA).



Joseph Hill
Carrollton, Georgia

Joseph Hill holds the position of Senior Product Development Engineer at AT&T Fitel Company. He was granted a B. Sc. degree in Ceramic Engineering from Clemson University. He joined AT&T Fitel in 1990, having the responsibilities of materials and cable development. Mr. Hill is a member of the American Ceramic Society (ACerS) and the National Institute of Ceramic Engineers (NICE).



Xavier Mann
AT&T Fitel Company
Carrollton, Georgia

Xavier Mann is currently the Senior Manager for International Markets at AT&T Fitel. He holds a Bachelor of Science and Master of Science in Ceramic Engineering from the Georgia Institute of Technology. Mr. Mann, who was with Siecor before Joining AT&T Fitel in 1987, has worked in the fiber optic cable industry for more than a decade, holding positions in engineering, product management, sales and marketing. Mr. Mann is a member of the Society of Cable Telecommunications Engineers (SCTE) and is a current member and past Chairman of the International Wire and Cable Symposium.

A NOVEL SYSTEM FOR THE INSTALLATION OF ALL-DIELECTRIC SELF-SUPPORTING OPTICAL CABLE ON HIGH VOLTAGE OVERHEAD POWER LINES.

AUTHORS: I. V. Nichols, C. A. Platt, S. M. Rowland, A. J. Taha.
Helsby Technology Centre, BICC Cables Ltd, Helsby, U.K.
C.N.Carter
The National Grid Company plc, Leatherhead, U.K.

ABSTRACT:

All-dielectric self-supporting (ADSS) cables hung on long-span, high voltage, overhead lines are subject to longitudinal electrical fields. These fields can lead to dry-band arc activity when the cable is polluted and wet, and ultimately damage to the cable. It has recently been shown that a threat exists in the worst cases, from the results of dry-band arc compression. The system described has been developed as a result of this new understanding, and extends the range of application of ADSS cables into the highest voltage applications. The proposed system incorporates a rod of defined resistivity which covers part of the cable length, adjacent to the towers, thereby controlling the current and the space potential over the whole cable length. This device can be installed under live-line conditions. The theoretical work on which the system is based is described and installation procedures briefly outlined.

1.0 INTRODUCTION:

Recent deregulation of electricity distribution companies and telecommunication networks has led to a world-wide increase in the use of fibre optic cables on long-span overhead power lines. Optical fibres can be installed on overhead lines using a variety of cable types[1,2]. The all-dielectric self-supporting (ADSS) cable is one of these. This cable typically has a pultruded glass or aramid fibre strength member, with a loose-tube optic fibre construction, and is sheathed[3].

ADSS cables are normally suspended from lattice towers, between the phase conductors so clashing cannot occur. Distributed capacitances between the optical cable, the phase conductors, the earth wires and ground, result in a voltage gradient along the dielectric cable's length. If the cable is dry, the voltage gradient does not present a problem. However, if the cable surface becomes conductive, due to moisture and the presence of pollution, a current is drawn along its length. The current is greatest at the tower, where the cable is clamped and at earth potential. This current will tend to dry the cable surface, inevitably leading to a first break in the previously continuous conductive surface. Experiments and calculations have previously shown that in some circumstances sufficient potential difference can result across such a dry-band to cause arcing [4,5]. Such arcing can be sufficient to degrade a cable sheath, through melting, formation of carbon tracks or erosion. Ultimately the strength member can also be damaged so that the cable may physically break.

The threat of dry-band arcing has been acknowledged for many years. The prime response of cable manufacturers has been to develop sheath materials which are resistant to ageing by arcs[6]. Ageing for these materials has generally been thought to be limited to gradual erosion. This has now been shown not to be the case. However, the general cause and effects of dry-band arcing on ADSS cables are now well documented[6,7].

Essentially, depending upon the local environment, the restriction of application has largely been based on the electric space-potential in which the cable may safely be hung. Typically, fairly arbitrary values of around 12 kV for mid-span potential have been used as limits of application. More correctly a current limit should be set. This may reasonably be taken as 1 mA to ground. Below this level, damage from dry-band arcing becomes very unlikely [8].

Two primary difficulties arise from this;

(i) the market is limited to most 132/150kV towers and some 275kV systems, but excludes most higher system voltages levels.

(ii) even on systems where cables may be safely hung, there may be tight tolerances on suspension points, adding surveying costs and requiring expensive metalwork to be manufactured.

A product is described which will enable the application of ADSS products into significantly higher space potential. This is possible because the current on the surface of the cable available for dry-band arcing is controlled. Eventually it may allow access to all large lattice systems. Such a product will provide a unique solution to the difficulties discussed above.

2.0 THE SOLUTION

The product consists of a standard ADSS cable installed in the normal way[1,2]. This allows live line installation of the cable. A rigid resistive rod is then applied to the outside of the cable so that it extends from the clamps over a significant proportion of the cable span length. This might be 50 m of a 366 m span. It is this rod which prevents stable dry-band arc formation on the cable.

The resistive rod is readily removed from the cable for maintenance, monitoring or replacement. Most importantly the rod is decoupled from strain on the cable or its sheath. The rod consists primarily of pultruded glass which provides stiffness, strength and abrasion resistance, and semiconductive fibres which are simultaneously pultruded with the glass. These fibres are embedded in the external surface of the rod for two reasons: firstly, any encapsulation increases effects of Joule heating; secondly, there will be less danger of a potential difference being built up between the fibres and moisture on the cable surface or earthing devices at the tower. The rod may equally well be installed on new or existing ADSS cable installations.

2.1 Installation Of The Resistive Rod

Figure 1 shows how the product lies over the cable adjacent to the clamp. The rod is attached to the cable with clips spaced 300 mm apart, Figure 2. The rod is firmly fixed to the clips to enable efficient application and removal. In addition a protrusion is glued to the end of the rod in the factory to prevent any possibility of clips slipping off when it is being removed from service. This is also designed to reduce local electric field at the rod tip.

The method of fixing the rod to the clamp is important, since the clamp provides the electrical earth and is the method by which longitudinal movement of the rod is prevented. The technique employs a preformed metallic spiral over the portion of the rod to be clamped. This reinforces the rod and provides an excellent electrical contact to the fibres. This is then clamped directly to the preformed armour wires of the cable clamp.

2.2 Installation Procedure

Because the ADSS cable is tensioned before the rod is attached, the majority of health and safety issues are easily overcome. Thus live-line installation is not inhibited. However, an earth is required on the resistive rod during installation. If it is not efficiently earthed during installation the rod may float to a substantial potential and may deliver up to a few milliamps to installation personnel. A 'bazooka' earth, which is essentially a split, open-ended tube, forms a running installation earth, Figure 3. Any exposed ADSS cable within reach of an operator from the tower will be wrapped in earthed metallic spiral guard wire. The 'bazooka' earth must also be used when the product is removed from service, but it is not required during the operational life of the cable; nor is it required if the rod is installed or removed with the circuits switched out.

Further details of installation techniques and experiences will be published separately. Two full scale mechanical installations have been completed on 366 m spans without difficulty.

3.0 THEORETICAL ANALYSIS

A model has been developed which allows calculation of the parameters which determine the efficacy of the system. This model is proprietary to BICC and has been verified as far as possible against the frequently quoted NGC programme, which allows the space potential in which an ADSS cable hangs and resultant currents to be calculated[4].

The model requires the following information:

(i) the co-ordinates of the conductor bundles and the span length
(ii) the phase and voltage of the conductors
(iii) the size and number of conductors in each bundle
(iv) the size and co-ordinates of the ADSS cable
(v) the resistance per unit length of Zone 1
(vi) the resistance per unit length of Zone 2
(vii) the length of Zone 1

where Zone 1 is the region covered by the resistive rod (Figure 1) and Zone 2 is beyond the resistive rod towards mid-span. The only variables which the cable supplier has control over are (iv), (v) and (vii). The model assumes parallel conductors and ADSS cable. This assumption is an approximation because the sags of the two types of catenary are not the same. Also blow-out of conductors and the cable in strong side winds will generally increase the severity of conditions. It will be seen that the important part of the model concerns the cable closest to the tower. This mitigates the issues of blow-out to some degree.

3.1 Variables of Concern

The issues are complicated in a system in which an all-dielectric cable has a resistive rod covering part of its length. These include dry-band arcing, heating effects in the rod, and the currents beyond the rod. The system will now be considered in various extreme conditions.

3.1.1 Dry System Figure 4a schematically shows a dry cable with a resistive rod. The maximum current in this system must be at x [4], the current accumulated over Zone 1. This is the minimum current (i_{min}) which the resistive rod will see and must be endured over its lifetime. The heat generated by the joule heating is given by $(i_{min})^2 R_e$, where R_e is the resistance per unit length of the rod. This level of heating must also be endured for the product's lifetime.

3.1.2 Completely Wet System, Figure 4b when the cable is completely wet, no issues arise. It should be noted that if the moisture imparts a resistance per unit length R_2 on Zone 2, the resistance in Zone 1, R_1, is $(1/R_e + 1/R_2)^{-1}$, not simply R_e, the rod's resistance per unit length. As previously, the current is greatest at x, so that a dry-band is most likely to form there first. Dry-band formation will also be slowed by the presence of the rod since the normal feedback effect of increasing resistance as moisture is dried out will be reduced. In this condition of a completely wet cable the maximum current possible is flowing to earth. That current i_{max} (R_e, R_2) is a function of R_e and R_2.

3.1.3 Dry-band at the Clamp, Figure 4(c). A dry-band at x has two implications. One is an increased voltage gradient across that gap. If this is sufficient, an arc will occur. Assuming continuity of current and resistance, the voltage gradient is simply given by the product of $i_{max}(R_e, R_2)$ and R_e.

The other limitation is the power generated in the resistive rod in the absence of an arc, since all the current must now flow through it to ground. This power per unit length is given by the product of $i_{max}^2(R_e, R_2)$ and R_e. The local resistance in the dry-band does not control the current. Any heating effect also reduces R_e (since it is a semiconductor), mitigating chances of thermal instability.

3.1.4 Dry-band away from the Clamp, Figure 4(d). A dry-band formed at y must be less onerous than at x, since the current must be lower.

3.1.5 Zone 1 Dry, Zone 2 Wet, no dry band. This case shown in Figure 4(e) resembles that of Figure 4(a). The prime difference is that a current, i_z, can now flow at point z. Therefore, the current at x will also increase. It will be seen that if Zone 1 is long enough this current at z may be very small. This is the basis of the rod's efficacy.

3.1.6 Dry-band between Zones 1 and 2, Zone 2 wet, Figure 4(f). This is the condition most likely to give rise to dry-band arcing if the system is poorly designed. For example if Zone 1 is very conductive (ie. if $R_e \rightarrow$ metallic levels), the situation is unchanged from that of a wholly dielectric system; it is simply as if the clamp has been shifted up the cable. The parameter determining whether or not a damaging arc can form is the current, i_z, available if no gap were present[8]. This is the current available to drive an arc.

3.1.7 Summary of Important parameters to system design The following have been identified as important system parameters:

(i) The maximum continuous power generation acceptable in the rod so that it does not age unacceptably = P^e_{max}; this will depend upon the rod design.

(ii) The maximum short-term power generation acceptable in the rod to prevent melting, etc. = P^e_{limit}; this will also depend upon the rod design.

(iii) The maximum voltage gradient acceptable on the rod so arcing cannot occur = V^e_{limit}.

(iv) The maximum current at the boundary with Zone 1 (i_z), so damaging dry-band arcing does not occur here.

3.2 Evaluation of Typical Parameters

The variables that need to be calculated are:

(i) maximum current drawn to earth when cable is dry, i_{min}, to ensure that

$$(i_{min})^2 R_e < P^e_{max} \quad (3.1)$$

(ii) maximum current drawn to earth when cable is wet, i_{max}, to ensure that

$$(i_{max})^2 R_e < P^e_{limit} \quad (3.2)$$

and that

$$(i_{max}) R_e < V^e_{limit} \quad (3.3)$$

(iii) the current drawn through z on a wet cable i_z available for arcing across a dry-band at z, to ensure damaging dry-band arcing will not occur beyond the rod end.

3.2.1 Operational Limits The following are conservative experimentally-determined parameters for the prototype resistive rod: P^e_{max} = 10 W/m, P^e_{limit} = 40 W/m, V^e_{limit} = 10 kV/m, if i_z is below 1 mA under all circumstances then dry-band arcing will not pose a threat [8].

3.2.2 Calculations of Parameters - Comparison of Systems with different Voltages. Arbitrarily, a UK L6 400 kV span, a UK L3 275 kV span, and a standard 132 kV span were all compared. The results of this are shown in Table 1. All were chosen to have symmetric phasing and the ADSS cable hung between the bottom four phase conductors due to mechanical stability. The span length was taken as 366 m in each case.

It should be noted that R_e is quoted in Table 1, not R_1. In the calculations it is important to remember that R_1 changes, depending on whether the cable is wet or dry. On this basis, one might conclude that, given R_e of 500kΩ/m, the problem of dry-band arcing is overcome. It is certain that in this case the 400kV system is the most severe. This system will now be considered in greater detail. In particular, the effects of a more conductive deposit on the cable must be considered.

3.2.3 L6, 400kV Symmetric Phasing In the extreme case the pollution could be assumed to have metallic conductivity. This is a worst case analysis which would not happen in reality and gives the system's theoretical maximum current. Figure 5 shows how the current on the cable at x, i_{max}, varies with the uniform cable conductivity. Severe pollution levels or coastal conditions might reduce the surface resistivity of a standard ADSS cable to 200 kΩ/m, resulting in 5mA in this case. Without an resistive rod present to control the current this is clearly enough to damage the cable [2,7].

Table 2 shows the effect of R_e, for a 50m long rod on (i) the continuous power generated in the rod ($i_{min}^2 R_e$), (ii) the short term maximum power generated in the rod in conditions of extreme pollution ($i_{max}^2 R_e$), (iii) the maximum voltage gradient along the rod ($i_{max} R_e$) and (iv) the current available for arcing at the end of the rod, (i_z), (assuming pollution on the cable gives a minimum resistance of 200 kΩ/m).

It is clear from this that with symmetric phasing and the ADSS cable suspended between the bottom four phase conductors, a solution exists if a rod can be provided with a resistance between 400-800 kΩ/m and a heat dissipation of better than 40 W/m. In this case the rod has a sufficiently low resistance so that it does not overheat, but at the same time, has a high enough resistance to prevent arcing at its end.

In this analysis no attempt has been made to optimise the position of the ADSS cable, so the situation might be optimised still further. It is also clear that every span may be different in terms of geometry and pollution conditions, therefore considerable effort is required in planning such a system, and deciding when it is necessary to employ resistive rods.

4.0 CONCLUSIONS

In order to combat the effects of dry-band arcing an add-on device incorporating a resistive rod can be used. The resistance per unit length of this device must be very carefully controlled and consistent along its length.

A practical form of the device is a pultruded rod, which is attached to the cable by conductive polymeric clips.

It has been shown both theoretically and in the laboratory that such a system can prevent the ADSS cable from being damaged in extreme conditions. Full scale live line trials will be reported shortly.

Acknowledgements:

The authors would like to thank BICC Cables Limited and The National Grid Company plc for permission to publish the material in this paper.

REFERENCES

[1] J R Martin
"Optical Fibres for Power Utilities" CIGRE (1993) Australia, Paper 5.2

[2] G Carlton, A Bartlett, C Carter and A Parkin
"UK Power Utilities Experience with Optical Telecommunications Cabling Systems", Power Eng. Journal Feb (1995) pp7-14.

[3]A J Davies, P Radage, S M Rowland and D J Walker
"The Selection of Materials for a Long Span, Dielectric, Aerial, Self-Supporting Cable for Optical Communications" Plastics In Telecoms VI, 27/1-27/10, London Sept (1992)

[4]C N Carter and M A Waldren
"Mathematical Model of Dry-Band Arcing on Self-Supporting, All-Dielectric, Optical Cables, Strung on Overhead Power Lines" IEE Proc-C 139 (1992) pp185-196.

[5]S M Rowland
"Sheathing Materials for Dielectric, Aerial Self-Supporting Cables for Application on High Voltage Power Lines", Proc 6th DMMA (1992) IEE Conf. Pub. No. 363 pp 53-56.

[6]S M Rowland and C N Carter
"The Evaluation of Sheathing Materials for an All-Dielectric, Self Supporting, Communication Cable for Use on Long Span Overhead Power Lines" Proc 5th DMMA (1988) IEE Conf. Pub. No. 289 pp77-80.

[7]S M Rowland and F Easthope - "Electrical ageing and testing of dielectric self-supporting cables for overhead power lines", IEE Proc A 140 (1993) 351-356.

[8]To be published, S M Rowland and I V Nichols.

System (kV)	R_e (kΩ/m)	R_2 (kΩ/m)	i_{min} (mA)	$i_{min}^2 R_e$ (W/m)	i_{max} (mA)	$i_{max}^2 R_e$ (W/m)	$i_{max} R_e$ V/m	I_z (mA)
400	500	500	2.9	2.2	3.4	2.9	858	0.88
275	500	500	2.4	1.5	2.8	1.9	697	0.69
132	500	500	0.72	0.13	0.83	0.17	208	0.20

Table 1: Comparison of spans of differing system voltages. In each case the resistive rod is 50 m long.

Re (kΩ/m)	i_z (mA)	i_{max} (mA).	$i_{min}^2 R_e$ (W/m)	$i_{max}^2 R_e$ (W/m)	$i_{max} R_e$ (V/m)
200	2.21	8.43	6.90	14.22	1686
400	1.19	7.60	7.92	23.13	3041
600	0.75	7.26	8.17	31.63	4356
800	0.51	7.07	8.25	40.02	5658
1000	0.37	6.96	8.27	48.37	6955
1200	0.27	6.87	8.28	56.69	8248

Table 2: Effects of resistive rod resistance on a symmetrically phased 400kV system.

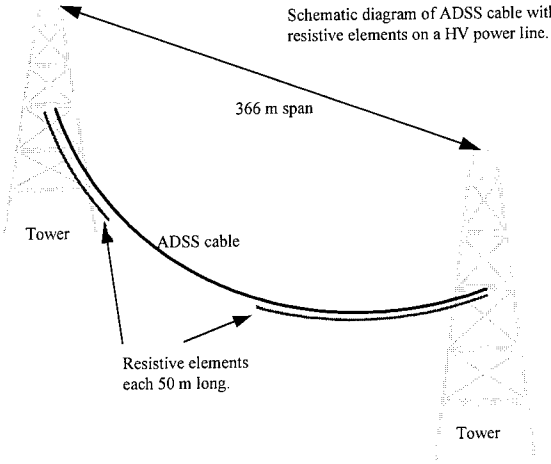


Figure 1 Position of resistive rod on span.

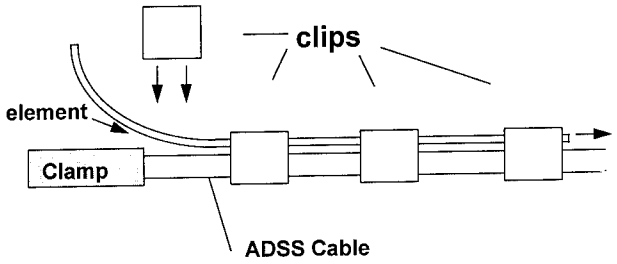


Figure 2 The resistive resistive rod is manually fed onto the installed cable. m is mid-span.

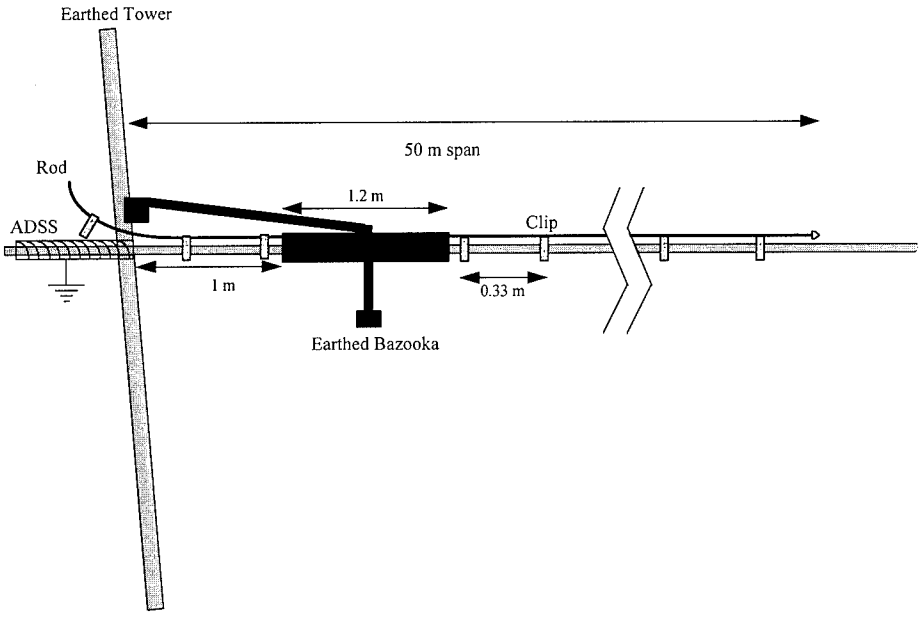


Figure 3 Schematic of installation technique.

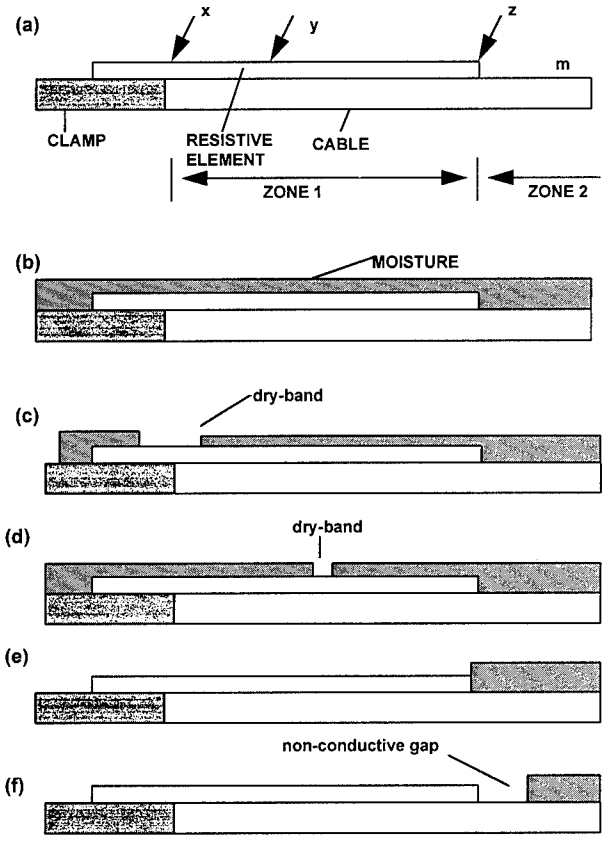


Figure 4 Schematics of the cable assembly. Point x is the boundary between cable and clamp. Point z is the end of the resistive rod and zone 1. Point y is an arbitrary location between the two.

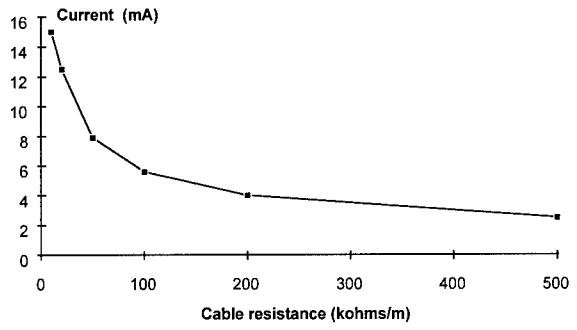


Figure 5 Current on cable as a function of uniform cable resistance.



Arif Taha
BICC Cables Ltd
Helsby Tech Centre
Helsby
Cheshire WA6 0DJ
United Kingdom

Arif Taha graduated from Manchester University in 1990 with a BSc Hons in Materials Science. He has since received an MSc in Instrumentation and a PhD in Electrical Engineering from the same institution. He is currently employed as a Research Engineer at BICC Cables Ltd. Arif is currently developing optical cable systems for application on long-span high voltage power distribution networks.

Small Aerial Optic Cable for Multimedia Network

Osamu Koyasu, Akira Sano, Kohichirou Watanabe, Akio Mogi and Matsuhiro Miyamoto

Fujikura Ltd. Opt-Electronics Lab.
Chiba, Japan

ABSTRUCT

We have designed and evaluated a new self-supporting aerial cable in which an optical fiber unit having 10 single-mode fibers is wound round a supporting wire. The number of fibers in the unit can be increased up to 12. Therefore, by increasing the number of units to be wound round the supporting wire, it is possible to make a higher-fiber-count cable as well. The outside diameter of the fiber unit is as small as 7 mm and the cable weight is as light as 35 g/m, so it is suitable for use as a small-size, lightweight self-supporting aerial cable. This feature contributes greatly to reducing installation costs as well as cable costs. Evaluation of some trial products showed that the new cable has good environmental and mechanical performance. In addition, results of a long-term reliability test in the field showed that the cable is stable in transmission loss and fiber strain. Being small-size, lightweight and flexible in fiber count, the new cable is best suited in terms of cable performance and economics for use in multimedia network construction.

1. INTRODUCTION

Optical fiber cable meets the demand of not only telecommunication networks but also CATVs, LANs, mobile telephone networks, radio information service, etc. This is because they posses performance of enabling high-grade transmission, multi-channel transmission or high-speed transmission. Optical fiber cables have been used so far for applications in main routes connecting large-demand areas and in subscriber networks in large cities.

Distant, small-demand areas and cities with a limited number of subscribers have little benefited from the high-grade performance the optical cables possesses. The cables to be used in these areas are required to be low in fiber count (most suitable for meeting demands), small-size and lightweight for easy installation. In Japan, aerial cables, which enable economical installation, are required to be small-size and lightweight. Having designed and evaluated an optical fiber cable having such , performance we will report the results of this evaluation.

2.CABLE STRUCTURE

The structure of the cable is shown in Fig. 1. Type A has one optical unit, and Type B has two optical units, wound round a supporting wire. The unit consists of a tube filled with 10 single-mode fibers and jelly. On both sides of this tube, one each is thin

wire arranged to reduce thermal contraction and strain. Table 1 shows the specifications of the cables.

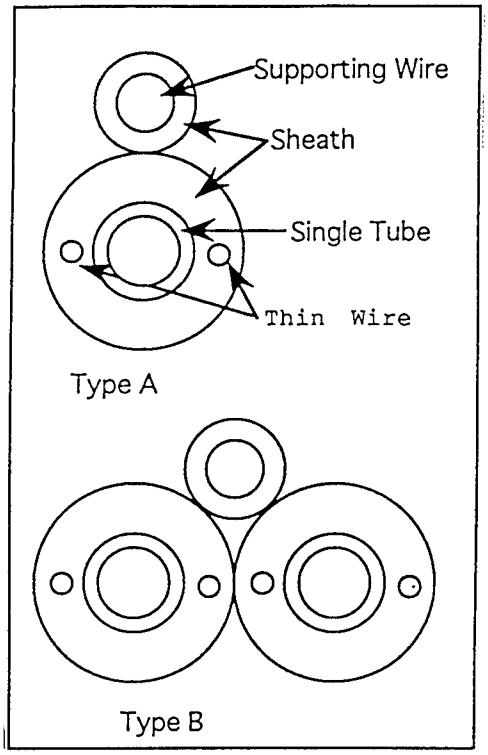


Fig. 1 Structure of Self-Supporting Cable

3. Design

3.1 Supporting Wire

In designing the supporting wire of the self-supporting cable, it is necessary to consider the effect of wind force. When a wind force is applied to the strung cable, the sum of the cable's own weight and the wind power acts on the wire. Hence, the effective weight of the cable can be considered to have increased. In the calculation model shown in Fig.2, tension is represented by equation (1):

$$T=\frac{WS^2}{8d}, \quad T_0=\frac{W_0S^2}{8d_0} \qquad (1)$$

Cable elongation is equal to the sum of thermal expansion and elongation by tension, so it is represented by equation (2):

$$\varepsilon=\alpha\,(t-t'_0)+\frac{T}{EA} \qquad (2)$$

Table 1 Spexification of Self-Supporting Cable

Outside diameter of tube	3.0mm
Diameter of Thin wire	0.45mm
Diameter of fiber unit	7.0mm
Diameter of supporting wire	4.6mm
Winding pitch	500mm
Weight of fiber unit	35g/m
Total weight, Type A	95g/m
Total weight, Type B	130g/m

Where

T and T_0: tension (Nf)
t and t_0: temperature (℃)
t'_0: temperature at cable fabrication, 20℃
W and W_0: cable weight (g/m)
S: span (m)
α: thermal expansion coefficient (/℃)
EA: product of Young's modulus and cross-sectional area
ε: cable elongation (%)
ε_0: permissible cable elongation (%)
d and d_0: sag (m)

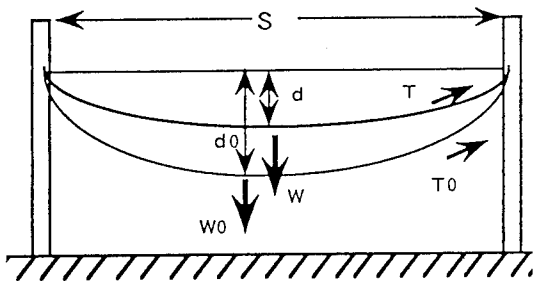


Fig. 2 Calculation Model of Supporting Wire

Fig.2 shows the relation between the ratio of supporting wire strength to effective cable weight and the span, for each level of permissible strain. In the case of stringing the cable under conditions of 40 m span, 0.2% permissible elongation and 35 cm sag, the strength of the supporting wire is

determined as EA/W = 1.349 E5 N/(N/m) from Fig.3. Assuming the wind force to be 540N/cm² (at a wind velocity of 20 m/min),

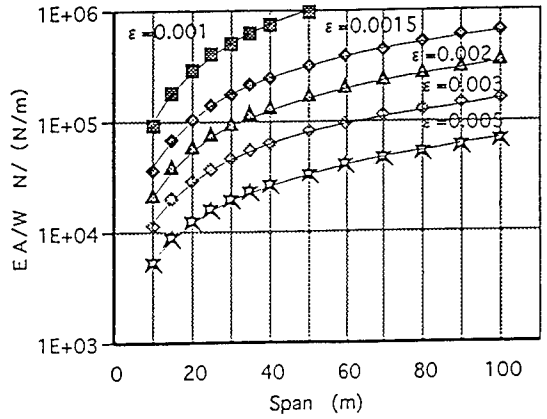
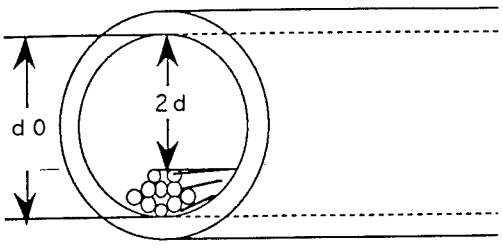


Fig.3 Design Diagram of Supporting Wire

the effective weight of Type A is 6.3 N/m and EA is 8.34 E5 N. Therefore, the outside diameter of the supporting wire is about 2.5mm. In the case of Type B, the effective weight is 7.93 N/m and EA is 10.695 E5 N. Therefore, the outside diameter of the wire is 2.8 mm.

3.2Tube Diameter and Winding Pitch

The inside diameter of the tube depends on the number of fibers, permissible fiber strain, minimum radius of curvature and winding pitch round the supporting wire. It is assumed that the 10 fibers in the tube move together, meandering like a sine wave in the longitudinal direction, as shown in the model of Fig.4.



d0: tube I.D. 2d: clearance

Fig.4 Design Model of Tube Diameter

It is assumed that the temperature range is from -30 to +70 ℃ and the permissible strain 0.2%, and that the stranded assembly of fibers has a circular section with a diameter of 0.75 mm that is three times as large as the fiber diameter. Meandering amplitude, permissible radius of curvature ρ and permissible percent excess length El for the group of fibers in the tube are represented by equation (3):

$$El = \frac{r}{4 \times \rho} \qquad (3)$$

Percent excess length El includes the effect of the tube being made longer than the supporting wire by winding the optical unit round the wire. Fig.7 shows the relation between the inside diameter of the tube and the radius of curvature, which depends on the winding pitch, under conditions that no strain is produced in the fiber even when a 0.2% strain is applied to the cable.

It follows from the figure that the inside diameter of the tube is 1.9 mm and the winding pitch 500 mm when the radius of curvature is from 30 to 40 mm.

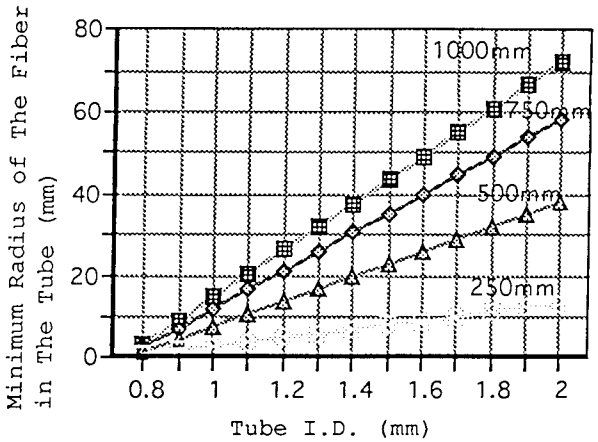


Fig.5 Minimum Radius by Tube I.D.

4.CABLE CHARACTERISTICS

We were tested trial cables for tensile, compressive, impact, etc.

4.1 In-process Change in Transmission Loss

Transmission losses in Type A in the fabrication process ranging from fiber to cabling stages are shown Fig.6. No loss increase was observed at both 1.55 μm and 1.31 μm wavelength, so the cable was confirmed to have been fabricated under stable conditions.

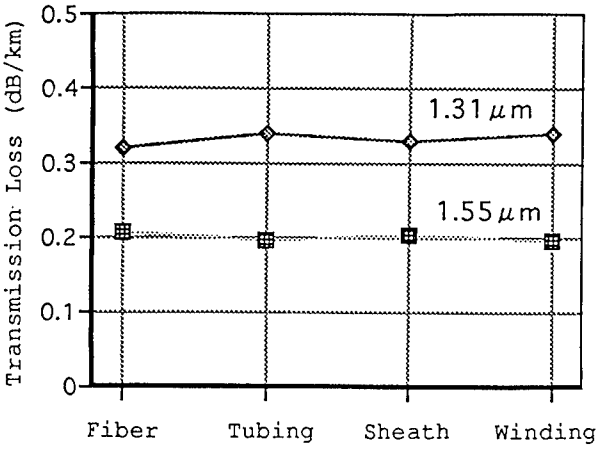


Fig. 6 In-process Change in Transmission Loss

4.2 Thermal Cycling

Transmission loss measurements were made after holding the cable for 24 hours at each temperature in the range of− 30 to +70 ℃. This measuring cycle was repeated twice. Fig.7 shows transmission losses at 1.55 μm at each temperature. Both Type A and Type B had good results with variation in loss.

4.3 Tensile Perormance

Fig. 8 shows the elongation and variation in loss of the cable when pulled by applying to it. The cable, when elongated as much 0.35%, showed a good result with virtually no variation in loss.

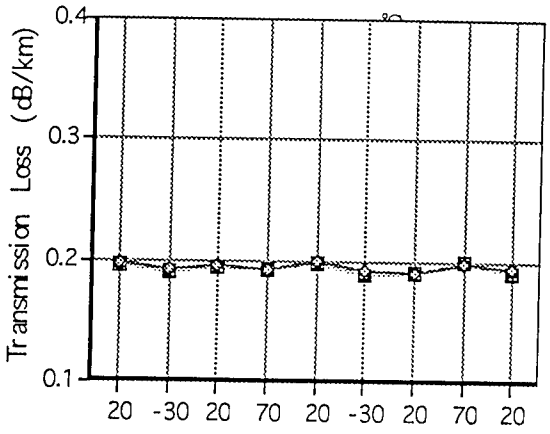


Fig. 7 Result of Thermal Cycles

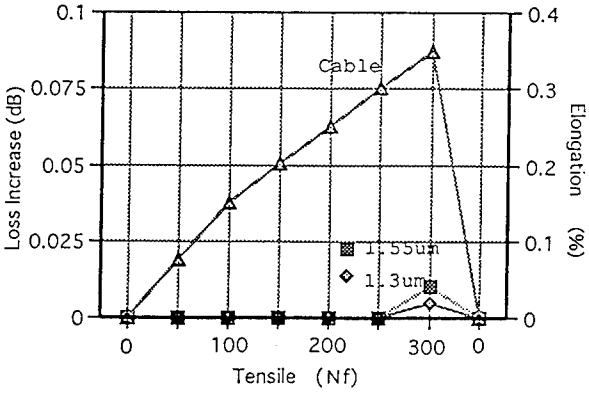


Fig. 8 Result of Tensile Test

4.4 Compression

Using a 50 mm wide plate, the cable was tested in two different positions, i.e., the position in which it was placed on the plate with the supporting wire upward, and the position in which it was placed with the wire sideways. In the case of Type B, however, with the wire upward, it gets between the fiber units and, with the wire sideways, the units vertically arranged above each other are horizontally arranged side by side. Therefore, only the test results of Type A are given here. The loss variation at 1.55 μm is shown in Fig.9 and the deformation in Fig. 10. With the

supporting wire sideways, the loss increase was less than 0.1 dB and the degree of flattening less than 40% under a compressive load of 2.94 kN per 50 mm. With the wire upward, no loss increase was observed and the degree of flattening was as low as 30%.

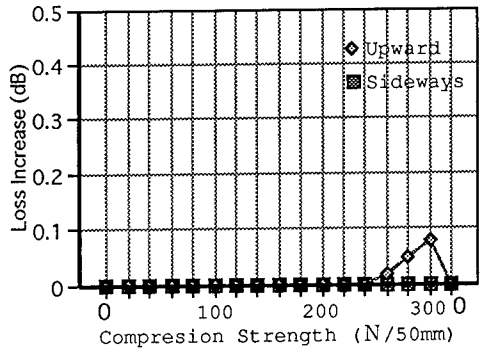


Fig. 9 Loss Increase by Compression Strength

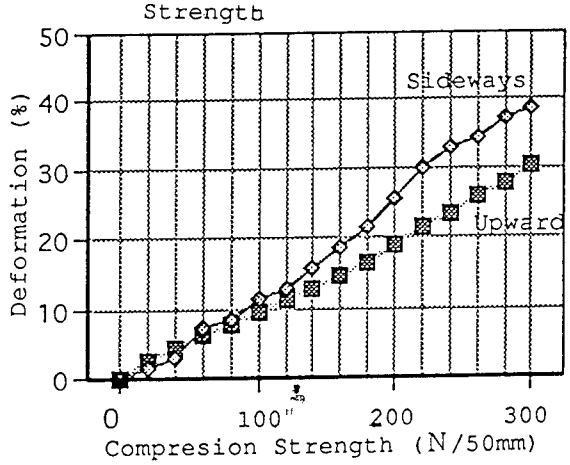


Fig. 10 Deformation by Compression Strength

Table 2 Test Results of Mechanical Properties

Test Item	Test Condition	Result (Type A&B)
Twisting	±360° 5turns	No loss increase (1.55,1.31μm)
Bending	30mmϕ ±90° 20 times	No loss increase (1.55,1.31μm)
Impact	20mmϕ 1kg load Drop heught 1.8m	<0.1 dB (at 1.55μm) <0.02dB(at 1.31μm)
Minimum Bending	30mmϕ 360° once	No loss increase (1.55,1.31μm)

4.5 Other Mechanical Charactaristics

Table 2 shows the test results of other mechanical properties. As seen in the table, both Type A and Type B had good results.

5. STRINGING PERFORMANCE



Fig. 11 Strung Cable

5.1 Stringing Conditions

The slack at 20℃ was determined as 35 cm. From equation (1), the stringing tension in this case is calculated as 530 N for Type A and 755 N for Type B, and the maximum tension at the maximum wind pressure (1.1 kN/cm²) is calculated as 1.67 kN for Type A and 2.45 kN for Type B. This tension causes the cable to elongate 0.2 to 0.3%, but it involves no problem in light of the tensile test results and because the tension at break of steel is 5.98 kN.

The cable actually strung is shown in Fig. 11 and method of anchoring it to poles in Fig. 12. Two kinds of hardware, suspender and winding grip, are used for anchoring.

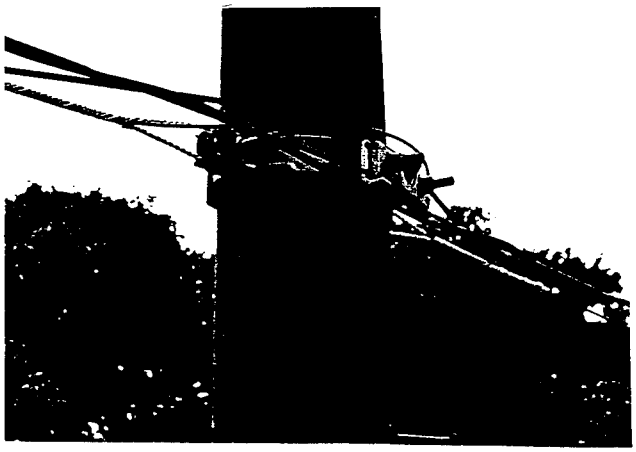


Fig. 12 Anchoring of Cable

5.2 Characteristics of Aerial Cable

Stringing was stracted in January 1995. In Japan, February is the lowest in temperature, so the results obtained during this one month are given below.

5.2.1 Transmission loss

The correlation between cable temperature and transmission loss for Type A is shown in Figs. 13 and 14. As seen from these figures, the loss is not correlated with the cable temperature, and its variation as ±0.025 dB at 1.55 μm and +0.03 to −0.02 dB at 1.3 μm.

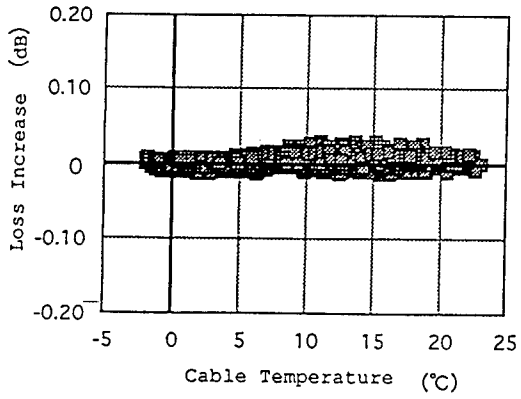


Fig. 13 Loss Increase by Cable Temerature(at 1.55 μm)

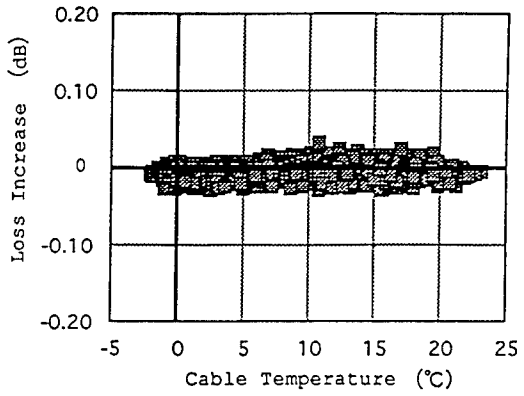


Fig.14 Loss Increase by Cable Temperature(at 1.3 μm)

5.2.2 Strain

Fig. 15 shows the correlation between cable temperature and tension of supporting wire. The supporting wire elongation calculated from tension is shown in Fig.16. The coefficient for it is 2.5E-6(/℃). As the thermal expansion coefficient of supporting wire is about 12.5E-6(/℃). So fiber strain calculated from thermal and tension is less than 0.05%.

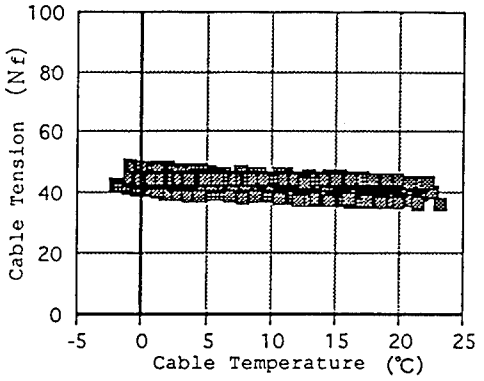


Fig. 15 Tension by Cable Temperature

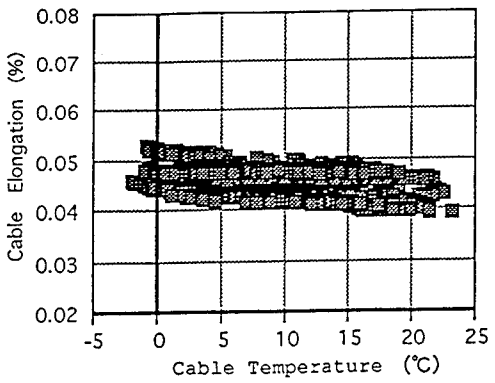


Fig. 16 Cable Elongation Calculated from tension by Cable Temperature

6. CONCLUSION

We devised a low-fiber-count, small-size, lightweight self-supporting aerial optic cable. Fibers were inserted with jelly into a tube, two thin steel wires were arranged along the tube to reduce thermal contraction and strain, and a polyethylene sheath was placed over the tube and strain, to form an optical fiber unit. By winding this unit round a supporting wire, we made the self-supporting aerial cable. The cable was tested for tensile, compressive, impact and thermal properties, and good results were obtained. Moreover, as a result of our continuous evaluation of the cable performance in the field, it was found that the cable exhibited good performance in winter.

In addition to these cable properties, the cable has the advantage of being low in fiber count, small-size and lightweight. Owing to these features, the cable is not only easy to make, but also easy to handle in the stringing work and able to be anchored with low tension without need for any special device, so it is economically excellent. We think that the cable will contribute greatly to the construction of multimedia networks which are expected to make fast progress in the future.

ACKNOWLEDGEMENT

We would like to thank many people at Fujikura who helped us in designing, manufacturing and testing this new self-supporting aerial optic cable.

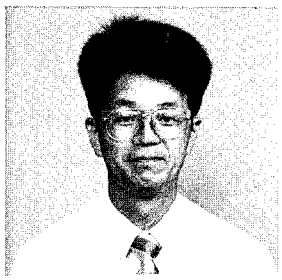
REFERENCE

{1}Y.Sugawara, H.Sinohara "DESIGN OF SUPPORTING WIRE FOR SELF-SUPPORTING CABLE" IEICE Transaction Vol.J65-B No.1 1982 pp116-117

{2}H.Sinohara, S.Tomita, M.Kawase "DESIGN OF SELF-SUPPORTING OPTICAL CABLE WITH SZ TWISTING STRUCTURE" IEICE Transaction Vol.J70-C No.6 1987 pp 802-809

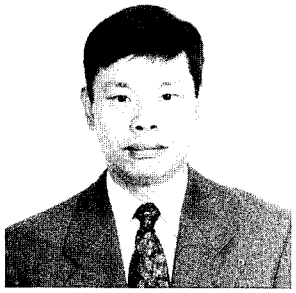
{3}J.P.BONICEL, O.TATAT, G.COUVRIE, L.RAPEBACH, P.ZAMZOW, J.BACHS, C.VERGEZ "AERIAL FIBER OPTIC CABLE FOR RAILWAY APPLICATIONS METALLIC OR DIELECTRIC SOLUTIONS" 43rd iwcs 1994 pp368-375

{4}A.Fargahi, C.Zehunder, A.Banfi, D.Schoepke, C.Theodossi, H.Hagmann, W.Nagele "DESIGN AND TEST OF A NEW METALLIC FIBER-OPTIC CABLE FOR AERIAL CABLEWAYS" 42nd IWCS 1993 pp 182-188



Osamu Koyasu
Opt-Electronics Laboratory
Fujikura Ltd.
1440, Mutuzaki, Sakura-shi, Chiba, 285, Japan

O.Koyasu was born in 1953.He joined Fujikura Ltd. from Kisarazu Technical Coleege in 1973 and has been engaged in research and development of transmission cable.He is now engineer in the Telecommunication Cable Section and a member of the IEICE of Japan.



Akira Sano
Opt-Electronics
Laboratory
Fujikura Ltd.

1440, Mutuzaki,
Sakura-shi, Chiba,
285, Japan

A.Sano was born in 1960. He joined Fujikura Ltd. after graduated from Kyouto University with a B.E. in 1983 and has been engaged in research and development of optical cable. He is now engineer in the Telecommunication Cable Section and a member of the IEICE of Japan.

Akio Mogi
Opt-Electronics
Laboratory
Fujikura Ltd.

1440, Mutuzaki,
Sakura-shi, Chiba,
285, Japan



Akio Mogi was born in 1946. He joined Fujikura Ltd. after his graduation fron Hneda Institute High School in 1967 and has been engaged in research and development of the metallic cables and optical cables. He is now the sub-maneger optical fiber cable section and a member of IEICE of Japan.



Kohichirou Watanabe
Opt-Electronics
Laboratory
Fujikura Ltd.

1440, Mutuzaki,
Sakura-shi, Chiba,
285, Japan

K.Watanabe was born 1959.He received a B.E. degree in electrical engineering from Tohoku University in 1982. Since joining Fujikura Ltd. in 1988, he has worked on the development of optical fiber cables. He is now sub-manager of the optical fiber cable section and a member of the IEICE of Japan.

Matsuhiro Miyamoto
Opt-Electronics
Laboratory
Fujikura Ltd.

1440, Mutuzaki,
Sakura-shi, Chiba,
285, Japan



Matsuhiro Miyamoto was born in 1953. He graduated from Nagoya INstitute of Technology with a B.E. degree of electrical engineering. He joined Fujikura Ltd. after his graduation from Tokyo Institute of Technology with a M.S. degree in 1978 and has been engaged in research and development of optical fiber and optical fiber cables. He is now a manager of the optical fiber cable section.

DESIGN AND RELIABILITY CONSIDERATIONS FOR LONG SPAN, HIGH VOLTAGE, ADSS CABLES

D. A. KELLER [1], O. TATAT [1], R. GIRBIG [1], M. ADAMS [2], R. BÖHME [3], C. LARSSON [4]

[1] ALCATEL CABLE - OFCCC, FRANCE - [2] ALCATEL ATC, USA -
[3] KABELRHEYDT, GERMANY - [4] ALCATEL IKO KABEL, SWEDEN

ABSTRACT

The evolution of the ADSS cable designs has generated reliable cable and hardware combinations, and anti-tracking jacket materials. The aramid design is superior in weight, loading and flexibility, however the increased compressibility requires hardware, designed for the radial compressive density of the cable. Three specific field tests for vibration, minimum sag, and field voltage are on-going. In an accelerated laboratory test, three samples of ADSS cable, two tensioned to 30 kN and one untensioned, have been subjected to up to 2000 hours of salt-fog testing at voltages ranging from 20 kV to 35 kV. All three cables completed the test without tracking or puncture, having only erosion of the jacket to a depth of less than 30% of the minimum wall thickness (IEEE spec < 50% min wall) indicating an estimated 20-30 year life for the cables.

BACKGROUND

The reliability of aerial dielectric cables is improving, however there is a customer need to extend the level of understanding of the failure mode of these cable designs. The theoretical tradeoffs of several designs are discussed. Selection of a design from these several possibilities was made and was followed by testing to explore the failure mode. High Voltage Salt-Fog testing, hardware selection and testing, and field experience are discussed.

DESIGN OPTIONS

When full dielectric cables were initially installed on "super high voltage lines" they could have suffered from one of three modes of failure: which are tracking, erosion, and rupture [1].

OPGW is often selected to avoid these problems; however, in some cases the ADSS is preferred, due to its lighter weight and centrally located position. Given the expertise, the OPGW can be installed on active or energized high voltage lines [2]; however, the ADSS is generally easier to install on hot lines.

Besides tracking resistance, the ADSS design faces four additional target zones, the cable's strength, strain window and weight, and compressibility or compatibility with the hardware.

To understand the cable assembly target zone options, four basic examples were chosen to represent some of the popular solutions available [3,4,5] and are illustrated as (1) Aramid design, the (2) Solid Core, the (3) GRP layer and the (4) Individual GRP design. All are shown in Fig. 1.

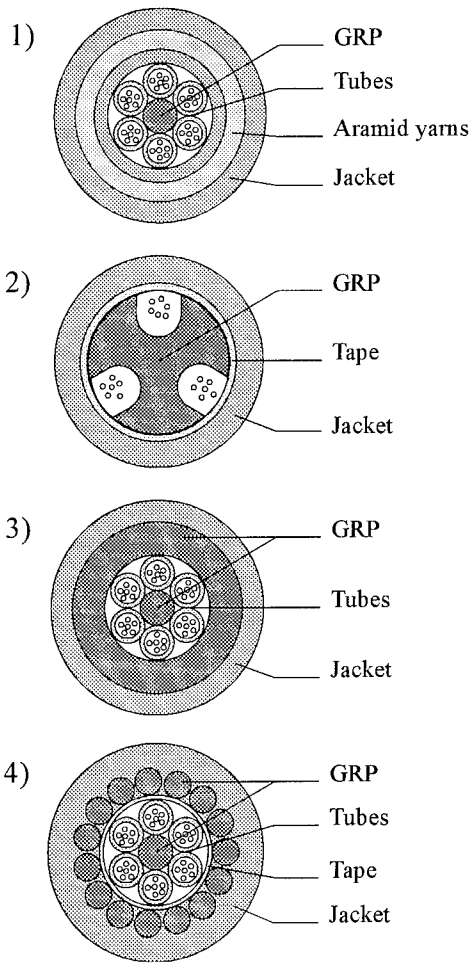


Fig. 1 : 4 Cable Designs

Each of the four designs was configured with a 13 mm outer diameter, leaving only the varied strengths and weights due to material variances.

These differences in weight, wind effects, probable ice loading, and effective spans are graphed in Fig. 2 and 3. In the following table the cable parameters are listed.

Parameters	ARAMID	SOLID CORE	GRP LAYER	INDIVID. GRPs
OD [mm]	13.02	13.10	12.95	13.15
St Window	0.8 %	0.8 %	0.8 %	0.8 %
Creep Allowance	0.1 %	0.1 %	0.1 %	0.1 %
Max Load [N]	20666	22235	19573	16407
Cable Break [N]	50400	61167	53846	45140
Cross Section [mm^2]	133.2	134.8	131.7	135.8
Cable Modulus [kN/mm^2]	18.4	19.7	17.7	14.2
Cable Weight [kg/km]	148	190	196	196
Thermal Elongation	$2*10^{-7}$	$9.5*10^{-6}$	$1.14*10^{-5}$	$1.3*10^{-5}$
Start Temp. [°C]	23	23	23	23
End Temp. [°C]	-10	-10	-10	-10
Initial Sag	1%	1%	1%	1%

Table 1 : Cable Parameters

The Solid Core design has the highest modulus for the total area of the four cables; however, the added weight of the solid (GRP) core reduces the allowable spans as compared to the longest overall span Aramid design as shown in Fig. 2 and 3.

The Solid Core design traditionally has a smaller strain window than the other three Loose Tube Core designs. Its 0.8% strain window includes 0.25% fiber elongation at maximum cable load where the Loose tube designs have 0% fiber elongation. If this elongation were to be subtracted in this exercise the Solid Core design would be further limited in span length.

The Aramid design has improved flexibility and has been flex cycled in excess of 40,000 cycles around a 6" (15.24 cm) mandrel without damage. There is very little compression from the preformed rods tension hardware for the Solid Core design, while the Aramid design has the greatest compression of all of the 4 examples. The GRP layer design has excellent strain window potential and excellent compression performance in the hardware, however accessing the fibers may be more difficult and it is not very flexible. The Individual GRP design combines improved compressibility, flexibility and accessibility to the fibers but the allowable spans for a given cable diameter are limited as compared to the other three designs.

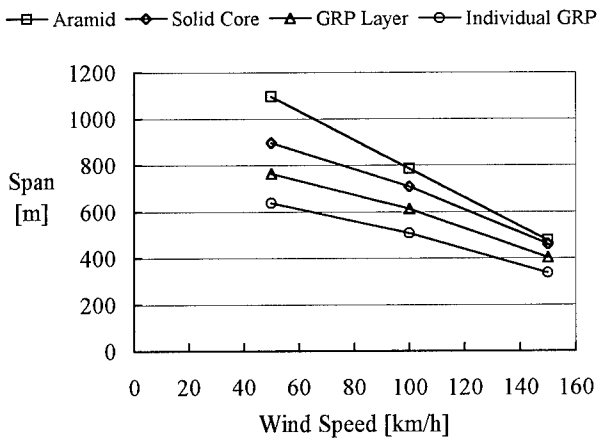


Fig. 2 : Span Ranges Four Designs
Ice Thickness : 0 mm

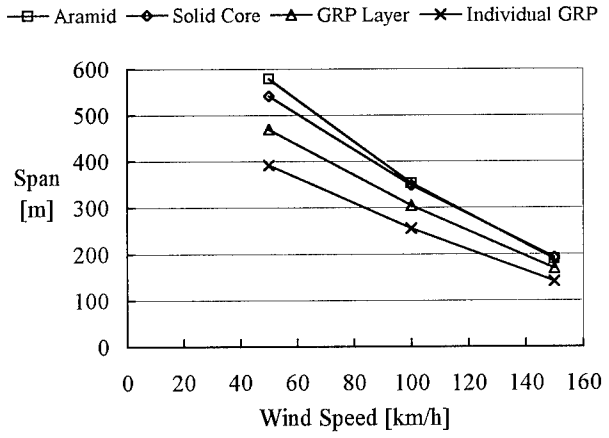


Fig. 3 : Span Ranges Four Designs
Ice Thickness : 12.5 mm

SAG AND TENSION COMPARISONS

An exact solution of the cable catenary given hyperbolic functions is difficult, especially in cases with long spans and / or height differences between suspension points.

One solution is to replace the catenary by a parabola and to solve parabolic equations instead of hyperbolic functions. The other, more accurate solution, is to use series approximations to the hyperbolic functions. To be accurate it is sufficient to use the first two terms of the series. The parabolic approximation can be used for spans of up to 500 m and a slope of 30° with the sag calculation error of less than 1%. Although the sag and tension error for relatively light ADSS cables compared to conductors or OPGWs is low, the use of

series approximations for longer spans or greater height differences and sags is recommended. [6,7,8].

In general, commercially available calculation programs use the series approximation and in case of the unloaded cable give the same results. For a loaded cable, with ice and wind load, the results differ from program to program. The main reasons are different assumptions for ice density and wind speed to wind load conversion.

ARAMID APPLICATION

The gripping strength of the hardware on the cable is directly related to the radial compressive density of the cable and the hardware design. Two important factors are the aramid packing during assembly combined with hardware designed to the compressibility of the cable.

In addition to yarn packing, attention can be paid to the relative lay lengths of each layer and the resulting torsion under tension to result in a "torsionless" cable.

Utilization of typical water blocking gels adds weight to the design and at +70°C can reduce the coefficient of friction between the aramid and the jacket via the compound. For the current design, the aramid yarns were finished with water in oil emulsion containing super-absorbing polymers. The coated aramid was cabled and then creep and tensile tested in high temperature and high humidity conditions. No reduction of cable strength was measured.

In addition to some internal guidelines as above, the IEEE ADSS draft [9] was used for the qualification testing.

HARDWARE EXPERIENCE

The armor rods (first layer hardware) must be preformed to the correct diameter to perform correctly at the maximum tensile strength. The Actual Ultimate Tensile Strength can be less than the Theoretical Ultimate Tensile Strength, however it is greater than the Max Rated Load (load before fiber strain) of the cable. Aramid cable having 20 to 40 kN max rated loads reach their break strength of 50 to 100 kN, while the larger designs are more difficult, due to increased compression.

For example, for a cable with maximum rated load of 57.7 kN, and a theoretical ultimate tensile strength of 150 kN, the actual maximum tensile strength obtainable at 23 °C is 130 kN. The Max Rated Load of the cable of 57.7 kN is well within the actual strength of 130 kN. A design with a max rated load of 93 kN and a theoretical break of 252 kN, reaches an actual 158 kN in the preformed grips. This allows for a 65 kN safety margin, sufficient for a cable of this type.

FIELD CONDITIONS AND EXPERIENCE

Aeolian vibration is a form of energy which must be dissipated in these cable designs. The ability of ADSS cables to dissipate a portion of the mechanical energy received from the wind is called "cable self-damping". A power technique can be used to measure self-damping [10]. A 17 mm diameter ADSS cable having aramid of about 600 kdtex was subjected to vibration angles of 5',10' and 20' (one angular minute ['] is 1/60 angular degree [°].) Automatic sweeping from 8 to 100 Hz was performed at 5 kN, 10 kN and 15 kN.

As seen in Fig. 7 the general tendency of the cable was an increase of the self damping as the vibration frequency increases and the vibration angle increases, however a decrease in the self damping was seen as the cable tension increases.

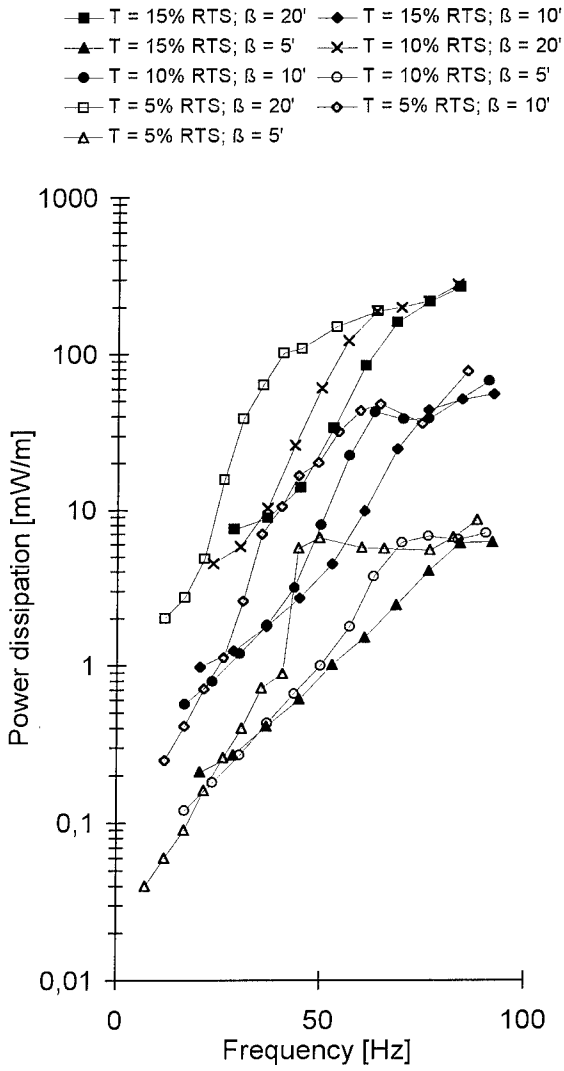


Fig. 7 : Cable Self Damping

Fig. 8 depicts an estimate of the maximum vibration level of the 17 mm ADSS cable, when power input of laminar wind is in balance with cable self-damping.

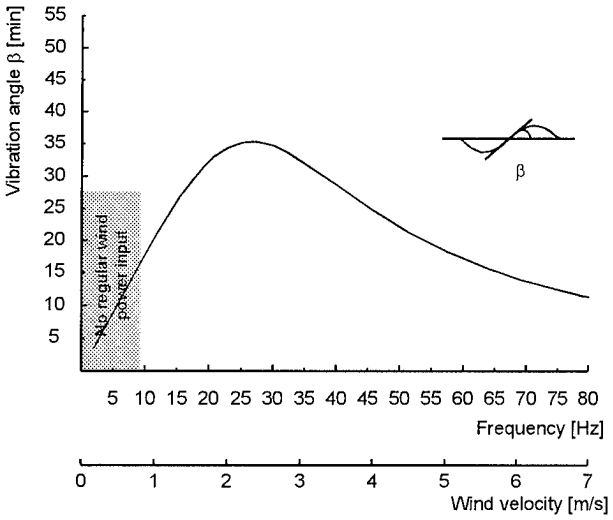


Fig. 8 : Free Span Vibration Angle

FIELD TESTING

MINERVOIS, FRANCE

An Electricité de France (EdF) test facility in Minervois, France was chosen to locate 2 ADSS cables across a 500 meter valley labeled span C and F. The cables were installed at a load of 10 kN each, without dampers of any kind. The cables were allowed to vibrate undamped for 10 months.

Span C and F were monitored for vibration activity for a period of one week in June 1995 using a non-contact measurement method [10] on the center section of the span. Aeolian wind vibration could only be observed during low turbulence wind found in the early morning or late evening. Of C and F, span F was chosen for the damper tests. The schedule was set as: "non-damper set-up" days 1 and 2, "3 spiral vibration dampers (SVDs) each side" days 3 and 6, and "2 Stockbridge dampers each side" days 4 and 5. All "captured" or recorded vibration instances are plotted in Fig. 9.

Conditions for days 1 and 2 did not produce significant vibrations for span F without dampers. Span F's highest vibrations were found with the Stockbridge dampers on days 4 and 5. The SVDs were tried on day 3 and 6 with lower vibration angles recorded. The wind conditions for days 3 through 6 were similar suggesting the SVDs dissipated more vibration energy as compared to the 1 type/positioning Stockbridge dampers that were used.

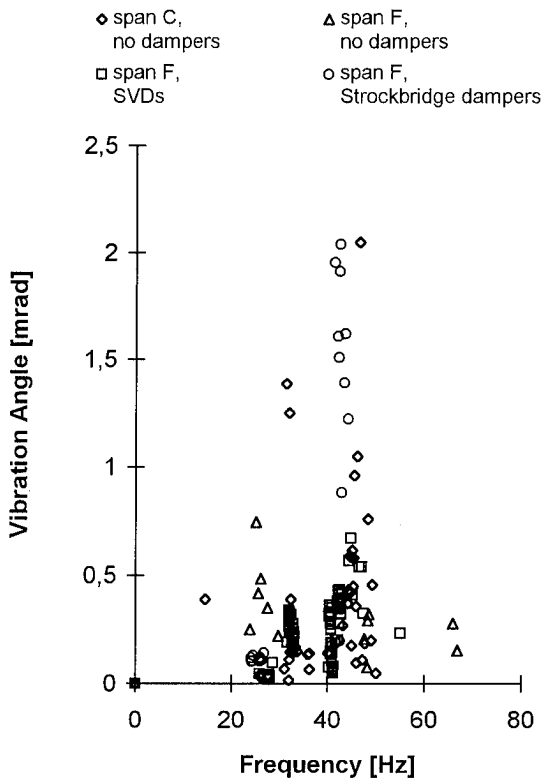


Fig. 9 : Vibration Intensity

SWEDEN

In one trial 30 km was installed with a 0.5 to 0.7% sag limit to reduce clashing between tightly spaced conductors. The installation was on wooden poles not originally designed for high tension ADSS cables. High aramid dtex counts, installed tension of approx. 15 kN and the cable's low weight provided minimum sag for the typical span of 300 m.

In another trial, four lengths, a total approx. 15 km, were installed by helicopter [11] during four working days. The cables were installed this way due to the very rocky topology of the area, which made it impossible to find locations to place the pulling and payout equipment. The helicopter operated with a ground level speed of 10 km/h, and the cable was strung dragfree with a tension of approx. 3 kN. In an installation of this type the wind speed must not exceed 10 m/s during the flight. Special sheaves, where the cable could snap-in, were used. During the snap-in process the helicopter was halted and turned towards the wind direction. The drum, fixed in a special combined payout and breaking equipment, normally hangs 10 m below the helicopter, although this had to be adjusted according to the height of the surrounding trees. The breaking tension can be electrically adjusted from the helicopter, to make the flight as smooth as possible. The helicopter used in this actual project was able to

carry a payload of 1750 kg. The combined payout and breaking equipment weighs 50 kg, which leaves 1700 kg for drum and cable (> 5 km of cable possible).

Both of these installations illustrated the advantages of the lightest weight and the most flexible cable.

FIELD VOLTAGE "POTENTIAL" AND DRY BAND ARCING BACKGROUND

The Field Voltage "Potential", not the Line Voltage, at the specific ADSS cable location on the tower, with respect to the conductor location, directly relates to the degradation resulting from Tracking and Dry Band Arcing. If the field voltage is less than 12 kV then ordinary PE compounds can be used. If the Field Voltage is between 12 to 20 kV, cross-linked anti-tracking compound must be used. The lifetime of the installation is dependent on the maximum line voltage, field potential at the ADSS cable location, the jacket material used, the level of pollution or low resistive material that can accumulate on the cable surface and the amount and type of rain that is experienced by the cable. Arcing across dry sections (dry-band arcing) requires a 25 kV field potential to be sufficiently aggressive to damage a properly designed sheath material [12]. In the case of a 400 kV line it is quite possible to locate the cable in a phase location of 20 kV or less and given the proper jacket material have an expected life of the cable of 20 years or greater. Further steps could be taken to install the cable in a lower field potential (5 kV i.e.) and further enhance the life of the cable [13,14].

TYPICAL CABLE LOCATION ON TOWERS AND LIFE TIME PREDICTIONS

Anti-tracking jackets performed well for 2.5 years with damage at the 3rd year at 25 kV for Fawley, with failures in 2-3 months at Hunterston at about the 60 kV level [2,12,14,15]. In a revised test performed at Hunterston, at 25 kV, the cable performed well without jacket damage for 9 months until a severe storm occurred resulting in a puncture to the cable jacket [2,16-18].

Field voltage calculation examples are readily made with several available sources of commercial software. As discussed in Carter and Waldren [15], the field will change when one field is switched off, therefore variations of the lifetime "actual reality" must be plotted to insure that the anti-tracking jacket remains within a field potential of <20 kV. A hypothetical situation is for the cable to be installed in a 5-10 kV field, which may increase to a 20 kV field when one side field is turned off

Modern sheath materials are able to withstand more arcing than those in the early trials [14]. During this same time period, cables have been installed on High Voltage Lines using anti-tracking material with good results. Dissado [18] discussed a method for life time prediction based on voltage level and failure probability. From [1] we can see that the 1 to 10 mA currents induced in the salt-fog test exceed the worse case 1 mA occurrence that caused the failure on the Hunterston, Scotland trial.

In an over simplified example we can compare the 1000 h Salt-Fog test to Carlton [14], where monitored arcing occurred much less often than expected, having only three periods of arcing activity in February 1992 which was noted as typical. These three periods of activity ranged from .6 to 1 mA as compared to a typical 1 to 10 mA current in the Salt-Fog test. Assuming 36 periods of arcing per year and 1.5 hour periods leads to an estimate of 54 hours of arcing per year for 1080 hours of arcing activity for a 20 year period.

The IEEE specification for salt water flow rate, droplet size, temperature NaCL content of water, nozzle capacity and nozzle pressure and exhaust was found to be a good optimization of pollution and dry-banding to generate continuous arcing. A 1000 h salt-fog test with continuous arcing to simulate a 20 year life and a 2000 h test to simulate a 30 year life was selected.

SALT-FOG - DRY BAND ARCING TEST RESULTS

The three common modes of failure due to dry band arcing, when full dielectric cables are installed on "super high voltage lines" are tracking, erosion, and rupture. Tracking (mode 1) is the deterioration of the polymer resulting in a carbon treeing effect. The carbon tracks are equivalent to an electrical extension of the grounded metal rods. Erosion (mode 2) still occurs when the cross-linked polymer bonds slowly give-way to the stress and strain and the heat generated from the dry band arcing activity. Jacket ruptures (3rd mode) are caused by a substantial arc generating sufficient heat to create a hole in the cable jacket.

Prior to IEEE Salt-Fog testing other laboratory testing was performed as illustrated in tables 3 and 4 to select the best jacket material types.

Material	Thick-ness [mm]	Aging [h]	Number of samples	1 arc 0,25 s, every 2 s, 10 mA	2 arcs 0,25 s, every 2 s, 10 mA	4 arcs 0,25 s, every 2 s, 10 mA	Continuous 10 mA
Black LDPE	5	500	5	17... 45 s			
	5	1000	5	6... 15 s			
PU	5	500	5	8... 15 s			
	5	1000	5	8... 13 s			
Thermo-plastic	5	500	10	P	P	10... 26 s	
X-linked	5	500	10	P	P	P	2... 10 s

P : PASSED

Table 3 : Dry Arc Resistance After Aging, ASTM D 495, 1000 h in WEATHEROMETER

Material	Black LDPE			PU				Thermo-plastic			X-linked			
Thickn. [mm]	3	5	3	3	5	5	5	3	5	3	3	5	5	5
Aging [h]			500			500	1000			500			500	500
Voltage [V]														
1000	P	P	P	P	P	P	P	P	P	P	P	P	P	P
1250	P	10	P	10	11	P	P	P	P	P	P	P	P	P
1500	P		P			P	P	P	P	P	P	P	P	P
1750	5		P			15	10	P	P	P	P	P	P	P
2000			18					55	P	P	P	P	P	P
2250									P	P	P	P	P	P
2500									P	P	P	P	P	P
2750									P	20	P	P	P	P
3000									P		P	P	P	P
3250									20		P	P	P	P
3500											20	38	P	P
3750													P	P
4000													P	P
4250													P	P
4500													P	P
4750													P	P
5000													P	P
5250													P	P
5500													P	45
5750													P	
6000													P	

P: PASSED

Table 4 : Tracking and Erosion Test,
ASTM D 2303 / IEC 587

Crosslinked materials typically perform much better in dry arc or salt-fog testing [17].

RESULTS FROM IEEE TEST

In IEEE Salt-Fog testing., three samples of ADSS cable, 2 tensioned to 30 kN and one untensioned, have been subjected to 1000 h to 2000 h salt-fog tests at voltages ranging from 20 kV to 35 kV. All three completed the test without tracking or puncture, having erosion only of the jacket to a depth of less than 30% of the minimum wall thickness.

SAMPLE 1

Tensioned at 30 kN, with annular electrode at earthed end [2].

200 h at 20 kV	.5 mA to 20 mA leakage current recorded 1st 20 h 1 mA to 30 mA recorded in 1st 100 h
204 h at 25 kV	at 260 h crazing pattern observed mean current 1 mA, discharge to 40 mA detected, peak leakage of 2 mA measured.
231 h at 30 kV	at 600 h erosion depth of .2 mm observed transient to 80 mA (peak)
365 h at 35 kV	erosion circumferential to depth of .5 mm

SAMPLE 2

Untensioned, without annular electrode at earthed end.

231 h at 30 kV	evidence of erosion at 100 h discharge of 10-20 mA
769 h at 35 kV	erosion marks circumferential pattern to .2 mm depth transient of 50 ma peak were recorded. transients of up to 80 mA peak by the end of the test

SAMPLE 3

Tensioned with annular electrode at earthed end

2000 h UV test (UV exposure ASTM G53-88) prior to the Salt-Fog test.

1st:	1000 h at 30 kV	erosion to depth of .2 mm
2nd:	1000 h at 30 kv	erosion to depth of .4 mm

Tension and annular electrodes were used in the 3rd sample due to the increased erosion seen in sample 1. Less severe erosion occurred in sample 2 although the sample remained at 35 kV for 769 hours as compared to only 365 hours for sample 1, confirming the more severe effect with annular electrodes as discussed in [18].

Sample 1 and 3 were both tensioned 1000 h with sample 1 finishing with 365 h at 35 kV. Sample 1 sustained a 0.5 mm erosion depth as compared to a 0.2 mm for sample 3 suggesting a severe effect from the additional 5 kV.

As a confirmation of the longevity of the jacket material the third cable sample was subjected to a second 1000 h at 30 kV under 30 kN tension resulting in total of 0.4 mm of degradation depth.

FIELD TESTING

NECKARWERKE, GERMANY

A continued monitoring 380 kV installation on a NECKARWERKE line, in ESSLINGEN, GERMANY, has completed two years duration with no evidence of any cable degradation. The ADSS cable has been installed in 5 and 20 kV field locations on the tower to demonstrate the effect different levels field potential in less severe environments having less than 54 hours of dry band arcing per year. No damage has been observed to date.

SUMMARY

The continued development of the lightweight aerial cable has resulted in the evolution of the ADSS cable designs and especially the jacket material.

Given a standard cable diameter, the aramid design is superior in weight and loading however the reverse is true for hardware

compatibility is more difficult due to the increased compressibility of the cable.

Field measurements indicate more vibration energy is dissipated using spiral vibration dampers. Field tests are on-going with no failures due to hardware vibration or field voltage.

Three samples of ADSS cable, tensioned to 30 kN and one untensioned, have been subjected to a 1000 - 2000 h salt-fog test at voltages ranging from 20 kV to 35 kV. These samples have completed the test without tracking or puncture, having erosion of the jacket of less than 30% of the minimum wall thickness indicating an estimated 20 - 30 year life for the cables.

From these results, the ADSS cable has proven to be a reliable solution for High Voltage line applications.

ACKNOWLEDGEMENTS

The authors would like to thank: H.J. Krispin of RIBE GmbH & Co, Schwabach, Germany, for his cooperation and support in the non-contact vibration measurements in Minervois. M. Marklove of GEC ALSTHOM, Stafford, UK, for his cooperation and support in the salt-fog cable testing.

REFERENCES

[1] A.J. Peacock, J.C.G. Wheeler, "Development of Aerial Fibre Optic Cables for Operation on 400 kV Power Lines", IEE Proceedings-A, Vol. 139, No. 6, November 1992, pp 304-314.

[2] G. Carlton, A. Bartlett, C. Carter, T. Parkin, "UK power utilities' experience with optical telecommunications cabling systems", Power Engineering Journal, February, 1995, pp 7-14.

[3] A.T.M. Grooten, E.J. Bresser, A.G.W.M. Berkers "Practical Experience with Metal-Free Self-Supporting Aerial Optical Fibre Cable in High Voltage Environments", International Wire & Cable Symposium Proceedings, 1987, pp 426-437.

[4] A.J. Davies, P. Radage, S.M. Rowland, and D.J. Walker "The selection of materials for long span, dielectric,aerial, self-supporting cable for optical communications", Plastics in Telecoms. VI, London, 1992, pp 27/1-27/10

[5] S.M. Rowland, K. Craddock, C.N. Carter, I. Houghton, D. Delme-Jones, "The Development of a Metal-Free, Self-Supporting Optical Cable For Use On Long Span, High Voltage Overhead Power Lines", International Wire & Cable Symposium Proceedings, 1987, pp 449-456.

[6] E. Maurer, "Die Berechnung der Freileitungen mit Rücksicht auf die mechanischen Verhältnisse der Leiter", SEV Bulletin Nr. 2, 1936, pp 41-53, SEV Bulletin Nr. 3, 1936, pp 65-73.

[7] P.F. Winkelman, "Sag-Tension Computations and Field Measurements of Bonneville Power Administration", AIEE Transactions, Vol. 78, February 1960, pp. 1532-1548.

[8] V.W. Kelsey, "Practical Solutions of Catenaries", 1984 14000 E. Linvale Pl.#201, Aurora, CO 80014.

[9] "Standard for All Dielectric Self-Supporting Fiber Optic Cable (ADSS) for Use on Overhead Utility Lines", IEEE P1222 Draft 1993, October 25

[10] G. Agelink, "Vibration Measurements on Live Overhead Lines by Means of a Non-Contact Measuring Method", CIGRE Symposium22-81 Stockholm, Paper 22-8/112-08 (1981)

[11] D.E. Mize, "Helicopter Installation of Fiberoptic Groundwire on Overhead Lines", ESMO '93, Las Vegas, Nevada, September 12 - 17, 1993

[12] C.N. Carter, "Arc control devices for use on all-dielectric self-supporting, optical cables", IEE Proceedings-A, , Vol. 140, No. 5, September 1993, pp 357-361.

[13] C.N. Carter, "Dry Band Electrical Activity on Optical Cables Separately Strung on Overhead Power Lines", International Wire & Cable Symposium Proceedings, 1988, pp 117-121.

[14] G Carlton, C N Carter, A J Peacock, R Sutehall, "Monitoring Trials on All-Dielectric, Self-Supporting, Optical Cable for Power Line Use", International Wire & Cable Symposium Proceedings, 1992, pp 59-63.

[15] C.N. Carter, M.A. Waldron, "Mathematical Model of Dry-Band Arcing on Self-Supporting, All-Dielectric, Optical Cables Strung on Overhead Power Lines.", IEE Proceedings-A, Vol. 139, No. 3, May 1992, pp 185-196.

[16] S. M. Rowland, F. Easthope, "Electrical ageing and testing of dielectric self-supporting cables for overhead powerlines", IEE Proceedings-A, Vol. 140, No. 5, September 1993, pp 351-356.

[17] J.C.G. Wheeler, M.L. Lissenburg, J.D.S. Winchliffe, M.E. Sleven, "The Development and Testing of a Track Resistant Sheathing Material for Aerial Optical Fibre Cables", 5th International Conference on Dielectric Materials, Measurements and Applications, Canterbury, June 88.

[18] L.A. Dissado, M.J. Parry, S.V. Wolfe, A.T. Summers, C.N. Carter, "A New Sheath Evaluation Technique For Self-Supporting Optical Fibre Cables on Overhead Power Lines", International Wire & Cable Symposium Proceedings, 1990, pp 743-751.

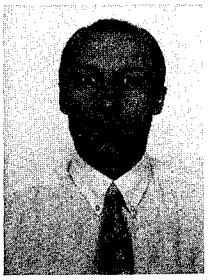
AUTHORS

David A. KELLER - ALCATEL CABLE
35, rue Jean Jaurès - 95871 Bezons ,FRANCE



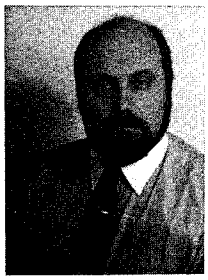
David A. KELLER born in Harrodsburg, KY, USA in 1960 received his B.Sc. degree in Mechanical Engineering from the University of Kentucky in 1983. He has held several US positions in both Optical Cable Process Engineering and Product Development before and after joining Alcatel in 1987. Since May 1993 he has held the position of Cable Development Project Engineer at the Alcatel Optical Fiber Cable Competence Center in Bezons, France.

Olivier TATAT - ALCATEL CABLE
35, rue Jean Jaurès - 95871 Bezons ,FRANCE



Olivier TATAT was born in 1959. He received his engineering degree from the Institut des Sciences de l'Ingénieur de Montpellier (ISIM) in 1982. He joined Les Câbles de Lyon, now Alcatel Câble, in 1985. Now he is working as a project engineer, in charge of the development of OPGW, in the Alcatel Optical Fiber Cable Competence Center in Bezons, France.

Reinhard GIRBIG - ALCATEL CABLE
35, rue Jean Jaurès - 95871 Bezons ,FRANCE



Reinhard GIRBIG (41) received his Dipl.-Ing. degree from the Ruhr University Bochum in 1982 and joined KABELRHEYDT in 1987 as a development engineer in the fiber optics area, responsible for the technical aspects of OTDR measurement. In 1991 he became head of the Optical Fiber Cable Installation Technique Group. Since May 1993 he is working as a project engineer and responsible for the Transmission and Characterization Group in the Alcatel Optical Fiber Cable Competence Center in Bezons, France.

Michael ADAMS - ALCATEL ATC
2515 Penny Road - Claremont NC, 28610, USA



Michael ADAMS received his B.S. degree in mechanical engineering from the university of Tennessee, Knoxville in 1991. He joined Alcatel ATC the same year and has been engaged in research and development of fiber-optic cables.

Ralf BÖHME - KABELRHEYDT AG
Bonnenbroicher Str. 2-14 - 41238 Mönchengladbach, GERMANY



Ralf BÖHME (41) received his Dipl.-Ing. degree from Bergische University Wuppertal in 1986. He joined KABELRHEYDT the same year. As a member of the development department for optical fiber cables he is responsible for the development and engineering of ADSS cables.

Christer LARSSON - ALCATEL IKO KABEL
S-514 81 Grimsås, SWEDEN



Christer LARSSON, born in 1957, graduated from Chalmers University of Technology, Gothenbourg, Sweden in 1983. He holds a M.Sc. in Engineering Physics and has since been active within various fields of optical fiber communications, with special focus on applications for the electrical power industry. He is today affiliated with Alcatel IKO Kabel, Sweden.

Mid-span Jointing of Optical Groundwire (OPGW)

F. Grajewski*, W. Stieb*, H. Haag**, G. Hög**

*ALCATEL KABELMETAL **KABEL RHEYDT AG

Abstract

A new technology for the jointing of optical fiber ground wire in the span is presented. The basic concept is based on the separation of the mechanical and electrical connections from the splicing of the fibers. This results in a splice closure for the optical fibers, concentrically arranged around the mechanical splice. This hermetically tight splice space has such an optimized mass and shape that investigations up to this time have not revealed any harmful influence on the mechanical and dynamic behaviour of the jointing system of the ground wire. The design of the joint and the results of our investigations are discussed in the presentation.

Introduction

Ground wires were originally intended to protect high voltage lines against lightning and short circuits. However, in some countries telecommunications over high voltage power lines using the ground wire play a major role. The ground wire has two functions: it protects the power lines against the effects of lightning and grounds short-circuit currents. Originally it was manufactured as a steel-reinforced aluminium conductor (SRAC) and it did not have any telecommunication function. Then, about 25 years ago, coaxial or symmetrically-paired copper telecommunication circuits began to be fitted into the ground wire core, so as to enable it to carry telecommunications. The telecommunication's role of the ground wire was strengthened when optical fiber replaced copper on lines installed from 1980 onwards. Incidentally, this also eliminated the problem of induced voltage on the copper circuits.

In Germany the Deutsche Telekom is expecting severe competition from power utilities, which are losing no time to install optical fiber ground wire. In many other countries power utility companies which are increasing the capacity of their high voltage lines, are equipping them with optical fiber ground wire at the same time.

In common practice optical fiber ground wires are connected from tower to tower. This means that the electrical and mechanical joint is performed on top of the tower. The ground wire with the fibres is lead down the tower and the fibres are spliced in a special metallic enclosure. This jointing technology requires that the length of the fiber-optical ground wire be accurately determined when production starts in the factory. This very often causes problems during planning and delivery of the materials into the field, especially in countries with under-developed infrastructure.

This paper deals with a completely new technology for jointing an optical fiber ground wire in mid-span. The influence of such a joint on the static and dynamic behaviour of the line will be discussed.

Design of the Mid-span Joint

The connection of an optical ground wire in mid-span is only possible if the mechanical and electrical connections are made separately from the fiber splicing operation. The second basic requirement for the joint is the implementation of well-known and approved technologies whereever possible. Figure 1 shows the basic design elements of a joint which completely fulfill these central requirements.

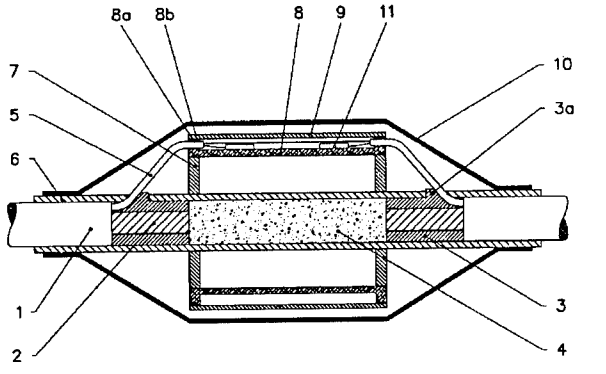


Fig. 1 Basic Design Elements of the Joint

The first layer of the OPGW (2) which carries the stainless steel tube with the optical fibers (5) is connected with a compression type steel joint (4).

Between the outer layer of aluminium alloy wires (1) and the compression type steel joint, guiding rings (3) are arranged to lead the stainless steel tube out of the core without falling below the bending radius of the fibers. In addition they protect the fibers from any mechanical damage in this area. The outer layer of aluminium alloy wires is rebuilt using a special design of an aluminium alloy helical joint (6).

In the section over the guide rings and the compression type steel joint the aluminium alloy helical joint is straightened by twisting back the helical rods. This allows for the separation of the aluminium wires through the protrusions (3a) of the guide rings which lead them out of the stainless steel tube. Up to this point we have used only well-known jointing technology to realize the mechanical and electrical connections.

The fiber splices require strong mechanical protection to maintain the proper bending radius of the fibers and a hermetically-sealed space to secure the splices. These requirements can be completely fulfilled with our new concentrical joint closure.

Fitting rings (7) are positioned onto the outer aluminium alloy helical joint at each end of the compression type steel joint. They carry an inner tube (8). This tube is equipped with a sealing device (8a) against the outer tube (9) and two inlet devices (8b) for the steel tube which carry the optical fibers. The fiber inlets must be impervious to moisture. All diameters are chosen in such a way that the minimum bending radius is respected throughout the joint. The splice carriers (11) can safely accommodate up to 36 splices. Recesses in the splice space serve to tie down excessive fiber lengths.

The outer closing consists of a thin-walled anti-corrosion steel shell (10) with a central cylindrical part and two conical parts at both ends of the joint. It is fixed onto the OPGW independently from the inner parts of the joint.

This new technology of a concentric, hermetically-sealed joint housing for the optical fiber splices yields the following advantages:

- complete separation of the mechanical and electrical connections from the fiber connection;

- the mechanical and electrical connections are made using known and approved technologies;

- sufficient space is provided for the splices of two concentrical tubes containing up to 36 fibres each;

- the volume and the mass of the joint are strictly minimized; they depend only on the bending radius of the fibers;

- no special care needs to be taken about sealing the ground wire, because moisture which comes into the joint has no chance to penetrate the optical splice space;

- the independant outer protection is bullet-proof without affecting the inner components;

- the outer protection cuts in half the heat energy attributed to the sun; it offers mechanical protection to the concentrical inner tubes and gives the joint its smooth shape without distributing the weight of the joint over a long length.

Mechanical Properties of the Joint

To analyze the mechanical properties of the above-described joint, we carried out a test series

under static load. The joint was installed between fiber optical ground wires with the following data:

Ground wire type:

ASLH-D(S)bb 1x12 E9/125 (Ay/Aw 99/49-10.8)

- Design:

core:	1 Aw-wire	4.1 mm
1st layer:	5 Aw-wires	3.0 mm
	1 Ay-wire	3.0 mm
	1 stainless steel tube with 12 E9/125	3.0 mm
2nd layer:	13 Ay-wires	3.0 mm
Diameter:		16.1 mm
Weight:		632 kg/km

- Technical Data according to German standard VDE 0210/12.85:

effective cross section:	147.5 mm²
rated tensile strength:	86.9 kN
modulus of elasticity:	91.7 kN/mm²
permissible max. working stress:	247.5 N/mm²
everyday stress (EDS):	94.3 N/mm²

To realize the mechanical and electrical connections the following accessories were used [1]:

- Compression type steel joint

length:	340 mm
outer diameter:	17 mm
inner diameter:	11 mm
hardness:	174-180 HB
corrosion protection:	hot dipped galvanized

The stainless steel tube was taken out of the core and substituted by an Aw-wire with 3 mm diameter.

- Aluminium alloy helical joint VAG 161 231 sim. consisting of 12 rods, 4.24 mm diameter.

The experimental set-up and the dimensions of the tested joint are shown in figure 2. To evaluate elongation the basic lengths l_a and l_b were provided with reference marks.

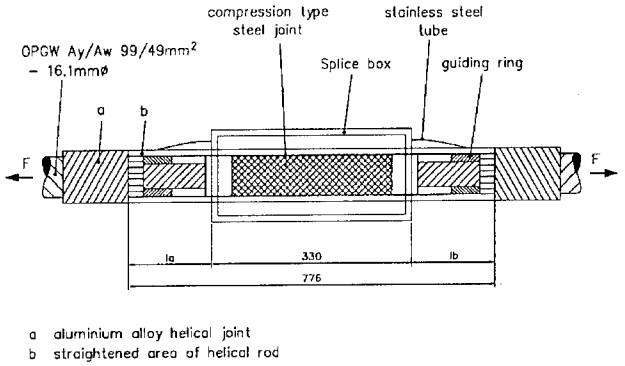


Fig. 2 Experimental Set-Up of Tensile Test of the Joint

Figure 3 represents the elongation behaviour of the joint. The tensile force was incrementally increased up to the VDE-required minimum failing load of 70.2 kN and the displacement between the joint and the reference mark was measured. The diagram shows the displacement vs. $l_a + l_b$ (in °/oo). Figure 3 makes it clear that there is no critical behaviour under the described conditions. After removing the load the permanent deformation was 1.9 °/oo or 0.5 mm in absolute value, which also is not critical.

While the joint was loaded the torque and the rotation angle of the guiding rings were measured, as shown in figures 4 and 5. Analysis of the disassembled connection reveals no damage or other harmful influence of the joint onto the mechanical connection. Even the rotation angle of about 60°, which occurs under maximum load, does not show any damage to the stainless steel tube. This is attributed to the circumferential freedom of movement of the guiding rings and the stainless steel tube.

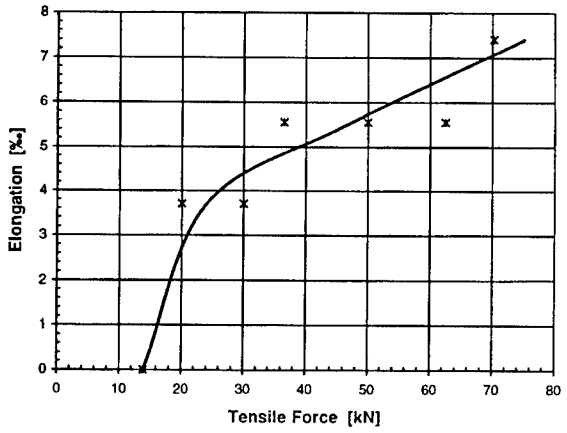


Fig. 3 Test Result "Tension Test": Elongation Behavior of the Joint

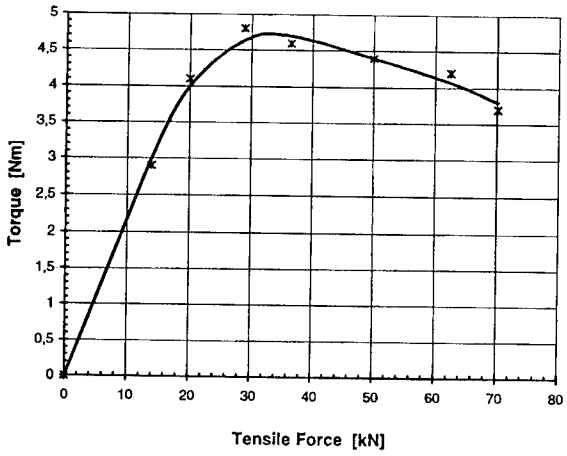


Fig. 4 Test Result "Tension Test": Torque in Dependence of Tensileforce

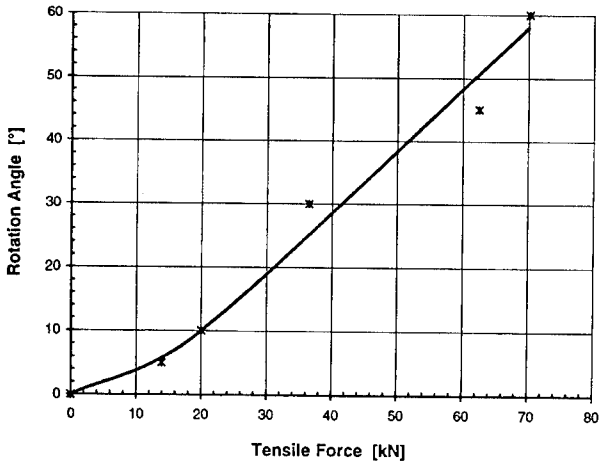
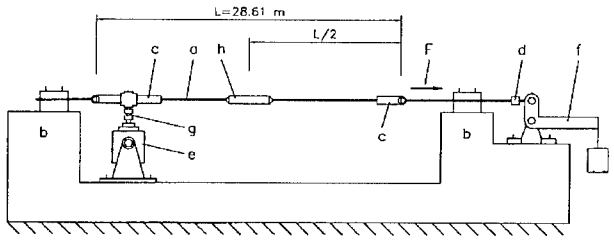


Fig. 5 Rotation Angle of Cable Going into the Joint Measured at the Guiding Ring for the Steel Tubes

These investigations prove that there is no harmful effect on a conventional mechanical connection of an optical ground wire by a concentrically arranged joint for optical fibers during static load. It demonstrates the validity of the concept of the separation between mechanical and optical connection.

Dynamical Behaviour of the Joint

To get an overview of the dynamic influences on a ground wire a frequency sweep was run in an indoor vibration test stand. The test set-up is shown in figure 6. The span length was 28.61 m. The joint with a weight of 2.8 kg was completely installed in the middle of the field. The applied load was the everyday stress (EDS) for such a ground wire: 13.19 kN. The span was excited by an electrodynamic excitator from one end. Figure 7 shows the mounting of the joint into the actual test set-up.



a OPWG
b abutment
c dead end fitting
d load cell
e excitator
f auxiliary device
g coupling device
h mid-span joint
F tensile force = 13.2 kN

Fig. 6 Test Set-Up "Frequency Sweep"

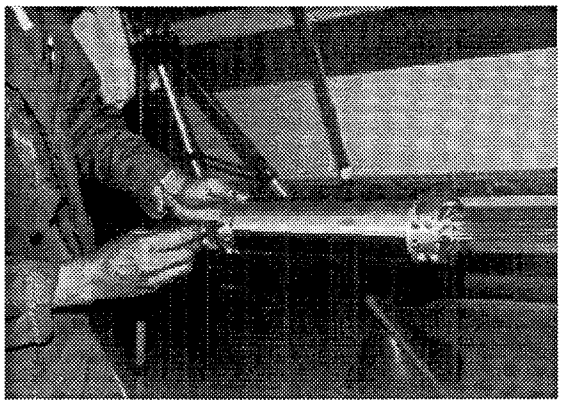


Fig. 7 Trial Station for Analysis of Dynamic Behaviour

Figure 8 presents the influence of the joint onto the resonant frequencies for the span in the test set-up. Curve 2 shows the measured resonant frequencies as a function of the harmonic coefficients. Only a slight shift toward the lower frequencies is to be seen. This means that the influence of the joint onto the dynamical behaviour is negligible.

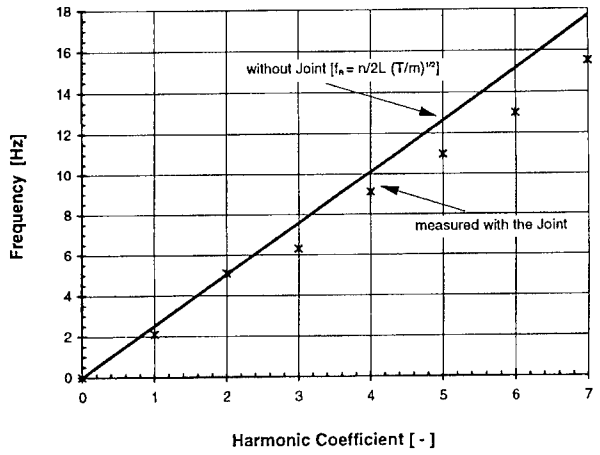


Fig. 8 Influence of the Joint on the Resonance Frequencies of the OPGW

This also confirms observations at higher harmonic coefficients, especially at frequencies in excess of 6 Hz, which are in reality those which are wind-stimulated[2] and which showed that the nodal point settled in the joint. This resulted in a slewing motion of the joint around this point which means that the wave propagation is not influenced by the joint.

The reason for this behaviour is that the long outer housing with its low weight is decoupled from the short mass of the joint itself.

Conclusions

The results presented here demonstrate very clearly that the described mid-span joint closure is an economically way to connect optical fiber ground wire without any technical disadvantages. The resulting separation of mechanical and electrical connection from the optical connection allows on one hand the use of well-proven connecting technologies of the ground wire and on the other hand an optimum of security for the optical connection in a concentrically arranged splicing space for the fibers. This is possible without affecting the mechanical strength of the ground wire or its dynamical behaviour.

With regard to dynamic behaviour, further tests, such as vibration fatigue tests, are in preparation.

Acknowledgements

The authors wish to thank Messrs. Richard Bergner GmbH & Co., especially Mr. Buchwald and Mr. Böhme, for providing the test facilities, and Mr. Hofheimer of Cable Consultants Corp./Larchmont NY for his valuable assistance in preparing this paper. The OPGW was produced from KABEL RHEYDT.

References

1. Richard Bergner GmbH & Co.
VE-Bericht K 6347

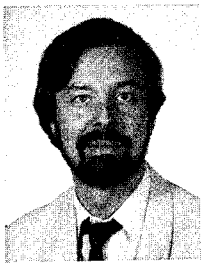
Elektroarmaturen Schwabach:
Spannfeldmuffe für Erdseil-LWL-Luftkabel

Buchwald: Ay/Aw 99/49 mm²-16.1 mm mit St-

Preßverbinder und Spirale VAG 161 231,
ähnl. 18.07.95

2. RIBE Mitteilungen 14

Hauszeitschrift der Firma Richard Bergner,
Elektroarmaturen, Schwabach b. Nürnberg



Franz Grajewski
ALCATEL KABELMETAL
31655 Stadthagen
Germany

Dr.-Ing. Franz Grajewski studied mechanical engineering at Aachen's Technical University. From 1984 to 1988 he assumed a scientific fellowship at the University's Institute of Polymer Processing. After graduation he joined ALCATEL KABELMETAL as Manager R&D/Heat-Srhink Technology. Since 1991 he is General Manager of the product group Accessories and Heat-Shrink Technology.



Werner Stieb
ALCATEL KABELMETAL
31655 Stadthagen
Germany

Dipl.-Ing. Werner Stieb, after receiving his electrical engineering degree from the University of Kaiserslautern in 1986, joined ALCATEL KABELMETAL as a development engineer in the field of telecommunication cables. Today he is responsible for product marketing of fibre optic accessories in the product group Accessories and Heat-Shrink Technology.



Helmut G. Haag
KABEL RHEYDT AG
41048 Mönchengladbach
Germany

Helmut G. Haag (46) is Director of the Sales Division for Telecommunications. After reaching his Dipl.-Physiker degree from the University of Stuttgart he joined KABEL RHEYDT in 1975 for the development of coaxial cables. Later he has been also responsible for the development of optical cables. From 1980 to 1983 he built up the production plant for these cables. From 1984 to 1989 he has been responsible for the technical sales department. Since 1990 he took over his present position.



Georg Hög
KABEL RHEYDT AG
41048 Mönchengladbach
Germany

Georg Hög was born in 1950. After studying electronics at the Technische Hochschule in Aachen he joined KABEL RHEYDT as a development engineer for copper cables in 1977. In 1980 he became responsible for the development of symmetrical telecommunication cables. In this position he was also busy in the standardization for copper cables for the German Telekom. In 1985 he became the head of the development for optical fibre cables. From 1987 to 1988 he was the head of the technique department of BETEFA (special cables for telecommunications). Since 1989 back to KABEL RHEYDT, he was responsible for the development and construction department for optical fibre cables. Since 1995 he is responsible for the technical sales department telecommunications cables. He is also responsible for the standardization for optical fibre cables for the DBP Telekom and a member in the standardization bodies in VDE ETSI and IEC for optical fibre cables.

LIGHTNING STRIKE RESISTANCE OF OPGW

J.P. BONICEL[1], O. TATAT[1], U. JANSEN[2], G. COUVRIE[1]

[1] ALCATEL CABLE-OFCCC, FRANCE- [2] KABEL RHEYDT, GERMANY

ABSTRACT

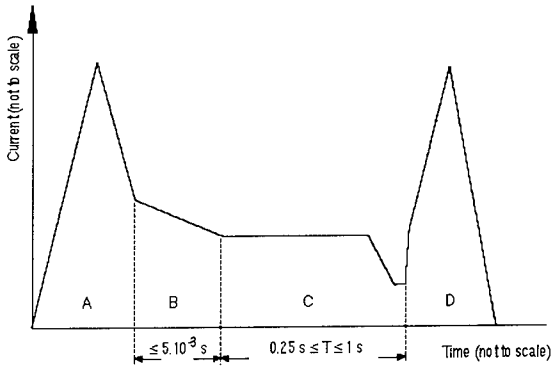
Optical Ground Wires (OPGW) are now used extensively worldwide on Very High Voltage (VHV) lines. The average optical fibre count is increasing in relation with the will of the power utilities to become operators.
Although telecommunications through OPGW is highly desired, one must remember that the purpose of OPGW is grounding.
A lightning strike hitting a conductor would certainly result in a short circuit and consequently a temporary power outage. The strikes, depending on their severity, may damage the GW.
The aim of this paper is to present the testing standards for lightning strike resistance applicable to the OPGW and the results obtained with various OPGW constructions in terms of armor and/or optical core designs.
The results are discussed. Severe damage to the armoring strands, even the largest ones, is generally obtained at level 3, when the smallest ones do not break at level 1. The results are discussed in order to establish the baselines of the OPGW design criteria for good lightning strike resistance.

1-INTRODUCTION

Optical Ground Wire (OPGW) designers are using the mechanical and electrical requirements of their customers in order to propose the most appropriate cable constructions.
Nevertheless, they must keep in mind the primary function of the cable : it is installed at the top of the Very High Voltage (VHV) lines in order to protect the conductors from lightning strikes. It is the "lightning getter" of the line and consequently it must have a good level of resistance to lightning impacts.
Lightning resistance for ground wires or OPGW is generally not specified. For instance IEEE 1138 (1) does not contain any test methods and requirements. This situation may change with the future IEC specification for OPGW.
When, rarely, a customer specifies lightning resistance, he often refers to the MIL STD 1757A test method (2).
The lightning resistance of OPGW having not yet been widely investigated, and in order for the designer to have more than simple rules such as "the biggest the armoring wires, the best the lightning resistance", we have conducted a series of tests with different OPGW designs.

2-TEST METHOD AND EQUIPMENT

The aeronautic industry has the highest experience with lightning strikes and laboratory simulation.
The Military Standard 1757A describes the "lightning qualification test techniques for aerospace vehicles and hardware".
There are different test methods dedicated to different parts of hardware depending upon if they have a low or high probability to be a strike attachment point or a swept stroke zone with high or low probability of flash hang-on.
Obviously, an OPGW is a high probability hardware for lightning attachment and transfer. As the cable is metallic, it may carry substantial amounts of electrical current by conduction, and as we are interested in the direct effects resulting from the lightning strike, we have decided to base our testing method on method T02 from MIL STD 1757A.
This is summarized by the graph in fig. 1. This graph presents the current waveform during a lightning strike.



Component A (initial stroke)
peak amplitude = 200 kA ± 10%
action integral = 2 x 10^6 A^2.s ± 20%
time duration ≤ 500 µs
Component B (intermediate current)
maximum charge transfer = 10 Coulombs
average amplitude = 2 kA ± 10%
Component C (continuing current)
charge transfer = 200 Coulomb ± 20%
amplitude = 200 - 800 A
Component D (restrike)
peak amplitude = 100 kA ± 10%
action integral = 0.25 x 10^6 A^2.s ± 20%
time duration ≤ 500 µs

For our tests, we considered only component A and component C and we have applied them using 3 levels of severity which are :

- level 1 : 30 kA component A coupled with 15 Coulomb component C
- level 2 : 100 kA component A coupled with 100 Coulomb component C
- level 3 : 200 kA component A coupled with 200 Coulomb component C

Prior to this tests, and in order to determine which component has the strongest effect on the cable, we performed a series of tests including only the peak component.

In order to better simulate the actual situation of an OPGW installed on a VHV line, the cable samples were tensioned during the tests. The tension level was chosen for each cable to be close to 20 % of its Ultimate Tensile Strength (UTS) which is an usual value for Every Day Stress (EDS) for such cables.
The length of the tensioned cable is about 1.5 meter and the lightning flash is applied in the middle of this section.

3-TEST 1 : Effect of the peak component

3.1-Sampling

Five cables with an outside armoring layer made of aluminium alloy were tested. The aluminium alloy wire diameters were :

- cable 1 : 2.0 mm
- cable 2 : 2.25 mm
- cable 3 : 2.5 mm
- cable 4 : 2.75 mm
- cable 5 : 3.0 mm

Two tests condition were used :

- condition 1 : peak current : 100 kA
  action integral : 3.10^6 A^2.s
  charge transfer : 50 Coulomb
- condition 2 : peak current : 220 kA
  action integral : 10.10^6 A^2.s
  charge transfer : 85 Coulomb

3.2-Results

None of the wires even the smallest one have been broken. It demonstrates that damages noticed during further tests including A and C components are due to the charge transfer during the long term component

4-TEST 2 : Peak + long term component

4.1-Sampling

As a simple rule, it is known that cables with larger armoring wire diameter have higher resistance to lightning impact.
Armoring wires can be made of aluminium or aluminium alloy, galvanized steel or Aluminium Clad Steel (ACS).
The armor can contain a single layer of wires or multiple layers. There are various optical core designs for OPGW.

In order to take all these options into account, we have tested 9 different OPGWs. For most of them, more details and characteristics have been presented in previous papers (3, 4)

These cables, called OPGW A to OPGW I, are presented in fig. 2 at the end of this paper and a description of their armor construction is given in fig. 3.

OPGW Reference	Armor descriptions	Diameter (mm)
A	14 ACS wires Ø 2 mm	11.3
B	12 ACS wires Ø 2.5 mm	12.3
C	9 ACS wires Ø 3.4 mm	13.6
D	14 galvanised steel wires Ø 2 mm 20 aluminium alloy wires Ø 2 mm	15.3
E	18 galvanised steel wires Ø 2 mm 19 aluminium alloy wires Ø 2.6 mm	19.2
F	18 ACS wires Ø 2 mm 24 ACS wires Ø 2 mm 24 aluminium alloy wires Ø 2.8 mm	23.6
G	12 ACS wires Ø 3.4 mm 18 aluminium alloy wires Ø 3.4 mm	23.6
H	1 ACS wire Ø 4.1 mm 5 ACS wires + 2 steel tubes Ø 3 mm 13 Aldrey wires Ø 3 mm 19 Aldrey wires Ø 3 mm	22.1
I	1 ACS wire Ø 4.1 mm 5 ACS wires + 2 steel tubes Ø 3 mm 13 Aldrey wires Ø 3 mm	16.1

Fig. 3 : OPGW A to I armor description

For each cable and each level of severity, the test is repeated 2 times.
After each test the fibres are checked for optical continuity.
During the test, we measured the attenuation of all the fibres (spliced together) of the cable at 1550 nanometers.
After the test, the cable sample was evaluated for damages.

4.2-Results

We never experienced fibre breakage during the tests.
Concerning attenuation variations during the test, it must be pointed out that due to the difficult conditions of measurement, we have not been in a position to get reliable results. Nevertheless and just to give an idea, for 90% of the tests, it was less than 0.05 dB. The remaining 10% showed attenuation variations (gain or loss) less than 0.3 dB that could be

due to the electrical environment effect on the test equipment. More tests will be perform in the future with a special care to the measurement conditions in order to get more reliable figures.

Fig. 4 to 6 are presenting the damages resulting from the strikes. They include a calculated breaking strength of the cable in percent of the original UTS. For this calculation, only the unbroken armoring wires are taken into account and surface pitting was not considered as reducing a wire tensile strength.

LEVEL 1 : 30 kA 15 Coulomb	strike 1	strike 2
OPGW A		
Optical core	-	-
Armor	ACS surface pitting	ACS surface pitting
Calculated residual tensile strength (%UTS)	100	100
OPGW B		
Optical core	-	-
Armor	ACS surface pitting	ACS surface pitting
Calculated residual tensile strength (%UTS)	100	100
OPGW C		
Optical core	-	-
Armor	ACS surface pitting	ACS surface pitting
Calculated residual tensile strength (%UTS)	100	100

LEVEL 2 : 100 kA 100 Coulomb	strike 1	strike 2
OPGW A		
Optical core	Al tube twisted and pitted	Al tube twisted and pitted
Armor	5 ACS wires broken	5 ACS wires broken
Calculated residual tensile strength (%UTS)	64	64
OPGW B		
Optical core	Plastic tubes melted (*)	Plastic tubes melted (*)
Armor	3 ACS wires broken	2 ACS wires broken
Calculated residual tensile strength (%UTS)	75	83
OPGW C		
Optical core	-	-
Armor	2 ACS wires broken	2 ACS wires broken
Calculated residual tensile strength (%UTS)	78	78

(*) : no damages to the fibres

LEVEL 3 : 200 kA 200 Coulomb	strike 1	strike 2
OPGW A		
Optical core	Al tube twisted and pitted	Al tube twisted and pitted
Armor	7 ACS wires broken	6 ACS wires broken
Calculated residual tensile strength (%UTS)	50	57
OPGW B		
Optical core	Plastic tubes melted (*)	Plastic tubes melted (*)
Armor	2 ACS wires broken	2 ACS wires broken
Calculated residual tensile strength (%UTS)	83	83
OPGW C		
Optical core	-	-
Armor	1 ACS wires broken	2 ACS wires broken
Calculated residual tensile strength (%UTS)	89	78

(*) : no damages to the fibres

Fig. 4 : Damages to single layer armored cables

LEVEL 1 : 30 kA 15 Coulomb	strike 1	strike 2
OPGW D		
Optical core	-	-
Armor	Al. alloy wire surface pitting	Al. alloy wire surface pitting
Calculated residual tensile strength (%UTS)	100	100
OPGW E		
Optical core	-	-
Armor	Al. alloy wire surface pitting	Al. alloy wire surface pitting
Calculated residual tensile strength (%UTS)	100	100
OPGW F		
Optical core	-	-
Armor	Al. alloy wire surface pitting	Al. alloy wire surface pitting
Calculated residual tensile strength (%UTS)	100	100

LEVEL 2 : 100 kA 100 Coulomb	strike 1	strike 2
OPGW D		
Optical core	-	-
Armor	6 al. alloy wires broken	8 al. alloy wires broken
Calculated residual tensile strength (%UTS)	93	90
OPGW E		
Optical core	-	-
Armor	6 al. alloy wires broken	6 al. alloy wires broken
Calculated residual tensile strength (%UTS)	91	91
OPGW F		
Optical core	-	-
Armor	3 al. alloy wires broken	5 al. alloy wires broken
Calculated residual tensile strength (%UTS)	97	95

LEVEL 3 : 200 kA 200 Coulomb	strike 1	strike 2
OPGW D		
Optical core	plastic tubes melted (*)	plastic tubes melted (*)
Armor	8 al. alloy wires broken	8 al. alloy wires broken 1 galvanised steel wire broken
Calculated residual tensile strength (%UTS)	90	85
OPGW E		
Optical core	-	-
Armor	7 al. alloy wires broken	6 al. alloy wires broken
Calculated residual tensile strength (%UTS)	89	91
OPGW F		
Optical core	-	-
Armor	7 al. alloy wires broken 2 ACS wires broken	6 al. alloy wires broken 3 ACS wires broken
Calculated residual tensile strength (%UTS)	89	90

(*) : no damages to the fibres

Fig. 5 : Damages to double layer armored cables (part 1)

5-DISCUSSION

5.1-Physical damages :

At level 1, the damage was limited in all of the cables to slight pitting on the surface of the outside layer of the armoring wires (ACS or aluminium alloy).
It does not affect the tensile strength of the cable.

LEVEL 1 : 30 kA 15 Coulomb	strike 1	strike 2
OPGW G		
Optical core	-	-
Armor	Al. alloy wire surface pitting	Al. alloy wire surface pitting
Calculated residual tensile strength (%UTS)	100	100
OPGW H		
Optical core	-	-
Armor	Al. alloy wire surface pitting	Al. alloy wire surface pitting
Calculated residual tensile strength (%UTS)	100	100
OPGW I	Not tested	

LEVEL 2 : 100 kA 100 Coulomb	strike 1	strike 2
OPGW G		
Optical core	-	-
Armor	3 al. alloy wires broken	3 al. alloy wires broken
Calculated residual tensile strength (%UTS)	95	95
OPGW H		
Optical core	-	-
Armor	6 al. alloy wires pitted	3 al. alloy wires broken
Calculated residual tensile strength (%UTS)	90	95
OPGW I	Not tested	

LEVEL 3 : 200 kA 200 Coulomb	strike 1	strike 2
OPGW G		
Optical core	-	-
Armor	5 al. alloy wires broken	4 al. alloy wires broken
Calculated residual tensile strength (%UTS)	92	94
OPGW H		
Optical core	-	
Armor	4al. alloy wires broken and 1 al alloy wire broken in the inside layer	
Calculated residual tensile strength (%UTS)	91	
OPGW I		
Optical core		steel tube pitted (*)
Armor		5 al. alloy wires broken
Calculated residual tensile strength (%UTS)		87

(*) : no damages to the fibres

Fig. 6 : Damages to double layer armored cables (part 2)

At level 2, each cable suffered broken wires at the outside layer (ACS or aluminium alloy). The number of wires broken depending upon their diameter is (average for 2 tests) :

aluminium alloy
- 3.4 mm : 3 wires broken
- 3.0 mm : 1.5 wire broken
- 2.8 mm : 4 wires broken
- 2.6 mm : 6 wires broken
- 2.0 mm : 7 wires broken

ACS
- 2.0 mm : 5 wires broken
- 2.5 mm : 2.5 wires broken
- 3.4 mm : 2 wires broken

The following equation (5) gives an estimation of the volume of material which will be melted for a given electrical charge.

$$V \text{ (in mm3)} = 20.10^9.Q/(d.(Cw.Tm+Cm))$$

V = volume of melted material
d = material density
Tm = material melting point
Cm = material fusion heat
Cw = material specific heat
Q = electrical charge

For aluminium, d = 2700 Kg/m3, Tm = 658°C, Cw = 908J/(kg.K), Cm = 397000 J/kg
For steel, d = 7700 Kg/m3, Tm = 1530°C, Cw = 469J/(kg.K), Cm = 272000 J/kg

For the same charge, 3 times more aluminium than steel will melt. This is not in good relation with our results. In reality, steel or ACS wires do not perform three times better than aluminium.
Essentially, the optical core of the single layer armored cable is damaged if a large number of wires are broken (twisting of the optical core) or if the cable structure does not include an aluminium tube as for example OPGW B. No damage was noted on double layer armored cable as for example OPGW D.

At level 3, wires from the outside but also from the inside layer may be broken and only big cables built with large wire diameters such as OPGW G or OPGW H will pass a 90% of the original UTS requirement after test.
Double layer cables without an aluminium tube such as OPGW D or a steel tube cable with only one armoring layer over the steel tube will present risks of damage of the optical core.
Single layer armored cables are not suitable for such a level of severity.

5.2-Representativity of the tests

Figure 7 (6) gives, on a logarithmic base, the cumulative distribution of several of the lightning parameters. These parameters are peak current and flash charge.
They show that our testing levels are representative of :
- -level 1 : more than 50% of the negative strikes
- -level 2 : more than 99% of the negative strikes
  more than 50% of the positive strikes
- -level 3 : more than 99% of the negative strikes
  more than 80% of the positive strikes

Positive strikes represents only less than 10% of the total strikes.

In addition figure 8 gives the keraunic distribution of the world. Such a map can be found in CCITT document (7). This map and the following empirical equation (8) which gives, for a known keraunic level, the average number of strikes (N) per 100 km of line, may be used to show that very big and strong OPGW (resistant to our testing level 3) can be reserved to exceptionally high risk regions.

$$N = (32.6\ Hs^{0.61} + W) \cdot 0.0023\ Td^{1.3}$$

Td : keraunic level
W : line effective width
Hs: structure effective height

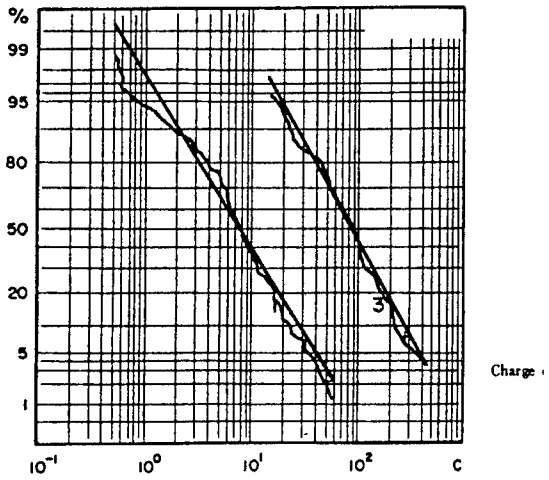


Figure 7.1 : cumulative distribution of several of the lightning parameters : Flash charge Q
(1) : negative first strokes ; (3) : positive strokes

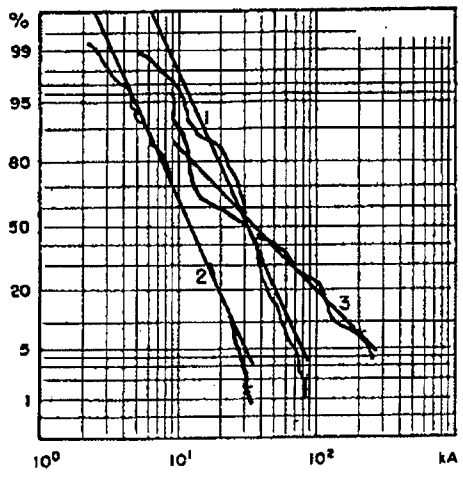


Figure 7.2 : cumulative distribution of several of the lightning parameters : Peak current I
(1) : negative first strokes ; (2) : negative following strokes ;
(3) : positive strokes

For example, W = 15 m, Hs = 40 m, Td = 20 (western Europe) or 180 (central Africa), give :
N = 37 flashes/100 km/year in Europe
N = 638 flashes/100km/year in central Africa
So that a cable giving a 95% level protection (resistant to our level 2) will suffer :
638x(1-0.95)=32 damages per 100 km and year in central Africa, but only 37x(1-0.95)=2 damages per year and 100 km in western Europe

It must be pointed out than for small damages to the outer layer of the cable, it is possible to repair it. Helical protecting rods are installed on the damaged part in order to recover the electrical and mechanical properties of the cable.
For more severe damages, a cable length might be changed.

6-CONCLUSIONS

For High Voltage lines already existing and where the conventional earthwire must be replaced by an OPGW, a big and heavy OPGW is generally not accepted because the towers have not been built to support additional loads.
In that case, the solution is generally to propose a small, ACS single layer armored OPGW. It must be pointed out that such OPGWs are able to withstand rather weak lightning strikes (at least 30 kA, 15 Coulomb but we will determine in further test which maximum level of severity they can withstand). Their integrity and consequently their tensile strength are affected at 100 kA, 100 Coulomb level and any cable of such kind will need to be replaced after such a strike. The main reason for that is because the reinforcing wires (ACS) are directly

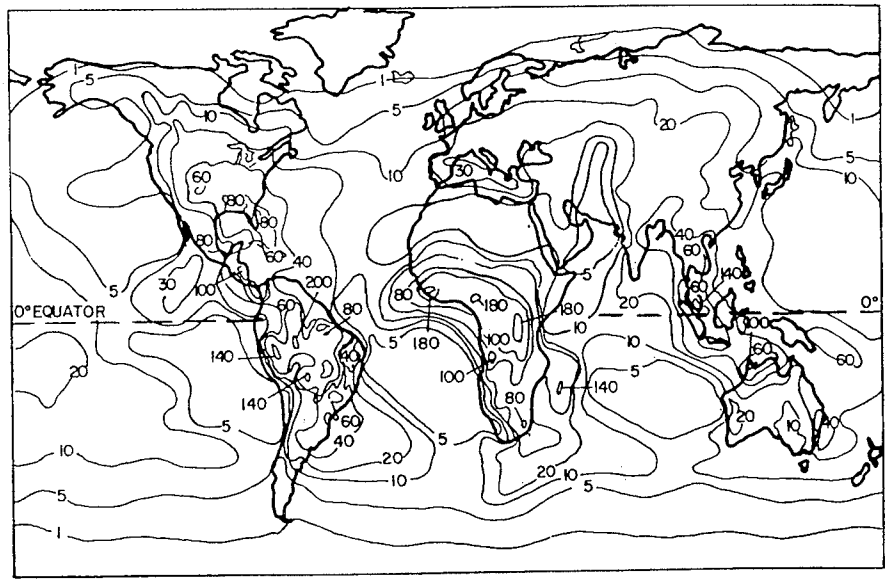


Figure 8 : keraunic distribution of the world

exposed on the outside layer. In addition, even if the ACS wires are not broken, there is a risk of surface pitting of the ACS wires which can further lead to corrosion (9) and affect the long term reliability. Nevertheless, for such lines, if a small ground wire gave satisfaction, there is no reason that a small Optical Ground Wire, using the same wire diameter, will suffer more breakage.

For the same reason, OPGWs whose armor is made of 2 layers but with the ACS wire layer on the outside must be avoided for medium or high lightning strike resistance.

For lightning strike resistance at level 2 or 3, any additional layer between the outside surface of the cable and the optical fibre, such as inner armoring layer or aluminium tube, is an advantage.

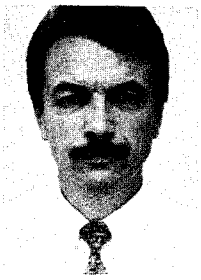
For new VHV lines the possibility exists to supply a rather big and strong OPGW because it is possible to design the towers in order to be strong enough to support high cable loading. In that case, a strong design must be preferred in order to withstand the highest level of severity for lightning strike.
A cable such as OPGW E will support strikes having a 100 kA peak and 100 Coulomb transfer charge which represents 95 % of the strikes in the field. Such a protection level is enough for most of the regions.
Cables such as OPGW G or OPGW H will support strikes having a 200 kA peak and 200 Coulomb charge transfer which represents more than 99 % of the strikes in the field. Their use is really justified only for very high keraunic level regions.

References :

(1) : IEEE Std 1138-1994 : "IEEE Standard Construction of Composite Fiber Optic Ground Wire (OPGW) for Use on Electric Power Utility Lines"
(2) : MIL-STD-1757A : "Lightning qualification test techniques for aerospace vehicles and hardware"
(3) : "Optical ground wires a worldwide technical survey and comparison", JP.Bonicel and al, IWCS 93
(4) : "Aerial fiber optic cables for railway application-metallic or dielectric solutions", JP.Bonicel and al, IWCS 1994
(5) : "Blitzgefährdung und Blitzprüfung von Erdseil-Luftkabeln", Prof.Dr. J. Wiesinger, E V U - F a c h t a g u n g Lichtwellenleitertechnik in Weimar, 8.-10.5.1995
(6) : "Parameters of lightning flashes", Berger and al., CIGRE Electra N°41
(7) : "The protection of telecommunication lines and equipment against lightning discharges", CCITT, 1978
(8) : "Lightning parameters for engineering applications", Anderson and Eriksson, CIGRE Electra N°69
(9) : "Effets des coups de foudre sur les cables de garde à fibres optiques", Meier, Nibio and Gaille, 13eme CIRED, 1995

Authors

Jean Pierre BONICEL
ALCATEL CABLE
35 rue Jean Jaures-95871 Bezons, FRANCE



Jean Pierre BONICEL was born in 1952. He received his engineering degree from the Institut des Sciences de l'Ingenieur de Montpellier (ISIM) in 1976. He joined Les Câbles de Lyon, now Alcatel Cable, in 1977 where he was in charge of material and mechanical problems for telecommunications cables. Now he is the head of the telecommunications cables laboratory, manager for the Alcatel Cable Optical Fiber Cable Competence center, and technical Director for the Telecommunications Department.

Gerard COUVRIE
ALCATEL CABLE
35 rue Jean Jaures-95871 Bezons, FRANCE



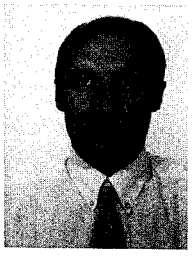
Gerard COUVRIE was born in 1949. He received his General Certificate of Education in 1968. After two years in Mathematics and Physics, he joined Alcatel Cable Outside plant Operations Department. He is now working on the development of OPGW in the Alcatel Cable Optical Fiber Cable Competence center.

Ulrich JANSEN
KABEL RHEYDT AG
Bonnenbroicher Str. 2-14- 41048, Mönchengladbach, GERMANY

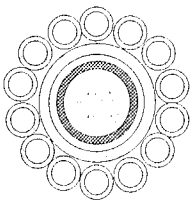


Ulrich JANSEN (31) received his Dipl. Ing. Degree from the University of Aachen in 1990. He joined KABEL-RHEYDT in the same year. As a member of the development department for optical fibre cables, he is responsible for development of OPGW.

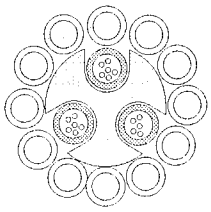
Olivier TATAT
ALCATEL CABLE
35 rue Jean Jaures-95871 Bezons, FRANCE



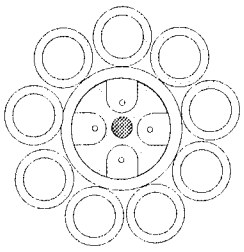
Olivier TATAT was born in 1959. He received his engineering degree from the Institut des Sciences de l'Ingenieur de Montpellier (ISIM) in 1982. He joined Les Câbles de Lyon, now Alcatel Cable, in 1985. Now he is working as project engineer, in charge of the development of OPGW, in the Alcatel Optical Fiber Cable Competence center.



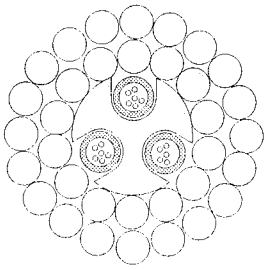
Cable A



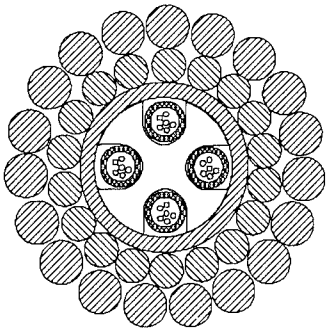
Cable B



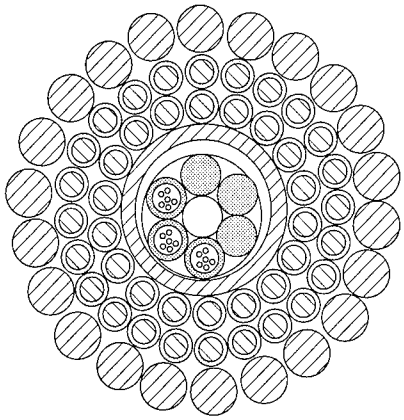
Cable C



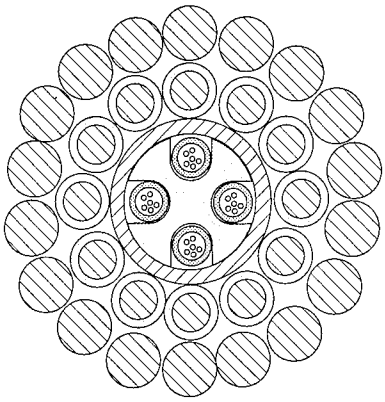
Cable D



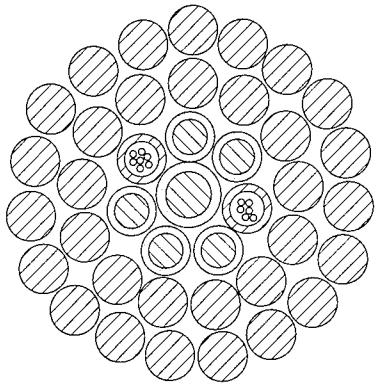
Cable E



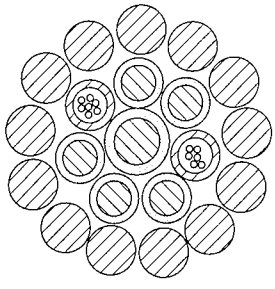
Cable F



Cable G



Cable H



Cable I

Fig. 2 : OPGW cables design

LAN MEDIA INSTALLERS AND MANUFACTURERS ROUNDTABLE

CHAIRPERSON
Irving Kolodny, Consultant, Bellerose Manor, NY

MODERATOR
Arlyn Powell, Senior Associate Editor
Cabling, Installation and Maintenance Magazine, Nashua, NH

OVERVIEW

This session, new to the Symposium, focuses on the installation issues that face both the copper and fiber optic cable manufacturers and installers. Three members of the installer community will present their experiences using cable, connectors and test equipment. They will be followed by representatives of the manufacturing community, who will answer installer concerns and present their own perspectives on the installation issues involved. Speakers will then have the opportunity to interact with each other, a lively interchange should result.

INSTALLER ABSTRACTS

EXPERIENCES WITH CABLE

Craig Thomasmeyer, Systems Consultant, Miller Information Systems (Pittsburgh, PA)

Cable installers see cable quality as generally good across the board, even for the relatively new Category 5 products. From the point of view of the installer, kinking and sheath tearing are problems that must be faced. A packaging consideration--reels versus boxes-- is another issue; 3000- to 5000-foot reels are much easier to use than boxes, which tend to be more difficult to secure. From the perspective of end users, the cable infrastructure is starting to be viewed as a commodity, as a result, price has become an important issue. Some 60% to 80% of Miller's installations are price-driven; no one can afford to pay price premiums today. End users also show little interest in exceeding the minimum specifications established by the Electronic Industries Association and Telecommunications Industry Association in their standards; they simply do with the minimum, which seems to be another reflection of the cable-as-commodity mindset.

EXPERIENCES WITH CONNECTORS

Sam Flaherty, President, Teledata Systems (Souderton, PA)

When it comes to connectors, patch panels and wallplates, the installer focus is on ease of use and by extension, identifying products that will be cost-effective in an installation. The installer looks for products that will make his or her job less troublesome and time-consuming. And yet, it is not uncommon for installers to encounter products where the emphasis seems to be on manufacturing production rather than customer needs. One example of this is the 110 keystone connector, which cannot be punched down in the wallplate. Also, it has no base outside of the wallplate and is therefore difficult to handle. As a result installing this product is very time-consuming. By contrast, certain fiber-optic connector and splice products have clearly been developed with the emphasis on ease of use. Unfortunately, such products tend to be expensive, which limits the penetration of optical fiber into the premises market.

EXPERIENCES WITH TEST EQUIPMENT

Larry Johnson, President, The Light Brigade (Kent, WA)

Field equipment for fiber-optic testing has had a reputation for being both complicated and expensive. In just the past few years, however, manufacturers have simplified their products and brought prices down substantially, in part to appeal to the emerging premises data-communications market. Cabling contractors need to understand the uses of the full range of fiber-optic test equipment available, so that they can match required product features and performance against their applications. They must also be prepared to field-test these devices against manufacturer product specifications. And finally, given the high cost of some fiber-optic equipment, it is prudent to consider leasing or rental as well as outright purchase in some cases.

MANUFACTURER ABSTRACTS

PERSPECTIVES ON CABLE

David Hess, Vice President of Technology, Berk-Tek, Inc. (New Holland, PA)

Installers are primarily concerned about cost. Driven by cost considerations attributable to this concern, data-communications cable designs have evolved rapidly from telecommunications cable formats. For example, the very successful IEEE 802.3 10 Base-T format sprang from a desire to implement local area networks over telephone wire, a low-cost and almost universally present infrastructure. The unique features of these cables, then, are arguably only enhancements or modifications of telecommunications cable designs. These modifications can be subtle--for instance, changing the length of the twists in twisted-pair cable or substituting multimode for singlemode optical fiber. Some enhancements may be invisible to the buyer--for instance, dimensional control in the manufacture of optical fiber is orders of magnitude more precise than it once was--but they take work, and so they cost more. Also, improvements in those cable features that an installer can see, such as flexibility and ruggedness, come with a price premium. After all, special packaging that saves work for the installer is bound to add work and cost for the manufacturer. Successful cable design achieves a balance between such features and cost. The forces driving standardization result in a smaller selection of features. As market forces shrink the number of options available, quality and reliability become the paramount cable attributes.

PERSPECTIVES ON CONNECTORS

Scott Miles, Product Manager for Office Products, Mod-Tap, Inc. (Harvard, MA)

The twin themes in the design and manufacture of telecommunications connectors are ease of use and low installed cost. To these ends, connectivity houses are pursuing many technological options. For example, rearward-facing, low-insertion-force connectors minimize punchdown time and installation cost. Standardizing color-coding lessens the chance of installation errors, and minimizing the number of loose parts to be assembled reduces confusion and lowers installation cost. Labeling connector products (or manufacturing them so that they can be easily labeled) lowers both installation and maintenance costs. Making larger wallplates will help installers with sheetrock problems. Rack-front management options, such as strain relief and cable guides, make installation of high-speed data cabling faster and keep the installation neater for its users. And finally, advances in modular-furniture design are increasing flexibility while decreasing cost for end-users.

PERSPECTIVES ON TEST EQUIPMENT

Jim Boedekker, Marketing Manager of the Cable Network Analysis Unit, Tektronix, Inc. (Beaverton, OR)

Manufacturers of test equipment have the challenge of developing tools that, on the one hand, are capable of making complex and accurate measurements and, on the other hand, are very easy to use. In fact, the ideal test tools should be so easy to use that an installer can push a button and the instrument will independently perform the full range of tests that are required. To make the equation even more complex, installers are looking for cost-effective test instruments as well. A new generation of test tools meets these seemingly conflicting installer requirements, but a question remains. With many choices available in test equipment, how can an installer make a decision about which is best? After narrowing down the choices using a checklist of needs, the final decision should depend on actually using the instrument. After making multiple tests of the same wire or fiber to check for accuracy, repeatability and ease of use, an informed decision can be made.

MFA: A NEW PERFLUOROPOLYMER FOR WIRE & CABLE APPLICATIONS

Giandomenico Vita, Massimo Pozzoli

AUSIMONT S.p.A.- Viale Lombardia 20, I-20021 BOLLATE ITALY

ABSTRACT

The new perfluoropolymer MFA is here presented. This material belongs to the generic class of perfluoroalkoxypolymers and its backbone, made with tetrafluoroethylene and perfluoromethylvinylether, confers to the material oustanding chemical resistance, very interesting optical properties in the UV region and excellent electrical and mechanical properties at high temperature. Main advantages of MFA for applications in the Wire and Cable Industry, especially in comparison to some other established perfluoropolymers, are the high temperature endurance with oustanding resistance to Thermal Stress Cracking and the very low electrical dissipation factor from 1 MHz to 1 GHz.

INTRODUCTION

MFA is a new perfluoropolymer, belonging to the generic class of perfluoroalkoxy-polymers (the so-called PFA polymers). After a brief presentation of the chemical structure of MFA and some highlights about its production, this paper will mainly point out the performance aspects of MFA in comparison to the already well known FEP and conventional PFA polymers.
Main difference from most typical commercial PFA's is the presence of a different comonomer in the polymer's backbone: while perfluoropropylvinylether (PFPVE) is the well known comonomer for pratically all most important commercial PFA's, MFA is basically a copolymer of TFE with perfluoromethylvinylether (PFMVE). Hence the name MFA, to distinguish it from conventional PFA's. The structure of MFA is a backbone where TFE and PFMVE are randomly polymerized to give a polymer with oustanding electrical, thermal and chemical resistance characteristics (as expected from a perfluoroalkoxypolymer), and at the same time with an optimized price/performance ratio.

1. OVERVIEW OF THE COMONOMER PREPARATION AND POLYMERIZATION

The launch of MFA in the market of perfluoropolymers has been feasible and economically attractive because of two major breakthroughs in the technology of monomers' preparation and polymerization. The first breakthrough is a new industrial process[1] for the production of perfluorovinylethers (PFVE). PFMVE is obtained according to this proprietary process in an easier and more straightforward way with respect to normal PFVE productions. In the literature the so-called "epoxide" process is generally known[2], where PFPVE is obtained starting from a HFP oxidation to an epoxide and then reaction of the epoxide with perfluorinated acyl fluorides to an alkoxyacyl fluoride. Finally the alkoxyacyl fluoride is converted into PFPVE by high temperature treatment in presence of a base. The second breakthrough in the technology of perfluorinated polymers is the use of a proprietary process for the polymer preparation. As a brief explanation, this new process makes possible, when compared to standard emulsion and suspension polymerizations (typically used for the polymerization of PFA and FEP polymers[3]), the presence of a number of polymerization loci much higher than in the two conventional cases[4]. Therefore

even a co-monomer with a relatively low reactivity can be successfully utilized and reacted easily with overall yields higher than those ones obtained with the conventional technologies.
Worth mentioning is that both the monomer and the polymer preparation made according ref.1) and ref.4) are in full compliance of the last regulations regarding use and consumption of ozone-depleting substances.

2. BASIC POLYMER CHARACTERISTICS

2.1 GENERAL PROPERTIES

Basic properties of MFA are listed in table 1.

GENERAL PROPERTIES	METHOD	UNIT	PFA	MFA	FEP
Specific Gravity	ASTM D 792	g/cm^3	2.12-2.17	2.12-2.17	2.12-2.17
Melting Temperature	ASTM D 2116	C	300-310	280-290	260-270
Linear Thermal Expan. coefficient	ASTM E 831	$1/K10^{-5}$	12 - 20	12 - 20	12 - 20
Specific Heat	-	kJ/kg K	1.0	1.1	1.2
Thermal Conductivity	ASTM D 696	W/K.m	0.19	0.19	0.19
Flammability	UL 94		V-O	V-O	V-O
Oxigen Index	ASTM D 2863	%	> 95	> 95	> 95
Hardness Shore D	ASTM D 2240		55-60	55-60	55-60
Friction coeff.(on steel)	-		0.2	0.2	0.2
Water Absorption	ASTM D 570	%	< 0.03	< 0.03	< 0.02

Table 1 : General properties of perfluorinated polymers

The melting point of MFA is 280-290 C, which is between the melting points of FEP and PFA (260 and 300 C). Typical general properties at room temperature confirm that MFA pratically behaves there like most perfluoropolymers. Throughout the paper the following descriptions will be used as references to typical commercialpolymer grades:
MFA low Melt Flow Rate(MFR):MFR of 2 to 4
PFA low MFR: MFR of 2 to 3
FEP very low MFR: MFR of 1.5-2.0
MFA high MFR: MFR of 12 to 15
PFA high MFR: MFR of 12 to 14
FEP medium MFR: MFR of 6 to 8
FEP plenum grades: MFR of 18 to 22

2.2 MECHANICAL PROPERTIES

Tensile properties of MFA have been compared to those of FEP and PFA.

Viscosity levels that were as homogeneous as possible for the three polymers were selected for these tests. Data for the low MFR grades are shown in Fig. 1.

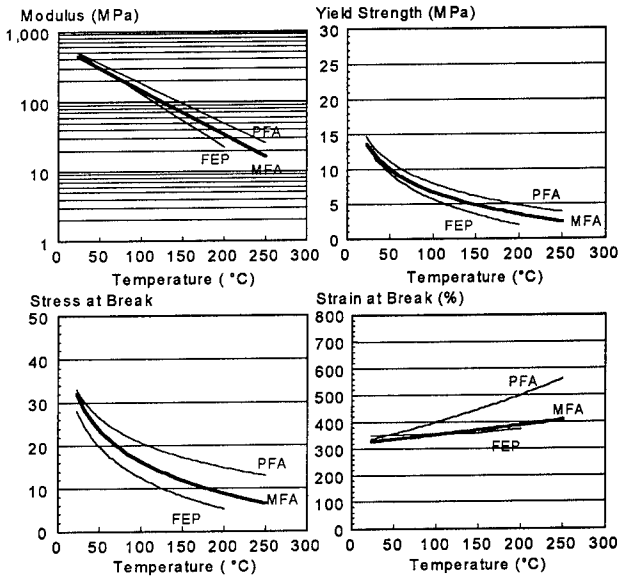


Fig. 1 : tensile properties as a function of temperatures for high viscosity grades. (ASTM D 1708 method)

While data at room temperature are very much comparable among the different polymers, MFA data at 200 C are intermediate between FEP and PFA.
At 250 C, while FEP cannot offer any tensile resistance at temperatures this close to its melting peak, MFA has roughly the same performance of FEP at 200 C. Abrasion resistance data carried out according to the Taber test procedure (ASTM D 1044) are listed in Table 2.

FLUOROPOLYMERS	TYPICAL MFR (g/10') ASTM D 2116	WEAR INDEX (mg/1000 cycles)
PFA low MFR	2 - 3	9 - 10.5
MFA low MFR	2 - 3	10 - 11.5
FEP very low MFR	1.5 - 2	14 - 15.5
PFA high MFR	12 - 14	15.5 - 17
MFA high MFR	12 - 15	15.5 - 17
FEP medium MFR	6 - 8	18.5 - 20

Table 2: Abrasion Taber Test (ASTM D 1044)

MFA shows an abrasion resistance at room temperature pratically comparable to that of PFA and significantly higher to that one of FEP. Abrasion resistance is

typically linked, for semicrystalline polymers, to the crystallinity.The MFA structure is, in such respect, closer to PFA than to FEP. The creep data at high temperature (200 C) are very interesting (Figures 2 and 3):

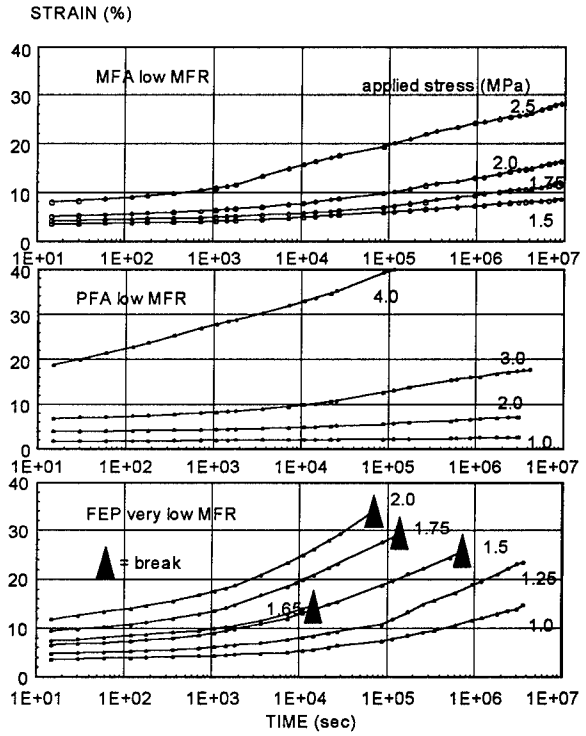


Fig. 2 : Tensile creep curves at 200°C

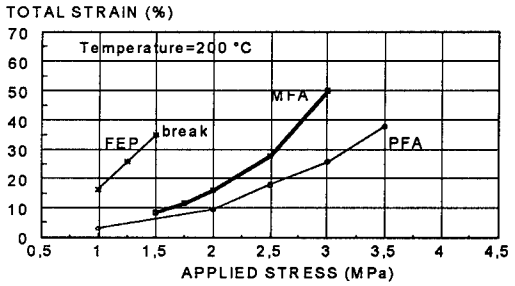


Fig. 3 : Isochronus stress-strain curves for 2000 hrs creep time

They show the basic and perhaps most important difference in behaviour between FEP on one side and PFA and MFA on the other side. The creep tests have been made according to ASTM D 2990.
Measurements carried out up to 2000 hrs at 200 C on MFA and PFA low MFR and FEP very low MFR show that, according to the applied load and to the test time, FEP specimens will undergo a partial and progressive embrittlement that eventually leads to cracking. This behaviour is generally known as Thermal Stress Cracking (TSC).
Fig. 4 shows the picture of a FEP cracked surface, where a progressive craze has been observed, with consequent decrease of the ligament and final failure by yielding due to its progressive and sharp reduction.

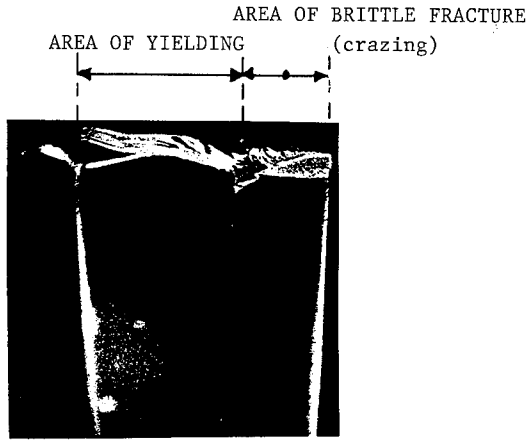


Fig. 4 : FEP cracked surface.

PFA and MFA do not show any of this transition and their behaviour, in the explored experimental range, is such that no hints of a similar embrittlement occur, even at longer times.
Fig. 2 and 3 show tests done on MFA low MFR, PFA low MFR and one grade of FEP very low MFR.
The same behaviour can be observed with high and medium MFR grades, as later discussed about tests done on wire insulations.

Izod impact tests data (not shown here) confirm, even for MFA, the oustanding tough behaviour even at low temperatures of perfluoropolymers, as dictated by the perfluorinated structure.

MIT flex endurance test data are reported on Fig. 5.
These test have been carried out according to ASTM D 2176 on 0.3 mm thick compression molded specimens.
MFA, especially for the low MFR grade, shows a behaviour much more similar to PFA than to FEP.

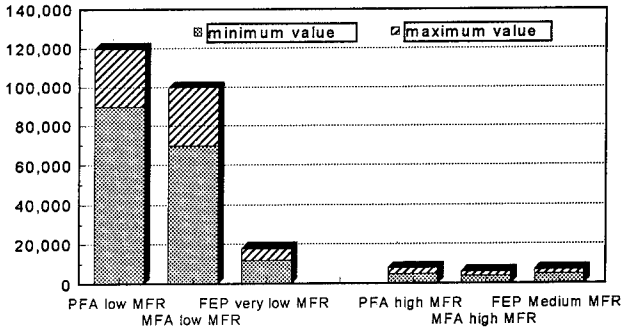


Fig. 5 : Flex-Life cycles at 23°C (thickness=0.3 mm). ASTM D 2176

2.3 ELECTRICAL PROPERTIES

Electrical properties measured on compression molded plaques are shown in Table 3:

PROPERTY	ASTM METHOD	UNIT	PFA	MFA	FEP
Volume Resistivity (fm 23 to 150°C)	D 257	ohm.cm	> 10^{17}	> 10^{17}	> 10^{17}
Surface Resistivity	D 257	ohm	> 10^{17}	> 10^{17}	> 10^{17}
Arc Resistance	D 495	sec.	> 200	> 200	> 200
Dielectric Strength (1 mm)	D 149	KV/mm	30-32	30-32	26-30

Table 3 : Electrical properties of HYFLON MFA resins (23°C)

Dielectric strength of MFA as a function of wall thickness is reported in Fig. 6.

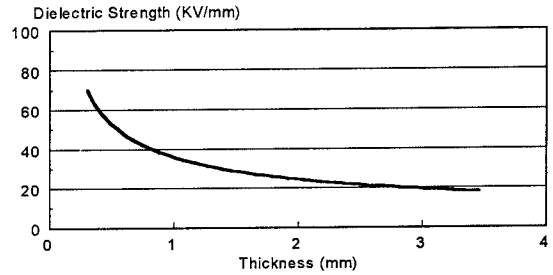


Fig. 6 : Effect of thickness on Dielectric Strength at 23°C of MFA resin.

All these data, carried out at room temperature, do not show big differences among the three polymers under comparison (FEP, PFA and MFA). Data of dielectric constant and dissipation factor show that MFA has a dissipation factor significantly lower than a typical FEP plenum grade, especially in the region between 1 and 100 Mhz. This can obviously lead to an improved design of cables in this frequency range. Data as a function of temperature and frequency are reported in table 4.

PROPERTIES AS A FUNCTION OF TEMPERATURE		
Electrical Properties	MFA high MFR	FEP plenum grade
DISSIPATION FACTOR (100 KHz)		
23 °C --> 200°C	< 10^{-3}	< 10^{-3}
DIELECTRIC CONSTANT (100 KHz)		
23 °C	2.0	2.1
50 °C	2.0	2.1
100 °C	2.0	2.1
200 °C	1.8	1.8
PROPERTIES AS A FUNCTION OF FREQUENCY (ROOM TEMPERATURE)		
Electrical Properties	MFA high MFR	FEP plenum grade
DISSIPATION FACTOR		
1 MHz	2.67 10^{-4}	7.25 10^{-4}
50 MHz	7.68 10^{-4}	8.68 10^{-4}
488 MHz	9.18 10^{-4}	9.64 10^{-4}
DIELECTRIC CONSTANT		
1 MHz	2.04	2.03
50 MHz	2.03	2.03
488 MHz	2.04	2.04

courtesy of Comm/Scope Inc., Network Cable Div., Claremont, NC.

Table 4 : Dielectric properties obtained on compression moulded specimens (0.5 mm thick)

2.4 RHEOLOGICAL AND PROCESSING PROPERTIES

Flow curves of two commercial grades of MFA are reported in Fig. 7. These curves are very close to those of PFA with same MFR level.

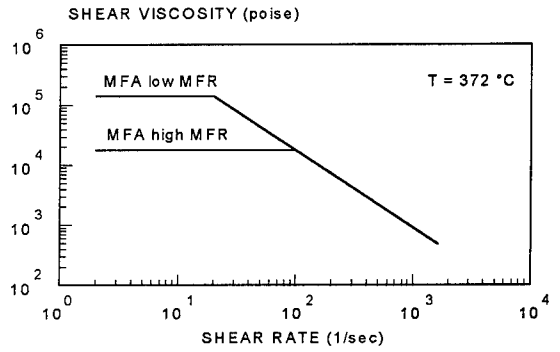


Fig. 7 : Flow curves of MFA resins

Processability and typical temperatures of processing of MFA are therefore very similar to those typical for PFA.
It must be remarked that the two MFA grades considered have better processability (so as higher line speeds), than do FEP very low MFR and FEP medium MFR. This is due to the higher MFR and also due to the fact that thermal stability of PFVE based copolymers (that

is PFA and MFA) is normally higher than that one of HFP-based polymers (FEP). In Fig. 8 (TGA data) typical isothermal TGA data at 380 C for 1 hour are shown.

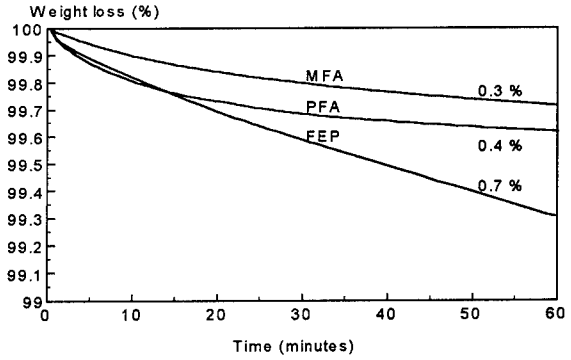


Fig. 8 : Thermogravimetric analysis in air at 380°C for 1 hours.

PFA and MFA behave pratically in the same way while FEP has a different slope and a higher final weight loss.
As a conclusion, it can be said that MFA has a processability behaviour quite overlapping the typical commercial PFA grades, both in terms of line speed and in terms of thermal stability during processing.

2.5 OPTICAL PROPERTIES

Even if optical properties are generally not relevant for Wire and Cable applications, it is worth mentioning that MFA shows a lower Haze value than FEP and PFA and that its trasmittance at UV frequency (between wavelength of 200 and 400 nm) is the lowest among all typical semicrystalline perfluoropolymers.
These properties are not obtained through a reduction of crystallinity.
As a matter of fact, X-rays and DSC data point out the higher cristallinity of MFA in comparison with FEP.

3. W&C APPLICATIONS; TYPICAL PROPERTIES OF MFA INSULATED WIRES AND CABLES.

From the basic structure and properties of MFA, it can be easily understood that its main applications in the Wire and Cable industry are for high temperature-resistant constructions and for medium-high frequency applications where a superior performance in comparison with conventional FEP dielectric core is sought. The high temperature resistant applications stem naturally from the considerations previously outlined:

- better tensile properties than FEP and only slightly lower than PFA above 200 C: data at 250 C are comparable to that of FEP at 200 C.
- virtual absence of tough-brittle transitions, that lead standard FEP polymers to severe thermal stress cracking when exposed to both stress and temperature.

The general characterization of the polymer has been integrated with the technological tests typical for the wire and cable industry to better assess the advantages of MFA over other insulations.

3.1 CUT THROUGH

Tests of cut through, according to ASTM D 3032, have been extensively done on different fluoropolymers and as a function of temperature.
Typical tested construction is a 20 AWG stranded conductor with 0.25 mm insulation wall thickness.Fig. 9 shows bar charts at 23, 150 and 200 C:

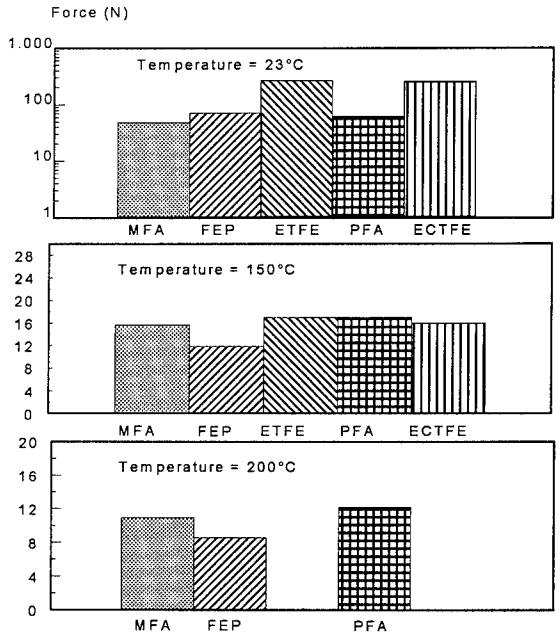


Fig. 9 : Cut through data obtained on 20 AWG insulated cables (0.25 mm thick)

Cut through resistance at room temperature is highest for ECTFE and ETFE polymers, followed by FEP medium MFR and then by MFA and PFA. At 120 °C there is a cross-over between FEP (medium MFR) and MFA (high MFR) and a cross-over between ETFE and MFA occur at about 150°C.

3.2 MANDREL TESTS

The mandrel test is another typical technological test widely used in the W&C industry to assess the high temperature performance of a plastic insulation. It can be done by using different methodologies and with different outer insulation diameter/mandrel diameter ratios.Generally, the higher the ratio, the more critical the test.
Tables 5 and 6 show the results of different tests done with different constructions and following different specification methods:

TEST method	1 int. method according to VDE 0207	2 int. method according to UL 758/1581	3 internal method
mandrel diameter (mm)			
- primary, WT=0.25 mm OD=1.5 mm	5	1.5	12
- jacket, WT=0.25 mm OD=4.5	-	12	25.4
Testing Temperature (°C)			
- PFA	290	260	290
- MFA	240	260	240
- FEP	240	232	240
Testing Time (hrs.)	6	1	16
number of cycles	1	1	10

Table 5 : operative conditions followed for the mandrel test

MANDREL TEST	PFA	MFA	FEP
PRIMARY INSULATION			
Internal method 1 according to VDE 0207	no cracks	no cracks	no cracks
Internal method 2 according to UL 758/1581	no cracks	no cracks	no cracks
Internal method 3	no cracks	no cracks	cracks after 8 cycles
JACKETING			
Internal method 2 according to UL 758/1581	-	no cracks	-
Internal method 3	-	no cracks	-

Table 6 : mandrel test results obtained on insulated and jacketed cables (wall thikness=0.25 mm).

All of them show the oustanding resistance to TSC of MFA, even at temperatures very close to the melting point.

3.3 THERMAL RATING ON INSULATED WIRES

Another important design parameter for selecting a high temperature insulating material is the thermal rating. The thermal rating is the temperature at which the cable can whistand 20000 hours of exposure. Tests are being carried out on 20 AWG wires with 0.25 mm insulation thickness of MFA high MFR. Tests are being carried out according to specification IEC 216 (part 1) and ASTM D 3032. These tests are not yet completed. Present data (June 1995) are reported on table 7:

THERMAL AGEING CONDITIONS:		
Temperature (°C)	Time for Cycle (days)	
250	21	
257	16	
270	7	
LAST UPDATING: 12.07.95		
Temperature (°C)	Number of cycles	Number of Failures
250	16 (8064 hrs.)	0/10
257	21 (8064 hrs.)	0/10
270	45 (7560 hrs.)	1/10

Table 7 : thermal rating test in progress according to ASTM D 3032 AWG 20 (nichel coated copper) insulated cable (t=0.25 mm)

MFA high MFR insulations have already passed, without any failure, more than 7000 hours at 257°C and more than 7000 hours at 270°C with only one failure out of ten specimens. 270°C is only 10°C below the melting peak. The same test carried out at 250°C with FEP medium MFR insulated wires was terminated at 1600 hours with the failure of all 10 specimens.
While testing is not yet complete, it is suggested to consider, as a safe figure, an MFA thermal rating @ 20000 hours between 235 and 245°C.

3.4 CREEP TESTS ON INSULATIONS

This test, though being borrowed from typical tests for rubber insulations, points out some remarkable differences among PFA, MFA and FEP.
The insulations (0.25 mm wall thickness over 20 AWG nickel-plated stranded conductors) were stripped off the conductor and loaded with a given weight in order to have a constant stress of 2 MPa across the cross-section of the insulation.

Fig. 10 shows the creep strain after 30 minutes of exposure at different temperatures for insulations made with: MFA high MFR, PFA high MFR, FEP medium MFR.

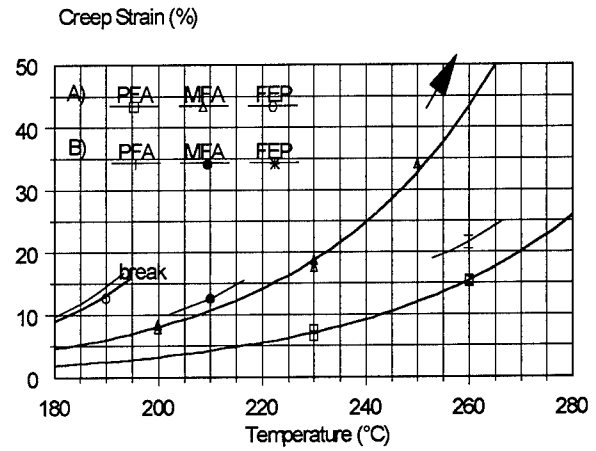


Fig. 10 : TENSILE CREEP TEST. Isochronus curves (t=30 min; L=2 MPa)
A) compression moulded specimens B) cable insulations

FEP tends to crack even at temperature lower than 200 C, while MFA and PFA creep continuously, in a ductile way, with increasing strains as temperature is increased. The higher creep of MFA, in comparison with PFA, particularly above 200 C, is due to its lower melting point.

3.5 ATTENUATION DATA ON A RG-58 CONSTRUCTION

Table 8 shows the attenuation data on RG-58 cables obtained with a standard FEP and MFA dielectric cores.

Electrical Properties	MFA high MFR	FEP plenum grade
Inside diameter (mm)	0.823	0.896
Outside diameter (mm)	2.778	2.799
ATTENUATION (db/100 ft)		
100 MHz	-4.086	-4.178
200 MHz	-6.032	-6.225
300 MHz	-7.672	-7.955
400 MHz	-9.059	-9.426
500 MHz	-10.431	-11.270
600 MHz	-11.665	-12.392
700 MHz	-12.764	-14.370
800 MHz	-13.949	-15.773
900 MHz	-14.976	-17.100
1000 MHz	-15.981	-18.369

courtesy of Comm/Scope Inc., Network Cable Div., Claremont, NC.

Table 8 : Attenuation data on RG-58 cables

The MFA cable shows a lower attenuation (2.388 db/100 ft gain, at 1 GHz), in spite of the fact that a smaller conductor was used for the construction with MFA and a smaller outer diameter was used to have same impedence.

CONCLUSION

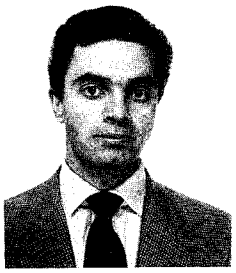
The new MFA perfluoropolymer has been presented together with its main performance characteristics and in comparison to already known melt-processable perfluoropolymers.
It has been shown how TSC resistance has been greatly improved over the most common FEP grades, to obtain a typical TSC and creep resistance very similar to conventional PFA polymers.
This aspect has made possible the design of MFA grades with lower viscosities (and hence better processability) than those ones typical of FEP grades used in high temperature applications.
The oustanding high temperature properties make MFA an ideal choice wherever high temperature wires and cables must be designed with a safety margin superior to the standard FEP insulations and also wherever PFA cables are not to be used at its uppermost temperature range.
Appliances wire, hook-up wires, cables for special constructions in the automotive industry and heat tracing cables are already current applications for MFA.
The oustanding dissipation characteristics make then MFA an ideal choice for wire and cables where high frequency signals must be trasmitted, with significant improvement to the standard FEP constructions and without the need to use the ultimate choice of PFA or PTFE.

ACKNOWLEDGEMENTS

Many thanks to Mr. R. Wessels of Commscope Inc, Clairemont, NC, for his help in measuring high frequency properties of MFA. Authors wish then aknowledge the help and support of Dr. G. Ajroldi and Dr. V. Arcella, both of AUSIMONT S.p.A. and Mr. B. Wright, of AUSIMONT USA.

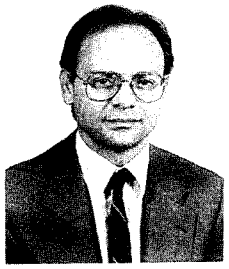
REFERENCES

1- US Patent 4900872
2- US Patent 3358003
3- US Patent 3132123
4- US Patent 4864006



Giandomenico Vita
Ausimont S.p.A.
Viale Lombardia 20,
I-20021 Bollate
ITALY

Born in Como (Italy). He holds a University degree in Chemical Engineering from Politecnico of Milano (Italy). He has been working 11 years in the field of fluorinated polymers. Since 1992 he has had the world-wide responsibility for the Applicative Development and Technical Service of AUSIMONT fluorinated melt-processable polymers.



Massimo Pozzoli
Ausimont S.p.A.
Viale Lombardia 20,
I-20021 Bollate
ITALY

Born in Monza (Italy). He holds a University degree in Chemical Engineering from Politecnico of Milano. He has been working in the Material Science Department for some years. Since 1993 he has worked in the melt-processable polymers Technical Service and Development Department where he has been acquiring particular expertise in W&C applications.

DEVELOPMENT OF IRRADIATED FLEXIBLE FLAT CABLE

T. Hosokawa, Y. Naruse, K. Tanaka, T. Kuga and Y. Takeda

Sumitomo Electric Industries, LTD.
Tochigi, Japan

Abstract

The demand of flat cable has been increased especially in the field of electronics equipment, owing to its flexibility and easiness of wiring. Recently, there are a lot of thing to be requested for the flat cable, and in these requests, flexibility, heat resistance and voltage resistance are very important properties. But up to now, there is no flat cable to satisfy these three properties, then we started to develop the flat cable which satisfied every property of flexibility, heat resistance and voltage resistance. And we have succeeded to develope the new flat cable which had excellent properties mentioned above by using new insulation material and the technique to cross-link the insulation by irradiation of electron beam.

1. Introduction

Up to now, many kinds of flat cable have been used for internal wiring materials of electronic equipment such a VCR and an audio set, etc. The reason why many flat cables have become to be used is that they have various advantages. For example, They are suitable for high dense wiring and wiring at the moving place, because of its flexibility.

Recently, the requirements for flat cable became various with improvement of the function and ability of electronic equipment. In those requirements, flexibility, heat resistance and voltage resistance are the most important properties, however, there is no flat cable which can satisfy these properties. This time we decided to use our own developed insulation material and the technique of cross-linking by irradiation of electron beam. As a result, new flat cable obtained here has excellent flexibility, heat resistance and voltage resistance. And as the other strong point, this flat cable has excellent and stable electrical properties in the wide temperature range, and has resistance for various chemical liquids.

We report about the progress of development, construction and properties of this developed new flat cable.

2. Developement

2-1 Current products

The construction of popular flat cable and the example of its wiring method are shown in Fig.1.

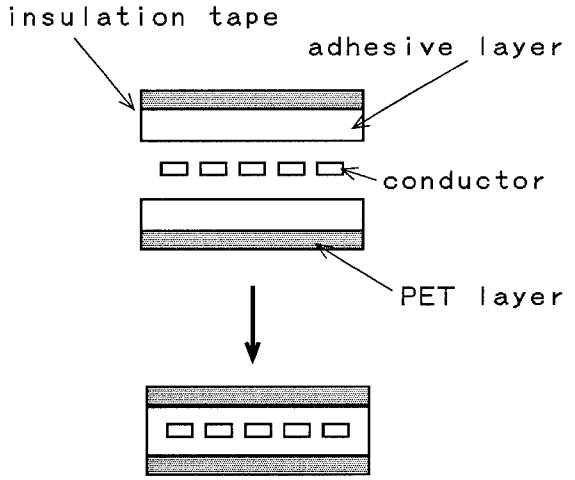


Fig. 1 Construction and wiring method

The insulation of flat cable consists of polyethylene-telephtalate(PET) firm layer and adhesive layer, and the flat cable is produced by using two sheets of insulation tape and flat conductors like Fig.2.

The current flat cable can classify roughly in two kinds shown in Table 1. One is standard product which is superior in flexibility, however its UL rating of 80 ℃ in temperature and 30V in voltage is not high. And the other is high rating product which has the UL rating of 105 ℃ and 300V, but this is poor in flexibility because of its thick insulation.

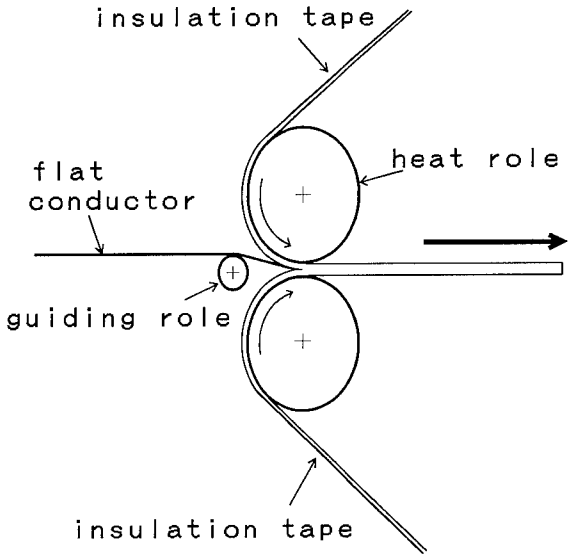


Fig. 2 Manufacturing method

Table 1 Construction of current flat cable

item		current standard	current high rating
UL rating	temperature	80 ℃	105 ℃
	voltage	30V	300V
insulation thickness (μ m)	PET layer	25	50
	adhesive layer (material)	45 (polyester)	60 (polyester)
	total	70	110
conductor thickness(μ m)		35 ~ 50	35 ~ 100
cable thickness(μ m)		175 ~ 240	255 ~ 320

2-2 Development of new flat cable

The flexibility of flat cable become less with increase of insulation thickness. So, we researched to decrease the insulation thickness of high rating product. The reason why the current product has thick insulation is that the current adhesive of insulation, which consists of thermoplastic polyester, doesn't have good electrical properties and heat resistance. Therefore, we concentrated to develop the new adhesive which has excellent properties.

As a result of various kinds of investigation, we have succeeded to decrease the insulation thickness from 110 μ m to 80 μ m and develop the target flat cable by using following technique.

1) using new material as the adhesive layer

We used special modified polyolefin as the material of adhesive layer. Because this material is superior to current adhesive in the point of electrical properties.

2) cross-linking of adhesive layer

We can't obtain heat resistance only by using above polyolefin material. So we tried to improve the heat resistance by cross-linking the adhesive. We decide to use the irradiation technique of electron beam as the method of cross-linking.

2-3 Construction of developed product

The construction of developed flat cable is shown in Table 2.

Table 2 Construction of current flat cable

item		current standard	developed
UL rating	temperature	80 ℃	105 ℃
	voltage	30V	300V
insulation thickness (μ m)	PET layer	25	30
	adhesive layer (material)	45 (polyester)	50 (cross-linked polyolefin)
	total	70	80
conductor thickness(μ m)		35 ~ 50	35 ~ 100
cable thickness(μ m)		175 ~ 240	195 ~ 260

3. Properties

3-1 Properties of developed adhesive layer

1) Heat resistance

The experimental result of heat resistance of adhesive is shown in Fig.3. This figure expresses the transformation rate of adhesives when the weight of 300g/c m^2 is added on the adhesive layer at 136 ℃. From this figure, it is found that the current adhesive transform perfectly, on the other hand, developed adhesive transform only 30%. Because developed polyolefin adhesive is cross-linked by irradiation.

Fig.4 shows the degradation of elongation property of adhesive after adhesive are aged at 136 ℃ . It is clear that the developed adhesive is hard to degrade.

2) Electrical properties

Temperature dependence of electrical resistance per unit volume is shown in Fig.5 and that of dielectric constant is shown in Fig 6. Electrical resistance of developed adhesive is higher and its dielectric constant is lower, and also their temperature dependence are much smaller than those of current adhesive.

This means developed adhesive has stable electrical properties in the wide temperature range.

3-2 Properties of developed product

1) UL rating

This developed product obtains UL recognition of 105 ℃ in temperature rating and 300V in voltage rating.

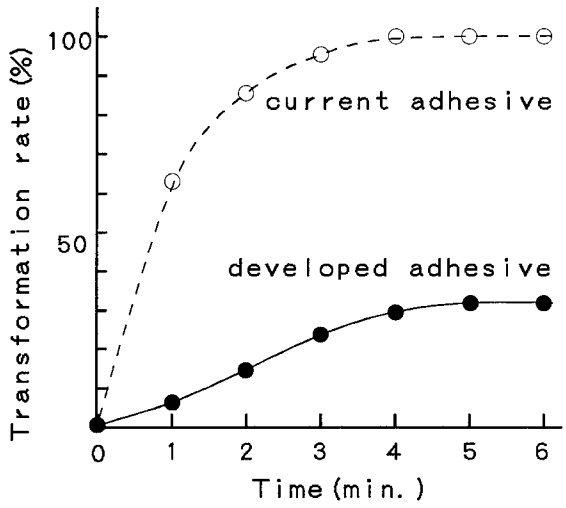


Fig. 3 Transformation rate of adhesive

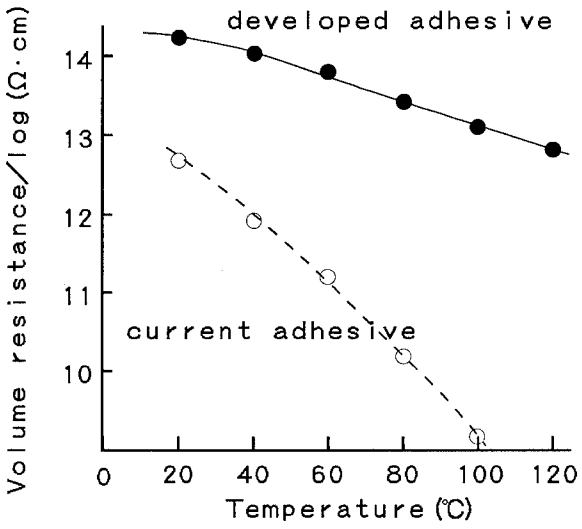


Fig. 5 Volume resistance of adhessive

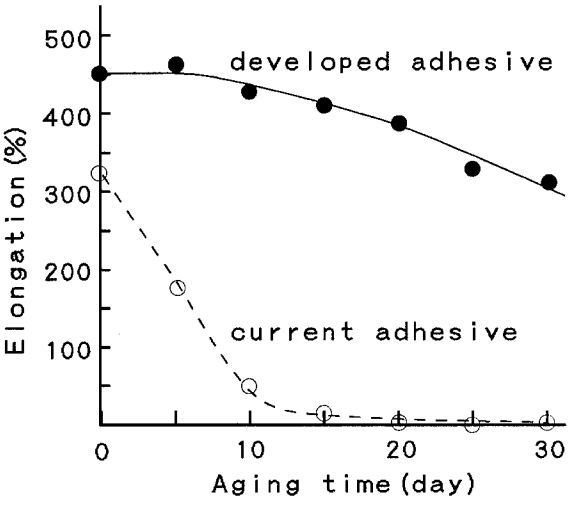


Fig. 4 Elongation of adhesive after aging

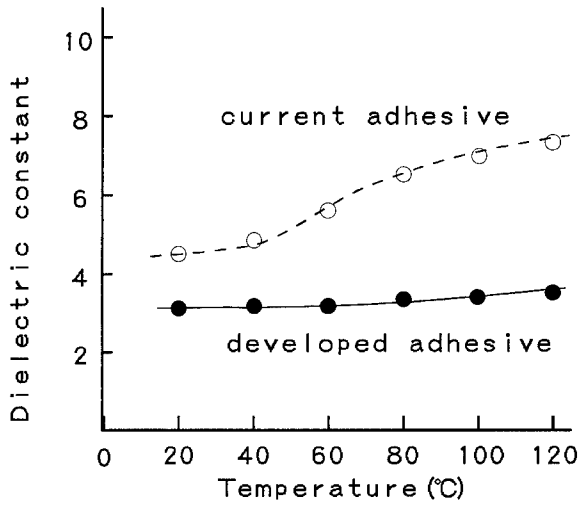


Fig. 6 Dielectric constant of adhesive

2) Flexibility

In order to test the flexibility of flat cable, we measured the force to bend the flat cable by the method shown in Fig.7. The results are shown in Table 3. The force of the developed product is about 1/4 of the current high rating product and became very close to the current standard product.

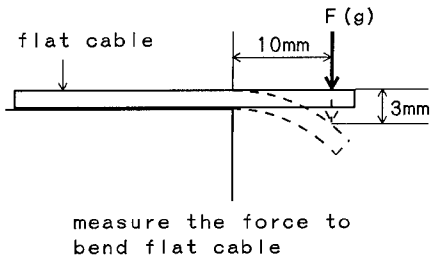


Fig. 7 How to measure bending force of flat cable

Table 3 The force to bend flat cable

sample	bending force(g)
current standard	10
current high rating	17
developed	60

3) The resistance for hot solder

We investigated the relation between the dipping time to the solder bath and the shrinkage of insulation, when the terminal conductor part was dipped into solder bath like Fig.8. That result is shown in Fig.9. It is found that the developed product has excellent property in the resistance for hot solder as compared with current product. This is the effect that adhesive is cross-linked.

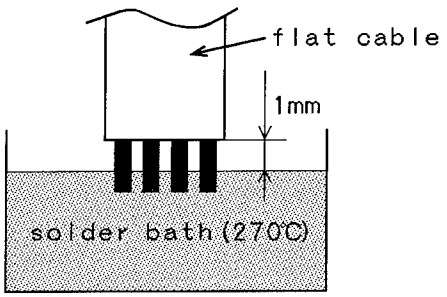


Fig. 8 Test method of resistance for hot solder

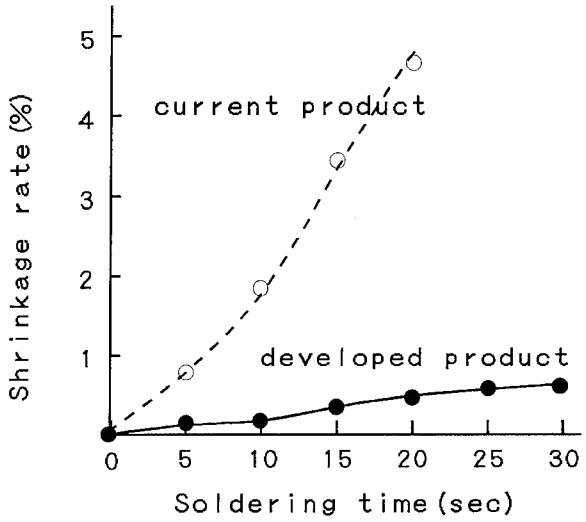


Fig. 9 Insulation shrinkage by soldering test

4) Electrical properties

We manufactured shielding flat cable shown in Fig.10, and measured the temperature dependence of capacitance between signal conductor and ground conductor. Fig.11 shows its result. This developed product has very small temperature dependence of capacitance as compared with current product, because of the difference of dielectric constant property between their adhesives.

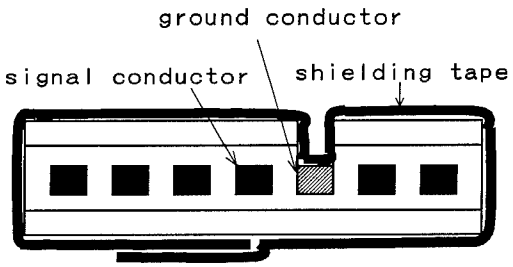


Fig. 10 Shielding construction of flat cable

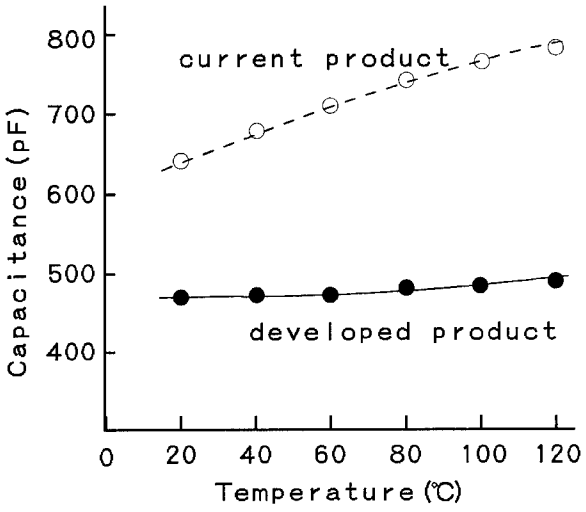


Fig. 11 Capacitance of shielding flat cable

5) Resistance for chemical liquids

Besides properties mentioned above, we investigated the resistance for various chemical liquids. These results are shown in Table 4. Developed product has excellent properties in resistance for organic solvent and acid. This effect is also obtained by using this developed adhesive.

Table 4 Resistance for chemical liquids

chemical liquid	current standard	current high rating	developed
ethanol	○	○	○
toluen	×	×	○
dichloro-ethane	×	×	○
hydrochloric acid	△	△	○
caustic soda	△	△	△

4. Conclusions

This development make it possible to supply the flat cable which is suitable for high dense wiring and superior to heat resistance and voltage resistance and to expand the field using flat cable.

We will keep up to develop the new product by using technology of materials and irradiation, in order to make it possible to use flat cable in the various field in the future



Takehiro Hosokawa

Sumitomo Electric Industries, Ltd.
3-3, Satuki-cho,
Kanuma-city,
Tochigi-prefecture
Japan

Takehiro Hosokawa received his M.S. degree in chemical engineering from Kobe University in 1989. He then joined Sumitomo Electric Industries, Ltd., and engaged in development and design of flat cables. Mr. Hosokawa is now a member of Electronics Wire Division.



Toru Kuga

Sumitomo Electric Industries, Ltd.
3-3, Satuki-cho,
Kanuma-city,
Tochigi-prefecture
Japan

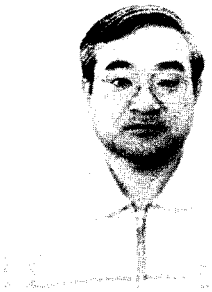
Toru Kuga received his B.S. degree in comunication engineering from Kyusyu University in 1975. He then joined Sumitomo Electric Industries, Ltd., and engaged in development and design of flat cables. Mr. Kuga is now a manager, Flat Components Section, Electronics Wire Division.



Youichi Naruse

Sumitomo Electric Industries, Ltd.
3-3, Satuki-cho,
Kanuma-city,
Tochigi-prefecture
Japan

Youichi Naruse received his M.S. degree in electronics engineering from Nagoya Institute of Technology in 1993. He then joined Sumitomo Electric Industries, Ltd., and engaged in development and design of flat cables. Mr. Naruse is now a member of Electronics Wire Division.



Yasuo Takeda

Sumitomo Electric Industries, Ltd.
3-3, Satuki-cho,
Kanuma-city,
Tochigi-prefecture
Japan

Yasuo Takeda received his B.S. degree in process chemical engineering from Hokkaido University in 1971. He then joined Sumitomo Electric Industries, Ltd., and engaged in development and design of flat cables. Mr. Takeda is now manager, Flat Components Department, Electronics Wire Division.



Keiichi Tanaka

Sumitomo Electric Industries, Ltd.
1-1-3, shimaya,
Konohana-ku,
Osaka-prefecture
Japan

Keiichi Tanaka received his B.S. degree in applied chemical engineering from Tohoku University in 1983. He then joined Sumitomo Electric Industries, Ltd., and engaged in development and design of flat cables. Mr. Takeda is now a senior staff of Osaka Research Laboratories.

LASER PRINTABLE BLACK CABLE JACKETING COMPOUNDS

L. Y. Lee, D. E. Roberts, B. L. Vest, and K. Tonyali

Quantum Chemical Company
Cincinnati, Ohio 45249

ABSTRACT

A new technology using a YAG laser to print high quality images and lettering onto polyolefin cable jacket surfaces has been developed. This technology offers fast, one-step printing, excellent image flexibility, and low maintenance cost to mark cables, particularly for black polyethylene jackets. The quality of laser printed images is superior to that of the current ink jet method in both abrasion resistance, contrast and resolution. A computerized gray-scale measuring method is used to evaluate image contrast quality. Laser printing depends on parameters such as laser pulse frequency, beam size, power setting, and material response. Specially formulated laser responsive polyethylene resins are UV resistant and suitable for outdoor applications. Weather-o-meter testing of laser printable resins is comparable to a commercial product at 4000 hours exposure time. The laser printable resin also has better electrical properties than a comparable non-laser printable resin.

INTRODUCTION

Cables are often required to be labeled with information such as manufacturer's name and logo, type of cable, and footage length. Current processes in marking cables mainly utilize ink jet[1] or mechanical stamping methods[2]. However, these methods generally suffer from a combination of drawbacks such as poor abrasion resistance, slow processing, lack of image flexibility, and the use of undesirable solvents. For example, the ink jet process (which is by far the most common way in labeling cables) uses dyes and solvents to produce markings which are often not very durable. Furthermore, the use of these chemicals usually incurs high maintenance cost and could pose as an environmental hazard in handling and waste disposal. Alternatively, mechanical stamping or indentation methods would produce abrasion-resistant marks but are inherently slow and limited in image flexibility. Hence, an environmentally friendly, direct, non-contact method to produce durable and legible images and lettering is highly desirable.

Laser beam marking has been practiced commercially in microelectronics and small molded products[3]. It offers advantages in mark durability and image resolution. Most commercial units are equipped with computer softwares that allow complex images and various lettering font types to be printed. Laser printing in the cable industry, however, is limited in PVC jackets in which CO_2 lasers are used. The main reason is that laser response is quite specific in the type of base resin and various types of additives commonly used. Attempts to mark polyethylene jackets, particularly black cable jackets, often resulted in illegible marks without much contrast. This report describes the important parameters in using a YAG laser to produce highly contrasting prints on black polyethylene surfaces. Various aspects in laser settings, material response, and subsequently a mechanism to account for the laser-polymer interaction are discussed. Based on these understandings, a family of laser printable polyethylene compounds was developed that are suitable for outdoor cable jacketing applications.

EXPERIMENTAL

Laser Beam Printing

A commercial Nd : YAG laser at 1064 nm wavelength was used to print an array of symbols (Figure 1) as a function of power setting and pulse frequency. Five power settings were used, ranging from 0% to 100% which correspond to 2-3 W at 0% and 25 W at 100%, respectively. Nine pulse frequencies from 1 kHz to cw100 (cw = continuous wave) were scanned to evaluate material response. In most cases, the best response was obtained at 10-15W and 10-25 kHz range. The symbol generated at 50% power level and 15 kHz was used for contrast measurement.

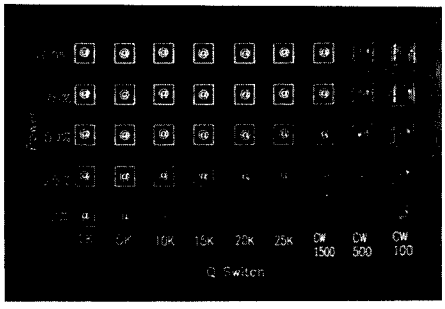


Figure 1. Array of Laser Printed Symbols

Image Analysis

The gray intensity contrast of laser printed symbols was determined by analyzing their photographic images with an image analysis software (Global Lab Image, v. 2.10) installed on an IBM PS/2 computer. The measured values were referenced against an internal standard using white and black tapes, and this ratio was expressed as the percent gray contrast. A rating system of 0-4 was assigned. A rating of 0 was assigned when there is no marking after laser beam exposure. Contrast percents of 0-10%, 10-20%, 20-30%, and greater than 30% were given the ratings of 1, 2, 3, and 4, respectively. The visual quality of the ratings is that a value of 4 is considered very good to excellent, a value of 3 is considered good, a value of 2 is considered fair, and a value of 1 is considered poor.

Sample Preparation

Laser printable samples were made by blending the components in a 240 cc Brabender mixer for 8 min. at a melt temperature applicable to the base resin. The resulting mixture was compression molded into 152 mm x 152 mm x 1.6 mm plaques.

RESULTS AND DISCUSSION

Laser Printing in PE Containing Carbon Black

Image Contrast as a Function of Carbon Black Levels

Polyethylene in its pure state is transparent to laser light in the UV-visible range such as the YAG laser. Pigments or light absorbing additives such as carbon black (CB) are needed to make PE laser responsive. A series of LLDPE plaques containing 0-2.0% N110 type CB was exposed to the 1064 nm laser beam and the resulting printed symbols were analyzed. Table 1 shows the contrast data and ratings. High contrasting prints were obtained at 0.1-0.5% CB levels with the optimum at 0.35% CB.

TABLE 1 CONTRAST DATA FOR N110/LLDPE

% CB	% CONTRAST	RATING
0.01	---	0
0.03	8.9	1
0.10	27.5	3
0.25	33.8	4
0.35	34.5	4
0.51	28.3	3
0.71	21.7	3
1.01	17.6	2
2.00	9.0	1

Image Contrast as a Function of CB Particle Size

In addition to N110 which has a mean diameter of 18-20 mμ, three other carbon blacks of different particle size (N326, N774, and N990) were used in LLDPE to evaluate the laser print. The contrast data in Table 2 generally show that particle size below 100 mμ does not have a significant effect on the print quality and CB level dependence; optimum contrast about 30% was achieved at about 0.3% CB. The only exception was N990, which has a diameter of 200-500 mμ, produced a slightly lower contrast (22%) at 0.35%.

TABLE 2. CONTRAST DATA FOR CB/LLDPE

CB TYPE	DIA. (nm)	%CB	%CONTRAST	RATING
N326	20-30	0.35	29.1	4
	20-30	0.50	25.9	3
	20-30	1.00	13.1	2
	20-30	1.50	11.8	2
	20-30	2.00	11.4	2
N774	60-70	0.35	32.2	4
	60-70	0.50	21.4	3
	60-70	1.00	15.6	2
	60-70	1.50	14.0	2
	60-70	2.00	9.9	1
N990	200-500	0.35	22.3	3
	200-500	0.50	13.1	2
	200-500	1.00	13.7	2
	200-500	1.50	12.6	2
	200-500	2.00	9.9	1

Image Contrast as a Function of Base Resin Type

In addition to LLDPE, four other polyolefins were laser printed with N110 CB added. These resins were polypropylene (PP), high density polyethylene (HDPE), ethylene vinyl silane copolymer (EVS), and ethylene n-butyl acrylate copolymer (EnBA). Contrast results relative to CB content are given in Table 3. The data indicate that CB level of 0.1-0.7% would provide good contrast in these resins. Specifically, HDPE appears to have better contrast than the other resins over a greater CB range (0.1-0.7%). Both EVS and LLDPE gave similar contrast over the same CB range. While PP gave good contrast at low CB level, it was poorer at higher levels. The EnBA appears to have the narrowest range, it gave good contrast only at 0.1% CB. Overall, there appears no consistent dependence of contrast performance to resin type. Since resin characteristics such as MI, melting point, and other properties were not well controlled in these experiments, it is difficult to offer any valid correlation between resin type and laser printability.

TABLE 3 CONTRAST DATA FOR N110/RESINS

RESIN	% CB	% CONTRAST	RATING
PP	0.05	36.2	4
	0.10	40.4	4
	0.30	26.5	3
	0.70	16.0	2
	1.00	11.3	2
HDPE	0.01	---	0
	0.05	5.5	1
	0.10	38.3	4
	0.35	39.3	4
	0.51	35.0	4
	0.71	31.1	4
	1.01	28.5	3
EVS	0.35	42.0	4
	0.50	24.4	3
	1.00	19.8	2
	1.50	12.4	2
	2.00	10.6	2
EnBA	0.05	1.6	1
	0.10	36.9	4
	0.30	17.9	2
	0.71	7.0	1
	1.01	1.9	1

Optical microscopy of the laser printed symbols in general identified three layers or regions. A schematic of a typical micrograph is shown in Figure 2. Region A is a white layer raised above the plaque surface, B is a region below the surface similar in appearance to A, and C located further below the surface but darker in appearance. The estimated thickness of these layers are 10-35 μm for A, 0-60 μm for B, and 17-70 μm for C. Regions A and B were not present in all the symbols depending on the laser parameters whereas C was present in all the symbols. Symbols that appeared the sharpest and brightest correspond to those with the thickest regions A and B combined. Based on these observations, the following conclusions can be drawn:

1. Regions A and B are layers of polymer that were resolidified during or after the laser beam exposure. Region C is the depth where the laser beam has penetrated from the surface.

2. Region A is the layer that is mainly responsible for the visual contrast quality. A layer raised above the polymer surface which is depleted with CB provides the best contrast because it reflects most of the light to our eyes.

3. In symbols where regions A and B are absent, the marks were indentation or crater formation with a color change . This results in poor contrast because most of the light is captured and not reflected back to our eyes.

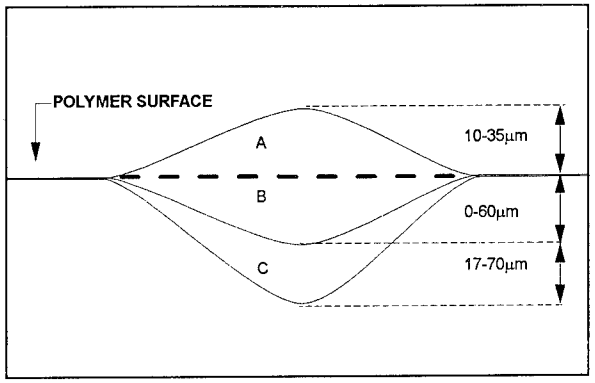


Figure 2. Schematic Drawing of A Laser Printed Mark

Laser Marking Mechanism in CB Added PE

A photophysical mechanism for laser beam printing of CB modified polyolefins can be developed based on the experimental observation. As the laser beam impinges on the polymer surface, it penetrates a depth which is inversely proportional to the CB content. Since the polymer is for the most part transparent to the laser beam, the light absorbing path is confined to the CB particles. CB light absorption can be expressed according to Beer's law:

$$J = J_0 e^{-\alpha d}$$

where J_0 is the energy density of laser beam which is the pulse energy divided by the beam size, α is the absorption coefficient and d is the particle diameter. The photo energy captured by a CB particle can be converted and dissipated in physical/chemical processes depending on the energy domain and kinetics of the processes. For a YAG laser with energy density usually less than 0.1 J/cm^2, the principle paths are thermal heating and possible ablation.

Thermal pathways can lead to reactions within the CB particle and to the surrounding polymer matrix. Five pathways can be identified:

1) conduction to the surrounding polymer matrix,
2) melting of the surrounding polymer matrix
3) oxidation of CB to produce CO_2
4) thermal decomposition of the polymer, and
5) ablation or etching

The temperature rise in the CB can be calculated based on the light energy density and properties of CB[4]:

$$T = J_0 (1 - e^{-\alpha d}) d^2 / \varphi d^3 C_p$$

A temperature rise of 3600 °K is estimated using appropriate values for the parameters where

J_0 = laser energy density = 0.05 J/cm^2
α = CB absorption coefficient = 10^{-5} cm^{-1}
d = particle size = 2 x 10^{-6} cm
φ = CB density = 1.8 g/cm^3
C_p = CB specific heat = 0.7 J/°Kg

At this high temperature, CB could be oxidized and vaporized (pathway 3). The temperature increase could also result in melting and vaporization of the surrounding polymer (pathways 1, 2, and 4). Using specific heat of 2.3 J/°Kg for polyethylene, an increase of 3600 °K would give 7600 J/g of energy. This value far exceeds the heat of fusion (100 J/g) and heat of vaporization (2500 J/g) for polyethylene. Thus, a partial conversion of the thermal energy could easily lead to phase transformation of the polymer. The extent of thermal effect on the surrounding polymer is also governed by its heat transfer property. Using the equation of the time constant of thermal diffusion[5]

$$x = (t D)^{1/2}$$

where t is the laser pulse width, D is the thermal diffusivity, x, the distance of thermal diffusion which can be determined for the duration of the polymer exposed to the laser beam. A value of 14 x 10^{-6} cm is calculated using typical values for t (200 ns) and D (10^{-3} cm^2/s). This value is about seven times the CB particle size (20 nm) which implies that a substantial amount of polymer is affected and a temperature gradient is developed quickly within each laser pulse.

Thermal diffusion into the surrounding polymer suggests that the CB particle-particle distance is an important parameter in determining the extent of thermal processes taking place in a polymer matrix. Based on a simple spherical geometry and idealized dispersion of the CB particles, the particle-particle distance as a function of CB content can be calculated as

$$x = (v/1.8\ W_f) - d$$

where v is the particle spherical volume, d the diameter, and 1.8 W_f the volume fraction multiplied by its specific gravity. Using a 20 nm diameter, the particle-particle distance is plotted against W_f in Figure 3. As seen, the greatest change in CB distances occurs below 0.5% which implies that any changes in the thermal effects should also be most noticeable in this range. The contrast data of laser prints as a function of CB level indeed reveal that the best contrast was obtained at 0.1-0.5% CB.

Photoablation of polymers (pathway 5) is a phenomenon in which the polymer surface is etched without detectable thermal damage[6]. Although quantitative models have not yet been fully developed to account for the complex mechanism(s), it is generally accepted that the laser energy is rapidly converted

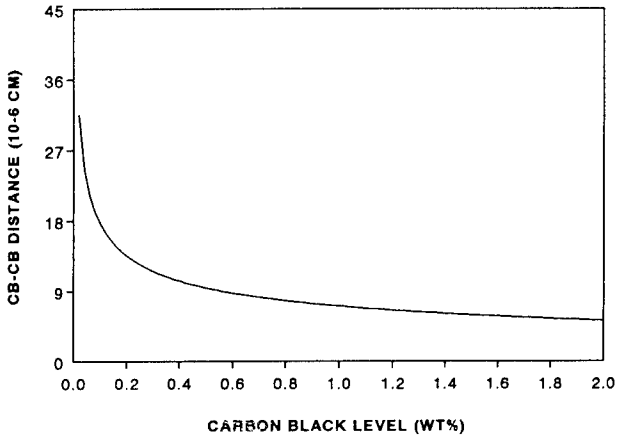


Figure 3. CB-CB Inter-particle Distance

and used to break bonds leading to fragmentation of the polymer. Photoablation is more common with higher energy sources such as excimer lasers. It is reasonable to assume that the YAG laser does not cause extensive ablation although some conversion to kinetic energy is possible. Thus, the apparent absence of CB in the raised layer could be due to an ablation effect in which CB particles being separated and/or expelled out from the hot deforming polymer into neighboring region, in addition to oxidation and vaporization. Both of these mechanisms require rapid conversion of photo energy into chemical or kinetic energy within the CB particle.

YAG Laser Parameters

Under normal operating conditions, the laser beam size and wavelength are fixed in each operational configuration, while the pulse frequency, power output, and beam velocity can be varied in each individual scan. These parameters are important in determining mark quality. For example, the resolution of a printed mark is a function of spot overlap produced by the beam. Figure 4 depicts degree of overlap as the pulse rate changes: Fig. 4a shows 0% overlap in which the laser marks are adjacent to each other. To obtain the appearance of a continuous line, overlap up to +50% is needed as shown in Fig. 4b. Fig. 4c shows -50% overlap in which a distance of the beam radius separating the circular marks to give a dot matrix appearance. In general, aesthetically acceptable marks are produced within these overlap parameters. Once the desirable overlap is set, beam velocity and pulse frequency are related linearly by beam size and overlap factor. The overlap factors are 0.5, 1, and 1.5 for 50%, 0%, and -50% overlap, respectively. Figure 5 depicts this relationship with two different beam sizes. If the marking process is dictated by the writing speed such as in cable manufacturing lines, the pulse frequency must be selected with the overlap window. Conversely, if the mark quality is dictated by the pulse frequency due to the polymer photo response, the writing speed is constrained by the overlap factor.

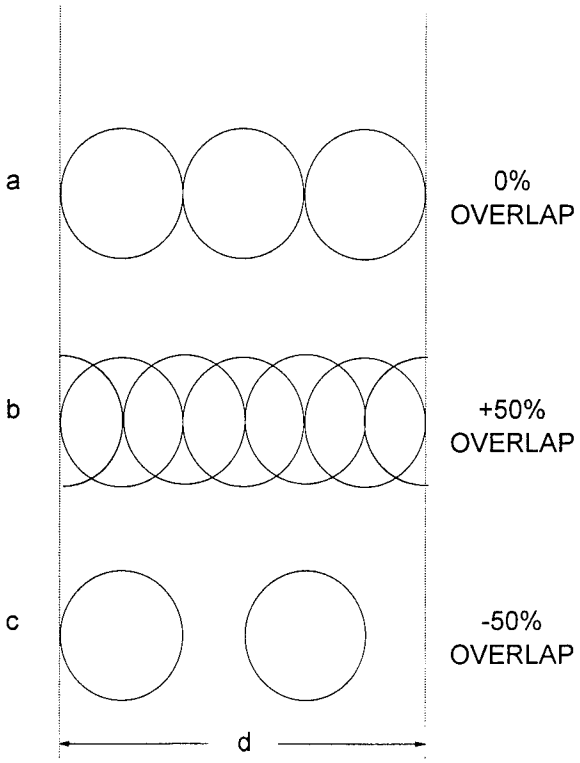


Figure 4. Degree of Overlap

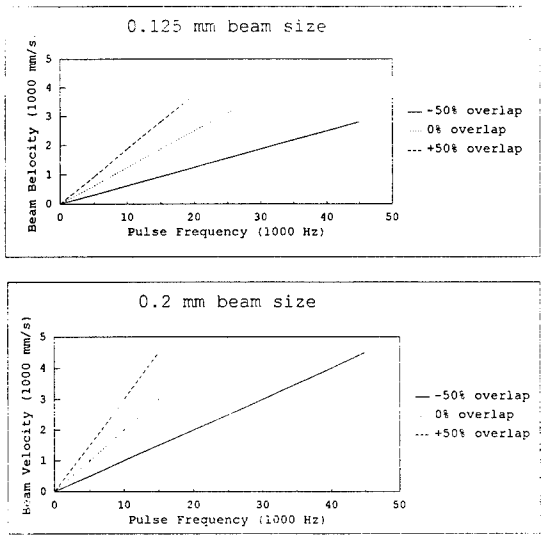


Figure 5. Laser Beam Scan Rates

UV Stabilized Laser Printable Resins

Most outdoor cables require protection from sun light. Current commercial jacketing compounds contain 2.6% N110 grade CB as required by the material specification. However, these products do not yield contrasting marks when exposed to YAG lasers. Good contrasting marks are possible only with much lower CB levels. To compensate for the loss of UV protection at lower CB levels, UV stabilizers are needed. A laser printable jacketing compound based on LLDPE was formulated with some commercial UV stabilizers. Tensile bars were prepared and exposed in a Weather-o-meter equipped with Xenon lamps and borosilicate filters in compliance with ASTM method G-26. Water spray was not used during the continuous exposure. Samples were measured for their elongation at break from 0-4000 hrs per 1000 hr interval. Table 4 reports this data compared to a non-laser printable commercial jacketing compound and a laser printable control sample which does not contain the UV additives.

Table 4. Weather-o-meter Data: Elongation Retention

SAMPLE	1000 HRS	2000 HRS	3000 HRS	4000 HRS
LASER PRINTABLE NO UV ADD.	99%	1%	0%	0%
LASER PRINTABLE WITH UV ADD.	109%	99%	107%	70%
NON-LASER PRINTABLE	114%	119%	107%	9%

As shown, the UV performance of the laser printable compound with added UV stabilizers is comparable to the non-laser printable product. Furthermore, the overall properties of the laser printable compound are comparable to the standard product as shown in Table 5 below. The superior electrical properties of the laser printable compound is clearly apparent. This is presumably due to the lower level of CB which often is a source of water absorption in cable resins.

Table 5. Comparison of Cable Jacket Properties

PROPERTY	NON-LASER PRINTABLE	LASER PRINTABLE
Density g/cc	0.93	0.921
MI g/10 min.	0.72	0.61
Tensile Strength at Break psi	2500	2340
Tensile Strength at Yield psi	1640	1685
Elongation %	710	730
DC 1 MHz	2.5	2.31
DF 1 MHz	0.0003	0.00015
ESCR, 10%	0/10/96	0/10/96
LTB,F50	<-76	<-76

SUMMARY

Laser printable polyethylene jacketing compounds suitable for outdoor applications were developed. Laser printing is achieved with a YAG laser in resins containing 0.1-0.7% carbon black with the optimum range of 0.1-0.4 for most resins. The print quality depends on laser parameters such as pulse frequency, beam velocity, beam size, and power setting. The optimal laser condition is at high pulse rates (15-25 kHz) and at 10-15 W power range. Print contrast performance is measured by a computerized gray-scale image analysis method. Laser beam and polymer interaction can be described with a thermal model that accounts for carbon black photo-absorption, temperature rise, and thermal diffusion to the surrounding polymer matrix. The UV resistance of laser printable resins is comparable to current commercial products based on Weather-o-meter testing.

REFERENCES

1. U.S. Patent No. 3,434,456
2. U.S. Patent No. 4,997,994
3. S.C. Tam, et al., Part B: J. of Eng. Mfg., 207, 179-192, (1993).
4. M. Hofmann et al., Proc. SPIE vol. 744, 156-180 (1987).
5. T.A. Znottins et al., Laser Focus/Electro-Optics, 54-70, (May 1987).
6. R. Srinivasan and B. Braren, Chem. Rev., vol. 89, No. 6, 1303-1316 (1989).

ACKNOWLEDGEMENTS

The authors wish to thank Mr. Larry Carter, Application Engineer at General Scanning Inc., TLSI Division, in Somerville, MA for his participation in conducting the laser printing experiments and his knowledge in laser operations.

BIOGRAPHY

Lester Lee is a Research Specialist of the Wire and Cable Group at Quantum Chemical Company. He holds a B.S. degree in chemistry from University of Washington and a Ph.D. degree in physical chemistry from Oregon Graduate Institute of Science & Technology. Since joining Quantum in 1988, he has worked in developing polyethylene products in flame retardant and other specialty applications.



USING AN NEW AGEING RATE DEFINITION FOR THERMAL ENDURANCE OF CABLE MATERIALS AT VARIABLE TEMPERATURES

Dr. Roland A. Widler, Richard T. Durham

Huber + Suhner AG, CH-8330 Pfäffikon, Switzerland

Abstract

The service life of electrical cables can depend heavily on the thermal endurance properties of the polymer insulation. The thermal endurance time of an insulation material is measured according to IEC 216, and the resulting thermal endurance curves - often linear - allow the evaluation of endurance times at different, but constant temperatures. Today there are however no practical methods available to predict the endurance time of an insulation material after exposure to varying temperatures. This work provides a solution by using a new ageing rate definition which is derived directly from the measured endurance curve. It allows the calculation of an endurance time for any temperature function to which an insulation material may be exposed.

Introduction

Polymeric insulation materials often have to maintain their function even at elevated temperatures. Important fields of use are

- power cables for construction and railways
- automotive leads "under the hood"
- appliance wiring, motor leads
- aircraft wiring

Whereas the use of high temperature thermoplastics is limited mainly to specialties such as aircraft applications, insulation materials used in many of the above systems are modified 'standard' thermoplastics and elastomers. Their **maximum service life** is limited by slow ageing processes which lead to irreversible deterioration of properties (eg. brittling). Other failure mechanisms due to mechanical deformation, abrasion, heat flow, ionizing radiation, chemical attack etc, may also shorten service life but will not be discussed here.

1. Thermal endurance at constant ageing temperatures

This section covers the basic procedures used to evaluate the thermal endurance of insulation materials according to the Standard IEC 216 [1]; these will be required in later sections.

The steps are:

a) choose one or more properties which are critical "for the function of the insulation in the actual application".
b) expose the well defined samples to three or more ageing temperatures to give endurance times in the range 100 to 5000 hours.
c) test the specimens using a non-destructive or destructive method until the measured property reaches a specified endpoint (eg. mechanical failure) or a specified degree of change.

The results of such exposure often show a linear relationship between the logarithm of the time taken to reach the defined endpoint and the reciprocal absolute temperature - the well known Arrhenius curve. It is characterised either by the regression coefficients a and b, or by the "temperature index" (TI) and the "halving interval" (HIC). Examples are shown in fig.1.

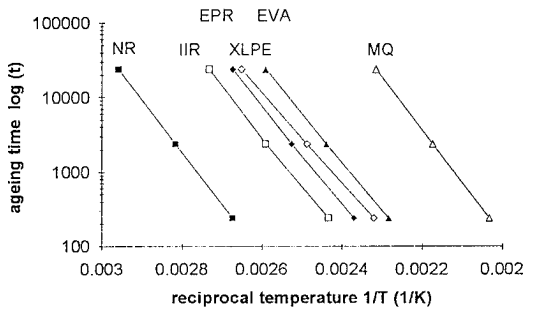


fig.1 Examples of Arrhenius curves based on data from ref. 2

The standard also mentions how to make use of nonlinear thermal endurance curves.

Thermal endurance curves are necessary for material selection and evaluation, as well as for quality control and specification. However, a correlation to the lifetime of a finished cable has to be proved separately because of additional factors. An Arrhenius curve allows us to find endurance times at different, but **constant temperatures.** In practice, however, the thermal stress on the material is not constant but varies significantly during the service life. The following sections show how to use a thermal endurance curve to estimate the endurance time of materials under **varying thermal conditions.**

2. Definition of an ageing rate

In many practical applications with periodic heating and cooling cycles it would be useful to predict the effect of the varying temperature on the expected lifetime. This requires a suitable ageing rate. To date there is no practical ageing rate definition available, since classical kinetic equations, which are based on clearly defined concentration changes, cannot be applied in bulk polymers.
The fact that simple linear endurance curves exist for a wide range of different polymers implies that the (unknown) rate determining step among the complicated system of consecutive and parallel chemical reactions must be simple.
We will describe at this point a novel definition for ageing rate which has the advantage of being applicable without knowledge of the chemistry of the involved processes, and which is based on the same experimental data collected whilst determining the thermal endurance curve of a material.
This definition is based on two premises. Firstly, the thermal endurance diagram must already contain the whole information on the time-temperature dependency of a selected property, and therefore no additional data are necessary. Secondly, the practical ageing rate is determined by energy conversion rather than concentration change.
This leads to the following definition:

The ageing rate of a selected property is proportional to the reciprocal endurance time at a given temperature.

Based on the Arrhenius equation (1),

$$\log(t_e) = a + b.(\frac{1}{T}) \qquad (1)$$

t_e = endurance time in hours at absolute temperature T
a, b = regression coefficients

rearrangement gives the temperature dependent ageing rate r(T), with constant c:

$$t_e = \exp(a + \frac{b}{T}) \qquad (2)$$

$$r(T) = c.\frac{1}{t_e} = c.\exp(-a - \frac{b}{T}) \qquad (3)\ (4)$$

In the following two sections we demonstrate the application of this definition for solving practical problems, before treating the topic more mathematically and before discussing the theoretical background.

3. Thermal endurance with cyclic temperature change

To show the use of the ageing rate definition we will use a case history. A customer needed to know whether a specific motor lead of our Radox-range would survive the minimum time required, if an accidental switch failure in a circuit caused the temperature to rise. A second switch limited the maximum temperature, so we had to consider a periodic temperature function T(t) as in fig. 2:

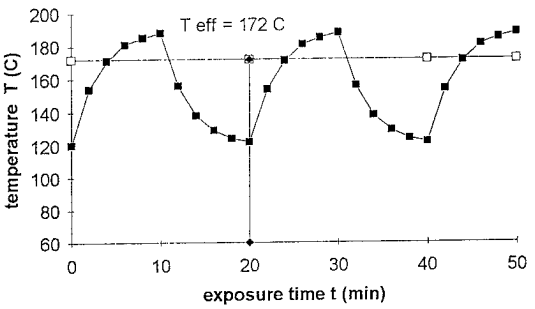


fig.2 Temperature function with period 20 min. between 120°C and 190°C

Since the thermal endurance curve of the material (based on crosslinked EVA) is known, the graphical procedure is as follows:

1. Set a number of points on the endurance curve in the temperature range of interest and determine the corresponding endurance times t_e. (The example is based on data from EVA curve in fig 1).
2. Calculate the ageing rate $r(T) = 1/t_e$ for the previously defined temperatures and plot the resulting ageing rate values versus time (see fig. 3).
3. Determine the mean ageing rate $\bar{r}$ by integrating the ageing rate function over a period. The area A1 in fig. 3 must be equal to area A2.

4. Calculate the mean endurance time t_e (reciprocal value of the mean ageing rate). This value could be directly compared with the minimum time required by the customer, and the question yes / no could be answered.

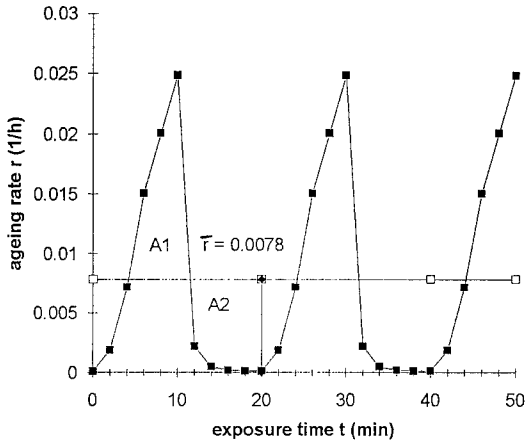


fig.3 Ageing rate function based on log (t_e) = (6502.2/T) - 12.5 and temperature function fig. 2

As was expected, the corresponding effective ageing temperature T_{eff} determined from the Arrhenius curve proved to be well above the arithmetic mean temperature (+ 17°C).

The method demonstrates how one can extract much more information than usual from the existing experimental ageing data. In our specific case the temperature range covered a part of the thermal endurance curve which is no longer linear (> 180°C). However, the general empirical treatment of the data is not influenced by deviation from linearity. This shows, that the proposed ageing rate definition can be used for any form of temperature function, as will be shown in the next section.

4. Thermal endurance with exposure to any temperature function

During the development of electro-technical products which have to meet severe requirements regarding security and service life, a construction engineer may use specifications based on temperature distributions. The specified service life of a system including its power or signal cables may cover periods of time at different temperature levels. For example, an insulation material based on crosslinked EVA with an Arrhenius curve according to fig. 1 is expected to be exposed during 40 % of its service life to a temperature T1 = 140°C, during 30 % to T2 = 160°C and 30 % to 180°C (see fig. 4).

The question is, whether it will meet the minimum endurance time requirement of 200 h.

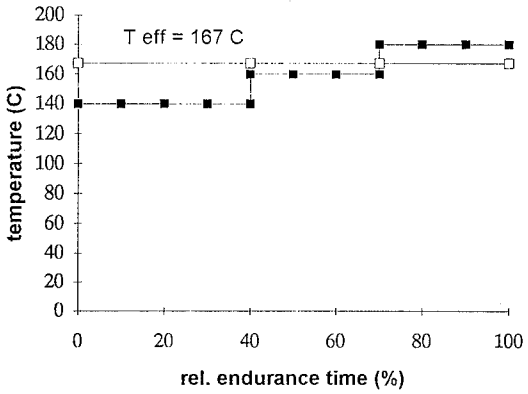


fig.4 Temperature function with three levels 140°C, 160°C, 180°C

The procedure used is analagous to that used before. We start by determining the endurance times at the three temperatures given and calculate the three ageing rates r(T1), r(T2) and r(T3). This gives the curve i Fig. 5.

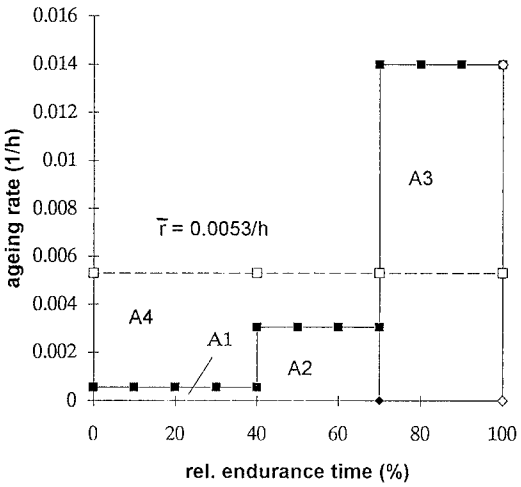


fig.5 Ageing rate function based on log (t_e) = (6502.2/T) - 12.5 and temperature function fig. 4

To find the mean ageing rate $\bar{r}$ an integration must be made over the whole period of interest; area A4 has to be equal to the sum of A1, A2 and A3. The reciprocal value $1/\bar{r}$ will then correspond to the mean endurance time t_e = 187 h. The insulation would not meet the requirement of 200 h.
The corresponding mean effective ageing temperature T_{eff} will be 167°C. Its value is higher than an arithmetic mean <= 160°C, as expected.
Neglecting this temperature difference of + 7°C, which corresponds to a factor 2 difference in endurance time (or to a "halving interval" respectively), could give an qualitatively different answer. (endurance time > 300 h).

A similar problem arises when one has to decide whether or not a cable has to be replaced after a certain time in service. An insulation material with known thermal endurance curve may have been exposed to an unknown temperature function T(t) during time t1 until inspection. What remaining endurance time t2 = (t_e - t1) is to be expected under the same conditions? (fig. 6)
The answer can be found by measuring the remaining endurance time t3 of a sample at arbitrary but constant temperature T3 (fig. 6 and 7).

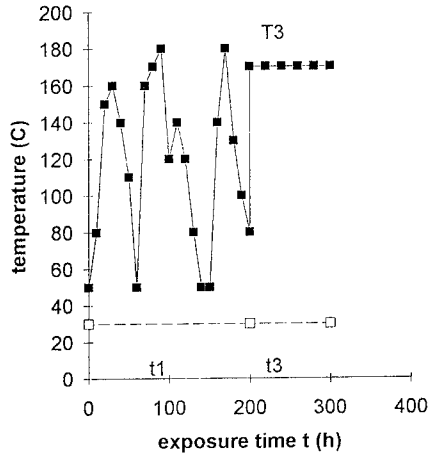


fig. 6 Temperature function with irregular period t1 and testing period t3

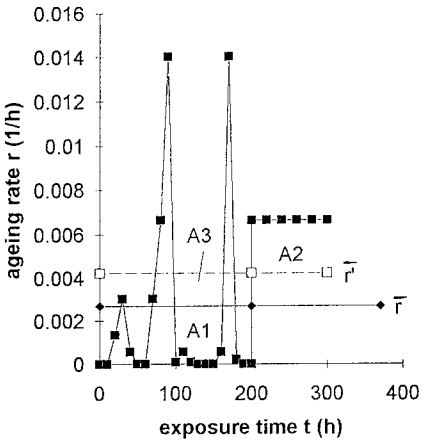


fig.7 Ageing rate function based on log (t_e) = (6502.2/T) - 12.5 and temperature function fig. 6

The total thermal endurance time t_e = t1 + t2 will correspond to an overall mean effective temperature T_{eff} with mean ageing rate $\bar{r} = 1/t_e$, whereas the measured endurance time t_e' = t1 + t3 will allow the calculation of a corresponding mean ageing rate $\bar{r}'$ for period t_e'. By setting the sum of the integrals A1 = $\bar{r}$. t1 and A2 = r3. t3 equal to the integral A3 = $\bar{r}'$. t_e' we can calculate the ageing rate of interest $\bar{r}$ during period t1. The reciprocal value $1/\bar{r}$ is the total endurance time t_e yielding the remaining time t2. From the endurance curve we can then obtain the mean effective temperature T_{eff}.
A verification of this procedure can be made using the three-level temperature function treated before (fig. 4 and 5), defining two of the three ageing temperatures as unknown.

5. Mathematical treatment

In view of the general aspects which restrict the use of thermal endurance data (see section 1) it may not be worthwhile in industrial practice to use sophisticated mathematical formalism. For qualitative evaluations - with decisions yes/no - the graphical method will usually be adequate. However, for basic material research and for future electronic data processing the mathematical approach will be treated here.

We start with the linear equation of Arrhenius, defined in section 2.

$$\log(t_e) = a + b.(\frac{1}{T}) \qquad (1)$$

and look how an endurance time t_e can be calculated from the regression coefficients a and b and a temperature function of general form T(t). For an irregular temperature function, as is often the case in practice, the possible endurance time of a material will vary continuously with time.
Nevertheless it must fit in an equation of the form (1), but with a mean effective temperature T_{eff}. Clearly, this effective temperature will itself depend on the temperature dependency of the property of interest, on the temperature function T(t) and on the exposure time t.

Using the ageing rate as defined in section 2, the actual ageing rate at time t and temperature T will be

$$r(T,t) = c.(\frac{1}{t_e}) \qquad (5)$$

c = constant

$$= c.\exp(-a - \frac{b}{T(t)}) \qquad (6)$$

To get the **mean ageing** rate at time t and temperature T we have to calculate the integral over the exposure time t_0 - t and normalize with that time:

$$\bar{r}(T,t) = \frac{1}{(t-t_0)} . \int_{t_0}^{t} c.\exp(-a - \frac{b}{T(t)}) . dt \qquad (7)$$

$$= \frac{c}{(t-t_0)} . \int_{t_0}^{t} \exp(-a - \frac{b}{T(t)}) . dt \qquad (8)$$

The specific temperature function T(t) must be used for the calculation. The corresponding actual endurance time will be its reciprocal value.
For an exposure time (= integration limit) to failure, t will be equal to t_e. The actual mean ageing rate and its reciprocal value will lead to the endurance time t_e, which is independent of the unknown rate constant c:

$$t_e = \frac{c}{\bar{r}} = (t_e - t_0) / (\int_{t_0}^{t_e} \exp(-a - \frac{b}{T(t)}) . dt) \qquad (9)$$

For a constant ageing temperature for example, the ageing rate will reduce to equation (3) and the endurance time to equation (2), as expected.

6. Discussion

The concept of an ageing rate definition directly derived from the thermal endurance curve may look strange, but it seems to work. Preliminary verification tests at Huber + Suhner support this approach, but much more data are necessary. The question regarding the chemical background remains, and also the discussion about the consequences of possible models.
As was mentioned in section 2, the ageing rate is associated in this treatment with an energy conversion, and the rate constant c introduced in equation (3) may then have the dimension Joule. As a consequence, the integration of an ageing rate over a period of time will correspond to a certain energy turnover during that period of ageing. Therefore an endurance time will also be related reciprocally to a certain amount of energy which has been turned over to reach the defined property change.
The idea for this energy approach comes from life sciences. In recent years several publications have indicated that the ageing of living biological cells is connected with their energy consumption.

What consequences may derive from the approach? Firstly, the endurance time must be dependent on the size of the measured sample. Therefore a thick insulation sample will be associated with a larger energy conversion for a certain property change than a thin wall sample. This is an observed fact mentioned in IEC 216. As the oxygen diffusion rate is also dependent on the sample geometry, the relationship endurance time - sample size will certainly not be linear. This work could therefore provide a basis for comparisons of thermal endurance data on samples with different dimensions or even for standardizing ageing data.
Secondly, thermal endurance data must reflect real bulk or system properties, since morphology, homogenity of mixtures etc, will all influence the chemical ageing reactions and therefore the mean ageing rate and endurance time. This is confirmed by our experience that ageing tests are also sensitive quality measurement tools. The demonstrated treatment of experimental data can therefore be applied not just to pure materials, but also to combinations of materials such as insulated conductors and cables. This could broaden the application of system tests such as the 'hookup-test' according to ASTM D 3032[3].

Acknowledgments

We thank our collegues in the physical testing department (headed by Dr. Eva Reck) and the head of the material development group, Dr. M. Egli, for practical support and discussions, and Dr. H. Schönbacher, CERN Geneva, for sharing his long experience with ageing tests.

Literature References

1 IEC 216, especially part 1 (1990), part 2 (1990) and part 5 (1990)
2 Electric cables Handbook, 2nd edition, BSP Professional Books (1990), p. 53
3 a) ASTM D 3032 (1993)
b) BritishStandard BS G 230 (1991)



Roland Widler obtained his degree in Chemistry at the Swiss Federal Institute (ETH), Zurich in 1977. He was awarded his doctorate by the Department of Chemical Technology at the same Institute in 1984. Since this time he has held various positions in the central Research and Development of Huber + Suhner AG, Switzerland. He is currently responsible for thermoplastic material development and member of national Technical Committee (IEC) TC 15B.

After gaining his honours degree in Polymer Chemistry and Technology at UWIST, Cardiff in 1982, Richard Durham worked as Principal Research Engineer at Standard Telecommunications Laboratories, Harlow, England, before moving to Huber + Suhner AG, Switzerland, where he leads the Rheology Group in the central Research and Development.

ECONOMIC & PRODUCT EFFICIENCY RELATIONSHIPS WITH NON-LEAD STABILIZERS FOR PVC

G.R. Bennett- Applied Research and Technical Service J.A. Caballero- Director of Technology and Business Development

Synergistics Industries (NJ) Inc. Farmingdale, New Jersey

ABSTRACT

The Society of Plastic Engineers reports that the first recorded formulation of PVC as a wire insulation occurred in 1935. Over the years many new stabilizer systems have been developed for use in PVC, it's Alloys and Blends.

The use of lead products as thermal stabilizers has been under attack by numerous environmental groups concerned with both responsible environmental care and employee safety. Whether they are right or wrong is not discussed in this paper. The reality is that the possibility exists that PVC compounds which serve the Wire and Cable industry may have to be reformulated with Non-lead stabilizers. In fact, some Wire and Cable companies have already made the commitment to reformulate lead out of their compounds. This brings with it both performance and economic trade offs. We will describe our experience in developing non-lead stabilized compounds in this paper.

DISCUSSION

The Wire and Cable industry has been a reluctant and distinct holdout to removing lead stabilizers from PVC compounds. The reasons are not always clearly understood or defined. The benefits of lead as a heat stabilizer have many dimensions. All of which have to be defined both in performance and cost.

A brief discussion of PVC degradation mechanisms is necessary to understand the functionality of lead in PVC compounds. There are three elements to the degradation of PVC. HCl evolution - "the zipper reaction theory" - proposes that HCl initially released acts autocatalytically (through loss of labile chlorine) causing the loss of additional HCl until the decomposition results in double bond structures called polyenes. As unsaturation and subsequent oxidation by air during processing and as well as under in-service conditions there is a general loss of properties. (Free radical degradation) Figure 1.

Heat stabilizers/systems are used to retard the chemical degradation of PVC during processing and throughout its expected useful life. They must function in three ways to be effective. The most significant is to scavenge the HCl during processing, thus, retarding the onset of dehydro-halogenation. They must provide moieties which are more stable to replace the labile chlorine. This has the effect of retarding the rate of unzipping of the polymer. Heat stabilizers must also function as antioxidants to inhibit the rate of oxidation.

It is during the processing of PVC that the major thermal damage takes place. Due to either induced heat or heat generated by shear, the loss of HCl occurs. Processing aids are required to minimize the generation of heat generated by shear. Lead, in addition to acting as a heat stabilizer, also functions as a processing aid.

LEAD STABILIZERS

Lead stabilizer systems are single component in nature. Once selected they provide the three functions mentioned above. In addition, they also act as a processing aid. Most importantly, they are low cost. The heart of all lead stabilizers is the lead content. Table 1 lists the major lead stabilizers and their properties. Effect on the electrical insulating properties of the final compound are, of course, an important consideration of any ingredient in a wire and cable compound. It is also one of the most difficult properties to equal. This is another of the compelling reasons why lead stabilizers were the stabilizers of choice over the past 50+ years. Table 1 shows the most common lead stabilizers, their lead levels and Specific Gravity. The lead soaps are used primarily as lubricants

NON-LEAD STABILIZERS

Non-lead stabilizer systems are multi-component in nature. They are generally based upon three ingredients:

- Alkaline earth metals and anions functioning to absorb HCl.

- The use of secondary and primary metal carboxylates which utilize coordination chemistry to function as displacements for labile chlorine atoms.
- Antioxidants which terminate free radicals.

Electrical properties of non-lead stabilizer systems have not been as effective or efficient as lead systems.

Because of the large number of non-lead systems being offered to compounders without proven end use performance and further lacking a method of classifying them on the basis of chemical nature, performance or other criteria, we decided not to include a listing of these products.

TRANSITION OF LEAD TO NON-LEAD STABILIZER SYSTEMS

Transition from lead to non-lead will require a cooperative effort on the part of the compounder and the wire and cable manufacturer. Both must recognize the need for compromise. Many adjustments in performance demands will be required in both process and end use. The inherent positive characteristics of lead stabilizers allowed us to establish performance parameters which, in many cases, were in excess of application and process requirements.

For instance, as a result of favorable economics, the industry has been able to over-stabilize vinyl compounds to allow for long periods of changeover and setup periods.

Weathering characteristics rarely have had to be addressed by the addition of other additives to protect the PVC system unlike other polymer systems.

SELECTION OF NON-LEAD STABILIZER SYSTEMS

PHYSICAL PROPERTIES

As the criteria for wire and cable applications increases in complexity, achievement of desired performance properties becomes more difficult. Stabilizer suppliers are scrambling to provide products to meet these more demanding application requirements.

ELECTRICAL PROPERTIES

As mentioned, this is the most difficult area for the non-lead stabilizers to compete. Lead stabilizers contribute positively toward the final electrical properties of the compound. The best that can be said to date is that some replacements do not adversely affect electricals. In the case of long term insulation resistance, non-lead stabilizer suppliers have not established a system with a reliable track record. This will require considerable partnering with compounders and wire and cable manufacturers.

THERMAL STABILIZING EFFICACY

Current replacements for lead stabilizers are not able to match the level of stability that lead systems achieve. Although many achieve levels of acceptable performance, it is always at a higher cost.

WEATHERING AND PERMANENCE

Formulators must guard against the tendency of many of the non-lead offerings to surface bloom giving a wax-like look and feel.

PROCESSABILITY

Each stabilizer package has its own characteristic effect on processing, whether classified as lubricating or non-lubricating. The system will affect the processing characteristics such as fusion, dispersion and distribution, melt homogeneity, and viscosity. So, whether you are extruding a hard or soft compound, the development of final product performance properties and appearance will be affected by the stabilizer system.

COLOR AND APPEARANCE

Lead stabilizers have strong pigmenting properties. Most replacements have negligible opacification. Thus, formulators are forced to add pigmenting materials. This is generally titanium dioxide.

WIRE AND CABLE APPLICATION

As a result of the diversity of wire and cable applications in the wire and cable market, the emphasis on the properties discussed above require different performances from the non-lead stabilizer system. This different emphasis is placed on the importance of UV stability, electrical performance, etc.. This will require the non-lead stabilizer systems to be tailored to the application unlike the more universal lead systems. Until recently, the broad application characteristics of lead stabilizers have been taken for granted.

ECONOMICS

No effective system exists today that costs less than twice the lead stabilizer product, on a pound for pound basis. The significant Specific Gravity difference partially alleviates the price problem but, to date, no simple direct answer exists.

Because of the cost/performance difference between current lead based and non-lead based systems, various sectors of the industry will be forced to make tough decisions on performance properties.

EXPERIMENTAL

To illustrate a portion of the interrelationship of economics, dynamic thermal stability and, thereby, cost efficiency, we have studied several non-lead systems designed primarily for basic jacket systems. This work is not application specific.

Dynamic thermal stability (DTS) was chosen because, to some extent, it resembles the extrusion and injection molding processes that the product will encounter. It provides an effective model that can predict problems that can occur during manufacturing. The test was performed on a HAAKE System 90 at 250°C with a charge size of 60 grams at 100 RPM.

The basic 60° C jacket formulation as shown below was used to evaluate a series of stabilizer systems. These systems were evaluated for efficacy in applications up to ratings of 90° C. Each stabilizer was used at three levels in the same base formulation. We compared the dynamic thermal stability results, raw material cost and the volume cost relative to the lead stabilized product.

Physical properties such as tensile strength, elongation, modulus, durometer and limiting oxygen index were performed, but the results are not being presented because no significant changes or trends could be detected.

Other factors related to non-lead stabilizers, such as weathering, color, appearance, electrical properties and lubrication, with these and numerous other systems, are under study and will be reported in future reports.

FORMULATION	
PVC Resin 68K	100.00
STABILIZER as noted	2.00/3.5/5.00
Di-isodecylphthalate (DIDP)	60.00
Calcium Carbonate (3 micron)	40.00
Wax (165 Microcrystaline)	0.40
Calcium Stearate	0.35

SYSTEM	Stabilizer Type
A	Tribasic Lead Sulphate
B	Calcium Zinc
C	Barium Calcium Zinc
D	Barium Calcium Zinc
E	Calcium Zinc
F	Barium Zinc
G	Mixed Metal Proprietary

RESULTS OF STUDIES

Effect of Specific Gravity:

As you can see in Figure 2, lead system (A) increases Specific Gravity significantly with small increases in PHR. While non-lead systems (B - G) have negligible effect on Specific Gravity.

Effect on Compound Costs:

Figure 3 shows the effect on compound cost per pound utilizing non-lead systems as expressed in cost difference in cents per pound. You will observe that the cost per pound is larger and would seemingly make the transition cost prohibitive.

Effect on Volume Costs:

Figure 4 shows the effect on compound volume cost per pound in cents. Here we see this impact of Specific Gravity on costs per unit volume. Now this cost penalty is lessened.

Effect on Dynamic Thermal Stability:

Figure 5 demonstrates the effect of increasing the loading of the stabilizer system. The lead stabilizer system provides almost linear improvement with increasing dosage. The non-lead systems' rate of improvement in dynamic stability often begins to taper off as dosage increases. None of the replacement stabilizers perform at the level of the lead stabilizer.

Relationship Between Dynamic Thermal Stability and Cost

Figure 6 shows that the relationship between cost and dynamic thermal stability must be carefully examined or an incorrect decision could be made. This could result in too high a price being paid for the stabilizer package. Conversely the degree of dynamic thermal stability could also be unsatisfactory.

CONCLUSIONS

The tables show that the Dynamic Thermal Stability of the lead stabilizer can be achieved using non-lead systems in most cases. The problem encountered is that, at equal levels of stability, the loading of non-lead stabilizer would be substantially higher. Based on an experience at equal performance levels, there is a premium attached to the use of the non-lead systems.

The hope that the difference in Specific Gravity would compensate for the increased cost of the non-lead system did not materialize. This is especially true when higher performance, application specific systems are designed.

SUMMARY

To minimize the increase in cost when formulating non-lead Vinyl compounds, we must consider the optimum level of stability required during both the compounding step and the final product fabrication. This, as discussed earlier, has been determined previously by the lower cost of lead stabilizers that then resulted in the overstabilization of many vinyl compounds. If the compounders and Wire and Cable manufacturers work together, the level of stabilizer required to securely stabilize the product can be determined allowing for the minimum cost increase.

The compounder must consider the optimum level of stability required during both compounding step and the final production fabrication which minimizes increase in overall unit volume costs. This consideration is also impacted by the many other properties and applications cited in discussion of selection of non-lead stabilizers.

The Wire and Cable manufacturer must recognize that current lead stabilized compounds have enjoyed the benefit of a low cost, versatile, stabilizer system which has allowed for the luxury of performance which has exceeded requirements. Transition to non-lead systems will require compromise.

Success can only be achieved by a cooperative adventure.

Figure 1

DEGRADATION

DEHYDROCHLORINATION

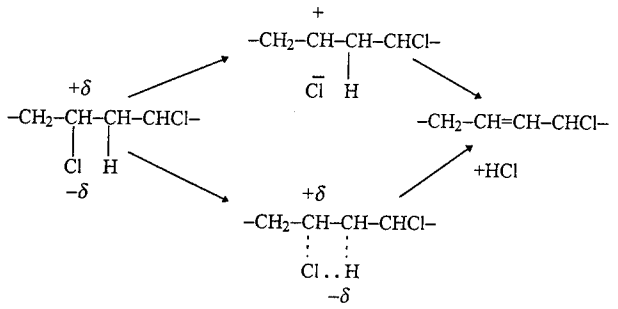


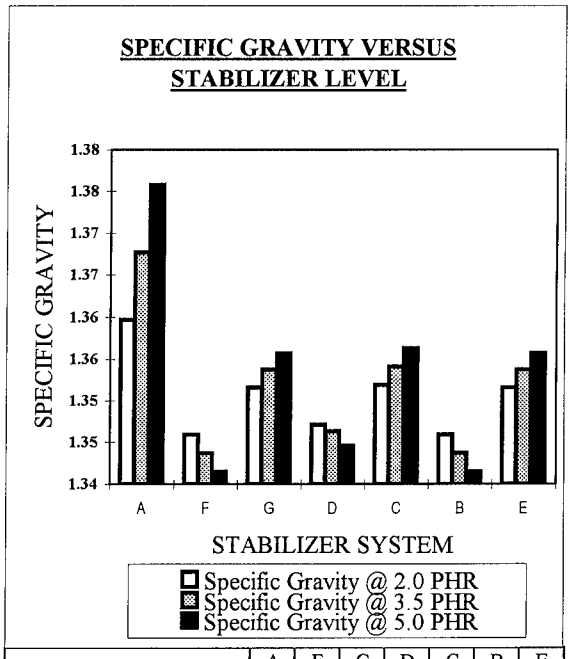
Table 1

LEAD STABILIZERS

LEAD STABILIZERS	% PbO	Specific Gravity
Tribasic Lead Sulfate $PbSo_4 \bullet 3PbO + H_2O$	88.7	6.9
Monobasic Lead Sulfate $PbSo_4 \bullet PbO$	84.5	6.7
Dibasic Lead Phosphate $PbHPO_3 \bullet 2PbO \bullet 1/H_2O$	90.2	6.9
Dibasic Lead Phthalate $Pb(C_6H_4)(CO_2)_2 \bullet 2PbO + 1/2H_2O$	78.5	4.5
Basic Lead Carbonate $2PbCO_3 \bullet Pb(OH)_2$	86.0	6.9
Dibasic Lead Stearate $Pb(c17\ H35\ COO)_2 \bullet 2PbO$	55.4	2.0
Various Co-Precipitates	80.0-85.0	≈ 5.4

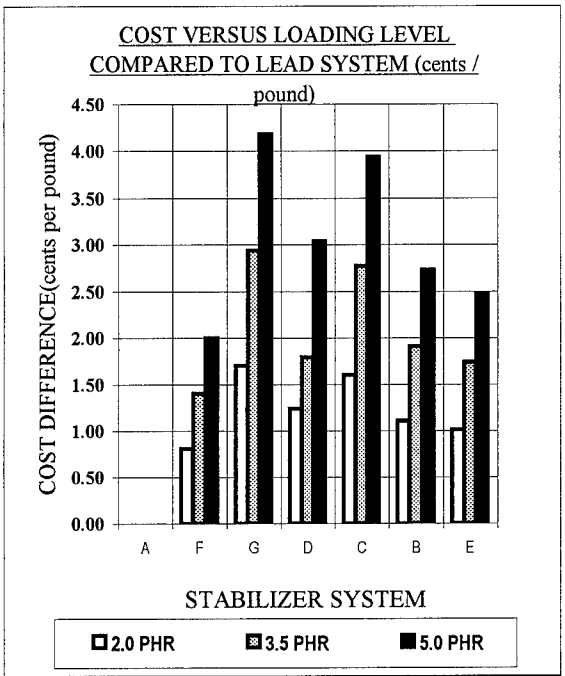
- This is a relatively small list of additives from which to choose.
- The list of non-lead stabilizers being offered is well over 100 and expanding.

FIGURE 2



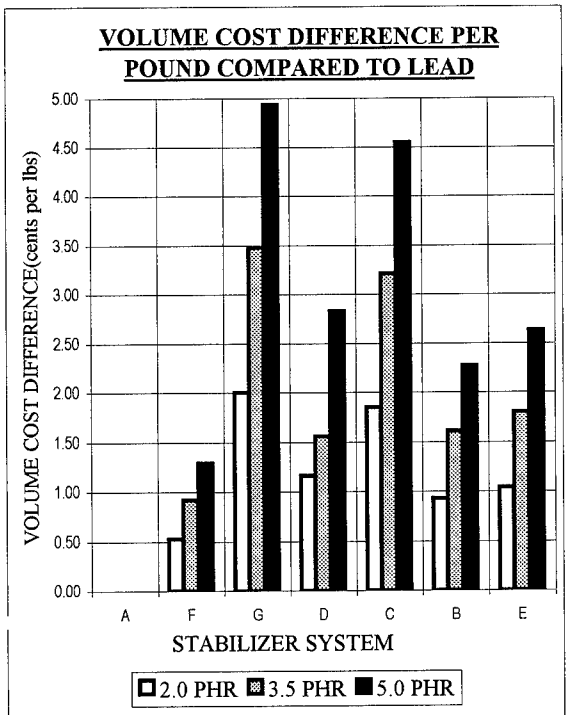
	A	F	G	D	C	B	E
Specific Gravity @ 2.0 PHR	1.36	1.35	1.35	1.35	1.35	1.35	1.35
Specific Gravity @ 3.5 PHR	1.37	1.34	1.35	1.35	1.35	1.34	1.35
Specific Gravity @ 5.0 PHR	1.38	1.34	1.36	1.34	1.36	1.34	1.36

FIGURE 3



	A	F	G	D	C	B	E
2.0 PHR		0.81	1.70	1.24	1.60	1.11	1.01
3.5 PHR		1.40	2.94	1.79	2.77	1.91	1.74
5.0 PHR		2.00	4.18	3.04	3.94	2.73	2.48

FIGURE 4



	A	F	G	D	C	B	E
2.0 PHR		0.53	2.00	1.16	1.85	0.93	1.04
3.5 PHR		0.92	3.48	1.56	3.21	1.61	1.80
5.0 PHR		1.29	4.93	2.83	4.55	2.27	2.63

FIGURE 5

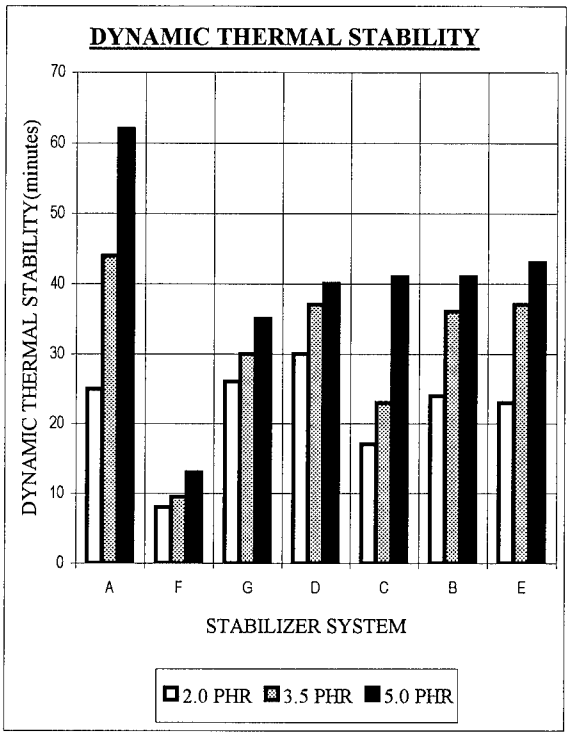
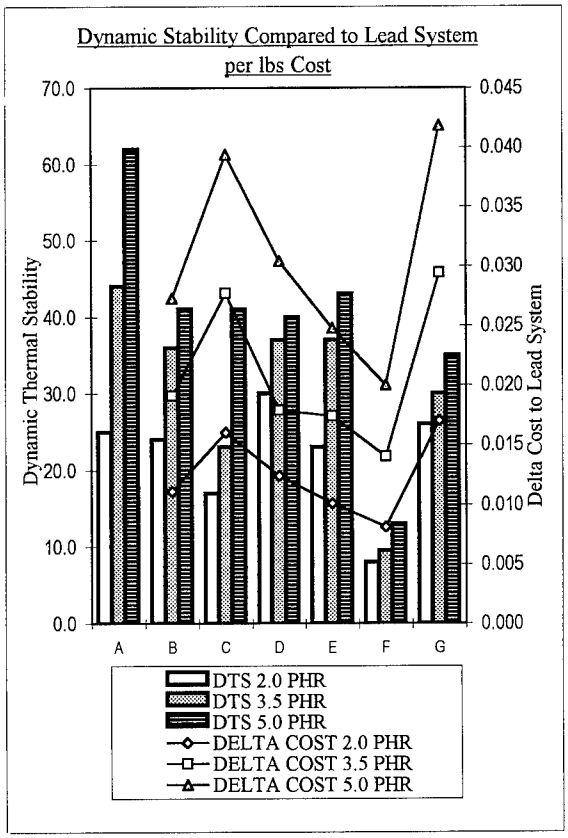


FIGURE 6



OPTICAL FIBER RELIABILITY AND HANDLEABILITY RESULTS FROM THE BIARRITZ FIELD TRIAL.

A. GOURONNEC, R. GOARIN, G. LE MOIGNE, J. MARTRET
M. BAPTISTE.

France Telecom, Centre National d'Etudes des Télécommunications.
CNET/LAB/QFE/CDO
Technopole Anticipa
2 avenue Pierre Marzin
22307 LANNION, France.

ABTRACT

The first experimental optical fiber network (fiber to the home CATV and video-phone) was installed in BIARRITZ (FRANCE) at the beginning of 1980. It appeared interesting to evaluate and expertise fibers reliability after more than 10 years of ageing in a real adverse field environment. In the paper we give a short description of the BIARRITZ field trial. After a first measurement of the mechanical parameters using normalised dynamic and static tests, we compared the results obtained with those of the equivalent tests used to evaluate these fibers before their installation in the field. We also have performed some fusion splices tests for evaluating the handleability of those fibers. In conclusion, the paper gives the ageing results measured on the BIARRITZ optical fibers after more than 10 years of service in real environment.

Keywords : Optical Fiber, Reliability, Handleability, Mechanical test.

1. BIARRITZ NETWORK STRUCTURE.

In 1979 the french government decided to test the fiber to the home (FTTH) network solution at the BIARRITZ location using multimode optical fibers. The first subscribers were connected in early 1984, and in 1986 one thousand were connected. In the last years FRANCE TELECOM decided to stop this experimentation. The CNET has made an evaluation of the quality of the fibers picked up from particular points of the network.

In the paper we give the optical fiber reliability and the first handleability results obtained from different types of optical cables from the BIARRITZ field trial.The FTTH network structure in BIARRITZ location was a star topology [1] using 50/125 µm multimode optical fibers with an epoxy acrylate coating of 180 µm diameter.

2. THE BIARRITZ OPTICAL FIBER CABLES.

1. The cables structures

In order to have a real representation of the distribution part of the network we have tested different cable elements as indicated in table 1. The structure of each tested cable is also given in this table. The 70 fibers duct cable is sheathed with an welded aluminum tube covered with polyethylene. It is composed of seven V-groove units, with one fiber per groove. Each unit is made of polypropylene surrounding a central steel member. The fifty fibers cable is a ribbon cored cable, ribbons are made of preformed ALUPE, each ribon contains five optical fibers. The ten ribbons are cabled inside a welded aluminum sheath

covered with polyethylene. The other cables are V-grooved structure with 2 or 10 fibers per unit, each of them have a steel central strength member. The 10 optical fibers cable is corrugated steel sheath. All the cables aren't gelly filled, and the fibers are free of tension in the V-groove. The cabling pitch is 30 cm, the unit diameter is 4 mm and the V-groove is 0.8 mm deep.

The cables were mesured in transmission losses by the backscattering technique. No variation was measured during the different phases of the pulling out and during the cable units preparation. Concerning the environmental conditions all the aerial and outdoor cables where in salty ambiance and two lengths of the 10 fibers cable were in wet condition.

3. THE OPTICAL FIBER MECHANICAL and HANDLEABILITY TESTS

The evaluation of the aged fibers is done firstly by repeating the same tests as those initially done. There was an axial dynamic tension on 55 cm long samples at a speed of 20 mm/mn, plus a static bending test on glass mandrels of 5 mm diameter. Then we have performed the actual tests usually done in our laboratory, an axial dynamic tension test on 50 cm long samples at 2, 5, 50, 500 mm/mn and a static bending test on 2.8, 3.0, 3.2, 3.4 mm diameter.

3.1. Fiber performance after 10 years in the field.

3.1.1. Dynamic Axial Tension test

On the fibers issued from the BIARRITZ field trial, we have made axial strenght tests.[2],[3] The initial values of the fibers mechanical performances where measured by SILEC at the end of 1983. The failure distribution is given in figure 1a for 20 cm sample length and an axial tension speed of 55 mm/mn(mean = 5.20 daN, St.Dev. = 5.94 daN). On the field aged fibers the tests were firstly performed by using similar methods than those made in 1983. Figure 1b shows the aged fibers failure cumulated distribution diagram for the 50 and 70 optical fibers cables. We have a mean value of 3.24 daN and a standard deviation of 1.74 daN. In this figure we can observe a distribution with two populations fibers. The cumulated distribution gives a n parameter of 15.14 . On the 10 optical fibers we have measured a n factor of 26.33, which is very high. Only a blunting phenomenum can explain these specific results[4],[6].

3.1.2. Static Fatigue bending test.

The bending fatigue test were performed on 5 mm diameter borosilicate glass mandrels, with one meter of fiber wounded around each mandrel.

The performances obtained in 70°C water give a mean time to failure of 190 hours with a standard deviation of 63 hours for the initials measurements (1983). After 10 years the same test gives 72 hours (Std. Dev. 49 H.). In ambiant air the meantime to failure was 17760 hours. Today we have observed only one sample failure on the tested "70" optical fibers cable. The relatively low stress level could explain the good resistance of those fibers according to this bending test.

3.1.3. Stripability test.

We have no information on the initial stripability values. So we have done only the specified test [5]. The mean value obtained for 10 tests is 2.03 N with a standard deviation of 0.73 N. These values are in conformity with our technical specification. Due to the outer coating diameter we have stripped the fibers with two tools: the first one with an oblique

stripping tool, the second with the specified tool with a central hole of 150 μm diameter.

3.2. Handleability of the BIARRITZ field aged fibers.

We haven't informations on the handleability of the fibers layed down in the BIARRITZ field trial. We can only say that for the BIARRITZ installation network no abnormal situation was reported. So for the tests we have compared the results obtained on aged field fibers to those of G 652 fibers. The first results are given in [7]. We have done complementary tests using different techniques in fiber preparation: chemical stripability, other stripability tools... We have used the same splicing conditions and the tests were performed by the same operator. The results show the degradation of the strength force of the spliced fibers in each case, even on the G 652 fibers. It principally shows that the actual stripability techniques are the main degradation factor during fibers handling. The figure 2 a and 2b shows some of the obtained results. The strength of the spliced fibers are lower than 1.0 Gpa, some values are as low as 0.2 GPa. We can observe that for chemical strippability the mean strength values obtained are slightly higher than those obtained by mechanical stripping for the highest pulling speeds. For the aged fibers the diameter of the stripping hole is 150 μm, the 180 μm tool was not suitable in this case. The results obtained with the different stripping tools are the same order.

3.3. General analysis of the results.

We have compared the mechanical results obtained on the initial measurement (1983) to those of the actual tests (1994 and 1995) on the field aged optical fibers and tested their handleability.

For the dynamic fatigue by axial tension in the figure 3 we give the Weibull plot with the slope m and the $\sigma(0)$ values ($\sigma(0)_{(1983)}$= 50 N) . We can see a degradation after 10 years in the field ($\sigma(0)_{(1994)}$= 22 N). In 1994' results, the extrinsic part of the curve is present, giving a low factor m (e) of 1.56 only.

For the 10 optical fibers cable tested we have obtained a very high **n** value (26.33), and a mean failure strength pratically equal to the initial one as given in figure 4. In this cable we have observed water inside when it was unsheathed. We could explain the **n** factor improvement by a blunting of the fibers, possibly due to the very low stress level on the fibers in the V-groove cable and the permanent humidity behaviour, giving a smoothed flaw corrosion. From those fibers, we have also observed a development of the extrinsic part in the Weibull plot, but not as important as we observed on the "50" and "70" optical fibers cables.

For the static bending fatigue tests we have operated four stress levels corresponding to mandrels of 2.8, 3.0, 3.2, 3.4 mm in diameter under a 0.5 N.winding force. The Weibull graph and the static **n** parameter are given in figure 5. We observe quite low static stress corrosion susceptibility parameter in this case compared to the G 652 fiber tested (>24). This could be induced by the observed extrinsic part of the Weibull plot. The figures 6a and 6b give the complete axial and bending comparisons results observed during our investigation measurements.

4. CONCLUSION.

We have tested from the mechanical and handleability points of view many optical fibers directly issued from the Plan Cable BIARRITZ network. The fibers tested were used in the field more than 10 years, and they were in a relatively harsh environment. The cable structures are based on V-groove construction, so the residual strain on the fibers was very low. The first results indicate that after 10 years a real degradation appears giving a dynamic **n** factor about 15 and a static **n**

parameter about 20. We observe an increase of flaws caracterized by the extrinsic part in the Weibull plot. On one cable with specific fiber behaviour, a blunting phenomenum can explain the specially high **n** value. After ageing, the results of mechanical tests in our laboratory on BIARRITZ fibers indicate that an extrinsic type degradation is appearing. We can also notice that for the intrinsic flaws, the variations are very low. So in the life time calculation models it is necessary to take into account the effect of the extrinsec weak flaws evolution with the time.

In handleability investigations the results show a general strength degradation of the spliced fiber : values lower than 1.0 Gpa. are measured. The stripability operation appears as the most critical parameter in preparation of fusion splices technique.

5. AKNOWLEDGMENTS.

The authors would like to present their best thanks to SILEC, particularly to Mr Faucher for the preparation of cables and for providing the initial measurements. They would thanks their colleague Mrs. BAPTISTE M. for tests preparation and measurements. They would also like to thank M. G. Desert for its help in results presentation.

6. REFERENCES.

[1] R. GOARIN, *Component Reliability Results from the BIARRITZ Field Trial and from "PLAN CABLE"* Volume Deployment., GLOBECOM 91, (p 558- p 563).

[2] J. ZARZYCKI, *Les verres et l'état vitreux*, ed MASSON, Paris 1982.

[3] IEC 86 A, (sec 261), *Determination of stress corrosion susceptibility parameters.* (document issued from IEC/ITU-SWG on mechanicals tests).

[4] W. GRIFFIOEN, *Stress Corrosion, Ageing and Blunting.* COST 246 communication. 16/02/93.

[5] European Norm *EN 188000* and France Telecom specification *STC 938 1010.*

[6] A. GOURONNEC, R. GOARIN, G. LE MOIGNE, M. BAPTISTE. *Optical fiber reliability results from the BIARRITZ field trial.*Proc. SPIE, Vol. 2290 (1994) 191.

[7] W. GRIFFIOEN, T. VOLOTINEN, P. WILSON, A. GOURONNEC, T.SVENSON. *Handleability of aged optical fibers.* Proc. IWCS 95.. SVENSON. Handleability of aged optical fibers. Proc. IWCS 95.

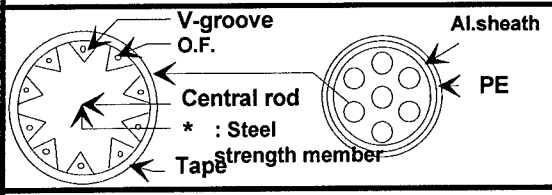
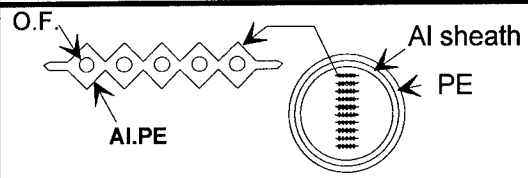
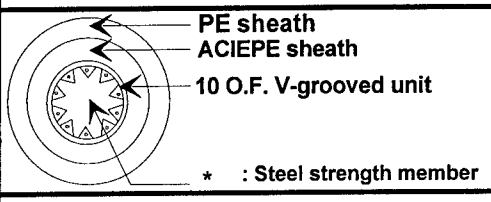
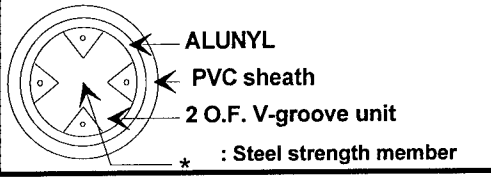
Cable	Type	Structure	Observation
70 O.F.	Duct		
50 O.F.	Duct		
10 O.F.	Duct of outdoor cables		Water in the cable
2 O.F.	Outdoor cables and/or Aerial		Salt air

Table 1 : Cable structure used in Biarritz trial.

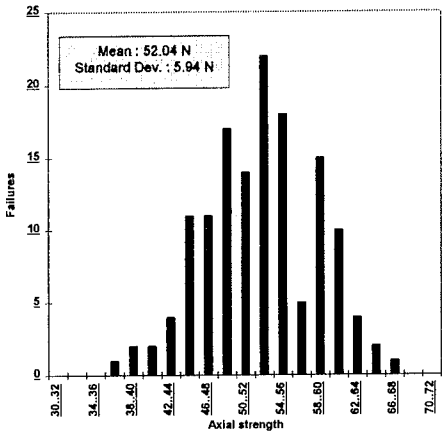


Fig.1a : Initial stength distribution (1983) (55 cm, 20 mm/mn).

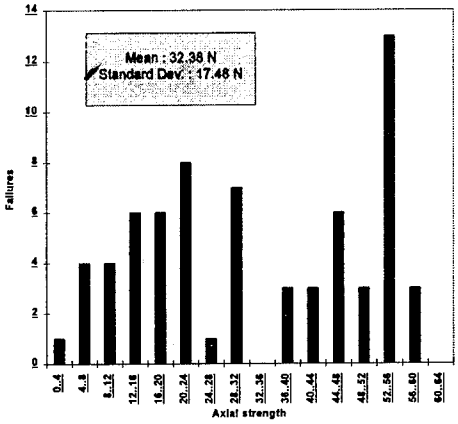


Fig.1b : Strength distribution (1994). (50, 70 O.F., 20 mm/mn, 55cm)

Fig. 1:Dynamic fatigue by axial tension test.

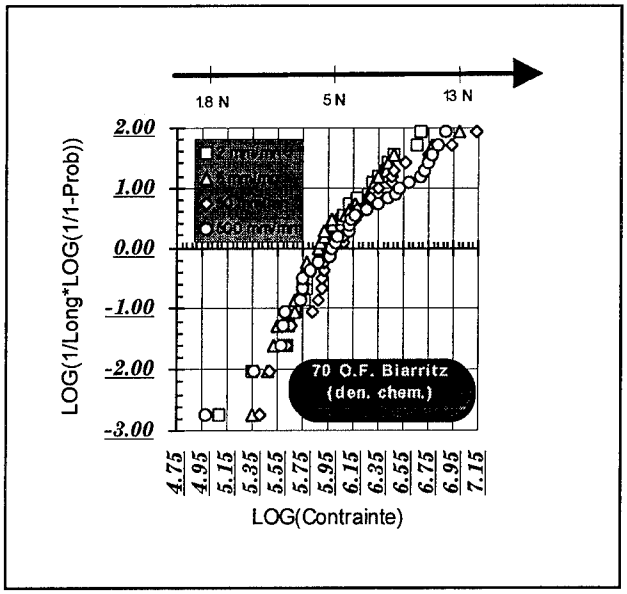


Fig 2a: Weibull plot for spliced fibers. (chimical stripping)

Mec.	Mean (N)	5.07	5.26	5.95	5.73
	σ(N)	2.48	2.54	2.85	2.03
Chem.	Mean (N)	5.37	5.47	6.21	6.26
	σ(N)	1.86	2.36	2.78	2.86

Fig 2b: Stripping influence on strength of spliced optical fibers.

Fig. 2: Handleability of the aged fiber

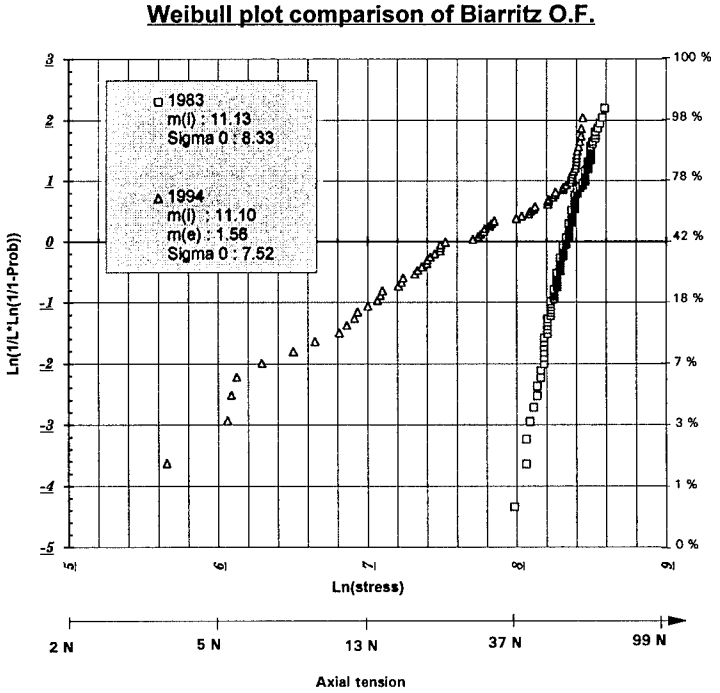


Fig.3 : Optical Fiber Axial Strength comparison between 1983 and 1994/5 (55 cm; 20 mm/mn)

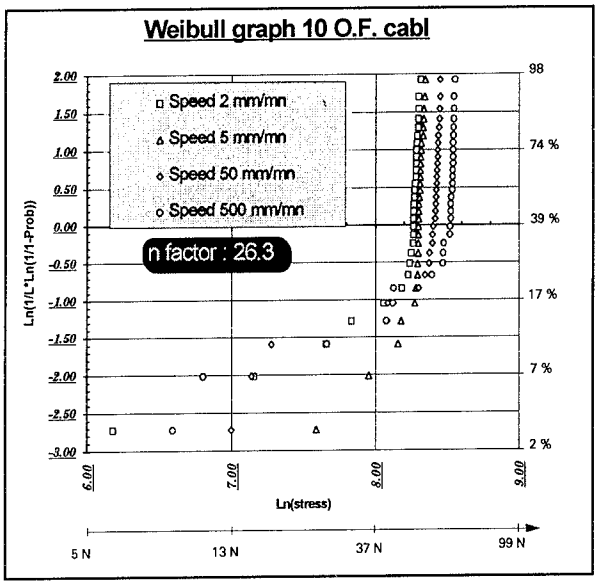


Fig.4 Optical fiber axial dynamic fatigue on the 10 O.F.

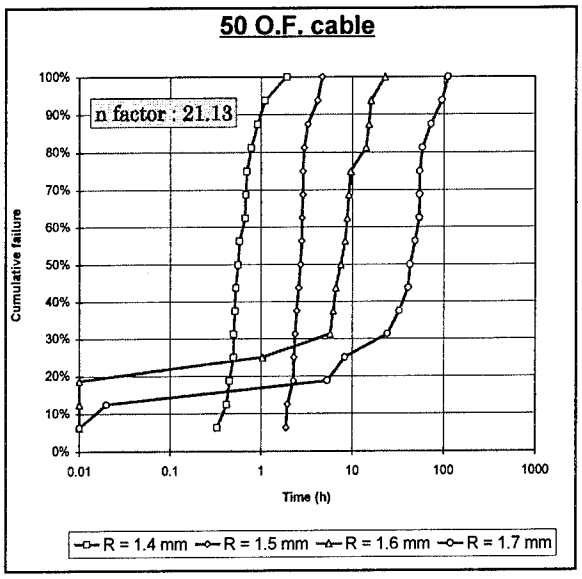


Fig.5 Optical fiber bending static fatigue on the 50 O.F.

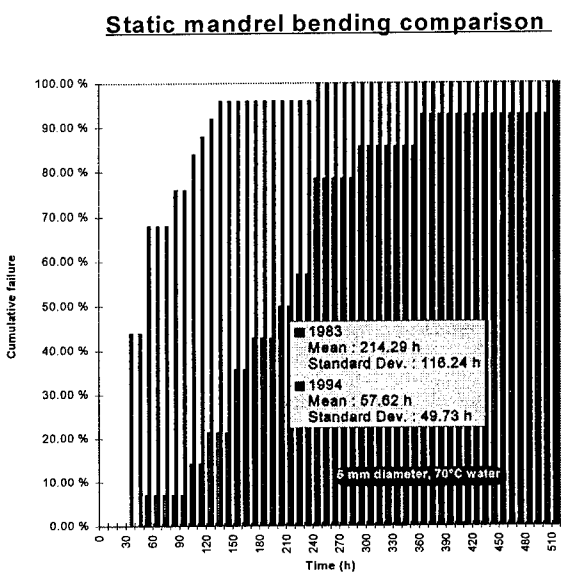


Fig.6a : Static Bending Fatigue comparison between 1983 and 1994 O.F.

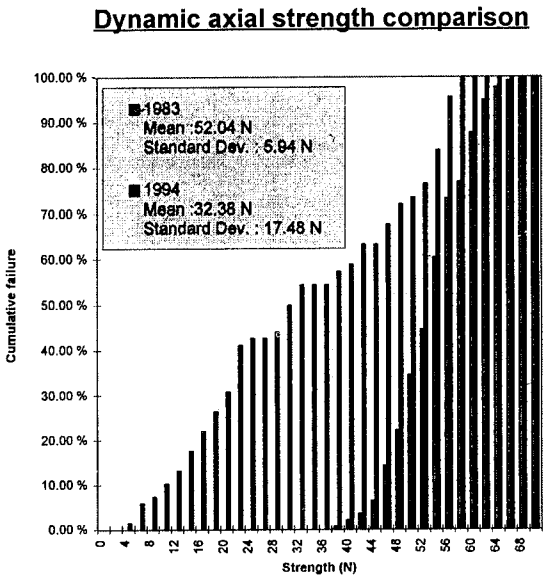
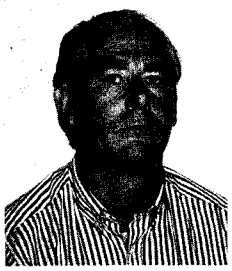


Fig.6b : Dynamic Axial Fatigue comparison between 1983 and 1994 O.F.

Fig 6:Static and Dynamic Fatigue Comparison between initial and field aged fibers.

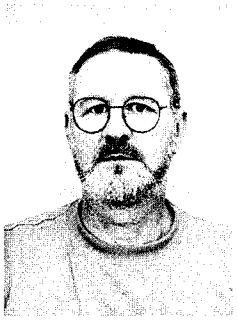
Authors BIOGRAPHIES



Alain GOURONNEC was born in 1946. He received his engineer degree from the CONSERVATOIRE NATIONAL DES ARTS ET METIERS in 1978. He joined the CNET in 1971 where he was in charge of the pulling and multipulling of optical fibers studies. In 1986 he started to work on development and specification of telecommunication cables; since 1993 he has been in charge of evaluation and qualification of optical fibers for France Telecom needs; he is also in charge of the optical fiber reliability studies in CNET.



Roland GOARIN was born in 1942. He received his doctorate in electronics in 1968 and joins the CNET during the same year. He is an international expert for components reliability. He is now the head of the "Components and Devices for Optronics" department.



Gerard LE MOIGNE was born in 1943. As a technician in electronics he joined the CNET in1965. Since 1984 he has been in charge of the mechanical reliability test for the CNET Laboratory for Evaluation and Qualification of Optical Fibers.



Jeanine MARTRET as technician is responsible for the dynamics fatigue tests in the Laboratory for Evaluation and Qualification of Optical Fibers.

Mechanical Behavior of Optical Fibers Removed From a Field-Aged Cable

Jeffrey L. Smith, Anurag Dwivedi*, and Patrick T. Garvey
Corning Incorporated, Corning, NY 14831.
(607) 974-2437

Abstract

Optical fiber handleability after exposure to field conditions is an important aspect for long term reliability. The attributes that control handleability of a fiber are mainly strength and strippability. In the present study optical fibers were removed from a nine year old cable that had been aged in the field for five years. The effect of zero stress aging on the strength of these fibers in these field conditions is studied. The surface roughness is measured using an Atomic Force Microscope (AFM). In addition, the strip force and Dynamic Mechanical Analysis (DMA) on coating materials was performed. Results show that these fibers are as handleable as their as-manufactured counterparts and the zero stress aging of the cabled fibers is not a reliability concern.

Introduction

Based on a 1993 Bellcore study, cable failures account for nearly 1/3 of the total telecommunication outages[1]. About 59% of these cable failures occurred as a result of accidental dig-ups. However, this paper is concerned with failure mechanisms for optical fiber that can be considered related to the long-term glass and coating degradation; namely, strength degradation due to fatigue eventually causing fiber breakage and the inability to handle the fiber in the field during stripping, cleaving, and splicing.

There are no cases reported so far where fiber fatigue was responsible for a network failure. This is indicative of the conservatism built into current cable designs and the care taken in avoiding stresses during cable deployment. It is still important to understand whether or not fibers would be handleable during re-entry and repair after several years of field aging.

The purpose of this study is to examine the handleability of fibers aged in a cable and to reflect on the significance of the results as they pertain to handleability of fibers during cable repair and re-entry. The role of coatings and the cable components in protecting the fibers from aging and strength degradation was also studied. Results are found to be consistent with studies[2] where fibers were aged in a cabled condition.

Background

Whereas there is an abundance of strength data on short fiber lengths after laboratory aging, there are only a few publications that examine the strength of fiber in the field-aged state.[2,3] Since there are no industry accepted models for translating accelerated laboratory aging behavior to field aging behavior, it is difficult to predict functional field performance from laboratory data. To study the degradation over time, an empirical approach should be followed and fibers from a field-deployed cable should be removed and tested.

An earlier study,[2] where fibers were removed from a severely aged cable, showed almost no degradation of mechanical characteristics of the optical fibers due to aging. Other recent studies have shown strength degradation of optical fiber due to accelerated laboratory aging[4,5]. These reports may seem contradictory, but a close examination of the experimental procedures reveals that most of the studies are based on the testing of

uncabled fibers aged in environments not commonly encountered in the field. Unfortunately, the results of such studies are almost always interpreted in terms of real field conditions which is misleading.

For example, in a 1988 work[4] a drop in strength was observed after aging in water. Fibers were tested in a 2-pt bend configuration after aging the uncabled fibers in 100°C water. In a more recent study[5] uncabled fibers were tested in 25°C, 40°C, 60°C, 80°C and 100°C water and a drop in strength was noted. Based on this work, an aging model was proposed which has the Arrhenius form,

$$t = t_0 \exp(E/RT) \quad \text{.....(1)}$$

where t is time required for a specific strength degradation, t_0 is a pre-exponential term, E is the activation energy of the reaction causing strength degradation, R is the gas constant, and T is the absolute temperature of the water. Another complication comes from the fact that different fibers yield different rates of strength degradation. After aging in ~40°C water, a more than 40% drop in strength was seen for the fiber tested by Kurkjian et. al.[5], whereas a less than 10% strength drop was observed for the fiber tested by Carr[6]. The strength degradation model proposed by Carr[6] has the following form.

$$S = S_0 \exp(-\alpha t^{1/2}) \quad \text{.....(2)}$$

Where S_0 is the initial strength and S is the strength after aging for time, t, in water, and α is a constant for a given material and aging condition.

Most aging models[5,6] suggested so far are based on aging studies of uncabled fiber in the liquid water (25-100°C) which is not a common environment for most applications. The results of the present study would be used to assess the handleability of field-aged fibers during re-entry and repair as well as to test the applicability of the proposed aging models to commonly encountered field conditions.

Cable Design

A schematic of the cable design used for this study is illustrated in Figure 1. The cable consisted of four gel-filled buffer tubes and one filler tube. Each buffer tube contained six fibers. Two of the buffer tubes contained single-mode fibers while the remaining two tubes contained multimode fibers. Only the single-mode fibers were used for the present study since mechanical attributes of optical fibers are assumed to be independent of their refractive index profiles. All fibers were coated with a dual layer acrylate coating and overcoated with a thin layer of thermally cured coloring ink. The loose tube cable design was an unarmored construction with interstitial compound for water blocking.

Cable History

The cable tested in the present study was installed in an underground conduit between buildings in Corning, NY. The cable was manufactured in 1985 and left in a warehouse in an uncontrolled environment for just over two years. It was first installed in September 1987, and then re-routed in April 1992. The segment tested in the present study was an excess piece that was removed during this re-routing. The underground conduit which held the cable is located within 150 meters of a river. Based on periodic inspections of the manhole, this conduit would frequently fill with water, often submerging the cable (Figures 2 & 3). The cable was dissected and fibers were carefully removed in 1994 for mechanical testing. At the time of testing, the fibers had been in the cable for about nine years and the cable had been in a field installed state for a period of five years. According to the National Weather Service, the average lowest temperature in the Corning NY region is 14°F and average highest temperature is 80°F.

Additional samples were also included in this study for comparative purposes. Three fibers that were manufactured in the same time frame as the cabled fibers were archived on fiber shipping spools. These archived fibers were stored in a box in a warehouse with uncontrolled temperature and humidity and

were tested at the same time as the cable-aged fiber. The results were compared with those of a recently manufactured fiber with the same glass and coating design. For simplicity these fibers will be referred to as "Cable-Aged", "Archived", and "Recently Manufactured," respectively, in the following discussion.

Experimental Testing

Fiber Removal:

The two buffer tubes containing the single-mode fibers were removed from an approximately 90-meter length of field-aged cable described above. The buffer tubes were cut into two-meter lengths to allow for easier fiber removal. The fibers were carefully pulled out of the buffer tubes, ensuring no coating or glass damage due to fiber removal. The filling compound was removed from the fibers by soaking a Kimwipe™ with D-Gel™ and carefully sliding the fiber through the wipe. After the fibers were cleaned, they were coiled and taped on the inner side of a cardboard folder. All specimens were prepared, preconditioned, and tested in a controlled environment of 50% Relative Humidity (RH) and 23°C.

Atomic Force Microscopy:

The surfaces of the aged and archived fibers were examined using an atomic force microscope (AFM). Optical fiber coatings were chemically removed by dipping in methylene chloride, boiling sulfuric acid, and water. A 2X2 μm^2 area was scanned. Surface topography and average surface roughness were recorded.

Strength Testing:

Strength testing was performed on a Rotating Capstan Fiber Tester (RCFT). Testing was done according to FOTP-28B[7] with a gauge length of 0.5 meter and a strain rate of 5%/min. Fibers were attached to the testing apparatus by wrapping the fiber a minimum of two times around 4 inch diameter capstans at each end of the gauge length.

Strip Force Testing:

Peak strip force was measured to determine the coating integrity and strippability after field aging. Strip force was performed according to FOTP-178[7] with a strip length of 30 mm, a stripping speed of 500 mm/min, and a data acquisition rate of 200 Hz.

Dynamic Mechanical Analysis (DMA):

Mechanical properties of viscoelastic materials such as optical fiber coatings are best characterized by Dynamic Mechanical Analysis (DMA). The response of a viscoelastic material to cyclic stress contains two elements, a) viscous, and b) elastic. The response varies with the frequency of the cyclic field. Though the detailed description of the fundamentals of dynamic mechanical testing can be found elsewhere[8,9], it is important to note that the mechanical response of a viscoelastic material is most commonly characterized by a complex modulus

$E^* = E' + iE''$,

Where E' is the storage modulus associated with the elastically stored energy, whereas E'' is the loss modulus associated with the energy loss due to viscous relaxation. The peak of E'' vs temperature curve typically exhibits a maxima at the glass transition temperature (T_g) of the glassy materials.

Composite tubes made of both inner and outer primary coatings were removed by stripping under liquid nitrogen temperature. These tube samples have several advantages[10] over films commonly used for dynamic mechanical characterization of optical fiber coating. Dynamic mechanical testing was performed at a stress field frequency of 1Hz on the composite tubes obtained from field-aged cabled fiber, archived fiber, and a recently manufactured fiber.

Visual Examination/Microscopy:

All specimens were examined both visually and microscopically. Microscopic examinations were done using 200X magnification on samples immersed in index matching liquid.

Results and Discussion

Atomic Force Microscopy (AFM):

AFM images of a cable-aged, an archived, and a recently manufactured fiber are shown in Figures 4, 5, and 6 respectively. As shown in Table 1, and Figures 4, 5, and 6, the average surface roughness values for all fibers measured in the present study are found to be within a narrow range.

The original three dimensional AFM plots showing the curved fiber surfaces have been Auto-flattened (the average horizontal offset is calculated and subtracted from each line) and Plane-fit in both X and Y directions (an average X and Y value has been measured and subtracted from the entire image). The Flattening and Plane-fit processing is necessary to avoid including the vertical distances resulting from curvature into the calculations for surface roughness.

Based on the surface roughness and the AFM micrographs, the surface topography was equivalent for the cable-aged, archived, and recently manufactured fibers.

Strength Experiments:

Several specimens were tested for strength immediately after 24-hour preconditioning in 23°C/50%RH. The strength values are shown in Figure 7 and Table 1 for fibers of different colors. The results show no dependence of fiber strength on various ink colors. The measured strength distribution for the cable-aged samples, with a median value range of 655-658 kpsi, is statistically the same as the archived samples, with a median value range of 656-669 kpsi. The median strength of recently manufactured fibers was found to be in the range 633-675 kpsi. It is therefore concluded that the aging of this cable has not degraded the strength distribution of the fibers contained within. The strength of these fibers is more than sufficient to handle the common field handling scenarios encountered during cable repair.

Results from the present study are schematically shown in Figure 8 along with the strength degradation plots reported in an earlier work[5]. Figure 8 illustrates the dramatic difference between the degree of strength degradation in liquid water as compared to degradation in field-aged cable. No strength degradation is observed in the field aged cables. Whereas, about 25% of the original strength degradation would be predicted from the room temperature liquid water aging data[5]. This suggests that to use an Arrhenius model such as described in Equation 1, for predicting ZSA, the application-specific pre-exponential term (t_0), and activation energy (E_a) must be obtained. Similarly, the constant α in Carr's model[6] need to be determined for specific application.

Table 1. Summary of test results

Fiber Type and aging	Peak strip force (lbf)	Median Strength (kpsi)	Surface roughness (nm)
Colored, cable-aged	0.88 - 0.99	655 - 658	0.26 - 0.50
Uncabled, archived	0.67 - 0.89	656 - 669	0.26 - 0.34
Recently manufac-tured	0.60 - 0.80	633 - 675	0.26 - 0.49

Strip Force Experiments:

The strip force results are summarized in Figure 9, and Table 1. The results indicate that there is no dependence of strip force between various ink colors. The mean peak strip force range for the colored cable-aged fibers, 0.88 - 0.99 lbf, was slightly higher than typical strip force values for uncabled archived fibers, 0.67 - 0.89 lbf, and a recently manufactured fiber, 0.60-0.80 lbf. The slightly higher strip force of cable-aged samples could be attributed to the coloring ink.

As shown in Figure 9, all measured strip force values were well within Bellcore's recommended range[11] of 0.3 - 2.0 lbf.

DMA Experiments:

Storage modulus (E'), and loss modulus (E") were measured in the temperature range -60°C to 60°C, at 1Hz. Typical results are shown in Figures 10 and 11. No change in the viscoelastic properties of various coating samples could be concluded from these DMA results. The glass transition temperature (T_g) of the inner primary coating for each sample was determined from the peak of the E" vs. temperature plot, the results of which are summarized in Table 2. All T_g values were found to fall within a narrow temperature range.

Table 2: T_g of inner primary coating obtained from DMA

Aging	T_g (°C)
Cabled, field-aged	-18.5
Cabled, field-aged	-20.3
Cabled, field-aged	-21.6
Cabled, field-aged	-16.8
Cabled, field-aged	-20.9
Cabled, field-aged	-19.3
Uncabled, archived	-16.5
Uncabled, archived	-16.7
Uncabled, archived	-17.1
Uncabled, Recently manufactured	-18.0

Visuals/Microscopy Experiments:

There were no coating defects observed during visual inspection of any of the cable-aged fibers. Also, there were no anomalies found in the coating during microscopic examination.

Summary and Conclusions

Actual field aging of a fiber-optic cable showed no degradation of the handleability or mechanical behavior of the optical fibers. All of the fiber coatings were handleable as shown by normal peak strip force, unchanged viscoelastic properties, and no observable coating anomalies. No degradation was observed for either fiber strength or fiber surface roughness even after five years of field aging and nine years after cabling. Based on the strength and AFM data obtained in this study, zero-stress-aging is not a reliability or handleability concern for fibers field-aged and protected by fill compound and other typical cable components. Models based on the strength of uncabled fibers after aging in liquid water, temperature ranging from 25-100°C, overestimate the strength degradation of fibers in normal field conditions. In conclusion, the cable-aged fibers remained handleable for cable repair nine years after the manufacture of the cable. These fibers were in the field for more than half of this nine year period.

Acknowledgments

The authors thank P.T. Cruttenden, D.W. Hill, J.K. Cox, J.W. Botelho, D. J. Lash, and D.G. Pickles for their technical advice and experimental assistance.

References

1. S.V. Lisle, "The History, Prevention, and Impact of Fiber Optic Cable Failures," pp 223-235 in Proceedings of the 1993 National Fiber Optic Engineers Conference (NFOEC '93) in San Antonio, TX, June 14-17, 1993.

2. Anurag Dwivedi, G. S. Glaesemann, and C. K. Eoll, "Optical Fiber Strength, Fatigue, and Handleability After Aging in a Cable", IWCS Proc., pp 728-735, 1994.

3. H. H. Yuce, et al., "Effects of the Environment on an Unprotected Reel of Optical Fiber," Proceedings 40th International Wire and Cable Symposium, pp 700-706 (1991).

4. M.J. Matthewson and C.R. Kurkjian, "Environmental Effects on the Static Fatigue of Silica Optical Fiber," J. Am. Ceram. Soc., **71** [3], pp 177-83 (1988).

5. C. R. Kurkjian, D. Biswas, H. H. Yuce, and M.J Matthewson, "Corrosion and Strength Degradation of Lightguide Fibers in Water at Room Temperature", NFOEC Proc., pp 125-130, 1995.

6. J. J. Carr, "A Zero-Stress Aging Relationship for Optical Fiber", IWCS Proceedings, pp 394-399, 1993.

7. TIA Fiber Optic Test Procedure (FOTP) 28B, and FOTP-178.

8. Fundamental Principles of Polymeric Materials, second edition, by Stephen L. Rosen John Wiley & Sons, Inc, pp 321-337, 1993.

9. O. S. Gebizlioglu, I. M. Pitz, R. A. Frantz, "Mechanical Properties of Aged Fiber Coatings by Dynamic Mechanical Analysis of Optical Fibers", IWCS Proc., pp 564-570, 1994.

10. John W. Botelho, "Fiber Coating Composite Tubes: a Novel Method for Evaluating Material Properties", OFC'95, Volume 8, 1995 Technical Digest Series, Conference Edition, pp 265-266.

11. Bellcore GR-20-CORE, Issue 1, Sep. 1994.

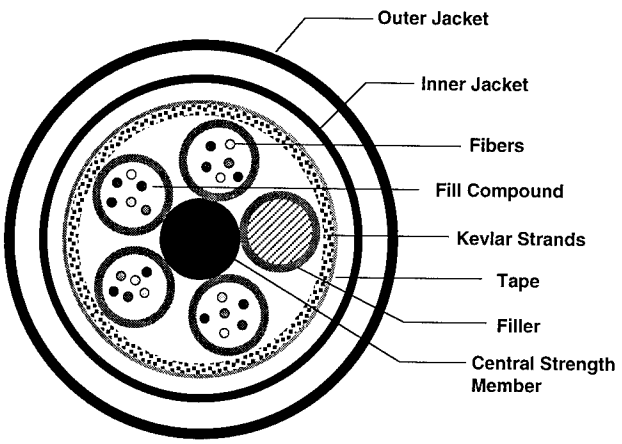


Figure 1: Schematic of the cable design

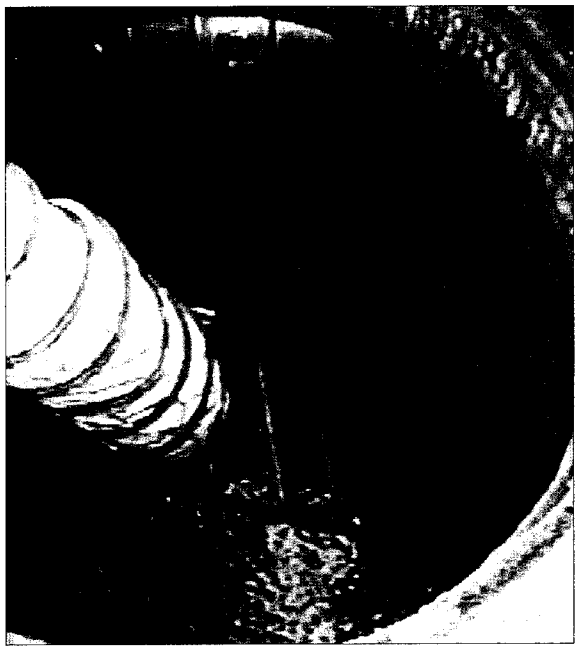


Figure 2: Conduits submerged in water inside the manhole.



Figure 3: Water being removed from the manhole using a water pump.

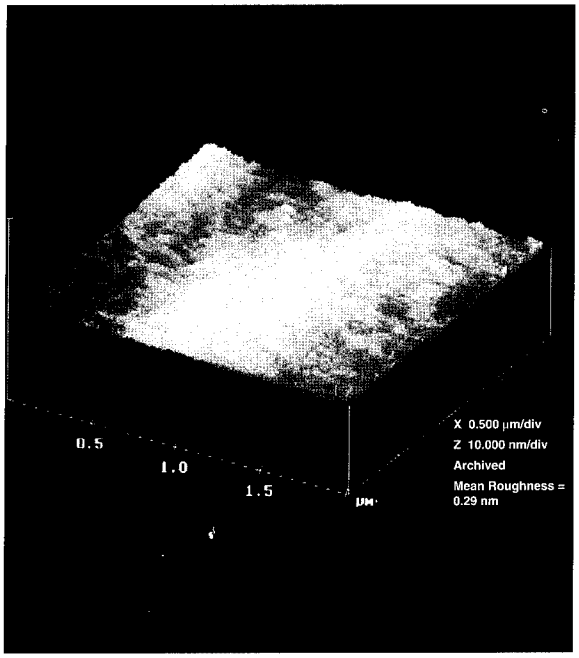


Figure 5: Auto-flattened and Plane-fit AFM scan of archived fiber.

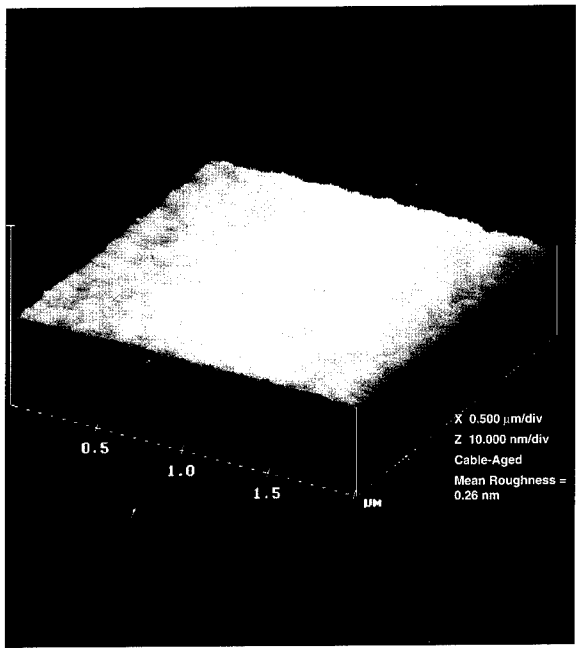


Figure 4: Auto-flattened and Plane-fit AFM scan of cable-aged fiber.

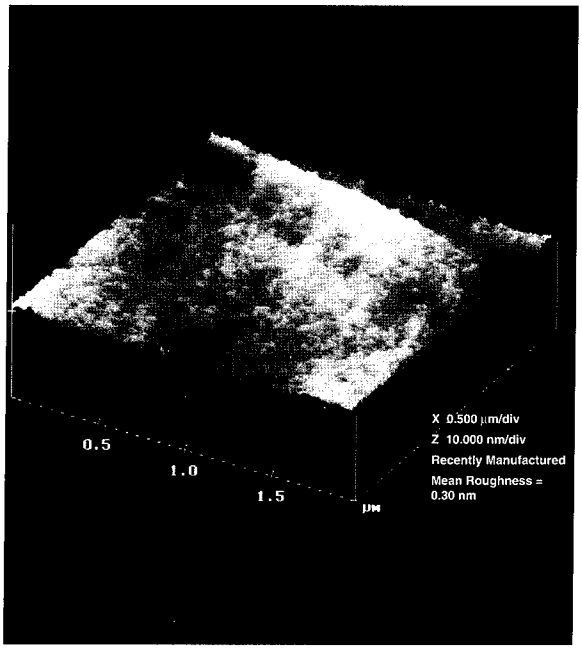


Figure 6: Auto-flattened and Plane-fit AFM scan of a recently manufactured fiber.

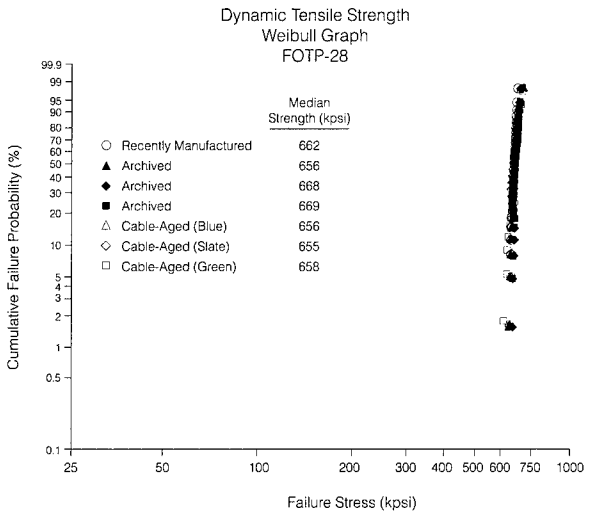


Figure 7: Strength distributions of cable-aged, archived, and recently manufactured fibers.

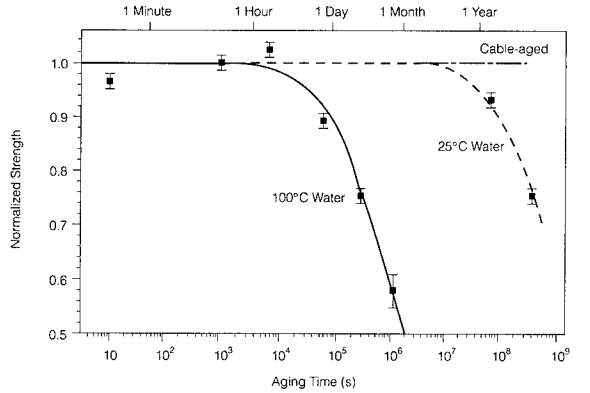


Figure 8: Comparison of strength degradation results obtained from fibers aged in the field and in laboratory[5] (liquid water).

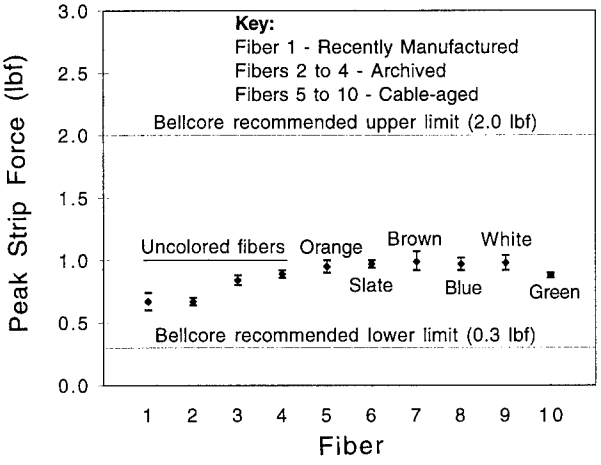


Figure 9: Peak strip force results for various fibers.

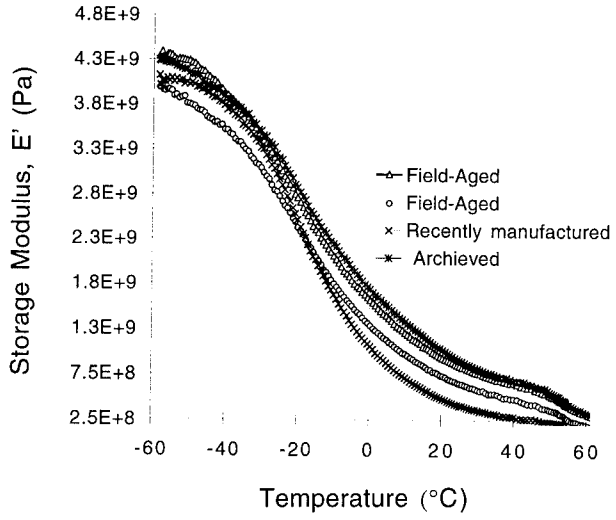


Figure 10: Coating Storage modulus (E') vs. temperature from DMA

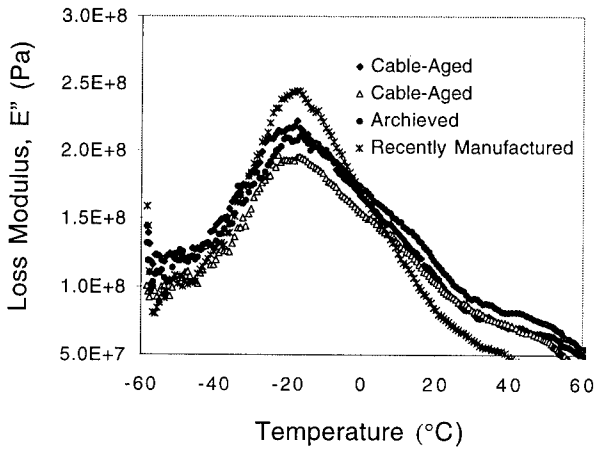


Figure 11: Coating Loss modulus (E") vs. temperature from DMA



Jeffrey L. Smith is an opto-mechanical technician at the Center for Fiber-Optic Testing (CFT), Corning Incorporated, Corning NY. Currently he is responsible for projects related to the mechanical performance of optical fiber products. He joined Corning in 1989 and has been involved with the development, design, implementation and documentation of new and/or enhanced mechanical test methods and equipment. Jeff holds an associate's degree in electronics technology, fiber-optic emphasis, from the Pennsylvania College of Technology and is currently pursuing a bachelor's degree in electrical engineering.



Patrick T. Garvey is currently a Sr. Applications Engineer with Corning Incorporated's Telecommunications Products Division in Corning, New York. He holds a B.S. in Chemical Engineering from Clarkson University (1984) and a M.S. in Mechanical Engineering from Union College (1990). He spent 7 years working in various engineering assignments at General Electric's Knolls Atomic Power Laboratory. In 1992 Pat joined Corning as a Team Leader at Corning's Center for Fiber-Optic Testing specializing in mechanical, environmental, and optical behavior of fiber ribbons and fiber coatings.



Anurag Dwivedi is a Senior Engineer at the Center for Fiber-Optic Testing (CFT), Corning Incorporated, Corning NY. Currently he is responsible for leading the ribbon, microbending and strip force testing team at CFT. He joined Corning in 1992 as a Senior Product Engineer. From 1991-1992 he was employed by Alfred University, Alfred, NY as a post-doctoral research associate.

Anurag received a Ph.D. in ceramics in 1991 and M.S. in ceramic Engineering in 1988 from Alfred University and a B.S. in ceramic engineering in 1986 from the Institute of Technology, Benaras Hindu University, Varanasi, India.

HANDLEABILITY OF AGED OPTICAL FIBERS

W. Griffioen[1], T. Volotinen[2], P. Wilson[3], A. Gouronnec[4], T. Svensson[5]

[1]KPN Research, St. Paulusstraat 4, 2264 XZ Leidschendam, The Netherlands
[2]Ericsson Cables, S-824 82 Hudiksvall, Sweden
[3]BT Laboratories, Martlesham Heath, Ipswich, Suffolk IP5 7RE, United Kingdom
[4]France Telecom CNET, 2, Route de Trégastel-BP40, F-22301 Lannion Cedex, France
[5]Telia Research, S-136 80 Haninge, Sweden
[1,2,3,4,5]Members of COST 246, WG1.1, SG1 "Handleability of aged fibers"

ABSTRACT

Current mechanical lifetime models for optical fibers are based on static-fatigue (spontaneous) fracture. In this paper the effect of fiber aging on handleability (spliceability) is studied in theory and by field experiments. It is concluded that handleability can only be defined on the high strength mode. Weak spots are not handleable. Zero-stress aging determines handleability, not stress corrosion. Estimations for handleability lifetimes can be performed with simple Arrhenius type of extrapolations. The earlier suggested criterion for handleability of aged fiber, a minimum strength of 2 GPa, has been compared to the results from tests on old fibers from BT's network and the Biarritz-trial (France Telecom). It is concluded that these naturally aged fibers can be spliced without problems, even when significantly weakened. Probably the strength distribution and the coating condition are also important factors. Further studies are necessary for a correct handleability criterion.

INTRODUCTION

Mechanical lifetime models for optical fibers have been studied by e.g. COST 218, COST 246 and EIA/TIA FO-6.68 (TSB-61). They are based on fracture at weak spots under a low static service tension, so called (spontaneous) static-fatigue fracture.[1] No statement is made about handleability of the fibers in these models. Recently reported laboratory and field tests, however, have shown that a risk may exist that the fibers at a dig-up of an older, aged cable can be so much weakened that the fibers cannot be spliced and handled, i.e. the handleability of the fibers may be the limiting factor for fiber lifetime.[2,3,4,5] Therefore a studygroup SG1 "Handleability of Aged Fibers" was established within COST 246, WG1.1.

During its service lifetime it may be necessary to subject the fiber to some handling, e.g. because of the necessity to reconnect, to repair or to upgrade at equipment interfaces, etc.. The fiber must survive this handling and splicing may not cause problems. Many effects must be studied for this, e.g. color changes, strippability and damaging of the coating and mechanical weakening of the fiber itself. This paper focuses upon weakening. The mechanisms for strength degradation of an optical fiber are stress corrosion and zero-stress aging.[1]

A clear criterion for handleability of aged, weakened fibers does not yet exist. However, it is suggested that a (median) minimum dynamic failure stress of about 2 GPa (1.4-2.2 GPa) could be used as the criterion.[2,3,4,5] This failure stress is usually defined at a strain rate of 5 %/min (0.07 GPa/s). It shall be noted that weak spots generally do not pass this criterion for weakening, e.g. a weak spot corresponding to a prooftest level of 0.72 GPa (1% elongation) is not strong enough. However, the probability of having a weak spot at a repair or connection point is small. Moreover, once such an event happens and fracture occurs (if that even happens) a new splice can be made without problems, because a new weak spot is not expected close to the previous one. Therefore it makes sense to define handleability only for the high strength mode.

STRENGTH DEGRADATION

The high strength mode flaws are, according to stress corrosion theory (e.g. power law), not affected by the low stresses which they are subjected to, because the service stress is determined by the weak spots. When aging and stress corrosion cause static-fatigue (spontaneous) fracture within the lifetime of the fibers, the handleability criterion is reached a few seconds before fracture (see Appendix A and B). Zero-stress aging determines weakening, not stress corrosion. A simple Arrhenius type of extrapolation can be used for handleability lifetime estimation (see Appendix B). This is illustrated with a numerical example (see Appendix C). In the following section handleability of field-aged fibers has been compared to dynamic-fatigue results. It is difficult to draw conclusions, because of the wide spread in dynamic failure stresses (see Section Discussion and Appendix D).

FIELD EVALUATION

BT's Network

BT has been deploying optical fiber in its network since 1984 and has, to date, installed over 2.5 million km of fiber. Recently BT Laboratories had the opportunity to recover Blown Fiber[11] units from trial sites in Leeds and York, installed in 1984 and 1986, respectively. The routes that the units were recovered from were chosen using local knowledge as being liable to sustained water immersion.

Leeds The fiber was taken from either side of a footway box (see Figure 1): on one side of the box the tubing was in very wet conditions and the ducting on the other side was dry. The tube that was exposed to the water had no metallic moisture barrier and the fiber unit in the tube was wet. The tube from the dry location contained an aluminum moisture barrier and did no show any sign of water ingress.

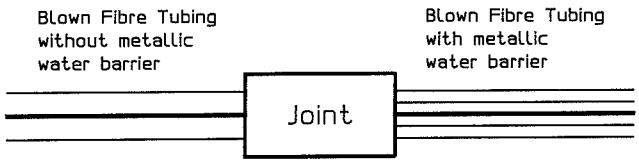


Figure 1 *Schematic of cable route recovered from Leeds.*

York The exchange in York (see Figure 2) is situated close to the river and some ductways leaving the exchange are continually flooded. The Blown Fiber unit enters the exchange from the duct in an external tube with an aluminum water barrier. The unit then passes through an internal tube (with no water barrier) and rises through the exchange to reach the equipment racks. There was no sign of water ingress into the cables. The bundle used was a 7-fiber bundle.

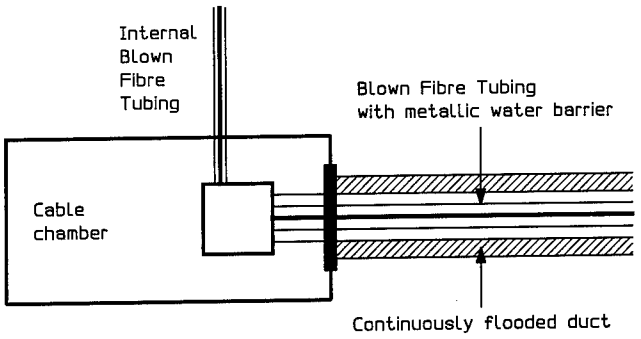


Figure 2 *Schematic of cable route recovered from York.*

Testing The fibers from two of the recovered units were stripped out and for each test about 30 samples with a length of 1 m were prepared. These samples were then broken using dynamic fatigue testing (10 mm/min). Some of the fibers recovered from Leeds exhibited coating delamination when being handled during testing. This will probably introduce an uncertainty into the results as very weak points could be introduced onto the fiber during handling. Samples from all three fiber units were also tested to see that they could still be spliced.

Results The results from the fiber samples recovered at Leeds show that there has been a significant strength degradation for the fibers that were subject to water ingress (see Figure 3). The median dynamic failure stress of the dry fibers is 4.89 GPa whilst this is 0.71 GPa for the wet fibers. Both graphs show a number of low-strength breaks, which may have been caused by nicking the fibers when removing them from the fiber unit. The early 7-fiber units did not have ripcords and thus the foam and skin were cut away using a blade. Fibers that were observed to have been damaged were not used for the strength testing. All 7-fiber samples survived standard splicing procedures (mechanical stripping, wiping, cleaving & splicing).

The fiber samples that were subject to water ingress exhibited very significant coating delamination with tubes of coating, up to 10 cm in length, coming away from the glass of the fiber. This is a documented problem for the first generation of dual-layer fiber coatings which were specially designed to have a low mechanical adhesion. This delamination mechanism will not occur with the vast majority of installed fiber and all currently produced fiber. Handling of the fiber with a damaged or missing primary coating will cause large flaws which will break at very low stress and it is probable that the low strength of these wet fiber samples is due to this problem.

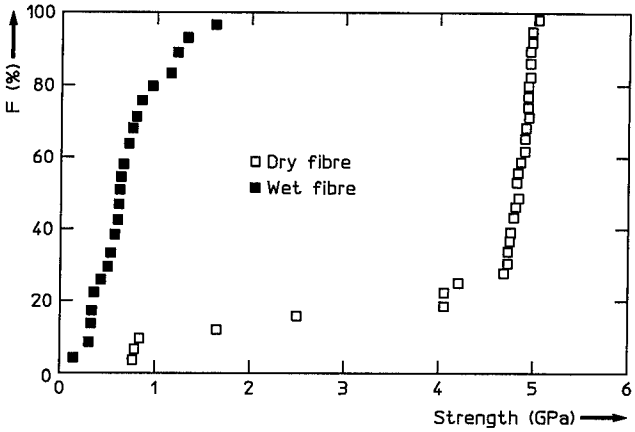


Figure 3 *Weibull plot for fiber recovered from Leeds.*

The results from the fiber samples recovered at York indicate that there is no significant strength degradation for those samples recovered from the wet location (see Figure 4). The fiber as being from a dry location came from the upper portion of the internal cabling (see Figure 2). The fiber as being from a wet location came from the first portion of the external tubing in the flooded duct. The median dynamic failure stress of the dry fibers is 5.00 GPa whilst this is 4.66 GPa for the wet fibers. Both graphs show a number of low-strength breaks, adding further credence to the theory that some damage occurred during the extraction of the fibers from the fiber units. All of the 7-fiber samples were spliced together successfully.

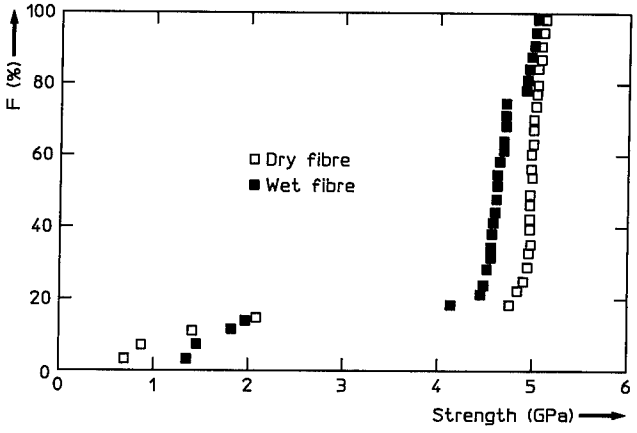


Figure 4 *Weibull plot for fiber recovered from York.*

The following conclusions can be drawn from the previous measurements. The strength distributions of the recovered fiber samples show the importance of the aluminum water barrier in protecting fibers from water ingress. The wet fiber recovered from Leeds shows a massive decrease in strength but it is not clear how much of this decrease is due to the action of the water as an aggressor on the glass or to the failure of the primary coating to protect the glass. If the main damage mechanism is the coating delamination then the magnitude of this effect will be negligible for the current fiber production. The fact that the wet samples from Leeds (median dynamic failure stress of 0.71 GPa) could be spliced casts doubt upon the 2 GPa threshold that has been proposed. Note, however, that it is the tail of the distribution that causes handleability problems, not the median (see Section Discussion).

Biarritz Trial (France Telecom)

The first experimental optical fiber network (fiber to the home CATV and video-phone) was installed in Biarritz at the beginning of 1980. Some parts of the first optical links have now been removed. When France Telecom decided to stop field trial services, it appeared interesting to evaluate and expertise the fiber reliability after more than 10 years of aging in a real adverse field environment. The conditions and constructions of the optical cables have been described in a paper by Gouronnec et al.[12] Here also cable preparation and tension tests have been described. In the current paper the first results of fusion-splice tests will be given. One of the field-aged fibers of the Biarritz trial (70-fiber cable) is used for these tests and compared with a G-652 fiber. The latter modern reference fiber has been chosen for comparison of todays handleability, i.e. using modern tools; aging has been studied more in detail in Ref.[12].

Testing The fiber strengths are evaluated by dynamic-fatigue testing at pulling speeds of 2, 5, 50 and 500 mm/min. At each speed 30 samples with a length of 0.5 m are tested. The failure stress is measured before and after fusion splicing. The coating of the spliced fibers is not restored. All splices have been made on a fusion splicer S-46999-M7-A60 from Siemens AG. The splicing program used is: pre-fusion current 14.7 mA, pre-fusion time 0.25 s, fusion current 17 mA and fusion time 1.2 s. The cleaver used is the York FK 11. All stripping and splicing tests were performed by one operator only. The tests were performed in a normal environment without temperature and air control. The dynamic-fatigue tests were performed immediately after splicing.

Results In Figure 5 and 6 the Weibull plots of dynamic failure stress σ_d are shown for the G-652 and Biarritz fiber, respectively. The values of the corrosion susceptibility n, obtained from these plots, are 20 and 16, respectively. At the tail of the distribution of the Biarritz fiber weakening well below the handleability criterion of 2 GPa can be seen. This behavior was also observed by Gouronnec et al.[12]

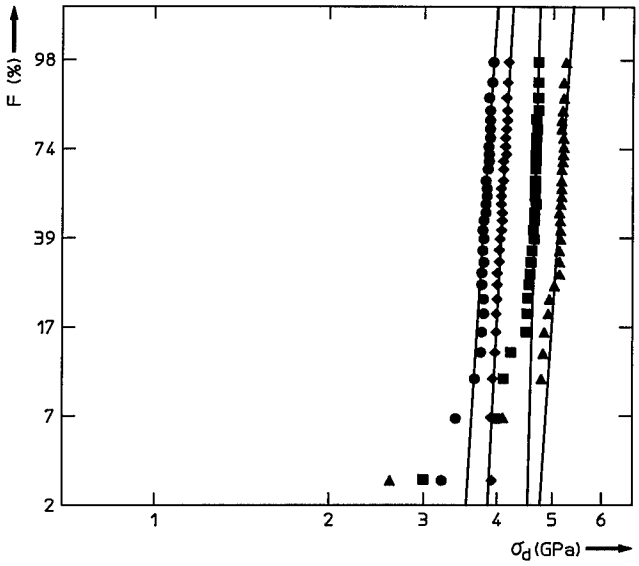


Figure 5 *Weibull plot for G-652 fiber.*

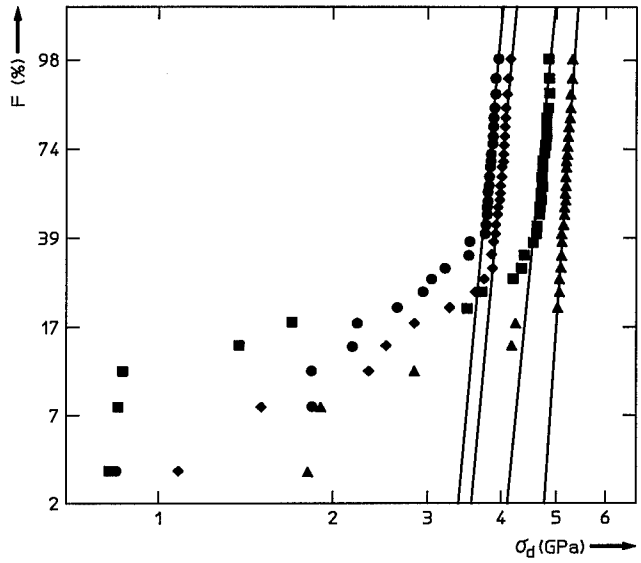


Figure 6 *Weibull plot for fiber recovered from Biarritz.*

In Figure 7 and 8 the Weibull plots of dynamic failure stress σ_d are shown for the spliced G-652 and Biarritz fiber, respectively. The splicing causes a clear weakening of the fibers, down to 0.2 GPa. The pulling speed effect is not observed. It seems that the stripping operation is the major parameter of the mechanical strength degradation of the spliced fiber. Also the aging of the fiber has no effect on the strength of the spliced fibers. Although the strength of some fibers before splicing was below the handleability criterion of 2 GPa (the median, however, is above 2 GPa), no problems occurred during splicing of the fibers.

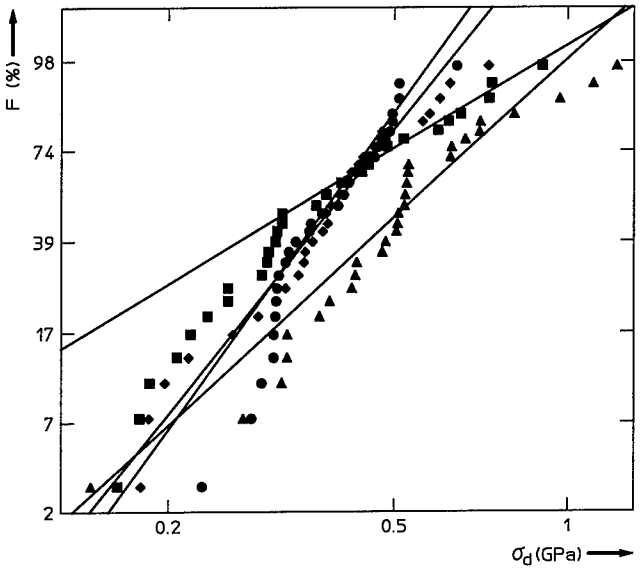


Figure 7 *Weibull plot for spliced G-652 fiber.*

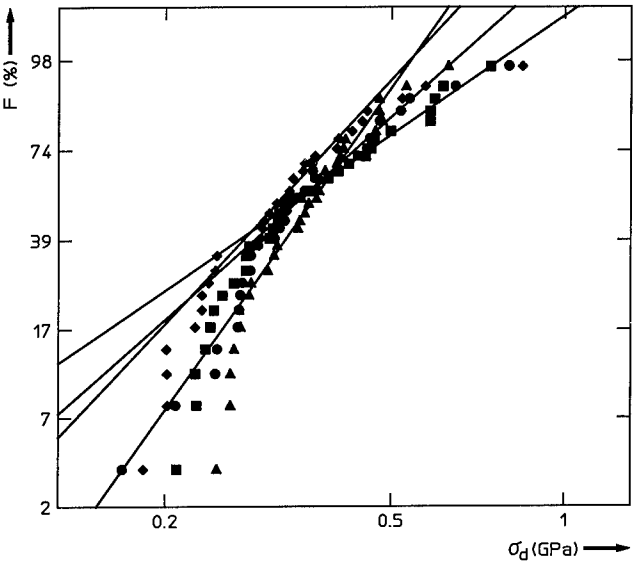


Figure 8 *Weibull plot for spliced fiber recovered from Biarritz.*

DISCUSSION

In this paper all field-aged fibers could be spliced without problems. This is also true for a fiber with median failure stress of 0.71 GPa (see Figure 3), well below the handleability criterion of 2 GPa. Note, however, that the strength distribution of this fiber (Figure 3) is sharp compared with the aged fibers from Ref.[4]. Because only a few fibers showed handleability problems in the latter reference, one must conclude that the tail of the distribution, not the median, is critical. Handleability problems can occur on a handling length of about one meter, but mainly on the few centimeters which are stripped from the primary coating. If the fiber is weak but only a few weak points exist, with low probability to find one on the stripped piece, the fiber may be spliced without problems. It must be further studied on which length handleability must be defined. The distribution of the strength of the aged fiber is an important factor (See Appendix D).

Even this observation does not explain the difference in handleability: the weakest fibers in Ref.[4] are of about the same strength as those from Figure 3. One explanation could be a difference in operator, stripping tool, or splice-condition. Another explanation is that the strength degradation of Figure 3 has been caused by coating delamination. The primary coating has an important protective function: buffering local stresses on the fiber surface during handling. Elasticity is also important for this. The coating can degrade in different ways: delamination but still elastic, brittle, etc.. It is not yet known how the state of the coating (strippability, adhesion, elasticity) affects the relation between measured dynamic failure stress and handleability. The handleability criterion must be further studied.

CONCLUSIONS

Weak spots in optical fibers are not handleable, not even from the start. For this reason handleability must be defined for the high strength mode. The high strength mode flaws are hardly affected by the low service stresses which they are subjected to. The service stress is determined by the weak spots and static fatigue. When aging and stress corrosion cause static-fatigue (spontaneous) fracture within the lifetime of the fibers, the handleability criterion is reached a few seconds before fracture. The nature of stress corrosion is such that either fracture occurs, or no measurable weakening occurs at all.

Zero-stress aging determines weakening, not stress corrosion. While static-fatigue fracture depends on weak spot statistics, prooftest parameters, applied stress and fiber/environment parameters, handleability mainly depends on the latter. No criterion for service stress follows for handleability (Note that, in principle, zero-stress aging slightly depends on stress; therefore zero-stress aging tests must be performed under the same low stress as during service). A simple Arrhenius type of extrapolation can be used for handleability lifetime estimation.

The earlier suggested criterion for handleability of aged fiber, a minimum strength of 2 GPa, has been compared to the experimental results of this work. From tests on old fibers from BT's network and the Biarritz-trial (France Telecom) it can be concluded that these naturally aged fibers can be spliced without problems, even when they were significantly weakened at some points. It is therefore suggested that the strength distribution of the aged fiber is an important factor for handleability and that mechanical strength alone cannot be used as handleability criterion. The coating condition and ability to protect the fiber surface during handling are also of great importance. Further studies are necessary to find a more complete criterion for handleability of aged fibers.

REFERENCES

1 W. Griffioen, "Mechanical lifetime model of optical fibers", Proc. 42nd *IWCS* (1993) 471.

2 H.H. Yuce, "Fiber reliability", Proc. 2nd *OFMC* (1993) 3.

3 T.T. Volotinen, H.H. Yuce, N. Bonanno, R.A. Frantz, S. Duffy, "Splicing of aged fibers", Proc. *SPIE*, Vol.1973 (1993) 186.

4 N.J. Bonanno, H.C. Hartman, R.W. Contreras, H.H. Yuce, T.T. Volotinen, J.P. Varachi, "Handling behavior of aged and unaged fibers during splicing operation", *Proc. 9th NFOEC* (1993).
5 A. Dwivedi, G.S. Glaesemann, C.K. Eoll, "Optical fiber strength, fatigue and handleability after aging in a cable", *Proc. 43rd IWCS* (1994) 728.
6 A.G. Evans, S.M. Wiederhorn, "Proof testing of ceramic materials- an analytical basis for failure prediction", *Int. J. Fract.*, Vol.10 (1974) 379.
7 D. Kalish, B.K. Tariyal, "Static and dynamic fatigue of polymer-coated fused silica optical fiber", *J. Am. Ceram. Soc.*, Vol.61 (1981) 518.
8 P.W. France, W.J. Duncan, D.J. Smith, K.J. Beales, "Strength and fatigue of multicomponent optical glass fibres", *J. Mater. Sci.*, Vol.18 (1983) 785.
9 P. Hasløv, K.B. Jensen, N.H. Skovgaard, "Degradation study for stressed optical fibres in water. New worst case lifetime estimation model", *Proc. 41th IWCS* (1992) 423.
10 W. Griffioen, "Mechanical lifetime model for optical fibers in water", Proc. *SPIE*, Vol.2074 (1993) 2.
11 M.H. Reeve, S.A. Cassidy, "Installation of optical fibre units using viscous drag of air", *Proc. ECOC* (1983).
12 A. Gouronnec, R. Goarin, G. Le Moigne, M. Baptiste, "Optical fiber reliability results from the Biarritz field trial", *Proc. SPIE*, Vol.2290 (1994) 191.
13 D. Inniss, Q. Zhong, C.R. Kurkjian, "Stress corrosion mechanism of pristine and corroded silica glass fibers", *Proc. 43rd IWCS* (1994) 736.
14 M.J. Matthewson, C.R. Kurkjian, "Strength measurement of optical fibers by bending", *J. Am. Ceram. Soc.*, Vol.69 (1986) 815.

APPENDIX A: STRESS CORROSION

Stress corrosion is usually modeled by means of a power law, where the rate at which a crack with size a grows is given by:[6]

$$\frac{da}{dt} = AK_I^n \qquad K_I = Y\sqrt{a}\cdot\sigma \tag{1}$$

Here A is a scale constant for the speed of crack growth, n the corrosion susceptibility, K_I the stress intensity factor, Y a geometrical constant (1.24 for an elliptical crack) and σ the applied stress. Catastrophic failure occurs at a critical value K_{Ic}, a material constant with a value of 8×10^5 N/m$^{3/2}$ for fused silica.[7] For this follows the (inert) strength S:

$$S = \frac{K_{Ic}}{Y\sqrt{a}} \tag{2}$$

Rewriting (1) with (2), the decrease of (inert) strength S of the fiber under the influence of stress σ follows as a function of time t:

$$S^{n-2} = S_I^{n-2} - \frac{1}{B}\int_0^t \sigma^n dt \tag{3}$$

Here S_I is the initial inert strength and $B = 2/(AY^2(n-2)K_{Ic}^{n-2})$. The time to fracture t_a under static (service) stress σ_a follows from (3), under the approximation that fracture occurs at $S = 0$:

$$t_a = \frac{BS_I^{n-2}}{\sigma_a^n} \tag{4}$$

The dynamic failure stress σ_d, i.e. for a stress $\sigma = d\sigma/dt \times t$, follows from (3), also under the approximation that fracture occurs at $S = 0$:

$$\sigma_d = \left[BS_I^{n-2}(n+1)d\sigma/dt\right]^{1/(n+1)} \tag{5}$$

Under the static stress σ_a the (inert) strength of the fiber decreases to a value S_h after a time t_{ah}, which can be found with (3):

$$S_h^{n-2} = S_I^{n-2} - \frac{\sigma_a^n t_{ah}}{B} \tag{6}$$

This decreased inert strength S_h can be measured as a decreased dynamic failure stress σ_{dh}, which follows from (3) analogously to the derivation of (5):

$$\sigma_{dh} = \left[BS_h^{n-2}(n+1)d\sigma/dt\right]^{1/(n+1)} \tag{7}$$

Combining (4), (5), (6) and (7) it follows:

$$\frac{t_{ah}}{t_a} = 1 - \left(\frac{\sigma_{dh}}{\sigma_d}\right)^{n+1} \tag{8}$$

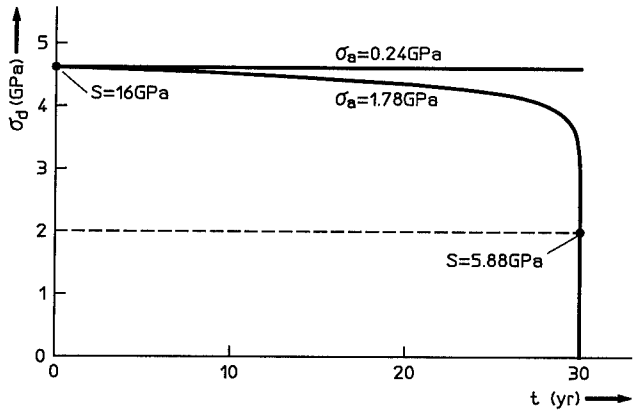


Figure A1 *Decrease of dynamic failure stress σ_d for a fiber under a stress σ_a of 1.78 GPa (failure of high strength mode) and under a stress σ_a of 0.24 GPa (failure of weak spots). The initial inert strength and the inert strength at the criterion for handleability, σ_d=2GPa, have been indicated.*

The criterion for handleability is usually a (median) dynamic failure stress of about 2 GPa (1.4-2.2 GPa) at a stress rate of 0.07 GPa/s (5%/min)[2,3,4,5], while this

value is around 5 GPa (same stress rate) for an unaged fiber (4.71 GPa for $B = 2\text{x}10^{-8}$ GPa^{2}s, $n = 20$, $S_I = 16$ GPa). From (8) it follows that handleability problems occur not earlier than 10 seconds before spontaneous fracture (after t_a of 30 years when $\sigma_a = 1.78$ GPa), when the inert strength has decreased to 5.88 GPa. The decay of the dynamic failure stress is shown in Figure A1. Hence it can be concluded that weakening of the fiber is not an issue when only stress corrosion occurs. The above proves that the nature of stress corrosion is such that either fracture occurs, or no measurable weakening occurs at all. This can also be understood from the strong dependency of failure time on applied stress. Consider a stress, exactly enough to cause fracture after the lifetime. For a slightly lower stress this would take much more time. Hence a slightly lower stress, applied the same time, will only have a small effect. Weakening is extremely bad luck!

This statement is general and becomes even stronger when realizing that in service no failure occurs for the high strength mode. The applied stress σ_a in service is specified in relation to weak spots (these spots cannot be considered for handleability because they are usually weaker than 2 GPa from the start). Usually one third of the prooftest level σ_p (often 0.72 GPa = 1%) is taken as a maximum. The service stress of 1.78 GPa giving fracture for the high strength mode in 30 years (previous general example) is much higher than the real service stress of 0.24 GPa. For the latter stress no weakening of the high strength mode occurs at all.

APPENDIX B: ZERO-STRESS AGING

When only stress corrosion occurs handleability is not an issue, because serious weakening coincides with static-fatigue (spontaneous) fracture for weak spots and does not occur at all for the high strength mode. When also zero-stress aging occurs it all becomes different. Now serious weakening can occur over the whole length of fiber, as is proved by many experiments. Three models exist that treat zero-stress aging in combination with stress corrosion, the France[8] model, the Hasløv/Jensen[9] model and the blunt-pit[10] model. In these models zero-stress aging determines the behavior in the beginning and stress corrosion only causes significant strength decrease towards the very end, just before fracture. This is not surprising after the conclusions from the previous section.

It becomes clear that weakening of the fiber is solely ruled by zero-stress aging. It depends on the fiber/environment parameters, prooftest parameters, weak spot statistics and the applied stress whether the fiber fractures (stress corrosion plus zero-stress aging on weak spots) before the handleability criterion is reached (determined by zero-stress aging alone, on high-strength mode). Note that for spontaneous failure, the handleability level of 2 GPa must also be passed, just before fracture occurs.

Zero-stress aging can be fitted with an Arrhenius type of law, which was also done in the mentioned models.[10] The rate at which a crack (or aging pit) with size a grows is given by:

$$\frac{da}{dt} = v_0 \exp\left(\frac{-E_a}{RT}\right) \qquad (9)$$

Here v_0 is a scale constant, E_a the zero-stress activation energy, R the gas constant and T the temperature. The parameters v_0 and E_a can be obtained by fitting measurements at different temperatures. Note that, in principle, also zero-stress aging may be influenced by stress (lowering of activation energy).[13] It is therefore recommended to perform the tests at the same (low) stress as the fiber is subjected to in service. Rewriting (9) expressed in strength S with (2), and carrying out the integration gives:

$$S^2 = S_I^{-2} + \left(\frac{Y}{K_{1c}}\right)^2 v_0 \exp\left(\frac{-E_a}{RT}\right) t \qquad (10)$$

Next this equation is transformed to a form with measurable dynamic failure stress, using (5) and a similar expression with S from (10) instead of S_I:

$$\frac{\sigma_{da}(t)}{\sigma_d} = \left[1 + \mathbb{C}\exp\left(\frac{-E_a}{RT}\right)\cdot t\right]^{\frac{-(n-2)}{2(n+1)}} \qquad \mathbb{C} = \left(\frac{YS_I}{K_{1c}}\right)^2 v_0 \qquad (11)$$

Here $\sigma_{da}(t)$ is the dynamic failure stress after aging during time t and σ_d is this stress at $t = 0$. E_a and $\mathbb{C}$ can be obtained by fitting data from zero-stress aging measurements at different temperatures. This kind of fit is also presented by Hasløv and Jensen.[9] The time t_{ah} follows from the handleability criterion $\sigma_{da}(t) = \sigma_{dh}$ by rewriting (11) again:

$$t_{ah} = \left[\left(\frac{\sigma_{dh}}{\sigma_d}\right)^{-2(n+1)/(n-2)} - 1\right]\cdot\frac{\exp\left(E_a/RT\right)}{\mathbb{C}} \qquad (12)$$

This formula represents a very simple lifetime estimation for handleability, obtained by a simple Arrhenius type of extrapolation. The stress, an important factor for spontaneous fracture, is not involved in the handleability model (but it is recommended to perform the aging tests under the same low stress as during service).

Care shall be taken that the accelerated (temperature) tests to obtain the zero-stress aging parameters are performed in the same regime as during service. There is a risk that a new mechanism is introduced when elevated temperatures are used. This can be recognized as kinks in the weakening as a function of temperature.[9]

APPENDIX C: NUMERICAL EXAMPLE

The zero-stress aging data from Ref.[10] will be fitted with (11) as an example. A nice fit is obtained for values $\mathbb{C}$ of 5×10^6 and E_a of 82 kJ. This differs somewhat from the fit of measured inert strengths after aging.[10] The time t_{ah} after which the dynamic failure stress of the fiber drops below the value of 2 GPa, the handleability criterion, is found with (12). This results in a handleability lifetime of 16.5 years for 20°C.

The handleability criterion can be compared with the condition for spontaneous failure. Mechanical lifetime models for spontaneous failure, as a result of a combined effect of zero-stress aging and stress corrosion, are given in Ref.[10]. An illustration is given with the Mitsunaga type of those "water models":[10]

$$\sigma_a = \sigma_p \left(\frac{t_p}{G(t_a)t_a}\right)^{1/n} \left\{\left[1 - \frac{\ln(1-F)}{LN_p}\right]^{n/m} - 1\right\}^{1/n} \qquad (13)$$

Here σ_a is the allowable static stress in service during lifetime t_a, σ_p is the prooftest level during time t_p, with failure number N_p per unit of length, F is the required failure probability on length L, m the Weibull parameter for the weak spot distribution (4 in Mitsunaga model)[10], and G a function that describes the effect of zero-stress aging ($G^{-1/n}$ is a measure for the strength decrease after zero-stress aging). Using the numbers from the numerical example in Ref.[10] with the values of $\mathbb{C}$ and E_a from this paper, the stress σ_a at which spontaneous failure occurs follows. Spontaneous failure (at 20°C), with a probability F of 1% on 1 km after 16.5 year, occurs at a service stress of 0.095 GPa.

In conclusion, the fiber from the example is not handleable anymore after 16.5 years, only depending on zero-stress aging parameters. For service stresses σ_a larger than 0.095 GPa, spontaneous failure with a probability F of 1% on 1 km occurs before the handleability criterion is reached (note that the handleability level of 2 GPa was also passed in this case, just before fracture). This example illustrates that spontaneous failure does not only depend on zero-stress aging parameters, but also on the stress corrosion parameters, the applied stress, the prooftest parameters and the weak spot statistics.

APPENDIX D: STATISTICS AGED FIBERS

The handleability is treated in this paper, sofar, without considering the strength distribution of the aged fiber. Because this distribution becomes much wider after aging, it should, in principle, be taken into account. When zero-stress aging is evaluated in lengths comparable with what is used in handling, the handleability estimation is of practical use. Therefore tensile testing of the aged fibers is to be preferred above 2-point bending (with effective test lengths of about 10 μm)[14]. Because (initial) weak spots do not appear in the handleability criterion, it is rather easy to take statistics of aged fibers into account. Note that for the spontaneous failure lifetime models, which include also weak spot statistics, such a job is extremely difficult.[10]

The distribution of dynamic failure stresses can be written as:[1]

$$\ln(1-F) = -0.69 \frac{L}{L_0}\left(\frac{\sigma_d}{\sigma_{dm}}\right)^{m_d} \qquad m_d = m\frac{n+1}{n-2} \qquad (14)$$

Here σ_{dm} is the median (50%-value) dynamic failure stress on length L_0, m the Weibull parameter for the inert strength distribution, m_d for dynamic fatigue and F the probability for fiber length L. Such an expression can also be written for the aged fiber, with $\sigma_{dam}(t)$ and $m_{da}(t)$:

$$\ln(1-F) = -0.69 \frac{L}{L_0}\left(\frac{\sigma_{da}}{\sigma_{dam}}\right)^{m_{da}} \qquad m_{da} = m_a\frac{n+1}{n-2} \qquad (15)$$

Because the distribution is sharp before aging, σ_{dm} can be used to characterize the strength. Now for $\sigma_{da}(t)$ can be written, with for σ_{dam}/σ_{dm} the expression from (11):

$$\frac{\sigma_{da}(t)}{\sigma_{dm}} = \left[-\frac{L_0}{L}\frac{\ln(1-F)}{0.69}\right]^{1/m_{da}} \left[1 + \mathbb{C}\exp\left(\frac{-E_a}{RT}\right)\cdot t\right]^{\frac{-(n-2)}{2(n+1)}} \qquad (16)$$

The time t_{ah} follows now with $\sigma_{da}(t) = \sigma_{dh}$:

$$t_{ah} = \left(\left\{\frac{\sigma_{dh}}{\sigma_{dm}}\left[\frac{-0.69\,L}{L_0\ln(1-F)}\right]^{1/m_{da}}\right\}^{\frac{-2(n+1)}{n-2}} - 1\right) \cdot \frac{\exp\left(E_a/RT\right)}{\mathbb{C}} \qquad (17)$$

Note that the requirements for the failure probability F for handleability differ from those for spontaneous fracture. For handleability one can afford rather high F: when fracture occurs during handling, just strip a new piece. Sometimes the distribution of strengths of an aged fiber cannot be described by a single Weibull distribution. In that case statistical extrapolations do not make sense and one is forced to test the fibers in lengths comparable to those during handling. Then 2-point bending is not a recommended test method anymore.

In the previous paragraph the strength distribution of aged fibers has been used for the handleability lifetime estimation. It is necessary to fit not only the strength decrease after aging, but also the width of the distribution (parameter m_{da}). Another, simpler, way is fitting with (11) of the tails of the strength distributions of aged fibers, at some chosen failure probability F. For lifetime estimation (12) can then be used. In this case a handleability criterion must be defined for a certain value of F, not the median. Again a test length comparable with the length used in handling is recommended. The handling length must still be defined (See Section Discussion).

BIOGRAPHIES



Willem Griffioen received his MS degree in physics and mathematics from Leiden University (Netherlands) in 1980 where he also worked until 1984. In 1984 he joined KPN Research at Leidschendam (Netherlands). His work included r&d of optical cables and installation techniques. Then he switched to reliability of optical fibers. Recently he received his PhD in this field from the Technical University of Eindhoven (Netherlands). He worked at Ericsson Cables in Hudiksvall (Sweden) in 1991/92 and at Telia Research in Haninge (Sweden) in 1994 in the scope of exchange/joint projects with KPN Research. Currently he is active in the field of outside-plant structures for the access network, especially concerning migration from copper to optical fiber. He is chairman of COST 246, WG1.2 and WG1.1, SG1.



Tarja Volotinen is a specialist in optical fibers at the Telecom Cables Division of Ericsson Cables AB, Hudiksvall (Sweden). She received her MSc from the University of Helsinki (Finland) in 1978. She worked for Nokia Cables from 1979 to 1986 on measurement techniques and quality control for optical fibers and cables. Since joining Ericsson in 1986, she has focused particularly on the performance and mechanical reliability of optical fibers. She received her PhD in Physics from the University of Helsinki (Finland) in 1991. In 1992-1993 she was a visiting scientist in the Fiber Distribution and Reliability Group at Bellcore, working on mechanical reliability of optical fibers. She is chairman of COST 246 Action "Materials and Reliability of Passive Optical Components and Fiber Amplifiers in Telecommunications Networks".



Peter Wilson graduated from the University of Nottingham (United Kingdom) in 1991 with a B.Eng (Hons.) in Electrical and Electronic Engineering with French. In 1991 he joined the Cables and Installation Group at BT Laboratories in Ipswich (United Kingdom) and since then he has worked in the fields of optical fibre and cable reliability and the design and specification of fibre cables for use in the access network. He is a member of COST 246.



Alain Gouronnec was born in 1946. He received his engineer degree from the Conservatoire National des Arts et Metiers in 1978. He joined the CNET in 1971 where he worked on the pulling and multipulling of optical fibers studies. Then in 1986 he started to work on development and specification of telecommunication cables; since 1993 he is in charge of the evaluation and the qualification of optical fibers for France Telecom needs; he is also in charge of the optical fiber reliability studies in CNET. He is a member of COST 246.



Torbjörn Svensson received his MS and Ph.D. from the Royal Institute of Technology, Stockholm (Sweden). During his employment at the Swedish Telecom Technology Dept, in 1985-91, and later at the Networks Outside Plant Division, he has been engaged in quality assurance and techniques for testing fibers and cables. He holds a number of patents, being the inventor of fiber optical test methods as the high-speed tensile test, the expander, the tube test, and the distributed strain technique. His present employment is at Telia Research AB, Sweden, where he is responsible for fiber mechanics and splicing technology. He is a member of COST 246.

INVESTIGATION ON INFLUENCE OF COATING MATERIALS TO ZERO STRESS AGING OF OPTICAL FIBER

Tomoyuki HATTORI, Akira URANO, Nobuhiro AKASAKA, and Yasuo MATSUDA

SUMITOMO ELECTRIC INDUSTRIES, LTD.
1, Taya-cho, Sakae-ku, Yokohama, 244 JAPAN

ABSTRACT

Fibers coated with several kinds of model primary coatings were aged in hot water or high temperature and high humidity, and their tensile strength were evaluated. It is proved that good adhesion of resin to glass reduces the degradation of fiber strength. For mechanical reliability of optical fiber, it is important to keep its adhesion stable in water with optimization of the composition of coating materials. It is also found that contact angle of water to silica glass substrate from which coating is peeled shows strong correlation with strength degradation in hot water. Contact angle will be useful for optimizing the coating materials to prevent strength degradation because it is influenced by the activity and coating residue of the silica surface in general.

1. INTRODUCTION

Optical fiber networks are now widely constructed in the world. In these application optical fiber is exposed in severer environment, such as high temperature and high humidity, than used to be. Reliability of optical fiber is of great interest for optical telecommunication systems. As for the mechanical reliability, it is well known that an optical fiber breaks under static stress. However according to recent studies, without any stresses, the optical fiber can be corroded chemically due to moisture attack, which is called "zero-stress aging"[1]. This makes predictions of the expected lifetime unreliable. The mechanism of zero-stress aging is proved to be owing to surface dissolution of silica[2], and to be affected by coating materials[3]. Low cure degree, alkalinity, and higher water absorption of coating materials makes fiber strength degrade in water at high temperature[4,5]. Coating delamination also cause fiber strength deterioration in severe environment[6]. Recently some studies have been carried out to increase mechanical lifetime of optical fiber by modification of coating materials. Matthewson et al. showed that the addition of nanosized particles of fumed silica to the coating materials improves long-term mechanical properties of the fiber[7]. In this paper, the influence of coating materials, especially the interaction between glass and primary coating, to zero-stress aging is investigated for the design of more reliable coating materials.

2. EXPERIMENTAL PROCEDURE

2-1 Coating

Several model primary coating materials, whose basic polymer compositions are same, have been prepared. The adhesion between glass and coating is controlled by varying the kind and content of monomer or some additives. Their modulus and water absorption are almost same.

The adhesion to glass of model coating materials was evaluated before and after aging in 85°C deionized

water. Peel strength and contact angle were used for evaluating the adhesion to glass. Test procedures are as follows.

Peel strength

Each model primary coating was applied on the surface of a glass plate with bar-coater to make a coating film with a thickness of about 250μm. The film was irradiated by a metal halide lamp in an atmosphere of nitrogen. The total irradiation energy was set to be 100mJ/cm^2. The peel strength was measured at a peel-off rate of 200mm/min.

Contact angle

Measuring diagram of contact angle is shown in Figure 1. Each model primary coating was applied on the surface of a silica glass disc with a thickness of about 30μm using spin-coater and cured by the metal halide lamp in an atmosphere of nitrogen at 100mJ/cm^2. The coated disc was immersed in 85°C deionized water. After aging, the cured film was removed from the disc, and contact angle of a deionized water drop on the disc was measured with the contact-angle meter type CA-D (Kyowa Kaimenkagaku Co., Ltd.).

2-2 Fiber

All fibers in this study were drawn and coated with model primary coatings and a standard secondary coating from some silica preforms. Drawing and coating conditions were maintained approximately constant for all test fibers. The glass fiber diameter is 125μm, and the outer coating diameter is almost 250μm.

Test fibers were aged in condition of 85°C deionized water and 85°C/85%RH. Before aging, gel fraction was measured for evaluation of curing degree of test fiber. Before and after aging, strip force and glass strength of test fibers were measured. Before evaluation, aged fibers were kept in the condition of 25°C/50%RH for 24hours. Test procedures are as follows.

MEK extraction test

All uncured components in coating materials are extracted by this test. About 0.15g of the coating material was weighed and extracted for 16hours with MEK (Methyl Ethyl Ketone) at 60°C. The gel fraction percentages (%GF) were calculated by the following equation :

$$\%GF = \frac{\text{weight (after extraction)}}{\text{weight (before extraction)}} \times 100$$

Strip force

The force required to remove the coating was measured with tensile tester using a commercial stripping tools. Stripped length were 10mm, and all tests were conducted at a rate of 10mm/min.

Glass strength

Test fibers were fractured on a gauge length of 500mm at a strain speed of 2.5%/min. A total of 15 samples was fractured in an ambient environment of

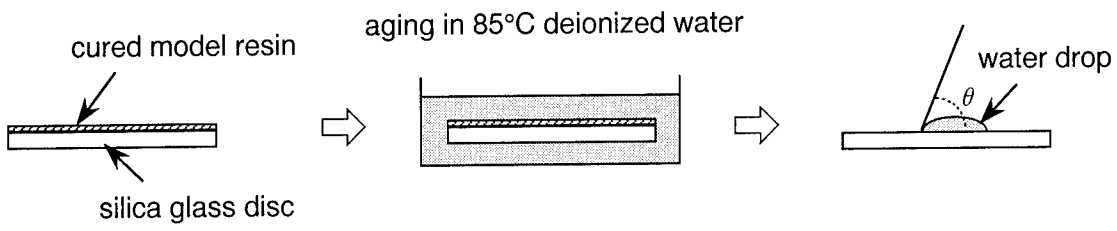


Figure 1 Measuring diagram of contact angle

Table 1 Characteristics of model resins and coated test fibers

fiber No.	1	2	3	4	5	6	7
primary coating	P-0	P-300	P-310	P-311	P-312	P-320	P-410
coating							
peel strength(g/cm)	9	5	20	23	30	23	9
contact angle(degree)	53	57	61	43	51	61	65
fiber							
gel fraction(%)	96.0	97.3	97.3	95.5	92.1	97.0	96.0
strip force(g)	252	342	441	473	250	563	349

25°C/50%RH for each aging time.

3. RESULTS

3-1 Characteristics of model coatings and test fibers

The initial characteristics of model coatings and test fibers are shown in Table 1. The initial strip force of each test fiber is almost proportional to peel strength of its primary coatings except for fiber 5. As indicated by low gel fraction of fiber 5, the low strip force may account for the poor curing property of P-312. Initial contact angles for primary coatings do not seem to be directly related to peel strength.

3-2 Aging behaviors of test fibers

Figure 2(a)~(g) show the changes of strength for aged fibers. In 85°C water, both strength of the fiber 1 and 2 were degraded remarkably. In 85°C/85%RH aging, there was no strength degradation in these primary coatings. Coating delamination was not observed in all aged fibers.

Strip forces of aged fibers in 85°C water are also shown in Figure 2. Those of fiber 3, 4, and 6 decrease at early stage, but after aging for longer time in 85°C

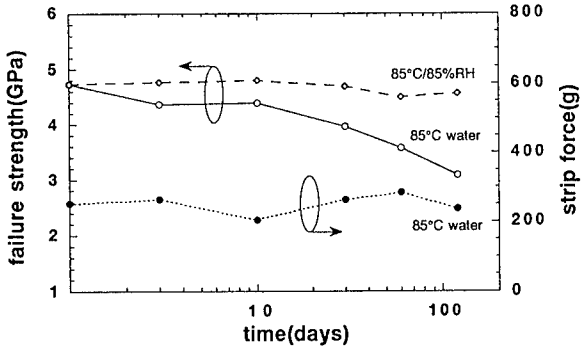


Figure 2(a) Aging behaviors for fiber 1

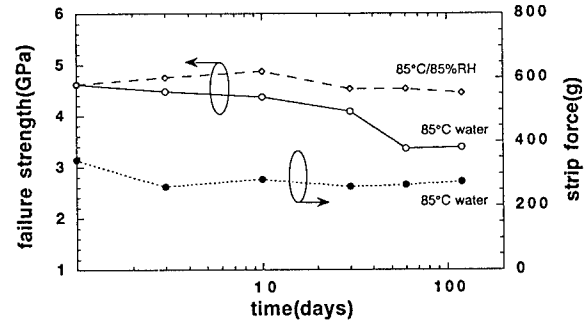


Figure 2(b) Aging behaviors for fiber 2

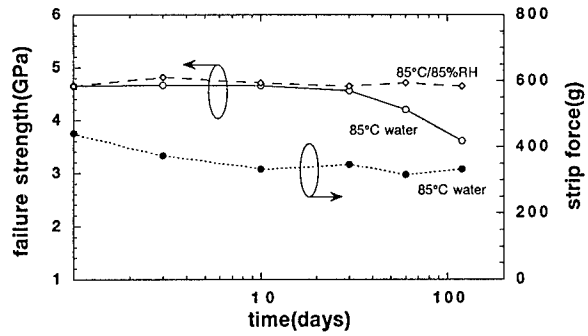


Figure 2(c) Aging behaviors for fiber 3

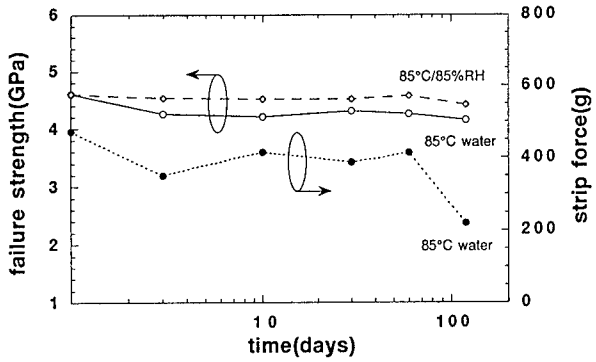


Figure 2(d) Aging behaviors for fiber 4

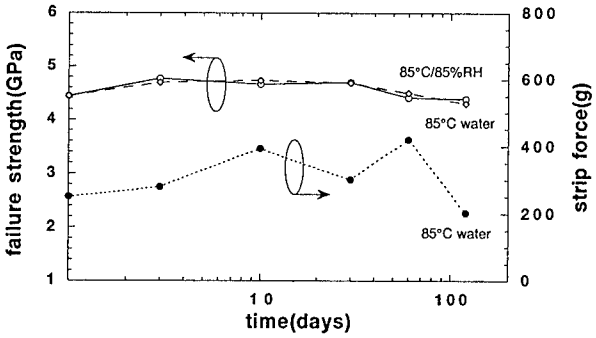


Figure 2(e) Aging behaviors for fiber 5

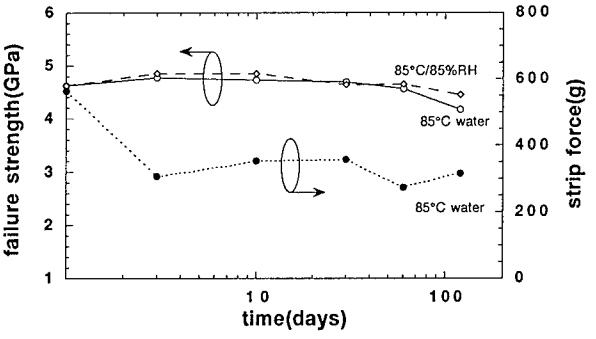


Figure 2(f) Aging behaviors for fiber 6

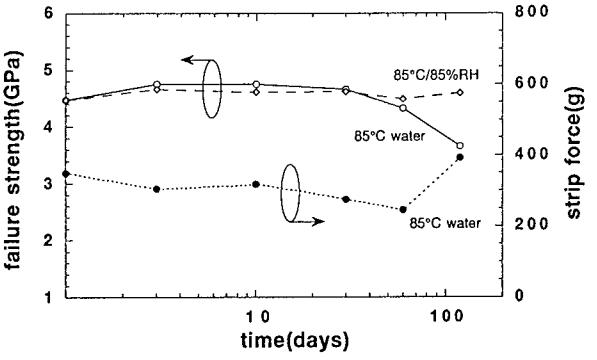


Figure 2(g) Aging behaviors for fiber 7

water they were stable.

The changes of peel strength are shown in Figure 3. In P-0, P-300, P-310 and P-410, small blisters appeared at the interface between glass and primary coating after 1 day aging. The blisters of P-300 and P-410 are smaller than those of P-0 and P-300. The generation and their size of blisters are seemed to be related to adhesion of resin to glass substrate. Contact angles are plotted in Figure 4. Contact angles for P-0, P-300 and P-410 decrease after aging. The increases of contact angle for P-311, P-312 and P-320 mean that the glass surfaces coated with them after aging become more hydrophobic. Small blisters, which were not observed in aged fibers, were also appeared after longer time aging for all coatings because of water penetration from the edge of sample pieces.

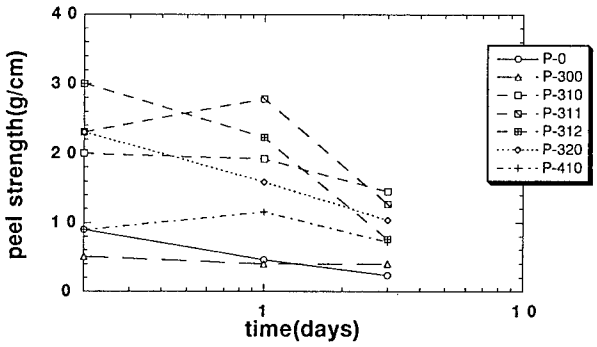


Figure 3 Peel strength change after aging in 85°C water

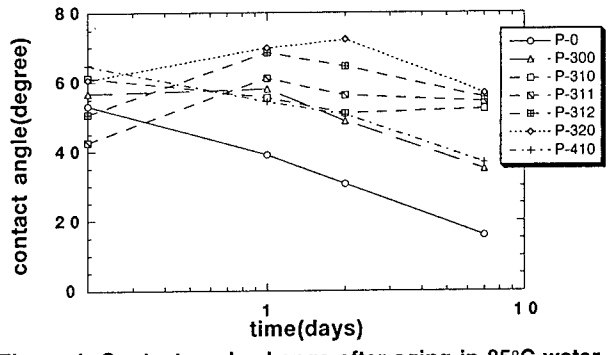


Figure 4 Contact angle change after aging in 85°C water

4. DISCUSSION

The relationship between the strength degradation and strip force after aging is presented in Figure 5. There is no correlation between the strength degradation and strip force, which is also pointed out by Frantz[8]. Because strip force is affected by many factors[9][10], strip force is not suitable for criteria of coating adhesion.

In the peel strength and contact angle experiments, blisters which were not observed in aged test fibers appeared at the interface between glass and coating after longer time aging because of water penetration from the edge of sample piece or effect of the difference in the coating structure and geometry. Therefore the short time values are used for the aging time in the discussion of relationship between strength degradation and adhesion. In peel strength, one day is adapted for the representative of the aging time. The peel strength is fairly related to the strength degradation as shown in Figure 6. As the adhesion to glass increases, the strength increases. It is possible to build up several hypotheses for the effect of adhesion. One is that the adhesion between glass and primary coating prevents water molecules from penetrating the glass surface. Another is that the adhesion lowers the activity of glass surface. The interesting result is obtained in contact angle measurements as indicated in Figure 7. Though the unaged contact angle is not related to the strength degradation, the contact angle after aging has strong correlation with the strength degradation. Contact angle of water to silica glass is generally influenced by the silica surface state, such as the activity of the surface, the adsorption of water molecule and coating residue. Since initial contact angle is not related to peel strength, as mentioned above, it seems likely that contact angle shows the another interaction between glass and primary coating in addition to the adhesion represented by peel strength. The origin of contact angle of peeled silica glass substrate is now under investigation with further chemical analysis.

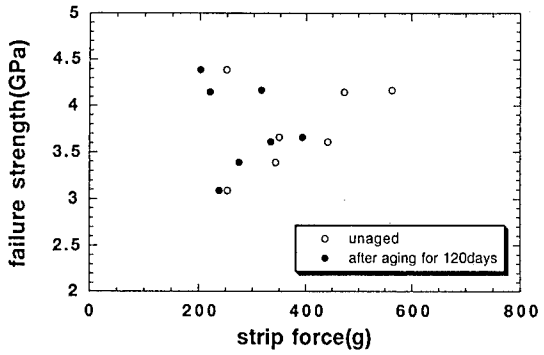


Figure 5 Relationship between strip force and failure strength after aging for 120days

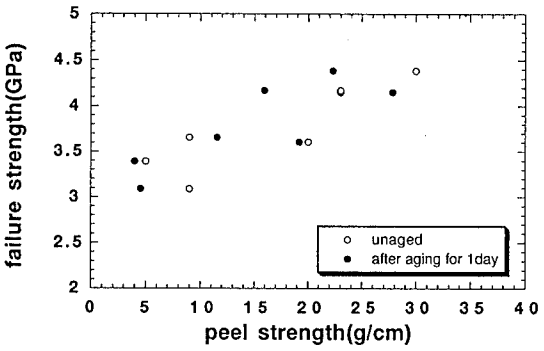


Figure 6 Relationship between peel strength and failure strength aging for 1day

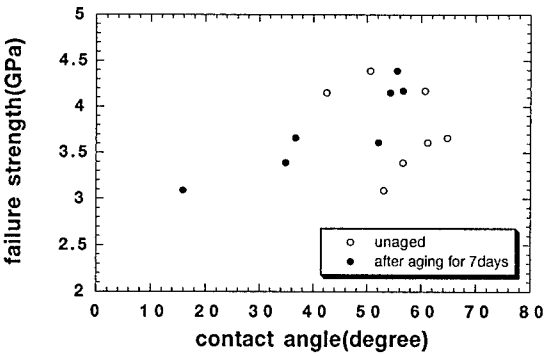


Figure 7 Relationship between contact angle and failure strength after aging for 7days

5. CONCLUSION

In summary, fibers coated with several kinds of model primary coatings were aged in hot water or high temperature and high humidity, and their tensile strength was evaluated. The strength of the fibers, whose adhesion become lower in hot water aging, degraded. On the other hand, in 85°C/85%RH aging, no strength degradation was observed for all fibers. It is proved that good adhesion of coating to glass reduces the degradation of fiber strength. It is important to optimize the composition of coating materials to keep stable adhesion in water. Contact angle will be useful for optimization of the composition of coating materials to prevent strength.

REFERENCES

[1] J. T Krause, "Zero stress strength reduction and transitions in static fatigue of fused silica fiber lightguides", J. Non-Cryst. Solids, **38&39**, 497 (1980)

[2] M. J. Matthewson and C. R. Kurkjian, "Environmental effects on the static fatigue of silica optical fiber", J. Am. Ceram. Soc., **71**, 17 (1988)

[3] H. H. Yuce, "Aging behavior of optical fibers", Proceeding of the 41st IWCS, 605 (1992)

[4] H. H. Yuce, I. M. Pitz, R. A. Frantz and M. Andrejco, "The effects of coating cure on the mechanical characteristics of optical fibers", Proceeding of the 39th IWCS, 715 (1990)

[5] N. Akasaka, T. Hattori, T Nonaka, K. Oishi and Y. Matsuda, "Design of optical fiber coating", Proceeding of the 19th ACOFT, 375 (1994)

[6] F. Cocchini, D. Cuomo, G. Ferri and A. Pudia, "Influence of glass-coating adhesion on the optical and mechanical performances of optical fibers in water", Proceeding of the 43rd. IWCS, 66 (1994)

[7] M. J. Matthewson, V. V. Rondinella and C. R. Kurkjian, "The influence of solubility on the reliability of optical fiber", Proceeding of SPIE, **1971** 52 (1992)

[8] R. A. Frantz, B. J. Keon, E. M. Vogel, T. N. Bowmer and H. H. Yuce, "The effects of optical fiber coating and ink materials on the corrosion of the glass surface", Proceeding of the 43rd. IWCS, 742 (1994)

[9] K. Nomura, N. Akasaka, T. Nonaka, T. Hattori and A. Nishimura, "A study for coating strippability of optical fiber", 1994 Spring National Convention Record, The Institute of Electronics, Information and Communication Engineers B-940 (1994)

[10] H. C. Chandan, J. R. Pretisce, J. W. Shea, C. R. Taylor, L. L. Blyler,D. Innis and L. Shepherd, "Fiber protective coating design for evolving telecommunication applications", Proceeding of the 41st. IWCS, 239 (1992)

Tomoyuki HATTORI



Sumitomo Electric Industries, Ltd.

1, Taya-cho, Sakae-ku Yokohama, JAPAN

Tomoyuki Hattori received his M.E. degree in Chemistry from Kyoto University in 1987. He joined Sumitomo Electric Industries, Ltd. in 1987, and has been engaged in research and development of optical fiber and cables. He is a member of Transmission Media Department in Yokohama Research Laboratories and a member of Institute of Electronics and Communication Engineers of Japan.

Akira URANO



Sumitomo Electric Industries, Ltd.

1, Taya-cho, Sakae-ku Yokohama, JAPAN

Akira Urano received his B.S. degree in material science from University of Tsukuba in 1984. He joined Sumitomo Electric Industries, Ltd. in 1984 and has been engaged in research and development of optical fiber. Mr. Urano is a member of Analytical Characterization Center in R&D Group, and a member of the Japan Society of Applied Physics.



Nobuhiro AKASAKA

Sumitomo Electric
Industries, Ltd.

1, Taya-cho, Sakae-ku
Yokohama, JAPAN

Nobuhiro Akasaka received his M.E. degree in Chemical Engineering from Tokyo University in 1983. He joined Sumitomo Electric Industries, Ltd. in 1983, and has been engaged in research and development of optical fiber and cables. He is a senior engineer of Transmission Media Department in Yokohama Research Laboratories.



Yasuo MATSUDA

Sumitomo Electric
Industries, Ltd.

1, Taya-cho, Sakae-ku
Yokohama, JAPAN

Yasuo Matsuda received his M.E. degree in Chemistry from Tokyo University in 1978. He joined Sumitomo Electric Industries, Ltd. in 1978, and has been engaged in research and development of optical fiber and cables. He is a chief research associate of Transmission Media Department in Yokohama Research Laboratories.

A NEW DUAL LAYER PRIMARY COATING FOR OPTICAL FIBRES WITH SUPERIOR AGEING BEHAVIOUR AND IMPROVED CABLING PERFORMANCE

G. Kuyt, J.W. Leclercq, A.H.E. Breuls

Plasma Optical Fibre B.V., Eindhoven, The Netherlands

ABSTRACT

A new, dual layer primary coating for optical fibres has been developed which is suitable for application in all cable concepts. Based upon a soft inner primary coating with a very low Tg, excellent microbending resistance is achieved and proven by temperature cycling tests on ribbons and tight buffered fibres. Smooth stripping in all conditions is ensured by a low but stable adhesion of the inner primary coating to the glass. Water soak tests on fibres and ribbons and a mineral oil soak test on fibres confirm the stable adhesion. Mechanical strength, the resistance to fatigue and to ageing in water is excellent as a result of an acid chemistry of the new coating. All results indicate that the new coating is suitable for application in both common loose tube cables and more demanding "tight" cable concepts like ribbon cables and tight buffered fibres.

INTRODUCTION

Optical fibres are now widely used in long-haul telecommunication systems. Also the use of optical fibres in the local loop and in local area networks (LAN's) is becoming economically competitive with copper because passive components are becoming cheaper. For the use of optical fibres in the local loop, other cable concepts than common long-haul loose tube and slotted core have been designed to meet higher requirements on mass splicing, connectorization and flexibility. Tight buffered fibres (rigidity, easy to handle) and fibre ribbons (high fibre density, mass splicing, easy connectorization) fulfil these requirements.

In tight cable concepts, like ribbons and tight buffering, fibres are exposed to lateral forces. These forces can cause additional optical attenuation due to microbending, especially at low temperatures when ribbon matrix material and tight secondary buffer shrink.

When installing fibres in the local loop, fibres will be exposed to wide range of harsh environments like water/high humidity and high/low temperature. It is obvious that more stringent requirements on fibre properties are imposed to ensure optical and mechanical reliability.

The primary coating of the fibre plays a major role in the optical and mechanical performance of fibres.

This paper presents a newly developed dual layer primary coating (DLPC-7). The new coating gives fibres excellent resistance to microbending, high and low temperatures and water or high humidity. The good handling characteristics and optical and mechanical performance of fibres with the new coating makes the new coating suitable for use in both loose tube/slotted core cables and "tight" cable concepts and is therefore a true multi-purpose coating.

FIBRE CHARACTERIZATION

All optical glass fibres used in tests in this paper are made with the plasma activated chemical vapour deposition process (PCVD). Fibres comply with the relevant ITU and IEC documents. Besides matched cladding single mode fibres (MCSM), also multi-mode with a 62.5 µm core (MM 62.5 µm) were tested since they are widely used in LAN's.

COATING CHARACTERIZATION

The new coating is designed to overcome the problems that occur when fibres with most standard coatings are used for ribbons and tight buffering. The inner primary of the standard coating has a relatively high E-modulus of 2.5 MPa and a relatively high glass transition temperature (Tg) of 0°C. Fibres with standard coating exhibit poor resistance to microbending in more demanding "tight" cable constructions at low temperatures.

Standard coatings show a high adhesion to the glass which causes a too high strip force of ribbons and tight buffered fibres. On the other hand, adhesion of standard coatings is not very stable in water and may cause delamination resulting in additional attenuation[1]. Rapid decrease of strength of standard coated fibres in hot water has been reported frequently[2,3,4,5]. This is a problem when fibres in the local loop are exposed to harsh environments.

The new coating is designed to overcome the above mentioned shortcomings of standard coatings. The new inner primary coating has a low E-modulus of 1.5 MPa and a very low Tg of -55°C. The tough outer primary has an E-modulus of 800 MPa and a Tg of 60 °C (all data derived from dynam-

ical mechanical analysis (DMA)). A good resistance to microbending can be predicted based upon the DMA data[6].
The adhesion of the new inner primary coating to the glass has been lowered. Unlike standard coatings, the adhesion level is stable in water and high temperatures. Smooth stripping of fibres, ribbons and tight buffered fibres is ensured under all conditions.
The chemistry of the new coating is more acidic than that of standard coatings. In the new coating, no base groups are present, as these would otherwise catalyze corrosion of the silica fibre. Fibre strength and ageing characteristics are predicted to be better as a result of this improved, balanced coating chemistry.

MICROBENDING SENSITIVITY

The sensitivity to microbending of MCSM and MM 62.5 µm fibres has been investigated. In the microbending test, fibres are wound on a 600 mm diameter drum, covered with sandpaper (40 µm Alox grade by 3M™). The winding force was kept constant at 4 N. Attenuation was measured before and after winding, see table I.

	Attenuation increase		
	MCSM 1310 nm [dB/km]	**MCSM 1550 nm [dB/km]**	**MM 62.5 µm 1300 nm [dB/km]**
New coating	0.8	1.5	5.2
Standard coating	3.2	6.7	9.2

Table I. Comparison microbending sensitivity.

It is clear that fibres with the new coating are far less sensitive to microbending.

TEMPERATURE CYCLING TESTS

The Tg of the new inner primary coating is -55°C. Therefore, temperature should not influence attenuation. To verify this, MCSM and MM 62.5 µm fibres were cycled between -60°C and +85°C. Attenuation was monitored continuously at 1300 (MM 62.5 µm) and 1550 nm (MCSM). Both fibre types showed a maximum increase in attenuation of less than 0.01 dB/km.
In a second test, tight buffered MM 62.5 µm fibres with the new coating were cycled between -55°C and +65°C. These fibres were tight buffered with PVC in one step from 245 µm to 900 µm. The results are shown in figure 1.

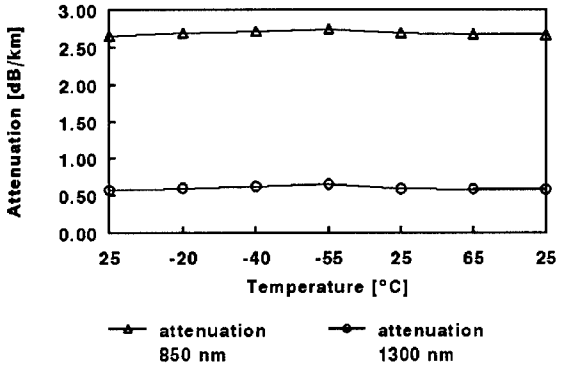


Figure 1. Temperature cycling of tight buffered MM 62.5 µm fibres with the new coating.

The increase in attenuation was less than 0.1 dB/km, indicating that indeed the inner primary stays soft at low temperatures. The inner primary provides good buffering to lateral forces originating from shrinkage of the tight secondary PVC buffer.

COATING STRIPPABILITY

In order to get smooth stripping and comfortable handling of fibre ribbons and tight buffered fibres, the adhesion of the new inner primary coating is lower than that of standard coating. Strip force measurements on fibres with the new coating have been made on both unaged and aged fibres to investigate strip force stability. All strip force measurements were done according to test methods IEC 793-1-B6 (average strip force) and FOTP-178 (peak strip force) at a strip speed of 500 mm/min.

Test condition	Strip force, average [N]	Strip force, peak [N]
23°C 55% relative humidity air, reference	1.4	4.2
Measured at 45°C	1.3	4.0
Measured at 0°C	1.3	3.6
60°C water 3 months	1.3	4.0
95°C 15 minutes	1.3	not available
85°C 85% R.H. 1 month	1.6	3.4
85°C 95% R.H. 1 month	1.6	3.5
70°C 55% R.H. 1 month	1.4	not available
70°C 7 tested filling gels 1 month	1.5-1.7	not available

Table II. Strip force of fibres with the new coating.

It can be concluded from table II that strip forces of the new coating are stable after exposure of fibres to harsh environments. It is also noteworthy that in none of the measurements any remaining particles were found on the glass surface. A clean surface is important as it avoids contamination and misalignments during (mass)-splicing.

ADHESION STABILITY

In the previous paragraph, the strip force of fibres with the new coating was stable in all tested harsh environments, indicating a stable adhesion of the inner primary to the glass. The adhesion stability can also be tested by monitoring attenuation while exposing fibre to a specific (harsh) environment. If adhesion would be affected, delamination of the coating could occur, resulting in a dramatic increase in attenuation.

Water soak test of UV-coloured fibres

MCSM fibres, which were coloured with a UV-curable ink, were immersed in water of 60°C. Attenuation was monitored at 1550 nm. From figure 2, a clear difference between the new and the standard coating is observed. While the fibre with the standard coating shows a maximum increase of 0.2 dB/km and does not relax fully, the fibre with the new coating does not show an attenuation increase at all.

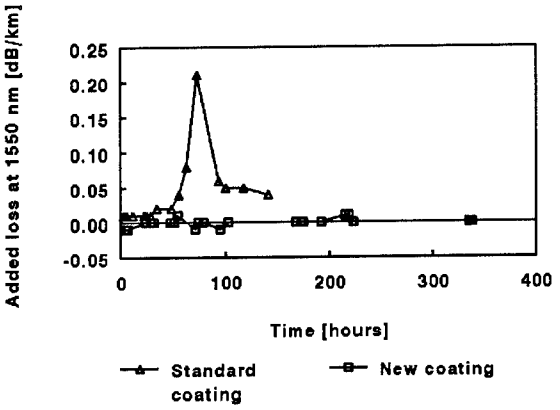


Figure 2. Water soak 60°C of UV-coloured fibres.

Mineral oil soak test

Besides stable adhesion in water, the adhesion in apolar environments like filling gels must be guaranteed. Behaviour in mineral oil is representative of fibre reaction to filling gels. A fibre with the new coating was immersed in mineral oil at 85°C for 7 days and afterwards temperature cycled seven times between -60°C and +85°C. This test is considered to be very severe. Attenuation was measured continuously at 1550 nm. The maximum attenuation increase during immersion at 85°C was 0.05 dB/km, the mean increase was 0.01 dB/km. After the immersion test, the maximum attenuation increase during temperature cycling was less then 0.01 dB/km.

APPLICATION OF FIBRES IN RIBBONS.

The use of optical fibre ribbons is increasing rapidly. The new coating is has been used extensively in ribbon applications. Ribbon processing of fibres and ribbon handling properties are good:

-Good fibre break out, leaving UV ink on the fibre.
-Good ribbon hot-stripping, also after temperature cycling and water soak.
-No remaining coating debris on the glass after stripping.

Temperature cycling of ribbons

It has already been mentioned that the low Tg of the new inner primary provides good buffering of lateral forces on the fibre. Buffering remains effective at temperatures down to -55°C. Temperature cycling between -40°C and +70°C of an encapsulated 4 MCSM fibre ribbon emphasizes the excellent resistance to microbending, see table III:

	Red	Blue	White	Green
Average attenuation increase @ 1550 nm [dB/km]	-0.01	-0.01	0.00	-0.01
Maximum attenuation increase @ 1550 nm [dB/km]	0.00	0.00	0.01	0.00

Table III. Temperature cycling of encapsulated 4-fibre ribbon, made of MCSM fibres with the new coating.

No significant attenuation increase can be observed in the temperature cycling test.

Ribbon water soak 60°C

The water soak test at 60°C is a very critical test for a ribbon. Usually, fibres in the ribbon show an irreversible increase in attenuation after a certain time. This increase is probably due to delamination of the inner primary coating. The high water temperature of 60°C accelerates possible delamination. A ribbon is considered to pass the test if no significant attenuation increase is observed in the first 20 days. Figure 3 shows the attenuation range during 60°C water soak of a four fibre ribbon made of MCSM fibres with the new coating.

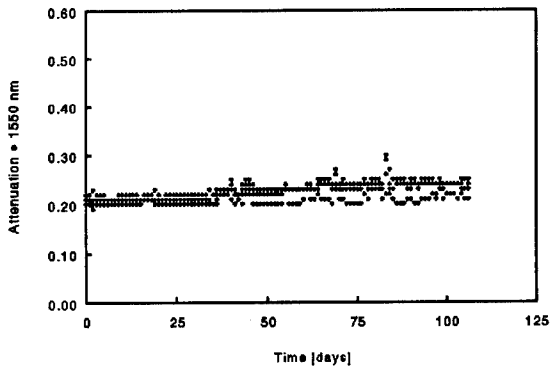


Figure 3. Water soak 60°C of a 4-fibre ribbon, made of MCSM fibres with the new coating.

Although the attenuation range broadens a little after 60 days, the maximum attenuation increase after 105 days was only 0.04 dB/km. These results indicate once again the very stable adhesion of the new inner primary coating.

FIBRE STRENGTH AND AGEING PROPERTIES

Dynamic two-point bending tests

The acid chemistry of the new coating and the absence of basic groups should improve mechanical fibre strength and ageing properties in comparison with standard coatings.
Fibre strength before and after ageing is researched by dynamic two-point bending [2,5]. The dynamic stress corrosion susceptibility factor n, or simply n-value, can be calculated from the dynamic two point bending results. A higher n-value means better resistance to fatigue. Table IV shows dynamic two point bending results for new and standard coating, before and after stress free ageing in water of 60°C and humid air of 85°C/85% R.H.

Coating	Ageing condition	Failure stress σ_f [GPa]	n-value [-]	m-value [-]
New coating	unaged	6.70	29	80-110
	60°C water 3 months	6.84	30	80-120
	85°C 85% R.H. 1 month	6.67	27	80-120
Standard coating	unaged	6.03	20	80-100
	60°C water 3 months	4.01	"28"	30-40

Table IV. Dynamic two point bending results.

Obviously, the new coating provides excellent protection against stress free ageing in hot and wet/humid conditions. On the contrary, standard coated fibres' strength degrades quickly to 4 GPa when immersed in water of 60°C and it was difficult to accurately calculate an n-value due to scattered measurements (low m-value)[7].

Dynamic tensile testing

A dynamic n-value of 32.5 was obtained from dynamic tensile testing of unaged fibres of 1 m length. The result complies with the two point bending test result.

Static fatigue in water of 85°C

Fibres, aged with known applied stresses in water of 85°C, suffer both fatigue (crack growth caused by applied stress) and zero stress ageing. In the corresponding plot of log (lifetime) versus log (applied stress), very often a transition in the slope or "fatigue knee" is observed[2,3]. At low applied stresses, the time to failure is mainly determined by zero

stress ageing. At high applied stresses, fatigue determines time to failure. In water of 85°C, this transition in slope for standard coated fibres occurs rapidly around 2.7 GPa applied stress / time to failure of around 12 days[3]. Figure 4 shows the static fatigue curves for the new coating, the standard coating and, for additional comparison, a prototype of the new coating[2].

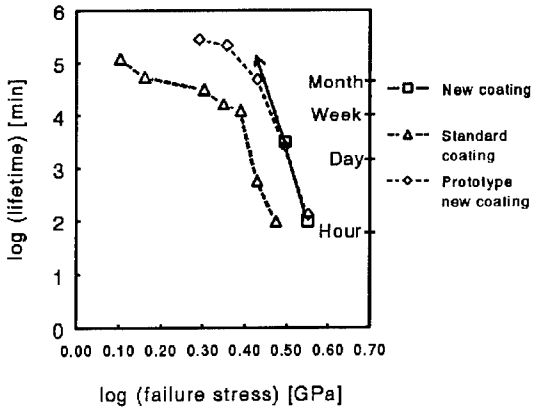


Figure 4. Static fatigue in water of 85°C.

The new coating shows very good resistance to fatigue and no fatigue knee is observed so far. After 70 days, only stress levels of 3.15 GPa and higher did cause break. It is obvious that the new coating provides excellent protection against both fatigue (result of high n-value) and stress free ageing. It seems that the results of the new coating are going to exceed the results of a prototype of the new coating.

CONCLUSION

The proposed dual layer primary coating (DLPC-7) gives fibres excellent resistance to microbending, also at low temperatures, and this resistance is demonstrated best by temperature cycling tests on ribbons and tight buffered fibres. Water soak tests of fibres and ribbons indicate a stable adhesion in hot water and mineral oil. The strip force remains stable after exposure to a wide range of harsh environments.

Furthermore, the new coating gives fibres excellent mechanical resistance against exposure to harsh environments. Both unaged and aged fibres show consistent high strength and high resistance to fatigue (high n-value).

All tests and also large scale field employment indicate that the new coating fulfils all more stringent requirements set by employment of optical fibres in more demanding cable structures. The new coating can be used for all cable concepts and is therefore a true multi-purpose coating.

REFERENCES

1. A. Abel, J. van Eekelen, "Dynamic water sensitivity of U-V acrylate inks and matrix coating, and its relationship to water soak performance of optical fibre ribbons, Proceedings of EFOC&N, p. 298-302, The Hague, The Netherlands, 1993.
2. J.W. Leclercq, A.H.E. Breuls, "Influence of adhesion promoters on the aging characteristics of optical fibers in water", SPIE conference "Fiber optic materials and components", Vol. 2290, p. 64-73, San Diego, USA, 1994.
3. E. Cuellar, M.T. Kennedy, D.R. Roberts, J.E. Ritter, "Zero stress aging and the static fatigue transition in optical fibers", SPIE conference "Fiber optics reliability and testing: Benign and adverse environments", Vol. 1791, p. 7-17, Boston, USA, 1992.
4. L. Oksanen, H. Knuuttila, "Two-point bending and tensile tests on aged fibers with different glass and coating compositions", SPIE conference "Fiber optic materials and components", Vol. 2290, p. 220-228, San Diego, USA, 1994.
5. P.C.P. Bouten, Lifetime of pristine optical fibres, thesis, University of Technology, Eindhoven, the Netherlands, 1987.
6. P.C.P Bouten, D.J. Broer, C.M.G. Jochem, T.P.M. Meeuwsen, H.J.M. Timmermans, "Doubly coated fibres with a low sensitivity to temperature and microbending", Journal of Lightwave Technology, Vol.7 No.4, p.680-686, 1989.
7. T. Svensson, A.H.E. Breuls, "Strength and fatigue of different kind of weak spots from the manufacture of optical glass fibers", SPIE conference "Fiber optic materials and components", Vol. 2290, p. 211-220, San Diego, USA, 1994.

BIOGRAPHY



Gerard Kuyt
Plasma Optical Fibre B.V.
Eindhoven, The Netherlands

Gerard Kuyt was born in Katwijk aan Zee, The Netherlands, in 1950. He received his B.Sc. degree in electronic engineering in 1973. In the same year, he started at Philips Research Laboratories in Eindhoven in a newly formed group on optical communication systems. In 1981, he joined Philips Optical Fibre B.V., now Plasma Optical Fibre B.V., in the measurement and application group. Currently, he is product manager. He is involved in international standardization in ITU SG15, IEC 86A en CECC WG28.



Jan-Willem Leclercq
Plasma Optical Fibre B.V.
Eindhoven, the Netherlands

Jan-Willem Leclercq was born in Eindhoven, the Netherlands, in 1968. He received his M.Sc. degree in chemical engineering in 1991. In 1992, he joined Philips Optical Fibre B.V., now Plasma Optical Fibre B.V. As a project leader in the research and development group, he is responsible for development of coatings for optical fibres.



Anton H.E. Breuls
Plasma Optical Fibre B.V.
Eindhoven, The Netherlands

Ton Breuls was born in Urmond, The Netherlands, in 1956. He received his M.Sc. degree in applied physics in 1982. He worked at PTT research Leidschendam, The Netherlands, from 1982 to 1984. In 1984 he joined the Philips Glass Division, Eindhoven, the Netherlands. Since 1987, he has been working at Philips Optical Fibre B.V., now Plasma Optical Fibre B.V. Since 1990, he has been manager of the research & development group of Plasma Optical Fibre. He is chairman of COST 246 work group 1.1.

AUTHORS INDEX

Name	Page
ABADIA, V.	569
ADAMS, M.	16, 786
AGRETTI, M.	675
AKASAKA, N.	865
ALADENIZE, B.	745
ALOISIO, JR., C. J.	139
ALVAREZ, R.	112
AMIN, S.	325
ANDREASSEN, J. S.	310
ANELLI, P.	756
AOUSTIN, H.	217
APPLEGATE, D.	176
ARAKI, S.	151, 616
ARIKAWA, T.	85
ARMBRUSTER II, P. F.	558
ASANO, K.	255
ASHBY, M.	366
ASIYA, F.	688
ATOBE, N.	169
AUVRAY, M.	359
AZUMA, Y.	372
BACON, F.	162
BAPTISTE, M.	840
BARRAUD, J. Y.	330
BASTIDE, C.	563
BEEBE, E.	58
BÉLANGER, M.	288
BENNETT, G. R.	835
BERTHELSEN, G.	47
BETTEN, E.	587
BILODEAU, J.	702
BISHOP, J.	192
BISWAS, D. R.	317
BIZEUL, J. C.	347
BJERKELI, T.	587
BLANCHARD, A. M.	217
BLUME, G. S.	490
BOEDEKKER, J.	808
BÖHME, R.	786
BOITEL, M.	217
BONICEL, J. P.	800
BONIORT, J. Y.	330, 343
BOSCHER, D.	347
BOSISIO, C.	756
BOTTANELLI, M.	675
BOTTMAN, J. S.	404
BOURRAT, G.	563
BOWMER, T. N.	720
BREHM, C.	343
BREULS, A. H. E.	872
BREWER, D. A.	387
BRICKEL, J. J.	58
BRINGUIER, A. G.	29
BRODE, F.	569
BÜHLER, F.	735
BURKE, B.	269
CABALLERO, J. A.	835
CAMARA, S.	668
CARRATT, M.	353
CARTER, C. N.	771
CAUDILL, L. M.	432
CESHNOY, J.	343
CHANG, T.-C.	507
CHAPIN, J. T.	432
CHARLES, Y.	199
CHAVEZ, O. G.	720
CHEN, K. Y.	445
CHEN, K.-Y.	502, 507, 554, 599
CHEN, W.-J.	507
CHEN, Y. W.	445
CHIBA, K.	104
CHIEN, W.-S.	445
CHOU, S.-H.	502
CHRAPLYVY, A. R.	42
CHUANG, H.-J.	445
CISTERNINO, F.	654
CLARK, L.	42
CLYBURN III, C. E.	29
COBB, T. R.	284
COCKRILL, K. J.	540
COMEZZI, G.	668
COMIZZOLI, R. B.	432
CONSONNI, E.	756
COSTELLO, M.	479
COTTINO, E.	654
COUVRIE, G.	563, 800
CRONK, B. J.	162
CROSS, J.	126
CURADO, P. J. P.	662
CURRAN, M.	52
CURTIS, D. I.	183
CUSANELLO, V. A.	335
D'AMICO, J. N.	720
DAEMS, D.	649
DAGUET, B.	583
DAI, Y.-D.	37
DALGOUTTE, D. G.	569
DANESHVAR, O.	763
DARSEY, J.	176
DAVIES, M. V.	540
DEBSKA, A.	479
DISSADO, L. A.	192

Name	Page
DIVITA, S.	325
DOBLE, I.	192
DRUEZ, J.	702
DUECKER, D. C.	528
DUNN, L. R.	42
DUPUY D'ANGEAC, G.	5
DURHAM, R. T.	829
DWIVEDI, A.	305, 848
ECKARD, A.	479
EMIG, K.	366
EMMERICH, M.	569
ENDO, S.	157
ETTER, H.	574
FANGMANN, R. E.	42
FARGAHI, A.	574
FEDOROFF, M.	366
FILHO, J. E.	662
FINAN, J. M.	728
FLAHERTY, S.	807
FLEISCH, K. A.	740
FRANTZ, R. A.	71, 146
FRIESEN, H. W.	261
FUJIMORI, A.	513
FUJITA, M.	22, 622
FURUKAWA, H.	239
FURUKAWA, S.	169, 640
GADONNA, M.	563
GAILLARD, P.	353, 668
GAILLE, F.	96
GALLAGHER, D.	366
GANDHI, P.	432
GAO, X.-P.	37
GARVEY, P. T.	848
GAUTUN, J. C.	668
GEBIZLIOGLU, O. S.	457, 519
GINOCCHIO, A.	756
GIRBIG, R.	786
GLESSNER, B.	546
GOARIN, R.	359, 840
GOFF, L. J.	728
GOTO, S.	169
GOURONNEC, A.	353, 359, 840, 857
GRAJEWSKI, F.	794
GREEN, J.	682
GRIFFIOEN, W.	857
GRIMADO, P. B.	519
GROLLEAU, G.	668
GRUNE, G. L.	269
GUEGUEN, J. J.	217
HAAG, H.	546, 794
HALE, P. G.	387
HAN, H. S.	449
HARA, M.	468
HASHIM, A.	397, 416
HASHIMOTO, D.	438
HATTORI, T.	865
HAYAMI, S.	627
HAYASHI, Y.	239
HAYES, T. M.	278
HEDE, J. C.	563
HERRERA, R.	112
HESS, D.	808
HEYDA, R.	176
HILL, J.	763
HOCHULI, M.	735
HOFFART, M.	546
HÖG, G.	546, 794
HOLDER, J.	16
HOLLENSETT, K.	52
HONDA, Y.	688
HONDO, H.	104, 468
HONJO, M.	79
HOOD, J. M.	4
HOPLAND, S.	212, 592
HORE, L. M.	720
HORIE, Y.	104
HOSOKAWA, S.	63
HOSOKAWA, T.	817
HOSOYA, H.	255
HSIAO, C.-M.	502, 507
HSIEH, C.-H.	599
HSU, H.-P.	502, 507, 599
HUFF, R. G.	42
HWANG, Y.-H.	599
IMAMURA, K.	22, 622
INUIZAWA, Y.	438
IRIE, S.	438
ISHIDA, K.	616
ITO, M.	485
IWATA, H.	627
IZUMITA, H.	372
JACKSON, K. W.	635
JACOBSON, M.	728
JACOBSON, N. J.	335
JANSEN, U.	800
JARVIS, D.	735
JOHANSEN, M.	47
JOHNSON, L.	807
JOHNSON, R.	569
JONES, M. E.	740
JUDY, A. F.	42
KALISH, D.	42, 176
KAMEI, Y.	438
KANAI, K.	250
KANAI, T.	232
KATSURA, H.	79
KAWANO, T.	485
KECK, D. B.	3
KELLER, D. A.	786
KEON, B. J.	146
KIKUCHI, Y.	85
KIM, P. K.	635

Name	Page
KIM, S. H.	449
KIMURA, T.	380
KING, W. W.	139
KISH, P.	134, 682
KLEIN, A.	176
KOBAYASHI, K.	151, 463, 616
KOEMAN, H.	404
KOKUBUN, T.	640
KOMIYA, T.	513
KOYAMA, T.	22
KOYAMADA, Y.	640
KOYASU, O.	205, 778
KUBO, Y.	157
KUBOTA, A.	535
KUGA, T.	817
KUMAR, N.	325
KUMMER, R. B.	42, 176
KURKJIAN, C. R.	317
KUSAYANAGI, T.	535
KUYT, G.	872
LAI, K.-H.	554
LAI, V. A.	497
LANG, I. D.	540
LANG, J. L.	183, 752
LARSSON, C.	786
LATINI, M. E.	662
LAUMER, J. W.	162
LE GOFF, G.	392
LE MARER, R.	217
LE MOIGNE, G.	359, 840
LE NIR, V.	288
LE ROUZIC, J.	392
LE SERGENT, C.	343
LEA-WILSON, N. D.	569
LECLERCQ, J. W.	872
LECOQ, D.	392
LEE, C.-C.	554
LEE, L. Y.	823
LESUEUR, P.	392
LIBERT, J.-F.	183, 199, 583, 745
LIGHT, M. C.	8
LIN, H.-F.	599
LIN, J.-C.	502
LIN, Y.-C.	502, 507, 599
LOCHKOVIC, G. A.	472
LOUBOUTIN, J. P.	347
MAGLIO, M.	224
MAHÉ, T.	217
MÄKITALO, O.	6
MAKWINSKI, M.	397
MANN, X.	763
MARRA, L.	176
MARTRET, J.	840
MARUOKA, T.	151
MATSUDA, Y.	865
MATSUMOTO, N.	627
MATSUO, N.	380
MATSUOKA, R.	468
MAUGUEN, C.	347
MCCALLUM, W. J.	8
MCCANN, G. R.	604
MCNUTT, C.	16
MEIXNER, A.	176
MENDES FILHO, M.	662
MILES, S.	808
MITSUHASHI, K.	616
MIYAMOTO, M.	205, 463, 616, 778
MIZUTANI, A.	157
MOGI, A.	205, 778
MOORE, K.	305
MOORE, R.	176
MOORE, R. C.	139
MOORMAN, M. L.	528
MORELLEC, D.	217
MORITA, S.	513
MOSER, J. M.	162
MURASE, T.	485
MURATA, A.	151
NAGANUMA, T.	513
NAGANUMA, Y.	157
NAGASAWA, S.	627
NAGAYAMA, A.	63
NAITO, Y.	513
NAKAMURA, E.	627
NARUSE, Y.	817
NEGISHI, K.	104
NEVEUX, JR., P. E.	490
NGUYEN, C.-T.	702
NICHOLS, I. V.	771
NISHIDA, Y.	232
NISHIMURA, A.	85
NISHIO, S.	169
NOMURA, Y.	239
NORRIS, J. C.	422
NOTHOFER, K.	546
NOUCHI, P.	343
NOVACK, J. C.	162
NOZAWA, M.	627
NUMATA, T.	169
OBI, K.	622
OCHSNER, J.-C.	96
OGUCHI, S.	63
OHIRA, F.	232
OKADA, N.	463, 616
OMURA, H.	380
OOHASHI, K.	151, 616
ORCEL, G.	330
OSAKA, K.	245
OTAKE, A.	468
OVERTON, R. J.	330
PATTERSON, R. J.	91
PECKHAM, D.	176

Name	Page
PECKHAM, D. W.	42
PÉCOT, A.	217, 392
PEI, C.-C.	599
PEINS, G. A.	432
PEREIRA NETTO, A. C.	662
PERETTA, P. G.	654
PERRIN, G.	217
PETNER, M. F.	91
PHILEN, D. L.	176
PITASSI, S.	224
PIXLEY, H. D.	694
PLATT, C. A.	771
PLITZ, I. M.	457, 519
POOLE, N. J.	540
POZZOLI, M.	809
PRITCHARD, R. C.	412
RABINE, B. A.	162
RAGNI, A.	569
RAUCHS, J.	668
REED, W. A.	42
REITH, L. A.	58, 71, 519
RICCARDI, E.	654
RIECH, V.	52
ROBERTS, D. E.	823
ROSENMAYER, T.	497
ROWLAND, S. M.	771
RUELLE, F.	745, 752
SAITO, K.	104
SAITO, M.	468
SAITO, Y.	157
SAITOH, T.	63
SAKAI, T.	485
SAKUYAMA, Y.	169
SANDERS, M. M.	192
SANO, A.	205, 463, 778
SANO, T.	245
SANSONETTI, P.	343
SASAKURA, K.	63
SATO, Y.	104
SAWANO, H.	616
SCHWIERING, C.	713
SCIACERO, J. R.	119
SEIDENBERG, J.	713
SEO, G. W.	449
SHAPIRO, S.	176
SHEN, G. X.	37
SHEU, T.-J.	445
SHIMOJI, N.	250
SHINMURA, K.	688
SHINODA, Y.	380
SHIONO, T.	485
SHIRAISHI, K.	485
SHOJI, T.	232
SHUSTACK, P. J.	740
SIBA, Y.	688
SIDDIQUI, S.	176
SIKORA, E.	212, 305
SINCLAIR, J. D.	432
SINGH, B.	325
SKULAND, K.	47
SLETTEN, G.	47
SLETTEN, G. M.	310
SMITH, J. L.	848
SOLLENBERGER, N. W.	635
SORDO, B.	654
SPANO, V.	224
STEMPFEL, O.	563
STIEB, W.	794
STOKES, S. R.	490
STUPAK, P. R.	335
SUDA, H.	640
SUPCZAK, M. J.	335
SUZUKI, R.	616
SVENSSON, T.	857
TAHA, A. J.	771
TAKAHASHI, I.	640
TAKEDA, T.	622
TAKEDA, Y.	817
TAKIZAWA, K.	85
TAMARU, N.	232
TANAKA, H.	22
TANAKA, K.	169, 817
TANIFUJI, T.	298, 579, 627
TANKA, H.	622
TATAT, O.	16, 786, 800
TAYLOR, C.	176
THALMAN, W.	479
THEODOSSI, C.	574
THOMAS, J. J.	42
THOMASMEYER, C.	807
THORNTON, J.	558
THROCKMORTON, R.	52
TKACH, R.	42
TONYALI, K.	823
TSAI, F.-Y.	445, 554
TSUTSUMI, M.	627
TUMINARO, R.	176
TURNER, K. T.	528
UEDA, T.	79
UKACHI, Z.	513
URANO, A.	865
VALLESTERO, N.	325
VENGSARKAR, A. M.	42
VEST, B. L.	823
VINTERMYR, I.	587
VITA, G.	809
VOGEL, E. M.	58, 146
VOLOTINEN, T.	857
VUILLAUME, G.	353
WAGMAN, R. S.	8, 472
WALKER, K. L.	42
WALLING, J.-H.	288, 702

Name	Page
WANG, C.-Y.	445
WARGOTZ, W. B.	192
WATANABE, K.	205, 463, 778
WATANABE, T.	245, 622
WHITE, K. T.	472
WIDLER, R. A.	829
WILLIAMS, R. H.	325
WILSON, P.	857
WOLFE, S. V.	192
WORTHINGTON, P.	183
YAGUCHI, S.	535
YAMAGUCHI, J.	232
YAMAMOTO, F.	640
YAMANISHI, T.	79
YANAGASE, H.	250
YANAGAWA, K.	126
YANG, H.	16
YAO, B.-S.	37
YASOUKA, T.	22
YEAP, T.	682
YOKOSUKA, H.	85, 239, 255
YOSHIDA, K.	372
YOSHINUMA, M.	535
YOSHIZAWA, N.	298, 579
YOSHIZAWA, T.	63
YUCE, H. H.	317
ZAMMIT, M. J.	457
ZAMZOW, P. E.	713
ZANCA, F.	569
ZHONG, Q.	192
ZIMMERMANN, H.	574
ZIMMERMANN, W. S.	735
ZUCCHINALI, A.	224

44TH INTERNATIONAL WIRE AND CABLE SYMPOSIUM (IWCS)
SYMPOSIUM COMMITTEE

IWCS STAFF

ELMER F. GODWIN
(President/Director)
GEF Associates
3A Buttonwood Drive
Shrewsbury, NJ 07702
Tel: (908) 741-8864 (Home)
Tel: (908) 389-0990 (Office)
Fax: (908) 389-0991 (Office)

IRVING KOLODNY
(Director's Assistant)
80-56 230th street
Bellerose Manor, NY 11427
Tel & Fax: (718) 464-9197

PAT HUDAK
(Administrative Assistant)
174 Main Street
Eatontown, NJ 07724
Tel: (908) 389-0990
Fax: (908) 389-0991

1995 OFFICERS

BRIAN D. GARRETT
(Chairman)
CommScope, Inc.
P.O. Box 879
Claremont, NC 28610
Tel: (704) 459-5003
Fax: (704) 459-5097

RICHARD ROSSI
(Vice-Chairman)
General Cable Co.
160 Fieldcrest Ave
Edison, NJ 08837
Tel: (908) 417-3132
Fax: (908) 225-3185

XAVIER MANN
(Secretary)
AT&T Fitel
201 Adamson Industrial Blvd
Carrollton, GA 30117
Tel: (770) 830-6616
Fax: (770) 836-8820

INGE B. KOVACS
(Treasurer)
Polycheck Ltd
264 Harvard Drive
Hackettstown, NJ 07840
Tel: (908) 852-1610
Fax: (908) 852-1518

1995 COMMITTEE MEMBERS

NILS ARTLOVE
Telia AB
Network Services
S-123 86 Farsta, Sweden
Tel: +46-8-7131212
Fax: +46-8-7132926

DR. STEPHEN HORNUNG
120/B67
British Telecom Laboratories
Martlesham Heath
Ipswich IP5 7RE
United Kingdom
Tel: +44-1473-644685
Fax: +44-1473-644142

DR. KOICHI INADA
Fujikura Ltd.
Opto-Electronics Laboratory
1440 mutsuzaki, sakura-shi
Chiba-ken 285, Japan
Tel: +81-43-484-3940
Fax: +81-43-484-3988

LAURENCE JONES
Borealis Compounds, Inc.
176 Thomas Road
Port Murray, NJ 07865
Tel: (908) 850-6200
Fax: (908) 850-6268

DR. FELIX P. KAPRON
Bellcore
445 South Street, MRE-2J174
Morristown, NJ 07960-6438
Tel: (201) 829-5225
Fax: (201) 829-5965

DR. MAREK KAPUSCINSKI)
Northern Telecom Ltd.
150, Montreal-Toronto Blvd
Lachine, Quebec
Canada H8S 1B6
Tel: (514) 639-2328
Fax: (514) 639-2337

DR. JOYCE P. (CHIP) KILMER
Optotec, N.A.A.
Suite 300
151 First Ave
New York, NY 10003
Tel: (212) 475-0093
Fax: (212) 475-0625

PAUL M. KOPERA
Anixter Inc.
4711 Golf Road
Skokie, IL 60076
Tel: (708) 677-2600
Fax: (708) 674-3045

JAMES R. LEECH
Union Carbide Corp
Weston Canal Center
P.O. Box 450
Somerset, NJ 08875-0450
Tel: (908) 271-7935
Fax: (908) 271-7949

MICHEL ROUSSEAU
Alcatel Cable
30, rue des Chasses
BP 309
92111 Clichy Cedex
France
Tel: +33-1-4756-6900
Fax: +33-1-4756-6739

JOHN R. SICOTTE
Corning Inc
35 W. Market St,; MP-RO-03
Corning, NY 14831
Tel: (607) 974-4447
Fax: (607) 974-7549

DR. HOWARD WICHANSKY
Cdr, US Army CECOM
ATTN: AMSEL-RD-ST-WL-AW
Fort Monmouth, NJ 07703-5203
Tel: (908) 427-4713
Fax: (908) 427-2150

ADVISORY

DR. PETER R. BARK
Siecor Corporation
P.O. Box 489
489 Siecor Park
Hickory, NC 28603
Tel: (704) 323-6205
Fax: (704) 323-6264

LEO CHATTLER
DCM Industries, Inc.
2930 Faber Street
Union City, CA 94587
Tel: (510) 429-9500
Fax: (510) 429-1250

MICHAEL A. DELUCIA
Naval Surface Warfare Center
Carderock Div, Annapolis Detach.
Energy R&D Office, Code 859
Annapolis, MD 21402-5067
Tel: (410) 293-9503
Fax: (410) 293-2875

DAVE FALLOWFIELD
AGT Limited
10020 100 St - Floor 22B
Edmonton, Alberta
Canada T5J 0N5
Tel: (403) 493-3807
Fax: (403) 493-4829

DIETER S. NORDMANN
(European Representative)
Kabelmetal Electro GmbH
P.O. Box 260; Kabelkamp 20
D30179 Hannover, Germany
Tel: +49-511-676-2020
Fax: +49-511-676-2664

MANUEL R. SANTANA
AT&T Bell Laboratories
2000 NE Expressway; Rm 1D32
Norcross, GA 30071
Tel: (770) 798-2754
Fax: (770) 798-4654

CONSULTANTS

DR. REINER J. GERDES
Gerdes Consulting & TransTel Group Inc.
812 Oakdale Rd., N.E.
Atlanta, GA 30307-1210
Tel: (770) 368-8343
Fax: (770) 368-8382

DR. RAYMOND E. JAEGER
SpecTran Corporation
50 Hall Road
Sturbridge, MA 01566
Tel: (508) 347-2261
Fax: (508) 347-2747

HANS A. MAYER
Olex Cables (A Division of Pacific Dunlop Ltd.)
207 Sunshine Road
Tottenham, VIC 3012
Melbourne, Australia
Tel: +61-3-9281-4240
Fax: +61-3-9314-1436

NOTES